ANL-5800
SECOND EDITION

1524

REACTOR PHYSICS CONSTANTS

July 1963

Prepared by
ARGONNE NATIONAL LABORATORY
Operated by
The University of Chicago
Under Contract with the U. S. Atomic Energy Commission

Published by
UNITED STATES ATOMIC ENERGY COMMISSION
Division of Technical Information

For sale by the Superintendent of Documents, U.S. Government Printing Office
Washington 25, D.C. - Price $6.00

PREFACE

The primary objective of the Reactor Physics Constants Center (RPCC), Argonne National Laboratory, is the periodic compilation and publication of the latest and best values of the constants, recipes, formulae, etc., which are necessary to calculate reactor characteristics. In addition to providing a unified compilation of pertinent data, the precepts of the RPCC are: (1) to encourage critical comparison of experiment with theory; (2) to encourage critical analysis of experimental techniques; (3) to encourage critical evaluations of contradictory data; and (4) to call attention to areas where further experimental and theoretical work will be most profitable; (5) to promote standardization in definitions of reactor physics parameters; and (6) to serve as a clearing house for reactor physics constants.

In this second edition of Reactor Physics Constants, the editors have assumed the prerogative to a somewhat greater degree than in the first edition (1958), of evaluating the data selected for publication. However, the absence of a particular set of data is not to be construed as an adverse judgment by the editors; in many instances, the editors were unaware of the existence of such information, or they may have decided that the information did not fit properly into the framework of the compilation. Furthermore, because of the wealth of material evaluated, and owing to space limitations for each subject, certain data are included and comparably good data are excluded. In such cases, the included data are intended to exemplify some facet of reactor physics.

More specifically, properties of elements and reactor materials, published in the 1958 edition (Section 9), have been excluded since these subjects are treated extensively in appropriate handbooks. Section 9 in this edition is devoted to a summary of constants necessary to the interpretation of counting data, and the properties of neutron sources.

The pronounced interest in high-speed computing machinery has justified the addition of a section on digital computer codes. The content of Section 10 does not exhaust the library of available codes; rather it is an outline of programs selected by the editors and their consultants on the basis of versatility and reasonably widespread usage by reactor physicists.

Other changes have been made in the constitution of data in some sections. For example, since reactor control and dynamics are pertinent to all reactor types, the treatment of these subjects has been almost completely removed from Sections 3 and 4 of the 1958 edition, and incorporated into a section entitled accordingly (Section 5) in this edition.

The editors recognize that certain topics in this edition have been and, in some cases, still are the subjects of more comprehensive, single-volume compilations by other AEC-affiliated sites and subcontractors. For example, much of the material in Sections 1 and 2 is compiled, evaluated, and published periodically by the Brookhaven Cross Section and Evaluation Group. These data have been included, in part, for the convenience of the reactor physicist who has occasional use for such information; they do not infer duplication of effort on the part of the RPCC. Whether this material will be updated in subsequent editions of Reactor Physics Constants will depend largely upon the degree of regularity with which the Brookhaven compendia are published.

In other instances, the data are abridged considerably in order to effect a smooth transition, with appropriate reference, to more comprehensive treatments of specific subjects. Section 8 on shielding constants falls within the scope of transition material and probably will be omitted from future editions by RPCC.

The compilation of the second edition is based on data available on March 15, 1961. More recent material has been included in some sections; however, the reader should not consider such data as

completely authoritative. Further, contributors from outside Argonne National Laboratory did not have the opportunity to review the text based on their contributions and are, therefore, not responsible for any misinterpretation of their data.

Section 1 contains data associated with the fission process, and as such is not confined to any particular reactor type; for example, values for the delayed neutron parameters do not include weighting factors for relative effectiveness. Effective values for the delayed neutron fraction are properties of a specific reactor and, hence, are included in the section which treats on that class of reactors.

The selected cross section data in Section 2 include, for convenience, some duplication of counterpart data available in the BNL publications. The fission cross sections and the angular distribution cross sections for various materials and energies are presented in a form especially suitable for reactor calculations. The scattering law at thermal energies is discussed at some length because of its importance in reactor physics analysis.

Sections 3 and 4 cover the statics of thermal homogeneous and heterogeneous reactors, respectively. In these sections, the problem of delineating the scope of the compilation becomes acute, since theory is much entwined with the constants necessary for the calculation of such reactors. In general, theory has been included to the extent considered necessary for exposition of the data. Also, certain criteria have been exercised with respect to the arrangement and possible overlap of material between the two sections. Unless specifically pertinent to the lattice structure of the reactor, the material is included in Section 3 on homogeneous systems. Some topics, resonance capture for example, are discussed in both sections. Certain considerations not related to the lumping of the fuel are given in Section 3. Resonance captures which primarily result from the lumping of fuel, are discussed in Section 4. The related material in Section 3 is not repeated, although it is of equal importance in the treatment of resonance capture in lumps.

Section 5 contains information pertinent to the analysis of control effectiveness, long-term changes, reactor kinetics, stability, and excursions in thermal reactors. With some exceptions, the theoretical aspects are defined as deemed necessary to the understanding of the data presented.

Sections 6 and 7 treat on multigroup calculation methods for intermediate and fast reactors. The scope of the compilation includes tables of representative multigroup constants, integral fast neutron physics data with emphasis on parameters for simple system analysis, and corresponding data for more complex reactor prototypes.

Section 8 is somewhat marginal within the scope of this compilation. The basic shielding constants are included for the convenience of the reactor physicist who occasionally utilizes such data although shielding problems may not be his primary interest. The basic data are supplemented by numerous references to more comprehensive manuals and reports available for the shielding specialist.

Section 9 summarizes those constants necessary for the interpretation of counting data, and the properties of neutron sources. The topics include a review of the perturbations caused by detecting foils, the interpretation of cadmium-covered counting data, scintillator constants and gas constants appropriate to counting chambers, along with range-energy relationships and atomic and molecular stopping cross sections. Constants related to the absorption and scattering of alpha and beta radiation in foil counting and of the charged recoil or reaction particles in neutron counting are outlined in Sections 9.5 and 9.6. Spectra and/or yields of both artificial and spontaneous fission neutron sources are presented in tabular form.

Section 10 describes computer programs used in reactor physics and reactor design. The intent of the descriptions of these programs is not only to show what is available in a given area, but also to permit a potential user to decide whether a given code suits his needs, or should be studied further and adapted to a specific problem.

The publication of the second edition represents the combined efforts of many people. The format and the guiding principles of the compilation were originated and exercised by a committee of Consultant Editors: W. C. Redman (Sections 1 and 9); H. H. Hummel (Sections 2 and 6); B. I. Spinrad (Sections 3 and 4); R. Avery (Sections 5 and 8); and D. Okrent (Sections 7 and 10). A group of editors, assisted by a number of Argonne staff members, conducted the literature search and prepared the manuscripts for the various sections. Unless otherwise indicated, the editors are members of the Reactor Engineering Division, ANL.

Section 1 was prepared by A. B. Smith. Information pertaining to the detailed formulation of fission product yields was supplied by S. Katcoff (BNL). Supplementary data were furnished by members of the Applied Nuclear Physics Section at Argonne.

Section 2 was prepared by P. J. Persiani. P. A. Moldauer contributed to Sections 2.3 and 2.4.2.

Section 3 was prepared by several authors. Sections 3.1 and 3.2 were written by C. N. Kelber; Sections 3.3 and 3.4 by B. J. Toppel; and Sections 3.5, 3.6, and 3.7, by D. H. Shaftman. E. F. Bennett collaborated in the writing of Section 3.7, and P. J. Persiani prepared Section 3.6.4.1.

Section 4 was prepared by C. N. Kelber. C. H. Westcott (Chalk River) contributed the information on spectral hardening. Additional information was provided by W. C. Redman, P. F. Gast (Hanford), A. Jeffry (Rolls-Royce Ltd.), I. Carlvik (AB Atomenergi), H. J. Wheeler, and B. J. Toppel.

Section 5 was prepared by E. M. Pennington, with contributions by K. K. Almenas, C. E. Cohn, J. W. Meadows, Z. A. Akcasu, V. Z. Jankus, and D. P. Moon.

Section 6 was written by B. J. Toppel. D. Callihan (ORNL), J. Stehn and H. B. Stewart (KAPL), R. Stark and P. Greebler (General Electric Co.), G. E. Hansen, W. H. Roach, G. Bell, and C. Mills (LASL), and R. Finke, E. Goldberg, and G. Grammens (Livermore), contributed unpublished experimental work, supplied preprints of unpublished experiments, and offered helpful advice.

Section 7 was prepared by W. B. Loewenstein and D. Meneghetti. Members of the ANL-ZPR-III staff supplied data prior to publication.

Section 8 was prepared by A. D. Rossin, with the assistance of A. E. McArthy, and of M. Grotenhuis (International Institute of Nuclear Science and Engineering, ANL). K. Shure (WAPD), F. Maienshein (ORNL), H. Goldstein (NDA), H. E. Hungerford (APDA), and C. C. Horton (Rolls-Royce, Ltd.) were particularly helpful in supplying data and suggestions.

Section 9 was prepared by R. Doerner. F. Helm contributed generously to the contents of Section 9.1. J. Schloser (Hanford) furnished tables of exponential integrals, and R. H. Ritchie (ORNL) supplied tables of his $g(\gamma,\tau)$ function.

Section 10 was prepared by Mrs. M. K. Butler of the Applied Mathematics Division, ANL, and H. Greenspan with the assistance of J. C. MacAlpine. In preparing Section 10, many of the authors of the computer programs were consulted and appreciation is expressed to them for their cooperation.

L. Templin acted as coordinator for the over-all project and, in collaboration with M. R. Sims, effected the final detailed editing for publication. The efforts of the stenographic staff who typed and proofread the several drafts of the manuscript are gratefully acknowledged. Especial acknowledgment is made of Miss J. Ludwig, Mrs. J. Fiene and Miss J. Schuster who supervised the clerical work as well as assisted in the typing of manuscripts.

Credit should be given to the Drafting Group of the Reactor Engineering Division, in particular, Miss K. C. Delaney, for the excellent rendition of the numerous illustrations; and to the ANL Graphics Arts Department for their assistance in photo-reduction or enlargement of the basic subjects extracted from the various publications.

Appreciation is expressed to the Editors for their permission to use data and illustrations from their respective copyrighted publications.

Hoylande D. Young, Director of the ANL Technical Information Division, assisted by E. N. Pettit, were instrumental in the expediting of publication.

It is not anticipated to publish a third edition for some time. Instead, as new data or improved correlations of various aspects of reactor physics are accumulated, RPCC Newsletters will be the preferred method of compiling. Additionally, errata in this second edition, as discovered, will be reported in the Newsletters.

The success of subsequent editions of the compilation depends very strongly upon the extent to which direct contributions are made to the RPCC. To assist in the preparation of future editions, contributions of new data, criticism of reported results, results of new analyses, comments on the organization and arrangement of presentation and on content of the compilation will be welcomed by the Reactor Physics Constant Center, Argonne National Laboratory, Argonne, Illinois.

L. J. Templin
April, 1961

CONTENTS

SECTION 1. FISSION PROPERTIES

		Page
1.1	INTRODUCTION: FISSION COMPILATION	1
1.2	FISSION ENERGETICS AND YIELDS	1
1.2.1	Fission Energetics	1
1.2.2	Prompt Fission Gamma-Ray Emission	1
1.2.3	Fission Product Yields	1
1.2.4	Fission Fragment Ranges	3
1.3	PROMPT FISSION NEUTRON ENERGY SPECTRUM	11
1.3.1	Experimental Determinations of Prompt Fission Neutron Spectra	11
1.3.2	The $U^{235} + n_{th}$ Prompt Fission Neutron Spectrum as a Function of the Lethargy, u	13
1.4	DELAYED FISSION NEUTRON EMISSION	14
1.4.1	Yields and Half-Lives of Delayed Neutron Groups	17
1.4.2	Delayed Neutron Energies	17
1.4.3	Delayed Photoneutrons in Be and D_2O	17
1.5	FISSION NEUTRON EMISSION	20
1.5.1	Tabulated $\bar{\nu}$ Values	20
1.5.2	Graphical Presentation of $\bar{\nu}$ Values	21
1.5.3	Distribution of ν	22
1.6	SPONTANEOUS FISSION HALF-LIVES	22

SECTION 2. SELECTED CROSS SECTION DATA

2.1	2200-meter/second NEUTRON CROSS SECTIONS FOR NATURALLY OCCURRING ELEMENTS	29
2.2	FISSION CROSS SECTIONS AND RELATED QUANTITIES AS FUNCTIONS OF ENERGY	29
2.2.1	Measurements of η and α	29
2.2.2	Dependence of Fission Cross Sections on Energy	35

SECTION 2. SELECTED CROSS SECTION DATA (Continued)

Page

2.3 CAPTURE CROSS SECTIONS AS FUNCTIONS OF ENERGY 37

2.4 SCATTERING CROSS SECTIONS AS FUNCTIONS OF ENERGY AND ANGLE . . . 40

2.4.1 Energy Transfer and Angular Distribution in the Low-Energy Region for Crystals, Gases, and Liquids 40
2.4.2 Energy Transfer in the kev-Mev Energy Region 47
2.4.3 Angular Distribution as a Function of Energy in the kev-Mev Region . . . 50

SECTION 3. CONSTANTS FOR THERMAL HOMOGENEOUS REACTORS

3.1 THERMAL NEUTRON SPECTRUM 75

3.1.1 The Integral Equation and Basic Solutions in Infinite Homogeneous Media . . 75
3.1.2 General Methods of Solution 76
3.1.3 Scattering Kernels 76
3.1.3.1 Hard Spheres of Unit Neutron Mass 77
3.1.3.2 Hard Spheres of Heavy Mass 77
3.1.3.3 Heavy Crystalline Moderator 77
3.1.3.4 Recent Work on Scattering in Water 77
3.1.3.5 Effective Mass Approximations to Chemical Binding in Water . . . 79
3.1.4 Solutions of the Neutron Thermalization Equations in Special Cases . . . 80
3.1.4.1 Moderation by Monatomic Hydrogen Gas 80
3.1.4.2 Moderation by a Monatomic, Heavy Gas: Asymptotic Solutions . . 80
3.1.4.3 Moderation by a Monatomic, Heavy Gas: Analytical Forms . . . 82
3.1.4.4 Variational Solutions of the Wilkins Equation 84
3.1.4.5 Hydrogen Bound in an Oscillator Potential Well 86
3.1.4.6 Heavy Crystalline Moderator 87
3.1.5 Special Problems in Discontinuous Media 87
3.1.5.1 Thermal Neutron Flux in a Medium with a Temperature Discontinuity 87
3.1.5.2 Effect of Spatial Distribution of Sources 88
3.1.6 Empirical Description of the Neutron Spectrum 89
3.1.6.1 Description of Spectra by Fitting to Monte Carlo Results 89
3.1.7 Experiments on Neutron Spectra 91
3.1.7.1 Measurement of Flux Spectrum in H_2O Poisoned with Boric Acid: Comparison with Theoretical Distribution 91
3.1.7.2 Spectra in Pure Water and in Multiplying Media 93
3.1.7.3 Spectra in Water, Polyethylene, and Zirconium Hydride 94
3.1.7.4 Neutron Spectra from Natural Uranium–Water Lattices 98

3.2 EFFECTIVE CROSS SECTIONS 99

3.2.1 A Variational Calculation for the Effective Thermal Cross Section . . . 99
3.2.2 Westcott's Convention and Effective Cross Section Compilation 101
3.2.3 Amster's Compilation of Thermal Cross Sections 102
3.2.4 Other Methods of Determining Cross Sections 104

3.3 THERMAL-GROUP DIFFUSION PARAMETERS 104

3.3.1 Diffusion Parameters of Thermal Neutrons in Non-Hydrogenous Moderators 105
3.3.1.1 Graphite (Reference Density: 1.60 gm/cm^3) 105
3.3.1.2 Beryllium (Reference Density: 1.85 gm/cm^3) 107
3.3.1.3 Beryllium Oxide (BeO; Reference Density: 2.96 gm/cm^3) . . . 109
3.3.1.4 Heavy Water (Reference Density: 1.1 gm/cm^3). 110

SECTION 3. CONSTANTS FOR THERMAL HOMOGENEOUS REACTORS (Continued)

Page

3.3 THERMAL-GROUP DIFFUSION PARAMETERS (Continued)

3.3.2 Diffusion Parameters in Water 111
3.3.2.1 Thermal Diffusion Length 111
3.3.2.2 Thermal Diffusion Coefficient and Transport Mean Free Path . . . 112
3.3.3 Diffusion Parameters for Thermal Neutrons in Other Hydrogeneous Moderators 115
3.3.4 Thermal-Group Diffusion Parameters in Mixtures of Moderators Containing Neutron Absorbers 118
3.3.5 Comments on Parameters for Thermal Neutrons in Non-Equilibrium Environments 121

3.4 SLOWING-DOWN PARAMETERS IN WELL-MODERATED MEDIA 123

3.4.1 Slowing-Down Kernels and Their Fourier Transforms 123
3.4.1.1 $\overline{P}_\infty(B^2,E)$ for Specific Cases 124
3.4.2 Moments of the Slowing-Down Distribution and Flux from Fission Sources . 125
3.4.3 Ages from Non-Fission Sources 132
3.4.4 Slowing Down of Fission Neutrons in Pure H_2O 135

3.5 NON-THERMAL PARAMETERS FOR MULTIGROUP DIFFUSION THEORY . . . 139

3.5.1 The MUFT 54-Group Library 139
3.5.2 Few-Group Cross Sections for Metal-H_2O Systems Fueled with U^{235} . . . 141
3.5.3 Parameters for One-Group and Two-Group Representations 143

3.6 THE INFINITE MULTIPLICATION FACTOR $k_\infty = \epsilon p_{res}(\eta f)_{eff}$ 149

3.6.1 The Neutron Chain and the Four-factor Formula $k_\infty = \epsilon p \eta f$ 149
3.6.2 The Fast Fission Factor, ϵ; The Fast Effect Factor 150
3.6.3 Epithermal Absorption in an Infinite Homogeneous Medium 155
3.6.3.1 The Integral Equation for the Neutron Collision Density . . . 156
3.6.3.2 Solutions for Special Cases 157
3.6.4 Resonance Absorption in an Infinite Homogeneous Medium 160
3.6.4.1 Resonance Integrals for Infinite Dilution 161
3.6.4.2 Narrow Resonance Approximations to the Collision Density, I_{eff}, and p 166
3.6.4.3 Narrow Resonance Approximations Including Effects of Doppler Broadening and of Scattering Interference 169
3.6.4.4 Effective Resonance Integrals (NN) in Mixtures of Moderators and Either U^{238} or Th^{232} 171
3.6.4.5 Numerical Comparisons of NN, Modified NN, NW, and Modified NW Approximations with Exact Calculations for U^{238}-H Mixtures 174
3.6.4.6 Methods of Computing Effective Resonance Integrals Over Isolated Resonances When First-Order Narrow Resonance Approximations are Unreliable 177
3.6.4.7 Modifications for Finite Media; Multigroup Cross Sections . . . 178
3.6.4.8 The Computation of p_{res} 179
3.6.5 The Effective Value of ηf: $(\eta f)_{eff}$ 179

SECTION 3. CONSTANTS FOR THERMAL HOMOGENEOUS REACTORS (Continued)

Page

3.7 INTEGRAL DATA 180

3.7.1 Critical-Parameter Studies of Uniform H_2O Solutions of Salts of Uranium Enriched in U^{235} 181

3.7.1.1 H_2O Solutions of Highly Enriched UO_2F_2 181

3.7.1.2 A Fitting Formula for Critical Dimensions of Cylinders Containing H_2O Solutions of Highly Enriched UO_2F_2 185

3.7.1.3 Critical Thickness of a Proton-Reflected, Infinite-Slab Solution of Enriched UO_2F_2 (93.2% U^{235}) 186

3.7.1.4 Graphical Summary of Critical Parameters of Aqueous Solutions of Enriched UO_2F_2 (93.2% U^{235}) in Uniform Cores 186

3.7.1.5 Aqueous Solutions of UO_2F_2 with 4.89 wt-% U^{235} Enrichment . . . 187

3.7.1.6 Aqueous Solutions of Highly Enriched $UO_2(NO_3)_2$ (>90% U^{235}) . . . 187

3.7.1.7 Los Alamos Water-Boiler Experiments 192

3.7.2 Effect of Composition and Thickness of Reflectors on the Critical Parameters of H_2O-Solutions of Uranium Salts Highly Enriched in U^{235} . . . 192

3.7.2.1 Aluminum-Walled Cylinders; Reflectors: Steel, Phosphoric Acid, Natural Uranyl Nitrate Solutions, Bismuth, and Water; Effects of Air Gaps in Reflector 192

3.7.2.2 Aluminum-Walled Slabs; Reflectors: Water and/or Styrofoam, Aluminum 192

3.7.2.3 Aluminum-Walled Vessels; Reflectors: Layers of Furfural, Concrete, Graphite, and Water 197

3.7.3 Annotated References for Reactivity Effects of Holes in Reflectors . . . 198

3.7.4 Critical Parameters of D_2O-Reflected H_2O Solutions of Highly Enriched UO_2SO_4: Effects of Temperature and of Reflector Level in HRE-1 199

3.7.5 Critical Parameters of Interacting Arrays of Regular Vessels Containing Aqueous Solutions of Highly Enriched UO_2F_2 202

3.7.6 Critical Parameters of Cylindrical Annular Cores Containing Aqueous Homogeneous Solutions of UO_2F_2 and of U_3O_8 204

3.7.7 Radial Flattening of Thermal Neutron Flux in a Cylindrical Core by Varying the Aqueous-Solution Concentration of Highly Enriched UO_2F_2 . . . 204

3.7.8 Critical Parameters of Highly Enriched UO_3-H_2O Slurries in an Aluminum Cylinder 208

3.7.9 Critical Parameters of Reactors Containing Mixtures of Paraffin and Enriched UF_4 (2 wt-% U^{235}) 209

3.7.10 Critical Parameters of Uniform D_2O Solutions of Natural or Enriched UO_2F_2 209

3.7.10.1 Extrapolations from Exponential Experiments Using D_2O Solutions of Natural UO_2F_2 211

3.7.10.2 Critical Parameters of Graphite-Reflected Cylindrical Cores Containing D_2O Solutions of Enriched UO_2F_2 (45.3 at-% U^{235}) . . . 211

3.7.11 Critical Parameters of Reactors Fueled with Thin Foils of Highly Enriched Uranium and Moderated with Beryllium Oxide 211

3.7.12 Critical Parameters of Reactors Fueled with Thin Foils of Highly Enriched Uranium and Moderated with Graphite 213

3.7.13 Critical Parameters of Aqueous Solutions of Uranium Highly Enriched in U^{233} 217

3.7.14 Critical Parameters of Aqueous Solutions of Plutonium Nitrate 220

SECTION 4. LATTICE CONSTANTS FOR THERMAL HETEROGENEOUS SYSTEMS

Page

4.1 THERMAL UTILIZATION 233

4.1.1 Diffusion Theory 233
4.1.1.1 Effects of Rod Size and Lattice Configuration 234
4.1.2 Spherical Harmonic Method – Isotropic Scattering 235
4.1.3 Spherical Harmonic Method – Linearly Anisotropic Scattering 250
4.1.4 Integral Transport Theory 250
4.1.4.1 Integral Transport Theory in Cylinders 256
4.1.4.2 Integral Transport Theory in Slab Geometry 264
4.1.4.3 Serber-Wilson Method in Slab Geometry 265
4.1.5 Disadvantage Factors from Considerations of Rod Blackness and Extrapolation Length 266
4.1.6 Spectral Hardening 269
4.1.7 Phenomenological and Approximate Formulae 271
4.1.7.1 Empirical Fit to Radial Power Distribution in Natural Uranium Rods in a Large Unit Cell of D_2O 272
4.1.7.2 Analytic Approximation to P_3 Method in Slab Geometry with Linearly Anisotropic Scattering 272
4.1.7.3 Thermal Self-Shielding Factor for Lumps 274

4.2 RESONANCE ESCAPE PROBABILITY 274

4.2.1 Formulae for the Resonance Integrals of Isolated Lumps 275
4.2.2 Equivalence Principles and the Method of Escape Probabilities 277
4.2.2.1 Equivalence Principles for Isolated Lumps 277
4.2.2.2 Equivalence Principles for Lattices 278
4.2.2.3 The Method of Escape Probabilities 278
4.2.3 Corrections to the Surface Area Arising from Shadowing: The Dancoff Correction 280
4.2.4 Monte Carlo Calculation of Resonance Escape 282
4.2.5 Doppler Broadening 293
4.2.6 Resonance Disadvantage Factors 295
4.2.7 Empirical Formulae 295

4.3 FAST EFFECT 296

4.3.1 Fast Fission Factor (ϵ), and Fast Fission Ratio (F) 296
4.3.2 Fast Conversion Ratio and ϵ in Terms of the Fast Fission Ratio (F) . . . 297
4.3.3 Effect of Fast Leakage 299
4.3.4 Interaction Fast Effect 300

4.4 MACROSCOPIC NEUTRON DIFFUSION IN LATTICES 301

4.4.1 Thermal Diffusion Length with No Anisotropy Assumed 301
4.4.2 Diffusion Length with Anisotropy Present 302
4.4.3 Effect of Holes in a Reactor 303
4.4.4 Small-Source Theory 309

4.5 INTEGRAL DATA 311

4.5.1 Light Water, Slightly Enriched Uranium Lattices 311
4.5.1.1 Studies of 1.524-cm Rods 311
4.5.1.2 Rod Diameters Other than 1.524-cm. 317
4.5.1.3 Correlative Plots of Data from Light Water-Uranium Lattices . . . 320

SECTION 4. LATTICE CONSTANTS FOR THERMAL HETEROGENEOUS SYSTEMS (Continued)

Page

4.5 INTEGRAL DATA (Continued)

4.5.2 Light Water–UO_2 Lattices 322
4.5.3 Natural Uranium–Graphite Lattices 327
4.5.3.1 Buckling Measurements for Natural Uranium Rods in Graphite . . 327
4.5.3.2 Measurements on Graphite Lattices 330
4.5.3.3 Exponential Experiments with Graphite-Moderated Uranium Metal Lattices 331
4.5.4 Heavy Water–Natural Uranium Lattices 333
4.5.4.1 Older Work (prior to 1955) 333
4.5.4.2 Recent Work 333
4.5.5 Light Water–ThO_2–UO_2 Lattices 346
4.5.6 Heavy Water–ThO_2–UO_2 Lattices 350
4.5.7 Beryllium–Uranium Lattices 355

SECTION 5. CONTROL AND DYNAMICS OF THERMAL REACTORS

5.1 REACTOR CONTROL 361

5.1.1 Linear Extrapolation Distance for Various Configurations 361
5.1.2 Effective Radii for Various Shapes of Black Bodies 372
5.1.3 Absorption Area Method 373
5.1.4 Reactivity Effects of a Black Cylindrical Rod 377
5.1.5 Interaction Effects of Control Rods 380
5.1.6 Multigroup Control Rod Calculations 387
5.1.7 Control Analysis in Heterogeneous Reactors Using Small-Source Theory . . 392

5.2 LONG-TERM CHANGES 394

5.2.1 Neutron Poisoning by Xe^{135} and Sm^{149} 394
5.2.2 Poisoning Due to Accumulation of Gross Fission Products 400
5.2.3 Isotope Buildup in Thorium Reactors 408
5.2.4 Studies of Isotope Concentration in Uranium–Thorium Reactors 415
5.2.5 Heavy Isotope Buildup and Reactivity Variation of Plutonium–Uranium Systems 418
5.2.6 Irradiation Dependence of σ_{eff} (Pu^{240}) 426
5.2.7 Plutonium Recycle 429
5.2.8 Burnable Poisons 436

5.3 REACTOR KINETICS 441

5.3.1 Effective Delayed Neutron Fraction and Prompt Neutron Lifetime 441
5.3.2 Relation Between Reactivity and Asymptotic Period 445
5.3.3 Reactor Transfer Function 451
5.3.4 Deviation of Observed Period from Asymptotic Period 452
5.3.5 Period Measurements with Source in Reactor 452
5.3.6 Effect of Source on Reactor Transfer Function 453
5.3.7 Fluctuation Experiments 453
5.3.8 Pulsed Neutron Experiments 470
5.3.9 Delayed Photoneutrons 474

5.4 REACTOR STABILITY 476

5.4.1 General Theory of Stability 476

SECTION 5. CONTROL AND DYNAMICS OF THERMAL REACTORS (Continued)

Page

5.4 REACTOR STABILITY (Continued)

5.4.2 Boiling Reactor Stability 480
5.4.3 Xenon Instability 490
5.4.4 Kinetics of Circulating Fuel Reactors 491

5.5 REACTOR EXCURSIONS 493

5.5.1 General Considerations 493
5.5.2 Excursions in Water Reactors 497
5.5.3 Reactor Excursions Limited by Large Prompt Negative Temperature Coefficients of Reactivity 508

SECTION 6. INTERMEDIATE REACTORS

6.1 CONSTANTS FOR INTERMEDIATE REACTOR CALCULATIONS 519

6.1.1 Age-Diffusion Equation 519
6.1.2 Resonance Self-Shielding Considerations 522
6.1.3 Multigroup Constants 523

6.2 REACTIVITY CONSIDERATIONS 525

6.2.1 Doppler Effect 525
6.2.2 Fission Product Capture Cross Section 530
6.2.3 Neutron Temperature Effects 530

6.3 INTEGRAL DATA 531

6.3.1 Beryllium-Moderated Reactors 531
6.3.2 Beryllium Oxide-Moderated Reactors 534
6.3.3 Graphite-Moderated Reactors 538
6.3.4 Hydrogen-Moderated Reactors 544
6.3.5 Deuterium-Moderated Reactors 548

6.4 PARAMETRIC SURVEYS 550

SECTION 7. FAST REACTORS

7.1 CONSTANTS FOR FAST REACTOR CALCULATIONS 555

7.1.1 Multigroup Notation 555
7.1.2 Multigroup Constants 558
7.1.3 Few-Group Constants 580

7.2 INTEGRAL DATA 581

7.2.1 Critical Mass (U^{235}, Pu^{239}, U^{233}, U^{238}, and Th Systems) 581
7.2.2 Shape Factor and Related Information 593
7.2.3 Effect of Inhomogeneity 596
7.2.4 Detector Ratios 596
7.2.5 Material Replacement Experiments 596
7.2.6 Buckling of Bare Systems for Mixtures of Fissile and Fertile Materials, and Diffusion Length in Natural Uranium 599

SECTION 7. FAST REACTORS (Continued)

Page

7.2 INTEGRAL DATA (Continued)

7.2.7 Extrapolation Distances and Reflector Savings for High-Density Uranium Systems 607
7.2.8 Calculated Extrapolation Distances and Reflector Savings for Some Dilute Systems 609
7.2.9 Spectrum-Averaged Cross Sections 611
7.2.10 Integral Measurement of the Capture-to-Fission Ratio (α) 612
7.2.11 Coupled Fast-Thermal Systems 612

7.3 FAST REACTOR DYNAMICS CONSIDERATIONS 617

7.3.1 Prompt Neutron Lifetime Measurements 617
7.3.2 Effective Delayed Neutron Fraction and Inhour Relation 618
7.3.3 Doppler Effect 620
7.3.4 Fast Reactor Kinetics 621

7.4 COMMENTS ON COMPUTATIONAL METHODS 622

7.4.1 Approximations to the Boltzmann Equation 622

SECTION 8. SHIELDING CONSTANTS

8.1 RADIATIONS FROM NUCLEAR EVENTS 629

8.1.1 Prompt Gamma Rays from Fission 629
8.1.2 Equilibrium Gamma Rays from Fission Products 629
8.1.3 Prompt Capture Gamma Rays 630
8.1.4 Inelastic Scattering Gamma Rays 634
8.1.5 Decay of Fission Product Gamma Rays 634
8.1.6 Decay of Gross Fission Product Energy Release 634
8.1.7 Activation Gamma-Ray Data 637
8.1.8 Cross Sections for Photoneutron Production 646

8.2 NEUTRON CONSTANTS 647

8.2.1 Attenuation of Fission Neutrons in Water 647
8.2.2 Removal Cross Section 648
8.2.3 Conversion Factors: Neutron Flux-to-Dose 650

8.3 GAMMA-RAY CONSTANTS 651

8.3.1 Total Gamma-Ray Attenuation Coefficient 651
8.3.2 Energy Absorption Coefficient 651
8.3.3 Buildup Factors 651
8.3.4 Conversion of Gamma-Ray Flux to Dose Rate 651

8.4 SHIELDING PROPERTIES OF CONCRETES 658

8.4.1 Physical Compositions 658
8.4.2 Nuclear Constants 658
8.4.3 Temperature Dependence of Removal Cross Section 658

8.5 CONVERSION FACTORS USEFUL IN SHIELDING CALCULATIONS 658

SECTION 9. CONSTANTS RELATED TO INTERPRETATION OF EXPERIMENTAL DATA

Page

9.1 FOIL ACTIVATION DATA 667

9.1.1 Cross Sections and Neutron Spectra 667
9.1.2 Self-Shielding Function 668
9.1.3 Self-Shielding in Resonance Activation 669
9.1.4 Outer Flux Perturbations 670
9.1.5 Integral Flux Perturbations 671
9.1.6 Flux Distribution Surrounding a Foil 672
9.1.7 Foil Covers 673
9.1.8 Exponential Integrals and Associated Functions 678
9.1.9 Foil Materials and Properties 678

9.2 CHARACTERISTICS OF PHOTOMULTIPLIER TUBES AND SCINTILLATORS . . . 681

9.2.1 Photomultiplier Tubes 681
9.2.2 Neutron-Detecting Scintillators 683
9.2.3 Gamma-Detecting Scintillators 684
9.2.4 Charged-Particle Detecting Scintillators 687

9.3 GAS CONSTANTS FOR NEUTRON DETECTORS 687

9.3.1 Diffusion Coefficients, Mobilities, and Drift Velocity of Heavy Ions . . . 689
9.3.2 Drift Velocity of Electrons 691
9.3.3 Ionization Potentials 691

9.4 RANGE-ENERGY RELATIONS AND ATOMIC STOPPING CROSS SECTIONS . . . 694

9.4.1 Energy Loss by Heavy Ions 694
9.4.2 Energy Loss by Electrons 694
9.4.3 Energy Loss by Fission Fragments 695
9.4.4 Stopping Power Conversion Factors 697
9.4.5 Range-Energy Relations 699

9.5 RADIATOR AND COUNTER PROPERTIES FOR NEUTRON DETECTION 702

9.5.1 Properties of Non-Fission Radiators 702
9.5.2 Properties of Fissionable Linings 702
9.5.3 Corrections for Thick Proton Recoil Radiators 702
9.5.4 Corrections for Thin Radiators 703

9.6 ABSOLUTE FOIL COUNTING 705

9.6.1 Absolute Beta Counting 705
9.6.2 Absolute Alpha Counting 707

9.7 NEUTRON SOURCES 709

9.7.1 Spectra of (α,n) Sources 709
9.7.2 Yields of (α,n) Sources 711
9.7.3 Photoneutron Sources 713
9.7.4 Spontaneous Fission Sources 714

SECTION 10. DIGITAL COMPUTER CODES

Page

10.1 PARAMETER EVALUATION AND WEIGHTING PROCEDURES 719

10.1.1 Resonance Escape and Resonance Region Averages 719
NUREP 720
QUERY 721

10.1.2 Slowing-Down Treatments 724
CASINO 13 724
MUFT-4 724
P1MG 726
PROGRAM 0159 727
PROGRAM 0329, 0366 728
RDR 5 728

10.1.3 Thermal Parameters and Spectrum Calculations 731
COGENT 731
ROUTINE II 732
SOFOCATE 732
SPECTRUM 733
SYZYGY 734
TEMPEST 735
TRAM 735

10.1.4 Flux Computations, Weighting, and Disadvantage Factors 739
CEPTR 739
FLIP 740
HOBO (RE 184) 741
I_2 741
IDIOT 742
RANCH 743
RDR 4 744
ROUTINE V 744
SLOP-1 745
TUT-T5 747

10.2 CRITICALITY SEARCH AND REACTIVITY CALCULATIONS 750

10.2.1 One-Dimensional Geometries 750
AIM-5 750
DMM 752
DSN 753
F2 755
FIRE 757
GNU II 758
PROD II 759
REX 761
UNCLE III, IV 762
VARI-1 763
WANDA 764
ZOOM 766

10.2.2 Two-Dimensional Geometries 773
ANGIE 773
CURE 774
EQUIPOISE 776
FLEER 778
MUG II 779
PDQ 2 781

SECTION 10. DIGITAL COMPUTER CODES (Continued)

Page

10.2 CRITICALITY SEARCH AND REACTIVITY CALCULATIONS (Continued)

TDC 783
UNCLE I, II 784

10.2.3 Three-Dimensional Geometries 789
TKO 789
TRIXY 791
UFO 792

10.3 REACTOR DYNAMICS AND CONTROL 796

10.3.1 Control Cells and Worth Evaluation 796
SCRAM I 796

10.3.2 Burnup 798
BOUT and BOUT II 798
BOX 798
BURNOUT 799
CANDLE 1 800
CUREBO 802
DRACO 803
GPR 805
TURBO 806

10.3.3 Isotope Production 810
CRUNCH 810

10.3.4 Reactor Kinetics and Transfer Functions 812
AIREK II, AIREK III 812
BUM, RE 132 813
K-CODE, ARK-1 814
RE 29, RE 129 815
RE 126, RE 135 816
RE 138 817
RE 171 818

10.4 REACTOR HAZARDS AND SAFETY 820

AX-1 820

10.5 SHIELDING 823

GRACE I 823
HIGH ENERGY SPECTRA MONTE CARLO PROGRAM 824
MIS 825
NIOBE 826
RE 34 826
RE 157 827
SHIELDING 09-0 828
SHIELDING 12-0 829
SPAN-2 829

SUBJECT INDEX 835

687863 O - 63 - 2

Section 1

FISSION PROPERTIES

1.1 INTRODUCTION: FISSION COMPILATION

This compilation of fission properties is limited to those characteristics of the fission process most often utilized in reactor design. The material is based primarily upon microscopic experimental measurements. Some theoretical extrapolation is employed to provide information where it is not experimentally available. The results of macroscopic measurements are omitted due to the usually uncertain interpretation of the experimental data. The neutron-induced fission process is considered only in the incident neutron range: 0 to 14 Mev. Spontaneous fission processes are considered where they are applicable to reactor work, or where their inclusion leads to a better understanding of other applicable fission processes. Charged particle-induced fission is not discussed as it is of no importance in reactor work. Throughout this compilation, a degree of selection is exercised in an effort to provide the "best" information. In so far as possible, such selection is done analytically.

Certainly, this compilation should not be construed as a definitive review of the fission process; the above principles preclude such an interpretation.

1.2 FISSION ENERGETICS AND YIELDS

1.2.1 FISSION ENERGETICS

All fission processes considered in this compilation are primarily binary.[1,2,3] The parent nucleus splits into two massive fragments of unequal size. Simultaneously, a relatively large amount of mass is converted into energy, most of which appears as a violent kinetic motion of the fragments. True ternary fission (less than one part in 10^5),[4] and binary fission accompanied by a light particle (one part in ~300),[5] is neglected. The most probable kinetic energies of the light and of the heavy fragments from known fission processes are summarized in Table 1-1. The total fragment kinetic energies and the ratio of heavy fragment to light fragment masses (M_H/M_L) are also given in the table.

1.2.2 PROMPT FISSION GAMMA-RAY EMISSION

Prompt gamma rays[16] ($T_{1/2} \lesssim 10^{-9}$ sec) are emitted at fission. The spectrum of these gamma rays is a monotonically decreasing function of their energy as shown in Fig. 1-1.[15–18] The number of prompt photons per fission and their average energies are given in Table 1-2. In addition to the prompt gamma-ray emission, about 9 Mev/fission is released in the form of prompt beta particles.[19]

1.2.3 FISSION PRODUCT YIELDS

Unless otherwise noted, the data in this section have been taken from a compilation by Katcoff.[12] References used in the compilation are repeated for convenience.

Table 1-1 — SUMMARY OF FISSION FRAGMENT PROPERTIES

(Numbers refer to "most probable" values)

	Z^2/A	Fragment Energy, Mev[a]			M_H/M_L Measurements		Primary Fragment Mass		Ref.[c]	Ref.[d]
		Light	Heavy	Total	Ion-Chamber[b]	Radiochemical	Heavy M_H	Light M_L		
$Th^{229} + n$	35.22	100.0	60.0	160 ± 3	1.57	—	—	—	6	—
$U^{233} + n$	36.17	97.0	66.0	163 ± 2	1.47 ± 0.02	1.46	139	95	7	12
$U^{235} + n$	35.86	98.0	67.0	165 ± 2	1.46 ± 0.02	1.45	140	96	7	12
$Pu^{239} + n$	36.82	100.0	72.0	172 ± 2	1.39 ± 0.02	1.39	140	100	7	12
$Pu^{241} + n$	36.51	101.0	73.0	174 ± 3	1.38 ± 0.02	—	140	102	9	—
Pu^{242} sp. fiss.	36.51	101.0	73.0	174 ± 3	1.38 ± 0.02	—	140	102	9	—
Cm^{242}	38.08	110.8	85.9	196.7	1.29	1.32	138	104	10	11
Cm^{244}	37.77	105.5	80.0	185.5 ± 5	1.32 ± 0.05	—	139	105	8	—
Cf^{252}	38.11	105.0	80.0	185 ± 4	1.33 ± 0.04	1.33	144	108	14,15	13
Fm^{254}	39.37	101.5	74.5	176 ± 6	1.36 ± 0.05	—	146	108	8	—

[a] All ionization chamber measurements corrected for an ionization defect of about 7 Mev per fragment.
[b] M_H/M_L from ion-chamber measurements refers to primary fragments.
[c] Refers to ion-chamber data.
[d] Refers to radiochemical data.

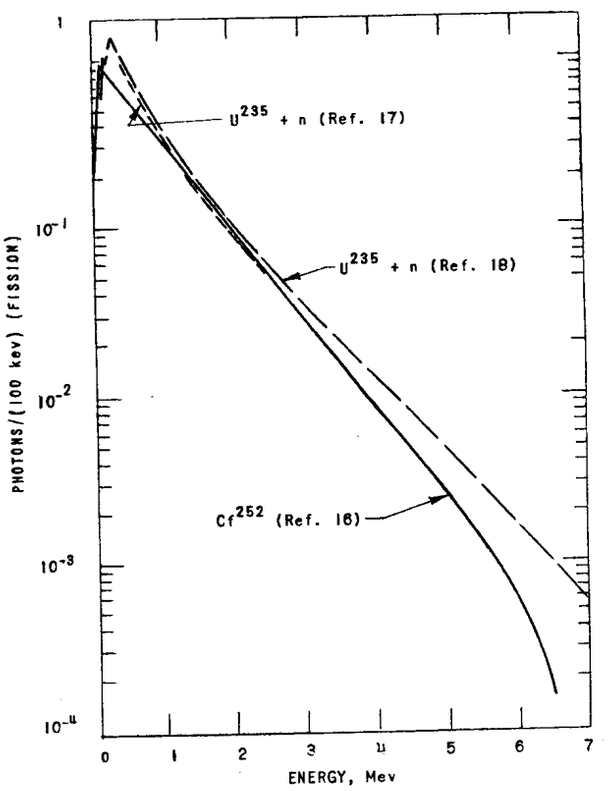

Fig. 1-1 — Photon spectrum from the fission of Cf^{252} and U^{235}.

In general, very few fission yields have been measured on an absolute basis. In most cases, yields have been determined relative to Ba^{140} whose absolute yield has been averaged to 6.44% for U^{235} thermal fission. Where the reported data have been based on an assumed yield for Ba^{140} other than 6.44%, the values given in the tables have been re-normalized to 6.44%. Yields which have been determined relative to an isotope other than Ba^{140} are indicated by footnotes in the tables.

Table 1-2—CHARACTERISTICS OF PROMPT GAMMA RAYS EMITTED IN FISSION

Fissioning Isotope	Total Photons per Fission	Total Energy of Photons, Mev	Ref.
U^{235} + n	7.4	7.2	18
Cf^{252}	10.3	8.2	16

Fission Product Chains. The fission product radioactive chains are shown schematically in Table 1-3.

Total Chain Yields from U^{235}-Thermal Neutron Fission. Table 1-4 lists the total integrated chain yield for each mass number from thermal neutron fissions in U^{235}. The fission product given uniquely characterizes the total chain yield for the respective mass number. Where an actively decaying isotope is indicated, no other isotope further along the chain is formed directly in fission. By definition, the integrated chain yield is equivalent to the total fission yield of nuclei having a particular mass.

Direct Yield of Some Primary U^{235} Fission Products. Table 1-5 gives the yield directly at fission of some primary products from U^{235} fission induced by both thermal and 14-Mev neutrons. As is evident from Table 1-3, some of these primary-yield nuclei can also be formed as the result of beta decay in a chain. In such cases, they are product members of the chain and, hence, are not primary yields. The ratio of the number of particular nuclei formed directly at fission, to the total yield of nuclei having the same mass, is denoted as the direct yield fraction of the chain yield.

Cumulative Yields of Various Fission Products from Thermal Neutron Fission. The cumulative yield of a fission product is the probability that, in one fission, the fission product is formed either directly or later in the decay chain.

Table 1-6 lists the cumulative fission yields of various isotopes from thermal neutron fission of U^{233}, U^{235}, and Pu^{239}. The data in Table 1-4, which also represent cumulative yields, are not repeated.

The cumulative yields in Table 1-6 do not necessarily represent total chain yields since a later member of the chain may also be formed directly from fission. In addition, as a result of isomerism, the yields for some U^{235} fission products are lower than their counterparts listed in Table 1-4 for the total chain yield. In the absence of isomerism, any discrepancy between values for the same isotope in Tables 1-4 and 1-6 (for U^{235} fission) is due to experimental error. The values in Table 1-4 are considered more reliable.

Cumulative Yields of Various Fission Products from Fast Fissions. The cumulative fission product yields from fission spectrum neutron-induced fissions in Pu^{239}, U^{238}, and Th^{232} are summarized in Table 1-7. Table 1-8 lists the yields from 14-Mev neutron-induced fissions in U^{235}, and 8-Mev neutron-induced fissions in Th^{232}.

The variation of yield for a given mass with incident energy for U^{235} fissions, shown in Fig. 1-2, is based on the data in Tables 1-4 and 1-8. The greatest change is the increase (by a factor of 100) in the probability of symmetric fission for 14-Mev neutrons. The peak yields drop slightly, but there is a small increase in the most asymmetric modes of fission.

1.2.4 FISSION FRAGMENT RANGES

The range of median-mass light and median-mass heavy fission fragments in representative materials is given in Figs. 1-3 and 1-4, respectively.[91] The residual energy after traversing the absorber was measured by a CsI(Tl) scintillator.

Table 1-3 — FISSION PRODUCT CHAINS

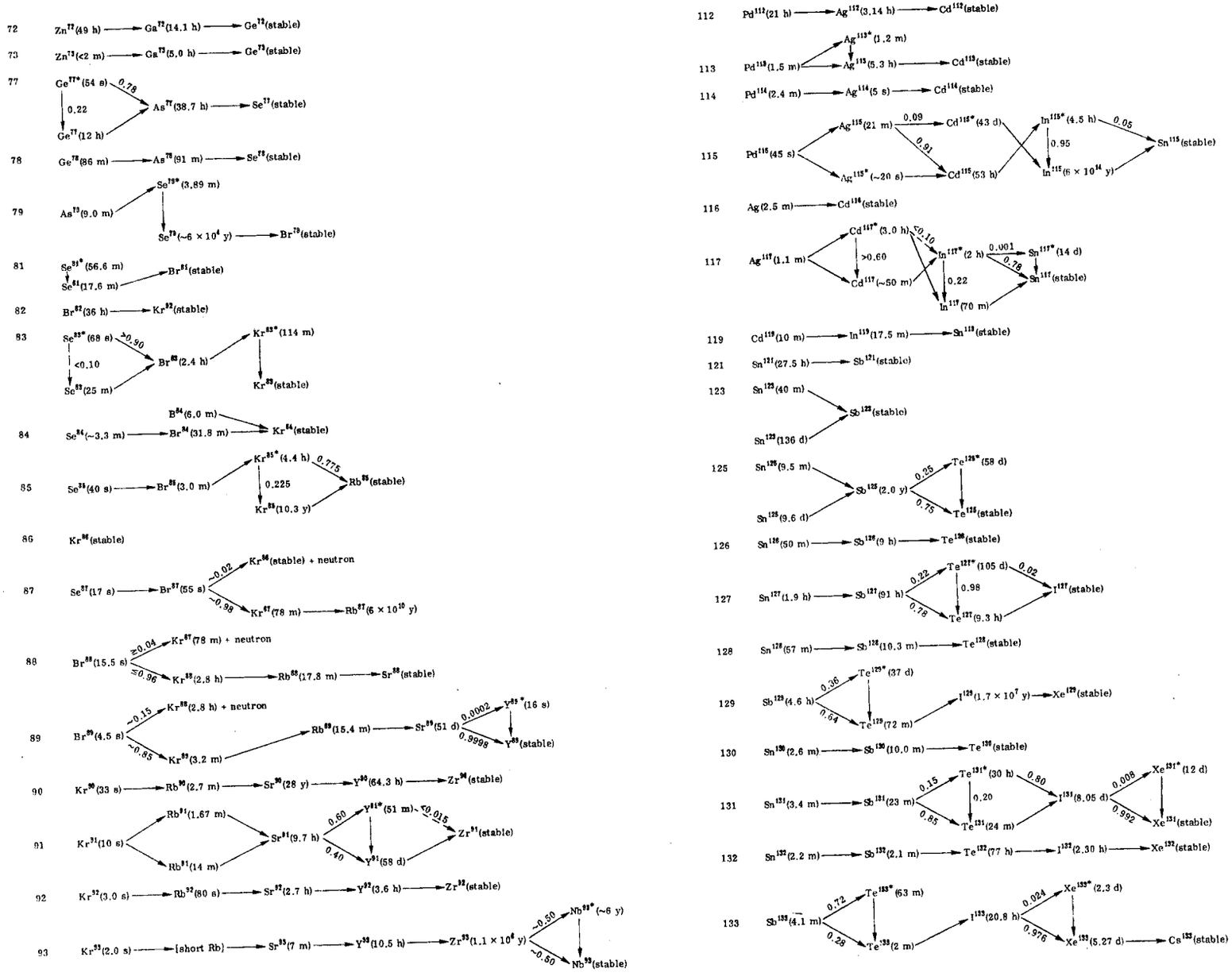

94 Kr^{94}(1.4 s) → [short Rb] → Sr^{94}(~2 m) → Y^{94}(16.5 m) → Zr^{94}(stable)

95 Y^{95}(10.5 m) → Zr^{95}(65 d) → 0.02 → Nb^{95*}(90 h); 0.98 → Nb^{95}(35 d); Nb^{95} → Mo^{95}(stable)

96 Nb^{96}(23 h) → Mo^{96}(stable)

96 Zr^{96}(stable)

97 Zr^{97}(17.0 h) → Nb^{97*}(60 s); ≤0.02 → Nb^{97}(73 m); Nb^{97} → Mo^{97}(stable)

98 Mo^{98}(stable)

99 Zr^{99}(30 s) → Nb^{99}(3 m) → Mo^{99}(66 h) → 0.87 → Tc^{99*}(6.0 h); 0.13 → Tc^{99}(2.1 × 10^5 y); Tc^{99} → Ru^{99}(stable)

100 Mo^{100}(stable)

101 Mo^{101}(14.6 m) → Tc^{101}(14.3 m) → Ru^{101}(stable)

102 Mo^{102}(11.5 m) → Tc^{102}(4.1 m); Mo^{102} → Tc^{102}(5 s); both → Ru^{102}(stable)

103 Tc^{103}(1.2 m) → Ru^{103}(39.7 d) → Rh^{103*}(57 m); ≤0.05 → Rh^{103}(stable)

104 [Mo^{104}(2.5 m)] → Tc^{104}(18 m) → Ru^{104}(stable)

105 [Mo^{105}(<2 m)] → Tc^{105}(10 m) → Ru^{105}(4.45 h) → Rh^{105*}(38 s); Rh^{105}(35.3 h) → Pd^{105}(stable)

106 Ru^{106}(1.0 y) → Rh^{106}(30 s) → Pd^{106}(stable)

107 [Tc^{107}(<1 m)] → Ru^{107}(4.8 m) → Rh^{107*}(6 s); Rh^{107} → Rh^{107}(22 m) → Pd^{107}(7 × 10^6 y) → Ag^{107}(stable)

108 [Tc^{108}(<1 m)] → Ru^{108}(4.4 m) → Rh^{108}(18 s) → Pd^{108}(stable)

109 Pd^{109}(13.4 h) → Ag^{109*}(39.2 s); Ag^{109}(stable)

111 SHORT [Rh^{111}] → ~0.01 → Pd^{111*}(5.5 h); ~0.99 → Pd^{111}(23 m); Pd^{111*} → 0.75 → Pd^{111}; Pd^{111*} → Ag^{111*}(74 s); Ag^{111*} → <0.01 → Cd^{111}(stable); Ag^{111*} → Ag^{111}(7.6 d) → Cd^{111}(stable)

134 Sb^{134}(0.8 m) → Te^{134}(44 m) → I^{134}(52.5 m) → Xe^{134}(stable)

135 Te^{135}(<0.5 m) → I^{135}(6.7 h) → 0.30 → Xe^{135*}(15.3 m); 0.70 → Xe^{135}(9.2 h); both → Cs^{135}(2.6 × 10^6 y) → Ba^{135}(stable)

136 Cs^{136}(13 d) → Ba^{136}(stable)

136 I^{136}(86 s) → Xe^{136}(stable)

137 I^{137}(24.0 s) → ~0.08 → Xe^{136}(stable) + neutron; ~0.92 → Xe^{137}(3.9 m) → Cs^{137}(29 y) → 0.92 → Ba^{137*}(2.57 m); 0.08 → Ba^{137}(stable)

138 I^{138}(5.8 s) → Xe^{137} (3.9 m) + neutron; Xe^{138}(17 m) → Cs^{138}(32.2 m) → Ba^{138}(stable)

139 I^{139}(2.7 s) → Xe^{139}(41 s) → Cs^{139}(9.5 m) → Ba^{139}(84 m) → La^{139}(stable)

140 Xe^{140}(16 s) → Cs^{140}(66 s) → Ba^{140}(12.8 d) → La^{140}(40.2 h) → Ce^{140}(stable)

141 Xe^{141}(1.7 s) → [short Cs] → Ba^{141}(18 m) → La^{141}(3.7 h) → Ce^{141}(33 d) → Pr^{141}(stable)

142 Ba^{142}(6 m) → La^{142}(75 m) → Ce^{142}(stable)

143 Xe^{143}(1 s) → [short Cs] → Ba^{143}(<0.5 m) → La^{143}(18 m) → Ce^{143}(33 h) → Pr^{143}(13.7 d) → Nd^{143}(stable)

144 Ce^{144}(285 d) → Pr^{144}(17.4 m) → Nd^{144}(5 × 10^{15} y)

145 Ce^{145}(3.0 m) → Pr^{145}(5.95 h) → Nd^{145}(stable)

146 Ce^{146}(13.9 m) → Pr^{146}(24.4 m) → Nd^{146}(stable)

147 Nd^{147}(11.1 d) → Pm^{147}(2.65 y) → Sm^{147}(1.3 × 10^{11} y)

148 Nd^{148}(stable)

148 Pm^{148}(5.3 d) → Sm^{148}(stable)

149 Nd^{149}(2.0 h) → Pm^{149}(54 h) → Sm^{149}(stable)

150 Nd^{150}(stable)

151 Nd^{151}(13 m) → Pm^{151}(27.5 h) → Sm^{151}(80 y) → Eu^{151}(stable)

152 Sm^{152}(stable)

153 Sm^{153}(47 h) → Eu^{153}(stable)

154 Sm^{154}(stable)

155 Sm^{155}(24 m) → Eu^{155}(1.9 y) → Gd^{155}(stable)

156 Sm^{156}(~10 h) → Eu^{156}(15.4 d) → Gd^{156}(stable)

157 Eu^{157}(15.4 h) → Gd^{157}(stable)

158 Eu^{158}(60 m) → Gd^{158}(stable)

159 Gd^{159}(18.0 h) → Tb^{159}(stable)

161 [Gd^{161}(3.6 m)] → Tb^{161}(6.9 d) → Dy^{161}(stable)

NOTE: When branching occurs, the fraction in each branch, if known, is indicated by the arrow. Dashed arrows are used when only the upper limits have been established. Brackets denote that the given nuclide probably occurs in fission but that it has not been so observed.

s = second m = minute h = hour d = day y = year * = metastable

Table 1-4—TOTAL CHAIN YIELD FROM THERMAL NEUTRON FISSIONS IN U^{235}

s = second m = minute h = hour d = day y = year * = metastable

Mass No.	Fission Product	% Yield	Ref.	Mass No.	Fission Product	% Yield	Ref.
72	Zn^{72} (49h)	0.000016	20, 21	125	Sb^{125} (2.0y)	0.021	42
73	Ga^{73} (5.0h)	0.00011	21	126	Sb^{126} (9h)	0.05[a]	43
77	As^{77} (38.7h)	0.0083	22, 23	127	Sb^{127} (91h)	0.13[b]	37, 44
78	As^{78} (91m)	0.021	22	128	Sn^{128} (57m)	0.37	36
79	As^{79} (9.0m)	0.056	24	129	I^{129} (1.7×10^7y)	0.9	45
81	Se^{81} (17.6m)	0.14	25	130	Sb^{130} (10m)	2.0	46
83	Kr^{83} (stable)	0.544	26, 27, 28	131	Xe^{131} (stable)	2.93, 2.88[a]	28
84	Kr^{84} (stable)	1.00	26, 27, 28	132	Xe^{132} (stable)	4.38, 4.31[a]	28
85	Rb^{85} (stable)	1.30	26	133	Cs^{133} (stable)	6.59, 6.49[a]	26
86	Kr^{86} (stable)	2.02	26, 27, 28	134	Xe^{134} (stable)	8.06, 7.9[a]	28
87	Rb^{87} (6×10^{10}y)	2.49	26	135	Cs^{135} (2.6×10^6y)	6.41, 6.31[a]	26
88	Sr^{88} (stable)	3.57[b]	26, 29	136	Xe^{136} (stable)	6.46, 6.36[a]	28
89	Sr^{89} (51d)	4.79	30	137	Cs^{137} (29y)	6.15, 6.05[a]	28
90	Sr^{90} (28y)	5.77[b]	26, 29	138	Ba^{138} (stable)	5.74	29
91	Zr^{91} (stable)	5.84	29	139	Ba^{139} (84m)	6.55[b]	30, 47
92	Zr^{92} (stable)	6.03	29	140	Ce^{140} (stable)	6.44[b,c]	26, 29
93	Zr^{93} (1.1×10^6y)	6.45	29	141	Ce^{141} (33d)	~6.0	48
94	Zr^{94} (stable)	6.40	29	142	Ce^{142} (stable)	5.95	49
95	Mo^{95} (stable)	6.27	29	143	Nd^{143} (stable)	5.98[b]	26, 29
96	Zr^{96} (stable)	6.33	29	144	Nd^{144} (5×10^{15}y)	5.67[b]	26, 29
97	Mo^{97} (stable)	6.09	29	145	Nd^{145} (stable)	3.95[b]	26, 29
98	Mo^{98} (stable)	5.78	29	146	Nd^{146} (stable)	3.07[b]	26, 29
99	Mo^{99} (66h)	6.06[b]	30, 31	147	Sm^{147} (1.3×10^{11}y)	2.38	26
100	Mo^{100} (stable)	6.30	29	148	Nd^{148} (stable)	1.70[b]	26, 29
101	Ru^{101} (stable)	5.0	29	149	Sm^{149} (stable)	1.13	26
102	Ru^{102} (stable)	4.1	29	150	Nd^{150} (stable)	0.67[b]	26, 29
103	Ru^{103} (39.7d)	3.0	32, 33	151	Sm^{151} (80y)	0.45	26
104	Ru^{104} (stable)	1.8	29	152	Sm^{152} (stable)	0.285	26
105	Ru^{105} (4.45h)	0.90[b]	34, 35	153	Sm^{153} (47h)	0.15[b]	37, 49
106	Ru^{106} (1.01y)	0.38	29, 32, 33	154	Sm^{154} (stable)	0.077	26
107	Rh^{107} (22m)	0.19	36	155	Sm^{155} (24m)	0.033	50
109	Pd^{109} (13.4h)	0.030	37	156	Eu^{156} (15.4d)	0.014[b]	37, 49, 51
111	Ag^{111} (7.6d)	0.019	37	157	Eu^{157} (15.4h)	0.0078	52
112	Pd^{112} (21h)	0.010[b]	37, 38	158	Eu^{158} (60m)	0.002	52
115	Cd^{115} (53h) + Cd^{115*} (43d)	0.011	39	159	Gd^{159} (18h)	0.00107[a]	49, 53
117	Cd^{117*} (3.0h)	0.011	40	161	Tb^{161} (6.9d)	0.000076	49, 53
121	Sn^{121} (27.5h)	0.015	41				

[a] Average of values in references cited.
[b] E. P. Steinberg, ANL, Private Communication. Based on a yield of (6.15 + 5.94)/2 = 6.05 for Cs^{137}.
[c] Measured absolute yield is 6.32%. The number 6.44% is used to normalize other yields.

Table 1-5 — DIRECT YIELD OF PRIMARY FISSION PRODUCTS FROM THERMAL AND 14-MEV NEUTRON-INDUCED FISSIONS IN U-235

s = second m = minute h = hour d = day y = year * = metastable

Mass No.	Fission Product	Thermal Neutrons			14-Mev Neutrons		
		% Yield	Fraction of Chain Yield	Ref.	% Yield	Fraction of Chain Yield	Ref.
78	As^{78} (91m)	0.0019	9×10^{-2}	25			
82	Br^{82} (36h)	4×10^{-5}	1.2×10^{-4} [a]	31, 56	0.003	3×10^{-3}	54
86	Rb^{86} (19d)	3×10^{-5}	1.5×10^{-5} [a]	31, 57			
90	Y^{90} (6.4h)	<0.0013	$<2.3 \times 10^{-4}$	58			
91	Y^{91} (58d)	<0.05	$<9 \times 10^{-3}$	58			
96	Nb^{96} (23h)	5.7×10^{-4}	9×10^{-5} [a]	31, 59	0.0034	6.4×10^{-4}	54
102	Rh^{102} (210d)	$<5 \times 10^{-7}$	$<1.2 \times 10^{7}$	60			
131	Te^{131*} (30h)	<0.15	$<5 \times 10^{-2}$	61	1.6	0.35	55
131	Te^{131} (24m)	<0.09	$<3 \times 10^{-2}$	61	<1.4	<0.30	55
131	I^{131} (8.05d)	<0.03	$<1 \times 10^{-2}$	61	<0.36	$<8 \times 10^{-2}$	55
132	I^{132} (2.3h)	<0.044	$<1 \times 10^{-2}$	61	0.8	0.16	55
133	Te^{133} (2m)	<0.66	<0.1	61	<2.2	<0.40	55
133	I^{133} (20.8h)	<0.33	$<5 \times 10^{-2}$	61	<2.2	<0.40	55
133	Xe^{133} (5.27d)	<0.0066	$<1 \times 10^{-3}$	62			
134	I^{134} (52.5m)	0.89	0.11	61	2.5	0.43	55
135	Xe^{135} (9.2h)	0.19	0.03	62, 63			
136	Xe^{136} (stable)	3.4	0.53	64			
136	Cs^{136} (13d)	0.006	9×10^{-4} [a]	31, 57	0.22	4×10^{-2}	54
140	La^{140} (40.2h)	<0.2	$<3 \times 10^{-2}$	65			
141	La^{141} (3.7h)	~0.1	$\sim 2 \times 10^{-2}$	66			
148	Pm^{148} (5.3d)	$<2 \times 10^{-4}$	$<1 \times 10^{-4}$	31			

[a] Average of values in references cited.

Table 1-6 — CUMULATIVE YIELDS OF VARIOUS FISSION PRODUCTS FROM THERMAL NEUTRON FISSIONS IN U^{233}, U^{235}, AND Pu^{239}

s = second m = minute h = hour d = day y = year * = metastable

Mass No.	Fission Product	U^{233}		U^{235}		Pu^{239}	Mass No.	Fission Product	U^{233}		U^{235}		Pu^{239}
		% Yield	Ref.	% Yield	Ref.	% Yield [a,b,c]			% Yield	Ref.	% Yield	Ref.	% Yield [a,b,c]
72	Zn^{72} (49h)					0.00012	127	Sb^{127} (91h)					0.39
77	Ge^{77} (12h)	0.010	31	0.0031[d]	22, 23		127	Te^{127*} (105d)			0.035	67	
77	As^{77} (38.7h)	0.019	31				129	Te^{129*} (37d)			0.35	44	
78	Ge^{78} (86m)			0.020[d]	22, 23		131	Sb^{131} (23m)			2.6	46	
81	Se^{81*} (57m)			0.0084	25		131	Te^{131*} (30h)			0.44	44	
83	Se^{83} (25m)			0.22	56		131	I^{131} (8.05d)	2.7	31	3.1[a]	37, 68	3.8
83	Br^{83} (2.4h)	0.79	31	0.51	57	0.085	131	Xe^{131} (stable)	3.74	67			2.87
83	Kr^{83} (stable)	1.14	67				132	Te^{132} (77h)			4.7	44	5.2
84	Br^{84} (31.8m)			0.90	58		132	Xe^{132} (stable)	5.10	67			4.02
84	Kr^{84} (stable)	1.90	67				133	Sb^{133} (4.1m)			4.0	44	
85	Kr^{85} (10.3y)	0.56	67	0.293[d]	26, 27, 28		133	Te^{133*} (63m)			4.9	44	
86	Kr^{86} (stable)	3.18	67				133	I^{133} (21h)			6.9	44	5.3
87	Br^{87} (55s)			3.1	59		133	Xe^{133} (5.27d)			6.62	69	5.27
89	Sr^{89} (51d)	6.5	31			1.9	133	Cs^{133} (stable)	6.18	67			5.27
90	Sr^{90} (28y)			5.8[d]	26, 29, 60, 61		134	Te^{134} (44m)			6.9[a]	44, 70	
91	Sr^{91} (9.7h)			5.8[d]	29, 60, 61	2.4	134	Xe^{134} (stable)	6.54	67			5.69
91	Sr^{91} (2.7h)			5.3	62		135	I^{135} (6.7h)	5.1	31	6.1[a]	44, 71, 72	5.8
91	Y^{91} (58d)			5.35	60	3.0	135	Cs^{135} (2.6×10^6y)	>4.9	67			5.53
91	Zr^{91} (stable)	6.53	68				136	I^{136} (86s)	1.7	64	3.1	73	2.1
92	Zr^{92} (stable)	6.70	68				136	Xe^{136} (stable)	<8.9	67			5.06
93	Zr^{93} (1.1×10^6y)	7.10	68				137	Cs^{137} (29y)	7.16	31	6.15	26, 74	5.24
94	Y^{94} (16.5m)			5.4	63		138	Cs^{138} (32m)			5.74	29, 75	
94	Zr^{94} (stable)	6.82	68				139	Ba^{139} (84m)					5.7
95	Zr^{95} (65d)	5.9	31	6.2	64	5.9	140	Ba^{140} (12.8d)	6.0	31	6.44[e]	29, 30, 70	5.68
95	Mo^{95} (stable)	6.10	68				140	Ce^{140} (stable)	5.6	69			5.68

96	Zr^{96} (stable)	5.60	68				141	Ce^{141} (33d)					5.2
97	Zr^{97} (17h)			5.9[d]	30, 64	5.7	142	Ce^{142} (stable)	5.6	69			6.69
97	Mo^{97} (stable)	5.35	68				143	Ce^{143} (33h)			5.7	26, 29, 77	5.4
98	Mo^{98} (stable)	5.18	68				143	Nd^{143} (stable)	5.2	69, 70			6.31
99	Mo^{99} (66h)	4.8	31			5.9	144	Ce^{144} (285d)	4.1	69, 70	6.0	26, 29	5.28
100	Mo^{100} (stable)	4.40	68				144	Nd^{144} (stable)	4.0	69, 70			5.29
101	Mo^{101} (14.6m)			~5.6	35		145	Nd^{145} (stable)	3.0	69, 70			4.24
101	Ru^{101} (stable)	3.00	68				146	Nd^{146} (stable)	2.3	69, 70			3.53
102	Mo^{102} (11.5m)			4.3	35		147	Nd^{147} (11d)			2.7	26, 78	
102	Ru^{102} (stable)	2.37	68				147	Sm^{147} (stable)	1.71	70			2.92
103	Ru^{103} (39.7d)	1.6	31			5.8	148	Nd^{148} (stable)	1.15	69, 70			2.28
104	Ru^{104} (stable)	0.96	68				149	Pm^{149} (5.6h)			1.4	26, 78	
105	Rh^{105} (35.3h)					3.9	149	Sm^{149} (stable)	0.61	70			1.89
106	Ru^{106} (1.01y)	0.28	31			5.0	150	Nd^{150} (stable)	0.48	69, 70			1.38
109	Pd^{109} (13.4h)	0.040	31	0.030	37	1.5	151	Sm^{151} (80y)	0.27	70			1.17
111	Ag^{111} (7.6d)	0.025	31			0.27	152	Sm^{152} (stable)	0.17	70			0.83
112	Pd^{112} (21h)	0.016	31			0.10	153	Sm^{153} (47h)	0.095	31			0.41
115	Ag^{115} (21m)			0.0077	39		154	Sm^{154} (stable)	0.037	70			0.32
115	Cd^{115*} (43d)	0.001	31	0.0007	39	0.003	155	Sm^{155} (24m)					0.22
115	Cd^{115} (53h)	0.019	31	0.0097	39	0.038	155	Eu^{155} (1.9y)			0.03	50, 51	
121	Sn^{121} (27.5h)	0.018	31			0.044	156	Sm^{156} (10h)			0.013	38, 49, 51	
123	Sn^{123} (136d)			0.0013	65		156	Eu^{156} (15.4h)					0.12
125	Sn^{125} (9.6d)	0.050	31	0.013	66	0.072							

[a] The Cs, Nd, and Sm yields were measured by Wiles, et al.,[79] and corrected to 5.6% yield for Ba^{140}. For some of the Ce and Nd isotopes, the ratios of yields per Ref. 80 were used.

[b] Most values are from Ref. 81, corrected to a Ba^{140} yield of $1.06 \times 5.32\% = 5.68\%$.

[c] The xenon isotope yields were determined by Fleming, et al.[82] These were normalized to corrected Cs yields at mass 133.

[d] Average of values in references cited.

[e] Measured value is 6.32%. The factor 1.06 is introduced to bring the total yield for light and heavy groups to 100% each.

Table 1-7—CUMULATIVE PERCENTAGE YIELDS FROM FISSION SPECTRUM NEUTRON-INDUCED FISSIONS IN Pu^{239}, U^{238}, AND Th^{232}

s = second m = minute h = hour d = day y = year * = metastable

Mass No.	Fission Product	Pu^{239}[a]	U^{238}[b]	Th^{232}[c]	Mass No.	Fission Product	Pu^{239}[a]	U^{238}[b]	Th^{232}[c]
72	Zn^{72} (49h)			0.00033	111	Ag^{111} (7.6d)		0.073	0.052
73	Ga^{73} (5.0h)			0.00045	112	Pd^{112} (21h)	0.14	0.046	0.057
77	Ge^{77} (12h)			0.009	115	Cd^{115*} (43d)		0.003	0.003
77	As^{77} (39h)		0.0038	0.020	115	Cd^{115} (53h)	0.069	0.037	0.072
83	Br^{83} (2.4h)			1.9	127	Sb^{127} (93h)		0.12	
83	Kr^{83} (stable)		0.40	1.99	131	I^{131} (8.05d)			1.2
84	Kr^{84} (stable)		0.85	3.65	131	Xe^{131} (stable)		3.2[d]	1.62
85	Kr^{85} (10.3y)		0.153	0.87	132	Te^{132} (77h)		4.7	2.4
86	Kr^{86} (stable)		1.38	6.0	132	Xe^{132} (stable)		4.7[d]	2.87
89	Sr^{89} (51d)		2.9	6.7	133	Cs^{133} (stable)		5.5 (8.08)[e]	
90	Sr^{90} (28y)	2.2	3.2	6.8	134	Xe^{134} (stable)		6.6[d]	5.38
91	Sr^{91} (9.7h)			7.2	135	Cs^{135} (2.6×10^6y)		6.0[e]	
95	Zr^{95} (65d)		5.7		136	Xe^{136} (stable)		5.9[d]	5.65
97	Zr^{97} (17h)	5.2		5.2	137	Cs^{137} (29y)	6.6	6.2 (7.11)[e]	6.3
99	Mo^{99} (67h)	5.9	6.3	2.7	140	Ba^{140} (12.8d)	5.0	5.7	6.2
103	Ru^{103} (40d)		6.6	0.16	141	Ce^{141} (33d)			9.0
105	Rh^{105} (35h)			0.07	144	Ce^{144} (290d)		4.9	7.1
106	Ru^{106} (1.0y)		2.7	0.042	153	Sm^{153} (47h)	0.48		
109	Pd^{109} (13.4h)	1.9	0.32	0.055	156	Eu^{156} (15.4d)		0.066	

[a] Values from Ref. 83.

[b] Most values are averages of data in Refs. 84 and 85 normalized to absolute yield of Mo^{99} in Ref. 86.

[c] Most values from Ref. 87. Kr and Xe yields measured by T. J. Kennett and H. G. Thode, and reported by private communication to S. Katcoff.

[d] Values from Ref. 88.

[e] Cs^{133} and Cs^{135} yields derived from ratios to Cs^{137} measured by R. H. Tomlinson and reported by private communication to S. Katcoff.

Table 1-8—CUMULATIVE PERCENTAGE YIELDS FROM 14-MEV NEUTRON-INDUCED FISSIONS IN U^{235} AND 8-MEV NEUTRON-INDUCED FISSIONS IN Th^{232}

s = second m = minute h = hour d = day y = year * = metastable

Mass No.	Fission Product	Cumulative % Yield in		Mass No.	Fission Product	Cumulative % Yield in	
		U^{235}	Th^{232}			U^{235}	Th^{232}
77	Ge^{77} (12h)		0.022	131	I^{131} (8.05d)	4.3	
83	Br^{83} (2.4h)	1.30		132	Te^{132} (77h)	4.3	2.0
83	Kr^{83} (stable)		2.7	132	I^{132} (2.3h)	5.0	
89	Sr^{89} (51d)	4.38	6.7	133	I^{133} (20.8h)	5.4	
91	Sr^{91} (9.7h)	4.19	5.6	133	Cs^{133} (stable)	5.6	
97	Zr^{97} (17h)	4.87	5.0	134	I^{134} (52.5m)	5.3	
99	Mo^{99} (66h)	5.17	3.1	134	Xe^{134} (stable)	5.9	
103	Ru^{103} (39.9d)	3.31	0.5	135	I^{135} (6.7h)	4.5	
105	Rh^{105} (35.3h)	1.86		135	Cs^{135} (2.6×10^6y)	5.7	
106	Ru^{106} (1.01y)	1.41	0.53	139	Ba^{139} (84m)	4.87	9.0
111	Ag^{111} (7.6d)	0.92	0.63	140	Ba^{140} (12.8d)	4.58	
115	Cd^{115} (53h)	0.89	0.76	143	Ce^{143} (33h)	3.72	
115	Total ^{115} chain	0.94		144	Ce^{144} (285d)	2.75	7.2
117	Cd^{117*} (3.0h)		0.4	156	Eu^{156} (15.4d)	0.11	
127	Sb^{127} (91h)	1.9					

Note: Most of the data by Ford and Gilmore,[89] and Turkevich, et al.[90] Iodine data by Wahl.[55] All values normalized to Mo^{99} as reported by Terrell.[86]

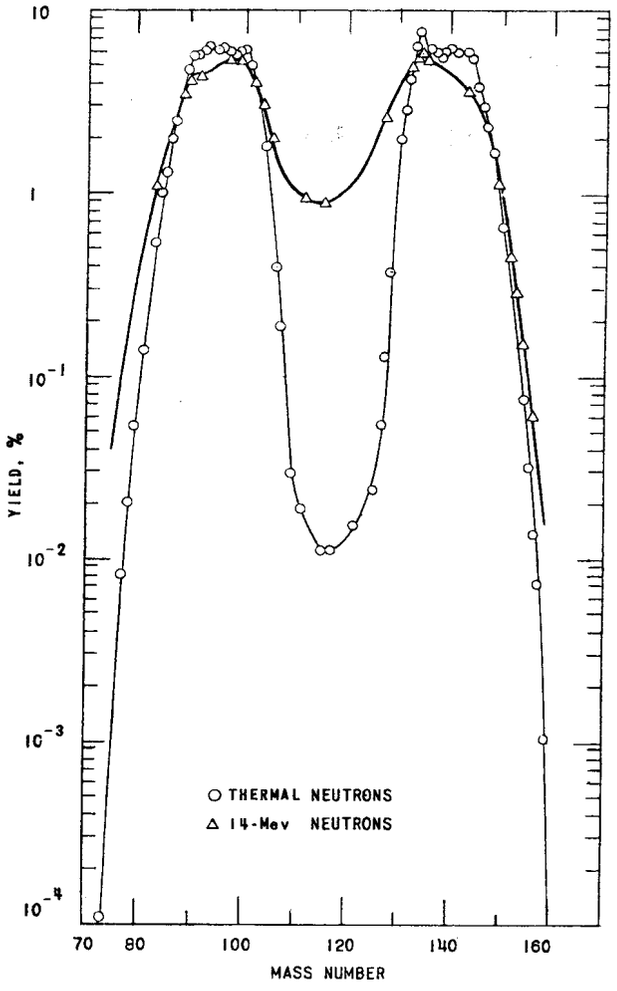

Fig. 1-2—Yield vs mass number for U^{235} fissions as a function of incident neutron energy.

1.3 PROMPT FISSION NEUTRON ENERGY SPECTRUM

Approximately 99% of the fission neutrons emitted at or immediately after fission ($\lesssim 10^{-10}$ sec) are defined as "prompt."[16,92,93] Most of these prompt neutrons are emitted isotropically from the moving fragment.[16,94] As a result, there is a correlation between the directions of the fragment and emitted neutron. The energy distribution of the prompt neutrons is described analytically by:[95,96]

$$N(E) = a\sqrt{E}\, e^{-E/T}$$

where E is the neutron energy in Mev; N(E) is the number of neutrons per unit energy interval; a is a constant dependent on the average number of neutrons emitted per fission; and T is a constant characteristic of the individual process.

1.3.1 EXPERIMENTAL DETERMINATIONS OF PROMPT FISSION NEUTRON SPECTRA

Experimental studies of prompt fission neutron spectra have been carried out by a number of workers.[97–109] Typical results of the measurement of $U^{235} + n_{th}$, $Pu^{239} + n_{th}$, and Cf^{252} spontaneous fission neutron spectra are shown in Figs. 1-5, 1-6, and 1-7, respectively. The average fission neutron energies obtained from Maxwellian spectral fits to existing measurements are summarized in

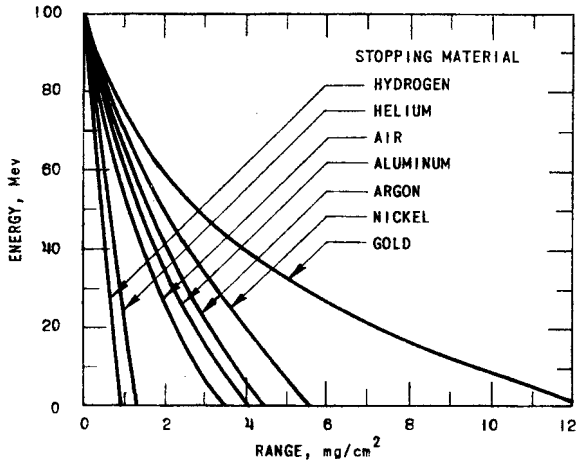

Fig. 1-3—Energy of median-mass light fission fragments of U^{235} (magnetically selected) as a function of range in various materials. *Reproduced from Ref. 91.*

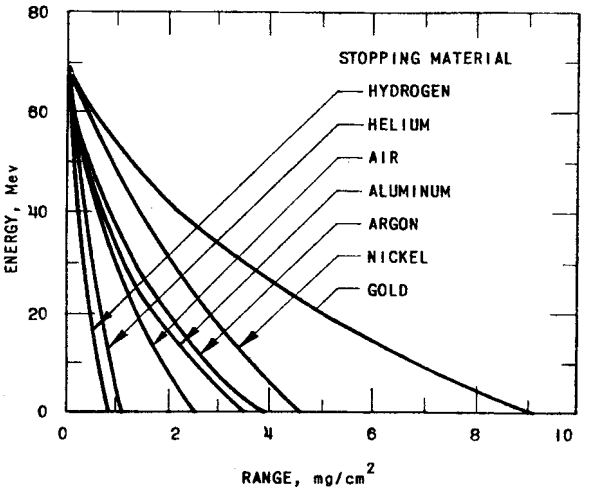

Fig. 1-4—Energy of median-mass heavy fission fragments of U^{235} (magnetically selected) as a function of range in various materials. *Reproduced from Ref. 91.*

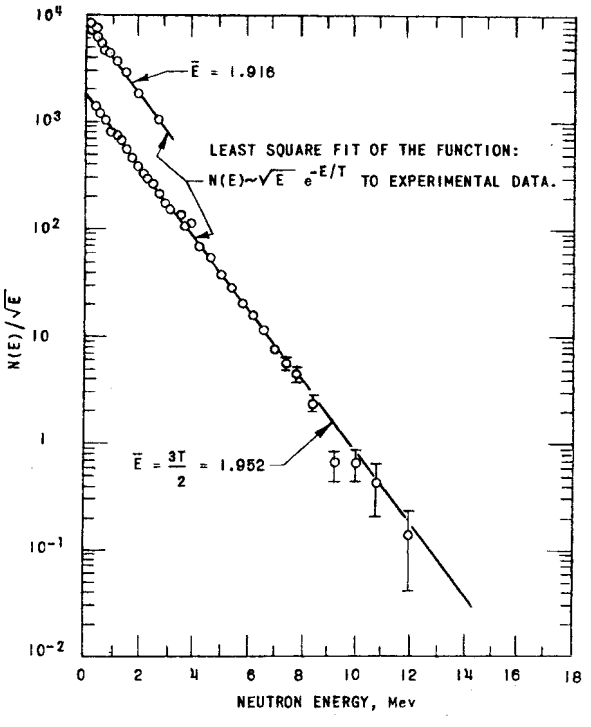

Fig. 1-5—Experimental determination of the fission neutron spectrum of $U^{235} + n_{th}$. *Reproduced from Ref. 97.*

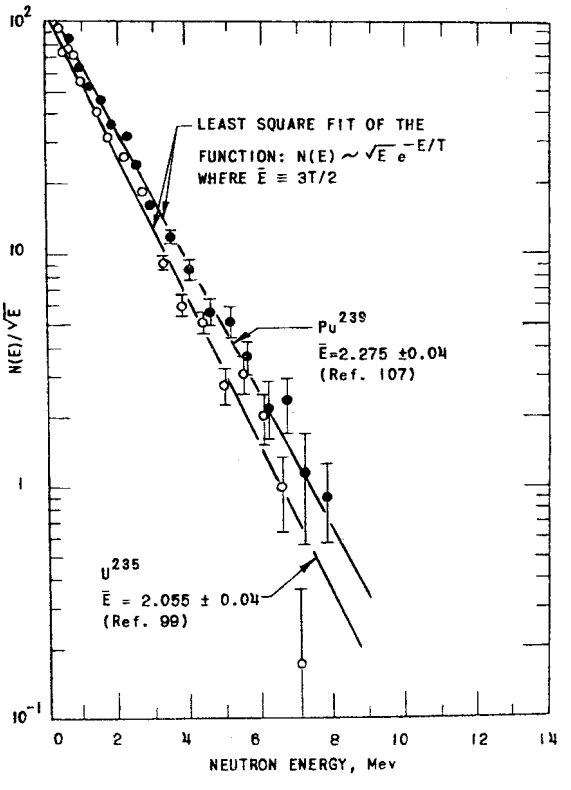

Fig. 1-6—Typical measured fission neutron spectra of $U^{235} + n_{th}$ and $Pu^{239} + n_{th}$. *Reproduced from Refs. 99 and 107.*

Table 1-9. Utilizing the relation $\overline{E} = 3T/2$ and the $\overline{\nu}$ values given in Section 1.5, the prompt fission neutron spectrum of each fission process can be generated. Average values of these necessary parameters for thermal neutron-induced fission processes are given in Table 1-10. The Maxwellian spectrum can be extrapolated to non-thermal incident neutron energies and to unmeasured neutron spectrum by utilizing the expression:[95]

$$\overline{E} = 0.78 + 0.621 \sqrt{\overline{\nu} + 1}$$

Suitable $\overline{\nu}$ values are given in Section 1.5. Qualitatively, the isotropy and incident neutron energy dependence of the prompt fission spectrum are small.

Table 1-9—AVERAGE ENERGY OF FISSION SPECTRUM NEUTRONS

Fissioning Nuclide	Energy Range, Mev	Method	$\overline{E}$, Mev[a] (Maxwellian)	$\overline{E}$[b], Mev	Ref.
$U^{235} + n_{th}$	0.35–12	Time of flight	1.916 ± 0.04	1.935 ± 0.05	97
	0.18–3	Photoplate	1.952 ± 0.013		97
	1.0–12	Photoplate	1.91 ± 0.04		98
	0.4–7	Photoplate	2.055 ± 0.04		99
	3.3–17	Prop. counter	1.854 ± 0.01		101
$U^{233} + n_{th}$	2.7	Threshold det.	$\overline{E}(U^{235})$ + 0.02 ± 0.01		103
	1.3–11	Prop. counter	2.17 ± 0.10		104
	2.0–8	Photoplate	2.23 ± 0.13		
	0.3–9	Time of flight and photoplate	1.87 ± 0.04	1.93 ± 0.06	106
	2.7	Threshold det.	$\overline{E}(U^{235})$ + 0.06 ± 0.02		105
	1.0–10	Photoplate	2.04 ± 0.06		98
$Pu^{239} + n_{th}$	2.7	Threshold det.	$\overline{E}(U^{235})$ + 0.07 ± 0.02	2.00 ± 0.05	103
	2.7	Threshold det.	$\overline{E}(U^{235})$ + 0.08 ± 0.02		105
	1.0–12	Photoplate	1.87 ± 0.05		98
	0.6–8	Photoplate	2.275 ± 0.04		107
Cf^{252} Spontaneous	2.0–10	Photoplate	2.12 ± 0.24	2.20 ± 0.1	108
	1.4–7	Photoplate	2.35 ± 0.08		109
	0.3–4	Time of flight	2.13 ± 0.05		

[a]Average energy given by least-squares fit to Maxwellian spectrum; the uncertainties are based on the standard deviations of the data points and do not include possible systematic errors in the energy scale.

[b]Average energy (arbitrarily weighted); uncertainties are over-all standard deviations.

1.3.2 THE $U^{235} + n_{th}$ PROMPT FISSION NEUTRON SPECTRUM AS A FUNCTION OF THE LETHARGY, u*

In some applications it is convenient to express the fission spectrum, F(u), in terms of the lethargy u. For $u = \ln (10/E)$:

$$F(u) = f(10\ e^{-u}) \left|\frac{dE}{du}\right|$$

and satisfies the normalization condition:

$$\int_{-\infty}^{\infty} F(u)\, du = 1$$

*Throughout the lethargy calculations, the average fission neutron energy, $\overline{E}$, is accepted as 1.98 Mev.

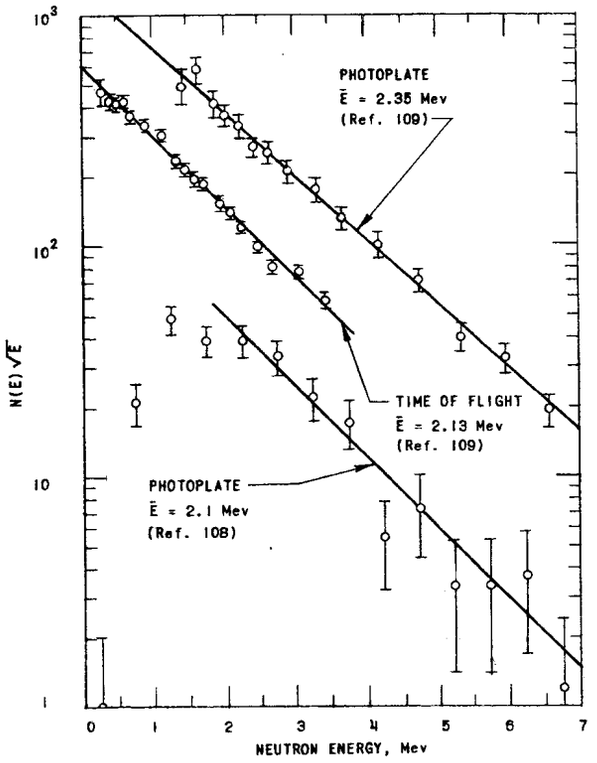

Fig. 1-7 — Least-squares fit of the spectral distribution $N(E) \sim \sqrt{E} \exp(-E/T)$ to the measured fission spectrum of Cf^{252}. *Reproduced from Refs. 108 and 109.*

Table 1-10 — PARAMETERS FOR THE PROMPT FISSION NEUTRON SPECTRUM

$N(E) = a\sqrt{E}\, e^{-E/T}$

Isotope	a	$T = \frac{2}{3}\bar{E}$
$U^{235} + n_{th}$	1.872	1.290
$U^{233} + n_{th}$	1.888	1.306
$Pu^{239} + n_{th}$	2.121	1.333
Cf^{252}	2.410	1.466

The integral of F(u),

$$I_F(u) = \int_{-\infty}^{u} F(x)\,dx = \int_{E}^{\infty} f(x)\,dx = I_f(E)$$

where E is the energy value corresponding to a given u.

Table 1-11 lists the values of u, f(E), and $I_f(E)$ for $0.05 \le E \le 20$ in intervals $\Delta E = 0.05$ for $0.05 \le E \le 6.0$, and in intervals $\Delta E = 1$ for $6 \le E \le 20$.

Table 1-12 lists the values of E, F(u), and $I_F(u)$ for $-0.7 \le u \le 20$ in intervals $\Delta u = 0.1$.

1.4 DELAYED FISSION NEUTRON EMISSION

Very soon after the discovery of fission neutron emission it was suggested,[110] and experimentally verified,[111] that ~1% of the fission neutrons was emitted long after the actual splitting of the parent nucleus. The importance of these delayed neutrons is out of proportion to their relatively small abundance due to the part they play in the control of multiplying systems. In this review, delayed neutrons are defined as those neutrons emitted an average time of $\gtrsim 10^{-3}$ seconds after the actual scission. Delayed neutron emission from U^{235}, U^{233}, U^{238}, Pu^{239}, Pu^{240}, and Th^{232} fission is described in terms of six exponentially decaying neutron groups. These groups are characterized by a half-life, T_i; a decay constant, λ_i; and a relative abundance, a_i. It is recognized that this six-group description of delayed neutron emission is a simplification of a very complex phenomena deeply rooted in the stability properties of neutron-rich nuclei. However, the six-group picture employed in the following is believed to be satisfactory for reactor design work.

Table 1-11—VALUES OF u, f(E), AND $I_f(E)$ VERSUS E

Note: Number in parentheses indicates the power of 10 by which the given value is to be multiplied.

E	u	f(E)	$I_f(E)$	E	u	f(E)	$I_f(E)$
5.000 (−2)	5.2983	1.4824 (−1)	9.9499 (−1)	3.550	1.0356	9.8615 (−2)	1.4357 (−1)
1.000 (−1)	4.6052	2.0285 (−1)	9.8611 (−1)	3.600	1.0217	9.5540 (−2)	1.3872 (−1)
1.500 (−1)	4.1997	2.4036 (−1)	9.7498 (−1)	3.650	1.0079	9.2548 (−2)	1.3402 (−1)
2.000 (−1)	3.9120	2.6847 (−1)	9.6223 (−1)	3.700	9.9425 (−1)	8.9637 (−2)	1.2946 (−1)
2.500 (−1)	3.6889	2.9031 (−1)	9.4824 (−1)	3.750	9.8083 (−1)	8.6806 (−2)	1.2505 (−1)
3.000 (−1)	3.5066	3.0755 (−1)	9.3328 (−1)	3.800	9.6758 (−1)	8.4052 (−2)	1.2078 (−1)
3.500 (−1)	3.3524	3.2121 (−1)	9.1755 (−1)	3.850	9.5451 (−1)	8.1376 (−2)	1.1664 (−1)
4.000 (−1)	3.2189	3.3200 (−1)	9.0120 (−1)	3.900	9.4161 (−1)	7.8774 (−2)	1.1264 (−1)
4.500 (−1)	3.1011	3.4041 (−1)	8.8439 (−1)	3.950	9.2887 (−1)	7.6245 (−2)	1.0877 (−1)
5.000 (−1)	2.9957	3.4683 (−1)	8.6720 (−1)	4.000	9.1629 (−1)	7.3789 (−2)	1.0502 (−1)
5.500 (−1)	2.9004	3.5157 (−1)	8.4973 (−1)	4.050	9.0387 (−1)	7.1403 (−2)	1.0139 (−1)
6.000 (−1)	2.8134	3.5485 (−1)	8.3206 (−1)	4.100	8.9160 (−1)	6.9086 (−2)	9.7874 (−2)
6.500 (−1)	2.7334	3.5687 (−1)	8.1427 (−1)	4.150	8.7948 (−1)	6.6836 (−2)	9.4476 (−2)
7.000 (−1)	2.6593	3.5780 (−1)	7.9640 (−1)	4.200	8.6750 (−1)	6.4652 (−2)	9.1189 (−2)
7.500 (−1)	2.5903	3.5778 (−1)	7.7850 (−1)	4.250	8.5567 (−1)	6.2533 (−2)	8.8010 (−2)
8.000 (−1)	2.5257	3.5692 (−1)	7.6063 (−1)	4.300	8.4397 (−1)	6.0476 (−2)	8.4935 (−2)
8.500 (−1)	2.4651	3.5534 (−1)	7.4282 (−1)	4.350	8.3241 (−1)	5.8480 (−2)	8.1962 (−2)
9.000 (−1)	2.4079	3.5311 (−1)	7.2511 (−1)	4.400	8.2098 (−1)	5.6545 (−2)	7.9086 (−2)
9.500 (−1)	2.3539	3.5031 (−1)	7.0752 (−1)	4.450	8.0968 (−1)	5.4667 (−2)	7.6306 (−2)
1.000	2.3026	3.4703 (−1)	6.9008 (−1)	4.500	7.9851 (−1)	5.2846 (−2)	7.3619 (−2)
1.050	2.2538	3.4331 (−1)	6.7282 (−1)	4.550	7.8746 (−1)	5.1081 (−2)	7.1021 (−2)
1.100	2.2073	3.3921 (−1)	6.5576 (−1)	4.600	7.7653 (−1)	4.9370 (−2)	6.8509 (−2)
1.150	2.1628	3.3478 (−1)	6.3891 (−1)	4.650	7.6572 (−1)	4.7712 (−2)	6.6083 (−2)
1.200	2.1203	3.3006 (−1)	6.2229 (−1)	4.700	7.5502 (−1)	4.6105 (−2)	6.3737 (−2)
1.250	2.0794	3.2510 (−1)	6.0591 (−1)	4.750	7.4444 (−1)	4.4547 (−2)	6.1471 (−2)
1.300	2.0402	3.1993 (−1)	5.8978 (−1)	4.800	7.3397 (−1)	4.3039 (−2)	5.9282 (−2)
1.350	2.0025	3.1458 (−1)	5.7392 (−1)	4.850	7.2361 (−1)	4.1577 (−2)	5.7167 (−2)
1.400	1.9661	3.0908 (−1)	5.5833 (−1)	4.900	7.1335 (−1)	4.0162 (−2)	5.5123 (−2)
1.450	1.9310	3.0346 (−1)	5.4301 (−1)	4.950	7.0320 (−1)	3.8791 (−2)	5.3150 (−2)
1.500	1.8971	2.9773 (−1)	5.2798 (−1)	5.000	6.9315 (−1)	3.7464 (−2)	5.1244 (−2)
1.550	1.8643	2.9193 (−1)	5.1324 (−1)	5.050	6.8320 (−1)	3.6179 (−2)	4.9403 (−2)
1.600	1.8326	2.8607 (−1)	4.9879 (−1)	5.100	6.7334 (−1)	3.4935 (−2)	4.7625 (−2)
1.650	1.8018	2.8017 (−1)	4.8463 (−1)	5.150	6.6359 (−1)	3.3731 (−2)	4.5908 (−2)
1.700	1.7720	2.7423 (−1)	4.7077 (−1)	5.200	6.5393 (−1)	3.2566 (−2)	4.4251 (−2)
1.750	1.7430	2.6829 (−1)	4.5721 (−1)	5.250	6.4436 (−1)	3.1439 (−2)	4.2651 (−2)
1.800	1.7148	2.6235 (−1)	4.4394 (−1)	5.300	6.3488 (−1)	3.0348 (−2)	4.1107 (−2)
1.850	1.6874	2.5642 (−1)	4.3097	5.350	6.2549 (−1)	2.9293 (−2)	3.9616 (−2)
1.900	1.6607	2.5052 (−1)	4.1830	5.400	6.1619 (−1)	2.8272 (−2)	3.8177 (−2)
1.950	1.6348	2.4465 (−1)	4.0592	5.450	6.0697 (−1)	2.7285 (−2)	3.6788 (−2)
2.000	1.6094	2.3882 (−1)	3.9383 (−1)	5.500	5.9784 (−1)	2.6330 (−2)	3.5448 (−2)
2.050	1.5847	2.3304 (−1)	3.8204 (−1)	5.550	5.8879 (−1)	2.5407 (−2)	3.4154 (−2)
2.100	1.5606	2.2732 (−1)	3.7053 (−1)	5.600	5.7982 (−1)	2.4515 (−2)	3.2906 (−2)
2.150	1.5371	2.2165 (−1)	3.5931 (−1)	5.650	5.7093 (−1)	2.3652 (−2)	3.1702 (−2)
2.200	1.5141	2.1606 (−1)	3.4836 (−1)	5.700	5.6212 (−1)	2.2817 (−2)	3.0541 (−2)
2.250	1.4917	2.1054 (−1)	3.3770 (−1)	5.750	5.5339 (−1)	2.2011 (−2)	2.9420 (−2)
2.300	1.4697	2.0509 (−1)	3.2731 (−1)	5.800	5.4473 (−1)	2.1232 (−2)	2.8339 (−2)
2.350	1.4482	1.9973 (−1)	3.1719 (−1)	5.850	5.3614 (−1)	2.0479 (−2)	2.7296 (−2)
2.400	1.4271	1.9445 (−1)	3.0733 (−1)	5.900	5.2763 (−1)	1.9751 (−2)	2.6291 (−2)
2.450	1.4065	1.8925 (−1)	2.9774 (−1)	5.950	5.1919 (−1)	1.9048 (−2)	2.5321 (−2)
2.500	1.3863	1.8415 (−1)	2.8841 (−1)	6.000	5.1083 (−1)	1.8368 (−2)	2.4386 (−2)
2.550	1.3665	1.7913 (−1)	2.7933 (−1)	7.000	3.5667 (−1)	8.7725 (−3)	1.1376 (−2)
2.600	1.3471	1.7421 (−1)	2.7049 (−1)	8.000	2.2314 (−1)	4.1039 (−3)	5.2211 (−3)
2.650	1.3280	1.6938 (−1)	2.6190 (−1)	9.000	1.0536 (−1)	1.8877 (−3)	2.3638 (−3)
2.700	1.3093	1.6464 (−1)	2.5355 (−1)	1.000 (1)	0.000	8.5618 (−4)	1.0577 (−3)
2.750	1.2910	1.6000 (−1)	2.4544 (−1)	1.100 (1)	−9.5310 (−2)	3.8368 (−4)	4.6862 (−4)
2.800	1.2730	1.5546 (−1)	2.3755 (−1)	1.200 (1)	−1.8232 (−1)	1.7016 (−4)	2.0576 (−4)
2.850	1.2553	1.5101 (−1)	2.2989 (−1)	1.300 (1)	−2.6236 (−1)	7.4777 (−5)	8.9680 (−5)
2.900	1.2379	1.4666 (−1)	2.2245 (−1)	1.400 (1)	−3.3647 (−1)	3.2597 (−5)	3.8830 (−5)
2.950	1.2208	1.4241 (−1)	2.1522 (−1)	1.500 (1)	−4.0547 (−1)	1.4107 (−5)	1.6690 (−5)
3.000	1.2040	1.3825 (−1)	2.0821 (−1)	1.600 (1)	−4.7000 (−1)	0	0.7130 (−5)
3.050	1.1874	1.3418 (−1)	2.0140 (−1)	1.700 (1)	−5.3063 (−1)	0	0
3.100	1.1712	1.3022 (−1)	1.9479 (−1)	1.800 (1)	−5.8779 (−1)	0	0
3.150	1.1552	1.2634 (−1)	1.8837 (−1)	1.900 (1)	−6.4185 (−1)	0	0
3.200	1.1394	1.2256 (−1)	1.8215 (−1)	2.000 (1)	−6.9315 (−1)	0	0
3.250	1.1239	1.1887 (−1)	1.7612 (−1)				
3.300	1.1087	1.1527 (−1)	1.7026 (−1)				
3.350	1.0936	1.1177 (−1)	1.6459 (−1)				
3.400	1.0788	1.0835 (−1)	1.5908 (−1)				
3.450	1.0642	1.0502 (−1)	1.5375 (−1)				
3.500	1.0498	1.0177 (−1)	1.4858 (−1)				

687863 O - 63 - 3

Table 1-12—VALUES OF E, F(u), AND $I_F(u)$ VERSUS u

Note: Number in parentheses indicates the power of 10 by which the given value is to be multiplied.

u	E	F(u)	$I_F(u)$	u	E	F(u)	$I_F(u)$	u	E	F(u)	$I_F(u)$
−7.000 (−1)	2.0138 (1)	3.5090 (−6)	2.1000 (−7)	6.000	2.4788 (−2)	2.6304 (−3)	9.9823 (−1)	1.300 (1)	2.2603 (−5)	0.0000	1.0000
−6.000 (−1)	1.8221 (1)	1.6610 (−5)	1.0800 (−6)	6.100	2.2429 (−2)	2.2675 (−3)	9.9848 (−1)	1.310 (1)	2.0452 (−5)		
−5.000 (−1)	1.6487 (1)	6.6142 (−5)	4.6900 (−6)	6.200	2.0294 (−2)	1.9544 (−3)	9.9869 (−1)	1.320 (1)	1.8506 (−5)		
−4.000 (−1)	1.4918 (1)	2.2543 (−4)	1.7890 (−5)	6.300	1.8363 (−2)	1.6843 (−3)	9.9887 (−1)	1.330 (1)	1.6745 (−5)		
−3.000 (−1)	1.3499 (1)	6.6786 (−4)	5.9120 (−5)	6.400	1.6616 (−2)	1.4514 (−3)	9.9903 (−1)	1.340 (1)	1.5151 (−5)	0.0000	1.0000
−2.000 (−1)	1.2214 (1)	1.7442 (−3)	1.7237 (−4)								
−1.000 (−1)	1.1052 (1)	4.0667 (−3)	4.4918 (−4)								
0.000	1.0000 (1)	8.5618 (−3)	1.0577 (−3)	6.500	1.5034 (−2)	1.2505 (−3)	9.9916 (−1)	1.350 (1)	1.3710 (−5)	0.0000	1.0000
1.000 (−1)	9.0484	1.6445 (−2)	2.2742 (−3)	6.600	1.3604 (−2)	1.0773 (−3)	9.9928 (−1)	1.360 (1)	1.2405 (−5)		
2.000 (−1)	8.1873	2.9086 (−2)	4.5053 (−3)	6.700	1.2309 (−2)	9.2805 (−4)	9.9938 (−1)	1.370 (1)	1.1224 (−5)		
3.000 (−1)	7.4062	4.7769 (−2)	8.2930 (−3)	6.800	1.1138 (−2)	7.9939 (−4)	9.9947 (−1)	1.380 (1)	1.0156 (−5)		
4.000 (−1)	6.7032	7.3399 (−2)	1.4291 (−2)	6.900	1.0078 (−2)	6.8852 (−4)	9.9954 (−1)	1.390 (1)	9.1898 (−6)	0.0000	1.0000
5.000 (−1)	6.0653	1.0624 (−1)	2.3214 (−2)	7.000	9.1188 (−3)	5.9299 (−4)	9.9960 (−1)	1.400 (1)	8.3153 (−6)	0.0000	1.0000
6.000 (−1)	5.4881	1.4573 (−1)	3.5762 (−2)	7.100	8.2510 (−3)	5.1068 (−4)	9.9966 (−1)	1.410 (1)	7.5240 (−6)		
7.000 (−1)	4.9659	1.9052 (−1)	5.2538 (−2)	7.200	7.4659 (−3)	4.3977 (−4)	9.9971 (−1)	1.420 (1)	6.8080 (−6)		
8.000 (−1)	4.4933	2.3854 (−1)	7.3974 (−2)	7.300	6.7554 (−3)	3.7869 (−4)	9.9975 (−1)	1.430 (1)	6.1601 (−6)		
9.000 (−1)	4.0657	2.8732 (−1)	1.0027 (−1)	7.400	6.1125 (−3)	3.2608 (−4)	9.9978 (−1)	1.440 (1)	5.5739 (−6)	0.0000	1.0000
1.000	3.6788	3.3426 (−1)	1.3138 (−1)	7.500	5.5308 (−3)	2.8077 (−4)	9.9981 (−1)	1.450 (1)	5.0435 (−6)	0.0000	1.0000
1.100	3.3287	3.7697 (−1)	1.6698 (−1)	7.600	5.0045 (−3)	2.4174 (−4)	9.9984 (−1)	1.460 (1)	4.5635 (−6)		
1.200	3.0119	4.1345 (−1)	2.0656 (−1)	7.700	4.5283 (−3)	2.0813 (−4)	9.9986 (−1)	1.470 (1)	4.1292 (−6)		
1.300	2.7253	4.4227 (−1)	2.4942 (−1)	7.800	4.0973 (−3)	1.7919 (−4)	9.9988 (−1)	1.480 (1)	3.7363 (−6)		
1.400	2.4660	4.6264 (−1)	2.9473 (−1)	7.900	3.7074 (−3)	1.5427 (−4)	9.9990 (−1)	1.490 (1)	3.3807 (−6)	0.0000	1.0000
1.500	2.2313	4.7436 (−1)	3.4165 (−1)	8.000	3.3546 (−3)	1.3281 (−4)	9.9991 (−1)	1.500 (1)	3.0590 (−6)	0.0000	1.0000
1.600	2.0190	4.7773 (−1)	3.8933 (−1)	8.100	3.0354 (−3)	1.1434 (−4)	9.9992 (−1)	1.510 (1)	2.7679 (−6)		
1.700	1.8268	4.7346 (−1)	4.3695 (−1)	8.200	2.7465 (−3)	9.8430 (−5)	9.9993 (−1)	1.520 (1)	2.5045 (−6)		
1.800	1.6530	4.6252 (−1)	4.8380 (−1)	8.300	2.4852 (−3)	8.4734 (−5)	9.9994 (−1)	1.530 (1)	2.2662 (−6)		
1.900	1.4957	4.4606 (−1)	5.2927 (−1)	8.400	2.2487 (−3)	7.2943 (−5)	9.9995 (−1)	1.540 (1)	2.0505 (−6)	0.0000	1.0000
2.000	1.3534	4.2525 (−1)	5.7286 (−1)	8.500	2.0347 (−3)	6.2791 (−5)	9.9996 (−1)	1.550 (1)	1.8554 (−6)	0.0000	1.0000
2.100	1.2246	4.0123 (−1)	6.1421 (−1)	8.600	1.8411 (−3)	5.4052 (−5)	9.9996 (−1)	1.560 (1)	1.6788 (−6)		
2.200	1.1080	3.7509 (−1)	6.5304 (−1)	8.700	1.6659 (−3)	4.6528 (−5)	9.9997 (−1)	1.570 (1)	1.5191 (−6)		
2.300	1.0026	3.4774 (−1)	6.8919 (−1)	8.800	1.5073 (−3)	4.0051 (−5)	9.9997 (−1)	1.580 (1)	1.3745 (−6)		
2.400	9.0718 (−1)	3.2000 (−1)	7.2257 (−1)	8.900	1.3639 (−3)	3.4476 (−5)	9.9998 (−1)	1.590 (1)	1.2437 (−6)	0.0000	1.0000
2.500	8.2085 (−1)	2.9251 (−1)	7.5320 (−1)	9.000	1.2341 (−3)	2.9676 (−5)	9.9998 (−1)	1.600 (1)	1.1254 (−6)	0.0000	1.0000
2.600	7.4274 (−1)	2.6578 (−1)	7.8110 (−1)	9.100	1.1167 (−3)	2.5544 (−5)	9.9998 (−1)	1.610 (1)	1.0183 (−6)		
2.700	6.7206 (−1)	2.4020 (−1)	8.0639 (−1)	9.200	1.0104 (−3)	2.1988 (−5)	9.9999 (−1)	1.620 (1)	9.2136 (−7)		
2.800	6.0810 (−1)	2.1603 (−1)	8.2919 (−1)	9.300	9.1424 (−4)	1.8926 (−5)	9.9999 (−1)	1.630 (1)	8.3368 (−7)		
2.900	5.5023 (−1)	1.9345 (−1)	8.4965 (−1)	9.400	8.2724 (−4)	1.6291 (−5)	9.9999 (−1)	1.640 (1)	7.5435 (−7)	0.0000	1.0000
3.000	4.9787 (−1)	1.7256 (−1)	8.6793 (−1)	9.500	7.4852 (−4)	1.4022 (−5)	9.9999 (−1)	1.650 (1)	6.8256 (−7)	0.0000	1.0000
3.100	4.5049 (−1)	1.5338 (−1)	8.8422 (−1)	9.600	6.7729 (−4)	1.2070 (−5)	9.9999 (−1)	1.660 (1)	6.1761 (−7)		
3.200	4.0762 (−1)	1.3591 (−1)	8.9867 (−1)	9.700	6.1283 (−4)	1.0389 (−5)	9.9999 (−1)	1.670 (1)	5.5883 (−7)		
3.300	3.6883 (−1)	1.2008 (−1)	9.1145 (−1)	9.800	5.5452 (−4)	8.9422 (−6)	9.9999 (−1)	1.680 (1)	5.0565 (−7)		
3.400	3.3373 (−1)	1.0583 (−1)	9.2274 (−1)	9.900	5.0175 (−4)	7.6969 (−6)	9.9999 (−1)	1.690 (1)	4.5753 (−7)	0.0000	1.0000
3.500	3.0197 (−1)	9.3054 (−2)	9.3267 (−1)	1.000 (1)	4.5400 (−4)	6.6250 (−6)	1.0000	1.700 (1)	4.1399 (−7)	0.0000	1.0000
3.600	2.7324 (−1)	8.1650 (−2)	9.4139 (−1)	1.010 (1)	4.1080 (−4)	5.7024 (−6)		1.710 (1)	3.7460 (−7)		
3.700	2.4724 (−1)	7.1510 (−2)	9.4904 (−1)	1.020 (1)	3.7170 (−4)	0.0000		1.720 (1)	3.3895 (−7)		
3.800	2.2371 (−1)	6.2523 (−2)	9.5573 (−1)	1.030 (1)	3.3633 (−4)	0.0000		1.730 (1)	3.0669 (−7)		
3.900	2.0242 (−1)	5.4583 (−2)	9.6158 (−1)	1.040 (1)	3.0432 (−4)	0.0000	1.0000	1.740 (1)	2.7751 (−7)	0.0000	1.0000
4.000	1.8316 (−1)	4.7586 (−2)	9.6668 (−1)	1.050 (1)	2.7536 (−4)	0.0000	1.0000	1.750 (1)	2.5110 (−7)	0.0000	1.0000
4.100	1.6573 (−1)	4.1435 (−2)	9.7113 (−1)	1.060 (1)	2.4916 (−4)			1.760 (1)	2.2720 (−7)		
4.200	1.4996 (−1)	3.6039 (−2)	9.7499 (−1)	1.070 (1)	2.2545 (−4)			1.770 (1)	2.0558 (−7)		
4.300	1.3569 (−1)	3.1313 (−2)	9.7836 (−1)	1.080 (1)	2.0400 (−4)			1.780 (1)	1.8602 (−7)		
4.400	1.2277 (−1)	2.7183 (−2)	9.8128 (−1)	1.090 (1)	1.8458 (−4)	0.0000	1.0000	1.790 (1)	1.6832 (−7)	0.0000	1.0000
4.500	1.1109 (−1)	2.3578 (−2)	9.8381 (−1)	1.100 (1)	1.6702 (−4)	0.0000	1.0000	1.800 (1)	1.5230 (−7)	0.0000	1.0000
4.600	1.0052 (−1)	2.0436 (−2)	9.8601 (−1)	1.110 (1)	1.5112 (−4)			1.810 (1)	1.3781 (−7)		
4.700	9.0953 (−2)	1.7701 (−2)	9.8791 (−1)	1.120 (1)	1.3674 (−4)			1.820 (1)	1.2469 (−7)		
4.800	8.2297 (−2)	1.5323 (−2)	9.8956 (−1)	1.130 (1)	1.2373 (−4)			1.830 (1)	1.1283 (−7)		
4.900	7.4466 (−2)	1.3257 (−2)	9.9099 (−1)	1.140 (1)	1.1195 (−4)	0.0000	1.0000	1.840 (1)	1.0209 (−7)	0.0000	1.0000
5.000	6.7379 (−2)	1.1463 (−2)	9.9222 (−1)	1.150 (1)	1.0130 (−4)	0.0000	1.0000	1.850 (1)	9.2374 (−8)	0.0000	1.0000
5.100	6.0967 (−2)	9.9083 (−3)	9.9329 (−1)	1.160 (1)	9.1661 (−5)			1.860 (1)	8.3584 (−8)		
5.200	5.5166 (−2)	8.5608 (−3)	9.9421 (−1)	1.170 (1)	8.2938 (−5)			1.870 (1)	7.5630 (−8)		
5.300	4.9916 (−2)	7.3938 (−3)	9.9501 (−1)	1.180 (1)	7.5046 (−5)			1.880 (1)	6.8433 (−8)		
5.400	4.5166 (−2)	6.3838 (−3)	9.9569 (−1)	1.190 (1)	6.7904 (−5)	0.0000	1.0000	1.890 (1)	6.1920 (−8)	0.0000	1.0000
5.500	4.0868 (−2)	5.5102 (−3)	9.9629 (−1)	1.200 (1)	6.1442 (−5)	0.0000	1.0000	1.900 (1)	5.6028 (−8)	0.0000	1.0000
5.600	3.6979 (−2)	4.7548 (−3)	9.9680 (−1)	1.210 (1)	5.5595 (−5)			1.910 (1)	5.0696 (−8)		
5.700	3.3460 (−2)	4.1019 (−3)	9.9724 (−1)	1.220 (1)	5.0305 (−5)			1.920 (1)	4.5872 (−8)		
5.800	3.0276 (−2)	3.5380 (−3)	9.9762 (−1)	1.230 (1)	4.5517 (−5)			1.930 (1)	4.1507 (−8)		
5.900	2.7394 (−2)	3.0509 (−3)	9.9795 (−1)	1.240 (1)	4.1186 (−5)	0.0000	1.0000	1.940 (1)	3.7557 (−8)	0.0000	1.0000
				1.250 (1)	3.7267 (−5)	0.0000	1.0000	1.950 (1)	3.3983 (−8)	0.0000	1.0000
				1.260 (1)	3.3720 (−5)			1.960 (1)	3.0749 (−8)		
				1.270 (1)	3.0511 (−5)			1.970 (1)	2.7823 (−8)		
				1.280 (1)	2.7608 (−5)			1.980 (1)	2.5175 (−8)		
				1.290 (1)	2.4981 (−5)	0.0000	1.0000	1.990 (1)	2.2779 (−8)		
								2.000 (1)	2.0612 (−8)	0.0000	1.0000

1.4.1 YIELDS AND HALF-LIVES OF DELAYED NEUTRON GROUPS

The properties of the delayed neutrons emitted following the thermal neutron-induced fission of U^{233}, U^{235}, and Pu^{239} are given in Table 1-13.[112] The characteristics of the delayed neutrons emitted following the fast neutron-induced fission of U^{233}, U^{235}, U^{238}, Pu^{239}, Pu^{240}, and Th^{232} are given in Table 1-14.[112] "Fast fission" is defined as fission induced by a continuous neutron spectra similar to a prompt fission neutron spectra.

Table 1-13—DELAYED NEUTRON YIELD FROM THERMAL FISSION IN U^{233}, U^{235}, AND Pu^{239}

Data from Ref. 112

Isotope	Delayed Neutrons/ Fission	Group Index, i	Half-Life, T_i	Decay Constant, λ_i	Relative Abundance, a_i	Absolute Group Yield, %
U^{233}	0.0066 ± 0.0003	1	55.00 ± 0.54	0.0126 ± 0.0002	0.086 ± 0.003	0.057 ± 0.003
		2	20.57 ± 0.38	0.0337 ± 0.0006	0.299 ± 0.004	0.197 ± 0.009
		3	5.00 ± 0.21	0.139 ± 0.006	0.252 ± 0.040	0.166 ± 0.027
		4	2.13 ± 0.20	0.325 ± 0.030	0.278 ± 0.020	0.184 ± 0.016
		5	0.615 ± 0.242	1.13 ± 0.40	0.051 ± 0.024	0.034 ± 0.016
		6	0.277 ± 0.047	2.50 ± 0.42	0.034 ± 0.014	0.022 ± 0.009
U^{235}	0.0158 ± 0.0005	1	55.72 ± 1.28	0.0124 ± 0.0003	0.033 ± 0.003	0.052 ± 0.005
		2	22.72 ± 0.71	0.0305 ± 0.0010	0.219 ± 0.009	0.346 ± 0.018
		3	6.22 ± 0.23	0.111 ± 0.004	0.196 ± 0.022	0.310 ± 0.036
		4	2.30 ± 0.09	0.301 ± 0.012	0.395 ± 0.011	0.624 ± 0.026
		5	0.61 ± 0.083	1.13 ± 0.15	0.115 ± 0.009	0.182 ± 0.015
		6	0.23 ± 0.025	3.00 ± 0.33	0.042 ± 0.008	0.066 ± 0.008
Pu^{239}	0.0061 ± 0.0003	1	54.28 ± 2.34	0.0128 ± 0.0005	0.035 ± 0.009	0.021 ± 0.006
		2	23.04 ± 1.67	0.0301 ± 0.0022	0.298 ± 0.035	0.182 ± 0.023
		3	5.60 ± 0.40	0.124 ± 0.009	0.211 ± 0.048	0.129 ± 0.030
		4	2.13 ± 0.24	0.325 ± 0.036	0.326 ± 0.033	0.199 ± 0.022
		5	0.618 ± 0.213	1.12 ± 0.39	0.086 ± 0.029	0.052 ± 0.018
		6	0.257 ± 0.045	2.69 ± 0.47	0.044 ± 0.016	0.027 ± 0.010

A comparison of the values in Tables 1-13 and 1-14 indicates only a slight shift in periods and yields as incident neutron energy is changed from thermal to an average energy of about 1.8 Mev. Actually, the fission product yields, and therefore the yield of delayed neutron precursors, depend on incident neutron energy.[113] This effect is clearly evident from Table 1-15 which presents the delayed neutron properties of Cf^{252} spontaneous fission.[114] This spontaneous process results in mass yields[115,116] appreciably different from those obtained from the fission processes given in Tables 1-13 and 1-14. As a result, the delayed neutron properties are markedly different.

The delayed neutron fraction, β, the relative number of delayed neutrons per fission, follows directly from Tables 1-13 and 1-14 and the known $\bar{\nu}$ values (see Section 1.5). The more useful β values are given in Table 1-16.

1.4.2 DELAYED NEUTRON ENERGIES

The measured mean energies of the delayed neutron groups from U^{235} fission are given in Table 1-17. The spectral shapes of these groups are not well known.

1.4.3 DELAYED PHOTONEUTRONS IN Be AND D_2O

The yield of photoneutrons from U^{235} fission products in D_2O has been measured.[120] Nine delayed neutron groups were resolved with the periods T_j and yields given in Table 1-18. The yields are established relative to the total yield of U^{235} delayed fission neutrons.[117]

The yields and periods of delayed neutrons present in Be-U^{235} reactive systems have been studied by several groups.[120,121,122] The results are summarized in twelve delayed neutron groups having the

Table 1-14—DELAYED NEUTRON YIELD FROM FAST FISSION IN U^{233}, U^{235}, U^{238}, Pu^{239}, Pu^{240}, AND Th^{232}

Isotope	Delayed Neutrons/ Fission	Group Index, i	Half-Life, T_i	Decay Constant, λ_i	Relative Abundance, a_i	Absolute Group Yield, %
U^{233}	0.0070 ± 0.0004	1	55.11 ± 1.86	0.0126 ± 0.0004	0.086 ± 0.003	0.06 ± 0.003
		2	20.74 ± 0.86	0.0334 ± 0.0014	0.274 ± 0.005	0.192 ± 0.009
		3	5.30 ± 0.19	0.131 ± 0.005	0.227 ± 0.035	0.159 ± 0.025
		4	2.29 ± 0.18	0.302 ± 0.024	0.317 ± 0.011	0.222 ± 0.012
		5	0.546 ± 0.108	1.27 ± 0.266	0.073 ± 0.014	0.051 ± 0.010
		6	0.221 ± 0.042	3.13 ± 0.675	0.023 ± 0.007	0.016 ± 0.005
U^{235}	0.0165 ± 0.0005	1	54.51 ± 0.94	0.0127 ± 0.0002	0.038 ± 0.003	0.063 ± 0.005
		2	21.84 ± 0.54	0.0317 ± 0.0008	0.213 ± 0.005	0.351 ± 0.011
		3	6.00 ± 0.17	0.115 ± 0.003	0.188 ± 0.016	0.310 ± 0.028
		4	2.23 ± 0.06	0.311 ± 0.008	0.407 ± 0.007	0.672 ± 0.023
		5	0.496 ± 0.029	1.40 ± 0.081	0.128 ± 0.008	0.211 ± 0.015
		6	0.179 ± 0.017	3.87 ± 0.369	0.026 ± 0.003	0.043 ± 0.005
U^{238}	0.0412 ± 0.0017	1	52.38 ± 1.29	0.0132 ± 0.0003	0.013 ± 0.001	0.054 ± 0.005
		2	21.58 ± 0.39	0.0321 ± 0.0006	0.137 ± 0.002	0.564 ± 0.025
		3	5.00 ± 0.19	0.139 ± 0.005	0.162 ± 0.020	0.667 ± 0.087
		4	1.93 ± 0.07	0.358 ± 0.014	0.388 ± 0.012	1.599 ± 0.081
		5	0.49 ± 0.023	1.41 ± 0.067	0.225 ± 0.013	0.927 ± 0.060
		6	0.172 ± 0.009	4.02 ± 0.214	0.075 ± 0.005	0.309 ± 0.024
Pu^{239}	0.0063 ± 0.0003	1	53.75 ± 0.95	0.0129 ± 0.0002	0.038 ± 0.003	0.024 ± 0.002
		2	22.29 ± 0.36	0.0311 ± 0.0005	0.280 ± 0.004	0.176 ± 0.009
		3	5.19 ± 0.12	0.134 ± 0.003	0.216 ± 0.018	0.136 ± 0.013
		4	2.09 ± 0.08	0.331 ± 0.012	0.328 ± 0.010	0.207 ± 0.012
		5	0.549 ± 0.049	1.26 ± 0.115	0.103 ± 0.009	0.065 ± 0.007
		6	0.216 ± 0.017	3.21 ± 0.255	0.035 ± 0.005	0.022 ± 0.003
Pu^{240}	0.0088 ± 0.0006	1	53.56 ± 1.21	0.0129 ± 0.0004	0.028 ± 0.003	0.022 ± 0.003
		2	22.14 ± 0.38	0.0313 ± 0.0005	0.273 ± 0.004	0.238 ± 0.016
		3	5.14 ± 0.42	0.135 ± 0.011	0.192 ± 0.053	0.162 ± 0.044
		4	2.08 ± 0.19	0.333 ± 0.031	0.350 ± 0.020	0.315 ± 0.027
		5	0.511 ± 0.077	1.36 ± 0.205	0.128 ± 0.018	0.119 ± 0.018
		6	0.172 ± 0.033	4.04 ± 0.782	0.029 ± 0.006	0.024 ± 0.005
Th^{232}	0.0496 ± 0.0020	1	56.03 ± 0.95	0.0124 ± 0.0002	0.034 ± 0.002	0.169 ± 0.012
		2	20.75 ± 0.66	0.0334 ± 0.0011	0.150 ± 0.005	0.744 ± 0.037
		3	5.74 ± 0.24	0.121 ± 0.005	0.155 ± 0.021	0.769 ± 0.108
		4	2.16 ± 0.08	0.321 ± 0.011	0.446 ± 0.015	2.212 ± 0.110
		5	0.571 ± 0.042	1.21 ± 0.090	0.172 ± 0.013	0.853 ± 0.073
		6	0.211 ± 0.019	3.29 ± 0.297	0.043 ± 0.006	0.213 ± 0.031

Table 1-15—DELAYED NEUTRONS FROM THE SPONTANEOUS FISSION OF Cf^{252}

Data from Ref. 114

Group Index	Half-Life, sec	Relative Abundance	Absolute Yield, neutrons/fission
1	20.5 ± 0.5	0.255 ± 0.01	0.22 ± 0.01
2	2.0 ± 0.4	0.338 ± 0.046	0.29 ± 0.04
3	0.5 ± 0.4	0.407 ± 0.12	0.35 ± 0.1
			TOTAL: 0.86 ± 0.1

Table 1-16—DELAYED NEUTRON FRACTION (β) FOR FAST AND THERMAL FISSION

Isotope	Fast Fission	Thermal Fission
U^{233}	0.0027 ± 0.0002	0.00264 ± 0.0002
U^{235}	0.0065 ± 0.0003	0.0065 ± 0.0003
U^{238}	0.0157 ± 0.0012	
Pu^{239}	0.0021 ± 0.0002	0.0021 ± 0.0002
Pu^{240}	0.0026 ± 0.0003	
Th^{232}	0.022	

Table 1-17—MEAN ENERGIES OF THE DELAYED NEUTRON GROUPS FOR U^{235} FISSION

Group Index, i	Half-Life, sec	Mean Energy, kev		
		Hughes, et al. *Ref. 117*	Burgy, et al. *Ref. 118*	Batchelor *Ref. 119*
1	55.7	250 ± 60	300 ± 60	250 ± 20
2	22.7	560 ± 60	670 ± 60	460 ± 10
3	6.2	430 ± 60	650 ± 100	405 ± 20
4	2.3	620 ± 60	910 ± 90	450 ± 20
5	0.61	420 ± 60	400 ± 70	
6	0.23			

yield fractions, β_i, and mean lives, τ_i, given in Table 1-19.[121] In addition to the tabulated values, some shorter periods may well appear in considerable intensity.[121]

Table 1-18—PHOTONEUTRON HALF-LIVES AND YIELDS FROM U^{235} FISSION PRODUCTS IN D_2O

Data from Ref. 120.

s = second m = minute h = hour

Group j	Half-Life, T_j	Yield-% Relative to Total Delayed Neutron Yield[a]
1	307h	0.0065
2	53h	0.0163
3	4.4h	0.0515
4	1.65h	0.370
5	27m	0.328
6	7.7m	0.534
7	2.4m	1.11
8	41s	3.24
9	2.5s	10.31

[a]Based on delayed neutron data of Hughes, et al.[117]

Table 1-19—DELAYED NEUTRON FRACTION IN Be

s = second m = minute

Group No.	Mean Life, τ_i	$\beta_i \times 10^5$
1	3814m	0.0628
2	576m	0.694
3	279m	0.479
4	158m	0.894
5	93m	1.15
6	29m	1.72
7	9.44m	2.63
8	269s	1.51
9	80.7s	35.7
10	31.7s	166.0
11	6.50s	233.0
12	3.12s	14.3

1.5 FISSION NEUTRON EMISSION

Fission neutrons are defined as all neutrons emitted at or following the actual scission. Experiment indicates that ~99% of these neutrons are emitted within $\lesssim$30 μsec of the actual splitting of the fissile nucleus.[112,124] The remaining ~1% of "delayed" neutrons is emitted following the fission with delays of up to $\lesssim 10^2$ seconds.[112] The properties of these delayed neutrons are discussed in Section 1.4. Experimental determinations of $\bar{\nu}$, the average number of neutrons released per fission, generally distinguish between "prompt" and "delayed" neutrons.[124] All experimental data presented here are corrected to include all fission neutrons, "delayed" and "prompt." The energy distribution of the fission neutrons is discussed in Sections 1.3 and 1.4.

Experiment indicates that the prompt neutrons are emitted after the actual scission with delays long compared to the characteristic nuclear time, but very short on a laboratory scale ($\sim 10^{-14}$ sec).[16,92,93] In addition, the prompt neutrons appear to be emitted isotropically from the moving fragment.[93,125,126] As a result, the correlation of the incident neutron-fragment axis is maintained, to some degree, by the prompt neutrons.[127,128] On the average, the light and the heavy fragment groups from binary fission contribute equally to the prompt fission neutron yield.[94] However, the heavier fragments from both the light and the heavy groups tend to emit prompt neutrons more copiously.[94]

1.5.1 TABULATED $\bar{\nu}$ VALUES

Tables 1-20, 1-21, and 1-22 summarize existing knowledge of fission neutron emission from both neutron-induced and spontaneous fission processes. The average number of neutrons, $\bar{\nu}$, (including delayed neutrons) emitted per fission is given. The energy of the incident neutron inducing the fission process is stated where applicable. In compiling this tabulation, only measurements made at discrete neutron energies have been considered. Values of $\bar{\nu}$ obtained at average incident neutron energies from a continuous spectrum are largely omitted due to the uncertainty in both the incident spectra and the energy dependence of the fission cross section. All $\bar{\nu}$ measurements involving ratio determinations of the type $\bar{\nu}(x)/\bar{\nu}(y)$ have been corrected to be consistent with the thermal neutron $\bar{\nu}$ values given in the tabulation. Where a particular measurement or set of measurements is absolute, it is accepted with its respective error despite the fact that evidence for a systematic shift may exist.

Table 1-20 —$\bar{\nu}$ OF U^{233} + n, U^{235} + n, U^{238} + n, Th^{232} + n, AND Pu^{239} + n

Isotope	E_n, Mev	$\bar{\nu}$	Ref.	Isotope	E_n, Mev	$\bar{\nu}$	Ref.
U^{233} + n	0.0	2.50 ± 0.02	129	U^{238} + n	1.50	2.60 ± 0.09	135
	4.0	2.998 ± 0.12	140		2.5	2.35 ± 0.018[a]	136
	14.1	3.78 ± 0.28	136		2.3	2.67 ± 0.08	137
	15.0	4.33 ± 0.17	145		4.0	3.05 ± 0.10	140
U^{235} + n	0.0	2.43 ± 0.02	129		4.25	3.04 ± 0.40	139
	0.7	2.48 ± 0.10	132		3.75	2.96 ± 0.10	137
		2.48 ± 0.06	133		14.0	3.43 ± 0.15[a]	140
	1.0	2.791 ± 0.35	133		14.1	4.05 ± 0.25	136
		2.791 ± 0.30	134		14.2	4.36 ± 0.35	142
	1.25	2.604 ± 0.09	135			4.46 ± 0.15	143
	1.5	2.605 ± 0.09	135	Pu^{239} + n	0.0	2.89 ± 0.03	129
	1.90	2.99 ± 0.55	134		−6.3	2.16 ± 0.026[b]	130
	2.0	2.80 ± 0.15	133			2.227 ± 0.045	124
	2.5	2.64 ± 0.19	136		2.1	3.12 ± 0.15	133
	4.0	3.05 ± 0.35	134		4.0	3.36 ± 0.11	140
		2.95 ± 0.12	140		4.25	3.59 ± 0.40	139
	4.25	3.07 ± 0.31	139		14.0	4.12 ± 0.15	140
	4.5	3.19 ± 0.31	137			4.41 ± 0.32	141
	4.8	3.14 ± 0.08	135		14.2	4.65 ± 0.40	143
	5.0	3.175 ± 0.35	134		15.0	4.61 ± 0.20	145
	14.0	4.43 ± 0.32	136	Th^{232} + n	1.50	2.6 ± 0.20	138
		4.05 ± 0.24	141		2.30	2.22 ± 0.10	137
	14.8	4.70 ± 0.50	144		3.75	2.39 ± 0.09	137
	15.0	4.419 ± 0.19	145		14.2	4.54 ± 0.20	143
					15.7	4.16 ± 0.13	137

[a]Points omitted in determining best value.
[b]Spontaneous fission of Pu^{240}.

Table 1-21 —$\bar{\nu}$ OF OTHER NEUTRON-INDUCED FISSION PROCESSES

Isotope	E_n, Mev	$\bar{\nu}$	Ref.
Pu^{241} + n	0	3.03 ± 0.06	146
		2.94 ± 0.059	130
		2.95 ± 0.10	147
		2.91 ± 0.10	148
		3.17 ± 0.12	149
	−6.1[a]	2.136 ± 0.09	131
Pu^{240} + n	1.47[b]	3.26 ± 0.21	150
	1.67[b]	3.37 ± 0.10	150
Np^{237} + n	1.4[b]	2.81 ± 0.09	150
	1.67[b]	2.9 ± 0.04	150
	2.50	2.72 ± 0.15	151

[a]Spontaneous fission of Pu^{242}.
[b]Average neutron energy not including effect of $\sigma_f(E)$.

1.5.2 GRAPHICAL PRESENTATION OF $\bar{\nu}$ VALUES

Figures 1-8, 1-9, and 1-10 show the $\bar{\nu}$ values of Tables 1-20, 1-21, and 1-22. The experimental data have been fitted, by the method of least squares, with a linear expression of the form:

$$\bar{\nu}(E) = \bar{\nu}(\text{thermal}) + \frac{d\bar{\nu}}{dE} E$$

where E is the incident neutron energy in Mev.

The individual measurements were weighted with the reciprocal of the experimental errors. The results of this fitting procedure are shown in the figures. The fit can be employed to determine $\bar{\nu}$ at any energy E. The necessary constants are listed in Table 1-23.

Table 1-22 —$\bar{\nu}$ OF SPONTANEOUS FISSION PROCESSES

Isotope	$\bar{\nu}$	Ref.	Isotope	$\bar{\nu}$	Ref.
U^{238} [a]	2.19 ± 0.08	143	Cm^{244}	2.61 ± 0.13	153
				2.80 ± 0.09	131
Th^{232}	2.37 ± 0.14	152		2.77 ± 0.059	124
Pu^{236}	1.89 ± 0.20	153		2.60 ± 0.11	155
	2.269 ± 0.19	131	Bk^{249}	3.67 ± 0.16	156
Pu^{238}	2.04 ± 0.10	153	Cf^{246}	2.88 ± 0.19	156
	2.299 ± 0.08	131			
Pu^{240}	2.227 ± 0.045	124	Cf^{252}	3.52 ± 0.16	153
	2.07 ± 0.11	131		3.53 ± 0.15	157
				3.77 ± 0.12	131
Pu^{242}	2.32 ± 0.16	153		3.818 ± 0.078	124
	2.15 ± 0.09	131		3.80 ± 0.16	158
				3.80 ± 0.035	130
Cm^{242}	3.0 ± 0.3	154			
	2.33 ± 0.11	153	Cf^{254}	3.90 ± 0.14	156
	2.61 ± 0.09	131	Fm^{254}	4.04 ± 0.19	159

[a] U^{238} spontaneous fission = 14.92 ± 0.2 n/(kg)(sec).[143]
Mean number of fissions/(kg U)(sec) = 6.82 ± 0.20.[143]

1.5.3 DISTRIBUTION OF ν

The distribution function, P_ν, is defined as the probability of emitting ν neutrons per fission. Although the experimental determinations pertain only to P_ν (prompt), the following distribution function can be applied to total fission neutron emission without measurable error.

In cumulative form, the distribution function P_ν is expressed by:[160]

$$\sum_{n=0}^{\nu} P_n = (2\pi)^{-1/2} \int_{-\infty}^{(\nu-\bar{\nu}+\frac{1}{2}+b)/\sigma} \exp(-t^2/2)\, dt$$

where $\sigma = 1.08$ for all fission processes utilized in applied work, and $b \lesssim 10^{-2}$ is nearly negligible. Experiments verify this distribution function for all measured cases with the exception of Cf^{252}. Measured values of P_i from the three most commonly utilized fission processes are given in Table 1-24.[124]

1.6 SPONTANEOUS FISSION HALF-LIVES

The measured spontaneous fission half-lives are given in Table 1-25.[162] The information is summarized graphically in Fig. 1-11; the dashed lines indicate the experimentally observed alpha half-life variation except for elements 102 and 104 where the curves are estimates.

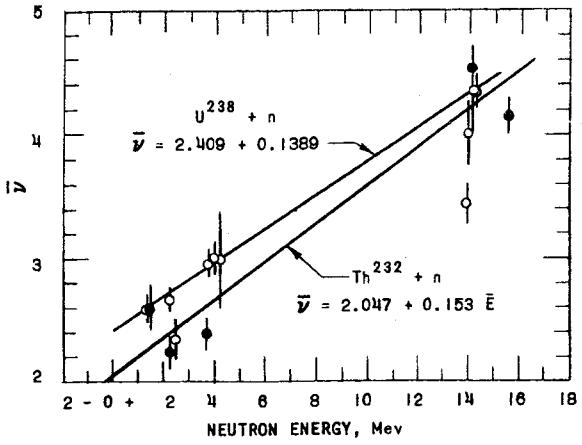

Fig. 1-8—Dependence of $\bar{\nu}(U^{238})$ and $\bar{\nu}(Th^{232})$ on incident neutron energy.

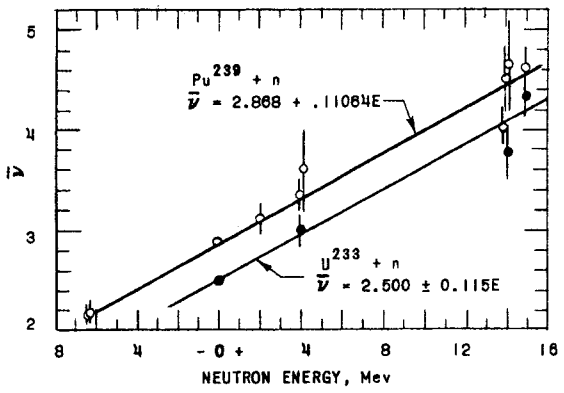

Fig. 1-9—Dependence of $\bar{\nu}(Pu^{239})$ and $\bar{\nu}(U^{233})$ on incident neutron energy.

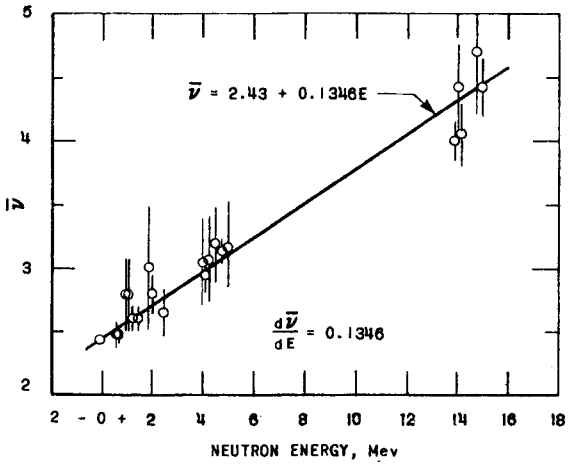

Fig. 1-10—Dependence of $\bar{\nu}(U^{235})$ on incident neutron energy.

Table 1-23—CONSTANTS FOR THE EXPRESSION $\bar{\nu}(E) = \bar{\nu}(\text{thermal}) + (d\bar{\nu}/dE)\, dE$

Isotope	$\bar{\nu}$(thermal)	$d\bar{\nu}/dE$, Mev^{-1}
U^{233} + n	2.500	0.115
U^{235} + n	2.43	0.1346
U^{238} + n	2.409	0.1385
Pu^{239} + n	2.868	0.1106
Th^{232} + n	2.047	0.153

Table 1-24—DISTRIBUTION FUNCTION (P_ν) FOR EMISSION OF PROMPT NEUTRONS IN VARIOUS ISOTOPES

Incident Neutron Energy = 80 kev

P_ν	U^{233}	U^{235}	Pu^{239}
P_0	0.010 ± 0.008	0.027 ± 0.004	−0.01 ± 0.01
P_1	0.151 ± 0.024	0.158 ± 0.010	0.11 ± 0.03
P_2	0.326 ± 0.037	0.339 ± 0.014	0.13 ± 0.06
P_3	0.301 ± 0.044	0.305 ± 0.015	0.56 ± 0.08
P_4	0.176 ± 0.041	0.133 ± 0.013	0.11 ± 0.08
P_5	0.042 ± 0.028	0.038 ± 0.009	0.06 ± 0.09
P_6	−0.010 ± 0.017	−0.001 ± 0.003	0.05 ± 0.08
P_7	0.006 ± 0.009	0.001 ± 0.002	0.00 ± 0.06
P_8	−0.002 ± 0.002	0.000 ± 0.000	−0.01 ± 0.03

Table 1-25—HALF-LIVES FOR SPONTANEOUS FISSION

h = hour d = day y = year

Isotope	Half-Life	Ref.	Isotope	Half-Life	Ref.
Th-230	$\geq 1.5 \times 10^{17}$y	161	Cm-250	$\sim 2 \times 10^{4}$y	177
Th-232	$>10^{20}$y	162	Bk-249	6×10^{8}y	178
	$>10^{21}$y	162		$>2 \times 10^{8}$y	179
U-232	$(8 \pm 5.5) \times 10^{13}$y	163		$>1.4 \times 10^{9}$y	180
U-234	1.6×10^{16}y	164	Cf-246	$(2.1 \pm 0.3) \times 10^{3}$y	181
U-235	1.8×10^{17}y	161	Cf-248	7×10^{3}y	182
				$>1.5 \times 10^{4}$y	183
U-236	2×10^{16}y	163	Cf-249	1.5×10^{9}y	184
U-238	8.04×10^{15}y	161		$>4.5 \times 10^{8}$y	180
U-238	$(5.9 \pm 0.14) \times 10^{15}$y	165	Cf-250	$(1.5 \pm 0.5) \times 10^{4}$y	179, 185, 186
U-238	$(1.3 \pm 0.2) \times 10^{16}$y	166	Cf-252	66 ± 10y	179, 185
Pu-236	3.5×10^{9}y	164		82 ± 6y	180
Pu-238	4.9×10^{10}y	167	Cf-254	56.2 ± 0.7d	177
Pu-239	5.5×10^{15}y	161		85 ± 15d	187
Pu-240	1.2×10^{11}y	168		55d	188
	1.32×10^{11}y	169		60 ± 12d	189
Pu-242	$(7.06 \pm 0.19) \times 10^{10}$y	170	E-253	3×10^{5}y	184, 190
	8.5×10^{10}y	171		$(7 \pm 3) \times 10^{5}$y	191
Pu-244	$(2.5 \pm 0.8) \times 10^{10}$y	172	E-254	1.5×10^{5}y	178
Cm-240	1.9×10^{6}y	164	Fm-254	200d	192
Cm-242	7.2×10^{6}y	173, 174		220 ± 40d	190
Cm-244	1.4×10^{7}y	164		246d	191
Cm-246	$(2 \pm 0.8) \times 10^{7}$y	175	Fm-255	>60y	178
Cm-248	$(4.6 \pm 0.5) \times 10^{6}$y	176	Fm-256	3h	193

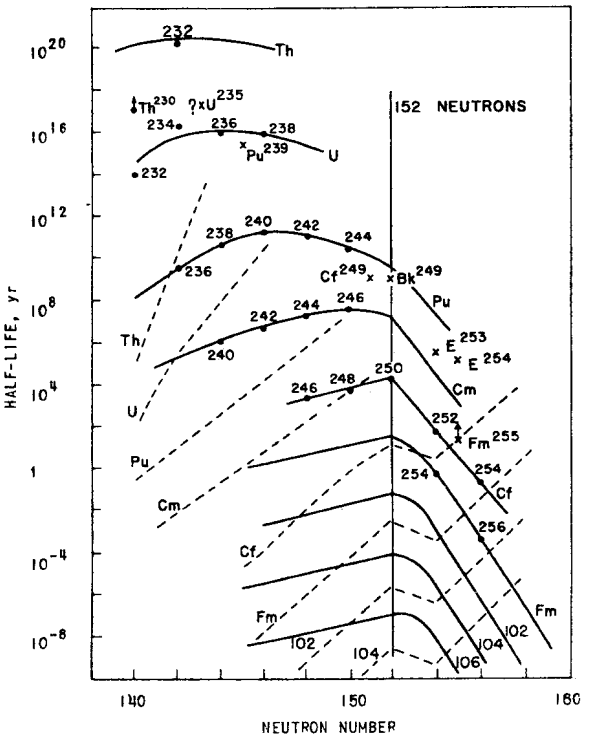

Fig. 1-11—Spontaneous fission half-life vs neutron number.
Reproduced from Ref. 2.

REFERENCES

1. N. Bohr and J. Wheeler, *Mechanism of Nuclear Fission*, Phys. Rev., 56: No. 5, 426, (1939).
2. E. K. Hyde, *A Review of Nuclear Fission – Part One – Fission Phenomena at Low Energy*, UCRL-9036, (1960).
3. I. Halpern, *Nuclear Fission*, Annual Review of Nuclear Science. Volume 9, (Palo Alto, California: Annual Reviews, Inc., 1959).
4. L. Rosen and A. Hudson, *Symmetrical Tripartition of U^{235} by Thermal Neutrons*, Phys. Rev., 78: No. 5, 533, (1950).
5. K. W. Allen and J. T. Dewan, *The Emission of Short-Range Charged Particles in the Slow Neutron Fission of Uranium*, Phys. Rev., 82: No. 4, 527, (1951).
6. A. Smith, et al., *Thermal-Neutron-Induced Fission of Th^{229}*, Phys. Rev., 111: No. 6, 1633, (1958).
7. W. E. Stein, *Velocities of Fragment Pairs from U^{233}, U^{235}, and Pu^{239} Fission*, Phys. Rev., 108: No. 1, 94, (1957).
8. A. B. Smith, et al., *An Experimental Study of Fission in the Actinide Elements*, Proc., 1958 Geneva Conference, 15: Paper No. 690, p. 392.
9. A. B. Smith, et al., *Fission Modes of $_{94}Pu^{242}$*, Phys. Rev., 106: No. 4, 779, (1957).
10. R. L. Shuey, *Instrumentation for Energy Determination of High-Energy Particles*, UCRL-793, (July, 1950).
11. E. P. Steinberg and L. E. Glendenin, *Radiochemical Investigation of the Spontaneous Fission of Cm^{242}*, Phys. Rev., 95: No. 2, 431, (1954).
12. S. Katcoff, *Fission-Product Yields from U, Th and Pu*, Nucleonics, 16: No. 4, 78, (April, 1958).
13. L. E. Glendenin and E. P. Steinberg, *Fission Yields in Spontaneous Fission of Cf^{252}*, J. Inorg. and Nuclear Chem., 1: No. 1, 45, (1955).
14. A. B. Smith, et al., *Spontaneous Fission Kinetics of Cf^{252}*, Phys. Rev., 102: No. 3, 813, (1956).
15. H. R. Bowman and S. G. Thompson, *The Prompt Radiations in the Spontaneous Fission of Californium-252*, Proc., 1958 Geneva Conference, 15: Paper No. 652, p. 212.
16. A. B. Smith, et al., *Prompt Gamma Rays Accompanying the Spontaneous Fission of Cf^{252}*, Phys. Rev., 104: No. 3, 699, (1956).
17. F. C. Maienschein, et al., *Gamma Rays Associated with Fission*, Proc., 1958 Geneva Conference, 15: Paper No. 670, p. 366.
18. J. Francis and R. Gamble, *Physics Division Semi-annual Progress Report for Period Ending March 20, 1955*, ORNL-1879, (October, 1955).
19. C. O. Muelhause and S. Oleksa, *Antineutrino Flux from a Reactor*, Phys. Rev., 105: No. 4, 1332, (1957).
20. C. D. Coryell and N. Sugarman (ed.), *Radiochemical Studies: The Fission Products*, National Nuclear Energy Series, (New York: McGraw-Hill Book Co., Inc., 1951), Div. IV, Vol. 9, (Three Books).
21. J. M. Siegel and L. E. Glendenin, *Zinc and Gallium Activities in Uranium Fission*, Ibid, Ref. 20, Book No. 2, Paper No. 53, pp. 549-65.
22. E. P. Steinberg and D. W. Engelkemeir, *Short-Lived Germanium and Arsenic Fission Activities*, Ibid, Ref. 20, Book No. 2, Paper No. 54, pp. 566-79.
23. N. Sugarman, *Genetics of the Ge^{78}–As^{78} Fission Chain*, Phys. Rev., 89: No. 3, 570, (1953).
24. J. G. Cuninghame, *The Chain As^{79}–Se^{79m} in Slow Neutron Fission of U^{235}*, Phil. Mag., 44: 900, (1953).
25. L. E. Glendenin, *Absence of Long-Lived Selenium in Fission. II. Search for Se^{79}*, Ibid, Ref. 20, Book 2, Paper No. 61, pp. 596-97
26. J. A. Petruska, H. G. Thode and R. H. Tomlinson, *The Absolute Fission Yields of Twenty-eight Mass Chains in the Thermal Neutron Fission of U^{235}*, Can. J. Phys., 33: No. 11, 693, (November, 1955).
27. A. T. Blades and H. G. Thode, *The Branching Ratio of Kr^{85m} from Fission Yield Studies*, Zeitung f. Naturforschung, 10a: Heft 11, 838, (1955).
28. A. T. Blades, W. H. Fleming and H. G. Thode, *The Ratio of Xenon to Krypton in U^{235} Fission*, Can. J. Chem., 34: No. 3, 233, (March, 1956).
29. E. P. Steinberg and L. E. Glendenin, *Survey of Radiochemical Studies of the Fission Process*, Proc., 1955 Geneva Conference, 7: Paper No. 614, p. 3.
30. G. W. Reed and A. Turkevich, *Uranium-235 Thermal Neutron Fission Yields*, Phys. Rev., 92: No. 6, 1473, (1953).
31. J. Terrell, et al., *Yield of Mo^{99} from Fission of U^{235} and U^{238}*, Phys. Rev., 92: No. 4, 1091, (1953).
32. W. H. Hardwick, *The Fission Yields of Ru^{103} and Ru^{106}*, Phys. Rev., 92: No. 4, 1072, (1953).
33. L. E. Glendenin and E. P. Steinberg, *Long-Lived Ruthenium-Rhodium Chains in Fission*, Ibid, Ref. 20, Book 2, Paper No. 103, pp. 793-804.
34. W. H. Sullivan, N. R. Sleight and E. M. Gladrow, *Characterization of 4.5h Ru Produced in Fission*, Ibid, Ref. 20, Book 2, Paper No. 105, pp. 808-12.
35. D. R. Wiles and C. D. Coryell, *Fission Yield Fine Structure in the Mass Region 99-106*, Phys. Rev., 96: No. 3, 696, (1954).
36. C. D. Coryell, *Fission Yields in the Mass Region 105-128*, Progress Report No. 37 for the Period June 1–August 31, 1955, Laboratory for Nuclear Science and Engineering, Massachusetts Institute of Technology, AECU-3121, (August, 1955), Part IV, p. 13.
37. D. W. Engelkemeir, et al., *Thermal-Neutron Fission Yields in U^{235}*, Ibid, Ref. 20, Book 3, Paper No. 217, pp. 1372-74.
38. J. A. Seiler, *Palladium-Silver Chains in Fission*, Ibid, Ref. 20, Book 2, Paper No. 119, pp. 860-70.
39. A. C. Wahl and N. A. Bonner, *Genetic Relationships and Fission Yields of Members of the Mass-115 Decay Chain*, Phys. Rev., 85: No. 4, 570, (1952).
40. R. P. Metcalf, *Study of the Chain 2.8h Cd^{117} – 1.95h In^{117}*, Ibid, Ref. 20, Book 2, Paper No. 128, pp. 905-909.
41. Editor's note of unpublished work of E. P. Steinberg, Ref. 20, Book 2, p. 913.
42. C. W. Stanley and L. E. Glendenin, *Study of Long-Lived Antimony in Fission*, Ref. 20, Book 2, Paper No. 134, pp. 947-57.
43. J. W. Barnes and A. J. Freedman, *Some New Isotopes of Antimony and Tin*, Letters to the Editor, Phys. Rev., 84: No. 2, 365, (1951).
44. A. C. Pappas, *A Radiochemical Study of Fission Yields in the Region of Shell Perturbations and the Effect of Closed Shells in Fission*, Technical Report No. 63, Laboratory for Nuclear Science and Engineering, Massachusetts Institute of Technology, AECU-2806, (September 15, 1953).
45. B. C. Purkayastha and G. R. Martin, *The Yields of I^{129} in Natural and in Neutron-Induced Fission of Uranium*, Can. J. Chem., 34: No. 3, 293, (1956).
46. A. C. Pappas and D. R. Wiles, *New Short-Lived Isotopes of Tin Found in Fission*, J. Inorg. and Nuclear Chem., 2: No. 2, 69, (1956).
47. A. P. Baerg and R. M. Bartholomew, *Yields in U^{235} Thermal Neutron Fission*, Can. J. Chem., 35: No. 9, 980, (1957).
48. W. H. Burgus and N. E. Ballou, *Characteristics of 28d Ce^{141}*, Ibid, Ref. 20, Book 2, Paper No. 180, pp. 1184-87.
49. H. G. Petrow and G. Rocco, *Fission Yield of Gd^{159} and Tb^{161}*, Phys. Rev., 96: No. 6, 1614, (1954).
50. L. Winsberg, *Study of 25m Sm^{155} in Fission*, Ibid, Ref. 20, Book 2, Paper No. 196, pp. 1284-91.
51. L. Winsberg, *Study of the Fission Chain 10h Sm^{156} – 15.4d Eu^{156}*, Ibid, Ref. 20, Book 2, Paper No. 198, pp. 1302-10; and *Study of 2y Eu^{155}, in Fission*, Ibid, Ref. 20, Book 2, pp. 1311-15.
52. L. Winsberg, *Study of 60m Eu^{158} and 15.4h Eu^{157} Activities in Fission*, Ibid, Ref. 20, Book 2, Paper No. 197, pp. 1292-1301.
53. E. C. Freiling, L. R. Bunney and N. E. Ballou, *Identification of Gadolinium and Terbium Radioisotopes as Fission Products of U^{235}*, Phys. Rev., 96: No. 1, 102, (1954).
54. G. P. Ford, *Nuclear Charge Distribution in U^{235} 14-Mev Neutron Fission*, AECD-3597, (November, 1953).

55. A. C. Wahl, *Fission of U^{235} by 14-Mev Neutrons: Nuclear Charge Distribution and Yield Fine Structure*, Phys. Rev., 99: No. 3, 730, (1955).
56. Editor's note on work of L. E. Glendenin, Ibid, Ref. 20, Book 2, p. 591.
57. J. R. Arnold and N. Sugarman, *Short-Lived Isomeric States of Se^{83} and Ge^{77}*, J. Chem. Phys., 15: No. 10, 703, (1947).
58. J. E. Sattizahn, M. Kahn and J. D. Knight, *Short-Lived Bromine and Selenium Nuclides from Fission*, Bull. Am. Phys. Soc., Series II, 2: No. 4, 197, (1957).
59. A. F. Stehney and N. Sugarman, *Characteristics of Br^{87}, A Delayed Neutron Activity*, Phys. Rev., 89: No. 1, 194, (1953).
60. G. W. Reed, *U^{235} Thermal Neutron Fission Yields at Masses 90 and 91*, Phys. Rev., 98: No. 5, 1327, (1955).
61. W. E. Grummitt and G. W. Milton, *The Independent Yields of La^{140}, Y^{90}, and Y^{91} in the Thermal Neutron Fission of U^{235} and U^{233}*, J. Inorg. and Nuclear Chem., 5: No. 2, 93, (1957).
62. E. J. Hoagland and S. Katcoff, *Fission Yield of 2.7h Sr^{92} and Radiations of 3.5h Y^{92}*, Ibid, Ref. 20, Book 2, Paper No. 73, pp. 660-62.
63. C. R. Dillard, et al., *Fission Yield of 20m Y*, Ibid, Ref. 20, Book 2, Paper No. 79, pp. 692-94.
64. C. D. Coryell, A. Y. Sakakura and A. M. Ross, *Fission Yields of 65-Day Zr^{95} and 17-Hr Zr^{97}; Search for Other Zr and Nb Fission Chains*, Phys. Rev., 77: No. 5, 755, (1950).
65. G. R. Leader, *Study of Long-Lived Tin in Fission*, Ibid, Ref. 20, Book 2, Paper No. 130, pp. 919-27.
66. J. A. Seiler, *Isotopes of Tin in Fission*, Ibid, Ref. 20, Book 2, Paper No. 129, pp. 910-918.
67. Editor's note on private communication of L. E. Glendenin, Ibid, Ref. 20, Book 2.
68. R. M. Bartholomew, et al., *The Fission Yield of I^{131} in the Thermal Neutron Fission of U^{235}*, Can. J. Chem., 31: No. 2, 120, (1953).
69. S. Katcoff and W. Rubinson, *Yield of Xe^{133} in the Thermal Neutron Fission of U^{235}*, Phys. Rev., 91: No. 6, 1458, (1953).
70. L. Yaffe, A. E. Day and B. A. Greer, *The Fission Yield of Te^{134}*, Can. J. Chem., 31: No. 1, 48, (1953).
71. L. E. Glendenin and R. P. Metcalf, *Characteristics of 6.7h I^{135} (I)*, Ibid, Ref. 20, Book 2, Paper No. 140, pp. 992-1004.
72. S. Katcoff, et al., *Characteristics of 6.7h I^{135} (II)*, Ibid, Ref. 20, Book 2, Paper No. 141, pp. 1005-14.
73. C. W. Stanley and S. Katcoff, *The Properties of 86-Second I^{136}*, J. Chem. Phys., 17: No. 7, 653, (1949).
74. F. Brown, *The Yield of Cs^{137} in the Pile Neutron Fission of Natural Uranium*, J. Inorg. and Nuclear Chem., 1: No. 4, 248, (1955).
75. R. M. Bartholomew and A. P. Baerg, *The Yield of Cs^{136} in Thermal Neutron Fission of U^{235}*, Can. J. Chem., 34: No. 3, 201, (1956).
76. L. Yaffe, et al., *Determination of the Absolute Fission Yield of Ba^{140} in Thermal Neutron Fission of U^{235}*, Can. J. Chem., 32: No. 11, 1017, (1954).
77. S. Katcoff, B. Finkle and N. Sugarman, *Fission Yield of the 33h Ce^{143}*, Ibid, Ref. 20, Book 2, Paper No. 176, p. 1167.
78. J. A. Marinsky and L. E. Glendenin, *Identification and Characteristics of 11d Nd^{147}*, Ibid, Ref. 20, Book 2, Paper No. 191, pp. 1229-42; and *Discovery, Identification, and Characteristics of 47h Pm^{149}*, Paper No. 193, pp. 1254-63.
79. D. M. Wiles, J. A. Petruska and R. H. Tomlinson, *Some Cumulative Yields of Isotopes Formed in the Thermal Neutron Fission of Pu^{239}*, Can. J. Chem., 34: No. 3, 227, (1956).
80. L. M. Krizhansky, et al., *Rare-Earth Isotope Yields in the Fission of Pu^{239} by Pile Neutrons*, Soviet Journal of Atomic Energy (English Trans.), 2: No. 3, 334, (1957).
81. E. P. Steinberg and M. S. Freedman, *Summary of Results of Fission-Yield Experiments*, Ibid, Ref. 20, Book 3, Paper No. 219, pp. 1378-90.
82. W. H. Fleming and H. G. Thode, *The Relative Yields of the Isotopes of Xenon in Plutonium Fission*, Can. J. Chem., 34: No. 3, 193, (1956).
83. D. W. Engelkemeir, et al., *Determination of Absolute Fast-Neutron Fission Yields in Pu^{239}*, Ibid, Ref. 20, Book 3, Paper No. 204, pp. 1331-33.
84. R. N. Keller, E. P. Steinberg and L. E. Glendenin, *Yields of Fission Products from U^{238} Irradiated with Fission Spectrum Neutrons*, Phys. Rev., 94: No. 4, 969, (1954).
85. D. W. Engelkemeir, et al., *Fission Yields in U^{238}*, Ibid, Ref. 20, Book 3, Paper No. 218, pp. 1375-77.
86. J. Terrell, et al., Internal Memorandum, Los Alamos Scientific Laboratory, LADC-1463, (1953).
87. A. Turkevich and J. B. Niday, *Radiochemical Studies on the Fission of Th^{232} with Pile Neutrons*, Phys. Rev., 84: No. 1, 52, (1951).
88. R. K. Wanless and H. G. Thode, *The Fission Yields of Isotopes of Xenon and Krypton in the Neutron Fission of U^{235} and U^{238}*, Can. J. Phys., 33: No. 9, 541, (1955).
89. G. P. Ford, et al., *Mass Yields from Fission by Neutrons Between Thermal and 14.7 Mev*, LA-1997, (1956).
90. A. Turkevich, J. B. Niday and A. Tompkins, *Radiochemical Studies on the Fission of Th^{232} with Li + D Neutrons*, Phys. Rev., 89: No. 3, 552, (1953).
91. C. B. Fulmer, *Scintillation Response of CsI(Tl) Crystals to Fission Fragments and Energy vs Range in Various Materials for Light and Heavy Fission Fragments*, Phys. Rev., 108: No. 5, 1113, (1957).
92. T. M. Snyder and R. W. Williams, *Upper Limit for the Time Between Fission and the Emission of Neutrons*, Phys. Rev., 81: No. 2, 171, (1951).
93. J. S. Fraser, *The Angular Distribution of Prompt Neutrons Emitted in Fission*, Phys. Rev., 88: No. 3, 536, (1952).
94. S. L. Whetstone, Jr., *Prompt-Neutron Emission from Single Fission Fragments*, Phys. Rev., 114: No. 2, 581, (1959).
95. J. Terrell, *Fission Neutron Spectra and Nuclear Temperatures*, Phys. Rev., 113: No. 2, 527, (1959).
96. J. M. Blatt and V. F. Weisskopf, *Theoretical Nuclear Physics*, (New York: John Wiley and Sons, Inc., 1952).
97. L. Cranberg, et al., *Fission Neutron Spectrum of U^{235}*, Phys. Rev., 103: No. 3, 662, (1956).
98. B. G. Erozolimskii, *Fission Neutrons*, Physics of Nuclear Fission, (New York: Pergamon Press, 1958), Chap. 6, p. 64.
99. N. Nereson, *Fission Neutron Spectrum of U^{235}*, Phys. Rev., 85: No. 4, 600, (1952).
100. T. W. Bonner, et al., *A Study of the Spectrum of the Neutrons of Low Energy from the Fission of U^{235}*, Phys. Rev., 87: No. 6, 1032, (1952).
101. B. E. Watt, *Energy Spectrum of Neutrons from Thermal Fission of U^{235}*, Phys. Rev., 87: No. 6, 1037, (1952).
102. D. L. Hill, *The Neutron Energy Spectrum from U^{235} Thermal Fission*, Phys. Rev., 87: No. 6, 1034, (1952).
103. J. A. Grundl and J. R. Neuer, *Comparison of U^{235} and Pu^{239} Fission Neutron Spectra*, Bull. Am. Phys. Soc., Series II, No. 2, 95, (1956).
104. K. Henry and M. Hayden, *Fission Neutron Spectrum of U^{233}*, Applied Nuclear Physics Division Annual Report for the Period Ending September 10, 1956, ORNL-2081, p. 108.
105. V. P. Kovalev, et al., *Fission Neutron Spectra in U^{233}, U^{235}, Pu^{239}*, Zhur. Eksp. i Teoret. Fiz., (USSR), 33: 1069, (1957).
106. A. B. Smith, et al., *Precise Determination of the U^{233} Fission Neutron Spectrum*, Phys. Rev., 114: No. 5, 1351, (1959).
107. N. Nereson, *Fission Neutron Spectrum of Pu^{239}*, Phys. Rev., 88: No. 4, 823, (1952).
108. E. Hjalmar, et al., *Photographic Emulsion Measurements of the Energy Distribution of Neutrons from Spontaneous Fission of Californium-252*, Arkiv för Fysik, 10: 357, (1956).
109. A. B. Smith, et al., *Spontaneous Fission Neutron Spectrum of Cf^{252}*, Phys. Rev., 108: No. 2, 411, (1957).
110. L. Szilard and W. H. Zinn, *Instantaneous Emission of Fast Neutrons in the Interaction of Slow Neutrons with Uranium*, Phys. Rev., 55: No. 8, 799, (1939).
111. R. B. Roberts, et al., *Further Observations on the Splitting of Uranium and Thorium*, Phys. Rev., 55: No. 5, 510, (1939).

112. G. R. Keepin, et al., *Delayed Neutrons from Fissionable Isotopes of Uranium, Plutonium and Thorium*, Phys. Rev., 107: No. 4, 1044, (1957).
113. S. A. Cox, ANL, private communication.
114. S. A. Cox, et al., *Delayed Neutrons from the Spontaneous Fission of Cf^{252}*, Phys. Rev., 112: No. 3, 960, (1958).
115. L. E. Glendenin and E. P. Steinberg, *Fission Yields in Spontaneous Fission of Cf^{252}*, J. Inorg. and Nuclear Chem., 1: 45, (1955).
116. J. G. Cuninghame, *The Mass Yield Curve for Fission of Am^{241} by Pile Neutrons*, J. Inorg. and Nuclear Chem., 4: 1, (1957).
117. D. J. Hughes, et al., *Energy of Delayed Neutrons from U^{235} Fissions*, Phys. Rev., 73: No. 2, 111, (1948).
118. M. Burgy, et al., *Energy of Delayed Neutrons from U^{235} Fissions*, Phys. Rev., 70: Nos. 1 and 2, 104, (1946).
119. R. Batchelor and H. R. McK. Hyder, *The Energy of Delayed Neutrons from Fission*, J. Nuclear Energy, 3: 7, (1956).
120. S. Bernstein, et al., *Yield of Photo-Neutrons from U^{235} Fission Products in Heavy Water*, Phys. Rev., 71: No. 9, 573, (1947).
121. A. K. Krasin, et al., *Physical Characteristics of Beryllium-Moderated Reactor*, Proc., 1958 Geneva Conference, 12: Paper No. 2146, p. 571.
122. P. Benoist, et al., *Critical and Subcritical Experiments on U-BeO Lattices*, Proc., 1958 Geneva Conference, 12: Paper No. 1192, p. 585.
123. W. K. Ergen, *Hard Gamma Emitters Among Fission Fragments*, ANP-59, (May, 1951).
124. B. C. Diven, et al., *Multiplicities of Fission Neutrons*, Phys. Rev., 101: No. 3, 1012, (1956).
125. K. Skarsvag, *Angular Correlation of Fission Neutrons*, Proc., 1955 Geneva Conference, 2: Paper No. 884, p. 185.
126. A. B. Smith, P. R. Fields and R. K. Sjoblom, *Angular Distribution and Energy Spectrum of Prompt Neutrons Resulting from the Spontaneous Fission of Cf^{252}*, Bull. Am. Phys. Soc., Series II, 4: No. 1, Part 2, p. 31, (1960).
127. A. Bohr, *On the Theory of Nuclear Fission*, Proc., 1955 Geneva Conference, 2: Paper No. 911, p. 151.
128. J. J. Griffin, *Energy Dependence of Fission Fragment Anisotropy*, Phys. Rev., 116: No. 1, 107, (1959).
129. D. J. Hughes and R. B. Schwartz, *Neutron Cross Sections*, World Weighted Averages, BNL-325, Second Edition, 1958, p. 28.
130. M. G. Sowerby, Fast Reactor Data Conference, Harwell, England, (1960), (Private communication).
131. D. A. Hicks, J. Ise and R. V. Pyle, *Probabilities of Prompt-Neutron Emission from Spontaneous Fission*, Phys. Rev., 101: No. 3, 1016, (1956).
132. V. I. Kalashnikova, et al., *Dependence of the Number of Neutrons Emitted in the Fission of Heavy Nuclei on the Excitation Energy of the Fissionable Nucleus*, Conference of the Academy of Sciences of USSR on Peaceful Uses of Atomic Energy, (1955), p. 127.
133. I. I. Bondarenko, et al., *Average Number and Spectrum of Prompt Neutrons in Fast-Neutron-Induced Fission*, Proc., 1958 Geneva Conference, 15: Paper No. 2187, p. 353.
134. J. L. Fowler, ORNL, unpublished report, (1956).
135. B. C. Diven, et al., unpublished. See Ref. 160.
136. I. Johnstone, unpublished report, AERE, Harwell, England.
137. B. D. Kuzminov, L. S. Kutsaeva and I. I. Bondarenko, *Prompt Neutron Numbers for the Fast Neutron Fission of U^{235}, U^{238}, Th^{232}, and Np^{237}*, Atomnaya Energiya, 4: No. 2, 187, (1958).
138. A. B. Smith, et al., *Number of Prompt Neutrons Emitted per Thorium-232 Fission*, Phys. Rev., 115: No. 5, 1242, (1959).
139. H. A. Bethe, et al., LASL report, (1955).
140. E. R. Graves, LASL, unpublished, (1954).
141. N. N. Florov and E. A. Tamanov, *Average Neutron Number $\bar{\nu}$ in Fission of the U^{238} by 14-Mev Neutrons*, Atomnaya Energiya, 5: No. 6, (1958).
142. N. N. Florov and V. M. Talyzin, *Average Neutron Number $\bar{\nu}$ in Fission of the U^{235} and U^{238} by 14-Mev Neutrons*, Atomnaya Energiya, 5: No. 6, (1958).
143. J. Leroy, CEN, Saclay, France, to be published.
144. A. N. Protopopov and M. V. Blinov, *Determination of Mean Number of Neutrons Emitted During Fission of U^{235} by 14.8-Mev Neutrons*, Atomnaya Energiya, 4: 374, (1958).
145. G. N. Smirenkin, et al., *Mean Number of Prompt Neutrons for Fission of U^{233}, U^{235} and Pu^{239} by 4- and 15-Mev Neutrons*, Atomnaya Energiya, 4: 188, (1958).
146. P. A. Egelstaff, K. W. Morton and S. E. Sanders, unpublished average value of UK, USA, and USSR values, reported from AERE, Harwell, (March, 1955).
147. A. B. Smith, ANL, unpublished, (1960).
148. A. H. Jaffey, *Thermal Neutron ν for Pu^{241}*, ANL-5396, (September, 1955).
149. G. deSaussure and E. G. Silver, *Number of Neutrons Released per Thermal Fission of Pu^{241}*, Applied Nuclear Physics Division Annual Report for Period Ending September 10, 1956, ORNL-2081, p. 105.
150. G. Hansen, LASL unpublished report. See R. B. Leachman, *Neutrons and Radiations from Fission*, Proc., 1958 Geneva Conference, 15: Paper No. 665, p. 331.
151. B. D. Kuzminov, L. S. Kutsaeva and I. I. Bondarenko, *Prompt Neutron Numbers for the Fast Neutron Fission of U^{235}, U^{238}, Th^{232}, and Np^{237}*, Atomnaya Energiya, 4: No. 2, 187, (1958).
152. F. R. Barclay, et al., *Neutrons from the Spontaneous Fission of Thorium*, Proc., Phys. Soc. (London), A65: 73, (1952).
153. W. W. T. Crane, et al., *Average Number of Neutrons per Fission for Several Heavy-Element Nuclides*, Phys. Rev., 101: No. 6, 1804, (1956).
154. F. R. Barclay and W. J. Whitehouse, *The Average Number of Neutrons Emitted in the Spontaneous Fission of Cm^{242}*, Proc., Phys. Soc. (London), A66: 447, (1953).
155. G. H. Higgins, et al., *Average Number of Neutrons per Spontaneous Fission of Cm^{244}*, Phys. Rev., 99: No. 1, 183, (1955).
156. R. V. Pyle, UCRL, unpublished results.
157. W. W. T. Crane, et al., *Average Number of Neutrons Emitted During the Spontaneous Fission of Cf^{252}*, Phys. Rev., 97: No. 6, 1727, (1955).
158. H. R. Bowman and S. G. Thompson, *The Prompt Radiations in the Fission of Cf^{252}*, Proc., 1958 Geneva Conference, 15: Paper No. 652, p. 212.
159. G. R. Choppin, et al., *Prompt Neutrons from the Spontaneous Fission of Fermium-254*, Phys. Rev., 102: No. 3, 766, (1956).
160. J. Terrell, *Distributions of Fission Neutron Numbers*, Phys. Rev., 108: No. 3, 783, (1957).
161. E. Segre, *Spontaneous Fission*, Phys. Rev., 86: No. 1, 21, (1952).
162. G. N. Flerov, et al., *The Spontaneous Fission of Thorium*, Zhur. Eksp. i Teoret Fiz., (USSR), 28: 503, (1955).
163. A. H. Jaffey and A. Hirsch, ANL, unpublished data, (1949).
164. A. Ghiorso, et al., *Spontaneous Fission of U^{234}, Pu^{236}, Cm^{240}, and Cm^{244}*, Phys. Rev., 87: No. 1, 163, (1952).
165. P. K. Kuroda and R. R. Edwards, *Radiochemical Measurement of the Natural Fission Rate of Uranium and the Natural Occurrence of Ba^{140}*, J. Inorg. and Nuclear Chem., 3: No. 6, 345, (1957).
166. N. A. Perfilov, *Periods of the Spontaneous Fission of Uranium and Thorium*, Zhur. Eksp. i Teoret. Fiz., (USSR), 17: 476, (1947).
167. A. H. Jaffey and A. Hirsch, ANL, unpublished data, (1947).
168. O. Chamberlain, et al., *$_{94}Pu^{240}$ and Its Spontaneous Fission*, Phys. Rev., 94: No. 1, 156, (1954).

169. E. M. Kinderman, *The Spontaneous Fission of Plutonium 240*, Atomic Energy Commission Declassified Report, HW-27660, (April, 1953).
170. J. Mech, et al., *Alpha and Spontaneous Fission Half-Lives of Plutonium-242*, Phys. Rev., 103: No. 2, 340, (1956).
171. E. K. Hyde, *A Review of Nuclear Fission, Part I. Fission Phenomena at Low Energy*, UCRL-9036, 98, (January, 1960), Value reported by M. Jones, et al., Knolls Atomic Power Laboratory.
172. P. R. Fields, et al., *Electron Capture Decay of Am^{244} and the Spontaneous Fission Half-Life of Pu^{244}*, Phys. Rev., 100: No. 1, 172, (1955).
173. A. Ghiorso and H. P. Robinson, UCRL, unpublished results, (1947).
174. G. C. Hanna, et al., *Spontaneous Fission in Cm^{242}*, Phys. Rev., 81: No. 3, 466, (1951).
175. S. M. Fried, et al., *Spontaneous Fission Half-Life of Cm^{246}*, J. Inorg. and Nuclear Chem., 2: 415, (1956).
176. J. P. Butler, et al., *Half-Lives and Alpha Energies of Cm^{248} and Cm^{246}*, Phys. Rev., 103: No. 4, 965, (1956).
177. J. Huizenga and H. Diamond, *Spontaneous-Fission Half-Lives of Cf^{254} and Cm^{250}*, Phys. Rev., 107: No. 4, 1087, (1957).
178. A. Ghiorso, et al., UCRL, unpublished results, (1955).
179. L. B. Magnusson, et al., *Berkelium and Californium Isotopes Produced in Neutron Irradiation of Plutonium*, Phys. Rev., 96: No. 6, 1576, (1954).
180. T. A. Eastwood, et al., *Isotopes of Berkelium and Californium Produced by Neutron Irradiation of Plutonium*, Phys. Rev., 107: No. 6, 1635, (1957).
181. E. K. Hulet, et al., *Spontaneous Fission Rate of Cf^{246}*, Phys. Rev., 89: No. 4, 878, (1953).
182. E. K. Hulet, *An Investigation of the Isotopes of Berkelium and Californium*, Ph. D. Thesis, University of California Unclassified Report UCRL-2283, (July, 1953).
183. E. K. Hulet, UCRL, unpublished results.
184. A. Ghiorso, et al., UCRL, unpublished results, (1954).
185. A. Ghiorso, et al., *New Isotopes of Americium, Berkelium and Californium*, Phys. Rev., 94: No. 4, 1081, (1954).
186. P. R. Fields, et al., *Spontaneous Fission Properties of Elements 97, 98, 99, and 100*, Nature 174: 265, (1954); (UCRL-9036, p. 99).
187. B. G. Harvey, et al., *Nuclide 99^{254}*, Phys. Rev., 99: No. 1, 337, (1955).
188. P. R. Fields, et al., *Transplutonium Elements in Thermonuclear Test Debris*, Phys. Rev., 102: No. 1, 180, (1956).
189. W. C. Bentley, et al., *The Formation of Higher Isotopes and Higher Elements by Reactor Irradiation of Pu^{239}; Some Nuclear Properties of the Heavier Isotopes*, Proc., 1955 Geneva Conference, 7: Paper No. 809, p. 261.
190. P. R. Fields, et al., *Additional Properties of Isotopes and Elements 99 and 100*, Phys. Rev., 94: No. 1, 209, (1954).
191. M. Jones, et al., *Isotopes of Einsteinium and Fermium Produced by Neutron Irradiation of Plutonium*, Phys. Rev., 102: No. 1, 203, (1956).
192. G. R. Choppin, et al., *Nuclear Properties of Some Isotopes of Californium, Elements 99 and 100*, Phys. Rev., 94: No. 4, 1080, (1954).
193. G. R. Choppin, et al., *Nuclear Properties of 100^{256}*, Phys. Rev., 98: No. 5, 1519, (1955).

Section 2

SELECTED CROSS SECTION DATA

2.1 2200-meter/second NEUTRON CROSS SECTIONS FOR NATURALLY OCCURRING ELEMENTS

Microscopic and macroscopic cross sections for 2200-meter/second neutrons are listed in Table 2-1. The cross section data are taken from BNL-325 and Supplement No. 1 (1960). Cross sections for some compounds are included.

Also tabulated, for easy reference, are the average logarithmic energy loss, ξ, and the transport scattering factor $(1 - \bar{\mu}_0)$.[1]

2.2 FISSION CROSS SECTIONS AND RELATED QUANTITIES AS FUNCTIONS OF ENERGY

2.2.1 MEASUREMENTS OF η AND α

The value of η (average neutron yield per neutron absorbed), as a function of neutron energy is presented for the fissionable isotopes U^{233}, U^{235}, and Pu^{239}. In the cases where η is computed from the measured value of α (capture to fission cross section ratio), the $\bar{\nu}$ used in the calculation is indicated in the text. The available measured values of α for U^{233}, U^{235}, and Pu^{239} are also included.

The computation includes data in BNL-325, along with recently published and unpublished measurements.[2] The α data in BNL-325 were converted to η by assuming $\bar{\nu}$ to be a constant in the electron-volt energy region. The values of $\bar{\nu}$ used for each of the isotopes were the world weighted-averaged values at 0.0253 ev.

U^{233}. Figures 2-1 and 2-2 show the variation of η for U^{233} as a function of energy. A value of $\bar{\nu} = 2.50 \pm 0.02$ was used to convert BNL-325 values to η values.

The value of η was measured by Sanders, et al.,[3] at Harwell using the crystal spectrometer. The crystals used were KCl and Cu, with the Cu crystal giving better resolution.

The measurements of η in the electron-volt region reported by USSR groups, Spivak, et al.,[4,5] were made by using a system of filters on the incident neutron beam. This resulted in an integrated value of η and is represented by the dashed block in the figures.

The η values for 30-, 140-, and 250-kev neutrons were obtained by using photoneutron sources (Sb + Be, Ga + D_2O, Na + D_2O, respectively). A Na + Be source was used for the 900-kev neutrons. Included are measurements of η in the 0.1 to 10-ev range by Magleby, et al.,[6] using the crystal spectrometer at the MTR.

The measurements of de Saussure[7] were obtained using the ORNL Fast Chopper. The η was determined from the ratio of the emission rate of fission neutrons from a thick foil and the incident flux of neutrons for each energy. The two values were measured simultaneously by allowing the incident

Table 2-1— CROSS SECTIONS FOR NATURALLY OCCURRING ELEMENTS

(2200-meter/second neutrons)

Atomic No.	Element or Compound	Atomic or Mol. Wt.	Density, gm/cm^3	Nuclei per Unit Vol. $\times 10^{-24}$	$1-\bar{\mu}_0$	ξ	Microscopic Cross Section, barn			Macroscopic Cross Section, cm^{-1}		
							σ_a	σ_s	σ_t	Σ_a	Σ_s	Σ_t
1	H	1.008	8.9[a]	5.3[a]	0.3386	1.000	0.33	38	38	1.7[a]	0.002	0.002
	H_2O	18.016	1	0.0335[b]	0.676	0.948	0.66	103	103	0.022	3.45	3.45
	D_2O	20.030	1.10	0.0331[b]	0.884	0.570	0.001	13.6	13.6	3.3[a]	0.449	0.449
2	He	4.003	17.8[a]	2.6[a]	0.8334	0.425	0.007	0.8	0.807	0.02[a]	2.1[a]	2.1[a]
3	Li	6.940	0.534	0.0463	0.9047	0.268	71	1.4	72.4	3.29	0.065	3.35
4	Be	9.013	1.85	0.1236	0.9259	0.209	0.010	7.0	7.01	124[a]	0.865	0.865
	BeO	25.02	3.025	0.0728[b]	0.939	0.173	0.010	6.8	6.8	73[a]	0.501	0.501
5	B	10.82	2.45	0.1364	0.9394	0.171	755	4	759	103	0.346	104
6	C	12.011	1.60	0.0803	0.9444	0.158	0.004	4.8	4.80	32[a]	0.385	0.385
7	N	14.008	0.0013	5.3[a]	0.9524	0.136	1.88	10	11.9	9.9[a]	50[a]	60[a]
8	O	16.000	0.0014	5.3[a]	0.9583	0.120	20[a]	4.2	4.2	0.000	21[a]	21[a]
9	F	19.00	0.0017	5.3[a]	0.9649	0.102	0.001	3.9	3.90	0.01[a]	20[a]	20[a]
10	Ne	20.183	0.0009	2.6[a]	0.9667	0.0968	<2.8	2.4	5.2	7.3[a]	6.2[a]	13.5[a]
11	Na	22.991	0.971	0.0254	0.9710	0.0845	0.525	4	4.53	0.013	0.102	0.115
12	Mg	24.32	1.74	0.0431	0.9722	0.0811	0.069	3.6	3.67	0.003	0.155	0.158
13	Al	26.98	2.699	0.0602	0.9754	0.0723	0.241	1.4	1.64	0.015	0.084	0.099
14	Si	28.09	2.42	0.0522	0.9762	0.0698	0.16	1.7	1.86	0.008	0.089	0.097
15	P	30.975	1.82	0.0354	0.9785	0.0632	0.20	5	5.20	0.007	0.177	0.184
16	S	32.066	2.07	0.0389	0.9792	0.0612	0.52	1.1	1.62	0.020	0.043	0.063
17	Cl	35.457	0.0032	5.3[a]	0.9810	0.0561	33.8	16	49.8	0.002	80[a]	0.003
18	A	39.944	0.0018	2.6[a]	0.9833	0.0492	0.66	1.5	2.16	1.7[a]	3.9	5.6[a]
19	K	39.100	0.87	0.0134	0.9829	0.0504	2.07	1.5	3.57	0.028	0.020	0.048
20	Ca	40.08	1.55	0.0233	0.9833	0.0492	0.44	3.0	3.44	0.010	0.070	0.080
21	Sc	44.96	2.5	0.0335	0.9852	0.0438	24	24	48	0.804	0.804	1.61
22	Ti	47.90	4.5	0.0566	0.9861	0.0411	5.8	4	9.8	0.328	0.226	0.555
23	V	50.95	5.96	0.0704	0.9869	0.0387	5	5	10.0	0.352	0.352	0.704
24	Cr	52.01	7.1	0.0822	0.9872	0.0385	3.1	3	6.1	0.255	0.247	0.501
25	Mn	54.94	7.2	0.0789	0.9878	0.0359	13.2	2.3	15.5	1.04	0.181	1.22
26	Fe	55.85	7.86	0.0848	0.9881	0.0353	2.62	11	13.6	0.222	0.933	1.15
27	Co	58.94	8.9	0.0910	0.9887	0.0335	38	7	45	3.46	0.637	4.10
28	Ni	58.71	8.90	0.0913	0.9887	0.0335	4.6	17.5	22.1	0.420	1.60	2.02
29	Cu	63.54	8.94	0.0848	0.9896	0.0309	3.85	7.2	11.05	0.326	0.611	0.937
30	Zn	65.38	7.14	0.0658	0.9897	0.0304	1.10	3.6	4.70	0.072	0.237	0.309
31	Ga	69.72	5.91	0.0511	0.9925	0.0283	2.80	4	6.80	0.143	0.204	0.347
32	Ge	72.60	5.36	0.0445	0.9909	0.0271	2.45	3	5.45	0.109	0.134	0.243
33	As	74.91	5.73	0.0461	0.9911	0.0264	4.3	6	10.3	0.198	0.277	0.475
34	Se	78.96	4.8	0.0366	0.9916	0.0251	12.3	11	23.3	0.450	0.403	0.853
35	Br	79.916	3.12	0.0235	0.9917	0.0247	6.7	6	12.7	0.157	0.141	0.298
36	Kr	83.80	0.0037	2.6[a]	0.9921	0.0236	31	7.2	38.2	81[a]	19[a]	99[a]
37	Rb	85.48	1.53	0.0108	0.9922	0.0233	0.73	12	12.7	0.008	0.130	0.138
38	Sr	87.63	2.54	0.0175	0.9925	0.0226	1.21	10	11.2	0.021	0.175	0.195
39	Yt	88.92	5.51	0.0373	0.9925	0.0223	1.31	3	4.3	0.049	0.112	0.160
40	Zr	91.22	6.4	0.0423	0.9927	0.0218	0.185	8	8.2	0.008	0.338	0.347
41	Nb	92.91	8.4	0.0545	0.9928	0.0214	1.16	5	6.16	0.063	0.273	0.336
42	Mo	95.95	10.2	0.0640	0.9931	0.0207	2.70	7	9.70	0.173	0.448	0.621
43	Tc	98	—	—	0.9932	0.0203	22	—	—	—	—	—
44	Ru	101.1	12.2	0.0727	0.9934	0.0197	2.56	6	8.56	0.186	0.436	0.622
45	Rh	102.91	12.5	0.0732	0.9935	0.0193	149	5	154	10.9	0.366	11.3
46	Pd	106.4	12.16	0.0689	0.9937	0.0187	8	3.6	11.6	0.551	0.248	0.799
47	Ag	107.88	10.5	0.0586	0.9938	0.0184	63	6	69	3.69	0.352	4.04
48	Cd	112.41	8.65	0.0464	0.9940	0.0178	2,450	7	2,457	114	0.325	114
49	In	114.82	7.28	0.0382	0.9942	0.0173	191	2.2	193	7.30	0.084	7.37
50	Sn	118.70	6.5	0.0330	0.9944	0.0167	0.625	4	4.6	0.021	0.132	0.152
51	Sb	121.76	6.69	0.0331	0.9945	0.0163	5.7	4.3	10.0	0.189	0.142	0.331
52	Te	127.61	6.24	0.0295	0.9948	0.0155	4.7	5	9.7	0.139	0.148	0.286
53	I	126.91	4.93	0.0234	0.9948	0.0157	7.0	3.6	10.6	0.164	0.084	0.248
54	Xe	131.30	0.0059	2.7[a]	0.9949	0.0152	35	4.3	39.3	95[a]	12[a]	0.001
55	Cs	132.91	1.873	0.0085	0.9950	0.0150	28	20	48	0.238	0.170	0.408
56	Ba	137.36	3.5	0.0154	0.9951	0.0145	1.2	8	9.2	0.018	0.123	0.142
57	La	138.92	6.19	0.0268	0.9952	0.0143	8.9	15	24	0.239	0.403	0.642
58	Ce	140.13	6.78	0.0292	0.9952	0.0142	0.73	9	9.7	0.021	0.263	0.283
59	Pr	140.92	6.78	0.0290	0.9953	0.0141	11.3	4	15.3	0.328	0.116	0.444
60	Nd	144.27	6.95	0.0290	0.9954	0.0138	46	16	62	1.33	0.464	1.79

Table 2-1—CROSS SECTIONS FOR NATURALLY OCCURRING ELEMENTS (Continued)

Atomic No.	Element or Compound	Atomic or Mol. Wt.	Density, gm/cm^3	Nuclei per Unit Vol. $\times 10^{-24}$	$1-\bar{\mu}_0$	ξ	Microscopic Cross Section, barn			Macroscopic Cross Section, cm^{-1}		
							σ_a	σ_s	σ_t	Σ_a	Σ_s	Σ_t
61	Pm	145	—	—	0.9954	0.0137	60	—	—	—	—	—
62	Sm	150.35	7.7	0.0309	0.9956	0.0133	5,600	5	5,605	173	0.155	173
	Sm_2O_3	348.70	7.43	0.0128[b]	0.974	0.076	16,500	22.6	16,500	211	0.289	211
63	Eu	152	5.22	0.0207	0.9956	0.0131	4,300	8	4,308	89.0	0.166	89.2
	Eu_2O_3	352.00	7.42	0.0127[b]	0.978	0.063	8,740	30.2	8,770	111	0.383	111
64	Gd	157.26	7.95	0.0305	0.9958	0.0127	46,000	—	—	1,403	—	—
65	Tb	158.93	8.33	0.0316	0.9958	0.0125	46	—	—	1.45	—	—
66	Dy	162.51	8.56	0.0317	0.9959	0.0122	950	100	1,050	30.1	3.17	33.3
	Dy_2O_3	372.92	7.81	0.0126[b]	0.993	0.019	2,200	214	2,414	27.7	2.7	30.4
67	Ho	164.94	8.76	0.0320	0.9960	0.0121	65	—	—	2.08	—	—
68	Er	167.27	9.16	0.0330	0.9960	0.0119	173	15	188	5.71	0.495	6.20
69	Tm	168.94	9.35	0.0333	0.9961	0.0118	127	7	134	4.23	0.233	4.46
70	Yb	173.04	7.01	0.0244	0.9961	0.0115	37	12	49	0.903	0.293	1.20
71	Lu	174.99	9.74	0.0335	0.9962	0.0114	112	—	—	3.75	—	—
72	Hf	178.5	13.3	0.0449	0.9963	0.0112	105	8	113	4.71	0.359	5.07
73	Ta	180.95	16.6	0.0553	0.9963	0.0110	21	5	26	1.16	0.277	1.44
74	W	183.86	19.3	0.0632	0.9964	0.0108	19.2	5	24.2	1.21	0.316	1.53
75	Re	186.22	20.53	0.0664	0.9964	0.0107	86	14	100	5.71	0.930	6.64
76	OS	190.2	22.48	0.0712	0.9965	0.0105	15.3	11	26.3	1.09	0.783	1.87
77	Ir	192.2	22.42	0.0703	0.9965	0.0104	440	—	—	30.9	—	—
78	Pt	195.09	21.37	0.0660	0.9966	0.0102	8.8	10	18.8	0.581	0.660	1.24
79	Au	197	19.32	0.0591	0.9966	0.0101	98.8	9.3	107.3	5.79	0.550	6.34
80	Hg	200.61	13.55	0.0407	0.9967	0.0099	380	20	400	15.5	0.814	16.3
81	Ti	204.39	11.85	0.0349	0.9967	0.0098	3.4	14	17.4	0.119	0.489	0.607
82	Pb	207.21	11.35	0.0330	0.9968	0.0096	0.170	11	11.2	0.006	0.363	0.369
83	Bi	209	9.747	0.0281	0.9968	0.0095	0.034	9	9	0.001	0.253	0.256
84	Po	210	9.24	0.0265	0.9968	0.0095	—	—	—	—	—	—
85	At	211	—	—	0.9968	0.0094	—	—	—	—	—	—
86	Rn	222	0.0097	2.6[a]	0.9970	0.0090	0.7	—	—	—	—	—
87	Fr	223	—	—	0.9980	0.0089	—	—	—	—	—	—
88	Ra	226.05	5	0.0133	0.9971	0.0088	20	—	—	0.266	—	—
89	Ac	227	—	—	0.9971	0.0088	510	—	—	—	—	—
90	Th	232.05	11.3	0.0293	0.9971	0.0086	7.56	12.6	20.2	0.222	0.369	0.592
91	Pa	231	15.4	0.0402	0.9971	0.0086	200	—	—	8.04	—	—
92	U	238.07	18.9	0.04783	0.9972	0.0084	7.68	8.3	16.0	0.367	0.397	0.765
	UO_2	270.07	10	0.0223[b]	0.9887	0.036	7.6	16.7	24.3	0.169	0.372	0.542
93	Np	237	—	—	0.9972	0.0084	170	—	—	—	—	—
94	Pu	239	19.74	0.0498	0.9972	0.0083	1,026	9.6	1,036	51.1	0.478	51.6
95	Am	242	—	—	0.9973	0.0082	8.000	—	—	—	—	—
96	Cm	245	—	—	0.9973	0.0081	—	—	—	—	—	—
97	Bk	249	—	—	0.9973	0.0081	500	—	—	—	—	—
98	Cf	249	—	—	0.9973	0.0079	900	—	—	—	—	—
99	E	253	—	—	0.9974	0.0079	160	—	—	—	—	—
100	Fm	256	—	—	0.9974	0.0078	—	—	—	—	—	—
101	Mv	260	—	—	0.9974	0.0077	—	—	—	—	—	—

[a] Value has been multiplied by 10^5.
[b] Molecules/cm^3.

687863 O - 63 - 4

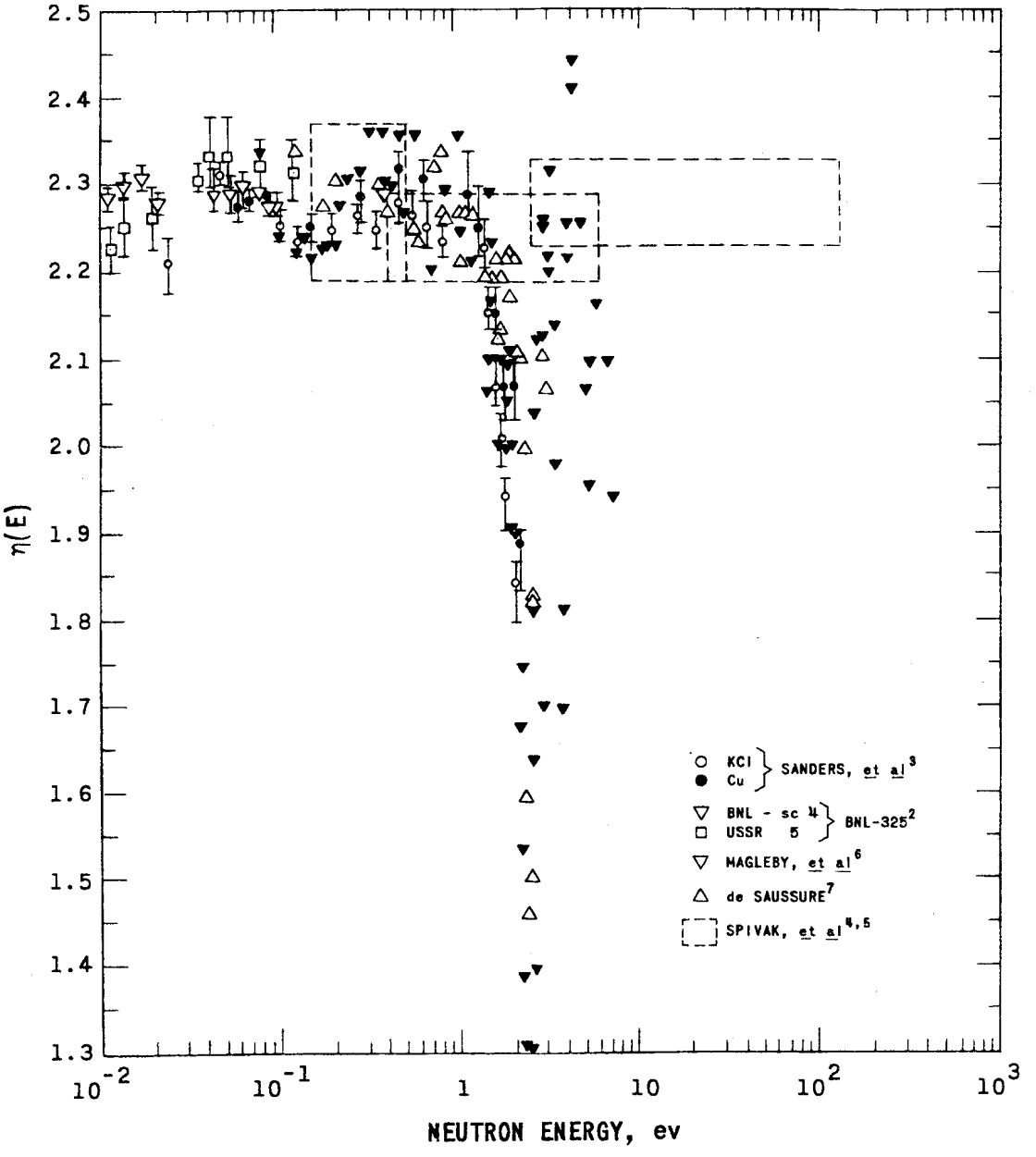

Fig. 2-1 — Neutron yield per neutron absorbed (η) for U^{233} as a function of energy.

beam to pass through a thin counter with known efficiency. The data were normalized to a value of $\eta = 2.30$ at 2200 meter/second.

In Table 2-2 are listed the values of α measured by Diven and Hopkins.[8] The α at each energy was measured directly by observing the capture and fission gamma-ray intensities. The value for η was computed using the linear energy dependence of $\bar{\nu}$ relation (see Section 1.5.2, Table 1-20):

$$\bar{\nu}(E) = \bar{\nu}(0.0253 \text{ ev}) + 0.12\ E(\text{Mev})$$

U^{235}. Figures 2-3 through 2-5 show the variation of η for U^{235} as a function of energy. Table 2-3 lists measured values for other than BNL-325 data. A value of $\bar{\nu} = 2.43 \pm 0.03$ was used to convert the α values in BNL-325 to η values. Included are the data (to be published) for η in the 0.001 to 0.5-ev range obtained by Bollinger and Saplakoglu using the Fast Chopper at ANL. The value $\eta/\bar{\nu}$ was in-

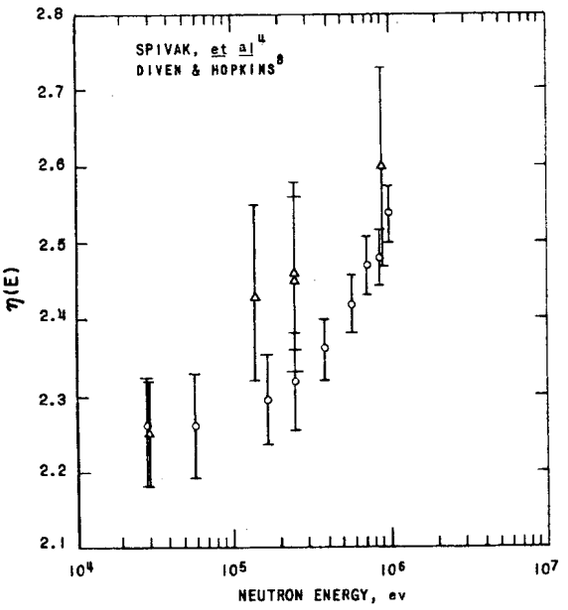

Fig. 2-2—Neutron yield per neutron absorbed (η) for U^{233} as a function of energy.

Table 2-2—VALUES OF α FOR U^{233} AS A FUNCTION OF NEUTRON ENERGY

Data from Ref. 8

Energy, kev	α
30	0.1085 ± 0.0220
60	0.1098 ± 0.0254
175	0.0983 ± 0.0202
250	0.0909 ± 0.0221
400	0.0780 ± 0.0103
600	0.0619 ± 0.0092
750	0.0472 ± 0.0086
900	0.0496 ± 0.0081
1000	0.0295 ± 0.0080

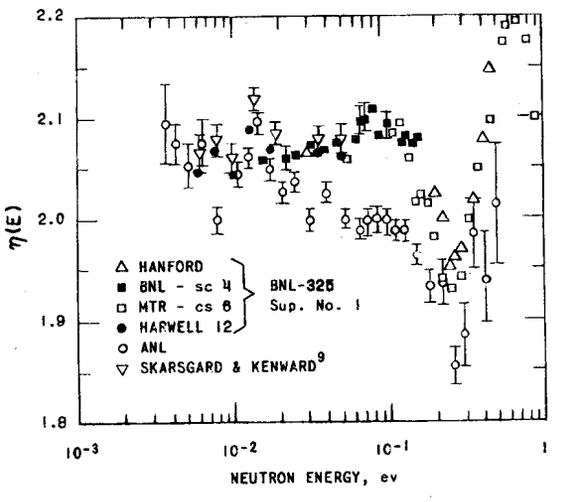

Fig. 2-3—Neutron yield per neutron absorbed (η) for U^{235} as a function of energy.

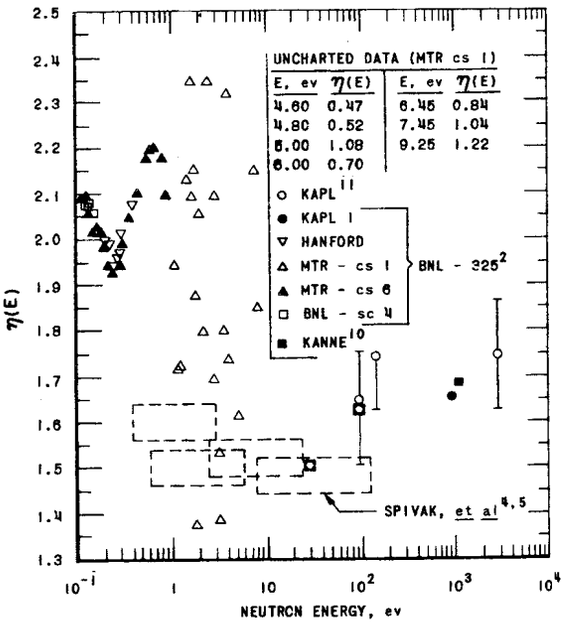

Fig. 2-4—Neutron yield per neutron absorbed (η) for U^{235} as a function of energy.

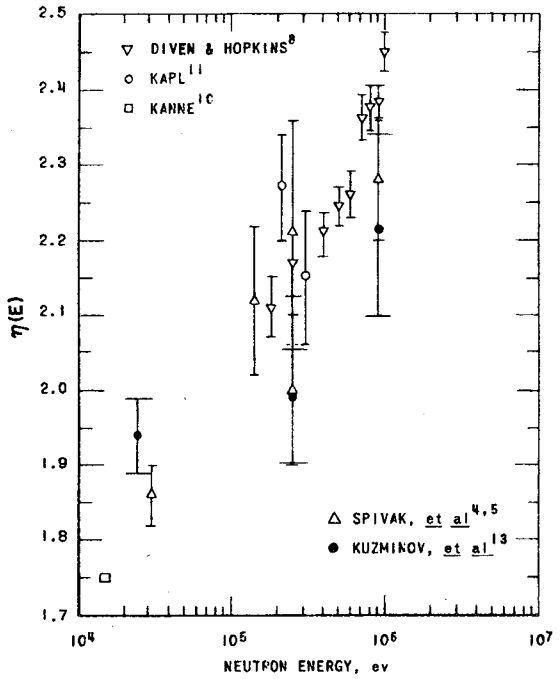

Fig. 2-5—Neutron yield per neutron absorbed (η) for U^{235} as a function of energy.

Table 2-3—VALUES OF α FOR U^{235} AS A FUNCTION OF NEUTRON ENERGY

Energy	α	Ref.
30 ev	0.65	10
100 ev	0.52	10,11
150 ev	0.42 ± 0.08	11
1200 ev	0.47	10
1500 ev	0.45 ± 0.09	11
3000 ev	0.42 ± 0.08	11
15 kev	0.41 ± 0.08	10
30 kev	0.3757 ± 0.0357	8
60 kev	0.3268 ± 0.0244	8
175 kev	0.2236 ± 0.0170	8
215 kev	0.1 ± 0.02	11
250 kev	0.2131 ± 0.0156	8
300 kev	0.17 ± 0.04	11
400 kev	0.1523 ± 0.0107	8
600 kev	0.1430 ± 0.0110	8
750 kev	0.1284 ± 0.0102	8
900 kev	0.1011 ± 0.0109	8
1000 kev	0.0868 ± 0.0077	8

ferred from direct measurements of σ_f and σ_t, using $\sigma_s \sim 12$ barns (constant). The cross sections reported were relative measurements (<3% error); η was normalized to 2.07 at 2200 meter/second.

Skarsgard and Kenward[9] used a crystal spectrometer to measure η in the 0.006 to 0.05-ev energy region. Within experimental error, η appeared to be constant in this range.

The KAPL measurements of α (Table 2-3), were made by Kanne, Stewart, and White[10] with appropriate shielded foils and mass spectrometer analysis. A theoretical analysis of α data has been made by Oleksa.[11] The value of η was computed using $\bar{\nu} = 2.43$ at the neutron energy 0.0253 ev, except for the 215- and 300-kev values where a correction in the energy dependence of $\bar{\nu}$ was made using the linear relation (see Section 1.5.2, Table 1-20; see also Ref. 12):

$$\bar{\nu}(E) = \bar{\nu}(0.0253 \text{ ev}) + 0.135\ E(\text{Mev})$$

The η values were computed from the Diven and Hopkins data on α (Table 2-3) using the above energy dependence of $\bar{\nu}$.

Pu^{239}. Figures 2-6 through 2-9 show the variation of η for Pu^{239} as a function of energy.

With reference to Fig. 2-7, the data on $(\eta/\bar{\nu})$ are given by Bollinger, et al.[14] The data points shown as open circles were obtained in a direct measurement of the fission neutrons using a sample 3mm thick. The data points shown as open squares were inferred from the individual cross sections. The η value may be computed using $\bar{\nu} = 2.89$ as a constant in this region.

With reference to Fig. 2-9, the set of data on η/η_0 (η_0 = thermal eta) in the energy region 6 to 60 ev was obtained by Farley[15] from a transmission-type experiment on two different thicknesses of samples after correcting for scattering.

Values of α reported by Kanne, Stewart, and White[10] are listed in Table 2-4. The value of η was computed using $\bar{\nu} = 2.89 \pm 0.03$. Errors associated with these results were not reported. The η values were computed from the α data of Divens and Hopkins[8] using the energy dependence of $\bar{\nu}$ as (see Section 1.5.2, Table 1-20):

$$\bar{\nu}(E) = \bar{\nu}(0.0253 \text{ ev}) + 0.11\ E(\text{Mev})$$

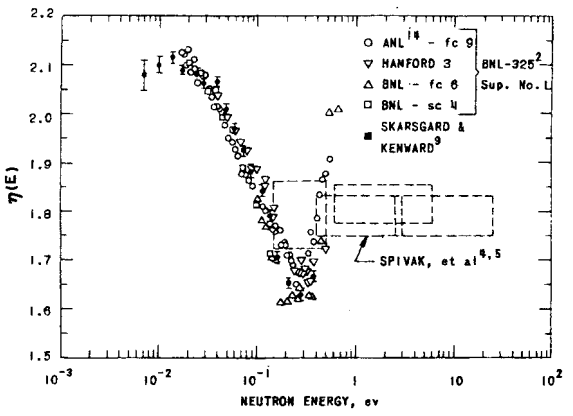

Fig. 2-6—Neutron yield per neutron absorbed (η) for Pu^{239} as a function of energy.

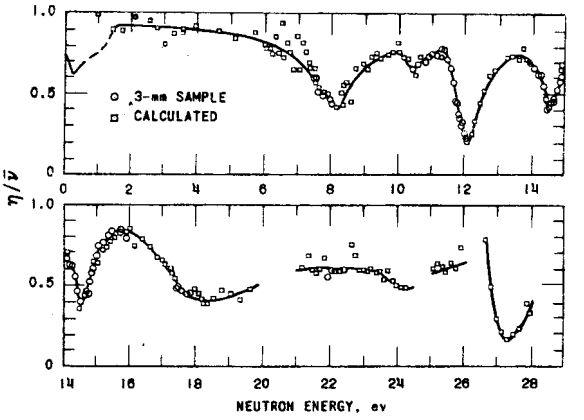

Fig. 2-7—Energy dependence of $\eta/\bar{\nu}$ for Pu^{239}. *Reproduced from Ref. 14.*

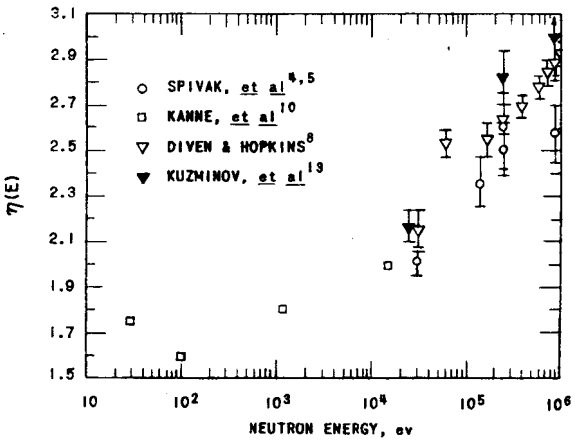

Fig. 2-8—Neutron yield per neutron absorbed (η) for Pu^{239} as a function of energy.

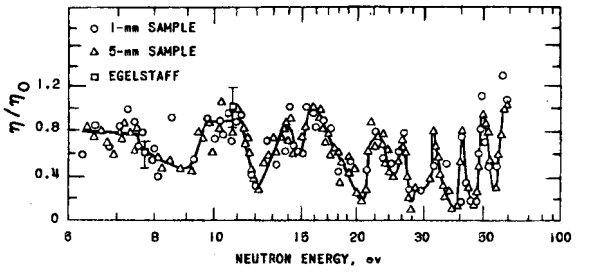

Fig. 2-9—Neutron yield per neutron absorbed (η) for Pu^{239} relative to thermal η as a function of energy. *Reproduced from Ref. 15.*

2.2.2 DEPENDENCE OF FISSION CROSS SECTIONS ON ENERGY

Figure 2-10 is a composite of fission cross section curves for even-odd fissile isotopes U^{233}, U^{235}, Pu^{239}, and Pu^{241} in the 0.1 to 10 Mev energy range. The data on U^{233}, U^{235}, and Pu^{239} are reproduced from BNL-325.[2] Included are values of Pu^{241} in the 0.12 to 21 Mev energy region, recently measured by Smith, et al.[16]

The fission cross sections for the even-even fissile isotopes are presented in Fig. 2-11. The data for U^{236}, U^{238}, and Th^{232} are taken from BNL-325.[2] Measurements on U^{238} and Th^{232} have been reported by Kalinin and Pankratov.[17] The values, in general, seem to be higher than those in BNL-325. The cross section data on Pu^{242} are the measured values of Butler.[18]

Fission cross section curves for odd-odd fissile nuclei are given in Fig. 2-12. The Am^{241} data are reported in BNL-325. The Am^{243} cross sections have been measured recently by Butler.[19] The Schmitt and Murray[20] measurements for Np^{237} and those of Kalinin and Pankratov[17] give generally higher values than those reported in BNL-325.

Table 2-4— VALUES OF α FOR Pu^{239} AS A FUNCTION OF NEUTRON ENERGY

Energy	α	Ref.
30 ev	0.65	10
100 ev	0.81	10
1200 ev	0.60	10
15 kev	0.45	10
30 kev	0.3427 ± 0.0383	8
60 kev	0.1446 ± 0.0165	8
175 kev	0.1423 ± 0.0229	8
250 kev	0.1063 ± 0.0162	8
400 kev	0.0892 ± 0.0085	8
600 kev	0.0648 ± 0.0090	8
750 kev	0.0457 ± 0.0096	8
900 kev	0.0354 ± 0.0118	8
1000 kev	0.0267 ± 0.0070	8

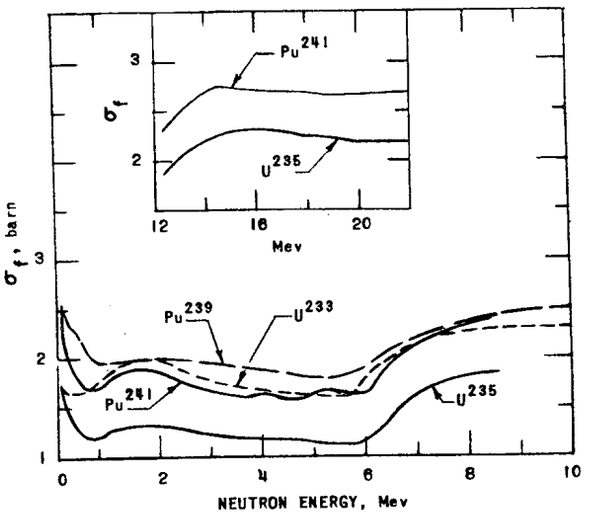

Fig. 2-10—Composite fission cross section curves.

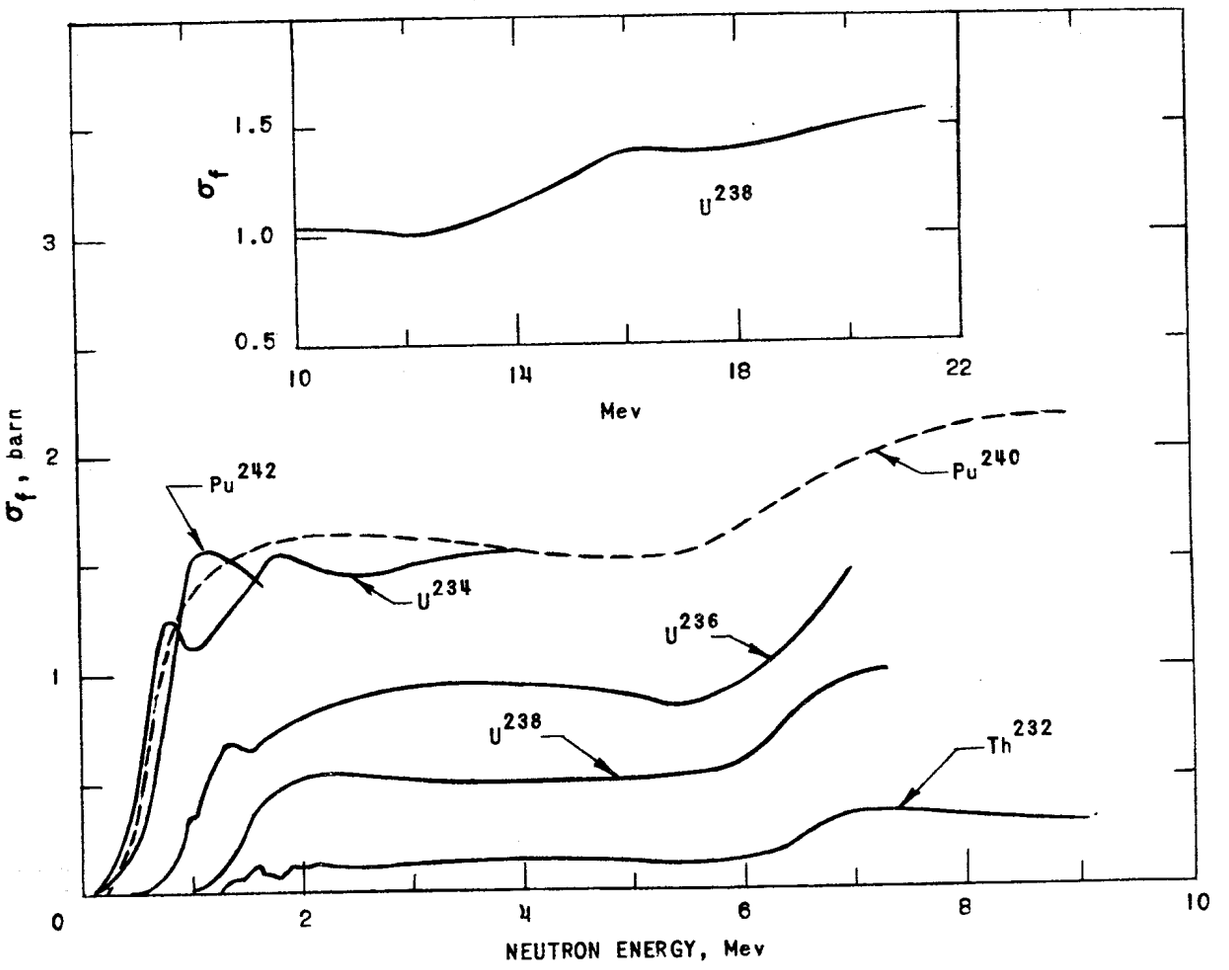

Fig. 2-11—Composite fission cross section curves.

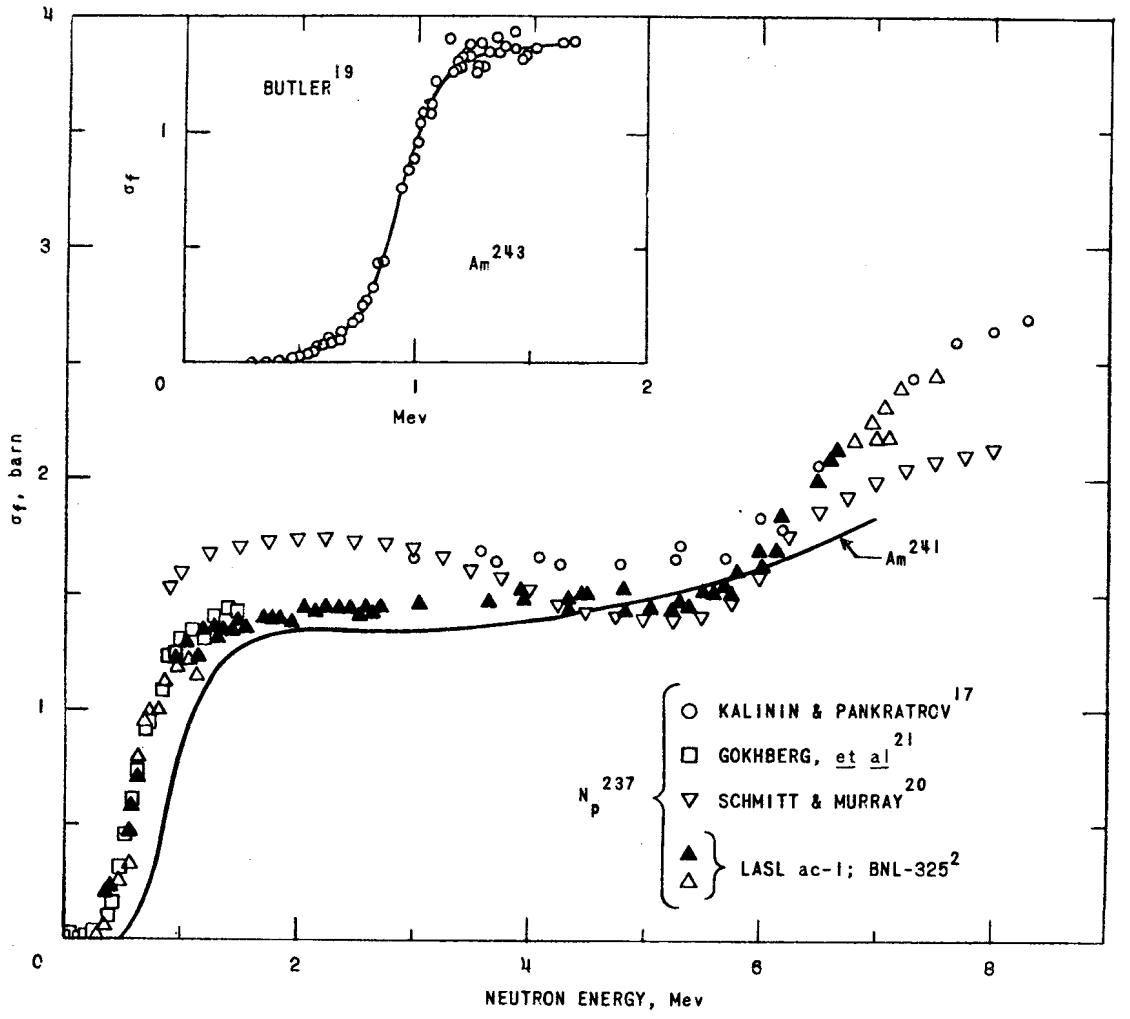

Fig. 2-12—Composite fission cross section curves.

2.3 CAPTURE CROSS SECTIONS AS FUNCTIONS OF ENERGY

Capture cross sections as deduced from available data and theoretical considerations by Yiftah, Okrent, and Moldauer[22] are reproduced as Fig. 2-13 through Fig. 2-26. The information is presented in two ways: first in the form of average cross section curves; secondly, in the form of contributions from known or suspected isolated resonances. The latter contributions are indicated by the positions of vertical bars at the resonance energies whose heights are proportional to the integrated resonance cross section:

$$f \int \sigma dE \qquad (2\text{-}1)$$

where f is the abundance of the isotope to which the resonance belongs; σ is the resonance capture cross section of the isotope; and the range of integration is several full resonance widths in the vicinity of the resonance energy.

The placement of the dashed resonance bars in these figures should be taken as an indication of the distribution of strong isolated capture resonances rather than their exact position.

It should be noted that the capture cross sections for Pu^{239} and U^{235} presented in Figs. 2-25 and 2-26 are based on the α data of Diven, Terrell, and Hemmendinger.[8]

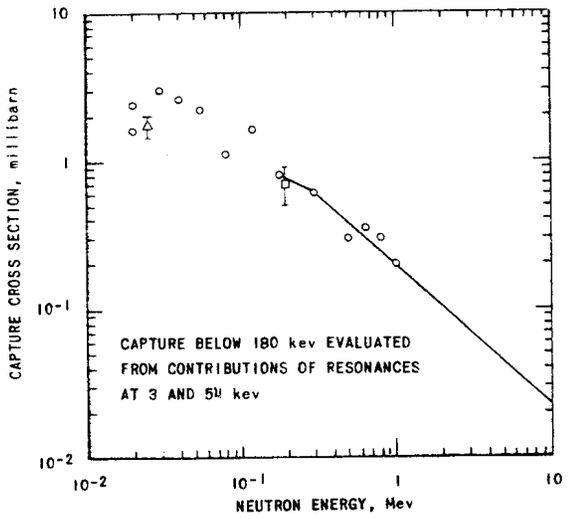

Fig. 2-13—Sodium: Capture cross section $\sigma_{n,\gamma}(E)$. *Data from Ref. 22.*

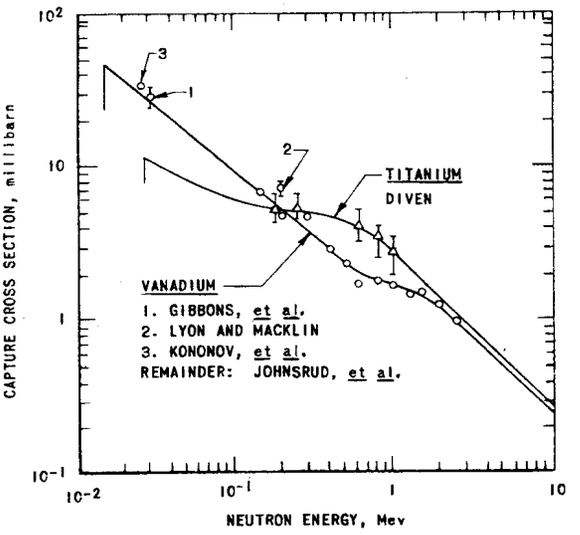

Fig. 2-14—Vanadium, Titanium: Capture cross sections $\sigma_{n,\gamma}(E)$. *Reproduced from Ref. 22.*

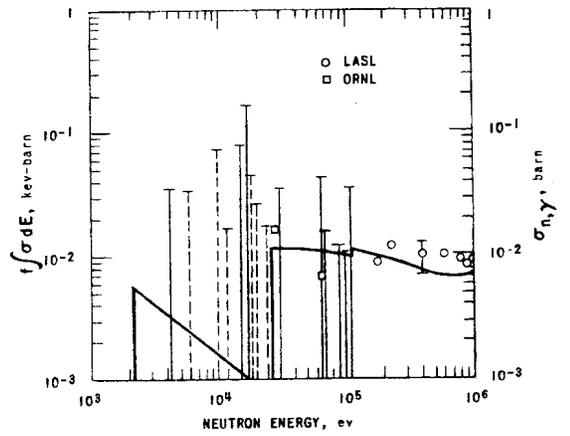

Fig. 2-15—Nickel: Capture cross section $\sigma_{n,\gamma}(E)$. Smooth curve defines cross section exclusive of isolated resonances specified by left-hand ordinate. *Reproduced from Ref. 22.*

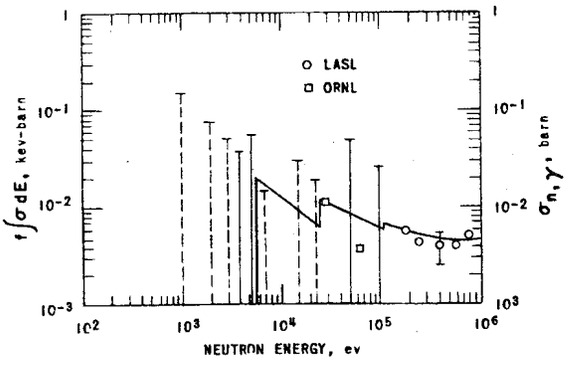

Fig. 2-16—Chromium: Capture cross section $\sigma_{n,\gamma}(E)$. Smooth curve defines cross section exclusive of isolated resonances specified by left-hand ordinate. *Reproduced from Ref. 22.*

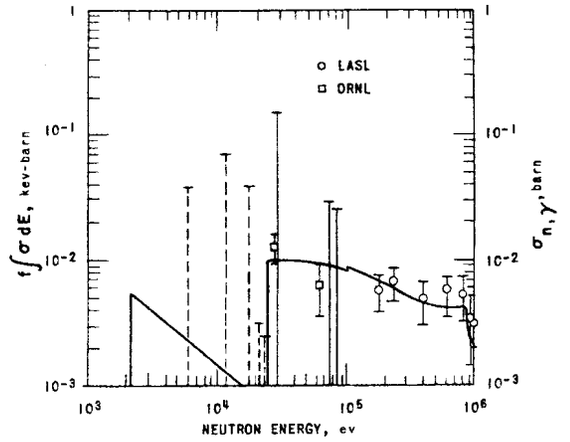

Fig. 2-17—Iron: Capture cross section $\sigma_{n,\gamma}(E)$. Smooth curve defines cross section exclusive of isolated resonances specified by left-hand ordinate. *Reproduced from Ref. 22.*

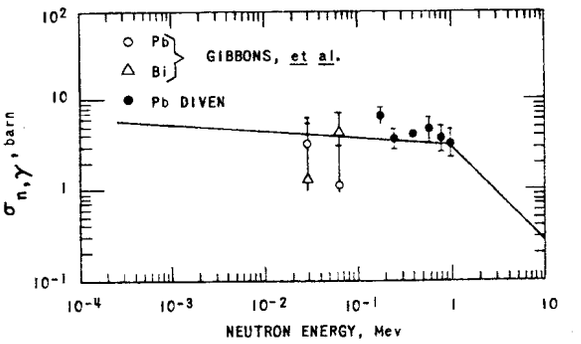

Fig. 2-18—Lead, Bismuth: Capture cross section $\sigma_{n,\gamma}(E)$. *Data from Ref. 22.*

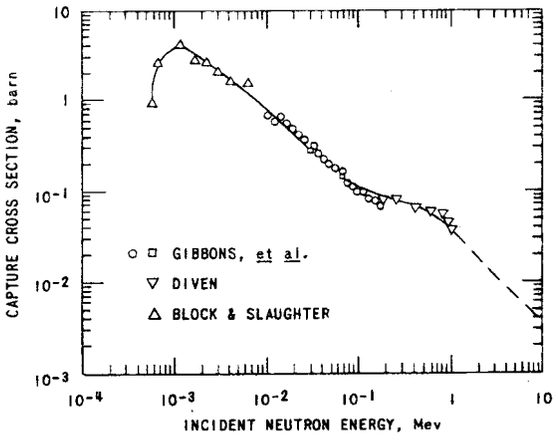

Fig. 2-19—Niobium: Capture cross section $\sigma_{n,\gamma}(E)$. *Data from Ref. 22.*

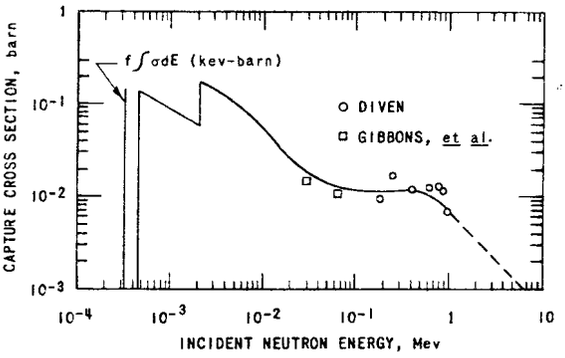

Fig. 2-20—Zirconium: Capture cross section $\sigma_{n,\gamma}(E)$. *Data from Ref. 22.*

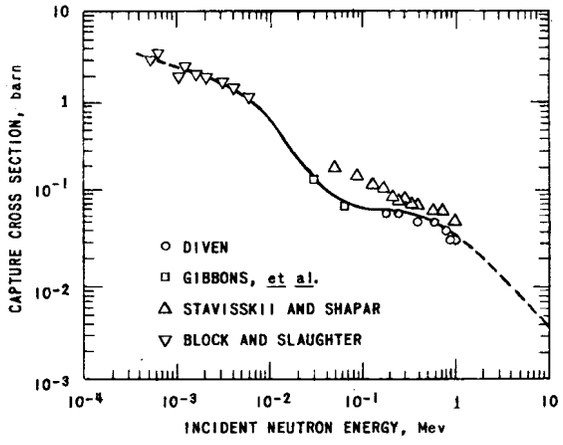

Fig. 2-21—Molybdenum: Capture cross section $\sigma_{n,\gamma}(E)$. *Data from Ref. 22.*

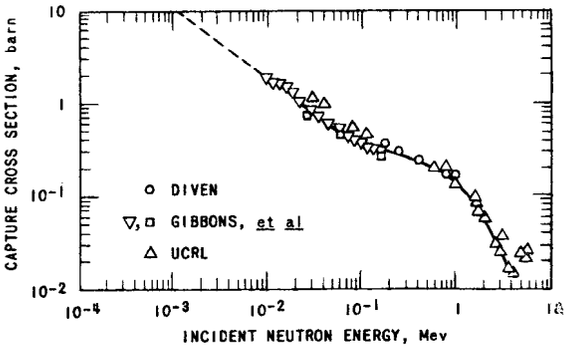

Fig. 2-22—Ta^{181}: Capture cross section $\sigma_{n,\gamma}(E)$. *Data from Ref. 22.*

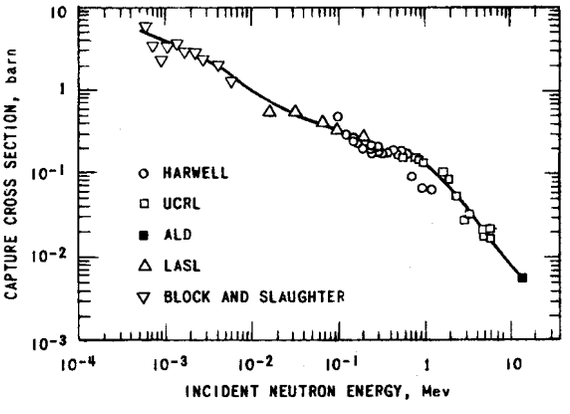

Fig. 2-23—Th^{232}: Capture cross section $\sigma_{n,\gamma}(E)$. *Data from Ref. 22.*

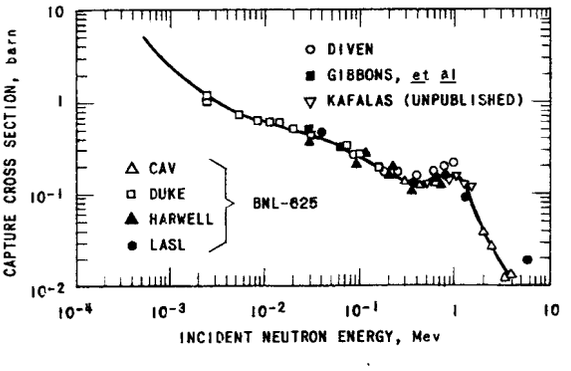

Fig. 2-24—U^{238}: Capture cross section $\sigma_{n,\gamma}(E)$. *Data from Ref. 22.*

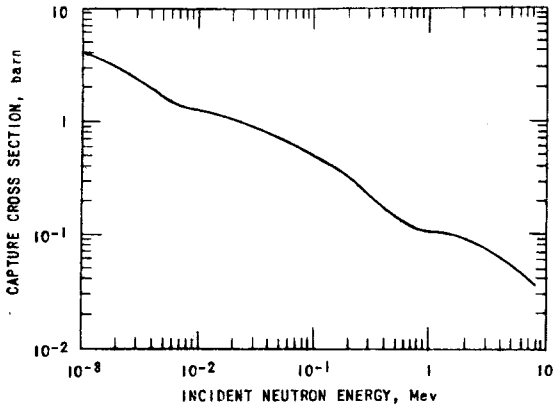

Fig. 2-25—Pu^{239}: Capture cross section $\sigma_{n,\gamma}(E)$. *Data from Ref. 22.*

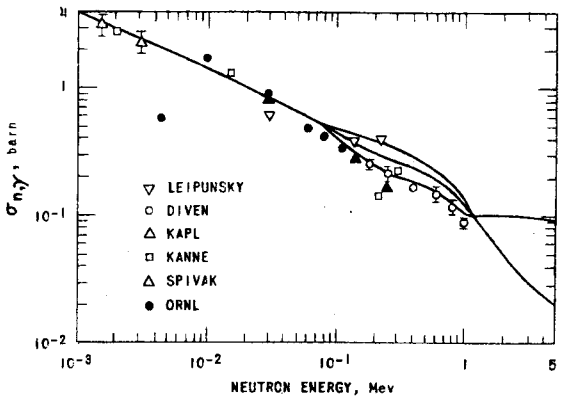

Fig. 2-26—U^{235}: Capture cross section $\sigma_{n,\gamma}(E)$. *Data from Ref. 22.*

2.4 SCATTERING CROSS SECTIONS AS FUNCTIONS OF ENERGY AND ANGLE

2.4.1 ENERGY TRANSFER AND ANGULAR DISTRIBUTION IN THE LOW-ENERGY REGION FOR CRYSTALS, GASES, AND LIQUIDS

The energy transfer and angular distribution of scattered neutrons may be described in terms of free atom scattering for incident neutron energies greater than the binding energy of atoms in a system. In the energy region where scattering nuclei do not act independently, the energy and angular distribution are affected by the state of the scattering system.

Van Hove[23] has presented a general theory of scattering for an arbitrary system of particles. The theory gives, in the Born approximation, the differential scattering cross section in terms of a space- and time-dependent correlation function, $G(\underline{r},t)$, for the scatterers. In this formalism, the differential cross section for a neutron with incident energy E_0 (wave vector $\underline{K}_0$), being scattered by a monatomic system of N nuclei into the elemental solid angle, $d\Omega$, about Ω, and into the energy interval, dE, about E (wave vector $\underline{K}$), is:

$$\frac{d^2\sigma}{d\Omega dE} = \frac{d^2\sigma_{coh}}{d\Omega dE} + \frac{d^2\sigma_{inc}}{d\Omega dE} \tag{2-2}$$

$$\frac{d^2\sigma_{coh}}{d\Omega dE} = \frac{K}{K_0}\frac{m_0^2}{\mu^2}\,Na_{coh}^2\,\frac{1}{2\pi\hbar}\int\int_{-\infty}^{\infty} d\underline{r}\,dt\,\exp\,[i\,(\underline{\kappa}\cdot\underline{r}-\omega t)]G(\underline{r},t)$$

$$\frac{d^2\sigma_{inc}}{d\Omega dE} = \frac{K}{K_0}\frac{m_0^2}{\mu^2}\,Na_{inc}^2\,\frac{1}{2\pi\hbar}\int\int_{-\infty}^{\infty} d\underline{r}\,dt\,\exp\,[i\,(\underline{\kappa}\cdot\underline{r}-\omega t)]G_s(\underline{r},t) \tag{2-3}$$

where $G(\underline{r},t) = G_s(\underline{r},t) + G_d(\underline{r},t)$

$G_s(\underline{r},t)$ = that part which describes the correlation between positions of one and the same particle at different times (self-diffusion)

$G_d(\underline{r},t)$ = pairs of distinct particles

$\underline{\kappa} = \underline{K}_0 - \underline{K}$

$\hbar\omega = E_0 - E$, being the momentum and energy transfer

m_0 and μ = neutron and reduced mass, respectively

The incoherent scattering, a_{inc}^2, due to isotope and spin effects, and the coherent scattering, a_{coh}^2, are defined as:

$$a_{coh}^2 = [\textstyle\sum_i p_i\,(w_{i+}\,a_{i+} + w_{i-}\,a_{i-})]^2$$

$$a_{inc}^2 = \textstyle\sum_i p_i\,(w_{i+}\,a_{i+}^2 + w_{i-}\,a_{i-}^2) - a_{coh}^2 \tag{2-4}$$

where p_i = abundance of the i*th* isotope, having the scattering amplitude a_{i+} for total spin $I_i + 1/2$, and a_{i-} for total spin $I_i - 1/2$, the weighting factors being

$$w_{i+} = \frac{I_i + 1}{2I_i + 1}$$

$$w_{i-} = \frac{I_i}{2I_i + 1} \tag{2-5}$$

Explicit expressions for the correlation function may be obtained in the case of crystals because of the harmonic nature of the forces, and in the case of gases where the inter-particle forces may be neglected. The results for these cases have been derived by many investigators[24–30] using the first Born approximation scattering formalism directly. The most complete formulation for scattering systems other than liquids is that of Zemach and Glauber.[27]

Monatomic Crystals. A crystalline substance may be represented by a system of coupled, harmonically oscillating nuclei in thermal equilibrium. The energy and angular distribution of the scattered neutron is expressed in terms of absorbing and emitting quanta (phonons) of vibrational energy from, or to, the system of scatterers (lattice). The differential cross section for a neutron being scattered by a monatomic system of nuclei vibrating about equilibrium positions is given by:

$$\frac{d^2\sigma_{inc}}{d\Omega dE} = \frac{K}{K_0}\frac{m_0^2}{\mu^2}\,Na_{inc}^2\,\exp(-2W)\,\frac{1}{2\pi\hbar}\int dt\,\exp\{-[i\omega t - \gamma(t)]\}$$

and

$$\frac{d^2\sigma_{coh}}{d\Omega dE} = \frac{K}{K_0}\frac{m_0^2}{\mu^2}\,Na_{coh}^2\,\exp(-2W)\,\frac{1}{2\pi\hbar}\int dt\,\exp(-i\omega t)\left\{\exp[\gamma(t)] + \sum_{j=1}^{N}\exp(i\,\underline{\kappa}\cdot\underline{r}_j)\,\exp[\gamma_j(\underline{r}_j,t)]\right\} \tag{2-6}$$

where $\underline{r}_j$ is the position vector of the jth nucleus from some arbitrary origin atom, and

$$\gamma(t) = \sum_{s=1}^{3N}\frac{\hbar(\underline{\kappa}\cdot\underline{e}_s)^2}{2mN\omega_s}\left\{\coth\frac{\hbar\omega_s}{2kT}\cos\omega_s t - i\sin\omega_s t\right\}$$

$$\gamma_j(\underline{r}_j,t) = \sum_{s=1}^{3N}\frac{\hbar(\underline{\kappa}\cdot\underline{e}_s)^2}{2mN\omega_s}\left\{\coth\frac{\hbar\omega_s}{2kT}\cos\omega_s t - i\sin\omega_s t\right\}\exp(i\underline{q}_s\cdot\underline{r}_j) \tag{2-7}$$

This form of the cross section is readily obtained from Zemach and Glauber's Eqs. (3-19) and (3-20), as given in Ref. 27, by substituting the generating function for the summation term in Eq. (3-19), and defining

$$\chi = \frac{\hbar(\underline{\kappa}\cdot\underline{e}_s)^2}{2mN\omega_s\sinh(\hbar\omega_s/2kT)}\exp(i\underline{q}_s\cdot\underline{r}_j)$$

as the argument of the Bessel function (see also Ref. 28).

The above cross section describes the process in which vibrational quanta (phonons) of frequencies, ω_s, and wave vectors, $\underline{q}_s$, having unit polarization vector, $\underline{e}_s$, have been exchanged between the neutron and lattice.

The phonon expansion approximation, used by many investigators, of the scattering cross section is obtained from Eq. (2-6) by writing the exponential terms involving $\gamma(t)$ and $\gamma_j(\underline{r}_j,t)$ in a power series:

$$\exp[\gamma(t)] = \sum_{\ell=0}^{\infty}\frac{1}{\ell!}[\gamma(t)]^{\ell}$$

$$\exp[\gamma_j(\underline{r}_j,t)] = \sum_{\ell=0}^{\infty}\frac{1}{\ell!}[\gamma_j(\underline{r}_j,t)]^{\ell} \tag{2-8}$$

Each term describes the process in which ℓ phonons have been exchanged by the neutron with a system of nuclei of mass m and temperature T. The exponent in the Debye-Waller intensity factor, $\exp(-2W)$,

is given by:

$$2W = \sum_{s=1}^{3N} \frac{\hbar(\underline{\kappa} \cdot \underline{e}_s)^2}{2mN\omega_s} \coth \frac{\hbar\omega_s}{2kT} \tag{2-9}$$

For a cubic lattice, and as an approximation for non-cubic lattices:

$$(\underline{\kappa} \cdot \underline{e}_s)^2 \approx \frac{1}{3} \kappa^2$$

The single-phonon approximation ($\ell = 1$), utilizing the Debye model, has been found in good agreement with experiments[31] on the total cross section (integrated differential cross section over energy and angle) for lead at 80°K in the neutron energy range 0.0013 to 0.02 ev. Also the total cross section measurements by Palevsky, Hughes, and Smith[32–34] on Fe, C, and Be in the range 0.0002 to 0.003 ev are in good agreement with the one-phonon theory. In this energy region (below Bragg cutoff), the coherent part of the cross section may be neglected (incoherent approximation).

For high temperatures of scattering material, and also at high neutron energies, the contribution due to multi-phonon processes becomes appreciable. Squires[35] considers higher-order processes and gets good agreement with experiment on total cross section as a function of material temperature for Ni and Mg at neutron wave lengths of 5.25 and 6.25 Å, respectively.

Kothari and Singwi[36] have studied the temperature variation of the total inelastic scattering cross section of graphite for 10 Å neutrons. The one-phonon and two-phonon processes are considered using the Krumhansl and Brooks[37] frequency distribution for graphite. The agreement with experiment is good.

Placzek[38] accounts for multi-phonon processes by rearranging the terms in the phonon-summation process as an expansion in the mass ratio m_0/m and finds the series for total cross section converges much more rapidly. Marshall and Stuart,[39] and Sjölander[28] use the above Placzek expansion in a study comparing the total cross sections computed based on the simple Debye frequency spectrum, and the observed, more detailed, frequency spectrum for Al, Mn, and V. The comparison in the above studies involves an integral quantity and depends only weakly upon the details of the model used for the frequency spectrum.

Sjölander,[28] and Schofield and Hassitt[40] have considered the general problem of multi-phonon processes. Their formalism reduces the incoherent inelastic differential cross section in terms of multiple integrals involving the frequency distribution, $\rho(\nu)$ of the scattering material. Schofield and Hassitt show that for the multi-phonon processes the multiple integrals may be approximated, using the central limit theory, by a Gaussian function. Sjölander further considers representing the multiple integrals in a Hermite polynomial expansion. This latter approximation is shown to give better results when compared with the exact calculations. Sjölander also shows that for a two-phonon process, a Debye frequency distribution approximation is in better agreement than the Gaussian when compared with computations based on the known frequency distribution of Al. The number of terms for which the multiple integrals would be computed exactly, however, will depend on the detailed structure of $\rho(\nu)$.

The details of the differential scattering cross section depend on the knowledge of the vibrational spectrum of the solid. Two theories have been advanced by Debye,[41] and by Born and von Karman.[42–44]

Debye's theory is based on the model in which a crystal is assumed to be a continuous medium. The number of allowable standing elastic waves in the solid is assumed to determine the frequency spectrum. The range of frequencies, from zero to a maximum, is determined by the interatomic spacings. Further, it is assumed that the velocity of sound is independent of frequency (dispersionless medium).

The theory of Born and von Karman is based on the concept of lattices and gives a more realistic wave dispersion relation than the Debye model. In this theory, the equations of motion of the atoms in the lattice are developed in terms of harmonic interatomic forces. The solution of these equations in terms of standing waves (normal coordinates), leads to the relations between frequencies and wave lengths (secular equation). The problem involves interatomic force constants which may be estimated if the elastic constants for the materials are known. The frequency distribution $\rho(\nu)d\nu$, the number of modes having frequencies in the range ν and $\nu + d\nu$, is then obtained from the dispersion relations.

Several investigators[45–49] have determined dispersion curves for some solids from the temperature diffuse scattering of X-rays.

Jacobsen[50] analyzed the dispersion curves for Cu at 300°K in terms of the force constants in the lattice theory for the first three nearest neighbor interactions. The force constants were chosen to give the best fit to the experimental dispersion curves for the three primary crystallographic axes. A

comparison of the vibrational spectra resulting from the central force, non-central force (generalized force) and Debye models is shown in Fig. 2-27.

In Fig. 2-28 is the frequency spectrum for Al at 300°K proposed by Walker.[51] The distribution is based on the first three nearest neighbor interactions. The force constants were selected to give the best fit to the dispersion curves, as well as to agree with the experimental data on the elastic constants. The histogram is obtained from 8,373 calculated eigenfrequencies. The smooth curve is obtained from the histogram after inclusion of the singularities arising from the critical points of the various branches.

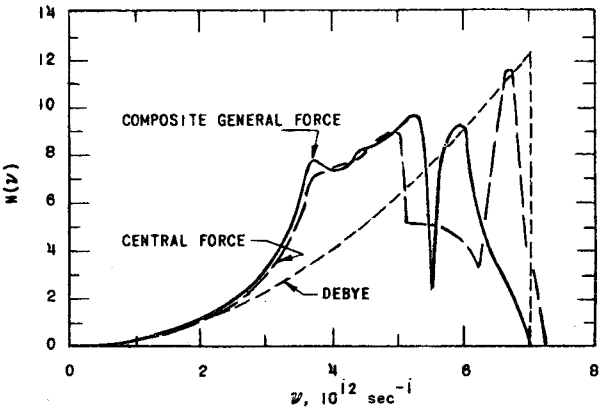

Fig. 2-27—Comparison of composite general force, central force, and Debye spectra for copper. Both the general force and central force spectra contain 3417 wave vector solutions. *Reproduced from Ref. 50.*

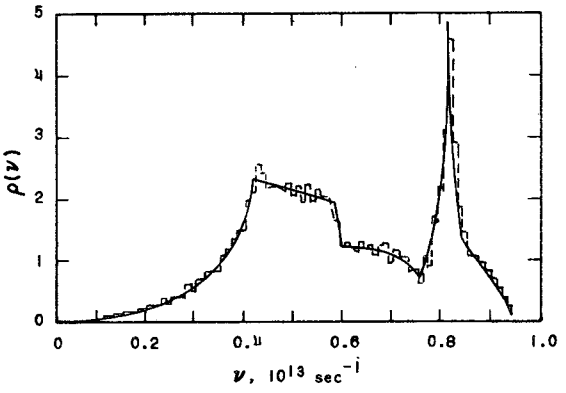

Fig. 2-28—Total vibrational frequency spectrum for aluminum at 300°K. *Reproduced from Ref. 51.*

Brockhouse and Stewart,[52] in a manner analogous to the X-ray scattering experiments, have studied inelastically scattered neutrons to determine dispersion curves for Al. Their results agree fairly well with the dispersion relations and force constants of Walker.

The vibration spectra of V and Mn-Co alloy as measured by Brockhouse and Stewart[52] are included in Figs. 2-29 and 2-30, respectively. In Fig. 2-29, curve (A) represents the combined histograms; curve (B) is a possible spectrum with the instrument resolution removed; and curve (C) is part of the Debye spectrum for $\theta_D = 338°K$ as determined by low-temperature specific heat measurements.

Baldock[53] calculated the frequency distribution of graphite by representing the normal modes as transverse modes in which the atoms move perpendicular to the planes, and planar modes with vibrations in the plane. The interaction between planar and transverse modes was neglected. The transverse modes were determined by the secular equation. For the planar modes, Baldock used the Krumhansl and Brooks[37] model and assumed the distribution to be given as:

$$\rho(\nu) = K_2\nu^2 \qquad 0 \le \nu \le 0.009\ \nu_{max}$$

$$\rho(\nu) = K_1\nu \qquad 0.009\ \nu_{max} \le \nu \le \nu_{max} \tag{2-10}$$

where K_2 and K_1 are normalizing constants, and ν_{max} is the maximum frequency corresponding to a Debye temperature of 2500°K. The linear dependence only was used in constructing the total normalized frequency distribution curve for graphite shown in Fig. 2-31.

Yoshimori and Kitano[54] have calculated the frequency distribution for the transverse and planar modes using a method developed by Houston[55] for a cubic lattice. In this method, the secular equation is solved along a given direction in the Brillouin zone. The frequency distribution along this direction is then expanded in spherical harmonics and only the first few terms are retained. The symmetry of the crystal determines the number of directions to choose. This method has the advantage of covering the whole of the Brillouin zone, as well as avoiding the laborious numerical computation of the secular equation for a large number of discrete points. However, divergences and shifts occur at critical frequencies due to the use of the improper summation procedure. The frequency spectrum for graphite, proposed by Yoshimori and Kitano, is given in Fig. 2-32.

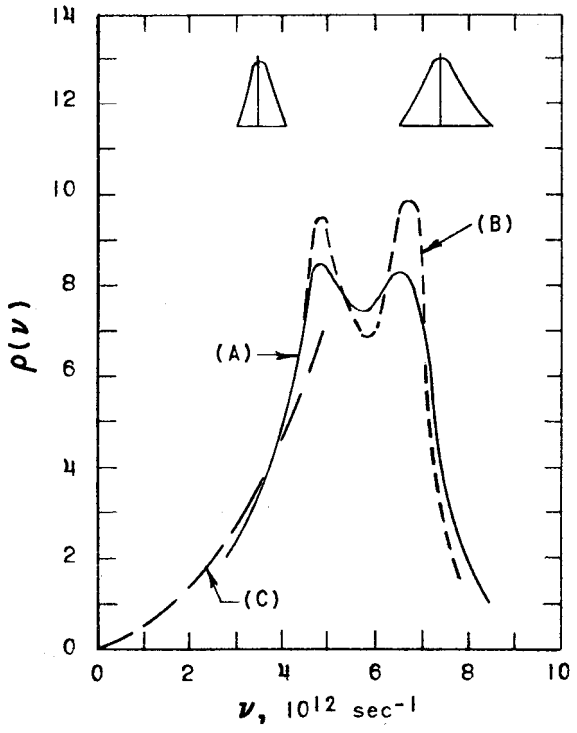

Fig. 2-29—Vibration spectrum of vanadium with the instrument resolution shown. *Reproduced from Ref. 52.*

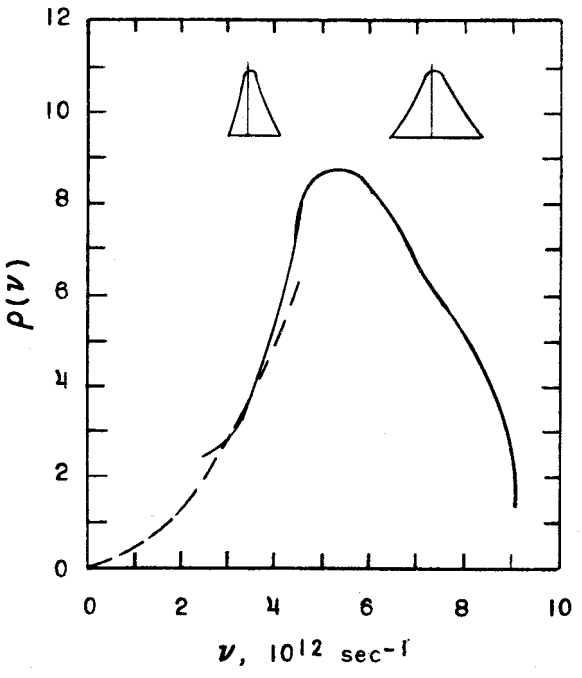

Fig. 2-30—Vibration spectrum for Mn-Co alloy. The dashed curve(C) was arbitrarily drawn for $\theta_D = 338°K$. *Reproduced from Ref. 52.*

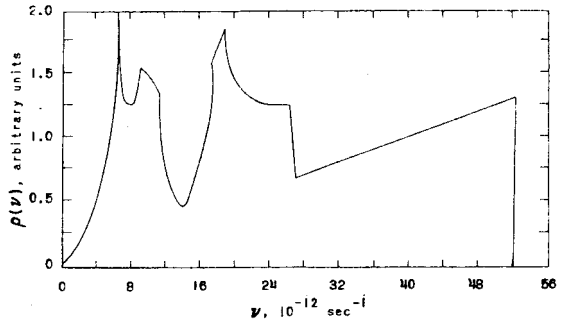

Fig. 2-31—Total vibrational frequency spectrum for graphite. *Data from Ref. 53.*

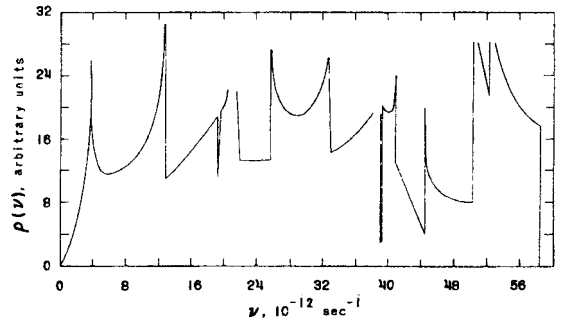

Fig. 2-32—Total vibrational frequency spectrum for graphite. *Data from Ref. 54.*

Recently, Egelstaff and Cocking[56] have reported measurements on neutron scattering by graphite for various temperatures. The frequency spectrum, Fig. 2-33, analyzed on the basis of Van Hove's formalism, was compared with the Baldock calculations. Because of the preliminary nature of the results and the low resolution reported, it is difficult to make a detailed comparison.

Monatomic Gases. The differential cross section for a system of independent scatterers of like mass having a Maxwellian velocity distribution is given by:[27]

$$\frac{d^2\sigma}{d\Omega dE} = \frac{K}{K_0}\frac{m_0^2}{\mu^2} Na^2 \frac{1}{2\pi\hbar}\int dt \exp(-i\omega t)\exp\left(-\frac{kT\kappa^2 t^2}{2m} - \frac{i\kappa^2\hbar t}{2m}\right) \qquad (2\text{-}11)$$

or

$$\frac{d^2\sigma}{d\Omega dE} = \frac{K}{K_0}\frac{m_0^2}{\mu^2} Na^2 \left(\frac{m}{2\pi kT\kappa^2\hbar^2}\right)^{1/2} \exp\left[-\left(\frac{m}{2kT\kappa^2\hbar^2}\right)\left(\hbar\omega + \frac{\kappa^2\hbar^2}{2m}\right)^2\right] \quad (2\text{-}12)$$

where

$$a^2 = a_{coh}^2 + a_{inc}^2$$

Equation (2-11) may also be obtained from Eqs. (2-6), (2-7), and (2-9), noting that in a system of non-interacting particles,

$$\sum_{j=1}^{N} \exp\,(i\,\underline{\kappa}\cdot\underline{r}_j) \exp\,[\gamma_j(\underline{r}_j,t)] \to 0$$

and by taking the limit, $\omega_s \to 0$ for all s.

The energy transfer cross section is obtained by integrating Eq. (2-12) over the solid angle, giving the Wigner-Wilkins[57] result

$$\sigma(v_0 \to v) = \frac{v}{v_0}\frac{mm_0}{\mu^2} Na^2\,\pi\,\{\exp\,[\beta^2(v_0^2 - v^2)]\,[\mathrm{erf}\,(\beta\theta v_0 - \beta\xi v) \pm \mathrm{erf}\,(\beta\theta v_0 + \beta\xi v)] + [\mathrm{erf}\,(\beta\theta v - \beta\xi v_0) \mp \mathrm{erf}\,(\beta\xi v_0 + \beta\theta v)]\} \quad (2\text{-}13)$$

where v_0 and v = initial and final neutron speeds

$\theta = (m + m_0)/2\sqrt{mm_0}$

$\xi = (m - m_0)/2\sqrt{mm_0}$

$\beta^2 = 1/2kT$

The upper and lower signs refer to the processes in which $v > v_0$ and $v < v_0$, respectively.

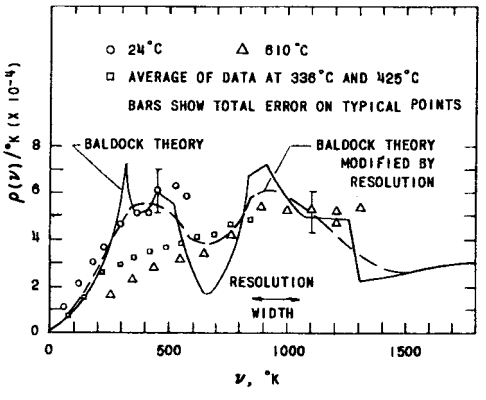

Fig. 2-33 — Comparison of theoretical and experimental frequency distributions for graphite. *Reproduced from Ref. 56.*

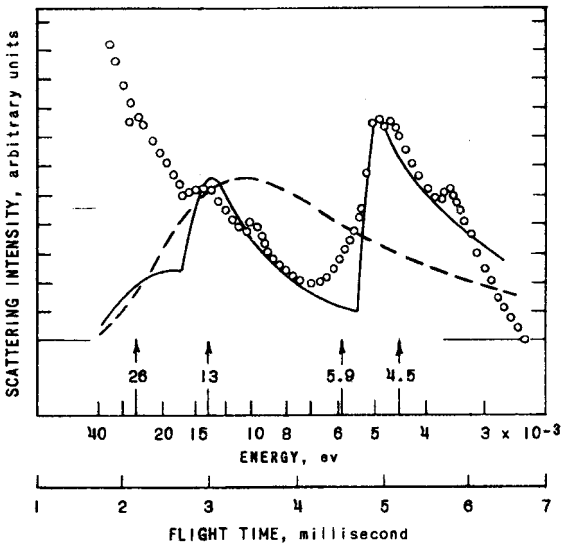

Fig. 2-34 — Differential scattering cross section of beryllium-filtered neutrons (cutoff at 3.96 Å) versus outgoing neutron energy for 90° scattering angle. *Reproduced from Ref. 65.*

Liquids. The motion of the atoms in liquids is not well understood at present and an explicit expression for the correlation function in Van Hove's formulation is difficult to construct. Vineyard[58] and Brockhouse[59] have proposed that a pure diffusive motion for atoms in a liquid, $G_d(\underline{r},t) = 0$, be assumed so that the self-correlation function may be taken as the solution of the classical diffusion equation.

The correlation function is taken as the Gaussian:

$$G_s(\underline{r},t) = \left[\frac{1}{4\pi\gamma(t)}\right]^{3/2} \exp\left[-r^2/4\,\gamma(t)\right] \tag{2-14}$$

where for pure classical diffusion,

$$\gamma(t) = D|t| \tag{2-15}$$

The term D is the self-diffusion coefficient, and $|t|$ is the time in which the atom will be displaced by distance $\underline{r}$. Vineyard considered also the case in which the atoms diffuse according to Langevin's equation. Schofield[60] modified this solution to be consistent with the quantum mechanical formalism.

Using the above model, the calculated energy spread of the scattered neutrons for light water does not appear to be verified by some recent experiments,[61,62] the calculated broadening being greater than that observed. Further, for purely diffuse motion the energy distribution of the scattered neutrons should show no structure. Hughes, et al.,[62] and Larsson, et al.,[63] observed definite peaks, indicating quantum effects similar to those describing the motion of atoms in a solid.

The liquid state has been considered a polycrystalline material by many investigators[64] studying specific heats as well as other thermodynamic quantities of liquids. Singwi and Sjölander,[65] calculated a differential scattering cross section for cold neutrons, using a model of liquid water in which a molecule in its equilibrium position performed an oscillatory motion for a mean time τ_0, then diffused for a mean time τ_1, and then repeated this kind of motion. They further estimated that for light water $\tau_0 \gg \tau_1$, so that a quasi-crystalline model for water may be used. The inelastic scattering of cold neutrons was then calculated for two models of water: the gas model (mass 18), Eq. (2-12), and the crystalline model, Eq. (2-6), assuming a Debye distribution of frequencies ($\theta_D = 135°K$). The results when compared with experiments,[62] Fig. 2-34, seem to substantiate the quasi-crystalline model for water. In the figure, the dashed lines are for the gas model, the solid line is based on the Debye spectrum, and the circles are the experimental points by Hughes.

Egelstaff, et al.,[66] reported their data and analysis to be consistent when the behavior of the atoms in H_2O and D_2O is represented by a combination of a diffusion and oscillatory motion.

Nelkin[67] assumed a model for water in which the motion of the hydrogen atom in water is considered in terms of the H_2O molecule as the basic dynamic unit. The internal vibrations of the molecule were assumed to be the same in the liquid state as in the vapor state. The energies of the molecular vibrations were taken to be 0.205 and 0.481 ev. The hindered rotations of the molecule were replaced by a single torsional oscillation having the energy 0.06 ev. The mass associated with this mode of vibration was taken as 2.32. The translational motion of the molecules was neglected. In Fig. 2-35 is the comparison of the calculated total cross section with experimental data. The agreement is good, but again the comparison involves an integrated quantity and depends only weakly upon the details of the model.

In Fig. 2-36 is a comparison of the calculated with experimental data on the energy distribution of neutrons of incident energy 0.065 ev after scattering through an angle of 90 degrees. The experimental

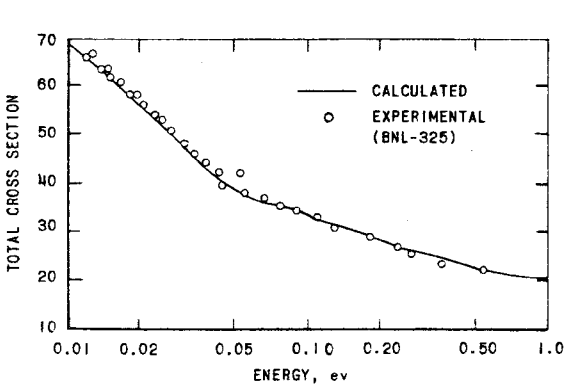

Fig. 2-35 — Total cross section of water in barns per hydrogen atom as a function of incident neutron energy. *Reproduced from Ref. 67.*

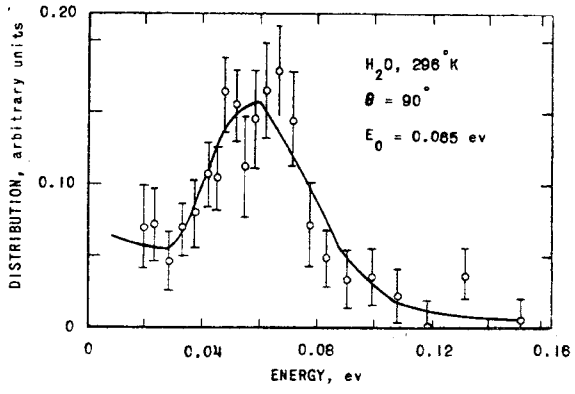

Fig. 2-36 — Energy distribution of neutrons of incident energy 0.065 ev after scattering through 90° by water. *Reproduced from Ref. 67.*

data are those of Brockhouse.[59] Here, both theory and experiment do not show the structure reported by the other investigators.[62,63] As pointed out by Nelkin, the model used would not show structure since the hindered translational modes were neglected. Frequencies associated with these modes are much lower than those associated with the internal vibrations.

2.4.2 ENERGY TRANSFER IN THE KEV-MEV ENERGY REGION

Figures 2-37 through 2-43 show the level excitation curves by neutron inelastic scattering for U^{233}, U^{235}, U^{238}, and Pu^{239}, at incident neutron energies up to 2 Mev.[22] With reference to the total inelastic curve of Fig. 2-42, the data point (△) was obtained by adding the partial cross sections of Cranberg. The data points (□) represent totals obtained by assuming the non-elastic cross section to be identical to that of U^{235} and subtracting fission and capture cross sections.

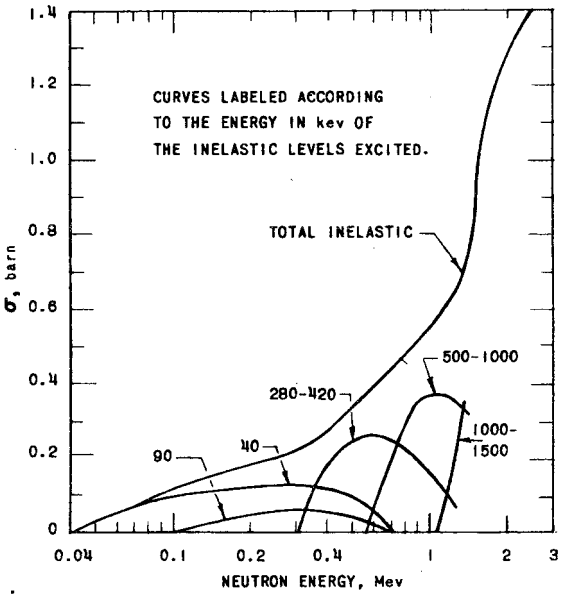

Fig. 2-37—U^{233}: Partial inelastic scattering cross sections. *Reproduced from Ref. 22.*

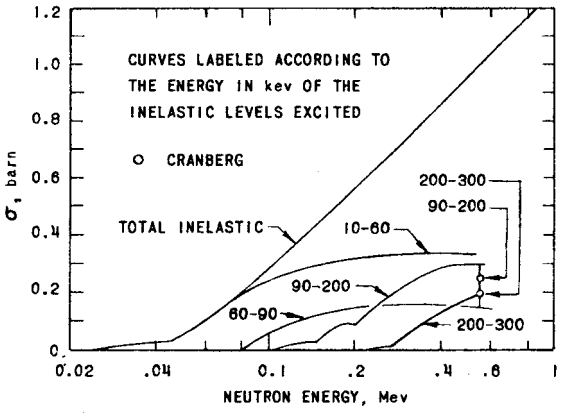

Fig. 2-38—U^{235}: Partial inelastic scattering cross sections below 550 kev. *Reproduced from Ref. 22.*

Above 2 Mev it is impractical to resolve individual level excitations, the levels being too numerous. The inelastic neutron spectra in this region can be determined by means of the statistical model. In this model, the energy distribution of the inelastically scattered neutrons is given by

$$N(E) = E\, e^{-E/\theta} \tag{2-16}$$

where N(E) is the probability that the energy of the emitted particle will be in a unit interval at E, and θ is the temperature of the residual nucleus obtained by Weisskopf[68] on the basis of his level spacing formula, $D = C \exp(-B\sqrt{E})$, as

$$\theta = \frac{2}{B}\sqrt{E} \tag{2-17}$$

where E is the incident energy, and B has been given by Weinberg and Wigner[69] as

$$B \approx 0.62\sqrt{A} \tag{2-18}$$

where A is the mass number.

687863 O - 63 - 5

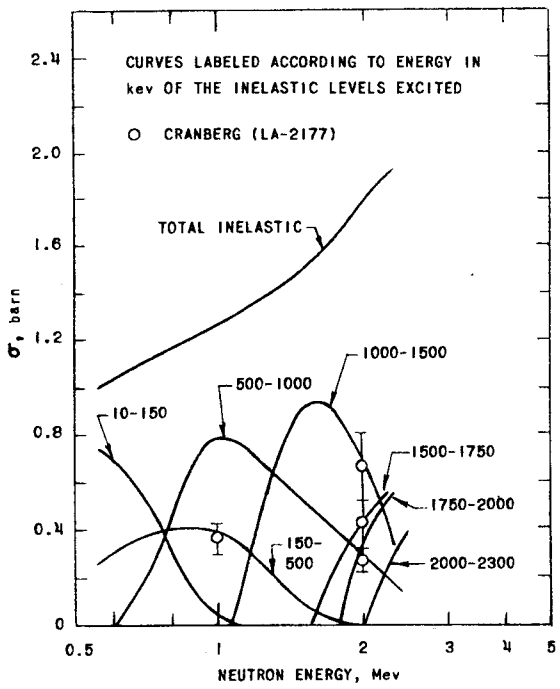

Fig. 2-39 — U^{235}: Partial inelastic scattering cross sections 550-2300 kev. *Reproduced from Ref. 22.*

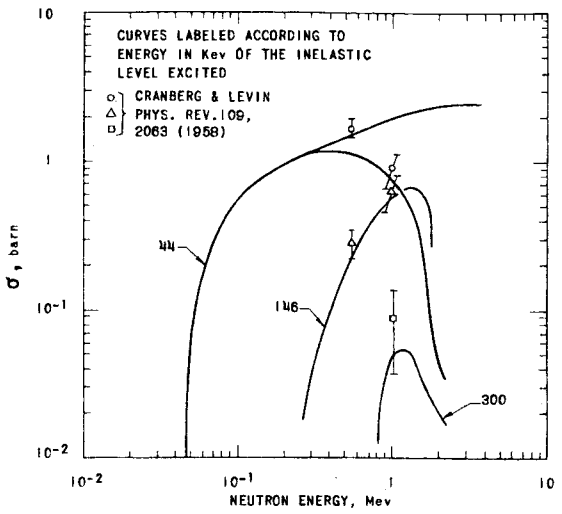

Fig. 2-40 — U^{238}: Partial inelastic scattering cross sections up to incident neutron energies of 2 Mev (Levels 44, 146, 300). *Reproduced from Ref. 22.*

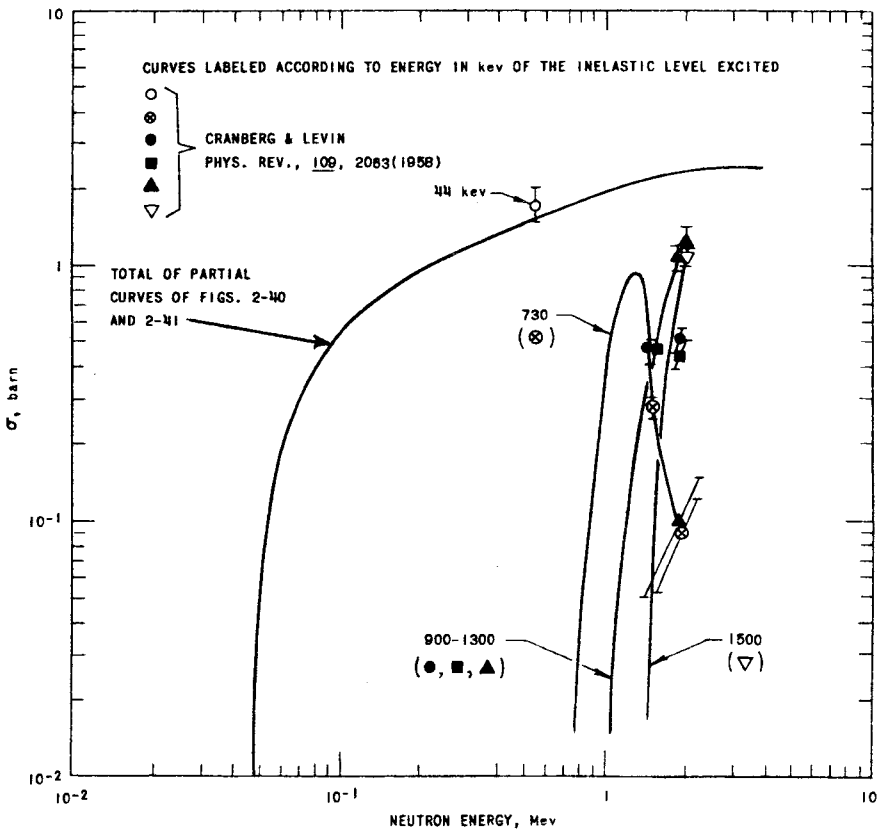

Fig. 2-41 — U^{238}: Partial inelastic scattering cross sections up to incident neutron energies of 2 Mev (Levels 730, 1000, 1500). *Reproduced from Ref. 22.*

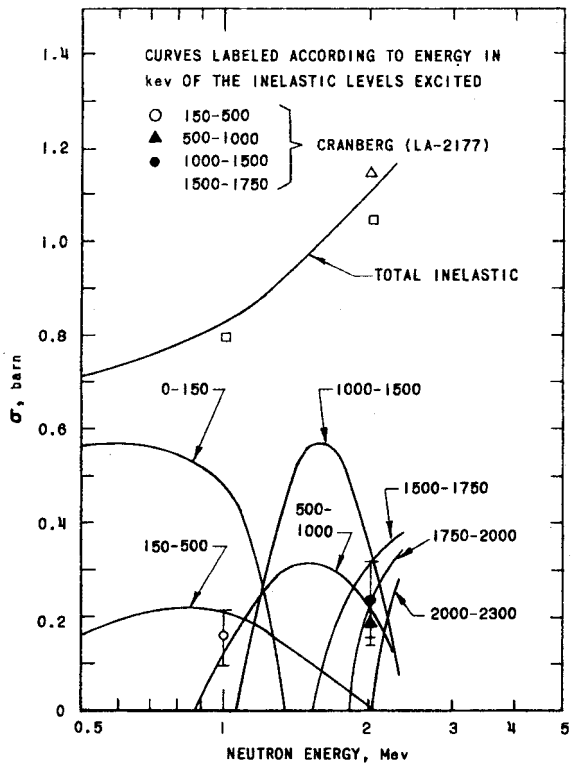

Fig. 2-42 — Pu^{239}: Partial inelastic scattering cross sections at incident neutron energies up to 2 Mev. *Reproduced from Ref. 22.*

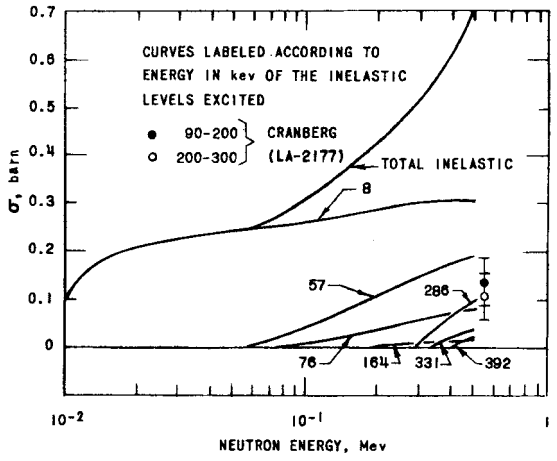

Fig. 2-43 — Pu^{239}: Partial inelastic scattering cross sections below 550 kev. *Reproduced from Ref. 22.*

The nuclear temperatures for U^{238} and other isotopes, as given in Ref. 22, are shown in Fig. 2-44. The total inelastic cross sections for U^{233}, U^{235}, U^{238}, and Pu^{239}, given by Howerton,[70] are shown in Fig. 2-45.

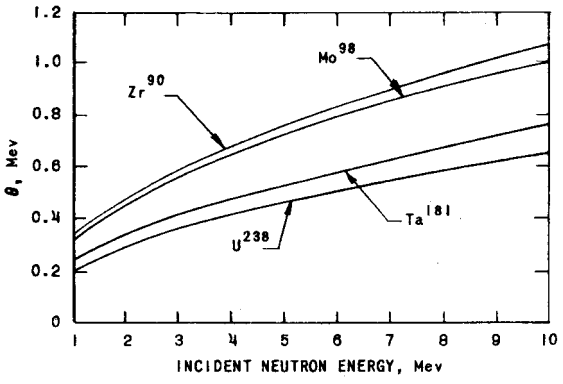

Fig. 2-44 — Nuclear temperatures of U^{238}, Ta^{181}, Mo^{98}, and Zr^{90}. *Reproduced from Ref. 22.*

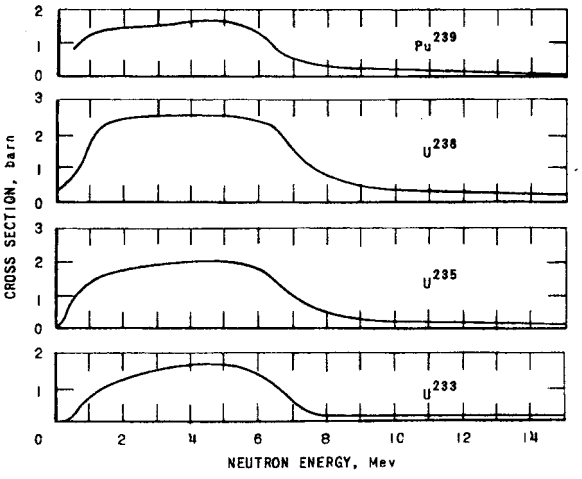

Fig. 2-45 — Total inelastic scattering cross sections for U^{233}, U^{235}, U^{238}, and Pu^{239}. *Reproduced from Ref. 70.*

2.4.3 ANGULAR DISTRIBUTION AS A FUNCTION OF ENERGY IN THE KEV-MEV REGION

The angular distribution cross section measurements are represented by an expansion in a series of Legendre Polynomials

$$\sigma_s(\mu) = \frac{\sigma_s}{4\pi} \sum_{\ell=0} \omega_\ell P_\ell(\mu) \tag{2-19}$$

where μ is the cosine of the scattering angle in the Laboratory System and σ_s is the total scattering cross section (i.e., the differential cross section integrated over the solid angle) and includes elastic and inelastic scattering. The data are presented in terms of the coefficients as a function of incident neutron energy, ω_0 being normalized to unity. The standard deviations of the polynomials are discussed in the referenced literature.

In the region of resonances, detailed curves obtained from the higher resolution experiments are presented separately. Included in addition to the ANL data[71–73] are the measurements of Wills, et al.,[74] on C, and the computation of Lustig, et al.,[75] for O^{16}.

The data in the form of polynomials are a more compact and practical description of the angular distribution than the usual cosine plots.[76] It is particularly advantageous in reactor design calculations since it is already in a form appropriate for spherical harmonics method of solution of the transport equation. Defining the transport scattering cross section as:

$$\sigma_{s,tr} = 2\pi \int_{-1}^{+1} (1-\mu)\ \sigma_s(\mu)\, d\mu = \sigma_s\left(1 - \frac{1}{3}\omega_1\right) \tag{2-20}$$

gives the average cosine of the scattering angle as a function of the energy; and assuming that the inelastic scattering is isotropic, then the transport cross section for elastic scattering is

$$\sigma_{el\ tr} = \sigma_{s,el}\left(1 - \frac{1}{3}\omega_1 \frac{\sigma_s}{\sigma_{s,el}}\right) \tag{2-21}$$

where $\sigma_{s,el}$ is the elastic scattering cross section integrated over the solid angle.

The coefficients presented are for scattering cross sections in the Laboratory System. To express these in the Center-of-Mass System, the following transformation matrix[77,78] may be used.

$$\omega_\ell^c = \sum_k T^{-1}_{\ell k}\, \omega_k^L \tag{2-22}$$

where L denotes Laboratory System,

$$T^{-1} = \begin{Bmatrix} 1 & 0 & 0 & 0 & 0 & 0 & 0 & \cdots \\ -2\gamma & 1-\frac{1}{5}\gamma^2 & \frac{2}{5}\gamma & \frac{3}{35}\gamma^2 & 0 & 0 & 0 & \cdots \\ 3\gamma^2 & -2\gamma & 1-\frac{9}{7}\gamma^2 & \frac{6}{7}\gamma & \frac{8}{21}\gamma^2 & 0 & 0 & \cdots \\ 0 & \frac{16}{5}\gamma^2 & -\frac{12}{5}\gamma & 1-\frac{14}{5}\gamma^2 & \frac{4}{3}\gamma & \frac{10}{11}\gamma^2 & 0 & \cdots \\ 0 & 0 & \frac{30}{7}\gamma^2 & -\frac{20}{7}\gamma & 1-\frac{370}{77}\gamma^2 & \frac{20}{11}\gamma & \frac{240}{143}\gamma^2 & \cdots \\ 0 & 0 & 0 & \frac{40}{7}\gamma^2 & -\frac{10}{3}\gamma & 1-\frac{95}{13}\gamma^2 & \frac{30}{13}\gamma & \cdots \\ 0 & 0 & 0 & 0 & \frac{3185}{429}\gamma^2 & -\frac{42}{11}\gamma & 1-\frac{567}{55}\gamma^2 & \cdots \\ \vdots & \vdots & \vdots & \vdots & \vdots & \vdots & \vdots & \end{Bmatrix} \tag{2-23}$$

where

$$\gamma \equiv \left[\frac{m_1\, m_3\, (m_3 + m_4)}{m_2\, m_4\, (m_1 + m_2)} \frac{E_r}{E_r + Q}\right]^{1/2} \tag{2-24}$$

and m_1 (incident particle), m_2 (target) are the masses of the reacting particles; m_3, m_4 are the masses of the reaction products; E_r is the energy of the relative motion in the Center-of-Mass System; and Q is the energy of the reaction. For an elastic scattering process $Q = 0$, $m_1 = m_3$, $m_2 = m_4$, and γ then becomes

$$\gamma = \frac{m_1}{m_2} \tag{2-25}$$

The inverse transformation matrix T is

$$T = \begin{Bmatrix}
1 & 0 & 0 & 0 & 0 & 0 & 0 & \cdots \\
2\gamma & 1 - \frac{3}{5}\gamma^2 & -\frac{2}{5}\gamma & \frac{9}{35}\gamma^2 & 0 & 0 & 0 & \cdots \\
\gamma^2 & 2\gamma & 1 - \frac{11}{7}\gamma^2 & -\frac{6}{7}\gamma & \frac{16}{21}\gamma^2 & 0 & 0 & \cdots \\
0 & \frac{8}{5}\gamma^2 & \frac{12}{5}\gamma & 1 - \frac{46}{15}\gamma^2 & -\frac{4}{3}\gamma & \frac{50}{33}\gamma^2 & 0 & \cdots \\
0 & 0 & \frac{18}{7}\gamma^2 & \frac{20}{7}\gamma & 1 - \frac{390}{77}\gamma^2 & -\frac{20}{11}\gamma & \frac{360}{143}\gamma^2 & \cdots \\
0 & 0 & 0 & \frac{80}{21}\gamma^2 & \frac{30}{9}\gamma & 1 - \frac{295}{39}\gamma^2 & -\frac{30}{13}\gamma & \cdots \\
0 & 0 & 0 & 0 & \frac{2275}{429}\gamma^2 & \frac{42}{11}\gamma & 1 - \frac{581}{55}\gamma^2 & \cdots \\
\vdots & \vdots & \vdots & \vdots & \vdots & \vdots & \vdots &
\end{Bmatrix} \tag{2-26}$$

The above matrices are a good approximation for $\gamma < 0.5$.

Figures 2-46 through 2-78 give the angular distribution for various materials of interest in reactor design. The values of σ_s may be obtained from the BNL-325 compilation.

The data of Refs. 71 and 72 were fitted to measurements made at five different scattering angles. In Ref. 73 the data represent a fitting to the measurements made at eight different angles. The data of Wills, et al.,[74] are fitted to measurements at nine angles.

The polynomials of Refs. 74 and 75 were transformed from the Center-of-Mass System to the Laboratory System using the ANL program PHY46D-B coded for the George Computer.

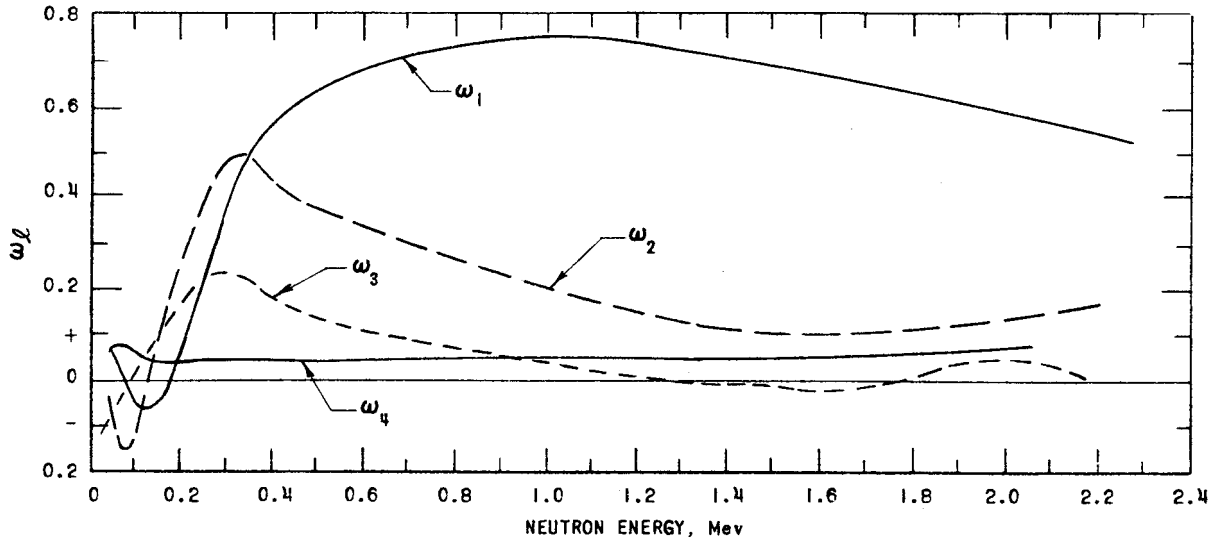

Fig. 2-46 — Coefficients of the Legendre polynomials of $_3Li^6$ as a function of neutron energy. *Data from Ref. 73.*

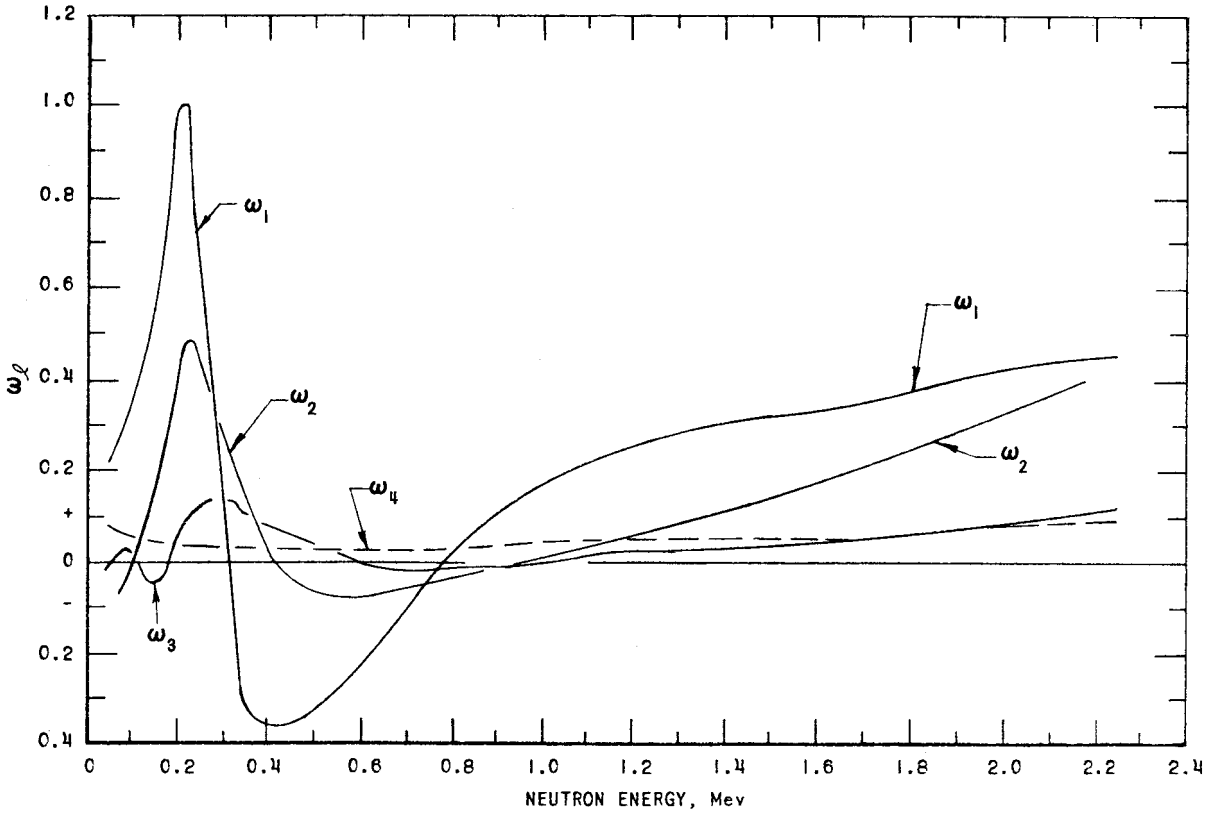

Fig. 2-47 — Coefficients of the Legendre polynomials of $_3Li^7$ as a function of neutron energy. *Data from Ref. 73.*

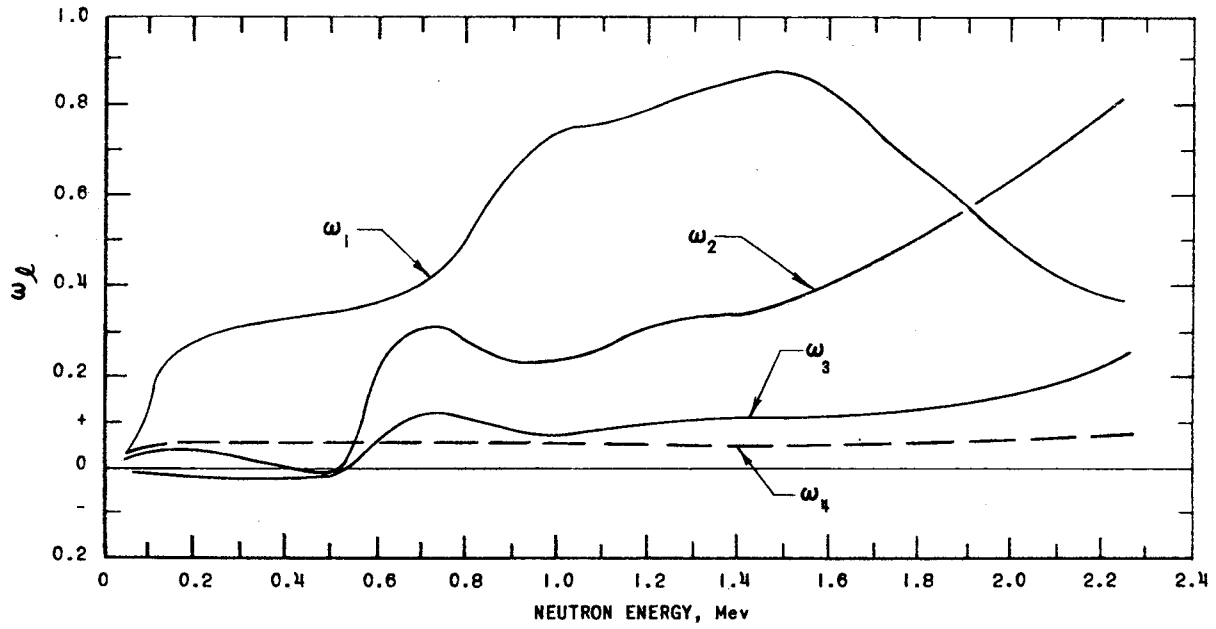

Fig. 2-48—Coefficients of the Legendre polynomials of $_4Be^9$ as a function of neutron energy. *Data from Ref. 73.*

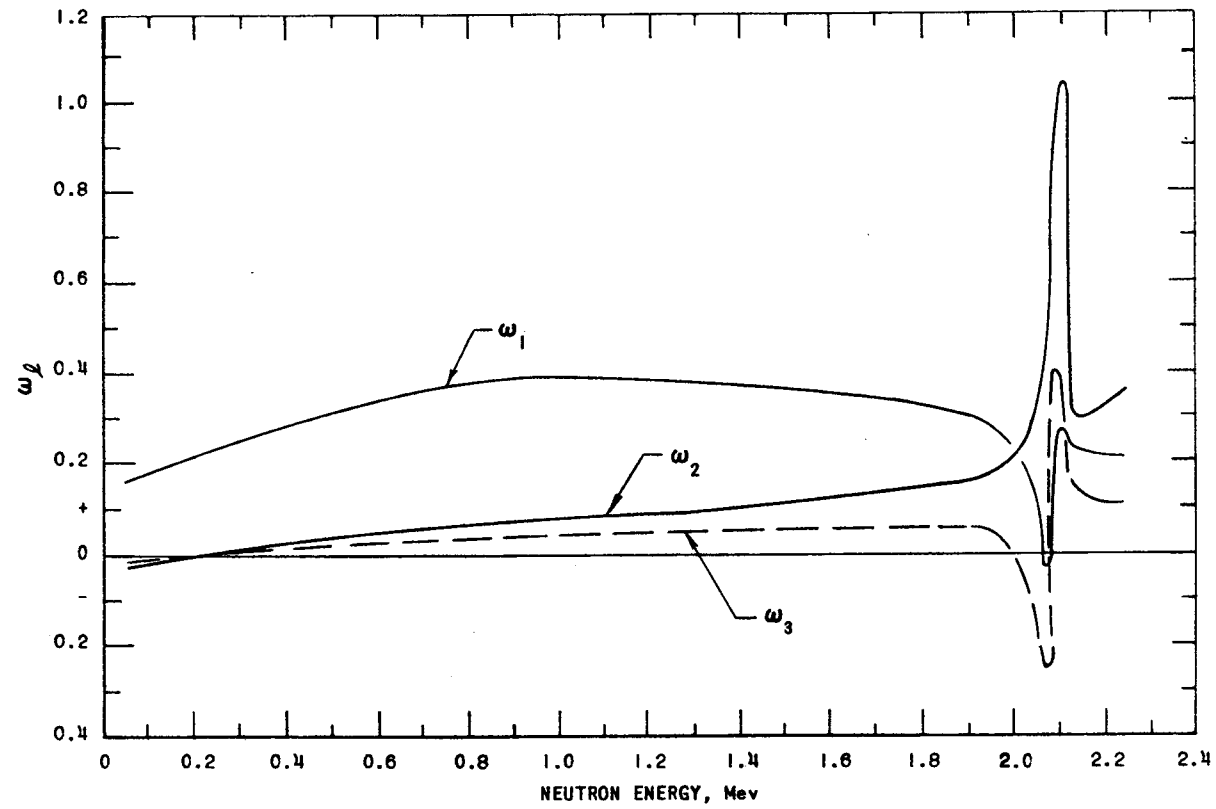

Fig. 2-49—Coefficients of the Legendre polynomials of $_6C^{12}$ as a function of neutron energy; broad resolution. *Data from Ref. 73.*

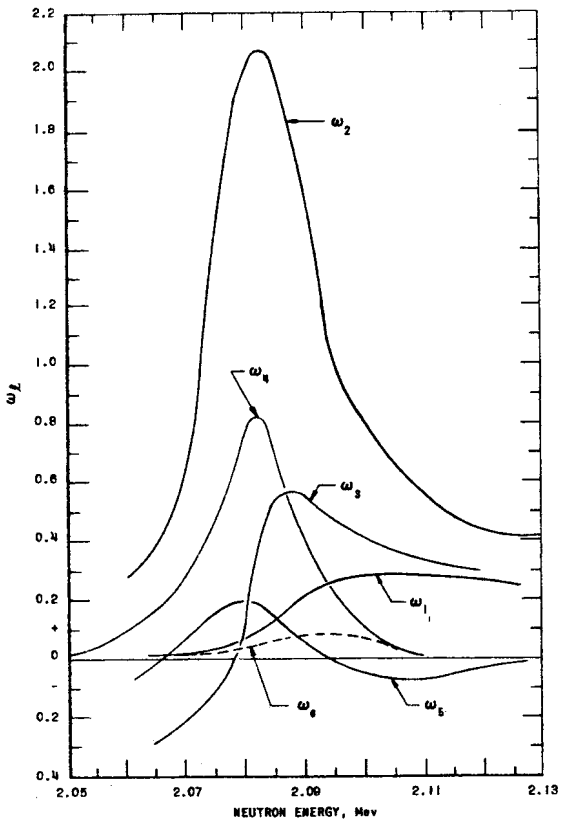

Fig. 2-50—Coefficients of the Legendre polynomials of $_6C^{12}$ as a function of neutron energy; resonance region. *Data from Ref. 73.*

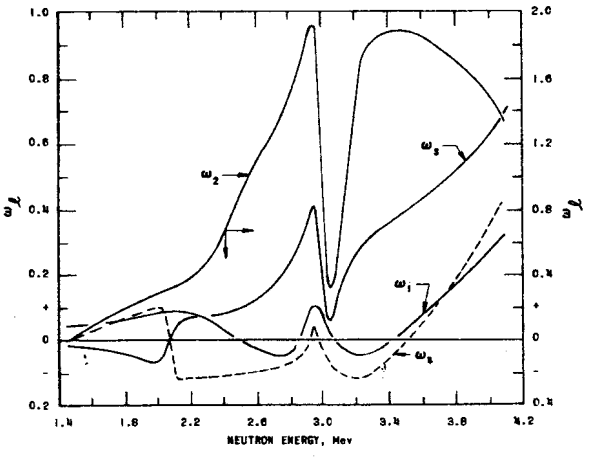

Fig. 2-51—Coefficients of the Legendre polynomials of $_6C^{12}$ as a function of neutron energy. *Data from Ref. 74.*

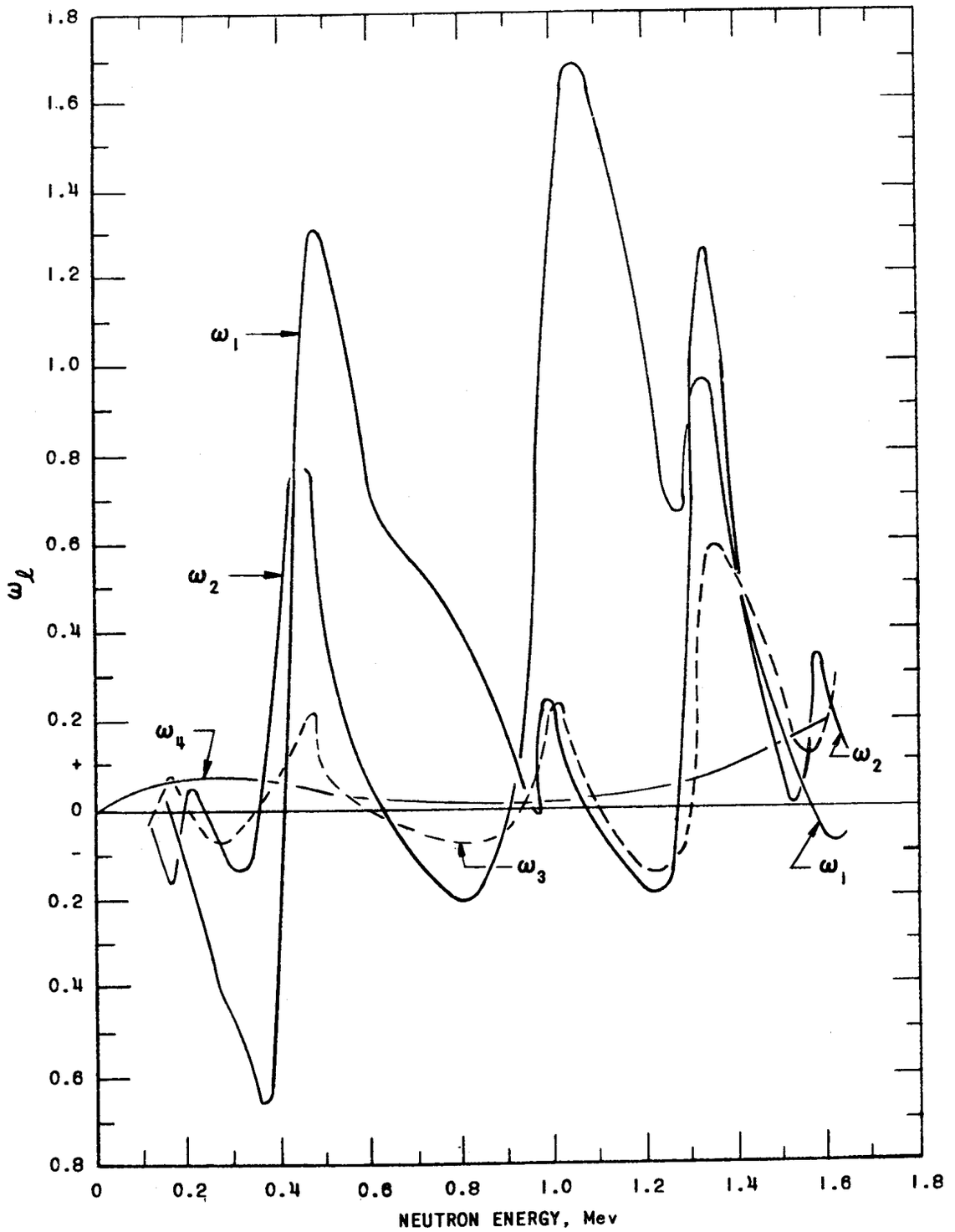

Fig. 2-52—Coefficients of the Legendre polynomials of $_8O^{16}$ as a function of neutron energy; broad resolution. *Data from Ref. 74.*

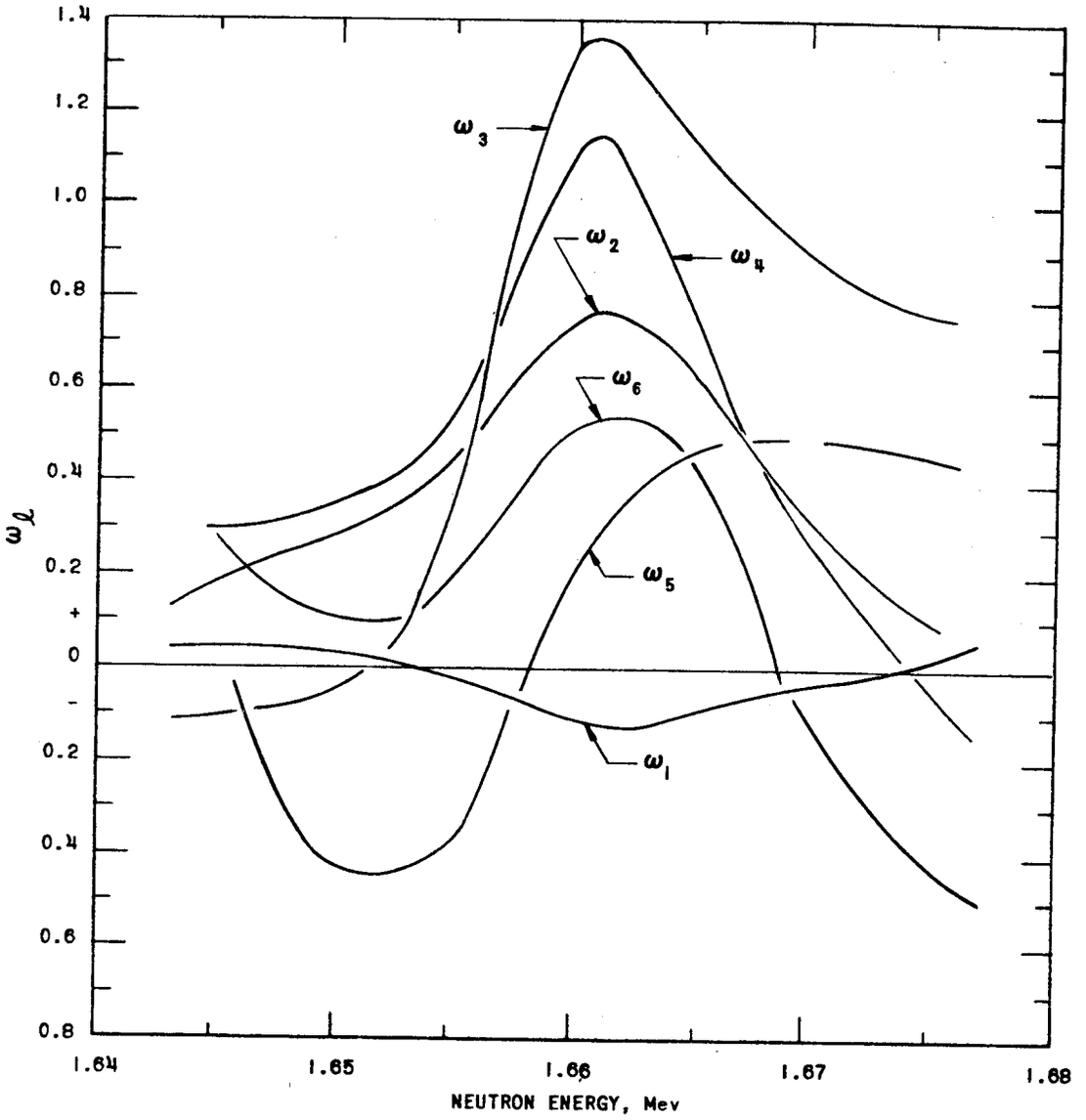

Fig. 2-53—Coefficients of the Legendre polynomials of $_8O^{16}$ as a function of neutron energy; resonance region. *Data from Ref. 75.*

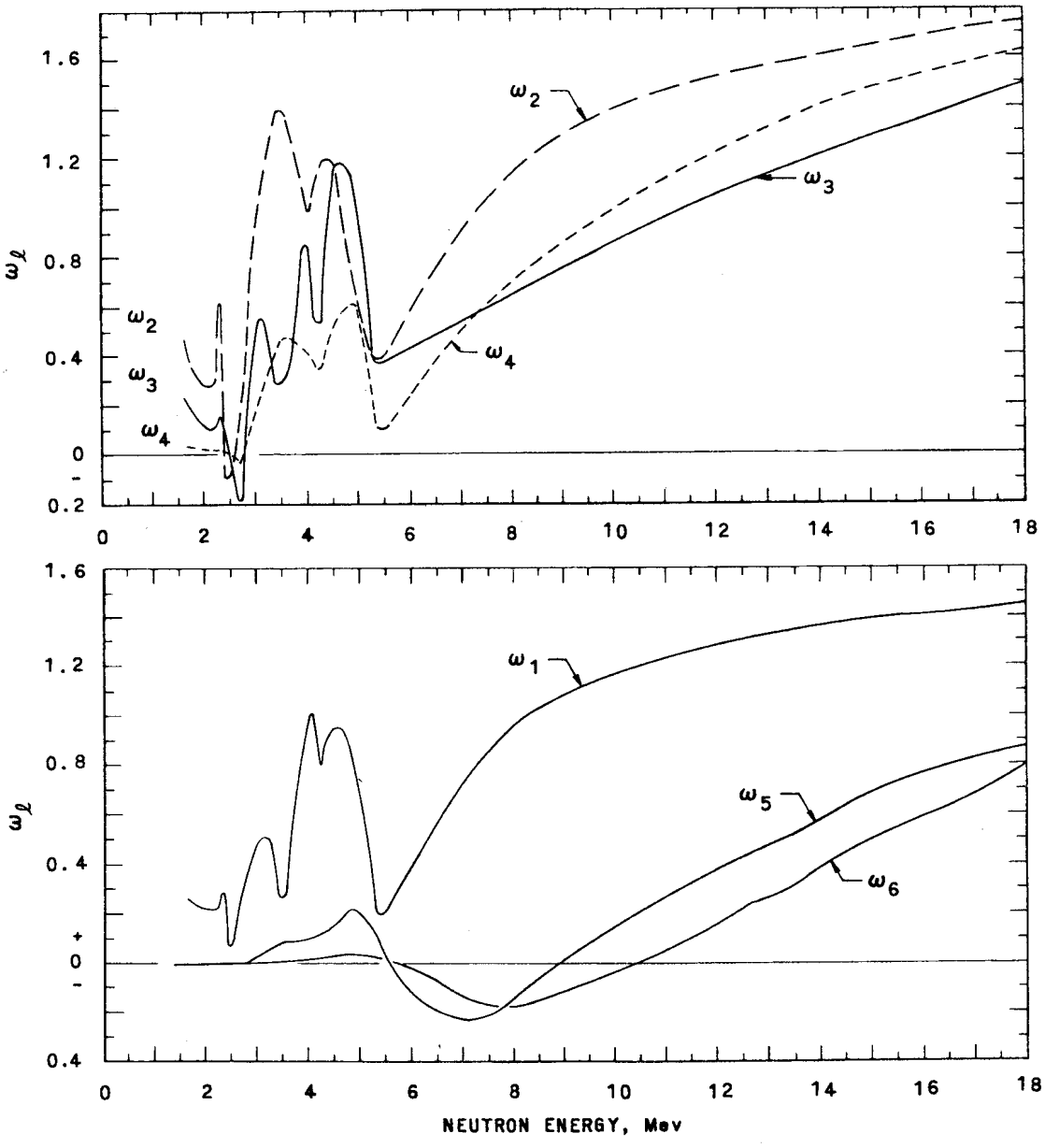

Fig. 2-54—Coefficients of the Legendre polynomials of $_8O^{16}$ as a function of neutron energy. *Data from Ref. 75.*

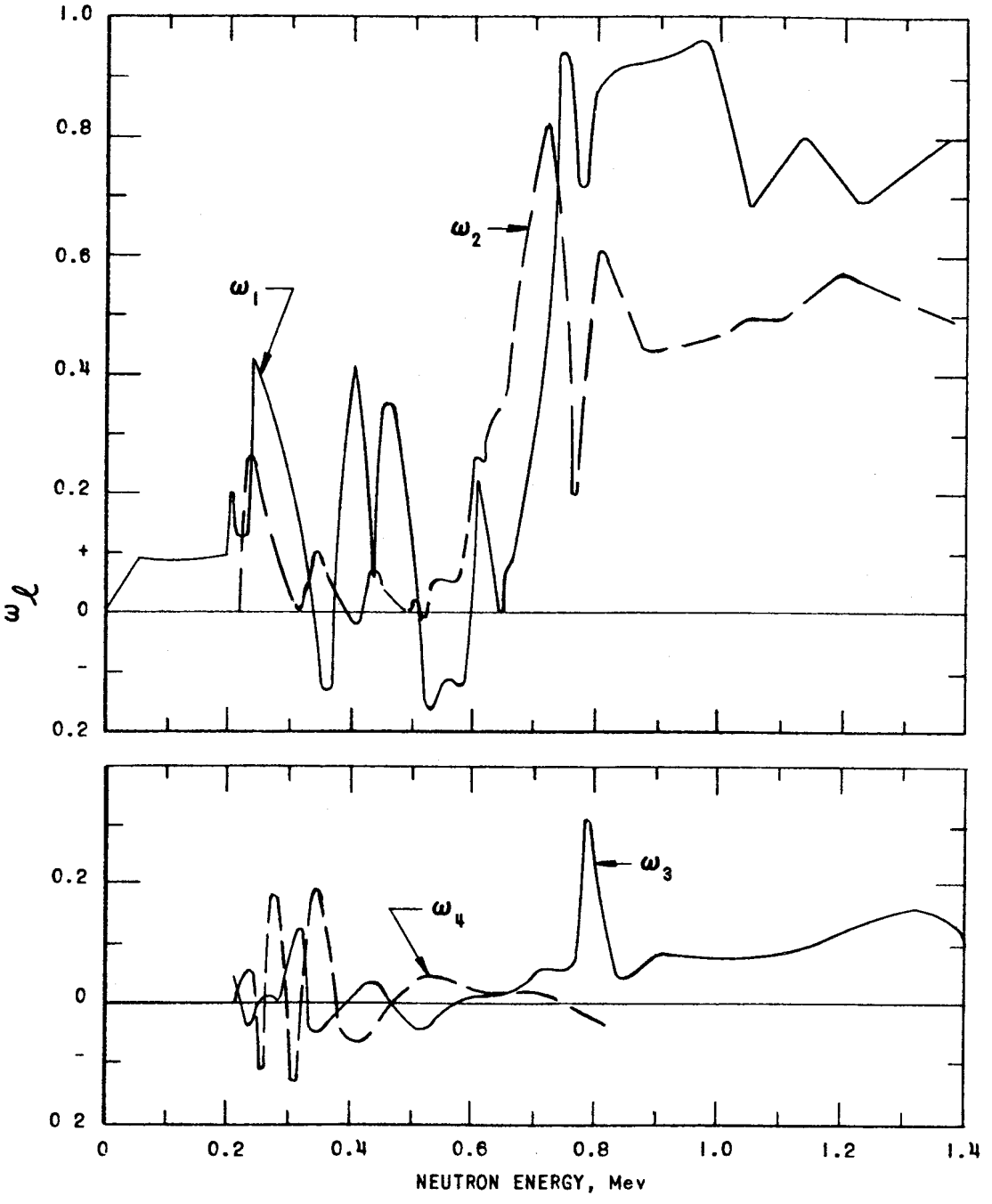

Fig. 2-55—Coefficients of the Legendre polynomials of $_{11}$Na as a function of neutron energy. *Data from Ref. 72.*

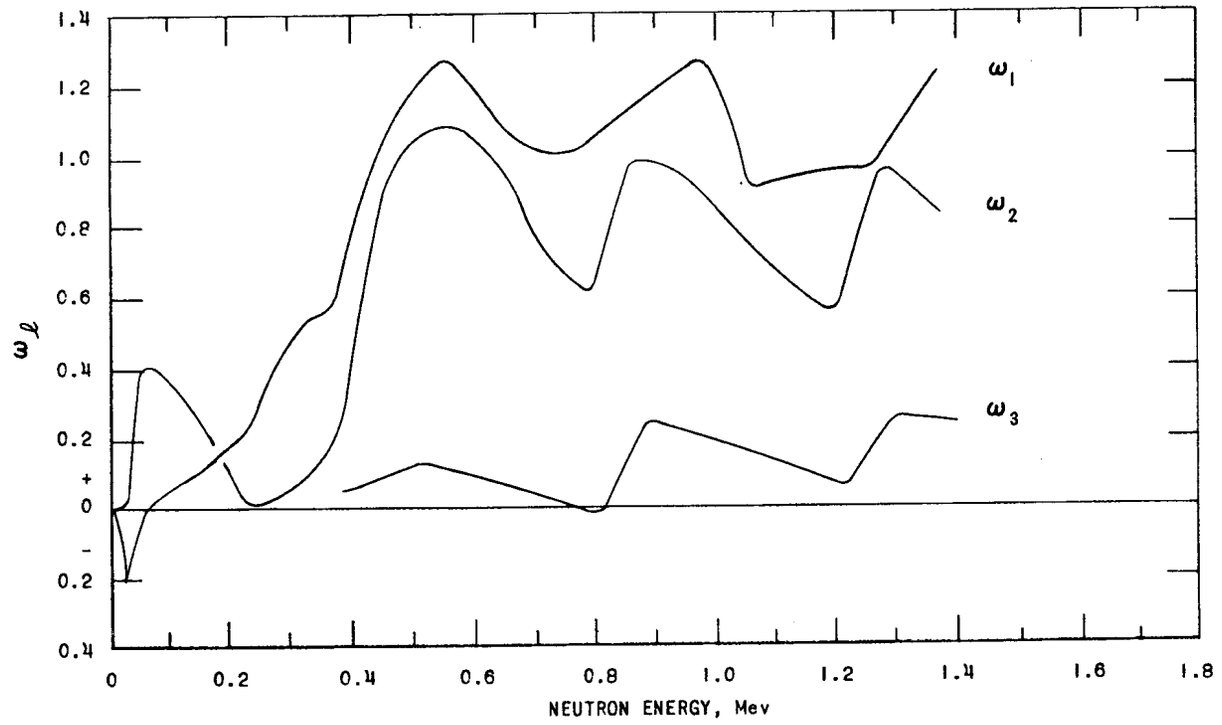

Fig. 2-56—Coefficients of the Legendre polynomials of $_{12}$Mg as a function of neutron energy. *Data from Ref. 71.*

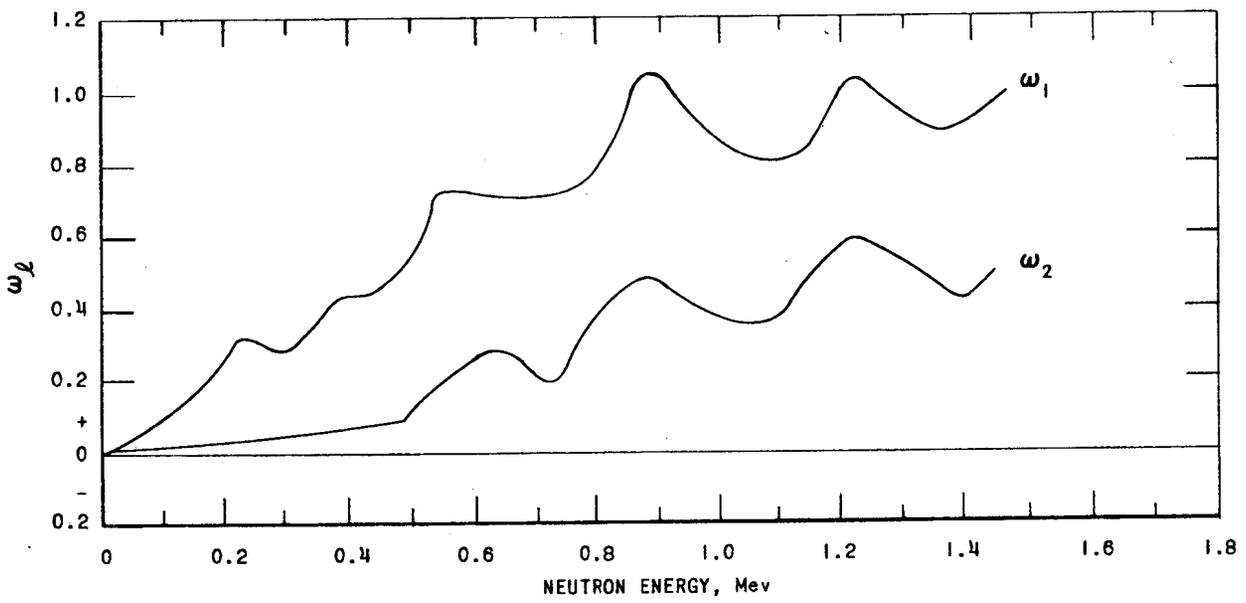

Fig. 2-57—Coefficients of the Legendre polynomials of $_{13}$Al as a function of neutron energy. *Data from Ref. 71.*

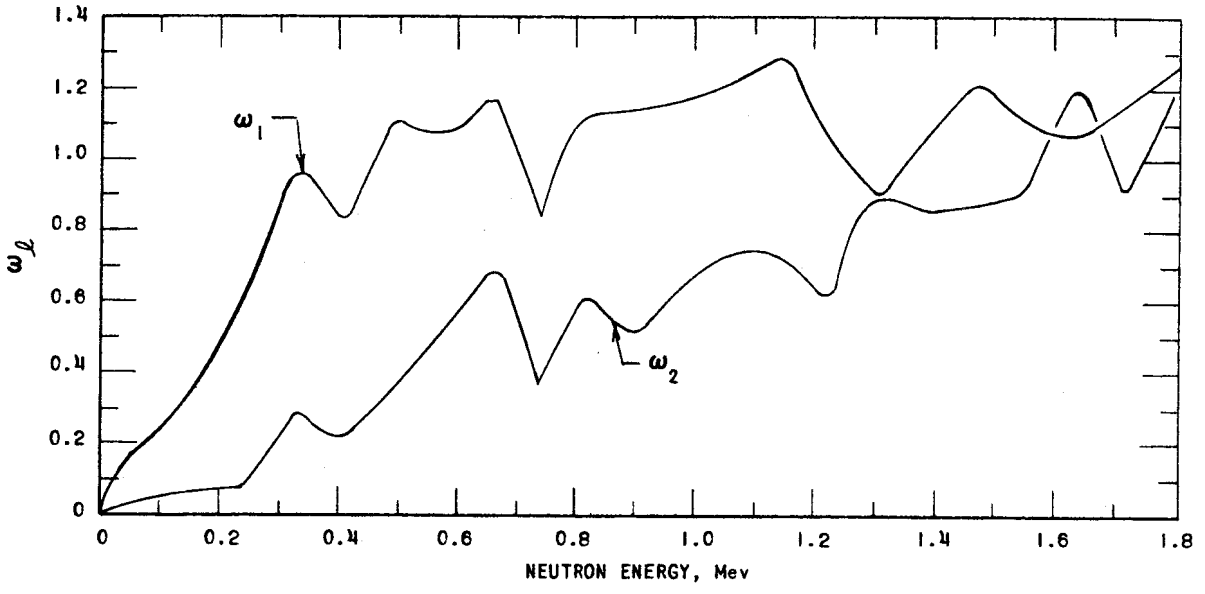

Fig. 2-58—Coefficients of the Legendre polynomials of $_{16}S$ as a function of neutron energy; broad resolution. *Data from Ref. 73.*

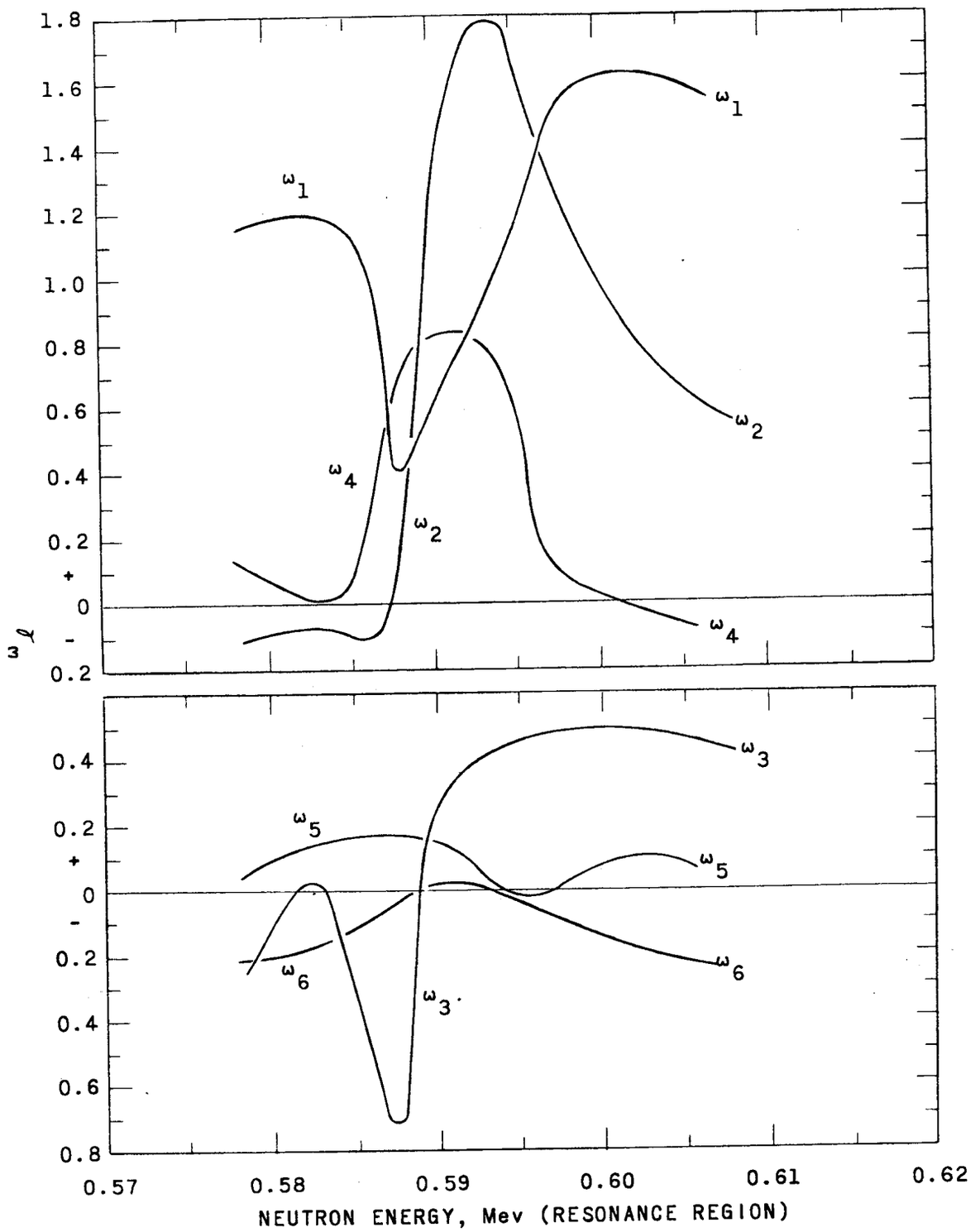

Fig. 2-59—Coefficients of the Legendre polynomials of $_{16}S$ as a function of neutron energy; resonance region. *Data from Ref. 73.*

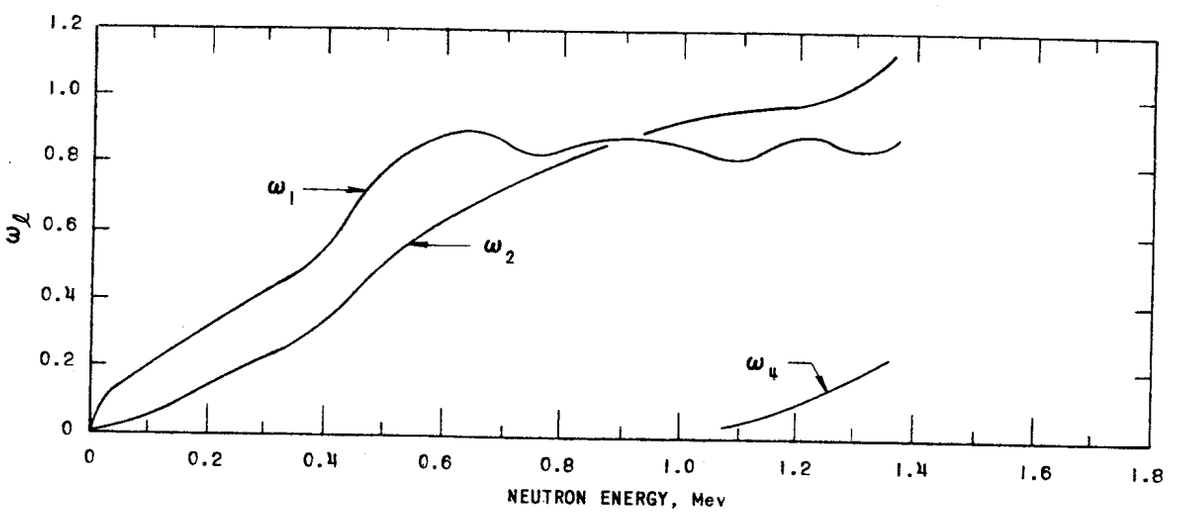

Fig. 2-60—Coefficients of the Legendre polynomials of $_{19}$K as a function of neutron energy. *Data from Ref. 71.*

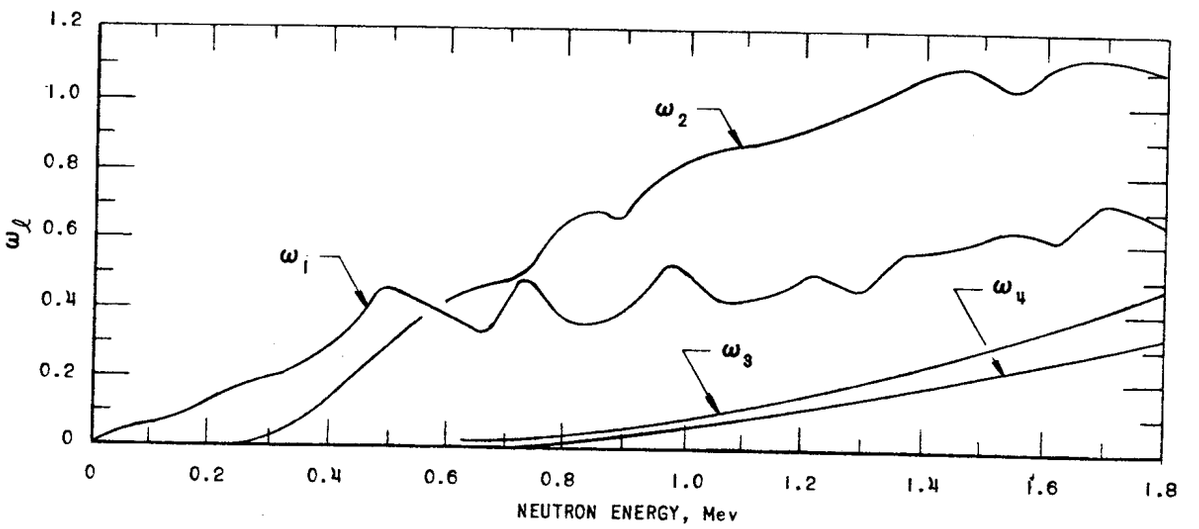

Fig. 2-61—Coefficients of the Legendre polynomials of $_{23}$V as a function of neutron energy. *Data from Ref. 71.*

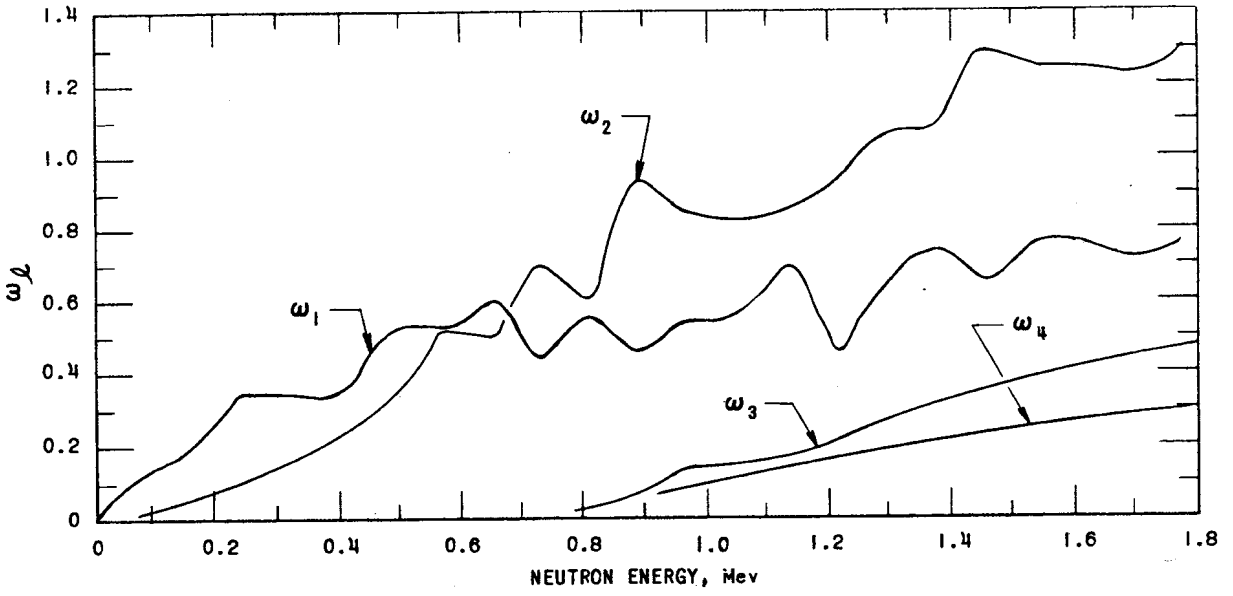

Fig. 2-62 — Coefficients of the Legendre polynomials of $_{24}$Cr as a function of neutron energy. *Data from Ref. 71.*

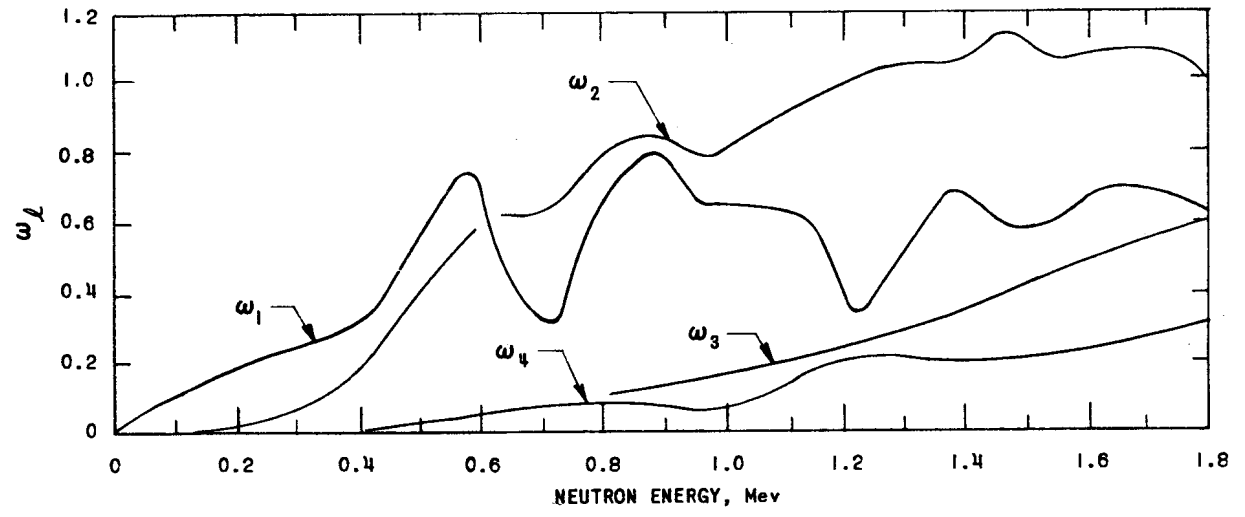

Fig. 2-63 — Coefficients of the Legendre polynomials of $_{26}$Fe as a function of neutron energy. *Data from Ref. 71.*

687863 O - 63 - 6

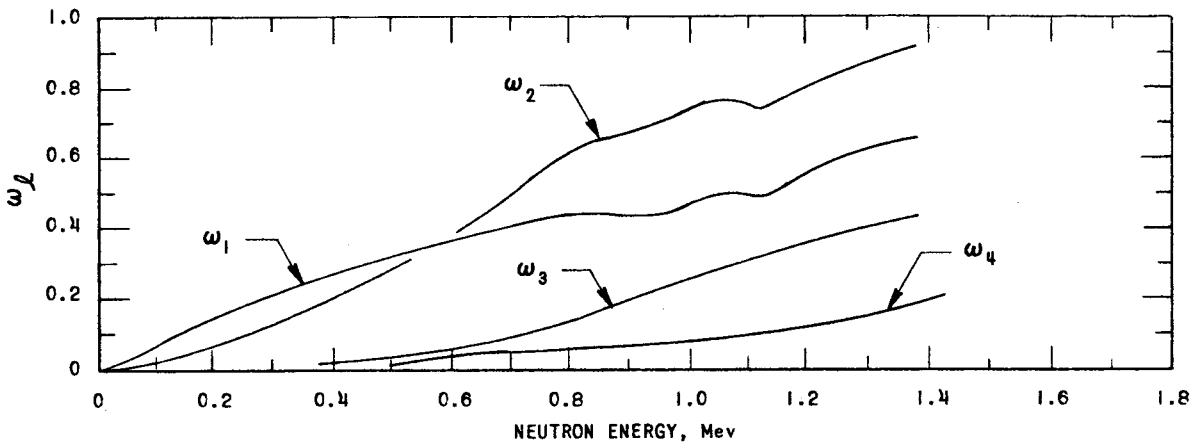

Fig. 2-64—Coefficients of the Legendre polynomials of $_{27}$Co as a function of neutron energy. *Data from Ref. 71.*

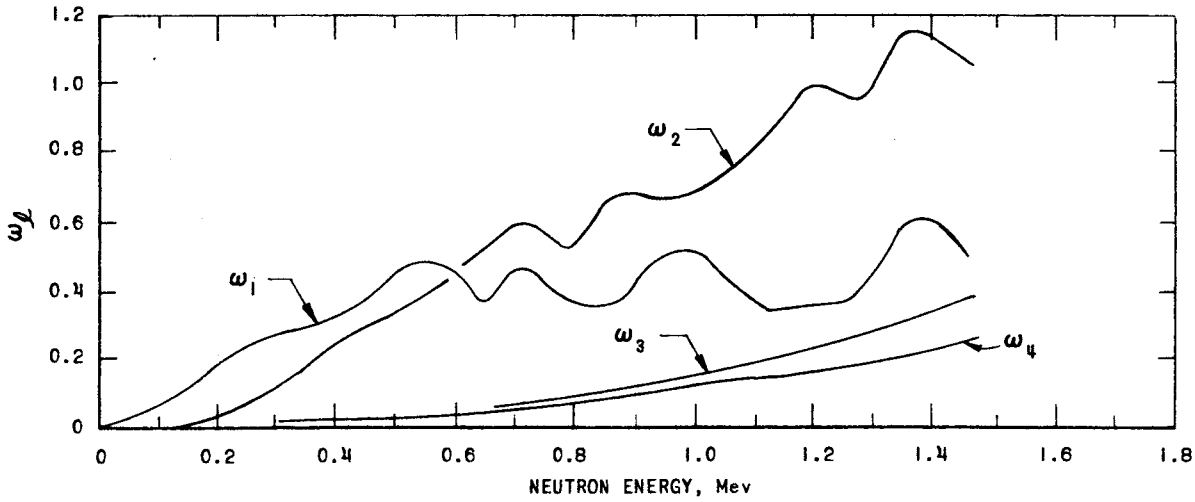

Fig. 2-65—Coefficients of the Legendre polynomials of $_{28}$Ni as a function of neutron energy. *Data from Ref. 71.*

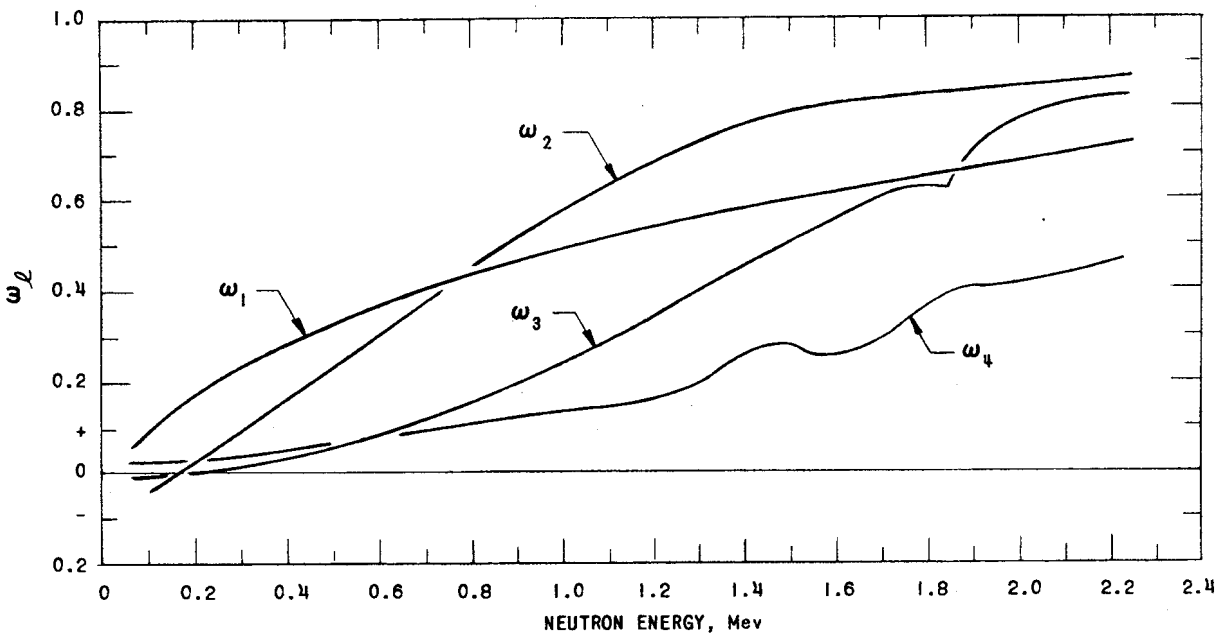

Fig. 2-66—Coefficients of the Legendre polynomials of $_{29}$Cu as a function of neutron energy. *Data from Ref. 73.*

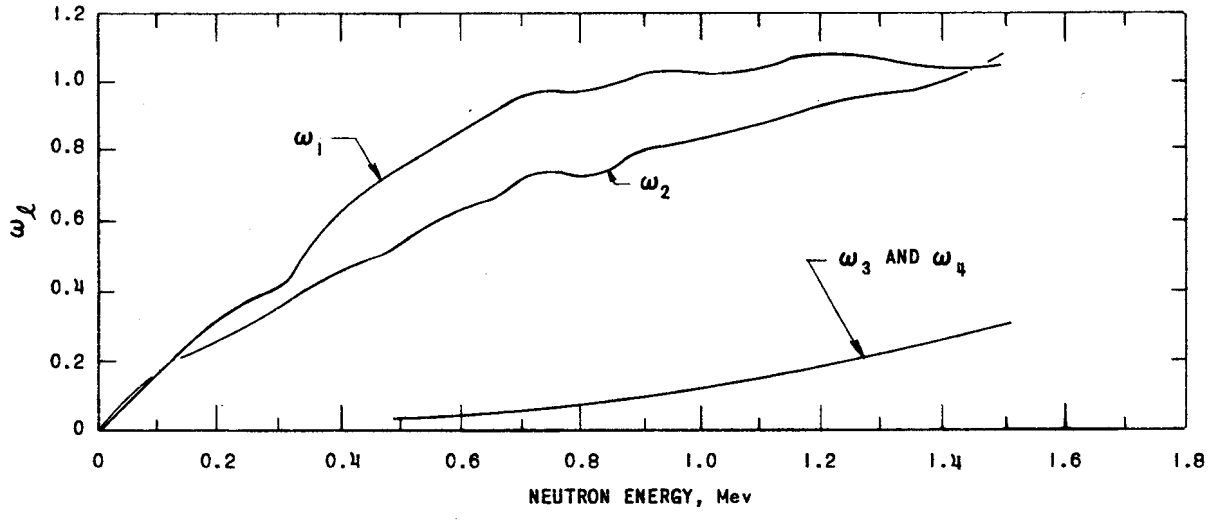

Fig. 2-67—Coefficients of the Legendre polynomials of $_{40}$Zr as a function of neutron energy. *Data from Ref. 71.*

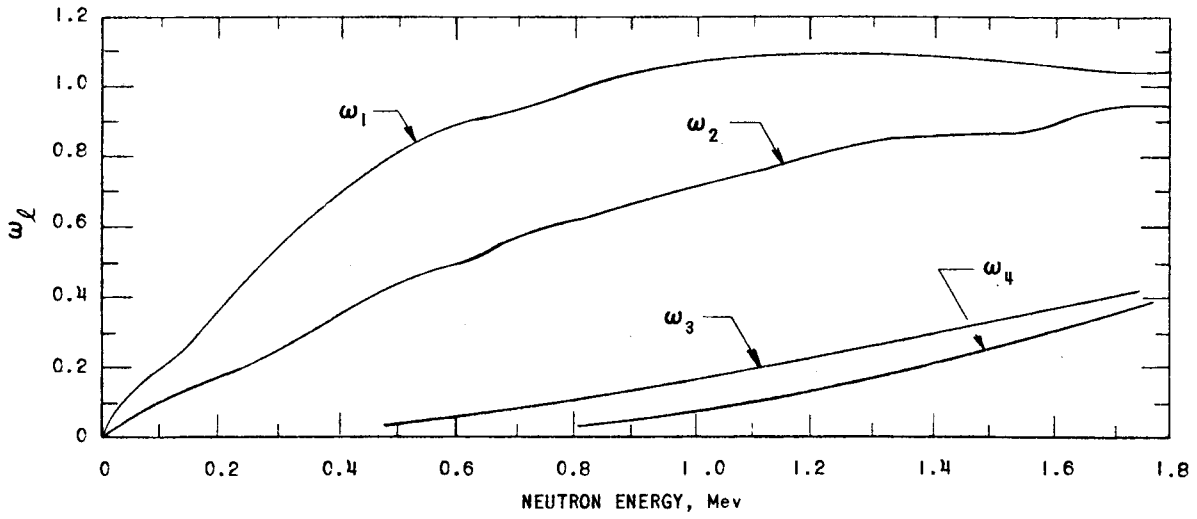

Fig. 2-68—Coefficients of the Legendre polynomials of $_{41}$Nb as a function of neutron energy. *Data from Ref. 71.*

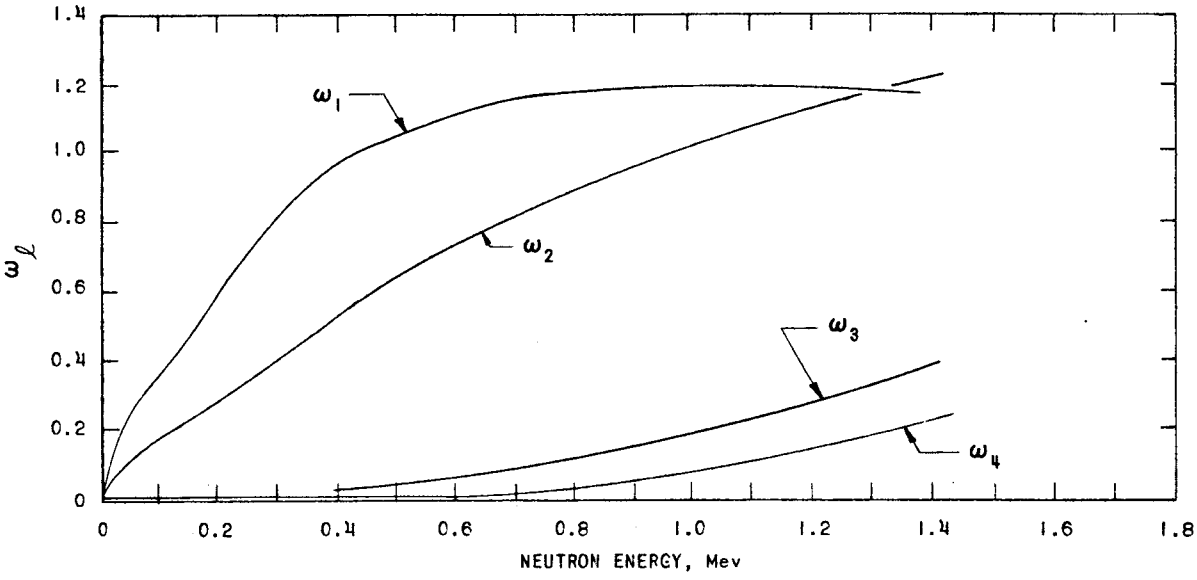

Fig. 2-69—Coefficients of the Legendre polynomials of $_{48}$Cd as a function of neutron energy. *Data from Ref. 71.*

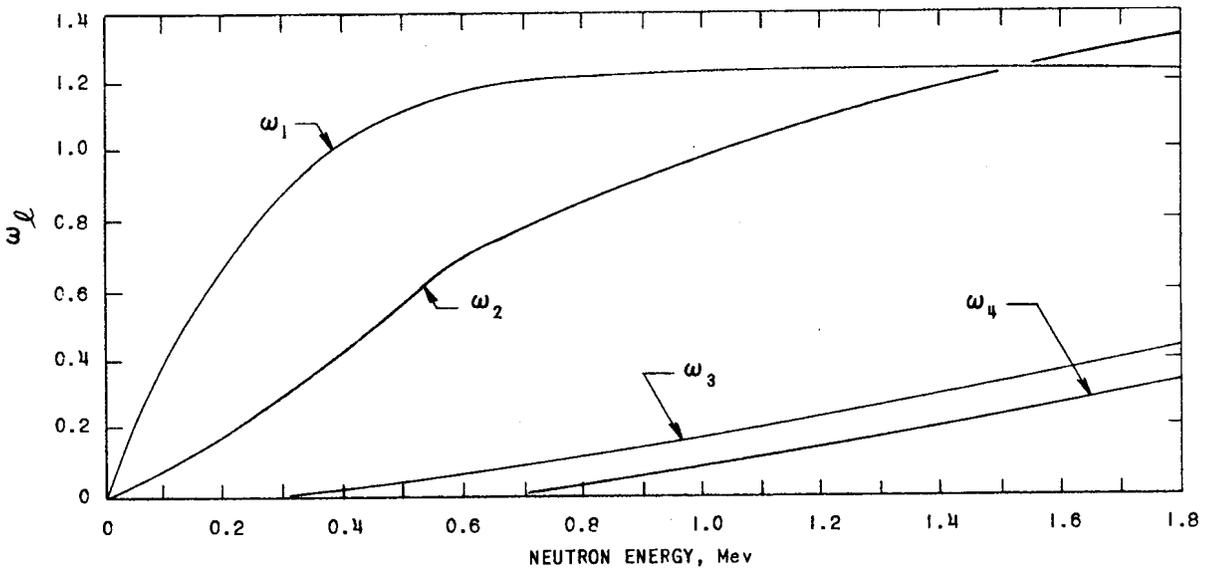

Fig. 2-70—Coefficients of the Legendre polynomials of $_{49}$In as a function of neutron energy. *Data from Ref. 71.*

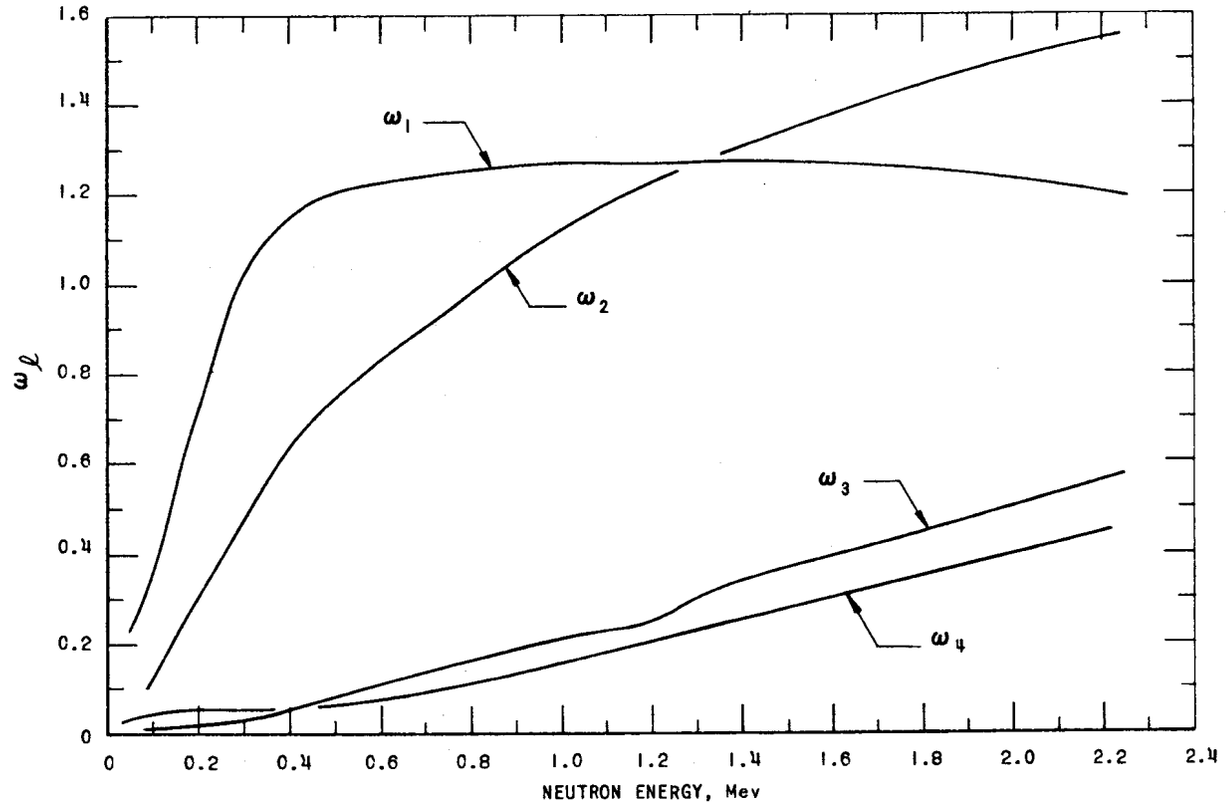

Fig. 2-71—Coefficients of the Legendre polynomials of $_{50}$Sn as a function of neutron energy. *Data from Ref. 73.*

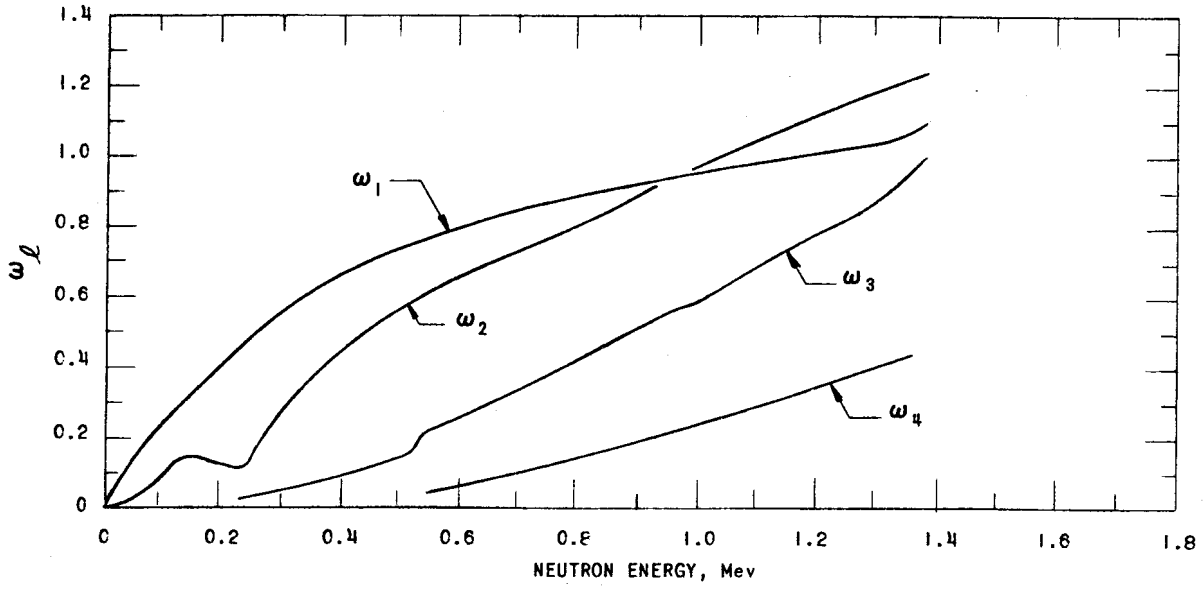

Fig. 2-72—Coefficients of the Legendre polynomials of $_{73}$Ta as a function of neutron energy. *Data from Ref. 71.*

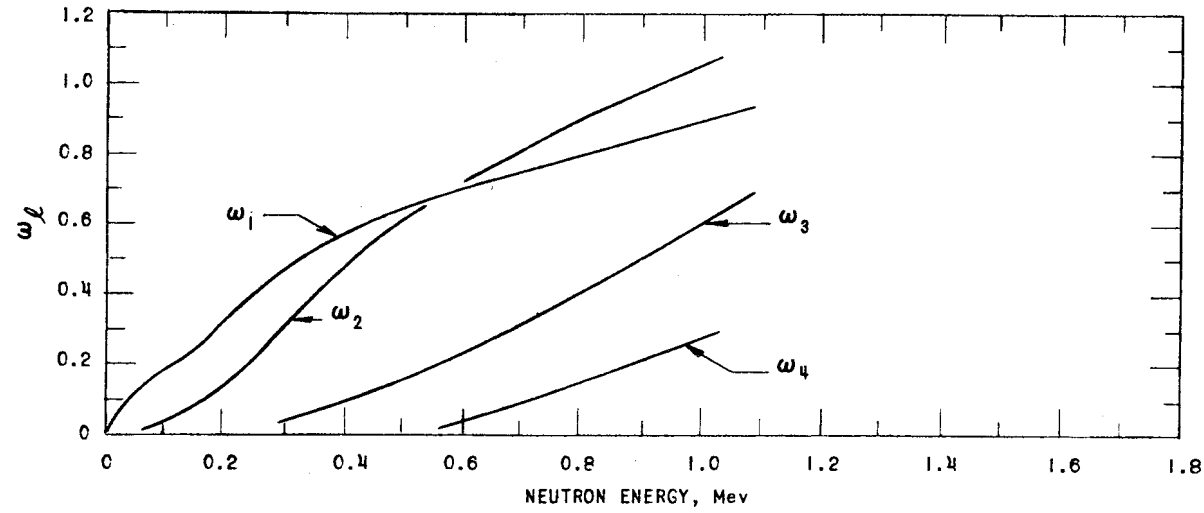

Fig. 2-73—Coefficients of the Legendre polynomials of $_{74}$W as a function of neutron energy. *Data from Ref. 71.*

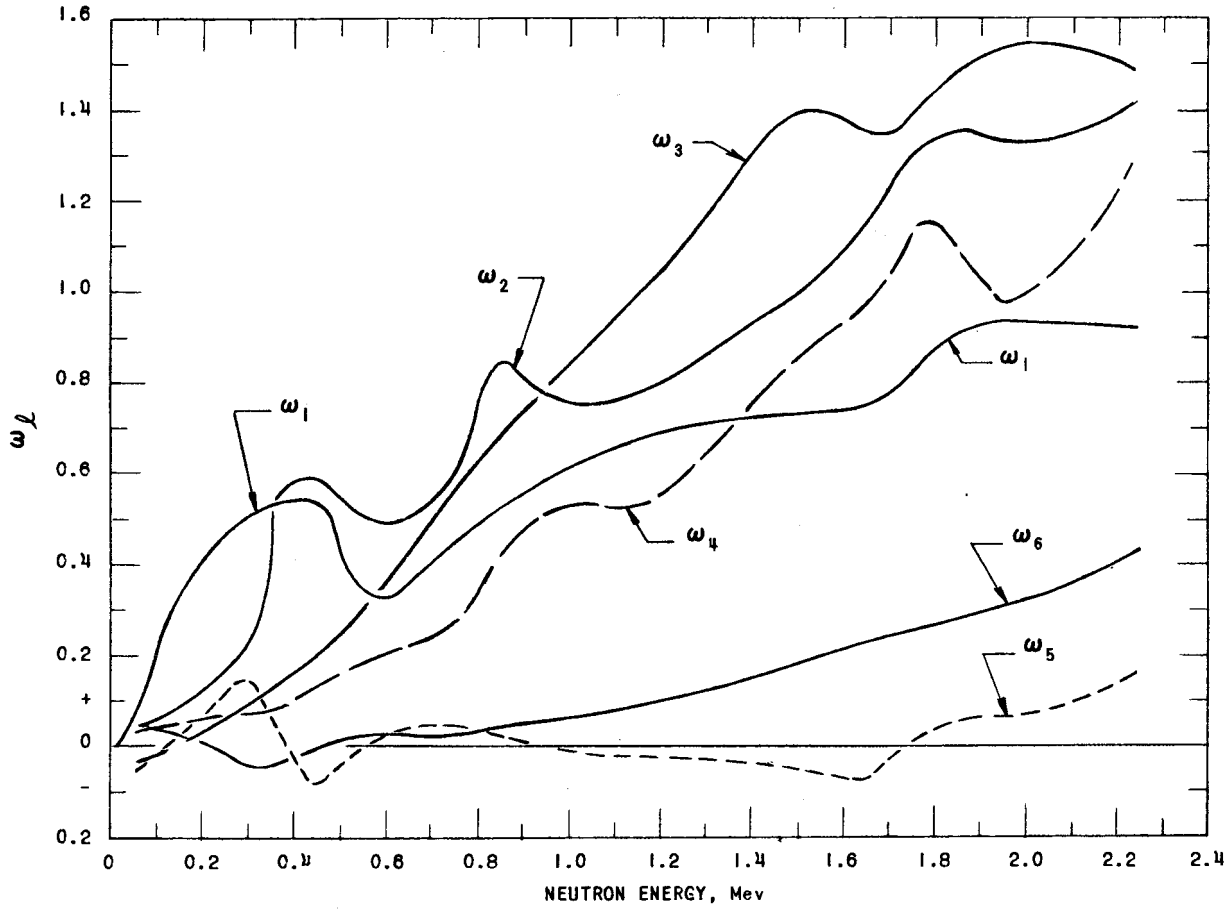

Fig. 2-74—Coefficients of the Legendre polynomials of $_{82}$Pb as a function of neutron energy. *Data from Ref. 73.*

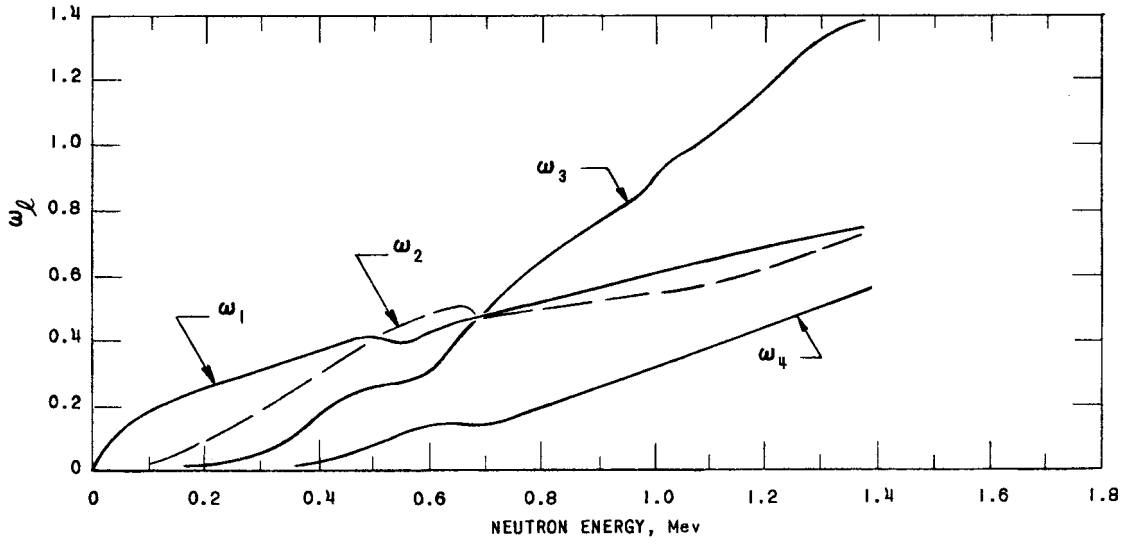

Fig. 2-75—Coefficients of the Legendre polynomials of $_{83}$Bi as a function of neutron energy. *Data from Ref. 71.*

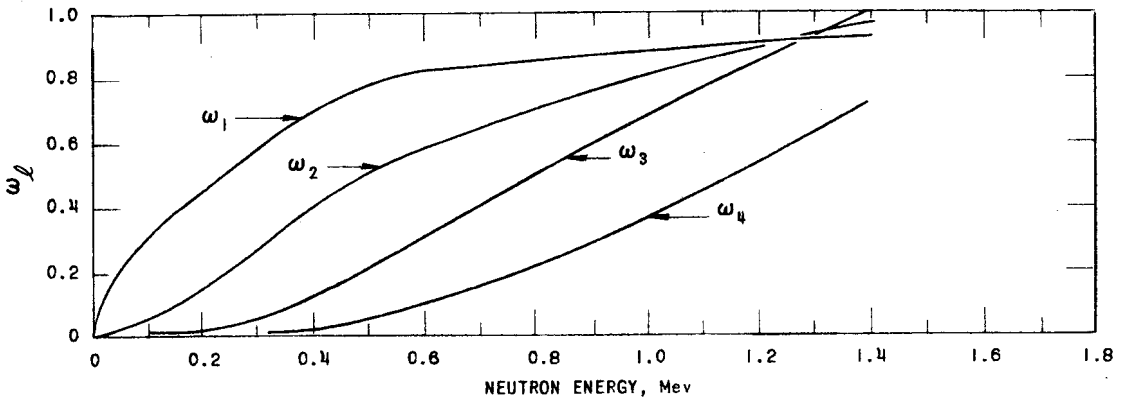

Fig. 2-76—Coefficients of the Legendre polynomials of $_{90}$Th as a function of neutron energy. *Data from Ref. 71.*

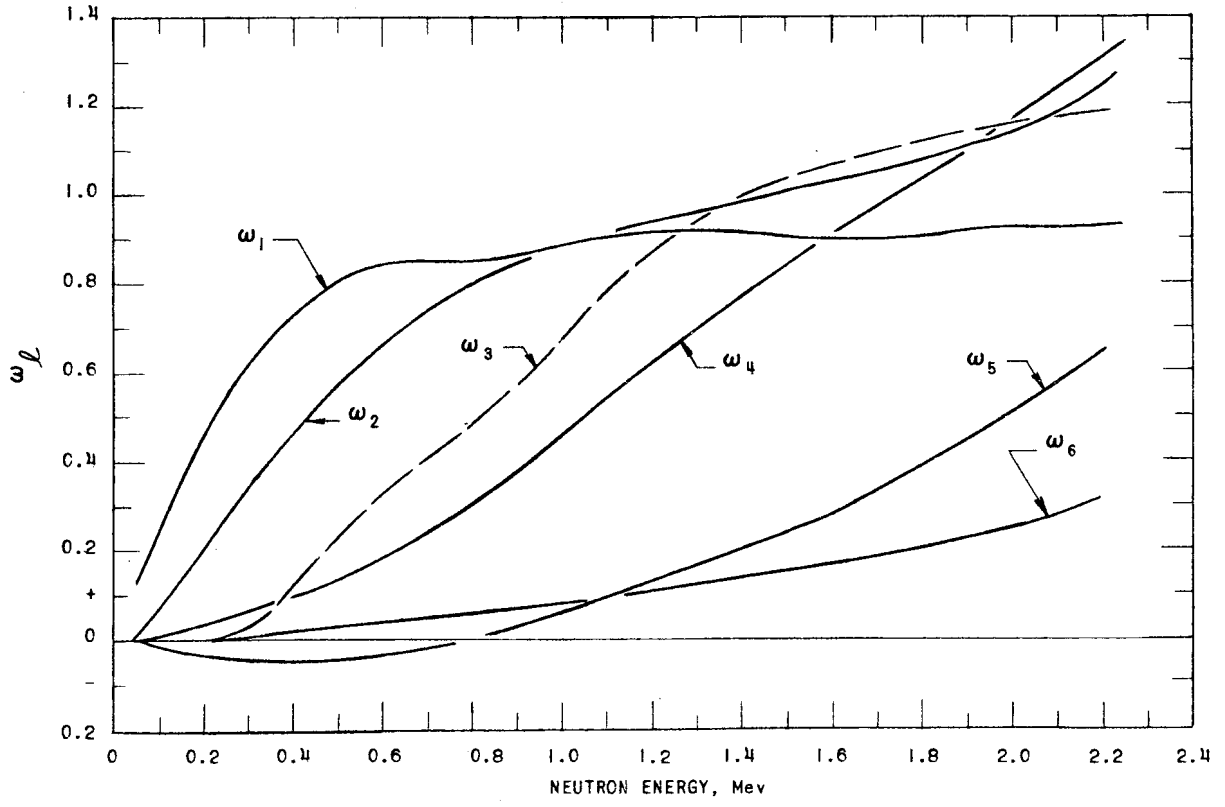

Fig. 2-77—Coefficients of the Legendre polynomials of $_{92}$U as a function of neutron energy. *Data from Ref. 73.*

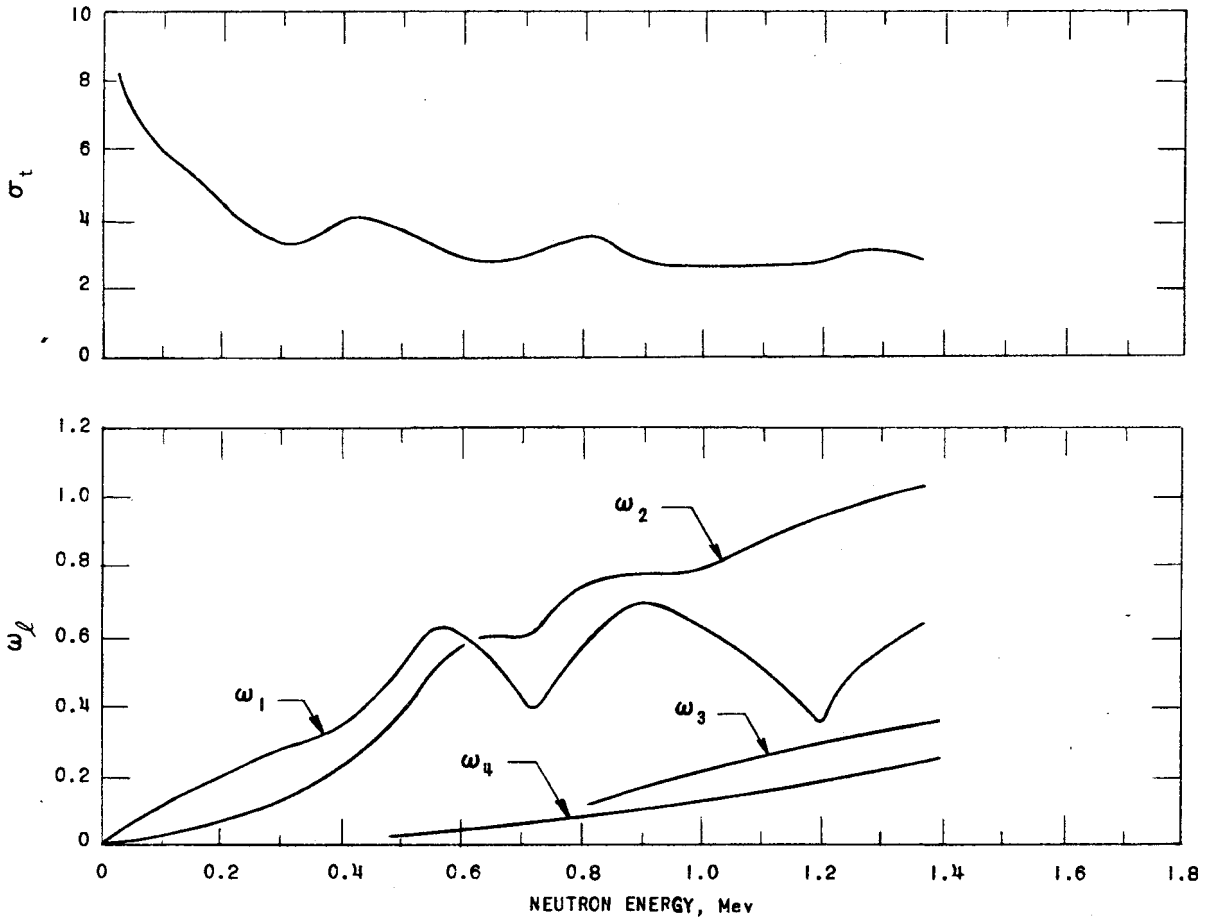

Fig. 2-78 — Coefficients of the Legendre polynomials and total cross section of stainless steel as a function of neutron energy.

REFERENCES

1. H. R. Kroeger, *Thermal Neutron Cross Sections and Related Data*, Nucleonics, 5: No. 4, 51, (1949).
2. D. J. Hughes and R. B. Schwartz, *Neutron Cross Sections*, BNL-325, Second Edition, (1958). See also Supplement I to Second Edition, (1960).
3. J. E. Sanders, H. M. Skarsgard and C. J. Kenward, *The Energy Dependence of the Fission-Neutron Yield per Neutron Absorbed in U^{233} Over the Range 0.025-2.2 ev*, J. Nuclear Energy, 5: No. 2, 186, (1957).
4. P. E. Spivak, et al., *Measurements of η for U^{233}, U^{235}, and Pu^{239} with Epithermal Neutrons*, J. Nuclear Energy, 4: No. 1, 70, (1957).
5. V. I. Kalashnikova, V. I. Lebedev and P. E. Spivak, *Relative Measurements of the Mean Number of Neutrons Emitted per Fission Induced in U^{233}, U^{235}, and Pu^{239} by Thermal Neutrons and Fission Neutrons*, J. Nuclear Energy, 5: No. 2, 226, (1957).
6. E. H. Magleby, et al., *Energy Dependence of η for Uranium-233 in the Region 0.1 to 4.0 eV*, Bull. Am. Phys. Soc., 1: 327, (1956). See also R. G. Fluharty, M. S. Moore and J. E. Evans, *The Total and Fission Cross Sections of Uranium-233 Below 1 kev*, Proc., 1958 Geneva Conference, 15: Paper No. 645, p. 111.
7. G. de Saussure, *A Report on the Measurements of Eta of U^{233} at ORNL*, Proc., Physics of Breeding Conference, ANL-6122, (1960), pp. 253-71.
8. B. C. Diven and J. C. Hopkins, *Capture-to-Fission Ratios for Fast Neutrons in U^{233}, U^{235}, Pu^{239}*, Bull. Am. Phys. Soc., Series II, 5: 494, (1960). See also, B. C. Diven, J. Terrell and A. Hemmendinger, *Capture-to-Fission Ratios for Fast Neutrons in U^{235}*, Phys. Rev., 109: No. 1, 144, (January 1, 1958).
9. H. M. Skarsgard and C. J. Kenward, *Measurements of the Energy Dependence of the Fission Neutron Yield per Neutron Absorbed in Pu^{239} and U^{235} in the Range 0.006-0.36 ev*, J. Nuclear Energy, 6: No. 3, 212, (1958).
10. W. R. Kanne, H. B. Stewart and F. A. White, *Capture-to-Fission Ratio of Pu^{239} and U^{235} for Intermediate Energy Neutrons*, Proc., 1955 Geneva Conference, 4: Paper No. 595, p. 315.
11. S. Oleksa, *The Variation of α of U^{235} with Energy in the Intermediate-Energy Range*, J. Nuclear Energy, 5: No. 1, 16, (1957).
12. J. Terrell, *Distributions of Fission Neutron Numbers*, Phys. Rev., 108: No. 3, 783, (1957).
13. B. D. Kuzminov, L. S. Kutsaeva and I. I. Bondarenko, *Prompt Neutron Numbers for the Fast Neutron Fission of U^{235}, U^{238}, Th^{232}, and Np^{237}*, Atomnaya Energiya, 4: No. 2, (1958), p. 187.
14. L. H. Bollinger, R. E. Coté and G. E. Thomas, *The Slow Neutron Cross Sections of Plutonium 239*, Proc., 1958 Geneva Conference, 15: Paper No. 687, p. 127.

15. F. J. M. Farley, *The Yield of Fission Neutrons per Neutron Absorbed for Pu^{239} up to 60 eV Incident Energy*, J. Nuclear Energy, 3: No. 1/2, (1956), p. 33.
16. L. Smith, K. Smith, R. L. Henkel and M. M. Thorpe, *Fission Cross Section of Pu-241*, Reports to the AEC Nuclear Cross Section Advisory Group, WASH-1028, (April 28-29, 1960), p. 33.
17. S. P. Kalinin and V. M. Pankratov, *Neutron-Induced Fission Cross Sections of Th^{232} and U^{238} in the Energy Range 3 to 11 Mev and of U^{233}, U^{235}, Np^{237} and Pu^{239} in the Energy Range of 3 to 8 Mev*, Proc., 1958 Geneva Conference, 16: Paper No. 2149, p. 136.
18. D. K. Butler, *Fission Cross Section of Plutonium-242*, Phys. Rev., 117: No. 5, 1305, (1960).
19. D. K. Butler, *Neutron-Induced Fission Cross Sections of Pu^{241} and Am^{243}*, Bull. Am. Phys. Soc., Series II, 6: No. 1, 8, (1961).
20. H. W. Schmitt and R. B. Murray, *Neutron-Induced Fission Cross Section of Np^{237}*, Phys. Rev., 116: No. 6, 1575, (1959).
21. B. M. Gochberg, G. A. Otroshchenko and V. A. Shigin, *Effective Cross Sections and Anisotropies of the Fission of Np^{237} and Th^{230}*. Soviet Physics, Doklady Akad. Nauk, SSSR, 128: No. 6, 1157, (September-October, 1959).
22. S. Yiftah, D. Okrent and P. A. Moldauer, *Fast Reactor Cross Sections*, (New York: Pergamon Press, 1960).
23. L. Van Hove, *Correlations in Space and Time and Born Approximation Scattering in Systems of Interacting Particles*, Phys. Rev., 95: No. 1, 249, (1954).
24. R. Weinstock, *Inelastic Scattering of Slow Neutrons*, Phys. Rev., 65: No. 1 and 2, 1, (1944).
25. P. O. Froman, *On Neutron Diffraction Phenomena According to the Kinematical Theory II*, Arkiv för Fysik, 4: 191, (1952).
26. A. Akhieser and I. Pomeranchuk, *Scattering of Slow Neutrons in Crystals*, Zhur. Eksp. i Teoret. Fiz., (USSR), 17: 769, (1947), No. 9.
27. A. C. Zemach and R. J. Glauber, *Dynamics of Neutron Scattering by Molecules*, Phys. Rev., 101: No. 1, 118-129, (1956).
28. A. Sjölander, *Multi-phonon Process in Slow Neutron Scattering by Crystals*, Arkiv för Fysik, 14: 315, (1958).
29. J. M. Cassels, *The Scattering of Neutrons by Crystals*, *Progress in Nuclear Physics*, (New York: Academic Press, Inc., 1950), Vol. 1, p. 185.
30. L. S. Kothari and K. S. Singwi, *Thermal Inelastic Scattering of Cold Neutrons in Polycrystalline Solids*, Proc., Roy. Soc. (London), A231: 293, (1955).
31. A. W. McReynolds, *Inelastic Scattering of Thermal Neutrons in Lead*, Phys. Rev., 91: No. 6, 1368, (1953).
32. G. W. Johnson, H. Palevsky and D. J. Hughes, *Inelastic Scattering of Low-Energy Neutrons in Graphite*, Phys. Rev., 82: No. 2, 345, (1951).
33. H. Palevsky and R. R. Smith, *Low-Energy Cross Section Measurements of Be with the Brookhaven Slow-Neutron Chopper*, Phys. Rev., 86: No. 4, 604, (1952).
34. H. Palevsky, D. J. Hughes and R. R. Smith, *Cross Section of Fe for Cold Neutrons*, Phys. Rev., 87: No. 1, 221, (1952).
35. G. L. Squires, *Multi-Oscillator Processes in the Scattering of Neutrons by Crystals*, Proc., Roy. Soc. (London), A212: 192, (1952).
36. L. S. Kothari and K. S. Singwi, *Thermal Inelastic Scattering of Cold Neutrons in Polycrystalline Graphite*, Phys. Rev., 106: No. 2, 230, (1957).
37. J. Krumhansl and H. Brooks, *The Lattice Vibration Specific Heats of Graphite*, J. Chem. Phys., 21: No. 10, 1663, (1953).
38. G. Placzek, *Incoherent Neutron Scattering by Polycrystals*, Phys. Rev., 93: No. 4, 895, (1954).
39. W. Marshall and R. N. Stuart, *The Scattering of Neutrons from Polycrystalline Materials*, UCRL-5568, (1959).
40. P. Schofield and A. Hassitt, *The Calculation of Thermal Neutron Spectra*, Proc., 1958 Geneva Conference, 16: Paper No. 18, p. 217.
41. P. Debye, *Zur Theorie der Spezifischem Wärmen*, Annalen der Physik, 39: 789, (1912). See also, *The Collected Papers of P. J. W. Debye*, (New York: Interscience Publishers, 1954), pp. 789-839.
42. M. Born and T. Von Karman, *Vibration in Space Gratings (Molecular Frequencies "Originalmitteilungen")*, Physik Zeit., 13: 297, (April 15, 1912). See also M. Born and K. Huang, *Dynamical Theory of Crystal Lattices*, (London: Oxford University Press, 1954).
43. M. Blackman, *Contributions to the Theory of Specific Heat of Crystals*, Proc., Roy. Soc. (London), A148: 365-85, (1935). See also, *On the Vibrational Spectrum of a Three-Dimensional Lattice*, Proc., Roy Soc. (London), A159: 416, (1937).
44. J. De Launay, *Solid State Physics*, (New York: Academic Press, Inc., 1956), Vol. 2, p. 219.
45. P. Olmer, *Dispersion des Vitesses des Ondes Acoustiques dans l'Aluminum*, Acta Cryst., 1: 57, (1948).
46. H. Cole and B. E. Warren, *Approximate Elastic Spectrum of Beta Brass from X-Ray Scattering*, J. Appl. Phys., 23: 335, (1952).
47. H. Cole, *Approximate Elastic Spectrum of Acoustic Waves in AgCl from X-Ray Scattering*, J. Appl. Phys., 24: No. 4, 482, (1953).
48. H. Curien, *Diffusion Thermique des Rayons X par des Monocristaux de fer-α et Dynamique du Réseau Cubique Centré*, Acta Cryst., 5: 393, (1952).
49. R. W. James, *The Optical Principles of the Diffraction of X-Rays*, (London: G. Bell and Sons, Ltd., 1948), Chapter 5. (This is a volume in the following set: *The Crystalline State-Vol. 2-Laurence Brigg.*).
50. E. H. Jacobsen, *Elastic Spectrum of Copper from Temperature-Diffuse Scattering of X-Rays*, Phys. Rev., 97: No. 3, 654, (1955).
51. C. B. Walker, *X-Ray Study of Lattice Vibrations in Aluminum*, Phys. Rev., 103: No. 3, 547, (1956). See also, G. L. Squires, *Relation Between the Vibration Frequencies of a Crystal and the Scattering of Slow Neutrons*, 103: No. 2, 304, (1956).
52. B. N. Brockhouse and A. T. Stewart, *Normal Modes of Aluminum by Neutron Spectrometry*, Rev. Mod. Phys., 30: No. 1, 236, (1958). See also, A. T. Stewart and B. N. Brockhouse, *Vibration Spectra of Vanadium and a Mn-Co Alloy by Neutron Spectrometry*, Rev. Mod. Phys., 30: No. 1, 250, (1958).
53. G. R. Baldock, *Lattice Vibrations and Specific Heat of Graphite*, Phil. Mag., Series 8, 1: No. 9, 789, (September, 1956).
54. A. Yoshimori and Y. Kitano, *Theory of the Lattice Vibration of Graphite*, J. Phys. Soc. (Japan), 11: No. 4, 352, (April, 1956).
55. W. V. Houston, *Normal Vibration of a Crystal Lattice*, Rev. Mod. Phys., 20: 161, (January, 1948).
56. P. A. Egelstaff and S. J. Cocking, *The Phonon Frequencies Distribution in Graphite at Several Temperatures*, IAEA Symposium on Inelastic Scattering of Neutrons in Solids and Liquids, Vienna, IS/8, (October, 1960).
57. E. P. Wigner and J. E. Wilkins, Jr., *Effect of the Temperature of the Moderator on the Velocity Distribution of Neutrons with Numerical Calculation for H as Moderator*, AECD-2275, (1944).
58. G. H. Vineyard, *Scattering of Slow Neutrons by a Liquid*, Phys. Rev., 110: No. 5, 999, (1958).
59. B. N. Brockhouse, *Structural Dynamics of Water by Neutron Spectrometry*, Nuovo Cimento Supplement, 9: 45, (1958).
60. P. Schofield, *Space-Time Correlation Function Formalism for Slow Neutron Scattering*, Phys. Rev. Letters, 4: No. 5, 239, (1960).
61. B. N. Brockhouse, *Diffusive Motions in Liquids and Neutron Scattering*, Phys. Rev. Letters, 2: No. 7, 287, (1959). See also, D. J. Hughes, et al., *Atomic Motions in Water by Scattering of Cold Neutrons*, Phys. Rev. Letters, 3: No. 2, 91, (1959).
62. D. J. Hughes, et al., *Atomic Motions in Water by Scattering of Cold Neutrons*, Phys. Rev., 119: No. 3, 872, (1960).
63. K. E. Larsson, S. Holmryd and K. Otnes, *An Experimental Study of the Scattering of Slow Neutrons from H_2O and D_2O*, Aktiebolaget Atomenergi, AE-47, (1960).
64. J. D. Bernal and R. H. Fowler, *A Theory of Water and Ionic Solutions with Particular Reference to Hydrogen and Hydrogen Ions*, J. Chem. Phys., 1: 515, (1933). See also, J. Leonard Jones and J. A. Pople, *Molecular Association in Liquids*, Proc., Roy. Soc. (London), A205: 155, (1951); J. Frenkel, *Kinetic Theory of Liquids*, (New Jersey: Oxford University Press, 1946).
65. K. S. Singwi and A. Sjölander, *Diffusive Motions in Water and Cold Neutron Scattering*, Phys. Rev., 119: No. 3, 863, (1960).
66. P. Egelstaff, et al., *The Thermal Neutron Scattering Law for Light and Heavy Water*, IAEA Symposium on Inelastic Scattering of Neutrons in Solids and Liquids, Vienna, IS/10, (October, 1960).
67. M. Nelkin, *Scattering of Slow Neutrons by Water*, Phys. Rev., 119: No. 2, 741, (1960).
68. J. M. Blatt and V. F. Weisskopf, *Theoretical Nuclear Physics*, (New York: John Wiley and Sons, 1952).
69. A. M. Weinberg and E. P. Wigner, *The Physical Theory of Neutron Chain Reactors*, (Chicago: University of Chicago Press, 1958).
70. R. J. Howerton, *Semi-Empirical Neutron Cross Sections*, UCRL-5351, Part II, Vol. I, (1958).

71. A. Langsdorf, Jr., R. O. Lane and J. E. Monahan, *Angular Distributions of Scattered Neutrons*, Phys. Rev., 107: No. 4, 1077, (1957). See also ANL-5567, *Neutron Scattering Angular Distribution*, (1956).
72. R. O. Lane and J. E. Monahan, *Differential Cross Sections for Neutron Resonance Scattering from Na^{23}*, Phys. Rev., 118: No. 2, 533, (1960).
73. R. O. Lane, et al., *The Angular Distributions of Neutrons Scattered from Various Nuclei*, Ann. Phys., 12: 135-71, (1961).
74. J. E. Wills, et al., *Scattering of Fast Neutrons from C^{12} and F^{19}*, Phys. Rev., 109: No. 3, 891, (1958).
75. H. Lustig, H. Goldstein and M. H. Kalos, *An Interim Report on the Neutron Cross Sections of Oxygen*, NDA086-2, (1958).
76. D. J. Hughes and R. S. Carter, *Neutron Cross Sections—Angular Distributions*, BNL-400, (1956).
77. P. F. Zweifel and H. Hurwitz, Jr., *Transformation of Scattering Cross Sections*, J. Appl. Phys., 25: No. 10, 1241, (1954).
78. R. O. Lane, W. F. Miller and K. E. Hillstrom, *Matrices for Transforming Legendre Polynomial Coefficients Between Laboratory and Center-of-Mass Systems*, ANL-6039, (1959).

Section 3

CONSTANTS FOR THERMAL HOMOGENEOUS REACTORS

3.1 THERMAL NEUTRON SPECTRUM

3.1.1 THE INTEGRAL EQUATION AND BASIC SOLUTIONS IN INFINITE HOMOGENEOUS MEDIA

The neutron-balance equation for the steady state takes the form:

$$[\sigma_a(E) + \sigma_s(E)]\ \phi(E)\ dE = dE \int_0^\infty dE'\,\sigma(E' \rightarrow E)\ \phi(E') + S(E)\ dE \qquad (3\text{-}1)$$

or, in terms of the number density N(v),

$$[V(v) + \gamma(v)]\ N(v)\ dv = dv \int_0^\infty G_s(v' \rightarrow v) N(v')\ dv' + S(v)\ dv \qquad (3\text{-}2)$$

where σ_a = neutron capture cross section of the moderating atoms
σ_s = neutron scattering cross section of the moderating atoms
$\sigma(E' \rightarrow E)dE$ = cross section for scattering neutrons from energy E′ to (E, E + dE)
$\phi(E)$ = neutron flux = Nv
v = neutron velocity
S(E) = source term
N(v)dv = number of neutrons per unit volume with velocities in the range v to v + dv
$G_s(v' \rightarrow v)dv'dv$ = probability per unit time that a neutron in velocity (v′, v′ + dv′) will be scattered into (v, v + dv)
V(v) = scattering probability per unit time
$\gamma(v)$ = capture probability per unit time
S(v)dv = number of source neutrons per unit volume per unit time in the range v to v + dv

Fundamental problems arising in the solution of Eqs. (3-1) and (3-2) are discussed in a number of references.[1–6] Each of the references cited here includes an extensive bibliography.

Two simple solutions exist. If σ_a [equivalently $\gamma(v)$] is zero, $\sigma_s(E)$ is constant, and the moderating atoms are stationary, conventional slowing-down theory is obtained. If σ_a is still set equal to zero but the moderating atoms are assumed to be in thermal equilibrium at temperature T, the neutron distribution will be the Maxwell distribution characterized by the temperature T; i.e.,

$$N(v) = \frac{4}{\sqrt{\pi}} \left(\frac{m}{kT}\right)^{3/2} \exp(-mv^2/2\ kT)\ v^2$$

where m = neutron mass
k = Boltzmann's constant

If σ_a [hence $\gamma(v)$] is not zero, it is difficult to make any general statements about the complete solution of Eqs. (3-1) and (3-2). In what follows, the discussion is limited to $\sigma_a v$ = constant.

Under very broad assumptions about $\sigma(E' \rightarrow E)$, Corngold[1] has shown that the flux may be represented asymptotically in energy by:

$$\phi(E) = \frac{1}{\sigma_f E}\left[\sum_{n=0,\frac{1}{2},\ldots}^{\infty}\left(\frac{T}{E}\right)^n \sum_{p=0}^{[n]} \tau_n^p \left(\frac{\Delta}{2}\right)^{2(n-p)}\right] \tag{3-3}$$

where σ_f = cross section for s-wave scattering of neutrons by a free moderator
$\Delta = (2/\mu)\,[\sigma_a(T)]/\sigma_f$
μ = ratio of neutron mass to scattering mass
$[n]$ = largest integer contained in n

The coefficients, τ_n^p, are defined through a recursive relation and depend on the properties of $\sigma(E' \rightarrow E)$.

Further specification of $\phi(E)$ is made by setting up a model for $\sigma(E' \rightarrow E)$. The results obtained from various specific models are described in the following sections.

3.1.2 GENERAL METHODS OF SOLUTION

Equation (3-1) can be solved, in general, by numerical methods once a suitable representation of $\sigma(E' \rightarrow E)$ and boundary conditions are given.

Monte Carlo methods are of wide applicability. An interesting series of problems have been solved this way by Brown,[7] and by Coveyou, Bate, and Osborn[8] (see also Section 3.1.6). A generally available code based on this method is ROUTINE II. TRAM is another Monte-Carlo code that is suitable for hydrogen-moderated assemblies and takes into account some spatial dependence. Both codes are described in Section 10.1.3.

By replacing the upper limit of the integral in the right-hand side of Eq. (3-1) by a finite cutoff energy, the integral may be approximated by a finite sum and the equation solved by an iterative procedure. A code used in performing this calculation is SPECTRUM, discussed in Section 10.1.3.

When the scattering kernel, $\sigma(E \rightarrow E')dE$, has the proper form, Eq. (3-1) may be converted to a second-order differential equation; these equations are usually solved by standard numerical methods. (Special forms of scattering kernels are discussed in Section 3.1.3.) Wigner and Wilkins[9] obtained such an equation for the case of moderation by hard spheres of unit (neutron) mass. This equation, for an arbitrary variation of absorption to scattering with energy, is solved by use of the codes SOFOCATE and TEMPEST (see Section 10.1.3). See also Section 3.1.4.

An approximation to the scattering kernel for hard spheres of larger mass leads to the Wilkins equation.[10] This equation is also solved by use of the TEMPEST code. See also Section 3.1.4.

Variational methods of solution for some specific cases are discussed in Section 3.1.4.

3.1.3 SCATTERING KERNELS

The kernel $\sigma(E \rightarrow E')$ is the cross section per unit energy range for scattering neutrons from energy E to E'; $\sigma(E \rightarrow E')dE$ as used here is identical to $d\sigma/dE$, as defined in Section 2.4.1. The evaluation of $d\sigma/dE$ from first principles requires a detailed knowledge of the quantum mechanical behavior of the scatterer. The use of specific models (e.g., monatomic crystals) allows the use of general representations such as Eqs. (2-6) and (2-7). These equations can be solved by approximating the sum over states:

$$\sum_{s=1}^{3n}$$

by an integral over a continuous distribution:

$$\int_0^{\infty} \rho(\nu)d\nu \ldots$$

Typical frequency distribution functions are discussed in Section 2.4.1. Information about these distributions may be derived from a variety of sources; however, the problem of utilizing the information to obtain $\sigma(E \rightarrow E')dE$ is complicated by numerous geometrical difficulties. These problems are considerably reduced for some special cases, as discussed next.

3.1.3.1 Hard Spheres of Unit Neutron Mass

If the spheres are in thermal equilibrium at a temperature, T, then

$$\sigma(E_0 \rightarrow E) = \frac{\sigma_s}{(E_0/kT)} 2\sqrt{E/kT} \begin{cases} \exp\left[(E_0 - E)/kT\right] \Theta\left(\sqrt{E_0/kT}\right) & \text{if } E_0 < E \\ \Theta\left(\sqrt{E/kT}\right) & \text{if } E_0 > E \end{cases}$$

where σ_s = free atom scattering cross section,
k = Boltzmann's constant,

$$\Theta(x) = \frac{2}{\sqrt{\pi}} \int_0^x \exp(-y^2)\, dy, \text{ a tabulated function.}$$

These results are obtained in Ref. 9 (see also Section 2.4.1).

3.1.3.2 Hard Spheres of Heavy Mass[9,10]

Again assume the spheres are in thermal equilibrium at temperature T. The equation is now sufficiently complicated to call for a condensed notation:

$$x = \sqrt{E/kT};\ x_0 = \sqrt{E_0/kT}$$

$$\theta = \frac{M+1}{2\sqrt{M}};\ \zeta = \frac{M-1}{2\sqrt{M}};\ \beta^2 = 1/2kT$$

then

$$\sigma(x_0 \rightarrow x) = \sigma_s \theta^2 x/x_0^2$$

$$\begin{cases} e^{-(x^2-x_0^2)} \left[\Theta(x_0 - \zeta x) + \Theta(x_0 + \zeta x)\right] + \Theta(x - \zeta x_0) - \Theta(x + \zeta x_0), & x_0 < x \\ e^{-(x^2-x_0^2)} \left[\Theta(\theta x_0 - \zeta x) - \Theta(\theta x_0 + \zeta x)\right] + \Theta(\theta x - \zeta x_0) + \Theta(\theta x + \zeta x_0), & x_0 > x \end{cases}$$

3.1.3.3 Heavy Crystalline Moderator

The calculation of the neutron spectrum in an infinite, homogeneous mixture of beryllium and a heavy absorber has been investigated by Nelkin.[6] The inelastic scattering cross section employed in the calculation was obtained from the Debye model, using the inverse mass and incoherent approximations (see Section 2). The resulting kernel for scattering from E to E′ is;

$$\sigma(E \rightarrow E') = \sigma_B \left(\frac{3T}{Ak^2\theta^3}\right) (E'/E)^{1/2} (E' + E) \frac{\Delta E}{kT} \left[\exp(\Delta E/kT) - 1\right]^{-1} \text{ for } \Delta E \leq k\theta$$

$$\sigma(E \rightarrow E') = 0 \text{ for } \Delta E > k\theta$$

where T = temperature of moderator
θ = Debye temperature of the crystal
k = Boltzmann's constant
σ_B = bound atom scattering cross section
A = mass of the scatterer in units of neutron mass

3.1.3.4 Recent Work on Scattering in Water

Nelkin[11] has used recent experimental results on the scattering of slow neutrons by water, together with molecular data from water vapor, to construct a model for scattering of slow neutrons by water.

If E_0 is the incident neutron energy, E the final neutron energy, and θ the angle through which the neutron is scattered, then Nelkin's model yields

$$\sigma(E_0, E, \theta) = \frac{\sigma_b}{4\pi}\left(\frac{E}{E_0}\right)^{1/2}\left(\frac{m}{2\pi\bar{E}K^2}\right)^{1/2}\exp\left(-\frac{K^2}{2A}\right)\sum_{n=-\infty}^{+\infty}\exp\left(-\frac{n\omega}{2T}\right) \times I_n\left(\frac{K^2}{2B}\right)\exp\left[-\frac{m}{2\bar{E}K^2}\left(E - E_0 - n\omega + \frac{K^2}{2m}\right)^2\right]$$

where K^2 = square of the momentum transfer
$m = 18$ = mass of water molecule
T = absolute temperature of the water
$\sigma_b = 81.2$ barns, is the bound hydrogen atom scattering cross section
$I_n(x)$ = Bessel function of imaginary argument

The other parameters depend on the range of incident neutron energy, and involve some constant coefficients in varying ways. The constant coefficients are:

$\omega_1 = 0.205$ ev, and $\omega_2 = 0.481$ ev, the frequencies of the two vibrational levels (the upper is doubly degenerate)
m_v = effective mass of vibrations = 1.95
$\alpha_v = \frac{1}{m_v}\left(\frac{1}{3\omega_1} + \frac{2}{3\omega_2}\right) = 0.65$ ev
$\omega_r = 0.06$ ev is the frequency of the hindered rotations
$m_r = 2.32$ is the mass of the hindered rotations

The values of $\bar{E}$, m, A, ω, and B for the various energy ranges are:

Set I: 0.01 ev ≤ E_0 ≤ 0.15 ev. Free translations and only elastic vibrational transitions are assumed for this energy range. Hindered rotations are treated properly.

$$m = M = 18$$
$$\bar{E} = T = 0.0255 \text{ ev}$$
$$A^{-1} = \alpha_v^{-1} + [m_r\omega_r \tanh(\omega_r/2T)]^{-1}; (A = 0.0971 \text{ ev})$$
$$B = m_r\omega_r \sinh(\omega_r/2T) = 0.206 \text{ ev}$$
$$\omega = \omega_r = 0.06 \text{ ev}$$

Set II: 0.20 ev ≤ E_0 ≤ 0.48 ev. The 0.205-ev vibrational level is treated properly in this energy range; only elastic transitions are considered for the higher level. The rotational level is treated in the high-energy limit.

$$m^{-1} = M^{-1} + m_r^{-1}, (m = 2.06)$$
$$\bar{E} = [(Tm_r + \bar{E}_r M)/(m_r + M)] = 0.0350 \text{ ev}$$
$$\bar{E}_r = [n(\omega_r/T) + 1/2]\,\omega_r = 0.036$$
$$n = [\exp(\omega_r/T) - 1]^{-1}$$
$$A = \alpha_v = 0.65 \text{ ev}$$
$$B = 3m_v\,\omega_1 \sinh(\omega_1/2T) = 33.31 \text{ ev}$$
$$\omega = \omega_1 = 0.205 \text{ ev}$$

0.15 ev ≤ E_0 ≤ 0.20 ev. In this energy range, the parameters are chosen from:

Set I if $\Delta E = |E - E_0| \leq 0.1$ ev

Set II if $\Delta E \geq 0.1$ ev

$E_0 \geq 0.48$. In this case, the upper vibrational level is considered, whereas the effect of the lower level is treated as though it were a free-atom motion with the proper kinetic energy.

$$m^{-1} = M^{-1} + m_r^{-1} + \frac{1}{3} m_v^{-1} \quad (m = 1.522)$$

$$\overline{E} = [(T/M) + (\overline{E}_r/m_r) + (\overline{E}_1/3m_v)]\, m = 0.0525 \text{ ev}$$

$$A = (3m_v\omega_2/2) = 1.402 \text{ ev}$$

$$B = \frac{2}{3} m_v\, \omega_2 \sinh(\omega_2/2T) = 8744 \text{ ev}$$

$$\omega = \omega_2 = 0.481 \text{ ev}$$

Spectra computed with this cross section, $\sigma(E_0, E, \theta)$, are compared with experimental results cited in Section 3.1.7.3.

3.1.3.5 Effective Mass Approximations to Chemical Binding in Water

Two examples of synthetic kernels which relate measured total cross sections to energy exchange are the work of Radkowsky,[12] and of Brown and St. John.[13] Radkowsky's treatment is based on Fermi's remark[14] that the ratio of the bound atom scattering cross section to the free atom scattering cross section is just the square of the ratio of the corresponding reduced masses. Then the effective mass of the proton bound in water can be calculated from the observed scattering cross section $\sigma_s(E)$ and is given by:

$$\frac{2M_{eff}(E)}{1 + M_{eff}(E)} = \sqrt{\frac{\sigma_s(E)}{\sigma_0}}$$

where σ_0 is the free atom scattering cross section. This method has been used to investigate the transport length in H_2O (see Section 3.3.2.1).

Brown and St. John[13] utilized a simplified model of the H_2O and D_2O molecule to take into account chemical binding effects in H_2O and D_2O, respectively. The H and D cross sections were fitted by expressions of the form:

$$\Sigma_s(v_r) = \Sigma_0 + \Sigma_{s1} \exp(-\alpha\, v_r^2)$$

where v_r is the relative velocity of the neutron and moderator atom. Further, it was assumed for spectrum calculations that at energies greater than some E_2, there is no absorption and $\Sigma_s(v_r) = \Sigma_0$. At energies between E_2 and an assumed E_1, the H(D) atoms were considered free and at rest. At energies below E_1, the molecules were treated as rigid rotators, and the H(D) atoms were given an effective mass, M_{eff}. A critique of this method has been given by Krieger and Nelkin.[15] Table 3-1 lists the values used by Brown and St. John.

Table 3-1—PARAMETER VALUES USED BY BROWN AND ST. JOHN

Data from Ref. 13.

	Σ_0, barn	Σ_{s1}, barn	α_1, (amu/ev)$^{1/2}$	E_2, ev	E_1, ev	M_{eff}
H_2O	20.7	13.1	4.5	2.87	0.226	1.9
D_2O	3.3	1.6	2.88	2.87	0.143	3.6

Note: M_{eff} is expressed in units of neutron masses.

In both cases, the effective mass obtained is used in conjunction with the hard sphere kernel (see Section 3.1.3.2).

687863 O - 63 - 7

3.1.4 SOLUTIONS OF THE NEUTRON THERMALIZATION EQUATIONS IN SPECIAL CASES

3.1.4.1 Moderation by Monatomic Hydrogen Gas

Wigner and Wilkins[9] solved Eq. (3-2) for the case of moderation by a monatomic gas of hard spheres of unit mass. The details of the procedure are also described in Ref. 2. The results are expressed as functions of $x = v/\sqrt{2kT}$ and the parameter $\beta\gamma \equiv (\sigma_a(E)\sqrt{E})/(\sigma_f\sqrt{2kT})$.

The asymptotic solution is:

$$N(x) = \frac{2\,\beta\gamma\ x\ C_0}{(x + \beta\gamma)^3}$$

$$C_0 = \int_0^\infty N(x)dx$$

This result has also been obtained by Corngold[1] as a special case.

Numerical calculations of N(x) in the range $0.1 \leq x \leq 10$ yield the plots shown in Fig. 3-1.

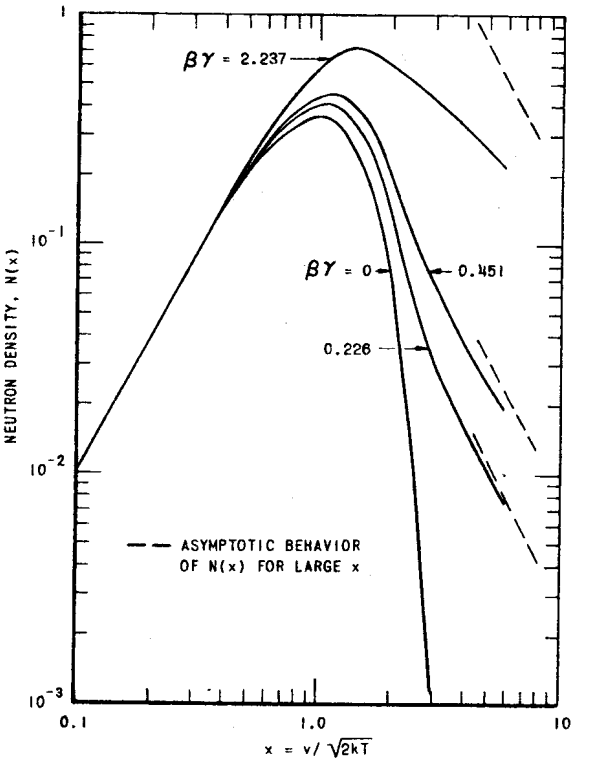

Fig. 3-1 —Neutron densities as a function of thermal velocities for several values of the ratio of absorption to scattering (β_γ) in monatomic hydrogen. *Reproduced from Ref. 9.*

3.1.4.2 Moderation by a Monatomic, Heavy Gas: Asymptotic Solutions

Asymptotic solutions [Eq. (3-3)] have been tabulated[1] for cases of moderation by hard spheres of mass 2 (deuterium), mass 9 (beryllium), and mass 12 (carbon). Table 3-2 lists the values of $\xi\tau_n^p$ for a gas model.

$$\xi = 1 + \left(\frac{1-\mu}{2\mu}\right)^2 \ln\left(\frac{1-\mu}{1+\mu}\right)$$

where μ is the ratio of neutron-to-moderator mass.

Table 3-2 — COEFFICIENTS $\xi\tau_n^p$ FOR GAS MODEL

Data from Ref. 1.

n	p = 0	p = 1	p = 2	p = 3
Deuterium				
0	1	—	—	—
1/2	−1.8	—	—	—
3/2	2.025	1.5	—	—
2	−1.83474	−3.92618	—	—
5/2	1.46658	5.85612	4.70722	—
3	−1.08040	−6.64188	−15.0004	—
7/2	0.751539	6.39462	26.4766	18.7909
	−0.501018	−5.52058	−34.7784	−69.7606
Beryllium				
0	1	—	—	—
1/2	−1.15384	—	—	—
1	0.712251	1.88889	—	—
3/2	−0.312829	−3.38584	—	—
2	0.109719	2.95915	5.68042	—
5/2	−0.0327020	−1.73038	−12.9480	—
3	0.00860901	0.773246	14.0189	22.7230
7/2	−0.00205461	−0.284096	−9.91963	−59.7909
Carbon				
0	1	—	—	—
1/2	−1.11428	—	—	—
1	0.653869	1.91667	—	—
3/2	−0.269027	−3.33391	—	—
2	0.0871875	2.78573	5.75922	—
5/2	−0.0287086	−1.53500	−12.7876	—
3	0.00562732	0.637788	13.2934	23.0364
7/2	−0.00119761	−0.215158	3.48693	−65.0395

If the recursion formula for the coefficients τ_n^p is formally expanded in terms of the mass ratio μ, and only the lowest order terms are retained, the recursion formula becomes a three-term inhomogeneous difference equation (in fact, it does so to all orders in μ for the gas case). The asymptotic series, Eq. (3-3), may then be associated with a series of second-order differential equations for the partial solutions $N_0(x)$, $N_1(x)$, etc.,

where $x = \sqrt{E/kT}$

$N(x) = \sum_k \mu^k N^{(k)}(x)$

$N_0(x) = N^{(0)}$

$N_1(x) = N^{(0)} + \mu N^{(1)}$, etc.

The equation for $N^{(0)}(x)$ is:

$$x\frac{d^2N^{(0)}}{dx^2} + (2x^2 - 1)\frac{dN^{(0)}}{dx} + (4x - \Delta)N^{(0)} = 0 \qquad (3\text{-}4)$$

The equation for $N^{(1)}(x)$ is:

$$x\frac{d^2N^{(1)}}{dx^2} + (2x^2 - 1)\frac{dN^{(1)}}{dx} + (4x - \Delta)N^{(1)} = \left(2x^{-2} + \frac{2\Delta}{3}x^{-1}\right)\frac{dN^{(0)}}{dx} - \left[4x^{-3} + 2\Delta x^{-2} + \left(\frac{\Delta^2}{3} - 4\right)x^{-1} - \frac{4}{3}\Delta\right]N^{(0)} \qquad (3\text{-}5)$$

Figure 3-2 is a comparison of solutions to Eqs. (3-4) and (3-5) for thermalization in gas of deuterium atoms ($\mu = 1/2$) when absorption is moderate ($\Delta = 1.86$), and when it is strong ($\Delta = 4.64$). The author states that the full asymptotic solution is nearly identical with N_1 over the entire range plotted.

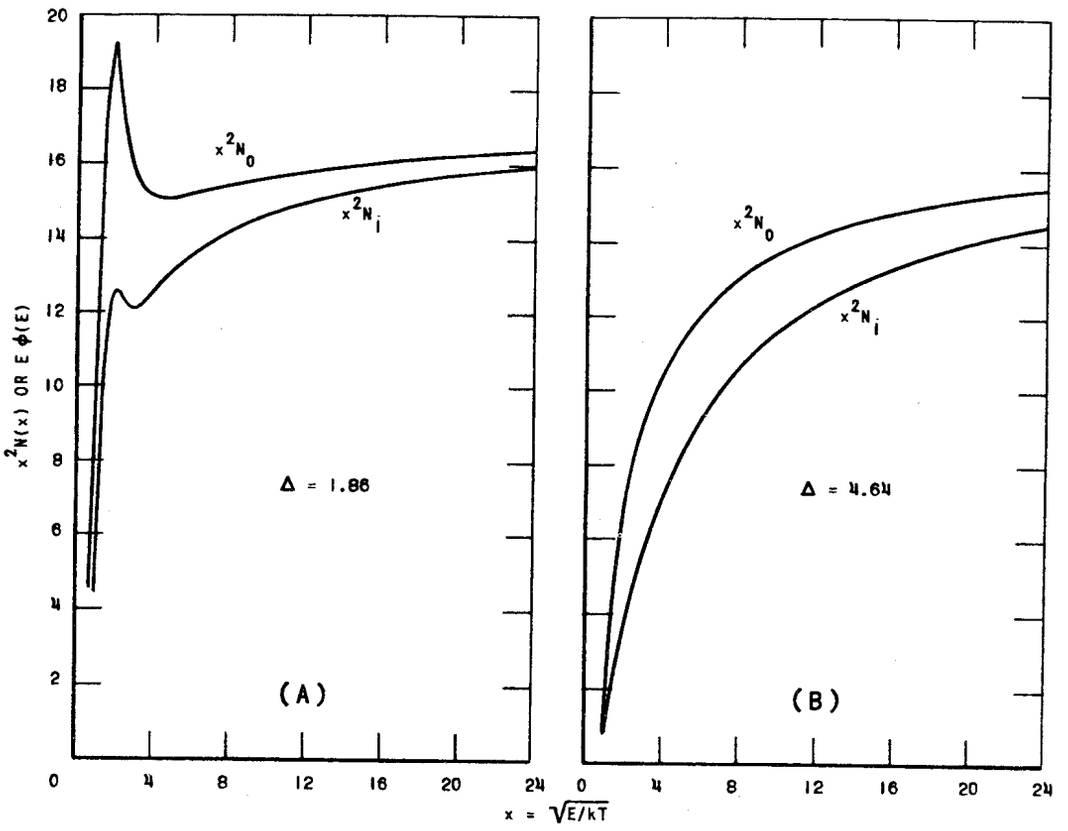

Fig. 3-2 — Comparison of solutions to first-order and zeroth-order differential equations for thermalization in gas of deuterium atoms with (A) moderate absorption, and (B) strong absorption. *Reproduced from Ref. 1.*

3.1.4.3 Moderation by a Monatomic, Heavy Gas: Analytical Forms

Equation (3-4), first proposed by Wilkins,[10] has been studied by a number of authors to obtain approximate analytical representations of the neutron spectrum. Hurwitz, Nelkin, and Habetler[5] found it convenient to represent the spectrum by two parameters: T, the absolute temperature of the moderator, and

$$\Delta = 2\sigma_a(E)\sqrt{(E/kT)}/\mu\sigma_0 = 4\sigma_a(kT)/\xi\sigma_0$$

where $\sigma_a(E)$ is assumed proportional to $1/\sqrt{E}$; μ is the mass ratio; and $\sigma_0 = \sigma_f$ = free atom scattering cross section. The spectrum was represented as a function of $E/kT = \epsilon$ by:

$$\epsilon\phi(E) = \epsilon^2 e^{-\epsilon} + \frac{H(\epsilon)\Delta}{4(1 - 0.79887\ \Delta)}, \quad \Delta \ll 1$$

$$H(\epsilon) \approx \frac{\sqrt{\pi}}{2} \sum_{n=0} \left(\frac{n!}{\epsilon^n}\right) + 0(-\epsilon)$$

A graph of $\epsilon^2 e^{-\epsilon} = M(\epsilon)$, and $H(\epsilon)$, is given in Fig. 3-3. Figure 3-4 is a graph of $\epsilon\phi(\epsilon)$ for various values of Δ; the plots were obtained by numerical integration of Eq. (3-4). Figure 3-5 is a comparison of the results of Hurwitz, Nelkin and Habetler, with the solutions of the Wigner-Wilkins equation (see Section 3.1.4.1). Here Δ is chosen numerically equal to $4\beta\gamma$ and the asymptotic solutions are matched.

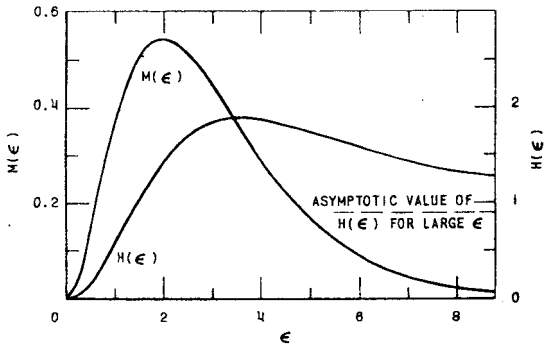

Fig. 3-3 —Energy distributions for small Δ. *Reproduced from Ref. 5.*

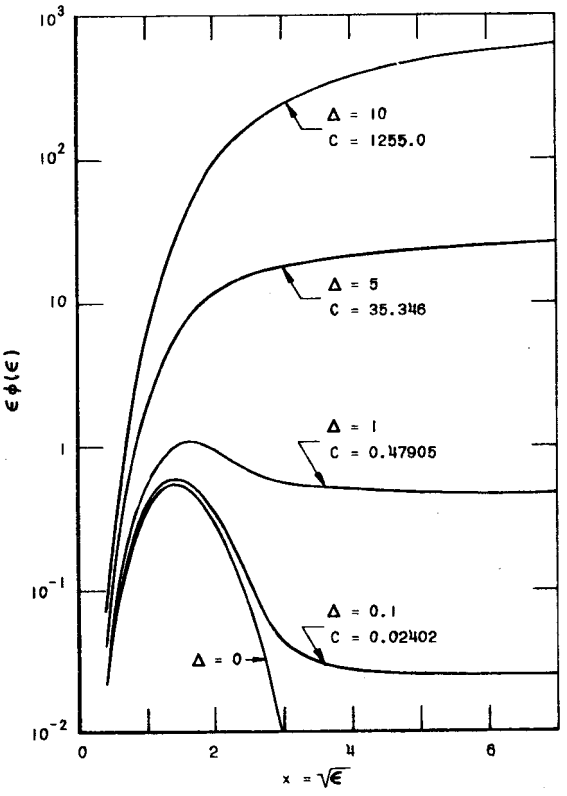

Fig. 3-4 —Energy distribution of neutrons thermalized by a heavy gaseous moderator in the presence of a 1/v absorber. *Reproduced from Ref. 5.*

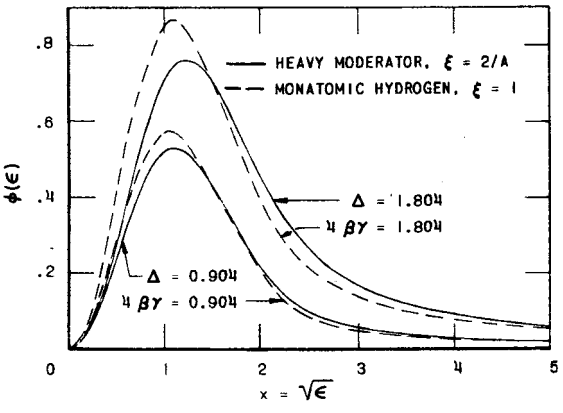

Fig. 3-5 —Energy distributions for moderators with 1/v absorption ($\sigma_a/\xi\sigma_s$ is constant). *Reproduced from Ref. 5.*

Cohen[3] has represented the solution of Eq. (3-4) correct to the second order in Δ (ϵ and Δ are the same as before) as a function of $x = \sqrt{\epsilon}$ by:

$$N(x) = x^2 e^{-x^2} [\mu_0(x) + \Delta\mu_1(x) + \Delta^2\mu_2(x) + \ldots]$$

where $\mu_0 = 4/\sqrt{\pi}$

$$\mu_1 = \frac{4x}{3\sqrt{\pi}}\left[1 + \frac{2x^2}{15} + \frac{4x^4}{175} + \frac{8x^6}{2205} + \frac{16x^8}{31185} + \frac{32x^{10}}{495495} + \cdots\right]$$

$$\mu_2 = \frac{x^2}{6\sqrt{\pi}}\left[1 + \frac{19x^2}{90} + \frac{157x^4}{3780} + \frac{1263x^6}{176400} + \cdots\right]$$

The asymptotic solution is $N(x) \sim C/x^2$, where C is bounded by:

$$\frac{\Delta}{2}\left[1 + 0.798873\,\Delta + 0.286606\,\Delta^2\right]$$

from below, and

$$\frac{\Delta}{2}\left[\frac{1 + 0.440129\,\Delta}{1 - 0.358744\,\Delta}\right]$$

from above.

3.1.4.4 Variational Solutions of the Wilkins Equation

Drozdov, et al.,[16] and Liebfried[17] have proposed linear functional forms for solution of the Wilkins equation (3-4). The work of Drozdov, et al., is summarized here.

The functional to be minimized is:

$$I(\Psi) = \int_0^{E_p} dE\ \Psi(E)\left[(\sigma_a + \sigma_s)\Psi - \int_0^{E_p} K(E,E')\ \Psi(E')\ dE' - 2\int_{E_p}^{\infty} K(E',E)\ \Psi^*(E')\ dE'\right]$$

where E_p = assumed thermal cutoff energy

$$\Psi(E) = \phi(E)/\sqrt{\phi_0(E)}$$

$$\phi_0(E) = E\exp(-E/kT) = E\exp(-\beta E)$$

$$K(E,E') = K(E',E) = [\phi_0(E')/\phi_0(E)]^{1/2}\ \sigma_s(E' \rightarrow E)$$

$$\Psi^*(E) = \left[\exp\left(-\int_E^{\infty} \frac{\sigma_a(E')\,dE'}{\xi E'\,\sigma_s(E')}\right)\right]\Big/\xi E\ \sigma_s(E);\ E > E_p$$

The trial function chosen is:

$$\phi(E) = CE\exp(-\gamma E);\ E < E_p$$

$$\phi(E) = \sqrt{\phi_0(E)}\ \Psi^*(E) = \phi^*(E);\ E > E_p$$

If σ_a is represented by $\lambda E^{-1/2}$ and is small (small Δ), and $E_p \gg kT$, the conditions of flux continuity and neutron conservation yield:

$$\frac{\exp(\gamma E_p)\,\lambda\sqrt{\pi}}{\xi E_p^2\,\sigma_s(E_p)\,2\gamma^{3/2}} = 1,\quad C = \frac{2}{\sqrt{\pi}}\frac{\gamma^{3/2}}{\lambda}$$

The extremum condition is given in terms of

$$Z = 1 - (\gamma/\beta)$$

and

$$x = [\beta - \gamma]\,E_p$$

Let $t \equiv dZ/dx$. In the case $Z \ll 1$, the extremum condition is:

$$Z^2\left(4\beta^4\,\eta_2 - \frac{1}{2}\,\beta^5\eta_3\right) - Z\,\beta^4\eta_2 - \theta\alpha\,\left(t\,\frac{\partial F}{\partial x} - \frac{3}{2}\,F\right) = 0$$

and

$$1/\theta = e^t/t^2$$

The auxiliary quantities, θ, α, η_2, η_3, and F, are:

$\theta = \lambda\sqrt{\pi\beta}\;2\xi\sigma_0$, where σ_0 = free atom scattering cross section

$\alpha = \dfrac{M+1}{4M}$, where M = scatterer mass

$\eta_2 = 2\int_0^\infty E^2 e^{-\beta E}\,dE \int_0^\infty \sigma_s(E \rightarrow E')(E'-E)dE'/\sigma_0$

$\eta_3 = -6\int_0^\infty E^2 e^{-\beta E}\,dE \int_0^\infty \sigma_s(E \rightarrow E')(E'-E)^2dE'/\sigma_0$

$F = 2\displaystyle\int_0^1 dt\left(1 - \frac{\delta}{t}\right)e^{xt}$

$\delta = [(M-1)/(M+1)]^2$

The temperature ratio is given by:

$$\frac{T_n}{T_0} = \frac{1}{1-Z} \approx 1 + Z$$

From the preceding formulae, it is seen that for sufficiently small $\sigma_a(kT_0)$, Z is determined by the first moments of the scattering cross section which are different from zero. For monatomic hydrogen gas

$$Z \approx C\,\frac{\sigma_a(kT_0)}{\sigma_0}$$

in the limit of small $\sigma_a(kT_0)$. C is reported to be in close agreement with the values found by Monte Carlo methods. Thus $C \approx 1.0$ (see Section 3.1.6.1).

Corngold and Zamick[18] have exhibited a rational variational principle well suited to the study of the problem of a pulse of neutrons incident on a finite sample of moderator. The functional $\Delta\{M\}$ is defined by:

$$\Delta\{M\} = -\,\frac{\int_0^\infty dx\,x^3\exp(-x^2)\,[(dM/dx)^2 - \beta M^2]}{\int_0^\infty dx\,x^2\exp(-x^2)\,M^2}$$

where M = flux divided by the Maxwellian flux component
$\beta = D\kappa^2/2\mu\sigma_s$
κ = relaxation length

The function M(x) which makes $\Delta\{M\}$ stationary, satisfies the Wilkins equation (3-4). If the flux is assumed proportional to $\exp(-\lambda t + \kappa Z)$, the stationary value of Δ is given by:

$$\Delta = \frac{4\sigma_a(kT)}{\xi\sigma_s} - 2\lambda$$

where λ is the eigenvalue. A suitable trial function is $M(x) = 1 + bx$, with b chosen to conserve neutrons. The eigenvalue is then estimated in the lowest mode as λ_0, which is given by:

$$2\lambda_0 = \frac{4\sigma_a(kT)}{\xi\sigma_s} - \left(\frac{2}{\sqrt{\pi}}\,\beta + 0.456\,\beta^2\right)$$

In the steady-state case, $\lambda \equiv 0$, the method may be used to estimate the relaxation length, κ, in terms of $\Delta = 4\sigma_a(kT)/\xi\sigma_0$. A similar method can be used for hydrogen gas problems.

The results are:

For pulses:

$$\Delta - 2\lambda_0 = 1.103\beta + 0.1470\beta^2$$

$$\Delta - 2\lambda_1 = -1.820 + 0.894\beta$$

$$\Delta - 2\lambda_2 = -2.937 + 1.001\beta$$

where λ_0 is the estimated eigenvalue of the lowest mode; λ_1 of the next lowest, etc. For the steady-state case:

$$\beta_0/4 = \sqrt{\pi}\,\Delta/8$$

$$\beta_1/4 = 0.354 + 0.194\Delta$$

$$\beta_2/4 = 0.457 + 0.177\Delta$$

where $\kappa_0^2 = (2\mu\sigma_s/D)\beta_0$ is the estimated eigenvalue of the lowest (most persistent) mode, $\kappa_1^2 = (2\mu\sigma_s/D)\beta_1$ of the next lowest, etc.

3.1.4.5 Hydrogen Bound in an Oscillator Potential Well

Cohen and Vaughan[19] considered the case of hydrogen bound in an isotropic, harmonic oscillator potential well. In this treatment, Eq. (3-1) is solved such that all collisions with atoms other than hydrogen are either purely elastic or lead to absorption. The oscillator quantum, $h\nu$, is taken to be 0.13 ev, and 1/v absorption of 10 barns per H atom is assumed present. The quantum 0.13 ev is taken to represent the state of affairs in ZrH_2. The result of their calculation is given in Fig. 3-6.

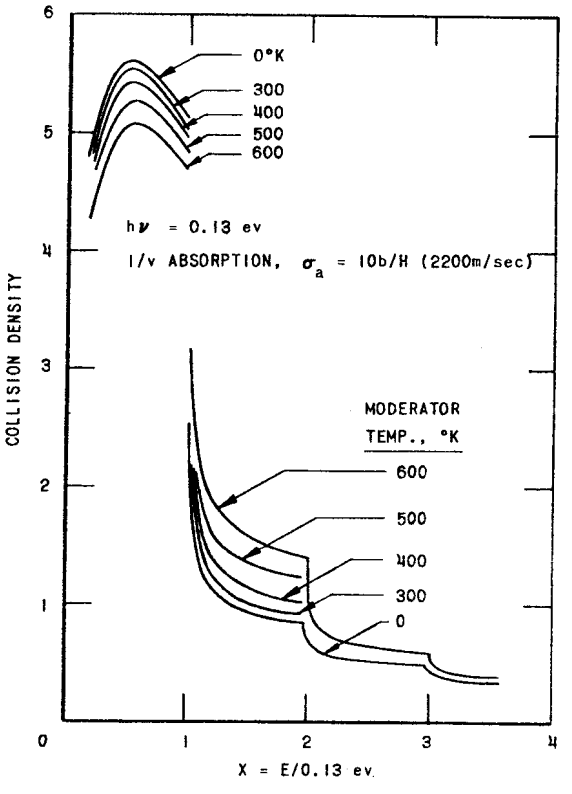

Fig. 3-6—Neutron collision density in infinite ZrH_2. *Reproduced from Ref. 19.*

3.1.4.6 Heavy Crystalline Moderator

In Fig. 3-7, the results of a numerical solution for the flux are compared for a Debye crystal (Section 3.1.3.3), and for a heavy gas.

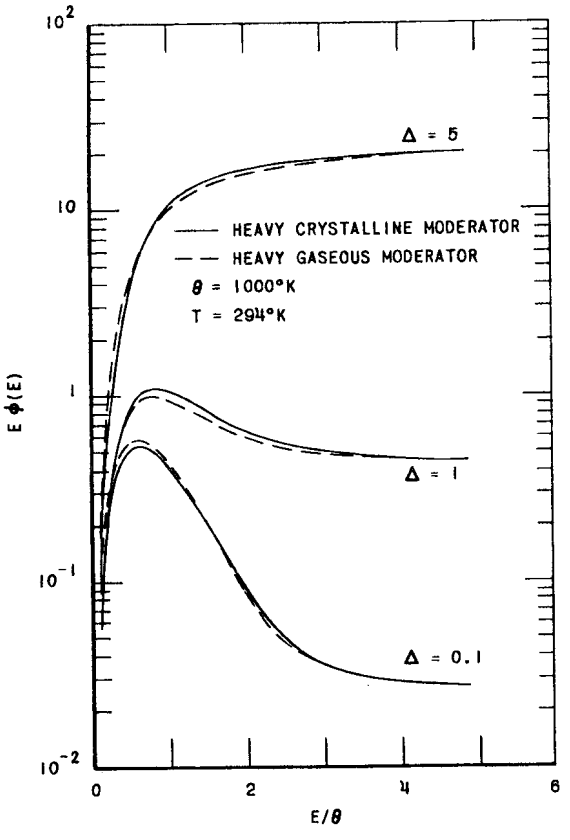

Fig. 3-7—Comparison of thermal spectra for 1/v absorption in a heavy crystalline moderator with spectra in a heavy gaseous moderator. *Reproduced from Ref. 6.*

3.1.5 SPECIAL PROBLEMS IN DISCONTINUOUS MEDIA

3.1.5.1 Thermal Neutron Flux in a Medium with a Temperature Discontinuity

Kottwitz[20] has solved the problem of determining the flux in a medium with a temperature discontinuity under the following assumptions: (1) no neutron absorption; (2) heavy monatomic gas moderation; (3) diffusion theory approximation is made; (4) slab geometry; and (5) the temperature of the medium, T, is given by:

$$T = T_1;\ x < 0$$

$$T = T_2;\ x > 0$$

where x is the distance from the origin. Then the equation to be solved is:

$$\frac{\partial^2 F}{\partial x^2} + 6\mu\sigma_0^2\left(1 + E\frac{\partial}{\partial E} + E\,T\frac{\partial^2}{\partial E^2}\right)F = 0$$

where μ is the neutron-to-moderator mass ratio, and σ_0 is the bound atom scattering cross section.

The temperature units are such that Boltzmann's constant (k) is unity. The solution is:

$$F(y,E) = \frac{E}{T^2} \exp\left(-\frac{E}{T}\right) \sum_{n=0}^{\infty} C_n \left(1 - \frac{T_0}{T}\right)^n L_n\left(\frac{E}{T}\right) \exp\left(-\sqrt{n}\,|y|\right)$$

where $y = \sigma_0 \sqrt{6\mu}\, x$

T = medium temperature

T_0 = temperature on other side of interface

$L_n(x)$ = Laguerre polynomial of order one. (The definition of Ref. 21 is used.)

The constants, C_n, for $0 \leq n \leq 20$ are listed in Table 3-3.

Table 3-3—CONSTANTS WHICH OCCUR IN THE TEMPERATURE DISCONTINUITY PROBLEM

Data from Ref. 20.

n	C_n	n	C_n
0	1.0000 0000 00	11	0.1234 4237 11
1	0.5000 0000 00	12	0.1166 3381 97
2	0.3535 5339 06	13	0.1106 9794 47
3	0.2803 3008 59	14	0.1054 6964 17
4	0.2355 4595 17	15	0.1008 2373 87
5	0.2049 8140 26	16	0.0966 6349 71
6	0.1826 2060 27	17	0.0929 1289 26
7	0.1654 5563 36	18	0.0895 1129 64
8	0.1518 0577 74	19	0.0864 0972 46
9	0.1406 5391 58	20	0.0835 6814 09
10	0.1313 4628 83		

3.1.5.2 Effect of Spatial Distributions of Sources

Michael[22] has studied the problem of determining the steady-state spatial distribution of neutrons in an absorbing medium with a spatially distributed source. The diffusion approximation was used; uniform temperature and the heavy monatomic gas moderation law were assumed; and σ_s was set equal to σ_{tr}. If the source of neutrons is distributed according to

$$S(x,E) = F(E) \exp(-k\,|x|)$$

the flux is given by:

$$\Psi(x,E) = 3\sigma_{tr}(E)\, M(E) \left[\exp(-k\,|x|) \sum_n \frac{H_n(E)}{\kappa_n^2 - k^2} \int_0^{\infty} 3\sigma_{tr}(E')\, F(E')\, H_n(E')\, dE' + \sum_n \frac{k}{\kappa_n} \frac{\exp(-\kappa_n |x|)}{k^2 - \kappa_n^2} \int_0^{\infty} 3\sigma_{tr}(E')\, F(E')\, H_n(E')\, dE' \right]$$

where $H_p(E) = \sum_m C_{pm} L_m^{(1)}(E)$

The first term in $\Psi(x,E)$ comes from the finite extent of the source. The second term is a sum of solutions of the homogeneous diffusion equation for which the κ_n are eigenvalues. (Rules for the case $\kappa_n^2 = k^2$ are given in the reference.)

The $L_m^{(1)}(E)$ are the associated Laguerre polynomials of order one.[21] The normalization used is:

$$\int_0^{\infty} dE\, L_n^{(1)}(E)\, L_m^{(1)}(E)\, M(E) = \delta_{mn}$$

where $M(E) = \frac{E}{T^2} e^{-E/T}$

The eigenvalues κ_n^2 are given via the equations for $\alpha_p \equiv \kappa_p^2/6\,\mu\sigma_s^2$, where μ is the neutron-to-moderator mass ratio.

The values of α_0, α_1, and α_2 are approximated as functions of $\Delta = 4\sigma_a(kT)/\xi\sigma_s$:

$$\alpha_0 = \frac{\sqrt{\pi}}{8}\Delta(1 - 0.034\Delta); \text{ for } \Delta < 2$$

$$\alpha_1 = 1 + 0.194\Delta - 0.004\Delta^2; \text{ for } \Delta < 2$$

$$\alpha_2 = 2 + 0.177\Delta - 0.001\Delta^2; \text{ for } \Delta < 2$$

The coefficients C_{pm} satisfy the equations:

$$\sum_{m=0}^{\infty} C_{pm}\left[\frac{\Delta}{4}V_{mn} + (m - \alpha_p)\delta_{mn}\right] = 0$$

$$V_{mn} = \int dE\, L_m^{(1)}(E)\, E^{-1/2}\, L_n^{(1)}(E)\, M(E)$$

In the limit k very large, the asymptotic solution is given by MH_0; the most probable energy occurs at $(1 + 0.07\Delta)kT$.

3.1.6 EMPIRICAL DESCRIPTION OF THE NEUTRON SPECTRUM

Cohen[2] has studied the properties of the following empirical description of the neutron spectrum:

(1) The neutron spectrum is Maxwellian, characterized by some temperature, T_n, to a cutoff energy.
(2) The spectrum is a slowing-down distribution beyond the cutoff energy.
(3) The neutron flux is continuous and neutrons are conserved.

He showed that if the average energy of the neutrons is set equal to that obtained by the heavy gas approximation, then

$$T_n/T_0 = 1 + C\Delta + \text{higher-order terms}$$

where $\Delta = \dfrac{4\sigma_a(kT_0)}{\xi\sigma_s} = 2A\sigma_a(kT_0)/\sigma_s$

T_0 = the moderator temperature

The mean energy is defined by:

$$\int dvN(v)/\int dvN(v)v^{-2}$$

The coefficient C is estimated in two ways. The first estimate is 0.3; the second is $1/\sqrt{\pi} = 0.56$. In a later article, Cohen[3] showed that any such prescription (at least in the heavy gas model) is arbitrary and there is no preferred method of specifying T_n.

3.1.6.1 Description of Spectra by Fitting to Monte Carlo Results

Coveyou, Bate and Osborn,[8] and Brown[7] have examined the results of Monte Carlo spectrum calculations to determine if there is an approximate relationship between T_n, T_0, and Δ $[= 2A\sigma_a(kT_0)/\sigma_s]$. The Coveyou, Bate and Osborn calculations were made in the monatomic gas approximation, for a variety of masses. The Brown calculations are based on the earlier calculations of Brown and St. John[13] in which a model of H_2O or D_2O was employed, including some of the features of chemical binding (Section 3.1.3.5). The least-squares method was used to fit a Maxwellian at some temperature, T_n, to the calculated spectrum over the range $0 \leq E \leq 3.6\ kT_0$. (Note: This is not the same as Cohen's fit mentioned in the introductory paragraph.)

Using a Monte Carlo method and the procedure of Section 3.1.3.5 for computing the scattering kernel, Brown[7] obtained the results shown in Figs. 3-8 through 3-10.

Coveyou, Bate and Osborn report that the formula $T_n/T_0 = (1 + 0.45\Delta)$ yields agreement to within 5% for the least-squares results for masses ranging between 1 and 25 and

$$\frac{\sigma_A(kT)}{\sigma_s} < 0.5$$

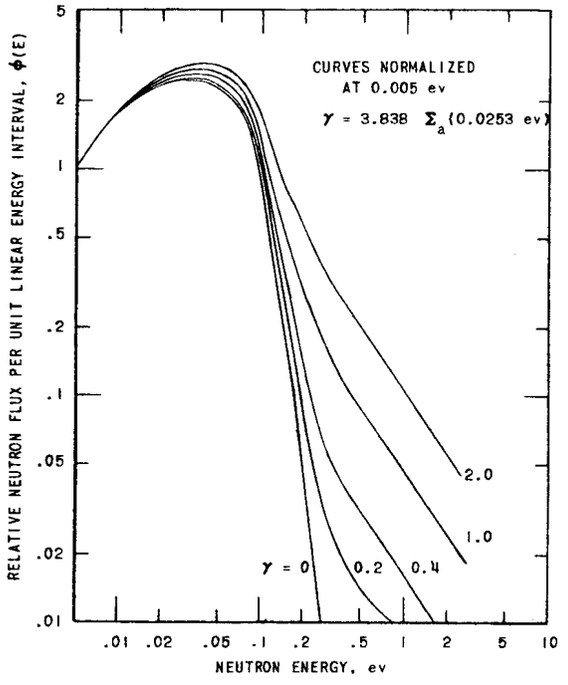

Fig. 3-8—Neutron distributions in H_2O at 80°C for different amounts of absorption. *Reproduced from Ref. 7.*

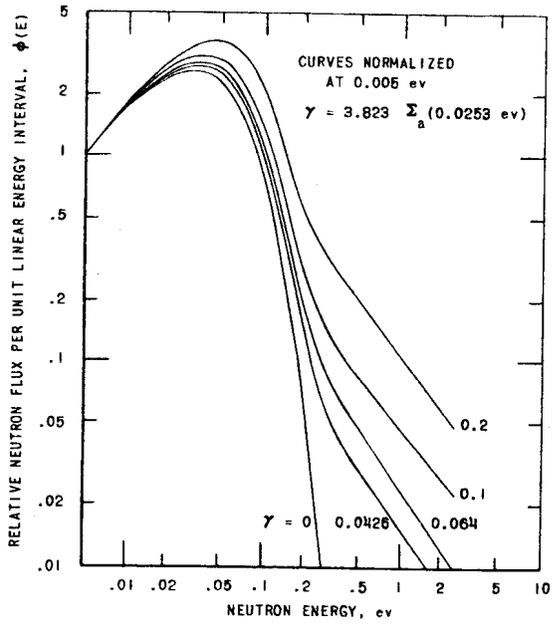

Fig. 3-9—Neutron distributions in D_2O at 80°C showing spectral hardening with varying neutron absorption. *Reproduced from Ref. 7.*

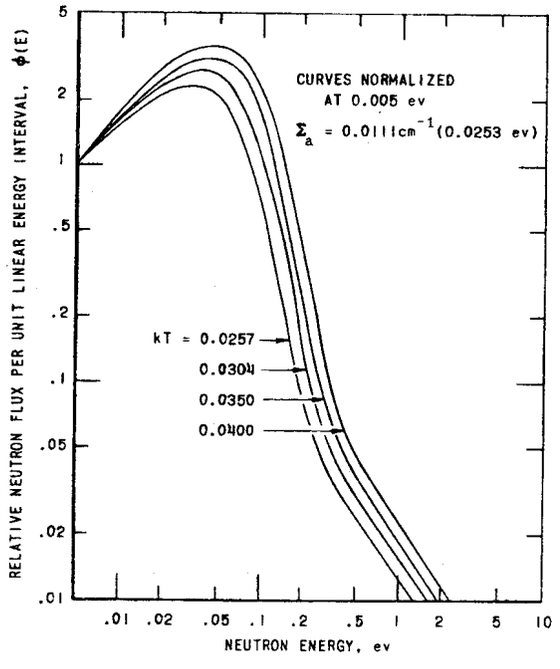

Fig. 3-10—Neutron distributions in D_2O showing spectral hardening with varying moderator temperatures. *Reproduced from Ref. 7.*

Brown[7] reports that in D_2O

$$\frac{T_n}{T_0} = 1 + 0.48\,\Delta;\ \Delta < 1.0$$

provides a 1% fit to the results of the least-squares fits. For H_2O, Brown reports that the coefficient is not independent of T_0 or $\sigma_a(kT_0)$. His results are given in Table 3-4.

Table 3-4—VALUES OF C IN $T_n/T_0 = 1 + C\Delta$ FOR H_2O

Data from Ref. 7.

kT_0, ev	Δ				
	0.0384	0.0687	0.137	0.384	0.687
0.0257	0.438	0.492	0.438	0.427	0.405
0.0304	0.402	0.402	0.402	0.372	0.342
0.035	—	0.328	0.352	0.328	0.295
0.040	—	0.307	0.307	0.281	0.254

3.1.7 EXPERIMENTS ON NEUTRON SPECTRA

3.1.7.1 Measurement of Flux Spectrum in H_2O Poisoned with Boric Acid: Comparison with Theoretical Distribution

Poole[23,24] employed pulsed-source, time-of-flight techniques to measure the thermal neutron flux in light-water containing various concentrations of boric acid.

Spectra in pure water at room temperature were measured at distances of 2, 5, 10, and 12.5 cm from the neutron source. These spectra, shown in Fig. 3-11, were normalized such that the integral of the flux in an identifiable Maxwellian flux component is unity. In all of these cases, a Maxwellian component was observed with temperature, T, equal (within experimental error) to the moderator temperature. A spectrum characterized by λ/E was observed above 0.2 ev. The value of λ closely approaches an asymptotic value of ≈ 0.015 at a distance of 10 cm from the source.

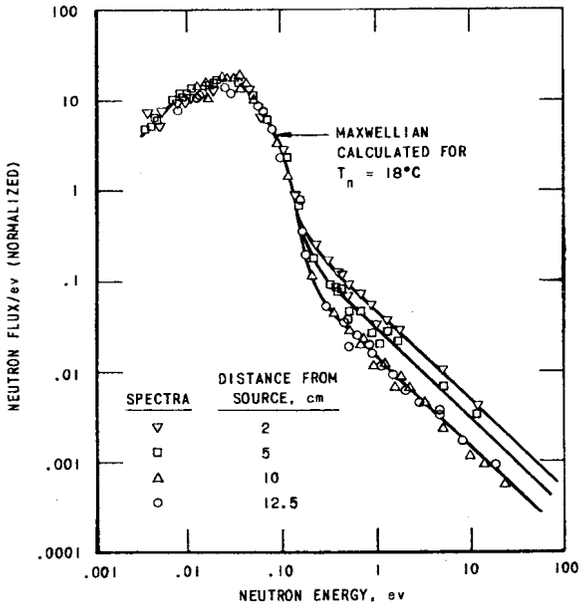

Fig. 3-11—Neutron flux spectrum in pure water. *Reproduced from Ref. 24.*

Neutron flux spectra were measured in boric acid solutions at room temperature and at elevated temperatures, with poisoning ranging from $\sigma_0 = 1.5$ barn to $\sigma_0 = 7.6$ barn, where σ_0 is the effective capture cross section per hydrogen atom at 2200 m/sec. The measured spectra, along with curves indicating the fitting of a hardened Maxwellian and the 1/E component at higher energies, are shown in Fig. 3-12.

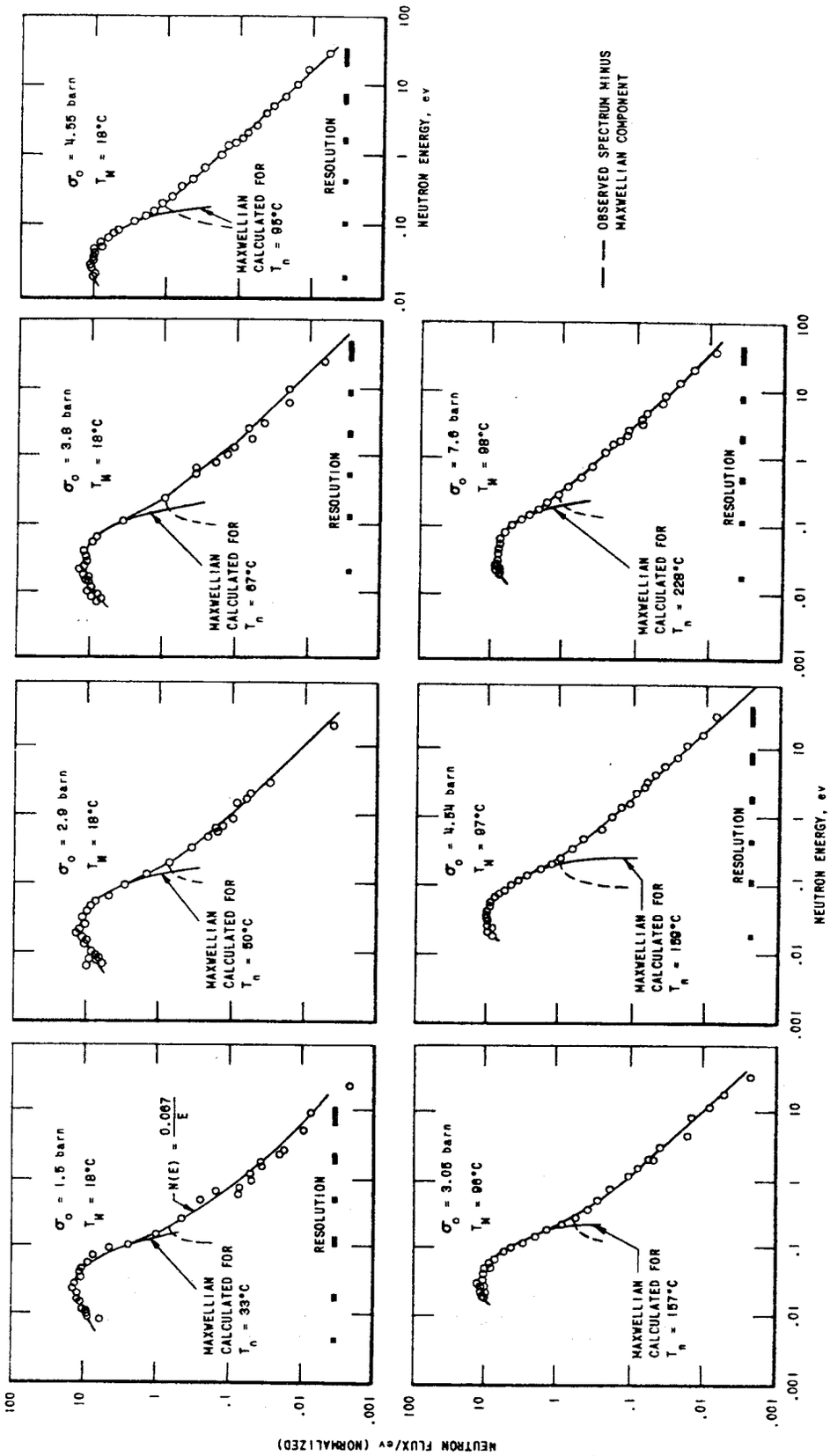

Fig. 3-12—Neutron flux spectra in boric acid solution. *Reproduced from Ref. 24.*

In the case of boric acid poisoning, Poole derived a general formula for λ given by:

$$\lambda = \frac{\sqrt{\pi}}{2}\sqrt{\frac{293}{T_n}}\frac{\sigma_0}{\sigma_s - 0.7\,\sigma_0}$$

where σ_s is the asymptotic scattering cross section for hydrogen, and T_n is the temperature of the Maxwellian component of the flux.

In Table 3-5 are listed the results of the experiments and the values obtained by the formulas of Coveyou, et al.,[8] and of Brown.[7] In Fig. 3-13, the ratios of the effective neutron temperature (T_n) in

Table 3-5—SUMMARIZED RESULTS ON T_n AND λ

Data from Ref. 24.

Moderator	σ_0, barn	T_M, °C	Position of probe, cm from source	Measured T_n, °C	Calculated T_n, °C			Measured λ, cm (All ± 10%)	Calculated λ, cm		
					Coveyou	Brown	Amster		Poole	Amster	Brown
Tap water	0.3	18	2	35 ± 30	—	—	—	0.048	—	—	—
Tap water	0.3	18	5	41 ± 30	—	—	—	0.033	—	—	—
Tap water	0.3	18	10	10 ± 30	—	—	—	0.016	—	—	—
Tap water	0.3	18	12.5	24 ± 30	—	—	—	0.015	—	—	—
Demineralized water	0.3	18	10	31 ± 30	—	—	—	0.018	—	—	—
Demineralized water	0.3	18	12.5	41 ± 30 Average 26 ± 15	—	—	—	0.016 Average 0.016 ± .001	—	—	—
Boric-acid solution	1.5	18	10	33 ± 30	40	40	30	0.067	0.069	0.072	—
Boric-acid solution	2.9	18	10	37 ± 30	59	57	47	0.130	0.137	0.139	—
Boric-acid solution	3.73	18	10	67 ± 30	72	69	—	0.13	0.19	0.180	—
Boric-acid solution	4.55	18	10	95 ± 35	80	75	68	0.214	0.214	0.215	0.240
Boric-acid solution	3.03	96	10	57 ± 40	—	—	—	0.121	0.125	—	—
Boric-acid solution	4.54	97	10	59 ± 40	—	—	44	0.236	0.19	—	—
Boric-acid solution	7.6	98	10	28 ± 50	—	93	79	0.328	0.356	0.34	0.35
Boric-acid solution	9.9	98	10	42 ± 50	—	—	—	0.44	—	—	—

the Maxwellian component, to the moderator temperature (T_M) are plotted on the basis of Poole's fitting and, also, in terms of the formulations of Coveyou and of Brown. Included are the parameters T_n and λ determined by Amster[25] by analyses of Wigner-Wilkins calculations of the neutron flux spectra in the boric acid solutions. Amster used the monatomic gaseous hydrogen model of neutron scattering and energy exchange.

In Fig. 3-14, comparisons are presented between the results of Wigner-Wilkins calculations by Amster and experimental results by Poole, the experimental results being normalized, as before, to unit area under a best-fit hardened Maxwellian component below the 1/E range. The solid lines are Wigner-Wilkins plots normalized to give the best fit at energies in the vicinity of maximum flux; the dashed lines are extrapolations to higher energies and are proportional to 1/E.

3.1.7.2 Spectra in Pure Water and in Multiplying Media

Slovacek and Stone[26] extracted a beam from pure water, and from water-moderated subcritical assemblies and measured, by use of a slow chopper, the spectra over the energy range 10^{-2} to 10 ev.

The details of the assemblies are given in Table 3-6.

The experimental results are plotted in Fig. 3-15. Also plotted are the spectra calculated by the SOFOCATE Code (see Section 10). The leakage correction was not included in the pure water cases.

The thermal self-shielding factor is just the fuel disadvantage factor calculated for the assemblies called Matrix I and Matrix II.

3.1.7.3 Spectra in Water, Polyethylene, and Zirconium Hydride

Beyster, et al.,[27] performed an extensive set of experiments on spectra in beams emerging from H_2O, $(CH_2)_n$, and $ZrH_{1.5}$. The moderators were poisoned with boron, cadmium, or samarium. The experimental data are displayed in Fig. 3-16. The calculations are described in Ref. 27 and involve a number of different models. Each curve is labeled with the absorption per H atom at 0.0253 ev.

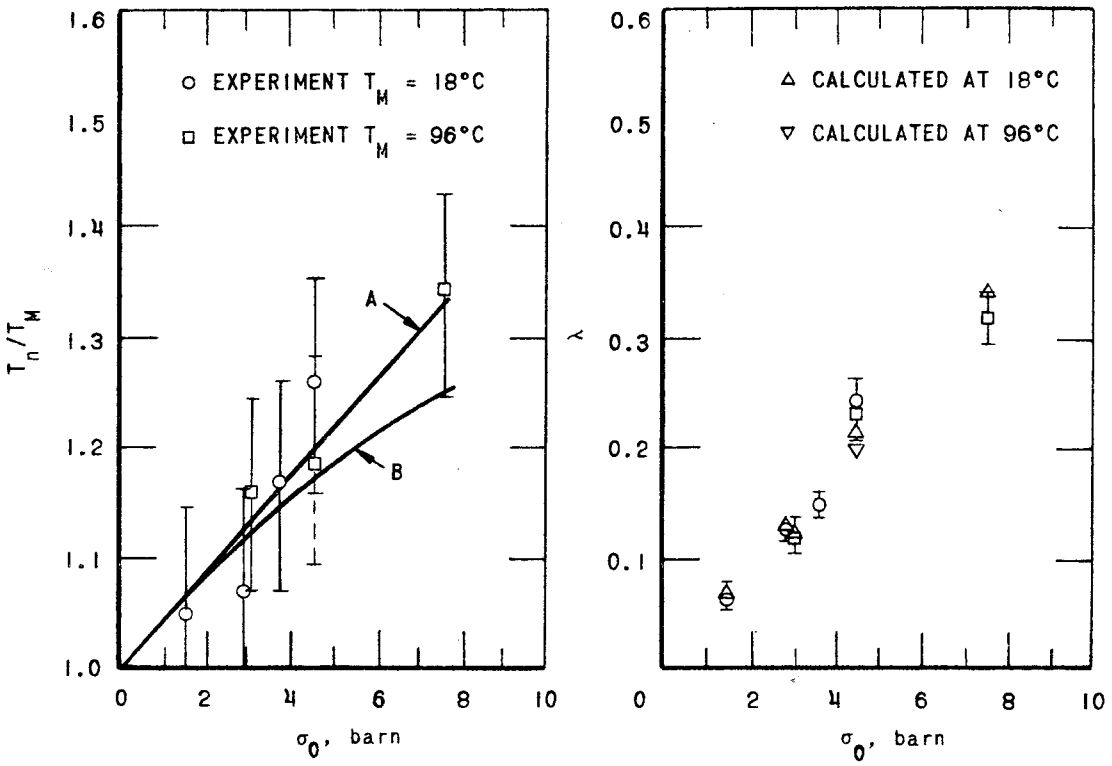

Fig. 3-13 — T_n/T_M and λ as a function of σ_0. Curve A is a plot of Coveyou's formula for T_M = 18°C; Brown's formula is ~3% lower. Curve B is a plot of Brown's formula for T_M = 96°C. *Reproduced from Ref. 24.*

Table 3-6 — SOURCE DATA

Data from Ref. 26.

Medium	T, °K	E_0, ev	α, cm^{-1}	γ, cm^{-1}	B^2, cm^{-2}	$D(E_0)B^2$, cm^{-1}	$\Sigma_a(E_0)$	$D(1\ ev)B^2$	$\Sigma_a(1\ ev)$
H_2O	298	0.0257	i(0.172 ± .02)	0.166 ± 0.001	−0.057 ± .01	−0.0064	0.0220	−0.033	0.00
H_2O	586	0.0505	0.112 ± .01	0.098 ± 0.001	0.003 ± .002	0.0007	0.0115	0.0025	0.00
Matrix I	298	0.0257	0.093 ± .006	0.056 ± 0.001	0.0055 ± .0011	0.0011	0.193	0.0056	0.03
Matrix I	586	0.0505	0.056 ± .004	0.036 ± 0.001	0.0018 ± .0014	0.0007	0.138	0.0024	0.03
Matrix II	298	0.0257	0.107 ± .007	0.062 ± 0.002	0.0077 ± .0015	0.0010	0.406	0.0066	0.06
Matrix III	586	0.505	0.063 ± .005	0.053 ± 0.002	0.0011 ± .0007	0.0003	0.290	0.0012	0.06

Nomenclature: T = water temperature.
E_0 = energy corresponding to T.
α,γ = measured constituents of the buckling $B^2 = \alpha^2 - \gamma^2$.
$D(E_0)B^2$ = equivalent absorption from leakage, calculated at $E = E_0$.
$\Sigma_a(E_0)$ = macroscopic absorption cross section of medium at E_0.
$D(1\ ev)B^2$ = equivalent absorption from leakage at 1 ev.
$\Sigma_a(1\ ev)$ = macroscopic absorption cross section of medium at 1 ev.

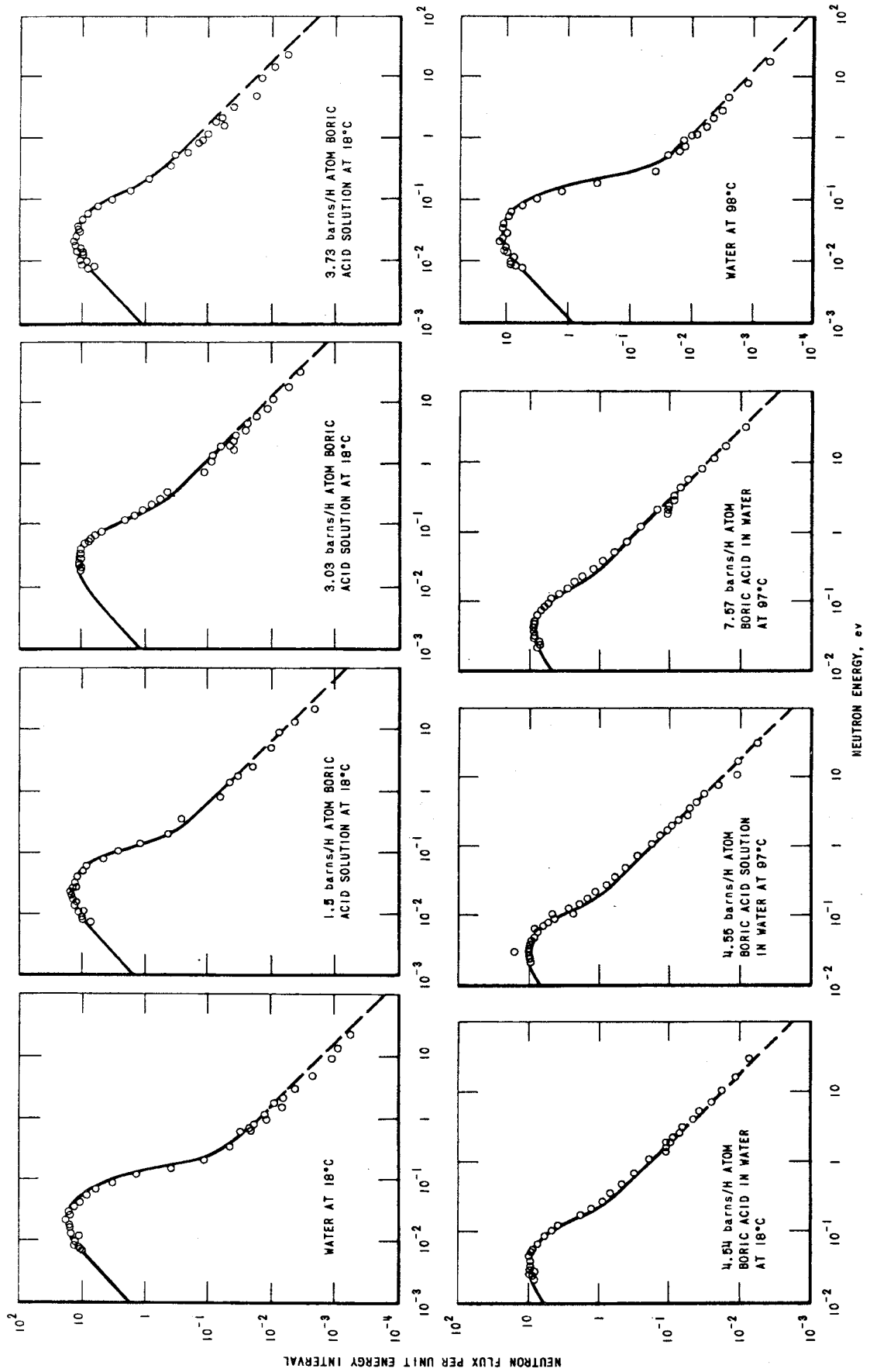

Fig. 3-14—Neutron flux spectra in solutions of boric acid and water. *Reproduced from Ref. 25.*

687863 O - 63 - 8

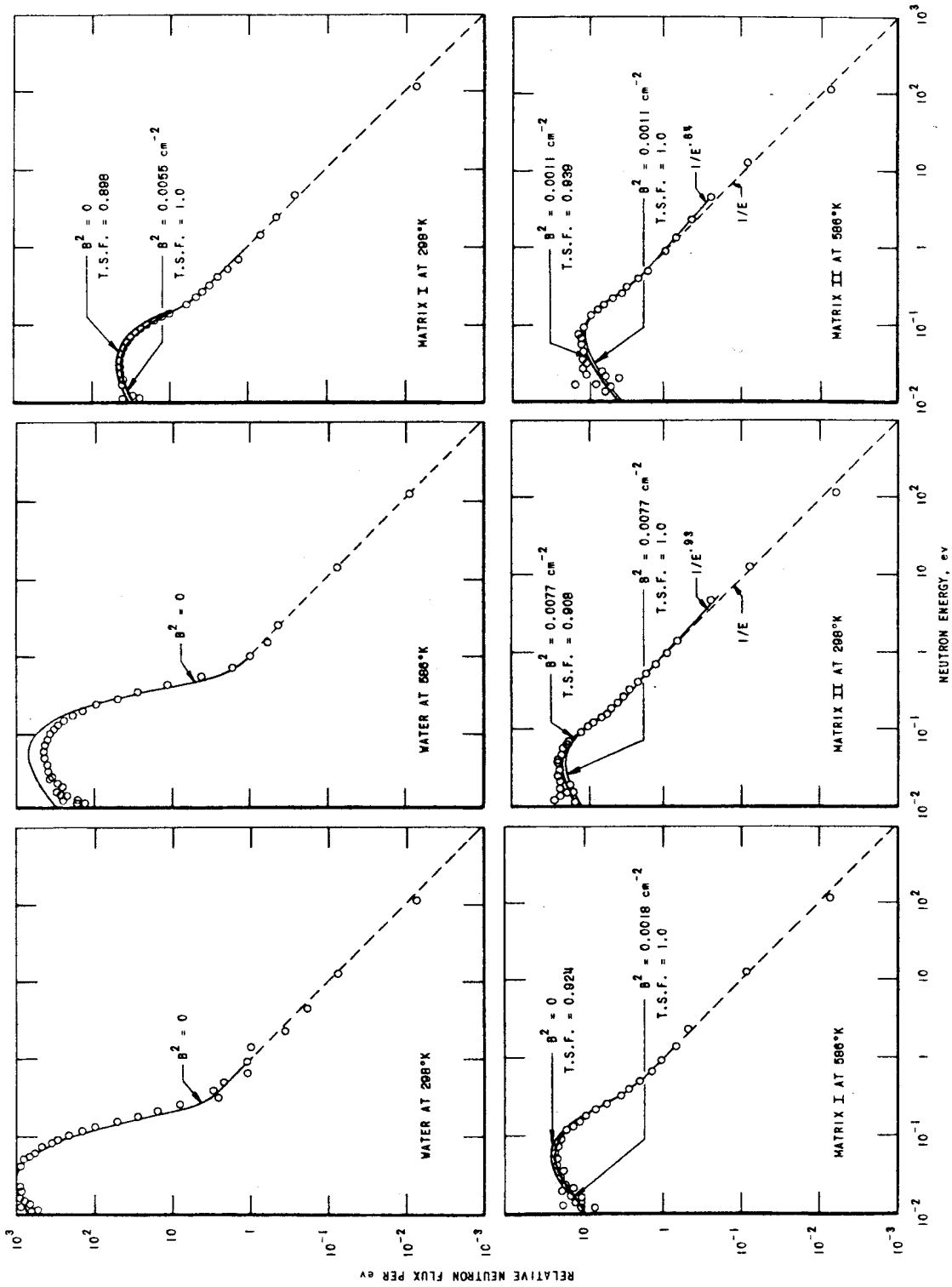

Fig. 3-15—Neutron spectra in water and multiplying media. Solid curves are SOFOCATE results for values of buckling (B^2) and thermal shielding factor (T.S.F.) indicated. *Reproduced from Ref. 26.*

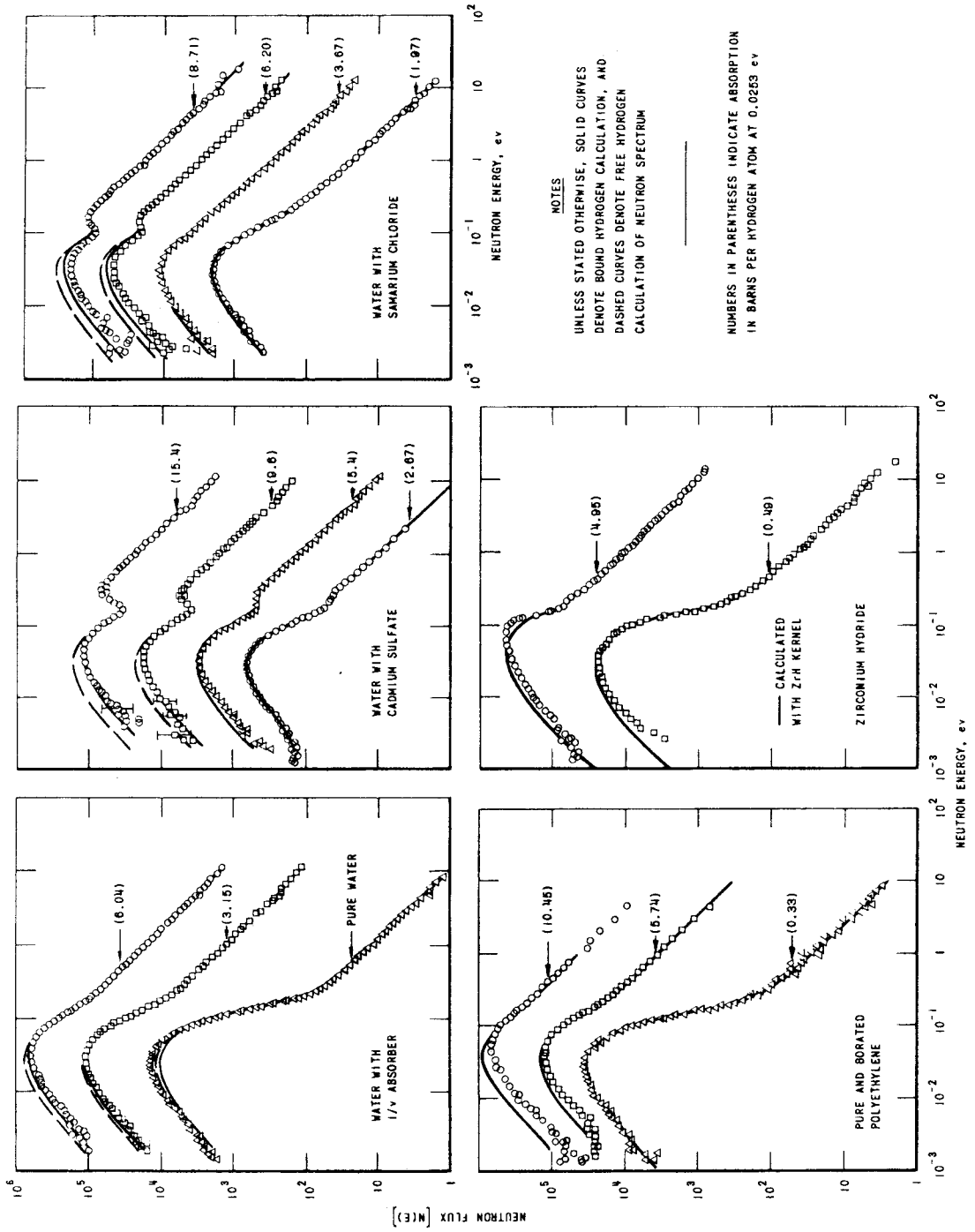

Fig. 3-16—Measured and calculated neutron flux spectra in water, polyethylene, and zirconium hydride. *Reproduced from Ref. 27.*

3.1.7.4 Neutron Spectra from Natural Uranium-Water Lattices*

Mostovoi, et al.,[28] used a slow chopper to measure the neutron spectrum emerging from subcritical assemblies fed by neutrons from the WWR.[29] Data are presented which represent the spectra from the WWR, and from the moderator (water) and fuel (natural uranium) of the subcritical assemblies.

The two lattices studied contained 3.5-cm-diameter, natural uranium rods in triangular arrays with spacings of 5.0 and 6.0 cm.

Plots of Nv^2 [$\propto E\,\phi(E)$] are reproduced in Fig. 3-17.

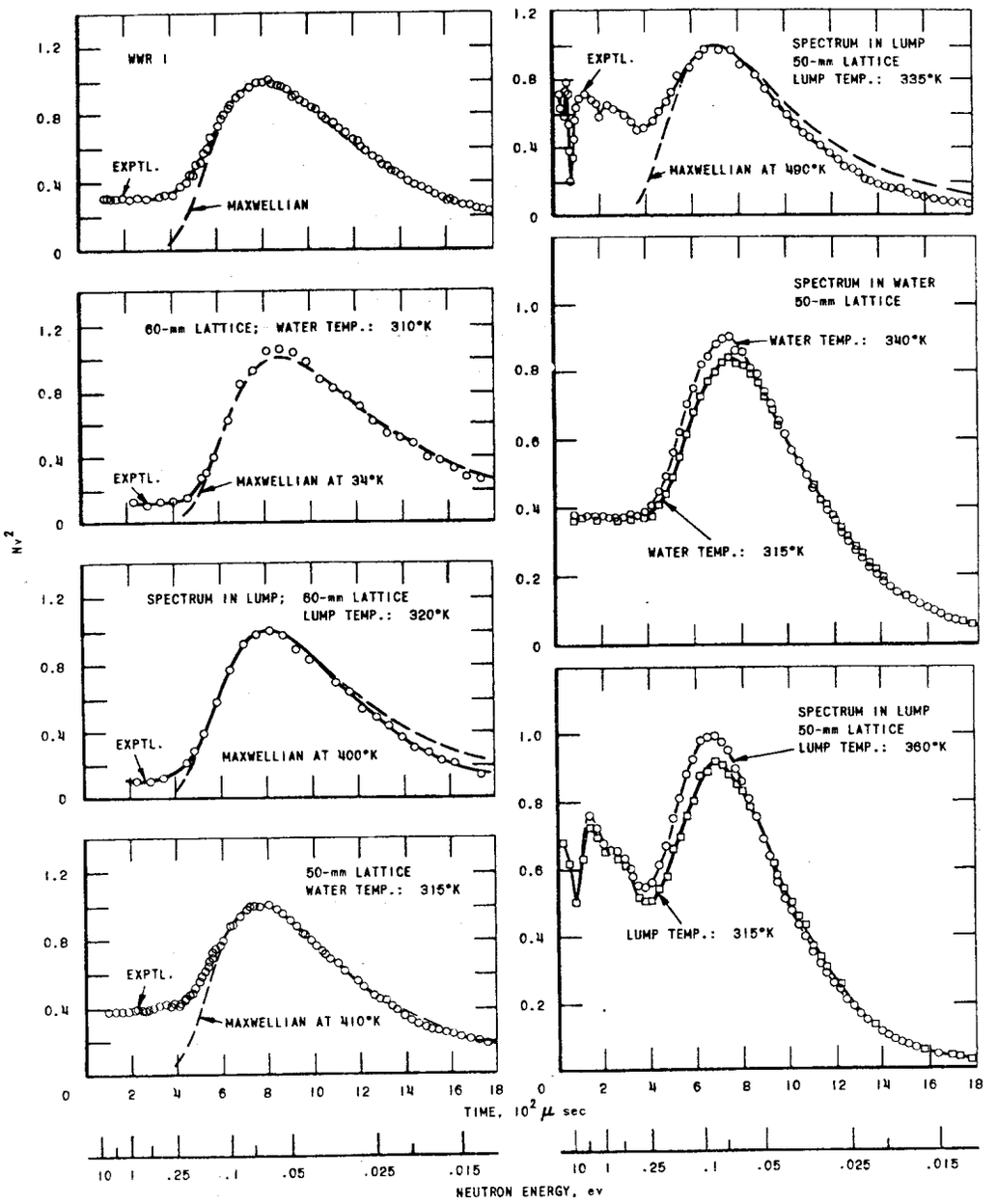

Fig. 3-17—Neutron spectra in uranium-water assemblies at various temperatures. *Reproduced from Ref. 28.*

* This work is included here because of its natural connection with the preceding material. Normally, it would appear in Section 4.

3.2 EFFECTIVE CROSS SECTIONS

3.2.1 A VARIATIONAL CALCULATION FOR THE EFFECTIVE THERMAL CROSS SECTION

Shimizu[30] has developed a variational method for calculating the effective thermal cross section of an isotope when the heavy monatomic gas model is employed. In his method, the majority of the capture is assumed to occur with a 1/v dependence; the cutoff energy, E_m, is selected at 10 kT, where T is the temperature of the medium; and the absorption parameter is given by:

$$\Delta^* = \sigma_a(kT)/\xi\sigma_s \quad \text{(one-fourth of the usual } \Delta\text{; see Section 3.1.1)}$$

The effective thermal cross section is defined by:

$$\hat{\sigma}_{th} = \int_0^{E_M} \phi(E)\sigma(E)dE \Big/ \int_0^{E_M} \sqrt{\frac{E_0}{E}}\,\phi(E)dE \tag{3-6}$$

where E is measured in units of kT. The following functional is introduced:

$$J\{\Psi(E),\ \chi(E)\} = \frac{\chi(E_M)\int_0^{E_M}\sigma_a^i M(E)\,\Psi(E)dE}{\int_0^{E_M}\left[\xi\sigma_s\ EM\frac{d\chi}{dE}\frac{d\Psi}{dE} + \sigma_a M(E)\,\chi(E)\right]dE} \tag{3-7}$$

where $M(E) = Ee^{-E}$, and $\sigma_a(E) = \xi\sigma_s\ \Delta^* 1/\sqrt{E}\ f(E,T) = \sigma_0\sqrt{E_0/E}\ f(E,T)$ is the capture cross section, with f(E,T) representing the departure from 1/v behavior.

$$\sigma_a^i = \xi\sigma_s\ \Delta^*\ 1/\sqrt{E}$$

is just the 1/v part of the absorption. Then the extremum values of Ψ and χ are such that $M\Psi$ satisfies the Wilkins equation (3-4) for absorption, σ_a, and χ satisfies

$$-\frac{d}{dE}\left(\xi\sigma_s\ EM\frac{d\chi}{dE}\right) + \sigma_a(E)M\chi = \left(\chi(E_m)\int_0^{E_M}\sigma_a M\Psi\ dE \Big/ \int_0^{E_M}\sigma_a^i(E)M\Psi\ dE\right)\sigma_a^i(E)\,M(E) \tag{3-8}$$

$M\chi$ is interpreted as a neutron spectrum arising from the external source given by the right member of Eq. (3-8). (If f(E,T) = constant, then $\chi = 1$.) The stationary value of J is

$$J\{\bar{\Psi},\chi\} = \hat{\sigma}_{th}/\sigma_0$$

The trial functions used are:

$$\chi = 1 + \alpha\ E$$

$$\Psi = 1 + \beta Q(E)$$

where

$$Q(E) = \int_0^E dZ\ Z^{-2}\ e^Z \int_0^Z dt\ \sqrt{t}\ e^{-t}$$

is the approximate iterative solution found by Hurwitz, et al.[5] The results are:

$$\frac{\sigma_{th}}{\sigma_0} = \frac{g_{th}(T) + s_{th}(T)\ \Delta^*}{1 + 0.4300\ \Delta^*}$$

where

$$g_{th} = \int_0^{E_M}\frac{1}{\sqrt{E}}\,f(E,T)M(E)\,dE \Big/ \int_0^{E_M}\frac{1}{\sqrt{E}}\,M(E)\,dE$$

$$s_{th} = 1.12857\int_0^{E_M}\frac{1}{\sqrt{E}}\,f(E,T)\,MQ\,dE - 2.34694\int_0^{E_M}\frac{1}{\sqrt{E}}\,f(E,T)\,M\,dE$$

and

$$E_M = 10\ kT$$

Table 3-7 lists values of g_{th} and s_{th} for selected isotopes.

It is estimated that the effective cross section obtained with the use of Table 3-7 is within 7% of the value obtained by a numerical computation, for all $\Delta^* < 1.0$.

Table 3-7—VALUES OF g_{th} AND s_{th} FOR SELECTED ISOTOPES

Data from Ref. 23.

T, °C	U^{235}				Pu^{239}				Pu^{241}	
	Absorption		Fission		Absorption		Fission		Absorption	
	g_{th}	s_{th}	g_{th}	s_{th}	g_{th}	s_{th}	g_{th}	s_{th}	g_{th}	s_{th}
20	0.9749	0.2842	0.9749	0.2780	1.0881	1.5153	1.0477	1.2350	1.02715	0.6580
40	0.96975	0.28935	0.9698	0.2812	1.1049	1.8642	1.0604	1.5095	1.0328	0.6799
80	0.9604	0.3055	0.9602	0.2932	1.1475	2.7929	1.09245	2.2474	1.2919	0.7264
120	0.9521	0.3203	0.9517	0.30475	1.2023	3.5914	1.1337	2.8830	1.3026	0.7767
160	0.94485	0.3284	0.9441	0.3103	1.2693	4.0836	1.1843	3.2735	1.3142	0.8314
200	0.9386	0.3318	0.9374	0.31145	1.3487	4.41165	1.2446	3.5335	1.3268	0.8910
240	0.9333	0.3328	0.9316	0.3101	1.4400	4.6516	1.3145	3.7239	1.3405	0.9562
280	0.9288	0.3318	0.9265	0.3071	1.5422	4.8312	1.3930	3.8671	1.3555	1.0280
320	0.9250	0.3289	0.92205	0.3031	1.6534	4.9620	1.4788	3.9718	1.3721	1.1074
360	0.9218	0.3245	0.9182	0.2983	1.7719	5.0496	1.5706	4.04265	1.3905	1.19575
400	0.9191	0.3190	0.9148	0.2927	1.8956	5.0981	1.6668	4.0826	1.4110	1.2947

An approximate value of the epithermal spectrum is obtained from the relation:

$$\phi(E)\hat{\phi}_{th} = \frac{\Delta_0^* P^*(E)}{E}\left(1 + b\frac{kT}{E}\right) + CM(E)$$

where

$$\hat{\phi}_{th} = \int_0^{E_M} \sqrt{E_0/E}\ \phi(E)dE$$

$$\Delta_0^* = \sqrt{T/T_0}\ \Delta^*\ (E_0 = kT_0 = 0.0253\ ev);\ E > E_M$$

$$P^*(E) = P(E)/P(E_M)$$

$$P(E) = \exp\left[-\int_E^{\infty} \frac{\sigma_a}{\xi\sigma_s E'}\left(1 + b\frac{kT}{E'}\right) dE'\right]$$

$$b = \frac{3.05 - 0.970\ \Delta^*}{1 + 0.097\ \Delta^*} \approx 3 - 1.2\ \Delta^*$$

and

$$C = \sqrt{T/T_0}\ (0.886078 + 0.085886\ \Delta^*)^{-1}$$

The effective cross section, σ_{eff}, is defined by:

$$\sigma_{eff} = \int_0^{\infty} \sigma(E)\ \phi(E)\ dE / \int_0^{E_M} \sqrt{E_M/E}\ \phi(E)\ dE$$

$$= \frac{\sigma_{th}}{\sigma_0} + \Delta_0^*\ S_R + a g_r$$

where

$$S_R = \frac{1}{\sigma_0} \int_{E_M}^{\infty} \sigma_a(E) \frac{P^*(E)}{E} \left(1 + b \frac{kT}{E}\right) dE$$

$$g_R = \int_{E_M}^{\infty} \frac{1}{\sqrt{E}} f(E,T)\, M dE \Big/ \int_0^{E_M} \frac{1}{\sqrt{E}} M\, dE$$

and

$$a = (1 + 0.09693\ \Delta^*)^{-1}$$

The term ag_r is generally negligible except when there is a resonance near E_M. The resonance integral, $\sigma_0 S_R$, includes 1/v capture down to E_M and has a correction for moderator motion.

Conversion factors to permit usage of other definitions of effective cross section are:

$$\int_0^{E_M} \sqrt{\frac{E_0}{E}}\, \phi(E)\, dE \Big/ \int_0^{E_M} \phi(E)\, dE = \sqrt{\frac{T_0}{T}}\ \frac{1 + 0.4300\ \Delta^*}{1.1280 + 1.4464\ \Delta^*}$$

and

$$\int_0^{\infty} \sqrt{\frac{E_0}{E}}\, \phi(E)\, dE \Big/ \int_0^{E_M} \sqrt{\frac{E_0}{E}}\, \phi(E) dE = \exp\left[\frac{2}{\sqrt{10}} \left(1 + \frac{b}{30}\right) \Delta^*\right] + \frac{0.0001681}{1 + 0.09693\ \Delta^*}$$

3.2.2 WESTCOTT'S CONVENTION AND EFFECTIVE CROSS SECTION COMPILATION

Westcott[31,32] has established an effective cross section convention and has published[32] an extensive compilation of coefficients for the determination of effective cross sections. His work is summarized here.

The 2200-meter/second flux is defined by nv_0, where

$$nv_0 = \int_0^{\infty} n(v) dv$$

$$v_0 = 2200 \text{ m/sec}$$

The effective cross section, $\hat{\sigma}$, is defined by:

$$\hat{\sigma} = \int_0^{\infty} \sigma(v)\, n(v) dv / nv_0$$

The spectrum, n(v), is represented as the sum of two components: (1) a Maxwellian distribution characterized by a neutron temperature, T; and (2) an epithermal component which is proportional to $1/v^2$ at large v. Four different analytical forms have been used for that part of the epithermal component which does not come from the Maxwellian tail. Westcott states a preference for the fourth form, $n_4(v)$ (epithermal):

$$n_4(v) = \left[1 - \frac{0.26}{(1 + v^2/16.4\ V_T^2)^5} + \left(4.75 \frac{V_T^2}{v^2}\right)^7\right]^{-1} \frac{V_T}{v^2}$$

where $V_T = v_0 \sqrt{T/T_0}$

$T = 293.6°K$

Under these assumptions, the effective cross section is given by:

$$\hat{\sigma} = \sigma_0[g(T) + r\, S_i(T)]$$

where σ_0 is the cross section at 2200 m/sec; g(T) is a measure of the departure of the cross section from 1/v dependence averaged over the Maxwellian component; and $S_i(T)$ is the contribution to the total reaction rate from the epithermal part of the spectrum minus the Maxwellian contribution. The

index i refers to the various analytical forms assumed for the epithermal component of the spectrum. The parameter r is used to normalize the relative contributions of the epithermal and Maxwellian components.

Operationally, r is defined by the cadmium ratio, R_{Cd}, of a thin "1/v" foil:

$$R_{Cd} = \frac{\text{Activity of bare foil}}{\text{Activity of Cd-covered foil}} = \frac{g + r\,S_i}{r}\left[S_i + \frac{1}{K}\left(\frac{T}{T_0}\right)^{1/2}\right]^{-1} \tag{3-9}$$

It is suggested[31] that an indicator such as thin gold foil be used; $K \approx 2$ and depends slightly on cadmium thickness.

Details of the range of applicability of Eq. (3-9) are discussed in Refs. 31 and 32. In Table 3-8, the g and S values are given for U^{235}, Pu^{239}, Pu^{240}, and Pu^{241}. The S values are based on the resonance integral at infinite dilution.

Formulae for Westcott's Spectral Index. Westcott's parameter, r, can be determined from the ratio of epicadmium to subcadmium activity, δ_{Cd}, in a sample which has nearly a 1/v cross section in the thermal range:

$$r = g\,\delta_{Cd}/[S + 2g\sqrt{4\,kT/\pi\,E_{Cd}}\;(1 + \delta_{Cd})]$$

where g and S are tabulated quantities; E_{Cd} is the cadmium cutoff energy; and T is the neutron temperature. This relationship has been pointed out by many authors; the particular one quoted here is taken from Ref. 33. If a strong resonance absorber with a resonance integral I and a 1/v thermal behavior is used, the relationship is:

$$r = \delta_{Cd}/\sqrt{4T/\pi\,T_0}\;[(I/\sigma_0) + 2\sqrt{kT_0/E_{Cd}}\;(1 + \delta_{Cd})]$$

where $T_0 = 293°K$, and σ_0 is the 2200 m/sec cross section.

3.2.3 AMSTER'S COMPILATION OF THERMAL CROSS SECTIONS

Amster[34] has prepared an extensive list of the average value of cross sections of a number of isotopes in the thermal energy range. The cross sections are averaged over spectra obtained by numerical integration of the Wigner-Wilkins equation (see Section 3.1.4). There are four independent variables which characterize each spectrum:

(1) Temperature, T, which takes on the values: 293°K, 400°K, 500°K, and 600°K.
(2) The 1/v absorption per hydrogen atom: σ_a/H atom ranges from 0 to 12 barns per atom at intervals of 2 barns per atom.
(3) U^{235} atoms per hydrogen atom; this variable ranges between 0 and 0.02 at intervals of 0.005.
(4) Pu^{239} atoms per H atom; this variable ranges between 0 and 0.01 at intervals of 0.0025.

Moderation is by free hydrogen with a constant cross section.

A typical page from the compilation is reproduced as Table 3-9. The energy interval over which the average is made is 0 to 0.625 ev. All average cross sections are in barns, the numbers themselves being in excess 50 floating points. Thus, YY.XXXXX is read: $(.XXXXX) \cdot 10^{YY-50}$.

Unit A is an artificial element whose absorption cross section is 1 barn at 0.0253 ev.; the energy dependence of the cross section is 1/v. The constant cross section of the moderator atoms (H) was set equal to 20.73 barns. Actually, this is the slowing-down power per H atom of a chemically unbound mixture of two H atoms and one oxygen atom; thus this compilation is directed toward water-moderated systems. Although the H scattering was assumed constant in computing the flux, its energy-dependent values were tabulated and averaged over the flux; these are reported as H_s. The transport cross section, H_{tr}, is an average of

$$\sigma_{tr} = \sigma_a + \sigma_s\,(1 - \bar{\mu})$$

where $\sigma_a = 0.05282\,E^{1/2}$; σ_s is taken from the H_s tabulation; and $\bar{\mu}$ is calculated from Radkowsky's scheme (see Section 3.1.3.5; Ref. 12).

Table 3-8—FACTORS g AND S FOR U^{235}, Pu^{239}, Pu^{240}, AND Pu^{241}

Data from Ref. 32.

T, °C	U^{235}						Pu^{240}			Pu^{239}						Pu^{241}[a]		
	Absorption			Fission			Absorption			Absorption			Fission			Fission		
	g	S_2	S_4	g	S_2	S_4	g	S_2	S_4	g	S_2	S_4	g	S_2	S_4	g	S_2	S_4
20	0.9780	0.0602	0.0497	0.9759	−0.0358	−0.0502	1.0270	33.63	33.74	1.0723	2.290	2.960	1.0487	1.794	2.329	1.0437	0.8211	1.0518
40	0.9733	0.0711	0.0614	0.9711	−0.0275	−0.0410	1.0335	34.74	34.95	1.0909	2.320	3.032	1.0623	1.820	2.389	1.0547	0.8195	1.0563
60	0.9689	0.0816	0.0725	0.9665	−0.0194	−0.0324	1.0397	35.82	36.10	1.1117	2.338	3.085	1.0777	1.835	2.432	1.0668	0.8132	1.0519
80	0.9648	0.0915	0.0828	0.9622	−0.0118	−0.0244	1.0458	36.87	37.23	1.1350	2.343	3.117	1.0952	1.840	2.460	1.0801	0.8016	1.0390
100	0.9610	0.1009	0.0923	0.9581	−0.0044	−0.0169	1.0518	37.88	38.33	1.1611	2.336	3.130	1.1150	1.836	2.471	1.0945	0.7845	1.0177
120	0.9575	0.1097	0.1010	0.9543	0.0025	−0.0100	1.0578	38.87	39.43	1.1903	2.318	3.122	1.1373	1.822	2.466	1.1101	0.7617	0.9882
140	0.9542	0.1180	0.1089	0.9507	0.0089	−0.0038	1.0638	39.83	40.52	1.2227	2.286	3.095	1.1623	1.797	2.445	1.1269	0.7333	0.9508
160	0.9511	0.1256	0.1159	0.9473	0.0149	0.0017	1.0699	40.77	41.62	1.2582	2.240	3.046	1.1898	1.761	2.407	1.1447	0.6993	0.9057
180	0.9483	0.1326	0.1222	0.9441	0.0204	0.0066	1.0760	41.68	42.72	1.2970	2.180	2.978	1.2200	1.713	2.352	1.1635	0.6601	0.8534
200	0.9457	0.1390	0.1276	0.9411	0.0253	0.0108	1.0823	42.58	43.84	1.3388	2.105	2.888	1.2528	1.653	2.280	1.1832	0.6161	0.7946
220	0.9433	0.1448	0.1323	0.9384	0.0298	0.0144	1.0888	43.45	44.97	1.3836	2.015	2.778	1.2880	1.581	2.192	1.2038	0.5679	0.7300
240	0.9412	0.1500	0.1364	0.9358	0.0338	0.0174	1.0953	44.31	46.13	1.4313	1.911	2.649	1.3255	1.497	2.088	1.2250	0.5161	0.6604
260	0.9392	0.1547	0.1397	0.9334	0.0373	0.0198	1.1021	45.15	47.30	1.4817	1.792	2.500	1.3653	1.402	1.969	1.2469	0.4615	0.5869
280	0.9373	0.1589	0.1425	0.9312	0.0404	0.0217	1.1089	45.97	48.50	1.5345	1.661	2.335	1.4071	1.297	1.836	1.2693	0.4046	0.5104
300	0.9357	0.1626	0.1448	0.9291	0.0431	0.0231	1.1160	46.78	49.73	1.5895	1.519	2.154	1.4507	1.182	1.690	1.2920	0.3464	0.4319
330	0.9335	0.1675	0.1474	0.9263	0.0464	0.0245	1.1268	47.97	51.61	1.6758	1.287	1.859	1.5193	0.996	1.452	1.3267	0.2579	0.3127
360	0.9316	0.1718	0.1492	0.9238	0.0492	0.0251	1.1380	49.12	53.56	1.7658	1.040	1.540	1.5910	0.796	1.195	1.3616	0.1700	0.1944
390	0.9299	0.1756	0.1505	0.9215	0.0515	0.0253	1.1496	50.24	55.55	1.8588	0.782	1.209	1.6651	0.588	0.927	1.3965	0.0847	0.0799
420	0.9285	0.1791	0.1517	0.9195	0.0536	0.0251	1.1617	51.33	57.58	1.9539	0.520	0.871	1.7410	0.376	0.654	1.4311	0.0034	−0.0289
450	0.9273	0.1825	0.1528	0.9177	0.0555	0.0249	1.1744	52.40	59.64	2.0505	0.259	0.536	1.8182	0.166	0.384	1.4652	−0.0727	−0.1304
480	0.9262	0.1860	0.1541	0.9161	0.0574	0.0248	1.1878	53.44	61.71	2.1477	0.004	0.210	1.8959	−0.040	0.120	1.4984	−0.1429	−0.2240
510	0.9252	0.1896	0.1558	0.9146	0.0594	0.0249	1.2020	54.46	63.76	2.2451	−0.241	−0.103	1.9738	−0.238	−0.133	1.5308	−0.2068	−0.3093
540	0.9244	0.1935	0.1581	0.9133	0.0616	0.0254	1.2173	55.45	65.79	2.3419	−0.475	−0.400	2.0514	−0.426	−0.373	1.5620	−0.2643	−0.3864
570	0.9236	0.1978	0.1607	0.9120	0.0641	0.0262	1.2339	56.42	67.78	2.4377	−0.695	−0.679	2.1281	−0.604	−0.598	1.5920	−0.3157	−0.4557
600	0.9229	0.2024	0.1639	0.9108	0.0669	0.0274	1.2521	57.36	69.72	2.5321	−0.900	−0.939	2.2037	−0.770	−0.808	1.6207	−0.3612	−0.5174
640	0.9220	0.2090	—	0.9093	0.0711	—	1.2797	58.59	—	2.6549	−1.151	—	2.3022	−0.972	—	1.6569	−0.4137	—
680	0.9211	0.2164	—	0.9079	0.0759	—	1.3117	59.77	—	2.7737	−1.378	—	2.3974	−1.154	—	1.6905	−0.4579	—
720	0.9202	0.2243	—	0.9065	0.0812	—	1.3495	60.91	—	2.8878	−1.581	—	2.4889	−1.318	—	1.7215	−0.4948	—
760	0.9192	0.2327	—	0.9050	0.0871	—	1.3944	62.01	—	2.9969	−1.764	—	2.5763	−1.465	—	1.7499	−0.5253	—
800	0.9182	0.2416	—	0.9036	0.0934	—	1.4478	63.07	—	3.1006	−1.928	—	2.6595	−1.598	—	1.7758	−0.5500	—
840	0.9171	0.2509	—	0.9021	0.1002	—	1.5113	64.08	—	3.1988	−2.076	—	2.7382	−1.717	—	1.7992	−0.5695	—
880	0.9159	0.2605	—	0.9006	0.1073	—	1.5867	65.03	—	3.2914	−2.209	—	2.8124	−1.824	—	1.8202	−0.5841	—
920	0.9146	0.2704	—	0.8990	0.1147	—	1.6758	65.93	—	3.3783	−2.329	—	2.8821	−1.920	—	1.8388	−0.5945	—
960	0.9133	0.2806	—	0.8973	0.1224	—	1.7804	66.78	—	3.4596	−2.436	—	2.9472	−2.006	—	1.8551	−0.6008	—
1000	0.9118	0.2910	—	0.8956	0.1304	—	1.9026	67.55	—	3.5353	−2.532	—	3.0079	−2.084	—	1.8693	−0.6040	—
1060	0.9095	0.3068	—	0.8930	0.1426	—	2.1230	68.58	—	3.6388	−2.659	—	3.0907	−2.185	—	1.8868	−0.6039	—
1120	0.9071	0.3229	—	0.8903	0.1551	—	2.3934	69.42	—	3.7305	−2.767	—	3.1640	−2.271	—	1.9001	−0.5989	—
1180	0.9045	0.3391	—	0.8875	0.1678	—	2.7195	70.06	—	3.8111	−2.858	—	3.2284	−2.344	—	1.9096	−0.5884	—
1240	0.9018	0.3554	—	0.8846	0.1807	—	3.1062	70.46	—	3.8812	−2.932	—	3.2843	−2.403	—	1.9158	−0.5712	—
1300	0.8987	0.3717	—	0.8813	0.1935	—	3.5567	70.61	—	3.9419	−2.998	—	3.3326	−2.455	—	1.9186	−0.5555	—

[a] It is assumed that $\sigma_\gamma/\sigma_f = 0.3765$, so that $\sigma_a = 1.3765\ \sigma_f$.

Table 3-9—SAMPLE PAGE FROM AMSTER'S COMPILATION

Data from Ref. 34.

Moderator temperature, °K = 53.4000
1/v barns per H atom at 0.0253 ev = 52.1000
U-235 atoms per H atom = 00.0000

Isotope or Element	Cross Section* for Pu-239 Atoms/H atom =				
	00.0000	48.2500	48.5000	48.7500	49.1000
Am-241	a = 53.6881	53.7052	53.7263	53.7479	53.7689
Au-197	a = 52.5664	52.5415	52.5215	52.5050	52.4913
Cd	a = 54.3086	54.2956	54.2842	54.2740	54.2650
Eu	a = 54.2750	54.2871	54.2970	54.3054	54.3125
Gd	a = 55.1681	55.1534	55.1417	55.1321	55.1241
H	s = 52.3387	52.3287	52.3206	52.3139	52.3083
H	tr = 52.2203	52.2087	52.1995	52.1918	52.1854
Hf	a = 52.6423	52.6240	52.6097	52.5982	52.5888
In	a = 53.1195	53.1164	53.1139	53.1119	53.1103
Np-237	a = 53.1645	53.1867	53.2054	53.2216	53.2357
Pu-239	a = 54.1250	54.1187	54.1141	54.1103	54.1071
Pu-239	f = 53.7672	53.7273	53.6975	53.6732	53.6524
Pu-240	a = 53.1089	53.1088	53.1089	53.1092	53.1095
Pu-241	f = 53.7578	53.7116	53.6750	53.6447	53.6188
Sm-149	a = 55.5474	55.5120	55.4827	55.4580	55.4370
U-233	a = 53.3333	53.3182	53.3062	53.2963	53.2879
U-233	f = 53.3016	53.2878	53.2768	53.2677	53.2601
U-235	a = 53.3504	53.3293	53.3125	53.2987	53.2870
U-235	f = 53.2975	53.2797	53.2655	53.2538	53.2440
Unit A	a = 50.5540	50.5267	50.5047	50.4867	50.4715
Xe-135	a = 57.1650	57.1526	57.1425	57.1342	57.1271

*a = absorption (capture plus fission); s = scattering; tr = transport; f = fission.

3.2.4 OTHER METHODS OF DETERMINING CROSS SECTIONS

There are numerous codes (Section 10) which prepare cross sections based on various models of thermalization. Effective thermal cross sections based on the Wigner-Wilkins model[9] are computed by SOFOCATE. Codes which prepare multithermal group cross sections are RE 145 and SLOP-1. These codes are described in Section 10.

Some work utilizing SLOP-1 has been reported recently by Goldsmith and Cantwell.[35] They observed that the use of four thermal groups gives almost as good an estimate of reaction rates as does the use of thirty-six groups. Since the problems treated and the methods of attack are highly specialized, this conclusion is properly regarded as qualitative.

3.3 THERMAL-GROUP DIFFUSION PARAMETERS

This section is devoted largely to the presentation of data for average diffusion parameters of thermal neutrons in moderators. In Sections 3.3.1 through 3.3.3, measured values of the average transport mean free path, $\overline{\lambda}_{tr}$, or of the diffusion constant, $\overline{D}_0 \equiv \overline{Dv}$, and the diffusion length, $\overline{L}$, are collected and compared. It is convenient to categorize the moderators in terms of "non-hydrogenous," "water," and "hydrogenous mixtures." Most of the measurements have been undertaken in pure moderators, and the emphasis is clear. In Section 3.3.4, the more general reactor condition of a mixture of materials containing neutron absorbers is discussed, and theoretical computations based on measurement are summarized. In Section 3.3.5, some brief comments are made on more recent methods of analysis of thermal neutron absorption and leakage in locally-homogeneous media where the neutron flux spectrum is non-equilibrium.

Several different types of experimental techniques have been employed to measure the average diffusion parameters of thermal neutrons in pure moderating media. In one approach, a fixed source (plane or "point") is placed in a medium that is large in comparison with the slowing-down length of the source neutrons and with the diffusion length of thermalized neutrons. The degree of activation of detectors by the thermal neutron flux is measured as a function of distance from the source. The average diffusion length, $\overline{L}$, is inferred from a fitting of the type: $f(r)\exp(-r/\overline{L})$. The function $f(r)$ depends upon the geometry of the source and upon the positions of the detectors.

For liquid moderators, a variation of the exponential attenuation method has been used to ascertain $\overline{\lambda}_{tr}$. The diffusion length is measured as a function of the macroscopic absorption cross section of a neutron absorber dissolved in the liquid (see Kash and Woods[36]). Approximately, $3/\overline{\lambda}_{tr}$ is the slope of $1/L^2$ as a function of the added poison, in the vicinity of zero poison. Brown, et al.,[37] have used the equation:

$$\frac{1}{L^2} = 3\overline{\Sigma}_a(\overline{\Sigma} - \overline{\mu}\,\overline{\Sigma}_s) - 3\,\overline{\Sigma}_a^2(1-\overline{\mu}c)\left(\frac{4}{5}+\overline{\mu}c\right) = \nu^2 - B_H^2$$

Here, $\overline{\mu}$ is the average cosine of the scattering angle; Σ is the total cross section; $c = \Sigma_s/\Sigma$; B_H^2 is the geometrical buckling in the direction normal to the axis of measurement of detector activity; and ν^2 is the square of the reciprocal relaxation length of detector activity. By rewriting the equation, $\overline{\Sigma}_{tr}$ for the pure moderator may be determined as the slope of a function linear in the neutron absorption cross section of the poisoned medium (see Section 3.3.3.1).

In a second approach, the linear extrapolation distance, d, is estimated from the variation of the activation in the vicinity of a black plane boundary, and the one-group transport theory formula: $d = 0.7104\,\overline{\lambda}_{tr}$, is used to determine an approximate value of the average transport mean free path of thermal neutrons in the medium. Typically, the experimenters then compute L^2 approximately as

$$L^2 \equiv \overline{L}^2 = \overline{\lambda}_{tr}/3\overline{\Sigma}_a$$

where $\overline{\Sigma}_a$ is the average macroscopic thermal absorption cross section of the medium.

Raievski and Horowitz[39] have inferred values of $\overline{\lambda}_{tr}$ from analyses of wave propagation from an oscillating source in a diffusing medium (see Sections 3.3.1.1 and 3.3.1.4). The theory of the method is discussed in Refs. 38 and 39.

Another method of determining diffusion parameters of thermal neutrons utilizes a pulsed neutron source.[40] The mathematical formulation is outlined in Section 5.3.8. In this procedure, thermal-neutron detectors usually are positioned so as to measure the time variation of the thermal neutron flux at a node of the fundamental flux mode. The time-asymptotic decay constant, $\overline{\lambda(B^2)}$, is determined as a function of the buckling of the medium. The $\overline{\lambda(B^2)}$ data are represented by a polynomial in the geometric buckling, usually taken to be of second order. Least-squares analysis yields the constant term, $\overline{\Sigma_a v}$; the coefficient of B^2, $\overline{Dv}$; and the coefficient of B^4, which involves $\overline{Dv}$, the diffusion cooling coefficient of the medium, and the variation of transport mean free path with energy.[40]

Approximately, $L^2 = \overline{Dv}/\overline{\Sigma_a v}$, and $\overline{\lambda}_{tr} = \overline{Dv}/\overline{v}$, where $\overline{v}$ is the average neutron velocity in an assumed Maxwellian distribution of thermal neutron flux with mode kT corresponding to the temperature of the medium. (Note that this choice of $\overline{v}$ is restricted to media that are very weak absorbers.)

3.3.1 DIFFUSION PARAMETERS OF THERMAL NEUTRONS IN NON-HYDROGENOUS MODERATORS

3.3.1.1 Graphite (Reference Density: 1.60 gm/cm^3)

It has been suggested by von Dardel and Sjöstrand,[40] Beckurts,[42] and Küchle and Beckurts[43] that polycrystalline graphites from different sources may show slightly different diffusion behavior. The evidence is marginal. It is based on disagreements beyond experimental error between the inferred mean free paths from pulsed-source experiments on different graphite types.

Table 3-10 summarizes these data, including also some results of Antonov, et al.[44]

Droulers, Lacour, and Raievski[41] studied the propagation of neutron waves in a large block of graphite, and measured the complex diffusion length as a function of the wave frequency of the source. The value $\overline{\lambda}_{tr} = 2.53\ (\pm 0.03)$ cm was inferred for room-temperature graphite of reference density (1.60 gm/cm^3). This result supersedes the value $\overline{\lambda}_{tr} = 2.55\ (\pm 0.09)$ cm reported earlier by Raievski and Horowitz[39] who used the same basic experimental method.

DeSaussure and Silver[45] have published data for AGHT graphite of density 1.65 ($\pm$ 0.01) gm/cm^3. Normalizing to reference density, $\overline{D}_0 = 2.10\ (\pm 0.06) \times 10^5$ cm^2/sec, and $\overline{\lambda}_{tr} = 2.53\ (\pm 0.08)$ cm.

Table 3-10—AVERAGE TRANSPORT MEAN FREE PATH FOR THERMAL NEUTRONS IN GRAPHITE AT 20°C[a]

Data from Refs. 42, 43, and 44.

Type of Graphite	Average Sample Density, gm/cm^3	$\bar{\lambda}_{tr}$,[b] cm	Ref.
Siemens-Plania (non-nuclear)	1.56	2.58 ± 0.02	42
Kropfmühl (natural, compacted)	2.05 – 2.08	2.57 ± 0.02	43
Pechiney, France (reactor grade)	1.70	2.53 ± 0.02[c]	43
Siemens-Plania (reactor grade)	1.69	2.52 ± 0.02	43
Russian	Not known	2.50 ± 0.04[d]	44

[a]Pulsed-source measurements.

[b]Adjusted to graphite density of 1.60 gm/cm^3.

[c]Also studied by Droulers, et al.,[41] who reported $\bar{\lambda}_{tr}$ = 2.53 (±0.03) cm from a different method of measurement (see text).

[d]$\bar{D}_0$ = 2.07 (±0.03) × 10^5 cm^2/sec, and $\bar{L}$ = 51.1 (±2.1) cm, also determined from this experiment.

The diffusion length, $\bar{L}$, of thermal neutrons in graphite has been measured in exponential experiments at various laboratories. Richey and Block[46] used graphite stacks of various sizes to determine whether the effective value of $\bar{L}$ varied significantly with the size of the medium. The experiments were prompted by other studies that had indicated a larger value of $\bar{L}$ in the moderators of the large Hanford reactors than was measured in the smaller Hanford Standard Pile. No significant variation of $\bar{L}$ with stack size was observed. Additional measurements were made with graphite media containing aluminum process tubes, similar to those used in the Hanford reactors. Corrections were applied for effects such as neutron streaming in the process tubes, absorption and scattering of neutrons by the aluminum in the tubes, and differences in the mean graphite density. Lee[47] re-evaluated the correction factors, and included the effects of neutron absorption by nitrogen in the machined openings and in the graphite pores. The diffusion lengths measured by Richey and Block, and the correction factors computed by Lee, are listed in Table 3-11, showing the relative importance of the perturbations.

Table 3-11—THERMAL DIFFUSION LENGTH ($\bar{L}$) IN THE GRAPHITE OF HANFORD REACTORS

Data from Refs. 46 and 47.

Reactor	Measured[a] $\bar{L}$, cm	Graphite Density, gm/cm^3	Correction[b] Factor for Absorptions in Al and N	Reciprocal of[c] Correction Factor for Streaming	Correction to Ref. Density (1.60 gm/cm^3)	Corrected $\bar{L}$, cm
Standard Pile	52.5 (±0.5)	1.658	—	—	1.0321	54.2
DR	51.6 (±1.0)	1.706	1.1076	1.1209	1.0586	54.0
H	55.0 (±1.0)	1.656	1.1115	1.1287	1.0310	55.8
C	53.63 (±0.75)	1.647	1.1249	1.1374	1.0260	54.42
KW	51.61 (±0.87)	1.647	1.1590	1.1311	1.0260	54.26
KE	50.94 (±0.76)	1.667	1.1576	1.1317	1.0370	54.03

[a]Ref. 46.

[b]Includes corrections for absorption of thermal neutrons by aluminum, using $\bar{\Sigma}_a^{Al}$ = 0.0145 cm^{-1}, and by nitrogen in the machined openings. Neutron absorption by nitrogen in the graphite pores is included in the "density" correction factor.

[c]This factor compensates for the overestimate in $\bar{L}$ arising from neutron streaming in the voids. Behrens' diffusion-theoretic formula[49] for streaming corrections was applied, using $\bar{\sigma}_{tr}$ = 4.95 barns for graphite.

Lloyd, et al.,[48] measured the dependence of $\bar{L}$ in graphite on the temperature of the medium. They noted that their data were well represented by a 1/v absorption cross section and a constant average λ_{tr}.

Laubenstein[50] measured $\bar{L}$ in graphite to be used for exponential experiments with lattices of clustered-fuel elements. The value $\bar{L}$ = 50.5 (± 0.8) cm was determined for graphite of density 1.713 gm/cm^3. Assuming that $\bar{L}$ is inversely proportional to the density, the result $\bar{L}$ = 54.1 (± 0.9) cm is deduced for ρ = 1.60 gm/cm^3.

Hendrie, et al.,[51] published data obtained in connection with work on LMFR (Liquid Metal Fuel Reactor) systems. From exponential experiments with graphite containing a thermal neutron absorber (copper), the values $\bar{L}$ = 57.2 (± 0.3) cm, and $\bar{\lambda}_{tr}$ = 2.77 (± 0.06) cm, were inferred for graphite of reference density. Hellstrand[52] has suggested that perhaps the thick (~5 ft) graphite zone separating the core of the source reactor from the exponential stack distorted the spectrum toward the lower-energy end. In this event, the larger $\lambda_{tr}(E)$ of neutrons with energies below the Bragg cutoff would be weighted more heavily, resulting in too high a value for $\bar{\lambda}_{tr}$ and, therefore, for $\bar{L}$.

In Table 3-12 are summarized the measured diffusion parameters for thermal neutrons in graphite, normalized to graphite of density 1.60 gm/cm^3.

Table 3-12— AVERAGE DIFFUSION PARAMETERS FOR THERMAL NEUTRONS IN ROOM-TEMPERATURE GRAPHITE (ρ = 1.60 gm/cm^3)

Diffusion Constant, $\bar{D}_0$, 10^5 cm^2/sec	$\bar{\lambda}_{tr}$, cm	$\bar{L}$, cm	Ref.
2.09 ± 0.03[a]	2.53 ± 0.03	—	41
2.13 ± 0.02[a]	2.58 ± 0.02[b]	—	42, 43
2.13 ± 0.02[a]	2.57 ± 0.02[b]	—	43
2.09 ± 0.02[a]	2.53 ± 0.02[b]	—	
2.08 ± 0.02[a]	2.52 ± 0.02[b]	—	
2.07 ± 0.03[a]	2.50 ± 0.04[b]	51.1 ± 2.1	44
2.10 ± 0.06	2.53 ± 0.08[c]	—	45
—	—	54.2[d]	46, 47
—	—	53.7 ± 0.5	48
—	—	54.1 ± 0.9	50
—	2.77 ± 0.06	57.2 ± 0.3	51

[a] Measured values for different types of graphite (see Table 3-11).

[b] Values computed from the relationship: $\bar{D}_0 = \bar{D}\bar{v}$, where $\bar{v} = (2/\sqrt{\pi})\, v(kT) = 2.48 \times 10^5$ cm/sec, and $\bar{D} = \bar{\lambda}_{tr}/3$.

[c] AGHT graphite.

[d] Value measured in the Hanford Standard Pile; it corresponds also to the average value for the graphite used in various Hanford reactors.

Singwi and Kothari[53] reported a calculated value of $\bar{D}_0 = 2.30 \times 10^5$ cm^2/sec for graphite (ρ = 1.60 gm/cm^3), corresponding to $\bar{\lambda}_{tr}$ = 2.76 cm.

3.3.1.2 Beryllium (Reference Density: 1.85 gm/cm^3)

Geraseva, et al.,[54] measured the distribution of thermal neutrons in a block (100 cm × 100 cm × 84 cm) of commercial beryllium of mean density 1.78 gm/cm^3. The beryllium was separated from a Ra-Be source of fast neutrons by a graphite parallelepiped of unspecified thickness. Analysis of the data for the thermal relaxation length in the direction normal to the graphite block indicated a value $\bar{L}$ = 22.1 (± 1.0) cm, or $\bar{L}$ = 21.3 (± 1.0) cm for beryllium of reference density.

Thermal neutron diffusion parameters in beryllium have been measured by pulsed-source techniques at a number of laboratories. Campbell and Stelson[55] determined the buckling dependence of the decay constant, λ, from the asymptotic time variation of thermal neutron leakage from small rectangular prisms of beryllium. The data from the pulsed-source measurements were represented by a function, $\lambda(B^2) = \bar{\Sigma}_a\bar{v} + \bar{D}_0B^2$, linear in B^2 in the range 0.012 cm^{-2} < B^2 < 0.036 cm^{-2}. The value $\bar{D}_0$ = 1.25 × 10^5 cm^2/sec was inferred for beryllium of reference density. Other authors have considered a

fitting of $\lambda(B^2)$ to terms of second order in B^2, thus including a diffusion-cooling (or diffusion-heating) effect (see Section 5.3.8).

Antonov, et al.,[44] performed pulsed-source experiments on rectangular prisms of beryllium with bucklings $0.0073\ cm^{-2} < B^2 < 0.0612\ cm^{-2}$. Normalizing to beryllium of density 1.85 gm/cm^3, $\overline{D}_0 = 1.17\ (\pm\ 0.05) \times 10^5\ cm^2/sec$ at room temperature.

Komoto and Kloverstrom[56] published data obtained from pulsed-source work with beryllium blocks in the buckling range $0.0034\ cm^{-2} < B^2 < 0.0412\ cm^{-2}$, the upper limit relating to a parallelepiped, 22.9 cm × 22.9 cm × 30.5 cm (9 in. × 9 in. × 12 in.). The value $\overline{D}_0 = 1.24\ (\pm\ 0.04) \times 10^5\ cm^2/sec$ was deduced for room-temperature beryllium of reference density. Assuming that the leakage spectrum was Maxwellian with peak neutron velocity 2.2×10^5 cm/sec, the diffusion coefficient is $\overline{D} = 0.50\ (\pm\ 0.02)$ cm.

DeSaussure and Silver[57] used the pulsed-source method to determine the dependence of $\overline{\lambda}_{tr}$ on the temperature of beryllium at ten different temperatures: $227°K \leq T \leq 784°K$. The measurements were made with an approximately cubical block, 51 cm (20 in.) on a side, corresponding to a buckling of $0.0105\ cm^{-2}$. In obtaining the results shown in Fig. 3-18, the decay constant, λ, was represented as

$$\lambda(B^2) = \overline{\Sigma}_a\,\overline{v} + \frac{\overline{\lambda}_{tr}}{3}\,\overline{v}\,B^2\,(1 - \overline{C}B^2)$$

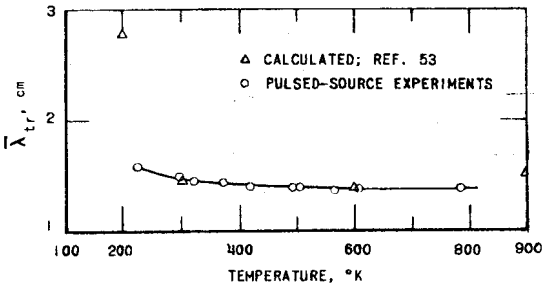

Fig. 3-18—Average transport mean free path ($\overline{\lambda}_{tr}$) of thermal neutrons in beryllium (ρ = 1.85 gm/cm^3) as a function of temperature. *Reproduced from Ref. 57.*

The term $B^2(1 - \overline{C}B^2)$ was taken to be invariant with the temperature, and the leakage spectrum was assumed to be Maxwellian. Included in the figure are values calculated by Singwi and Kothari[53] at four temperatures. Agreement between calculation and experiment is good at 300°K and at 600°K, the only calculated values at temperatures within the range of the experimental conditions. All values have been corrected to a density of 1.85 gm/cm^3.

DeSaussure and Silver[58] have also published room-temperature measurements in beryllium blocks with bucklings $0.008\ cm^{-2} < B^2 < 0.072\ cm^{-2}$. The value $\overline{D}_0 = 1.25\ (\pm\ 0.06) \times 10^5\ cm^2/sec$ was deduced.

Andrews[59] measured the decay constant, λ, of the fundamental mode of the neutron leakage from blocks of reference-density beryllium at five different temperatures: $292°K \leq T \leq 478°K$. Most of the stacks were cubical, ranging in size from 17.8 cm (7 in.) to 91.4 cm (36 in.), and in buckling from $0.0034\ cm^{-2}$ to $0.0753\ cm^{-2}$.

For each temperature, the parameters $\overline{\Sigma}_a\,\overline{v}$, $\overline{D}\,\overline{v}$, and $\overline{D}\,\overline{v}\,\overline{C}$ were computed from a least-squares fitting of the data, using

$$\lambda(B^2) = \overline{\Sigma}_a\,\overline{v} + \overline{D}\,\overline{v}\,B^2\,(1 - \overline{C}\,B^2)$$

and iterating to obtain an extrapolation distance $d = 2.13\,\overline{D}\,\overline{v}/\overline{v}$ consistent with the value of $\overline{D}\,\overline{v}$. In one approximation, the average velocity was assumed to be independent of the buckling: $\overline{v} = (2/\sqrt{\pi})\,v\,(kT)$. In a second approximation, the average velocity of the leakage spectrum was taken to be $(1 - \overline{C}B^2)$ times the infinite-medium $\overline{v}$, given above, thereby making the extrapolation distance buckling-dependent as well as temperature-dependent. The latter method yielded results for $\overline{D}$ in good agreement with those obtained using the buckling-independent extrapolation length, but the diffusion cooling coefficient was reduced slightly.

Andrew's results for $\overline{D}$, $\overline{\Sigma}_a\,\overline{v}$, and $\overline{L}$, are listed in Table 3-13. The beryllium was of high purity but appeared to contain some high-cross section impurities that contributed significantly to the absorption. The value of $\overline{\Sigma}_a\,\overline{v}$ decreased with increasing temperature, indicating a slightly non-1/v behavior of the net neutron absorption cross section even after corrections were made for the thermal expansion of the beryllium.

Bhandari[60] reported the result of a calculation of the diffusion constant, $\overline{D}_0$, for beryllium. Assuming a Debye frequency spectrum for beryllium, and without using the incoherent approximation

Table 3-13—NEUTRON-DIFFUSION PARAMETERS IN BERYLLIUM AT VARIOUS TEMPERATURES

(ρ = 1.85 gm/cm^3 at Room Temperature)

Data from Ref. 59.

Parameter	292°K	354°K	394°K	437°K	478°K
$\bar{\Sigma}_a\bar{v}$, sec^{-1}	285 ± 8	279 ± 6	278 ± 6	271 ± 6	269 ± 8
$\bar{D}_0 = \bar{D}\,\bar{v}$, 10^5 cm^2/sec	1.235 ± 0.013	1.318 ± 0.008	1.365 ± 0.008	1.430 ± 0.008	1.490 ± 0.010
$\bar{D}$, cm	0.499 ± 0.005	0.484 ± 0.003	0.475 ± 0.003	0.472 ± 0.003	0.471 ± 0.003
$\bar{L}$, cm	20.8 ± 0.3	21.7 ± 0.3	22.2 ± 0.3	23.0 ± 0.3	23.6 ± 0.4

made by Singwi and Kothari,[61] Bhandari computed the elastic and the one-phonon inelastic scattering cross sections as functions of neutron energy in the thermal range. The calculated total scattering cross section is in good agreement with the experimental results presented in BNL-325.[62] The value $\bar{D}_0 = 1.26 \times 10^5$ cm^2/sec was determined by averaging the calculated $\sigma_{tr}(E)$ with respect to a Maxwellian neutron distribution corresponding to a neutron temperature of 27°C. For beryllium of reference density,

$$\bar{D}_0 = 1.21 \times 10^5 \text{ cm}^2/\text{sec}$$

and

$$\bar{D} = 0.488 \text{ cm}.$$

The room-temperature neutron diffusion parameters for beryllium of density 1.85 gm/cm^3 are summarized in Table 3-14. (Data at other temperatures were presented in Fig. 3-18 and in Table 3-13).

Table 3-14—AVERAGE DIFFUSION PARAMETERS FOR THERMAL NEUTRONS IN ROOM-TEMPERATURE BERYLLIUM (ρ = 1.85 gm/cm^3)

Diffusion Constant, $\bar{D}_0$, 10^5 cm^2/sec	Diffusion Coefficient, $\bar{D}$, cm	Diffusion Length, $\bar{L}$, cm	Ref.
—	—	21.3 ± 1.0	54
1.25	0.50[a]	—	55
1.17 ± 0.05	0.47 ± 0.02[a]	—	44
1.24 ± 0.04	0.50 ± 0.02[a]	—	56
—	0.49[b]	—	57
1.25 ± 0.06	0.50 ± 0.02[a]	—	58
1.235 ± 0.013	0.499 ± 0.005	20.8 ± 0.3	59

[a] Values were computed from the published data, assuming that $\bar{D} = \bar{D}_0/[(2/\sqrt{\pi})\ 2.2 \times 10^5$ cm/sec].

[b] Measured at 300°K.

3.3.1.3 Beryllium Oxide (BeO; Reference Density: 2.96 gm/cm^3)

Diffusion parameters of thermal neutrons in beryllium oxide have been measured by the pulsed-source method and in exponential experiments.

Kloverstrom and Komoto, using the pulsed source method, obtained $\bar{D}_0 = 1.41\ (\pm 0.05) \times 10^5$ cm^2/sec in room-temperature beryllium oxide.[59]

Ramanna, et al.,[63] measured values of thermal parameters in blocks of BeO containing an impurity equivalent of less than 725 ppm of iron. Bursts of source neutrons were produced in a cascade

generator utilizing the D-Be reaction. The blocks varied in size from 30 cm × 30 cm × 30 cm, to 30 cm × 40 cm × 40 cm. The results were:

$$\overline{L} = 28.6\ (\pm\ 0.3)\ \text{cm}$$

$$\overline{D}_0 = 1.069\ (\pm\ 0.006) \times 10^5\ \text{cm}^2/\text{sec}$$

Iyengar, et al.,[64] measured $\overline{D}_0$ at various temperatures:

BeO Temp., °C	$\overline{D}_0$, 10^5 cm^2/sec
24	1.18 ± 0.02
80	1.36 ± 0.03
140	1.60 ± 0.03

Koechlin, et al.,[65] measured the spatial distributions of thermal neutron activation of Mn-Ni foils in a block (100 cm × 101 cm × 90 cm) of BeO separated from the thermal column of the Saclay reactor by a block of graphite 60 cm thick.

The distributions in planes parallel to the graphite-BeO interface were fitted by a product of two cosines. For BeO of reference density, the value $\overline{\lambda}_{tr} = 2.4\ (\pm\ 0.3)$ cm was inferred from the formula: Extrapolation length = $0.71\ \overline{\lambda}_{tr}$. This result is substantially higher than values obtained from the pulsed-source experiments described above. The authors suggest that the higher value may be due to selective filtering of neutrons from the reactor, both by the graphite and by the BeO itself, in which case the spectrum is biased toward the neutrons of energies below the Bragg cutoff, for which $\lambda_{tr}(E)$ is higher. [A similar discrepancy was noted by Hendrie, et al.,[51] in measurements with graphite blocks separated from the source by 5 ft of graphite (see Section 3.3.1.1).] Indeed, a consistent increase was observed in the value of $\overline{L}$ for BeO as a function of increasing distance from the graphite block. Normalizing to BeO of density 2.96 gm/cm^3:

Distance from Graphite Block, cm	$\overline{L}$, cm
10	31.9 (± 0.8)
20	32.4 (± 0.8)
30	33.1 (± 1.0)

3.3.1.4 Heavy Water (Reference Density: 1.1 gm/cm^3)

Applying the method of a modulated source, Raievski and Horowitz[66] measured $\overline{\lambda}_{tr} = 2.45$ (± 0.07) cm for pure D_2O at 13°C. Neutrons from an Sb-Be source were detected by BF_3 counters. Auger, et al.,[67] inferred a value $\overline{\lambda}_{tr} = 2.4\ (\pm\ 0.1)$ cm for thermal neutrons in pure D_2O from a least-squares linear fit of spatial activation distributions in the vicinity of a plane cadmium boundary. The detectors were BF_3 counters. Using these data, Kash and Woods[36] determined an extrapolation distance, and thereby the value $\overline{\lambda}_{tr} = 2.63\ (\pm\ 0.12)$ cm for D_2O. Hone[68] analyzed the same data, assuming a sinh function representation of the asymptotic flux, and obtained $\overline{\lambda}_{tr} = 2.60\ (\pm\ 0.10)$ cm for pure D_2O at 22°C; the stated error is based on the error estimate of Auger, et al.

Kash and Woods[36] reported upon a measurement yielding $\overline{\lambda}_{tr} = 2.52\ (\pm\ 0.04)$ cm for pure D_2O at room temperature. The experiment consisted of the measurement of activation distributions of bare and cadmium-covered indium foils in a cadmium-covered cylindrical tank of D_2O (99.7% pure), as a function of the macroscopic thermal neutron absorption cross section, $\overline{\Delta\Sigma}_a$, of an added 1/v neutron absorber. Assuming a sinh $[(h - z)/\overline{L}]$ fit to the subcadmium activation distributions, where h is the height of the tank of D_2O, $\overline{L}$ was determined as a function of $\overline{\Delta\Sigma}_a$, and $\overline{\lambda}_{tr}$ was found from the relationship: $1/\overline{L}^2 = (3\overline{\Sigma}_a)\,(1/\overline{\lambda}_{tr})$. The average thermal cross section, $\overline{\Sigma}_a$, was computed with respect to a Maxwellian distribution of thermal flux with mode corresponding to the moderator temperature, assuming that $\sigma_a^B = 750\ (\pm\ 10)$ barns for 2200-m/sec neutrons.

3.3.2 DIFFUSION PARAMETERS IN WATER

3.3.2.1 Thermal Diffusion Length

The thermal diffusion length, $\bar{L}$, has been measured in constant-source and in pulsed-source experiments.

Wilson, et al.,[69] used the relative activities of pairs of bare indium foils to fit an assumed exponential drop-off of neutron flux in a cylindrical tank of water located above the thermal column of CP-2. The tank was lined with cadmium on top and on the sides, and was separated from the thermal column by four inches of graphite. The measurements were made at various temperatures: $27°C < T < 93°C$. Assuming a linear dependence of $\bar{L}$ on the moderator temperature in that range, a least-squares fit yielded $\bar{L} = 2.644 + 0.0061T$, with $\bar{L}$ in centimeters, and T in degrees Centigrade.

Radkowsky[12] applied the Born approximation to determine an effective scattering mass, A, for hydrogen in the water molecule as a function of the incident neutron energy, writing:

$$\sigma_s^H \text{ (observed)} = M\mu^2$$

where M is a constant and the reduced mass, μ, is given by $\mu = Am/(A + 1)$, m being the mass of the proton. Using $\sigma_s^H = 20$ barns at high energy, A(E) was solved from

$$\{A(E)/[1 + A(E)]\}^2 = (1/2)\,[\sigma_s^{H_2O}(E) - \sigma_s^0]/80$$

Assuming isotropic scattering in the center-of-mass system, $\overline{\cos\theta} = 2/[3A(E)]$ was determined from the solution of the above equation, and thereby

$$\sigma_{tr}^{H_2O}(E) = \sigma_s^{H_2O}(E)\left(1 - \frac{2}{3A(E)}\,\frac{\sigma_s^{H_2O}(E) - \sigma_s^O}{\sigma_s^{H_2O}(E)}\right)$$

Assuming a Maxwellian distribution of neutron flux with mode corresponding to the moderator temperature, Radkowsky computed $\bar{\lambda}_{tr}$ and thence $\bar{L} = \bar{\lambda}_{tr}/3\bar{\Sigma}_a$, using $\sigma_s^O \equiv 3.73$ barns, $\sigma_a^H = 0.325$ barns at 0.025 ev, and a 1/v variation of σ_a^H. In Fig. 3-19, the temperature-dependent $\bar{L}$ computed by Radkowsky is compared with the results of Wilson, et al.[69] All values are adjusted to water of unit density.

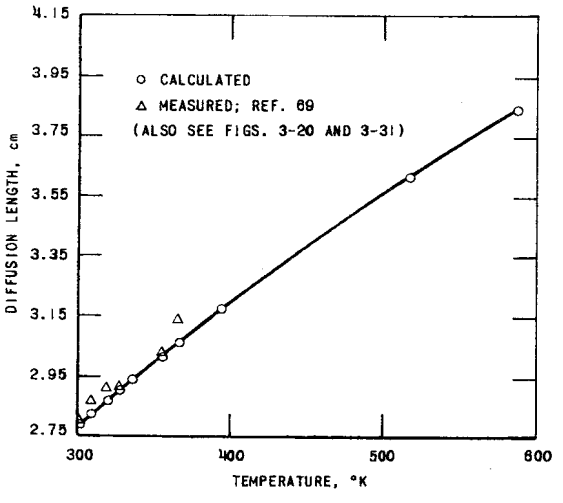

Fig. 3-19 — Average diffusion length ($\bar{L}$) of thermal neutrons in water as a function of temperature. (Normalized to water of unit density.) *Reproduced from Ref. 16.*

The Radkowsky "prescription" for the effective scattering mass of hydrogen in the water molecule has been applied to the computation of $\bar{\lambda}_{tr}$ in other hydrogeneous moderators (see Section 3.3.3). Deutsch[70] has suggested the formula:

$$\bar{L} = \frac{2.719}{\rho}\left[\frac{T + 273.1}{295.1}\right]^{1/2}\left[\frac{1.0614}{1 + 0.0614\left(\frac{T + 273.1}{295.1}\right)^{1/2}}\right]^{1/2}$$

687863 O - 63 - 9

where T is given in degrees Centigrade, $\overline{L}$ is in centimeters, and ρ is the density in units of grams per cubic centimeter. Deutsch stated that this formula is in good agreement with the results of Wilson, et al.,[69] and with the pulsed-source results of Antonov, et al.[44] Local least-squares linear fittings to the dependence of $\overline{L}$ on T yielded a temperature coefficient 0.0049 cm/°C for 10°C < T < 30°C, and 0.0059 cm/°C for 30°C < T < 90°C.

Von Dardel and Sjöstrand[71] reported the value $\overline{L}$ = 2.725 (± 0.03) cm at 22°C, obtained from pulsed-source data.

From other pulsed-neutron measurements, Dio and Schopper[72] derived the linear fitting: $\overline{L}$ = 2.70 + [0.0054 (± 0.0022)] (T-19) centimeters for 19°C < T < 75°C.

Rockey and Skolnik[73] applied two-group diffusion theory to analyze measured spatial distributions of foil activations for $\overline{L}$ in water. A small Sb-Be source supplied the neutrons, and the experiment was performed in a large vessel ($B^2 \approx 0$) at four different temperatures. Figure 3-20 shows their results compared with computations of $\rho\overline{L}$, based upon proportionality to $\overline{v}$ or upon the method of Radkowsky described above. Also included are data of Reier and De Juren,[74] and of Wright and Frost.[75]

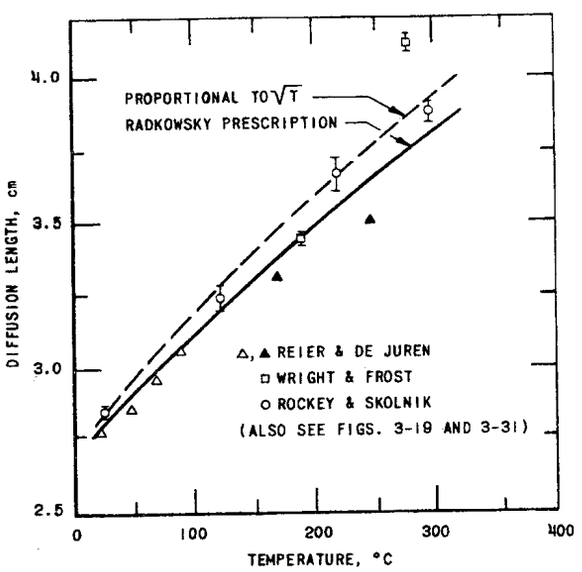

Fig. 3-20 — Average diffusion length ($\overline{L}$) of thermal neutrons in water. (Normalized to water of unit density.) *Reproduced from Ref. 73; additional data points from Ref. 74.*

The values for $\overline{L}$ discussed above are presented in Table 3-15. Also listed are published data of a number of other workers whose reports are not discussed in detail for lack of space. Two categories of experiments are tabulated: the so-called "exponential," and the "pulsed," the former relating to the measurement of the exponential attenuation of "thermal" neutrons far from a source.

3.3.2.2 Thermal Diffusion Coefficient and Transport Mean Free Path

The average transport mean free path, $\overline{\lambda}_{tr}$, for thermal neutrons in H_2O has been determined by fitting a measured distribution of detector activity to the theoretical distribution given by one-group neutron transport theory in the vicinity of a free plane boundary.

The thermal diffusion constant, $\overline{D}_0 \equiv \overline{D}\,\overline{v}$, has been measured as the coefficient of the buckling (B^2) in a polynomial fitting of the asymptotic decay of the thermal neutron flux in pulsed-source experiments. Approximately, $\overline{\lambda}_{tr} = 3\ \overline{D}_0/\overline{v}$, where $\overline{v}$ is the average thermal neutron velocity. If $\overline{D}_0$ and $\overline{v}$ are known, the diffusion coefficient, $\overline{D}$, and the average transport mean free path, $\overline{\lambda}_{tr}$, of the thermal neutrons may be calculated. Typically, when such a calculation is made by the experimenter, it is assumed that $\overline{v}$ is the average with respect to a Maxwellian distribution of thermal neutron flux:

$$\overline{v} = \int_0^\infty v\ \mathrm{Max}(v)dv \Big/ \int_0^\infty \mathrm{Max}(v)dv$$

although the leakage spectrum is not Maxwellian. Thus for a medium at room temperature, usually the value $\overline{v} \approx 2.482 \times 10^5$ cm/sec is used.

Sisk[77] has determined $\overline{\lambda}_{tr}$ = 0.48 (± 0.01) cm for demineralized water at 24°C by fitting the measured activity of indium foils to the solution of a one-dimensional problem of one-group neutron

Table 3-15—MEASURED DIFFUSION LENGTH OF THERMAL NEUTRONS IN H_2O

Note: Room* indicates that water temperature is not specified in the reference. Room temperature is assumed.

Type of Measurement	Water Temperature, °C	Size of Medium	Diffusion Length, $\bar{L}$, cm	Ref.
Exponential	27 to 93	Cylindrical tank; Dia. = 47 cm; filled to height of 56 cm	2.64 + 0.0061T (T in °C)	69
Exponential	Room	—	2.77 ± 0.04[a]	76
Exponential	24	$B^2 \approx 0$	2.67 ± 0.02	77,78
Exponential	22 ± 2 22 ± 2	Tank; Dia. = 107 cm	2.763 ± 0.015[b] 2.76 ± 0.07[c]	79
Pulsed source	22	$0.006\ cm^{-2} < B^2 < 0.018\ cm^{-2}$	2.85 ± 0.05	80
Pulsed source	22	$0.1\ cm^{-2} < B^2 < 0.7\ cm^{-2}$	2.725 ± 0.03	71
Pulsed source	23	Cylinder, Dia. = 18.6 cm; Hgt. = 2.75 to 20 cm	2.7 ± 0.1	44
Pulsed source	80	$0.086\ cm^{-2} < B^2 < 0.94\ cm^{-2}$	$3.1^{+0.2}_{-0.1}$	44
Pulsed source	Room*	$0.09\ cm^{-2} < B^2 < 0.96\ cm^{-2}$	2.66 ± 0.11	81
Pulsed source	Room*	$0.08\ cm^{-2} < B^2 < 1.1\ cm^{-2}$	2.69[d]	55
Exponential	25 190 277	30-cm-ID vessel	2.714 ± 0.010[e] 3.927 ± 0.023[e] 5.360 ± 0.037[e]	75
Exponential	19	Tank; Dia. = 80 cm; Hgt. = 100 cm	2.68 ± 0.02 2.69 ± 0.02[a]	82
Pulsed source	19 49	$0.093\ cm^{-2} < B^2 < 0.867\ cm^{-2}$ $0.16\ cm^{-2} < B^2 < 0.57\ cm^{-2}$	2.70 ± 0.05[f,g] 2.85 ± 0.07[f,g]	72
	75	$0.16\ cm^{-2} < B^2 < 0.63\ cm^{-2}$	3.00 ± 0.07[f,g]	83
Poison addition	20	Tank; Dia. = 50 cm; Hgt. = 60 cm	2.72 ± 0.03[h]	84
Exponential	23	—	2.779 ± 0.007	85
Pulsed source	22	$0.02\ cm^{-2} < B^2 < 0.42\ cm^{-2}$	2.80 ± 0.03	86
Exponential	25.9 122.7 218.5 295.3	$B^2 \approx 0$	2.859 ± 0.018 3.444 ± 0.039 4.078 ± 0.064 5.362 ± 0.049	73
Pulsed source	22 40 60 80	$0.1\ cm^{-2} < B^2 < 0.75\ cm^{-2}$	2.72 ± 0.04 2.76 ± 0.04 2.96 ± 0.05 3.04 ± 0.07	87,88
Exponential	23 49 70 90	Cylindrical tank; Dia. = Hgt. = 100 cm	2.775 ± 0.006[i] 2.862 ± 0.011 2.957 ± 0.013 3.051 ± 0.006	74
	166 244	$B^2 \approx 0$ $B^2 \approx 0$	3.302 ± 0.016 3.497 ± 0.020	

[a]Distilled water.

[b]Ra-Be source in distilled water. Von Dardel and Sjöstrand[71] have noted that a "diffusion heating" correction[89] must be made, reducing $\bar{L}$ by 0.035 cm to 2.728 (±0.015) cm, in excellent agreement with their result. On p. 206 of Ref. 79 are listed some other values of $\bar{L}$, determined in earlier experiments.

[c]Sb-Be source in distilled water.

[d]Computed from $\bar{L}^2 = \bar{D}_0/\bar{\Sigma}_a v$.

[e]Uncertainty limits refer only to errors in counting statistics.

[f]In Ref. 83, Dio states that an extrapolation distance of 0.32 cm was used. No statement was made of any variation of this value as a function of water temperature.

[g]Temperature coefficient of $\bar{L}$ is 0.0054 (±0.0022) cm/°C.

[h]The value of $\bar{L}$ at 20°C determined by Beckurts and Klüber[84] is 2.72 (±0.03) cm. Correcting for the slight hardening of the flux spectrum, $\bar{L}$ = 2.70 (±0.03) cm for a neutron temperature of 20°C. The latter value is to be compared to the results of pulsed-source experiments; the former value to the results of exponential experiments.

[i]The values quoted for $\bar{L}$ have been normalized to water of unit density. Measurements were made using In and Dy detectors; in some cases the value quoted for $\bar{L}$ is an average with respect to data from experiments with the two detectors.

transport. The foil activations were made in the neighborhood of, and normal to, a layer of cadmium bounding a slab face of a large H_2O medium.

The value of $\bar{\lambda}_{tr}$ may be inferred also from measurements of $\bar{L}$ by the formula:

$$\bar{\lambda}_{tr} = 3\bar{\Sigma}_a \bar{L}^2$$

provided $\bar{\Sigma}_a^{H_2O}$ is known, using, for example, the values of $\bar{L}$ listed in Table 3-15.

In most cases, the decay data from pulsed-source work have been fitted by a function of second order in the buckling, although Campbell and Stelson were able to represent their results well with a function linear in B^2. Unless otherwise stated, the measurements described in the following paragraphs and summarized in Table 3-16, have been analyzed in terms of a quadratic in B^2, yielding both the diffusion constant, $\bar{D}_0$, and the diffusion cooling coefficient.

Table 3-16— MEASURED VALUES OF $\bar{D}_0$ FOR THERMAL NEUTRONS IN H_2O

Note: Room* indicates that water temperature is not specified in the reference. Room temperature is assumed.

Type of Measurement	Water Temperature, °C	Size of Medium	Diffusion Constant, $\bar{D}_0$ 10^4 cm^2/sec	Temperature Coefficient of $\bar{D}_0$	Ref.
Pulsed source	Room*	0.006 cm^{-2} < B^2 < 0.018 cm^{-2}	3.850 ± 0.080[a]	—	80
Pulsed source	22	0.1 cm^{-2} < B^2 < 0.7 cm^{-2}	3.634 ± 0.075	—	40
	10 to 35			0.42 (± 0.04)%/°C	
Pulsed source	23	Cylinder; Dia. = 18.6 cm; Hgt. = 2.75 to 20 cm	3.5 ± 0.1	—	44
Pulsed source	80	0.086 cm^{-2} < B^2 < 0.94 cm^{-2}	$4.5^{+0.4}_{-0.2}$	—	44
Pulsed source	22	0.09 cm^{-2} < B^2 < 0.96 cm^{-2}	3.485 ± 0.110	—	81
Pulsed source	Room*	0.08 cm^{-2} < B^2 < 1.1 cm^{-2}	3.48	—	55
Pulsed source	19	—	3.505 ± 0.060	130 (± 30) cm^2/(sec) (°C)[b]	72
	49	—	3.855 ± 0.100	(19°C < T < 75°C)	83
	75	—	4.225 ± 0.100		
Poison addition	20	Tank; Dia. = 50 cm; Hgt. = 60 cm	3.530 ± 0.110	—	84
Pulsed source	22	—	3.540 ± 0.070	(footnote c)	87,88
	40	—	3.680 ± 0.050		
	60	—	4.050 ± 0.070		
	80	—	4.310 ± 0.170		
Pulsed source	22	0.02 cm^{-2} < B^2 < 0.42 cm^{-2}	3.680 ± 0.040		86

[a] Scott, et al.,[80] reported $\bar{\lambda}_{tr}$ = 0.525 (± 0.010) cm, measured in water at (presumably) room temperature, using a pulsed neutron source. However, von Dardel and Sjöstrand[40] list the result as $\bar{D}_0$ = 3.850 (± 0.080) × 10^4 cm^2/sec, and this appears to be consistent with the uninterpreted data of Scott, et al. (The value $\bar{\lambda}_{tr}$ = 0.525 cm is consistent with the value for $\bar{D}_0$ only if v(kT) = 2.2 × 10^5 cm/sec is used as the average velocity in the computation.)

[b] This value corresponds to 0.37 (± 0.09)%/°C, relative to the value of $\bar{D}_0$ at 19°C, from 19°C to 75°C.

[c] A straight line joining the values of $\bar{D}_0$ at 22°C and at 80°C has the slope 0.37%/°C, relative to $\bar{D}_0$ at 22°C. This linear representation yields $\bar{D}_0$ = 4.038 × 10^5 cm^2/sec at 60°C but overestimates the value at 40°C.

Antonov, et al.,[44] used the pulsed-source method to measure $\bar{D}_0$ in distilled water at 23°C and at 80°C. The value $\bar{D}_0$ = 3.5 (± 0.1) × 10^4 cm^2/sec was derived from a least-squares fitting of the decay of the fundamental mode.

Von Dardel and Sjöstrand[40] analyzed the results of Antonov, et al.,[44] and reported an average temperature coefficient of 0.5 (± 0.2) %/°C in that temperature range. They also reported independent measurements that yielded the value $\bar{D}_0$ = 3.634 (± 0.075) × 10^4 cm^2/sec, and an average temperature coefficient 0.42 (± 0.04) %/°C from 10°C to 35°C.

Dio and Schopper[72,83] have suggested the linear variation: $\bar{D}_0$ = [3.505 × 10^4 + (T-19) (130 ± 30)] cm^2/sec, for 19°C < T < 75°C.

Küchle[87,88] measured $\bar{D}_0$ in water at 22°C, 40°C, 60°C, and 80°C. The value $\bar{D}_0 = 3.540\ (\pm 0.070) \times 10^4$ cm²/sec at 22°C is in very good agreement with the results of Dio and Schopper. Küchle reported that

$$\rho\bar{\lambda}_{tr} \propto (T/T_0)^{0.4}$$

is as reasonable a representation as $(T/T_0)^{0.5}$ in the range 0.025 ev < kT < 0.030 ev; $kT_0 = 0.025$ ev and ρ is the density in grams per cubic centimeter.

3.3.3 DIFFUSION PARAMETERS FOR THERMAL NEUTRONS IN OTHER HYDROGENEOUS MODERATORS

Meadows and Whalen* have derived a value of $\bar{D}_0$ for thermal neutrons in zirconium hydride of density 3.48 gm/cm³ and composition $\sim ZrH_{1.7}$ [H: 1.79 (± 0.02) wt-%; Zr: 96.5 (± 0.2) wt-%; and Sn: 1.38 (± 0.01) wt-%]. Least-squares fitting of the data of $\lambda(B^2)$ obtained in pulsed-source experiments, with 0.03 cm^{-2} < B^2 < 0.39 cm^{-2}, yielded $\bar{D}_0 = 5.79\ (\pm 0.02) \times 10^4$ cm²/sec at a temperature of 25 (± 2)°C.

Measured diffusion parameters of thermal neutrons in polyethylene[90] and in paraffin[91–93] are listed in Table 3-17. Diffusion parameters in diphenyl, $(C_6H_5)_2$, and in Dowtherm A (or "Diphyl")† have been measured at several laboratories. In view of their possible importance as organic moderators for thermal reactors, some of the experiments are discussed below. Also, results of various calculations are presented.

Table 3-17—MEASURED VALUES OF DIFFUSION PARAMETERS FOR THERMAL NEUTRONS IN HYDROGENOUS MODERATORS

Note: Room* indicates that water temperature is not specified in the reference. Room temperature is assumed.

Type of Experiment	Temperature, °C	Size of Medium	$\bar{D}_0$, 10^4 cm²/sec	$\bar{\lambda}_{tr}$, cm	$\bar{L}$, cm	Ref.
Polyethylene (approximately CH_2^a; density: 0.918 (± 0.001) gm/cm³)						
Pulsed source	Room*	0.098 cm^{-2} < B^2 < 0.143 cm^{-2}	2.650 ± 0.060	0.320 ± 0.008	2.12 ± 0.03	90
Paraffin (approximately $C_{25}H_{52}$; reference density: 0.89 gm/cm³)						
Exponential	Room*	—	—	—	2.42 ± 0.04[b]	91, 92
Pulsed source	Room*	0.045 cm^{-2} < B^2 < 0.947 cm^{-2}	2.660 ± 0.050[c]	0.323 ± 0.005[d]	2.13 ± 0.04[c]	83
Pulsed source	Room*	—	2.639 ± 0.088	0.320 ± 0.011[d]	2.14 ± 0.07	88
Diphenyl						
Exponential	Not stated; presumably 35 to 190	Tank; Dia. = 94 cm; Hgt. = 100 cm	—	—	4.143 exp (0.0021 T) (T in °C)	97
Poison addition; exponential	85	Tank; Dia. = 69 cm; filled to height of 89 cm	—	0.79 ± 0.03	4.82 ± 0.07	37
Dowtherm A						
Exponential	Room*	—	—	—	$\sqrt{18.2 \pm 0.5}$	96
Exponential	36	Tank; Dia. = 94 cm; Hgt. = 100 cm	—	—	4.214 ± 0.006	97
	92		—	—	4.941 ± 0.002	
	146		—	—	4.934 ± 0.005	
	192		—	—	5.245 ± 0.004	
Pulsed source	20	Approximately 0.06 cm^{-2} < B^2 < 0.23 cm^{-2}	4.92 ± 0.08	—	4.14 ± 0.07	87, 88
	80		6.07 ± 0.13	—	4.71 ± 0.13	
	140		7.43 ± 0.24	—	5.35 ± 0.24	
	180		8.38 ± 0.29	—	5.76 ± 0.30	

[a]The carbon and hydrogen contents of polyethylene were measured, and the formula $CH_{2.005 \pm 0.010}$ is indicated.

[b]Ertaud and Zaleski[93] reported on measurements of the thermal relaxation length, stating that the value of $\bar{L}$ obtained by Tittle[91] for paraffin provided a good fit to their own data.

[c]In performing a least-squares analysis of the pulsed-source data, the bucklings were computed with an assumed extrapolation distance of 0.28 cm.

[d]Computed from $\bar{D}_0$ assuming a room-temperature Maxwellian distribution of the thermal neutron flux and using $\bar{v} = 2.482 \times 10^5$ cm/sec.

* Private communication from J. W. Meadows and J. F. Whalen, Argonne National Laboratory.

† A mixture of diphenyl and diphenyl oxide in the proportion approximately 26.5 wt-% to 73.5 wt-%.

Heintzé[94] measured the thermal relaxation distance in water and in various other hydrogenous materials. A graphite thermal column of the BNL reactor was used as a source of thermal neutrons, followed by a graphite cylinder 10 cm long and of the same diameter as the medium to be studied. The exposed surfaces were covered with cadmium to prevent streaming from the thermal column to the neutron detectors. The temperatures of the various media were approximately 20°C to 22°C. Bare and cadmium-covered indium foils were activated and the spatial distributions of sub-cadmium activation determined. The data are tabulated below.

Material	Density, gm/cm^3	$\bar{L}$, cm
H_2O	1.0	2.86 ± 0.03
Lucite ($C_8H_8O_2$)	1.18	3.14 ± 0.03
Furfural ($C_5H_4O_2$)	1.16	5.57 ± 0.14
Expanded plastic ($C_{7.47}H_{8.20}$)	0.504	6.73 ± 0.21

From these data, Heintzé computed effective average microscopic thermal neutron transport cross sections for hydrogen in the four media, obtaining approximately 31 barns in water and in Lucite, and approximately 35 barns in the other two materials. *It would appear that the effect of chemical binding on the effective transport cross section of the hydrogen is not greatly different in the hydrogenous compounds studied.*

Blackman, et al.,[95] made use of Heintzé's results to infer an effective thermal $\bar{\lambda}_{tr}$ for Dowtherm A. Using also a measured absorption cross section for that material at 0.025 ev, and assuming a Maxwellian distribution of thermal neutron flux, they computed $L^2 = 19\ (\pm 2)\ cm^2$. A direct measurement by Sanders and McCracken[96] indicated $L^2 = 18.2\ (\pm 0.5)\ cm^2$. (Blackman, et al., quoted Dowtherm A as being constituted of 26.5 vol-% diphenyl, not 26.5 wt-%).

Bata, et al.,[97] measured the spatial distributions of the activation of cadmium-covered silver foils, in Dowtherm A and in diphenyl, using a small ("point") Po-Be neutron source. The diffusion length was inferred from a fitting of the form:

$$\exp(-r/L) = a\,[n_1(r) - n_2(r)]$$

where $n_1(r)$ is the distribution of the activity of the foils; $n_2(r)$ is the distribution of the foil activity with a slab of cadmium separating the detector from the source; and a is constant.

The experiments were repeated at temperatures ranging from approximately 35°C to 190°C. In the case of Dowtherm A, the expression $\bar{L} = 4.002 \exp(0.0014\ T)$ cm was observed to fit the data for $36°C < T < 192°C$. Chemical analysis of the moderator indicated: 87.15% C, 5.97% H, and 6.88% O.

The experiments with diphenyl yielded the formula: $\bar{L} = 4.143 \exp(0.0021\ T)$ cm, with T in degrees Centigrade.

Brown, et al.,[37] measured $\bar{\lambda}_{tr} = 0.79\ (\pm 0.03)$ cm in pure diphenyl at 85°C by the poison-addition method (see Section 3.3). The thermal diffusion length in diphenyl at 85°C is 4.82 (± 0.07) cm. The diphenyl was contained in a cylindrical tank, 69 cm in diameter and filled to a height of 89 cm.

Williams, et al.,[98] computed $\bar{L}$ for diphenyl at 85°C by averaging $\lambda_{tr}(E)$ and $\Sigma_a(E)$ with respect to an assumed neutron flux distribution. The transport cross section for hydrogen in diphenyl was calculated as

$$\sigma_{tr}^{H}(E) = \left[1 - \frac{2}{3A(E)}\right]$$

The effective scattering mass, A(E), for hydrogen, was calculated by the method of Radkowsky, deriving the energy dependence of the hydrogen scattering cross section from the data of Melkonian[99] for C_4H_6. The computed average diffusion lengths were: $\bar{L} = 4.78$ cm for a Maxwellian spectrum, and $\bar{L} = 4.94$ for a Wigner-Wilkins spectrum with a cutoff of 10 kT.

Petrie, et al.,[100,101] published curves relating to computations of the same type for diphenyl. In Fig. 3-21, the measured total cross section of hydrogen in C_4H_6 and in water are compared. Figure 3-22 shows the transport cross section for hydrogen in the two moderators, as calculated by the Radkowsky prescription. Figure 3-23 displays the dependence of the diphenyl density on the temperature. Figure 3-24 gives $\bar{L}$ for diphenyl as a function of temperature, based on Wigner-Wilkins calculations described in some detail in Section 3.3.4 (see also Fig. 3-32).

Küchle[87,88] has reported on pulsed-source measurements of diffusion parameters for thermal neutrons in Dowtherm A at temperatures from 20°C to 180°C. The data are presented in Table 3-17. Figure 3-25 compares the values of $\overline{L}$ obtained by Bata, et al.,[97] and by Küchle. Figure 3-26 depicts the results of Küchle for ρ (gm/cm^3) times $\overline{\lambda}_{tr}$ (cm) for Dowtherm A as a function of temperature, and

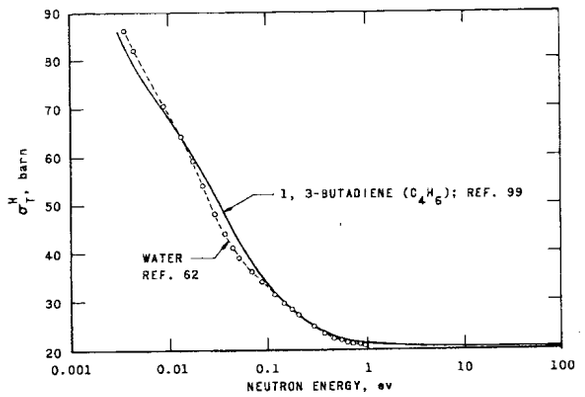

Fig. 3-21 — Measured microscopic total cross section of hydrogen in 1, 3-butadiene and in water. *Reproduced from Ref. 101.*

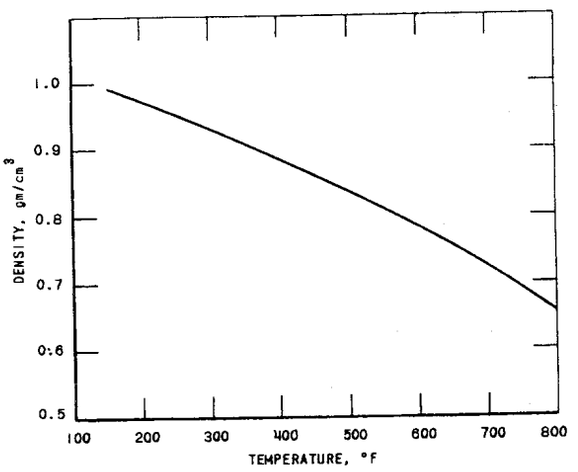

Fig. 3-23 — Density of diphenyl ($C_{12}H_{10}$) as a function of temperature. *Reproduced from Ref. 100.*

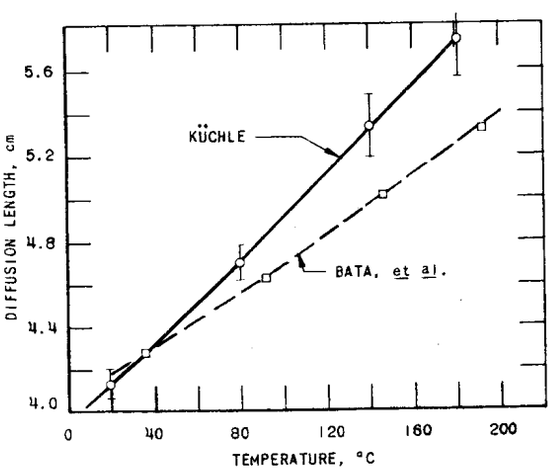

Fig. 3-25 — Measured average diffusion length ($\overline{L}$) of thermal neutrons in Dowtherm A as a function of temperature. *Reproduced from Ref. 88.*

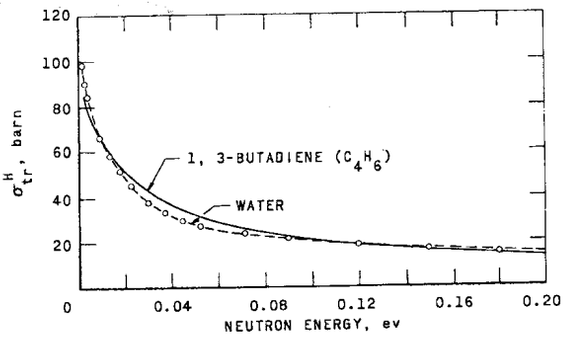

Fig. 3-22 — Calculated microscopic transport cross section of hydrogen in 1, 3-butadiene and in water. *Reproduced from Ref. 100.*

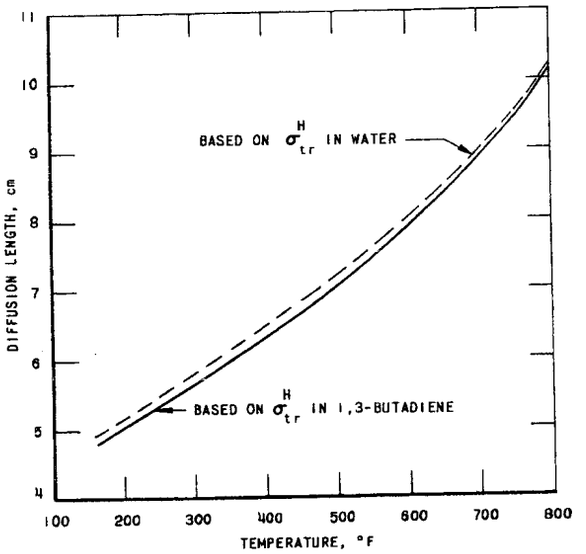

Fig. 3-24 — Calculated average diffusion length ($\overline{L}$) of thermal neutrons in diphenyl as a function of temperature. *Reproduced from Ref. 101.*

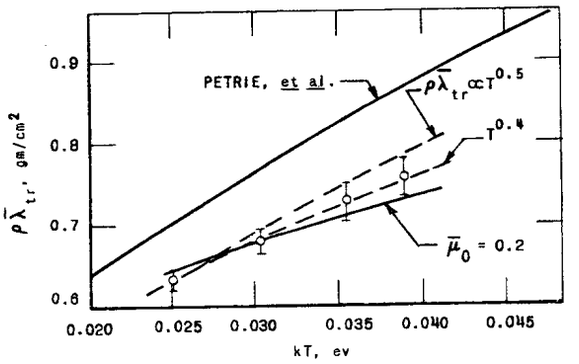

Fig. 3-26 — Product of density and average transport mean free path ($\rho\overline{\lambda}_{tr}$) of thermal neutrons in Dowtherm A as a function of neutron temperature. *Reproduced from Ref. 88.*

compares them with results of computations using the method of Petrie, et al.[100,101] Küchle's results are well represented by a $T^{0.4}$ variation for moderator kT in the range 0.025 ev to 0.039 ev:

$$\rho\bar{\lambda}_{tr} = 0.632 \left(\frac{T}{T_0}\right)^{0.4}$$

with $T_0 = 295°K$. Küchle observed that a $T^{0.4}$ variation represents the data of $\rho\bar{\lambda}_{tr}$ in water as well (see Section 3.3.2.2).

3.3.4 THERMAL-GROUP DIFFUSION PARAMETERS IN MIXTURES OF MODERATORS CONTAINING NEUTRON ABSORBERS

The preceding sections were concerned with average diffusion parameters for thermal neutrons in pure moderators. Mention was made of experiments wherein $\bar{L}$ was measured in liquids (H_2O, D_2O) in which neutron absorbers were dissolved. However, these experiments were performed primarily to yield values of $\bar{\lambda}_{tr}$ for the unpoisoned media (see Refs. 36, 37, 84, and 85).

Most of the experiments to date have been limited to the investigation of diffusion parameters in pure moderators of relatively low absorption where the thermal neutron flux spectrum is essentially Maxwellian. However, these experimental data are of relatively limited utility in computations of spatial distributions of thermal neutron flux in practical, finite, homogeneous reactor media. For these computations, $\bar{\lambda}_{tr}$ and $\bar{L}$ must be known.

In this section, the influence of neutron absorbers on $\bar{\lambda}_{tr}$ and $\bar{L}$ in *infinite*, homogeneous media with a uniform spatial source distribution is discussed.

Sections 3.1 and 3.2 deal with the thermal neutron flux spectrum, and average absorption cross sections for thermal neutrons in absorbing and scattering media. If the energy-dependent transport cross sections of the moderating materials are known, and if the thermal neutron flux spectrum is known, the usual procedure for determining the average thermal-group parameters is to compute $\bar{\lambda}_{tr}$ and $\bar{\Sigma}_a$, and thence L^2 from a formula derived from transport-theoretic analysis. For example:

$$L^2 = \bar{\lambda}_{tr}/3\bar{\Sigma}_a$$

when $\bar{\Sigma}_a$ is small in comparison with $\Sigma_s(1 - \bar{\mu})$. For a mixture of moderating materials,

$$\bar{\lambda}_{tr} \equiv \overline{(1/\Sigma_{tr})}$$

where $\Sigma_{tr}(E) = \Sigma_a^*(E) + \sum_i \alpha_i \Sigma_{tr,i}(E)$; $\Sigma_{tr,i}(E)$ and α_i are, respectively, the macroscopic transport cross section and the volume fraction of the ith pure material; and $\Sigma_a^*(E)$ is the cross section of the absorbing impurities.

Petrie, et al.,[100] have derived simplified formulas for diffusion parameters in hydrogenous mixtures on the basis of an assumed 1/v variation of the transport cross section for hydrogen in water and in hydrocarbons. Indeed, if the transport cross sections of the moderators and the absorption cross sections all vary as 1/v, then in a Maxwellian flux distribution,

$$\bar{\lambda}_{tr} = \left[\frac{1}{\bar{\lambda}_a^*} + \sum_i \alpha_i \frac{1}{\bar{\lambda}_{tr,i}}\right]^{-1}$$

where $\bar{\lambda}_a^*$ is the average absorption mean free path for the impurities; in this case $\bar{\lambda}_a^* = 1/\bar{\Sigma}_a^*$.

The following paragraphs are based upon the work of Conerty, Petrie, Storm, and Zweifel.[100,101]

Using Wigner-Wilkins thermal flux spectra, computed for various values of the parameter:

$$\beta\gamma = \frac{\Sigma_a(kT)}{\xi\bar{\Sigma}_{s,asymptotic}} \tag{3-10}$$

and for various values of the moderator temperature T, the authors evaluated the average value of a number of parameters of interest in the analysis of reactors moderated by hydrogenous mixtures. In Eq. (3-10), $\Sigma_a(kT)$ is the macroscopic absorption cross section at the energy kT; ξ is the average logarithmic energy decrement per collision; and $\Sigma_{s,asymptotic}$ is the free-atom macroscopic scattering cross section at energies near thermal.

For any 1/v absorber, the average absorption cross section is given by:

$$\overline{\sigma_{1/v}(\beta\gamma, kT)} = \sigma_{1/v}(E_0)\, E_0^{1/2}\, \overline{E^{-1/2}(\beta\gamma, kT)}$$

where E_0 is any convenient reference energy, and the averages are taken with respect to a Wigner-Wilkins spectrum cut off at 10 kT. Figure 3-27 is a plot of the average value, $\overline{E^{-1/2}(\beta\gamma, kT)}$, as a function of $\beta\gamma$ and kT. Tables listing the average thermal absorption cross sections relative to Wigner-Wilkins spectra have been published by Amster[34] (see Section 3.2.3) for a number of isotopes important to the field of thermal nuclear reactors.

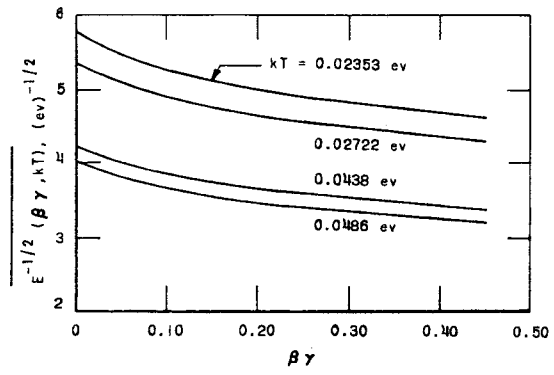

Fig. 3-27—Calculated average values of $E^{-1/2}$ as a function of $\beta\gamma$ and kT. *Reproduced from Ref. 100.*

The transport mean free path is given by:

$$\lambda_{tr}(E) = \left\{\sum_i N_i \left[\sigma_T^i(E) - \sigma_S^i(E)\, \overline{\mu(E)^i}\right]\right\}^{-1} \qquad (3\text{-}11)$$

where N_i, $\sigma_T^i(E)$, $\sigma_S^i(E)$, and $\overline{\mu(E)^i}$ are, respectively, the number of atoms per cm^3, the microscopic total cross section, the microscopic neutron scattering cross section, and the average cosine of the scattering angle for the ith nuclide. For isotopes of mass number A, other than bound hydrogen, $\overline{\mu(E)} = 2/(3A)$. The value of $\overline{\mu(E)}$ for bound hydrogen in water is assumed to be given by the Radkowsky prescription (see Section 3.3.2.1). [For hydrogen in other compounds, a similar formula is adopted, using the measured $\sigma_S(E)$.]

Figure 3-28 shows the resultant calculated $\bar{\lambda}_{tr}$ of water as a function of $\beta\gamma$ and kT. The corresponding averages for the hydrogen in water are shown in Fig. 3-29. Figure 3-30 gives the average

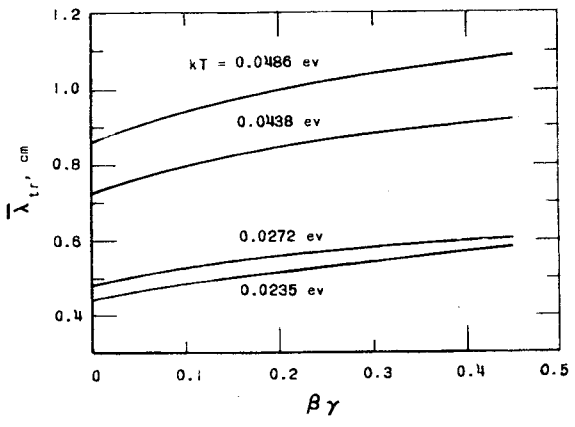

Fig. 3-28—Calculated average transport mean free path ($\bar{\lambda}_{tr}$) of thermal neutrons in water as a function of $\beta\gamma$ and kT. *Reproduced from Ref. 100.*

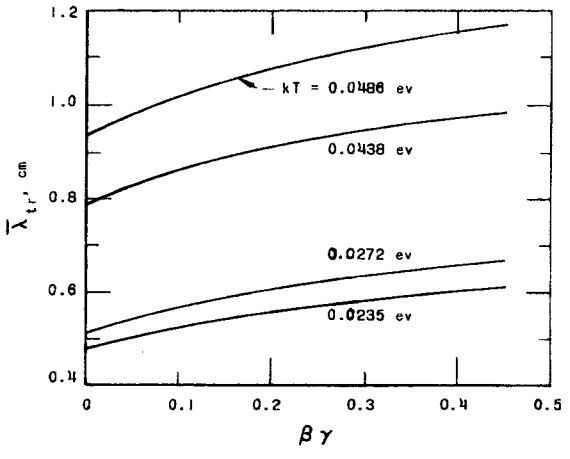

Fig. 3-29—Calculated average transport mean free path ($\bar{\lambda}_{tr}$) of thermal neutrons in hydrogen as a function of $\beta\gamma$ and kT. (Based on $\lambda_{tr}(E)$ of hydrogen in water.) *Reproduced from Ref. 100.*

of the hydrogen transport cross section, and Fig. 3-31 shows the average thermal diffusion length, $\bar{L}$, for water, which is taken as

$$\bar{L} = (\bar{\lambda}_{tr}/3\bar{\Sigma}_a)^{1/2}$$

Also given in Fig. 3-31 are some experimental values of the diffusion length of water at various temperatures.

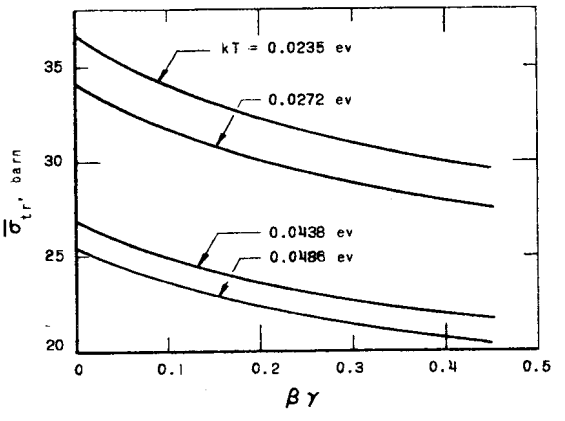

Fig. 3-30 — Calculated average microscopic transport cross section ($\bar{\sigma}_{tr}$) of hydrogen in water as a function of $\beta\gamma$ and kT. *Reproduced from Ref. 100.*

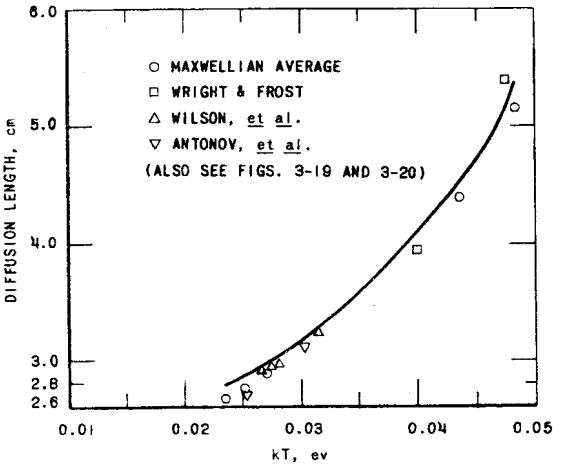

Fig. 3-31 — Average diffusion length ($\bar{L}$) of thermal neutrons in water as a function of temperature. *Reproduced from Ref. 100.*

To simplify the evaluation of $\bar{\lambda}_{tr}$ for mixtures of water and other substances, the authors[100,101] have derived series expansions which utilize the values of $\bar{\lambda}_{tr}$ for water (Fig. 3-28), or hydrogen in water (Fig. 3-29), or of $\bar{\sigma}_{tr}$ for hydrogen in water (Fig. 3-30), but which require no further integrations.

Equation (3-11) is rewritten in the form:

$$\lambda_{tr}(E) = [\Sigma^0_{tr}(E) + \Sigma'_a(E) + \Sigma'_{tr}]^{-1} \qquad (3\text{-}12)$$

where

$$\Sigma^0_{tr}(E) = N_0\,\sigma^0_{tr}(E)$$

$$\Sigma'_a(E) = \sum_m N_m\,\sigma^m_a(E)$$

$$\Sigma'_{tr} = \sum_m \left(1 - \frac{2}{3A_m}\right) N_m\,\sigma^m_s$$

The indices 0 and m refer to the hydrogenous and non-hydrogenous components of the mixture; σ_{tr} and σ_a denote microscopic transport and absorption cross sections; N, A, and σ_s are as defined after Eq. (3-11); and Σ'_{tr} is assumed to be energy independent.

If $\Sigma^0_{tr}(E) + \Sigma'_a(E) > \Sigma'_{tr}$ at thermal energies, then $\lambda_{tr}(E)$ may be expanded in a series

$$\lambda_{tr}(E) = [\Sigma^0_{tr}(E)\,R(E)]^{-1} + \sum_{n=1}^{\infty}(-1)^n\,(\Sigma'_{tr})^{n+1}\,R^{n+1}(E) \qquad (3\text{-}13)$$

where

$$R(E) \equiv 1 + [\Sigma'_a(E)/\Sigma^0_{tr}(E)]$$

is a slowly-varying function of energy in the range where the flux is high.

Assuming that in all but the first term of Eq. (3-13) $\Sigma'_{tr}(E)$ may be taken to be $1/v$, an average over the thermal flux range yields:

$$\bar{\lambda}_{tr} \approx \overline{(R^{-1})}\ \overline{\lambda^0_{tr}(\beta\gamma, kT)} - \sum_{n=1}^{\infty} \overline{(R^{-1})^{n+1}} \frac{(\Sigma'_{tr})^n}{[\Sigma^0_{tr}(E_0)]^{n+1}} \overline{\left(\frac{E}{E_0}\right)^{(n+1)/2}} \tag{3-14}$$

where an average value of R^{-1} has been used. By virtue of the assumption that $\Sigma^0_{tr}(E) + \Sigma'_a(E) > \Sigma'_{tr}$ at thermal energies, the infinite series on the right-hand side of Eq. (3-14) converges, provided the averaged terms involve integrations with a finite upper limit. If the series converges rapidly, so that only a few terms are needed, the upper limit may be extended to infinity for the terminated expansion. Petrie, et al., computed

$$\overline{\left(\frac{E}{E_0}\right)^{(n+1)/2}}$$

relative to a Maxwellian distribution, and calculated the first term on the right-hand side of Eq. (3-14) relative to a Wigner-Wilkins spectrum cut off at 10 kT. With these approximations,

$$\overline{\left(\frac{E}{E_0}\right)^{(n+1)/2}} = \Gamma\left(\frac{n+5}{2}\right)$$

The quantity $\overline{R^{-1}}$ may be obtained either as

$$\overline{R^{-1}} \approx \{1 + [\bar{\Sigma}'_a(kT)/\Sigma^0_{tr}(kT)]\}^{-1} \tag{3-15}$$

or

$$\overline{R^{-1}} \approx [1 + (\bar{\Sigma}'_a/\bar{\Sigma}^0_{tr})]^{-1} \tag{3-16}$$

Numerical examination has indicated that either Eq. (3-15) or Eq. (3-16) leads to essentially the same result for $\bar{\lambda}_{tr}$.

The accuracy of these approximations was checked for 100% water, using λ_{tr} for hydrogen in water as λ^0_{tr}. The agreement between a direct calculation and the series approximation was within 4% over a wide range of values of $\beta\gamma$ and of kT.

The above method may be applied to any hydrogenous mixture for which the deviation from $1/v$ behavior of the transport cross section of the hydrogenous component is small.

Figure 3-32 is a plot of the function $\rho\bar{\lambda}_{tr}$ in diphenyl for various values of $\beta\gamma$ and kT. (Other results derived for diphenyl are described in Section 3.3.3.)

3.3.5 COMMENTS ON PARAMETERS FOR THERMAL NEUTRONS IN NON-EQUILIBRIUM ENVIRONMENTS

In Sections 3.3.1 to 3.3.4, attention was focused on average parameters for a single thermal neutron group, covering the entire range of "thermal" energies. However, there are few thermal reactors without local inhomogeneities; for example: reflectors, or a water channel for a control rod. Through experiment and calculation,[102–106] it has become obvious that it is not simply diffusion theory that is inadequate to account for flux distributions in the vicinity of an interface separating two media with different temperatures and/or different moderating and absorbing characteristics. The concept of a single thermal group usually is inadequate, in these cases.

It has been suggested* that averaging cross sections over properly chosen spectra may yet make it feasible to use the concept of a single thermal group in the case of a water-gap calculation. Calame[104] has published a formula for the calculation of space-dependent cross sections in the neighborhood of water gaps, in terms of a spatially varying average of two equilibrium spectra. In a later paper, Calame[105] examined the implications of a simplified method used to estimate power peaking at a water gap in a thermal reactor. In this method, a single thermal group is used and flux computations are performed with cross sections averaged with respect to the equilibrium flux in an infinite, water-

*Private communication from G. H. Miley to G. P. Calame (see Ref. 105).

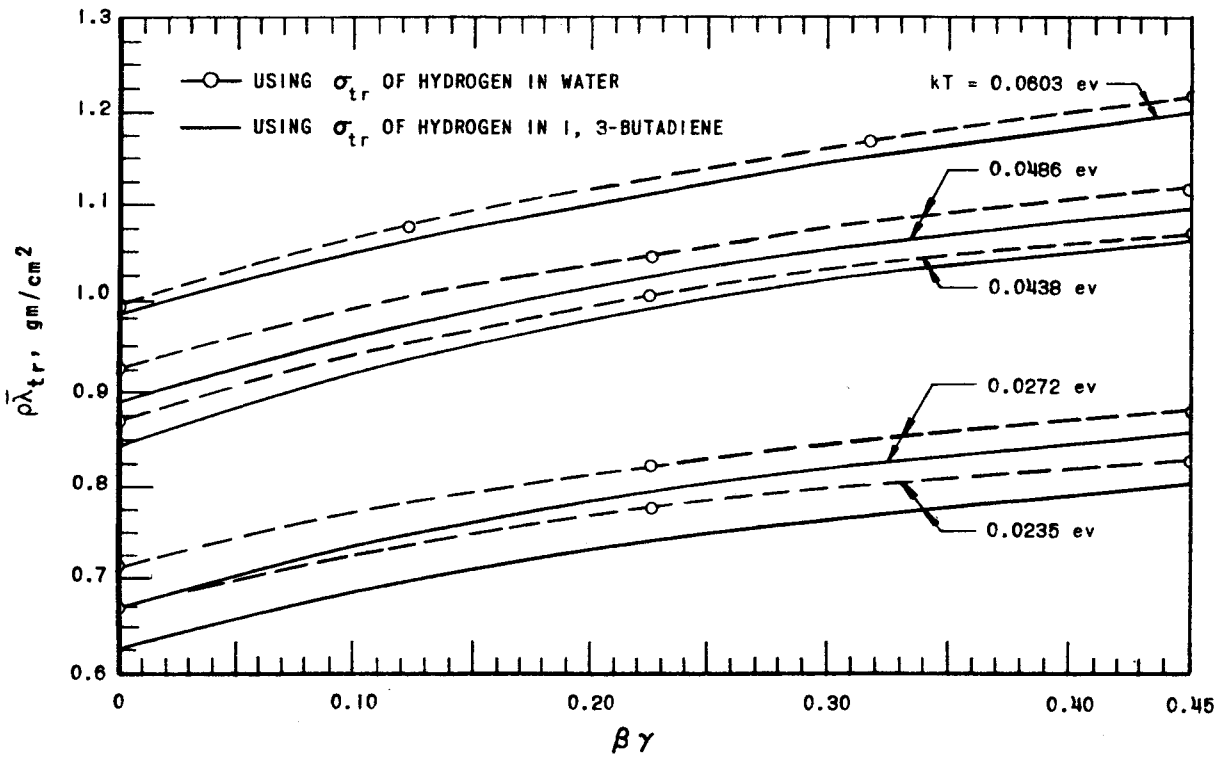

Fig. 3-32 — Product of density and calculated average transport mean free path ($\rho\bar{\lambda}_{tr}$) of thermal neutrons in diphenyl as a function of $\beta\gamma$ and kT. *Reproduced from Ref. 101.*

gap medium. Calame pointed out that an important limitation of the approximation is that the ratio of $\bar{\bar{\Sigma}}_{f,th}$ to $\bar{\bar{\Sigma}}_{a,th}$ in the core must be approximately independent of the flux spectrum over which the cross sections are averaged. Wright and Feiner[106] have proposed a formula for the thermal flux spectrum in the water gap and have compared experimental and calculated relaxation lengths in the large medium surrounding the gap.

The variation of the thermal neutron flux in the vicinity of a core-reflector interface has been calculated by Kelber and Kier,[107] using two thermal groups, characterized as the infinite-medium spectra in the two media, and assigning cross sections for transfer between the groups. Kottwitz[20] has computed the deviation from the asymptotic thermal neutron flux spectra in the vicinity of a plane interface between two semi-infinite media differing only in temperature. Following a suggestion by Selengut,[108] Kottwitz represented the thermal flux spectrum as a sum of two separable functions; for example:

$$\phi(y,E) = \left[1 - \frac{\exp(y)}{2}\right] M_1(E) + \frac{\exp(y)}{2} M_2(E) \text{ for } y \leq 0$$

where y is the space parameter; E is the energy parameter; $M_1(E)$ is a Maxwellian distribution with mode kT_1 corresponding to the temperature T_1 of the medium $y < 0$; and $M_2(E)$ is a Maxwellian with temperature T_2 of the medium $y > 0$. Analyses of this type provide insight to the problem of determining a few-region approximation with different average cross sections in each region.

Bennett and Heineman[109] have reported on the analysis of experiments simulating the two-medium model of Kottwitz to determine transfer cross sections between the two equilibrium groups, or "rethermalization" cross sections. The cross section for transfer between the groups was assumed to be independent of the direction of transfer. (Within each of the two groups, the diffusion and absorption cross sections are the averages with respect to the equilibrium spectrum.)

Fowler and Royston[110] have published results of spectrum calculations using Kottwitz's method, and have compared the absorption rates of a 1/v absorber and of Pu^{239} at the interface of the two media, thereby giving some notion of the influence of such a discontinuity.

Increasingly, efforts are being made to refine computations of thermal neutron absorption distributions and of thermal neutron leakage in thermal reactors. The discussion above is intended primarily to acknowledge the existence, the importance, and the gratifying success of these efforts.

3.4 SLOWING-DOWN PARAMETERS IN WELL-MODERATED MEDIA

3.4.1 SLOWING-DOWN KERNELS AND THEIR FOURIER TRANSFORMS

The critical properties of an unreflected thermal homogeneous reactor may be related to the Fourier transform of an appropriate slowing-down kernel. The slowing-down kernel, $P(\underline{r},\underline{r}', E)$, represents the probability per unit volume that a fission neutron originating at a point $\underline{r}'$ will reach the point $\underline{r}$ with an energy E. If $\phi(\underline{r}')$ represents the thermal flux at $\underline{r}'$, the thermal slowing-down density is given by:

$$q(\underline{r}, E_{th}) = \int_{Reactor} (k/p)\, \Sigma_a\, \phi(\underline{r}')\, P(\underline{r},\underline{r}', E_{th})\, d\underline{r}' \tag{3-17}$$

Equation (3-17) in conjunction with the thermal diffusion equation:

$$D\nabla^2\phi(\underline{r}) - \Sigma_a\, \phi(\underline{r}) + q\,(\underline{r}, E_{th}) = 0 \tag{3-18}$$

and the proper boundary conditions on q and ϕ specify the standard reactor model. Commonly used boundary conditions are:

$$\phi = q = 0$$

at the extrapolated boundary of the reactor, the extrapolation distance being assumed independent of energy, and

$$\partial\phi/\phi\partial\underline{0} = [-0.71\, \lambda_{tr}\, (E_{th})]^{-1}$$

$$\partial q/q\partial\underline{0} = [-0.71\, \lambda_{tr}\, (E)]^{-1}$$

at the physical boundary of the reactor, where $\partial/\partial\underline{0}$ is the derivative with respect to the outward normal $\underline{0}$, and λ_{tr} is the transport mean free path.

A solution of Eqs. (3-17) and (3-18) with given boundary conditions may be obtained by considering an infinite system of the same composition as the finite system.

In the infinite system, the slowing-down kernel, $P_\infty(\underline{r},\underline{r}',E)$, is a function of $|\underline{r} - \underline{r}'|$ and E only. This is not, in general, the case for $P(\underline{r},\underline{r}',E)$, but since P and P_∞ in most cases satisfy the same differential equation, P may be obtained by superimposing P_∞.

In the infinite medium, the slowing-down density, $q_\infty(\underline{r},E_{th})$, and the thermal flux, $\phi(\underline{r})$, satisfy

$$q_\infty(\underline{r}, E_{th}) = \int_{All\ space} (k/p)\, \Sigma_a\, \phi(\underline{r}')\, P_\infty(|\underline{r} - \underline{r}'|, E_{th})\, d\underline{r}' \tag{3-19}$$

and

$$D\nabla^2\phi(\underline{r}) - \Sigma_a\, \phi(\underline{r}) + q_\infty(\underline{r}, E_{th}) = 0 \tag{3-20}$$

It can be shown[111] that $\phi(\underline{r})$ in Eq. (3-20) is satisifed by any solution of $\nabla^2\phi(\underline{r}) + B^2\phi(\underline{r}) = 0$ provided B^2 is a root of

$$-DB^2 - \Sigma_a + (k/p)\, \Sigma_a\, \bar{P}_\infty(B^2, E_{th}) = 0 \tag{3-21}$$

and where $\bar{P}_\infty(B^2, E_{th})$ is the three-dimensional Fourier transform of $P_\infty(|\underline{r} - \underline{r}'|, E_{th})$; that is,

$$\bar{P}_\infty(B^2, E_{th}) = 4\pi \int_0^\infty \frac{\sin Br}{Br}\, P_\infty(r, E_{th})\, r^2\, dr \tag{3-22}$$

It also follows from Eq. (3-19) that

$$q_\infty(\underline{r}, E_{th}) = (k/p)\Sigma_a \bar{P}_\infty(B^2, E_{th})\, \phi(\underline{r})$$

and, consequently, $\bar{P}_\infty(B^2, E_{th})$ represents the non-leakage probability for neutrons in slowing down to thermal energy, E_{th}. Inönü has shown[112] that $\bar{P}_\infty(B^2, E_{th})$ represents the non-leakage probability quite accurately even when the size of the system is decreased to the order of the mean free path.

For a finite reactor in which the extrapolation distance is energy independent, and both P and P_∞ satisfy the same linear equation except for points close to the boundaries of the reactor, the solution for the flux from Eq. (3-20) is the same as the solution from Eq. (3-18). Further, the slowing-down densities are identical.

The criticality condition for the finite problem is obtained from Eq. (3-21) and

$$\frac{k}{p}\frac{\bar{P}_\infty(B^2, E_{th})}{1 + L^2B^2} = 1$$

B^2 being identified with the geometrical buckling of the reactor.

Commonly-used kernels that describe the slowing down of neutrons are:
Gaussian (Fermi) Kernel:

$$P_\infty(r,E) = \frac{\exp[-r^2/4\tau(E)]}{[4\pi\tau(E)]^{3/2}}$$

$P_\infty(B^2,E) = \exp[-B^2\tau(E)]$, where $\tau(E)$ is the Fermi age.

Diffusion (Yukawa) Kernel:

$$P_\infty(\underline{r},E) = \frac{\exp(-|\underline{r}|/L_1)}{4\pi L_1^2 |\underline{r}|}$$

$$\bar{P}_\infty(B^2,E) = 1/(1 + L_1^2 B^2)$$

Transport Kernel:

$$P_\infty(\underline{r}) = \Sigma_s \frac{\exp(-\Sigma|\underline{r}|)}{4\pi|\underline{r}|^2}$$

$$\bar{P}_\infty(B^2) = \frac{1}{B}\tan^{-1}\frac{B}{\Sigma}$$

Convolutions of these kernels give other representations for the slowing-down kernels.

3.4.1.1 $\bar{P}_\infty(B^2,E)$ for Specific Cases

Measurements and calculations of $\bar{P}_\infty(B^2,E)$ for H_2O are given in Section 3.4.4.

Mack and Zweifel[113] applied the Greuling-Goertzel method in the P_1 and B_1 approximations (Section 3.4.2) to calculate the non-leakage probability for a 2-Mev source to indium resonance in D_2O. Their results are given in Table 3-18. The Fourier transform of the Fermi kernel is included for comparison.

These authors also give the Fourier transform of the infinite medium, point source kernel which gives the flux of neutrons of lethargy u and displacement r from the 2-Mev source. This transform is denoted by $\phi_0(B^2,u)$. Table 3-19 gives $\phi_0(B^2,u)$ for $B^2 = 0.01$ and various u. Table 3-20 gives $\phi_0(B^2, 1.4$ ev) for various B^2.

Shapiro[115] cites a very good fit to the observed slowing-down density in D_2O by convolution of a Yukawa and a Gaussian kernel. The slowing-down density from a fission source to indium resonance was given by:

$$q(r) = \frac{A\exp(\tau_1/\tau_2)}{8\pi r\,\tau_2}\left\{\left[1 + \phi\left(\frac{r}{2\sqrt{\tau_1}} - \sqrt{\frac{\tau_1}{\tau_2}}\right)\right]\exp(-r/\sqrt{\tau_2}) - \left[1 - \phi\left(\frac{r}{2\sqrt{\tau_1}} + \sqrt{\frac{\tau_1}{\tau_2}}\right)\right]\exp(r/\sqrt{\tau_2})\right\}$$

where

$$\phi(x) = (2/\sqrt{\pi}) \int_0^x \exp(-y^2)\, dy$$

$$\tau_1 = 58 \text{ cm}^2$$

and

$$\tau_2 = 48 \text{ cm}^2$$

Table 3-18—$\bar{P}_\infty$ (B^2, 1.4 ev) FOR A 2-MEV SOURCE IN D_2O

Data from Ref. 113.

Note: Asterisks distinguish "consistent" Greuling-Goertzel method from the G-G method which assumes Fick's Law to be valid.

Approximation	$B^2 = 0.0025$	$B^2 = 0.01$	$B^2 = 0.0225$
P_1	0.7696	0.3618	0.1130
P_1^*	0.7694	0.3616	0.1136
B_1	0.7695	0.3714	0.1262
B_1^*	0.7693	0.3705	0.1268
$\exp(-B^2 \tau)$	0.7756	0.3619	0.1016

Table 3-19—COMPARISON OF FLUX $\phi_0(B^2, u)$, $B^2 = 0.01$

Data from Ref. 113.

Note: Asterisks distinguish "consistent" Greuling-Goertzel method from the G-G method which assumes Fick's Law to be valid.

u[a]	P_1	P_1^*	B_1	B_1^*
0	1.00	1.00	1.00	1.00
2	0.8714	0.8650	0.8744	0.8731
4	0.7593	0.7586	0.7647	0.7629
6	0.6616	0.6611	0.6686	0.6671
8	0.5765	0.5762	0.5847	0.5835
10	0.5023	0.5022	0.5113	0.5102
12	0.4378	0.4379	0.4471	0.4465
14.17	0.3770	0.3772	0.3864	0.3860

[a] u = 0 corresponds to 2 Mev.

Table 3-20—COMPARISON OF FLUX $\phi_0(B^2, 1.4 \text{ ev})$

Data from Ref. 113.

Note: Asterisks distinguish "consistent" Greuling-Goertzel method from the G-G method which assumes Fick's Law to be valid.

B^2	P_1	P_1^*	B_1	B_1^*
0.0025	0.7779	0.7776	0.7776	0.7776
0.01	0.3770	0.3772	0.3864	0.3860
0.0225	0.1237	0.1247	0.1375	0.1384

3.4.2 MOMENTS OF THE SLOWING-DOWN DISTRIBUTION AND FLUX FROM FISSION SOURCES

In Eq. (3-22), if (sin Br)/Br is expanded in a Taylor series and integrated term-by-term, there results

$$\bar{P}_\infty(B^2,E) = 4\pi \sum_{n=0}^{\infty} \frac{(-1)^n}{(2n+1)!} B^{2n} \int_0^\infty r^{2n} P_\infty(r,E)\, r^2\, dr$$

Normalizing $P_\infty(r,E)$ such that

$$4\pi \int_0^\infty P_\infty(r,E)\, r^2 dr = p = \bar{P}_\infty(0,E)$$

then

$$\bar{P}_\infty(B^2,E) = p \sum_{n=0}^{\infty} \frac{(-1)^n}{(2n+1)!}\, B^{2n}\, \overline{r_E^{2n}}$$

where $\overline{r_E^{2n}}$ is the 2nth moment of the slowing-down kernel; that is

$$\overline{r_E^{2n}} = \frac{\int_0^\infty r^{2n} P_\infty(r,E)\, r^2 dr}{\int_0^\infty P_\infty(r,E)\, r^2 dr}$$

The subscript E indicates the energy below which the neutrons have slowed down.

In the limit of vanishingly small B^2, one-sixth of the mean square distance from a point fission source for slowing down *past* energy E can be written

$$\frac{\overline{r_E^2}}{6} = \lim_{B^2 \to 0} \frac{1}{B^2} \left[1 - \frac{\bar{P}_\infty(B^2,E)}{\bar{P}_\infty(0,E)} \right] \tag{3-23}$$

where $\bar{P}_\infty(B^2,E)$ is the three-dimensional Fourier transform of $P_\infty(r,E)$. The quantity $\overline{r_E^2}/6$ is sometimes denoted as the "slowing-down age" at energy E.

Alternatively, let $K_\infty(r,E)$ be the infinite-medium, point-fission-source kernel which gives the flux of neutrons per unit energy at energy E and position $\underline{r}$ due to a unit point fission source at position $\underline{r}'$ (where again $r = |\underline{r} - \underline{r}'|$). Then, in the limit of vanishingly small B^2, one-sixth of the mean square distance from a point fission source of neutrons which *have* the energy E can be written

$$\frac{\overline{r^2}(E)}{6} = \lim_{B^2 \to 0} \frac{1}{B^2} \left[1 - \frac{\bar{K}_\infty(B^2,E)}{\bar{K}_\infty(0,E)} \right]$$

where $\bar{K}_\infty(B^2,E)$ is the three-dimensional Fourier transform of $\bar{K}_\infty(r,E)$, and the quantity $\overline{r^2}(E)/6$ is sometimes denoted as the "flux age" and referred to using the Greek τ.

The "flux age" will be larger than the "slowing-down age". In the common "age theory", they differ by the so-called last-flight correction.

In the case of a monoenergetic source having energy E_S, the "slowing-down age" would involve the use of $P_\infty(r,E_S,E)$, the infinite-medium, slowing-down kernel which gives the neutrons slowing down past energy E at $\underline{r}$ due to a unit point source of energy E_S at position $\underline{r}'$, where $r = |\underline{r} - \underline{r}'|$. The previous $P_\infty(r,E)$ is, of course, given by:

$$P_\infty(r,E) = \int_0^\infty f(E_S)\, P_\infty(r,E_S,E)\, dE_S$$

where $f(E_S)$ is the fission spectrum. Similarly, the "flux age" for a monoenergetic source involves $K_\infty(r,E_S,E)$. If E coincides with the source energy, the flux will include a component due to the virgin source neutrons, and the spatial distribution of slowing-down density is the distribution of first collisions. In both cases, there results the so-called first-flight correction in the common "age theory".

The critical equation for a reactor may be written in terms of the even moments of the slowing-down kernel as

$$\frac{k}{1 + L^2B^2} \sum_{n=0}^{\infty} \frac{(-1)^n}{(2n+1)!}\, B^{2n}\, \overline{r_E^{2n}} = 1$$

For a large thermal reactor, $B^2\, \overline{r_E^2} < 1$, and all the terms for $n > 1$ in this equation may be neglected. The criticality condition may then be written in terms of the 2nd moment $\overline{r_E^2}$.

Various methods have been employed to calculate the moments of slowing-down distributions. Marshak[116] derived formulas for the ratio of the second to the zeroth moment of the neutron density

under varying assumptions with regard to the cross section. Hurwitz and Zweifel,[117] and Hellens[118] used the P_1 and the B_1 approximations, and the Selengut-Goertzel method associated with these approximations, in their computations of slowing down and age.

Both the P_L and B_L methods start with the space Fourier transform of the Boltzmann equation. The kth Fourier component of the flux, $N(k,u,\mu)$, is expanded into a series of Legendre polynomials in μ, the cosine of the angle between the position and velocity vectors. Further, $\sigma(\mu_0,u',U)$, the cross section for scattering a neutron of lethargy u' through an angle $\cos^{-1}\mu_0$ with a logarithmic energy reduction $U = u-u'$, is expanded in Legendre polynomials in μ_0. Since

$$N(k,u,\mu) = \sum_{\ell=0}^{\infty} \frac{2\ell+1}{4\pi} N_\ell(k,u)\, P_\ell(\mu)$$

$$\sigma(\mu_0,u',U) = \sum_{\ell=0}^{\infty} \frac{2\ell+1}{4\pi} B_\ell(u',U)\, P_\ell(\mu_0)$$

and using the addition theorems for spherical harmonics, the term (in the Boltzmann equation)

$$\int d\Omega_0' \int_{u-q}^{u} \sigma(\mu_0,u',U)\, N(k,u',\mu')\, du'$$

becomes

$$\sum_{\ell=0}^{\infty} \frac{2\ell+1}{4\pi} P_\ell(\mu) \int_{u-q}^{u} N_\ell(k,u')\, B_\ell(u',U)\, du'$$

where $q = \ln[(1+\gamma)/(1-\gamma)]^2$, and γ is the ratio of neutron mass to the mass of the scattering nucleus. Finally, the Boltzmann equation for the jth Legendre component of N becomes

$$N_j(k,u) = \sum_{\ell=0}^{\infty} (2\ell+1)\, A_{\ell j}(k,u) \left[\sum^{\gamma} \int_{u-q}^{u} N_\ell(k,u')\, B_\ell^{\gamma}(u',U)\, du' + S_\ell(k,u) \right]$$

where $\sum^{\gamma}$ indicates sum over moderators present; S_ℓ is the Legendre expansion of the source term;

$$A_{j\ell} = A_{\ell j} = \frac{1}{2} \int_{-1}^{+1} d\mu \frac{P_j(\mu)\, P_\ell(\mu)}{\sigma_T(u) - ik\mu}$$

and σ_T is the total cross section. When the infinite set of equations for $N_j(k,u)$ is made finite by setting

$$J_\ell^{\gamma} \equiv \int_{u-q}^{u} N_\ell(k,u')\, B_\ell^{\gamma}(u',U)\, du'$$

equal to zero, and $S_\ell = 0$ for $\ell > L$, one obtains the B_L approximation.

The P_L approximation is obtained when an $(L+1)$-point Gauss integration formula is used in the equation for $A_{\ell j}$. This is equivalent to setting $N_\ell = 0$ for $\ell > L$.

In either the P_L or B_L methods, there are several ways of treating the system of equations for the $N_j(k,u)$. A common method is to evaluate J_ℓ^{γ} by a Taylor series expansion in u, u in the neighborhood of u'. In the P_1 approximation, if two terms are retained in the Taylor expansion for the N_0 component, and one term for the N_1 component of the flux, the age-diffusion approximation is obtained. If hydrogen is present, the above procedure may be modified.

One such modification, known as the Selengut-Goertzel (S-G) method, treats all elements other than hydrogen as outlined above. For hydrogen, the S-G method in effect treats correctly the energy loss of a neutron colliding with a proton but neglects the correlation between the loss of energy and the scattering angle.

Experimentally, one normally measures the "flux age". This is obtained by measuring in a medium the spatial distribution of neutrons corresponding to a given energy, e.g., at the indium resonance (1.44 ev). The activity of a Cd-covered In foil exposed at a distance r from the point source of fission neutrons can be written

$$A(r) \propto \int_{E_{Cd\ cutoff}}^{E_{fission}} \Sigma_{In}(E)\, \phi(E,r)\, dE$$

687863 O - 63 - 10

where $\Sigma_{In}(E)$ = macroscopic absorption cross section of indium
$\phi(E,r)$ = isotropic component of the neutron flux at the energy E and at a distance r from the source

Since the activation of the cadmium-covered indium foil is nearly zero except at the resonance, the "flux age" at 1.44 ev can be written as

$$\frac{\overline{r^2}\ (1.44\ \text{ev})}{6} = \frac{1}{6}\left[\int_0^\infty r^4\, A(r)\, dr \Big/ \int_0^\infty r^2\, A(r)\, dr\right] = \tau\ (\text{fission to } 1.44\ \text{ev})$$

The data on moments for various materials and mixtures follows:

Graphite and Graphite-Bismuth Mixtures. The flux age in graphite was measured by Hill, et al., at ORNL.[119] The results for the first three even moments corresponding to a point source and a graphite density of 1.60 gm/cm^3 were: $\overline{r^2}$ = 1864 cm^2; $\overline{r^4} = 6.89 \times 10^6$ cm^4; and $\overline{r^6} = 4.4 \times 10^{10}$ cm^6.

Alter, et al.,[120] used a Monte Carlo method and calculated a value for the flux age of 322 ± 6 cm^2 for graphite of the same density. The corresponding results for the first three even moments of the slowing-down kernel were: $\overline{r^2}$ = 1837 cm^2; $\overline{r^4} = 6.68 \times 10^6$ cm^4; and $\overline{r^6} = 4.2 \times 10^{10}$ cm^6.

Hendrie, et al.,[51] measured the flux age in stacks of graphite, and graphite containing blocks of bismuth located in 2 in. × 2 in. channels (graphite-bismuth ratio = 2 : 1). The results are given in Table 3-21. The value listed for this age in graphite at density 1.674 gm/cm^3 is 285.33 ± 0.4 cm^2. When converted by means of the inverse ratio of the densities squared, this becomes 312.5 ± 0.5 cm^2 (to indium resonance) at the density 1.60 gm/cm^3.

Table 3-21 — FLUX MOMENTS AND AGE TO INDIUM RESONANCE IN GRAPHITE AND A GRAPHITE–BISMUTH MIXTURE[a]

Data from Ref. 51.

Parameter	Units	Graphite[b]	Graphite–Bismuth (Stack B)
$\overline{z^2}$	cm^2	541.7 ± 0.9	842.6 ± 4.0
$\overline{z^4} \times 10^{-6}$	cm^4	1.003 ± 0.003	2.372 ± 0.02
$\overline{z^6} \times 10^{-10}$	cm^6	0.3669 ± 0.002	1.278 ± 0.009
$\overline{z^8} \times 10^{-14}$	cm^8	0.229	1.11
$\overline{z^{10}} \times 10^{-18}$	cm^{10}	0.215	1.38
$\overline{z^2_\infty}$	cm^2	570.66 ± 0.9	899.6 ± 3.0
τ	cm^2	285.33 ± 0.4	449.8 ± 2.0
Effective transverse dimensions of stack in measurements of $\overline{z^2}$, ... $\overline{z^{10}}$			
a	cm	124.14 ± 0.4	125.11 ± 0.2
b	cm	130.53 ± 0.4	132.9 ± 0.2

[a]Errors are statistical standard deviations.
[b]All values refer to an average stack density of 1.674 gm/cm^3.

Davey, et al.,[121] have measured the flux age to indium resonance in various stacks of graphite and bismuth. The bismuth elements measured 1.23 in. × 1.23 in. The graphite density was 1.649 gm/cm^3, and the bismuth density was 9.733 gm/cm^3. Owing to inelastic scattering in the natural uranium source rods used, a correction of 2.2% was added to the observed age. Table 3-22 summarizes the results for various graphite and bismuth volume ratios.

Carbon-Hydrogen Mixtures. Alter, et al.,[120] used a Monte Carlo method to calculate the ages and moments in carbon-hydrogen mixtures with ratios ranging from 0.5 to 2.0. All calculations were normalized to a mass density of unity. The results are summarized in Table 3-23.

Beryllium. Nobles and Wallace[122] measured the flux age to indium resonance in beryllium using a small piece of enriched uranium for a point source. The results were τ(In) = 80.2 ± 2 cm^2 and τ(thermal) = 97.2 cm^2.

Meneghetti and Hummel[123] calculated a flux age to 1.44 ev of 85 cm^2, including a first-flight correction of 4 cm^2. Inclusion of (n, 2n) and (n, α) reactions lowered the value to 71 cm^2.

D_2O and H_2O Admixtures. A series of measurements of age from fission to indium resonance in various D_2O-H_2O mixtures was made by Wade at the Savannah River Laboratory.[124] The data are summarized in Table 3-24.

Other measurements of τ(In) in D_2O are reported by Martin[125] as 107 ± 5 cm^2, and by Olcott[126] as 111 ± 1 cm^2.

Table 3-22— FLUX AGE IN GRAPHITE AND GRAPHITE–BISMUTH MIXTURES TO INDIUM RESONANCE

Data from Ref. 121.

Bi/C Vol. Ratio	τ(In), cm^2
0	318 ± 6
0.437	498 ± 10
1.053	738 ± 14
1.626	973 ± 20

Table 3-23— FLUX AGE AND MOMENTS FOR VARIOUS C/H RATIOS OF UNIT MASS DENSITY

Data from Ref. 120.

C/H	Flux Age, cm^2	Slowing-Down Kernel Moments		
		$\overline{r^2}$, cm^2	$\overline{r^4}$, $\times 10^4$ cm^4	$\overline{r^6}$, $\times 10^7$ cm^6
0.5	14.7 ± 0.2	87.1	2.89	2.88
1.0	36.2 ± 0.4	213	15.7	31.2
1.5	57.9 ± 0.6	341	38.2	104
2.0	81.1 ± 0.8	476	75.2	324

Table 3-24— FLUX AGE OF D_2O–H_2O MIXTURES

Data from Ref. 124.

Mole-% D_2O	τ(In), cm^2	λ^a, cm	Fraction Extrapolated Area
99.8	109 ± 3	9	0.13
99.0	107 ± 5	9	0.14
98.4	106 ± 3	9	0.15
95.3	93 ± 3	9	0.13
94.0	86 ± 3	8	0.08
91.8	78 ± 3	7	0.09
48.6	38.6 ± 1	7	0.02

[a] Extrapolation beyond 30 cm was based on an assumed distribution, $[\exp(-r/\lambda)]/r^2$, where λ has the value given.

Two sets of Monte Carlo calculations have been made of the flux ages in D_2O mixtures by Brown,[127] and by Coveyou and Sullivan.[128] In each case, the deuterium was assumed to scatter isotropically in the center-of-mass system. Brown also assumed isotropic scattering by oxygen. Coveyou and Sullivan, on the other hand, included the anisotropy of oxygen scattering. Table 3-25 lists the theoretical values. The values for pure D_2O are significantly higher than experiment, probably because of the neglect of the anisotropy in deuterium scattering (preferentially backwards for energies below 2 Mev).

Arnold[129] and Levine, et al.,[130] calculated the flux ages in various D_2O-H_2O mixtures by applying the Greuling-Goertzel approximation to a P_1 or B_1 calculation. The results by both methods are similar and are in good agreement with the experimental data of Wade. The data of Arnold are reproduced as Fig. 3-33. The MUFT 4 code used is described in Section 10.1.2.

Diphenyl. Brown[131] reported a measurement yielding $\tau(\text{In}) = 50.2$ cm^2 for diphenyl ($C_{12}H_{10}$) at 185°F. The quoted value should be increased 8% to account for the finite size of the tank facility employed: $\tau(\text{In}) = 54.2$ cm^2.

Table 3-25—THEORETICAL FLUX AGE TO INDIUM RESONANCE IN H_2O-D_2O MIXTURES BY MONTE CARLO CALCULATIONS

Data from Refs. 127 and 128.

Composition, % D_2O	τ(In), cm^2	
	Brown	Coveyou and Sullivan
100	119.5	126.0
90	77.0	—
87.5	—	72.7
75	52.0	54.6
62.5	—	45.1
50	36.7	39.0
37.5	—	35.0
25.0	—	31.4
12.5	—	28.4

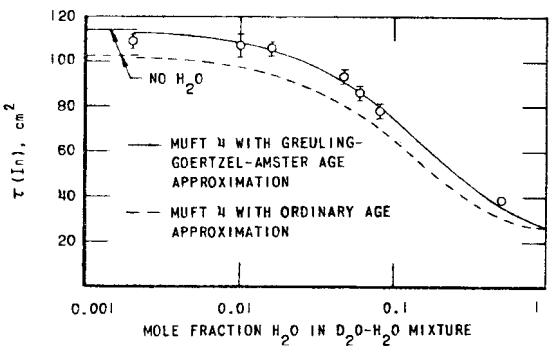

Fig. 3-33—Comparison between calculated flux ages in D_2O-H_2O mixtures and the experimental data of Wade. *Reproduced from Ref. 129.*

Francis, et al.,[132] have calculated the flux age using a Fourier transform method in B_1 approximation. Their results under various assumptions are compared in Table 3-26. Also shown is the approximate Selengut-Goertzel result for the age.

Alter, et al.,[120] used a Monte Carlo method and calculated a flux age of 46.4 ± 0.07 cm^2 in diphenyl at 185°F. They also reported values for the slowing-down kernel moments as follows: $\overline{r^n} = 2.727 \times 10^2$ cm^2 for n = 2; 2.348×10^5 cm^4 for n = 4; and 4.190×10^8 cm^6 for n = 6.

Table 3-26—FLUX AGE TO INDIUM RESONANCE IN DIPHENYL (185°F)

Data from Ref. 132.

Assumptions	τ(In), cm^2	
	Rigorous Theory	Selengut-Goertzel
No approximations	46.3	52.2
Isotropic carbon scattering	44.9	50.2
Isotropic carbon scattering; carbon slowing down neglected	53.5	59.6

H_2O-Natural Uranium. Barkov, et al.,[133] calculated the flux age from measured slowing-down distributions of fission neutrons in three different natural uranium-water lattices. The lattices consisted of 3.5-cm-diameter rods of natural uranium, canned in aluminum and covered with cadmium foils (0.6 mm thick) to suppress fission in the fuel. In the respective lattices, the rods were stacked

to form equilateral triangular networks with spacings 4.3, 5.0, and 6.0 cm, giving corresponding water-uranium volume ratios of 0.4, 1.0, and 2.0. The results are tabulated below.

H_2O-Nat. U Vol. Ratio	τ(In), cm^2 Exptl.	τ(In), cm^2 Corrected for epithermal fission
0.4	65 ± 3	58 ± 5
1.0	47 ± 2	44 ± 3
2.0	37 ± 2	35 ± 2

Matthes and Springer[134] used a Monte Carlo method to calculate the slowing-down age in U-H_2O lattices of 1.5-cm- and 3.0-cm-diameter U rods. Their results are plotted in Fig. 3-34.

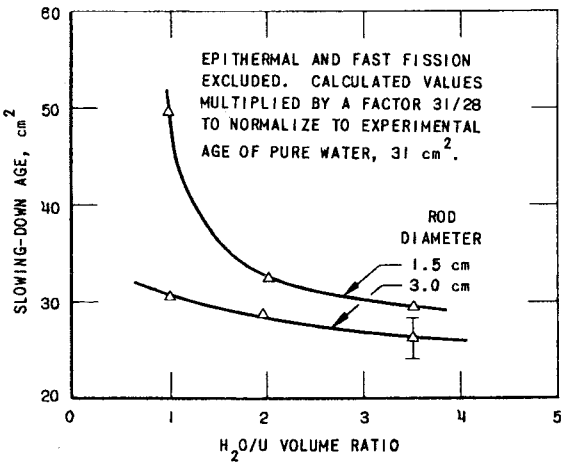

Fig. 3-34 — Slowing-down age at indium resonance in uranium-water lattices. *Data from Ref. 134.*

Thorium-H_2O and Thorium-Aluminum-H_2O. Pettus[135] measured the flux age to indium resonance in a number of Th-H_2O and Th-Al-H_2O lattices. The measurements were made in lattices containing thorium (56 mil thick) and aluminum (81 mil thick) plates two feet long and slightly less than three feet wide. The spacing of the plates was varied to change the relative volume fractions. The calculations were performed by the MUFT and "SPECTRAL" codes. The results are listed in Table 3-27.

Table 3-27 — MEASURED AND CALCULATED FLUX AGES IN Th–H_2O AND Th–Al–H_2O LATTICES

Data from Ref. 135.

Run	Lattice Volume Fraction Th	Al	H_2O	Experimental Age, cm^2 Measured	Corrected	Calculated Age, cm^2 MUFT	"Spectral" Code
a	0	0	1	26.5 ± 0.9	27.0 ± 0.9	25.1	28.9
1	0.173	0	0.827	30.9 ± 3.0	31.5 ± 3.0	30.2	36.1
2	0.290	0	0.710	36.8 ± 1.2	37.5 ± 1.2	34.6	39.3
2A	0.290	0	0.710	40.3 ± 2.0	40.3 ± 2.0	—	—
3	0.436	0	0.564	43.7 ± 2.0	44.6 ± 2.0	43.1	44.7
4	0.327	0.240	0.433	54.1 ± 1.7	55.2 ± 1.7	60.6	57.2
4A	0.327	0.240	0.433	63.1 ± 3.6	63.1 ± 3.6	—	—
5	0.239	0.179	0.5824	42.8 ± 1.4	43.7 ± 1.4	44.4	47.3
5A	0.239	0.179	0.582	41.1 ± 1.3	41.9 ± 1.3	—	—
6	0.198	0.299	0.503	53.7 ± 2.1	54.8 ± 2.1	53.4	54.5

Zirconium-H_2O. A measurement of the flux age in a zirconium-water mixture was performed at ORNL[136] using zirconium containing about 1% hafnium. The thermal neutron cross section was measured to be 0.85 barns. The metal was in the form of plates 36.0 in. × 6 in. × 0.080 in. Values of τ(In) = 30.03 cm^2 and 35.7 cm^2 were obtained for Zr/H_2O volume ratios of zero and 0.25, respectively.

Iron-H_2O. Sjöstrand and Story[137] have reported flux age measurements by Kendrick on Fe-H_2O mixtures with Fe/H_2O volume ratios of 1 and 2. The corresponding values of τ(In) are 40.7 cm^2 and 54.7 cm^2.

Aluminum-H_2O. The following flux age measurements in Al-H_2O mixtures were reported by Hill, et al.,[138] at ORNL:

Al/H_2O Vol. Ratio	τ(In), cm^2	τ(In → th), cm^2 (theoretical)	τ(th), cm^2
0	30.8	1	31.8
0.5	49.6	2	51.6
1.0	76.8	3	79.8

Owing to the disagreement between the calculated value and the currently accepted value for τ(In) in pure water (see Section 3.4.4), the results for other Al/H_2O ratios may also be considered questionable.

More recent calculations have been made* for Al-H_2O mixtures for various values of the buckling, B^2. The calculations were made using the MUFT 4 code (see Section 10.1.2) and the B_1 approximation. Also, the MUFT delayed neutron spectrum was used for one case. This calculation yields a "one-group age" which is, in terms of previously defined symbols,

$$\tau(\text{one-group}) = \frac{1}{B^2}\left(\frac{1}{\overline{P_\infty}\ (B^2,\ 0.625\ \text{ev})} - 1\right)$$

The results are summarized in Table 3-28.

Table 3-28— CALCULATED ONE-GROUP AGE TO INDIUM RESONANCE FOR VARIOUS Al–H_2O MIXTURES

Data from D. H. Shaftman, ANL, private communication.

Al/H_2O Vol. Ratio	B^2	Age, cm^2	
		Fission Spectrum	Delayed Neutron Spectrum
0.5	3.8×10^{-3}	42.2	18.6
	$10^{-3} - 10^{-5}$	42.0	—
1.0	10^{-3}	57.7	—
	10^{-4}	57.3	—

3.4.3 AGES FROM NON-FISSION SOURCES

Pure Water. The experimental results for the flux age in pure H_2O for various non-fission sources and detectors are given in Table 3-29.

Various theoretical calculations have been made of the flux age in pure H_2O for non-fission sources. Coveyou and Sullivan[139] used a Monte Carlo neutron age code to calculate the age to indium resonance for monoenergetic sources. Their results are given in Fig. 3-35.

Duggal, et al.,[146] used Marshak's formula[116] to calculate the value 59.6 cm^2 for the flux age to indium resonance for a Ra(α,n)Be source. This may be compared with their experimental value of 54.4 ± 2.1 cm^2.

Reier[151,157] used a Fourier transform method to compute the flux age to indium resonance for a Po(α,n)B source. Owing to uncertainties in the spectrum, calculated values ranging from 29.7 cm^2 to 35.5 cm^2 were obtained. These calculations are lower than the measured[151] value of 39.7 ± 1.2 cm^2.

The sensitivity of the second moment to variations in the cross sections is illustrated in Fig. 3-36. The effect of suppressing the capture and inelastic scattering cross sections of oxygen is clearly larger at higher energies. The relative insensitivity of the age to variations in the oxygen inelastic and capture cross section in the region of fission energies is also evident.

*Private communication, D. H. Shaftman, Argonne National Laboratory.

Table 3-29—FLUX AGES IN H_2O FOR NON-FISSION SOURCES

Source	Detector	τ, cm^2	Ref.	Footnote
Ra(α,n)Be	Dy	55	140	—
Ra(α,n)Be	Rh	54.5	141	—
Ra(α,n)Be	In Resonance	46.3	140	—
Ra(α,n)Be	In Resonance	48.5	142	—
Ra(α,n)Be	In Resonance	50.3	142	—
Ra(α,n)Be	In Resonance	45.4	143	—
Ra(α,n)Be	In Resonance	52.2	144	—
Ra(α,n)Be	In Resonance	48	145	—
Ra(α,n)Be	In Resonance	54.4	146	—
Ra(α,n)Be	I Resonance	45.5	145	—
Ra(α,n)Be	Rh Resonance	46.2	141	—
Po(α,n)Be	In Resonance	56.3	147	—
Po(α,n)Be	BF_2	58.5	148	—
Po(α,n)Be	BF_3(B^{10} 96%)	66.3	149	—
Po(α,n)Be	In Resonance	57.3 ± 2.0	150	—
Po(α,n)Be	In Resonance	55.4 ± 1.7	151	—
Po(α,n)Be	In Resonance	57.9 ± 1.7	151	—
Po(α,n)Be	In Resonance	55.7 ± 2	124	—
Be^9(d,n)	LiI	41 ± 1.6	152	1
Be^9(d,n)	LiI	28.4	63	1
T(d,n)	In Resonance	150 ± 6	153	2
T(d,n)	In Resonance	160.8	146	2
Ra(α,n)Be	In Resonance to Thermal	1.0	143	3
Po(α,n)Be	In Resonance to Thermal	0.3	147	4
Sb^{124}(γ,n)Be	In Resonance	5.5 ± 0.2	154	5
O^{17}(n,p)N^{17*}(n)N^{16}	BF_3	15 ± 4	155	6
Na^{24}(γ,n)Be	In Resonance	13.9 ± 0.2	156	7
Pu(α,n)Be	Ag^{109}	49.3	150	—
Pu(α,n)Be	In Resonance	52.8 ± 2.5	150	—
Pu(α,n)Be	Rh Resonance	53.7 ± 2.5	150	—
D(d,n)	In Resonance	34.6 ± 2.2	156	8
Po(α,n)B	In Resonance	39.7 ± 1.2	151	—

1. Maximum neutron energy is 4.5 Mev and peak of distribution occurs at 3.5 Mev. Density of BeO: 2.96 gm/cm^3.

2. Neutron energy 14.1 Mev.

3. Based on measured $M^2 = \tau(th) + L^2 = 54.7$ cm^2, assumed $L^2 = 8.3$ cm^2.

4. Based on measured $M^2 = \tau(th) + L^2 = 64.7$ cm^2, assumed $L^2 = 8.1$ cm^2.

5. Source energy is approximately 30 kev with a spread of 25%. See Section 9.

6. Delayed neutrons from N^{17} were produced by circulating water into the reactor, then into a disc-shaped coil which served as the source. Average energy of source neutrons was 0.9 Mev.

7. Source energy is 0.97 Mev.

8. The source emits neutrons anisotropically with energies from 3.12 Mev at 0° to the deuteron beam, to 2.00 Mev at 180°. The quoted age is the angle averaged value.

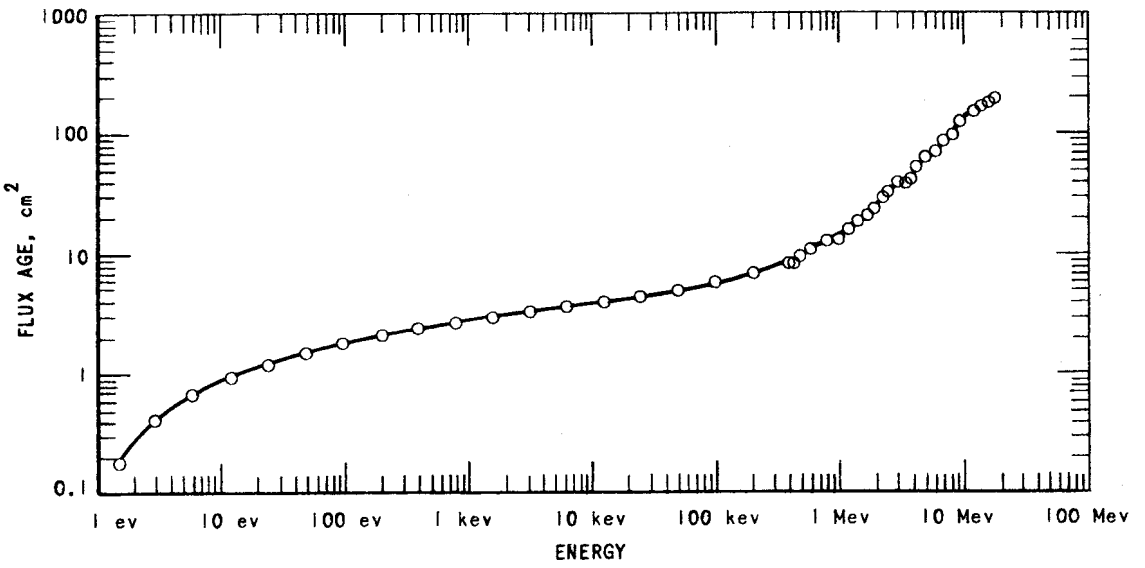

Fig. 3-35 — Flux age of neutrons from monoenergetic sources to indium resonance in H_2O (1% error). *Reproduced from Ref. 139.*

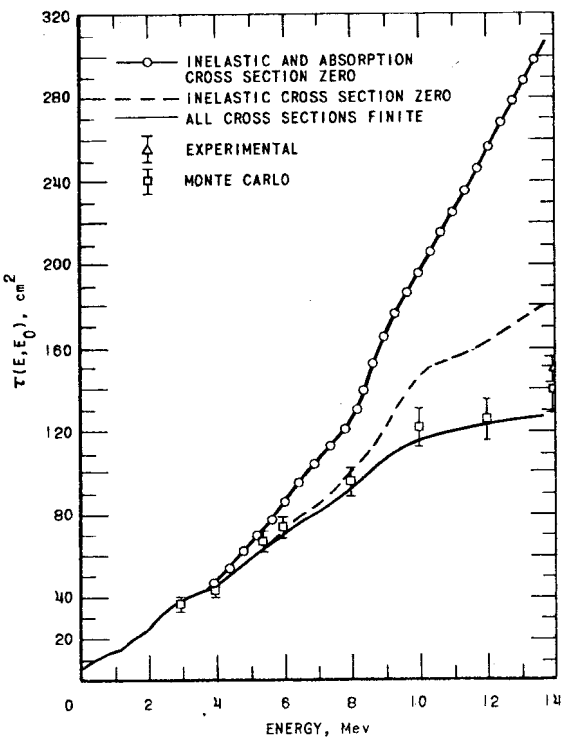

Fig. 3-36 — Flux age to indium resonance of neutrons of energy E(Mev) in pure water. *Reproduced from Ref. 151.*

Theoretical calculations of the age in water to In resonance for neutrons from a D-D source have been made by Zweifel[156] and Mullin.[158] For 100-kev and 150-kev incident deuterons, Zweifel calculated flux ages of 33.6 cm^2 and 33.8 cm^2, respectively. Mullin's Monte Carlo calculation assumed a 250-kev incident deuteron energy and yielded a slowing-down age of 35.8 ± 0.6 cm^2 with 68% confidence limits. The corresponding flux age to indium would be about 36.2 cm^2.

Media Other Than Pure Water. Table 3-30 summarizes the available experimental data on slowing-down distributions from various sources in media other than pure water.

A variety of methods have been employed to calculate the age of neutrons from monoenergetic sources in different media.[128,146,151] For radioactive sources, e.g., Po(α,n)Be, the uncertainty in the neutron spectrum is reflected in the calculated age. This is illustrated in Fig. 3-37 which compares theoretical with experimental values for several water-metal mixtures.

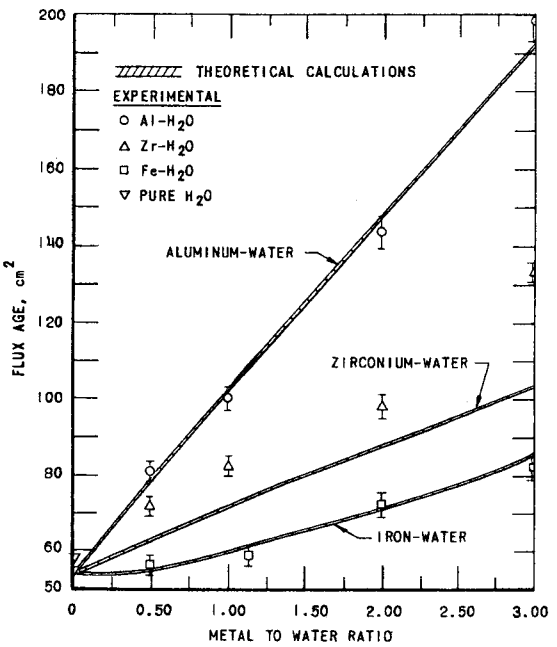

Fig. 3-37 — Theoretical and experimental flux ages to indium resonance. The bands represent the upper and lower limits obtained from the computations using four different measurements of the Po-Be spectrum. *Reproduced from Ref. 151.*

3.4.4 SLOWING DOWN OF FISSION NEUTRONS IN PURE H_2O

The long-standing disagreement between experimental and calculated values of the age of fission neutrons in light water has been evaluated in a review paper by Goldstein, et al.[128] They considered the possible sources of error in each instance and concluded that the major burden of proof lies with experiment.

A paper by Doerner, et al.,[165] overlaps the scope of the Goldstein review and includes recent results. This section presents these experimental and theoretical data in two parts: Fourier transforms of slowing-down kernels, and slowing-down moments.*

Fourier Transforms of Slowing-Down Kernels. Table 3-31 lists the different calculation methods employed, and the corresponding values obtained for $\bar{P}_\infty(B^2,E)$ in H_2O. The values $\bar{P}_\infty(B^2,E_{In})$ and $\bar{P}_\infty(B^2,E_{th})$ may also be calculated using the formulas:[168]

$$\bar{P}_\infty(B^2,E_{In}) = [(1 + 26.27\ B^2)\ (1 + 2.26\ B^2)^2]^{-1} \tag{3-24}$$

and

$$\bar{P}_\infty(B^2,E_{th}) = [(1 + 2.625\ B^2)^2\ (1 + 26.539\ B^2)]^{-1} \tag{3-25}$$

The constants given in Eqs. (3-24) and (3-25) are based on early data[138] and, hence, may not be completely reliable.

*Earlier measurements and calculations of the slowing-down moments from fission sources are included in a review paper by Wilkins, et al.[171] Data on the second moments of the slowing-down distribution from non-fission sources are presented in Section 3.4.3.

Table 3-30 — FLUX AGES FOR NON-FISSION SOURCES IN VARIOUS MEDIA

Source	Medium	Vol. Ratio (Room Temp.)	Detector	Age, cm^2	Reference	Footnote
Po(α,n)Be	H_2O : Fe	1 : 3	In Resonance	83.0 ± 2.5	151	11
Po(α,n)Be	H_2O : Fe	1 : 2	In Resonance	72.1 ± 2.2	151	11
Po(α,n)Be	H_2O : Fe	1 : 1	In Resonance	58.8 ± 1.8	151	11
Po(α,n)Be	H_2O : Fe	2 : 1	In Resonance	56.2 ± 2.2	151	11
Po(α,n)Be	H_2O : Fe	3 : 1	In Resonance	52.3	142	
Po(α,n)Be	H_2O : Fe	2 : 1	In Resonance	56.0	142	
Po(α,n)Be	H_2O : Fe	1 : 1	In Resonance	57.9	142	
Ra(α,n)	H_2O : Fe	1.3 : 1	In Resonance	53.2	140	1
Po(α,n)B	H_2O : Fe	1 : 2	In Resonance	73.9 ± 2.2	151	11
Po(α,n)B	H_2O : Fe	1 : 1	In Resonance	60.6 ± 1.8	151	11
Po(α,n)B	H_2O : Fe	2 : 1	In Resonance	46.9 ± 1.4	151	11
Sb^{124}(γ,n)Be	Graphite	100%	In Resonance	147	159	2
Sb^{124}(γ,n)Be	Graphite	100%	Au	128 ± 2	160	2
Ra(α,n)Be	Be	100%	In Resonance	120 ± 23	54	3
Po(α,n)Be	Be	100%	In Resonance	95 ± 11	54	3
Calculated	Be	100%	1.44 ev to thermal	20	161	
D(d,n)Be	BeO	100%	LiI counter	156	63	4
Ra(α,n)Be	SiO_2	100%	In Resonance	1900 ± 90	162	5
Ra(α,n)Be	$CaCO_3$	100%	In Resonance	461 ± 23	162	
Ra(α,n)Be	H_2O : Brine	894 : 106	In Resonance	55.3	144	6
Ra(α,n)Be	H_2O : Brine	894 : 106	I Resonance	52.2	144	6
Ra(α,n)Be	Furfural-"H_2O" : C	435 : 565	In Resonance	134.5	144	7
Ra(α,n)Be	H_2O : Sand	388 : 612	In Resonance	131.7	144	8
Po(α,n)Be	H_2O : Zr	4 : 1	BF_3	77.5	149	9
Po(α,n)Be	H_2O : Zr	2 : 1	BF_3	87.2	149	9
Po(α,n)Be	H_2O : Zr	1 : 1	BF_3	107.9	149	9
Po(α,n)Be	H_2O : Zr	1 : 3	In Resonance	133.0 ± 4.0	151	11
Po(α,n)Be	H_2O : Zr	1 : 2	In Resonance	98.0 ± 2.9	151	11
Po(α,n)Be	H_2O : Zr	1 : 1	In Resonance	82.5 ± 2.5	151	11
Po(α,n)Be	H_2O : Zr	2 : 1	In Resonance	71.4 ± 2.1	151	11
Po(α,n)B	H_2O : Zr	1 : 3	In Resonance	117.0 ± 3.5	151	11
Po(α,n)B	H_2O : Zr	1 : 2	In Resonance	95.6 ± 2.9	151	11
Po(α,n)B	H_2O : Zr	1 : 1	In Resonance	70.7 ± 2.1	151	11
Po(α,n)B	H_2O : Zr	2 : 1	In Resonance	53.1 ± 1.6	151	11
Ra(α,n)Be	H_2O : Bi	1 : 1	Dy	93.7	140	10
Ra(α,n)Be	H_2O : Bi	1 : 1	In Resonance	79.5	140	10
Ra(α,n)Be	H_2O : Bi	2 : 1	In Resonance	66.3	140	10
Ra(α,n)Be	H_2O : Bi	1 : 2	In Resonance	86.2	140	10
Ra(α,n)Be	H_2O : Pb	1 : 1	In Resonance	72.8	140	10
Po(α,n)Be	H_2O : Al	1 : 3	In Resonance	197.3 ± 5.9	151	11
Po(α,n)Be	H_2O : Al	1 : 2	In Resonance	143.5 ± 4.3	151	11
Po(α,n)Be	H_2O : Al	1 : 1	In Resonance	100.2 ± 3.0	151	11
Po(α,n)Be	H_2O : Al	2 : 1	In Resonance	81.2 ± 2.4	151	11
Po(α,n)B	H_2O : Al	1 : 3	In Resonance	166.5 ± 5.0	151	11
Po(α,n)B	H_2O : Al	1 : 2	In Resonance	130.3 ± 3.9	151	11
Po(α,n)B	H_2O : Al	1 : 1	In Resonance	86.3 ± 2.6	151	11
T(d,n)	H_2O : Al	1 : 1	In Resonance	198.4	146	12,13
T(d,n)	H_2O : Al	3 : 1	In Resonance	173	146	12,13
Ra(α,n)Be	H_2O : Al	1 : 1	In Resonance	101.9 ± 2.6	146	13
Ra(α,n)Be	H_2O : Al	3 : 2	In Resonance	82.1 ± 2.0	146	13
Ra(α,n)Be	H_2O : Al	2 : 1	In Resonance	80.3 ± 3.4	146	13
Ra(α,n)Be	H_2O : Al	4 : 1	In Resonance	69.1 ± 1.7	146	13
Po(α,n)Be	H_2O : D_2O	99.4 mole % D_2O	In Resonance	148 ± 3	124	
Po(α,n)Be	H_2O : D_2O	48.6 mole % D_2O	In Resonance	72 ± 5	124	
D(d,n)	D_2O	Not Given	In Resonance	116.8	163	14
Na^{24}(γ,n)Be	Kerosene	100%	In Resonance	13.8 ± 0.2	164	

1. Measurements were of heterogeneous assemblies of rods. Fe rods were 1.87 × 32 cm.
2. Graphite density: 1.652 gm/cm^3.
3. Beryllium density: 1.78 gm/cm^3.
4. Maximum neutron energy is 4.5 Mev and peak of distribution occurs at 3.5 Mev. Density of Be: 2.96 gm/cm^3.
5. Density of SiO_2: 1.61 gm/cm^3.
6. Approximately 900 pounds of salt were dissolved in water to give 47.4 cubic feet of solution. By chemical analysis, the average NaCl content was 292 milligrams per cubic centimeter of solution, corresponding to 92% saturation. Typical Analysis of Salt Used: Sodium chloride: 99.68%; calcium sulphate: 0.23%; calcium chloride: 0.09%; magnesium chloride: trace; iron and alumina: nil. Activation of iodide detector is due principally to neutrons of about 40 ev.
7. Furfural: $C_5H_4O_2$ ρ(equivalent water) = (Mass H_2O/Mass furfural) ρ(furfural) = 0.435.
8. The sand is "Flint Shot" (brand), Ottawa Silica Co., Ottawa, Illinois.
9. Measurements were of heterogeneous assemblies of rods varying in diameter from ½ in. to ¾ in.
10. Measurements were of heterogeneous assemblies of rods. Pb and Bi rods were 2 × 2 × 32 cm.
11. Measurements were of heterogeneous assemblies of rods of ⅝ in. diameter.
12. 200-kev deuterons incident on a tritium–titanium target.
13. Measurements were of heterogeneous assemblies of plates ¼ in. thick.
14. The stated age is an average value for 2-3 Mev neutrons.

Table 3-31—CALCULATED VALUES FOR $\bar{P}_\infty$ (B^2, E_{th})

B^2	Gauss	Yukawa-a	Yukawa-b	Greuling *Ref. 166*	Selengut-Goertzel *Ref. 167*	B_3 Method *Ref. 167*
0.005	0.859	0.889	0.868	0.887	0.868	0.890
0.010	0.738	0.800	0.767	0.794	0.770	0.805
0.015	0.634	0.727	0.687	0.716	0.689	0.735
0.020	0.544	0.667	0.622	0.649	0.622	0.675
0.030	0.402	0.571	0.523	0.543	0.520	0.580
0.040	0.296	0.500	0.451	0.462	0.439	0.504
0.050	0.219	0.444	0.397	0.399	0.378	0.443
0.075	0.102	0.348	0.305	0.290	0.272	0.333
0.100	0.048	0.286	0.248	0.220	0.202	0.260

Gauss Kernel: $\bar{P}_\infty (B^2, E_{th}) = \exp(-\tau B^2)$. $\tau = 30.4$ cm^2.

Yukawa Kernel: $\bar{P}_\infty (B^2, E_{th}) = (1 + L_1^2 B^2)^{-1}$. $L_1^2 = 25.0$ cm^2 and $L_1^2 = 30.4$ cm^2 for a and b, respectively.

Greuling Kernel: $\bar{P}_\infty (B^2, E_{th}) = [(1 + \tau_1 B^2)(1 + \tau_2 B^2)(1 + \tau_3 B^2)]^{-1}$ $\tau_1 = 20.2$ cm^2; $\tau_2 = 4.2$ cm^2; and $\tau_3 = 0.6$ cm^2.

Morriss and Zweifel[169] calculated $\bar{P}_\infty(B^2, E_{In})$ for delayed neutron sources following U^{235} thermal fission. The spectra are those of Batchelor and McK.Hyder.[170] Figure 3-38 shows $\bar{P}_\infty(B^2, E_{In})$ for fission neutrons and for each of four delayed neutron groups. The groups, a, b, c, and d represent the four longest-lived delayed neutron precursors from U^{235} thermal fission, in order of decreasing half-life.

Moments of the Slowing-Down Distribution from Fission Sources. Alter, et al.,[120] have calculated $\overline{r^n}$ for n = 2, 4, 6, using a Monte Carlo method. Their values are, respectively, 151 cm^2, 0.924×10^5 cm^4, and 1.793×10^8 cm^6.

Matthes and Springer[134] also used a Monte Carlo method and calculated $\overline{r^4} = 1.12 \times 10^5$ cm^4 and $\overline{r^6} = 1.9 \times 10^8$ cm^6.

Recent experimental values for the flux age to indium resonance of U^{235} fission neutrons are summarized in Table 3-32.

Pettus[135,172] compared the experimental age to indium resonance in water from U^{233} fission neutrons, with that of U^{235} fission neutrons. He reported a ratio of 0.948 ± 0.033 (U^{233} to U^{235}).

Faber and Zweifel[173] reported that the calculated age of U^{233} fission neutrons is (9 ± 12)% less than the age of U^{235} fission neutrons to indium resonance in water. This can be compared with the corresponding measured[135,172] value of (5 ± 3)%. The theoretical error results from uncertainties in the U^{233} fission spectrum.

Recent theoretical values for the flux age to indium resonance of U^{235} fission neutrons are summarized in Table 3-33.

The MUFT 4 code was used* in the B_1 approximation to calculate the one-group age to indium resonance for a buckling of 10^{-6}. The calculated value was 27.0 cm^2. The corresponding one-group age from the MUFT delayed neutron spectrum to indium resonance was 9.6 cm^2.

Morriss and Zweifel[169] have also calculated the age to indium resonance using MUFT 4 for the spectra corresponding to the four longest-lived delayed fission neutron groups.[170] The calculated values are, respectively, 7.1 cm^2, 9.1 cm^2, 8.6 cm^2, and 9.6 cm^2, in order of decreasing half-life.

*Private communication from D. H. Shaftman, Argonne National Laboratory.

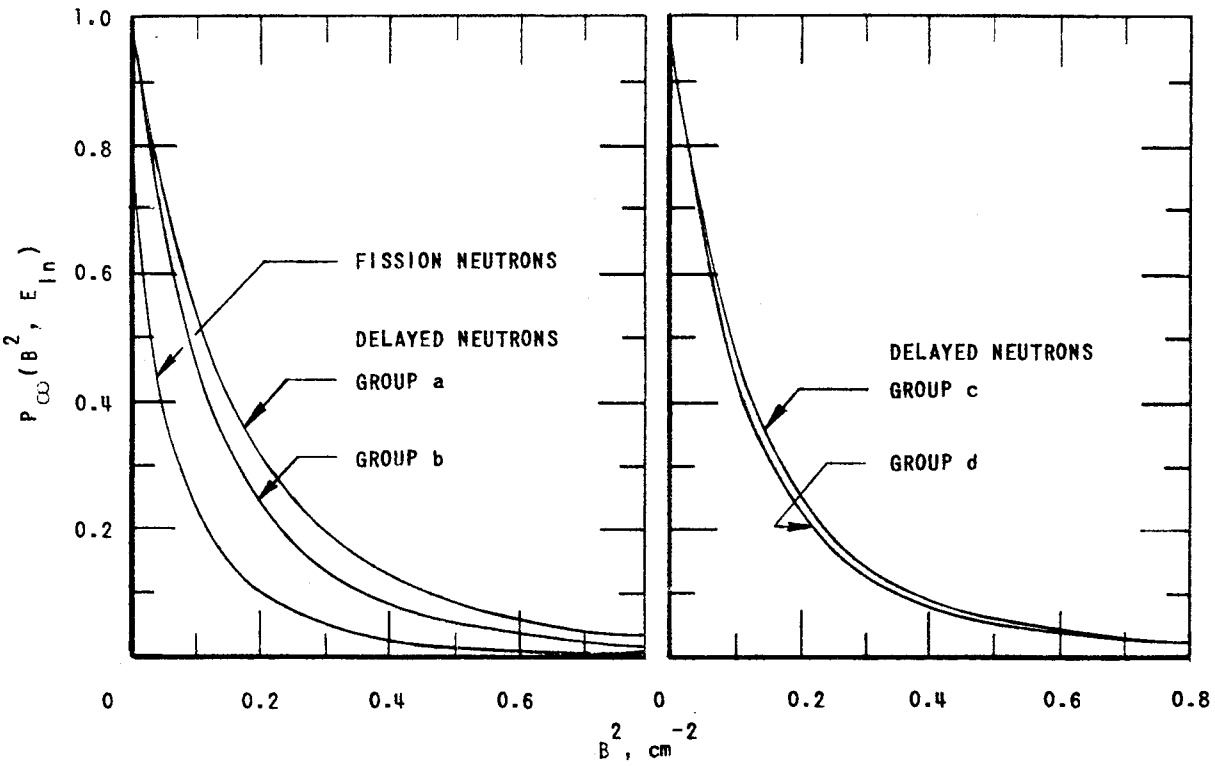

Fig. 3-38 — Fourier Transforms of slowing-down kernels in H_2O to indium resonance for fission neutrons and spectra of delayed neutrons. *Reproduced from Ref. 169.*

Table 3-32 — EXPERIMENTAL FLUX AGE OF U^{235} FISSION NEUTRONS TO INDIUM RESONANCE IN LIGHT WATER

Age, cm^2	Ref.
31.0 ± 1.0	124
26.7	174
27.3 ± 0.9	175
27.0 ± 0.9	135
27.86 ± 0.10	165

Table 3-33 — THEORETICAL FLUX AGE OF U^{235} FISSION NEUTRONS TO INDIUM RESONANCE IN LIGHT WATER

Age, cm^2	Ref.
25.6 ± 0.3	176
26.0	177
25.9	151
26.7	128
26.5	178
25.9 ± 0.03	128
28 ± 2[a]	134

[a] Slowing-down age.

3.5 NON-THERMAL PARAMETERS FOR MULTIGROUP DIFFUSION THEORY

3.5.1 THE MUFT 54-GROUP LIBRARY

The MUFT digital computer program[179] is discussed in Section 10. The program obtains a solution, in a multigroup P-1 or B-1 approximation, of the Fourier transform of the neutron slowing-down distribution from a plane source in an infinite homogeneous medium.

Associated with the program is a library of 54-group cross sections.[180] Table 3-34 gives the group structure of the set. The elements and isotopes available in the library as of April, 1960 are listed in

Table 3-34—GROUP STRUCTURE IN THE MUFT LIBRARY

Data from Ref. 180.

Group Number	Lower Energy, ev	Lower Lethargy	Lethargy Width	Group Number	Lower Energy, ev	Lower Lethargy	Lethargy Width
0	10×10^6	0		29	750	9.50	0.50
1	7.79	0.25	0.25	30	454	10.00	
2	6.07	0.50		31	275	10.50	
3	4.72	0.75		32	167	11.00	0.50
4	3.68	1.00		33	130	11.25	0.25
5	2.86	1.25		34	101	11.50	
6	2.23	1.50		35	78.7	11.75	
7	1.74	1.75		36	61.3	12.00	
8	1.35	2.00		37	47.8	12.25	
9	1.05×10^6	2.25	0.25	38	37.2	12.50	0.25
10	821×10^3	2.50	0.25	39	29.0	12.75	0.25
11	639	2.75		40	22.6	13.00	
12	498	3.00		41	17.6	13.25	
13	387	3.25		42	13.7	13.50	
14	302	3.50		43	10.7	13.75	
15	235	3.75		44	8.32	14.00	
16	183	4.00		45	6.50	14.25	
17	143	4.25		46	5.10	14.50	
18	111×10^3	4.50	0.25	47	3.97	14.75	0.25
19	86.5×10^3	4.75	0.25	48	3.06	15.00	0.25
20	67.4	5.00	0.25	49	2.38	15.25	0.25
21	40.9	5.50	0.50	50	1.855	15.50	0.25
22	24.8	6.00		51	1.440	15.7538	0.2538
23	15.0	6.50		52	1.125	16.00	0.2462
24	9.12	7.00		53	0.835	16.30	0.3000
25	5.53	7.50		54	0.625	16.5884	0.2884
26	3.35	8.00					
27	2.03	8.50					
28	1.23×10^3	9.00	0.50				

Table 3-35. In several instances, two representations of the same isotope are indicated. In such cases, the second representation is based on more recent and comprehensive nuclear data.

A discussion of the origin and limitations of the data is presented in Ref. 180.

For each of the isotopes, values are presented for the following parameters:

Symmetric Scattering

$$\langle \sigma_s \rangle_j \equiv \frac{1}{\Delta u_j} \int_{u_{j-1}}^{u_j} \int_{-1}^{1} 2\pi\sigma_s(u,\mu)\, du d\mu$$

Table 3-35— ELEMENTS AND ISOTOPES AVAILABLE ON THE MUFT PRODUCTION LIBRARY

Data from Ref. 180.

Element	Symbol*	Element	Symbol*
H	1	U-238	20
O	2	U-238	88
O	72	Pu-239	21
Zr	3	Pu-240	22
Zr	73	Pu-241	23
C	74	B-10	29
Fe	6	B-10	35
Ni	7	Be-9	40
Nb	8	Pb	48
Al	9	Hf-177	54
Cr	11	Hf-174	94
Hf (natural)	14	Hf-178	95
U-235	18	Hf-179	96
U-235	85	Hf-180	97

* Present IBM-704 identification.

where $2\pi\sigma_s(u,\mu)d\mu$ is the microscopic cross section for scattering through an angle having a cosine between μ and $\mu + d\mu$. The lethargy average is over group j.

Smooth Capture:

$$\bar{} < \sigma_c >_j \equiv \frac{1}{\Delta u_j} \int_{u_{j-1}}^{u_j} \sigma_c(u)du$$

where $\sigma_c(u)$ is the capture and charged particle (n, γ; n,p; n,α) cross section.

Total Inelastic:

$$< \sigma_{in} >_j \equiv \frac{1}{\Delta u_j} \int_{u_{j-1}}^{u_j} \sigma_{in}(u)du$$

where the n,2n cross section is included in the inelastic cross section, $\sigma_{in}(u)$.

Fission:

$$< \sigma_f >_j \equiv \frac{1}{\Delta u_j} \int_{u_{j-1}}^{u} \sigma_f(u)du$$

Anisotropic Scattering Cross Section:

$$< \sigma_{sl} >_j \equiv \frac{1}{\Delta u_j} \int_{u_{j-1}}^{u_j} \int_{-1}^{1} 2\pi\mu\sigma_s(u,\mu)dud\mu \equiv \bar{\mu}_j < \sigma_s >_j$$

where $\sigma_s(u,\mu)$ is the differential scattering cross section at lethargy u, and scattering angle $\cos^{-1}\mu$ in the laboratory system.

Number of Neutrons Per Fission:

$$< \nu >_j \equiv \frac{1}{\Delta u_j} \int_{u_{j-1}}^{u_j} \nu(u)du$$

where $\nu(u)$ is the number of neutrons emitted per fission at lethargy u.

Microscopic Slowing-Down Power:

$$< \xi \sigma_s >_j \equiv \frac{1}{\Delta u_j} \int_{u_{j-1}}^{u_j} \int_{-1}^{1} 2\pi U(\mu)\sigma_s(u,\mu)du d\mu \equiv \xi_j < \sigma_s >_j$$

where $U(\mu)$ is the lethargy gain due to an elastic scattering through $\cos^{-1}\mu$ in the laboratory system.

Resonance Parameters:

$$m_j \equiv \frac{\sigma_{0j}\Gamma_{aj}}{E_{0j}}; \quad r_j \equiv \frac{\sigma_{0j}\Gamma_{aj}}{\Gamma_j}$$

where σ_{0j} is the *total* cross section at the peak (occurring at energy E_{0j}) of the jth resonance (having absorption width Γ_{aj}, and total width Γ_j).

$$\Gamma_{aj} = \Gamma_{\gamma j} + \Gamma_{fj}$$

where $\Gamma_{\gamma j}$ is the radiative capture width, and Γ_{fj} is the width for fission. (See 3.6.4 for further discussion for the case of only radiative capture.) Resonance fission is accounted for by multiplying each contribution to the absorption by an appropriate fission to absorption ratio.

Inelastic Scattering Matrix:

The matrix is designated by $||\omega_{jn}||$, and the elements are defined by

$$\omega_{jn} \equiv \sigma_{jn}/\sum_n \sigma_{jn}$$

$$\sigma_{jn} \equiv \frac{1}{\Delta u_j} \int_{u_{n-1}}^{u_n} \int_{u_{j-1}}^{u_j} \sigma(u',u)du'du$$

where $\sigma(u',u)du$ is the cross section for inelastically scattering a neutron with lethargy u' into the interval between u and u + du.

All inelastically scattered neutrons are assumed to appear in the first 25 groups. Inelastic scattering which fails to remove a neutron from a given group is neglected (σ_{jj} taken equal to zero and the total inelastic scattering cross section in group j reduced accordingly).

The cross section for n-2n reactions is included in the inelastic scattering matrix. The current MUFT program uses a relationship based on neutron conservation; consequently, the second neutron is not accounted for.

In addition to the isotopes listed in Table 3-35, a set has been prepared* for deuterium which includes the parameters necessary to perform a Greuling-Goertzel calculation as extended by Amster.[114]

The MUFT library also includes two source spectra: the fission source, and a source representative of delayed neutrons. The data as presented give the source per unit lethargy for the different energy groups. Owing presumably to round-off errors, the normalizations for the two spectra are different, and each is slightly less than unity.

3.5.2 Few-Group Cross Sections for Metal-H_2O Systems Fueled with U^{235}

Three epithermal group parameters for use in four-group diffusion theory have been obtained[181] by fitting the results of a series of MUFT[179,180] calculations on various metal-water systems. The group structure is given in Table 3-36.

The group parameters computed are the transport ($\sigma_{tr,j}$), removal ($\sigma_{el,j} + \sigma_{in,j}$), absorption ($\sigma_c + \sigma_f$), and fission ($\sigma_f$) cross sections. Also given is the number of neutrons per fission, ν, for U^{235}.

Table 3-37 presents the three-group fitted microscopic cross sections for hydrogen, oxygen, zirconium, carbon, U^{235}, and B^{10}. The group-3 value of $\alpha(\sigma_c/\sigma_f)$ for U^{235} from Table 3-37 is 0.344. This value is perhaps somewhat low.

Ombrellaro[181] compared the results of using the fitted cross sections with the corresponding MUFT results for a variety of metal-water mixtures. In most cases, the fitted constants agreed with the MUFT constants to within 3%. Larger discrepancies were observed in the case of mixtures of uranium

*Private communication from W. H. Arnold, Jr., Westinghouse Electric Corporation.

oxide, water, and other elements, and for cases of zirconium-water mixtures of large metal-to-water ratios. These discrepancies presumably were due to alterations made in the MUFT cross sections to force agreement* with the old H_2O age to In value of 30 cm^2. They have been largely eliminated* by using the cross sections without alteration. As mentioned in Section 3.4.4, these MUFT cross sections yield an age to indium for H_2O of 27.0 cm^2.

Table 3-36—GROUP STRUCTURE

Data from Ref. 181.

Group Number	Lower Energy, ev	Lower Lethargy	Lethargy Width
0	10×10^6	0	—
1	821×10^3	2.50	2.50
2	5.53×10^3	7.50	5.00
3	0.625	16.5884	9.0884

Table 3-37—THREE-GROUP FITTED CROSS SECTIONS (barns)

Data from Ref. 181.

Group j	$\sigma_{tr,j}$	$\sigma_{in,j} + \sigma_{el,j}$	$\sigma_{c,j} + \sigma_{f,j}$	$\sigma_{f,j}$	ν_j
Hydrogen					
1	1.5659	1.4505	0.0000	0.0000	0.00
2	2.5837	2.2128	0.0002	0.0000	0.00
3	6.3389	2.2543	0.0142	0.0000	0.00
Oxygen					
1	1.2777	0.2371	0.0425	0.0000	0.00
2	3.9450	0.0889	0.0000	0.0000	0.00
3	4.2553	0.0450	0.0000	0.0000	0.00
Zirconium					
1	1.8906	0.0823	0.0000	0.0000	0.00
2	7.4082	0.0318	0.0000	0.0000	0.00
3	10.0029	0.0183	0.0077	0.0000	0.00
Carbon					
1	0.9797	0.2248	0.0000	0.0000	0.00
2	3.6306	0.1141	0.0000	0.0000	0.00
3	4.8184	0.0809	0.0000	0.0000	0.00
Uranium-235					
1	4.9349	0.1472	1.8186	1.3159	2.77
2	7.9809	0.0000	2.6953	1.9120	2.48
3	22.6183	0.0000	34.1205	25.3917	2.46
Boron-10					
1	0.4492	0.0000	0.4492	0.0000	0.00
2	2.2919	0.0000	2.2919	0.0000	0.00
3	172.0860	0.0000	172.0860	0.0000	0.00

*Private communication from B. I. Spinrad, Argonne National Laboratory, quoting verbal discussion from personnel at BAPD and KAPL.

3.5.3 PARAMETERS FOR ONE-GROUP AND TWO-GROUP REPRESENTATIONS

Fast Group Cross Sections for Water and Water-Uranium Mixtures with the Effect of Fast Capture Included. Hellens[118] calculated the various moderating properties of water, and H_2O-U and H_2O-UO_2 mixtures as a function of the amount of fast capture, fast fission, resonance capture, and buckling. Four computational schemes were used: the P_1 and B_1 methods, with and without the Selengut-Goertzel approximations.

In addition to the four means of approximating slowing down in hydrogen, three formulations of the two-group equations were considered:

$$D_F \nabla^2 \Phi_F - \Sigma_F \Phi_F + \nu k_F \Sigma_{fS} \Phi_S = 0$$

$$D_S \nabla^2 \Phi_S - \Sigma_{aS} \Phi_S + k_e \bar{\Sigma}_F \Phi_F = 0$$

Scheme A: $k_e = 1 \qquad k_F = \epsilon p$

B: $k_e = p \qquad k_F = \epsilon$

C: $k_e = \epsilon p \qquad k_F = 1$

Figure 3-39 shows the age in water as a function of buckling. Figure 3-40 is a graph of Σ_F as a function of buckling; the four approximations are much more consistent here. Figure 3-41 is a plot of

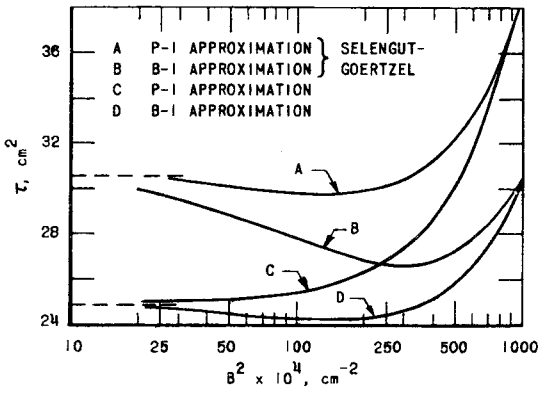

Fig. 3-39 — Two-group age (τ) as a function of buckling (B^2) in pure water. *Reproduced from Ref. 118.*

the age, $\tau = D_F/\Sigma_F$, in H_2O-U and H_2O-UO_2 mixtures. Figure 3-42 shows D_F for the various mixtures. Figures 3-43 and 3-44 give the fast fission factor, ϵ, and resonance escape probability, p, for the various mixtures according to Schemes A, B, and C. Figures 3-45 and 3-46 give the effects of using these constants on the age and on the fast removal constant, Σ_F, respectively.

Galanin[182] has presented a formula for the calculation of the age in a mixture of various materials which can be written as:

$$\frac{10^4}{\tau} = \sum_j \sum_{i \geq j} A_{ij} C_i C_j$$

where τ is the age in the mixture, and C_i is the equivalent full-density volume fraction of the ith substance in the mixture. Table 3-38 gives the densities assumed for the various substances considered, and the coefficients A_{ij}. When used with the above formula, the data for pure H_2O and D_2O yield ages of 31.0 cm^2 and 125 cm^2, respectively. The latter value has represented the Fermi age to thermal in D_2O for some time.[183] An age to 1.4 ev of 109 cm^2 is reported in Ref. 121.

687863 O - 63 - 11

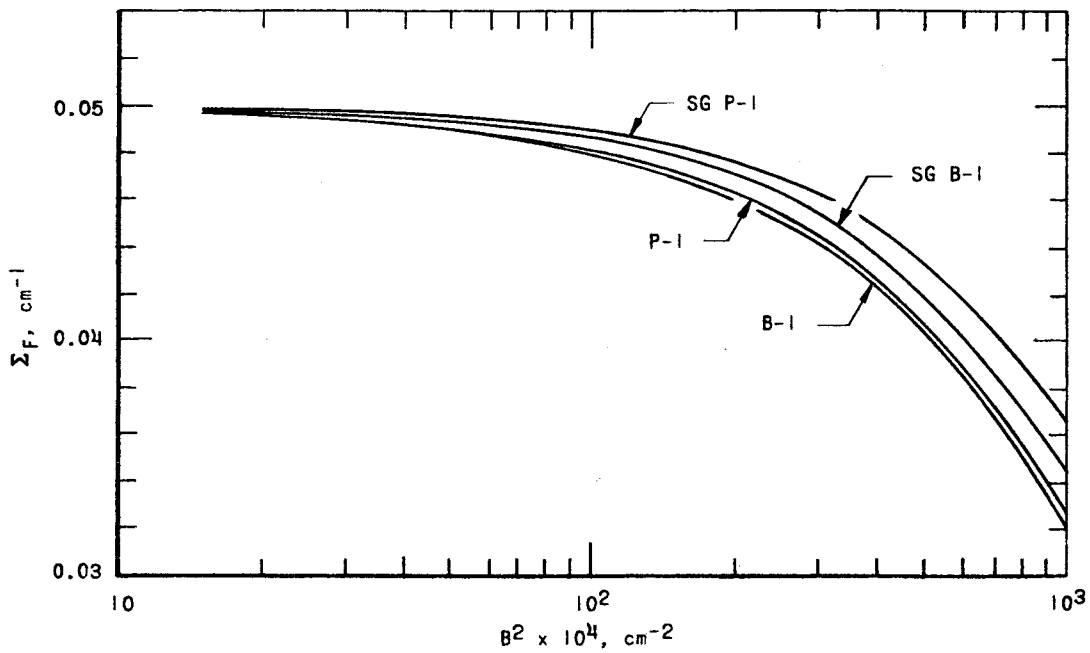

Fig. 3-40 — Fast removal cross section (Σ_F) in water as a function of buckling (B^2). *Reproduced from Ref. 118.*

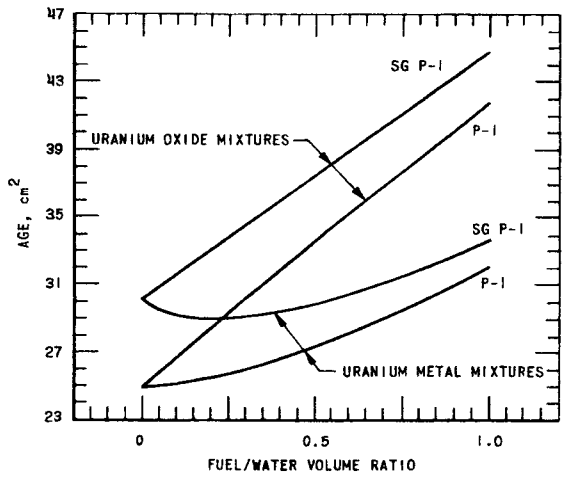

Fig. 3-41 — Age of fission neutrons in water mixtures of uranium metal and uranium oxide. *Reproduced from Ref. 118.*

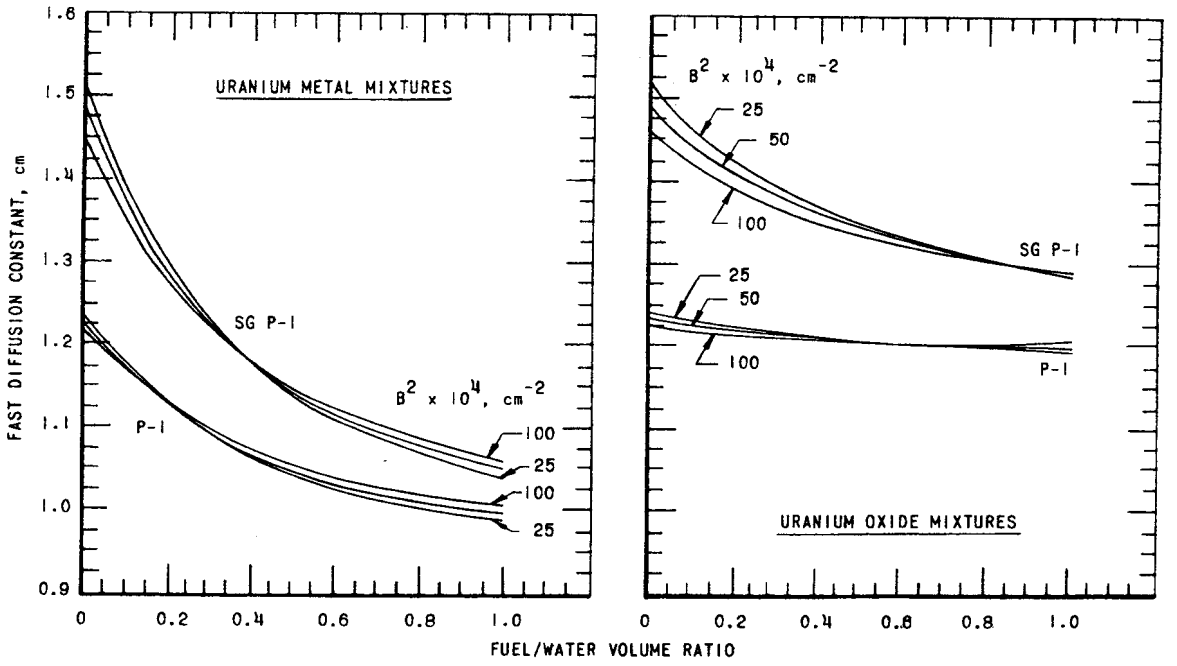

Fig. 3-42 — Fast diffusion constant (D_F) for various bucklings in water mixtures of uranium metal and uranium oxide. *Reproduced from Ref. 118.*

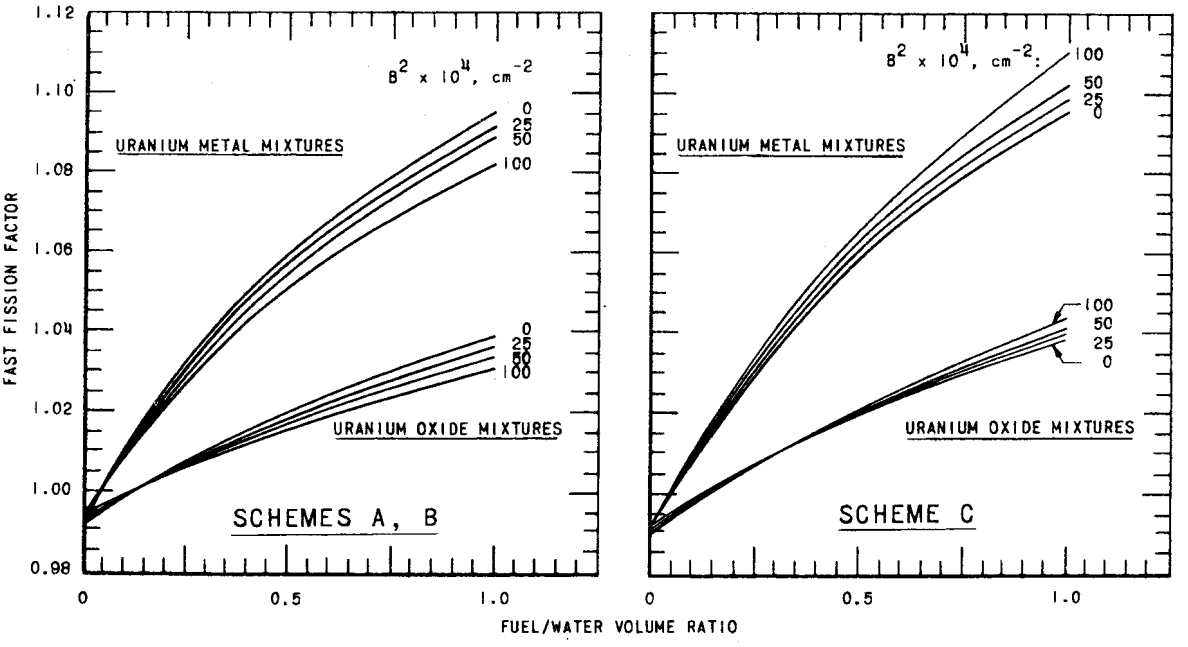

Fig. 3-43 — Fast fission factor (ϵ) in water mixtures of uranium metal and uranium oxide using various computational schemes and the P-1 approximation. *Reproduced from Ref. 118.*

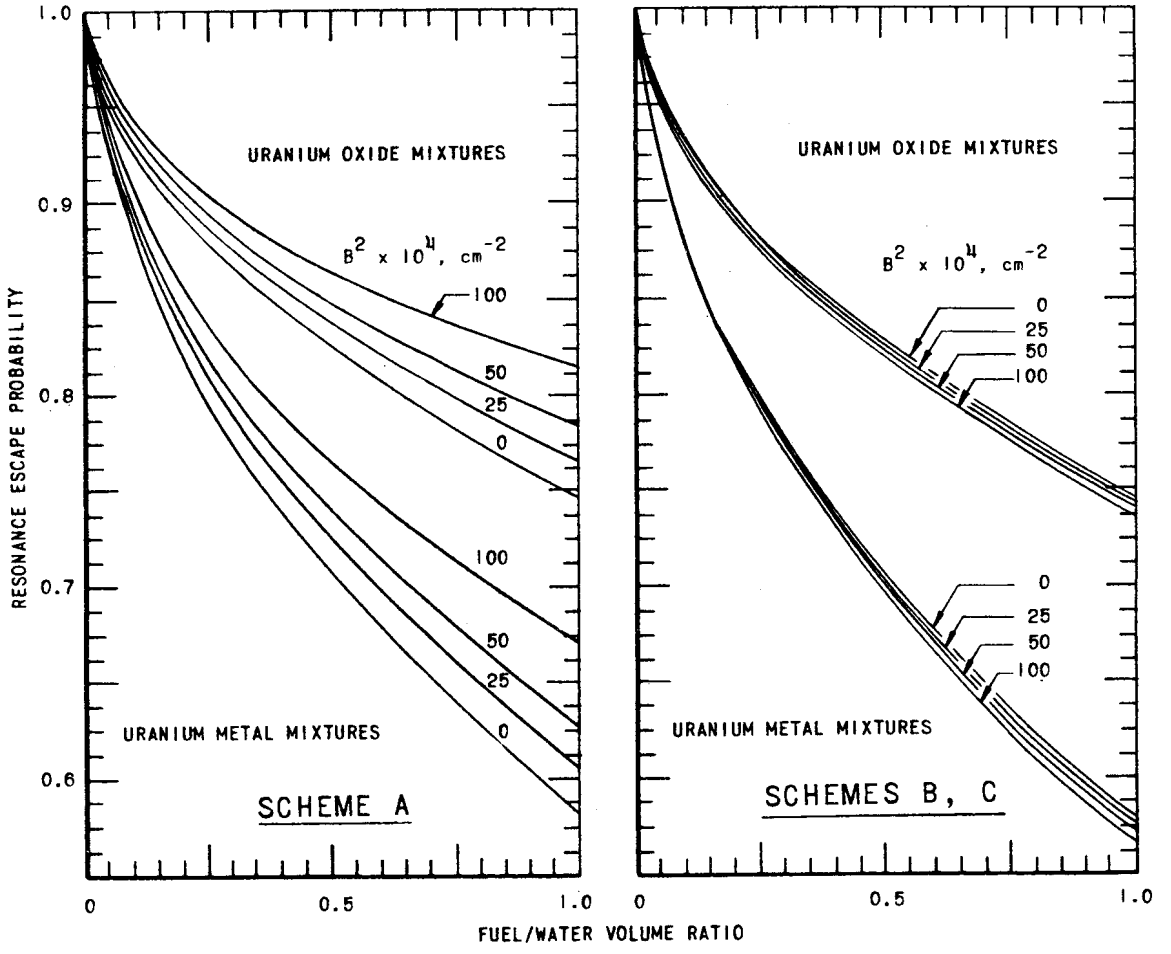

Fig. 3-44 — Resonance escape probability (p) in water mixtures of uranium metal and uranium oxide using various computational schemes and the P-1 approximation. *Reproduced from Ref. 118.*

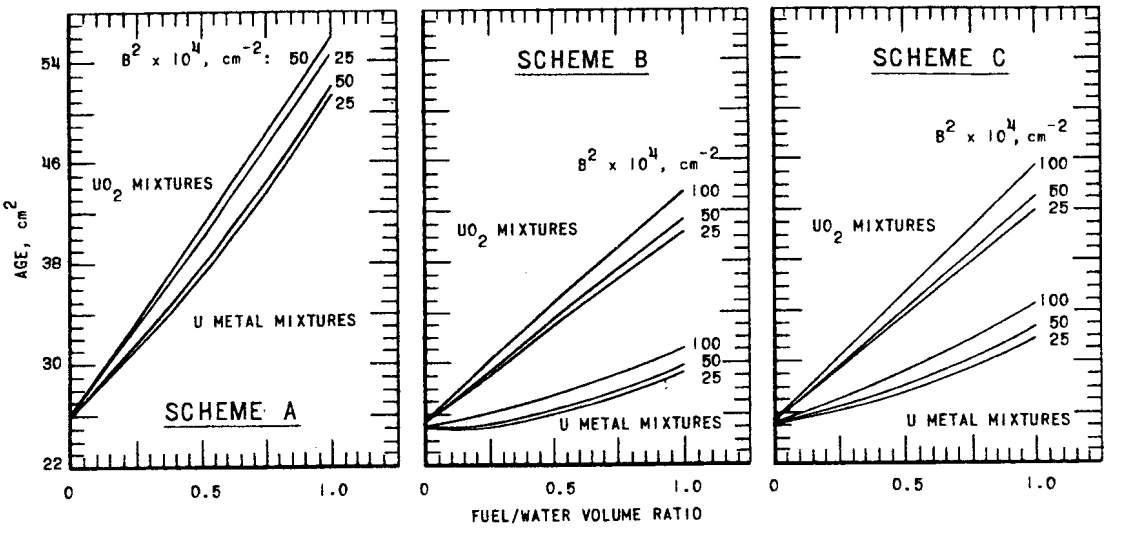

Fig. 3-45 — Age of fission neutrons in water mixtures of uranium metal and uranium oxide using various computational schemes and the P-1 approximation. *Reproduced from Ref. 118.*

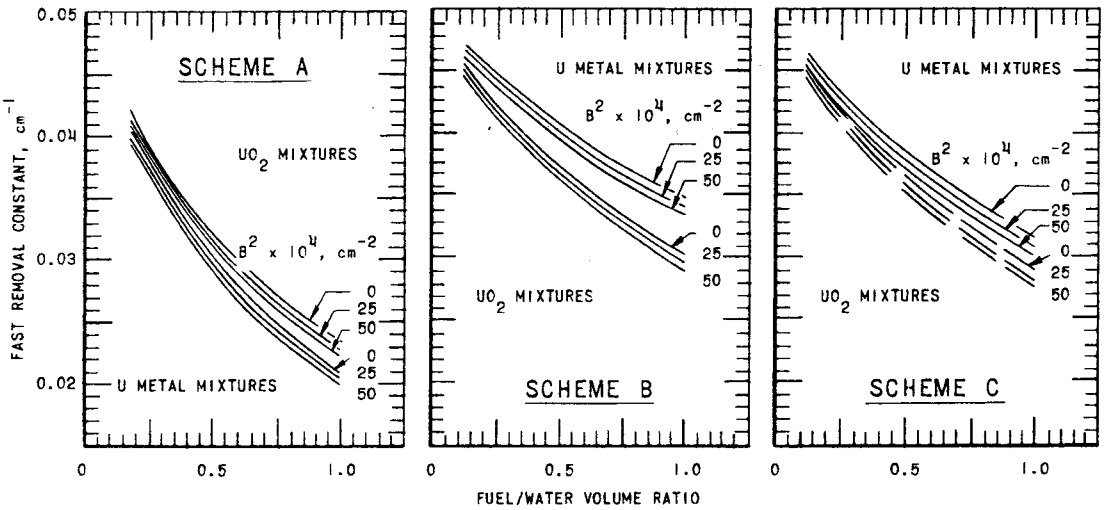

Fig. 3-46 — Fast removal constant (Σ_F) in water mixtures of uranium metal and uranium oxide using various computational schemes and the P-1 approximation. *Reproduced from Ref. 118.*

Table 3-38 — COEFFICIENTS A_{ij} FOR DETERMINING τ IN A MIXTURE OF VARIOUS SUBSTANCES

Reproduced from Ref. 182.

Density gm/cm³	i / j	H_2O	D_2O	Be	C	Na	Mg	Al	Fe	Zr	Bi	U
1.0	H_2O	323	—	—	—	—	—	—	—	—	—	—
1.1	D_2O	400	80	—	—	—	—	—	—	—	—	—
1.85	Be	730	220	116	—	—	—	—	—	—	—	—
1.67	C	440	130	120	32	—	—	—	—	—	—	—
0.93	Na	100	27	23	11	0.93	—	—	—	—	—	—
1.74	Mg	190	50	43	21	3.4	3.1	—	—	—	—	—
2.7	Al	110	29	24	12	1.9	3.4	0.93	—	—	—	—
7.8	Fe	1400	320	230	120	17	30	16	61	—	—	—
6.5	Zr	340	84	63	29	4	7.3	3.8	27	2.8	—	—
9.8	Bi	340	75	60	27	3.5	6.4	3.3	21	4.4	1.2	—
18.7	U	500	120	89	42	5.3	9.5	4.9	31	5.8	3.4	2.4

Spinrad reported* that the two-group age, $\tau_{2g} = 200$ cm², in the reflector of a D_2O moderated and reflected system gives good agreement with observed reflector savings,[184] provided the selected values of buckling and Fermi age, τ_f, satisfy

$$\exp(\tau_f B^2) = 1 + \tau_{2g} B^2$$

in the core.

Fast Group Constants for Metal-Water Mixtures by the Method of Equivalence Factors. A method is presented below for obtaining the constants for the upper two groups of a three-group formulation for mixtures of H_2O or D_2O and structural materials.

*Private communication from B. I. Spinrad, Argonne National Laboratory.

H_2O Mixtures[185]

The values below are for the following group structure:

Fast group	180 kev to 10 Mev
Epithermal group	1.4 ev to 180 kev

The age used for H_2O is 24 cm^2 for the fast group, and 6.9 cm^2 for the epithermal group. These values are not consistent with the latest experimental values (see Section 3.4.4).

Assuming that within each group the energy variations of material x and H_2O are sufficiently similar, define:

$$\alpha = \frac{\xi \Sigma_s(x)}{\xi \Sigma_s(H_2O)}$$

$$\beta = \frac{\Sigma_{tr}(x)}{\Sigma_{tr}(H_2O)}$$

$V(H_2O)$ = volume fraction of equivalent room temperature water

$V(x)$ = volume fraction of x

The value of τ and D for each group may be given in terms of τ and D for H_2O:

$$\tau = \frac{\tau(H_2O)}{V^2(H_2O)} \left\{\left[1 + \alpha \frac{V(x)}{V(H_2O)}\right]\left[1 + \beta \frac{V(x)}{V(H_2O)}\right]\right\}^{-1}$$

$$D = \frac{D(H_2O)}{V(H_2O)} \left[1 + \beta \frac{V(x)}{V(H_2O)}\right]^{-1}$$

Table 3-39 lists average microscopic transport cross sections for various materials in the two groups. Values for $D(H_2O)$ can be obtained from $\sigma_{tr}(H_2O)$. Values of α and β are given in Table 3-40. The above numbers are based on H_2O at STP. Straightforward corrections may be made for H_2O at other densities.

D_2O Mixtures

Equivalence factors[186] are given in Table 3-41 for various materials in D_2O mixtures. The group structure is the same as in the discussion on H_2O mixtures above. The D_2O constants are

Group	τ, cm^2	D, cm
Fast (180 kev to 10 Mev)	48	1.27
Epithermal (thermal to 180 kev)	79	1.24

Table 3-39— MICROSCOPIC TRANSPORT CROSS SECTIONS

Reproduced from Ref. 185.

Material	Fast Group	Epithermal Group
H_2O	6.03	16.44
Al	3.08	1.78
Cr	3.60	5.77
Fe	2.86	8.93
Ni	3.59	17.1
Zr	6.27	7.08
C	2.47	4.37
O	3.09	3.64
Polystyrene $(CH)_n$	3.94	10.77
Polyethylene $(CH_2)_n$	5.41	17.17
Furfural Alcohol $(C_5O_2H_4)$	27.35	67.53

Table 3-40— EQUIVALENCE FACTORS IN H_2O MIXTURES

Reproduced from Ref. 185.

Material	Fast Group		Epithermal Group	
	α	β	α	β
Al	0.103	0.922	0.006	0.195
Zr	0.107	1.33	0.005	0.547
Cr	0.176	1.47	0.014	0.862
Ni	0.224	1.62	0.041	2.82
Fe	0.186	1.20	0.021	1.39
C (1.6 gm/cm^3)	0.115	0.986	0.046	0.618
Polystyrene $(CH)_n$ (1.04 gm/cm^3)	0.756	0.943	0.737	0.930
Polyethylene $(CH_2)_n$ (0.91 gm/cm^3)	1.17	1.05	1.18	1.21
Furfural Alcohol $(C_5O_2H_4)$ (1.13 gm/cm^3)	0.664	0.943	0.640	0.850

Table 3-41— EQUIVALENCE FACTORS IN D_2O MIXTURES

Data from Ref. 186.

Material	Fast Group		Epithermal Group	
	α	β	α	β
Mg	0.067	0.480	0.057	0.445
Al	0.058	0.479	0.021	0.344
Zr	0.033	1.11	0.028	0.799
Stainless Steel	0.028	0.946	0.051	0.887

3.6 THE INFINITE MULTIPLICATION FACTOR $k_\infty = \epsilon p_{res}(\eta f)_{eff}$

3.6.1 THE NEUTRON CHAIN AND THE FOUR-FACTOR FORMULA $k_\infty = \epsilon p \eta f$

The concepts and approximations implied by the "four-factor formula," $k_\infty = \epsilon p \eta f$, for the infinite multiplication factor have greater validity for large, heterogeneous, low-enrichment thermal reactors than for practical homogeneous systems. The formula was developed originally for large, heterogeneous, graphite-moderated reactors fueled with natural uranium, where perhaps it is a reasonable approximation to ignore the interdependence, at all energies, of fission of U^{238}, resonance and 1/v capture by U^{238}, capture by and fission of U^{235}, and neutron leakage.

In the simplified description of the neutron chain process characterized by the four-factor formula, three spectral groupings of neutrons are considered, corresponding to the terms ϵ, p, and ηf. Starting with one primary neutron produced in fission events occurring at energies below the fission threshold of the fertile material (~1.4 Mev, for U^{238}), the total number of neutrons born below, or slowed down past, the fission threshold is termed the "fast fission factor," and is denoted by ϵ. This factor includes the fraction of fission neutrons born with subthreshold energies, and the neutrons arising from the net cascading process of capture and fission events at epithreshold energies. In assemblies containing beryllium, the contribution to neutron multiplication arising from (n, 2n) and (n, α) reactions may be significant. The factor ϵ should include these processes as well. For purposes of this presentation, the generalized function, ϵ, will be termed the "fast effect factor."

As the neutrons slow down through the resonance-absorption region of the fertile atoms, capture and fission processes occur and, per primary fission spectrum neutron, ϵp neutrons slow down to lower, or "thermal" energies. The remaining factor in this analysis, ηf, is characterized unambiguously as the number of fission neutrons produced during diffusion of thermal neutrons in the infinite medium. Though it is the product, ηf, that is averaged over the thermal flux spectrum, f has been designated as the "thermal utilization" of the fuel, and η is the average number of fission neutrons produced per thermal neutron absorption by the fuel.

In the section dealing with the fast effect factor (Section 3.6.2), various approximations to ϵ are discussed in which (typically) the capture and fission events with atoms of the thermally-fissionable isotope are ignored. Implicit to this omission is the assumption of low-enrichment fuel, so that there is little competition with capture and fission events in the fertile material. Otherwise, absorption by thermally-fissionable isotopes should be included.

In Section 3.6.4.1, infinite-dilution resonance integrals are tabulated, either measured or calculated as a sum of single-level Breit-Wigner terms plus contributions of unresolved resonances. In the bulk of the discussion in Section 3.6.4, the resonance escape probability, p, is computed, resonance-by-resonance, in various approximations. The effective "resonance escape probability" in an infinite, homogeneous reactor medium involves also neutron capture by fertile material between resonances, capture by the moderator, and capture and fission events in the fissionable isotopes. The choice has been made, in this presentation, to compute p by considering neutron capture in the resonances of the fertile material only, ignoring even the so-called 1/v absorption by that material between resonances. The resulting factor is denoted by p_{res}. All other absorptions in the resonance region are included in the definition of an effective value of ηf, denoted $(\eta f)_{eff}$, which includes all absorptions in the thermal energy range as well (see Section 3.6.5).

Accordingly, $k_\infty = \epsilon p_{res} (\eta f)_{eff}$.

3.6.2 THE FAST FISSION FACTOR, ϵ; THE FAST EFFECT FACTOR

The fast fission factor, ϵ, is related to the ratio, F, of fast fissions to thermal fissions by the expression

$$\epsilon = 1 + \frac{\nu_f - (1 + \alpha_f)}{\nu_{th}} F \tag{3-26}$$

where ν_{th} = average number of neutrons emitted per thermal fission
ν_f = average number of neutrons emitted per fast fission

and

$1 + \alpha_f$ = number of neutrons of epithreshold energies absorbed per fast fission event.

The factor F is given by a cascade process:

$$F = F_1 \sum_{n=0}^{\infty} \left(\frac{\nu_f}{\nu_{th}} F_1\right)^n = F_1/[1 - (\nu_f/\nu_{th}) F_1] \tag{3-27}$$

where F_1 is the ratio of first generation fast fission events per unit time and volume, to thermal fission events per unit time and volume. The ratio, F_1, can be expressed in the general form:

$$F_1 = \int_{E_*}^{E^*} \Sigma_f(E) \nu_{th} \phi(E) dE \tag{3-28}$$

where E^* is an upper limit for the computation; E_* is a lower limit, usually taken as a given threshold energy, $E_{threshold}$, for fast fission; $\phi(E)$ is the neutron flux arising from a source of one fission neutron per unit time and volume; and $\Sigma_f(E)$ is the energy-dependent fission cross section of the diluent.

Mozer[187] formulated an expression for ϵ (now denoted by $\bar{\epsilon}$ to avoid confusion) in terms of $\epsilon(E)$, the contribution to $\bar{\epsilon}$ at each energy above the threshold. The following description is a natural generalization of Mozer's work to include moderation by elements other than hydrogen and oxygen. The basic equation is:

$$\epsilon(E) = \nu P_f(E) \bar{\epsilon} + P_{in}(E) + P_{el}(E) \epsilon(E) + P_{mod} \tilde{\epsilon}_{mod}$$

In this equation, P_f, P_{in}, and P_{el} are the probabilities of fission, inelastic scattering, and elastic scattering in the fuel, as functions of neutron energy; P_{mod} is the probability of scattering in the moderator; $\bar{\epsilon}$ is defined by:

$$\bar{\epsilon} = \int_0^{\infty} \epsilon(E) \chi(E) dE$$

where $\chi(E)$ is the normalized fission spectrum; and $\tilde{\epsilon}_{mod}$ is a constant characterizing the contribution to $\epsilon(E)$ due to collisions with the moderator.

Three different approximations were proposed by Mozer to determine the contribution to $\bar{\epsilon}$ from the moderator:

(a) A collision with any moderator atom degrades the neutron energy to subthreshold values; then $\tilde{\epsilon}_{mod} = 1$, and

$$\epsilon(E) = \nu P_f(E)\,\bar{\epsilon} + P_{in}(E) + P_{el}(E)\,\epsilon(E) + P_{mod} \tag{3-29}$$

(b) A collision with any heavy atom present does not change the neutron energy; a collision with hydrogen leads to removal:

$$\epsilon(E) = \nu P_f(E)\,\bar{\epsilon} + P_{in}(E) + [P_{el} + P_{heavy}]\,\epsilon(E) + P_{hydrogen} \tag{3-30}$$

where P_{heavy} is the probability that a collision will result in a scattering by a heavy atom in the moderator, i.e., $P_{heavy} = P_{mod} - P_{hydrogen}$.

(c) A collision at energy E′ with a nucleus of mass A_i (measured in units of the neutron mass) of the moderator results in a uniform distribution of neutron energy E in the range $\alpha_i E' \le E \le E'$, where $\alpha_i = [(A_i - 1)/(A_i + 1)]^2$; then

$$\epsilon(E) = \nu P_f(E)\,\bar{\epsilon} + P_{in}(E) + P_{el}(E)\,\epsilon(E) + \sum_i \{P_{mod,i}[\int_{\alpha_i E}^{E} \epsilon(E')\,dE']/(1-\alpha_i)E\} \tag{3-31}$$

The results of calculations of $\bar{\epsilon}$ for homogeneous mixtures of uranium and various other materials are listed in Table 3-42. In this table, all columns otherwise not marked are based on "old" non-elastic cross sections for uranium, as indicated in Fig. 3-47 which also includes a graph of "new" cross sections.

Mozer proposed a correction for inelastic non-removal scattering by uranium, replacing $P_{in}(E)$ by $P_{in}(E)\,\tilde{\epsilon}_{in}(E)$ in Eqs. (3-29) through (3-31). The model for inelastic scattering was taken to be the decay of the compound nucleus by an evaporation process of neutron emission, yielding:

$$\tilde{\epsilon}_{in}(E) = \frac{1}{DE}\int_0^E \epsilon(E')\exp[-E'/\sqrt{DE}]\,E'\,dE'$$

where D = 0.025 Mev. Using the "old" non-elastic cross sections for uranium, $\bar{\epsilon} = 1.235$ was computed for pure uranium.

One-Group Formulations. In cases where the neutron flux spectrum is not much different from a fission spectrum in the lethargy region of importance for fast fissions, a simple one-group expression has been used to determine F_1:

$$F_1 = \frac{\nu_{th}\,\chi\Sigma_{ff}}{\Sigma_{ff} + \Sigma_{cf} + \Sigma_{if}}$$

Here, Σ_{ff}, Σ_{cf}, Σ_{if} are, respectively, cross sections for fission, for capture, and for scattering to below $E_{threshold}$, all averaged with respect to a fission spectrum above the threshold; and χ is the fraction of the fission spectrum above the threshold. Then

$$\epsilon = 1 + \frac{[\nu_f - (1+\alpha_f)]\,\chi\,\Sigma_{ff}}{\Sigma_{cf} + \Sigma_{if} - (\nu_f\chi - 1)\,\Sigma_{ff}}$$

Hellens[118] suggested the fitting formula:

$$\epsilon = 1 + \frac{[\nu_f - (1+\alpha_f)]\,\Sigma_{ff}}{\Sigma_{cf} + \Sigma_{if} - (\nu_f - 1)\,\Sigma_{ff}}$$

where Σ_{ff} is an average over the entire fission spectrum.

Using $\nu_f = 2.48$ for U^{238}, and $\Sigma_{cf}/\Sigma_{ff} = 0.14$ for U^{238}, Hellens was able to choose reasonable microscopic cross sections to fit computed values of $(\epsilon - 1)$, both for H_2O-U and for H_2O-UO_2 systems, to within 1% for non-water-to-water volume ratios from 0.25 to 1. These cross sections are given in Table 3-43.

Fleishman and Soodak[188] computed cross sections for a single epithreshold group ($E_{threshold}$ = 1.4 Mev) in a three-group formulation for the fast fission factor in heterogeneous systems. Except for the fission cross section of U^{238}, all cross sections listed in Table 3-44 were obtained as averages over

Table 3-42— FAST FISSION FACTOR ($\bar{\epsilon}$) IN INFINITE HOMOGENEOUS SYSTEMS

Data from Ref. 187.

Mod/U Vol. Ratio	U-H_2O old $\sigma^U_{non\text{-}el}$	U-H_2O new $\sigma^U_{non\text{-}el}$	U-D_2O	U-C	U-Pb[a]
$\bar{\epsilon}$ Corresponding to Eq. (3-29)					
0	1.227	1.170		1.227	
1/4	1.135	—		—	
1/2	1.100	1.097		1.122	
1/1	1.066	1.060		1.085	
2/1	1.039	1.037		1.053	
3/1	1.028	1.027		—	
5/1	1.018	1.018		1.025	
10/1	—	—		1.013	
$\bar{\epsilon}$ Corresponding to Eq. (3-30)					
0	1.227	1.170	1.227		
1/4	1.151	—	—		
1/2	1.117	1.100	—		
1/1	1.081	1.072	1.087		
2/1	1.051	1.048	—		
3/1	1.037	1.036	1.040		
5/1	1.024	1.024	1.026		
$\bar{\epsilon}$ = 1.2211 for the chemical composition UO_2					
$\bar{\epsilon}$ Corresponding to Eq. (3-31)					
0	1.227	1.170	1.227	1.227	1.227
1/4	1.162	—	—	—	—
1/2	1.130	1.110	—	1.193	—
1/1	1.093	1.081	1.102	1.164	1.143
2/1	1.060	1.055	—	1.133	1.107
3/1	1.044	1.042	1.050	—	—
5/1	1.028	1.028	1.032	1.078	1.063
10/1	—	—	—	1.044	1.037
$\bar{\epsilon}$ = 1.2028 for UO_2					

[a]Pb is assumed to slow neutrons by inelastic scattering only.

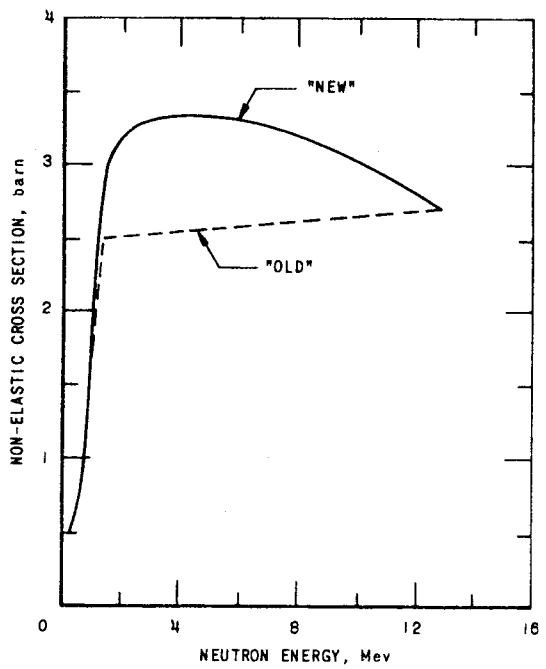

Fig. 3-47— Microscopic cross section for non-elastic scattering by uranium as a function of neutron energy. *Data from Ref. 187.*

Table 3-43 — ONE-GROUP "CROSS SECTIONS" FOR COMPUTATIONS OF ϵ IN H_2O-U AND IN H_2O-UO_2 MIXTURES (barns)

Data from Ref. 118.

Material	σ_{ff}	σ_{cf}	σ_{if}
H	0	0	1.38
O	0	0.024	0.171
U^{238}	0.30	0.042	2.32

Table 3-44 — ONE-GROUP PARAMETERS FOR ϵ COMPUTATIONS[a]

Data from Ref. 188.

Material	$\nu_f\sigma_{ff}$	σ_{ff}	σ_{cf}	σ_{if}[b]
U^{238}	1.56	0.549	0.054	2.07[c]
O	—	—	0.022	0
Mg	—	—	0.009	0.251
Al	—	—	0.007	0.319
Na	—	—	0.0005	0.225
Zr	—	—	0.029	0.960
Fe	—	—	0.004	0.686

[a]All cross sections are in units of barns.

[b]σ_{if} is defined to be the average cross section for scattering of a fission spectrum neutron from the range 1.4 Mev $\leq$ E $\leq$ 10 Mev to below 1.4 Mev. Only inelastic scattering is included in the values of this column.

[c]A value of $\sigma_{n,2n}$ = 0.02b has been added to account for the extra neutrons from the (n,2n) reaction with U^{238}.

a fission spectrum from 1.4 Mev to 10 Mev. To account for fissions of U^{238} atoms by neutrons of energy less than 1.4 Mev, the value of $\nu_f\sigma_{ff}$ for U^{238} was computed with the formula:

$$\nu_f\sigma_{ff} = \int_0^{10} \nu(E)\ \sigma_f(E)\ \phi(E)\ dE \Big/ \int_{1.4}^{10} \phi(E)\ dE$$

Fast Effect in Beryllium and in Uranium-Beryllium Mixtures. A cascade process similar to that determining the fast effect in U^{238} is present also in beryllium-moderated systems. In the Mev energy range, both (n,2n) and (n,α) reactions with Be are non-trivial and, because of the uncertainty in the data for the energy-dependent (n,2n) cross section, the magnitude of the fast effect in a Be-moderated system is difficult to assess.

Häfele[190] approximated the equilibrium flux spectrum in an infinite medium of beryllium containing a unit fission spectrum source by extrapolating from the sum of spectra from a finite number of successive elastic collisions. In Fig. 3-48, the normalized fission spectrum is compared with the equilibrium spectrum to indicate the dangers of performing naive one-group computations when the average cross sections depend decisively on the shape of the neutron flux spectrum. (A review of results not included in this section may be found in Ref. 190.)

Häfele[190] computed the fast effect factor for beryllium, using optimistic and pessimistic estimates of the energy dependence of the (n,2n) cross section. In another report, Häfele and Tsagaris[191] published the results of similar computations for BeO. These results appear in Table 3-45.

Häfele calculated ϵ from the formula:

$$\epsilon = 1 + \int_{E_{threshold}}^{\infty} S(E)\ \frac{\Sigma_{(n,2n)}(E) - \Sigma_{(n,\alpha)}(E)}{\Sigma_{total}(E)}\ dE$$

where S(E) is the approximate equilibrium spectrum in the material, and $E_{threshold}$ was taken to be 1 Mev.

Chernick and Moore[192] fitted two curves to the beryllium (n,2n) cross section data of Fischer[193], and of Marion and Cranberg,[194] and, for each curve, calculated ϵ for beryllium (see Table 3-45).

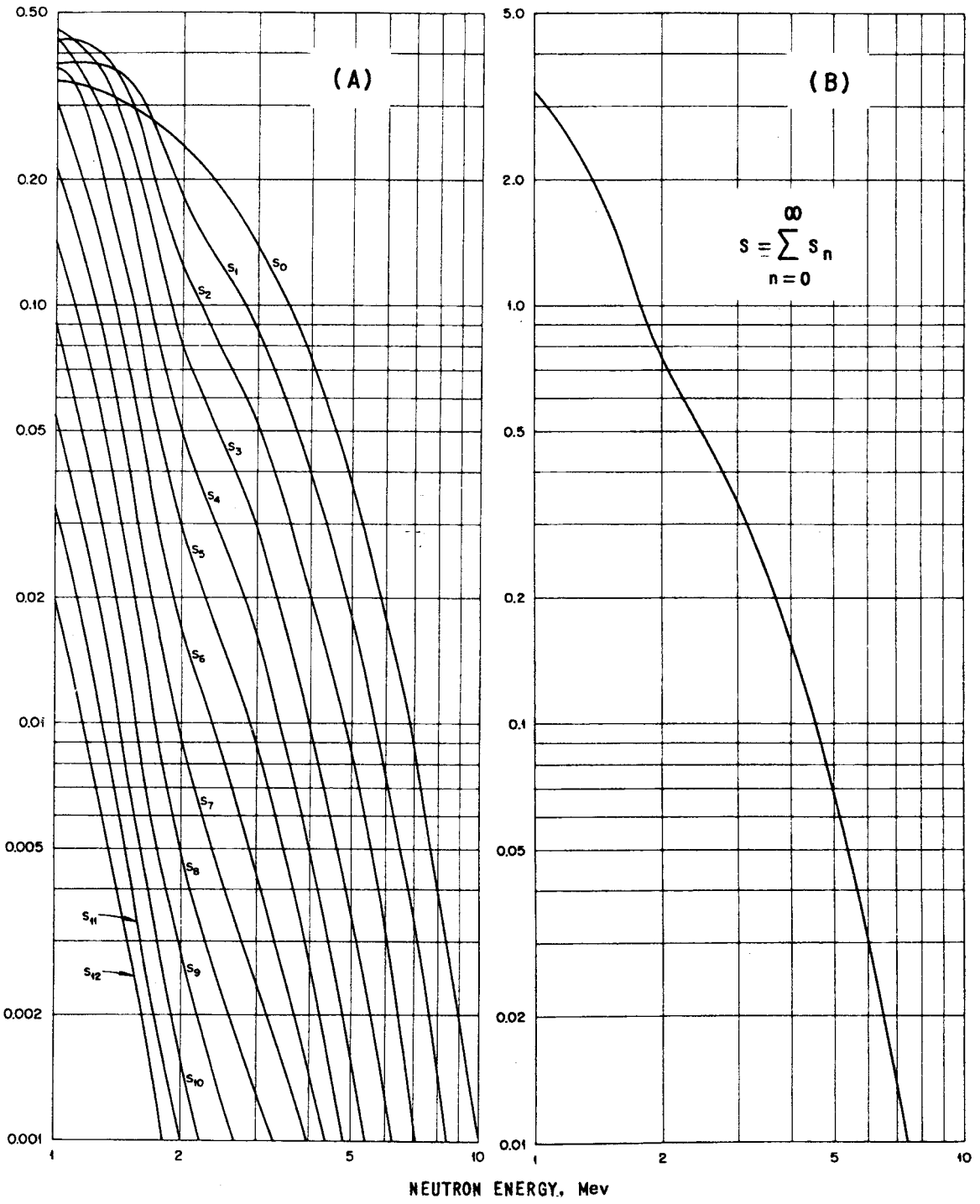

Fig. 3-48 — (A) Relative neutron flux spectrum (S_n) after n elastic collisions, and (B) relative final neutron flux spectrum (S), in an infinite medium of beryllium containing a uniform U^{235} fission spectrum source. *Data from Ref. 190.*

Table 3-45— FAST EFFECT FACTOR IN INFINITE HOMOGENEOUS SYSTEMS OF BERYLLIUM OR BERYLLIUM OXIDE

Data from Ref. 199.

(n,2n) reactions per source neutron[a]	(n,α) reactions per source neutron	ϵ	Ref.
Beryllium			
0.118	0.0422	1.076 (upper bound)	190
0.094	0.0422	1.051 (lower bound)	
0.105	0.039	1.066 (Marion and Cranberg data)	192
0.100	0.039	1.061 (Fischer data)	
0.242	0.049	1.19	195
0.164	0.049	1.12	
0.083	0.049	1.03	
0.121	0.0423	1.078	199
Beryllium Oxide			
0.0794	0.0336	1.046[b] (upper bound)	191
0.0603	0.0336	1.027[b] (lower bound)	
0.081	0.0348	1.046[b]	199

[a] Source neutrons are fission spectrum neutrons from U^{235}.
[b] The (n,α) reaction in O^{16} is included.

Anisotropy of the scattering was not included, nor did the analysis consider the contribution of the (n,2n) neutron output to the spectrum.

Aline, et al.,[195] fitted three curves to (n,2n) cross section data inferred from the work of Marion, et al.,[196] Bockelman, et al.,[197] and Fowler and Cohn,[198] and performed 18-group calculations for the neutron flux spectrum in beryllium above 0.71 Mev, the (n,α) threshold energy. In these computations, it was assumed that neutrons arising from (n,2n) reactions do not contribute to the epi-0.71-Mev spectrum. However, the anisotropy of elastic scattering by beryllium was explicitly included in the calculations of the elastic transfer cross sections. The values of ϵ ranged from 1.03 to 1.19, emphasizing the importance of the uncertainty in the (n,2n) curves for beryllium.

Rief[199,200] has written a Monte Carlo program (FF-MOCCA) for multigroup computations of the fast effect factor in homogeneous media, and in complex reactor lattices. Using cross section data reported in Refs. 192 and 200, Rief computed ϵ in infinite, homogeneous mixtures of natural uranium and beryllium containing a (U^{235}) fission spectrum source. For pure beryllium, $\epsilon = 1.078$, with a statistical error of ± 0.005. For natural uranium, the ratio of fast fissions to thermal fissions was determined to be 0.39; this value is low when compared to normalized data of Chezem.[201] Rief's results for Be and BeO are compared in Table 3-45 with the calculations of other authors.

In Table 3-46 are listed results for mixtures of natural uranium and beryllium wherein the minimum energy considered was 0.9 Mev.

3.6.3 EPITHERMAL ABSORPTION IN AN INFINITE HOMOGENEOUS MEDIUM

In this section, equations for the neutron collision density, the slowing-down density, and the probability that epithermal neutrons escape absorption are exhibited, and approximate solutions are presented. Considerable use has been made of the book by Weinberg and Wigner,[189] and the monograph on resonance absorption written by Dresner.[202] Since detailed derivations of analytical results are available in these works, in general only the solutions and conclusions are presented here.

Table 3-46— FAST-EFFECT DATA FOR INFINITE HOMOGENEOUS MIXTURES OF BERYLLIUM AND NATURAL URANIUM

Data from Ref. 199.

U/Be Vol. Ratio	$\gamma(U^{238})$	$\gamma(U^{235})$	γ(Be)	ϵ	$\Delta\epsilon$	No. of Histories	No. of Collisions
∞	0.4287	0.0175	0	1.2465	0.0143	1000	4424
2/1	0.2804	0.0074	0.0435	1.1929	0.0087	2000	7241
1/1	0.2127	0.0056	0.0630	1.1667	0.0080	2000	6914
1/2	0.1474	0.0037	0.0800	1.1384	0.0073	2000	6658
1/4	0.0878	0.0022	0.0948	1.113	0.0065	2000	6649
0	0	0	0.1209	1.078	0.0053	2000	6182

Notes: (a) γ of a material is defined to be the ratio of secondary fast neutrons to primary fast neutrons. For example, for U^{238}, γ is the ratio of U^{238} fission neutrons to primary U^{235} fission neutrons. (b) ϵ is the fast-effect factor, including all fission, (n,2n), and capture events. (c) $\Delta\epsilon$ is the statistical uncertainty in ϵ.

If not explicitly stated otherwise, the medium consists of a homogeneous mixture of an absorber, and of non-absorbing nuclides of constant scattering cross section. It is assumed that all neutron scattering is isotropic in the center-of-mass coordinate system and is elastic, and that neutrons cannot gain energy in the collision. In view of the linearity of the equations, it is sufficient to assume a monoenergetic, unit neutron source since the slowing-down density for an arbitrary source can be obtained as an appropriate superposition of solutions. The source energy, E_S, is taken to be the upper limit of the computation.

3.6.3.1 The Integral Equation for the Neutron Collision Density

The neutron collision density, F(E), is the solution of the integral equation:

$$F(E) = \int_E^{E_S} \sum_{j=0}^{k} \frac{\Sigma_{sj}(E')}{\Sigma(E')} F(E') P_{sj}(E' \rightarrow E)\, dE' + \delta(E_S - E) \qquad (3\text{-}32)$$

In Eq. (3-32) and in subsequent equations:

$F(E)$ = density of neutron events per second per unit energy at energy E, cm^{-3} sec^{-1}
$q(E)$ = neutron slowing-down density, cm^{-3} sec^{-1}
$\Sigma_{sj}(E)$ = macroscopic scattering cross section of the jth nuclide, cm^{-1}; for hydrogen, this will be written $\Sigma_S^H(E)$
$\Sigma_{pj}(E)$ = macroscopic potential scattering cross section of the jth nuclide, cm^{-1}
$\Sigma_s(E)$ = macroscopic scattering cross section of the medium, cm^{-1}
$\Sigma_p(E)$ = macroscopic potential scattering cross section of the medium, cm^{-1}
$\Sigma_a(E)$ = macroscopic absorption cross section of the medium, cm^{-1}
$\Sigma(E) \equiv \Sigma_s(E) + \Sigma_a(E)$
$P_{sj}(E' \rightarrow E)\,\Delta E$ = slowing-down kernel for the jth nuclide. It is the probability that, upon scattering by the jth nuclide, a neutron of energy E′ will have an energy $\tilde{E}$ in the interval $E < \tilde{E} < E + \Delta E$
ξ_j = average logarithmic energy loss of the neutron per collision with the jth nuclide.

With the assumption that scattering is elastic and is isotropic in the center-of-mass system, the slowing-down kernel has the form:

$$P_{sj}(E' \rightarrow E)\,\Delta E = \begin{cases} \dfrac{\Delta E}{(1-\alpha_j)E'}, & \alpha_j E' \le E \le E' \\ 0, & \text{otherwise} \end{cases}$$

where $\alpha_j = [(A_j - 1)/(A_j + 1)]^2$; and A_j is the mass of the jth nuclide in units of the neutron mass. The parameters ξ_j and α_j satisfy:

$$\xi_j = 1 + \frac{\alpha_j \log \alpha_j}{1 - \alpha_j}$$

3.6.3.2 Solutions for Special Cases

The Placzek Function. The solution to Eq. (3-32) in the case of a non-absorbing single nuclide of mass number A, with an energy-dependent scattering cross section, $\Sigma_s(E)$, has been investigated by Placzek.[203] Below source energy,

$$F(E) = (1/E_S)\, P_A\,(E/E_S)$$

where $P_A(E/E_S)$, the Placzek function, depends only on the relative energy E/E_S, and the mass number A. Figure 3-49 is a plot of $(1-\alpha)(E/E_S)\,P_A(E/E_S)$ versus $u/(\ln \alpha)$, where $u = \ln (E/E_S)$. Asymptotically, $P_A(E/E_S) = E_S/\xi E$, as $E \to 0$.

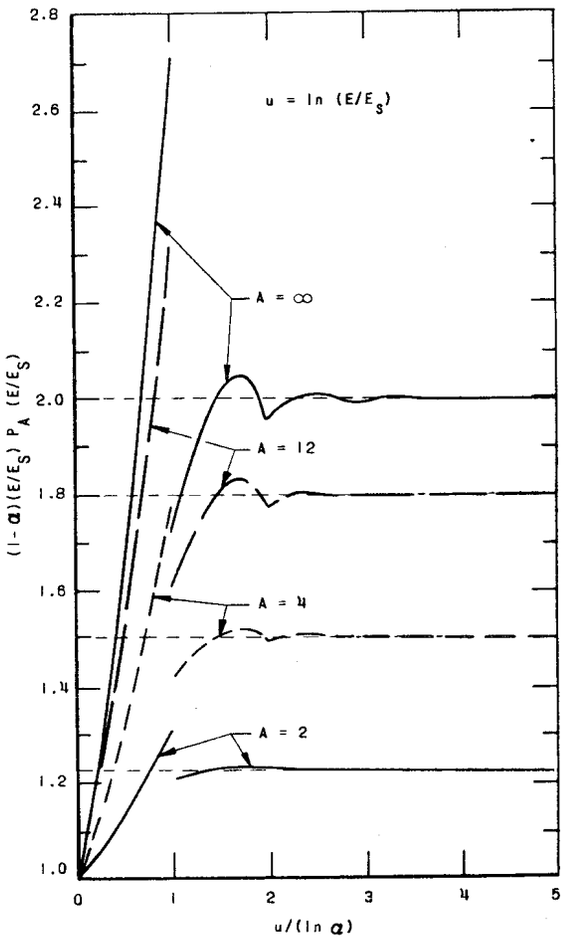

Fig. 3-49 — The Placzek Function $[P_A(E/E_S)]$ versus mass number of the nonabsorbing nuclide. *Data from Ref. 189.*

Solutions for Case of Proton Moderator plus Non-moderating Absorber. In this case, $P_{S0}(E' \to E) \equiv 0$ for the non-moderating nuclide, $j = 0$, and the solution is:

$$F(E) = \frac{\Sigma_s(E_S)}{\Sigma(E_S)} \frac{1}{E} \exp\left(-\int_E^{E_S} \frac{\Sigma_a(E')}{\Sigma(E')} \frac{dE'}{E'}\right) \tag{3-33}$$

where the scattering by the non-moderating absorber is not included.

The slowing-down density past energy E, q(E), may be shown to satisfy $q(E) = E\,F(E)$ in this special case. With the normalization of unit source, the function q(E) is the probability that the source neutron will escape absorption in slowing down from energy E_S past energy E. It is denoted by the term "absorption escape probability" and is written as $p(E,E_S)$. More generally, the slowing-down density past energy E (where E is lower than the minimum energy of a unit source distribution), is termed the absorption escape probability. Thus

$$p(E,E_S) = \exp\left(-\int_E^{E_S} \frac{\Sigma_a(E')}{\xi^H\, \Sigma(E')} \frac{dE'}{E'}\right) \tag{3-34}$$

If Σ_s^H is constant in the energy range $E \leq E' \leq E_S$, and provided that neutron absorption by the hydrogen is ignored, $p(E,E_S)$ may be written in the familiar form:

$$p(E,E_S) = \exp\left[-\frac{N_0}{\xi^H \Sigma_S^H} I_{eff}(E,E_S)\right] \tag{3-35}$$

where

$$I_{eff}(E,E_S) = \int_E^{E_S} \Sigma_{a0}(E') \frac{\Sigma_S^H}{\Sigma_s^H + \Sigma_{a0}(E')} \frac{dE'}{E'} \tag{3-36}$$

is the "effective absorption integral" of the absorber over the range $E \leq E' \leq E_S$; N_0 is the atom density of the absorber in the medium, and $\sigma_{a0}(E)$ its microscopic absorption cross section.

Asymptotic Solution in a Medium with a Slowly-Varying Ratio of Scattering to Absorption. For a medium consisting of a single nuclide of mass number A, and with $(\Sigma_s/\Sigma) = \beta$ (constant), the slowing-down density below source level is given by:

$$q(E) = (E/E_S)^{\lambda} \tag{3-37}$$

where λ is the real root of the equation:

$$1 - \lambda = \beta\left[\frac{1 - \alpha^{(1-\lambda)}}{1 - \alpha}\right] \tag{3-38}$$

and

$$\alpha = [(A-1)/(A+1)]^2$$

When β is close to unity (that is, for weak absorption), an expansion of λ in powers of $1 - \beta$ may be made, yielding:[202]

$$\lambda = \frac{1}{\xi}(1-\beta)\left[1 + \frac{\xi - \gamma}{\xi}(1-\beta) + \cdots\right] \tag{3-39}$$

The parameter γ is given by:

$$\gamma = 1 - \frac{\alpha(\ln \alpha)^2}{2(1-\alpha)\xi}$$

and $2\xi\gamma$ is the average squared lethargy change per scattering.

Hurwitz[202,204] applied the WKB method to obtain an approximation for the resonance escape probability in the case of a medium where β is slowly varying in energy. The procedure, in effect, makes use of the solution Eq. (3-37) [which may be rewritten $q(u) = \exp(-\lambda u)$, in terms of the lethargy, u] in that now

$$q(u) = \exp\left[-\int_0^u \lambda(u')\,du'\right]$$

where $\lambda(u')$ is a function of lethargy. The function $\lambda(u')$ is obtained as the solution of Eq. (3-38) for each value of u' upon introducing the lethargy-dependent value of β. In deriving this result, it was assumed that absorption is zero where the Placzek function is oscillating, that is, for lethargy $u < 3 \ln (1/\alpha)$.

To first order in $1 - \beta = \Sigma_a/(\Sigma_s + \Sigma_a)$, from Eq. (3-39),

$$\lambda(u') = \frac{\Sigma_a(u')}{\xi\,[\Sigma_s(u') + \Sigma_a(u')]}$$

and

$$p(u,0) \equiv q(u) \approx \exp\left(-\int_0^u \frac{\Sigma_a(u')}{\xi\,[\Sigma_s(u') + \Sigma_a(u')]}\,du'\right) \tag{3-40}$$

To second order in $1-\beta$,

$$\lambda(u') = \frac{\Sigma_a(u')}{\xi\Sigma_s(u') + \gamma\ \Sigma_a(u')}$$

yielding the Greuling-Goertzel approximation.[205]

The approximate solutions described above have been referred to as "synthetic-kernel" solutions, in the same sense that Hurwitz' WKB solution is synthetic. The solution with $\lambda(u') = \Sigma_a(u')/\xi\Sigma_s(u')$ has been labeled the Fermi "synthetic-kernel" solution. In Table 3-47 are presented comparison data from calculations of the absorption escape probability for neutrons slowing down from E_1 to E_2, where β is constant, $(E_2/E_1) = \exp(-5)$, and the various synthetic kernels have been applied. Other examples may be found in Refs. 202 and 206.

Table 3-47—COMPARISON OF ABSORPTION ESCAPE PROBABILITIES COMPUTED BY SYNTHETIC-KERNEL METHODS

$p(E_2,E_1) = (E_2/E_1)^{\lambda}$ for constant $1-\beta$; $(E_2/E_1) = \exp(-5)$

Data from Refs. 206 and 207.

Moderator Mass Number, A	$1-\beta$	Exact		$p(E_2/E_1)$ (Synthetic Kernels)		
		λ	$p(E_2,E_1)$	Fermi $\lambda=\Sigma_a/(\xi\Sigma_s)$	Wigner $\lambda=\Sigma_a/[\xi(\Sigma_s+\Sigma_a)]$	Greuling-Goertzel $\lambda=\Sigma_a/(\xi\Sigma_s+\gamma\Sigma_a)$
12	0.0005	0.003168	0.98429	—	—	—
	0.005	0.031588	0.85390	0.85346	0.85412	—
	0.05	0.306496	0.21600	0.2050	0.22110	—
	0.1	0.593757	5.137×10^{-2}	4.20×10^{-2}	5.607×10^{-2}	—
	0.2	1.118817	3.720×10^{-3}	1.77×10^{-3}	5.082×10^{-3}	3.76×10^{-3}
50	0.0005	0.012663	0.93865	—	0.93866	—
	0.005	0.126248	0.53193	0.5308	0.53248	—
	0.05	1.225912	2.177×10^{-3}	1.78×10^{-3}	2.401×10^{-3}	—
100	0.0005	0.025162	0.88178	0.88176	0.88182	—
	0.005	0.250831	0.28532	0.2841	0.28591	—

For a mixture of nuclides, the solutions described above may be generalized.[202] For example, Eq. (3-37) applies, with

$$1-\lambda = \beta\sum_{j=1}^{N}\frac{\Sigma_{sj}}{\Sigma_s}\frac{1-\alpha_j^{(1-\lambda)}}{1-\alpha_j}$$

Note that Eq. (3-40) in terms of the neutron lethargy, is identical to Eq. (3-34) (for hydrogen moderation), except that ξ replaces ξ^H. Indeed, if $A = 1$, $\xi = \gamma = 1$, and both the Wigner approximation and the Greuling-Goertzel approximation are exact.

Weinberg and Wigner[189], and, independently, Corngold,[208] have derived an equation for the collision density in terms of the Placzek function, $P_A(E/E')$:

$$F(u) = \frac{1}{\xi} - \frac{1}{\xi}\int_0^u [1-\beta(u')]\ F(u')\ [1-p_A(u-u')]\ du' \qquad (3\text{-}41)$$

where

$$1 - p_A(u-u') = \xi(E/E')\ P_A(E/E')$$

An approximate solution to Eq. (3-41) is

$$F(u) = \frac{1}{\xi-\xi_1(u)}\exp\left(-\int_0^u \frac{1-\beta(u')}{\xi-\xi_1(u')}\,du'\right) \qquad (3\text{-}42)$$

where

$$\xi_1(u) = \int_0^u du'\ [1-\beta(u')]\ p_A\ (u-u')\ \exp\left[\int_{u_1}^u \frac{1-\beta(u'')}{\xi}\,du''\right]$$

687863 O - 63 - 12

Then

$$p(u,0) \equiv q(u) = \exp\left(-\int_0^u \frac{1-\beta(u')}{\xi - \xi_1(u')}\,du'\right) \tag{3-43}$$

Corngold[208] has formulated a variational principle for p(u,0) exact for solutions of Eq. (3-41).

3.6.4 RESONANCE ABSORPTION IN AN INFINITE HOMOGENEOUS MEDIUM

Background material concerning nuclear resonance reactions is available in the book by Weinberg and Wigner,[189] in Dresner's monograph,[202] and in various textbooks and papers on nuclear physics, including the books by Blatt and Weisskopf,[209] and by Sachs,[210] and the article by Breit and Wigner.[211] Considerable use has been made of the publications of Dresner,[202] and Sampson and Chernick,[212] in the sections dealing with approximate formulas for the resonance escape probability over sharp resonances.

The discussion of this section is limited to the study of isolated resonances, with cross sections in the vicinity of the resonance represented by single-level Breit-Wigner formulas. For s-wave neutrons, and neglecting Doppler broadening, the microscopic cross section for radiative capture is

$$\sigma_{c,res}(E) = \frac{2\pi\hbar^2}{m} \frac{g_J\,\Gamma_n\,\Gamma_\gamma}{E_0^{1/2}\,E^{1/2}\left\{4(E-E_0)^2 + \left[\left(\frac{E}{E_0}\right)^{1/2}\Gamma_n + \Gamma_\gamma\right]^2\right\}} \tag{3-44}$$

or, at energies $E \approx E_0$

$$\sigma_{c,res}(E) \approx \frac{\Gamma_\gamma}{\Gamma}\,\frac{\sigma_0}{1+x^2} \tag{3-45}$$

The microscopic resonance total cross section in the vicinity of energy E_0 is given by:

$$\sigma_{t,res} = \frac{\sigma_0}{1+x^2} + \left(g_J\sigma_{p0}\,\frac{\Gamma_n}{\Gamma}\,\sigma_0\right)^{1/2}\,\frac{2x}{1+x^2} \tag{3-46}$$

where the second term on the right-hand side arises from scattering-interference effects.

In the above equations

E = energy of the incident neutron, ev

E_0 = energy at which the peak resonance total cross section, σ_0, is attained, ev

m = mass of the neutron

$g_J = \frac{2J+1}{2(2I+1)}$ is the statistical spin factor, where I is the spin of the target nucleus, and J is the total angular momentum of the compound nucleus. For s-wave neutrons, $J = I \pm (1/2)$; for nuclei of spin zero, $g_J = 1$.

Γ_n, Γ_γ = neutron width and radiative-capture width, respectively, of the resonance, ev. In these computations, it is assumed that the total width of the resonance, Γ, is the sum of Γ_n and Γ_γ.

$x \equiv \frac{E-E_0}{(\Gamma/2)}$

σ_{p0} = microscopic potential scattering cross section of the absorbing nuclide, barns

The infinite-dilution resonance integral for a single-level Breit-Wigner resonance is independent of the temperature of the absorber. However, if the potential scattering cross section per absorber atom, σ_{p0}, is not very large, the Doppler broadening of the resonance cross section arising from the thermal motion of the absorber atoms should be considered.

Including interference between potential and resonance scattering by the absorber, the effective Doppler-broadened cross sections in or in the vicinity of a sharp resonance are approximately:[202]

$$\sigma_{c,eff}(E) = \sigma_0\,\frac{\Gamma_\gamma}{\Gamma}\,\psi(\theta,x) \tag{3-47}$$

$$\sigma_{el,eff}(E) = \sigma_0\,\frac{\Gamma_n}{\Gamma}\,\psi(\theta,x) + \left(g_J\,\sigma_{p0}\,\frac{\Gamma_n}{\Gamma}\sigma_0\right)^{1/2}\chi(\theta,x) \tag{3-48}$$

In these equations,

$$\theta \equiv \frac{4\,E_0}{\Gamma^2}\frac{\mu\,kT}{M}$$

$\mu \equiv \frac{Mm}{M+m}$ is the reduced mass, where M is the mass of the absorbing nuclide

kT ≡ energy mode of the Maxwell distribution of absorber atom velocities, ev

$$\psi(\theta,x) \equiv \frac{1}{\sqrt{4\pi\theta}}\int_{-\infty}^{\infty}\frac{1}{1+y^2}\exp\left[-\frac{(x-y)^2}{4\theta}\right]dy \tag{3-49}$$

is the Doppler-broadened line shape

$$\chi(\theta,x) \equiv \frac{1}{\sqrt{4\pi\theta}}\int_{-\infty}^{\infty}\frac{2y}{1+y^2}\exp\left[-\frac{(x-y)^2}{4\theta}\right]dy \tag{3-50}$$

is the Doppler-broadened, interference-scattering line shape.

References to the literature concerning the function $\psi(\theta,x)$ are cited in the monograph by Dresner.[202] An extensive tabulation of values of $\psi(\theta,x)$ has been published by Rose, et al.[213] Formulas for the effective resonance integral, involving $\psi(\theta,x)$ and $\chi(\theta,x)$ are discussed in Section 3.6.4.2.

3.6.4.1 Resonance Integrals for Infinite Dilution

When a resonance absorber is placed in a moderator at a concentration approaching zero (infinite dilution), its absorption per atom is unaffected by energy self-shielding between levels, or by Doppler broadening. Under these circumstances, it absorbs neutrons in the slowing-down spectrum of the moderator. The gross feature of this spectrum in the epicadmium energy region is its dE/E dependence for the case of infinite source energy, elastic scattering that is isotropic in the center-of-mass system, and constant $\overline{\xi\Sigma_s}$. It is convenient to express the infinite-dilution resonance integral, which is proportional to the reaction rate, as:[189,212]

$$I_{inf} = \int_{E_C}^{E_{max}}\sigma(E)\frac{dE}{E} \tag{3-51}$$

The upper limit, E_{max}, generally is taken as 2 Mev, which is approximately the average energy of the fission spectrum. The lower energy limit is determined by the high-pass neutron filters, usually cadmium, and the type of experiment used in determining the integral. If the appropriate $\sigma(E)$ is used, then a subscript on I_{inf} is used to denote fission (f), capture (c), or absorption (a).

The resonance capture integral may be computed directly from the assigned resonance parameters for positive and negative energy levels. For nuclei without fission channels, the radiative microscopic capture cross section can be described by the sum of single-level Breit-Wigner terms.[214,215] For s-wave neutrons and positive energy levels, the cross section is written [see Eq. (3-44)]:

$$\sigma_c(E) = \frac{2\pi\hbar^2}{m}\sum_i \frac{g_{Ji}\,\Gamma_{ni}\,\Gamma_{\gamma i}}{E_i^{1/2}\,E^{1/2}\left\{4(E-E_i)^2 + \left[(E/E_i)^{1/2}\,\Gamma_{ni} + \Gamma_{\gamma i}\right]^2\right\}} \tag{3-52}$$

where E_i is the energy of the ith resonance level.

Substituting the formula for $\sigma_c(E)$, [Eq. (3-52)], into the integral of Eq. (3-51) and integrating over the energy range from cutoff, E_c, to infinity (the result being insensitive to the substitution of ∞ for E_{max}), the resonance integral, in the approximation that E_c/E_1 is much less than unity, may be written as:

$$I_{inf,c} = \frac{\pi\hbar^2}{2m}\sum_i g_{Ji}\frac{\Gamma_{ni}\,\Gamma_{\gamma i}}{E_i^{5/2}}\left[\frac{2}{E_c^{1/2}} + \frac{2\pi E_i^{1/2}}{\Gamma_i} - \frac{E_c^{1/2}}{E_i}\right] \tag{3-53}$$

Also, for most isotopes, the terms $E_c^{1/2}/E_i$ may be neglected and the integral may be written in the form:

$$I_{inf,c} = 2\,\sigma_c\left(E_T\right)\left(\frac{E_T}{E_c}\right)^{1/2} + \frac{\pi^2\hbar^2}{m}\sum_i g_{Ji}\frac{\Gamma_{ni}\,\Gamma_{\gamma i}}{E_i^2\,\Gamma_i} \tag{3-54}$$

where

$$\sigma_c(E_T) = \frac{\pi\hbar^2}{2mE_T^{1/2}} \sum_i g_{Ji} \frac{\Gamma_{ni}\,\Gamma_{\gamma i}}{E_i^{5/2}} \tag{3-55}$$

is the capture cross section at some "thermal" energy, $E_T \ll E_1$, due to resonances above E_c. The summation is performed over all positive energy levels of the compound nucleus above E_c.

To account for the unresolved levels at higher energies, the resonance integral is computed by summing over all the resolved levels, as above, and for the unresolved levels the summation is replaced by an integration after introducing a density distribution of levels. Dresner[216] assumed that the resonances are uniformly spaced and that the capture widths and the reduced neutron widths

$$\Gamma_{ni}^0 \equiv \Gamma_{ni}/E_i^{1/2}$$

are constant and are equal to the averaged values $\overline{\Gamma}_\gamma$ and $\overline{\Gamma_n^0}$ respectively. With these assumptions, the contribution of the unresolved levels to the second term of Eq. (3-54) is given by:

$$\frac{\pi^2\hbar^2 g}{m}\frac{\overline{\Gamma_n^0}\,\overline{\Gamma}_\gamma}{D}\int_{E_d}^{\infty}\frac{dE}{E^{3/2}\left[E^{1/2}\overline{\Gamma_n^0}+\overline{\Gamma}_\gamma\right]} = \frac{\pi\hbar^2}{m}g\left(\frac{2\pi\,\overline{\Gamma}_\gamma}{D}\right)\frac{1}{E_d}\left[\frac{B-\ln(1+B)}{B^2}\right] \tag{3-56}$$

where D is the average level spacing (1/D is the level density); E_d is the energy above which resonances are not resolved; and

$$B \equiv \overline{\Gamma}_\gamma/(\overline{\Gamma_n^0}\,E_d^{1/2}) \tag{3-57}$$

Kuhn[217] has revised the Dresner correction term by accounting for the fluctuations of the reduced neutron widths, using the distribution proposed by Porter and Thomas.[218] The multiplicative correction factor that is to be applied to the right-hand side of Eq. (3-56) is plotted in Fig. 3-50.

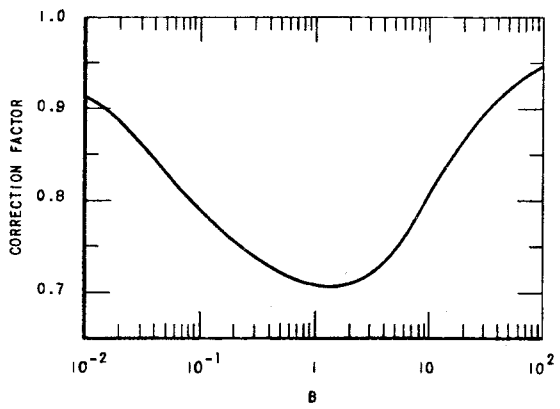

Fig. 3-50—Correction factor for fluctuations in neutron width. *Reproduced from Ref. 217.*

For a "pure 1/v absorber," indicating only positive levels, the measured capture cross section at neutron energy E_T, corresponding to a velocity of 2200 m/sec, is used for $\sigma_c(E_T)$ in the first term of Eq. (3-54). This takes into account the unresolved as well as the resolved levels.

For some nuclei, the introduction of one or more negative energy levels is needed to describe the capture cross section. These levels may or may not contribute to the resonance integral, depending upon the positioning of the levels and the magnitudes of the parameters. In the absence of assigned parameters for these levels, an upper limit to the resonance integral may be computed by evaluating the first term on the right-hand side of Eq. (3-54) at a neutron energy E_L, instead of at E_T. E_L is some energy below, but near, the first level.

In Table 3-48 are listed the measured and/or computed values of the resonance integral as defined by Eq. (3-51). The measured values are listed according to the method by which the measurement was made, i.e., activation method or absorption method. Brief comments, pertinent to the results, are indicated by literal superscripts, and they are presented at the end of the table. Listed are the low-energy cutoff values used by the investigators.

Table 3-48— RESONANCE INTEGRALS FOR INFINITE DILUTION (barns)

Notes: (c) = capture integral, (f) = fission integral; (c + f) = capture plus fission integrals

Element	Nat. Abund., %	Measured		Calculated	No. of Resonances	Lower Energy, ev	Ref.	Element	Nat. Abund., %	Measured		Calculated	No. of Resonances	Lower Energy, ev	Ref.
		Activation	Absorption							Activation	Absorption				
Li	—	—	28	—	—	0.4	222	Ga^{69}	60.2	9.2	—	—	—	0.4	222
B	—	—	280 ± 40	—	—	0.49	223	Ga^{71}	39.8	15	—	—	—	0.4	222
N	—	—	4.8 ± 2.4	—	—	0.49	223	Ge	—	—	3.5 ± 2.9	—	—	0.49	223
F^{19}	100	—	2.3 ± 0.5	—	—	0.49	223	As^{75}	100	36.8	33	170[f]	—	0.4	222
Na^{23}	100	~0.24	0.27	—	—	0.4	222	Se	—	—	9.6 ± 1.2	—	—	0.49	223
Na^{23}		0.30 ± 0.01	—	—	—	0.5	224	Se^{77}	7.58	—	—	33[g]	3	0.4	228
Mg	—	—	0.9	—	—	0.4	222	Se^{80}	49.82	—	—	0.9[g]	3	0.4	228
Mg	—	—	0.072[a]	—	—	—	219	Br	—	—	118 ± 14	—	—	0.49	223
Al^{27}	100	—	<0.18[a]	—	—	—	219	Br^{79}	50.52	147	—	—	—	0.4	222
Al^{27}	100	~0.16	0.18	—	—	0.4	222	Br^{81}	49.48	—	—	61.6[g]	2	0.4	228
Si	—	—	0.5	—	—	0.4	222	Kr^{82}	11.56	—	—	200[g]	1	0.4	228
P^{31}	100	—	<2	—	—	0.4	222	Kr^{83}	11.55	—	—	240[g]	2	0.4	228
S	—	—	0.6	—	—	0.4	222	Kr^{84}	56.90	—	—	3.4[g]	2	0.4	228
Cl	—	—	12	—	—	0.4	222	Rb	—	—	9.0 ± 2.8	—	—	0.49	223
Cl	—	—	12.8 ± 1.7	—	—	0.49	223	Rb^{85}	72.15	—	—	0.55[g]	4	0.4	228
K	—	—	3.5 ± 1.1	—	—	0.49	223	Rb^{87}	27.85	—	—	0.17[g]	4	0.4	228
Ca	—	—	2	—	—	0.4	222	Sr	—	—	16	—	—	0.4	222
Sc^{45}	100	~10.7	—	—	—	0.4	222	Sr	—	—	10.0 ± 2.6	—	—	0.49	223
Ti	—	—	3	—	—	0.4	222	Y^{89}	100	0.91	—	—	—	0.4	222
Ti	—	—	3.8 ± 0.9	—	—	0.49	223	Y^{89}	100	—	—	0.73[g]	3	0.4	228
V	—	—	4.1[a]	—	—	—	219	Zr	—	—	3	—	—	0.4	222
V	—	—	3.3 ± 0.8	—	—	0.49	223	Zr	—	—	0.69 ± 0.09	0.63[a,h]	—	—	219
V^{51}	99.76	~2.2	—	—	—	0.4	222	Zr	—	—	3.7 ± 0.5	—	—	0.49	223
Cr	—	—	2.6 ± 1.1	—	—	0.49	223	Zr^{91}	11.23	—	5.4 ± 1.6[c]	—	—	0.55	229
Mn^{55}	100	—	15.4[a,b]	—	—	—	219	Zr^{91}	11.23	—	—	5.6[g]	1	0.4	228
Mn^{55}	100	15.6 ± 0.6[c]	—	—	—	0.55	—	Nb^{93}	100	—	14[a]	16[a,i]	—	—	219
Mn^{55}	100	14.2 ± 0.6	—	—	—	0.5	224	Mo	—	—	20[a]	22[a,i]	—	—	219
Mn^{55}	100	14.0 ± 0.3[d]	—	—	—	—	—	Mo^{95}	15.70	—	107[a,j]	107[a,i]	—	—	219
Mn^{55}	100	—	—	17[e]	—	0.4	—	Mo^{96}	16.50	—	—	27[g]	1	0.4	228
Fe	—	—	2.1	—	—	0.4	222	Mo^{97}	9.45	—	—	15[g]	4	0.4	228
Fe	—	—	1.8[a]	—	—	—	219	Mo^{98}	23.75	—	—	12.45	—	0.5	230
Fe	—	—	2.3 ± 0.25	—	—	0.5	221	Mo^{98}	23.75	10.8 ± 2.5	—	—	—	0.5	224
Fe	—	—	2.3 ± 0.4	—	—	0.49	223	Mo^{100}	9.62	3.73 ± 0.20	—	—	—	0.5	231
Co^{59}	100	81 ± 4[e]	—	—	—	—	225	Tc[99]	—	—	72[a]	—	—	—	219
Co^{59}	100	75 ± 5	—	—	—	0.5	226	Rh^{103}	100	656	575	1146[f]	—	0.4	222
Co^{59}	100	72.3 ± 5	—	—	—	0.5	224	Rh^{103}	100	—	—	1095[g]	5	0.4	228
Ni	—	—	4	—	—	0.4	222	Pd	—	—	23	—	—	0.4	222
Ni	—	—	<3.1[a]	—	—	—	219	Ag	—	—	>650	—	—	0.4	222
Ni	—	—	3.2 ± 0.5	—	—	0.49	223	Ag	—	—	841[a]	761[a,i]	—	—	219
Cu	—	—	3.3 ± 0.3	—	—	0.5	221	Ag^{107}	51.35	74	—	—	—	0.4	222
Cu	—	3.7	4	—	—	0.4	222	Ag^{109}	48.65	1160	—	—	—	0.4	222
Cu	—	3.13	—	—	—	0.64	227	Ag^{109}	48.65	—	1910[a,j]	1440[a,i]	—	—	219
Cu	—	—	3.7 ± 0.8	—	—	0.49	223	In	—	—	3700[a]	3100[a,i]	—	—	219
Cu^{63}	69.1	4.4	—	—	—	0.4	222	In	—	—	—	3240[e,*]	—	0.4	—
Cu^{63}	69.1	5.1 ± 0.15	—	—	—	0.5	224	In^{113}	4.23	—	—	271[e]	—	—	—
Cu^{65}	30.9	2.2	—	—	—	0.4	222	In^{115}	95.77	2640[k]	—	—	—	0.4	222
Cu^{65}	30.9	2.3 ± 0.23	—	—	—	0.5	224	In^{115}	95.77	2630 ± 133	—	—	—	—	—
Zn	—	—	2	—	—	0.4	222	In^{115}	95.77	—	—	3370[e]	—	—	—
Zn	—	—	3.4 ± 0.8	—	—	0.49	223	Sn	—	—	8.8[a]	5.3[a,i]	—	—	219
Ga	—	—	11.7 ± 2.7	—	—	0.49	223	Sn	—	—	5.7 ± 0.7	—	—	0.49	223

Table 3-48 —RESONANCE INTEGRALS FOR INFINITE DILUTION (barns) (Continued)

Notes: (c) = capture integral, (f) = fission integral; (c + f) = capture plus fission integrals

Element	Nat. Abund., %	Measured		Calculated	No. of Resonances	Lower Energy, ev	Ref.
		Activation	Absorption				
Sn^{120}	32.97	—	—	0.82[g]	1	0.4	228
Sn^{124}	5.98	—	—	12[g]	1	0.4	228
Sb	—	—	106 ± 13	—	—	0.49	223
Sb	—	—	115 ± 12	—	—	0.5	221
Sb^{121}	57.25	162	—	—	—	0.4	222
Sb^{121}	57.25	—	—	203[g]	6	0.4	228
Sb^{123}	42.75	—	—	162[g]	4	0.4	228
Sb^{123}	42.75	~138	—	—	—	0.4	222
Te	—	—	~74[a,i]	>49[a,i]	—	—	219
Te	—	—	50.0 ± 6.0	—	—	0.49	223
Te^{122}	2.46	—	—	56[g]	1	0.4	228
Te^{123}	0.87	—	—	6765[g]	3	0.4	228
Te^{124}	4.61	—	—	5.5[g]	1	0.4	228
Te^{125}	6.99	—	—	24[g]	5	0.4	228
Te^{126}	18.71	—	—	9.0[g]	1	0.4	228
Te^{128}	31.79	—	—	10[g]	1	0.4	228
I^{127}	100	—	130 ± 18	—	—	0.5	221
I^{127}	100	—	183[a]	158[a,i]	—	—	219
I^{127}	100	140	—	—	—	0.4	222
I^{127}	100	—	—	173[m]	—	—	—
I^{129}	—	—	—	42[g]	6	0.4	228
I^{129}	—	36 ± 4	—	—	—	0.6	232
Xe^{129}	26.44	—	—	260[g]	2	0.4	228
Xe^{131}	21.18	—	—	810[g]	3	0.4	228
Cs^{133}	100	400 ± 25[c]	—	—	—	0.55	241
Cs^{133}	100	—	504[a]	394[a,i]	—	—	219
Cs^{135}	—	62 ± 2	—	—	—	0.6	232
Ba	—	—	12.6 ± 1.7	—	—	0.49	223
Ba^{136}	7.81	—	—	13[g]	2	0.4	228
La	—	—	11	—	—	0.4	222
La^{139}	99.911	—	—	13[g]	1	0.4	228
Ce	—	—	3.7 ± 1.7	—	—	0.49	223
Pr^{141}	100	—	—	25[g]	7	0.4	228
Pr^{141}	100	15.5 ± 3[c]	—	—	—	0.55	241
Nd	—	—	40 ± 6	—	—	0.5	221
Nd^{143}	12.32	—	<218[a]	>181[a,h]	—	—	219
Nd^{145}	8.29	—	156[a,j]	>273[a,h]	—	—	219
Pm^{147}	—	—	—	2190[g]	9	0.4	228
Sm	—	—	1790 ± 270	—	—	0.49	223
Sm^{147}	15.07	—	—	715[g]	13	0.4	228
Sm^{147}	15.07	—	<1385[a]	—	—	—	219
Sm^{152}	26.63	2740 ± 150[c]	—	—	—	0.55	241
Sm^{152}	26.63	—	—	2210[g]	1	0.4	228
Sm^{152}	26.63	—	2960[a]	—	—	—	219
Eu^{151}	47.77	—	<6900[a]	7320[a]	—	—	219
Eu^{153}	52.23	—	1500[a]	1760[a,i]	—	—	219
Gd	—	—	67 ± 8.0	—	—	0.49	223
Tb^{159}	100	—	—	393[g]	16	0.13	228
Dy^{164}	28.18	420 ± 50	—	416[e]	—	0.4	247
Dy^{164}	28.18	482 ± 33[d]	—	—	—	—	—

Element	Nat. Abund., %	Measured		Calculated	No. of Resonances	Lower Energy, ev	Ref.
		Activation	Absorption				
W^{184}	30.6	—	—	8.6[e]	—	—	—
W^{186}	28.4	355	—	—	—	0.4	222
W^{186}	28.4	—	—	481[e]	—	—	—
W^{186}	28.4	396 ± 59[d]	—	—	—	—	—
Re^{185}	37.07	1160	—	1630[f]	—	0.4	222
Re^{187}	62.93	305	—	310[a]	—	0.4	222
Os	—	—	180 ± 20	—	—	0.49	223
Ir	—	—	2000 ± 490	—	—	0.49	223
Ir^{191}	38.5	3500[k]	—	7680[f]	—	0.4	222
Ir^{193}	61.5	1370[k]	—	976[f]	—	0.4	222
Pt	—	—	69	—	—	0.4	222
Pt	—	—	~189[a,l]	114[a,l]	—	—	219
Au^{197}	100	—	1558[a]	1591[a,i]	—	—	219
Au^{197}	100	1533 ± 40	—	—	—	0.5	220
Au^{197}	100	1558	—	—	—	0.4	222
Au^{197}	100	1553	—	—	—	0.64	227
Au^{197}	100	—	—	1584[m]	—	0.4	—
Hg	—	—	73 ± 5	—	—	0.5	221
Hg	—	—	72.4 ± 8	—	—	0.49	223
Tl^{203}	—	129	—	—	—	0.4	222
Tl^{205}	—	0.5	—	—	—	0.4	222
Pb	—	—	0.1	—	—	0.4	222
Pb	—	—	0.13[a]	—	—	—	219
Bi^{209}	100	—	0.5	—	—	0.4	222
Bi^{209}	100	—	0.07[d]	—	—	—	219
Th^{232}	100	—	110[g,j]	108[a,i]	—	—	219
Th^{232}	100	85	—	—	—	0.5	226
Th^{232}	100	—	—	96[m]	—	—	—
Th^{232}	—	500 ± 150°	—	—	—	0.4	234
Th^{233}	—	400 ± 100	—	—	—	0.5	226
Pa^{233}	—	700 ± 200°	—	—	—	0.4	234
Pa^{233}	—	770 ± 90	—	—	—	0.6	232
U	—	—	224 ± 40	—	—	0.49	223
U^{233}	—	—	100 ± 4 (c)	—	—	0.4	234
U^{233}	—	—	1000 ± 200 (c + f)	—	—	0.4	234
U^{233}	—	—	—	813 (f)[p]	—	—	235
U^{233}	—	—	—	812 (f)[p]	—	0.4	236
U^{233}	—	870 (f)	—	—	—	—	237
U^{234}	0.0057	—	—	700 ± 70°	—	0.4	234
U^{235}	0.714	271 (f)	—	—	—	0.4	222
U^{235}	0.714	274 ± 11 (f)	—	—	—	0.5	238
U^{235}	0.714	—	—	340 (f)[p]	—	—	235
U^{238}	—	415 ± 40[c]	—	—	—	0.55	241
U^{238}	—	—	400 ± 50°	—	—	0.4	234
U^{238}	—	350 ± 90	—	340 ± 40[q]	—	0.4	239
U^{238}	99.3	280 ± 10°	—	—	—	0.4	234
U^{238}	99.3	—	287[a]	—	—	—	219
U^{238}	99.3	281 ± 20	—	—	—	0.4	240
U^{238}	99.3	—	—	279 ± 7[q]	—	0.4	239
Np^{237}	—	—	955[a,b]	—	—	—	219

Lu	—	—	720 ± 70	—	—	0.5	221	Pu^{239}	—	—	—	3600 ± 1000 (c + f)[o]	—	0.15	234
Lu^{175}	97.40	463 ± 15[d]	—	—	—	—	—	Pu^{239}	—	327 ± 22 (f)	—	—	—	0.5	238
Lu^{176}	2.60	887 ± 65[d]	—	—	—	—	—	Pu^{239}	—	—	—	1500 ± 300 (c)[o]	—	0.15	234
Hf	—	—	2800 ± 600	—	—	0.5	221	Pu^{239}	—	—	—	230 (f)[p]	—	—	241
Hf	—	—	2900[a]	2050[a,i]	—	—	219	Pu^{240}	—	—	11,450[a,b]	8450[a,i]	—	—	219
Hf^{180}	35.44	21.8	—	—	—	0.4	222	Pu^{240}	—	8700 ± 800	—	—	—	0.5	242
Ta	—	—	1110[a]	750[a,i]	—	—	219	Pu^{240}	—	—	—	8000 ± 400	—	0.4	239
Ta	—	—	474 ± 62	—	—	0.49	223	Pu^{240}	—	9000 ± 3000	—	—	—	0.4	243
Ta^{181}	99.988	590	—	555[n]	—	0.4	222	Pu^{240}	—	—	10,000 ± 2800	—	—	0.2	244
W	—	—	—	353[e]	—	—	—	Pu^{240}	—	—	—	8565[e]	—	—	—
W	—	—	290 ± 35	—	—	0.49	223	Pu^{241}	—	557 ± 33 (f)	—	—	—	0.5	238
W	—	—	340[a]	—	—	—	219	Pu^{242}	—	1275 ± 30	—	—	—	0.5	245
W^{182}	26.4	—	—	584[e]	—	—	—	Am^{243}	—	2290 ± 50		—	—	0.5	245
W^{183}	14.4	—	—	414[e]	—	—	—								

[a]The resonance integral given is not significantly dependent on what cutoff is used since the material has a cross section dependence that is close to 1/v in the cutoff region.

[b]Values were deduced from measurements in the DIMPLE Maxwellian spectrum and with the GLEEP oscillator.

[c]Gold resonance integral (including 1/v) of 1534b used as standard (private communication from F. Feiner, KAPL, 1961).

[d]Private communication from J. L. Crandall, Savannah River, 1960. Work done by G. M. Jacks.

[e]Calculated by P. J. Persiani of Argonne from level parameters given in Supplement 1, Second Edition, BNL-325, (1960); includes unresolved-level corrections. The Dy^{164} value includes the bound level. The parameters for this level were obtained from R. Sher, BNL (private communication).

[f]Estimated from parameters of the first large resonance and the thermal cross section; does not include correction for unresolved levels.

[g]Calculated from level parameters in the second edition of BNL-325, or its supplement (1960). The number of levels listed is the number of resonance levels for which separate calculations were carried out. If the number of resolved levels is three or more, the resonance integral listed includes a contribution from the unresolved resonances, calculated using average resonance parameters.

[h]Calculated from parameters of the first resonance only; includes unresolved-resonance contributions.

[i]Calculated from parameters given in BNL-325; includes unresolved-level contributions.

[j]Measurements on single solutions only, and corrected for screening.

[k]A resonance near thermal leads to considerable dependence on the details of the cadmium absorber that was used.

[l]Only one sample of these materials was available and the estimated screening was large. Values listed must be treated with caution.

[m]Calculated by P. J. Persiani of Argonne from level parameters given in Ref. 246; includes unresolved-level corrections.

[n]Estimated from level parameters; does not include corrections for unresolved levels.

[o]Values preferred from analysis of available data.

[p]Numerical integration of the fission cross section curves. In Ref. 241, the range of integration is from 1 ev to 50 kev.

[q]Calculated from level parameters and the thermal cross section; includes unresolved-level corrections.

Usually, the measured value in the activation method is obtained from the cadmium ratio of the unknown sample x, and of a reference standard s, using the relation:

$$I_{inf,c}(x) = I_{inf,c}(s) \frac{(CdR - 1)_s}{(CdR - 1)_x} \frac{\sigma_{cx}}{\sigma_{cs}} \quad (3\text{-}58)$$

where σ_{cx} and σ_{cs} are the capture cross sections at 2200 m/sec, and CdR is the cadmium ratio. The standards are usually gold or indium. This relationship is valid for nuclei whose cross sections have an energy dependence in the subcadmium region identical to that of the standard.

An expression independent of this assumption is obtained by replacing the ratio of cross sections by the cadmium-difference ratio (CdD_x/CdD_s), so that

$$I_{inf,c}(x) = I_{inf,c}(s) \frac{(CdR - 1)_s}{(CdR - 1)_x} \frac{CdD_x}{CdD_s} \frac{e_x}{e_s}$$

where e_x and e_s are the counter efficiencies for the unknown and the standard, respectively. The cadmium difference is defined as the difference between the activity of the bare foil and the cadmium-covered foil. It includes the proper irradiation and decay time correction factors.

In the pile oscillator method, the reactivity change caused by the absorption of cadmium-filtered neutrons is compared with the change produced by a standard, usually gold. The measurements reported by Tattersall, et al.,[219] and Jirlow and Johansson[220] involve the subtraction of the "1/v term" [the first term in Eq. (3-54)], from the measured value. However, the resonance integral given in Table 3-48 includes this term.

The measurements by Spivak, et al.,[221] were made by impinging a boron-collimated neutron beam onto an absorbing sample in a graphite cavity. An array of counters was embedded in the graphite wall, and the change in the total counting rate of all the counters between a known absorber and the unknown absorber was measured.

All data listed are total integral values. Corrections were applied to those data originally reported as "above 1/v". In general, computed values are not included unless they have been supported by measurements. Generally, only one computed result is listed as typical when a number of approximately equal values have been reported. In cases where only one measurement has been reported in the literature, the reported value has been included. When several values for a given material were found to be in marked disagreement and it was not possible to judge a preferred value, all values were listed. In cases for which values were in considerable disagreement and a selection was made, more credence was placed in recently measured values than in older data.

3.6.4.2 Narrow Resonance Approximations to the Collision Density, I_{eff}, and p

Asymptotically below source energies, and above thermal energies, the neutron collision density, F(E), in a weakly absorbing medium essentially is inversely proportional to the neutron energy. Within a resonance, F(E) may be sharply varying; in any event, it is difficult to calculate accurately. Formulas have been developed for the collision density in the context of the "narrow resonance approximation." In this approximation, it is assumed that the resonance is so sharp, or "narrow," that a collision of a resonance-energy neutron with a moderator atom degrades the neutron energy to below the resonance. The approximation is reasonable for mixtures of such important resonance absorbers as U^{238} and Th^{232} with most moderators.

Within the narrow resonance approximation, formulas for F(E) and for the effective resonance integral, I_{eff}, have been derived for finite-dilution media in terms of the narrowness of the resonance in comparison with the mean neutron energy loss in neutron-absorber collisions. Two extreme assumptions have appeared in the literature. A resonance may be sufficiently narrow that a scattering collision of a resonance-energy neutron with an absorber atom effectively removes the neutron from the region of the resonance. In this situation, no qualitative distinction need be made between collisions with moderator atoms or with absorber atoms. The designation "NR" approximation appears frequently in the literature for this case. Conversely, the resonance may be very wide with respect to the energy lost by the neutron in a collision with the absorber. In a homogeneous medium, such scatterings of resonance neutrons may be ignored. This approximation has been labeled variously as "NRIM" or "NRIA," meaning that, effectively, the absorber atoms are of infinite mass.

In the hope of reducing the ambiguities inherent in the symbols NR and NRIA, the following nomenclature has been adopted in Section 3. The "NN" approximation denotes the case where the resonance is narrow both with respect to moderator scatterings and to absorber scatterings. (This symbol re-

places "NR.") In the "NW" approximation, the resonance is narrow relative to neutron-moderator collisons but wide with respect to collisions with the absorber. (This symbol replaces "NRIA.")

Modifications of these approximations have appeared where better approximations to F(E) in the resonance have been developed, for example, by iterating once on F(E) in Eq. (3-32).

For accurate computations of p, the effects of Doppler broadening must be included. Nevertheless, there is much to learn from the detailed numerical studies made with various approximations to the evaluation of p. It is useful to examine the relative accuracy of these approximations in the absence of the complication of Doppler broadening.

NN Approximation for a Single Resonance. A parameter that has been found useful in determining whether a resonance is represented more reasonably in the one or in the other approximation is the "practical width" of the resonance, Γ_p. As defined by Wigner,[189] Γ_p is the energy band around E_0 in which the total macroscopic (Doppler-broadened) resonance cross section exceeds the macroscopic potential scattering cross section of the medium.

A single resonance, far below source energies and isolated from perturbing effects of higher-energy resonances, is said to be "narrow", relative to a mixture of nuclides, if, for each nuclide, $(1-\alpha)\,E_0 \gg \Gamma_p$. Somewhat more generally, the resonance is "narrow" if the overwhelming contribution to the collision density by slowing-down processes is from energy regions where Σ_a is very small and where the collision density essentially has regained its asymptotic, age-theory form: $F(E) \approx q_0/(\bar{\xi}E)$. In this case, $F(E) \approx q_0/(\bar{\xi}E)$ in the resonance also, where q_0 is the slowing-down density somewhat above the resonance, and now F(E) is the total collision density, including resonance scatterings. In deriving this formula for F(E), it has been assumed that, except for the anomalous scattering of the absorber at resonance energies, all Σ_{sj}'s are constant. Here,

$$\bar{\xi} = \sum_j \xi_j \,(\Sigma_{pj}/\Sigma_p)$$

the average being taken over all nuclides, including the absorber (see Section 3.6.3.1 for definitions of symbols).

Normalizing q_0 to unity at energy E* above the resonance, the resonance escape probability to energy E below the resonance is given by:

$$p(E,E^*) \approx 1 - \frac{N_0}{\bar{\xi}\Sigma_p} I_{eff}\,(E,E^*) \qquad \text{(NN approximation)} \tag{3-59}$$

where Σ_p = macroscopic potential scattering cross section of the medium, cm^{-1}
N_0 = density of absorber atoms in the medium, cm^{-3}

and the effective resonance integral is defined by:

$$I_{eff}(E,E^*) = \int_E^{E^*} \sigma_{a,res}(E') \frac{\Sigma_p}{\Sigma(E')} \frac{dE'}{E'} \qquad \text{(NN approximation)} \tag{3-60}$$

where $\Sigma(E')$ is the total cross section of the medium, cm^{-1}.

Neglecting Doppler broadening, the NN result for I_{eff} over a single resonance may be approximated by an integral over the entire energy spectrum to give:[202]

$$I_{eff} \approx \left[\frac{\pi}{2}\frac{\Sigma_p}{N_0}\frac{\Gamma\gamma}{E_0}\right] \Bigg/ \left[\Delta(1+\Delta-i)\right]^{1/2} \tag{3-61}$$

where

$$i \equiv g_J \frac{\Gamma_n}{\Gamma}\sigma_{p0}\frac{N_0}{\Sigma_p}$$

If $\Delta \gg 1 - i$, then

$$I_{eff} \approx I_\infty = \frac{\pi}{2}\sigma_0\,\Gamma_\gamma/E_0$$

where I_∞ is the infinite-dilution resonance integral discussed in Section 3.6.4.1.

If $p(E,E^*) \approx 1$, then

$$p(E,E^*) \approx \exp\left(-\frac{N_0}{\bar{\xi}\Sigma_p} I_{eff}(E,E^*)\right) \tag{3-62}$$

an approximation proposed initially by Wigner.

Modified Narrow Resonance (Mod. NN) Approximation. Spinney[248] modified the NN approximation for homogeneous mixtures of a heavy absorber, hydrogen, and other moderators, to treat neutron energy degradation by the absorber more accurately. This modification is of particular interest for a resonance narrow with respect to $(1-\alpha_j)E_0$ for $j > 0$, but so wide that a resonance-energy neutron may remain in the resonance region upon scattering by a heavy absorber atom (as is the situation for the low-lying resonances of U^{238}). In this formulation, the collision density within a narrow resonance is given approximately by:

$$F(E) \approx \frac{1}{\bar{\xi}E} \exp\left(-f\int_E^{E^*} \frac{\Sigma_a(E')}{\bar{\xi}\Sigma(E')}\frac{dE'}{E'}\right) \qquad \text{(Mod. NN approximation)} \tag{3-63}$$

where

$$f = \frac{\bar{\xi}}{1-\alpha_0}\left(1 - \frac{\Gamma}{\Gamma_\gamma}\sum_{j=0}^{k}\frac{\alpha_0-\alpha_j}{1-\alpha_j}\frac{\Sigma_{sj}}{\Sigma_p}\right) \tag{3-64}$$

$$\bar{\xi} = \frac{1}{\Sigma_p}\sum_{j=0}^{k}\xi_j\,\Sigma_{pj}$$

and α_0 is α for the heavy absorber atom.

The upper limit of integration, E^*, and the normalization of $F(E)$ were chosen so that $F(E) \approx 1/(\bar{\xi}E)$ for $E \geq E^*$.

The connection between the resonance escape probabilities in the NN and Mod. NN approximations is

$$1 - p\ (\text{Mod. NN}) = \frac{1}{f}\left[1 - \exp\left(-f\int_E^{E^*}\frac{\Sigma_a(E')}{\bar{\xi}\Sigma(E')}\frac{dE'}{E'}\right)\right] = \frac{1}{f}\left\{1 - [p(NN)]^f\right\} \tag{3-65}$$

Narrow Resonance Infinitely Heavy Absorber (NW) Approximations. The basis of the NW model is that the resonance is narrow relative to all moderating nuclides and that, effectively, neutron scatterings by the heavy absorber atoms do not result in a change of neutron energy. This model is most useful when $(1-\alpha_0)E_0 \ll \Gamma_p$, i.e, for resonances that are very wide in comparison with the energy loss suffered by resonance neutrons when scattered by absorber atoms. An example of this is the 6.68 ev resonance of U^{238}. Equations corresponding to Eqs. (3-59) and (3-60) may be obtained by deleting *all* scattering by the absorber atoms in the definition of $\bar{\xi}$ as well:

$$\left.\begin{aligned} p(E,E^*) &\approx 1 - \frac{N_0}{\bar{\xi}\Sigma_M} I_{eff}(E,E^*) \\ \text{where} \quad I_{eff}(E,E^*) &= \int_E^{E^*} \sigma_a(E')\frac{\Sigma_M}{\Sigma_a(E')+\Sigma_M}\frac{dE'}{E'} \end{aligned}\right\} \qquad \text{(NW approximation)} \tag{3-66}$$

Here $\Sigma_M \equiv$ macroscopic scattering cross section of the moderator, cm^{-1}.

As was done for Eq. (3-59), Eq. (3-66) was derived subject to the normalization of unit slowing-down-density past E^*.

Neglecting Doppler broadening effects, Chernick and Vernon[249] have obtained:

$$I_{eff}(-\infty,\infty) = I_\infty \Big/ \left[1 + \frac{\Sigma_0}{\Sigma_M}\frac{\Gamma_\gamma}{\Gamma}\right]^{1/2} \qquad \text{(NW approximation)} \tag{3-67}$$

It is to be noted that often it is the exponential formula that is identified as the "NW approximation" to the resonance escape probability, for $p(E,E^*) \approx 1$:

$$p(E,E^*) \approx \exp\left(-\frac{N_0}{\bar{\xi}(\Sigma_p - \Sigma_{p0})} I_{eff}(E,E^*)\right) \tag{3-68}$$

Chernick and Vernon[249] developed a "Modified NW" approximation by iterating once on the NW collision density, assuming that $\alpha_0 \approx 1$:

$$F^0(E) \approx \frac{\Sigma(E)}{\bar{\xi}E(\Sigma_a + \Sigma_M)} \tag{3-69}$$

to get

$$F^1(E) \approx \frac{1}{\bar{\xi}E} + \frac{1}{\bar{\xi}(1-\alpha_0)} \int_E^{E/\alpha_0} \frac{\Sigma_{s0}(E')}{\Sigma_a(E') + \Sigma_M} \frac{dE'}{(E')^2} \qquad \text{(Mod.NW)} \tag{3-70}$$

where $\Sigma_{s0}(E)$ is the total scattering cross section of the fuel in the medium, and $\bar{\xi}$ is an average with respect to moderator scatterings only. For an isolated Breit-Wigner resonance, with $g_J = 1$,

$$\bar{\xi}\,\Sigma_M\,E\,F^1(E) \approx \Sigma_p + \frac{\Sigma_{p0}}{G^2}\frac{\Gamma_n}{\Gamma}\left(1 - \frac{\Gamma_\gamma}{\Gamma_n}\frac{\Sigma_{p0}}{\Sigma_M}\right)\frac{1}{\epsilon}\left[\tan^{-1}(Z+\epsilon) - \tan^{-1} Z\right] \tag{3-71}$$

where

$$\epsilon \equiv \epsilon(E) = \frac{2(1-\alpha)E}{\alpha\Gamma G};\quad Z = \frac{2(E-E_0)}{\Gamma G};\quad G^2 = 1 + \frac{\Sigma_0}{\Sigma_M}\frac{\Gamma_\gamma}{\Gamma}$$

Neglecting Doppler broadening and scattering interference effects, the fractional change, $\Delta(1-p)$, in $(1-p)$ is:

$$\frac{\Delta(1-p)}{1-p(NW)} = \frac{\Gamma_n}{\Gamma}\frac{\Sigma_0}{\Sigma_p}\frac{1}{G^2}\left(1 - \frac{\Gamma_\gamma}{\Gamma_n}\frac{\Sigma_{p0}}{\Sigma_M}\right)\frac{1}{a(a+1)}\left\{\frac{a+1}{\epsilon(E_0)}\tan^{-1}\left[\frac{\epsilon(E_0)}{a+1}\right] - 1\right\} \tag{3-72}$$

where

$$a^2 = (1/G^2)\left[1 + (\Sigma_0/\Sigma_p)\right]$$

Spinney,[248] and Chernick and Vernon,[249] performed detailed computations of resonance absorption in homogeneous mixtures of hydrogen and U^{238}, using the various narrow resonance approximations described in the preceding paragraphs. These are discussed in Section 3.6.4.5.

3.6.4.3 Narrow Resonance Approximations Including Effects of Doppler Broadening and of Scattering Interference

To include the effects of the thermal motion of the resonance-absorber atoms, the Doppler-broadened line shape, $\Psi(\theta,x)$, is substituted for the natural line shape, and the effective resonance integral for a single narrow resonance becomes:

$$I_{eff} = \frac{\Sigma_p}{N_0}\frac{\Gamma_\gamma}{E_0}\int_0^\infty \frac{\Psi(\theta,x)}{\Delta + \Psi(\theta,x)}\,dx \tag{3-73}$$

The integral is designated as the function $J(\hat{\xi},\Delta)$, where $\hat{\xi} = 1/\sqrt{\theta}$. Values for $J(\hat{\xi},\Delta)$ are listed in Table 3-49. Blake[251] has published curves and tables, and Roe[252] has reported on analytical and numerical studies of the function:

$$f_H(\theta,\zeta) \equiv \frac{1}{\pi}\int_{-\infty}^\infty \frac{\Psi(\theta,x)}{1 + \zeta\Psi(\theta,x)}\,dx \tag{3-74}$$

Table 3-49 — THE INTEGRAL $J(\hat{\xi},\Delta) = \int_0^\infty \frac{\psi(\theta,x)}{\Delta + \psi(\theta,x)}\,dx$; $\hat{\xi} = 1/\sqrt{\theta}$

A. $J(\hat{\xi},\Delta)$; $\Delta = 2^k \times 10^{-5}$ *Data from Ref. 202.*

k	$\hat{\xi}$									
	0.1	0.2	0.3	0.4	0.5	0.6	0.7	0.8	0.9	1.0
0	4.979(2)[a]	4.970(2)	4.969(2)	4.968(2)	4.968(2)	4.968(2)	4.967(2)	4.967(2)	4.967(2)	4.967(2)
1	3.532	3.517	3.514	3.513	3.513	3.513	3.513	3.513	3.513	3.513
2	2.514	2.491	2.487	2.485	2.485	2.484	2.484	2.484	2.484	2.484
3	1.801	1.767	1.761	1.759	1.758	1.757	1.757	1.757	1.757	1.757
4	1.307	1.257	1.248	1.245	1.244	1.243	1.243	1.243	1.242	1.242
5	9.667(1)	8.993(1)	8.872(1)	8.831(1)	8.812(1)	8.802(1)	8.796(1)	8.792(1)	8.790(1)	8.788(1)
6	7.355	6.501	6.335	6.278	6.252	6.238	6.230	6.225	6.221	6.218
7	5.773	4.777	4.562	4.485	4.450	4.430	4.419	4.412	4.407	4.403
8	4.647	3.589	3.328	3.230	3.183	3.158	3.143	3.133	3.126	3.121
9	3.781	2.759	2.471	2.354	2.297	2.265	2.245	2.232	2.223	2.217
10	3.045	2.153	1.867	1.741	1.675	1.638	1.614	1.598	1.587	1.579
11	2.367	1.676	1.423	1.301	1.235	1.194	1.168	1.151	1.138	1.129
12	1.730	1.268	1.074	9.718(0)	9.119(0)	8.739(0)	8.484(0)	8.304(0)	8.174(0)	8.077(0)
13	1.164	9.081(0)	7.815(0)	7.087	6.629	6.322	6.107	5.950	5.833	5.744
14	7.172(0)	6.014	5.342	4.914	4.624	4.419	4.268	4.154	4.066	3.997
15	4.088	3.658	3.371	3.169	3.022	2.911	2.826	2.759	2.706	2.663
16	2.204	2.067	1.966	1.889	1.829	1.781	1.743	1.712	1.687	1.666
17	1.148	1.109	1.078	1.053	1.033	1.016	1.002	9.904(−1)	9.805(−1)	9.722(−1)
18	5.862(−1)	5.757(−1)	5.671(−1)	5.599(−1)	5.539(−1)	5.488(−1)	5.445(−1)	5.408	5.376	5.348
19	2.963	2.936	2.913	2.894	2.877	2.863	2.851	2.840	2.831	2.823
20	1.490	1.483	1.477	1.472	1.468	1.464	1.461	1.458	1.455	1.453
21	7.468(−2)	7.452(−2)	7.437(−2)	7.424(−2)	7.413(−2)	7.403(−2)	7.395(−2)	7.388(−2)	7.381(−2)	7.375(−2)
22	3.739	3.735	3.732	3.728	3.726	3.723	3.721	3.719	3.718	3.716
23	1.871	1.870	1.869	1.868	1.868	1.867	1.867	1.866	1.866	1.865
24	9.358(−3)	9.356(−3)	9.355(−3)	9.352(−3)	9.350(−3)	9.349(−3)	9.348(−3)	9.346(−3)	9.345(−3)	9.344(−3)
25	4.680	4.680	4.679	4.679	4.678	4.678	4.678	4.677	4.677	4.677
26	2.340	2.340	2.340	2.340	2.340	2.340	2.340	2.340	2.340	2.340
27	1.170	1.170	1.170	1.170	1.170	1.170	1.170	1.170	1.170	1.170
28	5.851(−4)	5.851(−4)	5.851(−4)	5.851(−4)	5.851(−4)	5.851(−4)	5.851(−4)	5.851(−4)	5.851(−4)	5.851(−4)
29	2.925	2.926	2.926	2.926	2.926	2.926	2.926	2.926	2.926	2.926
30	1.463	1.463	1.463	1.463	1.463	1.463	1.463	1.463	1.463	1.463
31	7.314(−5)	7.314(−5)	7.315(−5)	7.315(−5)	7.315(−5)	7.315(−5)	7.314(−5)	7.314(−5)	7.314(−5)	7.314(−5)

B. $J(\hat{\xi},k)$; $\Delta = 2^k$ *Data from Ref. 250.*

k	$\hat{\xi}$													
	0.02	0.03	0.04	0.05	0.10	0.15	0.20	0.25	0.30	0.35	0.40	0.45	0.50	∞
4.0	2.386(2)	1.856(2)	1.613(2)	1.501(2)	1.307(2)	1.269(2)	1.257(2)	1.251(2)	1.248(2)	1.246(2)	1.245(2)	1.245(2)	1.244(2)	1.242(2)
4.5	2.229	1.704	1.455	1.335	1.120	1.077	1.062	1.055	1.052	1.050	1.048	1.048	1.047	1.044
5.0	2.086	1.573	1.324	1.198	9.667(1)	9.168(1)	8.993(1)	8.914(1)	8.872(1)	8.817(1)	8.831(1)	8.820(1)	8.812(1)	8.780(1)
5.5	1.951	1.459	1.212	1.083	8.400	7.836	7.634	7.541	7.491	7.462	7.443	7.430	7.421	7.382
6.0	1.821	1.355	1.116	9.863(1)	7.355	6.733	6.501	6.393	6.335	6.301	6.278	6.263	6.252	6.207
6.5	1.692	1.257	1.030	9.022	6.491	5.819	5.559	5.436	5.369	5.328	5.302	5.284	5.272	5.219
7.0	1.563	1.164	9.508(1)	8.273	5.772	5.063	4.777	4.636	4.562	4.515	4.485	4.464	4.450	4.388
7.5	1.431	1.073	8.761	7.588	5.166	4.436	4.128	3.975	3.889	3.836	3.801	3.777	3.760	3.689
8.0	1.296	9.809(1)	8.036	6.944	4.647	3.911	3.589	3.423	3.328	3.269	3.230	3.203	3.183	3.101
8.5	1.158	8.881	7.319	6.323	4.191	3.468	3.139	2.964	2.861	2.796	2.753	2.722	2.701	2.606
9.0	1.018	7.940	6.600	5.713	3.781	3.088	2.759	2.579	2.471	2.401	2.354	2.321	2.297	2.190
9.5	8.771(1)	6.988	5.876	5.107	3.403	2.754	2.435	2.255	2.144	2.071	2.021	1.985	1.959	1.839
10.0	7.399	6.037	5.150	4.504	3.045	2.454	2.153	1.977	1.867	1.792	1.741	1.703	1.675	1.544
10.5	6.099	5.107	4.429	3.907	2.701	2.179	1.903	1.737	1.629	1.556	1.504	1.466	1.437	1.296
11.0	4.909	4.223	3.730	3.325	2.367	1.921	1.676	1.523	1.423	1.352	1.301	1.264	1.235	1.087
11.5	3.861	3.411	3.070	2.770	2.043	1.676	1.466	1.331	1.239	1.174	1.126	1.090	1.062	9.099(0)
12.0	2.973	2.691	2.468	2.257	1.731	1.442	1.268	1.154	1.074	1.015	9.718(0)	9.382(0)	9.119(0)	7.607
12.5	2.246	2.078	1.939	1.797	1.436	1.219	1.083	9.888(0)	9.217(0)	8.718(0)	8.337	8.039	7.802	6.345
13.0	1.671	1.574	1.491	1.400	1.165	1.011	9.082(0)	8.352	7.815	7.406	7.087	6.834	6.629	5.276
13.5	1.227	1.174	1.126	1.070	9.240(0)	8.199(0)	7.470	6.930	6.521	6.202	5.948	5.743	5.574	4.369
14.0	8.922(0)	8.634(0)	8.370(0)	8.033(0)	7.173	6.507	6.015	5.637	5.342	5.106	4.914	4.756	4.624	3.597
14.5	6.439	6.286	6.145	5.946	5.461	5.056	4.740	4.489	4.287	4.122	3.985	3.870	3.773	2.940
15.0	4.620	4.541	4.467	4.351	4.088	3.853	3.659	3.501	3.371	3.261	3.169	3.090	3.022	2.381
15.5	3.302	3.261	3.223	3.155	3.018	2.887	2.773	2.678	2.598	2.529	2.470	2.418	2.373	1.907
16.0	2.352	2.332	2.312	2.272	2.204	2.133	2.068	2.013	1.966	1.925	1.889	1.857	1.829	1.508
16.5	1.673	1.662	1.652	1.628	1.596	1.558	1.522	1.492	1.465	1.441	1.420	1.402	1.385	1.175
17.0	1.187	1.182	1.177	1.162	1.148	1.129	1.109	1.092	1.078	1.065	1.053	1.042	1.033	9.026(−1)
17.5	8.419(−1)	8.393(−1)	8.369(−1)	8.276(−1)	8.217(−1)	8.122(−1)	8.017(−1)	7.927(−1)	7.849(−1)	7.778(−1)	7.713(−1)	7.655(−1)	7.601(−1)	6.830
18.0	5.964	5.952	5.940	5.881	5.862	5.817	5.760	5.712	5.671	5.633	5.599	5.567	5.539	5.098
18.5	4.223	4.217	4.212	4.173	4.171	4.150	4.120	4.095	4.073	4.054	4.036	4.019	4.004	3.760
19.0	2.989	2.986	2.984	2.958	2.963	2.954	2.937	2.924	2.913	2.903	2.894	2.885	2.877	2.746
19.5	2.115	2.114	2.113	2.095	2.102	2.098	2.089	2.082	2.077	2.071	2.067	2.062	2.058	1.989
20.0	1.496	1.496	1.495	1.483	1.490	1.489	1.483	1.480	1.477	1.474	1.472	1.470	1.468	1.431

[a] Numbers in parentheses are powers of 10 which multiply the entry next to which they stand and all unmarked entries below it.

Figure 3-51 is a useful graphical representation of the behavior of $f_H(\theta,\zeta)$. Note that

$$J(\hat{\xi},\Delta) = \frac{\pi}{2\Delta} f_H\left(\theta,\frac{1}{\Delta}\right)$$

When the effects of the interference between the potential scattering and the resonance scattering of the absorber atoms are included:

$$I_{eff} = \frac{\Sigma_p}{N_0}\frac{\Gamma_\gamma}{E_0} J(\hat{\xi},\Delta) + \frac{1}{2} g_J \frac{\Gamma_n}{\Gamma}\frac{\Gamma_\gamma}{E_0}\frac{\sigma_{p0}}{\Delta^2}\frac{\pi}{4[\Delta(1+\Delta)]^{1/2}} f(\theta,\Delta) \qquad \text{(NN)} \qquad (3\text{-}75)$$

The notation is defined in Sections 3.6.4 and 3.6.4.2. The function $\Psi(\theta,x)$ is discussed in Section 3.6.4.

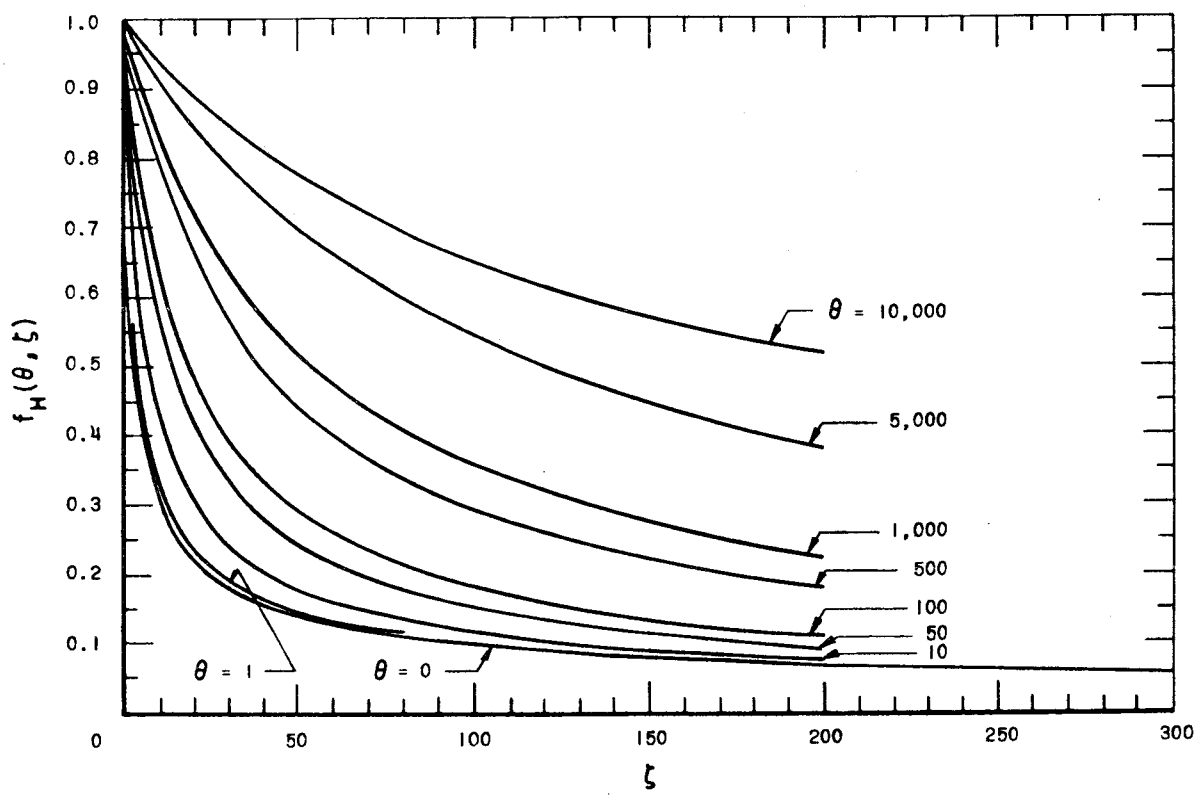

Fig. 3-51 — The function: $f_H(\theta,\zeta) = \frac{1}{\pi}\int_{-\infty}^{\infty}\{\psi(\theta,x)/[1+\zeta\psi(\theta,x)]\}dx$. *Reproduced from Ref. 251.*

The second term on the right-hand side of Eq. (3-75) represents the contribution of scattering-interference effects to the effective resonance integral. The function $f(\theta,\Delta)$ is the integral:[253]

$$f(\theta,\Delta) \equiv \frac{4}{\pi}[\Delta(1+\Delta)]^{1/2}\int_{-\infty}^{\infty}\frac{\Psi(\theta,x)\chi^2(\theta,x)}{[\Delta+\Psi(\theta,x)]^3}dx \qquad (3\text{-}76)$$

Rothenstein[253] has published graphs of $f(\theta,R)$, where $\Delta = 2^R \times 10^{-5}$; these are reproduced as Fig. 3-52.

3.6.4.4 Effective Resonance Integrals (NN) in Mixtures of Moderators and Either U^{238} or Th^{232}

Using Eq. (3-73) for each of the resolved resonances tabulated in BNL-325, Dresner[254] calculated the effective resonance integrals of U^{238} and Th^{232} for several values of σ_p. The formula:

$$I' = \sigma_p \frac{\Gamma_\gamma}{D}\int_{\Delta_1}^{\infty} J(\hat{\xi},\Delta)\frac{d\Delta}{\Delta} \qquad (3\text{-}77)$$

was used to determine the contribution (I′) of the unresolved, high-energy resonances. In Eq. (3-77),

D = average spacing of the resonances, ev

and

$$\Delta_1 \equiv \frac{\sigma_p}{\sigma_0} \text{ for the resolved resonance of highest energy } E_0$$

Dresner assumed that Γ_γ is constant, and that $\Gamma_n \gg \Gamma_\gamma$ in the vicinity of the highest E_0 of the resolved resonances. In this range, a constant value of $\xi = 0.1$ was used, both for U^{238} and for Th^{232}. (Note that Doppler broadening has been included, but not scattering interference effects.) The results are presented in Table 3-50.

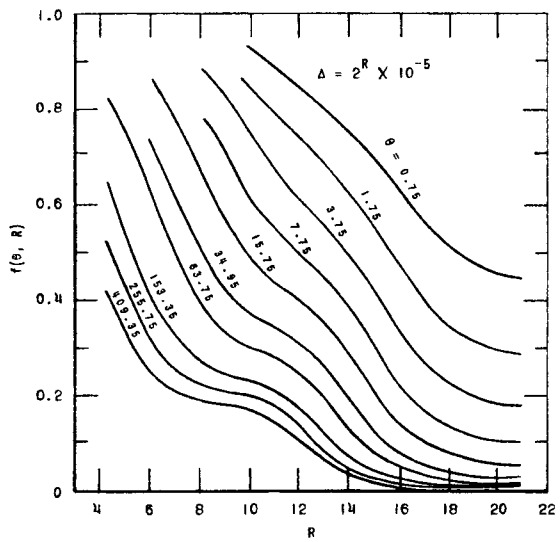

Fig. 3-52 — The function: $f(\theta,R) = \frac{4}{\pi}[\Delta(1+\Delta)]^{3/2} \times \int_{-\infty}^{\infty} \frac{\psi(\theta,x)\chi^2(\theta,x)}{[\Delta+\psi(\theta,x)]^3}\,dx$. *Reproduced from Ref. 253.*

Table 3-50 — CALCULATED EFFECTIVE RESONANCE INTEGRALS OF U^{238} AND Th^{232} IN HOMOGENEOUS MIXTURES[a]

Data from Ref. 254.

Fertile Material	Temp., °K	Potential Scattering per Atom of Fertile Material, σ_p, barn	Contribution of Resolved Resonances, barn	Contribution of Unresolved Resonances, barn	Sum [not including (1/v) Contribution], barn	(1/v) Contribution, barn
U^{238}	0	20	7.9	1.7	9.6	1.4
		200	24	4.8	28.8	1.4
		2000	74	11	85	1.4
	300	20	8.1	3.0	11.1	1.4
		80	17	6.6	23.6	1.4
		200	27	9.4	36.4	1.4
		2000	86	12	98	1.4
Th^{232}	0	20	3.7	2.2	5.9	3.5
		200	12	6.3	18.3	3.5
		2000	33	14	47	3.5
	300	20	4.0	4.0	8.0	3.5
		80	8.9	8.6	17.5	3.5
		200	15	12	27	3.5
		2000	42	20	62	3.5

[a]The interference effects between resonance scattering and potential scattering by the fertile material are not included.

Blake[251] published similar tables (Tables 3-51 and 3-52) for homogeneous mixtures of U^{238} (or Th^{232}) and moderators with energy-independent scattering cross sections. In his treatment, only s-wave captures were included; no correction was made for the statistical variation of the reduced

Table 3-51 — EFFECTIVE RESONANCE INTEGRAL, I_{eff} (NN), FOR HOMOGENEOUS MIXTURES OF U^{238} AND MODERATOR (barns)

Data from Ref. 251.

Temp., °K	$\sigma_p = 5$	10	20	30	40	50	100	200	300	400	600	800	1000	1500	2000	2500	3000	4000	5000	10,000	100,000
0	5.70	7.55	10.13	12.08	13.7	15.15	20.71	28.41	34.21	39.01	46.90	53.38	58.98	70.50	79.80	87.70	94.59	106.26	115.94	148.75	242.37
300	6.15	8.34	11.45	13.85	15.86	17.63	24.52	34.17	41.55	47.77	58.22	67.00	74.68	90.68	103.63	114.52	123.88	139.28	151.55	188.78	258.29
400	6.22	8.47	11.66	14.11	16.18	17.99	25.08	35.06	42.74	49.24	60.19	69.41	77.47	94.23	107.72	119.00	128.64	144.37	156.78	193.72	259.48
500	6.29	8.58	11.84	14.34	16.45	18.31	25.57	35.84	43.78	50.53	61.93	71.53	79.91	97.30	111.23	122.80	132.64	148.60	161.07	197.64	260.37
600	6.35	8.68	12.00	14.55	16.70	18.59	26.00	36.54	44.73	51.70	63.50	73.43	82.10	100.03	114.31	126.11	136.11	152.21	164.72	200.88	261.06
700	6.40	8.77	12.14	14.73	16.92	18.84	26.39	37.18	45.60	52.78	64.93	75.17	84.10	102.48	117.06	129.06	139.17	155.38	167.88	203.62	261.63
800	6.45	8.85	12.27	14.90	17.12	19.07	26.76	37.78	46.40	53.78	66.27	76.78	85.93	104.72	119.55	131.71	141.91	158.19	170.67	206.00	262.10
1000	6.55	9.00	12.50	15.20	17.48	19.49	27.42	38.86	47.88	55.60	68.69	79.68	89.22	108.70	123.94	136.33	146.67	163.01	175.42	209.95	262.85
1200	6.63	9.13	12.71	15.47	17.80	19.86	28.00	39.84	49.20	57.24	70.85	82.25	92.12	112.16	127.72	140.28	150.70	167.05	179.36	213.15	263.44
1400	6.70	9.25	12.90	15.71	18.09	20.19	28.54	40.74	50.42	58.74	72.81	84.58	94.73	115.16	130.96	143.65	154.11	170.43	182.63	215.72	263.81
1600	6.76	9.35	13.06	15.91	18.33	20.47	29.00	41.52	51.49	60.06	74.55	86.63	97.03	117.93	133.93	146.71	157.19	173.46	185.55	217.99	264.20
1800	6.83	9.46	13.21	16.12	18.58	20.76	29.46	42.30	52.54	61.35	76.22	88.60	99.21	120.45	136.62	149.46	159.96	176.15	188.13	219.96	264.53
2000	6.88	9.55	13.36	16.31	18.81	21.02	29.89	43.03	53.53	62.56	77.79	90.42	101.23	122.76	139.07	151.96	162.45	178.57	190.43	221.70	264.81
2500	7.02	9.76	13.69	16.73	19.32	21.62	30.88	44.70	55.79	65.31	81.31	94.51	105.72	127.85	144.40	157.35	167.80	183.70	195.28	225.29	265.38
3000	7.13	9.95	13.98	17.11	19.78	22.15	31.76	46.20	57.81	67.76	84.41	98.07	109.60	132.17	148.87	161.82	172.21	187.88	199.19	228.11	265.81

Note: $\sigma_p \equiv$ total potential scattering cross section per atom of U^{238}, $\Sigma_p/N^{U^{238}}$ (barns). I_{eff} includes 1/v capture above 0.4 ev. Approximately, this contribution is:

$$2\frac{\Sigma_p}{N^{U^{238}}}\log\left[1+\frac{\sigma_{a(1/v)}^{U^{238}}\ (0.4\text{ ev})}{\Sigma_p/N^{U^{238}}}\right]$$

Table 3-52 — EFFECTIVE RESONANCE INTEGRAL, I_{eff} (NN), FOR HOMOGENEOUS MIXTURES OF Th^{232} AND MODERATOR (barns)

Data from Ref. 251.

Temp., °K	$\sigma_p = 5$	10	20	30	40	50	100	200	300	400	600	800	1000	1500	2000	2500	3000	4000	5000	10,000	100,000
0	6.36	7.91	9.86	11.27	12.44	13.45	17.29	22.47	26.26	29.34	34.26	38.17	41.45	47.91	52.83	56.80	60.12	65.41	69.50	81.49	103.49
300	6.92	8.89	11.56	13.59	15.30	16.81	22.65	30.60	36.32	40.86	47.86	53.16	57.41	65.24	70.73	74.85	78.08	82.88	86.29	94.89	106.12
400	7.02	9.06	11.85	13.98	15.77	17.35	23.48	31.79	37.75	42.44	49.63	55.04	59.34	67.20	72.65	76.70	79.87	84.52	87.79	95.94	106.27
500	7.10	9.21	12.10	14.31	16.18	17.82	24.19	32.80	38.94	43.76	51.09	56.58	60.91	68.78	74.18	78.17	81.27	85.79	88.95	96.73	106.39
600	7.18	9.35	12.32	14.61	16.54	18.23	24.82	33.69	39.98	44.90	52.35	57.88	62.24	70.09	75.45	79.38	82.42	86.83	89.89	97.36	106.48
700	7.25	9.47	12.53	14.88	16.86	18.61	25.39	34.48	40.90	45.90	53.44	59.02	63.39	71.23	76.53	80.41	83.39	87.69	90.67	97.88	106.55
800	7.32	9.58	12.71	15.12	17.16	18.96	25.90	35.19	41.73	46.80	54.42	60.03	64.41	72.22	77.47	81.30	84.23	88.44	91.35	98.32	106.61
1000	7.43	9.78	13.05	15.57	17.70	19.57	26.82	36.45	43.17	48.36	56.11	61.76	66.14	73.89	79.05	82.78	85.62	89.67	92.44	99.03	106.71
1200	7.54	9.97	13.35	15.97	18.17	20.12	27.62	37.53	44.41	49.70	57.53	63.20	67.58	75.27	80.34	83.98	86.74	90.65	93.32	99.59	106.78
1400	7.64	10.13	13.63	16.32	18.60	20.61	28.33	38.49	45.50	50.86	58.76	64.45	68.82	76.43	81.42	84.98	87.67	91.47	94.03	100.04	106.84
1600	7.73	10.28	13.88	16.65	19.00	21.06	28.98	39.35	46.48	51.90	59.85	65.54	69.90	77.44	82.35	85.84	88.46	92.16	94.64	100.42	106.89
1800	7.81	10.43	14.11	16.95	19.36	21.47	29.57	40.14	47.36	52.83	60.82	66.52	70.85	78.33	83.17	86.59	89.16	92.75	95.17	100.74	106.93
2000	7.89	10.56	14.32	17.24	19.70	21.85	30.12	40.86	48.17	53.68	61.70	67.39	71.71	79.12	83.89	87.26	89.77	93.28	95.62	101.02	106.96
2500	8.07	10.86	14.81	17.87	20.45	22.72	31.34	42.45	49.92	55.52	63.59	69.27	73.53	80.79	85.40	88.63	91.02	94.35	96.56	101.58	107.03
3000	8.23	11.13	15.25	18.43	21.12	23.47	32.40	43.80	51.41	57.07	65.16	70.81	75.02	82.13	86.61	89.72	92.02	95.19	97.29	102.02	107.08

Note: $\sigma_p \equiv$ total potential scattering cross section per atom of Th^{232}, $\Sigma_p/N^{Th^{232}}$ (barns). I_{eff} includes 1/v capture above 0.4 ev. Approximately, this contribution is:

$$2\frac{\Sigma_p}{N^{Th^{232}}}\log\left[1+\frac{\sigma_{a(1/v)}^{Th^{232}}\ (0.4\text{ ev})}{\Sigma_p/N^{Th^{232}}}\right]$$

neutron width in the region of unresolved resonances; and interference between resonances and between resonance and potential scattering was neglected. The contributions from the individual resonances were computed, using Eq. (3-73), over 27 resolved resonances of U^{238} and 18 resolved resonances of Th^{232}. The parameters of 27 resolved resonances in U^{238} were taken largely from BNL-325, Second Edition.

The contribution (I_2) from the region of unresolved resonances ($E > \hat{E}$) was determined from the equation:

$$I_2 = \frac{\pi}{2}\frac{\Gamma_\gamma}{D}\frac{\Sigma_p}{N_0}\int_{\hat{E}}^{2\ \mathrm{Mev}} \zeta'(E)\, f_H(\theta',\xi')\frac{dE}{E} \tag{3-78}$$

assuming

Γ_γ = constant, ev

$\Gamma_n(E) = \Gamma_{n0}\sqrt{E}$; $\Gamma(E) = \Gamma_\gamma + \Gamma_n(E)$, ev

D = average resonance spacing, ev

Using the notation of Section 3.6.4,

$$\Delta = \frac{\Gamma_\gamma}{\Gamma_{n0}};\quad \theta' = \left(\frac{4E}{\Gamma^2}\right)\left(\frac{m}{M}kT\right)$$

$$\zeta'(E) = \left(\frac{2\pi\hbar^2}{m\frac{\Sigma_p}{N_0}}\right)\left(\frac{1}{(\Delta+\sqrt{E})\sqrt{E}}\right)$$

The values assigned to these parameters for Blake's computations are:

Γ_γ: 0.025 ev (U^{238}); 0.035 ev (Th^{232})

Γ_{n0}: 0.00175 ev (U^{238}); 0.00197 ev (Th^{232})

D: 20.1 ev (U^{238}); 16.9 ev (Th^{232})

Brooks and Tralli[255] computed the effective resonance integral in media containing U^{238}, and published curves for I_{eff} over individual resolved resonances up to and including E_0 = 530 ev. The calculations were on the basis of the NN or the NW model, depending upon the magnitude of

$$\frac{\Gamma_p}{[1-\alpha(U^{238})]E_0}$$

Doppler broadening, with kT = 0.025 ev, was included.

Bell[256] published some results to indicate the importance of including the effect of scattering interference for resonances where the practical width is relatively large and where $\Gamma_n \gtrsim \Gamma_\gamma$. Table 3-53 lists results of numerical calculations for an unbroadened U^{238} resonance, with E_0 = 103.5 ev, and with varying amounts of hydrogen scattering. Bell observed that Doppler broadening tends to decrease the effect of interference, and thus interference scattering provides a contribution to the temperature coefficient diminishing the effect of Doppler broadening.

3.6.4.5 Numerical Comparisons of NN, Modified NN, NW, and Modified NW Approximations with Exact Calculations for U^{238}-H Mixtures

The NN, Modified NN, and NW formulas for the resonance escape probability for isolated, narrow resonances have been tested against exact numerical calculations by Spinney.[248] Computations were made for individual resonances of U^{238} in homogeneous media of U^{238} and hydrogen.

In Table 3-54, resonance absorption probabilities are listed for H/U^{238} atomic ratios of 1 and 10. The cross sections were not corrected for Doppler broadening or for scattering-interference effects, and it was possible to perform the integrations analytically. The microscopic potential scattering

Table 3-53 — CAPTURE PROBABILITY IN THE 103.5-ev U^{238} RESONANCE[a]

Data from Ref. 256.

Σ_s^H/N_0, barn	Capture Probability		Ratio
	Interference Neglected	Interference Included	
10	0.0265	0.0358	1.35
20	0.0176	0.0224	1.27
40	0.0116	0.0143	1.21
80	0.00766	0.00883	1.15
200	0.00444	0.00485	1.09
800	0.00197	0.00205	1.04
2000	0.00115	0.00118	1.02

[a]The integration was carried out over the range 73 ev to 147 ev. $\Gamma_\gamma = 0.025$ ev; $\sigma_{p0} = 10$ barns; and the subscript "zero" refers to U^{238}.

cross sections were assumed to be 20 barns for H and 10 barns for U^{238}. Table 3-54 includes the results of Modified NW calculations by Chernick and Vernon[249] for the case of unit H/U^{238} ratio.

Additional comparisons for stationary fuel atoms (Table 3-55) indicate the magnitude of the error in terminating the computation at one practical width (Γ_p) around E_0. Spinney[248] notes that the neglect of absorption in the "wings" of the resonance probably leads to larger errors than are inherent in the NN approximation.

Similar computations, including the Doppler broadening effect for a moderator kT = 0.025 ev, are summarized in Table 3-56. The column labeled "exact" refers to detailed numerical solutions of the

Table 3-54 — RESONANCE ABSORPTION PROBABILITIES FOR SINGLE BREIT-WIGNER RESONANCES: HOMOGENEOUS MIXTURES OF H AND U^{238}

(Integrations Over Entire Energy Range)

Data from Refs. 248 and 249.

E_0, ev	H/U atom ratio = 1				H/U atom ratio = 10		
	NN	Mod. NN	NW	Mod. NW	NN	Mod. NN	NW
6.7	0.2104	0.07708	0.1806	—	0.06071	0.06215	0.06102
21.0	0.08780	0.07539	0.08401	—	0.02406	0.02955	0.02728
36.9	0.05625	0.11065	0.06946	—	0.01522	0.02654	0.02240
66.3	0.02236	0.02613	0.02595	0.0253	0.005961	0.006967	0.008183
81.3	0.006521	0.006300	0.005562	0.00627	0.001672	0.001675	0.001697
90	0.001137	0.001129	0.000968	0.00113	0.0002019	0.0002020	0.0002004
103.5	0.01390	0.02135	0.02174	0.0202	0.003691	0.004840	0.006807
117.5	0.008259	0.008361	0.008563	0.00840	0.002177	0.002248	0.002670
146	0.001782	0.001763	0.001498	0.00177	0.000419	0.0004189	0.000417
166	0.002976	0.002938	0.002632	0.00294	0.000761	0.000762	0.000796
192	0.005957	0.009141	0.01245	0.01043	0.001573	0.002006	0.003768
212	0.004684	0.005283	0.007058	—	0.001257	0.001362	0.002163
242	0.003842	0.004239	0.005788	—	0.001010	0.001077	0.001765
258	0.000900	0.000895	0.000763	—	0.000206	0.0002064	0.000207
278	0.002913	0.003041	0.003842	—	0.000763	0.000787	0.001170
297	0.002638	0.002743	0.003479	—	0.000690	0.000710	0.001057
368	0.002234	0.002574	0.004520	—	0.000585	0.000635	0.001315
418	0.001717	0.001827	0.002867	—	0.000446	0.000463	0.000841

Note: $\Gamma_\gamma = 0.025$ ev was assumed for all resonances. No corrections were made for Doppler broadening or for interference between resonance scattering and potential scattering.

687863 O - 63 - 13

Table 3-55 — RESONANCE ABSORPTION PROBABILITIES FOR SINGLE BREIT-WIGNER RESONANCES: HOMOGENEOUS MIXTURES OF H AND U^{238}

(Integrations Over One Practical Width Around E_0)

Data from Ref. 248.

E_0, ev	H/U Atom Ratio = 1			H/U Atom Ratio = 10		
	NN	Mod. NN	NW	NN	Mod. NN	NW
6.7	0.1775	0.07416	0.1468	0.05676	0.05799	0.05706
21.0	0.07281	0.06417	0.06892	0.02242	0.02715	0.02565
36.9	0.04651	0.08037	0.05974	0.01418	0.02371	0.02137
66.3	0.01840	0.02090	0.02196	0.005548	0.006412	0.007770
81.3	0.005333	0.005185	0.004399	0.001551	0.001553	0.001577
90	0.000901	0.000896	0.000734	0.000178	0.000178	0.000176
103.5	0.01142	0.01620	0.01924	0.003435	0.004419	0.006551
117.5	0.006783	0.006851	0.007079	0.002024	0.002086	0.002518
146	0.001454	0.001442	0.001172	0.000385	0.000385	0.000383
166	0.002439	0.002414	0.002097	0.000705	0.000706	0.000741
192	0.004893	0.006928	0.01137	0.001464	0.001834	0.003658
212	0.003846	0.004244	0.006206	0.001169	0.001259	0.002077
242	0.003154	0.003419	0.005088	0.000939	0.000997	0.001694
258	0.000733	0.000730	0.000597	0.000189	0.000189	0.000190
278	0.002391	0.002477	0.003315	0.000709	0.000730	0.001116
297	0.002165	0.002235	0.002999	0.000671	0.000690	0.001008
368	0.001833	0.002058	0.004110	0.000544	0.000587	0.001274
418	0.001409	0.001482	0.002552	0.000426	0.000442	0.000832

Note: $\Gamma_\gamma = 0.025$ ev was assumed for all resonances. No corrections were made for Doppler broadening or for interference between resonance scattering and potential scattering.

integral equation for the collision density. A measure of the accuracy of the NN approximation for a given isolated resonance in a U^{238}-H mixture is afforded (Fig. 3-53) by graphing $(1\text{-}p)_{NN}/(1\text{-}p)_{exact}$ as a function of the parameter y tabulated in Table 3-56:

$$y = \frac{\Gamma_p}{[1 - \alpha(U^{238})]\, E_0}\left(\frac{\Gamma_n}{\Gamma} - \frac{\Sigma_{p0}}{\Sigma_p}\right)$$

The critical value of Γ_n/Γ is essentially Σ_{p0}/Σ_p. The NN approximation underestimates the actual absorption when $(\Gamma_n/\Gamma) > (\Sigma_{p0}/\Sigma_p)$; similarly, the absorption predicted by NW is greater (or less) than that predicted by NN according to whether Γ_n/Γ is greater (or less) than Σ_{p0}/Σ_p.

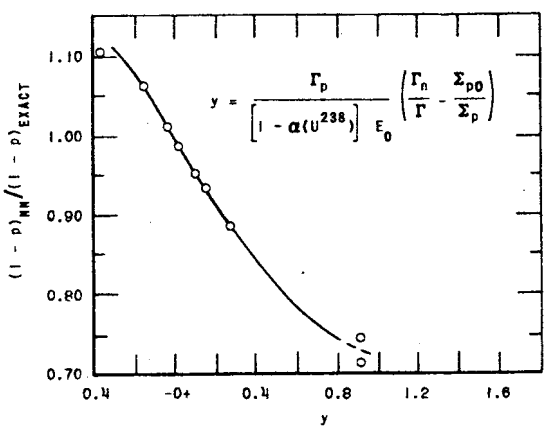

Fig. 3-53 — Relative error of resonance capture in the NN approximation as a function of the parameter y. *Reproduced from Ref. 248.*

Table 3-56—RESONANCE ABSORPTION AND ESCAPE PROBABILITIES FOR SINGLE BREIT-WIGNER RESONANCES: HOMOGENEOUS MIXTURE WITH UNIT ATOMIC RATIO H to U^{238}

Data from Ref. 248.

E_0, ev	$\frac{\Gamma_a}{\Gamma}$	$\frac{\Gamma_p\ (kT = 0.025\ ev)}{[1-\alpha(U^{238})]E_0}$	Probability for Resonance Absorption				y	Probability for Resonance Escape			
			EXACT	NN	Modified NN	NW		p(EXACT)	p(NN)	p(Mod. NN)	p(NW)
6.7	0.057	11.28	—	—	—	—	−3.06	(0.84707)	0.81429	0.84707	0.84707
21.0	0.263	5.57	0.06755	0.07455 +10.4%	0.06551 −3.0%	0.07059 +4.5%	−0.361	0.93245	0.92545	0.93449	0.92941
36.9	0.565	5.93	0.05820	0.04739 −18.6%	0.08295 +42.5%	0.06110 +5.0%	1.408	0.94180	0.95261	0.93890	0.93890
66.3	0.500	2.05	—	—	—	—	0.352	(0.97720)	0.98044	0.97759	0.97643
81.3	0.078	0.56	0.009596	0.010163 +5.9%	0.009632 +0.38%	0.008109 −15.5%	−0.140	0.99040	0.98984	0.99037	0.99189
90	0.0036	0.086	0.001104	0.001114 +0.91%	0.001106 +0.18%	0.000998 −9.6%	−0.0281	0.99890	0.99887	0.99889	0.99900
103.5	0.728	2.31	0.01593	0.01182 −25.8%	0.01698 +6.6%	0.02044 +28.3%	0.924	0.98407	0.98818	0.98302	0.97956
117.5	0.375	0.67	0.009170	0.009035 −1.5%	0.009157 −0.14%	0.009500 +3.6%	0.0319	0.99083	0.99097	0.99084	0.99050
146	0.035	0.28	—	—	—	—	−0.0818	(0.99624)	0.99611	0.99620	0.99678
166	0.138	0.35	—	—	—	—	−0.0672	(0.99451)	0.99436	0.99450	0.99525
192	0.848	1.77	0.007119	0.005068 −28.6%	0.007274 +2.2%	0.01228 +73%	0.920	0.99288	0.99493	0.99273	0.98772
212	0.706	0.74	0.005021	0.004440 −11.6%	0.004976 −0.9%	0.007689 +53%	0.282	0.99498	0.99556	0.99502	0.99231
242	0.706	0.62	—	—	—	—	0.234	(0.99590)	0.99630	0.99594	0.99352
258	0.049	0.17	—	—	—	—	−0.0486	(0.99789)	0.99785	0.99787	0.99814
278	0.615	0.40	0.003495	0.003318 −5.1%	0.003485 −0.29%	0.004936 +41%	0.116	0.99651	0.99668	0.99652	0.99506
297	0.615	0.37	—	—	—	—	0.107	(0.99681)	0.99696	0.99682	0.99571
368	0.839	0.64	—	—	—	—	0.326	(0.99767)	0.99798	0.99771	0.99494
418	0.762	0.37	0.001950	0.001816 −6.9%	0.001939 −0.56%	0.003855 +98%	0.160	0.99805	0.99818	0.99806	0.99615

Notes: (1) $\Gamma_\gamma = 0.025$ ev was assumed for all resonances.
(2) No correction was made for scattering interferences.
(3) Individual resonances were computed with Doppler-broadened cross sections (kT = 0.025 ev). Integrations were performed over one practical width (Γ_p) around E_0.
(4) Percentages stated give the deviation from the exact result.

3.6.4.6 Methods of Computing Effective Resonance Integrals Over Isolated Resonances When First-Order Narrow Resonance Approximations are Unreliable

Increasing attention is being paid to computations of absorption in resonances which do not fall into the category of NN or NW. This breakdown occurs even for heavy absorbers such as bismuth,[257] and, for certain resonances, U^{238}.

Various methods have been applied; some are described earlier in this section. Spinney[248] first solved for the collision density in the energy range from an energy E_1 above the resonance down to $\alpha(U^{238})E_1$. The function $(E')^{\kappa-1}$ appearing as a factor in an integrand in this solution was replaced by its first-order expansion around the lower limit, E, of the integral, permitting the continuation of the solution to lower energies. This is the basis of the Modified NN formula.

Chernick and Vernon[249] substituted the NW solution for the collision density in the source term of the integral equation to obtain the next-order approximation for the collision density, yielding the Modified NW results.

Rothenstein and Chernick[257] suggested a perturbation method to be applied to lattices of absorbing lumps in non-absorbing moderators. The deviation of the collision density from its asymptotic 1/E form is expanded in inverse powers of $(E-E_0)$, and the expansion is cut off after a few terms. Then the integral equation for the collision density perturbation is solved numerically at lower energies. This procedure should be useful for homogeneous mixtures, as well.

Bell[258] suggested a Neumann series solution for the collision density, and showed how Spinney's Modified NN result may be obtained as a first-order iterate. Spinrad, et al.,[259] also used a Neumann series approach to exhibit integration formulas which are accurate and rapidly converging for resonances of the NN and of the NW types.

Corngold[208] applied variational methods to the computation of the effective resonance integral. Goldstein and Cohen[260] proposed an iteration procedure to solve for the first iterate of the relative flux. They used a trial function of the form:

$$\phi^{(1)}(E) = \frac{\Sigma_M + \lambda\Sigma_p}{\Sigma_M + \Sigma_a(E) + \lambda\Sigma_s(E)} \frac{1}{E} \tag{3-79}$$

where λ is chosen so that the effective resonance integrals are equal for the trial function and its first iterate; $0 \leq \lambda \leq 1$, where $\lambda = 0$ and $\lambda = 1$ correspond, respectively, to the NW and the NN approximations.

Marchuk and Mikhailus[261] reported a numerical method of solving the integral equation for the collision density, $\psi(u)$, and the adjoint equation for the adjoint collision density (the resonance escape probability). The method is applied to a resonance that is very wide in comparison with the maximum energy loss of a resonance neutron scattered by the heavy absorber. Starting with a known (asymptotic) solution at sufficiently low lethargies, the function $\phi(u) = \psi(u)e^u$ is determined as an average over each interval of a uniform partition of the lethargy range at higher lethargies. Doppler broadening and scattering-interference contributions may be included in the computations.

3.6.4.7 Modifications for Finite Media; Multigroup Cross Sections

In a critical, uniform, unreflected reactor with total geometric buckling B^2, an approximate formula may be written for the ratio of the slowing-down density at E_2, to that at $E_1 \geq E_2$:

$$p^*(E_1 \rightarrow E_2, B^2) \approx \exp\left[-\int_{E_2}^{E_1} \frac{\Sigma_a(E) + DB^2}{\bar{\xi}\{\Sigma_s(E) + K[\Sigma_a(E) + DB^2]\}} \frac{dE}{E}\right] \tag{3-80}$$

This may be recognized as a generalization, to a finite medium, of the synthetic-kernel methods discussed earlier. The case $K = 1$ corresponds to the Wigner approximation for the case of zero buckling (the NN approximation).

Equation (3-80) is obtained with the diffusion theory representation of the net local neutron leakage, $DB^2\,\phi(\bar{r},E)$, by considering the leakage as an additional absorption-type removal process. The flux is assumed to be separable into a simple product of an energy-dependent function and a space-dependent function.

In Section 6.1.1, a prescription for an effective absorption cross section is given (for the case $B^2 = 0$), equating the absorption rate per unit energy in a flux of the form:

$$\phi(\bar{r},E) = \frac{q(\bar{r},E)}{\bar{\xi}\Sigma_s E} \text{ (Fermi)}$$

with the actual absorption rate per unit energy at E. An effective diffusion coefficient (D_{eff}) should be defined in an analogous fashion, for finite media, so as to retain the correct ratio of leakage to absorption and the correct attenuation rate, $p^*(E' \rightarrow E, B^2)$. (Note that the method described in Section 6.1.1 only approximately meets these two conditions.)

Thus in any multigroup formulation of the Boltzmann equation for the neutron flux, collision density, or slowing-down density, the effective group cross sections are functions not only of the lethargy width of the group, but also of the attenuation processes in that group. If the slowing-down density is reduced appreciably by these processes, or if the flux within the group is depressed severely by absorption and scattering resonances, the effective cross sections should reflect the flux perturbations. If the group is wide in comparison with the energy band occupied by any absorption resonances it contains, the group absorption cross section is most sensitive, although the group diffusion coefficient may be affected significantly by scattering resonances.

The variation of the effective resonance integral (I_{eff}) with the potential scattering per absorbing atom, and with the temperature of the mixture, has been discussed in detail earlier in this section. The ith group average value, $\bar{\sigma}_{r,i}$, for the reaction cross section, $\sigma_r(E)$, may be defined[258] as the ratio of the total reaction rate of that type in the group, to the integrated flux in the group. If the region of resonance absorption in the group occupies a small fraction of the group width: $\Delta_i = E_{i,u} - E_{i,l}$, if the

resonances are "narrow", and if the Wigner synthetic kernel is used, then the average value for the case $B^2 = 0$ becomes:

$$\bar{\sigma}_{r,i} \sim \left[\ln \frac{E_{i,u}}{E_{i,\ell}}\right]^{-1} \int_{E_{i,\ell}}^{E_{i,u}} \sigma_r(E) \frac{\Sigma_p^*}{\Sigma^*(E)} \frac{dE}{E}$$

where

$$\Sigma_p^* = \begin{cases} \Sigma_p & \text{(NN approximation)} \\ \Sigma_p - \Sigma_{p0} & \text{(NW approximation)} \end{cases}$$

and

$$\Sigma^*(E) = \begin{cases} \Sigma(E) & \text{(NN approximation)} \\ \Sigma_p^* + \Sigma_a(E) & \text{(NW approximation)} \end{cases}$$

The effective absorption cross section is

$$\bar{\sigma}_{a,i} \approx \sum_j I_{eff,ij} / \ln(E_{i,u}/E_{i,\ell})$$

where the sum is taken over all resonances in group i, and $I_{eff,ij}$ is the effective resonance integral of the jth resonance in group i.

Bell[258] computed group absorption and scattering cross sections for a particular group subdivision frequently used at the Los Alamos Scientific Laboratory; the nuclides Mo, W, U^{235}, U^{238}, and Pu^{239} are included. The more general form (for an infinite medium):

$$\bar{\sigma}_{r,i} = \left[\int_{\text{group } i} \frac{\sigma_r(E)}{\Sigma^*(E)} \frac{dE}{E}\right] \Bigg/ \left[\int_{\text{group } i} \frac{1}{\Sigma^*(E)} \frac{dE}{E}\right]$$

was used. Doppler broadening and scattering interference effects were included. (Refer to Section 6.2.1 for detailed tabulations of $\bar{\sigma}(n,\gamma)_i$ and $\bar{\sigma}(n,n)_i$, for various values of Σ_p/N_0 and kT_0.)

In the MUFT program,[179,180] the resonance integrals are calculated in the NW approximation, without Doppler broadening. For each resonance in each group, a factor may be specified as input information to provide for Doppler effects and for the preference of some other method of computing the effective resonance integral of individual resonances.

3.6.4.8 The Computation of p_{res}

The evaluation of the resonance escape probability for individual resonances has been discussed in the preceding sections. Some results have been presented for the effective resonance integrals of mixtures of U^{238} and moderators, or of Th^{232} and moderators. If $p_{res,j}$ is known, resonance-by-resonance, and if the absorption-escape probability, $p_{\text{unresolved res}}$, is known in the region of the unresolved resonances, then the over-all resonance escape probability, p_{res}, is calculated as the product of the individual values of p. [Note that Eq. (3-44) includes the 1/v absorption, and that it is rather an equation of the type Eq. (3-45), or similar formulas involving Doppler broadening, that should be used in the computation of p_{res}.]

As discussed in Section 3.6.1, p_{res} includes only *resonance* absorption characteristics of the fertile material. In Section 3.6.5, approximations to the appropriately defined $(\eta f)_{eff}$ are discussed.

3.6.5 THE EFFECTIVE VALUE OF ηf: $(\eta f)_{eff}$

If, as discussed in Section 3.6.1, all neutron production and removal events occurring in the resonance energy region were accounted for in the concept of p, the remaining factor, ηf, would characterize reactions in the "thermal" group. In that case, for a homogeneous medium, f is the "thermal utilization" of the fuel:

$$f = \left[\int_0^{E_c} \Sigma_a^{\text{fuel}}(E)\, \phi(E)\, dE\right] \Big/ \left[\int_0^{E_c} \Sigma_a^{\text{total}}(E)\, \phi(E)\, dE\right] \qquad (3\text{-}81)$$

where Σ_a^{fuel} and Σ_a^{total} are the macroscopic absorption cross sections of the fuel and of the entire medium, respectively, and E_c is an appropriately selected cutoff energy for the thermal group.

The average value of η, the number of neutrons emitted per absorption in fuel, is specified by the requirement that

$$\eta f = \left[\int_0^{E_c} \eta(E)\ \Sigma_a^{fuel}\ (E)\ \phi(E)\ dE\right] \Big/ \left[\int_0^{E_c} \Sigma_a^{total}\ (E)\ \phi(E)\ dE\right] \tag{3-82}$$

These are rather conventional definitions that ignore epithermal processes. Since, typically, important epithermal reactions are ignored in the computation of p, ηf should be redefined as $(\eta f)_{eff}$:

$$(\eta f)_{eff} = \left[\int_0^{E_{threshold}} \eta(E)\ \tilde{\Sigma}_a^{fuel}\ (E)\ \phi(E)\ dE\right] \Big/ \left[\int_0^{E_{threshold}} \tilde{\Sigma}_a^{total}\ (E)\ \phi(E)\ dE\right]$$

where $\tilde{\Sigma}_a^{total}(E)$ does not include $\Sigma_{a,res}(E)$ of the fertile material, and $E_{threshold}$ is the fast-fission threshold energy defined in Section 3.6.2. The computation of $\phi(E)$ may proceed in a step-by-step analysis of the absorption-escape probabilities over the unresolved resonance region, and over the resolved resonances, and should include the attenuation effects of intervening "1/v" absorption.

3.7 INTEGRAL DATA

The criteria adopted for the selection of data in this section are described in the following paragraphs.

The reactor fuel is distributed in an essentially homogeneous manner in cores of regular geometry, including pseudo-cylinders, pseudo-spheres, cylinders, spheres, and slabs. For beryllium-moderated and graphite-moderated systems, where data are scarce, the criteria were relaxed to include reactors fueled with thin foils of U^{235}.

An arbitrary division of reactors into "thermal" and "intermediate" systems was made. If the bulk of criticality data from a set of experiments concerned reactors wherein at least two-thirds of the fissions occurred below cadmium cutoff, these data have been included here. If most of the data from a given series of experiments did not meet this criterion, but the system could not be categorized as a fast reactor, the information was described in Section 6.3.

For water-moderated, U^{235}-fueled reactors,[262] the subdivision occurred at $H/U^{235} \sim 50$, corresponding to a partition ratio:

$$\frac{(\xi\Sigma_s)_{asymptotic}}{\text{atoms } U^{235}/cm^3} \sim 1030 \text{ barns}$$

which defines the magnitude of the macroscopic slowing-down power per atom of U^{235}. This same definition was applied to other moderators. Table 3-57 summarizes the respective atom ratios of moderator to U^{235}.

Table 3-57 — MODERATOR/FUEL ATOM RATIOS CORRESPONDING TO PARTITION RATIOS: $\dfrac{(\xi\Sigma_s)\text{ asymptotic}}{\text{fissile-atom density}}$

Data from Refs. 262 and 263.

Fuel	Atom Ratio					$\dfrac{(\xi\Sigma_s)\text{ asymptotic}}{X}$
	H/X[a] (H_2O)	D/X (D_2O)	C/X	Be/X	BeO/X	
U^{235}	50[b]	~380	~1350	~820	~600	~1030 barns
U^{233}	~100	~740	~2700	~1600	~1170	2000 barns[b]

[a] X denotes atom density of U^{235} or U^{233} in the core.

[b] Criterion from which the various atom ratios, moderator/X, were computed.

For U^{233}-fueled reactors, a partition ratio of 2000 barns was chosen, following Chernick's results.[263] The corresponding atom ratios of moderator to U^{233} are given in Table 3-57.

In the case of Pu^{239} data, the reactors investigated could be categorized unambiguously as "thermal" systems, or as non-thermal systems.

3.7.1 CRITICAL-PARAMETER STUDIES OF UNIFORM H_2O SOLUTIONS OF SALTS OF URANIUM ENRICHED IN U^{235}

Critical masses of aqueous solutions of various salts of uranium enriched in U^{235} have been investigated at several laboratories. The salts included (uranyl) oxyfluoride (UO_2F_2); nitrate [$UO_2(NO_3)_2$] with additional nitric acid to provide an acid medium; sulphate (UO_2SO_4); and phosphate [$(UO_2)_3(PO_4)_2$].

3.7.1.1 H_2O Solutions of Highly Enriched UO_2F_2

A series of critical experiments with solutions of UO_2F_2 (uranium enriched to 93.2–93.4 wt-% in U^{235}) has been performed at Oak Ridge National Laboratory. The walls of the containing vessels were either stainless steel, or aluminum coated to resist corrosion. Unreflected and water-reflected spherical cores, and unreflected or partially reflected cylindrical and slab cores were studied. Whenever a reflector was present, the lateral reflector thickness was at least 10 cm; the data were not corrected for the finiteness of these reflectors. A top reflector of at least 15 cm of H_2O was used for cylinders having such a reflector; in each case, a thin-walled tank made of the same material as the solution container was used to separate this water from the core.

Curves of solution density versus the atom ratio H/U^{235} are given in Fig. 3-54 for solutions of uranyl oxyfluoride and uranyl nitrate.

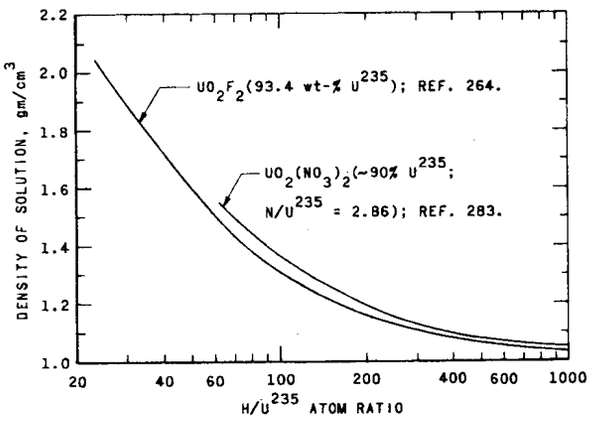

Fig. 3-54 — Density of uranyl oxyfluoride and uranyl nitrate solutions as a function of H/U^{235} atom ratio. *Data from Refs. 264 and 283.*

Data for cylindrical and slab cores are listed in Table 3-58. Since the experiments were continued over several years, and were performed by more than one group of experimenters, a column identifying the data by reference number has been added.

Table 3-59 lists critical parameters of UO_2F_2-H_2O solutions, with 93.2% U^{235} enrichment, in aluminum-walled spheres.

Thomas, et al.,[268] have published data on the temperature dependence of critical parameters of H_2O solutions of ~90% enriched UO_2F_2 in reflected and unreflected aluminum-walled spheres. Two spherical vessels of diameter 26.4 cm and 32.0 cm, with 0.13-cm-thick walls of 3S aluminum, were used as solution containers. The inside surfaces of the spheres were coated with plastic. The vessels were mounted in cylindrical tanks of such dimensions as to provide a reflector thickness of at least 15 cm of H_2O. The data are given in Table 3-60.

Table 3-58 — CRITICAL PARAMETERS OF UO_2F_2–H_2O SOLUTIONS

(Uranium is ~93.4% Enriched in U^{235})

Core Diameter, cm	H/U^{235} Atom Ratio	U^{235} Concentration, gm/cm^3 sol.	Critical Core Height, cm	Critical Mass, kg U^{235}	Ref.
Aluminum-Walled Cylinders and Slabs					
Water-Reflected					
15.2	27.1	0.8288	89.3	13.47	265
	43.2	0.537	70.1	6.87	266
	58.8	0.415	71.8	5.44	264
16.5	26.2	0.827	44.5	7.91	264
	44.3	0.5376	38.7	4.45	265
	78.7	0.315	42.6	2.87	267
	119.0	0.212	52.6	2.39	264
20.3	29.9	0.759	20.7	5.09	264
	49.5	0.488	18.8	2.97	267
	78.7	0.315	19.4	1.98	267
	192.0	0.134	28.1	1.22	264
	290.0	0.0881	40.1	1.15	264
25.4	27.1	0.8288	12.4	5.2	265
	43.2	0.537	12.5	3.40	266
	51.5	0.470	11.4	2.72	266
	127	0.199	14.4	1.45	267
	328.7	0.0787	22.4	0.893	264
	499	0.0522	35.2	0.0930	264
38.1	27.1	0.8288	7.7	7.3	265
	52.9	0.459	7.90	4.14	264
	221	0.116	11.30	1.49	264
	499	0.0522	16.90	1.01	264
	755	0.0343	27.10	1.02	264
	999	0.0260	44.30	1.31	264
76.2	27.1	0.8288	5.0 ± 1	18.9 ± 3.8	265
	44.3	0.5376	4.8 ± 1	11.8 ± 2.5	265
	72.4	0.3423	5.5 ± 1	8.6 ± 1.6	265
50.8 × 50.8 sq. cross section	27.1	0.8288	6.3 ± 1	13.5 ± 2.2	265
	44.3	0.5376	4.3 ± 1	6.0 ± 1.4	265
	72.4	0.3423	6.2 ± 1	5.5 ± 0.9	265
Partially Water Reflected[a]					
15.2	44.3	0.5376	75.0	7.34	265
19.1	44.3	0.5376	25.7	3.93	265
20.3	44.3	0.5376	23.6	4.12	265
	51.5	0.470	23.8	3.64	266
	72.4	0.3423	23.3	2.59	265
25.4	43.2	0.537	17.3	4.71	266
	72.4	0.3423	16.7	2.90	265
38.1	74.6	0.3314	12.0	4.5	265
Bare					
22.3	44.3	0.5376	219	45.8	265
	50.1	0.480	202.2	37.8	266
	55.4	0.437	171.6	29.2	266
	60.8	0.402	162.5	25.4	266
	66.1	0.373	159.8	23.2	266
	71.5	0.350	163.2	22.2	266
25.4	27.1	0.8288	38.9	16.4	265
	44.3	0.5376	35.1	9.6	265
	50.1	0.480	34.8	8.40	266
	52.9	0.459	34.0	7.90	264
	55.4	0.437	34.3	7.60	266
	60.8	0.402	34.1	6.96	266
	66.1	0.373	34.1	6.45	266
	73.4	0.3370	33.7	5.8	265
	83.1	0.300	34.4	5.22	266
	169	0.151	41.2	3.15	264
	328	0.0785	147.8	5.83	266
	331	0.0779	170.1	6.72	266
30.5	44.3	0.5376	23.2	9.1	265
	50.1	0.480	22.6	7.92	266
	55.4	0.437	22.7	7.25	266
	60.8	0.402	22.7	6.67	266
	331	0.0779	32.8	1.86	266
38.1	27.1	0.8288	18.5	17.5	265
	44.3	0.5376	17.9	11.0	265
	50.1	0.480	17.9	9.79	266
	74.6	0.3314	16.8	6.4	265
	169.0	0.151	18.5	3.18	264
	328.7	0.0787	21.7	1.95	264
	331	0.0779	22.9	2.03	266
	499	0.0522	27.4	1.63	264
	755	0.0343	43.6	1.70	264
50.8	27.1	0.8288	15.8	26.5	265
	44.3	0.5376	15.0	16.3	265
	50.1	0.480	15.4	14.9	266
	60.8	0.402	15.3	12.5	266
	73.4	0.3370	15.2	10.4	265
	325	0.0791	18.7	2.97	266
76.2	44.3	0.5376	13.7	33.6	265
	50.1	0.480	13.8	30.2	266
	72.4	0.3423	13.9 ± 0.5	21.6 ± 0.7	265
	331	0.0779	16.3	5.79	266

50.8	72.4	0.3423	10.6	7.3	265	50.8 × 50.8 sq. cross section	27.1	0.8288	15 ± 1	32 ± 2	265
							72.4	0.3423	14.3	12.6	265
76.2	72.4	0.3423	9.2	14.4	265		331	0.0779	17.9	3.60	266
76.2 × 152.4 cross section[b]	57.0	0.4240	8.4	41.5	265						
Stainless Steel Cylinders											
Water-Reflected						**Bare**					
15.2	44.3	0.5376	118.4	11.59	265	22.9	74.6	0.3314	59.0	8.1	265
16.5	31.6	0.724	49.0	7.59	264	25.4	43.9	0.538	32.3	8.80	264
	43.9	0.538	47.1	5.42	264		62.7	0.396	31.7	6.36	264
	86.4	0.288	53.8	3.31	264		86.4	0.288	31.9	4.65	264
17.8	31.6	0.724	34.0	6.11	264		123.2	0.205	34.3	3.56	264
	43.9	0.538	32.7	4.37	264		174	0.148	38.7	2.90	264
	86.4	0.288	36.0	2.57	264		226	0.114	46.6	2.69	264
	174	0.148	57.3	2.10	264	30.5	174	0.148	24.7	2.67	264
20.3	31.6	0.724	22.6	5.31	264		226	0.114	26.2	2.18	264
	43.9	0.538	21.9	3.82	264		320	0.0805	30.3	1.78	264
	56.7	0.424	22.2	3.05	264		499	0.0522	48.9	1.86	264
	86.4	0.288	23.8	2.22	264	38.1	56.7	0.424	17.1	8.26	264
	123.2	0.205	26.0	1.73	264		221	0.116	19.5	2.58	264
	174	0.148	30.1	1.44	264		499	0.0522	27.0	1.61	264
	226	0.114	36.3	1.34	264		755	0.0343	41.7	1.63	264
	320	0.0805	60.1	1.57	264	50.8	119	0.212	14.3	6.14	264
25.4	31.6	0.724	15.3	5.61	264		221	0.116	15.7	3.69	264
	43.9	0.538	14.9	4.06	264		329	0.0787	17.4	2.77	264
	62.7	0.396	15.2	3.05	264		499	0.0522	20.5	2.17	264
	86.4	0.288	15.4	2.25	264		755	0.0343	26.7	1.86	264
	123.2	0.205	16.8	1.74	264	**Cadmium-Lined (0.44 gm/cm^2) Water-Reflected**					
	174	0.148	18.1	1.36	264						
	226	0.114	20.0	1.15	264	20.3	43.9	0.538	51.5	8.98	264
	320	0.0805	25.0	1.02	264		62.7	0.396	48.4	6.21	264
30.5	62.6	0.394	12.3	3.53	264		86.4	0.288	56.5	5.28	264
	174	0.148	14.9	1.61	264	22.9	31.6	0.724	29.0	8.62	264
	226	0.114	16.5	1.37	264		43.9	0.538	28.8	6.36	264
	320	0.0805	18.5	1.09	264		62.7	0.396	28.3	4.61	264
	499	0.0522	26.3	1.00	264		86.4	0.288	29.2	3.45	264
	755	0.0343	48.7	1.22	264		123.2	0.205	32.0	2.69	264
38.1	56.7	0.424	10.1	4.88	264		174	0.148	37.3	2.26	264
	221	0.116	13.0	1.72	264	25.4	31.6	0.724	21.1	7.74	264
	499	0.0522	20.0	1.15	264		43.9	0.538	21.4	5.83	264
	755	0.0343	28.8	1.13	264		62.7	0.396	22.0	4.42	264
							86.4	0.288	22.0	3.21	264
							221	0.116	28.7	1.69	264
						30.5	56.7	0.424	15.8	4.89	264
							174	0.148	19.5	2.10	264
							226	0.114	20.9	1.74	264
							499	0.052	32.8	1.25	264

[a]Assemblies have no top reflector.
[b]This vessel was coated with Unichrome; others were coated with Heresite.

Table 3-59 — CRITICAL PARAMETERS OF $UO_2F_2-H_2O$ SOLUTIONS IN ALUMINUM-WALLED SPHERES[a]

Data from Ref. 269.

Core Diameter, cm	H/U^{235} Atom Ratio	U^{235} Concentration, gm/cm^3 sol.	Critical[b] Mass, kg U^{235}	Reflector[c]	Sphere Wall Thickness, cm
23.0	76.1	0.325	2.08	H_2O	0.16
23.6	126.5	0.199	1.39	H_2O	0.16
55.8	1112	0.0234	2.13	none	0.20
55.8	1270	0.0205	1.86	H_2O	0.20
69.2	1393	0.0186	3.25	none	0.32

[a]Uranium 93.2% enriched in U^{235}; spheres constructed of Type 1100 aluminum; no correction made for container thickness.
[b]Volume known to within ±0.5%; concentration to within ±1%.
[c]When present, water reflector was effectively infinite.

Table 3-60 — TEMPERATURE DEPENDENCE OF CRITICAL PARAMETERS OF WATER-REFLECTED $UO_2F_2-H_2O$ SOLUTIONS IN ALUMINUM-WALLED SPHERES[a]

Data from Ref. 268.

Core Diameter, cm	Temperature, °C	H/U^{235} Atom Ratio	U^{235} Concentration at 25°C, gm/cm^3 sol.	Critical Mass, kg U^{235}
(26.4)*	27.5	268.8	0.0951	0.918
	39.5	263.3	0.0971	0.935
26.6*	74.0	245.4	0.1041	0.990
	85.5	239.3	0.1068	1.010
(32.0)*	27.0[c]	515.1	0.0503	0.856
	43.0	502.6	0.0515	0.872
31.9[b]†	43.0	503.4	0.0514	0.871
	54.0	496.5	0.0521	0.879
	64.5	487.6	0.0531	0.890
	87.5	476.8	0.0543	0.900
	87.5	459.6	0.0563	0.932
(32.0)* 31.9[d]†	27.0	203.5	0.1252	2.129

[a]Uranium ~90% enriched in U^{235}. Spheres were constructed of Type 3S aluminum; no correction was made for container thickness.
[b]The values of the concentrations and masses measured with this sphere are believed to be about 2% high because of a systematic error.
[c]In this experiment, the reactor was critical with about 0.1% of the core unfilled and at a temperature 5°C lower than the values listed. Using measured expansion coefficients of the solution and of the container, an extrapolation was made to the temperature at which the full core would have been critical.
[d]No reflector.
*Values in parentheses are nominal dimensions, as reported in Ref. 268.
†Values based upon subsequent volumetric calibrations. Private communication from J. K. Fox, Phillips Petroleum Co., Idaho. (Also see Tables No. 3-105, 3-106, and 3-108.)

3.7.1.2 A Fitting Formula for Critical Dimensions of Cylinders Containing H_2O Solutions of Highly Enriched UO_2F_2

Some of the criticality data[264] given in Section 3.7.1.1 were fitted to an empirical formula by Schuske and Morfitt.[270–272] The formula: (D-a)(H-b) = c, relates critical core height and core diameter of water-reflected, cylindrical assemblies. The parameters a, b, and c, were determined empirically for H/U^{235} atom ratios in the range 31.6 to 400.0; they are listed in Table 3-61.

Table 3-61 — FITTING PARAMETERS FOR WATER-REFLECTED SOLUTIONS OF UO_2F_2 IN STAINLESS STEEL CYLINDERS[a]

Data from Ref. 270.

H/U^{235} Atom Ratio	(D-a)(H-b) = c		
	a, cm	b, cm	c, cm^2
31.6	14.22	6.42	99.0
50.0	14.10	5.85	102.6
100.0	14.58	6.24	104.1
200.0	16.10	7.60	104.9
300.0	17.88	9.25	108.4
400.0	20.02	11.54	104.1
			Avg.: 104.0

[a]Uranium enriched to ~93.2% U^{235}.

A mathematical justification for approximating to critical core dimensions by an equation of this type has been presented by Danzker.[273]

An approximate constant value for c is preferable to the variable c in Table 3-61. Accordingly, the average value of 104.0 cm^2 was chosen. Values of a and b, derived for this value of c, are given in Table 3-62.

The formula: (D-a)(H-b) = 104 cm^2, has been applied to calculations of the critical core height of solutions of highly enriched UO_2F_2 in water-reflected, stainless steel-walled cylinders. For H/U^{235} atom ratios ranging from 50 to at least 300, and for core diameters ranging from 16.5 cm to 38.1 cm, the average deviation of the calculated height from the experimental value was 1.4%. The maximum deviation was 5%.

In an extension of this technique, the (D-a)(H-b) = c formula, with c = 116 cm^2, was found to apply equally well for solutions in aluminum cylinders over the H/U^{235} range considered. Values of a and b are given in Table 3-63.

Macklin[274] has obtained an analytic expression for the functional dependence of a and b on the composition.

Table 3-62 — FITTING PARAMETERS FOR WATER-REFLECTED SOLUTIONS OF UO_2F_2 IN STAINLESS STEEL CYLINDERS[a]

Data from Ref. 270.

H/U^{235} Atom Ratio	(D-a)(H-b) = 104 cm^2	
	a, cm	b, cm
30	14.1	6.70
50	14.0	6.12
100	14.6	6.45
150	15.4	7.00
200	16.2	7.70
250	17.0	8.55
300	17.9	9.47
350	18.9	10.50
400	20.1	11.65

[a]Uranium enriched to ~93.2% U^{235}.

Table 3-63 — FITTING PARAMETERS FOR WATER-REFLECTED SOLUTIONS OF UO_2F_2 IN ALUMINUM-WALLED CYLINDERS[a]

Data from Ref. 271.

H/U^{235} Atom Ratio	(D-a)(H-b) = 116 cm^2	
	a, cm	b, cm
30	13.8	3.7
40	13.7	3.5
50	13.6	3.4
100	14.0	3.6
200	15.3	5.0
300	17.0	7.0
400	18.9	9.75

[a]Uranium enriched to ~93.2% U^{235} Wall thickness of cylinders = 0.16 cm.

3.7.1.3 Critical Thickness of a Proton-Reflected, Infinite-Slab Solution of Enriched UO_2F_2 (93.2% U^{235})

By extrapolation of measurements, Fox, et al.,[275] have determined a thickness of 4.47 (±0.18) cm for an infinite slab containing an aqueous solution of UO_2F_2. The slab was reflected by an effectively infinite medium of plastic and water. The uranium was enriched to 93.2% U^{235}, and the moderator-to-fuel atom ratio in the core was $H/U^{235} = 44.7$.

3.7.1.4 Graphical Summary of Critical Parameters of Aqueous Solutions of Enriched UO_2F_2 (93.2% U^{235}) in Uniform Cores

Paxton has published[276] curves relating to critical parameters of H_2O solutions of UO_2F_2 (93.2% U^{235}) in bare or water-reflected stainless steel spheres. The basic data obtained from critical mass studies of cylinders were converted to equivalent-sphere data by equating total geometric bucklings. Figures 3-55 through 3-58 show the effective extrapolation lengths used for the cylinder-

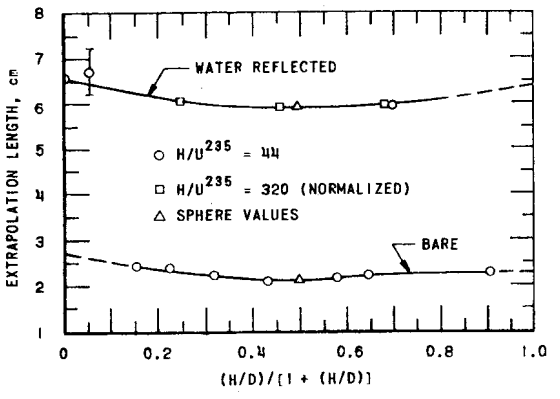

Fig. 3-55—Effective extrapolation lengths for aluminum-walled cylinders ($1/16$ in. wall) containing H_2O solutions of UO_2F_2 (uranium enriched to ~93.2% U^{235}). *Reproduced from Ref. 276.*

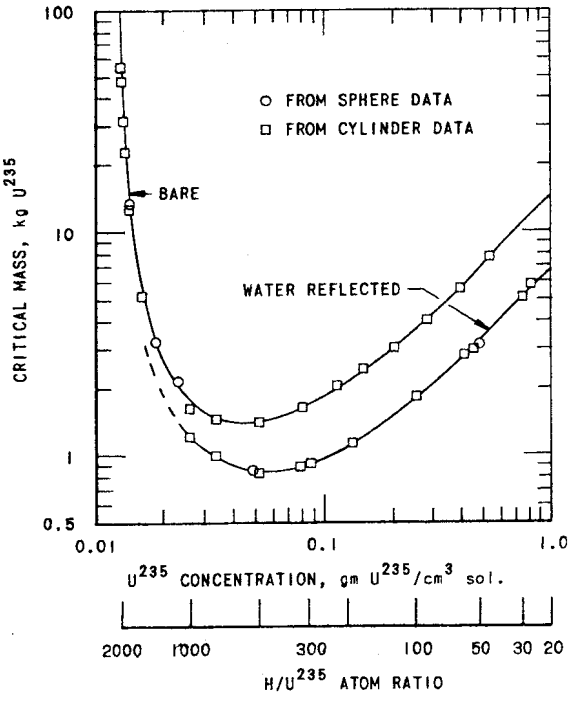

Fig. 3-56—Critical masses of H_2O solutions of UO_2F_2 (uranium enriched to ~93.2% U^{235}) in stainless steel spheres ($1/16$ in. wall). *Reproduced from Ref. 276.*

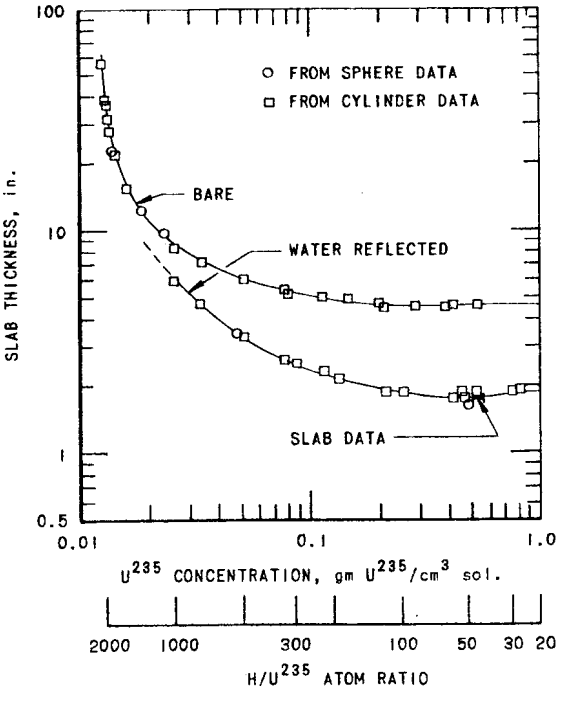

Fig. 3-57—Estimated critical thicknesses of infinite slabs containing H_2O solutions of UO_2F_2 (uranium enriched to ~93.2% U^{235}). Slab walls are stainless steel, $1/16$ in. thick. *Reproduced from Ref. 276.*

sphere equivalence, the actual and inferred sphere data, and estimates of the critical, infinite-slab thickness and infinite-cylinder diameter as a function of the H/U^{235} atom ratio.

Reference 277 is a companion report, intended for nuclear safety guidance.

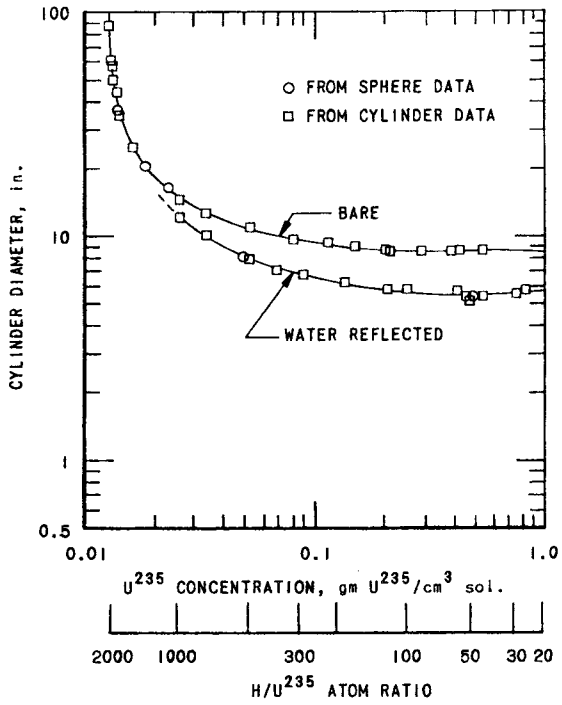

Fig. 3-58 — Estimated critical diameters of infinite cylinders containing H_2O solutions of UO_2F_2 (uranium enriched to ~93.2% U^{235}). Cylinder walls are stainless steel, $^1/_{16}$ in. thick. *Reproduced from Ref. 276.*

3.7.1.5 Aqueous Solutions of UO_2F_2 with 4.89 wt-% U^{235} Enrichment

Critical cores containing H_2O solutions of UO_2F_2 with a U^{235} enrichment of 4.89 wt-% have been investigated by Cronin.[278,279] The data are summarized in Table 3-64.

3.7.1.6 Aqueous Solutions of Highly Enriched $UO_2(NO_3)_2$ (>90% U^{235})

Critical masses of solutions of $UO_2(NO_3)_2$ in H_2O have been measured by Brown, et al.[280] The uranium was enriched to more than 90% in U^{235}, and the solution concentrations corresponded to H/U^{235} atom ratios in the range: 1633 to 1776. The solution container was a stainless steel cylindrical tank with a diameter of 91.5 cm (36 in.), a height of 183 cm (72 in.), and a radial wall thickness of 0.32 cm. The core was reflected below by a solid Lucite cylinder, 25 cm thick, contained within the core tank. There was no reflector above the core other than a steel control rod support plate (~ 2.5 cm thick), which was at least 50 cm above the core solution heights. The critical parameters, measured with and without a 20-cm radial H_2O reflector, are listed in Table 3-65.

The reactivity worth of the radial reflector was obtained by measuring the increment in critical solution height when the reflector was removed, and multiplying the differential height by the average worth per centimeter of solution height in that range. The results are presented in Table 3-66. Also included are the differential reactivity worths of solution height. Note that the reflector worth was essentially constant over the range of solution heights and H/U^{235} ratios examined.

Fox, et al.,[267] measured the critical parameters of aqueous solutions of uranyl nitrate in unreflected, stainless steel cylinders. The uranium was enriched to 92.8% in U^{235} and the N/U atom ratio was approximately 3.8. The results of that study are listed in Table 3-67.

Magnuson[281] published critical-concentration data for unreflected, aluminum spheres. One datum was reported earlier:[282] the 69.2-cm-diameter, unpoisoned sphere was quoted as having H/U^{235} = 1379. Additional experiments were performed, varying the H/U^{235} ratio in the core and maintaining criticality by the addition of boron to the core solution. The experimental parameters, calculated from data in Ref. 281, are listed in Table 3-68.

Callihan, et al.,[283] published the results of a series of critical experiments performed in 1950 at ORNL with solutions of uranyl nitrate highly enriched in U^{235}. Studies were made of the change in critical mass upon addition of nitric acid, or nitric acid plus phosphoric acid, to the core solution.

Table 3-64 — CRITICAL PARAMETERS OF URANYL FLUORIDE SOLUTIONS[a]

Data from Ref. 278.

H/U^{235} Atom Ratio	U^{235} Concentration, gm/cm^3 sol.	Critical Parameters		Container Description
		Height, cm	Mass, kg U^{235}	
Water-Reflected Assemblies				
524	0.04254	25.4	2.76	Aluminum vessel, 50.8 cm square cross section.[b]
		29.3	2.53	Stainless steel cylinder, 50.8 cm dia.
		44.78	2.17	Aluminum cylinder, 38.1 cm dia.
		50.37	2.44	Stainless steel cylinder, 38.1 cm dia.
643	0.03562	26.49	4.30	Aluminum cylinder, 76.2 cm dia.[c]
		28.4	2.61	Aluminum vessel, 50.8 cm square cross section.[b]
		37.4	2.70	Stainless steel cylinder, 50.8 cm dia.[c]
		34.7	2.50	Stainless steel cylinder, 50.8 cm dia.
		75.5	3.06	Stainless steel cylinder, 38.1 cm dia.
735	0.03179	26.7	3.87	Aluminum cylinder, 76.2 cm dia.[c]
		32.41	2.63	Aluminum vessel, 50.8 cm square cross section.[b]
		42.77	2.76	Stainless steel cylinder, 50.8 cm dia.[c]
		40.09	2.58	Stainless steel cylinder, 50.8 cm dia.
		153.01	5.54	Stainless steel cylinder, 38.1 cm dia.
991	0.02428	40.49	4.48	Aluminum cylinder, 76.2 cm dia.[c]
994	0.02422	89.4	4.40	Stainless steel cylinder, 50.8 cm dia.[c]
		85.72	4.21	Stainless steel cylinder, 50.8 cm dia.
1026	0.02352	62.69	3.76	Aluminum vessel, 50.8 cm square cross section.[b]
1099	0.02211	62.5	3.77	Aluminum sphere, 69.2 cm dia.[d]
Unreflected Assemblies				
524	0.04254	35.9	3.89	Aluminum vessel, 50.8 cm square cross section.[b]
		38.66	3.33	Stainless steel cylinder, 50.8 cm dia.
643	0.03562	28.85	4.69	Aluminum cylinder, 76.2 cm dia.[e]
		39.9	3.63	Aluminum vessel, 50.8 cm square cross section.[b]
		45.65	3.30	Stainless steel cylinder, 50.8 cm dia.
735	0.03179	31.50	4.58	Aluminum cylinder, 76.2 cm dia.[e]
		45.47	3.69	Aluminum vessel, 50.8 cm square cross section.[b]
		54.35	3.50	Stainless steel cylinder, 50.8 cm dia.
991	0.02428	44.75	4.96	Aluminum cylinder, 76.2 cm dia.[e]
1002	0.02404	64.60	4.14	Aluminum sphere, 69.2 cm dia.[d,f]
1025	0.02354	122-127[g]	7.3-7.7	Aluminum vessel, 50.8 cm square cross section.

[a] Uranium: 4.89 wt-% U^{235}.
[b] Inside measurement was 50.5 cm on a side; Al thickness: ~0.16 cm (nominal).
[c] Top surfaces of these cylinders were not reflected.
[d] Sphere was 98% filled.
[e] Supported by Plexiglas table top, 2.5 cm thick.
[f] At this concentration, the sphere with a water reflector was critical when 83% filled.
[g] Extrapolated.

Table 3-65—CRITICAL PARAMETERS OF AQUEOUS SOLUTIONS OF $UO_2(NO_3)_2$ IN STAINLESS STEEL CYLINDERS[a]

Data from Ref. 280.

H/U^{235} Atom Ratio	Critical Solution Height, cm		Critical Mass, kg U^{235}	
	Reflected Radially	Bare Radially	Reflected Radially	Bare Radially
1633 (±2)	58.7 (±0.05)	61.7 (±0.05)	5.91 (±0.04)	6.21 (±0.04)
1688	69.2	74.2	6.75	7.24
1710	75.2	81.5	7.24	7.85
1721	79.1	86.1	7.57	8.24
1739	86.6	95.3	8.20	9.03
1757	95.5	106.7	8.95	10.00
1773	106.2	120.9	9.87	11.24
1776	110.0	127.0	10.21	11.78

[a]Uranium enriched to >90% in U^{235}.

Table 3-66—REACTIVITY WORTH OF RADIAL WATER REFLECTOR

Data from Ref. 280.

H/U^{235} Atom Ratio	Critical Solution Height, cm		$\Delta\rho/\Delta H$, 10^{-4} cm^{-1}	Worth of Radial Water Reflector, 10^{-4} ρ
	Reflected Radially	Bare Radially		
1650	61.7	65.3	12.2	43.4
1670	65.3	69.9	10.3	47.2
1690	69.9	74.7	8.8	42.4
1710	75.4	81.8	7.3	46.5
1730	82.8	90.9	5.9	48.3
1750	91.7	101.9	4.7	47.6
1770	104.4	117.9	3.2	43.5

Table 3-67—CRITICAL PARAMETERS OF AQUEOUS SOLUTIONS OF $UO_2(NO_3)_2$ IN UNREFLECTED STAINLESS STEEL CYLINDERS[a]

Data from Ref. 267.

Core Diameter, cm	H/U^{235} Atom Ratio	U^{235} Concentration, gm/cm^3 sol.	Critical Core Height, cm	Critical Mass, kg U^{235}
50.8	1000	0.0259	38.3	2.01
154.7	1604	0.01613	45.1	13.68
154.7	1821	0.01422	72.7	19.45
154.7	1905	0.01359	105.2	26.88
154.7	1981	0.01307	203.3	49.95
274	1951	0.01324	90.9	70.8
274	2000	0.01292	122.4	92.3
274	2052	0.01261	241.2	178.8

[a]Uranium enriched to 92.8% in U^{235}; N/U ~ 3.8.

Table 3-68 — BORON-POISONED H_2O SOLUTIONS OF $UO_2(NO_3)_2$ IN BARE ALUMINUM-WALLED SPHERES[a]

Data from Ref. 281.

Core Diameter, cm	H/U^{235} Atom Ratio	U^{235} Concentration, gm/cm³ sol.	Boron Concentration, mg/cm³ sol.	Total NO_3 Concentration, gm/cm³ sol.	Critical[b] Mass, kg U^{235}	Cadmium[c] Ratio of U^{235} Foils
69.2	1378	0.0187	0	0.0192	3.25	0.0281
69.2	1177	0.0219	0.094	0.0219	3.80	—
69.2	1033	0.0249	~0.19	0.0246	4.32	—
69.2	972	0.0265	~0.23	0.0262	4.60	0.0381
121.9[d]	1835	0.0141	0	0.0116	13.38	0.0241

[a]Uranium enriched to ~93.2% in U^{235}.

[b]Actually, with this mass of U^{235} the reactor would be very slightly supercritical. Reference 281 gives $(k_{eff}-1) = 1.29 \times 10^{-3}$ for the larger, unpoisoned core and the deviation from criticality was even smaller for the other cases.

[c]The "cadmium ratio" definition used here is the ratio of the "epicadmium" activation to the "subcadmium" activation. Two U^{235} metal foils, ~0.005 cm thick and ~0.793 cm in diameter, one bare and one covered with cadmium (0.066 cm thick), were irradiated near the center of the core.

[d]The aluminum wall thickness was 0.77 cm for this sphere, and 0.32 cm for the smaller sphere.

Other experiments were devised to yield comparison of the reactivity effects of varying the thickness of special radial reflectors. The data in this section are limited to solutions of $UO_2(NO_3)_2$ in cores either unreflected radially, or with a water reflector at least 15 cm thick in all directions. Data from the latter experiments are presented in Section 3.7.2.

The core solutions were contained in right circular cylinders of various radii fabricated from Type 2S aluminum [wall thickness: 0.16 cm ($\frac{1}{16}$ in.)]. The aluminum was coated with Bakelite varnish.

The physical properties of some of the fuel solutions are listed in Table 3-69. The U^{235} enrichment inferred from the data is about 93%.

Table 3-69 — PHYSICAL PROPERTIES OF SOLUTIONS CONTAINING $UO_2(NO_3)_2$

Data from Ref. 283.

Atom Ratios			Fuel Content		Solution Density gm/cm³
H/U^{235}	N/U^{235}	P/U^{235}	gm U/gm sol.	gm U^{235}/cm³ sol.	
61.8	2.86	—	0.2485	0.359	1.55
88.0	7.48	—	0.1680	0.236	1.51
115	10.53	—	0.1339	0.187	1.50
128	6.97	15.8	0.0854	0.12	1.5
131	6.97	15.8	0.0846	0.120	1.52
157	5.37	15.8	0.0805	0.11	1.5
180	5.50	12.4	0.0812	0.11	1.5
230	7.48	—	0.0887	0.102	1.23
240	2.86	—	0.0963	0.105	1.16
316	2.90	53.1	0.0356	0.055	1.67
327	7.48	—	0.0673	0.073	1.17
352	2.86	—	0.0698	0.073	1.11
493	2.86	—	0.0524	0.053	1.08
733	2.86	—	0.0357	0.036	1.06

The critical parameters of solutions of uranyl nitrate with $N/U^{235} = 2.86$ are listed in Table 3-70. Similar data for solutions containing nitric acid and with $N/U^{235} = 7.48$ are given in Table 3-71. Results for cores containing solutions of uranyl nitrate plus phosphoric acid plus nitric acid are listed in Table 3-72.

In still another set of experiments, hexagonal arrays of aluminum tubes (O.D. ~ 2.5 cm) were placed in the core region to permit the introduction of various materials, including nitric acid, bismuth, and phosphorus. (For additional information see Ref. 283.)

Table 3-70—CRITICAL PARAMETERS OF H_2O SOLUTIONS OF HIGHLY ENRICHED URANYL NITRATE IN ALUMINUM-WALLED CYLINDERS

($N/U^{235} = 2.86$)

Data from Ref. 283.

Core Diameter, cm:	20.3		22.9		25.4		30.5		38.1	
H/U^{235} Atom Ratio	H_c, cm	M_c, kg	H_c, cm	M_c, kg	H_c, cm	M_c, kg	H_c, cm	M_c, kg	H_c, cm	M_c, kg
Water-Reflected (minimum of 15 cm of H_2O in all directions)										
61.8	25.5	2.97	19.7	2.90	16.6	3.02	—	—	9.4	3.85
240	36.7	1.24	25.3	1.08	20.1	1.06	15.1	1.15	12.2	1.45
352	—	—	35.0	1.04	26.2	0.96	19.3	1.02	14.4	1.20
493	—	—	—	—	37.0	1.00	24.6	0.95	17.9	1.08
733	—	—	—	—	—	—	43.2	1.11	26.7	1.07
Unreflected										
61.8	subcritical		subcritical		>40[a]	>7.3[a]	—	—	>18.0	>7.5
240	—	—	—	—	72.4	3.82	29.2	2.23	20.9	2.49
352	—	—	—	—	subcritical		36.8	1.94	24.0	1.99
493	—	—	—	—	—	—	49.5	1.91	28.3	1.71
733	—	—	—	—	—	—	subcritical		44.6	1.69

Note: H_c is the critical core height, and M_c is the critical mass of U^{235}.

[a]This system may be subcritical at infinite height; however, the lack of sufficient uranium precluded extension of the measurement above 27 cm and 4.8 kg.

Table 3-71—CRITICAL PARAMETERS OF H_2O SOLUTIONS OF HIGHLY ENRICHED URANYL NITRATE IN ALUMINUM CYLINDERS

(Nitric acid added; total $N/U^{235} = 7.48$)

Data from Ref. 283.

Core Diameter, cm:	22.9		25.4		30.5		38.1	
H/U^{235} Atom Ratio	H_c, cm	M_c, kg	H_c, cm	M_c, kg	H_c, cm	M_c, kg	H_c, cm	M_c, kg
Water-Reflected (minimum of 15 cm of H_2O in all directions)								
88.0	27.7	2.69	22.4	2.67	16.3	2.81	12.7	3.42
230	—	—	22.6	1.17	16.8	1.25	13.2	1.53
327	—	—	28.2	1.05	20.0	1.07	15.1	1.26
Unreflected								
88.0	—	—	>81.0	>9.7	35.2	6.06	22.6	6.09
230	—	—	>105	>5.4	32.9	2.44	22.7	2.63
327	—	—	subcritical		40.2	2.15	25.1	2.09

Note: H_c is the critical core height, and M_c is the critical mass of U^{235}.

Table 3-72—CRITICAL PARAMETERS OF H_2O SOLUTIONS OF HIGHLY ENRICHED URANYL NITRATE IN ALUMINUM CYLINDERS

(Nitric acid and phosphoric acid added)

Data from Ref. 283.

Core Diameter, cm	Atom Ratios			Critical Core Hgt., cm	Critical Mass, kg U^{235}
	H/U^{235}	N/U^{235}	P/U^{235}		
Water-Reflected (a minimum of 15 cm of H_2O in all directions)					
25.4	157	5.4	15.8	>27	>1.5
	157	5.4	15.8	>27[a]	>1.6[a]
	316	2.9	53.1	>105	>2.9
30.5	316	2.9	53.1	43.5	1.75
38.1	316	2.9	53.1	26.8	1.69
	316	2.9	53.1	29.5[a]	1.86[a]
	180	5.5	12.4	18.9[a]	2.5[a]
	180	5.5	12.4	15.4	2.0
Unreflected					
25.4	157	5.4	15.8	>57	>3.2
38.1	316	2.9	53.1	43.2	2.72
	180	5.5	12.4	>25	>3.3

[a]Without top water reflector.

687863 O - 63 - 14

3.7.1.7 Los Alamos Water-Boiler Experiments

Some early experiments with aqueous solutions of uranium enriched to ~14% or to ~89% U^{235} are described in Refs. 284 through 287. The solutions were contained in 30.5-cm-diameter stainless steel spheres, reflected by BeO and/or graphite. Typically, additional steel was present in the cores, in the form of pipes and/or cooling coils.

3.7.2 EFFECT OF COMPOSITION AND THICKNESS OF REFLECTORS ON THE CRITICAL PARAMETERS OF H_2O-SOLUTIONS OF URANIUM SALTS HIGHLY ENRICHED IN U^{235}

3.7.2.1 Aluminum-Walled Cylinders; Reflectors: Steel, Phosphoric Acid, Natural Uranyl Nitrate Solutions, Bismuth, and Water; Effects of Air Gaps in Reflector

Experiments by Callihan, et al.,[283] partially described in Section 3.7.1.6, have provided data on the effect of various reflector compositions and thicknesses on the critical mass of U^{235} in solutions of uranyl nitrate with ~93% U^{235} enrichment. The solutions were contained in right circular cylinders of various radii, and with 0.16-cm ($^1/_{16}$ in.)-thick walls of Type 3S aluminum coated with Bakelite varnish. Radial reflectors of varying thicknesses of H_2O, stainless steel, stainless steel and H_2O, phosphoric acid solutions, bismuth subcarbonate ($Bi_2O_2CO_3$, dry or in an H_2O slurry), or solutions of natural uranyl nitrate, were employed. Pertinent properties of these reflectors are listed in Table 3-73.

Table 3-73 — PROPERTIES OF SPECIAL RADIAL REFLECTORS

Data from Ref. 283.

Material	Concentrations	Remarks
$UO_2(NO_3)_2$ (solution)	0.426 gm U/cm^3	Natural isotopic concentration
$UO_2(NO_3)_2$ (solution)	0.217 gm U/cm^3	Natural isotopic concentration
$Bi_2O_2CO_3$ (dry)	0.52 gm Bi/cm^3	USP powder
$Bi_2O_2CO_3$ (slurry)	0.85 gm Bi/cm^3 0.82 gm H_2O/cm^3	Water slurry
H_3PO_4 (solution)	0.465 gm P/cm^3	86.7% H_3PO_4
Stainless steel	7.9 gm/cm^3	AISI Type 347

Concentric cylindrical shells of Type 3S aluminum (wall thickness: 0.16 cm), were constructed to contain the liquid partial reflectors. Four shells, each of outside thickness 2.54 cm, were made to fit around the 25.4-cm-diameter core. A fifth shell, of outside thickness 5.08 cm, was used outside the four smaller shells. These annular containers were used for the annular-void experiments as well; in these experiments, the minimum water reflector thickness in any direction was 10 cm.

The critical parameters of the fuel solutions are given in Tables 3-74 through 3-79. In each case, the core solution had N/U^{235} = 2.86 (atom ratio). The other properties of the core solution are described in Table 3-69.

A number of reflector experiments with critical solutions of highly enriched UO_2F_2 are described in Ref. 266. One set of experiments, in particular, indicates that, at least for the first 3.8 cm of Plexiglas, various slab thicknesses of Plexiglas followed by a large H_2O region are essentially equivalent to water in their reflecting properties. Other experiments dealt with partial reflectors. Table 3-80 lists the measured critical solution height versus the void thickness immediately above the solution in an aluminum cylinder (25.4 cm dia.; 0.16 cm wall), otherwise totally reflected by water.

3.7.2.2 Aluminum-Walled Slabs; Reflectors: Water and/or Styrofoam, Aluminum

Fox and Gilley have investigated the effectiveness of various reflectors for thin slab cores containing solutions of UO_2F_2 in H_2O. The uranium was enriched to 93.2% U^{235}. The nominal horizontal cross section of the cores was 15.2 cm × 122 cm, with aluminum walls 0.32 cm thick.

One set of experiments[288] was designed to compare the reflecting properties of Styrofoam, water, and Styrofoam followed by water. The H/U^{235} atom ratio in the core was 293. Physical properties of the materials and criticality data are summarized in Table 3-81.

In another group of experiments,[266] the critical height of a solution with H/U^{235} = 50.1 was measured as a function of the thickness of aluminum bounding the narrow dimension (15.2 cm). (Otherwise the core was unreflected.) The results are presented in Table 3-82.

Table 3-74 — CRITICAL PARAMETERS OF H_2O SOLUTIONS OF HIGHLY ENRICHED $UO_2(NO_3)_2$ IN ALUMINUM CYLINDERS (RADIAL H_2O REFLECTOR)

Data from Ref. 283.

Core Diameter, cm	H/U^{235} Atom Ratio	Thickness of H_2O Radial Reflector, cm	Critical Height of Core Solution, cm	Critical Mass, kg U^{235}
25.4	61.8	0	>40	>7.3
		2.24	28.6	5.20
		4.45	24.6	4.47
		6.68	23.3	4.24
		8.89	22.9	4.16
	240	0	72.4	3.82
		2.24	33.6	1.78
		4.45	28.4	1.51
		6.68	26.9	1.42
		8.89	26.6	1.41
	352	0	subcritical	
		2.24	43.9	1.61
		4.45	35.3	1.30
		8.89	32.5	1.20
30.5	352	0	36.8	1.94
		2.24	28.6	1.52
		4.45	26.0	1.38
		11.43	24.8	1.31
	493	0	49.5	1.91
		2.24	35.2	1.36
		11.43	30.0	1.16

Table 3-75 — CRITICAL PARAMETERS OF H_2O SOLUTIONS OF HIGHLY ENRICHED $UO_2(NO_3)_2$ IN ALUMINUM CYLINDERS (RADIAL STAINLESS STEEL REFLECTOR)

Data from Ref. 283.

Core Diameter, cm	H/U^{235} Atom Ratio	Thickness of Radial SST Reflector, cm	Critical Height of Core Solution, cm	Critical Mass, kg U^{235}
20.3	61.8	0	subcritical	—
		3.81	47.8	5.56
		5.08	39.7	4.63
		7.62	33.2	3.86
		8.89	31.5	3.66
25.4	61.8	0	>40	>7.3
		2.54	28.0	5.09
		6.35	21.2	3.85
	240	0	72.4	3.82
		0.64	47.3	2.51
		1.27	39.5	2.09
		2.54	32.8	1.73
		6.35	26.8	1.42
	352	0	subcritical	
		1.27	58.7	2.15
		1.91	48.6	1.78
		3.81	37.3	1.37
		6.35	33.1	1.22
	493	6.35	47.6	1.28

Table 3-76 — CRITICAL PARAMETERS OF H_2O SOLUTIONS OF HIGHLY ENRICHED $UO_2(NO_3)_2$ IN ALUMINUM CYLINDERS (RADIAL REFLECTOR OF STAINLESS STEEL BEYOND WHICH IS AN EFFECTIVELY INFINITE H_2O MEDIUM)

Data from Ref. 283.

Core Diameter, cm	H/U^{235} Atom Ratio	Thickness of Radial SST Reflector, cm	Critical Height of Core Solution, cm	Critical Mass, kg U^{235}
20.3	61.8	0	25.5	2.97
		0.30	29.6	3.44
		0.64	32.8	3.81
		1.27	34.7	4.04
		1.91	34.0	3.96
		2.54	33.1	3.85
		3.81	29.5	3.43
		5.08	27.4	3.18
		8.89	24.2	2.82
25.4	61.8	0	16.6	3.02
		1.27	18.6	3.39
		2.54	18.0	3.27
		6.35	16.4	2.98
	240	0	20.1	1.06
		0.64	23.4	1.24
		1.27	23.6	1.25
		2.54	22.8	1.20
		6.35	20.4	1.08
	352	0	26.2	0.96
		1.27	31.3	1.15
		1.91	30.7	1.13
		3.81	28.4	1.04
		6.35	26.5	0.97
	493	0	37.0	1.00
		6.35	38.9	1.04

Table 3-77 — CRITICAL PARAMETERS OF H_2O SOLUTIONS OF HIGHLY ENRICHED $UO_2(NO_3)_2$ IN ALUMINUM CYLINDERS (RADIAL REFLECTOR OF PHOSPHORIC ACID SOLUTION, OR OF BISMUTH SUBCARBONATE AND H_2O)

Data from Ref. 283.

Core Diameter, cm	Core Parameters			Radial Reflector	
	H/U^{235} Atom Ratio	Critical Height of Core solution, cm	Critical Mass, kg U^{235}	Composition	Thickness, cm
25.4	61.8	>40	>7.3	phosphoric acid solution; 0.465 gm P/cm^3	0
		>31.1	>5.6		2.24
		25.8	4.68		4.45
		23.6	4.28		6.68
		22.6	4.11		8.89
		16.0[a]	2.91[a]		
	240	72.4	3.82		0
		34.6	1.83		2.24
		29.2	1.55		4.45
		28.3	1.50		8.89
25.4	61.8	>40	>7.3	dry bismuth subcarbonate; 0.52 gm Bi/cm^3	0
		>36	>6.4		8.89
		21.8[a]	3.96[a]		8.89
	240	72.4	3.82		0
		53.6	2.84		4.45
		48.8	2.58		8.89
30.5	352	36.8	1.94		0
		35.4	1.87		2.24
		33.5	1.77		11.43
30.5	352	36.8	1.94	bismuth subcarbonate slurry; 0.85 gm Bi/cm^3, 0.82 gm H_2O/cm^3	0
		28.7	1.52		2.24
		24.7	1.31		11.43
	493	49.5	1.91		0
		30.1	1.17		11.43

[a] Values obtained with core and reflector enclosed in water.

Table 3-78—CRITICAL PARAMETERS OF H_2O SOLUTIONS OF HIGHLY ENRICHED $UO_2(NO_3)_2$ IN ALUMINUM CYLINDERS (RADIAL REFLECTOR OF SOLUTION OF NATURAL URANYL NITRATE)

Data from Ref. 283.

Core Diameter, cm	Core			Radial Reflector	
	H/U^{235} Atom Ratio	Critical Height of Core Solution, cm	Critical Mass, kg U^{235}	Concentration, gm U/cm^3 sol.	Thickness, cm
25.4	61.8	>40	>7.3	0.426	0
		29.9	5.40		2.24
		25.3	4.60		4.45
		23.6	4.29		6.68
		23.0	4.17		8.89
	240	72.4	3.82	0.426	0
		34.8	1.84		2.24
		29.0	1.53		4.45
		27.3	1.45		6.68
		26.4	1.40		8.89
	352	subcritical		0.426	0
		47.1	1.73		2.24
		36.1	1.33		4.45
		32.0	1.17		8.89
	352	subcritical		0.217	0
		44.7	1.64		2.24
		35.7	1.31		4.45
		32.5	1.20		8.89
30.5	493	49.5	1.91	0.217	0
		35.2	1.36		2.24
		29.8	1.15		11.43

Table 3-79—CRITICAL PARAMETERS OF H_2O SOLUTIONS OF ~93% ENRICHED $UO_2(NO_3)_2$ IN ALUMINUM CYLINDER[a] (ANNULAR VOID BETWEEN CORE AND WATER REFLECTOR)

Data from Ref. 283.

H/U^{235} Atom Ratio	Thickness of Annular Void, cm	Critical Height of Core Solution, cm	Critical Mass, kg U^{235}
61.8	0	16.6	3.02
	2.54	19.0	3.45
	5.08	21.0	3.81
	7.62	22.4	4.08
	10.16	23.6	4.28
	∞	>40	>7.3
240	0	20.1	1.06
	2.54	24.0	1.27
	5.08	26.5	1.40
	10.16	29.6	1.57
	∞	72.4	3.82

[a] N/U^{235} atom ratio = 2.86; cylinder diameter = 25.4 cm.

Table 3-80—CRITICAL PARAMETERS OF SOLUTIONS OF ENRICHED UO_2F_2 VERSUS THICKNESS OF CYLINDRICAL VOID SEPARATING THE CORE FROM THE TOP WATER REFLECTOR[a]

Data from Ref. 286.

Void Thickness, cm	Critical Height of Core Solution, cm
0	12.5
1	13.6
2	13.8
4	14.3
6	14.5

[a] H/U^{235} atom ratio = 43.2. Core solution contained in an aluminum cylinder (25.4 cm dia.; 0.16 cm wall), otherwise totally reflected by water.

Table 3-81—RELATIVE EFFECT OF WATER AND STYROFOAM REFLECTORS ON CRITICAL MASS OF AN H_2O SOLUTION OF ENRICHED UO_2F_2 IN A THIN ALUMINUM SLAB CONTAINER

Data from Ref. 288.

Properties of Materials	
Concentration of core solution:	0.0878 gm U^{235}/cm^3 sol. (93.2% U^{235} enrichment)
H/U^{235} atom ratio:	293
Density of Styrofoam:	0.028 gm/cm^3
Criticality Data	
Reflector Conditions	**Critical Height of Core Solution, cm**
No reflector	69.2
H_2O reflector on bottom and on all sides to height of solution	20.55
7.6 cm Styrofoam on each face	58.2
15.2 cm Styrofoam on each face	55.5
7.6 cm Styrofoam on each face, plus H_2O reflector on bottom and on all four sides of slab assembly to height of core solution	27.5
15.2 cm Styrofoam on each face, plus H_2O reflector on bottom and on all four sides of slab assembly to height of solution	31.8

Table 3-82—CRITICAL HEIGHT OF HIGHLY ENRICHED UO_2F_2 SOLUTION[a] VS. THICKNESS OF ALUMINUM WALLS BOUNDING SLAB CORE 15.2 cm THICK

Data from Ref. 266.

Wall Thickness, cm	Critical Height, cm
0.32	32.7
0.64	31.3
0.95	30.2

[a] H/U^{235} atom ratio = 50.1.

Measurements were made[266] of the increase in critical height of a solution ($H/U^{235} = 328$) as the distance of the core from a thick concrete wall was increased. In some of these experiments a sheet of Boral (~150 cm × 120 cm × 0.64 cm) was interposed between the core and the concrete, either at the boundary of the core or at the face of the concrete wall. The data are given in Fig. 3-59.

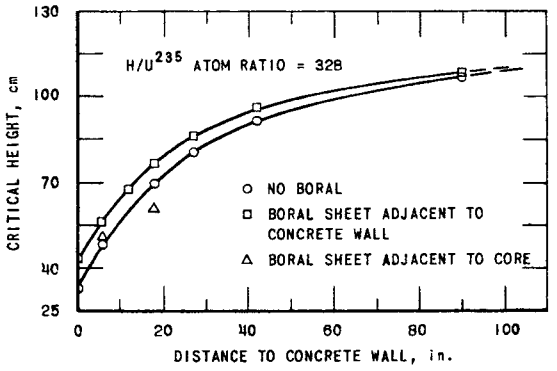

Fig. 3-59—Critical height of H_2O solutions of enriched UO_2F_2 in an aluminum-walled slab (6 in. thick), as a function of distance from a parallel concrete wall (5 ft thick). Aluminum wall thickness: 1/8 in.; no water between core and concrete wall. *Reproduced from Ref. 266.*

3.7.2.3 Aluminum-Walled Vessels; Reflectors: Layers of Furfural, Concrete, Graphite, and Water

Fox and Gilley[265,289] have reported on the variation of the critical parameters of H_2O solutions of highly enriched UO_2F_2 (~93% U^{235}) as a function of the composition and of the thickness of reflectors. The relative reflector effectiveness of furfural, concrete, and graphite were compared with that of water. The results, reported in Tables 3-83 through 3-85, have not been corrected for vessel structure, for absence of part of the reflector, etc., the purpose of the experiments being to make a *qualitative* comparison of reflector materials.

Table 3-83—EFFECT OF THICKNESS OF RADIAL REFLECTOR OF WATER OR FURFURAL ON CRITICAL PARAMETERS OF AN AQUEOUS SOLUTION OF ENRICHED UO_2F_2[a]

Data from Ref. 265.

Reflector Thickness, cm	Water Reflector		Furfural Reflector	
	Core Height, cm	Critical Mass, kg U^{235}	Core Height, cm	Critical Mass, kg U^{235}
0	34.2	5.85	34.2	5.85
2.24	24.7	4.23	26.0	4.46
4.45	21.4	3.66	22.7	3.88
6.68	20.3	3.47	21.0	3.60
8.89	20.0	3.42	20.1	3.44

[a] H/U^{235} atom ratio = 73.4.

The relative worths of furfural and water were measured as a function of their thickness as a radial reflector of a solution of UO_2F_2 contained in a 25.4-cm-diameter aluminum cylinder. The fuel concentration in the core was 0.337 gm U^{235}/cm^3, corresponding to an H/U^{235} atom ratio of 73.4. Concentric, aluminum-walled, annular "cans", 2.54 cm thick (including a total wall thickness of 0.32 cm), were used to contain the liquid reflector. The critical height of the core solution was determined in each case. The critical height data, given in Table 3-83, indicate that H_2O, with a hydrogen density 2.4 times that of furfural (C_4H_3OCHO), was more effective as a reflector than furfural for thicknesses less than 8.9 cm. At greater thicknesses, the two materials were essentially equivalent as reflectors.

The effectiveness of concrete as a neutron reflector was measured by determining the critical mass of an enriched uranium solution contained in a stainless steel cylinder (22.9 cm diameter) as a function of the distance from the cylinder to a concrete wall. The U^{235} concentration was 0.3314 gm/cm^3, corresponding to an H/U^{235} atom ratio of 74.6. The concrete wall (122 cm × 122 cm × 15 cm thick) consisted of blocks of shielding concrete having a density of 2.14 gm/cm^3. As shown in Table 3-84, little interaction occurred after the edge-to-edge separation was increased to 60 cm.

Measurements were made of the relative effectiveness of reflectors consisting of layers of water and/or carbon and/or water placed against the bottom of a 50.8-cm-diameter aluminum cylinder. The cylinder contained an aqueous solution of highly enriched UO_2F_2(~ 93.2% U^{235}). The U^{235} concentration was 0.8288 gm/cm^3, corresponding to H/U^{235} = 27.1. (An examination of the effectiveness of various thicknesses of firebrick in the layered reflector was also carried out in connection with possible hazards in casting operations.) The dependence of the critical solution height on the composition and thicknesses of the layers is shown in Table 3-85.

Table 3-84—CRITICAL PARAMETERS OF AN AQUEOUS SOLUTION OF ENRICHED UO_2F_2 VS. DISTANCE TO A WALL OF SHIELDING CONCRETE[a]

Data from Ref. 265.

Distance from Core Edge to Concrete Wall, cm	Critical Height of Solution, cm	Critical Mass, kg U^{235}
0	41.3	5.64
15.2	52.3	7.14
30.5	56.5	7.71
45.7	58.0	7.92
61.0	58.5	7.99
∞	59.0	8.05
0[b]	40.3	5.50
0	20.6	2.81[c]
∞	20.7	2.83[c]

[a] H/U^{235} atom ratio = 74.6; solution contained in a 22.9-cm-diameter stainless steel pipe; concrete density = 2.14 gm/cm^3; concrete wall 15 cm thick.

[b] In this case, the concrete thickness was 30.5 cm (12 in.).

[c] In these experiments, the concrete displaced water in an effectively infinite radial water reflector. There was no reflector on top of the cylinder of solution.

Table 3-85—CRITICAL PARAMETERS OF AN AQUEOUS SOLUTION OF ENRICHED UO_2F_2 VS. STRUCTURE OF BOTTOM REFLECTOR[a]

Data from Ref. 265.

Approximate Reflector Thickness, cm			Critical Height of Solution, cm	Critical Mass, kg U^{235}
Water	Carbon	Water		
0	0	0	15.4	25.9
0	1.3	0	14.8	24.8
0	2.5	0	14.3	23.9
0	5.1	0	13.4	22.5
0	8.9	0	12.7	21.3
0	14.0	0	12.3	20.6
0	0	15	12.1	20.3
0	7.6	15	11.3	19.0
0	14.0	15[b]	10.9	18.3
0.63	14.0	∞	10.8	18.2
1.2	14.0	∞	10.7	18.0
1.91	14.0	∞	10.9	18.3
2.54	14.0	∞	11.0	18.5

[a] H/U^{235} atom ratio = 27.1.

[b] Essentially infinite.

3.7.3 ANNOTATED REFERENCES FOR REACTIVITY EFFECTS OF HOLES IN REFLECTORS

Reactivity effects of experimental holes in the reflectors of critical assemblies constitute an important topic in the design and analysis of research reactors. The BSR (Bulk Shielding Reactor) at ORNL has been used for a number of experiments intended to supply such data for typical swimming-

pool reactors. In these cases, the fuel assemblies were positioned to present relatively flat core faces near voided reflector regions. Because of the typically unsymmetrical cores and/or reflectors appearing in this and in other reactors, detailed listings of experimental data are not given here. Instead, an annotated bibliography for some of these data is included.

Martin and Mann[290] reported on the reactivity effects of experimental holes in the reflector of critical assemblies constructed to test designs for the MTR. The core was comprised of an aqueous solution of highly enriched UO_2F_2 in which was inserted a uniform array of thin aluminum plates to mock-up an Al/H_2O volume ratio of approximately 0.65. The cores were reflected laterally by 30 cm of beryllium, in some cases backed by 30 cm of graphite. The cores were unreflected axially. The experiments were carried out on rectangular-parallelepiped cores of various sizes. Criticality was achieved by substituting thin stainless steel strips for some of the aluminum strips normally in place in the core.

Johnson, et al.,[291] described a set of experiments on the Bulk Shielding Reactor (BSR) designed to yield information on reactivity changes due to the presence of partial reflectors and of beam holes in the reflector of a swimming pool research reactor. The beam holes were cylindrical ducts, ranging in diameter from ~11 cm to 45 cm, and in length from ~30 cm to ~120 cm. The ducts were filled with air, or with borated water. Reactivity changes as large as 9.3% were reported for aggregates of experimental holes in the reflector.

Johnson, et al.,[292] measured the reactivity effects of large voids adjacent to one face of the BSR. The measurements were made with or without a curtain of cadmium or Boral between the core and the void. Iron slabs of various thicknesses were inserted into the void to simulate the presence of experimental equipment.

Reactivity effects of large voids in the water reflector of the Pool Critical Assembly (PCA) were studied by Reynolds, et al.[293] The PCA was fueled with BSR-type fuel assemblies, arranged to present a flat face of seven assemblies to the voided reflector. Four effects were investigated, including the variation of reactivity effect with: (1) void size; (2) void position on the core-reflector interface; (3) distance between the void and the core; and (4) the superposition of void reactivity effects. It was found that for voids separated by at least 10 cm of water, the reactivity effects were essentially additive. When voids were separated by ~5 cm of H_2O, the sum of the separately determined void reactivities exceeded the measured effect of the multiple-void case. For zero-separation, the single large void was more effective than the superposition of the individual void components.

A theoretical correlation, using one-group perturbation theory and treating the void at the core-reflector interface as a gray absorber, yielded satisfactory agreement with experiment when measured real fluxes were used together with a cosine approximation to the adjoint flux. A method based on two-group diffusion theory was developed to compute the reactivity worth of a void covering an entire slab face of a rectangular-parallelepiped core.

3.7.4 CRITICAL PARAMETERS OF D_2O-REFLECTED H_2O SOLUTIONS OF HIGHLY ENRICHED UO_2SO_4: EFFECTS OF TEMPERATURE AND OF REFLECTOR LEVEL IN HRE-1

Visner and Wood[294] have reported upon the dependence of the critical fuel concentration in 50.0-liter HRE-1 cores on core temperature, reflector temperature, reflector height, and fuel pressure. The core was comprised of an aqueous solution of UO_2SO_4 with uranium enriched to approximately 93 wt-% U^{235}, and contained in a Type 347 stainless steel sphere (45.7 cm ID; 0.48 cm wall thickness). The reflector vessel was fabricated of mild steel (7.6 cm wall thickness), with spherical sides (99-cm ID), and a cylindrical top and bottom. The reflecting material was D_2O of purity 99.1 wt-% (as determined by a mass spectrometer measurement at the conclusion of the experimental work).

Criticality measurements were made with and without fuel circulation at core temperatures below 105°C; the results are given in Tables 3-86 and 3-87. Thus the effect of delayed neutrons on reactivity, due to fuel circulation, may be studied. In the first set of measurements with circulating fuel (Table 3-86), only the high-pressure system was used. Subsequently, criticality measurements were made at elevated core temperatures, with the high- and low-pressure systems connected together; these results are given in Table 3-88. The temperature coefficient of reactivity at room temperature was -3.7×10^{-2} %/°C; at 220°C the value was −0.115%/°C. The uniform-pressure coefficient of reactivity was 0.16%/1000 psi at 23.5°C.

The reflector was calibrated at room temperature as a function of reflector height, in terms of the net loss in "reactivity", Δk_{eff}, of a reference reactor as the reflector level was lowered. For the reference reactor, the core temperature was 25°C, and the reflector level was at 100% (full). Measurements were made with non-circulating fuel (Table 3-89), and with circulating fuel.

When the fuel is circulating, there is a loss in reactivity because some of the delayed neutrons are effectively lost to the core during the transit of the core solution. When a correction was made for this effect, at room temperature, the reactivity variation with reflector level was essentially the same as in the reactor with non-circulating fuel. The reactivity coefficient of reflector level was approximately constant in the region defined by the top and bottom of the core.

Table 3-86—CRITICAL FUEL CONCENTRATION WITH CIRCULATION: REFLECTOR FULL, RODS WITHDRAWN, HIGH-PRESSURE SYSTEM ALONE[a]

Data from Ref. 294.

Fuel Concentration, gm U^{235}/kg H_2O	Core Temperature, °C	Reflector Temperature, °C	Fuel Pressure, psig
25.98	67	64	100
25.94	68	60	100
26.33	79	25	100
26.40	80	79	100
26.48	82	79	120
26.81	92	87	260
26.48	83	79	120
26.86	93	92	100
26.97	96	94	120
27.09	101	95	300
27.11	101	95	100
27.10	102	98	600
27.14	102	100	100
27.17	102	100	300
27.16	103	100	910
27.33	104	100	120
27.36	105	102	120

[a]A fit to the critical fuel concentration as a function of core temperature, $22°C \leq T \leq 67°C$ has been developed: (gm U^{235}/kg H_2O) $\approx 24.73 + 0.028\ (T-22)$. The reflector temperature was 25°C and the fuel pressure was 100 psig.

Table 3-87—CRITICAL FUEL CONCENTRATION WITHOUT CIRCULATION: REFLECTOR FULL, RODS WITHDRAWN, HIGH-PRESSURE SYSTEM ALONE (100 psig)

Data from Ref. 294.

Fuel Concentration, gm U^{235}/kg H_2O	Critical Core Temperature, °C	Approximate Reflector Temperature, °C
24.97	35.2	35
25.11	40	40
25.75	63.9	64
26.19	77.6	76
26.57	91.6	88
26.71	93.4	91
26.92	100.7	97
26.94	101.2	100
27.09	103.5	100
27.09	104.0	101

Table 3-88 — CRITICAL FUEL CONCENTRATION WITH CIRCULATION: REFLECTOR FULL, RODS WITHDRAWN, HIGH- AND LOW-PRESSURE SYSTEMS CONNECTED TOGETHER

Data from Ref. 294.

Fuel Concentration, gm U^{235}/kg H_2O	Core Temperature, °C	Reflector Temperature, °C	Fuel Pressure, psig
27.11	96	89	520
27.13	98	90	440
27.15	99	92	460
27.22	100	93	600
27.24	101	93	600
27.30	103	94	420
27.39	103	95	430
27.43	105	100	520
27.45	106	101	530
28.38	120	138	460
28.44	126	123	450
29.41	144	145	380
29.46	145	147	440
30.44	164	165	440
31.64	177	184	500
32.27	198	178	1000
33.35	201	176	560
33.39	201	186	540
33.35	201	186	560
33.36	201	186	560
33.58	202	201	580
35.09	217	203	460
35.24	217	200	450
35.21	217	203	460
27.46	102	94	500
33.94	204	198	500
37.38	222	200	500
37.34	229	207	500
37.17	225	200	500
39.24	244	190	1000

Table 3-89 — D_2O-REFLECTOR CALIBRATION FOR AN HRE CORE WITH NON-CIRCULATING FUEL AT ROOM TEMPERATURE

Data from Ref. 294.

Percentage Reduction[a] in Reflector Height	Reactivity[b] Change, %	Percentage Reduction in Reflector Height	Reactivity Change, %
0 (check point)	−0.02	41.5	−0.88
20.0	−0.01	43.6	−1.15
30.0	−0.12	45.5	−1.12
33.7	−0.20	50.7	−1.69
34.0	−0.28	55.3	−2.20
39.5	−0.58	68.5	−3.16
39.5	−0.57	68.7	−3.27
41.3	−0.88	74.4	−3.75

[a] The range of the level indicator is 76.2 cm.

[b] Characteristics of the reference reactor: shim, control, and safety rods withdrawn; core temperature 25°C; fuel concentration 24.88 gm U^{235}/kg H_2O; reflector level 100%.

The effectiveness of the HRE reflector at ~225°C is shown in Fig. 3-60. The various points indicated were obtained from calibrations involving changes in fuel concentration or temperature. Two separate temperature runs are indicated.

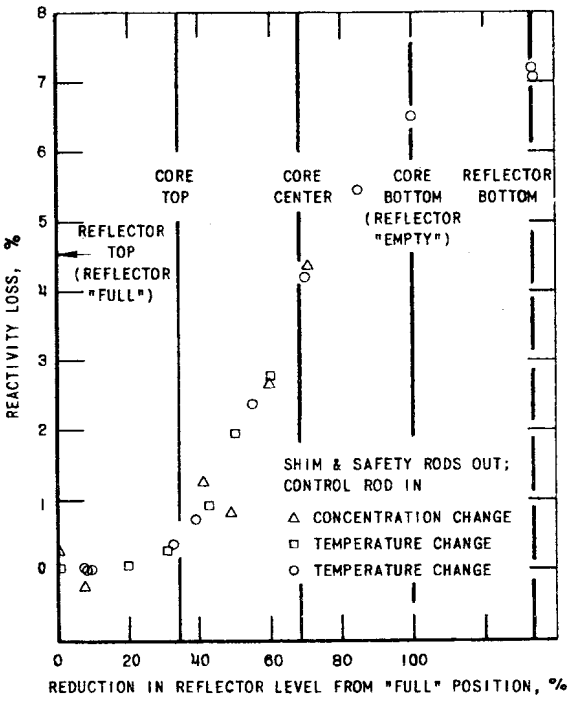

Fig. 3-60—Calibration of D_2O reflector at 225°C (HRE-1). *Reproduced from Ref. 294.*

3.7.5 CRITICAL PARAMETERS OF INTERACTING ARRAYS OF REGULAR VESSELS CONTAINING AQUEOUS SOLUTIONS OF HIGHLY ENRICHED UO_2F_2

Fox, et al.,[265] published criticality data for arrays of aluminum cylinders having parallel axes and containing an aqueous solution of uranium enriched to 93.2% U^{235}. The H/U^{235} atom ratio was 44.3. The results were summarized by the authors as follows:

> "In these (experiments) it was found that a hexagonal array of seven (one in the center) water-reflected, cadmium-wrapped 6-in.-diameter cylinders would be subcritical at any solution height with an edge-to-edge spacing of the cylinders greater than 2 in. A similar array of unreflected 8-in.-diameter cylinders required a spacing of about 18 in. Three unreflected 8-in.-diameter cylinders arranged in the geometry of an equilateral triangle required an edge-to-edge spacing of about 9 in. A water-reflected, cadmium-wrapped 8-in.-diameter cylinder became critical at a height of approximately 24.5 in. Water-reflected 6-in.-diameter cylinders arranged in straight-line arrays were effectively isolated at edge-to-edge spacings greater than 12 in. Two unreflected 8-in.-diameter cylinders required a spacing of 3 in. to remain subcritical at any height. When three water-reflected 8-in.-diameter cylinders were arranged in an isosceles-triangle geometry, it was found that the common critical height was essentially constant for vertex angles greater than 90 degrees. As would be expected, it was found that the angular dependence was much greater in an unreflected system."

There was no top reflector in these experiments. The core vessels, aluminum with a wall thickness of 0.16 cm., were coated with Heresite on the inside. Some of the results are summarized in Fig. 3-61. Similar data for H/U^{235} ~300 are given in Fig. 3-62. In the latter experiments, the arrays were isolated so far as possible from reflecting material, whereas in the earlier set the cylinders were positioned in a ~240-cm-diameter steel tank which acted as a reflector for the so-called unreflected arrays.

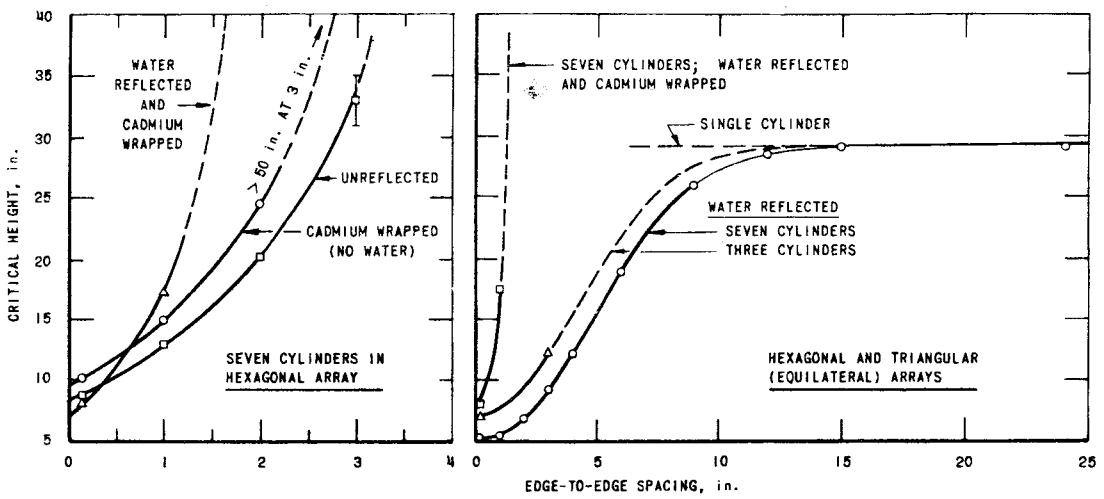

Fig. 3-61 — Critical solution height as a function of edge-to-edge spacing of aluminum cylinders (6 in. dia.) containing H_2O solutions of UO_2F_2 (uranium enriched to 93.2% U^{235}; H/U^{235} atom ratio = 44.3). *Reproduced from Ref. 265.*

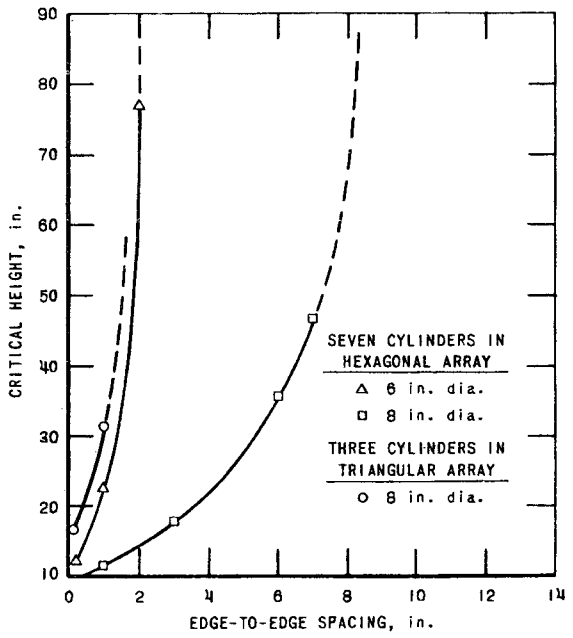

Fig. 3-62 — Critical solution height as a function of edge-to-edge spacing of unreflected aluminum cylinders containing H_2O solutions of UO_2F_2 (uranium enriched to 93.2% U^{235}; H/U^{235} atom ratio = 309). *Reproduced from Ref. 265.*

Figures summarizing the results for various arrays of 20.3-cm- and 24.1-cm-diameter cylinders, and straight-line arrays of 15.2-cm-diameter cylinders, may be found in Refs. 265 and 295. Cited below are other references to experiments dealing with interacting cores containing aqueous solutions of highly enriched UO_2F_2:

Containing Vessels	Geometry	Ref.
Aluminum pipes; ID ~10.2 cm, 12.7 cm, or 19.0 cm.	Pipes intersecting in "cross" or "Y" geometry; reflected or unreflected.	265
Five stainless steel pipes; ID ~10.2 cm; length ~180 cm; cadmium wrapped.	Pipes in a linear array, center-to-center spacing ~38 cm.	296
Aluminum or stainless steel cylinders.	Pairs of cylinders with parallel axes; water-reflected or unreflected.	274
Aluminum slabs and cylinders.	Various arrays of slabs or cylinders; included are slabs in "T" or "L" geometry.	266

Henry, et al.,[297] described methods of calculating the critical parameters of arrays of core cylinders, and compared calculations with experiments. Other methods include those reported by Avery[298,299] and by Stewart.[300]

3.7.6 CRITICAL PARAMETERS OF CYLINDRICAL ANNULAR CORES CONTAINING AQUEOUS HOMOGENEOUS SOLUTIONS OF UO_2F_2 AND OF U_3O_8

Some measurements of the critical parameters of cylindrical, annular cores containing aqueous solutions of UO_2F_2, with uranium enriched to 93.2% U^{235}, have been reported.[265,301] The containing vessels were formed by the concentric fitting of Type 2S aluminum cylinders with a wall thickness of 0.16 cm.

Data from Ref. 265 relate to solutions with H/U^{235} atom ratios of ~73. Variations of the content of the inner cylinder included: (1) leaving the inner cylinder empty; (2) filling it with water; (3) lining it with a sheet of cadmium 0.05 cm thick; and (4) lining it with cadmium and filling it with water. Critical parameters were measured with and without a water reflector on the sides and bottom; no reflector was used above the solution. The bottom plates of the annular containers were aluminum, ~1.3 cm thick. The data reported in Table 3-90 were not corrected for the effect of this aluminum partial reflector on the extrapolation length at the bottom of the core, or for the absence of a top reflector. Figures 3-63 and 3-64 are graphical representations of these datum points.

In an extension of these experiments, Fox and Gilley[301] measured the critical parameters of H_2O solutions of UO_2F_2 with atom ratios of 50.4 and 309. The dimensions of the cylinders ranged from 5.1 cm I.D. to 61.0 cm I.D., and from 25.4 cm O.D. to 76.2 cm O.D. All measurements were made with the inner cylinder lined with cadmium (0.05 cm thick), and filled with water to a height of ~122 cm. The data are presented in Table 3-91. No corrections were made for the aluminum bottom core plate (1.3 cm thick), or for the absence of a top reflector.

Callihan and Cronin[302] reported measurements in cylindrical, annular cores fueled with U_3O_8 in glycerol tri-stearate. The uranium was enriched to 5% in U^{235}.

3.7.7 RADIAL FLATTENING OF THERMAL NEUTRON FLUX IN A CYLINDRICAL CORE BY VARYING THE AQUEOUS-SOLUTION CONCENTRATION OF HIGHLY ENRICHED UO_2F_2

Morfitt[262,303] experimentally investigated the theoretical equivalence relationship between minimum critical mass and flat thermal neutron core flux in a thermal reactor wherein the moderator and reflector have identical slowing-down properties. Measurements were made in a cylindrical reactor, bare axially and reflected radially by an effectively infinite water medium. Aqueous solutions of UO_2F_2, with uranium enriched to 93.2% U^{235}, were used as fuel in a step-function approximation to the theoretical continuous curve for the radially-varying fuel concentration.

The core was divided into five regions radially, with a Type 2S aluminum wall (thickness: 0.064 cm) between adjacent regions. In each annular zone, the fuel concentration was taken to be the average value of the theoretical distribution. The dimensions and fuel concentrations are listed in Table 3-92.

Table 3-90 — CRITICAL PARAMETERS OF CYLINDRICAL ANNULAR CORES CONTAINING H_2O SOLUTIONS OF HIGHLY ENRICHED UO_2F_2 (93.2% U^{235})

Data from Ref. 265.

Core Diameter,[a] cm		Contents of Inner Cylinder	H/U^{235}[b] Atom Ratio	Critical Hgt. of Solution, cm		Critical Mass, kg U^{235}	
O.D.	I.D.			Reflected[c]	Unreflected	Reflected[c]	Unreflected
20.3	0	—	72.4	24.0	—	2.66	—
	5.1	H_2O	72.4	27.1	—	2.83	—
	10.2	H_2O	72.4	50.0	—	4.18	—
25.4	0	—	73.4	17.5	33.3	3.00	5.70
	5.1	H_2O	73.4	17.8	—	2.92	—
	10.2	H_2O	74.6	23.8	300[d]	3.36	42
	15.2	H_2O	74.6	64.1	—	6.93	—
	5.1	Air	74.6	20.7	49.6	3.37	8.01
	10.2	Air	74.6	27.6	—	3.90	—
	15.2	Air	74.6	76.8	—	8.30	—
	5.1	Cd Liner	74.6	20.4	70.0	3.30	11.3
	10.2	Cd Liner	74.6	31.9	—	4.52	—
	15.2	Cd Liner	74.6	[e]	—	—	—
	5.1	H_2O + Cd Liner	74.6	20.5	138.2	3.31	22.3
	10.2	H_2O + Cd Liner	74.6	45.4	[e]	6.43	—
	15.2	H_2O + Cd Liner	74.6	[e]	—	—	—
38.1	0	—	74.6	12.7	16.4	4.79	6.21
	5.1	H_2O	74.6	12.9	17.0	4.77	6.33
	10.2	H_2O	72.4	13.9	—	5.11	—
	15.2	H_2O	74.6	16.0	25.2	5.08	8.01
	20.3	H_2O	72.4	21.0	—	5.87	—
	25.4	H_2O	72.4	41.6	—	9.01	—
	5.1	Air	74.6	13.3	17.6	4.95	6.52
	15.2	Air	74.6	17.5	29.9	5.56	9.50
	5.1	Cd Liner	74.6	—	18.0	—	6.69
	15.2	Cd Liner	74.6	—	33.2	—	10.6
	5.1	H_2O + Cd Liner	74.6	—	18.2	—	6.76
	15.2	H_2O + Cd Liner	74.6	—	54.3	—	17.3
50.8	0	—	72.4	11.3	—	7.83	—
	5.1	H_2O	72.4	11.4	—	7.79	—
	15.2	H_2O	72.4	12.6	—	7.96	—
	25.4	H_2O	72.4	16.4	—	8.51	—
	38.1	H_2O	72.4	44.3	—	13.4	—

[a] Reference 265 lists dimensions in inches. Metric equivalents have been rounded off to the nearest 0.1 cm; e.g., 5.1 cm corresponds to 2 in. Walls of the cylindrical annuli are Type 25 aluminum, 0.16 cm thick.

[b] Solution Concentrations

H/U^{235} Atom Ratio:	72.4	73.4	74.6
gm U^{235}/cm^3 solution:	0.3423	0.3370	0.3314

[c] Effectively infinite water reflector axially below and radially beyond outer cylinder.

[d] Extrapolated from a maximum experimental core solution height of 142.5 cm.

[e] Apparently these annuli would have been subcritical at any height, on the basis of an extrapolation of the reciprocal neutron multiplication from that at solution heights ranging up to at least 120 cm.

Table 3-91—CRITICAL PARAMETERS OF CYLINDRICAL ANNULAR CORES CONTAINING H_2O SOLUTIONS OF HIGHLY ENRICHED UO_2F_2 (93.2% U^{235})

Note: Inner cylinder lined with cadmium and filled with H_2O.

Data from Ref. 301.

Core Diameter,[a] cm		H/U^{235} Atom Ratio[b]	Critical Hgt. of Solution, cm		Critical Mass, kg U^{235}	
O.D.	I.D.		Reflected[c]	Unreflected[d]	Reflected[c]	Unreflected[d]
25.4	5.1	50.4	20.2	101.5	4.7	23.7
	10.2	50.4	40.9	—	8.4	—
	5.1	309	39.1	—	1.59	—
30.5	5.1	50.4	16.0	27.8	5.4	9.5
	10.2	50.4	21.8	[e]	6.8	—
	15.2	50.4	48.7	—	12.8	—
	5.1	309	24.0	46.2	1.42	2.74
	10.2	309	46.6	—	2.53	—
38.1	5.1	50.4	—	19.2	—	10.4
	10.2	50.4	15.4	24.9	7.9	12.7
	15.2	50.4	19.5	50.5	9.0	23.3
	20.3	50.4	31.1	[e]	12.2	—
	25.4	50.4	[e]	—	—	—
	5.1	309	18.3	25.8	1.71	2.42
	10.2	309	22.7	42.9	2.01	3.80
	15.2	309	34.6	[e]	2.77	—
	20.3	309	[e]	—	—	—
50.8	15.2	50.4	13.3	19.2	11.8	17.0
	20.3	50.4	15.0	23.1	12.3	18.9
	25.4	50.4	18.4	36.3	13.5	26.6
	30.5	50.4	26.0	[e]	16.2	—
	35.6	50.4	93.3	—	46.4	—
	15.2	309	18.5	25.5	2.85	3.93
	20.3	309	21.4	35.0	3.04	4.98
	25.4	309	30.4	[e]	3.86	—
	30.5	309	88.3	—	9.57	—
76.2	38.1	50.4	13.4	18.8	22.0	31.0
	50.8	50.4	19.0	38.8	23.2	47.3
	61.0	50.4	91[f]	—	—	—
	38.1	309	18.1	24.2	5.17	6.92
	50.8	309	31.6	—	6.70	—

[a] Reference 301 lists dimensions in inches. Metric equivalents have been rounded off to the nearest 0.1 cm. Walls of the cylindrical annuli are Type 2S aluminum, 0.16 cm thick.

[b] Solution Concentrations

H/U^{235} Atom Ratio:	50.4	309
gm U^{235}/cm^3 solution:	0.4813	0.0836

[c] Effectively infinite outside water reflector to level corresponding to top of fuel solution.

[d] No radial water reflector.

[e] Extrapolation of the reciprocal source neutron multiplication curve from the multiplication at a solution height of at least 91 cm indicated that these assemblies would have been subcritical at any height.

[f] Extrapolation of the reciprocal multiplication curve from the value at a solution height of 77.4 cm indicated that this assembly could not have been made critical at a height less than 91 cm, if at all.

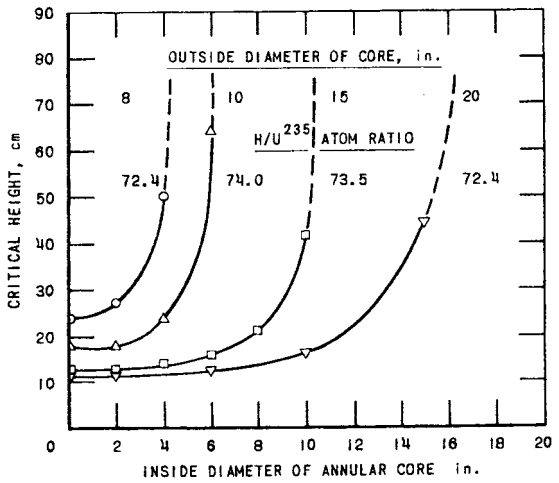

Fig. 3-63 — Critical solution height as a function of inside diameter of aluminum-walled annular cores containing H_2O solutions of UO_2F_2 (uranium enriched to 93.2% U^{235}). Inner cylinder filled with water; core reflected radially and at bottom with water. *Reproduced from Ref. 265.*

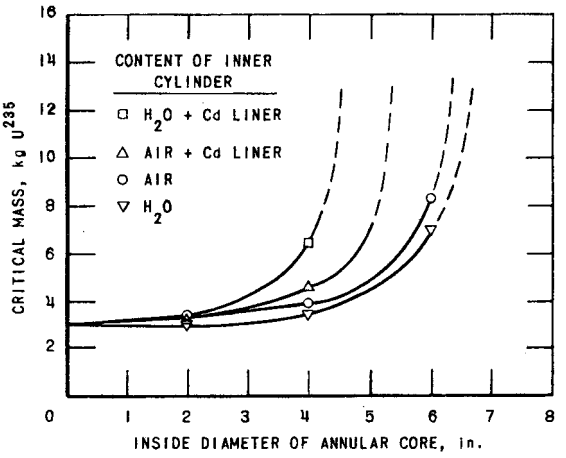

Fig. 3-64 — Critical mass as a function of inside diameter of water-reflected, aluminum-walled annular core (10 in. O.D.) containing H_2O solution of UO_2F_2 (uranium enriched to 93.2% U^{235}; H/U^{235} atom ratio = 74.6). *Reproduced from Ref. 265.*

Table 3-92 — SPECIFIED CHARACTERISTICS OF ANNULAR REGIONS IN MINIMUM-CRITICAL-MASS EXPERIMENT

Data from Ref. 303.

Annular Region Number	Radii of Annulus,[a] cm		Fuel Concentration, gm U^{235}/cm^3 H_2O
	Inner	Outer	
1	0	5.48	0.0678
2	5.54	8.08	0.0545
3	8.14	10.21	0.0418
4	10.27	12.49	0.0288
5	12.56	15.10	0.0153

[a] The inner and outer radii of the annulus correspond to the inner surfaces of the aluminum rings bounding the annulus. The measured average thickness of each radial zone was within ±0.03 cm of the specified thickness. The average thickness of the aluminum partitions was 0.064 cm.

687863 O - 63 - 15

A core and reflector height of 41.6 cm was specified in the computations. The measured height of core and radial reflector was 42.7 cm. Other comparison data of experiment and multigroup calculation are presented in Table 3-93.

In Fig. 3-65, the thermal neutron flux shape obtained from a two-group diffusion theory computation is compared with an experimental "subcadmium activity" curve, normalized to the same average value in the core.

Table 3-93—COMPARISON OF CALCULATED AND EXPERIMENTAL CRITICAL MASSES OF THE MINIMUM-CRITICAL-MASS REACTOR

Data from Ref. 303.

	Critical Mass, kg U^{235}		Reduction in Critical Mass, %
	Uniform Fuel Loading	Minimum-Mass Loading	
Experiment	1.162	1.061	8.7
Calculation	1.192	1.038[a]	12.9

[a]Obtained by correcting the calculated mass (1.024 kg U^{235}) for the non-ideal aspects of the experiment, e.g., for the aluminum radial partitions.

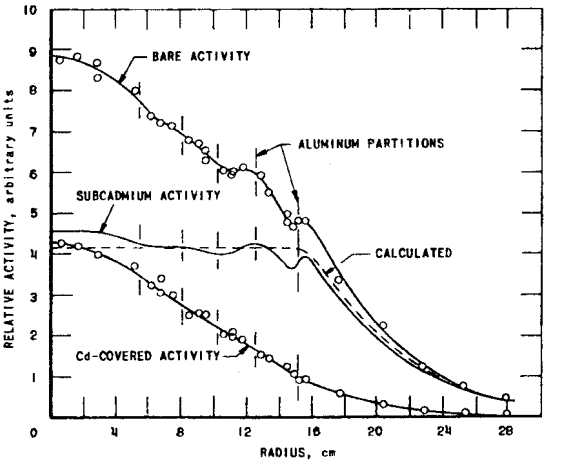

Fig. 3-65—Radial activities of bare and cadmium-covered indium detectors in the minimum-critical-mass experiment. *Data from Ref. 303.*

3.7.8 CRITICAL PARAMETERS OF HIGHLY ENRICHED UO_3-H_2O SLURRIES IN AN ALUMINUM CYLINDER

Cronin and Callihan[304] reported critical mass measurements for aqueous slurries of UO_3 enriched to 93.2% in U^{235}. The slurries were contained in an aluminum cylinder (30.5 cm dia.; 0.32 cm wall thickness), with a hemispherical bottom. The cylinder, in turn, was mounted in a steel tank (~275 cm dia.), into which water could be pumped to provide a radial and lower end reflector. In some experiments, the reactor was brought to criticality without a water reflector.

A stainless steel stirrer and aluminum baffles were used to maintain essentially vertical circulation of the slurry with little surface disturbance or vortex formation. In Table 3-94 are listed the criticality data for reflected cores at stirrer speeds of 200 rpm and 600 rpm.

Table 3-94 — CRITICAL PARAMETERS FOR UO_3-H_2O SLURRIES IN A 30.5-cm-DIAMETER ALUMINUM CYLINDER

Data from Ref. 304.

H/U^{235} Atom Ratio	U^{235} Concentration,[a] gm U^{235}/cm^3	Stirrer Speed: 600 rpm			Stirrer Speed: 200 rpm		
		Critical[b] Core Height, cm	Reflector Height, cm	Critical Mass, kg U^{235}	Critical Core Height,[b] cm	Reflector Height, cm	Critical Mass, kg U^{235}
90.2	0.278	21.1	21.1	3.20	20.1	20.2	3.03
136	0.186	22.6	26.0	2.35	—	—	—
204	0.125	24.3	27.6	1.73	23.1	27.6	1.62
251	0.102	24.1	24.1	1.40	23.2	23.2	1.34
259	0.0994	24.3	28.0	1.37	—	—	—
366	0.0707	30.3	31.5	1.29	—	—	—
413	0.0627	28.5	28.5	1.05	27.8	27.8	1.02
467	0.0554	30.8	33.0	1.02	—	—	—
511	0.0507	33.8	33.8	1.04	—	—	—
523	0.0496	34.0	34.0	1.03	32.0	34.0	0.96
538	0.0484	33.8	33.3	0.99	30.7	33.3	0.89
610	0.0425	37.0	38.0	0.97	—	—	—
632	0.0412	35.1	35.1	0.89	32.4	32.4	0.81
668	0.0388	41.3	54.0	1.01	—	—	—

[a] The laboratory analyses were reported as mass of uranium per unit mass of slurry sample. The specific gravity of the slurry was calculated using a UO_3-H_2O crystal density of 6 gm/cm^3.

[b] The temperature of the slurry was 29°C. A water reflector was present laterally, and at the bottom.

3.7.9 CRITICAL PARAMETERS OF REACTORS CONTAINING MIXTURES OF PARAFFIN AND ENRICHED UF_4 (2 wt-% U^{235})

An experimental group at ORNL[305–307] published critical mass data for cylindrical and for square-base-parallelepiped cores containing mixtures of paraffin ($C_{25}H_{52}$) and UF_4 enriched to 2 wt-% in U^{235}. The size of the UF_4 particles averaged 0.020 in. Four mixtures were used:

Fuel concentration		
wt-% UF_4 in paraffin	gm U/cm^3	H/U^{235} Atom Ratio
92.1	3.1	195
88.6	2.6	294
84.8	2.2	404
~82	1.97	501

In other experiments, blocks of 92.1 wt-% UF_4 and 88.6 wt-% UF_4 were alternated to give an effective H/U^{235} atom ratio of 245.

The reflected cores were surrounded with an effectively infinite mixture of paraffin and Plexiglas.

Graphic results of the experiments are reproduced as Figs. 3-66 and 3-67, giving the critical mass as a function of the width of the base of the core. Curves of the minimum critical mass versus the H/U^{235} atom ratio have been deduced from the experimental work; they appear in Fig. 3-68.

The infinite multiplication factor, k_∞, for a UF_4-paraffin medium, with uranium enriched to 2% U^{235} and with H/U^{235} = 195, has been inferred from a measurement in the PCTR at Hanford.[308] The result is $k_\infty = 1.216 \pm 0.013$.

3.7.10 CRITICAL PARAMETERS OF UNIFORM D_2O SOLUTIONS OF NATURAL OR ENRICHED UO_2F_2

This section contains data pertaining to well-moderated D_2O solutions of UO_2F_2. Critical-parameter investigations of D_2O solutions of highly enriched UO_2F_2 in stainless steel-walled spheres have been carried out by Olcott[126] for D/U^{235} atom ratios ranging from 34 to 856, plus a few experiments at D/U^{235} = 2081. These studies are described in Section 6.3 for, in the majority of the experiments, the D/U^{235} ratio was so low that more than one-third of the fissions occurred above cadmium-cutoff values.

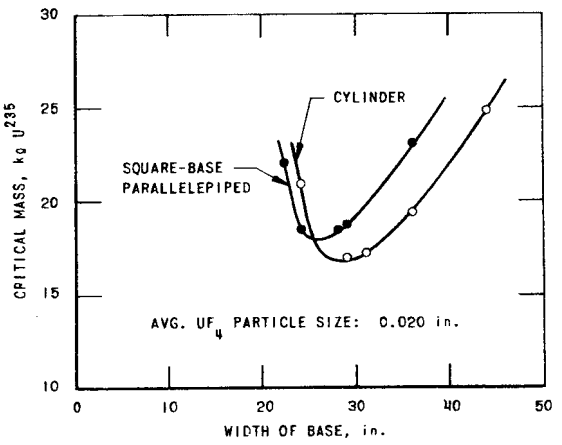

Fig. 3-66—Critical masses in reflected cores containing homogeneous mixture of paraffin and UF_4 (uranium enriched to 2% U^{235}; H/U^{235} atom ratio = 195). *Reproduced from Ref. 269.*

Fig. 3-67—Critical masses in cores containing homogeneous mixture of paraffin and UF_4 (uranium enriched to 2% U^{235}; H/U^{235} atom ratio = 294). *Reproduced from Ref. 269.*

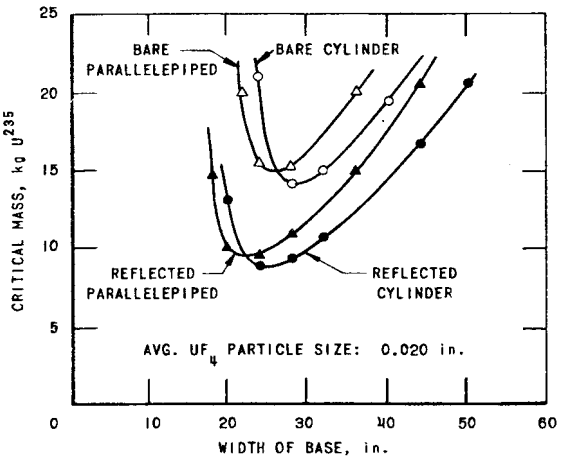

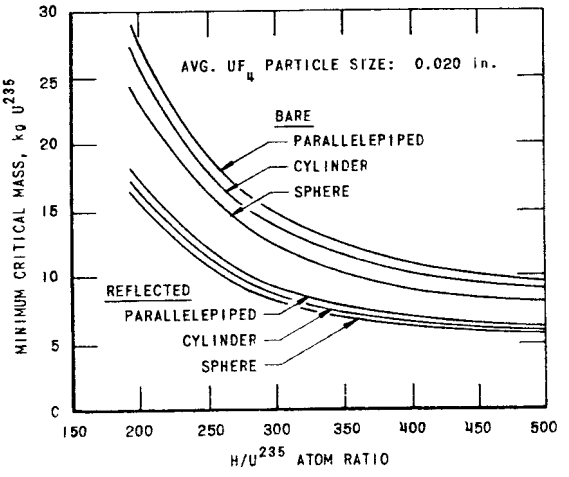

Fig. 3-68—Minimum critical masses as a function of H/U^{235} atom ratio in cores containing a homogeneous mixture of paraffin and UF_4 (uranium enriched to 2% U^{235}). *Reproduced from Ref. 307.*

3.7.10.1 Extrapolations from Exponential Experiments Using D_2O Solutions of Natural UO_2F_2

Measurements were made of the spatial variation of the activity of cadmium-covered indium foils irradiated in an exponential assembly located on top of the thermal column of the CP-2 reactor at Argonne.[309] The assembly consisted of a steel cylindrical tank containing a D_2O solution of natural uranyl oxyfluoride (UO_2F_2).

Using standard fitting procedures, the spatial activity distributions were analyzed to obtain the material buckling as a function of the fuel concentration. Calculated critical parameters of bare spheres of equivalent buckling are listed in Table 3-95.

Table 3-95 — CRITICAL PARAMETERS OF UNREFLECTED SPHERES CONTAINING NATURAL UO_2F_2 IN D_2O

Inferred from Exponential Experiments, Ref. 309.

Fuel Concentration, gm UO_2F_2/cm^3 solution	D_2O Purity, isotopic-%	Critical Sphere Radius, cm	Critical Mass, kg U	Volume of D_2O, 10^6 cm^3
0.0238	99.83	452	6602	358
0.0734	99.81	247	3583	62.7
0.1484	99.81	208	4348	37.3
0.2004	99.81	205	5598	35.4
0.2493	99.79	209	7343	37.1
0.2986	99.78	228	11438	47.9
0.3476	99.77	244	14586	52.2

3.7.10.2 Critical Parameters of Graphite-Reflected Cylindrical Cores Containing D_2O Solutions of Enriched UO_2F_2 (45.3 at-% U^{235})

Harrison, et al.,[310] have published criticality data obtained from measurements in H.A.Z.E.L. (Homogeneous Assembly Zero Energy). Radially-reflected, cylindrical cores containing D_2O solutions of UO_2F_2 with uranium enriched to 45.3 at-% U^{235} were brought to criticality by varying the core solution height. The fuel concentrations ranged from 0.007 to 0.025 gm U/gm solution; the corresponding critical core heights ranged from 200 cm to 70 cm. The D_2O purity was 99.83 molar-%.

The core tank was a right-circular, stainless steel cylinder (61 cm O.D., 214 cm high, 0.21 cm wall thickness), which rested on a steel base plate (2.7 cm thick) and supporting structure. The inside surface of the tank base was slightly dished. A vertical tube of stainless steel (1.9 cm I.D., 0.14 cm wall thickness) was an integral part of the core and passed through the center of the core. No corrections were made to the critical mass data for the reactivity effects of this tube. The top of the tank was fabricated of stainless steel plate (1.9 cm thick), and contained fittings of various kinds.

The reflector was comprised of a twelve-sided approximation to a cylindrical annulus of graphite with an over-all thickness of 46.6 (±0.9) cm. The reflector height was adjusted to match the core solution height to within ±2.5 cm.

Table 3-96 contains the criticality data and the temperature coefficient, in terms of the critical core height per degree centigrade, $\partial H_c/\partial T$, at room temperature. It is estimated that the error in fuel concentration is less than ±0.3%, that the error in critical height is less than ±0.1%, and that the error in critical mass is less than ±0.5%.

It was observed that a linear functional relationship:

$$\frac{1}{H_c} = \frac{9.95 \times 10^{-5}}{\text{gm U/gm sol.}} + 0.01824$$

provided a good fit to the experimental data. The reciprocal of the temperature coefficient of critical core height varied roughly as a linear function of the fuel concentration.

3.7.11 CRITICAL PARAMETERS OF REACTORS FUELED WITH THIN FOILS OF HIGHLY ENRICHED URANIUM AND MODERATED WITH BERYLLIUM OXIDE

Critical experiments on near-homogeneous, unreflected cores, fueled with thin foils of highly enriched uranium and moderated with BeO, have been reported by Kloverstrom, et al.[311] The uranium,

Table 3-96 — CRITICAL PARAMETERS OF CYLINDRICAL CORES CONTAINING D_2O SOLUTIONS OF UO_2F_2 AND RADIALLY REFLECTED WITH GRAPHITE

Data from Ref. 310.

Fuel Concentration, gm U/gm sol.	D/U^{235} [a] Atom Ratio	Solution Density at 18°C, gm/cm³	Critical Core Height at 18°C, cm	Reflector Height, cm	Critical Mass, kg U^{235}	$\partial H_c/\partial T$, cm/°C	Temp. Range, °C	Epicd.-to-Subcd.[b] Ratio at Core Center	
								Indium Foil	Manganese Foil
0.02585	1939	1.140	69.53[c]	64.5	2.699[c]	—	—	—	—
0.02009	2515	1.133	74.56	74.7	2.234	0.099	13.4	0.45	—
0.01700	2984	1.130	81.03	79.2	2.048	0.134[d]	9.3	0.37	—
0.01422	3580	1.126	89.12	89.4	1.877	0.173	6.5	0.32	0.087
0.01231	4146	1.123	99.47	99.1	1.808	0.242	6.3	0.32	0.079
0.00988	5183	1.120	121.67	123.9	1.769	0.454	5.5	0.24	0.068
0.00906	5658	1.119	137.50	138.5	1.832	0.60[d]	6.0	0.21	0.061
0.00850	6035	1.119	152.94	153.9	1.911	0.756	2.3	0.21	0.056
0.00784	6549	1.117	179.18	183.4	2.059	0.920	2.9	0.20	0.053
0.00764	6722	1.117	192.13	193.5	2.154	0.968	2.2	0.20	0.051

[a] Assuming 100% purity of D_2O.
[b] Epicadmium = activity above Cd cutoff; subcadmium = activity below Cd cutoff. Foils: 0.013 cm thick and 0.64 cm diameter; cadmium boxes: 0.051 cm thick.
[c] Extrapolated values; the reactor with this concentration was not taken to criticality.
[d] Interpolated values.

enriched to 93.2% U^{235}, was introduced into the core in a heterogeneous, parallel array of 13.3-cm-square foils with nominal thicknesses of 0.0025 cm and 0.0051 cm. The foils were coated with Teflon (~0.92 gm/foil). Foils of half-area and of quarter-area were used when a reduced spacing between fuel planes was desired.

The reactor cores were parallelepipeds built up with blocks of BeO having nominal base dimensions of ~15 cm × 15 cm (6 in. × 6 in.), and a thickness of ~1.3 cm or ~2.5 cm. On one face of each block was a 0.038-cm-deep, 13.65-cm-wide groove where fuel foils could be placed. The density of BeO was 2.86 gm/cm³.

Criticality data are given in Table 3-97. The data were corrected for the presence of a steel diaphragm, separating two zones of the reactor, on the basis of measurements with diaphragms of three different thicknesses. Reactivity corrections for the Teflon coating of the uranium foils and for

Table 3-97 — CRITICAL PARAMETERS OF UNREFLECTED BeO-U^{235} CORES[a]

Data from Ref. 311.

Equivalent Number of 0.0025-cm-thick Foils Stacked to give a Foil "Plane"	Approximate Spacing Between Foil Planes, cm	Be/U^{235} Atom Ratio	Average U^{235} Concentration, gm/cm³	Base Dimensions, cm × cm	Critical Core Height, cm	Critical[b] Buckling, 10^{-3} cm^{-2}
8	2.5 (1 inch)	247	0.109	61.0 × 61.0	51.3	8.28 ± 0.04
4	2.5	493	0.0545	61.0 × 61.0	55.9	7.77 ± 0.04
8	5.1	493	0.0545	61.0 × 61.0	56.6	7.70 ± 0.04
2	2.5	986	0.0272	61.0 × 61.0	63.5	7.15 ± 0.05
4	5.1	986	0.0272	61.0 × 61.0	65.5	7.01 ± 0.05
6	7.6	986	0.0272	61.0 × 61.0	69.9	6.77 ± 0.05
1	2.5	1920	0.0140	76.2 × 76.2	53.6	6.30 ± 0.08
2	5.1	1920	0.0140	76.2 × 76.2	54.9	6.17 ± 0.08
2	5.1	1920	0.0140	76.2 × 61.0	66.0	6.13 ± 0.08
3	7.6	1920	0.0140	76.2 × 61.0	69.3	5.94 ± 0.08
1[c]	2.5	3830	0.00702	91.4 × 91.4	58.2	4.91 ± 0.10
2[c]	5.1	3830	0.00702	91.4 × 91.4	61.5	4.64 ± 0.10
1	5.1	3830	0.00702	91.4 × 91.4	57.7	4.95 ± 0.10
2	10.2	3830	0.00702	91.4 × 91.4	61.5	4.64 ± 0.10
1[d]	2.5	7660	0.00351	91.4 × 91.4	91.9	3.34 ± 0.12

[a] Density of BeO = 2.86 gm/cm³.
[b] Computed using an extrapolation distance of 1.3 cm.
[c] Half-area fuel foils (triangular).
[d] Quarter-area fuel foils (triangular).

the 1.3-cm-diameter source hole were of opposite sign and were believed to be small—and were not made. No correction was applied for the 10-cm-thick aluminum structure (with a mean density of 0.37 gm/cm^3) located at the bottom of the stack.

In Table 3-98 are given estimates of critical bucklings of unreflected, homogeneous, BeO-enriched U systems, as determined by linear extrapolations of the data of Table 3-97.

Table 3-99 lists critical heights for assemblies with a base of 61.0 cm × 61.0 cm, and with an air gap separating the core into two halves at the vertical median plane. The Be/U^{235} atom ratio was 493; the foil planes were 0.010 cm thick and were spaced 2.5 cm apart.

Table 3-98—ESTIMATES OF CRITICAL BUCKLINGS OF UNREFLECTED, HOMOGENEOUS CORES CONTAINING BeO AND URANIUM ENRICHED TO 93.2% U^{235}

Data from Ref. 311.

Be/U^{235} Atom Ratio	Estimated Critical Buckling, 10^{-3} cm^{-2}	
	Linear Extrapolation	Parabolic Extrapolation
247	8.35	—
493	7.85	—
986	7.30	7.21
1920	6.42	6.38
3830	5.18	5.04
7660	3.8	3.5

Table 3-99—CRITICAL HEIGHTS OF UNREFLECTED ASSEMBLIES WITH A GAP AT THE VERTICAL MID-PLANE

Data from Ref. 312.

Gap Thickness, cm	Gap Content	Critical Core Height,[a] cm
0	—	56.4 ± 0.5
1.19	Hexcell[b]	62.3 ± 0.5
2.39	Hexcell	70.0 ± 0.5

[a] Over-all height = gap thickness + critical core height.

[b] Hexcell is an aluminum grid structure of mean density = 0.053 gm/cm^3.

Notes: Be/U^{235} atom ratio = 493; foil planes were 0.010 cm thick and spaced 2.5 cm apart.

Kloverstrom and Kraft[313] performed additional experiments on BeO-U^{235}-foil assemblies, with graphite reflectors of various thicknesses above and below the core. In some experiments, slabs of varying composition and thickness were positioned at the vertical mid-plane of the core, and between the core and the top and bottom reflectors. Table 3-100 lists critical heights of a core with base dimensions 61.0 cm × 61.0 cm, as a function of graphite reflector thickness at the top of the core. The reactor was reflected on the bottom by an equal thickness of graphite, of density 1.73 gm/cm^3; it was unreflected radially. The BeO/U^{235} ratio in the core was 247.

3.7.12 CRITICAL PARAMETERS OF REACTORS FUELED WITH THIN FOILS OF HIGHLY ENRICHED URANIUM AND MODERATED WITH GRAPHITE

Criticality data for graphite-moderated reactors fueled with thin foils of uranium, enriched to 93.2% in U^{235}, have been reported by Reynolds.[314,315] The graphite (ATJ), made by the National Carbon Company, had a density of 1.645 gm/cm^3 except in one experiment where the density was 1.640 gm/cm^3. The graphite was machined into solid plates and grooved plates (~15 cm square, ~1.3 cm thick), with a 0.025-cm recess milled in the top to contain the fuel foils. The grooved plates had a void

volume fraction of 0.40; they were used to implement the moderator stacking, generally in the ratio of one grooved plate to eleven solid plates. The foils were of the same type and size as described in Section 3.7.11. The reflector material was Standard QMV solid beryllium with a density of 1.84 gm/cm^3.

Table 3-101 lists data from nine experiments with various C/U^{235} atom ratios in the core. The first two experiments, with C/U^{235} ratios ≤ 600, perhaps are better suited to the scope of Section 6; they are included here for convenience of presentation. The C/U^{235} atom ratios and the critical masses listed have been corrected for the presence of a control void, for boron content of the graphite (10 to 15 ppm), for the porosity of the graphite blocks, for room return, for resonance absorption in U^{235}, and for the important heterogeneity effects of the fuel lumping. The corresponding, uncorrected data are included to afford a comparison with the inferred final, homogeneous, clean-reactor values.

Reynolds[314] published data on critical assemblies installed in the LASL "Honeycomb" system. This machine was made up of two stacks of tubes of Type 2S aluminum, each tube being 7.6 cm square and 91.5 cm long with 0.120-cm-thick walls. The average aluminum content of the machine was 0.165 gm/cm^3.

Table 3-100—CRITICAL HEIGHT OF A BeO-MODERATED, U^{235}-FOIL-FUELED CORE AS A FUNCTION OF THE THICKNESS OF GRAPHITE AXIAL REFLECTORS

Data from Ref. 313.

Graphite Thickness, cm	Critical Core Height, cm
0	51.3
15.2	40.1
30.5	36.3
45.7	36.1

Critical assemblies were constructed by inserting fuel subassemblies and reflector materials into the aluminum tubes. Each fuel subassembly consisted of graphite plates 40.6 cm long and ~7.4 cm wide, interleaved with 0.0051-cm-thick, or 0.0127-cm-thick uranium foils (enriched to 93.2% U^{235}) to yield the desired C/U^{235} atom ratio. The graphite (CS) had a boron content of less than 1 ppm, and was essentially free of moisture.

Two series of experiments were performed. The first series was confined to graphite-moderated, beryllium-reflected, pseudo-cylinders. Data from these experiments are listed in Section 6.3.

The second series of experiments was performed on graphite-moderated, graphite-reflected, rectangular parallepipeds. The data are listed in Table 3-102.

The effect of self-shielding of the 0.0025-cm-thick "Oralloy" (uranium enriched to 93.2 wt-% U^{235}) foils was estimated from substitution measurements with 0.0051-cm-thick foils. (Apparently a linear extrapolation was used to correct back to a homogeneous core.) The last column of Table 3-102 contains the reported estimates of k_{eff} for homogeneous cores. The values of the critical mass and of the C/U^{235} atom ratio were computed from the published data, assuming that there are approximately 0.933 atoms of U^{235} per atom of the uranium. The values of k_{eff} for Experiments No. 3, 4, and 6 were estimated to be between 1.01 and 1.03.

Finke and Grammens* used the "Hot Box" Facility at UCRL (Nevada) to study the temperature dependence of the critical mass of a graphite-moderated reactor fueled with foils (0.0051 cm thick) of uranium enriched to 93.2% in U^{235}. The core dimensions were 122 cm × 91.5 cm × 186.7 cm. A graphite reflector (30.5 cm thick) was positioned at each face of the core in the 91.5-cm direction; otherwise the reactor was unreflected. The graphite contained 5 ppm boron; the effective graphite density was 1.46 gm/cm^3.

At room temperature, the critical reactor contained ~19 kg U^{235} with approximately 0.86 kg of Type 347 stainless steel present per kilogram of uranium. With each additional kilogram of uranium, 1.71 kg of Type 347 stainless steel was introduced. The results are listed in Table 3-103.

In the following paragraphs are presented integral data from TREAT (Transient Reactor Test Facility),[316–320] a graphite-reflected reactor with a cylindrical core consisting of Zircaloy-clad,

* Private communication from R. G. Finke, UCRL.

Table 3-101—CRITICAL PARAMETERS FOR GRAPHITE-MODERATED, U^{235} FOIL-FUELED REACTORS[a]

Data from Ref. 314.

Experiment Number	Dimensions of[b] Core Base, cm × cm	Reflector[c] Composition and Thickness	Foil-Plane Thickness, cm	C/U^{235} Atom Ratio		Critical Core Hgt., cm[d]		Critical Mass, kg U^{235}		Critical[e] Buckling, 10^{-4} cm^{-2}
				Uncorrected	Corrected	Uncorrected	Corrected	Uncorrected	Corrected	
1	108.0 × 108.0	—	0.0102	297	301	119.6	112.8	149.7	140.1	23.07 ± 0.1
2	123.2 × 123.2	—	0.0051	600	603	101.9	95.5	82.26	77.4	22.26 ± 0.1
3	123.2 × 123.2	—	0.0051	1200	1206	107.4	102.4	43.57	41.5	21.01 ± 0.1
4	123.2 × 123.2	—	0.0025	2340	2355	120.9	113.5	25.14	23.6	19.42 ± 0.1
5	123.2 × 92.7	15.2 cm C on 2 sides	0.0051	1200	1206	108.7	103.4	32.97	31.5	—
6	92.7 × 92.7	15.2 cm C on 4 sides	0.0051	1200	1206	110.5	104.9	25.16	23.9	—
7	123.2 × 92.7	7.6 cm Be on 2 sides	0.0025	2340	2355	122.2	114.6	19.05	17.8	—
8	123.2 × 92.7	15.2 cm Be on 2 sides	0.0025	2340	2355	104.1	97.5	16.23	15.2	—
9	92.7 × 92.7	15.2 cm Be on 4 sides	0.0025	2340	2355	93.5	87.6	10.91	10.2	—

[a] Core graphite density was 1.645 gm/cm^3 except in Experiment No. 1 where it was 1.640 gm/cm^3. The control void was ignored in this assessment of graphite density. The Be density was 1.84 gm/cm^3.

[b] Dimensions listed ±0.1 cm.

[c] Base of core plus reflector was a square in all cases except Experiment No. 7 where it was 123.2 cm × 108.0 cm.

[d] The uncertainty in critical core height is ±0.25 cm.

[e] An extrapolation length of 1.90 cm was assumed at all unreflected faces.

Table 3-102 — CRITICAL DATA FOR GRAPHITE-REFLECTED, GRAPHITE-U^{235} RECTANGULAR PARALLELEPIPEDS

Data from Ref. 314.

Expt. No.	C/U^{235} Atom Ratio	Critical Mass,[a] kg U^{235}	Average[b] Density of Core Graphite, gm/cm^3	Dimensions of Critical Core, cm × cm × cm	Estimated k_{eff} for Homogeneous Core
1	7128	7.44	1.50	121.92 × 121.92 × 121.92	1.0666
2	5292	7.11	1.50	99.06 × 106.68 × 121.92	1.0465
3	3365	7.38	1.50	91.44 × 91.44 × 101.60	—
4	2535	8.24	1.50	83.82 × 83.82 × 101.60	—
5	4680	9.07	1.34	115.82 × 114.30 × 121.92	1.0480
6	2969	9.52	1.34	99.06 × 106.68 × 101.60	—

[a] The mass of U^{235} was computed with the assumption that the Oralloy contained 93.2 wt-% U^{235}. The average density of Type 2S aluminum in the assembly was 0.165 gm/cm^3.

[b] There was a graphite reflector of thickness ~30.5 cm on all sides; graphite density ~1.55 gm/cm^3.

Table 3-103 — TEMPERATURE-DEPENDENCE OF CRITICAL MASS OF GRAPHITE-MODERATED, U^{235}-FUELED REACTORS[a]

Private communication from R. Finke, UCRL.

Temperature, °C	Approximate C/U^{235} Atom Ratio	Critical Mass, kg U^{235}
20	3140	19.0
180	2830	21.1
401	2520	23.7
638	2290	25.9

[a] Effective graphite density = 1.46 gm/cm^3.

homogeneous, urania-graphite fuel elements. An upper (axial) graphite reflector, 64.8 cm thick, and a lower graphite reflector, 60.7 cm thick, both clad with aluminum, were employed. A temporary radial reflector extended from the core to an outer boundary that formed a square, 193 cm on a side. The temporary reflector was comprised of dummy fuel elements containing graphite, the first layer of dummies adjacent to the core being clad with Zircaloy, 0.064 cm thick, and the remainder with aluminum. Beyond this was a permanent reflector of unclad graphite with an outer boundary that formed a square, 325 cm on a side.

Table 3-104 lists the averaged core and reflector compositions for the critical reactor without experimental access slots. The measured critical mass was 5.171 kg U^{235}, corresponding to a critical core radius of 67.8 cm, and a core height of 121.0 cm.

Table 3-104 — AVERAGED TREAT COMPOSITION

Private communication from C. E. Dickerman, ANL.

Element	Atom Density in Core, 10^{24} atom/cm^3	Atom Density in Reflector, 10^{24} atom/cm^3	
		Temporary Reflector	Permanent Reflector
U^{235}	7.574×10^{-6}	—	—
U^{238}	5.543×10^{-7}	—	—
Zirconium	1.190×10^{-3}	1.953×10^{-4}	—
Boron	5.047×10^{-7}	1.596×10^{-7}	1.680×10^{-7}
Iron	3.344×10^{-5}	7.893×10^{-5}	2.184×10^{-5}
Aluminum	—	2.605×10^{-3}	1.135×10^{-3}
Carbon	0.07603	0.07222	0.07585

Epicadmium-to-subcadmium ratios measured[319] in the center of the TREAT core are tabulated below.

Detector	Epicadmium to Subcadmium Ratio*
Cu	0.122 ± 0.007
U^{235}	0.058 ± 0.003
Pu^{239}	0.054 ± 0.003

*Epicadmium = activity above Cd cutoff; Subcadmium = activity below Cd cutoff.

The temperature dependence of the temperature coefficient of reactivity in TREAT was deduced from an analysis of transient data.[320] A linear approximation to the temperature coefficient is provided by:

$$[(\Delta k/k)/°K] \approx \begin{cases} -0.000258 + 4.2 \times 10^{-7}\,(T-300), & 300°K \le T \le 400°K \\ -0.000216 + 2.2 \times 10^{-7}\,(T-400), & 400°K \le T \le 600°K \end{cases}$$

where T is the average temperature of the graphite in the core, in degrees Kelvin.

3.7.13 CRITICAL PARAMETERS OF AQUEOUS SOLUTIONS OF URANIUM HIGHLY ENRICHED IN U^{233}

The experiments discussed in this section fall into two major categories: those performed to obtain information relating to nuclear safety,[321] and experiments carried out to provide data for detailed theoretical analyses.[267–269,281,282,322] In the latter category, comparison experiments with aqueous solutions of U^{235} were made in containers of the same size and shape, and the ratio $\overline{\eta}(U^{233})/\overline{\eta}(U^{235})$ at thermal energies was inferred.

Experiments apparently belonging to the category of nuclear safety were performed by Fox, et al.,[321] using solutions of UO_2F_2 and $UO_2(NO_3)_2$ with the uranium enriched to 98.7 wt-% U^{233}. The relationship between the solution density and the H/U^{233} atom ratio is shown in Fig. 3-69. The core solutions were contained in cylindrical and spherical vessels of Type 3S aluminum. The aluminum was lined with a plastic (Heresite or Unichrome) to reduce corrosion. The diameters of the cylinders ranged from 12.7 cm to 30.5 cm, with H/U^{233} atom ratios ranging from 34.2 to 775. Two spheres

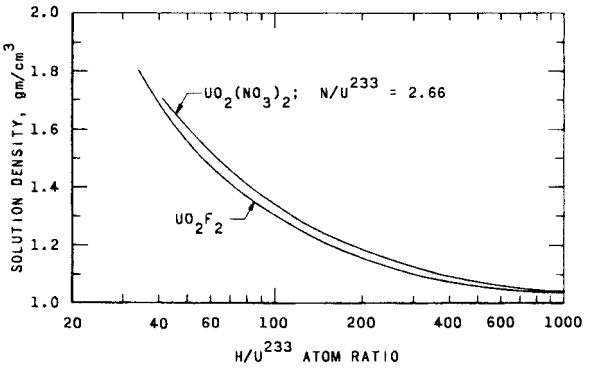

Fig. 3-69 — Density as a function of H/U^{233} atom ratio in H_2O solutions of uranyl fluoride and of uranyl nitrate (uranium enriched to 98.7% U^{233}). *Data from Ref. 321.*

were used, 26.4 cm and 32.0 cm in diameter, with H/U^{233} ratios in the range 381 to 663. In all but two criticals, the cores were reflected radially, and at the bottom, by an effectively infinite medium of water or of paraffin; in most cases, they were fully reflected at the top also.

The estimated critical parameters are shown in Tables 3-105 and 3-106. The results from the criticals with UO_2F_2 in Heresite-lined vessels were estimated to be correct to within ±1%. An error margin of ±3% was reported for solutions of $UO_2(NO_3)_2$ in the same vessels. Critical masses listed for the solutions in Unichrome-lined vessels were stated to be approximately 2% high because of a bias. Critical masses listed for the 13.7-cm- and the 16.7-cm-diameter cylinders were reported to

Table 3-105 — ESTIMATES OF CRITICAL PARAMETERS FOR AQUEOUS SOLUTIONS OF $UO_2(NO_3)_2$ WITH URANIUM HIGHLY ENRICHED IN U^{233}[a]

(Numbers in parentheses represent extrapolated values derived from source neutron multiplication curves of subcritical assemblies.)

Data from Ref. 321.

H/U^{233} Atom Ratio	Reflector	Critical Parameters			Maximum Parametric Values for Experimental Subcritical Assemblies		
		Height, cm	Volume, liter	Mass, kg U^{233}	Height, cm	Volume, liter	Mass, kg U^{233}
	Cylinder: 12.7 cm diameter[b]						
57.5	Paraffin	[c]	—	—	51	6.40	2.44
67.0	Paraffin	[c]	—	—	59	7.40	2.49
84.4	Paraffin	[c]	—	—	61	7.65	2.10
145	Paraffin	[c]	—	—	55	6.90	1.15
	Cylinder: 15.1 cm diameter[b]						
57.5	Paraffin	27.9	5.00	1.91	—	—	—
67.0	Paraffin	29.0	5.20	1.75	—	—	—
84.4	Paraffin	30.7	5.50	1.51	—	—	—
120	Paraffin	(38.5 ± 0.5)	(6.9 ± 0.1)	(1.37 ± 0.02)	36.8	6.60	1.30
151	Paraffin	(46.8 ± 0.5)	(8.4 ± 0.1)	(1.34 ± 0.02)	45.4	8.15	1.31
193	Paraffin	(73 ± 2)	(13.0 ± 0.4)	(1.65 ± 0.08)	55.4	9.80	1.24
	Cylinder: 19.1 cm diameter						
57.5	Paraffin	16.3	4.65	1.77	—	—	—
67.0	Paraffin	16.2	4.60	1.55	—	—	—
145	Paraffin	18.6	5.30	0.89	—	—	—
	Cylinder: 20.5 cm diameter						
42.2	Paraffin	(16.1 ± 0.2)	(5.30 ± 0.06)	(2.6 ± 0.03)	14.0	4.60	2.25
57.5	Paraffin	14.4	4.75	1.81	—	—	—
84.4	Paraffin	14.7	4.85	1.33	—	—	—
120	Paraffin	16.4	5.40	1.07	—	—	—
145	Paraffin	16.7	5.51	0.92	—	—	—
151	Paraffin	16.7	5.51	0.88	—	—	—
193	Paraffin	18.8	6.20	0.79	—	—	—
213	Paraffin	19.3	6.37	0.75	—	—	—
247	Paraffin	(21.2 ± 0.3)	(7.0 ± 0.1)	(0.70 ± 0.01)	19.9	6.56	0.66
	Cylinder: 21.5 cm diameter						
247	Paraffin	19.4	7.00	0.70	—	—	—
297	Paraffin	21.5	7.78	0.65	—	—	—
	Cylinder: 22.9 cm diameter						
356	Paraffin	21.3	8.75	0.62	—	—	—
379	Paraffin	22.9	9.39	0.62	—	—	—
	Cylinder: 25.5 cm diameter						
394	Paraffin	19.3	9.82	0.63	—	—	—
461	Paraffin	22.5	11.45	0.63	—	—	—
514	Paraffin	(25.2 ± 0.1)	(12.9 ± 0.05)	(0.63 ± 0.03)	25.1	12.77	0.63
514	Water	(25.5 ± 0.1)	(13.0 ± 0.05)	(0.64 ± 0.03)	25.1	12.77	0.63
	Cylinder: 30.5 cm diameter						
582	Paraffin	21.1	15.40	0.68	—	—	—
630	Paraffin	23.8	17.40	0.70	—	—	—
757	Paraffin	30.4	22.20	0.75	—	—	—
	Sphere: 26.6 cm diameter						
405	Water	Full	9.66	0.60	—	—	—

[a] $N/U^{233} = 2.66$.

[b] No reflector on the top surface.

[c] Apparently this assembly could not be made critical at any height.

Note: In Ref. 321, vessel diameters in English units are nominal dimensions.

Table 3-106—ESTIMATES OF CRITICAL PARAMETERS FOR AQUEOUS SOLUTIONS OF UO_2F_2 HIGHLY ENRICHED IN U^{233}

(Numbers in parentheses represent extrapolated values derived from source neutron multiplication curves of subcritical assemblies.)

Data from Ref. 321.

H/U^{233} Atom Ratio	Reflector	Critical Parameters			Maximum Parametric Values for Experimental Subcritical Assemblies		
		Height, cm	Volume, liters	Mass, kg U^{233}	Height, cm	Volume, liters	Mass, kg U^{233}
Cylinder: 11.2 cm diameter[a,b]							
34.2	Paraffin	[c]	—	—	29.9	2.95	2.02
39.4	Paraffin	[c]	—	—	34.9	3.43	2.07
45.9	Paraffin	[c]	—	—	42.6	4.19	2.18
53.7	Paraffin	[c]	—	—	49.0	4.82	2.18
74.1	Paraffin	[c]	—	—	68.5	6.76	2.24
Cylinder: 12.7 cm diameter							
34.2	Paraffin	(38 ± 2)	(4.8 ± 0.25)	(3.3 ± 0.2)	23.8	2.99	2.05
39.4	Paraffin	(41 ± 2)	(5.1 ± 0.25)	(3.1 ± 0.2)	27.6	3.46	2.08
45.9	Paraffin	(41 ± 1)	(5.2 ± 0.1)	(2.7 ± 0.1)	32.4	4.07	2.11
74.1	Paraffin	(56.5 ± 0.5)	(7.1 ± 0.06)	(2.36 ± 0.02)	53.3	6.70	2.22
Cylinder: 13.7 cm diameter[a,b]							
74.1	Paraffin	(48.7 ± 0.5)	(7.13 ± 0.06)	(2.37 ± 0.02)	46.3	6.77	2.25
Cylinder: 15.1 cm diameter[a,b]							
74.1	Paraffin	24.0	4.31	1.43	—	—	—
Cylinder: 16.7 cm diameter[b]							
34.2	Paraffin	(20 ± 1)	(4.4 ± 0.2)	(3.0 ± 0.15)	13.5	2.94	2.01
39.4	Paraffin	(16.7 ± 0.2)	(3.66 ± 0.04)	(2.20 ± 0.03)	16.3	3.55	2.13
45.2	Paraffin	(17.4 ± 0.2)	(3.79 ± 0.04)	(2.01 ± 0.03)	16.9	3.69	1.96
45.9	Paraffin	16.9	3.67	1.91	—	—	—
47.9	Paraffin	(17.7 ± 0.2)	(3.85 ± 0.04)	(1.94 ± 0.03)	16.9	3.69	1.86
53.7	Paraffin	(18.0 ± 0.3)	(3.93 ± 0.06)	(1.77 ± 0.03)	16.9	3.69	1.66
74.1	Paraffin	(19.1 ± 0.4)	(4.15 ± 0.09)	(1.38 ± 0.04)	16.9	3.69	1.23
Cylinder: 19.1 cm diameter							
154	Paraffin	18.4	5.25	0.87	—	—	—
Cylinder: 20.5 cm diameter							
250	Paraffin	(20.2 ± 0.05)	(6.66 ± 0.02)	(0.68 ± 0.02)	20.1	6.63	0.68
Cylinder: 21.5 cm diameter							
329	Paraffin	(22.2 ± 0.1)	(8.04 ± 0.04)	(0.63 ± 0.05)	21.6	7.80	0.61
Cylinder: 22.9 cm diameter							
396	Paraffin	(23.1 ± 0.1)	(9.47 ± 0.04)	(0.61 ± 0.05)	22.6	9.26	0.60
Cylinder: 25.5 cm diameter							
522	Water	(25.9 ± 0.1)	(13.18 ± 0.05)	(0.65 ± 0.05)	25.6	13.05	0.64
154	None	(24.0 ± 0.05)	(12.22 ± 0.03)	(2.02 ± 0.05)	23.8	12.15	2.01
Cylinder: 30.5 cm diameter							
775	Paraffin	30.5	22.8	0.74	—	—	—
Sphere: 31.9 cm diameter							
381	None	[d]	16.98	1.14	—	—	—

[a] No reflector on the top surface.

[b] Vessels coated with Unichrome; masses about 2% high because of impurities.

[c] Apparently this assembly could not be made critical at any height in the absence of a top reflector and in the presence of Unichrome.

[d] There was a 40-cm^3 void above the critical solution.

Note: In Ref. 321, vessel diameters in English units are nominal dimensions.

be high by a percentage not well known, but probably less than 10%. Many of the data were obtained from extrapolation of curves of neutron multiplication in subcritical media; accordingly, the maximum parametric values for the subcritical assemblies from which the extrapolation was made are included.

Criticality data from the second category of experiments have been published in various ORNL reports (Refs. 267-269, 281, 282, 322). They are listed in Tables 3-107 and 3-108.

Paxton[276] has interpreted and summarized in graphical form much of the data presented in Tables 3-105 through 3-108. The curves, similar to those included for U^{235}, are reproduced as Figs. 3-70 through 3-72.

3.7.14 CRITICAL PARAMETERS OF AQUEOUS SOLUTIONS OF PLUTONIUM NITRATE

Critical parameters of homogeneous aqueous solutions of plutonium nitrate in H_2O-reflected, right circular cylinders, and in bare or H_2O-reflected, spherical vessels have been measured at Hanford.[323] Much of the experimental work was performed to determine the dependence of the critical mass of Pu on the concentrations of poisons in the core solution. The emphasis was upon the effect of the presence of nitric acid in the core. Poisonings by lithium, bismuth, phosphate, or sulfate were examined also; however, the data are not included here. Another important area of experimentation was the variation of critical mass with the percentage of Pu^{240} in the plutonium, in the range 0.54 wt-% to 4.4 wt-% Pu^{240}.

In most of the experiments, the reflector temperature and, consequently, the core temperature, was held at 27°C; some data were obtained at temperatures ranging from 20°C to 50°C.

With one exception, the spherical cores were fabricated from Type 347 stainless steel (0.13 cm wall thickness). One vessel was fabricated from 20-gauge, type 2S aluminum and measured 33 cm in diameter. A fuel feed tube of stainless steel (0.95 cm O.D.) was attached to the base of each sphere. A stainless steel supporting neck (5.4 cm O.D.; 0.32 cm wall thickness) was used to suspend the core vessel in the reflector vessel.

The cylinders were made from stainless steel sheet (0.16 cm thick). A water-filled piston was used to provide an effectively infinite top water reflector; the cylinder wall-piston annulus did not exceed 0.13 cm. Except for the presence of the various support structure, fuel feed lines, etc., reflected reactors were surrounded by an effectively infinite water medium.

The data reported were not corrected for the various perturbations of the feed lines, the support neck, etc. The critical masses stated were obtained as the product of the core volume and the plutonium concentration, corrected only for penetration of control rods. In Fig. 3-73 are curves describing the relationship between the critical mass of plutonium and the nitrate concentration for reflected spheres of various sizes. The Pu^{240} isotopic content was held at 3.12 wt-%; the temperature was maintained at 27°C.

Kruesi, et al.,[323] observed that a linear relationship appeared to exist between the $\log_{10}$ (critical mass) and the nitrate concentration for each of the reflected spheres. Linear fits of this type were proposed (and seem reasonable in view of experimental uncertainties) for data from measurements of unreflected steel spheres 40.6 cm in diameter and 45.7 cm in diameter, with Pu containing 4.2 wt-% Pu^{240}. In the case of the 40.6-cm-diameter sphere, the fit: $\log_{10} m \sim 3.072 + 0.455\,(n-0.080)$ was displayed, where n is the nitrate concentration in gm/cm^3, and m is the mass in grams.

Figure 3-74 is a graphical summary of similar data for other Pu^{240} contents in a water-reflected, 33.0-cm-diameter, stainless steel sphere at 27°C.

Criticality data for reflected stainless steel spheres containing aqueous solutions of plutonium nitrate, with 3.12 wt-% Pu^{240} in Pu, are plotted in Fig. 3-75.

Table 3-109 lists criticality data for reflected, cylindrical cores wherein the percentages of Pu^{240} in Pu ranged from 2.85 wt-% to 2.9 wt-%; temperatures ranged from 20°C to 50°C; and core nitrate concentrations were varied between 0.107 gm/cm^3 and 0.300 gm/cm^3.

Additional papers on plutonium solution criticals have been published by Horton and McCullen,[324] Callihan,[325], Callihan, et al.,[302] and Paxton.[276] Figures 3-76 and 3-77 have been taken from Ref. 276.

Table 3-107— CRITICAL PARAMETERS OF UNREFLECTED AQUEOUS SOLUTIONS OF HIGHLY ENRICHED $UO_2(NO_3)_2$ (97.25%-97.70% U^{233}) IN ALUMINUM-WALLED SPHERES AND IN A STAINLESS STEEL-WALLED CYLINDER

Data from Refs. 267 and 322.

H/U^{233} Atom Ratio	Critical Core Height, cm	Atom density, 10^{20} atom/cm^3						
		U^{233}	U^{234}	U^{235}	U^{238}	N	H	B
Type 1100 aluminum-walled sphere: 69.2 cm diameter; 0.32 cm wall thickness								
1324	Full	0.50066	0.00827	0.00021	0.00327	1.363	663.00	0.0508
1368	Full	0.48455	0.00801	0.00021	0.00311	1.319	663.15	0.0383
1417	Full	0.46798	0.00772	0.00018	0.00301	1.274	663.29	0.0259
1470	Full	0.45120	0.00744	0.00018	0.00291	1.224	663.45	0.0133
1533	Full	0.43284	0.00716	0.00018	0.00281	1.178	663.60	—
Type 1100 aluminum-walled sphere: 122.0 cm diameter; 0.77 cm wall thickness								
1986	Full	0.33460	0.00525	0.00010	0.00256	0.753	664.67	—
Type 316 stainless steel-walled cylinder: 154.7 cm diameter; ~0.33 cm wall thickness								
1819	49.5	0.36517	0.00556	—	0.00410	0.826	664.39	—
1900	59.2	0.34978	0.00525	—	0.00395	0.849	664.44	—
1966	77.7	0.33292	0.00507	—	0.00375	0.802	664.59	—
2106	138.9	0.31567	0.00481	—	0.00354	0.795	664.70	—

An average value $\bar{\eta}_{th}(U^{233}) = 2.284 \pm 0.015$ was inferred from a theoretical analysis of these experiments.

Table 3-108— TEMPERATURE-DEPENDENCE OF CRITICAL PARAMETERS OF AQUEOUS SOLUTIONS OF HIGHLY ENRICHED UO_2F_2 (98.7% U^{233}) IN ALUMINUM-WALLED SPHERES[a]

Data from Ref. 268.

Sphere, Dia., cm	Water-Reflector[b] Thickness	H/U^{233} Atom Ratio	Temperature, °C	Critical Mass, kg U^{233}
(26.4)*	effectively infinite	418	32.0	0.591[c]
		415	39.5	0.596
26.6†		401	65.5	0.611
		390	83.2	0.623
		378	96.5	0.638
(32.0)*	effectively infinite	663	26.3	0.659
		643	56.0	0.673
31.9[d]†		603	99.5	0.703
	0	381	27.0	1.146

[a]The aluminum (Type 3S) wall thickness was 0.13 cm. The inside surface of the core was coated with a plastic to reduce corrosion.

[b]The spherical core containers were mounted in cylinders of such dimensions that a water reflector at least 15 cm thick could be introduced.

[c]The critical mass for the full sphere was obtained, in this case, by extrapolating 0.1% in core volume and 5°C in temperature.

[d]The values of the uranium content and critical masses measured in this sphere are believed by the experimenters to be ~2% high because of a systematic error.

*Values in parentheses are nominal dimensions, as reported in Ref. 268.

†Values based upon subsequent volumetric calibrations. Private communication from J. K. Fox, Phillips Petroleum Co., Idaho. (Also see Tables 3-60, 3-105, and 3-106.)

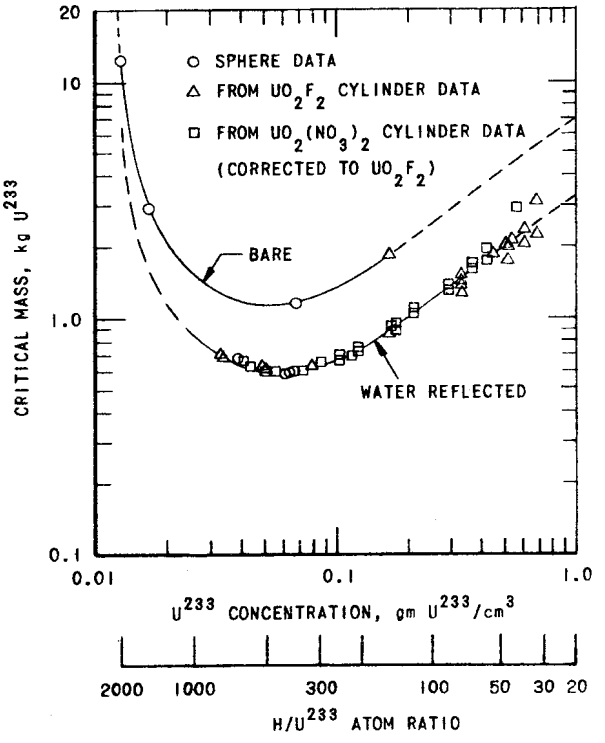

Fig. 3-70— Critical masses of H_2O solutions of UO_2F_2 (uranium highly enriched in U^{233}) in stainless steel spheres ($\frac{1}{16}$ in. wall). *Reproduced from Ref. 276.*

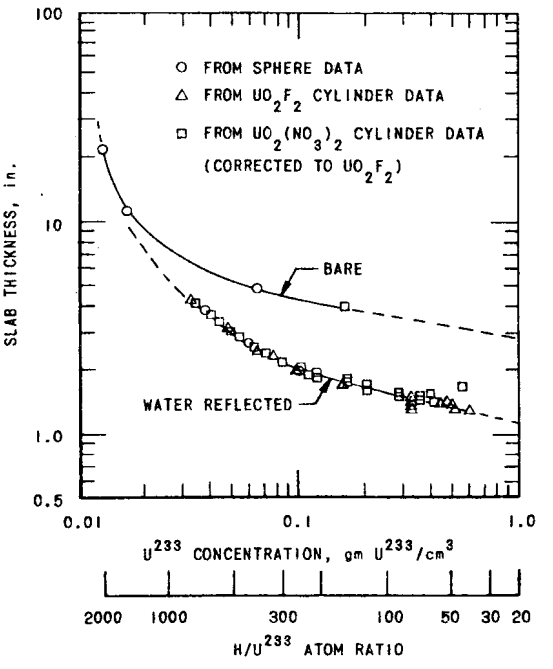

Fig. 3-71--Estimated critical thicknesses of infinite slabs containing H_2O solutions of UO_2F_2 (uranium highly enriched in U^{233}). Slab walls are stainless steel, $\frac{1}{16}$ in. thick. *Reproduced from Ref. 276.*

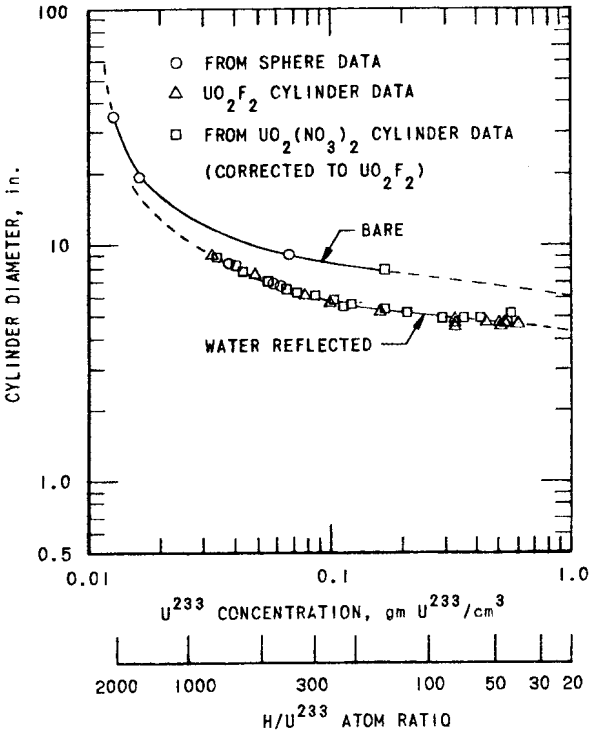

Fig. 3-72— Estimated critical diameters of infinite cylinders containing H_2O solutions of UO_2F_2 (uranium highly enriched in U^{233}). Cylinder walls are stainless steel, $\frac{1}{16}$ in. thick. *Reproduced from Ref. 276.*

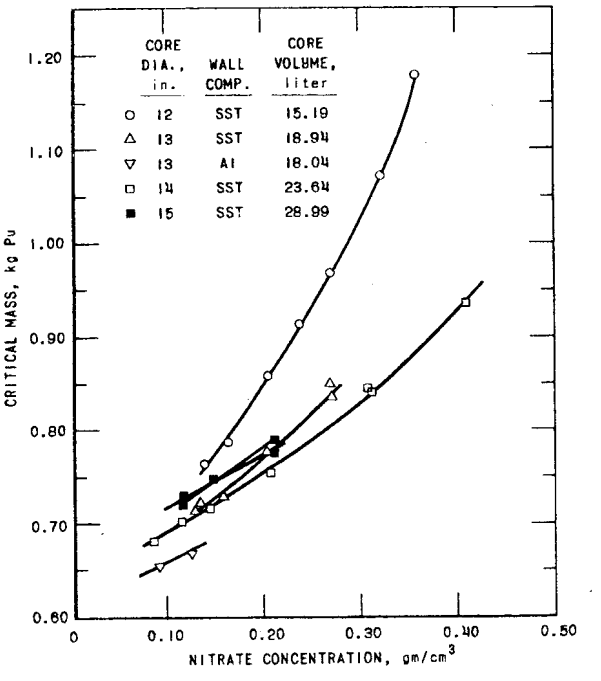

Fig. 3-73— Critical mass of plutonium as a function of plutonium nitrate concentration in homogeneous solutions contained in reflected spheres (3.12 wt-% Pu^{240} in Pu; 27°C). *Reproduced from Ref. 323.*

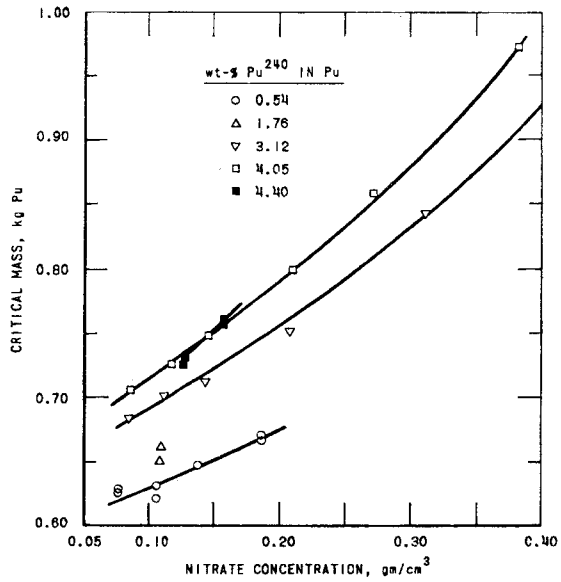

Fig. 3-74—Critical mass of plutonium as a function of Pu^{240} content and nitrate concentration in homogeneous aqueous solutions contained in a reflected stainless sphere (14 in. dia.). *Reproduced from Ref. 323.*

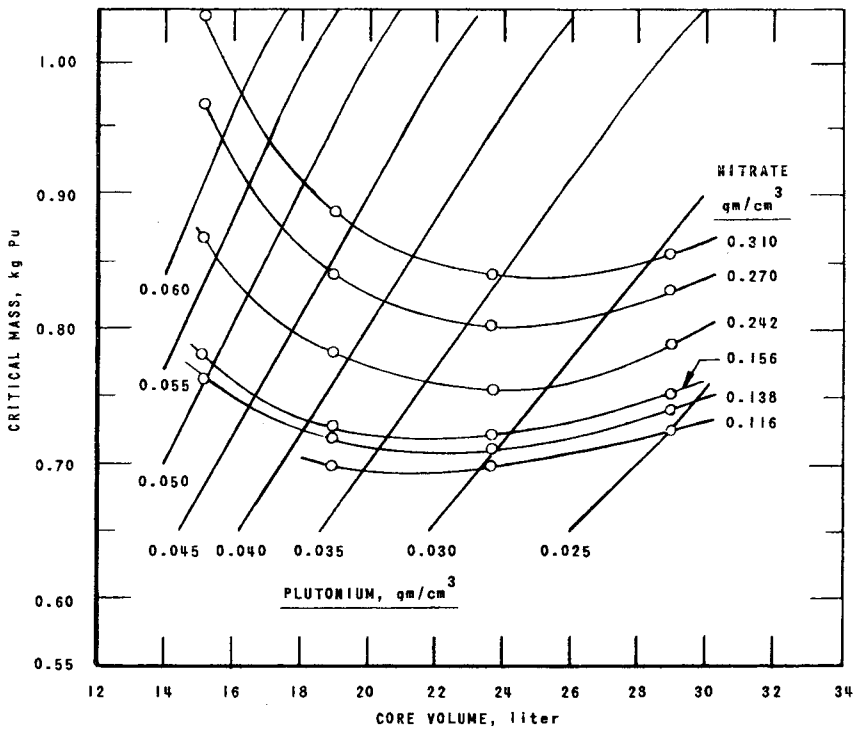

Fig. 3-75—Interdependence of critical mass of plutonium, core volume, plutonium concentration, and nitrate concentration, in homogeneous solutions contained in reflected stainless steel spheres (3.12 wt-% Pu^{240} in Pu; 27°C). *Reproduced from Ref. 323.*

687863 O - 63 - 16

Table 3-109—CRITICALITY DATA FOR HOMOGENEOUS AQUEOUS SOLUTIONS OF PLUTONIUM NITRATE IN REFLECTED STAINLESS STEEL CYLINDERS

Data from Ref. 323.

Core Diameter; Isotopic Pu^{240} Content	H/Pu^{239}[a] Atom Ratio	Pu Concentration, gm Pu/cm^3 sol.	Nitrate Concentration, gm$(NO_3)/cm^3$ sol.	Reflector Temperature, °C	Critical Core Height, cm	Critical Mass, kg Pu
22.9 cm; 2.85 wt-%	234	0.1092	0.166[b]	27.5	29.87	1.337
	261	0.0991	0.137	26.7	30.71	1.249
	301	0.0851	0.151[b]	26.9	32.33	1.128
	353	0.0739	0.126	27.2	35.41	1.073
	421	0.0615	0.134[b]	27.2	40.08	1.011
	478	0.0545	0.120	26.4	44.58	0.997
25.4 cm; 2.85 wt-%	331	0.0774	0.152[b]	28.6	25.22	0.989
	333	0.0769	0.152[b]	28.3	24.74	0.964
	412	0.0625	0.146[b]	28.3	27.25	0.860
	524	0.0493	0.142[b]	28.9	32.69	0.816
	662	0.0391[c]	0.138[b]	17.8	41.25	0.817
	662	0.0391	0.138[b]	28.3	41.76	0.827
	662	0.0391[c]	0.138[b]	50.0	44.42	0.879
27.9 cm; 2.9 wt-%	406	0.0640	0.121	26.9	22.81	0.895
	527	0.0490	0.139	26.9	25.96	0.780
	535	0.0488[c]	0.116	20.8	25.86	0.773
	535	0.0488[c]	0.116	45.6	26.72	0.799
27.9 cm; 2.85 wt-%	478	0.0544	0.120	26.9	25.60[d]	0.856
	553	0.0472	0.117	26.9	28.17[d]	0.815
	553	0.0472	0.117	26.9	27.08	0.784
	602	0.0417	0.215	27.5	32.63	0.835
	662	0.0391	0.138[b]	29.6	31.19	0.747
	665	0.0369	0.300	27.5	43.00	0.973
	773	0.0335	0.137[b]	30.0	39.55	0.813
	842	0.0308	0.136[b]	28.6	47.12[e]	0.889
30.5 cm; 2.9 wt-%	535	0.0488	0.116	29.2	22.35	0.799
	614	0.0423	0.127	28.9	25.25	0.779
	718	0.0365	0.107	27.2	28.47	0.758
	840	0.0311	0.114	28.1	33.43	0.759
	840	0.0311[c]	0.114	19.4	33.10	0.752
	840	0.0311[c]	0.114	47.0	34.52	0.784
	976	0.0265	0.134[b]	25.8	44.45	0.858
30.5 cm; 2.85 wt-%	234	0.1092	0.166[b]	27.8	17.32	1.380

[a] Computed with the assumption that the plutonium consisted solely of Pu^{239} and Pu^{240}.

[b] Estimates based on log book entries.

[c] Plutonium concentrations for temperature-coefficient experiments have not been corrected to the temperature at which the experiment was made.

[d] In these experiments, a 0.17-cm-thick layer of stainless steel was placed around the cylinder. The ends of the cylinder were not changed.

[e] Estimated by an extrapolation from subcritical count data.

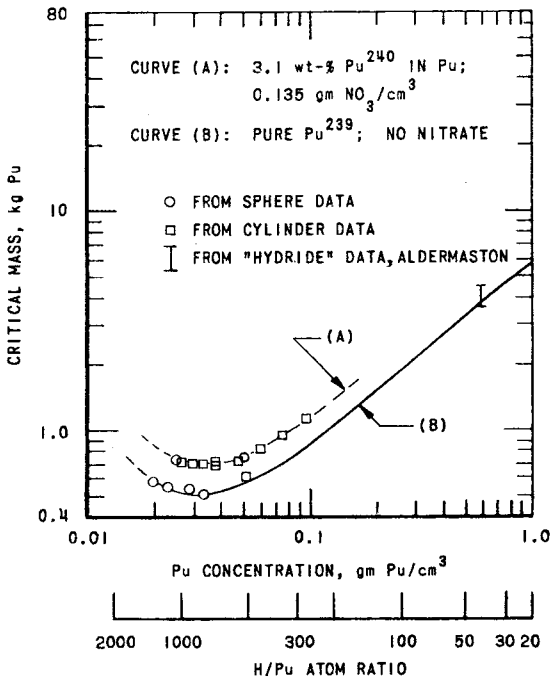

Fig. 3-76—Critical masses of homogeneous aqueous solutions of Pu^{239} in water-reflected stainless steel spheres. *Reproduced from Ref. 276.*

Fig. 3-77—Estimated critical dimensions of water-reflected infinite slabs and infinite cylinders containing homogeneous aqueous solutions of Pu^{239} (no nitrate; stainless steel containers, $\frac{1}{16}$ in. wall). *Reproduced from Ref. 276.*

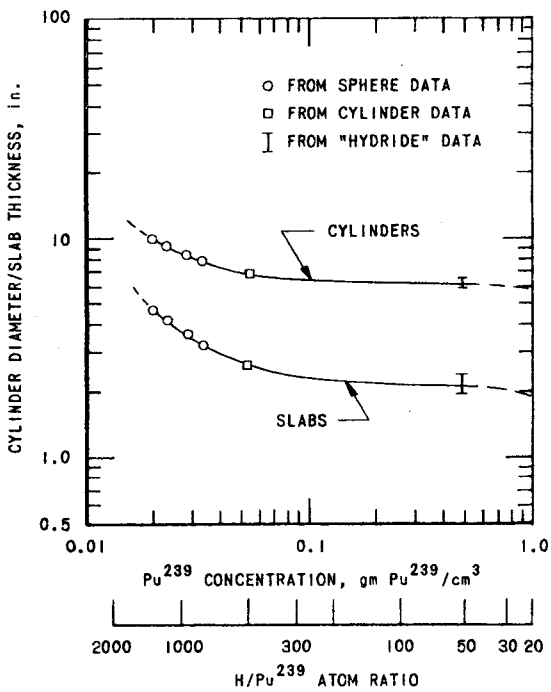

REFERENCES

1. N. Corngold, *Thermalization of Neutrons in Infinite Homogeneous Systems*, Ann. Phys., 6: No. 4, 368-398, (1959).
2. E. R. Cohen, *A Survey of Neutron Thermalization Theory*, Proc. 1955 Geneva Conference, 5: Paper No. 611, p. 405.
3. E. R. Cohen, *The Neutron Velocity Spectrum in a Heavy Moderator*, Nuclear Sci. and Eng., 2: No. 3, 227-245, (May, 1957).
4. N. Corngold, *Chemical Binding Effects in the Thermalization of Neutrons*, Ann. Phys., 11: No. 3, 338-358, (1960).
5. H. Hurwitz, Jr., M. S. Nelkin and G. J. Habetler: *Neutron Thermalization—I: Heavy Gaseous Moderator*, Nuclear Sci. and Eng., 1: No. 4, 280-312, (August, 1956).
6. M. S. Nelkin, *Neutron Thermalization—II: Heavy Crystalline Moderator*, Nuclear Sci. and Eng., 2: No. 2, 199-212, (April, 1957).
7. H. D. Brown, *Neutron Energy Spectra in Water*, DP-64, (February, 1956).
8. R. R. Coveyou, R. R. Bate and R. K. Osborn, *Effect of Moderator Temperature Upon Neutron Flux in Infinite, Capturing Medium*, J. Nuclear Energy, 2: No. 3, 153, (1956); see also, ORNL-1958, (October, 1955).
9. E. P. Wigner and J. E. Wilkins, Jr., *Effect of the Temperature of the Moderator on the Velocity Distribution of Neutrons with Numerical Calculations for H as the Moderator*, AECD-2275, (September, 1944).
10. J. E. Wilkins, Jr., *Effect of the Temperature of the Moderator on the Velocity Distribution of Neutrons for a Heavy Moderator*, CP-2481, (November, 1944).
11. M. Nelkin, *Scattering of Slow Neutrons by Water*, Phys. Rev., 119: No. 2, 741-746, (1960).
12. A. Radkowsky, *Temperature Dependence of Thermal Transport Mean Free Path*, Physics Division Quarterly Report (April, May, and June, 1950), ANL-4476, (July, 1950), pp. 89-100.
13. H. D. Brown and D. S. St. John, *Neutron Energy Spectrum in D_2O*, DP-33, (February, 1954).
14. E. Fermi, *Sul moto dei Neutroni nelle sostanze idrogenate*, Ricera Scientifica, 7(2): 13, (1936).
15. T. J. Krieger and M. S. Nelkin, *The Scattering of Slow Neutrons by Hydrogenous Moderators*, KAPL-1597, (August, 1956).
16. S. I. Drozdov, et al., *On the Calculation of Thermal Neutron Spectra*, Proc. 1958 Geneva Conference, 16: Paper No. 2033, p. 223.
17. G. Liebfried, *A Remark on Neutron Thermalization Theory*, Proc. Neutron Thermalization Conference, April 28-30, 1958, Gatlinburg, Tenn., ORNL-2739, (September, 1959).
18. N. Corngold and L. Zamick, *Decay Constants in the Thermalization of Neutrons by Monatomic Gases*, Trans. Am. Nuclear Soc., 3: No. 2, 504, (December, 1960).
19. E. R. Cohen and E. U. Vaughan, *Thermal Neutron Spectrum in Harmonically Bound Hydrogen Moderators*, Proc. Neutron Thermalization Conference, April 28-30, 1958, Gatlinburg, Tenn., ORNL-2739, (September, 1959).
20. D. A. Kottwitz, *Thermal Neutron Flux in a Medium With a Temperature Discontinuity*, Nuclear Sci. and Eng., 7: No. 4, 345, (April, 1960).
21. A. Erdelyi, et al., *Higher Transcendental Functions*, (New York: McGraw-Hill Book Co., Inc., 1955), Vol. III.
22. P. Michael, *Thermal Neutron Flux Distribution in Space and Energy*, Nuclear Sci. and Eng., 8: No. 5, 426-431, (November, 1960).
23. M. J. Poole, M. S. Nelkin and R. S. Stone, *The Measurement and Theory of Reactor Spectra*, Progress in Nuclear Energy, (London: Pergamon Press, Ltd., 1958), Series I: Physics and Mathematics, Vol. 2, Chap. 3.
24. M. J. Poole, *Measurement of Neutron Spectra in Moderators and Reactor Lattices—I: Aqueous Moderators*, J. Nuclear Energy, 5: No. 314, 325-341, (1957).
25. H. J. Amster, *The Wigner-Wilkins Calculated Thermal Neutron Spectra Compared with Measurements in a Water Moderator*, Nuclear Sci. and Eng., 2: No. 3, 394-404, (May, 1957).
26. R. E. Slovacek and R. S. Stone, *Low Energy Spectra Measurements*, Proc. Neutron Thermalization Conference, April 28-30, 1958, Gatlinburg, Tenn., ORNL-2739, (September, 1959).
27. J. R. Beyster, et al., *Measurements of Neutron Spectra in Water, Polyethylene, and Zirconium Hydride*, Nuclear Sci. and Eng., 9: No. 2, 168-184, (February, 1961).
28. V. I. Mostovoi, et al., *Neutron Spectrum Measurements in Uranium-Water Lattices*, Proc. 1958 Geneva Conference, 16: Paper No. 2152, p. 254.
29. Y. G. Nikolaev, *The Experimental Nuclear Reactor with Ordinary Water and Enriched Uranium*, Proc. 1955 Geneva Conference, 2: Paper No. 621, p. 392.
30. A. Shimizu, *Calculation of the Effective Thermal Cross Section and Its Temperature Coefficient—I*, J. Atomic Energy Soc. (Japan), 2: 10, 611-617, (1960).
31. C. H. Westcott, *Effective Cross-Section Values for Well-Moderated Thermal Reactor Spectra*, CRRP-960, (November, 1960).
32. C. H. Westcott, W. H. Walker and T. K. Alexander, *Effective Cross Sections and Cadmium Ratios for the Neutron Spectra of Thermal Reactors*, Proc. 1958 Geneva Conference, 16: Paper No. 202, p. 70.
33. K. H. Puechl, *An Approach to Reactor Using Results of Integral Experiments*, Nuclear Sci. and Eng., 9: No. 2, 241-259, (February, 1961).
34. H. J. Amster, *A Compendium of Thermal Neutron Cross Sections Averaged Over the Spectra of Wigner and Wilkins*, WAPD-185, (January, 1958).
35. M. Goldsmith and R. M. Cantwell, *Thermal Neutron Absorption in Thin Regions*, Trans. Am. Nuclear Soc., 3: No. 2, 509-510, (December, 1960).
36. S. W. Kash and D. C. Woods, *Measurement of the Transport Mean Free Path of Thermal Neutrons in D_2O by a Boron-Poisoning Method*, Phys. Rev., 90: No. 4, 564, (1953).
37. W. W. Brown, et al., *Exponential Experiments with Organic-Moderated Uranium Lattices*, Proc. 1958 Geneva Conference, 12: Paper No. 595, p. 514.
38. A. M. Weinberg and H. C. Schweinler, *Theory of Oscillating Absorber in a Chain Reactor*, Phys. Rev., 74: No. 8, 851, (1948).
39. V. Raievski and J. Horowitz, *Determination of the Mean Transfer Free Path of Thermal Neutrons by Measurement of the Complex Diffusion Length*, Proc. 1955 Geneva Conference, 5: Paper No. 360, p. 42.
40. G. von Dardel and N. G. Sjöstrand, *Diffusion Measurements with Pulsed Neutron Sources*, Progress in Nuclear Energy, (London: Pergamon Press, Ltd., 1958), Series I: Physics and Mathematics, Vol. 2, Chap. 5.
41. Y. Droulers, J. Lacour and V. Raievski, *Mesure du libre parcours moyen de transport des neutrons dans la graphite*, J. Nuclear Energy, 7: No. 3, 210, (1958).
42. K. H. Beckurts, *Measurements with a Pulsed Neutron Source*, Nuclear Sci. and Eng., 2: No. 4, 516-522, (July, 1957).
43. M. Küchle and K. H. Beckurts, *A Remark on the Transport Mean Free Path of Thermal Neutrons in Graphite*, J. Nuclear Energy, Part A, 10: 157, (1959).
44. A. V. Antonov, et al., *A Study of Neutron Diffusion in Beryllium, Graphite and Water by the Impulse Method*, Proc. 1955 Geneva Conference, 5: Paper No. 661, p. 3.
45. G. deSaussure and E. G. Silver, *Time-Dependent Neutron-Diffusion Measurements*, Applied Nuclear Physics Division Annual Progress Report for Period Ending September 1, 1957, ORNL-2389, (November, 1957), p. 119.
46. C. R. Richey and E. Z. Block, *Graphite Diffusion Length Measurements at Hanford*, HW-45035, (September, 1956).
47. M. T. Lee, *Re-evaluation of Graphite Diffusion Lengths*, HW-51175, (June, 1957).
48. R. C. Lloyd, E. D. Clayton and C. R. Ritchie, *Variation of Graphite Diffusion Length with Temperature*, Nuclear Sci. and Eng., 4: No. 5, 690, (November, 1958).

49. D. J. Behrens, *The Migration Length of Neutrons in a Reactor*, AERE-T/R-877, (February, 1952).
50. R. A. Laubenstein, *Exponential Experiments on Graphite Lattices Which Contain Multi-rod Fuel Elements*, Proc. 1958 Geneva Conference, 12: Paper No. 594, p. 689.
51. J. M. Hendrie, et al., *Slowing Down and Diffusion Lengths of Neutrons in Graphite-Bismuth Systems*, Proc. 1958 Geneva Conference, 12: Paper No. 601, p. 695.
52. Ibid, Ref. 51. Private communication from E. Hellstrand to J. M. Hendrie, et al.
53. K. S. Singwi and L. S. Kothari, *Transport Cross Section of Thermal Neutrons in Solid Moderators*, Proc. 1958 Geneva Conference, 16: Paper No. 1638, p. 325.
54. L. A. Geraseva, et al., *The Study of Beryllium as a Neutron Moderator*, Proc. 1955 Geneva Conference, 5: Paper No. 662, p. 13.
55. E. C. Campbell and P. H. Stelson, *Experiments with Pulsed-Neutron Source*, Physics Division Semiannual Progress Report for Period Ending March 10, 1956, ORNL-2076, (July, 1956), p. 32.
56. T. T. Komoto and F. Kloverstrom, *Diffusion Cooling in Beryllium and Graphite*, Trans. Am. Nuclear Soc., 1: No. 1, 94, (June, 1958).
57. G. deSaussure and E. G. Silver, *Measurements of the Transport Mean Free Path of Thermal Neutrons in Beryllium as a Function of Temperature*, Nuclear Sci. and Eng., 6: No. 2, 159, (August, 1959).
58. G. deSaussure and E. G. Silver, *Time-Dependent Neutron Diffusion Measurements*, Neutron Physics Division Annual Progress Report for Period Ending September 1, 1958, ORNL-2609, (October, 1958), p. 59.
59. W. M. Andrews, *Measurement of the Temperature Dependence of Neutron Diffusion Properties in Beryllium Using a Pulsed Neutron Technique*, UCRL-6083, (August, 1960), p. 193.
60. R. C. Bhandari, *Scattering of Thermal Neutrons in Beryllium*, J. Nuclear Energy, 6: Nos. 1/2, 104-112, (1957).
61. K. S. Singwi and L. S. Kothari, *Slowing Down of Neutrons in Beryllium from 1.44 ev to Thermal Energy*, J. Nuclear Energy, 5: No. 2, 342, (1957).
62. D. J. Hughes and J. A. Harvey, *Neutron Cross Sections*, BNL-325, (July, 1955).
63. R. Ramanna, et al., *On the Determination of Diffusion and Slowing Down Constants of Ordinary Water and Beryllium Oxide Using a Pulsed Neutron Source*, Proc. 1955 Geneva Conference, 5: Paper No. 872, p. 24.
64. S. B. D. Iyengar, et al., *Slowing Down and Diffusion of Neutrons in Beryllium Oxide*, (p. 215); and *Temperature Dependence of the Slowing Down and Diffusion Constants of Neutrons in Beryllium Oxide*, (p. 224), Proc. Ind. Acad. Sci., 45: Section A, (1957).
65. J. C. Koechlin, et al., *Measurements of the Diffusion Length of Thermal Neutrons in Beryllium Oxide*, Proc. 1955 Geneva Conference, 5: Paper No. 359, p. 20.
66. V. Raievski and J. Horowitz, *Mesure du libre parcours moyen de transport des neutrons thermiques dans l' eau lourde au moyen d'une source modulée*, Comptes Rendus, 238: 1993, (May, 1954).
67. P. Auger, A. M. Munn and B. Pontecorvo, *The Transport Mean Free Path of Thermal Neutrons in Heavy Water*, Can. J. Research, A25: 143, (1947).
68. D. W. Hone, *The Value of Transport Mean Free Path for D_2O*, J. Nuclear Energy, Part A, 11: No. 1, 34, (1959).
69. V. C. Wilson, E. W. Bragdon and H. Kanner, *The Temperature Coefficient of the Diffusion Length for Thermal Neutrons in Water*, CP-2306, (October, 1944).
70. R. W. Deutsch, *Temperature Dependence of the Thermal Diffusion Length in Water*, Nuclear Sci. and Eng., 1: No. 3, 252, (July, 1956).
71. G. von Dardel and N. G. Sjöstrand, *Diffusion Parameters of Thermal Neutrons in Water*, Phys. Rev., 96: No. 5, 1245, (1954).
72. W. H. Dio and E. Schopper, *Temperature Dependence of the Diffusion Coefficient and the Diffusion Length of Thermal Neutrons in Water*, Nuclear Phys., 6: 175-176, (1958).
73. K. S. Rockey and W. Skolnik, *Measurements on the Diffusion Length of Thermal Neutrons in Water from 25 to 296°C*, Nuclear Sci. and Eng., 8: No. 1, 62-65, (July, 1960).
74. M. Reier and J. A. DeJuren, *Diffusion Length of Thermal Neutrons in Water from 23°C to 244°C*, J. Nuclear Energy, 14: No. 1, 18, (1961).
75. W. B. Wright and R. T. Frost, *Preliminary Diffusion Length Measurements in Hot Water*, KAPL-M-WBW-2, (October, 1956).
76. A. Berthelot, R. Cohen and H. Reel, *La longeur de diffusion des neutrons thermiques dans l'eau*, Comptes Rendus, 225: 406, (September, 1947).
77. F. J. Sisk, *Transport Parameters for Thermal Neutrons in Water*, ORNL-933, (March, 1951).
78. F. J. Sisk and E. C. Campbell, *Thermal Neutron Transport in Water*, Bull. Am. Phys. Soc., 26: No. 1, 58, (February, 1951).
79. J. A. DeJuren and H. Rosenwasser, *Diffusion Length of Thermal Neutrons in Water*, J. Research Natl. Bur. Standards, 51: No. 4, 203, (October, 1953).
80. F. R. Scott, D. B. Thomson and W. Wright, *Thermal Neutron Capture Cross Sections of Hydrogen, Boron, and Silver*, Phys. Rev., 95: No. 2, 582, (1954).
81. A. Bracci and C. Coceva, *The Diffusion Parameters of Thermal Neutrons in Water*, Nuovo Cimento, Vol. IV, No. 1, 59, (July, 1956).
82. L. M. Barkov, V. K. Makarin and K. N. Mukhin, *Measurement of the Slowing Down of Neutrons in the Energy Range 1.46-0.025 ev in Water*, J. Nuclear Energy, Part II, 4: No. 1, 94-102, (1957).
83. W. H. Dio, *Über Untersuchungen der Diffusion thermischer Neutronen in Wasser und Paraffin mit einer gepulsten Quelle*, Nukleonik, 1: 13, (1958/59).
84. K. H. Beckurts and D. Klüber, *Bestimmung der Diffusionsparameter thermischer Neutronen in Wasser nach einer Vergiftungsmethode*, Z. Naturforsch., Band 13 a, Heft 10, 822, (1958).
85. M. Reier and J. A. DeJuren, *Diffusion Length Measurements in Water Poisoned with Boron*, Technical Progress Report, Reactor Physics and Mathematics for the Period September 1, 1959 to December 1, 1959, WAPD-MRJ-8, p. 4.
86. W. M. Lopez, et al., *A Preliminary Report on Measurements of Diffusion Parameters by the Pulsed-Neutron Method*, GA-1584, (September, 1960).
87. M. Küchle, *Measurements of the Temperature Dependence of Thermal Neutron Diffusion Parameters in Water and Dowtherm A*, Nuclear Sci. and Eng., 8: No. 1, 88, (July, 1960).
88. M. Küchle, *Messung der Temperaturabhängigkeit der Neutronendiffusion in Wasser und Diphyl mit der Impulsmethode*, Nukleonik, 2: No. 4, 131, (1960).
89. H. Hurwitz, Jr. and M. S. Nelkin, *The Thermal Spectrum in a Diffusing Medium*, Nuclear Sci. and Eng., 3: No. 1, 1, (January, 1958).
90. N. G. Sjöstrand, J. Mednis and T. Nilsson, *Geometric Buckling Measurements Using the Pulsed Neutron Source Method*, Arkiv Fysik, 15: 471, (1959).
91. C. W. Tittle, *The Thermal Neutron Diffusion Length of Paraffin*, Phys. Rev., 80: No. 4, 756, (1950).
92. B. S. Smith and J. H. Tait, *Thermal Neutron Distribution in a Slab of Paraffin*, Nature, 165: No. 4188, 196, (February 4, 1950).
93. A. Ertaud and P. Zaleski, *Mesure des densités de neutrons par autoradiographie de détecteurs*, Comptes Rendus, 234: 1969, (1952).
94. L. R. Heintzé, *Thermal-Neutron Diffusion Lengths for Water, Lucite, Furfural, and an Expanded Plastic*, Nucleonics, 14: No. 5, 108, (May, 1956).
95. T. E. Blackman, J. R. A. Lakey and G. Preston, *The Measurement of the Moderating Properties of Dowtherm A*, AERE R/R 2345, (August, 1957).
96. L. G. Sanders and A. K. McCracken, unpublished (see Ref. 95, p. 8).
97. L. Bata, I. Kiss and L. I. Pal, *Investigations on the Moderating Parameters of "Dowtherm A" at Different Temperatures*, Proc. 1958 Geneva Conference, 12: Paper No. 1730, p. 509.

98. R. O. Williams, Jr., et al., *Reactor Analysis of the Organic Moderated Reactor Experiment and Comparison of Experimental Results*, Proc. 1958 Geneva Conference, 12: Paper No. 630, p. 518.
99. E. Melkonian, *Slow Neutron Velocity Spectrometer Studies of O_2, N_2, A, H_2, H_2O, and Seven Hydrocarbons*, Phys. Rev., 76: No. 12, 1750, (1949).
100. C. D. Petrie, M. L. Storm and P. F. Zweifel, *Calculation of Thermal Group Constants for Mixtures Containing Hydrogen*, Nuclear Sci. and Eng., 2: No. 6, 728-744, (November, 1957).
101. M. C. Conerty, et al., *Calculation of Fast and Thermal Group Constants with Applications to Diphenyl*, KAPL-1643, (October, 1956).
102. M. Goldsmith, et al., *Theoretical Analysis of Highly Enriched Light Water Moderated Critical Assemblies*, Proc. 1958 Geneva Conference, 12: Paper No. 2376, p. 435.
103. M. Goldsmith and T. M. Ryan, *Thermal Activation Shapes in a Water-Moderated Critical Assembly*, Nuclear Sci. and Eng., 5: No. 5, 299-305, (May, 1959).
104. G. P. Calame, *A Few-Group Theory of Water Gap Peaking*, Nuclear Sci. and Eng., 8: No. 5, 400-404, (November, 1960).
105. G. P. Calame, *On the Calculation of Water Gap Peaking*, Nuclear Sci. and Eng., 10: No. 1, 90, (May, 1961).
106. W. B. Wright and F. Feiner, *Note on Position-Dependent Spectra*, Nuclear Sci. and Eng., 6: No. 1, 81, (July, 1959).
107. C. N. Kelber and P. Kier, *Few Group Analysis of D_2O-U^{235} Assemblies*, Nuclear Sci. and Eng., 8: No. 1, 1, (July, 1960).
108. D. S. Selengut, *Thermal Flux in a Cell with Temperature Discontinuities*, Nuclear Physics Research Quarterly Report, April, May, and June, 1958, HW-56919, (July, 1958), p. 13.
109. R. A. Bennett and R. E. Heineman, *Neutron Rethermalization Cross Section Measurements in Graphite*, Nuclear Sci. and Eng., 8: No. 4, 294, (October, 1960).
110. E. J. Fowler and R. J. Royston, *Spectrum Calculations in Non-Absorbing Media Using Kottwitz's Method*, AERE-M 503, (August, 1959).
111. A. M. Weinberg and L. C. Noderer, *Theory of Neutron Chain Reactions*, ORNL-CF-51-5-98, Vol. II, Part I, Chap. V, (August, 1951).
112. E. Inönü, *On the Validity of the Second Fundamental Theorem for Small Reactors*, Nuclear Sci. and Eng., 5: No. 4, 248, (April, 1959).
113. R. J. Mack and P. F. Zweifel, *Greuling-Goertzel Calculations in Heavy Water*, Nuclear Sci. and Eng., 7: No. 2, 144, (February, 1960).
114. E. Greuling, F. Clark and G. Goertzel, *A Multigroup Approximation to the Boltzmann Equation for Critical Reactors*, NDA 10-96; H. J. Amster, *Heavy Moderator Approximations in Neutron Transport Theory*, J. Appl. Phys., 29: No. 4, 623, (1958); G. Goertzel and E. Greuling, *An Approximate Method for Treating Neutron Slowing Down*, Nuclear Sci. and Eng., 7: No. 1, 69, (January, 1960).
115. M. M. Shapiro, *Reactor Statics*, Reactor Handbook (AECD-3645), 1: Chap. 1.5, 504, (1955).
116. R. E. Marshak, *Theory of the Slowing Down of Neutrons by Elastic Collisions with Atomic Nuclei*, Revs. Modern Phys., 19: No. 3, 185, (1947).
117. H. Hurwitz, Jr. and P. F. Zweifel, *Slowing Down of Neutrons by Hydrogenous Moderators*, KAPL-1269, (February, 1955).
118. R. L. Hellens, *Neutron Slowing Down in Group Diffusion Theory*, WAPD-114, (May, 1956).
119. J. E. Hill, et al., *The Slowing Down of Fission Neutrons in Graphite*, ORNL-187, (January, 1949).
120. H. Alter, J. Dudek and G. Joanou, *Monte Carlo Calculation of the Slowing Down Moments in Hydrocarbons*, NAA-SR-Memo 5655, (April, 1961).
121. W. G. Davey, et al., *An Experimental Study of the Slowing Down of Fission Neutrons and the Diffusion of Thermal Neutrons in Graphite and in Heterogeneous Mixtures of Bismuth and Graphite*, AERE R/R 2501, (March, 1958).
122. R. Nobles and J. Wallace, *The Diffusion Length and Age in Beryllium*, ANL-4076, (October, 1947), p. 10.
123. D. Meneghetti and H. H. Hummel, *Effect of (n,2n) and (n,α) Reactions on Age Calculations for Beryllium*, Nuclear Sci. and Eng., 6: No. 1, 57, (July, 1959).
124. J. W. Wade, *Neutron Age in Mixtures of Light and Heavy Water*, DP-163, (June, 1956); and *Neutron Age in Mixtures of D_2O and H_2O*, Nuclear Sci. and Eng., 4: No. 1, 12, (July, 1958).
125. E. Martin, *Lattice Measurements in Borated D_2O*, NAA-SR-925, (January, 1954), p. 11.
126. R. N. Olcott, *Homogeneous Heavy Water Moderated Critical Assemblies. Part I. Experimental*, Nuclear Sci. and Eng., 1: No. 4, 327, (August, 1956).
127. M. Tobias, *Review of Experimental and Theoretical Studies Concerning the Age of Fission Neutrons in Heavy Water*, ORNL-2575, (October, 1958).
128. H. Goldstein, P. F. Zweifel and D. G. Foster, Jr., *The Slowing Down of Neutrons in Hydrogeneous Media—Status of Theory and Experiment*, Proc. 1958 Geneva Conference, 16: Paper No. 2375, p. 379.
129. W. H. Arnold, Jr., *Age in D_2O–H_2O Mixtures*, Nuclear Sci. and Eng., 6: No. 5, 456, (November, 1959).
130. M. M. Levine, et al., *The Slowing Down of Neutrons by Deuterium*, Nuclear Sci. and Eng., 7: No. 1, 14, (January, 1960).
131. W. W. Brown, *Neutron Age and Diffusion Length Measurements in Diphenyl*, NAA-SR-Memo-1706, (1956).
132. N. C. Francis, M. L. Storm and P. F. Zweifel, *Neutron Age in Diphenyl*, Nuclear Sci. and Eng., 2: No. 6, 745, (November, 1957).
133. M. L. Barkov, et al., *The Slowing Down of Fission Neutrons in Uranium-Water Media*, J. Nuclear Energy, 4: 103, (1957).
134. W. Matthes and T. Springer, *The Computation of the Fermi Age in a Heterogeneous Reactor by the Monte Carlo Method*, J. Nuclear Energy, Part A, 10: No. 3-4, 158, (1959).
135. W. G. Pettus, *Neutron Age Measurements in Water and in Metal-Water Lattices*, BAW-146, (July, 1960).
136. J. I. Hoover and T. I. Arnette, *The Resonance Integral of Zirconium (~1% Hafnium) and the Slowing Down Length in a Mixture (4 : 1 by volume) of Light Water and Zirconium Metal*, ORNL-641, (July, 1950).
137. N. G. Sjöstrand and J. S. Story, *Nuclear Data for Reactor Design*, (London: Pergamon Press, Ltd.), (to be published).
138. J. E. Hill, L. D. Roberts and T. E. Fitch, *Slowing Down Distribution of U^{235} Fission Neutrons from a Point Source in Light Water*, J. Appl. Phys., 26: No. 8, 1013, (1955).
139. R. R. Coveyou and J. G. Sullivan, *Calculations of Neutron Ages in Various Media*, ORNL-2609, (October 28, 1958), p. 82.
140. A. M. Munn and B. Pontecorvo, *Spatial Distributions of Neutrons in Hydrogenous Media Containing Bismuth, Lead, and Iron*, Can. J. Res., A25: 157, (1947).
141. E. Amaldi and E. Fermi, *On the Absorption and the Diffusion of Slow Neutrons*, Phys. Rev., 50: 899, (1936).
142. D. Fieno, *Slowing Down Distribution to Indium Resonance of Neutrons from a Ra-α-Be Source in Water-Iron Mixtures*, NACA-RM-E54H04, (August, 1954).
143. J. H. Rush, *Range of Ra-α-Be Neutrons in Water*, Phys. Rev., 73: 271, (1948).
144. J. Dacey, R. Paine, Jr. and C. Goodman, *Nuclear Shielding Studies—III. Shielding Properties of Various Materials Against Neutrons and Gamma Rays*, NP-1243—Technical Report No. 23, (October, 1949).
145. C. W. Tittle, et al., *Nuclear Shielding Studies—I. The Slowing Down and Diffusion of Neutrons in Hydrogenous Media*, NP-1418—Technical Report No. 21, (August, 1949).
146. V. P. Duggal, S. M. Puri and K. Sri Ram, *Experiments on Fast Neutron Distributions in Water and Neutron Age in Water-Aluminum Mixtures*, Proc. 1958 Geneva Conference, 13: Paper No. 1640, p. 85.
147. R. H. Graham, et al., *Migration Area of Polonium-Beryllium Neutrons in Water*, MTA-45, (May, 1953).
148. J. W. T. Spinks and G. A. R. Graham, *Preparation and Characteristics of a Polonium-Beryllium Neutron Source*, Can. J. Research, 28: Sec. A, No. 1, 60, (1950).

149. W. Baer, *Spatial Distribution of Thermal Neutrons from a Polonium-Beryllium Source in Water-Zirconium Mixtures*, WAPD-99, (December, 1953).
150. F. A. Valente and R. E. Sullivan, *The Age of Plutonium-Beryllium Neutrons in Light Water*, Nuclear Sci. and Eng., 6: No. 2, 162, (August, 1959).
151. M. Reier, *The Age of Polonium-Beryllium and Polonium-Boron Neutrons in Various Metal-Water Mixtures – A Comparison Between Theory and Experiment*, Proc. 1958 Geneva Conference, 13: Paper No. 635, p. 91; M. Reier, F. Obenshain and R. L. Hellens, *The Age of Polonium-Beryllium Neutrons in Various Metal-Water Mixtures*, Nuclear Sci. and Eng., 4: No. 1, 1, (July, 1958).
152. R. Ramanna and M. Navalkar, *On the Determination of the Slowing Down Length in Ordinary Water Using a Pulsed Neutron Source*, Proc. Ind. Acad. Sci., Vol. XLV, Section A, 74, (1957).
153. R. S. Caswell, et al., *Attenuation of 14.1-Mev Neutrons in Water*, Nuclear Sci. and Eng., 2: No. 2, 143, (April, 1957).
154. L. M. Barkov and K. N. Mukhin, *The Slowing Down of Fission Neutrons in Water*, J. Nuclear Energy, 4: No. 1, Pt. 1, 91, (1957).
155. K. Shure and P. A. Roys, *Spatial Distribution of Thermal Neutrons from an N^{17} Source in Water*, Nuclear Sci. and Eng., 2: No. 2, 170-180, (April, 1957).
156. V. Spiegel, Jr., D. W. Oliver and R. S. Caswell, *Age to Indium Resonance for D-D Neutrons in Water*, Nuclear Sci. and Eng., 4: No. 4, 546, (October, 1958).
157. M. Reier, *The Age of Polonium-Boron Neutrons in Water*, Nuclear Sci. and Eng., 3: No. 3, 374, (March, 1958).
158. C. R. Mullin, *Monte Carlo Analysis of a Water Age Experiment*, KAPL-2003, (January, 1959).
159. L. D. Roberts, J. E. Hill and G. McCammon, *A Study of the Slowing Down Distribution of Sb^{124}-Be Photo-Neutrons in Graphite and of the Use of Indium Foils*, ORNL-201, (February, 1950).
160. W. L. Carlson, *Neutron Age Measurements in Graphite with Gold Resonance Detection*, ORNL-784, (September, 1950).
161. L. S. Kothari and K. S. Singwi, *Slowing Down of Neutrons in Beryllium from 1.44 eV to Thermal Energy*, J. Nuclear Energy, 5: No. 3-4, Pt. 1, 342, (1957).
162. J. Tittman, *Neutron Moderation in SiO_2*, Phys. Rev., 95: No. 2, 660, (1954).
163. A. C. B. Richardson, *Age to Indium Resonance for D-D Neutrons in Heavy Water*, Trans. Am. Nuclear Soc., 2: No. 1, 148, (June, 1959).
164. D. G. Foster, Jr., *Age of Na-Be Neutrons in Water and Kerosene*, Nuclear Sci. and Eng., 8: No. 2, 148, (August, 1960).
165. R. C. Doerner, et al., *Age of Fission Neutrons to Indium Resonance in Water*, Nuclear Sci. and Eng., 9: No. 2, 221, (February, 1961).
166. E. Greuling, et al., *Theory of Water-Tamped Water Boiler*, LA-399, (September, 1945).
167. H. Hurwitz, Jr. and R. Ehrlich, *Highly Enriched Intermediate and Thermal Assemblies*, Progress in Nuclear Energy, (New York: McGraw-Hill Book Co. Inc., 1956) Series 1: Physics and Mathematics, p. 343.
168. D. K. Trubey, H. S. Moran and A. M. Weinberg, *An Estimate of the Non-Leakage Probability for Bare Aqueous Homogeneous U^{235} Reactors*, ORNL-CF-57-11-15, (November, 1957).
169. V. W. Morriss and P. F. Zweifel, *Slowing-Down Kernel for Delayed Neutron Groups*, Reactor Technology Report No. 7—Physics, KAPL-2000-4, (1958), p. 15.
170. R. Batchelor and H. R. McK.Hyder, *The Energy of Delayed Neutrons from Fission*, J. Nuclear Energy, 3: No. 1/2, 7, (1956).
171. J. E. Wilkins, Jr., R. L. Hellens and P. F. Zweifel, *Status of Experimental and Theoretical Information on Neutron Slowing Down Distribution in Hydrogenous Media*, Proc. 1955 Geneva Conference, 5: Paper No. 597, p. 62.
172. W. G. Pettus, *Age of U^{233} Fission Neutrons in Water*, Nuclear Sci. and Eng., 8: No. 2, 171 (August, 1960).
173. M. Faber and P. F. Zweifel, *The Age of U^{233} Fission Neutrons in Water*, Nuclear Sci. and Eng., 6: No. 1, 81 (July, 1959).
174. T. V. Blosser and D. K. Trubey, *An Investigation of the Slowing Down of Fission Neutrons in Water*, Neutron Physics Annual Progress Report for Period Ending September 1, 1959, ORNL-2842, (November, 1959), p. 109.
175. D. B. Lombard and C. H. Blanchard, *Fission-to-Indium Age in Water*, Nuclear Sci. and Eng., 7: No. 5, 448, (May, 1960).
176. R. R. Coveyou, *Monte Carlo Calculations of Neutron Age in Water*, Applied Nuclear Division Annual Report for Period Ending September 10, 1956, ORNL-2081, (November, 1956), p. 144.
177. J. Certaine, *The Age of Fission Neutrons in Water at the Indium Resonance*, NDA-15-94, (August, 1957).
178. H. Goldstein and J. Certaine, *Some Recent Calculations of the Age of Fission Neutrons in Water*, ORNL-2389, (September, 1957), p. 22.
179. H. Bohl, Jr., E. M. Gelbard and G. H. Ryan, *MUFT-4 Fast Neutron Spectrum Code for the IBM-704*, WAPD-TM-72, (July, 1957).
180. A. F. Henry, *54 Group Library for P-1 Programs*, WAPD-TM-224, (April, 1960).
181. P. A. Ombrellaro, *Effective Fast Group Cross Sections in Four Group Theory*, WAPD-TM-63, (May, 1957).
182. A. D. Galanin, *Thermal Reactor Theory*, Second Revised and Authorized Edition, J. B. Sykes (trans.), (New York: Pergamon Press, 1960), p. 395.
183. M. Shapiro, op. cit., Ref. 115, p. 485.
184. M. Shapiro, op. cit., Ref. 115, p. 494.
185. R. W. Deutsch, *Computing 3-Group Constants for Neutron Diffusion*, Nucleonics, 15: No. 1, 47-51, (January, 1957).
186. C. N. Kelber, *Equivalence Factors for D_2O*, Nuclear Sci. and Eng., 3: No. 5, 633, (May, 1958).
187. B. Mozer, *A Study of the Fast Effect*, BNL-2741, (April, 1954).
188. M. R. Fleishman and H. Soodak, *Methods and Cross Sections for Calculating the Fast Effect*, Nuclear Sci. and Eng., 7: No. 3, 217-227, (March, 1960).
189. A. M. Weinberg and E. P. Wigner, *The Physical Theory of Neutron Chain Reactors*, (Chicago: University of Chicago Press, 1958).
190. W. Häfele, *The Fast-Neutron Multiplication Effect of Beryllium in Reactors*, ORNL-2779, (September, 1959).
191. W. Häfele and M. Tsagaris, *The Fast Multiplication Effect of Beryllium Oxide in Reactors*, ORNL-2849, (December, 1959).
192. J. Chernick and S. Oleksa Moore, *Breeding Potential of Thermal Reactors*, Nuclear Sci. and Eng., 6: No. 6, 537-544, (December, 1959).
193. G. J. Fischer, *Cross Section for the (n,2n) Reaction in Be^9*, Phys. Rev., 108: No. 1, 99, (1957).
194. V. L. Sailor, *Reports to the AEC Nuclear Cross-Sections Advisory Group*, WASH-1013, (November, 1958).
195. P. G. Aline, P. E. Novak and B. Wolfe, *On the Fast Effect in Beryllium*, Nuclear Sci. and Eng., 7: No. 4, 392-394, (April, 1960).
196. J. B. Marion, J. S. Levin and L. Cranberg, *Elastic and Nonelastic Neutron Cross Sections for Beryllium*, Phys. Rev., 114: No. 6, 1584, (1959).
197. D. J. Hughes and R. B. Schwartz, *Neutron Cross Sections*, BNL-325, 2nd Edition, (1958); data from C. K. Bockelman, et al.
198. J. L. Fowler and H. O. Cohn, *Scattering of Neutrons from Beryllium*, Bull. Am. Phys. Soc., 4: Series II, 385, (1959).
199. H. Rief, *The Fast Effect in Uranium and Beryllium Systems*, Nuclear Sci. and Eng., 10: No. 1, 83-89, (May, 1961).
200. H. Rief, *An IBM-704 Monte Carlo Code to Calculate the Fast Effect in Homogeneous and Heterogeneous Systems*, BNL-647, (January, 1961).
201. C. G. Chezem, *A Uranium-Metal Exponential Experiment*, Nuclear Sci. and Eng., 8: No. 6, 652-669, (December, 1960).
202. L. Dresner, *Resonance Absorption in Nuclear Reactors*, (New York: Pergamon Press, 1960).
203. G. Placzek, *On the Theory of the Slowing Down of Neutrons in Heavy Substances*, Phys. Rev., 69: Nos. 9 and 10, 423, (May 1, and 15, 1946).

204. J. C. Stewart and P. F. Zweifel, *A Review of Self-Shielding Effects in the Absorption of Neutrons*, Proc. 1958 Geneva Conference, 16: Paper No. 631, p. 650.
205. S. Glasstone and M. C. Edlund, *The Elements of Nuclear Reactor Theory*, (New York: D. Van Nostrand Company, Inc., 1952).
206. H. Soodak, F. Adler and E. Greuling, *Kinetic Theory of Neutrons*, Reactor Handbook (AECD-3645), 1: Chap. 1.3, 504, (1955).
207. A. M. Weinberg and L. C. Noderer, *Theory of Neutron Chain Reactions*, ORNL-CF-51-5-98, Vol. I, Chap. IV, (May, 1951).
208. N. Corngold, *Slowing Down of Neutrons in Infinite Homogeneous Media*, Proc. Phys. Soc. (London), A70, 793, (1957).
209. J. M. Blatt and V. F. Weisskopf, *Theoretical Nuclear Physics*, (New York: John Wiley and Sons, 1952).
210. R. G. Sachs, *Nuclear Theory*, (Cambridge, Mass.: Addison-Wesley Publishing Co., 1953).
211. G. Breit and E. P. Wigner, *Capture of Slow Neutrons*, Phys. Rev., 49: 519, (1936).
212. J. B. Sampson and J. Chernick, *Resonance Escape Probability in Thermal Reactors*, Progress in Nuclear Energy, (London: Pergamon Press, Ltd., 1958), Series I: Physics and Mathematics, Vol. II, Chap. 6.
213. M. E. Rose, et al., *A Table of the Integral:*

$$\psi(x,t) = \frac{1}{2\sqrt{\pi t}} \int_{-\infty}^{\infty} \frac{exp\left[-\frac{(x-y)^2}{4t}\right]}{1+y^2} dy,$$ WAPD-SR-506, Vols. 1 and 2, (October, 1954); see also BNL-257, (September, 1953).

214. C. W. Reich and M. S. Moore, *Multilevel Formula for the Fission Process*, Phys. Rev., 111: No. 3, 929, (1958).
215. L. M. Bollinger, *Slow Neutron Resonances*, Nuclear Spectroscopy, (New York: Academic Press, Inc., 1960), Part A, Chap. 3.
216. L. Dresner, *The Estimation of Resonance Integrals*, J. Nuclear Energy, 2: No. 2, 118, (1955).
217. E. Kuhn and L. Dresner, *The Effects of Fluctuations in the Reaction Widths on Resonance Integrals*, J. Nuclear Energy, 7: 69, (1958).
218. C. E. Porter and R. G. Thomas, *Fluctuations of Nuclear Reaction Widths*, Phys. Rev., 104: No. 2, 483, (1956).
219. R. B. Tattersall, et al., *Pile Oscillator Measurements of Resonance Absorption Integrals*, AERE-R/2887, (August, 1959).
220. K. Jirlow and E. Johansson, *The Resonance Integral of Gold*, J. Nuclear Energy, 11: No. 2-4, 101-107, (1960).
221. P. E. Spivak, et al., *Measurements of the Resonance Absorption Integrals for Various Materials and ν_{eff} - the Multiplication Coefficient of Resonance Neutrons for Fissionable Isotopes*, Proc. 1955 Geneva Conference, 5: Paper No. 659, p. 91.
222. R. L. Macklin and H. S. Pomerance, *Resonance Capture Integrals*, Proc. 1955 Geneva Conference, 5: Paper No. 833, p. 96.
223. V. B. Klimentov and V. M. Griazev, *Some Neutron Resonance Absorption Integrals*, J. Nuclear Energy, 9: No. 1-4, 20-27, (1959).
224. R. Dahlberg, et al., *Measurements of Some Resonance Activation Integrals*, J. Nuclear Energy, 14: No. 1, 53, (1961).
225. F. Feiner and L. J. Esch, *Cobalt Resonance Integral*, KAPL-2000-12, (December, 1960), p. I.37.
226. F. J. Johnston, et al., *The Thermal Neutron Absorption Cross Section of Th^{233} and the Resonance Integrals of Th^{232}, Th^{233} and Co^{59}*, J. Nuclear Energy, 11: No. 2-4, 95-100, (1960).
227. R. A. Bennett, *Effective Resonance Integrals of Cu and Au*, HW-63576, (January, 1960).
228. W. H. Walker, *Yields and Effective Cross Sections of Fission Products and Pseudo Fission Products*, CRRP-913, (March, 1960).
229. F. Feiner, *A Measurement of the Resonance Integral of Zr^{91}*, KAPL-2000-8, (December, 1959).
230. M. J. Cabell, *The Purification and Absolute Determination of Mo^{99} and the Neutron Capture Cross Section of Mo^{98}*, AERE-R-3647, (February, 1961).
231. M. J. Cabell, *The Thermal Neutron Capture Cross Section and the Resonance Capture Integral of Mo^{100}*, J. Nuclear Energy, Part A, 12: 172-176, (1960).
232. T. A. Eastwood, et al., *Radiochemical Methods Applied to the Determination of Cross Sections of Reactor Interest*, Proc. 1958 Geneva Conference, 16: Paper No. 203, p. 54.
233. H. M. Eiland, et al., *Determination of Thermal Cross Sections and Resonance Integrals of Some Fission Products*, KAPL-2000-11, (September, 1960).
234. J. Halperin and R. W. Stoughton, *Some Cross Sections of Heavy Nuclides Important to Reactor Operation*, Proc. 1958 Geneva Conference, 16: Paper No. 1072, p. 64.
235. S. Terasawa, *The Effect of Epithermal Fission on Aqueous Homogeneous Reactors*, ORNL-2553, (August, 1958).
236. R. G. Fluharty, et al., *The Total and Fission Cross Sections of U^{233} Below 1 kev*, Proc. 1958 Geneva Conference, 15: Paper No. 645, p. 111.
237. J. Halperin, et al., *The Resonance Integral for Neutron Fission of U^{233}*, ORNL-2983, (September, 1960).
238. J. Hardy, Jr., et al., *The Resonance Fission Integrals of U^{235}, Pu^{239}, and Pu^{241}*, Nuclear Sci. and Eng., 9: No. 3, 341-345, (March, 1961).
239. J. A. Harvey and R. B. Schwartz, *Thermal and Resonance Cross Sections of Heavy Nuclei*, Progress in Nuclear Energy, (London: Pergamon Press, Ltd., 1958), Series 1: Physics and Mathematics, Vol. II, Chap. 2.
240. R. L. Macklin and H. S. Pomerance, *Resonance Activation Integrals of U^{238} and Th^{232}*, J. Nuclear Energy, 2: No. 4, 243-246, (1956).
241. L. M. Bollinger, et al., *The Slow Neutron Cross Sections of Plutonium-239*, Proc. 1958 Geneva Conference, 15: Paper No. 687, p. 127.
242. F. W. Cornish and M. Lounsbury, *Cross Sections of Pu^{239} and Pu^{240} in the Thermal and Epi-Cadmium Regions*, CRC-633, (March, 1956).
243. B. F. Erozolimsky, et al., *Measurement of the Average Number ν_{eff} of Neutrons Emitted Per Single Capture Event for Samples of Pu^{239} with Impurities of the Isotope Pu^{240} and the Effective Resonance Capture Integral of Pu^{240}*, Soviet J. Atomic Energy, No. 3, 311-315, (1956); also J. Nuclear Energy, 4: No. 1, Pt. 2, 86, (1957).
244. P. A. Krupchinsky, *The Thermal Neutron Absorption Cross Section and Resonance Absorption Integral of Pu^{240}*, J. Nuclear Energy, 6: No. 1/2, Pt. 2, 155-162, (1957).
245. J. P. Butler, et al., *The Neutron Capture Cross Sections of Pu^{238}, Pu^{242}, and Am^{243} in the Thermal and Epicadmium Regions*, Can. J. Phys., 35: No. 2, 147, (February, 1957).
246. J. A. Harvey, *Reports to the AEC Nuclear Cross Sections Advisory Group, Argonne National Laboratory, September 19-21, 1960*, WASH-1029, (October, 1960).
247. V. Weinstock and K. Sher, *Activation Cross Section of Dy-164*, Trans. Am. Nuclear Soc., 3: No. 2, 463, (December, 1960).
248. K. T. Spinney, *Resonance Absorption in Homogeneous Mixtures*, J. Nuclear Energy, 6: Nos. 1/2, 53, (1957).
249. J. Chernick and R. Vernon, *Some Refinements in the Calculation of Resonance Integrals*, Nuclear Sci. and Eng., 4: No. 5, 649-672, (November, 1958).
250. F. T. Adler, G. W. Hinman and L. W. Nordheim, *The Quantitative Evaluation of Resonance Integrals*, Proc. 1958 Geneva Conference, 16: Paper No. 1988, p. 155.
251. J. P. H. Blake, *Resonance Integral Calculations for High Temperature Reactors*, AEEW-R25, (February, 1960).
252. G. M. Roe, *The Absorption of Neutrons in Doppler Broadened Resonances*, KAPL-1241, (October, 1954).
253. W. Rothenstein, *Collision Probabilities and Resonance Integrals for Lattices*, Nuclear Sci. and Eng., 7: No. 2, 162-171, (February, 1960).
254. L. Dresner, *The Effective Resonance Integrals of U^{238} and Th^{232}*, Nuclear Sci. and Eng., 1: No. 1, 68, (March, 1956).
255. W. L. Brooks and N. Tralli, *Theoretical Methods for the Calculation of D_2O Lattices*, NDA-84-24, 1: (July, 1959).

256. G. I. Bell, *Effect of Interference Between Resonance and Potential Scattering on Resonance Absorption*, Nuclear Sci. and Eng., 9: No. 3, 409, (March, 1961).
257. W. Rothenstein and J. Chernick, *Resonance Capture of Neutrons in Non-Heavy Absorbers*, Nuclear Sci. and Eng., 7: No. 5, 454-457, (May, 1960).
258. G. I. Bell, *Theory of Effective Cross Sections*, LA-2322, (June, 1959).
259. B. I. Spinrad, J. Chernick and N. Corngold, *Resonance Capture in Uranium and Thorium Lumps*, Proc. 1958 Geneva Conference, 16: Paper No. 1847, p. 191.
260. R. Goldstein and E. R. Cohen, *Neutron Resonance Absorption Integrals*, Trans. Am. Nuclear Soc., 3: No. 1, (June, 1960).
261. G. I. Marchuk and F. F. Mikhailus, *Resonance Absorption of Neutrons in an Infinite Homogeneous Medium*, J. Nuclear Energy, Part II, 9: 267-280, (1959).
262. A. D. Callihan, et al., *Small Thermal Homogeneous Critical Assemblies*, Proc. 1955 Geneva Conference, 5: Paper No. 834, p. 145.
263. J. Chernick, *Breeding Potential of Thermal Reactors*, Proc. Conference on the Physics of Breeding, October 19-21, 1959, ANL-6122, p. 285.
264. C. K. Beck, et al., *Critical Mass Studies, Part III*, K-343, (April, 1949).
265. J. K. Fox, et al., *Critical Mass Studies, Part IX Aqueous U^{235} Solutions*, ORNL-2367, (March, 1958).
266. J. K. Fox and L. W. Gilley, *Critical Parameters of Aqueous Solutions of U^{235}*, ORNL-2389, (November, 1957), p. 71.
267. J. K. Fox, et al., *Critical Parameters of U^{235} and U^{233} Solutions in Simple Geometry*, ORNL-2842, (November, 1959), p. 76.
268. J. T. Thomas, et al., *A Direct Comparison of Some Nuclear Properties of U^{233} and U^{235}*, Nuclear Sci. and Eng., 1: No. 1, 20, (March, 1956).
269. J. K. Fox, et al., *Critical Parameters of Uranium Solutions in Simple Geometry*, ORNL-2609, (October, 1958), p. 42.
270. C. L. Schuske and J. W. Morfitt, *An Empirical Study of Some Critical Mass Data*, Y-533, (December, 1949).
271. C. L. Schuske and J. W. Morfitt, *Empirical Studies of Critical Mass Data, Part II*, Y-829, (December, 1951).
272. T. R. Running, *Empirical Formulas*, (New York: John Wiley and Sons, 1917).
273. M. Danzker, *An Interpretation of Data on Enriched Hydrogeneous Thermal Reactors*, WAPD-26, (January, 1951).
274. A. D. Callihan, et al., *Critical Mass Studies, Part IV*, K-406, (November, 1949).
275. J. K. Fox, et al., *Critical Parameters of a Proton-Moderated and Proton-Reflected Slab of U^{235}*, Nuclear Sci. and Eng., 3: No. 6, 694, (June, 1958).
276. H. C. Paxton, *Critical Data for Nuclear Safety Guidance*, LAMS-2415, (February, 1960).
277. A. D. Callihan, et al., *Nuclear Safety Guide*, TID-7016, (1958).
278. D. F. Cronin, *Critical Mass Studies, Part X: Uranium of Intermediate Enrichments*, ORNL-2968, (1960), (unpublished).
279. D. F. Cronin and J. T. Thomas, *Critical Parameters of Slightly Enriched Uranium Solutions in Spherical Geometry*, Physics Division Semiannual Progress Report for Period Ending March 10, 1955, ORNL-1926, (September, 1955), p. 7.
280. J. R. Brown, et al., *Critical Experiments on a Highly Enriched Homogeneous Reactor*, WAPD-128, (May, 1955).
281. C. W. Nestor, Jr., *A Comparison of Elementary Criticality Calculations with Experimental Results*, Appendix by D. W. Magnuson, ORNL-CF-59-6-45, (June, 1959).
282. D. W. Magnuson, *Determination of η of U^{233} by Comparison of Critical Experiments in a 69.2 cm Diameter Sphere*, Neutron Physics Division Annual Progress Report for Period Ending September 1, 1958, ORNL-2609, (October, 1958), p. 29.
283. A. D. Callihan, et al., *Critical Mass Studies, Part V*, K-643, (June, 1950).
284. *An Enriched Homogeneous Nuclear Reactor*, AECD-3059, (January, 1951).
285. C. P. Baker, et al., *Waterboiler*, AECD-3063, (September, 1944).
286. R. E. Carter, et al., *Water Tamper Measurements*, LA-241, (March, 1945).
287. L. D. P. King, *The Los Alamos Homogeneous Reactor, SUPO Model*, LA-1301, (February, 1952).
288. J. K. Fox and L. W. Gilley, *Some Studies of Water, Styrofoam, and Plexiglass Reflectors*, ORNL-2609, (October, 1958), p. 38.
289. J. K. Fox and L. W. Gilley, *Critical Experiments with Aqueous Solutions of U^{235}*, ORNL-2081, (November, 1956), p. 61.
290. A. B. Martin and M. M. Mann, *Critical Experiments for the High Flux Reactor*, ORNL-167, (October, 1948).
291. E. B. Johnson, et al., *Reactivity Measurements with the Bulk Shielding Reactor; Control Rod Calibrations; Beam Hole Coefficients; Partial Reflector Coefficients*, ORNL-1871, (September, 1955).
292. E. B. Johnson, et al., *The Reactivity Effect of an Air Tank Against One Face of the Bulk Shielding Reactor*, ORNL-2179, (March, 1957).
293. A. B. Reynolds, et al., *Reactivity Effects of Large Voids in the Reflector of a Light-Water-Moderated and -Reflected Reactor*, Nuclear Sci. and Eng., 7: No. 1, 1, (January, 1960).
294. S. Visner and P. M. Wood, *Low-Power Criticality Experiments on the Homogeneous Reactor Experiment HRE-1*, ORNL-1858, (April, 1957).
295. J. K. Fox and L. W. Gilley, *Critical Parameters of Unreflected Arrays of Interacting Cylinders Containing Aqueous Solutions of U^{235}*, ORNL-2842, (November, 1959), p. 82.
296. J. D. Roarty, *Design of a Non-Critical Dump Tank Assembly for the Boiling Homogeneous Reactor*, CF-52-3-211, (March, 1952).
297. H. F. Henry, et al., *General Application of a Theory of Neutron Interaction*, K-1309, (November, 1956).
298. R. Avery, *Two Group Diffusion Theory for a Ring of Cylindrical Rods*, Nuclear Sci. and Eng., 3: No. 5, 504, (May, 1958).
299. R. Avery, *Theory of Coupled Reactors*, Proc. 1958 Geneva Conference, 12: Paper No. 1858, p. 182.
300. J. C. Stewart, *Interaction of Weakly Coupled Reactor Systems, With Application to the "Convergatron"*, Proc. 1958 Geneva Conference, 12: Paper No. 632, p. 192.
301. J. K. Fox and L. W. Gilley, *Critical Parameters for Poisoned Annular Cylinders Containing Aqueous Solutions of U^{235}*, ORNL-2609, (October, 1958), p. 31; also ORNL-CF-58-8-5 (unpublished).
302. A. D. Callihan and D. F. Cronin, *Ring Tamping*, Y-B23-22, (November, 1952).
303. J. W. Morfitt, *Minimum Critical Mass and Uniform Thermal Neutron Core Flux in an Experimental Reactor*, Y-1023, (December, 1953).
304. D. F. Cronin and A. D. Callihan, *Critical Mass Studies, Part VII, Aqueous Uranium Slurries*, ORNL-1726, (July, 1954).
305. J. J. Lynn, et al., *Homogeneous Hydrogen-Moderated Critical Assemblies with 2% U^{235} Enriched Uranium*, ORNL-2609, (October, 1958), p. 40.
306. J. T. Mihalczo and J. J. Lynn, *Homogeneous Critical Assemblies of 2% U^{235} Enriched UF_4 in Paraffin*, Neutron Physics Division Annual Progress Report for Period Ending September 1, 1960, ORNL-2842 (November, 1959), p. 85.
307. J. T. Mihalczo and J. J. Lynn, *Homogeneous Critical Assemblies of 2% U^{235} Enriched UF_4 in Paraffin*, ORNL-3016, (December, 1960), p. 71.
308. V. I. Neeley, *k_∞ Measurements of 2 Per Cent Enriched UF_4 in Paraffin*, Trans. Am. Nuclear Soc., 2: No. 1, 67, (1959).
309. A. Wattenberg, et al., *Exponential Experiments with D_2O and Solutions of UO_2F_2*, CP-3364, (November, 1945).
310. J. R. Harrison, et al., *Critical Assemblies with Heavy Water Solutions of Uranyl Fluoride (H.A.Z.E.L.)*, AERE R/R 2703, Pt. 2, (November, 1958).
311. F. A. Kloverstrom, et al., *Critical Measurements on Near-Homogeneous BeO-Moderated, Enriched-Uranium Fueled Systems*, Nuclear Sci. and Eng., 8: No. 3, 221, (September, 1960).

312. E. Goldberg, et al., *Critical Experiments Involving Gaps in Simple Configurations*, Trans. Am. Nuclear Soc., 3: No. 2, 331, (December, 1960).
313. F. A. Kloverstrom and D. E. Kraft, *Critical Measurements on Near-Homogeneous, BeO-Moderated, Oralloy-Fueled Systems*, UCRL-5369, Pt. 2, (July, 1959).
314. H. L. Reynolds, *Critical Measurements and Calculations for Enriched-Uranium Graphite-Moderated Systems*, UCRL-5175, (March, 1958), and Errata (May, 1958).
315. H. L. Reynolds, *Critical Measurements and Calculations for Enriched-Uranium Graphite-Moderated Systems*, Proc. 1958 Geneva Conference, 12: Paper No. 2408, p. 632.
316. H. P. Iskenderian, *Physics Analyses of the TREAT Reactor Design*, ANL-6025, (August, 1959).
317. G. A. Freund, et al., *Design Summary Report on the Transient Reactor Test Facility (TREAT)*, ANL-6034, (February, 1960).
318. H. P. Iskenderian, *Post Criticality Studies on the TREAT Reactor*, ANL-6115, (February, 1960).
319. F. Kirn, et al., *Reactor Physics Measurements in TREAT*, ANL-6173, (October, 1960).
320. D. Okrent, et al., *The Reactor Kinetics of the Transient Reactor Test Facility (TREAT)*, ANL-6174, (September, 1960).
321. J. K. Fox, et al., *Critical Mass Studies, Part VIII: Aqueous Solutions of U^{233}*, ORNL-2143, (September, 1959).
322. R. Gwin and D. W. Magnuson, *Critical Experiments for Reactor Physics Studies*, ORNL-CF-60-4-12, (September, 1960).
323. F. E. Kruesi, et al., *Critical Mass Studies of Plutonium Solutions*, HW-24514 (del.), (May, 1952).
324. C. C. Horton and J. D. McCullen, *Plutonium-Water Critical Assemblies*, Proc. 1955 Geneva Conference, 5: Paper No. 428, p. 156.
325. A. D. Callihan, *Nuclear Safety in Processing Reactor Fuel Solutions*, Nucleonics, 14: No. 7, 39, (July, 1956).
326. M. Nelkin, *Scattering of Slow Neutrons by H_2O*, Phys. Rev., 119: No. 2, pp. 741-46, (1960).

Section 4

LATTICE CONSTANTS FOR THERMAL HETEROGENEOUS SYSTEMS

4.1 THERMAL UTILIZATION

The thermal utilization, f, is the rate at which thermal neutrons are absorbed in fissile material, divided by the total rate at which thermal neutrons are absorbed. The main problem in computing thermal utilization in heterogeneous reactors arises from the non-uniform spatial distribution of the thermal flux. The thermal flux is depressed in a heavily absorbing region.

Although the term "thermal utilization" is used, the formulae presented apply to any single-energy group, provided appropriate constants are used.

The thermal utilization of a lattice is usually obtained through consideration of a unit cell. Macroscopic diffusion effects are ignored so that zero current at the cell boundary is assumed. The thermal utilization of a unit cell consisting of a fuel (U) and moderator (M) region is given by:

$$f = \frac{\bar{\Phi}_U \Sigma_{a,U} V_U}{\bar{\Phi}_U \Sigma_{a,U} V_U + \bar{\Phi}_M \Sigma_{a,M} V_M} = \frac{\Sigma_{a,U} V_U}{\Sigma_{a,U} V_U + (\bar{\Phi}_M / \bar{\Phi}_U) \Sigma_{a,M} V_M}$$

where $\Sigma_{a,U}$ and $\Sigma_{a,M}$ are the macroscopic absorption cross sections; V_U and V_M are the volumes; and $\bar{\Phi}_U$ and $\bar{\Phi}_M$ are the average thermal fluxes in the fuel and moderator, respectively. The quantity $\bar{\Phi}_M / \bar{\Phi}_U$ is referred to as the disadvantage factor in the following discussion.

Various calculation methods may be applied in order to obtain the average fluxes. Usually the following two approximations are made: (1) the unit cell has simple geometry, e.g., a square array of cylindrical rods would be considered to have a unit cell of cylindrically radial symmetry; and (2) the source for thermal neutrons in any region of the cell is constant within that region. The effects of rod size and lattice configuration in various geometries are estimated by formulae given at the end of Section 4.1.1.

4.1.1 DIFFUSION THEORY[1]

For the case of a cell containing a fuel region with zero source, surrounded by a moderator region with constant source, diffusion theory gives:

$$\frac{1}{f} = 1 + \frac{V_M \Sigma_{a,M}}{V_U \Sigma_{a,U}} G + (E - 1)$$

If there is also a constant source in the fuel region, the expression for f takes the form:

$$\frac{1}{f} = 1 + \left\{ \frac{\left(1 + \frac{S_U V_U}{S_M V_M}\right)\left(E + G \frac{V_M \Sigma_{a,M}}{V_U \Sigma_{a,U}}\right)}{1 + \frac{S_U V_U}{S_M V_M}\left[E + (G-1)\frac{V_M \Sigma_{a,M}}{V_U \Sigma_{a,U}}\right]} - 1 \right\}$$

where S_U and S_M are the relative source strengths in the fuel and moderator regions, respectively.

The expressions for G and E in slab, cylindrical, and spherical geometry are given in Table 4-1. In the case of no source in the fuel region, G is the ratio of the flux at the surface of the fuel region to the average flux in the fuel.

Table 4-1 — DIFFUSION THEORY CALCULATIONS OF THERMAL UTILIZATION (f)

Cell Geometry	G	E[a]
Infinite Slab	$\kappa_U t_U \coth \kappa_U t_U$	$\kappa_M t_M \coth \kappa_M t_M$
Infinite Cylinder	$\frac{\kappa_U r_U}{2} \frac{I_0(\kappa_U r_U)}{I_1(\kappa_U r_U)}$	$\frac{\kappa_M (r_M^2 - r_U^2)}{2 r_U}\left[\frac{I_0(\kappa_M r_U)K_1(\kappa_M r_M) + K_0(\kappa_M r_U) I_1(\kappa_M r_M)}{I_1(\kappa_M r_M)K_1(\kappa_M r_U) - K_1(\kappa_M r_M) I_1(\kappa_M r_U)}\right]$
Sphere	$\frac{\kappa_U r_U^2}{3} \frac{\tanh \kappa_U r_U}{\kappa_U r_U - \tanh \kappa_U r_U}$	$\frac{\kappa_M (r_M^3 - r_U^3)}{3 r_U}\left[\frac{1 - \kappa_M r_M \coth \kappa_M (r_M - r_U)}{1 - \kappa_M^2 r_M r_U - \kappa_M (r_M - r_U) \coth \kappa_M (r_M - r_U)}\right]$

Nomenclature:

t_U = half-thickness of fuel
t_M = half-thickness of moderator
r_U = radius of fuel region
r_M = outer radius of moderator = radius of cell
$\kappa^2 = \Sigma_a / D$, where D is the diffusion coefficient
I_0, I_1, K_0, K_1 are Bessel functions

[a]For cylinders, if $\kappa_M r_M \ll 1$, then: $E - 1 \approx \frac{(\kappa_M r_M)^2}{2}\left\{\frac{1}{1 - (r_U/r_M)^2} \ln(r_M/r_U) - \frac{3}{4} + \frac{1}{4}(r_U/r_M)^2\right\}$

4.1.1.1 Effects of Rod Size and Lattice Configuration

Neumann[2] investigated the effect of rod size on thermal utilization. He obtained the thermal utilization, f, for several lattice configurations, from the equation:

$$\frac{1}{f} = \frac{\Sigma_{a,M} V_M G}{\Sigma_0 V_0} + \frac{\Sigma_{a,M} V_M}{2\pi a D \lambda} \frac{K_0(\lambda a) + J I_0(\lambda a)}{K_1(\lambda a) - J I_1(\lambda a)}$$

where K_0, K_1, I_0, I_1 are Bessel functions
λ = inverse of the moderator diffusion length
$\Sigma_{a,M}$ = moderator absorption cross section
D = moderator diffusion coefficient
V_M = moderator volume per unit height
a = fuel rod radius
V_0 = rod volume per unit height
Σ_0 = the fuel absorption cross section
G = the ratio of surface to average flux in the fuel
J = a lattice property depending upon the lattice configuration

It may be computed as follows: Let

$\gamma = 0.57721 \ldots$ (Euler's constant)

$\alpha = \lambda \ell / 2\pi$, $\alpha_1 = \lambda a_1 / 2\pi$, $\alpha_2 = \lambda a_2 / 2\pi$

$\beta = \lambda \ell / 4\pi$, $\delta = \sqrt{3}\, \lambda \ell / 4\pi$ and $\tau = 3\lambda \ell / 4\pi$

where a_1, a_2, and ℓ, are lattice parameters in the appropriate geometries.

Define:

$$A(p) \equiv \sum_{s=1}^{\infty} \left[\frac{1}{(s^2 + p^2)^{1/2}} - \frac{1}{s}\right]$$

$$B(p,x) \equiv \sum_{s=1}^{\infty} [\coth x(s^2 + p^2)^{1/2} - 1)]/(s^2 + p^2)^{1/2}$$

These are very rapidly convergent series.

For a square lattice, spacing ℓ:

$$J_S = \frac{2}{\alpha} \coth \pi\alpha + \gamma + \ln\left(\frac{\alpha}{2}\right) + A(\alpha) + B(\alpha,\pi)$$

For a rectangular array, spacings a_1 and a_2:

$$J_r = \frac{1}{2}\left[\frac{1}{2\alpha_1} \coth \pi\alpha_2 + \frac{1}{2\alpha_2} \coth \pi\alpha_1 + 2\gamma + \ln(\alpha_1\alpha_2) + A(\alpha_1) + A(\alpha_2) + B(\alpha_1, \pi a_2/a_1) + B(\alpha_2, \pi a_1/a_2)\right]$$

For an equilateral triangle array, spacing l:

$$J_{rh} = \frac{1}{8\beta} \coth \pi\delta + \frac{1}{8\delta} \coth \pi\beta + \gamma + \ln\beta + \frac{1}{4} \ln 3 + \frac{1}{2} A(2\beta) + \frac{1}{2} A(2\delta) + \frac{1}{4} B(\beta, \pi\sqrt{3}) + \frac{1}{4} B(\delta, \pi/\sqrt{3})$$
$$+ \frac{1}{2} \sum_{s=0}^{\infty} \left[\frac{\tanh\left(\frac{\pi\sqrt{3}}{2}\sqrt{(2s+1)^2 + 4\beta^2}\right) - 1}{\sqrt{(2s+1)^2 + 4\beta^2}} + \frac{\tanh\left(\frac{\pi}{2\sqrt{3}}\sqrt{(2s+1)^2 + 4\delta^2}\right) - 1}{\sqrt{(2s+1)^2 + 4\delta^2}}\right]$$

For a hexagonal lattice, spacing ℓ:

$$J_h = J_{rh} - \pi/(2\sqrt{3}\,\lambda\ell) \cosh(\lambda\ell/4)/\sinh(3\lambda\ell/4)$$
$$- \frac{\pi}{6\lambda\ell} \cosh(\sqrt{3}\,\lambda\ell/4) - \frac{1}{4} \sum_{n=1}^{\infty} \frac{\cos\left(\frac{2\pi}{3} n\right) \coth\left(\frac{\pi}{\sqrt{3}}\sqrt{n^2 + \tau^2}\right)}{\sqrt{n^2 + \tau^2}}$$
$$- \frac{1}{4} \sum_{n=1}^{\infty} \frac{\coth(\pi\sqrt{3}\sqrt{n^2 + \delta^2}) \cosh\left(\frac{2\pi}{\sqrt{3}}\sqrt{n^2 + \delta^2}\right) - \sinh\left(\frac{2\pi}{\sqrt{3}}\sqrt{n^2 + \delta^2}\right)}{\sqrt{n^2 + \delta^2}}$$
$$+ \frac{1}{2} \sum_{n=0}^{\infty} \frac{\cos\frac{\pi}{3}(2n+1) \tanh\left[\frac{\pi}{2\sqrt{3}}\sqrt{(2n+1)^2 + 4\tau^2}\right]}{\sqrt{(2n+1)^2 + 4\tau^2}}$$
$$+ \frac{1}{2} \sum_{n=0}^{\infty} \frac{\tanh\left[\frac{\pi\sqrt{3}}{2}\sqrt{(2n+1)^2 + 4\delta^2}\right] \cosh\left[\frac{\pi}{\sqrt{3}}\sqrt{(2n+1)^2 + 4\delta^2}\right] - \sinh\left[\frac{\pi}{\sqrt{3}}\sqrt{(2n+1)^2 + 4\delta^2}\right]}{\sqrt{(2n+1)^2 + 4\delta^2}}$$

For the linear chain with rod spacing ℓ,

$$J_{lc} = \frac{1}{4\beta} + \gamma + \ln\beta + A(2\beta)$$

4.1.2 SPHERICAL HARMONIC METHOD – ISOTROPIC SCATTERING

The Spherical Harmonic Method may be used to obtain results more accurate than those given by diffusion theory. In plane geometry, with isotropic scattering and constant isotropic source, the one-velocity Boltzmann equation takes the form:

$$\mu \frac{d\Psi(x,\mu)}{dx} + \frac{\Psi(x,\mu)}{\ell} = \frac{c}{2\ell} \int_{-1}^{1} \Psi(x,\mu')\, d\mu' + \frac{Q}{2} \qquad (4\text{-}1)$$

where μ = cosine of the angle between the neutron velocity vector and the x axis
$\Psi(x,\mu)$ = angular neutron flux per unit μ interval (integrated over the azimuthal angle)
ℓ = total mean free path in the medium
$c = \frac{\Sigma_s}{\Sigma_s + \Sigma_c}$ mean number of secondaries per collision
Q = total source strength per unit volume per second

The term, $\Psi(x,\mu)$, may be expanded as:

$$\Psi(x,\mu) = \sum_{n=0}^{\infty} \Psi_n(x) \frac{2n+1}{2} P_n(\mu) \tag{4-2}$$

where the $P_n(\mu)$ are the Legendre Polynomials; $\Psi_0(x)$ is the total neutron flux; and $\Psi_1(x)$ the total neutron current.

Substitution of Eq. (4-2) into Eq. (4-1) yields the set of equations:

$$(n+1)\frac{d\Psi_{n+1}(x)}{dx} + n\frac{d\Psi_{n-1}(x)}{dx} + \frac{(2n+1)\Psi_n(x)}{\ell} = \left[\frac{c\Psi_0(x)}{\ell} + Q\right]\delta_{0,n}$$

where $\delta_{0,n}$ is the Kronecker delta function;

$\delta_{0,n} = 1$, if $n = 0$
$= 0$, otherwise

It is only necessary to consider the homogeneous system of equations ($Q = 0$), since for each region the general solution can be obtained by adding to the solution of the homogeneous system, the particular solution:

$$\Psi_n(x) = \frac{\ell Q}{1-c}\delta_{0,n}$$

The P_N approximation is obtained by retaining only the first N + 1 equations and setting

$$\frac{d\Psi_{N+1}(x)}{dx} = 0$$

in the last of these equations. A solution of the form:

$$\Psi_j(x) = \Psi_j^0 \exp(\nu x/\ell)$$

is assumed, and a determinental equation for ν results from the condition that the determinant of the coefficients must vanish.

The roots of the equation in the P_N approximation are the roots of:

$$G_{N+1}(\nu) = 0$$

where

$$G_0(\nu) = 1$$

$$G_1(\nu) = \frac{c-1}{\nu}$$

and $G_m(\nu)$ satisfies the recursion formula:

$$(m+1)G_{M+1}(\nu) + \frac{2m+1}{\nu}G_m(\nu) + mG_{m-1}(\nu) = 0$$

In general, the odd-order approximations (N odd) are used.[3] The roots of ν are then real, and occur in pairs with opposite sign. Designating the positive roots ν_i, the general solution is given by:

$$\Psi_n(x) = \sum_{i=1}^{(N+1)/2} G_n(\nu_i)(-1)^n A_i \exp(-\nu_i x/\ell) + B_i \exp(\nu_i x/\ell)$$

where A_i and B_i are arbitrary constants.

Values of ν_i and $G_n(\nu_i)$ for various odd P_N approximations are listed in Tables 4-2 and 4-3, respectively.

Table 4-2— VALUES FOR ν_i FOR N = 1, 3, 5, 7, 9, 11, 13

Data from Refs. 3 and 4.

	N = 1	3		5			7				
c	i = 1	1	2	1	2	3	1	2	3	4	
1.0	0.0	0.0	1.972027	0.0	1.225211	3.202945	0.0	1.103185	1.591779	4.458086	
0.9	0.547723	0.525560	2.055185	0.525430	1.240875	3.296688	0.525430	1.108937	1.615640	4.554851	
0.8	0.774597	0.711876	2.145773	0.710456	1.260956	3.393117	0.710413	1.116799	1.642629	4.652966	
0.7	0.948683	0.834508	2.241834	0.829085	1.286086	3.491504	0.828671	1.127655	1.672473	4.752078	
0.6	1.095445	0.922637	2.341383	0.909562	1.316073	3.591190	0.907696	1.142345	1.704602	4.851871	
0.5	1.224745	0.988751	2.442706	0.964672	1.349619	3.691603	0.959481	1.160900	1.738235	4.952060	
0.4	1.341641	1.039801	2.544478	1.002603	1.384742	3.792265	0.992327	1.181880	1.772515	5.052401	
0.3	1.449138	1.080124	2.645751	1.029086	1.419574	3.892788	1.012964	1.203058	1.806656	5.152683	
0.2	1.549193	1.112590	2.745892	1.048012	1.452833	3.992862	1.026230	1.222733	1.840027	5.252727	
0.1	1.643168	1.139170	2.844500	1.061917	1.483848	4.092252	1.035120	1.240155	1.872179	5.352384	
0.0	1.732051	1.161256	2.941340	1.072421	1.512380	4.190778	1.041352	1.255230	1.902832	5.451533	

	N = 9					N = 11					
c	i = 1	2	3	4	5	1	2	3	4	5	6
1.0	0.0	1.0594261	1.2978139	1.9873301	5.7211751	0.0	1.0386324	1.1831795	1.5191503	2.3941942	6.9878995
0.99	0.1725111	1.0596650	1.2987909	1.9899798	5.7309358	0.1725111	1.0387660	1.1837036	1.5204261	2.3970617	6.9977390
0.98	0.2429826	1.0599113	1.2997877	1.9926522	5.7407063	0.2429826	1.0389037	1.1842401	1.5217202	2.3999456	7.0075851
0.97	0.2963814	1.0601651	1.3008049	1.9953472	5.7504865	0.2963814	1.0390457	1.1847896	1.5230329	2.4028458	7.0174376
0.96	0.3408292	1.0604269	1.3018428	1.9980647	5.7602764	0.3408292	1.0391922	1.1853523	1.5243642	2.4057621	7.0272964
0.95	0.3794852	1.0606971	1.3029017	2.0008044	5.7700756	0.3794852	1.0393434	1.1859286	1.5257143	2.4086944	7.0371614
0.94	0.4139755	1.0609759	1.3039821	2.0035662	5.7798839	0.4139755	1.0394995	1.1865189	1.5270832	2.4116423	7.0470325
0.93	0.4452699	1.0612637	1.3050842	2.0063500	5.7897011	0.4452699	1.0396608	1.1871236	1.5284711	2.4146056	7.0569094
0.92	0.4740023	1.0615610	1.3062085	2.0091553	5.7995270	0.4740023	1.0398274	1.1877430	1.5298780	2.4175843	7.0667920
0.91	0.5006145	1.0618682	1.3073554	2.0119821	5.8093614	0.5006145	1.0399997	1.1883775	1.5313039	2.4205780	7.0766803
0.90	0.5254295	1.0621857	1.3085251	2.0148302	5.8192041	0.5254295	1.0401779	1.1890276	1.5327490	2.4235865	7.0865740
0.85	0.6295015	1.0639456	1.3147274	2.0293788	5.8685338	0.6295015	1.0411679	1.1925253	1.5402617	2.4388426	7.1361198
0.80	0.7104118	1.0660454	1.3215437	2.0444137	5.9180388	0.7104118	1.0423564	1.1964717	1.5482503	2.4544310	7.1857824
0.75	0.7755167	1.0685719	1.3289950	2.0598908	5.9676942	0.7755163	1.0438007	1.2009145	1.5567013	2.4703172	7.2355455
0.70	0.8286377	1.0716317	1.3370818	2.0757595	6.0174764	0.8286350	1.0455770	1.2058921	1.5655883	2.4864639	7.2853938
0.65	0.8720803	1.0753468	1.3457793	2.0919641	6.0673627	0.8720671	1.0477840	1.2114252	1.5748719	2.5028322	7.3353127
0.60	0.9073932	1.0798392	1.3550355	2.1084453	6.1173317	0.9073425	1.0505415	1.2175072	1.5845005	2.5193821	7.3852878
0.55	0.9357346	1.0851963	1.3647618	2.1251416	6.1673629	0.9355764	1.0539755	1.2240955	1.5944117	2.5360731	7.4353059
0.50	0.9580876	1.0914203	1.3748573	2.1419913	6.2174373	0.9576809	1.0581768	1.2311088	1.6045351	2.5528650	7.4853540
0.45	0.9753900	1.0983842	1.3851970	2.1589337	6.2675366	0.9745204	1.0631334	1.2384312	1.6147959	2.5697184	7.5354200
0.40	0.9885786	1.1058343	1.3956522	2.1759105	6.3176439	0.9870070	1.0686761	1.2459248	1.6251187	2.5865954	7.5854921
0.35	0.9985516	1.1134524	1.4060983	2.1928669	6.3677431	0.9960921	1.0745029	1.2534462	1.6354303	2.6034599	7.6355595
0.30	1.0061005	1.1209406	1.4164230	2.2097522	6.4178193	1.0026663	1.0802839	1.2608630	1.6456630	2.6202779	7.6856117
0.25	1.0118638	1.1280772	1.4265319	2.2265208	6.4678585	1.0074612	1.0857624	1.2680652	1.6557568	2.6370181	7.7356387
0.20	1.0163241	1.1347299	1.4363501	2.2431317	6.5178477	1.0110183	1.0907913	1.2749705	1.6656601	2.6536515	7.7856314
0.15	1.0198316	1.1408404	1.4458225	2.2595495	6.5677747	1.0137136	1.0953161	1.2815245	1.6753306	2.6701520	7.8355808
0.10	1.0226359	1.1464016	1.4549120	2.2757435	6.6176283	1.0158016	1.0993416	1.2876967	1.6847353	2.6864963	7.8854788
0.05	1.0249141	1.1514368	1.4635965	2.2916880	6.6673979	1.0174535	1.1029038	1.2934761	1.6938491	2.7026637	7.9353175
0.00	1.0267926	1.1559847	1.4718662	2.3073619	6.7170743	1.0187858	1.1060512	1.2988655	1.7026553	2.7186361	7.9850897

	N = 13										
c	i = 1	2	3	4	5	6	7				
1.0	0.0	1.0271063	1.1250576	1.3302236	1.7523053	2.8067398	8.2565967				
0.99	0.1725111	1.0271891	1.1253744	1.3309598	1.7537706	2.8097363	8.2664817				
0.98	0.2429826	1.0272745	1.1256994	1.3317097	1.7552515	2.8127450	8.2763714				
0.97	0.2963814	1.0273626	1.1260329	1.3324734	1.7567478	2.8157658	8.2862656				
0.96	0.3408292	1.0274534	1.1263751	1.3332512	1.7582597	2.8187986	8.2961643				
0.95	0.3794852	1.0275471	1.1267264	1.3340433	1.7597870	2.8218431	8.3060674				
0.94	0.4139755	1.0276439	1.1270870	1.3348500	1.7613298	2.8248992	8.3159747				
0.93	0.4452699	1.0277439	1.1274574	1.3356714	1.7628880	2.8279667	8.3258862				
0.92	0.4740023	1.0278471	1.1278377	1.3365077	1.7644616	2.8310453	8.3358018				
0.91	0.5006145	1.0279539	1.1282283	1.3373592	1.7660503	2.8341350	8.3457213				
0.90	0.5254295	1.0280644	1.1286296	1.3382260	1.7676544	2.8372356	8.3556447				
0.85	0.6295015	1.0286786	1.1308087	1.3427970	1.7758997	2.8528936	8.4053168				
0.80	0.7104118	1.0294174	1.1333108	1.3477763	1.7845083	2.8687921	8.4550719				
0.75	0.7755163	1.0303188	1.1361870	1.3531755	1.7934586	2.8849042	8.5048990				
0.70	0.8286348	1.0314357	1.1394892	1.3589941	1.8027218	2.9012023	8.5547874				
0.65	0.8720656	1.0328405	1.1432624	1.3652166	1.8122625	2.9176581	8.6047266				
0.60	0.9073340	1.0346308	1.1475341	1.3718103	1.8220394	2.9342428	8.6547066				
0.55	0.9355401	1.0369280	1.1523010	1.3787244	1.8320065	2.9509278	8.7047180				
0.50	0.9575581	1.0398566	1.1575163	1.3858923	1.8421148	2.9676847	8.7547515				
0.45	0.9741899	1.0434861	1.1630856	1.3932350	1.8523134	2.9844858	8.8047984				
0.40	0.9862941	1.0477436	1.1688747	1.4006672	1.8625520	3.0013044	8.8548502				
0.35	0.9948305	1.0523776	1.1747303	1.4081032	1.8727813	3.0181146	8.9048989				
0.30	1.0007630	1.0570471	1.1805043	1.4154629	1.8829554	3.0348921	8.9549368				
0.25	1.0049079	1.0614652	1.1860742	1.4226762	1.8930319	3.0516138	9.0049566				
0.20	1.0078622	1.0654690	1.1913524	1.4296853	1.9029733	3.0682584	9.0549512				
0.15	1.0100249	1.0690058	1.1962864	1.4364462	1.9127469	3.0848059	9.1049141				
0.10	1.0116531	1.0720890	1.2008534	1.4429276	1.9223252	3.1012382	9.1548390				
0.05	1.0129114	1.0747631	1.2050521	1.4491100	1.9316856	3.1175387	9.2047199				
0.00	1.0139069	1.0770815	1.2088956	1.4549837	1.9408106	3.1336924	9.2545507				

Table 4-3—VALUES OF $G_n(\nu_i)$ FOR N = 1, 3, 5, 7, 9, 11, 13

Data from Refs. 3 and 4.

c	n	N = 1	3		5			7			
		i = 1	1	2	1	2	3	1	2	3	4
1.0	0	1.000000	1.000000	1.000000	1.000000	1.000000	1.000000	1.000000	1.000000	1.000000	1.000000
	1	0.0	0.0	0.0	0.0	0.0	0.0	0.0	0.0	0.0	0.0
	2		0.0	−0.500000	0.0	−0.500000	−0.500000	0.0	−0.500000	−0.500000	−0.500000
	3		0.0	0.422577	0.0	0.680155	0.260177	0.0	0.755388	0.523523	0.186926
	4				0.0	−0.596483	0.232846	0.0	−0.823284	−0.200561	0.301623
	5				0.0	0.332190	−0.338997	0.0	0.738992	−0.192022	−0.271324
	6							0.0	−0.542027	0.388296	−0.139774
	7							0.0	0.279046	−0.288438	0.290791
0.9	0	1.000000	1.000000	1.000000	1.000000	1.000000	1.000000	1.000000	1.000000	1.000000	1.000000
	1	−0.182574	−0.190273	−0.048657	−0.190320	−0.080588	−0.030333	−0.190320	−0.090176	−0.061895	−0.021955
	2		0.043058	−0.464487	0.043327	−0.402583	−0.486198	0.043328	−0.378023	−0.442535	−0.492770
	3		−0.009698	0.409117	−0.010552	0.594450	0.266024	−0.010557	0.628264	0.497775	0.194946
	4				0.002649	−0.536413	0.223434	0.002666	−0.707938	−0.207269	0.294678
	5				−0.000633	0.302555	−0.334814	−0.000688	0.646497	−0.167299	−0.272409
	6							0.000179	−0.478863	0.362566	−0.135920
	7							−0.000044	0.247814	−0.273362	0.288912
0.8	0	1.000000	1.000000	1.000000	1.000000	1.000000	1.000000	1.000000	1.000000	1.000000	1.000000
	1	−0.258199	−0.280948	−0.093206	−0.281509	−0.158610	−0.058943	−0.281526	−0.179083	−0.121756	−0.042983
	2		0.091987	−0.434834	0.094356	−0.311222	−0.473943	0.094428	−0.259469	−0.388816	−0.486143
	3		−0.028064	0.399890	−0.033677	0.517229	0.272092	−0.033849	0.506610	0.475676	0.202789
	4				0.012187	−0.484338	0.215126	0.012561	−0.599246	−0.215157	0.288338
	5				−0.003936	0.277604	−0.331794	−0.004747	0.560546	−0.144771	−0.273775
	6							0.001782	−0.420819	0.340876	−0.132410
	7							−0.000591	0.219320	−0.261302	0.287513
0.7	0	1.000000	1.000000	1.000000	1.000000	1.000000	1.000000	1.000000	1.000000	1.000000	1.000000
	1	−0.316228	−0.359493	−0.133819	−0.361845	−0.233266	−0.085923	−0.362026	−0.266039	−0.179375	−0.063130
	2		0.146177	−0.410462	0.154658	−0.227935	−0.463086	0.155312	−0.146117	−0.339123	−0.480073
	3		−0.052280	0.394366	−0.069671	0.450897	0.278336	−0.071022	0.393319	0.457529	0.210460
	4				0.031065	−0.442592	0.207808	0.033501	−0.500801	−0.224396	0.282551
	5				−0.011707	0.258732	−0.329802	−0.015951	0.484741	−0.124517	−0.275393
	6							0.007373	−0.370754	0.323490	−0.129213
	7							−0.002851	0.195105	−0.252480	0.286548
0.6	0	1.000000	1.000000	1.000000	1.000000	1.000000	1.000000	1.000000	1.000000	1.000000	1.000000
	1	−0.365148	−0.433540	−0.170839	−0.439772	−0.303934	−0.111384	−0.440676	−0.350157	−0.234659	−0.082442
	2		0.204838	−0.390552	0.225248	−0.153590	−0.453476	0.228232	−0.040213	−0.293507	−0.474512
	3		−0.080996	0.391900	−0.119559	0.397128	0.284714	−0.125285	0.292108	0.443414	0.217961
	4				0.061095	−0.412874	0.201365	0.070370	−0.417332	−0.235093	0.277269
	5				−0.025259	0.246987	−0.328700	−0.039319	0.423905	−0.106481	−0.277233
	6							0.020773	−0.332542	0.310434	−0.126302
	7							−0.008799	0.177277	−0.246944	0.285973

0.5	0	1.000000	1.000000	1.000000	1.000000	1.000000	1.000000	1.000000	1.000000	1.000000	1.000000	1.000000	1.000000
	1	−0.408248	−0.505688	−0.204691	−0.518311	−0.370475	−0.135442	−0.521115	−0.430700	−0.287648	−0.100968		
	2		0.267162	−0.374305	0.305938	−0.088245	−0.444966	0.314683	0.056509	−0.251776	−0.469416		
	3		−0.113210	0.391850	−0.183030	0.355958	0.291186	−0.199211	0.206006	0.433175	0.225299		
	4				0.102579	−0.395374	0.195688	0.127329	−0.352926	−0.247275	0.272444		
	5				−0.044979	0.242548	−0.328365	−0.079502	0.382414	−0.090478	−0.279269		
	6							0.045802	−0.309817	0.301491	−0.123647		
	7							−0.020508	0.167844	−0.244562	0.285744		
0.4	0	1.000000	1.000000	1.000000	1.000000	1.000000	1.000000	1.000000	1.000000	1.000000	1.000000	1.000000	1.000000
	1	−0.447214	−0.577033	−0.235805	−0.598442	−0.433294	−0.158217	−0.604640	−0.507666	−0.338502	−0.118755		
	2		0.332419	−0.360990	0.395333	−0.030641	−0.437419	0.413972	0.144312	−0.213541	−0.464743		
	3		−0.148136	0.393657	−0.258216	0.325742	0.297719	−0.292196	0.134938	0.426457	0.232478		
	4				0.154205	−0.388683	0.190677	0.204818	−0.308036	−0.260884	0.268034		
	5				−0.070276	0.244648	−0.328680	−0.137766	0.361187	−0.076236	−0.281474		
	6							0.083842	−0.303577	0.296255	−0.121225		
	7							−0.038826	0.167436	−0.245055	0.285823		
0.3	0	1.000000	1.000000	1.000000	1.000000	1.000000	1.000000	1.000000	1.000000	1.000000	1.000000	1.000000	1.000000
	1	−0.483046	−0.648074	−0.264575	−0.680216	−0.493106	−0.179820	−0.691042	−0.581851	−0.387456	−0.135862		
	2		0.400000	−0.350000	0.491486	0.021043	−0.430710	0.523297	0.225465	−0.178310	−0.460452		
	3		−0.185164	0.396863	−0.342514	0.304032	0.304285	−0.400306	0.075551	0.422797	0.239504		
	4				0.213844	−0.390582	0.186242	0.299097	−0.278997	−0.275806	0.263997		
	5				−0.100029	0.252027	−0.329545	−0.211240	0.356991	−0.063448	−0.283826		
	6							0.133070	−0.311519	0.294223	−0.119012		
	7							−0.062904	0.174895	−0.248061	0.286174		
0.2	0	1.000000	1.000000	1.000000	1.000000	1.000000	1.000000	1.000000	1.000000	1.000000	1.000000	1.000000	1.000000
	1	−0.516398	−0.719043	−0.291344	−0.763350	−0.550648	−0.200358	−0.779552	−0.654272	−0.434776	−0.152302		
	2		0.469419	−0.340847	0.592570	0.068526	−0.424732	0.639440	0.302635	−0.145568	−0.456508		
	3		−0.223830	0.401113	−0.433471	0.288487	0.310860	−0.518793	0.023669	0.421704	0.246382		
	4				0.279395	−0.398890	0.182304	0.405101	−0.260852	−0.291895	0.260296		
	5				−0.133095	0.263418	−0.330871	−0.295511	0.366069	−0.051817	−0.286304		
	6							0.190337	−0.329997	0.294875	−0.116986		
	7							−0.091154	0.188299	−0.253203	0.286765		
0.1	0	1.000000	1.000000	1.000000	1.000000	1.000000	1.000000	1.000000	1.000000	1.000000	1.000000	1.000000	1.000000
	1	−0.547723	−0.790048	−0.316400	−0.847524	−0.606531	−0.219928	−0.869464	−0.725716	−0.480723	−0.168149		
	2		0.540294	−0.333152	0.697162	0.113133	−0.419386	0.759946	0.377772	−0.114842	−0.452876		
	3		−0.263780	0.406136	−0.529172	0.277282	0.317424	−0.643961	−0.023884	0.422718	0.253120		
	4				0.349185	−0.411867	0.178798	0.518736	−0.249626	−0.309000	0.256898		
	5				−0.168548	0.277795	−0.332584	−0.386876	0.381422	−0.041087	−0.288890		
	6							0.252928	−0.355838	0.297735	−0.115129		
	7							−0.122179	0.205938	−0.260126	0.287567		
0	0	1.000000	1.000000	1.000000	1.000000	1.000000	1.000000	1.000000	1.000000	1.000000	1.000000	1.000000	1.000000
	1	−0.577350	−0.8611136	−0.339981	−0.932470	−0.661209	−0.238619	−0.960290	−0.796666	−0.525532	−0.183435		
	2		0.612334	−0.326619	0.804249	0.155797	−0.414591	0.883235	0.452016	−0.085724	−0.449528		
	3		−0.304747	0.411728	−0.628250	0.269116	0.323962	−0.773409	−0.069066	0.425439	0.259721		
	4				0.422005	−0.428246	0.175662	0.637294	−0.242723	−0.326796	0.253772		
	5				−0.205712	0.294396	−0.334619	−0.482849	0.403317	−0.031046	−0.291568		
	6							0.318992	−0.386798	0.302392	−0.113424		
	7							−0.155019	0.226576	−0.266520	0.289555		

687863 O - 63 - 17

Table 4-3— VALUES OF $G_n(\nu_i)$ FOR N = 1, 3, 5, 7, 9, 11, 13 (Continued)

Data from Refs. 3 and 4.

c	n	N = 9					c	n	N = 9				
		i = 1	2	3	4	5			i = 1	2	3	4	5
1.0	0	1.0	1.0	1.0	1.0	1.0	0.60	0	1.0	1.0	1.0	1.0	1.0
	1	0.0	0.0	0.0	0.0	0.0		1	−0.4408232	−0.3704255	−0.2951957	−0.1897132	−0.0653880
	2	0.0	−0.50	−0.50	−0.50	−0.50		2	0.2287192	0.0145565	−0.1732232	−0.3650333	−0.4839665
	3	0.0	0.7865894	0.6421054	0.4193231	0.1456577		3	−0.1262209	0.2244833	0.4098585	0.4150241	0.1754486
	4	0.0	−0.9243180	−0.4908286	0.0057532	0.3304460		4	0.0718905	−0.3747176	−0.3994071	−0.0706931	0.3127839
	5	0.0	0.9411752	0.1670693	−0.3406693	−0.2204913		5	−0.0416327	0.4450357	0.2026778	−0.2716679	−0.2323943
	6	0.0	−0.8584356	0.1730165	0.3094768	−0.2047159		6	0.0242077	−0.4433096	0.0586203	0.2951313	−0.1910058
	7	0.0	0.6980908	−0.3907849	0.0027989	0.2554551		7	−0.0138602	0.3809593	−0.2540659	−0.0270969	0.2571820
	8	0.0	−0.4843681	0.4131921	−0.2734329	0.0954094		8	0.0074584	−0.2735902	0.3002657	−0.2341432	0.0883022
	9	0.0	0.2430721	−0.2540115	0.2574006	−0.2585625		9	−0.0032058	0.1399421	−0.1927280	0.2338475	−0.2558719
0.99	0	1.0	1.0	1.0	1.0	1.0	0.50	0	1.0	1.0	1.0	1.0	1.0
	1	−0.0579673	−0.0094369	−0.0076995	−0.0050252	−0.0017449		1	−0.5218729	−0.4581186	−0.3636741	−0.2334276	−0.0804190
	2	0.0040311	−0.4866416	−0.4911077	0.4962121	−0.4995433		2	0.3170541	0.1296181	−0.1032234	−0.3365346	−0.4805984
	3	−0.0003003	0.7716929	0.6353444	0.4189424	0.1464401		3	−0.2036246	0.1074776	0.3675817	0.4174734	0.1824434
	4	0.0000232	−0.9094429	−0.4877368	0.0037387	0.3299405		4	0.1341410	−0.2695448	−0.3904622	−0.0886734	0.3090971
	5	−0.0000018	0.9274707	0.1676810	−0.3385357	−0.2207814		5	−0.0891167	0.3585584	0.2171383	−0.2594629	−0.2354409
	6	0.0000001	−0.8467541	0.1697540	0.3087714	−0.2043222		6	0.0587437	−0.3776745	0.0358375	0.2959692	−0.1881565
	7	0.0	0.6899025	−0.3864580	0.0020134	0.2554530		7	−0.0374822	0.3353089	−0.2345274	−0.0342135	0.2580087
	8	0.0	−0.4782704	0.4093755	−0.2720721	0.0952049		8	0.0219528	−0.2455770	0.2884855	−0.2290241	0.0868290
	9	0.0	0.2400662	−0.2518547	0.2564611	−0.2584484		9	−0.0099629	0.1269605	−0.1878756	0.2323741	−0.2557201
0.95	0	1.0	1.0	1.0	1.0	1.0	0.40	0	1.0	1.0	1.0	1.0	1.0
	1	−0.1317574	−0.0471388	−0.0383759	−0.0249899	−0.0086654		1	−0.6069320	−0.5425768	−0.4299065	−0.2757466	−0.0949721
	2	0.0208007	−0.4333380	−0.3448188	−0.4812651	−0.4977473		2	0.4209162	0.2359739	−0.0379510	−0.3099095	−0.4774507
	3	−0.0035166	0.7123271	0.6086655	0.4175530	0.1495496		3	−0.3050107	0.0060680	0.3319248	0.4212102	0.1892717
	4	0.0006164	−0.8502354	−0.4756685	−0.0042631	0.3279538		4	0.2242484	−0.1865831	−0.3877353	−0.1063309	0.3056594
	5	−0.0001105	0.8729855	0.1702187	−0.3302071	−0.2219462		5	−0.1643021	0.2988526	0.2345300	−0.2490071	−0.2385047
	6	0.0000201	−0.8003588	0.1568730	0.3061207	−0.2027756		6	0.1178269	−0.3399738	0.0150334	0.2984122	−0.1855039
	7	−0.0000037	0.6530511	−0.3695069	−0.0011061	0.2555045		7	−0.0805192	0.3147942	−0.2210301	−0.0412607	0.2589636
	8	0.0000007	−0.4540880	0.3944919	−0.2668191	0.0944018		8	0.0496192	−0.2362729	0.2837904	−0.2255561	0.0854586
	9	−0.0000001	0.2281499	−0.2434662	0.2528777	−0.2580184		9	−0.0232354	0.1237636	−0.1876134	0.2324794	−0.2557408
0.90	0	1.0	1.0	1.0	1.0	1.0	0.30	0	1.0	1.0	1.0	1.0	1.0
	1	−0.1903205	−0.0941455	−0.0764219	−0.0496320	−0.0171845		1	−0.6957556	−0.6244755	−0.4942026	−0.3167776	−0.1090713
	2	0.0433283	−0.3670494	−0.4123954	−0.4630500	−0.4955704		2	0.5373053	0.3356493	0.0233634	−0.2849685	−0.4745074
	3	−0.0105574	0.6386978	0.5762154	0.4161228	0.1533917		3	−0.4262418	−0.0827420	0.3019774	0.4261175	0.1959407
	4	0.0026664	−0.7769970	−0.4613245	−0.0141399	0.3255486		4	0.3384213	−0.1225611	−0.3906176	−0.1237348	0.3024518
	5	−0.0006886	0.8057556	0.1736231	−0.3202660	−0.2234122		5	−0.2644713	−0.2630015	0.2548175	−0.2401032	−0.2415810
	6	0.0001805	−0.7432372	0.1411791	0.3031995	−0.2009047		6	0.1999063	−0.3280129	−0.0043060	0.3023153	−0.1830324
	7	−0.0000478	0.6088404	−0.3491903	−0.0049564	0.2556130		7	−0.1423138	0.3180127	−0.2127693	−0.0482722	0.2600340
	8	0.0000127	−0.4244096	0.3768269	−0.2606871	0.0934308		8	0.0903024	−0.2449292	0.2854225	−0.2235664	0.0841830
	9	−0.0000032	0.2135377	−0.2335678	0.2487980	−0.2575388		9	−0.0430358	0.1300505	−0.1915006	0.2340125	−0.2559180

0.85	0	1.0	1.0	1.0	1.0	1.0	0.20	0	1.0	1.0	1.0	1.0	1.0
	1	−0.2382838	−0.1409846	−0.1140921	−0.0739142	−0.0255600		1	−0.7871505	−0.7050136	−0.5569673	−0.3566442	−0.1227399
	2	0.0677917	−0.3012333	−0.3698300	−0.4453668	−0.4934668		2	0.6617610	0.4319578	0.0816485	−0.2615092	−0.4717530
	3	−0.0206292	0.5658705	0.5448911	0.4150423	0.1571849		3	−0.5604528	−0.1644413	0.2765708	0.4320664	0.2024577
	4	0.0065049	−0.7048307	−0.4479181	−0.0238795	0.3232275		4	0.4687182	−0.0703642	−0.3982008	−0.1409488	0.2994561
	5	−0.0020968	0.7397473	0.1773341	−0.3108534	−0.2248884		5	−0.3817793	0.2431704	0.2777592	−0.2325489	−0.2446654
	6	0.0006860	−0.6873335	0.1259800	0.3007234	−0.1991010		6	0.2980880	−0.3342429	−0.0226933	0.3075218	−0.1807276
	7	−0.0002265	0.5656881	−0.3299561	−0.0087549	0.2557686		7	−0.2174608	0.3386031	−0.2087379	−0.0552771	0.2612082
	8	0.0000745	−0.3954999	0.3603347	−0.2550441	0.0924952		8	0.1403630	−0.2670370	0.2923414	−0.2228763	0.0829944
	9	−0.0000222	0.1993218	−0.2244041	0.2451700	−0.2571210		9	−0.0675731	0.1435334	−0.1989021	0.2368141	−0.2562371
0.80	0	1.0	1.0	1.0	1.0	1.0	0.10	0	1.0	1.0	1.0	1.0	1.0
	1	−0.2815268	−0.1876093	−0.1511338	−0.0978276	−0.0337950		1	−0.8800786	−0.7850652	−0.6185941	−0.3954751	−0.1360004
	2	0.0944302	−0.2360207	−0.3282257	−0.4282233	−0.4914342		2	0.7908973	0.5272122	0.1377645	−0.2393324	−0.4691732
	3	−0.0338542	0.4940701	0.5148344	0.4143187	0.1609301		3	−0.7022657	−0.2430972	0.2545807	0.4389279	0.2088294
	4	0.0125723	−0.6340407	−0.4355790	−0.0334857	0.3209877		4	0.6085890	−0.0243175	−0.4095386	−0.1580272	0.2966559
	5	−0.0047716	0.6753111	0.1814100	−0.3019726	−0.2263740		5	−0.5093998	0.2326594	0.3030118	−0.2261506	−0.2477542
	6	0.0018370	−0.6330002	0.1113185	0.2986994	−0.1973619		6	0.4060703	−0.3518059	0.0405427	0.3138757	−0.1785760
	7	−0.0007123	0.5239027	−0.3119282	−0.0125045	0.2559691		7	−0.3008097	0.3704947	−0.2079731	−0.0622980	0.2624755
	8	0.0002726	−0.3675843	0.3451587	−0.2498936	0.0915935		8	0.1962221	−0.2981334	0.3034976	−0.2233135	0.0818857
	9	−0.0000917	0.1856186	−0.2160674	0.2419986	−0.2567625		9	−0.0950513	0.1618961	−0.2091611	0.2407284	−0.2566844
0.70	0	1.0	1.0	1.0	1.0	1.0	0	0	1.0	1.0	1.0	1.0	1.0
	1	−0.3620400	−0.2799469	−0.2243692	−0.1445254	−0.0498548		1	−0.9739065	−0.8650634	−0.6794096	−0.4333954	−0.1488743
	2	0.1553648	−0.1081486	−0.2482923	−0.3955620	−0.4875725		2	0.9227409	0.6225019	0.1923960	−0.2182526	−0.4667546
	3	−0.0711305	0.3548305	0.4590747	0.4139545	0.1682800		3	−0.8485013	−0.3207971	0.2350802	0.4465798	0.2150625
	4	0.0336968	−0.4983352	−0.4146272	−0.0523190	0.3167403		4	0.7540760	0.0187658	−0.4237996	−0.1750153	0.2940357
	5	−0.0162932	0.5531801	0.1909177	−0.2857951	−0.2293701		5	−0.6431181	0.2274173	0.3302161	−0.2207323	−0.2508439
	6	0.0079674	−0.5310939	0.0837467	0.2960165	−0.1940685		6	0.5198877	−0.3763104	−0.0581457	0.3212308	−0.1765654
	7	−0.0038910	0.4462339	−0.2799640	−0.0198732	0.2564973		7	−0.3890682	0.4096310	−0.2096765	−0.0693522	0.2638260
	8	0.0018329	−0.3160542	0.3193172	−0.2410633	0.0898873		8	0.2555659	−0.3351474	0.3179828	−0.2247202	0.0808505
	9	−0.0007194	0.1604338	−0.2022410	0.2370266	−0.2562133		9	−0.1243010	0.1835172	−0.2216976	−0.2456104	−0.2572477

Table 4-3 — VALUES OF $G_n(\nu_i)$ FOR N = 1, 3, 5, 7, 9, 11, 13 (Continued)

Data from Refs. 3 and 4.

c	n	N = 11						c	n	N = 11					
		i = 1	2	3	4	5	6			i = 1	2	3	4	5	6
1.0	0	1.0	1.0	1.0	1.0	1.0	1.0	0.60	0	1.0	1.0	1.0	1.0	1.0	1.0
	1	0.0	0.0	0.0	0.0	0.0	0.0		1	−0.4408478	−0.3807560	−0.3285402	−0.2524455	−0.1587691	−0.0541617
	2	0.0	−0.50	−0.50	−0.50	−0.50	−0.50		2	0.2288006	0.0436568	−0.0952301	−0.2610173	−0.4054714	−0.4889994
	3	0.0	0.8023372	0.7043169	0.5485523	0.3480642	−0.1192538		3	−0.1263775	0.1845766	0.3493889	0.4428496	0.3740808	0.1464622
	4	0.0	−0.9768643	−0.6667308	−0.2569101	0.1205877	0.3451349		4	0.0721450	−0.3402117	−0.4307762	−0.2933419	0.0442615	0.3320442
	5	0.0	1.0510833	0.4508604	−0.1344359	−0.3691115	−0.1843057		5	−0.0420203	0.4352581	0.3573616	−0.0210420	−0.3308877	−0.1980982
	6	0.0	−1.0412574	−0.1429979	0.3763311	0.1821541	−0.2392583		6	0.0247834	−0.4760730	−0.1791382	0.2687980	0.2038996	−0.2275274
	7	0.0	0.9609080	−0.1619993	−0.3448294	0.1750869	0.2215629		7	−0.0147092	0.4685214	−0.0330588	−0.2970136	0.1333151	0.2270137
	8	0.0	−0.8235873	0.3818456	0.0963134	−0.2965032	0.1499011		8	0.0087106	−0.4196502	0.2076576	0.1162693	−0.2776292	0.1414515
	9	0.0	0.6436608	−0.4655986	0.1867603	0.0782921	−0.2374643		9	−0.0050588	0.3380738	−0.2927826	0.1254070	0.0896483	−0.2379681
	10	0.0	−0.4362386	0.4040170	−0.3202631	0.2047213	−0.0703447		10	0.0027537	−0.2337519	0.2700146	−0.2550200	0.1822578	−0.0660847
	11	0.0	0.2166960	−0.2286205	0.2326872	−0.2344160	0.2350948		11	−0.0011949	0.0174447	−0.1572257	0.1932553	−0.2196064	0.2334175
0.99	0	1.0	1.0	1.0	1.0	1.0	1.0	0.50	0	1.0	1.0	1.0	1.0	1.0	1.0
	1	−0.0579673	−0.0096268	−0.0084481	0.0065771	−0.0041718	−0.0014290		1	−0.5220946	−0.4725108	−0.4061379	−0.3116167	−0.1958584	−0.0667971
	2	0.0040311	−0.4860987	−0.4892945	−0.4935113	−0.4973894	−0.4996937		2	0.3177483	0.1697994	−0.0051559	−0.2086850	−0.3849185	−0.4866144
	3	−0.0003003	0.7863476	0.6945637	0.5453639	0.3486139	0.1199658		3	−0.2049192	0.0475670	0.2777387	0.4245103	0.3818706	0.1528795
	4	0.0000232	−0.9601790	−0.6598795	−0.2575766	0.1185328	0.3447691		4	0.1361440	−0.2060153	−0.3909338	−0.3064821	0.0269149	0.3292191
	5	−0.0000018	1.0347444	0.4477955	−0.1313516	−0.3678997	−0.1846562		5	−0.0919528	0.3123864	0.3493921	0.0042096	−0.3244739	−0.2014708
	6	0.0000001	−1.0260865	−0.1436510	0.3730313	0.1826017	−0.2389296		6	0.0625762	−0.3695425	−0.1945269	0.2505919	0.2105910	−0.2250045
	7	0.0	0.9475502	−0.1584469	−0.3430565	0.1738705	0.2216867		7	−0.0425316	0.3808021	−0.0060327	−0.2936517	0.1249210	0.2285137
	8	0.0	−0.8125275	0.3766764	0.0966573	−0.2957793	0.1496639		8	0.0285166	−0.3513995	0.1793990	0.1238825	−0.2760178	0.1396387
	9	0.0	0.6352307	−0.4602377	0.1848577	0.0785230	−0.2374534		9	−0.0184390	0.2887718	−0.2698892	0.1151869	0.0931872	−0.2383604
	10	0.0	−0.4306216	0.3997333	−0.3179989	0.2039611	−0.0702250		10	0.0109173	−0.2022420	0.2550675	−0.2478921	0.1790603	−0.0651721
	11	0.0	0.2139333	−0.2262967	0.2312362	−0.2338252	0.2350252		11	−0.0050003	0.1023516	−0.1501815	0.1902290	−0.2186210	0.2333130
0.95	0	1.0	1.0	1.0	1.0	1.0	1.0	0.40	0	1.0	1.0	1.0	1.0	1.0	1.0
	1	−0.1317574	−0.0481073	−0.0421611	−0.0327715	−0.0207581	−0.0071051		1	−0.6078984	−0.5614424	−0.4815700	−0.3692038	−0.2319652	−0.0790984
	2	0.0208007	−0.4305706	−0.4466734	−0.4677808	−0.4870730	−0.4984855		2	0.4238512	0.2880438	0.0797741	−0.1592214	−0.3654804	−0.4843586
	3	−0.0035166	0.7225245	0.6558480	0.5328442	0.3508630	0.1227970		3	−0.3104524	−0.0749273	0.2143332	0.4094279	0.3901399	0.1591544
	4	0.0006164	−0.8936265	−0.6327885	−0.2603387	0.1103906	0.3433270		4	0.2325551	−0.0933364	−0.3608786	−0.3214741	0.0101553	0.3265515
	5	−0.0001105	0.9696187	0.4357667	−0.1191342	−0.3631845	−0.1860555		5	−0.1757478	0.2171509	0.3498983	0.0285261	−0.3191789	−0.2048126
	6	0.0000201	−0.9656548	−0.1463303	0.3601033	0.1844390	−0.2376343		6	0.1326499	−0.2947460	−0.2141306	0.2357142	0.2177657	−0.2226252
	7	−0.0000037	0.8943711	−0.1443637	−0.3362129	0.1690955	0.2221891		7	−0.0989517	0.3260795	0.0192646	−0.2938189	0.1172290	0.2300586
	8	0.0000007	−0.7685187	0.3562837	0.0980926	−0.2930131	0.1487294		8	0.0719082	−0.3142062	0.1583729	0.1327471	−0.2755232	0.1379306
	9	−0.0000001	0.6016990	−0.4391480	0.1774137	0.0794727	−0.2374228		9	−0.0496576	0.2655122	−0.2572259	0.1068793	0.0970002	−0.2388431
	10	0.0	−0.4082855	0.3829124	−0.3092200	0.2010231	−0.0697534		10	0.0308740	−0.1892688	0.2497265	−0.2444298	0.1767187	−0.0643126
	11	0.0	0.2029494	−0.2171815	0.2256346	−0.2315754	0.2347621		11	−0.0145740	0.0967364	−0.1488063	0.1899784	−0.2186130	0.2333160
0.90	0	1.0	1.0	1.0	1.0	1.0	1.0	0.30	0	1.0	1.0	1.0	1.0	1.0	1.0
	1	−0.1903205	−0.0961374	−0.0841023	−0.0652423	−0.0412612	−0.0141112		1	−0.6981386	−0.6479778	−0.5551753	−0.4253605	−0.2671472	−0.0910793
	2	0.0433283	−0.3613640	−0.3939020	−0.4361517	−0.4744627	−0.4970131		2	0.5444231	0.3997327	0.1604706	−0.1122896	−0.3470693	−0.4822241
	3	−0.0105574	0.6431015	0.6082028	0.5177535	0.3537889	0.1262982		3	−0.4395332	−0.1847242	0.1579994	0.3972964	0.3988568	0.1652924
	4	0.0026664	−0.8109340	−0.5997209	−0.2640259	0.1003866	0.3415710		4	0.3588204	−0.0005566	−0.3396464	−0.3382683	−0.0060817	0.3240313
	5	−0.0006886	0.8888184	0.4213204	−0.1041413	−0.3575883	−0.1877981		5	−0.2925326	0.1487068	0.3584775	0.0521553	−0.3149076	−0.2081233
	6	0.0001805	−0.8907811	−0.1498565	0.3445857	0.1868439	−0.2360582		6	0.2358666	−0.2519042	−0.2381986	0.2237871	0.2253999	−0.2203801
	7	−0.0000478	0.8285641	−0.1270708	−0.3282506	0.1633298	0.2228324		7	−0.1861310	0.3055918	0.0435797	−0.2972500	0.1101668	0.2316438
	8	0.0000128	−0.7141167	0.3315048	0.1000339	−0.2898479	0.1475928		8	0.1416842	−0.3099857	0.1436175	0.1428605	−0.2760573	0.1363202
	9	−0.0000034	0.5602836	−0.4136766	0.1685012	0.0807189	−0.2374133		9	−0.1014643	0.2703765	−0.2538897	0.1002472	0.1010763	−0.2394090
	10	0.0000009	−0.3807150	0.3626779	−0.2989050	0.1975826	−0.0691800		10	0.0647537	−0.1965502	0.2533318	−0.2443148	0.1751597	−0.0635027
	11	−0.0000002	0.1893967	−0.2062423	0.2191135	−0.2290192	0.2344671		11	−0.0310517	0.1015401	−0.1527645	0.1922895	−0.2195060	0.2334185

0.85	0	1.0	1.0	1.0	1.0	1.0	1.0	0.20	0	1.0	1.0	1.0	1.0	1.0	1.0
	1	−0.2382838	−0.1440690	−0.1257835	−0.0973860	−0.0615046	−0.0210198		1	−0.7912815	−0.7334125	−0.6274655	−0.4802901	−0.3014714	−0.1027534
	2	0.0677917	−0.2924413	−0.3417851	−0.4051596	−0.4621719	−0.4955817		2	0.6739869	0.5085512	0.2382118	−0.0674777	−0.3295906	−0.4802033
	3	−0.0206292	0.5641762	0.5615326	0.5033339	0.3568440	0.1297581		3	−0.5835485	−0.2880954	0.1069152	0.3877119	0.4079854	0.1712992
	4	0.0065049	−0.7289391	−0.5676958	−0.2680035	0.0905742	0.3398655		4	0.5045903	0.0807896	−0.3254086	−0.3567352	−0.0218606	0.3216490
	5	−0.0020969	0.8088693	0.4076550	−0.0894695	−0.3523240	−0.1895335		5	−0.4315254	0.0971591	0.3738788	0.0753374	−0.3115600	−0.2114030
	6	0.0006862	−0.8168427	−0.1536302	0.3298295	0.1893714	−0.2345284		6	0.3620161	−0.2306236	−0.2664421	0.2143582	0.2334653	−0.2182604
	7	−0.0002270	0.7636950	−0.1101672	−0.3209978	0.1577884	0.2234922		7	−0.2951097	0.3093723	0.0676364	−0.3035755	0.1036621	0.2332652
	8	0.0000757	−0.6605722	0.3076417	0.1021580	−0.2870089	0.1464903		8	0.2305363	−0.3299955	0.1336693	0.1541654	−0.2775270	0.1348010
	9	−0.0000254	0.5195715	−0.3893597	0.1600506	0.0820326	−0.2374348		9	−0.1068392	0.2964452	−0.2581544	0.0950185	0.1054017	−0.2400512
	10	0.0000084	−0.3536374	0.3434728	−0.2893737	0.1943998	−0.0686239		10	0.1089754	−0.2193686	0.2644072	−0.2471354	0.1743073	−0.0627390
	11	−0.0000025	0.1760937	−0.1958956	0.2131662	−0.2267485	0.2342085		11	−0.0526929	0.1144408	−0.1612272	0.1968730	−0.2212199	0.2336124
0.80	0	1.0	1.0	1.0	1.0	1.0	1.0	0.10	0	1.0	1.0	1.0	1.0	1.0	1.0
	1	−0.2815269	−0.1918730	−0.1671582	−0.1291781	−0.0814853	−0.0278327		1	−0.8859998	−0.8186718	−0.6989223	−0.5342086	−0.3350088	−0.1141338
	2	0.0944303	−0.2238857	−0.2904361	−0.3748477	−0.4502011	−0.4941900		2	0.8083260	0.6170392	0.3141540	−0.0243687	−0.3129485	−0.4782891
	3	−0.0338543	0.4858955	0.5160118	0.4896362	0.3600299	0.1331773		3	−0.7355866	−0.3896866	0.0593385	0.3802464	0.4174883	0.1771799
	4	0.0125726	−0.6478500	−0.5369093	−0.2723041	0.0809509	0.3382090		4	0.6610074	0.1575479	−0.3162574	−0.3767002	−0.0372431	0.3193958
	5	−0.0047724	0.7300277	0.3949294	−0.0751275	−0.3473907	−0.1912614		5	−0.5828356	0.0537893	0.3946080	0.0982758	−0.3090371	−0.2146517
	6	0.0018387	−0.7441236	−0.1577192	0.3158810	0.1920238	−0.2330436		6	0.5010705	−0.2209924	−0.2982676	0.2069728	0.2419307	−0.2162578
	7	−0.0007160	0.7000503	−0.0937019	−0.3145076	0.1524688	0.2241678		7	−0.4165106	0.3272224	0.0919323	−0.3123898	0.0976452	0.2349190
	8	0.0002809	−0.6081486	0.2848452	0.1044868	−0.2844955	0.1454207		8	0.3303723	−0.3647312	0.1271226	0.1665682	−0.2798393	0.1333668
	9	−0.0001105	0.4797795	−0.3663991	0.1520868	0.0834151	−0.2374862		9	−0.2440974	0.3358168	−0.2681905	0.0909272	0.1099607	−0.2407636
	10	0.0000428	−0.3272051	0.3254820	−0.2806778	0.1914734	−0.0680846		10	0.1592356	−0.2521365	0.2813054	−0.2524566	0.1740867	−0.0620183
	11	−0.0000145	0.1631177	−0.1862491	0.2078328	−0.2247627	0.2339850		11	−0.0773595	0.1325663	−0.1732433	0.2034151	−0.2236746	0.2338907
0.70	0	1.0	1.0	1.0	1.0	1.0	1.0	0.0	0	1.0	1.0	1.0	1.0	1.0	1.0
	1	−0.3620412	−0.2869229	−0.2487785	−0.1916213	−0.1206533	−0.0411783		1	−0.9815606	−0.9041173	−0.7699027	−0.5873180	−0.3678315	−0.1252334
	2	0.1553691	−0.0883762	−0.1905464	−0.3164065	−0.4272139	−0.4915217		2	0.9451919	0.7261420	0.3891252	0.0174136	−0.2970500	−0.4764749
	3	−0.0711392	0.3321551	0.4292069	0.4645820	0.3667953	0.1398967		3	−0.8918982	−0.4914510	0.0139542	0.3744998	0.4273282	0.1829399
	4	0.0337126	−0.4896514	−0.4799587	−0.2820006	0.0622560	0.3350372		4	0.8231474	0.2329699	−0.3106449	−0.3979735	−0.0522859	0.3172633
	5	−0.0163207	0.5772292	0.3730548	−0.0474417	−0.3385046	−0.1946949		5	−0.7408257	0.0140231	0.4193360	0.1211267	−0.3072443	−0.2178695
	6	0.0080152	−0.6040811	−0.1671944	0.2905557	0.1977081	−0.2302036		6	0.6471804	−0.2173855	−0.3330171	0.2012214	0.2507641	−0.2143645
	7	−0.0039747	0.5781946	−0.0622723	−0.3040006	0.1424784	0.2255633		7	−0.5447505	0.3529867	0.1167234	−0.3233302	0.0920513	0.2366014
	8	0.0019804	−0.5082870	0.2431201	0.1098449	−0.2804351	0.1433762		8	0.4362903	−0.4081778	0.1228918	0.1799580	−0.2829050	0.1320119
	9	−0.0009813	0.4042960	−0.3254661	0.1376944	0.0863903	−0.2376740		9	−0.3246853	0.3833107	−0.2824709	0.0877378	0.1147369	−0.2415400
	10	0.0004676	−0.2772196	0.2939953	−0.2659665	0.1863775	−0.0670543		10	0.2128655	−0.2910999	0.3026000	−0.2598692	0.1744271	−0.0613379
	11	−0.0001853	0.1386260	−0.1695562	0.1991450	−0.2216361	0.2336384		11	−0.1037177	0.1539863	−0.1879741	0.2116150	−0.2267932	0.2342466

Table 4-3 — VALUES OF $G_n(\nu_i)$ FOR N = 1, 3, 5, 7, 9, 11, 13 (Continued)

Data from Refs. 3 and 4.

c	n	N = 13						
		i = 1	2	3	4	5	6	7
1.0	0	1.0	1.0	1.0	1.0	1.0	1.0	1.0
	1	0.0	0.0	0.0	0.0	0.0	0.0	0.0
	2	0.0	−0.50	−0.50	−0.50	−0.50	−0.50	−0.50
	3	0.0	0.8113409	0.7407028	0.6264611	0.4755640	0.2969044	0.1009294
	4	0.0	−1.0073755	−0.7771454	−0.4491524	−0.0999384	0.1898804	0.3536078
	5	0.0	1.1163493	0.6508067	0.1066043	−0.2777927	−0.3592963	−0.1578327
	6	0.0	−1.1531480	−0.4128984	0.2273700	0.3739200	0.0764550	−0.2596273
	7	0.0	1.1281720	0.1237409	−0.4088094	−0.1581830	0.2573801	0.1936827
	8	0.0	−1.0504928	0.1550619	0.3772835	−0.1579212	−0.2388370	0.1831903
	9	0.0	0.9290780	−0.3703294	−0.1723483	0.3108375	−0.0680490	−0.2140714
	10	0.0	−0.7732182	0.4858574	−0.0933847	−0.1949076	0.2610185	−0.1156093
	11	0.0	0.5925707	−0.4877801	0.2907028	−0.0702327	−0.1156771	0.2213416
	12	0.0	−0.3970034	0.3856209	−0.3332595	0.2554857	−0.1602734	0.0545935
	13	0.0	0.1963312	−0.2088887	0.2134454	−0.2155540	0.2165924	−0.2170309
0.99	0	1.0	1.0	1.0	1.0	1.0	1.0	1.0
	1	−0.0579673	−0.0097353	−0.0088859	−0.0075134	−0.0057020	−0.0035591	−0.0012097
	2	0.0040311	−0.4857836	−0.4881560	−0.4915324	−0.4951231	−0.4981000	−0.4997805
	3	−0.0003003	0.7946988	0.7288775	0.6205201	0.4743333	0.2978334	0.1015709
	4	0.0000232	−0.9895736	−0.7673152	−0.4472357	−0.1019712	0.1880741	0.3533330
	5	−0.0000018	1.0983252	0.6441939	0.1084288	−0.2748075	−0.3587526	−0.1581939
	6	0.0000001	−1.1356527	−0.4100189	0.2233409	0.3722506	0.0773551	−0.2593600
	7	0.0	1.1118219	0.1244652	−0.4045757	−0.1586428	0.2563730	0.1938624
	8	0.0	−1.0357900	0.1513935	0.3745259	−0.1561103	−0.2387692	0.1829682
	9	0.0	0.9164189	−0.3647428	−0.1719017	0.3091535	−0.0673709	−0.2141303
	10	0.0	−0.7628964	0.4795509	−0.0916766	−0.1944315	0.2604500	−0.1154549
	11	0.0	0.5847794	−0.4819283	0.2877725	−0.0693976	−0.1157178	0.2213275
	12	0.0	−0.3918378	0.3812015	−0.3303739	0.2540724	−0.1598085	0 0545166
	13	0.0	0.1937922	−0.2065529	0.2117143	−0.2145408	0.2161947	−0.2169848
0.95	0	1.0	1.0	1.0	1.0	1.0	1.0	1.0
	1	−0.1317574	−0.0486596	−0.0443763	−0.0374800	−0.0284125	−0.0177189	−0.0060197
	2	0.0208007	−0.4289674	−0.4409222	−0.4578574	−0.4757818	−0.4905812	−0.4989129
	3	−0.0035166	0.7282187	0.6818014	0.5970038	0.4695472	0.3015648	0.1041233
	4	0.0006164	−0.9184927	−0.7282633	−0.4397575	−0.1100994	0.1809168	0.3522470
	5	−0.0001105	1.0263896	0.6179948	0.1157535	−0.2630224	−0.3566553	−0.1596337
	6	0.0000201	−1.0658575	−0.3986734	0.2073882	0.3657644	0.0809526	−0.2583045
	7	−0.0000037	1.0466208	0.1274094	−0.3879256	−0.1605516	0 2524271	0.1945829
	8	0.0000007	−0.9771791	0.1368157	0.3637655	−0.1489810	−0.2385611	0.1820915
	9	−0.0000001	0.8659703	−0.3426160	−0.1702373	0.3026231	−0.0646913	−0.2143721
	10	0.0	−0.7217730	0.4546197	−0.0849298	−0.1926520	0.2582628	−0.1148451
	11	0.0	0.5537441	−0.4588246	0.2763006	−0.0661149	−0.1159150	0.2212801
	12	0.0	−0.3712645	0.3637688	−0.3191183	0.2486065	−0.1580086	0.0542132
	13	0.0	0.1836812	−0.1973438	0.2049752	−0.2106455	0.2146808	−0.2168103
0.90	0	1.0	1.0	1.0	1.0	1.0	1.0	1.0
	1	−0.1903205	−0.0972702	−0.0886030	−0.0747258	−0.0565721	−0.0352456	−0.0119680
	2	0.0433283	−0.3580777	−0.3822426	−0.4162408	−0.4519939	−0.4813662	−0.4978515
	3	−0.0105574	0.6453514	0.6235328	0.5682160	0.4638858	0.3062642	0.1072831
	4	0.0026664	−0.8299770	−0.6801387	−0.4308762	−0.1202574	0.1721217	0.3509194
	5	−0.0006886	0.9368949	0.5858960	0.1249834	−0.2486508	−0.3542089	−0.1614226

c	n	N = 13						
		i = 1	2	3	4	5	6	7
0.60	0	1.0	1.0	1.0	1.0	1.0	1.0	1.0
	1	−0.4408520	−0.3866113	−0.3485735	−0.2915855	−0.2195342	−0.1363214	−0.0462176
	2	0.2288142	0.0605062	−0.0443619	−0.1811671	−0.3192677	−0.4303118	−0.4919897
	3	−0.1264037	0.1602726	0.2968131	0.4144974	0.4383986	0.3353005	0.1255559
	4	0.0721877	−0.3164687	−0.4193713	−0.3928935	−0.1816145	0.1227586	0.3436046
	5	−0.0420853	0.4223586	0.4203673	0.1839313	−0.1713012	−0.3435462	−0.1719074
	6	0.0248801	−0.4846823	−0.3221147	0.0815993	0.3237084	0.1123510	−0.2499219
	7	−0.0148517	0.5079740	0.1609883	−0.2681237	−0.1831154	0.2233589	0.2009779
	8	0.0089209	−0.4964741	0.0188054	0.2950740	−0.0948069	−0.2410349	0.1751408
	9	−0.0053699	0.4548627	−0.1740552	−0.1679645	0.2610546	−0.0433775	−0.2168715
	10	0.0032161	−0.3884850	0.2712626	−0.0329305	−0.1868982	0.2450195	−0.1100161
	11	−0.0018852	0.3033173	−0.2930530	0.1985230	−0.0414947	−0.1199816	0.2214237
	12	0.0010342	−0.2057878	0.2408138	−0.2471862	0.2149731	−0.1462284	0.0518117
	13	−0.0004518	0.1025143	−0.1330536	0.1632668	−0.1885912	0.2065891	−0.2159037
0.50	0	1.0	1.0	1.0	1.0	1.0	1.0	1.0
	1	−0.5221615	−0.4808356	−0.4319594	−0.3607784	−0.2714272	−0.1684815	−0.0571118
	2	0.3179580	0.1936085	0.0597667	−0.1095169	−0.2789819	−0.4148419	−0.4902147
	3	−0.2053104	0.0102442	0.2019170	0.3722233	0.4333623	0.3452983	0.1313981
	4	0.1367497	−0.1624466	−0.3500948	−0.3878778	−0.2024557	0.1075141	0.3413957
	5	−0.0928113	0.2730010	0.3828826	0.2059979	−0.1488628	−0.3414496	−0.1753103
	6	0.0637377	−0.3459460	−0.3146833	0.0507263	0.3168662	0.1213407	−0.2477846
	7	−0.0440639	0.3838451	0.1766993	−0.2445446	−0.1918546	0.2167375	0.2028285
	8	0.0305114	−0.3894211	−0.0108780	0.2864635	−0.0819784	−0.2431091	0.1733719
	9	−0.0210191	0.3661838	−0.1393148	−0.1730598	0.2545973	−0.0379201	−0.2176980
	10	0.0142462	−0.3186030	0.2384679	−0.0205595	−0.1888171	0.2430757	−0.1087888
	11	−0.0092944	0.2520344	−0.2666551	0.1856482	−0.0357700	−0.1218961	0.2216301
	12	0.0055449	−0.1724979	0.2229437	−0.2379022	0.2102999	−0.1440933	0.0512019
	13	−0.0022556	0.0863648	−0.1242516	0.1587477	−0.1865243	0.2058928	−0.2158287
0.40	0	1.0	1.0	1.0	1.0	1.0	1.0	1.0
	1	−0.6083378	−0.5726592	−0.5133142	−0.4283673	−0.3221387	−0.1999131	−0.0677595
	2	0.4251872	0.3198464	0.1587287	−0.0412537	−0.2405667	−0.4000869	−0.4885216
	3	−0.3129344	−0.1270132	0.1158826	0.3346663	0.4300253	0.3554493	0.1371229
	4	0.2363549	−0.0277402	−0.2925420	−0.3871934	−0.2236143	0.0928099	0.3392914
	5	−0.1810034	0.1492676	0.3577918	0.2298498	−0.1279158	−0.3400212	−0.1786689
	6	0.1394885	−0.2380705	−0.3173972	0.0218107	0.3122544	0.1303588	−0.2457507
	7	−0.1075041	0.2940401	0.1976114	−0.2259329	−0.2017055	0.2107834	0.2046865
	8	0.0823189	−0.3178908	−0.0392672	0.2833602	−0.0701691	−0.2457464	0.1716898
	9	−0.0620928	0.3117296	−0.1121991	−0.1813001	0.2504550	−0.0327011	−0.2185679
	10	0.0455287	−0.2791952	0.2177196	−0.0090913	−0.1923385	0.2418734	−0.1076224
	11	−0.0316783	0.2253303	−0.2535963	0.1772096	−0.0305420	−0.1241243	0.2219013
	12	0.0198259	−0.1562741	0.2162591	−0.2341591	0.2077397	−0.1424501	0.0506224
	13	−0.0094149	0.0788354	−0.1217088	0.1579158	−0.1862977	0.2058508	−0.2158260
0.30	0	1.0	1.0	1.0	1.0	1.0	1.0	1.0
	1	−0.6994663	−0.6622222	−0.5929669	−0.4945379	−0.3717560	−0.2306507	−0.0781692
	2	0.5483996	0.4397247	0.2534495	0.0240736	−0.2038517	−0.3860005	−0.4869062
	3	−0.4469915	−0.2518410	0.0374847	0.3013459	0.4282733	0.3657464	0.1427343
	4	0.3703392	0.0871432	−0.2456550	−0.3906226	−0.2451442	0.0786012	0.3372861
	5	−0.3085090	0.0530804	0.3445802	0.2556659	−0.1082745	−0.3392157	−0.1819842

	6	0.0001805	−0.9791045	−0.3849407	0.1878397	0.3581041	0.0854440	−0.2570146		6	0.2565527	−0.1646815	−0.3304235	−0.0056242	0.3097079	0.1394141	−0.2438144
	7	−0.0000478	0.9656466	0.1312175	−0.3678058	−0.1631041	0.2476793	0.1954869		7	−0.2116554	0.2438341	0.2244604	−0.2117630	−0.2126556	0.2054445	0.2065505
	8	0.0000128	−0.9044451	0.1188307	0.3509762	−0.1403321	−0.2384435	0.1810207		8	0.1720678	−0.2884188	−0.0673908	0.2854341	−0.0592373	−0.2489140	0.1700897
	9	−0.0000034	0.8034073	−0.3155143	−0.1684599	0.2949381	−0.0614157	−0.2146879		9	−0.1366310	0.2986483	−0.0916904	−0.1926687	0.2484512	−0.0276956	−0.2194779
	10	0.0000009	−0.6708032	0.4242072	−0.0767009	−0.1907215	0.2557271	−0.1141005		10	0.1045399	−0.2772314	0.2082257	0.0017318	−0.1973866	0.2413614	−0.1065133
	11	−0.0000003	0.5152952	−0.4307206	0.2625656	−0.0621437	−0.1162387	0.2212404		11	−0.0752140	0.2291982	−0.2533841	0.1728176	−0.0257384	−0.1266500	0.2222328
	12	0.0000001	−0.3457850	0.3426038	−0.3057489	0.2422105	−0.1558926	0.0538427		12	0.0482221	−0.1614597	0.2205208	−0.2355984	0.2071369	−0.1412630	0.0500717
	13	0.0	0.1711615	−0.1861758	0.1970035	−0.2061436	0.2129612	−0.2166140		13	−0.0232358	0.0821747	−0.1253420	0.1605648	−0.1877920	0.2064198	−0.2158909
0.85	0	1.0	1.0	1.0	1.0	1.0	1.0	1.0	0.20	0	1.0	1.0	1.0	1.0	1.0	1.0	1.0
	1	−0.2382838	−0.1458181	−0.1326484	−0.1117071	−0.0844642	−0.0525782	−0.0178458		1	−0.7937593	−0.7508430	−0.6715058	−0.5595637	−0.4203948	−0.2607342	−0.0883495
	2	0.0677917	−0.2873707	−0.3240439	−0.3752152	−0.4286579	−0.4723553	−0.4968153		2	0.6813510	0.5570599	0.3454750	0.0870841	−0.1686280	−0.3725331	−0.4853645
	3	−0.0206292	0.5628105	0.5660314	0.5401849	0.4586013	0.3110031	0.1104093		3	−0.5975535	−0.3708224	−0.0356388	0.2715235	0.4279513	0.3761814	0.1482365
	4	0.0065049	−0.7419318	−0.6329374	−0.4225845	−0.1304196	0.1634934	0.3496240		4	0.5265479	0.1912694	−0.2067558	−0.3976702	−0.2670789	0.0648424	0.3353745
	5	−0.0020969	0.8479970	0.5546728	0.1343205	−0.2346915	−0.3519567	−0.1631995		5	−0.4623499	−0.0264721	0.3408958	0.2834553	−0.0897343	−0.3389851	−0.1852570
	6	0.0006862	−0.8930422	−0.3718201	0.1687647	0.3509646	0.0899308	−0.2557570		6	0.4022393	−0.1138412	−0.3522970	−0.0320924	0.3090162	0.1485136	−0.2419702
	7	−0.0002270	0.8854148	0.1352115	−0.3485403	−0.1658562	0.2431351	0.1963944		7	−0.3448885	0.2211188	0.2569827	−0.2012741	−0.2246588	0.2006669	0.2084191
	8	0.0000757	−0.8324573	0.1011476	0.3390113	−0.1319825	−0.2384845	0.1799770		8	0.2896620	−0.2895112	−0.0961902	0.2920473	−0.0490328	−0.2525762	0.1685668
	9	−0.0000254	0.7415464	−0.2891438	−0.1670677	0.2878075	−0.0582205	−0.2150183		9	−0.2363036	0.3167023	−0.0759195	−0.2069402	0.2483666	−0.0228790	−0.2204249
	10	0.0000086	−0.6204467	0.3947904	−0.0687166	−0.1891353	0.2534104	−0.1133750		10	0.1847786	−0.3042001	0.2076496	0.0121735	−0.2038490	0.2414863	−0.1054584
	11	−0.0000029	0.4773337	−0.4036480	0.2495760	−0.0583229	−0.1166487	0.2212219		11	−0.1351860	0.2571498	−0.2637319	0.1718719	−0.0212834	−0.1294552	0.2226205
	12	0.0000010	−0.3206405	0.3222728	−0.2932468	0.2363199	−0.1539245	0.0534818		12	0.0877047	−0.1837353	0.2339505	−0.2415742	0.2082982	−0.1404948	0.0495480
	13	−0.0000003	0.1588099	−0.1754658	0.1895934	−0.2020683	0.2114330	−0.2164411		13	−0.0425602	0.0942569	−0.1341973	0.1662917	−0.1908525	0.2075544	−0.2160188
0.80	0	1.0	1.0	1.0	1.0	1.0	1.0	1.0	0.10	0	1.0	1.0	1.0	1.0	1.0	1.0	1.0
	1	−0.2815269	−0.1942847	−0.1764741	−0.1483926	−0.1120757	−0.0697158	−0.0236544		1	−0.8896330	−0.8394825	−0.7494670	−0.6237319	−0.4681830	−0.2902067	−0.0983087
	2	0.0944303	−0.2169010	−0.2664267	−0.3348473	−0.4057928	−0.4635479	−0.4958035		2	0.8190783	0.6745515	0.4361679	0.1484025	−0.1346744	−0.3596335	−0.4838923
	3	−0.0338543	0.4806943	0.5094611	0.5130022	0.4537130	0.3157821	0.1135026		3	−0.7563170	−0.4890010	−0.1057136	0.2444076	0.4288855	0.3867452	0.1536332
	4	0.0125726	−0.6545001	−0.5868636	−0.4149645	−0.1405947	0.1550298	0.3483603		4	0.6940003	0.2922959	−0.1730698	−0.4077224	−0.2894326	0.0514884	0.3335514
	5	−0.0047724	0.7598785	0.5245271	0.1437972	−0.2211552	−0.3498978	−0.1649645		5	−0.6297575	−0.0995538	0.3439911	0.3130929	−0.0720935	−0.3392807	−0.1884885
	6	0.0018387	−0.8078833	−0.3594637	0.1502015	0.3443684	0.0944146	−0.2545306		6	0.5629228	−0.0733372	−0.3809437	−0.0580362	0.3099499	0.1576628	−0.2402131
	7	−0.0007161	0.8061551	0.1394542	−0.3302220	−0.1688235	0.2387921	0.1973054		7	−0.4935937	0.2123713	0.2942871	−0.1936689	−0.2376456	0.1963974	0.2102910
	8	0.0002812	−0.7614481	0.0838115	0.3279721	−0.1239378	−0.2386838	0.1789598		8	0.4222702	−0.3072508	−0.1261711	0.3024431	−0.0394111	−0.2566963	0.1671168
	9	−0.0001111	0.6806068	−0.2636479	−0.1661174	0.2812526	−0.0551039	−0.2153627		9	−0.3496839	0.3525637	−0.0631270	−0.2237681	0.2499661	−0.0182280	−0.2214060
	10	0.0000441	−0.5708957	0.3665764	−0.0609942	−0.1879110	0.2513107	−0.1126681		10	0.2767031	−0.3483020	0.2134340	0.0224518	−0.2115931	0.2421942	−0.1044544
	11	−0.0000175	0.4400128	−0.3778274	0.2374126	−0.0546545	−0.1171449	0.2212239		11	−0.2042721	0.2997161	−0.2819247	0.1737203	−0.0171055	−0.1325214	0.2230605
	12	0.0000068	−0.2959363	0.3029571	−0.2817121	0.2309539	−0.1521026	0.0531302		12	0.1333671	−0.2165517	0.2543285	−0.2513366	0.2110155	−0.1401088	0.0490497
	13	−0.0000023	0.1466795	−0.1653141	0.1828112	−0.1984374	0.2100947	−0.2162909		13	−0.0649621	0.1117820	−0.1470498	0.1746143	−0.1953084	0.2092088	−0.2162054
0.70	0	1.0	1.0	1.0	1.0	1.0	1.0	1.0	0	0	1.0	1.0	1.0	1.0	1.0	1.0	1.0
	1	−0.3620413	−0.2908567	−0.2632759	−0.2207515	−0.1664150	−0.1034054	−0.0350681		1	−0.9862838	−0.9284349	−0.8272013	−0.6872929	−0.5152486	−0.3191124	−0.1080549
	2	0.1553694	−0.0770118	−0.1534291	−0.2563438	−0.3615302	−0.4465366	−0.4938511		2	0.9591336	0.7929870	0.5263930	0.2085573	−0.1017783	−0.3472509	−0.4824862
	3	−0.0711399	0.3183456	0.3999294	0.4615471	0.4451881	0.3254608	0.1195921		3	−0.9191074	−0.6081047	−0.1742541	0.2192953	0.4309009	0.3974284	0.1589283
	4	0.0337138	−0.4823668	−0.4991300	−0.4020842	−0.1610206	0.1385851	0.3459241		4	0.8670261	0.3932846	−0.1425441	−0.4201782	−0.3122033	0.0384957	0.3318119
	5	−0.0163229	0.5871212	0.4685098	0.1633265	−0.1953730	−0.3463513	−0.1684591		5	−0.8039549	−0.1707667	0.3516461	0.3443776	−0.0651686	−0.3400547	−0.1916797
	6	0.0080191	−0.6416109	−0.3378475	0.1147366	0.3328744	0.1033794	−0.2521685		6	0.7311791	−0.0370699	−0.4144971	−0.0837800	0.3122829	0.1668656	−0.2385380
	7	−0.0039814	0.6520004	0.1490450	−0.2967883	−0.1754608	0.2306964	0.1991363		7	−0.6501745	0.2102888	0.3353524	−0.1882439	−0.2515331	0.1925847	0.2121652
	8	0.0019922	−0.6238323	0.0503669	0.3090834	−0.1087694	−0.2395524	0.1770016		8	0.5625744	−0.3336378	−0.1574474	0.3158926	−0.0302436	−0.2612377	0.1657355
	9	−0.0010023	0.5628808	−0.2159757	−0.1657884	0.2699335	−0.0490979	−0.2160918		9	−0.4701323	0.3981806	0.0520808	−0.2427701	0.2530195	−0.0137207	−0.2224185
	10	0.0005052	−0.4754294	0.3147907	−0.0463874	−0.1866072	0.2477514	−0.1113079		10	0.3746823	−0.4021271	0.2235571	0.0327197	−0.2204799	0.2434330	−0.1034984
	11	−0.0002527	0.3682656	−0.3310562	0.2158810	−0.0477763	−0.1183945	0.2212867		11	−0.2780985	0.3507745	−0.3056958	0.1777685	−0.0131413	−0.1358296	0.2235490
	12	0.0001214	−0.2485197	0.2682917	−0.2619474	0.2218526	−0.1488886	0.0524539		12	0.1822522	−0.2555867	0.2797439	−0.2641695	0.2150843	−0.1400692	0.0485754
	13	−0.0000484	0.1234192	−0.1471963	0.1714002	−0.1925630	0.2079788	−0.2160560		13	−0.0889714	0.1325460	−0.1628280	0.1850634	−0.2009886	0.2113385	−0.2164468

For a unit cell containing two regions (denoted $\alpha = 1,2$) with half-thicknesses t_α, mean free paths ℓ_α, secondaries per collision c_α, and sources Q_α, the solution for the flux in each region is given by

$$\Psi_{\alpha,m}(x_\alpha) = \frac{Q_\alpha}{1-c}\,\delta_{0,m} + \sum_{i=1}^{(N+1)/2} A_{\alpha,i}\, G_m(\nu_{\alpha,i}) \cosh \nu_{\alpha,i}(x_\alpha/\ell_\alpha) \qquad m \text{ even}$$

$$\Psi_{\alpha,m}(x_\alpha) = \sum_{i=1}^{(N+1)/2} A_{\alpha,i}\, G_m(\nu_{\alpha,i}) \sinh \nu_{\alpha,i}(x_\alpha/\ell_\alpha) \qquad m \text{ odd}$$

where $m = 0, 1, \ldots N$. x is measured from the midplane of each region; and the boundary condition of symmetry at the midplanes is used. Continuity of $\Psi_m(x)$ at the interface may be used to determine the $A_{\alpha,i}$.

$$\sum_{i=1}^{(N+1)/2} A_{1,i} G_m(\nu_{1,i}) \cosh \frac{\nu_{1,i} t_1}{\ell_1} - \sum_{i=1}^{(N+1)/2} A_{2,i} G_m(\nu_{2,i}) \cosh \frac{\nu_{2,i} t_2}{\ell_2} = \left(\frac{Q_2}{1-c_2} - \frac{Q_1}{1-c_1}\right)\delta_{0,m}, \qquad m \text{ even}$$

$$\sum_{i=1}^{(N+1)/2} A_{1,i} G_m(\nu_{1,i}) \sinh \frac{\nu_{1,i} t_1}{\ell_1} + \sum_{i=1}^{(N+1)/2} A_{2,i} G_m(\nu_{2,i}) \sinh \frac{\nu_{2,i} t_2}{\ell_2} = 0, \qquad m \text{ odd}$$

where $m = 1, 2, \ldots N$.

The values Ψ_n can now be determined; in particular Ψ_0 (the total neutron flux), and hence, the thermal utilization and the disadvantage factor. Tables 4-4 and 4-5 give results of P_3 and P_5 calculations on thick and thin slabs, respectively, along with an indication of the rate of convergence of the method. A constant source was assumed in the non-capturing moderator, and a zero source in the fuel.

Table 4-4 — FLUX DISADVANTAGE FACTOR ($\bar{\Phi}_M/\bar{\Phi}_U$) FOR SLAB LATTICES (THICK SLABS)[a]

$1-c$	(t_U/ℓ_U)[b]	(t_M/ℓ_M)[b]	$(\bar{\Phi}_M/\bar{\Phi}_U)$	
			P_3	P_5
0.10	2	2	1.2784	1.2897
—	—	5	1.4200	1.4250
—	—	10	1.6645	1.6681
0.50	2	2	2.3331	2.3905
—	—	5	3.0499	3.0757
—	—	10	4.2754	4.2946
0.90	2	2	3.3206	3.4268
—	—	5	4.6226	4.6723
—	—	10	6.8326	6.8701
0.10	5	2	1.9776	1.9926
—	—	5	2.3045	2.3094
—	—	10	2.9060	2.9091
0.25	5	2	3.2470	3.2919
—	—	5	4.0816	4.0987
—	—	10	5.5913	5.6030
0.50	5	2	5.0944	5.2015
—	—	5	6.8010	6.8471
—	—	10	9.8328	9.8668

[a] J. Chernick, BNL, private communication.
[b] These values are for total thickness.

The Spherical Harmonic Method may be easily generalized to include anisotropic scattering (see Section 4.1.3). The extension to spherical geometry is also relatively easy, but the extension to cylindrical geometry is considerably more difficult.

Spherical Geometry. In spherical geometry, the P_N equations have the solution (Ref. 3, pp. 146-156):

$$\Psi_k(n) = \sum_{i=1}^{(N+1)/2} G_k(-\nu_i)\left(\frac{2}{\pi\nu_i r}\right)^{1/2}\left[A_i\nu_i K_{m+1/2}(\nu_i r) + B_i I_{m+1/2}(-\nu_i r)\right]$$

The space variable, r, is measured in mean free paths as in the plane case. The functions G_k and ν_i are the same as in the case of plane symmetry. The A's and B's are arbitrary constants, and the I's and K's are the modified Bessel functions of the first and second kind. The relationship:

$$K_s(x) = \frac{1}{2}\pi[I_{-s}(x) + I_s(x)]\csc(s\pi)$$

defines the K functions uniquely in terms of the I's.

Table 4-5— FLUX DISADVANTAGE FACTOR $(\bar{\Phi}_M/\bar{\Phi}_U)$ FOR SLAB LATTICES (THIN SLABS)[a]

1 − c	(t_U/ℓ_U)[b]	(t_M/ℓ_M)[b]	$(\bar{\Phi}_M/\bar{\Phi}_U)$	
			P_3	P_5
0.10	0.25	0.50	1.0093	1.0133
0.25	—	—	1.0233	1.0332
0.50	—	—	1.0465	1.0664
0.10	0.25	1.00	1.0150	1.0201
0.25	—	—	1.0374	1.0503
0.50	—	—	1.0748	1.1005
0.10	0.50	0.50	1.0243	1.0334
0.25	—	—	1.0606	1.0833
0.50	—	—	1.1209	1.1659
0.10	0.50	1.00	1.0348	1.0445
0.25	—	—	1.0869	1.1112
0.50	—	—	1.1735	1.2217
0.10	1.00	0.50	1.0692	1.0885
0.25	—	—	1.1717	1.2191
0.50	—	—	1.3386	1.4312
0.10	1.00	1.00	1.0870	1.1032
0.25	—	—	1.2162	1.2563
0.50	—	—	1.4282	1.5070

[a] J. Chernick, BNL, private communication.
[b] These values are for total thickness.

*Cylindrical Geometry.** In cylindrical geometry, the problems are more difficult by virtue of the dependence on two angular coordinates. The notation adopted here is that of Mark.[5] The coordinate system is defined by the distance from the cylinder axis on the polar angle, $\theta(=\cos^{-1}\mu)$, and the azimuthal angle, ϕ. The direction of the neutron path is given by a vector, $\tilde{\Omega}$, whose components are:

$$\Omega^1 = \sin\theta\sin\phi \qquad \Omega^2 = \sin\theta\cos\phi \qquad \Omega^3 = \cos\theta$$

The superscripts are used to indicate a contra-variant tensor. The corresponding space variables are: $X^1 = Z$, $X^2 = \phi$, $X^3 = r$. Let g^{ij} be the metric tensor in this space. Then form the spherical harmonic tensor:

$$T^i = \Omega^i$$

$$T^{ij} = \frac{1}{2}(3\Omega^i\Omega^j - g^{ij})$$

$$T^{ijk} = \frac{1}{2}(5\Omega^i\Omega^j\Omega^k - g^{ij}\Omega^k - g^{ik}\Omega^j - g^{kj}\Omega^i), \text{ etc.}$$

* See also Section 4.1.7.2.

Then

$$\Psi^{i\ldots k} = \int \Psi T^{i\ldots k}\, d\Omega$$

where the integration is over a unit sphere about the field point. If $\Psi^{\ell}\ T_{\ell}$ denotes the scalar product $\Psi^{i_1\ldots i_\ell} T_{i_1\ldots i_\ell}$, (summation convention)

then

$$\Psi = \frac{1}{4\pi} \sum_{\ell=0}^{\infty} \frac{(2\ell+1)2^{\ell}\,(\ell!)^2}{(2\ell)!}\, \Psi^{\ell}\ T_{\ell}$$

In the P_3 approximation, the non-zero elements of the various tensor components of Ψ are given by:

$$\Psi_0 = \sum_{i=1}^{2} \{A_i I_0[\nu_i(r)] + B_i\ K_0\ (\nu_i r)\}$$

$$\Psi^3 = \sum_{i=1}^{2} G_1(\nu_i)\ [A_i I_1(\nu_i r) - B_i K_1(\nu_i r)]$$

$$\Psi^{11} = \sum_{i=1}^{2} \left(-\frac{1}{2}\right) G_2(\nu_i)\ [A_i I_0(\nu_i r) + B_i K_0(\nu_i r)] + M I_0(\beta r) + N K_0(\beta r)$$

$$\Psi^{11} + 2\ \Psi^{33} = \sum_{i=1}^{2} \frac{3}{2}\, G_2(\nu_i)\ [A_i I_2(\nu_i r) + B_i K_2(\nu_i r)] + M I_2(\beta r) + N K_2(\beta r)$$

$$\Psi^{113} = \sum_{i=1}^{2} \left(-\frac{1}{2}\right) G_3(\nu_i)\ [A_i I_1(\nu_i r) - B_i K_1(\nu_i r)] - \frac{5}{3\beta}\,[M I_1(\beta r) - N K_1(\beta r)]$$

$$3\Psi^{113} + 4\Psi^{333} = \sum_{i=1}^{2} \frac{5}{2}\, G_3(\nu_i)\ [A_i I_3(\nu_i r) - B_i K_3(\nu_i r)] - \frac{5}{\beta}\,[M I_3(\beta r) - N K_3(\beta r)]$$

where $\beta = \sqrt{7}$; r is measured in mean free paths; and A_i, B_i, M, N, are undetermined coefficients.

Yvon's Method.[6] Sometimes called the Double P_N Method, this approximation is similar to the Spherical Harmonics Method outlined above. It differs in that the angular flux is described by two functions: one for $\mu < 0$ and one for $\mu > 0$. It is well suited to problems involving thin regions and can be expected to give better approximations at the interface than the full-range approximation.

Starting with Eq. (4-1), define the solutions:

$$\Psi^{+} = \Psi,\ 0_+ \le \mu \le 1 \qquad \Psi^{-} = \Psi,\ -1 \le \mu \le 0_-$$
$$= 0,\ -1 \le \mu \le 0_- \qquad = 0,\ 0_+ \le \mu \le 1$$

Then the expansion of $\Psi\ (x,\mu)$ is:

$$\Psi^{\pm}(x,\mu) = \sum_{n=0}^{\infty}\ (2n+1)\ B_n^{\pm}(x)\ P_n^{\pm}(\mu)$$

$$P_n^{+}(\mu) = P_n(2\mu - 1),\ 0_+ \le \mu \le 1$$
$$= 0, \qquad -1 \le \mu \le 0_-$$
$$P_n^{-}(\mu) = P_n(2\mu + 1),\ -1 \le \mu \le 0_-$$
$$= 0, \qquad 0_+ \le \mu \le 1$$

where $P_n(2\mu \pm 1)$ is the full-range Legendre polynomial of argument $(2\mu \pm 1)$. It follows from these definitions that:

$$\int_0^1 P_n^{+}(\mu)\ P_m^{+}(\mu)\ d\mu = \int_{-1}^{0} P_n^{-}(\mu)\ P_m^{-}(\mu)\, d\mu = \frac{\delta_{n,m}}{2n+1}$$

Moreover,

$$2(2n+1)\mu\ P_n^{\pm}(\mu) = (n+1)\ P_{n+1}^{\pm}(\mu) \pm (2n+1)\ P_n^{\pm}(\mu) + n P_{n-1}^{\pm}(\mu)$$

The total flux is given by:

$$\Psi_0(x) = \int_{-1}^{1} \Psi(x,\mu)\, d\mu = B_0^+(x) + B_0^-(x)$$

and the total current by:

$$\Psi_1(x) = \int_{-1}^{1} \Psi\mu(x,\mu)\, d\mu = \frac{B_1^+(x) + B_1^-(x)}{2} + \frac{B_0^+(x) - B_0^-(x)}{2}$$

Making use of the orthogonality relation of the $P_n^{\pm}$,

$$\frac{d}{dx}\left[n B_{n-1}^{\pm} \pm (2n+1) B_n^{\pm} + (n+1) B_{n+1}^{\pm}\right] + \frac{2(2n+1)}{\ell} B_n^{\pm} = \frac{c}{\ell}\left(B_0^{\pm} + B_0^{-}\right)\delta_{n,0} + 2(2n+1)\int^{\pm} S(x,\mu)\, P_n^{\pm}(\mu)\, d\mu$$

where the limits on the integral denoted by + are 0 to 1, and those denoted by − are −1 to 0.

As before, only the case $S(x,\mu) = 0$ need be considered. Then, for $n = 0$,

$$\frac{d}{dx}\left(\pm B_0^{\pm} + B_1^{\pm}\right) + \frac{2-c}{\ell} B_0^{\pm} - \frac{c}{\ell} B_0^{\pm} = 0$$

and for $n > 0$,

$$\frac{d}{dx}\left(n B_{n-1}^{\pm} \pm (2n+1) B_n^{\pm} + (n+1) B_{n+1}^{\pm}\right) + \frac{2(2n+1)}{\ell} B_n^{\pm} = 0$$

If the most general solution for $B_n^{\pm}(x)$ is inserted, the equations for the A's are:

$$B_n^{\pm}(x) = \textstyle\sum_i A_{n,i}^{\pm} \exp\left[\alpha_i (x/\ell)\right], \text{ which gives}$$

$$\alpha_i\left(\pm A_{0,i}^{\pm} + A_{1,i}^{\pm}\right) + (2-c) A_{0,i}^{\pm} - c A_{0,i}^{\pm} = 0$$

and

$$\alpha_i\left[n A_{n-1,i}^{\pm} \pm (2n+1) A_{n,i}^{\pm} + (n+1) A_{n+1,i}^{\pm}\right] + 2(2n+1) A_{n,i}^{\pm} = 0$$

From these equations the A's can be determined as follows: Let

$$G_n^{\pm}(\alpha) = -\frac{1}{\alpha n}\frac{A_n^{\pm}}{A_{n-1}}$$

then

$$G_n^{\pm} = \left\{(2n+1)(2 \pm \alpha) - \left[\frac{\alpha^2 (n+1)^2}{(2n+3)(2 \pm \alpha) - \{\alpha^2 (n+2)^2 / [(2n+5)(2 \pm \alpha) - \alpha^2 (n+3)^2 / \ldots]\}}\right]\right\}^{-1}$$

and

$$A_{0,i}^{\pm}\left[2 - c \pm \alpha_i - \alpha_i^2 G_1^{\pm}(\alpha_i)\right] - c A_{0,i}^{\pm} = 0$$

The eigenvalue equation for α_i is then

$$\left[2 - c + \alpha - \alpha^2 G_1^{+}(\alpha)\right]\left[2 - c - \alpha - \alpha^2 G_1^{-}(\alpha)\right] - c^2 = 0$$

Also,

$$A_{0,i}^{-} = A_{0,i}^{+}\frac{1}{c}\left[2 - c + \alpha - \alpha^2 G_1^{+}(\alpha)\right]$$

The N*th* order approximation is now made by requiring that all $A_n^{\pm} = 0$ for $n > N$. In the $P_0^{\pm}$ approximation:

$$\alpha_1 = 2(1-c)^{1/2}$$

In the $P_1^{\pm}$ approximation:

$$\alpha_1 = \sqrt{6}\left[2 - c + \sqrt{3 - 3c + c^2}\right]^{1/2}$$

$$\alpha_2 = \sqrt{6}\left[2 - c - \sqrt{3 - 3c + c^2}\right]^{1/2}$$

In the $P_2^{\pm}$ approximation, the eigenvalues are the solutions of:

$$\alpha^6 - 12\,\alpha^4\,(7 - 2c) + 20\,\alpha^2\left(21 - \frac{43}{3}c\right) - 400\,(1 - c) = 0$$

Further details may be obtained from Ref. 6.

4.1.3 SPHERICAL HARMONIC METHOD-LINEARLY ANISOTROPIC SCATTERING[7]

When the scattering function $f(\Omega,\Omega')$ is expanded in Legendre polynomials and approximated by

$$f(\Omega,\Omega') = \frac{1}{4\pi}\left[1 + 3b_1 P_1(\Omega\Omega')\right]$$

the treatment of the preceding section can be extended to include the term in b_1. The mean cosine of the scattering angle, usually denoted by $\bar{\mu}$, is just b_1. Tables 4-6 and 4-7 list the values of ν_i and $G_n(\nu)$ for N = 1, 3, 5, 7, and b_1 = 0.04, 0.08, $\frac{1}{3}$ and $\frac{2}{3}$. The notation is that of Section 4.1.2.

4.1.4 INTEGRAL TRANSPORT THEORY

Integral transport theory has been widely used in calculating flux depressions in cylindrical geometry. In general, any approximate treatment of cylindrical geometry is subject to serious error in the limit of small radii or thin regions since the boundary conditions are usually inexact. Thus, some caution is in order in making calculations in cylindrical geometry. For example, Newmarch[8] has shown that when a regular space-filling lattice of cylindrical rods is approximated by cylindrical cells with perfect reflection at the boundaries, the following theorem applies to transport theory calculations:

> "For the case of a constant thermal neutron source in the moderator and zero source in the fuel, the cylindrical cell approximation results in the average flux in the moderator being higher than the average flux in the fuel even where the cell dimensions, in units of mean free paths, tend to zero."

It is further estimated that in a typical light-water-moderated lattice, the flux ratios can be incorrect by a factor of two. Also it is shown that if the total mean free path in the moderator is large compared to the cell size and the fuel mean free path, the ratio of moderator flux to fuel flux is overestimated in the cylindrical cell approximation.

With these reservations in mind, one may also list the various approximations made in the several applications of integral transport theory quoted here and in Section 4.1.5.

In general, the results of an integral transport theory calculation of thermal utilization depend on the assumptions made concerning (a) the angular distribution of the flux directed into the rod, and (b) the shape of the flux in the fuel rod. An assumption is usually made that the flux in the moderator is determined by diffusion theory.

Amouyal and Benoist[9,10] and Theys[11] assume an isotropic flux directed into the rod (incoming current proportional to cos θ). Amouyal and Benoist show that their results are not sensitive to the angular dependence of the entering current, the possible error in the capture fraction of the rod being of the order of 1%. The source of uncollided neutrons (zero generation neutrons) in the fuel is assumed to be uniform and isotropic in Refs. 9, 10, and 11. Two methods are then used to calculate successive collision densities. In the first method, the first collision density is calculated exactly and in successive generations the non-uniform part of the sources is replaced by the average value of the first collision density. In the second method, the second generation captures are calculated exactly and all successive generations are calculated using the average value of the source arising from the first collision density. The calculations by Theys were based on the second method.

In calculations by McLennan,[12] the source from all generations is assumed to be uniform and isotropic, and formulae are given for angular distributions of flux directed into the rod either isotropic or proportional to cos θ.

Table 4-6 — VALUES OF ν_i FOR N = 1, 3, 5, 7

Data from Ref. 7.

	N = 1	3		5			7			
c	i = 1	1	2	1	2	3	1	2	3	4
					$b_1 = 0.04$					
1.0	0.0	0.0	1.972027	0.0	1.225211	3.202945	0.0	1.103185	1.591779	4.458086
0.99	0.169741	0.169061	1.979957	0.169061	1.226603	3.212176	0.169061	1.103686	1.594022	4.467690
0.98	0.240100	0.238174	1.987972	0.238174	1.228030	3.221438	0.238174	1.104200	1.596294	4.477311
0.97	0.294122	0.290580	1.996070	0.290578	1.229490	3.230732	0.290578	1.104729	1.598595	4.486946
0.96	0.339694	0.334233	2.004249	0.334228	1.230986	3.240055	0.334228	1.105273	1.600926	4.496597
0.95	0.379868	0.372227	2.012509	0.372217	1.232518	3.249408	0.372217	1.105832	1.603287	4.506263
0.9	0.537773	0.516069	2.054963	0.515952	1.240751	3.296594	0.515951	1.108879	1.615536	4.554800
0.8	0.762102	0.700648	2.144995	0.699361	1.260418	3.392792	0.699326	1.116521	1.642227	4.652791
0.7	0.935307	0.823282	2.240364	0.818331	1.284842	3.490890	0.817983	1.126922	1.671640	4.751746
0.6	1.082220	0.912320	2.339275	0.900239	1.313977	3.590297	0.898639	1.140912	1.703305	4.851382
0.5	1.212436	0.979837	2.440157	0.957260	1.346803	3.690498	0.952665	1.158716	1.736556	4.951447
0.4	1.330864	1.032548	2.541771	0.997131	1.381598	3.791058	0.987711	1.179272	1.770640	5.051723
0.3	1.440417	1.074653	2.643215	1.025348	1.416598	3.891621	1.010105	1.200566	1.804836	5.152018
0.2	1.542984	1.108947	2.743868	1.045744	1.450497	3.991902	1.024647	1.220828	1.838542	5.252171
0.1	1.639878	1.137359	2.843326	1.060878	1.482535	4.091678	1.034449	1.239130	1.871308	5.352047
0	1.732051	1.161256	2.941341	1.072421	1.512380	4.190778	1.041352	1.255230	1.902832	5.451533
					$b_1 = 0.08$					
1.0	0.0	0.0	1.972027	0.0	1.225211	3.202945	0.0	1.103185	1.591779	4.458086
0.99	0.166205	0.165539	1.979955	0.165539	1.226602	3.212175	0.165539	1.103685	1.594021	4.467690
0.98	0.235151	0.233266	1.987962	0.233266	1.228025	3.221434	0.233266	1.104198	1.596289	4.477308
0.97	0.288125	0.284658	1.996048	0.284656	1.229480	3.230722	0.284656	1.104724	1.598586	4.486941
0.96	0.332842	0.327497	2.004211	0.327493	1.230967	3.240039	0.327493	1.105264	1.600909	4.496588
0.95	0.372290	0.364812	2.012450	0.364803	1.232489	3.249383	0.364803	1.105818	1.603261	4.506249
0.9	0.527636	0.506396	2.054742	0.506291	1.240630	3.296499	0.506290	1.108822	1.615432	4.554749
0.8	0.749400	0.689218	2.144222	0.688055	1.259896	3.392468	0.688026	1.116254	1.641830	4.652616
0.7	0.921738	0.811866	2.238905	0.807354	1.283641	3.490279	0.807064	1.126228	1.670821	4.751413
0.6	1.068831	0.901840	2.337182	0.890695	1.311951	3.589408	0.889328	1.139561	1.702032	4.850894
0.5	1.200000	0.970795	2.437622	0.949654	1.344067	3.689396	0.945600	1.156643	1.734906	4.950836
0.4	1.320000	1.025205	2.539076	0.991516	1.378517	3.789853	0.982904	1.176752	1.768791	5.051045
0.3	1.431642	1.069130	2.640687	1.021526	1.413661	3.890456	1.007138	1.198118	1.803035	5.151353
0.2	1.538311	1.105280	2.741848	1.043438	1.448176	3.990943	1.023019	1.218936	1.837068	5.251616
0.1	1.636582	1.135542	2.842153	1.059831	1.481225	4.091104	1.033767	1.238107	1.870440	5.351710
0	1.732051	1.161256	2.941340	1.072421	1.512380	4.190778	1.041352	1.255230	1.902832	5.451533
					$b_1 = 1/3$					
1.0	0.0	0.0	1.972027	0.0	1.225212	3.202945	0.0	1.103185	1.591779	4.458086
0.99	0.141774	0.141208	1.979940	0.141208	1.226595	3.212168	0.141208	1.103682	1.594014	4.467686
0.98	0.200997	0.199392	1.987902	0.199392	1.227997	3.221408	0.199392	1.104186	1.596263	4.477294
0.97	0.246779	0.243826	1.995914	0.243825	1.229416	3.230663	0.243825	1.104696	1.598526	4.486910
0.96	0.285650	0.281103	2.003975	0.281101	1.230854	3.239935	0.281101	1.105213	1.600804	4.496533
0.95	0.320156	0.313782	2.012085	0.313778	1.232310	3.249224	0.313778	1.105738	1.603097	4.506163
0.9	0.458257	0.440105	2.053365	0.440056	1.239901	3.295906	0.440056	1.108487	1.614793	4.554429
0.8	0.663324	0.611414	2.139459	0.610846	1.256894	3.390440	0.610839	1.114776	1.639447	4.651517
0.7	0.830662	0.734591	2.229932	0.732222	1.276904	3.486455	0.732137	1.122574	1.665962	4.749325
0.6	0.979795	0.831305	2.324277	0.824891	1.300619	3.583845	0.824423	1.132608	1.694489	4.847826
0.5	1.118034	0.910348	2.421923	0.896839	1.328490	3.682498	0.895129	1.145774	1.725079	4.946989
0.4	1.249000	0.976516	2.522300	0.952521	1.360480	3.782301	0.947926	1.162834	1.757662	5.046781
0.3	1.374773	1.032851	2.624859	0.995257	1.395961	3.883138	0.985663	1.183760	1.792050	5.147167
0.2	1.496663	1.081460	2.729143	1.027920	1.433864	3.984898	1.011607	1.207327	1.827949	5.248112
0.1	1.615549	1.123877	2.941341	1.072421	1.512380	4.190778	1.041352	1.255230	1.902832	5.451533
0	1.732051	1.161256	2.941341	1.072421	1.512380	4.190778	1.041352	1.255230	1.902832	5.451533
					$b_1 = 2/3$					
1.0	0.0	0.0	1.972027	0.0	1.225211	3.202945	0.0	1.103185	1.591779	4.458086
0.99	0.100995	0.100592	1.979920	0.100592	1.226586	3.212159	0.100592	1.103678	1.594005	4.467681
0.98	0.144220	0.143076	1.987823	0.143076	1.227961	3.221373	0.143076	1.104170	1.596229	4.477275
0.97	0.178325	0.176207	1.995739	0.176207	1.229335	3.230586	0.176207	1.104660	1.598450	4.486868
0.96	0.207846	0.204564	2.003668	0.204563	1.230711	3.239800	0.204563	1.105150	1.600669	4.496460
0.95	0.234520	0.229906	2.011613	0.229905	1.232089	3.249015	0.229905	1.105640	1.602889	4.506051
0.9	0.346410	0.332972	2.051616	0.332961	1.239039	3.295136	0.332961	1.108101	1.614002	4.554012
0.8	0.529150	0.489098	2.133517	0.488937	1.253616	3.387829	0.488937	1.113264	1.636615	4.650088
0.7	0.692820	0.615767	2.218796	0.614949	1.269900	3.481550	0.614937	1.119161	1.660324	4.746617
0.6	0.848528	0.724946	2.308200	0.722267	1.288975	3.576713	0.722179	1.126434	1.685795	4.843850
0.5	1.0	0.820928	2.402191	0.814147	1.312083	3.673636	0.813695	1.136035	1.713655	4.942000
0.4	1.148913	0.905922	2.500972	0.891550	1.340495	3.772560	0.889830	1.149368	1.744469	5.041241
0.3	1.296148	0.981384	2.604526	0.954875	1.375142	3.873654	0.949811	1.168131	1.778679	5.141714
0.2	1.442221	1.048453	2.712660	1.004929	1.416114	3.977026	0.993373	1.193253	1.816530	5.243533
0.1	1.587451	1.108116	2.825061	1.043359	1.462432	4.082731	1.022550	1.223360	1.858010	5.346785
0	1.732051	1.161256	2.941341	1.072421	1.512380	4.190778	1.041352	1.255230	1.902832	5.451533

Table 4-7 — $G_n(\nu_i)$ FOR $b_1 = 0.04, 0.08, 1/3, 2/3$

Data from Ref. 7.

		N = 1	3		5			7			
c	n	i = 1	1	2	1	2	3	1	2	3	4
					$b_1 = 0.04$						
1.0	0	1.0	1.0	1.0	1.0	1.0	1.0	1.0	1.0	1.0	1.0
	1	0.0	0.0	0.0	0.0	0.0	0.0	0.0	0.0	0.0	0.0
	2	—	0.0	−0.5	0.0	−0.5	−0.5	0.0	−0.5	−0.5	−0.5
	3	—	0.0	0.422577	0.0	0.680155	0.260177	0.0	0.755388	0.523523	0.186926
	4	—	—	—	0.0	−0.596483	0.232846	0.0	−0.823284	−0.200561	0.301623
	5	—	—	—	0.0	0.332190	−0.338997	0.0	0.738992	−0.192022	−0.271324
	6	—	—	—	0.0	—	—	0.0	−0.542027	0.388296	−0.139774
	7	—	—	—	0.0	—	—	0.0	0.279046	−0.288438	0.290791
0.99	0	1.0	1.0	1.0	1.0	1.0	1.0	1.0	1.0	1.0	1.0
	1	−0.058913	−0.059150	−0.005051	−0.059150	−0.008153	−0.003113	−0.059150	−0.009061	−0.006273	−0.002238
	2	—	0.004030	−0.496325	0.004030	−0.490425	−0.498604	0.004030	−0.488174	−0.494330	−0.499278
	3	—	−0.000292	0.421158	−0.000294	0.671808	0.260781	−0.000294	0.743227	0.521041	0.187747
	4	—	—	—	0.000022	−0.590652	0.231879	0.000022	−0.812328	−0.201278	0.300918
	5	—	—	—	−0.000002	0.329316	−0.338562	−0.000002	0.730243	−0.189546	−0.271436
	6	—	—	—	—	—	—	0.0	−0.536067	0.385734	−0.139380
	7	—	—	—	—	—	—	0.0	0.276103	−0.286939	0.290597
0.98	0	1.0	1.0	1.0	1.0	1.0	1.0	1.0	1.0	1.0	1.0
	1	−0.083299	−0.083972	−0.010061	−0.083972	−0.016286	−0.006208	−0.083972	−0.018113	−0.012529	−0.004467
	2	—	0.008118	−0.492707	0.008120	−0.480887	−0.497222	0.008120	−0.476359	−0.488688	−0.498562
	3	—	−0.000829	0.419780	−0.000841	0.663511	0.261386	−0.000841	0.731086	0.518585	0.188566
	4	—	—	—	0.000090	−0.584870	0.230923	0.000090	−0.801398	−0.202003	0.300219
	5	—	—	—	−0.000010	0.326471	−0.338138	−0.000010	0.721521	−0.187087	−0.271549
	6	—	—	—	—	—	—	0.000001	−0.530129	0.383204	−0.138990
	7	—	—	—	—	—	—	0.0	0.273172	−0.285463	0.290408
0.97	0	1.0	1.0	1.0	1.0	1.0	1.0	1.0	1.0	1.0	1.0
	1	−0.101998	−0.103242	−0.015030	−0.103243	−0.024400	−0.009286	−0.103243	−0.027156	−0.018766	−0.006686
	2	—	0.012266	−0.489144	0.012272	−0.471386	−0.495856	0.012272	−0.464558	−0.483074	−0.497851
	3	—	−0.001528	0.418442	−0.001563	0.655267	0.261992	−0.001563	0.718967	0.516155	0.189383
	4	—	—	—	0.000206	−0.579137	0.229979	0.000206	−0.790496	−0.202736	0.299525
	5	—	—	—	−0.000027	0.323656	−0.337726	−0.000029	0.712829	−0.184647	−0.271665
	6	—	—	—	—	—	—	0.000004	−0.524215	0.380706	−0.138604
	7	—	—	—	—	—	—	0.0	0.270234	−0.284011	0.290224
0.96	0	1.0	1.0	1.0	1.0	1.0	1.0	1.0	1.0	1.0	1.0
	1	−0.117753	−0.119677	−0.019958	−0.119679	−0.032494	−0.012345	−0.119679	−0.036190	−0.024986	−0.008896
	2	—	0.016473	−0.485637	0.016488	−0.461925	−0.494504	0.016488	−0.452771	−0.477489	−0.497147
	3	—	−0.002360	0.417145	−0.002433	0.647076	0.262600	−0.002433	0.706871	0.513753	0.190198
	4	—	—	—	0.000372	−0.573456	0.229044	0.000372	−0.779625	−0.203476	0.298838
	5	—	—	—	−0.000056	0.320871	−0.337325	−0.000058	0.704167	−0.182225	−0.271784
	6	—	—	—	—	—	—	0.000009	−0.518326	0.378241	−0.138221
	7	—	—	—	—	—	—	−0.000001	0.267349	−0.282584	0.290045
0.95	0	1.0	1.0	1.0	1.0	1.0	1.0	1.0	1.0	1.0	1.0
	1	−0.131625	−0.134327	−0.024845	−0.134330	−0.040567	−0.015387	−0.134330	−0.045215	−0.031186	−0.011096
	2	—	0.020739	−0.482186	0.020768	−0.452505	−0.493167	0.020760	−0.440999	−0.471932	−0.496447
	3	—	−0.003308	0.415887	−0.003438	0.638943	0.263210	−0.003438	0.694800	0.511378	0.191011
	4	—	—	—	0.000589	−0.567829	0.228121	0.000590	−0.768785	−0.204225	0.298156
	5	—	—	—	−0.000100	0.318118	−0.336935	−0.000104	0.695538	−0.179821	−0.271905
	6	—	—	—	—	—	—	0.000018	−0.512463	0.375810	−0.137841
	7	—	—	—	—	—	—	−0.000003	0.264459	−0.281181	0.289870
0.9	0	1.0	1.0	1.0	1.0	1.0	1.0	1.0	1.0	1.0	1.0
	1	−0.185952	−0.193772	−0.048663	−0.193816	−0.080596	−0.030334	−0.193817	−0.090181	−0.061899	−0.021955
	2	—	0.042941	−0.465758	−0.043187	−0.406071	−0.486694	0.043189	−0.382402	−0.444597	−0.493030
	3	—	−0.009497	0.410192	−0.010296	0.599195	0.266282	−0.010301	0.634878	0.499934	0.195043
	4	—	—	—	0.002531	−0.540573	0.223665	0.002547	−0.715145	−0.208097	0.294835
	5	—	—	—	−0.000594	0.304871	−0.335151	−0.000643	0.652963	0.168089	−0.272550
	6	—	—	—	—	—	—	0.000164	−0.483604	0.364164	−0.135993
	7	—	—	—	—	—	—	−0.000040	0.250254	−0.274550	0.289063

Table 4-7 — $G_n(\nu_i)$ FOR $b_1 = 0.04, 0.08, \frac{1}{3}, \frac{2}{3}$ (Continued)

Data from Ref. 7.

		N = 1	3		5			7			
c	n	i = 1	1	2	1	2	3	1	2	3	4
					$b_1 = 0.08$						
1.0	0	1.0	1.0	1.0	1.0	1.0	1.0	1.0	1.0	1.0	1.0
	1	0.0	0.0	0.0	0.0	0.0	0.0	0.0	0.0	0.0	0.0
	2	—	0.0	−0.5	0.0	−0.5	−0.5	0.0	−0.5	−0.5	−0.5
	3	—	0.0	0.422577	0.0	0.680155	0.260177	0.0	0.755388	0.523523	0.186926
	4	—	—	—	0.0	−0.596483	0.232846	0.0	−0.823284	−0.200561	0.301623
	5	—	—	—	0.0	0.332190	−0.338997	0.0	0.738992	−0.192022	−0.271324
	6	—	—	—	—	—	—	0.0	−0.542027	0.388296	−0.139774
	7	—	—	—	—	—	—	0.0	0.279046	−0.288438	0.290791
0.99	0	1.0	1.0	1.0	1.0	1.0	1.0	1.0	1.0	1.0	1.0
	1	−0.060167	−0.060409	−0.005051	−0.060409	−0.008153	−0.003113	−0.060409	−0.009061	−0.006273	−0.002238
	2	—	0.004028	−0.496477	0.004029	−0.490820	−0.498661	0.004029	−0.488661	−0.494564	−0.499308
	3	—	−0.000286	0.421286	−0.000288	0.672345	0.260811	−0.000288	0.743964	0.521286	0.187758
	4	—	—	—	0.000021	−0.591123	0.231906	0.000021	−0.813131	−0.201372	0.300936
	5	—	—	—	−0.000002	0.329579	−0.338601	−0.000002	0.730964	−0.189635	−0.271452
	6	—	—	—	—	—	—	0.0	−0.536596	0.385916	−0.139389
	7	—	—	—	—	—	—	0.0	0.276375	−0.287073	0.290614
0.98	0	1.0	1.0	1.0	1.0	1.0	1.0	1.0	1.0	1.0	1.0
	1	−0.085052	−0.085739	−0.010061	−0.085739	−0.016286	−0.006208	−0.085739	−0.018113	−0.012529	−0.004467
	2	—	0.008114	−0.493004	0.008115	−0.481666	−0.497336	−0.008115	−0.477324	−0.489150	−0.498621
	3	—	−0.000811	0.420031	−0.000823	0.664572	0.261445	−0.000823	0.732543	0.519068	0.188588
	4	—	—	—	0.000086	−0.585800	0.230976	0.000087	0.802986	−0.202188	0.300254
	5	—	—	—	−0.000009	0.326989	−0.338215	−0.000009	0.722947	−0.187264	−0.271581
	6	—	—	—	—	—	—	0.000001	−0.531175	0.383562	−0.139007
	7	—	—	—	—	—	—	0.0	0.273710	−0.285729	0.290442
0.97	0	1.0	1.0	1.0	1.0	1.0	1.0	1.0	1.0	1.0	1.0
	1	−0.104121	−0.105390	−0.015030	−0.105390	−0.024401	−0.009286	−0.105390	−0.027156	−0.018767	−0.006686
	2	—	0.012255	−0.489582	0.012261	−0.472541	−0.496023	0.012261	−0.465989	−0.483757	−0.497938
	3	—	−0.001495	0.418812	−0.001528	0.656837	0.262079	−0.001528	0.721128	0.516871	0.189416
	4	—	—	—	0.000197	−0.580514	0.230056	0.000197	−0.792851	−0.203010	0.299578
	5	—	—	—	−0.000026	0.324423	−0.337839	−0.000026	0.714943	−0.184909	−0.271712
	6	—	—	—	—	—	—	0.000003	−0.525766	0.381237	−0.138628
	7	—	—	—	—	—	—	0.0	0.271052	−0.284405	0.290274
0.96	0	1.0	1.0	1.0	1.0	1.0	1.0	1.0	1.0	1.0	1.0
	1	−0.120177	−0.122138	−0.019958	−0.122140	−0.032495	−0.012346	−0.122140	−0.036190	−0.024986	−0.008896
	2	—	0.016454	−0.486210	0.016467	−0.463444	−0.494723	0.016467	−0.454657	−0.478387	−0.497260
	3	—	−0.002309	0.417629	−0.002378	0.649143	0.262715	−0.002378	0.709719	0.514694	0.190241
	4	—	—	—	0.000356	−0.575269	0.229146	0.000356	−0.782729	−0.203836	0.298907
	5	—	—	—	−0.000053	0.321880	−0.337474	−0.000055	0.706953	−0.182569	−0.271846
	6	—	—	—	—	—	—	0.000008	−0.520369	0.378939	−0.138253
	7	—	—	—	—	—	—	−0.000001	0.268401	−0.283102	0.290111
0.95	0	1.0	1.0	1.0	1.0	1.0	1.0	1.0	1.0	1.0	1.0
	1	−0.134304	−0.137057	−0.024845	−0.137060	−0.040568	−0.015388	−0.137060	−0.045215	−0.031186	−0.011096
	2	—	0.020709	−0.482889	0.020735	−0.454379	−0.493437	0.020735	−0.443328	−0.473040	−0.496587
	3	—	−0.003238	0.416481	−0.003359	0.641492	0.263351	−0.003359	0.698319	0.512538	0.191063
	4	—	—	—	0.000564	−0.570064	0.228246	0.000564	−0.772620	−0.204669	0.298241
	5	—	—	—	−0.000094	0.319363	−0.337118	−0.000097	0.698980	−0.180246	−0.271982
	6	—	—	—	—	—	—	0.000017	−0.514987	0.376670	−0.137881
	7	—	—	—	—	—	—	0.000003	0.265759	−0.281820	0.289951
0.9	0	1.0	1.0	1.0	1.0	1.0	1.0	1.0	1.0	1.0	1.0
	1	−0.189525	−0.197474	−0.048668	−0.197515	−0.080604	−0.030335	−0.197515	−0.090186	−0.061903	−0.021955
	2	—	0.042824	−0.467030	0.043050	−0.409561	−0.487190	0.043051	−0.386782	−0.446659	−0.493290
	3	—	−0.009294	0.411268	−0.010040	0.603942	0.266541	−0.010044	0.641494	0.502094	0.195141
	4	—	—	—	0.002416	−0.544734	0.223896	0.002429	−0.722353	−0.208925	0.294992
	5	—	—	—	−0.000556	0.307188	−0.335487	−0.000600	0.659432	−0.168880	−0.272691
	6	—	—	—	—	—	—	0.000150	−0.488347	0.365764	−0.136066
	7	—	—	—	—	—	—	−0.000035	0.252696	−0.275738	0.289214

Table 4-7 — $G_n(\nu_i)$ FOR $b_1 = 0.04, 0.08, \frac{1}{3}, \frac{2}{3}$ (Continued)

Data from Ref. 7.

		N = 1	3		5			7			
c	n	i = 1	1	2	1	2	3	1	2	3	4
					$b_1 = \frac{1}{3}$						
1.0	0	1.0	1.0	1.0	1.0	1.0	1.0	1.0	1.0	1.0	1.0
	1	0.0	0.0	0.0	0.0	0.0	0.0	0.0	0.0	0.0	0.0
	2	—	0.0	−0.5	0.0	−0.5	−0.5	0.0	−0.5	−0.5	−0.5
	3	—	0.0	0.422577	0.0	0.680155	0.260177	0.0	0.755388	0.523523	0.186926
	4	—	—	—	0.0	−0.596483	0.232846	0.0	−0.823284	−0.200561	0.301623
	5	—	—	—	0.0	0.332190	−0.338997	0.0	0.738992	−0.192022	−0.271324
	6	—	—	—	—	—	—	0.0	−0.542027	0.388296	−0.139774
	7	—	—	—	—	—	—	0.0	0.279046	−0.288438	0.290791
0.99	0	1.0	1.0	1.0	1.0	1.0	1.0	1.0	1.0	1.0	1.0
	1	−0.070535	−0.070818	−0.005051	−0.070818	−0.008153	−0.003113	−0.070818	−0.009061	−0.006273	−0.002238
	2	—	0.004021	−0.497436	0.004021	−0.493320	−0.499026	0.004021	−0.491750	−0.496045	−0.499496
	3	—	−0.000243	0.422097	−0.000245	0.675746	0.261000	−0.000245	0.748630	0.522836	0.187829
	4	—	—	—	0.000015	−0.594106	0.232076	0.000015	−0.818216	−0.201966	0.301049
	5	—	—	—	−0.000001	0.331240	−0.338848	−0.000001	0.735528	−0.190204	−0.271554
	6	—	—	—	—	—	—	0.0	−0.539943	0.387065	−0.139441
	7	—	—	—	—	—	—	0.0	0.278099	−0.287928	0.290724
0.98	0	1.0	1.0	1.0	1.0	1.0	1.0	1.0	1.0	1.0	1.0
	1	−0.099504	−0.100305	−0.010061	−0.100305	−0.016287	−0.006208	−0.100305	−0.018113	−0.012529	−0.004467
	2	—	0.008083	−0.494888	0.008083	−0.486605	−0.498053	0.008083	−0.483432	−0.492072	−0.498992
	3	—	−0.000691	0.421624	−0.000698	0.671289	0.261818	−0.000698	0.741772	0.522128	0.188727
	4	—	—	—	0.000062	−0.591691	0.231310	0.000062	−0.813043	−0.203360	0.300478
	5	—	—	—	−0.000006	0.330370	−0.338702	−0.000005	0.731974	−0.188386	−0.271783
	6	—	—	—	—	—	—	0.000001	−0.537796	0.385832	−0.139111
	7	—	—	—	—	—	—	0.0	0.277119	−0.287415	0.290658
0.97	0	1.0	1.0	1.0	1.0	1.0	1.0	1.0	1.0	1.0	1.0
	1	−0.121566	−0.123039	−0.015031	−0.123039	−0.024402	−0.009286	−0.123039	−0.027157	−0.018767	−0.006686
	2	—	0.012186	−0.492356	0.012189	−0.479854	−0.497083	0.012189	−0.475048	−0.488084	−0.498488
	3	—	−0.001273	0.421157	−0.001294	0.666785	0.262631	−0.001294	0.734815	0.521401	0.189621
	4	—	—	—	0.000142	−0.589238	0.230549	0.000142	−0.807768	−0.204745	0.299909
	5	—	—	—	−0.000016	0.329281	−0.338557	−0.000016	0.728332	−0.186570	−0.272010
	6	—	—	—	—	—	—	0.000002	−0.535586	0.384596	−0.138782
	7	—	—	—	—	—	—	0.0	0.276108	0.286901	0.290594
0.96	0	1.0	1.0	1.0	1.0	1.0	1.0	1.0	1.0	1.0	1.0
	1	−0.140032	−0.142297	−0.019960	−0.142298	−0.032498	−0.012346	−0.142298	−0.036192	−0.024987	−0.008896
	2	—	0.016332	−0.489840	0.016339	−0.473069	−0.496113	0.016339	−0.466598	−0.484079	−0.497982
	3	—	−0.001968	0.420698	−0.002010	0.662236	0.263438	−0.002010	0.727761	0.520653	0.190511
	4	—	—	—	0.000256	−0.586750	0.229793	0.000256	−0.802391	−0.206120	0.299342
	5	—	—	—	−0.000033	0.328274	−0.338416	−0.000033	0.724601	−0.184755	−0.272238
	6	—	—	—	—	—	—	0.000004	−0.533313	0.383358	−0.138455
	7	—	—	—	—	—	—	−0.000001	0.275065	−0.286385	0.290531
0.95	0	1.0	1.0	1.0	1.0	1.0	1.0	1.0	1.0	1.0	1.0
	1	−0.156174	−0.159346	−0.024850	−0.159348	−0.040574	−0.015388	−0.159348	−0.045219	−0.031190	−0.011096
	2	—	0.020520	−0.487341	0.020534	−0.466252	−0.495146	0.020534	−0.458083	−0.480058	−0.497476
	3	—	−0.002759	0.420245	−0.002834	0.657642	0.264240	−0.002834	0.720609	0.519887	0.191396
	4	—	—	—	0.000405	−0.584227	0.229042	0.000406	−0.796912	−0.207485	0.298777
	5	—	—	—	−0.000058	0.327249	−0.338277	−0.000059	0.720783	−0.182940	0.272464
	6	—	—	—	—	—	—	0.000009	−0.530979	0.382118	−0.138129
	7	—	—	—	—	—	—	−0.000001	0.273991	−0.285867	0.290468
0.9	0	1.0	1.0	1.0	1.0	1.0	1.0	1.0	1.0	1.0	1.0
	1	−0.218218	−0.227219	−0.048701	−0.227244	−0.080652	−0.030341	−0.227244	−0.090213	−0.061927	−0.219566
	2	—	0.042097	−0.475097	0.042217	−0.431701	−0.490334	0.042217	−0.414547	−0.459732	−0.494938
	3	—	−0.007940	0.418092	−0.008396	0.634057	0.268178	−0.008397	0.683435	−0.515786	0.195757
	4	—	—	—	0.001727	−0.571134	0.225358	0.001732	−0.768048	−0.214173	0.295985
	5	—	—	—	−0.000345	0.321886	−0.337618	−0.000365	0.700436	−0.173891	−0.273585
	6	—	—	—	—	—	—	0.000078	−0.518416	0.375902	−0.136526
	7	—	—	—	—	—	—	−0.000016	0.268173	−0.283269	0.290172

Table 4-7 — $G_n(\nu_i)$ FOR $b_1 = 0.04,\ 0.08,\ 1/3,\ 2/3$ (Continued)

Data from Ref. 7.

		N = 1	3		5			7			
c	n	i = 1	1	2	1	2	3	1	2	3	4
					$b_1 = 2/3$						
1.0	0	1.0	1.0	1.0	1.0	1.0	1.0	1.0	1.0	1.0	1.0
	1	0.0	0.0	0.0	0.0	0.0	0.0	0.0	0.0	0.0	0.0
	2	—	0.0	−0.5	0.0	−0.5	−0.5	0.0	−0.5	−0.5	−0.5
	3	—	0.0	0.422577	0.0	0.680155	0.260177	0.0	0.755388	0.523523	0.186926
	4	—	—	—	0.0	−0.596483	0.232846	0.0	−0.823284	−0.200561	0.301623
	5	—	—	—	0.0	0.332190	−0.338997	0.0	0.738922	−0.192022	−0.271324
	6	—	—	—	—	—	—	0.0	−0.542027	0.388296	−0.139774
	7	—	—	—	—	—	—	0.0	0.279046	−0.288438	0.290791
0.99	0	1.0	1.0	1.0	1.0	1.0	1.0	1.0	1.0	1.0	1.0
	1	−0.099015	−0.099411	−0.005051	−0.099411	−0.008153	−0.003113	−0.099411	−0.009061	−0.006274	−0.002238
	2	—	0.004010	−0.493699	0.004010	−0.496610	−0.499506	0.004010	−0.495813	−0.497993	−0.499744
	3	—	−0.000173	0.423165	−0.000173	0.680222	0.261250	−0.000173	0.754769	0.524876	0.187922
	4	—	—	—	0.000008	−0.598031	0.232299	0.000008	−0.824907	−0.202747	0.301199
	5	—	—	—	0.0	0.333426	−0.339173	0.0	0.741534	−0.190952	−0.271689
	6	—	—	—	—	—	—	0.0	−0.544349	0.388578	−0.139517
	7	—	—	—	—	—	—	0.0	0.280367	−0.289051	0.290868
0.98	0	1.0	1.0	1.0	1.0	1.0	1.0	1.0	1.0	1.0	1.0
	1	−0.138677	−0.139786	−0.010061	−0.139786	−0.016287	−0.006209	−0.139786	−0.018113	−0.012530	−0.004467
	2	—	0.008042	−0.497368	0.008043	−0.493103	−0.498998	0.008043	−0.491470	−0.495918	−0.499481
	3	—	−0.000493	0.423720	−0.000496	0.680129	0.262309	−0.000496	0.753915	0.526155	0.188910
	4	—	—	—	0.000032	−0.599443	0.231750	0.000032	−0.826278	−0.204903	0.300773
	5	—	—	—	−0.000002	0.334587	−0.339342	−0.000002	0.743853	−0.189863	−0.272048
	6	—	—	—	—	—	—	0.0	−0.546509	0.388818	−0.139247
	7	—	—	—	—	—	—	0.0	0.281605	−0.289633	0.290943
0.97	0	1.0	1.0	1.0	1.0	1.0	1.0	1.0	1.0	1.0	1.0
	1	−0.168232	−0.170255	−0.015032	−0.170255	−0.024403	−0.009286	−0.170255	−0.027158	−0.018768	−0.006686
	2	—	0.012097	−0.496008	0.012097	−0.489479	−0.498477	0.012097	−0.486970	−0.493777	−0.499210
	3	—	−0.000913	0.424244	−0.000921	0.679878	0.263356	−0.000921	0.752826	0.527362	0.189891
	4	—	—	—	0.000073	−0.600720	0.231198	0.000073	−0.827398	−0.207029	0.300345
	5	—	—	—	−0.000006	0.335676	−0.339502	−0.000006	0.745951	−0.188756	−0.272403
	6	—	—	—	—	—	—	0.0	−0.548509	0.389017	−0.138984
	7	—	—	—	—	—	—	0.0	0.282761	−0.290185	0.291014
0.96	0	1.0	1.0	1.0	1.0	1.0	1.0	1.0	1.0	1.0	1.0
	1	−0.192450	−0.195538	−0.019963	−0.195538	−0.032502	−0.012346	−0.195538	−0.036194	−0.024990	−0.008896
	2	—	0.016174	−0.494620	0.016176	−0.485739	−0.497942	0.016176	−0.482315	−0.491570	−0.498932
	3	—	−0.001418	0.424737	−0.001434	0.679471	0.264390	−0.001434	0.751504	0.528497	0.190866
	4	—	—	—	0.000132	−0.601864	0.230645	0.000132	−0.828267	−0.209125	0.299915
	5	—	—	—	−0.000012	0.336691	−0.339656	−0.000012	0.747827	−0.187631	−0.272753
	6	—	—	—	—	—	—	−0.000001	−0.550348	0.389174	−0.138720
	7	—	—	—	—	—	—	0.0	0.283835	−0.290705	0.291083
0.95	0	1.0	1.0	1.0	1.0	1.0	1.0	1.0	1.0	1.0	1.0
	1	−0.213201	−0.217481	−0.024856	−0.217481	−0.040582	−0.015389	−0.217481	−0.045223	−0.031194	−0.011096
	2	—	0.020276	−0.493204	0.020279	−0.481885	−0.497395	0.020279	−0.477504	−0.489296	−0.498646
	3	—	−0.001998	0.425201	−0.002026	0.678908	0.265411	−0.002026	0.749949	0.529561	0.191833
	4	—	—	—	0.000210	−0.602875	0.230089	0.000210	−0.828887	−0.211191	0.299483
	5	—	—	—	−0.000022	0.337634	−0.339802	−0.000022	0.749483	−0.186487	−0.273099
	6	—	—	—	—	—	—	0.000002	0.552028	0.389291	−0.138456
	7	—	—	—	—	—	—	0.0	0.284827	−0.291195	0.291148
0.90	0	1.0	1.0	1.0	1.0	1.0	1.0	1.0	1.0	1.0	1.0
	1	−0.288675	−0.300326	−0.048742	−0.300336	−0.080708	−0.030348	−0.300336	−0.090245	−0.061958	−0.021959
	2	—	0.041174	−0.485745	0.041210	−0.460918	−0.494474	0.041210	−0.451136	−0.476967	−0.497107
	3	—	−0.005876	0.427098	−0.006056	0.673799	0.270335	−0.006056	0.738705	0.533836	0.196569
	4	—	—	—	0.000922	−0.605975	0.227285	0.000923	−0.828269	−0.221092	0.297293
	5	—	—	—	−0.000140	0.341285	−0.340423	−0.000144	0.754478	−0.180498	−0.274762
	6	—	—	—	—	—	—	0.000023	−0.558046	0.389270	−0.137132
	7	—	—	—	—	—	—	−0.000004	0.288573	−0.293198	0.291433

687863 O - 63 - 18

In Section 4.1.5 integral transport theory is used to obtain formulae applicable to cases where experimental flux plots are available. All authors quoted in this section, with the exception of Stuart and Woodruff,[13] assume that the flux directed into the rod is isotropic and that the neutron flux in the rod is distributed in the shape predicted by diffusion theory.

Stuart and Woodruff[13] calculate the rod blackness for neutron flux directed into the rod to be isotropic or proportional to cos θ. As in Refs. 9, 10, and 14 they find that successive generations quickly forget their initial angular distribution. Initially isotropic sources are calculated exactly through five generations, while those proportional to cos θ are calculated exactly through two generations. Succeeding generations are supposed to have the same source shape as that arising from the last exactly calculated source. In addition, the case is studied where the exit flux has the same functional form as the entrance flux, which is assumed to be that of diffusion theory. In this case, the ratio of the amplitude of the cos θ term to the isotropic term in the entering flux is given by $\beta/(2-\beta)$, where β is the blackness.

4.1.4.1 Integral Transport Theory in Cylinders

Amouyal and Benoist[9,10] give formulas for the thermal utilization of a rod of fissionable or absorbing material (source = 0) of radius a, which is surrounded by a cooling gap of width c – a (which may be 0) and, finally, by an outer annular region of moderator (constant source); the outer radius is denoted by b. The thermal utilization is given by:

$$\frac{1}{f} - 1 = \frac{b^2 - c^2}{a^2} \frac{\Sigma_{c,M}}{\Sigma_{c,U}} \left[G + a\,\Sigma_{c,U} \left(1 - \frac{a}{c}\right)\right] + \kappa_M^2\, b^2\, C + \frac{b^2 - c^2}{c}\,\Sigma_{c,M}\left(\frac{3}{2}\lambda - 1\right)$$

where $\kappa_M^2 = 3\,\Sigma_{t,M}\,\Sigma_{c,M}$

$\Sigma_{t,M}$ = total cross section of moderator

$\Sigma_{c,M}$ = capture cross section of moderator

$\Sigma_{c,U}$ = capture cross section of fissionable material

$\Sigma_{t,U}$ = total cross section of fissionable material

$$C = \frac{1}{2}\left[\frac{b^2/c^2}{(b^2/c^2) - 1} \ln\left(\frac{b}{c}\right) - (3/4) + \frac{1}{4b^2/c^2}\right]$$

λ = a parameter

and

$$G = \frac{\Phi(a)}{\Phi_U}$$

where Φ_U is the average flux in the uranium. Isotropic incident flux is assumed. Three approximations to G in order of increasing accuracy are:

$$G = 1 + \frac{\Sigma_{c,U}}{\Sigma_{t,U}}\, A \left[1 + \alpha\frac{\Sigma_{s,U}}{\Sigma_{t,U}} + \beta\left(\frac{\Sigma_{s,U}}{\Sigma_{t,U}}\right)^2\right] \tag{4-3}$$

$$G = 1 + \frac{\Sigma_{c,U}}{\Sigma_{t,U}}\, B \tag{4-4}$$

$$G = 1 + (1 - \tau)\,\frac{1 - \sqrt{1 - 2\tau(1 - P_c)\,B}}{\tau\,(1 - P_c)} \tag{4-5}$$

where Σ_{sU} is the scattering cross section of the fissionable material; P_c is the collision probability tabulated in Ref. 12; A is defined by:

$$P_c = \frac{A + \eta}{A + \eta - 1}$$

$$\eta = a\,\Sigma_{t,U}$$

$$\tau = \Sigma_{s,U}/\Sigma_{t,U}$$

$$B = \frac{1}{1 - P_c}\left\{(a\Sigma_{t,U})^2\left[I_0\,(a\Sigma_{t,U})\,K_0\,(a\Sigma_{t,U}) + I_1\,(a\Sigma_{t,U})\,K_1\,(a\Sigma_{t,U})\right]\right.$$

$$\left. + a\Sigma_{t,U}\,I_0\,(a\Sigma_{t,U})\,K_1\,(a\Sigma_{t,U}) - a\Sigma_{t,U}\right\} - 1$$

Values of λ are given in Table 4-8; A in Table 4-9; B in Table 4-10; and α, β in Fig. 4-1. A comparison of values of G calculated from Eqs. (4-3) and (4-5) with experimental results for various rods is given in Table 4-11.

McLennan[12] has published a number of formulas and auxiliary data for a cosine angular, and a cosine squared angular incident distribution in a variety of cylindrical configurations. The source is zero in the fuel or absorber, and constant in the moderator. The "total current matching" boundary conditions are recommended.

Table 4-8 — VALUES OF λ

$c\Sigma_{t,M}$	λ	$c\Sigma_{t,M}$	λ
0.0	1.32	2.5	0.815
0.5	1.04	3.0	0.80
1.0	0.94	3.5	0.78
1.5	0.88	4.0	0.775
2.0	0.846	—	—

Table 4-9 — VALUES OF $A = (P_c/1 - P_c) - a\Sigma_{t,U}$

Data from Ref. 9.

$a\Sigma_{t,U}$	A	δ	$a\Sigma_{t,U}$	A	δ	$a\Sigma_{t,U}$	A	δ	$a\Sigma_{t,U}$	A	δ	$a\Sigma_{t,U}$	A	δ	$a\Sigma_{t,U}$	A	δ
0.00	0.00000	628	1.00	0.4561	131	2.00	1.2292	174	3.00	2.1402	187	4.00	3.0998	195	5.00	4.078	19
0.02	0.00628	599	.02	0.4692	131	.02	1.2466	172	.02	2.1589	188	.02	3.1193	193	.02	4.097	20
.04	0.01227	587	.04	0.4823	133	.04	1.2638	176	.04	2.1777	189	.04	3.1386	197	.04	4.117	20
.06	0.01814	587	.06	0.4956	134	.06	1.2814	175	.06	2.1966	190	.06	3.1583	193	.06	4.137	20
.08	0.02401	591	.08	0.5090	135	.08	1.2989	175	.08	2.2156	191	.08	3.1776	191	.08	4.157	18
0.10	0.02992	598	1.10	0.5225	137	2.10	1.3164	175	3.10	2.2347	188	4.10	3.1967	194	5.10	4.175	21
.12	0.03590	608	.12	0.5362	138	.12	1.3339	177	.12	2.2535	188	.12	3.2161	198	.12	4.196	19
.14	0.04198	620	.14	0.5500	138	.14	1.3516	176	.14	2.2723	193	.14	3.2359	195	.14	4.215	21
.16	0.04818	633	.16	0.5638	141	.16	1.3692	176	.16	2.2916	190	.16	3.2554	198	.16	4.236	19
.18	0.05451	648	.18	0.5779	141	.18	1.3868	177	.18	2.3106	189	.18	3.2752	195	.18	4.255	20
0.20	0.06099	661	1.20	0.5920	141	2.20	1.4045	178	3.20	2.3295	191	4.20	3.2947	192	5.20	4.275	19
.22	0.06760	677	.22	0.6061	144	.22	1.4223	178	.22	2.3486	190	.22	3.3139	195	.22	4.294	20
.24	0.07437	694	.24	0.6205	144	.24	1.4401	180	.24	2.3676	191	.24	3.3334	191	.24	4.314	19
.26	0.08131	711	.26	0.6349	146	.26	1.4581	179	.26	2.3867	191	.26	3.3525	203	.26	4.333	20
.28	0.08842	727	.28	0.6495	146	.28	1.4760	178	.28	2.4058	191	.28	3.3728	191	.28	4.353	21
0.30	0.09569	74	1.30	0.6641	148	2.30	1.4938	181	3.30	2.4249	192	4.30	3.3919	194	5.30	4.374	18
.32	0.1031	77	.32	0.6789	149	.32	1.5119	178	.32	2.4441	191	.32	3.4113	191	.32	4.392	21
.34	0.1108	77	.34	0.6938	149	.34	1.5297	180	.34	2.4632	191	.34	3.4304	202	.34	4.413	19
.36	0.1185	80	.36	0.7087	151	.36	1.5477	181	.36	2.4823	191	.36	3.4506	197	.36	4.432	20
.38	0.1265	81	.38	0.7238	151	.38	1.5658	183	.38	2.5014	190	.38	3.4703	194	.38	4.452	20
0.40	0.1346	84	1.40	0.7389	152	2.40	1.5841	180	3.40	2.5204	195	4.40	3.4897	197	5.40	4.472	19
.42	0.1430	84	.42	0.7541	153	.42	1.6021	184	.42	2.5399	190	.42	3.5094	192	.42	4.491	20
.44	0.1514	87	.44	0.7694	155	.44	1.6205	182	.44	2.5589	194	.44	3.5286	196	.44	4.511	20
.46	0.1601	89	.46	0.7849	155	.46	1.6387	179	.46	2.5783	188	.46	3.5482	199	.46	4.531	19
.48	0.1690	90	.48	0.8004	156	.48	1.6566	186	.48	2.5971	193	.48	3.5681	195	.48	4.550	20
0.50	0.1780	92	1.50	0.8160	156	2.50	1.6752	180	3.50	2.6164	192	4.50	3.5876	198	5.50	4.570	20
.52	0.1872	93	.52	0.8316	158	.52	1.6932	183	.52	2.6356	192	.52	3.6074	193	.52	4.590	20
.54	0.1965	96	.54	0.8474	158	.54	1.7115	184	.54	2.6548	195	.54	3.6267	197	.54	4.610	20
.56	0.2061	97	.56	0.8632	159	.56	1.7299	186	.56	2.6743	190	.56	3.6464	192	.56	4.630	20
.58	0.2158	98	.58	0.8791	161	.58	1.7485	183	.58	2.6933	193	.58	3.6656	195	.58	4.650	19
0.60	0.2256	101	1.60	0.8952	160	2.60	1.7668	186	3.60	2.7126	193	4.60	3.6851	198	5.60	4.669	19
.62	0.2357	102	.62	0.9112	161	.62	1.7854	183	.62	2.7319	196	.62	3.7049	193	.62	4.688	19
.64	0.2459	104	.64	0.9273	163	.64	1.8037	185	.64	2.7515	190	.64	3.7242	196	.64	4.708	20
.66	0.2563	105	.66	0.9436	162	.66	1.8222	184	.66	2.7705	194	.66	3.7438	200	.66	4.728	20
.68	0.2668	107	.68	0.9598	164	.68	1.8406	187	.68	2.7899	193	.68	3.7638	194	.68	4.749	21
0.70	0.2775	109	1.70	0.9762	164	2.70	1.8593	186	3.70	2.8092	191	4.70	3.7832	197	5.70	4.768	19
.72	0.2884	110	.72	0.9926	165	.72	1.8779	184	.72	2.8283	195	.72	3.8029	192	.72	4.787	19
.74	0.2994	111	.74	1.0091	166	.74	1.8963	187	.74	2.8478	194	.74	3.8221	194	.74	4.807	20
.76	0.3105	114	.76	1.0257	166	.76	1.9150	186	.76	2.8672	192	.76	3.8415	198	.76	4.826	19
.78	0.3219	115	.78	1.0423	168	.78	1.9336	188	.78	2.8864	195	.78	3.8613	202	.78	4.847	21
0.80	0.3334	116	1.80	1.0591	166	2.80	1.9524	187	3.80	2.9059	194	4.80	3.8815	195	5.80	4.867	20
.82	0.3450	118	.82	1.0757	170	.82	1.9711	188	.82	2.9253	192	.82	3.9010	199	.82	4.885	18
.84	0.3568	119	.84	1.0927	168	.84	1.9899	186	.84	2.9445	196	.84	3.9209	192	.84	4.907	22
.86	0.3687	120	.86	1.1095	169	.86	2.0085	185	.86	2.9641	194	.86	3.9401	195	.86	4.926	19
.88	0.3807	123	.88	1.1264	171	.88	2.0270	190	.88	2.9835	191	.88	3.9596	199	.88	4.946	20
0.90	0.3930	124	1.90	1.1435	170	2.90	2.0460	187	3.90	3.0026	196	4.90	3.9795	202	5.90	4.965	19
.92	0.4054	124	.92	1.1605	171	.92	2.0647	190	.92	3.0222	193	.92	3.9997	195	.92	4.985	20
.94	0.4178	127	.94	1.1776	171	.94	2.0837	187	.94	3.0415	197	.94	4.0192	198	.94	5.005	20
.96	0.4305	127	.96	1.1947	173	.96	2.1024	189	.96	3.0612	194	.96	4.0390	191	.96	5.025	20
.98	0.4432	129	.98	1.2120	172	.98	2.1213	189	.98	3.0806	192	.98	4.0581	20	.98	5.045	19
1.00	0.4561		2.00	1.2292		3.00	2.1402		4.00	3.0998		5.00	4.078		6.00	5.064	

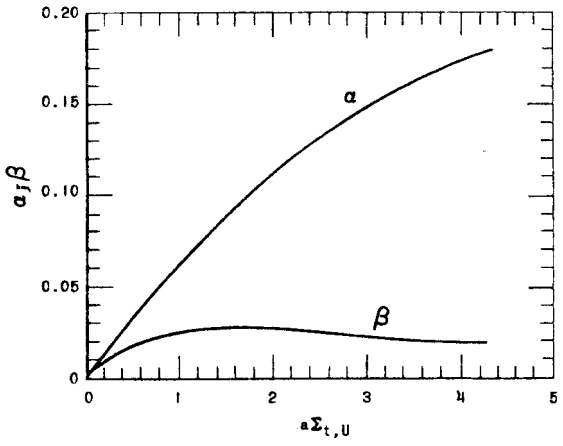

Fig. 4-1—Values of α and β. *Reproduced from Ref. 9.*

Table 4-10—VALUES OF B AS A FUNCTION OF $a\Sigma_{t,U}$

Data from Ref. 9.

$a\Sigma_{t,U}$	B	δ	$a\Sigma_{t,U}$	B	δ	$a\Sigma_{t,U}$	B	δ	$a\Sigma_{t,U}$	B	δ	$a\Sigma_{t,U}$	B	δ	$a\Sigma_{t,U}$	B	δ
0.00	0.00000	678	1.00	0.5603	148	2.00	1.3941	181	3.00	2.3327	188	4.00	3.306	20	5.00	4.293	20
.02	0.00678	704	.02	0.5751	148	.02	1.4122	179	.02	2.3515	198	.02	3.326	20	.02	4.313	20
.04	0.01382	726	.04	0.5899	150	.04	1.4301	183	.04	2.3713	192	.04	3.346	20	.04	4.333	19
.06	0.02108	748	.06	0.6049	151	.06	1.4484	186	.06	2.3905	192	.06	3.366	19	.06	4.352	20
.08	0.02856	770	.08	0.6200	151	.08	1.4670	180	.08	2.4097	194	.08	3.385	20	.08	4.372	20
0.10	0.03626	790	1.10	0.6351	153	2.10	1.4850	186	3.10	2.4291	192	4.10	3.405	19	5.10	4.392	20
.12	0.04416	813	.12	0.6504	154	.12	1.5036	179	.12	2.4483	192	.12	3.424	20	.12	4.412	19
.14	0.05229	833	.14	0.6658	154	.14	1.5215	189	.14	2.4675	195	.14	3.444	20	.14	4.431	21
.16	0.06062	852	.16	0.6812	156	.16	1.5404	181	.16	2.4870	191	.16	3.464	20	.16	4.452	20
.18	0.06914	873	.18	0.6968	156	.18	1.5585	184	.18	2.5061	197	.18	3.484	19	.18	4.472	19
0.20	0.07787	891	1.20	0.7124	157	2.20	1.5769	184	3.20	2.5258	193	4.20	3.503	20	5.20	4.491	20
.22	0.08678	910	.22	0.7281	158	.22	1.5953	188	.22	2.5451	195	.22	3.523	19	.22	4.511	20
.24	0.09588	93	.24	0.7439	159	.24	1.6141	186	.24	2.5646	191	.24	3.542	20	.24	4.531	19
.26	0.1052	95	.26	0.7598	159	.26	1.6327	180	.26	2.5837	194	.26	3.562	20	.26	4.550	20
.28	0.1147	97	.28	0.7757	161	.28	1.6507	187	.28	2.6031	197	.28	3.582	19	.28	4.570	20
0.30	0.1244	98	1.30	0.7918	161	2.30	1.6694	185	3.30	2.6228	192	4.30	3.601	20	5.30	4.590	20
.32	0.1342	100	.32	0.8079	163	.32	1.6879	187	.32	2.6420	198	.32	3.621	20	.32	4.610	20
.34	0.1442	102	.34	0.8242	163	.34	1.7066	184	.34	2.6618	190	.34	3.641	20	.34	4.630	20
.36	0.1544	104	.36	0.8405	164	.36	1.7250	188	.36	2.6808	190	.36	3.661	19	.36	4.650	19
.38	0.1648	106	.38	0.8569	165	.38	1.7438	188	.38	2.6998	200	.38	3.680	20	.38	4.669	20
0.40	0.1754	107	1.40	0.8734	163	2.40	1.7626	186	3.40	2.7198	205	4.40	3.700	20	5.40	4.689	20
.42	0.1861	109	.42	0.8897	166	.42	1.7812	187	.42	2.7403	182	.42	3.720	20	.42	4.709	20
.44	0.1970	110	.44	0.9063	170	.44	1.7999	191	.44	2.7585	198	.44	3.740	19	.44	4.729	20
.46	0.2080	112	.46	0.9233	164	.46	1.8190	184	.46	2.7783	197	.46	3.759	20	.46	4.749	20
.48	0.2192	114	.48	0.9397	169	.48	1.8374	191	.48	2.7980	191	.48	3.779	20	.48	4.769	20
0.50	0.2306	115	1.50	0.9566	167	2.50	1.8565	185	3.50	2.8171	185	4.50	3.799	20	5.50	4.789	19
.52	0.2421	117	.52	0.9733	170	.52	1.8750	189	.52	2.8356	207	.52	3.819	19	.52	4.808	20
.54	0.2538	119	.54	0.9903	171	.54	1.8939	189	.54	2.8563	191	.54	3.838	20	.54	4.828	20
.56	0.2657	119	.56	1.0074	169	.56	1.9128	197	.56	2.8754	202	.56	3.858	20	.56	4.848	20
.58	0.2776	122	.58	1.0243	170	.58	1.9325	182	.58	2.8956	188	.58	3.878	19	.58	4.868	20
0.60	0.2898	122	1.60	1.0413	172	2.60	1.9507	191	3.60	2.9144	191	4.60	3.897	20	5.60	4.888	19
.62	0.3020	125	.62	1.0585	172	.62	1.9698	187	.62	2.9335	209	.62	3.917	20	.62	4.907	20
.64	0.3145	125	.64	1.0757	174	.64	1.9885	191	.64	2.9544	189	.64	3.937	20	.64	4.927	20
.66	0.3270	127	.66	1.0931	172	.66	1.0076	186	.66	2.9733	192	.66	3.957	20	.66	4.947	20
.68	0.3397	129	.68	1.1103	174	.68	2.0262	190	.68	2.9925	200	.68	3.977	19	.68	4.967	20
0.70	0.3526	130	1.70	1.1277	175	2.70	2.0452	196	3.70	3.0125	197	4.70	3.996	20	5.70	4.987	20
.72	0.3656	131	.72	1.1452	175	.72	2.0648	189	.72	3.0322	190	.72	4.016	20	.72	5.007	20
.74	0.3787	132	.74	1.1627	176	.74	2.0837	194	.74	3.0512	195	.74	4.036	19	.74	5.027	19
.76	0.3919	134	.76	1.1803	175	.76	2.1031	186	.76	3.0707	192	.76	4.055	20	.76	5.046	20
.78	0.4053	135	.78	1.1978	175	.78	2.1217	193	.78	3.0899	201	.78	4.075	20	.78	5.066	21
0.80	0.4188	136	1.80	1.2153	177	2.80	2.1410	188	3.80	3.1100	196	4.80	4.095	20	5.80	5.087	19
.82	0.4324	138	.82	1.2330	177	.82	2.1598	192	.82	3.1296	204	.82	4.115	20	.82	5.106	20
.84	0.4462	138	.84	1.2507	179	.84	2.1790	193	.84	3.1500	199	.84	4.135	19	.84	5.126	20
.86	0.4600	140	.86	1.2686	182	.86	2.1983	190	.86	3.1699	204	.86	4.154	20	.86	5.146	20
.88	0.4740	141	.88	1.2868	177	.88	2.2173	189	.88	3.1903	180	.88	4.174	20	.88	5.166	20
0.90	0.4881	142	1.90	1.3045	176	2.90	2.2362	199	3.90	3.2083	196	4.90	4.194	20	5.90	5.186	19
.92	0.5023	143	.92	1.3221	180	.92	2.2561	188	.92	3.2279	199	.92	4.214	20	.92	5.205	20
.94	0.5166	145	.94	1.3401	181	.94	2.2749	196	.94	3.2478	195	.94	4.234	20	.94	5.225	20
.96	0.5311	146	.96	1.3582	182	.96	2.2945	190	.96	3.2673	196	.96	4.254	19	.96	5.245	20
.98	0.5457	146	.98	1.3764	177	.98	2.3135	192	.98	3.2869	20	.98	4.273	20	.98	5.265	20
1.00	0.5603		2.00	1.3941		3.00	2.3327		4.00	3.306		5.00	4.293		6.00	5.285	

The formulae and auxiliary data are reproduced in Tables 4-12 through 4-16, and Figs. 4-2 and 4-3. The nomenclature used is defined as follows:

R = fuel rod radius (no void channel)
t = transmission factor
$\Phi_U(r)$ = total flux at a point $r < R$
$\bar{\Phi}_U(r)$ = average total flux in fuel
$\Sigma = \Sigma_t$ = total cross section
Σ_s = scattering cross section
N = normalization: two choices are available, depending on whether the boundary condition preserves flux or total current
R_1 = fuel rod radius (when void is present)
$g(\sigma)$, $h(\sigma,\beta)$, $g_2(\sigma)$, $h_2(\sigma,\beta)$ are tabulated functions
N.B. : when a void channel is present, R is the *inner* radius of the moderator shell
$\bar{\Phi}_M(R)$ = flux in moderator computed by diffusion theory
S = source density in moderator (except in the case of a fuel shell in the center of a void annulus)

Table 4-11 — COMPARISON OF CALCULATED WITH EXPERIMENTAL VALUES OF G FOR URANIUM RODS

Data from Ref. 10.

U density, gm/cm^3:	18.80		18.88		18.83	
Enrichment (atom ratio):	0.4962×10^{-2}		0.7205×10^{-2}		0.9124×10^{-2}	
$\Sigma_{c,U}$, cm^{-1}:	0.2557		0.3200		0.3763	
Radius, cm:	1.27	2.54	0.952	1.27	1.59	1.27
P_1 approximation	1.098	1.358	1.076	1.133	1.202	1.166
Eq. (4-3)	1.137	1.369	1.120	1.178	1.245	1.216
Eq. (4-5)	1.143	1.394	1.123	1.185	1.256	1.225
Experimental	1.162 ± 0.012	1.420 ± 0.014	1.133 ± 0.011	1.190 ± 0.012	1.290 ± 0.013	1.238 ± 0.012

Note: Rods in an effectively infinite bath of D_2O.

Table 4-12 — CELL CALCULATION FORMULAS FOR HOMOGENEOUS FUEL CYLINDER (COSINE ANGULAR ENTRANCE DISTRIBUTION)

Symbol	Formula for Calculation
t	$1 - \dfrac{(1-\alpha)\ g(\sigma)}{1-\alpha[1-(1/2\sigma)\ g(\sigma)]}$, $\quad \alpha = \Sigma_s/\Sigma_t;\ \sigma = \Sigma_t R$
$\Phi_U(r)$	$N\left\{4h(\sigma,\beta) + \dfrac{2\alpha}{\sigma}\ g(\sigma)\ \dfrac{1-h(\sigma,\beta)}{1-\alpha[1-(1/2\sigma)\ g(\sigma)]}\right\}$, $\quad \beta = r/R$
$\bar{\Phi}_U$	$N\left\{\dfrac{(2/\sigma)\ g(\sigma)}{1-\alpha[1-(1/2\sigma)\ g(\sigma)]}\right\}$
N	$\dfrac{AK_0(\mu R) + B\ I_0(\mu R) + (S/\Sigma_{a,M})}{\dfrac{(2\alpha/\sigma)\ g(\sigma) + 4(1-\alpha)\ h(\sigma,1)}{1-\alpha[1-(1/2\sigma)\ g(\sigma)]}}$, Matched Fluxes $\dfrac{\Phi_M(R)}{4} + \dfrac{\lambda_{tr,M}}{6}\dfrac{\partial\Phi_M(R)}{\partial r}$, Matched Total Currents
$g(\sigma)$	$\dfrac{4}{3}\sigma^2\left\{I_0(\sigma)K_1(\sigma) - I_1(\sigma)K_0(\sigma) + \dfrac{I_1(\sigma)K_1(\sigma)}{\sigma} + 2\sigma[I_0(\sigma)K_0(\sigma) + I_1(\sigma)K_1(\sigma)] - 2\right\}$ Plotted in Fig. 4-3
$h(\sigma,\beta)$	$\sigma\int_\sigma^\beta \dfrac{dt}{t}\ I_0(\beta t)\ K_1(t)$ Numerical values given in Fig. 4-2, and Table 4-16.

Table 4-13—CELL CALCULATION FORMULAS FOR HOMOGENEOUS FUEL CYLINDER (COSINE SQUARED ANGULAR ENTRANCE DISTRIBUTION)[a]

Symbol	Formula for Calculation
t	$1 - \frac{(1-\alpha)\ g_2(\sigma)}{1-\alpha[1-(1/2\sigma)\ g(\sigma)]}$, $\alpha = \Sigma_s/\Sigma_t$; $\sigma = \Sigma_t R$
$\Phi_U(r)$	$N\left[4h_2(\sigma,\beta) + \frac{2\alpha}{\sigma}\ g_2(\sigma)\ \frac{1-h(\sigma,\beta)}{1-\alpha[1-(1/2\sigma)\ g(\sigma)]}\right]$, $\beta = r/R$
$\bar{\Phi}_U$	$N\left[\frac{(2/\sigma)\ g_2(\sigma)}{1-\alpha[1-(1/2\sigma)\ g(\sigma)]}\right]$
N	$\frac{AK_0(\mu R) + BI_0(\mu R) + (S/\Sigma_{a,M})}{4h_2(\sigma,1) + \frac{2\alpha}{\sigma}\ g_2(\sigma)\ \frac{1-h(\sigma,1)}{1-\alpha[1-(1/2\sigma)\ g(\sigma)]}}$, Matched Fluxes $\frac{\Phi_M(R)}{4} + \frac{\lambda_{tr,M}}{6}\ \frac{\partial\Phi_M(R)}{\partial r}$, Matched Total Currents
$g_2(\sigma)$	$\frac{\sigma}{30}\left\{124 - \frac{32}{\sigma} - \sigma[109\ I_0(\sigma)K_0(\sigma) + 124\ I_1(\sigma)K_1(\sigma) + 15\ I_2(\sigma)K_2(\sigma)]\right.$ $\left. - \frac{8}{\sigma}[I_1(\sigma)K_1(\sigma) - 3\ I_2(\sigma)K_2(\sigma)] - \frac{30}{\sigma^2}\ I_2(\sigma)K_1(\sigma) + 154\ I_1(\sigma)K_0(\sigma)\right\}$ $g_2(\sigma)$ has not been calculated as a function of σ.
$h_2(\sigma,\beta)$	$\frac{3}{2}\int_\sigma^a \left\{\left(t - \frac{\sigma^2}{t}\right) 2\ K_1(t)I_0(\beta t) - \beta[K_2(t) + K_0(t)]\ I_1(\beta t)\right\} dt$ The numerical integration of $h_2(\sigma,\beta)$ has not been carried out.
$g(\sigma)$; $h(\sigma,\beta)$	As defined in Table 4-12.

[a]Note that if the detailed pattern of flux in the fuel element is desired, $h_2(\sigma,\beta)$ must be calculated by a numerical integration. Using the "flux matching" boundary condition, one can calculate Φ_M/Φ_U by calculating $h_2(\sigma,1)$ without getting into the tedious work involved in finding $h_2(\sigma,\beta)$. Note further that if the "total current matching" boundary conditions are used, $\bar{\Phi}_M/\bar{\Phi}_U$ can be calculated from the formulas that are given, and no numerical integrations need to be carried out.

Table 4-14—CELL CALCULATION FORMULAS FOR THE HOMOGENEOUS FUEL CYLINDER IN THE CENTER OF A VOID ANNULUS (COSINE ANGULAR ENTRANCE DISTRIBUTION)

Symbol	Formula for Calculation
t	$1 - \frac{R_1}{R}\left\{\frac{(1-\alpha)\ g(\sigma_1)}{1-\alpha\ [1-(1/2\sigma_1)\ g(\sigma_1)]}\right\}$, $\alpha = \Sigma_s/\Sigma_t$; $\sigma_1 = \Sigma R_1$
$\Phi_U(r)$	$N\left[4h(\sigma_1,\beta_1) + \frac{2\alpha}{\sigma_1}\ g(\sigma_1)\ \frac{1-h(\sigma_1,\beta_1)}{1-\alpha[1-(1/2\sigma_1)\ g(\sigma_1)]}\right]$, $\beta_1 = r/R_1$
$\bar{\Phi}_U$	$N\left\{\frac{(2/\sigma_1)\ g(\sigma_1)}{1-\alpha[1-(1/2\sigma_1)\ g(\sigma_1)]}\right\}$
N	$\frac{\Phi_M(R)}{4} + \frac{\lambda_{tr,M}}{6}\ \frac{\partial\Phi_M(R)}{\partial r}$

The functions $g(\sigma_1)$ and $h(\sigma_1,\beta_1)$ are as defined in Table 4-12.

Table 4-15—CELL CALCULATION FORMULAS FOR THE CYLINDRICAL SHELL OF FUEL IN THE CENTER OF A VOID ANNULUS (COSINE ANGULAR ENTRANCE DISTRIBUTION)

Symbol	Formula for Calculation
t	$1-\frac{R_1}{R}(1-\alpha)\,S\,\frac{\bar{k}(S)}{1-\alpha\,\bar{f}(S)}$, $\quad \alpha=\Sigma_s/\Sigma_t;\ S=\Sigma\epsilon$
$\Phi_U(r)$	$N\left[k(S,\eta)+\alpha\,\frac{\bar{k}(S)\,f(S,\eta)}{1-\alpha\,\bar{f}(S)}\right]$, $\quad \eta=\frac{1}{\epsilon}(r-R_1)$
$\bar{\Phi}_U$	$N\left[\frac{\bar{k}(S)}{1-\alpha\,\bar{f}(S)}\right]$
$k(S,\eta)$	$2\{2\,e^{-S}\cosh S\eta - S(1-\eta)\,E_1[S(1-\eta)] - S(1+\eta)\,E_1[S(1+\eta)]\}$, $\quad E_1(x)=\int_x^\infty \frac{e^{-y}}{y}dy$
$\bar{k}(S)$	$\frac{1}{S}\left[1+(2S-1)\,e^{-2S}-4S^2\,E_1(2S)\right]$
$f(S,\eta)$	$\frac{1}{2}\left\{S(1+\eta)\,E_1[S(1+\eta)] - S\eta\,E_1(S\eta) + e^{-S\eta}(1-e^{-S})\right\}$
$\bar{f}(S)$	$\frac{1}{2S}\left[\frac{1}{2}+(S-1)\,e^{-S}-\frac{1}{2}(2S-1)\,e^{-2S}+2S^2E_1(2S)-S^2E_1(S)\right]$
N	$\frac{\Phi_M(R)}{4}+\frac{\lambda_{tr}}{6}\frac{\partial\Phi_M(R)}{\partial r}$

In the case of a cylindrical fuel shell in a central void annulus:

R_1 = inner radius of fuel shell
R_2 = outer radius of fuel shell
$\epsilon = R_2 - R_1$
$\eta = r/\epsilon$, $R_1 \le r \le R_2$
$h,k,\bar{k},f,\bar{f}$ = auxiliary functions
μ^{-1} = diffusion length in moderator

Table 4-16—$h(\sigma,\beta) = \sigma\int_\sigma^\beta K_1(t)\,I_0(\beta t)\,\frac{dt}{t}$

σ	β = 0.0	0.1	0.2	0.3	0.4	0.5	0.6	0.7	0.8	0.9	1.0
0.0	1.000	1.000	1.000	1.000	1.000	1.000	1.000	1.000	1.000	1.000	1.000
0.5	0.5064	0.5078	0.5120	0.5191	0.5295	0.5436	0.5619	0.5856	0.6166	0.6591	0.7334
1.0	0.2736	0.2755	0.2812	0.2910	0.3055	0.3253	0.3519	0.3872	0.4351	0.5041	0.6353
1.4	0.1705	0.1723	0.1782	0.1881	0.2032	0.2243	0.2529	0.2920	0.3470	0.4295	0.5968
1.6	0.1352	0.1370	0.1425	0.1524	0.1671	0.1879	0.2168	0.2565	0.3137	0.4009	0.5841
1.8	0.1074	0.1091	0.1145	0.1238	0.1381	0.1583	0.1868	0.2268	0.2852	0.3764	0.5741
2.0	0.0854	0.0870	0.0922	0.1010	0.1146	0.1340	0.1618	0.2016	0.2606	0.3548	0.5661
2.2	0.0682	0.0696	0.0743	0.0826	0.0953	0.1140	0.1410	0.1800	0.2376	0.3359	0.5596
2.4	0.0544	0.0557	0.0600	0.0676	0.0797	0.0973	0.0232	0.1614	0.2202	0.3187	0.5543
2.6	0.0435	0.0447	0.0487	0.0556	0.0668	0.0832	0.1081	0.1450	0.2033	0.3032	0.5498
3.0	0.0272	0.0281	0.0314	0.0372	0.0466	0.0611	0.0832	0.1177	0.1744	0.2757	0.5428
3.5	0.0161	0.0167	0.0190	0.0236	0.0390	0.0429	0.0621	0.0928	0.1466	0.2479	0.5364
4.0	0.0072	0.0077	0.0096	0.0127	0.0184	0.0285	0.0446	0.0719	0.1222	0.2224	0.5317

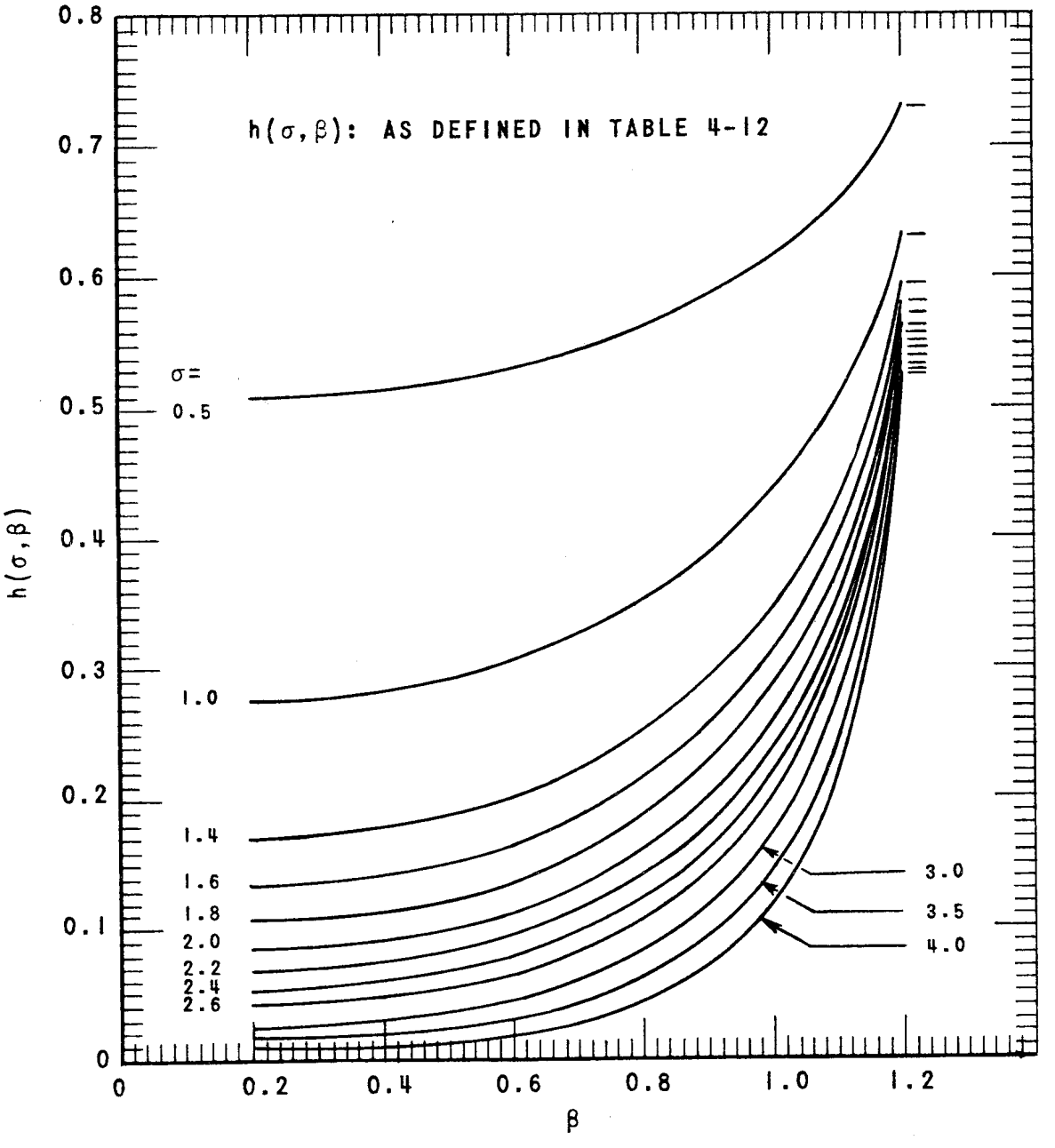

Fig. 4-2—Curves of the function $h(\sigma,\beta)$. *Reproduced from Ref. 12.*

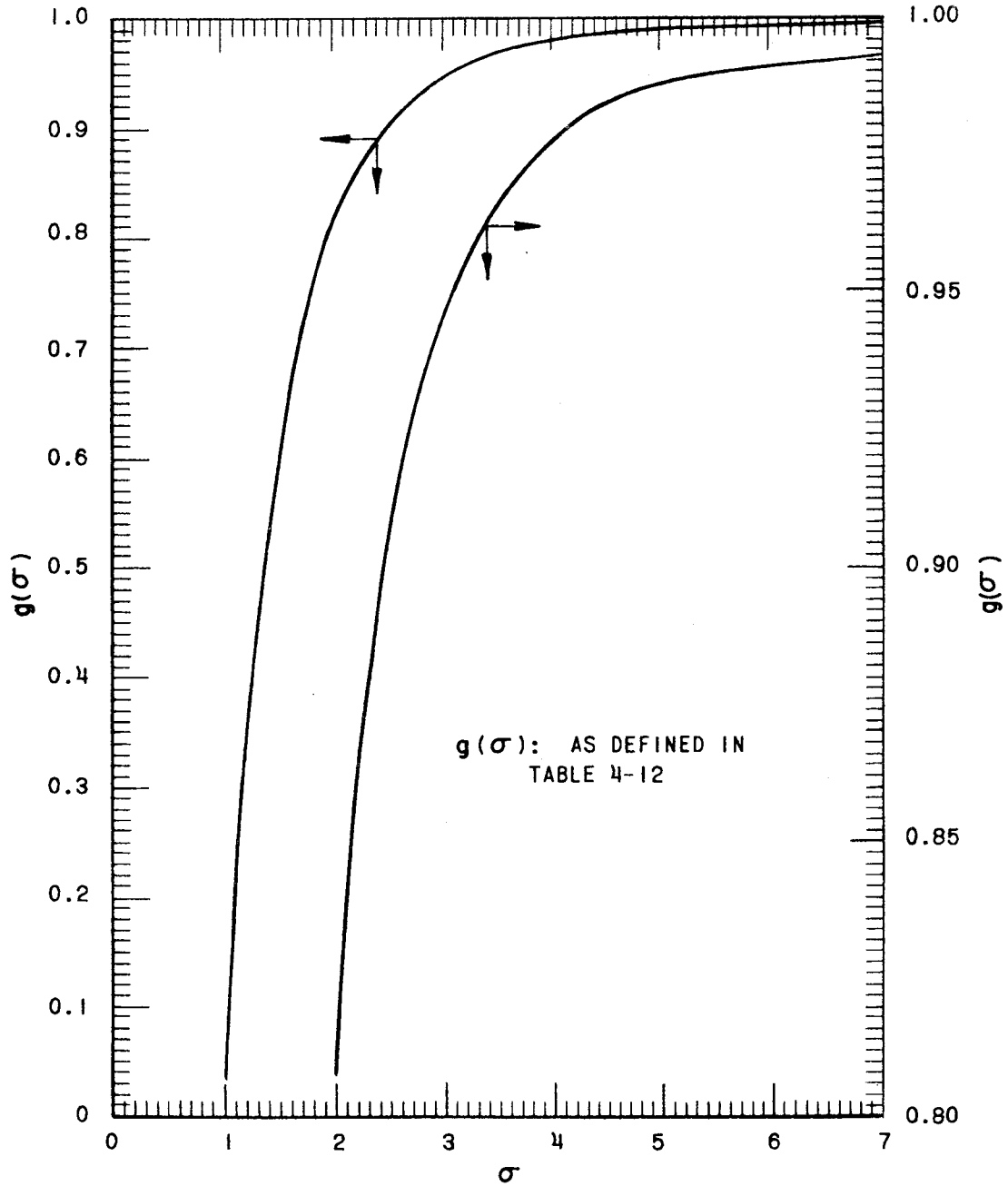

Fig. 4-3—Curves of the function g(σ). *Reproduced from Ref. 12.*

4.1.4.2 Integral Transport Theory in Slab Geometry.[11]

In slab geometry let:

$\overline{\phi}_M$ = average value of flux in the moderator
$\overline{\phi}_U$ = average value of flux in the fuel
ϕ_a = value of the flux at the interface
Σ_c = macroscopic cross section for capture
Σ_s = macroscopic cross section for scattering
Σ_{tr} = macroscopic cross section for transport
Σ_t = total macroscopic cross section
a = half-thickness of fuel region
b = half-thickness of moderator region

With the assumption of isotropic incident flux, and neutron balance, the following formulae are obtained:

$$G = \phi_a/\overline{\phi}_0 = 1 + \frac{\Sigma_{c,U}}{\Sigma_{t,U}} A^*$$

or, more accurately,

$$G = 1 + \frac{\Sigma_{c,U}}{\Sigma_{t,U}} A^* \left[1 + \alpha^* \frac{\Sigma_{s,U}}{\Sigma_{t,U}} + \beta^* \left(\frac{\Sigma_{s,U}}{\Sigma_{t,U}}\right)^2\right]$$

$$\overline{\phi}_M/\overline{\phi}_U = G + a\Sigma_{c,U}[\Sigma_{tr,M}(b - a) + 0.13]$$

Then the thermal utilization, f, is found from

$$\frac{1}{f} = 1 + \frac{(b - a)\,\Sigma_{c,M}}{a\Sigma_{c,U}} \frac{\overline{\phi}_M}{\overline{\phi}_U}$$

The function A^* is given in Table 4-17; and α^* and β^* are plotted in Fig. 4-4.

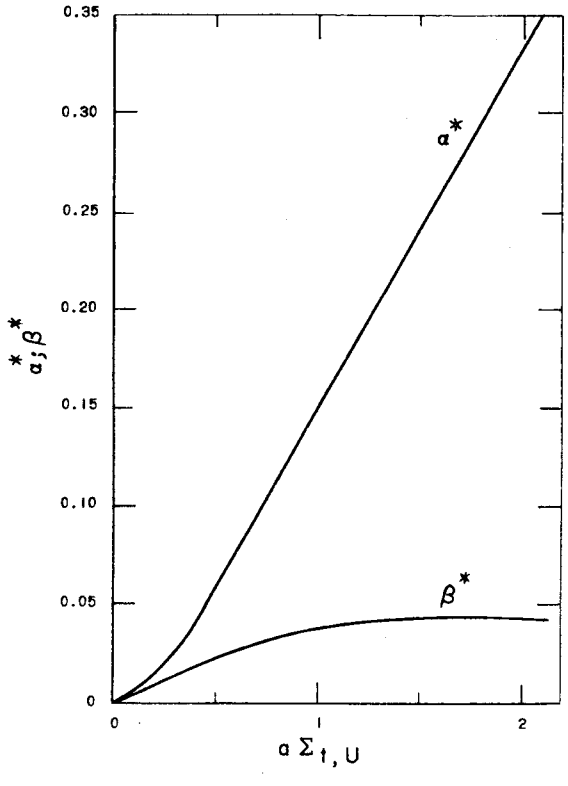

Fig. 4-4—α^* and β^* as a function of $a\Sigma_{t,U}$. *Reproduced from Ref. 11.*

Table 4-17 — TABLE OF $A^* = [P_c/(1 - P_c)] - 2a\Sigma_{t,U}$ FOR SLABS OF HALF-THICKNESS a

Data from Ref. 11.

$a\Sigma_{t,U}$	A*	$a\Sigma_{t,U}$	A*	$a\Sigma_{t,U}$	A*	$a\Sigma_{t,U}$	A*	$a\Sigma_{t,U}$	A*
0.00	0.0	0.46	0.5161	1.34	1.8236	2.26	3.5462	3.18	5.3624
0.01	0.0309	0.47	0.5277	1.36	1.8604	2.28	3.5891	3.20	5.4041
0.02	0.0506	0.48	0.5388	1.38	1.8961	2.30	3.6251	3.22	5.4466
0.03	0.0670	0.49	0.5504	1.40	1.9307	2.32	3.6623	3.24	5.4902
0.04	0.0814	0.50	0.5621	1.42	1.9672	2.34	3.7009	3.26	5.5178
0.05	0.0946	0.52	0.5861	1.44	2.0024	2.36	3.7407	3.28	5.5634
0.06	0.1068	0.54	0.6096	1.46	2.0359	2.38	3.7820	3.30	5.6100
0.07	0.1185	0.56	0.6341	1.48	2.0714	2.40	3.8246	3.32	5.6402
0.08	0.1297	0.58	0.6593	1.50	2.1087	2.42	3.8593	3.34	5.6890
0.09	0.1405	0.60	0.6843	1.52	2.1443	2.44	3.8952	3.36	5.7209
0.10	0.1508	0.62	0.7099	1.54	2.1817	2.46	3.9419	3.38	5.7718
0.11	0.1610	0.64	0.7357	1.56	2.2171	2.48	3.9804	3.40	5.8054
0.12	0.1710	0.66	0.7617	1.58	2.2544	2.50	4.0200	3.42	5.8399
0.13	0.1809	0.68	0.7886	1.60	2.2935	2.52	4.0610	3.44	5.8752
0.14	0.1906	0.70	0.8154	1.62	2.3303	2.54	4.0929	3.46	5.9304
0.15	0.2004	0.72	0.8430	1.64	2.3645	2.56	4.1364	3.48	5.9676
0.16	0.2100	0.74	0.8701	1.66	2.4004	2.58	4.1706	3.50	6.0056
0.17	0.2196	0.76	0.8976	1.68	2.4381	2.60	4.2167	3.55	6.1045
0.18	0.2291	0.78	0.9268	1.70	2.4776	2.62	4.2532	3.60	6.2092
0.19	0.2384	0.80	0.9549	1.72	2.5141	2.64	4.2908	3.65	6.2985
0.20	0.2481	0.82	0.9832	1.74	2.5523	2.66	4.3296	3.70	6.3929
0.21	0.2576	0.84	1.0128	1.76	2.5873	2.68	4.3696	3.75	6.4925
0.22	0.2671	0.86	1.0422	1.78	2.6239	2.70	4.4108	3.80	6.5976
0.23	0.2767	0.88	1.0714	1.80	2.6622	2.72	4.4532	3.85	6.7083
0.24	0.2864	0.90	1.1017	1.82	2.7021	2.74	4.4969	3.90	6.8006
0.25	0.2960	0.92	1.1330	1.84	2.7384	2.76	4.5297	3.95	6.8978
0.26	0.3058	0.94	1.1637	1.86	2.7763	2.78	4.5759	4.00	7.0000
0.27	0.3156	0.96	1.1935	1.88	2.8158	2.80	4.6108	4.05	7.1075
0.28	0.3254	0.98	1.2259	1.90	2.8511	2.82	4.6467	4.10	7.1934
0.29	0.3353	1.00	1.2571	1.92	2.8940	2.84	4.6836	4.15	7.3113
0.30	0.3451	1.02	1.2890	1.94	2.9325	2.86	4.7348	4.20	7.4067
0.31	0.3551	1.04	1.3195	1.96	2.9664	2.88	4.7740	4.25	7.5068
0.32	0.3652	1.06	1.3523	1.98	3.0081	2.90	4.8144	4.30	7.6117
0.33	0.3754	1.08	1.3855	2.00	3.0451	2.92	4.8422	4.35	7.6913
0.34	0.3857	1.10	1.4168	2.02	3.0835	2.94	4.8847	4.40	7.8056
0.35	0.3960	1.12	1.4504	2.04	3.1234	2.96	4.9283	4.45	7.8936
0.36	0.4068	1.14	1.4842	2.06	3.1581	2.98	4.9732	4.50	7.9856
0.37	0.4170	1.16	1.5156	2.08	3.2012	3.00	5.0048	4.55	8.1149
0.38	0.4277	1.18	1.5493	2.10	3.2388	3.02	5.0519	4.60	8.2162
0.39	0.4383	1.20	1.5826	2.12	3.2779	3.04	5.0855	4.65	8.2874
0.40	0.4492	1.22	1.6182	2.14	3.3111	3.06	5.1199	4.70	8.3970
0.41	0.4600	1.24	1.6508	2.16	3.3530	3.08	5.1705	4.75	8.5114
0.42	0.4711	1.26	1.6856	2.18	3.3889	3.10	5.2069	4.80	8.5939
0.43	0.4819	1.28	1.7198	2.20	3.4339	3.12	5.2444	4.85	8.7175
0.44	0.4930	1.30	1.7533	2.22	3.4727	3.14	5.2828	4.90	8.8078
0.45	0.5044	1.32	1.7889	2.24	3.5047	3.16	5.3222	4.95	8.9020
								5.00	9.0000

4.1.4.3 Serber-Wilson Method in Slab Geometry

Bengston[16] has generalized the Serber-Wilson Method to derive expressions for the average fluxes in a slab array of pure absorber alternating with pure moderator and scattering. Let the thickness of the absorber be $2t_U$ (mean free paths), and the thickness of the scatterer be $2t_M$ (mean free paths).

The average flux in the absorber, $\overline{\phi}_U$ is given by $\overline{\phi}_U = t_M/t_U$. The average flux in the moderator is given by:

$$\overline{\phi}_M = \left\{-1 + t_M^2 + \frac{t_M(1 - 3\,K_1) + 3\,J_2}{J_0}\right\}$$

The functions J_0, J_1 and K_1 are defined by:

$$2\,J_0 = \sum_{m=0}^{\infty} \{E_3\,[2m(t_M + t_U)] - E_3\,[2t_M + 2m(t_M + t_U)] - E_3\,[(2t_U + 2m(t_U + t_M)] + E_3\,[2(m + 1)\,(t_M + t_U)]\}$$

The functions $E_n(x)$ are defined and tabulated in Ref. 15.

$2J_2$ = same series as J_0 but replace E_3 by E_5

$$2K_1 = \frac{1}{3} + \sum_{m=0}^{\infty} \{E_4\,[2t_m + 2m(t_M + t_U)] - E_4\,[2t_U + 2m(t_M + t_U)]\}$$

$$J_1 = [2\,t_U\,(t_U + t_M) - t_U^2]\,\frac{J_0}{2} - J_2 + t_M K_1$$

4.1.5 DISADVANTAGE FACTORS FROM CONSIDERATIONS OF ROD BLACKNESS AND EXTRAPOLATION LENGTH*

Kushneriuk[14,17] gives results for thermal utilization in rods similar to those obtained in Section 4.1.4, but which involve concepts of rod blackness and extrapolation length. In his formulation, G has its usual definition: the ratio of surface flux to average flux in the rod; α is $\phi_{as}(a)/\phi(a)$, where $\phi(a)$ is the actual flux at the surface of the rod; $\phi_{as}(a)$ is the value at the surface of the rod of the asymptotic flux in the moderator as determined by diffusion theory with appropriate boundary conditions at the surface of the rod; and β (see also Ref. 13) is the probability that a neutron incident on the rod surface will be absorbed before escaping the rod, and is called the blackness of the rod. The extrapolation length is given by

$$\lambda = \phi_{as}(a)/\phi'_{as}(a)$$

The integral transport theory result for the blackness is:

$$\beta = \frac{(1 - c)\,P_1(a/\ell)}{(1 - c)\,P_C(\nu)}$$

where c = ratio of scattering to total cross section in the rod
$P_C(\nu)$ = the collision probability tabulated in Ref. 12
$\nu = \ell/L$ is the root of $2\nu = c\,\ln[(1 + \nu)/(1 - \nu)]$
ℓ = mean free path in the rod
L = thermal diffusion length in rod

$$P_1\left(\frac{a}{\ell}\right) = \frac{4a}{3\ell}\left\{I_1\left(\frac{a}{\ell}\right)K_1\left(\frac{a}{\ell}\right) - 1 - \frac{2a}{\ell} + \frac{2a^2}{\ell^2}\left[I_0\left(\frac{a}{\ell}\right)K_0\left(\frac{a}{\ell}\right) + I_1\left(\frac{a}{\ell}\right)K_1\left(\frac{a}{\ell}\right) + \frac{\ell}{a}\,I_0\left(\frac{a}{\ell}\right)K_1\left(\frac{a}{\ell}\right)\right]\right\}$$

and I_n and K_n are the modified Bessel functions of the first and second kind.

The values of G computed by the methods given in Section 4.1.4 are in good agreement with those given in Ref. 14, and can be used in the present case. (For further details on the calculation of G, see Ref. 14). One useful and simple approximation for G in the range $1.001 < G < 1.10$ is:

$$G(\text{approx.}) = a\,[2 - \beta]/\beta\ell_a$$

* Refer to remarks at the beginning of Section 4.1.4.

where ℓ_a is the absorption mean free path in the rod. Define:

$$P_0\left(\frac{a}{\ell}\right) = 1 + I_1\left(\frac{a}{\ell}\right) K_1\left(\frac{a}{\ell}\right) - \frac{3\ell}{4a} P_1\left(\frac{a}{\ell}\right)$$

and

$$g\left(\frac{a}{\ell_a}\right) = 2 - P_0(a/\ell_a)/P_1(a/\ell_a)$$

A result of integral transport theory is:

$$\alpha = \left\{\left[2 - \frac{3}{2} P_1(a/\ell_a)\, g\,(a/\ell_t)\right] \Big/ [2 - P_0(a/\ell_a)]\right\} \Big/ (G/g)$$

where ℓ_t is the transport mean free path in the rod. The function $G(a/\ell_t)$ is given in Table 4-18.

Table 4-18 — VALUES OF g(x)

Data from Ref. 14.

x	g(x)	x	g(x)
0.07	0.114	1.0	0.413
0.10	0.139	1.5	0.466
0.15	0.175	2.5	0.524
0.2	0.204	5.0	0.571
0.3	0.251	8.0	0.590
0.5	0.314	12.0	0.598
0.7	0.361	∞	0.623

The extrapolation length, λ, permits the determination of ϕ_{as}, and thus, the amount of capture in the moderator. Values of λ, or references thereto, are given for a series of cases.

Black cylinders: (See Refs. 18 and 19.) Gray cylinders of small radius with or without air gaps: (See Refs. 20 and 21.)

Homogeneous, purely absorbing cylinder in an infinite bath of pure, isotropic scatterer:

$$\lambda/\ell_t = [4/3P_1(a/\ell_a)] - g(a/\ell_t)$$

ℓ_a = absorption mean free path in the rod

ℓ_t = transport mean free path of moderator

Non-homogeneous purely absorbing rod with radial symmetry, in an infinite bath of pure. isotropic scatterer:

$$\lambda/\ell_t = [4/3\eta(a)] - g(a/\ell_t)$$

$$\eta(a) = 1 - \frac{4}{\pi}\int_0^{\pi/2} Ki_3(\tau)\, d\phi$$

$$\tau(\overline{AB}) = \int_B^A [1/\ell_a(s)]\, ds$$

$\overline{AB}$ = average chord of the cylinder in units of absorption mean free paths

$$Ki_3(x) = \int_0^\infty \cosh^{-3} u \exp(-x \cosh u)\, du$$

and is tabulated in Section 4.2.3.

ϕ = angle between the outward normal and the chord.

Rod with radius a, air gap of width (b – a):

$$\frac{\lambda}{\ell_t} = \left[\frac{4b}{3aP_1(a/\ell_a)}\right] - g\left(\frac{b}{\ell_t}\right)$$

Gap is a weakly capturing sheath of thickness (b – a), and total mean free path, ℓ_{sh}.

$$\eta(b) = \frac{a}{b} P_1\left(\frac{a}{\ell_a}\right) T + \frac{2}{b\ell_{sh}}(b^2 - a^2) - \frac{a}{b} P_1\left(\frac{a}{\ell_a}\right)(1 - T)$$

$$T = 1 - \frac{2(b-a)}{\ell_{sh}},\quad 2(b-a) \ll \pi^2 a$$

Homogeneous rod, c > 0

$$\frac{\lambda}{\ell_t} = \frac{4}{3\beta} - g\left(\frac{a}{\ell_t}\right)$$

If $a/\ell_a \to \infty$:

$$\left.\begin{aligned}\frac{\lambda}{\ell_t}\\ \frac{\lambda}{\ell_t}\end{aligned}\right\} \begin{aligned}&\to 0.7104 + 0.2046c && c \ll 1\\ &\to 1/\sqrt{3(1-c)} && c \to 1\end{aligned}$$

If there is an air gap of width (b – a):

$$\frac{\lambda}{\ell_t} = \frac{4b}{3a\beta} - g\left(\frac{b}{\ell_t}\right)$$

N sheaths:

$$\frac{\lambda(R)}{\ell_t} = \frac{4}{3\eta(R)} - g\left(\frac{R}{\ell_t}\right)$$

R = outside radius of assembly

$\eta(R)$ = total assembly blackness

$$\eta = \frac{a}{R}\beta\prod_{i=1}^{N} T_i + \frac{2}{\pi R}\sum_{i=1}^{N}\left(\frac{A_i}{\ell_i}\right) - \frac{a}{R}\beta\left[\sum_{i=1}^{N}(1 - T_i)\right]$$

$$T_i = 1 - \frac{2}{\pi\ell_i}\left[\sqrt{a_i^2 - a^2} - \sqrt{a_{i-1}^2 - a^2} + \left(\frac{a_i^2}{a}\right)\sin^{-1}\frac{a}{a_i} - \frac{a_{i-1}^2}{a}\sin^{-1}\frac{a}{a_{i-1}}\right]$$
$$+ (a_i^2/a)\sin^{-1}(a/a_i) - (a_{i-1}^2/a)\sin^{-1}(a/a_{i-1})$$

where a_i = outer radius of *ith* sheath
$a_N = R$
a = inner rod radius
A_i = cross-sectional area of *ith* sheath
ℓ_i = absorption mean free path in *ith* sheath; for an air gap, $\ell_i \to \infty$

Water Sheath:

G = G(approx.), and use two-group diffusion theory

Rod Clusters, widely separated:

The cluster is viewed as a single homogeneous rod with c > 0. The effective cross section of each rod in the cluster may be determined by considering it in an infinite array of rods arranged as in the cluster.

4.1.6 SPECTRAL HARDENING

When the spectrum is hardened by capture in the rod, the problem becomes more complex.[22] The calculation of thermal utilization may be simplified with the assumption of no energy transfer in the rod or in the moderator. The system may then be considered to be made up of many independent energy groups, and the formulation of Section 4.1.5 used for the study of spectral hardening.

An equivalent set of diffusion constants is obtained by setting

$$\rho(E,x) = C(E)I_0[\kappa(E)ax]$$

where ρ is the neutron density at energy E and at a distance ax centimeters from the center of the rod (x = 1 is the rod boundary). These solutions are used to compute the capture in the rod at each energy, and the consequent hardening. Then:

$$2\pi a J_{in}(E)\,\beta(E) = 2\pi a C(E)\,\Sigma_a(E) I_1[a\kappa(E)]/\kappa(E)$$

$$C(E) = a\Sigma_a(E)\,\{[2 - \Sigma(E)]/\beta(E)\} = \frac{a\kappa(E)I_0[a\kappa(E)]}{2I_1[a\kappa(E)]} = \text{ratio of surface}$$

to average flux in the rod which can be used to find C(E) and $\kappa(E)$; $\Sigma_a(E)$ is the macroscopic absorption cross section in the rod; and $J_{in}(E)$ is the current into the rod. It is convenient to specify:

$$J_{in}(E) = D\frac{E}{(kT)^2}\exp(-E/kT) + J_{in}^F(E)\Delta(E)$$

$$\Delta(E) = 0,\ E < 5kT$$

$$= 1,\ E > 5kT$$

The fast component, $J_{in}^F(E)$, is usually represented by a constant divided by E. This constant is found by asserting that the slowing-down density is equal to the rate of neutron absorption. This formulation can be extended to rods whose compositions vary radially; this is done in Ref. 17.

If an initially Maxwellian spectrum (temperature T = °K) falls on one face of a slab of non-scattering, absorbing material, a hardened spectrum is produced. Considered here is the case of such a spectrum isotropically incident (cosine incident law) on one side of a plane slab of material with a 1/v absorption law. The thickness times the absorption cross section at 1 ev is denoted by K; the transmission of the slab (the fraction of the neutron density remaining)* is t; and the mean velocity of the hardened distribution is given by $\bar{v} = x\,v_0$. For the initial spectrum

$$x = (4T/\pi T_0)^{1/2}$$

where

$$T_0 = 293.6°K.$$

Values of t and x for different values of K and T are given in Table 4-19.

The average cross section

$$\bar{\sigma} = \int\sigma(v)n(v)\,vdv/\int vn(v)dv$$

is given by $\bar{\sigma} = \hat{\sigma}/x$.

For a neutron density distribution function n(v), $\hat{\sigma}$ is defined by:

$$\hat{\sigma} = \int\sigma(v)n(v)vdv/v_0\int n(v)dv$$

where v_0 is equal to 2200 meters/second.

---

* The fraction of initial neutron density is also the fraction of initial reaction rate for a 1/v-detector, so that this quantity is the flux depression or thermal disadvantage factor as measured with a 1/v-law detector.

With respect to hardening, $\hat{\sigma}$ is invariant for substances, e.g., U^{238}, which follow a 1/v-law in the thermal region (to ~1% accuracy), but will vary for non-1/v substances, e.g., Pu^{239} (see Table 4-19).

Westcott[22] has reformulated the preceding material to yield a least-squares fit for the ratio of the cross section in the hardened spectrum, $\hat{\sigma}_H$, to that in the unhardened Maxwellian, $\hat{\sigma}_M$. Only the Maxwellian part of the incident spectrum is considered. The cross section data used in the least-squares fit post-date those used in preparing the Pu^{239} data given in Table 4-19. The formula is:

Table 4-19 — RESULTS OF SPECTRAL HARDENING CALCULATION (AND $\hat{\sigma}$ FOR Pu^{239})

Unhardened Values	Hardened Values				
T = 20°C x = $2/\sqrt{\pi}$ = 1.12838 $\hat{\sigma}$ = 776.61	K = 0.0059645 t = 0.854024 x = 1.15679 $\hat{\sigma}$ = 780.32	0.0119290 0.764130 1.17509 782.86	0.0178935 0.693949 1.19036 785.07	0.0238580 0.635847 1.20385 787.09	0.0357870 0.543065 1.22749 790.78
	K = 0.0477161 t = 0.470986 x = 1.24818 $\hat{\sigma}$ = 794.17	0.0596451 0.412827 1.26687 797.37	0.0715741 0.364748 1.28406 800.43	0.0894676 0.306418 1.30773 804.84	0.1073611 0.260197 1.32942 809.08
T = 100°C x = 1.27286 $\hat{\sigma}$ = 824.75	K = 0.0059645 t = 0.866207 x = 1.30220 $\hat{\sigma}$ = 831.20	0.0119290 0.782374 1.32124 835.70	0.0178935 0.716237 1.33717 839.62	0.238580 0.661007 1.35128 843.22	0.0357870 0.571849 1.37602 849.83
	K = 0.0477161 t = 0.501675 x = 1.39773 $\hat{\sigma}$ = 855.94	0.0596451 0.444394 1.41735 861.74	0.715741 0.396534 1.43542 867.31	0.0894676 0.337761 1.46033 875.38	0.1073611 0.290545 1.48319 883.20
T = 180°C x = 1.40249 $\hat{\sigma}$ = 900.47	K = 0.0059645 t = 0.875349 x = 1.43259 $\hat{\sigma}$ = 911.09	0.0119290 0.796215 1.45225 918.54	0.0178935 0.733287 1.46872 925.05	0.0238580 0.680392 1.48333 931.04	0.0357870 0.594300 1.50899 942.06
	K = 0.0477161 t = 0.525870 x = 1.53153 $\hat{\sigma}$ = 952.26	0.0596451 0.469522 1.55192 961.95	0.0715741 0.422063 1.57073 967.32	0.0894676 0.363250 1.59666 984.77	0.1073611 0.315511 1.62048 997.86
T = 260°C x = 1.52092 $\hat{\sigma}$ = 1005.22	K = 0.0059645 t = 0.882512 x = 1.55164 $\hat{\sigma}$ = 1021.10	0.0119290 0.807182 1.57181 1032.25	0.0178935 0.746898 1.58875 1042.02	0.0238580 0.695962 1.60377 1050.99	0.0357870 0.612514 1.63021 1067.48
	K = 0.0477161 t = 0.545668 x = 1.65344 $\hat{\sigma}$ = 1082.74	0.0596451 0.490242 1.67449 1097.19	0.0715741 0.443263 1.69391 1111.09	0.0894676 0.384622 1.72070 1131.16	0.1073611 0.336633 1.74533 1150.58

$$(\hat{\sigma}_H/\hat{\sigma}_M) - 1 = [A_1 + B_1 T^* + C_1 (T^*)^2](1 - t) + [A_2 + B_2 T^* + C_2 (T^*)^2](1 - t)^2 + [A_3 + B_3 T^* + C_3 (T^*)^2](1 - t)^3 \quad (4\text{-}6)$$

where $T^* = (T - 140)/100$; T = temperature of incident Maxwellian in degrees Kelvin; and t is transmission. Values of t for various cases are given in Table 4-19.

Values of the coefficients A_n, B_n, and C_n are given in Table 4-20, together with an estimate of the least-squares error. The fit was made for temperatures in the range 20°C to 260°C. Interpolation of t is facilitated by the fact that t is a function of $K/\sqrt{T}$.

Table 4-20—COEFFICIENTS A_n, B_n, C_n FOR EQUATION (4-6)

Element or Isotope	n	Isotropic Incidence		
		A_n	B_n	C_n
Cadmium	1	0.222338	0.021142	−0.017296
	2	−0.101890	0.041830	0.029551
	3	0.355480	−0.027930	−0.055144
	10^6_a	—	951.3	—
Indium	1	0.022792	0.005404	0.000101
	2	−0.008207	0.000406	−0.000024
	3	0.030691	0.005274	0.000090
	10^6_a	—	121.9	—
Samarium	1	0.202744	−0.028937	−0.007852
	2	−0.051100	0.045962	0.003030
	3	0.207240	−0.115945	−0.009800
	10^6_a	—	1134.9	—
Gadolinium	1	−0.069330	−0.032842	−0.000004
	2	0.028880	−0.003085	−0.000370
	3	−0.128740	−0.028772	0.003553
	10^6_a	—	278.5	—
Lutecium	1	0.222867	0.013849	−0.018258
	2	−0.099070	0.039455	0.021230
	3	0.351580	−0.046343	−0.048840
	10^6_a	—	734.4	—
$_{92}U^{235}$ absorption	1	−0.032014	−0.001680	0.001376
	2	0.008351	−0.002863	−0.000345
	3	−0.031019	0.004998	0.002013
	10^6_n	—	79.4	—
$_{92}U^{235}$ fission	1	−0.032552	−0.002168	0.001186
	2	0.009001	−0.002591	−0.000203
	3	−0.031982	0.003702	0.001739
	10^6_n	—	196.2	—
$_{94}Pu^{239}$ absorption	1	0.103402	0.051637	0.007309
	2	−0.044810	−0.013841	−0.015280
	3	0.186150	0.089771	0.022820
	10^6_a	—	916.0	—
$_{94}Pu^{239}$ fission	1	0.078761	0.044352	0.007973
	2	−0.034610	−0.013384	−0.012610
	3	0.143960	0.079131	0.021800
	10^6_a	—	763.6	—
$_{94}Pu^{241}$ fission	1	0.064395	0.027778	0.003316
	2	−0.025980	−0.005447	−0.007148
	3	0.106900	0.043535	0.009553
	10^6_a	—	401.4	—

Note: In this table, "a" is the least-squares error in fitting the 63 (or 70) calculated values using Eq. (4-6).

4.1.7 PHENOMENOLOGICAL AND APPROXIMATE FORMULAE

The formulae listed in this section are either analytic approximations, empirical correlations, or representations of standard formulae in terms of data obtainable from experiments without theoretical interpretation.

687863 O - 63 - 19

4.1.7.1 Empirical Fit to Radial Power Distribution in Natural Uranium Rods in a Large Unit Cell of D_2O

A set of empirical equations has been derived which summarizes experimental data on the radial distribution of thermal neutrons in fuel rods.[23]

Let $\rho = a\Sigma_a$, where a is the rod radius, and Σ_a is the macroscopic absorption cross section of the rod. The axis-to-surface ratio of neutron density is:

$$A(\rho) = 1/(1 + 0.69713\rho + 0.48598\ \rho^2 + 0.33879\ \rho^3) \tag{4-7}$$

The radial distribution of neutron density, normalized to unity at the surface of the rod, is given by:

$$n(r, \rho) = A(\rho)\ [1 + 0.69713\ \rho(r/a)^2 + 0.48598\rho^2\ (r/a)^4 + 0.33879\ \rho^3\ (r/a)^6] \tag{4-8}$$

The ratio of average-to-surface neutron density taken over the cross section of the rod is given by:

$$G^{-1} = A(\rho)\ [1 + 0.34856\rho + 0.16199\rho^2 + 0.08469\rho^3] \tag{4-9}$$

Equations (4-7) through (4-9) are valid in the range $0 \leq \rho \leq 2$.

Accuracy of the Fit. An analysis of the sources of errors indicates the following relative errors in the determination of the neutron density distribution in an absorbing rod as given by Eq. (4-7):

ρ	Relative Error, % (RMS Error of Fit)
0 – 0.5	1.0
0.5 – 1.0	3.0
1.0 – 2.0	5.0

4.1.7.2 Analytic Approximation to P_3 Method in Slab Geometry with Linearly Anisotropic Scattering[24]

The case considered is a two-region slab cell consisting of a thin fuel region and a relatively thick moderator region. It is assumed that the neutron source is zero in the fuel region, and is constant and isotropic in the moderator region. Scattering anisotropy is taken into account by including a linear anisotropic term, $P_1(\mu)$. The only space variable is in the direction perpendicular to the slab plane, x; angular dependence of the neutron velocity vector is given in terms of μ, the cosine of the angle between the neutron velocity vector and the x axis.

The following notation and symbols are used in the analysis:

V = half-thickness of region

Σ_s = macroscopic scattering cross section

Σ_a = macroscopic absorption cross section

$\Sigma_t = \Sigma_s + \Sigma_a$ = total macroscopic cross section

$$a = 1 - \frac{\Sigma_s}{\Sigma_t} = \frac{\Sigma_a}{\Sigma_t}$$

$$b = a\left(1 - \overline{\mu}\,\frac{\Sigma_s}{\Sigma_t}\right)$$

$\overline{\mu}$ = average cosine of scattering angle

$$\nu_1^2 = +\left(\frac{3}{2}b + \frac{14}{9}a + \frac{35}{18}\right) - \left[\left(\frac{3}{2}b + \frac{14}{9}a + \frac{35}{18}\right)^2 - \frac{35}{3}b\right]^{1/2}$$

$$\nu_2^2 = +\left(\frac{3}{2}b + \frac{14}{9}a + \frac{35}{18}\right) + \left[\left(\frac{3}{2}b + \frac{14}{9}a + \frac{35}{18}\right)^2 - \frac{35}{3}b\right]^{1/2}$$

$\kappa_1 = \nu_1\ \Sigma_t$

$\kappa_2 = \nu_2\ \Sigma_t$

$Y = \Sigma_t\ V$

All of the symbols carry an additional subscript: U for the fuel region, and M for the moderator region.

The result of the analysis for the ratio of the average fluxes in the fuel and moderator regions is given in the form:

$$\frac{\bar{\phi}_M}{\bar{\phi}_U} = G + (E-1)\frac{V_U \Sigma_{a,U}}{V_M \Sigma_{a,M}} \tag{4-10}$$

If V_U is small:

$$G = 1 + \frac{1}{3}\xi\, Y_U^2 + \ldots \tag{4-11}$$

where

$$\xi = \frac{3b_U(\nu_{U,1}^2 + \nu_{U,2}^2) - \nu_{U,1}^2\,\nu_{U,2}^2 + \left(\frac{1}{\nu_{M,2}} 3b_U + \frac{2}{5}\frac{a_U}{Y_M}\right)\nu_{U,1}^2\,\nu_{U,2}^2\,Y_U}{3b_U + \frac{1}{\nu_{M,2}}\nu_{U,1}^2\,\nu_{U,2}^2\,Y_U}$$

In diffusion theory (P_1 approximation) $\xi = 3b_U$. The limits of validity of Eq. (4-10) are $Y_U < \frac{1}{2}$, $\nu_{M,2} Y_M > 3$. In Eq. (4-10):

$$E - 1 = \frac{1 - t_{M,1}}{t_{M,1}}(1 + \Psi_U \Psi_M)$$

where

$$t_{k,i} = \frac{\tanh \kappa_{k,i} V_k}{\kappa_{k,i} V_k}$$

$k = U, M$

$i = 1, 2$

In the P_1 approximation:

$$E - 1 = \frac{1 - t_{M,1}}{t_{M,1}}$$

Under the conditions of validity of Eq. (4-11), Ψ_U is well approximated by:

$$\Psi_U = \frac{1}{a_U}\left[\frac{(3b_U - \nu_{U,1}^2)(\nu_{U,2}^2 - 3b_U)}{3b_U + \frac{1}{\nu_{M,2}}\nu_{U,1}^2\,\nu_{U,2}^2\,Y_U}\right]$$

There are four conditions on $\nu_{M,2} Y_M$, and $\nu_{M,1} Y_M$ in which different approximations for Ψ_M hold:

(1) $\nu_{M,2} Y_M \ll 1$; $\quad \Psi_M = \frac{1}{\sqrt{35}}\frac{a_M}{b_M}\nu_{M,2}^2 Y_M$

(2) $\nu_{M,2} Y_M \leq 3$; $\quad \nu_{M,1} Y_M \ll 1$; $\Psi_M = \frac{3}{\sqrt{35}}\frac{a_M}{b_M}(1 - t_{M,2})\frac{1}{Y_M}$

(3) $\nu_{M,2} Y_M > 3$; $\quad \nu_{M,1} Y_M < 1$

$$\Psi_M = \frac{3}{\sqrt{35}}\frac{a_M}{b_M}\left(1 - \frac{27}{35} b_M\right)\left(1 + \frac{1}{15}\nu_{M,1}^2 Y_M^2 - \frac{1}{\nu_{M,2} Y_M}\right)\frac{1}{Y_M}$$

(4) Infinite Moderator ($V_M \to \infty$); $\Psi_M = \sqrt{\frac{3}{35}}\frac{a_M}{\sqrt{b_M}}$

A comparison of the results of this approximation with the full P_3 method is shown in Table 4-21.

Table 4-21—COMPARISON OF ANALYTIC APPROXIMATION AND P_3 METHOD

	Fuel	Moderator
Σ_s	0.3924 cm^{-1}	0.4572 cm^{-1}
Σ_a	0.56504 cm^{-1}	0.0002852 cm^{-1}
$\bar{\mu}$	0.95744 —	0.457525 —
V	0.2972 cm	4.000 cm

	G	$(E-1)\ (V_U\Sigma_{a,U}/V_M\Sigma_{a,M})$
Approximate method	1.0795	0.3945
P_3 approximation	1.07973	0.3950

4.1.7.3 Thermal Self-Shielding Factor for Lumps

The thermal self-shielding factor for lumps is given approximately by:[25]

$$F = 1 - \{1/[1 + 0.314(S/V)/\Sigma_a]\}$$

where Σ_a is the absorption cross section of the material in the lump averaged over an estimated hardened Maxwellian; S/V is the surface to volume ratio; and F is such that if ϕ_H is the flux calculated in a homogenized system, $F\phi_H\Sigma_{aV}$ thermal captures occur in the lump. This approximation is limited to $\Sigma_{tot}\,(4\ V/S) \leq 4$.

4.2 RESONANCE ESCAPE PROBABILITY

In the process of slowing down, neutrons collide with nuclei and may be absorbed in resonances. The infinite dilution resonance integral is given by:

$$(R.I.) = \int \sigma_a(E)\,\frac{dE}{E}$$

where $\sigma_a(E)$ is the microscopic absorption cross section of the material under consideration, and the integral extends over an energy range encompassing all the resonances. The usefulness of the resonance integral arises from the fact that in a slowing-down medium the flux has a characteristic 1/E dependence. If a sizable number of resonance absorber atoms are present however, there is, in general, a depletion of the flux at the resonances. The effective resonance integral is then defined by:

$$(R.I.)_{eff} = \int \sigma_a(E)\ \bar{\phi}(E)dE$$

where $\bar{\phi}(E)$ is the average over all the atoms of the sample of the resonance depleted flux normalized to 1/E away from the resonances. In a homogeneous mixture, if σ_a is small or has narrow, well-separated resonances, then

$$\bar{\phi}\,(E) = \frac{\Sigma_{pot}(E)}{\Sigma_s(E) + \Sigma_a(E)}\,\frac{1}{E}$$

where $\Sigma_s(E)$, $\Sigma_a(E)$, and Σ_{pot} are the macroscopic scattering, absorption, and potential scattering cross sections of the mixture, respectively. The effective resonance integral is then given by:

$$(R.I.)_{eff} = \int \sigma_a(E)\,\frac{\Sigma_{pot}(E)}{\Sigma_s(E) + \Sigma_a(E)}\,\frac{dE}{E}$$

and the resonance escape probability is given by:

$$p = \exp\,[-(N_a/\xi\Sigma_s)(R.I.)_{eff}]$$

where N_a is the number of absorber atoms per unit volume and $\xi\Sigma_s$ is the slowing-down power.

In a heterogeneous array, the effective resonance integral is a complicated function of the geometry and composition of the system. It is usually given in a form that involves both the volume and surface of the fuel lump and is considered in Section 4.2.1. In the heterogeneous case, p is given by:

$$p = \exp\left[-(N_a V_a/\xi \Sigma_{s,M} V_M)(\bar{\phi}_a/\bar{\phi}_M)(R.I.)_{eff}\right]$$

where V_a and V_M are the volume of the absorber and of moderator, respectively, and $\bar{\phi}_a$ and $\bar{\phi}_M$, the average flux in the absorber and the moderator. The ratio, $\bar{\phi}_M/\bar{\phi}_a$, is called the resonance disadvantage factor, and can be calculated in the same way as the corresponding thermal quantity. There are some reservations about the use of the resonance disadvantage factor; see for example, the work of Corngold,[26] and Spinrad, Chernik, and Corngold.[27] Usually, $\bar{\phi}_a/\bar{\phi}_M$ is set equal to one; in lattices with pitch large compared to the slowing-down length, this may not be adequate.[28]

Parametric Representation of Resonance Integrals in Heterogeneous Systems. Systematic expositions of methods of computing resonance integrals have been made by many authors; a comprehensive review article is that by Spinrad, Chernik and Corngold.[27] Briefly, the results of the various modes of calculations are such that the effective resonance integral for any given resonance may be represented by one of two formulae: the narrow resonance (N.R.) or narrow resonance infinite mass (N.R.I.M.) approximation. The parameter:

$$\zeta = (S/4\, N_a V \sigma_0)$$

is introduced; S is the surface area of the lump, V the volume of the lump, N_a the atomic density of absorbing atoms, σ_0 the potential scattering of the absorbing atoms, and ζ is the reciprocal mean chord length of the lump measured in terms of mean free path off-resonance. Then the N.R. formula leads to $(R.I.)_{eff}$ proportional to $\sqrt{\zeta + 1}$, and the N.R.I.M. formula to $(R.I.)_{eff}$ proportional to $\sqrt{\zeta}$. The flux $\bar{\phi}(E)$ can be reasonably represented by a linear combination of N.R. and N.R.I.M. approximations so that the total

$$(R.I.)_{eff} = \int \frac{dE}{E} \sigma_a (P\phi_{NR} + Q\,\phi_{NRIM})$$

In this case, the effective resonance integral is proportional to $\sqrt{\zeta + P}$.

In Section 4.2.1, formulae are given for the effective resonance integrals of isolated lumps of U^{238} and Th^{232}. That part of the absorption cross section which is proportional to $(E)^{-1/2}$ is nearly constant across each resonance. The resonance integrals tabulated in Section 4.2.1 represent the sum of the contributions from individual resonances and the *"1/v" capture is thus not included in the resonance integral.*

4.2.1 FORMULAE FOR THE RESONANCE INTEGRALS OF ISOLATED LUMPS

This section includes parametric representations of the effective resonance integrals of isolated lumps of U^{238}, UO_2, UC, and Th. Methods of extending these formulae to other compositions are given in Section 4.2.2 and the corrections necessary to extend the formulae to lumps in lattices are given in Section 4.2.3.

For U^{238} Vernon[29] gives the fitted formulae:

$$(R.I.)_{eff} = 27.8\sqrt{S/M + 0.04} \quad \text{(experimental)}$$
$$= 28.5\sqrt{S/M + 0.06} \quad \text{(theoretical)}$$

No 1/v contribution is included (see Section 4.2); the temperature is 300°K. Extension to UO_2 and UC is made by using the formulae:

$$(S/M)_{UO_2} = 0.881\,(S/M)_U - 0.068$$
$$(S/M)_{UC} = 0.952\,(S/M)_U - 0.046$$

The results are given graphically in Fig. 4-5; a tabular representation is given in Table 4-22.

For Th^{232} Vernon[30] gives:

$$(R.I.)_{eff} = 20.1\sqrt{S/M + 0.15} \quad \text{at } 300°K$$
$$= 24.8\sqrt{S/M + 0.12} \quad \text{at } 1000°K \text{ (1/v contribution not included)}$$

These are stated to be tentative values.

Hellstrand[31] gives:

$$(R.I.)_{eff} = 17.3\ \sqrt{S/M + 0.06} \quad \pm 5\% \text{ as a result of activation measurements}$$

Rothman and Ward[32] give:

$$(R.I.)_{eff} = (3.1 \pm 1.2) + (18.2 \pm 2)\ \sqrt{S/M} \quad \text{(no 1/v contribution)}$$

as a result of reactivity measurements. The Rothman and Ward measurements may also be represented by:

$$(R.I.)_{eff} = 20.3\ \sqrt{(S/M) + 0.10}$$

in good agreement with the theoretical value.

Table 4-22—RESONANCE INTEGRALS FOR U^{238}

Temp., °K	Source	S/M, cm²/gm													
		0	0.01	0.05	0.10	0.20	0.30	0.40	0.50	0.60	0.70	0.80	0.90	1.00	1.20
300	NRIM	0.04	2.07	4.58	6.46	9.15	11.25	13.04	14.64	16.08	17.42	18.70	19.90	21.05	23.19
	NR	1.62	1.60	1.70	1.90	2.29	2.65	2.98	3.27	3.55	3.79	4.03	4.25	4.46	4.84
	$\ell = 0$	1.64	1.53	1.42	1.45	1.57	1.69	1.80	1.89	1.97	2.04	2.10	2.16	2.20	2.28
	Total	4.93	6.83	9.33	11.44	14.64	17.22	19.45	21.43	23.23	24.88	26.46	27.94	29.34	31.94
500	NRIM	0.04	2.07	4.59	6.50	9.27	11.44	13.32	15.02	16.57	18.01	19.37	20.67	21.92	24.29
	NR	1.81	1.78	1.90	2.13	2.58	2.98	3.34	3.66	3.96	4.24	4.48	4.72	4.95	5.36
	$\ell = 0$	1.75	1.66	1.56	1.59	1.71	1.84	1.94	2.02	2.10	2.16	2.21	2.27	2.31	2.38
	Total	5.23	7.14	9.68	11.85	15.19	17.89	20.23	22.33	24.26	26.04	27.69	29.29	30.81	33.66
800	NRIM	0.04	2.08	4.62	6.57	9.44	11.74	13.74	15.55	17.22	18.81	20.33	21.77	23.09	25.47
	NR	2.02	1.99	2.12	2.38	2.88	3.32	3.72	4.07	4.40	4.70	4.98	5.24	5.48	5.92
	$\ell = 0$	1.87	1.78	1.69	1.71	1.84	1.96	2.06	2.14	2.21	2.26	2.31	2.35	2.39	2.44
	Total	5.56	7.48	10.06	12.29	15.79	18.65	21.15	23.39	25.46	27.40	29.25	30.99	32.59	35.46
1000	NRIM	0.04	2.08	4.63	6.62	9.55	11.92	14.00	15.89	17.64	19.29	20.87	22.37	23.80	26.48
	NR	2.13	2.09	2.24	2.51	3.03	3.51	3.92	4.30	4.64	4.94	5.23	5.50	5.76	6.21
	$\ell = 0$	1.93	1.84	1.75	1.78	1.90	2.02	2.12	2.19	2.25	2.31	2.35	2.39	2.42	2.47
	Total	5.73	7.64	10.25	12.54	16.11	19.08	21.67	24.01	26.16	28.17	30.08	31.89	33.61	36.79
1200	NRIM	0.04	2.08	4.65	6.65	9.66	12.10	14.25	16.21	18.04	19.76	21.39	22.96	24.46	27.31
	NR	2.21	2.18	2.33	2.61	3.17	3.66	4.09	4.49	4.84	5.16	5.46	5.73	5.99	6.45
	$\ell = 0$	1.97	1.89	1.80	1.83	1.95	2.07	2.16	2.24	2.29	2.35	2.39	2.42	2.45	2.50

Note: $\ell = 0$ denotes the contribution from the statistical region.

INFINITE DILUTION	
(6)[a] NRIM	251.39
(48)[a] NR	12.46
$\ell = 0$	2.83
$\ell = 1$, $j = 1/2$	0.25
$\ell = 1$, $j = 3/2$	0.58
E > 30K	0.80
	268.3

[a]Number of narrow resonances

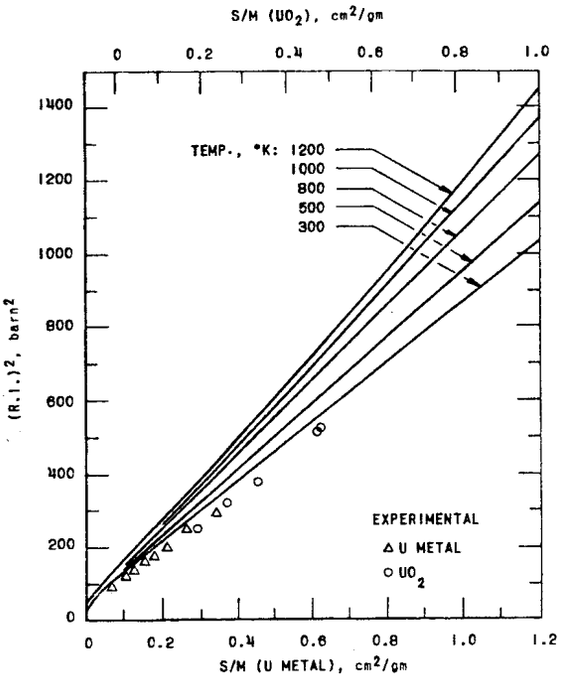

Fig. 4-5—Effective resonance integrals for uranium. *Reproduced from Ref. 29.*

Temperature Dependence. The temperature dependence of the U^{238} resonance integral has been calculated and is given in graphical form in Fig. 4-5. In Ref. 29, the temperature dependence is further analyzed and the representation is given analytically by:

$$(R.I.)_{eff} = I_0(1 + \alpha\sqrt{T})$$

where T is the temperature in degrees Kelvin, and I_0 and α depend on S/M. There is no necessary connection between I_0 and the resonance integral at T = 0. Values of α and I_0 as a function of S/M are given in Table 4-23. The analytical form of the resonance integral is to be understood as a fitting function; any theoretical interpretation is obscure.

Energy Dependence of the Resonance Integral. If the resonance integral is defined over a range whose lower limit, E, is allowed to vary, the effective resonance integral may be plotted as a function of E. This plot is given in Fig. 4-6.

Table 4-23—I_0 AND α VS. S/M FOR URANIUM METAL

S/M	I_0	α
0.05	8.2	0.008
0.5	18.3	0.010
1.0	24.2	0.012

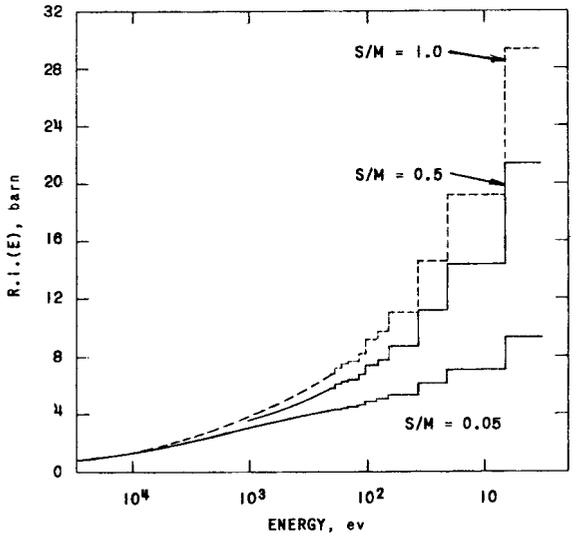

Fig. 4-6—Energy dependence of R.I. for various lump sizes. *Reproduced from Ref. 29.*

4.2.2 EQUIVALENCE PRINCIPLES AND THE METHOD OF ESCAPE PROBABILITIES

A detailed consideration of the resonance integral shows that under some broad assumptions the resonance integrals for: (a) homogeneous mixtures of an absorber with moderator, (b) isolated lumps of absorber mixed with varying amounts of scatterer, and (c) lattices of such lumps, have the same functional representation. Under these conditions, a parameter can be defined which may be evaluated in each of the cases (a), (b), and (c). Systems having equal values of this parameter have equal resonance integrals.

4.2.2.1 Equivalence Principles for Isolated Lumps

In Ref. 33 an equivalence principle is defined for isolated lumps under these assumptions:

(1) The resonance integral for any resolved resonance is adequately represented by either the N.R. or N.R.I.M. approximation.

(2) The probability, P_0, that a neutron which was scattered into an energy interval dE about E in the lump makes its next collision in the lump, is given by Wigner's rational approximation:

$$1 - P_0 = 1/[1 + (\ell_0/\lambda_0)]$$

where $\ell_0 = 4$ V/S is the mean chord length in the lump, and $\lambda_0 = 1/\sigma_t$ is the mean free path in the lump. Under these conditions, a parameter σ_e can be defined:

$$\sigma_e = \sigma_0 + (1/N_a\ell_0)$$

where N_a is the density of absorber atoms in the lump, and σ_0 is the total scattering off-resonance in the lump per absorber atom. That is, if an absorber atom has a potential scattering, σ_{pot}, and the macroscopic scattering cross section of all other atoms in the lump is Σ_1, then

$$\sigma_e = \sigma_{pot} + (1/N_a)\,[\Sigma_1 + (S/4V)]$$

Systems having equal values of σ_e have equal resonance integrals. A comparison of a wide variety of measurements of resonance integrals as functions of σ_e is made in Ref. 34. In U^{238} mixtures, whether homogeneous or in isolated lumps, Vernon's result (see Section 4.2.1) yields:

$$(R.I.)_{eff} = 2.87\sqrt{\sigma_e + (5.93 - \sigma_0)}$$

4.2.2.2 Equivalence Principles for Lattices[33]

In addition to the two assumptions made in Section 4.2.2.1, two new assumptions must be made to derive an equivalence principle for lattices:

(1) *Principle of Reciprocity:* the ratio of escape probability from fuel to moderator, to that from moderator to fuel, is inversely proportional to the respective total cross sections. In Ref. 35, this is shown to be exact under the weak assumption of isotropic uniform distribution of neutrons in a fuel lump.

(2) *Condition of Detailed Equivalence:* The collision probability, P_0, at a given energy for the fuel in a lattice is equal to the collision probability at the same energy for an isolated lump of dimensions $(C)^{-1}$ times as large, where C is the flux reduction, or Dancoff factor. This condition is not exact but provides a close approximation to the actual probabilities for a lattice. Formulae for, and numerical values of, the Dancoff factor, C, are found in Section 4.2.3.

In lattices, the equivalence parameter is given by:

$$\sigma_e = \sigma_{pot} + \frac{1}{N_a}\left[\Sigma_1 + \frac{S(1-C)}{4V}\right]$$

Systems with the same value of σ_e have equal resonance integrals whether the fuel is homogeneously mixed, in an isolated lump, or in a lattice.

4.2.2.3 The Method of Escape Probabilities[33,35]

For an isolated lump, the method of escape probabilities yields the following formulae for the resonance integral in the N.R. approximation:

$$R.I. = \int \left(\frac{S}{4N_aV}\,\frac{\sigma_a + \sigma_s}{\sigma_t}\,G + \sigma_0\right)\frac{\sigma_a}{\sigma_t}\,\frac{dE}{E}$$

where σ_a is the absorption cross section, σ_s the anomalous scattering cross section, $\sigma_t = \sigma_a + \sigma_s + \sigma_0$; and G is the lump-penetrability factor and is related to the escape probability by: $1 - P_0(E)$ = escape probability = $(\lambda_0/\ell_0)\,G$.

In the N.R.I.M. approximation

$$R.I. = \int \left[\frac{S}{4N_aV}\left(\frac{G\sigma_a/\sigma_t}{1 - P_0p_{s0}}\right)\right]\frac{dE}{E}$$

where $p_{s0} = (\sigma_0 + \sigma_s)\,\sigma_t$.

In Sections 4.2.2.1 and 4.2.2.2 results were quoted which utilized Wigner's rational approximation: $G_a = (\ell_0/\lambda_0)/(1 + \ell_0/\lambda_0)$. Here, corrections to this approximation arising from the neglect of geometrical factors are discussed. Table 4-24 is a comparison of G_a with exact values of G for various sizes.

If the cross sections at 0°K are used, and interference between potential and anomalous scattering is neglected, it is possible to compute a resonance integral for spheres for a single resonance using the exact G and the approximate value G_a. Then the ratio of the resonance integral for a finite sphere, to that of an infinite sphere, is a function of $\lambda_0 m/\ell_0$ where $\lambda_0 m = 1/N_a\sigma_0$. Figure 4-7 gives I_{exact}, the value of the ratio of resonance integrals using exact values of G, and I_{approx}, the ratio obtained using

approximate values of G_a. The correction is never larger than 10.5%. Figure 4-7 should provide a good indication of the geometric correction in general.

Lattices. In lattices, the use of the Wigner's rational approximation together with the Dancoff correction leads to further errors. In slab lattices with fuel zones of width a, and moderator zones of width b,

$$G = 1 - 2\sum_{m=0}^{\infty} \{E_3[(m+1)\Sigma_U a + m\Sigma_M b] + E_3[m\Sigma_U a + (m+1)\Sigma_M b] - 2E_3[(m+1)(\Sigma_U a + \Sigma_M b)]\}$$

For an array of cylindrical fuel rods of radius a, imbedded in a concentric cylinder of moderator, radius b:

$$G = 1 - \frac{4}{\pi}\sum_{m=0}^{\infty}\int_0^{\pi/2} \{Ki_3[2(m+1)A + 2mB] + Ki_3[2mA + 2(m+1)B] - 2Ki_3[2(m+1)(A+B)]\}\cos\Psi d\Psi$$

where $A = \Sigma_U a \cos\Psi$

$B = \Sigma_M(\sqrt{b^2 - a^2\sin^2\Psi} - a\cos\Psi)$

Σ_U, Σ_M = total cross sections for fuel and moderator, respectively

The functions Ki_3 are discussed further in Section 4.2.3.

Wigner's rational approximation to $1 - P_0 = \lambda_0 G/\ell_0$ is:

$$1 - P_0 = 1/[1 + (\ell_0/\lambda_0)/(1 - C)]$$

Table 4-24 — PENETRABILITY FACTOR G

l_0/λ_0	Sphere	Cylinder	Slab	Approximate G_a (Wigner)
0.0	0.0	0.0	0.0	0.0
0.04	0.0391	0.0390	0.0381	0.0384
0.08	0.0765	0.0760	0.0734	0.0741
0.20	0.179	0.177	0.167	0.167
0.40	0.323	0.317	0.296	0.286
0.80	0.531	0.522	0.485	0.444
1.0	0.606	0.596	0.557	0.500
2.0	0.822	0.814	0.781	0.667
3.0	0.912	0.906	0.888	0.750
4.0	0.945	0.944	0.940	0.800
6.0	0.975	0.977	0.982	0.857
8.0	0.986	0.988	0.999	0.889
∞	1	1	1	1

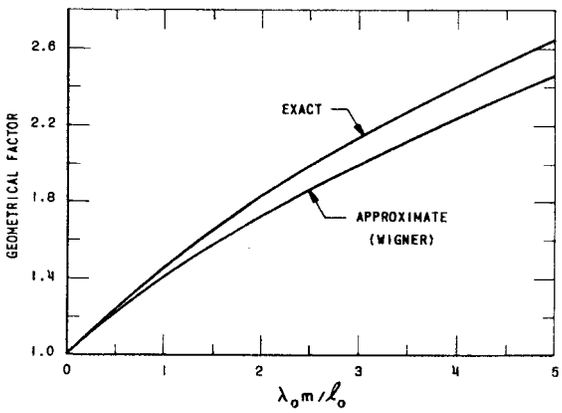

Fig. 4-7 — Comparison of exact with approximate geometrical factors. *Reproduced from Ref. 33.*

Rothenstein[35] has suggested an improved rational approximation:

$$1 - P_0 = \left[\left(1+\frac{\ell_0/\lambda_0}{1-C}\right)-\left(\frac{K\ell_0/\lambda_0}{K\ell_0/\lambda_0+1}\right)\right]^{-1}$$

where K is an adjustable parameter. For cylinders:

$$K = \tfrac{1}{3} \text{ in the limit } \ell_0/\lambda_0 \to 0$$
$$= \tfrac{4}{3} \text{ in the limit } \ell_0/\lambda_0 \to \infty$$

For slabs

$$K = \infty \text{ in the limit } \ell_0/\lambda_0 \to \infty$$
$$= \tfrac{5}{8} + \tfrac{1}{4}\{\gamma + \log[(\ell_0/\lambda_0)/2]\} \text{ in the limit } \ell_0/\lambda_0 \to 0$$

Bell[36] has proposed the following approximation:

$$1 - P_0 \approx 1/\{1 + [(\ell_0/\lambda_0)/f_1]\}$$

where $f_1 = 1/[1 + (\lambda_1/\ell_1)]$
λ_1 = mean free path in moderator
ℓ_1 = mean chord length in the moderator

Exact calculations have been carried out for slab lattices, and Monte Carlo calculations for cylinders.[33] The significant results of the study are:

(1) The Wigner and Bell approximations give the correct trends but underestimate the collision probabilities for most of the range by 10% and 15%, respectively.

(2) Rothenstein's method for cylinders using K = 4/3 agrees well with the exact calculation over most of the range. In those portions of the range for which K = 4/3 does not agree well with calculation, K = 1/3 does give good agreement. The discrepancies are such that the average, over the entire range, of the results from K = 4/3 and K = 1/3 is very little in error.

(3) The equivalence relationship for lattices shows excellent agreement over a wide range. It estimates the resonance integral to within 1.5% for 1 − C = 0.54, and to within 0.5% for 1 − C = 0.8; the agreement is better than 0.1% for 1 − C = 0.9 or more. In contrast, the Wigner and Bell approximations to the escape probability underestimate the resonance integral by 6 to 8%. Rothenstein's method overestimates by 3 or 4% for K = 4/3, and underestimates by the same amount for K = 1/3.

Variational Methods. Corngold[37] has presented a variational principle for the resonance escape probability. The method is presented for homogeneous mixtures; equivalence methods can be used to extend the method to heterogeneous systems.

4.2.3 CORRECTIONS TO THE SURFACE AREA ARISING FROM SHADOWING: THE DANCOFF CORRECTION

In a lattice of rods, the presence of one rod depletes the flux at the peak of the resonance which is incident on another rod, and thus leads to a *reduction* of the effective surface. In the formula for the effective resonance integral, the factor which multiplies the surface area, S, is $(1 - \sum C_i)$, where the summation for any rod extends over all other rods, and C_i is a function of both the size of the rods and the distance to rod i.

Bell's Approximation.[36] Bell's approximation to the flux reduction (Dancoff) factor has been indirectly referred to in Section 4.2.2.3. In his approximation, the surface area of a fuel lump is multiplied by:

$$1/[1 + (S/4V_M\Sigma_M)]$$

where V_M is the volume of the moderator, and Σ_M is the moderator macroscopic scattering cross section.

The Dancoff Factor. The formula for C given by Dancoff and Ginsburg[38] is:

$$C = \frac{\rho d_i^2}{\lambda^3 \pi^2} \int\int d\theta\, d\theta' \frac{Ki_3(|\vec{\rho} - \vec{\rho}'|/\lambda)}{|\vec{\rho} - \vec{\rho}'|^3/\lambda^3} \left\{\cos\theta - \frac{\rho}{d_i}[1 + \cos(\theta + \theta')]\right\} \left\{\cos\theta - \frac{\rho}{d_i}[1 + \cos(\theta + \theta')]\right\}$$

$$|\vec{\rho} - \vec{\rho}'| = \sqrt{d^2 - 2d\rho\,(\cos\theta + \cos\theta') + 2\rho^2\,[1 + \cos(\theta + \theta')]}$$

where $\vec{\rho}, \vec{\rho}'$ are the radius vectors of the rod under consideration, and rod i, respectively, measured in each case from the center of the rod to its circumference in a plane perpendicular to the rod axis; θ and θ' are the angle these vectors make with the line of centers between the reference rod and rod i; λ is the moderator mean free path; d_i is the distance between the center of the rods; and Ki_3 is discussed in Ref. 39. Limits on θ and θ' are such that a straight line joining the points of integration does not pass through the interior of either rod in the interval included between the two points. The mean value theorem of integral calculus shows that C may be written in the form:

$$C = \frac{4}{\pi^2} Ki_3 \left[\delta\left(\frac{d}{\rho}\right)\frac{\rho}{\lambda}\right] f\left(\frac{\rho}{d}\right) \tag{4-12}$$

As $\lambda \to \infty$

$$C \to \sin^{-1}(\rho/d)/\pi$$

$$Ki_3 \to \pi/4$$

$$f(\rho/d) \to \sin^{-1}(\rho/d)$$

and $\delta(d/\rho)$ is obtained by comparison of Eq. (4-12) with values of C obtained by numerical integration.* The results are shown in Fig. 4-8. Note that d/ρ must be greater than 2. If $d/\rho > 3.8$, the following asymptotic form may be used:

$$C = \frac{\lambda^2}{\rho d}\sqrt{\frac{\pi\lambda}{2d}}\, e^{-d/\lambda}\left\{\frac{-2(\rho/\lambda)}{\pi}\int_0^{\pi/2} d\theta\, \cos\theta \exp[(\rho\cos\theta)/\lambda]\right\}^2$$

$$C = \frac{4}{\pi^2}\left(\sin^{-1}\frac{\rho}{d}\right) Ki_3\left[\left(\frac{d}{\rho} - 1.78\right)\frac{\rho}{\lambda}\right] \text{ is a fit to Eq. (4-12)}$$

The surface correction term for slabs is:

$$1 - C = [1 - 2\,E_3(\Sigma_s d)]$$

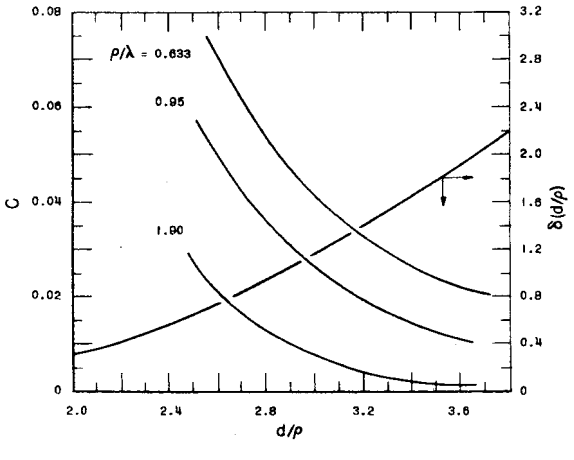

Fig. 4-8—Dancoff-Ginsburg correction factor. *Data from Ref. 38.*

*The use of the mean value theorem and the graph of $\delta(d/\rho)$ was suggested by J. A. Thie; B. J. Toppel of ANL suggested the use of the expression $\delta(d/\rho) = (d/\rho) - 1.78$.

where d = distance between fuel plates
Σ_s = scattering cross section in the moderator
$E_3(x) = \int_1^\infty e^{-xU} U^{-3}\, dU$

Values of $E_n(x)$ are tabulated in Ref. 12.

For a hollow rod[40] of outer surface area S_0 and an inner surface area S_i, with moderator in the center hole, replace S by

$$S_0 + \gamma S_i$$

where $\gamma = 2R_i \Sigma_s P_c(R_i \Sigma_s)$
R_i = inner radius
Σ_s = scattering cross section of the moderator
P_c = collision probability tabulated in Ref. 12

The formula:

$$C = \frac{4}{\pi}\int_0^{\pi/2} \mathrm{Ki}_3\left(\frac{2\rho}{\lambda}\sin x\right)\sin x\, dx$$

has also been suggested. The integral can be computed using Table 4-26.

Values of C, as defined by the Dancoff-Ginsburg equation, are given in Table 4-25. Values of $\mathrm{Ki}_3(x)$ are given in Table 4-26, as well as in Ref. 39. The data for Table 4-25 were supplied by I. Carlvik (AB Atomenergi, Stockholm), while Table 4-26 was computed by H. J. Wheeler (Argonne National Laboratory).

4.2.4 MONTE CARLO CALCULATION OF RESONANCE ESCAPE[41]

The Monte Carlo calculation of resonance escape gives a useful numerical check on the accuracy of computations made by analytical methods (e.g., the N.R. and N.R.I.M. approximations discussed in Section 4.2.1).

Histories of neutrons are followed through the neutron energy range $E_{max} \geq E \geq E_{min}$ where E_{min} might be chosen as the "Cd cutoff" energy, and E_{max} of the order of 0.01 to 0.1 Mev.

Each cell consists of a number of regions. Each region is a homogeneous mixture of isotopes.

Neutron histories start with injection into the assembly at an energy $E \leq E_{max}$ and with velocity determined by the assumption that the flux above E_{max} has a 1/E energy dependence and is isotropic.

Elastic scatterings are assumed to be isotropic in the center-of-mass system. Nuclei are in thermal motion which results in the Doppler broadening of the resonances.

Treatment of Isotopes Other than U^{238}.

σ_s = constant

$\sigma_a(E) = \sigma_a(1\text{ ev})/\sqrt{E}$

where E is measured in ev.

Treatment of U^{238}.

σ_s potential = 10.75 barns

background $\sigma_a(E)$ = background $\sigma_a(1\text{ ev})/\sqrt{E}$

At resonance:

$$\sigma_a(E,T) = \sqrt{E_0/E}\ \sigma_{ra}\ \psi(x,\theta)$$

$$\sigma_s(E,T) = \sigma_{rs}\ \psi(x,\theta) + \sqrt{\sigma_{pot}\sigma_{rs}}\ \chi(x,\theta)$$

$$\sigma_{ra} = 4\pi\lambda_0^2\, g[(\Gamma_n/\Gamma_\gamma)/\Gamma^2]$$

$$\sigma_{rs} = 4\pi\lambda_0^2\, g\,(\Gamma_n^2/\Gamma^2)$$

Table 4-25 — SHADOWING IN THE CASE OF TWO PARALLEL CIRCULAR CYLINDERS

(Dancoff-Ginsburg Correction Factor, C)

Note: Values of C are correct to three decimal places.

$\frac{d}{\rho}$	$\frac{\rho}{\lambda} = 0.00$	0.05	0.10	0.15	0.20	0.25	$\frac{d}{\rho}$	$\frac{\rho}{\lambda} = 0.00$	0.05	0.10	0.15	0.20	0.25
2.00	0.1817	0.1792	0.1767	0.1744	0.1721	0.1699	5.00	0.0646	0.0523	0.0426	0.0349	0.0287	0.0236
2.05	0.1749	0.1718	0.1688	0.1659	0.1632	0.1605	5.10	0.0633	0.0510	0.0413	0.0366	0.0274	0.0225
2.10	0.1691	0.1654	0.1620	0.1586	0.1554	0.1523	5.20	0.0620	0.0497	0.0400	0.0324	0.0263	0.0214
2.15	0.1638	0.1597	0.1558	0.1520	0.1484	0.1449	5.30	0.0608	0.0484	0.0388	0.0312	0.0252	0.0204
2.20	0.1590	0.1544	0.1501	0.1460	0.1420	0.1382	5.40	0.0597	0.0472	0.0376	0.0301	0.0241	0.0194
2.25	0.1545	0.1495	0.1448	0.1404	0.1361	0.1320	5.50	0.0586	0.0460	0.0364	0.0290	0.0231	0.0185
2.30	0.1503	0.1450	0.1399	0.1351	0.1306	0.1262	5.60	0.0575	0.0449	0.0353	0.0279	0.0222	0.0176
2.35	0.1464	0.1407	0.1354	0.1303	0.1255	0.1209	5.70	0.0565	0.0438	0.0343	0.0269	0.0213	0.0168
2.40	0.1427	0.1368	0.1311	0.1258	0.1207	0.1159	5.80	0.0555	0.0428	0.0332	0.0260	0.0204	0.0160
2.45	0.1393	0.1330	0.1271	0.1216	0.1163	0.1113	5.90	0.0545	0.0418	0.0323	0.0251	0.0196	0.0153
2.50	0.1360	0.1294	0.1232	0.1174	0.1119	0.1068	6.00	0.0536	0.0408	0.0313	0.0242	0.0188	0.0146
2.55	0.1329	0.1260	0.1196	0.1136	0.1080	0.1027	6.10	0.0527	0.0399	0.0304	0.0234	0.0180	0.0139
2.60	0.1300	0.1228	0.1162	0.1100	0.1042	0.0988	6.20	0.0518	0.0390	0.0296	0.0226	0.0173	0.0133
2.65	0.1272	0.1198	0.1129	0.1066	0.1006	0.0951	6.30	0.0509	0.0381	0.0287	0.0218	0.0166	0.0127
2.70	0.1245	0.1169	0.1098	0.1033	0.0972	0.0916	6.40	0.0501	0.0373	0.0279	0.0211	0.0160	0.0122
2.75	0.1219	0.1141	0.1069	0.1002	0.0940	0.0883	6.50	0.0493	0.0364	0.0272	0.0104	0.0154	0.0116
2.80	0.1195	0.1115	0.1041	0.0972	0.0910	0.0851	6.60	0.0486	0.0357	0.0264	0.0197	0.0148	0.0111
2.85	0.1171	0.1089	0.1014	0.0944	0.0880	0.0821	6.70	0.0479	0.0349	0.0257	0.0191	0.0142	0.0107
2.90	0.1149	0.1065	0.0988	0.0917	0.0852	0.0793	6.80	0.0472	0.0342	0.0251	0.0185	0.0137	0.0102
2.95	0.1128	0.1041	0.0963	0.0891	0.0826	0.0766	6.90	0.0465	0.0335	0.0244	0.0179	0.0132	0.0098
3.00	0.1107	0.1019	0.0939	0.0867	0.0801	0.0740	7.00	0.0458	0.0328	0.0238	0.0173	0.0127	0.0094
3.05	0.1087	0.0997	0.0916	0.0843	0.0776	0.0715	7.10	0.0451	0.0321	0.0232	0.0168	0.0123	0.0090
3.10	0.1068	0.0977	0.0894	0.0820	0.0753	0.0692	7.20	0.0445	0.0315	0.0226	0.0163	0.0118	0.0086
3.15	0.1050	0.0957	0.0873	0.0798	0.0731	0.0669	7.30	0.0439	0.0309	0.0220	0.0158	0.0114	0.0083
3.20	0.1032	0.0937	0.0853	0.0777	0.0709	0.0648	7.40	0.0433	0.0303	0.0214	0.0153	0.0110	0.0079
3.25	0.1014	0.0919	0.0834	0.0757	0.0689	0.0627	7.50	0.0427	0.0297	0.0209	0.0149	0.0106	0.0076
3.30	0.0998	0.0901	0.0815	0.0738	0.0669	0.0608	7.60	0.0422	0.0291	0.0204	0.0144	0.0102	0.0073
3.35	0.0982	0.0884	0.0797	0.0719	0.0650	0.0589	7.70	0.0416	0.0286	0.0199	0.0140	0.0099	0.0070
3.40	0.0966	0.0867	0.0779	0.0701	0.0632	0.0570	7.80	0.0411	0.0280	0.0194	0.0135	0.0095	0.0067
3.45	0.0951	0.0851	0.0762	0.0684	0.0615	0.0553	7.90	0.0405	0.0275	0.0189	0.0131	0.0092	0.0064
3.50	0.0937	0.0835	0.0746	0.0667	0.0598	0.0536	8.00	0.0400	0.0270	0.0184	0.0127	0.0088	0.0062
3.55	0.0923	0.0820	0.0730	0.0651	0.0582	0.0520	8.10	0.0395	0.0265	0.0180	0.0123	0.0085	0.0059
3.60	0.0909	0.0805	0.0715	0.0636	0.0566	0.0505	8.20	0.0390	0.0260	0.0176	0.0120	0.0082	0.0057
3.65	0.0896	0.0791	0.0700	0.0620	0.0551	0.0490	8.30	0.0385	0.0255	0.0172	0.0116	0.0079	0.0055
3.70	0.0883	0.0777	0.0685	0.0606	0.0536	0.0476	8.40	0.0381	0.0250	0.0167	0.0113	0.0077	0.0052
3.75	0.0871	0.0764	0.0672	0.0592	0.0522	0.0462	8.50	0.0376	0.0246	0.0163	0.0110	0.0074	0.0050
3.80	0.0859	0.0751	0.0658	0.0578	0.0509	0.0449	8.60	0.0372	0.0242	0.0160	0.0107	0.0072	0.0048
3.85	0.0847	0.0738	0.0645	0.0565	0.0496	0.0436	8.70	0.0367	0.0237	0.0156	0.0103	0.0069	0.0046
3.90	0.0836	0.0726	0.0632	0.0552	0.0483	0.0423	8.80	0.0363	0.0233	0.0152	0.0101	0.0067	0.0045
3.95	0.0825	0.0714	0.0620	0.0540	0.0471	0.0412	8.90	0.0359	0.0229	0.0149	0.0098	0.0065	0.0043
4.00	0.0814	0.0702	0.0608	0.0528	0.0459	0.0400	9.00	0.0355	0.0225	0.0146	0.0095	0.0062	0.0041
4.05	0.0803	0.0691	0.0597	0.0516	0.0448	0.0389	9.10	0.0351	0.0221	0.0142	0.0092	0.0060	0.0040
4.10	0.0793	0.0680	0.0585	0.0505	0.0437	0.0378	9.20	0.0347	0.0218	0.0139	0.0090	0.0058	0.0038
4.15	0.0783	0.0669	0.0574	0.0494	0.0426	0.0368	9.30	0.0344	0.0214	0.0136	0.0087	0.0057	0.0037
4.20	0.0773	0.0659	0.0564	0.0484	0.0416	0.0358	9.40	0.0340	0.0211	0.0133	0.0085	0.0055	0.0035
4.25	0.0764	0.0649	0.0553	0.0473	0.0406	0.0348	9.50	0.0336	0.0207	0.0130	0.0083	0.0053	0.0034
4.30	0.0754	0.0639	0.0543	0.0463	0.0396	0.0339	9.60	0.0333	0.0204	0.0127	0.0080	0.0051	0.0033
4.35	0.0745	0.0629	0.0534	0.0454	0.0386	0.0330	9.70	0.0329	0.0200	0.0124	0.0078	0.0050	0.0032
4.40	0.0737	0.0620	0.0524	0.0444	0.0377	0.0321	9.80	0.0326	0.0197	0.0122	0.0076	0.0048	0.0030
4.45	0.0728	0.0611	0.0515	0.0435	0.0369	0.0313	9.90	0.0323	0.0194	0.0119	0.0074	0.0046	0.0029
4.50	0.0720	0.0602	0.0506	0.0426	0.0360	0.0305	10.00	0.0319	0.0191	0.0116	0.0072	0.0045	0.0028
4.60	0.0704	0.0585	0.0488	0.0409	0.0344	0.0289							
4.70	0.0688	0.0568	0.0472	0.0393	0.0328	0.0274							
4.80	0.0673	0.0553	0.0456	0.0377	0.0313	0.0261							
4.90	0.0659	0.0538	0.0441	0.0363	0.0300	0.0248							

Table 4-25 — SHADOWING IN THE CASE OF TWO PARALLEL CIRCULAR CYLINDERS (Continued)

(Dancoff-Ginsburg Correction Factor, C)

Note: Values of C are correct to three decimal places.

$\frac{d}{\rho}$	$\frac{\rho}{\lambda} = 0.30$	0.35	0.40	0.45	0.50	$\frac{d}{\rho}$	$\frac{\rho}{\lambda} = 0.30$	0.35	0.40	0.45	0.50
2.00	0.1678	0.1658	0.1638	0.1619	0.1601	5.00	0.0191	0.0156	0.0128	0.0107	0.0091
2.05	0.1579	0.1554	0.1530	0.1506	0.1483	5.10	0.0181	0.0147	0.0120	0.0100	0.0085
2.10	0.1493	0.1464	0.1436	0.1409	0.1383	5.20	0.0171	0.0138	0.0112	0.0093	0.0079
2.15	0.1416	0.1383	0.1352	0.1322	0.1293	5.30	0.0162	0.0129	0.0105	0.0087	0.0073
2.20	0.1345	0.1310	0.1276	0.1243	0.1212	5.40	0.0153	0.0121	0.0098	0.0080	0.0068
2.25	0.1280	0.1242	0.1206	0.1171	0.1138	5.50	0.0145	0.0114	0.0091	0.0075	0.0063
2.30	0.1220	0.1180	0.1142	0.1105	0.1070	5.60	0.0137	0.0107	0.0085	0.0069	0.0058
2.35	0.1165	0.1123	0.1083	0.1045	0.1008	5.70	0.0129	0.0100	0.0079	0.0064	0.0054
2.40	0.1113	0.1070	0.1028	0.0989	0.0951	5.80	0.0122	0.0094	0.0074	0.0060	0.0050
2.45	0.1065	0.1020	0.0978	0.0937	0.0899	5.90	0.0116	0.0088	0.0068	0.0055	0.0047
2.50	0.1019	0.0973	0.0929	0.0888	0.0849	6.00	0.0109	0.0083	0.0064	0.0051	0.0043
2.55	0.0977	0.0929	0.0885	0.0343	0.0803	6.10	0.0104	0.0077	0.0059	0.0047	0.0040
2.60	0.0937	0.0888	0.0843	0.0801	0.0761	6.20	0.0098	0.0072	0.0055	0.0044	0.0037
2.65	0.0899	0.0850	0.0804	0.0761	0.0721	6.30	0.0093	0.0068	0.0051	0.0041	0.0035
2.70	0.0863	0.0813	0.0767	0.0724	0.0684	6.40	0.0088	0.0064	0.0047	0.0038	0.0032
2.75	0.0829	0.0779	0.0733	0.0690	0.0649	6.50	0.0083	0.0060	0.0044	0.0035	0.0030
2.80	0.0797	0.0747	0.0700	0.0657	0.0617	6.60	0.0079	0.0056	0.0041	0.0032	0.0028
2.85	0.0767	0.0716	0.0669	0.0626	0.0586	6.70	0.0075	0.0052	0.0038	0.0030	0.0026
2.90	0.0738	0.0687	0.0640	0.0597	0.0558	6.80	0.0071	0.0049	0.0035	0.0028	0.0024
2.95	0.0710	0.0659	0.0613	0.0570	0.0531	6.90	0.0067	0.0046	0.0033	0.0026	0.0023
3.00	0.0684	0.0633	0.0587	0.0544	0.0505	7.00	0.0063	0.0043	0.0030	0.0024	0.0021
3.05	0.0659	0.0608	0.0562	0.0520	0.0481	7.10	0.0060	0.0040	0.0028	0.0022	0.0020
3.10	0.0636	0.0585	0.0539	0.0497	0.0458	7.20	0.0057	0.0038	0.0026	0.0020	0.0019
3.15	0.0613	0.0562	0.0516	0.0475	0.0437	7.30	0.0054	0.0035	0.0024	0.0019	0.0017
3.20	0.0592	0.0541	0.0495	0.0454	0.0417	7.40	0.0051	0.0033	0.0022	0.0017	0.0016
3.25	0.0571	0.0521	0.0475	0.0434	0.0398	7.50	0.0049	0.0031	0.0020	0.0016	0.0015
3.30	0.0551	0.0501	0.0456	0.0416	0.0379	7.60	0.0046	0.0029	0.0019	0.0015	0.0014
3.35	0.0533	0.0482	0.0438	0.0398	0.0362	7.70	0.0044	0.0026	0.0017	0.0013	0.0014
3.40	0.0514	0.0465	0.0420	0.0381	0.0346	7.80	0.0041	0.0024	0.0015	0.0012	0.0013
3.45	0.0497	0.0448	0.0404	0.0365	0.0331	7.99	0.0039	0.0022	0.0014	0.0011	0.0012
3.50	0.0481	0.0431	0.0388	0.0350	0.0316	8.00	0.0036	0.0021	0.0012	0.0010	0.0011
3.55	0.0465	0.0416	0.0373	0.0335	0.0302	8.10	0.0034	0.0019	0.0011	0.0009	0.0010
3.60	0.0450	0.0401	0.0359	0.0322	0.0289	8.20	0.0032	0.0017	0.0010	0.0008	0.0009
3.65	0.0435	0.0387	0.0345	0.0309	0.0277	8.30	0.0031	0.0016	0.0009	0.0007	0.0009
3.70	0.0421	0.0373	0.0332	0.0296	0.0265	8.40	0.0029	0.0014	0.0008	0.0006	0.0008
3.75	0.0407	0.0360	0.0319	0.0284	0.0253	8.50	0.0027	0.0013	0.0006	0.0005	0.0008
3.80	0.0395	0.0348	0.0307	0.0273	0.0243	8.60	0.0025	0.0012	0.0006	0.0005	0.0007
3.85	0.0382	0.0336	0.0296	0.0262	0.0232	8.70	0.0024	0.0011	0.0005	0.0004	0.0007
3.90	0.0370	0.0324	0.0285	0.0251	0.0223	8.80	0.0022	0.0010	0.0004	0.0003	0.0006
3.95	0.0359	0.0313	0.0274	0.0241	0.0213	8.90	0.0021	0.0008	0.0003	0.0003	0.0006
4.00	0.0347	0.0302	0.0264	0.0232	0.0205	9.00	0.0020	0.0007	0.0002	0.0002	0.0006
4.05	0.0337	0.0292	0.0255	0.0223	0.0196	9.10	0.0019	0.0006	0.0002	0.0002	0.0005
4.10	0.0326	0.0282	0.0245	0.0214	0.0188	9.20	0.0017	0.0006	0.0001	0.0001	0.0005
4.15	0.0316	0.0273	0.0236	0.0206	0.0180	9.30	0.0016	0.0005	0.0000	0.0001	0.0005
4.20	0.0307	0.0264	0.0228	0.0198	0.0173	9.40	0.0015	0.0004	0.0000	0.0000	0.0004
4.25	0.0298	0.0255	0.0220	0.0190	0.0166	9.50	0.0014	0.0003	0.0001	0.0000	0.0004
4.30	0.0289	0.0247	0.0212	0.0183	0.0159	9.60	0.0013	0.0002	0.0001	0.0000	0.0004
4.35	0.0280	0.0239	0.0204	0.0176	0.0153	9.70	0.0012	0.0002	0.0002	0.0001	0.0004
4.40	0.0272	0.0231	0.0197	0.0169	0.0147	9.80	0.011	0.0001	0.0002	0.0001	0.0003
4.45	0.0264	0.0223	0.0190	0.0163	0.0141	9.90	0.0010	0.0000	0.0003	0.0001	0.0003
4.50	0.0256	0.0216	0.0183	0.0157	0.0135	10.00	0.0010	0.0000	0.0003	0.0002	0.0003
4.60	0.0241	0.0202	0.0171	0.0145	0.0125						
4.70	0.0227	0.0189	0.0159	0.0135	0.0115						
4.80	0.0215	0.0177	0.0148	0.0125	0.0107						
4.90	0.0203	0.0166	0.0138	0.0116	0.0099						

Table 4-25 — SHADOWING IN THE CASE OF TWO PARALLEL CIRCULAR CYLINDERS (Continued)

(Dancoff-Ginsburg Correction Factor, C)

Note: Values of C are correct to three decimal places.

$\frac{d}{\rho}$	$\frac{\rho}{\lambda}=0.55$	0.60	0.65	0.70	0.75	$\frac{d}{\rho}$	$\frac{\rho}{\lambda}=0.55$	0.60	0.65	0.70	0.75
2.00	0.1583	0.1566	0.1549	0.1533	0.1517	5.00	0.0075	0.0062	0.0051	0.0043	0.0036
2.05	0.1461	0.1440	0.1419	0.1399	0.1379	5.10	0.0069	0.0057	0.0047	0.0039	0.0033
2.10	0.1357	0.1332	0.1308	0.1285	0.1263	5.20	0.0064	0.0052	0.0043	0.0036	0.0030
2.15	0.1264	0.1237	0.1211	0.1185	0.1160	5.30	0.0059	0.0048	0.0039	0.0032	0.0027
2.20	0.1181	0.1152	0.1123	0.1096	0.1069	5.40	0.0054	0.0044	0.0036	0.0029	0.0025
2.25	0.1106	0.1074	0.1045	0.1016	0.0988	5.50	0.0050	0.0040	0.0032	0.0027	0.0022
2.30	0.1036	0.1004	0.0973	0.0943	0.0914	5.60	0.0046	0.0037	0.0029	0.0024	0.0020
2.35	0.0973	0.0940	0.0908	0.0877	0.0848	5.70	0.0042	0.0033	0.0027	0.0022	0.0018
2.40	0.0915	0.0881	0.0848	0.0817	0.0787	5.80	0.0039	0.0031	0.0024	0.0020	0.0016
2.45	0.0862	0.0827	0.0794	0.0763	0.0733	5.90	0.0036	0.0028	0.0022	0.0018	0.0015
2.50	0.0812	0.0776	0.0743	0.0711	0.0681	6.00	0.0033	0.0025	0.0020	0.0016	0.0013
2.55	0.0766	0.0730	0.0697	0.0655	0.0634	6.10	0.0030	0.0023	0.0018	0.0014	0.0012
2.60	0.0723	0.0688	0.0654	0.0622	0.0592	6.20	0.0028	0.0021	0.0016	0.0013	0.0011
2.65	0.0683	0.0648	0.0614	0.0582	0.0553	6.30	0.0026	0.0019	0.0015	0.0012	0.0010
2.70	0.0646	0.0611	0.0577	0.0546	0.0516	6.40	0.0024	0.0018	0.0013	0.0010	0.0009
2.75	0.0612	0.0576	0.0543	0.0512	0.0483	6.50	0.0022	0.0016	0.0012	0.0009	0.0008
2.80	0.0579	0.0544	0.0511	0.0481	0.0452	6.60	0.0020	0.0015	0.0011	0.0008	0.0007
2.85	0.0549	0.0514	0.0481	0.0451	0.0423	6.70	0.0019	0.0013	0.0010	0.0008	0.0007
2.90	0.0520	0.0486	0.0454	0.0424	0.0397	6.80	0.0017	0.0012	0.0009	0.0007	0.0006
2.95	0.0494	0.0459	0.0428	0.0399	0.0372	6.90	0.0016	0.0011	0.0008	0.0006	0.0005
3.00	0.0469	0.0435	0.0404	0.0376	0.0349	7.00	0.0015	0.0010	0.0008	0.0006	0.0005
3.05	0.0445	0.0412	0.0381	0.0353	0.0328	7.10	0.0014	0.0010	0.0007	0.0005	0.0005
3.10	0.0423	0.0390	0.0360	0.0333	0.0308	7.20	0.0013	0.0009	0.0006	0.0005	0.0004
3.15	0.0402	0.0370	0.0340	0.0314	0.0289	7.30	0.0012	0.0008	0.0006	0.0005	0.0004
3.20	0.0382	0.0350	0.0322	0.0296	0.0272	7.40	0.0011	0.0008	0.0005	0.0004	0.0004
3.25	0.0363	0.0332	0.0304	0.0279	0.0256	7.50	0.0010	0.0007	0.0005	0.0004	0.0003
3.30	0.0346	0.0315	0.0288	0.0263	0.0241	7.60	0.0010	0.0006	0.0004	0.0004	0.0003
3.35	0.0329	0.0299	0.0273	0.0248	0.0227	7.70	0.0009	0.0006	0.0004	0.0003	0.0003
3.40	0.0314	0.0284	0.0258	0.0235	0.0214	7.80	0.0008	0.0005	0.0004	0.0003	0.0003
3.45	0.0299	0.0270	0.0244	0.0222	0.0201	7.90	0.0007	0.0005	0.0003	0.0002	0.0002
3.50	0.0285	0.0257	0.0232	0.0210	0.0190	8.00	0.0007	0.0004	0.0003	0.0002	0.0002
3.55	0.0271	0.0244	0.0220	0.0198	0.0179	8.10	0.0006	0.0004	0.0002	0.0002	0.0002
3.60	0.0259	0.0232	0.0208	0.0187	0.0169	8.20	0.0006	0.0003	0.0002	0.0002	0.0002
3.65	0.0247	0.0221	0.0198	0.0177	0.0159	8.30	0.0005	0.0003	0.0002	0.0001	0.0001
3.70	0.0236	0.0210	0.0187	0.0168	0.0150	8.40	0.0005	0.0003	0.0002	0.0001	0.0001
3.75	0.0225	0.0200	0.0178	0.0159	0.0142	8.50	0.0004	0.0002	0.0001	0.0001	0.0001
3.80	0.0215	0.0190	0.0169	0.0150	0.0134	8.60	0.0004	0.0002	0.0001	0.0001	0.0001
3.85	0.0205	0.0181	0.0160	0.0142	0.0127	8.70	0.0004	0.0002	0.0001	0.0001	0.0001
3.90	0.0196	0.0172	0.0152	0.0135	0.0120	8.80	0.0003	0.0002	0.0001	0.0001	0.0001
3.95	0.0187	0.0164	0.0145	0.0128	0.0113	8.90	0.0003	0.0002	0.0001	0.0001	0.0001
4.00	0.0179	0.0157	0.0137	0.0121	0.0107	9.00	0.0003	0.0001	0.0001	0.0001	0.0001
4.05	0.0171	0.0149	0.0131	0.0115	0.0101	9.10	0.0003	0.0001	0.0001	0.0000	0.0001
4.10	0.0163	0.0142	0.0124	0.0109	0.0096	9.20	0.0003	0.0001	0.0001	0.0000	0.0001
4.15	0.0156	0.0136	0.0118	0.0103	0.0091	9.30	0.0002	0.0001	0.0000	0.0000	0.0001
4.20	0.0149	0.0129	0.0112	0.0098	0.0086	9.40	0.0002	0.0001	0.0000	0.0000	0.0001
4.25	0.0143	0.0123	0.0107	0.0093	0.0081	9.50	0.0002	0.0001	0.0000	0.0000	0.0001
4.30	0.0137	0.0118	0.0102	0.0088	0.0077	9.60	0.0002	0.0001	0.0000	0.0000	0.0000
4.35	0.0131	0.0113	0.0097	0.0084	0.0073	9.70	0.0002	0.0001	0.0000	0.0000	0.0000
4.40	0.0125	0.0107	0.0092	0.0079	0.0069	9.80	0.0001	0.0000	0.0000	0.0000	0.0000
4.45	0.0120	0.0102	0.0088	0.0075	0.0065	9.90	0.0001	0.0000	0.0000	0.0000	0.0000
4.50	0.0115	0.0098	0.0083	0.0072	0.0062	10.00	0.0001	0.0000	0.0000	0.0000	0.0000
4.60	0.0105	0.0089	0.0076	0.0064	0.0056						
4.70	0.0097	0.0081	0.0063	0.0058	0.0050						
4.80	0.0089	0.0074	0.0062	0.0053	0.0045						
4.90	0.0082	0.0068	0.0056	0.0047	0.0040						

Table 4-25— SHADOWING IN THE CASE OF TWO PARALLEL CIRCULAR CYLINDERS (Continued)

(Dancoff-Ginsburg Correction Factor, C)

Note: Values of C are correct to three decimal places.

$\frac{d}{\rho}$	$\frac{\rho}{\lambda} = 0.80$	0.85	0.90	0.95	1.00	$\frac{d}{\rho}$	$\frac{\rho}{\lambda} = 0.80$	0.85	0.90	0.95	1.00
2.00	0.1501	0.1486	0.1472	0.1458	0.1444	5.00	0.0030	0.0025	0.0021	0.0017	0.0015
2.05	0.1360	0.1341	0.1323	0.1305	0.1288	5.10	0.0027	0.0022	0.0019	0.0016	0.0013
2.10	0.1241	0.1219	0.1198	0.1178	0.1159	5.20	0.0025	0.0020	0.0017	0.0014	0.0012
2.15	0.1136	0.1113	0.1090	0.1068	0.1047	5.30	0.0022	0.0018	0.0015	0.0012	0.0010
2.20	0.1044	0.1019	0.0995	0.0971	0.0949	5.40	0.0020	0.0016	0.0013	0.0011	0.0009
2.25	0.0961	0.0935	0.0910	0.0886	0.0862	5.50	0.0018	0.0014	0.0012	0.0010	0.0008
2.30	0.0886	0.0859	0.0833	0.0809	0.0785	5.60	0.0016	0.0013	0.0010	0.0008	0.0007
2.35	0.0819	0.0792	0.0766	0.0741	0.0717	5.70	0.0014	0.0011	0.0009	0.0007	0.0006
2.40	0.0759	0.0731	0.0705	0.0680	0.0656	5.80	0.0013	0.0010	0.0008	0.0006	0.0005
2.45	0.0704	0.0677	0.0650	0.0625	0.0801	5.90	0.0011	0.0009	0.0007	0.0006	0.0005
2.50	0.0652	0.0624	0.0598	0.0573	0.0550	6.00	0.0010	0.0008	0.0006	0.0005	0.0004
2.55	0.0606	0.0578	0.0553	0.0528	0.0505	6.10	0.0009	0.0007	0.0005	0.0004	0.0004
2.60	0.0564	0.0537	0.0511	0.0487	0.0464	6.20	0.0008	0.0006	0.0005	0.0004	0.0003
2.65	0.0524	0.0498	0.0473	0.0449	0.0427	6.30	0.0007	0.0005	0.0004	0.0003	0.0003
2.70	0.0489	0.0462	0.0438	0.0415	0.0393	6.40	0.0006	0.0005	0.0004	0.0003	0.0002
2.75	0.0456	0.0430	0.0406	0.0383	0.0362	6.50	0.0006	0.0004	0.0003	0.0002	0.0002
2.80	0.0425	0.0400	0.0377	0.0355	0.0334	6.60	0.0005	0.0004	0.0003	0.0002	0.0002
2.85	0.0397	0.0373	0.0350	0.0328	0.0309	6.70	0.0005	0.0003	0.0003	0.0002	0.0002
2.90	0.0371	0.0347	0.0325	0.0304	0.0285	6.80	0.0004	0.0003	0.0002	0.0002	0.0001
2.95	0.0347	0.0324	0.0302	0.0282	0.0264	6.90	0.0004	0.0003	0.0002	0.0002	0.0001
3.00	0.0325	0.0302	0.0281	0.0262	0.0244	7.00	0.0004	0.0003	0.0002	0.0001	0.0001
3.05	0.0304	0.0282	0.0262	0.0243	0.0226	7.10	0.0003	0.0002	0.0002	0.0001	0.0001
3.10	0.0285	0.0263	0.0244	0.0226	0.0209	7.20	0.0003	0.0002	0.0002	0.0001	0.0001
3.15	0.0267	0.0246	0.0227	0.0210	0.0194	7.30	0.0003	0.0002	0.0001	0.0001	0.0001
3.20	0.0250	0.0230	0.0212	0.0195	0.0180	7.40	0.0003	0.0002	0.0001	0.0001	0.0001
3.25	0.0234	0.0215	0.0197	0.0181	0.0167	7.50	0.0002	0.0002	0.0001	0.0001	0.0001
3.30	0.0220	0.0201	0.0184	0.0169	0.0155	7.60	0.0002	0.0002	0.0001	0.0001	0.0001
3.35	0.0207	0.0188	0.0172	0.0157	0.0144	7.70	0.0002	0.0001	0.0001	0.0001	0.0001
3.40	0.0194	0.0176	0.0161	0.0146	0.0133	7.80	0.0002	0.0001	0.0001	0.0001	0.0001
3.45	0.0182	0.0165	0.0150	0.0136	0.0124	7.90	0.0002	0.0001	0.0001	0.0001	0.0000
3.50	0.0171	0.0155	0.0140	0.0127	0.0115	8.00	0.0001	0.0001	0.0001	0.0000	0.0000
3.55	0.0161	0.0145	0.0131	0.0118	0.0107	8.10	0.0001	0.0001	0.0000	0.0000	0.0000
3.60	0.0152	0.0136	0.0123	0.0111	0.0100	8.20	0.0001	0.0001	0.0000	0.0000	0.0000
3.65	0.0143	0.0128	0.0115	0.0103	0.0093	8.30	0.0001	0.0001	0.0000	0.0000	0.0000
3.70	0.0134	0.0120	0.0107	0.0096	0.0086	8.40	0.0001	0.0000	0.0000	0.0000	0.0000
3.75	0.0126	0.0113	0.0101	0.0090	0.0080	8.50	0.0001	0.0000	0.0000	0.0000	0.0000
3.80	0.0119	0.0106	0.0094	0.0084	0.0075	8.60	0.0001	0.0000	0.0000	0.0000	0.0000
3.85	0.0112	0.0099	0.0088	0.0078	0.0070	8.70	0.0001	0.0000	0.0000	0.0000	0.0000
3.90	0.0106	0.0093	0.0083	0.0073	0.0065	8.80	0.0000	0.0000	0.0000	0.0000	0.0000
3.95	0.0100	0.0088	0.0077	0.0069	0.0061	8.90	0.0001	0.0000	0.0000	0.0000	0.0000
4.00	0.0094	0.0082	0.0073	0.0064	0.0057	9.00	0.0000	0.0000	0.0000	0.0000	0.0000
4.05	0.0088	0.0078	0.0068	0.0060	0.0053	9.10	0.0000	0.0000	0.0000	0.0000	0.0000
4.10	0.0083	0.0073	0.0064	0.0056	0.0049	9.20	0.0000	0.0000	0.0000	0.0000	0.0000
4.15	0.0079	0.0069	0.0060	0.0052	0.0046	9.30	0.0000	0.0000	0.0000	0.0000	0.0000
4.20	0.0074	0.0065	0.0056	0.0049	0.0043	9.40	0.0000	0.0000	0.0000	0.0000	0.0000
4.25	0.0070	0.0061	0.0053	0.0046	0.0040	9.50	0.0000	0.0000	0.0000	0.0000	0.0000
4.30	0.0066	0.0057	0.0050	0.0043	0.0038	9.60	0.0000	0.0000	0.0000	0.0000	0.0000
4.35	0.0062	0.0054	0.0046	0.0040	0.0035						
4.40	0.0059	0.0051	0.0044	0.0038	0.0033						
4.45	0.0056	0.0048	0.0041	0.0035	0.0031						
4.50	0.0053	0.0045	0.0039	0.0033	0.0029						
4.60	0.0047	0.0040	0.0034	0.0029	0.0025						
4.70	0.0042	0.0035	0.0030	0.0026	0.0022						
4.80	0.0038	0.0032	0.0027	0.0023	0.0019						
4.90	0.0034	0.0028	0.0023	0.0020	0.0017						

Table 4-25 — SHADOWING IN THE CASE OF TWO PARALLEL CIRCULAR CYLINDERS (Continued)

(Dancoff-Ginsburg Correction Factor, C)

Note: Values of C are correct to three decimal places.

$\frac{d}{\rho}$	$\frac{\rho}{\lambda}$ = 1.05	1.10	1.15	1.20	1.25	$\frac{d}{\rho}$	$\frac{\rho}{\lambda}$ = 1.05	1.10	1.15	1.20	1.25
2.00	0.1430	0.1417	0.1404	0.1392	0.1380	5.00	0.0012	0.0010	0.0009	0.0007	0.0006
2.05	0.1271	0.1255	0.1239	0.1223	0.1208	5.10	0.0011	0.0009	0.0008	0.0006	0.0005
2.10	0.1139	0.1121	0.1103	0.1085	0.1068	5.20	0.0010	0.0008	0.0007	0.0006	0.0005
2.15	0.1026	0.1006	0.0986	0.0967	0.0948	5.30	0.0009	0.0007	0.0006	0.0005	0.0004
2.20	0.0927	0.0906	0.0885	0.0865	0.0848	5.40	0.0007	0.0006	0.0005	0.0004	0.0003
2.25	0.0840	0.0818	0.0796	0.0776	0.0756	5.50	0.0007	0.0005	0.0004	0.0004	0.0003
2.30	0.0762	0.0739	0.0718	0.0697	0.0677	5.60	0.0006	0.0005	0.0004	0.0003	0.0003
2.35	0.0694	0.0671	0.0650	0.0629	0.0610	5.70	0.0005	0.0004	0.0003	0.0003	0.0002
2.40	0.0632	0.0610	0.0589	0.0569	0.0549	5.80	0.0004	0.0003	0.0003	0.0002	0.0002
2.45	0.0578	0.0556	0.0535	0.0515	0.0496	5.90	0.0004	0.0003	0.0002	0.0002	0.0002
2.50	0.0527	0.0505	0.0485	0.0465	0.0446	6.00	0.0003	0.0002	0.0002	0.0002	0.0001
2.55	0.0483	0.0461	0.0441	0.0422	0.0404	6.10	0.0003	0.0002	0.0002	0.0001	0.0001
2.60	0.0443	0.0422	0.0402	0.0384	0.0366	6.20	0.0002	0.0002	0.0001	0.0001	0.0001
2.65	0.0406	0.0386	0.0367	0.0349	0.0332	6.30	0.0002	0.0002	0.0001	0.0001	0.0001
2.70	0.0372	0.0353	0.0335	0.0317	0.0301	6.40	0.0002	0.0001	0.0001	0.0001	0.0001
2.75	0.0342	0.0324	0.0306	0.0289	0.0274	6.50	0.0001	0.0001	0.0001	0.0001	0.0000
2.80	0.0315	0.0297	0.0280	0.0264	0.0249	6.60	0.0001	0.0001	0.0001	0.0001	0.0000
2.85	0.0290	0.0272	0.0256	0.0241	0.0227	6.70	0.0001	0.0001	0.0001	0.0000	0.0000
2.90	0.0267	0.0250	0.0234	0.0220	0.0206	6.80	0.0001	0.0001	0.0000	0.0000	0.0000
2.95	0.0246	0.0230	0.0215	0.0201	0.0188	6.90	0.0001	0.0001	0.0000	0.0000	0.0000
3.00	0.0227	0.0212	0.0197	0.0184	0.0172	7.00	0.0001	0.0001	0.0000	0.0000	0.0000
3.05	0.0210	0.0195	0.0181	0.0168	0.0157	7.10	0.0001	0.0001	0.0000	0.0000	0.0000
3.10	0.0194	0.0179	0.0166	0.0154	0.0143	7.20	0.0001	0.0001	0.0000	0.0000	0.0000
3.15	0.0179	0.0165	0.0153	0.0141	0.0131	7.30	0.0001	0.0001	0.0000	0.0000	0.0000
3.20	0.0165	0.0152	0.0141	0.0130	0.0120	7.40	0.0001	0.0000	0.0000	0.0000	0.0000
3.25	0.0153	0.0141	0.0129	0.0119	0.0110	7.50	0.0001	0.0001	0.0000	0.0000	0.0000
3.30	0.0142	0.0130	0.0119	0.0109	0.0100	7.60	0.0001	0.0000	0.0000	0.0000	0.0000
3.35	0.0131	0.0120	0.0110	0.0100	0.0092	7.70	0.0001	0.0000	0.0000	0.0000	0.0000
3.40	0.0121	0.0111	0.0101	0.0092	0.0084	7.80	0.0001	0.0000	0.0000	0.0000	0.0000
3.45	0.0113	0.0102	0.0093	0.0085	0.0077	7.90	0.0000	0.0000	0.0000	0.0000	0.0000
3.50	0.0104	0.0095	0.0086	0.0078	0.0071	8.00	0.0000	0.0000	0.0000	0.0000	0.0000
3.55	0.0097	0.0087	0.0079	0.0072	0.0065						
3.60	0.0090	0.0081	0.0073	0.0066	0.0060						
3.65	0.0083	0.0075	0.0067	0.0061	0.0055						
3.70	0.0077	0.0069	0.0062	0.0056	0.0050						
3.75	0.0072	0.0064	0.0057	0.0051	0.0046						
3.80	0.0067	0.0059	0.0053	0.0047	0.0042						
3.85	0.0062	0.0055	0.0049	0.0044	0.0039						
3.90	0.0058	0.0051	0.0045	0.0040	0.0036						
3.95	0.0054	0.0047	0.0042	0.0037	0.0033						
4.00	0.0050	0.0044	0.0039	0.0034	0.0030						
4.05	0.0046	0.0041	0.0036	0.0032	0.0028						
4.10	0.0043	0.0038	0.0033	0.0029	0.0026						
4.15	0.0040	0.0035	0.0031	0.0027	0.0024						
4.20	0.0038	0.0033	0.0029	0.0025	0.0022						
4.25	0.0035	0.0030	0.0026	0.0023	0.0020						
4.30	0.0033	0.0028	0.0024	0.0021	0.0019						
4.35	0.0030	0.0026	0.0023	0.0020	0.0017						
4.40	0.0028	0.0024	0.0021	0.0018	0.0016						
4.45	0.0026	0.0023	0.0019	0.0017	0.0015						
4.50	0.0025	0.0021	0.0018	0.0016	0.0014						
4.60	0.0021	0.0018	0.0016	0.0013	0.0012						
4.70	0.0019	0.0016	0.0013	0.0011	0.0010						
4.80	0.0016	0.0014	0.0012	0.0010	0.0008						
4.90	0.0014	0.0012	0.0010	0.0008	0.0007						

687863 O - 63 - 20

Table 4-25 — SHADOWING IN THE CASE OF TWO PARALLEL CIRCULAR CYLINDERS (Continued)

(Dancoff-Ginsburg Correction Factor, C)

Note: Values of C are correct to three decimal places.

$\frac{d}{\rho}$	$\frac{\rho}{\lambda} = 1.30$	1.35	1.40	1.45	1.50	$\frac{d}{\rho}$	$\frac{\rho}{\lambda} = 1.30$	1.35	1.40	1.45	1.50
2.00	0.1368	0.1356	0.1345	0.1334	0.1323	5.00	0.0005	0.0004	0.0004	0.0003	0.0003
2.05	0.1193	0.1179	0.1165	0.1151	0.1137	5.10	0.0004	0.0004	0.0003	0.0003	0.0002
2.10	0.1051	0.1034	0.1018	0.1003	0.0987	5.20	0.0004	0.0003	0.0003	0.0002	0.0002
2.15	0.0930	0.0913	0.0896	0.0879	0.0863	5.30	0.0003	0.0003	0.0002	0.0002	0.0002
2.20	0.0827	0.0809	0.0791	0.0773	0.0757	5.40	0.0003	0.0002	0.0002	0.0002	0.0001
2.25	0.0737	0.0718	0.0701	0.0683	0.0666	5.50	0.0002	0.0002	0.0002	0.0001	0.0001
2.30	0.0658	0.0639	0.0621	0.0604	0.0587	5.60	0.0002	0.0002	0.0001	0.0001	0.0001
2.35	0.0590	0.0572	0.0554	0.0537	0.0520	5.70	0.0002	0.0001	0.0001	0.0001	0.0001
2.40	0.0530	0.0512	0.0495	0.0478	0.0462	5.80	0.0002	0.0001	0.0001	0.0001	0.0001
2.45	0.0478	0.0460	0.0443	0.0427	0.0412	5.90	0.0001	0.0001	0.0001	0.0001	0.0000
2.50	0.0428	0.0411	0.0395	0.0379	0.0364	6.00	0.0001	0.0001	0.0001	0.0000	0.0000
2.55	0.0387	0.0370	0.0354	0.0339	0.0325	6.10	0.0001	0.0001	0.0000	0.0000	0.0000
2.60	0.0350	0.0334	0.0319	0.0304	0.0291	6.20	0.0001	0.0000	0.0000	0.0000	0.0000
2.65	0.0316	0.0301	0.0286	0.0272	0.0259	6.30	0.0001	0.0000	0.0000	0.0000	0.0000
2.70	0.0286	0.0271	0.0257	0.0244	0.0232	6.40	0.0000	0.0000	0.0000	0.0000	0.0000
2.75	0.0259	0.0245	0.0232	0.0220	0.0208	6.50	0.0000	0.0000	0.0000	0.0000	0.0000
2.80	0.0235	0.0222	0.0209	0.0198	0.0187						
2.85	0.0213	0.0201	0.0189	0.0178	0.0167						
2.90	0.0194	0.0182	0.0170	0.0160	0.0150						
2.95	0.0176	0.0165	0.0154	0.0144	0.0135						
3.00	0.0160	0.0149	0.0140	0.0130	0.0122						
3.05	0.0146	0.0136	0.0126	0.0118	0.0110						
3.10	0.0133	0.0123	0.0114	0.0106	0.0099						
3.15	0.0121	0.0112	0.0104	0.0096	0.0089						
3.20	0.0110	0.0102	0.0094	0.0087	0.0080						
3.25	0.0101	0.0093	0.0085	0.0079	0.0072						
3.30	0.0092	0.0084	0.0077	0.0071	0.0065						
3.35	0.0084	0.0077	0.0070	0.0064	0.0059						
3.40	0.0077	0.0070	0.0064	0.0059	0.0054						
3.45	0.0070	0.0064	0.0058	0.0053	0.0048						
3.50	0.0064	0.0058	0.0053	0.0048	0.0044						
3.55	0.0059	0.0053	0.0048	0.0044	0.0040						
3.60	0.0054	0.0049	0.0044	0.0040	0.0036						
3.65	0.0049	0.0044	0.0040	0.0036	0.0033						
3.70	0.0045	0.0041	0.0036	0.0033	0.0029						
3.75	0.0041	0.0037	0.0033	0.0030	0.0027						
3.80	0.0038	0.0034	0.0030	0.0027	0.0024						
3.85	0.0035	0.0031	0.0028	0.0025	0.0022						
3.90	0.0032	0.0028	0.0025	0.0022	0.0020						
3.95	0.0029	0.0026	0.0023	0.0020	0.0018						
4.00	0.0027	0.0024	0.0021	0.0019	0.0016						
4.05	0.0025	0.0022	0.0019	0.0017	0.0015						
4.10	0.0023	0.0020	0.0017	0.0015	0.0014						
4.15	0.0021	0.0018	0.0016	0.0014	0.0012						
4.20	0.0019	0.0017	0.0015	0.0013	0.0011						
4.25	0.0018	0.0015	0.0013	0.0012	0.0010						
4.30	0.0016	0.0014	0.0012	0.0011	0.0009						
4.35	0.0015	0.0013	0.0011	0.0010	0.0008						
4.40	0.0014	0.0012	0.0010	0.0009	0.0008						
4.45	0.0013	0.0011	0.0009	0.0008	0.0007						
4.50	0.0012	0.0010	0.0009	0.0007	0.0006						
4.60	0.0010	0.0008	0.0007	0.0006	0.0005						
4.70	0.0008	0.0007	0.0006	0.0005	0.0004						
4.80	0.0007	0.0006	0.0005	0.0004	0.0004						
4.90	0.0006	0.0005	0.0004	0.0004	0.0003						

Table 4-25—SHADOWING IN THE CASE OF TWO PARALLEL CIRCULAR CYLINDERS (Continued)

(Dancoff-Ginsburg Correction Factor, C)

Note: Values of C are correct to three decimal places.

$\frac{d}{\rho}$	$\frac{\rho}{\lambda}$ = 1.60	1.70	1.80	1.90	2.00	$\frac{d}{\rho}$	$\frac{\rho}{\lambda}$ = 1.60	1.70	1.80	1.90	2.00
2.00	0.1302	0.1282	0.1263	0.1244	0.1227	5.00	0.0002	0.0001	0.0001	0.0000	0.0000
2.05	0.1111	0.1085	0.1061	0.1038	0.1016	5.10	0.0001	0.0001	0.0000	0.0000	0.0000
2.10	0.0958	0.0929	0.0902	0.0877	0.0852	5.20	0.0001	0.0001	0.0000	0.0000	0.0000
2.15	0.0831	0.0801	0.0773	0.0746	0.0720	5.30	0.0001	0.0000	0.0000	0.0000	0.0000
2.20	0.0724	0.0694	0.0665	0.0638	0.0612	5.40	0.0001	0.0000	0.0000	0.0000	0.0000
2.25	0.0634	0.0603	0.0574	0.0547	0.0522	5.50	0.0001	0.0000	0.0000	0.0000	0.0000
2.30	0.0554	0.0524	0.0496	0.0470	0.0445	5.60	0.0001	0.0000	0.0000	0.0000	0.0000
2.35	0.0489	0.0459	0.0432	0.0407	0.0383	5.70	0.0000	0.0000	0.0000	0.0000	0.0000
2.40	0.0431	0.0403	0.0377	0.0353	0.0331	5.80	0.0000	0.0000	0.0000	0.0000	0.0000
2.45	0.0382	0.0355	0.0330	0.0308	0.0287	5.90	0.0000	0.0000	0.0000	0.0000	0.0000
2.50	0.0336	0.0310	0.0287	0.0265	0.0245						
2.55	0.0298	0.0273	0.0251	0.0231	0.0218						
2.60	0.0265	0.0242	0.0221	0.0202	0.0185						
2.65	0.0235	0.0213	0.0194	0.0176	0.0161						
2.70	0.0209	0.0188	0.0170	0.0154	0.0139						
2.75	0.0186	0.0167	0.0150	0.0135	0.0122						
2.80	0.0166	0.0148	0.0132	0.0119	0.0106						
2.85	0.0148	0.0131	0.0117	0.0104	0.0093						
2.90	0.0132	0.0117	0.0103	0.0091	0.0081						
2.95	0.0118	0.0104	0.0091	0.0080	0.0071						
3.00	0.0106	0.0092	0.0081	0.0071	0.0062						
3.05	0.0095	0.0082	0.0071	0.0062	0.0054						
3.10	0.0085	0.0073	0.0063	0.0055	0.0048						
3.15	0.0076	0.0065	0.0056	0.0048	0.0042						
3.20	0.0068	0.0058	0.0050	0.0043	0.0037						
3.25	0.0061	0.0052	0.0044	0.0038	0.0032						
3.30	0.0055	0.0046	0.0039	0.0033	0.0028						
3.35	0.0049	0.0041	0.0035	0.0029	0.0025						
3.40	0.0044	0.0037	0.0031	0.0026	0.0022						
3.45	0.0040	0.0033	0.0027	0.0023	0.0019						
3.50	0.0036	0.0029	0.0024	0.0020	0.0017						
3.55	0.0032	0.0026	0.0021	0.0018	0.0015						
3.60	0.0029	0.0023	0.0019	0.0016	0.0013						
3.65	0.0026	0.0021	0.0017	0.0014	0.0012						
3.70	0.0023	0.0019	0.0015	0.0012	0.0010						
3.75	0.0021	0.0017	0.0013	0.0011	0.0009						
3.80	0.0019	0.0015	0.0012	0.0010	0.0008						
3.85	0.0017	0.0013	0.0011	0.0009	0.0007						
3.90	0.0015	0.0012	0.0009	0.0008	0.0006						
3.95	0.0014	0.0011	0.0008	0.0007	0.0006						
4.00	0.0013	0.0010	0.0007	0.0006	0.0005						
4.05	0.0011	0.0009	0.0007	0.0005	0.0004						
4.10	0.0010	0.0008	0.0006	0.0005	0.0004						
4.15	0.0009	0.0007	0.0005	0.0004	0.0003						
4.20	0.0008	0.0006	0.0005	0.0004	0.0003						
4.25	0.0008	0.0006	0.0004	0.0003	0.0003						
4.30	0.0007	0.0005	0.0004	0.0003	0.0002						
4.35	0.0006	0.0004	0.0003	0.0002	0.0002						
4.40	0.0005	0.0004	0.0003	0.0002	0.0002						
4.45	0.0005	0.0003	0.0003	0.0002	0.0002						
4.50	0.0004	0.0003	0.0002	0.0002	0.0001						
4.60	0.0004	0.0002	0.0002	0.0001	0.0001						
4.70	0.0003	0.0002	0.0001	0.0001	0.0001						
4.80	0.0002	0.0002	0.0001	0.0001	0.0001						
4.90	0.0002	0.0001	0.0001	0.0001	0.0000						

Table 4-25 — SHADOWING IN THE CASE OF TWO PARALLEL CIRCULAR CYLINDERS (Continued)

(Dancoff-Ginsburg Correction Factor, C)

Note: Values of C are correct to three decimal places.

$\frac{d}{\rho}$	$\frac{\rho}{\lambda} = 2.10$	2.20	2.30	2.40	2.50	2.60	2.70	2.80	2.90	3.00
2.00	0.1210	0.1193	0.1178	0.1163	0.1148	0.1134	0.1120	0.1107	0.1095	0.1082
2.05	0.0994	0.0973	0.0954	0.0934	0.0916	0.0898	0.0881	0.0864	0.0848	0.0832
2.10	0.0828	0.0805	0.0784	0.0763	0.0742	0.0723	0.0704	0.0686	0.0669	0.0652
2.15	0.0695	0.0672	0.0649	0.0628	0.0607	0.0588	0.0569	0.0551	0.0533	0.0517
2.20	0.0587	0.0564	0.0541	0.0520	0.0500	0.0481	0.0462	0.0445	0.0428	0.0412
2.25	0.0498	0.0475	0.0454	0.0434	0.0414	0.0396	0.0378	0.0361	0.0345	0.0330
2.30	0.0422	0.0399	0.0379	0.0359	0.0341	0.0324	0.0307	0.0292	0.0273	0.0264
2.35	0.0361	0.0340	0.0321	0.0303	0.0286	0.0270	0.0255	0.0241	0.0228	0.0215
2.40	0.0310	0.0290	0.0272	0.0255	0.0240	0.0225	0.0211	0.0199	0.0187	0.0176
2.45	0.0267	0.0249	0.0232	0.0216	0.0202	0.0189	0.0176	0.0165	0.0155	0.0146
2.50	0.0227	0.0210	0.0194	0.0180	0.0167	0.0155	0.0144	0.0133	0.0124	0.0115
2.55	0.0196	0.0180	0.0166	0.0153	0.0141	0.0130	0.0120	0.0111	0.0102	0.0094
2.60	0.0170	0.0155	0.0142	0.0131	0.0120	0.0110	0.0101	0.0093	0.0085	0.0079
2.65	0.0146	0.0133	0.0121	0.0110	0.0101	0.0092	0.0084	0.0077	0.0070	0.0064
2.70	0.0126	0.0114	0.0103	0.0094	0.0085	0.0077	0.0070	0.0064	0.0058	0.0052
2.75	0.0109	0.0098	0.0089	0.0080	0.0072	0.0065	0.0059	0.0053	0.0048	0.0043
2.80	0.0095	0.0085	0.0076	0.0069	0.0062	0.0055	0.0050	0.0045	0.0040	0.0036
2.85	0.0082	0.0073	0.0065	0.0058	0.0052	0.0047	0.0042	0.0037	0.0033	0.0030
2.90	0.0072	0.0063	0.0056	0.0050	0.0044	0.0039	0.0035	0.0031	0.0028	0.0025
2.95	0.0062	0.0055	0.0048	0.0043	0.0038	0.0033	0.0029	0.0026	0.0023	0.0020
3.00	0.0054	0.0048	0.0042	0.0037	0.0032	0.0028	0.0025	0.0022	0.0019	0.0017
3.05	0.0047	0.0041	0.0036	0.0031	0.0028	0.0024	0.0021	0.0018	0.0016	0.0014
3.10	0.0041	0.0036	0.0031	0.0027	0.0023	0.0020	0.0018	0.0015	0.0013	0.0012
3.15	0.0036	0.0031	0.0027	0.0023	0.0020	0.0017	0.0015	0.0013	0.0011	0.0010
3.20	0.0031	0.0027	0.0023	0.0020	0.0017	0.0015	0.0013	0.0011	0.0009	0.0008
3.25	0.0027	0.0023	0.0020	0.0017	0.0015	0.0013	0.0011	0.0009	0.0008	0.0007
3.30	0.0024	0.0020	0.0017	0.0015	0.0013	0.0011	0.0009	0.0008	0.0007	0.0006
3.35	0.0021	0.0018	0.0015	0.0013	0.0011	0.0009	0.0008	0.0007	0.0006	0.0005
3.40	0.0018	0.0015	0.0013	0.0011	0.0009	0.0008	0.0007	0.0006	0.0005	0.0004
3.45	0.0016	0.0013	0.0011	0.0009	0.0008	0.0007	0.0006	0.0005	0.0004	0.0003
3.50	0.0014	0.0012	0.0010	0.0008	0.0007	0.0006	0.0005	0.0004	0.0003	0.0003
3.55	0.0012	0.0010	0.0008	0.0007	0.0006	0.0005	0.0004	0.0003	0.0003	0.0002
3.60	0.0011	0.0009	0.0007	0.0006	0.0005	0.0004	0.0004	0.0003	0.0002	0.0002
3.65	0.0009	0.0008	0.0006	0.0005	0.0005	0.0004	0.0003	0.0002	0.0002	0.0002
3.70	0.0008	0.0007	0.0006	0.0005	0.0004	0.0003	0.0003	0.0002	0.0002	0.0001
3.75	0.0007	0.0006	0.0005	0.0004	0.0003	0.0003	0.0002	0.0002	0.0001	0.0001
3.80	0.0006	0.0005	0.0004	0.0003	0.0003	0.0002	0.0002	0.0001	0.0001	0.0001
3.85	0.0006	0.0004	0.0004	0.0003	0.0002	0.0002	0.0002	0.0001	0.0001	0.0001
3.90	0.0005	0.0004	0.0003	0.0002	0.0002	0.0002	0.0001	0.0001	0.0001	0.0001
3.95	0.0004	0.0003	0.0003	0.0002	0.0002	0.0001	0.0001	0.0001	0.0001	0.0001
4.00	0.0004	0.0003	0.0002	0.0002	0.0001	0.0001	0.0001	0.0001	0.0001	0.0000
4.05	0.0003	0.0002	0.0002	0.0002	0.0001	0.0001	0.0001	0.0001	0.0000	0.0000
4.10	0.0003	0.0002	0.0002	0.0001	0.0001	0.0001	0.0001	0.0000	0.0000	0.0000
4.15	0.0003	0.0002	0.0001	0.0001	0.0001	0.0001	0.0001	0.0000	0.0000	0.0000
4.20	0.0002	0.0002	0.0001	0.0001	0.0001	0.0001	0.0000	0.0000	0.0000	0.0000
4.25	0.0002	0.0001	0.0001	0.0001	0.0001	0.0001	0.0000	0.0000	0.0000	0.0000
4.30	0.0002	0.0001	0.0001	0.0001	0.0001	0.0000	0.0000	0.0000	0.0000	0.0000
4.35	0.0002	0.0001	0.0001	0.0001	0.0001	0.0000	0.0000	0.0000	0.0000	0.0000
4.40	0.0001	0.0001	0.0001	0.0001	0.0000	0.0000	0.0000	0.0000	0.0000	0.0000
4.45	0.0001	0.0001	0.0001	0.0000	0.0000	0.0000	0.0000	0.0000	0.0000	0.0000
4.50	0.0001	0.0001	0.0001	0.0000	0.0000	0.0000	0.0000	0.0000	0.0000	0.0000
4.60	0.0001	0.0001	0.0000	0.0000	0.0000					
4.70	0.0001	0.0000	0.0000	0.0000	0.0000					
4.80	0.0000	0.0000	0.0000	0.0000	0.0000					
4.90	0.0000	0.0000	0.0000	0.0000	0.0000					
5.00	0.0000	0.0000	0.0000	0.0000	0.0000					

Table 4-25 — SHADOWING IN THE CASE OF TWO PARALLEL CIRCULAR CYLINDERS (Continued)

(Dancoff-Ginsburg Correction Factor, C)

Note: Values of C are correct to three decimal places.

$\frac{d}{\rho}$	$\frac{\rho}{\lambda}$ = 3.10	3.20	3.30	3.40	3.50	3.60	3.70	3.80	3.90	4.00
2.00	0.1070	0.1059	0.1048	0.1037	0.1026	0.1016	0.1006	0.0996	0.0987	0.0978
2.05	0.0817	0.0802	0.0788	0.0774	0.0760	0.0747	0.0735	0.0722	0.0710	0.0699
2.10	0.0636	0.0620	0.0605	0.0590	0.0576	0.0563	0.0549	0.0537	0.0524	0.0512
2.15	0.0500	0.0485	0.0470	0.0456	0.0442	0.0429	0.0416	0.0404	0.0392	0.0381
2.20	0.0397	0.0382	0.0368	0.0355	0.0342	0.0330	0.0318	0.0307	0.0296	0.0286
2.25	0.0316	0.0303	0.0290	0.0278	0.0267	0.0256	0.0245	0.0235	0.0225	0.0216
2.30	0.0250	0.0238	0.0226	0.0215	0.0204	0.0198	0.0192	0.0185	0.0177	0.0165
2.35	0.0204	0.0192	0.0182	0.0172	0.0163	0.0154	0.0147	0.0141	0.0134	0.0126
2.40	0.0165	0.0155	0.0146	0.0138	0.0130	0.0122	0.0115	0.0109	0.0102	0.0097
2.45	0.0137	0.0128	0.0120	0.0113	0.0106	0.0100	0.0094	0.0088	0.0081	0.0074
2.50	0.0107	0.0099	0.0092	0.0086	0.0079	0.0074	0.0069	0.0064	0.0059	0.0055
2.55	0.0087	0.0080	0.0074	0.0069	0.0064	0.0059	0.0054	0.0050	0.0047	0.0043
2.60	0.0072	0.0066	0.0061	0.0056	0.0052	0.0048	0.0044	0.0041	0.0038	0.0035
2.65	0.0058	0.0053	0.0049	0.0045	0.0041	0.0038	0.0034	0.0032	0.0029	0.0026
2.70	0.0048	0.0043	0.0039	0.0036	0.0033	0.0030	0.0027	0.0025	0.0022	0.0020
2.75	0.0039	0.0035	0.0032	0.0029	0.0026	0.0024	0.0022	0.0020	0.0018	0.0016
2.80	0.0033	0.0029	0.0026	0.0024	0.0022	0.0019	0.0018	0.0016	0.0014	0.0013
2.85	0.0027	0.0024	0.0021	0.0019	0.0017	0.0015	0.0014	0.0012	0.0011	0.0010
2.90	0.0022	0.0019	0.0017	0.0015	0.0014	0.0012	0.0011	0.0010	0.0009	0.0008
2.95	0.0018	0.0016	0.0014	0.0012	0.0011	0.0010	0.0009	0.0008	0.0007	0.0006
3.00	0.0015	0.0013	0.0012	0.0010	0.0009	0.0008	0.0007	0.0006	0.0006	0.0005
3.05	0.0012	0.0011	0.0009	0.0008	0.0007	0.0006	0.0006	0.0005	0.0004	0.0004
3.10	0.0010	0.0009	0.0008	0.0007	0.0006	0.0005	0.0005	0.0004	0.0003	0.0003
3.15	0.0008	0.0007	0.0006	0.0006	0.0005	0.0004	0.0004	0.0003	0.0003	0.0002
3.20	0.0007	0.0006	0.0005	0.0004	0.0004	0.0003	0.0003	0.0003	0.0002	0.0002
3.25	0.0006	0.0005	0.0004	0.0004	0.0003	0.0003	0.0003	0.0002	0.0002	0.0002
3.30	0.0005	0.0004	0.0003	0.0003	0.0002	0.0002	0.0002	0.0002	0.0001	0.0001
3.35	0.0004	0.0003	0.0003	0.0002	0.0002	0.0002	0.0002	0.0001	0.0001	0.0001
3.40	0.0003	0.0003	0.0002	0.0002	0.0002	0.0001	0.0001	0.0001	0.0001	0.0001
3.45	0.0003	0.0002	0.0002	0.0002	0.0001	0.0001	0.0001	0.0001	0.0002	0.0001
3.50	0.0002	0.0002	0.0002	0.0001	0.0001	0.0001	0.0001	0.0001	0.0001	0.0000
3.55	0.0002	0.0002	0.0001	0.0001	0.0001	0.0001	0.0001	0.0001	0.0001	0.0000
3.60	0.0002	0.0001	0.0001	0.0001	0.0001	0.0001	0.0001	0.0001	0.0000	0.0000
3.65	0.0001	0.0001	0.0001	0.0001	0.0001	0.0001	0.0001	0.0000	0.0000	0.0000
3.70	0.0001	0.0001	0.0001	0.0001	0.0001	0.0001	0.0000	0.0000	0.0000	0.0000
3.75	0.0001	0.0001	0.0001	0.0001	0.0000	0.0000	0.0000	0.0000	0.0000	0.0000
3.80	0.0001	0.0001	0.0001	0.0000	0.0000	0.0000	0.0000	0.0000	0.0000	0.0000
3.85	0.0001	0.0001	0.0000	0.0000	0.0000					
3.90	0.0001	0.0000	0.0000	0.0000	0.0000					
3.95	0.0000	0.0000	0.0000	0.0000	0.0000					
4.00	0.0000	0.0000	0.0000	0.0000	0.0000					

where Γ_n, Γ_γ are the neutron and gamma-ray half-widths; g is the statistical weight (assumed equal to 1 for U^{238}); E = energy of the neutron; E_0 = energy of neutron at the center of the resonance; Γ is the full width of the resonance at half-maximum and is the absolute temperature.

$$x = 2(E - E_0)/\Gamma$$

$$\theta = 4E_0kT/(238\Gamma^2)$$

$$\psi(x,\theta) = \frac{1}{2\sqrt{\pi\theta}} \int_{-\infty}^{\infty} \frac{\exp\left[-(x-y)^2/4\theta\right]}{1+y^2}\, dy$$

$$\chi(x,\theta) = \frac{1}{2\sqrt{\pi\theta}} \int_{-\infty}^{\infty} \frac{2y \exp\left[-(x-y)^2/4\theta\right]}{1+y^2}\, dy$$

At energy E, where $E_0 \leq E \leq E_0'$, the sum of the background cross section and the contributions for the resonances centered at E_0 and E_0' is used for the cross section. Thus interference is considered between the potential scattering and resonance scattering, but not between resonances.

Table 4-26 — $Ki_3(x)$ VS. x

Note: The number X.XXX...XE-YY is read: $(X.XXX...X)10^{-YY}$

x	$Ki_3(x)$	x	$Ki_3(x)$	x	$Ki_3(x)$
0.1	6.92543316E-01	4.1	7.81301898E-03	8.1	1.13865457E-04
0.2	6.12064469E-01	4.2	7.01824850E-03	8.2	1.02564318E-04
0.3	5.41862953E-01	4.3	6.30502588E-03	8.3	9.23886693E-05
0.4	4.80375445E-01	4.4	5.66489351E-03	8.4	8.32259881E-05
0.5	4.26358271E-01	4.5	5.09028310E-03	8.5	7.49750352E-05
0.6	3.78791869E-01	4.6	4.57441980E-03	8.6	6.75447398E-05
0.7	3.36825266E-01	4.7	4.11123878E-03	8.7	6.08531743E-05
0.8	2.99739411E-01	4.8	3.69530857E-03	8.8	5.48266166E-05
0.9	2.66921371E-01	4.9	3.32176462E-03	8.9	4.93987453E-05
1.0	2.37845096E-01	5.0	2.98624876E-03	9.0	4.45098716E-05
1.1	2.12056711E-01	5.1	2.68485588E-03	9.1	4.01062858E-05
1.2	1.89162892E-01	5.2	2.41408643E-03	9.2	3.61396503E-05
1.3	1.68821591E-01	5.3	2.17080331E-03	9.3	3.25664619E-05
1.4	1.50734425E-01	5.4	1.95219420E-03	9.4	2.93475649E-05
1.5	1.34640437E-01	5.5	1.75573710E-03	9.5	2.64477187E-05
1.6	1.20310906E-01	5.6	1.57917042E-03	9.6	2.38351965E-05
1.7	1.07544945E-01	5.7	1.42046560E-03	9.7	2.14814410E-05
1.8	9.61658275E-02	5.8	1.27780277E-03	9.8	1.93607417E-05
1.9	8.60178423E-02	5.9	1.14954910E-03	9.9	1.74499516E-05
2.0	7.69636005E-02	6.0	1.03423938E-03	10.0	1.57282341E-05
2.1	6.88817322E-02	6.1	9.30558610E-04	10.1	1.41768239E-05
2.2	6.16648960E-02	6.2	8.37326455E-04	10.2	1.27788259E-05
2.3	5.52180654E-02	6.3	7.53483284E-04	10.3	1.15190272E-05
2.4	4.94570369E-02	6.4	6.78077793E-04	10.4	1.03837270E-05
2.5	4.43071324E-02	6.5	6.10255748E-04	10.5	9.36058915E-06
2.6	3.97020695E-02	6.6	5.49250054E-04	10.6	8.43850148E-06
2.7	3.55829740E-02	6.7	4.94371712E-04	10.7	7.60745782E-06
2.8	3.18975192E-02	6.8	4.45001841E-04	10.8	6.85844469E-06
2.9	2.85991672E-02	6.9	4.00584531E-04	10.9	6.18334424E-06
3.0	2.56465060E-02	7.0	3.60620311E-04	11.0	5.57484394E-06
3.1	2.30026618E-02	7.1	3.24660406E-04	11.1	5.02635753E-06
3.2	2.06347883E-02	7.2	2.92301542E-04	11.2	4.53195113E-06
3.3	1.85136092E-02	7.3	2.63181302E-04	11.3	4.08627969E-06
3.4	1.66130224E-02	7.4	2.36973995E-04	11.4	3.68452772E-06
3.5	1.49097441E-02	7.5	2.13386813E-04	11.5	3.32235658E-06
3.6	1.33829950E-02	7.6	1.92156592E-04	11.6	2.99585810E-06
3.7	1.20142262E-02	7.7	1.73046736E-04	11.7	2.70151040E-06
3.8	1.07868725E-02	7.8	1.55844513E-04	11.8	2.43614036E-06
3.9	9.68613565E-03	7.9	1.40358672E-04	11.9	2.19688883E-06
4.0	8.69879127E-03	8.0	1.26417202E-04	12.0	1.98117948E-06

The parameters of the 27 low-energy resonances have been measured, but for energies above 530 ev only a statistical description of the resonance structure of U^{238} is known. The description which is used is:

$$z = \sqrt{\Gamma_n^0/\Gamma_{n,avg}^0}; \quad \Gamma_n^0 = \Gamma_n/E_0$$

and the probability density, z, is given by:

$$z = (1/\sqrt{2\pi}) \exp(-Z^2/2) \quad \text{(Porter and Thomas distribution)}$$

For convenience, it is assumed that these resonances are uniformly spaced and have a constant Γ_γ. For speed of computation, a value of θ is used which is represented in the relatively sparse collection of tables of $\psi(x,\theta)$ and $\chi(x,\theta)$ rather than the value of θ corresponding to the selection of Γ_n, etc.

Results and Conclusions. An example of the results of a run on a 4-to-1 (by volume) uranium oxide-to-water lattice follows. This run is of only 5120 histories but serves to illustrate some of the capabilities and limitations of the method. The rods have radius 0.7629 cm, 0.0829 cm cladding (treated as vacuum), 2.36 cm pitch (center-to-center distance between neighbors), and are in hexagonal array. The system is at room temperature. The results are shown in Table 4-27.

Table 4-27—RESULTS OF MONTE CARLO RESONANCE ABSORPTION CALCULATIONS

Energy Band, ev	U Absorptions/Source Neutron	
	Outer Annulus of Rod, 10% of Rod	Inner Region of Rod, 90% of Rod
0.45–8.44	0.013069	0.033671
–15.6	0.000154	0.001730
–28.9	0.006484	0.013964
–51.55	0.004453	0.015106
–73.7	0.002434	0.003918
–85.55	0.000195	0.002014
–96.5	0.000011	0.000403
–110	0.000826	0.003405
–131.5	0.000985	0.002122
–156	0.000003	0.001281
–178.5	0.000013	0.000961
–201	0.000555	0.002114
–381.5	0.001210	0.005945
–539	0.000810	0.003076
–10,000	0.003879	0.018572

The percentage of source neutrons absorbed at energy < 539 ev is 0.1209, and in the energy interval 539 ev < E < 10,000 ev, the percentage is 0.0225. The value of p is:

$$p = 0.8566 \pm 0.0025$$

All energy bands except the last three cover only one resonance. There are eight resonances in the interval 201–381.5 ev, seven more to 539 ev, and above that, the resonance parameters are determined by sampling based on the statistical model.

The lattice on which this calculation is based has a measured value of $p = 0.838 \pm 0.003$; thus the Monte Carlo calculation underestimates 1-p by about 12%. This discrepancy may be caused by neglect of resonances above 10,000 ev.

4.2.5 DOPPLER BROADENING

When the temperature of the resonance absorber is increased, there is a change in the effective resonance integral of the absorber. The effect of temperature on the resonance integral has been included in the formulae in Section 4.2.1. The detailed calculation of the resonance integral, in which the temperature enters as a parameter, is described in several papers. Reference 42 includes extensive tables for numerical computation.

Vernon[29] reports an average value for the fractional increase with temperature of the resonance integral of U^{238}:

$$\left(\frac{\Delta R.I.}{R.I.}\right)_{avg} = 1.6\ 10^{-4}/°C \text{ for } S/M = 0.05 \text{ for } 20°C < T < 1200°C$$

Rodeback[43] reports average values of $\Delta R.I./R.I.$:

U^{238} $S/M = 0.12$, $(\Delta R.I./R.I.)_{avg} = 0.9\ 10^{-4}/°C$

Th^{232} $S/M = 0.19$, $(\Delta R.I./R.I.)_{avg} = 2.5\ 10^{-4}/°C$

These values were obtained by activation analysis.

Recent experimental data in the range 20°C to 270°C have been reported by Small.[44] These data, obtained by oscillating heated bars of U^{238} and Th^{232} in the reactor DIMPLE, are given in Tables 4-28 and 4-29, and graphically in Fig. 4-9.

Table 4-28—DOPPLER CHANGE IN RESONANCE ABSORPTION PER DEGREE CENTIGRADE RISE IN TEMPERATURE FOR URANIUM BARS OF VARIOUS S/M RATIOS

(Based on $\sigma_{R.I.} = 2.81 + 2.47\sqrt{S/M}$ excluding 1/v)

U Bar						
Diameter, in.	Length, in.	S/M	$\sigma_{R.I.}$, barn	$\Sigma_{R.I.} = VN\sigma_{R.I.}$	$\frac{\Delta\Sigma_{R.I.}}{\Delta t}$	Corrected Coefficient $\frac{1}{\Sigma_{R.I.}}\frac{\Delta\Sigma_{R.I.}}{\Delta t}$
0.976	3.0	0.100	10.62	1.89	4.24×10^{-4}	$(2.07 \pm 0.18) \times 10^{-4}$
0.612	4.5	0.147	12.27	1.26	2.73×10^{-4}	$(1.99 \pm 0.23) \times 10^{-4}$
0.543	3.0	0.169	12.96	0.703	1.55×10^{-4}	$(1.99 \pm 0.23) \times 10^{-4}$
0.543	4.5	0.165	12.84	1.041	2.51×10^{-4}	$(2.20 \pm 0.27) \times 10^{-4}$
0.230	3.0	0.399	18.42	0.170	6.10×10^{-5}	$(3.22 \pm 0.37) \times 10^{-4}$
0.230	4.5	0.376	17.95	0.243	7.13×10^{-5}	$(2.62 \pm 0.37) \times 10^{-4}$

Table 4-29—DOPPLER CHANGE IN RESONANCE ABSORPTION PER DEGREE CENTIGRADE RISE IN TEMPERATURE FOR THORIUM BARS OF VARIOUS S/M RATIOS

Th Bar							
Diameter, in.	Length, in.	S/M	$\sigma_{R.I.}$, barn	$\Sigma_{R.I.} = VN\sigma_{R.I.}$	$\frac{\Delta\Sigma_{R.I.}}{\Delta t}$	Coefficient $\frac{1}{\Sigma_{R.I.}}\frac{\Delta\Sigma_{R.I.}}{\Delta t}$ Excluding 1/v	Coefficient Including 3.2b 1/v Contribution to $\sigma_{R.I.}$
0.612	3.0	0.253	10.1	0.48	1.86×10^{-4}	$(3.9 \pm 0.3) \times 10^{-4}$	3.0×10^{-4}
0.543	3.0	0.276	11.2	0.35	1.49×10^{-4}	$(3.9 \pm 0.3) \times 10^{-4}$	3.0×10^{-4}
0.230	3.0	0.653	16.7	0.098	2.56×10^{-5}	$(2.6 \pm 0.5) \times 10^{-4}$	2.2×10^{-4}

Note: Data taken from the unrevised report AERE R/R 2774 (Ref. 44).

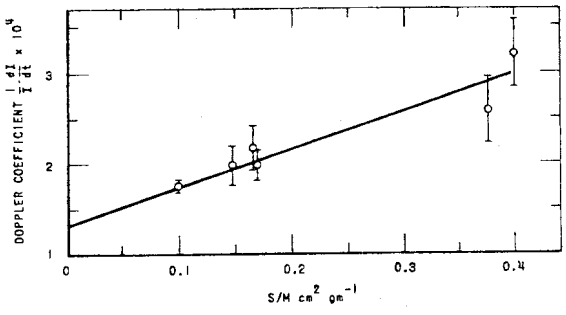

Fig. 4-9—Measured Doppler Coefficients vs. S/M for Uranium Bars. *Reproduced from Ref. 44.*

4.2.6 RESONANCE DISADVANTAGE FACTORS

In general, disadvantage factors are not used in resonance integral calculations since the theoretical formulation includes the depression of the flux in the sample. In large cells there may be excessive removal or capture in the moderator and this leads to a non-uniform source in the moderator. This problem has been studied by Tralli, et al.[28]

The disadvantage factor, $\overline{\phi}_M/\overline{\phi}_a$, can be calculated as in Section 4.1.1, but there are two marked differences. One is that in the present instances the diffusion theory results are more likely to be applicable. The other is that the resonance group constants are not nearly so well known as are the thermal constants, since there is much uncertainty as to the appropriate width to be assigned to the resonance region. The transport mean free path for moderators is usually constant over the resonance band, and hence is readily calculated.

The term $\xi\Sigma_s/\Delta u$ is the removal cross section by elastic scattering out of the resonance group which has been assigned a logarithmic width, Δu. The appropriate value for Δu may be estimated from the resonance absorber diffusion length, $1/\kappa$, for resonance neutrons by the relation

$$\Delta u \approx \frac{N_a 3\ \Sigma_s (R.I.)_{eff}}{\kappa^2}$$

where the simple approximation of diffusion theory, $\kappa^2 = 3\Sigma_a\Sigma_s$, has been made. However, κ^2 in the resonance region has been measured only for U, and therefore estimates for other materials are extremely uncertain: Δu is sometimes taken equal to 5.6 for natural uranium. The magnitude of Δu is usually not too important, however, since the spatial distribution of the flux is almost flat (Ref. 1, p. 273).

In the moderator, the diffusion theory parameters

$$\kappa_M^2 = (3\Sigma_{tr,M}\,\xi\Sigma_{s,M})/\Delta u$$

and

$$D_M = 1/3\,\Sigma_{tr,M}$$

can be applied, where

$$\xi\Sigma_{s,M}/\Delta u = (\Sigma_a)_{eff}$$

Clusters of Rods. For lattices consisting of widely separated rod clusters, each cluster may be replaced by an equivalent rod having as its outer boundary the circumscribed surface of the cluster. The shadowing of rods within the cluster is described in Section 4.2.3. In this way an $(R.I.)_{eff}$ is found for each rod. This yields an effective absorption cross section, $(\Sigma_a)_{eff}$, which is then homogenized with the $(\Sigma_a)_{eff}$ of the moderator within the circumscribed surface. Flux weighting, i.e., disadvantage factors, should be employed for the unit cell within the cluster if necessary; Σ_{tr} is similarly homogenized and the cluster can now be treated as one large rod. Another disadvantage factor calculation may then be applied to determine the proper flux-weighting factors for the homogenized cluster and the surrounding moderator. In this calculation, the source is assumed to be constant in each region and proportional to the moderator volume fraction.

4.2.7 EMPIRICAL FORMULAE

Formulae derived from integral experiments and similar sources are presented. The following were obtained from Ref. 81.

In U^{238},

$$R.I. = (A/G_0) + 47\ (S/M)_{eff} - 70\ (S/M)_{eff}^2$$

where A = 6.2 for plates, and A = 6.0 for rods.

$$(S/M)_{eff} = (S_0/M) + (1/G_0)\ (S_i/M)$$

where the terms S_0 and S_i refer to the bounding area of a clump, and the area inside the perimeter of

the clump, respectively, and G_0 is the ratio of the resonance flux at the surface of the assembly to that in the interior. If the assembly has a cross section A_T, and the uranium a cross section A_U:

$$G_0 = (\kappa R/2)\,[I_0(\kappa R)/I_1(\kappa R)]$$

$$\kappa = \sqrt{A_U/A_T}\,\kappa_U;\ \kappa_U = 0.420$$

$$R = \sqrt{A_T/\pi}$$

In UO_2 lattices,

$$R.I. = (12.9/G_0) + 15.3\ (S/M)_{eff}$$

4.3 FAST EFFECT

Neutrons with energy greater than about 1 Mev can cause fissions in U^{238}. The fast fission factor, ϵ, is defined as the number of neutrons injected into the moderator at energies below the fast fission threshold of U^{238} per neutron born in thermal fission. This definition, based on arguments given in Ref. 45 differs from that often given and includes effects associated with fast capture by U^{238}. The formulation presented follows Ref. 46, which is more general than that presented in Ref. 45.

4.3.1 FAST FISSION FACTOR (ϵ), AND FAST FISSION RATIO (F)

Three groups of neutrons are considered, defined as follows:

Group 1: That portion of the fission spectrum with energies above 1.4 Mev, the U^{238} effective fast fission threshold. The fission spectrum is considered to be:

$$\phi(E) = \exp(-E/0.965)\sinh\sqrt{2.29\,E}$$

Group 2: The sub-threshold portion of the fission spectrum.

Group 3: Those neutrons which have been scattered out of group 1. The spectrum is taken to be:

$$\phi(E) = Ee^{-E};\ E < 1.4\ \text{Mev}$$

The pertinent cross sections are:

$\sigma_{f,1}$ = fission by a group-1 neutron
$\sigma_{c,1}$ = capture of a group-1 neutron
$\sigma_{s,1,1}$ = scattering of a group-1 neutron, the scattered neutron remaining in group 1
$\sigma_{s,1,3}$ = scattering of a group-1 neutron, the scattered neutron being in group 3
$\sigma_{t,1} = \sigma_{f,1} + \sigma_{c,1} + \sigma_{s,1,1} + \sigma_{s,1,3}$ total cross section for a group-1 neutron
$\sigma_{c,2}$ = capture of a group-2 neutron
$\sigma_{s,2,2}$ = scattering of a group-2 neutron, the neutron remaining in group 2
$\sigma_{t,2} = \sigma_{c,2} + \sigma_{s,2,2}$ = total cross section for a group-2 neutron
$\sigma_{c,3}$ = capture of a group-3 neutron
$\sigma_{s,3,3}$ = scattering of a group-3 neutron, the neutron remaining in group 3
$\sigma_{t,3} = \sigma_{c,3} + \sigma_{s,3,3}$ = total cross section for a group-3 neutron

Fission of U^{238} by neutrons below the somewhat arbitrary 1.4-Mev threshold is not considered explicitly. This contribution is accounted for by adjustment of ν to give the correct number of neutrons from fast fission. (For details, see Ref. 46). Only that part of the scattering cross section that is due to scattering which is isotropic in the laboratory system is considered.

Since interaction effects are not considered, the following will not apply to close-packed lattices, such as occur in H_2O–moderated reactors. For these, the mean free path for group-1 neutrons is of the order of several centimeters and the formulae used in homogeneous systems can be applied (see Section 3.6.2, and Table 4-34).

The fast fission factor is given by,

$$\epsilon - 1 = C_1 G_1 - C_2 L_2 - C_3 L_3$$

where C_i is the number of collisions per original fast neutron for the *ith* group; and G_1, L_2, and L_3 are the gains and losses, respectively, per collision for groups 1, 2, and 3.

$$C_1 = \frac{f_1 \, P\left(a_1, \frac{\kappa R}{a_1}\right)}{1 - P\,(a_1,0)\,\frac{\nu_1 f_1 \sigma_{f,1} + \sigma_{s,1,1}}{\sigma_{t,1}}}$$

$$C_2 = \frac{f_2}{1 - \frac{\sigma_{s,2,2}}{\sigma_{t,2}}\,P(a_2,0)}\left[P\left(a_2, \frac{\kappa R}{a_2}\right) + \frac{\nu_1 \sigma_{f,1}}{\sigma_{t,1}}\,C_1\,P(a_2,0)\right]$$

$$C_3 = \frac{P(a_3,0)}{1 - \frac{\sigma_{s,3,3}}{\sigma_{t,3}}\,P(a_3,0)}\,\frac{\sigma_{s,1,3}}{\sigma_{t,1}}\,C_1$$

$$G_1 = \frac{(\nu_1 - 1)\,\sigma_{f,1} - \sigma_{c,1}}{\sigma_{t,1}}$$

$$L_2 = \sigma_{c,2}/\sigma_{t,2}$$

$$L_3 = \sigma_{c,3}/\sigma_{t,3}$$

where ν_1 = average number of neutrons emitted per U^{238} fission
f_1 = fraction of fission neutrons born in group 1
$f_2 = 1 - f_1$ = fraction of fission neutrons born in group 2

$P\left(a_i, \frac{\kappa R}{a_i}\right)$ = collision probability in fuel for a group i source distributed as the thermal flux

κ = inverse thermal neutron diffusion length, cm^{-1}
R = measure of size of fuel lump, cm
$a_i = R/\lambda_i$, where λ_i = total mean free path in fuel lump for group i neutrons
$P(a_i,0)$ = collision probability in fuel for a uniformly distributed source of group i neutrons

The fast fission ratio, F, is usually defined as the ratio of fast fissions to thermal fissions. If interaction between fuel lumps is negligible, this is equivalent to defining F as the ratio of U^{238} fast fissions prior to the neutrons leaving the fuel lump, to fissions subsequent to the neutrons leaving the fuel lump. From the latter definition,

$$F = \nu_s\,(\sigma_{f,1}/\sigma_{t,1})\,C_1$$

where ν_s is the number of fission neutrons (assumed to be thermal fissions), per subsequent fission.

In addition to the cross sections in Table 4-30, the following parameters are used: $\nu_1 = 2.84$, $\nu_s = 2.47$, $f_1 = 0.561$. The collision probabilities[12] for some simple geometries are given in Tables 4-31 and 4-32, together with an indication of the effect of a non-uniform source distribution.

4.3.2 FAST CONVERSION RATIO AND ϵ IN TERMS OF THE FAST FISSION RATIO (F)

If, in the previous subsection, all of the collision probabilities are assumed to be equal, the following formula for ϵ is obtained:

$$\epsilon - 1 = \frac{3.939\,F}{(1 - 2.170\,F)^2}\,[F^2 - 0.8165\,F + 0.1639] \approx \frac{3.939\,F}{1 - 2.17\,F}\,(0.7719 - 2.17\,F)$$

Associated with fast fission is fast conversion, which may be accounted for as follows:

One thermal fission coming from $1 + \alpha_{th}$ absorptions in fissionable material, gives F fast fissions, or $F(\nu_1 - 1)$ extra neutrons, or $\nu_{th} + F(\nu_1 - 1)$ total neutrons produced. Of these, $\nu_{th}\epsilon$ neutrons reenter the chain reaction. Hence $\nu_{th}(1 - \epsilon) + F(\nu_1 - 1)$ neutrons are absorbed in the fast region.

The fast conversion ratio, FCR, is then:

$$FCR = \frac{\nu_{th}(1 - \epsilon) + F(\nu_1 - 1)}{1 + \alpha_{th}}$$

Table 4-30— FAST EFFECT CROSS SECTIONS (barns)

Data from Ref. 46.

Material	Group 1						Group 2			Group 3		
	$\nu_1\sigma_{f,1}$	$\sigma_{f,1}$	$\sigma_{t,1}$	$\sigma_{s,1\to1}$	$\sigma_{s,1\to3}$	$\sigma_{c,1}$	$\sigma_{t,2}$	$\sigma_{s,2\to2}$	$\sigma_{c,2}$	$\sigma_{t,3}$	$\sigma_{s,3\to3}$	$\sigma_{c,3}$
U^{238}	1.56	0.549	4.541	1.89[a]	2.07[a]	0.032	6.05	5.91	0.138	5.66	5.53	0.135
O	—	—	1.63	1.60	0	0.022	4.24	4.24	0	4.24	4.24	0
Mg	—	—	1.26	1.00	0.251	0.009	3.77	3.77	0.0005	3.36	3.36	0.0005
Al	—	—	1.83	1.51	0.319	0.007	3.35	3.35	0.001	3.13	3.13	0.0009
Na	—	—	1.38	1.15	0.225	0.0005	3.52	3.52	0.0005	3.45	3.45	0.0005
Zr	—	—	3.18	2.19	0.960	0.029	5.27	5.24	0.028	4.97	4.97	0.028
Fe	—	—	2.14	1.45	0.686	0.004	2.72	2.72	0.005	2.57	2.56	0.005
D[b]	—	—	1.59	0.32	1.27	0	2.05	2.05	0	2.03	2.03	0
Teflon	—	—	9.40	7.96	1.28	0.163	19.82	19.82	0.002	18.35	18.35	0.002
D_2O[b]	—	—	4.80	2.24	2.54	0.022	8.34	8.34	0	8.30	8.30	0
UO_2	1.56	0.549	7.796	5.10[a]	2.07[a]	0.077	14.54	14.40	0.138	14.15	14.01	0.135

[a] A value of $\sigma^{238}_{n,2n} = 0.02$b has been added to account for the extra neutrons from the (n,2n) reaction in U^{238}.

[b] Deuterium is the only listed element for which transfer by elastic scattering was considered. The formulas used for calculating this effect were for isotropic scattering in the center-of-mass system which is known not to be the case at these energies. In any case, the listed deuterium cross sections may be used to obtain an estimate of the effect on ϵ of the presence of deuterium in the fuel element.

Table 4-31— COLLISION PROBABILITY FOR CYLINDERS: P(a,0)

Data from Ref. 12.

a	P(a,0)	a	P(a,0)	a	P(a,0)	a	P(a,0)
0.00	0.00000	0.50	0.40405	1.00	0.59285	1.50	0.69843
0.02	0.02561	0.52	0.41424	1.02	0.59826	1.52	0.70164
0.04	0.04967	0.54	0.42414	1.04	0.60354	1.54	0.70479
0.06	0.07248	0.56	0.43377	1.06	0.60870	1.56	0.70788
0.08	0.09421	0.58	0.44314	1.08	0.61375	1.58	0.71091
0.10	0.11498	0.60	0.45225	1.10	0.61869	1.60	0.71389
0.12	0.13487	0.62	0.46112	1.12	0.62352	1.62	0.71681
0.14	0.15396	0.64	0.46975	1.14	0.62825	1.64	0.71968
0.16	0.17231	0.66	0.47816	1.16	0.63287	1.66	0.72250
0.18	0.18996	0.68	0.48634	1.18	0.63740	1.68	0.72526
0.20	0.20697	0.70	0.49432	1.20	0.64183	1.70	0.72798
0.22	0.22336	0.72	0.50209	1.22	0.64616	1.72	0.73065
0.24	0.23918	0.74	0.50966	1.24	0.65041	1.74	0.73327
0.26	0.25446	0.76	0.51704	1.26	0.65457	1.76	0.73585
0.28	0.26923	0.78	0.52424	1.28	0.65864	1.78	0.73838
0.30	0.28351	0.80	0.53126	1.30	0.66263	1.80	0.74087
0.32	0.29733	0.82	0.53811	1.32	0.66654	1.82	0.74331
0.34	0.31070	0.84	0.54479	1.34	0.67038	1.84	0.74572
0.36	0.32366	0.86	0.55131	1.36	0.67413	1.86	0.74808
0.38	0.33621	0.88	0.55767	1.38	0.67781	1.88	0.75040
0.40	0.34838	0.90	0.56389	1.40	0.68142	1.90	0.75269
0.42	0.36019	0.92	0.56996	1.42	0.68495	1.92	0.75493
0.44	0.37164	0.94	0.57588	1.44	0.68842	1.94	0.75714
0.46	0.38276	0.96	0.58167	1.46	0.69182	1.96	0.75931
0.48	0.39356	0.98	0.58733	1.48	0.69516	1.98	0.76145

The ratio $\frac{P(a,\kappa R/a)}{P(a,0)}$ is a little less than 1. In particular,

$$\left.\begin{aligned} \text{at } a = 1,\ &\frac{P(a,\ \kappa R/a)}{P(a,0)} \approx 1 - 0.012\,\frac{\kappa R}{a} \\ \text{at } a = 0.5,\ &\frac{P(a,\ \kappa R/a)}{P(a,0)} \approx 1 - 0.009\,\frac{\kappa R}{a} \end{aligned}\right\} \quad 0 < \frac{\kappa R}{a} < 4$$

$$\text{as } a \to 0,\ \frac{P(a,\ \kappa R/a)}{P(a,0)} \to 1$$

which, using $\alpha_{th} = 0.183$, becomes

$$FCR = \frac{0.03814\ F}{(1 - 2.170\ F)^2}\left[5.441 - 0.9461\ F - 23.57\ F^2\right] \approx \frac{0.2075\ F\ (2F + 1)}{1 - 2.17\ F}$$

Table 4-32—COLLISION PROBABILITY P(a,0) FOR SLABS, CYLINDERS AND SPHERES WITH UNIFORM SOURCE

Data from Ref. 12.

a = half-thickness for slabs
a = radius for cylinders or spheres, in mean free paths

a	Slab	Cylinder	Sphere
0.00	0.0000	0.0000	0.0000
0.02	0.0831	0.0256	0.0148
0.04	0.1390	0.0497	0.0294
0.06	0.1849	0.0725	0.0436
0.08	0.2246	0.0942	0.0575
0.10	0.2597	0.1150	0.0712
0.15	0.3335	0.1632	0.1040
0.20	0.3932	0.2070	0.1352
0.25	0.4432	0.2469	0.1649
0.30	0.4859	0.2835	0.1931
0.35	0.5229	0.3172	0.2199
0.40	0.5554	0.3484	0.2454
0.45	0.5841	0.3772	0.2696
0.50	0.6097	0.4040	0.2927
0.60	0.6533	0.4522	0.3357
0.70	0.6890	0.4943	0.3748
0.80	0.7187	0.5313	0.4104
0.90	0.7437	0.5639	0.4430
1.00	0.7651	0.5928	0.4728
1.50	0.8363	0.6984	0.5890
2.00	0.8757	0.7636	0.6676
2.50	0.9002	0.8068	0.7230
3.00	0.9167	0.8371	0.7636
4.00	0.9375	0.8765	0.8183
5.00	0.9500	0.9008	0.8530

Note: A useful approximation is Wigner's rational approximation:

$$P_0 = \frac{(4V/S)}{1 + (4V/S)}$$

where V is the volume of the lump, and S is the surface area of the lump.

4.3.3 EFFECT OF FAST LEAKAGE

Kouts and Sher[47] point out that leakage in the energy region of fast fission can affect the value of ϵ. Assuming the non-leakage probability, P, in this region to be $P = 1/(1 + L_f^2 B^2)$, the effect can be estimated. An estimate of L_f^2 can be obtained by equating L_f^2 to the value of $\bar{r}^2/6$ at the U^{238} fission threshold. In Ref. 47, where a lattice of 0.6-inch rods of uranium in H_2O is studied, L_f^2 is estimated by taking the total age to indium, and subtracting from it the age from U^{238} fission threshold to 1.44 ev. The latter quantity can be evaluated by assuming that in pure water this age is 11 cm^2 and that in the lower energy group the uranium and aluminum are regarded as having infinite mass in computing the space logarithmic decrement, so that,

$$L_f^2 = \tau_{H_2O} - 11\ (1 + V_{metal}/V_{water})$$

In Ref. 47, $\tau_{H_2O} = 26$ cm^2 was used. It can then be shown that

$$\frac{\epsilon}{\epsilon_\infty} = 1 - F\left(\frac{1}{P} - 1\right)\frac{\nu(U^{238})}{\nu(U^{235})}$$

where ϵ_∞ is the fast fission factor for an infinite array. The chief error actually is not in the estimation of P, but in $\alpha(U^{238})$ = capture to fission ratio in U^{238} above fission threshold and in $\nu(U^{238})$.

4.3.4 INTERACTION FAST EFFECT[48]

In Section 4.3.1 it was tacitly supposed that if a neutron escapes from a rod it is degraded below fast fission threshold in the moderator. It may, however, penetrate into a neighboring rod while still above the threshold. The effect resulting from the direct interaction with neighboring rods without the neutron suffering any intervening moderator collision should be considered. This requires a redefinition of the collision probabilities to include collision in neighboring fuel elements. For a slab array it is found that:

$$P_0 = 1 - \int_0^1 t_U^{-1}\,\mu\,\frac{[1 - \exp(-t_U/\mu)]\,[1 - \exp(-t_M/\mu)]}{1 - \exp(-t_U/\mu)\exp(t_M/\mu)}\,d\mu$$

where P_0 is the collision probability in fuel for a uniform source in the fuel; t_U is the width of the fuel slab in mean free paths; and t_M is the width of the moderator slab in mean free paths.

Setting b = thickness of fuel slab (cm)

$$S = (t_M/t_U)\,(\sigma_U/\sigma_M)$$

$$\sigma_{tot\ M} = T(\sigma_{tot\ U})$$

and

$$\sigma_{nat\ U} = \sigma(cm^{-1})$$

Clark[48] has shown that

$$P_0 = P_0(TS, \sigma b)$$

The homogeneous case is $\sigma b = 0$. Table 4-33 gives a list of values of the ratio of $P_0(TS,\sigma b)$ to $P_0(TS,0)$ for various values of TS,σb.

Table 4-33—COLLISION PROBABILITY IN A SLAB ARRAY

Data from Ref. 48.

TS	$P_0(TS,\sigma b)/P_0(TS,0)$			
	$\sigma b = 1$	2	3	∞
0.0	1.0	1.0	1.0	1.0
0.5	1.13	1.22	1.28	1.5
1.0	1.35	1.55	1.68	2.0
2.0	1.88	2.30	2.51	3.0
∞	∞	∞	∞	∞

In computing the fast effect in which the interaction is large (e.g., typical light-water lattices), the fast fission factor should first be computed as though the system were homogeneous, and then the corrections for heterogeneity applied. The factor ϵ thus found is then defined slightly differently than the factor defined in Sections 4.3.1 and 4.3.2. Section 3.6.2 contains a definition of ϵ in homogeneous systems, and formulae for its calculation.

The corrections, $\Delta\epsilon$, to the fast effect for heterogeneous systems of 0.75-inch rods in a hexagonal H_2O lattice, and 0.375-inch slabs in the H_2O lattices, compared to homogeneous systems of the same

composition, are given in Table 4-34. The fast fission factor, ϵ, is calculated for a homogeneous assembly; $\epsilon + \Delta\epsilon$ is the fast effect in the heterogeneous array.

In calculating the fast effect in tightly-packed lattices, especially light-water lattices, the effects of heterogeneity can be estimated by utilizing the results of Clark (Table 4-33) for a slab lattice of the same water-to-metal ratio as the given lattice. Alternatively, Monte Carlo techniques are being developed (see, e.g., H. Rief, "The Fast Effect in Uranium and Beryllium Systems," Nuclear Sci. and Eng., to be published), or multigroup transport theory techniques can be employed using the same group structure and neutron inventory techniques as outlined in Section 4.3.1.

Table 4-34—CHANGES $\Delta\epsilon$ IN ϵ TO ACCOUNT FOR HETEROGENEITY

Data from Ref. 49.

V_{H_2O}/V_U	ϵ	$\Delta\epsilon$	
		0.75-in. rods, hex. lattice	0.375-in. slabs
0	1.227	0.0	0.0
1	1.098	0.011	0.010
2	1.065	0.011	0.010
3	1.048	0.012	0.011
4	1.038	0.014	0.012

4.4 MACROSCOPIC NEUTRON DIFFUSION IN LATTICES

The lattice constants f, ϵ, and p, were all obtained by considering the system to consist of an infinite array of unit cells. Over-all neutron diffusion which results from the finiteness of the system must also be considered. The usual (but not the only) treatment is to reduce, on the basis of the unit cell calculations, the heterogeneous composition to an equivalent homogeneous one, and then to treat the finite system by the methods of Section 3.

A typical problem arising in the analysis of a heterogeneous reactor is that of determining the diffusion theory parameters for a homogeneous system which is equivalent to the original system in the sense of exhibiting the same reactivity and macroscopic neutron flux shapes. In the multigroup theory, these parameters include the diffusion coefficient, $\overline{D}$, and the average cross sections, $\overline{\Sigma}$.

4.4.1 THERMAL DIFFUSION LENGTH WITH NO ANISOTROPY ASSUMED

In the thermal energy region, the thermal migration area, $\overline{L^2} = \overline{D}/\Sigma_a$ is required. In a homogeneous system, L^2 is obtained from the volume-weighted macroscopic absorption and scattering cross sections. In reactors describable as lattice systems, consisting, for example, of periodically distributed slab, cylindrical, or spherical fuel elements in a moderating medium, it has been found reasonably accurate to obtain the average cross section by flux weighting. Thus

$$\overline{\Sigma}_{tr} = \frac{\sum_i \Phi_i \Sigma_{tr,i}}{\sum_i \Phi_i}; \quad \overline{\Sigma}_a = \frac{\sum_i \Phi_i \Sigma_{a,i}}{\sum_i \Phi_i}$$

where the index i refers to the various homogeneous areas of which the lattice cell is composed, and Φ_i is the spatially integrated flux in the ith area:

$$\Phi = \int_{\text{area } i} \Phi dV$$

The thermal migration area, $\overline{L^2}$, may be obtained from the average cross sections, $\overline{\Sigma}_{tr}$ and $\overline{\Sigma}_a$ in the usual way for homogeneous mixtures; $\overline{L^2} = (3\Sigma_{tr}\Sigma_a)^{-1}$. The diffusion coefficient, $\overline{D}$, is then related to $\overline{L^2}$, by the usual relation $\overline{D} = \overline{\Sigma}_a \overline{L^2}$.

In the case of reactors where $\overline{\phi}_{mod} \gg \overline{\phi}_{fuel}$, a widely used approximate formula is:

$$\overline{L} = L_1 \sqrt{1 - f}$$

where L_1 is the diffusion length in the pure moderator, and f is the thermal utilization of the lattice.

4.4.2 DIFFUSION LENGTH WITH ANISOTROPY PRESENT

Homogenization procedures of the preceding type (Section 4.4.1) are applicable to reactors that are essentially similar in all directions, e.g., spheres of uranium distributed uniformly in a large natural uranium-graphite reactor. In most reactors of current interest, however, the fuel is fabricated into plates or into right circular cylinders. The diffusion lengths would be expected to exhibit a dependence on the direction of neutron transport.

Diffusion Theory Analysis. Spinrad[50] has obtained formulae, within the structure of diffusion theory, for diffusion lengths in directions parallel and perpendicular to slab and cylindrical lattices. The assumptions involved lead to more accurate results as the degree of heterogeneity increases. The formula are:

Slab Lattice (two-region cell):

(a) Direction parallel to plate

$$D_1\left(\kappa_{\|}^2-\kappa_1^2\right)^{1/2}\tan\left(\kappa_{\|}^2-\kappa_1^2\right)^{1/2}\frac{t_1}{2}=D_2\left(\kappa_2^2-\kappa_{\|}^2\right)^{1/2}\tanh\left(\kappa_2^2-\kappa_{\|}^2\right)^{1/2}\frac{t_2}{2}$$

where D_i = diffusion coefficient of region i
κ_i^2 = reciprocal of thermal migration area in region i; i = 1,2
t_i = thickness of region i
$\kappa_{\|}^2$ = reciprocal of average thermal migration area in direction parallel to the plates

(b) Direction perpendicular to plate

$$\cosh\kappa_{\perp}\,(t_1+t_2)=(\cosh\kappa_1t_1)\,(\cosh\kappa_2t_2)+\frac{1}{2}\left[\frac{\kappa_1D_1}{\kappa_2D_2}+\frac{\kappa_2D_2}{\kappa_1D_1}\right](\sinh\kappa_1t_1)\,(\sinh\kappa_2t_2)$$

where $\kappa_{\perp}^2$ is the reciprocal of average thermal migration area in direction perpendicular to the plate.

Cylindrical Lattice (two-region cell):

(a) Direction parallel to rods:

$$D_1\left(\kappa_1^2-\kappa_{\|}^2\right)^{1/2}\frac{I_1\left[\left(\kappa_1^2-\kappa_{\|}^2\right)^{1/2}a\right]}{I_0\left[\left(\kappa_1^2-\kappa_{\|}^2\right)^{1/2}a\right]}=-D_2\,k\,\frac{J_1(kA)Y_1(ka)-J_1(ka)Y_1(kA)}{J_1(kA)Y_0(ka)-J_0(ka)Y_1(kA)}$$

where $\kappa_{\|}^2$ = reciprocal of average thermal migration area in direction parallel to the rods
$k=\left[k_{\|}^2-k_2^2\right]^{1/2}$
a = radius of inner region
A = radius of outer region

A difficult numerical problem must be solved to determine $\kappa_{\perp}^2$ in this case. (For details see Ref. 50.)

Transport Theory Analysis. In a more recent report, Davison[51] presented a somewhat different formulation of the problem. Davison restricts his attention to a reactor made up of parallel slabs of two different materials, a so-called "sandwich" reactor of materials 1 and 2.

(a) Direction Perpendicular to Slabs:

$L_{\perp}^2$, the thermal migration area in the direction perpendicular to the slabs, is given for two cases.

Case I: The thickness of each slab is small compared to the neutron mean free path in it.

$$L_{\perp}^2=f_1L_1^2\frac{\bar{\ell}^2}{\ell_1^2}+f_2L_2^2\frac{\bar{\ell}^2}{\ell_2^2}$$

where L = thermal neutron diffusion length
t = total thickness of a slab
ℓ = total mean free path in each material
$\bar{\ell}=[t_1+t_2]/[t_1/\ell_1+t_2/\ell_2]$
f_1 = fraction of thermal neutron captures occurring in each material
$f_2=1-f_1$

Case II: The thickness of each slab is large compared to the mean free path in it.

$$L_\perp^2 = f_1 L_1^2 + f_2 L_2^2$$

An approximation sometimes used for a case intermediate between Case I and Case II is:

$$L_\perp^2 = f_1 L_1^2 \frac{\bar{\ell}}{\ell_1} + f_2 L_2^2 \frac{\bar{\ell}}{\ell_2}$$

(b) Direction parallel to the slabs:

The formula is complicated; for details see Ref. 51, and related subjects in literature by Trlifaj,[52] Laletin,[53] and Beeler.[54,55]

Anisotropy Effect on Slowing-Down Area. Wade[56] has reported that in an Al–D_2O lattice, the age in the direction along the Al rods was 140 cm^2, and transverse to the rods, 108 cm^2.

The lattice consisted of 2S Al rods (1 in. dia. × 5 ft long), suspended in clusters of four rods in contact; the clusters formed a hexagonal lattice. The clusters were housed in 63S Al tubes. The cross-sectional area of the metal in the tube was 0.732 $in.^2$, the area of the four rods, 3.14 $in.^2$. The total area of a unit cell was 42.4 $in.^2$, so that the volume ratio of Al/D_2O was 0.1. No other measurements have been reported which yield a similar effect.

The effect of neutron streaming in voids is distinguished from the anisotropic effects introduced by heterogeneities in composition by virtue of the complete lack of scattering in the former. The effects of voids are considered in Section 4.4.3.

4.4.3 EFFECT OF HOLES IN A REACTOR

Diffusion Theory Results. The theoretical discussion is based on Ref. 57.

The effect of holes in a reactor, such as cooling gaps, is to increase migration areas. Let L_0^2 be the diffusion area without holes, and L^2 the diffusion area with holes of any single-energy group. Assuming no anisotropy, it is found that:

$$\frac{L^2}{L_0^2} = 1 + 2\phi + \left\{ \phi^2 \frac{(2r)}{(\phi\lambda)} \left[\exp\left(2r/\phi\lambda\right) - 1\right]^{-1} \right\} + Q\, r\phi/\lambda$$

where ϕ = volume of holes/volume of material
$v\phi$ = volume of each hole
s = surface area of each hole
r = hydraulic radius
= $2\, v\phi/s$ for cylinders
= $3\, v\phi/s$ for holes totally within the reactor volume
λ = mean free path through solid material of reactor
Q = the mean square chord length through the hole divided by the square of the mean chord length and is given in Table 4-35 for various shaped holes

In all cases, L^2/L_0^2 is at least as great as $(1 + \phi)^2$, the density correction. The values of L^2/L_0^2 for a square lattice of cylindrical holes are given in Table 4-36.

In most cases, L^2 becomes an anisotropic function. Diffusion area formulae, taking into account anisotropic effects for cylindrical holes are:

$$3\, L_\parallel^2/L_0^2 = 1 + 2\,\phi + \left\{ \phi^2 \left(\frac{2\,r}{\phi\lambda}\right) \left[\exp\left(\frac{2\,r}{\phi\lambda}\right) - 1\right]^{-1} \right\} + \frac{3}{2} Qr\ \phi/\lambda$$

$$3\, L_\perp^2/L_0^2 = 1 + 2\,\phi + \left\{ \phi^2 \left(\frac{2\,r}{\phi\lambda}\right) \left[\exp\left(\frac{2\,r}{\phi\lambda}\right) - 1\right]^{-1} \right\} + \frac{3}{4} Qr\ \phi/\lambda$$

Some experimental results are given in Table 4-37 and compared with calculations by these formulae.

The results of some experiments on graphite reactors with arrays of square holes (25% void) are given in Ref. 58 (Table 4-37). A comparison of Behren's theory with Monte Carlo calculations, as well as other modes of calculation, is reported in Ref. 59.

687863 O - 63 - 21

Table 4-35 — VALUES OF Q FOR PARTICULAR SHAPES OF HOLES

Data from Ref. 57.

	Q
Spherical hole	1.125
Regular tetrahedron hole	1.583
Infinite cylinder of circular section	1.333
Infinite cylinder of regular hexagonal section	1.397
Infinite cylinder of square section	1.487
Infinite cylinder of equilateral triangular section	1.648
Spherical shell	$1.125 \times f(\mu)$
Cylinder shell	$1.333 \times F(\mu)$

(where μ = inner-radius/outer-radius, and f and F are tabulated below)

μ	$f(\mu)$	$F(\mu)$	μ	$f(\mu)$	$F(\mu)$
0.0	1.000	1.0000	0.6	1.11	1.2023
0.1	1.001	1.0258	0.7	1.18	1.2604
0.2	1.005	1.0536	0.8	1.27	1.3422
0.3	1.016	1.0839	0.9	1.43	1.53
0.4	1.04	1.1178	1.0	∞	∞
0.5	1.07	1.1567	—	—	—

Table 4-36 — L^2/L_0^2 FOR A SQUARE LATTICE OF CYLINDRICAL HOLES

Data from Ref. 57.

$\frac{\text{Lattice spacing}}{\text{Hole diameter}}$ =	10	5	3	2
r/λ very small	1.016 (1.000)	1.066 (1.000)	1.200 (1.000)	1.548 (1.000)
r/λ = 1/3	1.019 (1.003)	1.079 (1.012)	1.234 (1.028)	1.609 (1.039)
r/λ = 1	1.026 (1.010)	1.108 (1.039)	1.319 (1.099)	1.815 (1.172)
r/λ = 3	1.047 (1.031)	1.194 (1.066)	1.574 (1.312)	2.466 (1.593)

Note: In each case, the upper figure is the value of L^2/L_0^2. The figure in parentheses is the ratio of this value to the simple density correction $(1 + \phi)^2$.

Table 4-37 — DIFFUSION AREAS IN GRAPHITE REACTORS WITH LATTICES OF SQUARE HOLES

Data from Ref. 58.

Reactor size, cm	167.6 × 165.1 × 185.4
Hole size, cm	9.68 × 9.68
Spacing between holes (center-to-center), cm	19.36
$L_{\parallel}$, cm	94.0 ± 3.0
$L_{\perp}$, cm	82.2 ± 2.5
$\epsilon = L_{\parallel}^2/L_{\perp}^2$	1.305 ± 0.03
Graphite diffusion length, L_0, cm	54.7 ± 1.8
ϵ from Behren's formula	1.284

Integral Transport Theory. Benoist[60] has treated in a more rigorous manner the case of cylindrical geometry with annular cavities. The major improvements over the previous theory of Behrens[57] are twofold. Benoist considers the contributions of cross terms to the diffusion length. In general, these terms cancel only in the case of both isotropic scattering and homogeneous media. Benoist also takes into account the difference in mean free paths in fuel and in moderator. This aspect of his method makes it useful when the cell contains control material instead of fuel.

The formulas which follow are applicable to cylindrical cells with rotational symmetry. The cell consists of a central rod u, an annular cavity c, and moderator M. The neutrons are assumed monoenergetic. The subscript k takes on the values r,z.

The diffusion coefficient D_k is given (in terms of auxiliary functions) by

$$\frac{D_k}{\frac{1}{3}\lambda_M} = 1 + \frac{\phi_M}{\phi_t}\left\{\frac{V_c}{V_t} + \frac{V_u}{V_t}\left(1 - \frac{\lambda_M}{\lambda_u}\right) + \frac{V_c \phi_c}{V_t \phi_M}\frac{b-a}{\lambda_M}(Q_k + Q'_k - q_k)\right.$$

$$\left. + \frac{V_c}{V_t}\frac{a}{\lambda_M}\left[\frac{\phi_c}{\phi_M}\left(1 - \frac{\lambda_M}{\lambda_u}\right) + \frac{\phi_u}{\phi_M} - \frac{\lambda_M}{\lambda_u}\right]W_k + \frac{V_u a}{V_t \lambda_M}\left(1 - \frac{\lambda_M}{\lambda_u}\right)\left(\frac{\phi_u}{\phi_M} - \frac{\lambda_M}{\lambda_u}\right)T_k\right\}$$

The auxiliary functions Q_k, Q'_k, q_k, W_k, and T_k are defined in detail in the reference. In the case considered here, these functions depend on one or two of three parameters: α, the ratio of rod radius to the outer annular radius; η, the rod radius in fuel mean free paths; and γ, the outer annular radius in the moderator mean free paths.

Symbols appearing in the formula are defined as follows:

λ_i = the total mean free path in region i, cm
V_i = the volume of region i, cm^3; i = u,c
V_t = the total cell volume, cm^3
ϕ_i = average flux in region i; i = u, c, M

$\phi_t = \dfrac{V_M \phi_M + V_0 \phi_c + V_u \phi_u}{V_t}$, the average flux in the cell

a = radius of rod u, cm
b = outer radius of annulus c, cm

$\alpha = \dfrac{a}{b}$

$\eta = a/\lambda_u$
$\gamma = b/\lambda_u$

If the neutrons are fast, the flux may be assumed flat: $\phi_u = \phi_c = \phi_M$. Then,

$$\frac{D_k}{\frac{1}{3}\lambda_M} = 1 + \frac{V_c}{V_t} + \frac{V_u}{V_t}\left(1 - \frac{\lambda_M}{\lambda_u}\right) + \frac{V_c}{V_t}\frac{b-a}{\lambda_M}(Q_k + Q'_k - q_k) + 2\frac{V_c}{V_t}\frac{a}{\lambda_M}\left(1 - \frac{\lambda_M}{\lambda_u}\right)W_k + \frac{V_u}{V_t}\frac{a}{\lambda_M}\left(1 - \frac{\lambda_M}{\lambda_u}\right)^2 T_k$$

Q_k is evaluated by means of a function $F(\alpha)$ given in Table 4-38 and the relations:

$Q_z = 2F(\alpha)$

$Q_r = F(\alpha)$

$Q'_k(\eta,\alpha)$ is given by Figs. 4-10 and 4-11

$q_r(\gamma,\alpha)$ is given by Fig. 4-12. $q_z = 0$

$W_k(\eta,\alpha)$ is given by Figs. 4-13 and 4-14

$T_k(\eta)$ is given by Fig. 4-15

The mean flux, ϕ_c, in the cavity is given by

$$\frac{\phi_c}{\phi_u} = G + a\Sigma_{c,u}\,\overline{N}(\alpha)$$

Table 4-38 — F(α)

α	F(α)	ΔF	α	F(α)	ΔF	α	F(α)	ΔF	α	F(α)	ΔF
0.0	1.0000	25	0.25	1.0683	31	0.50	1.1566	42	0.75	1.2972	80
0.01	1.0025	25	0.26	1.0714	31	0.51	1.1608	44	0.76	1.3052	84
0.02	1.0050	25	0.27	1.0745	31	0.52	1.1652	44	0.77	1.3136	87
0.03	1.0075	26	0.28	1.0776	31	0.53	1.1696	45	0.78	1.3223	91
0.04	1.0101	26	0.29	1.0807	32	0.54	1.1741	45	0.79	1.3314	95
0.05	1.0127	25	0.30	1.0839	32	0.55	1.1786	46	0.80	1.3409	100
0.06	1.0152	26	0.31	1.0871	32	0.56	1.1832	48	0.81	1.3509	105
0.07	1.0178	27	0.32	1.0903	33	0.57	1.1880	49	0.82	1.3614	111
0.08	1.0205	26	0.33	1.0936	33	0.58	1.1929	50	0.83	1.3725	118
0.09	1.0231	27	0.34	1.0969	33	0.59	1.1979	50	0.84	1.3843	124
0.10	1.0258	27	0.35	1.1002	34	0.60	1.2029	52	0.85	1.3967	134
0.11	1.0285	27	0.36	1.1036	35	0.61	1.2081	53	0.86	1.4101	142
0.12	1.0312	27	0.37	1.1071	35	0.62	1.2134	54	0.87	1.4243	153
0.13	1.0339	27	0.38	1.1106	36	0.63	1.2188	56	0.88	1.4396	167
0.14	1.0366	28	0.39	1.1142	36	0.64	1.2244	57	0.89	1.4563	182
0.15	1.0394	28	0.40	1.1178	35	0.65	1.2301	58	0.90	1.4745	20
0.16	1.0422	28	0.41	1.1213	37	0.66	1.2359	60	0.91	1.494	23
0.17	1.0450	28	0.42	1.1250	38	0.67	1.2419	62	0.92	1.517	25
0.18	1.0478	29	0.43	1.1288	38	0.68	1.2481	64	0.93	1.542	30
0.19	1.0507	29	0.44	1.1326	38	0.69	1.2545	65	0.94	1.572	34
0.20	1.0536	29	0.45	1.1364	39	0.70	1.2610	68	0.95	1.606	43
0.21	1.0565	29	0.46	1.1403	40	0.71	1.2678	69	0.96	1.649	54
0.22	1.0594	29	0.47	1.1443	41	0.72	1.2747	72	0.97	1.703	—
0.23	1.0623	30	0.48	1.1484	41	0.73	1.2819	75	0.98	1.78	—
0.24	1.0653	30	0.49	1.1525	41	0.74	1.2894	78	0.99	1.85	—
0.25	1.0683		0.50	1.1566		0.75	1.2972		1.0	∞	

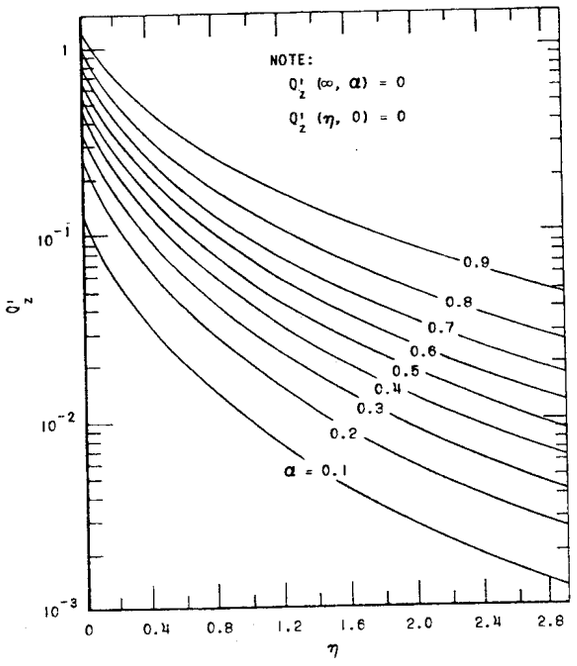

Fig. 4-10 — $Q'_z(\eta,\alpha)$. *Reproduced from Ref. 60.*

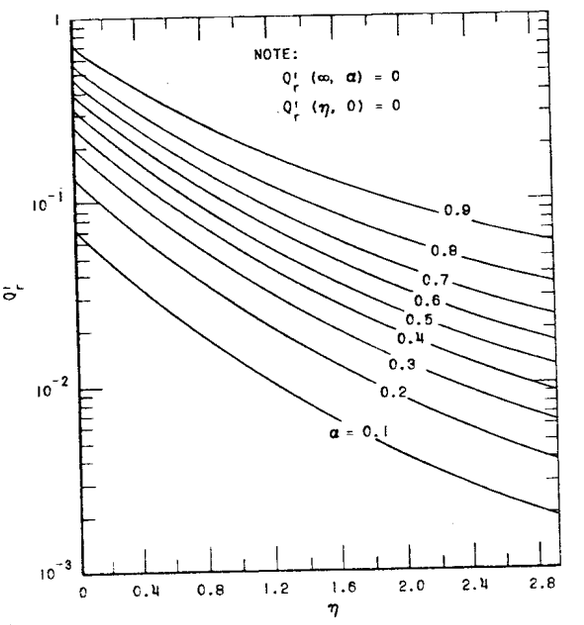

Fig. 4-11 — $Q'_r(\eta,\alpha)$. *Reproduced from Ref. 60.*

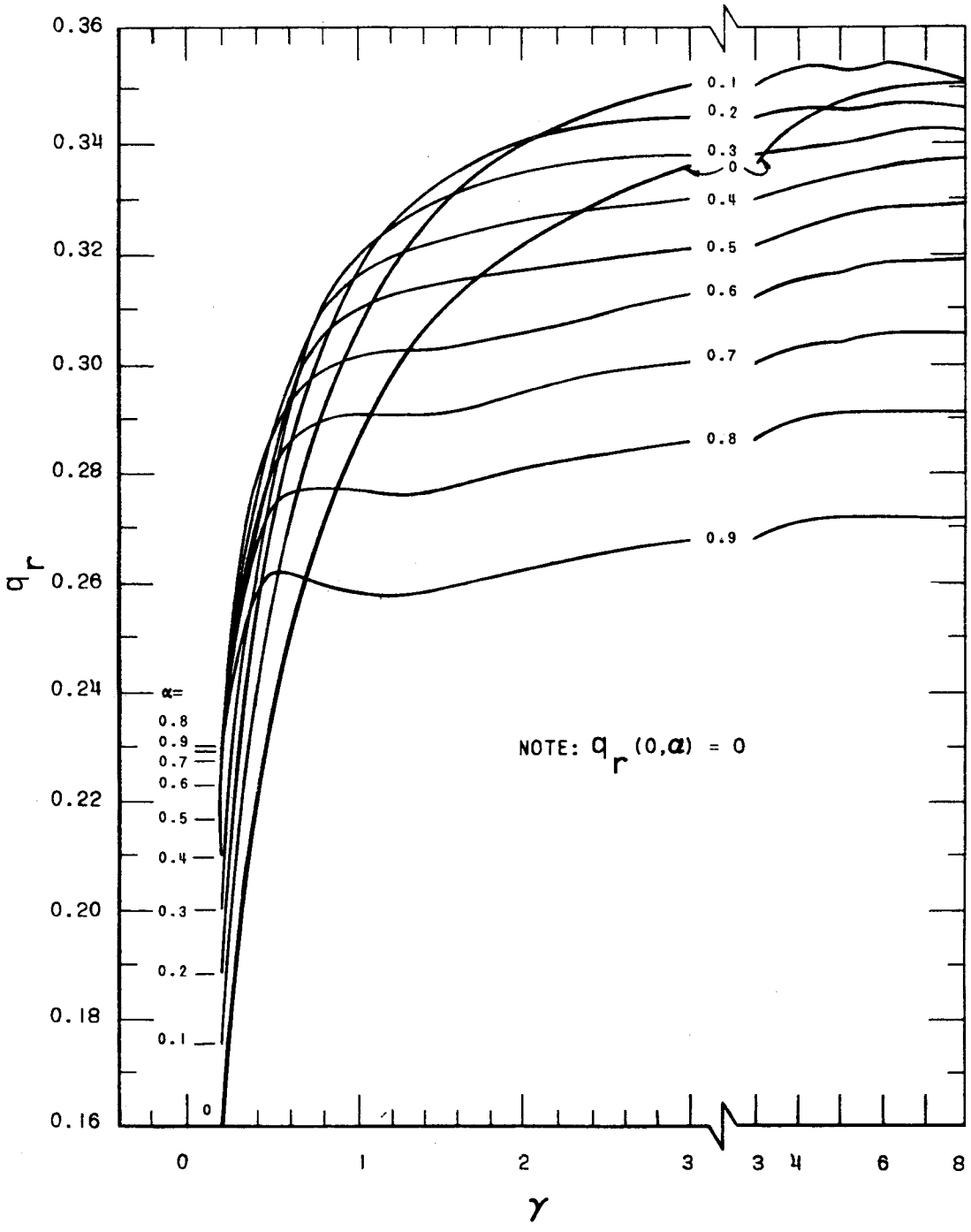

Fig. 4-12—$q_r(\gamma,\alpha)$. *Reproduced from Ref. 60.*

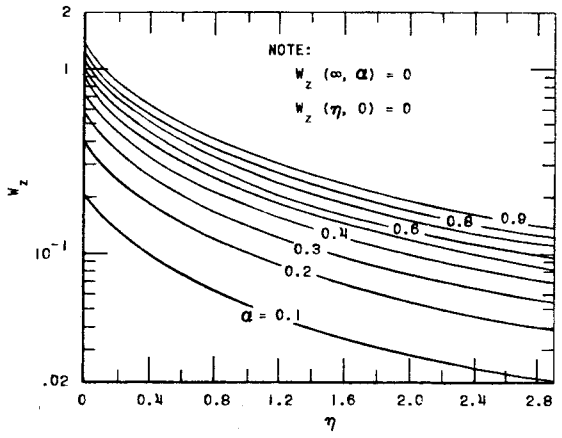

Fig. 4-13—$W_z(\eta,\alpha)$. *Reproduced from Ref. 60.*

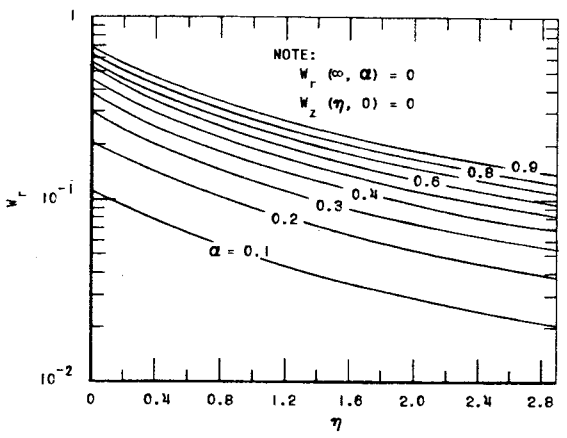

Fig. 4-14—$W_r(\eta,\alpha)$. *Reproduced from Ref. 60.*

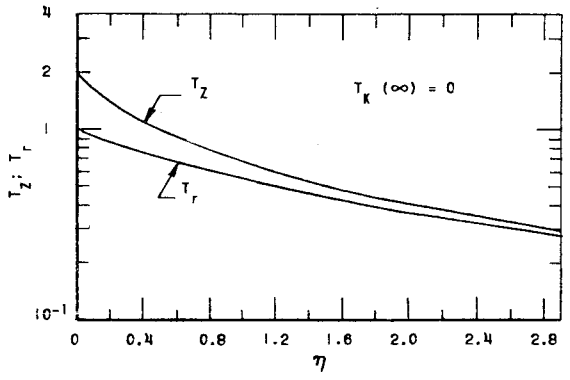

Fig. 4-15—$T_z(\eta)$; $T_r(\eta)$. *Reproduced from Ref. 60.*

where G, the ratio of surface flux to average flux in the rod, is given in Section 4.1.4; $\Sigma_{c,u}$ is the macroscopic capture cross section in region u; and the auxiliary function, $\bar{N}(\alpha)$ is given in Table 4-39.

Approximations

Usually $\phi_t \approx \phi_M$.

$$\bar{N}(\alpha) \approx 1 - \alpha \text{ in the usual cells}$$

The T_k term is usually negligible, except when the central rod is very transparent.
The error in setting $\phi_u = \phi_c = \phi_M$ is not great and permits a quick estimate.
Thin metallic cladding usually has a negligible effect on D_k.

Other Correction Terms. If the axial buckling B_z^2 is positive,

$$\delta Q_z = \frac{3\pi}{4} B_z(a + b)\, \bar{N}(\alpha)$$

The effect of radial buckling is negligible.

If the lattice spacing becomes as small as six mean free paths, the interaction between cells becomes significant. The equations for the corrections are rather involved and may be found in Ref. 60.

If $\phi_u \ll \phi_M$, a correction for the non-uniformity of the flux in the cavity should be considered (see Appendix 3 of Ref. 60).

For cases in which the cell is to be treated as a non-circular cylinder, see the analytical formulation in Ref. 60.

Table 4-39—$\bar{N}(\alpha) = \left(1 - \frac{2\phi_0}{\pi} - \frac{1}{\pi}\sin 2\phi_0\right) \frac{1}{1-\alpha^2}$

α	$\bar{N}(\alpha)$	α	$\bar{N}(\alpha)$	α	$\bar{N}(\alpha)$	α	$\bar{N}(\alpha)$
0.0	1	0.31	0.6767474	0.62	0.4297912	0.93	0.1628217
0.01	0.9873666	0.32	0.6680346	0.63	0.4222191	0.94	0.1501966
0.02	0.9749269	0.33	0.6593948	0.64	0.4146418	0.95	0.1366154
0.03	0.9626749	0.34	0.6508255	0.65	0.4070559	0.96	0.1217543
0.04	0.9506049	0.35	0.6423242	0.66	0.3994577	0.97	0.1050663
0.05	0.9387113	0.36	0.6338883	0.67	0.3918435	0.98	0.0854822
0.06	0.9269886	0.37	0.6255156	0.68	0.3842093	0.99	0.0602320
0.07	0.9154317	0.38	0.6172035	0.69	0.3765508	1.0	0.0
0.08	0.9040355	0.39	0.6089497	0.70	0.3688635		
0.09	0.8927950	0.40	0.6007518	0.71	0.3611426		
0.10	0.8817057	0.41	0.5926075	0.72	0.3533830		
0.11	0.8707628	0.42	0.5845144	0.73	0.3455791		
0.12	0.8599622	0.43	0.5764702	0.74	0.3377250		
0.13	0.8492994	0.44	0.5684726	0.75	0.3298140		
0.14	0.8387703	0.45	0.5605193	0.76	0.3218392		
0.15	0.8283710	0.46	0.5526080	0.77	0.3137927		
0.16	0.8180975	0.47	0.5447363	0.78	0.3056661		
0.17	0.8079460	0.48	0.5369021	0.79	0.2974499		
0.18	0.7979129	0.49	0.5291029	0.80	0.2891335		
0.19	0.7879946	0.50	0.5213363	0.81	0.2807051		
0.20	0.7781876	0.51	0.5136002	0.82	0.2721515		
0.21	0.7684885	0.52	0.5058919	0.83	0.2634575		
0.22	0.7588941	0.53	0.4982092	0.84	0.2546058		
0.23	0.7494010	0.54	0.4905496	0.85	0.2455763		
0.24	0.7400063	0.55	0.4829106	0.86	0.2363457		
0.25	0.7307069	0.56	0.4752896	0.87	0.2268864		
0.26	0.7214996	0.57	0.4676840	0.88	0.2171654		
0.27	0.7123818	0.58	0.4600912	0.89	0.2071426		
0.28	0.7033504	0.59	0.4525084	0.90	0.1967688		
0.29	0.6944027	0.60	0.4449327	0.91	0.1859817		
0.30	0.6855359	0.61	0.4373614	0.92	0.1747013		

4.4.4 SMALL-SOURCE THEORY

When the rod size is small compared to the lattice pitch, small-source theory may be used.

The solution of control problems in heterogeneous thermal reactors often may be obtained with sufficient accuracy by first replacing the lattice by an equivalent homogeneous mixture, and then applying the techniques described in Section 5.1. Other methods have been developed to deal with the case of isolated neutron sinks in lattice reactors difficult to analyze by homogenization procedures. The "small source" theory, proposed by Horning,[61] was also presented at the 1955 Geneva Conference in a somewhat different form by Feinberg[62] and Galanin,[63] and has been applied to a variety of problems. Lanning[64] has reported on a small source-small sink method applicable to radially symmetric reactors unreflected axially (see Section 5.1.7). The following is a summary of Galanin's results:

The time-independent, one-group neutron diffusion equation is, for a system of rods at r_k, in a moderating medium:

$$D\nabla^2\phi(r) - \Sigma_a\,\phi(r) + \eta\gamma\textstyle\sum_k W(r,r_k)\phi(r_k) - \gamma\sum_k \delta(r - r_k)\phi(r) = 0 \qquad (4\text{-}13)$$

where D and Σ_a are the diffusion constant and macroscopic absorption cross section, respectively, of the moderator; and γ is the number of thermal neutrons captured in a rod per unit flux at the surface of the rod. Thus,

$$\gamma = \Sigma_{au}\, G^{-1}\, \pi\rho^2$$

where G is the ratio of surface flux to average flux in the rod, defined in Section 4.1.1; ρ is the rod radius; $W(r,r_k)$ is the probability that a neutron born in fission at r_k is thermalized at r; and η is the number of fission neutrons produced in a rod per thermal neutron captured.

It has been assumed that the rods are small compared with the lattice spacing. If the area of a lattice cell is denoted by a^2, and the parameter $q_0 = a^2\Sigma_a/\gamma$ is introduced, Eq. (4-13) can be reduced to:

$$q_0\ \phi(r) = \sum_k H(|r - r_k|)\ \phi(r_k) \tag{4-14}$$

In the event there is an infinite reflector having the same diffusion properties as the moderator, the kernel $H(|r|)$ has the form:

$$H(|r|) = \frac{a^2}{2\pi L^2}\left\{\left[\eta e^{\tau/L^2}\int_{\tau/L^2}^{\infty} - \int_0^{\infty}\right]\exp - \left(Z + \frac{r^2}{4L^2Z}\right)\right\}\frac{dZ}{2Z}$$

where τ is the Fermi age in the moderator; age theory (Section 3) has been assumed.

If the solution $\phi(r_k) = \exp[i\ (B_x\ X_k + B_y\ Y_k)]$ is introduced, Eq. (4-14) yields the critical equation:

$$q_0 = \sum_k H(r_k)\exp\ [i\ (B_x\ X_k + B_y\ Y_k)] \tag{4-15}$$

for the buckling $B^2 = B_x^2 + B_y^2$. Under the assumptions that $\tau/a^2 \ll 1$, and $Ba/2\pi \ll 1$, a critical equation can be obtained in the form:

$$q_0 = \eta\ \{[\exp\ (-B^2\tau) - 1]/(1 + L^2B^2)\} - q_1$$

The new quantity, q_1, is the capture rate of thermal neutrons in the moderator per thermal neutron captured in the rod, in excess of the capture rate when the thermal flux is flat throughout the cell. That is, q_1 is the quantity, E-1, introduced in Section 4.1.1. Since q_0 is the capture rate in the moderator per neutron captured in the rod when the flux is flat in the cell, an equation may be written:

$$\frac{1}{f} = 1 + q_0 + q_1 \text{ as in Section 4.1.1}$$

If the definition $q = q_0 + q_1$ is introduced, the critical equation takes the form:

$$1 = \eta f\ \exp\ (-B^2\tau)/(1 + B^2L_p^2)$$

where

$$f = \frac{1}{1 + q}$$

and

$$L_p^2 = \frac{q}{1 + q}\ L^2 = (1 - f)L^2 \text{ as in Section 4.4.1}$$

In addition, q_0 should be modified in the same order of approximation, to be:

$$q_0 = \frac{\Sigma_a}{\gamma}\ [a^2 - \pi\rho^2]$$

Galanin[63] applied small-source theory to a synthetic problem with the following properties: $a = \sqrt{\tau} = 1$; $L^2 = 49$; $q_0 = 0.015$; $\rho = 0.1$; and $q_1 = 0.0033$. The infinite lattice multiplication factor was then found: $k_{het} = \eta(1 + q_0 + q_1)$, for reactors consisting of 4, 12, 24, and 32 rods imbedded in an infinite medium. Using standard homogenization techniques and the thermal utilization computed by the diffusion theory approximation, a homogenized model of the reactor was obtained, and the corresponding infinite medium multiplication factor, k_{hom}, was found.

In Table 4-40, the percentage error in $(k_{het} - k_{hom})$ is listed as a function of the number of rods. For a small number of rods, the difference is appreciable, but decreases as the number of rods increases. In this example, the difference is not large; in Ref. 63 it is pointed out that, in general, systems of more than about 30 rods show negligible differences between the modes of calculation.

There is an extensive bibliography on small-source theory (see Refs. 65 through 68). In addition, a machine code HERESEY, which utilizes small-source theory to analyze lattices, is discussed in a sequence of reports from Technical Research Group.[69]

The inclusion of resonance capture and fission poses a problem. Assuming that resonance capture and fission occur at single energies corresponding to lethargies τ_0 and τ_1, respectively, Zink[67] has shown that the critical equation for an infinitely high, bare cylindrical reactor is:

$$\theta = -\frac{1}{2\pi D} K_0\left(\frac{a}{L}\right) + \frac{L^2}{Db^2}\left[1 - \frac{\rho_1}{L} K_1\left(\frac{\rho_1}{L}\right)\right] + \frac{1}{Db^2}\left[\frac{\left(\frac{h_0}{1-\gamma_{f/b^2}}\right)(1-\gamma/b^2)\exp(-B^2\tau_t) - 1}{B^2 + 1/L^2}\right]$$

where K_0, K_1 are the Bessel functions

$\theta = \phi/Q$, where ϕ is the thermal flux at the surface of a fuel rod, and Q the absorption rate per unit length of rod

D = diffusion coefficient for the moderator material

L = diffusion length for the moderator material

τ_t = the age of thermal neutrons which have slowed down from fission energy in the moderator

a = fuel rod radius

b = distance between fuel rods

B^2 = radial buckling

$\rho_1 = b/\sqrt{\tau}$

h_0 = the number of neutrons produced in a fuel element per thermal neutron absorbed in the element

γ_0 is proportional to the resonance blackness: the resonance absorption escape probability, p, is given by $p = 1 - \gamma_0/b^2$

γ_1 is defined in the same fashion as γ_0, but for the resonance fission process

$\gamma = \gamma_0 + \gamma_1$

$\gamma_f = h'\gamma_1$, where h' is number of source neutrons produced per resonance absorption which leads to fission

Table 4-40 — PERCENT ERROR IN $(k_{het} - k_{hom})$ VERSUS NUMBER OF RODS

Data from Ref. 63.

No. of Rods	k_{het}	k_{hom}	$\bar{k} = \frac{1}{2}(k_{het} + k_{hom})$	$(k_{het} - k_{hom})/\bar{k}$, %
4	2.290	2.310	2.300	−0.87
12	1.532	1.514	1.523	1.18
24	1.311	1.301	1.306	0.77
32	1.250	1.242	1.246	0.64

4.5 INTEGRAL DATA

Data taken from exponential and critical experiments on various lattices are reported here. In general, only those data are given which are derived from the experiments without the use of a specific model of neutron diffusion or other reactor theory detail. The exceptional cases are those wherein the calculation is direct, exhibits internal consistency, and leads to derived numbers of considerable interest. Authors' calculations are included when they are useful for purposes of comparison.

The data are organized, in part, on the basis of place of origin since variations in experimental techniques often make the direct comparison of data from different laboratories difficult. In some cases (notably the later work on $U-H_2O$ and UO_2-H_2O), a concerted effort has been made to use standard techniques.

4.5.1 LIGHT WATER, SLIGHTLY ENRICHED URANIUM LATTICES

4.5.1.1 Studies of 1.524-cm Rods

Tables 4-41 through 4-50, and Figs. 4-16 through 4-21, are taken from Kouts and Sher.[47] They represent a compilation of data gleaned from experiments on lattices of 1.524-cm rods of uranium (slightly enriched) in normal water. The rods are clad with 0.07112 cm of aluminum, and an air gap of

Table 4-41 — INTRACELL FLUX AVERAGES

(The flux is assumed flat in the air gap.)

H_2O/U Vol. Ratio	Enrichment, % U^{235}	$\bar{\phi}_M$	$\bar{\phi}_U$	$\bar{\phi}_{Al}$
1.0	1.3	1.446	1.125	1.258
1.5	1.3	1.536	1.134	1.270
2.0	1.3	1.618	1.134	1.260
3.0	1.3	1.684	1.136	1.265
4.0	1.3	1.810	1.144	1.295
1.0	1.15	1.421	1.119	1.245
1.5	1.15	1.449	1.124	1.250
2.0	1.15	1.591	1.150	1.303
3.0	1.15	1.632	1.126	1.255
4.0	1.15	1.722	1.137	1.283
1.0	1.0	1.410	1.103	1.220
1.5	1.0	1.478	1.119	1.243
2.0	1.0	1.506	1.111	1.230
3.0	1.0	1.614	1.115	1.230
4.0	1.0	1.706	1.123	1.252

$\bar{\phi}_M$ = Average flux in moderator
$\bar{\phi}_U$ = Average flux in uranium
$\bar{\phi}_{Al}$ = Average flux in aluminum sheath

Table 4-42 — THERMAL UTILIZATION, f

H_2O/U Vol. Ratio	Enrichment, % U^{235}		
	1.3	1.15	1.0
1.0	0.946	0.942	0.937
1.5	0.920	0.917	0.909
2.0	0.893	0.887	0.881
3.0	0.845	0.836	0.825
4.0	0.795	0.787	0.773

Table 4-43 — RATIO OF U^{238} FISSIONS TO THERMAL FISSION

H_2O/U Vol. Ratio	Enrichment, % U^{235}		
	1.3	1.15	1.0
1.0	0.1780	0.1784	0.1918
1.5	0.1346	0.1370	0.1461
2.0	0.1100	0.1094	0.1202
3.0	0.0871	0.0816	0.0914
4.0	0.0734	0.0739	0.0708

Table 4-44 — EPICADMIUM CAPTURE RATIO FOR U^{238}

H_2O/U Vol. Ratio	$R_a = \frac{\text{EpiCd Rate}}{\text{Total Rate}}$
1	1.50 ± 0.05
2	1.99 ± 0.02
3	2.26 ± 0.03
4	2.66 ± 0.13

Table 4-45 — GOLD CADMIUM RATIOS

H_2O/U Vol. Ratio	R_a
1.0	1.18
1.5	1.24
2.0	1.32
3.0	1.47
4.0	1.55

Table 4-46 — EPICADMIUM FISSION FRACTIONS IN U^{235}

H_2O/U Vol. Ratio	Enrichment, % U^{235}		
	1.3	1.15	1.0
1.0	0.207	0.174	0.144
1.5	0.155	0.105	0.116
2.0	0.117	0.082	0.078
3.0	0.062	0.054	0.045
4.0	0.048	0.040	0.032

Table 4-47—INFINITE MULTIPLICATION FACTOR, k_∞, CALCULATED BY VARIOUS METHODS

Enrichment, % U^{235}	H_2O/U Vol. Ratio	One Group	Two Group	Three Group			Age	Age Diffusion
				L_1^2 = 5 cm^2	L_1^2 = 7.5 cm^2	L_1^2 = 10 cm^2		
1.3	1.0	1.118	1.118	1.119	1.119	1.119	1.120	1.120
1.3	1.5	1.191	1.191	1.192	1.192	1.191	1.194	1.193
1.3	2.0	1.217	1.216	1.216	1.216	1.216	1.218	1.217
1.3	3.0	1.200	1.198	1.198	1.198	1.197	1.197	1.196
1.3	4.0	1.156	1.157	1.158	1.158	1.158	1.159	1.159
1.15	1.0	1.079	1.079	1.079	1.079	1.079	1.078	1.079
1.15	1.5	1.148	1.149	1.148	1.148	1.148	1.147	1.148
1.15	2.0	1.171	1.171	1.170	1.170	1.170	1.169	1.169
1.15	3.0	1.154	1.154	1.153	1.152	1.152	1.149	1.150
1.15	4.0	1.112	1.113	1.113	1.113	1.113	1.112	1.113
1.0	1.0	1.037	1.037	1.037	1.037	1.036	1.036	1.036
1.0	1.5	1.109	1.110	1.109	1.109	1.108	1.106	1.107
1.0	2.0	1.128	1.128	1.127	1.127	1.127	1.123	1.125
1.0	3.0	1.109	1.109	1.107	1.107	1.106	1.103	1.104
1.0	4.0	1.065	1.066	1.065	1.065	1.065	1.063	1.064

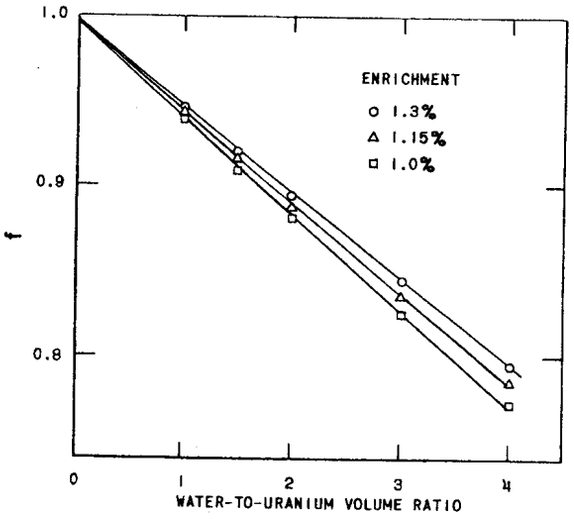

Fig. 4-16—Thermal utilization (f) for uranium lattices. *Data from Ref. 47.*

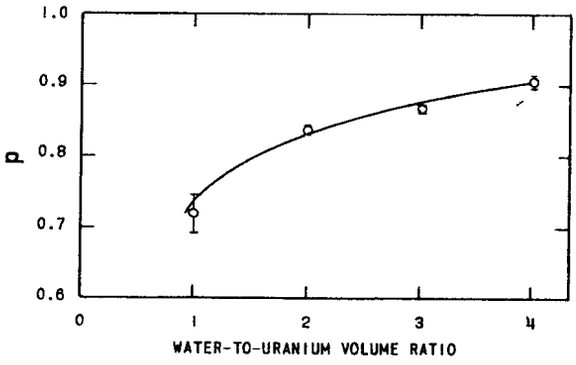

Fig. 4-17—Resonance escape probability (p) for uranium-water lattices. *Interpreted data; Ref. 47.*

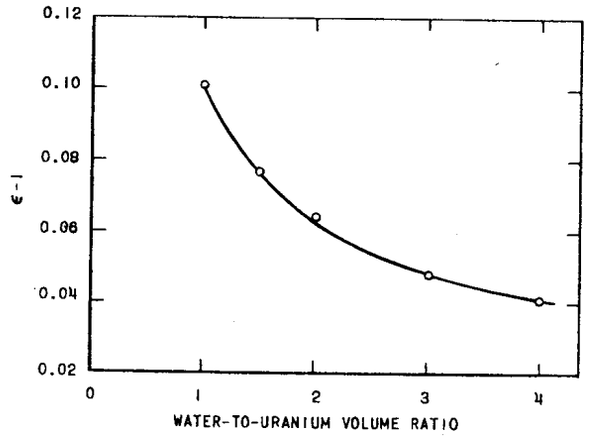

Fig. 4-18—Fast effect (ϵ) for uranium-water lattices. *Interpreted data; Ref. 47.*

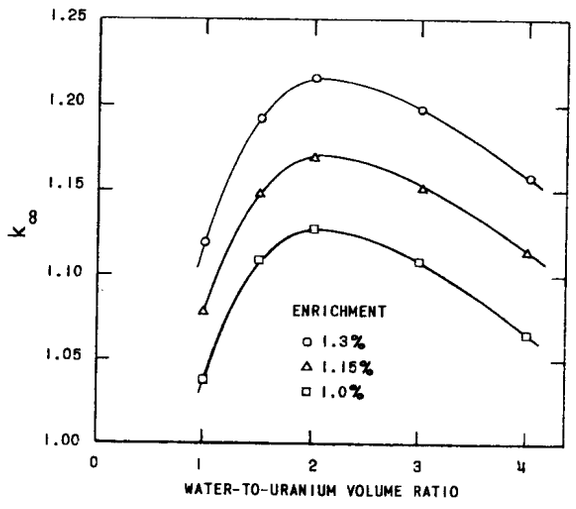

Fig. 4-19—Infinite multiplication factor (k_∞) for uranium-water lattices. *Interpreted data; Ref. 47.*

Table 4-48—RESULTS OF M^2 ANALYSES

H_2O/U Vol. Ratio	Method			Combined Analysis
	Enrichment Variation	Poison Variation with 1.3% Enrichment	Poison Variation with 1.15% Enrichment	
M^2, cm^2, One-Group Theory				
1.0	34.20	35.93	36.87	36.85 ± 0.95
1.5	38.41	38.50	36.57	36.81 ± 0.89
2.0	34.98	36.92	34.80	35.45 ± 0.90
3.0	36.05	33.10	31.91	32.76 ± 1.18
4.0	34.20	32.17	30.74	31.04 ± 1.17
L_f^2, cm^2, Two-Group Theory				
1.0	31.85	33.29	34.38	34.41
1.5	35.89	35.48	33.76	34.00
2.0	32.36	33.96	31.68	32.27
3.0	32.88	29.41	28.23	29.12
4.0	30.59	28.26	27.25	27.48
L_2^2, cm^2, Three-Group Theory with L_1^2 = 5 cm^2				
1.0	26.31	27.62	29.16	29.05
1.5	29.63	29.55	28.31	28.38
2.0	26.00	27.86	26.07	26.51
3.0	26.54	23.52	22.60	23.32
4.0	24.14	22.54	22.02	22.07
L_2^2, cm^2, Three-Group Theory with L_1^2 = 7.5 cm^2				
1.0	23.54	24.99	26.53	26.42
1.5	26.68	26.70	25.65	25.66
2.0	23.05	24.96	23.36	23.75
3.0	22.86	20.76	19.91	20.56
4.0	21.87	19.79	19.45	19.43
L_2^2, cm^2, Three-Group Theory with L_1^2 = 10 cm^2				
1.0	20.95	22.35	24.04	23.85
1.5	23.80	23.96	22.89	22.89
2.0	20.24	22.16	20.74	21.06
3.0	20.78	18.05	17.27	17.86
4.0	19.21	17.14	16.90	16.84
M^2, cm^2, Age Theory				
1.0	31.90	33.40	35.83	35.32
1.5	33.20	34.52	34.57	34.10
2.0	29.91	32.36	32.30	32.28
3.0	30.84	29.54	29.37	29.52
4.0	30.52	29.26	29.78	29.36
τ, cm, Age Diffusion Theory				
1.0	29.84	31.10	33.48	33.07
1.5	31.34	32.07	32.06	31.68
2.0	27.96	30.06	29.58	29.61
3.0	28.47	26.58	26.23	26.53
4.0	27.63	25.97	26.50	26.16

Table 4-49 — BUCKLING, B^2, AND REFLECTOR SAVINGS, λ (CLEAN LATTICES)

Enrichment, % U^{235}	H_2O/U Vol. Ratio	B^2, $cm^{-2} \times 10^4$	λ, cm
1.3	1.0	32.11 ± 0.54	7.94 ± 0.10
1.3	1.5	51.87 ± 0.50	7.44 ± 0.10
1.3	2.0	61.08 ± 0.32	7.04 ± 0.06
1.3	3.0	60.99 ± 0.26	6.70 ± 0.05
1.3	4.0	50.38 ± 0.27	6.64 ± 0.07
1.15	1.0	21.33 ± 0.41	8.10 ± 0.12
1.15	1.5	40.23 ± 0.30	7.50 ± 0.08
1.15	2.0	48.22 ± 0.31	7.10 ± 0.08
1.15	3.0	47.12 ± 0.33	6.68 ± 0.10
1.15	4.0	36.03 ± 0.16	6.43 ± 0.06
1.0	1.0	9.90 ± 0.54	8.76 ± 0.15
1.0	1.5	29.63 ± 0.42	7.47 ± 0.13
1.0	2.0	36.07 ± 0.39	7.04 ± 0.15
1.0	3.0	33.15 ± 0.31	6.51 ± 0.16
1.0	4.0	20.96 ± 0.26	6.46 ± 0.17

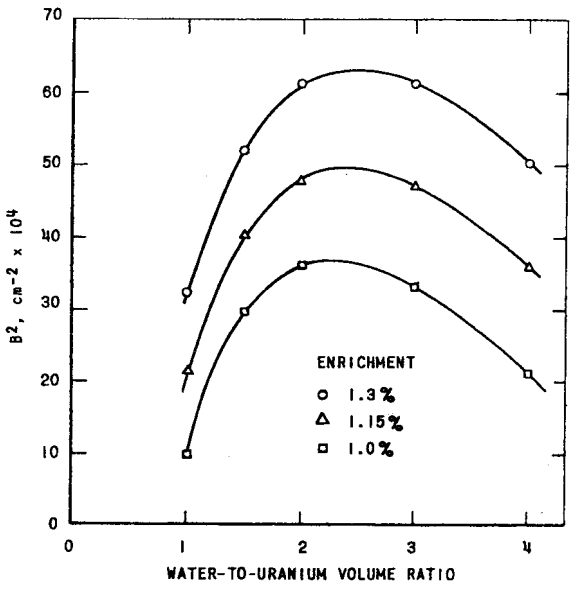

Fig. 4-20 — Buckling (B^2) for uranium-water lattices. *Data from Ref. 47.*

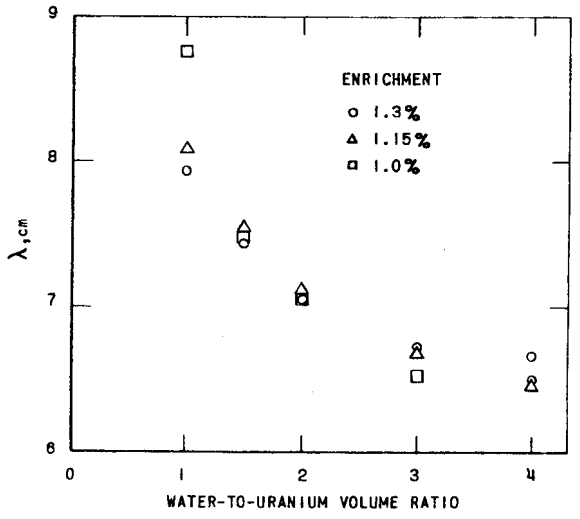

Fig. 4-21 — Reflector savings (λ) for uranium-water lattices. *Data from Ref. 47.*

about 0.0127 cm separates the U from the Al. The tables of M^2 and k_∞ were computed on the basis of one-group, two-group, and three-group age, and age diffusion theory. In each case, the results were internally consistent, and there is no obvious basis for a choice between the methods.

In the calculations summarized in Tables 4-46 and 4-47, the measured or calculated values of f, η, ϵ, and p were plotted against buckling to obtain the group constants. For example, in two-group theory,

$$V = f\eta/(1 + L_S^2B^2)$$

is plotted against B^2, using

$$L_S^2 = f\ L_{S,fuel}^2 + (1 - f)\ L_{S,H_2O}^2$$

where L_S^2 is the thermal diffusion area. The critical equation:

$$k_\infty = \eta\epsilon pf = (1 + L_S^2B^2)(1 + L_2^2B^2)$$

shows that the slope of V vs. B^2 is just L_2^2. From the determination of L_2^2, k_∞ can be calculated.

Table 4-50— BUCKLING, B^2, AND REFLECTOR SAVINGS, λ (POISONED LATTICES)

Enrichment, % U^{235}	H_2O/U Vol. Ratio	B_2O_3, mg/ml	B^2, $cm^{-2} \times 10^4$	λ, cm
1.3	1.0	2.587	10.67 ± 1.48	6.32 ± 0.27
1.3	1.5	1.039	38.63 ± 1.13	6.56 ± 0.26
1.3	1.5	3.452	10.84 ± 1.22	5.82 ± 0.24
1.3	2.0	2.587	16.38 ± 0.34	5.90 ± 0.10
1.3	3.0	1.724	12.87 ± 0.83	6.08 ± 0.12
1.3	4.0	0.500	33.21 ± 0.81	5.90 ± 0.16
1.3	4.0	0.855	16.93 ± 1.00	6.65 ± 0.25
1.3	4.0	1.059	10.97 ± 1.30	6.31 ± 0.25
1.15	1.0	2.98	−2.54 ± 0.58	6.16 ± 0.15
1.15	1.0	3.327	−6.44 ± 0.46	6.23 ± 0.10
1.15	1.5	2.022	13.17 ± 0.43	6.47 ± 0.10
1.15	1.5	3.926	−8.18 ± 0.40	5.76 ± 0.09
1.15	2.0	1.911	12.36 ± 0.62	6.52 ± 0.17
1.15	2.0	3.00	−5.96 ± 1.00	5.95 ± 0.10
1.15	3.0	1.308	7.70 ± 0.58	6.22 ± 0.18
1.15	4.0	0.344	22.16 ± 0.36	6.36 ± 0.16
1.15	4.0	0.746	5.58 ± 0.48	6.78 ± 0.24
1.15	4.0	1.300	−13.57 ± 0.46	6.53 ± 0.21

In three-group theory,

$$V = f\eta/(1 + L_S^2B^2)\ (1 + L_1^2B^2)$$

and L_1^2 is assumed to equal 5, 7.5, or 10 cm^2; L_S^2 is defined as before; and L_2^2 determined once again as the slope of V vs. B^2. The other critical equations such as: one group, $k_\infty = 1 + M^2B^2$; age, $k_\infty = \exp(\tau B^2)$; and age diffusion, $k_\infty = [\exp(\tau B^2)]\ (1 + L_S^2B^2)$, are handled similarly.

For Table 4-48 variations in f and L_S^2 were obtained by uniform poisoning of the water. The method of obtaining L_2^2 or M^2, or τ, is essentially the same as in the preceding example except that V is plotted against the value of the poison concentration. The column "Enrichment Variation" represents results obtained by varying the enrichment with no added poison. Poison was added only to lattices with enrichments of 1.15% and 1.3%. The column "Combined Analysis" lists the weighted average of the results obtained by: (a) varying the enrichment, (b) varying the poison in 1.3% enrichment lattices, and (c) varying the poison in 1.15% enrichment lattices.

Table 4-51 lists data on 1.524-cm rods at 3.063% enrichment.

Table 4-51—CRITICAL APPROACH MEASUREMENTS OF 1.524-cm (0.600-in.) RODS (3.063% ENRICHMENT)

Data from Ref. 70.

Lattice Spacing, in.	h, cm	H_2O/U Vol. Ratio	N_c, rods	R_c, cm	λ, cm	B^2, 10^{-6} cm^{-2}
1.000	40.64	2.06	152.1	16.45	6.37	14,572
1.000	81.28	2.06	114.9	14.30	—	—
1.100	40.64	2.71	118.6	15.97	6.22	15,243
1.100	81.28	2.71	91.2	14.01	—	—
1.200	40.64	3.41	104.5	16.36	6.08	15,026
1.200	81.28	3.41	79.9	14.30	—	—
1.300	40.64	4.18	98.9	17.24	5.94	14,340
1.300	81.28	4.18	74.1	14.92	—	—
1.420	40.64	5.18	100.3	18.97	5.78	13,067
1.420	81.28	5.18	73.8	16.27	—	—
1.600	40.64	6.84	122.0	23.57	5.54	10,515
1.600	81.28	6.84	82.4	19.37	—	—

4.5.1.2 Rod Diameters Other than 1.524-cm

In addition to 1.524-cm (0.6-in.) rod lattices, which have been studied extensively, other rod sizes have been used at a variety of enrichments in less complete studies. The results reported here are arranged in order of descending rod sizes.

Studies of 2.35-cm (0.925-in.) rods with 3.063% enrichment are summarized in Table 4-52.

Studies of 0.983-cm (0.387-in.) rods are reported in Ref. 71. Critical mass parameters are given in Table 4-53. Table 4-54 lists the thermal utilization, f; the ratio of U^{238} fission rate to U^{235} fission rate, δ_{28}; the epicadmium to subcadmium fission rate in U^{235}, δ_{25}; the epicadmium to subcadmium capture ratio in U^{238}, ρ_{28}; and the zero thickness of gold cadmium ratio, R_{Au}.

Lattices of 0.762-cm (0.3-in.) rods have been reported in Ref. 70. The results are given in Table 4-55.

Table 4-52—CRITICAL PARAMETERS: 2.35-cm (0.925-in.) RODS (3.063% ENRICHMENT)

Data from Ref. 70.

Lattice Spacing, in.	h, cm	H_2O/U Vol. Ratio	N_c, rods	R_c, cm	λ, cm	B^2, 10^{-6} cm^{-2}
1.500	40.64	1.893	72.11	16.98	7.16	13,189
1.500	60.96	1.89	60.0	15.50	—	—
1.600	40.64	2.29	63.5	17.01	6.96	13,384
1.600	60.96	2.29	52.4	15.45	—	—
1.700	40.64	2.72	58.6	17.35	6.79	13,229
1.700	60.96	2.72	49.2	15.90	—	—
1.800	40.64	3.17	56.7	18.08	6.66	12,839
1.800	60.96	3.17	46.9	16.44	—	—
1.950	40.64	3.89	60.4	20.21	6.56	11,484
1.950	60.96	3.89	48.6	18.13	—	—

Studies of 0.635-cm (0.250-in.) rods have been reported in Ref. 71. The available data are given in Table 4-56. The notation is the same as in Table 4-54.

Studies of 0.445-cm (0.175-in.) rods of 3.063% enrichment have been reported in Ref. 70. The results are given in Table 4-57.

Table 4-53 — CRITICAL MASS PARAMETERS: 0.983-cm (0.387-in.) RODS

Data from Ref. 71.

H_2O/U Vol. Ratio	U^{235}, wt-%	mg B_2O_3 / ml H_2O	B^2, 10^{-4} cm^{-2}	λ, cm
1.0	1.3	0.0	20.90 ± 0.46	8.56 ± 0.11
	1.15	0.0	12.03 ± 0.91	8.60 ± 0.13
	1.0	0.0	3.23 ± 0.80	8.61 ± 0.16
	1.15	0.627	5.40 ± 0.89	7.99 ± 0.14
	1.15	1.119	3.64 ± 1.57	7.67 ± 0.31
1.5	1.3	0.0	40.51 ± 0.30	8.07 ± 0.09
	1.15	0.0	31.21 ± 0.35	7.81 ± 0.11
	1.0	0.0	19.70 ± 0.34	8.00 ± 0.12
	1.15	0.793	24.15 ± 0.90	6.54 ± 0.19
	1.15	1.493	12.87 ± 1.02	6.65 ± 0.22
	1.15	2.93	−0.50 ± 0.54	6.03 ± 0.14
2.0	1.3	0.0	52.19 ± 0.36	7.56 ± 0.08
	1.15	0.0	42.26 ± 0.51	7.12 ± 0.15
	1.0	0.0	29.02 ± 0.34	7.32 ± 0.12
	1.15	0.793	28.17 ± 1.00	6.58 ± 0.22
	1.15	1.493	16.74 ± 0.57	6.28 ± 0.10
	1.15	3.66	−13.85 ± 0.71	5.77 ± 0.13
3.0	1.3	0.0	59.25 ± 0.33	6.94 ± 0.07
	1.15	0.0	46.18 ± 0.37	6.81 ± 0.11
	1.0	0.0	31.39 ± 0.19	6.88 ± 0.12
	1.15	0.793	26.43 ± 1.01	6.02 ± 0.18
	1.15	1.499	7.31 ± 0.54	6.15 ± 0.11
	1.15	2.247	−6.97 ± 0.67	5.78 ± 0.14
4.0	1.3	0.0	54.69 ± 0.36	6.81 ± 0.08
	1.15	0.0	40.14 ± 0.17	6.80 ± 0.05
	1.0	0.0	25.68 ± 0.24	6.39 ± 0.20
	1.15	0.358	29.48 ± 0.52	6.20 ± 0.17
	1.15	0.793	15.76 ± 0.85	5.83 ± 0.21
	1.15	1.501	−9.50 ± 0.46	6.34 ± 0.11

Table 4-54 — EXPERIMENTAL DATA: 0.983-cm (0.387-in.) RODS

Data from Ref. 71.

Enrich., wt-%	H_2O/U Vol. Ratio	f	δ_{28}	δ_{25}	ρ_{28}	R_{Au}
1.0	1.0	0.941	0.183 ± 0.010	0.24	2.44 ± 0.10	1.15
	1.5	0.916	0.129 ± 0.006	0.096	1.61 ± 0.05	1.23
	2.0	0.891	0.114 ± 0.003	—	1.35 ± 0.05	1.31
	3.0	0.842	0.086 ± 0.004	0.053	0.93 ± 0.03	1.43
	4.0	0.802	0.079 ± 0.005	0.037	0.73 ± 0.03	1.76
1.15	1.0	0.945	0.177 ± 0.005	0.22	—	—
	1.5	0.920	0.127 ± 0.004	0.15	—	—
	2.0	0.898	0.108 ± 0.002	0.10	—	—
	3.0	0.852	0.077 ± 0.001	0.089	—	—
	4.0	0.808	0.066 ± 0.001	—	—	—
1.3	1.0	0.949	0.173 ± 0.004	0.24	—	—
	1.5	0.927	0.134 ± 0.001	0.17	—	—
	2.0	0.904	0.109 ± 0.001	0.12		
	3.0	0.865	0.086 ± 0.001	0.073	—	—
	4.0	0.823	0.073 ± 0.001	0.052	—	—

Table 4-55— EXPERIMENTAL DATA: 0.762-cm (0.3-in.) RODS (3.063% ENRICHMENT)

Data from Ref. 70.

Lattice Spacing, in.	h, cm	H_2O/U Vol. Ratio	N_c, rods	R_c, cm	λ, cm	B^2, 10^{-6} cm^{-2}
0.500	81.28	2.06	624	16.7	6.80	13,607
0.600	40.64	3.41	387.5	15.75	6.42	15,216
0.600	81.28	3.41	298.1	13.82	—	—
0.700	40.64	5.00	296.9	16.09	6,08	15,311
0.700	81.28	5.00	230.0	14.16	—	—
0.800	40.64	6.84	271.9	17.59	6.00	13,952
0.800	81.28	6.84	199.9	15.09	—	—
0.900	40.64	8.92	285.7	20.79	5.97	11,958
0.900	81.28	8.92	203.8	17.14	—	—

Table 4-56— EXPERIMENTAL DATA: 0.635-cm (0.250-in.) RODS

Data from Ref. 71.

Enrichment, % U^{235}	H_2O/U Vol. Ratio	δ_{28}	δ_{25}	ρ_{28}	R_{Au}
1.0	1.5	0.129 ± 0.003	0.14	2.35 ± 0.06	—
	2.0	0.105 ± 0.003	0.095	2.00 ± 0.04	1.27
	3.0	0.086 ± 0.003	0.056	1.27 ± 0.02	1.40
	4.0	0.063 ± 0.002	0.050	1.02 ± 0.01	1.59
1.15	1.5	0.136 ± 0.002	—	—	—
	2.0	0.106 ± 0.002	—	—	—
	3.0	0.080 ± 0.007	—	—	—
	4.0	0.063 ± 0.002	—	—	—

Table 4-57— EXPERIMENTAL DATA: 0.445-cm (0.175-in.) RODS (3% ENRICHMENT)

Data from Ref. 70.

Lattice Spacing, in.	h, cm	H_2O/U Vol. Ratio	N_c, rods	R_c, cm	λ, cm	B^2, 10^{-6} cm^{-2}
0.300	59.69	2.24	1786	16.9	7.5	11,477
0.375	59.69	4.06	873.3	14.78	6.91	14,121
0.450	59.69	6.29	628.3	15.04	6.53	14,292
0.500	59.69	8.00	569.7	15.92	6.40	13,492
0.550	59.69	9.89	554.2	17.27	6.32	12,281
0.600	59.69	11.96	572.5	19.15	6.30	10,821

687863 O - 53 - 22

4.5.1.3 Correlative Plots of Data from Light Water-Uranium Lattices

Whereas material in the preceding sections was organized by rod size and enrichment, the material presented in this section is in the form of correlative plots. Figure 4-22 and Fig. 4-23 are from Ref. 25; the ordinate $\rho(U^{238})$, in both figures is the ratio of epicadmium to subcadmium captures in U^{238}.* Figure 4-24 is from Ref. 70, and shows the maximum buckling and minimum mass vs. rod diameter for 3.06% enriched uranium.

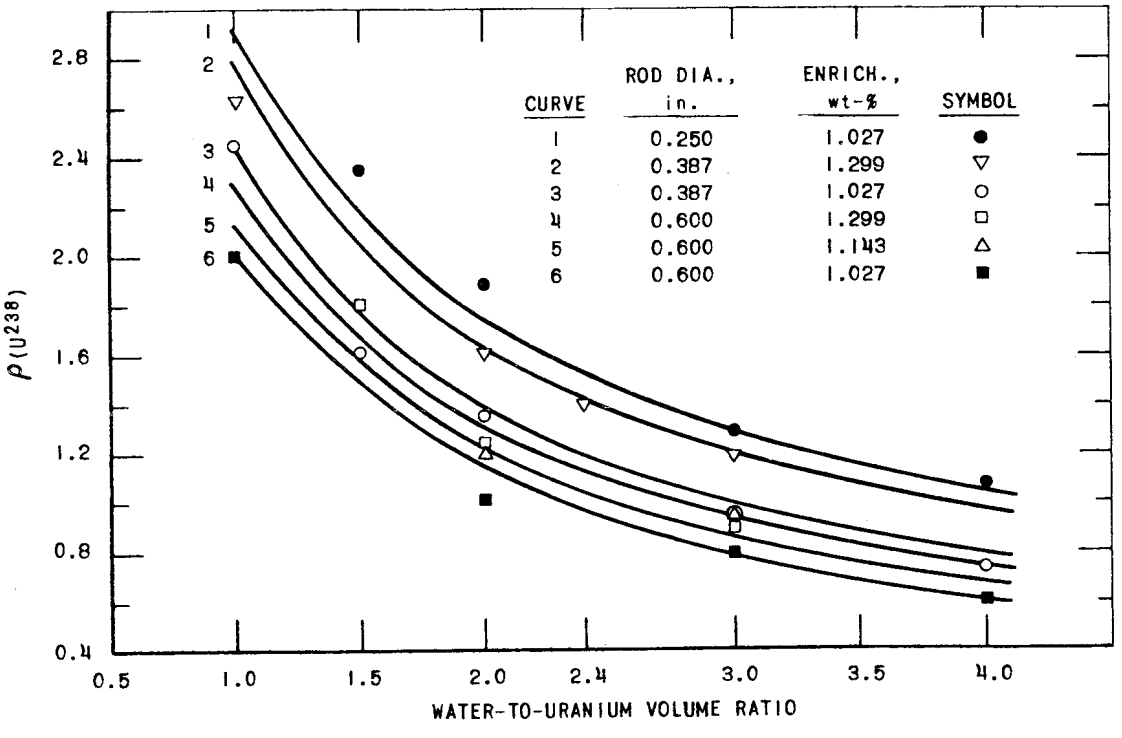

Fig. 4-22—Variation in capture ratios in U^{238} with water-to-uranium volume ratio. *Reproduced from Ref. 25.*

*$\rho(U^{238})$ = capture rate in U^{238} of neutrons with energies above cadmium cutoff, divided by the rate of capture of neutrons with energies below cadmium cutoff.

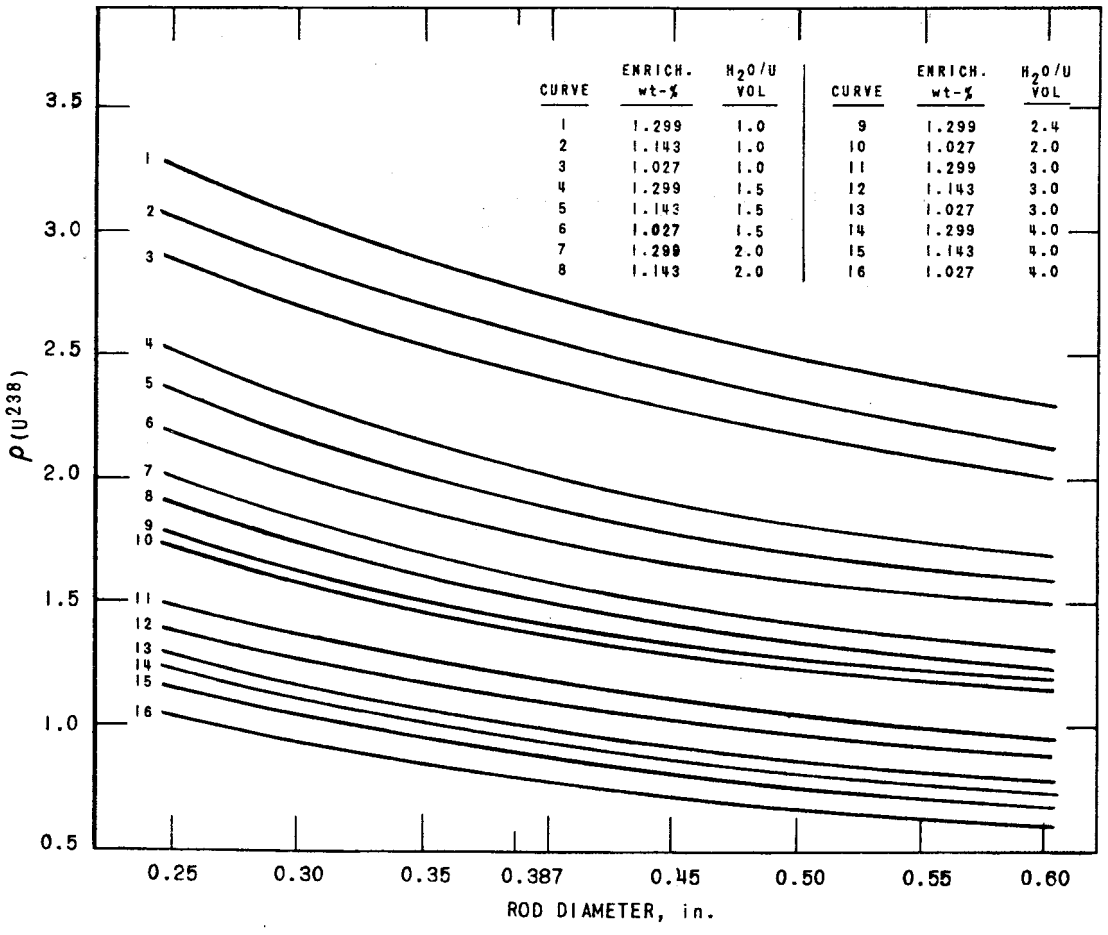

Fig. 4-23 — Variation in capture ratios in U^{238} with rod diameter. *Reproduced from Ref. 25.*

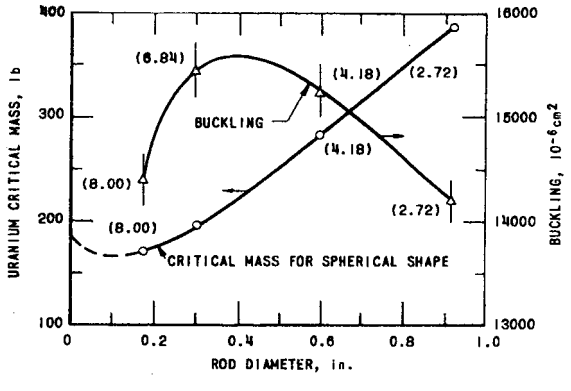

Fig. 4-24 — Maximum buckling and minimum mass vs. uranium rod diameter; 3.06% enriched uranium. Values in parentheses are H_2O/U volume ratios. *Data from Ref. 70.*

4.5.2 LIGHT WATER-UO_2 LATTICES[72–77]

Experiments similar to those of Kouts and Sher (Section 4.5.1), but utilizing UO_2 as fuel, were performed by a group at the Bettis Plant. In these experiments, the enrichment was nominally 1.3% U^{235}. Some lattices of metal rods, such as used by Kouts and Sher, were also reported. The data are summarized in Tables 4-58 through 4-62. Later work on UO_2 lattices is reported in Ref. 81 and is summarized in Tables 4-63 and 4-64, and Figs. 4-25 through 4-28.

Table 4-58 — THERMAL UTILIZATION OF UO_2 LATTICES

Reproduced from Ref. 72.

Rod Dia., in.	Fuel	Fuel Density, gm/cm^3	Enrichment, % U^{235}	H_2O/U Vol. Ratio	H_2O/UO_2 Vol. Ratio	Disadvantage Factor, $\bar{\phi}_m/\bar{\phi}_u$	Thermal Utilization, f
0.600	Metal	—	1.3	1.5	—	1.39 ± 0.04	0.918 ± 0.004
0.600	Metal	—	1.3	2.0	—	1.45 ± 0.04	0.890 ± 0.004
0.600	Metal	—	1.3	3.0	—	1.49 ± 0.04	0.843 ± 0.003
0.600	Metal	—	1.15	2.0	—	1.45 ± 0.04	0.881 ± 0.004
0.600	Metal	—	1.15	3.0	—	1.45 ± 0.04	0.835 ± 0.005
0.387	Metal	—	1.3	2.0	—	1.21 ± 0.04	0.904 ± 0.003
0.387	Metal	—	1.3	3.0	—	1.31 ± 0.04	0.857 ± 0.004
0.600	Oxide	7.53	1.3	3.0	1.07	1.09 ± 0.03	0.873 ± 0.004
0.600	Oxide	7.53	1.3	4.0	1.40	1.14 ± 0.03	0.837 ± 0.005
0.600	Oxide	7.53	1.3	5.0	1.76	1.16 ± 0.03	0.805 ± 0.005
0.384	Oxide	7.53	1.3	4.0	1.39	1.10 ± 0.01	0.836 ± 0.004
0.384	Oxide	7.53	1.3	4.9	1.73	1.10 ± 0.01	0.807 ± 0.004
0.384	Oxide	10.53	1.3	2.9	1.42	1.10 ± 0.01	0.874 ± 0.004
0.384	Oxide	10.53	1.3	3.6	1.78	1.13 ± 0.01	0.848 ± 0.004
0.384	Oxide	10.53	1.3	4.9	2.40	1.13 ± 0.01	0.809 ± 0.004

Table 4-59 — U^{238} CAPTURE FRACTION IN UO_2 LATTICES

Reproduced from Ref. 72.

Rod Dia., in.	Fuel	Fuel Density, gm/cm^3	Enrichment, % U^{235}	H_2O/U Vol. Ratio	H_2O/UO_2 Vol. Ratio	Capture Fraction,[a] ρ
0.600	U metal	—	1.3	1.5	—	1.80 ± 0.18
0.600	U metal	—	1.3	2.0	—	1.24 ± 0.12
0.600	U metal	—	1.3	3.0	—	0.89 ± 0.09
0.600	U metal	—	1.15	2.0	—	1.20 ± 0.03
0.600	U metal	—	1.15	3.0	—	0.93 ± 0.04
0.387	U metal	—	1.3	2.0	—	1.59 ± 0.03
0.387	U metal	—	1.3	3.0	—	1.18 ± 0.03
0.600	UO_2	7.53	1.3	3.0	1.07	1.19 ± 0.04
0.600	UO_2	7.53	1.3	4.0	1.40	0.994 ± 0.013
0.600	UO_2	7.53	1.3	5.0	1.76	0.807 ± 0.014
0.384	UO_2	7.53	1.3	4.0	1.39	1.04 ± 0.05
0.384	UO_2	7.53	1.3	5.0	1.73	0.901 ± 0.02
0.384	UO_2	10.53	1.3	2.9	1.42	1.43 ± 0.01
0.384	UO_2	10.53	1.3	3.6	1.78	1.15 ± 0.01
0.384	UO_2	10.53	1.3	4.9	2.40	0.934 ± 0.01

[a] $\rho = \dfrac{\text{radiative capture in } U^{238} \text{ above cadmium cutoff energy}}{\text{radiative capture in } U^{238} \text{ below cadmium cutoff energy}}$

Table 4-60—U^{238}-TO-U^{235} FISSION RATIOS IN UO_2 LATTICES

Reproduced from Ref. 72.

Rod Dia., in.	Enrichment, % U^{235}	Fuel	Fuel Density, gm/cm^3	H_2O/U Vol. Ratio	H_2O/UO_2 Vol. Ratio	Fission Ratio,[a] δ_{28}
0.600	1.15	Metal	—	2.0	—	0.104 ± 0.010
0.600	1.15	Metal	—	3.0	—	0.081 ± 0.008
0.387	1.3	Metal	—	2.0	—	0.099 ± 0.010
0.387	1.3	Metal	—	3.0	—	0.078 ± 0.008
0.600	1.3	UO_2	7.53	3.0	1.07	0.071 ± 0.007
0.600	1.3	UO_2	7.53	4.0	1.40	0.059 ± 0.006
0.600	1.3	UO_2	7.53	5.0	1.76	0.051 ± 0.004
0.384	1.3	UO_2	7.53	4.0	1.39	0.063 ± 0.003
0.384	1.3	UO_2	7.53	5.0	1.73	0.054 ± 0.003
0.384	1.3	UO_2	10.53	2.9	1.42	0.078 ± 0.009
0.384	1.3	UO_2	10.53	3.6	1.78	0.070 ± 0.004
0.384	1.3	UO_2	10.53	4.9	2.40	0.057 ± 0.003

[a] δ_{28} is the ratio of fissions in U^{238} to fissions in U^{235}.

Table 4-61—RESULTS OF BUCKLING AND REFLECTOR SAVINGS MEASUREMENTS

Reproduced from Ref. 73.

Lattice Designation		Critical No. of Fuel Rods at 20°C	Critical Buckling, $10^4 \times cm^{-2}$		Radial Ref. Svgs., cm		Total Axial Ref. Svgs., cm
Fuel	H_2O/U Vol. Ratio		Bettis (20°C)	BNL	Bettis	BNL	
U Metal; 1.3%; 0.600 in.	2.0	335 ± 1	61.12[a]	61.08 ± 0.32	—	7.04 ± 0.06	—
	3.0	264 ± 1	61.09[a]	60.99 ± 0.26	—	6.70 ± 0.05	—
U Metal; 1.15%; 0.600 in.	2.0	464 ± 1	48.31[a]	48.22 ± 0.31	—	7.10 ± 0.25	—
	3.0	377 ± 1	47.26[a]	47.12 ± 0.33	—	6.68 ± 0.10	—
U Metal; 1.3%; 0.387 in.	2.0	904 ± 2	53.55 ± 0.48	52.56 ± 0.39	7.40(2)[b] ± 0.17	7.46 ± 0.09	14.07(1) ± 0.71
	3.0	630 ± 2	58.2 ± 1.00	59.25 ± 0.33	7.22(1) ± 0.31	6.94 ± 0.07	14.23(1) ± 0.82
UO_2; 7.53 gm/cm^3; 1.3%; 0.601 in.	3.0	1269 ± 3	28.37 ± 0.06	—	8.55(5) ± 0.06	—	17.82(5) ± 0.23
	4.0	1027 ± 3	30.17 ± 0.06	—	8.36(4) ± 0.06	—	16.72(4) ± 0.19
	5.0	987 ± 3	29.06 ± 0.07	—	7.92(4) ± 0.07	—	15.90(5) ± 0.22
UO_2; 7.52 gm/cm^3; 1.3%; 0.388 in.	4.0	3045 ± 3	25.28 ± 0.10	—	8.41(4) ± 0.12	—	17.06(6) ± 0.51
	5.0	2784 ± 3	25.21 ± 0.10	—	8.08(4) ± 0.12	—	15.37(3) ± 0.26
UO_2; 10.53 gm/cm^3; 1.3%; 0.383 in.	3.0	2173 ± 3	32.59 ± 0.15	—	7.86(6) ± 0.12	—	15.27(11) ± 0.41
	3.6	1755 ± 3	35.47 ± 0.18	—	7.41(5) ± 0.13	—	14.69(8) ± 0.43
	5.0	1575 ± 3	34.22 ± 0.13	—	7.10(7) ± 0.10	—	14.52(8) ± 0.17

[a] Calculated from number of fuel rods using BNL values of radial reflector savings and assuming the axial reflector savings is twice the radial value.

[b] Number of measurements indicated in parentheses.

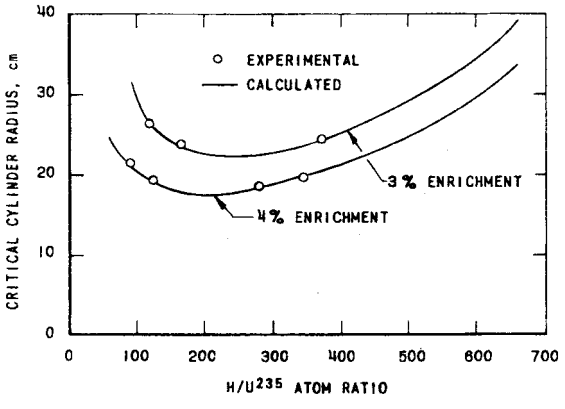

Fig. 4-25—Critical experiment data; low-enriched UO_2 fuel pins; stainless steel clad; pin height = 168.9 cm. *Reproduced from Ref. 74.*

Table 4-62—TEMPERATURE COEFFICIENT RESULTS OF UO_2 LATTICES

Reproduced from Ref. 73.

Lattice Designation		Temperature Coefficient, $\partial\rho/\partial\theta$ ($°C^{-1}$) × 10^4	
Fuel	H_2O/U Vol. Ratio	20°C	40°C
U Metal; 1.3%; 0.600 in.	2.0	−0.36(2)[a] ± 0.02	−0.76 ± 0.02
	3.0	+0.10(6) ± 0.02	−0.19 ± 0.02
U Metal; 1.15%; 0.600 in.	2.0	−0.40(12) ± 0.02	−0.74 ± 0.02
	3.0	+0.11(4) ± 0.02	−0.14 ± 0.02
U Metal; 1.3%; 0.387 in.	2.0	−0.46(8) ± 0.04	−0.82 ± 0.04
	3.0	−0.47(6) ± 0.02	−0.78 ± 0.02
UO_2; 7.53 gm/cm^3; 1.3%; 0.601 in.	3.0	−0.71(10) ± 0.02	−0.93 ± 0.02
	4.0	−0.66(6) ± 0.02	−0.87 ± 0.02
	5.0	−0.55(6) ± 0.02	−0.83 ± 0.02
UO_2; 7.52 gm/cm^3; 1.3%; 0.388 in.	4.0	−0.85(5) ± 0.02	−1.02 ± 0.02
	5.0	−0.90(4) ± 0.03	−1.01 ± 0.03
UO_2; 10.53 gm/cm^3; 1.3%; 0.383 in.	3.0	−0.57(27) ± 0.07	−0.89 ± 0.07
	3.6	−0.69(38) ± 0.05	−0.87 ± 0.05
	5.0	−0.72(10) ± 0.02	−0.87 ± 0.02

[a]Number of measurements at all temperatures indicated in parentheses.

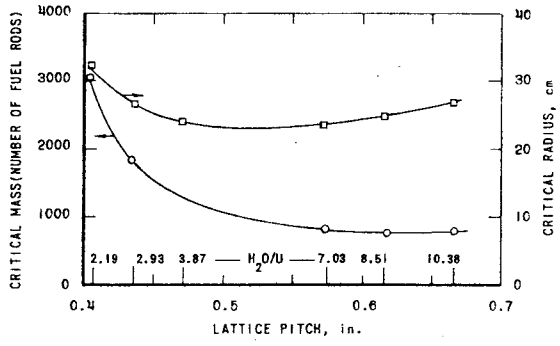

Fig. 4-26—Critical mass and radius as a function of lattice pitch for a clean core. *Reproduced from Ref. 75.*

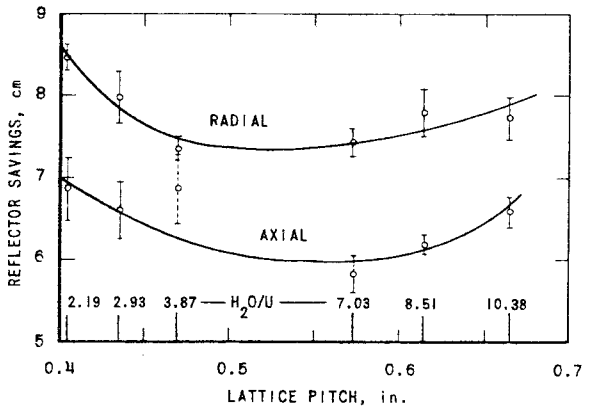

Fig. 4-27—Radial and axial reflector savings as a function of lattice pitch. *Reproduced from Ref. 75.*

The fuel in the earlier experiments (Tables 4-58 through 4-62) is in the form of Al-clad cylindrical rods, 48 in. long. The rod diameters and fuel density are given in the tables. The aluminum clad is 0.028 in. thick and there is an 0.005-inch radial air gap between the fuel and the Al.

The compositions and sizes of the fuel used in the experiments summarized in Table 4-63 do not include the fuel used in the Yankee critical experiments. This fuel is described in detail in Fig. 4-28.

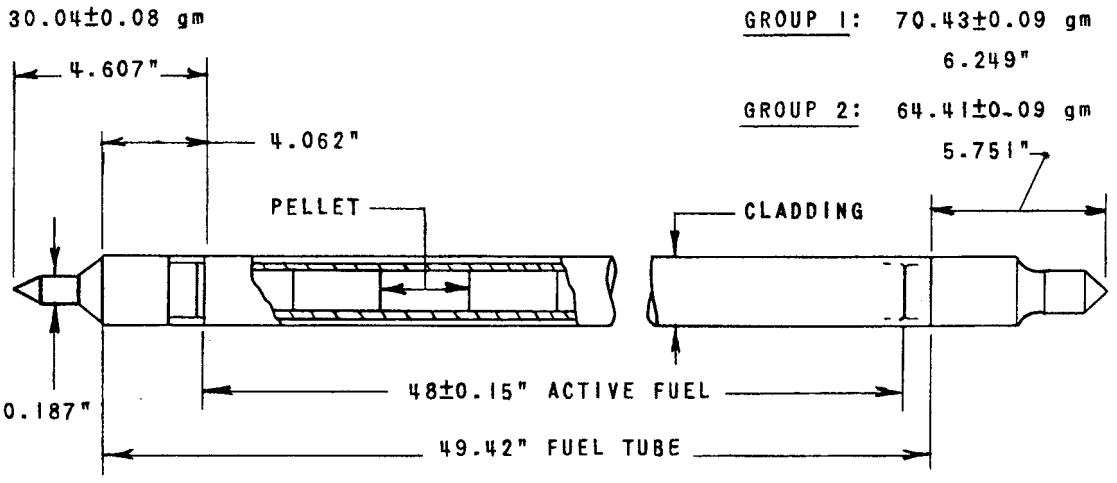

DIMENSIONS

FUEL		CLADDING	
ENRICHMENT	2.700±0.017 wt-%	TYPE	SST 304
FORM	SINTERED UO_2 PELLETS	TUBING	
PELLET		ID	0.3062±0.0009 in.
DIAMETER	0.3000±0.0002 in.	WALL	0.0161±0.0003 in.
LENGTH	0.5989±0.0034 in.	LENGTH	49.420±0.007 in.
DENSITY	10.2±0.1 gm/cm^3	WEIGHT	104.5±1.4 gm
WEIGHT	7.07±0.13 gm	END PLUGS	SST 304
PELLETS/ROD	80		
LENGTH/ROD	48.00±0.15 in.		
WEIGHT/ROD	566.0±4.6 gm		

Fig. 4-28—Yankee Critical Assembly fuel rods. Dimensions are derived from measurements of existing rods and do not represent manufacturing tolerances. *Reproduced in part from Ref. 77.*

Figure 4-25 is a graph of critical radii as measured by Ball and MacKinney (see Table 4-63). The calculated lines are included to indicate the probable trend of the data.

Figures 4-26 and 4-27 are correlations of "Yankee" critical experiments,[77] as are the data in Table 4-64.

Table 4-63—UO_2 FUEL PINS IN WATER (RADIALLY REFLECTED SYSTEMS)

Fuel Radius, cm		Clad Thickness, cm	Fuel Density, gm/cm^3	N_{25}/N_{28}	Pin/H_2O Vol. Ratio	H/U^{235} Ratio	Fuel Height, cm	Experimental Critical Cylinder Radius, cm	Ref.
Pin	Pellet								
0.8460	0.7635	0.071 Al[a]	7.53	0.01348	0.700 HP[b]	524	121.9	41.4	71
0.8460	0.7635	0.071 Al	7.53	0.01348	0.877 HP	418	121.9	39.7	71
0.8460	0.7635	0.071 Al	7.53	0.01348	1.150 HP	319	121.9	41.2	71
0.5755	0.4930	0.071 Al	7.52	0.01348	0.787 HP	518	121.9	45.7	71
0.5755	0.4930	0.071 Al	7.52	0.01348	0.980 HP	416	121.9	45.1	71
0.5755	0.4865	0.071 Al	10.53	0.01348	0.585 HP	511	121.9	37.6	71
0.5755	0.4865	0.071 Al	10.53	0.01348	0.787 HP	380	121.9	36.3	71
0.5755	0.4865	0.071 Al	10.53	0.01348	0.987 HP	303	121.9	38.2	71
0.6350	0.5640	0.071 SS	9.45	0.03128	0.355 SP	373	168.9	24.2	76
0.6350	0.5640	0.071 SS	9.45	0.03128	0.807 SP	164	168.9	23.8	76
0.6350	0.5640	0.071 SS	9.45	0.03128	1.102 SP	120	168.9	26.7	76
0.6350	0.5640	0.071 SS	9.45	0.04213	0.288 SP	345	168.9	19.8	76
0.6350	0.5640	0.071 SS	9.45	0.04213	0.355 SP	280	168.9	18.6	76
0.6350	0.5640	0.071 SS	9.45	0.04213	0.807 SP	123	168.9	19.3	76
0.6350	0.5640	0.071 SS	9.45	0.04213	1.102 SP	90	168.9	21.7	76
0.4329	0.3796	0.053 SS	10.20	0.0470	0.932 SP	91	142.5	20.0	77[c]
0.4329	0.3796	0.053 SS	10.20	0.0470	0.704 SP	121	142.5	18.5	77
0.4298	0.3810	0.041 SS	10.20	0.0281	1.214 SP	113	121.9	32.0	77
0.4298	0.3810	0.041 SS	10.20	0.0281	0.906 SP	151	121.9	26.8	77
0.4298	0.3810	0.041 SS	10.20	0.0281	0.687 SP	199	121.9	24.3	77

[a]The symbol Al means aluminum cladding and the symbol SS means stainless steel cladding.
[b]The symbol HP means hexagonal pitch and the symbol SP means square pitch.
[c]See also the material in Table 4-64 and Figs. 4-26, 4-27, and 4-28.

Table 4-64—SUMMARY OF CLEAN CRITICAL MASSES (NUMBER OF FUEL RODS) AS A FUNCTION OF LATTICE PITCH

(For 2.73% enriched UO_2, stainless steel-clad fuel rods in cylindrical configurations with a height of 121.9 cm)

Data from Refs. 74 and 77.

Ratio, W/U	Pitch, in.	Temp., °C	No. of Fuel Rods	Radius, cm
2.19	0.405	20.0	3043	32.01
2.93	0.435	20.0	1851	26.82
3.87	0.470	20.0	1301	24.27
7.03	0.573	22.5	826	23.60
8.51	0.615	23.0	789.9	24.77
10.38	0.665	23.0	813	27.17

Note: The data reported in Table 4-64 and Figs. 4-26 and 4-27 are taken in large part from critical experiments for the "Yankee" reactor. The properties of the fuel rods used in these experiments are given in Fig. 4-28. The data reported here are for clean systems with no control rods in the core.

4.5.3 NATURAL URANIUM–GRAPHITE LATTICES

4.5.3.1 Buckling Measurements for Natural Uranium Rods in Graphite

Exponential measurements have been performed at Hanford on a variety of rod sizes. In Table 4-65 are listed the rod sizes and associated characteristics, together with references for each case. Constituent ratios (by volume) are given in Table 4-66.

Hollow rods. Davenport[79] has reported on the bucklings of lattices of natural uranium tubes (1.66 in. O.D., and 0.81 in. I.D. or 1.11 in. I.D.). The clad was Al, and the center hole was filled with water. Figure 4-29 gives the results of buckling measurements with lattices of tubes imbedded in graphite, and the material volume ratios. Bucklings for the various Hanford lattices are given in Figs. 4-30 through 4-35.

Table 4-65—ROD AND TUBE SIZES

(Dimensions are in cm)

Fuel Element Diameter	Can		Process Tube		Graphite Hole Diameter	Ref.
	O.D.	I.D.	O.D.	I.D.		
6.35	6.55	6.37	8.00	7.67	8.07	78
4.88	5.08	4.90	6.10	5.72	6.13	78
4.22	4.40	4.26	none used		4.42	79
3.45	3.66	3.48	4.40	4.04	4.42	79
2.98	3.18	3.0	3.82	3.50	3.844	79
2.35	2.54	2.36	3.1	2.80	3.13	79

Table 4-66—DESCRIPTION OF MATERIAL IN SOLID SLUG EXPONENTIAL EXPERIMENTS

(Ratios of Al, H_2O, and C atoms, to U atoms per cell)[a]

Slug Diameter, cm	H_2O/U	Al/U	Lattice Spacing, in.	C/U
2.35 (0.925 in.)	0.174	0.686	5.1875	69.9
			6.1875	100.7
			7	129.0
			7.5	148.7
2.98 (1.175 in.)	0.180	0.551	6.1875	61.0
			7.5	90.6
3.45 (1.36 in.)	0.191	0.630	5.1875	32.4
			6.1875	47.3
			7	61.1
			7.5	70.7
			8	80.9
			8.375	89.4
			10.375	139.0
			12.375	198.8
4.22 (1.66 in.)	no water	0.088	6.1875	29.0
			7.5	43.4
			12.375	122.0
			15	179.2
4.88 (1.92 in.)	0.288	0.264	6.1875	11.64
			8.375	22.65
			10.375	35.60
			12.375	51.31
6.35 (2.50 in.)	0.185	0.403	8.375	12.67
			10.375	20.31
			12.375	29.58
			14.5625	41.58

[a]The quality of the graphite used in these experiments is such that the diffusion length at density 1.6 gm/cm^3 is 54.4 cm^2. Densities of graphite range from 1.647 gm/cm^3 to 1.658 gm/cm^3.

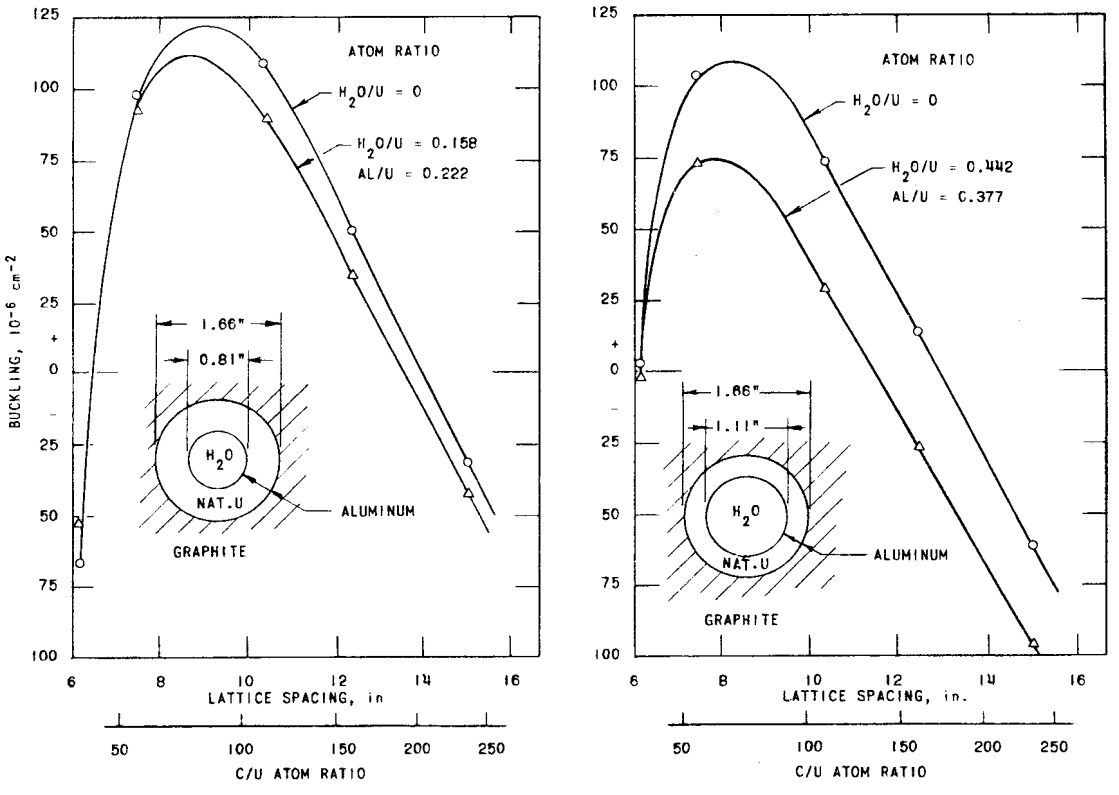

Fig. 4-29—Bucklings of lattices of internally cooled natural uranium tubes. *Reproduced from Ref. 79.*

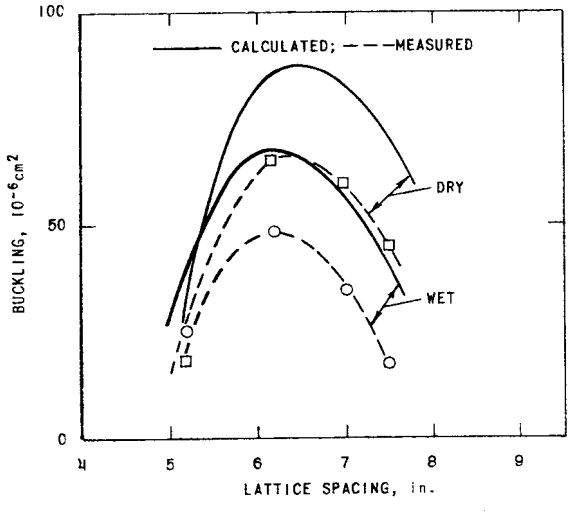

Fig. 4-30—Buckling values for 0.925-inch fuel rods. *Reproduced from Ref. 78.*

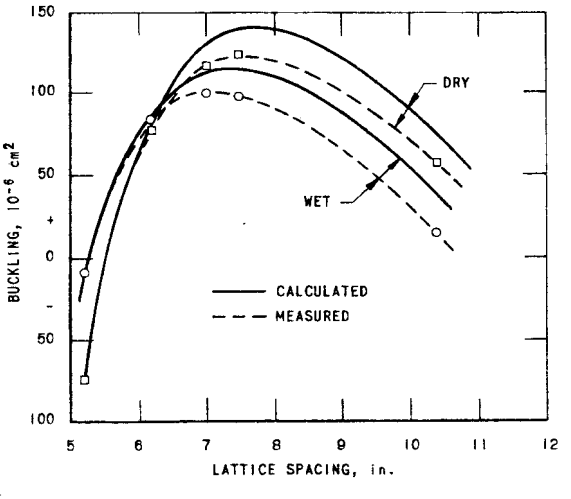

Fig. 4-31—Buckling values for 1.175-inch fuel rods. *Reproduced from Ref. 78.*

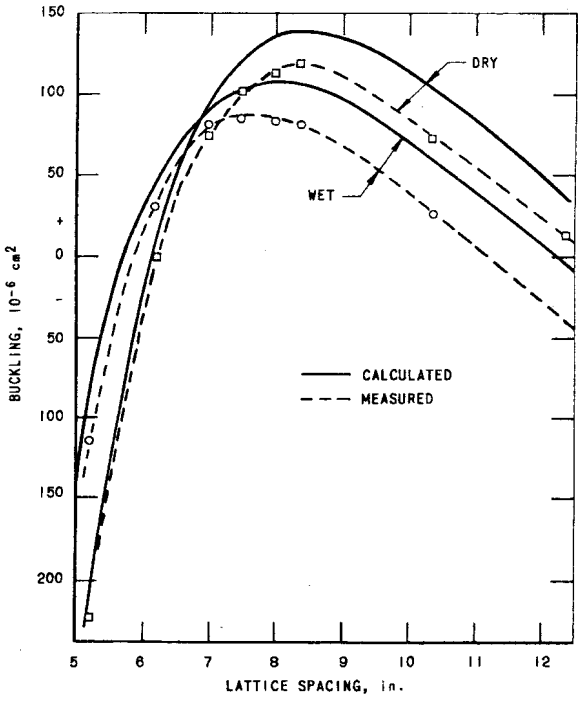

Fig. 4-32—Buckling values for 1.36-inch fuel rods. *Reproduced from Ref. 78.*

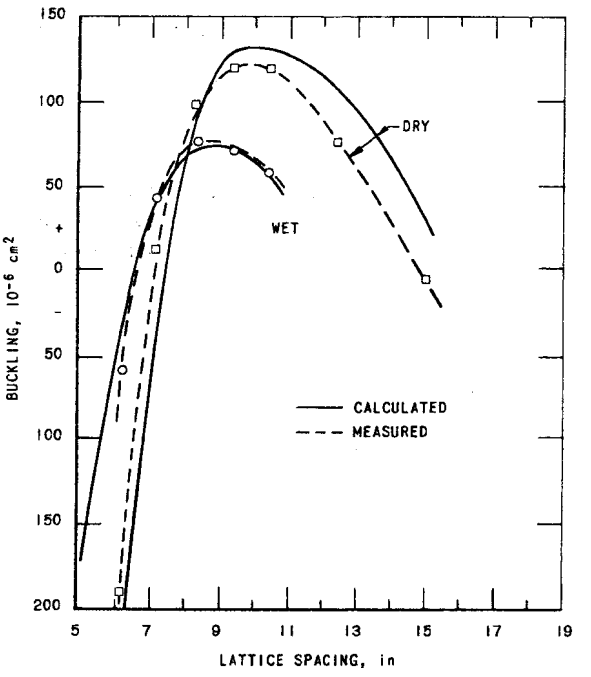

Fig. 4-33—Buckling values for 1.66-inch fuel rods. *Reproduced from Ref. 78.*

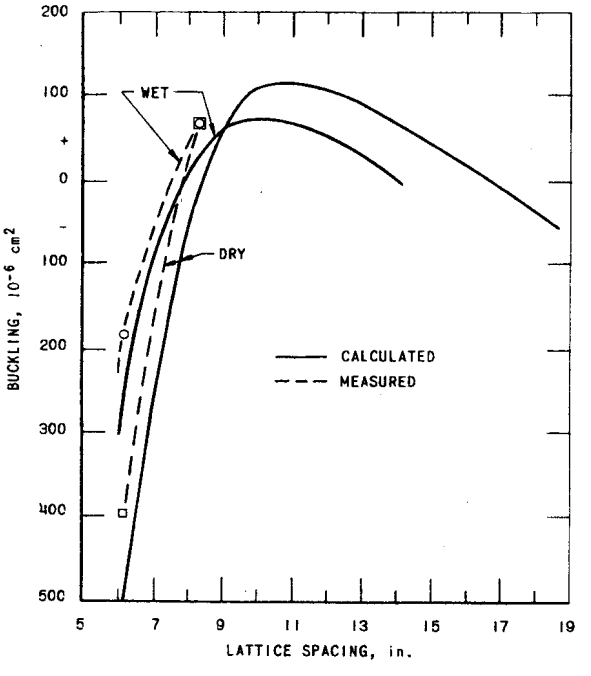

Fig. 4-34—Buckling values for 1.92-inch fuel rods. *Reproduced from Ref. 78.*

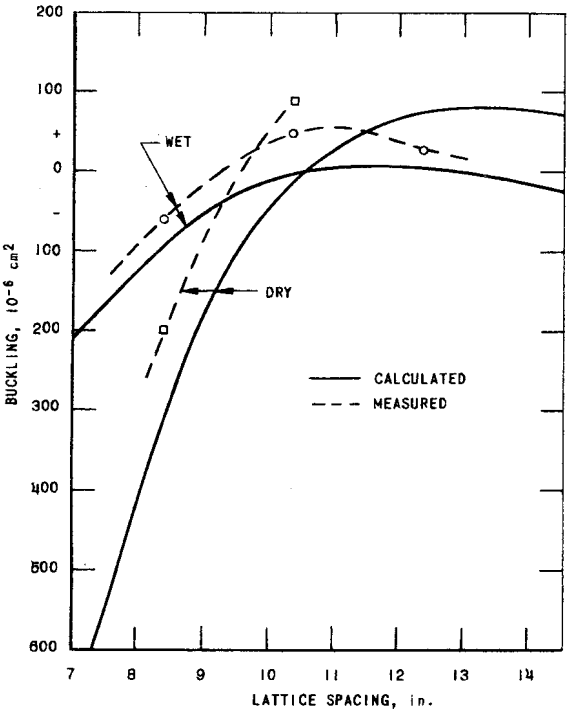

Fig. 4-35—Buckling values for 2.5-inch fuel rods. *Reproduced from Ref. 78.*

4.5.3.2 Measurements on Graphite Lattices

Measurements of the buckling of graphite moderated systems in the United Kingdom are reported in Ref. 80. The results are given in Table 4-67.

Table 4-67 — BUCKLING MEASUREMENTS IN GRAPHITE-MODERATED LATTICES

Lattice Pitch[a]	Uranium		Aluminium Can		Air Channel Diameter, in.	Axial Buckling (α^2), m^{-2}	Radial Buckling (β^2), m^{-2}
	Rod Diameter, in.	Enrichment,[b] Co.	Outside Diameter, in.	Inside Diameter, in.			
8.91	1.2	1.0	1.445	1.365	1.91	−0.932	1.910
8.25	1.2	1.0	1.445	1.365	3.77	−1.248	2.193
8.25	1.2	1.0	1.445	1.365	1.59	−1.187	2.223
7 × 8.167	1.2	1.0	1.445	1.365	1.75	−1.263	2.296
7.875	1.2	1.0	1.445	1.365	3.75	−1.132	2.465
7.875	1.2	1.3	1.445	1.365	3.75	1.274	0.877
7.875	1.2	1.0	1.445	1.365	1.50	2.116	−0.723
7.875	1.2	1.3	1.445	1.365	1.50	2.040	1.264
7.875	1.2	1.6	1.445	1.365	1.50	2.098	2.708
7.875	1.2	1.0	1.445	1.365	3.75	1.974	−1.526
7.875	1.2	1.3	1.445	1.365	3.75	2.058	0.088
7.875	1.2	1.6	1.445	1.365	3.75	2.024	0.881
7.875	1.2	1.6	1.445	1.365	3.75	−1.912	5.844
7.875	1.2	1.3	1.445	1.365	3.75	−0.840	3.334
5.0	1.2	1.6	1.445	1.365	1.50	2.060	−0.797
5.0	1.2	1.6	1.445	1.365	1.50	2.076	0.817
5.0	1.2	1.0	1.445	1.365	1.50	2.060	−3.546
8.25	1.2	1.0	1.445	1.365	3.77	1.092	−0.470
8.25	1.0	1.0	1.264	1.060	3.77	−1.384	2.201
8.25	1.0	1.0	1.264	1.060	1.59	−1.661	2.223
7 × 8.167	1.0	1.0	1.445	1.365	1.75	−1.434	2.296
7.875	1.0	1.0	1.264	1.060	3.75	−1.300	2.461
7.875	1.0	1.0	1.264	1.060	2.75	−1.354	2.477
7.875	1.0	1.0	1.264	1.060	1.50	−1.419	2.468
7.0	1.0	1.0	1.264	1.060	3.75	−1.841	2.961
7.0	1.0	1.0	1.264	1.060	2.75	−1.842	3.019
7.0	1.0	1.0	1.264	1.060	1.50	1.116	−0.008
6.3	1.0	1.0	1.445	1.365	1.88	−2.317	3.297
6.2	1.0	1.0	1.264	1.060	1.50	−2.882	3.868
5.0	1.0	1.0	1.264	1.060	2.75	−5.637	5.657
5.0	1.0	1.0	1.264	1.060	1.50	−5.917	5.749
7.875	1.0	1.045	1.264	1.060	3.75	−1.135	2.484
8.25	1.0	1.0	1.264	1.060	3.77	1.158	−0.818
8.25	1.0	1.0	1.264	1.060	1.59	1.170	−0.615
7.875	1.0	1.0	1.264	1.060	3.75	1.183	−0.593
7.875	1.0	1.0	1.264	1.060	2.75	1.178	−0.315
7.0	1.0	1.0	1.264	1.060	3.75	1.116	−0.776
7.0	1.0	1.0	1.264	1.060	2.75	1.147	−0.258
5.0	1.0	1.0	1.264	1.060	2.75	1.889	−2.793
5.0	0.522	1.0	No Can		1.5	2.062	−1.159
6.2	0.522	1.0	No Can		1.5	2.012	−1.813

Note: The error in the total buckling ($\alpha^2 + \beta^2$) is always about ±0.03 m^{-2}.

[a] Square unless otherwise stated.

[b] The enrichment is in terms of multiples of the abundance of U^{235} in natural uranium. Thus, Co = 1 corresponds to 0.712% U^{235} atoms per U atom; Co = 1.6 corresponds to 1.6 × 0.712 = 1.14% U^{235} atoms/U atom.

4.5.3.3 Exponential Experiments with Graphite-Moderated Uranium Metal Lattices

Experiments conducted at Atomics International[81] on graphite lattices correspond closely to D_2O-U lattice experiments described earlier (see Section 4.5.4.1).

Three fuel enrichments of U^{235} were used: 0.4962 at-%, 0.705 at-%, and 0.9124 at-%. The fuels with these enrichments are referred to as depleted, natural, and enriched, respectively. The density of the fuel varies slightly with enrichment (see Table 4-68).

Table 4-68 — MATERIAL DENSITIES FOR THE EXPONENTIAL LATTICES

Material	Density, gm/cm^3
Depleted Uranium: 0.4962 at-% U^{235}	18.80
Natural Uranium: 0.7205 at-% U^{235}	18.88
Enriched Uranium: 0.9124 at-% U^{235}	18.83
Aluminum	2.668
AGOT Graphite:	
Lattice Spacing, in.: 7.0	1.709
9.5	1.734
12.0	1.705

Each fuel element was composed of 15 uranium metal slugs (1 in. O.D., 4 in. long) housed in an aluminum tube (1.080 in. O.D., 0.030 in. wall), effecting an annular clearance of ~0.010 in. The aluminum tubes, in turn, fitted into the graphite fuel channels with approximately 0.005 in. clearance on a radius.

Material bucklings derived from flux maps are given in Table 4-69; μ is the root buckling in the horizontal direction, and ν the root buckling in the vertical direction: $B^2 = 2\mu^2 - \nu^2$.

Table 4-69 — MATERIAL-BUCKLING MEASUREMENTS

(Errors are standard deviations)

Lattice,[a] in.	μ, m^{-1}	ν, m^{-1}	B^2, m^{-2}
7.0 (D)	2.835 ± 0.007	4.130 ± 0.011	−1.010 ± 0.086
7.0 (N)	2.835 ± 0.007	3.777 ± 0.008	+1.778 ± 0.071
7.0 (E)	2.835 ± 0.007	3.495 ± 0.012	+3.833 ± 0.083
9.5 (D)	2.512 ± 0.004	3.792 ± 0.007	−1.759 ± 0.050
9.5 (N)	2.512 ± 0.004	3.496 ± 0.005	+0.401 ± 0.040
9.5 (E)	2.513 ± 0.004	3.279 ± 0.006	+1.866 ± 0.039
12.0 (N)	2.486 ± 0.003	3.621 ± 0.005	−0.749 ± 0.028
12.0 (E)	2.486 ± 0.003	3.461 ± 0.005	+0.378 ± 0.028

[a] D = depleted U; N = natural U; E = enriched U.

Material bucklings can be derived from single rod measurements using small source theory. The results of such measurements, together with the results given in Table 4-69, are shown graphically in Fig. 4-36.

Thermal utilizations are given in Table 4-70 and resonance escape probabilities in Table 4-71.

A summary of calculated and measured lattice parameters for these systems is given in Table 4-72. In Table 4-72, p is the resonance escape probability when 1/v capture is included.

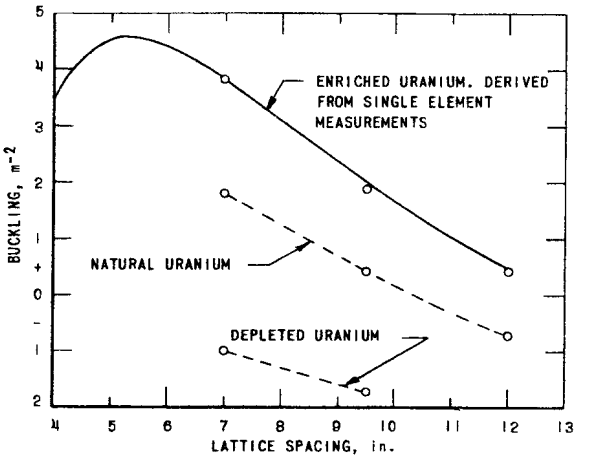

Fig. 4-36—Material buckling of uranium-graphite lattices. *Data from Ref. 81.*

Table 4-70—THERMAL UTILIZATION

Lattice,[a] in.	Experiment	Theory (S_4)
7.0 (D)	0.8791 ± 0.0050	0.8779
7.0 (N)	0.8932 ± 0.0044	0.8912
7.0 (E)	0.9046 ± 0.0041	0.8988
9.5 (D)	0.7928 ± 0.0076	0.7886
9.5 (N)	0.8115 ± 0.0072	0.8085
9.5 (E)	0.8263 ± 0.0067	0.8200
12.0 (N)	0.7187 ± 0.0095	0.7278
12.0 (E)	0.7363 ± 0.0098	0.7034

[a]D = depleted U; N = natural U; E = enriched U.

Table 4-71—RESONANCE ESCAPE SUMMARY

Lattice Spacing Natural Fuel, in.	p		I_{eff}^{res}[a], barn
	Measured, Including 1/v	Corrected for 1/v	
7	0.865 ± 0.004	0.8773	10.9 ± 0.7
9.5	0.927 ± 0.003	0.9343	10.8 ± 0.6
12	0.962 ± 0.002	0.9669	8.4 ± 0.05

[a]Average, 10.02 ± 0.40.

Table 4-72—SUMMARY OF LATTICE PARAMETERS

Lattice,[a] in.	Calculated					Measured			
	η	ϵ	L^2, cm^2	τ, cm^2	p	B^2, m^{-2}	f	P_1	P
7 (D)	1.444	1.024	301.20	302.3	0.9132	−1.010	0.8791	—	—
7 (N)	1.330	1.024	268.82	302.3	0.9090	+1.778	0.8932	0.8669	0.8799
7 (E)	1.439	1.024	250.00	302.3	0.9231	+3.833	0.9046	—	—
9.5 (D)	1.444	1.024	515.46	291.6	0.9301	−1.759	0.7928	—	—
9.5 (N)	1.330	1.024	467.29	291.6	0.9326	+0.401	0.8115	0.9287	0.9361
9.5 (E)	1.439	1.024	440.53	291.6	0.9385	+1.866	0.8263	—	—
12 (N)	1.330	1.024	689.66	300.0	0.9471	−0.749	0.7187	0.9620	0.9669
12 (E)	1.439	1.024	657.89	300.0	0.9555	+0.371	0.7363	—	—

[a](D) = depleted U; (N) = natural U; (E) = enriched U.

4.5.4 HEAVY WATER–NATURAL URANIUM LATTICES

4.5.4.1 Older Work (prior to 1955)

The results of older experiments[82] on D_2O-uranium lattices are summarized in Table 4-73. The data include buckling, ratio of flux at the surface of the fuel to the average flux in the fuel, and the ratio of the average flux in the moderator to the average flux in the fuel. These lattices are similar to those reported in Section 4.5.3.3.

Table 4-73—SUMMARY OF D_2O-URANIUM LATTICES

Square lattices; Al clad is 0.1 cm thick

Data from Ref. 82.

Enrichment, % U^{235}	Rod Diameter, in.	Cell Side, in.	D_2O/U Volume	Buckling, 10^4 cm^{-2}	Surface Flux / Avg. Rod. Flux	Avg. Mod. Flux / Avg. Rod Flux
0.4962	1.00	4.50	24.82	1.76	1.162	1.537
		4.90	29.64	2.10		1.563
		7.50	71.02	1.60		1.633
		12.00	183.7	0.105		1.792
	2.00	7.25	15.71	1.61	1.420	2.427
		9.00	24.80	2.25		2.594
		12.00	44.94	1.2		2.796
0.7205	0.75	3.00	19.35	7.60	1.133	1.406
		4.50	45.09	7.48		1.474
		6.00	81.13	5.40		1.508
	1.00	3.625	15.69	7.31	1.190	1.520
		4.50	24.82	8.47		1.578
		4.90	29.64	8.36		1.598
		6.00	45.03	7.25		1.657
		7.50	71.02	5.36		1.718
		9.00	102.8	3.92		1.789
		12.00	183.7	2.11		1.901
	1.25	4.50	15.47	8.32	1.290	1.809
		6.00	28.39	8.30		1.918
		7.50	44.99	6.84		1.976
		9.00	65.29	5.35		2.064
		12.00	117.0	2.92		2.237
	1.50	6.00	19.36	8.65	1.356	2.139
		7.25	28.79	7.94		2.221
		9.00	44.97	6.29		2.341
		12.00	80.81	3.69		2.527
	2.00	7.25	15.71	8.23	1.502	2.560
		9.00	24.80	7.22		2.806
		12.00	44.94	4.76		3.174
0.9124	1.00	3.625	15.69	12.6	1.238	1.721
		4.90	29.64	12.5		1.829
		6.00	45.03	10.6		1.924
		7.50	71.02	7.81		1.968
		9.00	102.8	5.85		2.0069
		12.00	183.7	3.13		2.131

4.5.4.2 Recent Work

References 83 and 84 are summaries of recent work on D_2O-natural uranium lattices. Some work on UO_2 lattices is also included. The uranium was coated with lacquer; there was no other clad-

ding. The UO_2 was in the form of pellets of density 10.1 gm/cm^3, and 0.370 in. diameter.* These pellets were loaded into aluminum tubes of 0.500 in. O.D. and 0.049 in. wall thickness.

The different fuel assemblies studied are shown in Fig. 4-37. Figures 4-38 through 4-52 depict graphically the results reported in Ref. 83. Tables 4-74 through 4-78 summarize the results reported

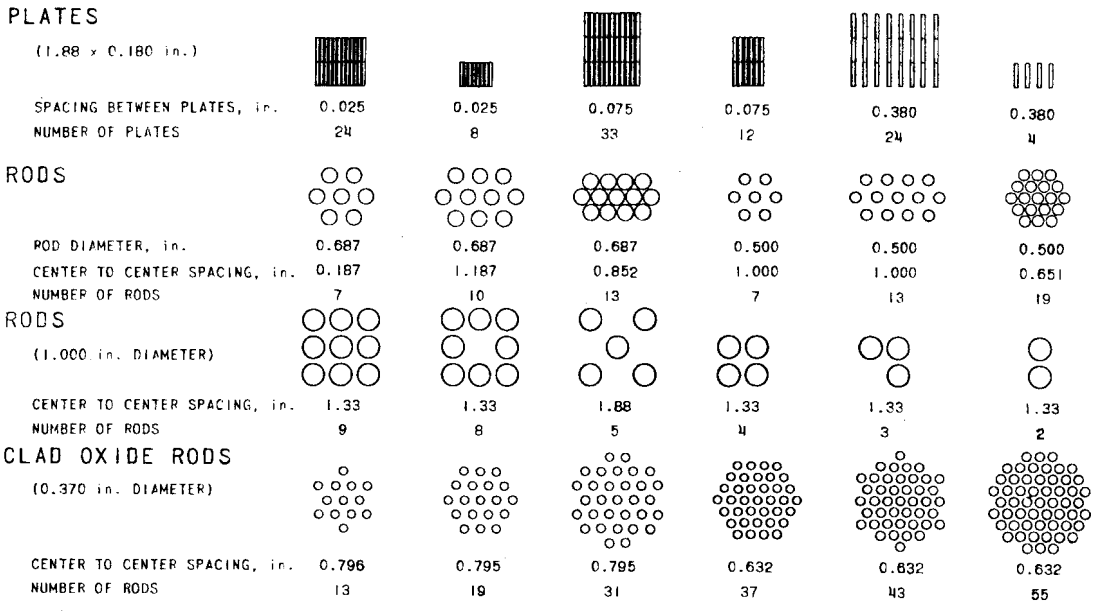

Fig. 4-37—Cross section of typical fuel assemblies used in buckling measurements. *Reproduced from Ref. 83.*

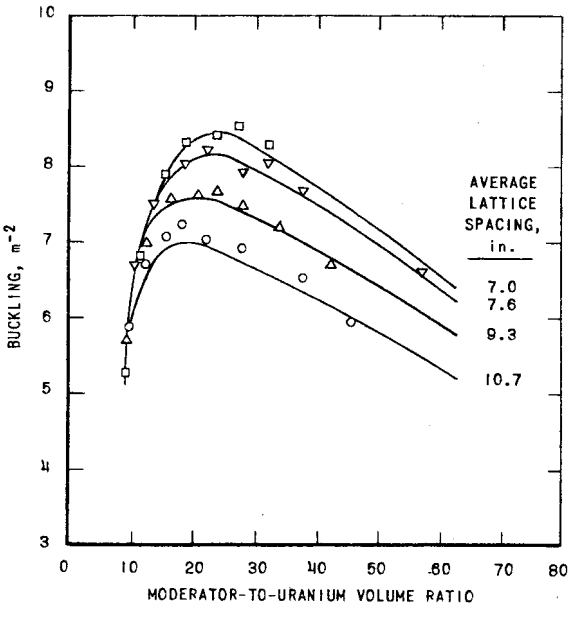

Fig. 4-38—Buckling vs. moderator-to-fuel ratio. Plate assemblies with 0.025-inch water channels; water purity: 99.75 mol-% D_2O. *Reproduced from Ref. 83.*

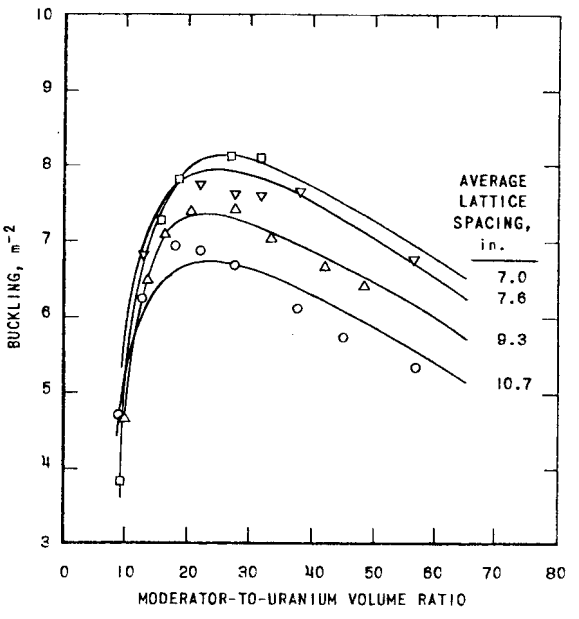

Fig. 4-39—Buckling vs. moderator-to-fuel ratio. Plate assemblies with 0.075-inch water channels; water purity: 99.75 mol-% D_2O. *Reproduced from Ref. 83.*

*The quoted density of 10.1 gm/cm^3 is an average density; in some calculations 10.32 gm/cm^3 was used. (Private communication from N. P. Baumann, Savannah River Laboratory.)

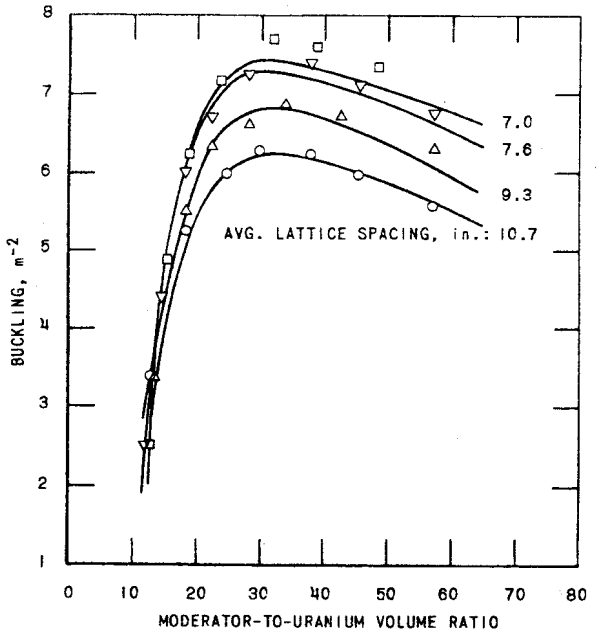

Fig. 4-40 — Buckling vs. moderator-to-fuel ratio. Plate assemblies with 0.380-inch water channels; water purity: 99.75 mol-% D_2O. *Reproduced from Ref. 83.*

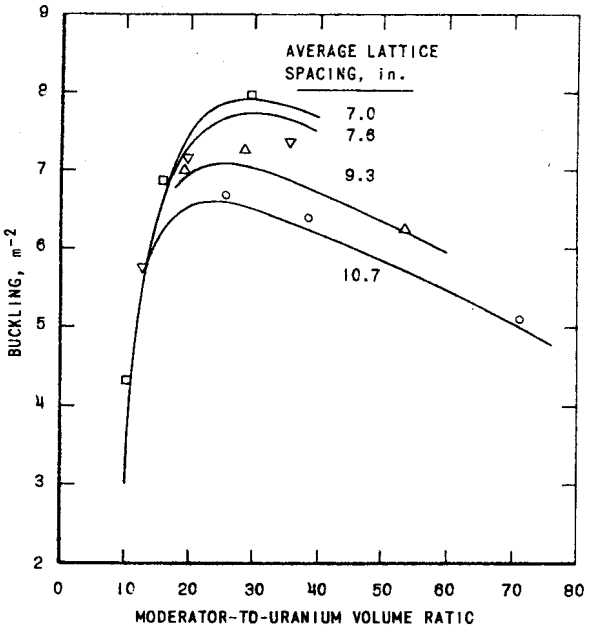

Fig. 4-41 — Buckling vs. moderator-to-fuel ratio. Metal rod assemblies with 0.500-inch rods and 0.651-inch center-to-center rod spacings; water purity: 99.75 mol-% D_2O. *Reproduced from Ref. 83.*

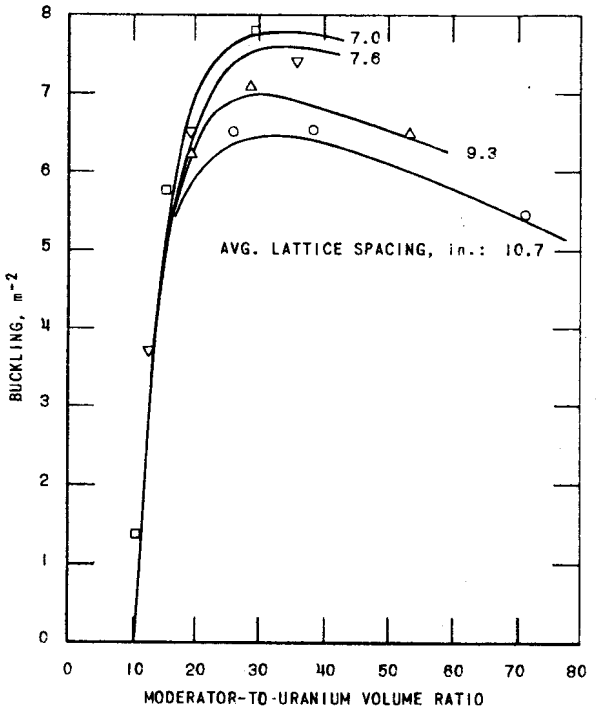

Fig. 4-42 — Buckling vs. moderator-to-fuel ratio. Metal rod assemblies with 0.500-inch rods and 1.000-inch center-to-center rod spacings; water purity: 99.75 mol-% DO_2. *Reproduced from Ref. 83.*

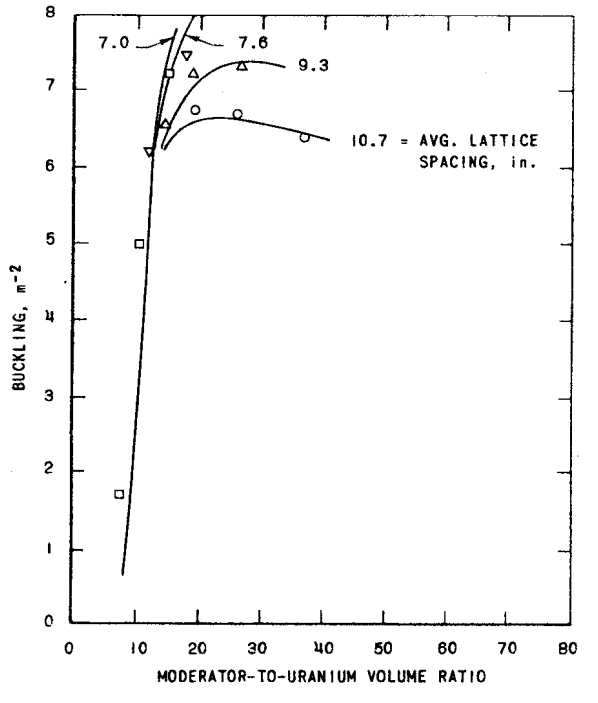

Fig. 4-43 — Buckling vs. moderator-to-fuel ratio. Metal rod assemblies with 0.687-inch rods and 0.852-inch center-to-center rod spacings; water purity: 99.75 mol-% D_2O. *Reproduced from Ref. 83.*

687863 O - 63 - 23

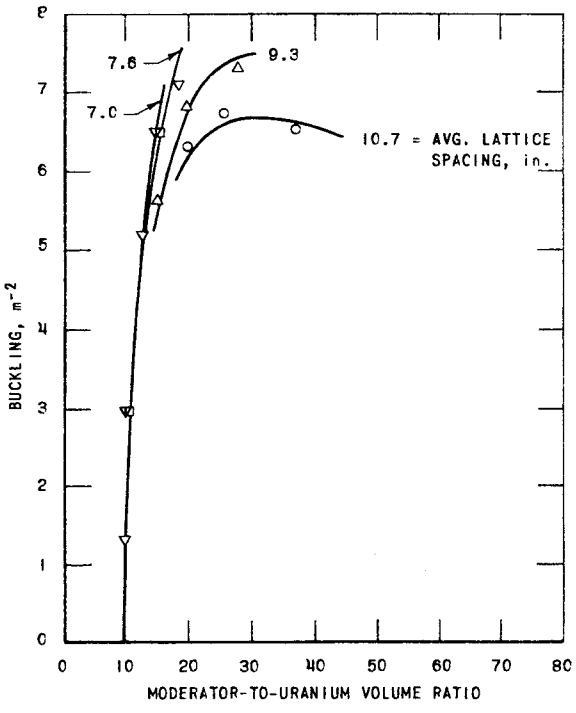

Fig. 4-44—Buckling vs. moderator-to-fuel ratio. Metal rod assemblies with 0.687-inch rods and 1.187-inch center-to-center rod spacings; water purity: 99.75 mol-% D_2O. *Reproduced from Ref. 83.*

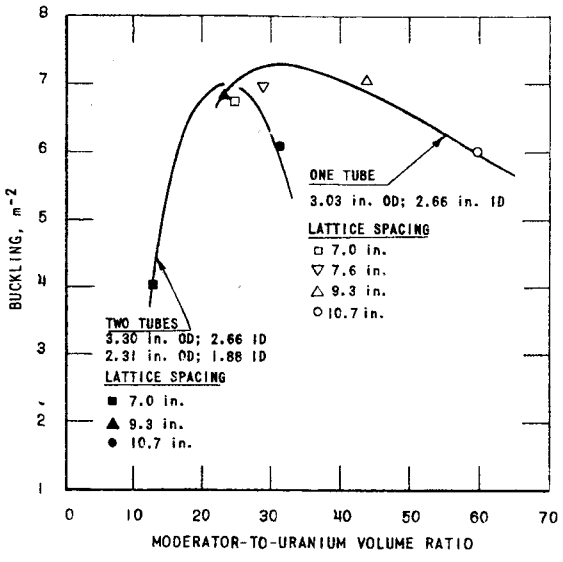

Fig. 4-45—Buckling vs. moderator-to-fuel ratio. Metal tube assemblies; water purity: 99.75 mol-% D_2O. *Reproduced from Ref. 83.*

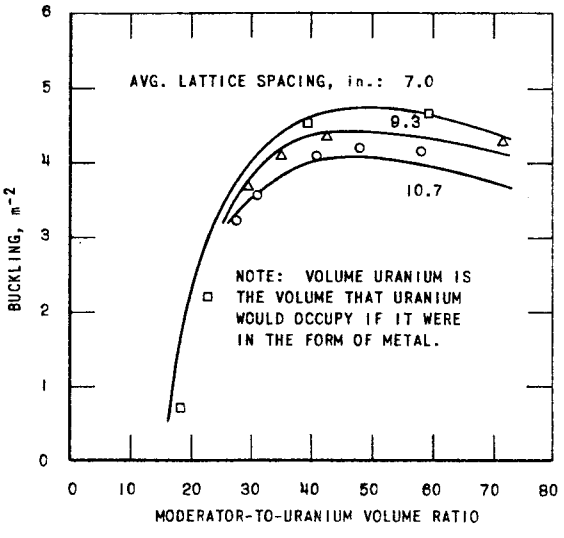

Fig. 4-46—Buckling vs. moderator-to-fuel ratio. Clad oxide assemblies with 0.632-inch center-to-center rod spacings; water purity: 99.75 mol-% D_2O. *Reproduced from Ref. 83.*

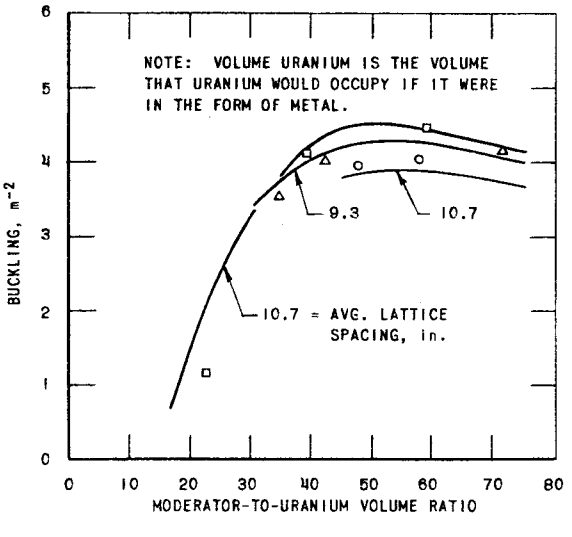

Fig. 4-47—Buckling vs. moderator-to-fuel ratio. Clad oxide rod assemblies with 0.795-inch center-to-center rod spacings; water purity: 99.75 mol-% D_2O. *Reproduced from Ref. 83.*

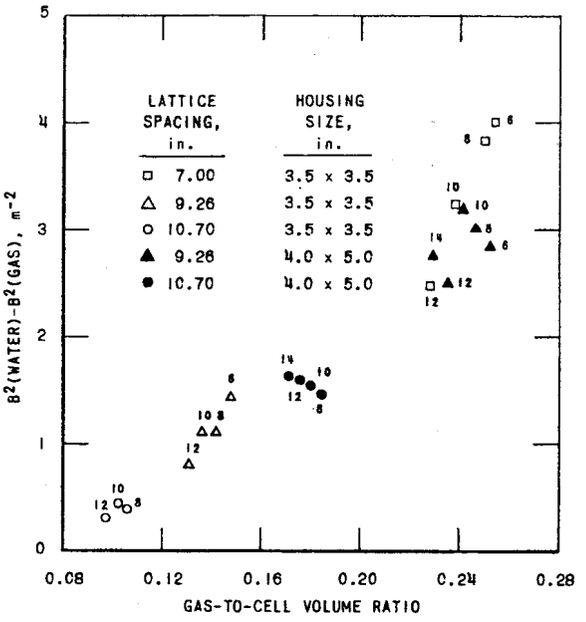

Fig. 4-48 — Measured buckling difference between water-cooled and gas-cooled lattices; 0.380-inch plate spacing. Numbers adjacent to data points refer to number of plates per assembly. *Reproduced from Ref. 83.*

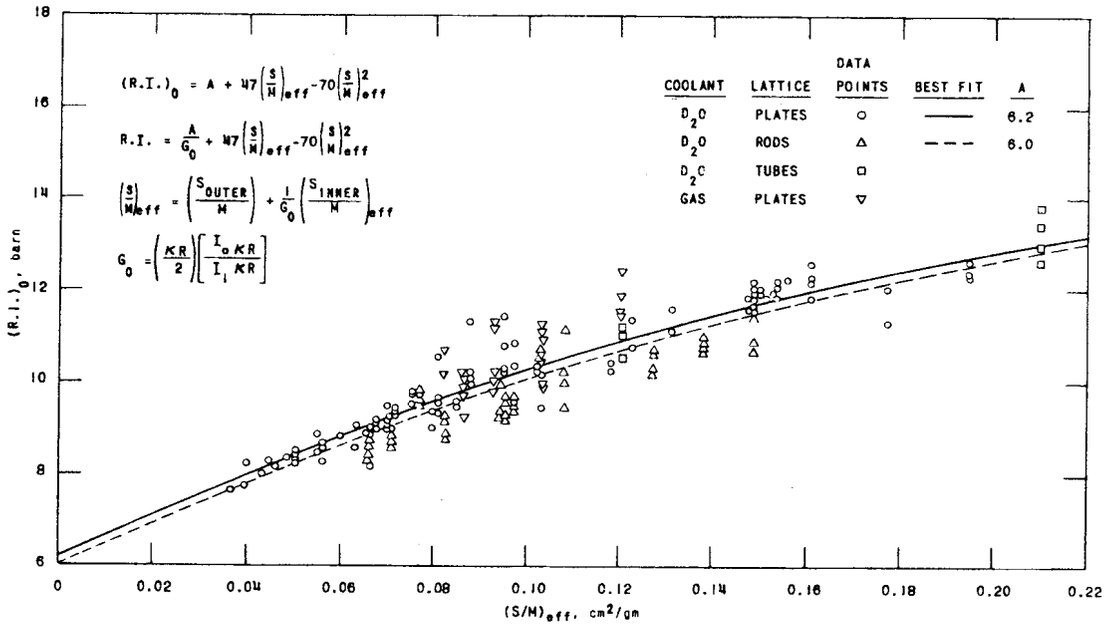

Fig. 4-49 — Effective resonance integral of uranium metal. *Reproduced from Ref. 83.*

Table 4-74—NUCLEAR PARAMETERS FOR D_2O-MODERATED CLUSTERS OF NATURAL URANIUM PLATES

Lattice Description				Lattice Parameters, 99.75% D_2O							Corrections Applied to B^2, m^{-2}			Resonance Integral Parameters	
Plate Spacing, in.	Triangular Lattice Pitch, in.	Plates per Assembly	V_M/V_F	f	ϵ	p	L^2, cm^2	τ, cm^2	B^2, m^{-2}	k_∞	D_2O Purity	Small Sample	Non-uniform Spacing	I_0, barn	(S_{eff}/M), cm^2/gm
0.025	10.69	46	9.1	0.9893	1.0761	0.8134	112	133.2	5.87	1.1491	0.06	−0.25	1.07	7.14	0.0392
		36	11.9	0.9872	1.0715	0.8450	135	130.1	6.72	1.1861	0.17		0.82	7.33	0.0406
		28	15.5	0.9852	1.0656	0.8684	155	127.7	7.07	1.2098	0.26		0.65	7.71	0.0456
		24	18.3	0.9840	1.0620	0.8822	167	126.6	7.23	1.2233	0.29		0.53	7.93	0.0485
		20	22.1	0.9814	1.0588	0.8973	195	125.4	7.03	1.2373	0.38		0.44	8.12	0.0520
		16	27.9	0.9786	1.0540	0.9162	224	124.3	6.91	1.2540	0.46		0.32	8.17	0.0579
		12	37.6	0.9744	1.0499	0.9348	268	123.2	6.52	1.2691	0.55		0.21	8.34	0.0642
		10	45.2	0.9715	1.0464	0.9358	298	122.7	5.93	1.2623	0.69		0.18	9.74	0.0683
	9.26	34	9.2	0.9910	1.0710	0.8052	95	133.0	5.70	1.1341	0.04	−0.35	0.97	7.76	0.0414
		26	12.4	0.9891	1.0645	0.8434	115	129.7	6.99	1.1783	0.17		0.71	7.98	0.0464
		20	16.4	0.9869	1.0588	0.8730	138	127.3	7.56	1.2106	0.29		0.52	8.24	0.0520
		16	20.7	0.9848	1.0540	0.8921	160	125.8	7.60	1.2288	0.36		0.40	8.60	0.0579
		14	23.8	0.9838	1.0511	0.9019	169	125.0	7.66	1.2376	0.41		0.35	8.85	0.0631
		12	28.0	0.9815	1.0499	0.9147	193	124.3	7.48	1.2508	0.47		0.27	8.93	0.0642
		10	33.7	0.9793	1.0464	0.9257	217	123.6	7.19	1.2588	0.52		0.21	9.26	0.0683
		8	42.4	0.9761	1.0421	0.9361	250	122.8	6.70	1.2636	0.59		0.16	9.85	0.0745
	7.56	20	10.6	0.9922	1.0588	0.8243	83	131.3	6.73	1.1492	0.00	—	0.42	7.99	0.0520
		16	13.5	0.9907	1.0540	0.8496	98	128.9	7.50	1.1773	0.10	—	0.33	8.33	0.0579
		12	18.3	0.9885	1.0499	0.8780	121	126.6	8.05	1.2092	0.22	—	0.25	8.95	0.0642
		10	22.2	0.9870	1.0464	0.8955	137	125.4	8.22	1.2273	0.30	—	0.20	9.14	0.0683
		8	27.9	0.9848	1.0421	0.9088	160	124.3	7.92	1.2376	0.37	—	0.16	9.85	0.0745
		7	32.1	0.9833	1.0400	0.9251	176	123.7	8.05	1.2554	0.43	—	0.12	9.25	0.0777
		6	37.6	0.9813	1.0375	0.9314	196	123.2	7.65	1.2583	0.48	—	0.10	9.81	0.0834
		4	56.9	0.9749	1.0313	0.9505	263	122.1	6.60	1.2682	0.61	—	0.06	10.46	0.1042
	7.00	20	8.9	0.9936	1.0588	0.7939	68	133.5	5.24	1.1081	−0.11	—	—	8.06	0.0520
		16	11.3	0.9925	1.0540	0.8272	80	130.6	6.81	1.1483	0.00	—	—	8.29	0.0579
		12	15.5	0.9906	1.0499	0.8600	99	127.7	7.90	1.1870	0.11	—	—	8.87	0.0642
		10	18.7	0.9893	1.0464	0.8795	112	126.4	8.32	1.2081	0.20	—	—	9.04	0.0683
		8	23.7	0.9874	1.0421	0.8993	132	125.1	8.41	1.2279	0.29	—	—	9.05	0.0745
		7	27.2	0.9861	1.0400	0.9131	145	124.4	8.52	1.2426	0.34	—	—	9.22	0.0777
		6	31.9	0.9844	1.0375	0.9228	163	123.8	8.26	1.2507	0.40	—	—	9.52	0.0834
		4	48.5	0.9789	1.0313	0.9472	220	122.5	7.42	1.2690	0.55	—	—	9.67	0.1042
0.075	10.69	45	9.3	0.9908	1.0634	0.7944	97	132.9	4.69	1.1107	0.04	−0.25	1.23	7.90	0.0536
		33	13.0	0.9882	1.0583	0.8387	124	129.2	6.23	1.1640	0.19		0.87	8.10	0.0594
		24	18.3	0.9852	1.0521	0.8758	156	126.6	6.91	1.2047	0.34		0.60	8.31	0.0683
		20	22.1	0.9832	1.0482	0.8892	176	125.4	6.83	1.2162	0.40		0.49	8.64	0.0687
		16	27.9	0.9804	1.0461	0.9034	205	124.3	6.63	1.2295	0.49		0.39	9.38	0.0739
		12	37.6	0.9763	1.0415	0.9160	247	123.2	6.07	1.2359	0.58		0.28	10.70	0.0836
		10	45.2	0.9734	1.0394	0.9235	278	122.7	5.71	1.2399	0.64		0.24	11.58	0.0898
		8	56.9	0.9690	1.0366	0.9363	324	122.1	5.31	1.2480	0.72		0.17	11.95	0.0921
	9.26	33	9.5	0.9920	1.0583	0.7928	85	132.6	4.69	1.1045	0.00	−0.35	1.05	8.39	0.0593
		24	13.5	0.9898	1.0521	0.8386	108	128.9	6.46	1.1588	0.15		0.75	8.79	0.0683
		20	16.4	0.9883	1.0482	0.8624	124	127.3	7.07	1.1856	0.22		0.60	8.88	0.0687
		16	20.7	0.9861	1.0461	0.8842	146	125.8	7.37	1.2103	0.34		0.41	9.19	0.0739

		12	28.0	0.9830	1.0415	0.9105	179	124.3	7.41	1.2370	0.45		0.30	9.37	0.0836
		10	33.7	0.9808	1.0394	0.9167	202	123.6	7.00	1.2402	0.51		0.25	10.32	0.0898
		8	42.4	0.9774	1.0366	0.9310	237	122.8	6.64	1.2517	0.59		0.18	10.63	0.0921
		7	48.7	0.9755	1.0350	0.9367	257	122.5	6.38	1.2549	0.63		0.16	11.10	0.0951
	7.56	20	10.6	0.9931	1.0482	0.8104	74	131.3	5.67	1.1195	−0.05	—	0.46	8.58	0.0686
		16	13.5	0.9917	1.0461	0.8392	89	128.9	6.88	1.1553	0.07	—	0.36	8.96	0.0739
		12	18.3	0.9896	1.0415	0.8713	110	126.6	7.75	1.1917	0.19	—	0.27	9.43	0.0836
		10	22.2	0.9881	1.0394	0.8833	126	125.4	7.73	1.2038	0.25	—	0.22	10.18	0.0898
		8	27.9	0.9858	1.0366	0.8985	149	124.3	7.60	1.2184	0.36	—	0.18	10.96	0.0921
		7	32.1	0.9844	1.0350	0.9093	164	123.7	7.57	1.2294	0.40	—	0.15	11.18	0.0951
		6	37.6	0.9825	1.0328	0.9268	184	123.2	7.64	1.2479	0.47	—	0.12	10.46	0.1013
		4	56.9	0.9763	1.0286	0.9491	249	122.1	6.76	1.2648	0.61	—	0.07	10.74	0.1147
	7.00	20	8.9	0.9945	1.0482	0.7769	60	133.5	3.80	1.0747	−0.14	—	—	8.67	0.0686
		16	11.3	0.9933	1.0461	0.8132	72	130.6	5.83	1.1213	0.04	—	—	8.92	0.0739
		12	15.5	0.9915	1.0415	0.8498	91	127.7	7.24	1.1644	0.09	—	—	9.51	0.0836
		10	18.7	0.9902	1.0395	0.8692	104	126.4	7.78	1.1872	0.17	—	—	9.80	0.0898
		8	23.7	0.9884	1.0366	0.8896	124	125.1	8.01	1.2095	0.26	—	—	9.89	0.0921
		7	27.2	0.9871	1.0350	0.9014	136	124.4	8.10	1.2220	0.32	—	—	10.46	0.0951
		6	31.9	0.9855	1.0328	0.9158	154	123.8	8.08	1.2369	0.39	—	—	10.38	0.1013
		4	48.5	0.9802	1.0286	0.9428	208	122.5	7.48	1.2615	0.54	—	—	10.49	0.1147
0.380	10.69	33	13.0	0.9931	1.0276	0.7907	78	129.2	3.36	1.0708	−0.04	−0.25	1.31	10.29	0.1344
		24	18.3	0.9901	1.0270	0.8352	109	126.6	5.23	1.1270	0.15		0.91	10.87	0.1406
		18	24.7	0.9869	1.0261	0.8674	142	124.9	5.97	1.1657	0.31		0.64	11.46	0.1459
		15	29.9	0.9846	1.0255	0.8874	166	124.0	6.24	1.1890	0.41		0.51	11.55	0.1473
		12	37.6	0.9815	1.0236	0.9065	198	123.2	6.20	1.2085	0.51		0.37	11.87	0.1553
		10	45.2	0.9785	1.0226	0.9174	228	122.7	5.94	1.2182	0.60		0.30	12.50	0.1593
		8	56.9	0.9742	1.0215	0.9312	274	122.1	5.54	1.2297	0.69		0.21	12.86	0.1665
	9.26	33	9.5	0.9958	1.0276	0.7276	52	132.6	−0.65	0.9880	−0.25	−0.35	1.52	10.80	0.1344
		24	12.5	0.9935	1.0270	0.7900	74	129.6	3.37	1.0697	−0.07		1.09	10.53	0.1406
		18	18.3	0.9911	1.0261	0.8351	98	126.6	5.49	1.1270	0.10		0.78	11.36	0.1459
		15	22.2	0.9894	1.0255	0.8601	116	125.4	6.31	1.1581	0.21		0.61	11.74	0.1473
		12	28.0	0.9870	1.0236	0.8817	140	124.3	6.60	1.1820	0.33		0.46	12.29	0.1553
		10	33.7	0.9848	1.0226	0.9031	164	123.6	6.86	1.2068	0.43		0.35	11.99	0.1593
		8	42.4	0.9814	1.0215	0.9212	198	122.8	6.69	1.2255	0.54		0.24	12.10	0.1665
		6	57.0	0.9762	1.0206	0.9432	252	122.1	6.28	1.2471	0.69		0.14	11.57	0.1763
	7.56	18	11.9	0.9952	1.0261	0.7725	57	130.1	2.48	1.0469	−0.17	—	0.58	11.24	0.1459
		15	14.4	0.9940	1.0255	0.8046	69	128.3	4.39	1.0883	−0.07	—	0.47	11.44	0.1473
		12	18.3	0.9924	1.0236	0.8384	85	126.6	5.97	1.1302	0.05	—	0.36	11.76	0.1553
		10	22.2	0.9909	1.0226	0.8604	101	125.4	6.68	1.1569	0.15	—	0.29	12.14	0.1593
		8	27.9	0.9886	1.0215	0.8860	124	124.3	7.22	1.1873	0.27	—	0.22	12.28	0.1665
		6	37.6	0.9850	1.0206	0.9147	161	123.2	7.37	1.2202	0.43	—	0.14	12.18	0.1763
		5	45.3	0.9829	1.0175	0.9250	183	122.6	7.08	1.2276	0.50	—	0.12	12.76	0.1971
		4	56.9	0.9792	1.0174	0.9395	220	122.1	6.72	1.2420	0.60	—	0.09	12.80	0.1972
	7.00	18	10.0	0.9963	1.0261	0.7315	46	132.0	−0.43	0.9924	−0.27	—	—	11.37	0.1459
		15	12.2	0.9953	1.0255	0.7729	56	129.8	2.50	1.0469	−0.18	—	—	11.48	0.1473
		12	15.5	0.9940	1.0236	0.8130	69	127.7	4.86	1.0977	−0.06	—	—	11.75	0.1553
		10	18.7	0.9927	1.0226	0.8417	83	126.4	6.20	1.1339	0.04	—	—	11.81	0.1593
		8	23.7	0.9908	1.0215	0.8700	102	125.1	7.13	1.1684	0.17	—	—	11.62	0.1665
		6	31.9	0.9877	1.0206	0.9020	133	123.8	7.67	1.2067	0.33	—	—	12.06	0.1763
		5	38.6	0.9859	1.0175	0.9159	152	123.1	7.58	1.2193	0.40	—	—	12.37	0.1971
		4	48.5	0.9827	1.0174	0.9316	183	122.5	7.33	1.2360	0.52	—	—	12.55	0.1972

Table 4-75 — NUCLEAR PARAMETERS FOR D_2O-MODERATED CLUSTERS OF NATURAL URANIUM RODS

Lattice Description					Lattice Parameters, 99.75% D_2O							Lattice Parameters, 99.12% D_2O				Resonance Integral Parameters		
																I_0, barns, using		
Rod Diameter, in.	Rod Spacing, in.	Rods per Cluster	Triangular Lattice Pitch, in.	V_M/V_F	f	ϵ	p	L^2, cm^2	τ, cm^2	B^2, m^{-2}	k_∞	f	L^2, cm^2	τ, cm^2	B^2, m^{-2}	(V_M/V_F)	(V_{cell}/V_F)	(S_{eff}/N), cm^2/gm
0.500	0.151	7	7.00	29.8	0.9867	1.0277	0.9087	143.68	123.9	7.92	1.2230	0.9674	137.27	121.3	7.52	10.18	10.52	0.1089
		7	7.56	35.1	0.9839	1.0277	0.9168	172.92	123.3	7.38	1.2302	0.9607	164.53	120.7	6.87	11.17	11.49	0.1089
		7	9.26	53.0	0.9747	1.0277	0.9469	270.96	122.2	6.25	1.2586	0.9387	254.29	119.6	5.50	9.90	10.09	0.1089
		7	10.69	71.1	0.9653	1.0277	0.9590	365.97	121.7	5.14	1.2624	0.9171	312.16	119.1	4.42	9.34	9.47	0.1089
		13	7.00	15.6	0.9921	1.0340	0.8461	86.87	127.2	6.85	1.1518	0.9806	83.67	124.5	6.79	9.38	9.98	0.0945
		13	7.56	19.4	0.9903	1.0340	0.8625	106.11	125.9	7.12	1.1720	0.9761	101.92	123.3	6.93	9.92	10.43	0.0945
		13	9.26	28.0	0.9840	1.0340	0.9083	172.05	124.2	7.26	1.2263	0.9609	163.72	121.6	6.77	9.28	9.61	0.0945
		13	10.69	37.7	0.9777	1.0340	0.9275	240.12	123.1	6.39	1.2442	0.9456	226.31	120.5	5.71	9.26	9.51	0.0945
		19	7.00	10.4	0.9945	1.0380	0.7915	62.55	130.5	4.29	1.0843	0.9863	60.54	127.8	4.46	8.79	9.63	0.0827
		19	7.56	12.2	0.9930	1.0380	0.8211	77.49	129.1	5.79	1.1230	0.9828	74.74	126.4	5.83	8.86	9.59	0.0827
		19	8.28	14.91	0.9912	1.0380	0.8390	96.59	127.5	6.28	1.1456	0.9783	92.88	124.8	6.16	9.58	10.22	0.0827
		19	9.26	18.9	0.9881	1.0380	0.8729	129.26	126.0	7.05	1.1880	0.9708	123.75	123.4	6.75	9.20	9.69	0.0827
		19	10.69	25.5	0.9830	1.0380	0.8979	183.68	124.0	6.68	1.2157	0.9583	174.49	121.4	6.17	9.13	9.49	0.0827
	0.500	7	7.00	29.8	0.9891	1.0179	0.8989	122.58	123.9	7.78	1.2009	0.9732	117.54	121.3	7.50	11.33	11.71	0.1484
		7	7.56	35.1	0.9867	1.0179	0.9043	148.09	123.3	7.21	1.2052	0.9673	141.48	120.7	6.95	12.14	12.49	0.1484
		7	9.26	53.0	0.9785	1.0179	0.9416	234.21	122.2	6.52	1.2445	0.9477	221.05	119.6	5.86	10.78	10.98	0.1484
		7	10.69	71.1	0.9693	1.0179	0.9536	321.22	121.7	5.36	1.2486	0.9284	299.81	119.1	4.56	10.59	10.74	0.1380
		13	7.00	15.6	0.9944	1.0208	0.8250	67.35	127.2	5.58	1.1112	0.9862	65.10	124.5	5.69	10.60	11.28	0.1380
		13	7.56	19.4	0.9930	1.0208	0.8465	82.93	125.9	6.43	1.1386	0.9862	79.96	123.3	6.40	10.84	11.40	0.1380
		13	9.26	28.0	0.9878	1.0208	0.8928	137.17	124.2	7.12	1.1947	0.9700	131.16	121.6	6.68	10.93	11.32	0.1380
		13	10.69	37.7	0.9824	1.0208	0.9146	193.96	123.1	6.53	1.2172	0.9570	183.97	120.5	5.95	10.88	11.17	0.1380
		19	7.00	10.4	0.9967	1.0216	0.7573	44.16	130.5	1.33	1.0233	0.9918	42.83	127.8	1.73	10.06	11.03	0.1272
		19	7.56	12.2	0.9956	1.0216	0.7915	55.29	129.1	3.66	1.0684	0.9892	53.54	126.4	3.92	10.16	10.99	0.1272
		19	8.28	14.9	0.9943	1.0216	0.8133	69.81	127.5	4.78	1.0963	0.9858	67.45	124.8	4.83	10.97	11.71	0.1272
		19	9.26	18.9	0.9919	1.0216	0.8499	95.06	126.0	6.25	1.1428	0.9799	91.54	123.4	6.14	10.68	11.24	0.1272
		19	10.69	25.5	0.9877	1.0216	0.8803	138.07	124.0	6.54	1.1787	0.9699	132.00	121.4	6.20	10.65	11.07	0.1272

0.687	0.165	7	7.00	15.2	0.9918	1.0377	0.8511	89.97	127.4	7.20	1.1624	0.9797	86.64	124.7	7.10	9.47	10.09	0.0778
		7	7.56	17.9	0.9899	1.0377	0.8685	109.81	126.3	7.46	1.1838	0.9751	105.39	123.6	7.24	9.79	10.34	0.0778
		7	9.26	27.4	0.9835	1.0377	0.9110	177.51	124.2	7.35	1.2337	0.9596	168.75	121.6	6.85	9.55	9.90	0.0778
		7	10.69	36.8	0.9769	1.0377	0.9280	247.25	123.2	6.37	1.2483	0.9438	232.78	120.6	5.68	9.61	9.87	0.0778
		10	7.00	10.4	0.9942	1.0420	0.8001	66.54	130.5	4.95	1.0999	0.9856	64.33	127.8	5.09	8.52	9.34	0.0710
		10	7.56	12.3	0.9928	1.0420	0.8207	82.13	129.0	5.83	1.1267	0.9821	79.20	126.3	6.23	8.68	9.39	0.0710
		10	9.26	19.0	0.9877	1.0420	0.8779	136.36	126.0	7.24	1.1989	0.9699	130.39	123.4	6.93	8.79	9.25	0.0710
		10	10.69	25.7	0.9825	1.0420	0.9009	193.14	124.5	6.71	1.2239	0.9573	183.21	121.7	6.20	8.93	9.28	0.0710
		13	7.00	7.74	0.9953	1.0450	0.7472	52.51	134.0	1.67	1.0313	0.9885	50.89	131.2	1.98	8.33	9.51	0.0664
		13	7.56	9.58	0.9941	1.0450	0.7876	65.51	131.2	4.28	1.0857	0.9855	63.34	128.4	4.41	8.27	9.14	0.0664
		13	9.26	14.2	0.9898	1.0450	0.8477	111.31	127.8	6.58	1.1635	0.9448	106.82	125.1	6.37	8.68	9.29	0.0664
		13	10.69	19.4	0.9851	1.0450	0.8782	157.88	125.9	6.72	1.1996	0.9636	152.37	123.3	6.25	8.63	9.08	0.0664
	0.500	7	7.00	15.2	0.9926	1.0258	0.8394	74.91	127.4	6.44	1.1342	0.9817	72.31	124.7	6.46	10.31	10.99	0.1028
		7	7.56	17.9	0.9908	1.0258	0.8589	88.84	126.3	7.10	1.1584	0.9773	85.56	123.6	7.00	10.65	11.24	0.1028
		7	9.26	27.4	0.9847	1.0258	0.8996	151.00	124.2	7.32	1.2058	0.9625	144.09	121.6	6.91	10.52	10.92	0.1028
		7	10.69	36.8	0.9784	1.0258	0.9235	212.32	123.2	6.52	1.2299	0.9475	200.92	120.6	5.91	10.45	10.73	0.1028
		10	7.00	10.4	0.9957	1.0276	0.7768	52.08	130.5	2.96	1.0546	0.9893	50.46	127.8	3.31	9.39	10.29	0.0975
		10	7.56	12.3	0.9945	1.0276	0.8037	64.90	129.0	4.55	1.0899	0.9863	62.76	126.3	5.12	9.46	10.23	0.0975
		10	9.26	19.0	0.9901	1.0276	0.8650	110.25	126.0	6.83	1.1678	0.9757	105.82	123.4	6.62	9.68	10.19	0.0975
		10	10.69	25.7	0.9855	1.0276	0.8922	158.43	124.5	6.72	1.1990	0.9646	151.01	121.7	6.29	9.65	10.03	0.0975
		13	7.00	7.74	0.9970	1.0290	0.7154	38.92	134.0	−1.51	0.9740	0.9925	37.76	131.2	−1.04	9.24	10.43	0.0962
		13	7.56	9.58	0.9960	1.0290	0.7615	49.20	131.2	1.96	1.0356	0.9900	47.65	128.4	2.29	9.16	10.12	0.0962
		13	9.26	14.2	0.9925	1.0290	0.8290	86.19	127.8	5.61	1.1235	0.9813	83.04	125.1	5.57	9.65	10.33	0.0962
		13	10.69	19.4	0.9886	1.0290	0.8637	126.29	125.9	6.33	1.1660	0.9720	121.00	123.3	6.04	9.57	10.06	0.0962
0.687	—	1	4.00[a]	42.1	0.9853	1.0197	0.9234	156.22	122.8	7.86	1.2311	0.9641	148.95	120.2	7.39	11.99	12.27	0.1225
0.687	—	1	3.00[a]	23.3	0.9920	1.0197	0.8752	85.95	124.9	7.97	1.1748	0.9803	82.83	122.3	7.85	10.80	11.26	0.1225
0.687	—	1	2.00[a]	9.8	0.9966	1.0197	0.7536	37.23	131.1	0.96	1.0163	0.9917	36.10	128.4	1.29	9.12	10.05	0.1225
0.500	—	1	3.00[a]	44.8	0.9861	1.0145	0.9219	148.26	122.6	7.85	1.2238	0.9659	141.53	120.0	7.46	12.63	12.91	0.1681
0.500	—	1	2.00[a]	19.4	0.9940	1.0145	0.8430	65.10	125.9	6.52	1.1280	0.9852	62.96	123.3	6.57	11.36	11.95	0.1681
0.500	—	1	1.50[a]	10.4	0.9967	1.0145	0.7417	36.61	131.5	−0.29	0.9951	0.9919	35.50	128.7	0.15	10.01	10.98	0.1681

[a]Square lattice.

Table 4-76 — NUCLEAR PARAMETERS FOR D_2O-MODERATED CLUSTERS OF NATURAL URANIUM PLATES IN GAS-FILLED TUBES

Lattice Description					Lattice Parameters, 99.75% D_2O							Corrections Applied to B^2, m^{-2}			Resonance Integral Parameters	
Gas Tube, in.	Triangular Lattice Pitch, in.	Plates per Assembly	V_M/V_F	$\frac{V_{void}}{V_{cell}}$	f	ϵ	p	L^2, cm^2	τ, cm^2	B^2, m^{-2}	k_∞	D_2O Purity	Non-uniform Spacing	Housing Tube	I_0, barn	(S_{eff}/M), cm^2/gm
4.0 × 5.0	9.26	14	17.9	0.228	0.9920	1.034	0.8519	161	259	3.65	1.159	0.05	0.25	0.53	10.13	0.0825
		12	20.9	0.235	0.9911	1.032	0.8743	190	270	3.88	1.186	0.08	0.18	0.56	9.99	0.0870
		10	25.1	0.241	0.9900	1.030	0.8812	222	278	3.68	1.192	0.11	0.15	0.59	11.27	0.0938
		8	31.4	0.246	0.9879	1.028	0.9065	278	291	3.70	1.222	0.15	0.10	0.64	11.07	0.1039
		6	41.9	0.252	0.9846	1.025	0.9271	363	302	3.44	1.242	0.19	0.06	0.69	11.45	0.1204
	10.69	14	26.2	0.172	0.9871	1.034	0.8898	212	218	4.56	1.206	0.21	0.35	0.51	10.62	0.0825
		12	30.6	0.176	0.9855	1.032	0.9110	246	226	4.62	1.230	0.24	0.25	0.53	10.04	0.870
		10	36.7	0.180	0.9843	1.030	0.9170	273	232	4.39	1.234	0.25	0.20	0.59	11.19	0.0938
		8	45.9	0.185	0.9813	1.028	0.9337	339	240	4.08	1.250	0.29	0.14	0.62	11.19	0.1039
		6	61.2	0.189	0.9767	1.025	0.9493	432	247	3.64	1.261	0.32	0.09	0.67	11.39	0.1204
3.5 × 3.5	7.00	12	11.6	0.228	0.9952	1.032	0.7934	93	238	2.40	1.081	−0.08	0.00	0.58	9.20	0.0870
		10	13.9	0.238	0.9945	1.030	0.8180	113	251	3.00	1.112	−0.03	0.00	0.63	9.78	0.0938
		8	17.4	0.249	0.9935	1.028	0.8415	144	266	3.29	1.139	0.01	0.00	0.69	10.90	0.1039
		6	23.2	0.254	0.9916	1.025	0.8747	190	279	3.69	1.180	0.08	0.00	0.79	12.41	0.1204
	9.26	12	24.0	0.131	0.9890	1.032	0.8899	152	187	5.81	1.207	0.20	0.36	0.58	9.86	0.0870
		10	28.8	0.136	0.9877	1.030	0.9050	177	191	5.75	1.223	0.25	0.28	0.62	10.19	0.0938
		8	36.0	0.142	0.9853	1.028	0.9265	217	197	5.60	1.245	0.30	0.18	0.68	9.88	0.1039
		6	48.0	0.148	0.9816	1.025	0.9337	279	203	4.84	1.247	0.33	0.13	0.75	11.83	0.1204
	10.69	12	33.7	0.098	0.9830	1.032	0.9185	212	170	5.89	1.237	0.38	0.36	0.51	9.65	0.0870
		10	40.4	0.102	0.9809	1.030	0.9294	244	174	5.53	1.244	0.43	0.27	0.48	10.03	0.0938
		8	50.5	0.106	0.9776	1.028	0.9444	295	181	5.17	1.260	0.48	0.18	0.64	9.91	0.1039

Table 4-77 — NUCLEAR PARAMETERS FOR D_2O-MODERATED CLUSTERS OF ALUMINUM-CLAD UO_2 RODS

Lattice Description				Lattice Parameters, 99.75% D_2O							Lattice Parameters, 99.2% D_2O				Resonance Integral Parameters	
Rod Spacing, in.	Triangular Lattice Pitch, in.	Rods per Assembly	V_M/V_F[a]	f	ϵ	p	L^2, cm^2	τ, cm^2	B^2, m^{-2}	k_∞	f	L^2, cm^2	τ, cm^2	B^2, m^{-2}	I_0, barn	(S_{eff}/M), cm^2/gm
0.132	10.69	61	27.6	0.9352	1.016	0.8645	125.5	149.9	3.20	1.0900	0.9229	121.2	147.7	2.98	16.07	0.1899
		55	31.0	0.9340	1.016	0.8769	138.7	147.0	3.56	1.1042	0.9203	133.4	144.8	3.29	15.96	0.1936
		43	40.7	0.9308	1.015	0.9034	173.4	141.2	4.09	1.1326	0.9132	166.4	139.0	3.69	15.60	0.2096
		37	47.9	0.9285	1.015	0.9158	198.0	138.4	4.18	1.1453	0.9082	189.5	136.2	3.70	15.56	0.2125
		31	57.9	0.9353	1.014	0.9302	230.8	135.7	4.17	1.1582	0.9014	220.0	133.5	3.61	15.18	0.2217
	9.26	43	29.6	0.9355	1.015	0.8746	122.9	148.1	3.67	1.1020	0.9235	118.7	145.9	3.46	16.30	0.2096
		37	35.0	0.9339	1.015	0.8904	141.4	144.2	4.08	1.1200	0.9197	136.2	142.0	3.78	16.35	0.2125
		31	42.5	0.9315	1.014	0.9071	165.9	140.4	4.33	1.1370	0.9148	159.4	138.2	3.95	16.32	0.2217
		19	71.7	0.9231	1.013	0.9452	255.4	133.1	4.29	1.1729	0.8966	242.7	130.9	3.68	15.30	0.2461
	7.00	37	18.4	0.9401	1.015	0.8030	73.5	163.0	0.71	1.0168	0.9338	71.4	160.8	0.79	17.43	0.2125
		31	22.7	0.9389	1.014	0.8346	87.4	155.6	2.21	1.0544	0.9310	84.8	153.4	2.18	17.32	0.2217
		19	39.4	0.9340	1.013	0.9005	138.6	141.8	4.52	1.1306	0.9204	133.6	139.6	4.22	16.70	0.2461
		13	59.3	0.9287	1.011	0.9311	195.9	135.3	4.66	1.1601	0.9085	187.5	133.1	4.17	16.72	0.2806
0.395	10.69	37	47.9	0.9294	1.008	0.9072	175.5	138.4	3.95	1.1278	0.9128	168.6	136.2	3.58	17.06	0.2978
		31	57.9	0.9264	1.008	0.9222	207.5	135.7	4.03	1.1428	0.9063	198.6	133.5	3.56	16.83	0.3060
	9.26	37	35.0	0.9341	1.008	0.8788	124.7	144.2	3.56	1.0980	0.9232	120.6	142.0	3.37	17.98	0.2978
		31	42.5	0.9319	1.008	0.8982	148.8	140.4	4.02	1.1196	0.9183	143.4	138.2	3.73	17.81	0.3060
		19	71.7	0.9237	1.007	0.9382	236.3	133.1	4.13	1.1580	0.9005	225.4	130.9	3.60	17.19	0.3264
	7.00	37	18.4	0.9396	1.008	0.7787	65.3	163.0	−0.94	0.9787	0.9356	63.6	160.8	−0.75	19.46	0.2978
		31	22.7	0.9385	1.008	0.8183	78.3	155.6	1.16	1.0273	0.9327	76.2	153.4	1.22	18.94	0.3060
		19	39.4	0.9338	1.007	0.8922	128.1	141.8	4.09	1.1133	0.9225	123.8	139.6	3.88	18.06	0.3264
		13	59.3	0.9285	1.007	0.9244	184.4	135.3	4.44	1.1469	0.9109	177.0	133.1	4.03	18.32	0.3532

[a]The fuel volume, V_F, is that for natural uranium metal having the same total number of uranium atoms per assembly.

Table 4-78—NUCLEAR PARAMETERS FOR D_2O-MODERATED TUBES OF NATURAL URANIUM

Lattice Description			Lattice Parameters, 99.75% D_2O							Corrections Applied to B^2, m^{-2}				Resonance Integral Parameters	
No. of Tubes Per Assembly	Triangular Lattice Pitch, in.	V_M/V_F	f	ϵ	p	L^2, cm^2	τ, cm^2	B^2, m^{-2}	k_∞	D_2O Purity	Small Sample	Non-uniform Spacing	Cladding	I_0, barn	(S_{eff}/M), cm^2/gm
1	10.69	59.8	0.935	1.014	0.932	231	122.0	4.72	1.1729	0.84	−0.25	0.22	1.27	12.92	0.2088
	9.26	43.8	0.943	1.014	0.919	167	122.7	5.51	1.1658	0.64	−0.35	0.27	1.52	12.58	0.2088
	7.56	28.9	0.952	1.014	0.874	103	124.0	5.12	1.1196	0.31	0.00	0.26	1.82	13.74	0.2088
	7.00	24.6	0.954	1.014	0.859	85	124.7	4.77	1.1024	0.17	0.00	0.00	1.96	13.36	0.2088
2	10.69	31.2	0.956	1.029	0.901	207	123.7	5.13	1.1764	0.41	−0.25	0.39	0.94	10.95	0.1212
	9.26	23.1	0.962	1.029	0.871	123	125.0	5.62	1.1442	0.23	−0.35	0.53	1.21	11.14	0.1212
	7.00	12.8	0.970	1.029	0.791	59	128.7	2.51	1.0476	−0.21	0.00	0.00	1.49	10.52	0.1212

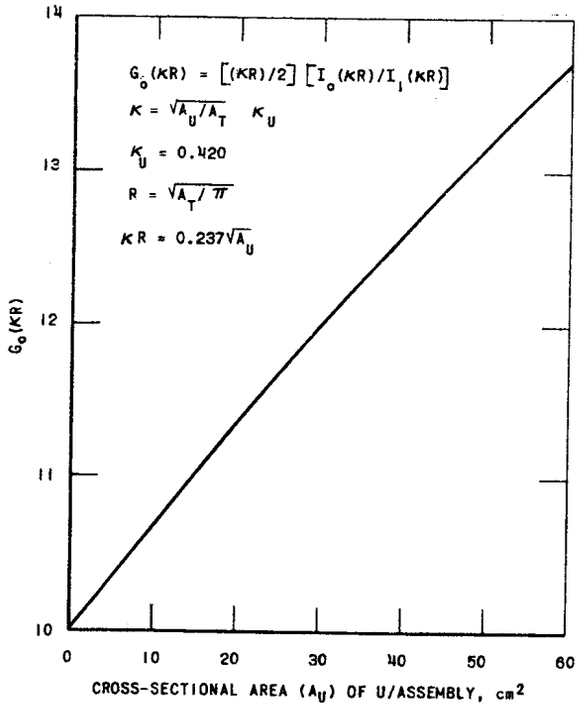

Fig. 4-50—Ratio (G_0) of surface flux to interior flux. *Reproduced from Ref. 83.*

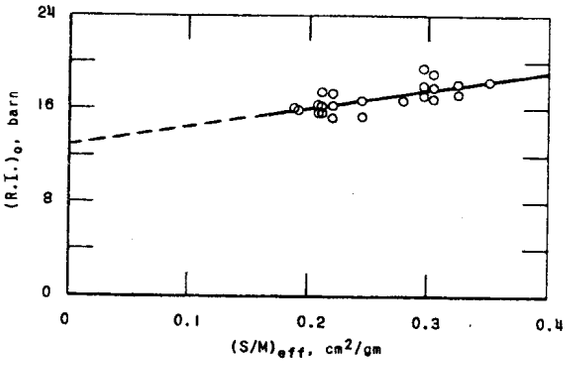

Fig. 4-51—Effective resonance integral of uranium dioxide. *Data from Ref. 83.*

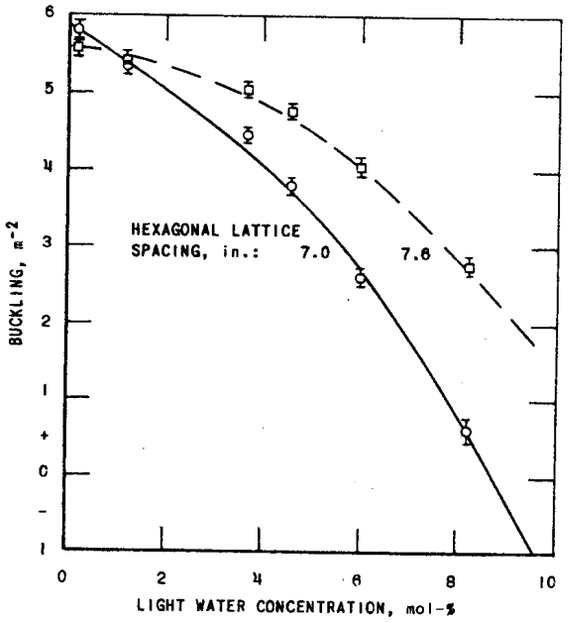

Fig. 4-52—Calculated buckling as a function of H_2O concentration for two hexagonal lattices of four-rod clusters. Fuel assemblies are four-rod clusters of 1-inch metal rods (see Fig. 4-37). *Reproduced from Ref. 83.*

in Refs. 83 and 84. [The 13th and 14th columns of Tables 4-74, 4-76, and 4-78, are corrections to the buckling for the small number of lattice cells in the assembly (small sample), and for irregularities in the spacing.] The lattice parameters have been derived by a variety of methods; the details are given in the references. The theoretical curves shown in Figs. 4-38 through 4-47 result from semi-empirical theory.[83] These are reported to yield a standard deviation from the data less than the value 0.25 m^{-2} indicated by an independent estimate of experimental accuracy. There is one exception: metal plate lattices yield a standard deviation of 0.28 m^{-2}. Thus the calculated curves should, for the most part, yield a good estimate of the trend of the data.

4.5.5 LIGHT WATER–ThO_2–UO_2 LATTICES[85]

Recent work on H_2O–ThO_2–UO_2 lattices has been summarized in Ref. 85. Five clean cores were studied: 15A, 15B, 15D, $25\sqrt{2}$B, 25D. Table 4-79 is a list of the lattice pitch (p), the over-all

Table 4-79 — CORE VOLUME RATIOS AND VOLUME FRACTIONS

Core	Volume Ratios				Volume Fractions		
	Pitch, p		M/W	W/F	Water	Fuel Pellets	Aluminum
	in.	cm					
15A	0.3850	0.9779	1.024	1.379	0.4942	0.3582	0.0875
15B	0.4027	1.0229	0.860	1.642	0.5376	0.3274	0.0800
15D	0.4810	1.2217	0.480	2.945	0.6759	0.2295	0.0561
$25\sqrt{2}$ B	0.5694	1.4463	0.301	5.794	0.7687	0.1326	0.0906
25D	0.4810	1.2217	0.480	3.636	0.6759	0.1859	0.1269

metal-to-water volume ratio (M/W), the water to fuel volume ratio (W/F), and the volume fractions in the core of water, fuel pellets and aluminum. The radial reflector was water.

Fuel pins with Th : U^{235} ratios of 15 : 1 and 25 : 1 were used in the studies. Table 4-80 is a list of fuel pin properties.

Table 4-80 — PROPERTIES OF FUEL PINS

Properties	15 : 1 Pins	25 : 1 Pins
O.D. in.	0.309	0.309
Clad material	Al-2S	Al-2S
Clad thickness, in.	0.014	0.034
I.D., in.	0.281	0.241
Active pin length, in.	60.0	60.0
Pellet diameter, in.	0.260	0.234
Effective pellet density, gm/cm^3	8.35	8.45
$M(U^{235})$/pin, gm	24.04	12.04
$N(Th)/N(U^{235})$	15.00	25.34
$M(ThO_2)$/pin, gm	405.0	341.8
M(Pellets)/pin, gm	434.6	356.8

Table 4-81 summarizes the results of the clean critical experiments: C is the cadmium ratio; k_2/k_1 is the k_{eff} in the thermal group, divided by the epithermal k_{eff}; $\overline{\phi}_W/\overline{\phi}_F$ is the ratio of average flux in the water, to that in the fuel; P is the resonance escape probability; and the other symbols have their usual meaning.

Table 4-82 is a detailed list of the results of clean core flux traverses: δ is the radial reflector savings, and λ the *total* vertical reflector savings.

Experiments were performed to determine migration areas and k_∞ as functions of water height and boron concentration. The results are summarized in Table 4-83; N_B is the boric acid concentration in grams of boron per liter of water.

Correlative plots of buckling and reflector savings versus M/W ratios are given in Fig. 4-53 and Fig. 4-54. Reflector savings versus radius are given in Fig. 4-55.

Table 4-81—SUMMARY OF RESULTS

Core	M/W	$\frac{N(Th)}{N(U^{235})}$	$\frac{N(H)}{N(U^{235})}$	R_c, cm	M_c, kg	B_m^2, 10^{-3} cm^{-2}	C_U	C_{Th}	k_2/k_1	$\bar{\phi}_W/\bar{\phi}_F$	P_{Th}	P_U
$25\sqrt{2}$ B	0.301	25.34	528	27.3	13.46	5.355	19.8	2.82	18.8	1.22	0.916	0.960
25 D	0.480	25.34	329	23.5	13.99	6.401	12.8	2.26	11.8	1.16	0.878	0.933
15 D	0.480	15.00	165	15.5	9.73	11.42	8.7	1.78	7.7	1.22	0.870	0.886
15 B	0.860	15.00	131	17.0	20.79	9.425	5.5	1.48	4.5	1.12	0.810	0.816
15 A	1.024	15.00	78.0	18.1	25.96	8.531	4.8	1.37	3.8	1.22	0.756	0.786

Nomenclature: M/W: Over-all metal-to-water ratio by volume.
$N(Th)/N(U^{235})$: Ratio of atomic density of Th to U^{235}.
$N(H)/N(U^{235})$: Ratio of atomic density of H to U^{235}.
R_c: The critical radius of a fully reflected cylinder, 5 ft high.
M_c: The critical mass fully reflected cylinder, 5 ft high.
C_U: The ratio of total absorptions to epicadmium absorptions in U^{235} (fission activation only).
C_{Th}: The ratio of total absorptions to epicadmium absorptions in Th.
k_2/k_1: The k_{eff} in the thermal group divided by the epithermal $k_{eff} = (C_U - 1)$. (Two and one-half group theory).
$\bar{\phi}_W/\bar{\phi}_F$: Ratio of average thermal flux in the water to the average in the fuel.
P_{Th}: Resonance escape probability with respect to Th. (Calculated from C_{Th} and theoretical results).
P_U: Resonance escape probability with respect to U. (Calculated from C_U and theoretical results).

Table 4-82—SUMMARY OF RESULTS: CLEAN CORE FLUX TRAVERSES

Properties	Core Identification				
	$25\sqrt{2}$ B	25D	15D	15B	15A
Pitch, in.	0.5694	0.4810	0.4810	0.4027	0.3850
M/W	0.301	0.480	0.480	0.860	1.024
W/F	5.794	3.630	2.945	1.642	1.379
No. fuel pins	1146.0	1176.0	514.0	880.0	1108.0
Effective radius, cm	27.62	23.64	15.63	17.12	18.37
Core height, cm	137.79	143.06	139.52	135.14	128.91
Critical height, cm	135.27	140.50	135.05	133.44	127.21
$\overline{B}_r \pm \sigma$, $cm^{-1} \times 10^{-4}$	701.25 ± 0.73	773.50 ± 2.96	1048.01 ± 3.21	945.61 ± 1.52	896.00 ± 1.46
$\overline{B}_z \pm \sigma$, $cm^{-1} \times 10^{-4}$	205.74 ± 0.92	200.78 ± 0.54	202.93 ± 2.09	217.30 ± 0.78	221.59 ± 0.48
$\overline{B}_{z\,crit} \pm \sigma$, $cm^{-1} \times 10^{-4}$	209.17 ± 0.92	204.40 ± 0.54	208.97 ± 2.09	219.88 ± 0.78	224.29 ± 0.48
$\delta \pm \sigma$, cm	6.67 ± 0.04	7.45 ± 0.12	7.32 ± 0.07	8.31 ± 0.04	8.47 ± 0.04
$\lambda \pm \sigma$, cm	14.92 ± 0.68	13.41 ± 0.42	15.29 ± 1.61	9.44 ± 0.51	12.86 ± 0.31
$B^2 \pm \sigma$, $cm^{-2} \times 10^{-4}$	53.55 ± 0.11	64.01 ± 0.46	114.20 ± 0.70	94.25 ± 0.29	85.31 ± 0.26
Critical radius, cm (Full water height)	27.3	23.5	15.5	16.97	18.13
No. fuel rods (Full water height)	1118.0	1162.0	506.0	865.0	1080.0
Critical mass, kg	13.46	13.99	9.73	20.79	25.96

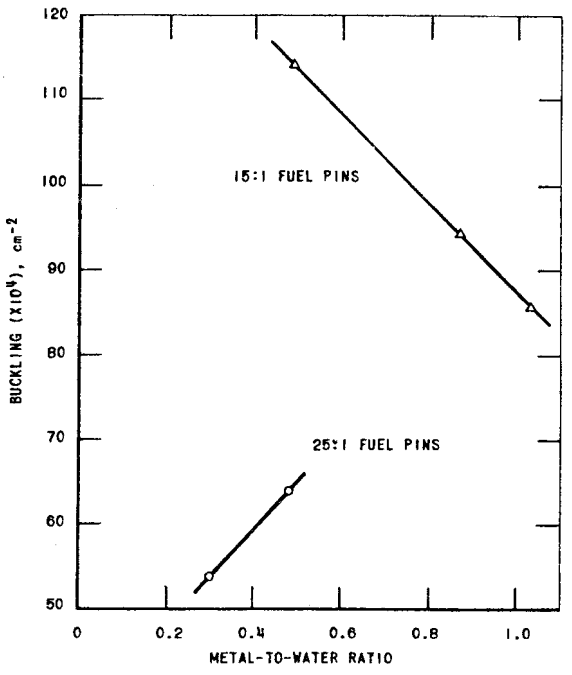

Fig. 4-53—Buckling vs. metal-to-water ratio for clean cores. *Reproduced from Ref. 85.*

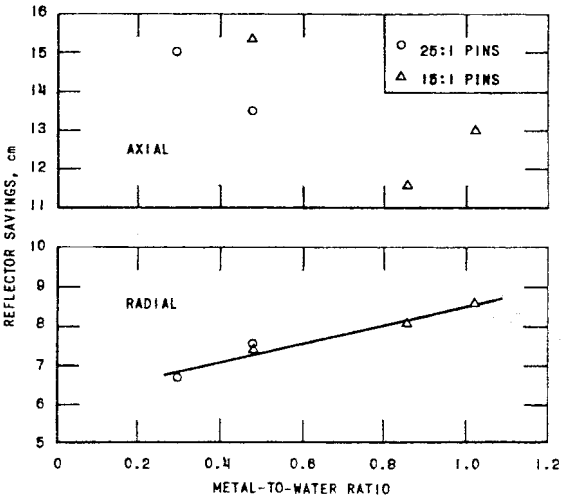

Fig. 4-54—Reflector savings vs. metal-to-water ratios for clean cores. *Data from Ref. 85.*

Table 4-83 — M^2 AND k_∞ OBTAINED FROM LEAKAGE EXPERIMENTS

Core & Series	N_B	B_r^2	B_z^2	$B_r^2 + B_z^2$	M_z^2/M_r^2	One-Group Model					Gaussian Model				
						M_z^2	M_r^2	M_{eff}^2 [a]	M_{eff}^2 [b]	k_∞	M_z^2	M_r^2	M_{eff}^2 [a]	M_{eff}^2 [b]	k_∞
25D	0.0	58.30	5.46	63.76	1.02	42.4 ± 0.8	41.6 ± 0.8	41.7 ± 0.8	—	1.266 ± 0.005	33.5 ± 0.6	32.8 ± 0.6	32.9 ± 0.6	—	1.234 ± 0.005
15A	0.0	80.34	5.93	86.27	1.15	65.3 ± 1.6	56.8 ± 1.6	57.4 ± 1.6	—	1.49 ± 0.01	43.7 ± 1.0	38.0 ± 1.0	38.4 ± 1.0	—	1.39 ± 0.01
15B-1	0.070	84.56	7.03	91.59	1.05	62.3 ± 1.0	59.3 ± 1.0	59.5 ± 1.0	—	—	40.3 ± 0.6	38.4 ± 0.6	38.5 ± 0.6	—	—
-2	0.322	77.04	6.99	84.03	1.05	58.5 ± 1.3	55.7 ± 1.3	55.9 ± 1.3	54.4	1.49 ± 0.03	39.8 ± 0.8	37.9 ± 0.8	38.0 ± 0.8	37.7	1.41 ± 0.01
-3	0.586	69.99	6.30	76.29	1.05	57.5 ± 0.9	54.8 ± 0.9	55.0 ± 0.9	±2.8	—	40.5 ± 0.6	38.5 ± 0.6	38.7 ± 0.6	±0.8	—
-4	0.823	63.86	6.34	70.20	1.05	49.4 ± 1.0	47.0 ± 1.0	47.2 ± 1.0	—	—	37.1 ± 0.7	35.3 ± 0.7	35.5 ± 0.7	—	—
15D-1	0.0	103.8	10.0	113.8	1.02	32.4 ± 1.0	31.8 ± 1.0	31.9 ± 1.0	—	—	23.8 ± 0.7	23.3 ± 0.7	23.3 ± 0.7	—	—
-2	0.235	91.5	9.02	100.5	1.02	43.4 ± 0.9	42.5 ± 0.9	42.6 ± 0.9	36.6	1.42 ± 0.03	30.4 ± 0.6	29.8 ± 0.6	29.9 ± 0.6	28.5	1.38 ± 0.01
-3	0.432	80.3	8.45	88.8	1.02	37.0 ± 0.9	36.3 ± 0.9	36.3 ± 0.9	±2.3	—	28.0 ± 0.7	27.4 ± 0.7	27.4 ± 0.7	±0.7	—
-4	0.635	72.6	5.28	77.9	1.02	36.3 ± 0.6	35.6 ± 0.6	35.6 ± 0.6	—	—	28.7 ± 0.5	28.1 ± 0.5	28.1 ± 0.5	—	—

[a] From differential-reactivity measurements.
[b] From least-squares fits to the critical equation.

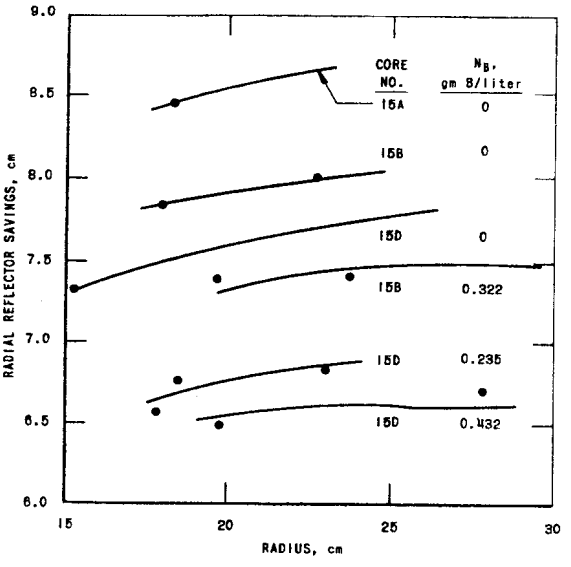

Fig. 4-55—Radial reflector savings vs. radius. *Data from Ref. 85.*

4.5.6 HEAVY WATER–ThO_2–UO_2 LATTICES

Experiments on lattices of ThO_2–UO_2 fuel in D_2O are reported in Ref. 86. The fuel was the same as that reported on in Section 4.5.5. The tank containing the D_2O was 205.74 cm ($6\frac{3}{4}$ ft) in diameter. The D_2O concentration varied from 99.1% to 97.1% in a roughly linear fashion, while the experiments were in progress. In the experiments involving clusters, two types of tubes were used to contain the fuel pins: Large –6.191 cm ($2\frac{7}{16}$ in.), and Small–6.0425 cm ($2\frac{3}{8}$ in.). These were used as much as possible in the same ratio –about 3 : 1.

Details of the fuel pin design are given in Table 4-84.

The critical heights of uniform lattices are given in Table 4-85; clustered cores were also studied.

Table 4-84—PROPERTIES OF FUEL PINS

Properties	15 : 1 Pins	25 : 1 Pins
O.D., in.	0.309	0.309
Clad material	Al-2S	Al-2S
Clad thickness, in.	0.014	0.034
I.D., in.	0.281	0.241
Active pin length, in.	60.0	60.0
Pellet diameter, in.	0.260	0.234
Effective pellet density, gm/cm^3	8.35	8.45
M_{25}/pin, gm	24.04	12.04
N(Th)/N(U^{235})	15.00	25.34
M(ThO_2)/pin, gm	405.0	341.8
M(Pellets)/pin, gm	434.6	356.8

Table 4-85—CLEAN CRITICALS OF SINGLE FUEL RODS IN UNIFORM GEOMETRY

Loading No.	D_2O Conc., at-%	No. of Rods	Height, cm	Temperature, °C
25:1 Fuel, $\frac{3}{4}$-inch Pitch				
90	98.5	665	150.88	—
89	98.5	685	145.40	—
455	97.15	685	159.13	21.7
91	98.5	745	132.84	—
233	97.95	745	135.08	20.0
456	97.15	745	139.09	21.9
92	98.5	805	123.53	—
93	98.5	867	115.95	—
161	98.35	925	111.05	23.1
94	98.5	926	110.03	—
162	98.35	945	109.30	25.0
95	98.5	1009	103.30	—
25:1 Fuel, $1\frac{1}{8}$-inch Pitch				
103	98.5	325	148.22	19.4
231	97.95	325	157	—
104	98.5	353	133.79	19.7
105	98.5	375	125.20	20.0
232	97.95	375	132.21	21.1
106	98.5	405	115.81	20.0
107	98.5	421	111.85	20.6
108	98.5	461	103.70	20.0
25:1 Fuel, $1\frac{1}{2}$-inch Pitch				
117	98.5	—	154.97	19.4
118	98.5	266	147.61	19.4
457	97.15	266	178	22.2
119	98.5	283	137.08	20.0
120	98.5	299	129.35	19.7
458	97.15	299	178	22.2
463	97.1	331	148.74	22.2
464	97.1	339	143.66	22.3
25:1 Fuel, ~$2\frac{1}{4}$-inch Pitch				
178	98.15	932	113.61	24.4
244	97.8	1082	104.33	19.7
15:1 Fuel, $\frac{3}{4}$-inch Pitch				
388	98.2	345	132.97	26.4
385	98.2	366	123.04	25.8
381	98.2	421	104.58	25.3
382	98.2	495	90.16	25.6
384	98.2	593	78.90	25.8
383	98.2	687	71.78	26.2
15:1 Fuel, $1\frac{1}{8}$-inch Pitch				
403	97.3	163	150.81	25.8
402	97.3	190	115.47	25.6
401	97.3	321	72.38	23.0
400	97.3	429	59.73	26.1
15:1 Fuel, $1\frac{1}{2}$-inch Pitch				
407	97.25	139	127.32	25.3
405	97.25	163	103.05	25.6
404	97.25	247	72.79	25.4
15:1 Fuel, $2\frac{1}{4}$-inch Pitch				
411	97.25	134	137.15	25.1
410	97.25	147	122.10	25.1
409	97.25	176	103.58	24.7

687863 O - 63 -

The mechanical details of the clustered fuel arrangements allow the substitution of light water or air for the heavy water normally present within the cluster of fuel. Figures 4-56 through 4-59 provide a brief review of the core geometry. Figure 4-56 shows the arrangement of fuel clusters for the cores of maximum size assembled with $4\frac{1}{4}$-inch and $5\frac{7}{64}$-inch square lattice spacings. Cores of 24, 32, 44 and 52 clusters were studied with the $4\frac{1}{4}$-inch spacing, and arrays of 21, 25, 29, 37 and 49 clusters in the $5\frac{7}{64}$-inch pattern. Figure 4-57 is a photograph of a core with 44 clusters arranged with a $4\frac{1}{4}$-inch spacing. The pattern of fuel pins within the cluster tubes is shown in Fig. 4-58. Measurements were

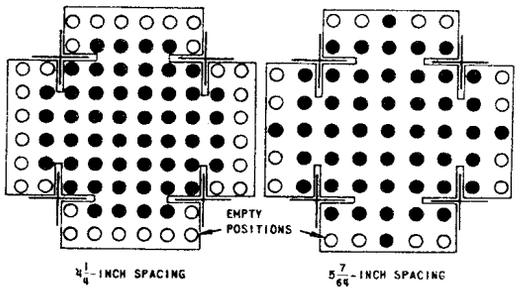

Fig. 4-56—Patterns of cluster tubes in cores of maximum diameter.

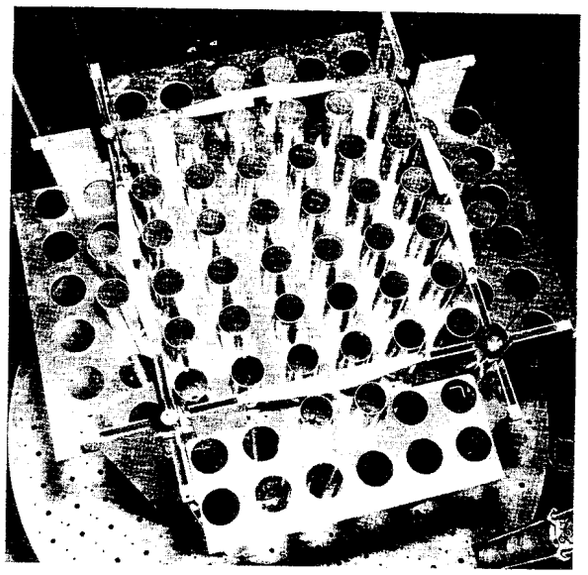

Fig. 4-57—Clustered core: 10.8 cm square spacing.

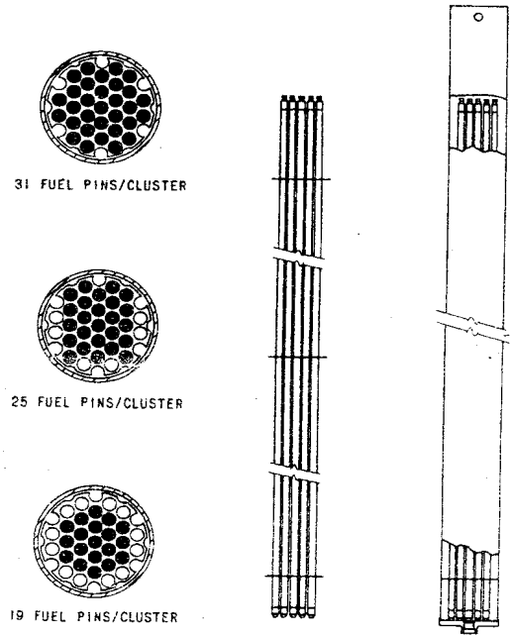

Fig. 4-58—Arrangement of fuel in cluster tubes.

made with assemblies of 19, 25, and 31 fuel pins in each cluster. Figure 4-59 is a photograph of a cluster of 31 fuel pins and a cluster tube. Three small circular grids of perforated sheet were used to achieve the clustering and spacing of fuel pins as shown. The aluminum clustered tubes had removable bottom plugs, and removable sleeves around the clustered tubes insured precise location of these tubes within holes in a top grid plate. Table 4-86 and Table 4-87 give criticality and reactivity results for clustered lattices of 25:1 (Th:U^{235} ratio) pins. Similar data for 15:1 pins are shown in Table 4-88 and in Fig. 4-60.

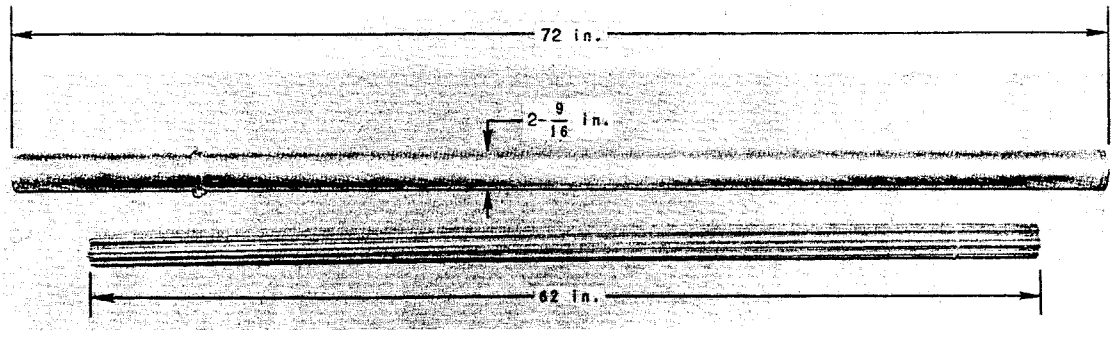

Fig. 4-59 — Cluster and shroud.

Table 4-86 — CRITICALITY DATA FOR 4¼-in. SQUARE LATTICE

D_2O Conc., at-%	Loading No.	No. of Clusters (Small – Large)	Contents of Clusters	Rc, cm	Hc, cm
31 Fuel Pins/Cluster					
97.65	297	44 (11-33)	D_2O	40.41	86.54
97.6	298	32 (8-24)	D_2O	34.44	108.84
97.6	299	24 (6-18)	D_2O	29.85	147.80
97.55	334	24 (6-18)	D_2O	29.85	148.49[a]
97.65	296	44 (11-33)	Air	40.41	109.13
97.65	295	32 (8-24)	Air	34.44	145.53
97.65	294	24 (6-18)	Air	29.85	170.00
97.65	293	24 (6-18)	H_2O	29.85	123.01[b]
97.55	335	24 (6-18)	H_2O	29.85	125.26[c]
25 Fuel Pins/Cluster					
97.6	300	32 (8-24)	D_2O	34.44	114.50
97.6	301	32 (8-24)	Air	34.44	168.86
97.6	303	32 (8-24)	H_2O	34.44	136.04[d]
19 Fuel Pins/Cluster					
97.6	320	52 (13-39)	D_2O	43.92	89.87
97.6	321	44 (11-33)	D_2O	40.41	100.03
97.6	322	32 (8-24)	D_2O	34.44	133.48
97.6	319	52 (13-39)	Air	43.92	123.74
97.6	318	52 (13-39)	H_2O	43.92	170.00[e]

[a]Repeat of Loading No. 299, 23 days later; T = 21.1°C.

[b]From three pairs of D_2O–H_2O critical levels: 126.11 and 109.22; 122.73 and 125.73; 123.00 and 123.19 cm.

[c]Repeat of Loading No. 293, 29 days later; T = 21.4°C.

[d]From three pairs of D_2O–H_2O critical levels: 141.20 and 114.30; 135.23 and 153.67; 135.94 and 137.16 cm.

[e]H_2O at 152.40 cm.

Table 4-87 — CRITICALITY DATA FOR $5\frac{7}{64}$-in. SQUARE LATTICE

D_2O Conc., at-%	Description		Contents of Clusters	R_c, cm	H_c, cm
	Loading No.	No. of Clusters (Small–Large)			
31 Fuel Pins/Cluster					
97.65	278	49 (12-37)	D_2O	51.26	75.74
97.65	279	37 (6-31)	D_2O	44.53	86.56
97.65	282	29 (6-23)	D_2O	39.42	100.58
97.65	283	21 (5-16)	D_2O	33.55	136.68
97.65	277	49 (12-37)	Air	51.26	84.56[a]
97.65	280	37 (6-31)	Air	44.53	98.95
97.65	281	29 (6-23)	Air	39.42	116.26[b]
97.63	290	29 (6-23)	H_2O	39.42	108.71[c]
97.63	287	21 (5-16)	H_2O	33.55	161.71[d]
25 Fuel Pins/Cluster					
97.60	309	49 (12-37)	D_2O	51.26	81.58[e]
97.60	308	37 (9-28)	D_2O	44.53	94.31
97.60	306	25 (6-19)	D_2O	36.60	131.65[f]
97.60	307	21 (5-16)	D_2O	33.55	167.54
97.60	310	49 (12-37)	Air	51.26	94.32
97.60	311	37 (9-28)	Air	44.53	110.90
97.60	304	37 (9-28)	H_2O	44.53	141.90[g]
19 Fuel Pins/Cluster					
97.60	315	49 (12-37)	D_2O	51.26	95.01
97.60	314	37 (9-28)	D_2O	44.53	113.46
97.60	316	29 (7-22)	D_2O	39.42	143.94
97.60	312	49 (12-37)	Air	51.26	110.38
97.60	313	37 (9-28)	Air	44.53	134.67
97.60	317	49 (12-37)	H_2O	51.26	170.00[h]

[a] At least 3 tubes leaked (through bottom plugs).

[b] One cluster out of position ~5 cm at base of core.

[c] From three pairs of D_2O-H_2O critical levels: 108.51 and 144.78, 108.67 and 119.38, 108.71 and 109.22 cm.

[d] H_2O at 144.78 cm.

[e] Corrected by −0.29 cm for one voided cluster at periphery.

[f] Corrected by −1.50 cm for foils present.

[g] From two pairs of D_2O-H_2O: 142.47 and 137.16; 141.86 and 142.24 cm.

[h] H_2O at 152.40 cm.

Table 4-88 — CRITICAL HEIGHTS FOR 15 : 1 CLUSTERED CORES OF $5\frac{7}{64}$-in. SQUARE PITCH

No. of Clusters (Large–Small)	Void		D_2O Filled	
	Loading No.	H_c, cm	Loading No.	H_c, cm
31-Rod Clusters				
37 (28-9)	415	60.45	—	—
29 (22-7)	416	66.83	—	—
25 (19-6)	417	75.29	429	64.41
21 (16-5)	418	79.22	—	—
16 (12-4)	422	101.12	427	85.83
13 (10-3)	419	118.59	—	—
12 (9-3)	423	139.17	425	116.97
11 (9-2)	421	157.33	—	—
19-Rod Clusters				
37 (28-9)	438	72.67	441	63.70
25 (19-6)	437	90.86	440	78.64
16 (12-4)	436	137.26	439	115.82

Temperature range: 23.2–24.9°C

D_2O Concentration: 97.2 at-%

Cluster patterns:

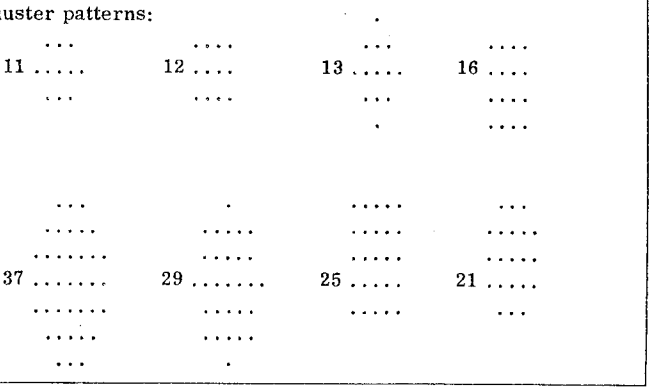

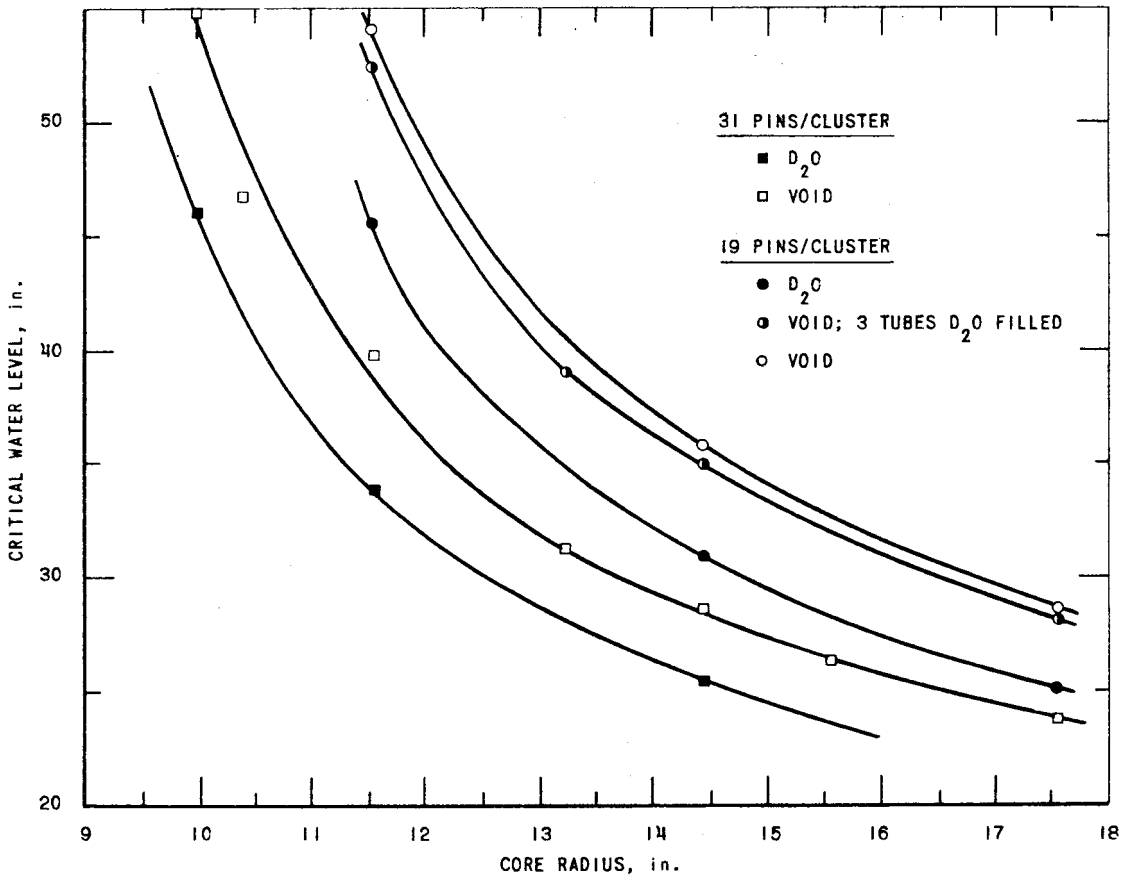

Fig. 4-60—Critical assemblies for 15:1 clustered cores ($5^7/_{64}$ in. square lattice). *Reproduced from Ref. 86.*

4.5.7 BERYLLIUM–URANIUM LATTICES

Reference 87 is a report on beryllium lattices with fuel of 10% U^{235} and 90% U^{238}. The lattices were composed of cells 10.7 × 6.4 cm. In the center of each cell there was a vertical channel 1.7 cm in diameter; at a radius of 2.0 cm from this there were six channels 1.45 cm in diameter. The fuel could thus be placed in as many as seven holes in the cell. There were horizontal holes in the cell, 3.1 cm in diameter, forming a rectangular lattice 10.7 × 8.0 cm. The fuel elements were made of U_3O_8 powder (ρ = 3.23 gm/cm^3). The powder was contained in co-axial stainless steel tubes 1.34 (× 0.02) cm and 0.90 (× 0.04) cm in diameter.

Three configurations were examined: in *variation "a"*, there was no water in the core or reflector; in *variation "b"*, the centers of the fuel tubes were filled with water [N(H)/N(U^{235}) = 76]; in *variation "c"*, water filled the fuel elements and horizontal holes. In *variation "c"*, the water was in aluminum tubes 3 cm in diameter and 0.05 cm thick.

Figure 4-61 shows the critical mass as a function of the ratio of beryllium atoms to U^{235} atoms (C_{Be}/C_{25}) in unreflected systems.

Figure 4-62 shows the buckling of the bare assemblies.

In Fig. 4-63 the critical mass of reflected assemblies is given. The reflector was radial only and composed of Be, or Be and H_2O.

Table 4-89 lists the radial reflector savings, δ, as a function of the core radius, R, and the reflector thickness, d.

Tables 4-90, 4-91, and 4-92 list critical masses for different reactor conditions.

687863 O - 63 - 24

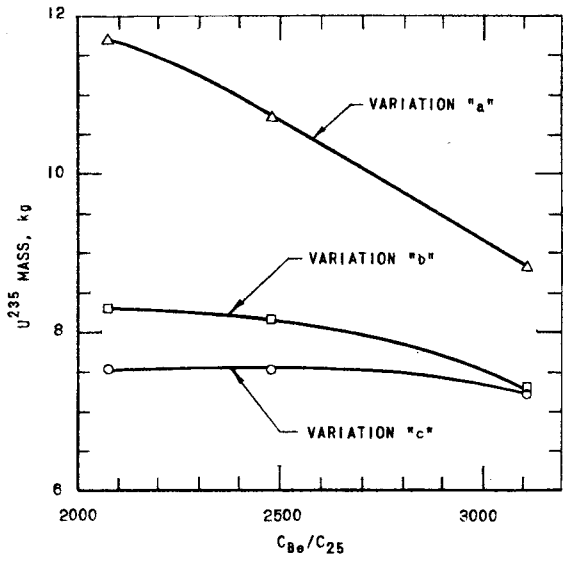

Fig. 4-61—Critical mass as a function of C_{Be}/C_{25} for non-reflected assemblies. *Reproduced from Ref. 87.*

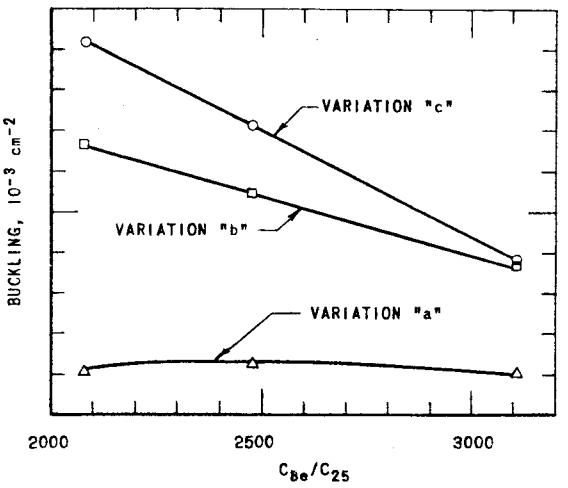

Fig. 4-62—Buckling of non-reflected critical assemblies as a function of C_{Be}/C_{25}. *Reproduced from Ref. 87.*

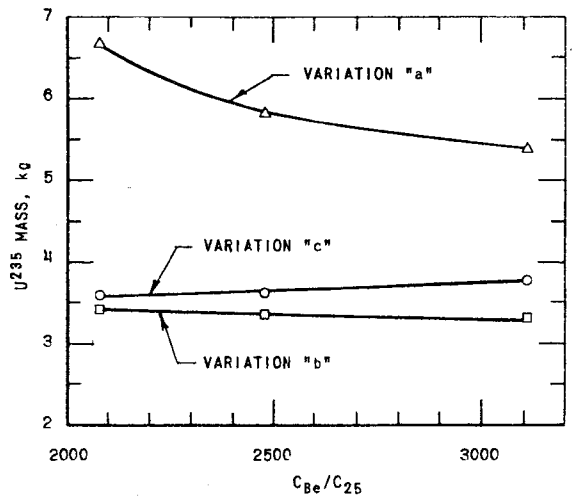

Fig. 4-63—Critical mass of reflected assemblies as a function of C_{Be}/C_{25}. *Reproduced from Ref. 87.*

Table 4-89 — RADIAL REFLECTOR SAVINGS (δ) VS. CORE RADIUS (R) AND REFLECTOR THICKNESS (d)

$\frac{C_{Be}}{C_{25}}$	Variation "a"			Variation "b"			Variation "c"		
	R, cm	d, cm	δ, cm	R, cm	d, cm	δ, cm	R, cm	d, cm	δ, cm
2080	36.5	15.5	14.7	26.2	25.8	15.5	26.8	25.2	12.1
2480	37.5	14.5	13.4	28.4	23.6	15.0	28.2	23.8	13.0
3112	40.4	11.6	11.1	31.5	20.5	15.7	33.7	18.3	12.3

Table 4-90 — URANIUM-BERYLLIUM REACTORS WITH AND WITHOUT A SIDE REFLECTOR

The holes in the beryllium cylinder are filled with graphite slugs. There are no end reflectors.

Number of Fuel Elements per Cell	Thickness of Side Reflector, cm	Core Radius, cm	Crit. Mass, kg U^{235}	$\frac{C_{Be}}{C_{25}}$	$\frac{C_C}{C_{25}}$	Reactor Height, cm
4	11.6	40.4	5.46	3112	463	96
4	0.0	52.0	8.78	3112	463	90
5	14.5	37.5	5.86	2486	337	96
5	0.0	52.0	10.70	2486	337	88
6	15.5	36.5	6.66	2075	255	96
6	0.0	52.0	11.70	2075	255	89
7	14.4	37.6	8.26	1777	113	96

Table 4-91 — URANIUM-WATER-BERYLLIUM REACTORS WITH AND WITHOUT A SIDE REFLECTOR

The central tubes of the fuel elements are filled with water. The holes in the beryllium cylinder are filled with graphite slugs. There are no end reflectors.

Number of Fuel Elements per Cell	Thickness of Side Reflector, cm	Core Radius, cm	Crit. Mass, kg U^{235}	$\frac{C_{Be}}{C_{25}}$	$\frac{C_C}{C_{25}}$	$\frac{C_H}{C_{25}}$	Reactor Height, cm
4	20.5	31.5	3.31	3112	401	72	96
4	0.0	52.0	7.23	3112	401	72	74
5	23.6	28.4	3.36	2486	273	72	96
5	0.0	52.0	8.16	2486	273	72	67
6	25.8	26.2	3.42	2075	190	72	96
6	0.0	52.0	8.30	2075	190	72	63
7	27.4	24.6	3.53	1777	113	72	96

Table 4-92 — URANIUM-WATER-BERYLLIUM REACTORS WITH AND WITHOUT A SIDE REFLECTOR

The central tubes of the fuel elements and the horizontal holes in the beryllium cylinder are filled with water. The holes in the beryllium cylinder are filled with graphite slugs. There are no end reflectors.

Number of Fuel Elements per Cell	Thickness of Side Reflector, cm	Core Radius, cm	Crit. Mass, kg U^{235}	$\frac{C_{Be}}{C_{25}}$	$\frac{C_C}{C_{25}}$	$\frac{C_H}{C_{25}}$	Reactor Height, cm
4	18.3	33.7	3.78	3112	202	242	96.0
4	0.0	52.0	7.20	3112	202	242	73.7
5	23.8	28.2	3.62	2486	115	208	96.0
5	0.0	52.0	7.55	2486	115	208	62.0
6	25.2	26.8	3.60	2075	58	186	96.0
6	0.0	52.0	7.51	2075	58	186	57.0
7	26.9	25.1	3.69	1777	0	170	96.0

REFERENCES

1. S. Glasstone and M. C. Edlund, *The Elements of Nuclear Reactor Theory*, (New York: D. Van Nostrand Co., Inc., 1952).
2. H. Neumann, *Thermal Utilization, Thermal Flux, and Lattice Cell Shape*, HW-52048, (August, 1957).
3. B. Davison, *Neutron Transport Theory*, (Oxford: Clarendon Press, 1957).
4. A. Jeffery, *Tables of Characteristic Roots and Functions for the Spherical Harmonic Method*, Mathematical Tables and Better Aids to Computation, XIII, 321, (October, 1959).
5. J. C. Mark, *The Spherical Harmonic Method-I*, Chalk River Laboratory, CRT-340, (June, 1949).
6. S. Ziering and D. Schiff, *Yvon's Method for Slabs*, Nuclear Sci. and Eng., 3: No. 6, 635-647, (June, 1958).
7. A. Jeffery, Rolls Royce, Ltd.; Unpublished data.
8. D. A. Newmarch, *Errors Due to the Cylindrical Cell Approximation in Lattice Calculations*, AEEW-R34, (June, 1960).
9. A. Amouyal and P. Benoist, *New Method of the Determination of the Thermal Utilization Factor of a Cell*, CEA-571, (April, 1956).
10. A. Amouyal and P. Benoist, *Calcul Du La Placien D'Une Barre D'Uranium Dans Une Cellue*, CEA-209, (1957).
11. M. H. Theys, *Integral Transport Theory of Thermal Utilization Factor in Slab Geometry*, Nuclear Sci. and Eng., 7: No. 1, 58-63, (January, 1960).
12. J. A. McLennan, *Reactor Cell Calculations for Some Cylindrically Symmetric Fuel Elements Surrounded by Moderator*, APEX-362, (August, 1955).
13. G. W. Stuart and R. W. Woodruff, *Method of Successive Generations*, Nuclear Sci. and Eng., 3: No. 3, 339-373, (March, 1958).
14. S. A. Kushneriuk, *Neutron Capture by Long Cylindrical Bodies Surrounded by Predominantly Scattering Media*, CRT-712, (June, 1957).
15. K. M. Case, F. DeHoffman and G. Placzek, *Introduction to the Theory of Neutron Diffusion*, (Washington, D. C.: Government Printing Office, 1953).
16. J. Bengston, *Neutron Self-Shielding in a Single Plane Lattice*, Nuclear Sci. and Eng., 3: No. 1, 71-76, (January, 1958).
17. S. A. Kushneriuk, *Effective Cross Sections and Neutron Flux Distributions in a Natural Uranium Rod Application to Rod 683*, CRT-725, (September, 1957).
18. B. Davison, *Influence of a Black Sphere and of a Black Cylinder Upon the Neutron Density in an Infinite Non-Capturing Medium*, Proc. Phys. Soc. (London), 64: Section A., Part 10, (October, 1951).
19. B. Davison and S. A. Kushneriuk, *Linear Extrapolation Lengths for a Black Sphere and a Black Cylinder*, MT-214, (March, 1946).
20. B. Davison and S. A. Kushneriuk, *Linear Extrapolation Lengths for a Small Black Cylinder with a Small Air-Gap and a Small Imperfectly Absorbing Cylinder With and Without a Small Air Gap*, CRT PI-45, (AECL-124), (July, 1947).
21. R. J. Royston, *The Linear Extrapolation Length at the Surface of an Imperfectly Absorbing Cylinder*, J. Nuclear Sci. and Eng., 1: No. 3, 194, (1954-1955).
22. C. H. Westcott, *Effective Fission and Capture Cross Sections for Hardened Maxwellian Neutron Spectra*, J. Nuclear Energy, Part A: Reactor Science, 12: No. 3, 113-121, (June, 1960).
23. F. R. Taraba and S. H. Paine, *The Radial Distribution of Thermal Neutron Flux in Cylindrical Fuel Specimens During Neutron Irradiation*, ANL-5872, (August, 1959).
24. M. Copic, *The Spherical Harmonic Method-Approximate Analytical Expressions for the Disadvantage Factor in P_3 Approximation in the Slab Geometry*, Special Project Report, International School of Nuclear Science and Engineering, Argonne National Laboratory.
25. K. H. Puechl, *An Approach to Reactor Physics Using Results of Integral Experiments*, Nuclear Sci. and Eng., 9: No. 2, 241, (February, 1961).
26. N. C. Corngold, *Resonance Escape Probability in Slab Lattices*, J. Nuclear Energy, 4: No. 3, 293, (1957).
27. B. I. Spinrad, J. Chernick and N. Corngold, *Resonance Capture in Uranium and Thorium Lumps*, Proc., 1958 Geneva Conference, Vol. 16: Paper No. 1847, pp. 191-206.
28. N. Tralli, J. Agresta and W. Seibyl, *Multigroup Diffusion Calculation of K_∞ for D_2O Lattices*, Nuclear Sci. and Eng., 6: No. 2, 157-159, (August, 1959).
29. A. R. Vernon, *Calculation of the Effective Resonance Integral of U-238*, Nuclear Sci. and Eng., 7: No. 3, 252-259, (March, 1960).
30. A. R. Vernon, *Calculation of Resonance Integrals for Uranium and Thorium Lumps*, Trans. Am. Nuclear Sci. and Eng., 1: No. 2, 22-23, (1958).
31. E. Hellstrand and J. Weitman, *The Resonance Integral of Thorium Metal Rods*, Nuclear Sci. and Eng., 9: No. 4, 507, (April, 1961).
32. A. Rothman and C. Ward, Argonne National Laboratory, Private Communication.
33. P. Bakshi, *Equivalence Principles and Resonance Integrals*, BNL-4381, (September, 1959).
34. M. Levine, *Generalized Resonance Integral Representation*, Nuclear Sci. and Eng., 8: No. 4, 363-364, (October, 1960).
35. W. Rothenstein, *Collision Probabilities and Resonance Integrals for Lattices*, BNL-563, (T-151), (June, 1959).
36. G. I. Bell, *A Simple Treatment for Effective Resonance Absorption Cross Section in Dense Lattices*, Nuclear Sci. and Eng., 5: No. 2, 138-139, (February, 1959).
37. N. Corngold, *Slowing Down of Neutrons in Infinite Homogeneous Media*, Proc. Phys. Soc. (London) LXX: Section A—Part II, 793, (November, 1957).
38. S. M. Dancoff and M. Ginsburg, *Surface Resonance Absorption in a Close-Packed Lattice*, CP-2157, (October, 1944).
39. W. G. Bickley and J. Naylor, *A Short Table of the Functions $Ki_n(x)$ from $n = 1$ to $n = 16$*, Phil. Mag., 20: Series F, 343, (August, 1935).
40. E. Hellstrand, *Measurements of the Effective Resonance Integral in Uranium Metal and Oxide in Different Geometries*, J. Appl. Phys., 28: No. 12, 1493, (December, 1957).
41. R. D. Richtmeyer, R. Van Norton and A. Wolfe, *The Monte Carlo Calculation of Resonance Capture in Reactor Lattices*, Proc., 1958 Geneva Conference, Vol. 16, Paper No. 2489, pp. 180-186.
42. F. T. Adler and L. W. Nordheim, *Tables for Computation of Resonance Integrals*, GA-377, (June, 1958).
43. G. W. Rodeback, *Temperature Coefficients of Uranium and Thorium Resonance Integrals*, NAA-SR-1641, (September, 1956).
44. V. G. Small, *An Experimental Determination of the Increase with Temperature of the Resonance Absorption in Uranium and Thorium*, AERE R/R 2774, (April, 1959). V. G. Small, *Measurements of the Temperature Coefficients of the Resonance Integrals of Uranium and Uranium Oxide by the Pile Oscillator Technique*, AAEW-R 59, (May, 1961).
45. B. I. Spinrad, *Fast Effect in Lattice Reactors*, Nuclear Sci. and Eng., 1: No. 6, 455, (December, 1956).
46. M. R. Fleischman and H. Soodak, *Methods and Cross Sections for Calculating the Fast Effect*, Nuclear Sci. and Eng., 7: No. 3, 217-227, (March, 1960).
47. H. Kouts and R. Sher, *Experimental Studies of Slightly Enriched Uranium, Water Moderated Lattices*, Part I: 0.600-in. Diameter Rods, BNL-486, (September, 1957).
48. F. H. Clark, *Variation of Fast Fission Effect with Homogeneity in Infinite Slab Reactor*, KAPL-743, (March, 1957).
49. J. Chernick, *The Theory of Uranium Water Lattices*, Proc., 1955 Geneva Conference, Vol. 5, Paper No. 603, p. 215.
50. B. I. Spinrad, *Anisotropic Diffusion Lengths in Diffusion Theory*, J. Appl. Phys., 26: No. 5, 548, (May, 1955).
51. B. Davison, *Effective Thermal Diffusion Length in a Sandwich Reactor*, CRT-715, (July, 1957).
52. L. Trlifaj, *A Variational Method for the Homogenization of a Heterogeneous Medium*, J. Nuclear Energy, 6: 142-154, (1958).

53. N. I. Laletin, *Passage of Neutrons in a Heterogeneous Medium*, Proc., 1958 Geneva Conference, Vol. 16: Paper No. 2189, pp. 601-610.
54. J. R. Beeler, *Diffusion Tensor for Slab Geometry*, APEX-488, December, 1958.
55. J. R. Beeler, *Diffusion Anisotropy in Singly- and Doubly-Periodic Lattices*, Trans. Am. Nuclear Soc., 3: No. 1, 266-276, (June, 1960).
56. J. W. Wade, *Neutron Age in Mixtures of Light and Heavy Water*, DP-163, (June, 1956).
57. D. J. Behrens, *The Effect of Holes in a Reacting Material on the Passage of Neutrons*, Proc. Phys. Soc. (London), 62: Series A, 607, (1949).
58. L. Seren, *An Experimental Test of Behren's Theory; Measurement of Anisotropic Diffusion Lengths in Graphite Containing 25% Void*, Trans. Am. Nuclear Soc., 1: No. 2, 31, (December, 1958).
59. C. Carter, *Streaming Due to Holes In A Reactor*, AERE-R3367, (November, 1960).
60. P. Benoist, *Formulation Generale et Calcul Pratique du Coefficient de Diffusion Dans un Reseau Comportant des Cavites*, CEA-1354, (1959).
61. W. A. Horning, *Small Source Model of a Thermal Pile*, HW-24282, (February 26, 1957); also, *A Summary of Small Source Theory Applied to Thermal Reactors*, HW-34021, (December, 1954).
62. S. M. Feinberg, *Heterogeneous Methods for Calculating Reactors: Survey of Results and Comparison with Experiment*, Proc., 1955 Geneva Conference, 5: Paper No. 669, p. 484.
63. A. D. Galanin, *The Thermal Coefficient in a Heterogeneous Reactor*, Proc., 1955 Geneva Conference, 5: Paper No. 666, p. 477.
64. D. D. Lanning, *Heterogeneous Reactor Critical Conditions Using Small Source Theory*, Reactor Control Meeting held in Los Angeles, Calif., March 6-8, 1957, TID-7532, Part 1, p. 61, (October, 1957).
65. S. M. Feinberg, *Heterogeneous Methods for Calculating Reactors*, Progress in Nuclear Energy, (New York: McGraw-Hill Book Co., 1956), Series I, 1: 311-342.
66. D. C. Leslie, *The Method of Feinberg-Galanin*, AEEW-M18, (October 1959).
67. J. W. Zink, *An Extension of Small Source Theory to Include Epithermal Fission*, NAA-SR-4457, (January 15, 1960).
68. K. Meetz, *Exact Treatment of Heterogeneous Core Structures*, Proc., 1958 Geneva Conference, 16: Paper No. 968, pp. 611-626.
69. C. N. Klahr, *Heterogeneous Reactor Calculation Methods*, NYO-2673, (June 30, 1959); NYO-2674, (September 30, 1959); NYO-2675, (December 31, 1959); NYO-2676, (March 31, 1960).
70. Nuclear Physics Research Quarterly Report—Jan., Feb., March, 1960, (Hanford Works), HW-64866, (June, 1960).
71. H. Kouts, et al., *Physics of Slightly Enriched Normal Water Lattices*, Proc., 1958 Geneva Conference, 12: Paper No. 1841, pp. 446-482.
72. D. Klein, et al., *Measurements of Thermal Utilization, Resonance Escape Probability, and Fast Effect in Water-Moderated, Slightly Enriched Uranium, and Uranium Oxide Lattices*, Nuclear Sci. and Eng., 3: No. 4, 403-427, (April, 1958).
73. J. R. Brown, et al., *Kinetic and Buckling Measurements on Lattices of Slightly Enriched Uranium or UO_2 Rods in Light Water*, WAPD-176, (January, 1958).
74. D. B. Wehmeyer and K. E. Roach, *Nuclear Safety of $UO_2-ThO_2-H_2O$ Systems*, BAW-150, (November, 1960).
75. V. E. Grob, et al., *Multi-Region Reactor Lattice Studies: Results of Critical Experiments in Loose Lattices of UO_2 Rods in H_2O*, WCAP-1412, (March, 1960).
76. A. L. MacKinney and R. M. Ball, *Reactivity Measurements on Unperturbed Slightly Enriched Uranium Dioxide Lattices*, Trans. Am. Nuclear Soc., 3: No. 1, (June, 1960).
77. P. W. Davison, et al., *Measurements on Lattices of Stainless Steel Clad, Slightly Enriched Uranium Dioxide Fuel Rods in Light Water*, Yankee Critical Experiments, YAEC-94, (April, 1959).
78. D. E. Wood, *Review of Solid Rod Buckling Measurements in Graphite-Uranium Exponentials*, Nuclear Physics Research Quarterly Report—Jan., Feb., March, 1959, HW-60220, (April, 1959).
79. D. E. Davenport, *Exponential Experiments in Graphite Systems*, Proc., 1955 Geneva Conference, 5: Paper No. 599, p. 309.
80. C. G. Campbell and I. S. Grant, *Critical and Sub-Critical Experiments with a Two-Group Correlation of Results*, Proc., 1958 Geneva Conference, 12: Paper No. 40, pp. 728-746.
81. R. W. Campbell and R. K. Paschall, *Exponential Experiments with Graphite-Moderated Uranium-Metal Lattices*, NAA-SR-5409, (September, 1960).
82. E. R. Cohen, *Exponential Experiments on D_2O-Uranium Lattices*, Proc., 1955 Geneva Conference, 5: Paper No. 605, p. 268.
83. G. Dessauer, *Physics of Natural Uranium Lattices in Heavy Water*, Proc., 1958 Geneva Conference, 12: Paper No. 590, pp. 320-340.
84. N. P. Baumann, *Process Development Pile Measurements of Lattice Parameters of Natural Uranium in Heavy Water*, DP-407, (July, 1959).
85. N. L. Snidow, et al., *Thorium Uranium Physics Experiments*, Final Report, BAW-1191, (May, 1960).
86. W. C. Redman, et al., *Critical Experiments with Thoria-Urania Fuel In Heavy Water*, ANL-6378, (December, 1961).
87. A. K. Krasin, et al., *Physical Characteristics of a Beryllium-Moderated Reactor*, Proc., 1958 Geneva Conference, 12: Paper No. 2146, pp. 571-579.

Section 5

CONTROL AND DYNAMICS OF THERMAL REACTORS

5.1 REACTOR CONTROL

5.1.1 LINEAR EXTRAPOLATION DISTANCE FOR VARIOUS CONFIGURATIONS

In the study of control rods inserted into homogeneous reactors, it is often convenient to describe their effects on the behavior of the asymptotic neutron flux at large distances from the rod. As is well known, in one-group analysis the asymptotic transport theory and the diffusion theory neutron fluxes exhibit the same spatial dependence. Thus, if the logarithmic derivative of the diffusion theory flux at the rod is set equal to that of the asymptotic transport theory flux, the two fluxes would be expected to coincide asymptotically and, therefore, to facilitate diffusion theory computations of greater accuracy. The linear extrapolation distance, λ, at the surface of a rod is defined as the reciprocal of the logarithmic derivative of the flux evaluated at that surface.

The condition on the flux at the rod surface may be replaced by the stipulation that the flux vanishes at a radius r_{eff}. This radius, denoted "effective rod radius," is smaller than the actual radius r of the rod, and is given approximately by: $r_{eff} = r - \lambda$, where λ is the linear extrapolation distance.

In the following descriptions, λ and the rod radii are given in units of the total mean free path of the external medium, unless otherwise specified.

Linear Extrapolation Distances for Black Cylinders and Black Spheres.[1] A body is said to be black to neutrons of a given velocity if the albedo of the body is zero, or equivalently, if no neutron entering the body re-enters the source medium. In the following formulas, the black body is assumed to be placed in an isotropically and elastically scattering, non-absorbing, infinite, homogeneous medium.

For a large, black sphere of radius a:[2]

$$\lambda_a = 0.7104 + \frac{0.5047}{a} + \frac{0.2336}{a^2} - \left(\frac{\ln a}{4} + 0.1704\right)\frac{1}{a^3} + O\left(\frac{\ln^2 a}{a^4}\right)$$

For a small, black sphere of radius a:[3]

$$\lambda_a = \frac{4}{3} - \frac{5}{9}a - \left[\frac{2}{3}\left(\frac{\pi^2}{4} - 1\right)\ln a + 1.4002\right]a^2 + O(a^3 \ln^2 a)$$

For an infinitely long, large, black cylinder of radius a:[4]

$$\lambda_a = 0.7104 + \frac{0.2524}{a} + \frac{0.0949}{a^2} - \left[\frac{5}{64}\ln a + 0.02561\right]\frac{1}{a^3} + O\left(\frac{\ln^2 a}{a^4}\right)$$

For an infinitely long, small, black cylinder of radius a:[5]

$$\lambda_a = \frac{4}{3} + \left[\left(1 - \frac{16}{3\pi^2}\right) \ln a - 0.2164\right] a + O(a^2 \ln^2 a)$$

The symbol O indicates that the error terms are of the order of the quantity following in parentheses. It may be observed that the limiting cases for large spheres and large cylinders are both $\lambda = 0.7104$, the linear extrapolation distance at the surface of an infinite, black slab.

These asymptotic results were combined into smooth curves, $\lambda(a)$, by application of the spherical harmonics (P_L) approximations to the neutron transport equation. Table 5-1 lists the results of $P_L (L = 1,2,\ldots,8)$ computations[6] for black spheres. The results for black cylinders in the P_3 approximation[7] are shown in Table 5-2.

Table 5-1 — LINEAR EXTRAPOLATION DISTANCE FOR BLACK SPHERES: P_L APPROXIMATION OF λ_a

Reproduced from Ref. 1.

a	P_L Approximation							
	P_1	P_2	P_3	P_4	P_5	P_6	P_7	P_8
0.00	0.5774	∞	0.6395	∞	0.6537	∞	—	—
0.05	0.5774	16.7746	0.6894	8.7173	0.7499	6.0648	—	—
0.10	0.5774	8.7746	0.7306	4.7543	0.8211	3.4482	—	—
0.20	0.5774	4.7746	0.7922	2.7867	0.9116	2.1655	1.0140	1.3390
0.30	0.5774	3.4413	0.8332	2.1391	0.9585	1.7508	—	—
0.40	0.5774	2.7746	0.8598	1.8189	0.9806	1.5471	—	—
0.50	0.5774	2.3746	0.8764	1.6280	0.9886	1.4248	1.0291	1.1271
0.70	0.5774	1.9175	0.8909	1.4096	0.9842	1.2807	—	—
1.00	0.5774	1.5746	0.8891	1.2417	0.9604	1.1614	0.9874	—
1.50	0.5774	1.3079	0.8676	1.1008	0.9183	1.0507	—	—
2.00	0.5774	1.1746	0.8443	1.0222	0.8847	0.9843	0.9000	—
2.50	0.5774	1.0946	0.8246	0.9707	0.8589	0.9393	—	—
3.00	0.5774	1.0413	0.8087	0.9341	0.8389	0.9069	—	—
4.00	0.5774	0.9460	0.7853	0.8857	0.8104	0.8633	—	—
5.00	0.5774	0.9346	0.8552	0.7914	0.8356	0.8028	—	—
∞	0.5774	0.7746	0.6940	0.7297	0.7039	0.7197	0.7069	0.7159

Table 5-2 — LINEAR EXTRAPOLATION DISTANCE FOR BLACK CYLINDERS: P_3 APPROXIMATION OF λ_a

Reproduced from Ref. 1.

a	P_3 Approx.	a	P_3 Approx.
0.1014	0.8354	2.0284	0.8079
0.2028	0.8905	3.0426	0.7775
0.4057	0.9171	4.0567	0.7605
0.6085	0.9074	4.8681	0.7516
1.0142	0.8709	6.0851	0.7426
1.5213	0.8335	10.142	0.7277

Davison[1] observed that the P_{2k+1} approximations underestimated λ, and the P_{2k} approximations converged on λ from above. Apparently, even the P_7 computations were not sufficiently accurate to permit unquestionable fits between the asymptotic cases. In Figs. 5-1 and 5-2 are graphed the various asymptotic formulae and the P_L results as well as a "probable shape" for the transition regions. For the case of the long, black cylinder, Zaretsky[8] has computed values of $\lambda = 0.99$ for $a = 0.5$, and $\lambda = 0.889$ for $a = 1$, by accurate numerical integration of the transport equation.

Linear Extrapolation Distance at the Outer Surface of a Small Air Gap Surrounding a Small, Black Cylinder.[9] The following formula, correct to the order indicated, applies to the linear extrapolation

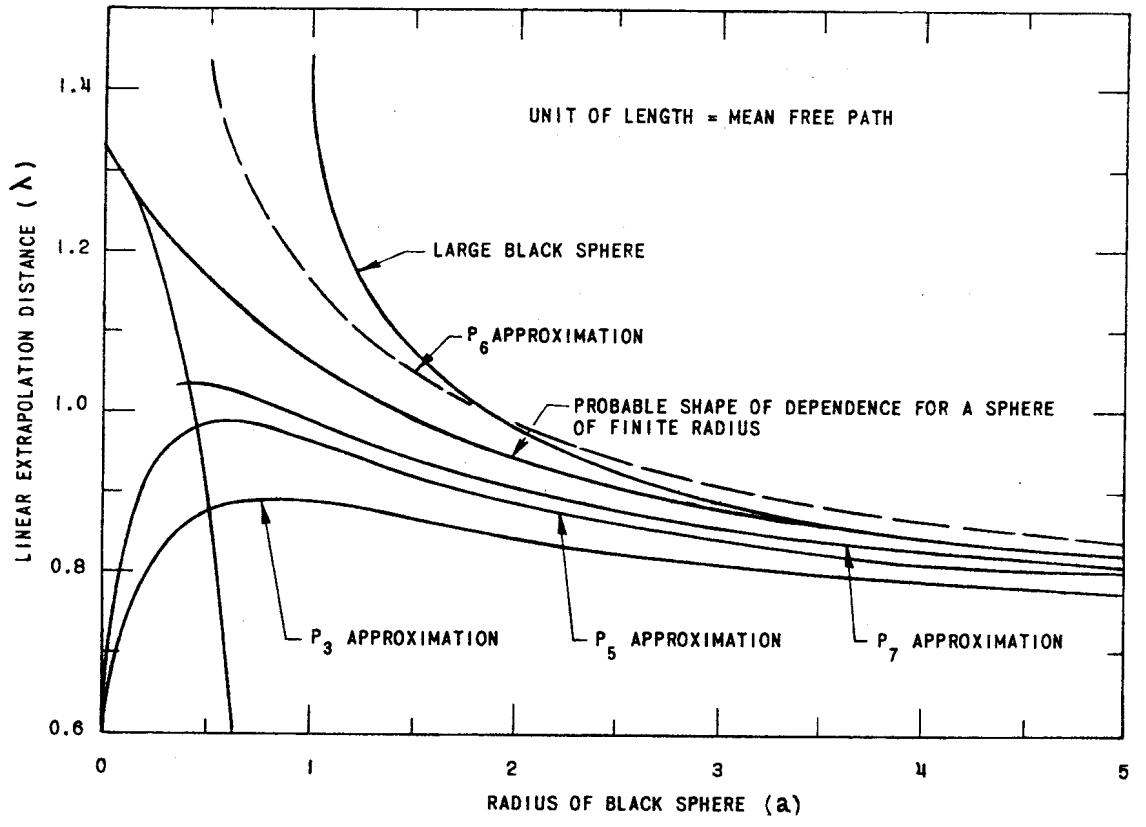

Fig. 5-1 — Linear extrapolation distance at the surface of a black sphere. *Reproduced from Ref. 1.*

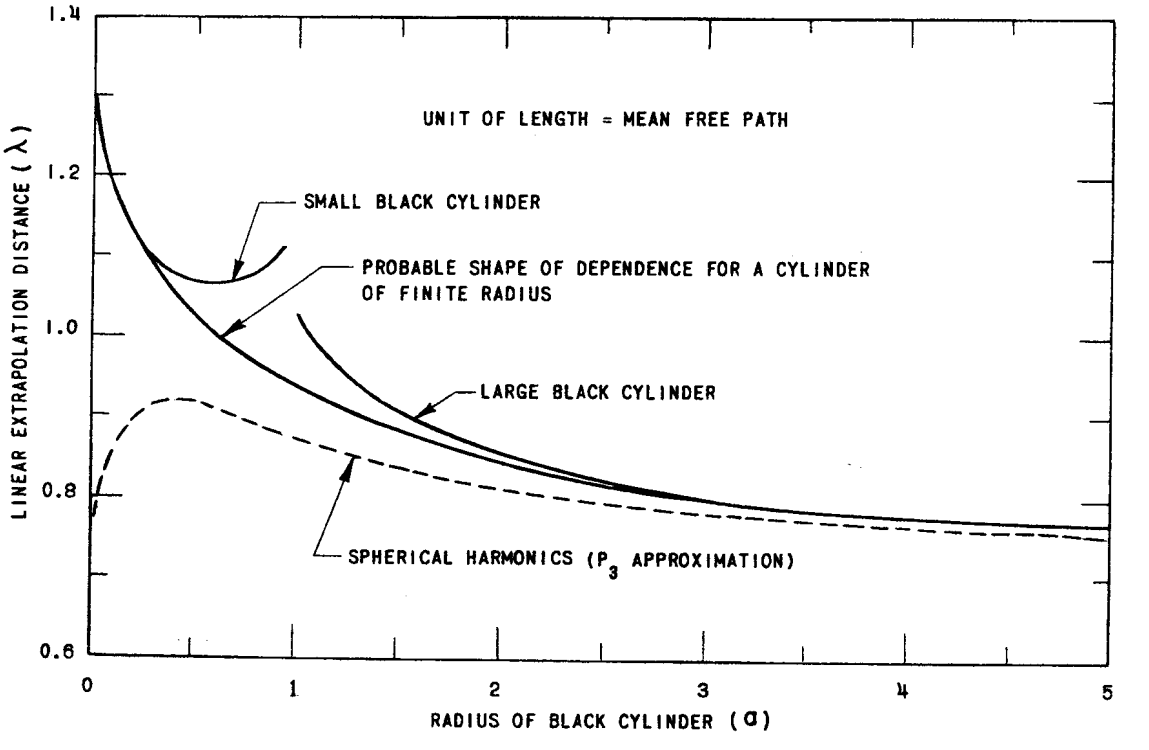

Fig. 5-2 — Linear extrapolation distance at the surface of a black cylinder. *Reproduced from Ref. 1.*

distance, λ_b, at the outer surface of an air gap surrounding a purely absorbing, black cylinder of radius a. The radius, a, and the air-gap thickness (b – a), measured in units of the total mean free path of the surrounding purely scattering medium, are assumed to be small. Then:

$$\lambda_b = \frac{4}{3}\frac{b}{a} + \left(1 - \frac{16}{3\pi^2}\right) b \ln b - 0.0735b - 0.1429\frac{a^2}{b} + O(ab \ln^2 b)$$

which reduces to the linear extrapolation distance at the surface of the small, black cylinder if b = a.

Linear Extrapolation Distance at the Surface of a Small, Black Sphere Surrounded by an Air Gap of Arbitrary Thickness.[10] For a small, black sphere of radius a:

$$\lambda_a = \frac{4}{3} - \frac{5}{9}a + O(a^2 \ln^n a) \tag{5-1}$$

It has been shown that the effect on the asymptotic neutron density of surrounding a small, black sphere of radius a with an air gap of thickness (b – a), is the same as the effect induced by the replacement of this sphere by a sphere of radius a′ without an air gap:

$$a' = a + \frac{a^2}{6}\left[1 - \frac{3}{2}\frac{a}{b + \sqrt{b^2 - a^2}} + \frac{1}{2}\frac{a^3}{\left(b + \sqrt{b^2 - a^2}\right)^3}\right] + O(a^3 \ln^n a)$$

In the presence of the air gap, the linear extrapolation distance at the surface of the black sphere is:

$$\lambda_a = \frac{4}{3} - a\left[1 - \frac{2}{3}\frac{a}{b + \sqrt{b^2 - a^2}} + \frac{2}{9}\frac{a^3}{\left(b + \sqrt{b^2 - a^2}\right)^3}\right] + O(a^2 \ln^n a)$$

By $O(a^2 \ln^n a)$ it is meant that the error terms are of order $a^2 \ln^n a$, n = 0, 1, 2 ... In particular, there is an error term of order a^2, as may be observed by passing to the limit b = a and comparing the resultant formula with the formula for the small, black sphere without an air gap.

No restriction is placed on the size of the air gap in the case of a black sphere, as contrasted with the formula for the small, black cylinder with an air gap, Eq. (5-1).

Linear Extrapolation Distance at the Free Boundary of a Homogeneous Half-Space.[11] The linear extrapolation distance at a free plane boundary has been obtained for various restrictive assumptions concerning the scattering properties of the medium. For a linear scattering law in a purely scattering medium, the emergent angular distribution, and the linear extrapolation distance (in units of the transport mean free path), are the same as for the isotropic case. In the case of an isotropically scattering medium with zero absorption, $\lambda = 0.7104\, \ell_s$, where ℓ_s is the scattering mean free path.

If the medium is capturing and multiplying, and if scattering is linearly anisotropic, the microscopic scattering cross section is given by:

$$\sigma_s(\mu) = \frac{\sigma_{so}}{2}(1 + 3b\mu)$$

where μ is the cosine of the scattering angle, and σ_{so} is the total scattering cross section. Then the distance z_0' (in scattering mean free paths) to the plane where the asymptotic solution vanishes may be obtained as a function of (1 + f), the average number of neutrons emerging per collision, from Table 5-3. In that table may be found the coefficient, κ', of the argument of the asymptotic flux:

$$F_0^{as}(z) \propto \sin \kappa'(z + z_0')$$

By definition of λ,

$$\frac{1}{\lambda} = \frac{d}{dz} \log F_0^{as}(z)\Big|_{z=0}$$

or

$$\lambda = \frac{\tan \kappa' z_0'}{\kappa'}$$

Table 5-3—DIFFUSION LENGTH AND LINEAR EXTRAPOLATION DISTANCE FOR MILNE'S PROBLEM

(Anisotropic Scattering)

Data from Ref. 12.

$1+f$	$(1+f)z_0'$	$(\kappa')^2$
0.0	$1-3b$	-1
0.2	$0.7843-1.2197b$	$-0.99982+0.00350b$
0.4	$0.7300-0.1624b$	$-0.9714+0.1660b$
0.6	$0.7154+0.3305b$	$-0.8233+0.4009b$
0.8	$0.7113+0.5757b$	$-0.5047+0.3902b$
1.0	$0.7104+0.7104b$	0
1.2	$0.7106+0.7897b$	$0.6965-0.8201b$
1.4	$0.7117+0.8386b$	$1.5871-2.0921b$
1.6	$0.7130+0.8693b$	$2.6732-3.8270b$
1.8	$0.7142+0.8881b$	$3.9554-6.0305b$
2.0	$0.7152+0.8998b$	$5.4341-8.7063b$
2.2	$0.7162+0.9059b$	$7.1096-11.856b$
2.4	$0.7173+0.9084b$	$8.9819-15.483b$
2.6	$0.7184+0.9092b$	$11.051-19.585b$
2.8	$0.7194+0.9077b$	$13.318-24.166b$
3.0	$0.7203+0.9047b$	$15.781-29.224b$

Linear Extrapolation Distance at the Surface of a Purely Absorbing, Gray Cylinder.[9] The linear extrapolation distance at the surface of a purely absorbing, small, gray cylinder is given by:

$$\lambda_a(\text{Small Gray Cylinder}) = \frac{4}{3}\left[\frac{1}{g(a^*)} - 1\right] + \lambda_a\ (\text{Small Black Cylinder})$$

where a^* is the radius of the cylinder, measured in capture mean free paths of the absorbing cylinder, and $g(a^*) = 2(1-P_c)a^*$. The escape probability, P_c, is the average probability that a neutron arising from a uniform source within the cylinder will suffer a collision (in this case, a capturing collision) in its first traverse of the cylinder; P_c is listed as a function of a^* in Table 5-4.[13] Royston[14] has extended the domain of λ_a to gray cylinders of larger radius by the use of the P_3 approximation. These results are given in Fig. 5-3.

The effect of a small air gap of outer radius b around a small, gray cylindrical rod has been investigated.[9] Denoting by λ_b the linear extrapolation distance at the outer surface of the air gap:

$$\lambda_b(\text{Small Gray Cylinder}) = \frac{4}{3}\frac{b}{a}\left[\frac{1}{g(a^*)} - 1\right] + \lambda_b\ (\text{Small Black Cylinder})$$

The linear extrapolation distance at the absorber surface is given by:

$$\lambda_a(\text{Small Gray Cylinder}) = \frac{a}{b}\left[\lambda_b\ (\text{Small Gray Cylinder})\right] - a\ \ln\left(\frac{b}{a}\right)$$

Linear Extrapolation Distance into a Purely Absorbing, Gray Slab.[15] Consider a purely absorbing, gray slab of half-thickness a^* (measured in capture mean free paths, ℓ_2, in that medium), located in an infinite homogeneous medium. The infinite medium absorbs and scatters neutrons, and contains a uniform distribution of sources.

Let ℓ_1 denote the total mean free path in the external medium, and let α be the probability that a collision in that medium will result in a neutron capture. Then in the P_1 (spherical harmonics) approximation to the one-group problem, the linear extrapolation distance, λ, at the surface of the gray slab is given by:

$$\lambda = \frac{2}{3}\frac{1 + 3E_4(2a^*)}{1 - 2E_3(2a^*)}$$

Table 5-4 — COLLISION PROBABILITY P_c FOR INFINITE CYLINDER OF RADIUS a*

Reproduced from Ref. 13.

a*	P_c	a*	P_c	a*	P_c	a*	P_c
0.00	0.00000	1.10	0.61869	2.20	0.78282	3.30	0.85130
.02	0.02561	.12	0.62352	.22	0.78459	.32	0.85216
.04	0.04967	.14	0.62825	.24	0.78633	.34	0.85301
.06	0.07248	.16	0.63287	.26	0.78805	.36	0.85385
.08	0.09421	.18	0.63740	.28	0.78974	.38	0.85468
0.10	0.11498	1.20	0.64183	2.30	0.79140	3.40	0.85550
.12	0.13487	.22	0.64616	.32	0.79304	.42	0.85632
.14	0.15396	.24	0.65041	.34	0.79465	.44	0.85712
.16	0.17231	.26	0.65457	.36	0.79624	.46	0.85792
.18	0.18996	.28	0.65864	.38	0.79781	.48	0.85870
0.20	0.20697	1.30	0.66263	2.40	0.79936	3.50	0.85948
.22	0.22336	.32	0.66654	.42	0.80088	.52	0.86025
.24	0.23918	.34	0.67038	.44	0.80239	.54	0.86101
.26	0.25446	.36	0.67413	.46	0.80387	.56	0.86177
.28	0.26923	.38	0.67781	.48	0.80532	.58	0.86251
0.30	0.28351	1.40	0.68142	2.50	0.80677	3.60	0.86325
.32	0.29733	.42	0.68495	.52	0.80818	.62	0.86398
.34	0.31070	.44	0.68842	.54	0.80958	.64	0.86471
.36	0.32366	.46	0.69182	.56	0.81096	.66	0.86542
.38	0.33621	.48	0.69516	.58	0.81233	.68	0.86613
0.40	0.34838	1.50	0.69843	2.60	0.81367	3.70	0.86683
.42	0.36019	.52	0.70164	.62	0.81500	.72	0.86752
.44	0.37164	.54	0.70479	.64	0.81630	.74	0.86821
.46	0.38276	.56	0.70788	.66	0.81759	.76	0.86889
.48	0.39356	.58	0.71091	.68	0.81886	.78	0.86956
0.50	0.40405	1.60	0.71389	2.70	0.82012	3.80	0.87023
.52	0.41424	.62	0.71681	.72	0.82136	.82	0.87089
.54	0.42414	.64	0.71968	.74	0.82258	.84	0.87154
.56	0.43377	.66	0.72250	.76	0.82379	.86	0.87219
.58	0.44314	.68	0.72526	.78	0.82498	.88	0.87283
0.60	0.45225	1.70	0.72798	2.80	0.82616	3.90	0.87346
.62	0.46112	.72	0.73065	.82	0.82732	.92	0.87409
.64	0.46975	.74	0.73327	.84	0.82847	.94	0.87471
.66	0.47816	.76	0.73585	.86	0.82960	.96	0.87533
.68	0.48634	.78	0.73838	.88	0.83071	.98	0.87594
0.70	0.49432	1.80	0.74087	2.90	0.83182	4.00	0.87654
.72	0.50209	.82	0.74331	.92	0.83291	.02	0.87714
.74	0.50966	.84	0.74572	.94	0.83399	.04	0.87773
.76	0.51704	.86	0.74808	.96	0.83505	.06	0.87832
.78	0.52424	.88	0.75040	.98	0.83610	.08	0.87890
0.80	0.53126	1.90	0.75269	3.00	0.83714	4.10	0.87947
.82	0.53811	.92	0.75493	.02	0.83816	.12	0.88004
.84	0.54479	.94	0.75714	.04	0.83917	.14	0.88061
.86	0.55131	.96	0.75931	.06	0.84017	.16	0.88117
.88	0.55767	.98	0.76145	.08	0.84116	.18	0.88173
0.90	0.56389	2.00	0.76355	3.10	0.84214	4.20	0.88228
.92	0.56996	.02	0.76562	.12	0.84310	.22	0.88282
.94	0.57588	.04	0.76765	.14	0.84405	.24	0.88336
.96	0.58167	.06	0.76966	.16	0.84500	.26	0.88389
.98	0.58733	.08	0.77163	.18	0.84593	.28	0.88443
1.00	0.59285	2.10	0.77357	3.20	0.84685	4.30	0.88495
.02	0.59826	.12	0.77548	.22	0.84776	.32	0.88547
.04	0.60354	.14	0.77736	.24	0.84866	.34	0.88598
.06	0.60870	.16	0.77921	.26	0.84955	.36	0.88650
.08	0.61375	.18	0.78103	.28	0.85043	.38	0.88701

Table 5-4—COLLISION PROBABILITY P_c FOR INFINITE CYLINDER OF RADIUS a* (Continued)

Reproduced from Ref. 13.

a*	P_c	a*	P_c	a*	P_c	a*	P_c
4.40	0.88751	4.80	0.89671	5.20	0.90453	5.60	0.91126
.42	0.88801	.82	0.89713	.22	0.90489	.62	0.91157
.44	0.88850	.84	0.89755	.24	0.90525	.64	0.91188
.46	0.88899	.86	0.89796	.26	0.90560	.66	0.91219
.48	0.88948	.88	0.89837	.28	0.90595	.68	0.91250
4.50	0.88996	4.90	0.89878	5.30	0.90631	5.70	0.91280
.52	0.89044	.92	0.89919	.32	0.90665	.72	0.91310
.54	0.89091	.94	0.89959	.34	0.90700	.74	0.91340
.56	0.89138	.96	0.89999	.36	0.90734	.76	0.91369
.58	0.89184	.98	0.90038	.38	0.90768	.78	0.91399
4.60	0.89230	5.00	0.90077	5.40	0.90802	5.80	0.91429
.62	0.89276	.02	0.90116	.42	0.90835	.82	0.91457
.64	0.89321	.04	0.90155	.44	0.90868	.84	0.91487
.66	0.89366	.06	0.90193	.46	0.90902	.86	0.91515
.68	0.89411	.08	0.90231	.48	0.90934	.88	0.91544
4.70	0.89455	5.10	0.90268	5.50	0.90967	5.90	0.91572
.72	0.89499	.12	0.90306	.52	0.90999	.92	0.91600
.74	0.89542	.14	0.90343	.54	0.91031	.94	0.91628
.76	0.89585	.16	0.90381	.56	0.91063	.96	0.91656
.78	0.89628	.18	0.90417	.58	0.91095	.98	0.91684
						6.00	0.91711

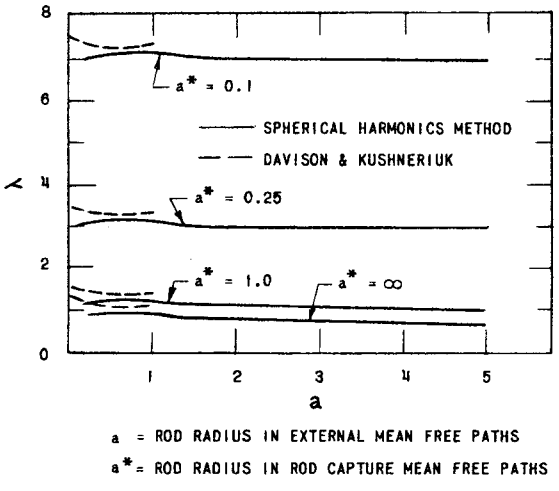

Fig. 5-3—Linear extrapolation distance at the surface of a purely absorbing gray cylinder. *Reproduced from Ref. 14.*

where

$$E_n(z) = z^{n-1} \int_z^\infty (e^{-x}/x^n)\, dx$$

is the exponential integral of order n.

P_1, P_3 and P_5 computations that have been made for various values of α in a particular system where $\ell_1/\ell_2 = 1.2$ and $a^* = 0.2$, are listed in Table 5-5.

Table 5-5—λ AS A FUNCTION OF α FOR A SLAB WITH $\ell_1/\ell_2 = 1.2$ AND $a^* = 0.2$

α	Order of Approximation		
	P_1	P_3	P_5
0.00094	2.1526	2.2890	2.2919
0.1	2.1526	2.7364	2.7575
0.1667	2.1526	3.0864	3.1602
0.3	2.1526	3.9462	4.3461

Linear Extrapolation Distance at the Plane Interface of Two Homogeneous Half-Spaces.[16] The linear extrapolation distance, λ, into an absorbing, non-multiplying half-space which scatters isotropically from a non-absorbing, isotropically scattering medium, may be obtained from Fig. 5-4. In that figure, the abscissa is c, the ratio of scattering to total cross section in the capturing medium,

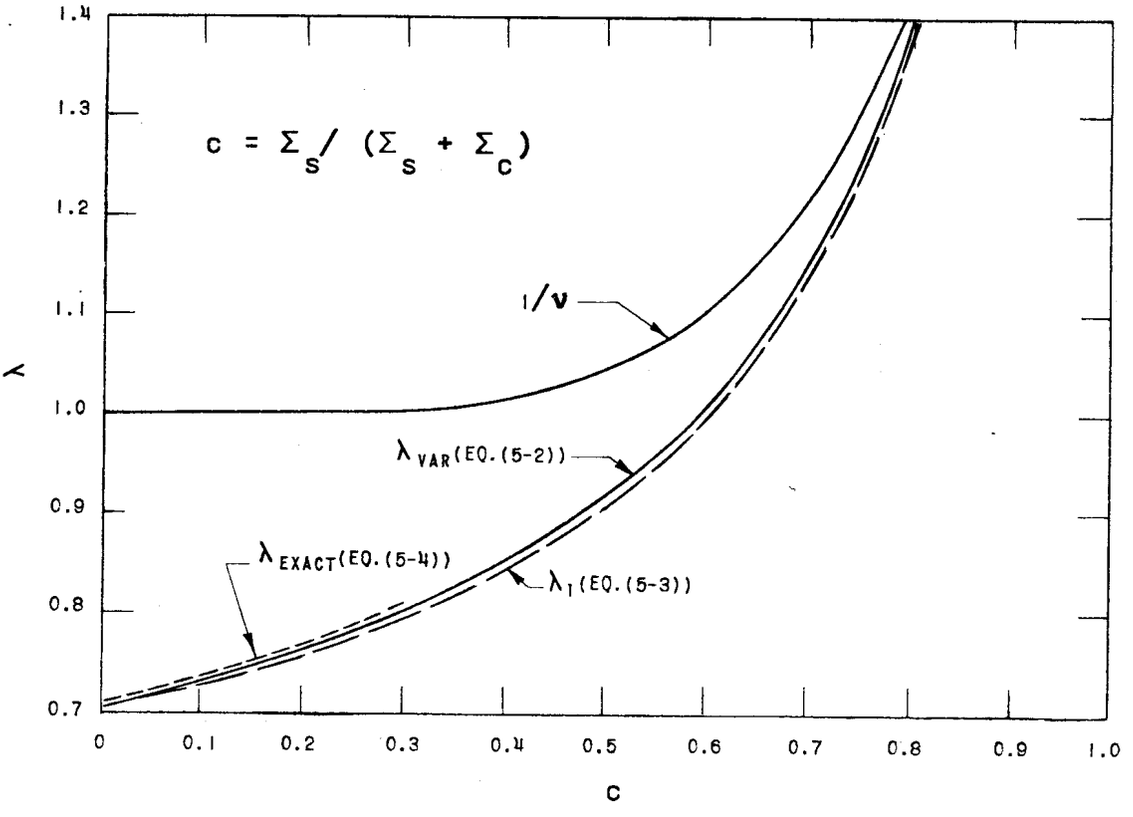

Fig. 5-4 — Linear extrapolation distance at interface of two semi-infinite media: (1) pure scatterer; and (2) scatterer and absorber. *Reproduced from Ref. 16.*

and the ordinate is λ for the scattering medium. The curve marked λ_{var} was obtained by substitution of the trial function $[\nu/3(1-c)]e^{\nu x}$ for the flux in the capturing half-space, $x < 0$. Then:

$$\lambda_{var} = 0.70711 + 0.22953\ c + 0.21134\ c^2 + 0(c^3) \tag{5-2}$$

For c near unity, i.e., for small ratios of capture to scattering,

$$\lambda \approx 1/\nu \approx [c/3(1-c)]^{1/2}$$

The function λ_1 was obtained by assuming a linear variation, $x + a$, of the neutron flux in the positive half-space (the purely scattering medium), again using the trial function $[\nu/3(1-c)]e^{\nu x}$ in the negative half-space, and applying variational techniques to estimate the value of λ_1. For small c,

$$\lambda_1 = 0.6667 + 0.2046\ c\ (1 + c) + 0(c^3) \tag{5-3}$$

The so-called "λ_{exact}" was found by solving the integral equation for the neutron density distribution in the positive half-space. Approximately:

$$\lambda_{exact} = 0.71045 + 0.25000\ c + 0.19885\ c^2 + 0.16991\ c^3 + 0(c^4) \tag{5-4}$$

Linear Extrapolation Distance at the Surface of a Scattering and Capturing Cylinder.[16] Consider a homogeneous cylinder of radius a which captures and scatters neutrons isotropically and elastically. Suppose that this cylinder is surrounded by N homogeneous purely absorbing annuli, and that these N + 1 regions are embedded in an infinite, purely scattering medium, which scatters isotropically and elastically. Let:

a = radius of cylinder (all measurements are in units of the total mean free path of the infinite medium)

$$\alpha_t = \frac{\Sigma_c(\text{cylinder}) + \Sigma_s(\text{cylinder})}{\Sigma_s(\text{infinite medium})}$$

$$c = \frac{\Sigma_s(\text{cylinder})}{\Sigma_{total}(\text{cylinder})} = \text{average number of neutrons generated per collision in the cylinder}$$

$$\alpha_i = \frac{\Sigma_c(i\textit{th annulus})}{\Sigma_s(\text{infinite medium})}$$

A_i = cross-sectional area of the i*th* annulus

a_i = outer radius of the i*th* annulus

τ_i = thickness of the i*th* annulus

$R = a_N = a + \sum_{i=1}^{N} \tau_i$

Then the linear extrapolation distance at the outermost surface (at radius R) is given by:

$$\lambda = \frac{4}{3}\frac{1}{P(a\alpha_t,\alpha_i,a_i)} - 4T(R) + f(R)$$

where

$$P(a\alpha_t,\alpha_i,a_i) = \frac{a}{R}P(a\alpha_t)\prod_{i=1}^{N} T_i + \frac{2}{\pi R}\sum_{i=1}^{N}\alpha_i A_i - \frac{a}{R}P(a\alpha_t)\sum_{i=1}^{N}(1 - T_i)$$

with

$$P(a\alpha_t) = \frac{(1-c)\ P_1(a,\alpha_t)}{1 - c\ P_c(a\alpha_t,\nu)}$$

$$P_1(a\alpha_t) = \frac{4}{3}a\alpha_t\left\{\begin{array}{l} K_1(a\alpha_t)\ I_1(a\alpha_t) - 1 - 2a\alpha_t \\ \\ +2(a\alpha_t)^2\left[I_0(a\alpha_t)K_0(a\alpha_t) + I_1(a\alpha_t)\ K_1(a\alpha_t) + \dfrac{I_0(a\alpha_t)K_1(a\alpha_t)}{a\alpha_t}\right] \end{array}\right\}$$

$P_c(a\alpha_t,\nu)$ satisfies the relationship:

$$\frac{c}{1-c}\left[1 - P_c(a\alpha_t,\nu)\right] = 3a\ c\ B\ I(a,\alpha_t,c)$$

where

$$I(a,\alpha_t,c) = a\int_1^\infty \frac{du}{u(\nu^2-u^2)}\ K_1(a\alpha_t u)\left[\nu\ I_1(a\alpha_t\nu)\ I_0(a\alpha_t u) - u\ I_0(a\alpha_t\nu)\ I_1(a\alpha_t u)\right]$$

and

$$B = \frac{\alpha_t\nu}{3(1-c)\ a\ I_1(a\alpha_t\nu)}$$

ν satisfying the transcendental equation $2\nu = c\ \log\left(\frac{1+\nu}{1-\nu}\right)$; and

$$T_i = 1 - 2\frac{\alpha_i}{\pi}\left[\sqrt{a_i^2-a^2} - \sqrt{a_{i-1}^2-a^2} + \frac{a_i^2}{a}\ \text{arc sin}\frac{a}{a_i} - \frac{a_{i-1}^2}{a}\ \text{arc sin}\frac{a}{a_{i-1}}\right]$$

The functions 4T(R) and $P_1(a\alpha_t)$ are plotted in Fig. 5-5, and are tabulated in Table 5-6.

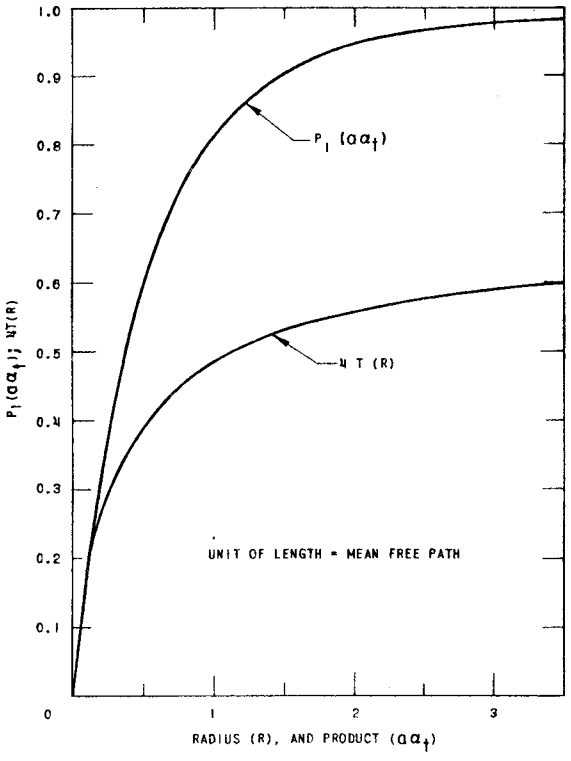

Fig. 5-5 — Functions $P_1(a\alpha_t)$ and 4T(R). *Reproduced from Ref. 16.*

Table 5-6 — VALUES OF $P_1(a\alpha)$, 4T(a), AND f(a)

Reproduced from Ref. 16.

$a\alpha$	$P_1(a\alpha)$	a	4T(a)	f(a)
0.0	0.0	0.0	0.0	0.0
0.1	0.1770	0.07	0.1439	0.035
0.2	0.3127	0.10	0.1844	0.045
0.3	0.4299	0.15	0.2303	0.055
0.5	0.5960	0.2	0.2662	0.062
0.7	0.7080	0.3	0.3206	0.070
0.8	0.7499	0.5	0.3919	0.078
1.0	0.8143	0.7	0.4380	0.077
1.3	0.8771	1.0	0.4837	0.074
1.6	0.9155	1.5	0.5297	0.064
2.0	0.9458	2.5	0.5760	0.052
2.5	0.9662	5.0	0.6152	0.044
3.0	0.9772	8.0	0.6344	0.044
4.0	0.9877	12.0	0.6420	0.044
5.0	0.9921	—	—	—

The function f(a) has been approximated for two cases of a homogeneous cylinder of radius a:

$\alpha = 1$, i.e., Σ_{total}(cylinder) = Σ_{total}(infinite medium)

and

$\alpha = \infty$, i.e., black cylinder

These two approximations are plotted in Fig. 5-6 as a function of a, together with a plot of f(a) which Kushneriuk and McKay have suggested as an approximation of wider applicability. The suggested variation of f(a) is to be used also for the case where there are absorbing annuli, in which event Fig. 5-6 is to be interpreted as a plot of f(R) vs. R. Table 5-6 lists the suggested function f(a) for various values of the parameter a.

The special case of a homogeneous purely absorbing cylinder in an infinite scattering medium has been examined in detail. In Fig. 5-7, the linear extrapolation distance is shown as a function of the cylinder radius for various values of $a\alpha$.

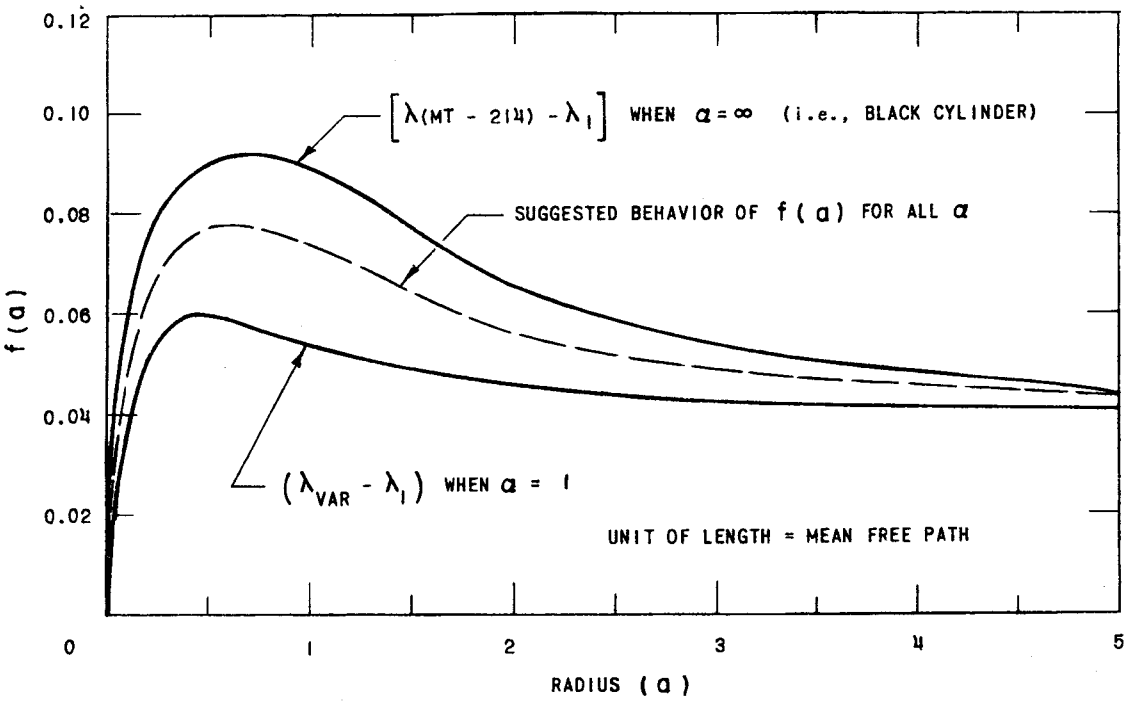

Fig. 5-6—Various approximations for f(a). *Reproduced from Ref. 16.*

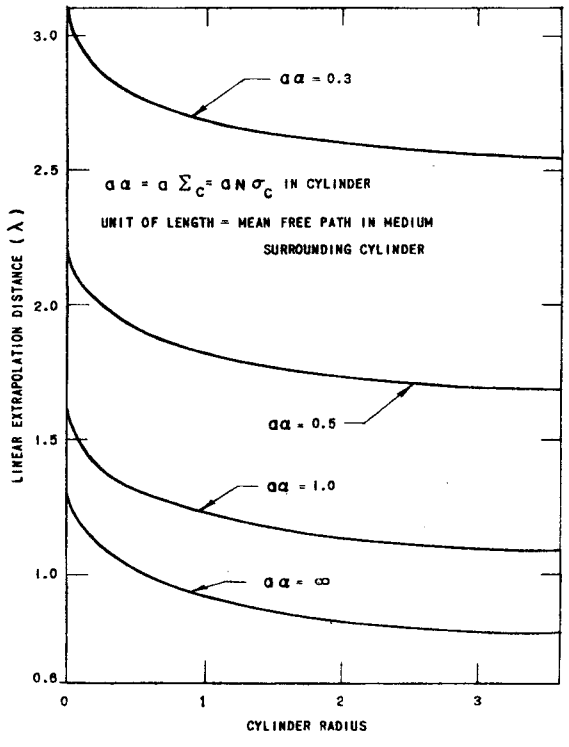

Fig. 5-7—Linear extrapolation distance at the surface of a purely absorbing cylinder. *Reproduced from Ref. 16.*

687863 O - 63 - 25

5.1.2 EFFECTIVE RADII FOR VARIOUS SHAPES OF BLACK BODIES

There is considerable overlap between this section and Section 5.1.3 dealing with the concept of absorption area. In both sections, equivalence relationships between black bodies either are directly stated or may be inferred. However, the absorption area may be used directly for reactivity analyses, whereas the correlation between the reactivity effects of a black body and of an equivalent cylindrical rod is only a step to the final result.

This section is devoted to the presentation of results taken from work of Wheeler.[17]

The effective radius, r_{eff}, of a black body in an infinite homogeneous medium is defined as the radius of a cylindrical rod which has the same effect on the asymptotic neutron density. In determining this asymptotic neutron density, the condition is used that the density vanishes at the surface of the equivalent rod.

In Table 5-7, formulae for r_{eff} are given for various shapes of purely absorbing black bodies in holes of various sizes.[18] In Table 5-8 are listed measured and theoretical values of relative rod ef-

Table 5-7—EFFECTIVE RADIUS, r_{eff}, OF BLACK CONTROL BARS

Data from Ref. 18.

Nomenclature

r = actual rod radius, cm
r_{eff} = effective rod radius, cm
ℓ = transport mean free path in the external medium, cm
λ = linear extrapolation distance for a purely absorbing black cylinder in an infinite homogeneous medium, in units of the total mean free path in the external medium
r_0 = outer radius of the hole in which the black body is located, cm
s = perimeter, cm, determined by putting a measuring tape once about the bar and drawing it tight; in general, the tape will not touch the bar at all points
w = span of the thin bar, or of the cross formed from two thin bars, cm

Case	r_{eff}
(1) Large, snugly-embedded rod of radius r	$r \exp(-0.71\ell/r)$
(2) Snugly-embedded rod of radius r	$r \exp(-\lambda\ell/r)$
(3) Small compared to ℓ, snugly-embedded bar of perimeter s	$0.46\,\ell \exp(-8\pi\ell/3s)$
(4) Small compared to ℓ, snugly-embedded rod of radius r	$0.46\,\ell \exp(-4\ell/3r)$
(5) Bar in a considerably larger hole of radius r_0	$r_0 \exp(-8\pi\ell/3s)$
(6) Rod in a considerably larger hole of radius r_0	$r_0 \exp(-4\ell/3r)$
(7) Embedded strip of small thickness compared to ℓ, but with w comparable with or larger than ℓ	$w/4 \exp\{-[Y(1 - 0.114\,Y + 0.048\,Y^2)]^{-1}\}$ where $Y = w\sqrt{3}/\pi\ell$
(8) Embedded cross formed of two thin strips of width $w/\sqrt{2}$	same as preceding
(9) Large, embedded, rectangular bar	See Fig. 5-7

Table 5-8—EFFECT OF CONTROL ELEMENT SHAPE

Data from Ref. 18.

Shape of Element	Perimeter, cm	Observed[a] Effectiveness Relative to + bar	In-hole Calculation[b]		Embedded Calculation[c]	
			r_{eff}, cm	Relative Effectiveness	r_{eff}, cm	Relative Effectiveness
–	18.1	0.90	1.65	0.87	1.28	0.82
+	25.6	1.00	2.38	1.00	2.24	1.00
0	28.4	1.06	2.58	1.03	3.20	1.06

[a] All bars had a maximum extension of 9.05 cm and were located in a square hole equivalent in area to a circle of radius r_1 = 5.74 cm.

[b] Using case (5) of Table 5-7.

[c] Using Table 5-7: case (7) for rectangular shape (–); case (8) for cross shape (+); and case (1), but with a value 0.58 instead of 0.71, for cylindrical (0) elements.

fectiveness for various shapes of black bodies.[18] Figure 5-8 is a nomogram for the effective radius of a black rectangular bar.

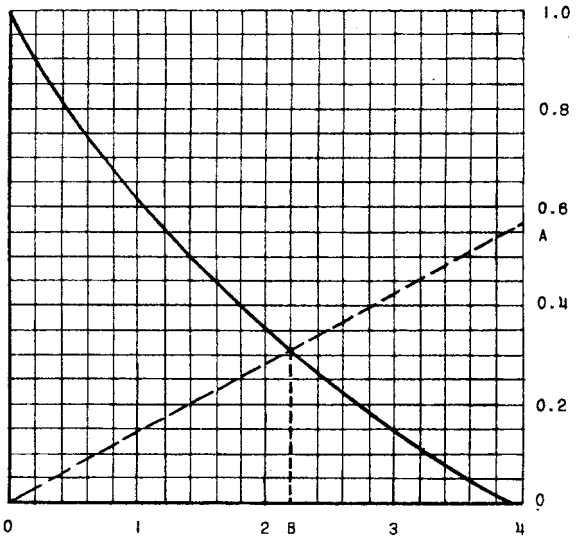

Fig. 5-8—Effective radius of rectangular bar. *Reproduced from Ref. 18.* Remove a layer of thickness 0.71(1) all around the bar to obtain a smaller effective rectangle of width w and thickness Aw. Plot A on right scale of graph and connect to lower left corner by a straight line intersecting curve. Below intersection, read $B = w/r_{eff}$ on bottom scale.

5.1.3 ABSORPTION AREA METHOD[19]

The absorption area of a source-free, black body is defined as the ratio of the rate of neutron absorption by the body per unit height, to the source intensity in the external medium. The concept of absorption area introduced by Hurwitz and Roe[19] may be used as a characterization of equivalence between black bodies of irregular shape, i.e., two black bodies may be termed equivalent if they have equal absorption area.

Consider a black body in a homogeneous infinite medium containing a uniform distribution of neutron sources, and let L^2 be the thermal diffusion area of the infinite medium. Then for L large, compared with the dimensions of the body, the absorption area is given by:

$$C \text{ (limit of large L)} \approx 2\pi\, L\, r_{eff}[K_1(r_{eff}/L)/K_0(r_{eff}/L)]$$

Note that this equation would be exact in the framework of diffusion theory for a cylindrical rod of radius r_{eff}, with the flux vanishing at the surface of the rod.

In Table 5-9, the value of r_{eff} is listed for several regular bodies.

Table 5-9—r_{eff} FOR SIMPLE SHAPES

Reproduced from Ref. 19.

Bar	$r_{eff} = a/2$, where a is the half-width of the bar.							
Symmetrical cross	$r_{eff} = a/\sqrt{2}$, where a is the distance of the end of an arm from the axis.							
Rectangle[a]	d′/d = 0.0	0.0432	0.2219	0.3968	0.5085	0.6418	0.8030	1.000
	r_{eff}/d = 0.25	0.2732	0.3939	0.4038	0.4401	0.4820	0.5314	0.5902
Ellipse	$r_{eff} = [(a + b)/2]$, where a and b are semi-major and semi-minor axes.							

[a]The terms d′ and d are, respectively, the short and long sides of the rectangle. For the rectangle: $r_{eff}/d = [4\kappa^2 B(\kappa^2)]^{-1}$, where κ is determined by the implicit relationship: $d'/d = [(1-\kappa^2)/\kappa^2][B(1-\kappa^2)/B(\kappa^2)]$, where $B(\kappa^2)$ is a complete elliptical integral.

If the boundary of the black body has a radius of curvature which is large everywhere in comparison with L, then the boundary may be approximated by a polygon whose sides are large in comparison with L, and the interaction between vertices of this polygon may be neglected. In this case, the absorption area is:

$$C \text{ (limit of small L)} = L \cdot \text{perimeter} + L^2 \sum_{\text{corners}} D(\phi_i) + O(L^3)$$

where ϕ_i is the external angle at corner i.

The function $D(\phi)$ is given by:

$$D(\phi) = 4 \sum_{n=1}^{n_0} (-1)^n \cot n\phi + \frac{4}{\phi} \int_0^\infty \frac{\tanh x \sinh (x\pi/\phi) \cos (\pi^2/2\phi)\, dx}{\sinh^2 (x\pi/\phi) + \sin^2 (\pi^2/2\phi)}$$

where n_0 is the largest integer less than $\pi/2\phi$.

In Table 5-10, $D(\phi)$ is listed for several values of ϕ. This function is shown in Fig. 5-9, together with the results obtained in the limit $\phi \to 0$:

$$D(\phi) = \frac{4 \ln 2}{\phi}$$

$$\text{For } \phi \approx \pi,\ D(\phi) = \frac{(\phi - \pi)}{2}$$

Table 5-10—VALUES OF $D(\phi)$ FOR CERTAIN ANGLES

Reproduced from Ref. 19.

ϕ	$D(\phi)$
2π	1
$3\pi/2$	$\frac{4}{3\pi}\left(\frac{4\pi}{3\sqrt{3}} - 1\right)$
π	0
$\pi/2$	$-4/\pi$
$\pi/3$	$-4/\sqrt{3}$

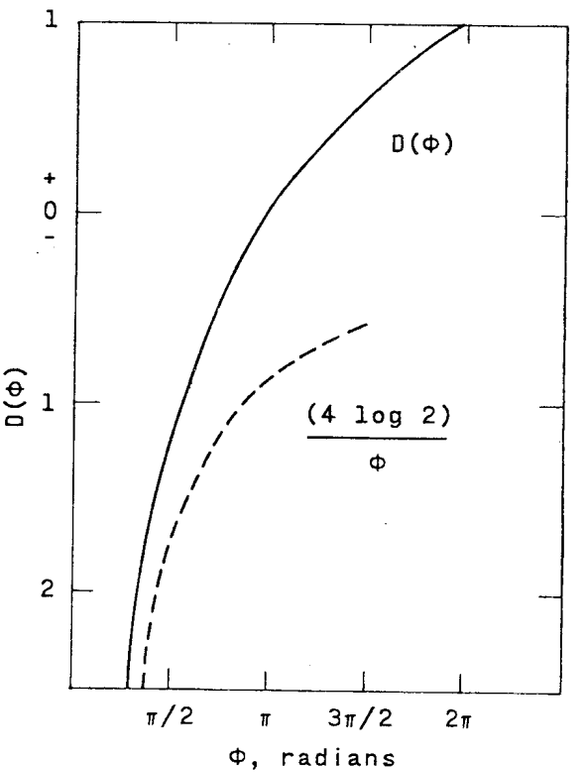

Fig. 5-9—Absorption area correction for corners of exterior angle ϕ. *Reproduced from Ref. 19.*

For intermediate values of L, approximate absorption area formulae for a bar and for a symmetrical cross rod have been obtained by variational methods. The bar is a black slab of zero thickness and of finite width 2a centimeters.

The ratio of the absorption area to 4aL is listed in Table 5-11 for black bars. The absorption area is obtained in four approximations:

Column 1. In the limit of large L:

$$\frac{C}{4aL} = \frac{\pi}{4}\frac{K_1(a/2L)}{K_0(a/2L)}$$

Column 2. In the limit of small L:

$$C = L\,[\text{perimeter} + 2L]$$

or

$$\frac{C}{4aL} = 1 + \frac{L}{2a}$$

Column 3. A variational lower bound

Column 4. A variational upper bound

Table 5-11—C/4aL FOR BLACK BAR

$\frac{L}{2a}$	Large L Limit $r_{eff} = a/2$	Small L Limit $\Sigma D(\phi) = 2$	Variational Lower Bound	Variational Upper Bound
0.2	1.061	1.200	1.175	1.200
0.5	1.4073	1.500	1.468	1.496
1.0	1.909	2.000	1.934	1.965
2.0	2.786	3.000	2.782	2.819
5.0	5.021	6.000	4.984	5.054
10.0	8.2440	11.000	8.15	8.367

This table is useful in examining the range of validity of the asymptotic formulae. To facilitate such an examination, in Fig. 5-10 the ratios C/C(limit of large L) are plotted for the various approximate formulae, together with a "Best Estimate" curve. The absolute value of C/4aL is graphed in Fig. 5-11, together with the curve of C(limit of large L)/4aL.

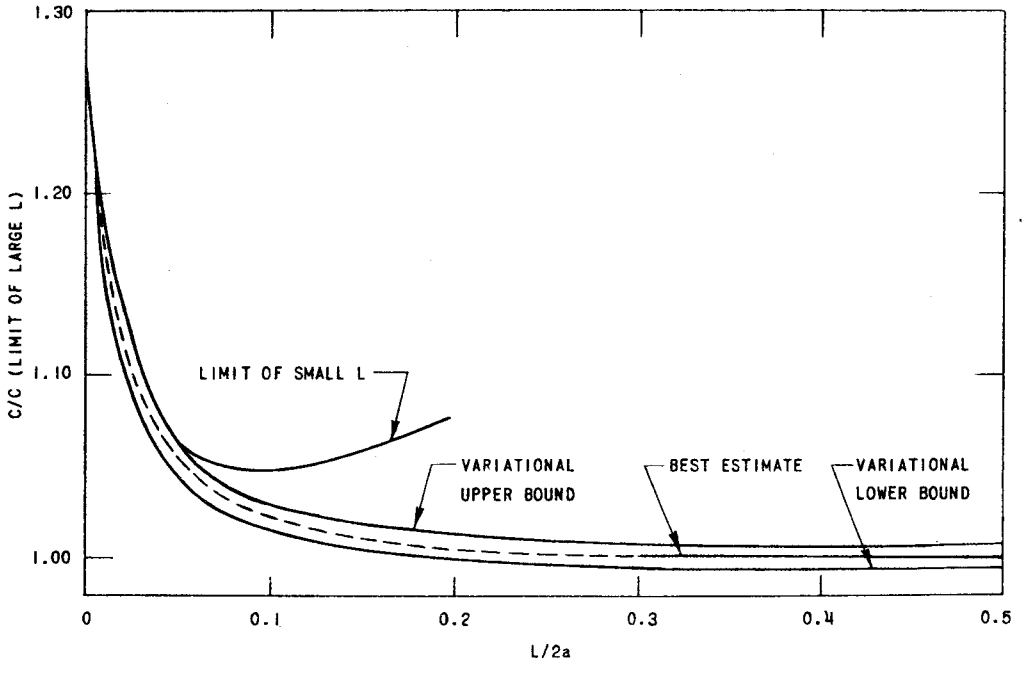

Fig. 5-10—Ratio of absorption area for black bar to absorption area calculated from the formula of the limit of large L. *Reproduced from Ref. 19.*

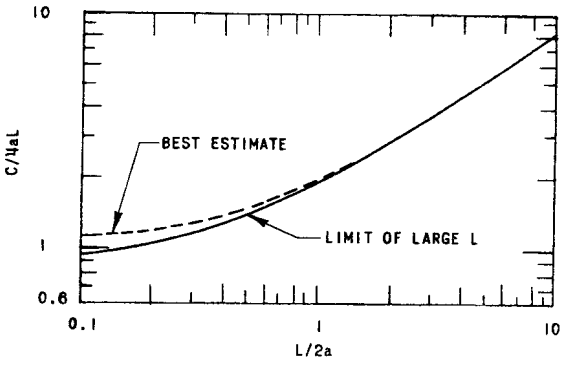

Fig. 5-11 — Absorption area for black bar. *Reproduced from Ref. 19.*

The cross rod has a full span of 2a centimeters, i.e., each of the four arms is 1 cm wide. Table 5-12 is analogous to Table 5-11 for the control bar. In the limit of large L,

$$C/8aL = [(\pi\sqrt{2}/8)][K_1(a/\sqrt{2L})/K_0(a/\sqrt{2L})]$$

In the limit of small L,

$$C/8aL = 1 - 0.273(L/2a)$$

Table 5-12 — C/8aL FOR SYMMETRICAL CROSS ROD

$\frac{L}{2a}$	Large L Limit $r_{eff} = a/\sqrt{2}$	Small L Limit $\Sigma D(\phi) = -1.093$	Variational Lower Bound	Variational Upper Bound
0.1	0.6295	0.9727	—	0.9732
0.2	0.6973	0.9454	—	0.9598
0.5	0.8802	0.8635	—	1.0254
1.0	1.1478	0.727	1.1850	1.2319
2.5	1.8328	—	1.8212	—
10.0	4.5291	—	4.44	—

Columns 4 and 5 are, respectively, variational lower and upper bounds of C/8aL. Figures 5-12 and 5-13 are analogous to those described for the control bar.

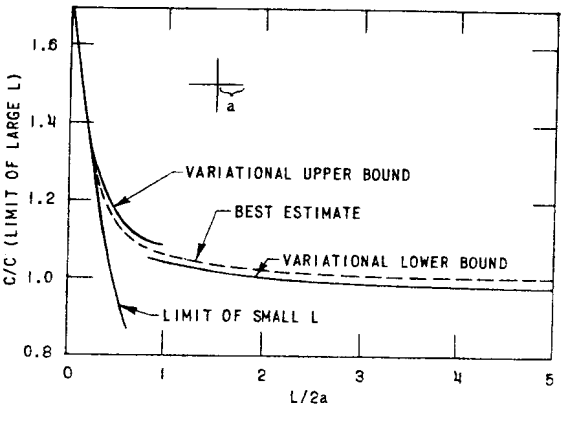

Fig. 5-12 — Ratio of absorption area for black cross to absorption area calculated from the formula of the limit of large L. *Reproduced from Ref. 19.*

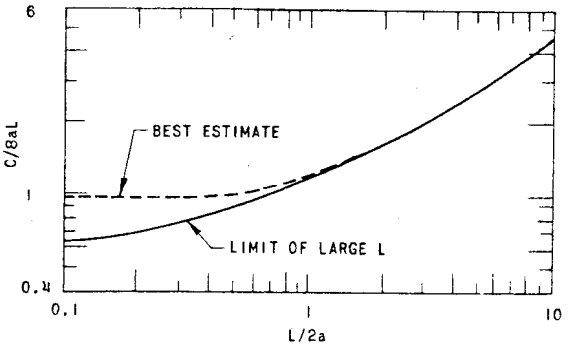

Fig. 5-13 — Absorption area for black cross. *Reproduced from Ref. 19.*

Experimental confirmation of the equivalence relationship between a control bar and a symmetrical cross rod has been obtained by Bach and Kitchen.[20] Measurements were made in a cylindrical critical assembly (Flexible Plastic Reactor), moderated with polyethylene and fueled with uranium highly enriched in U^{235}. Although the absorption area was defined earlier for black rods, the concept is meaningful for source-free, gray rods as well. It is of special significance that the one-group equivalence relationship for black crosses and bars was shown experimentally to apply to gray bodies which are strong absorbers of neutrons over a wide energy range.

In Fig. 5-14, the reactivity effects of the various absorbers are shown as a function of the span of the absorber. In order to demonstrate the geometrical dependence of the absorption area, the experimentally-obtained reactivities are normalized to the reactivity effect of the 0.027-in. thick cadmium body with a span of 2 in. The experimental data were corrected for the effect of non-zero absorber thickness on the assumption that the fractional absorption area of the edge is proportional to the fractional geometric area of the edge. This correction was made in order to provide a meaningful comparison with the zero-thickness results of Hurwitz and Roe.[19] The magnitude of this correction is shown in Fig. 5-15, in terms of the relative reactivity effects of 0.100-in. thick and 0.200-in. thick hafnium bars. Figure 5-14 shows the "best estimate" and the "small L limit" curves of Hurwitz and Roe, normalized to the 2-inch span cadmium bodies, and based on a measured diffusion length L = 0.6 in.

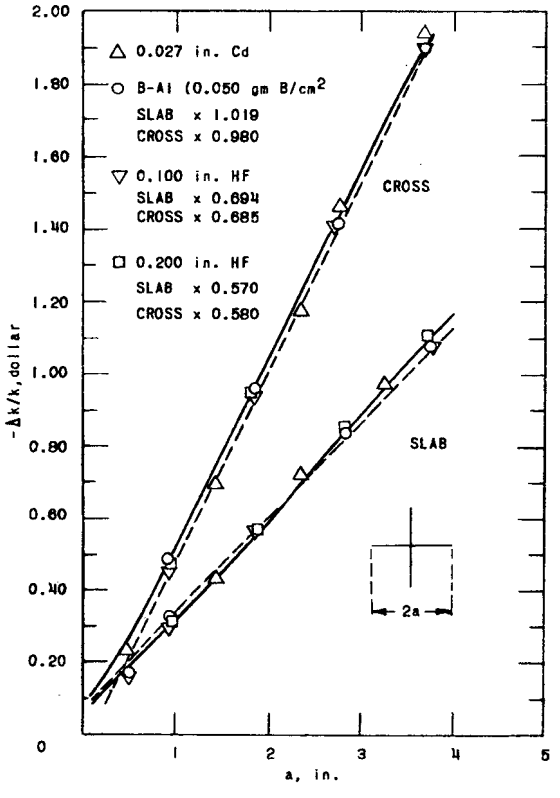

Fig. 5-14—Relative reactivity effects of slab and cross rods. Slab and cross data normalized to a = 2 in. *Reproduced from Ref. 20.*

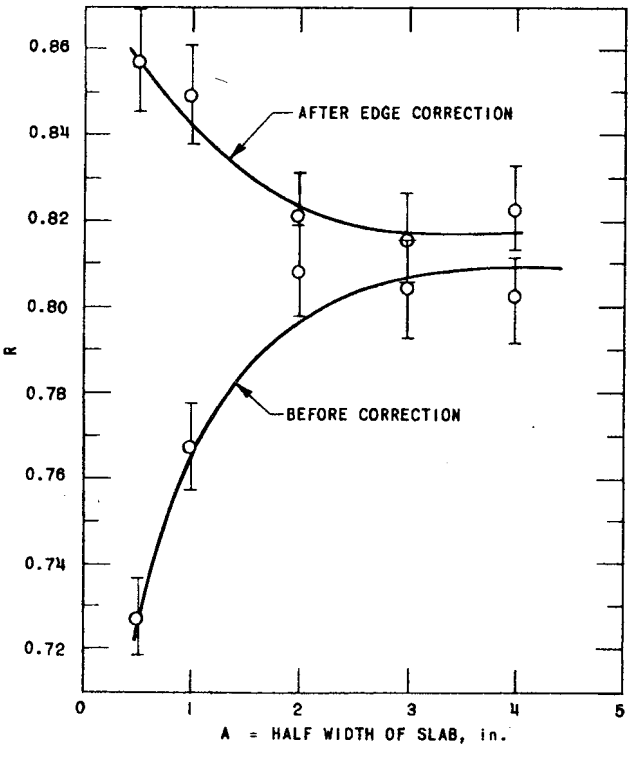

Fig. 5-15—The ratio: R = (Δk/k 0.100-in. Hf slab/ Δk/k 0.200-in. Hf slab) showing effect of edge correction. *Reproduced from Ref. 20.*

5.1.4 REACTIVITY EFFECTS OF A BLACK CYLINDRICAL ROD

In one-group diffusion theory analysis of a small, circular cylinder at the center of an unreflected, cylindrical reactor, the variation of the excess effective multiplication factor, $\Delta k_{eff} = k_{eff} - 1$, with effective rod radius, r_{eff}, is given approximately by:[21]

$$\Delta k_{eff} = \frac{7.5\ M^2}{(1 + M^2B^2)\ R^2} \left[\frac{1}{0.116 + \ln (R/2.4\ r_{eff})}\right]$$

where r_{eff} = the rod radius minus the linear extrapolation distance
M^2 = neutron migration area, cm^2

and

$$B^2 \approx [(2.4/R)^2 + (\pi/H)^2],\ cm^{-2}$$

where R and H are the radius and height, respectively, of the core.

With the approximation that the linear extrapolation distance for thermal neutrons may be computed as if all neutrons were thermal, an approximate formula for k_{eff} may be obtained from two-group neutron diffusion theory:[22]

$$k_{eff} = \frac{7.5\ M^2}{(1 + L^2B^2)\ (1 + \tau B^2)R^2}\left[0.116\left(1 + \frac{\tau}{L^2}\right) + \frac{\tau}{L^2}\ln\left(\frac{L\sqrt{\tau}}{M\ r_{eff}}\right) + \ln\left(\frac{R}{2.4\ r_{eff}}\right)\right]^{-1}$$

where $M^2 = (L^2 + \tau)$, cm^2
τ = age to thermal, cm^2
L^2 = thermal diffusion area, cm^2

In the derivation of this formula, it was assumed that the rod was transparent to neutrons in the fast group.

Adler[23] has applied one-group diffusion theory to the analysis of the variation of effectiveness of a cylindrical rod with distance from the center of the core. He has shown[24] that the critical buckling determined by two-group diffusion theory may be obtained by a modified one-group diffusion theory. For applicability of the modified one-group method, absorbing rods must be at least one diffusion length apart, and at least one diffusion length from the core-reflector interface. The variation of effectiveness of a black, cylindrical rod with distance, d, from the axis of an unreflected cylinder of radius R, is shown in Fig. 5-16. In that figure, a comparison is presented with the curve of effectiveness predicted by the weighting of the rod worth with the square of the unperturbed flux, the result of lowest order one-group perturbation theory. It may be observed that the perturbation theory approximation overestimates rod effectiveness by 10% to 25% when the rod is off center by 25% or more of the way from the center to the edge of the core.

The effect of a radial reflector on the worth of a single rod is illustrated[25] in Fig. 5-17. The change in critical buckling is shown as a function of rod position for two reactors having the same buckling in the absence of the rod, one reflected and the other unreflected radially.

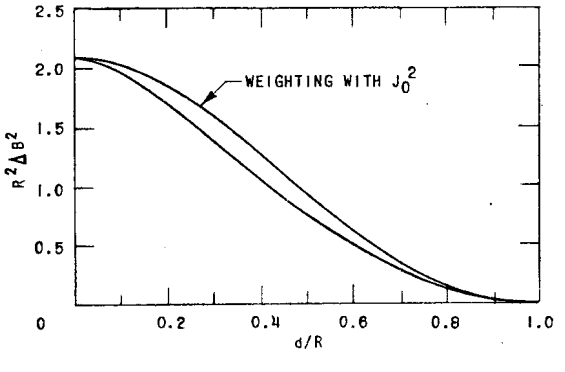

Fig. 5-16—Effectiveness of eccentric cylindrical control rod of radius r_{eff} = 0.01R. *Reproduced from Ref. 18.*

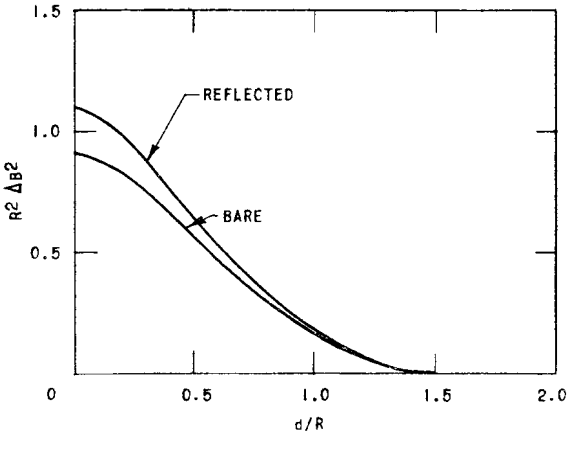

Fig. 5-17—Control rod effectiveness in bare vs. reflected reactors. *Reproduced from Ref. 25.*

The preceding paragraphs have dealt with the problem of a fully inserted cylindrical rod. The relative effectiveness of a small, black cylindrical rod in a bare reactor has been calculated[25] as a function of the fractional penetration of the rod into the reactor. In Fig. 5-18, this curve is presented for one set of rod and reactor dimensions, together with a curve based on lowest-order, one-group

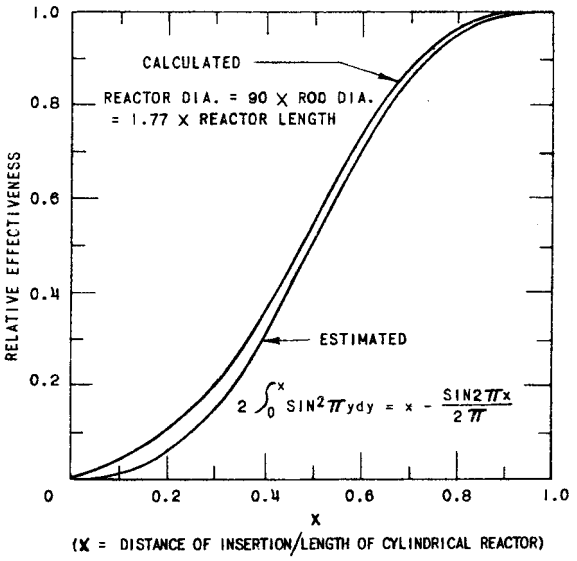

Fig. 5-18—Effectiveness of partially withdrawn axial control rod relative to effectiveness when completely inserted. *Reproduced from Ref. 25.*

perturbation theory weighting with the square of the unperturbed axial flux distribution. It may be observed that the perturbation theory curve lies below the more accurate curve along its entire length.

Schindler[26] has treated the problem of a partially inserted rod along the axis of a cylindrical reactor by determining the buckling, B^2, as the solution of the variational problem derived from the neutron flux equation $(\nabla^2 + B^2)\phi = 0$. Table 5-13 gives the results of his calculations for the ratio, Δ, of the change in buckling from the critical reactor when the rod is partially inserted, to the change when

Table 5-13—COMPARISON OF VALUES OF Δ

Data from Ref. 26.

	$R/r_{eff} = 50$		$R/r_{eff} = 75$		$R/r_{eff} = 100$		$R/r_{eff} = 125$		$50 \leq R/r_{eff} \leq 150$	
x	Δ_1(calc)	Δ_2(calc)	Δ_1(calc)	Δ_2(calc)	Δ_1(calc)	Δ_2(calc)	Δ_1(calc)	Δ_2(calc)	Δ_1(appr)	Δ_2(appr)
0	0.0000	0.0000	0.0000	0.0000	0.0000	0.0000	0.0000	0.0000	0.0000	0.0000
1/4	0.0892	0.1095	0.0912	0.1095	0.0938	0.1108	0.0940	0.1108	0.0908	0.1104
1/3	0.1922	—	0.1962	—	0.2022	—	0.2016	—	0.1955	—
1/2	0.4946	0.5561	0.5010	0.5552	0.5099	0.5581	0.5100	0.5566	0.5000	0.5556
2/3	0.8011	—	0.8050	—	0.8109	—	0.8104	—	0.8045	—
3/4	0.9073	0.9271	0.9093	0.9312	0.9125	0.9276	0.9124	0.9269	0.9092	0.9288
1	1.0000	1.0000	1.0000	1.0000	1.0000	1.0000	1.0000	1.0000	1.0000	1.0000

the rod is fully inserted. Thus Δ corresponds to the relative effectiveness used in Fig. 5-18; Δ_1(calc) and Δ_2(calc) are first and second approximations to Δ, while Δ_1(appr) and Δ_2(appr) are given by the following approximate formulae for Δ_1(calc) and Δ_2(calc):

$$\Delta_1(\text{appr}) = x - \frac{1}{2\pi} \sin 2\pi x$$

$$\Delta_2(\text{appr}) = x - \frac{1}{2\pi} \sin 2\pi x + \frac{1}{18} \sin^3 \pi x$$

It is seen that Δ_1(appr) is the same as the perturbation theory result mentioned in connection with Fig. 5-18. The approximation for Δ_2 is accurate to less than 0.5% for $50 \leq (R/r_{eff}) \leq 150$ for any reactor height and represents closely the calculated results of Murray given in Fig. 5-18.

A curve similar to Fig. 5-18 has been obtained by one-group, two-dimensional calculations on an IBM-704 using the CURE code.[27] The rod radius was varied over a range up to 20% of the bare core radius. In Fig. 5-19, the fractional reactivity change as a function of the rod penetration is plotted for various rod radii. The curve is almost independent of rod radius over the range examined.

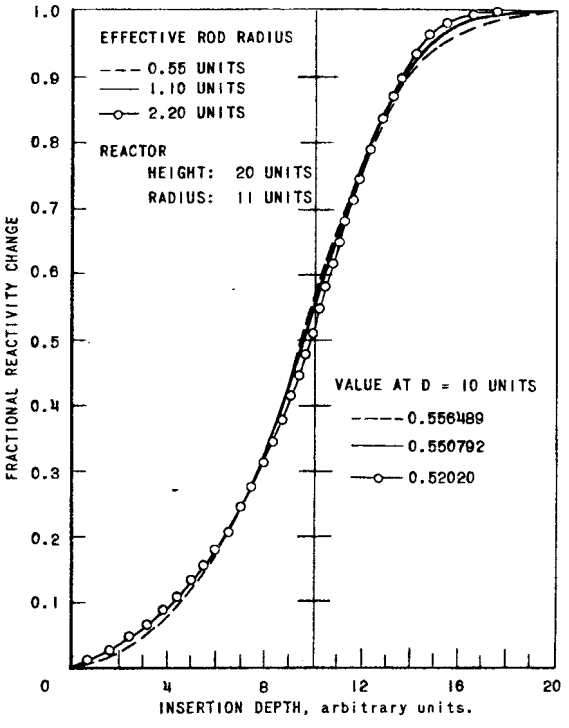

Fig. 5-19 — Fractional reactivity change as a function of rod radius and depth of insertion. *Reproduced from Ref. 27.*

These computations were extended to rod radii as large as 50% of the bare core radius.[28] The fractional change in critical buckling required when the rod is inserted halfway is plotted in Fig. 5-20 as a function of R/r_{eff}. For $R/r_{eff} < 5$, the drop is very sharp.

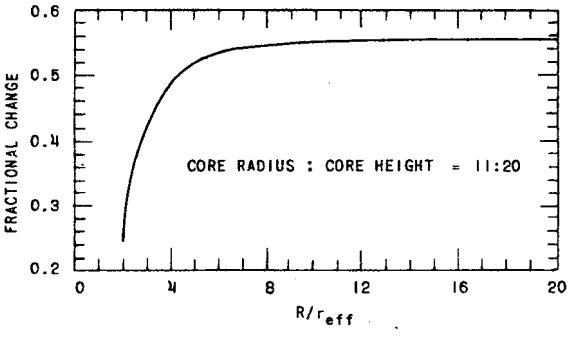

Fig. 5-20 — Dependence of fractional change in critical buckling on ratio of radius of core to radius of central black control rod inserted halfway. *Reproduced from Ref. 28.*

5.1.5 INTERACTION EFFECTS OF CONTROL RODS

The methods discussed in this section have been devised to describe the effect of discrete control regions in an otherwise uniform medium. Another method, based on the small-source, small-sink analysis, is described in Section 5.1.7.

It is well known that the reactivity effect of a set of closely spaced, black control rods fully inserted into a reactor is smaller than the sum of the worths of the individual rods. This result may be ascribed to what is generally known as the "shadowing" of each control rod by the other rods, or the "interference" between rods, i.e., the flux depression in the neighborhood of a rod is enhanced by the presence of nearby rods. Beyond certain separation distances, however, the combined rod effectiveness may exceed the sum of the isolated parts. This occurs because the flux depression in the vicinity of each rod is countered partially by the rise in flux outside the region of influence of the other rods.

Interaction of Plane Control Sheets in a Slab Reactor. Several papers[29–31] treat the effectiveness of a number of plane control sheets in a reactor. Wolfe[30] sets up the problem in a general way for N arbitrarily spaced sheets by using matrix multiplication methods to find the critical determinant. If the sheet spacing is large compared with the smaller of L and $\sqrt{\tau}$, approximations can be made to simplify the algebra involved. The cases of equally spaced sheets throughout the core, or an arbitrary number of equally spaced sheets anywhere in the core, are considered in detail using the approximations referred to above. Wilf[32] has simplified the critical equation by Wolfe for the case of N equally spaced sheets. McWhorter, Russell and Wolfe[31] apply the work of Wolfe to a detailed discussion of three special cases involving thermally black control sheets: (a) a single control sheet at the midplane of a slab reactor; (b) an infinite reactor containing an array of equally spaced control sheets; and, (c) two symmetrically placed control sheets in a slab reactor. Various conclusions are reached on the effectiveness of the sheets depending on the relative values of τ, L^2, and the distance between sheets.

Generalizations of the Nordheim-Scalettar Method[33] for Cylindrical Rods. A commonly used method is the Nordheim-Scalettar[33] scheme of two-group diffusion theory. In this method, the flux is written as a linear combination of regular solutions of the wave equation and of irregular terms with singularities at the positions of the control rods. Either a linear extrapolation distance or a logarithmic derivative condition is employed for the thermal flux at the surface of the thermally black rod. In various versions or modifications of the Nordheim-Scalettar method[34–43] the two-group fast flux is assumed to be finite at the center of the rod, or to vary in the neighborhood of the rod in a manner described by a fast linear extrapolation distance. The original Nordheim-Scalettar (N-S) condition[33] is that the fast flux is finite at the center of the rod. For large control rods and for reactors where the ratio of fast to thermal flux is large, the N-S condition implies that the gradient of fast neutrons at the rod surface is appreciable and, therefore, perhaps a poor approximation to the physical situation.[39] For example, in the SPERT-I reactor the central control blade was shown experimentally to be worth 3.4% in the reflected reactor.[38] The application of the original N-S condition to the computation of an equivalent-round rod in an equivalent bare reactor yielded 6.9%. This disagreement is attributed primarily to the use of the N-S condition. The use of a boundary condition, reported variously in its essential import as "Codd-Rennie,"[36–39,44] (C-R), or "Murray-Niestlie Hollow-Shell,"[44–46] namely, that the fast current into the rod is zero, led to a value of 3.2% in the reflected core and in the equivalent-bare core.

A further modification of the fast flux boundary condition which is applicable to moderator-filled control rods has been made by Perry,[39] and Murray and Niestlie[45] (M-N). The method consists of diffusion theory calculation of a moderator-filled centrally-positioned, round rod in the reactor. The regular solution $I_0(\kappa r)$ of the wave equation is used in conjunction with the usual diffusion theory boundary conditions for the fast group: continuity of flux and of current at the rod boundary, r = a. The fast extrapolation distance is defined by:

$$d_1 = \frac{D_{core}\, I_0(\kappa a)}{D_{rod}\, \kappa I_1(\kappa a)}$$

where D_{core}, D_{rod} are, respectively, the fast diffusion coefficients outside and inside the rod, and:

$$\kappa^2 = \frac{1}{\tau} + \frac{(\pi)^2}{H}$$

τ = age to thermal in the rod material

H = extrapolated height of the reactor core

A generalization[47] of the Nordheim-Scalettar analysis to a two-group diffusion theory of a ring of uniformly spaced cylindrical rods in an otherwise homogeneous reactor may be applied to gray rods, to rods containing a fissionable material, etc. In this treatment, diffusion theory is considered to be applicable both inside and outside the rods.

Adler[23] has reduced the two-group Nordheim-Scalettar calculation to an equivalent one-group calculation. This one-group method was applied to the computation of the worth of rods in a bare reactor. In Fig. 5-21, a comparison is shown between the reactivity effect per rod in a four-rod ring, and the effect of an isolated rod at that distance. Figure 5-22 shows the effect of a reflector on the worth of the ring of four rods; the comparison is made between a reflected and an equivalent bare reactor.

Simplifications[34–43] of the critical determinants are possible if the control rods are distributed uniformly in rings, with the center at the radial axis of a cylindrical core.

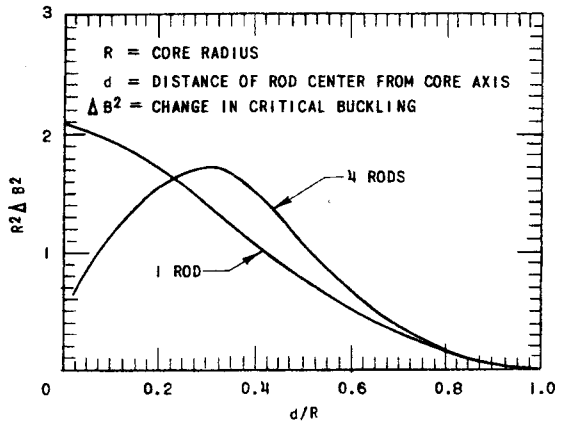

Fig. 5-21 — Comparison between the effect per control rod of a ring of four rods and that of a single eccentric rod at the same distance from the center of a bare system. *Reproduced from Ref. 23.*

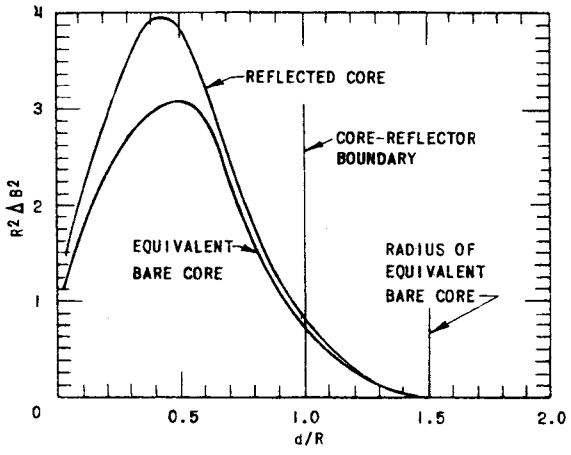

Fig. 5-22 — Comparison of the effect of a ring of four rods in bare and in reflected systems having the same critical buckling if no rods are present. Radius of control rod = 0.01R. *Reproduced from Ref. 23.*

Murray[35] has reported results of two-group diffusion theory investigations of multiple control rod configurations in bare cylindrical reactors. For a ring of M symmetrically spaced, round rods concentric with the core axis, the critical buckling, μ^2, is given by the formula:

$$\psi(\mu R) = \psi(\mu a)$$

where

$$\psi(\mu R) \approx \left[M \sum_{k=-\infty}^{\infty} \frac{J_{Mk}^2(\mu d)\, Y_{Mk}(\mu R)}{J_{Mk}(\mu R)} - \sum_{m=2}^{M} Y_0(\mu r_{1m}) \right]^{-1}$$

$$\psi(\mu a) \approx \frac{a_1 a_2 - a_3 a_4}{a_5 a_2 - a_3 a_6}$$

and

$$a_1 = \frac{J_0(\mu a)}{d_1} - J_0'(\mu a) \qquad a_4 = S_1\left[\frac{J_0(\mu a)}{d_2} - J_0'(\mu a)\right]$$

$$a_2 = S_2\left[\frac{K_0(\nu a)}{d_2} - K_0'(\nu a)\right] \qquad a_5 = \frac{Y_0(\mu a)}{d_1} - Y_0'(\mu a)$$

$$a_3 = \frac{K_0(\nu a)}{d_1} - K_0'(\nu a) \qquad a_6 = S_1\left[\frac{Y_0(\mu a)}{d_2} - Y_0'(\mu a)\right]$$

In these formulae:

d = radius of locus of centers of the rods, cm
r_{1m} = distance from center of rod No. 1 to center of rod No. m
R = core radius, cm
a = rod radius, cm
d_1, d_2 are the fast and thermal linear extrapolation distances at the rod
μ^2, ν^2 are the usual bucklings of the two-group diffusion theory
S_1, S_2 are the ratios of fast to thermal flux in the two components of those fluxes (cf. Kurath and Spinrad)[48]

The prime symbol represents differentiation with respect to a.

Murray has reported on comparisons of theory with experiment. A control rod of radius 1.74 cm, located 12.75 cm from the axis of the BSF (Bulk Shielding Facility) reactor at ORNL, was found to be

worth 1.37%, in comparison with ~1.38% determined by measurement. The calculation was performed on an equivalent bare core. A calculation which included the effect of a reflector gave a value of ~1.5%. The latter calculation predicted that a fuel mass of 52 gm U^{235} would compensate for the reactivity loss engendered in a fully inserted rod $\frac{5}{8}$-in. off center in the Raleigh Research Reactor. The experimental value was 57 gm.

Using only the terms where k = 0 in the formula for $\psi(\mu R)$, the critical equation reduces to:

$$\frac{J_0(\mu R)}{Y_0(\mu R)} \approx \frac{M\psi(\mu a)}{1 + I\psi(\mu a)} \cdot J_0^2(\mu d)$$

where

$$I = \sum_{m=2}^{M} Y_0(\mu r_{1m})$$

Using the approximate critical equation, the reactivity values of 1, 2, 3, 4, and 5 rods were computed for the equivalent bare BSF core. The results are presented in Fig. 5-23. In Fig. 5-24, the reactivity effect of a ring of two diametrically opposite rods is shown as a function of the distance of the ring of centers from the core axis.

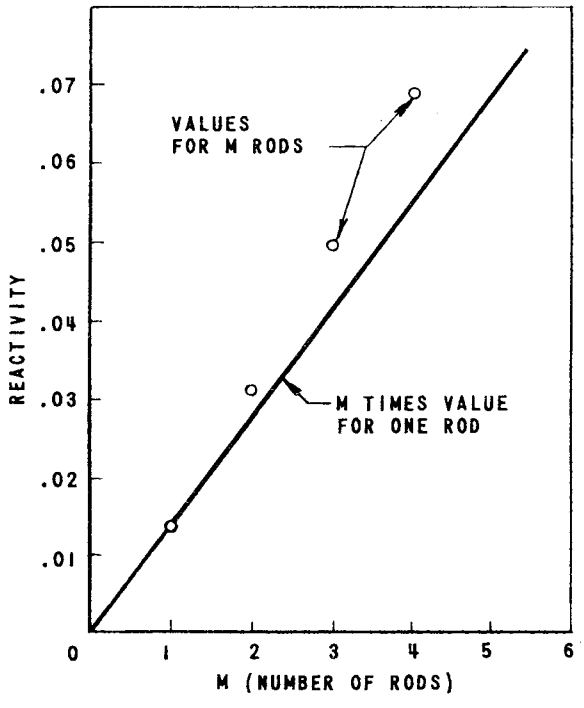

Fig. 5-23 — Reactivity vs. number of cylindrical rods. *Reproduced from Ref. 35.*

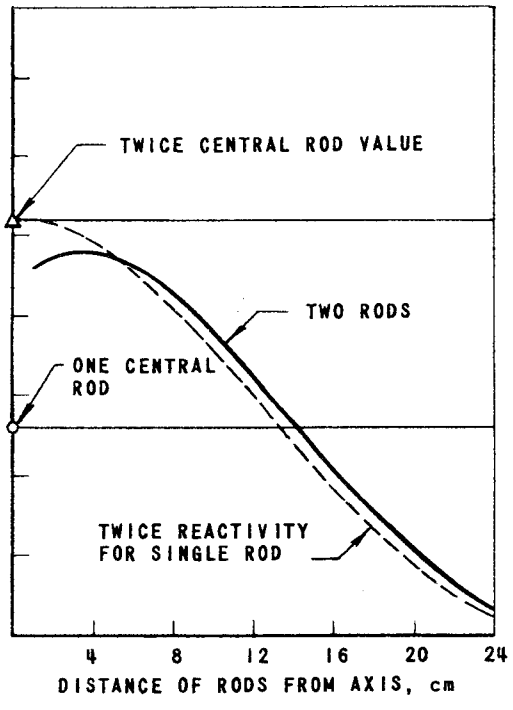

Fig. 5-24 — Interaction of two cylindrical control rods. *Reproduced from Ref. 35.*

The interaction effects of five water-filled, black annuli in the APPR are described[39] in Table 5-14. The control system consists of a ring of four rods around a central rod. For each rod configuration, criticality was attained experimentally by varying the number of boron-containing plates, and separately, by varying the fuel loading. In Table 5-14, calculated results obtained by the various (N-S, C-R, M-N) fast flux boundary conditions are compared with experiment. In the table, $W = k_{eff} - 1$, the excess k held down by the rod configuration indicated; $\sum_i W_i$ is the sum of the values of the individual rods in the combination, taken separately. It may be noted that the (M-N) boundary condition, which is the most applicable from physical considerations, agrees better with experiment than the (N-S) or (C-R) boundary conditions.

Murray, Price and Birken[40] have developed two-group diffusion theory formulae to calculate the critical buckling of several control rod configurations in bare cylindrical reactors, and have extended their work to reactors reflected radially. Variational methods have been employed by Gyftopoulos and

Table 5-14—COMPARISON OF CALCULATED AND EXPERIMENTAL ROD VALUES IN APPR

Reproduced from Ref. 39.

Configuration[a]	Calculated Worth		Experimental Worth				Calculation Method
			Uniform Poison		Fuel Addition		
	W	$W/\Sigma_i W_i$	W	$W/\Sigma_i W_i$	W	$W/\Sigma_i W_i$	
X	0.026	—	0.027	—	0.026	—	M-N
0	0.058	—	0.063	—	0.059	—	M-N
0	0.122	—	—	—	—	—	N-S
0	0.026	—	—	—	—	—	C-R
X + 0	0.099	1.18	0.089	0.99	0.085	1.00	M-N
2X	0.068	1.26	—	—	—	—	M-N
2X + 0	0.147	1.31	—	—	—	—	M-N
3X	0.118[b]	1.51	—	—	—	—	M-N
3X + 0	0.188[b]	1.38	0.166	1.15	—	—	M-N
4X	0.171	1.64	0.173	1.60	—	—	M-N
4X + 0	0.241	1.49	0.229	1.34	—	—	M-N

[a]X signifies an off-center rod position; 0 signifies the central rod position; all rods are fully inserted.

[b]In the calculation, the three off-center rods are located at the corners of an equilateral triangle.

de Sobrino[41] to calculate the reactivity worth of an eccentric control rod, or a ring of control rods, in a cylindrical reactor using both one- and two-group theory.

Partitioning of Reactor Core into Control Cells. A method of control analysis used frequently in reactor design is to partition the reactor core into an integral number of smaller units, one unit associated with each control rod. Each unit is treated as a cell in an infinite lattice, and the cell boundary conditions on flux and current appropriate to the configuration are applied. In general, this method works best when the number of control cells is large. In each cell, the approximation is made that the actual absorbing rod may be replaced by a round rod or by some other shape which is amenable to calculation.

Henry[49] has reported on a simplified analysis for cross rods from which is obtained the ratio $[\Sigma_p/(\Sigma + \Sigma_p)]$, where Σ_p is the homogeneous poison cross section equivalent in control worth to the actual rod; and Σ is the average macroscopic absorption cross section in the cell medium outside of the rod. Thus $\Sigma_p/(\Sigma + \Sigma_p)$ is essentially the reactivity held down by the control rod. Let the diagram represent a quarter-section of the control cell.

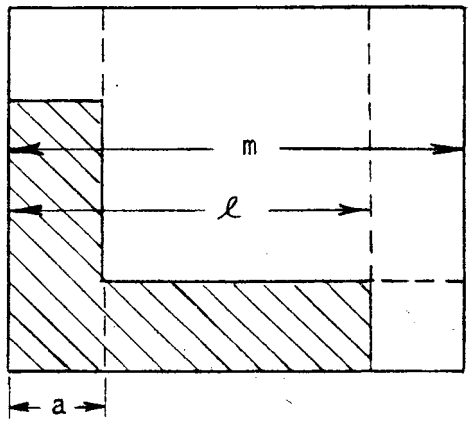

Then treating each arm of the cross as an infinite black slab of half-thickness a, in a slab cell of half-thickness m, a cell computation yields the neutron current into the rod:

$$\frac{q}{h\,\Sigma + (1/L)\coth\left[(m-a)/L\right]}$$

Then it is assumed that

$$\frac{\Sigma_p}{\Sigma + \Sigma_p} = \frac{1}{q}\left[\frac{\text{total exposed perimeter of rod}}{\text{total area of source region}}\right]\frac{q}{h\,\Sigma + (1/L)\coth\left[(m-a)/L\right]}$$

or

$$\left(\frac{\Sigma_p}{\Sigma + \Sigma_p} = \frac{2\ell}{m^2 - 2a\ell' + a^2}\right)\left[h\,\Sigma + \frac{1}{L}\coth\left(\frac{m-a}{L}\right)\right]^{-1}$$

where q = source density, neutrons/(cm^2)(sec), assumed to be constant in the region outside the rod, and to be zero inside the rod

L = diffusion length of the medium outside the rod

h = linear extrapolation distance into the rod/D (for a black slab, h = 3 × 0.7104)

and the other terms are defined in the diagram. The diffusion length is assumed to be given by:

$$L = \sqrt{D/\Sigma}$$

where D is the diffusion coefficient in the medium.

In Table 5-15 a comparison is presented between Σ_p's calculated by this method and also by two-dimensional calculations on a digital computer. It was assumed that the rods were black, with a value h = 2.13.

Table 5-15—VALUES OF Σ_p CORRESPONDING TO VARIOUS CROSS-SHAPED RODS IN VARIOUS SQUARE CELLS

Reproduced from Ref. 49.

Cell Width (2m), cm:	20.16	20.16	20.16	21.36	21.36	21.36	21.36	19.05	19.05
Square of Thermal Diffusion Length of Medium (L^2), cm^2:	1.544	1.544	1.544	2.515	2.881	4.567	5.315	6.337	11.36
Ratio of thermal diffusion length to rod span half size (L/ℓ):	0.261	0.178	0.143	0.270	0.289	0.364	0.392	0.396	0.531
Values of equivalent poison cross section (Σ_p), cm^{-1}:									
Two-Dimensional Machine Code Solution	0.0140	0.0219	0.0293	0.0182	0.0168	0.0192	0.0179	0.0233	0.0244
Slab Cell Approximation	0.0138	0.0216	0.0293	0.0191	0.0177	0.0208	0.0193	0.0233	0.0268
$\frac{\Sigma_p\text{ (exact)} - \Sigma_p\text{ (cell method)}}{\Sigma_p\text{ (exact)}}$	0.014	0.014	0.000	−0.049	−0.054	−0.082	−0.078	−0.045	−0.098

In a more recent report by Henry,[50] the above analysis is modified slightly in that the outer edge of the cell for the infinite slab calculation is taken as one-half the distance from the surface of the control blade to the actual outer edge of the cell. This is plausible, as one-half the area of the cell supplies neutrons to each blade of the cross. As a result of this modification, coth [(m − a)/L] should be replaced by coth [(m − a)/2L] in the expression for $[\Sigma_p/(\Sigma + \Sigma_p)]$.

If the cross rod fills the cell, it may be convenient to envision the cell as a square, black annulus around the core medium. Stewart and Smith[51] have obtained an infinite series representation for the flux distribution in this square cell. The problem solved was a one-group diffusion theory cell calculation with constant source and vanishing of the thermal flux at the surface of the black boundary. The flux is given by:

$$\phi(x,y) = \sum_{\substack{n,m\geq 1\\ \text{odd}}} a_{mn}\sin\left(\frac{m\pi x}{w}\right)\sin\left(\frac{n\pi y}{w}\right)$$

where w = length of one side of the square core medium, cm

$$a_{mn} = S\left(\frac{2}{\pi}\right)^4\left(\frac{W}{L}\right)^2\frac{1}{mn}\left[m^2 + n^2 + (W/\pi L)^2\right]^{-1}$$

L = thermal diffusion length in the core medium, cm

S = neutron source strength per unit volume, divided by the macroscopic absorption cross section of the core medium

Defining C* to be the fraction of all neutrons absorbed by the rod,

$$C^* = 1 - \frac{64}{\pi^4}\,\nu^2\,f(\nu)$$

where

$$\nu = \frac{\kappa W}{\pi};\ \kappa = \frac{1}{L};\ f(\nu) = \sum_{\substack{m,n\geq 1\\ \text{odd}}} \frac{1}{m^2 n^2}\cdot\frac{1}{m^2 + n^2 + \nu^2}$$

For large ν:

$$f(\nu) = \frac{\pi^4}{64\,\nu^2}\left[1 - \frac{4}{\pi\nu} + \frac{16}{\pi^3\nu^2}\right] + 0\,[\exp\,(-\pi\nu)]$$

For small ν:

$$f(\nu) = \frac{1}{\nu^2 + 2} + 0.0282 - 0.0024\,\nu^2 + 0.0002\,\nu^4 + 0(\nu^6)$$

It is of interest to determine the size of a cylindrical cell, bounded by black material, which is equivalent to the square cell in the sense that

$$C^*\ (\text{circle}) = C^*\ (\text{square})$$

where

$$C^*\ (\text{circle}) = \frac{2I_1(\kappa r)}{\kappa r\ I_0(\kappa r)}$$

Applying the same boundary condition, vanishing of the flux at the outer boundary, leads to the equivalence relationship described in Fig. 5-25 between $\nu_s \equiv (\kappa w)/\pi$ and $\nu_c \equiv (\kappa r)/\pi$, where r = radius of the

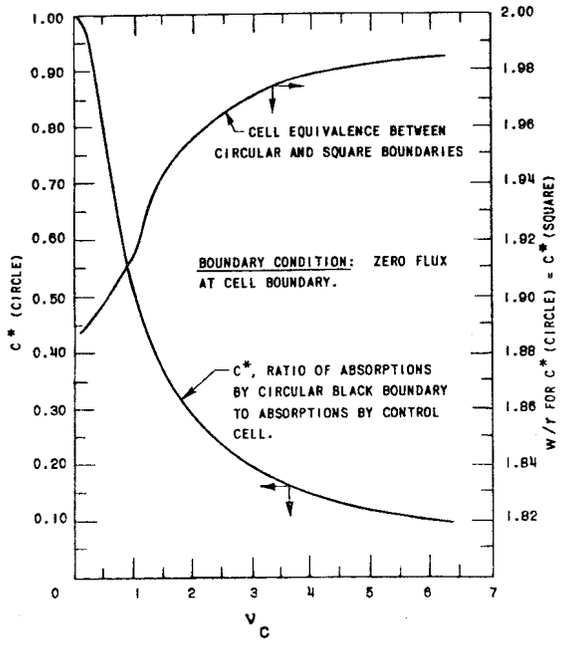

Fig. 5-25—One-group diffusion theory calculations of rod worth.

circle. The inscribed circle provides a very good approximation to equivalence even for relatively small values of ν_c. This may be compared with the assumption frequently made that the equivalent circle has approximately the same geometric area as the square. In the case of equal area, $(\nu_s/\nu_c) = 1.77$, whereas actually $\nu_s/\nu_c = 2$ in the limit as $\nu_c \to \infty$.

There is a relation between this work and the Absorption Area Method discussed in Section 5.1.3 for small values of L. For small L, the value of C* is 4L/W if the approximation:

$$f(\nu) = (\pi^2/64\ \nu^2)(1 - 4/\pi\nu)$$

is used. The value of C in the Absorption Area Method for small L is approximately L times the perimeter, or 4LW for the case discussed here. Inspection shows the definitions of C and C* differ by a factor of W^2; therefore, the results of the two methods are in agreement.

Carlvik, McCririck, and Brimberg[43] have compared the results of a cell-type calculation and a Nordheim-Scalettar-type calculation for a bare, cylindrical, heavy-water, natural uranium reactor having (1) a ring of four control rods, or (2) a ring of four rods plus a ring of eight rods with the twelve rods forming a square lattice. The results of the calculations are shown in Fig. 5-26. It is seen that agreement is better for the 12-rod case than for the 4-rod case, as might be expected, since a cell-type calculation should work better when the number of rods is large.

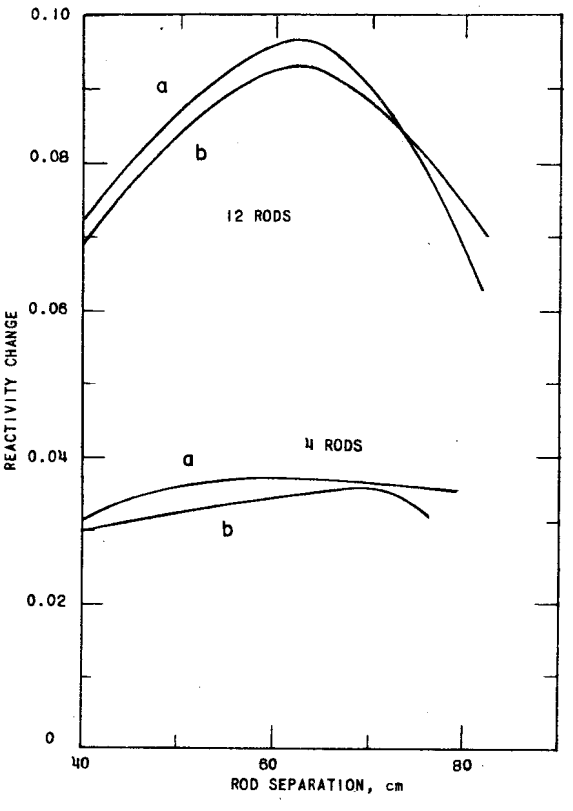

Fig. 5-26 — Variation of reactivity with rod separation. A comparison between (a) the cell method, and (b) the Nordheim-Scalettar method. *Reproduced from Ref. 43.*

5.1.6 MULTIGROUP CONTROL ROD CALCULATIONS

Multigroup diffusion techniques have been applied to control rod calculations to obtain a more realistic representation of the problem than is possible in the one-group description.

Stevens[52] has extended the absorption-area concept (Section 5.1.3) to control rods that are not black and have epithermal as well as thermal absorption. It is assumed that the slowing-down age is much larger than the square of the thermal diffusion length. For slab geometries, the thermal absorption area for the case where epithermal absorption is neglected is given by the small L formulae of Hurwitz and Roe except that L is replaced by L′ = LF. The quantity F is given by F = 1/(1 + d/L) where the extrapolation distance, d, may be written as

$$d = \frac{2}{3}\lambda\frac{(1 + T)}{(1 - T)}$$

687863 O - 63 - 26

In this expression, $\lambda/3$ is the thermal diffusion coefficient in the external medium, and T is the transmission probability of the control slab. The transmission probability of the slab can be expressed as

$$T = 1 - 2\Sigma ft = 1 - 2f\xi$$

where Σ is the macroscopic absorption cross section of the slab; t is its thickness; and the transport theory expression for the self-shielding factor is

$$f = \frac{1}{2\xi}\left[1 - 2\,E_3(\xi)\right] = \frac{1}{2\xi}\left[1 - e^{-\xi} + \xi e^{-\xi} - \xi^2 \int_{\xi}^{\infty} \frac{e^{-u}}{u}\,du\right]$$

Similar results are obtained for cylinders and spheres of radius r. The modified absorption areas are:

Cylinder: $C = (2\pi Lr)/\{[K_0(r/L)/K_1(r/L)] + \Delta/L\}$

Sphere: $C = (4\pi r^2 L)/[r/(r + L) + (\Delta/L)]$

where $\Delta = \lambda\left[\frac{\Delta'}{\lambda} + \frac{1 - 2f\xi}{2f\xi}\right]$

and $\xi = \Sigma r$ for a cylinder, and $\xi = 2\Sigma r/3$ for a sphere.

The self-shielding factors for cylinders and spheres are:

Cylinder: $f = \frac{1}{2\xi}\left(1 - \frac{3}{16\xi^2} - \frac{15}{128\xi^4} - \frac{575}{4096\xi^6} \cdots\right)$

Sphere: $f = \frac{2}{9\xi^3}\left[\frac{9\xi^2}{4} - \frac{1}{2} + e^{-3\xi}\left(\frac{1}{2} + \frac{3}{2}\,\xi\right)\right]$

Formulae of Δ'/λ are:

Cylinder: $\Delta'/\lambda = 0.7104 + 0.5047\,\lambda/2r$

Sphere: $\Delta'/\lambda = 0.7104 + 0.5047\,\lambda/r$

When both thermal and epithermal absorption are considered, diffusion equations are written for both groups with a constant source in the epithermal group from slowing down of fast neutrons. These equations yield absorption areas for both thermal and epithermal groups. Formulae for slab control rods are given by Stevens.[52] The use of these absorption areas in conjunction with three-group theory for a core with uniformly distributed control cells, yields a value of k_{eff}:

$$k_{eff} = \frac{\nu\left[f_2 \frac{\Sigma_{f2}}{\Sigma_{s1,2}} + \frac{f_2 f_3}{1 + L_3^2 B^2}\frac{\Sigma_{f3}}{\Sigma_{a3}}\right]}{(1 + L_1^2 B^2)(1 + L_2^2 B^2)\left(1 + \frac{\Sigma_{a2}}{\Sigma_{s1,2}}\right)}$$

where subscripts 1, 2, 3, denote fast, epithermal, and thermal groups, respectively. In this expression, ν is the number of fast neutrons produced per fission; L_1^2, L_2^2, and L_3^2 are the migration areas of the three groups; $\Sigma_{s1,2}$ is the slowing-down cross section from group 2; Σ_{a2} and Σ_{a3} are absorption cross sections; Σ_{f2} and Σ_{f3} are the corresponding fission cross sections; B^2 is the buckling; and f_2 and f_3 are defined by:

$$f_i = (A_c - A_i)/A_c$$

where A_c is the cell area, and A_i is the absorption area of group i.

The results for computations of single cross rod (1.88 in. half-width) experiments conducted in the Flexible Plastic Reactor (FPR) are tabulated below. The heading "1-Group" refers to thermal absorption only, while "2-Group" refers to both thermal and epithermal absorption. In the case of hafnium, which has significant epithermal absorption, the two-group approach gives much better agreement with experiment than does the one-group calculation.

Absorber Sample	Reactivity Change, dollar		
	Experiment	1-Group	2-Group
B-Al (0.05 gm B/cm^2)	0.994 ± 0.015	1.008	1.027
Cd (0.027 in. thick)	0.956 ± 0.015	1.076	1.023
Hf (0.100 in. thick)	1.396 ± 0.022	0.901	1.452
Hf (0.200 in. thick)	1.710 ± 0.028	1.024	1.726

A similar comparison between experiment and calculations with control rod absorptions in two groups for single, long, thin slabs (1.8 in. wide by $15\frac{1}{32}$ in. long) in the Advanced Test Reactor (ATR), is given below. Since the absorber worth depends upon the test location, only the relative experimental measurements have interpretative values. The calculated and measured values were arbitrarily normalized for the 0.205-in. thick hafnium sample.

Absorber Sample	Reactivity Change, dollar	
	Experiment	2-Group
Cd (0.125 in. thick)	0.326	0.311
Hf (0.050 in. thick)	0.285	0.271
Hf (0.103 in. thick)	0.380	0.369
Hf (0.205 in. thick)	0.470	0.470 (normalized)
7% B-SS (0.205 in. thick)	0.252	0.221

Greebler,[53] Pearlstein,[54] and Deutsch[55] have also applied absorption area theory to non-black rods with epithermal and thermal absorption.

Wolfe[56] extends the absorption area concept by writing the absorption area for a control element black to any number of groups, in terms of a linear combination of the Hurwitz-Roe one-group absorption areas calculated as a function of the migration length of each group. The linear combination is chosen to take into account the different importances of the various groups. In a later paper,[57] the work is extended to non-black control elements.

Wolfe and Fischer[58] have used two-group perturbation theory to determine the reactivity change produced by a thermally black control element inserted in a reactor. The expression derived involves the Hurwitz-Roe absorption area. They extend their work[59] to second-order perturbation theory and compare results of the perturbation calculations to exact two-group calculations for a cylindrical rod on the axis of a bare, cylindrical reactor. The second-order perturbation theory results agree well with the exact calculations for the entire range of rod radii considered.

Tonks[29] has made a study of control slabs in a reactor which establishes a sounder theoretical basis for the "absorption area" concept and provides correction terms.

The control-cell method described in Section 5.1.5 has been extended by Henry[50] to include epithermal absorption. Two-group diffusion theory with a constant source in the higher energy group is used. The expression for the epithermal poison cross section is of the same form as that derived for the thermal cross section, except for appropriate substitutions. The thermal constants are replaced by the corresponding epithermal constants and the thermal absorption cross section is replaced by the epithermal total removal cross section. For the thermal group, the poison cross section is given by:

$$\frac{\Sigma_{p2}}{\Sigma_{p2}+\Sigma_2} = \frac{2\ell}{m^2 - 2a\ell + a^2}\frac{\left(1-\frac{\Sigma_{p1}}{\Sigma_1}\Delta\right)}{\left[h_2\,\Sigma_2 + \frac{1}{L_2}\coth\left(\frac{m-a}{2L_2}\right)\right]}$$

where

$$\Delta = \frac{m^2 - 2a\ell + a^2}{2\ell}\cdot\frac{1}{L_1^2 - L_2^2}\left[L_1\coth\left(\frac{m-a}{2L_1}\right) - L_2\coth\left(\frac{m-a}{2L_2}\right)\right] - 1$$

the subscripts 1 refer to the epithermal group, and subscripts 2 refer to the thermal group. The quantity Σ_1 is the total removal cross section from the epithermal group. The other notation is the same as in Section 5.1.5.

There is a close relationship between the Absorption Area Method for cross rods and the Cell Method of Henry. Both the thermal and epithermal currents into the rods will be the same in the two

methods provided: (1) the corner effects are neglected in the absorption area method; and (2) the thickness of the rod and the deviation of the coth terms from unity are neglected in the method of Henry.

Voorhis and Ryan[60] and Voorhis, et al.,[61] have examined the effect of absorbing membranes of cadmium and gold[60,61] and boron-polyethylene[61] which bisected a highly enriched slab core. A "thin region" procedure is described whereby the membranes are replaced by fictitious diffusion regions whose net effect on the surrounding core is the same as the actual membrane. This method is outlined as follows. The solution to the transport equation for an absorbing slab is combined with a P_1 approximation outside the slab and the appropriate boundary conditions to yield the equations:

$$\alpha(u) = \frac{j^+ + j^-}{\phi^+ + \phi^-} = \frac{1 - 2E_3(z)}{2[1 + 3E_4(z)]}$$

and

$$\beta(u) = \frac{j^+ - j^-}{\phi^+ - \phi^-} = \frac{1 + 2E_3(z)}{2[1 - 3E_4(z)]}$$

where u is the lethargy; j^+ and j^- are the net currents *into* the rod on either side of it; ϕ^+ and ϕ^- are the corresponding fluxes; and $z = 2\Sigma_a(u)t$, where $\Sigma_a(u)$ is the absorption cross section of the slab for lethargy u, and t is its half-thickness. The expression for α is in agreement with the expression for the linear extrapolation distance into a purely absorbing, gray slab given in Section 5.1.1. Combination of these expressions for α and β with diffusion theory expressions for flux and current inside the slab yields the equations:

$$\Sigma_a = \frac{\sqrt{<\alpha><\beta>}}{2t} \ln\left(\frac{1 + \sqrt{<\alpha>/<\beta>}}{1 - \sqrt{<\alpha>/<\beta>}}\right)$$

and

$$D\Sigma_a = <\alpha><\beta>$$

which can be solved for the effective D and Σ_a of the slab. The notation $<\alpha>$ and $<\beta>$ is used to signify that α and β are to be averaged over the energy group in question. Details of the averaging process are given in Ref. 50.

After the diffusion theory group constants for the fictitious diffusion region are determined, one-dimensional, 2- or 4-group diffusion calculations are performed in the direction normal to the membrane. In the calculation, the core, reflector (water), and thin fictitious region are taken as separate diffusing media. The transverse leakage is accounted for in the calculation by increasing the group absorption by the term $D_i B_T^2$, where D_i is the *ith* group diffusion constant, and B_T^2 is the transverse buckling.

The diffusion calculations were compared with experiment in two ways. The first determined how closely the critical size of each assembly could be predicted; the second compared experimental activation traverses through each assembly with computed neutron fluxes. Good agreement was obtained in the latter case when the activation data were arbitrarily normalized to the calculated flux plot near the core-water boundary. Table 5-16 compares selected experimental and calculated values for k_{eff} for cores of various dimensions with various membranes. The experimental values of k_{eff} are not exactly unity because control rods were not completely withdrawn, and the values quoted represent extrapolation to completely withdrawn rods. It is seen that there is good agreement between experimental and 4-group calculated values of k_{eff}.

Comparisons of "thin region" and "absorption area" calculations have been made by French and Ruane[62] for the Plastic Moderated Critical Assembly (PMA-3A). In the "thin region" calculations, effective diffusion constants are calculated for the rod in a manner similar to that described above.[50,60,61] The case studied was an annular core with eight boral cross rods, and the calculations were performed using 3-group diffusion theory with the aid of the two-dimensional CURE code. The values determined by the two methods were in good agreement and were within 1.4% Δk of experiment.

Age-diffusion theory has been used by Uberall[63] to study the effect of a slab control rod at the center of a reactor. The age-diffusion treatment gives a more detailed picture of epithermal control rod absorption since it considers the energy dependence of quantities, such as neutron flux and current, which are represented only by average values in two-group theory. Uberall compares the epithermal absorption with that calculated by two-group theory and concludes that two-group theory overestimates epithermal absorption by about 10%.

Table 5-16—COMPARISON OF EXPERIMENTAL AND THEORETICAL REACTIVITY

Selected data from Ref. 61.

Absorbing Membrane	Experimental k_{eff} with Membrane	Calculated k_{eff} With Membrane,		Calculated k_{eff} Without Membrane, 4-Group	Calculated Worth Δk_{eff} of Membrane, 4-Group
		4-Group	2-Group		
20-mil Cd	1.002	1.013	1.022	1.157	0.144
10-mil Au	1.000	1.008	1.024	1.073	0.065
30-mil Au	1.001	1.011	1.023	1.132	0.121
50-mil Au	1.000	1.018	1.025	1.160	0.142
Boron	1.001	1.016	1.031	1.043	0.027
None	1.001	1.005	1.026	—	—

The treatment of control rods given so far in this section has not considered the effects of water channels. In a heterogeneous water reactor, the removal of a control rod creates a water channel which produces a peaking of the thermal flux. Even when the control rod is inserted, the channel may be wide enough so that an extrapolation distance calculated by treating the surrounding core as a homogeneous medium may not be quite accurate. Little has been published on the effects of water channels. In his thesis, Jackson[64] reports experiments and calculations to determine the reactivity effects of a thin-walled Al cylinder (0.875″ ID) left void or filled with water, or with water plus boric acid. The cylinder was inserted along the axis of the Raleigh Reactor which is homogeneous and water moderated. Calculations were performed using a one-group, two-region, diffusion theory, or a two-group one-region theory in which fast and thermal extrapolation distances were used at the rod boundary. The values calculated for the reactivity difference between water and boric acid rods or water and void were less than values determined by experiment.

Dannels and Eich[65] performed a water-slot experiment to study the peaking in a water channel produced by omitting the center row of fuel rods in a Yankee reactor core. Calculations were made using slab geometry with a water slot of width equal to the pitch of the square lattice, and a homogenized fuel region; different numbers of groups (2 or 4); different sets of fast and thermal constants; and both WANDA (diffusion theory) and SNG (S4 transport theory) codes. Fast constants were calculated by hand or by the MUFT 4 code. Thermal constants were taken to be Maxwellian, or calculated with the SOFOCATE code which uses the Wigner-Wilkins free-gas theory (Section 3.1.2). References to all of the codes are given in Section 10.

Results of the calculations are given in Table 5-17. In this table, $\overline{P}_{rod}$ is the average of the fission density values obtained at each edge of a slab which is adjacent to the water slot and whose width

Table 5-17—WATER SLOT EXPERIMENT

Power Peaking Factors Obtained by Various Calculational Methods in Slab Geometry

Reproduced from Ref. 65.

Input Description				No. of Groups	Code	$\frac{\overline{P}_{rod}}{\overline{P}_0}$
Water		Fuel				
Fast Constants	Thermal Constants	Fast Constants	Thermal Constants			
HAND	SOF-W.W.	HAND	SOF-W.W.	2	WANDA	1.426
HAND	Maxwellian	HAND	SOF-W.W.	2	WANDA	1.405
HAND	Maxwellian	HAND	Maxwellian	2	WANDA	1.529
MUFT 4	SOF-W.W.	MUFT 4	SOF-W.W.	2	WANDA	1.489
MUFT 4	Maxwellian	MUFT 4	SOF-W.W.	2	WANDA	1.462
MUFT 4	Maxwellian	MUFT 4	Maxwellian	2	WANDA	1.605
MUFT 4	SOF-W.W.	MUFT 4	SOF-W.W.	4	WANDA	1.502
MUFT 4	Maxwellian	MUFT 4	SOF-W.W.	4	WANDA	1.481
MUFT 4	Maxwellian	MUFT 4	Maxwellian	4	WANDA	1.615
MUFT 4	SOF-W.W.	MUFT 4	SOF-W.W.	4	SNG-S4	1.682
MUFT 4	Maxwellian	MUFT 4	Maxwellian	4	SNG-S4	1.893
				Experimental Result: 1.47		

equals the experimental pitch (1.028 cm); and $\overline{P}_0$ is the amplitude of the cosine that best fits the fission density values in the region 5 to 18 cm. The best agreement with experiment is given by the combination MUFT-SOFOCATE-Diffusion Theory. Transport theory predicts peaking considerably higher than diffusion theory and experiment. The MUFT and SOFOCATE codes were also used to calculate the constants in similar work by Goldsmith and Ryan.[66]

5.1.7 CONTROL ANALYSIS IN HETEROGENEOUS REACTORS USING SMALL-SOURCE THEORY

The application of small-source theory to criticality calculations for nuclear reactors without control rods has been discussed in Section 4.4.4. The following is a summary of the work of Lanning[67] who used the methods of small-source theory in the study of control rod problems. The reactor under consideration is radially symmetric, unreflected axially, of infinite radius, and has the same slowing-down properties throughout.

The time-independent, one-group neutron diffusion equation is:

$$D\left(\nabla^2 - \frac{1}{L^2}\right)\phi = \sum_{i=1}^{N} Q_i(z)\,\delta(|\vec{\rho} - \vec{\rho}_i|) - \sum_{i=1}^{N} S_i(z)\,q(z,|\vec{\rho} - \vec{\rho}_i|,\tau)$$

where N = total number of sources plus sinks
D = diffusion coefficient of the moderator
L^2 = diffusion area of the moderator
τ = age to thermal energy
$Q_i(z)$ = strength of the i*th* sink (neutrons absorbed per second per unit length of rod)
$S_i(z)$ = strength of the i*th* source (fast neutrons emitted per second per unit length of rod)
$q(z,|\vec{\rho} - \vec{\rho}_i|,\tau)$ = probability that a fast neutron emitted by the i*th* source rod will be slowed to thermal at (z,ρ); it is the solution of the age equation: $\nabla^2 q = \partial q/\partial\tau$

If the reactor core is a right circular cylinder of effective height H, is unreflected at the top and bottom, and is of infinite radius, then the i*th* source rod contributes:

$$q_i = \{S_i^0 \cos(\kappa z) \exp(-\kappa^2\tau) \exp - [(\vec{\rho} - \vec{\rho}_i)^2/4\tau]\}/4\pi\tau$$

Let

$$\lambda^2 = (1/L^2) + \kappa^2;\ \kappa^2 = \pi^2/H^2;$$

$$S_i(z) = S_i^0 \cos \kappa z;\ Q_i(z) = Q_i^0 \cos \kappa z$$

The solution of the diffusion equation may be obtained[68] by using the two-dimensional Fourier transform and its inverse, along with certain integral relations involving Bessel functions. Then for the flux at any point (z,ρ):

$$\phi(z,\vec{\rho}) = (\cos \kappa z)\left[\sum_{i=1}^{N} -Q_i^0 \frac{K_0(\lambda|\vec{\rho} - \vec{\rho}_i|)}{2\pi D} + \sum_{i=1}^{N} S_i^0 \exp(-\kappa^2\tau) G\left(\frac{\lambda}{\tau}|\vec{\rho} - \vec{\rho}_1|\right)\right]$$

where

$$G\left(\frac{\lambda}{\tau}\rho\right) = \frac{1}{2\pi D}\int_0^\infty \frac{s \exp(-s^2\tau) J_0(s\rho)\,ds}{s^2 + \lambda^2}$$

Now G satisfies the differential equation

$$\frac{\partial G}{\partial\tau} - \lambda^2 G = \frac{-1}{2\pi D}\int_0^\infty s \exp(-s^2\tau)\, J_0(s\rho)\,ds$$

$$= \frac{-1}{2\pi D}\int_0^\infty s \exp(-s^2\tau) \sum_{n=0}^{\infty} \frac{(-1)^n (s\rho)^{2n}}{2^{2n}\, n!\, n!}\,ds$$

$$= \frac{-1}{4\pi D\tau}\sum_{n=0}^{\infty} \frac{(-1)^n}{n!}\left(\frac{\rho^2}{4\tau}\right)^n$$

$$= -\frac{1}{4\pi D}\exp(-\rho^2/4\tau)$$

which has the solution

$$G\left(\begin{matrix}\lambda \\ \tau\end{matrix}\rho\right) = \frac{e^{\lambda^2\tau}}{4\pi D}\int_{\lambda^2\tau}^{\infty} \exp\left[-\left(s + \frac{\lambda^2\rho^2}{4s}\right)\right]\frac{ds}{s}$$

$$= \frac{e^{\lambda^2\tau}}{4\pi D}\left[2K_0(\lambda\rho) - \int_0^{\lambda^2\tau} \exp\left[-\left(s + \frac{\lambda^2\rho^2}{4s}\right)\right]\frac{ds}{s}\right]$$

$$= \frac{e^{\lambda^2\tau}}{4\pi D}\left[2K_0(\lambda\rho) - \int_{\rho^2/4\tau}^{\infty} \exp(-t)\,\frac{dt}{t}\left(1 - \frac{\lambda^2\rho^2}{4t} + \frac{\lambda^4\rho^4}{32t^2} + \cdots\right)\right]$$

$$= \frac{e^{\lambda^2\tau}}{4\pi D}\left[2K_0(\lambda\rho) - E_1\left(\frac{\rho^2}{4\tau}\right) + \lambda^2\,\tau E_2\left(\frac{\rho^2}{4\tau}\right) - \frac{(\lambda^2\tau)^2}{2}E_3\left(\frac{\rho^2}{4\tau}\right) + \cdots\right)\right]$$

where

$$K_0(\lambda\rho) = \int_0^{\infty} \exp\left[-\left(s + \frac{\lambda^2\rho^2}{4s}\right)\right]\frac{ds}{2s}$$

and the definition

$$E_n(x) = x^{n-1}\int_x^{\infty} \frac{e^{-t}\,dt}{t^n}$$

This form for G is convenient for calculations since $E_n(x)$ can be found in tables.

The term $S_i^0 = h_i\,Q_i^0$, where h_i is the number of fast neutrons produced per thermal neutron absorbed in the rod. Diffusion theory gives the following relation between Q_i^0, ϕ_i and β_i:

$$Q_i^0 = \beta_i J_{in,i}\;2\pi a_i = \frac{\pi a_i\,\beta_i}{2-\beta_i}\,\phi_i$$

where $\beta_i J_{in,i}$ is the net current into the i*th* rod
β_i is the thermal blackness[69] of the i*th* rod
a_i is the radius of the i*th* rod
$\phi_i = \phi(a_i)$ is the thermal neutron flux evaluated at the surface of the i*th* rod

Each rod has its own Q_i^0; hence, there will be as many boundary conditions as there are rods in the reactor, unless certain symmetry relations can be established. Since $\phi_i(a_i)$ contains the Q_i^0, boundary conditions on Q_i^0 give a homogeneous set of equations in the Q_i^0 and therefore specify a critical determinant.

The multiplication factor is obtained by integrating the diffusion equation over the reactor.

$$k_{eff} = \frac{\sum_{i=1}^{N} S_i^0\,e^{-\kappa^2\tau}}{\sum_{i=1}^{N} Q_i^0 + \int_{\text{reactor volume}} \phi\,\frac{D}{L^2}\,dV + \int_{\text{reactor surface}} J_{out}\,dS}$$

Lanning[67] reported on the application of this method to an annular loading of 30 or 32 fuel rods in a large, graphite medium, plus eight special control rods made of Cd and U^{235}, and having "open" and "closed" positions. These control rods were located in the graphite outside the fuel annulus. The mass of fuel required to counter the neutron losses in these control rods was calculated and also determined experimentally.

For this case

$h_{fuel} = 2.03$
$\beta_{fuel} = 0.465$

The moderator was graphite: $L = 54.4$ cm; $\tau = 352$ cm^2
For the control rods open, $h = 0.662$; $\beta = 0.897$
For the control rods closed, $h = 0.055$; $\beta = 0.897$

The additional fuel required to maintain criticality was:

	ΔM_{calc} (kg U^{235})	ΔM_{obs} (kg U^{235})
Rods present and open–rods replaced by graphite	1.29	1.34
Rods present and closed–rods present and open	1.14	0.96

5.2 LONG-TERM CHANGES

5.2.1 NEUTRON POISONING BY Xe^{135} AND Sm^{149}

Xenon-135. The fission product chain of mass number 135 is: (Section 1.)

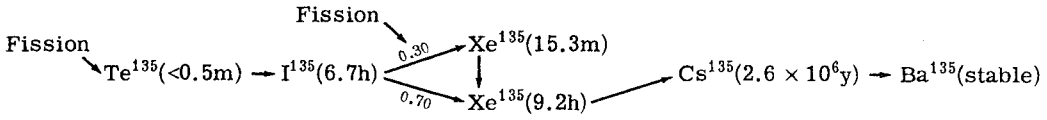

Since the Te^{135} has so short a half-life, I^{135} is considered as arising directly from fission. The yield of I^{135} and direct yield of Xe^{135} from thermal fission are summarized below:

Fissionable Isotope	U^{233}	U^{235}	Pu^{239}
Yield of I^{135}	0.051	0.061	0.055
Yield of Xe^{135} (direct)	—	0.003	—

The concentrations of I^{135} and of Xe^{135} in a reactor are given by:

$$\frac{dI(t)}{dt} = \phi\,\Sigma_f\,Y^I - \lambda^I I \tag{5-5}$$

$$\frac{dX(t)}{dt} = \phi\,\Sigma_f\,Y^X + \lambda^I I - (\lambda^X + \phi\sigma_a^X)X \tag{5-6}$$

where I, X = the concentrations (atoms per cubic centimeter) of I^{135} and Xe^{135}, respectively
$\phi\Sigma_f$ = the fission rate (fissions per cubic centimeter per second)
Y^I = fission yield of I^{135} (actually of Te^{135})
Y^X = direct fission yield of Xe^{135}
$\lambda^I = 2.89 \times 10^{-5}$/sec is the decay constant of I^{135}
$\lambda^X = 2.09 \times 10^{-5}$/sec is the decay constant of Xe^{135} and time, t, is in seconds

The microscopic absorption cross section of Xe^{135}, σ_a^X, is given as 2.72×10^6 barns at 2200 m/sec.[70] In addition, g-factors[71] are presented for the capture cross section of Xe^{135} for various values of the neutron temperature. The absorption cross section of iodine is small enough that it is ignored in Eq. (5-5).

The general solutions of Eqs. (5-5) and (5-6) for a time interval $t_0 \le t_0 + t \le t_1$ over which $\phi\Sigma_f$ and $\phi\sigma_a^X$ are essentially constant, are as follows:

$$I(t_0 + t) = \frac{\phi\Sigma_f Y^I}{\lambda^I}\left[1 - \exp(-\lambda^I t)\right] + I(t_0)\exp(-\lambda^I t) \tag{5-7}$$

and

$$X(t_0 + t) = \frac{\phi\Sigma_f(Y^I + Y^X)}{\lambda^X + \phi\sigma_a^X} + \left[X(t_0) - \frac{\phi\Sigma_f(Y^I + Y^X)}{\lambda^X + \phi\sigma_a^X} - \frac{(\lambda^I I(t_0) - \phi\Sigma_f Y^I)}{\lambda^X + \phi\sigma_a^X - \lambda^I}\right]\exp\left[-(\lambda^X + \phi\sigma_a^X)\,t\right] + \left[\frac{\lambda^I I(t_0) - \phi\Sigma_f Y^I}{\lambda^X + \phi\sigma_a^X - \lambda^I}\right]\exp(-\lambda^I t) \tag{5-8}$$

Since in general reactor applications, $\phi\Sigma_f$ and $\phi\sigma_a^X$ are slowly varying in time, the complete time dependence of the iodine and xenon concentrations may be found approximately by a sequence of solutions of this type.

The general solution of Eq. (5-6) may be simplified considerably in two special cases. Starting with fresh fuel, so that $I(t_0) = X(t_0) = 0$, with $t_0 = 0$,

Case 1: $\phi\sigma_a^X \ll \lambda^X$, or $\phi \ll 10^{13}$ n/(cm^2) (sec)

$$X(t) \approx \frac{\phi\Sigma_f(Y^I + Y^X)}{\lambda^X}\left[1 - \exp(-\lambda^X t)\right] - \phi\Sigma_f Y^I\left[\frac{\exp(-\lambda^X t) - \exp(-\lambda^I t)}{\lambda^I - \lambda^X}\right]$$

Case 2: $\phi\sigma_a^X \gg \lambda^X$ and for $t > 1$ hr

$$X(t) \approx \frac{\phi\Sigma_f(Y^I + Y^X)}{\phi\sigma_a^X} - \frac{\phi\Sigma_f Y^I}{\phi\sigma_a^X}\exp(-\lambda^I t) \approx \frac{\phi\Sigma_f(Y^I + Y^X)}{\phi\sigma_a^X}\left[1 - \exp(-\lambda^I t)\right]$$

since $Y^I \gg Y^X$.

Thus

$$\frac{X(t)}{X_{eq}} \approx \left[1 - \exp(-\lambda^I t)\right]$$

where X_{eq} is the equilibrium concentration:

$$X_{eq} = \frac{\phi\Sigma_f(Y^I + Y^X)}{\lambda^X + \phi\sigma_a^X}$$

Therefore, for very high flux, the xenon concentration is proportional to the iodine concentration, reaching 50% of its equilibrium level in one half-life of I^{135} (6.7 hr), 95% in one day, and 99% in two days.

Starting with an unpoisoned fuel, if Σ_f decreases linearly with time, but $\phi\Sigma_f$ is constant, then a good approximation to X(t) may be obtained as a generalization to Case 2 above, i.e., for $\phi\sigma_a^X \gg \lambda^X$ and for $t > 1$ hour:

$$X(t) = \frac{(\phi\Sigma_f)_0(1 - Ct)}{(\phi\sigma_a^X)_0}\left[(Y^I + Y^X) - Y^I\exp(-\lambda^I t)\right]$$

where $(\phi\Sigma_f)_0$ and $(\phi\sigma_a^X)_0$ are the values at time zero, and $\Sigma_f = \Sigma_{f0}(1 - Ct)$.

Since $Y^X \ll Y^I$,

$$\frac{X(t)}{X_{eq}} \approx \left[1 - \exp(-\lambda^I t)\right](1 - Ct)$$

where X_{eq} is the saturation concentration for the case in which the fuel concentration is maintained at its initial level.

If the change in flux and the fractional burnup of fuel is small in a time comparable to the half-life of Xe^{135}, then the iodine and xenon concentrations approach the saturation levels:

$$I_{eq} = \frac{\phi\Sigma_f Y^I}{\lambda^I}$$

$$X_{eq} = \frac{\phi\Sigma_f(Y^I + Y^X)}{\lambda^X + \phi\sigma_a^X}$$

and

$$\frac{X_{eq}}{I_{eq}} = \left(\frac{Y^I + Y^X}{Y^I}\right)\left(\frac{\lambda^I}{\lambda^X + \phi\sigma_a^X}\right)$$

It is convenient to describe the xenon poisoning effect as the ratio:

$$\left(\frac{\phi\Sigma_a^X}{\phi\Sigma_f}\right)_{eq} = \frac{(Y^I + Y^X)\,\phi\sigma_a^X}{\lambda^X + \phi\sigma_a^X}$$

This ratio is graphed in Fig. 5-27 for a thermal reactor where fission events occur only in U^{235}.

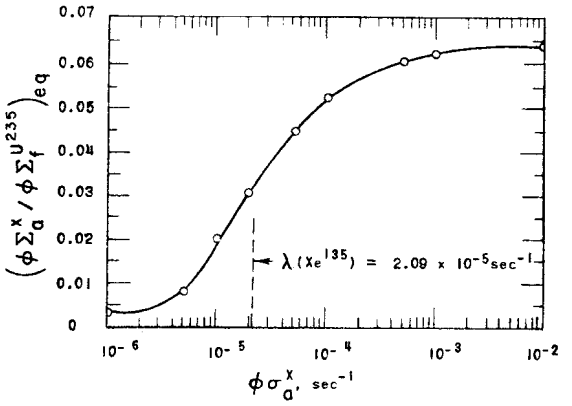

Fig. 5-27 — Relative neutron absorption by equilibrium xenon in a highly enriched (U^{235}) thermal reactor.

If, after I^{135} and Xe^{135} have attained their equilibrium values for flux ϕ, the flux is instantaneously set equal to 0 at t = 0, then

$$I(t) = I_{eq} \exp(-\lambda^I t)$$

$$X(t) = X_{eq} \exp(-\lambda^X t) - \lambda^I I_{eq}\left[\frac{\exp(-\lambda^I t) - \exp(-\lambda^X t)}{\lambda^I - \lambda^X}\right] \qquad (5\text{-}9)$$

The xenon concentration will increase after shutdown from equilibrium operation if $(dX(t)/dt)_{t=0} > 0$, i.e., if $\phi\sigma_a^X > (Y^X\lambda^X/Y^I)$. Differentiating Eq. (5-9) and solving for the time at which the xenon concentration is maximum:

$$t_{max} = \frac{1}{\lambda^X - \lambda^I} \log\left\{\frac{\lambda^X}{\lambda^I}\left[1 + \left(\frac{\lambda^I - \lambda^X}{\lambda^I}\right)\left(\frac{X_{eq}}{I_{eq}}\right)\right]\right\}$$

t_{max} asymptotically approaches 11.3 hr as ϕ is increased.

Buildup of xenon after a step change in flux level from an equilibrium concentration may be obtained easily from the solution of Eq. (5-6) by using the following initial conditions:

$I(0) = I_{eq}$
$X(0) = X_{eq}$
$\phi\Sigma_f$ = fission rate at the new flux level

Figures 5-28 and 5-29, prepared by MacRae and Parr,[72] show the times to reach maximum xenon concentration following a step function change in the flux from one non-zero value to a second non-zero value. A value of $\sigma_a^X = 3.5 \times 10^6$ barns was used in the calculations.

Clark and English[73] have published tables of numbers that permit rapid calculation of the time-dependence of xenon concentration following a step change in flux level.

Ward[74] has prepared a so-called "universal xenon curve". This is explained as follows: In Eq. (5-9), write $t = t' - t^*$, where

$$t^* = \frac{\ln[1 + (z/\lambda^I)(\lambda^I - \lambda^X)]}{\lambda^I - \lambda^X} \qquad (5\text{-}10)$$

and $z = X_{eq}/I_{eq}$.

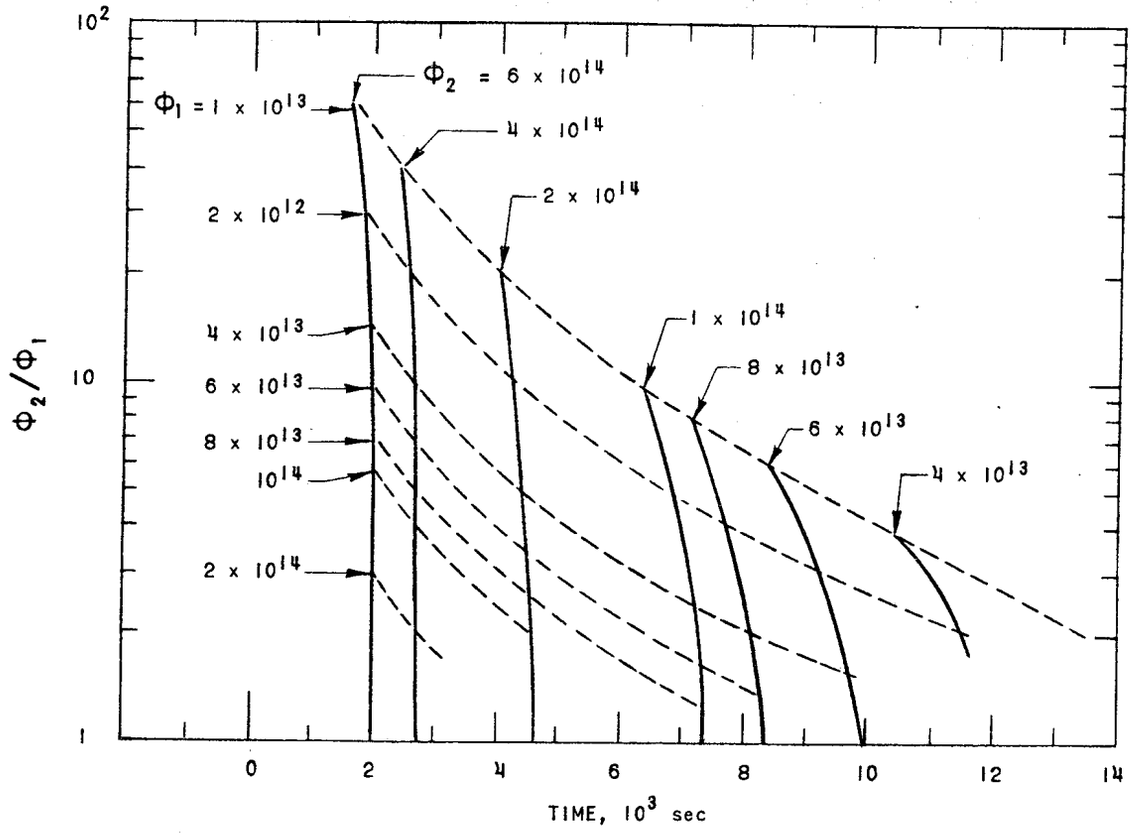

Fig. 5-28 — Time to reach maximum xenon poisoning after flux increase from ϕ_1 to ϕ_2. *Reproduced from Ref. 72.*

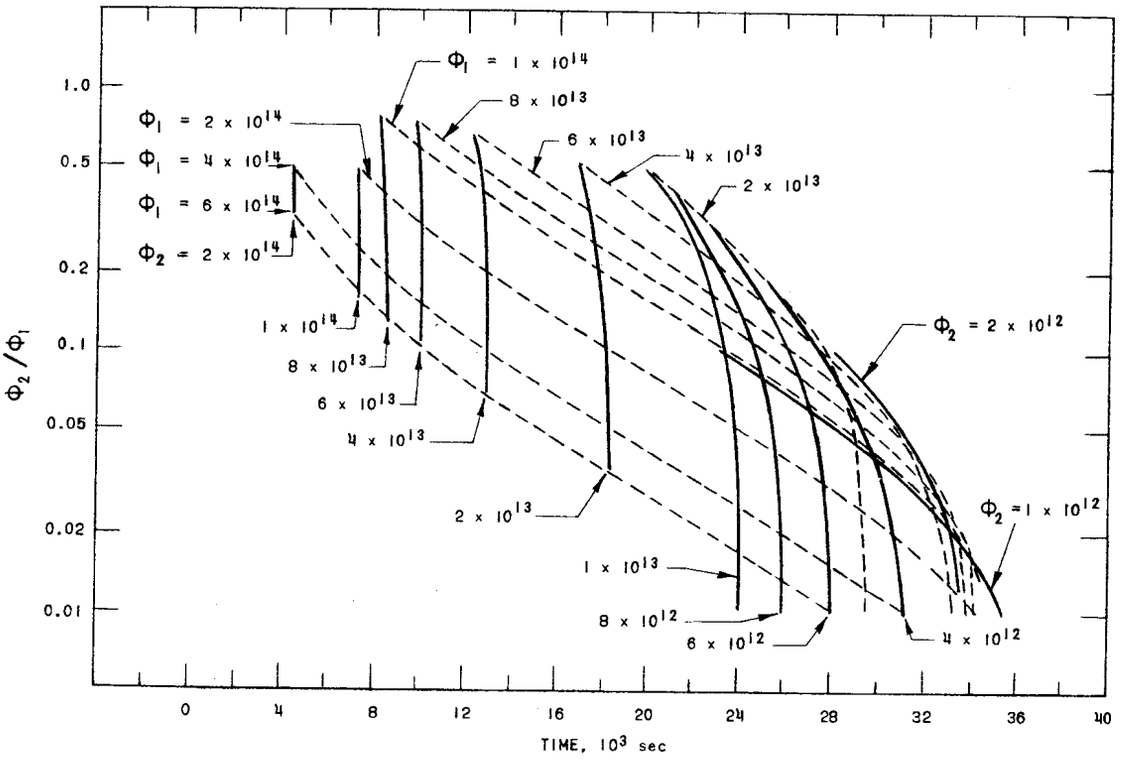

Fig. 5-29 — Time to reach maximum poisoning after flux decrease from ϕ_1 to ϕ_2. *Reproduced from Ref. 72.*

This gives

$$X(t,z) = X^*(t',z) = \frac{I_{eq}\,\lambda^I}{\lambda^I - \lambda^X}\left[1 + \frac{z}{\lambda^I}(\lambda^I - \lambda^X)\right]^{\lambda^I/(\lambda^I-\lambda^X)} (e^{-\lambda^X t'} - e^{-\lambda^I t'})$$

Now $X^*(t',z)$ has a maximum value $X^*(T,z)$ for $T = [\ln(\lambda^I/\lambda^X)]/(\lambda^I - \lambda^X)$. Therefore,

$$\frac{X^*(t',z)}{X^*(T,z)} = \frac{\lambda^X e^{\lambda^I T}}{\lambda^I - \lambda^X}(e^{-\lambda^X t'} - e^{-\lambda^I t'}) = \left(\frac{X}{X_{max}}\right)^*$$

Also,

$$\frac{X(t,z)}{X(0,z)} = \frac{[X^*(t',z)/X^*(T,z)]}{[X^*(t^*,z)/X^*(T,z)]} \tag{5-11}$$

The term $X(t,z)/X(0,z)$ is obtained by calculating t^* from Eq. (5-10), and then using that portion of Fig. 5-30 for $t' \geq t^*$. Figure 5-30 is a plot of $(X/X_{max})^*$ as a function of t'. Figure 5-31 is a plot of z vs. t^*, that is, a graph of Eq. (5-10). Both curves were prepared by Ward, using a microscopic absorption cross section of 3.4×10^6 barns and ignoring direct production of xenon from fission.

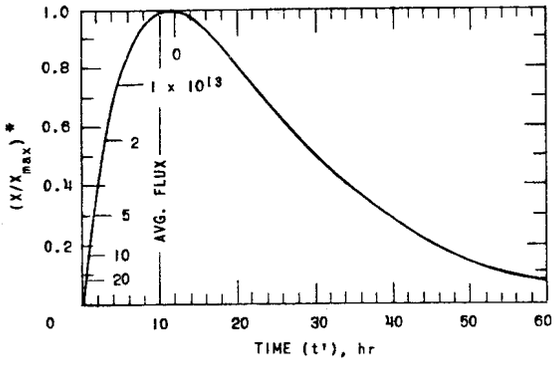

Fig. 5-30 — Flux-independent curve of xenon concentration as a function of time after complete shutdown. *Reproduced from Ref. 74.*

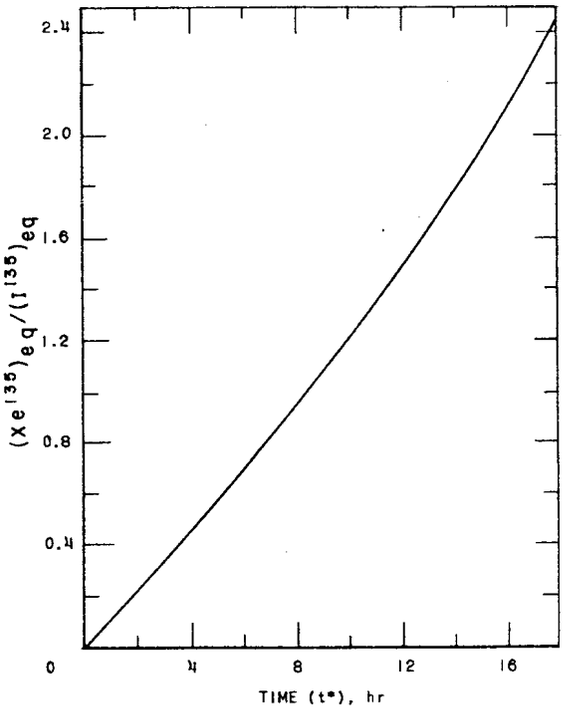

Fig. 5-31 — Translation time (t*) as a function of ratio of equilibrium concentration of Xe^{135} to I^{135}. *Reproduced from Ref. 74.*

Samarium-149. Samarium-149 is a stable isotope arising from beta decay of promethium-149 (Pm^{149}), which is formed directly from fission, and also from the beta decay of the fission product neodymium-149. The neodymium isotope has so short a half-life (2.0 hr) in comparison with that of Pm^{149} (54 hr), that the simplified chain for Sm^{149} is written:

$$\text{Fission} \rightarrow Pm^{149}\ (54\ \text{h}) \rightarrow Sm^{149}\ (\text{stable})$$

The cumulative yields of Sm^{149} from thermal fission are:

	U^{233}	U^{235}	Pu^{239}
Y =	0.0066	0.0113	0.019

The dynamic balance equations for the simplified model are:

$$\frac{dPm}{dt} = \phi\Sigma_f Y^{Pm} - \lambda^{Pm} Pm$$

$$\frac{dSm}{dt} = \lambda^{Pm} Pm - \phi\sigma_a^{Sm} Sm$$

$$\lambda^{Pm} = 3.56 \times 10^{-6}/\text{sec}$$

Pm = concentration of promethium-149

Sm = concentration of samarium-149

Over a time interval of constant $\phi\Sigma_f$ and $\phi\sigma_a^{Sm}$,

$$Pm(t) = \frac{\phi\Sigma_f Y^{Pm}}{\lambda^{Pm}} [1 - \exp(-\lambda^{Pm} t)] + Pm(0) \exp(-\lambda^{Pm} t)$$

$$Sm(t) = \frac{\phi\Sigma_f Y^{Pm}}{\phi\sigma_a^{Sm}} + \left[Sm(0) - \frac{\phi\Sigma_f Y^{Pm}}{\phi\sigma_a^{Sm}} - \frac{\lambda^{Pm} Pm(0) - \phi\Sigma_f Y^{Pm}}{\phi\sigma_a^{Sm} - \lambda^{Pm}}\right] \exp(-\phi\sigma_a^{Sm} t)$$

$$+ \left[\frac{\lambda^{Pm} Pm(0) - \phi\Sigma_f Y^{Pm}}{\phi\sigma_a^{Sm} - \lambda^{Pm}}\right] \exp(-\lambda^{Pm} t)$$

Thus the equilibrium concentration of Sm^{149} is

$$Sm_{eq} = \frac{\phi\Sigma_f Y^{Pm}}{\phi\sigma_a^{Sm}}$$

which is independent of the magnitude of the flux.

For $\phi\sigma_a^{Sm} \ll \lambda^{Pm}$, or $\phi \ll 10^{14}$ n/(cm^2)(sec), and Pm(0) = Sm(0) = 0, after a few days:

$$Sm(t) \approx \frac{\phi\Sigma_f Y^{Pm}}{\phi\sigma_a^{Sm}} [1 - \exp(-\phi\sigma_a^{Sm} t)]$$

For $\phi\sigma_a^{Sm} \gg \lambda^{Pm}$ (or $\phi \gg 10^{14}$ n/cm^2 sec) and Pm(0) = Sm(0) = 0 after about one day:

$$Sm(t) \approx \frac{\phi\Sigma_f Y^{Pm}}{\phi\sigma_a^{Sm}} [1 - \exp(-\lambda^{Pm} t)]$$

After a shutdown from equilibrium at t = 0 from flux ϕ_0 to flux zero:

$$Sm(t) = \frac{\phi_0\Sigma_f Y^{Pm}}{\lambda^{Pm}} [1 - \exp(-\lambda^{Pm} t)] + \frac{\phi_0\Sigma_f Y^{Pm}}{\phi_0\sigma_a^{Sm}}$$

and

$$Sm(\infty) = \phi_0\Sigma_f Y^{Pm} \left(\frac{1}{\lambda^{Pm}} + \frac{1}{\phi_0\sigma_a^{Sm}}\right)$$

Figure 5-32 shows the number of atoms of Sm^{149} per initial atom of U^{235}, as a function of irradiation time for several values of flux. In preparing this figure, Blomeke and Todd[75] used the values $Y^{Pm} = 0.013$, and $\sigma_a^{Sm^{149}} = 50{,}000$ barns.

687863 O - 63 - 27

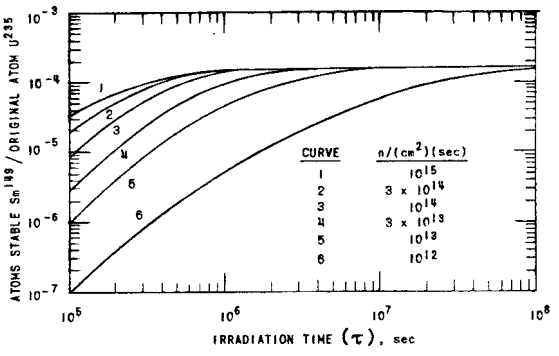

Fig. 5-32—Effect of irradiation time and flux on amount of stable Sm^{149} formed in fission of U^{235}. *Reproduced from Ref. 75.*

5.2.2 POISONING DUE TO ACCUMULATION OF GROSS FISSION PRODUCTS

Poisoning effects of fission products in reactors have been treated by many investigators.[75–90] The time-dependent concentration of a given fission fragment is obtained from the solution of the equation

$$\frac{dN_i}{dt} = Y_i N_f \hat{\sigma}_f \phi - N_i \hat{\sigma}_i \phi + N_{i-1} \hat{\sigma}_{i-1} \phi - \lambda_i N_i + \lambda_k N_k \qquad (5\text{-}12)$$

where N_i is the number of atoms per unit volume of the fission product of species i; N_f is the number of fuel atoms per unit volume; Y_i is the direct yield from fission of the fission product ($\sum Y_i = 2$); λ_i and λ_k are decay constants, with k indicating the precursor fission product; $\hat{\sigma}_f$ is the effective microscopic fission cross section of the fuel; $\hat{\sigma}_i$ is the effective microscopic absorption cross section of the fission product; ϕ is the flux; and i – 1 indicates the fission product leading to i under neutron capture. Frequently, fission products are assigned to two groups according to half-life, such that all nuclei in the short half-life group are assumed to decay at once and all nuclei in the long half-life group are assumed to be stable. In this approximation, the last two terms in Eq. (5-12) disappear. This permits the independent variable of Eq. (5-12) to be changed from the time, t, to the flux time $\int_0^t \phi(t)dt$, the variable $\int_0^t \hat{\sigma}_f \phi(t)dt$, or the fuel burnup,

$$\beta = 1 - \exp\left[-\hat{\sigma}_a \int_0^t \phi(t)dt\right]$$

where $\hat{\sigma}_a$ is the microscopic absorption cross section of the fuel.

In most of the earlier work,[75–81,89,90] thermal poisoning alone was considered. More recently, the treatment has been extended to consider epithermal absorption as well.[82–88] Usually this is done in the framework of Westcott's g and s factor formulation, (Section 3.2.2). Thus in Eq. (5-12) the effective cross sections, $\hat{\sigma}$, are given by $\hat{\sigma} = \sigma_0 (g + rs)$; ϕ is the "2200 m/sec flux", i.e., the total neutron density times 2200 m/sec; and σ_0 is the cross section at 2200 m/sec.

The work of most investigators involves the calculation of $\sum_i N_i \hat{\sigma}_i$ as a function of time, flux-time, or fuel burnup. Frequently, the fission products are divided into high and low thermal cross section groups with the high cross section group including Xe^{135}, Sm^{149}, Sm^{151}, Eu^{155}, Cd^{113}, Gd^{157} and, sometimes, several others. Xe^{135} and Sm^{149} are usually treated separately, as in Section 5.2.1. For small irradiation times, only the high cross section group is of importance. For longer irradiation times, the poisoning of the high cross section group saturates; therefore, many authors consider only the low cross section group in calculating $\sum_i N_i \hat{\sigma}_i$. This low cross section group is often referred to as non-saturating poisons or "slag".

Poisoning calculations have been performed for the fission products of U^{235}, U^{233}, Pu^{239}, and Pu^{241}. Figures 5-33 through 5-35, which are taken from the work of Walker,[78] show the poisoning in U^{233}, U^{235}, and Pu^{239} by fission products of known cross section except Xe^{135} and Sm^{149}. Figures 5-36 through 5-38 give results including Xe^{135} and Sm^{149}. Thermal poisoning alone is considered. In these figures, Case I refers to the number of fissile atoms remaining fixed during the irradiation, while in Case II the fuel burns up according to

$$N_f = N_f(0) \exp(-\hat{\sigma}_a \phi t)$$

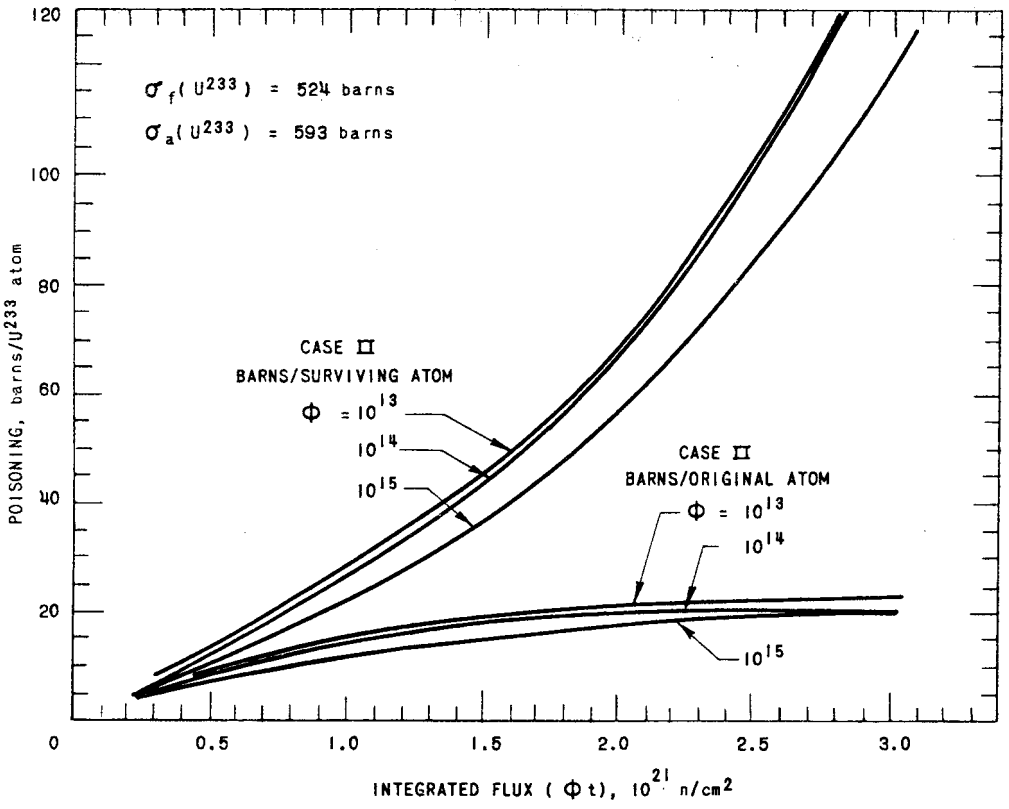

Fig. 5-33 — Poisoning in U^{233} by fission products for which σ_c is known except Xe^{135} and Sm^{149}. *Reproduced from Ref. 78.*

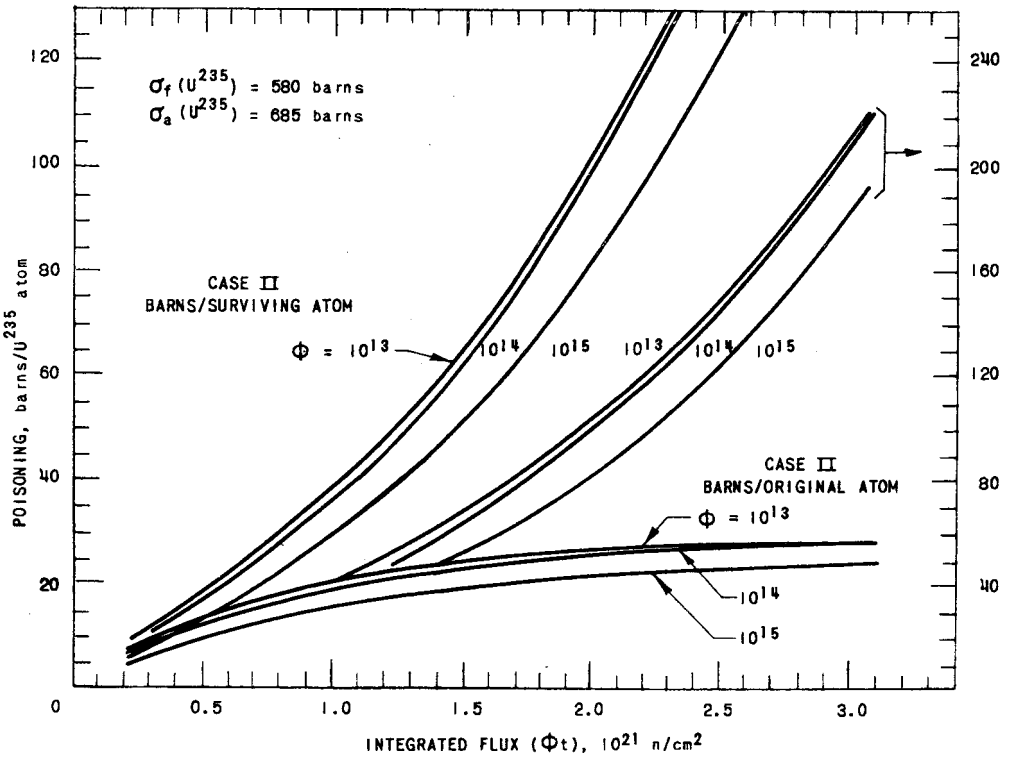

Fig. 5-34 — Poisoning in U^{235} by fission products for which σ_c is known except Xe^{135} and Sm^{149}. *Reproduced from Ref. 78.*

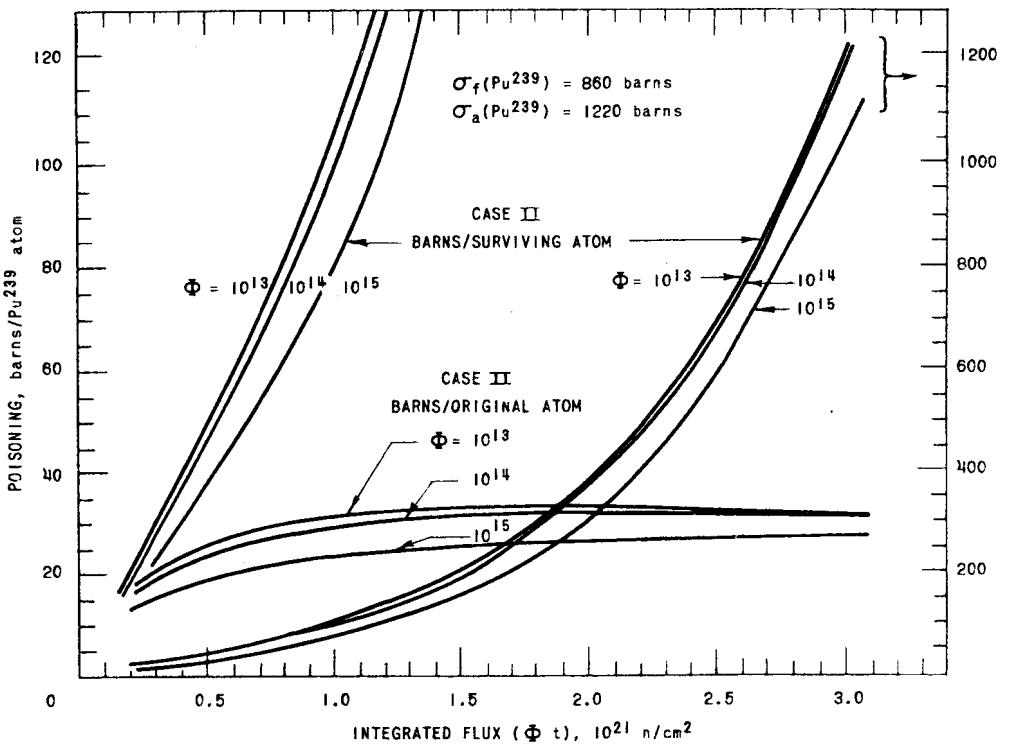

Fig. 5-35 — Poisoning in Pu^{239} by fission products for which σ_c is known except Xe^{135} and Sm^{149}. *Reproduced from Ref. 78.*

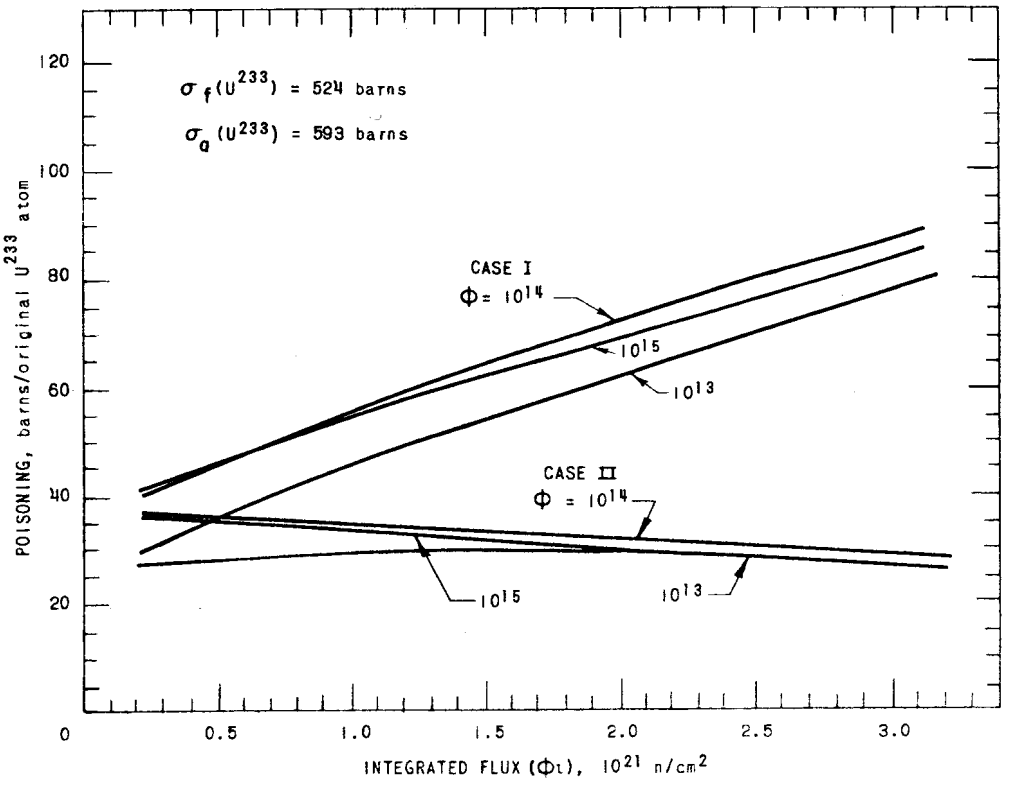

Fig. 5-36 — Poisoning in U^{233} by fission products for which σ_c is known. *Reproduced from Ref. 78.*

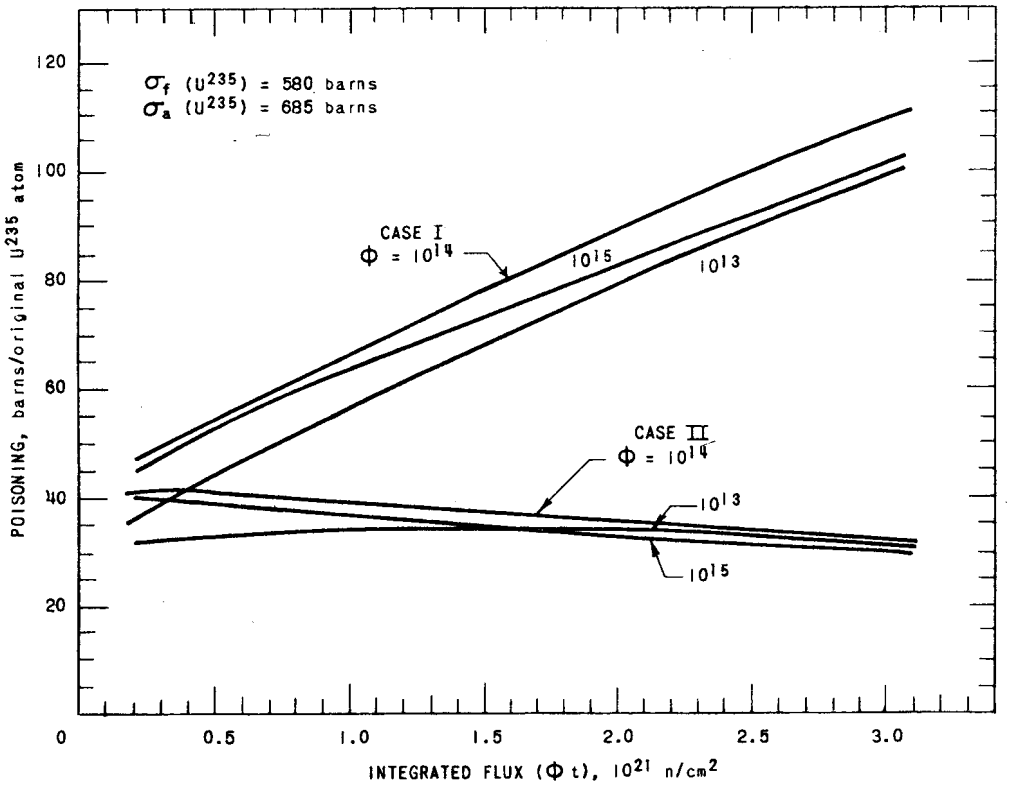

Fig. 5-37 — Poisoning in U^{235} by fission products for which σ_c is known. *Reproduced from Ref. 78.*

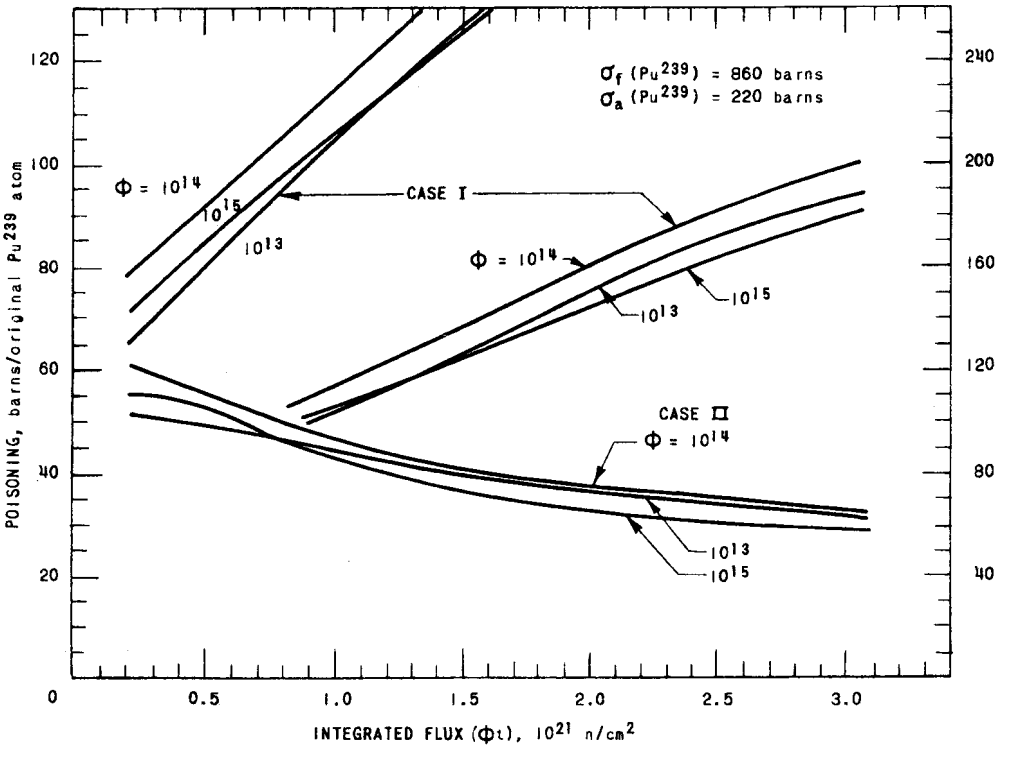

Fig. 5-38 — Poisoning in Pu^{239} by fission products for which σ_c is known. *Reproduced from Ref. 78.*

Blomeke and Todd[75,81] present a vast array of data for thermal poisoning by U^{235} fission products. Their calculations assume constant flux, replenishment of fuel, and include the β-decay terms in Eq. (5-12).

Reference 75 contains

(1) Tables of yields and cross sections.
(2) Equilibrium concentrations of the various radioactive isotopes as a function of flux levels.
(3) Curves of the fraction of equilibrium concentration of radioactive isotopes as a function of flux level and of time after startup.
(4) Curves of the concentrations of radioactive isotopes as a function of time after shutdown, for various levels of flux prior to shutdown.
(5) Curves of the buildup of individual stable fission products as a function of flux level and of irradiation time.
(6) Curves describing the total poisoning effects of fission products as a function of flux and time.

Reference 81 presents tables giving the results of summations of the data of Ref. 75 on a "per chain" and a "per element" basis, and for the rare-gas and rare-earth groups.

Curves of the total poisoning effect of fission product buildup (including Xe^{135} and Sm^{149}) as a function of the flux level and of irradiation time are shown in Fig. 5-39.

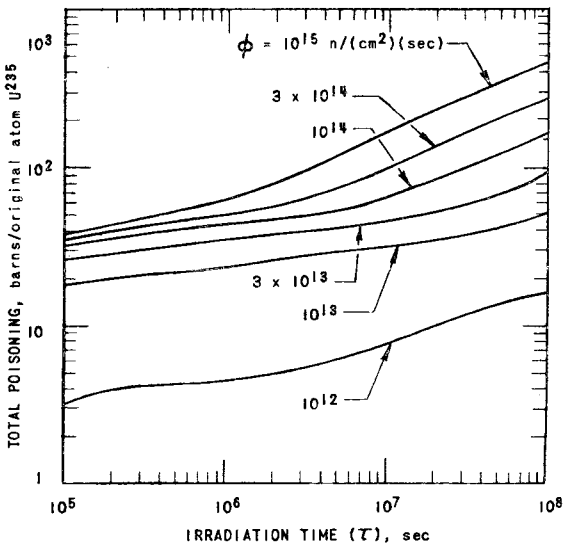

Fig. 5-39 — Buildup of total fission product poisoning with irradiation time and thermal neutron flux. *Reproduced from Ref. 75.*

Hurst[79,80] introduces the idea of pseudo-fission products. An expression of the form

$$\frac{\hat{\sigma}^{fp}}{\text{fission}} = \sum_{i=1}^{3} (\hat{\sigma}_i Y_i e^{-\hat{\sigma}_i x}) \tag{5-13}$$

is chosen to represent the effective cross section of fission products resulting from one average fission at time zero at a flux time x later. The values of $\hat{\sigma}_i$ and Y_i are chosen to fit the data of the complete calculations.

Table 5-18 gives values of Y_i for thermal poisoning for two ranges of irradiation. The cross sections, $\hat{\sigma}_i$, are $\hat{\sigma}_1$ = 25 barns, $\hat{\sigma}_2$ = 300 barns, and $\hat{\sigma}_3$ = 600 barns.

The total cross section of fission products at operating time t_0 may be found by integration of Eq. (5-13).

$$\Sigma^{fp}(t_0) = \int_0^{t_0} dt\, \Sigma_f(t)\, \phi(t) \frac{\hat{\sigma}^{fp}(x)}{\text{fission}} \tag{5-14}$$

where $\Sigma_f(t)$ is the macroscopic fission cross section; and

$$x = \int_t^{t_0} \phi(t')dt'$$

Table 5-18—FRACTIONAL YIELDS OF PSEUDO-FISSION PRODUCTS

Data from Ref. 80.

Nuclide	$\phi t = 0 - 3 \times 10^{21}$ n/cm^2			$\phi t = 0 - 10 \times 10^{21}$ n/cm^2		
	25b Y_1	300b Y_2	600b Y_3	25b Y_1	300b Y_2	600b Y_3
U^{233}	0.678	0.1008	−0.0097	0.695	0.0976	−0.0089
U^{235}	0.809	0.1223	−0.0154	0.852	0.1137	−0.0129
Pu^{239}	1.087	0.2196	−0.0537	1.220	0.1927	−0.0456
Pu^{241}	1.163	0.2147	−0.0540	1.287	0.1904	−0.0469

Note:

1. For fission products of unknown cross section, the assumption was made that these isotopes and the higher order isotopes in that chain have the same distribution of intermediate and low cross sections as the chains where the cross sections are known. The total cross section of the known products, therefore, was multiplied by the factor: [2/(total yield of products of known cross section)].
2. The results may be used for reactors where the flux level is less than, or of the order of 10^{13} n/(cm^2)(sec).
3. Primary fission products with $\sigma_a > 1000$ b are omitted, but their (n,γ) daughters are included.

Data are also available on fission product poisoning where resonance absorption is considered. Reference 83 gives data on thermal fission yields of U^{233}, U^{235}, and Pu^{239} fission products, and cross section data on fission products, including resonance integrals. Most of these data were compiled from papers presented at the 1958 Geneva Conference. Reference 85 presents extensive tables of yields of fission products for U^{233}, U^{235}, Pu^{239}; estimated yields for Pu^{241}; cross section data for fission products, including both thermal cross sections and resonance integrals; and β-decay half-lives of fission products. Also, the numbers involved in the pseudo-fission product treatment[79,80] are brought up to date, including resonance absorption considerations. Table 5-19 gives fractional yields of pseudo-fission products as a function of $r\sqrt{T/T_0}$, where r is the quantity defined by Westcott (Section 3.2.2) which indicates the epithermal contribution to the spectrum; T is the temperature of the Maxwellian distribution; and T_0 is 293°K. The cross sections of the pseudo-fission products have been

Table 5-19—VARIATION OF PSEUDO-FISSION PRODUCT YIELDS WITH $r\sqrt{T/T_0}$

Data from Ref. 85.

Nuclide	$r\sqrt{T/T_0}$	50b Y_1	300b Y_2	800b Y_3
U^{233}	0.03	0.5691	0.0850	−0.00292
	0.05	0.5769	0.0981	−0.00415
	0.07	0.5833	0.1107	−0.00497
	0.09	0.5842	0.1224	−0.00522
U^{235}	0.03	0.6860	0.0845	−0.00511
	0.05	0.6929	0.1012	−0.00678
	0.07	0.6976	0.1175	−0.00790
	0.09	0.6968	0.1321	−0.00829
Pu^{239}	0.03	0.8148	0.1210	−0.0181
	0.05	0.8108	0.1501	−0.0216
	0.07	0.8016	0.1783	−0.0244
	0.09	0.7862	0.2037	−0.0258
Pu^{241}	0.03	0.8190	0.1173	−0.00946
	0.05	0.8183	0.1439	−0.0116
	0.07	0.8174	0.1683	−0.0128
	0.09	0.8056	0.1916	−0.0129

changed to 50, 300, and 800 barns from the corresponding values in Table 5-18. For zero irradiation [x = 0 in Eq. (5-13)], and $r\sqrt{T/T_0} = 0.07$, which is typical of the NRX reactor, the epithermal absorption increases the value of $\hat{\sigma}^{fp}$ per fission over the value for thermal absorption alone by amounts ranging from 23% for Pu^{239}, to 42% for U^{233}.

Greenhow and Hansen[84] consider poisoning, including epithermal effects, in U^{235} reactors for the case of constant power operation and linear burnup. Figure 5-40 shows the ratio of the effective cross

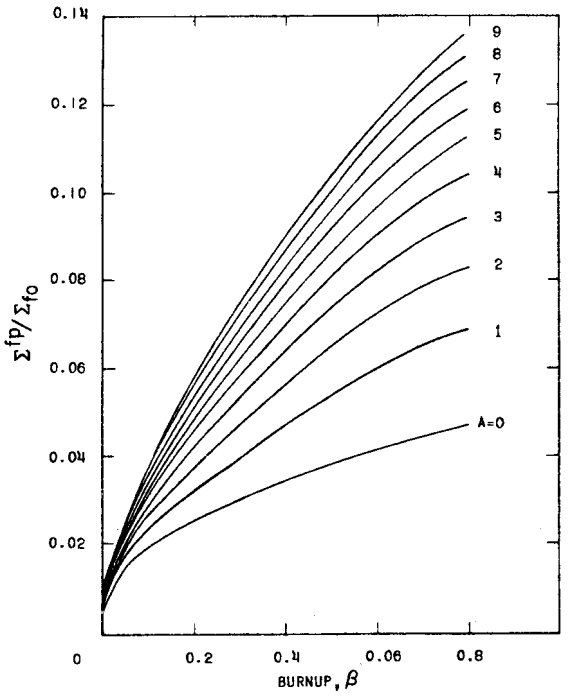

Fig. 5-40—Effective cross section of fission products as a function of burnup and values of A. *Reproduced from Ref. 84.*

section of fission products, Σ^{fp}, to the initial macroscopic fission cross section, Σ_{f0}, as a function of burnup, β, for various values of the ratio A, of the epithermal to the thermal flux. For A = 0 the results are in fair agreement with those of Deutsch[77] which were calculated in a similar manner but with poorer data. This work considers U^{236} and its associated chain as fission products.

Nephew[86] presents data on fission product poisoning of U^{233}, U^{235}, and Pu^{239} reactors. The high cross section fission products Xe^{135}, Sm^{149}, and Sm^{151}, Gd^{155}, Eu^{155}, Cd^{113}, and Gd^{157} are omitted from the calculations. The case of a neutron temperature of 1000°K and continuous fuel replenishment is considered. Four pseudo-elements are defined so that the poison cross section (in barns per average fission) is given approximately by

$$\hat{\sigma}^{fp} = \sum_i \frac{N_i \hat{\sigma}_i}{N_f F} = \sum_i Y_i \hat{\sigma}_i \frac{(1 - e^{-\alpha_i F})}{\alpha_i F} \tag{5-15}$$

where

$$F = \int \hat{\sigma}_f \phi(t) dt$$

and

$$\alpha_i = \frac{\hat{\sigma}_i}{\hat{\sigma}_f} = (1 - P) \frac{g\sigma_0}{g_f \sigma_f} + \frac{P\Sigma_\mu}{\Sigma_f}$$

Here, the Westcott formalism is used and P is the fraction of fissions due to the epithermal flux; $g\sigma_0$ is the effective thermal absorption cross section of the pseudo-element; $g_f\sigma_f$ is the effective thermal fission cross section of the fuel; Σ_μ is the total resonance integral of the pseudo-element above the

thermal cutoff at μkT; and Σ_f is the corresponding fission resonance integral of the fuel. The quantity Σ_μ may be written

$$\Sigma_\mu = I_T + \left(\frac{4T_0}{\mu T}\right)^{1/2} g\sigma_0$$

where I_T is the resonance integral, excluding the 1/v contribution (excess resonance integral). Table 5-20 lists the fuel constants involved in calculating $\hat{\sigma}^{fp}$ for the three fissionable species, while Table 5-21 presents the necessary data on the pseudo-elements.

Table 5-20—FUEL CONSTANTS FOR PSEUDO-ELEMENT CALCULATIONS (T = 1000°K)

Data from Ref. 86.

	U^{233}	U^{235}	Pu^{239}
g_f	1.0376	0.912	2.4613
σ_f, barn	527	580	746
Σ_f, barn	805	271 ± 25	319

Table 5-21—PSEUDO-ELEMENT CONSTANTS (T = 1000°K)

Data from Ref. 86.

Isotope	Pseudo-element Number:	1	2	3	4
U^{233}	Y	0.0943	0.181	0.0513	0.0175
	$g\sigma_0$	228.31	30.88	147.56	134.29
	I_T	113.89	284.48	836.25	2812.0
	I_T < 100 ev	18.494	240.280	807.020	2726.11
U^{235}	Y	0.1124	0.210	0.0582	0.0295
	$g\sigma_0$	216.81	31.52	140.94	129.15
	I_T	71.0	283.1	905.54	2449.83
	I_T < 100 ev	17.62	243.33	851.375	2365.08
Pu^{239}	Y	0.117	0.2027	0.086	0.06
	$g\sigma_0$	204.70	31.52	169.65	146.83
	I_T	90.86	277.4	918.38	2399.33
	I_T < 100 ev	16.070	233.000	890.47	2336.83

Note: Units for $g\sigma_0$ and I_T are barns per average fission.

For F = 0, the data of Table 5-21 give effective thermal cross sections of 37, 43, and 54 barns per fission for U^{233}, U^{235}, and Pu^{239}, respectively. The corresponding excess resonance integrals below 100 ev are 134, 172, and 266 barns.

In connection with fission product absorption in the resonance region, theoretical work has been done[87,88] on estimating the average fission product cross section per fission as a function of energy in the energy range from 100 to 10^6 electron volts. These treatments make use of statistical distribution of neutron resonances. A comparison of the results for U^{235} of Greebler, et al.[87] and Gordeev and Pupko[88] is given in Table 5-22.

Table 5-22—U^{235} FISSION PRODUCT CROSS SECTIONS IN BARNS/FISSION

E, ev:	10^2	10^3	10^4	10^5	10^6
$\sum_i Y_i\sigma_i$ (Ref. 87)	15.4	2.8	0.49	0.10	0.09
$\sum_i Y_i\sigma_i$ (Ref. 88)	15.2	2.78	0.54	0.230	0.106

Gordeev and Pupko[88] determined the total absorption resonance integral per pair of fission fragments in the energy range from 100 to 10^6 ev to be 23 barns.

Fission product poisoning in reactors with circulating fuel has also been considered. Lock[89] develops the mathematical treatment and gives formulae for the calculation of the amount of any fission product after any time of reactor operation under varying conditions. Various efficiencies of removing fission product gases are considered. Davidge and Lock[90] make calculations of poisoning from fission product gases in liquid-fueled reactors under various conditions of halogen removal and chemical processing of the reactor solution.

5.2.3 ISOTOPE BUILDUP IN THORIUM REACTORS

The nuclear reactions occurring during neutron irradiation of Th^{232} are diagrammed in Fig. 5-41.

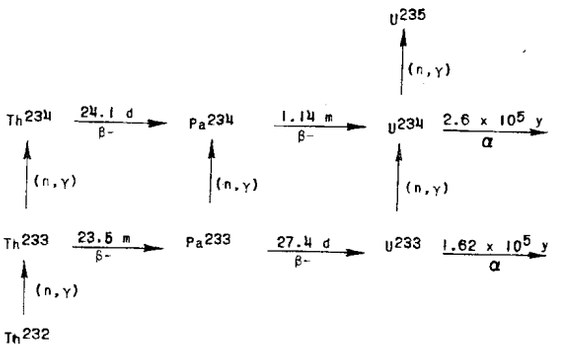

Fig. 5-41 — Nuclear reactions under thermal irradiation of Th^{232}.

Thorium slugs (about 4 cm OD, 16 cm long) have been irradiated[91] in the Low Intensity Test Reactor (LITR) of Oak Ridge National Laboratory, and in a graphite reactor. Using 12.5b for the resonance integral of thorium in the slugs, and 7.0b for the thermal capture cross section of thorium, a value of 8.0b was selected as an effective capture cross section of the thorium in the two reactors. (In both reactors at the site of irradiation, the ratio of resonance to thermal absorption was 0.13.) Using this value for thorium, the differential equations representing the reaction rates in thorium and in Pa^{233} were solved for the effective capture cross section of Pa^{233}. The results for each of seven irradiated slugs are listed in Table 5-23. The weighted average value, 151b, may be compared with an average of 129b, based on five slugs irradiated in the graphite reactor.

Table 5-23 — U^{233} AND U^{234} YIELDS AND DERIVED CROSS SECTIONS FOR LITR IRRADIATIONS

Data from Ref. 91.

Time in Reactor, day	$\frac{U^{233}\ \text{Chain}}{Th^{232}}$ ($\times 10^{-6}$)	$\frac{U^{234}\ \text{Chain}}{U^{233}\ \text{Chain}}$ ($\times 10^{-2}$)	$\sigma_c(Pa^{233})_{eff}$, barns
62	134.0	0.090	138
113	329.0	0.202	149
175	488.0	0.259	145
35	36.7	0.032	154
42	65.8	0.055	152
63	107	0.078	140
133	196	0.135	172

Aluminum-jacketed, solid thorium slugs have been irradiated in the Materials Testing Reactor (MTR) for periods up to 18 months.[92] The reactivity effect of each irradiated slug was determined by period measurements in the Reactivity Measurements Facility (RMF) at the MTR site. The results are shown in Table 5-24. A detailed mass spectrographic analysis was made of a thorium slug (1.33 ID;

Table 5-24—SUMMARY OF DATA ON THORIUM SLUGS IN MTR IRRADIATION

Data from Ref. 92.

Slug No.	% Δk/k	gm U^{233}	nvt ($\times 10^{-20}$)
51	0.107	10.6	11.6
52	0.115	10.9	12.0
53	0.118	10.9	10.1
54	0.115	11.4	13.0
56	0.056	1.5	1.3
57	0.085	3.2	2.9
58	0.090	4.7	4.5
59	0.082	4.4	4.1
60	0.042	3.1	2.8
61	0.050	2.3	2.0
62	0.076	4.5	4.3
63	0.080	6.3	6.3
64	0.062	6.1	6.0
65	0.034	4.9	4.7
66	0.064	4.9	4.7
67	0.074	6.1	6.1
68	0.065	5.2	4.9
69	0.058	4.9	4.7

6.5 inch long) clad with 0.05 in. of aluminum[93,94] The slug had been irradiated in the MTR for one year to an nvt of approximately 10^{21} n/cm^2, and had then cooled for 3.5 years prior to analysis. The average distributions of uranium isotopes at various distances from the slug axis are shown in Table 5-25.

Table 5-25—AVERAGE RADIAL DISTRIBUTION OF URANIUM IN IRRADIATED THORIUM SLUG

Reproduced from Ref. 94.

Radial Interval, cm	U^{233}, wt-%	Isotopic Distribution, % of Total Uranium		
		U^{233}	U^{234}	U^{235}
0.0 – 0.5	0.33	98.50	1.45	0.06
0.5 – 0.9	0.34	98.45	1.50	0.05
0.9 – 1.3	0.36	98.26	1.65	0.09
1.3 – 1.6	0.37	98.23	1.65	0.12
1.6 – 1.7	0.40	98.15	1.72	0.14

Theoretical studies have been made by Taraba,[95] Gresky and Arnold,[96,97] Nisle,[98] and Schuman and Tromp,[99] of the buildup of heavy isotopes during neutron irradiation of thorium.

In most of the work,[95–98] only thermal cross sections are considered, although Ref. 99 allows for epithermal absorption. The cross sections used are listed in each of the references. In Ref. 99, the resonance flux per lethargy interval is taken to be $^1/_{12}$ of the thermal flux (typical of MTR fuel), and the cross sections used are compared with those for such a spectrum later recommended by Stoughton and Halperin[100] (see Section 5.2.5). Thermal cross sections may be compared with those in the latest edition of BNL-325.[70,101] The greatest uncertainty lies in the absorption cross section of Pa^{233}. Stoughton and Halperin recommend a 2200-m/sec value of 70 ± 20 barns, an effective resonance integral of 1200 ± 400 barns, and an effective capture cross section for the spectrum in Ref. 99, of 170 ± 40 barns. Values used by the various investigators in the buildup calculations[95–99] varied from 90 to 150 barns.

Gresky and Arnold consider both batch[97] and continuous[96] irradiation of thorium. In batch irradiation, the concentration of Th^{232} is held constant and the higher isotopes build up from initially zero concentrations. For example, the equation for the buildup of Pa^{233} is

$$\frac{dN_{13}}{dt} = N_{02}\,\phi\sigma_{02} - N_{13}\,\phi\sigma_{13} - N_{13}\,\lambda_{13}$$

where notation is standard. The solution of this equation is

$$\frac{N_{13}}{N_{02}} = \frac{\phi\sigma_{02}}{\phi\sigma_{13} + \lambda_{13}} \{1 - \exp [-(\phi\sigma_{13} + \lambda_{13})\, t]\}$$

In continuous irradiation, the equilibrium concentrations are considered for a continuous irradiation and continuous chemical processing of the heavy isotopes formed from a mole of thorium which is kept constant. Thus for the Pa^{233} concentration, the differential equation is

$$\frac{dN_{13}}{dt} = N_{02}\, \phi\sigma_{02} - N_{13}\, \phi\sigma_{13} - N_{13}\, \lambda_{13} - N_{13}C = 0$$

which has the solution

$$\frac{N_{13}}{N_{02}} = \frac{\phi\sigma_{02}}{\phi\sigma_{13} + \lambda_{13} + C}$$

where C is the chemical processing rate, i.e., the inverse of the processing period.

Figures 5-42 through 5-46 show the buildup of the heavy isotopes for batch irradiation at various fluxes. Figure 5-47 shows the effect of neutron flux and irradiation time on the Pa^{233}/U^{233} ratio.

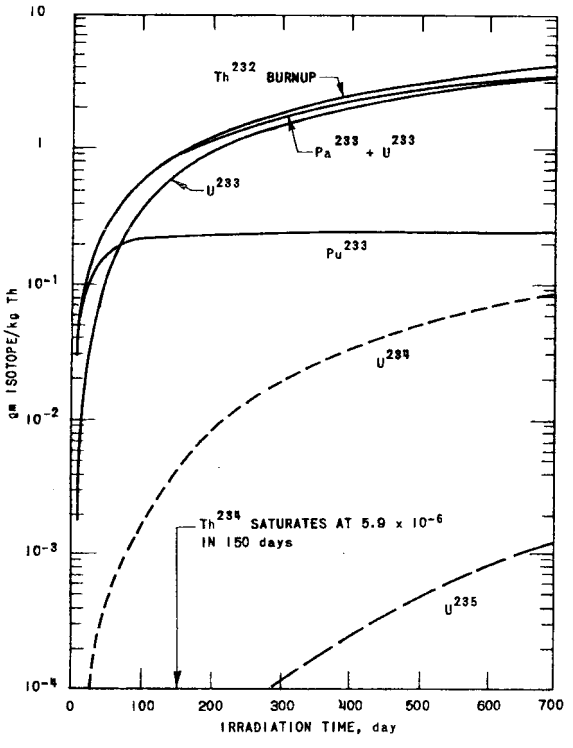

Fig. 5-42 — Concentration of heavy isotopes produced by long-term irradiation of Th^{232} at flux of 10^{13} n/(cm²)(sec). *Reproduced from Ref. 97.*

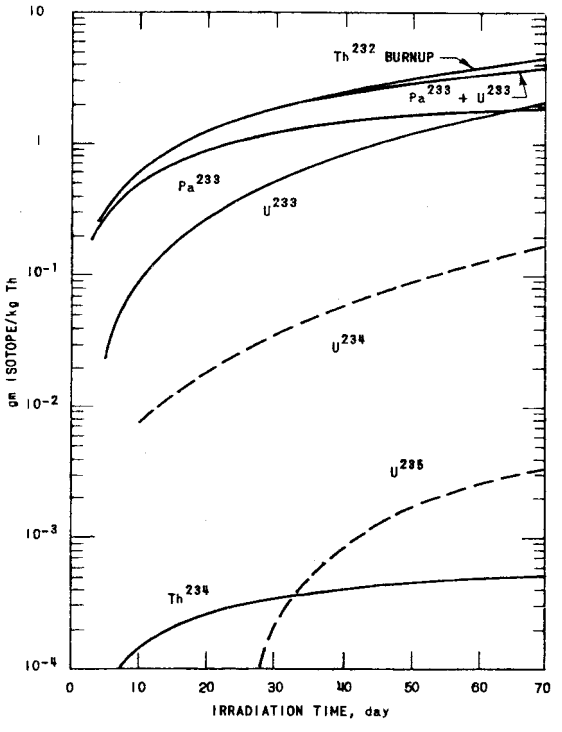

Fig. 5-43 — Concentrations of heavy isotopes produced by short-term irradiation of Th^{232} at flux of 10^{14} n/(cm²)(sec). *Reproduced from Ref. 97.*

Figure 5-48 summarizes the data of Figs. 5-42 through 5-46. Figures 5-49 and 5-50 for continuous irradiation[96] are analogous to Figs. 5-47 and 5-48 for batch irradiation.

Nisle[98] has compared the heavy isotope production from irradiation of Th^{232} for cycled and for uninterrupted irradiation. For cycled irradiation, the fuel is irradiated for 16 days and then allowed to decay for 5 days, giving a 21-day cycle (MTR cycle). Table 5-26 compares the isotopic production at the end of 25 cycles with that for uninterrupted irradiation.

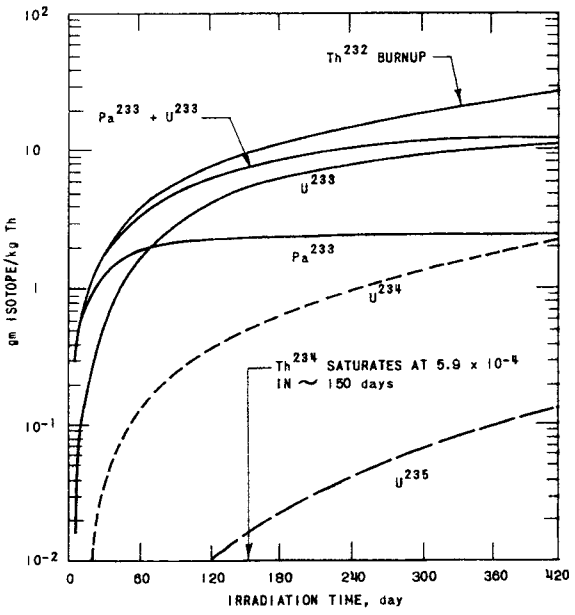

Fig. 5-44—Concentrations of heavy isotopes produced by long-term irradiation of Th^{232} at flux of 10^{14} n/(cm^2)(sec). *Reproduced from Ref. 97.*

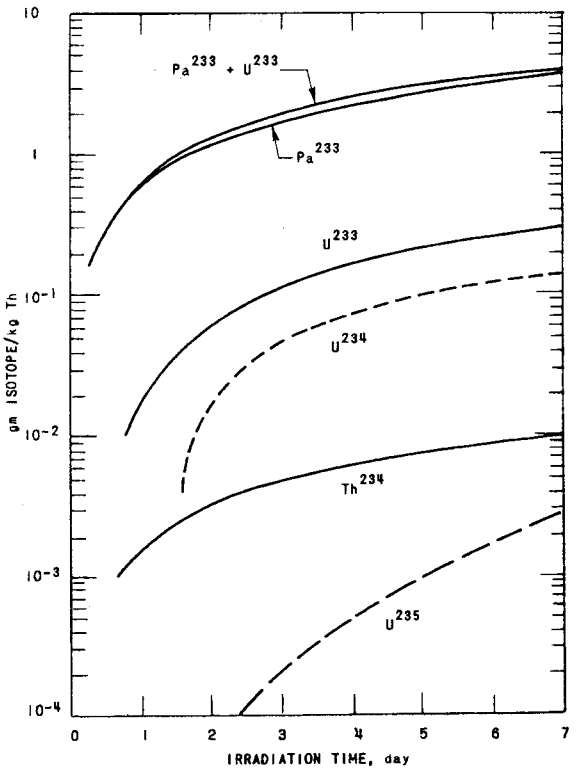

Fig. 5-45—Concentrations of heavy isotopes produced by short-term irradiation of Th^{232} at flux of 10^{15} n/(cm^2)(sec). *Reproduced from Ref. 97.*

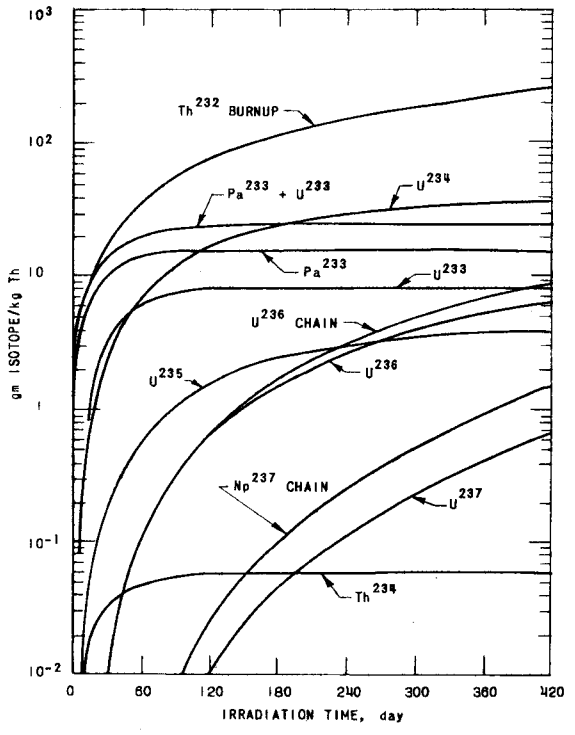

Fig. 5-46—Concentrations of isotopes produced by long-term irradiation of Th^{232} at flux of 10^{15} n/(cm^2)(sec). *Reproduced from Ref. 97.*

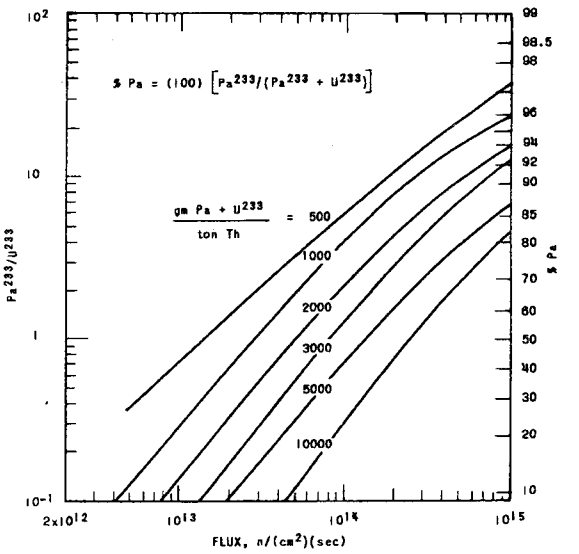

Fig. 5-47—Effect of neutron flux and extent of irradiation on Pa^{233}/U^{233} ratio. *Reproduced from Ref. 97.*

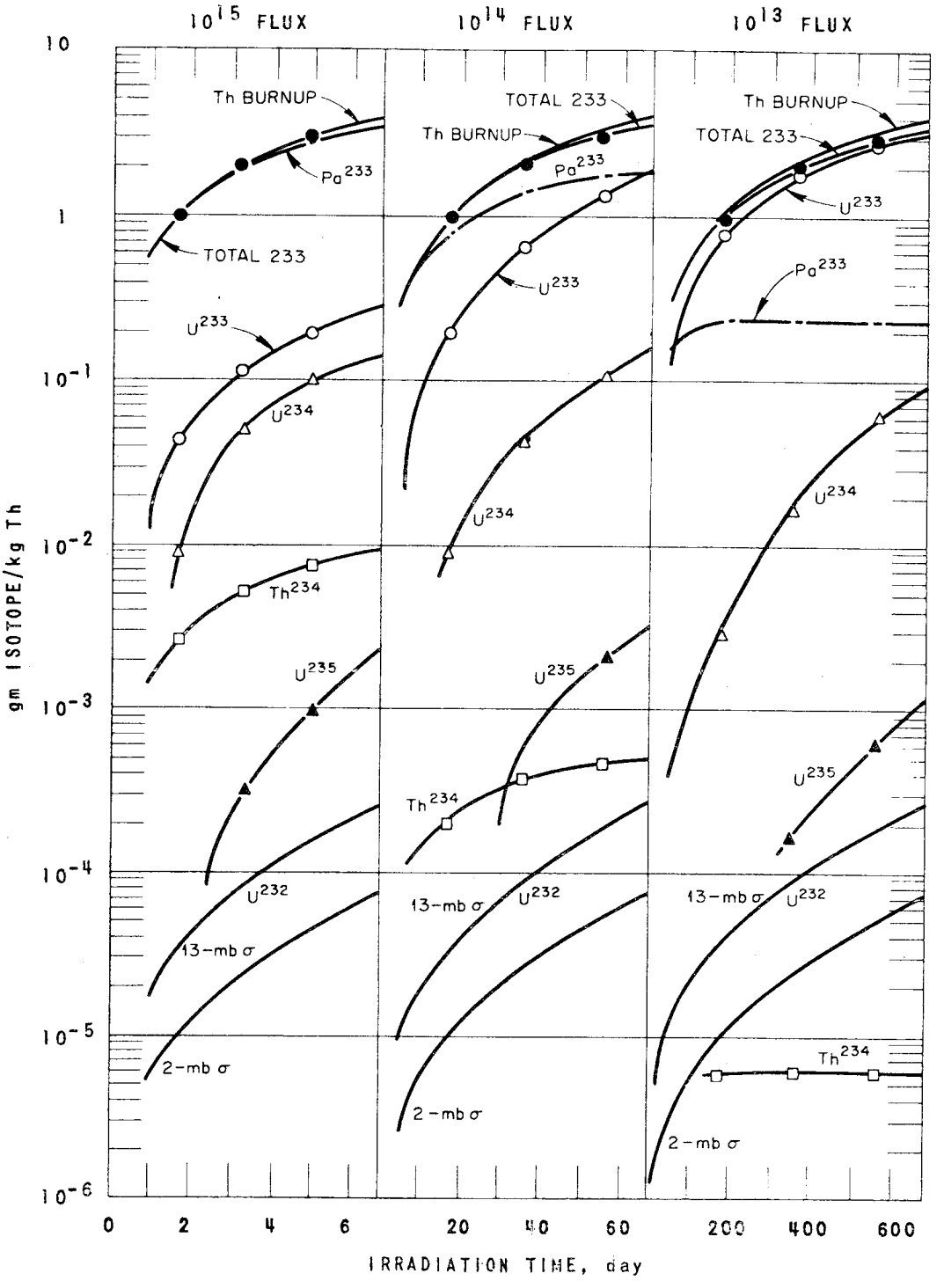

Fig. 5-48 — Summary of Th^{232} neutron irradiation data. *Reproduced in part from Ref. 97.*

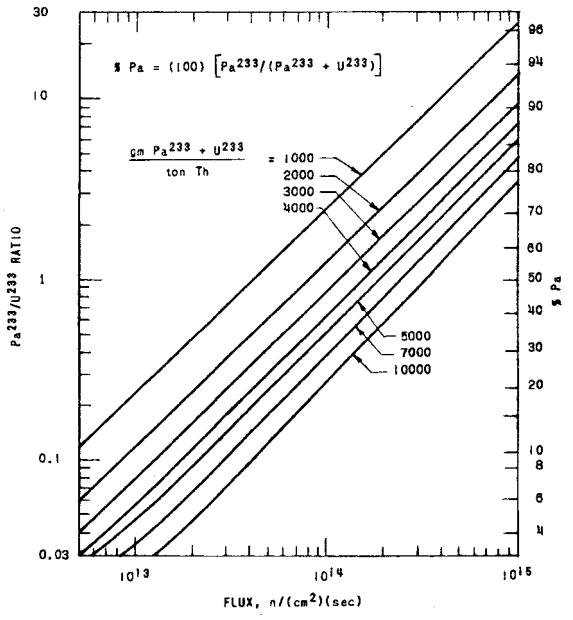

Fig. 5-49 — Effect of neutron flux and (gm/ton) level on Pa^{233}/U^{233} ratio. *Reproduced from Ref. 96.*

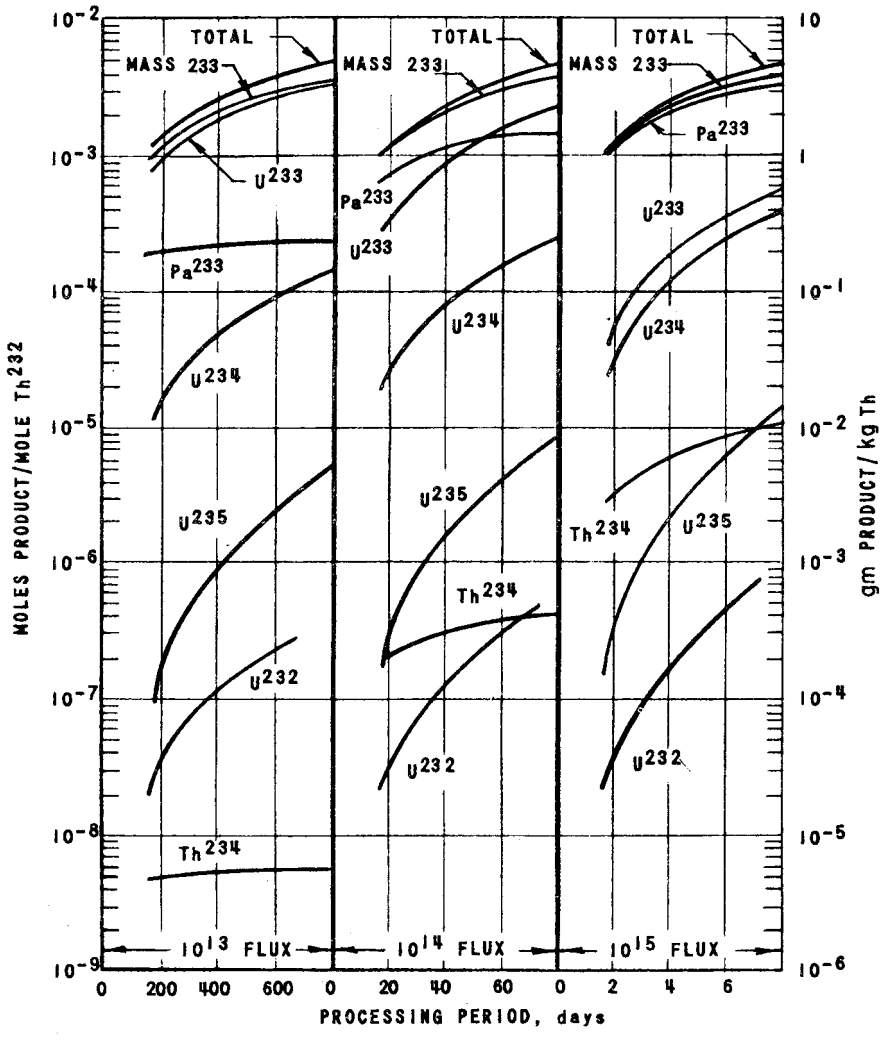

Fig. 5-50 — Effect of reactor processing period, and neutron flux, on products formed by irradiation of Th^{232}.

Table 5-26—COMPARISON OF ISOTOPE PRODUCTION FOR CYCLED VS. UNINTERRUPTED IRRADIATION

Data from Ref. 98.

25 MTR Cycles; Flux = 10^{13} nv; Initial Th^{232} = 3×10^{22} nuclei

Isotope	25 Cycles Irradiation	Uninterrupted Irradiation
Pa^{233}	6.3373×10^{18} nuclei	7.8411×10^{18} nuclei
U^{233}	6.6552×10^{19}	6.5286×10^{19}
$U^{233} + Pa^{233}$	7.2889×10^{19} (Item 1)	7.3127×10^{19} (Item 2)
U^{234}	9.1488×10^{17}	9.4016×10^{17}
U^{235}	6.776×10^{15}	7.7368×10^{15}
U^{233} fissioned	5.9219×10^{18}	5.6463×10^{18}
U^{235} fissioned	8.4572×10^{15}	8.0003×10^{14}
$U^{233} + U^{235}$ fissions	5.9208×10^{18} (Item 3)	5.6471×10^{18} (Item 4)
Th^{232}	2.9220×10^{22}	2.9920×10^{22}
Difference in eventual U^{233} (Item 1 − Item 2) = -0.238×10^{18} (loss)		
Difference in fissioned nuclei (Item 3 − Item 4) = 0.283×10^{18} (gain)		

Note: Cumulative irradiation is the same for both the cycled and uninterrupted irradiation cases.

Schuman and Tromp[99] have calculated the composition of many reactor-irradiated heavy nuclides in a flux with an epithermal component. Figures 5-51 through 5-53 present the thorium data for three values of thermal flux. The fast flux is stated on these figures because it is involved in the Th^{232} (n,2n) reaction.

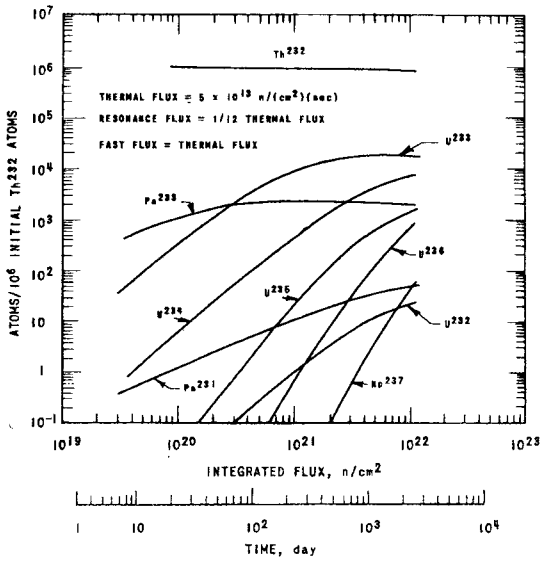

Fig. 5-51—Composition of reactor-irradiated thorium. *Reproduced from Ref. 99.*

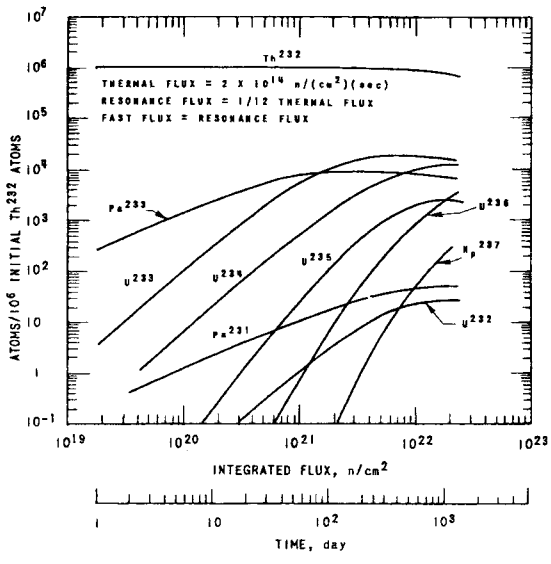

Fig. 5-52—Composition of reactor-irradiated thorium. *Reproduced from Ref. 99.*

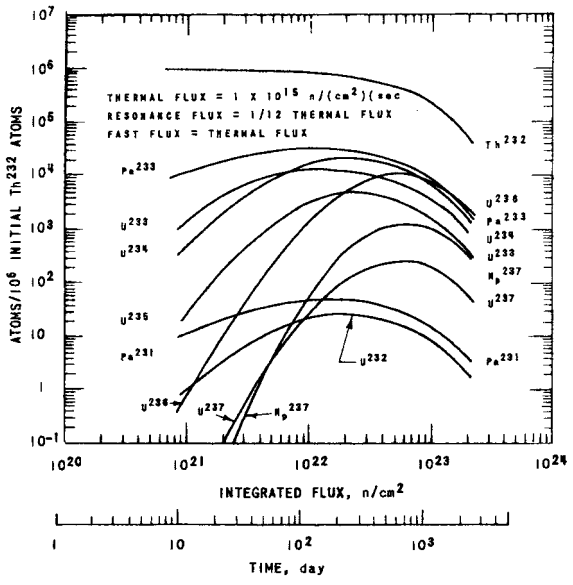

Fig. 5-53—Composition of reactor-irradiated thorium. *Reproduced from Ref. 99.*

5.2.4 STUDIES OF ISOTOPE CONCENTRATION IN URANIUM-THORIUM REACTORS

Typical conceptual designs of U^{233} breeder reactors involve irradiation of a thorium blanket and the chemical processing of this thorium to obtain U^{233} for replenishment of the fuel in the core. Discussions of such reactor cycles have been published,[102–110] and include curves for isotope buildup, reactivity effects of irradiation, refueling requirements, etc.

Stoughton and Halperin[111] have reported studies of five different cases involving the replenishment of core fuel, initially either U^{233} or U^{235}, with U^{233} either pure or containing 5% U^{234}. Long and Lock[112] have published tables showing the amounts produced of these higher isotopes in a reactor where the U^{233} concentration is held fixed, and the various isotopes are exposed continuously to a constant flux of 10^{15} n/(cm^2)(sec). These computations are summarized in Table 5-27. Resonance absorption was neglected in these calculations.

Davey[113] has applied the g and s factors (see Section 3.2.2 for discussion of Westcott's notation: $\hat{\sigma} = \sigma_0$ (g + rs)) given by Campbell and Freemantle[114] (in Ref. 114, the related notation $\bar{S}$ and S^1 is used), to the computation of effective cross sections as a function of the ratio of epithermal to thermal absorptions in the system. Using an effective neutron temperature of 475°C, Davey computed the effective cross sections of U^{233}, U^{234}, U^{235}, and U^{236} as a function of λ, where

$$r = \frac{1.345\,\lambda}{1 + 1.345\,\lambda}$$

is based on an epithermal flux consisting of a Maxwellian plus a 1/E flux beginning at ~2.81 kT_{eff}. The factor λ plays the part of the factor β used by Westcott. The results are shown in Table 5-28.

Table 5-29 gives the equilibrium quantities of the uranium isotopes as calculated by Davey, using the above cross sections.

Schuman and Tromp[99] calculated the composition of reactor-irradiated U^{233} in a spectrum having a resonance flux per lethargy interval equal to $1/12$ of the thermal flux. In general, the results (Fig. 5-54), are independent of the flux as long as $\phi_{res}/\phi_{thermal} = 1/12$; there is a slight dependence of $U^{237} + Np^{237}$ on the flux.

Carter[115] has published a collection of graphs, derived from analog computer calculations, describing the buildup of various heavy isotopes arising from constant power operation of low enrichment, fixed fuel systems. The systems were initially fueled with U^{235} and contained thorium as fertile material. The effects of three parameters were studied: power level, initial U^{235} enrichment, and the probability of escaping resonance capture by Th^{232}. The report includes curves of the variation of η during irradiation, where η is the number of neutrons produced per thermal neutron absorbed in the materials present in the fuel rod. Spinrad, et al.,[105] have also reported on similar studies.

687863 O - 63 - 28

Table 5-27 — AMOUNTS OF HIGHER ISOTOPES PRODUCED FROM U^{233} AFTER VARIOUS TIMES IN A FLUX OF 10^{15} n/(cm^2)(sec)

Reproduced from Ref. 112.

Results expressed as a fraction of original fissile material ($\times 10^{-3}$)

Time, days:	1	3	10	30	100	300	1000	∞
U								
N_{24}/N_{23}	4.500	13.400	43.50	123.00	334.0	611.0	721.0	721.0
N_{25}/N_{23}	0.041	0.116	1.15	7.08	30.4	62.7	74.1	75.6
N_{26}/N_{23}	—	—	—	0.28	12.6	96.1	421.0	900.0
N_{27}/N_{23}	—	—	—	0.002	0.08	0.66	3.17	6.44
N_{28}/N_{23}	—	—	—	—	—	0.0	1.12	21.0
N_{29}/N_{23}	—	—	—	—	—	—	—	0.001
Total N_U/N_{23}	4.541	13.516	44.65	130.36	377.08	770.47	1,220.4	1,724.0
Np								
N_{37}/N_{23}	—	—	—	—	0.1709	3.151	19.89	47.4
N_{38}/N_{23}	—	—	—	—	0.0052	0.095	0.602	1.4
N_{39}/N_{23}	—	—	—	—	—	—	0.004	0.07
N_{30}/N_{23}	—	—	—	—	—	—	0.00	0.00
Total N_{Np}/N_{23}	0.000	0.000	0.000	0.000	0.1761	3.146	20.50	48.9
Pu								
N_{48}/N_{23}	—	—	—	—	0.0459	0.847	5.35	12.74
N_{49}/N_{23}	—	—	—	—	0.0186	0.342	2.17	5.39
N_{40}/N_{23}	—	—	—	—	0.0106	0.196	1.25	3.08
N_{41}/N_{23}	—	—	—	—	0.0049	0.073	0.46	1.14
N_{42}/N_{23}	—	—	—	—	0.05	0.92	5.86	14.50
N_{43}/N_{23}	—	—	—	—	—	—	—	0.01
Total N_{Pu}/N_{23}	0.00	0.00	0.00	0.00	0.130	2.38	15.09	36.83
Am								
N_{53}/N_{23}	—	—	—	—	—	0.23	1.47	3.63
N_{54}/N_{23}	—	—	—	—	—	—	—	0.007
Total N_{Am}/N_{23}	0.00	0.00	0.00	0.00	0.00	0.23	1.47	3.64
Cm								
N_{64}/N_{23}	—	—	—	—	—	—	—	0.05
Total N_{Cm}/N_{23}	0.00	0.00	0.00	0.00	0.00	0.00	0.00	0.05

Legend: $N_{2j} \equiv U^{23j}$ atoms, j = 3 to 9; $N_{3k} \equiv Np^{23k}$, k = 7 to 9; $N_{30} \equiv Np^{240}$; $N_{48} \equiv Pu^{238}$; $N_{49} \equiv Pu^{239}$; $N_{4n} \equiv Pu^{24n}$, n = 0, 1, 2, 3; $N_{5j} \equiv Am^{24j}$, j = 3, 4; $N_{64} \equiv Cm^{244}$.

Table 5-28—EFFECTIVE CROSS SECTIONS AND ETA VALUES

Reproduced from Ref. 113.

U^{233}	$\lambda = 0$	0.05	0.10	0.15	0.20	0.25
σ_a	590.0	658.2	718.3	771.7	819.4	862.2
σ_f	538.0	600.2	655.0	703.7	747.2	786.2
σ_c	52.00	58.01	63.31	68.01	72.22	76.00
η	2.289	2.289	2.289	2.289	2.289	2.289
U^{234}						
σ_a	92.0	151.9	204.7	251.6	293.5	331.1
U^{235}						
σ_a	626.8	632.6	637.6	642.2	646.2	649.8
σ_f	530.4	531.2	531.9	532.6	533.2	533.7
σ_c	96.4	101.4	105.7	109.6	113.0	116.1
η	2.075	2.059	2.046	2.034	2.024	2.014
U^{236}						
σ_a	6.0	31.25	53.54	73.30	90.97	106.8

Table 5-29—EQUILIBRIUM QUANTITIES OF THE URANIUM ISOTOPES

Data from Ref. 113.

$\frac{\text{Atoms}}{\text{cc}}$	$\lambda = 0$	0.05	0.10	0.15	0.20	0.25
N_{23}	1000	1000	1000	1000	1000	1000
N_{24}	565	382	309	270	246	230
N_{25}	83	92	99	106	112	117
N_{26}	1334	299	195	158	139	127
Total:	2982	1773	1603	1534	1497	1474

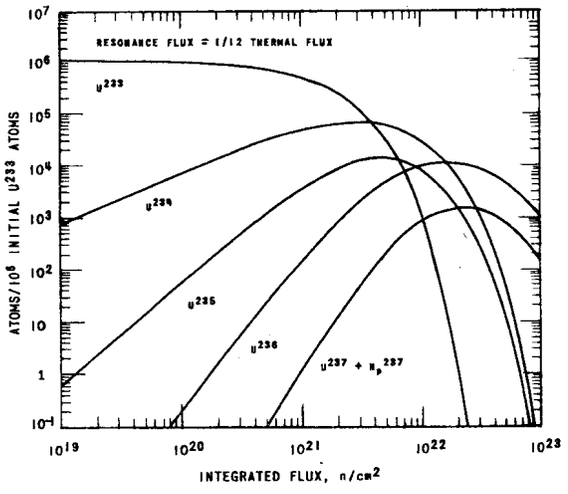

Fig. 5-54—Composition of reactor-irradiated U^{233}. *Reproduced from Ref. 99.*

Carter and Howard[116] extended the analog computation (Ref. 115) to mixtures of enriched thorium (i.e., $Th^{232} + U^{235}$), with or without natural uranium. These calculations assumed a neutron temperature of 650°K while the earlier calculations were for room temperature. Also, calculations without fission products, and with fission products having an effective cross section of 50 barns per fission were compared. The results for cases without natural uranium are shown in Fig. 5-55. The quantity μ appearing on these graphs is given by $\mu = \epsilon(1 - p)L$, where ϵ is the fast fission factor; p is the resonance escape probability; and L is the fast non-leakage probability. The fission products have a large effect on η/η_0 for long irradiations. A comparison of all the graphs given in Ref. 116 shows that the variations in $Th^{232}-U^{235}$ fuel are very roughly a mirror image of the η variations in $U^{238}-U^{235}$ fuel. Thus it is concluded that a reactor loaded with a mixture of natural uranium and thorium can have a rather flat curve of reactivity versus irradiation time over its lifetime.

References 105, 109, and 110 make comparisons between U^{235}–Th systems and $U^{238}-U^{235}$ systems. Some of the material given below may be compared with that on $U^{238}-U^{235}$ systems given in the following sections. Figure 5-56 from Ref. 110 shows the change of fuel composition with cumulative burnup in uranium recycle operation for a light-water reactor initially fueled with $ThO_2 + U^{235}O_2$. Each cycle is fueled with make-up thorium mixed with recovered uranium, and enough makeup of U^{235} to provide a burnup of 6000 Mwd/ton. The slight increase in U^{233} concentration from the end of one cycle of operation to the beginning of the next is due to the decay of Pa^{233} prior to chemical processing. The decreases in concentration of U^{234} and U^{236} between cycles reflect processing losses. Figure 5-57 is similar to Fig. 5-56 but is for a heavy-water reactor initially fueled with $Th + U^{235}$. The U^{235} content for the loading of each cycle is chosen to give a burnup of 31,000 Mwd/ton.

5.2.5 HEAVY ISOTOPE BUILDUP AND REACTIVITY VARIATION OF PLUTONIUM-URANIUM SYSTEMS

The nuclear reactions among the heavy isotopes under neutron irradiation are given in Fig. 5-58.

The cross sections required for the calculation of isotope buildup are reported in the literature in two general classes: basic and effective cross sections. The effective cross sections (e.g., identified by $\hat{\sigma}_i$ in the Westcott notation), when multiplied by a certain flux (i.e., $\phi = nV_0$, where $V_0 = 2200$ m/sec), provide the correct reaction rate; thus in their interpretation, the spectrum of the reactor in question and the definition of the flux must be taken into account. Effective cross sections and their use are discussed in Refs. 91, 100, 117–121, and many others.

Basic Constants. Besides the standard BNL-325 data, some excellent survey reports are available which summarize the best values of the constants.[100,117,121] Usually the 2200-m/sec values, I_∞ (the infinite dilution resonance integral), and some other helpful constants are given. In Table 5-30, the effective cross sections are defined as

$$\sigma_{eff} = \sigma_{th} + \frac{\phi_{res}}{\phi_{th}} I_\infty$$

and give the correct reaction rate for an infinitely dilute substance when multiplied by the thermal (2200 m/sec) flux. The lower limit for I_∞ is the cadmium cutoff energy.

Irradiation of Plutonium. Plutonium samples irradiated in the NRX and MTR reactors have been analyzed to determine the Pu isotopic distributions and their effective cross sections. Fields, et al.,[122] applied a method of successive approximations to determine σ_{eff}^{241} and σ_{eff}^{240}. The concentrations of the isotopes used as points of reference in this analysis were obtained by mass spectrometric methods from three samples of Pu irradiated in the NRX reactor for periods of six months, one year, and two years. The experimental concentrations are given in Table 5-31, together with an isotopic description of the starting material (CW-3), one of the original samples irradiated by Fermi in 1944. The results of the theoretical analysis for the effective cross sections of Pu^{241} in the NRX reactor are listed in Table 5-32. The NRX reactor is D_2O moderated, fueled with natural uranium, and operated at 60°C. In the Westcott[121] notation the reactor spectrum is characterized by

$$\hat{\sigma}_{NRX} = g\sigma_0 + 0.079\, I_{eff}$$

where I_{eff} is the effective (self-shielding corrected) resonance integral.

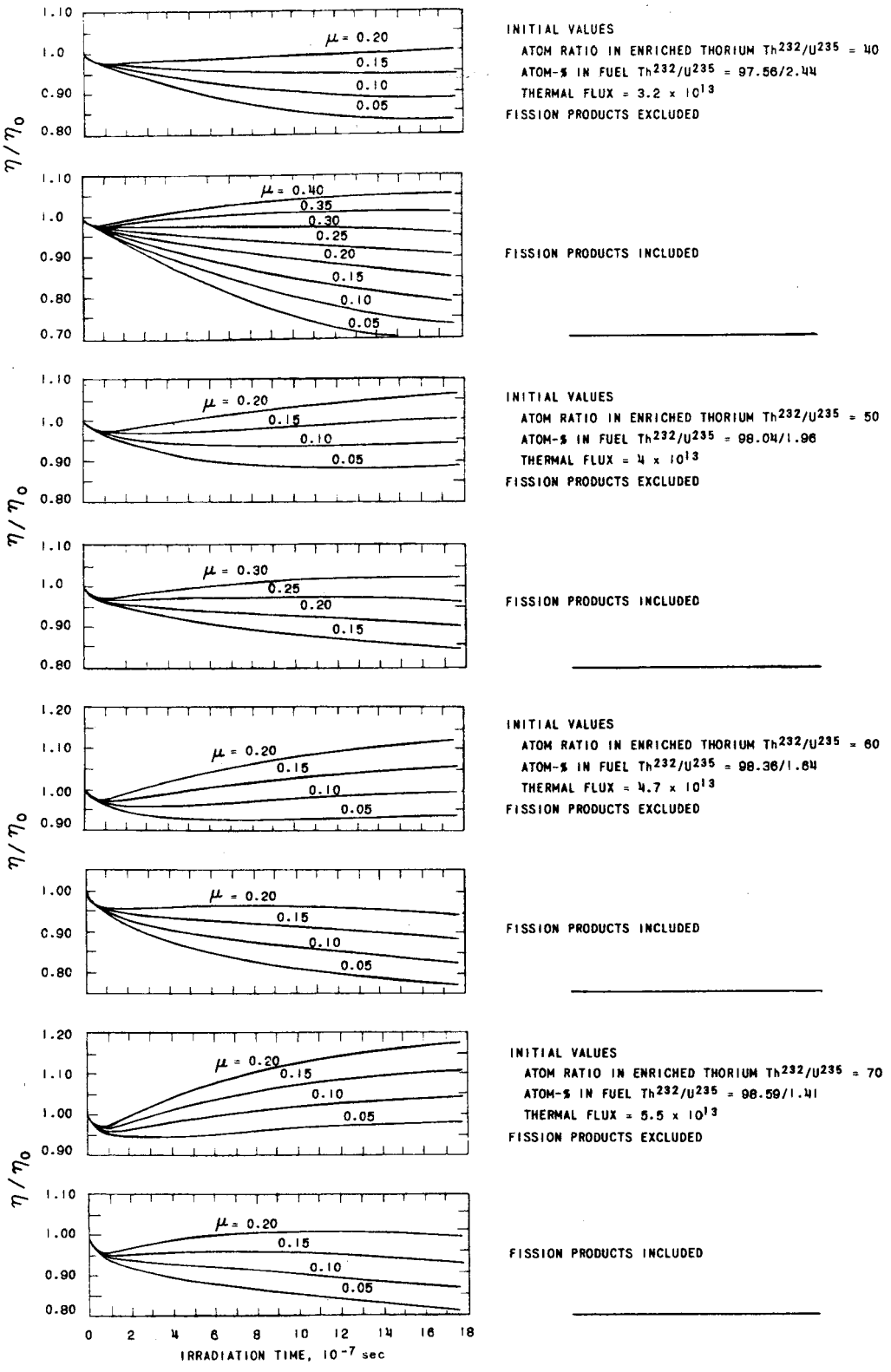

Fig. 5-55—Variation of η in Th^{232}/U^{235} systems for initial values cited, with and without fission products. Constant specific power = 20 Mw/ton; Mwd/ton = $(1.574)(10^{-4})$(Mw/ton)(sec). *Reproduced from Ref. 116.*

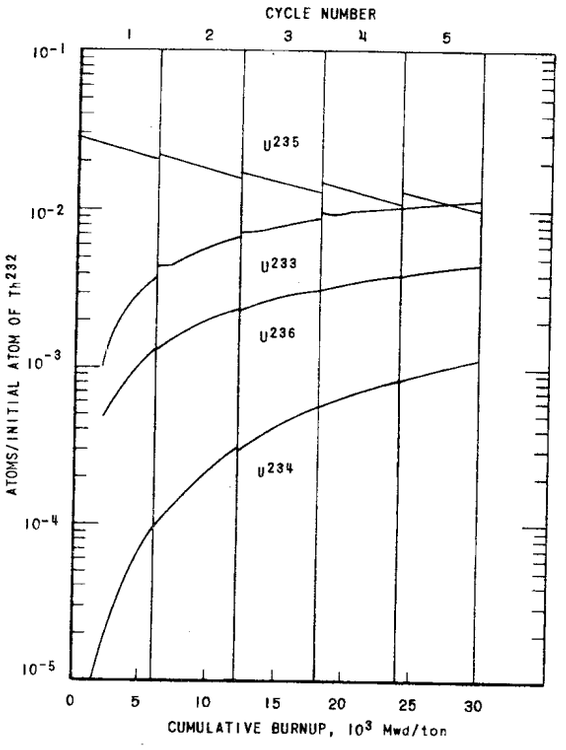

Fig. 5-56 — Change of fuel composition with cumulative burnup in uranium recycle operation for thorium oxide-fueled, light-water reactor. Burnup/cycle = 6,000 Mwd/ton. *Reproduced from Ref. 110.*

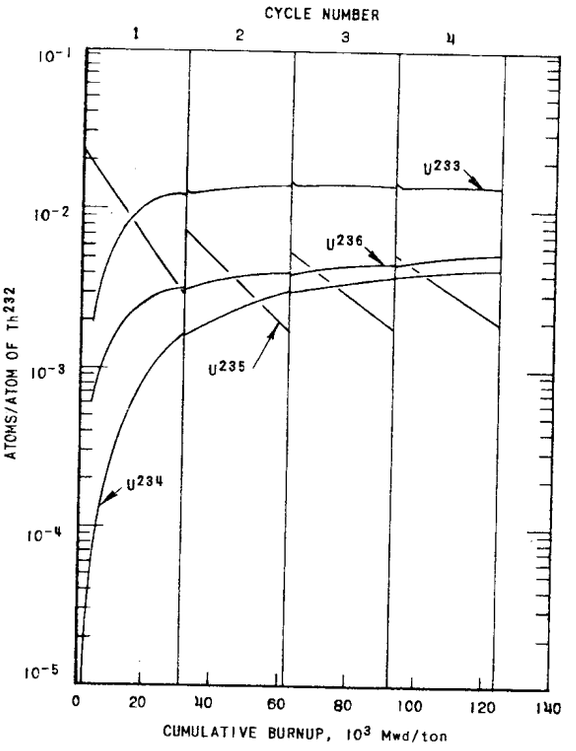

Fig. 5-57 — Change in fuel composition with cumulative burnup in uranium recycle operation for thorium-fueled, heavy-water reactor. Burnup/cycle = 31,000 Mwd/ton. *Reproduced from Ref. 110.*

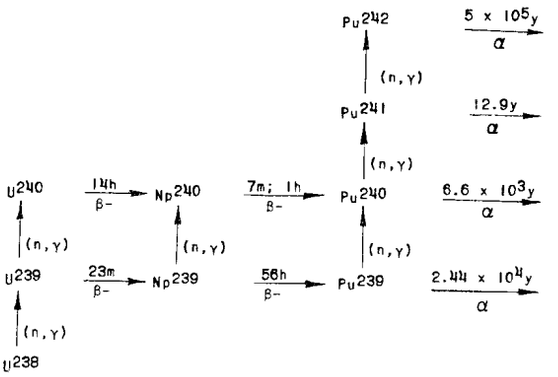

Fig. 5-58 — Nuclear reactions under neutron irradiation of U^{238}.

Table 5-30—PREFERRED VALUES OF HEAVY NUCLIDE CROSS SECTIONS (in barns)

(σ_{eff} values are for $\Phi_r/\Phi_{th} = 1/12$ and $E_m = 0.03$ ev)

Reproduced from Ref. 100.

Nuclide	Process[a]	σ_0 (2200 meters/sec)	$(g\sigma_0)^b$	I_∞	σ_{eff}
Th^{232}	C	7.45 ± .15	7.45 ± .15	85 ± 10	14.5 ± 1.5
Th^{233}	C	1450 ± 300	1450 ± 100	400 ± 100	1500 ± 150
Pa^{233}	C	70 ± 20	70 ± 20	1200 ± 400	170 ± 40
U^{233}	C	52 ± 5	48 ± 10	300 ± 100	70 ± 20
	A	580 ± 15	580 ± 30	1200 ± 200	680 ± 50
	F	530 ± 15	535 ± 20	900 ± 100	610 ± 50
U^{234}	C	95 ± 10	95 ± 10	700 ± 100	150 ± 20
U^{235}	C	110 ± 15	110 ± 15	150 ± 50	125 ± 20
	A	695 ± 15	685 ± 20	450 ± 100	720 ± 30
	F	580 ± 15	570 ± 20	300 ± 50	595 ± 30
U^{236}	C	6 ± 2	6 ± 2	400 ± 100	40 ± 10
U^{238}	C	2.72 ± 0.05	2.74 ± 0.05	280 ± 15	26 ± 2
U^{239}	C	—	25 ± 15	—	25 ± 15
	F	—	15 ± 10	—	15 ± 10
Np^{239}	C	45 ± 15	45 ± 15	—	80 ± 20
Pu^{239}	C	280 ± 30	350 ± 40	1500 ± 300[c]	480 ± 50
	A	1030 ± 40	1160 ± 50	3500 ± 500[c]	1460 ± 100
	F	750 ± 30	810 ± 40	2000 ± 200[c]	980 ± 60
Pu^{240}	C	280 ± 20	300 ± 30	9000 ± 1500	1100 ± 200
Pu^{241}	C	375 ± 50	410 ± 50	1000 ± 300[c]	500 ± 100
	A	1400 ± 100	1510 ± 150	2800 ± 500[c]	1750 ± 200
	F	1025 ± 50	1100 ± 50	1800 ± 300[c]	1250 ± 100
Pu^{242}	C	25 ± 10	25 ± 10	1300 ± 200	130 ± 30

[a]Here C, A, and F represent capture, absorption (i.e., capture plus fission), and fission respectively.

[b]σ_{th} values may be calculated on the assumption of a 1/v behavior out to the Cd cutoff by adding 0.45 $\sigma_0\Phi_r/\Phi_{th}$ to the $g\sigma_0$ values. (This should not be done in the case of Pu^{239} or Pu^{241}.)

[c]Values obtained by integrating from 0.15 ev to about 1 Mev.

Table 5-31—MASS SPECTROMETER ANALYSIS OF PLUTONIUM SAMPLES IRRADIATED IN THE NRX REACTOR (in per cent)[a]

Data from Ref. 122.

Sample	Pu^{239}	Pu^{240}	Pu^{241}	Pu^{242}	Approx. nvt
CW-3	92.63 ± 0.07	6.96 ± 0.07	0.406 ± 0.005	—	1×10^{20}
CR-1	74.31 ± 0.22	21.96 ± 0.20	3.39 ± 0.07	0.337 ± 0.01	7×10^{20}
CR-2	53.3 ± 0.3	35.6 ± 0.2	9.17 ± 0.04	1.96 ± 0.03	1×10^{21}
CR-3	23.82 ± 0.16	49.35 ± 0.40	17.07 ± 0.24	9.76 ± 0.07	3×10^{21}

[a]The measured Pu^{241} concentration was corrected for decay and all the isotopic values were then readjusted to 100%.

Table 5-32—NEUTRON ABSORPTION AND CAPTURE CROSS SECTIONS OF Pu^{240} AND Pu^{241}[a] (in barns)

Reproduced from Ref. 122.

Sample	$\sigma_{a,eff}(Pu^{240}) = \sigma_{c,eff}(Pu^{240})$	$\sigma_{a,eff}(Pu^{241})$	$\sigma_{c,eff}(Pu^{241})$	$\sigma_{f,eff}(Pu^{241})$
CR-1	560 ± 55	1450 ± 250	390 ± 80	1060 ± 210
CR-2	550 ± 55	1450 ± 250	390 ± 80	1060 ± 210
CR-3	495 ± 50	1450 ± 250	390 ± 80	1060 ± 210

[a]The values are based on $\sigma_{a,eff}(Pu^{239}) = 1150$ barns; $\sigma_{c,eff}(Pu^{239}) = 385$ barns; $\sigma_{f,eff}(Pu^{240}) = 0$; and $\sigma_{a,eff}(Pu^{242}) = 30$ barns.

Irradiations of Pu^{239} samples in a thermal neutron flux at 3×10^{14} n/(cm^2)(sec) were carried out in the MTR[123] up to an integrated flux of 1.4×10^{22} n/cm^2. A segment of the results is presented in Table 5-33. By measuring the concentrations of the various heavy isotopes as a function of exposure level (n/cm^2), it was possible to derive effective cross sections of the heavier plutonium and transplutonium isotopes. The results are reported in Refs. 122 and 123. Using these effective cross sections, computations were made of the heavy isotope buildup during irradiations in a thermal neutron flux of 3×10^{14} n/(cm^2)(sec); the results are summarized in Fig. 5-59.

Table 5-33—PRODUCTS FROM PLUTONIUM IRRADIATIONS IN THE CORE OF THE MATERIALS TESTING REACTOR

Reproduced from Ref. 123.

Sample No.:	MTR-1	MTR-2	MTR-3
Mass of Pu^{239} inserted, mg	350	350	170
nvt, n/cm^2	4×10^{21}	1.1×10^{22}	1.4×10^{22}
Mass of Pu after irradiation, mg[a]	50	20	6
Isotopic composition of the Pu, mol-%[b]			
Pu^{238}	—	0:216 ± 0.004	0.16 ± 0.02
Pu^{239}	5.33 ± 0.05	0.087 ± 0.002	0.068 ± 0.004
Pu^{240}	39.0 ± 0.4	2.02 ± 0.02	0.633 ± 0.006
Pu^{241}	21.6 ± 0.3	1.31 ± 0.01	0.308 ± 0.006
Pu^{242}	34.1 ± 0.3	96.33 ± 0.02	98.77 ± 0.03
Pu^{244}	0.0018 ± 0.0001	0.037 ± 0.002	0.052 ± 0.004

[a]Approximate yield; efficiency of recovery not determined accurately.
[b]Measured by mass spectrometer.

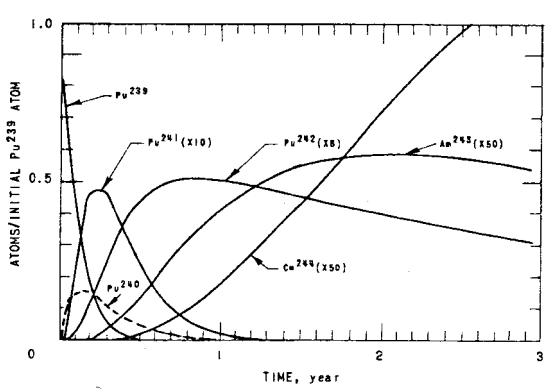

Fig. 5-59—Growth and decay of the heavier plutonium isotopes, Am^{243}, Cm^{244}, as functions of time of exposure of Pu^{239} to a thermal neutron flux of 3×10^{14} n/(cm^2)(sec). *Reproduced from Ref. 122.*

Irradiation of Natural Uranium. A considerable effort has been expended on irradiation effects of natural uranium. A systematic, long-range program in this field has been carried on at Chalk River with cooperation of Harwell and ANL. More recent are investigations of Gunst[124] and co-workers who have irradiated UO_2 up to 15,600 Mwd/ton in the MTR reactor.

Chalk River U Irradiation. The Chalk River data have been analyzed by various groups in many diverse ways. The early work, in particular a thorough analysis of NRX Rod No. 683, is given in Refs. 91, 119, 122, and 125–129. Some later reports are of a survey nature, collecting and correlating the data. Especially detailed are the set of CRRP-761 reports,[130–132] and Ref. 133. A short summary of the work is given in Ref. 134.

The Chalk River group has emphasized the study of the changes in effective cross sections of the heavy nuclides (especially Pu^{239} and Pu^{240}) with irradiation. Kushneriuk[120,135] has developed theoretical methods which take into account the effect of self-shielding and spectrum changes on heavy isotope buildup. This is illustrated by the effective cross sections listed for the NRX and GLEEP reactors in Tables 5-34 and 5-35. The thermal neutron temperature and the irradiation steps considered are identical. The difference between the values in the two tables is caused by the higher epithermal component (higher by a factor of 1.57) in the GLEEP reactor.[133]

Table 5-34—EFFECTIVE TIME-AVERAGE CROSS SECTIONS FOR NRX (in barns)

Data from Ref. 133.

Irradiation (I), n/cm^2 ($\times 10^{21}$)	Pu^{239}		Pu^{240}
	$\hat{\sigma}^{239}$	$\hat{\sigma}_f^{239}$	$\hat{\sigma}^{240}$
0.0	1301	884	1035
0.1	1295	880.6	1020
0.2	1287	875.9	952.5
0.3	1280	872.3	876
0.4	1275	869.3	809
0.5	1271	866.8	753
0.6	1267	864.5	705
0.7	1263	862.6	665

U^{235}: $\hat{\sigma}^{235} = 665.8$; $\hat{\sigma}_f^{235} = 556.6$; for all I.
Pu^{241}: $\hat{\sigma}^{241} = 1500$; $\hat{\sigma}_f^{241} = 1100$; for all I.

Table 5-35—EFFECTIVE CROSS SECTIONS FOR ANALYSIS OF THE GLEEP OSCILLATOR EXPERIMENTS (in barns)

Data from Ref. 133.

Irradiation (I), n/cm^2 ($\times 10^{21}$)	Pu^{239}		Pu^{240}
	$\hat{\sigma}^{239}$	$\hat{\sigma}_f^{239}$	$\hat{\sigma}^{240}$
0.0	1383	929	1473
0.1	1364.9	918.2	1393
0.2	1349.5	909.6	1251
0.3	1336.3	902.6	1105
0.4	1327.7	897.2	984
0.5	1319.5	892.4	889
0.6	1312.7	888.7	816
0.7	1307	885.7	711

U^{235}: $\hat{\sigma}^{235} = 666.9$; $\hat{\sigma}_f^{235} = 555.6$; for all I.
Pu^{241}: $\hat{\sigma}^{241} = 1500$; $\hat{\sigma}_f^{241} = 1100$; for all I.

The isotopic changes of irradiated samples have been analyzed extensively.[130] Tables 5-36 and 5-37 give the changes in the Pu and U chains up to burnups of 0.633×10^{21} n/cm^2.

Table 5-38 lists the radial concentration of Pu isotopes in a section of NRX Rod No. 683 taken from near the midplane of the reactor.[126] This rod had generated about 100 Mwd of energy before re-

Table 5-36— BUILDUP OF PLUTONIUM ISOTOPES

Data from Ref. 130.

Sample	Irradiation, n/cm^2 ($\times 10^{21}$)	$\frac{\text{Atoms Pu}}{\text{Atoms U}}$ ($\times 10^3$)	$\frac{\text{Atoms U}}{\text{Initial atoms U}}$	$\frac{\text{Atoms Pu}}{\text{Initial atoms } U^{235}}$	Isotopic Analysis, %		
					Plutonium Isotope	Uncorrected for Pu^{241} Decay	Corrected for Pu^{241} Decay
8	0.0347	0.1273	0.99972	0.01767	239	99.268 ± .008	99.267
					240	0.727 ± .017	0.727
					241	0.005 ± .005	0.006
5	0.0924	0.3338	0.99926	0.04629	239	98.146 ± .017	98.139
					240	1.824 ± .016	1.824
					241	0.030 ± .007	0.037
9	0.2268	0.7611	0.99818	0.10546	239	95.209 ± .012	95.156
					240	4.537 ± .011	4.535
					241	0.245 ± .005	0.302
11	0.3840	1.2129	0.99679	0.1678	239	92.241 ± .017	92.109
					240	7.163 ± .016	7.153
					241	0.596 ± .007	0.708
4	0.6326	1.8145	0.99525	0.25067	239	87.295 ± .052	87.116
					240	11.267 ± .051	11.250
					241	1.320 ± .010	1.516
					242	0.118 ± .005	0.118

Table 5-37— BURNUP OF U^{235}

Data from Ref. 130.

(1)	(2)	(3)	(4)	(5)	(6)	(7)
Sample	Irradiation, n/cm^2 ($\times 10^{21}$)	$\frac{\text{Atoms } U^{238}}{\text{Initial atoms } U^{238}}$	$\frac{\text{Atoms } U^{235}}{\text{Atoms } U^{238}}$ ($\times 10^2$)	$\frac{\text{Atoms } U^{235} \text{ Burned}}{\text{Initial Atoms } U^{235}}$		% Difference $100 \times [(5)-(6)/(6)]$
			Measured	Calculated	Measured	
8	0.0347	0.9999	0.7116 ± .0010	0.02276	0.0196 ± .0014	+16 ± 7
5	0.0924	0.9997	0.6841 ± .0010	0.05946	0.0576 ± .0014	+3.2 ± 2.4
9	0.2268	0.9992	0.6218 ± .0010	0.1396	0.1439 ± .0014	−3.0 ± 1.0
11	0.3840	0.9986	0.5671 ± .0016	0.2245	0.2197 ± .0022	+2.2 ± 1.0
4	0.6326	0.9977	0.4764 ± .0012	0.3414	0.3451 ± .0017	−1.1 ± 0.5

Table 5-38— RADIAL CONCENTRATION OF PLUTONIUM ISOTOPES IN A SECTION OF NRX ROD NO. 638 (in mg/gm U)

Data from Ref. 126.

Radial Depth, 10^{-3} in.	Total Pu	Pu^{239}	Pu^{240}	Pu^{241}	Pu^{242}
000–002	4.128	3.456	0.567	0.096	0.010
002–004	3.169	2.655	0.433	0.073	0.007
004–006	2.581	2.164	0.351	0.059	0.006
006–008	2.522	2.116	0.342	0.057	0.006
040–043	2.157	1.828	0.280	0.045	0.005
140–145	1.871	1.611	0.225	0.032	0.003
305–310	1.669	1.461	0.182	0.024	0.002
480–485	1.560	1.375	0.162	0.021	0.002

moval. The values in Table 5-38 are based on a combination of alpha counting and mass spectrometric analysis.

Measurements of the relative reactivity change with burnup for the same samples referred to in Tables 5-36 and 5-37, have been made at Harwell using the GLEEP oscillator.[128,136] The unit employed to measure the relative reactivity is defined as follows:

$$\Sigma^{app} = \frac{\text{Signal from irrad. sample} - \text{signal from unirrad. sample}}{\text{Signal from boron standard}} \times \Sigma_a^{\text{boron standard}}$$

That is, the reactor is calibrated by oscillating a boron sample of known absorption cross section; then the irradiated and unirradiated samples are oscillated and the amplitudes of the obtained signals are compared. The cross section obtained is fictitious in the sense that it combines the reactivity effects of changes in absorption and fission cross sections and relates them to a change in absorption cross section only.

The cross section obtained is divided by the number of initial fissile atoms and the resulting new unit is called the "bifa" (barns per initial fissile atom). The results of the oscillator measurements are compared in Fig. 5-60 with a theoretical curve obtained using the cross sections given in Table 5-35.

Assuming some of the better known nuclear constants to be correct, some of the more uncertain ones can be inferred from the experimental data. For example,[133] with $\alpha^{25} = 0.194$, 0.058 U^{238} fissions per thermal fission, and fission energy ≈200 Mev, an initial production rate of plutonium of 0.918 gm/Mwd is obtained. Further, with $\sigma_{eff}^{25} = 665$ barns, the effective cross section of U^{238} is $\sigma_{eff}^{28} = 3.67 \pm 0.04$ barns. Since for thermal neutrons only $\sigma_{th}^{28} = 2.73 \pm 0.03$, this indicates that 25.6 ± 1.1% of Pu is produced by epithermal capture.

MTR UO_2 Irradiation: In the MTR, natural UO_2 has been irradiated up to 15,600 Mwd/ton by Gunst, et al.[124] The experimental and evaluation programs of this group centered around accurate relative reactivity measurements as a function of irradiation and also as a function of post-irradiation cooling time. The measurements of the relative reactivity (η/η_0, where η is the number of fission neutrons produced per thermal neutron absorbed in the sample) were done in the RMF (Reactivity Measurement Facility) reactor.[137] The outstanding feature of these measurements is that the fission and absorption effects on the relative reactivity are separated. This can be done since the RMF facility is calibrated with a series of known absorptive and fissionable standards. The measured asymptotic η/η_0 (with respect to cooling time) at 15,600 Mwd/ton is 0.77. For example, Fig. 5-61 shows a comparison between the calculated and measured cooling transient of η/η_0 for a UO_2 sample irradiated to

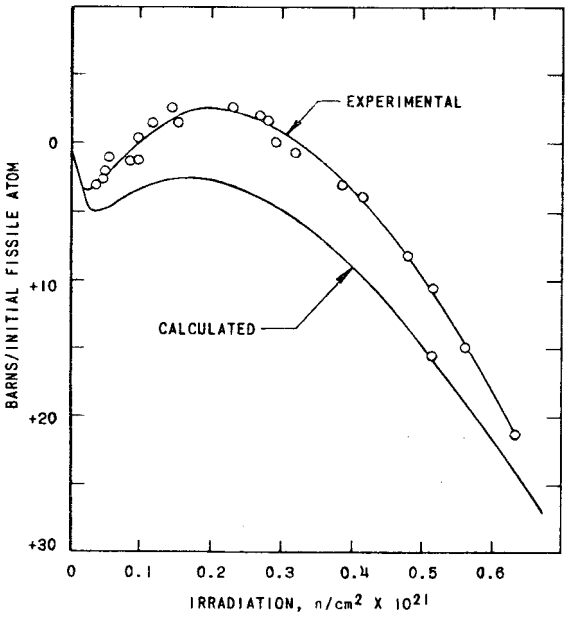

Fig. 5-60 — Reactivity change of irradiated natural uranium. *Reproduced from Ref. 130.*

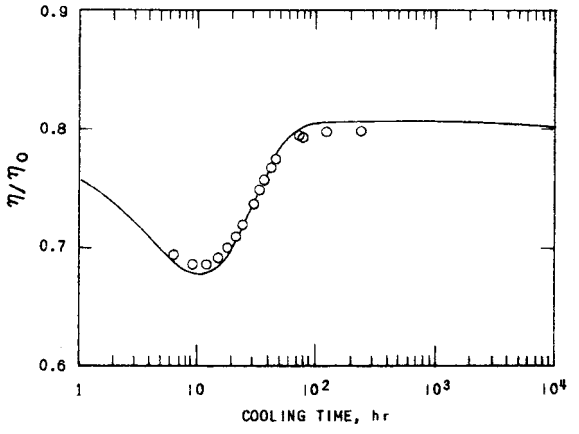

Fig. 5-61 — Experimental points and theoretical curve for the cooling transient of a UO_2 sample irradiated to 13,300 Mwd/ton. *Reproduced from Ref. 124.*

13,300 Mwd/ton. The agreement is excellent, both during the Xe transient as well as in the asymptotic range. Such close agreement was achieved by considering all of the important transient fission products as Xe^{135}, Sm^{149}, I^{135}, and also the short-lived heavy isotope intermediaries as Np^{239} and U^{237}. A compendium of constants used in this type of calculation is given in Table 5-39. The code used in the calculation is detailed in Ref. 138.

Gunst[139] observed that ignoring the 2.33-day Np^{239} precursor to Pu^{239} can lead, in some cases, to significant errors in the calculated relative reactivity. The error is emphasized in reactors having high rates of Pu^{239} formation. As an example, a PWR blanket fuel rod at 115°F with a $\phi_{res}/\phi_{th} \approx 3$ is taken, and the effect of the correct Np^{239} decay along with the usual practice of ignoring Np^{239} is compared. The results on η/η_0 are shown in Fig. 5-62 and, as observed, the error can reach 2.3% in η/η_0 at 500 Mwd/ton.

Slightly Enriched U-Reactors. At the present time, irradiation data from reactors of this type are limited to a recent analysis of blanket rods from the Shippingport reactor. The data are listed in Table 5-40.

5.2.6 IRRADIATION DEPENDENCE OF σ_{eff} (Pu^{240})

Because Pu^{240} has an extremely high resonance at 1 ev, the effective cross section is spectrum and concentration dependent, and is quite sensitive to irradiation history.[119] This is illustrated in Table 5-41 where the effective Pu^{240} cross section (σ^{40}_{eff}) has been inferred from measured Pu isotope distributions in a graphite reactor.[125]

A theoretical analysis of this cross section has been made by Crowther and Weil.[141] The objective of the study was to determine a constant value for the cross section which could be used for the entire irradiation time, and would yield approximately correct results at the end of the exposure. Reactor parameters investigated included lattice spacing, U^{235} enrichment, and the levels of the integrated thermal neutron flux. The epithermal absorption in U^{235}, Pu^{239}, and Pu^{241}, and epithermal 1/v capture in U^{238} was ignored. Resonance absorption in Pu^{240} was included by defining an effective microscopic capture cross section:

$$\hat{\sigma}^{40}_{eff} = \hat{\sigma}^{40}_{th} + \frac{\epsilon \sum_i \eta_i N_i \sigma^i_a}{(1 + \tau B^2)\, N^{fuel}} \frac{p^{28}(1 - p^{40})}{M^{40}} = \hat{\sigma}^{40}_{th} + \hat{\sigma}^{40}_{res}$$

where $\hat{\sigma}^{40}_{th}$ is the effective thermal cross section; p^{40} is the resonance escape probability for Pu^{240}; p^{28} is the resonance escape probability for U^{238}; N_i is the atomic density of material i in the fuel lump; N^{fuel} is the total atomic density of the fuel lump; M^{40} is the atom fraction of Pu^{240} in the fuel lump; and other symbols have their usual meanings. A simplified formula for p^{40} was used:

$$p^{40} = \exp\left[\frac{-M^{40} I^{40}}{S}\right]$$

where

$$I^{40} \approx I^{40}_{\infty}/[1 + (I^{40}_{\infty} M^{40})/\sigma^{fuel}_s] = \text{effective resonance integral of } Pu^{240}$$

The infinite dilution resonance integral, I^{40}_{∞}, was assumed to be 9000 barns, and

$$S = \left(\frac{\xi \Sigma_s}{N^{fuel}}\right)\left(\frac{V^{mod}}{V^{fuel}}\right) F = \text{(moderating power per fuel atom)}$$

where F is the resonance disadvantage factor.

With this formulation of σ^{40}_{eff}, a number of burnup calculations were made for a range of H_2O/UO_2 lattices. As is evident from the results (Fig. 5-63), σ^{40}_{eff} is strongly dependent on the fuel-to-water ratio; for extremely tight lattices, the effective cross section actually increases with exposure. This is due to the progressively hardening neutron spectrum and the increased importance of the 1-ev resonance. However, for all realistic fuel-to-moderator ratios, σ^{40}_{eff} decreases with irradiation, the progressively increasing self-shielding overshadowing all other effects.

In order to make the correlation independent of the actual reactor configuration, a dimensionless parameter, S/Z, was evolved, where S is defined above, and

$$Z = \frac{\epsilon \sum_i \eta_i N_i \sigma^i_a}{(1 + \tau B^2)\, N^{fuel}}$$

Table 5-39 — INPUT PARAMETERS USED IN CODE CALCULATIONS OF ISOTOPIC CONCENTRATIONS DURING IRRADIATION OF NATURAL URANIUM, AND FOR TRANSIENT BEHAVIOR FOLLOWING IRRADIATION[a,b]

Reproduced from Ref. 124.

Isotope	Initial Isotopic Concentration (N_0), atoms/specimen	Total Decay Constant (λ), sec^{-1}	Effective Maxwellian-Averaged Thermal Cross Sections for		Effective Resonance Integrals for Energy Range 0.17 ev to Infinity for		Fission Energy (Q), Mev/fission	Neutrons per Fission	Direct Fractional Yields upon Fission of			
			Absorption (σ_a), barn	Capture (σ_γ), barn	Absorption (R_a), barn	Capture (R_γ), barn			U^{235}	U^{238}	Pu^{239}	Pu^{241}
U^{235}	3.16×10^{21}	0	570.0	91.6	921	333	205	2.47	—	—	—	—
U^{236}	0	0	5.1	5.1	295	295	—	—	—	—	—	—
U^{237}	0	1.19×10^{-6}	0	0	0	0	—	—	—	—	—	—
Np^{237}	0	0	146	146	468	468	—	—	—	—	—	—
U^{238}	4.33×10^{23}	0	2.31	2.31	23	23	205	2.59	—	—	—	—
Np^{239}	0	3.44×10^{-6}	60	60	0	0	—	—	—	—	—	—
Pu^{239}	0	0	957	282	2600	1030	205	2.90	—	—	—	—
Pu^{240}	0	0	260	260	8550	8550	—	—	—	—	—	—
Pu^{241}	0	1.67×10^{-9}	1270	346	2440	1330	205	3.06	—	—	—	—
I^{135}	0	2.88×10^{-5}	7.0	7.0	0	0	—	—	0.061	0.061	0.058	0.058
Xe^{135}	0	2.11×10^{-5}	2.46×10^{6}	2.46×10^{6}	2.83×10^{5}	2.83×10^{5}	—	—	0.002	0.002	0.002	0.002
Nd^{149}	0	9.63×10^{-5}	0	0	0	0	—	—	0.0113	0.02	0.0189	0.02
Pm^{149}	0	3.63×10^{-6}	0	0	0	0	—	—	0	0	0	0
Sm^{149}	0	0	5.96×10^{4}	5.96×10^{4}	6970	6970	—	—	0	0	0	0

[a] Moderator temperature is assumed to be 115°F both during and following irradiation. Symbols defined in the table are identical to those used in Ref. 138.

[b] Probability for fast fission per atom of U^{238} is given by $\delta^{28}\,\phi$ (Ref. 138), where ϕ is the thermal flux and δ^{28} is 0.028 barn for the case considered. Fast fission is almost negligible. Effective thermal absorption cross section of stable fission products is assumed to be 50 barns/fission.

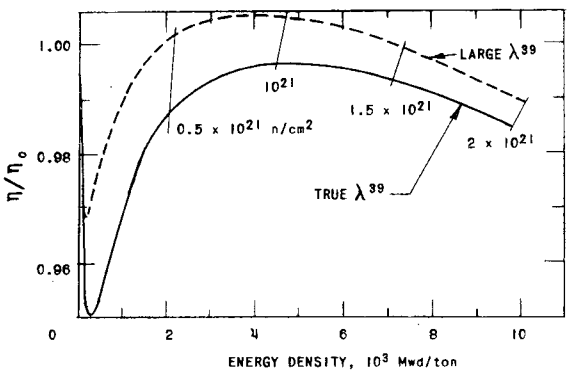

Fig. 5-62 — Calculated η/η_0 as a function of Mwd/ton for two values of λ^{39}. η is the regeneration factor as a function of irradiation, and η_0 is the pre-irradiation value. Several time-integrated thermal fluxes are indicated. The epithermal flux $\phi_R = 0.2\phi$, where ϕ is the thermal flux, and ϕ_R is the epithermal flux per unit lethargy. *Reproduced from Ref. 139.*

Table 5-40 — COMPOSITION OF UO_2 FUEL RODS IRRADIATED IN SHIPPINGPORT REACTOR

Data from Ref. 140.

	Rod No. 1	Rod No. 2
Pre-irradiation U, gm	135.30	133.43
Post-irradiation:		
U total, gm	133.67 + 0.12	132.35 + 0.14
U^{235} (wt-% of U)	0.3059 + .0004	0.4397 + .0004
U^{236}	0.0667 + .0007	0.0479 + .0003
U^{238}	99.622 + .0008	99.512 + .0005
Pu total, gm	0.617 + 0.012	0.506 + 0.012
Pu^{239} (wt-% of Pu)	69.71 + 0.04	79.84 + 0.06
Pu^{240}	22.20 + 0.02	15.20 + 0.05
Pu^{241}	6.68 + 0.02	4.45 + 0.03
Pu^{242}	1.41 + 0.02	0.51 + 0.02
Conversion ratio	1.06	1.24
α	0.203	0.219
Mwd/ton	6,350	3,800

Table 5-41 — EFFECTIVE CAPTURE CROSS SECTION OF Pu^{240} VS. PLUTONIUM ISOTOPIC COMPOSITION

Sample No.	Atom-% Pu^{240}	Atom-% Pu^{241} (Corr. for decay)	σ_{eff}^{40}, barn
114-42	0.49	0.008	2480
114-46	1.29	0.035	1550
114-52	2.01	0.084	1520
114-57	2.68	0.132	1340
114-61	5.77	0.488	1030

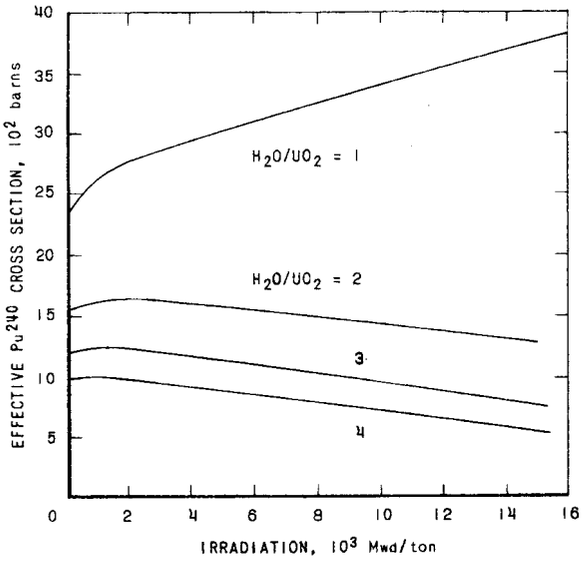

Fig. 5-63—Effective Pu^{240} cross sections as a function of irradiation and lattice spacing for a uniform lattice of 0.5 in. diameter UO_2 rods in H_2O.

The effective constant cross section as a function of the S/Z parameter is shown for a practical range of burnups in Fig. 5-64.

The method of determining the appropriate σ^{40}_{eff} for a specific burnup is: (1) to estimate the time-average number of fuel atoms (N^{fuel}), during the irradiation; (2) from this compute the average S/Z; and (3) choose the effective constant σ^{40}_{eff} at the appropriate burnup from Fig. 5-64.

As might be expected, for long burnups Pu^{240} tends to saturate and its effective cross section becomes constant with irradiation and a function of the reactor parameters only. Thus for long burnups, Fig. 5-65 can be used and the approximate range of error should not exceed ±100 barns.

Although Figs. 5-64 and 5-65 were calculated for H_2O-UO_2 systems, they are applicable, within limits, to other systems.

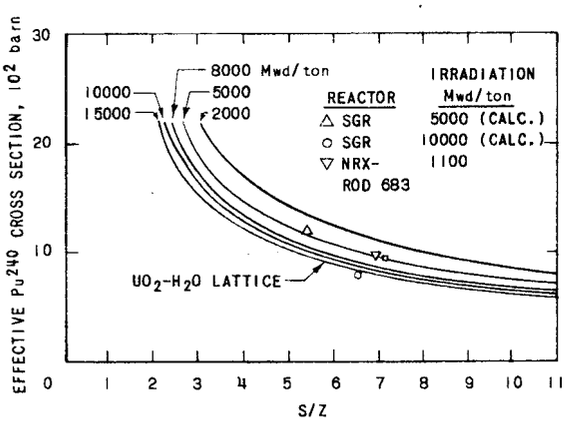

Fig. 5-64—Summary of effective Pu^{240} cross sections showing irradiation dependence.

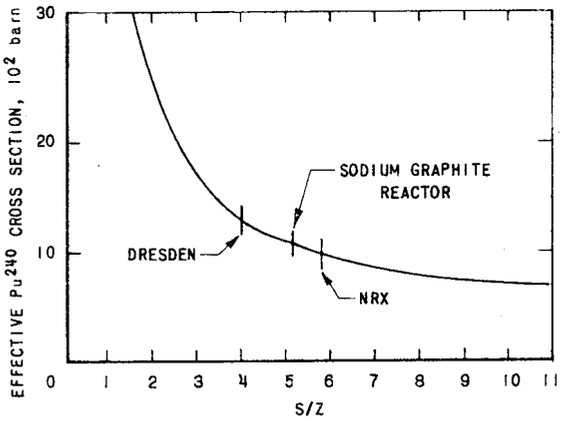

Fig. 5-65—Effective Pu^{240} cross sections for long-term reactivity calculations.

5.2.7 PLUTONIUM RECYCLE

The final choice of a fuel cycle is based on economical consideration; however, many of the difficulties and the bulk of the work in choosing a cycle lie in the realm of physics.

Two examples of fuel recycle management plans are given in Figs. 5-66 and 5-67. Obviously, many more variations are possible: enriched U might be employed, the Pu does not have to be blended into the U but can be used in integral elements in the form of spikes, etc.

In all cases, the use of Pu recycle will extend the effective cycle time, or reduce the required feed enrichments. The interrelation of both of these effects for a sodium-graphite reactor[118] is shown in

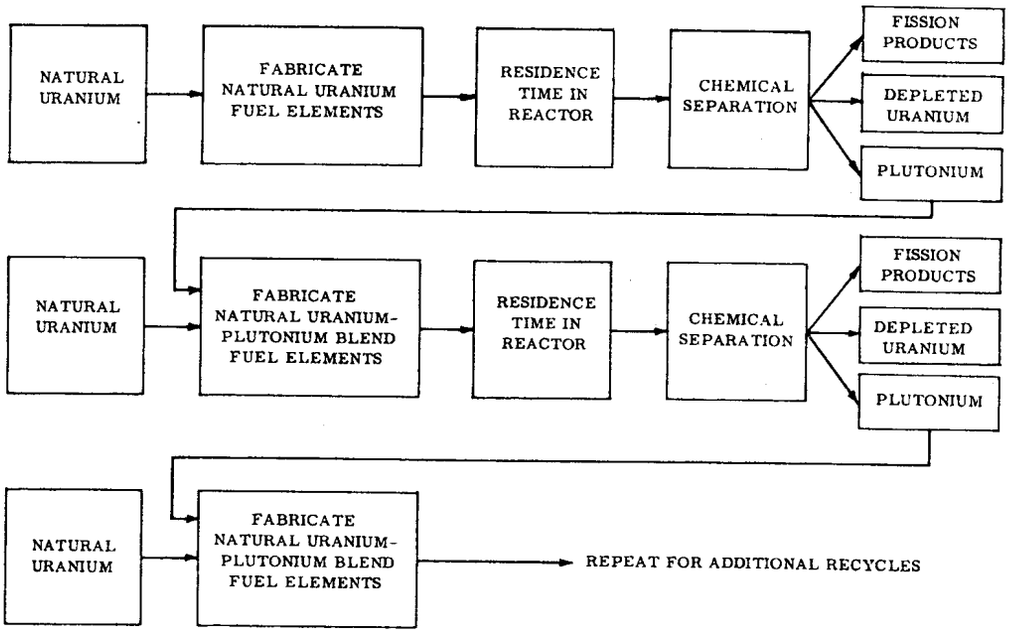

Fig. 5-66 — Natural uranium feed plutonium recycle scheme. Depleted uranium rejected at end of cycle. *Reproduced from Ref. 148.*

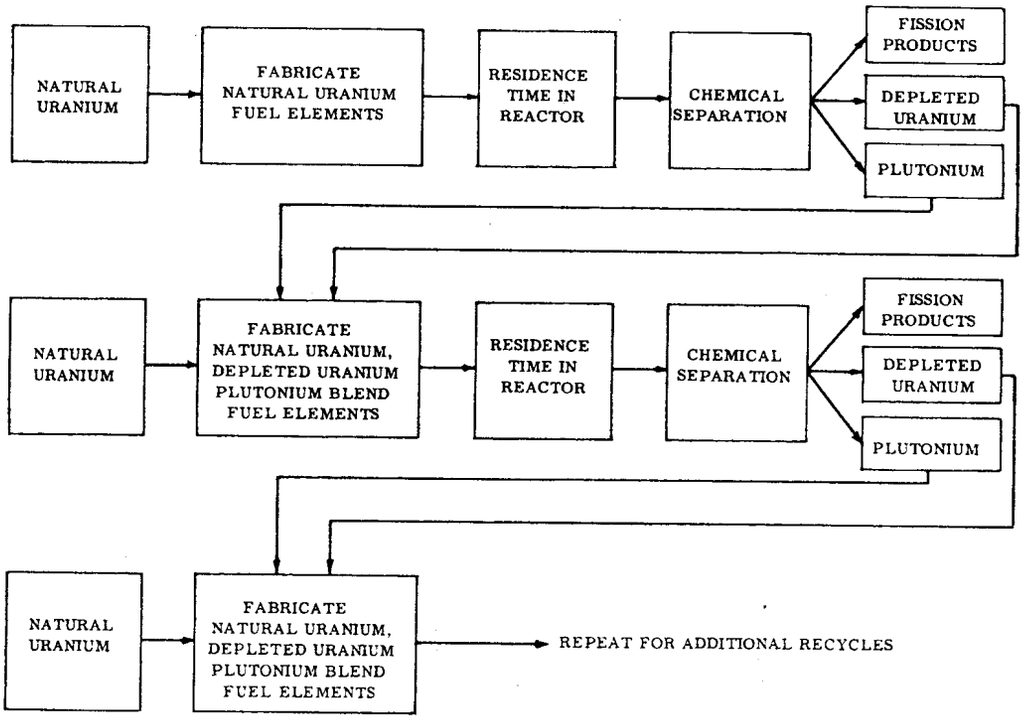

Fig. 5-67 — Natural uranium feed plutonium recycle scheme. Some depleted uranium also recycled. *Reproduced from Ref. 148.*

Fig. 5-68. (The U^{235} enrichments required to enable the reactor to reach the burnup levels are indicated along the abscissa.) The subject of Pu recycle has been treated extensively in the open literature. Some specific calculational models are given in Ref. 142–145; larger scale studies of a survey nature are presented in Refs. 110, 118, 146, 147.

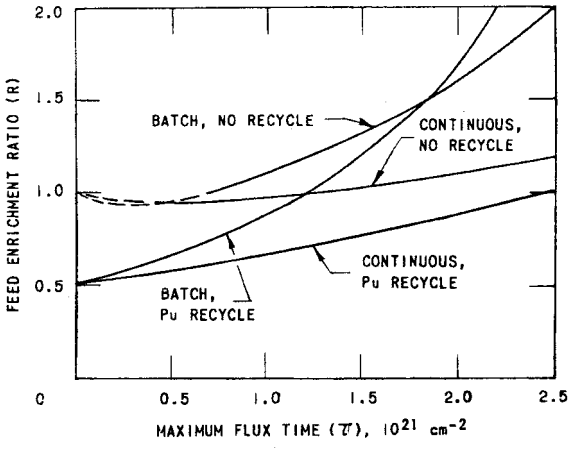

Fig. 5-68 — Feed enrichment ratio vs. Maxwellian flux time for unmixed fuel. *Reproduced, by permission, from "Nuclear Chemical Engineering," M. Benedict and T. Pigford. Copyright 1957, McGraw-Hill Book Company, Inc.*

Gas-Cooled Graphite Reactors. Reactors of this type are usually fueled with natural uranium which limits the no-cycle reactivity lives attainable to about 3,000 Mwd/ton. Reactivity life here is used to mean the exposure in Mwd/ton which the fuel has sustained at the time when the reactor can no longer be kept critical. The recycle of the Pu produced in the initial cycles can extend considerably the useful reactivity lives of the subsequent cycles. This fueling scheme has been analyzed by several investigators.[147–150] Figure 5-69 shows the calculated results for a Calder Hall-type reactor after six cycles. From an initial cycle of 2700 Mwd/ton, the useful reactivity life of the fuel is seen to increase quickly to an asymptotic value of about 8700 Mwd/ton.

The isotopic buildups occurring under a recycle scheme are, in principle, no different from the one-cycle cases; however the eventual burnups are usually an order of magnitude larger (i.e., 60,000 vs 6,000 Mwd/ton). Under these long irradiations, different parameters become important. For example, the effective Pu^{240} cross section, because of its rapid change, is very troublesome at relatively short burnups, reaches its equilibrium value at ~8,000 Mwd/ton, and is constant over most of a 60,000 Mwd/ton cycle. On the other hand, Pu^{242} becomes increasingly more significant and the parameters governing its buildup (i.e., α of Pu^{241}) become very important. The constituency of the plutonium isotopes through a number of cycles is given in Fig. 5-70. As the Pu^{242} builds up, the whole character of the Pu changes and its worth as a thermal fuel begins to decrease. It probably would be advantageous to interrupt such saturated Pu recycle fuels and use the material in fast reactors. This is suggested by the fact that Pu^{240} is fissionable for fast neutrons, and Pu^{241} is a good fast reactor fuel.

Since the cycles indicated also cover rather long periods (i.e., about 70 years for the ~40,000 Mwd/ton-burnup shown in Fig. 5-69), it becomes necessary to consider the decay constants (half-life = 13 years) for Pu^{241}. If neglected, the decay constants can lead to substantial errors in reactivity.

D_2O Moderated Reactors. A long-term program systematically exploring the Pu recycle concept was initiated at Hanford in 1956.[151] The Plutonium Recycle Test Reactor (PRTR)[152] was constructed at the Hanford Site for the express purpose of experimentally testing the numerous Pu recycle schemes. The first loading tested consisted of UO_2 elements interspersed with Pu spikes. The results of an analysis[153] on recycle are given in Fig. 5-71 which compares the no-cycle and the equilibrium Pu-recycle reactivity lives for a range of reactor sizes and thermal efficiencies. The thermal utilization factor, f, is plotted along the abscissa, and curves for a range of the material dependent parameter, k_∞/ϵ, are given. Larger values of k_∞/ϵ are required for reactors of smaller size. Since the burnups attainable per cycle are in some cases large (~10,000 Mwd/ton), it must be cautioned that consideration has been given only to reactivity limits on fuel cycles and not to any metallurgical (radiation damage) limits.

Figure 5-72 gives the fuel cycle and the isotope buildup history for a total of five cycles and a cumulative burnup of 53,000 Mwd/ton. The Pu isotopes, with the exception of Pu^{242}, build up extremely fast, with the Pu^{239} concentration exceeding the U^{235} concentration for portions of even the second cycle.

Summaries of the programmatic effort at Hanford are given in Refs. 153–155.

687863 O - 63 - 29

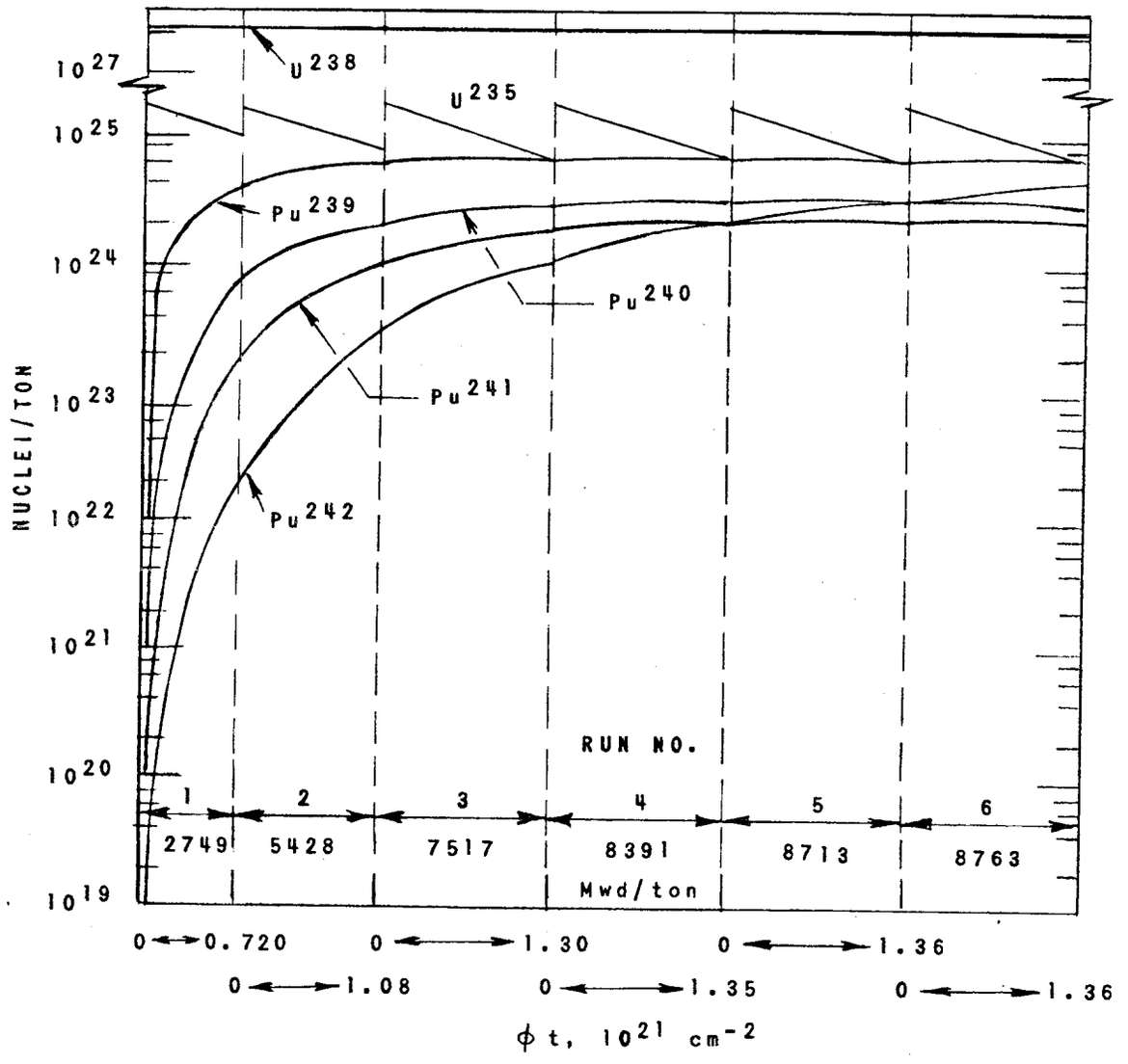

Fig. 5-69 — Isotopic Concentration vs. flux time. *Reproduced from Ref. 148.*

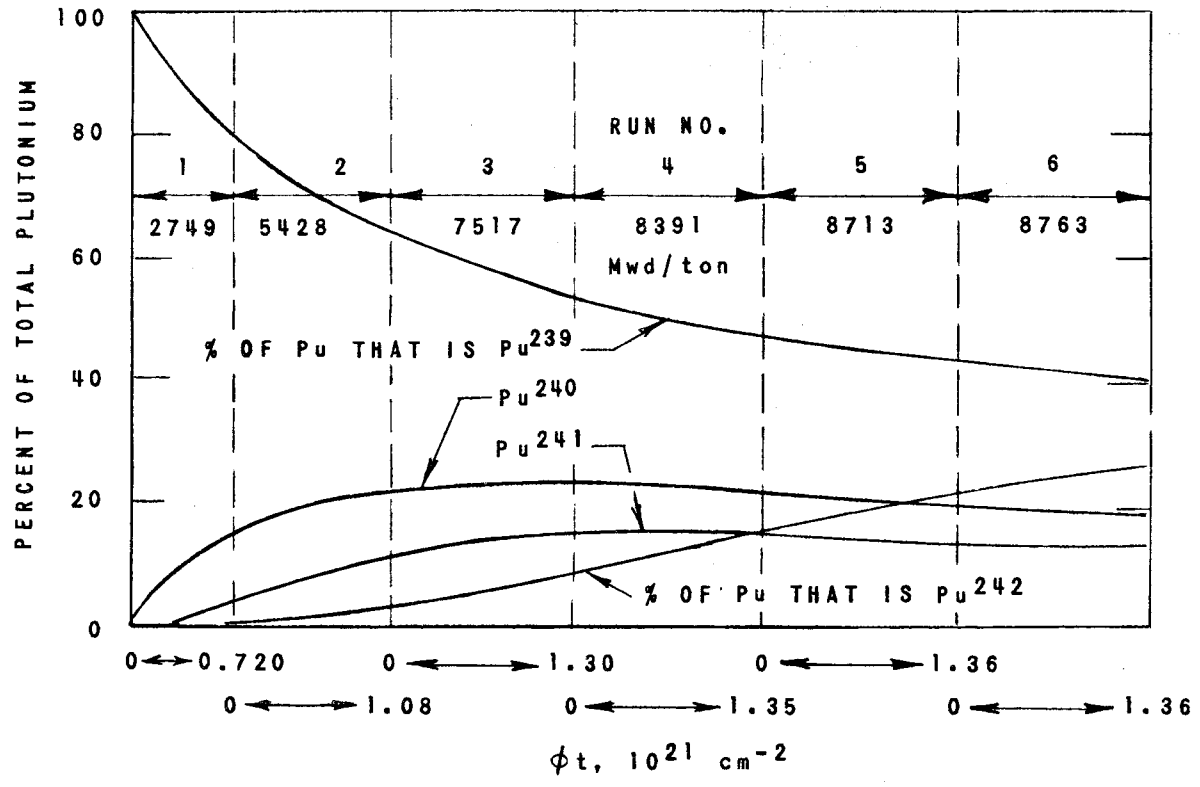

Fig. 5-70 — Isotopic constituency of the plutonium. *Reproduced from Ref. 148.*

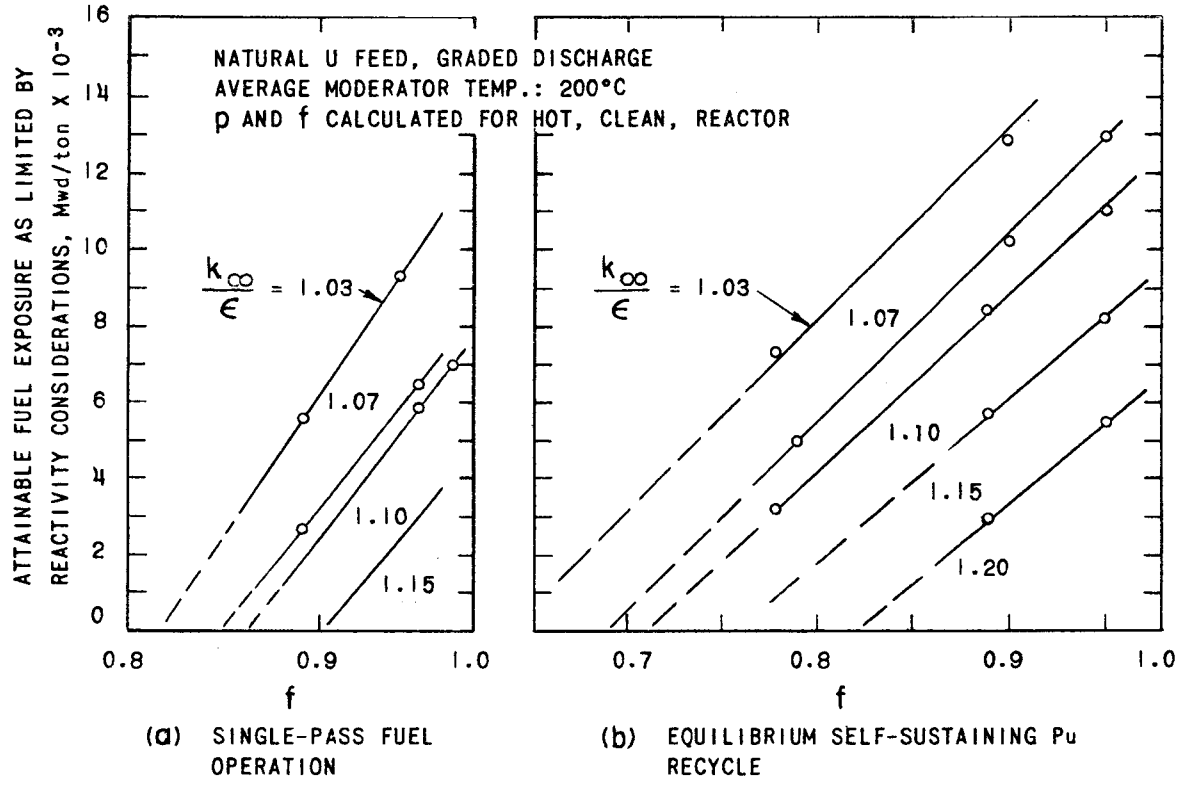

Fig. 5-71 — Variation of reactor design parameters with exposure. *Reproduced from Ref. 153.*

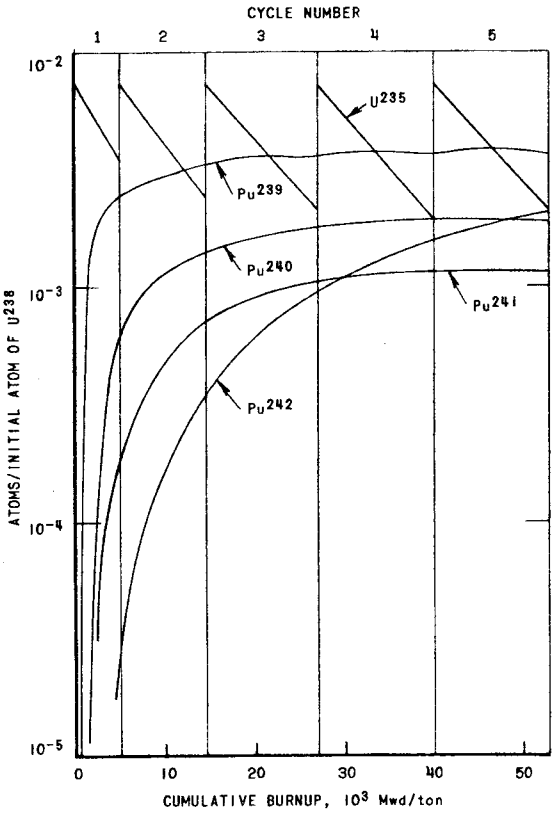

Fig. 5-72 — Change of fuel composition with cumulative burnup in plutonium recycle operation of heavy-water reactor fueled with natural uranium. *Reproduced from Ref. 110.*

Light-Water Moderated Reactors. The accuracy of available basic data does not yet permit an answer to a major question about this important type of reactor: Can an equilibrium Pu recycle scheme be sustained with only natural uranium feed? However, enriched uranium requirements can be reduced several fold by employing Pu recycle. This has been investigated for a range of boiling water reactors by Greebler, et al.[156] The range of parameters covered was:

$\frac{\text{Volume (water)}}{\text{Volume (fuel)}}$ = 1.5 to 2.3 (with ~2.0 appearing to be most advantageous)
Initial enrichments = 0.72 to 1.5%
Make-up enrichments = 0.72 to 1.15%
Cycle times = 4000 to 10000 Mwd/ton

The discharge reactivity of three different enriched fuels irradiated for a total of ten cycles of 8,000 Mwd/ton each, is given in Fig. 5-73. In this particular scheme, 20% of the fuel is discharged after reaching 8,000 Mwd/ton. The Pu is separated, mixed with uranium of the indicated enrichments, and recycled into the reactor. As shown in Fig. 5-73, between 0 and 15,000 Mwd/ton a transient occurs which carries the reactor reactivity well below the required operating minimum k_{eff} of 1.04. (The excess above k_{eff} = 1 is necessary to compensate for Xe and Sm poisoning.) Thus, none of the make-up enrichments is satisfactory for the initial cycles, although quite acceptable at the asymptotic burnups above 15,000 Mwd/ton. This could be compensated by using shorter initial cycles as was done for the D_2O and graphite reactors, but this would disregard the flexibility which enriched feed provides. In general, it is more advantageous to maintain a uniform fuel cycle (i.e., the indicated 8,000 Mwd/ton) and to vary the enrichment of the make-up feed. The required variation for the same reactor and the same burnup is given in Fig. 5-74 and is seen to approach the constant asymptotic value by 15,000 Mwd/ton.

The isotopic history covering a burnup of 60,000 Mwd/ton for a PWR-type, light-water reactor[110] is given in Fig. 5-75. Variable enrichment of the make-up feed is employed. The relatively slow approach to equilibrium of light-water reactors is demonstrated by a comparison of Fig. 5-75 with equivalent results for the graphite (Fig. 5-69) and the D_2O (Fig. 5-72) reactors.

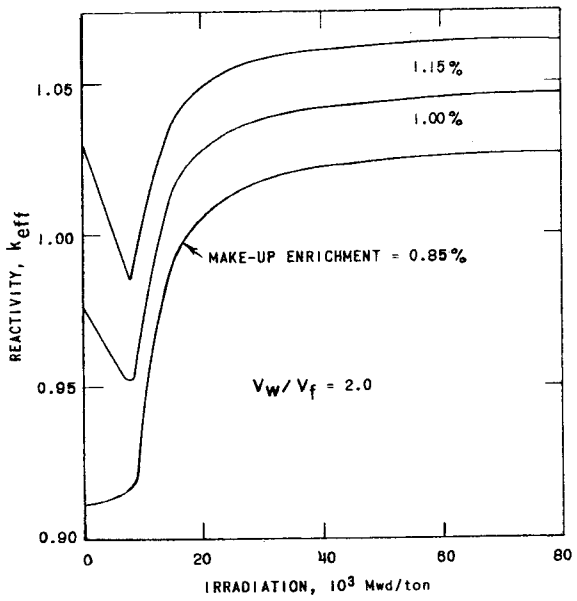

Fig. 5-73 — Discharge reactivity for constant make-up enrichment, 8,000 Mwd/ton cycle. *Reproduced from Ref. 156.*

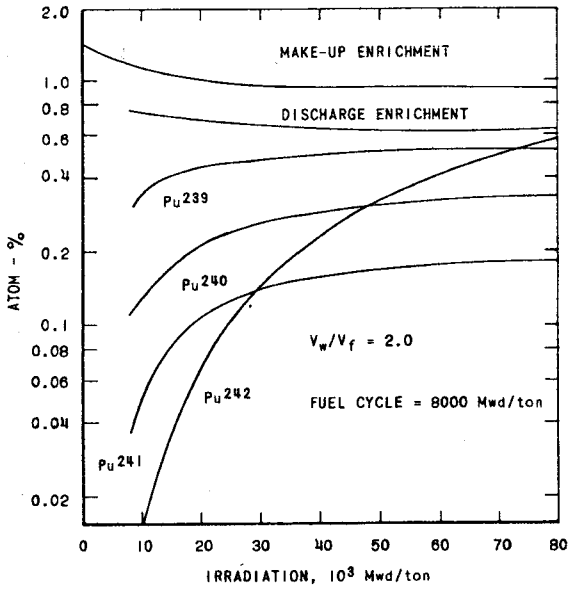

Fig. 5-74 — Initial enrichment and discharge fuel compositions for constant end-of-cycle reactivity, k_{eff} = 1.040. *Reproduced from Ref. 156.*

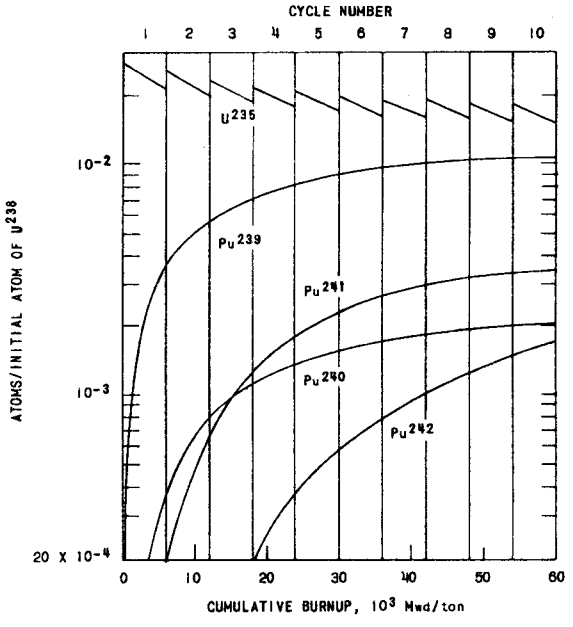

Fig. 5-75 — Change of fuel composition with cumulative burnup in plutonium recycle operation in uranium-fueled, light-water reactor; burnup/cycle = 6,000 Mwd/ton. *Reproduced from Ref. 110.*

5.2.8 BURNABLE POISONS

Burnable poisons are materials which have a large absorption cross section and are included in a reactor in order to limit the maximum available reactivity in the system. During reactor operation, the burnable poisons are changed by neutron capture into elements of low capture cross section which tends to compensate for reactivity losses as the fuel is burned.

Consider the case of one species of burnable poison with the fuel and poison uniformly distributed and unshielded and with only thermal neutron absorption. The spatial dependence of the flux is neglected. Concentrations of the fuel and poison nuclei are given by:

$$\frac{dN_F}{dt} = -\sigma_a^F \, N_F(t) \, \phi(t) \tag{5-16}$$

$$\frac{dN_B}{dt} = -\sigma_a^B N_B(t) \, \phi(t) \tag{5-17}$$

where N_F and N_B are the concentrations of fuel and poison, respectively, in nuclei/cc; σ_a^F and σ_a^B are the corresponding microscopic absorption cross sections; and $\phi(t)$ is the thermal flux. The solutions of these equations are

$$N_F = N_{F,0} \exp(-\sigma_a^F \, T) \tag{5-18}$$

and

$$N_B = N_{B,0} \exp(-\sigma_a^B T) \tag{5-19}$$

where the zero subscripts denote initial concentrations; and T is the flux time, that is

$$T = \int_0^t \phi(t) \, dt$$

Thus the relation

$$\frac{N_B}{N_{B,0}} = \left(\frac{N_F}{N_{F,0}}\right)^{\sigma_a^B/\sigma_a^F} \tag{5-20}$$

holds true. Equations (5-18) and (5-19) may be written in a more explicit form for the cases where the reactor is operated at constant flux or constant power. If the flux is constant,

$$N_F = N_{F,0} \exp(-\sigma_a^F \, \phi t) \tag{5-21}$$

and

$$N_B = N_{B,0} \exp(-\sigma_a^B \, \phi t) \tag{5-22}$$

If the power is constant

$$N_F \phi(t) = N_{F,0} \, \phi_0$$

then

$$N_F = N_{F,0} \, (1 - \sigma_a^F \, \phi_0 \, t) \tag{5-23}$$

and

$$N_B = N_{B,0} \, (1 - \sigma_a^F \phi_0 \, t)^{\sigma_a^B/\sigma_a^F} \tag{5-24}$$

Using two-group theory, write the value of k_{eff} for the reactor as

$$k_{eff} = \frac{\epsilon \eta p}{1 + \tau B^2} \frac{f(t)}{1 + B^2 L(t)} \tag{5-25}$$

where the notation used is standard and only f and L^2 are considered to be time-dependent. Equation (5-25) may be rewritten

$$k_{eff} = \frac{\epsilon \eta p}{1 + \tau B^2} \left\{ 1 + \frac{DB^2 + \Sigma_a^C}{\Sigma_a^{F,0}} \exp\left(\sigma_a^F T\right) + \frac{\Sigma_a^{B,0}}{\Sigma_a^{F,0}} \exp\left[(\sigma_a^F - \sigma_a^B)T\right] \right\}^{-1} \tag{5-26}$$

by using the relation

$$f = \Sigma_a^F / (\Sigma_a^F + \Sigma_a^B + \Sigma_a^C) \tag{5-27}$$

and

$$L^2 = D / (\Sigma_a^F + \Sigma_a^B + \Sigma_a^C) \tag{5-28}$$

where Σ_a^C is the macroscopic absorption cross section for materials whose cross sections do not vary with time; and D, the diffusion coefficient, is assumed to be constant. The absorption by xenon is included in Σ_a^C as it is a fairly good approximation to assume constant xenon absorption over the reactor life. It is seen from Eq. (5-26) that k_{eff} will have a maximum at a value of T given by the solution of the equation

$$\frac{(\Sigma_a^C + DB^2)}{\Sigma_a^{B,0}} \frac{\sigma_a^F}{\sigma_a^B - \sigma_a^F} = \exp\left(-\sigma_a^B T\right) \tag{5-29}$$

provided the constants involved are such that the left-hand side of the equation has a value less than unity. The variation of k_{eff} with time will behave qualitatively as shown in Fig. 5-76.[157]

The use of more than one species of burnable poison does not add any significant complication to the analysis. It is merely necessary to write an equation similar to Eq. (5-17) for each species and proceed as before.

Consider the use of self-shielded poisons. If boron without self-shielding is used, the reactivity rise (or "mismatch") in the early part of the reactor life may exceed the design value of the control rods. This is due to the relatively rapid depletion of poison. However, if the boron is used in lumps, self-shielding will cause it to burn more slowly and permit a reduction in the mismatch. In a typical case with heavy self-shielding, the behavior of the reactivity as a function of time would be given by a curve as shown in Fig. 5-77. Initially, the reactivity decreases because the poison is so heavily self-

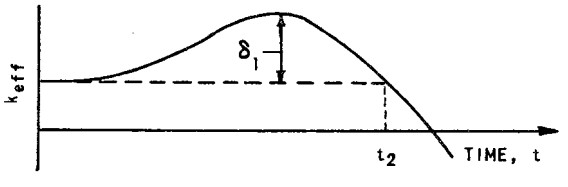

Fig. 5-76 — Time dependence of k_{eff} with lightly shielded burnable poison. *Reproduced from Ref. 157.*

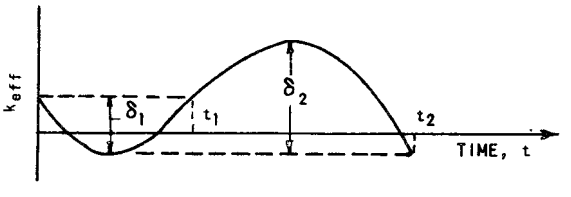

Fig. 5-77 — Time dependence of k_{eff} with heavily shielded burnable poison. *Reproduced from Ref. 157.*

shielded that its effectiveness does not decrease significantly with burnup. However, as the poison is depleted, its self-shielding decreases, and it burns out faster than the fuel, causing a reactivity rise.

The self-shielding factor, g, gives the ratio of the effective macroscopic absorption cross section of a lump, to the cross section it would have if there were no self-shielding. It may be written as[157]

$$g^{-1} = 1 + \sum_{i=1}^{\infty} a_i \left(2t\, \Sigma_a\right) \tag{5-30}$$

where the a_i are coefficients depending only on the geometry and properties of the medium external to the lump; t is the thickness or other characteristic dimension of the lump; and Σ_a is the unshielded macroscopic absorption cross section. In general, the a_i decrease rapidly with increasing i and only one term of the series is used. Thus g may be written

$$g = \left\{1 + \left[\gamma N(T)/N_0\right]\right\}^{-1} \tag{5-31}$$

where γ is independent of time and is a function of lump geometry; and N(T) and N_0 are the total number of absorber atoms in the lump at flux times T and 0, respectively.

The differential equations corresponding to Eqs. (5-16) and (5-17) for the self shielded case are

$$\frac{dN_F}{dt} = \frac{-\sigma_a^F N_F(t)\phi(t)}{1 + \gamma_F (N_F(t)/N_{F,0})} \tag{5-32}$$

and

$$\frac{dN_B}{dt} = \frac{-\sigma_a^B N_B(t)\phi(t)}{1 + \gamma_B (N_B(t)/N_{B,0})} \tag{5-33}$$

The solutions of these equations are

$$T = -\frac{\gamma_F}{\sigma_a^F}\left[\frac{N_F(T)}{N_{F,0}} + \frac{1}{\gamma_F}\ln\left(\frac{N_F(T)}{N_{F,0}}\right) - 1\right] \tag{5-34}$$

and

$$T = -\frac{\gamma_B}{\sigma_a^B}\left[\frac{N_B(T)}{N_{B,0}} + \frac{1}{\gamma_B}\ln\left(\frac{N_B(T)}{N_{B,0}}\right) - 1\right] \tag{5-35}$$

Figure 5-78 shows the ratio of the effective poison cross section at T, to its value at T = 0:

$$[\Sigma_a^B(T)\, g(T)]/[\Sigma_a^B(0)\, g(0)]$$

for a range of values of the self-shielding parameter, γ, as calculated from Eq. (5-35) with $\sigma_a^B = 2575$ barns.

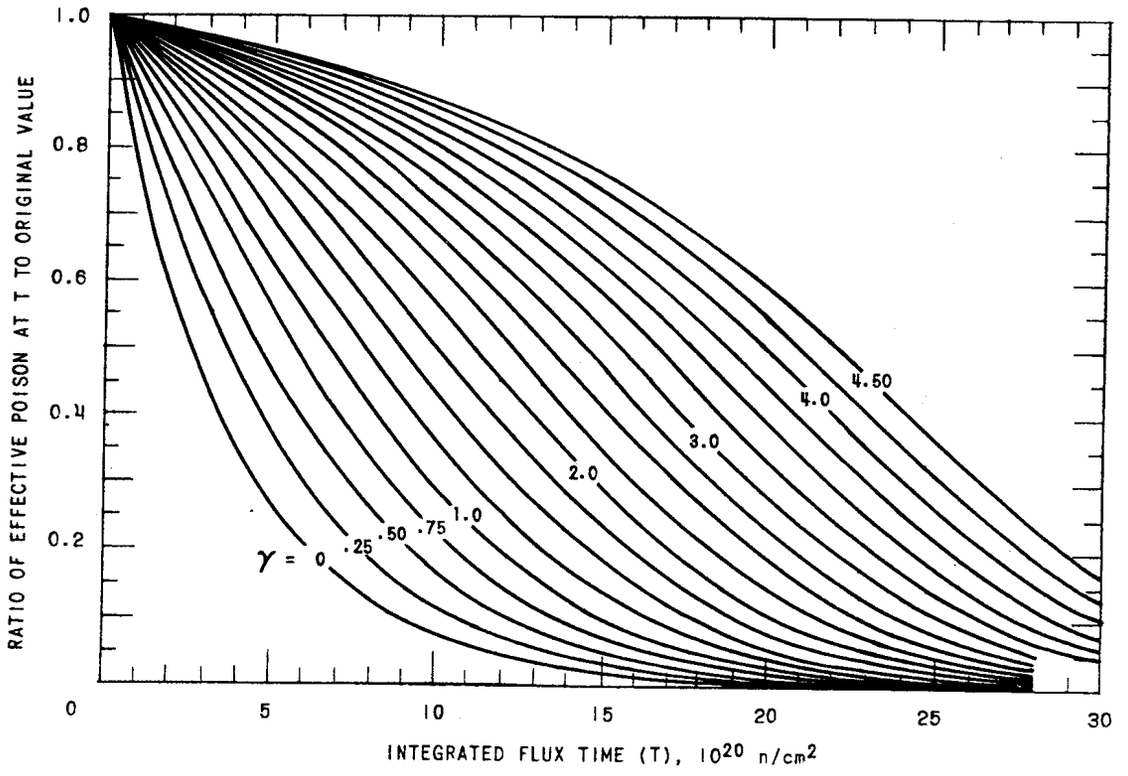

Fig. 5-78—Effective burnable poison concentration. *Reproduced from Ref. 157.*

The reactivity mismatch may be reduced further by using a combination of burnable poison elements of two different self-shielding factors. If most of the poison is placed in one set of elements which are heavily shielded, and the remaining rods are lightly shielded, the positive reactivity increment of the lightly shielded poison (Fig. 5-76) can be arranged to coincide with the initial dip of Fig. 5-77. Also, the sharp fall in reactivity in Fig. 5-76 after time t_2 can be made to occur near the peak of the positive reactivity loop of Fig. 5-76.

Equations (5-32) and (5-33) can be modified to allow for epithermal and thermal absorption by adding to the right-hand side a second term of the same form as the first term but with σ_a, γ, and ϕ referring to epithermal rather than thermal quantities.[158] Figure 5-79 is a plot similar to Fig. 5-78

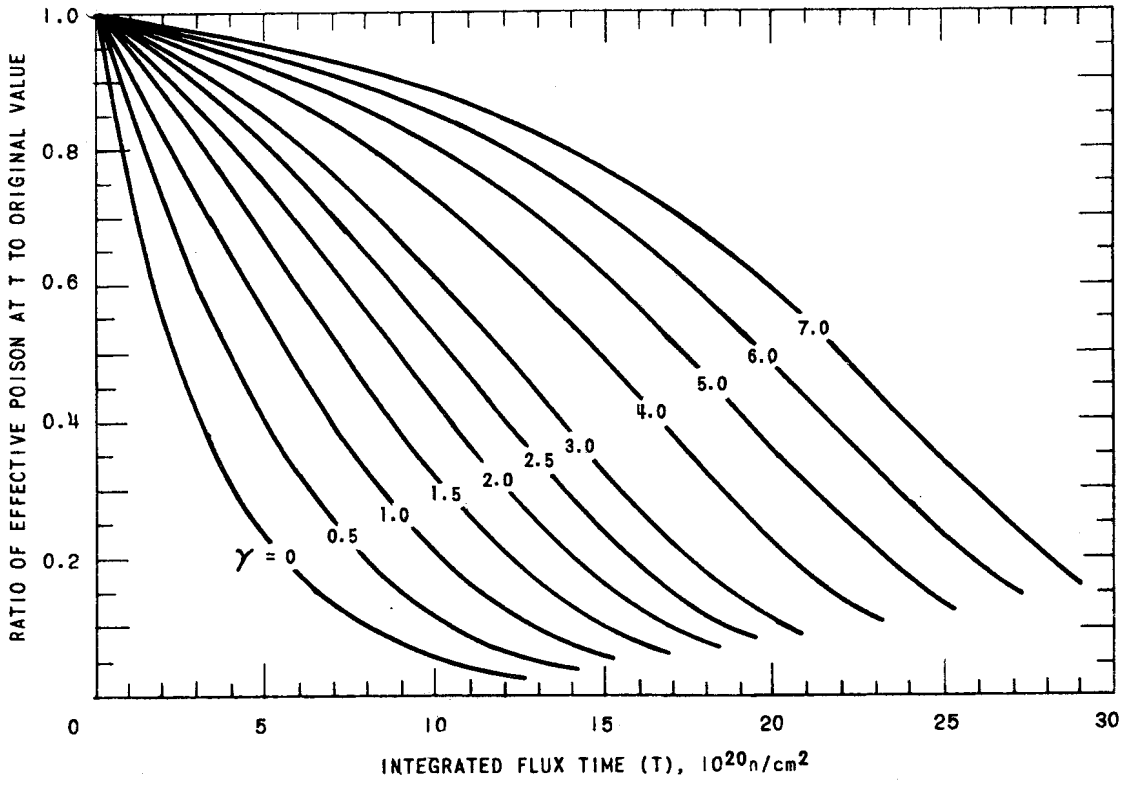

Fig. 5-79—Effective burnable poison concentration, including epithermal absorption. *Reproduced from Ref. 157.*

but with epithermal absorption included. In calculating the curves of Fig. 5-79, the values σ_a^B (thermal) = 2604 barns, σ_a^B (epithermal) = 172 barns, ϕ (epithermal)/ϕ (thermal) = 1.65 and γ_B (epithermal) = 0, were used. Comparison with Fig. 5-78 shows the marked reduction of the effective shielding of poison as a result of the epithermal absorption.

In the discussion above, the spatial dependence of the fluxes and macroscopic cross sections has been ignored. The non-uniformity of fuel burnup in a reactor usually results in an increased rate of loss of reactivity because the fuel burns out most rapidly in regions of high thermal flux which, usually, also have high statistical weight. The poison will burn out most rapidly in the same regions as does the fuel. This tends to offset the reactivity loss due to non-uniform fuel burnup.

Figures 5-80 and 5-81 show the results of some non-uniform burnup calculations by Knolls Atomic Power Laboratory.[157] The phenomena are typical of small, light-water moderated reactors with zirconium fuel elements highly enriched in U^{235}, light-water reflectors, and boron as the burnable poison. The calculations were performed using one-dimensional, four-group codes. Reactor control was effected by movement of central rods into the top of the core. In Fig. 5-80, Case A applies to a core where initially the fuel and burnable poison are uniformly distributed. In Case B, the same amount of fuel and poison is used but the poison extends to only $\frac{3}{4}$ the height of the core. It is seen that the burnup in Case B is much more uniform. In Case A, there is no significant burnup of the fuel and poison in the region normally occupied by control rods. On the other hand, in Case B almost all the poison is depleted, thus producing a longer core life than in Case A.

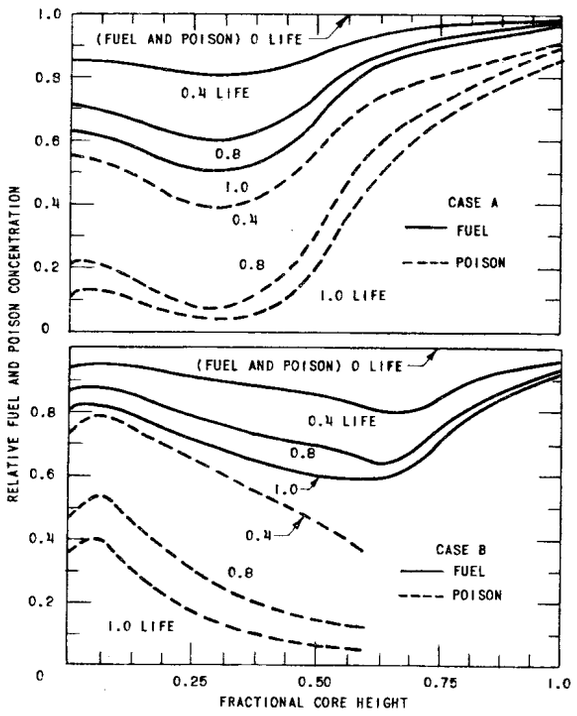

Fig. 5-80 — Fuel and burnable distributions (axial) for full and partial length poison. *Reproduced from Ref. 157.*

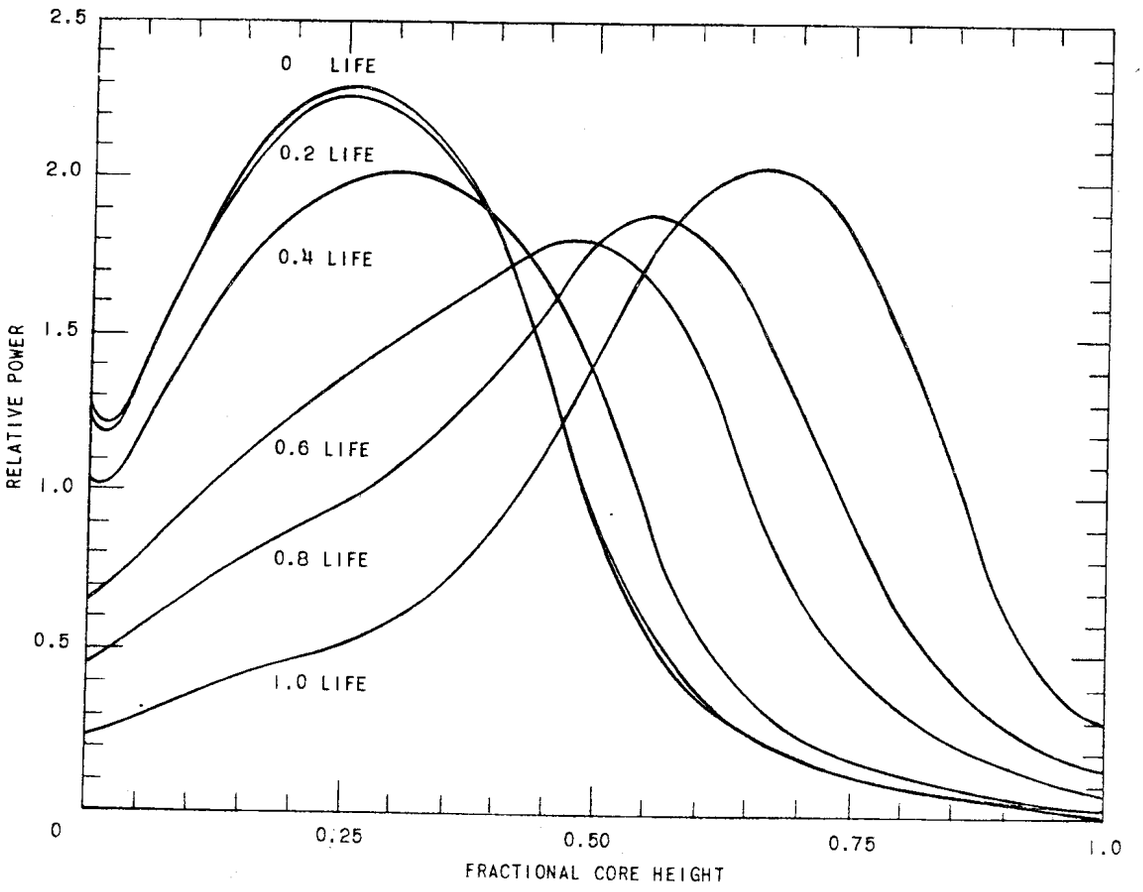

Fig. 5-81 — Time-dependent power distributions, partial poison length: 3/4. *Reproduced from Ref. 157.*

Figure 5-81 shows power distribution as a function of time for a core with $^3/_4$ poison height. The value of the power density peak to average is quite stable although the position of the peak shifts with burnup.

Figure 5-82 illustrates power flattening obtained by non-uniform distribution of burnable poisons. The reactor is divided into two radial zones with V_2 the volume of the outer zone in which the burnable poison concentration is lowered, and V_T the total core volume; β is the ratio of poison density in the outer zone, to that in the inner zone.

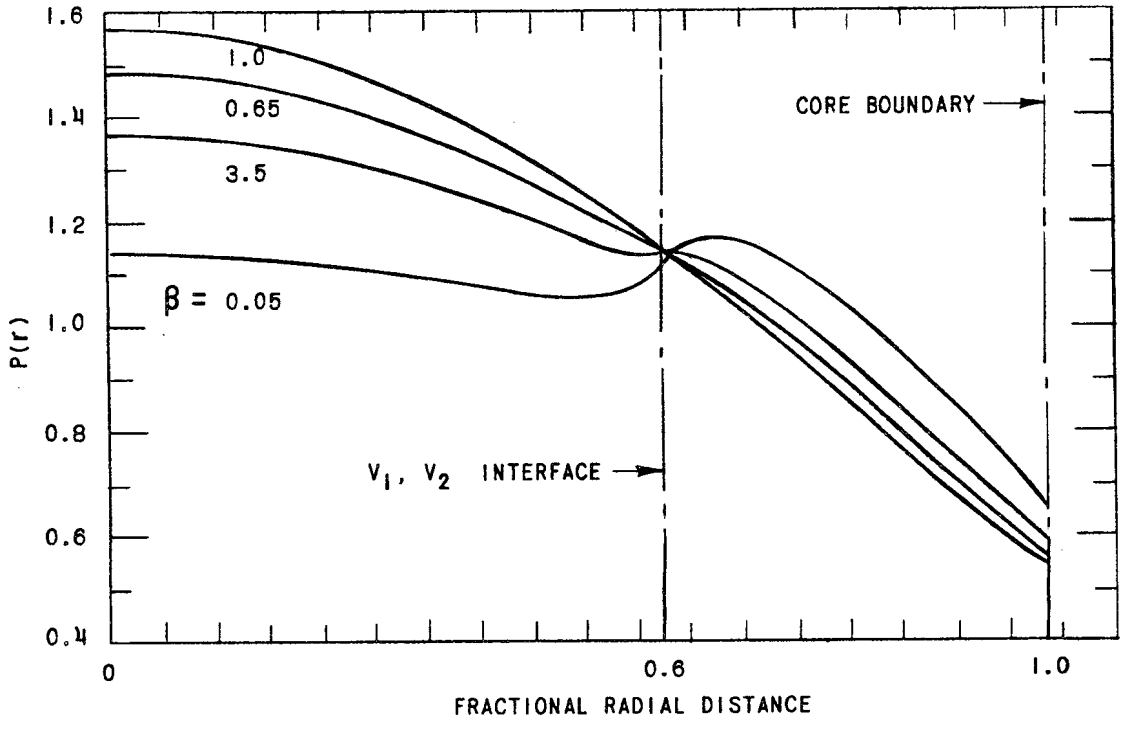

Fig. 5-82 — Power density as a function of core radius for $V_2/V_T = 0.65$, and various β. *Reproduced from Ref. 157.*

In the treatment so far, the problem of burnup was solved analytically only for the case of an average or non-space-dependent flux while space-dependent problems were solved by computer techniques. Some analytical work has been done on space- and time-dependent problems involving long-term reactivity changes with or without burnable poisons.[159–161] The analytical work assumes that the thermal flux may be expressed as the product of a function of space and a function of time and involves the use of two-group perturbation theory. Although the work is restricted to simple geometries, it can yield greater insight into the problems than computer methods. Further details are given in the above mentioned references.

In addition to boron, several other materials have been considered for use as burnable poisons.[162] Some of these materials are dysprosium, lutecium, lithium, mercury, and europium.

5.3 REACTOR KINETICS

5.3.1 EFFECTIVE DELAYED NEUTRON FRACTION AND PROMPT NEUTRON LIFETIME

Effective Delayed Neutron Fraction. Since delayed neutrons are born with a lower average energy than that of prompt neutrons, they will have a different probability of leaking or undergoing various nuclear events than will the prompt neutrons. Thus it is necessary to define an effective delayed neutron fraction which is used in adjusting the ordinary delayed neutron fractions for use in the inhour equation. This is done most readily by using the equations of multigroup theory along with perturbation

theory. For a reactor containing two fissionable species, say U^{235} and U^{238}, the diffusion equations for the multigroup fluxes and delayed neutron precursor densities are

$$\text{div}\,(D_i \text{ grad } \phi_i) - (\Sigma_{a,i} + \Sigma_{sl,i})\,\phi_i + \Sigma_{sl,i-1}\,\phi_{i-1} + (1-\beta^{25})\,\chi^{25}_{p,i}\,\nu^{25}\sum_j \Sigma^{25}_{f,j}\,\phi_j + (1-\beta^{28})\,\chi^{28}_{p,i}\,\nu^{28}\sum_j \Sigma^{28}_{f,j}\,\phi_j + \chi^{25}_{d,i}\sum_j \lambda^{25}_j\,C^{25}_j + \chi^{28}_{d,i}\sum_j \lambda^{28}_j\,C^{28}_j = \frac{1}{v_i}\frac{\partial \phi_i}{\partial t} \tag{5-36}$$

$$\frac{\partial C^{25}_i}{\partial t} = -\lambda^{25}_i\,C^{25}_i + \beta^{25}_i\,\nu^{25}\sum_j \Sigma^{25}_{f,j}\,\phi_j \tag{5-37}$$

$$\frac{\partial C^{28}_i}{\partial t} = -\lambda^{28}_i\,C^{28}_i + \beta^{28}_i\,\nu^{28}\sum_j \Sigma^{28}_{f,j}\,\phi_j \tag{5-38}$$

where D_i = diffusion constant of energy group i
ϕ_i = flux of neutrons in energy group i
$\Sigma_{a,i}$ = macroscopic absorption (capture plus fission) cross section for energy group i
$\Sigma_{sl,i}$ = macroscopic slowing down cross section for energy group i
β^{25} = fraction of U^{235} fission neutrons which are delayed
$\chi^{25}_{p,i}$ = fraction of prompt neutrons emitted into energy group i for U^{235}
ν^{25} = average number of neutrons produced by a U^{235} fission
$\Sigma^{25}_{f,j}$ = macroscopic fission cross section due to U^{235}
$\chi^{25}_{d,i}$ = fraction of delayed neutrons from U^{235} fission emitted into energy group i
λ^{25}_i = decay constant for delayed neutron emitter C^{25}_i which arises from U^{235} fission
v_i = average neutron velocity of energy group i
β^{25}_i = fraction of U^{235} fission neutrons which are delayed and arise from decay of delayed neutron emitter C^{25}_i
C^{25}_i = number of atoms per cm^3 of delayed neutron emitter having decay constant λ^{25}_i

The quantities β^{28}, ν^{28}, $\Sigma^{28}_{f,j}$, $\chi^{28}_{p,i}$, $\chi^{28}_{d,i}$, λ^{28}_i, β^{28}_i, C^{28}_i have definitions similar to the above except that the superscript 25 is replaced by the superscript 28, denoting U^{238}.

Assuming time dependences proportional to $e^{\lambda t}$ for the ϕ_i, C^{25}_i and C^{28}_i, and then substituting C^{25}_i and C^{28}_i from Eqs. (5-37) and (5.38) into Eq. (5-36),

$$\begin{aligned}\text{div}\,(D_i \text{ grad } \phi_i) - (\Sigma_{a,i} + \Sigma_{sl,i})\,\phi_i + \Sigma_{sl,i-1}\,\phi_{i-1} &+ \left[\chi^{25}_{p,i}\,(1-\beta^{25}) + \beta^{25}\,\chi^{25}_{d,i}\right]\nu^{25}\sum_j \Sigma^{25}_{f,j}\,\phi_j \\ &+ \left[\chi^{28}_{p,i}\,(1-\beta^{28}) + \beta^{28}\,\chi^{28}_{d,i}\right]\nu^{28}\sum_j \Sigma^{28}_{f,j}\,\phi_j \\ &= \lambda\left[\frac{\phi_i}{v_i} + \chi^{25}_{d,i}\sum_k \frac{\beta^{25}_k}{\lambda+\lambda^{25}_k}\,\nu^{25}\sum_j \Sigma^{25}_{f,j}\,\phi_j \right. \\ &\left. + \chi^{28}_{d,i}\sum_k \frac{\beta^{28}_k}{\lambda+\lambda^{28}_k}\,\nu^{28}\sum_j \Sigma^{28}_{f,j}\,\phi_j\right]\end{aligned} \tag{5-39}$$

The corresponding adjoint flux equation is:

$$\begin{aligned}\text{div}\,(D_i \text{ grad } \phi^*_i) - (\Sigma_{a,i} + \Sigma_{sl,i})\,\phi^*_i + \Sigma_{sl,i}\,\phi^*_{i+1} &+ \nu^{25}\,\Sigma^{25}_{f,i}\sum_j \left[\chi^{25}_{p,j}\,(1-\beta^{25}) + \beta^{25}\,\chi^{28}_{d,j}\right]\phi^*_j \\ &+ \nu^{28}\,\Sigma^{28}_{f,i}\sum_j \left[\chi^{28}_{p,j}\,(1-\beta^{28}) + \beta^{28}\,\chi^{28}_{d,j}\right]\phi^*_j \\ &= \lambda\left[\frac{\phi^*_j}{v_i} + \nu^{25}\,\Sigma^{25}_{f,i}\sum_j \chi^{25}_{d,j}\,\phi^*_j\sum_k \frac{\beta^{25}_k}{\lambda+\lambda^{25}_k}\right. \\ &\left. + \nu^{28}\,\Sigma^{28}_{f,i}\sum_j \chi^{28}_{d,j}\,\phi^*_j\sum_k \frac{\beta^{28}_k}{\lambda+\lambda^{28}_k}\right]\end{aligned} \tag{5-40}$$

In Eqs. (5-39) and (5-40), the symbols ϕ_i and ϕ_i^* now refer to the spatial dependences of the fluxes and adjoints only; that is, the $e^{\lambda t}$ time dependences are not included.

According to the results of first-order perturbation theory:[163]

$$\lambda = \left(\int < \phi_0^* | \delta Q | \phi_0 > dV\right) \Big/ \left(\int < \phi_0^* | \alpha | \phi_0 > dV\right) \tag{5-41}$$

where Eq. (5-39) has been rewritten in matrix form as

$$(Q + \delta Q)|\phi> = \lambda\alpha|\phi> \tag{5-42}$$

and

$$Q|\phi_0> = 0 \tag{5-43}$$

The terms Q,δQ, and α, are square matrices of order N determined from Eq. (5-39),

where N = number of energy groups

$|\phi_0>$ = column vector of order N having elements ϕ_{i0}

$<\phi_0^*|$ = row vector of order N having elements ϕ_{i0}^*

and $\int dV$ signifies integration over the reactor volume

In evaluating the right-hand side of Eq. (5-41) explicitly for the case where δQ arises only from changes from the critical reactor in $\delta\nu^{25}$ and $\delta\nu^{28}$ such that

$$\frac{\delta\nu}{\nu} = \frac{\delta\nu^{25}}{\nu^{25}} = \frac{\delta\nu^{28}}{\nu^{28}}$$

$$\frac{\delta\nu}{\nu} = \frac{\lambda \int \left[\sum_i \frac{\phi_i^* \phi_i}{v_i} + \sum_k \sum_i \sum_j \frac{\beta_k^{25}}{\lambda + \lambda_k^{25}} (\chi_{d,i}^{25} \phi_i^*)(\nu^{25} \Sigma_{f,j}^{25} \phi_j) + \sum_k \sum_i \sum_j \frac{\beta_k^{28}}{\lambda + \lambda_k^{28}} (\chi_{d,i}^{28} \phi_i^*)(\nu^{28} \Sigma_{f,j}^{28} \phi_j)\right] dV}{\int \sum_i \sum_j \{[\chi_{p,i}^{25}(1-\beta^{25}) + \beta^{25}\chi_{d,i}^{25}]\, \phi_i^* \nu^{25} \Sigma_{f,j}^{25} \phi_j + [\chi_{p,i}^{28}(1-\beta^{28}) + \beta^{28}\chi_{d,i}^{28}]\, \phi_i^* \nu^{28} \Sigma_{f,j}^{28} \phi_j\} dV} \tag{5-44}$$

where the zero subscripts of ϕ_i and ϕ_i^* have been removed to simplify the notation. In comparing Eq. (5-44) with the usual inhour equation,[164] and using the fact that $\lambda_k^{25} = \lambda_k^{28}$, the contribution from delayed neutrons may be written[165]

$$\rho = \beta_{eff} \sum_k \frac{\bar{A}_k}{1 + \lambda_k/\lambda} \tag{5-45}$$

where

$$\beta_{eff} = \frac{\int [\beta^{25} \sum_i \sum_j (\chi_{d,i}^{25} \phi_i^*)(\nu^{25} \Sigma_{f,j}^{25} \phi_j) + \beta^{28} \sum_i \sum_j (\chi_{d,i}^{28} \phi_i^*)(\nu^{28} \Sigma_{f,j}^{28} \phi_j)]\, dV}{\int \{\sum_i \sum_j [\chi_{p,i}^{25}(1-\beta^{25}) + \beta^{25}\chi_{d,i}^{25}]\, \phi_i^* \nu^{25} \Sigma_{f,j}^{25} \phi_j + \sum_i \sum_j [\chi_{p,i}^{28}(1-\beta^{28}) + \beta^{28}\chi_{d,i}^{28}]\, \phi_i^* \nu^{28} \Sigma_{f,j}^{28} \phi_j\} dV} \tag{5-46}$$

and

$$\bar{A}_k = \frac{\int [\beta_k^{25} \sum_i \sum_j (\chi_{d,i}^{25} \phi_i^*)(\nu^{25} \Sigma_{f,j}^{25} \phi_j) + \beta_k^{28} \sum_i \sum_j (\chi_{d,i}^{28} \phi_i^*)(\nu^{28} \Sigma_{f,j}^{28} \phi_j)]\, dV}{\int [\beta^{25} \sum_i \sum_j (\chi_{d,i}^{25} \phi_i^*)(\nu^{25} \Sigma_{f,j}^{25} \phi_j) + \beta^{28} \sum_i \sum_j (\chi_{d,i}^{28} \phi_i^*)(\nu^{28} \Sigma_{f,j}^{28} \phi_j)]\, dV} \tag{5-47}$$

Even though the above relations were obtained for the case of scattering into the next lower group only, Eqs. (5-44) through (5-47) are valid for an arbitrary scattering matrix.

Gwin[166] has accounted for the increased importance of the delayed neutrons in a bare reactor by using age theory and distinguishing the prompt and delayed neutrons by means of their different ages. If τ_p and τ_d are, respectively, the age to thermal of the prompt and the delayed neutrons,

$$k_{eff} = \frac{(1-\beta) k_\infty \exp(-\tau_p B^2)}{1 + L^2 B^2} + \frac{\beta k_\infty \exp(-\tau_d B^2)}{1 + L^2 B^2}$$

and

$$\frac{\beta_{eff}}{\beta} = \{(1-\beta) \exp[-(\tau_p - \tau_d) B^2] + \beta\}^{-1}$$

where k_∞ = the infinite medium multiplication constant
B^2 = the buckling
L^2 = the square of the diffusion length

For an infinite system (so that $B^2 = 0$), or if τ_p is taken equal to τ_d, β_{eff} and β become identical.

For an aqueous solution of UO_2F_2 (enriched to about 90% in U^{235}) containing 0.0763 gm/cm^3 of U^{235}, and having a hydrogen to U^{235} ratio of 337, Gwin[166] obtained the values $\tau_p = 25.4$ cm^2; $\tau_d = 14.1$ cm^2; and $\beta_{eff} = 0.0096$. The analysis depended upon the experimental values of critical height, and change in reactivity with height, of the bare critical solution.

From analysis of an oscillator experiment, de Hoffmann[167] obtained the value $\beta_{eff} = 0.00855$ for the Los Alamos Water Boiler.

Prompt Neutron Lifetime. The following expression for the prompt neutron lifetime, ℓ, can be obtained from perturbation considerations by comparing Eq. (5-44) with the usual inhour equation, and ignoring the differences between $\chi^{25}_{p,i}$, $\chi^{28}_{p,i}$, $\chi^{25}_{d,i}$, and $\chi^{28}_{d,i}$:

$$\ell = \frac{\int \sum_i \frac{\phi_i^* \phi_i}{v_i} dV}{\int [\sum_i \sum_j \chi_i \phi_i^* \nu^{25} \Sigma^{25}_{f,j} \phi_j + \sum_i \sum_j \chi_i \phi_i^* \nu^{28} \Sigma^{28}_{f,j} \phi_j] dV} \tag{5-48}$$

By inserting a uniform 1/v absorber of magnitude C/v into a critical reactor, and using the multigroup perturbation theory given above, it is easily shown that

$$\ell = \frac{\delta\nu/\nu}{C} \tag{5-49}$$

where $\delta\nu/\nu$ is the change in reactivity produced by the absorber. This "1/v method" may be performed either by computation or by experiment.

In the case of a bare core, Eq. (5-48) yields results in terms of the various reactor quantities such as, diffusion length, buckling, etc. The lifetime in one-group theory is given by:

$$\ell = \frac{\ell_0}{1 + L^2B^2}$$

where $\ell_0 = 1/v\Sigma_a$; L is the diffusion length; B^2 is the buckling; v is the neutron velocity, and Σ_a is the macroscopic absorption cross section.

The analogous expression in two-group theory is given by

$$\ell = \frac{\ell_{0,f}}{1 + L_f^2 B^2} + \frac{\ell_{0,s}}{1 + L_s^2 B^2}$$

where f and s refer to the fast and slow groups, respectively, and

$$\ell_{0,f} = \frac{1}{v_f \Sigma_{a,f}}$$

$$\ell_{0,s} = \frac{1}{v_s \Sigma_{a,s}}$$

where L_s is the slow-group diffusion length and L_f^2 corresponds to the age of the slow-group neutrons; v_f and v_s are the fast and slow-group velocities, respectively; $\Sigma_{a,s}$ is the slow-group macroscopic absorption cross section; and $\Sigma_{a,f}$ is the fast group macroscopic slowing-down plus absorption cross section.

Measurements of the lifetime, ℓ, only yield values for ℓ/β_{eff}. This ratio has been measured for the Zero Power Thermal Source Reactor (ZPR-IV') at Argonne by three methods which are based on the statistical nature of the neutron chain. Using a special least square analysis, and assuming a value $\beta_{eff} = 0.007$, Cohn[168] obtained a value of $\ell = 69.2 \pm 3.0$ (μsec). The method used is the same as that discussed by Moore[169] who pointed out that an analysis of the power spectrum of the statistical fluctuations in neutron level of the reactor can yield the high-frequency portion of the reactor transfer function.

The Rossi Alpha Method,[170,171] used by Kato and McMahon[172] yielded the value $\ell = 68.5 \pm 7.0$ (μsec). Luckow[174] employed the method suggested by de Hoffmann[173] and obtained values of ℓ ranging from 67.5 to 72.0 μsec. The latter two measurements were also based on a value $\beta_{eff} = 0.007$.

5.3.2 RELATION BETWEEN REACTIVITY AND ASYMPTOTIC PERIOD

In the space-dependent, one-energy group model, the time behavior of the neutron density in a reactor is related to the reactivity, prompt neutron lifetime, and delayed neutron precursors, by the following set of first-order differential equations:

$$\frac{dn}{dt} = [k(1-\beta) - 1]\frac{n}{\ell} + \sum_i^N \lambda_i C_i$$

$$\frac{dC_i}{dt} = \frac{k\beta_i n}{\ell} - \lambda_i C_i \qquad (5\text{-}50)$$

where n = neutron density
C_i = density of precursors for the *i*th delayed neutron group
k = effective multiplication constant
β = delayed neutron fraction
a_i = relative yield of *i*th delayed neutron group, $\sum a_i = 1$
$\beta_i = \beta a_i$, delayed neutron fraction for *i*th delayed neutron group
λ_i = decay constant for *i*th delayed neutron group
ℓ = prompt neutron lifetime
N = number of delayed neutron groups

Further notation used is:

$\Delta k = k - 1$
$\rho = \Delta k/k\beta$, reactivity in dollars
T = period (e-folding time) of the neutron density

The above equations do not include the possible variation in effectiveness of the delayed neutrons relative to prompt neutrons. Such variation is dependent on the details of the reactor and is discussed for various types in the appropriate section.

An alternate, commonly used version of the kinetic equations[175] is obtained from Eqs. (5-50) by replacing ℓ by ℓk. The equations then become:

$$\frac{dn}{dt} = (\rho - 1)\,\beta\frac{n}{\ell} + \sum_i \lambda_i C_i$$

$$\frac{dC_i}{dt} = \beta_i\frac{n}{\ell} - \lambda_i C_i \qquad (5\text{-}51)$$

The following discussion and numerical values are based on Eq. (5-50).

For a constant value of k, the following relation exists between the reactivity in dollars, and the asymptotic period, T, of the neutron density:

$$\rho = \frac{\ell}{\beta(\ell + T)} + \frac{T}{\ell + T}\sum_i \frac{a_i}{1 + \lambda_i T}$$

The relationship between reactivity and asymptotic periods for prompt neutron lifetimes in the range 10^{-8} sec $\leq \ell \leq 10^{-3}$ sec is presented in both tabular and graphical form. The numerical results for positive reactivities using the thermal fission delayed neutron data for U^{233}, U^{235}, and Pu^{239}, are given in Tables 5-42, 5-43, and 5-44, respectively. The results for negative reactivities and $\ell = 10^{-8}$ sec, are given in Table 5-45. Figures 5-83 through 5-86 show the data in graphical form.

Table 5-42—REACTIVITY VS. ASYMPTOTIC PERIOD (T) FOR VARIOUS NEUTRON LIFETIMES (ℓ) FOR U^{233}

T, sec	Reactivity, dollar					
	ℓ (sec) = 10^{-8}	10^{-7}	10^{-6}	10^{-5}	10^{-4}	10^{-3}
1.00 (−7)	3.5874 (1)	—	—	—	—	—
2.00 (−7)	1.9267 (1)	—	—	—	—	—
4.00 (−7)	1.0356 (1)	—	—	—	—	—
6.00 (−7)	7.2888	—	—	—	—	—
8.00 (−7)	5.7360	—	—	—	—	—
1.00 (−6)	4.7982	—	—	—	—	—
2.00 (−6)	2.9085	—	—	—	—	—
4.00 (−6)	1.9566	—	—	—	—	—
6.00 (−6)	1.6383	7.2888	—	—	—	—
8.00 (−6)	1.4789	5.7360	—	—	—	—
1.00 (−5)	1.3832	4.7982	—	—	—	—
2.00 (−5)	1.1917	2.9085	—	—	—	—
4.00 (−5)	1.0959	1.9566	—	—	—	—
6.00 (−5)	1.0639	1.6383	7.2888	—	—	—
8.00 (−5)	1.0479	1.4789	5.7360	—	—	—
1.00 (−4)	1.0383	1.3832	4.7981	—	—	—
2.00 (−4)	1.0191	1.1917	2.9085	—	—	—
4.00 (−4)	1.0095	1.0958	1.9565	—	—	—
6.00 (−4)	1.0062	1.0638	1.6381	7.2886	—	—
8.00 (−4)	1.0046	1.0477	1.4787	5.7358	—	—
1.00 (−3)	1.0036	1.0381	1.3830	4.7979	—	—
2.00 (−3)	1.0014	1.0186	1.1912	2.9080	—	—
4.00 (−3)	9.9985 (−1)	1.0085	1.0948	1.9555	—	—
6.00 (−3)	9.9898 (−1)	1.0047	1.0623	1.6366	7.2871	—
8.00 (−3)	9.9827 (−1)	1.0026	1.0457	1.4767	5.7338	—
1.00 (−2)	9.9762 (−1)	1.0011	1.0356	1.3805	4.7954	—
2.00 (−2)	9.9473 (−1)	9.9646 (−1)	1.0137	1.1863	2.9031	—
4.00 (−2)	9.8939 (−1)	9.9026 (−1)	9.9889 (−1)	1.0852	1.9460	—
6.00 (−2)	9.8432 (−1)	9.8490 (−1)	9.9065 (−1)	1.0482	1.6226	7.2733
8.00 (−2)	9.7945 (−1)	9.7988 (−1)	9.8420 (−1)	1.0274	1.4583	.7156
1.00 (−1)	9.7475 (−1)	9.7509 (−1)	9.7855 (−1)	1.0131	1.3580	4.7731
2.00 (−1)	9.5329 (−1)	9.5347 (−1)	9.5519 (−1)	9.7246 (−1)	1.1450	2.8620
4.00 (−1)	9.1749 (−1)	9.1757 (−1)	9.1844 (−1)	9.2707 (−1)	1.0134	1.8743
6.00 (−1)	8.8769 (−1)	8.8775 (−1)	8.8832 (−1)	8.9408 (−1)	9.5163 (−1)	1.5262
8.00 (−1)	8.6186 (−1)	8.6190 (−1)	8.6234 (−1)	8.6665 (−1)	9.0982 (−1)	1.3409
1.00	8.3893 (−1)	8.3897 (−1)	8.3931 (−1)	8.4277 (−1)	8.7730 (−1)	1.2223
2.00	7.5104 (−1)	7.5106 (−1)	7.5123 (−1)	7.5296 (−1)	7.7023 (−1)	9.4287 (−1)
4.00	6.4059 (−1)	6.4060 (−1)	6.4069 (−1)	6.4155 (−1)	6.5019 (−1)	7.3656 (−1)
6.00	5.6909 (−1)	5.6909 (−1)	5.6915 (−1)	5.6973 (−1)	5.7549 (−1)	6.3308 (−1)
8.00	5.1698 (−1)	5.1698 (−1)	5.1703 (−1)	5.1746 (−1)	5.2178 (−1)	5.6498 (−1)
1.00 (1)	4.7642 (−1)	4.7643 (−1)	4.7646 (−1)	4.7681 (−1)	4.8027 (−1)	5.1483 (−1)
2.00 (1)	3.5396 (−1)	3.5396 (−1)	3.5398 (−1)	3.5415 (−1)	3.5588 (−1)	3.7317 (−1)
4.00 (1)	2.4430 (−1)	2.4430 (−1)	2.4431 (−1)	2.4440 (−1)	2.4526 (−1)	2.5391 (−1)
6.00 (1)	1.8947 (−1)	1.8947 (−1)	1.8948 (−1)	1.8954 (−1)	1.9011 (−1)	1.9588 (−1)
8.00 (1)	1.5558 (−1)	1.5558 (−1)	1.5559 (−1)	1.5563 (−1)	1.5606 (−1)	1.6039 (−1)
1.00 (2)	1.3230 (−1)	1.3230 (−1)	1.3230 (−1)	1.3234 (−1)	1.3269 (−1)	1.3615 (−1)
2.00 (2)	7.6335 (−2)	7.6335 (−2)	7.6337 (−2)	7.6354 (−2)	7.6527 (−2)	7.8257 (−2)
4.00 (2)	4.1618 (−2)	4.1618 (−2)	4.1619 (−2)	4.1627 (−2)	4.1714 (−2)	4.2579 (−2)
6.00 (2)	2.8645 (−2)	2.8645 (−2)	2.8646 (−2)	2.8652 (−2)	2.8709 (−2)	2.9286 (−2)
8.00 (2)	2.1845 (−2)	2.1845 (−2)	2.1845 (−2)	2.1850 (−2)	2.1893 (−2)	2.2325 (−2)
1.00 (3)	1.7655 (−2)	1.7656 (−2)	1.7656 (−2)	1.7659 (−2)	1.7694 (−2)	1.8040 (−2)
2.00 (3)	9.0153 (−3)	9.0153 (−3)	9.0155 (−3)	9.0172 (−3)	9.0345 (−3)	9.2076 (−3)
4.00 (3)	4.5567 (−3)	4.5567 (−3)	4.5568 (−3)	4.5576 (−3)	4.5663 (−3)	4.6528 (−3)
6.00 (3)	3.0489 (−3)	3.0489 (−3)	3.0489 (−3)	3.0495 (−3)	3.0553 (−3)	3.1130 (−3)
8.00 (3)	2.2909 (−3)	2.2909 (−3)	2.2909 (−3)	2.2913 (−3)	2.2957 (−3)	2.3389 (−3)
1.00 (4)	1.8347 (−3)	1.8347 (−3)	1.8348 (−3)	1.8351 (−3)	1.8386 (−3)	1.8732 (−3)

Note: The base number is to be multiplied by 10 raised to the power indicated within the parentheses.

Table 5-43—REACTIVITY VS. ASYMPTOTIC PERIOD (T) FOR VARIOUS NEUTRON LIFETIMES (ℓ) FOR U^{235}

T, sec	Reactivity, dollar					
	ℓ (sec) 10^{-8}	10^{-7}	10^{-6}	10^{-5}	10^{-4}	10^{-3}
1.00 (−7)	1.5114 (1)	—	—	—	—	—
2.00 (−7)	8.3929	—	—	—	—	—
4.00 (−7)	4.7866	—	—	—	—	—
6.00 (−7)	3.5451	—	—	—	—	—
8.00 (−7)	2.9167	—	—	—	—	—
1.00 (−6)	2.5371	—	—	—	—	—
2.00 (−6)	1.7724	8.3929	—	—	—	—
4.00 (−6)	1.3872	4.7866	—	—	—	—
6.00 (−6)	1.2583	3.5451	—	—	—	—
8.00 (−6)	1.1938	2.9167	—	—	—	—
1.00 (−5)	1.1551	2.5371	—	—	—	—
2.00 (−5)	1.0776	1.7724	8.3928	—	—	—
4.00 (−5)	1.0388	1.3871	4.7866	—	—	—
6.00 (−5)	1.0258	1.2583	3.5451	—	—	—
8.00 (−5)	1.0194	1.1938	2.9166	—	—	—
1.00 (−4)	1.0155	1.1551	2.5371	—	—	—
2.00 (−4)	1.0077	1.0775	1.7723	8.3928	—	—
4.00 (−4)	1.0037	1.0386	1.3870	4.7864	—	—
6.00 (−4)	1.0023	1.0256	1.2581	3.5448	—	—
8.00 (−4)	1.0016	1.0191	1.1935	2.9163	—	—
1.00 (−3)	1.0011	1.0151	1.1547	2.5367	—	—
2.00 (−3)	9.9997 (−1)	1.0070	1.0768	1.7716	8.3921	—
4.00 (−3)	9.9878 (−1)	1.0023	1.0372	1.3855	4.7850	—
6.00 (−3)	9.9785 (−1)	1.0002	1.0235	1.2559	3.5427	—
8.00 (−3)	9.9699 (−1)	9.9873 (−1)	1.0162	1.1906	2.9135	—
1.00 (−2)	9.9616 (−1)	9.9756 (−1)	1.0115	1.1511	2.5332	—
2.00 (−2)	9.9219 (−1)	9.9289 (−1)	9.9988 (−1)	1.0697	1.7645	8.3853
4.00 (−2)	9.8466 (−1)	9.8501 (−1)	9.8851 (−1)	1.0234	1.3718	4.7716
6.00 (−2)	9.7751 (−1)	9.7774 (−1)	9.8007 (−1)	1.0034	1.2358	3.5229
8.00 (−2)	9.7068 (−1)	9.7086 (−1)	9.7260 (−1)	9.9007 (−1)	1.1645	2.8877
1.00 (−1)	9.6413 (−1)	9.6427 (−1)	9.6567 (−1)	9.7964 (−1)	1.1192	2.5016
2.00 (−1)	9.3478 (−1)	9.3485 (−1)	9.3555 (−1)	9.4254 (−1)	1.0124	1.7075
4.00 (−1)	8.8745 (−1)	8.8748 (−1)	8.8783 (−1)	8.9133 (−1)	9.2628 (−1)	1.2749
6.00 (−1)	8.4939 (−1)	8.4941 (−1)	8.4964 (−1)	8.5197 (−1)	8.7528 (−1)	1.1080
8.00 (−1)	8.1724 (−1)	8.1725 (−1)	8.1743 (−1)	8.1918 (−1)	8.3666 (−1)	1.0113
1.00	7.8929 (−1)	7.8930 (−1)	7.8944 (−1)	7.9083 (−1)	8.0482 (−1)	9.4459 (−1)
2.00	6.8645 (−1)	6.8646 (−1)	6.8653 (−1)	6.8723 (−1)	6.9423 (−1)	7.6419 (−1)
4.00	5.6524 (−1)	5.6524 (−1)	5.6528 (−1)	5.6563 (−1)	5.6913 (−1)	6.0415 (−1)
6.00	4.9085 (−1)	4.9085 (−1)	4.9088 (−1)	4.9111 (−1)	4.9345 (−1)	5.1681 (−1)
8.00	4.3854 (−1)	4.3854 (−1)	4.3856 (−1)	4.3873 (−1)	4.4049 (−1)	4.5801 (−1)
1.00 (1)	3.9891 (−1)	3.9892 (−1)	3.9893 (−1)	3.9907 (−1)	4.0047 (−1)	4.1450 (−1)
2.00 (1)	2.8488 (−1)	2.8488 (−1)	2.8489 (−1)	2.8496 (−1)	2.8566 (−1)	2.9268 (−1)
4.00 (1)	1.8966 (−1)	1.8966 (−1)	1.8966 (−1)	1.8970 (−1)	1.9005 (−1)	1.9356 (−1)
6.00 (1)	1.4436 (−1)	1.4436 (−1)	1.4436 (−1)	1.4438 (−1)	1.4462 (−1)	1.4696 (−1)
8.00 (1)	1.1711 (−1)	1.1711 (−1)	1.1711 (−1)	1.1713 (−1)	1.1731 (−1)	1.1906 (−1)
1.00 (2)	9.8734 (−2)	9.8734 (−2)	9.8736 (−2)	9.8750 (−2)	9.8890 (−2)	1.0030 (−1)
2.00 (2)	5.5734 (−2)	5.5734 (−2)	5.5734 (−2)	5.5741 (−2)	5.5812 (−2)	5.6515 (−2)
4.00 (2)	2.9945 (−2)	2.9946 (−2)	2.9946 (−2)	2.9949 (−2)	2.9985 (−2)	3.0336 (−2)
6.00 (2)	2.0495 (−2)	2.0495 (−2)	2.0495 (−2)	2.0497 (−2)	2.0521 (−2)	2.0755 (−2)
8.00 (2)	1.5582 (−2)	1.5582 (−2)	1.5582 (−2)	1.5584 (−2)	1.5601 (−2)	1.5777 (−2)
1.00 (3)	1.2570 (−2)	1.2570 (−2)	1.2570 (−2)	1.2572 (−2)	1.2586 (−2)	1.2726 (−2)
2.00 (3)	6.3935 (−3)	6.3935 (−3)	6.3936 (−3)	6.3943 (−3)	6.4013 (−3)	6.4716 (−3)
4.00 (3)	3.2249 (−3)	3.2249 (−3)	3.2250 (−3)	3.2253 (−3)	3.2288 (−3)	3.2640 (−3)
6.00 (3)	2.1563 (−3)	2.1563 (−3)	2.1563 (−3)	2.1566 (−3)	2.1589 (−3)	2.1824 (−3)
8.00 (3)	1.6196 (−3)	1.6196 (−3)	1.6197 (−3)	1.6198 (−3)	1.6216 (−3)	1.6392 (−3)
1.00 (4)	1.2969 (−3)	1.2969 (−3)	1.2969 (−3)	1.2970 (−3)	1.2984 (−3)	1.3125 (−3)

Note: The base number is to be multiplied by 10 raised to the power indicated within the parentheses.

687863 O - 63 - 30

Table 5-44—REACTIVITY VS. ASYMPTOTIC PERIOD (T) FOR VARIOUS NEUTRON LIFETIMES (ℓ) FOR Pu^{239}

T, sec	Reactivity, dollar					
	ℓ (sec) = 10^{-8}	10^{-7}	10^{-6}	10^{-5}	10^{-4}	10^{-3}
1.00 (−7)	4.4199 (1)	—	—	—	—	—
2.00 (−7)	2.3628 (1)	—	—	—	—	—
4.00 (−7)	1.2590 (1)	—	—	—	—	—
6.00 (−7)	8.7900	—	—	—	—	—
8.00 (−7)	6.8665	—	—	—	—	—
1.00 (−6)	5.7049	—	—	—	—	—
2.00 (−6)	3.3641	—	—	—	—	—
4.00 (−6)	2.1850	—	—	—	—	—
6.00 (−6)	1.7907	8.7900	—	—	—	—
8.00 (−6)	1.5932	6.8665	—	—	—	—
1.00 (−5)	1.4747	5.7049	—	—	—	—
2.00 (−5)	1.2375	3.3641	—	—	—	—
4.00 (−5)	1.1188	2.1850	—	—	—	—
6.00 (−5)	1.0792	1.7906	8.7900	—	—	—
8.00 (−5)	1.0594	1.5932	6.8665	—	—	—
1.00 (−4)	1.0475	1.4747	5.7048	—	—	—
2.00 (−4)	1.0237	1.2374	3.3641	—	—	—
4.00 (−4)	1.0117	1.1186	2.1849	—	—	—
6.00 (−4)	1.0077	1.0790	1.7905	8.7898	—	—
8.00 (−4)	1.0057	1.0591	1.5930	6.8663	—	—
1.00 (−3)	1.0044	1.0472	1.4744	5.7045	—	—
2.00 (−3)	1.0017	1.0230	1.2368	3.3634	—	—
4.00 (−3)	9.9977 (−1)	1.0105	1.1173	2.1836	—	—
6.00 (−3)	9.9867 (−1)	1.0058	1.0771	1.7885	8.7879	—
8.00 (−3)	9.9777 (−1)	1.0031	1.0566	1.5904	6.8638	—
1.00 (−2)	9.9695 (−1)	1.0012	1.0440	1.4712	5.7014	—
2.00 (−2)	9.9328 (−1)	9.9542 (−1)	1.0168	1.2305	3.3572	—
4.00 (−2)	9.8654 (−1)	9.8761 (−1)	9.9830 (−1)	1.1052	2.1715	—
6.00 (−2)	9.8017 (−1)	9.8088 (−1)	9.8801 (−1)	1.0593	1.7708	8.7704
8.00 (−2)	9.7408 (−1)	9.7461 (−1)	9.7996 (−1)	1.0334	1.5673	6.8409
1.00 (−1)	9.6824 (−1)	9.6866 (−1)	9.7294 (−1)	1.0157	1.4429	5.6734
2.00 (−1)	9.4196 (−1)	9.4217 (−1)	9.4431 (−1)	9.6570 (−1)	1.1794	3.3064
4.00 (−1)	8.9932 (−1)	8.9943 (−1)	9.0050 (−1)	9.1119 (−1)	1.0181	2.0846
6.00 (−1)	8.6483 (−1)	8.6490 (−1)	8.6561 (−1)	8.7274 (−1)	9.4403 (−1)	1.6557
8.00 (−1)	8.3556 (−1)	8.3562 (−1)	8.3615 (−1)	8.4150 (−1)	8.9497 (−1)	1.4290
1.00	8.1002 (−1)	8.1006 (−1)	8.1049 (−1)	8.1477 (−1)	8.5755 (−1)	1.2849
2.00	7.1522 (−1)	7.1525 (−1)	7.1546 (−1)	7.1760 (−1)	7.3899 (−1)	9.5284 (−1)
4.00	6.0146 (−1)	6.0148 (−1)	6.0158 (−1)	6.0265 (−1)	6.1335 (−1)	7.2033 (−1)
6.00	5.3013 (−1)	5.3014 (−1)	5.3021 (−1)	5.3092 (−1)	5.3806 (−1)	6.0939 (−1)
8.00	4.7902 (−1)	4.7902 (−1)	4.7907 (−1)	4.7961 (−1)	4.8496 (−1)	5.3847 (−1)
1.00 (1)	4.3966 (−1)	4.3966 (−1)	4.3971 (−1)	4.4013 (−1)	4.4442 (−1)	4.8723 (−1)
2.00 (1)	3.2254 (−1)	3.2254 (−1)	3.2257 (−1)	3.2278 (−1)	3.2492 (−1)	3.4633 (−1)
4.00 (1)	2.1942 (−1)	2.1942 (−1)	2.1943 (−1)	2.1954 (−1)	2.2061 (−1)	2.3132 (−1)
6.00 (1)	1.6851 (−1)	1.6852 (−1)	1.6852 (−1)	1.6859 (−1)	1.6931 (−1)	1.7645 (−1)
8.00 (1)	1.3736 (−1)	1.3736 (−1)	1.3736 (−1)	1.3742 (−1)	1.3795 (−1)	1.4331 (−1)
1.00 (2)	1.1614 (−1)	1.1614 (−1)	1.1614 (−1)	1.1618 (−1)	1.1661 (−1)	1.2090 (−1)
2.00 (2)	6.5911 (−2)	6.5911 (−2)	6.5913 (−2)	6.5935 (−2)	6.6149 (−2)	6.8291 (−2)
4.00 (2)	3.5492 (−2)	3.5492 (−2)	3.5493 (−2)	3.5503 (−2)	3.5611 (−2)	3.6682 (−2)
6.00 (2)	2.4305 (−2)	2.4305 (−2)	2.4305 (−2)	2.4312 (−2)	2.4384 (−2)	2.5098 (−2)
8.00 (2)	1.8483 (−2)	1.8483 (−2)	1.8484 (−2)	1.8489 (−2)	1.8543 (−2)	1.9078 (−2)
1.00 (3)	1.4913 (−2)	1.4913 (−2)	1.4913 (−2)	1.4917 (−2)	1.4960 (−2)	1.5389 (−2)
2.00 (3)	7.5867 (−3)	7.5867 (−3)	7.5870 (−3)	7.5891 (−3)	7.6105 (−3)	7.8248 (−3)
4.00 (3)	3.8272 (−3)	3.8272 (−3)	3.8273 (−3)	3.8283 (−3)	3.8391 (−3)	3.9462 (−3)
6.00 (3)	2.5591 (−3)	2.5591 (−3)	2.5591 (−3)	2.5599 (−3)	2.5670 (−3)	2.6384 (−3)
8.00 (3)	1.9222 (−3)	1.9222 (−3)	1.9222 (−3)	1.9228 (−3)	1.9281 (−3)	1.9817 (−3)
1.00 (4)	1.5391 (−3)	1.5391 (−3)	1.5392 (−3)	1.5396 (−3)	1.5439 (−3)	1.5867 (−3)

Note: The base number is to be multiplied by 10 raised to the power indicated within the parentheses.

Table 5-45 — NEGATIVE REACTIVITY VS. NEGATIVE ASYMPTOTIC PERIOD (T) FOR U^{233}, U^{235}, Pu^{239}, AND $\ell = 10^{-8}$ sec

T, sec	Reactivity, dollar			T, sec	Reactivity, dollar		
	U^{233}	U^{235}	Pu^{239}		U^{233}	U^{235}	Pu^{239}
−7.86 (1)	—	—	−9.66	−9.60 (1)	−5.74 (−1)	−3.19 (−1)	−3.44 (−1)
−7.87	—	—	−7.26	−9.80 (1)	−5.26	−2.95	−3.23
−7.88	—	—	−5.83	−1.00 (2)	−4.86	−2.76	−3.05
−7.89	—	—	−4.89	−1.10 (2)	−3.59	−2.13	−2.43
−7.90 (1)	—	—	−4.22	−1.20 (2)	−2.90 (−1)	−1.77 (−1)	−2.05 (−1)
−7.91 (1)	—	—	−3.72	−1.30 (2)	−2.45 (−1)	−1.53 (−1)	−1.78 (−1)
−7.92	—	—	−3.33	−1.40	−2.13	−1.35 (−1)	−1.58
−7.93	—	—	−3.02	−1.50	−1.89	−1.22 (−1)	−1.43
−7.94	—	—	−2.76	−1.75	−1.49	−9.74 (−2)	−1.15 (−1)
−7.95 (1)	—	—	−2.55	−2.00 (2)	−1.23 (−1)	−8.16 (−2)	−9.64 (−2)
−7.96 (1)	—	—	−2.37	−2.25 (2)	−1.05 (−1)	−7.03 (−2)	−8.31 (−2)
−7.97	—	—	−2.22	−2.50	−9.15 (−2)	−6.18	−7.31
−7.98	—	—	−2.09	−2.75	−8.12	−5.51	−6.53
−7.99	—	—	−1.97	−3.00	−7.30	−4.98	−5.90
−8.00 (1)	—	—	−1.87	−3.50 (2)	−6.09 (−2)	−4.17 (−2)	−4.95 (−2)
−8.01 (1)	−9.50	—	−1.78	−4.00 (2)	−5.22 (−2)	−3.59 (−2)	−4.26 (−2)
−8.02	−8.39	—	−1.70	−4.50	−4.57	−3.16	−3.75
−8.03	−7.51	—	−1.62	−5.00	−4.06	−2.81	−3.34
−8.04	−6.81	—	−1.56	−6.00	−3.33	−2.31	−2.74
−8.05 (1)	−6.23	—	−1.50	−7.50 (2)	−2.62 (−2)	−1.83 (−2)	−2.17 (−2)
−8.06 (1)	−5.74	—	−1.44	−1.00 (3)	−1.93 (−2)	−1.35 (−2)	−1.60 (−2)
−8.07	−5.32	−8.64	−1.39	−2.00	−9.43 (−3)	−6.63 (−3)	−7.87 (−3)
−8.08	−4.97	−6.60	−1.35	−3.00	−6.24	−4.39	−5.21
−8.09	−4.66	−5.35	−1.30	−4.00	−4.66	−3.28	−3.90
−8.10 (1)	−4.38	−4.51	−1.26	−5.00 (3)	−3.72 (−3)	−2.62 (−3)	−3.11 (−3)
−8.20 (1)	−2.80	−1.83	−9.83 (−1)	−6.00 (3)	−3.09 (−3)	−2.18 (−3)	−2.59 (−3)
−8.30	−2.08	−1.20	−8.20	−7.00	−2.65	−1.87	−2.22
−8.40	−1.67	−9.15 (−1)	−7.13	−8.00	−2.32	−1.63	−1.94
−8.50	−1.41	−7.53 (−1)	−6.37	−9.00	−2.06	−1.45	−1.72
−8.60 (1)	−1.22	−6.47 (−1)	−5.79 (−1)	−1.00 (4)	−1.85 (−3)	−1.31 (−3)	−1.55 (−3)
−8.70 (1)	−1.08	−5.73 (−1)	−5.34 (−1)				
−8.80	−9.76 (−1)	−5.17	−4.98				
−9.00	−8.21	−4.39	−4.42				
−9.20	−7.14	−3.87	−4.01				
−9.40 (1)	−6.35 (−1)	−3.48 (−1)	−3.70 (−1)				

Note: The base number is to be multiplied by 10 raised to the power indicated within the parentheses.

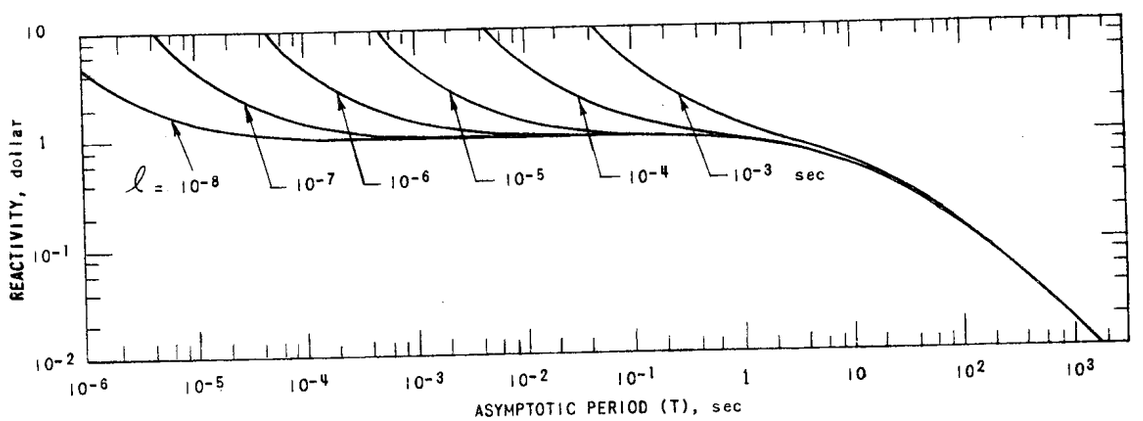

Fig. 5-83 — Reactivity vs. asymptotic period for various neutron lifetimes (ℓ) for U^{233}.

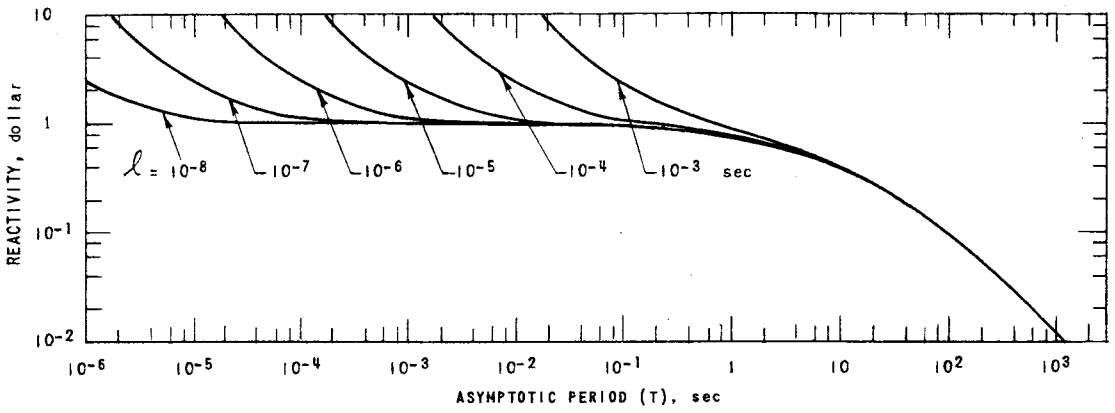

Fig. 5-84—Reactivity vs. asymptotic period for various neutron lifetimes (ℓ) for U^{235}.

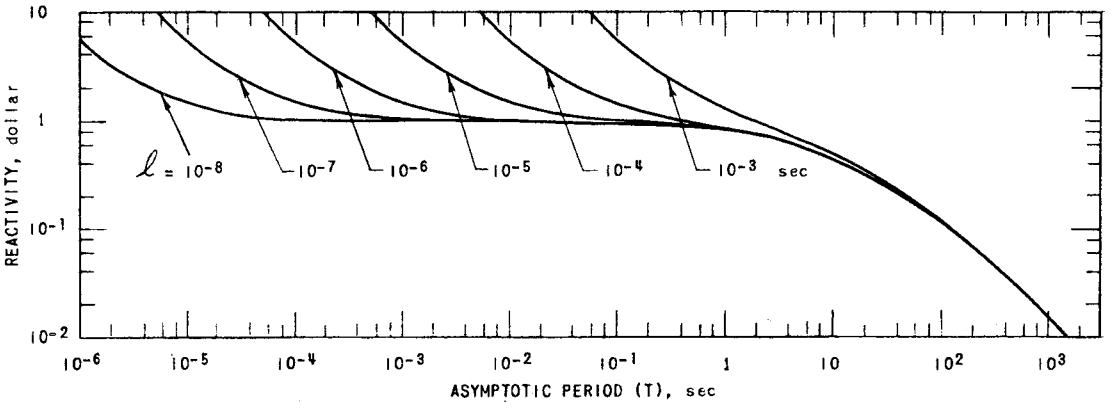

Fig. 5-85—Reactivity vs. asymptotic period for various neutron lifetimes (ℓ) for Pu^{239}.

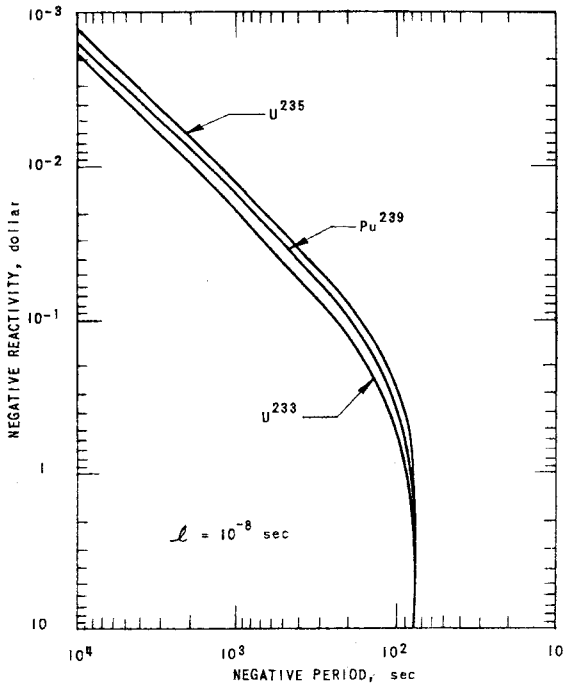

Fig. 5-86—Negative reactivity vs. negative asymptotic period (T) for U^{233}, U^{235}, and Pu^{239}.

5.3.3 REACTOR TRANSFER FUNCTION

The reactor transfer function (zero power transfer function) is a measure of the response of the neutron density to a sinusoidal time variation in reactivity.

In Eq. (5-50) set

$$k - 1 = \Delta k(t) \ll 1$$

$$n = n_1(t) + n_0$$

$$C_i = C_{i,1}(t) + C_{i,0}$$

If $n_1(t) \ll n_0$, the terms involving $n_1(t)\Delta k(t)$ may be ignored. The Laplace transform of Eq. (5-50) is

$$\frac{N(s)}{n_0 R(s)} = \frac{1 - s\sum_i \frac{\beta_i}{s + \lambda_i}}{s\left(\ell + \sum_i \frac{\beta_i}{s + \lambda_i}\right)} = \frac{1}{\beta} M(s) \tag{5-52}$$

where $N(s)$ = Laplace transform of $n_1(t)$
$R(s)$ = Laplace transform of $\Delta k(t)$

The quantity $M(s)$ is usually called the reactor transfer function although sometimes $\frac{1}{\beta}(Ms)$ is used.

The initial values of $C_{i,1}$ and n_1 were taken to be zero since non-zero values would appear only in terms not involving $\Delta k(t)$ when the inverse transform of Eq. (5-52) is taken. Since the asymptotic response of the reactor to the function $\Delta k(t)$, is of immediate interest, the other terms are not considered.

On taking inverse Laplace transforms of Eq. (5-52)

$$\frac{n_1(t)}{n_0} = \frac{1}{\ell} \sum_k \left[\frac{1 - \sum_i \frac{s_k \beta_i}{s_k + \lambda_i}}{Z'(s_k)}\right] \int_0^t \exp\left[s_k (t - t')\right] \Delta k(t')dt' \tag{5-53}$$

where

$$Z(s) = \frac{s}{\ell}\left(\ell + \sum_i \frac{\beta_i}{s + \lambda_i}\right)$$

$Z(s_k) = 0$, and $Z'(s_k)$ denotes differentiation. Substitution of $\delta \exp(i\omega t')$ for $\Delta k(t')$ in Eq. (5.53) gives

$$\frac{n_1(t)}{n_0} = \frac{\delta}{\ell} \sum_k \left[\frac{1 - \sum_i \frac{s_k \beta_i}{s_k + \lambda_i}}{Z'(s_k)}\right]\left(\frac{\exp(i\omega t) - \exp(s_k t)}{i\omega - s_k}\right)$$

Since the reactor was originally critical, all $\exp(s_k t)$ will approach zero after a short time except the one for $s_k = 0$. Thus

$$\frac{n_1(t)}{n_0} = \frac{\delta}{\ell}\left[\sum_k \frac{\left(1 - \sum_i \frac{s_k \beta_i}{s_k + \lambda_i}\right)\exp(i\omega t)}{Z'(s_k)(i\omega - s_k)} - \frac{1}{i\omega Z'(0)}\right]$$

$$= \delta \frac{M(i\omega)}{\beta} \exp(i\omega t) - \frac{\delta}{i\omega \ell Z'(0)}$$

$$= \delta \frac{|M(i\omega)|}{\beta} \exp\left[i(\omega t + \theta)\right] - \frac{\delta}{i\omega \ell Z'(0)}$$

A reactivity input of $\Delta k(t) = \delta \cos \omega t$ yields a variation in neutron density of

$$\frac{n_1(t)}{n_0} = \delta \frac{|M(i\omega)|}{\beta} \cos(\omega t + \theta)$$

For the case where $\omega \ll \lambda_i$ for all i, θ is almost -90° and

$$|M(i\omega)| \approx \beta \Big/ \left[\omega\left(\ell + \sum_i \frac{\beta_i}{\lambda_i}\right)\right]$$

When $\omega \gg \lambda_i$ for all i, θ is given approximately by:

$$\theta = -\tan^{-1}\frac{\omega\ell}{\beta}$$

and

$$|M(i\omega)| = \beta(1-\beta)/(\beta^2 + \ell\omega^2)^{1/2}$$

If Eq. (5-51) had been used to derive the transfer function, the numerator in the middle expression in Eq. (5-52) would have been unity.

Tables 5-46, 5-47, and 5-48 give for U^{233}, U^{235}, and Pu^{239}, respectively, the magnitude and phase angle of the reactor transfer function for the frequency range $10^{-3} < \omega < 10^6$ radians per second, for prompt neutron lifetimes in the range 10^{-8} sec $\leq \ell \leq 10^{-3}$ sec. The definition based on Eq. (5-50) is used in these tables. Figures 5-87 through 5-92 give the corresponding data in graphical form.

5.3.4 DEVIATION OF OBSERVED PERIOD FROM ASYMPTOTIC PERIOD[176]

The worth of a step change in reactivity in a reactor system may be obtained by observation of the kinetics behavior of the system. This is usually done by use of the inhour equation which relates the reactivity and the asymptotic period.

The introduction of a step change in reactivity into a critical reactor results in an observed rate of reactor power change characteristic of the amount and sign of the reactivity step, and of the general kinetic characteristics of the reactor. A premature observation of the change in reactor power with time may show a period which is in considerable error owing to the presence of transient terms. Following a step change in reactivity the waiting time to observe a period within 1%, 5%, or 10% of the asymptotic value is shown in Figs. 5-93, and 5-94 for a reactor without a source. The delayed neutron data used are those of Keepin (see Section 1.4.1).

Figure 5-95 shows the error in reactivity given by the inhour equation as a result of an error in the asymptotic period.

5.3.5 PERIOD MEASUREMENTS WITH SOURCE IN REACTOR[176]

The reactor kinetics equations are:

$$\frac{dn}{dt} = [k(1-\beta) - 1]\frac{n}{\ell} + \sum_i \lambda_i C_i + S$$

$$\frac{dC_i}{dt} = \frac{k\beta_i n}{\ell} - \lambda_i C_i$$

where S is the source. The other symbols are defined in Section 5.3.2. The complete solution for the experimentally interesting case of $k \neq 1$ is:

$$\frac{n(t)}{n_0} = \sum_{j=1}^{N+1} (A_j + B_j)\exp(s_j t) + C$$

where the s_j are the N + 1 roots of the inhour equation:

$$\rho = \frac{k-1}{k} = \frac{\ell s + s\sum_{i=1}^{N} \frac{\beta_i}{s+\lambda_i}}{1+\ell s}$$

and

$$A_j = (1-\rho)\frac{\ell + k_0 \sum_{i=1}^{N} \frac{\beta_i}{s_j + \lambda_i}}{\ell(1-\rho) + \sum_{i=1}^{N} \frac{\beta_i \lambda_i}{(s_j + \lambda_i)^2}}$$

$$B_j = (1-\rho)\frac{1-k_0}{s_j\left[\ell(1-\rho) + \sum_{i=1}^{N} \frac{\beta_i \lambda_i}{(s_j + \lambda_i)^2}\right]}$$

$$C = \frac{\rho - 1}{\rho}(1 - k_0)$$

The subscript 0 refers to initial values which obtain until $t = 0$ at which time the effective multiplication constant is changed abruptly from k_0 to the final k. Owing to the normalization used, the results do not depend explicitly upon S, but rather upon k_0.

The deviation from the critical state of an assembly is reflected sensitively in the accuracy of measurements of periods subsequent to the introduction of the step change in reactivity. If the initial value of k were unity, i.e., if there were no detectable effect from built-in neutron sources, then the only inaccuracy in a period measurement would be occasioned by a premature observation of the period. If a source is present, the error in period is considerably more severe, even after a long time has elapsed.

The influence of the extraneous source is illustrated for various degrees of initial subcriticality in Figs. 5-96 through 5-100.

The effect of varying the prompt neutron lifetime is illustrated in Table 5-49 where the deviation of the observed period from the asymptotic period is given at various times after a reactivity step.

The effect of varying the delayed neutron parameters is illustrated in Table 5-51. In this calculation, use was made of the data of Keepin, et al., (see Section 1.4.1), and the early data of Hughes,[177] and a set of parameters (Table 5-50) representative of a D_2O-moderated reactor in which account is taken of the delayed photoneutrons.

5.3.6 EFFECT OF SOURCE ON REACTOR TRANSFER FUNCTION

The effect of various degrees of subcriticality in a reactor with a source, upon the reactor transfer function is plotted in Figs. 5-101 through 5-104. The delayed neutron data used are those of Keepin given in Section 1.4.1. Figures 5-101 through 5-104 are from the data of Toppel.* The transfer function as defined here, is $1/\beta$ times the transfer function defined in Section 5.3.3.

5.3.7 FLUCTUATION EXPERIMENTS

The term "noise" is used in describing the discreteness of the neutrons and the statistical nature of nuclear reactions. These effects are usually manifested by a random fluctuation in the neutron population of the reactor. Since the properties of the noise depend upon the kinetic properties of the particular reactor, observation of noise offers a convenient method for studying these properties. The following discussion will use the conventional zero-power, space-independent, one-energy-group kinetics model.

The noise observed from a given critical reactor can be completely characterized by its "power spectrum." This is given by:[178]

$$\langle |I(f)|^2 \rangle = 2\frac{Q^2 \epsilon n}{\ell}\left[1 + \frac{\epsilon}{(2\pi f L)^2 + B^2}\left(\frac{\overline{\nu^2} - \bar{\nu}}{\bar{\nu}}\right)\right] \tag{5-54}$$

where $\langle |I(f)|^2 \rangle$ is the spectral density of the current fluctuations in a neutron-sensitive ionization chamber at the reactor, i.e., the mean square amplitude of these fluctuations per unit bandwidth at the frequency f; n is the total number of neutrons in the reactor; Q is the charge which passes through the

*B. J. Toppel, ANL, private communication.

Table 5-46— MAGNITUDE (|M|) AND PHASE ANGLE (θ) OF ZERO POWER TRANSFER FUNCTION FOR U^{233}

ω, rad/sec	ℓ(sec) = 10^{-3}		10^{-4}		10^{-5}		10^{-6}		10^{-7}		10^{-8}	
	|M|	θ	|M|	θ	|M|	θ	|M|	θ	|M|	θ	|M|	θ
(1/10) (−2)	5.3247 (1)	−87.509	5.4246 (1)	−87.462	5.4347 (1)	−87.457	5.4358 (1)	−87.457	5.4359 (1)	−87.457	5.4359 (1)	−87.457
(1/8)	4.2639 (1)	−86.890	4.3439 (1)	−86.832	4.3521 (1)	−86.826	4.3529 (1)	−86.825	4.3530 (1)	−86.825	4.3530 (1)	−86.825
(1/6)	3.2046 (1)	−85.866	3.2648 (1)	−85.788	3.2710 (1)	−85.780	3.2716 (1)	−85.779	3.2716 (1)	−85.779	3.2716 (1)	−85.779
(1/4)	2.1490 (1)	−83.848	2.1895 (1)	−83.731	2.1936 (1)	−83.719	2.1940 (1)	−83.718	2.1941 (1)	−83.718	2.1941 (1)	−83.718
(1/2)	1.1064 (1)	−78.179	1.1276 (1)	−77.949	1.1297 (1)	−77.926	1.1299 (1)	−77.924	1.1300 (1)	−77.923	1.1300 (1)	−77.923
(1/10) (−1)	6.0465	−69.117	6.1670	−68.681	6.1792	−68.636	6.1805	−68.632	6.1806	−68.631	6.1806	−68.631
(1/8)	5.0803	−65.636	5.1838	−65.105	5.1944	−65.051	5.1955	−65.045	5.1956	−65.045	5.1956	−65.045
(1/6)	4.1272	−60.927	4.2146	−60.249	4.2235	−60.180	4.2244	−60.173	4.2245	−60.172	4.2245	−60.172
(1/4)	3.1852	−54.067	3.2575	−53.118	3.2648	−53.020	3.2656	−53.010	3.2656	−53.010	3.2656	−53.009
(1/2)	2.2588	−43.327	2.3201	−41.651	2.3263	−41.478	2.3269	−41.461	2.3270	−41.459	2.3270	−41.459
(1/10) (0)	1.7312	−36.534	1.7930	−33.670	1.7992	−33.373	1.7998	−33.343	1.7998	−33.340	1.7998	−33.339
(1/8)	1.5965	−34.899	1.6593	−31.516	1.6655	−31.164	1.6662	−31.128	1.6662	−31.125	1.6662	−31.124
(1/6)	1.4444	−32.897	1.5089	−28.696	1.5152	−28.256	1.5158	−28.212	1.5159	−28.208	1.5159	−28.207
(1/4)	1.2717	−30.291	1.3397	−24.533	1.3461	−23.924	1.3468	−23.863	1.3468	−23.857	1.3468	−23.856
(1/2)	1.0740	−27.741	1.1571	−17.505	1.1639	−16.402	1.1646	−16.291	1.1647	−16.280	1.1647	−16.278
(1/10) (1)	9.3844 (−1)	−31.110	1.0696	−12.578	1.0776	−10.486	1.0783	−10.276	1.0784	−10.254	1.0784	−10.252
(1/8)	8.9140 (−1)	−33.912	1.0518	−11.660	1.0605	−9.078	1.0612	−8.817	1.0613	−8.791	1.0613	−8.789
(1/6)	8.2072 (−1)	−38.732	1.0327	−10.954	1.0427	−7.560	1.0435	−7.217	1.0436	−7.182	1.0436	−7.179
(1/4)	6.9757 (−1)	−47.358	1.0110	−10.894	1.0241	−5.889	1.0250	−5.382	1.0251	−5.331	1.0251	−5.326
(1/2)	4.5157 (−1)	−63.398	9.7882 (−1)	−13.867	1.0056	−4.113	1.0067	−3.115	1.0068	−3.015	1.0068	−3.005
(1/10) (2)	2.4937 (−1)	−75.570	9.2459 (−1)	−22.453	9.9823 (−1)	−3.779	9.9991 (−1)	−1.795	1.0000	−1.596	1.0000	−1.576
(1/8)	2.0224 (−1)	−78.328	8.9249 (−1)	−26.741	9.9689 (−1)	−4.021	9.9899 (−1)	−1.543	9.9909 (−1)	−1.295	9.9910 (−1)	−1.270
(1/6)	1.5335 (−1)	−81.168	8.3399 (−1)	−33.362	9.9526 (−1)	−4.622	9.9824 (−1)	−1.323	9.9836 (−1)	−0.992	9.9837 (−1)	−0.959
(1/4)	1.0306 (−1)	−84.074	7.1516 (−1)	−44.222	9.9220 (−1)	−6.128	9.9768 (−1)	−1.190	9.9782 (−1)	−0.695	9.9783 (−1)	−0.645
(1/2)	5.1780 (−2)	−87.025	4.5912 (−1)	−62.597	9.7854 (−1)	−11.196	9.9722 (−1)	−1.422	9.9750 (−1)	−0.431	9.9751 (−1)	−0.331

(1/10) (3)	2.5922 (−2)	−88.511	2.5081 (−1)	−75.437	9.3007 (−1)	−21.178	9.9658 (−1)	−2.363	9.9741 (−1)	−0.381	9.9743 (−1)	−0.182
(1/8)	2.0740 (−2)	−88.809	2.0302 (−1)	−78.256	8.9814 (−1)	−25.781	9.9616 (−1)	−2.880	9.9740 (−1)	−0.404	9.9742 (−1)	−0.156
(1/6)	1.5557 (−2)	−89.107	1.5370 (−1)	−81.136	8.3906 (−1)	−32.729	9.9526 (−1)	−3.764	9.9738 (−1)	−0.463	9.9741 (−1)	−0.133
(1/4)	1.0372 (−2)	−89.404	1.0316 (−1)	−84.063	7.1856 (−1)	−43.910	9.9272 (−1)	−5.556	9.9735 (−1)	−0.615	9.9740 (−1)	−0.119
(1/2)	5.1864 (−3)	−89.702	5.1793 (−2)	−87.024	4.6005 (−1)	−62.533	9.7935 (−1)	−10.916	9.9721 (−1)	−1.134	9.9740 (−1)	−0.142
(1/10) (4)	2.5932 (−3)	−89.851	2.5923 (−2)	−88.511	2.5096 (−1)	−75.427	9.3083 (−1)	−21.051	9.9665 (−1)	−2.219	9.9739 (−1)	−0.236
(1/8)	2.0746 (−3)	−89.881	2.0741 (−2)	−88.808	2.0310 (−1)	−78.251	8.9883 (−1)	−25.687	9.9624 (−1)	−2.765	9.9739 (−1)	−0.288
(1/6)	1.5559 (−3)	−89.911	1.5558 (−2)	−89.106	1.5373 (−1)	−81.134	8.3963 (−1)	−32.668	9.9535 (−1)	−3.677	9.9738 (−1)	−0.377
(1/4)	1.0373 (−3)	−89.940	1.0372 (−2)	−89.404	1.0317 (−1)	−84.063	7.1892 (−1)	−43.880	9.9281 (−1)	−5.499	9.9735 (−1)	−0.557
(1/2)	5.1865 (−4)	−89.970	5.1864 (−3)	−89.702	5.1795 (−2)	−87.023	4.6014 (−1)	−62.526	9.7944 (−1)	−10.889	9.9721 (−1)	−1.105
(1/10) (5)	2.5932 (−4)	−89.985	2.5932 (−3)	−89.851	2.5924 (−2)	−88.511	2.5098 (−1)	−75.426	9.3091 (−1)	−21.039	9.9666 (−1)	−2.204
(1/8)	2.0746 (−4)	−89.988	2.0746 (−3)	−89.881	2.0741 (−2)	−88.808	2.0311 (−1)	−78.250	8.9890 (−1)	−25.678	9.9625 (−1)	−2.754
(1/6)	1.5559 (−4)	−89.991	1.5559 (−3)	−89.911	1.5558 (−2)	−89.106	1.5373 (−1)	−81.133	8.3968 (−1)	−32.662	9.9536 (−1)	−3.669
(1/4)	1.0373 (−4)	−89.994	1.0373 (−3)	−89.940	1.0372 (−2)	−89.404	1.0317 (−1)	−84.063	7.1895 (−1)	−43.877	9.9282 (−1)	−5.493
(1/2)	5.1865 (−5)	−89.997	5.1865 (−4)	−89.970	5.1864 (−3)	−89.702	5.1795 (−2)	−87.023	4.6015 (−1)	−62.526	9.7945 (−1)	−10.886
(1/10) (6)	2.5932 (−5)	−89.999	2.5932 (−4)	−89.985	2.5932 (−3)	−89.851	2.5924 (−2)	−88.511	2.5098 (−1)	−75.426	9.3092 (−1)	−21.038
(1/8)	2.0746 (−5)	−89.999	2.0746 (−4)	−89.988	2.0746 (−3)	−89.881	2.0741 (−2)	−88.808	2.0311 (−1)	−78.250	8.9891 (−1)	−25.677
(1/6)	1.5559 (−5)	−89.999	1.5559 (−4)	−89.991	1.5559 (−3)	−89.911	1.5558 (−2)	−89.106	1.5373 (−1)	−81.133	8.3969 (−1)	−32.661
(1/4)	1.0373 (−5)	−89.999	1.0373 (−4)	−89.994	1.0373 (−3)	−89.940	1.0372 (−2)	−89.404	1.0317 (−1)	−84.063	7.1896 (−1)	−43.877
(1/2)	5.1865 (−6)	−90.000	5.1865 (−5)	−89.997	5.1865 (−4)	−89.970	5.1864 (−3)	−89.702	5.1795 (−2)	−87.023	4.6015 (−1)	−62.526
(1/10) (7)	2.5932 (−6)	−90.000	2.5932 (−5)	−89.999	2.5932 (−4)	−89.985	2.5932 (−3)	−89.851	2.5924 (−2)	−88.511	2.5098 (−1)	−75.426

Note: The base number is to be multiplied by 10 raised to the power indicated within the parentheses.

Table 5-47— MAGNITUDE (|M|) AND PHASE ANGLE (θ) OF ZERO POWER TRANSFER FUNCTION FOR U^{235}

ω, rad/sec	ℓ(sec) = 10^{-3}		10^{-4}		10^{-5}		10^{-6}		10^{-7}		10^{-8}	
	|M|	θ	|M|	θ	|M|	θ	|M|	θ	|M|	θ	|M|	θ
(1/10) (−2)	7.6017 (1)	−87.970	7.6837 (1)	−87.948	7.6921 (1)	−87.946	7.6929 (1)	−87.945	7.6930 (1)	−87.945	7.6930 (1)	−87.945
(1/8)	6.0856 (1)	−87.465	6.1513 (1)	−87.438	6.1580 (1)	−87.435	6.1587 (1)	−87.435	6.1587 (1)	−87.435	6.1587 (1)	−87.435
(1/6)	4.5711 (1)	−86.628	4.6205 (1)	−86.592	4.6255 (1)	−86.588	4.6260 (1)	−86.588	4.6261 (1)	−86.588	4.6261 (1)	−86.588
(1/4)	3.0603 (1)	−84.976	3.0935 (1)	−84.922	3.0969 (1)	−84.916	3.0972 (1)	−84.916	3.0972 (1)	−84.916	3.0972 (1)	−84.916
(1/2)	1.5630 (1)	−80.284	1.5801 (1)	−80.176	1.5818 (1)	−80.165	1.5820 (1)	−80.164	1.5820 (1)	−80.164	1.5820 (1)	−80.164
(1/10) (−1)	8.3462	−72.448	8.4406	−72.242	8.4501	−72.221	8.4511	−72.219	8.4512	−72.219	8.4512	−72.219
(1/8)	6.9336	−69.255	7.0134	−69.004	7.0215	−68.979	7.0223	−68.976	7.0224	−68.976	7.0224	−68.976
(1/6)	5.5458	−64.751	5.6117	−64.429	5.6184	−64.396	5.6190	−64.393	5.6191	−64.392	5.6191	−64.392
(1/4)	4.1958	−57.965	4.2488	−57.509	4.2542	−57.463	4.2547	−57.459	4.2548	−57.458	4.2548	−57.458
(1/2)	2.8793	−47.584	2.9227	−46.787	2.9271	−46.706	2.9275	−46.698	2.9276	−46.697	2.9276	−46.697
(1/10)	2.1053	−40.601	2.1461	−39.283	2.1502	−39.148	2.1507	−39.135	2.1507	−39.133	2.1507	−39.133
(1/8)	1.9130	−38.619	1.9533	−37.075	1.9573	−36.918	1.9578	−36.902	1.9578	−36.900	1.9578	−36.900
(1/6)	1.6994	−36.013	1.7393	−34.115	1.7432	−33.920	1.7436	−33.901	1.7437	−33.899	1.7437	−33.899
(1/4)	1.4598	−32.113	1.4992	−29.542	1.5031	−29.277	1.5035	−29.251	1.5035	−29.248	1.5035	−29.248
(1/2)	1.2011	−25.677	1.2429	−21.135	1.2467	−20.664	1.2471	−20.616	1.2472	−20.612	1.2472	−20.611
(1/10) (1)	1.0631	−22.952	1.1171	−14.583	1.1214	−13.704	1.1218	−13.615	1.1219	−13.607	1.1219	−13.606
(1/8)	1.0285	−23.241	1.0902	−13.035	1.0948	−11.954	1.0952	−11.846	1.0953	−11.835	1.0953	−11.834
(1/6)	9.8558 (−1)	−24.552	1.0620	−11.383	1.0669	−9.969	1.0674	−9.827	1.0674	−9.813	1.0674	−9.812
(1/4)	9.2105 (−1)	−28.434	1.0321	−9.700	1.0378	−7.627	1.0383	−7.418	1.0383	−7.397	1.0383	−7.395
(1/2)	7.6367 (−1)	−41.056	1.0005	−8.775	1.0089	−4.729	1.0095	−4.321	1.0095	−4.280	1.0095	−4.276
(1/10) (2)	5.2699 (−1)	−58.176	9.8021 (−1)	−11.137	9.9746 (−1)	−3.175	9.9814 (−1)	−2.367	9.9819 (−1)	−2.286	9.9820 (−1)	−2.278
(1/8)	4.4738 (−1)	−63.353	9.7219 (−1)	−12.849	9.9579 (−1)	−2.959	9.9654 (−1)	−1.950	9.9660 (−1)	−1.849	9.9660 (−1)	−1.839
(1/6)	3.5343 (−1)	−69.216	9.5747 (−1)	−15.918	9.9435 (−1)	−2.881	9.9525 (−1)	−1.538	9.9531 (−1)	−1.403	9.9532 (−1)	−1.390
(1/4)	2.4548 (−1)	−75.716	9.2109 (−1)	−22.158	9.9299 (−1)	−3.168	9.9430 (−1)	−1.155	9.9437 (−1)	−0.953	9.9437 (−1)	−0.933
(1/2)	1.2602 (−1)	−82.718	7.8002 (−1)	−38.295	9.9015 (−1)	−4.932	9.9370 (−1)	−.914	9.9379 (−1)	−0.512	9.9379 (−1)	−0.471

(1/10) (3)	6.3444 (−2)	−86.341	5.3463 (−1)	−57.451	9.8113 (−1)	−9.109	9.9346 (−1)	−1.129	9.9364 (−1)	−0.323	9.9365 (−1)	−0.243
(1/8)	5.0797 (−2)	−87.071	4.5223 (−1)	−62.928	9.7461 (−1)	−11.232	9.9338 (−1)	−1.306	9.9362 (−1)	−0.299	9.9363 (−1)	−0.198
(1/6)	3.8123 (−2)	−87.802	3.5590 (−1)	−69.012	9.6098 (−1)	−14.728	9.9322 (−1)	−1.632	9.9361 (−1)	−0.289	9.9362 (−1)	−0.155
(1/4)	2.5427 (−2)	−88.534	2.4632 (−1)	−75.647	9.2499 (−1)	−21.418	9.9279 (−1)	−2.330	9.9359 (−1)	−0.317	9.9361 (−1)	−0.116
(1/2)	1.2717 (−2)	−89.267	1.2614 (−1)	−82.707	7.8267 (−1)	−38.028	9.9052 (−1)	−4.514	9.9357 (−1)	−0.494	9.9360 (−1)	−0.091
(1/10) (4)	6.3589 (−3)	−89.633	6.3459 (−2)	−86.338	5.3551 (−1)	−57.388	9.8163 (−1)	−8.903	9.9347 (−1)	−0.919	9.9360 (−1)	−0.113
(1/8)	5.0872 (−3)	−89.707	5.0805 (−2)	−87.069	4.5276 (−1)	−62.892	9.7511 (−1)	−11.069	9.9340 (−1)	−1.138	9.9360 (−1)	−0.131
(1/6)	3.8154 (−3)	−89.780	3.8126 (−2)	−87.801	3.5616 (−1)	−68.995	9.6147 (−1)	−14.610	9.9326 (−1)	−1.506	9.9360 (−1)	−0.163
(1/4)	2.5436 (−3)	−89.853	2.5428 (−2)	−88.534	2.4641 (−1)	−75.641	9.2545 (−1)	−21.345	9.9284 (−1)	−2.246	9.9359 (−1)	−0.233
(1/2)	1.2718 (−3)	−89.927	1.2717 (−2)	−89.267	1.2615 (−1)	−82.706	7.8295 (−1)	−38.002	9.9058 (−1)	−4.472	9.9357 (−1)	−0.452
(1/10) (5)	6.3590 (−4)	−89.963	6.3589 (−3)	−89.633	6.3460 (−2)	−86.338	5.3559 (−1)	−57.381	9.8168 (−1)	−8.883	9.9348 (−1)	−0.898
(1/8)	5.0872 (−4)	−89.971	5.0872 (−3)	−89.707	5.0806 (−2)	−87.069	4.5282 (−1)	−62.888	9.7517 (−1)	−11.053	9.9341 (−1)	−1.121
(1/6)	3.8154 (−4)	−89.978	3.8154 (−3)	−89.780	3.8126 (−2)	−87.801	3.5618 (−1)	−68.993	9.6153 (−1)	−14.598	9.9326 (−1)	−1.493
(1/4)	2.5436 (−4)	−89.985	2.5436 (−3)	−89.853	2.5428 (−2)	−88.534	2.4641 (−1)	−75.641	9.2549 (−1)	−21.338	9.9284 (−1)	−2.238
(1/2)	1.2718 (−4)	−89.993	1.2718 (−3)	−89.927	1.2717 (−2)	−89.267	1.2615 (−1)	−82.706	7.8298 (−1)	−37.999	9.9058 (−1)	−4.468
(1/10) (6)	6.3590 (−5)	−89.996	6.3590 (−4)	−89.963	6.3589 (−3)	−89.633	6.3461 (−2)	−86.338	5.3560 (−1)	−57.381	9.8169 (−1)	−8.881
(1/8)	5.0872 (−5)	−89.997	5.0872 (−4)	−89.971	5.0872 (−3)	−89.707	5.0806 (−2)	−87.069	4.5282 (−1)	−62.888	9.7517 (−1)	−11.052
(1/6)	3.8154 (−5)	−89.998	3.8154 (−4)	−89.978	3.8154 (−3)	−89.780	3.8126 (−2)	−87.801	3.5618 (−1)	−68.993	9.6153 (−1)	−14.597
(1/4)	2.5436 (−5)	−89.999	2.5436 (−4)	−89.985	2.5436 (−3)	−89.853	2.5428 (−2)	−88.534	2.4642 (−1)	−75.641	9.2550 (−1)	−21.337
(1/2)	1.2718 (−5)	−89.999	1.2718 (−4)	−89.993	1.2718 (−3)	−89.927	1.2717 (−2)	−89.267	1.2615 (−1)	−82.706	7.8298 (−1)	−37.999
(1/10) (7)	6.3590 (−6)	−90.000	6.3590 (−5)	−89.996	6.3590 (−4)	−89.963	6.3589 (−3)	−89.633	6.3461 (−2)	−86.338	5.3560 (−1)	−57.381

Note: The base number is to be multiplied by 10 raised to the power indicated within the parentheses.

Table 5-48—MAGNITUDE (|M|) AND PHASE ANGLE (θ) OF ZERO POWER TRANSFER FUNCTION FOR Pu^{239}

ω, rad/sec	ℓ(sec) = 10^{-3}		10^{-4}		10^{-5}		10^{-6}		10^{-7}		10^{-8}	
	|M|	θ	|M|	θ	|M|	θ	|M|	θ	|M|	θ	|M|	θ
(1/10) (−2)	6.2872 (1)	−87.987	6.4612 (1)	−87.931	6.4791 (1)	−87.925	6.4809 (1)	−87.925	6.4811 (1)	−87.925	6.4811 (1)	−87.925
(1/8)	5.0329 (1)	−87.486	5.1722 (1)	−87.416	5.1866 (1)	−87.409	5.1880 (1)	−87.408	5.1882 (1)	−87.408	5.1882 (1)	−87.408
(1/6)	3.7798 (1)	−86.655	3.8845 (1)	−86.562	3.8953 (1)	−86.552	3.8964 (1)	−86.551	3.8965 (1)	−86.551	3.8965 (1)	−86.551
(1/4)	2.5295 (1)	−85.010	2.5996 (1)	−84.871	2.6069 (1)	−84.857	2.6076 (1)	−84.855	2.6077 (1)	−84.855	2.6077 (1)	−84.855
(1/2)	1.2893 (1)	−80.294	1.3254 (1)	−80.020	1.3291 (1)	−79.992	1.3295 (1)	−79.989	1.3295 (1)	−79.988	1.3295 (1)	−79.988
(1/10) (−1)	6.8563	−72.190	7.0534	−71.660	7.0737	−71.605	7.0757	−71.600	7.0759	−71.599	7.0759	−71.599
(1/8)	5.6897	−68.790	5.8557	−68.139	5.8728	−68.072	5.8745	−68.065	5.8747	−68.065	5.8747	−68.065
(1/6)	4.5510	−63.914	4.6873	−63.069	4.7013	−62.982	4.7027	−62.973	4.7029	−62.972	4.7029	−62.972
(1/4)	3.4601	−56.462	3.5697	−55.250	3.5809	−55.125	3.5820	−55.112	3.5821	−55.111	3.5821	−55.111
(1/2)	2.4383	−45.202	2.5303	−43.010	2.5397	−42.782	2.5406	−42.759	2.5407	−42.757	2.5407	−42.756
(1/10)	1.8532	−38.878	1.9463	−35.150	1.9557	−34.756	1.9566	−34.717	1.9567	−34.713	1.9567	−34.712
(1/8)	1.7020	−37.493	1.7968	−33.107	1.8062	−32.642	1.8072	−32.595	1.8073	−32.590	1.8073	−32.590
(1/6)	1.5297	−35.905	1.6272	−30.494	1.6368	−29.916	1.6377	−29.858	1.6378	−29.852	1.6378	−29.851
(1/4)	1.3285	−33.991	1.4316	−26.672	1.4414	−25.880	1.4424	−25.800	1.4425	−25.792	1.4425	−25.791
(1/2)	1.0852	−32.582	1.2106	−19.930	1.2211	−18.518	1.2221	−18.376	1.2222	−18.361	1.2222	−18.360
(1/10) (1)	9.0612 (−1)	−37.111	1.0971	−15.040	1.1095	−12.403	1.1106	−12.136	1.1107	−12.109	1.1107	−12.106
(1/8)	8.4480 (−1)	−40.213	1.0726	−14.124	1.0861	−10.883	1.0873	−10.554	1.0874	−10.522	1.0874	−10.518
(1/6)	7.5728 (−1)	−45.250	1.0460	−13.435	1.0616	−9.197	1.0628	−8.767	1.0630	−8.724	1.0630	−8.720
(1/4)	6.1834 (−1)	−53.694	1.0153	−13.486	1.0356	−7.279	1.0370	−6.646	1.0371	−6.583	1.0372	−6.576
(1/2)	3.7849 (−1)	−68.084	9.6882 (−1)	−17.120	1.0096	−5.162	1.0113	−3.922	1.0115	−3.798	1.0115	−3.786
(1/10) (2)	2.0370 (−1)	−78.279	8.9177 (−1)	−27.171	9.9894 (−1)	−4.733	1.0016	−2.276	1.0017	−2.030	1.0017	−2.005
(1/8)	1.6459 (−1)	−80.538	8.4864 (−1)	−32.013	9.9696 (−1)	−5.023	1.0002	−1.956	1.0004	−1.649	1.0004	−1.618
(1/6)	1.2443 (−1)	−82.852	7.7436 (−1)	−39.224	9.9452 (−1)	−5.754	9.9912 (−1)	−1.674	9.9931 (−1)	−1.264	9.9932 (−1)	−1.223
(1/4)	8.3431 (−2)	−85.209	6.3756 (−1)	−50.327	9.8988 (−1)	−7.597	9.9830 (−1)	−1.499	9.9852 (−1)	−0.884	9.9854 (−1)	−0.823
(1/2)	4.1862 (−2)	−87.597	3.8545 (−1)	−67.283	9.6936 (−1)	−13.782	9.9761 (−1)	−1.773	9.9804 (−1)	−0.546	9.9806 (−1)	−0.423

(1/10) (3)	2.0950 (−2)	−88.798	2.0494 (−1)	−78.150	8.9975 (−1)	−25.631	9.9664 (−1)	−2.931	9.9791 (−1)	−0.478	9.9794 (−1)	−0.232
(1/8)	1.6762 (−2)	−89.038	1.6525 (−1)	−80.469	8.5643 (−1)	−30.884	9.9599 (−1)	−3.570	9.9789 (−1)	−0.505	9.9792 (−1)	−0.198
(1/6)	1.2572 (−2)	−89.278	1.2472 (−1)	−82.821	7.8084 (−1)	−38.513	9.9462 (−1)	−4.660	9.9787 (−1)	−0.578	9.9791 (−1)	−0.168
(1/4)	8.3820 (−3)	−89.519	8.3519 (−2)	−85.199	6.4139 (−1)	−50.004	9.9074 (−1)	−6.870	9.9782 (−1)	−0.764	9.9790 (−1)	−0.150
(1/2)	4.1911 (−3)	−89.759	4.1874 (−2)	−87.595	3.8632 (−1)	−67.224	9.7061 (−1)	−13.431	9.9760 (−1)	−1.405	9.9790 (−1)	−0.177
(1/10) (4)	2.0956 (−3)	−89.880	2.0951 (−2)	−88.797	2.0507 (−1)	−78.141	9.0084 (−1)	−25.480	9.9675 (−1)	−2.747	9.9789 (−1)	−0.293
(1/8)	1.6765 (−3)	−89.904	1.6762 (−2)	−89.038	1.6532 (−1)	−80.464	8.5738 (−1)	−30.775	9.9612 (−1)	−3.423	9.9788 (−1)	−0.357
(1/6)	1.2574 (−3)	−89.928	1.2573 (−2)	−89.278	1.2475 (−1)	−82.819	7.8156 (−1)	−38.445	9.9476 (−1)	−4.550	9.9787 (−1)	−0.467
(1/4)	8.3824 (−4)	−89.952	8.3821 (−3)	−89.519	8.3528 (−2)	−85.199	6.4180 (−1)	−49.973	9.9089 (−1)	−6.797	9.9783 (−1)	−0.690
(1/2)	4.1912 (−4)	−89.976	4.1911 (−3)	−89.759	4.1875 (−2)	−87.595	3.8641 (−1)	−67.218	9.7075 (−1)	−13.396	9.9762 (−1)	−1.368
(1/10) (5)	2.0956 (−4)	−89.988	2.0956 (−3)	−89.880	2.0951 (−2)	−88.797	2.0508 (−1)	−78.140	9.0095 (−1)	−25.465	9.9677 (−1)	−2.728
(1/8)	1.6765 (−4)	−89.990	1.6765 (−3)	−89.904	1.6762 (−2)	−89.038	1.6533 (−1)	−80.463	8.5748 (−1)	−30.764	9.9614 (−1)	−3.408
(1/6)	1.2574 (−4)	−89.993	1.2574 (−3)	−89.928	1.2573 (−2)	−89.278	1.2475 (−1)	−82.819	7.8164 (−1)	−38.438	9.9477 (−1)	−4.539
(1/4)	8.3824 (−5)	−89.995	8.3824 (−4)	−89.952	8.3821 (−3)	−89.519	8.3529 (−2)	−85.198	6.4184 (−1)	−49.970	9.9090 (−1)	−6.790
(1/2)	4.1912 (−5)	−89.998	4.1912 (−4)	−89.976	4.1911 (−3)	−89.759	4.1875 (−2)	−87.595	3.8642 (−1)	−67.218	9.7076 (−1)	−13.393
(1/10) (6)	2.0956 (−5)	−89.999	2.0956 (−4)	−89.988	2.0956 (−3)	−89.880	2.0951 (−2)	−88.797	2.0509 (−1)	−78.140	9.0096 (−1)	−25.464
(1/8)	1.6765 (−5)	−89.999	1.6765 (−4)	−89.990	1.6765 (−3)	−89.904	1.6762 (−2)	−89.038	1.6533 (−1)	−80.463	8.5749 (−1)	−30.763
(1/6)	1.2574 (−5)	−89.999	1.2574 (−4)	−89.993	1.2574 (−3)	−89.928	1.2573 (−2)	−89.278	1.2475 (−1)	−82.819	7.8164 (−1)	−38.437
(1/4)	8.3824 (−6)	−90.000	8.3824 (−5)	−89.995	8.3824 (−4)	−89.952	8.3821 (−3)	−89.519	8.3529 (−2)	−85.198	6.4184 (−1)	−49.970
(1/2)	4.1912 (−6)	−90.000	4.1912 (−5)	−89.998	4.1912 (−4)	−89.976	4.1911 (−3)	−89.759	4.1875 (−2)	−87.595	3.8642 (−1)	−67.218
(1/10) (7)	2.0956 (−6)	−90.000	2.0956 (−5)	−89.999	2.0956 (−4)	−89.988	2.0956 (−3)	−89.880	2.0951 (−2)	−88.797	2.0509 (−1)	−78.140

Note: The base number is to be multiplied by 10 raised to the power indicated within the parentheses.

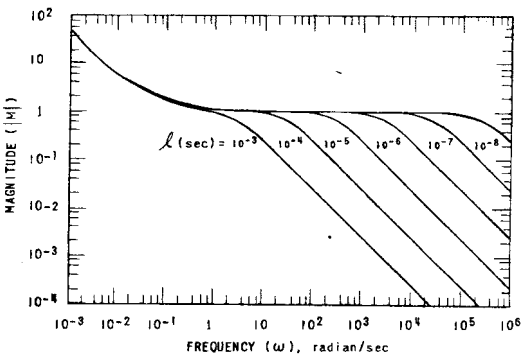

Fig. 5-87 — Magnitude of zero power reactor transfer function vs. frequency for various neutron lifetimes (ℓ) for U^{233}.

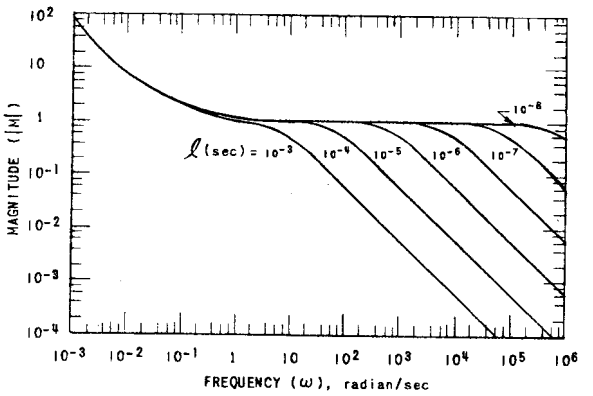

Fig. 5-88 — Magnitude of zero power reactor transfer function vs. frequency for various neutron lifetimes (ℓ) for U^{235}.

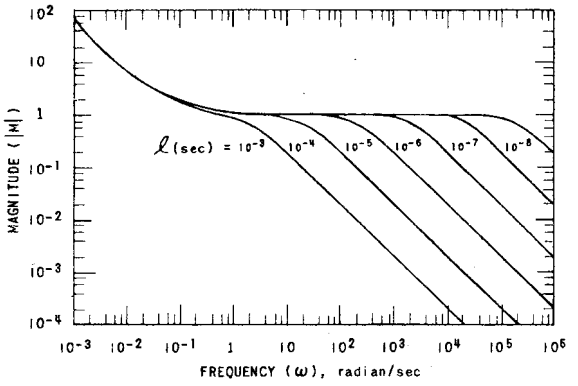

Fig. 5-89 — Magnitude of zero power reactor transfer function vs. frequency for various neutron lifetimes (ℓ) for Pu^{239}.

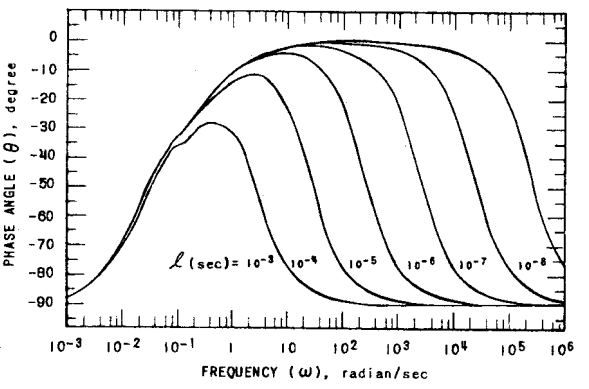

Fig. 5-90 — Phase angle of zero power reactor transfer function vs. frequency for various neutron lifetimes (ℓ) for U^{233}.

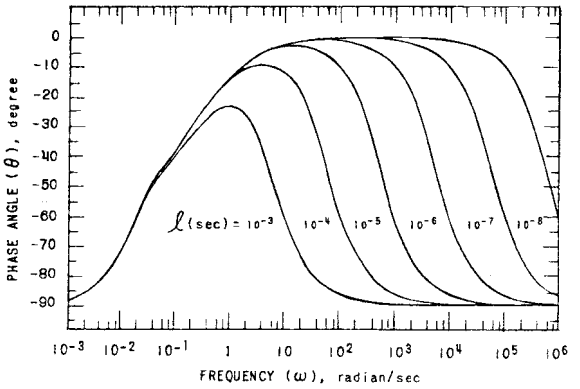

Fig. 5-91 — Phase angle of zero power reactor transfer function vs. frequency for various neutron lifetimes (ℓ) for U^{235}

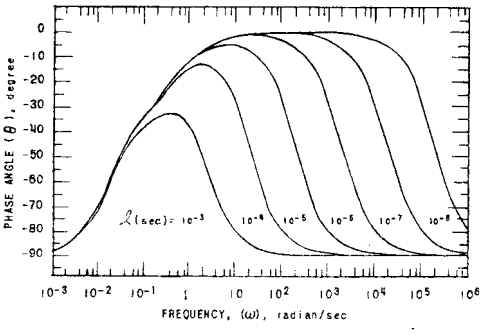

Fig. 5-92 — Phase angle of zero power reactor transfer function vs. frequency for various neutron lifetimes (ℓ) for Pu^{239}.

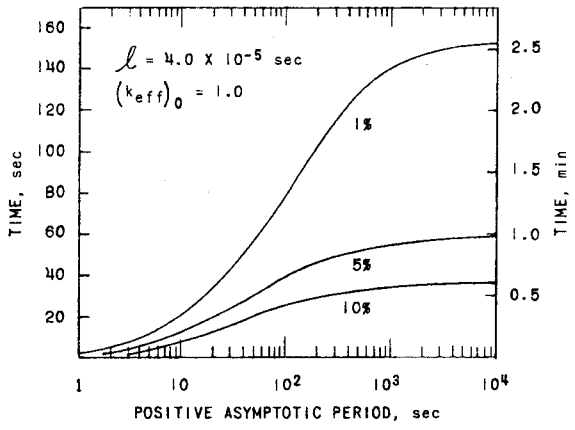

Fig. 5-93 — Time after positive step change in reactivity to observe a period within 1%, 5%, and 10% of the asymptotic value, as a function of positive asymptotic period.

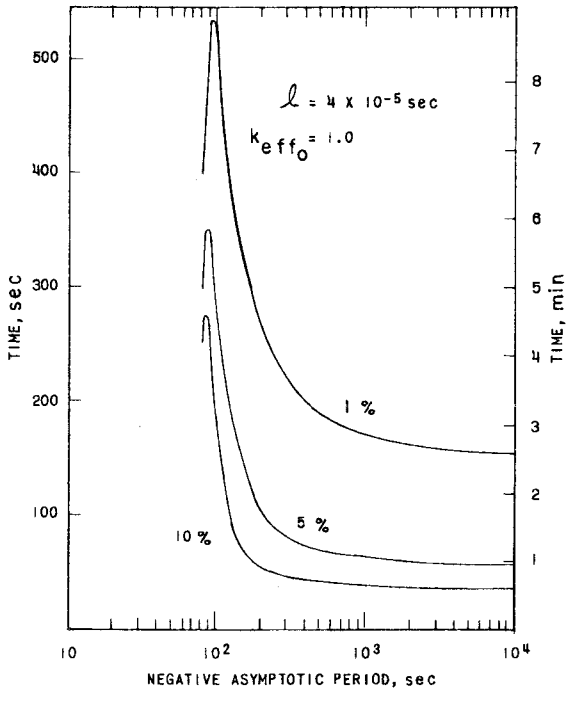

Fig. 5-94 — Time after negative step change in reactivity to observe a period within 1%, 5%, and 10% of the asymptotic value, as a function of negative asymptotic period.

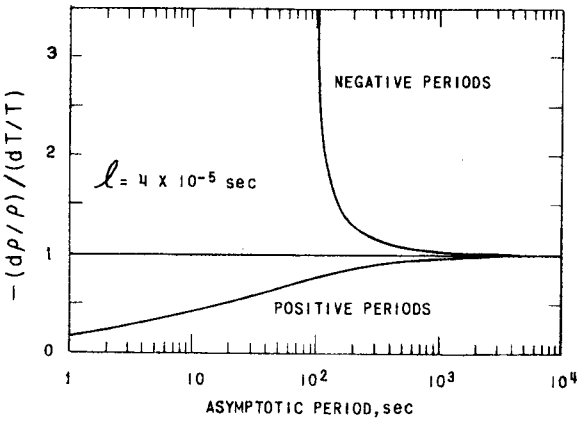

Fig. 5-95 — Relative error in reactivity and asymptotic period as a function of asymptotic period for both positive and negative periods.

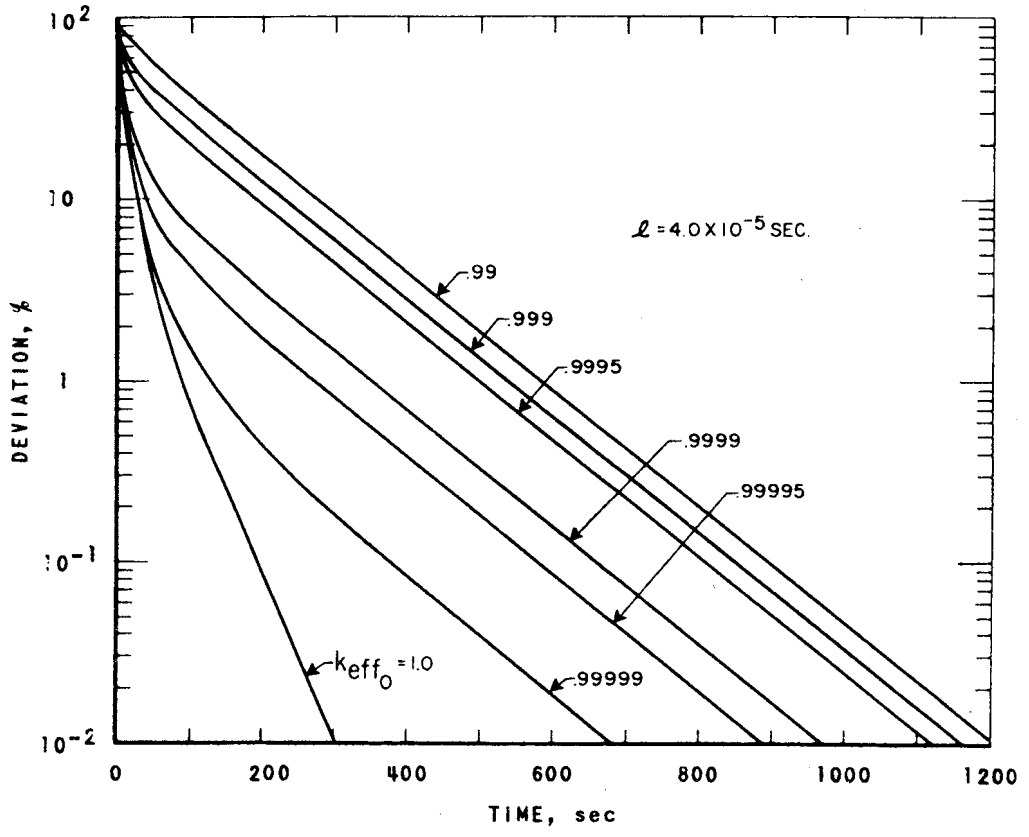

Fig. 5-96—Deviation of observed period from asymptotic period as a function of time after positive step change in reactivity to $\rho = 5 \times 10^{-4}$ for various values of k.

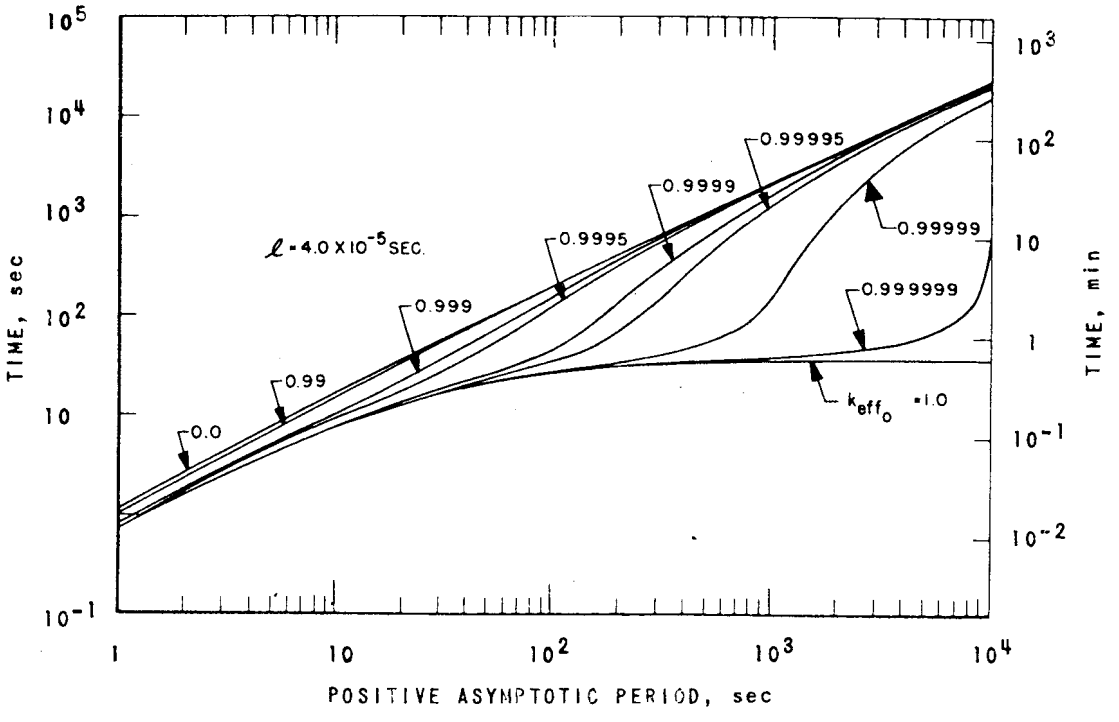

Fig. 5-97—Waiting time after positive change in reactivity to observe a period within 10% of the asymptotic period, as a function of positive asymptotic period for various initial values of k.

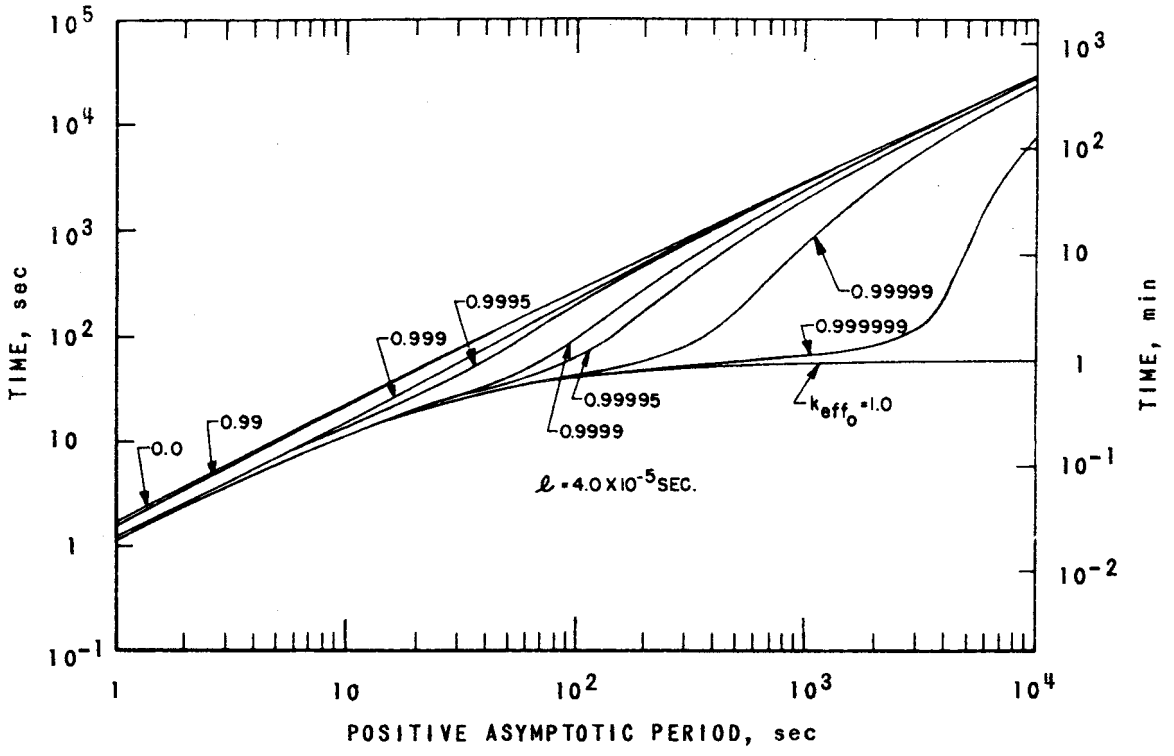

Fig. 5-98—Waiting time after positive step change in reactivity to observe a period within 5% of the asymptotic value, as a function of positive asymptotic period for various initial values of k.

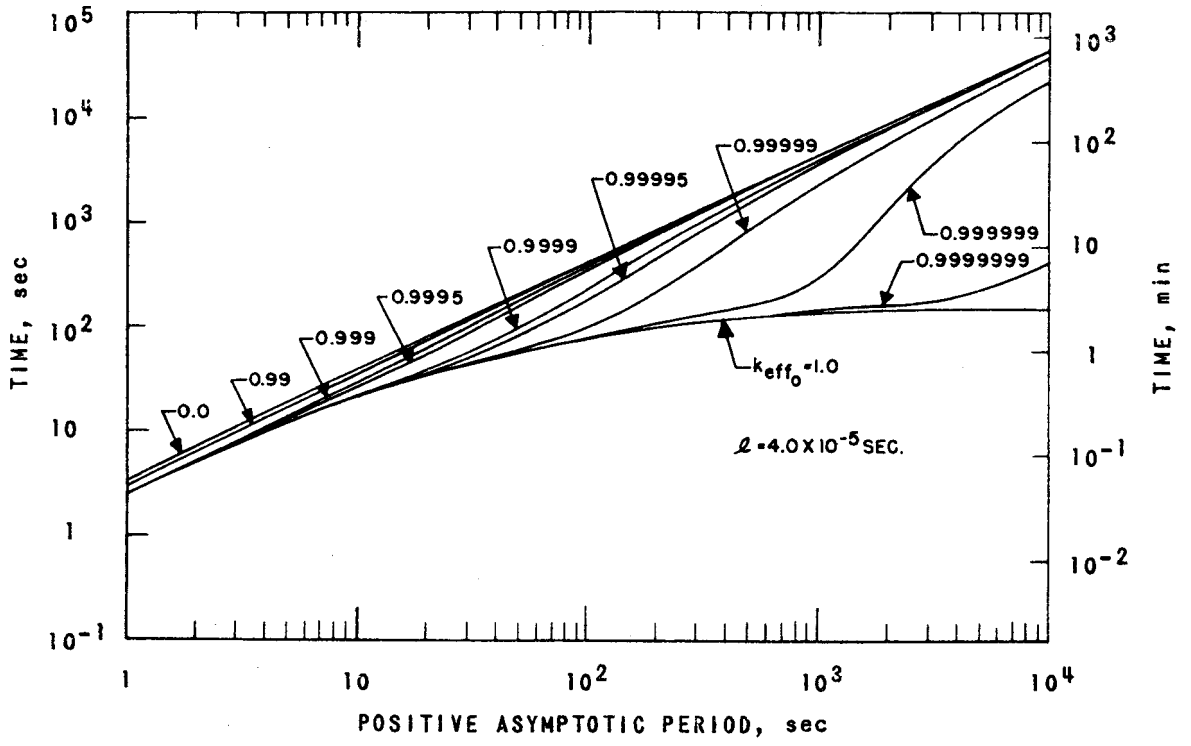

Fig. 5-99—Waiting time after positive step change in reactivity to observe a period within 1% of the asymptotic value, as a function of positive asymptotic period for various initial values of k.

687863 O - 63 - 31

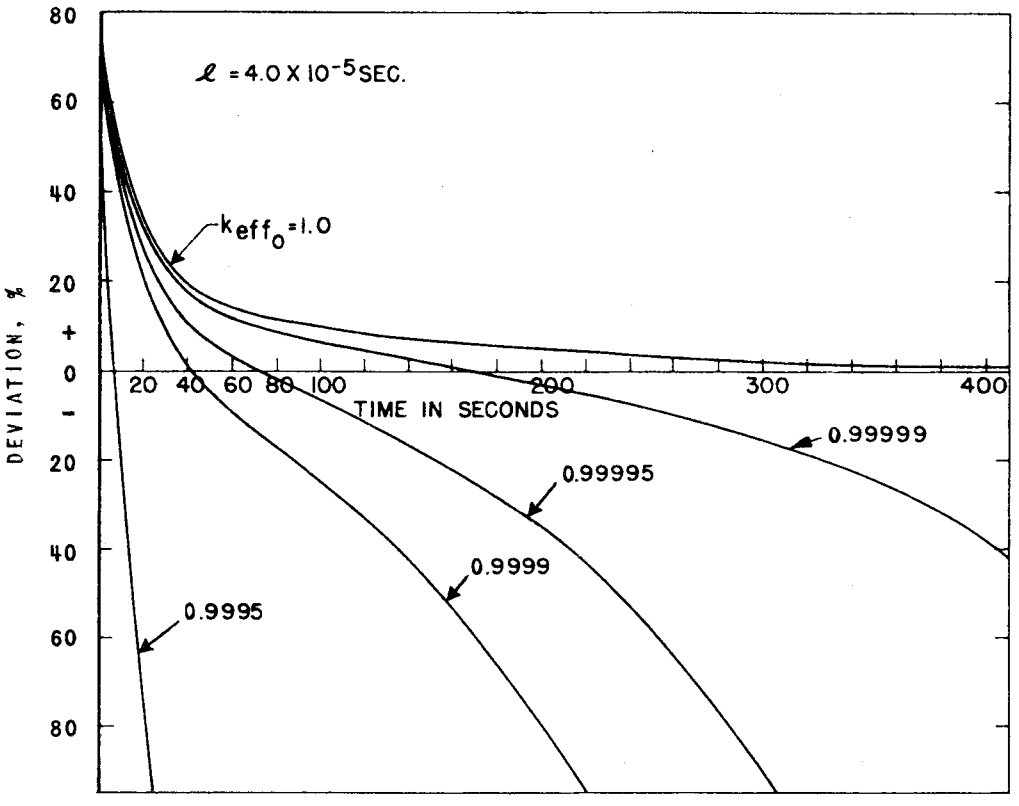

Fig. 5-100—Deviation of observed period from the reciprocal of the algebraically largest root of the inhour equation, as a function of time after a step change in reactivity to $\rho = -1.0 \times 10^{-3}$ for various initial values of k.

Table 5-49—INFLUENCE OF VARYING PROMPT NEUTRON LIFETIME[a]

Data from Ref. 176.

ℓ, sec	Deviation, %	t, sec
$\rho = 1 \times 10^{-4}$		
1×10^{-3}	1.167	3000
4×10^{-5}	1.113	3000
1×10^{-7}	1.111	3000
1×10^{-3}	43.510	100
4×10^{-5}	43.399	100
1×10^{-7}	43.394	100
$\rho = 1 \times 10^{-3}$		
1×10^{-3}	1.222	100
4×10^{-5}	1.149	100
1×10^{-7}	1.146	100
1×10^{-3}	43.882	4
4×10^{-5}	42.886	4
1×10^{-7}	42.844	4

[a] $k_0 = 0.9999$

Table 5-50 — DELAYED NEUTRON PARAMETERS

Data from Ref. 176.

i	λ_i, sec^{-1}	β_i	i	λ_i, sec^{-1}	β_i
1	6.26×10^{-7}	2.90×10^{-7}	9	1.69×10^{-2}	1.42×10^{-4}
2	3.63×10^{-6}	7.10×10^{-7}	10	3.05×10^{-2}	1.53×10^{-3}
3	4.37×10^{-5}	2.24×10^{-6}	11	1.11×10^{-1}	1.37×10^{-3}
4	1.17×10^{-4}	1.61×10^{-5}	12	2.77×10^{-1}	4.50×10^{-4}
5	4.28×10^{-4}	1.43×10^{-5}	13	3.01×10^{-1}	2.75×10^{-3}
6	1.50×10^{-3}	2.33×10^{-5}	14	1.14	8.00×10^{-4}
7	4.81×10^{-3}	4.83×10^{-5}	15	3.01	2.90×10^{-4}
8	1.24×10^{-2}	2.30×10^{-4}			

Table 5-51 — INFLUENCE OF DELAYED NEUTRON PARAMETERS

($\ell = 4.0 \times 10^{-5}$ sec for all cases)

Asymptotic Period, sec	k_0	Source of Delayed Parameters	Waiting Time to Achieve Accuracy Indicated, sec		
			1%	5%	10%
8289	1.0	a	152.9	58.0	36.5
		b	15390	6980	5160
		c	156.5	57.1	35.8
1075	1.0	a	141.7	55.2	35.0
		b	2525	1164	640
		c	145.2	54.3	34.6
134	1.0	a	88.4	41.8	27.8
		b	237	83.6	44.9
		c	89.4	41.0	27.9
10.5	1.0	a	22.3	11.68	7.44
		b	23.8	12.59	8.08
		c	22.7	11.90	7.72
8289	0.9999	a	37370	24000	18245
		b	34090	21000	15440
		c	37250	23900	18175
1075	0.9999	a	4309	2580	1837
		b	3990	2332	1630
		c	4264	2531	1785
134	0.9999	a	350.7	142.7	67.5
		b	357.0	157.8	83.1
		c	338.8	134.3	60.9
10.5	0.9999	a	23.7	12.36	7.91
		b	24.9	13.13	8.43
		c	24.0	12.60	8.13

[a] Data from Sec. 1.4.1.
[b] Data from Table 5-50.
[c] Data of Hughes, et al.[177]

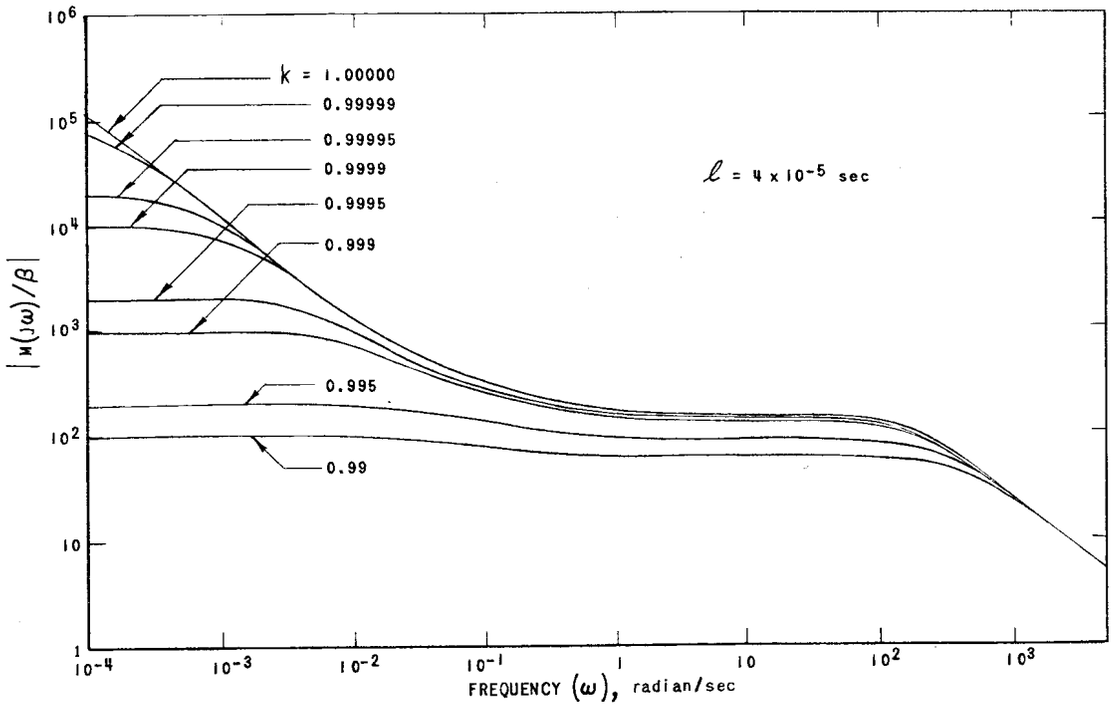

Fig. 5-101 — Magnitude of the transfer function vs. frequency for various degrees of subcriticality in reactor with source.

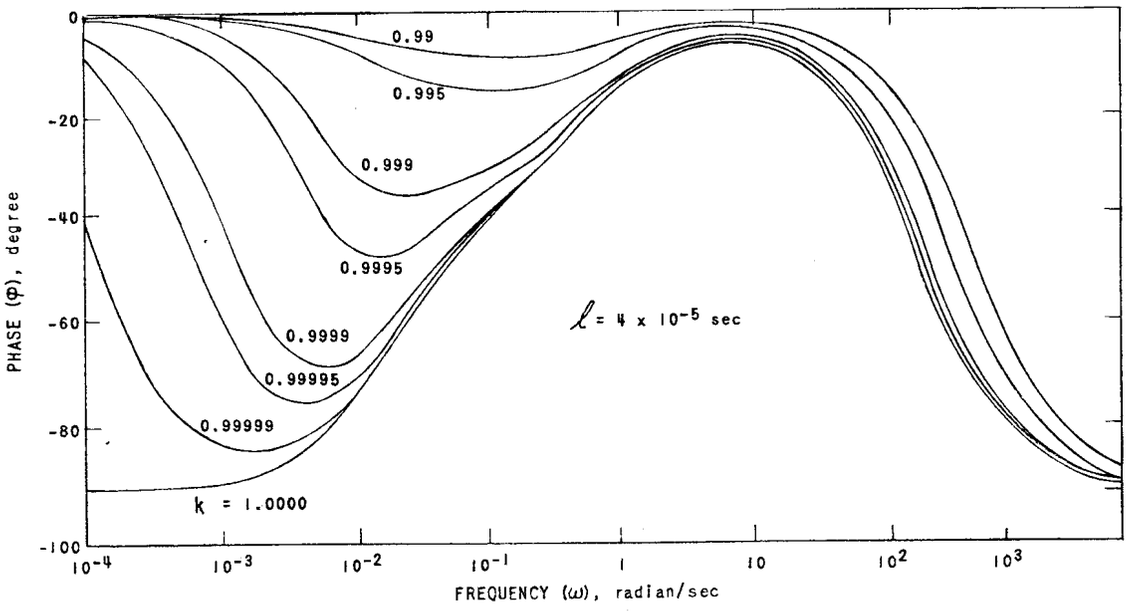

Fig. 5-102 — Phase of the transfer function vs. frequency for various degrees of subcriticality in reactor with source.

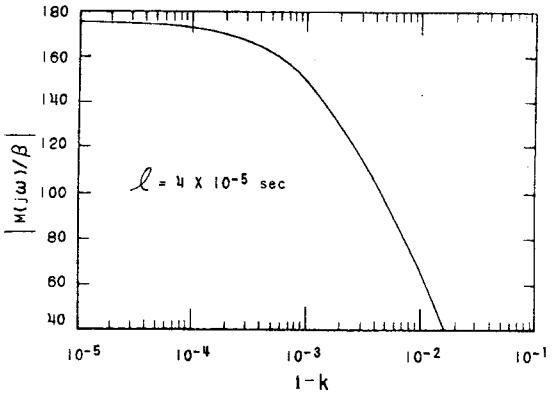

Fig. 5-103 — Magnitude of transfer function in reactor with source as a function of 1-k for $\omega = 1$ radian/sec.

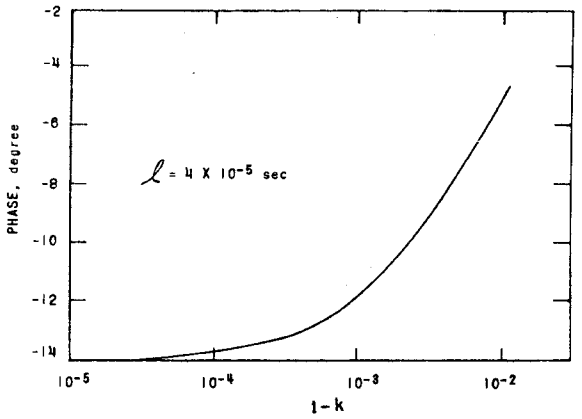

Fig. 5-104 — Phase (ϕ) of the transfer function as a function of 1-k for $\omega = 1$ radian/sec.

chamber for each neutron absorbed in it; and ϵ is the fraction of all neutrons disappearing from the reactor, whether by absorption or leakage, that is absorbed by the chamber. The quantity $(\overline{\nu^2} - \overline{\nu})/\overline{\nu}$ is a measure of the fluctuations in the number of neutrons produced in fission. For U^{235}, the values $\overline{\nu^2} = 7.32 \pm 0.15$, and $\overline{\nu} = 2.47 \pm 0.03$ are reported in Ref. 179. L and B are given by:

$$L = \ell + \sum_i \frac{\lambda_i \beta_i}{(2\pi f)^2 + \lambda_i^2}$$

$$B = \beta - \sum_i \frac{\lambda_i^2 \beta_i}{(2\pi f)^2 + \lambda_i^2} \qquad (5\text{-}55)$$

and approach the prompt lifetime, ℓ, and the total delayed neutron fraction, β, respectively, as the frequency becomes large compared to the delayed neutron precursor decay constants λ_i. β_i is the delayed neutron fraction for the *ith* group.

The first term in the brackets of Eq. (5-54) represents the noise produced by the statistics of neutron detection in the chamber; the second term gives the noise originating in the reactor. The noise has a spectrum with the same shape as the square modulus of the reactor oscillating-source transfer function; it has a roll-off around a frequency given by the "Rossi Alpha" ($\alpha = \beta/\ell$), followed by a tail in which the amplitude decreases by a factor of two for every increase of a factor of two in frequency. For this second term to be observable, it is necessary to have an ϵ greater than about 5×10^{-5}. The spectrum given by Eq. (5-54) has been observed[180] in a number of reactors and used to determine α. Equation (5-54) assumes that the chamber and associated equipment have a flat frequency response over the range being measured. If this is not the case, it can be compensated for easily.[180] Equation (5-54) is a complete description of pile noise; the results of other noise experiments can be derived by transforming it according to the prescriptions of random noise theory.

One of the earliest statistical experiments to be developed was the Rossi Alpha Experiment. A pulse counter is used and coincidences are recorded between pairs of pulses separated in time. The probability, $P(t)\Delta t$, that a count in interval Δt at a time t follows a count at $t = 0$ is given by:[170]

$$P(t)\Delta t = C\Delta t + \frac{\epsilon}{2}\left(\frac{\overline{\nu^2} - \overline{\nu}}{\overline{\nu}}\right)\frac{(1-\beta)^2}{\beta} e^{-\alpha t}\,\Delta t \qquad (5\text{-}56)$$

where C is the average count rate. If the experiment is done with the reactor subcritical, as is sometimes necessary due to maximum count rate limitations, the quantity β must be replaced with $(1 - k_p)$, where k_p is the prompt multiplication factor, and $\alpha = [(1 - k_p)/\ell]$

Another early experiment is the variance-to-mean measurement. A pulse counter is also used and a series of measurements are made of the number of counts in intervals of duration τ. The variance of this group is calculated, and the parameter $[Y(\tau) + 1]$, the ratio of the variance to the mean of the group

is obtained. This quantity is unity for a system with pure Poisson statistics and no correlations. The function $Y(\tau)$ is given by:[181]

$$Y(\tau) = \frac{\epsilon}{(1-k_p)^2}\left(\frac{\overline{\nu^2}-\overline{\nu}}{\overline{\nu}^2}\right)\left[1-\left(\frac{1-e^{-\alpha\tau}}{\alpha\tau}\right)\right] \tag{5-57}$$

Equation (5-57) assumes that the delayed neutron precursor lifetimes are long compared to τ. If delayed neutrons are taken explicitly into account, the function $Y(\tau)$ is modified considerably and diverges at large values of τ for a critical reactor.[182]

In Fig. 5-105, the quantity $\sigma'(\tau)$, which is related to $Y(\tau)$ in the manner described in Ref. 182, is plotted against τ.

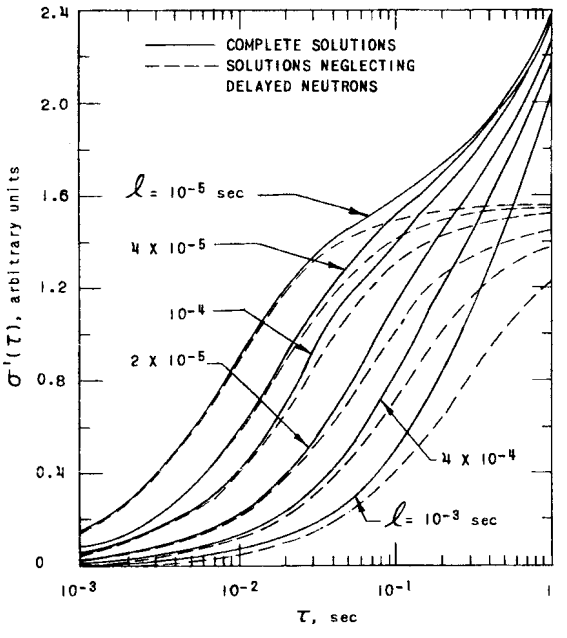

Fig. 5-105 — $\sigma'(\tau)$ vs τ for various neutron lifetimes and including the delayed neutron contribution. *Reproduced from Ref. 182.*

Another experiment involving variance which does not diverge in this way is discussed in Ref. 182. The integrated signal from a detector for two successive time intervals of duration τ is used, and the difference between them taken; this gives

$$\Delta I(\tau) = \frac{\int_t^{t+\tau} I(t')\,dt' - \int_{t-\tau}^{t} I(t')\,dt'}{\int_t^{t+\tau} I(t')\,dt'} \tag{5-58}$$

where $I(t)$ is the current from an ionization chamber or the count rate from a pulse counter. Numerous samples of $\Delta I(\tau)$ are taken and the mean square is calculated:

$$\rho(\tau) = \overline{[\Delta I(\tau)]^2} \tag{5-59}$$

It has been shown[183] that for a detector efficiency $\epsilon > 10^{-4}$,

$$\rho(\tau) = \frac{2\,k_p^2}{F_0\tau}\left(\frac{\overline{\nu^2}-\overline{\nu}}{\overline{\nu}}\right)\frac{G(\tau)}{\gamma^2} \tag{5-60}$$

where F_0 is the number of fissions per second in the reactor; γ is the effectiveness factor for the delayed neutrons (i.e., the ratio between the value of β characterizing the kinetics of the particular reactor, and that value characteristic of the fissionable isotope used); and $G(\tau)$ is a function depending on the delayed neutron parameters (and the prompt neutron lifetime, for small τ). The function $G(\tau)$ for U^{235} is plotted in Fig. 5-106. Thus a measurement of $\rho(\tau)$ yields an experimental relationship between F_0 and γ, and allows one to be determined if the other is known or assumed.

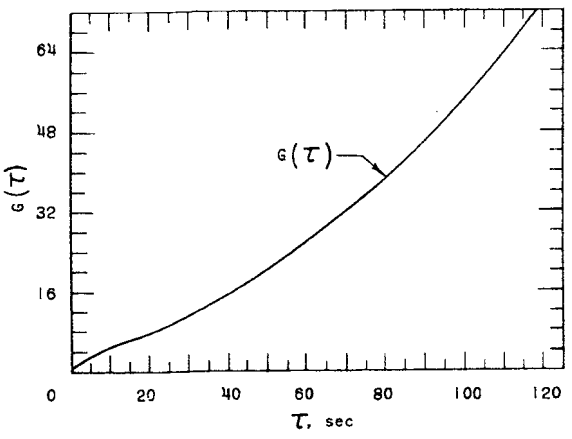

Fig. 5-106—G(τ) vs. τ(U^{235} fuel). *Data from Ref. 183.*

Another important noise function is the autocorrelation function which is given by:

$$\chi(\tau) = \frac{1}{T}\int_0^T I(t)I(t+\tau)\,dt \tag{5-61}$$

where the averaging time T is very long compared to the lag τ. If the delayed neutron precursor lifetimes are assumed long compared to τ, the function has an $e^{-\alpha\tau}$ or "Rossi Alpha" dependence. Calculated values[183] of χ(τ) are shown on Fig. 5-107.

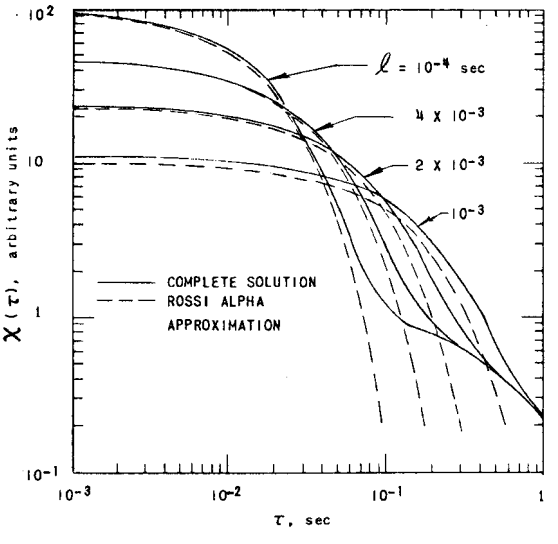

Fig. 5-107—Autocorrelation function [χ(τ)] vs. τ. *Reproduced from Ref. 183.*

Besides being of interest as a phenomenon, pile noise is the ultimate limitation on the accuracy of other types of experiments. The same theory used previously will still apply. For example, the error in a criticality measurement, where the reactor is held at steady power and the position of a control element is observed, is given by:[178]

$$\sigma^2(t) = \frac{\ell}{nt}\left(\frac{\overline{\nu^2} - \overline{\nu}}{\overline{\nu}}\right) \tag{5-62}$$

where σ(t) is the standard deviation in average reactivity for an averaging time t. This may be written in the convenient forms (for U^{235}):

$$\sigma(t) = 0.89/\sqrt{R}$$

or

$$\sigma(t) = 5.1 \times 10^{-6}/\sqrt{Pt} \tag{5-63}$$

where R is the total number of fissions occurring during the measurement time t, and P is the reactor power in watts.

A common method for reactivity measurements is the alternate insertion and removal of a sample by a pile oscillator. The insertions and removals are made rapidly to reduce the uninteresting traversing effects.[184] If the output from a detector is multiplied by a sine function synchronous with the oscillation, and integrated, the signal-to-noise ratio in the output is given by:[185]

$$Y = \frac{|\Delta|}{\pi}\left[\frac{2\,\epsilon\,F_0\,N\tau|W(i\omega)|^2}{\bar{\nu}+\epsilon|W(i\omega)|^2}\right]^{1/2} \tag{5-64}$$

where $\omega = 2\pi/t$ = angular frequency of the oscillations
N = number of cycles observed
$|W(i\omega)|$ = reactor transfer function
Δ = reactivity difference between sample-in and sample-out positions

5.3.8 PULSED NEUTRON EXPERIMENTS

The basic technique in the pulsed-source method consists of irradiating a sample of moderating material with a short burst of neutrons, and then following the time dependence of the neutron flux after the end of the burst. This problem has been studied by a number of investigators.[186–191] For most purposes, diffusion theory and the age approximation are adequate although the multigroup formulation has been found useful for illustrating some points.[188,189] The following presentation is based, in part, on papers by Antonov, et al.[189] and von Dardel and Sjöstrand.[190]

The neutron density, $n(\bar{r},t)$, satisfies the time-dependent diffusion equation:

$$D_0(t)\,\nabla^2 n(\bar{r},t) - \frac{n(\bar{r},t)}{\ell} = \frac{\partial n(\bar{r},t)}{\partial t} \tag{5-65}$$

where

$$D_0(t) = \frac{\frac{1}{3}\int v\,\lambda_{tr}(v)\,n(\bar{r},v,t)dv}{\int n(\bar{r},v,t)dv} \tag{5-66}$$

and

$$\frac{1}{\ell} = \frac{\int v\Sigma_a(v)\,n(\bar{r},v,t)dv}{\int n(\bar{r},v,t)dv} \tag{5-67}$$

The term $D_0(t)$ is the usual diffusion coefficient relating the current to the flux gradient multiplied by the average neutron velocity, and ℓ corresponds to the prompt neutron lifetime.

If the absorption cross section follows a 1/v-law, then $1/\ell$ is constant in time and may be eliminated from Eq. (5-65) by the substitution:

$$n(\bar{r},t) = e^{-t/\ell}\,n_0(\bar{r},t) \tag{5-68}$$

A further simplification is obtained by introducing the generalized neutron age:

$$\tau_g(t) = \int_0^t D_0(t')dt' \tag{5-69}$$

Then Eq. (5-65) takes the form of the usual age equation:

$$\nabla^2 n_0(\bar{r},\tau_g(t)) = \frac{\partial n_0(\bar{r},\tau_g(t))}{\partial \tau_g(t)} \tag{5-70}$$

The general solution of Eq. (5-65) may be written

$$n(\bar{r},t) = e^{-t/\ell}\sum_{lmn} A_{lmn}\,R_{lmn}(\bar{r})\exp\left[-B^2_{lmn}\,\tau_g(t)\right] \tag{5-71}$$

where $R_{\ell mn}(\bar{r})$ and $B^2_{\ell mn}$ are eigenfunctions and eigenvalues corresponding to the geometry of the system. At times greater than the slowing-down time, t_s, the diffusion coefficient D_0 approaches an asymptotic value, D_0'. Then, for large t

$$\tau_g(t) = \int_0^{t_s} D_0(t)dt - D_0' t_s + D_0' t$$
$$= \tau - D_0' t_s + D_0' t = \tau_m + D_0' t \qquad (5\text{-}72)$$

where

$$\tau_m = \int_0^{t_s} (D_0(t) - D_0') \, dt$$
$$= \int_0^{\infty} (D_0(t) - D_0') \, dt \qquad (5\text{-}73)$$

is the Fermi age of the neutrons in the moderating material. Equation (5-71) may now be written

$$n(\bar{r},t) = e^{-t/\ell} \sum_{\ell mn} A_{\ell mn} R_{\ell mn}(\bar{r}) \exp\left[-B^2_{\ell mn} (\tau_m + D_0' t)\right] \qquad (5\text{-}74)$$

Since $B^2_{\ell mn}$ for the higher modes will always be larger than B^2 for the fundamental, after a sufficiently long time Eq. (5-74) reduces to

$$n(\bar{r},t) = A \, R(\bar{r}) \exp\left[-B^2 \tau_m - \left(\frac{1}{\ell} + D_0' B^2\right) t\right] \qquad (5\text{-}75)$$

Andrews[192] has plotted the time necessary after a pulse for the establishment of the fundamental mode as a function of buckling for beryllium. Figure 5-108 shows the results of his work, and the work of two other groups of experimenters. The values shown in Fig. 5-108 were determined experimentally from the waiting times, t, for which Eq. (5-75) is an acceptable approximation of Eq. (5-74).

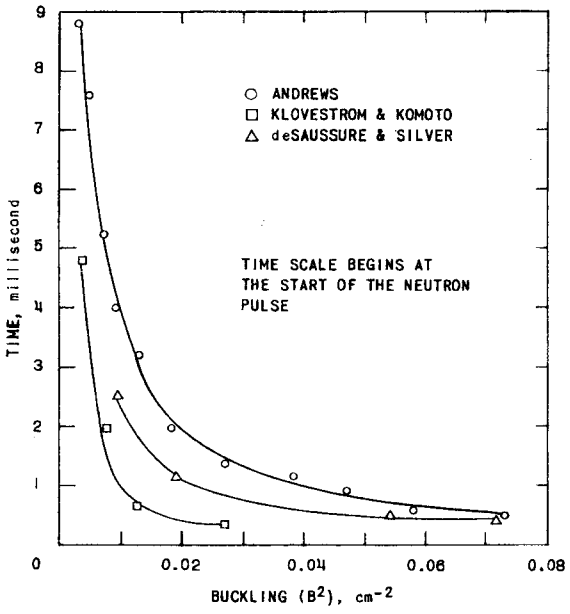

Fig. 5-108 — Approximate time required for the establishment of a normal mode distribution, as a function of the buckling for beryllium. *Reproduced from Ref. 192.*

The asymptotic value of D will depend on the geometric buckling since the leakage probability depends on the neutron velocity, being larger for neutrons with high velocity. Thus the average velocity of the remaining neutrons will be smaller than in an infinite medium. This process has been named diffusion cooling. The following treatment assumes that near equilibrium, the neutron velocity spectrum is Maxwellian and may be characterized by a temperature. This is not a good approximation for small systems where the leakage probability is high, or when the neutron "temperature" is much greater than T_0.

The following considerations of diffusion cooling are essentially those of Beckurts.[193] At equilibrium, the neutrons lose as much energy by leakage as they gain from the moderator. The average energy of a neutron escaping from the moderator is given by:

$$\bar{E}_a = \frac{\int_S \int_v \frac{\lambda_{tr}}{3} v\,(\text{grad } n)_\perp \, dS \, \frac{1}{2} mv^2 \, dv}{\int_S \int_v \frac{\lambda_{tr}}{3} v\,(\text{grad } n)_\perp \, dS \, dv} \tag{5-76}$$

where v and m denote the neutron velocity and mass, respectively, and $(\text{grad } n)_\perp$ denotes the component of the gradient of the neutron density perpendicular to the element of surface dS. For the case λ_{tr} = constant, $\bar{E}_a$ may be written

$$\bar{E}_a = \frac{m}{2} \frac{\int_0^\infty v^3 n(v) dv}{\int_0^\infty v\, n(v) dv} \tag{5-77}$$

where the divergence theorem is used and $\nabla^2 n = -B^2 n$.

If a Maxwellian of temperature T_n is substituted for n(v), $\bar{E}_a$ is easily evaluated to be $2kT_n$. The rate of energy loss per neutron by leakage is given by:

$$\frac{dE}{dt} = D_0' B^2 \left[\bar{E}_a - \frac{3}{2} kT_n \right] \tag{5-78}$$

since $\frac{3}{2} kT_n$ is the average energy for a Maxwellian of temperature T_n, and $D_0' B^2$ is the leakage probability per unit time. This rate of energy loss is balanced by the rate of energy gain from the moderator which may be written

$$-\frac{dE}{dt} = \left(\frac{1}{\tau_{th}^0} \right) \frac{3}{2} k(T_n - T_0) \tag{5-79}$$

where τ_{th}^0 is the thermalization time constant for an infinite moderator.[194,195] Thus the equilibrium energy balance is expressed by:

$$D_0' B^2 \left[\bar{E}_a - \frac{3}{2} kT_n \right] = \frac{-1}{\tau_{th}^0} \frac{3}{2} k(T_n - T_0) \tag{5-80}$$

On using a Maxwellian to evaluate D_0'

$$D_0' = \frac{\lambda_{tr}}{3} \sqrt{\frac{2kT_n}{m}}$$

and

$$\frac{\partial D_0'}{\partial T_n} = \frac{D_0'}{2T_n}$$

Substituting these expressions along with $\bar{E}_a = 2kT_n$ in Eq. (5-80) gives

$$T_n - T_0 = -\frac{2}{3} \tau_{th}^0 B^2 T_n^2 \frac{\partial D_0'}{\partial T_n} \tag{5-81}$$

If the diffusion coefficient is expanded in a Taylor series,

$$D_0'(T_n) = D_0(T_0) + (\partial D_0'/\partial T_n)_{T_n = T_0} (T_n - T_0) + \cdots \tag{5-82}$$

Now, on setting

$$D_0'(T_n) = D_0(T_0) - CB^2 \tag{5-83}$$

there results

$$C = (2/3)\tau_{th}^0 \, T_0^2 \, (\partial D_0'/\partial T_n)^2_{T_n=T_0} \tag{5-84}$$

to first approximation if T_n is close to T_0.

Equation (5-84) may also be written

$$C = (1/6)D_0^2 \, \tau_{th}^0 \tag{5-85}$$

The decay constant of the time-dependent exponential term in Eq. (5-75) may be written

$$\lambda = \frac{1}{\ell} + D_0 B^2 - CB^4 \tag{5-86}$$

Experimental Measurements of Diffusion Parameters and Thermalization Times. By measuring the decay constant, λ, of the fundamental mode of several values of B^2 and then fitting the experimental data to Eq. (5-86) by the method of least squares, it is possible to obtain ℓ, D_0, C and the diffusion length $L = \sqrt{D_0 \ell}$. The usual method is as follows: The moderator is given some elementary shape for which the geometric buckling is easily calculated. The neutron source and detector are placed outside the moderator in order not to influence the geometry and are usually placed in positions calculated to suppress the higher harmonics. The counting rate is measured as a function of time after the source pulse by a time analyzer. Keepin[196] has surveyed the types of sources, intensities, detectors, and time analyzers needed for these measurements.

At least one investigator[197] has measured the time dependence of the neutron spatial distribution with the detector inside the moderator. The decay constants of the higher modes and, consequently, higher values of B^2, are obtained by a Fourier analysis of the spatial distributions.

The technique just described for measuring ℓ, D_0, and C can be used to measure bucklings of unusual geometric shapes and the changes in buckling caused by the insertion of absorbing rods into moderators.[193,205,206] In making such buckling measurements, ℓ, D_0, and C are known and B^2 is determined from Eq. (5-86) and measured values of λ.

The thermalization time constant may be found by measuring the time dependence of the neutron transmission coefficient through a 1/v absorber and relating this to the neutron temperature. Thermalization time constants may also be estimated from Eq. (5-85), using experimental values of D_0 and C. However, these estimates are apt to be uncertain due to the rather large experimental error often quoted for C and the frequent disagreement between various experimenters. [Also, Singwi and Kothari[194] have shown that the relation between C and τ_{th}^0 is a very sensitive function of $\lambda_{tr}(v)$.] For materials where $\lambda_{tr}(v)$ is not a constant, Eq. (5-84) may be used by replacing $\partial D_0/\partial T_n$ with $\partial D_0/\partial T_0$. Over small temperature ranges, these may not be too different from one another.

Several attempts have been made to compute D_0, C, and τ_{th}^0 for specific moderators (see Refs. 186, 187, 190, 194, 195, and 198–202). In general, the agreement between theory and experiment for C and τ_{th} has not been too good. (The notation τ_{th} without the zero superscript signifies the thermalization time constant for the finite, rather than the infinite medium.) The most rigorous attempt has been made by Singwi[202] who expands the neutron spectrum in Laguerre polynomials and discards the concept of a neutron "temperature." His values of C for beryllium are in good agreement with the experimental results of deSaussure and Silver,[203] but differ from values of Andrews[192] by a factor of 2 although they do show the same temperature dependence. For beryllium oxide, Singwi's value of C is a factor of 2 lower than the experimental value of Iyengar, et al.,[204] at room temperature, and the theoretical temperature dependence is completely at variance with the experimental results. On the other hand, the experimental result for carbon[189,193] is in very good agreement with Singwi's predicted value.

Values of D_0 and L for various moderators measured by pulsed-source techniques as well as other methods are given in Section 3.3. Thermalization time constants, τ_{th}, are listed in Table 5-52.

Measurement of Effective Cross Section. According to Eq. (5-67), the lifetime, ℓ, may be defined by:

$$1/\ell = N(\overline{v\sigma}) = N \, v_0 \, \hat{\sigma} \tag{5-87}$$

where N is the atomic density; $(\overline{v\sigma})$ is $v\sigma(v)$ averaged over the neutron spectrum; and $\hat{\sigma}$ is the Westcott effective cross section. The effective cross section of a moderating material may be obtained by a

Table 5-52—THERMALIZATION TIME CONSTANTS (τ_{th})

(Measured by transmission methods except where otherwise indicated)

Moderator	T, °C	B^2, cm^{-2}	τ_{th}, μsec	Ref.
H_2O	−175	~0.08	20	190
	Room	~0.08	7	190
D_2O	20	0	66[a]	
Dowtherm A	20	0	14[b]	
	180	0	3[b]	
Be	Room	0	$53 < \tau_{th} < 126$[a]	
BeO	24	0.037	140	204
C	Room	0.0014	209 ± 30	189
		0.008	185 ± 45	193
		0.026	154 ± 65	189

[a] Calculated from experimental values of D_0 and C, using Eq. (5-85).
[b] Calculated from experimental values of D_0, C, and dD_0/dT_0, using Eq. (5-84).

measurement of $1/\ell$. By measuring $1/\ell$ for an aqueous solution, the effective cross section of the solute may be obtained from the relation

$$1/\ell = (1/\ell)_{H_2O} + (1/\ell)_s \tag{5-88}$$

where the subscript s refers to the solute. This has been done in a variety of ways,[207–211] but the simplest method has been developed by von Dardel and Sjöstrand,[209] and applied by Meadows and Whalen[211] to a number of elements. Two decay curves are measured under identical experimental conditions, one for pure water and one for a dilute solution of the material to be measured. It may be seen from Eq. (5-74) and Eq. (5-88) that the point-by-point ratio of the two curves will yield a pure exponential curve whose decay constant is given by $(1/\ell)_s$.

Slowing-Down Time Spectrometer. Bergman, et al.,[212] have developed a spectrometer based on the fact that a short burst of monoenergetic fast neutrons slowed down by a heavy moderator will have a very narrow energy spread. The time distribution of neutron capture γ-rays emitted from samples placed in the moderator is measured and the peaks are related to capture resonances. The authors used about 110 tons of lead as a moderator. They estimate that the method is applicable over the energy range of 1 ev to 10 kev, with a resolution equivalent to a spectrometer with a 6-meter flight path.

Age Measurements. The value of τ_m can be determined from Eq. (5-75) by measuring A $R(\bar{r})$ exp $(-B^2\tau_m)$ at several values of B^2 under conditions such that A $R(\bar{r})$ can be calculated. Then the age to thermal is given by:[213]

$$\tau = \tau_m + D_0' t_s \tag{5-89}$$

where t_s is the slowing-down time.

5.3.9 DELAYED PHOTONEUTRONS

In a reactor moderated by heavy water or beryllium, delayed photoneutrons are produced by (γ,n) reactions with the deuterium or beryllium. The gamma rays involved in the production result from the decay of fission products and consequently the photoneutrons have the half-lives of the fission products. The energy of the gamma rays must be above the threshold for the (γ,n) reaction, which is 2.3 Mev for deuterium,[214] and 1.63 Mev for beryllium.[215]

The yield of photoneutrons for U^{235} fission products has been measured in D_2O and in Be by Bernstein, et al.[216,217] Implicit in both of these measurements are the details of yield and half-life of delayed neutrons from U^{235} fissions. The delayed neutron data for U^{235} of Hughes, et al.,[177] were used.

For the D_2O measurement it was possible to resolve the data into eight groups of photoneutrons.[216] To each of these groups there corresponds a half-life T_j, and a yield relative to the total yield of delayed neutrons. These are listed in Table 5-53.

Table 5-53—PHOTONEUTRON HALF-LIVES AND YIELDS FROM U^{235} FISSION PRODUCTS IN D_2O

Data from Ref. 216.

Group j	Half-Life,[a] T_j	Yield, %, Relative to Total Delayed Neutron Yield[b]
1	53 h	0.0163
2	4.4 h	0.0515
3	1.65 h	0.370
4	27 m	0.328
5	7.7 m	0.534
6	2.4 m	1.11
7	41 s	3.24
8	2.5 s	10.31

[a] m = minute; h = hour; s = sec.
[b] Based on delayed neutron data of Hughes, et al.[177]

The experimental data for the yield of photoneutrons from U^{235} fission products in Be could not be resolved into sums of exponentials[217] as was the case in the D_2O data.

Figure 5-109 shows the relative yield of photoneutrons from U^{235} fission products in Be for t_e = 15 minutes. Figure 5-110 shows the relative yield for t_e = 74 hours. Figure 5-111 compares yields

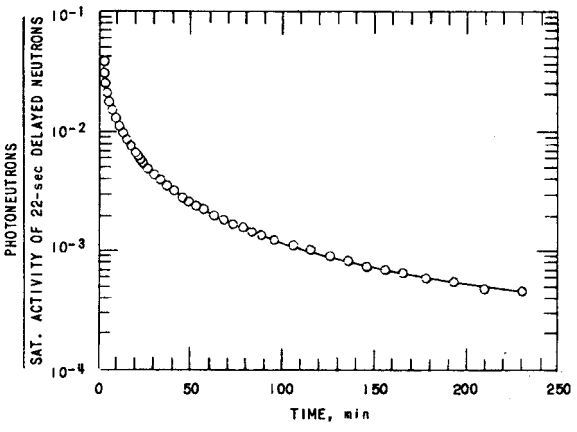

Fig. 5-109—Relative yield of photoneutrons from U^{235} fission products in Be after 15-minute exposure. *Reproduced from Ref. 217.*

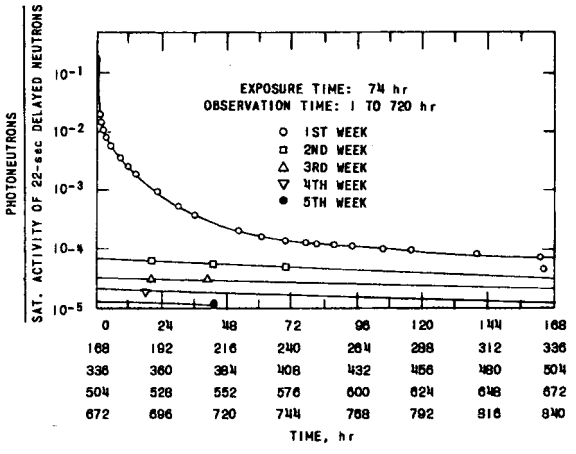

Fig. 5-110—Relative yield of photoneutrons from U^{235} fission products in Be. *Reproduced from Ref. 217.*

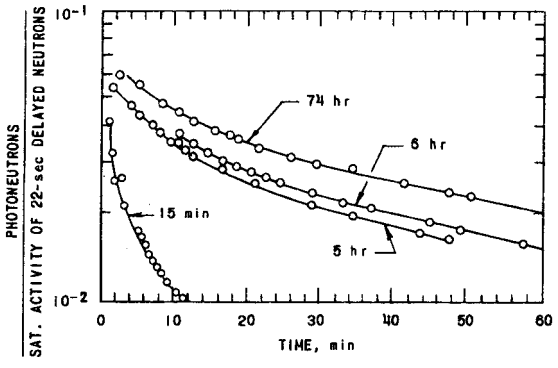

Fig. 5-111—Relative yield of photoneutrons from U^{235} fission products in Be for various exposure times. *Reproduced from Ref. 217.*

for t_e = 15 minutes, 5 hours, 6 hours, and 74 hours. Figure 5-112 compares the yields of photoneutrons from U^{235} fission products in D_2O with those in Be for t_e = 6 hours. Ergen[218] has correlated the above results on the photoneutrons from D_2O and Be, with known, hard gamma emitters among the fission fragments. Corresponding to an exposure time t_e, the corrected experimental yield relative to the 22-second delayed neutron half-life is plotted as a function of time after irradiation.

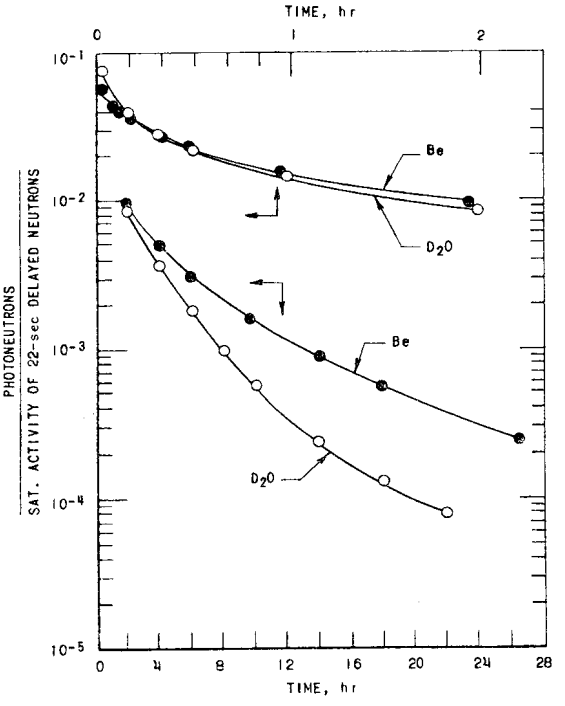

Fig. 5-112—Comparison of photoneutron activities of D_2O and Be after 6-hour exposure. *Reproduced from Ref. 217.*

A study of the yields of photoneutrons in a heavy water reactor has been made by Johns and Sargent[219] using the ZEEP reactor. In this work, the reactor was operated at a constant power level for a time and then suddenly made subcritical by the insertion of control rods. The neutron intensity was measured as a function of time after shutdown, and the kinetic equations were used in an analysis to give the yields and half-lives of delayed neutrons and photoneutrons.

The same experimental method can be used to obtain the relative photoneutron effectiveness factor, by assuming values for the relative yields of delayed neutrons and photoneutrons. The effectiveness factor is defined for a reactor as the ratio between the value of β_i, which would appear in the kinetic equations describing the reactor, and the value of β_i characteristic of the fission process, or in the case of photoneutrons, of an infinitely dilute core of infinite extent. By assuming that all ordinary delayed neutrons have the same effectiveness factor E_d, and that all photoneutrons have the same effectiveness factor E_p, the relative photoneutron effectiveness factor may be defined by $E = E_p/E_d$. The value of E would be unity for photoneutrons having the same energy as ordinary delayed neutrons and for infinitely dilute fuel. If the photoneutrons have a lower energy than the ordinary delayed neutrons and thus have fewer losses by leakage in slowing-down in a finite core, E will tend to be greater than unity (see Section 5.3.1). However, fuel elements of finite size absorb some of the gamma rays that would otherwise produce photoneutrons. This effect tends to make E less than unity.

Maxon and Cohn[220] have measured values of E in the THUD critical assembly at Argonne National Laboratory. This assembly has fuel rods consisting of enriched uranium oxide plus thorium oxide and a heavy-water moderator. The experimental values ranged from 0.42 for a closely-spaced, clustered lattice, to 1.15 for a widely-spaced, uniform lattice.

5.4 REACTOR STABILITY

5.4.1 GENERAL THEORY OF STABILITY

General Consideration. The theory of stability deals with the time behaviour of the reactor power in an *autonomous* reactor system following a *perturbation*. A reactor system is said to be

autonomous if the equations which describe the time dependence of reactor power (equations of motion) are unaltered by a translation of time origin.[221] This definition implies that all the external variables through which the performance of the reactor can be affected (control rod position, inlet temperature and flow rate of the coolant, steam load, etc.) are constant. To be specific, only one external variable, namely, reactivity input (control rod position) will be considered in the following treatment. The equation of motion of the reactor system can be written in the form of an integro-differential equation if the concentrations of delayed neutron precursors are eliminated. This is accomplished by using Laplace transform methods on the conventional reactor kinetics equations (Section 5.3.2).

$$\frac{\ell}{\beta}\frac{dN(t)}{dt} = N(t)\,(k_{ex} - 1 - k_f) + \int_0^\infty N(t-u)\,D(u)\,du \tag{5-90}$$

where ℓ is the prompt neutron lifetime; β is the fraction of all delayed neutrons; N(t) is the reactor power; k_{ex} is the externally controlled excess reactivity in dollars (reactivity input); k_f is the *negative* reactivity due to the feedback mechanism; and D(u) is the power due to the delayed neutrons emitted, per unit time at t, by the precursors produced by a unit fission energy at (t-u):

$$D(u) = \sum_i \frac{\beta_i \lambda_i}{\beta} e^{-\lambda_i u}; \quad \int_0^\infty D(u)\,du = 1$$

where β_i is the delayed neutron fraction for the *ith* group; and λ_i is the decay constant of the *ith* delayed neutron precursor.

The feedback mechanism refers to all physical phenomena through which reactor power variations can affect the excess reactivity. It is described mathematically by a set of equations which determine the functional dependence of reactivity on the reactor power:

$$k_f = k_f\,[N(t)]$$

Usually, the value of k_f at a given time t depends on the entire past history of N(t). If $k_f[N(t)]$ is given by a convolution integral as

$$k_f = \int_0^\infty N(t-u)\,K(u)\,du \tag{5-91}$$

then the feedback mechanism is said to be *linear*. In this case, the feedback is characterized by a single kernel, K(u), which is the negative reactivity at t due to unit fission energy released in the reactor at (t-u). (Note that K(u) = 0 for u < 0.) In the general case where the feedback is non-linear, no general form for $k_f[N(t)]$ similar to Eq. (5-91) can be given. A special non-linear feedback model will be discussed later.

The *equilibrium state* of an autonomous reactor system corresponding to a constant reactivity input, k_0, is defined as the time-independent solution of Eq. (5-90), $N(t) \equiv N_0$, if it exists. The equilibrium power, N_0, is a root of

$$k_0 - k_f\,(N_0) = 0 \tag{5-92}$$

The existence of a finite positive equilibrium state and its uniqueness will be assumed in the following treatment. For the case of linear feedback, Eq. (5-92) becomes

$$k_0 - N_0 \int_0^\infty K(u)\,du = 0 \tag{5-93}$$

where the integral can be identified as the negative power-reactivity coefficient.

It proves convenient to express Eq. (5-90) in terms of deviations from the equilibrium state:

$$[1 + z(t)]\,\rho_f + \frac{\ell}{\beta}\dot{z} + \int_0^\infty \dot{z}(t-u)\,D_1(u)\,du = 0 \qquad t > 0 \tag{5-94}$$

where the dot denotes differentiation with respect to time, and where

$$\rho_f = k_f - k_0, \quad z(t) = [N(t) - N_0]/N_0$$

$$D_1(u) = \textstyle\sum_i (\beta_i/\beta) \exp(-\lambda_i u) \tag{5-95}$$

As stated earlier, the theory of stability deals with the time behavior of a reactor following a perturbation. The term *perturbation* can now be clarified. Consider a reactor which is operated at equilibrium until a time $t = -t_1$, and perturbed continuously by changing the control rod position until $t = 0$.

The reactor system becomes autonomous for $t \geq 0$. In general, the system will not be in its equilibrium state. (The new equilibrium state does not, in general, correspond to the original equilibrium state). Since the feedback reactivity depends on the past history of the power, the behavior of z(t) for $t > 0$ can be determined only by knowing z(t) for $t \leq 0$. Therefore, the term *perturbation* will refer to the power variations prior to $t = 0$.

Concept of Stability for Reactor System. The question of stability concerns deviations of reactor power about the equilibrium state $z = 0$, particularly for large values of t. The purpose of stability analysis is to determine the necessary and sufficient conditions on the system parameters and perturbation functions which insure stability according to a specified stability definition.[222] In the following, *asymptotic stability* will be treated, which implies

$$\lim_{t\to\infty} z(t) = 0 \tag{5-96}$$

Asymptotic stability does not set any restriction on the magnitude of power excursions which may be so large as to cause permanent damage to the reactor. Therefore, it may be further required that the power excursion should never exceed a preassigned value determined by safety requirements.[223] Another type of stability is the *orbital*[222,223] stability which applies to reactor systems whose equilibrium state is a periodic function of time (limit cycle). The magnitude of this stable periodic equilibrium state may be small enough to be permitted from the safety point of view. But a reactor which has orbital stability may not be stable in the sense of asymptotic stability. Stability analysis so far has been confined mostly to the asymptotic stability.

Linear Stability. The kinetics equations can be linearized if the perturbation is so small that z(t) in Eq. (5-94) is always negligible compared to unity. In this case, linear feedback as given by Eq. (5-91) also may be assumed since the feedback equations can be linearized for small power variations. Hence, Eq. (5-94) becomes

$$N_0 \int_0^\infty z(t-u)\, K(u)\, du + \frac{\ell}{\beta}\dot{z} + \int_0^\infty \dot{z}(t-u)\, D_1(u)\, du = 0, \qquad t > 0 \tag{5-97}$$

Defining

$$z(t) \equiv z_-(-t) + z_+(t) \tag{5-98}$$

where $z_-(t) = z_+(t) \equiv 0$ for $t \leq 0$, it readily follows that

$$z(t) \equiv z_+(t) \text{ for } t > 0, \text{ and } z(t) \equiv z_-(-t) \text{ for } t < 0$$

Hence, $z_-(t)$ is the perturbation function.

The Laplace transform of Eq. (5-97), gives

$$\bar{z}_+(s) = \frac{(\ell/\beta)\, z(0) - \bar{K}_1(s)}{[1/Z(s)] + N_0\, \bar{K}(s)} \tag{5-99}$$

where $\bar{K}_1(s)$ is the Laplace transform of

$$K_1(t) \equiv \int_0^\infty z_-(u)\, [D_1(t+u) + N_0\, K(t+u)]\, du$$

and

$$\frac{1}{Z(s)} \equiv s\left[\frac{\ell}{\beta} + \frac{1}{\beta}\sum \frac{\beta_i}{\lambda_i + s}\right] \tag{5-100}$$

where Z(s) is the neutron kinetics transfer function (Section 5.3.3). The Laplace transform of K(t) is $\bar{K}(s)$ and is called the feedback transfer function.

It follows from Eq. (5-99) that $\lim_{t\to\infty} z_+(t) = 0$ for any sufficiently small perturbation function $z_-(t)$, if all the roots of $1 + N_0 Z(s)\bar{K}(s) = 0$, the characteristic equation of the system, have negative real parts. This condition is obviously necessary and sufficient, and follows from the inverse Laplace transform of Eq. (5-99) where a root with a positive real part gives rise to an exponentially increasing term. There are several techniques in servomechanisms theory to investigate the linear stability without actually solving the characteristic equation. Bode, Nyquist, and root-locus plots are graphical methods which are commonly used.[224] Routh's criterion can also be used analytically when the characteristic equation is in a polynomial form.[224]

Non-Linear Stability. The non-linearity of a reactor system is, in the first place, due to the product term $[z(t)\rho_f]$ in the neutron kinetics equation, Eq. (5-94). In addition, the feedback mechanism may be non-linear. Stability analyses of non-linear reactor systems so far have yielded only sufficient conditions for stability.[221,225–232] It proves convenient to distinguish between linear and non-linear feedback.

Linear Feedback. In this case, the feedback mechanism is characterized by the feedback transfer function $\bar{K}(s)$. The stability criterion is stated as follows:[226,227,231]

> "If the feedback transfer function $\bar{K}(s)$ is a positive real function, then $\lim_{t\to\infty} z(t) = 0$ for any bounded perturbation function $z_-(t)$."

The sufficient and necessary conditions for a function $\bar{K}(s)$, which is real for real s, to be positive real are: (1) it is analytic in the right-half s plane; (2) any poles on the imaginary axis are simple with real positive residues; and (3) its real part is non-negative on the imaginary axis, i.e.,

$$\text{Re } \bar{K}(j\omega) \geq 0 \tag{5-101}$$

for all real values of ω.[233]

When $\bar{K}(s)$ has no poles on the imaginary axis, the positive realness reduces to Eq. (5-101), which is known as Welton's stability criterion.[232] Note that $\bar{K}(s)$ is real for real s since K(t) is real.

It must be emphasized that the above criterion is sufficient and much too restrictive. Many important reactor types, such as boiling water reactors, do not fall within the region of application of this criterion. In fact, Welton's criterion does not apply to reactor systems which may become unstable in the linearized treatment at a certain power level. As an illustrative example, consider a reactor with a single temperature coefficient, i.e., in terms of incremental values

$$\rho_f = aT, \quad \dot{T} = bz(t) - cT \tag{5-102}$$

Eliminating T with Laplace transforms yields the feedback transfer function, $\bar{K}(s) = ab/(s + c)$. Positive realness of $\bar{K}(s)$ requires $ab > 0$, $c > 0$.

Non-Linear Feedback. In this case, the following stability criterion is proved:[231]

> "If the feedback mechanism is such that the integral
>
> $$\int_0^t \rho_f(t')\, z\,(t')\, dt', \quad t > 0 \tag{5-103}$$
>
> has a lower bound for any continuous function $z(t) \geq -1$ defined in $-\infty < t < +\infty$, the equilibrium state $z(t) \equiv 0$ is asymptotically stable for any bounded perturbation function $z_-(t)$."

The condition $z(t) \geq -1$ follows from the positiveness of reactor power, [see Eq. (5-95)]. The following example illustrates the application of the criterion. Consider a non-linear feedback[234] characterized by

$$\rho_f = f(T), \quad \dot{T} = zg(z) - h(T), \quad g(z) \neq 0 \tag{5-104}$$

where g(z), h(T) and f(T) are arbitrary functions; and T is the incremental temperature measured from the equilibrium value. The integral, Eq. (5-103), becomes

$$\int_0^t \frac{f(T)\, h(T)}{g(z)}\, dt + \int_0^T \frac{f(T')}{g(z)}\, dT' \tag{5-105}$$

Sufficient conditions which insure that Eq. (5-105) has zero as a lower bound are:

$$g(z) > 0, \qquad T\, h(T) \geq 0, \qquad T\, f(T) \geq 0$$

687863 O - 63 - 32

It is interesting to note that the linear feedback model given by Eq. (5-102) is a special case of the non-linear feedback in Eq. (5-104) with $f(T) \equiv aT$, $g(z) \equiv b$, $h(T) \equiv cT$. Substitution of these values in Eq. (5-105) yields $acb > 0$ and $ab > 0$, which are the same conditions as those obtained from the conditions of positive realness. In fact, the criterion for non-linear feedback which implies that the feedback can be represented by a *passive* non-linear electric network,[231] yields the positive realness condition when the feedback is linear.[233,235,236] This can also be proved directly by substituting

$$\rho_f \equiv \int_0^\infty z(t-u)\, K(u)\, du$$

into Eq. (5-103).

5.4.2 BOILING REACTOR STABILITY

General Considerations. This section treats the dynamic behavior and inherent stability of the reactor part of a boiling reactor system. The remainder of the plant, which is conventional for the most part, can be designed for over-all stability once the dynamic behavior of the reactor proper is sufficiently understood. Inlet coolant, steam load and control rod position, which constitute the link between the reactor proper and the remainder of the plant, will be regarded as external variables. These variables are assumed to be constants when the inherent stability of the reactor is considered. From the standpoint of the control system of the entire plant, however, the reactor power response to the variations in these external variables is of prime importance.

Conventional neutron kinetics equations are derived by ignoring spatial changes in the neutron flux during transients; therefore the analysis excludes the so-called "flux tilt instability" which comprises the long-term xenon oscillations and the short-term spatial instabilities.[237] Flux tilt instabilities are expected to be of importance only in large reactor cores; however, neither type of flux tilt instability has been observed in the boiling reactors constructed to date. Tests on the Dresden reactor, the first large reactor with effective local monitoring, have shown no evidence of spatial flux instability.[238]

The principal reactivity feedback in a boiling water reactor is due to the steam volume in the core, which locally reduces both the absorption and moderation and increases the leakage. The void-reactivity coefficient is a function of position in the core. It is for the most part negative, but it may be positive in the center of a light-water boiling reactor, where the effect of loss of absorption may more than offset the effect of loss of moderation and increased leakage.[239]

The feedback due to the metal and moderator temperature variations proves to be of minor importance, as compared with the void effects, in boiling reactors. The metal temperature coefficient includes the density variations with temperature as well as the Doppler effect.

The hydrodynamics of steam and water flow in the core and in the reactor vessel also play an important role in the dynamic behavior of a boiling reactor. The fundamental hydrodynamic equations which describe the steam and water flow are for the most part non-linear. They can be linearized by neglecting the second- and higher-order increments of the various variables; for example, in the dynamic behavior of the reactor for small perturbations (small signal or linearized theory). By application of Laplace transforms to the linearized set of equations the whole feedback mechanism may be characterized by a single function H(s), the feedback transfer function. Upon multiplying H(s) by the Laplace transform of the incremental power variations, the Laplace transform of the incremental reactivity variation is obtained. Obviously, H(s) is a function of the operating power level P_0. To be all-inclusive, H(s) contains the temperature feedback as well as the void-reactivity feedback.

The stability of the reactor is determined by the roots of the characteristic equation of closed loop, i.e., $P_0 Z(s)\, H(s) = 1$, where Z(s) is the zero-power transfer function obtained from the linearized kinetic equations. If all the roots of this equation have negative real parts, then the system is inherently stable for small perturbations.

The critical power level, P_c, where instability occurs, is defined as $P_c Z(j\omega_c)\, H(j\omega_c) = 1$, where ω_c is the circular frequency of the spontaneous oscillations.

The value of H(0) is the power-reactivity coefficient. Ignoring the temperature feedback, H(0) can be approximated by the slope α_v, of the reactivity in voids versus power curve, at the operating power level. Then, the stability condition can be expressed as

$$P_0 \alpha_v < X \tag{5-106}$$

where $X = |H(0)/H(j\omega_c)\, Z(j\omega_c)|$. The value of X depends mainly upon the geometry of the reactor, and, to a lesser degree, upon the distribution of the voids in the core. As a crude approximation, it may be assumed to be independent of power and pressure.

Published results for a number of boiling reactors show that, in practice, X varies between 2 and 8 for different designs.[240] It may be deduced that the stability of a boiling reactor depends largely upon the value of $P_0\alpha_v$. The important point is that the criterion does not involve the total amount of reactivity held in voids. The value of $P_0\alpha_v$ is smaller than the total reactivity in voids, since the curve representing reactivity in voids vs. power is concave to the power axis, as observed from the experimental results.[239] Another conclusion is that the specific volume of steam, and thus $P_0\alpha_v$, decreases with increasing pressure for the same power density. Hence, there will be a monotonically increasing boundary curve of power vs. pressure for a given geometry, which separates the stable and unstable regions. Physical interpretation of this boundary lies in the fact that the reduction in the specific steam volume with pressure is balanced by the increase in power density approximately giving rise to the same void condition as at a lower pressure and power. Experiments on EBWR at different powers and pressures verified this conclusion.[241] In a boiling reactor, the critical power level determined by Eq. (5-106) is often lower than the economical power limit set by the burnout effects unless the pressure is increased up to 70 atm, or more.

Theoretical Feedback Model. An explicit form for the feedback transfer function, H(s), in terms of the design parameters, is needed to predict the reactor stability. Extensive theoretical work has been done in this field.[242–250] The model described below[249] is based on the following main assumptions:

(1) A single representative channel is considered.

(2) Variations of kinetic and potential energies in the two-phase flow are ignored.

(3) The vertical pressure gradient is neglected.

(4) The vertical flux distribution is represented by a sinusoidal curve whose half-wave length is taken slightly shorter than the actual core height to account for flux depressions near the top of the core.

(5) First power (linear) flux weighting is adopted for the importance.

(6) An average uniform steam velocity is assumed.

(7) The distributed time constant transfer functions are simplified to single time-constant (or lumped time-constant) transfer functions.

General expressions for any flux and steam velocity distribution, and for any weighting function are also available if higher numerical accuracy is desirable.

Figure 5-113 shows the block diagram of the inherent feedback mechanism in a natural circulation, boiling water reactor. Analytical expressions for the various gains and time constants appearing in the diagram are given in Table 5-54. Table 5-55 lists the reactor parameters that enter the feedback model. If they can be determined by basic core calculations and out-of-pile measurements, then the dynamic behavior, as well as the stability of the reactor can be predicted in the design stage.

A brief, qualitative description of the feedback model (Fig. 5-113) follows. Consider a step change in the nuclear power. The resulting transients in the rate of heat transfer from the fuel element into the channel is determined by the geometry, thermal properties of the fuel material, and the film coefficient of heat transfer between the element and coolant. Due to the difference in the film coefficients in the boiling and subcooled sections of the channel, the transient behavior is slightly different in these two regions. The transfer functions G_9 and G_{10} represent the heat transfer rate in the boiling and subcooled regions, respectively. The average fuel plate temperatures are characterized by G_1 and G_2.

A step increase in the heat transfer rate in the subcooled region lowers the position of the boiling boundary (which is assumed as a horizontal interface separating the boiling and non-boiling regions), and increases the average water temperature. The transients are determined by the thermal properties and velocity of the water in the channel. The boxes G_{11} and G_3 represent the boiling boundary variations and average water temperatures in the subcooled region, respectively.

In the boiling region, a step increase in the heat transfer rate causes a step change in the steam production rate, but does not affect the water temperature. The increase in steam production rate is characterized by the box $[1/(H_s - H_w)]$. The total steam volume in the core does not increase immediately due to the finite steam transit time in the core. The transient in the resulting steam volume change (with the proper weighting) is represented by G_8.

The steam production rate is also affected by the shift in the boiling boundary since the latter changes the height of the boiling region and thus the portion of power available for steam production. The box $[-Q^0\ (L_{nb})]$ represents this effect. It should be noted that the shifts of boiling boundary due to the pressure changes (box G_{12}) are excluded at the input of this box, since they are included in G_{14}.

Any mismatch between the steam generation rate and the steam load causes the steam pressure in the vessel to rise or to fall. The rate of change of pressure may be calculated by assuming that steam in the vessel obeys the ideal gas law (Beckjord,[246] op. cit., p. 27). The initial rate of change of pressure following a step change in the heat transfer rate is reduced by the shift in the boiling boundary position due to the change in the saturation temperature with pressure. This decrease is compensated

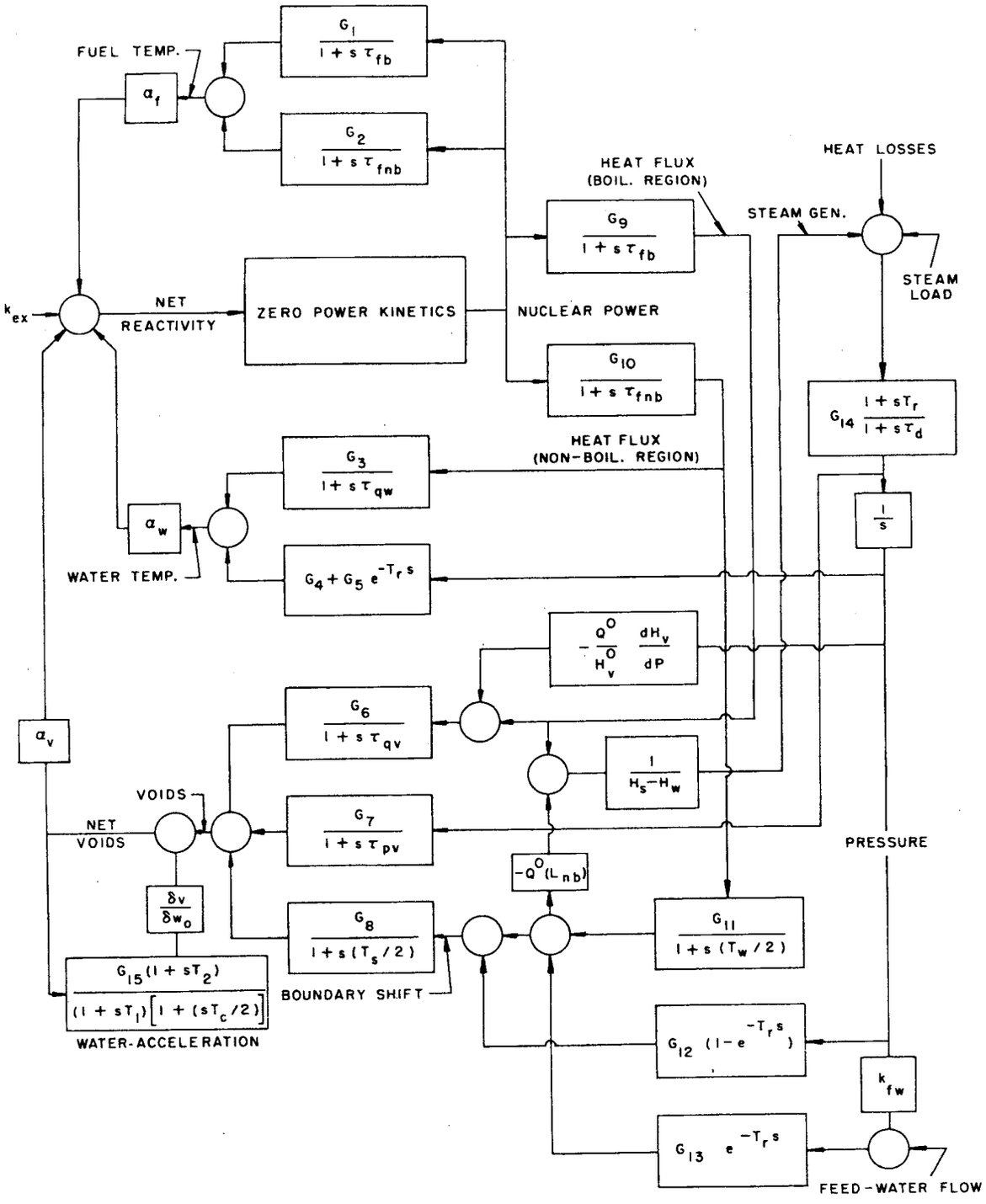

Fig. 5-113 —Internal feedback diagram of boiling water reactors.

Table 5-54—EXPLICIT FORMS OF TIME CONSTANTS AND GAINS

Time Constants

Fuel plate time constant

$$\tau_f = \tau_1\left[\frac{R_2 + R_3}{R_1} + \frac{1}{3} + \frac{\tau_2}{\tau_1}\left(\frac{1}{2} + \frac{R_3}{R_2}\right)\right]$$

Note: τ_{fb} and τ_{fnb} signify τ_f in the boiling and non-boiling regions, respectively.

Water temperature time constant

$$\tau_{qw} = 2\,\frac{(1-\cos\beta)^2}{\beta(2\beta-\sin 2\beta)}\,T_w$$

Power-void time constant

$$\tau_{qv} = \frac{2(1-\cos\alpha)^2}{\alpha(2\alpha-\sin 2\alpha)}\,T_s;\left[\text{multiply by 0.8 if } \alpha \geq \left(\frac{2}{3}\right)\pi\right]$$

Pressure-void time constant

$$\tau_{pv} = \frac{2\alpha-4\sin\alpha+\sin 2\alpha+4(K_1/K_2)(\alpha-\sin\alpha)}{2\alpha[2(K_1/K_2)(1-\cos\alpha)-\sin^2\alpha]}\,T_s$$

where

$$K_1 = \frac{AL}{2H_v\omega_s}\left[\left(\rho_w\frac{dH_w}{dP}-\rho_s\frac{dH_s}{dP}\right)\frac{Q^0\cos\alpha}{2U_0AH_v}-\rho_w\frac{dH_w}{dP}\right]$$

and

$$K_2 = -\frac{Q^0L}{4U_0H_v^2\omega_s}\left(\rho_w\frac{dH_w}{dP}-\rho_s\frac{dH_s}{dP}\right)$$

Steam mass-pressure rate time constant [Eqs. (4) and (5) in Ref. 250]

$$\tau_d = T_r\Big/\left[1+\left(\frac{M_w}{H_s-H_w}\frac{dH_w}{dP}\Big/\frac{M_s}{P}-\frac{M_s}{\theta_s}\frac{d\theta_s}{dP}+\frac{M_s}{H_s-H_w}\frac{dH_s}{dP}\right)\right]$$

(θ_s is in degrees Rankine).

Water acceleration time constants.

$$T_c = L_c/U^0\ (L_b)\ \text{(Chimney transit time)}$$

$$T_1 = M'/2BW_0^0$$

$$T_2 = \frac{T_c/2}{1+2(L_c/L_b)}$$

Table 5-54— EXPLICIT FORMS OF TIME CONSTANTS AND GAINS (Continued)

Gains

$$\left.\begin{matrix} G_1 \\ G_2 \end{matrix}\right\} = \frac{\pi^2}{8V_f}\left(\frac{L'}{L}\right)\left[d_1\left(\frac{R_1}{3} + R_2 + R_3\right) + d_2\left(\frac{R_2}{2} + R_3\right)\right]\left\{\begin{matrix} \left[\alpha + \frac{1}{2}\sin 2\beta\right] \\ \left[\alpha - \frac{1}{2}\sin 2\beta\right] \end{matrix}\right.$$

$$G_3 = \frac{1}{4c_w \dot{M}_t}(1-\cos\beta)$$

$$G_4 = \frac{d\theta_s}{dP}\frac{(1-\cos\alpha)}{2}$$

$$G_5 = \frac{d\theta_s}{dP}\frac{(1+\cos\alpha)}{2}$$

$$G_6 = \frac{\pi(1-\cos\alpha)}{4H_v\alpha}T_s$$

$$G_7 = \frac{K_2}{4}(2\alpha - 4\sin\alpha + \sin 2\alpha) + K_1(\alpha - \sin\alpha)$$

$$G_8 = -\frac{Q^0(L_{nb})}{H_v}\frac{\pi(1-\cos\alpha)}{2\alpha}T_s$$

$G_9 = \frac{1-\cos\alpha}{2}$ (Power in the boiling region/power in the whole channel)

$G_{10} = \frac{1+\cos\alpha}{2}$ (Power in the nonboiling region/power in the whole channel)

$$G_{11} = -\frac{1}{Q^0(L_{nb})}$$

$$G_{12} = \frac{dH_w}{dP}\frac{\dot{M}_t}{Q^0(L_{nb})}T_r$$

$$G_{13} = \frac{H_w - H_{fw}}{Q^0(L_{nb})}$$

$$G_{14} = 1\Big/\left(\frac{M_s}{P} - \frac{M_s}{\theta_s}\frac{d\theta_s}{dP} + \frac{M_s}{H_s - H_w}\frac{dH_s}{dP} + \frac{M_w}{H_s - H_w}\frac{dH_w}{dP}\right)$$

(θ_s is in degrees Rankine); (G_{14} is given as Eq. (5) in Ref. 250).

$$G_{15} = \frac{g\rho_w}{2BW_0^0}\left(1 + \frac{2L_c}{L_b}\right)$$

$\frac{\delta V}{\delta w_0}$ = Slope of the steam volume in the core versus inlet water velocity curve evaluated at the operating point.

Table 5-55 — FEEDBACK PARAMETERS

A	Channel cross-sectional area
A_d	Downcomer cross-sectional area
B	Over-all friction coefficient relative to inlet water velocity in the circulation loop
c_1, c_2, c_w	Specific heats of fuel section, cladding, and water
d_1, d_2	Half-thickness of the fuel section and the thickness of cladding
g	Acceleration due to gravity
H_{fw}	Enthalpy of feed water
H_s	Saturation enthalpy of steam
H_w	Saturation enthalpy of water
H_v	Latent heat per unit volume of steam
k_1, k_2	Thermal conductivities of the fuel and cladding materials
k_{fw}	Reactivity due to feed water
L, L'	Reduced and actual core height
L_{nb}	Length of nonboiling region
L_b, L_b'	Reduced and actual length of the boiling region
L_c	Length of the chimney
M_w	Water mass in the vessel
M_s	Steam mass in the vessel
M_d	Water mass in the downcomer
M_{nb}	Water mass in the nonboiling region of the core
M'	$M_b + M_{nb} + M_d(A/A_d)$
M_b	Total mass in the boiling region (water + steam)
$\dot{M}_t = \dot{M}_r + \dot{M}_{fw}$	Total water flow rate at the core inlet
$\dot{M}_{fw}$	Feed water mass flow rate
$\dot{M}_r$	Mass flow rate of the recirculation water
P	Pressure
Q^0	Thermal power delivered to the whole channel
$Q^0(x)$	Thermal power per unit height of the channel
R_1, R_2, R_3	Thermal resistances of the half fuel section, the cladding and the film
s	Laplace transform variable
T_r	Recirculation time
T_s	Steam transit time, $T_s = (L/U_0)$
T_w	Water transit time, $T_w = (L_{nb}/W_0^0)$
$U^0(x)$	Steam velocity
U_0	Average steam velocity
V	Steam volume in the core
V_f	Volume of the fuel plates
$W_0 = W_0^0 + w_0(t)$	Water velocity in the nonboiling region
W_0^0	Water velocity in the nonboiling region, at steady state

Greek Symbols

α, β	$(\pi L_b/L)$ and $(\pi L_{nb}/L)$
$\alpha_v, \alpha_f, \alpha_w$	Void-, fuel temperature-, and water temperature-reactivity coefficients
θ_s	Saturation temperature
$\rho_1, \rho_2, \rho_s, \rho_w$	Densities of fuel material, cladding, steam, and water
τ_1, τ_2	$(\rho_1 c_1 d_1^2/k_1)$ and $(\rho_2 c_2 d_2^2/k_2)$
ω_s, ω_w	(α/T_s) and (β/T_w)

Note: Where appearing, a dot above a symbol denotes a time derivative of the function.

continuously by the arrival of recirculation water whose temperature follows the saturation temperature at the top of the core with a time delay T_r, the circulation time. G_{14} represents the transients in the rate of change of pressure due to unbalance in the steam generation and load.

Flashing of saturated water into steam, as well as steam condensation in the core due to the pressure changes, is represented by G_7.

The boiling boundary position is also affected by the flow and enthalpy variations of the feedwater as indicated by G_{13}. The possibility of feed-water variations due to pressure variations in the vessel is taken into account by K_{fw}.

The effect of pressure variations on the water temperature in the boiling and in the subcooled regions is represented by G_4 and G_5, respectively.

The effect of shifts of the boiling boundary on the steam volume in the core is given by G_8.

The inlet water velocity at the bottom of the core has been assumed to be constant in the derivation of the above transfer functions. However, any increase in the steam volume in the core and in the chimney increases the pressure head in the circulation loop, and thus the water velocity. An increase in the water velocity reduces the steam residence time, thereby decreasing the initial steam volume. This effect of water acceleration on the steam volume is taken into account by the loop containing the boxes G_{15} and $(\partial V/\partial W_0)$. The effect of the water acceleration is accentuated by a long chimney.

Finally, α_w, α_f, and α_v convert the water temperature, fuel temperature and void volume variations into reactivity variations.

The model described above can be readily extended to forced circulation boiling reactors by modifying the boxes related with circulation water effects. Numerical applications (Table 5-56) show

Table 5-56—NUMERICAL VALUES FOR EBWR AT 20 Mw AND 41 atm

Reactor Parameters	
$A = 7831.5\ cm^2$	$R_{3nb} = 7376\ (cm^2)(sec)(°C)/cal$
$c_w = 1\ cal/(kg)(°C)$	$T_r = 9\ sec$
$c_1 = 0.037\ cal/(kg)(°C)$	$T_s = 0.35\ sec$
$c_2 = 0.069\ cal/(kg)(°C)$	$T_w = 0.64\ sec$
$d_1 = 0.216\ cm$	$\dot{M}_t = 476.3\ kg/sec$
$d_2 = 0.0488\ cm$	$r = 2$
$H_w - H_{fw} = 111.2\ cal/kg$	$V_f = 493\ ℓ$
$H_v = 8.5 \times 10^{-3}\ cal/cm^3$	$W_0^0 = 76.5\ cm/sec$
$L' = 121.9\ cm$	$dH_w/dP = 7.096\ (kw)(sec)/(kg)(atm)$
$L = 107.3\ cm$	$dH_s/dP = 0.659\ (kw)(sec)/(kg)(atm)$
$L_{nb} = 48.77\ cm$	$dT_s/dP = 1.38\ °C/atm$
$M_w = 8981.3\ kg$	$\lambda = 6 \times 10^{-5}\ sec^{-1}$
$M_s = 326.6\ kg$	$\beta = 0.0073$
$R_1 = 3647\ (cm^2)(sec)(°C)/cal$	$\alpha_f = -0.27\ cents/°C$
$R_2 = 1127\ (cm^2)(sec)(°C)/cal$	$\alpha_w = -2.9\ cents/°C$
$R_{3b} = 365\ (cm^2)(sec)(°C)/cal$	$\alpha_v = -3.9\ cents/ℓ$
Time Constants and Gains	
$\tau_{fb} = 0.38\ sec$	$G_3 = 3.88 \times 10^{-3}\ °C/(cal)(sec)$
$\tau_{fnb} = 0.44\ sec$	$G_4 = 2.54 \times 10^{-1}\ °C/(cal)(sec)$
$\tau_{qw} = 0.25\ sec$	$G_5 = 1.32 \times 10^{-1}\ °C/(cal)(sec)$
$\tau_{pv} = 0.03\ sec$	$G_6 = 2.25 \times 10^{-2}\ ℓ/(cal)(sec)$
$\tau_{qv} = 0.11\ sec$	$G_7 = -12.89\ ℓ/(atm)(sec)$
$\tau_d = 1.46\ sec$	$G_8 = -2.6\ ℓ/cm$
$T_r/2 = 4.5\ sec$	$G_9 = 0.65$
$T_s/2 = 0.175\ sec$	$G_{10} = 0.34$
$T_w/2 = 0.32\ sec$	$G_{11} = -1.23 \times 10^{-2}\ cm/(cal)(sec)$
$G_1 = 1.39 \times 10^{-3}\ °C/cal/sec$	$G_{12} = 14.06\ cm/atm$
$G_2 = 5.18 \times 10^{-3}\ °C/cal/sec$	$G_{14} = 2.39 \times 10^{-2}\ atm/kg$

that temperature effects are negligible in comparison with void effects.[249] Moreover, at high pressures, pressure-void effects prove to be important only at lower frequencies (typically, lower than 1 rad/sec in EBWR). Therefore, temperature and pressure effects can be disregarded when exploring the high-frequency response of the reactor which contains the resonance peak. Results for EBWR obtained with the power-void transfer function only; i.e., G_9, G_{10}, G_{11}, G_8, G_6 and α_v, have been encourag-

ing for the properties of the resonance peak at high pressures[247] (Table 5-57). Figures 5-114 and 5-115 compare the experimental and calculated amplitude and phase responses of the closed loop transfer function of EBWR at 20 Mw and 41 atm in the low, as well as the high-frequency regions. The calculated transfer function was obtained by neglecting the temperature and water acceleration effects which are numerically small. The agreement is satisfactory in view of the uncertainties of the numerical values used in calculations. Where parameters in the theory are matched to the experimental data, much better agreement is possible.

Table 5-57—CHARACTERISTICS OF THE RESONANCE IN THE EBWR TRANSFER FUNCTION

	20 Mw		50 Mw	
	Calculated	Measured	Calculated	Measured
Frequency, cps	1.11	1	1.59	1.7
Half-width, cps	4.06	1.8	1.29	0.4
Maximum gain, db	45.4	46.1	48.6	55.4

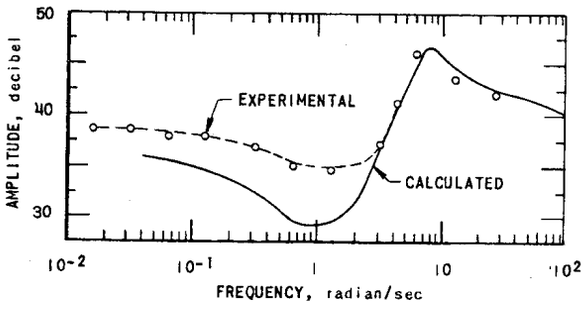

Fig. 5-114—Amplitude response of EBWR transfer function at 20 Mw and 41 atm.

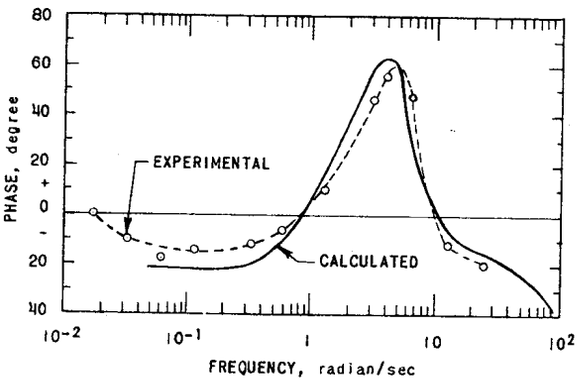

Fig. 5-115—Phase response of EBWR transfer function at 20 Mw and 41 atm.

Hydraulic Instabilities. Although feedback models similar to that represented in Fig. 5-113 have been successful in the interpretation of boiling reactor behavior at high pressures, they become inadequate at low pressures. When the steam pressure is so low that it is comparable with the static pressure drop in the vertical channel due to the weight of water, the dominant mechanism for instability changes from the nuclear feedback to the purely hydraulic instability. The instability ("chugging") observed in the original low-pressure boiling reactor experiments is an example of hydraulic instability. Experiments on BORAX-I and SPERT-I reactors indicated that the onset of the hydraulic instability is sensitive to the height of water in the reactor tank above the core.[251,252] Hydraulic instability has been observed also in out-of-reactor tests where the heating elements were electrically heated.[253] It was found in these experiments that the hydraulic instability had a sharp threshold at 75% exit voids. Preliminary theoretical models predict that the hydraulic instabilities are accompanied by a reversal of flow in the convection circuit enabling large void fraction changes to take place within the reactor core.[254] Further work in this area is under way at Ramo-Wooldridge[255] and at Argonne. Undoubtedly, the nuclear feedback reacts to the hydraulic instability, but does not play an important role in its onset. Forced circulation is currently believed to reduce the possibility of hydraulic instability. There is considerable evidence, obtained from the performance of existing boiling water reactors to support the conclusion that hydraulic instability is not important in high-pressure power reactors.

Prediction of Reactor Performance at Higher Powers. The performance at high powers, as well as the instability threshold, of a reactor can be predicted with some confidence by extrapolating information obtained at low powers under a variety of conditions. The behavior of the reactor at a given power and pressure can be determined by varying one of the external variables and observing the cor-

responding change in power or in any other reactor parameter (temperature, pressure, etc.). The commonly used technique is to investigate the amplitude and phase response of the reactor power to a sinusoidal reactivity input.[241] Although other modes of reactivity input (e.g., step, ramp, and square wave), can be used, sinusoidal input is usually preferred, for it directly yields the closed loop transfer function of the system. Reactor noise analysis may also be used to obtain some information about the dynamic behavior of the reactor.

The theoretical model can be improved by adjusting values of various feedback parameters for the best agreement between experimental and theoretical power responses. Due to the large number of feedback parameters, only those parameters are considered which affect the stability most, e.g., void-reactivity coefficient, steam transit time, and recirculation time. Most of the remaining parameters (e.g., fuel plate time constant) can be estimated with sufficient reliability from either basic calculations, or by out-of-reactor measurements. Extrapolation of the adjusted values of feedback parameter from the low-power measurements yields the feedback transfer function at the desired high power. Measurements of time constants at reduced pressures also can be used to predict the time constants at a higher power and pressure, since, as mentioned earlier, the void conditions are approximately similar in both cases (DeShong and Lipinski,[250] op. cit., p. 32).

Another method of extrapolation which does not require an accurate feedback model is to assume a form for H(s):

$$H(s) = \frac{\alpha \Pi_i (1 + s\tau_{-i})}{\Pi_i (1 + s\tau_i)}, \quad i = 1,2,... \tag{5-107}$$

and to determine the phenomenological time constants, τ_i, and power-reactivity coefficient, α, from the experimental feedback transfer function. The latter is given by:

$$P_0^{-1} [Z(s)^{-1} - Q(s)^{-1}]$$

where Q(s) is the experimental closed loop transfer function. The time constants are determined by resolving the experimental amplitude and phase responses into the Bode diagram (break frequency method).[250] The number of time constants to be included depends on the desired accuracy in describing the experimental curve by Eq. (5-107). Although the time constants in Eq. (5-107) do not have to correspond to actual time constants, some of them may be so identified. Extrapolation of τ_i and α to higher powers then gives the phenomenological feedback transfer function at the desired power level. A combination of this method with a specific feedback model was used successfully to predict the 40-Mw performance of EBWR[250] (see Fig. 5-116).

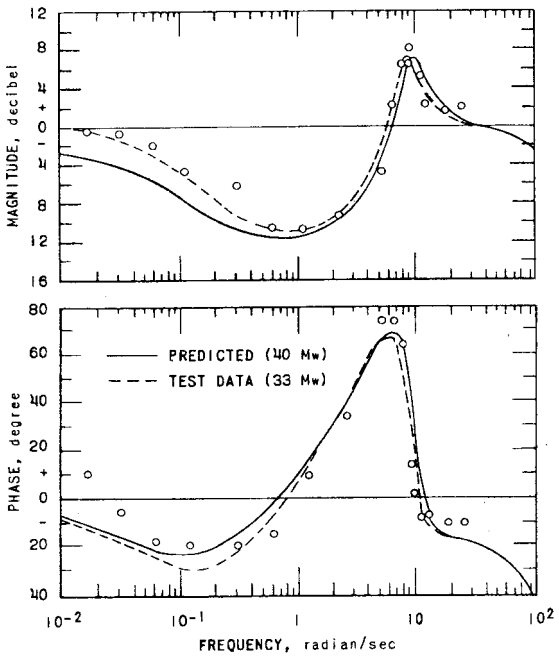

Fig. 5-116 — Predicted power transfer function of EBWR at 40 Mw.

The instability threshold can be predicted by extrapolating from low-power measurements a quantity which approaches zero at the threshold. The "gain" and "phase" margins are two examples which have been used to predict the instability threshold of EBWR.[250] The former is equal to $(1 - |ZHP_0|)$ at a frequency for which the phase of ZH is 180°, and the latter measures the deviation from 180° of the phase of ZH when $|P_0ZH| = 1$. Extrapolation on the basis of either the gain or phase margin requires a complete knowledge of the feedback transfer function at different powers and frequencies. There are other quantities suitable for extrapolation, however, which can be measured directly. For example, the half-width of the resonance peak in the amplitude response of the closed-loop transfer function which also approaches zero at the instability threshold can be obtained easily by making a Fourier analysis of the reactor noise (i.e., via the autocorrelation function). For cases of interest to stability where the resonance peak is narrow, knowledge of the core internal statistics and feedback loops is not required in the experimental determination of the half-width[256] (see Table 5-57). Use of the inverse of the root mean square (r.m.s.) value of the power fluctuations to predict the instability threshold has been proposed recently.[257] The success of the extrapolation process involved in these techniques depends on the monotonic variation of the above quantities with power. Experimental curves for EBWR have indicated that phase and gain margin, as well as the inverse of the r.m.s. value, are monotonically decreasing with power and thus allow an extrapolation to be made[250] as shown in Fig. 5-117.

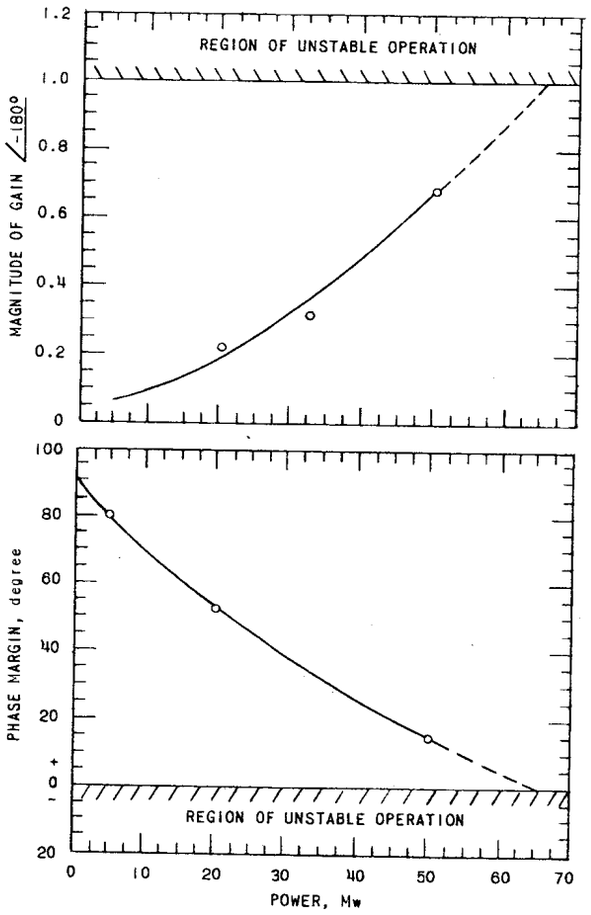

Fig. 5-117— Prediction of unstable operation in EBWR.

Effect of Reactor Noise on Stability. The theory discussed so far has consisted essentially of analyses resulting in systems of differential equations with constant coefficients. However, in a specific boiling reactor, the reactor parameters, and thus the coefficients of the differential equations describing the reactor system, are randomly varying as a result of the random nature of boiling, random fluctuations in the inlet velocity and enthalpy, random disturbances on the water surface above the core, etc. The first consequence of the parameter variations is random fluctuations in the reactor power at steady operation (reactor noise).[258] The presence of reactor noise is not of great importance from the standpoint of the control system of the entire power plant, since the r.m.s. value of the noise is usually less than 10% of the average value. However, reactor noise sets a limit on the accuracy of

the kinetic experiments (e.g., transfer function measurements), thereby requiring the use of statistical methods to increase the accuracy.[259]

The second and important consequence of reactor noise is that it influences the reactor stability in such a way that very large amplitude oscillations may arise even when the system with constant parameters is stable. This type of instability is known as "mean square or stochastic" instability.[257,260] Preliminary investigations show[257] that the stochastic instability is likely to occur only when the conventional instability threshold, as previously defined, is approached. The difference between the conventional and stochastic instability thresholds will probably fall within the accuracy of the conventional instability predictions mentioned in previous sections. Stochastic instability may play an important role during the initial rise of reactor power, since it occurs at a lower power than the conventional instability. The method of extrapolation of the inverse of r.m.s. of the reactor noise previously mentioned predicts directly the stochastic instability. Preliminary application of this method to EBWR has been encouraging.[257]

5.4.3 XENON INSTABILITY

A reactor that has been operating at a steady power level for a sufficiently long time will contain an equilibrium amount of xenon. The xenon concentration will vary immediately with the flux level, but the production rate will not change for some time. The xenon poison will continue to decrease whenever the flux is increased, and to increase whenever the flux is decreased. This will tend to emphasize the flux distortion. Eventually, the increased flux will result, through the production term, in increased xenon which will tend to lower the flux. It is possible that such flux distortions are unstable so that the flux distribution can oscillate continually even though the mean power is kept constant by the use of control rods. The problem of xenon instability is most important for large, high-flux reactors with small migration areas.

Ward[261] has investigated the kinetic behavior of a reactor with migration area M^2 (unpoisoned) and critical buckling κ^2. In the analysis, the time-dependent equations for neutron flux, delayed neutron precursor density, iodine concentration, and xenon concentration are considered. Steady-state values are assumed to be perturbed by small quantities proportional to $\exp(\omega t)$ for $t > 0$, and spatially to a function f_i, where the f_i are solutions of

$$\nabla^2 f_i + \kappa_i^2 f_i = 0$$

and $f_i = 0$ at the outer boundary of the reactor.

Retaining only the first order of small quantities and utilizing the orthogonality properties of the f_i, the following equation can be found for ω

$$(k - 1 - M^2\kappa_j^2 - A\overline{X}_j) + \left[\frac{-\omega}{\lambda} - k\beta\left(1 - \sum_d \frac{\beta_d\lambda_d}{\omega + \lambda_d}\right)\right] + \frac{A\overline{\phi}_j\,\sigma_a^{Xe}}{\lambda_{Xe} + \omega + \overline{\phi}_j\sigma_a^{Xe}}\left(\overline{X}_j - \frac{\lambda_I}{\lambda_I + \omega}\right) = 0 \qquad (5\text{-}108)$$

where λ is the reciprocal neutron lifetime in the unpoisoned infinite reactor; β, the total delayed neutron fraction; β_d, λ_d, the relative delayed neutron fractions (i.e., $\sum_d \beta_d = 1$) and reciprocal lifetimes; λ_I the reciprocal lifetime of I^{135}; λ_{Xe}, the same quantity for Xe^{135}; σ_a^{Xe}, the Xe^{135} absorption cross section; $\overline{\phi}_j$, the projection of $\overline{\phi}_0$ on f_j defined in the same fashion as $\overline{X}_j$ is defined subsequently (ϕ is the neutron flux). The first term in the equation is the amount below critical of the jth mode: AX is the local change in k due to xenon poison, where A is the ratio of xenon absorption at equilibrium to core absorption for very high flux (i.e., the xenon decay rate is neglected with respect to loss through neutron capture); and

$$\overline{X}_j = \int f_j^2\, X_0 dv$$

where X_0 is the unperturbed value of X, and the f_j are normalized to $\int f_j^2\, dv = 1$. The second term in the equation is the change in k necessary to make the perturbation grow with reciprocal period, ω. Finally, the third term is a measure of the reactivity effect of the xenon.

For the higher modes, the first term of Eq. (5-108) is negative and large compared to the second term. With the approximation that the sum of the first two terms is a constant K_j, Eq. (5-108) may then be written as a quadratic:

$$\omega^2 + b\omega + c = 0$$

where

$$b = \lambda_{Xe} + \lambda_I + \lambda_n + \frac{A}{K_j}\lambda_n \bar{X}_j$$

and

$$c = \lambda_I \left[\lambda_{Xe} + \lambda_n - \frac{A\lambda_n}{K_j}(1 - \bar{X}_j)\right]$$

with

$$\lambda_n = \bar{\phi}_j \sigma_a^{Xe}$$

Since λ_I, λ_{Xe}, and λ_n are all greater than zero, $0 < \bar{X} < 1$ and $K_j < 0$; therefore $c > 0$. For $b^2 < 4c$, the roots of the quadratic are conjugate complex, corresponding to oscillatory behaviour of the flux perturbation with exponentially increasing or decreasing amplitude, depending on whether $b < 0$ or $b > 0$. The condition for undamped oscillation is $b = 0$, which yields an oscillation frequency, f, given by:

$$(2\pi f)^2 = \frac{\lambda_I [\lambda_{Xe} + \lambda_n + \lambda_I(1 - \bar{X}_j)]}{\bar{X}_j}$$

Substituting the explicit form of K_j into the expression $-b > 0$, it is noted that a necessary condition for instability is that the unpoisoned reactor be large enough to be above critical for the j*th* mode, i.e., $k - 1 - \kappa_j^2 M^2 > 0$. For very high flux reactors, i.e., $\lambda_n \gg \lambda_{Xe}$, this criterion is also a sufficient condition. Furthermore, if $\lambda_n \gg \lambda_{Xe}$, it follows that

$$2\pi f \approx (\lambda_I \lambda_n)^{1/2}$$

Randall and St. John[262] extended the work of Ward[261] to cases where the stationary reactor power distribution is much different from the fundamental geometrical mode. The stability criterion is of the same form but somewhat more difficult to analyze since the actual flux shape and the fundamental mode shape are involved. Also, the effects of a power coefficient, and direct formation of Xe^{135} are included.

For a bare, one-dimensional reactor with zero power coefficient and height H, the threshold flux for onset of oscillation depends on the ratio H^2/M^2 and is 1.52×10^{13} n/(cm^2)(sec) for $H^2/M^2 = 2500$, and 5×10^{13} n/(cm^2)(sec) for $H^2/M^2 = 1250$. The periods in these cases are 29.4 and 22.1 hr, respectively.

Xenon oscillations have also been considered in Refs. 263 to 265. Henry and Germann[263] treated a one-dimensional slab reactor having two fuel regions with flat fluxes of different magnitudes separated by a moderator region. Wick[264] studied an annular seed-blanket type of reactor. He used a Laplace transform analysis and introduced the concept of a "xenon transfer function". Also, a preliminary investigation was made of the effect of using two-group diffusion theory rather than one-group theory. Mochizuki and Takeda[265] analyzed a Calder Hall-type reactor, using transfer function methods and making detailed considerations involving heat transfer problems.

5.4.4 KINETICS OF CIRCULATING FUEL REACTORS

Studies of the kinetics of circulating fuel reactors have been made by Ergen,[230,266,267] Ergen and Weinberg,[229,268] Walton,[269,270] and Fleck.[271–273] All of these investigators except Fleck formulate the problem in terms of equations involving integral operations on the past history of the reactor flux. Fleck begins his treatment by writing partial differential equations for the space and time dependence of the neutron flux, and either the delayed neutron precursor densities or the temperature. As this method is more straightforward, it will be briefly outlined here. Two simplified cases are considered: (a) Low-Power Kinetics with Delayed Neutrons; and (b) Temperature-Dependent Kinetics without Delayed Neutrons.

Case (a): Low-Power Kinetics with Delayed Neutrons. The objective is to derive the inhour equation for the circulating fuel reactor, and to compare it with the inhour equation for a stationary fuel reactor. It is assumed that the reactor core is a cylinder of height h and the circulating fuel circuit is a closed loop with the same cross-sectional area as the core. The length of the circuit outside

the core is h_e. The neutron flux is described by the one-velocity model, and the hydrodynamics is described by a one-dimensional flow ("slug flow"). Fissions are considered to take place only in the core. The following differential equations describe the circulating fuel reactor:

$$D\nabla^2\phi - \Sigma_a\,\phi + (1-\beta)\,\nu\,\Sigma_f\,pe^{-\tau B^2}\,\phi + pe^{-\tau B^2}\sum_i \lambda_i C_i = \frac{1}{V}\frac{d\phi}{dt} \tag{5-109}$$

$$\frac{\partial C_i}{\partial t} + q\,\frac{\partial C_i}{\partial z} = \nu\beta_i\,\Sigma_f\,\phi - \lambda_i C_i,\quad 0 \le z \le h \tag{5-110}$$

$$\frac{\partial C_i}{\partial t} + q\,\frac{\partial C_i}{\partial z} = -\lambda_i C_i,\quad h \le z \le h + h_e \tag{5-111}$$

The notation is standard except that q is the velocity of the circulating fuel, and z is the distance around the circuit measured from the core inlet. Equations (5-110) and (5-111) are the usual delayed neutron precursor density equations modified by the continuity equation of hydrodynamics. The solutions of Eqs. (5-109) through (5-111) may be obtained by using Laplace transform methods along with the assumption that the axial flux varies as

$$\phi(z,t) = \phi_0 e^{\omega t}\sin\left(\frac{\pi z}{h}\right)$$

Using a few approximations, the following equation may be derived for the reactivity ρ:

$$\rho = \frac{\ell\omega}{\ell\omega+1} + \frac{1}{\ell\omega+1}\sum_i \frac{\beta_i}{\omega+\lambda_i}\{\omega + \lambda_i\,[1 - a_i(\omega)]\} \tag{5-112}$$

where

$$a_i(\omega) = 1 - \frac{q}{h}\,\frac{\left\{1-\exp\left[-(\omega+\lambda_i)\,\frac{h_e}{q}\right]\right\}\left\{1-\exp\left[-(\omega+\lambda_i)\,\frac{h}{q}\right]\right\}}{(\omega+\lambda_i)\left\{1-\exp\left[-(\omega+\lambda_i)\,\frac{(h+h_e)}{q}\right]\right\}} \tag{5-113}$$

and is the fraction of precursors of type i that are in the core. The reactivity, ρ, of the system is defined as that which would exist in the case of no circulation. This expression for ρ may be compared with the expression for the case of a stationary fuel reactor.[274] For $q = 0$, $a_i(\omega) = 1$, and the two expressions agree as expected. For steady-state conditions, $\omega = 0$, and

$$\rho(\omega = 0) = \rho_0 = \textstyle\sum_i \beta_i[1 - a_i(0)]$$

Assuming that $\omega \ll \lambda_i$, and $\lambda_i(h + h_e) \ll q$, it follows that

$$\rho - \rho_0 \approx \frac{\ell\omega}{\ell\omega+1} + \frac{1}{\ell\omega+1}\sum_i \frac{h}{(h+h_e)}\,\frac{\beta_i\omega}{\omega+\lambda_i} \tag{5-114}$$

Equation (5-114) shows that for long reactor periods and fast flow, the effective delayed neutron fraction is the actual delayed neutron fraction, β_i, multiplied by the transit time through the core divided by the transit time through the whole loop. A circulating fuel reactor will exhibit shorter asymptotic periods for a given $\rho - \rho_0$ than will a stationary fuel reactor.

Case (b): Temperature-Dependent Kinetics without Delayed Neutrons. The one-velocity model and slug flow are used as in Case (a) and the prime interest is stability considerations. The calculation is performed for an open-loop circuit, i.e., the entrance conditions to the core are constant in time, so that the external loop removes all the heat generated in the core. Fluid particles and heat are transported with uniform speed q, and thermal equilibrium and density changes of the fuel occur instantaneously. The equations to be solved are

$$D\nabla^2\phi - \Sigma_a\,\phi + \nu\,\Sigma_f\,pe^{-\tau B^2}\,\phi = \frac{1}{V}\frac{\partial\phi}{\partial t} \tag{5-115}$$

$$\frac{\partial T}{\partial t} + q\frac{\partial T}{\partial z} = \frac{E\Sigma_f \phi}{C} \tag{5-116}$$

where T is the temperature; E is the energy released in one fission; C is the heat capacity of the fuel; and other notation is as used in Case (a). Equation (5-116) is simply the continuity equation in heat transport. The change in local effective multiplication factor may be expressed

$$\delta k = \delta k_0 - \alpha\,[T(z,t) - T(0,t)]$$

where α is the temperature coefficient of reactivity, and $T(0,t) = T(0,0)$ is the temperature at the core inlet. By using Laplace transform methods on Eqs. (5-115) and (5-116) and assuming that $\phi(z,t) = \phi(t) \sin(\pi z/h)$, the following equations may be derived for $t > t_1$, where $t_1 = h/q$:

$$\ell\,\frac{dP}{dt}(t) = -\alpha P(t)\,\theta(t) \tag{5-117}$$

and

$$\frac{d\theta(t)}{dt} = \frac{1}{C}\left[P(t) - \frac{1}{t_1}\int_0^{t_1} P(t-s)\,ds\right] \tag{5-118}$$

where

$$P(t) = E\Sigma_f \phi(t)$$

and the effective temperature is given by:

$$\theta(t) = -\frac{\delta k_0}{\alpha} + \frac{1}{C}\int_0^{t_1} P(t-s)\left(1 - \frac{s}{t_1}\right) ds \tag{5-119}$$

Equations (5-117) and (5-118) are of the same form as those used by Ergen, Weinberg, and Welton in their stability considerations. On using the linearized form of Eqs. (5-117) and (5-118) with $P(t) = P(0)\,[1 + p(t)]$, where $p(t) \ll 1$, and assuming that p(t) is proportional to $e^{\omega t}$, it may be shown that $\mathrm{Re}(\omega) \leq 0$. Therefore, the power oscillations are damped unless the transit time through the core has certain resonance values. For these resonance values, p(t) represents a steady, undamped, sinusoidal oscillation.

Fleck[273] has carried out numerical solutions of the kinetic equations for Case (b). The constants used are typical of the Brookhaven U-Bi LMFR design. Graphs are given of the neutron density and temperature at the core exit as functions of time for various conditions. The temperature variations are mild, although in some cases the neutron density variations are quite extreme.

Meghreblian and Holmes[275] treat both Cases (a) and (b), essentially following the development of Fleck.

Ergen, Ergen and Weinberg, and Welton, consider the case where the oscillations are non-linear. Plausibility arguments, rather than rigorous proofs, are used to show that the oscillations are damped unless the transit time has resonance values as mentioned above. In the case where both the temperature coefficient of reactivity and delayed neutrons are taken into account, indirect methods have been used[230] to show that the non-linear oscillations are damped.

5.5 REACTOR EXCURSIONS

5.5.1 GENERAL CONSIDERATIONS

It has been shown[175,276,277] that when only small reactivity changes are involved and no large spatial variation of the flux shape is expected, the space and energy dependence in the neutronic equations can be eliminated and the temporal variation of the neutron population can be described as a function of reactivity by the ordinary differential kinetics equations. The reactivity can be considered composed of two parts: (1) reactivity that is inserted mechanically (usually either as a step function,

or as a ramp function), and (2) feedback reactivity that is produced by the reactor system, usually as a result of heat generation. In general, it is difficult to eliminate with proper justification the space dependency from the equations determining the reactivity. However, this can be done for very slow and very fast excursions and at least qualitative features of an intermediate excursion can be inferred.

Simplified Kinetics Equations. The usual kinetics equations accounting for the delayed neutrons have been given in Section 5.3.2. The equations can be simplified if the excess reactivity is small and if terms of the order of the delayed neutron fraction are ignored compared to unity.

$$\begin{cases} \dot{\phi} = \dfrac{k_{ex}}{\ell}\,\phi - \sum_i \dot{C}_i \\ \dot{c}_i = \dfrac{\beta_i}{\ell}\,\phi - \lambda_i C_i \end{cases}$$

where ϕ is the neutron density, and the other quantities are as defined in Section 5.3.2. The delayed neutron precursors then do not depend on the reactivity explicitly and can be eliminated from the equations in a simple fashion,[278] yielding an integro-differential relation between the flux and the reactivity:

$$\ell\dot{\phi} = (k_{ex} - \beta)\,\phi + \left[\int_{-\infty}^{t} dt'\ \phi(t')\right] \sum_i \beta_i\lambda_i \exp\left[\lambda_i(t' - t)\right] \qquad (5\text{-}120)$$

If the burst is narrow, compared with the $1/\lambda$ values, the preceding relation can be simplified to give the flux at times fairly long after the burst at $t = 0$:[279]

$$\ell\dot{\phi} = (k_{ex} - \beta)\,\phi + \left(\int \phi\ dt\right) \sum_i \beta_i\lambda_i \exp(-\lambda_i t)$$

A still simpler relation, valid during a narrow burst, can be obtained by replacing $\exp \lambda_i (t' - t)$ in Eq. (5-120) by unity:

$$\ell\dot{\phi} = (k_{ex} - \beta)\,\phi + \sum_i \beta_i\lambda_i \int_{-\infty}^{t} \phi\ dt$$

On the other hand, if the burst is very long compared with the $1/\lambda$ values, the following relation is obtained by taking three terms in the Taylor series expansion of $\dot{\phi}(t)$:

$$\left[\ell + \sum_i (\beta_i/\lambda_i)\right] \dot{\phi} = k_{ex}\,\phi + \ddot{\phi} \sum_i (\beta_i/\lambda_i^2)$$

Thus the behavior of the reactor is governed by the delayed neutrons.

The relationship between the reactivity and the flux in wide bursts is obscured by the role played by the delayed neutrons. The behavior of the burst and reactivity reduction mechanism has then to be studied numerically.

Excursions Above Prompt Critical. When the reactivity exceeds prompt critical, the effect of the delayed neutrons is recognized only after the burst, and the behaviour of the flux during the burst is determined by simple relationships with the reactivity. Usually it can be assumed that the reactivity is inserted at an essentially constant rate. When the burst is large, however, the behaviour of the flux in the neighborhood of its peak can be described by the maximum reactivity inserted. The latter can be quite adequately determined without a detailed knowledge of the reactivity reduction mechanism. Thus, the effect of the reactivity reduction mechanism on the excursion may be considered as the case where the reactivity is inserted suddenly. The following discussions pertain to reactivity insertion at a constant rate and the determination of maximum reactivity that may be inserted this way. Subsequently, simple models for reactivity reduction mechanisms and the behaviour of the associated fluxes are discussed.

Reactivity Insertion at Constant Rate without Feedback. Usually there is no effective reactivity reduction mechanism during the initial period of a large burst, and the reactivity simply increases linearly. Analytical solutions for the flux applicable to this case have been found by Smets[280] and others.[277] Approximate formulae valid for fast rates of reactivity insertion were derived earlier.[281,282] If the reactivity insertion starts while the reactor is below critical, $k_s < 1$, and operating at a power level, P_s, due to the presence of sources, the power level at delayed critical, P_d, will be[281]

$$P_d \approx \frac{1 + \beta - k_s}{\beta}\,P_s \qquad (5\text{-}121)$$

If the reactivity insertion is continued at the rate a, the power level at prompt critical, P_p, is given by:

$$P_p \approx P_d \ (\pi\beta/2\ell a)^{1/2} \tag{5-122}$$

For continued reactivity insertion the presence of the delayed neutrons can be neglected. Therefore, at time t_1, at which time an integrated energy Q_1 has been developed, the reactivity, k_0, above prompt critical, is roughly proportional to the square root of the reactivity insertion rate, a, and the prompt lifetime:[283]

$$k_0 = (\ell^{-1} a t_1^2)^{1/2} \ (\ell a)^{1/2} \tag{5-123}$$

The coefficient

$$\ell^{-1} a t_1^2 = \ln (Q_1^2 P_p^{-2} \ell^{-1} a) + \ln \ln (Q_1^2 P_p^{-2} \ell^{-1} a) \tag{5-124}$$

if it is large, is very insensitive to the exact values of the parameters. Thus even if Q_1 is only approximately known, k_0 as determined from Eq. (5-123) does not change appreciably.

Reactivity Insertion at Constant Rate with Feedback. Reactivity insertion at a constant rate with accompanying reactivity reduction proportional to the total energy generated has been considered by Fuchs.[284] In this case, the solution can be obtained by quadratures. Since the kinetics equation in the case of no delayed neutrons is

$$\ell \frac{\dot{\phi}}{\phi} = at - b \int \phi \, dt$$

the explicit dependence on time can be eliminated by differentiation:

$$\ell \frac{d^2}{dt^2} (\ln \phi) = a - b \exp (\ln \phi)$$

which is the equation of motion of a point particle with coordinate $(\ln \phi)$ in a potential

$$a \ln \phi - b \exp (\ln \phi)$$

The flux changes periodically with an average value $\bar{\phi} = (a/b)$. Therefore, if the lowest flux is known numerically, the highest flux can be obtained numerically from the "conservation of energy integral." For large excursions in reactivity, the reduction mechanism is effective only for a short time. For the case where delayed neutrons are considered, numerical calculations show[285] that the oscillations in power damp out and the power tends toward a constant level (for a time scale short compared to the delayed neutron periods). The delayed neutron precursors build up and the reactivity oscillates with decreasing amplitude about prompt critical.

Step Insertion of Reactivity. For a step insertion of reactivity, the kinetics equations simplify considerably since time does not come into them explicitly. For excursions above prompt critical they can be solved analytically for some important reactivity reduction mechanisms.

The reactivity reduction mechanisms can be separated into three overlapping classes:

First, the "quasi-static" case, where the reactivity reduction is a function of the total heat generated. Into this class would fall reactivity reduction by heating the moderator in a thermal reactor and thereby changing its scattering cross section for energy transfer in the thermal region and effective thermal absorption and fission cross sections. Doppler broadening also falls into this class.

Second, the "long delay" case, where the excursion is so fast that heating of the fuel does not result immediately in its uniform expansion, or expansion and expulsion of the moderator is hampered by thermal inertia. The reactivity reduction can be described approximately by a function of delayed values of the energy input. The shape of the power burst as well as the magnitude will be different in this case.

Finally, the "mass inertia" case, where the burst is so short that mechanical inertia prevents the reactor from expanding. In this case, the shape of the burst will be similar to the second case but the energy generated per unit volume will depend strongly upon the details of the reactor system.

687863 O - 63 - 33

It is instructive to consider the behavior of the burst assuming that the reactivity reduction is proportional to the n*th* power of the energy developed. The kinetics equation for the "quasi-static" case is

$$\ell \frac{\ddot{E}}{\dot{E}} = k_0 - b^n E^n$$

Integrating with respect to energy

$$\ell \dot{E} = k_0 E - \frac{1}{n+1} b^n E^{n+1}$$

The peak power, $\dot{E}_{max}$, is obtained from

$$(k_0)^{-1/n} \frac{\ell}{k_0} b \dot{E}_{max} = n/(n+1)$$

The total energy, E_t, is obtained when the power vanishes, and is given by:

$$(k_0)^{-1/n} bE_t = (n+1)^{1/n}$$

The "width" of the burst in terms of initial period is given by:

$$(k_0 E_t)/(\ell \dot{E}_{max}) = (n+1)^{1+(1/n)} n^{-1} \qquad (5\text{-}125)$$

For the "long delay" case, the kinetics equation is

$$\ell \frac{\ddot{E}}{\dot{E}} = k_0 - \{bE_0 \exp[(k_0/\ell)(t-\tau)]\}^n$$

Integrating with respect to time

$$\ell \ln[(\ell \dot{E})/(k_0 E_0)] = k_0 t - \frac{(E_0 b)^n \ell}{n k_0} \exp[n(k_0/\ell)(t-\tau)]$$

The maximum power is given by:

$$(k_0)^{-1/n}(\ell/k_0)\, b \exp[-(k_0\tau)/\ell]\, \dot{E}_{max} = \exp(-1/n)$$

The total energy is obtained by integrating over the power

$$(k_0)^{-1/n} b \exp(-k_0\tau/\ell)\, E_t = n^{1/n}\, \Gamma[1 + (1/n)]$$

where

$$\Gamma(x) = \int_0^\infty u^{x-1} e^{-u}\, du$$

The "width" of the burst is given by:

$$(k_0 E_t)/(\ell E_{max}) = (en)^{1/n}\, \Gamma\left(1 + \frac{1}{n}\right) \qquad (5\text{-}126)$$

The kinetics equations for the mass inertia model,

$$k = \ell\, \ddot{E}/\dot{E}$$

$$\ddot{k} = -CE^n \qquad (5\text{-}127)$$

have to be solved by numerical integration. However, by introducing proper scaling factors for the excess reactivity and the time, it can be shown that

$$(\ell^2 C/k_0^3)^{1/n}\, E_t$$

and

$$(\ell^2 C/k_0^3)^{1/n}\ (\ell/k_0)\ \dot{E}_{max}$$

are functions of n only where k_0 is the step reactivity initially inserted. Thus the maximum power and the total energy are proportional to a higher power of k_0 than in the case of the previous two models. The calculations have been performed numerically and the results for the burst width $(k_0 E_t)/(\ell \dot{E}_{max})$ are listed in Table 5-58 along with the results for the previous two models. The close agreement with the "long delay" model indicates that only a small underestimate in the maximum power and the total energy will result if the mass inertia is treated as a long delay.

Table 5-58—BURST WIDTH, $[(k_0 E_t)/(\ell \dot{E}_{max})]$, IN TERMS OF INITIAL PERIOD FOR VARIOUS MODELS

n	Quasi-Static	Long Delayed	Mass Inertia
0.5	6.75	3.71	3.98
1.0	4.00	2.71	2.90
1.5	3.07	2.30	2.42
2.0	2.60	2.08	2.16
2.5	2.31	1.91	1.98
3.0	2.12	1.80	1.86
3.5	1.98	1.71	1.76
4.0	1.87	1.65	1.69
4.5	1.79	1.59	1.63
5.0	1.72	1.55	1.58

The comparison of the two models is further illustrated by the following. On integrating the second of Eqs. (5-127) twice with respect to time,

$$k = k_0 - \int_{-\infty}^{t} dt' C E^n(t')(t - t')$$

The substitution of the approximation: $E = A \exp(k_0 t/\ell)$, where A is a constant in the integral, yields

$$k = k_0 - A^n C \left(\frac{\ell}{n k_0}\right)^2 \exp\left(\frac{n k_0 t}{\ell}\right) = \ell \frac{\ddot{E}}{\dot{E}}$$

which is of a form similar to the kinetics equation for the "long delay" model.

Between small reactivity insertions, where the quasi-static model is applicable, and very large insertions where mass inertia effects are dominant, there is a wide region where reactivity should be determined from more detailed "hydrodynamical" calculations. The energy yield will be larger than that obtained by extrapolating the quasi-static and mass inertia models.

5.5.2 EXCURSIONS IN WATER REACTORS

A step insertion of reactivity in a water-moderated reactor will cause an exponential power rise of constant period which is terminated when one or more shutdown mechanisms become important. The particular shape and magnitude of the power burst will depend on the characteristics of the system and the amount of reactivity inserted. A ramp insertion of reactivity will give rise to a similar power burst except that the period of the rising exponential will decrease continuously until the shutdown mechanism becomes operative.

Five cores with differing nuclear characteristics have been tested in the SPERT-I reactor to evaluate the severity of excursions in heterogeneous reactors. The parameters studied were the magnitude and speed of reactivity insertion, initial H_2O temperature, and initial power level. The static characteristics of these cores are given in Table 5-59. Also indicated are the reciprocal period, α, and the step reactivity insertion for which the cladding temperatures reach the melting point of aluminum at the hottest spot in the core.

Figures 5-118 and 5-119 show the burst behavior of core A-17/28 for several different initial asymptotic periods. The initial water temperature was 20°C and the initial power 5 watts in all cases.

Table 5-59— CHARACTERISTICS OF SPERT-I CORES

Reproduced, in part, from Ref. 280.

Core:	B-12/64	B-16/40	A-17/28	B-24/32	P-18/19
Number of fuel assemblies	64	40	28	32	19
Number of fuel plates per assembly	12	16	17	24	18
Plate spacing, cm	0.483	0.483/0.165	0.297	0.165	0.338
Clad material	Al	Al	Al	Al	SS
Clad thickness, cm	0.0508	0.0508	0.0508	0.0508	0.0127
Critical mass, kg U^{235}	4.3	3.6	3.9	4.3	7.6
Total U^{235} loaded, kg	5.4	4.5	4.7	5.4	9.3
H/U ratio	760	540	320	270	120
Metal-to-water ratio	0.46	0.63	0.79	1.14	0.3
Available excess reactivity, $	4.3	5.6	5.2	6.6	4.9
Reactivity loss at 20°C–95°C, $	1.44	1.67	1.47	1.73	1.48
Temperature coefficient at 20°C, $/°C	-1.8×10^{-2}	-1.7×10^{-2}	-0.67×10^{-2}	-1.1×10^{-2}	-0.25×10^{-2}
Temperature coefficient at 95°C, $/°C	-2.0×10^{-2}	-3.4×10^{-2}	-2.7×10^{-2}	-3.4×10^{-2}	-3.4×10^{-2}
Central void coefficient, $/cm^3	$+0.8 \times 10^{-4}$	-4.7×10^{-4}	-9.3×10^{-4}	-17×10^{-4}	-18×10^{-4}
Average void coefficient, (C_v), $/cm^3	-0.93×10^{-4}	-2.9×10^{-4}	-4.6×10^{-4}	-7.3×10^{-4}	-9.9×10^{-4}
Average void coefficient, $/1% void	−0.16	−0.26	−0.34	−0.40	—
Prompt neutron lifetime (ℓ), sec[a]	0.75×10^{-4}	0.72×10^{-4}	0.48×10^{-4}	0.49×10^{-4}	0.14×10^{-4}
(ℓ/β), sec	11×10^{-3}	10×10^{-3}	7×10^{-3}	7×10^{-3}	2×10^{-3}
($C_v\beta/\ell$), % $\Delta k/(cm^3)(sec)$	0.9	3	7	10	50
α (melting), sec^{-1}	200	300	370	400	—
Step reactivity insertion to initiate melting, % $\Delta k/k$	2.2	3.0	2.4	2.6	—

[a] Using $\beta = 0.007$.

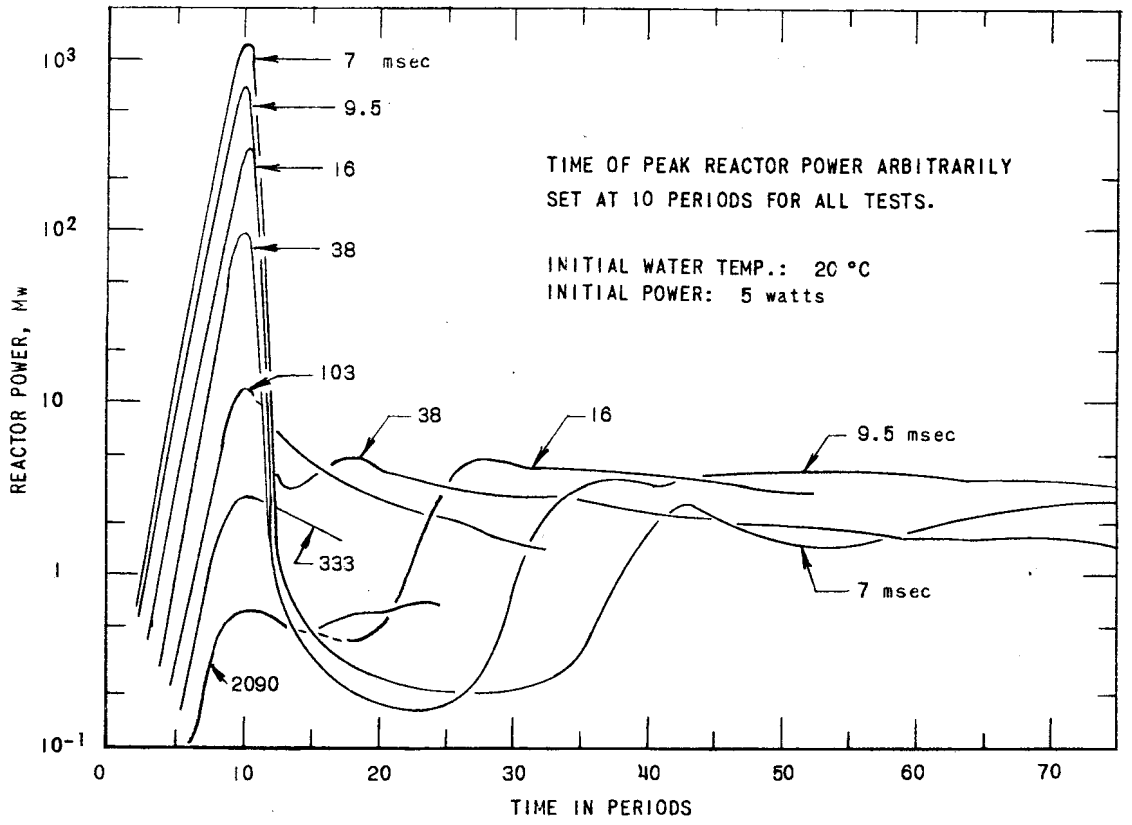

Fig. 5-118—Reactor power behavior as a function of reactor period for SPERT-I core A-17/28. *Reproduced from Ref. 287.*

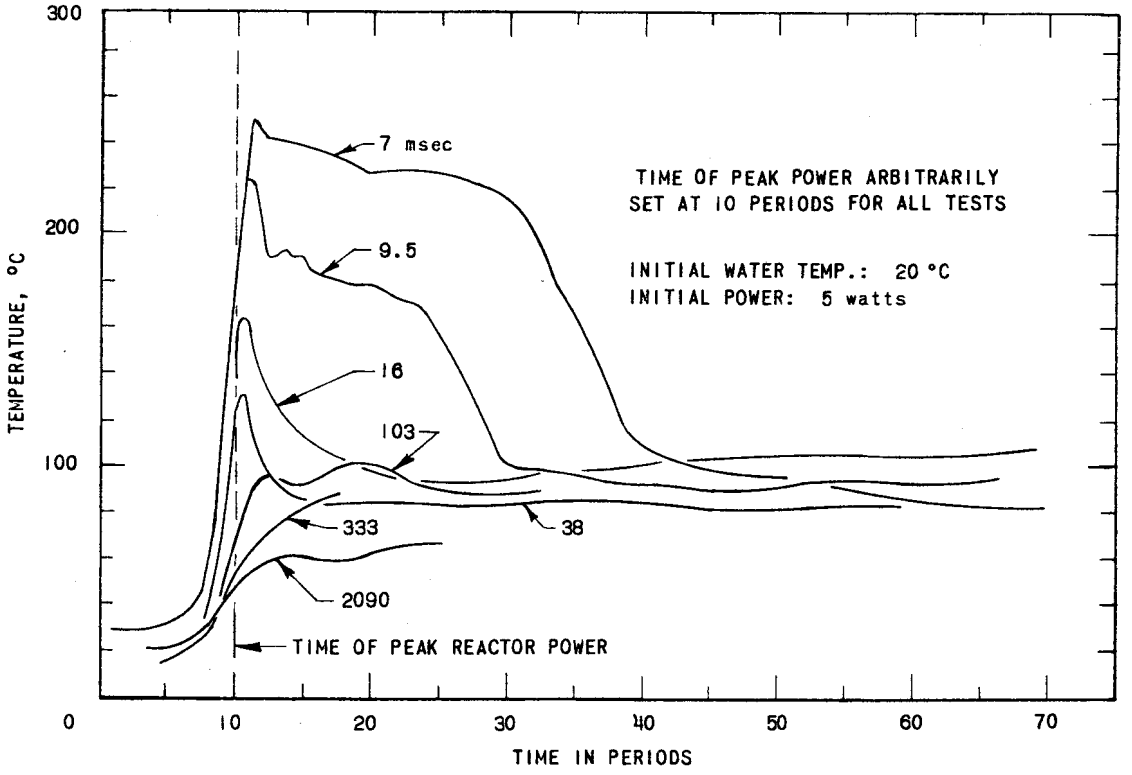

Fig. 5-119—Fuel plate temperature behavior as a function of reactor period for SPERT-I core A-17/28. *Reproduced from Ref. 287.*

Figures 5-120 through 5-139 show the experimental results for the maximum reactor power, the energy release up to the time of peak power, fuel cladding temperature rise, and maximum pressure as functions of the initial asymptotic reciprocal period for the five cores. The effect of differing initial temperatures, θ_i, is evident.

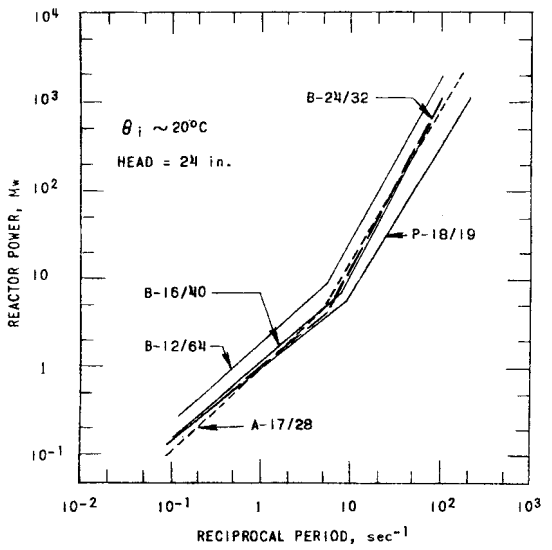

Fig. 5-120—Maximum reactor power vs. reciprocal period for SPERT-I cores. *Reproduced from Ref. 286.*

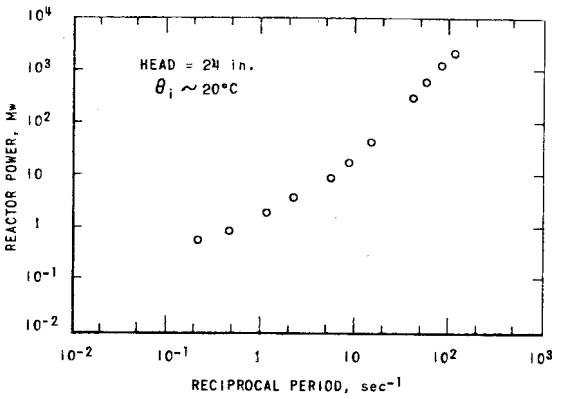

Fig. 5-121—Maximum reactor power vs. reciprocal period for SPERT-I core B-12/64. *Reproduced from Ref. 288.*

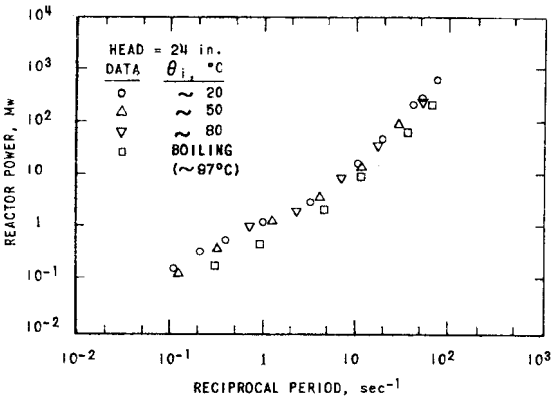

Fig. 5-122—Maximum reactor power vs. reciprocal period for SPERT-I core B-16/40. *Reproduced from Ref. 288.*

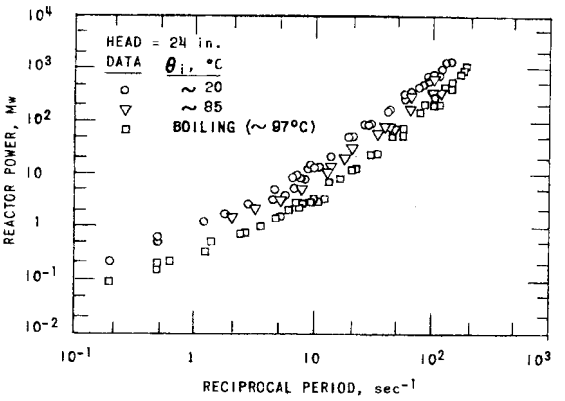

Fig. 5-123—Maximum reactor power vs. reciprocal period for SPERT-I core A-17/28. *Reproduced from Ref. 288.*

Fig. 5-124—Maximum reactor power vs. reciprocal period for SPERT-I core B-24/32. *Reproduced from Ref. 288.*

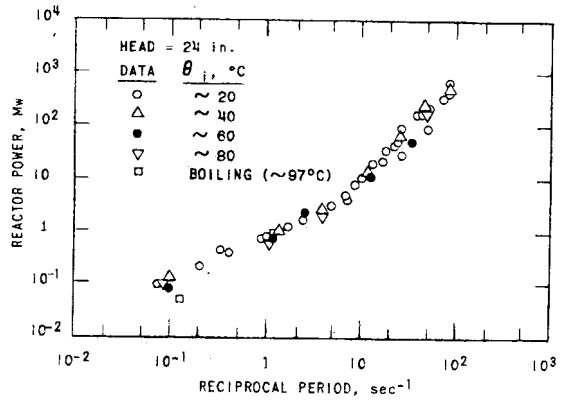

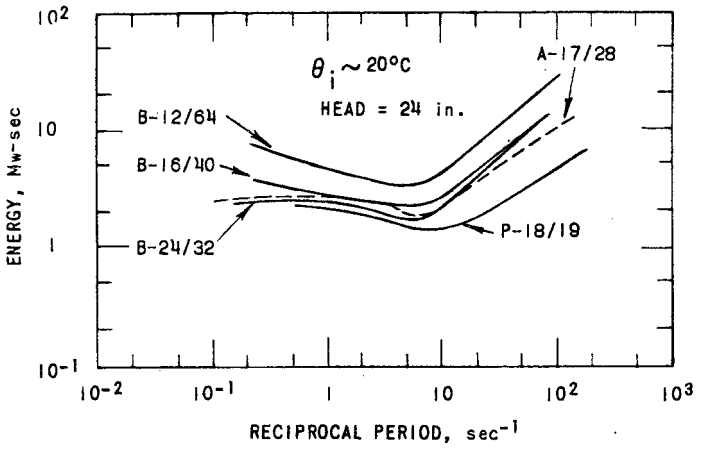

Fig. 5-125—Energy to time of peak power vs. reciprocal period for SPERT-I cores. *Reproduced from Ref. 286.*

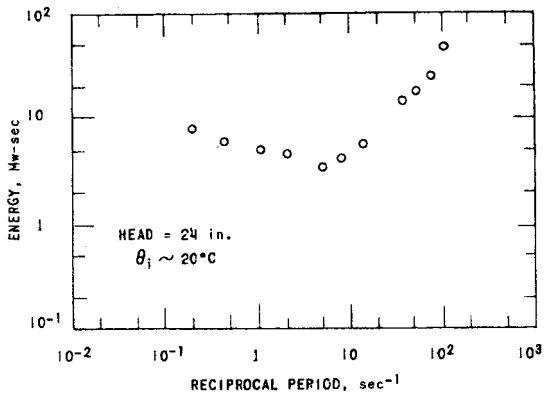

Fig. 5-126—Energy to peak of power excursion vs. reciprocal period for SPERT-I core B-12/64. *Reproduced from Ref. 288.*

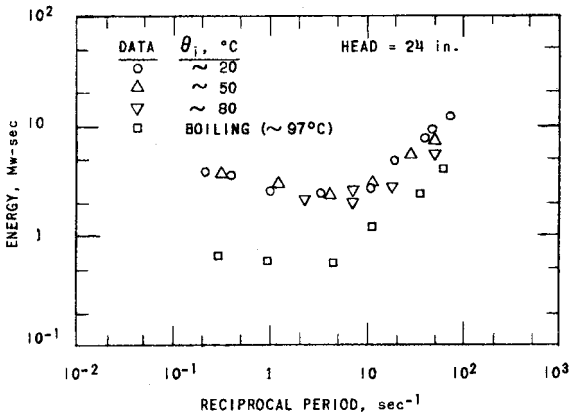

Fig. 5-127—Energy to peak of power excursion vs. reciprocal period for SPERT-I core B-16/40. *Reproduced from Ref. 288.*

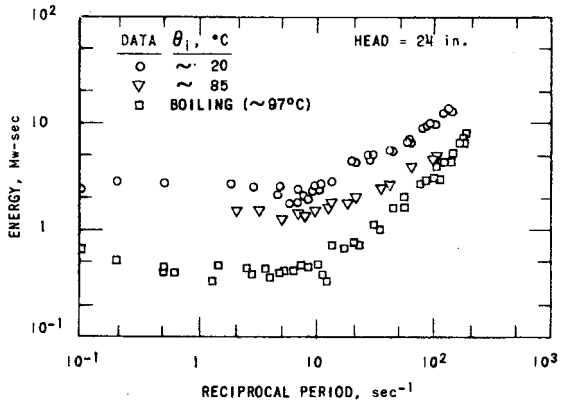

Fig. 5-128—Energy to peak of power excursion vs. reciprocal period for SPERT-I core A-17/28. *Reproduced from Ref. 288.*

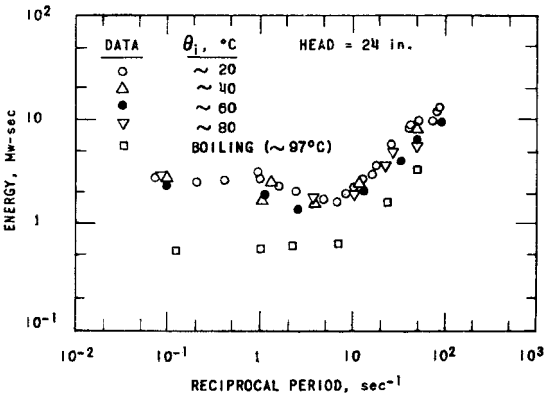

Fig. 5-129—Energy to peak of power excursion vs. reciprocal period for SPERT-I core B-24/32. *Reproduced from Ref. 288.*

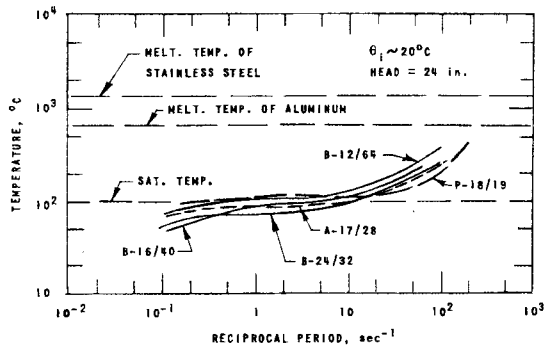

Fig. 5-130 — Maximum fuel plate surface temperature vs. reciprocal period for SPERT-I cores. *Reproduced from Ref. 286.*

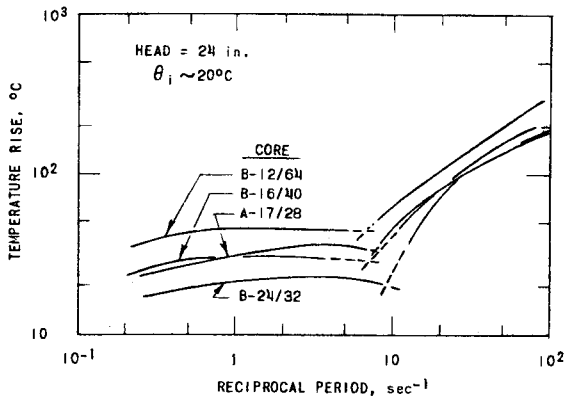

Fig. 5-131 — Fuel plate surface temperature rise at the time of maximum reactor power vs. reciprocal period for SPERT-I cores. *Reproduced from Ref. 288.*

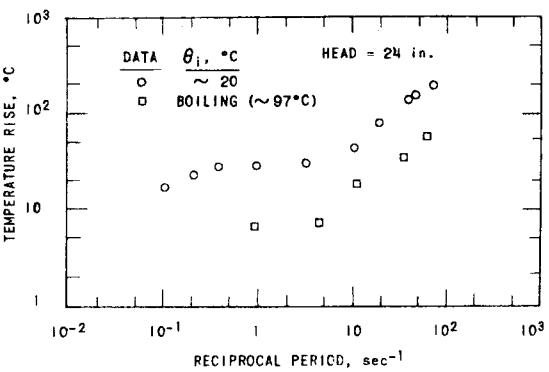

Fig. 5-132 — Fuel plate surface temperature rise at the time of maximum reactor power vs. reciprocal period for SPERT-I core B-16/40. *Reproduced from Ref. 288.*

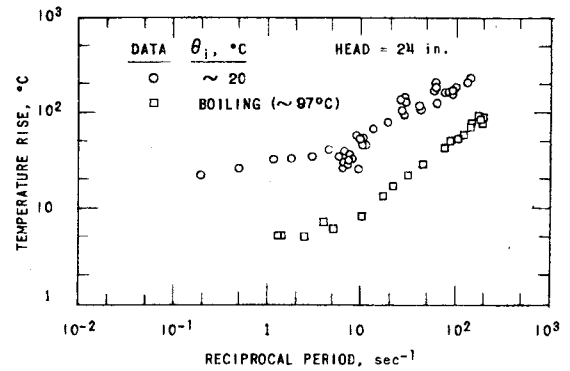

Fig. 5-133 — Fuel plate surface temperature rise at the time of maximum reactor power vs. reciprocal period for SPERT-I core A-17/28. *Reproduced from Ref. 288.*

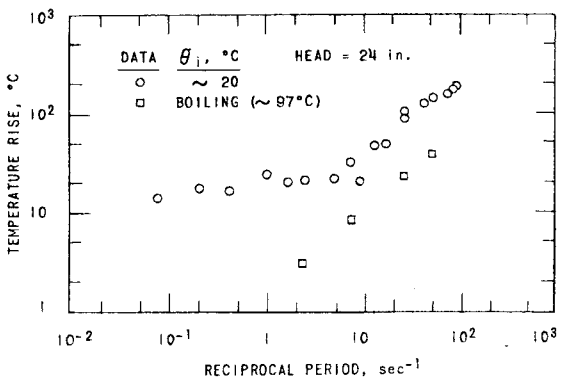

Fig. 5-134 — Fuel plate surface temperature rise at the time of maximum reactor power vs. reciprocal period for SPERT-I core B-24/32. *Reproduced from Ref. 288.*

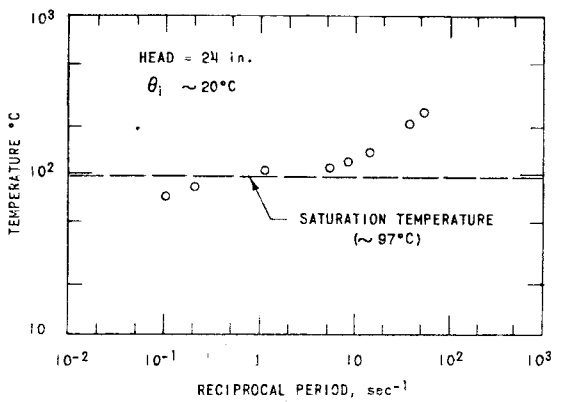

Fig. 5-135 — Maximum fuel plate surface temperature vs. reciprocal period for SPERT-I core B-12/64. *Reproduced from Ref. 288.*

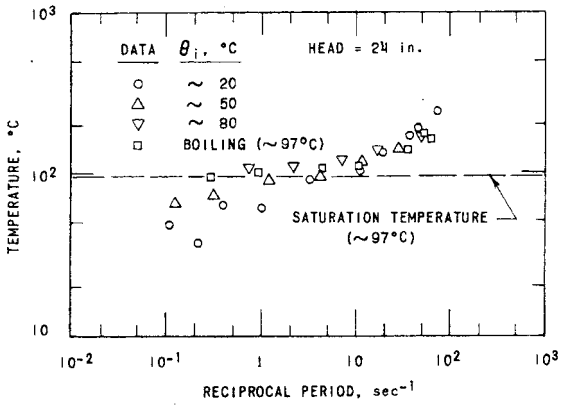

Fig. 5-136—Maximum fuel plate surface temperature vs. reciprocal period for SPERT-I core B-16/40. *Reproduced from Ref. 288.*

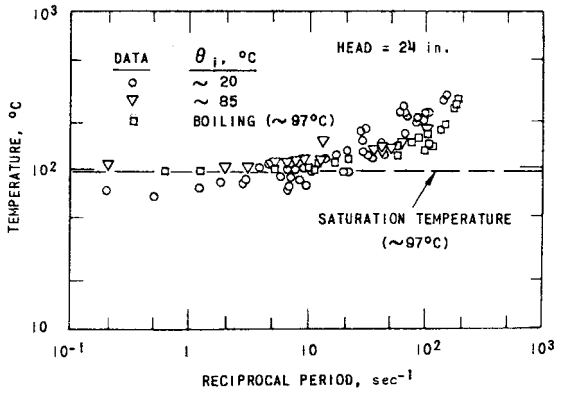

Fig. 5-137—Maximum fuel plate surface temperature vs. reciprocal period for SPERT-I core A-17/28. *Reproduced from Ref. 288.*

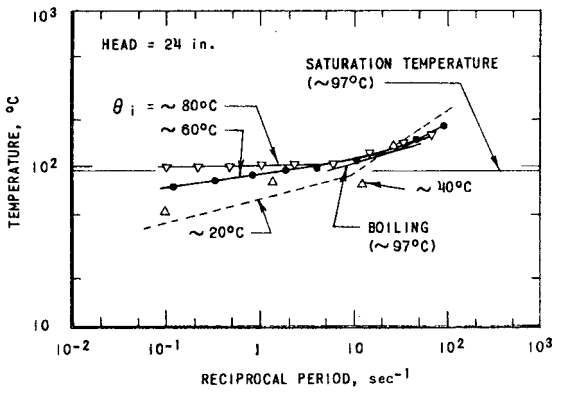

Fig. 5-138—Maximum fuel plate surface temperature vs. reciprocal period for SPERT-I core B-24/32. *Reproduced from Ref. 288.*

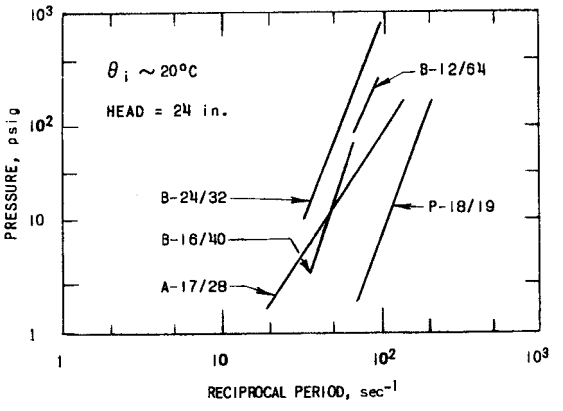

Fig. 5-139—Maximum pressure vs. reciprocal period for SPERT-I cores. *Reproduced from Ref. 286.*

Forbes, et al.,[286] have pointed out that the behavior of all SPERT-I cores, on the basis of α, is remarkably similar notwithstanding the wide range of static characteristics involved. The differences which do exist can be characterized by the use of a parameter, b, which involves the average void coefficient and the prompt neutron lifetime. The power- or energy-ratio of two cores at constant α has been shown to vary inversely as the square root of the ratio of the void coefficient to the neutron lifetime.

For ramp insertions of reactivity the most important parameter is the rate of reactivity insertion (Fig. 5-140); the reactivity coefficient, b, and the initial power are secondary effects.

The ramp and step excursions are approximately equivalent when the maximum α in the ramp case equals the constant α in the step case. This can be seen for the maximum power in Fig. 5-141.

Miller[289] has obtained the reactivity as a function of time during an excursion by analyzing the experimental power data. Figure 5-142 shows the compensated reactivity at peak power, $k_c(t_m)$, as a function of the reciprocal period. This function has well-defined asymptotes for small and large α and exhibits a characteristic dip near the α corresponding to prompt critical. Forbes[290] has shown that while the observed minimum in the $k_c(t_m)$ curve is due principally to the effect of delayed neutrons, it is also dependent to a limited extent on the nature of the reactor shutdown process.

Several theoretical models have been postulated as a means of correlation and/or explanation of the data obtained from SPERT-I and BORAX tests. A completely accurate model would have to show agreement with data on at least the following points: (1) shape of power pulse; (2) maximum power; (3) compensated reactivity at peak power; (4) energy released; (5) variation in cladding temperature; and (6) peak temperature.

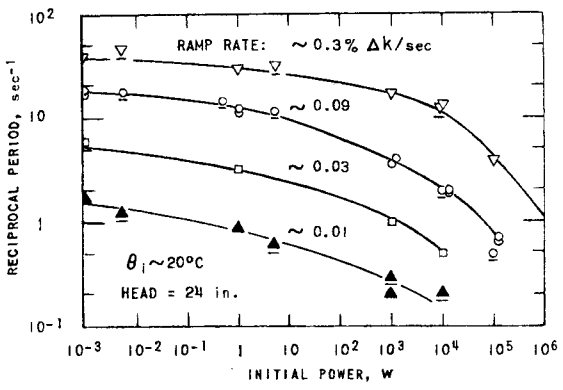

Fig. 5-140—Maximum reciprocal period vs. initial power level as a function of ramp rate for SPERT-I core A-17/28. *Reproduced from Ref. 288.*

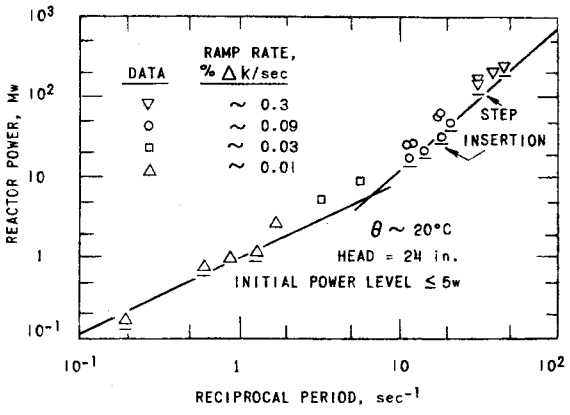

Fig. 5-141—Maximum reactor power vs. maximum reciprocal period during ramp rate tests on SPERT-I core A-17/28. *Reproduced from Ref. 288.*

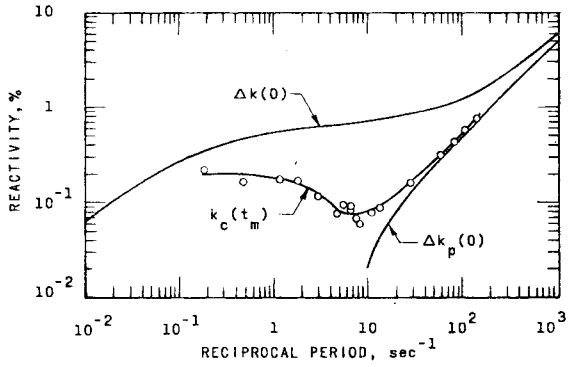

Fig. 5-142—Compensated reactivity at peak power vs. reciprocal period. *Reproduced from Ref. 289.*

Corben[291] has shown that some of the properties of a power burst are independent of the shutoff mechanism and may be described quantitatively with no assumptions other than that the pile kinetic equations are non-linear. He obtains a kinetic equation of the form

$$\phi(t) = \phi_1 \exp(\alpha t) - \phi_2 \exp(2\alpha t) \qquad \phi_2 \ll \phi_1$$

Differentiation gives

$$\exp(\alpha t_m) = \phi_1/2\phi_2$$

$$\phi_m = \phi_1^2/4\phi_2$$

Hence,

$$\phi_m = (\phi_1/2) \exp(\alpha t_m)$$

or the maximum power is one-half of the initial power extrapolated to the time of maximum power. This result is in fair agreement with the faster SPERT-I and KEWB transients (Table 5-60).

The energy to peak power, $E(\phi_m)$, is obtained by integrating $\phi(t)$

$$E(\phi_m) = (3\phi_1^2)/(8\alpha\phi_2) = (3\tau\phi_m)/2$$

where

$$\tau = 1/\alpha$$

Table 5-60—COMPARISON OF CORBEN MODEL WITH EXPERIMENT

Data from Ref. 291.

Reactor	Period, ms	ϕ_m, Mw (Exptl.)	$(\phi_1/2) \exp(\alpha t_m)$
SPERT	12	520	460
	100	13.3	13
KEWB	1.97	550	580
	5.11	128	118
BEPO	28,000	68	15
GODIVA	0.09	2.6×10^{18} fissions/sec	3×10^{18} fissions/sec

This is compared to SPERT-I data in Fig. 5-143. A similar comparison with BORAX data is shown in Fig. 5-144.

Corben[291] has derived the burst width (width at half maximum) to be equal to $1.76/\alpha$. For the faster transients ($\alpha \geq 30$ sec^{-1}), this is in agreement with experiment within the accuracy of observation.

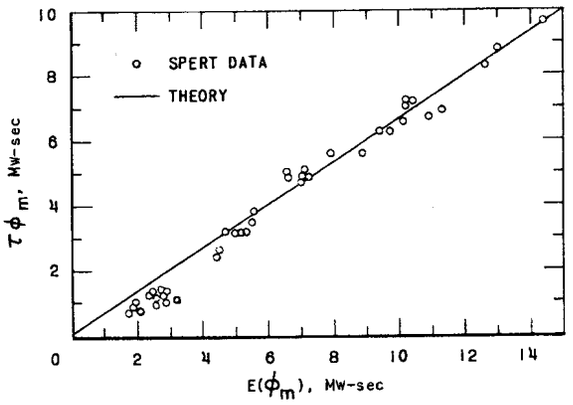

Fig. 5-143—Maximum reactor power times reactor period ($\tau\phi_m$) vs. energy to peak of power burst [$E(\phi_m)$] for SPERT-I reactor. *Reproduced from Ref. 291.*

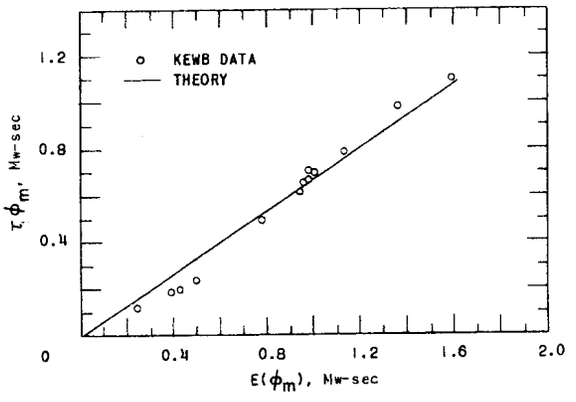

Fig. 5-144—Maximum reactor power times reactor period ($\tau\phi_m$) vs. energy to peak of power burst [$E(\phi_m)$] for KEWB reactor. *Reproduced from Ref. 291.*

Fuch's[284,292] model for reactor burst behavior assumes a shutdown effect which is proportional to the energy released up to any instant. Forbes[293] extended this model to include a delay time, τ, between energy production and its appearance in the form of a shutdown effect which is proportional to the nth power of the energy. His kinetic equation takes the form

$$\frac{\dot{\phi}(t)}{\phi(t)} = \alpha - b\,[E(t-\tau)]^n$$

where b is the reactivity coefficient.

Comparison of the results of this model with a limited amount of experimental data shows a good fit for power burst shape and reactivity compensation for n between 1.5 and 2.

The peak power versus reciprocal period data can be matched using a time delay which is almost constant in terms of reactor periods. The effect of delayed neutrons has been neglected in this analysis and assumptions have been made which limit the applicability of the equation to $t \leq t_m$.

Forbes has postulated the Conduction Boiling Model[294] in which heat transfer rates are assumed to be characteristic of conduction to stagnant water, rather than of boiling, during a rapid transient. This model can be made to correlate a wide range of experimental data using an arbitrary factor, f_{as}, for the fraction of transported energy which goes into steam formation. Figure 5-145 shows the cor-

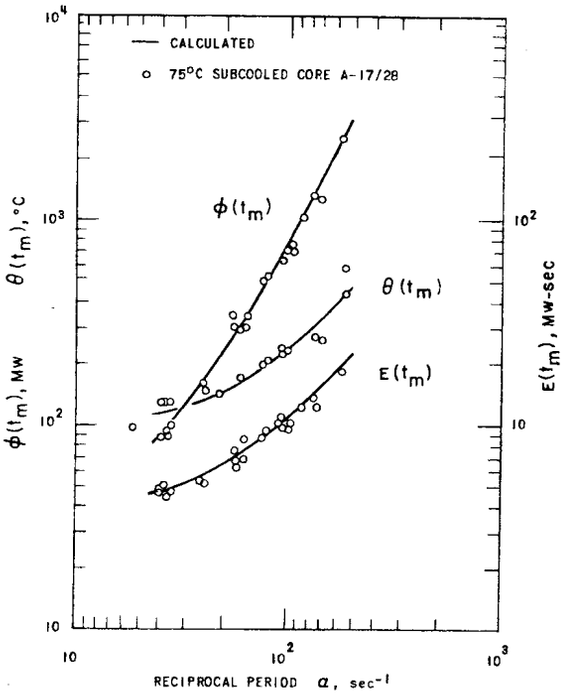

Fig. 5-145 — Power, energy, and temperature at time of peak power vs. reciprocal period. *Reproduced from Ref. 294.*

relation of data for the SPERT-I core A-17/28 by this model. The arbitrary constant must range from 0.00044 to 0.0050 to fit data for different cores and amount of subcooling; no physical basis for the selection of f_{as} has been determined.

Forbes[295] has used Corben's two-term expansion in terms of exponentials as an analytic expression for the burst shape, but without restricting coefficients in the exponents to integers. With this analytic model, expressions for the energy content of the fuel plates and the diffusion of heat from the plates to the water moderator are obtained. The reactivity effects due to thermal expansion of the fuel plates, thermal expansion of the moderator, and steam formation can then be determined. Again, the magnitude of the steam reactivity effect depends upon an arbitrary constant f_{as}. The compensated reactivity at peak power, $k_c(t_m)$, as a function of α can be fit well by this model as is shown in Fig. 5-146. However, convective circulation effects, which would be important for small α, as well as

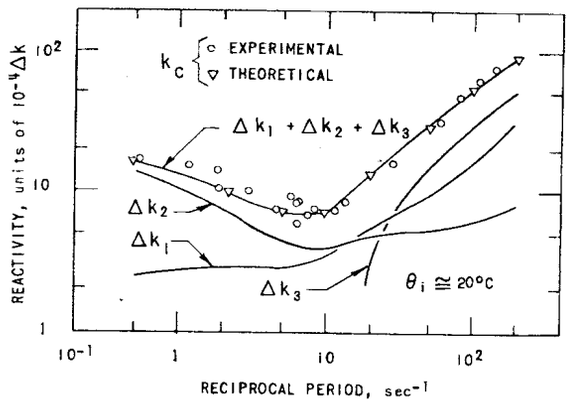

Fig. 5-146 — Compensated reactivity at peak power vs. reciprocal period for SPERT-I core A-17/28. *Reproduced from Ref. 295.*

neutron temperature effects have been neglected. The contributions from the individual effects of plate expansion, Δk_1; moderator heating, Δk_2; and steam formation, Δk_3; are also shown in Fig. 5-146.

A good fit to the experimental compensated reactivity data can be obtained assuming steam formation to be the primary shutdown mechanism for large α, and water and metal expansion to be secondary mechanisms. However, relatively little is known about the dynamics of these mechanisms and it is not absolutely certain that steam formation is the dominant effect. French[290] has found that the excursion behavior of a SPERT core with fuel plates insulated by a thin layer of Lithcotec LC-34, is indistinguishable from the behavior of a core with bare plates. Calculations indicate that a tempera-

ture above saturation should not have occurred on the surface of the insulated plates for certain of the short period excursions until after peak power was reached. Reference 296 gives the results of investigations of reactor shutdown mechanisms by capsule-type experiments and by photographic methods. These results indicate that rapid onset of boiling does occur for bare plates and is the most likely shutdown mechanism.

Reference 297 contains a summary and analysis of the SPERT program, including recommendations as to future programs.

References 296 and 298-304 describe several non-empirical methods for reactor excursion analysis which have been used to compare a wide variety of reactors. In general, a set of coupled equations which describe the core hydrodynamics, heat transfer, void formation, reactivity, and neutron kinetics must be solved. Using appropriate approximations, fair agreement with experimental data can be obtained.

References 279 and 305 through 311 give further information about excursions in heterogeneous, water-moderated reactors.

Homogeneous Reactors. According to Ref. 312, the shutdown mechanisms operative during an excursion in a homogeneous water reactor are radiolytic gas formation and temperature effects. The KEWB experiments have shown that the initial temperature, initial pressure, initial power, and initial void volume, have relatively little effect on the behavior of the reactor.[312] Since shutdown is accomplished before boiling can occur, both the peak power (Fig. 5-147) and the energy released (Fig. 5-148) during the excursion are less than for the corresponding excursion in a heterogeneous reactor.

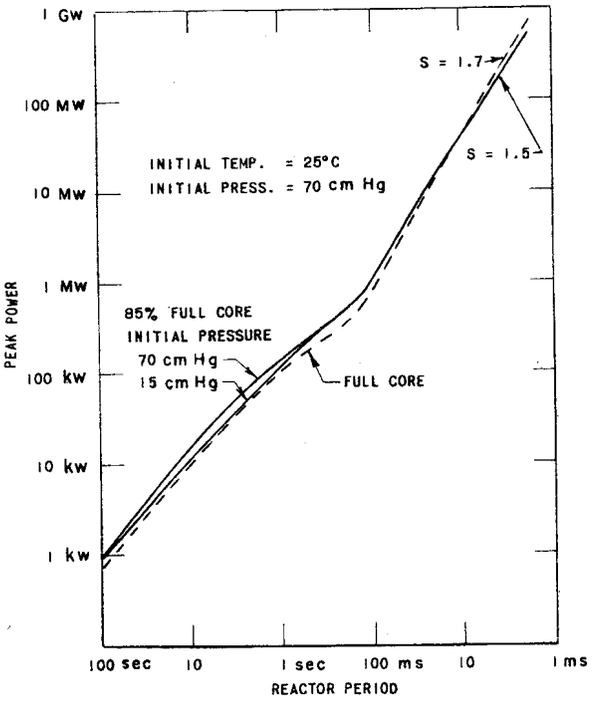

Fig. 5-147—Peak power vs. reactor period. *Reproduced from Ref. 312.*

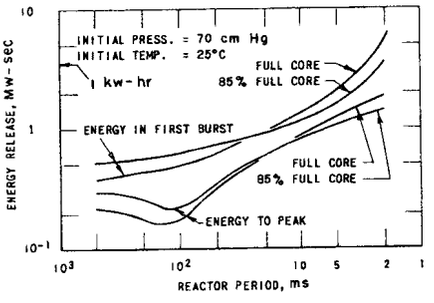

Fig. 5-148—Energy release vs. reactor period. *Reproduced from Ref. 312.*

The limiting feature with respect to reactivity addition in a homogeneous reactor is the maximum permissible pressure rise within the reactor system. Figure 5-149 shows the maximum pressure measured at the top and bottom of the spherical KEWB core, as a function of the initial asymptotic period. The peak power and energy release for the cylindrical KEWB core are almost identical with those for the spherical core, but the peak pressure is somewhat lower.[313]

Ramp additions of reactivity to the homogeneous reactor can be correlated well with step insertions using the maximum reciprocal period as was done for SPERT data.

Reference 312 describes a mathematical model which is based on the assumption that the rate of formation of radiolytic voids is proportional to the product of the instantaneous power and the concentration of previously formed gas (as measured by the energy released). The model has been used to

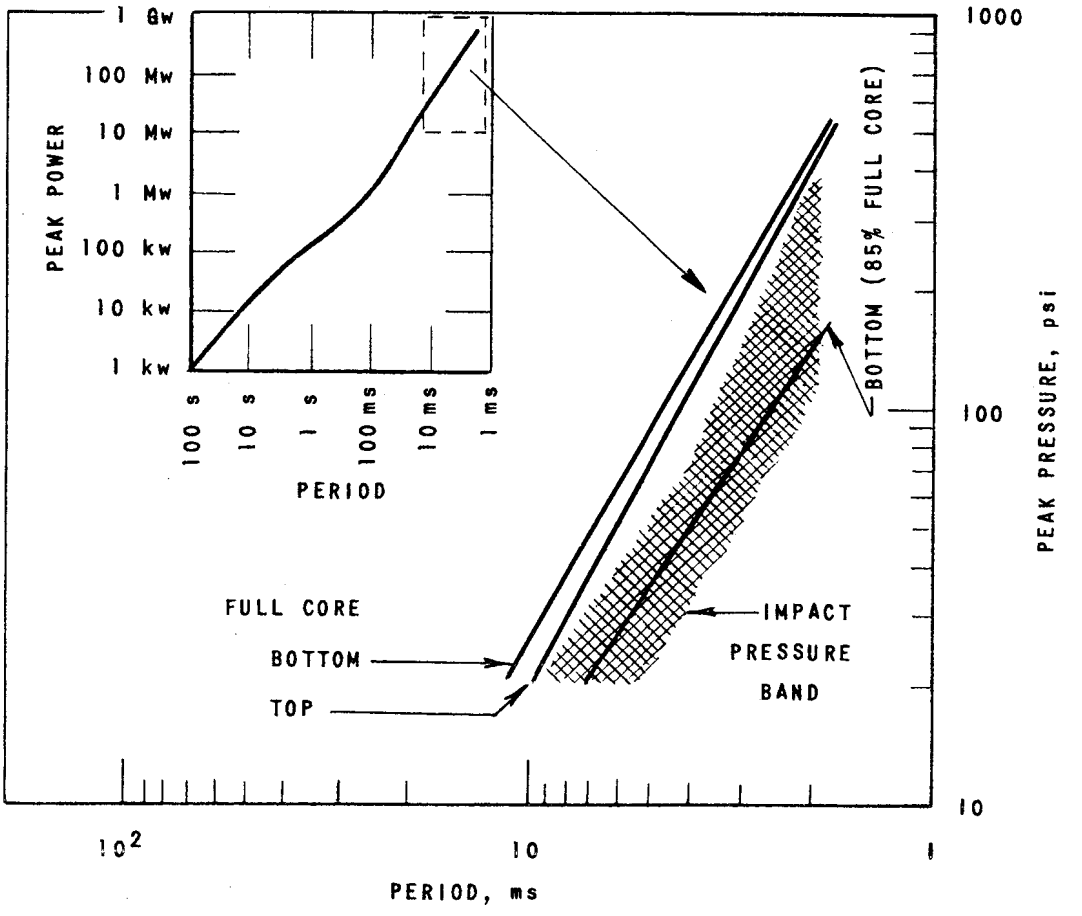

Fig. 5-149 — Peak pressure vs. reactor period. *Reproduced from Ref. 312.*

derive equations for the peak power and the energy release as functions of the neutron lifetime, delayed neutron fraction, step reactivity input, temperature and void volume coefficients of reactivity, heat capacity of the core, and void formation coefficient. One value of the proportionality constant affords a good fit to experimental data for transients with periods less than 10 ms.

Postulation of the existence of reflector-delayed neutrons in KEWB, having a mean decay time of 2 ms and an effective abundance of 2.3%, results in a reduction in the amount of reactivity to be compensated at peak power for transients with periods less than 10 ms.[313] Hence a smaller radiolytic void formation rate can account for the short period transient behavior. The interaction model (Ref. 312) is then not necessary to explain the void formation behavior. A more conservative model which results in a void volume proportional to the time integral of the energy, leads to reasonably good agreement with experimental data.

5.5.3 REACTOR EXCURSIONS LIMITED BY LARGE PROMPT NEGATIVE TEMPERATURE COEFFICIENTS OF REACTIVITY

TRIGA. The Training Research Isotope Production Reactor (General Atomics) is a light-water cooled reactor with fuel-moderator elements composed of uranium and zirconium-hydride enclosed in a close fitting, unbonded aluminum tube.[314–316] This type of reactor exhibits a negative prompt temperature coefficient of reactivity resulting almost entirely from the heating of the zirconium hydride. Even though tightly bound, hydrogen is effective in transferring energy to the thermal neutrons within the fuel, thus increasing the thermal neutron leakage from the core and decreasing the fission probability. During rapid excursions in TRIGA, there have been no other apparent reactivity-compensating mechanisms.

Characteristics of TRIGA are listed in Table 5-61. The results of transient experiments utilizing step insertions of reactivity are summarized in Table 5-62.

Table 5-61—CHARACTERISTICS OF THE TRIGA REACTOR

Data from Refs. 314 and 315.

Prompt average temperature coefficient of reactivity	-1.3×10^{-4}/°C
Prompt neutron lifetime	8×10^{-5} sec
Delayed neutron fraction	0.008
Critical mass	2 kg U^{235}
Volume fraction of H_2O in core	0.35
Zr:H atomic ratio in fuel	1:1
Uranium (20% U^{235}) in fuel	8 wt-%

Table 5-62—SUMMARY OF TRIGA TRANSIENT EXPERIMENTS

Data from Refs. 314 and 316.

Reactivity Inserted in step, $	Minimum Reactor Period, sec	Peak Power, Mw	Maximum Fuel Temperature, °C	Burst Width, ms	Energy Release Prompt Burst, Mw-sec
0.74	1.74	0.2	122	—	—
0.91	0.47	0.58	153	—	—
1.06	0.15	1.6	177	—	—
1.16	0.069	5	193	—	—
1.30	0.034	20	222	—	—
1.69	0.013	100	285	—	—
2.00	0.0098	250	360	40	10
3.90	0.0028	2200	~600	10	~20

A detailed thermal model has been used for digital computation of the excursion behavior of the reactor.[314] Agreement with experiment is excellent. The Fuch's model[284] can also be used to predict accurately the shape and magnitude of a prompt burst.

Figure 5-150 shows the maximum power reached during an excursion, as a function of the minimum period obtained during the excursion. This may be compared to similar curves for the SPERT cores (Fig. 5-120) and for KEWB (Fig. 5-147).

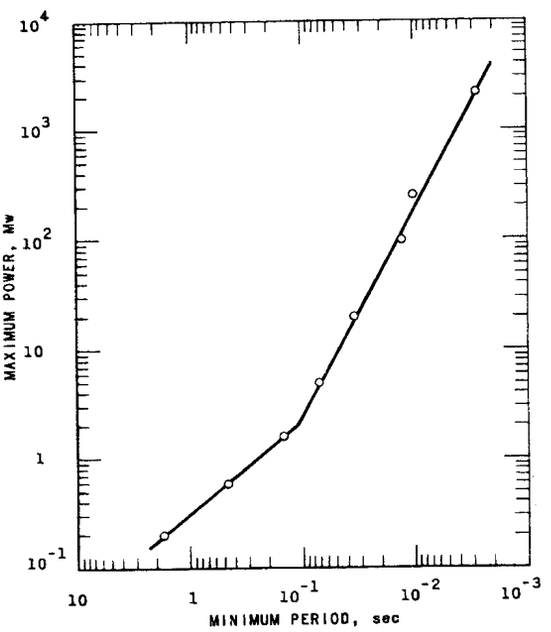

Fig. 5-150—Maximum power as a function of minimum period for the TRIGA reactor.

TREAT. The Transient Reactor Test Facility[317,318] is a pulsed, graphite-moderated reactor used primarily to generate safely, very large integrated bursts of thermal neutrons over a large sample volume. In order to maximize the immediately available heat capacity, the core comprises a uniform dispersion of uranium oxide within a graphite matrix. The graphite moderator serves as a heat sink, absorbing the energy generated in the 20-micron uranium particles with time lags on the order of one millisecond. Heating of the graphite causes a rise in the average thermal neutron energy, which increases the neutron leakage probability, thereby generating a sizeable negative temperature coefficient.

Characteristics of TREAT are listed in Table 5-63. The results of transient experiments utilizing step insertions of reactivity are summarized in Table 5-64.

Table 5-63 — CHARACTERISTICS OF THE TREAT REACTOR

Data from Refs. 317 and 318.

Prompt temperature coefficient of reactivity (60°C to 170°C), per average °C change in core	-2.2×10^{-4}
Prompt temperature coefficient of reactivity (60°C to 170°C), per °C change at core center	-1.3×10^{-4}
Prompt neutron lifetime	8.8×10^{-4} sec
Delayed neutron fraction	0.0072
Minimum critical mass	5.2 kg U^{235}
Carbon-U^{235} atom ratio	10,000 : 1
Calculated prompt average temperature coefficient (20°C to 320°C)	-2.5×10^{-4}/°C

Table 5-64 — SUMMARY OF RESULTS OF TREAT TRANSIENT EXPERIMENTS

Data from Ref. 318.

Reactivity Inserted in Step, % Δk	Minimum Reactor Period, sec	Peak Power, Mw	Total Energy Release, Mw-sec	Temperature Rise of Core Center, °C	Burst Width, sec
0.42	4.3	1.85	82	54.5	~40
0.60	1.37	7.0	120	72	~20
0.71	0.76	14	142	86	~7
0.95	0.31	54	200	119	~1.5
1.15	0.19	140	247	142	~0.7
1.55	0.105	380	315	176	0.4
1.90	0.075	860	440	237	0.35

Satisfactory agreement has been obtained between experiment and theory for shapes of the power curves, integrated transient power values, and maximum reactor temperatures. The theoretical model employs a single feedback mechanism due to the prompt negative temperature coefficient of reactivity.

Figure 5-151 shows the maximum power reached during an excursion, as a function of the minimum period obtained during the excursion. A comparison of this figure with similar data for SPERT (Fig. 5-120), KEWB (Fig. 5-147), and TRIGA (Fig. 5-150), reveals that the slopes of the curves plotted on log-log scales for periods shorter than those at prompt critical are very nearly the same (1.8 to 1.9) for all four reactors. The slopes of curves for periods longer than prompt critical differ more widely, ranging from 0.85 (TRIGA), to 0.98 (SPERT), to 1.07 (KEWB), to 1.15 (TREAT).

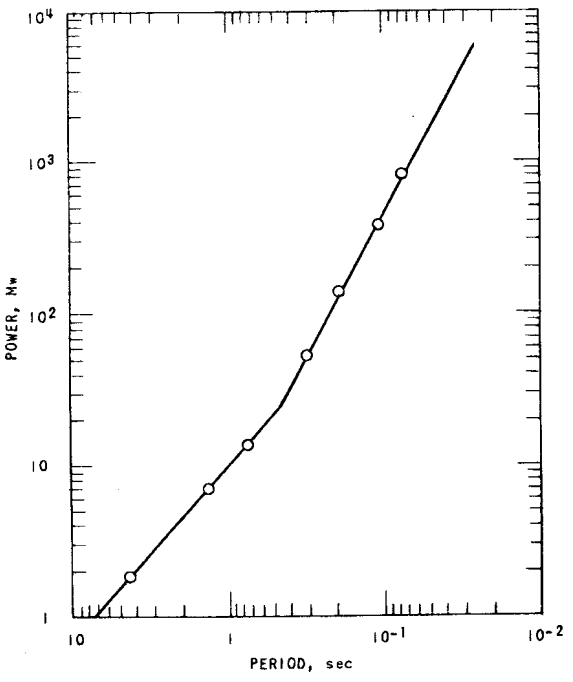

Fig. 5-151—Maximum power as a function of minimum period for the TREAT reactor.

REFERENCES

1. B. Davison and S. A. Kushneriuk, *Linear Extrapolation Length for a Black Sphere and a Black Cylinder*, MT-214, (March, 1946).
2. B. Davison, *Influence of a Large Black Sphere upon the Neutron Density in an Infinite Non-Capturing Medium*, MT-93, (November, 1944).
3. B. Davison, *Influence of a Small Black Sphere upon the Neutron Density in an Infinite Non-Capturing Medium*, MT-88, (November, 1944).
4. B. Davison, *Influence of a Large Black Cylinder upon the Neutron Density in an Infinite Non-Capturing Medium*, MT-135, (April, 1945).
5. W. P. Seidel, B. Davison and S. A. Kushneriuk, *Influence of a Small Black Cylinder upon the Neutron Density in an Infinite Non-Capturing Medium*, MT-207, (February, 1946).
6. C. Mark, *The Spherical Harmonics Method II. General Development of the Theory*, CRT-340, (MT-97), (May, 1945).
7. C. Mark, *The Spherical Harmonics Method I. General Development of the Theory*, CRT-340, (MT-92), (November, 1945).
8. D. F. Zaretsky, *Effective Boundary Conditions for 'Grey' Bodies*, Proc., 1955 Geneva Conference, 5: Paper No. 667, p. 525.
9. B. Davison and S. A. Kushneriuk, *Linear Extrapolation Lengths for a Small Black Cylinder with a Small Air-Gap and a Small Imperfectly Absorbing Cylinder with and without an Air-Gap*, TPI-45, (AECL 124), (July 1947).
10. B. Davison, *Influence of an Air-Gap Surrounding a Small Black Sphere upon the Linear Extrapolation Length of the Neutron Density in the Surrounding Medium*, MT-232, (April, 1946).
11. H. Soodak, F. Adler and E. Grueling, *Kinetic Theory of Neutrons*, Reactor Handbook, AECD-3645, Vol. 1: Chap. 1.3, pp. 391-392, (March, 1955).
12. Ibid, *Diffusion Length and Extrapolation Length for Milne's Problem for Anisotropic Scattering*, Table 1.3.12, p. 392.
13. K. M. Case, F. deHoffman and G. Placzek, *Introduction to the Theory of Neutron Diffusion: Volume I*, (Washington, D. C.: U. S. Government Printing Office, 1953).
14. R. J. Royston, *The Linear Extrapolation Length at the Surface of an Imperfectly Absorbing Cylinder*, J. Nuclear Energy, 1: No. 3, p. 194 ff., (1954-1955).
15. R. J. Royston, *The Behavior of a Flux of Neutrons in the Neighborhood of a Control Plate*, AERE T/R 2211, (March, 1957).
16. S. A. Kushneriuk and C. McKay, *Neutron Density in an Infinite, Non-Capturing Medium Surrounding a Long Cylindrical Body which Scatters and Captures Neutrons*, CRT-566 (AECL 137), (July, 1954).
17. J. A. Wheeler, *Principles of Nuclear Power*, N-2292, Chap. 22, (June, 1944).
18. Gerald Goertzel, *Reactor Dynamics*, Reactor Handbook, AECD-3645, Vol. 1: Chap. 1.6, p. 531, (March, 1955).
19. H. Hurwitz, Jr. and G. M. Roe, *Absorption of Neutrons by Black Control Rods*, KAPL-1336, (March, 1955); or J. Nuclear Energy, 2: No. 2, p. 85 ff., (1955-1956).
20. D. R. Bach and S. W. Kitchen, *Effects of Rod Shape on Control Rod Worth*, Reactor Control Meeting held in Los Angeles, California, March 6-8, 1957, TID-7532, Part I, 138, (October, 1957).
21. S. Glasstone and M. C. Edlund, *The Elements of Nuclear Reactor Theory*, (New York: D. Van Nostrand Co., Inc., 1952), Eq. 11.21.1, p. 321.
22. Ibid, Eq. 11.31.1, p. 325.
23. F. T. Adler, *Efficiency of Control Rods as a Function of Their Position in a Cylindrical Pile in the One-Group Picture*, MT-222, (February, 1947), (Issued as AECL-253, February, 1956).
24. F. T. Adler, *Reduction of the Two-Group Model to an Equivalent One-Group Model*, MT-201, (March, 1946).
25. Gerald Goertzel, *Reactor Dynamics*, Reactor Handbook, AECD-3645, Vol. 1: Fig. 1.6.38, p. 604, and Fig. 1.6.39, p. 605, (March, 1955).

687863 O - 63 - 34

26. G. M. Schindler, *On the Efficiency of a Concentric Cut-off Rod of a Thermal Reactor as a Function of the Inserted Length of the Rod*, J. Nuclear Energy, 8: 18, (1958).
27. *Quarterly Reactor Technology Report No. 3, July-September, 1957*, KAPL-1868.
28. J. P. Jewett, C. R. Mullin and J. H. Smith, *Calculation of the Worth of a Partially Inserted Control Rod*, Paper presented at the Meeting of the American Nuclear Society held in New York, October 29, 1957.
29. L. Tonks, *Uniformly Spaced Control Elements in a Reactor: Theoretical Basis of Application of 'Absorption Area' to Reactor Control Evaluation*, Nuclear Sci. and Eng., 6: No. 3, p. 202, (September, 1959).
30. B. Wolfe, *The General Theory of Control Sheets*, Nuclear Sci. and Eng., 4: No. 5, 635, (November, 1958).
31. R. J. McWhorter, J. Russell and B. Wolfe, *The Use of Thermally Black Control Sheets*, Nuclear Sci. and Eng., 5: No. 6, 382, (June, 1959).
32. H. S. Wilf, *Concerning the Theory of Control Sheets*, Nuclear Sci. and Eng., 5: No. 2, 137, (February, 1959).
33. L. E. Nordheim and R. Scalettar, *Theory of Pile Control Rods*, MDDC-42, (June, 1946).
34. H. L. Garabedian, *Control Rod Theory for A Cylindrical Reactor*, AECD-3666, (August, 1950).
35. R. L. Murray, *Reactivity Values of Multiple Reactor Control Rods*, Preprint 83, Paper presented at the Nuclear Engineering and Science Congress sponsored by Engineers Joint Council, December 12-16, 1955, at Cleveland, Ohio. Published by American Institute of Chemical Engineers, New York.
36. J. Codd and C. A. Rennie, *Two-Group Theory of Control Rods in a Thermal Reactor*, AERE R/R 818, (1952).
37. T. Auerbach, *Formulas for Control Rod Worth in Thermal Reactors*, Reactor Control Meeting held in Los Angeles, March 6-8, 1957, TID-7532, Part I, p. 11, (October, 1957).
38. R. E. Lightle, *Multiple Control Rod Calculations*, TID-7532, Part I, p. 49, (October, 1957).
39. A. M. Perry, *APPR Control Rods – Theory and Experiment*, TID-7532, Part I, p. 111, (October, 1957).
40. R. L. Murray, W. T. Price and S. H. Birken, *Control Rod Theory for Asymmetrical Arrays and Reflected Cores*, Nuclear Sci. and Eng., 8: No. 3, 254-259, (September, 1960).
41. E. P. Gyftopoulos and L. de Sobrino, *Variational Calculation of Control Rod Reactivity*, Nuclear Sci. and Eng., 6: No. 2, 135-139, (August, 1959).
42. G. V. Sinyutin and V. N. Semenov, *Determination of Control Rod Effectiveness in Cylindrical Reactor*, Proc., 1958 Geneva Conference, 11: Paper No. 2469, p. 523.
43. I. Carlvik, H. McCririck and S. Brimberg, *Calculations of the Influence of a Large Number of Control Rods on the Reactivity of a Thermal Reactor*, Proc., 1958 Geneva Conference, 11: Paper No. 152, p. 532.
44. D. R. Metcalf, *Central Control Rod Calculations for SPERT Reactors*, TID-7532, Part I, Table I, p. 229.
45. R. L. Murray and J. W. Niestlie, *Reactor Control Rod Theories*, Nucleonics, 13: No. 2, 18, (1955).
46. P. F. Gast, *Experimental Checks of Control Rod Theory*, Proc., 1955 Geneva Conference, 5: Paper No. 612, p. 389.
47. R. Avery, *Two-Group Diffusion Theory for a Ring of Cylindrical Rods*, Nuclear Sci. and Eng., 3: No. 5, 504, (May, 1958).
48. B. I. Spinrad and D. Kurath, *Computation Forms for Solution of Critical Problems by Two-Group Diffusion Theory*, ANL-4352, (March, 1952).
49. A. F. Henry, *Review of Methods Used in Control Rod Analyses for Reactor Design at Bettis*, TID-7532, Part I, p. 3.
50. A. F. Henry, *A Theoretical Method for Determining the Worth of Control Rods*, WAPD-218, (August, 1959).
51. J. C. Stewart and J. H. Smith, *Interaction of Black Control Rods*, KAPL-1471, (January, 1956).
52. H. E. Stevens, *Half-Group Theories for Control Rods*, TID-7532, Part I, p. 16.
53. P. Greebler, *Control Rod Calculations for Determination of Reactivity and Power Distribution*, Nuclear Sci. and Eng., 3: No. 4, 445, (April, 1958).
54. S. Pearlstein, *Application of the Absorption Area Method to Three-Group Diffusion Theory Problems*, KAPL-M-SP-10, (July, 1957), or Nuclear Sci. and Eng., 4: No. 3, 322, (September, 1958).
55. R. W. Deutsch, *Evaluation of a Bank of Slab-Type Control Rods*, Nuclear Sci. and Eng., 5: No. 3, 150, (March, 1959).
56. B. Wolfe, *Epithermal Effects on Control Element Worth*, J. Nuclear Energy, 7: 71-80, (1958).
57. B. Wolfe, *The Effect of a Current Boundary Condition on Control Rod Effectiveness*, J. Nuclear Energy, 8: 63-65, (1958).
58. B. Wolfe and D. L. Fischer, *Perturbation Theory of Control Elements I*, Nuclear Sci. and Eng., 4: No. 6, 785, (December, 1958).
59. B. Wolfe and D. L. Fischer, *Perturbation Theory of Control Elements II*, Nuclear Sci. and Eng., 5: No. 1, 5, (January, 1959).
60. A. D. Voorhis and T. M. Ryan, *Investigation of Absorbing Membranes in Slab Reactors*, TID-7532, Part I, p. 202.
61. A. D. Voorhis, et al., *Experimental and Theoretical Study of Critical Slabs. Effect of Absorbing Membranes of Cadmium, Gold and Boron*, WAPD-170, (April, 1957).
62. N. E. French and T. F. Ruane, *Analysis of a Plastic Moderated Critical Assembly (PMA-3A) Using Two Methods of Control Rod Representation*, KAPL-M-NEF-4, (June, 1958).
63. H. Uberall, *Neutron Absorption by Control Rods of Varying Transparency*, Nuclear Sci. and Eng., 7: No. 3, 228, (March, 1959).
64. T. L. Jackson, *Measurement and Analysis of Reactivity Values of Control Rods*, NP-6604, (1958).
65. R. A. Dannels and W. J. Eich, *Neutron Flux Peaking and Power Shapes: A Comparison of Theory and Experiment*, YAEC-151, (October, 1959).
66. M. Goldsmith and T. M. Ryan, *Thermal Activation Shapes in a Water-Moderated Critical Assembly*, Nuclear Sci. and Eng., 5: No. 5, 299, (May, 1959).
67. D. D. Lanning, *Heterogeneous Reactor Critical Conditions Using Small Source Theory*, TID-7532, Part I, p. 61, (October, 1957).
68. R. V. Meghreblian and D. K. Holmes, *Reactor Analysis*, (New York: McGraw-Hill Book Co., Inc., 1960), pp. 707-708.
69. G. W. Stuart, *A Chart of Neutron Blackness for Solid Cylindrical Rods*, HW-34187, (January 7, 1956).
70. D. J. Hughes and R. B. Schwartz, *Neutron Cross Sections*, BNL-325, Second Edition, (July, 1958).
71. C. H. Westcott, *Effective Cross Section Values for Well-Moderated Thermal Reactor Spectra*, CRRP-680, (AECL-407), (January, 1957); CRRP-787, (AECL-670), (August, 1958); CRRP-862, (AECL-869), (with D. A. Roy), (August, 1959); see also C. G. Campbell and R. G. Freemantle, *Effective Cross Section Data for Thermal Reactor Calculations*, AERE-RP/R 2031, (August, 1956).
72. W. MacRae and R. Parr, *Xenon Poisoning Transients Following Changes in Reactor Power, and Their Effect on Reactivity*, AERE ED/R 1590, (January, 1954).
73. H. K. Clark and J. C. English, *Xenon Tables*, DP-200, (May, 1957).
74. A. G. Ward, *A Universal Curve for the Prediction of Xenon Poison after a Reactor Shutdown*, CRRP-685, (AECL-411), (January, 1957).
75. J. O. Blomeke and Mary F. Todd, *U^{235} Fission Product Production as a Function of Thermal Neutron Flux, Irradiation Time and Decay Time*, ORNL-2127, Part I, Vols. 1 and 2, (August, 1957).
76. J. B. Sampson, et al., *Poisoning in Thermal Reactors Due to Stable Fission Products*, KAPL-1226, (October, 1954).
77. R. W. Deutsch, *Fission Product Buildup in Enriched Thermal Reactors*, Nucleonics, 14: No. 9, 89, (September, 1956).
78. W. H. Walker, *Fission Products Accumulation*, CRRP-634, (AECL-309), (March, 1956).
79. D. G. Hurst, *Calculated Cross Sections of Irradiated Fission Products*, CRRP-659, (AECL-346), (July, 1956).
80. D. G. Hurst, J. M. Kennedy and W. H. Walker, *Cross Sections and Yields of Pseudo-Fission Products*, CRRP-760, (AECL-715), (October, 1958).

81. J. O. Blomeke and Mary F. Todd, *U^{235} Fission Product Production as a Function of Thermal Neutron Flux, Irradiation Time and Decay Time II. Summations of Individual Chains, Elements and the Rare-Gas and Rare-Earth Groups*, ORNL-2127, Part II, Vol. 1, (December, 1957); Vol. 2, (June, 1958); Vol. 3, (November, 1958).
82. N. J. Pattenden and H. Rose, *Stable and Long-Lived Fission Products of Importance to Reactors*, AERE N/P and R/R 2651, (July, 1958).
83. N. J. Pattenden, *Fission Product Poisoning Data*, ORNL-2778, (October, 1959).
84. C. R. Greenhow and E. C. Hansen, *Reactor Spectra Effects on Fission Fragment Cross Sections*, KAPL-2057, (December, 1959).
85. W. H. Walker, *Yields and Effective Cross Sections of Fission Products and Pseudo-Fission Products*, CRRP-913, AECL-1054, (March, 1960).
86. E. A. Nephew, *Thermal and Resonance Absorption Cross Sections of the U^{233}, U^{235}, and Pu^{239} Fission Products*, ORNL-2869, (March, 1960).
87. P. Greebler, H. Hurwitz, Jr. and M. L. Storm, *Statistical Evaluation of Fission-Product Absorption Cross Sections at Intermediate and High Energies*, Nuclear Sci. and Eng., 2: No. 3, 334-351, (May, 1957).
88. L. V. Gordeev and V. Y. Pupko, *Evaluation of the Absorption Cross Section of U^{235} Fission Fragments in the Energy Range 0.025 ev to 1 Mev and Calculation of Fragment Effects in Intermediate Reactors*, Proc., 1958 Geneva Conference, 16: Paper No. 2223, p. 141.
89. C. J. L. Lock, *Mathematics of Fission-Product Formation in Reactors with Circulating Fuel*, AERE C/M 278, (May, 1956).
90. P. C. Davidge and C. J. L. Lock, *Neutron Poison by Gaseous Fission Products*, J. Nuclear Energy, 6: No. 3, 191, (1958).
91. J. Halperin, et al., *Effective Capture Cross Sections of Pa^{233} and Np^{239} for Thermal Reactor Neutrons*, Proc., 1955 Geneva Conference, 7: Paper No. 732, p. 258.
92. E. Fast and D. R. deBoisblanc, *Measurements of MTR-Irradiated Thorium Slugs in the Reactivity Measurement Facility*, IDO-16255, (March, 1956).
93. B. E. Paige, P. Goris and J. E. Rein, *Determination of Uranium in Irradiated Thorium*, IDO-14411, (June, 1957).
94. R. S. Nisle and E. Fast, *Distribution of U^{233} in an Irradiated Thorium Slug*, IDO-16419, (October, 1957).
95. F. R. Taraba, *Thermal Neutron Irradiation of Natural Thorium*, ANL-5335, (July, 1954).
96. A. T. Gresky and E. D. Arnold, *Products Produced in Continuous Neutron Irradiation of Thorium*, ORNL-1817, (February, 1956).
97. A. T. Gresky and E. D. Arnold, *Products Produced in Batch Neutron Irradiation of Thorium*, ORNL-1818, (December, 1955).
98. R. G. Nisle, *Calculation of Isotope Production by the Cyclic Irradiation of Thorium*, IDO-16504, (March, 1959).
99. R. P. Schuman and R. L. Tromp, *Calculation of the Composition of Reactor Irradiated Heavy Nuclides*, IDO-16571, (December, 1959).
100. R. W. Stoughton and J. Halperin, *Heavy Nuclide Cross Sections of Particular Interest to Thermal Reactor Operation: Conventions, Measurements and Preferred Values*, Nuclear Sci. and Eng., 6: No. 2, 100, (August, 1959).
101. D. J. Hughes, B. A. Magurno and M. K. Brussel, *Neutron Cross Sections, Supplement Number 1*, BNL-325, Second Edition, (January, 1960).
102. S. Visner, *Neutron Chain Reactions in Aqueous Homogeneous Systems*, Reactor Handbook, AECD-3646, Vol. 2: Chap. 4.2, p. 511, (May, 1955).
103. W. H. L. Porter, *Estimated Concentrations of the Heavy Elements in a Liquid Metal-Fueled Reactor with Continuous Chemical Processing*, AERE M/R 1950, (June, 1956).
104. M. Tobias, M. W. Rosenthal and T. B. Fowler, *Time Dependent Studies of the Nuclear Characteristics of HRE-3*, CF-57-12-1, (December, 1957).
105. B. I. Spinrad, J. C. Carter and C. Eggler, *Reactivity Changes and Reactivity Lifetimes of Fixed-Fuel Elements in Thermal Reactors*, Proc., 1955 Geneva Conference, 5: Paper No. 835, p. 125.
106. B. P. Rastogi, *The Dependence of Breeding Gain and Power on the Level of U^{233} in the Blanket of a Two-Region Homogeneous Reactor*, J. Nuclear Energy, 6: 99, (1957).
107. A. M. Perry, C. A. Preskitt and E. C. Halbert, *A Study of Graphite Moderated Th-U^{233} Breeder Systems*, ORNL-2666, (February, 1960).
108. D. Baroncini, et al., *A Study on a Two-Core Converter Reactor*, Proc., 1958 Geneva Conference, 12: Paper No. 1379, p. 623.
109. D. Ciuffa and L. Sani, *Considerations on the Use of Thorium in Power Reactors*, Proc., 1958 Geneva Conference, 13: Paper No. 1380, p. 470.
110. T. H. Pigford, et al., *Fuel Cycles in Single-Region Thermal Power Reactors*, Proc., 1958 Geneva Conference, 13: Paper No. 1016, p. 198.
111. R. W. Stoughton and J. Halperin, *Heavy Isotope Buildup in the Core of a U^{235} Breeder*, J. Nuclear Energy, 4: 279, (March, 1957).
112. G. Long and C. J. L. Lock, *The Rates of Buildup of Higher Isotopes and Elements in a High Flux Reactor*, AERE C/R 1881, Part I, (March, 1956).
113. W. G. Davey, *The Buildup of Uranium Isotopes by Irradiation of U^{233}*, AERE R/M 98, (October, 1956).
114. C. G. Campbell and R. G. Freemantle, *Effective Cross Section Data for Thermal Reactor Calculations*, AERE RP/R 1923, (May, 1956).
115. J. C. Carter, *The Regeneration Factor as a Function of Time in a $Th^{232}-U^{235}$ Thermal Reactor*, ANL-5283, (September, 1954).
116. J. C. Carter and R. C. Howard, *Isotopic Abundance and the Variation of η in Irradiated Nuclear Fuels Consisting Initially of Combinations of Th^{232}, U^{238}, and U^{235}*, ANL-6067, (October, 1959).
117. J. Halperin, J. O. Blomeke and D. A. Mrkvicka, *Effective Reactor Cross Sections in MTR Fuel Assemblies*, Nuclear Sci. and Eng., 3: No. 4, 395, (April, 1958).
118. M. Benedict and T. Pigford, *Fuel Cycles in Thermal Nuclear Reactors*, Nuclear Chemical Engineering, (New York: McGraw Hill Book Company, Inc., 1957), p. 65-128.
119. R. W. Stoughton and J. Halperin, *On the Effective Capture Cross Section of Pu^{240} for Reactor Neutrons*, Nuclear Sci. and Eng., 2: No. 4, 481, (July, 1957).
120. S. A. Kushneriuk, *Effective Cross Sections and Neutron Flux Distribution in a Natural Uranium Rod*, CRT-725, (1957).
121. C. H. Westcott, *Effective Cross Section Values for Well-Moderated Thermal Reactor Spectra*, CRRP-960 (AECL-1101), (November, 1960).
122. P. R. Fields, et al., *Pile Neutron Cross Sections of the Heavier Plutonium Isotopes*, Nuclear Sci. and Eng., 1: No. 1, 62, (March, 1956).
123. W. C. Bentley, et al., *The Formation of Higher Isotopes and Higher Elements by Reactor Irradiation of Pu^{239}; Some Nuclear Properties of the Heavier Isotopes*, Proc., 1955 Geneva Conference, 7: Paper No. 809, p. 261.
124. S. B. Gunst, E. D. McGarry and J. J. Scoville, *The Reactivity of Natural UO_2 Irradiated to 6×10^{21} n/cm^2*, Nuclear Sci. and Eng., 7: No. 5, 407, (May, 1960).
125. D. W. Osborne (Ed.), *Chemistry Division, Section C-I, Summary Report: January–March, 1951*, ANL-4667, (May, 1951).
126. D. G. Gurst, et al., *NRX Rod No. 683, Analysis of Irradiated Uranium and Estimation of Effective Cross Sections*, CRR-622, Rev. (AECL-447), (May, 1957).
127. B. I. Spinrad, *Reactivity Gains in NRX Irradiated Slugs*, Nuclear Sci. and Eng., 1: No. 6, 541, (December, 1956).
128. D. J. Littler, *Measurements of the Change in Cross Section of Irradiated Uranium Made by Modulating the Power of a Nuclear Reactor*, AERE RS/R 2092, (1956).

129. D. J. Littler, *Long-Term Reactivity Changes in Natural Uranium Reactors*, Proc., 1955 Geneva Conference, 5: Paper No. 432, p. 141.
130. A. G. Ward and D. S. Craig, *Analysis of Measurements of the Reactivity Change with Irradiation for Natural Uranium Samples*, CRRP-761-C, (AECL-814), (April, 1960).
131. R. G. Hart, et al., *Chemical and Isotopic Analysis of Irradiated Uranium Slugs from Demountable Slug Rod A.G.W.-1*, CRRP-761-B, (AECL-813), (September, 1959).
132. A. G. Ward and D. S. Craig, *Measurements of the Reactivity Change with Irradiation for Natural Uranium Samples Irradiated in NRX*, CRRP-761-A, (AECL-812), (May, 1959).
133. D. S. Craig, et al., *Long Irradiation of Natural Uranium*, Proc., 1958 Geneva Conference, 16: Paper No. 205, p. 83.
134. A. G. Ward, *Reactivity Life of Natural Uranium*, Nucleonics, 18: No. 10, 69, (October, 1960).
135. S. A. Kushneriuk, *Distribution of Resonant Neutron Capture in a Natural Uranium Rod*, J. Nuclear Energy, Part A, Reactor Science, 10: p. 133, (September, 1959).
136. H. Rose, et al., *The Use of the Pile Oscillator in Thermal Reactor Problems*, AERE R/R 2681, (1958).
137. D. R. deBoisblanc, et al., *The Reactivity Measurement Facility and Its Applications*, Proc., 1958 Geneva Conference, 13: Paper No. 1842, p. 75.
138. S. B. Gunst, *Isotopic Concentrations for a Time Varying Irradiation of U or Pu*, WAPD-TM-191, (August, 1959).
139. S. B. Gunst, *Reactivity Associated with the Decay of Np^{239} in Irradiated Natural Uranium Dioxide*, Nuclear Sci. and Eng., 6: No. 5, 376, (November, 1959).
140. P. S. Lacy and J. H. Leonard, *Isotopic Analyses of Irradiated UO_2 Fuel Rods from Shippingport*, Trans. Am. Nuclear Soc., 3: No. 2, 401, (December, 1960).
141. R. L. Crowther and J. W. Weil, *The Effective Cross Section of Pu^{240} in Long-Term Reactivity Calculations*, Nuclear Sci. and Eng., 3: No. 6, 747, (June, 1958).
142. W. B. Lewis, *Attainable Burnup of U with Pu Recycling*, DR-38, (February, 1956).
143. M. F. Duret, *Reactivity and Fuel Balance in Recycled Pu Reactors*, RPI-12, (October, 1955).
144. R. E. Heineman, *Parameters Characterizing the Equilibrium State in Pu-Fed-Back Reactors*, HW-43923, (June, 1956).
145. R. E. Peterson and G. S. Busselman, *A Generalized Calculation of Material and Reactivity Balance in Recycled Pu Reactors*, HW-54074, (January, 1958).
146. D. P. Herron, et al., *Fuel Cycles for Nuclear Power Reactors*, Proc., 1958 Geneva Conference, 13: Paper No. 1044, p. 189.
147. Symposium, *Nuclear Fuel Cycles*, Nuclear Eng., 4: No. 36, 113, (March, 1959).
148. L. Barbieri, J. Webster and K. Chow, *Plutonium Recycle in the Calder Hall Type Reactor*, Nuclear Sci. and Eng., 5: No. 2, 105, (February, 1959).
149. S. E. Lewis and C. S. Lowthian, *Theoretical Aspects of Fuel Cycling in Industrial Calder Hall Type Reactors*, Proc., 1958 Geneva Conference, 13: Paper No. 311, p. 229.
150. P. J. Grant, *Fuel Cycle Optimization in Power Station Design*, Nuclear Power, 4: No. 39, 73, (July, 1959).
151. *The Plutonium-Recycle Program*, HW-50700, (June, 1957).
152. N. G. Wittenbrock, et al., *Plutonium Recycle Test Reactor*, HW-61236, (October, 1959).
153. *Plutonium Recycle Program Annual Report*, HW-62000, (October, 1959).
154. *Plutonium Recycle Program Annual Report*, HW-52000, (September, 1957).
155. *Plutonium Recycle Program Annual Report*, HW-58000, (October, 1958).
156. P. Greebler, et al., *Recycle of Pu in Low Enrichment Light Water Reactors*, Proc., 1958 Geneva Conference, 13: Paper No. 2167, p. 251.
157. A. Radkowsky, *Theory and Application of Burnable Poisons*, Proc., 1958 Geneva Conference, 13: Paper No. 1900, p. 426.
158. R. C. Dahlberg and F. D. Judge, *The Depletion of Burnable Poisons in Endurance Calculations*, KAPL-2058, (March 1, 1960).
159. G. B. Melese, *Analyses of Reactor Control by Burnable Poisons for Rectanguloid, Cylindrical and Spherical Geometries*, Trans. Am. Nuclear Soc., (November, 1959), p. 198.
160. B. Wolfe, *Predicting Reactivity at High Burnup*, Nucleonics, 16: No. 3, 116, (March, 1958).
161. R. L. Murray, S. A. Hasnain and A. L. Mowery, Jr., *Reactor Fuel Cycle Analyses by Series Methods*, Nuclear Sci. and Eng., 6: No. 1, 18, (July, 1959).
162. H. E. Stevens and W. K. Anderson, *Study of Several Potential Burnable Poison Materials for Power Reactor Applications*, Nuclear Sci. and Eng., 2: No. 2, Suppl., 202, (November, 1959).
163. H. L. McMurry, *Perturbation Theory and Applications, I Theoretical*, IDO-16252, (January, 1956).
164. S. Glasstone and M. C. Edlund, *The Elements of Nuclear Reactor Theory*, (New York: D. Van Nostrand Co., Inc., 1952), Formula 10.29.1, p. 301.
165. J. K. Long, et al., *Fast Neutron Power Reactor Studies with ZPR-III*, Proc., 1958 Geneva Conference, 12: Paper No. 598, p. 119.
166. R. Gwin, *Determination of Reactor Parameters from Period Measurements*, Applied Nuclear Physics Division Annual Report for Period Ending September 10, 1956, ORNL-2081, (September, 1956), p. 84.
167. F. deHoffmann, *Criticality of the Water Boiler and Effective Number of Delayed Neutrons*, AECD-3051, (December, 1944).
168. C. E. Cohn, *The Determination of Reactor Transfer Functions by Pile Noise Analysis*, Trans. Am. Nuclear Soc., (June, 1958), p. 162.
169. M. N. Moore, *The Determination of Reactor Transfer Functions from Measurements at Steady Operation*, Nuclear Sci. and Eng., 3: No. 4, 387, (April, 1958).
170. J. D. Orndoff, *Prompt Neutron Periods of Metal Critical Assemblies*, Nuclear Sci. and Eng., 2: No. 4, 450, (July, 1957).
171. G. S. Brunson, et al., *Measuring the Prompt Period of a Reactor*, Nucleonics, 15: 132, No. 11, (November, 1957).
172. W. Y. Kato and J. P. McMahon, *Neutron Lifetime Measurements in Thermal Reactors*, Trans. Am. Nuclear Soc., (June, 1958), p. 41.
173. F. deHoffmann, *Statistical Aspects of Pile Theory*, Science and Engineering of Nuclear Power, (Reading, Massachusetts: Addison Wesley Pub. Co., Inc., 1949), Vol. II, Chap. 9, p. 103.
174. W. K. Luckow, *The Evaluation of Nuclear Reactor Parameters from Measurements of Neutron Statistics*, Unpublished Ph. D. Thesis, University of Michigan, (1958).
175. A. F. Henry, *The Application of Reactor Kinetics to the Analysis of Experiments*, Nuclear Sci. and Eng., 3: No. 1, 52, (January, 1958).
176. B. J. Toppel, *Sources of Error in Reactivity Determinations by Means of Asymptotic Period Measurements*, Nuclear Sci. and Eng., 5: No. 2, 88, (February, 1959).
177. D. J. Hughes, et al., *Delayed Neutrons from Fission of U^{235}*, Phys. Rev., 73: No. 2, 111, (1948).
178. C. E. Cohn, *A Simplified Theory of Pile Noise*, Nuclear Sci. and Eng., 7: No. 5, 472, (May, 1960).
179. B. C. Diven, et al., *Multiplicities of Fission Neutrons*, Phys. Rev., 101: No. 3, 1012, (February 1, 1956).
180. C. E. Cohn, *Determination of Reactor Kinetic Parameters by Pile Noise Analysis*, Nuclear Sci. and Eng., 5: No. 5, 331, (May, 1959).
181. R. Feynmann, F. deHoffman, and R. Serber, *Dispersion of the Neutron Emission in U-235 Fission*, J. Nuclear Energy, 3: 64, (1956).
182. E. F. Bennett, *The Rice Formulation of Pile Noise*, Nuclear Sci. and Eng., 8: No. 1, 53, (July, 1960).
183. E. F. Bennett (ANL), unpublished data.

184. F. Feiner, et al., *Pile Oscillator Techniques and the Error Analysis of Oscillator Measurements,* KAPL-1703, (October 26, 1956).
185. O. R. Frisch and D. J. Littler, *Pile Modulation and Statistical Fluctuations in Piles,* Phil. Mag., 45: Series 7, 126, (February, 1954).
186. G. F. von Dardel, *The Interaction of Neutrons with Matter Studied with a Pulsed Neutron Source,* Trans. Roy. Inst. Tech. (Stockholm), No. 75, (1954).
187. G. F. von Dardel, *A Study of the Interaction of Neutrons with Moderating Materials,* Phys. Rev., 94: No. 5, 1272, (1954).
188. S. B. D. Iyengar and G. S. Mani, *Thermal Neutron Distribution Due to Time-Dependent Fast Neutron Source in Non-Multiplying Media,* Proc. Indian Acad. Science, 42A: 175, (1955).
189. A. V. Antonov, et al., *A Study of Neutron Diffusion in Beryllium, Graphite and Water by the Impulse Method,* Proc., 1955 Geneva Conference, 5: Paper No. 661, p. 3.
190. G. von Dardel and N. G. Sjöstrand, *Diffusion Measurements with Pulsed Neutron Sources,* Progress in Nuclear Energy, Vol. II, Series I, p. 183, (1958).
191. N. G. Sjöstrand, *On the Theory Underlying Diffusion Measurements with Pulsed Neutron Sources,* Arkiv för Fysik, 15: No. 12, 147, (1959).
192. W. M. Andrews, *Measurement of the Temperature Dependence of Neutron Diffusion Properties in Be Using a Pulsed Neutron Technique,* UCRL-6083, (August, 1960).
193. K. H. Beckurts, *Measurements with a Pulsed Neutron Source,* Nuclear Sci. and Eng., 2: No. 4, 516, (July, 1957).
194. K. S. Singwi and L. J. Kothari, *Diffusion Cooling of Neutrons in a Finite Solid Moderator Assembly,* J. Nuclear Energy, 8: 59, (1958).
195. M. Nelkin, *The Diffusion Cooling of Neutrons in a Finite Moderator,* J. Nuclear Energy, 8: 48, (1958).
196. G. R. Keepin, *Pulsed Source Techniques,* LAMS 2215, (March, 1958).
197. W. M. Lopez, et al., *A Preliminary Report on Measurements of Diffusion Parameters in Water by the Pulsed Neutron Method,* GA-1584, (September, 1960).
198. L. J. Kothari and K. S. Singwi, *Slowing Down of Neutrons in Beryllium from 1.44 ev to Thermal Energy,* J. Nuclear Energy, 5: 342, (1957).
199. R. C. Bhandari, *Scattering of Thermal Neutrons in Beryllium,* J. Nuclear Energy, 6: 104, (1957).
200. R. C. Bhandari, L. J. Kothari and K. S. Singwi, *Scattering of Thermal Neutrons in Beryllium Oxide,* J. Nuclear Energy, 7: 45, (1958).
201. L. S. Kothari and K. S. Singwi, *Slowing Down of Neutrons Near Thermal Equilibrium in Beryllium and Beryllium Oxide,* Proc., 1958 Geneva Conference, 16: Paper No. 1639, p. 316.
202. K. S. Singwi, *On the Theory of Diffusion Cooling of Neutrons in a Finite Solid Moderator Assembly,* J. Nuclear Energy, Part A, Reactor Science, 11: 19, (1959); Arkiv för Fysik, 16: 385, (1959-60).
203. G. de Saussure and E. G. Silver, *Determination of the Neutron Diffusion Parameters in Room-Temperature Beryllium,* ORNL-2641, (February, 1959).
204. S. B. D. Iyengar, et al., *Temperature Dependence of the Slowing Down and Diffusion Constants of Neutrons in Beryllium Oxide,* Proc. Indian Acad. Science, 45: Section A, 224, (1957).
205. N. G. Sjöstrand, J. Mednis and T. Nilsson, *Geometric Buckling Measurements Using the Pulsed Neutron Source Method,* Arkiv för Fysik, 15: No. 35, 471, (1959).
206. G. de Saussure and E. G. Silver, *An Application of the Pulsed Neutron Technique to Reactor Theory,* Trans. Am. Nuclear Soc., 3: No. 1, 155, (1960).
207. G. von Dardel and A. W. Waltner, *Determination of the Neutron Proton Capture Cross Section,* Phys. Rev., 91: 1284, (1953).
208. F. R. Scott, D. B. Thompson and W. Wright, *Thermal Neutron Capture Cross Sections of Hydrogen, Boron, and Silver,* Phys. Rev., 95: 582, (1954).
209. G. von Dardel and N. G. Sjöstrand, *Absorption Cross Section of Boron for Thermal Neutrons,* Phys. Rev., 96: No. 6, 1566, (1954).
210. C. H. Collie, R. E. Meads and E. E. Lockett, *The Capture Cross Section of Neutrons by Boron,* Proc. Phys. Soc., (London), A69: 464, (1956).
211. J. W. Meadows and J. F. Whalen, *Thermal Neutron Absorption Cross Sections by the Pulsed Source Method,* Nuclear Sci. and Eng., 9: No. 2, 132, (February, 1961).
212. A. A. Bergman, et al., *A Neutron Spectrometer Based on Measuring the Slowing Down Time of Neutrons in Lead,* Proc., 1955 Geneva Conference, 4: Paper No. 642, p. 135.
213. S. B. D. Iyengar, et al., *Slowing Down and Diffusion of Neutrons in Beryllium Oxide,* Ibid, Ref. 204; p. 215.
214. W. F. Hornyak, et al., *Energy Levels of Light Nuclei III,* Revs. Modern Phys., 22: 291, (October, 1950).
215. E. Guth and C. J. Mullin, *Theory of the Photo- and Electrodisintegration of Be^9,* Phys. Rev., 76: No. 2, 234, (1949).
216. S. Bernstein, et al., *Yield of Photoneutrons from U^{235} Fission Products in Heavy Water,* Phys. Rev., 71: No. 9, 573, (1947).
217. S. Bernstein, et al., *Yield of Photoneutrons from U^{235} Fission Products in Be,* AECD-1833, (February 20, 1948).
218. W. K. Ergen, *Hard Gamma Emitters Among Fission Products,* ANP-59, (May 3, 1951).
219. M. W. Johns and B. W. Sargent, *Photoneutrons in a Heavy Water Pile,* Can. J. Phys., 32: 136, (February, 1954).
220. B. S. Maxon and C. E. Cohn (ANL), unpublished data.
221. T. A. Welton, *Kinetics of Stationary Reactor Systems,* Proc., 1955 Geneva Conference, 5: Paper No. 610, p. 377.
222. R. E. Kalman and J. E. Bertram, *Control System Analysis and Design Via the 'Second Method' of Lyapunov,* ASME-AIEE-IRE-ISA National Automatic Control Conference, Dallas, Texas, (November 4-5, 1959).
223. L. B. Robinson, *Concept of Stability for Nuclear Reactors,* J. Appl. Phys., 25: 516, (1954).
224. H. Chestnut and R. Mayer, *Servomechanism and Regulating System Design,* (New York: John Wiley and Sons, Inc., 1955).
225. W. K. Ergen, H. J. Lipkin and J. A. Nohel, *Applications of Liapounov's Second Method in Reactor Dynamics,* J. Math. and Phys., 36: 36, (1957).
226. H. B. Smets, *On Welton's Stability Criterion for Nuclear Reactors,* J. Appl. Phys., 30: 1623, (1959).
227. E. P. Gyftopoulos and J. Devooght, *Boundedness and Stability in Nonlinear Reactor Dynamics,* Nuclear Sci. and Eng., 7: No. 6, 533, (June, 1960).
228. H. B. Smets, *Un Critere de Stabilite Non-lineaire des Reacteurs Nucleaires,* Bull. Acad. Sci., (Belgium), 45: No. 2, 104, (1959).
229. W. K. Ergen and A. M. Weinberg, *Some Aspects of Non-Linear Reactor Dynamics,* Physica, 20: 413, (1954).
230. W. K. Ergen, *Kinetics of Circulating-Fuel Nuclear Reactors,* J. Appl. Phys., 25: No. 6, 702, (1954).
231. A. Z. Akcasu and A. Dalfes, *A Study of Non-Linear Dynamics,* Nuclear Sci. and Eng., 8: No. 2, 89, (August, 1960).
232. T. A. Welton, *A Stability Criterion for Reactor Systems,* ORNL-1894, (July, 1955).
233. D. F. Tuttle, *Network Synthesis,* (New York: John Wiley and Sons, Inc., 1958), Vol. 1, p. 107.
234. V. M. Popov, *Notes on the Inherent Stability of Nuclear Reactors,* Proc., 1958 Geneva Conference, 11: Paper No. 2458, p. 245.
235. N. Balabanian, *Network Synthesis,* (New York: Prentice-Hall, Inc., 1958), p. 27.
236. R. M. Foster, *Passive Network Synthesis,* Proc., Symposium on Modern Network Synthesis, New York, April 13-15, 1955, p. 4.
237. J. N. Grace, *Analysis of a Reactivity Instability Experiment with Boiling and Non-Linear Analysis of Spatial Stability and Flux Tilt Transients,* Proc., Conference on Transfer Function Measurement and Reactor Stability Analysis, ANL-6205, (May, 1960), p. 174.

238. E. S. Beckjord and W. H. Harker, *The Dynamics of Large Boiling Reactors,* ANL-6205, (May, 1960), p. 189.
239. A. W. Kramer, *Boiling Water Reactors,* (Reading, Massachusetts: Addison-Wesley Pub. Co., Inc., 1958).
240. A. Hitchcock, *Nuclear Reactor Stability,* (London: Temple Press Limited, 1960).
241. J. A. DeShong, Jr., *Power Transfer Functions of EBWR Obtained Using a Sinusoidal Reactivity Driving Function,* ANL-5798, (January, 1958).
242. T. Snyder and J. Thie, *Physics of Boiling Reactors,* Proc., 1958 Geneva Conference, 11: Paper No. 2402, p. 433.
243. J. A. Thie, *Theoretical Reactor Statics and Kinetics of Boiling Reactors,* Proc., 1958 Geneva Conference, 11: Paper No. 638, p. 440.
244. J. A. Thie, *Stability of Bubbling Reactors,* ANL-5601, (December, 1956), p. 31.
245. J. A. Thie, *Boiling Water Reactor Instability,* Nucleonics, 16: No. 3, 102, (March, 1958).
246. E. S. Beckjord, *Dynamic Analysis of Natural Circulation Boiling Water Power Reactors,* ANL-5799, (March, 1958).
247. J. A. Thie, *Dynamic Behavior of Boiling Reactors,* ANL-5849, (May, 1959).
248. J. W. Weil, *Boiling Water Reactor Stability,* NP-7608, (1957).
249. A. Z. Akcasu, *Theoretical Feedback Analysis in Boiling Water Reactors,* ANL-6221, (October, 1960).
250. J. A. DeShong, Jr. and W. C. Lipinski, *Analyses of Experimental Power Reactivity Feedback Transfer Functions for a Natural Circulation Boiling Water Reactor,* ANL-5850, (July, 1958).
251. J. R. Dietrich, et al., *Design and Operating Experience of a Prototype Boiling Reactor,* Proc., 1955 Geneva Conference, 3: Paper No. 851, pp. 56, 70.
252. S. G. Forbes, F. Schroeder and W. E. Nyer, *Instability in SPERT-I,* Nucleonics, 15: No. 1, 41, (January, 1957).
253. P. A. Lottes, et al., *Experimental Studies of Natural Circulation Boiling and Their Application to Boiling Reactor Performance,* Proc., 1958 Geneva Conference, 7: Paper No. 1983, p. 784.
254. J. A. Fleck, *The Dynamic Behavior of Boiling Water Reactors,* J. Nuclear Energy, Part A, Reactor Science, 11: 114, (1960).
255. S. M. Zivi, *Calculations of Void Compensated Reactivity in Spert IA from Experimental Data,* Kinetics Studies of Heterogeneous Water Reactors, Annual Summary Report–1959, App. D., RWD-RL-167, (February, 1960).
256. J. A. Thie, *Statistical Analysis of Power Reactor Noise,* Nucleonics, 17: No. 10, 102, (October, 1959).
257. A. Z. Akcasu, *Mean Square Instability in Boiling Reactors,* Nuclear Sci. and Eng., 10: 337, (August, 1961).
258. J. A. Thie, *Methods of Investigating Noisy Power Reactors,* Proc., Conference on Transfer Function Measurements and Reactor Stability Analysis, Part I, ANL-6205, (1960), p. 90.
259. A. Z. Akcasu, *Methods of Investigating Noisy Power Reactors,* Proc., Conference on Transfer Function Measurements and Reactor Stability Analysis, Part II, ANL-6205, (1960), p. 97.
260. H. Harker, *Stochastic Instability in Reactors,* Trans. Am. Nuclear Soc., 3: 475, (1960).
261. A. G. Ward, *The Problem of Flux Instability in Large Power Reactors,* CRRP-657, (July, 1956), (AECL-345).
262. D. Randall and D. S. St. John, *Xenon Spatial Oscillations,* Nucleonics, 16: No. 3, 82, (March, 1958).
263. A. F. Henry and J. D. Germann, *Oscillations in the Power Distribution Within a Reactor,* Nuclear Sci. and Eng., 2: No. 4, 469, (July, 1957).
264. R. S. Wick, *Space and Time-Dependent Flux Oscillations (and Instability) in Thermal Reactors Due to Nonuniform Formation and Depletion of Xenon,* WAPD-TM-138, (August, 1958).
265. K. Mochizuki and A. Takeda, *An Analysis of Neutron Flux Spatial Oscillation Due to Xenon Build-Up in a Large Power Reactor Core,* Nuclear Sci. and Eng., 7: No. 4, 336, (April, 1960).
266. W. K. Ergen, *The Inhour Formula for a Circulating-Fuel Nuclear Reactor with Slug Flow,* CF-53-12-108, (December, 1953).
267. W. K. Ergen, *The Behavior of Certain Functions Related to the Inhour Formula of Circulating Fuel Reactors,* CF-54-1-1, (January, 1954).
268. A. M. Weinberg and W. K. Ergen, *Some Aspects of Non-Linear Reactor Kinetics,* Proc., Kjeller Conference on Heavy Water Reactors, (August, 1953), p. 62.
269. T. A. Welton, *A Stability Criterion for Reactor Systems,* ORNL-1894, (October 17, 1952); and *Kinetics of Stationary Reactor Systems,* Proc., 1955 Geneva Conference, 5: Paper No. 610, p. 377.
270. T. A. Welton, *Kinetics of Homogeneous Reactors,* Proc., Second Fluid Fuels Development Conference held at Oak Ridge, April 17-18, 1952, CF-52-4-197 (Rev.), (April, 1952), p. 4.
271. J. A. Fleck, Jr., *Theory of Low-Power Kinetics of Circulating Fuel Reactors with Several Groups of Delayed Neutrons,* BNL-334 (T-57), (April, 1955).
272. J. A. Fleck, Jr., *The Theory of Circulating Reactor Kinetics at Low Power,* BNL-1933, (April, 1954); also *Kinetics of Circulating Reactors at Low Power,* Nucleonics, 12: No. 10, 52, (October, 1954).
273. J. A. Fleck, Jr., *The Temperature-Dependent Kinetics of Circulating Fuel Reactors,* BNL-357 (T-65), (July, 1955).
274. S. Glasstone and M. C. Edlund, *The Elements of Nuclear Reactor Theory,* (Princeton, New Jersey: D. Van Nostrand Company, Inc., 1952), Eq. 10.24.3, p. 298.
275. R. V. Meghreblian and D. K. Holmes, *Reactor Analysis,* (New York: McGraw Hill Book Company, 1960), pp. 590-610.
276. L. N. Ussachoff, *Equation for the Importance of Neutrons, Reactor Kinetics and the Theory of Perturbation,* Proc., 1955 Geneva Conference, 5: Paper No. 656, p. 503.
277. E. R. Cohen, *Some Topics in Reactor Kinetics,* Proc., 1958 Geneva Conference, 11: Paper No. 629, p. 302.
278. H. C. Corben, *The Computation of Excess Reactivity from Power Traces,* Nuclear Sci. and Eng., 5: No. 2, 127, (February, 1959).
279. R. E. Kemp, *Some Notes on the Coherent Detection of Small Signals in the Presence of Noise,* Kinetic Studies of Heterogeneous Water Reactors, Annual Summary Report–1959, App. E, RWD-RL-167, (February, 1960).
280. H. B. Smets, *Reactor Dynamics at Low Power,* Proc., 1958 Geneva Conference, 11: Paper No. 107, p. 237.
281. R. A. Daane, et al., *Progress Report on the Study of Low Probability, High Hazard, Fast Reactor Accidents,* NDA 14-107, (November, 1955).
282. R. A. Daane, *Fast Reactor Accident Scaling Laws,* NDA-14-84, (May, 1955).
283. W. J. McCarthy, Jr., et al., *Studies of Nuclear Accidents in Fast Power Reactors,* Proc., 1958 Geneva Conference, 12: Paper No. 2165, p. 207.
284. K. Fuchs, *Efficiency for Very Slow Assembly,* LA-596, (1946).
285. R. O. Brittan, *Some Problems in the Safety of Fast Reactors,* ANL-5577, (May, 1956).
286. S. G. Forbes, et al., *Analysis of Self-Shutdown Behavior in the SPERT I Reactor,* IDO-16528, (July, 1959).
287. J. C. Haire, *Subcooled Transient Tests in the SPERT I Reactor–Experimental Data,* IDO-16342, (July, 1958).
288. W. E. Nyer and S. G. Forbes, *SPERT I Reactor Safety Studies,* Proc., 1958 Geneva Conference, 11: Paper No. 2428, p. 470.
289. R. W. Miller, *Calculations of Reactivity Behavior During SPERT I Transients,* IDO-16317, (June, 1957).
290. J. H. Norberg (Ed.), *Quarterly Progress Report, (January, February, March, 1959),* IDO-16539.
291. H. C. Corben, *Power Bursts in Nuclear Reactors,* RWC 22-127, (September, 1958).
292. G. O. Bright, et al., *An Elementary Model for Reactor Burst Behavior,* IDO-16393, (August, 1957).
293. G. O. Bright (Ed.), *Quarterly Progress Report, (January, February, March, 1958),* IDO-16452.
294. G. O. Bright (Ed.), *Quarterly Progress Report, (April, May, June, 1958),* IDO-16489.
295. G. O. Bright (Ed.), *Quarterly Progress Report, (July, August, September, 1958),* IDO-16512.

296. E. Janssen, W. H. Cook and K. Hikido, *Metal-Water Reactions: I. A Method for Analyzing a Nuclear Excursion in a Water Cooled and Moderated Reactor*, GEAP-3073, (May, 1958).
297. W. E. Nyer and S. G. Forbes, *SPERT Program Review*, IDO-16634, (October, 1960).
298. J. I. Owens, *Metal-Water Reactions: II. An Evaluation of Severe Nuclear Excursions in Light Water Reactors*, GEAP-3178, (June, 1959).
299. K. Hikido, *Metal-Water Reactions: IV. Heat Transfer Conditions During Severe Nuclear Excursions in Water Cooled Reactors*, GEAP-3204, (September, 1959).
300. S. E. Golian, et al., *Transient Response of Plane Parallel Fuel Assemblies to Exponential Power Excursions*, NRL-4495, (January, 1955).
301. B. H. Noordhoff, C. F. Foreman and J. W. Haskins, *Comparison of Two Methods for Analyzing Accidental Power Transients*, WAPD-TM-31, (January, 1957).
302. E. R. Sanford, *Accidental Power Transients in Metal-Water Reactors, Part I*, WAPD-SC-581, (August, 1956).
303. L. Gartner and R. Daane, *The Self-Regulation by Moderator Boiling in Stainless Steel-UO_2-H_2O Reactors*, NDA-16, (June, 1955).
304. L. Gartner, *The Improvement in Self-Regulating Ability of Water Moderated Reactors by Means of Graphite and D_2O Reflectors*, NDA-18, (August, 1955).
305. W. A. Horning and H. C. Corben, *Theory of Power Transients in the SPERT I Reactor*, IDO-16446, (August, 1957).
306. G. W. Griffing and L. I. Deverall, *Kinetic Studies of the SPERT I Reactor: Initial Behavior by the Energy Model*, IDO-16397, (April, 1958).
307. G. O. Bright and S. G. Forbes, *Miscellaneous Tests With the SPERT I Reactor*, IDO-16551, (October, 1959).
308. W. E. Nyer, et al., *Experimental Investigations of Reactor Transients*, IDO-16285, (April, 1956).
309. W. H. Zinn, et al., *Transient and Steady-State Characteristics of a Boiling Reactor*, ANL-5211, (February, 1954).
310. J. R. Dietrich, *Experimental Investigation of the Self-Limitation of Power During Reactivity Transients in a Subcooled, Water Moderated Reactor*, ANL-5323, (1954).
311. J. A. Thie, *An Experimental Investigation of Boiling Reactor Safety*, ANL-6135, (To be published).
312. *Annual Technical Progress Report, AEC Unclassified Programs, Fiscal Year 1959*, NAA-SR-3850, (August, 1959).
313. *Annual Technical Progress Report, AEC Unclassified Programs, Fiscal Year 1960*, NAA-SR-5350, (August, 1960).
314. R. S. Stone, et al., *Transient Behavior of TRIGA, a Zirconium-Hydride, Water Moderated Reactor*, Nuclear Sci. and Eng., 6: No. 4, 255-259, (October, 1959).
315. General Atomics Division, *Hazards Report for Torrey Pines TRIGA Reactor*, GA-722, (May, 1959).
316. *Application to United States Atomic Energy Commission for Construction Permit and Utilization Facility License for the FLAIR Reactor to be Constructed at the TRIGA Facility of the John Jay Hopkins Laboratory, San Diego, California*, GA-1263, (March, 1960).
317. D. Okrent, et al., *The Reactor Kinetics of the Transient Reactor Test Facility (TREAT)*, ANL-6174, (September, 1960).
318. F. Kirn, et al., *Reactor Physics Measurements in TREAT*, ANL-6173, (October, 1960).

Section 6

INTERMEDIATE REACTORS

Intermediate reactors are those reactors whose median-energy-of-fission-producing neutrons lie in a range of a few electron volts to a few thousand electron volts. They are also called "resonance" reactors because the bulk of the neutron flux lies in the resonance region of the heavy element cross sections.

The criterion for inclusion of data in Section 6, rather than in Sections 3 or 4, was based on an arbitrary division between "thermal" and "intermediate" systems. The assumed moderator atom-to-fuel atom ratios corresponding to this division are given below for U^{235} and U^{233} fuels and various moderators (see Section 3.7).

X	H/X	D/X	C/X	Be/X	BeO/X
U^{235}	~50	~380	~1390	~820	~600
U^{233}	~100	~740	~2700	~1600	~1170

This section also includes the reflector-moderated reactor. The core contains little or no moderator but is well reflected with a material of low mass number—commonly Be. The median energy of fission may vary from the thermal range at the reflector fuel interface, to the intermediate range in parts of the fuel region well removed from the reflector.

6.1 CONSTANTS FOR INTERMEDIATE REACTOR CALCULATIONS

6.1.1 AGE-DIFFUSION EQUATION

The age-diffusion equation, for purposes of multigroup calculations, is reduced to a set of linear differential equations:[1,2]

$$-\left(\frac{\Delta u_i}{3\xi\Sigma_{s,i}\,\Sigma_{tr,i}}\right)\nabla^2(q_i)_{avg} + \left(\frac{\Delta u_i\,\Sigma_{ne,i}}{\xi\Sigma_{s,i}}\right)(q_i)_{avg} + q_i^0 = q_i^I + Q_{f,i} + Q_{in,i} \qquad (6\text{-}1)$$

where Δu_i = lethargy width of group i

$u = \ln[10/E\ (\text{Mev})]$

$\Sigma_{s,i}$ = scattering cross section in group i

$\Sigma_{ne,i}$ = total non-elastic cross section for group i

$= \Sigma_{f,i} + \Sigma_{c,i} + \Sigma_{in,i}$, where $\Sigma_{f,i}$ is fission cross section of group i; $\Sigma_{c,i}$ is capture cross section of group i; $\Sigma_{in,i}$ is inelastic removal cross section for group i

$\Sigma_{tr,i} = \Sigma_{ne,i} + \Sigma_{s,i}\,(1-\bar{\mu})$, where $\bar{\mu}$ is the average cosine of scattering angle

ξ = average logarithmic energy loss per collision

$Q_{f,i}$ = source into group i from fission
$Q_{in,i}$ = source into group i from inelastic scattering
q_i^I = elastic slowing down density into group i
q_i^0 = elastic slowing down density out of group i
$(q_i)_{avg}$ = average elastic slowing down density in group i

In order to solve Eq. (6-1), it is necessary to provide a relationship between q_i^0, q_i^I, and $(q_i)_{avg}$. This relationship is selected by Ehrlich and Hurwitz[1] to be:

$$(q_i)_{avg} = \omega_1 q_i^I + \omega_2 q_i^0 \tag{6-2}$$

There remains the choice of ω_1 and ω_2. Three schemes are cited below. Schemes A and B have been used at KAPL.

Scheme A. $\omega_1 = 0$, and ω_2 is chosen by trial and error for each region and group so that the product of ω_2 and the spatial average of $(q_i^0)_{avg}$ gives a reasonable value of the spatial average of $(q_i)_{avg}$.

In addition to the more general trial and error method, there is an approximation procedure* which provides a simple formula for calculating ω_2. In the diffusion approximation model with continuous slowing down in a region of homogeneous composition, and for an energy range in which elastic scattering constitutes the only source of neutrons,

$$-\frac{1}{3\Sigma_{tr}}\nabla^2\left(\frac{q}{\xi\Sigma_s}\right)+\frac{\Sigma_a}{\xi\Sigma_s}q=-\frac{\partial q}{\partial u} \tag{6-3}$$

Let B_T^2 be the total buckling and approximate: $\nabla^2 q = -B_T^2 q$; then Eq. (6-3) becomes an ordinary differential equation with the solution:

$$q = q_0 \exp\left[-\int_{u_0}^{u}\left(\frac{\Sigma_a}{\xi\Sigma_s}+\frac{B_T^2}{3\Sigma_{tr}\xi\Sigma_s}\right)du\right] \tag{6-4}$$

For a lethargy group $u_0 \leq u \leq u_1$ chosen so that the integrand of Eq. (6-4) is approximately constant through the interval, q may be written:

$$q = q_0 \exp\left(-y\,\frac{u-u_0}{u_1-u_0}\right)$$

where

$$y = \int_{u_0}^{u_1} du\,\left(\frac{\Sigma_a}{\xi\Sigma_s}+\frac{B_T^2}{3\xi\Sigma_{tr}\Sigma_s}\right)$$

The average of q in the group will be

$$\bar{q}_i = \frac{1}{\Delta u_i}\int_{u_0}^{u_1} q\,du$$

$$= \frac{q_0}{y}(1-e^{-y}) \tag{6-5}$$

and

$$q_1 = q_0\,e^{-y}$$

ω_2 is then just the ratio of $\bar{q}_i$ and q_i, so that

$$\omega_2 = \frac{(e^y-1)}{y} \tag{6-6}$$

*Private communication, R. Stark, Vallecitos Atomic Laboratory.

Some modification is necessary to extend this procedure to energy regions containing inelastic scattering and fission sources; however, good results are obtained by using $\omega_1 = 0$ and $\omega_2 = 1$.

Scheme B. $\omega_1 = \omega_2 = \frac{1}{2}$

Scheme C. Scheme C, in use at ORNL,[1,2] assumes a linear relationship of ϕ in the group. It relates ω_1 and ω_2 with the values of the reciprocal of $\xi\Sigma_s$ at the high end of the group, $(1/\xi\Sigma_s)^I$; at the low end of the group, $(1/\xi\Sigma_s)^0$; and the average over the group, $(1/\xi\Sigma_s)_{avg}$.

$$\left.\begin{aligned}\omega_1 &= \frac{(1/\xi\Sigma_s)^I}{(2/\xi\Sigma_s)_{avg}} \\ \omega_2 &= \frac{(1/\xi\Sigma_s)^0}{(2/\xi\Sigma_s)_{avg}}\end{aligned}\right\} \tag{6-7}$$

The criteria for choosing one particular scheme are summarized as follows:

(1) When a small number of groups is used, $\omega_1 = 0$ and ω_2 is estimated for each group and region of the assembly with the aim of making the spatial average of $(\omega_2 q)$ approximately equal to the average of the spatial averages of q^0 and q^I.

(2) When the variation of flux with position is not too rapid, then $\omega_1 = \omega_2 = \frac{1}{2}$ is a convenient form to assume.

(3) When ϕ^I, ϕ^0, and ϕ_{avg} are continuous across the interface between regions, the ORNL scheme tends to reduce oscillations at the interface between very dissimilar regions.

For greater precision, corrections to the ω values may be needed. Once ω_1 and ω_2 are chosen, the multigroup age-diffusion equation is solved. The flux values thus obtained are used to calculate the degradation from group to group at any reactor point compared to the average degradation in the group. New values of ω_1 and ω_2 can be deduced and adjustments made as indicated. If necessary, the procedure may be repeated.

The applicability of Eq. (6-1) to cases for which the $\Sigma_{ne,i}$ are not much smaller than the $\Sigma_{s,i}$ is considered in Refs. 3 and 4. The space-independent solution of the age-diffusion equation in a source-free-energy range is compared with the corresponding solution of the Boltzmann equation. The results of this comparison have been used to indicate a means by which the absorption cross sections may be adjusted in order to establish equivalence between the slowing-down processes as calculated by the two methods.

Equation (6-4) with $B_T^2 = 0$ is the space-independent solution of the age-diffusion equation. It is shown in Refs. 3 and 4 that an approximate solution of the Boltzmann equation is given by:

$$q(u) = q_0 \exp\left[-\int_0^u \lambda(u')\, du'\right] \tag{6-8}$$

where $\lambda(u)$ is related to $P(u)$, the probability that a neutron scattered into the lethargy u will be captured before being scattered again, by the expression

$$\frac{1}{1-\overline{P}(u)} = \frac{1-\alpha^{(1-\lambda)}}{(1-\alpha)(1-\lambda)} \tag{6-9}$$

In Eq. (6-9), $\alpha = (A-1)^2/(A+1)^2$, where A is the mass of the scattering material in units of the neutron mass. $\overline{P}(u)$ is the average value of $P(u)$ when the spacing of the absorption resonances is small compared to the average energy loss in a scattering collision. $\overline{P}(u)$ is chosen such that

$$\overline{P}(u)\,\Delta u = \sum_{\substack{\text{resonances} \\ \text{in } \Delta u}} f_i \frac{\int_i \Sigma_a\, du}{\Sigma_s} \tag{6-10}$$

where the index i goes over the resonances in the interval Δu; f_i is the self-shielding factor for the i*th* resonance (see Section 6.1.2); $\int_i \Sigma_a\, du$ is the integral of the absorption cross section over the region of the i*th* resonance; and Σ_a and Σ_s are macroscopic cross sections averaged over structural inhomogeneities. The solution Eq. (6-8) is based on the condition that $\overline{P}(u)$ is either small compared to unity, or a slowly varying function of u.

Comparison of Eqs. (6-8) and (6-4) with $B_T^2 = 0$ indicates that if Σ_a of Eq. (6-4) is replaced by a $(\Sigma_a)_{eff}$ so chosen that

$$\frac{(\Sigma_a)_{eff}}{\xi\Sigma_s} = \lambda \tag{6-11}$$

the desired correspondence between the two solutions of the space-independent problem would obtain. Equation (6-9) can be written

$$\lambda(\overline{P}) = \frac{\overline{P}}{\xi}\beta(\overline{P}) \tag{6-12}$$

where $\beta(\overline{P})$ is a correction factor which is unity when $\overline{P}$ is small. In the Greuling-Goertzel approximation[5]

$$\beta = \frac{1}{1 - [1 - (\gamma/\xi)]\,\overline{P}} \tag{6-13}$$

where γ is a function of α. Comparing Eqs. (6-12) and (6-11), one may write

$$(\Sigma_a)_{eff} = f\beta\,(\overline{P})\,\Sigma_a \tag{6-14}$$

where the self-shielding factor, f, is defined as (see Section 6.1.2)

$$f = \frac{\overline{P}\,\Sigma_s}{\Sigma_a} \tag{6-15}$$

The factor $\beta(\overline{P})$ corrects for the error in age theory when the absorption is large.

Hofmann and Storm[4] point out that for most practical cases it is sufficient to let $\beta = 1$ since typical values of β for U^{235}-fueled assemblies were found at KAPL to be in the neighborhood of 1.02.

6.1.2 RESONANCE SELF-SHIELDING CONSIDERATIONS*

This section follows closely the discussion given by H. Hurwitz, Jr. in the appendix to KAPL-1241.[3]

It is assumed that the nuclear resonances have an energy width which is small compared to the average energy loss experienced by a neutron following a scattering collision. Consequently, the number of neutrons scattered from higher energies into the energy range dE at E will be taken to be independent of E over the resonance.

A function $P[\Sigma_a(E)]$ of the total resonance cross section, $\Sigma_a(E)$, is defined which gives the probability that a neutron having energy E will be absorbed by the material having the resonance cross section before it is scattered out of the resonance energy region. Then if ϵ is independent of energy, the self-shielding factor f of a resonance is defined by

$$f = \int_{res} P[\Sigma_a\,(E)]\,dE \Big/ \lim_{\epsilon \to 0} \frac{1}{\epsilon} \int_{res} P[\epsilon\Sigma_a\,(E)]\,dE \tag{6-16}$$

For example, in the case of a homogeneous medium

$$P[\Sigma_a(E)] = \Sigma_a(E)/[\Sigma + \Sigma_a(E)] \tag{6-17}$$

and hence

$$f = \int_{res} \frac{\Sigma_a(E)}{\Sigma + \Sigma_a(E)}\,dE \Big/ \int_{res} \frac{\Sigma_a(E)}{\Sigma}\,dE \tag{6-18}$$

In Eqs. (6-17) and (6-18), Σ refers to the other materials in the medium and is explicitly assumed to be independent of E over the region of the resonance. Under the assumptions presented above, Eq. (6-18) is seen to be just the ratio of the effective resonance integral, to the infinite dilution integral for the resonance in question.

The above formalism may be applied to reactor problems by phrasing the theory employed in the calculation to make use of the ratio of the number of neutrons undergoing a resonance process, to the total number of neutrons scattered out of the region of the resonance per unit energy. This ratio can

*For a discussion of monoenergetic self-shielding effects, see Section 9.1.

then be written as the product of the self-shielding factor and the elementary linear expression for the ratio which is valid in the limit of infinite dilution [the denominator of Eq. (6-18)].

Tables and curves useful for evaluation of f in the case of Doppler-broadened resonances are given in Section 3.6.4.

6.1.3 MULTIGROUP CONSTANTS

Multigroup cross sections for use in intermediate reactor calculations are given in Table 7-2. The values for the uranium, plutonium, and thorium isotopes refer to the case of infinite dilution. For finite dilutions, the group cross section curves given in Figs. 6-1 through 6-8,[7] and 6-9,* must be used and the transport cross sections recomputed. The abscissa of these curves gives the potential scatter-

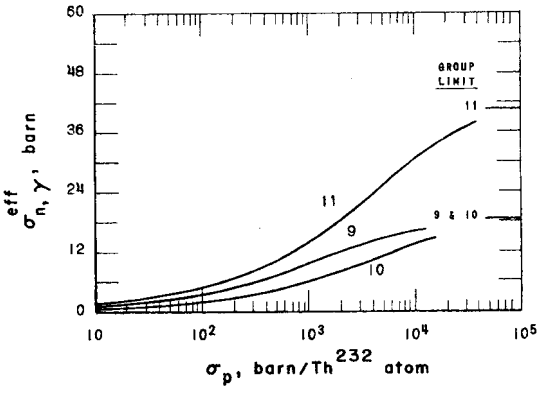

Fig. 6-1—Effective group capture cross section of Th^{232} as a function of total material scattering cross section. *Reproduced from Ref. 7.*

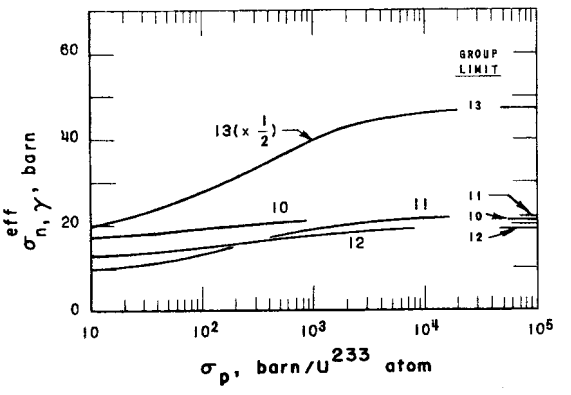

Fig. 6-2—Effective group capture cross section of U^{233} as a function of total material scattering cross section. *Reproduced from Ref. 7.*

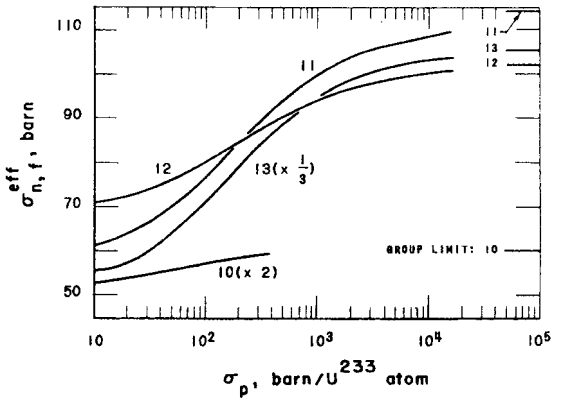

Fig. 6-3—Effective group fission cross section of U^{233} as a function of total material scattering cross section. *Reproduced from Ref. 7.*

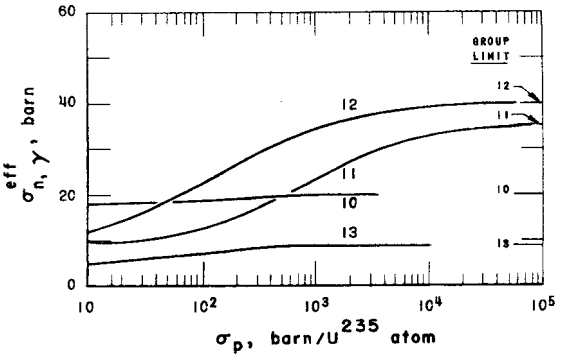

Fig. 6-4—Effective group capture cross section of U^{235} as a function of total material scattering cross section. *Reproduced from Ref. 7.*

ing cross section, σ_p, of the medium per absorber atom. The curves are based on the narrow resonance approximation and neglect the effects of Doppler broadening, resonance scattering, and resonance overlap. The numbers on the various curves refer to the group in question (Table 7-2). Above the region of the resolved resonances, the theoretical Porter and Thomas[6] distribution of neutron widths was assumed.

*Private communication, G. E. Hansen and W. H. Roach, Los Alamos Scientific Laboratory.

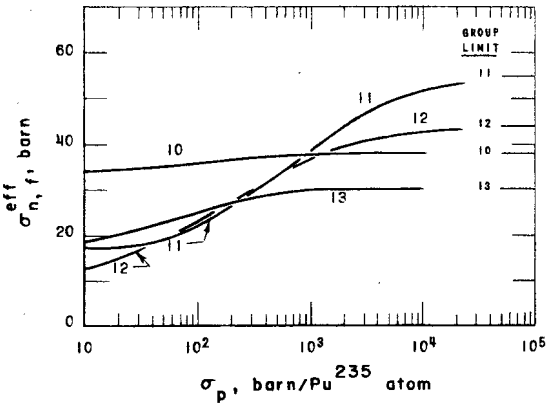

Fig. 6-5—Effective group fission cross section of U^{235} as a function of total material scattering cross section. *Reproduced from Ref. 7.*

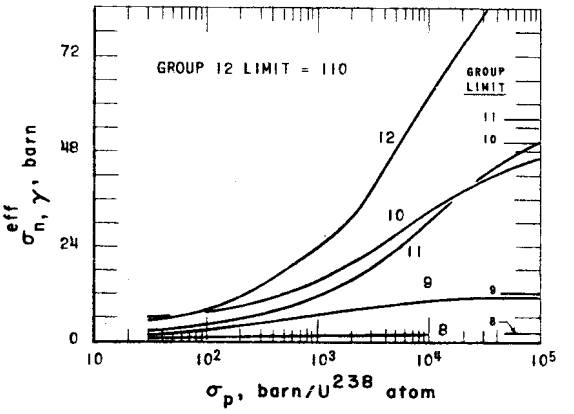

Fig. 6-6—Effective group capture cross section of U^{238} as a function of total material scattering cross section. *Reproduced from Ref. 7.*

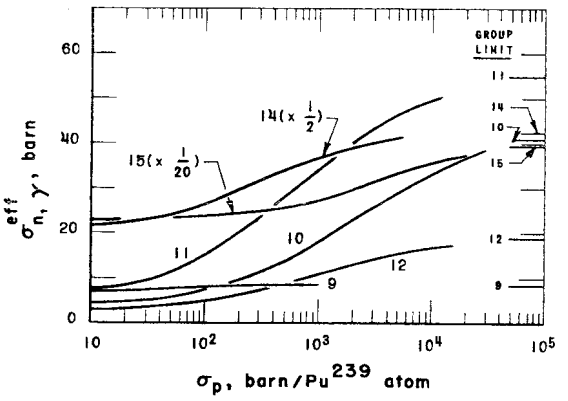

Fig. 6-7—Effective group capture cross section of Pu^{239} as a function of total material scattering cross section. *Reproduced from Ref. 7.*

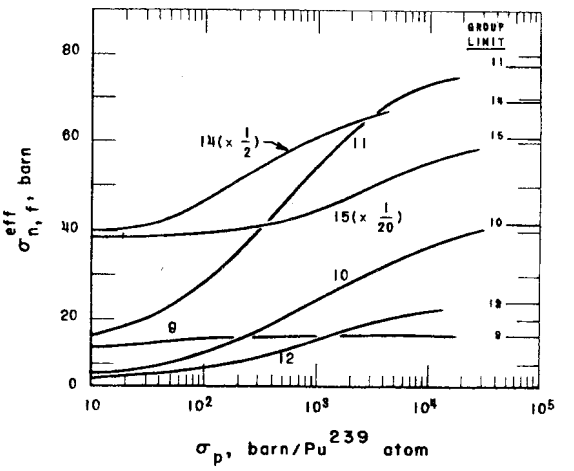

Fig. 6-8—Effective group fission cross section of Pu^{239} as a function of total material scattering cross section. *Reproduced from Ref. 7.*

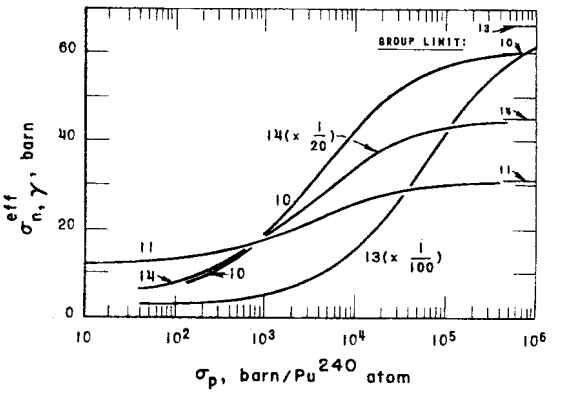

Fig. 6-9—Effective group capture cross section of Pu^{240} as a function of total material scattering cross section.

Although the curves given in Figs. 6-1 through 6-9 were intended for use with homogeneous systems, they may be applied also to heterogeneous systems. In this case, the appropriate value of σ_p may be determined using the techniques described in Sections 4.2.2 and 4.2.3.

The cross sections given in Table 7-2 have been used* to calculate several experimental systems. The results are given in Table 6-1. The calculations were made using the SNG code (Section 10) in the S4 approximation.

Table 6-1 — SYSTEMS CALCULATED USING CROSS SECTIONS IN TABLE 7-2

System[a]	Moderator Uranium	Geometry	B^2, cm^{-2}	Equiv. Crit. Sphere Radius, cm	k	Ref.
U-235 + BeO	247	Parallelepiped	8.35×10^{-3}	33.07	1.0097	8
U-235 + BeO	493	Parallelepiped	7.85×10^{-3}	34.16	1.0058	8
U-235 + BeO	1920	Parallelepiped	6.42×10^{-3}	38.02	1.0274	8
U-235 + BeO	3830	Parallelepiped	5.18×10^{-3}	41.95	1.0362	8
U-235 + Graphite	301	Parallelepiped	23.07×10^{-4}	63.51	1.0176	9
U-235 + Graphite	2355	Parallelepiped	19.42×10^{-4}	69.39	1.0197	9
Oralloy (93.2% U-235); Water Reflected	—	Sphere (r = 6.78 cm)		—	r_c (calc.) = 6.69 cm	10

[a]Unreflected except as noted.

6.2 REACTIVITY CONSIDERATIONS

6.2.1 DOPPLER EFFECT

The Doppler coefficient has been measured in two beryllium-moderated intermediate reactors at KAPL. Three materials were considered: UO_2 (highly enriched), $UO_2(U^{238})$, and hafnium. The experimental methods are described by Frost, et al.[11,12] The theoretical aspects of Doppler coefficients are discussed in detail by Bethe,[13] Feshbach, et al.,[14] and Nicholson.[15] The results of the experiments are summarized in Table 6-2.

Table 6-2 — DOPPLER COEFFICIENTS OF UO_2 AND HAFNIUM IN INTERMEDIATE REACTORS

Reproduced from Ref. 11.

Material	Thickness, $mole/cm^2$	PPA-21A		PPA-20	
		Temp. Range, °C	T dK/dT[a] per mole	Temp. Range, °C	T dK/dT[a] per mole
UO_2 (Highly Enriched)[b]	1.1×10^{-3}[c]	400–750	-0.26×10^{-4}[d] -0.17×10^{-4}[e]	325–725	-0.23×10^{-4}[d] -0.15×10^{-4}[e]
$UO_2(U^{238})$[b]	1.0×10^{-3}[c]	400–750	-2.07×10^{-4}[d]	320–700	-2.2×10^{-4}[d] -1.1×10^{-4}[e]
Hafnium	1.8×10^{-3} (0.86-mm wire)	400–750	-1.46×10^{-4}[d]	340–760	-2.1×10^{-4}[d]

[a]The error for all values of T dk/dT is ±15%; T in degrees Kelvin.

[b]The coefficient was measured for two positions in the reactors.

[c]The oxide samples were distributed as an annulus enclosed in stainless steel. The center of the annulus was MgO.

[d]Measured at center of assembly.

[e]Measured in Ring No. 5.

Note: Median energy of fission: PPA-20 = 50 ev; PPA-21A = 125 ev.

*Private communication, W. H. Roach, Los Alamos Scientific Laboratory.

Table 6-3—EFFECTIVE CROSS SECTIONS

	σ_p	$\bar{\sigma}_{n,f}$	$\bar{\sigma}_{n,\gamma}$	$\bar{\sigma}_{n,n}$	$\bar{\sigma}_{n,f}$	$\bar{\sigma}_{n,\gamma}$	$\bar{\sigma}_{n,n}$	$\bar{\sigma}_{n,f}$	$\bar{\sigma}_{n,\gamma}$	$\bar{\sigma}_{n,n}$	$\bar{\sigma}_{n,f}$	$\bar{\sigma}_{n,\gamma}$	$\bar{\sigma}_{n,n}$	$\bar{\sigma}_{n,f}$	$\bar{\sigma}_{n,\gamma}$	$\bar{\sigma}_{n,n}$	$\bar{\sigma}_{n,f}$	$\bar{\sigma}_{n,\gamma}$	$\bar{\sigma}_{n,n}$	$\bar{\sigma}_{n,f}$	$\bar{\sigma}_{n,\gamma}$	$\bar{\sigma}_{n,n}$	$\bar{\sigma}_{n,\gamma}$	$\bar{\sigma}_{n,n}$
		0.414 ≤ E ≤ 1.13 ev			1.13 ≤ E ≤ 3.06 ev			3.06 ≤ E ≤ 8.31 ev			8.31 ≤ E ≤ 22.6 ev			22.6 ≤ E ≤ 36 ev			0.41 – 36 ev Resonance Integral							
Uranium-235 T = 0.0253 ev	0.1	56.39	10.22	11.58	16.23	4.51	10.36	8.87	5.49	9.24	13.74	10.14	9.60	14.23	7.16	10.24	3.15	1.33						
	10	56.93	10.35	11.59	17.58	5.06	10.38	11.03	7.36	9.25	17.18	13.01	9.66	19.83	10.25	10.35	23.52	9.55						
	32	57.79	10.56	11.60	19.20	5.73	10.40	13.44	9.69	9.26	21.08	16.49	9.76	25.60	13.51	10.51	52.77	22.73						
	100	59.14	10.89	11.61	21.29	6.59	10.43	16.58	13.19	9.28	27.33[a]	22.56[a]	9.94	34.22[a]	18.58[a]	10.80	92.32	41.31						
	200	59.98	11.10	11.62	22.46	7.06	10.45	18.55	15.61	9.30	31.62[a]	27.03[a]	10.11	39.49[a]	21.77[a]	11.05	118.33	55.47						
	400	60.62	11.27	11.63	23.35	7.40	10.46	20.32	17.88	9.31	36.70[a]	32.38[a]	10.31	44.86[a]	25.06[a]	11.33	141.50	69.75						
	1600	61.30	11.44	11.63	24.27	7.75	10.47	22.75	21.05	9.33	47.41[a]	43.26[a]	10.75	53.56[a]	30.30[a]	11.84	174.91	93.41						
	10^4	61.53	11.51	11.64	24.59	7.86	10.47	23.89	22.54	9.34	55.66[a]	51.08[a]	11.08	58.46[a]	33.15[a]	12.16	193.7	107.9						
	∞	61.58	11.52	11.64	24.66	7.89	10.47	24.16	22.89		58.15	53.36		59.71	33.86		198.8	111.9						
		0.414 ≤ E ≤ 1.13 ev			1.13 ≤ E ≤ 3.06 ev			3.06 ≤ E ≤ 8.31 ev			8.31 ≤ E ≤ 22.6 ev			22.6 ≤ E ≤ 36 ev			0.41 – 36 ev Resonance Integral							
Uranium-235 T = 0.050 ev	0.1	56.47	10.25	11.58	16.31	4.59	10.36	9.07	5.70	9.24	14.96	11.22	9.63	15.91	8.10	10.30	3.13	1.33						
	10	57.01	10.38	11.59	17.66	5.14	10.38	11.30	7.67	9.25	18.52	14.27	9.70	22.11	11.58	10.42	23.62	10.16						
	32	57.87	10.59	11.60	19.27	5.80	10.40	13.75	10.09	9.26	22.47	17.90	9.80	28.20	15.08	10.60	53.33	23.40						
	100	59.22	10.92	11.61	21.33	6.63	10.43	16.91	13.64	9.28	28.75[a]	24.17[a]	9.99	36.90[a]	20.27[a]	10.91	93.58	42.68						
	200	60.04	11.13	11.62	22.48	7.07	10.45	18.85	16.03	9.30	33.07[a]	28.73[a]	10.17	42.03[a]	23.38[a]	11.16	120.0	57.25						
	400	60.69	11.29	11.63	23.34	7.39	10.46	20.55	18.20	9.31	38.14[a]	34.05[a]	10.38	47.09[a]	26.46[a]	11.43	143.4	71.70						
	1600	61.36	11.47	11.63	24.24	7.70	10.47	22.78	21.08	9.33	48.44[a]	44.29[a]	10.80	54.80[a]	31.05[a]	11.91	176.4	94.65						
	10^4	61.59	11.53	11.64	24.54	7.81	10.47	23.76	22.35	9.34	55.74[a]	50.97[a]	11.08	58.81[a]	33.34[a]	12.18	193.8	107.7						
	∞	61.63	11.54	11.64	24.60	7.83	10.47	23.99	22.64	9.34	57.81	52.79		59.78	33.89		198.3	111.1						
		0.414 ≤ E ≤ 1.13 ev			1.13 ≤ E ≤ 3.06 ev			3.06 ≤ E ≤ 8.31 ev			8.31 ≤ E ≤ 22.6 ev			22.6 ≤ E ≤ 36 ev			0.41 – 36 ev Resonance Integral							
Uranium-235 T = 0.10 ev	0.1	56.64	10.30	11.59	16.47	4.74	10.36	9.47	6.16	9.24	17.04	13.06	9.69	18.68	9.64	10.39	3.12	1.37						
	10	57.17	10.43	11.59	17.81	5.29	10.38	11.84	8.34	9.25	20.62	16.30	9.76	25.52	13.53	10.51	23.77	10.50						
	32	58.03	10.64	11.60	19.41	5.93	10.40	14.36	10.89	9.26	24.55	20.09	9.87	31.65	17.12	10.70	54.08	24.42						
	100	59.36	10.97	11.61	21.42	6.70	10.43	17.49	14.41	9.28	30.81[a]	26.54[a]	10.07	39.83[a]	22.05[a]	11.02	95.24	44.56						
	200	60.18	11.18	11.62	22.53	7.10	10.45	19.35	16.66	9.30	35.14[a]	31.10[a]	10.25	44.49[a]	24.88[a]	11.27	122.2	59.53						
	400	60.81	11.34	11.63	23.36	7.39	10.46	20.93	18.61	9.31	40.13[a]	36.24[a]	10.46	48.96[a]	27.58[a]	11.54	145.8	74.00						
	1600	61.47	11.51	11.63	24.20	7.67	10.47	22.88	21.07	9.33	49.65[a]	45.34[a]	10.85	55.44[a]	31.38[a]	11.98	177.9	95.73						
	10^4	61.70	11.56	11.64	24.49	7.76	10.47	23.68	22.08	9.34	55.74[a]	50.70[a]	11.08	58.56[a]	33.15[a]	12.20	193.7	107.1						
	∞	61.74	11.58	11.64	24.55	7.78	10.47	23.86	22.30	9.34	57.36[a]	52.07[a]		59.28[a]	33.56[a]		197.6	109.9						
		0.414 ≤ E ≤ 1.13 ev			1.13 ≤ E ≤ 3.06 ev			3.06 ≤ E ≤ 8.31 ev			8.31 ≤ E ≤ 22.6 ev			22.6 ≤ E ≤ 36 ev			0.41 – 36 ev Resonance Integral							
Uranium-235 T = 0.20 ev	0.1	56.94	10.40	11.59	16.75	4.97	10.36	10.14	6.94	9.23	20.10	15.85	9.77	22.47	11.80	10.50	3.09	1.39						
	10	57.47	10.53	11.59	18.08	5.51	10.38	12.66	9.38	9.24	23.36	18.95	9.85	29.57	15.94	10.62	23.93	10.91						
	32	58.31	10.73	11.60	19.64	6.12	10.40	15.21	12.06	9.26	27.12	22.77	9.97	35.45	19.48	10.81	54.92	25.63						
	100	59.63	11.06	11.61	21.59	6.82	10.43	18.19	15.44	9.28	33.33[a]	29.35[a]	10.19	42.94[a]	24.08[a]	11.12	97.14	46.80						
	200	60.43	11.26	11.62	22.64	7.17	10.45	19.86	17.43	9.30	37.64[a]	33.87[a]	10.37	47.13[a]	26.64[a]	11.36	124.6	62.20						
	400	61.04	11.42	11.63	23.42	7.42	10.46	21.21	19.08	9.31	42.47[a]	38.69[a]	10.57	51.05[a]	28.98[a]	11.61	148.5	76.65						
	1600	61.69	11.58	11.64	24.20	7.66	10.47	22.79	21.01	9.33	50.93[a]	46.45[a]	10.90	56.47[a]	32.09[a]	11.99	179.6	97.02						
	10^4	61.91	11.64	11.64	24.46	7.74	10.47	23.40	21.76	9.33	55.75[a]	50.52[a]	11.08	58.92[a]	33.45[a]	12.18	193.8	106.8						
	∞	61.95	11.65	11.64	24.51	7.76	10.47	23.53	21.92	9.33	56.95	51.50		59.48	33.75		197.1	109.1						

		0.414 ≤ E ≤ 1.13 ev			1.13 ≤ E ≤ 3.06 ev			3.06 ≤ E ≤ 8.31 ev			8.31 ≤ E ≤ 22.6 ev			22.6 ≤ E ≤ 36 ev			0.41 – 36 ev Resonance Integral				
Uranium-235 T = 0.50 ev	0.1	57.66	10.64	11.59	17.36	5.45	10.36	11.75	8.92	9.23	25.31	21.07	9.93	29.17	15.77	10.64	3.04	1.44			
	10	58.17	10.76	11.60	18.63	5.94	10.38	14.33	11.56	9.24	27.83	23.59	10.01	34.33	18.97	10.75	24.09	11.57			
	32	58.97	10.96	11.60	20.12	6.46	10.40	16.76	14.16	9.26	31.28	27.19	10.14	39.16	21.96	10.91	56.05	27.39			
	100	60.24	11.28	11.62	21.93	7.03	10.43	19.36	17.07	9.29	37.36[a]	33.60[a]	10.36	45.31[a]	25.74[a]	11.20	99.79	49.82			
	200	61.00	11.47	11.62	22.88	7.30	10.44	20.70	18.61	9.30	41.49[a]	37.81[a]	10.54	48.75[a]	27.81[a]	11.42	128.0	65.66			
	400	61.60	11.62	11.63	23.56	7.49	10.45	21.71	19.79	9.31	45.82[a]	41.99[a]	10.72	51.94[a]	29.66[a]	11.65	151.9	79.93			
	1600	62.22	11.78	11.64	24.22	7.68	10.46	22.79	21.07	9.32	52.49[a]	47.89[a]	10.97	56.19[a]	32.05[a]	11.97	181.4	98.56			
	10^4	62.43	11.83	11.64	24.44	7.74	10.47	23.17	21.53	9.33	55.75[a]	50.57[a]	11.09	58.04[a]	33.05[a]	12.12	193.7	106.6			
	∞	62.47	11.84	11.64	24.48	7.75	10.47	23.25	21.62	9.33	56.51	51.17		58.44	33.27		196.4	108.4			

		0.414 ≤ E ≤ 1.13 ev			1.13 ≤ E ≤ 3.06 ev			3.06 ≤ E ≤ 8.31 ev			8.31 ≤ E ≤ 22.6 ev			22.6 ≤ E ≤ 61.4 ev			61.4 ≤ E ≤ 167 ev			167 ≤ E ≤ 419 ev			0.41 – 419 ev Resonance Integral	
Uranium-238 T = 0.0253 ev	0.1		0.619	8.75		0.500	8.57		1.35	8.11		0.54	8.03		0.37	9.55		0.17	10.28		0.10	10.67	0.54	
	10		0.624	8.75		0.501	8.57		3.56	8.24		1.60	8.32		1.38	10.63		1.19	11.53		0.78	12.51	8.09	
	20		0.624	8.75		0.502	8.57		4.73	8.32		2.15	8.51		1.84	11.18		1.72	12.08		1.16	13.20	11.24	
	80		0.625	8.75		0.502	8.57		8.91	8.60		4.19	9.18		3.50	12.79		3.69	13.77		1.40[a]	15.31	21.26	
	200		0.625	8.75		0.502	8.57		14.19	8.93		6.90	10.01		5.58	14.56		4.16[a]	15.72		2.23[a]	17.72	32.47	
	400		0.625	8.75		0.502	8.57		20.62	9.31		10.28	11.04		8.10	16.60		5.80[a]	17.99		3.18[a]	20.37	47.42	
	2000		0.625	8.75		0.502	8.57		48.86	10.97		21.40[a]	15.69		12.55[a]	25.96		11.78[a]	27.15		6.03[a]	28.79	100.4	
	10^4		0.625	8.75		0.502	8.57		89.41[a]	13.45		42.33[a]	23.26		27.28[a]	44.74		18.40[a]	38.58		8.14[a]	36.16	186.9	
	∞		0.625	8.75		0.502	8.57		126.92			63.39			47.47			22.76			9.19[a]		273.4	

		0.414 ≤ E ≤ 1.13 ev			1.13 ≤ E ≤ 3.06 ev			3.06 ≤ E ≤ 8.31 ev			8.31 ≤ E ≤ 22.6 ev			22.6 ≤ E ≤ 61.4 ev			61.4 ≤ E ≤ 167 ev			167 ≤ E ≤ 419 ev			0.41 – 419 ev Resonance Integral	
Uranium-238 T = 0.050 ev	0.1		0.619	8.75		0.500	8.57		1.35	8.11		0.54	8.04		0.37	9.57		0.17	10.35		0.10	10.99	0.54	
	10		0.624	8.75		0.502	8.57		3.59	8.24		1.62	8.34		1.39	10.66		1.30	11.64		0.88	12.77	8.29	
	20		0.624	8.75		0.502	8.57		4.79	8.32		2.19	8.54		1.87	11.21		1.92	12.23		1.32	13.48	11.63	
	80		0.625	8.75		0.502	8.57		9.26	8.62		4.41	9.25		3.65	12.89		4.24	14.10		1.59[a]	15.78	22.52	
	200		0.625	8.75		0.502	8.57		15.16	8.99		7.53	10.19		6.02	14.82		4.74[a]	16.35		2.51[a]	18.45	35.05	
	400		0.625	8.75		0.502	8.57		22.50	9.42		11.54	11.38		8.94	17.13		6.59[a]	18.98		3.52[a]	21.33	52.16	
	2000		0.625	8.75		0.502	8.57		54.22	11.27		24.64[a]	16.83		13.98[a]	27.77		12.91[a]	28.97		6.21[a]	29.84	111.41	
	10^4		0.625	8.75		0.502	8.57		94.97[a]	13.78		46.42[a]	24.72		28.99[a]	46.90		19.04[a]	39.91		7.96[a]	36.41	198.65	
	∞		0.625	8.75		0.502	8.57		126.87			64.38			46.22			22.56			8.73		272.5	

		0.414 ≤ E ≤ 1.13 ev			1.13 ≤ E ≤ 3.06 ev			3.06 ≤ E ≤ 8.31 ev			8.31 ≤ E ≤ 22.6 ev			22.6 ≤ E ≤ 61.4 ev			61.4 ≤ E ≤ 167 ev			167 ≤ E ≤ 419 ev			0.41 – 419 ev Resonance Integral	
Uranium-238 T = 0.200 ev	0.1		0.619	8.75		0.500	8.57		1.36	8.13		0.56	8.10		0.37	9.66		0.19	10.74		0.10	11.78	0.54	
	10		0.624	8.75		0.502	8.57		3.77	8.27		1.72	8.44		1.46	10.80		1.74	12.11		1.22	13.56	9.11	
	20		0.624	8.75		0.502	8.57		5.19	8.37		2.42	8.67		2.03	11.41		2.66	12.82		1.91	14.44	13.27	
	80		0.625	8.75		0.502	8.57		11.10	8.74		5.49	9.61		4.44	13.44		6.04	15.37		2.31[a]	17.53	27.75	
	200		0.625	8.75		0.502	8.57		19.55	9.24		9.99	10.94		7.87	16.05		6.55[a]	18.58		3.56[a]	21.03	45.19	
	400		0.625	8.75		0.502	8.57		30.06	9.85		15.59	12.62		12.05	19.34		8.97[a]	22.20		4.70[a]	24.44	68.82	
	2000		0.625	8.75		0.502	8.57		69.44	12.16		31.86[a]	19.44		18.74[a]	33.85		15.88[a]	33.81		7.06[a]	32.72	141.22	
	10^4		0.625	8.75		0.502	8.57		105.89[a]	14.42		52.30[a]	26.81		34.09[a]	53.37		20.73[a]	42.92		8.24[a]	37.63	222.35	
	∞		0.625	8.75		0.502	8.57		126.21			64.08			45.48			22.83			8.68		271.0	

		0.414 ≤ E ≤ 1.13 ev			1.13 ≤ E ≤ 3.06 ev			3.06 ≤ E ≤ 8.31 ev			8.31 ≤ E ≤ 22.6 ev			22.6 ≤ E ≤ 61.4 ev			61.4 ≤ E ≤ 167 ev			167 ≤ E ≤ 419 ev			0.41 – 419 ev Resonance Integral	
Uranium-238 T = 2.0 ev	0.1		0.619	8.74		0.502	8.56		1.50	8.23		0.60	8.55		0.39	10.74		0.33	13.64		0.17	14.60	0.57	
	10		0.625	8.74		0.504	8.57		5.94	8.45		2.59	9.04		2.27	12.05		3.94	14.89		2.70	16.55	13.57	
	20		0.625	8.74		0.504	8.57		9.18	8.64		4.15	9.45		3.51	12.95		5.76	15.96		3.82	17.92	21.37	
	80		0.625	8.74		0.504	8.57		22.99	9.42		11.11	11.37		8.72	16.71		11.13	20.46		4.22[a]	22.72	49.67	
	200		0.625	8.74		0.504	8.57		40.36	10.42		20.07	14.06		15.27	21.93		11.37[a]	25.75		5.58[a]	27.14	81.96	
	400		0.625	8.74		0.504	8.57		57.95	11.45		29.13	16.99		21.85	28.09		14.28[a]	30.71		6.52[a]	30.57	119.20	
	2000		0.625	8.74		0.504	8.57		98.92	13.91		46.54[a]	24.69		29.85[a]	47.70		19.83[a]	41.08		7.93[a]	36.45	197.96	
	10^4		0.625	8.74		0.504	8.57		118.41[a]	15.14		58.28[a]	28.92		40.94[a]	61.81		22.07[a]	45.60		8.41[a]	38.64	248.98	
	∞		0.625	8.74		0.504	8.57		125.44			62.46			45.59			22.77			8.55		268.56	

687863 O - 63 - 35

Table 6-3—EFFECTIVE CROSS SECTIONS

Table 6-3—EFFECTIVE CROSS SECTIONS (Continued)

	σ_p	$\tilde{\sigma}_{n,f}$	$\tilde{\sigma}_{n,\gamma}$	$\tilde{\sigma}_{n,n}$	$\tilde{\sigma}_{n,f}$	$\tilde{\sigma}_{n,\gamma}$	$\tilde{\sigma}_{n,n}$	$\tilde{\sigma}_{n,f}$	$\tilde{\sigma}_{n,\gamma}$	$\tilde{\sigma}_{n,n}$	$\tilde{\sigma}_{n,f}$	$\tilde{\sigma}_{n,\gamma}$	$\tilde{\sigma}_{n,n}$	$\tilde{\sigma}_{n,f}$	$\tilde{\sigma}_{n,\gamma}$	$\tilde{\sigma}_{n,n}$	$\tilde{\sigma}_{n,f}$	$\tilde{\sigma}_{n,\gamma}$	$\tilde{\sigma}_{n,n}$	$\tilde{\sigma}_{n,f}$	$\tilde{\sigma}_{n,\gamma}$	$\tilde{\sigma}_{n,n}$	$\tilde{\sigma}_{n,\gamma}$	$\tilde{\sigma}_{n,n}$
		0.025 ≤ E ≤ 0.056 ev			0.056 ≤ E ≤ 0.414 ev			0.414 ≤ E ≤ 1.13 ev			1.13 ≤ E ≤ 3.06 ev			3.06 ≤ E ≤ 8.31 ev			8.31 ≤ E ≤ 22.6 ev			22.6 ≤ E ≤ 43 ev				
Plutonium-239 T = 0.0253 ev	0.1	588.1	269.9	9.43	666.9	392.2	9.55	75.22	31.21	13.00	19.25	2.86	11.10	8.92	2.34	9.36	8.94	5.11	10.22	1.68	1.20	10.72		
	10	588.2	269.9	9.43	668.2	393.2	9.55	77.85	32.86	13.03	19.90	3.02	11.13	9.42	2.92	9.38	13.33	7.79	10.33	2.80	2.92	10.92		
	32	588.3	270.0	9.43	671.2	395.3	9.56	82.65	35.89	13.11	20.53	3.18	11.15	10.19	3.89	9.40	18.52	11.14	10.51	3.81	4.66	11.16		
	100	588.8	270.2	9.43	680.0	401.7	9.59	92.62	42.27	13.25	21.11	3.34	11.19	11.81	5.97	9.47	27.30	17.24	10.88	5.24[a]	7.37[a]	11.54		
	200	589.4	270.4	9.43	691.9	410.4	9.63	101.53	48.03	13.38	21.33	3.40	11.20	13.48	8.10	9.55	34.82	22.86	11.23	6.22[a]	9.42[a]	11.86		
	400	590.3	270.7	9.43	712.9	425.6	9.69	111.74	54.68	13.52	21.47	3.44	11.21	15.84[a]	11.10[a]	9.57	43.94[a]	29.93[a]	11.69	7.37[a]	11.95[a]	12.26		
	1600	592.7	271.5	9.43	794.4	484.1	9.96	130.30	66.88	13.75	21.59	3.47	11.22	22.41[a]	19.38[a]	10.04	63.84[a]	46.38[a]	12.83	9.71[a]	17.60[a]	13.21		
	10^4	594.6	272.2	9.43	937.9	586.2	10.44	141.79	74.50	13.89	21.62	3.48	11.22	30.17[a]	29.12[a]	10.47	81.07[a]	60.89[a]	13.86	11.41[a]	22.26[a]	14.05		
	∞	595.2	272.4	9.43	1022.3	645.9		144.84	76.52		21.63	3.49	11.22	33.36	33.13		86.80	65.69		11.91	23.72			
		0.025 ≤ E ≤ 0.056 ev			0.056 ≤ E ≤ 0.414 ev			0.414 ≤ E ≤ 1.13 ev			1.13 ≤ E ≤ 3.06 ev			3.06 ≤ E ≤ 8.31 ev			8.31 ≤ E ≤ 22.6 ev			22.6 ≤ E ≤ 43 ev				
Plutonium-239 T = 0.050 ev	0.1	588.3	270.0	9.41	668.8	393.5	9.58	75.31	31.28	12.99	19.25	28.6	11.10	8.92	2.35	9.36	9.04	5.19	10.24	1.70	1.24	10.73		
	10	588.4	270.1	9.41	670.2	394.5	9.59	77.96	32.94	13.03	19.90	30.2	11.12	9.44	2.94	9.38	13.52	7.97	10.36	2.90	3.13	10.94		
	32	588.6	270.1	9.41	673.2	396.6	9.60	82.77	35.99	13.10	20.53	31.8	11.15	10.23	3.94	9.40	18.92	11.51	10.57	4.00	5.07	11.19		
	100	589.1	270.3	9.41	682.0	403.0	9.63	92.80	42.41	13.24	21.11	33.4	11.19	11.94	6.13	9.47	28.16	18.07	10.99	5.58[a]	8.07[a]	11.62		
	200	589.7	270.5	9.41	694.0	411.7	9.67	101.8	48.21	13.37	21.34	34.0	11.20	13.73	8.40	9.56	36.13	24.13	11.39	6.66[a]	10.35[a]	11.99		
	400	590.6	270.8	9.41	715.1	427.0	9.74	112.1	54.93	13.51	21.47	34.4	11.21	16.26[a]	11.62[a]	9.69	45.65[a]	31.61[a]	11.92	7.89[a]	13.08[a]	12.43		
	1600	592.9	271.6	9.41	796.7	485.7	10.03	130.9	67.32	13.75	21.59	34.7	11.22	23.11[a]	20.24[a]	10.07	65.67[a]	48.11[a]	13.12	10.20[a]	18.65[a]	13.38		
	10^4	594.9	272.3	9.41	939.2	587.1	10.53	142.6	75.10	13.89	21.63	34.8	11.22	30.48[a]	29.51[a]	10.48	81.65[a]	61.22[a]	14.08	11.67[a]	22.57[a]	14.08		
	∞	595.4	272.5	9.41	1022.1	645.8		145.8	77.17		21.63	34.8	11.22	33.26	33.00		86.64	65.23		12.06	23.68			
		0.025 ≤ E ≤ 0.056 ev			0.056 ≤ E ≤ 0.414 ev			0.414 ≤ E ≤ 1.13 ev			1.13 ≤ E ≤ 3.06 ev			3.06 ≤ E ≤ 8.31 ev			8.31 ≤ E ≤ 22.6 ev			22.6 ≤ E ≤ 43 ev				
Plutonium-239 T = 0.10 ev	0.1	588.8	270.4	9.34	672.7	396.1	9.57	75.51	31.43	12.99	19.25	2.86	11.10	8.94	2.36	9.37	9.20	5.36	10.26	1.74	1.32	10.74		
	10	588.9	270.4	9.34	674.1	397.1	9.58	78.18	33.10	13.03	19.90	3.02	11.13	9.47	2.97	9.39	13.88	8.34	10.38	3.08	3.51	10.96		
	32	589.0	270.5	9.34	677.1	399.2	9.59	83.03	36.18	13.10	20.53	3.19	11.16	10.31	4.03	9.41	19.62	12.25	10.60	4.31	5.76	11.26		
	100	589.5	270.7	9.34	686.0	405.7	9.62	93.19	42.68	13.24	21.11	3.34	11.19	12.17	6.40	9.49	29.55	19.53	11.04	6.10[a]	9.23[a]	11.75		
	200	590.1	270.9	9.34	698.0	414.5	9.66	102.31	48.58	13.37	21.34	3.41	11.20	14.14	8.91	9.58	38.04	26.16	11.46	7.33[a]	11.83[a]	12.17		
	400	591.0	271.2.	9.34	719.3	429.8	9.73	112.82	55.44	13.51	21.48	3.45	11.21	16.92[a]	12.43[a]	9.72	48.04[a]	34.14[a]	11.98	8.69[a]	14.84[a]	12.68		
	1600	593.4	272.0	9.34	801.0	488.6	10.03	132.19	68.20	13.74	21.59	3.48	11.22	24.04[a]	21.40[a]	10.11	67.83[a]	50.36[a]	13.09	11.02[a]	20.43[a]	13.65		
	10^4	595.3	272.7	9.34	941.7	588.8	10.54	144.42	76.31	13.89	21.63	3.49	11.22	30.84[a]	29.96[a]	10.49	82.15[a]	61.75[a]	13.89	12.32[a]	23.91[a]	14.29		
	∞	595.9	272.9	9.34	1021.7	645.5		147.70	78.50		21.64	3.50	11.23	33.15	32.87		86.32	64.96		12.64	24.82			
		0.025 ≤ E ≤ 0.056 ev			0.056 ≤ E ≤ 0.414 ev			0.414 ≤ E ≤ 1.13 ev			1.13 ≤ E ≤ 3.06 ev			3.06 ≤ E ≤ 8.31 ev			8.31 ≤ E ≤ 22.6 ev			22.6 ≤ E ≤ 43 ev				
Plutonium-239 T = 0.20 ev	0.1	589.8	271.1	9.33	680.2	401.0	9.55	75.90	31.72	12.99	19.26	2.87	11.10	8.97	2.38	9.38	9.54	5.69	10.30	1.81	1.47	10.77		
	10	589.8	271.1	9.33	681.6	402.0	9.55	78.62	33.43	13.02	19.91	3.03	11.13	9.53	3.03	9.40	14.58	9.05	10.45	3.36	4.05	11.01		
	32	590.0	271.2	9.33	684.6	404.2	9.56	83.56	36.57	13.09	20.54	3.19	11.15	10.45	4.18	9.43	20.89	13.53	10.69	4.77	6.70	11.34		
	100	590.5	271.3	9.33	693.6	410.8	9.59	93.96	43.23	13.24	21.12	3.35	11.19	12.54	6.83	9.52	31.80	21.83	11.20	6.80[a]	10.67[a]	11.93		
	200	591.1	271.5	9.33	705.8	419.6	9.63	103.37	49.33	13.36	21.35	3.41	11.20	14.76	9.65	9.62	40.92	29.10	11.66	8.17[a]	13.57[a]	12.42		
	400	591.9	271.8	9.33	727.2	435.2	9.71	114.31	56.48	13.50	21.48	3.45	11.21	17.81[a]	13.53[a]	9.78	51.27[a]	37.38[a]	12.20	9.62[a]	16.76[a]	12.96		
	1600	594.3	272.6	9.33	808.9	493.9	9.99	134.83	70.03	13.73	21.60	3.48	11.22	25.06[a]	22.67[a]	10.17	70.27[a]	52.61[a]	13.25	11.86[a]	21.99[a]	13.88		
	10^4	596.2	273.3	9.33	945.8	591.6	10.49	148.13	78.88	13.87	21.64	3.49	11.22	31.09[a]	30.27[a]	10.50	82.59[a]	62.00[a]	13.90	12.97[a]	24.74[a]	14.38		
	∞	596.7	273.5	9.33	1020.9	644.9		151.76	81.30		21.65	3.50	11.22	32.94	32.60		85.93	64.46		13.22	25.40			
		0.025 ≤ E ≤ 0.056 ev			0.056 ≤ E ≤ 0.414 ev			0.414 ≤ E ≤ 1.13 ev			1.13 ≤ E ≤ 3.06 ev			3.06 ≤ E ≤ 8.31 ev			8.31 ≤ E ≤ 22.6 ev			22.6 ≤ E ≤ 43 ev				
Plutonium-239 T = 0.50 ev	0.1	592.7	273.2	9.35	700.8	414.9	9.61	77.14	32.64	12.98	19.27	2.88	11.10	9.04	2.44	9.41	10.64	6.72	10.43	2.03	1.87	10.86		
	10	592.8	273.2	9.35	702.3	415.9	9.61	80.00	34.45	13.02	19.92	3.04	11.12	9.67	3.16	9.43	16.62	11.03	10.61	4.00	5.26	11.14		
	32	593.0	273.2	9.35	705.4	418.2	9.63	85.24	37.80	13.09	20.56	3.21	11.15	10.75	4.50	9.47	24.08	16.72	10.93	5.71	8.53	11.54		
	100	593.4	273.4	9.35	714.5	424.8	9.66	96.41	45.00	13.23	21.14	3.37	11.18	13.21	7.63	9.57	36.65	26.72	11.53	8.07[a]	13.20[a]	12.23		
	200	594.0	273.6	9.35	726.8	433.8	9.71	106.73	51.73	13.35	21.37	3.43	11.20	15.77	10.88	9.69	46.63	34.79	12.05	9.57[a]	16.41[a]	12.78		
	400	594.8	273.9	9.35	748.4	449.5	9.79	119.03	59.81	13.50	21.51	3.47	11.21	19.12[a]	15.14[a]	9.85	57.17[a]	43.11[a]	12.60	11.03[a]	19.63[a]	13.34		
	1600	597.0	274.7	9.35	828.5	507.3	10.12	143.22	75.86	13.75	21.63	3.50	11.22	26.07[a]	23.94[a]	10.22	74.14[a]	56.14[a]	13.49	13.03[a]	24.24[a]	14.15		
	10^4	598.9	275.3	9.35	954.1	597.3	10.63	160.02	87.08	13.90	21.67	3.51	11.22	30.83[a]	29.95[a]	10.48	83.50[a]	62.86[a]	13.95	13.90[a]	26.33[a]	14.53		
	∞	599.5	275.5	9.35	1017.8	642.6		164.82	90.30		21.67	3.51	11.22	32.12	31.59		85.83	64.47		14.09	26.80			

		0.414 ≤ E ≤ 1.125 ev			1.125 ≤ E ≤ 3.06 ev			3.06 ≤ E ≤ 8.32 ev			8.32 ≤ E ≤ 22.6 ev			22.6 ≤ E ≤ 61.4 ev			61.4 ≤ E ≤ 167 ev			167 ≤ E ≤ 454 ev			0.414–454 ev Resonance Integral
Molybdenum	20		0.611	5.48		0.359	5.48		0.212	5.46		0.166	5.38		1.89[a]	6.80		1.15[a]	6.21		0.427[a]	6.23	3.73
T = 0.0253 ev	40		0.611	5.48		0.359	5.48		0.212	5.46		0.166	5.38		2.44[a]	7.28		1.45[a]	6.38		0.535[a]	6.41	5.06
	100		0.611	5.48		0.359	5.48		0.212	5.46		0.166	5.38		3.59[a]	8.24		1.99[a]	6.72		0.706[a]	6.76	7.28
	200		0.611	5.48		0.359	5.48		0.212	5.46		0.166	5.38		4.86[a]	9.30		2.51[a]	7.08		0.840[a]	7.08	9.41
	400		0.611	5.48		0.359	5.48		0.212	5.46		0.166	5.38		6.52[a]	10.69		3.13[a]	7.53		0.961[a]	7.41	11.98
	1000		0.611	5.48		0.359	5.48		0.212	5.46		0.166	5.38		9.15[a]	12.87		3.96[a]	8.15		1.081[a]	7.78	15.78
	2000		0.611	5.48		0.359	5.48		0.212	5.46		0.166	5.38		11.09[a]	14.48		4.48[a]	8.54		1.138[a]	7.96	18.45
	4000		0.611	5.48		0.359	5.48		0.212	5.46		0.166	5.38		12.65	15.78		4.85[a]	8.82		1.173[a]	8.07	20.54
	∞		0.611	5.48		0.359	5.48		0.212	5.46		0.166	5.38					5.33			1.212		23.70

		0.414 ≤ E ≤ 1.125 ev			1.125 ≤ E ≤ 3.06 ev			3.06 ≤ E ≤ 8.32 ev			8.32 ≤ E ≤ 22.6 ev			22.6 ≤ E ≤ 61.4 ev			61.4 ≤ E ≤ 167 ev			167 ≤ E ≤ 255 ev			0.414–255 ev Resonance Integral
Tungsten	0.1		3.80	5.15		3.15	4.96		6.51	5.77		6.21	16.88		1.01	22.11		0.29	11.14		0.57	20.66	0.59
T = 0.0253	10		3.83	5.15		3.18	4.96		9.90	5.85		10.67	22.09		3.29	24.00		1.13	12.00		2.57	24.21	19.72
	20		3.84	5.15		3.18	4.96		12.07	5.92		13.75	26.39		4.26	25.40		1.52	12.64		3.52	26.66	27.88
	80		3.85	5.15		3.18	4.96		20.04	6.21		25.37	45.08		7.23	30.25		1.41[a]	15.08		3.26[a]	35.63	50.81
	200		3.85	5.15		3.19	4.96		29.47	6.57		39.07	70.00		6.93[a]	35.18		1.94[a]	17.92		4.45[a]	46.03	74.34
	400		3.85	5.15		3.19	4.96		39.55	6.95		53.88	99.19		8.96[a]	40.07		2.47[a]	20.83		5.52[a]	57.00	102.8
	2000		3.85	5.15		3.19	4.96		70.12[a]	8.08		104.66	218.6		15.09[a]	54.77		3.90[a]	29.17		8.16[a]	91.19	195.7
	10^4		3.85	5.15		3.19	4.96		96.04[a]	8.97		155.45	434.1		19.71[a]	66.30		4.99[a]	35.80		9.99[a]	120.4	283.9
	∞		3.85	5.15		3.19	4.96		108.95			184.92			21.76			5.52			10.85		332.8

[a]Calculated using narrow resonance approximation.

Bell* has calculated effective cross sections for the energy regions of the resolved resonances of Mo, W, U^{235}, U^{238}, and Pu^{239}. The calculations were made for the homogeneous case from the narrow resonance and narrow resonance infinite mass theories as given in LA-2322,[16] with cross sections given by Devaney, et al.[17] Interference between resonance and potential scattering, as well as Doppler broadening, was included. Table 6-3 gives the effective cross sections in barns as functions of energy group, moderator cross section (σ_p in barns) per absorber atom, and temperature (for U^{235}, U^{238}, and Pu^{239}). Resonance integrals over the resolved resonances are also given, except for Pu^{239}. The effective scattering cross sections, $\tilde{\sigma}_{n,n}$, were computed using the narrow resonance approximation.

The tabulated results may be applied to non-homogeneous systems by using the techniques described in Sections 4.2.2 and 4.2.3 to determine the appropriate value of σ_p.

6.2.2 FISSION PRODUCT CAPTURE CROSS SECTION

A calculation of the fission product capture cross section, σ^{fp} in the intermediate to fast energy range has been made by Moldauer.[18]

$$\sigma^{fp} = \frac{\sum_i Y_i \sigma_i}{\sum_i Y_i}$$

where σ_i represents the isotopic capture cross sections, and Y_i the isotopic yields. His results are plotted in Fig. 6-10, along with earlier estimates of the capture cross section. The curve by Moldauer is dashed above 200 kev to indicate the decreased reliability of the calculations at higher energy. For lower energies, extrapolation of Fig. 6-10 down to about 5 ev assuming a 1/v dependence for σ should be valid.†

6.2.3 NEUTRON TEMPERATURE EFFECTS

For elevated temperature systems, modification of the thermal group cross sections is necessary in order to account for interaction between the neutrons and the hot moderator.

Mills‡ has used 12-group thermal cross sections obtained using the gas model, together with higher-energy-group cross sections similar to those in Table 7-2, to calculate elevated temperature systems studied by UCRL.§ Table 6-4 gives a comparison between calculated and measured§ values for graphite experiments.

A high-temperature BeO experiment on Hot Box[19] performed by UCRL§ having a BeO/U^{235} molar ratio of about 560/1 indicates an average nuclear temperature coefficient of reactivity between 90°F and 950°F of −\$0.39 ± \$0.05/100°F. Near 900°F, the measured nuclear temperature coefficient was −\$0.37 ± \$0.04/100°F. Mills,‡ using the cross sections mentioned above, calculated an average temperature coefficient of \$0.40. (Δk = 0.0080 corresponds to \$1.00).

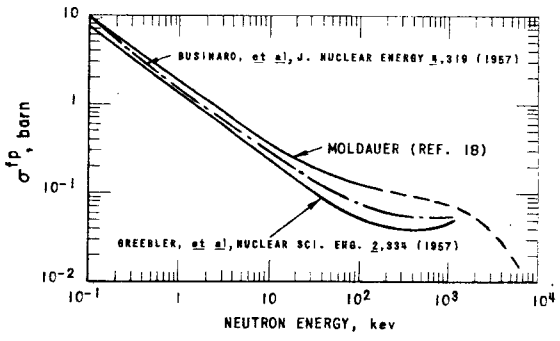

Fig. 6-10—Fission product capture cross section as a function of energy. *Reproduced from Ref. 18.*

Table 6-4—COMPARISON OF CALCULATED WITH MEASURED CRITICAL MASSES FOR HIGH-TEMPERATURE GRAPHITE ASSEMBLIES

Temp., °K	Critical Mass, kg U^{235}	
	Measured[a]	Calculated
293.2	19.01	—
452.7	21.06	20.91
674.9	23.68	23.84
911.0	25.92	25.58

[a] Core 4 × 3 × 6.125 ft^3; 1-foot C reflector on each end of 3-foot dimension. ρ(C) = 1.46 gm/cc, 6 ppm B assumed; 2-mil Oy foils. Room-temperature system has 0.855 kg SS-347/kg Oy (93.2% U^{235}). For each kg of Oy added to the higher temperature systems, there is 1.71 kg of SS-347 added. The C/U^{235} atomic ratio is 4250/1 for the room-temperature case including effects of self-shielding.

*Private communication, G. Bell, Los Alamos Scientific Laboratory.

†Private communication, P. Moldauer, Argonne National Laboratory.

‡Private communication, C. Mills, Los Alamos Scientific Laboratory. The calculations were made using the diffusion theory code FIRE (see Section 10).

§Private communication, R. Finke, Livermore Laboratory, UCRL.

6.3 INTEGRAL DATA

6.3.1 BERYLLIUM-MODERATED REACTORS

Unreflected. Two beryllium-moderated, unreflected reactors known as CA-1 and CA-18 are reported from ORNL.[20] System CA-1 is an intermediate reactor, while CA-18 has a slower spectrum, approaching that of a thermal reactor. The pertinent characteristics of both systems are given in Table 6-5.

Table 6-5 — CHARACTERISTICS OF ORNL REACTORS CA-1 AND CA-18

Reproduced from Ref. 20.

	CA-1	CA-18
Dimensions, in.	21.0 × 21.0 × 23.2	24.0 × 28.4 × 24.1
Spacing of 0.010-inch fuel discs, in.	1	4
U^{235} loading, kg	18.08	7.65
Observed reactivity	1.0054	1.0020
Be : U^{235} atomic ratio	390	1560
Volume fractions		
U	0.0064	0.0016
Be	0.9060	0.9128
Al	0.0610	0.0611
Stainless Steel	0.0004	0.0003
Void	0.0262	0.0242
Observed fraction of fissions caused by neutrons below Cd cutoff	0.46 ± 0.1	0.87 ± 0.03

Beryllium Reflected. A series of critical experiments with beryllium moderators, unreflected, and with beryllium reflectors, was performed on the KAPL "honeycomb" assembly.[21–25] In addition to the various reflector compositions, some of the assemblies were blanketed with natural uranium or lead.

The KAPL "honeycomb" is a hexagonal array of 2-inch aluminum or steel tubes.[26] The core and reflector sizes are measured in terms of the number of rings of tubes filled with a particular composition. The fuel is comprised of thin (0.020-inch) discs, spaced with thick (0.10- to 0.80-inch) beryllium discs. The distribution of the discs results in an assembly as homogeneous as can be obtained.

The loading and other pertinent information on the assemblies studied is given in Table 6-6. The reactors were made critical with one exception: PPA-6 was subcritical.

The spectrum, characterized by the median energy of fission (MEF), is shown by these experiments to be a parameter which can be adjusted by changing the ratio of fuel to moderator.[27] When the MEF is changed, a number of quantities which are energy sensitive also change. Among the more important of such quantities are (1) the fraction of fissions below Cd cutoff; and (2) the ratio of the effective absorption cross section per absorber atom, to the effective fission cross section per fuel atom. The subcadmium fraction is easily measured by standard techniques. The cross section ratio is derived from reactivity or "danger" coefficients.

An understanding of the physical effects occurring in the reactivity-coefficient measurements is obtained by normalizing the adjoint function to the iterated fission probability as developed by Hurwitz.[28] The iterated fission probability, $F(\underline{r},E)$, is the average number of fissions produced per generation, an infinite number of generations after a neutron of energy E has been introduced into a critical reactor at position $\underline{r}$. The reactivity change brought about by a change in material composition is then proportional to the number of neutrons added to (or removed from) the assembly, multiplied by their effectiveness represented by the iterated fission probability. The total fission rate, f_T, and the fission spectrum average of $F(\underline{r},E)$, denoted $F_H(\underline{r})$, are related as follows:

$$f_T = \iint \phi(\underline{r},E)\,\Sigma_f\,dE\,dV = \nu \iint \phi(\underline{r},E)\Sigma_f\,F_H(\underline{r})\,dE\,dV$$

where $\phi(\underline{r},E)$ = neutron flux per unit energy at position $\underline{r}$ and energy E
ν = average number of neutrons per fission
Σ_f = macroscopic fission cross section

Table 6-6—BERYLLIUM-MODERATED INTERMEDIATE REACTORS

Assembly:	PPA-1	PPA-2[a]	PPA-3[b]	PPA-4[b]	PPA-5[b]	PPA-6	PPA-7	PPA-8	PPA-9	PPA-10	PPA-11	PPA-21[a]	PPA-25	PPA-26
CORE														
No. of rings	5	6	5	5.5[c]	5.5[c]	5.5[c]	5.5[c]	6.5[c]	6.5[c]	5.5[c]	5	8	7	7
Core length, in.	16.5	20.1	17.2	18.6	18.6	17.1	17.1	17.1	18.1	18.1	17.1	27.3	27.7	27.7
Core volume, liter	—	~112	~62	85.0	85.1	78.0	78.0	111.9	118.6	86.0	62.6	273.0	208.2	208.2
Void, vol-%	—	15.7	15.7	15.5	15.5	6.2	6.4	6.3	6.4	6.0	7.4	13.1	15.1	15
Be : U atom ratio	218	134	48	45	33	45.4	23.6	50.1	55.2	4.13	1.73	92.9	113.7	113.7
Be, kg	87.8	161.2	77.4	82.7	72.6	78.7	60.3	112.1	119.5	19.9	8.2	220.6	206.6	206.6
vol-%	—	74.96	62.4	52.9	47.1	54.6	41.8	54.1	54.4	12.5	7.1	43.7	53.8	53
Mg, kg	—	—	—	—	—	—	—	—	—	—	—	98.4	—	—
vol-%	—	—	—	—	—	—	—	—	—	—	—	20.7	—	—
Na, kg	0	0	6.2	19.2	24.2	12.0	17.7	18.5	18.2	32.9	24.3	—	—	—
vol-%	—	—	9.8	23.2	28.37	15.8	23.4	16.9	15.8	39.4	40.0	—	—	—
Al, kg	3.4	2[e]	2[e]	2[e]	2[e]	13.9	13.9	19.9	21.1	15.3	11.1	124.2	95.4	95.4
vol-%	—	0.74	0.74	0.01	0.72	6.5	6.5	6.5	6.4	6.4	6.4	16.5	17.3	17.3
Fe, kg[d]	24.3	39.4	17.3	29.2	30.0	5.8	7.5	9.0	8.8	14.5	1.2	—	—	—
vol-%	—	5.2	2.87	0.293	4.35	1.0	1.4	1.0	1.0	2.2	2.2	—	—	—
Stainless Steel, kg	—	—	—	—	—	82.6	102.0	113.8	130.4	191.5	130.5	93.9	211.3	211.3
vol-%	—	—	—	—	—	12.6	15.8	12.4	13.4	25.4	25.8	4.3	13.3	16.0
U^{235}, kg	10.5	31.3	42.4	47.5	58.1	45.2	66.6	58.3	56.4	125.4	123.6	61.9	47.4	47.4
vol-%	—	1.54	3.47	2.99	3.57	3.1	4.6	2.8	2.6	7.8	10.6	1.2	2.0	2.0
U^{238}, kg	—	1.6	2.2	2.6	3.1	2.4	3.6	3.1	3.0	6.7	6.5	4.38	3.30	3.3
vol-%	—	0.1	0.21	0.18	0.22	0.2	0.2	0.2	0.1	0.4	0.6	0.1	0.1	0.1
Fuel thickness, in. (foils)	—	0.02	0.02	0.02	0.02	—	—	—	—	—	0.04	—	—	—
Poison	—	—	—	—	—	—	—	—	—	—	—	Pyrex Rods	—	—
END REFLECTOR[f]														
Thickness, in.	—	—	—	—	—	7.6	7.6	—	7.2	7.2	9.7	17.5	17.4	17.4
Volume, liters	—	—	—	—	—	27.4	27.4	39.3	36.9	27.0	28.1	175	130.8	130.8
% Void	—	—	—	—	—	5.0	5.0	5.1	5.7	6.2	5.3	13.5	12.8	12.8
Be, kg	—	—	—	—	—	35.8	35.8	51.3	47.4	34.1	27.6	140.5	104.7	104.7
vol-%	—	—	—	—	—	70.3	70.3	70.4	69.2	68.2	52.9	—	—	—
Mg, kg	—	—	—	—	—	—	—	—	—	—	—	117.6	—	—
Na, kg	—	—	—	—	—	2.8	2.8	4.0	4.0	3.0	6.8	—	—	—
vol-%	—	—	—	—	—	10.6	10.6	10.6	11.2	11.6	24.7	—	—	—
Al, kg	—	—	—	—	—	5.0	5.0	7.2	6.7	4.9	5.2	—	134.7	134.7
vol-%	—	—	—	—	—	6.6	6.6	6.6	6.6	6.6	6.6	—	—	—
Fe, kg	—	—	—	—	—	1.4	1.4	2.0	2.0	1.5	3.3	—	—	—
vol-%	—	—	—	—	—	0.6	0.6	0.6	0.7	0.7	1.5	—	—	—
Stainless Steel, kg	—	—	—	—	—	14.9	14.9	21.3	20.0	14.6	20.4	61.3	45.3	45.3
vol-%	—	—	—	—	—	6.8	6.8	6.7	6.7	6.8	8.9	—	—	—

SIDE REFLECTOR														
No. of rings	—	—	1	1.5	1.5	1.5	1.5	1.5	1.5	1.5	1.5	4	4	4
Volume, liters	—	—	—	—	—	52.4	52.4	61.6	65.3	52.2	49.3	518.1	463.5	463.5
% Void	—	—	21.7	21.0	21.0	5.8	5.8	5.7	5.7	5.7	5.6	13	12.8	12.8
Be, kg	76.8	—	71.3	143.4	143.4	72.7	72.7	88.0	90.6	74.2	67.2	793.4	710.3	710.3
vol-%	—	—	—	—	—	77.0	77.0	77.0	74.9	76.7	73.4	—	—	—
Na, kg	—	—	—	0.416	—	1.9	1.9	2.2	3.7	2.2	3.5	—	—	—
vol-%	—	—	—	—	—	3.7	3.7	3.7	5.8	4.2	7.4	—	—	—
Al, kg	—	—	1.9	3.0	6.6	9.3	9.3	10.9	11.6	9.3	9.0	—	—	—
vol-%	—	—	—	—	—	6.6	6.6	6.6	6.4	6.4	6.4	—	—	—
Fe, kg	—	—	25.4	19.0	46.9	0.91	0.91	1.08	1.79	0.99	1.7	—	—	—
vol-%	—	—	—	—	—	0.22	0.22	0.22	0.35	0.25	0.44	—	—	—
Stainless Steel, kg	—	—	—	—	—	28.5	28.5	33.4	35.4	28.2	10.9	184.1	159.2	159.2
vol-%	—	—	—	—	—	6.8	6.8	6.7	6.7	6.7	6.8	—	—	—
Poison	—	—	—	—	—	—	—	—	—	—	—	B_4C Rods in curtain at interface; 4.40 kg B_4C		B_4C rods at interface
$ of Poison	—	—	—	—	—	—	—	—	—	—	—	~12	—	8.4
BLANKET														
Material	Pb	U	U	U	—	U	U	U	U	U	U	—	—	—
Thickness, in.	—	12	12	12	—	—	—	—	—	—	—	—	—	—
End, vol-%	—	—	—	—	—	17.0	25.2	17.1	18.8	48.9	53.6	—	—	—
Side, vol-%	—	—	—	—	—	69.5	69.5	56.3	55.1	66.7	56.5	—	—	—

[a] No reflector.
[b] Weights include end reflector.
[c] Tube ring contains 50% core slugs and 50% reflector slugs.
[d] Includes iron in sodium containers.
[e] Aluminum present for shimming.
[f] Cores PPA-1 to PPA-5 had no end reflectors.

When a pure absorber is inserted in a void space in the reactor, the resultant reactivity change is given by:

$$\Delta k/k = -N \int \phi(\underline{r},E)\, \sigma_a(E)\, F(\underline{r},E)\, dE/f_T$$

where N = number of absorber atoms
σ_a = microscopic absorption cross section of the absorber

The reactivity coefficient, RC_a, can then be defined for one mole of absorber, and expressed in cents/mole by:

$$(RC_a) = \frac{-N_0 F_L(\underline{r}) \int \phi\, \sigma_a dE}{cf_T} = -\frac{\Delta_a F_L}{cf_T}$$

where c = one hundredth of the reactivity difference between delayed and prompt critical = 1 cent
$\Delta_a = N_0 \int \phi \sigma_a\, dE$ = absorption rate in one mole of absorber at $\underline{r}$
N_0 = Avogadro's number
$F_L(\underline{r})$ = iterated fission probability averaged over the absorption spectrum of the sample

$$= \frac{\int \phi(\underline{r},E)\, \sigma_a(E)\, F(\underline{r},E)\, dE}{\int \phi(\underline{r},E)\, \sigma_a(E)\, dE}$$

The term $F_L(\underline{r})$ can be evaluated in a critical assembly by observing the reactivity change associated with a resonance absorber such as gold or manganese, and measuring the neutron absorption rate by the foil activation. The total fission rate, f_T, can also be measured. The ratio of effective absorber cross section to effective fission cross section for U^{235} as fuel is then given by:

$$\frac{\bar{\sigma}_a(\underline{r})}{\bar{\sigma}_f(\underline{r})} \equiv \frac{N_0 \int \phi(\underline{r},E)\sigma_a(E)\, dE}{N_0 \int \phi(\underline{r},E)\sigma_f(E)\, dE} = \frac{\Delta_a(\underline{r})}{\Delta_f(\underline{r})} = \frac{-RC_a}{(235/M)\,[P(\underline{r})/P_{avg}][F_L(\underline{r})/c]}$$

where $\Delta_f(\underline{r})$ = fission rate in one mole of fuel at $\underline{r}$
M = total fuel load in grams
$\frac{P(\underline{r})}{P_{avg}}$ = ratio of power density at $\underline{r}$, to the average power density

The results for typical intermediate assemblies are summarized in Table 6-7. The ratios $\bar{\sigma}_a(0)/\bar{\sigma}_f(0)$ for a number of materials at the centers of the cores given in Table 6-7 were deduced from central "danger" coefficient results, using the listed values of $F_L(0)/c$ and $P(0)/P_{avg}$. The median-energy-of-fission given in Table 6-7 is defined as the energy E_{med} for which

$$\int_0^{E_{med}} \sigma_f(E)\phi(\underline{r},E)F(\underline{r},E)dE = \int_{E_{med}}^{\infty} \sigma_f(E)\phi(\underline{r},E)F(\underline{r},E)dE$$

An additional study of PPA-21 critical assemblies (Table 6-8) is of interest because of the variations in the basic loading. The boron curtain consisted of B_4C rods placed in the interstices between the circular tubes on the periphery of the core. Other changes are self-evident in the table.

6.3.2 BERYLLIUM OXIDE–MODERATED REACTORS

A series of BeO-moderated, Oralloy-fueled (93.2% U^{235}), graphite-reflected assemblies has been studied at UCRL.[29] Figure 6-11 is a schematic of the basic system for the assemblies having a core BeO/U^{235} atomic ratio of 247. Table 6-9 gives a description of the various "X" materials used. The results of the critical measurements are given in Table 6-10. Figure 6-12 summarizes the measurements in Reactors No. 1 through No. 4.

Figure 6-13 and Table 6-11 give results[29] for unreflected systems having a core BeO/U^{235} atomic ratio of 493.

The effect of temperature on BeO-moderated systems has been investigated.* The results are summarized in Table 6-12.

Other studies have included BeO-moderated, graphite-reflected systems containing gaps between the core and reflector.† Figure 6-14 shows the configurations utilized. The results are summarized in Table 6-13.

*Private communication, R. Finke and G. Grammens, Livermore Laboratory, UCRL.
†Private communication, E. Goldberg, Livermore Laboratory, UCRL.

Table 6-7 — SUMMARY OF SPECTRUM-SENSITIVE QUANTITIES IN PPA REACTORS

Data from Ref. 27.

Critical assembly	PPA-11[a]	PPA-5	PPA-20a	PPA-12
Core volume, liter	62.6	85.1	293.9	272
Equivalent core dia., cm	42.8	47.9	73.4	70.8
Fuel inventory, kg	123.6	58.1	51.7	39.8
Be : U^{235} atom ratio	1.73 : 1	33 : 1	137.5 : 1	178.5 : 1
Median-energy-of-fission (at core center)	235 kev	1500 ev	82 ev	40 ev
Fraction of fissions below Cd cutoff (at core center)	<0.01	0.02	0.09	0.24
Side reflector composition	Be	Be	Be + B	Be + Void
$F_L(0)/c$	0.86×10^4	0.97×10^4	1.45×10^4	1.42×10^4
$P(0)/P_{avg}$	1.09	1.12	1.60	1.77
$\bar{\sigma}_a/\bar{\sigma}_f$ of Selected Materials (at core center)				
B	0.17	0.56	0.75	1.02
Cr	—	0.0010	0.0036	0.0044
Mn	—	0.071	0.031	0.022
Co	—	0.14	0.123	—
Ni	—	0.0063	0.0066	—
Nb	0.032	0.092	0.036	0.034
Mo	0.041	0.072	0.048	0.043
Rh	0.27	0.43	0.78	0.90
Pd	0.10	0.18	—	0.10
Ag	—	0.57	1.21	0.45
Cd	—	0.22	1.83	2.22
Cs	—	0.26	0.30	0.63
Sm	—	0.90	4.2	—
Ta	0.17	0.39	1.14	0.47
W	—	0.20	0.40	—
Au	0.17	0.76	1.64	—

[a]The samples used in this assembly were all sufficiently thin so that self-shielding effects were negligible.

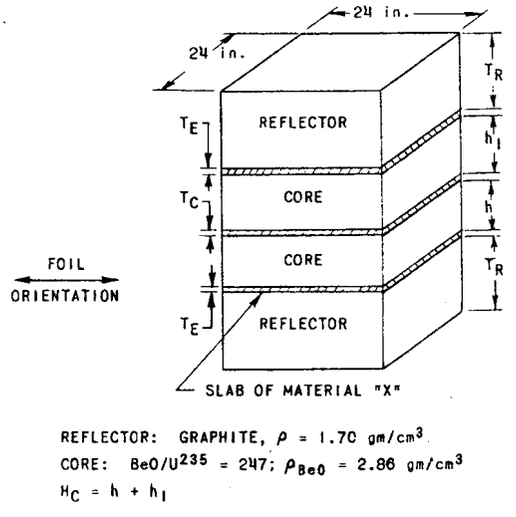

Fig. 6-11 — Basic sandwich system. *Reproduced from Ref. 29.*

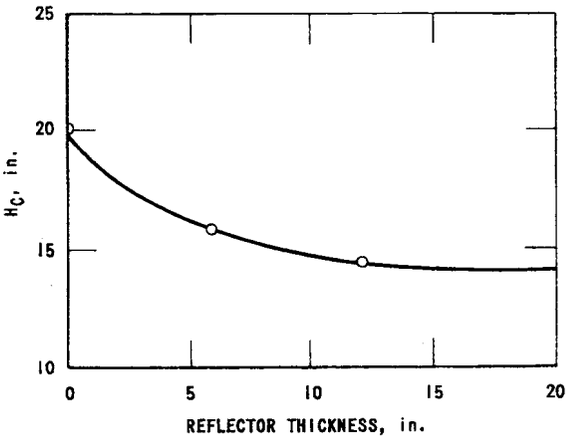

Fig. 6-12 — Critical core height vs. graphite reflector thickness for sandwich systems. *Reproduced from Ref. 29.*

Table 6-8—COMPOSITION CHANGES IN PPA-21

Data from Ref. 11.

PPA	Description	Composition, mol			Be : U^{235}	Approx. Reactivity Value of Boron, $[a]	
		Cd	Be	U^{235}		Core	Curtain
21A	Half of interstices filled with U-Al alloy rods (4.99 kg interstitial fuel). Boron curtain at core-reflector boundary to balance excess reactivity.	—	24454	263.27	92.9	—	15.00
21B	Second half of interstices filled with beryllium (1654 mols Be added). Increase in reactivity balanced by additional boron rods at core reflector boundary.	—	26108	263.27	99.2	—	19.00
21C	Beryllium (added in PPA 21B) balanced by boron rods distributed through core. Fuel removed from interstices to make room for boron rods.	—	26108	261.10	100	4.00	15.00
21D	Beryllium (added in PPA 21B) balanced by cadmium distributed through core (4.55 kg of Cd).	40.5	26108	261.10	100	—	15.00
21E	Interstitial beryllium removed; 4.8 kg interstitial fuel added. Loss of reactivity balanced by removal of cadmium (3.17 kg of Cd in core).	28.22	24454	280.82	87.1	—	15.00
21F	All cadmium removed from core. Excess reactivity balanced by addition of boron curtain.	—	24454	280.82	87.1	—	17.50
21G	All boron removed from curtain. All interstitial fuel removed (9.78 kg). Excess reactivity balanced by cadmium distributed through core.	108.1	24454	242.04	101	—	—

[a] $1 = 0.0087 Δk/k.

Table 6-9—COMPOSITION OF "X" MATERIALS IN BeO-MODERATED REACTORS

Data from Ref. 29

"X"	In Reactor No.	Density, gm/cm^3	Comments
Gold	16, 17	19.0 ± 0.1	Allegedly "pure"; no chemical analysis.
Hastelloy	18-20	—	Available in sheets which average 0.0266 in. thick, and which bear the legend: Heat RV 7329, ... R-235. No chemical analysis.
Molybdenum	12-15	10.2	Available in sheets averaging 0.0402 in. thick. Chemical analysis: 0.004% B; 0.004% Cd; 0.04% Gd.
Molybdenum	53-56	10.2	Strips average 1.017 × 0.266 in. cross section. No chemical analysis.
Boron-stainless steel	28-31	8.0	18-8 stainless steel (type 304); 2.1 wt-% B.
Inconel	10, 11	8.3	71.9%, Ni; 15.14%, Cr; 0.005%, B.
Calcium Oxide	24	—	Powder
Platinum	25, 26	21.2	Allegedly "pure."
Boral	8, 34-36, 44, 45	2.53	Boron-aluminum sandwich containing 17.5 wt-% boron.
Aluminum	5, 6	—	Type 6061 or 61S. Alloying elements: 0.6%, Si; 0.25%, Cu; 1.0%, Mg; 0.25%, Cr.
Polyethylene	9, 42-46	0.94	CH_2
Rhodium	27	—	No chemical analysis.
Hexcell	21-23, 58-60	0.053	Aluminum honeycomb used to simulate voids.
Cadmium	37, 38	—	No chemical analysis.
Styrofoam	40, 41	0.032	C_6H_6. Used to simulate voids.
Graphite	51-56, 60	1.73	ATJ graphite as described in text of Ref. 29.

Table 6-10—RESULTS OF CRITICAL MEASUREMENTS OF "SANDWICH" REACTORS

Reactor No.	T_R, in.	Material "X"	T_c, in.	h, in.	T_E, in.	H_c, in.
1	0	—	—	—	—	20.2
2	6	—	—	—	—	15.8
3	12	—	—	—	—	14.3_5
4	18	—	—	—	—	14.2
5	12	Aluminum	—	—	0.25	14.6_5
6	12	Aluminum	—	—	0.75	15.5
7	12	Cadmium	—	—	0.032	17.2
8	12	Boral	—	—	0.25	19.0
9	6	Polyethylene	—	—	0.25	14.2
10	12	Inconel	—	—	0.050	14.7
11	12	Inconel	0.10	7.5	—	15.0
12	12	Molybdenum	0.120	7.5	—	16.3_5
13	12	Molybdenum	0.080	7.5	—	15.8
14	12	Molybdenum	0.040	7.5	—	15.2
15	12	Molybdenum	—	—	0.040	15.0
16	12	Gold	0.010	7.5	—	17.4
17	12	Gold	0.002	7.5	—	15.4_5
18	12	Hastelloy	0.150	7.5	—	15.8
19	12	Hastelloy	0.075	7.5	—	15.1
20	12	Hastelloy	—	—	0.075	14.8_5
21	12	Hexcell	0.47	8	—	16.5_5
22	12	Hexcell	0.94	8.5	—	19.0
23	12	Hexcell	—	—	0.47	15.5
24	12	Calcium Oxide	0.47	8.5	—	16.3_5
25	12	Platinum[a]	0.020	7.5	—	15.4
26	12	Platinum[b]	0.020	7.5	—	15.7
27	12	Rhodium[b]	0.0115	7.5	—	16.2

[a]12 in. square centered in the 24 in. square.
[b]12 in. × 24 in. rectangle centered in the 24 in. square.

Table 6-11—MEASURED CRITICAL DIMENSIONS IN FOUR UNREFLECTED BeO/U^{235} "SANDWICH" SYSTEMS

(BeO/U^{235} atom ratio = 493)

Reactor No.	Material "X"	T_c, in.	h, in.	H_c, in.
57	—	—	—	22.2
58	Hexcell	0.47	13	24.8
59	Hexcell	0.94	13	27.6
60	0.5 in. Hexcell; 0.5 in. Graphite	0.97	13	25.5

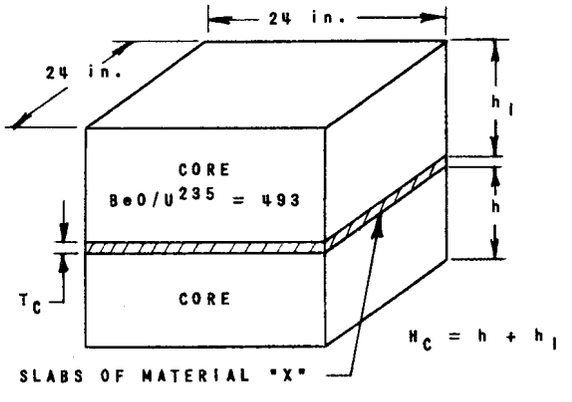

Fig. 6-13—Unreflected sandwich system. *Reproduced from Ref. 29.*

Table 6-12—EFFECT OF TEMPERATURE ON BeO-MODERATED CRITICAL ASSEMBLIES

(BeO/U^{235} atom ratio = 373)

Temperature, °F:	90[a]	950[a]
Critical mass, kg U^{235}	15.20	16.18
Density, atom/cm^3 ($\times 10^{-24}$)		
U^{235}	0.0001787[b]	0.0001776[b]
Moderator	0.0677	0.0673
Fe	0.00122	0.00121
Reactor dimensions, cm		
Length	86.52	91.60
Width	60.84	60.96
Height	60.23	60.35
Equiv. sphere radius, cm	38.75	39.18

[a]Experimental nuclear temperature coefficient average 35¢/100°F; Stainless-steel/Oralloy (93.2% U^{235}) weight ratio 210.6/245.2 gm/gm (SS-347); foils doubled, 2-mil Oy and 2-mil SS-347 on each side; Oralloy foils 22.92 × 8.72 in., dimensions reduced from inhomogeneous reactors by diffusion theory equivalent thickness means; iron absorption equal to SS-347 absorption.

[b]4-mil foils.

Table 6-13—RESULTS FOR BeO ASSEMBLIES CONTAINING GAPS

No.	Description	Ref. Fig. 6-14	BeO/U^{235} Atom Ratio	T_c, in.	T_E, in.	H_c^a, in.	"Void Content"
1	Bare BeO	(a)	493	—	—	22.2	—
2	Bare BeO	(a)	493	0.470	—	24.53	Hexcell; Al (ρ = 0.053)
3	Bare BeO	(a)	493	0.937	—	27.56	Hexcell; Al (ρ = 0.053)
4	Bare BeO	(a)	493	0.970	—	25.53	Hexcell; ½ in. graphite (ρ = 1.70)
5	Sandwich	(b)	247	—	—	14.4	—
6	Sandwich	(b)	247	0.470	—	16.54	Hexcell; Al (ρ = 0.053)
7	Sandwich	(b)	247	0.937	—	18.96	Hexcell; Al (ρ = 0.053)
8	Sandwich	(b)	247	—	0.47	15.47	Hexcell; Al (ρ = 0.053)
9	Box	(c)	247	—	—	16.25	Styrofoam (ρ = 0.032)
10	Box	(c)	247	—	0.50	16.6	Styrofoam (ρ = 0.032)
11	Box	(c)	247	—	1.00	17.0	Styrofoam (ρ = 0.032)
12	Box	(c)	247	—	1.063	17.3	Air

[a]H_c is the critical height not including the gaps, T_c or T_E.

6.3.3 GRAPHITE-MODERATED REACTORS

ORNL Thin Graphite Reflector Experiment. A graphite-moderated assembly was studied on a honeycomb assembly at ORNL.[30] The graphite was in the form of square blocks which varied in length. The fuel consisted of circular discs held in place by skewers.

The core size was 45 × 45 × 44.1 in. The over-all assembly, including 3-inch side reflectors, measured 51 × 51 × 44.1 in. The thin reflector was equivalent to an additional fueled region of equal size.

The total uranium loading (44.449 kg fuel, or 41.515 kg U^{235}) was critical with a 10.4 × 3 × 3-in. gap in the center (control rod withdrawal). If compensation is made for the void, and extra fuel is added for the reflector, the equivalent bare reactor would be critical with M_c = 52.48 kg U^{235}. The details of the reactor core are given in Table 6-14.

LASL Graphite Reflector Experiments. A series of multiplication experiments was performed at LASL[31] to ascertain the critical properties of some uranium-graphite systems.

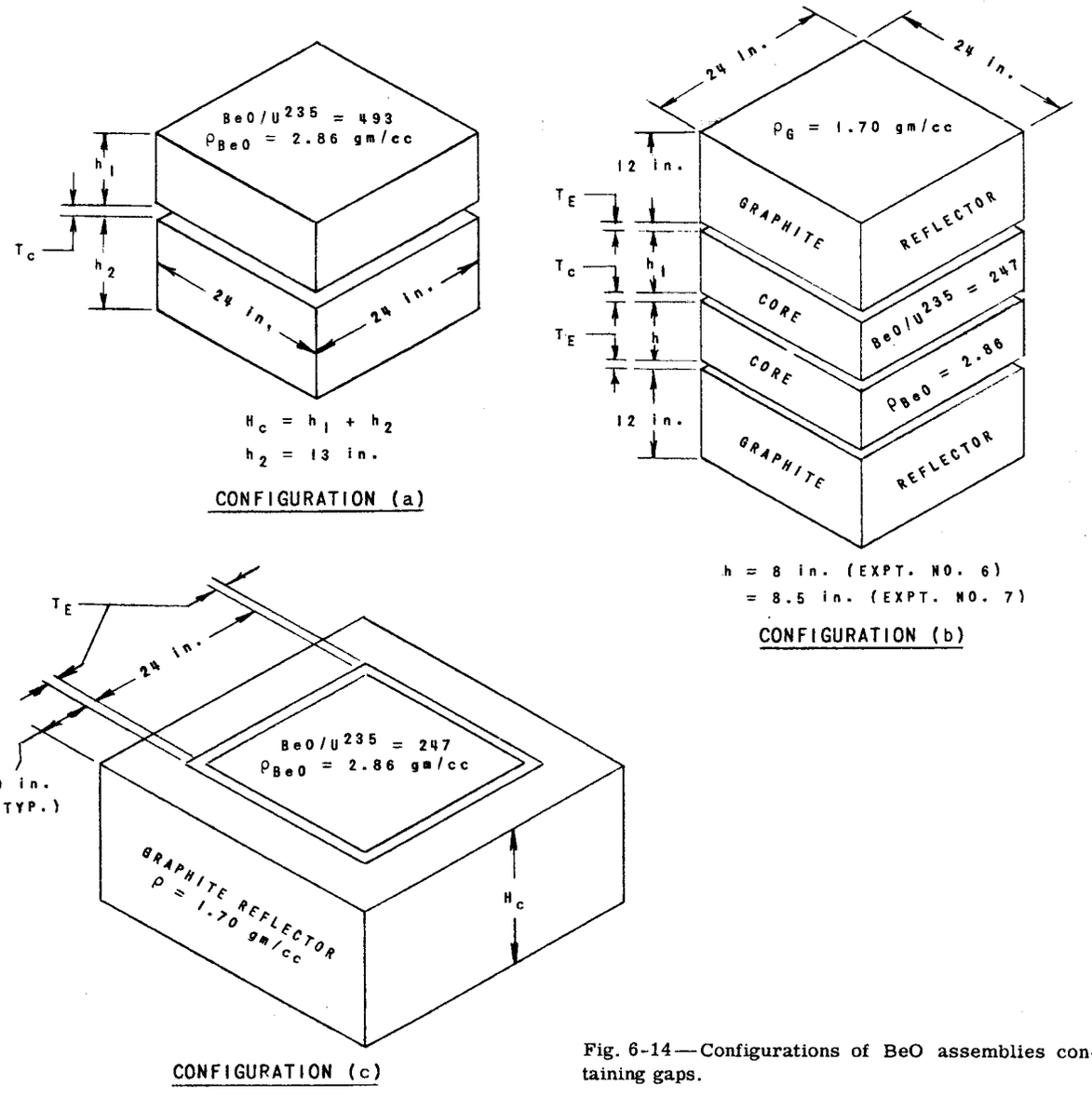

Fig. 6-14—Configurations of BeO assemblies containing gaps.

Table 6-14—GRAPHITE-MODERATED REACTOR

Data from Ref. 30.

Material	Vol-%	Density, gm/cm^3	Mass, kg
U (enriched)	—	—	44.449
U^{235}	—	—	41.515
U^{235} in equivalent bare core (core + 3-inch reflector)	0.162	18.7	53.234
Graphite	89.48	1.717	2889.7
Graphite impurities	0.014	—	—
Aluminum	6.08	2.71	310
Stainless Steel[a]	0.031	7.93	4.663
Void	4.26	—	—
Median energy of fission = 0.15 ev % Thermal Fission = 27.7			

[a]Impurities in aluminum and graphite are treated as stainless steel.

The core was composed of U^{235} discs (10.5-in. dia.) of various thicknesses, interleaved with graphite discs of various thicknesses. The resulting reactors were quite heterogeneous and the spectra of some of these assemblies were nearly as fast as some all-metal, fast reactors. The carbon-to-uranium ratio yielded a spectrum comparable to the system PPA-11 (see Table 6-7) in which the median energy of fission is 235 kev.

The reflector was added, separately, to the top, bottom, and sides. Each loading continued until all the U was used. The critical mass was then determined by an extrapolation of the reciprocal multiplication curves.

The critical data for the series of experiments are summarized in Table 6-15.

Table 6-15—SUMMARY OF URANIUM-GRAPHITE CORE CONFIGURATIONS

Data from Ref. 31.

U[a] Plate Thick., in.	Graphite Plate Thick., in.	U + Graphite,[a] gm/cm^3	U,[a] gm/cm^3	U(max.),[a] kg	Mult., (max.)	1/Mult.	M_c, kg U^{235}	H_c, cm
Solid	0	18.82	18.82	50.5	18.08	0.055	49.8	5.08
0.315	0.5	8.33	7.29	67.4	6.44	0.155	75.2	19.84
0.315	1.0	5.79	4.52	67.4	1.55	0.645	—	—
0.315	2.0	4.05	2.57	67.4	—	—	—	—
0.630	0.5	11.26	10.51	67.4[b]	28.89[b]	0.035	58.3	10.64
0.630	1.0	8.32	7.29	67.4	7.73	0.129	73.0	19.25
0.630	2.0	5.82	4.52	67.4	2.01	0.498	—	—
0.945	0.5	12.92	12.33	50.5	8.96	0.112	53.6	8.36
0.945	1.0	10.12	9.16	50.5	5.59	0.179	59.7	12.32
0.945	2.0	7.22	6.05	50.5	3.10	0.323	74.1	23.52

[a] U = 93.2% U^{235}.

[b] A complete assembly of this amount of uranium in this configuration would have become critical. The maximum multiplication was obtained with a 0.425-in. (including 0.063 in. steel support plate) separation between the two halves. A correction was made for obtaining the critical mass M_c.

LASL Beryllium Reflector Experiments. The honeycomb assembly at LASL was used to conduct a series of experiments on graphite-moderated, beryllium-reflected reactors.[32] The general configuration of the assemblies studied was that of a mock cylinder (Fig. 6-15).

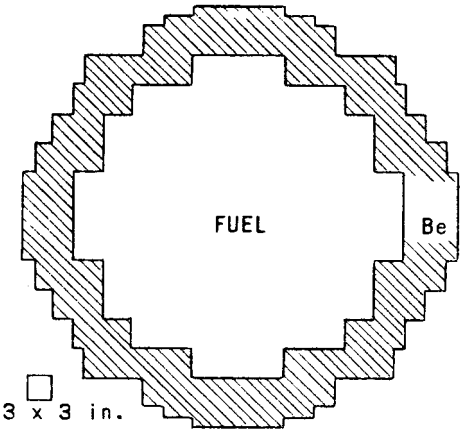

Fig. 6-15—Cross section of assembly No. 8 (Table 6-16). *Reproduced from Ref. 32.*

The series of experiments, summarized in Table 6-16, established a relation between the critical mass and the carbon-to-U^{235} atom ratio.[32] The experiments listed in Table 6-17 were performed to establish the minimum core volume consistent with the material available. The results of these surveys are shown graphically in Fig. 6-16.

Assembly No. 8, shown in Fig. 6-15, was studied extensively with respect to fission rates and cadmium ratio as a function of position within the assembly. The cadmium ratios with U^{235} foils varied on the axial center from ~3.2 at one core-end reflector interface to ~1.5 at the radial midplane of the

assembly. Radially, the minima were at the axial center and had the values ~1.7 and ~1.5 at positions 3 in. and 8 in., respectively, from the end reflector. The cadmium ratios with indium foils varied radially from ~1.15 at the center, to about 1.25 at the core edge, and were almost independent of axial position.

Table 6-16 — CRITICAL CONDITIONS FOR VARIABLE C/U^{235} SERIES[a]

Data from Ref. 32.

Assembly No.	C/U^{235}	Crit. Mass, kg U^{235}	Fuel Region: Effective Graphite Density, gm/cm³	Fuel Region: Radius, cm	Fuel Region: Length, cm	Wall Reflector: Effect. Be Density, gm/cm³	Wall Reflector: Thick., cm	East End Reflector: Graphite[b] Thick. in ΔEF, cm	East End Reflector: Be Thick., cm	West End Reflector: Graphite[b] Thick. in ΔWF, cm	West End Reflector: Be Thick., cm
1	124	53.6	1.42_1	31.3_0	77.7	1.65_9	12.4	2.5_4	10.1	1.0_2	20.2
2	124	53.6	1.42_1	31.3_0	77.7	1.65_9	13.7	2.5_4	10.1	1.0_2	10.1
3	395	28.7	1.42_1	40.5_6	78.7_4	1.66_6	12.9_6	2.5_4	11.4_7	0	8.1_2
4	395	33.6	1.29_0	46.1_0	78.7_4	1.65_5	14.0	2.5_4	7.6_0 + 3.2_2^c	0	7.6_0 + 3.2_2^c
5	399	37.6	1.29_8	48.8_3	78.7_4	1.66_1	12.8	2.5_4	8.5_3	0	8.5_3^d
6	1018	16.22	1.47_7	48.8_3	76.2	1.66_4	12.0	2.5_4	9.7_6	2.5_4	23.0_3
7	1018	16.22	1.47_7	48.8_3	76.2	1.66_4	12.0	2.5_4	9.7_6	2.5_4	9.7_6
8	410	30.1	1.50	40.56	81.28	1.66	13.08	—	10.16	—	10.16
9	410	30.1	1.50	40.56	81.28	1.66	16.74	—	10.16	—	0
10	410	30.1	1.50	40.56	81.28	1.66	29.90[e]	—	0	—	0

[a] Unless otherwise specified, mean densities of graphite and beryllium in the east and west face reflectors are the same as listed in fuel and wall reflector regions.

[b] Small carbon regions designated ΔEF and ΔWF about the east and west faces of the core. The density and area is the same as the carbon in the core.

[c] Graphite at 1.42 gm/cm³.

[d] Graphite at 1.47_7 gm/cm³.

[e] Extrapolated value. Actual critical configuration with 27.58 cm Be + 5.75 cm graphite ($\bar{\rho} = 1.56$).

Note: Assemblies 6 and 7 contained 0.002-in. foils only; assemblies 1-5 contained ~17.5 kg U^{235} as 0.002-in. foils, and the remainder as 0.005-in. foils; assemblies 8-10 contained 0.005-in. foils only.

Table 6-17 — CRITICAL DATA FOR SMALL-CORE ASSEMBLIES

Data from Ref. 32.

Assembly No.	Critical Mass, kg U^{235}	C/U^{235} Atomic Ratio	$\bar{\rho}_{C'}$, gm/cm³	$\bar{\rho}_C$, gm/cm³	Core Length: 76.2 cm: Be Island Radius, cm	Core Length: 76.2 cm: Core Outside Radius, cm	Wall	Reflector Thickness, cm: East End	Reflector Thickness, cm: West End
11	11.94	330	1.42	1.66	—	25.25	24.71	2.54 C + 10.16 Be	2.54 C + 20.32 Be
12	15.56	327	1.41	1.66	—	28.83	23.65	2.54 C[a]	2.54 C + 20.32 Be
13	8.27[b]	332	1.38	1.66	19.38	28.83	19.99	2.54 C[a]	2.54 C + 20.32 Be

[a] Peripheral beryllium extends 4 in. beyond core.

[b] A safety rod fuel tube in east beryllium island was considered beryllium.

Note: These assemblies contained 0.002-in. uranium foils only.

UCRL Graphite and Beryllium Reflector Experiments. A series of critical experiments on graphite-moderated, graphite- and beryllium-reflected assemblies was performed* at the University of California Radiation Laboratory (Livermore). The assemblies were stacked on a low-mass honeycombed aluminum table (density = 3 lb/ft³). The fuel (93.5% U^{235}) was in the form of 5.25-in. square foils, 0.001 in. and 0.002 in. thick. In addition, each foil was coated with ~0.92 gm of Teflon. The ATJ-graphite moderator had a density of 1.73 gm/cm³, and the average density of the core was adjusted by varying the void fraction. The density of the beryllium in the reflector was 1.84 gm/cm³. The nominal carbon/U^{235} atom ratio varied from 600 to 2340. The assemblies were controlled by poisoned rods.

A summary of the basic assembly and the critical data is given in Table 6-18.

*Private communication, P. Greebler, APED, General Electric Co.

The relation between the radial buckling of an octagon and a circle of equivalent area is given by B^2(octag) = 1.009 B^2(circle). The bucklings shown in Table 6-19 were obtained using this relation. The corrected value of the bucklings, when the corrections are applied by various means to eliminate the effect of the control rod channels, are also given. These are summarized as follows (corresponding to columns in Table 6-19):

(1) The control channel was successively displaced from the center and the critical height measured. These results were then extrapolated to complete removal of the control channel.

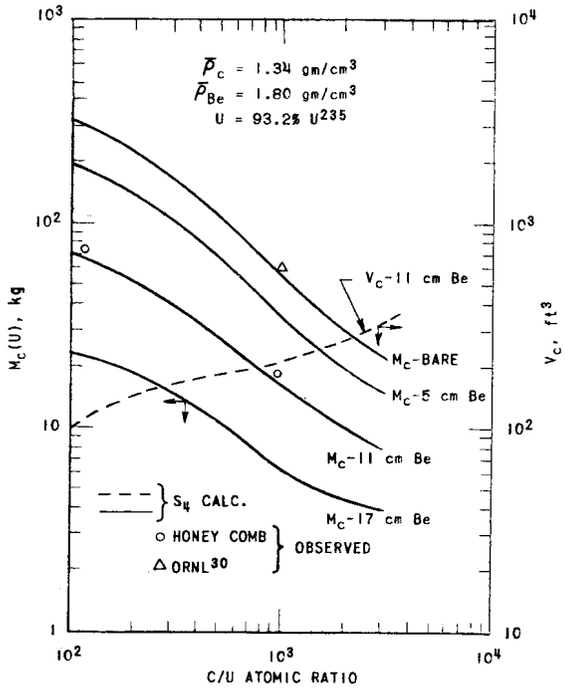

Fig. 6-16 — Critical parameters of spherical uranium–graphite core with beryllium reflector. *Reproduced from Ref. 32.*

Table 6-18 — SUMMARY OF CRITICAL MASS DATA FOR THE BASIC GRAPHITE-MODERATED SYSTEMS

Core Size, cm		Reflector Thickness, cm	$(C/U)_{abs}$	$(C/U)^a_{eff}$	U^{235}, kg
Radial Dimensions	Height				
Core Geometry: Right Octagonal Cylinder					
238[b]	133	0	600	675	89.3
214[b]	153	0	600	675	79.1
191[b]	167	0	600	675	76.5
167[b]	240	0	—	—	~112
144[b]	175	15-C (8 sides)	600	—	40.5
Core Geometry: Parallelepiped					
191 × 191	152	0	600	675	82.3
191 × 191	167	0	1200	1379	43.5
191 × 144	169	15-C (2 sides)	1200	—	33.0
144 × 144	171	15-C (4 sides)	1200	—	25.3
191 × 191	187	0	2340	2586	25.1
191 × 144	161	15-Be (2 sides)	2340	—	16.2
144 × 144	145	15-Be (4 sides)	2340	—	11.0

[a] $(C/U)_{eff} = \dfrac{(C/U)_{abs}}{\text{Disadvantage Factor}}$.

[b] Flat-to-flat diameter of octagon.

(2) Considering the control channel void as a perturbation, δ, on the buckling, and applying the results to the experiments of (1), the observed buckling is given by:

$$B^2_{obs} = B^2_0 - \phi^2 \delta$$

where ϕ is the flux at the position of the void.

(3) Usual two-group perturbation on B^2 due to reduced density of the center region.

(4) Plugs were placed in one-half the channels and the change in B^2 observed. Total effect = 2 × effect in one-half the channels.

In addition to the foregoing, the disadvantage factors for fuel foils of various thicknesses were determined, and are given in Fig. 6-17.

Table 6-19 — SUMMARY OF BUCKLING DATA FOR THE BASIC GRAPHITE-MODERATED SYSTEMS

Core Size, cm				Correction by							
				(1) Extrapolation of Channel Position		(2) ϕ^2 Perturbation		(3) Two-Group Perturbation		(4) Doubling Void Effect	
Radial Dimensions	Height	C/U (Nominal)	$B^{2a}_{obs} \times 10^4$, cm^{-2}	H, cm	$B^2 \times 10^4$, cm^{-2}	H, cm	$B^2 \times 10^4$, cm^{-2}	H, cm	$B^2 \times 10^4$, cm^{-2}	H, cm	$B^2 \times 10^4$, cm^{-2}
Core Geometry: Right Octagonal Cylinder											
191	167	600	20.96	—	—	—	—	—	—	—	—
214	153	600	20.99	—	—	—	—	—	—	—	—
238	133	600	21.26	—	—	—	—	—	—	—	—
Core Geometry: Parallelepiped											
191	152	600	21.11	152	21.69	153.5	21.53	152.5	21.64	—	—
191	167	1200	20.17	161.2	20.69	162	20.62	161.2	20.69	158.0	21.03
191	187	2340	18.57	181	18.98	181	18.98	180.5	19.04	178.3	19.18

[a] $B^2_{obs} = \left(\frac{\pi}{H + 2\delta}\right)^2 + 1.009\left(\frac{2.048}{R + \delta}\right)^2$, where δ = 1.92 cm extrapolation distance.

Note: Density of graphite for homogeneous system = 1.636 gm/cm^3.

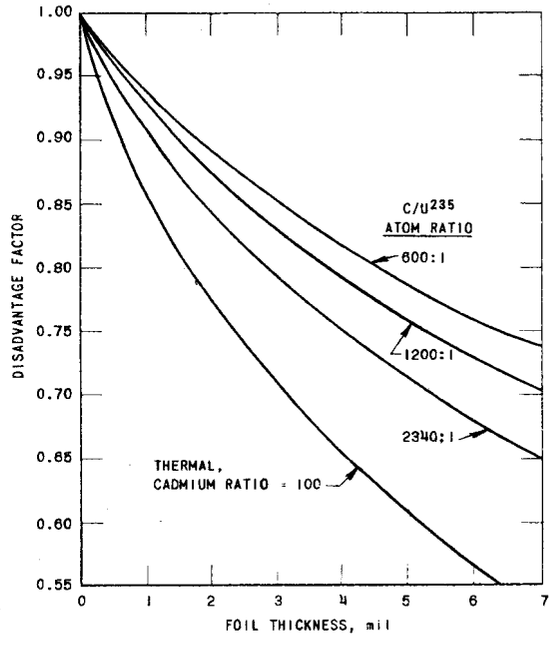

Fig. 6-17 — Disadvantage factor vs. uranium foil thickness.

687863 O - 63 - 36

A series of graphite-moderated, graphite-reflected systems containing gaps between core and reflector has been studied at UCRL.* The facility is described in detail in UCRL-5175.[9] Figure 6-18

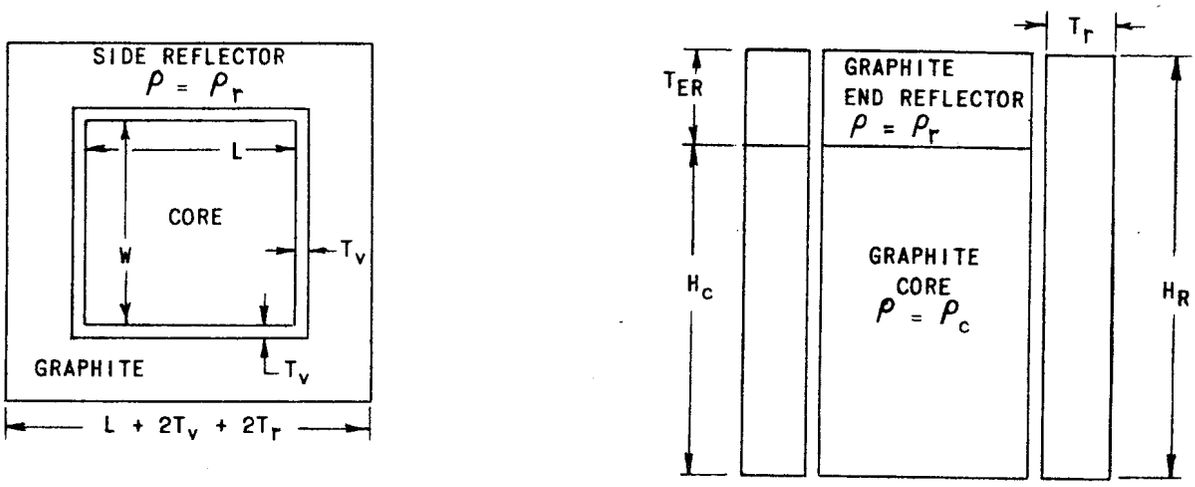

Fig. 6-18 — Critical assembly configuration of Table 6-20. *Reproduced from Ref. 9.*

shows a schematic of the system used for the gap studies. The results are summarized in Table 6-20. In the geometry considered, the reactivity worth of the core–side reflector gaps was measured to be $\Delta k_{eff}/\Delta T_{void} \cong -0.020$ in.$^{-1}$.

Table 6-20 — CRITICAL ASSEMBLIES CONTAINING CORE-SIDE REFLECTOR GAPS

Expt. No.	L, in.	W, in.	H_c, in.	H_c(corr.),[a] in.	T_r, in.	T_v^b, in.	ρ_c, gm/cm^3	ρ_r, gm/cm^3	C/U^{235}	Comments
92	48.5	48.5	35.9	35.57	—	—	1.633	—	296	
93	42.5	42.1	32.11	31.92	6.0	—	1.632	1.70	295	
94	42.5	42.5	29.16	28.97	12.0	—	1.636	1.70	295	
97	42.5	42.5	33.32	33.13	6.0	1.0	1.632	1.70	295	
99	42.5	42.5	34.44	34.25	6.0	2.0	1.632	1.70	295	
103	42.5	42.5	35.49	35.30	6.0	3.0	1.632	1.70	295	
105	42.5	42.5	28.85	28.66	6.0	2.0	1.632	1.70	295	6.0 in. end reflector[c,e]
106	42.5	42.5	28.63	28.44	6.0	2.0	1.632	1.70	295	7.0 in. end reflector, H_R = 30.3 in.
107	42.5	42.5	29.63	29.44	6.0	2.0	1.632	1.70	295	6.0 in. end reflector, H_R = 29.65 in.
111	42.5	42.5	34.2	34.01	6.0	3.0	1.632	1.70	295	Material in gap[d]
112	42.5	42.5	33.2	33.01	6.0	2.0	1.632	1.70	295	Material in gap[d]
113	42.5	42.5	32.3	32.11	6.0	1.0	1.632	1.70	295	Material in gap[d]
119	36.5	36.5	36.06	35.73	6.0	—	1.635	1.70	298	
122	36.5	36.5	40.6	40.27	6.0	2.0	1.635	1.70	298	

[a] Corrected for vane slot voids.
[b] Density of aluminum honeycomb in gap: 0.018 gm/cm^3.
[c] H_c + 6.0 in. = H_R, where H_R is the height of the side reflector.
[d] Stainless steel, 0.122 in. thick; aluminum, 0.72 in. thick; polyethylene, 0.124 in. thick.
[e] ρ(end reflector) = ρ(side reflector) for Expt. Nos. 105, 106, and 107.

6.3.4 HYDROGEN-MODERATED REACTORS

Studies were made by Dow Chemical[33,34] on a series of reflected and bare cylindrical assemblies consisting of plutonium metal sheet moderated with Plexiglas (see Fig. 6-19). The results are listed in Tables 6-21 through 6-25. The H : Pu atom ratio was calculated assuming the metal and Plexiglas to be homogeneously mixed in each assembly.

*Private communication, E. Goldberg, Livermore Laboratory.

Bare cylindrical assemblies containing boron carbide-impregnated Epolene-n $[(CH_2)_n]$ discs were also studied.[35] Figure 6-20 is a schematic of the boron-containing assemblies. The results are summarized in Table 6-26.

Experiments were performed at ORNL[36] on bare and totally reflected assemblies containing enriched U^{235} (UO_2F_2) solutions. The totally reflected systems used an effectively infinite water reflector. The results are summarized in Table 6-27.

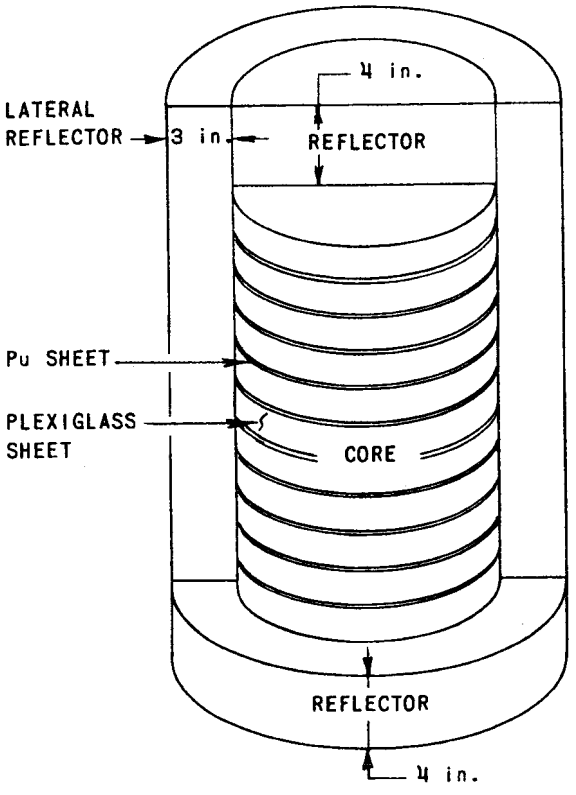

Fig. 6-19—Schematic of Plexiglass and plutonium metal assemblies. *Reproduced from Ref. 33.*

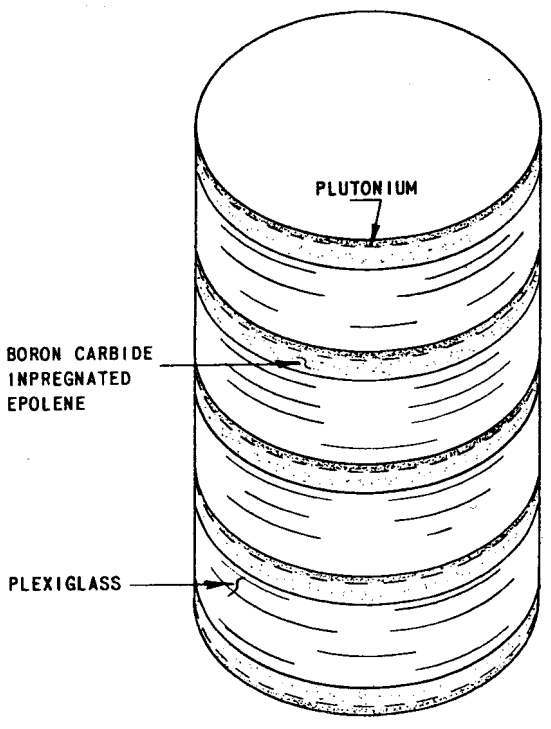

Fig. 6-20—Schematic of experimental assembly containing boron.

Table 6-21—UNTAMPED CYLINDERS–12.5 in. DIAMETER

Data from Ref. 33.

H : Pu	Extrapolated Critical Height, cm	Mass in Experiment, kg	Extrapolated Critical Mass, kg	ρ_{Pu}, gm/cm^3	Sheet Thickness, in.	
					Plutonium	Plexiglas
1.62	9.57	40.42	56.46	7.423	0.1152	0.115
5.52	14.98	35.17	39.93	3.27	0.0632	0.243
5.89	15.59	29.40	38.44	3.10	0.1152	0.472
6.07	15.83	29.40	38.12	3.03	0.0576	0.243
11.39	18.89	20.21	26.64	1.77	0.0576	0.472
11.62	21.77	22.05	30.14	1.74	0.1728	1.442
11.69	20.03	22.05	27.59	1.73	0.1152	0.970
16.78	20.57	16.54	20.42	1.248	0.0576	0.715
35.60	25.60	10.67	12.55	0.614	0.0366	0.970
39.84	40.94	14.48	18.42	0.551	0.0632	1.940
72.25	66.34	12.92	16.36	0.309	0.0366	1.940
6.07[a]	—	—	37.8	3.03	—	—
11.6[a]	—	—	24.7	1.74	—	—

[a]Homogeneous cylinders; extrapolated critical values.

Table 6-22 — UNTAMPED CYLINDERS–12.5 in. DIAMETER

Data from Ref. 34.

H : Pu	Extrapolated Critical Height, cm	Mass in Experiment, kg	Extrapolated Critical Mass, kg	ρ_{Pu}, gm/cm^3	Sheet Thickness, cm	
					Plutonium	Plexiglas
20.3	26.6	16.05	22.2	1.056	0.0400	0.6172
47.6	27.7	8.56	10.3	0.470	0.0400	1.4910
45.7	30.6	9.63	11.9	0.492	0.0801	2.982
92.9	29.3	4.99	5.9	0.254	0.0238	1.816
94.2	37.8	5.35	7.4	0.247	0.0400	3.015
90.7	42.3	6.65	8.5	0.254	0.0476	3.632

Table 6.23 — UNTAMPED CYLINDERS–18 in. DIAMETER

Data from Ref. 34.

H : Pu	Extrapolated Critical Height, cm	Mass in Experiment, kg	Extrapolated Critical Mass, kg	ρ_{Pu}, gm/cm^3	Sheet Thickness, cm	
					Plutonium	Plexiglas
19.4	18.1	24.88	32.0	1.075	0.0400	0.5829
18.7	17.4	25.95	32.0	1.120	0.0801	1.165
18.1	17.1	25.95	32.8	1.166	0.1202	1.749
48.5	20.0	12.31	15.1	0.459	0.0238	0.8801
46.4	20.2	12.96	15.7	0.474	0.0476	1.7602
45.6	19.9	13.84	15.8	0.483	0.0639	2.3876
94.1	20.2	6.48	8.0	0.241	0.0238	1.7767
88.6	22.5	7.78	9.6	0.260	0.0476	3.5534
87.0	29.3	9.72	13.0	0.270	0.0715	5.3304

Table 6.24 — TAMPED CYLINDERS–12.5 in. DIAMETER

Data from Ref. 33.

H : Pu	Extrapolated Critical Height, cm	Mass in Experiment, kg	Extrapolated Critical Mass, kg	ρ_{Pu}, gm/cm^3	Sheet Thickness, in.	
					Plutonium	Plexiglas
0	1.70	14.48	21.94	15.8	0.670	0
0.500	2.39	17.21	22.56	11.75	0.350	0.243
0.992	2.94	18.18	22.13	9.35	0.342	0.472
2.36	4.35	16.55	21.21	5.98	0.0632	0.115
4.89	6.03	14.48	17.69	3.60	0.0632	0.243
9.11	7.71	10.34	13.55	2.15	0.0632	0.472
16.09	9.37	8.30	9.70	1.30	0.0366	0.472
30.78	11.48	5.93	6.46	0.706	0.0366	0.970

Table 6-25 — TAMPED CYLINDERS–12.5 in. DIAMETER

Data from Ref. 34.

H : Pu	Calculated[a] Critical Height, cm	Mass in Experiment, kg	Extrapolated Critical Mass, kg	ρ_{Pu}, gm/cm^3	Sheet Thickness, cm	
					Plutonium	Plexiglas
19.6	11.47	7.49	9.8	1.079	0.0400	0.6172
18.5	10.86	8.56	9.8	1.140	0.0801	1.2344
46.2	14.0	4.32	5.3	0.478	0.0238	0.9093
43.3	13.65	4.65	5.5	0.509	0.0476	1.8186
42.0	13.52	4.34	5.6	0.523	0.0639	2.3977
87.3	14.31	2.66	3.3	0.256	0.0238	1.8160
92.2	18.71	2.67	3.6	0.243	0.0400	3.0140
82.2	18.57	3.32	4.0	0.272	0.0476	3.6312

[a] Calculated using critical mass and density.

Table 6-26 — UNREFLECTED BORON-CONTAINING ASSEMBLIES

Data from Ref. 35.

Cylindrical Core Diameter, in.	Extrapolated Critical Mass, kg	Mass of Boron in Core, gm	Calculated Critical Height, cm	Density of Pu in Core, gm/cm^3	H : Pu Ratio	Density of Boron in Core, gm/cm^3
12.5	24.6	23.6	20.1	1.544	13.4	0.00148
12.5	19.3	18.5	27.2	0.897	24.1	0.00086
12.5	18.4	17.6	36.9	0.630	35.0	0.00060
12.5	33.8	32.4	92.4	0.462	48.2	0.00044
18.0	62.5	1011.2	33.8	1.126	18.9	0.01850
18.0	45.4	372.5	25.2	1.099	19.4	0.00900
18.0	38.9	638.6	52.0	0.456	48.8	0.00750
18.0	47.6	780.6	126.6	0.229	98.7	0.00380

Materials (for cylindrical assemblies of plutonium)

Fuel

Plutonium discs, average density 15.8 gm/cm^3

Diameter, in.	Thickness, in.	Mass, gm
12.5	0.0576	1837.4
18.0	0.0158	535.1

Moderator

Plexiglas, Type R, average density ~1.2 gm/cm^3

Diameter, in.	Thickness, in.
12.5	0.115
12.5	0.243
12.5	0.472
18.0	0.117
18.0	0.230
18.0	0.470

Boron Carbide-Impregnated Epolene-n[a]

$(CH_2)_n$ + boron carbide

Diameter, in.	Thickness, in.	Mass $(CH_2)_n$, gm	Mass B_4C, gm
12.5	~0.060	120.6	2.1
18.0	~0.090	284.1	21.4

Boron carbide ~82.8% boron (some elemental boron as inclusions)

[a] Epolene-n – Eastman Chemical Products, Inc., Kingsport, Tennessee.

Table 6-27 — CRITICAL PARAMETERS OF ENRICHED U^{235} SOLUTIONS IN SIMPLE GEOMETRY

Container Material and Geometry	Solution Concentration		Critical Values		
	$H:U^{235}$ Atom Ratio	U^{235}, gm/cm^3	Height, cm	Volume, liter	Mass, kg U^{235}
Totally Water-Reflected					
Aluminum					
6 in. dia. cylinder	27.1	0.8288	89.3	16.25	13.47
6.5 in. dia. cylinder	44.3	0.5376	38.7	8.28	4.45
10 in. dia. cylinder	27.1	0.8288	12.4	6.3	5.2
15 in. dia. cylinder	27.1	0.8288	7.7	8.8	7.3
30 in. dia. cylinder[a]	27.1	0.8288	5.0 ± 1	22.8 ± 4.6	18.9 ± 3.8
	44.3	0.5376	4.8 ± 1	21.9 ± 4.6	11.8 ± 2.5
	72.4	0.3423	5.5 ± 1	25.1 ± 4.6	8.6 ± 1.6
20 × 20 in. square[a]	27.1	0.8288	6.3 ± 1	16.3 ± 2.6	13.5 ± 2.2
	44.3	0.5376	4.3 ± 1	11.1 ± 2.6	6.0 ± 1.4
	72.4	0.3423	6.2 ± 1	16.0 ± 2.6	5.5 ± 0.9
9 in. dia. sphere	47.3	0.5061	—	6.32[b]	3.20
Stainless Steel					
6 in. dia. cylinder	44.3	0.5376	118.4	21.55	11.59
No Reflector					
Aluminum					
8.76 in. dia. cylinder	44.3	0.5376	219	85.2	45.8
9.5 in. dia. cylinder	44.3	0.5376	44.4	20.3	10.9
10 in. dia. cylinder	27.1	0.8288	38.9	19.8	16.4
	44.3	0.5376	35.1	17.8	9.6
	73.4	0.3370	33.7	17.1	5.8
12 in. dia. cylinder	44.3	0.5376	23.2	16.9	9.1
15 in. dia. cylinder	27.1	0.8288	18.5	21.1	17.5
	44.3	0.5376	17.9	20.4	11.0
	74.6	0.3314	16.8	19.2	6.4
20 in. dia. cylinder	27.1	0.8288	15.8	32.0	26.5
	44.3	0.5376	15.0	30.4	16.3
	73.4	0.3370	15.2	30.8	10.4
30 in. dia. cylinder	44.3	0.5376	13.7	62.5	33.6
	72.4	0.3423	13.9 ± 0.5	63 ± 2	21.6 ± 0.7
20 × 20 in. square	27.1	0.8288	15 ± 1	38 ± 3	32 ± 2
	72.4	0.3423	14.3	36.9	12.6
Stainless Steel					
9 in. dia. cylinder	74.6	0.3314	59.0	24.3	8.1

[a]The accuracy of the results of these critical volumes is unusually poor for the following reasons: vessels of these dimensions were difficult to level in order to assure that the lower surface of the liquid was horizontal and that the liquid-level measuring device was properly "zeroed"; it was difficult to simultaneously measure the position of the upper liquid surface and properly locate the top reflector in contact with that surface; the uncertainty in the effect on critical height of the thick container bottom plate affected significantly the measurements in slab-like volumes.

[b]Sphere lacked 80 cm^3 being full; the data extrapolate to a critical mass and concentration of 3.09 kg of U^{235} and 0.483 gm U^{235}/cm^3 ($H:U^{235} = 49.9$) in a full sphere of capacity 6.4 liter.

6.3.5 DEUTERIUM-MODERATED REACTORS

Critical mass measurements have been made at Los Alamos Scientific Laboratory on ten critical assemblies of enriched uranyl-fluoride, heavy-water solutions. The isotopic concentration of the deuterium ranged from an initial 99.8%, to about 99.0% at the end of the series. The uranium was approximately 90% U^{235}. The experiments were performed at room temperature.

Six critical measurements were made in D_2O-reflected core assemblies. The six cores were stainless steel spheres (0.040-in. wall thickness) with diameters ranging from 13.5 to 18.5 in. The re-

flector thickness depended upon the core diameter, the outside diameter of the stainless steel reflector vessel being 35 in. The results are listed in Table 6-28.

Four measurements were made in unreflected, stainless steel cylinders ($\frac{1}{8}$-in. wall thickness), and then corrected for the effect of the glory hole. The critical parameters for corresponding spherical cores were then calculated. The experimental results, and the reduced data obtained by calculation, are given in Table 6-29.

Table 6-28 — CRITICAL DATA FOR D_2O-REFLECTED SPHERICAL $U^{235}O_2F_2$–D_2O CORES

Reproduced from Ref. 37.

Sphere Diameter, in.	Critical Volume, liter	Critical Mass, kg U^{235}	D/U^{235} Atom Ratio	U^{235} Density, gm/cm^3	D_2O Reflector Thickness, in.
13.5	20.9	14.2	34.2	0.679	10.7
14.5	26.1	11.6	53.7	0.443	10.2
15.5	31.7	9.6	81.2	0.302	9.7
16.5	38.1	7.0	135.3	0.185	9.2
17.5	45.9	4.8	243	0.104	8.7
18.5	53.8	3.2	431	0.060	8.2

Table 6-29 — CRITICAL DATA FOR BARE CYLINDRICAL $U^{235}O_2F_2$–D_2O CORES

Reproduced from Ref. 37.

D/U^{235} Atom Ratio	U^{235} Density, gm/cm^3	Cyl. Inside Radius, cm	Axial Glory Hole		Critical Height, cm (Measured)	Critical Volume, liter (Measured)
			O.D. in.	Matl.		
230	0.1094	31.6	1	SST	71.45	223.8
419	0.0610	31.6	1	SST	78.74	246.6
856	0.0301	38.1	1	SST	61.09	278.0
856	0.0301	38.1	1.125	Al	60.83	276.8
2081	0.0124	38.1	1.125	Al	84.75	385.8
Reduced Data						
D/U^{235} Atom Ratio	Cyl. Critical Radius (glory hole removed), cm	Cyl. Critical Volume (glory hole removed), liter	Critical Vol.[a] of Sphere in $\frac{1}{8}$ in. SST, liter		Critical Vol.[a] of Ideal Bare Sphere, liter	Critical Mass of Bare Sphere, kg U^{235}
230	31.55	223.1	194.4		197.7	21.6
419	31.53	245.5	208.2		211.7	12.9
856	38.04	275.9	243.3		247.0	7.4
2081	38.04	384.6	335.4		340.1	4.2

[a]Assumes equivalent stainless steel thickness of 0.2 cm, extrapolation distance of 2.5 cm (critical volume is increased 1.1 to 1.2% for extrapolation distance of 3.9 cm). There has been no correction for ~1 at-% H^1 contamination of the D in these solutions.

It is estimated that errors of values of critical volume are less than ±1% for the existing conditions, and that errors of corresponding U^{235} concentrations or D/U^{235} ratios are within ±2%. For the unreflected systems, the standard solution and the D_2O levels to which critical volumes were adjusted were selected to compensate for the effect of the filling tube channel through the reflector and for asphericity of the outer reflector surface.

The critical systems were not ideal in two principal respects: (1) neutron absorption by the stainless steel spheres in the reflected assemblies is estimated to increase critical volumes a maximum of ~2% above values for non-absorbing containers; and (2) light-water contamination of the D_2O solutions. Other contaminants were minor and the reflector contamination by normal water is of slight significance. In the spherical cores, the deuterium was probably between 99.6 and 99.8 at-%, and the main effect of the normal hydrogen is an increase in moderation. The correction to pure D_2O would require

~1% increase in critical volume at nominal D/U^{235}. The large-volume cylindrical solutions contained D_2O which had been incompletely protected against water vapor. Spot checks suggest that the normal hydrogen contamination averaged about 1 at-%. In this case, the correction to pure D_2O, requires a 2-3% increase in critical volume at nominal D/U^{235}.

6.4 PARAMETRIC SURVEYS

Parametric surveys based solely on calculations serve to demonstrate the effect of changes in a reactor even though certain absolute quantities cannot be verified experimentally.

The results of critical mass calculations by Safanov[38] for bare, spherical, homogeneous U^{235} reactors involving several moderators are shown graphically in Fig. 6-21.

Figure 6-22 gives the calculated median fission energy for various BeO/U^{235} ratios in bare homogeneous systems.[39]

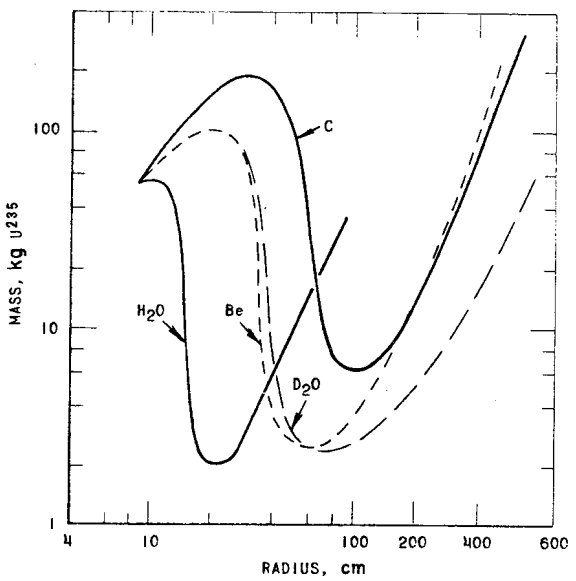

Fig. 6-21—Critical mass of U^{235} vs. critical radius for bare, homogeneous, spherical reactors with various moderators. *Reproduced from Ref. 38.*

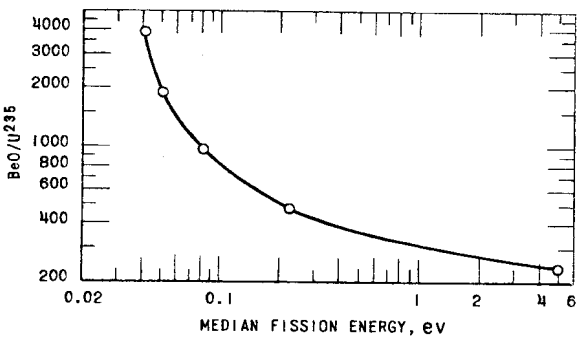

Fig. 6-22—Calculated median fission energy vs. BeO/U^{235} ratio for bare, homogeneous critical systems. *Reproduced from Ref. 39.*

Mandl[40–42] and Whipple[43] have calculated Pu-Be systems. The variation of critical radius with median energy of fission is shown in Fig. 6-23 for a bare homogeneous sphere, and in Fig. 6-24 for a

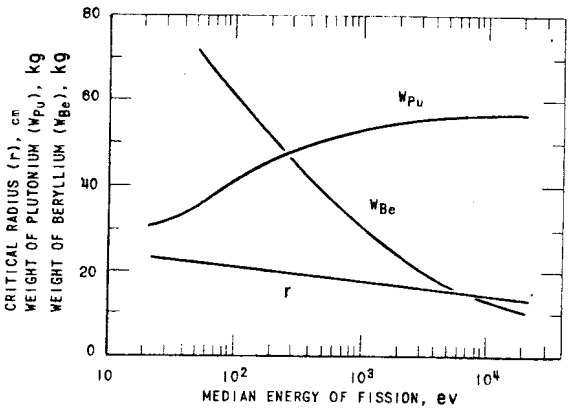

Fig. 6-23—Critical parameters of Pu–Be systems. *Reproduced from Ref. 42.*

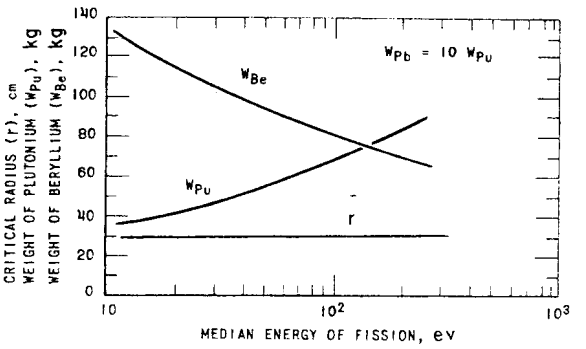

Fig. 6-24—Critical parameters for Pu–Be–Pb systems. *Reproduced from Ref. 40.*

bare homogeneous sphere with Pb coolant added. Figure 6-25 shows the variation of the ratio of moderator volume to volume of coolant and fuel, with median energy of fission.

Several simplifying assumptions have been made for the nuclear parameters in Figs. 6-23 through 6-26; in particular, η has been assumed equal to ν, when in fact it is smaller ($\sim 0.7\ \nu$). Thus, the figures serve only to establish trends.

Mills* has calculated D_2O-, Be-, and BeO-moderated-U^{235} spherical systems, and graphite-moderated U^{233}, U^{235}, and Pu^{239} spherical systems. The calculations were made using the DSN code in the S4 approximation (see Section 10). His results are given in Tables 6-30 and 6-31.

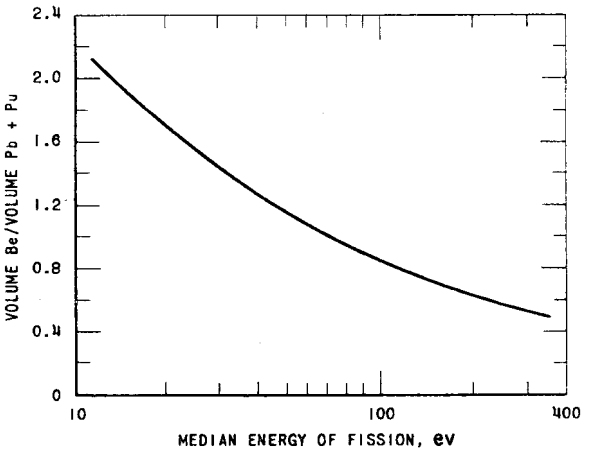

Fig. 6-25 — Volume ratio of moderator to coolant and fuel for bare, homogeneous, spherical Pu–Be–Pb critical systems. *Reproduced from Ref. 40.*

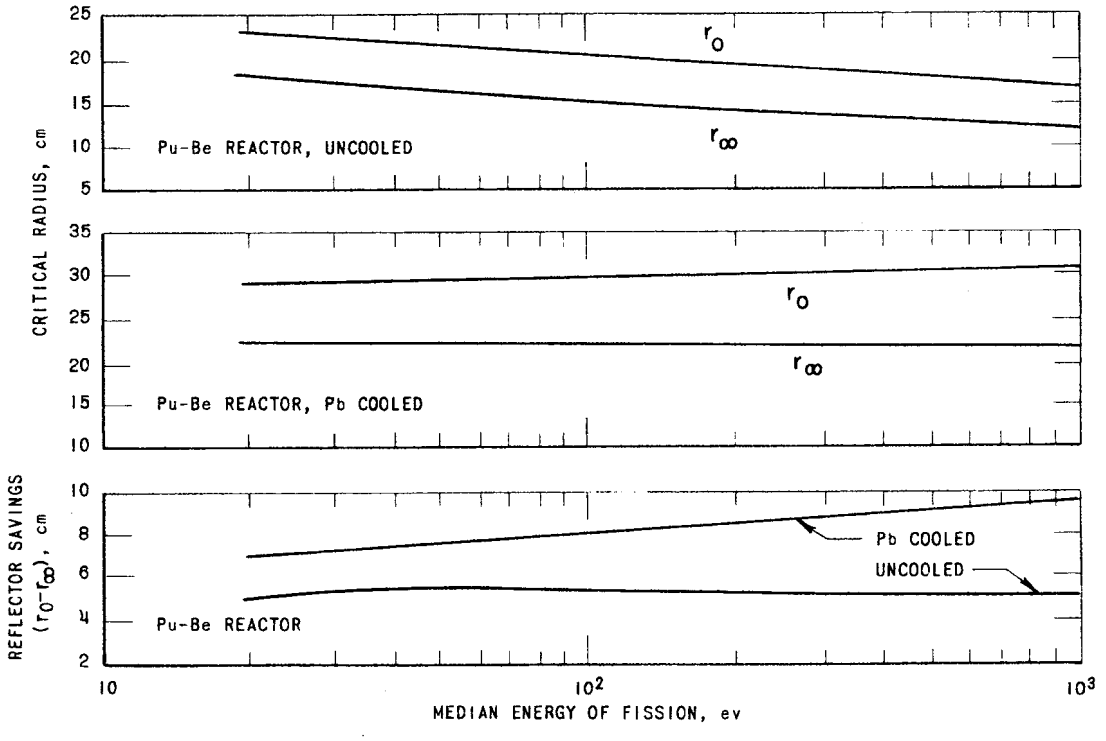

Fig. 6-26 — Critical radii of Pu–Be–Pb systems without reflector (r_0) and with infinite reflector (R_∞). *Reproduced from Ref. 41.*

*Private communication, C. Mills, Los Alamos Scientific Laboratory.

Table 6-30 — CRITICAL PARAMETERS OF D_2O-, Be-, AND BeO-MODERATED U^{235} BARE SPHERICAL SYSTEMS

Moderator/U^{235} Atom Ratio	Critical Radius, cm	Critical Mass, kg U^{235}	Critical Conc. kg U^{235}/liter
D_2O-Moderated			
1	12.2	82.7	10.87
3	18.0	100.8	5.92
10	22.4	107.6	2.29
30	29.2	86.5	0.829
100	34.8	45.3	0.257
300	36.7	17.89	0.0864
1000	39.5	6.71	0.0260
3000	45.8	3.49	0.00867
Be-Moderated			
1	10.7	68.5	13.35
3	13.4	85.4	8.47
10	17.4	82.1	3.72
30	22.1	64.6	1.43
100	27.4	39.0	0.453
300	29.5	16.5	0.153
1000	30.4	5.44	0.0463
3000	33.2	2.37	0.0155
BeO-Moderated			
1	11.5	70.1	11.01
3	14.6	78.7	6.03
10	20.2	80.7	2.34
30	26.3	64.7	0.849
100	31.5	34.5	0.263
300	33.6	14.07	0.0885
1000	35.3	4.91	0.0267
3000	39.8	2.35	0.00889

Table 6-31 — CRITICAL PARAMETERS OF GRAPHITE MODERATED–U^{233}, U^{235}, AND Pu^{239} BARE SPHERICAL SYSTEMS

Atom Ratio C/x	Critical Radius, cm	Critical Mass, kg	Critical Conc., kg/liter
U^{233}			
1	9.1	37.1	11.75
3	13.1	63.7	6.77
10	21.9	119.9	2.73
30	32.2	140.8	1.007
100	42.8	103.1	0.314
300	50.8	58.2	0.106
1000	57.3	25.1	0.0319
3000	63.8	11.58	0.01064
10000	76.4	5.96	0.00319
U^{235}			
1	12.4	94.6	11.85
3	17.5	153.2	6.83
10	27.6	242.1	2.75
30	40.4	280.6	1.016
100	54.5	214.8	0.317
300	65.3	124.5	0.1068
1000	67.2	40.9	0.0322
3000	70.5	15.75	0.01073
10000	81.2	7.23	0.00322
Pu^{239}			
1	8.1	27.3	12.26
3	12.1	51.7	7.01
10	21.3	113.6	2.81
30	34.0	170.2	1.034
100	49.4	162.7	0.322
300	60.4	100.2	0.1086
1000	67.0	41.2	0.0327
3000	70.2	15.8	0.01091
10000	76.5	6.14	0.00328

REFERENCES

1. R. Ehrlich and H. Hurwitz, Jr., *Multigroup Methods for Neutron Diffusion Problems*, Nucleonics, 12: No. 2, 23, (February, 1954).
2. C. B. Mills, *The General Methods of Reactor Analysis Used in the ANP Physics Group*, ORNL-1493, (November, 1953).
3. G. M. Roe, *The Absorption of Neutrons in Doppler Broadened Resonances*, KAPL-1241, (October, 1954).
4. P. L. Hofmann and M. L. Storm, *Self-shielding Calculations for SIR-Type Reactors*, The Physics of Intermediate Spectrum Reactors, J. R. Stehn, (Ed.); UC-81, (September, 1958), p. 11-1.
5. G. Goertzel and E. Greuling, *An Approximate Method for Treating Neutron Slowing Down*, Nuclear Sci. and Eng., 7: No. 1, 69-72, (January, 1960).
6. C. E. Porter and R. G. Thomas, *Fluctuations of Nuclear Reaction Widths*, Phys. Rev., 104: No. 2, 483, (October, 1956).
7. W. H. Roach, *Computational Survey of Idealized Fast Breeder Reactors*, Nuclear Sci. and Eng., 8: No. 6, 621, (December, 1960).
8. F. A. Kloverstrom, R. M. R. Deck and A. J. Reyenga, *Critical Measurements on Near-Homogeneous BeO-Moderated, Oralloy Fueled Systems*, UCRL-5369, Part 1—Revised, (July, 1959).
9. H. L. Reynolds, *Critical Measurements and Calculations for Enriched—Uranium Graphite-Moderated Systems*, UCRL-5175, (March 1958).
10. H. C. Paxton, *Critical Data for Nuclear Safety Guidance*, LAMS-2415, (February, 1960).
11. R. T. Frost, *Report of the Project Physics Section for June, July, August, 1954*, KAPL-1207, (1954), p. 62.
12. R. T. Frost, W. Y. Kato and D. K. Butler, *Measurement of Doppler Temperature Coefficient in Intermediate and Fast Assemblies*, Proc., 1958 Geneva Conference, 12: Paper No. 1777, p. 79.
13. H. A. Bethe, *Nuclear Physics*, Revs. Modern Phys., 9: No. 2, 69-244, (April, 1937).
14. H. Feshbach, G. Goertzel and H. Yamauchi, *Estimation of Doppler Effect in Fast Reactors*, Nuclear Sci. and Eng., 1: No. 1, 4-19, (March, 1956).
15. R. B. Nicholson, *The Doppler Effect in Fast Neutron Reactors*, APDA-139, (June, 1960).
16. G. Bell, *Theory of Effective Cross Sections*, LA-2322, (June, 1959).
17. J. Devaney, M. Goldstein and B. Fagen, *Pu^{239} Cross Sections and Their Temperature Dependence*, LA-2127, (1957); J. Devaney and B. Fagen, *U^{238} Cross Sections and Their Temperature Dependence*, LA-2144, (1958); J. Devaney, M. Devaney and D. Coward, *Tungsten Cross Sections and Their Temperature Dependence*, LA-2289, (1958); J. Devaney, D. Coward and R. Anderson, *Molybdenum Cross Sections and Their Temperature Dependence*, LA-2373, (1960); J. Devaney, et al., *Calculations of U^{235} Cross Sections and Their Temperature Dependence*, (unpublished).
18. P. A. Moldauer, *On the Estimation of Fast Neutron Cross Sections*, Proc., Conference on the Physics of Breeding, ANL-6122, (October, 1959), p. 67.
19. H. L. Reynolds and C. E. Walter, *Hot Box, A High-Temperature Critical Facility*, UCRL-5483, (March, 1959).
20. H. Hurwitz, Jr. and R. Ehrlich, *Comparison of Theory and Experiment for Intermediate Assemblies*, Proc., 1955 Geneva Conference, 5: Paper No. 608, p. 423.
21. R. Ehrlich, *Multigroup and Adjoint Calculations for SAPL-2 and SAPL-3*, KAPL-347, (July, 1950).
22. R. Ehrlich, *Further Multigroup Results with Moderated Blankets*, KAPL-M-RE-3, (August, 1948).
23. R. Ehrlich, *Further Multigroup Results on Pile 2 and Aluminum Alloy Piles*, KAPL-M-RE-5, (August, 1948).
24. R. Ehrlich, H. Hurwitz, Jr. and J. R. Stehn, *A Multigroup Method for Computing Critical Masses of Intermediate Piles*, A-4315, (May, 1947).
25. H. Hurwitz, Jr. and R. Ehrlich, *Multigroup Methods*, Reactor Sci. and Tech., TID-2009, 3: No. 2, 13-42, (June, 1953).
26. T. Snyder, *The Critical Assembly—A Nuclear Design Tool*, Proc., 1955 Geneva Conference, 5: Paper No. 602, p. 162.
27. H. B. Stewart, P. L. Hofmann and M. L. Storm, *Physics Considerations in the Design of Intermediate Energy Spectrum Reactors*, Proc., 1958 Geneva Conference, 12: Paper No. 2381, p. 142.
28. H. Hurwitz, Jr., *Note on the Theory of Danger Coefficients*, KAPL-98, (September, 1948).
29. F. A. Kloverstrom and D. E. Kraft, *Critical Measurements on Near-Homogeneous, BeO Moderated, Oralloy Fueled Systems*, UCRL-5369, Part 2, (July, 1960).
30. E. L. Zimmerman, *A Graphite-Moderated Critical Assembly—CA-4*, Y-881, (December, 1952).
31. J. C. Hoogterp, *Critical Masses of Graphite-Tamped Heterogeneous Oy-Graphite Systems*, LA-1732, (May, 1954).
32. G. E. Hansen, et al., *Beryllium-Reflected, Graphite-Moderated Critical Assemblies*, LA-2141, (July, 1957).
33. C. L. Schuske, et al., *Plutonium Plexiglas Assemblies*, RFP-178, (January, 1960).
34. G. H. Bidinger, et al., *Plutonium Plexiglas Assemblies*, Part II, RFP-190, (April, 1960).
35. G. H. Bidinger, et al., *Nuclear Safety Experiments on Plutonium and Enriched Uranium Hydrogen Moderated Assemblies Containing Boron*, RFP-201, (October, 1960).
36. J. K. Fox, et al., *Critical Mass Studies, Part IX. Aqueous U^{235} Solutions*, ORNL-2367, (March, 1958).
37. R. N. Olcott, *Homogeneous Heavy Water Moderated Critical Assemblies. Part I. Experimental*, Nuclear Sci. and Eng., 1: No. 4, 327, (August, 1956).
38. George Safanov, *A Brief Description of Some RAND Reactor Studies*, RM-847, (May, 1952).
39. S. P. Stone and R. E. Lingenfelter, *Neutron Diffusion Theory Programs and Their Application to Simple Critical Systems*, UCRL-5913, (March, 1960).
40. (Mrs.) M. E. Mandl, *Preliminary Estimate of the Critical Radius of a Bare Pu-Be Intermediate Reactor with Pb Coolant*, AERE T/M-48, (June, 1951).
41. (Mrs.) M. E. Mandl, *Preliminary Estimate of the Critical Radius of a Pu-Be Intermediate Reactor with an Infinite Reflector, with and without Pb Coolant*, AERE T/M-59, (February, 1952).
42. (Mrs.) M. E. Mandl, *Preliminary Estimate of the Critical Radius of a Bare Pu-Be Intermediate Reactor*, AERE T/R-529, (August, 1950).
43. R. T. P. Whipple, *The Critical Radius of a Spherical Intermediate Reactor Consisting of a Homogeneous Core Surrounded by an Infinite Reflector of Heavy Material*, AERE T/R-920, (April, 1952).

Section 7

FAST REACTORS

7.1 CONSTANTS FOR FAST REACTOR CALCULATIONS

Multigroup constants for fast reactor calculations must be obtained by suitably averaging microscopic cross section information, as a function of neutron energy, over the energy interval of interest. Generally, this is done by assuming a neutron spectrum as a function of energy throughout the energy interval. Whether the assumed spectrum is the correct one can be determined by analyzing spectra calculated using such multigroup constants; for example, by analyzing spectra with a finer group structure, or by examination of a smooth curve fit through the multigroup spectrum. The calculated neutron spectrum may or may not agree with that assumed originally to generate the multigroup constants. If agreement is not satisfactory, the same iterative process may be continued until agreement is obtained.

It may be possible to arrive at a set of constants averaged over a spectrum which agrees with subsequent calculated spectra. However, if the energy interval representing a group is large, such constants may not be applicable to a new system with different spectral properties. Furthermore, even though a spectrum calculation at one point may be substantially in agreement with that originally assumed to generate the multigroup constants, it may not be assumed that those same constants are always adequate to describe the spectrum throughout the system.

In order to ensure that the multigroup constants are essentially independent of the spectrum within the group, the use of a large number of energy groups, each representing a small energy interval, suggests itself. However, many of the detailed cross sections are unknown. Therefore, there is considerable difference of opinion as to the optimum number of energy groups for analysis of various types of assemblies.

Few-group calculations have been used with reasonable success for a wide variety of criticality determinations. However, for a more complete study, multigroup sets using more than ten-energy groups have been used frequently for fast reactor analysis. A minimum of fifteen fast energy groups may be required for an exhaustive study of fast neutron systems with pronounced spectral degradation. Generally, one, two, or three groups above the U^{238} fission threshold (~1.4 Mev) are adequate. Groups below the U^{238} fission threshold usually are selected to cover unit or half-unit lethargy intervals down to about 10 kev.

7.1.1 MULTIGROUP NOTATION

The diffusion theory multigroup equations may be written as a set of equations of the form:

$$D_j \nabla^2 \phi_j - \Sigma_{a,j} \phi_j + Q_{s,j} + Q_{f,j} = 0$$

where j = 1, ... N labels the energy group

ϕ_j = the total flux in group j

$\Sigma_{a,j} = \Sigma_{f,j} + \Sigma_{c,j} + \Sigma_{in,j} + \Sigma_{er,j}$ = total removal cross section from group j

$\Sigma_{f,j}$ = fission cross section of group j

$\Sigma_{c,j}$ = capture cross section of group j

$\Sigma_{in,j} = \sum_{k \neq j} \Sigma_{in,j \to k}$ = inelastic removal cross section from group j

$\Sigma_{er,j} = \sum_{k \neq j} \Sigma_{er,j \to k}$ = elastic removal cross section from group j

$Q_{s,j} = \sum_{k \neq j} (\Sigma_{in,k \to j} + \Sigma_{er,k \to j})\ \phi_k$ = scattering source into group j

$Q_{f,j} = \chi_j \sum_{k=1}^{N} (\nu \Sigma_f)_k\ \phi_k$ = fission source into group j

χ_j = fraction of fission neutrons born into group j

and

D_j = diffusion coefficient of group j, related to transport cross section, $\Sigma_{tr,j}$, by some prescription; for simple diffusion theory:

$$D_j = 1/3\Sigma_{tr,j}$$

The group macroscopic cross sections $\Sigma_{f,j}$, $\Sigma_{c,j}$, $\Sigma_{in,j \to k}$ and $\Sigma_{er,j \to k}$ may be obtained from the corresponding group microscopic cross sections for individual materials, e.g., for reaction q in material z,

$$\Sigma_{q,j} = \sum_z N^z\ \sigma^z_{q,j}$$

where N^z = atoms/cm^3 of material z.

The group microscopic cross sections are obtained, in principle at least, from fundamental cross sections which, using the notation of Goldstein,[1] may be written:

for any type of parasitic capture:

$$\sigma_{n,\gamma}(E),\ \sigma_{n,\alpha}(E),\ \text{etc}$$

for fission:

$$\sigma_{n,f}(E)$$

for total elastic scattering, including moderation and angular distribution:

$$\sigma_{n,n}(E),\ \sigma_{n,n}(E \to E'),\ \sigma_{n,n}(E \to E',\ \theta)$$

and for total inelastic scattering, including angular distribution:

$$\sigma_{n,n'}(E \to E'),\ \sigma_{n,n'}(E \to E',\ \theta)$$

Multigroup microscopic cross sections may now be defined for group capture:

$$\sigma^z_{c,j} = \frac{\int_{E_{jL}}^{E_{jH}} [\sigma^z_{n,\gamma}(E) + \sigma^z_{n,\alpha}(E) + \ldots]\ \phi(E)\ dE}{\int_{E_{jL}}^{E_{jH}} \phi(E)\ dE}$$

for group fission:

$$\sigma^z_{f,j} = \frac{\int_{E_{jL}}^{E_{jH}} \sigma^z_{n,f}(E)\ \phi(E)\ dE}{\int_{E_{jL}}^{E_{jH}} \phi(E)\ dE}$$

for scattering, whether within or out of group j:

$$\sigma^z_{\left\{\begin{matrix}in\\el\end{matrix}\right\}j \to k} = \frac{\int_{E'=E_{kL}}^{E_{kH}} \int_{E=E_{jL}}^{E_{jH}} \sigma^z_{\left\{\begin{matrix}n,n'\\n,n\end{matrix}\right\}} (E \to E')\ \phi(E)\ dE\ dE'}{\int_{E_{jL}}^{E_{jH}} \phi(E)\ dE}$$

where E_{jL} and E_{jH} are the lower and upper limits of group j, respectively, and $\phi(E)$ is the flux per unit energy interval at E.

The cross section for fission neutron production by group j neutrons is given by:

$$(\nu\Sigma_f)_j = \sum_z N^z (\nu\sigma_f)_j^z$$

and

$$(\nu\sigma_f)_j^z = \frac{\int_{E_{jL}}^{E_{jH}} \nu^z(E)\, \sigma_{n,f}^z(E)\, \phi(E)\, dE}{\int_{E_{jL}}^{E_{jH}} \phi(E)\, dE}$$

The group transport cross section, $\Sigma_{tr,j}$, may be obtained from:

$$\Sigma_{tr,j} = \sum_z N^z \sigma_{tr,j}^z \tag{7-1}$$

where

$$\frac{1}{\sigma_{tr,j}^z} = \frac{\left[\int_{E_{jL}}^{E_{jH}} \phi(E)\, dE/\sigma_{tr}^z(E)\right]}{\int_{E_{jL}}^{E_{jH}} \phi(E)\, dE}$$

and

$$\begin{aligned}\sigma_{tr}^z(E) = {} & \sigma_{n,\gamma}^z(E) + \sigma_{n,\alpha}^z(E) + \ldots \sigma_{n,f}^z(E) + \int_0^{E_{jL}} [\sigma_{n,n'}^z(E \to E') + \sigma_{n,n}^z(E \to E')]\, dE' \\ & + \int_{E_{jH}}^{\infty} [\sigma_{n,n'}^z(E \to E') + \sigma_{n,n}^z(E \to E')]\, dE' \\ & + \int_{E_{jL}}^{E_{jH}} \int_{-1}^{1} [\sigma_{n,n'}^z(E \to E', \theta) + \sigma_{n,n}^z(E \to E', \theta)]\, (1 - \cos\theta)\, d(\cos\theta)\, dE'\end{aligned}$$

In the absence of pronounced resonance effects due to capture and/or scattering within an energy group, an alternative prescription for $\sigma_{tr,j}$ is given by:

$$\sigma_{tr,j}^z = \frac{\int_{E_{jL}}^{E_{jH}} \sigma_{tr}^z(E)\, \phi(E)\, dE}{\int_{E_{jL}}^{E_{jH}} \phi(E)\, dE} = \sigma_{c,j}^z + \sigma_{f,j}^z + \sum_{k \neq j} \sigma_{in,j\to k}^z + \sigma_{er,j\to k}^z$$

$$+ \frac{\int_{E_{jL}}^{E_{jH}} \int_{E_{jL}}^{E_{jH}} \int_{-1}^{1} \phi(E)\, [\sigma_{n,n'}^z(E \to E', \theta) + \sigma_{n,n}^z(E \to E', \theta)]\, (1 - \cos\theta)\, d(\cos\theta)\, dE\, dE'}{\int_{E_{jL}}^{E_{jH}} \phi(E)\, dE} \tag{7-2}$$

The last term may be denoted by:

$$(\sigma_{in,j\to j}^z + \sigma_{el,j\to j}^z)\, (1 - \bar{\mu})$$

where $\bar{\mu}$ is the average cosine of the scattering angle. It cannot be said that Eq. (7-1) is superior to Eq. (7-2) since in neither case is the really correct average (which involves the mixture) applied:

$$\frac{1}{\Sigma_{tr,j}} = \left[\int_{E_{jL}}^{E_{jH}} \left\{[\phi(E)\, dE] \Big/ \sum_z N^z \sigma_{tr}^z(E)\right\}\right] \Big/ \int_{E_{jL}}^{E_{jH}} \phi(E)\, dE$$

The application of the S_n and DSN methods[2,3,4] to the solution of fast reactor problems requires some recombination of the previously defined constants. In the case of plane geometry, and the assumption of isotropic scattering in the transport approximation, the transport equation is written:

$$\left(\mu \frac{\partial}{\partial x} + \Sigma_{tr,j}\right) N_j(x,\mu) = S_j(x)$$

where $N_j(x,\mu)$ is the angular neutron flux per unit μ interval, and μ is the direction cosine with respect to x. The source term, $S_j(x)$, may be expressed in terms of the previously defined $\phi_j(x)$ where:

$$\phi_j(x) = \frac{1}{2} \int_{-1}^{+1} N_j(x,\mu)\, d\mu$$

Then $S_j(x)$ appears as:

$$S_j(x) = \chi_j \sum_{k=1}^{J} \nu_k \Sigma_{f,k} \phi_k + \sum_{k=1}^{J} \Sigma_{k\to j} \phi_k$$

The first term on the right hand side is the $Q_{f,j}$ defined earlier. The second term differs from the previous $Q_{s,j}$ only in that the $k = j$ term is included in the sum. $\Sigma_{k\to j}$ for $k \neq j$ is the same as defined previously. $\Sigma_{k\to k}$ may be defined by:

$$\Sigma_{k\to k} = \Sigma_{tr,k} - \Sigma_{c,k} - \Sigma_{f,k} - \Sigma_{in,k} - \Sigma_{er,k}$$

7.1.2 MULTIGROUP CONSTANTS

Three sets of multigroup constants: ANL-16,[5] LASL-16,[6,7] and ANL-11,[8] are given in Tables 7-1, 7-2, and 7-3, respectively. The primary motivation for including these particular sets of constants is the versatility afforded by their combined use. For instance, the LASL 16-group compilation may be used for both fast and intermediate systems. It can also be used as a 6-group, all-fast set. The ANL 16-group set contains the most recent microscopic cross section information. Comparison between theory and experiment shows that this set of constants tends to underpredict critical mass. The ANL 11-group set has been found suitable for the analysis of fast neutron systems having critical masses of less than about 225 kg U^{235}.

The format of the LASL constants differs somewhat from the ANL constants. In the LASL constants, microscopic data are represented as they will appear in the reactor calculation. Thus

$$\sigma_{i\to i} = \sigma_{tr} - \sigma_f - \sigma_{n,\gamma} - \sum_{k\neq 1} \sigma_{i\to k}$$

and

$$\sigma_{i\to i+1}$$

include the inelastic component as well as that due to elastic moderation. In the ANL constants, inelastic events within a group that result in scattering to the same group are accounted for but not explicitly represented.

A number of sets of multigroup constants are described and identified in Table 7-4. In addition to giving details concerning materials and group structure, some editorial comments concerning origin and/or application of the sets are given below. The latter are not to be considered all-inclusive on the basis of all experience that has been obtained with the various sets of constants.

(1) The ANL 4-group set[9,14] features two fast groups. This set (see Table 7-41) has been adjusted to predict criticality and spectrum of the coupled reactor experiment on ZPR-III.

(2) The LASL 6-group set[10] has been selectively adjusted to give good agreement on virtually all the high-density plutonium and uranium critical assemblies at LASL. The five high-energy group constants for U^{233}, U^{235}, U^{238}, and Pu^{239} of the LASL 16-group set (Table 7-2) are obtained from this six-group set.

(3) Both of the 9-group sets[11] from the USSR demonstrate good agreement between theory and experiment. In general, the constants tend to be too reactive and thus underpredict critical masses.* A special feature is the use of a fission spectrum for high-energy fission which differs somewhat from that of low-energy fission.

(4) The LASL 10-group set[12] shows good agreement between theory and experiment on the high-density LASL systems, and has been similarly successful for some of the smaller ZPR-III systems. These constants have not been tested against the larger (>200 kg U^{235}) ZPR-III systems. The set has been used in conjunction with LAMPRE-size critical experiments.

(5) A number of 10-group sets have been used at ANL.[13] These represent early attempts to predict the small (100-200 kg U^{235}) ZPR-III cores. In general, the constants were not sufficiently reactive for reasonable prediction. Structural and coolant materials exhibited too much reactivity. One set was constructed specifically for analyzing EBR-II-type systems with respect to both criticality and reactivity behavior of coolant and structural materials.

(6) Other 10-group sets were assembled to improve agreement between calculation and measurement for moderately large cores (200-300 kg U^{235}). Two of these sets were used for the analysis of the

*Unpublished data, D. Meneghetti, ANL.

Table 7-1 — MULTIGROUP CONSTANTS FOR FAST REACTOR ANALYSIS (ANL 16-GROUP)

(Microscopic cross sections in barns)

Fission Spectrum and Energy/Lethargy Structure

j	E_L, Mev	Δu	Fission Spectrum (χ)
1	3.668	—	0.132
2	2.225	0.5	0.213
3	1.35	0.5	0.232
4	0.825	0.5	0.179
5	0.5	0.5	0.116
6	0.3	0.5	0.067
7	0.18	0.5	0.034
8	0.11	0.5	0.017
9	0.067	0.5	0.010
10	0.0407	0.5	0
11	0.025	0.5	0
12	0.015	0.5	0
13	0.0091	0.5	0
14	0.0055	0.5	0
15	0.0021	1.0	0
16	0.0005	—	0

Boron-10 ($N = 0.1364 \times 10^{24}$)					Boron ($N = 0.1364 \times 10^{24}$)				
j	E_L	σ_{tr}	$\sigma_{n,\alpha}$	σ_{er}	j	E_L	σ_{tr}	$\sigma_{n,\alpha}$	σ_{er}
1	3.668	0.74	0.06	0.330	1	3.668	0.71	0.012	0.314
2	2.225	1.46	0.19	0.502	2	2.225	1.20	0.039	0.426
3	1.35	2.12	0.3	0.629	3	1.35	2.01	0.07	0.620
4	0.825	2.27	0.23	0.661	4	0.825	2.07	0.037	0.675
5	0.5	2.55	0.44	0.684	5	0.5	2.02	0.074	0.654
6	0.3	4.1	0.7	1.21	6	0.3	3.51	0.18	1.090
7	0.18	4.68	1.0	1.24	7	0.18	3.51	0.20	1.035
8	0.11	4.53	1.55	1.00	8	0.11	3.78	0.32	1.076
9	0.067	4.49	2.2	0.708	9	0.067	4.16	0.45	1.057
10	0.0407	4.73	2.9	0.543	10	0.0407	4.45	0.59	1.056
11	0.025	5.07	3.6	0.446	11	0.025	4.73	0.73	1.126
12	0.015	6.06	4.5	0.446	12	0.015	4.93	0.91	1.064
13	0.0091	6.55	4.9	0.471	13	0.0091	4.94	1.00	1.042
14	0.0055	7.82	5.8	0.575	14	0.0055	5.23	1.18	1.071
15	0.0021	10.21	7.1	0.308	15	0.0021	5.43	1.44	0.365
16	0.0005	18.33	11.	—	16	0.0005	5.87	2.23	—

Carbon ($N = 0.0828 \times 10^{24}$)												
					$\sigma_{n,n',j \to j+k}$							
j	E_L	σ_{tr}	$\sigma_{n,\gamma}$	σ_{er}	$\sigma_{n,n'}$	k = 0	1	2	3	4	5	6
1	3.668	0.90	0	0.35	0.08	0.002	0.029	0.037	0.006	0.006	—	—
2	2.225	1.50	—	0.50	—	—	—	—	—	—	—	—
3	1.35	1.81	—	0.53	—	—	—	—	—	—	—	—
4	0.825	2.21	—	0.67	—	—	—	—	—	—	—	—
5	0.5	2.73	—	0.84	—	—	—	—	—	—	—	—
6	0.3	3.31	—	0.99	—	—	—	—	—	—	—	—
7	0.18	3.75	—	1.07	—	—	—	—	—	—	—	—
8	0.11	4.10	—	1.16	—	—	—	—	—	—	—	—
9	0.067	4.31	—	1.12	—	—	—	—	—	—	—	—
10	0.0407	4.41	—	1.10	—	—	—	—	—	—	—	—
11	0.025	4.44	—	1.14	—	—	—	—	—	—	—	—
12	0.015	4.53	—	1.09	—	—	—	—	—	—	—	—
13	0.0091	4.53	—	1.09	—	—	—	—	—	—	—	—
14	0.0055	4.53	—	1.09	—	—	—	—	—	—	—	—
15	0.0021	4.53	—	0.37	—	—	—	—	—	—	—	—
16	0.0005	4.4	0	0	—	—	—	—	—	—	—	—

687863 O - 63 - 37

Table 7-1 — MULTIGROUP CONSTANTS FOR FAST REACTOR ANALYSIS (ANL 16-GROUP) (Continued)
(Microscopic cross sections in barns)

Oxygen ($N = 0.096 \times 10^{24}$)

j	E_L	σ_{tr}	$\sigma_{n,\alpha}$	σ_{er}	$\sigma_{n,n',j\to j+k}$							
					$\sigma_{n,n'}$	k = 0	1	2	3	4	5	6
1	3.668	1.14	0.052	0.337	0.018	0	0.005	0.011	0.002	—	—	—
2	2.225	1.72	—	0.430	—	—	—	—	—	—	—	—
3	1.35	2.56	—	0.559	—	—	—	—	—	—	—	—
4	0.825	3.51	—	0.793	—	—	—	—	—	—	—	—
5	0.5	3.47	—	0.797	—	—	—	—	—	—	—	—
6	0.3	4.09	—	0.914	—	—	—	—	—	—	—	—
7	0.18	3.35	—	0.715	—	—	—	—	—	—	—	—
8	0.11	3.35	—	0.710	—	—	—	—	—	—	—	—
9	0.067	3.35	—	0.651	—	—	—	—	—	—	—	—
10	0.0407	3.35	—	0.626	—	—	—	—	—	—	—	—
11	0.025	3.35	—	0.643	—	—	—	—	—	—	—	—
12	0.015	3.35	—	0.605	—	—	—	—	—	—	—	—
13	0.0091	3.35	—	0.605	—	—	—	—	—	—	—	—
14	0.0055	3.54	—	0.639	—	—	—	—	—	—	—	—
15	0.0021	3.64	—	0.227	—	—	—	—	—	—	—	—
16	0.0005	3.64	—	—	—	—	—	—	—	—	—	—

Sodium ($N = 0.022 \times 10^{24}$)

j	E_L	σ_{tr}	$\sigma_{n,\gamma}$	σ_{er}	$\sigma_{n,n',j\to j+k}$							
					$\sigma_{n,n'}$	k = 0	1	2	3	4	5	6
1	3.668	1.30	0.0005	0.137	0.633	0.158	0.166	0.141	0.084	0.046	0.027	0.011
2	2.225	1.47	0.0001	0.164	0.57	0.238	0.228	0.029	0.038	0.016	0.014	0.007
3	1.35	1.96	0.0001	0.215	0.541	0.27	0.271	0	0	0	0	0
4	0.825	2.89	0.0002	0.374	0.480	0.061	0.284	0.135	0	0	0	0
5	0.5	3.93	0.0003	0.594	0.236	0	0.127	0.056	0.030	0.012	0.011	0
6	0.3	3.22	0.0005	0.5	—	—	—	—	—	—	—	—
7	0.18	3.49	0.0007	0.518	—	—	—	—	—	—	—	—
8	0.11	3.10	0	0.458	—	—	—	—	—	—	—	—
9	0.067	3.46	0	0.468	—	—	—	—	—	—	—	—
10	0.0407	4.77	0.003	0.619	—	—	—	—	—	—	—	—
11	0.025	3.88	0	0.518	—	—	—	—	—	—	—	—
12	0.015	4.10	0	0.515	—	—	—	—	—	—	—	—
13	0.0091	5.01	0	0.629	—	—	—	—	—	—	—	—
14	0.0055	7.23	0	0.907	—	—	—	—	—	—	—	—
15	0.0021	22.81	0.377	0.969	—	—	—	—	—	—	—	—
16	0.0005	5.93	0	—	—	—	—	—	—	—	—	—

Aluminum ($N = 0.0603 \times 10^{24}$)

j	E_L	σ_{tr}	$\sigma_{n,\gamma}$	σ_{er}	$\sigma_{n,n',j\to j+k}$							
					$\sigma_{n,n'}$	k = 0	1	2	3	4	5	6
1	3.668	1.37	0.0263	0.118	0.711	0.177	0.187	0.159	0.095	0.051	0.030	0.012
2	2.225	1.60	0.0003	0.162	0.491	0.116	0.198	0.083	0.071	0	0.023	0
3	1.35	2.00	0.0004	0.216	0.222	0.008	0.115	0.078	0.021	0	0	0
4	0.825	2.48	0.0004	0.332	0.056	0	0.014	0.026	0.010	0.004	0.002	0
5	0.5	2.97	0.0007	0.404	—	—	—	—	—	—	—	—
6	0.3	3.17	0.0011	0.420	—	—	—	—	—	—	—	—
7	0.18	3.82	0.0017	0.484	—	—	—	—	—	—	—	—
8	0.11	5.02	0.0023	0.632	—	—	—	—	—	—	—	—
9	0.067	5.98	0.0030	0.690	—	—	—	—	—	—	—	—
10	0.0407	2.78	0	0.308	—	—	—	—	—	—	—	—
11	0.025	6.34	0.0039	0.721	—	—	—	—	—	—	—	—
12	0.015	0.75	0	0.081	—	—	—	—	—	—	—	—
13	0.0091	1.13	0	0.121	—	—	—	—	—	—	—	—
14	0.0055	1.51	0.0923	0.161	—	—	—	—	—	—	—	—
15	0.0021	1.37	0	0.0507	—	—	—	—	—	—	—	—
16	0.0005	1.37	0	0	—	—	—	—	—	—	—	—

Table 7-1—MULTIGROUP CONSTANTS FOR FAST REACTOR ANALYSIS (ANL 16-GROUP) (Continued)

(Microscopic cross sections in barns)

Potassium (N = 0.0134×10^{24})

					$\sigma_{n,n',j\to j+k}$							
j	E_L	σ_{tr}	$\sigma_{n,\gamma}$	σ_{er}	$\sigma_{n,n'}$	k = 0	1	2	3	4	5	6
1	3.668	2.05	0.109	0.165	0.7	0.07	0.16	0.18	0.13	0.09	0.04	0.03
2	2.225	2.19	0.1054	0.216	0.08	0	0	0.025	0.023	0.02	0.012	0
3	1.35	2.03	0.0583	0.181	—	—	—	—	—	—	—	—
4	0.825	1.53	0.0236	0.141	—	—	—	—	—	—	—	—
5	0.5	1.50	0.0009	0.141	—	—	—	—	—	—	—	—
6	0.3	1.87	0.0015	0.171	—	—	—	—	—	—	—	—
7	0.18	2.19	0.0021	0.191	—	—	—	—	—	—	—	—
8	0.11	2.04	0.0027	0.177	—	—	—	—	—	—	—	—
9	0.067	2.75	0.0033	0.218	—	—	—	—	—	—	—	—
10	0.0407	3.46	0.0045	0.264	—	—	—	—	—	—	—	—
11	0.025	3.27	0.0057	0.256	—	—	—	—	—	—	—	—
12	0.015	1.92	0.0072	0.142	—	—	—	—	—	—	—	—
13	0.0091	2.32	0.0699	0.171	—	—	—	—	—	—	—	—
14	0.0055	3.74	0	0.276	—	—	—	—	—	—	—	—
15	0.0021	3.54	0.3465	0.090	—	—	—	—	—	—	—	—
16	0.0005	3.15	0	—	—	—	—	—	—	—	—	—

Titanium (N = 0.0566×10^{24})

					$\sigma_{n,n',j\to j+k}$							
j	E_L	σ_{tr}	$\sigma_{n,\gamma}$	σ_{er}	$\sigma_{n,n'}$	k = 0	1	2	3	4	5	6
1	3.668	2.04	0.0005	0.077	1.31	0.173	0.309	0.339	0.241	0.138	0.066	0.044
2	2.225	2.76	0.0009	0.158	0.92	0.237	0.364	0.228	0.051	0.040	0	0
3	1.35	2.93	0.0015	0.203	0.30	0	0.155	0.1	0.045	—	—	—
4	0.825	2.47	0.0025	0.179	—	—	—	—	—	—	—	—
5	0.5	2.42	0.0038	0.184	—	—	—	—	—	—	—	—
6	0.3	2.03	0.0044	0.150	—	—	—	—	—	—	—	—
7	0.18	2.98	0.0048	0.210	—	—	—	—	—	—	—	—
8	0.11	2.78	0.0056	0.195	—	—	—	—	—	—	—	—
9	0.067	4.26	0.0072	0.273	—	—	—	—	—	—	—	—
10	0.0407	9.45	0.009	0.583	—	—	—	—	—	—	—	—
11	0.025	15.3	0.011	0.969	—	—	—	—	—	—	—	—
12	0.015	76.6	0.023	4.57	—	—	—	—	—	—	—	—
13	0.0091	29.8	0	1.78	—	—	—	—	—	—	—	—
14	0.0055	14.8	0	0.882	—	—	—	—	—	—	—	—
15	0.0021	15	0.377	0.309	—	—	—	—	—	—	—	—
16	0.0005	4.5	0	—	—	—	—	—	—	—	—	—

Vanadium (N = 0.0704×10^{24})

					$\sigma_{n,n',j\to j+k}$							
j	E_L	σ_{tr}	$\sigma_{n,\gamma}$	σ_{er}	$\sigma_{n,n'}$	k = 0	1	2	3	4	5	6
1	3.668	2.12	0.0005	0.0548	1.60	0.194	0.370	0.418	0.304	0.174	0.085	0.055
2	2.225	2.32	0.0008	0.0550	1.66	0.294	0.457	0.407	0.266	0.139	0.061	0.036
3	1.35	2.16	0.0012	0.0484	1.49	0.383	0.437	0.332	0.191	0.089	0.037	0.021
4	0.825	2.47	0.0015	0.0948	1.07	0.268	0.268	0.139	0.139	0.139	0.086	0.031
5	0.5	2.64	0.0019	0.151	0.63	0.05	0.236	0.168	0.176	0	0	0
6	0.3	3.54	0.0028	0.246	0.38	0	0	0.210	0.105	0.043	0.022	0
7	0.18	4.95	0.0044	0.328	—	—	—	—	—	—	—	—
8	0.11	5.55	0.007	0.366	—	—	—	—	—	—	—	—
9	0.067	6.6	0.010	0.399	—	—	—	—	—	—	—	—
10	0.0407	6.41	0.017	0.372	—	—	—	—	—	—	—	—
11	0.025	8.38	0.026	0.499	—	—	—	—	—	—	—	—
12	0.015	21.2	0.039	1.19	—	—	—	—	—	—	—	—
13	0.0091	49.5	0.059	2.78	—	—	—	—	—	—	—	—
14	0.0055	25.2	0.168	1.39	—	—	—	—	—	—	—	—
15	0.0021	30.3	0.303	0.584	—	—	—	—	—	—	—	—
16	0.0005	7.1	0	—	—	—	—	—	—	—	—	—

Table 7-1—MULTIGROUP CONSTANTS FOR FAST REACTOR ANALYSIS (ANL 16-GROUP) (Continued)

(Microscopic cross sections in barns)

Chromium ($N = 0.0801 \times 10^{24}$)												
					$\sigma_{n,n',j\to j+k}$							
j	E_L	σ_{tr}	$\sigma_{n,\gamma}$	σ_{er}	$\sigma_{n,n'}$	k = 0	1	2	3	4	5	6
1	3.668	1.84	0.0007	0.057	1.300	0.152	0.297	0.340	0.249	0.144	0.070	0.048
2	2.225	2.45	0.0013	0.096	1.140	0.197	0.311	0.280	0.185	0.097	0.043	0.027
3	1.35	2.34	0.002	0.103	0.706	0	0	0.431	0.148	0	0.127	—
4	0.825	2.31	0.004	0.161	—	—	—	—	—	—	—	—
5	0.5	2.31	0.007	0.163	—	—	—	—	—	—	—	—
6	0.3	2.77	0.008	0.190	—	—	—	—	—	—	—	—
7	0.18	2.44	0.0085	0.160	—	—	—	—	—	—	—	—
8	0.11	5.45	0.009	0.355	—	—	—	—	—	—	—	—
9	0.067	4.29	0.0098	0.256	—	—	—	—	—	—	—	—
10	0.0407	3.89	0.014	0.223	—	—	—	—	—	—	—	—
11	0.025	2.59	0.013	0.153	—	—	—	—	—	—	—	—
12	0.015	2.98	0.0187	0.165	—	—	—	—	—	—	—	—
13	0.0091	6.24	0.020	0.346	—	—	—	—	—	—	—	—
14	0.0055	17.17	0.036	0 953	—	—	—	—	—	—	—	—
15	0.0021	13.98	0.057	0.268	—	—	—	—	—	—	—	—
16	0.0005	4.30	0.143	0	—	—	—	—	—	—	—	—

Iron ($N = 0.0847 \times 10^{24}$)												
					$\sigma_{n,n',j\to j+k}$							
j	E_L	σ_{tr}	$\sigma_{n,\gamma}$	σ_{er}	$\sigma_{n,n'}$	k = 0	1	2	3	4	5	6
1	3.668	1.99	0.0058	0.052	1.400	0.148	0.310	0.369	0.277	0.162	0.080	0.054
2	2.225	2.19	0.0010	0.074	1.120	0.204	0.615	0.118	0.086	0.058	0.007	0.032
3	1.35	2.01	0.0017	0.076	0.792	0.141	0.395	0.256	0	0	0	—
4	0.825	1.98	0.0030	0.102	0.334	0	0.079	0.076	0.093	0.056	0.030	—
5	0.5	2.30	0.0042	0.151	—	—	—	—	—	—	—	—
6	0.3	2.97	0.0047	0.190	—	—	—	—	—	—	—	—
7	0.18	2.42	0.0060	0.148	—	—	—	—	—	—	—	—
8	0.11	2.89	0.0078	0.176	—	—	—	—	—	—	—	—
9	0.067	6.02	0.0103	0.335	—	—	—	—	—	—	—	—
10	0.0407	4.36	0.0100	0.233	—	—	—	—	—	—	—	—
11	0.025	12.51	0.0199	0.687	—	—	—	—	—	—	—	—
12	0.015	2.24	0.0046	0.116	—	—	—	—	—	—	—	—
13	0.0091	5.66	0.0138	0.293	—	—	—	—	—	—	—	—
14	0.0055	8.79	0.0131	0.454	—	—	—	—	—	—	—	—
15	0.0021	5.76	0.0030	0.103	—	—	—	—	—	—	—	—
16	0.0005	8.00	0.02	0	—	—	—	—	—	—	—	—

Nickel ($N = 0.0913 \times 10^{24}$)												
					$\sigma_{n,n',j\to j+k}$							
j	E_L	σ_{tr}	$\sigma_{n,\gamma}$	σ_{er}	$\sigma_{n,n'}$	k = 0	1	2	3	4	5	6
1	3.668	2.10	0.0015	0.061	1.380	0.138	0.301	0.364	0.277	0.164	0.081	0.055
2	2.225	2.34	0.0025	0.083	1.000	0.156	0.266	0.251	0.170	0.090	0.041	0.026
3	1.35	2.67	0.0045	0.134	0.232	0	0.009	0.103	0.054	0.049	0.008	0.009
4	0.825	2.97	0.0074	0.176	—	—	—	—	—	—	—	—
5	0.5	3.17	0.0066	0.194	—	—	—	—	—	—	—	—
6	0.3	3.86	0.0074	0.235	—	—	—	—	—	—	—	—
7	0.18	5.19	0.0090	0.302	—	—	—	—	—	—	—	—
8	0.11	5.98	0.010	0.346	—	—	—	—	—	—	—	—
9	0.067	7.82	0.0127	0.414	—	—	—	—	—	—	—	—
10	0.0407	7.48	0.0126	0.381	—	—	—	—	—	—	—	—
11	0.025	11.03	0.0138	0.577	—	—	—	—	—	—	—	—
12	0.015	31.78	0.0347	1.563	—	—	—	—	—	—	—	—
13	0.0091	27.65	0.0165	1.360	—	—	—	—	—	—	—	—
14	0.0055	14.90	0.0114	0.733	—	—	—	—	—	—	—	—
15	0.0021	23.85	0.1783	0.405	—	—	—	—	—	—	—	—
16	0.0005	15.00	0.04	0	—	—	—	—	—	—	—	—

Table 7-1—MULTIGROUP CONSTANTS FOR FAST REACTOR ANALYSIS (ANL 16-GROUP) (Continued)

(Microscopic cross sections in barns)

Zirconium ($N = 0.0425 \times 10^{24}$)

j	E_L	σ_{tr}	$\sigma_{n,\gamma}$	σ_{er}	$\sigma_{n,n',j\to j+k}$							
					$\sigma_{n,n'}$	k = 0	1	2	3	4	5	6
1	3.668	2.64	0.001	0.040	1.800	0.089	0.301	0.470	0.419	0.274	0.143	0.104
2	2.225	3.01	0.002	0.0674	1.35	0.04	0.46	0.32	0.24	0.15	0.09	0.05
3	1.35	3.54	0.003	0.117	0.6	0	0.21	0.18	0.11	0.05	0.03	0.02
4	0.825	4.44	0.006	0.172	0.14	0	0	0.07	0.04	0.02	0.01	0
5	0.5	5.86	0.007	0.236	—	—	—	—	—	—	—	—
6	0.3	7.06	0.008	0.277	—	—	—	—	—	—	—	—
7	0.18	6.87	0.009	0.263	—	—	—	—	—	—	—	—
8	0.11	7.65	0.010	0.283	—	—	—	—	—	—	—	—
9	0.067	7.72	0.013	0.263	—	—	—	—	—	—	—	—
10	0.0407	8.10	0.018	0.266	—	—	—	—	—	—	—	—
11	0.025	8.73	0.025	0.294	—	—	—	—	—	—	—	—
12	0.015	7.99	0.035	0.253	—	—	—	—	—	—	—	—
13	0.0091	7.27	0.054	0.230	—	—	—	—	—	—	—	—
14	0.0055	8.21	0.076	0.260	—	—	—	—	—	—	—	—
15	0.0021	7.78	0.110	0.0852	—	—	—	—	—	—	—	—
16	0.0005	6.40	0.080	0	—	—	—	—	—	—	—	—

Niobium ($N = 0.0545 \times 10^{24}$)

j	E_L	σ_{tr}	$\sigma_{n,\gamma}$	σ_{er}	$\sigma_{n,n',j\to j+k}$							
					$\sigma_{n,n'}$	k = 0	1	2	3	4	5	6
1	3.668	2.44	0.007	0.0331	1.73	0.074	0.272	0.447	0.412	0.274	0.145	0.106
2	2.225	2.77	0.012	0.0333	2.08	0.182	0.455	0.550	0.434	0.256	0.123	0.080
3	1.35	3.70	0.02	0.0817	1.58	0.253	0.418	0.403	0.269	0.140	0.061	0.036
4	0.825	4.64	0.033	0.121	0.804	0	0.099	0.281	0.265	0.092	0.067	—
5	0.5	5.83	0.05	0.206	—	—	—	—	—	—	—	—
6	0.3	6.82	0.052	0.260	—	—	—	—	—	—	—	—
7	0.18	7.73	0.065	0.282	—	—	—	—	—	—	—	—
8	0.11	8.40	0.086	0.304	—	—	—	—	—	—	—	—
9	0.067	8.65	0.12	0.287	—	—	—	—	—	—	—	—
10	0.0407	8.28	0.18	0.264	—	—	—	—	—	—	—	—
11	0.025	7.56	0.27	0.248	—	—	—	—	—	—	—	—
12	0.015	7.06	0.42	0.218	—	—	—	—	—	—	—	—
13	0.0091	7.21	0.65	0.219	—	—	—	—	—	—	—	—
14	0.0055	7.20	1.02	0.212	—	—	—	—	—	—	—	—
15	0.0021	7.17	1.85	0.055	—	—	—	—	—	—	—	—
16	0.0005	7.0	3.27	—	—	—	—	—	—	—	—	—

Molybdenum ($N = 0.0640 \times 10^{24}$)

j	E_L	σ_{tr}	$\sigma_{n,\gamma}$	σ_{er}	$\sigma_{n,n',j\to j+k}$							
					$\sigma_{n,n'}$	k = 0	1	2	3	4	5	6
1	3.668	2.74	0.006	0.030	2.17	0.086	0.331	0.557	0.521	0.351	0.187	0.137
2	2.225	2.95	0.010	0.036	2.09	0.166	0.441	0.553	0.447	0.268	0.129	0.086
3	1.35	3.36	0.017	0.062	1.72	0.246	0.440	0.447	0.309	0.163	0.072	0.043
4	0.825	4.08	0.028	0.106	1.04	0.137	0.446	0.278	0.110	0.016	0.053	0
5	0.5	5.50	0.047	0.180	0.34	0.134	0.143	0.026	0.033	0.004	0	0
6	0.3	6.33	0.055	0.230	0.21	0	0.132	0.042	0.036	0	0	0
7	0.18	7.60	0.060	0.270	0.06	0	0	0.038	0.022	0	0	0
8	0.11	8.17	0.070	0.289	—	—	—	—	—	—	—	—
9	0.067	7.94	0.085	0.257	—	—	—	—	—	—	—	—
10	0.0407	7.58	0.120	0.236	—	—	—	—	—	—	—	—
11	0.025	7.37	0.160	0.236	—	—	—	—	—	—	—	—
12	0.015	7.02	0.220	0.211	—	—	—	—	—	—	—	—
13	0.0091	6.94	0.300	0.209	—	—	—	—	—	—	—	—
14	0.0055	6.75	0.380	0.203	—	—	—	—	—	—	—	—
15	0.0021	6.62	0.480	0.0688	—	—	—	—	—	—	—	—
16	0.0005	7.00	0.980	0	—	—	—	—	—	—	—	—

Table 7-1 — MULTIGROUP CONSTANTS FOR FAST REACTOR ANALYSIS (ANL 16-GROUP) (Continued)

(Microscopic cross sections in barns)

Tantalum ($N = 0.0553 \times 10^{24}$)												
					$\sigma_{n,n',j\to j+k}$							
j	E_L	σ_{tr}	$\sigma_{n,\gamma}$	σ_{er}	$\sigma_{n,n'}$	k = 0	1	2	3	4	5	6
1	3.668	3.11	0.033	0.0115	2.67	0.021	0.188	0.535	0.700	0.583	0.354	0.289
2	2.225	3.80	0.056	0.0199	2.87	0.086	0.398	0.711	0.723	0.500	0.263	0.189
3	1.35	4.23	0.092	0.0268	2.65	0.205	0.545	0.715	0.583	0.341	0.161	0.100
4	0.825	4.58	0.114	0.0455	2.16	0.616	0.974	0.343	0.125	0.058	0.044	0
5	0.5	5.09	0.14	0.0673	1.62	0.484	0.612	0.275	0.082	0.115	0.052	0
6	0.3	6.16	0.19	0.0852	0.9	0.253	0.391	0.204	0.034	0.018	0	0
7	0.18	6.94	0.24	0.0962	0.5	0	0.225	0.027	0.228	0.020	0	0
8	0.11	7.54	0.3	0.133	—	—	—	—	—	—	—	—
9	0.067	8.08	0.4	0.130	—	—	—	—	—	—	—	—
10	0.0407	8.77	0.54	0.131	—	—	—	—	—	—	—	—
11	0.025	9.47	0.8	0.142	—	—	—	—	—	—	—	—
12	0.015	10.3	1.15	0.148	—	—	—	—	—	—	—	—
13	0.0091	11.2	1.7	0.146	—	—	—	—	—	—	—	—
14	0.0055	13.2	2.2	0.178	—	—	—	—	—	—	—	—
15	0.0021	15.4	2.9	0.073	—	—	—	—	—	—	—	—
16	0.0005	23.6	7.0	—	—	—	—	—	—	—	—	—
Lead ($N = 0.033 \times 10^{24}$)												
					$\sigma_{n,n',j\to j+k}$							
j	E_L	σ_{tr}	$\sigma_{n,\gamma}$	σ_{er}	$\sigma_{n,n'}$	k = 0	1	2	3	4	5	6
1	3.668	3.86	0.0007	0.040	2.23	0.012	0.128	0.411	0.582	0.510	0.320	0.267
2	2.225	4.44	0.001	0.0604	1.1	0.22	0.40	0.18	0.11	0.09	0.06	0.04
3	1.35	4.20	0.0017	0.0570	0.6	0.03	0.36	0.15	0.03	0.02	0.01	0
4	0.825	4.50	0.003	0.0728	0.2	0	0.06	0.08	0.02	0.02	0.01	0.01
5	0.5	4.65	0.0032	0.0815	0.02	0	0	0.005	0.006	0.005	0.003	0.001
6	0.3	4.92	0.0034	0.0839	—	—	—	—	—	—	—	—
7	0.18	6.69	0.0035	0.109	—	—	—	—	—	—	—	—
8	0.11	8.85	0.0036	0.143	—	—	—	—	—	—	—	—
9	0.067	9.95	0.0037	0.148	—	—	—	—	—	—	—	—
10	0.0407	10.1	0.0039	0.144	—	—	—	—	—	—	—	—
11	0.025	9.95	0.004	0.146	—	—	—	—	—	—	—	—
12	0.015	10.5	0.0042	0.145	—	—	—	—	—	—	—	—
13	0.0091	10.5	0.0043	0.145	—	—	—	—	—	—	—	—
14	0.0055	10.9	0.0045	0.150	—	—	—	—	—	—	—	—
15	0.0021	11.0	0.0046	0.0523	—	—	—	—	—	—	—	—
16	0.0005	11.0	0.005	—	—	—	—	—	—	—	—	—
Bismuth ($N = 0.0281 \times 10^{24}$)												
					$\sigma_{n,n',j\to j+k}$							
j	E_L	σ_{tr}	$\sigma_{n,\gamma}$	σ_{er}	$\sigma_{n,n'}$	k = 0	1	2	3	4	5	6
1	3.668	3.69	0.0003	0.0338	2.30	0.012	0.131	0.422	0.600	0.526	0.331	0.278
2	2.225	4.29	0.0004	0.0615	1.07	0.102	0.578	0.290	0.088	0.012	0	0
3	1.35	3.75	0.0007	0.0552	0.38	0	0.162	0.140	0.078	0	0	0
4	0.825	3.77	0.0012	0.0614	0.13	0	0	0.092	0.020	0.009	0.009	—
5	0.5	4.58	0.0013	0.0794	—	—	—	—	—	—	—	—
6	0.3	6.00	0.0014	0.101	—	—	—	—	—	—	—	—
7	0.18	7.21	0.0014	0.116	—	—	—	—	—	—	—	—
8	0.11	8.39	0.0014	0.134	—	—	—	—	—	—	—	—
9	0.067	9.05	0.0015	0.133	—	—	—	—	—	—	—	—
10	0.0407	9.38	0.0016	0.132	—	—	—	—	—	—	—	—
11	0.025	10.4	0.0016	0.151	—	—	—	—	—	—	—	—
12	0.015	12.8	0.0017	0.174	—	—	—	—	—	—	—	—
13	0.0091	12.8	0.0017	0.174	—	—	—	—	—	—	—	—
14	0.0055	9.14	0.0018	0.125	—	—	—	—	—	—	—	—
15	0.0021	9.52	0.0018	0.0448	—	—	—	—	—	—	—	—
16	0.0005	11.0	0.002	—	—	—	—	—	—	—	—	—

Table 7-1—MULTIGROUP CONSTANTS FOR FAST REACTOR ANALYSIS (ANL 16-GROUP) (Continued)

(Microscopic cross sections in barns)

Thorium ($N = 0.03 \times 10^{24}$)														
							$\sigma_{n,n',j\to j+k}$							
j	E_L	σ_f	ν	σ_{tr}	$\sigma_{n,\gamma}$	σ_{er}	$\sigma_{n,n'}$	k = 0	1	2	3	4	5	6
1	3.668	0.160	2.94	3.87	0.0197	0.0191	2.73	0.011	0.128	0.464	0.699	0.655	0.415	0.358
2	2.225	0.126	2.6	4.68	0.0394	0.0291	2.80	0.034	0.255	0.605	0.745	0.582	0.330	0.249
3	1.35	0.081	2.4	4.72	0.0744	0.03	2.69	0.522	0.820	0.998	0.242	0.032	0.076	—
4	0.825	—	—	4.90	0.12	0.0484	1.60	0.966	0.549	0.077	0.008	—	—	—
5	0.5	—	—	5.58	0.17	0.0780	1.60	1.106	0.467	0.016	0.011	—	—	—
6	0.3	—	—	6.57	0.18	0.101	1.00	0.675	0.316	0.009	0	—	—	—
7	0.18	—	—	8.54	0.21	0.126	0.8	0.474	0.326	0	0	—	—	—
8	0.11	—	—	10.0	0.27	0.147	0.63	0.278	0.249	0.103	0	—	—	—
9	0.067	—	—	11.2	0.36	0.151	0.34	0	0.251	0.054	0.035	—	—	—
10	0.0407	—	—	12.2	0.43	0.158	—	—	—	—	—	—	—	—
11	0.025	—	—	12.9	0.5	0.171	—	—	—	—	—	—	—	—
12	0.015	—	—	13.7	0.53	0.171	—	—	—	—	—	—	—	—
13	0.0091	—	—	14.4	0.56	0.180	—	—	—	—	—	—	—	—
14	0.0055	—	—	14.2	0.64	0.177	—	—	—	—	—	—	—	—
15	0.0021	—	—	14.2	0.82	0.061	—	—	—	—	—	—	—	—
16	0.0005	—	—	15.0	2.0	—	—	—	—	—	—	—	—	—
U^{233} ($N = 0.048 \times 10^{24}$)														
							$\sigma_{n,n',j\to j+k}$							
j	E_L	σ_f	ν	σ_{tr}	$\sigma_{n,\gamma}$	σ_{er}	$\sigma_{n,n'}$	k = 0	1	2	3	4	5	6
1	3.668	1.64	3.11	4.18	0.013	0.017	1.72	0.007	0.082	0.292	0.440	0.413	0.261	0.225
2	2.225	1.84	2.85	4.81	0.023	0.024	1.49	0.018	0.136	0.322	0.396	0.310	0.176	0.132
3	1.35	1.92	2.72	4.87	0.039	0.025	1.19	0.029	0.230	0.440	0.165	0.134	0.058	0.134
4	0.825	1.95	2.64	4.91	0.077	0.032	0.58	0.023	0.175	0.138	0.093	0.040	0.089	0.022
5	0.5	2.02	2.59	5.61	0.129	0.041	0.43	0.029	0.158	0.118	0.052	0.041	0.032	0
6	0.3	2.24	2.55	7.04	0.160	0.059	0.29	0.102	0.050	0.052	0.032	0.024	0.018	0.012
7	0.18	2.32	2.53	8.83	0.197	0.083	0.2	0.115	0.077	0.008	0	0	0	0
8	0.11	2.47	2.51	10.60	0.247	0.108	0.17	0.070	0.080	0.010	0.007	0.003	0	0
9	0.067	2.75	2.50	12.37	0.322	0.123	0.1	0.025	0.043	0.032	—	—	—	—
10	0.0407	3.13	2.50	13.71	0.416	0.129	—	—	—	—	—	—	—	—
11	0.025	3.63	2.50	14.46	0.535	0.126	—	—	—	—	—	—	—	—
12	0.015	4.27	2.50	15.29	0.669	0.122	—	—	—	—	—	—	—	—
13	0.0091	5.01	2.50	16.20	0.833	0.126	—	—	—	—	—	—	—	—
14	0.0055	5.79	2.50	16.58	1.126	0.121	—	—	—	—	—	—	—	—
15	0.0021	7.57	2.50	18.50	1.395	0.038	—	—	—	—	—	—	—	—
16	0.0005	9.00	2.50	22.01	2.550	—	—	—	—	—	—	—	—	—
U^{235} ($N = 0.048 \times 10^{24}$)														
							$\sigma_{n,n',j\to j+k}$							
j	E_L	σ_f	ν	σ_{tr}	$\sigma_{n,\gamma}$	σ_{er}	$\sigma_{n,n'}$	k = 0	1	2	3	4	5	6
1	3.668	1.21	3.15	3.88	0.020	0.017	1.98	0.008	0.093	0.337	0.507	0.475	0.301	0.259
2	2.225	1.29	2.84	4.73	0.035	0.024	1.95	0.023	0.177	0.421	0.520	0.405	0.230	0.174
3	1.35	1.31	2.67	4.86	0.058	0.025	1.65	0.040	0.318	0.611	0.229	0.186	0.080	0.186
4	0.825	1.27	2.58	5.08	0.115	0.032	1.32	0.066	0.405	0.292	0.211	0.214	0.132	0
5	0.5	1.22	2.52	5.58	0.193	0.041	1.07	0.340	0.394	0.119	0.105	0.059	0.053	0
6	0.3	1.29	2.48	6.81	0.240	0.059	0.88	0.431	0.347	0.073	0.022	0.007	0	0
7	0.18	1.42	2.45	8.54	0.296	0.082	0.63	0.289	0.243	0.061	0.020	0.016	0.001	0
8	0.11	1.62	2.44	10.10	0.370	0.106	0.44	0.150	0.206	0.038	0.033	0.009	0.004	0
9	0.067	1.86	2.43	11.50	0.483	0.121	0.23	0.051	0.125	0.040	0.010	0.004	0	0
10	0.0407	2.15	2.43	12.60	0.624	0.126	0.07	0	0.042	0.021	0.007	0	0	0
11	0.025	2.51	2.42	13.60	0.803	0.136	—	—	—	—	—	—	—	—
12	0.015	2.95	2.42	14.30	1.003	0.134	—	—	—	—	—	—	—	—
13	0.0091	3.49	2.42	15.10	1.249	0.131	—	—	—	—	—	—	—	—
14	0.0055	4.33	2.42	18.70	1.689	0.163	—	—	—	—	—	—	—	—
15	0.0021	4.98	2.42	22.30	2.092	0.068	—	—	—	—	—	—	—	—
16	0.0005	8.5	2.42	28.00	3.825	—	—	—	—	—	—	—	—	—

Table 7-1—MULTIGROUP CONSTANTS FOR FAST REACTOR ANALYSIS (ANL 16-GROUP) (Continued)

(Microscopic cross sections in barns)

U^{238} ($N = 0.048 \times 10^{24}$)

j	E_L	σ_f	ν	σ_{tr}	$\sigma_{n,\gamma}$	σ_{er}	$\sigma_{n,n',j\to j+k}$							
							$\sigma_{n,n'}$	k = 0	1	2	3	4	5	6
1	3.668	0.609	3.20	3.90	0.010	0.017	2.500	0.010	0.118	0.425	0.640	0.600	0.380	0.327
2	2.225	0.581	2.87	4.63	0.022	0.025	2.550	0.031	0.232	0.551	0.678	0.530	0.301	0.227
3	1.35	0.430	2.68	4.87	0.057	0.029	2.330	0.452	0.710	0.865	0.210	0.028	0.065	—
4	0.825	0.024	2.56	5.01	0.129	0.044	1.930	1.010	0.551	0.272	0.089	0.008	—	—
5	0.5	—	—	5.59	0.139	0.060	1.580	1.110	0.470	0	0	—	—	—
6	0.3	—	—	6.88	0.127	0.082	1.280	0.824	0.456	0	0	—	—	—
7	0.18	—	—	8.48	0.161	0.104	0.988	0.492	0.496	0	0	—	—	—
8	0.11	—	—	10.10	0.227	0.131	0.697	0.254	0.244	0.199	0	—	—	—
9	0.067	—	—	11.50	0.290	0.140	0.400	0	0.292	0.064	0.044	—	—	—
10	0.0407	—	—	12.50	0.370	0.151	0.105	0	0	0.076	0.029	—	—	—
11	0.025	—	—	13.60	0.450	0.169	—	—	—	—	—	—	—	—
12	0.015	—	—	14.30	0.520	0.166	—	—	—	—	—	—	—	—
13	0.0091	—	—	15.00	0.602	0.174	—	—	—	—	—	—	—	—
14	0.0055	—	—	15.10	0.660	0.174	—	—	—	—	—	—	—	—
15	0.0021	—	—	16.00	0.93	0.063	—	—	—	—	—	—	—	—
16	0.0005	—	—	14.00	2.000	—	—	—	—	—	—	—	—	—

Pu^{239} ($N = 0.048 \times 10^{24}$)

j	E_L	σ_f	ν	σ_{tr}	$\sigma_{n,\gamma}$	σ_{er}	$\sigma_{n,n',j\to j+k}$							
							$\sigma_{n,n'}$	k = 0	1	2	3	4	5	6
1	3.668	1.83	3.45	3.97	0.054	0.0165	1.4	0.006	0.066	0.238	0.358	0.336	0.213	0.183
2	2.225	1.99	3.22	4.99	0.0798	0.0300	1.27	0.015	0.116	0.274	0.338	0.264	0.150	0.113
3	1.35	1.96	3.10	5.14	0.0965	0.0314	1.05	0.035	0.210	0.323	0.203	0.112	0.054	0.113
4	0.825	1.81	3.02	5.07	0.104	0.0338	0.84	0.323	0.302	0.082	0.051	0.040	0.042	0
5	0.5	1.70	2.97	6.09	0.129	0.0510	0.76	0.423	0.263	0.050	0.024	0	0	0
6	0.3	1.70	2.94	7.27	0.182	0.0711	0.64	0.427	0.154	0.033	0.012	0.007	0.004	0.003
7	0.18	1.70	2.92	8.66	0.290	0.0947	0.46	0.342	0.112	0.005	0	0	0	0.001
8	0.11	1.70	2.91	10.20	0.409	0.115	0.28	0.202	0.063	0.014	0.001	0	0	0
9	0.067	1.80	2.91	11.50	0.534	0.119	—	—	—	—	—	—	—	—
10	0.0407	1.93	2.90	12.70	0.686	0.126	—	—	—	—	—	—	—	—
11	0.025	2.17	2.90	13.80	0.892	0.137	—	—	—	—	—	—	—	—
12	0.015	2.40	2.90	14.60	1.084	0.134	—	—	—	—	—	—	—	—
13	0.0091	2.45	2.90	15.20	1.211	0.140	—	—	—	—	—	—	—	—
14	0.0055	2.41	2.90	16.10	1.280	0.148	—	—	—	—	—	—	—	—
15	0.0021	3.28	2.90	18.00	1.891	0.0533	—	—	—	—	—	—	—	—
16	0.0005	6.00	2.90	13.50	4.020	—	—	—	—	—	—	—	—	—

Pu^{240} ($N = 0.048 \times 10^{24}$)

j	E_L	σ_f	ν	σ_{tr}	$\sigma_{n,\gamma}$	σ_{er}	$\sigma_{n,n',j\to j+k}$							
							$\sigma_{n,n'}$	k = 0	1	2	3	4	5	6
1	3.668	1.54	3.85	3.90	0.018	0.017	1.482	0.006	0.070	0.252	0.379	0.356	0.225	0.194
2	2.225	1.63	3.51	4.63	0.039	0.025	1.383	0.017	0.126	0.299	0.368	0.288	0.163	0.122
3	1.35	1.59	3.32	4.87	0.100	0.029	1.058	0.205	0.323	0.393	0.095	0.013	0.029	—
4	0.825	1.39	3.21	5.01	0.226	0.037	0.511	0.267	0.146	0.072	0.024	0.002	—	—
5	0.5	0.76	3.15	5.59	0.243	0.060	0.733	0.515	0.218	0	0	—	—	—
6	0.3	0.191	3.10	6.88	0.222	0.082	0.897	0.578	0.319	0	0	—	—	—
7	0.18	0.041	3.07	8.48	0.282	0.104	0.6	0.299	0.301	0	0	—	—	—
8	0.11	—	—	10.10	0.397	0.131	0.208	0.076	0.073	0.059	0	—	—	—
9	0.067	—	—	11.50	0.508	0.140	—	—	—	—	—	—	—	—
10	0.0407	—	—	12.50	0.648	0.151	—	—	—	—	—	—	—	—
11	0.025	—	—	13.60	0.788	0.169	—	—	—	—	—	—	—	—
12	0.015	—	—	14.30	0.910	0.166	—	—	—	—	—	—	—	—
13	0.0091	—	—	15.00	1.054	0.174	—	—	—	—	—	—	—	—
14	0.0055	—	—	15.10	1.155	0.174	—	—	—	—	—	—	—	—
15	0.0021	—	—	16.00	1.435	0.063	—	—	—	—	—	—	—	—
16	0.0005	—	—	14.00	3.500	—	—	—	—	—	—	—	—	—

Table 7-1—MULTIGROUP CONSTANTS FOR FAST REACTOR ANALYSIS (ANL 16-GROUP) (Continued)

(Microscopic cross sections in barns)

Pu^{241} ($N = 0.048 \times 10^{24}$)														
							$\sigma_{n,n',j\to j+k}$							
j	E_L	σ_f	ν	σ_{tr}	$\sigma_{n,\gamma}$	σ_{er}	$\sigma_{n,n'}$	k = 0	1	2	3	4	5	6
1	3.668	1.65	3.53	4.19	0.013	0.0165	1.72	0.007	0.082	0.292	0.440	0.413	0.261	0.225
2	2.225	1.83	3.31	4.73	0.023	0.0231	1.49	0.018	0.136	0.322	0.396	0.310	0.176	0.132
3	1.35	1.89	3.18	4.83	0.039	0.0249	1.19	0.029	0.230	0.440	0.165	0.134	0.058	0.134
4	0.825	1.83	3.10	4.73	0.077	0.0338	0.58	0.023	0.175	0.138	0.093	0.040	0.089	0.022
5	0.5	1.70	3.06	5.59	0.129	0.0510	0.43	0.029	0.158	0.118	0.052	0.041	0.032	0
6	0.3	1.83	3.03	7.07	0.160	0.0711	0.29	0.114	0.151	0.025	0	0	0	0
7	0.18	2.05	3.01	9.17	0.197	0.0947	0.2	0.101	0.091	0.008	0	0	0	0
8	0.11	2.27	3.00	10.76	0.247	0.115	0.17	0.053	0.087	0.024	0.006	0	0	0
9	0.067	2.75	2.99	12.40	0.322	0.119	0.1	0	0.065	0.022	0.013	0	0	0
10	0.0407	3.13	2.99	13.63	0.416	0.126	—	—	—	—	—	—	—	—
11	0.025	3.70	2.98	14.82	0.535	0.137	—	—	—	—	—	—	—	—
12	0.015	4.43	2.98	16.03	0.669	0.134	—	—	—	—	—	—	—	—
13	0.0091	5.29	2.98	17.63	0.833	0.140	—	—	—	—	—	—	—	—
14	0.0055	5.99	2.98	19.58	1.126	0.148	—	—	—	—	—	—	—	—
15	0.0021	6.91	2.98	21.11	1.395	0.0533	—	—	—	—	—	—	—	—
16	0.0005	9.0	2.98	20.49	2.550	—	—	—	—	—	—	—	—	—

Pu^{242} ($N = 0.048 \times 10^{24}$)														
							$\sigma_{n,n',j\to j+k}$							
j	E_L	σ_f	ν	σ_{tr}	$\sigma_{n,\gamma}$	σ_{er}	$\sigma_{n,n'}$	k = 0	1	2	3	4	5	6
1	3.668	1.54	3.85	3.90	0.018	0.017	1.482	0.006	0.070	0.252	0.379	0.356	0.225	0.194
2	2.225	1.37	3.51	4.63	0.039	0.025	1.643	0.020	0.150	0.355	0.437	0.342	0.194	0.145
3	1.35	1.45	3.32	4.87	0.100	0.029	1.198	0.232	0.365	0.444	0.108	0.014	0.035	—
4	0.825	1.57	3.21	5.01	0.226	0.037	0.331	0.173	0.095	0.047	0.015	0.001	—	—
5	0.5	0.66	3.15	5.59	0.243	0.060	0.833	0.585	0.248	0	0	—	—	—
6	0.3	0.179	3.10	6.88	0.222	0.082	0.909	0.585	0.324	0	0	—	—	—
7	0.18	0.053	3.07	8.48	0.282	0.104	0.588	0.293	0.295	0	0	—	—	—
8	0.11	0.023	3.06	10.10	0.397	0.131	0.185	0.068	0.065	0.052	—	—	—	—
9	0.067	—	—	11.50	0.508	0.140	—	—	—	—	—	—	—	—
10	0.0407	—	—	12.50	0.648	0.151	—	—	—	—	—	—	—	—
11	0.025	—	—	13.60	0.788	0.169	—	—	—	—	—	—	—	—
12	0.015	—	—	14.30	0.910	0.166	—	—	—	—	—	—	—	—
13	0.0091	—	—	15.00	1.054	0.174	—	—	—	—	—	—	—	—
14	0.0055	—	—	15.10	1.155	0.174	—	—	—	—	—	—	—	—
15	0.0021	—	—	16.00	1.435	0.063	—	—	—	—	—	—	—	—
16	0.0005	—	—	14.00	3.500	—	—	—	—	—	—	—	—	—

Table 7-2 — MULTIGROUP CONSTANTS FOR FAST REACTOR ANALYSIS (LASL 16-GROUP)

(Microscopic cross sections in barns)

Group	Neutron Energy Range	Δu	Avg. Neutron Velocity, 10^8 cm/sec	Fission Spectrum (χ)
1	3 – ∞ Mev		28.5	0.204
2	1.4 – 3 Mev	0.762	19.9	0.344
3	0.9 – 1.4 Mev	0.442	14.7	0.168
4	0.4 – 0.9 Mev	0.811	11.0	0.180
5	0.1 – 0.4 Mev	1.386	6.7	0.090
6	17 – 100 kev	1.772	2.70	0.014
7	3 – 17 kev	1.735	1.14	0
8	0.55 – 3 kev	1.696	0.480	0
9	100 – 550 ev	1.705	0.206	0
10	30 – 100 ev	1.204	0.101	0
11	10 – 30 ev	1.099	0.0566	0
12	3 – 10 ev	1.204	0.0319	0
13	1 – 3 ev	1.099	0.0179	0
14	0.4 – 1 ev	0.916	0.0109	0
15	0.1 – 0.4 ev	1.386	0.00606	0
16	Thermal (0.025 ev)		0.00218	0

Pu^{239}

Group	σ_f	$\sigma_{n,\gamma}$	σ_{tr}	$\nu\sigma_f$	$\sigma_{i\to i}$	$\sigma_{i\to i+1}$	$\sigma_{i\to i+2}$	$\sigma_{i\to i+3}$	$\sigma_{i\to i+4}$	$\sigma_{i\to i+5}$
1	1.90	0.03	4.25	6.612	1.05	0.20	0.27	0.45	0.31	0.04
2	1.95	0.05	4.5	6.026	1.42	0.18	0.50	0.35	0.05	—
3	1.83	0.07	4.8	5.472	2.09	0.45	0.30	0.06	—	—
4	1.70	0.11	5.7	4.981	3.55	0.29	0.05	—	—	—
5	1.67	0.17	8.4	4.810	6.51	0.05	—	—	—	—
6	1.92	0.38	13.2	5.491	10.85	0.05	—	—	—	—
7	2.5	1.0	13.5	7.150	9.96	0.04	—	—	—	—
8	4.2	2.5	16.7	12.012	9.96	0.04	—	—	—	—
9	16.5	8.6	35.1	47.19	9.96	0.04	—	—	—	—
10	42	41	93	120.12	9.94	0.06	—	—	—	—
11	78	55	143	223.08	9.93	0.07	—	—	—	—
12	24	19	53	68.64	9.94	0.06	—	—	—	—
13	20	3	33	57.2	9.93	0.07	—	—	—	—
14	139	85	234	397.54	9.92	0.08	—	—	—	—
15	1221	792	2023	3492.06	9.94	0.06	—	—	—	—
16	705	275	990	2016.3	10.0	—	—	—	—	—

Pu^{240}

Group	σ_f	$\sigma_{n,\gamma}$	$\sigma_{s,el}$	σ_{tr}	$\nu\sigma_f$	$\sigma_{i\to i}$	$\sigma_{i\to i+1}$	$\sigma_{i\to i+2}$	$\sigma_{i\to i+3}$	$\sigma_{i\to i+4}$	$\sigma_{i\to i+5}$
1	1.60	0.05	—	4.25	5.952	1.03	0.24	0.33	0.55	0.40	0.05
2	1.54	0.08	—	4.5	5.267	1.62	0.22	0.58	0.40	0.06	—
3	1.39	0.11	—	4.65	4.587	2.24	0.50	0.35	0.06	—	—
4	0.77	0.15	—	5.45	2.487	4.07	0.40	0.06	—	—	—
5	0.05	0.23	—	8.2	0.159	7.87	0.05	—	—	—	—
6	0	0.45	11	11.45	0	10.95	0.05	—	—	—	—
7	0	0.7	11	11.7	0	10.95	0.05	—	—	—	—
8	0	2.0	11	13	0	10.95	0.05	—	—	—	—
9	0	11	11	22	0	10.95	0.05	—	—	—	—
10	0	60	11	71	0	10.92	0.08	—	—	—	—
11	0	31	12	43	0	11.91	0.09	—	—	—	—
12	0	24	15	39	0	14.90	0.10	—	—	—	—
13	1.4	6640	508	7149.4	4.2	504.14	3.86	—	—	—	—
14	0.2	898	38	936.2	0.6	37.65	0.35	—	—	—	—
15	0	140	11	151	0	10.93	0.07	—	—	—	—
16	0.03	252	11	263.03	0.09	11	—	—	—	—	—

Table 7-2—MULTIGROUP CONSTANTS FOR FAST REACTOR ANALYSIS (LASL 16-GROUP) (Continued)

(Microscopic cross sections in barns)

U^{233}

Group	σ_f	$\sigma_{n,\gamma}$	σ_{tr}	$\nu\sigma_f$	$\sigma_{i\to i}$	$\sigma_{i\to i+1}$	$\sigma_{i\to i+2}$	$\sigma_{i\to i+3}$	$\sigma_{i\to i+4}$	$\sigma_{i\to i+5}$
1	1.75	0.04	4.25	5.285	1.19	0.20	0.27	0.45	0.31	0.04
2	1.83	0.06	4.5	4.941	1.53	0.18	0.50	0.35	0.05	—
3	1.89	0.08	4.6	4.933	1.82	0.45	0.30	0.06	—	—
4	1.94	0.11	5.3	4.986	2.91	0.29	0.05	—	—	—
5	2.24	0.15	8.1	5.667	5.66	0.05	—	—	—	—
6	3.5	0.42	12.5	8.785	8.54	0.04	—	—	—	—
7	6	0.84	16.5	15.06	9.61	0.05	—	—	—	—
8	9	3	23	22.59	10.94	0.06	—	—	—	—
9	19	13	44	47.69	11.94	0.06	—	—	—	—
10	30	21	63	75.30	11.91	0.09	—	—	—	—
11	114	22	148	286.14	11.91	0.09	—	—	—	—
12	102	19	133	256.02	11.91	0.09	—	—	—	—
13	316	94	422	793.16	11.91	0.09	—	—	—	—
14	133	15	160	333.83	11.89	0.11	—	—	—	—
15	200	23	235	502	11.92	0.08	—	—	—	—
16	467	46	525	1172.2	12.0	—	—	—	—	—

U^{235}

Group	σ_f	$\sigma_{n,\gamma}$	σ_{tr}	$\nu\sigma_f$	$\sigma_{i\to i}$	$\sigma_{i\to i+1}$	$\sigma_{i\to i+2}$	$\sigma_{i\to i+3}$	$\sigma_{i\to i+4}$	$\sigma_{i\to i+5}$
1	1.21	0.05	4.25	3.557	1.20	0.27	0.37	0.65	0.44	0.06
2	1.22	0.08	4.50	3.196	1.77	0.24	0.67	0.45	0.07	—
3	1.22	0.11	4.65	3.087	2.30	0.55	0.40	0.07	—	—
4	1.20	0.15	5.2	2.988	3.42	0.35	0.08	—	—	—
5	1.43	0.23	7.9	3.518	6.16	0.08	—	—	—	—
6	2.5	0.65	12.4	6.125	9.2	0.05	—	—	—	—
7	4.2	1.3	15.1	10.29	9.55	0.05	—	—	—	—
8	7.9	3.2	21.1	19.36	9.95	0.05	—	—	—	—
9	18.7	8.5	37.2	45.815	9.95	0.05	—	—	—	—
10	38	20	68	93.1	9.95	0.05	—	—	—	—
11	55	35	100	134.75	9.95	0.05	—	—	—	—
12	44	40	94	107.8	9.95	0.05	—	—	—	—
13	30	9	49	73.5	9.95	0.05	—	—	—	—
14	70	10	90	171.5	9.95	0.05	—	—	—	—
15	185	39	234	453.25	9.96	0.04	—	—	—	—
16	516	95	621	1264.2	10.0	—	—	—	—	—

U^{238}

Group	σ_t	σ_f	$\sigma_{n,\gamma}$	σ_{tr}	$\nu\sigma_f$	$\sigma_{i\to i}$	$\sigma_{i\to i+1}$	$\sigma_{i\to i+2}$	$\sigma_{i\to i+3}$	$\sigma_{i\to i+4}$	$\sigma_{i\to i+5}$
1	7.53	0.616	0.02	4.00	1.725	1.254	0.33	0.46	0.79	0.53	0.07
2	7.20	0.485	0.05	4.4	1.213	1.825	0.35	0.96	0.64	0.09	—
3	6.78	0.044	0.10	4.5	0.108	2.906	0.80	0.55	0.10	—	—
4	7.56	0	0.14	5.25	0	4.53	0.50	0.08	—	—	—
5	9.86	0	0.16	8.2	0	7.96	0.08	—	—	—	—
6	13	0	0.45	12.0	0	11.45	0.10	—	—	—	—
7	14	0	0.7	14	0	13.24	0.06	—	—	—	—
8	15	0	2	15	0	12.94	0.06	—	—	—	—
9	22	0	11	22	0	10.95	0.05	—	—	—	—
10	59	0	50	59	0	8.94	0.06	—	—	—	—
11	65	0	56	65	0	8.94	0.06	—	—	—	—
12	119	0	110	119	0	8.94	0.06	—	—	—	—
13	9.4	0	0.4	9.4	0	8.94	0.06	—	—	—	—
14	9.55	0	0.55	9.55	0	8.94	0.06	—	—	—	—
15	10.0	0	1.00	10.0	0	8.95	0.05	—	—	—	—
16	11.44	0	2.44	11.44	0	9.0	—	—	—	—	—

Table 7-2 — MULTIGROUP CONSTANTS FOR FAST REACTOR ANALYSIS (LASL 16-GROUP) (Continued)

(Microscopic cross sections in barns)

Th^{232}

Group	σ_f	$\sigma_{n,\gamma}$	σ_{tr}	$\nu\sigma_f$	$\sigma_{i\to i}$	$\sigma_{i\to i+1}$	$\sigma_{i\to i+2}$	$\sigma_{i\to i+3}$	$\sigma_{i\to i+4}$	$\sigma_{i\to i+5}$
1	0.16	0.02	4.00	0.384	1.64	0.33	0.46	0.79	0.53	0.07
2	0.10	0.05	4.22	0.230	2.03	0.35	0.96	0.64	0.09	—
3	0.009	0.07	4.32	0.021	2.791	0.80	0.55	0.10	—	—
4	0	0.13	5.04	0	4.33	0.50	0.08	—	—	—
5	0	0.21	7.87	0	7.58	0.08	—	—	—	—
6	0	0.48	13.48	0	12.936	0.064	—	—	—	—
7	0	0.60	14.5	0	13.83	0.07	—	—	—	—
8	0	1.9	14.5	0	12.536	0.064	—	—	—	—
9	0	18.0	30	0	11.94	0.06	—	—	—	—
10	0	18.0	30	0	11.915	0.085	—	—	—	—
11	0	40.7	52.7	0	11.906	0.094	—	—	—	—
12	0	0.5	12.5	0	11.915	0.085	—	—	—	—
13	0	0.9	12.9	0	11.906	0.094	—	—	—	—
14	0	1.5	13.5	0	11.887	0.113	—	—	—	—
15	0	2.7	14.7	0	11.926	0.074	—	—	—	—
16	0	7.6	19.6	0	12.0	—	—	—	—	—

H^1

Group	σ_t	σ_c	$\sigma_{s,in}$	$\sigma_{s,el}$	$\sigma_{tr,el}$	σ_{tr}	$\sigma_{i\to i}$	$\sigma_{i\to i+1}$	$\sigma_{i\to i+2}$	$\sigma_{i\to i+3}$	$\sigma_{i\to i+4}$	$\sigma_{i\to i+5}$
1	1.8	0	0	1.8	0.60	0.60	−0.84	0.769	0.239	0.239	0.144	0.049
2	2.9	0	0	2.9	0.97	0.97	−0.961	0.690	0.690	0.415	0.116	0.020
3	4.0	0	0	4.0	1.33	1.33	−1.906	1.796	1.076	0.300	0.052	0.012
4	5.5	0	0	5.5	1.83	1.83	−1.9375	2.827	0.781	0.132	0.022	0.0055
5	9.0	0	0	9.0	3.00	3.00	−1.8681	4.041	0.684	0.117	0.0216	0.0045
6	15.6	0	0	15.6	5.20	5.20	−2.0961	6.022	1.045	0.187	0.0296	0.0125
7	19	0	0	19.0	6.33	6.33	−2.6912	7.372	1.349	0.209	0.0608	0.0304
8	20	0.001	0	19.999	6.666	6.666	−2.969	7.880	1.220	0.360	0.1220	0.0520
9	20	0.004	0	19.996	6.665	6.669	−2.9420	6.719	1.920	0.680	0.1920	0.0960
10	20	0.008	0	19.992	6.664	6.672	−4.9798	7.757	2.719	0.780	0.2319	0.1559
11	20	0.014	0	19.986	6.662	6.676	−5.4489	8.494	2.418	0.719	0.360	0.1199
12	20.4	0.025	0	20.375	6.792	6.817	−5.0470	7.906	2.364	1.182	0.387	—
13	20.4	0.045	0	20.355	6.785	6.830	−5.550	7.409	3.684	1.242	—	—
14	20.4	0.070	0	20.330	6.777	6.847	−6.539	9.982	3.334	—	—	—
15	20.5	0.130	0	20.370	6.790	6.920	−4.230	11.020	—	—	—	—
16	20.7	0.29	0	20.41	6.8	7.09	6.8	—	—	—	—	—

Hydrogen Anisotropic: Modification I

Group	σ_{tr}	$\sigma_{i\to i}$	$\sigma_{i\to i+1}$	$\sigma_{i\to i+2}$	$\sigma_{i\to i+3}$	$\sigma_{i\to i+4}$	$\sigma_{i\to i+5}$
1	1.45	0.01	0.769	0.239	0.239	0.144	0.049
2	2.175	0.244	0.69	0.69	0.415	0.116	0.020
3	3.3	0.064	1.796	1.076	0.300	0.052	0.012
4	4.125	0.357	2.827	0.781	0.132	0.022	0.006
5	6.75	1.881	4.041	0.684	0.117	0.022	0.005
6	11.7	4.404	6.022	1.045	0.187	0.030	0.012
7	14.25	5.229	7.372	1.349	0.209	0.061	0.030
8	15.0	5.365	7.880	1.220	0.360	0.122	0.052
9	15.0	5.389	6.719	1.920	0.680	0.192	0.096
10	15.0	3.348	7.757	2.719	0.780	0.232	0.156
11	15.0	2.875	8.494	2.418	0.719	0.360	0.120
12	15.0	3.136	7.906	2.364	1.182	0.387	—
13	15.0	2.620	7.409	3.684	1.242	—	—
14	18.0	4.730	9.90	3.30	—	—	—
15	25.0	19.87	5.00	—	—	—	—
16	45.0	44.71	—	—	—	—	—

Table 7-2—MULTIGROUP CONSTANTS FOR FAST REACTOR ANALYSIS (LASL 16-GROUP) (Continued)

(Microscopic cross sections in barns)

Hydrogen Anisotropic: Modification I (Continued)

Group	σ_{tr}	$\sigma_{i\to i}$	$\sigma_{i\to i+1}$	$\sigma_{i\to i+2}$	$\sigma_{i\to i+3}$	$\sigma_{i\to i+4}$	$\sigma_{i\to i+5}$
For 6 groups							
2	2.175	0.244	0.69	0.69	0.415	0.136	
3	3.3	0.064	1.796	1.076	0.364	—	
4	4.125	0.357	2.827	0.941	—	—	
5	6.75	1.881	4.869	—	—	—	
6	11.7	11.7	—	—	—	—	

Hydrogen Anisotropic: Modification II

Group	σ_{tr}	$\sigma_{i\to i}$	$\sigma_{i\to i+1}$	$\sigma_{i\to i+2}$	$\sigma_{i\to i+3}$	$\sigma_{i\to i+4}$	$\sigma_{i\to i+5}$
1	1.45	0.015	0.569	0.128	0.096	0.036	0.006
2	2.175	0.130	0.511	0.397	0.148	0.020	0.001
3	3.3	0.022	1.365	0.507	0.068	0.005	0.000
4	4.125	0.178	1.849	0.248	0.016	0.001	0.000
5	6.75	1.226	2.356	0.155	0.012	0.001	0.000
6	11.7	2.86	3.372	0.248	0.019	0.001	0.000
7	14.25	3.41	4.15	0.325	0.023	0.004	0.001
8	15.0	3.52	4.444	0.310	0.051	0.010	0.002
9	15.0	3.54	3.998	0.637	0.128	0.020	0.006
10	15.0	2.18	4.964	0.987	0.158	0.028	0.011
11	15.0	1.82	5.445	0.863	0.152	0.045	0.005
12	15.0	1.91	5.076	0.896	0.268	0.028	—
13	15.0	1.59	4.942	1.474	0.160	—	—
14	18.0	4.00	6.4	0.6	—	—	—
15	25.0	10.0	2.0	—	—	—	—
16	45.0	12.0	—	—	—	—	—
For 6 groups							
2	2.175	0.130	0.511	0.397	0.148	0.021	
3	3.3	0.022	1.365	0.507	0.073	—	
4	4.125	0.178	1.849	0.265	—	—	
5	6.75	1.226	2.524	—	—	—	
6	11.7	6.50	—	—	—	—	

D^2

Group	σ_t	σ_c	$\sigma_{s,in}$	$\sigma_{s,el}$	$\sigma_{tr,el}$	σ_{tr}	$\sigma_{i\to i}$	$\sigma_{i\to i+1}$	$\sigma_{i\to i+2}$	$\sigma_{i\to i+3}$
1	1.86	0	0	1.86	1.18	1.18	−0.191	0.849	0.265	0.257
2	2.55	0	0	2.55	1.73	1.73	+0.010	0.730	0.730	0.260
3	2.85	0	0	2.85	2.21	2.21	−0.403	1.683	0.930	—
4	3.0	0	0	3.0	2.44	2.44	+0.055	2.134	0.251	—
5	3.25	0	0	3.25	2.44	2.44	0.868	1.539	0.033	—
6	3.4	0	0	3.4	2.27	2.27	0.903	1.336	0.031	—
7	3.4	0	0	3.4	2.27	2.27	0.880	1.353	0.037	—
8	3.4	0	0	3.4	2.27	2.27	0.853	1.380	0.037	—
9	3.4	0	0	3.4	2.27	2.27	0.859	1.234	0.177	—
10	3.4	0	0	3.4	2.27	2.27	0.472	1.482	0.316	—
11	3.4	0	0	3.4	2.27	2.27	0.373	1.625	0.272	—
12	3.4	0	0	3.4	2.27	2.27	0.4722	1.482	0.309	0.0068
13	3.4	0	0	3.4	2.27	2.27	0.3730	1.625	0.272	—
14	3.4	0.00010	0	3.3999	2.267	2.2671	0.1860	1.877	0.204	—
15	3.4	0.00016	0	3.39984	2.267	2.26716	0.6210	1.646	—	—
16	3.4	0.0004	0	3.3336	2.222	2.2224	2.222	—	—	—

Table 7-2 — MULTIGROUP CONSTANTS FOR FAST REACTOR ANALYSIS (LASL 16-GROUP) (Continued)

(Microscopic cross sections in barns)

Li^6									
Group	σ_t	σ_c	$\sigma_{s,in}$	$\sigma_{s,el}$	$\sigma_{tr,el}$	σ_{tr}	$\sigma_{i\to i}$	$\sigma_{i\to i+1}$	$\sigma_{i\to i+2}$
1	2.00	0.11	—	1.89	0.92	1.03	0.434	0.486	—
2	1.50	0.23	—	1.27	0.77	1.00	0.438	0.298	0.034
3	1.40	0.26	0	1.14	0.86	1.12	0.270	0.590	—
4	1.90	0.50	0	1.40	1.20	1.70	0.702	0.498	—
5	4.95	1.95	0	3.00	2.52	4.47	1.909	0.611	—
6	1.75	0.85	0	0.9	0.80	1.65	0.648	0.152	—
7	2.5	1.4	0	0.9	0.80	2.2	0.645	0.155	—
8	5.2	4.3	0	0.9	0.80	5.1	0.642	0.158	—
9	10.6	9.7	0	0.9	0.80	10.5	0.642	0.158	—
10	20.8	19.9	0	0.9	0.80	20.7	0.577	0.223	—
11	35.5	34.6	0	0.9	0.80	35.4	0.555	0.245	—
12	61	60.1	0	0.9	0.80	60.9	0.577	0.223	—
13	110	109.1	0	0.9	0.80	109.9	0.555	0.245	—
14	172	171.1	0	0.9	0.80	171.9	0.507	0.293	—
15	310	309.1	0	0.9	0.80	309.9	0.606	0.194	—
16	838	837.1	0	0.9	0.80	837.9	0.800	—	—

Li^7									
Group	σ_t	σ_c	$\sigma_{s,in}$	$\sigma_{s,el}$	$\sigma_{tr,el}$	σ_{tr}	$\sigma_{i\to i}$	$\sigma_{i\to i+1}$	$\sigma_{i\to i+2}$
1	2.19	—	—	2.19	1.10	1.10	0.43	0.67	—
2	1.76	0	0.09	1.67	1.05	1.14	0.67	0.45	0.02
3	1.55	0	0.18	1.37	1.06	1.24	0.41	0.83	—
4	1.27	0	0.04	1.23	1.07	1.11	0.692	0.416	0.002
5	3.50	0	0	3.50	2.99	2.99	2.37	0.62	—
6	1.04	0	0	1.04	0.94	0.94	0.79	0.15	—
7	1.07	0	0	1.07	0.97	0.97	0.81	0.16	—
8	1.07	0	0	1.07	0.97	0.97	0.81	0.16	—
9	1.07	0	0	1.07	0.97	0.97	0.81	0.16	—
10	1.07	0.001	0	1.069	0.967	0.968	0.736	0.231	—
11	1.07	0.001	0	1.069	0.967	0.968	0.714	0.253	—
12	1.07	0.002	0	1.068	0.966	0.968	0.735	0.231	—
13	1.07	0.004	0	1.066	0.965	0.969	0.712	0.253	—
14	1.07	0.006	0	1.064	0.963	0.969	0.661	0.302	—
15	1.07	0.012	0	1.058	0.957	0.969	0.758	0.199	—
16	1.07	0.029	0	1.041	0.938	0.967	0.938	—	—

Boron (natural)							
Group	σ_t	σ_c	$\sigma_{s,el}$	$\sigma_{tr,el}$	σ_{tr}	$\sigma_{i\to i}$	$\sigma_{i\to i+1}$
1	1.6	0.04	1.56	1.48	1.52	0.81	0.67
2	1.9	0.06	1.84	1.73	1.79	1.31	0.42
3	2.4	0.04	2.36	2.10	2.14	1.22	0.88
4	2.6	0.08	2.72	2.19	2.27	1.69	0.50
5	3.6	0.27	3.33	2.89	3.16	2.51	0.38
6	4.31	0.61	3.7	3.47	4.08	3.11	0.36
7	5.2	1.5	3.7	3.47	4.97	3.10	0.37
8	7.1	3.4	3.7	3.47	6.87	3.09	0.38
9	11.7	8.0	3.7	3.47	11.47	3.09	0.38
10	20.1	16.4	3.7	3.47	19.87	2.94	0.53
11	32.7	29	3.7	3.47	32.47	2.89	0.58
12	55.7	52	3.7	3.47	55.47	2.94	0.53
13	95.7	92	3.7	3.47	95.47	2.89	0.58
14	154.7	151	3.7	3.47	154.47	2.77	0.70
15	276.7	273	3.7	3.47	276.47	3.01	0.46
16	673	669.3	3.7	3.47	672.77	3.47	—

Table 7-2 — MULTIGROUP CONSTANTS FOR FAST REACTOR ANALYSIS (LASL 16-GROUP) (Continued)

(Microscopic cross sections in barns)

Be^9

Group	σ_t	σ_c	$\sigma_{s,el}$	$\sigma_{n,2n}$	$\sigma_{tr,el}$	σ_{tr}	$\sigma_{i\to i}$	$\sigma_{i\to i+1}$	$\sigma_{i\to i+2}$
1	2.1	0.041	1.709	0.35	0.90	1.291	0.432	0.818	0.35
2	2.2	0.032	2.048	0.12	1.323	1.475	0.934	0.509	0.12
3	3.0	0	3.0	0	2.38	2.38	1.173	1.207	—
4	3.7	0	3.7	0	3.31	3.31	2.397	0.913	—
5	4.5	0	4.5	0	3.94	3.94	3.306	0.634	—
6	5.6	0	5.6	0	5.18	5.18	4.525	0.655	—
7	5.7	0	5.7	0	5.28	5.28	4.60	0.68	—
8	5.8	0	5.8	0	5.37	5.37	4.66	0.71	—
9	5.85	0	5.85	0	5.42	5.42	4.71	0.71	—
10	5.9	0	5.9	0	5.46	5.46	4.45	1.01	—
11	5.9	0	5.9	0	5.46	5.46	4.35	1.11	—
12	5.9	0	5.9	0	5.46	5.46	4.45	1.01	—
13	5.9	0.001	5.899	0	5.46	5.46	4.349	1.11	—
14	5.9	0.002	5.898	0	5.46	5.46	4.128	1.33	—
15	5.9	0.004	5.896	0	5.46	5.46	4.576	0.88	—
16	6.01	0.009	6.00	0	5.56	5.569	5.56	—	—

C^{12}

Group	σ_t	σ_c	$\sigma_{s,el}$	σ_{tr}	$\sigma_{i\to i}$	$\sigma_{i\to i+1}$
1	1.65	0	1.65	1.23	0.715	0.515
2	1.9	0	1.9	1.42	1.106	0.314
3	2.5	0	2.5	2.26	1.404	0.856
4	3.1	0	3.1	2.93	2.326	0.604
5	3.8	0	3.8	3.59	3.157	0.433
6	4.5	0	4.5	4.25	3.849	0.401
7	4.7	0	4.7	4.44	4.012	0.428
8	4.6	0	4.6	4.34	3.912	0.428
9	4.6	0	4.6	4.34	3.912	0.428
10	4.6	0	4.6	4.34	3.737	0.603
11	4.6	0	4.6	4.34	3.678	0.662
12	4.7	0	4.7	4.44	3.824	0.616
13	4.7	0	4.7	4.44	3.763	0.677
14	4.7	0	4.7	4.44	3.627	0.813
15	4.7	0.001	4.699	4.44	3.903	0.536
16	4.7	0.003	4.697	4.44	4.437	—

O^{16}

Group	σ_t	σ_c	$\sigma_{s,in}$	$\sigma_{s,el}$	$\sigma_{tr,el}$	σ_{tr}	$\sigma_{i\to i}$	$\sigma_{i\to i+1}$
1	1.9	0.040	0	1.86	1.29	1.33	0.866	0.424
2	1.7	0	0	1.7	1.18	1.18	0.989	0.191
3	4.5	0	0	4.5	3.23	3.23	2.328	0.902
4	4.5	0	0	4.5	3.63	3.63	3.074	0.556
5	3.8	0	0	3.8	3.71	3.71	3.373	0.337
6	3.4	0	0	3.4	3.26	3.26	3.029	0.231
7	3.7	0	0	3.7	3.55	3.55	3.295	0.255
8	3.8	0	0	3.8	3.64	3.64	3.370	0.270
9	3.8	0	0	3.8	3.64	3.64	3.370	0.270
10	3.8	0	0	3.8	3.64	3.64	3.260	0.380
11	3.8	0	0	3.8	3.64	3.64	3.226	0.414
12	3.8	0	0	3.8	3.64	3.64	3.260	0.380
13	3.8	0	0	3.8	3.64	3.64	3.226	0.414
14	3.8	0	0	3.8	3.64	3.64	3.142	0.498
15	3.8	0	0	3.8	3.64	3.64	3.309	0.331
16	3.8	0.0002	0	3.7998	3.641	3.6412	3.641	—

Table 7-2—MULTIGROUP CONSTANTS FOR FAST REACTOR ANALYSIS (LASL 16-GROUP) (Continued)

(Microscopic cross sections in barns)

F^{19}

Group	σ_t	σ_c	$\sigma_{s,in}$	$\sigma_{s,el}$	$\sigma_{tr,el}$	σ_{tr}	$\sigma_{i\to i}$	$\sigma_{i\to i+1}$	$\sigma_{i\to i+2}$	$\sigma_{i\to i+3}$
1	1.9	0.10	0.4	1.4	0.9	1.4	0.88	0.42	—	—
2	2.4	0	0.9	1.5	1.0	1.9	1.28	0.32	0.21	0.09
3	2.5	0	1.0	1.5	1.09	2.09	1.41	0.68	—	—
4	4.0	0.0002	1.6	2.4	1.60	3.2002	2.14	1.06	—	—
5	5.3	0.0002	1.8	3.5	2.81	4.6102	3.953	0.65	0.007	—
6	4.2	0	0	4.2	3.78	3.78	3.53	0.25		—
7	3.7	0	0	3.7	3.57	3.57	3.36	0.21	—	—
8	3.7	0	0	3.7	3.57	3.57	3.35	0.22	—	—
9	3.6	0	0	3.6	3.47	3.47	3.25	0.22	—	—
10	3.4	0	0	3.4	3.28	3.28	2.99	0.29	—	—
11	3.1	0	0	3.1	2.99	2.99	2.71	0.28	—	—
12	3.3	0	0	3.3	3.18	3.18	2.90	0.28	—	—
13	3.4	0.001	0	3.339	3.28	3.279	2.97	0.31	—	—
14	3.4	0.002	0	3.338	3.28	3.278	2.91	0.37	—	—
15	3.6	0.004	0	3.596	3.47	3.276	3.21	0.26	—	—
16	3.6	0.008	0	3.592	3.46	3.272	3.46	—	—	—

Na^{23}

Group	σ_t	σ_c	$\sigma_{s,in}$	$\sigma_{s,el}$	$\sigma_{tr,el}$	σ_{tr}	$\sigma_{i\to i}$	$\sigma_{i\to i+1}$	$\sigma_{i\to i+2}$	$\sigma_{i\to i+3}$
1	2.3	0.030	0.143	2.127	1.434	1.607	1.137	0.440	—	—
2	2.5	0	0.963	1.537	1.297	2.260	1.704	0.556	—	—
3	3.2	0.0002	0.869	2.3308	2.121	2.9902	1.799	1.191	—	—
4	3.2	0.0005	0.420	2.78	2.70	3.1194	2.4709	0.604	0.036	0.008
5	3.2	0.0009	0	3.20	3.11	3.1072	2.9113	0.195	(1×10^{-8})	—
6	4.0	0.001	0	4.0	3.88	3.884	3.695	0.188	—	—
7	6.28	0.001	0	6.27	6.088	6.089	5.787	0.301	—	—
8	4.69	0.001	0	4.68	4.544	4.545	4.310	0.234	—	—
9	3.10	0.005	0	3.095	3.005	3.010	2.850	0.155	—	—
10	3.10	0.011	0	3.089	2.999	3.010	2.783	0.216	—	—
11	3.12	0.018	0	3.102	3.012	3.030	2.776	0.236	—	—
12	3.16	0.032	0	3.128	3.037	3.069	2.818	0.219	—	—
13	3.19	0.057	0	3.133	3.042	3.099	2.804	0.238	—	—
14	3.30	0.10	0	3.20	3.11	3.21	2.816	0.294	—	—
15	3.44	0.19	0	3.25	3.16	3.35	2.962	0.198	—	—
16	3.85	0.447	0	3.4	3.3	3.747	3.30	—	—	—

Al^{27}

Group	σ_t	σ_c	$\sigma_{s,in}$	$\sigma_{s,e}$	$\sigma_{tr,el}$	σ_{tr}	$\sigma_{i\to i}$	$\sigma_{i\to i+1}$	$\sigma_{i\to i+2}$	$\sigma_{i\to i+3}$
1	2.4	0.0159	0.7	1.68	1.09	1.8059	1.10	0.56	0.10	0.03
2	2.94	0.00035	0.3	2.64	1.722	2.02235	1.662	0.23	0.11	0.02
3	2.97	0.00038	0.2	2.77	1.94	2.14038	1.61	0.38	0.14	0.01
4	3.63	0.0007	0	3.63	2.72	2.7207	2.47	0.25	—	—
5	3.33	0.002	0	3.33	2.83	2.832	2.69	0.14	$(\sigma_{2\to6} = 0.0009)$	
6	1.5	0.005	0	1.50	1.43	1.435	1.36	0.07	—	—
7	1.5	0.002	0	1.498	1.461	1.463	1.398	0.063	—	—
8	1.4	0.001	0	1.399	1.364	1.365	1.304	0.060	—	—
9	1.4	0.003	0	1.397	1.363	1.366	1.303	0.060	—	—
10	1.4	0.006	0	1.394	1.360	1.366	1.276	0.084	—	—
11	1.4	0.010	0	1.390	1.356	1.366	1.264	0.092	—	—
12	1.42	0.017	0	1.403	1.368	1.385	1.284	0.084	—	—
13	1.45	0.03	0	1.42	1.38	1.41	1.286	0.094	—	—
14	1.5	0.05	0	1.45	1.41	1.46	1.295	0.115	—	—
15	1.5	0.08	0	1.42	1.38	1.46	1.306	0.074	—	—
16	1.6	0.20	0	1.4	1.36	1.56	1.36	—	—	—

Table 7-2—MULTIGROUP CONSTANTS FOR FAST REACTOR ANALYSIS (LASL 16-GROUP) (Continued)

(Microscopic cross sections in barns)

K

Group	σ_t	σ_c	$\sigma_{s,el}$	$\sigma_{tr,el}$	σ_{tr}	$\sigma_{i\to i}$	$\sigma_{i\to i+1}$
1	3.1	0	3.1	2.11	2.11	1.795	0.315
2	3.2	0	3.2	2.22	2.22	2.071	0.149
3	2.3	0	2.3	1.69	1.69	1.495	0.195
4	2.15	0	2.15	1.84	1.84	1.724	0.116
5	2.0	0	2.0	1.97	1.97	1.898	0.072
6	1.90	0.001	1.899	1.866	1.867	1.813	0.053
7	1.45	0.003	1.447	1.422	1.425	1.380	0.042
8	1.55	0.008	1.542	1.515	1.523	1.470	0.045
9	1.73	0.017	1.713	1.683	1.700	1.633	0.050
10	1.90	0.038	1.862	1.830	1.868	1.752	0.078
11	2.0	0.068	1.932	1.898	1.966	1.809	0.089
12	2.15	0.12	2.03	1.99	2.11	1.905	0.085
13	2.3	0.21	2.09	2.05	2.26	1.954	0.096
14	2.4	0.36	2.04	2.00	2.36	1.888	0.112
15	2.7	0.61	2.09	2.05	2.66	1.975	0.075
16	4.04	1.75	2.29	2.25	4.00	2.25	—

Fe

Group	σ_t	σ_c	$\sigma_{s,el}$	$\sigma_{s,in}$	$\sigma_{tr,el}$	σ_{tr}	$\sigma_{i\to i}$	$\sigma_{i\to i+1}$	$\sigma_{i\to i+2}$	$\sigma_{i\to i+3}$
1	3.5	0.003	2.247	1.25	0.99	2.243	1.630	0.61	—	—
2	2.9	0.005	2.05	0.845	1.35	2.20	1.575	0.40	0.20	0.02
3	2.34	0.010	1.89	0.44	1.51	1.96	1.47	0.23	0.23	0.02
4	2.91	0.010	2.84	0	2.28	2.29	2.157	0.123	(1×10^{-8})	
5	2.85	0.010	2.69	0	2.43	2.44	2.359	0.071	—	—
6	4.43	0.010	2.33	0	2.22	2.23	2.17	0.05	—	—
7	6.01	0.010	5.74	0	5.64	5.65	5.52	0.120	—	—
8	7.2	0.011	7.189	0	7.103	7.114	6.952	0.151	—	—
9	11.1	0.027	11.073	0	10.941	10.968	10.708	0.233	—	—
10	11.5	0.055	11.445	0	11.309	11.364	10.977	0.332	—	—
11	11.5	0.098	11.402	0	11.266	11.364	10.901	0.365	—	—
12	11.5	0.17	11.33	0	11.20	11.37	10.871	0.329	—	—
13	11.5	0.31	11.19	0	11.06	11.37	10.702	0.358	—	—
14	11.5	0.51	10.99	0	10.86	11.37	10.431	0.429	—	—
15	11.7	0.91	10.79	0	10.66	11.57	10.390	0.270	—	—
16	13.2	2.24	10.96	0	10.8	13.04	10.8	—	—	—

Ni

Group	σ_t	σ_c	$\sigma_{s,in}$	$\sigma_{s,el}$	$\sigma_{tr,el}$	σ_{tr}	$\sigma_{i\to i}$	$\sigma_{i\to i+1}$	$\sigma_{i\to i+2}$	$\sigma_{i\to i+3}$
1	3.4	0.01	1.41	1.98	0.87	2.29	1.37	0.91	—	—
2	3.2	0.01	0.67	2.51	1.65	2.33	1.72	0.30	0.21	0.09
3	3.2	0.01	0	3.16	2.52	2.53	2.32	0.20	—	—
4	3.1	0.01	0	3.05	2.44	2.45	2.34	0.10	—	—
5	3.8	0.01	0	3.74	3.37	3.38	3.29	0.08	—	—
6	5.6	0.02	0	5.42	5.15	5.17	5.05	0.10	—	—
7	14.9	0.04	0	14.72	14.5	14.54	14.21	0.29	—	—
8	16	0.04	0	15.82	15.64	15.68	15.32	0.32	—	—
9	17	0.05	0	16.82	16.63	16.68	16.30	0.33	—	—
10	17.0	0.10	0	16.82	16.63	16.73	16.16	0.47	—	—
11	17.5	0.18	0	17.32	17.12	17.30	16.59	0.53	—	—
12	17.5	0.31	0	17.19	17.00	17.31	16.52	0.48	—	—
13	17.7	0.56	0	17.14	16.95	17.51	16.42	0.53	—	—
14	18.4	0.94	0	17.46	17.26	18.20	16.62	0.64	—	—
15	19.2	1.6	0	17.60	17.40	19.00	16.97	0.43	—	—
16	21.4	4.6	0	16.8	16.61	21.21	16.61	—	—	—

687863 O - 63 - 38

Table 7-2—MULTIGROUP CONSTANTS FOR FAST REACTOR ANALYSIS (LASL 16-GROUP) (Continued)

(Microscopic cross sections in barns)

Zr										
Group	σ_t	σ_c	$\sigma_{s,el}$	$\sigma_{s,in}$	$\sigma_{tr,el}$	σ_{tr}	$\sigma_{i\to i}$	$\sigma_{i\to i+1}$	$\sigma_{i\to i+2}$	$\sigma_{i\to i+3}$
1	4.1	0.003	2.537	1.56	1.753	3.316	2.454	0.813	0.032	0.014
2	4.9	0.005	4.035	0.87	2.943	3.818	3.232	0.372	0.204	0.005
3	6.6	0.007	6.383	0.23	5.288	5.525	5.026	0.302	0.150	0.040
4	8.3	0.012	8.288	0	8.227	8.239	8.005	0.222	—	—
5	8.6	0.015	8.585	0	8.522	8.537	8.387	0.135	—	—
6	8.8	0.015	8.785	0	8.721	8.736	8.614	0.107	—	—
7	7.7	0.015	7.685	0	7.629	7.644	7.533	0.096	—	—
8	6.6	0.015	6.585	0	6.537	6.552	6.453	0.084	—	—
9	6.4	0.015	6.385	0	6.338	6.353	6.257	0.081	—	—
10	6.2	0.015	6.185	0	6.140	6.155	6.028	0.112	—	—
11	6.2	0.015	6.185	0	6.140	6.155	6.018	0.122	—	—
12	6.2	0.015	6.185	0	6.140	6.155	6.029	0.111	—	—
13	6.2	0.022	6.178	0	6.133	6.155	6.011	0.122	—	—
14	6.2	0.036	6.164	0	6.119	6.155	5.973	0.146	—	—
15	6.2	0.065	6.135	0	6.090	6.155	5.994	0.096	—	—
16	6.2	0.159	6.041	0	5.997	6.156	5.997	—	—	—

Mo									
Group	σ_t	σ_c	$\sigma_{s,in}$	$\sigma_{s,el}$	σ_{tr}	$\sigma_{i\to i}$	$\sigma_{i\to i+1}$	$\sigma_{i\to i+2}$	$\sigma_{i\to i+3}$
1	3.91	0	0.66	3.25	2.91	2.39	0.52	—	—
2	4.9	0	0.92	3.98	3.82	3.10	0.35	0.25	0.12
3	6.4	0	0.10	6.3	5.32	5.00	0.30	0.02	—
4	7.8	0	0	7.8	7.75	7.55	0.20	—	—
5	8.8	0	0	8.8	8.74	8.61	0.13	—	—
6	8.5	0	0	8.5	8.44	8.34	0.10	—	—
7	7.1	0.1	0	7.0	7.05	6.87	0.08	—	—
8	8.1	1.5	0	6.6	8.05	6.47	0.08	—	—
9	9.2	2.9	0	6.3	9.16	6.18	0.08	—	—
10	19.4	13.4	0	6.0	19.36	5.86	0.10	—	—
11	5.6	0.05	0	5.55	5.56	5.41	0.10	—	—
12	5.7	0.08	0	5.62	5.66	5.48	0.10	—	—
13	6.0	0.15	0	5.85	5.96	5.70	0.11	—	—
14	6.5	0.25	0	6.25	6.46	6.07	0.14	—	—
15	6.7	0.90	0	5.80	6.86	5.87	0.09	—	—
16	7.6	2.50	0	5.10	7.56	5.06	—	—	—

Table 7-3—MULTIGROUP CONSTANTS FOR FAST REACTOR ANALYSIS (ANL 11-GROUP)

(Microscopic cross sections in barns)

Pu^{239} ($N = 0.048 \times 10^{24}$)														
									$\sigma_{in,j\to j+k}$					
j	χ	E_L	Δu	σ_{tr}	ν	σ_f	α^*	σ_{er}	σ_{in}	k = 1	2	3	4	5	6
1	0.338	2.25	—	4.6	3.18	2.0	0.02	0.0142	1.35	0.513	0.382	0.221	0.120	0.0648	0.0486
2	0.236	1.35	0.5	4.6	3.09	1.95	0.04	0.0238	1.0	0.457	0.264	0.143	0.0780	0.0358	0.0195
3	0.178	0.825	0.5	5.26	3.02	1.86	0.05	0.0438	0.7	0.331	0.179	0.0980	0.0490	0.0245	0.0182
4	0.116	0.5	0.5	5.9	2.97	1.75	0.07	0.0559	0.7	0.336	0.183	0.0917	0.0446	0.0340	0.0084
5	0.066	0.3	0.5	7.1	2.95	1.70	0.10	0.0811	0.4	0.200	0.100	0.0512	0.0371	0.00884	0.00248
6	0.033	0.18	0.5	8.5	2.93	1.68	0.16	0.106	0.23	0.115	0.0591	0.0428	0.0101	0.00276	—
7	0.017	0.11	0.5	9.5	2.92	1.73	0.23	0.124	0	—	—	—	—	—	—
8	0.008	0.067	0.5	10.8	2.91	1.80	0.30	0.142	0	—	—	—	—	—	—
9	0.006	0.025	1.0	12.3	2.91	2.0	0.37	0.0803	0	—	—	—	—	—	—
10	0.002	0.0091	1.0	16.4	2.91	2.25	0.47	0.110	0	—		—	—	—	—
11	0	0	—	16.8	2.91	3.5	0.60	0	0	—		—	—	—	—

*$\alpha = \sigma_c/\sigma_f$

Table 7-3—MULTIGROUP CONSTANTS FOR FAST REACTOR ANALYSIS (ANL 11-GROUP) (Continued)

(Microscopic cross sections in barns)

U^{233} ($N = 0.048 \times 10^{24}$)

j		σ_{tr}	ν	σ_f	α^*	σ_{er}	$\sigma_{in,j\to j+k}$						
							σ_{in}	k = 1	2	3	4	5	6
1		4.3	2.8	1.80	0.028	0.0141	1.25	0.479	0.359	0.208	0.112	0.0625	0.030
2		4.5	2.65	1.85	0.043	0.0237	1.00	0.457	0.264	0.143	0.078	0.039	0.019
3		4.8	2.59	1.94	0.057	0.0336	0.75	0.355	0.192	0.105	0.0525	0.0262	0.0195
4		5.5	2.55	2.04	0.074	0.0497	0.35	0.168	0.0917	0.0458	0.0234	0.0168	0.0042
5		5.7	2.53	2.21	0.090	0.0536	0.10	0.0501	0.0250	0.0128	0.00927	0.00221	0.00062
6		7.0	2.52	2.27	0.10	0.0756	0	—	—	—	—	—	—
7		9.0	2.52	2.43	0.10	0.106	0	—	—	—	—	—	—
8		11.0	2.51	2.57	0.10	0.137	0	—	—	—	—	—	—
9		15.0	2.51	3.0	0.10	0.0983	0	—	—	—	—	—	—
10		20.0	2.51	4.2	0.10	0.129	0	—	—	—	—	—	—
11		25.0	2.51	7.0	0.10	0	0	—	—	—	—	—	—

U^{235} ($N = 0.048 \times 10^{24}$)

j		σ_{tr}	ν	σ_f	α^*	σ_{er}	$\sigma_{in,j\to j-k}$						
							σ_{in}	k = 1	2	3	4	5	6
1		4.5	2.77	1.3	0.077	0.00941	2.3	0.881	0.660	0.382	0.207	0.115	0.0552
2		4.5	2.65	1.28	0.078	0.0192	1.85	0.845	0.488	0.265	0.144	0.0712	0.0361
3		4.8	2.58	1.25	0.08	0.0386	1.15	0.544	0.294	0.161	0.0805	0.0402	0.0299
4		5.1	2.53	1.20	0.12	0.0429	1.2	0.576	0.314	0.157	0.0798	0.0582	0.0144
5		6.3	2.51	1.28	0.15	0.0694	0.7	0.351	0.175	0.0896	0.0649	0.0155	0.00434
6		7.9	2.49	1.42	0.18	0.0978	0.4	0.200	0.103	0.0744	0.0176	0.0048	0
7		9.65	2.48	1.6	0.20	0.130	—	—	—	—	—	—	—
8		10.9	2.47	1.9	0.25	0.143	—	—	—	—	—	—	—
9		12.25	2.47	2.3	0.30	0.0778	—	—	—	—	—	—	—
10		13.5	2.47	3.4	0.35	0.0748	—	—	—	—	—	—	—
11		14.3	2.47	6.0	0.42	0	—	—	—	—	—	—	—

U^{238} ($N = 0.048 \times 10^{24}$)

j		σ_{tr}	ν	σ_f	σ_c	σ_{er}	$\sigma_{in,j\to j+k}$						
							σ_{in}	k = 1	2	3	4	5	6
1		4.7	2.65	0.59	0.015	0.0144	2.87	1.06	0.46	0.66	0.39	0.12	0.18
2		4.5	2.55	0.45	0.062	0.0234	2.44	0.62	0.89	0.52	0.16	0.10	0.15
3		5.0	2.47	0.003	0.13	0.0616	1.20	0.52	0.35	0.22	0.11	0	0
4		5.5	0	0	0.143	0.0826	0.44	0.44	0	—	—	—	—
5		6.7	0	0	0.13	0.102	0.47	0.47	0	—	—	—	—
6		8.25	0	0	0.15	0.127	0.55	0.50	0.05	—	—	—	—
7		9.65	0	0	0.20	0.150	0.55	0.55	0	—	—	—	—
8		10.9	0	0	0.30	0.171	0.40	0.38	0.02	—	—	—	—
9		12.25	0	0	0.40	0.0991	0.05	0.03	0.02	—	—	—	—
10		13.5	0	0	0.61	0.108	0	—	—	—	—	—	—
11		14.3	0	0	0.80	0	0	—	—	—	—	—	—

Th^{232} ($N = 0.03 \times 10^{24}$)

j		σ_{tr}	ν	σ_f	σ_c	σ_{er}	$\sigma_{in,j\to j+k}$						
							σ_{in}	k = 1	2	3	4	5	6
1		4.3	2.4	0.135	0.03	0.0102	3.3	1.22	0.53	0.76	0.45	0.14	0.20
2		4.5	2.3	0.10	0.04	0.0244	2.8	0.71	1.02	0.60	0.18	0.12	0.17
3		4.6	0	0	0.08	0.0569	1.25	0.54	0.37	0.23	0.11	0	0
4		5.1	0	0	0.15	0.0786	0.43	0.43	0	0	0	0	0
5		6.6	0	0	0.20	0.104	0.40	0.40	0	0	0	0	0
6		8.0	0	0	0.25	0.127	0.45	0.40	0.05	—	—	—	—
7		9.2	0	0	0.32	0.147	0.43	0.43	—	—	—	—	—
8		10.5	0	0	0.38	0.171	0.32	0.32	—	—	—	—	—
9		11.6	0	0	0.50	0.0966	0	—	—	—	—	—	—
10		13.5	0	0	0.60	0.112	0	—	—	—	—	—	—
11		14.0	0	0	0.80	0	0	—	—	—	—	—	—

*$\alpha = \sigma_c/\sigma_f$

Table 7-3—MULTIGROUP CONSTANTS FOR FAST REACTOR ANALYSIS (ANL 11-GROUP) (Continued)

(Microscopic cross sections in barns)

Pu^{240} ($N = 0.048 \times 10^{24}$)

	C[a]							$\sigma_{in,j\to j+k}$							
j	σ_{tr}	σ_{er}	σ_{tr}	ν	σ_f	σ_c	σ_{er}	σ_{in}	k = 1	2	3	4	5	6	7
1	1.4	0.311	4.6	2.65	1.6	0.02	0.0127	1.9	0.701	0.304	0.437	0.258	0.0798	0.120	—
2	1.8	0.515	4.6	2.55	1.5	0.08	0.0237	1.45	0.368	0.529	0.309	0.0957	0.0594	0.0885	—
3	2.17	0.690	5.3	2.47	1.35	0.18	0.0516	0.70	0.303	0.204	0.128	0.0644	0	0	—
4	2.97	0.944	5.9	2.47	0.7	0.20	0.0764	0.45	0.45	0	0	0	0	0	—
5	3.24	1.030	7.1	2.47	0.18	0.20	0.105	0.45	0.45	0	0	0	0	0	—
6	3.79	1.204	8.5	2.47	0.03	0.20	0.131	0.45	0.410	0.040	0	0	0	0	—
7	3.98	1.265	9.5	0	0	0.30	0.147	0.45	0.45	0	0	0	0	0	—
8	4.16	1.322	10.8	0	0	0.45	0.170	0.25	0.238	0.012	0	0	0	0	—
9	4.25	0.675	12.3	0	0	0.70	0.0974	0	—	—	—	—	—	—	—
10	4.36	0.693	16.4	0	0	1.0	0.129	0	—	—	—	—	—	—	—
11	4.33	0	16.8	0	0	1.5	0	0	—	—	—	—	—	—	—

Na ($N = 0.022 \times 10^{24}$)

	O[b]						$\sigma_{in,j\to j+k}$							
j	σ_{tr}	σ_{er}	σ_{tr}		σ_c	σ_{er}	σ_{in}	k = 1	2	3	4	5	6	7
1	1.05	0.178	1.9		0.0003	0.167	0.50	0.32	0.065	0.04	0.03	0.015	0.03	—
2	1.6	0.348	2.5		0.0003	0.337	0.30	0.30	0	0	0	0	0	—
3	3.6	0.871	3.3		0.0005	0.494	0.40	0.284	0.116	0	0	0	0	—
4	3.0	0.726	3.2		0.0006	0.477	0.40	0.08	0.128	0.076	0.044	0.044	0.028	—
5	5.7	1.379	3.3		0.0008	0.562	0	—	—	—	—	—	—	—
6	3.35	0.811	3.6		0.001	0.613	0	—	—	—	—	—	—	—
7	3.26	0.789	3.5		0.001	0.596	0	—	—	—	—	—	—	—
8	3.26	0.789	3.3		0.001	0.562	0	—	—	—	—	—	—	—
9	3.26	0.394	4.9		0.003	0.417	0	—	—	—	—	—	—	—
10	3.26	0.394	4.9		0.001	0.417	0	—	—	—	—	—	—	—
11	3.26	0	10.0		0.005	0	0	—	—	—	—	—	—	—

Mo ($N = 0.0640 \times 10^{24}$)

					$\sigma_{in,j\to j+k}$							
j		σ_{tr}		σ_c	σ_{er}	σ_{in}	k = 1	2	3	4	5	6	7
1		2.5		0.010	0.0320	1.40	0.35	0.40	0.30	0.15	0.10	0.10	—
2		3.2		0.017	0.0886	0.84	0.411	0.33	0.099	0	0	0	—
3		4.0		0.024	0.150	0.40	0	0.108	0.117	0.068	0.042	0.065	—
4		5.3		0.034	0.221	—	—	—	—	—	—	—	—
5		6.4		0.040	0.267	—	—	—	—	—	—	—	—
6		7.2		0.046	0.300	—	—	—	—	—	—	—	—
7		7.8		0.057	0.325	—	—	—	—	—	—	—	—
8		7.9		0.066	0.329	—	—	—	—	—	—	—	—
9		7.4		0.090	0.154	—	—	—	—	—	—	—	—
10		7.1		0.120	0.147	—	—	—	—	—	—	—	—
11		7.2		0.200	0	—	—	—	—	—	—	—	—

Fe ($N = 0.0847 \times 10^{24}$)

					$\sigma_{in,j\to j+k}$							
j		σ_{tr}		σ_c	σ_{er}	σ_{in}	k = 1	2	3	4	5	6	7
1		2.05		0.005	0.0432	1.18	0.450	0.206	0.196	0.122	0.0802	0.0448	0.0814
2		2.0		0.005	0.0864	0.65	0.39	0.26	0	0	0	0	0
3		1.9		0.005	0.107	0.4	0	0.170	0.104	0.0592	0.0332	0.0332	0
4		2.2		0.005	0.157	0	—	—	—	—	—	—	—
5		3.0		0.006	0.214	0	—	—	—	—	—	—	—
6		3.5		0.007	0.249	0	—	—	—	—	—	—	—
7		4.3		0.008	0.306	0	—	—	—	—	—	—	—
8		5.3		0.008	0.378	0	—	—	—	—	—	—	—
9		6.8		0.025	0.242	0	—	—	—	—	—	—	—
10		4.0		0.012	0.142	0	—	—	—	—	—	—	—
11		8.0		0.014	0	0	—	—	—	—	—	—	—

[a] ($N = 0.0838 \times 10^{24}$)
[b] ($N = 0.096 \times 10^{24}$)

Table 7-3—MULTIGROUP CONSTANTS FOR FAST REACTOR ANALYSIS (ANL 11-GROUP) (Continued)

(Microscopic cross sections in barns)

Al ($N = 0.0603 \times 10^{24}$)													
						$\sigma_{in,j\to j+k}$							
j		σ_{tr}		σ_c	σ_{er}	σ_{in}	k = 1	2	3	4	5	6	7
1		1.45		0.0003	0.0930	0.54	0.211	0.108	0.081	0.0648	0.0270	0.0324	0.0162
2		1.8		0.0004	0.197	0.30	0.147	0.123	0.030	0	0	0	0
3		2.0		0.0005	0.279	0.09	0.018	0.0279	0.0189	0.0135	0.0117	0	0
4		2.85		0.0007	0.416	0	—	—	—	—	—	—	—
5		3.1		0.0015	0.452	0	—	—	—	—	—	—	—
6		4.1		0.0018	0.598	0	—	—	—	—	—	—	—
7		5.6		0.0040	0.817	0	—	—	—	—	—	—	—
8		4.0		0.0035	0.583	0	—	—	—	—	—	—	—
9		5.5		0.0090	0.401	0	—	—	—	—	—	—	—
10		1.8		0.0080	0.131	0	—	—	—	—	—	—	—
11		1.6		0.0120	0	0	—	—	—	—	—	—	—
			Ta ($N = 0.0553 \times 10^{24}$)										
						$\sigma_{in,j\to j+k}$							
j		σ_{tr}		σ_c	σ_{er}	σ_{in}	k = 1	2	3	4	5	6	7
1		3.7		0.07	0.0174	2.5	0.95	0.708	0.410	0.222	0.120	0.09	—
2		4.5		0.09	0.0438	2.2	1.005	0.581	0.315	0.172	0.0847	0.0429	—
3		5.0		0.10	0.0748	1.5	0.710	0.384	0.21	0.105	0.0525	0.039	—
4		5.2		0.14	0.0937	0.8	0.384	0.210	0.105	0.0532	0.0388	0.0096	—
5		5.6		0.20	0.119	0	—	—	—	—	—	—	—
6		6.3		0.25	0.133	0	—	—	—	—	—	—	—
7		7.5		0.30	0.158	0	—	—	—	—	—	—	—
8		8.1		0.35	0.170	0	—	—	—	—	—	—	—
9		9.9		0.40	0.104	0	—	—	—	—	—	—	—
10		10.0		0.70	0.102	0	—	—	—	—	—	—	—
11		17.0		1.50	0	0	—	—	—	—	—	—	—

Table 7-4—MULTIGROUP CONSTANTS FOR FAST REACTORS– A DESCRIPTIVE SUMMARY

Origin	No. of Groups	No. of Materials	Materials	Above 1.4 Mev	0.5-1.4 Mev	0.1-0.5 Mev	Below 0.1 Mev	Thermal & Resonance Groups?	Ref.
ANL	4	6	U-235; U-238; Fe; Al; H_2O; Be	1	1	1	2	Yes	9, 14
LASL	6	4	U-235; Pu-239; U-233; U-238	2	2	1	1	No	10
USSR	9	3	U-235; U-238; Pu-239	1	2	2	4	No	11
USSR	9	9	U-235; U-238; Pu-239; Fe; Ni; K; Na; Mo; Be	1	2	2	4	No	11
LASL	10	7	U-235; U-238; Pu-239; Pu-240; C; Fe; Ni	1	1	2	6	Yes	12
ANL	10[a]	6	U-235; U-238; Pu-239; Fe; Al; Na	1	1(2)	3	5(4)	No	13
	10	5	U-235; U-238; Pu-239; Fe; Al	1	2	3	4	No	13, 14
ANL	11	13	Pu-239; Pu-240; U-235; U-233; U-238; Th; Ta; Mo; Fe; Al; Na; O; C	2	2	3	4	No	8
ANL	13	7	Pu-239; U-235; U-238; Zr; Na; Be; Al	1	1	2	9	Yes	16
LASL	16	22	Pu-239; Pu-240; U-233; U-235; U-238; Th; Mo; Zr; Ni; Fe; K; Al; Na; F; O; C; Be; B; Li-7; Li-6; D; H	2	2	1	11	Yes	6, 7
ANL	16	26	Pu-239; Pu-240; Pu-241; Pu-242; U-233; U-235; U-238; Th; Bi; Pb; Ta; Mo; Nb; Zr; Ni; Fe; Cr; V; Ti; K; Al; Na; O; C; B; B-10	3	2	3	8	No	5

[a]Two variations of this set are reported. In the first variation, numbers outside the parentheses indicate the number of groups in the designated energy range. The numbers inside the parentheses indicate the corresponding number of groups in the second variation.

fast core of the fast-thermal critical assembly (ZPR-V).[14] The "revised" set differs from the "standard" set in that the "revised" set is based upon measurements of inelastic scattering excitation cross sections for the low-lying levels of U^{238} reported by Cranberg and Levin.[15] The revised set has given reasonable criticality predictions for ZPR-III cores having large uranium volume fractions and large ratios of U^{238} to U^{235}.

(7) The ANL 11-group set[8] was evolved from experience with some of the 10-group sets. The change from ten to eleven groups was prompted by the consistent discrepancy between measured and predicted values of the $\sigma_f(U^{238})/\sigma_f(U^{235})$ ratio.[13] This set is adequate for estimating criticality of the smaller systems (>225 kg U^{235}). Critical masses of larger, high-density uranium systems are overestimated, while critical masses of larger cores having appreciable diluent materials, i.e., aluminum and steel, tend to be underestimated. For example, the Fermi critical configuration was slightly underestimated. These major problems are currently attributed to insufficient reactivity contributed by U^{238}, and too much reactivity held by coolant (Na) or coolant-mockup (Al), and structural materials (Fe).

(8) The ANL 13-group[16] set has been used extensively to predict the properties of coupled fast-thermal reactor systems. However, criticality of the coupled experiment on ZPR-III[9] is better predicted by the 4-group set cited in (1) above. Because Be and C in such systems would see a very degraded neutron flux, removal of neutrons from above to below the U^{238} fission threshold is about twice as large as in the corresponding cross sections of all-fast multigroup constants.

(9) The LASL 16-group set[6,7] has been used extensively in the analysis of fast and intermediate systems. The fast groups are essentially those of the 6-group set cited in (2) above. The 16-group constants have given good agreement between theory and experiment on the high-density systems investigated at LASL,[6] as well as the moderate size (<250 kg U^{235}) ZPR-III systems.*

(10) The ANL 16-group set[5] is a recent addition to the library of multigroup constants. It has been assembled without recourse to results from critical experiments. Preliminary results on criticality determinations suggest good agreement between theory and experiment for the largest uranium systems assembled on ZPR-III; however, large systems having much coolant and structure (Fermi) are appreciably underestimated. Underestimation of critical mass also occurs for the smaller ZPR-III systems, as well as the small, high-density LASL systems. This set of constants includes more materials than have been used in the past. Details of group cross section assignment are described in the original work.[5]

The preceding remarks are, and are intended to be, qualitative. They do not constitute either editorial endorsement or rejection of any particular set of multigroup constants. The comments are simply intended to convey the editorial impression that, currently, there is no single set of multigroup constants that may be used on a routine basis and, at the same time, exhibits a fixed, and known, uncertainty.

In general, agreement of calculations based upon available microscopic cross section data with integral measurements has been limited. Most of the characteristics of fast neutron systems can be predicted semi-quantitatively. From an immediate and practical point of view, various multigroup parameters may be adjusted (within measured cross section uncertainties and, at times, ad hoc), to force quantitative agreement with experiments over a limited range of systems. This approach is used frequently (and has met with some success) to predict systems that are similar to systems investigated experimentally. Adjustment of multigroup constants in this manner does inject limitations on the types of conceptual systems whose neutronics may be predicted with confidence.

More basic and long range approaches are two-fold: (1) determination of improved microscopic cross sections and fission data; and (2) improved calculational procedures. An example of the latter is the accounting for the effects of the detailed energy variation of the group flux, considering resonance effects (both scattering and absorption) upon the multigroup cross section parameters.

7.1.3 FEW-GROUP CONSTANTS

The variations of cross sections with energy are such that if only a few groups are used, the group cross sections are, for the most part, limited to the neutron spectrum for which the cross section parameters are evaluated. Because of the resultant simplification in calculation, however, few-group constants are still of great utility.

The three sets of few-group constants listed in Table 7-5 were obtained by averaging calculated spectra based on multigroup calculations. They were averaged in fairly hard reactor spectra and

*Private communication, R. Campise, Atomics International.

Table 7-5—ONE-, TWO-, AND THREE-GROUP CONSTANTS

(Microscopic cross sections in barns)

Group	j	Energy Range, Mev	Fission Spectrum	Pu^{239}						U^{235}					
				ν	σ_f	σ_c	σ_{tr}	$\sigma_{in,j\to j+1}$	$\sigma_{in,j\to j+2}$	ν	σ_f	σ_c	σ_{tr}	$\sigma_{in,j\to j+1}$	$\sigma_{in,j\to j+2}$
One	1	0 – ∞	1.0	2.98	1.85	0.26	6.8	—	—	2.6	1.4	0.25	6.8	—	—
Two	1	1.35 – ∞	0.575	3.10	1.95	0.10	4.6	0.90	—	2.7	1.29	0.08	4.5	1.50	—
	2	0 – 1.35	0.425	2.93	1.78	0.30	7.0	—	—	2.5	1.44	0.28	7.2	—	—
Three	1	1.35 – ∞	0.575	3.10	1.95	0.10	4.6	0.45	0.45	2.7	1.29	0.08	4.5	1.00	0.50
	2	0.4 – 1.35	0.326	2.98	1.75	0.12	6.0	0.50	—	2.53	1.27	0.13	5.7	0.50	—
	3	0 – 0.4	0.099	2.91	1.80	0.35	10.0	—	—	2.47	1.77	0.49	10.0	—	—
				U^{238}						Fe					
				ν	σ_f	σ_c	σ_{tr}	$\sigma_{in,j\to j+1}$	$\sigma_{in,j\to j+2}$		σ_c	σ_{tr}	$\sigma_{in,j\to j+1}$	$\sigma_{in,j\to j+2}$	
One	1	0 – ∞	1.0	2.6	0.095	0.16	6.9	—	—		0.006	2.7	—	—	
Two	1	1.35 – ∞	0.575	2.6	0.524	0.036	4.6	2.05	—		0.005	2.0	0.70	—	
	2	0 – 1.35	0.425	2.47	0.005	0.19	7.1	—	—		0.006	2.8	—	—	
Three	1	1.35 – ∞	0.575	2.6	0.524	0.036	4.6	1.41	0.64		0.005	2.0	0.60	0.10	
	2	0.4 – 1.35	0.326	2.47	0.01	0.13	5.8	0.25	—		0.006	2.13	0.22	—	
	3	0 – 0.4	0.009	—	—	0.26	9.6	—	—		0.006	3.24	—	—	
				Au	Na					Np^{237}	Al				
				σ_c	σ_c	σ_{tr}	$\sigma_{in,j\to j+1}$	$\sigma_{in,j\to j+2}$		σ_f	σ_c	σ_{tr}	$\sigma_{in,j\to j+1}$	$\sigma_{in,j\to j+2}$	
One	1	0 – ∞	1.0	—	0.0008	3.3	—	—		—	0.002	3.1	—	—	
Two	1	1.35 – ∞	0.575	—	0.0005	2.0	0.30	—		—	0.004	1.8	0.38	—	
	2	0 – 1.35	0.425	—	0.0008	3.5	—	—		—	0.002	3.5	—	—	
Three	1	1.35 – ∞	0.575	0.07	0.0005	2.0	0.24	0.06		1.42	0.004	1.8	0.33	0.05	
	2	0.4 – 1.35	0.326	0.192	0.001	3.2	0.18	—		0.68	0.0006	2.4	0.2	—	
	3	0 – 0.4	0.099	0.65	0.001	3.7	—	—		0	0.002	3.8	—	—	

NOTE: The group inelastic removal $\sigma_{in,j\to k}$ includes inelastic and elastic removal.

were used principally in the analysis of small, high-density systems, i.e., Godiva, Topsy, Jezebel, and Popsy, as well as the Jemima assemblies and EBR-II. (See Section 7.2 for description of these assemblies.)

The effective U^{238} fission cross section must be considered a variable with core enrichment and dilution when one-group analysis is used.

A set of two-group cross sections may be used in the analytical treatment of fast reactor problems without recourse to high-speed computing equipment. The group structure is such that group 1 represents all the neutrons above, while group 2 represents all those below, the U^{238} fission threshold (1.4 Mev).

Three-group calculations are helpful in analyzing critical experiments. The threshold detectors $U^{238}(n,f)$ and $Np^{237}(n,f)$, or $Pu^{240}(n,f)$, combined with a detector give an approximate integral of the flux, i.e., $U^{235}(n,f)$ or $Pu^{239}(n,f)$. They facilitate an experimental division of the flux into three approximate energy groups. The group boundaries are about 1.35 Mev and 0.4 Mev.

7.2 INTEGRAL DATA

7.2.1 CRITICAL MASS (U^{235}, Pu^{239}, U^{233}, U^{238}, AND Th SYSTEMS)

There is considerable experimental information on a variety of fast neutron systems. The results cited here have been investigated in relatively simple geometry; thus much of the data are amenable to calculation in spherical geometry.

Table 7-6 describes critical experiments performed with high-density plutonium cores. Jezebel is an unreflected plutonium critical assembly at LASL. Popsy has essentially the same core composition, but is reflected with a natural uranium blanket and has a much lower critical mass. The other assemblies represent experiments performed at UCRL. Table 7-7 describes three critical experiments using appreciable amounts of Pu^{240}.

Table 7-8 describes critical configurations involving U^{233} and Pu^{239} in various reflectors, including enriched uranium. It is from such data, when correlated with calculations, that an unreflected sphere of U^{233} is expected to be critical with about 16 kg of that material.

Table 7-6 — OBSERVED CRITICAL MASSES: HIGH-DENSITY SPHERICAL PLUTONIUM CORES

Density of Pu in core, gm/cm^3	Reflector			Critical Mass, kg Pu	Ref.
	Composition	Density, gm/cm^3	Thick., cm		
15.44	—	—	—	16.28[a]	18
15.54	Nat. U	18.8	24.1	5.73[b]	18
15.8	Nat. U	18.8	5.0	8.06	19
15.8	Nat. U	18.8	2.0	10.68	19
15.8	Beryllium	1.86	5.0	7.48	19
15.8	Beryllium	1.86	2.0	10.35	19
15.8	Carbon	1.63	5.0	10.05	19
15.8	Carbon	1.63	2.0	12.75	19
19.25	Beryllium	1.84	5.22	5.43	20
19.25	Beryllium	1.84	32.0	2.47	20
19.25	Beryllium	1.84	21.0	3.22	20
19.25	Beryllium	1.84	13.0	3.93	20
19.25	Beryllium	1.84	8.17	4.66	20

[a]Jezebel Assembly
[b]Popsy Assembly

Table 7-7 — CRITICAL EXPERIMENTS WITH NATURAL URANIUM-REFLECTED SPHERICAL Pu^{240} CORES

Data from Ref. 17.

Spherical core radius, cm	2.73		
Core No.	I	II	III
Weight of materials, gm			
Pu	1615.45	1610.30	1611.19
Ni	10.89	11.76	14.10
Oy (93.2% U^{235})[a]	9521	9755	10618
Isotopic composition of Pu			
Pu^{239}	0.9756	0.9497	0.8047
Pu^{240}	0.0234	0.0473	0.161
Pu^{241}	0.0010	0.0030	0.0292
Pu^{242}	—	—	0.0051
Spherical radius of natural uranium[b] reflector, cm		24.1	

[a]Density ≈ 18.75 gm/cm^3
[b]Density = 18.8 gm/cm^3

Table 7-8 — OBSERVED CRITICAL CONFIGURATIONS: SPHERICAL CORES OF U^{233} AND Pu^{239} IN VARIOUS SPHERICAL REFLECTORS

Data from Ref. 21.

Core					Critical Reflector Thickness,[a] cm			
Material	Diameter, cm	Mass, kg	Density, gm/cm^3	Enrichment, wt-%	Enriched Uranium	Natural Uranium	Be	Tungsten Alloy
U^{233}	9.200	7.601	18.62	98.25	1.981	5.309	4.196	5.791
U^{233}	10.089	10.012	18.62	98.25	1.214	2.301	2.045	2.438
Pu^{239}	10.084	8.386	15.62[b]	b	1.656	4.128	3.688	4.699

[a]Reflector Densities, gm/cm^3:
Enriched Uranium (93%) = 18.8
Natural Uranium = 18.92
Be (98 wt-%) = 1.83
W-Alloy (91.3 wt-% W) = 17.21

[b]Density is for Pu. This contains 4.9 at-% Pu^{240}, and 0.31 at-% Pu^{241}.

Table 7-9 summarizes critical experiments with unreflected plutonium cores. The plutonium is diluted with varying amounts of depleted uranium, steel, thorium, aluminum, and air.

Table 7-9 — OBSERVED CRITICAL MASSES: UNREFLECTED PLUTONIUM CORES

Data from Ref. 22.

Diluent	Nominal Pu/Diluent Ratio	Average Density, gm/cm^3			Cylindrical Critical Mass, kg Pu	Critical L/D Ratio	Est. Spherical Critical Mass, kg Pu
		Pu	Diluent	Ni			
None	—	14.27	—	0.651	21.39	0.546	17.5
Depleted U	2 : 1	9.83	5.97	0.448	27.3	0.955	24.7
Steel	2 : 1	9.78	2.50	0.446	32.8	1.23	28.6
Thorium	2 : 1	9.78	3.62	0.446	35.2	1.32	30.1
Aluminum	2 : 1	9.69	0.83	0.441	37.0	1.40	31.1
Air	2 : 1	9.98	—	0.455	77.1	2.82	43.7

Tables 7-10 and 7-11 describe plutonium core configurations in thick, natural uranium, and thorium reflectors, respectively. The range of core dilution with fertile and structural materials is larger than for unreflected cores since a limited supply of fissionable material could be better utilized due to the effectiveness of the reflectors.

Data in Tables 7-9, 7-10, and 7-11, are as reported. The diluted cores are quite heterogeneous and this must be recognized when contemplating a comparison between theory and experiment. Corrections for heterogeneity (Section 7.2.3) must be applied for precise comparison.

Table 7-10 — OBSERVED CRITICAL MASSES: NATURAL URANIUM REFLECTED[a] PLUTONIUM CORES

Data from Ref. 22.

Diluent	Nominal Pu/Diluent Ratio	Average Density, gm/cm³			Cylindrical Critical Mass, kg Pu	Critical L/D Ratio	Est. Spherical Critical Mass, kg Pu
		Pu	Diluent	Ni			
None	—	14.23	—	0.652	8.96	0.23	6.8
Depleted U	2 : 1	9.77	5.94	0.447	10.35	0.387	8.8
	1 : 1	7.44	9.05	0.339	11.96	0.588	11.0
	1 : 2	5.06	12.27	0.231	16.91	1.22	15.5
	1 : 3	3.81	13.87	0.174	30.13	2.98	19.2
Steel	2 : 1	9.76	2.51	0.447	10.88	0.407	9.5
	1 : 1	7.45	3.80	0.339	13.55	0.664	12.7
	1 : 2	5.01	5.11	0.228	21.78	1.59	19.3
Thorium	2 : 1	9.76	3.63	0.447	11.13	0.417	9.9
	1 : 1	7.51	5.57	0.343	14.25	0.694	13.7
	1 : 2	5.07	7.49	0.231	25.15	1.81	21.7
Aluminum	2 : 1	9.76	0.840	0.447	11.04	0.414	9.9
	1 : 1	7.50	1.28	0.342	13.70	0.667	13.2
	1 : 2	5.05	1.75	0.230	22.36	1.62	20.2
Air	2 : 1	9.92	—	0.453	11.25	0.414	10.4
	1 : 1	7.62	—	0.348	14.58	0.70	14.6
	1 : 2	5.12	—	0.233	24.85	1.77	24.9

[a]Reflector thickness = 19 cm; reflector density ≈ 18.9 gm/cm³

Table 7-11 — OBSERVED CRITICAL MASSES: THORIUM REFLECTED[a] PLUTONIUM CORES

Data from Ref. 22.

Diluent	Nominal Pu/Diluent Ratio	Average Density, gm/cm³			Cylindrical Critical Mass, kg Pu	Critical L/D Ratio	Est. Spherical Critical Mass, kg Pu
		Pu	Diluent	Ni			
None	—	14.5	—	0.659	12.75	0.322	9.7
Depleted U	2 : 1	9.91	5.99	0.451	14.65	0.541	12.5
	1 : 1	7.42	9.04	0.339	17.56	0.865	16.2
	1 : 2	5.06	12.27	0.231	30.78	2.222	21.3
Steel	2 : 1	9.76	2.50	0.446	16.02	0.60	14.1
	1 : 1	7.43	3.80	0.339	21.55	1.061	20.6
Thorium	2 : 1	9.82	3.63	0.447	16.61	0.618	15.1
	1 : 1	7.45	5.52	0.340	23.16	1.136	21.3
Aluminum	2 : 1	9.95	0.851	0.453	16.45	0.604	15.0
	1 : 1	7.59	1.30	0.346	22.80	1.098	21.2
Air	2 : 1	9.95	—	0.453	17.35	0.638	16.5
	1 : 1	7.65	—	0.349	25.75	1.23	24.5

[a]Reflector thickness = 19 cm; reflector density ≈ 11.3 gm/cm³

Table 7-12 describes critical experiments performed with high-density uranium systems. The core alloy is highly enriched uranium. The Godiva assembly is a spherical, unreflected system. Topsy is reflected with a natural uranium blanket, and has a much lower critical mass than Godiva. Uranium hydride cores with natural uranium and nickel reflectors are also given.

Table 7-12—OBSERVED CRITICAL MASSES: SPHERICAL URANIUM CORES HIGHLY ENRICHED IN U^{235}

Enrich., %	Density of Core Alloy, gm/cm³	Reflector			Critical Mass, kg U^{235}	Ref.
		Composition	Density, gm/cm³	Thick., cm		
93.9	18.75[a]	—	—	—	48.8	10, 23
94.1	18.75[b]	Nat. U	18.8	20.32	16.28	10, 23
93.5	18.75	Nat. U	18.8	5.08	23.75	23, 25
93.5	18.75	Nat. U	18.8	4.75	24.5	23, 25
93.9	18.55	Graphite	1.69	43.2	16.9	24, 25
93.9	18.55	Water	1.0	∞	23.2	24, 25
93.9	18.55	Paraffin	0.89	∞	22.2	24, 25
93.15	7.40[c]	Nat. U	19.0	20.32	12.61	24
93.15	7.40[c]	Nickel	8.8	20.32	12.63	24

[a]Godiva; [b]Topsy; [c]Hydride core ($UH_{2.97}C_{1.11}O_{0.25}$).

Table 7-13 summarizes the effectiveness of various reflectors around a spherical, enriched uranium core. Such data are basic to nuclear safety analyses. They can be very useful toward the determination of high-energy constants of these reflector materials in multigroup analyses.

Table 7-13—CRITICAL MASSES OF ENRICHED URANIUM SPHERES IN VARIOUS REFLECTORS[a]

(in kg enriched uranium; mass of U^{235} = 93.5 × cited values)

Reflector	Reflector[b] Density, gm/cm³	Reflector Thickness			
		2.54 cm	5.08 cm	10.16 cm	∞
Be	1.84	29.2 kg	20.8 kg	14.1 kg	—
BeO	2.69	—	21.3	15.5	~8.9 kg
WC	14.7	—	21.3	16.5	~16.0
U	19.0	30.8	23.5	18.4	16.1
W-alloy[c]	17.4	31.2	24.1	19.4	—
Paraffin	0.91	32.6	—	—	21.8
H_2O	—	—	~24.0	22.9	22.8
D_2O	—	—	(27)	21.0	~13.6
Cu	8.88	32.4	25.4	20.7	—
Ni	8.88	33.0	25.7	(21.5)	~19.6
Al_2O_3	2.76	35.1	—	—	—
Graphite[d]	1.69	35.5	29.5	24.2	~16.7
Fe	7.87	36.0	29.3	25.3	23.2
Zn	7.04	—	29.8	25.0	—
Th	11.48	—	33.3	—	—
Al	2.70	39.3	(35.5)	(32)	<30.0
Ti	4.50	39.7	—	—	—
Mg	1.77	41.0	—	—	—

[a]Data from Refs. 25 and 26.
[b]Density of enriched uranium = 18.8 gm/cm³.
[c]About 92 wt-% W.
[d]CS-312

NOTE: Parentheses indicate interpolated data.

Table 7-14 lists critical data for uranium cores of various enrichments, and dilutions with structural, moderator, and coolant materials. The Jemima assemblies are stacks of alternately highly enriched and natural uranium plates. The ZPR-III assemblies consist of small plates of the basic constituent materials arranged in a two-half honeycomb machine. The Jemima and ZPR-III results are given as measured and reported. The effect of inhomogeneity (Section 7.2.3) must be determined for a precision comparison between theory and experiment. (Note: The designations in the first column of Table 7-14 will be used to identify the respective assemblies in subsequent sections treating spectral indices, central material replacement experiments and prompt neutron lifetime measurements.)

A number of empirical correlations to predict criticality of a wide range of systems have been attempted. Some of these are:[30]

(1) The effect of changing the density of an enriched uranium core surrounded by a thick, natural uranium reflector is given by: Critical Mass $\approx$ (core density)$^{-1.2}$

(2) The effect of changing the U^{235} enrichment in the core is given by: (Critical Mass of U^{235} + U^{238}) $\approx$ (U^{235} enrichment)$^{-1.7}$

(3) Critical masses of Pu^{239} and U^{233} for small, high-density cores can be approximated by scaling U^{235} critical masses downward by a factor of 3.

A number of fast reactor critical experiments have been performed which do not readily lend themselves to criticality calculations in simple geometry. In many cases, the objective was to obtain design information for a specific reactor system. Other cases were investigated to provide physics information for core meltdown analyses or nuclear safety standards. Some systems were constructed to investigate spherical geometrical effects.

EBR-II-size systems were studied on ZPR-III to determine the effect of: (1) core geometry and (2) low-density radial and central blankets, on critical mass. The results are given in Table 7-15.

A number of critical configurations with extremely high and low ratios of core height to diameter were investigated at LASL and ANL. The studies at ANL included rectangular core geometry. The ANL results are listed in Table 7-16. These particular data are basic to the construction of the shape factor curves (Section 7.2.2). LASL experiments, basic to the construction of the shape factor curves (Section 7.2.2), deal with highly enriched uranium cores reflected by various thicknesses of natural uranium. The experimental data, corrected to a core alloy density of 18.8 gm/cm^3, are summarized in Table 7-17. Actual experiments were performed with a core alloy of slightly lower density.

Special critical experiments in extreme geometry (very high or very low L/D ratio) have been reported.[31,32] Table 7-18 lists data for reflected, highly enriched uranium cores. Table 7-19 contains similar data for reflected plutonium cores. Table 7-20 is a summary of data on bare and on reflected, 46% enriched cores in extreme cylindrical geometry.

Other critical experiments were performed to investigate the influence on critical mass of highly enriched, high-density uranium core geometry. These cores were reflected with water or graphite. The results are given in Table 7-21.

Table 7-22 is a summary of critical experiments performed to study the influence of various reflector materials on annular, high-density, highly enriched uranium cores.

Mock-up experiments have been carried out for EBR-I, Mark II;[13] EBR-I, Mark III;[13] LAMPRE;[33] EBR-II;[13,28] UKAEA Fast Reactor;[34] and the Enrico Fermi Reactor.[28,35] The EBR-I, EBR-II, and Fermi mock-ups were investigated on the ZPR-III facility. The UKAEA Fast Reactor was investigated in four distinct cylindrical core configurations on the UKAEA-ZEUS facility. The UKAEA also studied several configurations on the ZEPHYR facility.[34,36] The LAMPRE critical experiments were performed in a number of configurations on a LASL basic assembly machine. The USSR has reported critical and reactor experiments with four distinct systems.[11]

The four cylindrical cores investigated on the ZEUS facility are typical of critical experiments designed to provide data for reactor configuration. Data on the various core compositions and dimensions employed are summarized in Table 7-23. All cores were reflected radially with blanket elements 112 cm in over-all length; the composition is listed in Table 7-24. The axial blanket thickness was 15.7 cm. This, in turn, was reflected by about 31 cm of magnesium, and about 10 cm of steel. Cores No. 1, 2, and 3, featured the same upper and lower axial blankets, while various axial blanket configurations were employed on core No. 4 (Table 7-25).

An engineering mock-up of EBR-II on ZPR-III yielded much detailed design information. Although several reactor systems were included in the experimental program, only the "clean" core mock-up having a uniform core, will be described here. The "clean" core did not include the compositional and geometrical asymmetries due to the control and safety rods of the actual EBR-II design. This EBR-II mock-up consisted of a cylindrical core with a radial reflector in three annular regions. Axially, the

Table 7-14—OBSERVED CRITICAL MASSES: URANIUM CORES OF VARIOUS ENRICHMENTS AND DILUTIONS

Assembly	Sphere or Cylinder L/D	Critical Core Dimensions, cm Length & Diameter or Diameter	Core Composition (Volume Fraction)[a]							Reflector[c] Identification	Fuel Worth[d] at Core Edge, inhours/kg U^{235}	Critical Mass, kg U^{235}	Ref.
			U^{235}	U^{238}	SST (Fe)	Al	C	O[b]	Na				
Jemima-53	0.58	15.49 × 26.67	0.535	0.465	—	—	—	—	—	A	—	86.7	6, 27
-37	1.0	25.50 × 26.67	0.377	0.623	—	—	—	—	—	A	—	100.7	6, 27
-29	1.18	34.16 × 29.01	0.29	0.71	—	—	—	—	—	A	—	123.0	6, 27
-16	—	— —	0.162	0.829	—	—	—	—	—	B	—	—	6
ZPR-III-6F	Sphere	45.6 —	0.14	0.159	0.123	0.314	—	—	—	C′	75	131.1	13
-9A	Sphere	50.4 —	0.117	0.380	0.142	0.215	—	—	—	C	61	146.2	13
-2A	0.97	40.8 × 42.0	0.14	0.01	0.275	0.314	—	—	—	C′	69	147.7	13
-13	1.00	40.8 × 40.6	0.14	0.1586	0.1174	0.3044	—	—	—	C	75	138.6	13, 28
-10	1.04	45.9 × 44.25	0.119	0.579	0.193	—	—	—	—	C	49	155.8	13
-22	0.88	51.0 × 58.7	0.094	0.701	0.093	—	—	—	—	C	31	243.7	13, 29
-24	0.93	71.3 × 76.9	0.076	0.729	0.093	—	—	—	—	C	10	460.7	29
-25	0.90	76.3 × 85.20	0.071	0.741	0.093	—	—	—	—	C	11	581.6	29
-16	0.92	51.0 × 55.9	0.095	0.50	0.092	—	0.204	—	—	C	41	204.8	13
-12	0.87	45.9 × 52.75	0.095	0.355	0.092	—	0.357	—	—	C	45	176.8	13
-17	0.93	45.9 × 49.5	0.095	0.206	0.092	—	0.510	—	—	C	70	156.5	13
-14	0.99	45.9 × 46.3	0.094	0.007	0.093	—	0.745	—	—	C	74	136.1	13
ZPR-III-15	0.89	51.0 × 57.4	0.095	0.315	0.177	0.194	—	—	—	C	45	220.4	13
-23	0.84	51.0 × 60.7	0.093	0.007	0.092	0.428	—	—	—	C	38	258.1	29
-29	0.79	71.3 × 90.0	0.0497	0.0997	0.248	0.244	—	0.145	—	C	20	421.0	28
-30	0.75	62.2 × 82.8	0.0592	0.0906	0.246	0.234	—	0.072	—	C	20	395.0	28
-31	0.69	62.2 × 90.4	0.0581	0.0914	0.245	0.235	—	—	—	C	18	463.0	28
-32	1.17	61.1 × 52.2	0.093	0.007	0.81	—	—	—	—	C	46	227.5	28
-33	1.14	61.1 × 53.4	0.073	0.007	0.636	—	—	—	0.158	C	46	238.0	28
-34	0.94	86.5 × 91.9	0.0467	0.103	0.246	0.255	0.106	—	—	C	18	503.0	28
-36	1.43	71.27 × 49.76	0.0937	0.495	0.127	—	—	—	0.182	C	42	242.7	28

[a]Core Material: U^{235} U^{238} Al C SST(Fe) Na
Ref. density, gm/cm³: 18.75 19.0 2.7 1.43 7.85 0.97

[b]Assumed atomic density = N = 0.096×10^{24} atom/cm³

[c]A = Unreflected; B = Natural uranium, 7.62 cm thick;
C = Standard ZPR-III Reflector, 30 cm thick

Volume Fractions:	Depleted U	SST	Al
C′	0.834	0.073	0.023
C	0.834	0.073	—

[d]Approximate worth of core given in inhours/kg of contained U^{235}. Values listed are extremely sensitive to intra-drawer plate configuration.

Table 7-15— EFFECT OF CORE GEOMETRY AND BLANKET DENSITY ON EBR-II-SIZE CRITICAL ASSEMBLIES

Data from Ref. 13.

Assembly Description	ZPR-III Assembly No.	Critical Core Dimensions, cm		Core Composition, vol-%				Reflector Composition, vol-%					Critical core Mass kg U^{235}
		Length	Diameter	U^{235}	U^{238}	Al	SST(304)	Region[a]	U^{235}	U^{238}	SST(304)	Al	
Cylindrical core in high-density reflector	2	40.8	40.1	14.0	15.7	31.5	12.3	Central	—	—	—	—	136.0
								Inner	0.19	83.3	7.31	2.27	—
								Outer	0.19	83.3	7.31	2.27	—
Annular core; low density central blanket; high-density reflector	3	40.8	17.1 (Inside)	14.2	15.9	31.0	12.1	Central	0.08	39.7	7.31	24.6	176.9
		40.8	48.6 (Outside)	—	—	—	—	Inner	0.19	83.3	7.31	2.27	—
								Outer	0.19	83.3	7.31	2.27	—
Annular core; low-density central and inner reflector; high-density outer reflector	4	40.8	17.1 (Inside)	14.0	15.9	31.5	12.2	Central	0.08	39.7	7.31	24.6	201.1
		40.8	51.9 (Outside)	—	—	—	—	Inner	0.08	39.7	7.31	24.67	—
								Outer	0.19	83.3	7.31	2.27	—
Cylindrical core in low-density reflector, surrounded by high-density reflector	5	40.8	43.6	1.40	15.9	31.5	12.2	Central	—	—	—	—	159.5
								Inner	0.08	39.7	7.31	24.6	—
								Outer	0.19	83.3	7.31	2.27	—

[a]Inner reflector thickness = 18.1 cm.
Outer reflector thickness > 12 cm.
Central reflector diameter = 17.1 cm.

Table 7-16—EFFECT OF CHANGING CORE DIMENSIONS ON REFLECTED CRITICAL ASSEMBLIES[a]

Data from Ref. 13.

Assembly Description	ZPR-III Assembly Number	Critical Core Dimensions, cm (length × diameter or length × depth × width)	Core Composition, vol-%				Critical Core Mass, kg U^{235}
			U^{235}	U^{238}	Al	SST(304)	
Cylinder	6C	18 × 72.1	14.0	15.9	31.4	12.3	221.0
	6B	20.55 × 65.6	14.0	15.9	31.4	12.3	183.0
	1B	30.7 × 46.6	14.1	16.0	31.5	12.4	137.1
	2	40.8 × 40.1	14.0	15.7	31.5	12.3	136.0
	6D	56.1 × 35.7	14.0	15.7	31.4	12.3	147.4
	6E	71.4 × 33.55	14.0	15.9	31.4	12.3	164.2
Rectangular	1A	30.7 × 38.73 × 45.4	14.1	16.0	31.5	12.4	142.4
Parallelepiped	1C	30.7 × 33.20 × 56.2	14.1	16.0	31.5	12.4	151.0
	1D	30.7 × 27.65 × 82.5	14.0	15.9	31.5	12.4	183.4
	6A	40.8 × 22.17 × 81.4	14.0	15.9	31.4	12.3	194.5
Cylinder	9B[b]	25.6 × 66.8	11.6	37.8	21.3	14.4	193.3
	9	48.8 × 46.5	11.7	38.0	21.6	15.0	151.9

[a]Reflector composition (vol-%): 0.19 U^{235}; 83.3 U^{238}; 2.27 Al; and 7.31 SST(304). Reflector thickness >23 cm for assemblies 1A, 1B, 1C, 1D, 9, 9B; >30 cm for assemblies 2, 6A, 6B, 6C, 6D, 6E.

[b]Reflector of this assembly identical to No. 9, except that it does not contain Al.

Table 7-17—CRITICAL DATA ON NATURAL URANIUM REFLECTED CYLINDRICAL CORES OF ENRICHED URANIUM[a]

Data from Ref. 25.

Enriched Uranium Density = 18.8 gm/cm^3
Natural Uranium Density = 18.9 gm/cm^3

Reflector Thickness, cm	Critical L/D Ratio	Critical Mass, kg enriched uranium
0	1.76	68.7
0	0.953	57.4
0	0.723	57.8
0	0.61	60.5
2.844	3.51	51.8
2.844	1.38	34.5
2.844	0.84	32.8
2.844	0.565	34.0
2.844	0.46	37.0
2.844	0.41	39.9
5.08	2.15	31.2
5.08	1.03	25.8
5.08	0.67	26.2
5.08	0.47	28.8
~20.3	3.08	22.8
~22.9	1.00	17.77
~21.6	0.31	21.7
~19.7	0.18	27.4

[a]93.5% enriched in U^{235}.

Table 7-18—CRITICAL PARAMETERS FOR HIGHLY ENRICHED URANIUM CORES IN EXTREME GEOMETRY

Data from Ref. 31.

Core				Reflector		
Height, cm	Diameter, cm	Density, gm/cm^3	Mass,[a] kg	Material	Thickness, cm	Density, gm/cm^3
70.61	8.23	18.70	70.3	Depleted Uranium	6.99	18.9
55.88	8.23	18.70	55.5	Graphite	12.32	1.60
40.89	8.23	18.70	40.7	Graphite	14.61	1.60
36.32	8.23	18.70	36.1	Graphite	15.88	1.60
66.04	8.23	18.70	65.8	Polyethylene	10.16	0.92
100.33	8.23	18.70	100	Water	∞	1.00
8.26	38.1	17.70	165.7	None	—	—
4.98	38.1	17.70	100.5	Beryllium	2.54	1.80
3.43	38.1	17.70	69.5	Beryllium	5.08	1.80
2.59	38.1	17.70	52.5	Beryllium	7.62	1.80
2.01	38.1	17.70	40.5	Beryllium	10.16	1.80
1.61	38.1	17.70	32.5	Beryllium	12.70	1.80
3.48	38.1	17.70	70.0	Natural Uranium	7.62	18.9
2.77	38.1	17.70	55.8	Graphite	17.78	1.60
3.63	38.1	17.70	73.2	Polyethylene	5.08	0.92
3.12	38.1	17.70	63.2	Water	∞	1.00

[a]kg of enriched uranium.
Cores with 8.23 cm diameter have 93.2% enrichment in U^{235}.
Cores with 38.1 cm diameter have 93.4% enrichment in U^{235}.

Table 7-19 — CRITICAL PARAMETERS FOR HIGH-DENSITY PLUTONIUM CORES IN EXTREME GEOMETRY

Data from Ref. 31.

Core				Reflector		
Height, cm	Diameter, cm	Density, gm/cm^3	Mass,[a] kg Pu	Material	Thickness, cm	Density, gm/cm^3
50.22	5.72	15.44	20.0	Depleted Uranium	7.62	18.7
40.92	5.72	15.44	16.3	Graphite	17.8	1.60
83.82	5.61	15.44	32.2	Polyethylene	10.2	0.92
70.61	5.61	15.44	27.1	Water	∞	1.00
74.68	5.61	15.44	28.6	Polyethylene + Water	10.2 + ∞	—
3.91	15.24	14.3	10.14	Natural Uranium	7.62	18.7
5.92	15.24	14.3	15.44	Graphite	2.54	1.60
4.14	15.24	14.3	10.8	Graphite	17.8	1.60
4.24	15.24	14.3	11.1	Water	∞	1.00
2.67	27.94[b]	13.1[b]	21.4	Water	∞	1.00
2.01	40.64[b]	13.1[b]	34.1	Water	∞	1.00

[a] 96% Pu^{239} in Pu.
[b] Estimates based on critical mass.

Table 7-20 — CRITICAL EXPERIMENTS ON 46% ENRICHED URANIUM CORES IN EXTREME CYLINDRICAL GEOMETRY

Data from Ref. 32.

L/D Ratio	Core Radius, cm	Critical Thickness, cm	Critical[a] Mass, kg U^{235}	Reflector Description
0.282	14.71	8.31	48.0	Natural uranium
0.139	21.49	5.99	73.7	Radial: 15.24 cm at full density
0.091	28.07	5.11	107.3	Axial: 2.54 cm at full density, followed by 14.48 cm at 85% of full density
				Full density = 18.83 gm/cm^3
0.259	14.71	7.62	43.9	Graphite
0.127	21.49	5.44	66.9	Thickness = 15.24 cm in all directions
0.081	28.07	4.52	94.9	Density = 1.8 gm/cm^3
0.325	14.71	9.55	55.0	Radial: 15.24 cm of graphite
0.165	21.49	7.11	87.5	Axial: 20.32 cm of borated graphite (5 wt-% B)
0.109	28.07	6.10	128.1	Density ≈ 1.8 gm/cm^3
0.38	14.71	11.18	64.4	Aluminum
0.19	21.49	8.15	100.3	Thickness ≥ 15.24 cm in all directions
0.123	28.07	6.91	145.1	Density = 2.75 gm/cm^3
0.355	14.71	10.46	60.3	Steel
0.176	21.49	7.57	93.2	Thickness ≥ 15.24 cm in all directions
0.116	28.07	6.53	137.1	Density = 8.0 gm/cm^3
0.627	14.71	18.44	106.3	Unreflected
0.323	21.49	13.89	170.9	

[a] Density of core alloy = 18.44 gm/cm^3

Table 7-21 — CRITICAL MASS OF WATER AND GRAPHITE REFLECTED HIGHLY ENRICHED URANIUM CORES IN CYLINDRICAL GEOMETRY

Data from Refs. 24 and 30.

Diameter, cm	Height, cm	L/D Ratio	Critical Mass,[a] kg U	Reflector[b]
10.11	19.21	1.90	28.5	Water
12.06	11.82	0.98	25.3	Water
13.97	9.22	0.66	26.0	Water
16.19	7.45	0.46	27.6	Water
17.78	6.49	0.37	29.5	Water
19.05	5.72	0.30	30.9	Water
8.26	24.37	2.95	24.0	Graphite
10.11	13.14	1.30	19.5	Graphite
12.07	9.83	0.81	18.7	Graphite
13.97	6.92	0.50	19.7	Graphite
16.19	5.59	0.35	21.3	Graphite
19.05	4.48	0.24	24.1	Graphite
13.69	(Sphere)	—	24.9	Water
12.49	(Sphere)	—	18.1	Graphite

[a]Core alloy enrichment of U^{235} in U is between 93.4% and 94%.
Core alloy density = 18.5 gm/cm^3.

[b]Water reflector essentially infinite. Graphite thickness = 43 cm; density = 1.69 gm/cm^3.

Table 7-22 — CRITICAL MASSES OF HIGH-DENSITY ENRICHED URANIUM CORES IN ANNULAR CYLINDRICAL GEOMETRY[a]

Data from Ref. 25.

Reflector Thickness, Material	Critical Mass, kg Enriched Uranium	Critical Core Height, cm
2.54 cm, natural uranium	82.7 ± 0.3	7.65
7.62 cm, natural uranium	55.9 ± 0.3	5.16
7.62 cm, polyethylene	60.6 ± 0.3	5.59
5.08 cm, graphite (CS-312)	78.5 ± 0.3	7.26
2.54 cm, natural uranium in 5.08 cm polyethylene	54.5 ± 0.3	5.03
2.54 cm, natural uranium in 5.08 cm polyethylene (no inner reflector)	60.8 ± 0.3	5.61

[a]Inner Core Diameter = 15.24 cm.
Outer Core Diameter = 31.10 cm.
Core Uranium ~ 93% enriched in U^{235}
Core Uranium density ≈ 18.8 gm/cm^3
Except where noted, inner reflector region filled with reflector material.

687863 O - 63 - 39

Table 7-23 — CORE COMPOSITION FOR THE ZEUS CRITICAL EXPERIMENTS (in vol-%)

Data from Ref. 34.

		Effective[a] Radius, cm	U^{235}	U^{238}	Nb	V	Ni	Steel	Al	C	Critical Mass, kg U^{235}
Core 1	Main Region	22.9	12.9	36.2	5.8	—	2.6	0.1	11.9	—	—
	Outer Region	23.59	0.4	47.4	6.4	—	2.1	—	11.8	—	201.2
Core 2	Main Region	22.9	12.0	19.0	—	—	—	0.1	11.9	29.4	—
	Outer Region	23.59	0.2	31.9	—	—	—	—	12.2	31.2	189.6
Core 3A	Inner Region	12.51	13.0	27.9	6.7	2.1	—	6.9	14.2	—	—
	Outer Region	—	12.2	16.0	4.2	0.1	1.6	24.1	13.3	—	—
	Core Average	23.59	12.4	19.4	4.9	0.6	1.1	19.3	13.5	—	207.1
Core 3B	Inner Region	12.51	15.6	25.4	7.4	1.1	0.5	6.9	14.2	—	—
	Outer Region	—	10.1	18.1	3.6	0.8	1.3	24.1	13.3	—	—
	Core Average	23.59	11.7	20.1	4.7	0.8	1.1	19.3	13.5	—	193.6
Core 4A, 4B	Inner Region	12.51	15.6	24.9	6.2	1.0	1.4	6.7	14.3	—	—
	Outer Region	—	10.8	17.4	4.0	0.6	1.2	23.7	13.4	—	—
	Core Average	23.59	12.1	19.5	4.6	0.7	1.3	18.9	13.6	—	200.3
Core 4C1	Inner Region	12.51	15.6	24.9	6.2	1.0	1.4	6.7	14.3	—	—
	Outer Region	—	10.7	17.5	4.0	0.6	1.2	23.7	13.4	—	—
	Core Average	23.59	12.1	19.6	4.6	0.7	1.3	18.9	13.6	—	200.2
Core 4C4	Inner Region	12.51	16.3	24.2	6.2	0.8	1.7	6.7	14.2	—	—
	Outer Region	—	11.0	17.2	4.1	0.5	1.2	23.7	13.4	—	—
	Core Average	23.59	12.5	19.2	4.7	0.6	1.3	18.9	13.6	—	205.8

[a]Core height = 53.3 cm except for Core 2 with a height of 54.61 cm.

Table 7-24 — RADIAL BLANKET COMPOSITION OF ZEUS EXPERIMENTS (in vol-%)

Data from Ref. 34.

	Core Designation[a]		
		3B, 4	
	1,2,3A,3B	Inner Blanket	Outer Blanket
Natural uranium	63.8	56.7	56.7
Steel	7.2	10.0	14.3
Aluminum	8.4	12.7	8.4
Inner radius, cm	26.37	26.37	36.91
Outer radius, cm	96.65	36.91	43.94

[a]Core 3B was investigated for two different blanket dimensions, as indicated.

Table 7-25 — AXIAL BLANKET COMPOSITION IN ZEUS ASSEMBLIES (in vol-%)

Data from Ref. 34.

Core	Natural Uranium	Steel	Mg	Al
1,2,3,4[a]				
4A[b]	—	40.8	—	18.3
4B[b]	—	2.7	37.1	20.9
4C1[b]	45.3	2.7	—	9.4
4C4[b]	43.7	4.9	—	5.6

[a]Compositions are identical to core compositions except that enriched is replaced by natural uranium.

[b]Upper reflector only.

reflector consisted of structural gaps followed by a depleted uranium blanket. Figure 7-1 shows a section through the central axis of the assembly, the composition and geometry of the various regions, and the observed critical mass.

An engineering mock-up of the Enrico Fermi Fast Breeder Reactor (EFFBR) was also performed on ZPR-III. Again, only the results pertaining to the "clean" core mock-up will be cited. Figure 7-2 shows a section of a portion of the reactor (axial and azimuthal symmetry prevail), along with other pertinent data.

It is to be noted that the engineering mock-ups described here do not represent, in detail, the actual engineering configurations.

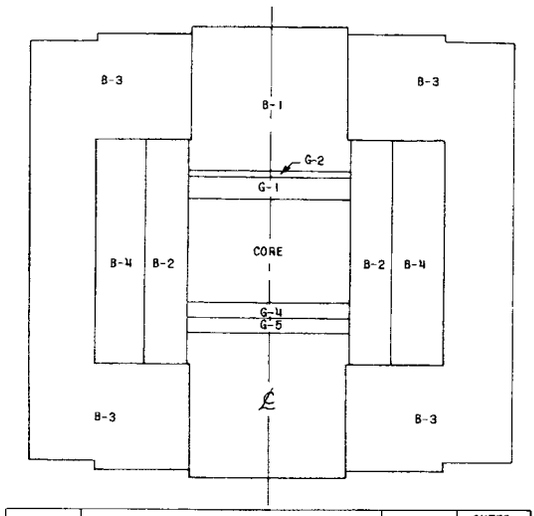

REGION	COMPOSITION, vol-%				LENGTH, cm	OUTER BOUNDARY RADIUS, cm
	U^{235}	U^{238}	Al	SST		
CORE	13.93	15.84	26.48	19.35	35.76	22.81
G-1	-	-	27.0	30.0	7.62	22.81
G-2	-	-	9.0	56.3	2.54	22.81
G-3	-	-	29.0	24.6	5.08	22.81
G-4	-	-	22.3	40.5	5.08	22.81
B-1	0.06	29.90	17.93	19.52	48.3	25.17
B-2	0.13	61.28	6.44	19.81	76.2	39.37
B-3	0.13	59.59	1.10	7.31	145.	80.52
B-4	0.15	66.36	8.11	15.72	76.2	55.1

CRITICAL MASS = 152.7 kg U^{235}

Fig. 7-1 — Geometry, composition, and critical mass of an EBR-II mock-up on ZPR-III (Assembly No. 8). *Reproduced from Refs. 13 and 28.*

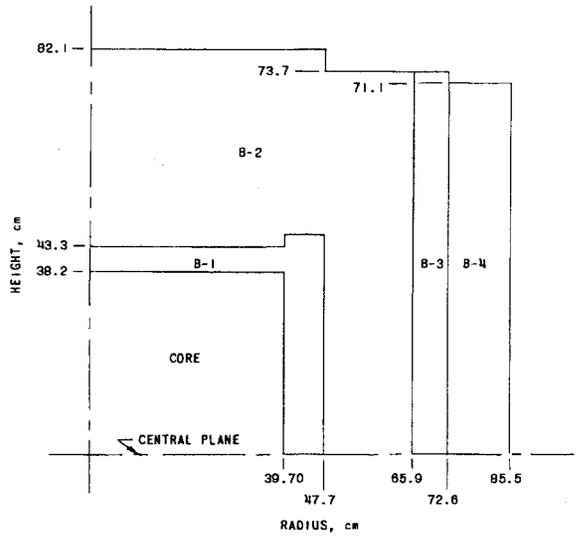

REGION	COMPOSITION, vol-%					
	U^{235}	U^{233}	Al	SST	Mo	Zr
CORE	6.09	18.97	25.14	14.32	5.03	4.32
B-1	0.10	45.39	10.08	19.42	2.46	
B-2	0.11	48.70	13.47	21.00		
B-3	0.11	46.35	0.86	16.65		
B-4	0.14	59.59	1.10	7.31		

CRITICAL MASS=431.5kg U^{235}

Fig. 7-2 — Geometry, composition, and critical mass of an EFFBR mock-up on ZPR-III (Assembly No. 20). *Reproduced from Ref. 28.*

7.2.2 SHAPE FACTOR AND RELATED INFORMATION

The shape factor for an assembly is defined as the ratio of the spherical critical mass of a system with similar core composition and reflector parameters to the critical mass of a given assembly. Figure 7-3 shows the shape factors determined for cylindrical assemblies with various core height-to-diameter ratios (L/D). The shape factors for ZPR-III assemblies (Table 7-16) having critical masses between 130 kg and 220 kg U^{235}, correspond very closely to the shape factors for high-density and highly enriched uranium cores reflected with natural uranium (2.8 cm thick).

The experimental shape factor data (Fig. 7-3) were obtained on systems with a core volume less than 100 liters. Since fast power reactor design usually requires larger core volumes, two-dimensional diffusion theory shape factor analyses for the latter types of systems were carried out for two distinct cases:[88]

(1) A relatively high-density uranium core and thick reflector (similar to ZPR-III assemblies No. 24 and No. 25) with a core volume of less than 600 liters and critical mass of about 600 kg U^{235} in optimum geometry.

(2) A relatively low-density system with core volumes of about 900 liters and a critical mass of about 800 kg U^{235} in optimum geometry. The core composition is very similar to that of the EBR-II

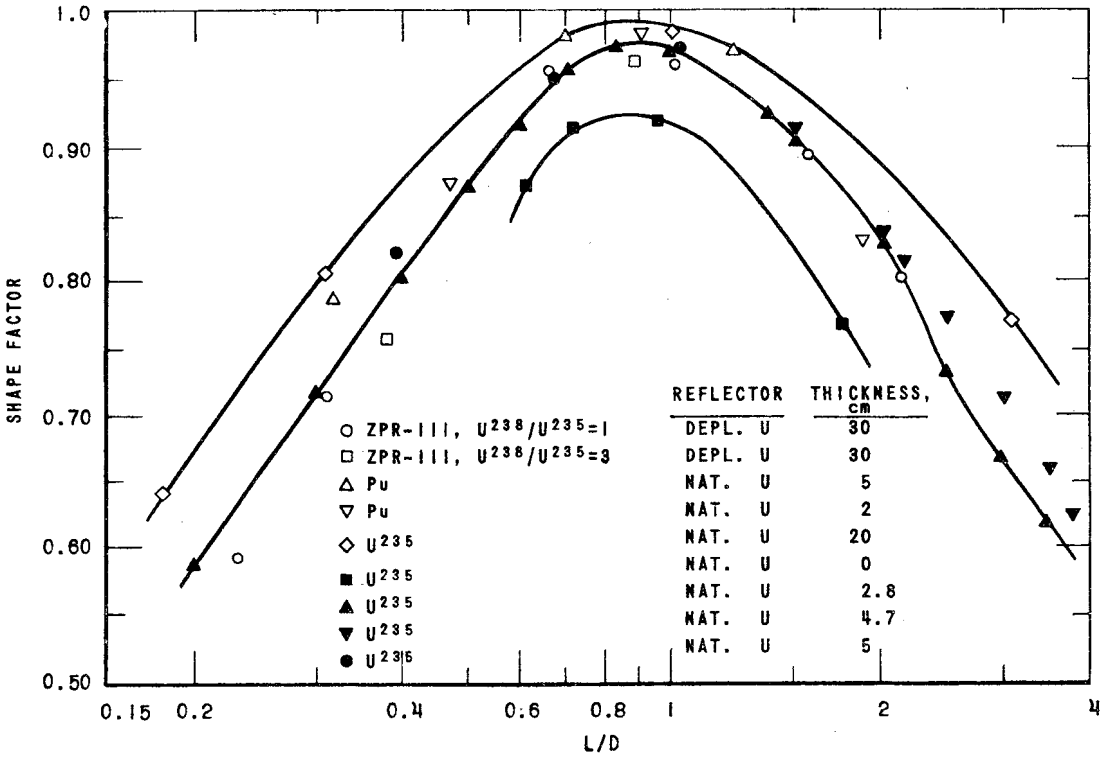

Fig. 7-3 —Shape factor as a function of L/D for various cylindrical assemblies. *Experimental data from Refs. 13, 19, 23, and 25.*

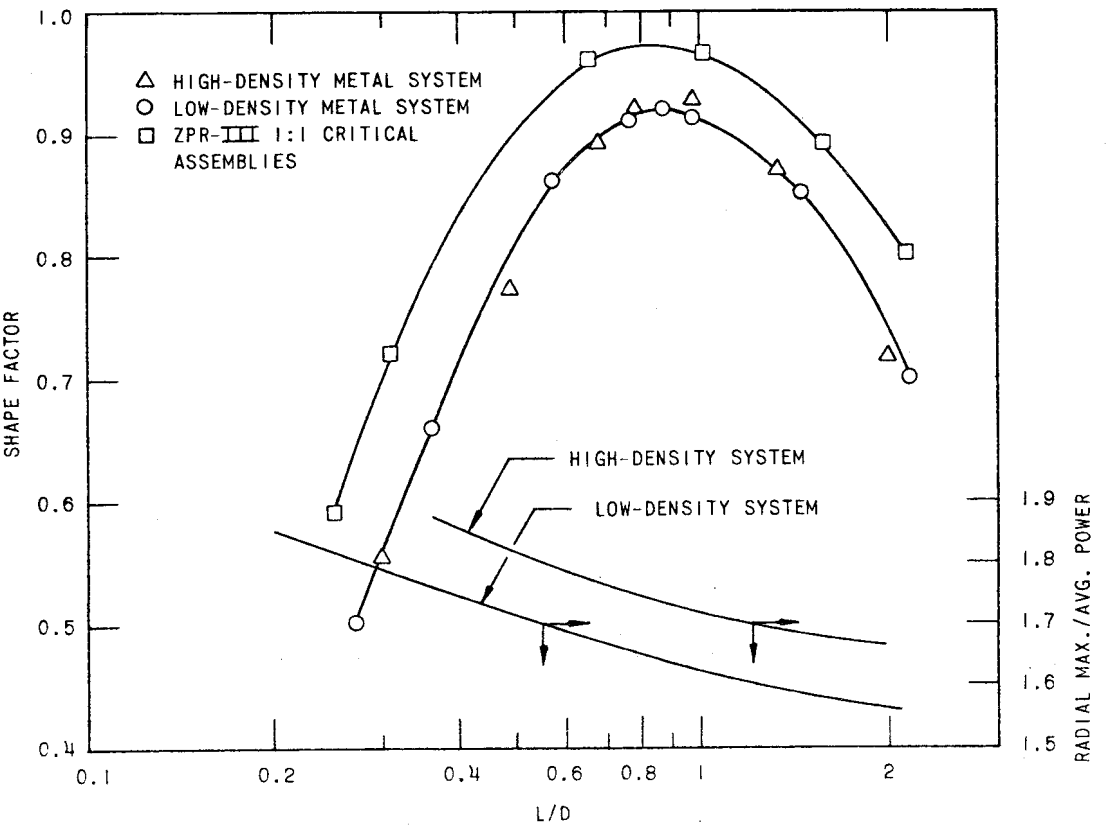

Fig. 7-4 — Predicted shape factors for cylindrical fast neutron systems.

except at a very much lower enrichment of U^{235} in U, and the thick reflector composition is essentially that of the EBR-II radial blanket.

The range of L/D ratios investigated varied from about 0.2 to 2.0. In addition to the shape factor data, other results of interest to reactor design were extracted from the calculations. For both cases, the variation of maximum power density to average core power density as a function of L/D is very small. Similarly, the variation of the ratio of total reflector power (thick reflector) to core power as a function of L/D is very small. However, there is a significant variation of the ratio of maximum power density to average radial core power density (center plane of core) as a function of L/D.

The results of the shape factor calculations are summarized in Fig. 7-4. The experimental data from ZPR-III ($U^{238}/U^{235} = 1$) are superimposed for comparison. The calculated results on the radial maximum to average core power density are also given. Specific data pertinent to the two systems investigated are given in Table 7-26. Table 7-27 summarizes some power distribution data extracted from the calculations.

The information in Section 7.2.1, when used in conjunction with Figs. 7-3 and 7-4, affords an estimate of the critical masses of a large number of systems of varying geometries.

Table 7-26 — SHAPE FACTOR CALCULATIONS: SYSTEM DESCRIPTION

System	L/D Ratio	Critical Mass, kg U^{235}	Region	Composition (Volume Fraction)			
				U^{235}	U^{238}	Fe	Na
High density	0.90	585	Core	0.07	0.74	0.09	0
			Reflector	0.002	0.83	0.07	0
Low density	0.90	725	Core	0.045	0.25	0.20	0.50
			Reflector	0	0.60	0.20	0.20

Table 7-27 — SHAPE FACTOR CALCULATIONS: PERTINENT RESULTS OF POWER DISTRIBUTION, P

System	L/D Ratio	$(P_{max}/P_{avg})^a$ (in core)	$(P_{reflector}/P_{core})$	$(P_{max}/P_{rad\ avg})^b$
High density	0.36	2.21	0.053	1.78
	0.54	2.18	0.045	1.70
	0.72	2.18	0.045	1.67
	1.00	2.17	0.044	1.62
	1.35	2.18	0.044	1.59
	2.02	2.23	0.044	1.57
	Sphere	2.07	0.038	—
Low density	0.20	2.09	0.052	1.75
	0.37	2.00	0.050	1.66
	0.56	1.97	0 046	1.60
	0.74	1.96	0.045	1.56
	0.87	1.95	0.044	1.54
	0.93	1.96	0.044	1.52
	1.39	1.98	0.044	1.49
	2.10	2.02	0.045	1.46
	Sphere	1.85	0.044	—

[a] (P_{avg}) in core $= \int_{core} P(r,z)dv / \int_{core} dv$.

[b] For cylinder, $P_{rad\ avg} = \int_{core} P(r,0)r\,dr / \int_{core} r\,dr$.

7.2.3 EFFECT OF INHOMOGENEITY

In some cases, experimentally observed critical masses given in Section 7.2.1 require corrections if they are to be interpreted as corresponding to homogeneous systems. Experiments were performed to estimate the effect upon reactivity of using finite fuel plate thickness for various ZPR-III assemblies.[13,28] These experiments determined the sensitivity of a system for various degrees of heterogeneity, i.e., bunching of fuel plates. With increased heterogeneity, an increase in reactivity was observed as shown in Table 7-28. The indicated mass correction from the standard configuration to an idealized homogeneous composition is from results of SNG and DSN slab cell calculation for Δk_{eff}.[13,37]

Calculations[37] have been made for a projected large U^{235}-fueled fast assembly having a spherical critical mass of about 1000 kg. A reflector savings of 20 cm was assumed. The average atomic densities of the core (in units of 10^{24} atoms per cm^3) were: $N(U^{235}) = 0.00172$; $N(U^{238}) = 0.00626$; N(Fe) = 0.0207; and N(Al) = 0.0207. All core materials other than those contained in 93 atom-% enriched fuel plates were homogenized as diluent. For the case of an assumed 7.07 cm thickness of diluent between equally spaced 0.32 cm thick fuel plates, the deviation from homogeneous was $1.3 \pm 0.2\%$ k. For the case of one-half as much diluent thickness between equally spaced 0.16 cm thick fuel plates, the deviation was $0.5 \pm 0.1\%$ k.

Reference 37 includes DSN calculations of reactivity changes, flux variations, and detector response variations in heterogeneities caused by various intra-drawer configurations of fuel and diluent, and deviations of reactivities from ideal homogeneous cores.

7.2.4 DETECTOR RATIOS

Currently, there is little experimental information on the characteristic neutron spectra of a fast reactor other than may be inferred from measured detector ratios in such systems. For instance, a measurement of $\sigma_f^{U^{238}}/\sigma_f^{U^{235}}$ makes it possible to estimate the fraction of the neutron flux above the U^{238} fission threshold (~1.4 Mev). Similarly, a measurement of $\sigma_f^{U^{234}}/\sigma_f^{U^{235}}$ can be used to determine the fraction of neutrons above the fission threshold of U^{234} (~0.5 Mev). In addition, $\sigma_c^{U^{238}}/\sigma_f^{U^{235}}$ is important toward determining the conversion ratio of a system fueled with enriched uranium.

Table 7-29 lists the experimentally determined cross section ratios at the core center of some high-density systems. The reported values, particularly for $\sigma_f^{U^{235}}/\sigma_f^{U^{238}}$, represent a variety of experimental techniques. Different methods do not always give the same value for the same quantity. A range for which experimental values have been reported is given along with the most probable measured value.

Table 7-30 summarizes the experimentally obtained cross section ratios for many of the ZPR-III assemblies. Where more than one measurement is reported, the more probable value is given, followed by the less probable value in parentheses.

The data in Tables 7-29 and 7-30 have been extensively studied by comparing them with predictions from multigroup diffusion theory and SNG calculations. In general, it is possible to obtain fair agreement between measured and calculated values. The observed variation in a single central detector ratio as a function of core composition (and reflector composition for small cores) can be estimated semi-quantitatively. However, certain deviations are observed when the required precision of comparison between theory and experiment is narrowed. The predicted values for $\sigma_{n,\gamma}^{U^{238}}/\sigma_f^{U^{235}}$ always appear to exceed the measured values, often by as much as 20%.[5,8]

Calculated U^{238}/U^{235} fission cross section ratios tend to be less than the measured values listed in Table 7-29, whereas calculated U^{238}/U^{235} fission cross section ratios tend to exceed the measured values listed in Table 7-30. A consistent trend is observed in the case of Np^{237}/U^{238}, or U^{234}/U^{235} fission cross section ratios. The former are underestimated whereas the latter are overestimated (by as much as 15%).

It is concluded that calculated neutron spectra tend to be more energetic (harder) than measured spectra. This conclusion is more firmly established when comparisons are made between calculated and measured neutron lifetimes. Measurement is usually based on the Rossi α technique (see Section 7.3.1).

7.2.5 MATERIAL REPLACEMENT EXPERIMENTS

Tables 7-31, 7-32, and 7-33 list material replacement experiments in various fast neutron systems. The experimental data are given in either cents/mole, or inhours/kilogram. A cent is $1/100$ of a

Table 7-28—EFFECT OF CORE HETEROGENEITY ON CRITICAL MASS FOR VARIOUS ZPR-III ASSEMBLIES

Assembly Number	Periodic Configuration of Plates in Drawers of Core[a]	Full Worth at[b] Core Edge, Inhour/kg U^{235}	Reactivity Relative to Reference		Critical Mass Change Relative to Reference, kg U^{235}	Calculated or Estimated Reactivity Deviation from Homogeneous, $\%k_{eff}$	Calculated or Estimated Critical Mass Deviation from Homogeneous, kg U^{235}
			Inhour[c]	$\%k_{eff}$			
2	|AEADAAEADASAEADA|	76	Reference		(C.M. = 136.0)[d]	0.8[d]	−3.9[d]
	|AAAADDDEEEAASAAA|			1.8[d]	−9.2[d]	—	—
2A	|AEASAAEASASAEASA|	69.3	Reference		(C.M. = 147.7)[d]	0.8[d]	−3.8[d]
	|AAAASSSEEEAASAAA|			2.0[d]	−9.9[d]	—	—
14	|CCCCECCCCCCECCCC|	~83	Reference		(C.M. = 136.0)[b]	1.2 ± 0.2[e]	−6[f]
	|CCCCCCCEECCCCCCC|		424	1.35[g]	−5.0[b]	—	—
20[h]	|AZASDEAAADLAMAAD|	51.6 (mean value over core)	Reference		(C.M. ≅ 431.5)[i]	—	−5 to −6[f]
	|AZASDelAAADelAAAAD|		−191	−0.4[g]	3.7[j]	—	—
	|AZASDeEAAADlAAAAD|		349	0.8[g]	−6.8[j]	—	—
	|AZASAADEDAAAMAAD|		83.5	0.2[g]	−1.6[j]	—	—
	|AZASAAPPPAAAMAAD|		−194	−0.4[g]	3.8[j]	—	—
	|AZAPSAAPAAAPMAAD|		−452	−1.0[g]	8.6[j]	—	—
22	|DDDEDDDDDDDDEDDD|	30.9	Reference		(C.M. = 243.7)[k]	0.8 ± 0.2[e]	−14[f]
	|DDDDDDDEEDDDDDDD|		415.3	0.9[g]	−13.4[h]	—	—
	|DeDDDDeDDDDeDDDDeD|		−182	−0.4[g]	5.9[h]	—	—
23	|AAAEAAAAAAAAEAAA|	38.4	Reference		(C.M. = 258.1)[k]	1.1 ± 0.3[e]	−13[f]
	|AAAAAAAEEAAAAAAA|		468.6	1.1[g]	−12.2[j]	—	—
	|AeAAAAeAAAAeAAAAeA|		−160	−0.4[g]	+4.2[j]	—	—
24	|DDEDDDDDDDDDDEDD|	10.3	Reference		(C.M. = 460.7)[k]	—	—
	|DDDDDDDEDDDDDDDD|						
	|DEDDDDDDDDDEDDDD|						
	|DDDDEDDDDDDDDEDD|						
	|DDDDDDDDEDDDDDDD|						
	|DDDDDDDDDDDDDDDD|						
	|DEEDDDDDDDDDDDDD|						
	|DDDDDEEDDDDDDDDD|		399		−38.7[j]	—	—
	|DDDDDDDDEEDDDDDD|						
	|DDDDDDDDDDDDDEED|						

[a]Order of plates in a core drawer. Capital letters denote 0.32 cm thick regions, and small letters denote 0.16 cm thick regions. Key to order of pieces: E—93% enriched U^{235} D—Depleted U A—63% density aluminum (perforated) C—Graphite M—Molybdenum P—31% enriched U^{235} S—Stainless steel 304 L—Aluminum (non-perforated) Z—Zirconium

[b]Worth of core material at radial edge of core expressed as inhours per kilogram of contained U^{235}, experimentally obtained by ZPR-III Experimental Group (Ref. 28).

[c]Experimental inhour values obtained by ZPR-III Experimental Group or extrapolated from such values (Ref. 28).

[d]Ref. 13.

[e]Ref. 37.

[f]Unpublished data, D. Meneghetti, ANL.

[g]Significant figures in $\%k_{eff}$ based on the possible estimated uncertainty range in calculated values of inhours/percent.

[h]Composition and geometry in Fig. 7-2 (all other assemblies described in Table 7-14).

[i]Ref. 28.

[j]Obtained from experimental reactivity and experimental fuel worth measurements of Ref. 28.

[k]Ref. 29.

Table 7-29—MEASURED DETECTOR RATIOS AT CORE CENTER: HIGH-DENSITY URANIUM AND PLUTONIUM SYSTEMS

Assembly	$\sigma_f^{U^{235}}/\sigma_f^{U^{238}}$	$\sigma_f^{Np^{237}}/\sigma_f^{U^{238}}$	$\sigma_f^{Pu^{239}}/\sigma_f^{U^{235}}$	$\sigma_f^{U^{234}}/\sigma_f^{U^{235}}$	$\sigma_f^{U^{233}}/\sigma_f^{U^{235}}$	$\sigma_{n,\gamma}^{U^{238}}/\sigma_f^{U^{238}}$	Ref.
Jezebel	5.0(4.6,5.1)	4.6	—	—	—	—	18
Popsy	5.7	—	1.41	—	—	0.449	18
Godiva	6.17–6.54	5.1	1.43	0.823	1.67	0.458	10
Topsy	7.3(6.6,6.8)	5.2	1.44	0.754	1.63	0.529	10
Jemima (53)	8.7–9.6	5.3	—	—	—	0.816	10
Jemima (37)	10.1–10.9	5.9	—				10
Jemima (29)	12.9–13.7	—	—				10
Jemima (16)	18.2(17.0,20.4)	6.3, 7.1	—				10
Jemima (09)	28–30	—	1.26				38
Jemima (06)	36	—	—				38
Jemima (05)	42–44	—	1.23				38
Jemima (04)	47–48	—	1.11				38
Natural Uranium	243	14.5	1.14				38,39,40
Uranium Hydride	~20	—	—				24

Table 7-30—MEASURED DETECTOR RATIOS AT CORE CENTER: ZPR-III ASSEMBLIES

Assembly No.	Nominal $N^{U^{238}}/N^{U^{235}}$	$\sigma_f^{U^{235}}/\sigma_f^{U^{235}}$ Fission Counter	$\sigma_f^{U^{238}}/\sigma_f^{U^{235}}$ Radio Chemical	$\sigma_f^{U^{234}}/\sigma_f^{U^{235}}$	$\sigma_f^{Pu^{239}}/\sigma_f^{U^{235}}$	$\sigma_f^{U^{233}}/\sigma_f^{U^{235}}$	$\sigma_f^{Pu^{240}}/\sigma_f^{U^{235}}$	$\sigma_{n,\gamma}^{U^{238}}/\sigma_f^{U^{235}}$	Ref.
6F	1	—	0.069	—	—	—	—	0.084	13
9A	3	0.051	—	0.43	1.30	—	—	—	13
5	1	0.074	0.075	0.56	1.24	—	—	0.087	13
2A	0	0.088	0.088	0.57	1.28	—	—	—	13
13(2)	1	0.071(0.064)	0.077(0.060)	0.44(0.47)	1.22(1.16)	1.53	0.513	0.082(0.06)	13,28
10	5	0.044	0.048	0.33	1.22	1.52	—	0.093	13
22(11)	7	0.036	0.036(.041)	0.293(0.299)	1.16(1.17)	1.53(1.51)	0.333	0.091	13,29
24	9.6	0.0284	0.0282	0.246	1.14	1.44	—	0.092	28,29
25	10.4	0.0292	—	0.253	1.17	—	—	0.092	28,29
16	5	0.041	—	0.297	—	—	—	—	13
12	3.5	0.044	0.046	0.293	1.10	1.46	—	0.100	13
17	2	0.049	0.046	0.298	1.08	1.46	—	0.104	13
14	0.07	0.055	0.060	0.305	1.05	1.45	—	0.109	13
15	3	0.052	0.052	0.356	1.22	1.54	—	0.080	13
23	0.07	0.067 – 0.069	0.079	0.399 – 0.407	1.18	1.48	0.228	0.089	28,29
30	1.5	0.043	—	0.300	1.12	1.49	0.328	—	28
31	1.6	0.044	—	0.335	1.18	1.52	—	—	28
29	2	0.036	—	0.259	1.06	1.47	0.289	0.115	28
20	3	0.038	—	0.30	1.15	1.52	0.332	0.100	28,35
19	1	0.075	0.073	0.433	—	—	—	0.080	16
32	0.07	0.045	—	0.367	1.20	1.51	0.382	—	28
33	0.07	0.047	—	0.370	1.21	1.51	0.400	—	28
34	2.2	0.034	0.04	0.247	1.07	1.45	0.271	0.12	28
36	5	0.041	—	0.312	1.20	1.47	0.335	—	28

dollar, the dollar being the amount of reactivity required to bring a system from delayed to prompt critical. An inhour is the amount of reactivity which will give a stable period of 3600 seconds.

The material replacement data become useful upon conversion of the relative reactivity measurements in terms of reactor period or control mechanism movement, to absolute reactivity. This can be accomplished by assigning a conversion factor, based largely on analysis (see Section 7.3.2), between reactor period and absolute reactivity. Presentation of data in cents/mole or inhours/kilogram, both related to reactor period through the decay constants of the delayed neutron groups, then requires the definition of the dollar in terms of reactivity. Most of the systems cited in Tables 7-31, 7-32, and 7-33 have a significant number of U^{238} fissions. Since the delayed neutron fraction of U^{238} is greater than that of either U^{235} or Pu^{239}, the specification of this conversion factor, depending also on the importance of delayed versus prompt neutrons, becomes a complex analytical problem. Such values have been obtained for the various systems and are given at the bottom of the Tables 7-31, 7-32, and 7-33.

Table 7-31 lists experimental material replacement data for Jezebel, Godiva, and four Topsy assemblies. Two Topsys have high-density, highly enriched uranium cores with either a nickel or uranium reflector. The other two Topsys are fueled with highly enriched uranium hydride. These results are only a fraction of the data reported.[24,41] Values given are those measured near the center and the boundary of the core in the various systems.

Table 7-32 summarizes material replacement experiments at the core center of the various ZPR-III assemblies.

Table 7-33 summarizes a variety of material replacement experiments performed on mock-ups of the EBR-II, Fermi (EFFBR), and other systems, installed in the ZPR-III facility. Such reactivity effects vary, to some extent, with the nature of each substitution. In general, these variations in reactivity introduce uncertainties ranging from 5 to 15%. In the most extreme case observed, the substitution of a sodium sample near the center of ZPR-III-8 gave 25 or 40 inhours/kilogram, depending on whether the surrounding coolant volume was made up of low-density aluminum or sodium respectively. The phenomena associated with these substitutions are not completely understood.

7.2.6 BUCKLING OF BARE SYSTEMS FOR MIXTURES OF FISSILE AND FERTILE MATERIALS, AND DIFFUSION LENGTH IN NATURAL URANIUM

Multigroup constants from Table 7-3 were used to calculate the bucklings of U^{235}-U^{238}, Pu^{239}-U^{238}, U^{233}-Th, Pu^{239}-Th, and Pu^{239}-Pu^{240} mixtures. The results are given in Figs. 7-5 and 7-6 as a function of enrichment of the fissionable material in the mixture.

The bucklings for U^{235}-U^{238} mixtures (Fig. 7-5) were obtained by using two sets of multigroup constants. The first of these calculations, "consistent with natural uranium exponential experiments", utilized the 10-group constants of Refs. 14 and 42. The other calculations utilized the 11-group constants in Table 7-3.

The calculated multigroup fluxes were used to obtain pertinent cross section ratios as a function of mixture composition. These spectral results, along with some experimental data for U^{235}-U^{238} mixtures, are plotted in Figs. 7-7 and 7-8. The experimental data were obtained from Godiva and the Jemima assemblies.[10]

Asymptotic transport theory was used to obtain the buckling.[43] The convention for the sign of the buckling value is such that the diffusion equation is written:

$$\nabla^2\phi + K^2\phi = 0$$

Thus, $K^2 > 0$ defines a multiplying medium.

For simplicity, $N = 0.048 \times 10^{24}$ atoms/cm^3 was assumed for all materials except thorium ($N = 0.03 \times 10^{24}$). The buckling of less dense systems can be estimated since $K^2 \sim N^2$.

To emphasize the range where $K^2 \approx 0$, it was found useful to have a logarithmic representation; for $K^2 < 0$, $-K^2$ is plotted.

Measurements of average cross sections, etc., in a natural uranium equilibrium spectrum are generally carried out by Snell experiments.[39,44] In addition, the presence of natural uranium blankets in numerous reactor systems has enabled measurements of spectra and detector responses at positions, within the blankets, approaching the equilibrium spectrum.

Snell block experiments consist of measuring the responses of various detectors at positions within a large block of natural uranium. One face of the block is fed by neutrons diffusing from a neu-

Table 7-31—EFFECT OF MATERIAL REPLACEMENT ON REACTIVITY OF VARIOUS FAST ASSEMBLIES
(cents/mole for compounds; gram-atoms for elements)

Data from Refs. 24 and 41.

	Topsy[a]		Topsy[b]		Godiva[c]		Jezebel[d]		Uranium Hydride[e]		Uranium Hydride[f]	
	Near Center	Near Core Boundary	Near Center	Near Core Boundary	Near Center	Near Core Boundary	Near Center	Near Core Boundary	Near Center	Near Core Boundary	Near Center	Near Core Boundary
H	—	—	—	—	—	—	—	—	29.5	4	34	7
Be	8.8	12.6	—	—	6.7	9.4	13.1	67.1	7.5	4	9	5
BeO	10.7	23.0	—	—	—	—	5.25	134.0	—	—	—	—
B	−9.6	4.7	−6.7	—	−6.3	7.9	—	—	46	−4	−52.5	−9
C	−2.9	11.5	5.4	13.9	2.2	9.7	−5.8	68.0	3.5	4	3.5	4.5
CH_2	125.0	65.0	—	—	88.6	24.5	100.7	151.1	—	—	—	—
CD_2	46.3	—	—	—	—	—	−14.7	183.7	—	—	—	—
CF_2	11.9	39.7	—	—	—	—	−36.8	—	—	—	—	—
Mg	2.1	—	—	—	—	—	—	—	7.5	4	9	6
MgF_2	14.2	39.5	—	—	—	—	—	—	—	—	—	—
Al	1.4	10.8	4.0	13.6	0.4	8.1[g]	−11.9	71.3	2	2.5	3.5	4
O	—	—	—	—	—	—	—	—	4	4	3	4
Al_2O_3	9.3	—	—	—	—	—	—	—	—	—	—	—
S	−7.2	6.9	—	—	—	—	−59.0	—	−1.0	1	−0.5	1
Ca	−5.0	—	—	—	—	—	—	—	—	—	—	—
Ti	−0.7	10.6	—	—	—	—	−21.8	73.5	2.5	6	5.5	5.5
V	1.2	14.8	—	—	—	—	−13.0	87.8	2.5	8	3.5	6.5
Cr	−0.5	11.8	—	—	—	—	—	—	2.5	4	—	—
Fe	−0.45	10.8	2.5	14.7	−0.1	9.0[g]	−18.1	73.5	2	4.5	3.5	4
Mn	0.2	13.1	—	—	—	—	—	—	−1.5	6.5	−1.5	4.5
Co	−1.2	12.7	—	—	−0.5	11.1	−20.6	79.7	−7.5	4	−6.5	3
Ni	−4.38	10.4	−1.9	11.9	−4.0	9.6[g]	−40.2	78.0	−0.5	6	1.0	4.5
Cu	−1.67	11.8	1.7	15.9	−1.6	10.5[g]	−27.5	83.9	1.5	4	2.5	5
Zn	−2.88	12.7	—	—	−2.3	11.6[g]	−33.9	84.8	3	5	2.5	5
Ga	−2.3	13.0	3.7	18.1	—	—	—	—	—	—	—	—
Ge	−2.7	—	—	—	—	—	—	—	2.5	—	—	—
As	0.0	19.2	—	—	—	—	—	—	−10	4	−7.5	3
Zr	−0.6	19.0	—	—	—	—	−30.0	133.7	11	—	—	—
Nb	−5.1	16.4	—	—	—	—	—	—	−4	5	−2.5	4
Mo	−1.5	20.6	—	—	—	—	−37.0	115.3	−2	6	−0.5	7
Rh	−10.9	11.4	—	—	—	—	—	—	−30.5	1	—	—
Pd	−7.8	13.2	—	—	—	—	—	—	−15.5	3	−13.5	1.5
Te	—	—	—	—	—	—	—	—	−4	3	−3.5	2
Ag	−14.9	9.4	—	—	−9.2	13.7	−78.2	95.4	−38	−0.5	−39	−4.5
Cd	−6.9	13.8	—	—	—	—	−55.0	108.3	−14.5	2.5	−13	2.5
In	−21.0	7.2	—	—	—	—	—	—	−41	−1	−43.5	−7
Sn	−2.5	15.6	—	—	—	—	−36.6	108.0	−0.5	4	1.5	6
Sb	−11.3	12.0	—	—	—	—	—	—	−24.5	−0.5	−24.5	−2.5
I	−10.3	—	—	—	—	—	—	—	−41	1	—	—
La	~0.0	—	—	—	—	—	−30.5	101.5[h]	—	—	—	—
Ce	−2.5	—	—	—	—	—	−28.2	118.7[h]	25.5	12	—	—
Nd	−6.0	—	—	—	—	—	—	—	2.5	—	—	—

Ta	−13.6	12.9	—	—	—	—	−84.1	121.1	−53	−1.5	−53	−7
Tl	—	—	—	—	—	—	—	—	−1	6	−3.5	5
W	−7.7	18.0	—	—	−3.6	—	−60.9	129.1	−17	4	−17.5	2.5
Ir	−16.9	—	—	—	—	—	—	—	—	—	—	—
Pt	−7.8	16.9	—	—	—	—	—	—	−19	4	−16	2.5
Au	−12.4	13.5	−2.9	21.0	−6.7	17.8	−73.0	125.9	−31.5	1.5	−31	−1
Pb	0.4	21.2	—	—	—	—	—	—	3	8	5.5	9
Bi	−1.7	22.6	5.1	26.2	−1.5	19.8	−19.7	147.1	5.5	7.5	6	9
Th	−4.8	20.2	5.1	27.2	−1.2	20.0[g]	−54.4	149.1	—	—	—	—
Nat. U	24.5	30.1	33.1	35.1	21.9	22.6 (21.2)[g]	94.4	172.1	9	7.5	13.5	7.5
Enriched U												
(93.4%)	—	—	—	—	—	—	676.9	251.6	—	—	—	—
(95.4%)	184.6	105.6	186.3	85.8	135.5[i]	33.2 (30.6)[g]	—	—	—	—	—	—
(92%)	—	—	—	—	—	—	—	—	91.5	39	103.5	33
U-233												
(98.2%)	328.1	172.1	320.7	132.4	—	—	1227.0	642.7[h]	—	—	—	—
Np-237	160.0	—	—	—	—	—	699.0	—	—	—	—	—
Pu-239												
(98.5%)	377.1	187.9	371.9	144.3	279.6	42.6[g]	—	—	—	—	—	—
(94%)	—	—	—	—	—	—	—	—	169.5	63	187	53
(95.3%)	—	—	—	—	—	—	1438.7	675.8	—	—	—	—
Pu-240	268.0	—	—	—	168.0	—	—	—	—	—	—	—
Li_2SO_4	−0.5	—	—	—	—	—	—	—	—	—	—	—
$Li_2^6SO_4$ (89.42%)	−99.6	—	—	—	—	—	—	—	—	—	—	—
B^{10} (85%)	—	—	−58.7	—	−42.1	6.6 (6.2)[g]	−199.2	—	—	—	—	—
Si	—	—	—	—	—	—	−13.7	72.7	2.5	3.5	2.5	2.5
SiO_2	—	—	—	—	—	—	−31.3	211.8	—	—	—	—
WC	—	—	—	—	—	—	—	—	−19	7.5	−17	5
TiN	—	—	—	—	—	—	−21.8	73.5	—	—	—	—
Dy_2O_3	—	—	—	—	—	—	−175.0	—	—	—	—	—
Ho_2O_3	—	—	—	—	—	—	−282.1	440.4[h]	—	—	—	—
Yb_2O_3	—	—	—	—	—	—	−156.5	—	—	—	—	—
β_{eff}	0.0072		0.0066		0.0066		0.0019		0.0068		0.0068	

[a] Enriched uranium in thick natural uranium reflector (core radius = 6.05 cm). Central measurements at r = 1.12 cm. Some measurements at r = 1.30 cm. Boundary measurements at r = 5.21 cm. Some measurements at r = 5.18 and 5.23 cm.

[b] Enriched uranium in thick Ni reflector (core radius = 6.48 cm). Central measurements at r = 2.1 cm. Boundary measurements at r = 6.07 cm.

[c] Bare enriched uranium core (radius = 8.74 cm). Central measurements at r = 0.076 cm. Boundary measurements at r = 7.98 cm.

[d] Bare Pu core (radius = 6.30 cm). Central measurements at r = 0. Boundary measurements at r = 5.79 cm.

[e] Natural uranium reflector (central and boundary measurements at 2.03 and 8.51 cm, respectively; core radius = 7.77 cm).

[f] Nickel reflector (central and boundary measurements at 2.03 and 8.51 cm, respectively; core radius = 7.80 cm).

[g] r = 8.14 cm.

[h] r = 4.52 cm.

[i] 93.7%.

Table 7-32—EFFECT OF MATERIAL REPLACEMENT AT CENTER OF DILUTE ZPR-III FAST NEUTRON SYSTEMS (inhours/kilogram)

Data from Refs. 13, 28, and 29.

Material	Assembly[a]										
	7[b]	1B[c]	13[c]	2[c]	2A[d]	2B[d]	5[d]	8[c] (EBR-II)	9[c]	9A[c]	11[c]
Li	—	—	—	—	—	—	−141	—	—	—	—
Be	—	—	—	231	—	—	—	—	—	—	—
B^{10}	—	−3540[e]	−2840[f]	—	—	—	—	—	—	−3060[f]	−2760[f]
C	—	—	—	—	138	106	85.5	—	—	—	33.1
Al	—	—	4.0	—	—	—	—	2.1	—	−11.4	—
Na	—	—	—	—	—	—	52.9	—	—	—	—
Si	—	—	—	—	—	—	8.5	—	—	—	—
S	—	—	—	—	—	—	−32.2	—	—	—	—
K	—	—	—	—	—	—	41.1	—	—	—	—
Ca	—	—	—	—	—	—	66.9	—	—	—	—
Ti	—	—	—	—	—	—	2.2	—	—	—	—
V	—	—	—	—	—	—	8.4	12.1	—	—	—
Cr	—	—	—	—	—	—	−6.3	—	—	—	—
Mn	—	—	—	—	—	—	3.9	—	—	−5.0	—
SST	—	—	−7.1	−9.4[g]	−2.5	—	−7.2[c]	−5.4	—	−12.8	−15.4
Fe	—	—	—	—	—	—	−8.0	—	—	−12.7	—
Inconel X	—	—	—	—	—	—	—	—	—	—	—
Co	—	—	—	—	—	—	1.8	—	—	—	—
Ni	—	—	—	—	−4.4	−13.1	—	—	—	—	—
Cu	—	—	—	—	−0.35	−12.0	—	—	—	−16.8	—
Zn	—	—	—	—	−2.0	−11.8	—	—	—	—	—
As	—	—	—	—	—	—	−29.8	—	—	—	—
Se	—	—	—	—	—	—	−3.6	—	—	—	—
Y	—	—	—	—	—	—	—	—	—	—	—
Zr	—	—	—	—	6.1	−1.3	—	—	—	—	—
Nb(Cb)	—	—	—	—	—	—	−27.8	−21.6	—	—	−35.7
Mo	—	—	−15.6	—	—	—	−17.6	—	—	−23.4	−24.3
Ru	—	—	—	—	—	—	−35.1	—	—	—	−48.7
Pd	—	—	—	—	—	—	−57.7	—	—	—	—
Ag	—	—	−76.8	—	−64.3[h]	−76.2	—	—	—	−89.4	—
Cd	—	—	—	—	−22.6	−33.8	−30.4	—	—	—	—
In	—	−79	—	—	—	—	—	—	−94.8	—	—
Sn	—	—	—	—	−6.8	−11.7	—	—	—	—	—
Sb	—	—	—	—	—	—	−35.5	—	—	—	—
Te	—	—	—	—	—	—	−11.9	—	—	—	—
I	—	—	—	—	—	—	−43.0	—	—	—	—
Ba	—	—	—	—	—	—	15.2	—	—	—	—
Ce	—	—	—	—	—	—	−1.9	—	—	—	—
Hf	—	—	—	—	—	—	−34.3	—	—	—	—
Ta	—	—	−43	—	—	—	−39.5	—	—	—	−49.4
W	—	—	—	—	—	—	−17.9	—	—	—	—
Hg	—	—	—	—	—	—	−9.0	—	—	—	—
Pb	—	—	—	−2.0[g]	1.6	—	—	—	—	—	—
Bi	—	—	—	—	1.0	−1.4	—	—	—	—	—
Th	—	—	—	—	−12.2	−22.4	—	—	—	—	—
U^{233}	—	—	519	—	—	—	—	504	—	—	507
Enriched U	864	—	—	—	—	—	—	—	—	—	—
(93.2%)	812	264	251	—	229[i]	257[i]	258[i]	257	—	—	254
Pu (~95% Pu^{239})		498	502	—	446[i]	494[i]	498[i]	497	—	—	459
Depleted U[j]	—	—	—	2.4[g]	8.0	—	2.6 (3.6[h])	— 3.2	—	—	—
B_4C	—	—	—	−2450[k]	—	—	−430[h]	—	—	—	—
CH_2	—	—	—	—	—	—	3060[l]	—	—	—	—
Al_2O_3	—	—	—	—	—	—	—	28.2	—	—	—
Physicum I[m]	—	—	—	—	—	—	—	−7.0	—	—	—
Physicum II[m]	—	—	—	—	—	—	—	−12.4	—	—	—
β_{eff}	0.0068	0.0074	0.0074	0.0074	0.0073	0.0074	0.0074	0.0074	0.0073	0.0074	0.0073
Inhours/%Δk	437	430	430	430	410	430	415	415	436	440	470

[a] Reactor compositions and sizes may be obtained from Tables 7-14, 7-15, 7-16, and Figs. 7-1 and 7-2. Over-all core compositions of assemblies: 1B, 2, 2B, 13, and 6F are essentially identical; 9 and 9A are essentially identical; 11 and 22 are essentially identical.

[b] EBR-I Mock-up, Ref. 13.

[c] Relative to void except as noted.

[d] Relative to 56% Al (192 gm Al) except as noted.

[e] 84.6% B^{10}.

[f] 94% B (92% enriched in B^{10}).

[g] Relative to 56% Al.

[h] Relative to 96 gm Al.

[i] Relative to void.

[j] ~0.22% U^{235}.

[k] ~87% enriched in B^{10}.

[l] Relative to 45 gm Al.

[m] Fission product mock-up, Ref. 13.

Table 7-32 — EFFECT OF MATERIAL REPLACEMENT AT CENTER OF DILUTE ZPR-III FAST NEUTRON SYSTEMS (inhours/kilogram) (Continued)

Data from Refs. 13, 28, and 29.

Material	Assembly[a]														
	22[c]	16[c]	12[c]	14[c]	20[c] (Fermi)	23[c]	24[c]	25[c]	29[c]	30[c]	31[c]	32[c]	33[c]	34[c]	36[c]
Li	—	—	—	—	—	—	—	—	—	—	—	—	—	−81.4	—
Be	−18.3	—	—	—	34.5	149	−48.6	—	—	—	—	—	—	84.8	38.4
B^{10}	—	—	−4160[f]	—	−1800[f]	—	—	—	—	—	—	—	—	—	—
C	−31	4.1	34.6	143.8	6.6	65.5	35.6	−37.2	39.5	43.0	36.4	173	143	36.5	0.51
Al	−16.8	—	−7.1	—	−4.0	2.6	−12.5	−12.8	3.0	1.7	1.0	31.5	23.5	0.93	−13.1
Na	—	—	—	—	—	—	—	—	17.7	12.0	12.1	—	40.5	7.14	16.5
Si	—	—	—	—	—	—	—	—	—	—	—	—		—	—
S	—	—	—	—	—	—	−18.7	—	—	—	—	—	−1.8	—	—
K	—	—	—	—	—	—	—	—	—	—	—	—	—	—	—
Ca	—	—	—	—	—	—	—	—	—	—	—	—	—	—	—
Ti	—	—	—	—	—	—	—	—	—	—	—	—	—	—	—
V	—	—	—	—	—	—	−8.3	—	—	—	—	—	—	—	—
Cr	—	—	—	—	—	—	—	—	—	—	—	—	4.35	−0.60	—
Mn	—	—	—	—	—	—	—	—	—	—	—	—	—	—	—
SST	−14.7	—	−11.2	—	−4.1	0.3	−8.5	−8.1	−1.3	−2.0	−0.54	1.6	1.08	−1.45	−22.1
Fe	—	—	—	—	—	—	—	−6.5	—	—	—	—	−0.24	−1.3	—
Inconel X	—	—	—	—	−5.0	—	—	—	—	—	—	—	—	—	—
Co	—	—	—	—	—	—	—	—	—	—	—	—	—	—	—
Ni	—	—	−19.3	—	—	—	—	—	—	—	—	—	1.35	−2.75	
Cu	—	—	—	—	—	—	—	—	—	—	—	—	—	—	—
Zn	—	—	—	—	—	—	—	—	—	—	—	—	—	—	—
As	—	—	—	—	—	—	—	—	—	—	—	—	—	—	—
Se	—	—	—	—	—	—	—	—	—	—	—	—	—	—	—
Y	−11.4	—	—	—	—	4.0	−7.2	—	—	—	—	—	—	−14.9	−7.47
Zr	−13.1	—	—	—	−3.7	3.2	−7.6	−7.3	—	—	—	7.4	—	−1.21	−7.92
Nb(Cb)	—	—	−45.5	—	—	—	−20.4	−16.2	—	—	—	—	−11.6	−16.0	−28.7
Mo	—	—	−30.5	—	−10.8	—	−15.8	−13.0	—	—	—	—	−6.0	−9.45	−20.8
Ru	—	—	−66.7	—	—	—	−32.7	—	—	—	—	—	—	—	—
Pd	—	—	—	—	—	—	—	—	—	—	—	—	—	—	—
Ag	−73.9	—	—	—	—	−42.0	−47.3	−39.4	—	—	—	—	—	−44.0	−68.5
Cd	—	—	—	—	—	—	—	—	—	—	—	—	—	—	—
In	—	—	—	—	—	—	—	—	—	—	—	—	—	—	—
Sn	—	—	—	—	—	—	−10.2	—	—	—	—	—	—	—	—
Sb	—	—	—	—	—	—	—	—	—	—	—	—	—	—	—
Te	—	—	—	—	—	—	—	—	—	—	—	—	—	—	—
I	—	—	—	—	—	—	—	—	—	—	—	—	—	—	—
Ba	—	—	—	—	—	—	−23.4	—	—	—	—	—	—	—	—
Ce	—	—	—	—	—	—	—	—	—	—	—	—	—	—	—
Hf	—	—	—	—	—	—	−23.2	—	—	—	—	—	—	—	—
Ta	—	—	−66.8	—	−24.6	−18.6	−32.5	−26.2	—	—	—	—	−30.5	−28.7	−40.1
W	—	—	—	—	—	—	—	—	—	—	—	—	—	—	—
Hg	—	—	—	—	−4.9	—	−7.3	—	—	—	—	—	—	−5.05	—
Pb	—	—	—	—	—	—	−1.8	—	—	—	—	—	1.49	−0.093	−2.14
Bi	−4.5	—	—	—	—	1.6	−2.5	−1.8	—	—	—	—	—	−0.37	−2.15
Th	—	—	—	—	—	—	−15.9	—	—	—	—	—	−14.1	−12.8	−21.6
U^{233}	486	—	548	—	—	283	304	271	244	238	201	412	367	206	432
Enriched U (93.2%)	242	—	269	—	126	144	156	135	121	115	108	213	197	107	241
Pu (~95% Pu^{239})	466	—	480	—	228	275	273	239	206	211	197	405	349	182	384
Depleted U^{j}	−11.7	—	−11.5	—	−5.5	3.7	−7.7	−7.2	−6.5	−2.9	−2.7	−2.3	−0.75	−5.78	−9.2
B_4C	−1870	—	—	—	−1275	−1280	−1148	−989	—	—	—	−218	−1960	−1278	−1737
CH_2	—	—	—	—	—	—	—	—	—	—	—	—	—	—	946
Al_2O_3	—	—	—	—	—	—	−17.7	−17.5	—	—	—	—	92.1	8.02	−7.88
Physicum I[m]	—	—	—	—	−20.4	—	−21.2	−22.2	—	—	—	—	−0.13	−14.1	−22.5
Physicum II[m]	—	—	—	—	—	—	−25.5	−20.6	—	—	—	—	0.0	−12.6	−22.3
β_{eff}	0.0073	—	0.0075	—	0.0069	—	0.0073	0.0072	—	—	—	—	—	—	—
Inhours/%Δk	470	—	427	—	448	—	471	486	—	—	—	—	—	—	—

Table 7-33—REACTIVITY WORTH OF MATERIALS SUBSTITUTED IN VARIOUS CORES[a] (inhours/kilogram)

Data from Refs. 13 and 28.

Material	Distributed Throughout Core of:								Radial Core Boundary of:	
	ZPR-III-8 (EBR-II)	ZPR-III-5	ZPR-III-2	ZPR-III-2A	ZPR-III-13	ZPR-III-20 (Fermi)	ZPR-III-32	ZPR-III-34	ZPR-III-20 (Fermi)	ZPR-III-33
C	—	—	—	—	—	—	—	16.3	—	—
O	79.7	—	—	—	—	10.5	—	—	—	—
Al	~30.0	26 – 32	28 – 29	29.0	23.2	3.8 – 4.0	26.5	4.65	10.3	32.0
Be	—	—	—	—	—	—	—	—	21.2	—
Al_2O_3	54.3	—	—	—	—	—	—	—	—	—
Na	45 – 50	47 – 52	—	—	—	6.7	42.8	—	—	60.4
V	24.6	—	—	—	—	—	—	—	—	—
SST	9.3	10.5	8.7	10.8	—	0.93	6.82	1.66	4.2	7.6
Nb	1.2	—	—	—	—	—	—	—	—	—
Zr	—	—	—	—	—	2.25	—	—	5.1	—
Mo	9.9	—	—	—	—	−1.29	—	—	2.7	—
Ru	−0.83	—	—	—	—	—	—	—	—	—
Rh	−23.1	—	—	—	—	—	—	—	—	—
Pd	−8.4	—	—	—	—	—	—	—	—	—
Ta	—	—	—	—	−18.5	—	—	—	—	—
Physicum I[b]	13.6	—	—	—	—	—	—	—	5.1	—
Physicum II[b]	10.5	—	—	—	—	—	—	—	—	—
B^{10}	—	—	—	—	—	—	—	—	~ −383.0	—
$B_4^{10}C$	—	—	—	—	—	—	—	—	~ −258.0	—
Enriched U	—	—	—	—	—	—	—	44.1	—	—
Depleted U	—	—	—	—	—	—	—	−0.846	—	—

[a]Cores are described in Table 7-14; where determined, β_{eff} is given in Table 7-32.
[b]Fission product mock-ups (Ref. 13).

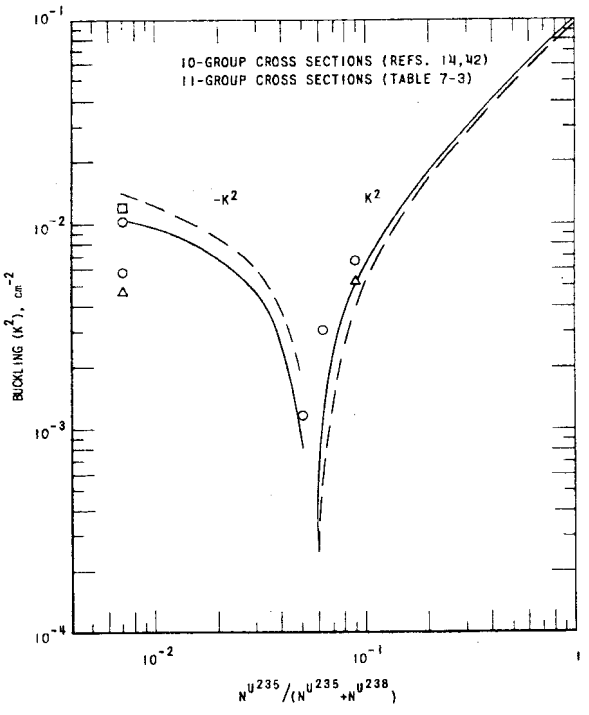

Fig. 7-5 — Buckling for bare U^{235}-U^{238} systems, assuming $N^{U^{235}} + N^{U^{238}} = 0.048 \times 10^{24}$.

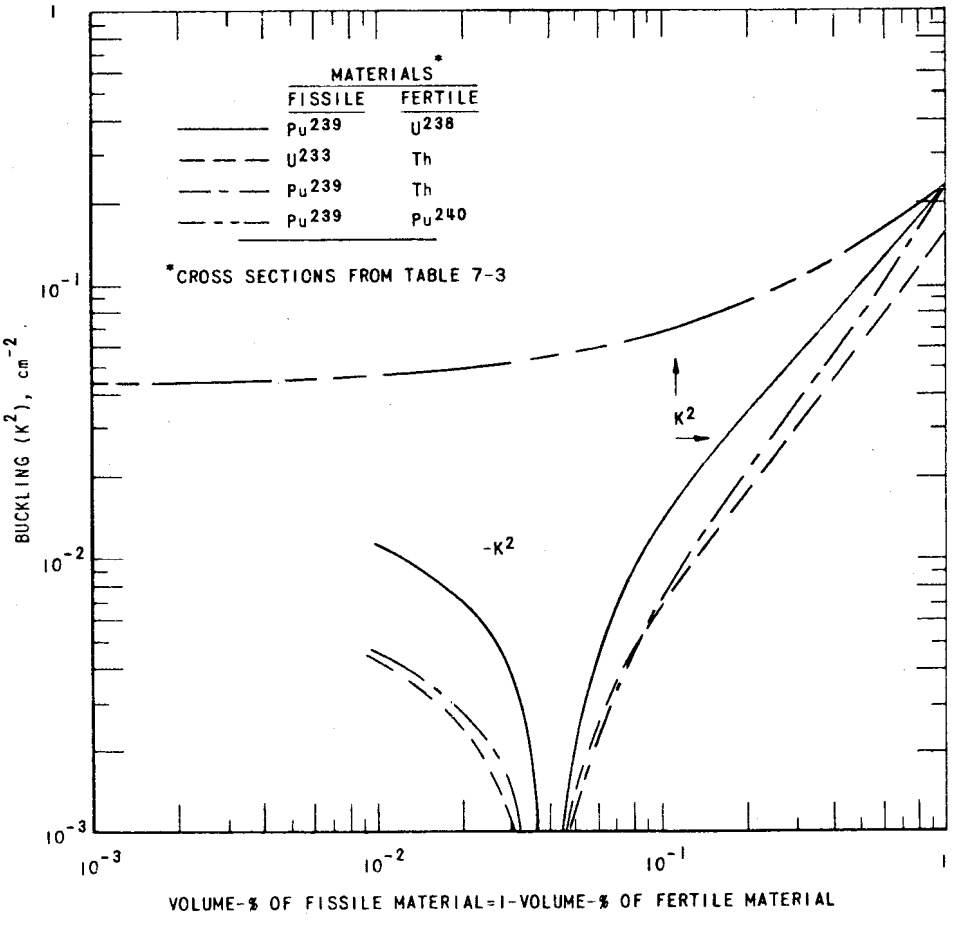

Fig. 7-6 — Buckling for bare systems containing U^{233}, U^{238}, Pu^{239}, Pu^{240}, Th.

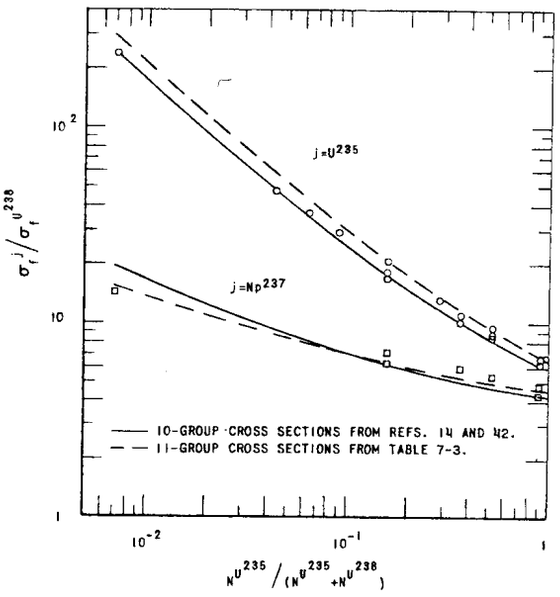

Fig. 7-7— Fission ratios for bare U^{235}-U^{238} systems. *Experimental data from Ref. 10.*

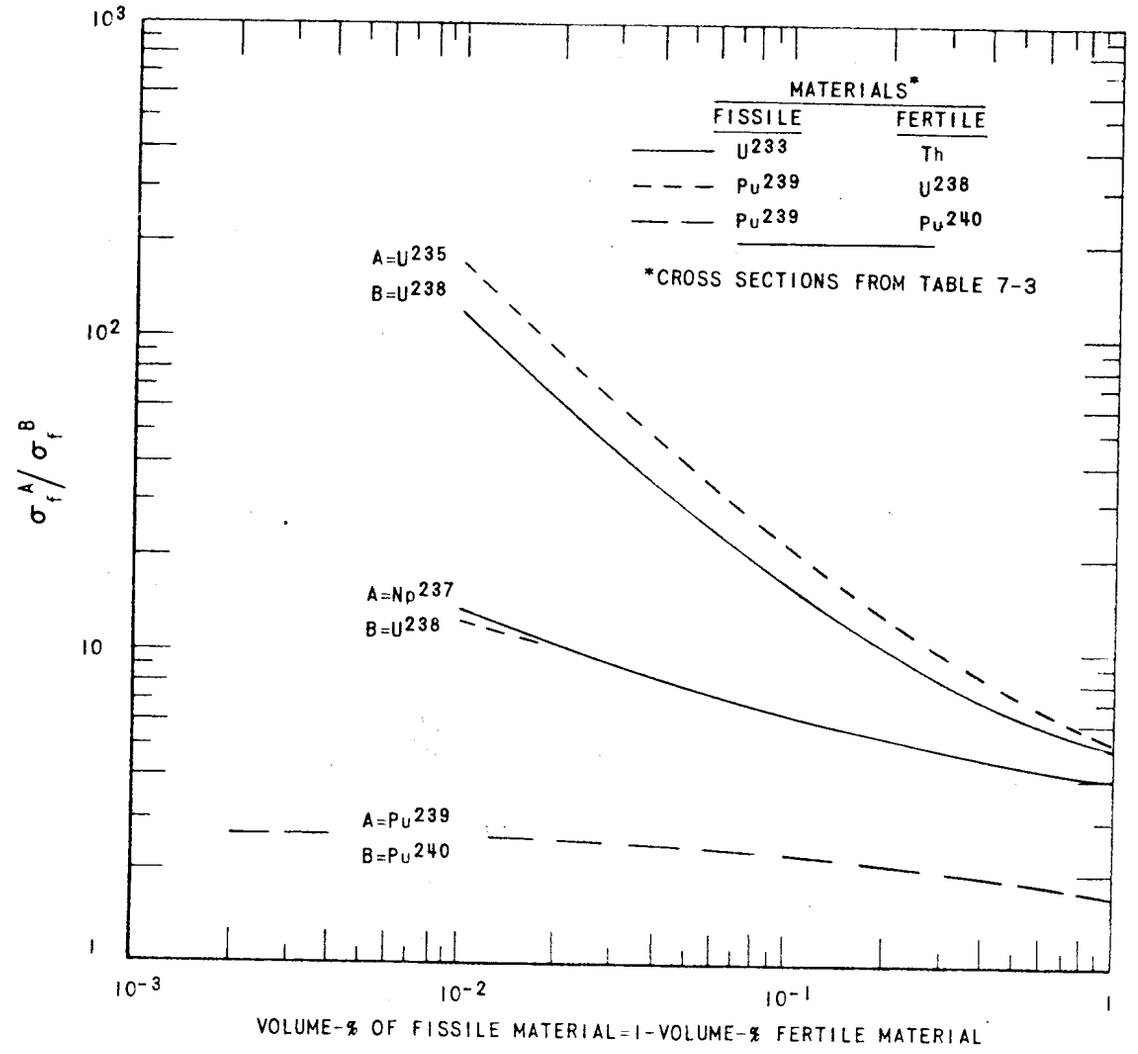

Fig. 7-8 — Fission ratios for bare systems containing U^{233}, U^{238}, Pu^{238}, Pu^{240}, Th. *Experimental data from Ref. 10.*

tron source, i.e., a reactor. The neutrons diffusing into the block cause fission and give rise to a fast neutron source a short distance into the block. Knowledge of the energy responses of the detectors allows an estimate of the equilibrium natural uranium flux spectrum. Measured relative responses of the detectors give an average value of the detector cross sections in an equilibrium spectrum. Traverses of the detectors through regions of the block having an equilibrium spectrum give a measure of the relaxation or "diffusion" length of the equilibrium spectrum neutrons.

Snell experiments are described in a series of ORNL reports.[45] Recently, measurements in depleted uranium have been made in the Soviet Union.[11] Measurements in natural uranium have been made in France, and at Los Alamos.[39]

The various reported values of diffusion length and detector responses, as summarized by Chezem,[39] are listed in Table 7-34.

Table 7-34 — SUMMARY OF URANIUM EQUILIBRIUM SPECTRUM FLUX PARAMETER MEASUREMENTS

Data from Ref. 39.

Experiment	Method of Observation	Diffusion Length, cm	$\bar{\sigma}_f^{U^{235}}/\bar{\sigma}_f^{U^{238}}$	$\bar{\sigma}_f^{Np^{237}}/\bar{\sigma}_f^{U^{238}}$	$\bar{\sigma}_f^{Pu^{239}}/\bar{\sigma}_f^{U^{238}}$	$\bar{\sigma}_{in}^{U^{238}}$
Pajarito (Present)	Foil activation	9.17 ± 0.18	238 ± 6	15 ± 2	—	1.99 ± 0.05
	Radiochemistry	—	240 ± 12	—	—	2.00 ± 0.08
	Fission chambers	—	243 ± 15	14.5 ± 0.1	250 ± 16	2.02 ± 0.09
	Fission chambers[a]	—	241 ± 13	—	—	—
Chicago (Met. Lab.)	Fission chambers	—	200[b]	—	—	—
Oak Ridge	Foil activation	9.6[b]	—	—	—	—
	Fission chambers	—	336[b]	—	—	—
Argonne Fast Exponential	Fission chambers	10.0 ± 0.2	363 ± 40	—	—	—
	Radiochemistry	—	220[c]	—	—	—
Pajarito (Indoors)	Foil activation	13.18[d]	220 ± 22	—	—	—
	Foil activation	10.35[e]	—	—	—	—
	Radiochemistry	—	200 ± 10	—	228 ± 12	—
	Fission chambers	—	210 ± 10	15.9 ± 0.8	—	—
Russian (Depleted U)	Fission chambers	—	249 ± 20[f]	—	230[b,f]	—
Saclay	Foil activation	8.9[b]	—	—	—	—
	Foil activation	10.3[b,g]	—	—	—	—
	Fission chambers	—	221 ± 11[h]	—	—	—

[a] By G. J. Fischer, Argonne National Laboratory.
[b] No uncertainty quoted by experimenters.
[c] Approximate value; uncertainty large.
[d] 15-inch diameter column; no uncertainty quoted.
[e] 21-inch diameter column; no uncertainty quoted.
[f] Derived value.
[g] Considered a perturbed value.
[h] Maximum observation.

7.2.7 EXTRAPOLATION DISTANCES AND REFLECTOR SAVINGS FOR HIGH-DENSITY URANIUM SYSTEMS

Observed reflector savings, δ_r, on 93.5% enriched uranium spheres for various thicknesses of reflectors are given in Table 7-35. These experimental reflector savings are the difference in critical radii between an unreflected and reflected core.

Figure 7-9 shows the correspondence between δ_r(Pu) and δ_r(93.5% enriched uranium) for thin reflectors of identical composition and thickness, for small, high-density, 93.5% enriched uranium and plutonium cores.

687863 O - 63 - 40

Table 7-35—REFLECTOR SAVINGS (δ_r) ON 93.5% ENRICHED URANIUM SPHERES FOR VARIOUS REFLECTOR THICKNESSES (t)

Data from Ref. 10.

Reflector Material	Density, gm/cm^3	Observed Reflector Savings, cm			
		t = ½ in.	1 in.	2 in.	4 in.
U (normal)	18.9	0.81	1.31	1.87	2.40
W-alloy	17.4	0.82	1.29	1.82	2.29
Fe	7.78	0.59	0.92	1.36	1.70
Al	2.70	0.43	0.68	—	—
Be	1.84	0.90	1.46	2.14	2.94

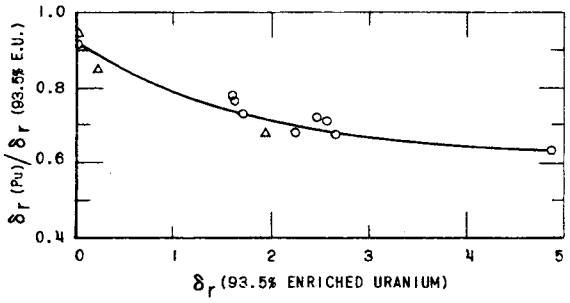

Fig. 7-9—Reflector savings ratio for plutonium and 93.5% enriched uranium critical assemblies having the same reflector material and thickness, plotted against the reflector savings of 93.5% enriched uranium. *Reproduced from Ref. 10.*

"Effective extrapolation lengths" are given in Refs. 11 and 36 for reflected cylinders of 93.5% enriched uranium and of Pu having various height to diameter ratios for various reflectors. (The "effective extrapolation distance" as defined in Ref. 31 is the λ_c which satisfies the relation

$$B^2(\text{sphere}) = \left(\frac{2.405}{\frac{d}{2} + \lambda_c}\right)^2 + \left(\frac{\pi}{h + 2\lambda_c}\right)^2$$

for a cylinder of diameter d and height h, when bare-sphere extrapolation distances are chosen as 2.15 cm for 93.5% enriched uranium, and 2.06 cm for plutonium).

Figure 7-10 shows the calculated extrapolation distances, δ_e, for solid, bare U^{235}-U^{238} cores having various enrichments and calculated reflector savings, δ_r, for analogous cores surrounded by thick,

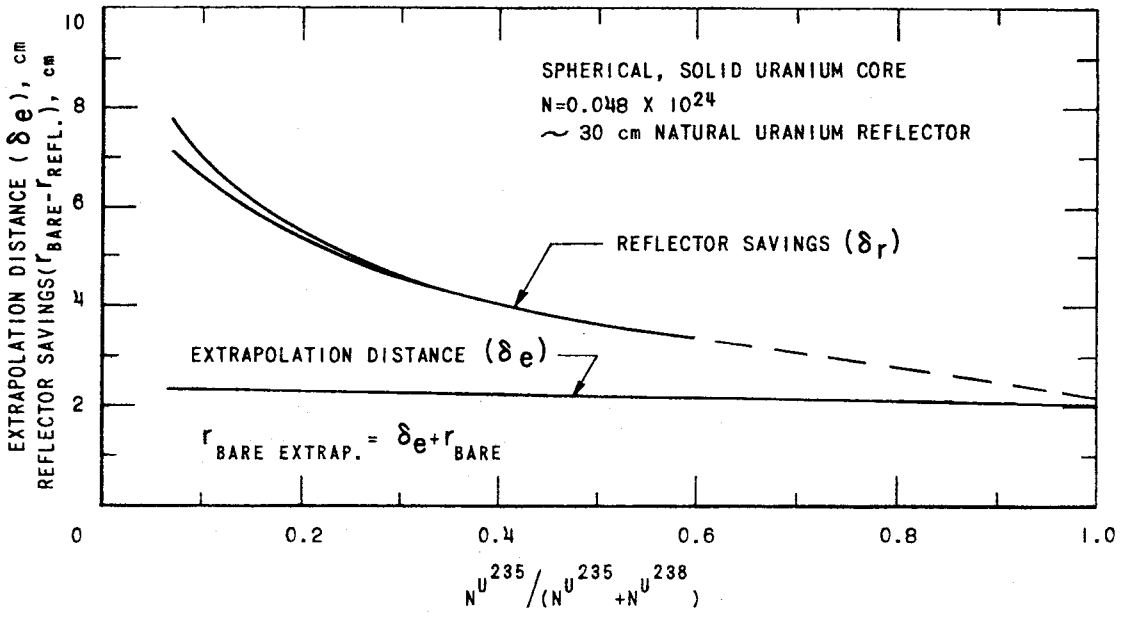

Fig. 7-10—Calculated extrapolation distances and reflector savings for high-density uranium systems.

solid, natural uranium reflectors. The calculated extrapolation distance is here obtained by the defining relation:

$$\delta_e = \frac{\pi}{\kappa^2} - r$$

where r is the critical radius of a spherical bare core of given composition as obtained by the S_4 method, and κ^2 is the material buckling obtained by multigroup fundamental mode analysis employing the transport leakage term. The calculated reflector savings is here defined as the difference between spherical bare and reflected critical dimensions, both obtained by the S_4 method; i.e., bare does not refer here to the extrapolated bare size. The breadth of the reflector savings curve represents the spread of uncertainty resulting from equivalent calculations using various multigroup cross section sets (Refs. 8 and 14).

Calculated extrapolation distances for bare, high-density spherical cores are listed in Table 7-36.

Table 7-36 — CALCULATED EXTRAPOLATION DISTANCES (δ_e) FOR HIGH-DENSITY SYSTEMS OF VARIOUS ENRICHMENTS

Based on cross sections of Refs. 13 and 42.

$N^{U^{235}} + N^{U^{238}} = N^{Pu^{239}} + N^{U^{238}} = 0.048 \times 10^{24}$ atom/cm^3

$N^{Pu^{239}}/(N^{Pu^{239}} + N^{U^{238}})$	δ_e, cm
1.00	1.68
0.80	1.81
0.60	1.95
0.40	2.12
0.20	2.30
0.10	2.38
0.06	2.38
$N^{U^{235}}/(N^{U^{235}} + N^{U^{238}})$	δ_e, cm
1.00	2.065
0.80	2.13
0.60	2.21
0.40	2.29
0.20	2.35
0.12	2.37
0.08	2.35

7.2.8 CALCULATED EXTRAPOLATION DISTANCES AND REFLECTOR SAVINGS FOR SOME DILUTE SYSTEMS

Figure 7-11 shows the calculated bare core extrapolation distance and reflector savings for spherical fast systems with U^{235} fuel and U^{238} fertile material. Figure 7-12 shows similar data for systems with Pu^{239} fuel and U^{238} fertile material. Each system contained 0.5 total volume fraction of fuel and fertile material; Fe and Al represent structural and coolant materials. The calculations were carried out by the S_4 method, using the 11-group fast neutron cross section set in Table 7-3.

Owing to cross section uncertainties, the calculated reflector savings values are only indicative for cores of this size and composition. Extrapolation is unreliable; therefore independent calculations should be undertaken for other core sizes and compositions.

Table 7-37 gives the calculated reflector savings for a series of compositions similar to those investigated on the ZPR-III facility. The results are based on a 10-group set of cross sections and are given for spherical, slab, and cylindrical geometries. In the latter two cases, the system was assumed infinite in the transverse directions.

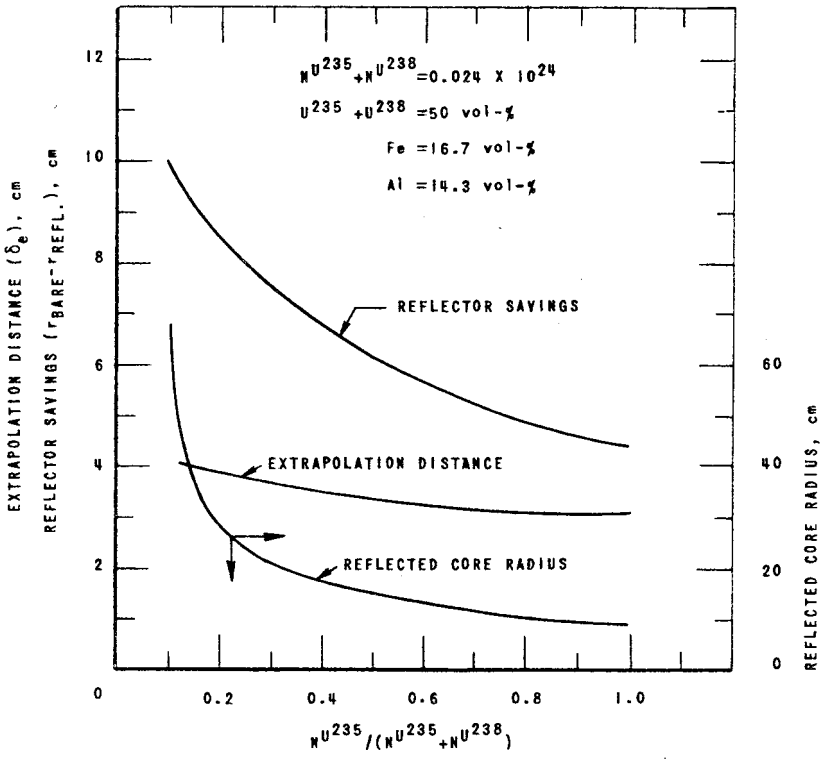

Fig. 7-11— Bare core extrapolation distance and correspondence of reflector savings with reflected core radius calculated for spherical fast systems with U^{235} fuel and U^{238} fertile material. Reflector thickness: ~50 cm; composition (vol-%): 40 U^{238}, 23.2 Al, 20 Fe.

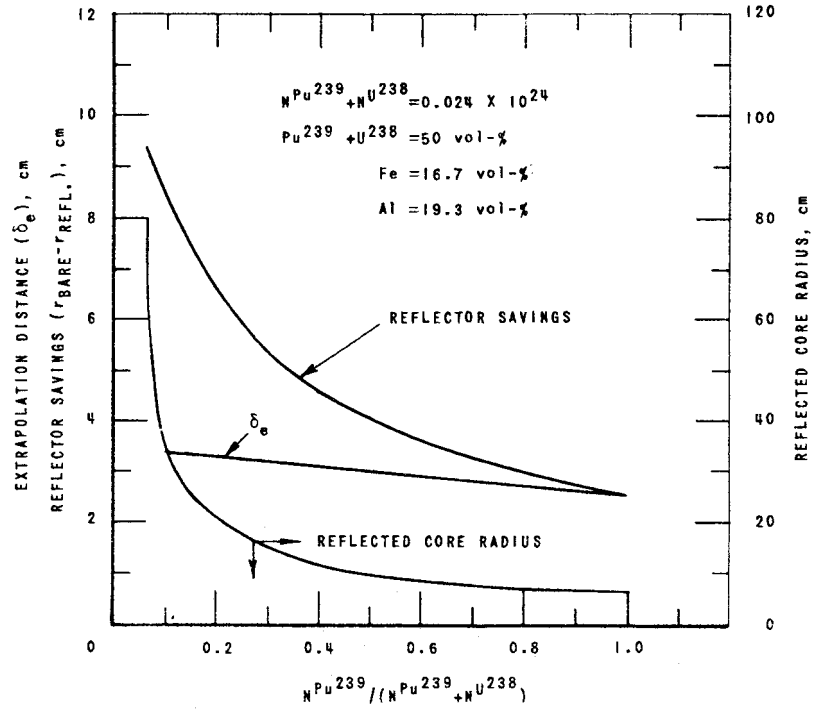

Fig. 7-12— Bare core extrapolation distance and correspondence of reflector savings with reflected core radius calculated for spherical fast systems with Pu^{239} fuel and U^{238} fertile material. Reflector thickness: ~50 cm; composition (vol-%): 40 U^{238}, 23.2 Al, 20 Fe.

Table 7-37—CALCULATED REFLECTOR SAVINGS FOR SMALL DILUTE URANIUM SYSTEMS

Based on cross sections in Table 15, Ref. 13.

Note: Reflector in each system is high-density, depleted uranium (83 vol-%) in a stainless steel matrix (9 vol-%).

Core Composition (Volume Fraction)				Reflector Savings, cm			Critical Dimension of Reflected Core, cm		
U^{235}	U^{238}	Fe	Al	Sphere	Cylinder	Slab	Sphere Radius	Cylinder Radius	Slab Half-Thickness
0.14	0.16	0.12	0.31	11.1	11.0	9.0	21.9	13.9	5.4
0.14	0.01	0.28	0.31	11.2	11.3	9.5	23.1	14.0	5.7
0.12	0.38	0.14	0.22	7.9	8.7	7.7	25.5	16.3	7.6

7.2.9 SPECTRUM-AVERAGED CROSS SECTIONS

Measurements of threshold detector responses, with and without a spherical shell of the specimen material between the neutron source and the detector, permit the determination of effective cross sections averaged over the energy region above the detector threshold. The experimental arrangement consists of a neutron source placed some distance from the shell, and a detector placed at the center of the shell. On the basis of reciprocity arguments, Bethe[46] has shown that this arrangement is equivalent to the one with source and detector interchanged, the latter arrangement being more amenable to analysis.

Average cross sections for fission spectrum neutrons above the fission threshold of U^{238} (~1.4 Mev) are given in Table 7-38; corresponding values for the region above the fission threshold of Np^{237} (~0.5 Mev) are given in Table 7-39. The inelastic cross section includes all processes other than fission for removal from energies above the threshold.

Table 7-38—AVERAGE CROSS SECTIONS FOR FISSION SPECTRUM NEUTRONS ABOVE THE U^{238} FISSION THRESHOLD (in barns)

Data from Refs. 5, 48, and 49.

Element	σ_{in}	σ_{tr}	Element	σ_{in}	σ_{tr}	σ_f
Aluminum	0.319	1.68	Cadmium	1.52	3.11	—
Titanium	0.563	2.47	Tin	1.12	3.00	—
Vanadium	0.575	2.34	Tungsten	2.23	3.82	—
Iron	0.686	2.13	Gold	2.04	3.93	—
Nickel	0.713	2.26	Lead	0.712	3.84	—
Copper	0.900	2.35	Bismuth	0.728	4.05	—
Zinc	0.955	2.32	U^{238}	2.061	4.62	0.555
Zirconium	0.960	3.06	U^{235}	1.58	4.77	1.285
Silver	1.66	3.07	Pu^{239}	0.80	—	—

Leachman and Schmitt[47] have measured the average cross section for fission of U^{238} by neutrons from the fission of U^{235}. The value in terms of ν, the average number of neutrons per thermal fission of U^{235}, was:

$$\bar{\sigma}_f(U^{238}) = (0.756 \pm 0.008)/\nu \text{ barns}$$

Using a value of $\nu = 2.43 \pm 0.02$

$$\bar{\sigma}_f(U^{238}) = 0.311 \pm 0.006$$

Activation cross sections in fission and reactor spectra have been measured for a large number of elements. The data are listed in Table 7-40.

Table 7-39—AVERAGE CROSS SECTIONS FOR FISSION SPECTRUM NEUTRONS ABOVE THE Np^{237} FISSION THRESHOLD (in barns)

Data from Refs. 5, 48, and 49.

Element	σ_{in}	σ_{tr}	Element	σ_{in}	σ_{tr}
Aluminum	0.087	2.07	Silver	0.840	3.42
Titanium	0.187	2.24	Cadmium	0.658	3.50
Vanadium	0.224	2.35	Tin	0.369	3.51
Iron	0.276	2.01	Tungsten	1.080	3.70
Nickel	0.276	2.38	Gold	1.00	3.63
Copper	0.304	2.64	Lead	0.208	4.16
Zinc	0.305	2.58	Bismuth	0.197	4.38
Zirconium	0.302	3.99	U^{238}	1.04	4.56
			Pu^{239}	1.09	—

7.2.10 INTEGRAL MEASUREMENT OF THE CAPTURE-TO-FISSION RATIO (α)

Mass spectrometric techniques have been employed to measure the capture-to-fission ratio (α) for U^{235} and Pu^{239}, as a function of position in EBR-I.[52] The results are plotted in Figs. 7-13 and 7-14. These data have been compared[5] with measurements of α as a function of neutron energy, such as those reported in Section 2.2.1.

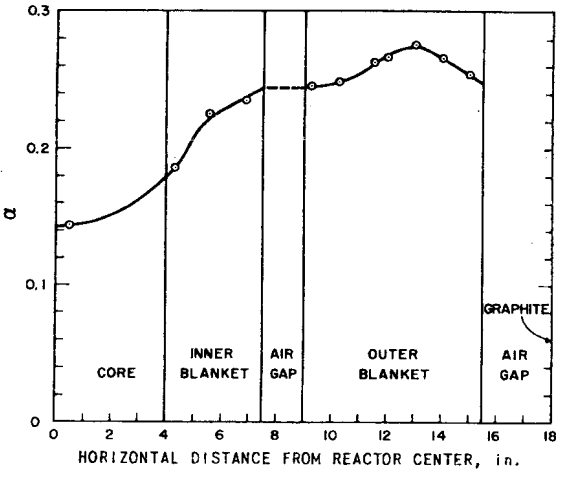

Fig. 7-13—Ratio of capture to fission (α) for U^{235} in EBR-I. *Reproduced from Ref. 52.*

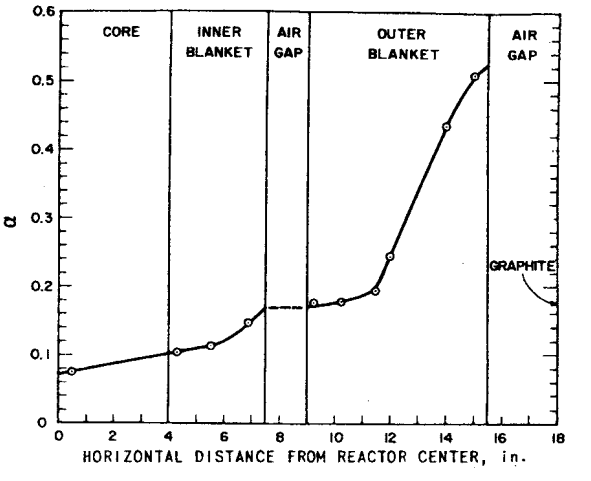

Fig. 7-14—Ratio of capture to fission (α) for Pu^{239} in EBR-I. *Reproduced from Ref. 52.*

7.2.11 COUPLED FAST-THERMAL SYSTEMS

A fast-thermal system consists of a fast assembly and a thermal assembly coupled together in the sense that some of the neutrons born in one assembly cause fissions in the other.[53] Each of the assemblies is subcritical when uncoupled from the other. In particular, the system is not critical on fast neutrons alone.

A coupled fast-thermal power breeder critical experiment[9] was performed in the ZPR-III facility. The primary interest in such a system arises from the possibility of obtaining an assembly, only slightly subcritical on fast neutrons, which combines the breeding ratio of a fast reactor with essentially the same, long, neutron lifetime of a thermal reactor.

The composition and geometry of the radially symmetric critical system are described in Fig. 7-15. The fast core and depleted uranium blankets are similar to those in the all-fast system, ZPR-III-5 (Table 7-15). The main difference in the composition of these regions between the coupled experiment and ZPR-III-5 is that most of the stainless steel in the latter experiment was replaced by aluminum because of its much lower absorption cross section for thermal and near-thermal neutrons.

Table 7-40 — MEASURED ACTIVATION CROSS SECTIONS IN FISSION AND REACTOR SPECTRA (in barns)

Nucleus	Half-Life	Fission Spectrum (Ref. 50)	Godiva (Ref. 51)	Jezebel (Ref. 51)	Zephyr (Ref. 34)	Zeus (Ref. 34)	BR-1[a] (Ref. 11)	BR-2 (Ref. 11)
Na^{23}	15 hr	0.00026	—	—	0.00054	0.00055	—	—
Mg^{26}	9.6 min	0.0006	—	—	0.0003	0.00026	—	—
Al^{27}	2.3 min	0.00037	—	—	0.00057	0.00081	—	—
Si^{30}	2.7 hr	0.0011	—	—	—	—	—	—
Cl^{37}	38 min	0.00074	—	—	0.00074	0.00078	—	—
A^{40}	1.8 hr	0.00093	—	—	—	—	—	—
K^{41}	12.4 hr	0.0029	—	—	0.0053	0.0081	—	—
Ca^{48}	8.5 min	0.0019	—	—	—	—	—	—
Tl^{50}	6 min	0.0019	—	—	—	—	—	—
V^{51}	3.9 min	0.0018	0.0029 ± .0002	0.0029	—	—	—	—
Mn^{55}	2.6 hr	0.00382	0.0033 ± .0002	0.0029	—	—	—	—
Co^{59}	11 min	0.0046 } 0.011	0.0371 ± .0030	—	—	—	—	—
	5 yr	... }						
Ni^{64}	2.6 hr	0.0051	—	—	0.0056	0.0043	—	—
Cu^{63}	12.9 hr	0.0114	0.0144 ± .0006	0.0122	—	—	—	—
Cu^{65}	4.3 min	0.006	0.0088 ± .0005	—	—	—	—	—
Zn^{68}	52 min	0.008 } 0.0232	—	—	—	—	—	—
	14 hr	0.0152 }	—	—	—	—	—	—
Ga^{60}	20 min	0.0209	—	—	—	—	—	—
Ge^{74}	82 min	0.012	—	—	—	—	—	—
As^{75}	27 hr	0.0225	0.0562 ± .0040	—	0.078	0.118	—	—
Br^{79}	18 min	0.029 } 0.0425	0.0571 ± .0050	—	—	—	—	—
	4.4 hr	0.0135 }	0.0311 ± .0020	—	—	—	—	—
Br^{81}	36 hr	0.017	0.045 ± .004	—	0.081	0.175	—	—
Kr^{84}	4 hr	0.0019 } <.010	—	—	—	—	—	—
	10 yr	<0.008 }	—	—	—	—	—	—
Kr^{86}	78 min	0.0024	—	—	—	—	—	—
Rb^{85}	19.5 day	0.0231	0.0619 ± 0.0030	—	—	—	—	—
Rb^{87}	17.5 min	0.0018	0.0041 ± 0.0008	—	—	—	—	—
Sr^{88}	53 day	0.0021	—	—	—	—	—	—
Y^{89}	61 hr	0.007	0.0086 ± 0.0007	—	—	—	—	—
Nb^{93}	6.6 min	0.041	0.0371 ± 0.0030	0.0276	—	—	—	—
Mo^{98}	67 hr	0.0104	—	—	0.040	0.042	—	—
Mo^{100}	15 min	0.0123	—	—	0.021	0.034	—	—
Ru^{102}	42 day	0.030	—	—	—	—	—	—
Ru^{104}	4 hr	0.031	—	—	—	—	—	—
Rh^{103}	44 sec	0.094 } 0.109	—	—	—	—	—	—
	4.2 min	0.0154 }	0.0190 ± 0.0015	0.0155	—	—	—	—
Pd^{108}	13 hr	0.108	—	—	—	—	—	—
Ag^{107}	2.3 min	0.085	0.180 ± 0.018	0.153	—	—	—	—
Ag^{109}	25 sec	0.174 } 0.178	—	—	—	—	—	—
	225 day	... }	—	—	—	—	—	—
In^{115}	13 sec	0.057 } 0.223	—	—	—	—	—	—
	54 min	0.166 }	0.146 ± 0.010	0.139	0.277	0.302	—	—
Sn^{120}	27.5 hr	0.014 } >0.014						
	>400 day	... }	—	—	—	—	—	—
Sn^{122}	40 min	0.012 } >0.012	—	—	—	—	—	—
	126 day	... }	—	—	—	—	—	—
Sn^{124}	9.5 min	0.015 } 0.019	—	—	—	—	—	—
	9.4 day	0.004 }	—	—	—	—	—	—
Sb^{121}	2.8 day	0.090	0.106 ± 0.008	0.093	—	—	—	—
I^{127}	27 min	0.105	0.104 ± 0.010	—	0.160	0.196	—	—
Xe^{136}	3.9 min	0.001	—	—	—	—	—	—
Ba^{138}	86 min	0.0023	—	—	—	—	—	—
La^{139}	40 hr	0.005	0.0091 ± 0.0007	0.0082	—	—	—	—
Ce^{140}	28 day	0.0054	—	—	—	—	—	—
Ce^{142}	33 hr	0.0042	—	—	—	—	—	—
Pr^{141}	19 hr	0.011	—	—	0.025	0.031	—	—
Nd^{146}	11 day	0.040	—	—	—	—	—	—
Nd^{148}	1.7 hr	0.080	—	—	—	—	—	—
Lu^{175}	3.7 hr	0.158 } 0.158	—	—	—	—	—	—
	10^{10} yr	... }	—	—	—	—	—	—
Lu^{176}	6.7 day	0.330	—	—	—	—	—	—
Ta^{181}	16 min	... } 0.142	0.0018 ± 0.0002	—	0.232	0.292	—	—
	117 day	0.142 }	0.152 ± 0.015	—	—	—	—	—
W^{186}	25 hr	0.071	—	—	0.060	0.076	—	—
Re^{185}	90 hr	0.180	0.232 ± 0.010	—	—	—	—	—
Re^{187}	18 hr	0.165	0.179 ± 0.015	—	—	—	—	—
Pt^{198}	31 min	0.064	—	—	0.051	0.099	—	—
Au^{197}	2.7 day	0.120	0.1230 ± 0.0025	0.1012	0.183	0.234	0.150	0.150
Hg^{204}	5.5 min	0.102	—	—	—	—	—	—
Pb^{208}	3.3 hr	0.002	—	—	0.00065	0.0009	—	—
Bi^{209}	5 day	0.0034	0.0014 ± 0.0001	—	—	—	—	—
Th^{232}	—	—	—	—	0.167	0.165	—	—
U^{238}	—	—	—	—	0.112	0.151	0.094	0.105

[a] Uranium reflector.

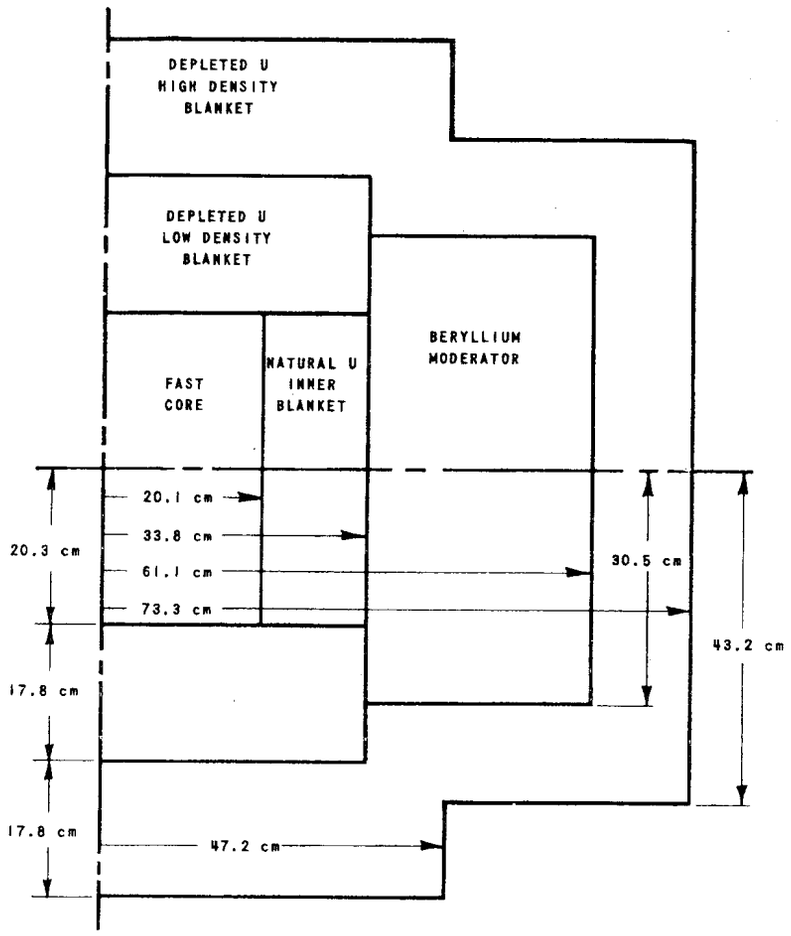

MATERIAL	COMPOSITION (VOLUME FRACTION)				
	FAST CORE	NAT. U INNER BLANKET	DEPL. U L-DENSITY BLANKET	Be MODERATOR	DEPL. U H-DENSITY BLANKET
U^{235}	0.140	0.003	0.0008	-	0.0019
U^{238}	0.159	0.394	0.397	-	0.833
Al	0.414	0.311	0.316	0.073	0.073
Be	-	-	-	0.835	-

Fig. 7-15—Geometry and composition of the coupled fast-thermal critical facility. *Data from Ref. 9.*

The critical mass of the fast core was determined to be 137 kg of U^{235}. The prompt neutron lifetime measured by a 1/v method was 12.3×10^{-6} seconds, while the Rossi α method yielded 16.5×10^{-6} seconds. The effective delayed neutron fraction, $\beta_{eff} = 0.0074$, was estimated by methods similar to those described in Section 7.3.2. A ratio of fast fissions to thermal fissions of 7.3 was obtained by integrating detector responses throughout the system.

Table 7-41 lists the 4-group cross sections used in the two-dimensional (r,z) analysis of the coupled power breeder critical experiment. Also listed are the 4-group cross sections for H_2O used in the two-dimensional (x,y) analysis of the coupled fast-thermal experiment, ZPR-V.

Table 7-41 — ANL 4-GROUP MICROSCOPIC CROSS SECTIONS (in barns)

Data from Refs. 9 and 14.

j	Lower Energy, E_L	Lethargy, $U = \ln \frac{10}{E_L\ (Mev)}$	Fission Spectrum	$\frac{10^7}{v\ cm/sec}$	H_2O		
					σ_{tr}	σ_c	$\sigma_{j\to j+1}$
1	1.353 Mev	2	0.575	0.0041	3.08	0	2.81
2	9.12 kev	7	0.425	0.020	10.52	0	4.04
3	0.4 ev	17.03	0	2.3	16.55	0.035	4.14
4	0	—	0	39.2	68.6	0.57	0

	U^{235}						Be			
j	σ_{tr}	ν	σ_f	σ_c	σ_{in}	σ_{er}	σ_{tr}	σ_c	σ_{in} (n,2n)	σ_{er}
1	4.7	2.65	1.3	0.1	1.4	0	1.53	0.06	0.07	0.47
2	7.0	2.55	1.4	0.3	0	0	4.0	0	($\sigma_{1\to 2}^{n,2n} = 0.22$)	0.21
3	51.0	2.5	23.0	18.0	0	0.01	—	—	—	—
4	597.0	2.5	490	97	0	0	5.56	0	0	0.088
							6.5	0.009	0	0

	U^{238}						Al			
j	σ_{tr}	ν	σ_f	σ_c	σ_{in}	σ_{er}	σ_{tr}	σ_c	σ_{in}	σ_{er}
1	4.7	2.65	0.53	0.04	2.1	0	1.8	0.0003	0.3	0.08
2	7.0	—	0	0.18	0	0	3.0	0.0024	0	0.002
3	11.0	—	0	0.8	0	0.01	1.4	0.01	0	0.008
4	13.0	—	0	2.4	0	0	1.6	0.20	0	0

The ZPR-V reactor consisted of a central, unmoderated core region, a blanket of natural uranium, and an outer, annular, water-moderated, U^{235}-fueled region. The geometry and regional compositions for the ZPR-V are shown in Fig. 7-16. The extrapolated bare height of the annular and water regions was taken to be 75 cm, corresponding to a reflector savings of about 7 cm. The extrapolated bare height of the fast core and blanket regions was taken to be 100 cm, corresponding to a reflector savings of about 19.5 cm.

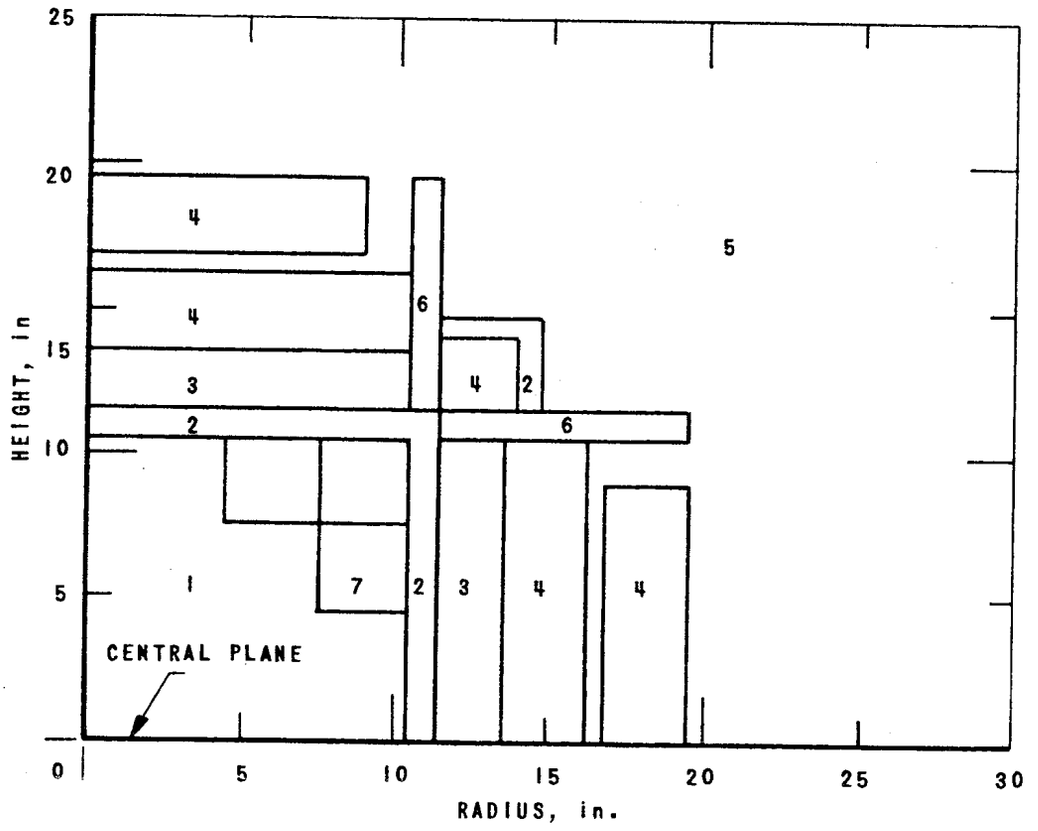

REGION	N, atoms/cm^3 ($\times 10^{-24}$)				
	U^{235}	U^{238}	Fe	Al	H_2O
1	0.0027	0.01364	0.00859	0.00929	-
2	-	-	0.0847	-	-
3	0.000337	0.0470	-	-	-
4	0.000128	-	-	0.0205	0.0221
5	-	-	-	-	0.03345
6	-	-	0.0212	0.0452	-
7	0.000117	0.016356	0.00859	0.00929	-

Fig. 7-16—Geometry (quarter section) and composition of ZPR-V. U^{238}:U^{235} core ratio = 5:1; 2 in. blanket. *Reproduced from Ref. 14.*

7.3 FAST REACTOR DYNAMICS CONSIDERATIONS

7.3.1 PROMPT NEUTRON LIFETIME MEASUREMENTS

Various methods have been used to measure the prompt neutron lifetime of a system. The 1/v poison method is based upon a determination of the loss of reactivity associated with the insertion of a 1/v absorber uniformly into the system. The measurement may be made by small sample insertions. The cumulative effect is then deduced from integration of the results. The prompt neutron lifetime, ℓ, is given by $\ell = \rho/c$, where ρ is the reactivity loss which accompanies the insertion of a 1/v absorber with macroscopic value c/v.

Prompt neutron lifetime may also be determined by the Rossi-α method, which gives the ratio of the over-all lifetime of the system and the effective delayed neutron fraction. The Rossi-α is the average decay constant of the population in a prompt neutron chain. It is determined experimentally by measurements of the statistical variation in the number of pairs of detected neutron events, as a function of the time interval between them. Such measurements must be done at extremely low reactor power so that the prompt neutron chains do not overlap excessively.[54,55,56] Table 7-42 lists the Rossi α values for various fast systems.

Table 7-42—ROSSI-α AT DELAYED CRITICAL[a]

Assembly[b]	α, $sec^{-1} \times 10^{-4}$	Assembly[b]	α, $sec^{-1} \times 10^{-4}$
Popsy[b]	−20	ZPR-III-6F	−9.85
Jezebel	−65	ZPR-III-5	−8.45
	—	ZPR-III-9	−9.0
Topsy	−37	ZPR-III-10	−10.8
Godiva	−1.10	ZPR-III-11(or 22)	−10.4
Jemima Oy(53.5)	−63	ZPR-III-12	−6.85
Jemima Oy(37.5)	−46	ZPR-III-17	−5.35
Jemima Oy(29.0)	−37	ZPR-III-14	−3.85
Jemima Oy(16.2)	−17.5	ZPR-III-13	−9.35
Uranium Hydride	−4.21	ZPR-III-19	−37.5
(Uranium reflector)		ZPR-III-20	−4.47
Uranium Hydride	−2.86	ZPR-III-23	—
(Nickel reflector)		ZPR-III-24	−8.51
		ZPR-III-25	−9.1
		EBR-I Mock-up	−17.4
		ZPR-III-29	−3.48
		ZPR-III-34	−2.92
		ZPR-III-36	−9.40

[a]ZPR-III and EBR-I data from Ref. 13, and/or private communications with G. S. Brunson, ANL (Idaho Div.). Data on other assemblies are from Refs. 10 and 24; these assemblies are described in Section 7.2.1.

[b]Popsy, Topsy, and Jemima Oy(16.2) cores were surrounded by natural uranium reflectors. Jezebel, Godiva, and 53%, 38%, and 29% Jemimas were unreflected. All ZPR-III cores were surrounded by a high-density, depleted uranium reflector except ZPR-III-5. The latter was surrounded by a less dense reflector (~17 cm thick) which, in turn, was surrounded by a high-density reflector.

A pulsed neutron method of measuring the prompt neutron decay constant consists of introducing short pulses of neutrons and observing the subsequent leakage current as a function of time.

The prompt neutron decay constant may also be determined by analyzing the variance-to-mean ratio of the neutron population fluctuation as a function of various intervals of time, and by analyzing neutron statistics by frequency analysis.

The foregoing methods are described and evaluated in a review paper by Bengston.[56]

7.3.2 EFFECTIVE DELAYED NEUTRON FRACTION AND INHOUR RELATION

A typical fast power reactor contains large quantities of U^{238}, both in the core and breeder blanket, reflector. The neutron spectrum is such that anywhere between 15% and 30% of the fissions occur in U^{238}.

The evaluation of the effective delayed neutron fraction of the system is complicated by: (1) the spatial distribution of the U^{238} fissions which differs from that of the fuel (U^{235} or Pu^{239}) fissions; and (2) the delayed neutron characteristics of U^{238} which differ from that of the fuel. The evaluation may be carried out by determining the fraction of total importance production rate of all fission neutrons which results from the delayed neutron.

For the case of two fissionable species (U^{235} and U^{238}) in a system having multigroup flux and adjoint solutions $[\phi_i(r)]$ and $[\phi_i^+(r)]$, the effective delayed neutron fraction may be expressed in the form:[87]

$$\beta_{eff} = \frac{D}{D + P}$$

where

$$D = \frac{\left[\int \sum_{i=1}^{J} (\nu \Sigma_f)_i^{25} \phi_i \, dV\right]\left\{\int\left[\sum_{i=1}^{J} (\nu \Sigma_f)_i^{25} \phi_i\right]\left(\sum_{j=1}^{J} \chi_{Dj}^{25} \phi_j^+\right) dV\right\} (1/\bar{\nu}^{25}) (n/F)^{25}}{\int\left[\sum_{i=1}^{J} (\nu \Sigma_f)_i^{25} \phi_i\right]\left(\sum_{j=1}^{J} \chi_j \phi_j^+\right) dV}$$

$$+ \frac{\left[\int \sum_{i=1}^{J} (\nu \Sigma_f)_i^{25} \phi_i \, dV\right]\left\{\int\left[\sum_{i=1}^{J} (\nu \Sigma_f)_i^{28} \phi_i\right]\left(\sum_{j=1}^{J} \chi_{Dj}^{28} \phi_j^+\right) dV\right\} (1/\bar{\nu}^{28}) (n/F)^{28}}{\int\left[\sum_{i=1}^{J} (\nu \Sigma_f)_i^{25} \phi_i\right]\left(\sum_{j=1}^{J} \chi_j \phi_j^+\right) dV}$$

and

$$P = \frac{\left[\int \sum_{i=1}^{J} (\nu \Sigma_f)_i^{25} \phi_i \, dV\right][\bar{\nu}^{25} - (n/F)^{25}]}{\bar{\nu}^{25}}$$

$$+ \frac{\left[\int \sum_{i=1}^{J} (\nu \Sigma_f)_i^{25} \phi_i \, dV\right]\left\{\int\left[\sum_{i=1}^{J} (\nu \Sigma_f)_i^{28} \phi_i\right]\left(\sum_{j=1}^{J} \chi_j \phi_j^+\right) dV\right\}[\bar{\nu}^{28} - (n/F)^{28}]}{\left\{\int\left[\sum_{i=1}^{J} (\nu \Sigma_f)_i^{25} \phi_i\right]\left(\sum_{j=1}^{J} \chi_j \phi_j^+\right) dV\right\} \bar{\nu}^{28}}$$

The above definitions follow essentially those in Ref. 13.

Table 7-43 lists the fraction of the delayed neutrons, χ_{Dj}^{25} and χ_{Dj}^{28}, emitted into energy group j of the multigroup energy divisions of the 11-group cross section set (Table 7-3). These values are based

Table 7-43—MULTIGROUP DISTRIBUTION OF DELAYED FISSION NEUTRONS

Data from Ref. 87. Values based on data from Refs. 57 and 58.

$E_{j\ lower}$, Mev	Group j	χ_{Dj}^{25}	χ_{Dj}^{28}
2.25	1	0	0
1.35	2	0	0
0.825	3	0	0
0.500	4	0	0
0.300	5	0.962	0.987
0.180	6	0.038	0.013
0.110	7	0	0
0.067	8	0	0
0.025	9	0	0
0.0091	10	0	0
0	11	0	0

$(n/F)^{25}$ = 0.0165 = average number of delayed neutrons/U^{235} fission.
$(n/F)^{28}$ = 0.0412 = average number of delayed neutrons/U^{238} fission.
$\bar{\nu}^{25}$ = 2.56 = average number of neutrons emitted/U^{235} fission.
$\bar{\nu}^{28}$ = 2.62 = average number of neutrons emitted/U^{238} fission.

on the delayed neutron abundances data of Keepin, et al.,[57] and the reported average energies of the delayed groups.[58] The average number of delayed neutrons per U^{235} fission, $(n/F)^{25}$, the average number of delayed neutrons per U^{238} fission $(n/F)^{28}$, the average number of neutrons emitted per U^{235} fission, $\bar{\nu}^{25}$, and the average number of neutrons emitted per U^{238} fission, $\bar{\nu}^{28}$, are the values given by Keepin, et al.[57]

Calculated or estimated β_{eff} for a number of fast systems are given in Table 7-44.

Table 7-44 — CALCULATED OR ESTIMATED EFFECTIVE DELAYED NEUTRON FRACTIONS AND INHOURS/% OF REACTIVITY FOR VARIOUS ASSEMBLIES[a]

Assembly	Calc. U^{238} Fissions per U^{235} Fission	β_{eff}	Inhours/% of Reactivity[b]	Volume Fractions			
				Core		Blanket	
				U^{235}	U^{238}	Uranium	Vol-%
ZPR-III-2A	0.19	0.0073	410	0.14	0	Depleted	0.84
ZPR-III-6F	0.26	0.0074	430	0.14	0.16	Depleted	0.84
ZPR-III-5 (like EBR-II)	0.23	0.0074	415	0.14	0.16	Depleted	—
						Inner Region	0.40
						Outer Region	0.84
ZPR-III-9A	0.32	0.0074	440	0.12	0.38	Depleted	0.84
PBR (Conceptual 800-liter core)	0.27	0.0072	450	0.05	0.027	Depleted	0.70
EBR-I	0.18	0.0068	440	0.50	0	Natural	—
						Inner Region	0.48
						Outer Region	0.82
ZPR-III-10	0.32	0.0074	440	0.12	0.58	Depleted	0.84
ZPR-III-11(and 22)	0.35	0.0073	470	0.095	0.72	Depleted	0.84
ZPR-III-12	0.30	0.0075	430	0.094	0.354	Depleted	0.84
ZPR-III-24	0.39	0.0073	480	—	—	Depleted	0.84
ZPR-III-25	0.37	0.0072	485	—	—	Depleted	0.84
Godiva	0.01	0.0066	—	0.938	0.062	Bare Core	—
Topsy	—	0.0072	—	0.941	0.059	Natural	~1.0
Jemima (53)	0.096	0.0073	—	0.53	0.47	Bare Core	—
Jemima (37)	0.15	0.0075	—	0.37	0.63	Bare Core	—
Jemima (29)	0.19	0.0076	—	0.29	0.71	Bare Core	—
Jemima (16)	—	0.0076	—	0.16	0.84	Natural	~1.0
Jezebel	—	0.0019	—	Pu Core		Bare Core	—

[a] ZPR-III and EBR-I calculations from Refs. 13 and 87. Los Alamos β_{eff} values from Ref. 10.
[b] Estimated error about 5 to 10%.

The reactivities versus asymptotic periods may be calculated using the delayed group abundances, a_i^{25} and a_i^{28}, and decay constants, λ_i^{25} and λ_i^{28}, corrected to the adjoint-weighted effective delayed neutron yields from U^{235} and U^{238}.

The reactivity versus asymptotic period is:

$$\rho \cong \left(\sum_{i=1}^{6} \frac{\beta_i^{25}}{1 + \lambda_i^{25} T} + \sum_{i=1}^{6} \frac{\beta_i^{28}}{1 + \lambda_i^{28} T} \right)$$

with

$$\beta_i^{25} = \beta_{eff} C^{25} a_i^{25}$$

where β_{eff} is the effective delayed neutron fraction; and a_i^{25} is the fraction of the delayed neutrons from a U^{235} fission which is emitted in delayed group i and having decay constant λ_i^{25}.

$$C^{25} \equiv \frac{D^{25}}{D^{25} + D^{28}}$$

where D^{25} is the effective delayed neutron yield from U^{235} fission per U^{235} fission, and D^{28} is the effective delayed neutron yield from U^{238} fission per U^{235} fission.

$$\beta_i^{28} = \beta_{eff} C^{28} a_i^{28}$$

with analogous definitions.

Calculation of reactivity in inhours versus asymptotic period for a series of ZPR-III assemblies of widely differing composition yields the inhour curve (Fig. 7-17), which is independent of composition for a large range of period.

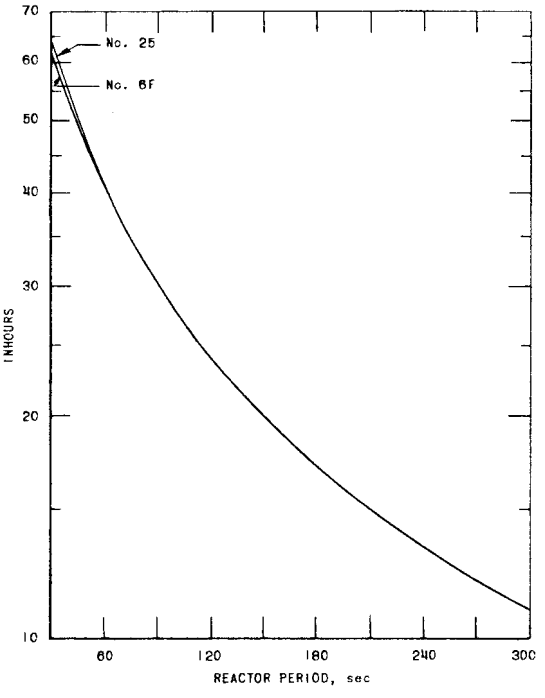

Fig. 7-17—Calculated inhours vs. reactor period for ZPR-III assemblies No. 6F, 9A, 22(11), and 25. *Data from Ref. 87.*

Calculated and estimated inhours/% of reactivity for various ZPR-III fast systems are given in Tables 7-32 and 7-44. As this quantity is sensitive to cross section parameters, in contrast to the inhour versus period which is insensitive, the accuracy of the listed (inhour/%k) is about 5 to 10%. This accuracy estimate does not include uncertainties in the determination of delayed neutron yields for pure materials.

7.3.3 DOPPLER EFFECT

Knowledge of the prompt temperature coefficient of reactivity for fast reactors is of great importance because of its role in the safety of these systems. One component of the prompt temperature coefficient is due to the Doppler effect which arises from a change in the relative velocity distribution of the neutrons and nuclei following a change in temperature. Doppler broadening of the cross section resonances leads to a lessening of flux depletion at these same resonances, with a consequent increase in the interaction rate.

The positive component of a change in the reactivity is due to an increase in the fission rate of U^{233}, U^{235}, Pu^{239}, and Pu^{241}, as a result of the Doppler effect. The negative component of a change in reactivity is due primarily to the increase in the neutron capture rate of Th, U^{238}, and Pu^{240}, as well as the thermally fissile isotopes cited above. The magnitude and sign of the net Doppler coefficient of reactivity are a function of the relative densities of fissionable and fertile materials, the neutron spectrum and the operating temperature of the reactor.

The Doppler temperature coefficient is a difficult quantity to calculate accurately for fast reactors because of the uncertainty of the resonance parameters and level distribution of fissionable and fertile materials in the tens and hundreds of kilovolt energy region. A number of theoretical estimates of the coefficient have been made using nuclear theory and low-energy resonance data. Goertzel, et al.,[59,60] made the first estimate of the effect in the region of interest for fast reactors (fueled with U^{235} and U^{238}) based on statistical theory. A similar approach, with more emphasis on details of the resonance parameters, was made by Lane, et al.[61] With additional low-energy resonance parameters, Bethe[62] (in 1957) re-evaluated the coefficient of reactivity for the Fermi and the EBR-I reactors. Nicholson[63] (in 1960) extended the analysis to cover the energy region of 1 kev to 200 kev, using the same methods as developed by Bethe. Nicholson used a different method for evaluating the effect of

U^{238}, and included the effect of inelastic scattering. The major differences in these four theoretical studies of the Doppler effect has been in the treatment of the resonance parameters and level distribution of U^{235} and U^{238}. Some of the results of these studies are given in Table 7-45.

Table 7-45—CALCULATED DOPPLER TEMPERATURE COEFFICIENTS

Reactor	Y[a]	T(°K)	$d\rho/dT$	Ref.
EBR-I	0	680	0.79×10^{-6}	62
Fermi	2.8	680	-2.44×10^{-6}	62
Fermi	2.7	560	-1.7×10^{-6}	63

[a] $Y \equiv N^{U^{238}}/N^{U^{235}}$, where N = number of atoms per unit volume.

Doppler reactivity effects have also been calculated for some large dilute PuO_2-UO_2 fueled fast reactors.[64] Calculations by Greebler, and Hutchins[65] indicate that a fast oxide breeder reactor may have a Doppler coefficient of -1.0×10^{-5} $(\Delta k/k)/°C$ at 900°C. Eighty percent of this coefficient is due to neutron capture effects between 500 and 5000 ev, even though only 15% of the fission power is caused by neutrons of energy less than 5000 ev. With 12% Pu^{239} in the fuel alloy, its positive Doppler coefficient of reactivity represented about 40% of the negative Doppler coefficient from the U^{238}. This study indicates that the magnitude of the Doppler coefficient of reactivity will change appreciably upon varying the ratio of coolant to fuel plus structural material.

Two experiments have been done to measure the Doppler coefficient. Kato and Butler[66] attempted to measure the Doppler effect of U^{235} in a highly enriched EBR-I mock-up in ZPR-III. A helix made of U^{235} was electrically thermal cycled between 50°C and 170°C, and the change in reactivity was determined using pile oscillator techniques. Because of the uncertainties introduced into the experiment by expansion of the uranium upon heating, they were able only to set an upper limit of 0.83×10^{-8} $(\Delta k/k)/°C$ for the Doppler effect of the 506-gram U^{235} sample at an average temperature of 106°C. Extrapolation of this value to the entire critical mass of the EBR-I results in a Doppler coefficient no greater than 1.6×10^{-6} $(\Delta k/k)/°C$ at 20°C.

Another measurement of the Doppler effect in a fast reactor was made by Baker and Jaques.[67] They oscillated heated samples of natural uranium and enriched uranium (93% U^{235}) in the central channel of ZEUS-3B core which was surrounded by material having a U^{238}/U^{235} ratio of 1.63. The ZEUS-3B core was a two-region assembly with an average U^{238}/U^{235} ratio of 1.72. The accuracy of their experiments was also limited by the corrections necessary for the thermal expansion effect of the sample. Baker and Jaques observed a small negative temperature coefficient corresponding to increased capture in U^{238} with increasing temperature of

$$\frac{d\sigma_c}{dT} = 0.0006 \pm 0.0002 \text{ mb/°C}$$

They estimate that the Doppler temperature coefficient for the entire ZEUS reactor was zero, within experimental error. An upper limit for the magnitude of the Doppler coefficient, either positive or negative, was placed at 1×10^{-6} $(\Delta k/k)/°C$.

7.3.4 FAST REACTOR KINETICS

Zero, or low-power fast reactor kinetics below prompt critical are determined principally by the delayed neutrons (Section 5.3). Kinetic behavior above prompt critical is determined principally by the prompt neutron lifetime (Section 7.3.1). The influence of fertile fissions on the zero-power kinetics of a U^{235}- or Pu-fueled fast reactor is described in Section 7.3.2. Calculations of the effective delayed neutron fraction for a number of fast neutron systems are summarized in Tables 7-31 and 7-32.

Experimental information pertaining to the power kinetics of fast neutron systems is limited to those reactors which have operated on nuclear heat over a large power range. Systematic experimental investigations have been reported for Godiva neutron pulses[68] and extended periods of operation with EBR-I.[69]

Godiva Bursts. The Godiva-I assembly is one of the simplest and most thoroughly investigated spherical, critical systems. Godiva-II, the successor to Godiva-I, is a cylindrical reactor, but has most of the Godiva-I properties and behavior. Criticality, spectrum, and material replacement data

are given in Tables 7-12, 7-29, 7-31, and 7-42. Godiva-I was subjected to a series of self-limiting bursts.[68] Each burst was initiated by a step change in reactivity. Following the retirement of Godiva-I after an accidental burst which damaged the reactor, Godiva-II was designed specifically for the reliable production of super-prompt-critical fission bursts.

The self-limiting nature of the Godiva bursts is due to expansion of the core which accompanies the heating associated with high power levels. This expansion provides a shutdown mechanism (loss of reactivity) by slightly reducing the effective density of the core.

Analysis of the Godiva bursts is an interesting prerequisite to analyzing the excursion behavior of more complicated fast reactor systems. A number of analytical methods have been applied to such investigations. References 68, 70, 71, 72, and 73 contain the more significant attempts on this problem. Empirical analysis has demonstrated that the following relationships apply to the Godiva-I bursts:[72]

Reciprocal Period of Initial Excess Reactivity (sec^{-1}) $\equiv \alpha$
Total Number of Fissions in Burst, $F = 9 \times 10^{10}\ \alpha$
Maximum Fission Rate (sec^{-1}), $(dF/dt)_{max} = 2.22 \times 10^{10}\ \alpha^2 = \frac{1}{4}\ F\alpha$
Temperature Rise (°C), $\Delta\theta = 4.6 \times 10^{-4}\ \alpha$
Width of Burst (sec) $= 3.5/\alpha$
Half Width × Peak Height = Half Width × $(dF/dt)_{max} = \frac{7}{8}\ F$

The above relations were obtained from ten different experiments. These ranged from bringing the reactor 1 cent to 30 cents above prompt critical. (One cent = 0.01 dollar $\approx 6.6 \times 10^{-3}\%\ \Delta k/k$). Initial reactor periods, before shutdown coefficients became operative, ranged from 3.8×10^{-2} seconds to 1.2×10^{-5} seconds.

EBR-I Kinetics and Stability. Extended periods of power operation with the EBR-I Mark-I, -II, and -III cores[69] have yielded much experimental information on fast power reactor kinetics and stability. The appearance of a large resonance in the power reactor transfer function, in addition to the occurrence of spontaneous oscillations under certain operating conditions, in the Mark-II core has stimulated considerable analytical effort. This effort is designed to give a precise understanding of the dynamic relationship between power, temperature distribution, and reactivity. The density changes and structural deformations which occur as reactor power level or coolant flow is varied are translated into reactivity effects. These effects are fed back into the kinetic equations which determine reactor power changes in the presence of delayed neutrons and deviations from criticality.

Several different methods have been applied to the kinetic and stability analysis of the EBR-I Mark-II and Mark-III core loadings. All methods utilize similar physical concepts, although they differ in complexity. A summary of recent experimental and analytical work is given in Reference 74. An extremely detailed analytical model for EBR-I Mark-III is described in Reference 75. Less detailed analyses are described in References 76, 77, and 78. The non-linear aspects of such studies are treated in Reference 79. The fuel pin time constant is treated in Reference 80.

A summary of experimental stability studies on the EBR-I, Mark-III core is given in Reference 81.

7.4 COMMENTS ON COMPUTATIONAL METHODS

7.4.1 APPROXIMATIONS TO THE BOLTZMANN EQUATION

Table 7-46, prepared by Carlson,[2,3,82] lists the relative accuracy of various approximations to the solution of the one-velocity Boltzmann equation in spherical geometry.

The systems studied feature a core surrounded by a reflector. The modified diffusion method, MDM,[83] is similar to the extrapolated endpoint method, EEM,[84] except that the extrapolated endpoint correction is applied only at the outer boundary rather than at each interface. Both methods are applicable strictly to slab geometry, or to spherical geometry with constant mean free path. The effect of departing from constant mean free path in the modified diffusion method for spherical geometry can be seen in Table 7-46.

A comparison of diffusion theory with the SNG method in multigroup form has been carried out,[43] using both three-group and ten-group sets over a wide range of reactor sizes and with some variance in composition. In each calculation, the radius of the core was varied until criticality was reached. The transport approximation was used in these calculations. Figure 7-18 shows the ratio of critical radius by diffusion theory, relative to that by the S_4 method, as a function of critical radius by the S_4 method.

Table 7-46—RELATIVE ACCURACY OF VARIOUS CALCULATION METHODS FOR THE CRITICAL CORE RADIUS OF A REFLECTED SPHERE

$f = [(\nu - 1)\sigma_f - \sigma_c]/\sigma_{tr}$, excess number of neutrons emerging from a collision

1 + f Core	1 + f Reflect.	Reflect. Thick. m.f.p.	(1) Core m.f.p. = Reflector m.f.p.					(2) Core m.f.p. = ¾ Reflector m.f.p.					(3) Core m.f.p. = ½ Reflector m.f.p.				
			Exact[a] Crit. Core Radius m.f.p.	% Error				Exact[b] Crit. Core Radius m.f.p.	% Error				Exact[b] Crit. Core Radius m.f.p.	% Error			
				SWM[c]	MDM[d]	S_2	S_4		SWM[c]	MDM[d]	S_2	S_4		SWM[c]	MDM[d]	S_2	S_4
1.3	1.00	1.5	1.896	−2.2	−1.5	−4.4	−0.9	1.825	−2.5	−2.8	−4.0	−0.8	1.999	−2.0	1.4	−4.7	−0.9
1.3	0.95	1.5	1.973	−2.1	−1.8	−4.2	−0.7	1.917	−2.4	−3.4	−4.2	−0.8	2.057	−1.9	1.3	−4.4	−0.8
1.3	0.80	1.5	2.132	−2.2	−2.6	−3.7	−0.6	2.103	−2.4	−4.7	−3.8	−0.7	2.184	−2.2	0.4	−4.0	−0.8
1.7	1.00	1.5	1.044	−1.6	−4.1	−5.7	−1.2	0.997	−1.6	−6.9	−5.4	−1.0	1.103	−1.4	1.2	−5.7	−1.1
1.7	0.95	1.5	1.075	−1.6	−4.4	−5.6	−1.1	1.035	−1.6	−7.5	−5.3	−1.0	1.125	−1.3	1.1	−5.3	−1.0
1.7	0.80	1.5	1.148	−1.8	−5.5	−5.1	−1.0	1.122	−1.8	−9.0	−4.9	−0.9	1.180	−1.7	0.3	−5.0	−0.9
1.3	1.00	3.0	1.752	−1.9	−1.7	−4.6	−0.9	1.651	−2.2	−3.5	−4.1	−0.8	1.893	−1.7	1.5	−4.7	−0.9
1.3	0.95	3.0	1.886	−2.0	−2.0	−4.3	−0.9	1.811	−2.2	−4.1	−4.3	−0.8	1.996	−2.0	1.2	−4.6	−0.9
1.3	0.80	3.0	2.108	−2.2	−2.8	−3.7	−0.7	2.074	−2.4	−5.1	−3.8	−0.7	2.165	−2.2	0.5	−4.0	−0.7
1.7	1.00	3.0	0.992	−1.5	−4.5	−5.5	−1.0	0.934	−1.7	−7.7	−5.4	−1.1	1.068	−1.4	0.7	−5.5	−1.0
1.7	0.95	3.0	1.043	−1.6	−4.8	−5.5	−1.1	0.995	−1.6	−8.1	−5.3	−1.0	1.104	−1.4	0.8	−5.3	−1.0
1.7	0.80	3.0	1.137	−1.8	−5.6	−5.0	−1.1	1.109	−1.8	−9.4	−4.8	−0.9	1.174	−1.8	0.2	−4.9	−0.9

Note: m.f.p. ≡ mean free path.

[a]The core radius assumed to be correct; obtained by Extrapolated End Point Method (EEM) known to be in error by about −0.1%. Errors for core in column (1) are relative to these values.

[b]Obtained by extrapolation from S_2 and S_4, using the case of core m.f.p. = reflector m.f.p. as a guide; errors for core m.f.p. and reflector m.f.p. are relative to these values.

[c]Serber-Wilson Method.

[d]Modified Diffusion Method, similar to EEM but with interface correction only at the outside boundary.

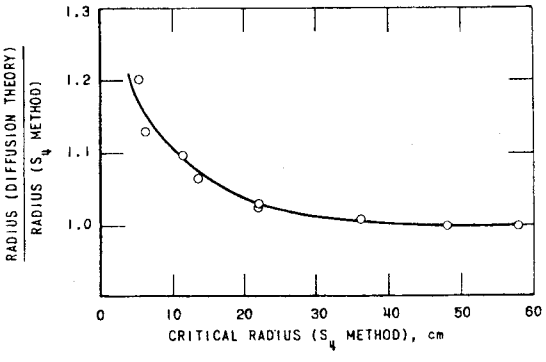

Fig. 7-18—Ratio of critical radii (Diffusion Theory-to-S_4 Method) as a function of critical radius (S_4 Method). *Reproduced from Ref. 43.*

Other comparisons between diffusion theory and the SNG method indicate that slight variations from Fig. 7-18 may be obtained as the properties of the reflector relative to the core are varied. In particular, as core leakage is increased for a given size core (possibly by introducing a less effective reflector), the difference between diffusion theory and the SNG method tends to increase. Some specific calculations of this nature are summarized in Table 7-47. Similar calculations by multigroup Serber-Wilson method, SWM,[85,86] give an error in critical radius, relative to the S_4 method, of −0.05 to −1.0% over the range of core radii up to 22 cm.

Improvements in the SNG method may be obtained by using successively larger values of N. Kiehn[12] systematically studied this effect with a solid plutonium assembly similar to Jezebel. Figure 7-19 shows the results of the 10-energy group calculations. In the S_4 approximation, the calculated error in critical radius is about −1%, reflected systems giving similar results.

A detailed comparison of fluxes calculated by multigroup diffusion theory, Serber-Wilson method, and S_4 for three power reactors similar to EBR-I and EBR-II, and a large-scale power reactor, is given in a paper by Okrent, et al.[43]

There is a valuable multigroup technique which can be readily performed in a few hours with the aid of a desk computer.[43] Specifically, the flux behavior in an unreflected fast system can be characterized rather well by use of a single spatial mode. (This would be rigorous if the extrapolation distance were energy independent.) Therefore, the neutron energy spectrum and material buckling (B^2) of

Table 7-47 — COMPARISON OF CALCULATED CRITICAL PARAMETERS: DIFFUSION THEORY VS. S_4 METHOD

Data from Ref. 8.

System Description	Approximate Core Volume, liter	$\left[\frac{k(D.T.) - k(S_4)}{k(S_4)}\right]^a$	$\left[\frac{R(D.T.) - R(S_4)}{R(S_4)}\right]^b$
ZPR-III-2A	56	−0.025	—
-6F	50	−0.024	—
-5	61	−0.033	—
-9A	67	−0.018	—
-10	70	−0.015	—
-11	135	−0.009	—
-12	100	−0.015	—
-14	77	−0.020	—
-15	125	−0.011	—
Metal Core, Metal Reflector	400	—	0.016
Oxide Core, Metal Reflector	400	—	0.019
Metal Core, Metal Reflector	800	—	0.010
Oxide Core, Metal Reflector	800	—	0.013
Carbide Core, Metal Reflector	800	—	0.014
Oxide Core, Oxide Reflector	800	—	0.020

[a] $k(D.T.)$ and $k(S_4)$ are calculated multiplication constants obtained from diffusion theory and S_4 analyses, respectively.

[b] $R(D.T.)$ and $R(S_4)$ are calculated critical radii obtained from diffusion theory and S_4 analyses, respectively.

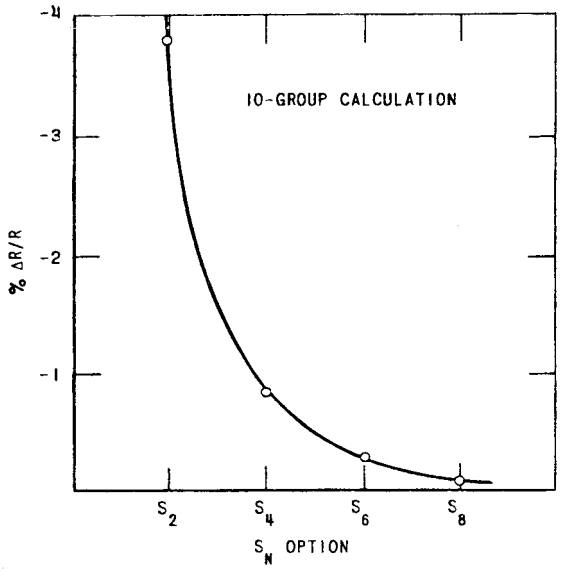

Fig. 7-19 — Relative error in critical radius as a function of SNG option. *Reproduced from Ref. 12.*

such a system can be determined by space-independent calculations. The more general equations are limited by assuming:

$$\nabla^2 \phi_j(r) = -B^2 \phi_j(r)$$

and

$$\phi_j(r) = \phi_j F(r)$$

for all j, resulting in a set of N algebraic equations. Here N is the total number of groups and $\phi_j(r)$ is the total flux in group j at the general spatial coordinate position r. These can now be solved by as-

signing an arbitrary fission source, making a first guess on buckling, and iterating on the latter until the calculated fluxes produce the assigned fission source within the desired accuracy.

The value of this method is not limited to bare cores. For a reflected fast reactor of simple geometry and of intermediate or large size, the flux in most of the core is characterized by the fundamental mode and the true average core spectrum is similar to that predicted by analysis of the equivalent bare core. The core spectra obtained in this manner can be used for assigning cross sections in one- or two-group, multi-dimensional calculations.

For analyses of small, bare, fast critical assemblies, the diffusion theory fundamental mode solution is replaced by the corresponding asymptotic solution of the Boltzmann equation; i.e., the diffusion theory group leakage term,

$$B^2/3\Sigma_{tr,j}$$

is replaced by

$$\{B/[\tan^{-1}(B/\Sigma_{tr,j})]\} - \Sigma_{tr,j}$$

where $\Sigma_{tr,j}$ is the macroscopic transport cross section for group j. This describes the spectrum and flux shape near the center of such an assembly quite well.

REFERENCES

1. H. Goldstein, *A Proposed Nomenclature Scheme for Experimental Nuclear Cross Sections*, NDA 2-33, (January, 1957).
2. B. G. Carlson, *Solution of the Transport Equation by S_N Approximations*, LA-1891, (February, 1955).
3. B. G. Carlson and G. I. Bell, *Solution of the Transport Equation by the S_N Method*, Proc., 1958 Geneva Conference, 16: Paper No. 2386, p. 535.
4. B. G. Carlson, et al., *The DSN and TDC Neutron Transport Codes*, LAMS-2346, (February, 1960).
5. S. Yiftah, D. Okrent and P. Moldauer, *Fast Reactor Cross Sections—A Study Leading to a Sixteen Group Set*, (New York: Pergamon Press, 1960).
6. W. H. Roach, *Computational Survey of Idealized Fast Breeder Reactors*, Nuclear Sci. and Eng., 8: No. 6, 621, (December, 1960).
7. G. E. Hansen and W. H. Roach, *Six and Sixteen Group Cross Sections for Fast and Intermediate Critical Assemblies*, LAMS-2543, (December, 1961).
8. W. B. Loewenstein and D. Okrent, *The Physics of Fast Power Reactors*, Proc., 1958 Geneva Conference, 12: Paper No. 637, p. 16.
9. R. Avery, et al., *Coupled Fast-Thermal Power Breeder Critical Experiment*, Proc., 1958 Geneva Conference, 12: Paper No. 2160, p. 151.
10. G. E. Hansen, *Properties of Elementary Fast Neutron Critical Assemblies*, Proc., 1958 Geneva Conference, 12: Paper No. 592, p. 84.
11. A. I. Leipunsky, et al., *Studies in the Physics of Fast Neutron Reactors*, Proc., 1958 Geneva Conference, 12: Paper No. 2038, p. 3; also private communication from author.
12. R. M. Kiehn, *Some Applications of the S_N Method*, Nuclear Sci. and Eng., 4: No. 2, 166, (August, 1958).
13. J. K. Long, et al., *Fast Neutron Power Reactor Studies with ZPR-III*, Proc., 1958 Geneva Conference, 12: Paper No. 598, p. 119.
14. H. H. Hummel, et al., *Experimental and Theoretical Studies of the Coupled Fast-Thermal System ZPR-V*, Proc., 1958 Geneva Conference, 12: Paper No. 599, p. 166.
15. L. Cranberg, *Fast Neutron Scattering by U^{235}, Pu^{239}, and U^{238}*, Proc., Conference on the Physics of Breeding, ANL-6122, (October, 1959), pp. 51-63; see also L. Cranberg and J. Levin, *Fast Neutron Scattering by U^{235}, Pu^{239}, and U^{238}*, International Conference on Interaction of Neutrons with Nucleus, New York, September, 1957.
16. R. Avery, *Coupled Fast-Thermal Power Breeder*, Nuclear Sci. and Eng., 3: No. 2, 129, (February, 1958).
17. D. M. Barton, W. Bernard and G. E. Hansen, *Critical Masses of Composition of Oy and Pu-239-240 in Flattop Geometry*, LAMS-2489, (1961).
18. G. A. Jarvis, et al., *Two Plutonium-Metal Critical Assemblies*, Nuclear Sci. and Eng., 8: No. 6, 525, (December, 1960).
19. F. Kloverstrom, *Spherical and Cylindrical Plutonium Critical Masses*, UCRL-4957, (September, 1957).
20. H. R. Ralston, *Critical Parameters of Spherical Systems of Alpha-Phase Plutonium Reflected by Beryllium*, UCRL-5349, (September, 1958).
21. E. A. Plassmann and D. P. Wood, *Critical Reflector Thicknesses for Spherical U^{233} and Pu^{239} Systems*, Nuclear Sci. and Eng., 8: No. 6, 615, (December, 1960).
22. D. Wood, C. Beyers and L. Osborn, *Critical Masses of Cylinders of Plutonium Diluted with Other Metals*, Nuclear Sci. and Eng., 8: No. 6, 578, (December, 1960).
23. V. Josephson, R. W. Paine, Jr. and L. L. Woodward, *Oralloy Shape Factor Measurements*, LA-1155, (August, 1950).
24. E. C. Mallary, *Oralloy Cylindrical Shape Factor and Critical Mass Measurements in Graphite, Paraffin, and Water Tampers*, LA-1305, (October, 1951); also G. A. Linenberger, J. D. Orndoff and H. C. Paxton, *Enriched-Uranium Hydride Critical Assemblies*, Nuclear Sci. and Eng., 7: No. 1, 44, (January, 1960).
25. H. C. Paxton, *Critical Data for Nuclear Safety Guides*, LAMS-2415, (February, 1960); also private communication from author.
26. G. A. Graves and H. C. Paxton, *Critical Masses of Oralloy Assemblies*, Nucleonics, 15: No. 6, 90, (June, 1957).
27. H. C. Paxton, et al., *Bare Critical Assemblies of Oralloy at Intermediate Concentrations of U^{235}*, LA-1671, (May, 1954).
28. J. K. Long, et al., *Experimental Results on Large Dilute Fast Critical Systems with Metallic and Ceramic Fuels*, Paper presented at IAEA Seminar on Physics of Fast and Intermediate Reactors, Vienna, August, 1961; also unpublished ZPR-III data.
29. W. P. Keeney and J. K. Long, *Dilute Fast Critical Experiments in ZPR-III*, Trans. Am. Nuclear Soc., 3: No. 2, 327, (1960).
30. H. C. Paxton and G. A. Graves, *Critical Masses of Fissionable Metals as Basic Nuclear Safety Data*, LA-1958, (April, 1956).
31. G. Hansen, H. Paxton and D. Wood, *Critical Plutonium and Enriched-Uranium-Metal Cylinders of Extreme Shape*, Nuclear Sci. and Eng., 8: No. 6, 570, (December, 1960).

32. J. R. Dominey, R. C. Lane and A. F. Thomas, *Critical Mass Studies with Slabs of 46% Enriched Uranium*, NR/A-1/61, (1961).
33. H. G. Barkmann, et al., *Preliminary Critical Experiments on a Mock-up of the Los Alamos Molten Plutonium Reactors*, LA-2142, (June, 1957).
34. R. D. Smith and J. E. Sanders, *Experimental Work with Zero Energy Fast Reactors*, Proc., 1958 Geneva Conference, 12: Paper No. 39, p. 89; also private communication from R. D. Smith.
35. E. L. Alexanderson, E. Garelis and J. B. Nims, *Critical Experiment Calculation for the Enrico Fermi Reactor*, Trans. Am. Nuclear Soc., 1: No. 2, 98, (1958).
36. J. E. R. Holmes, et al., *Experimental Studies on Fast Neutron Reactors at A.E.R.E.*, Proc., 1955 Geneva Conference, 5: Paper No. 404, p. 331.
37. D. Meneghetti and M. F. Loomis, *Calculation of Heterogeneity Effects in ZPR-III Fast Assemblies Using the DSN Program*, ANL-6218, (November, 1960); also D. Meneghetti, *Calculation of Heterogeneity Effects in Fast Assemblies*, Trans. Am. Nuclear Soc., 3: No. 2, (1960).
38. J. J. Neuer, et al., *Preliminary Survey of Uranium Metal Exponential Column*, LA-2023, (January, 1956).
39. C. G. Chezem, *A Uranium Exponential Experiment*, Nuclear Sci. and Eng., 8: No. 6, 652, (December, 1960).
40. F. C. Beyer, et al., *The Fast Exponential Experiments*, Proc., 1955 Geneva Conference, 5: Paper No. 598, p. 342.
41. L. B. Engle, G. E. Hansen and H. C. Paxton, *Reactivity Contributions of Various Materials in Topsy, Godiva and Jezebel*, Nuclear Sci. and Eng., 8: No. 6, 543, (December, 1960).
42. D. Meneghetti, H. H. Hummel and W. B. Loewenstein, *Ten-Group Calculated Equilibrium Neutron Spectrum and Diffusion Length in Natural Uranium*, Nuclear Sci. and Eng., 3: No. 2, 151, (February, 1958).
43. D. Okrent, R. Avery and H. H. Hummel, *A Survey of the Theoretical and Experimental Aspects of Fast Reactor Physics*, Proc., 19 Geneva Conference, 5: Paper No. 609, p. 347.
44. A. H. Snell, et al., *Studies in a Five-Ton Metal Pile*, CF-589, (April, 1943).
45. J. E. Brolley, et al., *Neutron Multiplication in a Mass of Uranium Metal*, CF-1627, (April 1, 1944).
46. H. A. Bethe, *The Reciprocity Theorem in Neutron Scattering*, LA-1428, (June, 1952).
47. R. B. Leachman and H. W. Schmitt, *Average Fission Cross Section of U^{238} for Fission Neutrons*, LA-1624, (January, 1953).
48. H. A. Bethe, J. R. Beyster and R. E. Carter, *Inelastic Cross Sections for Fission Spectrum Neutrons*, LA-1429, (December, 1955).
49. R. E. Carter and J. R. Beyster, *Inelastic Collision Cross Sections for Fission Spectrum Neutrons*, Phys. Rev., 90: No. 2, 389, (April, 1953).
50. D. J. Hughes, R. C. Garth and J. S. Levin, *Fast Neutron Cross Sections and Nuclear Level Density*, Phys. Rev., 91: 6, 1423, (September, 1953).
51. C. C. Byers, *Cross Sections of Various Materials in the Godiva and Jezebel Critical Assemblies*, Nuclear Sci. and Eng., 8: No. 6, 608, (December, 1960).
52. P. Kafalas, M. Levenson and C. M. Stevens, *Determination of the Ratio of Capture to Fission Cross Sections in EBR-I*, Nuclear Sci. and Eng., 2: No. 5, 657, (September, 1957).
53. R. Avery, *Theory of Coupled Reactors*, Proc., 1958 Geneva Conference, 12: Paper No. 1858, p. 182.
54. J. D. Orndoff, *Prompt Neutron Periods of Metal Critical Assemblies*, Nuclear Sci. and Eng., 2: No. 4, 450, (July, 1957).
55. G. S. Brunson, et al., *Measuring the Prompt Period of a Reactor*, Nucleonics, 15: No. 11, 132, (November, 1957).
56. J. Bengston, *Determination of Prompt Neutron Decay Constants of Multiplying Systems*, Proc., 1958 Geneva Conference, 12: Paper No. 1783, p. 63.
57. G. R. Keepin, T. F. Wimett and R. K. Zeigler, *Delayed Neutrons from Fissionable Isotopes of Uranium, Plutonium, and Thorium*, LA-2118, (February, 1957).
58. H. Goldstein, *The Attenuation of Gamma Rays and Neutrons in Reactor Shields*, (Washington, D. C.: U. S. Government Printing Office, May, 1957), p. 40.
59. G. Goertzel, *An Estimation of Doppler Effect in Intermediate and Fast Neutron Reactors*, Proc., 1955 Geneva Conference, 5: Paper No. 613, p. 472.
60. G. Feshbach, G. Goertzel and H. Yamauchi, *Estimation of Doppler Effect in Fast Reactors*, Nuclear Sci. and Eng., 1: No. 1, 4, (March, 1956).
61. A. M. Lane, J. E. Lynn and J. S. Story, *An Estimation of the Doppler Effect in Fast Neutron Reactors*, AERE T/M 137, (July, 1956).
62. H. A. Bethe, *On the Doppler Effect in Fast Reactors*, APDA-119, (March, 1957).
63. R. B. Nicholson, *The Doppler Effect in Fast Neutron Reactors*, APDA-139, (June, 1960).
64. P. Greebler, B. A. Hutchins and J. R. Sueoka, *Calculation of Doppler Coefficient and Other Safety Parameters for a Large Fast Oxide Reactor*, GEAP-3646, (March, 1961).
65. P. Greebler and B. A. Hutchins, *Calculation of Doppler Reactivity Effects in a PuO_2-UO_2 Fueled Fast Reactor*, Trans. Am. Nuclear Soc., 4: No. 1, 17, (June, 1961).
66. W. Y. Kato and D. K. Butler, *Measurement of the Doppler Temperature Effect in an EBR-I Type Assembly*, Nuclear Sci. and Eng., 5: No. 5, 320, (May, 1959); also ANL-5809, (July, 1958).
67. A. R. Baker and T. A. J. Jaques, *A Measurement of the Contribution of the Doppler Effect to the Temperature Coefficient of Reactivity in a Fast Reactor*, AERE R/M 168, (June, 1958).
68. T. F. Wimett and J. D. Orndoff, *Applications of Godiva-II Neutron Pulses*, Proc., 1958 Geneva Conference, 10: Paper No. 419, p. 449.
69. F. W. Thalgott, et al., *Stability Studies on EBR-I*, Proc., 1958 Geneva Conference, 12: Paper No. 1845, p. 242.
70. G. E. Hansen, *Burst Characteristics Associated with the Slow Assembly of Fissionable Materials*, LA-1441, (July, 1952).
71. K. Fuchs, *Efficiency for Very Slow Assembly*, LA-596, (1946).
72. R. O. Brittan, *Some Problems in the Safety of Fast Reactors*, ANL-5577, (May, 1956).
73. W. R. Stratton, T. H. Colvin and R. B. Lazarus, *Analysis of Prompt Excursions in Simple Systems and Idealized Fast Reactors*, Proc., 1958 Geneva Conference, 12: Paper No. 431, p. 196.
74. *Proceedings of the Conference on Transfer Function Measurement and Reactor Stability Analysis*, ANL-6205, (May, 1960): R. R. Smith, *Recent EBR-I Stability Studies*, p. 232; F. Storrer, *Analysis of the Power Feedback Relations in Fast Reactors*, p. 251; and D. Okrent and H. H. Hummel, *Kinetics Studies on EBR-I and EBR-II*, p. 269.
75. J. C. Carter, D. W. Sparks and J. H. Tessier, *The Internal Feedback of EBR-I Mark-III*, Nuclear Sci. and Eng., 8: No. 4, 326, (October, 1960); also ANL-6124, (February, 1960).
76. H. A. Bethe, *Reactor Safety and Oscillator Tests*, APDA-117, (October, 1956).
77. G. H. Kinchin, *The Stability of Fast Reactors*, AERE RP/M83, (June, 1956).
78. R. T. Ackroyd, et al., *Stability Considerations in the Design of Fast Reactors*, Proc., 1958 Geneva Conference, 12: Paper No. 1462, p. 230.
79. H. A. Sandmeier, *Nonlinear Treatment of Large Perturbation in Power Reactor Stability*, Nuclear Sci. and Eng., 6: No. 2, 85, (August, 1959); also H. A. Sandmeier, *The Kinetics and Stability of Fast Reactors with Special Considerations of Non-linearities*, ANL-6014, (June, 1959).
80. H. A. Sandmeier and D. M. O'Shea, *Time Constant of Cylindrical Fuel Pin with Axial Coolant Flow*, Nuclear Sci. and Eng., 5: No. 3, 186, (March, 1959).
81. R. R. Smith, et al., *Instability Studies with EBR-I Mark-III*, ANL-6266, (December, 1960).

82. B. G. Carlson, *Solution of the Transport Equation by S_N Approximations*, LA-1599, (October, 1953).
83. J. Codd, L. R. Shepherd and J. H. Tait, *The Physics of Fast Reactors*, Progress in Nuclear Energy (New York: McGraw-Hill Book Co. Inc., 1956), Series I: Physics and Mathematics, p. 264.
84. S. Frankel and E. Nelson, *Methods of Treatment of Displacement Integral Equations*, AECD-3497, (September, 1953).
85. H. M. Melvin, *A Method of Calculating the Critical Dimensions of Spherically Symmetrical Reactors; Part II: Systems with a Finite Tamper*, AERE T/R-587, (October, 1950).
86. B. Davison, *Neutron Transport Theory*, (Oxford: Clarendon Press, 1957).
87. D. Meneghetti, *Recent Advances and Problems in Theoretical Analyses of ZPR-III Fast Critical Assemblies*, Paper presented at IAEA Seminar on Physics of Fast and Intermediate Reactors, Vienna, August, 1961.
88. W. B. Loewenstein and G. W. Main, *Fast Reactor Shape Factors and Shape-Dependent Variables*, ANL-6403, (November, 1961).

Section 8

SHIELDING CONSTANTS

Effort has been made to supply a concise selection of data on standard shielding materials for the use of the shield designer. The collection of data on the typical concrete mixes is expected to provide a basis for their comparison as well as some constants for use in determining nominal values for shielding calculations.

Geometry, multilayer effects, and considerations of the general shielding problem are not included since detailed discussions of these subjects are readily available in the open literature.[1–6]

8.1 RADIATIONS FROM NUCLEAR EVENTS

The spectra of gamma radiation from various sources are of primary interest in reactor shielding design. To facilitate calculations, these gamma rays may be treated conveniently as a set of monoenergetic sources, and are presented in the form of line spectra. An effective value of the gamma-ray energy, M(E), and the number of photons, N(E), is associated with each discrete energy E of the line spectrum. N(E) and M(E) are related by $M(E) = EN(E)$. Data related to fission are based on U^{235} thermal fission. Data on the fission neutron energy spectrum and neutron yield per fission for various nuclei are presented in Section 1.

8.1.1 PROMPT GAMMA RAYS FROM FISSION

The energy distribution of prompt gamma rays born directly in fission is given in Table 8-1 in terms of several line spectra with varying degrees of detail. The coarser breakdowns are included for convenience in performing approximate calculations.

Roos[9] combines data on the energy released within 5×10^{-8} seconds of fission as reported by Maienschein, et al.,[10] and by Sklyarevskii,[11] to give a total prompt energy release of about 7.9 Mev/fission.

In a report by Carver,[12] the "prompt" gamma rays from fission are totaled as 7.535 Mev/fission. This value includes the low-energy data of Maienschein's group,[13] as tabulated by Smith,[14] and later work by the same group.[15]

8.1.2 EQUILIBRIUM GAMMA RAYS FROM FISSION PRODUCTS

The energy distribution of equilibrium fission product gamma rays is given in Table 8-2 for two different line spectra. The equilibrium condition refers to the typical reactor situation in which the reactor is assumed to have been operating for a sufficiently long time so that fission product activities are essentially at their saturation values.

In a report by McBean,[16] the best synthesis of data from Howlett, et al.,[17] Blomeke and Todd,[18] Burris and Dillon,[19] Perkins and King,[20] Maienschein, et al.,[13] and Zobel, et al.,[21] gives the average gamma-energy residue subsequent to fission as 7.0 ± 1 Mev/fission. Radiations classified as prompt in Section 8.1.1 are specifically excluded from this section.

Table 8-1 — PROMPT FISSION GAMMA-RAY SPECTRA

Spectrum A[a]			Spectrum B		Spectrum C	
E, Mev	N(E), γ/fission	M(E), Mev/fission	E, Mev	M(E), Mev/fission	E, Mev	M(E), Mev/fission
0.5	3.1	1.55	—	—	—	—
1.0	1.9	1.90	1.0	3.450	1.0	3.451
1.5	0.84	1.26	—	—	—	—
2.0	0.55	1.10	2.0	2.360	2.0	3.085
2.5	0.29	0.725	—	—	—	—
3.0	0.15	0.450	3.0	1.175	—	—
3.5	0.062	0.217	—	—	—	—
4.0	0.065	0.260	4.0	0.477	4.0	1.035
4.5	0.024	0.108	—	—	—	—
5.0	0.019	0.095	5.0	0.203	—	—
5.5	0.017	0.094	—	—	—	—
6.0	0.007	0.042	6.0	0.136	6.0	0.256
6.5	0.004	0.026	7.0	0.026	—	—
—	7.028	7.827	—	7.827	—	7.827

[a]Reproduced from Ref. 4, Table 3.2 (from data of Gamble[7]).

Note: In addition, Bertini, et al.,[8] estimate the effective prompt capture gamma-ray source from U^{235} in a thermal reactor to be 1.18 Mev per fission, based on a value of 0.184 for α of U^{235}.

Table 8-2 — EQUILIBRIUM FISSION PRODUCT GAMMA-RAY SPECTRA

	Spectrum A				Spectrum B		
			M(E)			M(E)	
Energy Group	Energy Range, Mev	Effective Energy, Mev	Mev[a] per Fission	Mev/(sec)(watt)[b] of Reactor Power	Effective Energy, Mev	Mev[a] per Fission	Mev/(sec)(watt) of Reactor Power
1	0.1–0.4	0.4	0.645	2.0×10^{10}			
2	0.4–0.9	0.8	3.87	1.2×10^{11}	1	5.16	1.6×10^{11}
3	0.9–1.35	1.3	0.645	2.0×10^{10}			
4	1.35–1.8	1.7	1.06	3.3×10^{10}	2	1.737	5.38×10^{10}
5	1.8–2.2	2.18	0.677	2.1×10^{10}			
6	2.2–2.6	2.5	0.290	9.0×10^{9}	3	0.322	1.0×10^{10}
7	2.6	2.8	0.032	1.0×10^{9}			
Total			7.219	2.24×10^{11}			

[a]3.1×10^{10} fissions/(watt)(sec) assumed.
[b]Data from Ref. 4, Table 3.5.

Based on work by Smith,[22] and using the data of Maienschein, et al.,[13] along with the results given by Knabe and Putnam,[23] Carver[12] reports a value of 6.522 Mev/fission for delayed fission-product gamma rays.

8.1.3 PROMPT CAPTURE GAMMA RAYS

Table 8-3 is a compilation, prepared by Troubetzkoy and Goldstein,[24] of data on radiative capture gamma-ray spectra for numerous nuclei. The compilation lists the yields of the capture gamma rays in seven energy intervals. In the self-contained bibliography of Table 8-3, the authors have listed the primary references for the data.

Table 8-3—TABULATION OF GAMMA-RAY SPECTRA FROM THERMAL-NEUTRON CAPTURE

Reproduced, in part, from Data of Ref. 24.

Target Nucleus	Photons/100 Captures 0–1 Mev	1–2 Mev	2–3 Mev	3–5 Mev	5–7 Mev	7–9 Mev	>9 Mev	Highest Energy Gamma Ray, Mev	Average[a] Number of Photons per Capture	References[b]
1 H	0	0	100	0	0	0	0	2.230	—	3, 16, 36, 65
1 D	0	0	0	0	100	0	0	6.244	—	43
2 He	—	—	—	—	—	—	—	—	—	—
3 Li	—	—	—	—	~40	~60	0	7.26	—	7
4 Be	0	0	0	54	73	0	0	6.80	—	27, 45, 50, 54
5 B^{10}	0	0	0	>110	>28	≥6	0.8	11.43	—	7
6 C	0	0	0	100	0	0	0	4.95	1.3	30, 44, 45, 50
7 N^{14}	—	—	—	>54	≥11	15	12	10.833	—	7, 30, 50
8 O	—	—	—	—	—	—	—	—	—	—
9 F	—	>100[c]	—	—	≥111	0	0	6.600	—	19, 30
10 Ne	—	—	—	—	—	—	—	—	—	—
11 Na	>96	127	187	70	31	0	0	6.41	<2	10, 17, 18, 27,[d] 30, 51,[e] 61, 64
12 Mg	—	—	>28	>72	10	3.3	0.57	11.089	—	17, 19, 30, 46, 59
13 Al	>236	195[f]	69	62	19	19	0	7.724	~2	10, 17, 28, 34, 37, 45, 49, 51,[e] 53
14 Si	>100	63	30	89	11	4.1	0.1	10.59	—	2, 17, 45, 49, 53, 59
15 P	>290	97	55	98	27	7.2	0	7.94	—	10, 17, 30, 53,[e] 59
16 S	>70	32	72	70	44	6.5	0	8.64	—	10, 17, 27, 49, 53,[e] 59, 78, 79
17 Cl	>49	85	41	47	55	24	0	8.55	3.1	10, 17, 27,[d] 30, 34, 37, 38, 53,[e] 58, 61, 68, 69, 74, 78, 79, 80
18 A	—	—	—	—	—	—	—	—	—	—
19 K	>100	81	57	106	37	4.7	0	9.36	—	3, 10, 11, 12, 17, 38, 53,[e] 58
20 Ca	>14	191	77	85	64	1.8	0	7.83	—	3, 10, 17, 38, 49, 53,[e] 78, 79
21 Sc	>52	59	38	65	29	12	0	8.85	—	10, 14,[e] 30, 38
22 Ti	>54	160	16	24	78	1.3	0.2	10.47	—	2, 9, 17, 38, 57, 63, 70, 72, 78, 79
23 V	>83	132[g]	11.4	21	67	16	0	7.98	2.5	10, 14,[e] 15,[e] 17, 28, 38, 70
24 Cr	>85	41	21	12	23	39	6.4	9.716	>2	10, 17, 30, 38, 48,[e] 70, 78, 79
25 Mn	>125[h]	91[i]	60[j]	50	34	17	0	7.261	2.6	10, 14,[e] 28, 35, 37, 38, 58, 66, 70
26 Fe	>75	60	27	23	25	38	2.1	10.16	1.7	2, 10, 34, 35, 37, 38, 48,[e] 58, 60 70, 78, 79
27 Co	>61	26	17	42	52	8.5	0	7.486	—	10, 14,[e] 26, 28, 35, 38, 58, 68, 70
28 Ni	>84	40	23	23	34	62	0.8	8.997	—	3, 10, 17, 38, 48,[e] 78, 79
29 Cu	>68	47	26	30	27	43	0	7.914	2.6	10, 14,[e] 30, 58, 60, 70, 76, 78, 79
30 Zn	>156	93	67	48	29	16	1	9.51	—	10, 48[e]
31 Ga	—	—	—	57	34	0.2	0	7.73	—	19
32 Ge	—	—	—	—	—	—	—	—	—	—
33 As	—	—	—	47	22	1	0	7.30	2.7	13
34 Se	—	—	—	65	27	9	1.7	10.483	—	47
35 Br	—	—	—	79	41	6.4	0	7.879	—	19, 34
36 Kr	—	—	—	—	—	—	—	—	—	—
37 Rb	—	—	—	—	—	—	—	—	—	—
38 Sr	—	—	—	69	51	14	0.1	9.22	—	47
39 Y	>71	23	6	50	59	0	0	6.850	—	8
40 Zr	—	—	—	113	35	4	0	8.66	—	47
41 Nb	—	—	—	54	14	0.4	0	7.19	2.6	13
42 Mo	>137	>18	—	84	26	3	0.03	9.15	—	41, 47
43 Tc	—	—	—	—	—	—	—	—	—	—
44 Ru	—	—	—	—	—	—	—	—	—	—
45 Rh	>91	99	61	38	10	0	0	6.792	—	13, 23, 24, 26, 30, 38
46 Pd	—	—	—	—	—	—	—	—	—	—
47 Ag	>92	87	64	70	17	0.5	0	7.27	2.9	13, 23, 24, 25, 30, 35, 41, 58, 76
48 Cd	>135	92	96	73	17	1	0.1	9.046	4.1	1,[g] 4, 17, 23, 30, 31, 34, 35, 38, 40 47, 58, 61, 62, 64, 67, 69, 77, 80
49 In	>102[k]	197[i]	78[m]	36	4	0	0	5.86	3.3	13, 23, 30, 35, 38, 76
50 Sn	>216	153	67	139	33	4	0.4	9.35	—	32, 47
51 Sb	150	99	58	36	12	0	0	6.80	—	13, 23, 24, 25, 32
52 Te	>58	—	—	—	—	—	—	—	—	23, 24, 38, 41
53 I	>30	—	—	97	22	0	0	6.71	—	5, 6, 23, 24, 26, 55, 58, 70
54 Xe	—	—	—	—	—	—	—	—	—	—
55 Cs	>46	—	—	61	25	0	0	6.702	—	5, 6, 41, 55
56 Ba	—	—	—	75	14	1.4	0.1	9.23	—	47
57 La	>21.7	8.2	—	>35	>12.5	0	0	5.045	—	30, 34, 38
58 Ce	—	—	—	—	—	—	—	—	—	—
59 Pr	—	—	—	34	8	0	0	5.83	—	13
60 Nd	>105	—	—	—	—	—	—	—	—	21, 41
61 Pm	—	—	—	—	—	—	—	—	—	—
62 Sm	>167	150	109	45	5	1	0	7.89	5.6	1,[g] 23, 26, 30, 31, 40, 47, 58
63 Eu	106	153	109	56	6.5	0	0	6.05	—	23, 30, 75
64 Ga	194	117	100	23	34	0.3	0	7.33	3.9	20, 22, 23, 24, 31, 47, 56, 58, 75

Table 8-3—TABULATION OF GAMMA-RAY SPECTRA FROM THERMAL-NEUTRON CAPTURE (Continued)

Reproduced, in part, from Data of Ref. 24.

Target Nucleus	Photons/100 Captures							Highest Energy Gamma Ray, Mev	Average[a] Number of Photons per Capture	References[b]
	0–1 Mev	1–2 Mev	2–3 Mev	3–5 Mev	5–7 Mev	7–9 Mev	>9 Mev			
65 Tb	>7	—	—	—	—	—	—	—	—	23
66 Dy	90	102	106	43	10	0	0	5.87	—	23, 24, 29, 31, 40, 75
67 Ho	—	98	77	49	8	0	0	6.1	—	23, 24, 33, 75
68 Er	225	145	133	103	14	0	0	6.680	—	23, 29, 75
69 Tm	—	91	73	55	10	0	0	6.5	—	23, 24, 33, 75
70 Yb	—	—	—	—	—	—	—	—	—	
71 Lu	—	—	—	—	—	—	—	—	—	—
72 Hf	>137	137	85	52	12	0.5	0	7.62	—	19, 23, 29, 75
73 Ta	>137	99	66	55	5	0	0	6.04	—	9, 13, 23, 24, 29, 75
74 W	>68	82	59	53	15	0.5	0	7.42	—	30, 34, 47, 58
75 Re	124	88	62	51	10.5	0	0	6.14	—	23, 30
76 Os	—	—	—	—	—	—	—	—	—	
77 Ir	98	85	58	51	19.6	0	0	6.088	—	5, 6, 23, 30, 55, 58
78 Pt	>109	92	64	45	15	1	0	7.920	—	23, 24, 27, 30
79 Au	>100	69	33	68	38	0.1	0	6.494	3.5	13, 23, 26, 30, 34, 39, 58, 70, 71
80 Hg	>94	122	55	86	41	0	0	6.446	3.3	1,[g] 26, 30, 34, 47, 58, 73
81 Tl	—	—	—	76	62	0	0	6.54	—	13
82 Pb	0	0	0	0	7	93	0	7.38	—	1, 52, 60
83 Bi	0	0	0	100	0	0	0	4.17	—	30, 52, 55
84 Po	—	—	—	—	—	—	—	—	—	—
85 At	—	—	—	—	—	—	—	—	—	—
86 Em	—	—	—	—	—	—	—	—	—	—
87 Fr	—	—	—	—	—	—	—	—	—	—
88 Ra	—	—	—	—	—	—	—	—	—	—
89 Ac	—	—	—	—	—	—	—	—	—	—
90 Th	>118	140	64	17	0	0	4.92	—	—	18, 30
91 Pa	—	—	—	—	—	—	—	—	—	—
92 U^{238}	254	178	91	34	0	0	4.062	—	—	20, 42
93 Np	—	—	—	—	—	—	—	—	—	—
94 Pu	—	—	—	—	—	—	—	—	—	—

[a] All values in this column are taken from C. O. Muehlhause, Phys. Rev. 79: 277, (1950). They may therefore differ from the multiplicities deduced from the spectra directly.

[b] See bibliography. The Chalk River compilation (Ref. 10) and Soviet compilation (Ref. 30) are referred to only in those cases when either new or revised data are reported there.

[c] Includes a 100%, 1.63-Mev gamma ray in Ne^{20} following 11s decay of F^{20}.

[d] The data have been revised by the authors; revised data are given in Ref. 30.

[e] The data have been revised by the authors; revised data are given in Ref. 10.

[f] Includes a 100%, 1.78-Mev gamma ray in Si^{28} following 2.3m decay of Al^{28}.

[g] Includes a 99.75%, 1.43-Mev gamma ray in Cr^{52} following 3.8m decay of V^{52}.

[h] Includes a 99%, 0.85-Mev gamma ray in Fe^{56} following 2.6h decay of Mn^{56}.

[i] Includes a 23%, 1.80-Mev gamma ray in Fe^{56} following a 2.6h decay of Mn^{56}.

[j] Includes a 15%, 2.13-Mev gamma ray in Fe^{56} following 2.6h decay of Mn^{56}.

[k] Includes a 5%, 0.41-Mev and an 8%, 0.82-Mev gamma ray in Sn^{116} following 54m decay of In^{116}.

[l] Includes a 36%, 1.09-Mev and a 63%, 1.29-Mev gamma ray in Sn^{116} following 54m decay of In^{116}.

[m] Includes an 11%, 2.12-Mev gamma ray in Sn^{116} following 54m decay of In^{116}.

1. B. P. Adyasevich, L. V. Groshev and A. M. Demidov, Conf. Academy of Sciences of the USSR on the Peaceful Uses of Atomic Energy, (July 1, 1955). Session on Physico-Mathematical Sciences (Akad. Nauk S.S.S.R., Moscow, 1955). Translation by Consultants Bureau, Inc., New York, 1955, p. 195.
2. B. P. Adyasevich, L. V. Groshev and A. M. Demidov, *Atomnaya Energiya*, 1: 40, (1956). Translation: *J. Nuclear Energy*, 3: 258, (1956) and *Soviet Journal of Atomic Energy*, 1: No. 2, 183, (Consultants Bureau, Inc., New York, 1956).
3. B. P. Adyasevich, et al., *Atomnaya Energiya*, 1: 28, (1956). Translation: *J. Nuclear Energy*, 3: 325, (1956), and *Soviet Journal of Atomic Energy*, 1: No. 2, 171, (Consultants Bureau, Inc., New York, 1956).
4. M. L. Alexandrova, *Doklady Akad. Nauk, S.S.S.R.*, 69: 763, (1949).
5. R. Balzer, et al., *Nuovo cimento XI*, 609, (1959).
6. R. Balzer, et al., *Helv. Phys. Acta*, 32: 264, (1959).
7. G. A. Bartholomew and P. J. Campion, *Can. J. Phys.*, 35: 1347, (1957).
8. G. A. Bartholomew, et al., *Nuclear Phys.*, 10: 590, (1959).
9. G. A. Bartholomew, et al., Proc. Int. Conf. on the Neutron Interaction with the Nucleus, Columbia University, New York, (1957); USAEC Report TID-7547, (1957), p. 252.
10. G. A. Bartholomew and L. A. Miggs, "Compilation of Thermal Neutron Capture γ-Rays," CRGP-784, AECL-669, (1958).
11. G. A. Bartholomew and B. B. Kinsey, *Can. J. Phys.*, 31: 327, (1953).
12. G. A. Bartholomew and B. B. Kinsey, *Can. J. Phys.*, 31: 927, (1953).
13. G. A. Bartholomew and B. B. Kinsey, *Can. J. Phys.*, 31: 1025, (1953).
14. G. A. Bartholomew and B. B. Kinsey, *Phys. Rev.*, 89: 386, (1953).
15. G. A. Bartholomew and B. B. Kinsey, *Phys. Rev.*, 93: 1434, (1954).
16. R. E. Bell and L. G. Elliot, *Phys. Rev.*, 79: 282, (1950).

17. T. H. Braid, *Phys. Rev.*, 102: 1109, (1956).
18. N. A. Bugrov and G. V. Danilian, *Izvest. Akad. Nauk, S.S.S.R., Ser. Fiz.*, 20: 941, (1956).
19. P. J. Campion and G. A. Bartholomew, *Can. J. Phys.*, 35: 1361, (1957).
20. P. J. Campion, et al., *Can. J. Phys.*, 37: 377, (1959).
21. P. J. Campion, J. W. Knowles and G. A. Bartholomew, *Bull. Am. Phys. Soc., Series II*, 4: 247, (1959).
22. E. L. Church and M. Goldhaber, *Phys. Rev.*, 88: 943, (1952).
23. J. E. Draper, *Phys. Rev.*, 114: 268, (1959).
24. J. E. Draper and C. K. Bockelman, *Bull. Am. Phys. Soc., Series II*, 3: 177, (1958).
25. D. L. Edens, et al., *Bull. Am. Phys. Soc., Series II*, 4: 97, (1959).
26. I. V. Estulin, L. F. Kalinkin and A. S. Melioranskiy, *J. Exptl. Theoret. Phys. (U.S.S.R.)*, 32: 979, (1957). Translation: *Soviet Physics–JETP*, 5: 801, (1957).
27. L. V. Groshev, B. P. Adyasevich and A. M. Demidov, *Proc., 1955 Geneva Conference*, 2: Paper No. 651, p. 39.
28. L. V. Groshev, et al., *Atomnaya Energiya*, 3: 187, (1957). Translation: *Soviet Journal of Atomic Energy*, 3: No. 9, (Consultants Bureau, Inc., New York, 1957).
29. L. V. Groshev, et al., *Atomnaya Energiya*, 4: 5, (1958). Translation: *J. Nuclear Energy*, 9: 50, (1959).
30. L. V. Groshev, et al., "Atlas of γ-Ray Spectra from Radiative Capture of Thermal Neutrons," Atomizdat, Moscow, 1958. Translation by J. B. Sykes, (New York: Pergamon Press, 1959).
31. L. V. Groshev, A. M. Demidov and V. A. Naidenov, *Izvest. Akad. Nauk S.S.S.R., Ser. Fiz.*, 21: 1619, (1957).
32. L. V. Groshev, B. I. Gavrilov and A. M. Demidov, *Atomnaya Energiya*, 6: 281, (1959).
33. L. V. Groshev, A. M. Demidov and V. I. Pelekhov, unpublished, (1959).
34. B. Hamermesh, *Phys. Rev.*, 80: 415, (1950).
35. B. Hamermesh, *Phys. Rev.*, 81: 487, (1951).
36. B. Hamermesh and R. J. Culp, *Phys. Rev.*, 92: 211, (1953).
37. B. Hamermesh and V. Hummel, *Phys. Rev.*, 83: 663, (1951).
38. B. Hamermesh and V. Hummel, *Phys. Rev.*, 88: 916, (1952).
39. B. Hamermesh, D. Rose and R. K. Smither, *Bull. Am. Phys. Soc.*, 1: 346, (1956).
40. C. T. Hibdon and C. O. Muehlhause, *Phys. Rev.*, 88: 943, (1952).
41. L. F. Kalinkin, A. S. Melioranskii and I. V. Estulin, "Gamma Radiation From Radiative Capture of Thermal Neutrons by Mo^{95} Ag^{107}, Te^{123}, and Cs^{133} Nuclei," *Soviet Physics–JETP*, 35: 410, (1959).
42. R. W. Kenney and J. T. Mattingley, *Bull. Am. Phys. Soc., Series II*, 1: 389, (1956).
43. B. B. Kinsey and G. A. Bartholomew, *Phys. Rev.*, 80: 918, (1950).
44. B. B. Kinsey and G. A. Bartholomew, *Can. J. Phys.*, 31: 49, (1953).
45. B. B. Kinsey and G. A. Bartholomew, *Can. J. Phys.*, 31: 537, (1953).
46. B. B. Kinsey and G. A. Bartholomew, *Can. J. Phys.*, 31: 901, (1953).
47. B. B. Kinsey and G. A. Bartholomew, *Can. J. Phys.*, 31: 1051, (1953).
48. B. B. Kinsey and G. A. Bartholomew, *Phys. Rev.*, 89: 375, (1953).
49. B. B. Kinsey and G. A. Bartholomew, *Phys. Rev.*, 93: 1260, (1954).
50. B. B. Kinsey, G. A. Bartholomew and W. H. Walker, *Can. J. Phys.*, 29: 1, (1951).
51. B. B. Kinsey, G. A. Bartholomew and W. H. Walker, *Phys. Rev.*, 83: 519, (1951).
52. B. B. Kinsey, G. A. Bartholomew and W. H. Walker, *Phys. Rev.*, 82: 380, (1951).
53. B. B. Kinsey, G. A. Bartholomew and W. H. Walker, *Phys. Rev.*, 85: 1012, (1952).
54. B. B. Kinsey, G. A. Bartholomew and W. H. Walker, *Can. J. Phys.*, 31: 1, (1953).
55. H. Knoepfel, P. Scherrer and P. Stoll, *Z. Physik*, 156: 293, (1959).
56. J. W. Knowles, G. A. Bartholomew and P. J. Campion, *Bull. Am. Phys. Soc., Series II*, 4: 246, (1959).
57. J. W. Knowles, et al., *Phys. Rev.*, 114: 1065, (1959).
58. H. E. Kubitschek and S. M. Dancoff, *Phys. Rev.*, 76: 531, (1949).
59. G. Manning and G. A. Bartholomew, *Phys. Rev.*, 115: 401, (1959).
60. W. E. Meyerhoff, H. Roderick and L. G. Mann, *Phys. Rev.*, 83: 203A, (1951).
61. C. H. Miller, A. W. Cameron and M. Glicksman, *Can. J. Research*, A.28: 475, (1950).
62. C. D. Moak and J. W. T. Dabbs, *Phys. Rev.*, 75: 1770, (1949).
63. H. T. Motz, *Phys. Rev.*, 93: 925, (1954).
64. H. T. Motz, *Phys. Rev.*, 104: 1353, (1956).
65. D. M. Van Patter and W. Whaling, *Rev. Modern Phys.*, 26: 402, (1954).
66. R. W. Pringle and G. Isford, *Phys. Rev.*, 83: 467, (1951).
67. R. W. Pringle, H. W. Taylor and K. I. Roulston, *Phys. Rev.*, 87: 1016, (1952).
68. W. A. Reardon, R. W. Krone and R. Stump, *Phys. Rev.*, 91: 334, (1953).
69. A. L. Recksiedler and B. Hamermesh, *Phys. Rev.*, 96: 109, (1954).
70. M. Reiser and M. H. Shamos, *Phys. Rev.*, 100: 1302, (1955).
71. D. Rose, H. Ostrander and B. Hamermesh, *Rev. Sci. Instr.*, 28: 233, (1957).
72. R. E. Segel, *Bull. Am. Phys. Soc., Series II*, 2: 230, (1957).
73. R. E. Segel, *Bull. Am. Phys. Soc., Series II*, 3: 64, (1958).
74. R. E. Segel, *Phys. Rev.*, 113: 844, (1959).
75. V. V. Sklyarevskii, E. P. Stepanov and B. A. Obiniakov, *Atomnaya Energiya*, 4: 22, (1958). Translation: *J. Nuclear Energy*, 9: 69, (1959).
76. V. V. Sklyarevskii, E. P. Stepanov and B. A. Obinyakov, *Atomnaya Energiya*, 5: 454, (1958). Translation: *J. Nuclear Energy*, A.10: 183, (1959).
77. W. A. Thornton, et al., *Phys. Rev.*, 86: 604, (1952).
78. G. Trumpy, "On the Determination of Nuclear Spins by the Study of Neutron Capture Gamma Rays," JENER-Pub-13, (1957).
79. G. Trumpy, *Nuclear Phys.*, 2: 664, (1957).
80. R. Wilson, *Phys. Rev.*, 80: 90, (1950).

8.1.4 INELASTIC SCATTERING GAMMA RAYS

Table 8-4 gives the differential cross sections of several elements for the production of gamma rays in the energy range 2 to 11 Mev, from inelastic scattering of 14-Mev neutrons. All data are normalized to a value of 15.9 mb/steradian for carbon, obtained by using the data of Anderson, et al.[25]

The production cross sections for oxygen are 11 ± 4 mb/steradian for the 6.14-Mev gamma rays, and a total of 6.5 ± 2 mb/steradian for the gamma rays from the unresolved 6.91- and 7.12-Mev levels.

Other data on production of gamma rays by inelastic scattering in iron, silicon, aluminum, and oxygen are given by Troubetzkoy.[26]

Table 8-4—CROSS SECTIONS FOR GAMMA-RAY PRODUCTION FROM INELASTIC SCATTERING OF 14-Mev NEUTRONS

Data from Ref. 30.

Gamma-Ray Energy Range, Mev	Cross Section at 90°, mb/steradian						
	Mg	Al	Si	P	S	Ca	Fe
2-3	16.1	30.9	17.0	43.0	26.4	27.8	42.6
3-4	11.7	12.7	12.0	12.4	11.7	18.2	23.4
4-5	7.5	7.5	8.5	7.5	7.3	8.3	13.9
5-6	4.8	5.3	6.4	4.7	4.4	5.8	10.0
6-7	3.7	3.9	5.7	2.7	2.5	3.7	8.5
7-8	3.0	2.7	4.7	0.8	1.1	1.7	5.7
8-9	2.0	0.7	3.0	—	0.1	0.1	2.8
9-10	1.0	—	1.3	—	—	—	0.6
10-11	0.1	—	0.1	—	—	—	—
Integrated cross section from 2 to 11 Mev	49.9	63.7	58.7	71.1	53.5	65.6	107.5
Nonelastic cross section	77.2	78.8	81.2	89.9	90.7	108	109
Ratio: $\frac{\text{integrated cross section}}{\text{nonelastic cross section}}$	0.65	0.81	0.72	0.79	0.59	0.61	0.99

8.1.5 DECAY OF FISSION PRODUCT GAMMA RAYS

The activity of fission products after reactor shutdown is discussed extensively in the literature. Blomeke[18] presents an extensive tabulation of fission product data, including gross and individual activities, as functions of operation time, time after shutdown, reactor flux level, etc.

Avery, et al.,[3] have plotted a set of recommended curves (Fig. 8-1) for fission product gamma-ray decay using six energy groups. These curves were developed by utilizing results obtained by Maienschein, et al.,[13] Perkins and King,[20] Scoles,[27] Stehn and Clancy,[28] and Clark.[29] The highest energy group (Γ_6) is divided into four subgroups, and the data given in Fig. 8-2.

The curves of Perkins and King[20] for decay of gamma activity for various periods of reactor operation were presented in the first edition of ANL-5800.

An experimental determination of gamma rays from fission products between 125 and 1600 seconds after fission is reported by Zobel and Love.[31]

8.1.6 DECAY OF GROSS FISSION PRODUCT ENERGY RELEASE

Figure 8-3 shows the rate of total fission product energy release (gamma plus beta) as a function of time after shutdown following reactor operation for an infinite period of time. Figure 8-4 gives the integrated energy release as a function of time from the time of reactor shutdown.

The simple expression suggested by Way and Wigner[32] for the decay of gamma radiation after fission:

$$\Gamma(t) = 1.26\ t^{-1.2}\ \text{Mev/sec per fission}$$

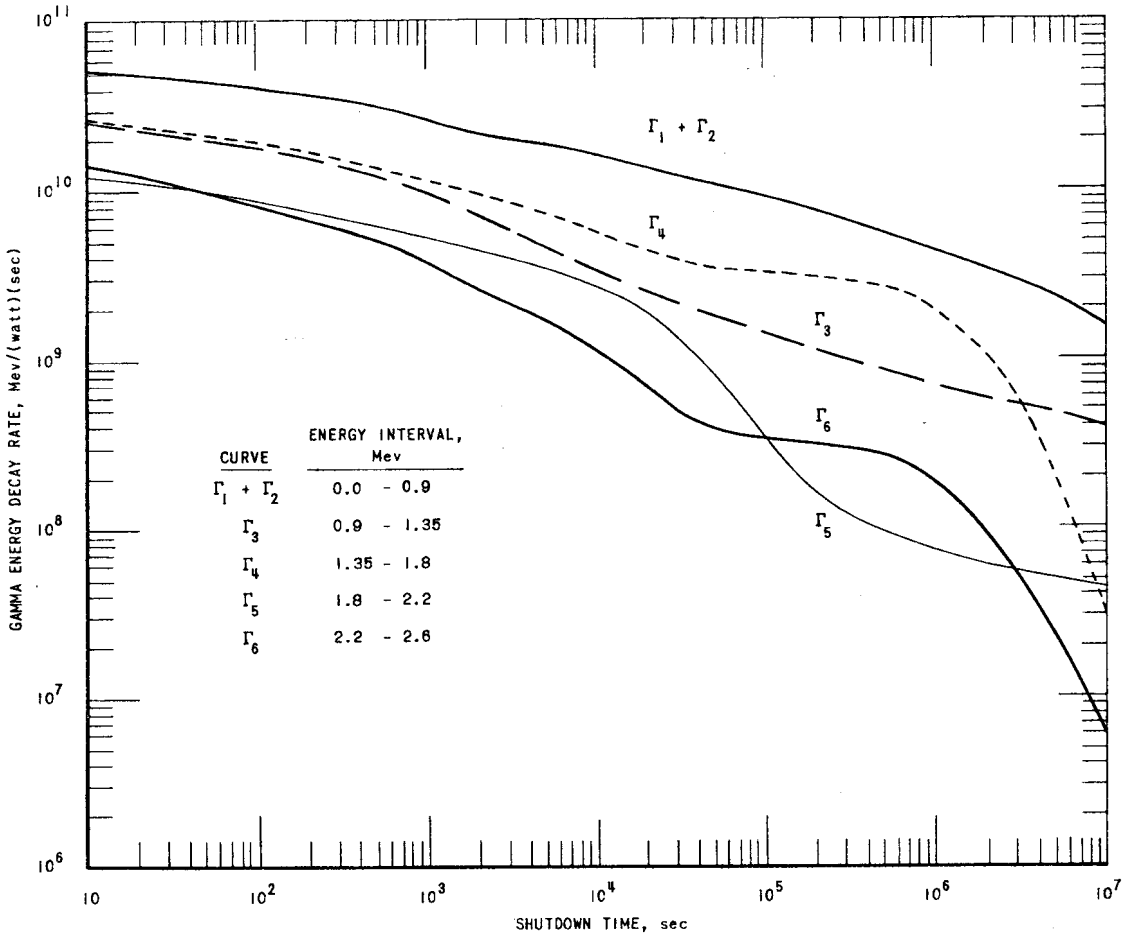

Fig. 8-1 — Fission product gamma energy spectra below 2.6 Mev (infinite irradiation). *Reproduced from Ref. 3.*

where t is the time after fission in seconds, has been shown to be fairly accurate for t greater than 100 seconds. For a reactor which has been operating for a finite time T, the fission product power per watt of reactor power, D(T,t), is given by:

$$D(T,t) = 3.1 \times 10^{10} \int_t^{T+t} d\tau \Gamma(\tau) \text{ Mev/sec per watt}$$

Thus

$$P_0 D(T,t) = 1.95 \times 10^{11} P_0 \{1 - [1 + (T/t)]^{-0.2}\} t^{-0.2} \text{ Mev/sec}$$

where P_0 is the reactor operating power in watts.

Butler and Grotenhuis[33] suggest a graphical expedient for determining D for any combination of T and t. The two functions that make up the right-hand member of the above equation are plotted in Fig. 8-5. The function

$$f(t,T) = 1 - [1 + (T/t)]^{-0.2}$$

represents a correction term to adjust the fission product power after an infinite operating time to that for a finite operating time.

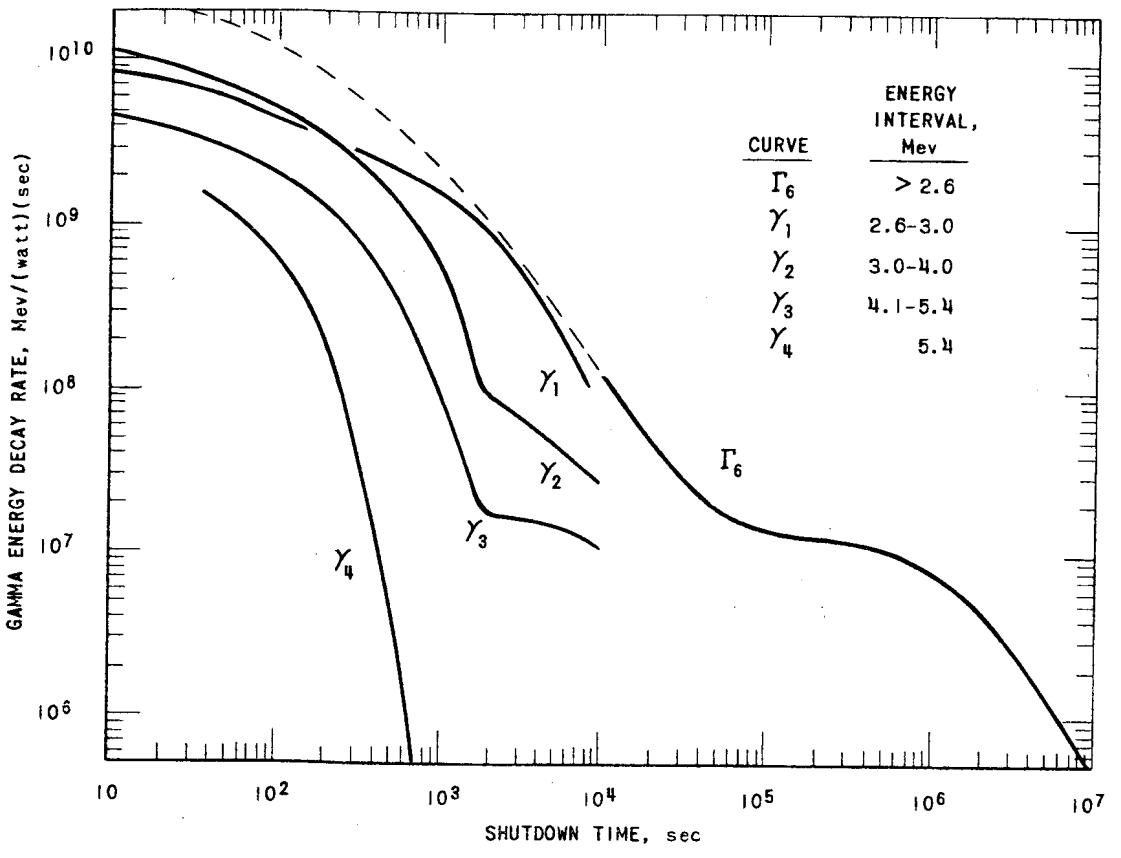

Fig. 8-2 — Fission product gamma energy spectra above 2.6 Mev (infinite irradiation). *Reproduced from Ref. 3.*

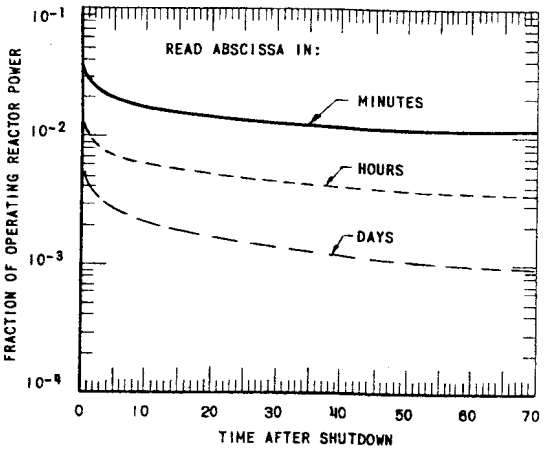

Fig. 8-3 — Fission product power vs. time after shutdown following infinite operation.

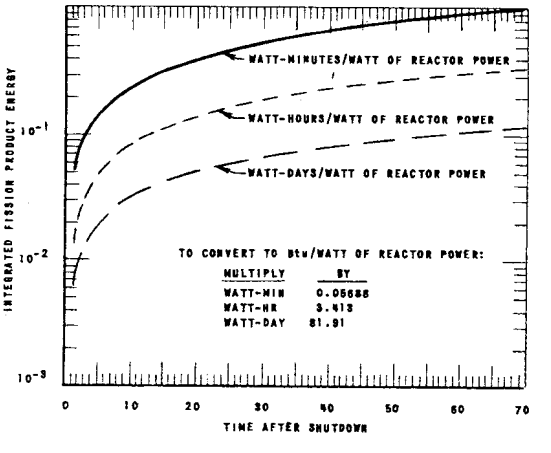

Fig. 8-4 — Integrated fission product energy generated vs. time after shutdown following infinite operation.

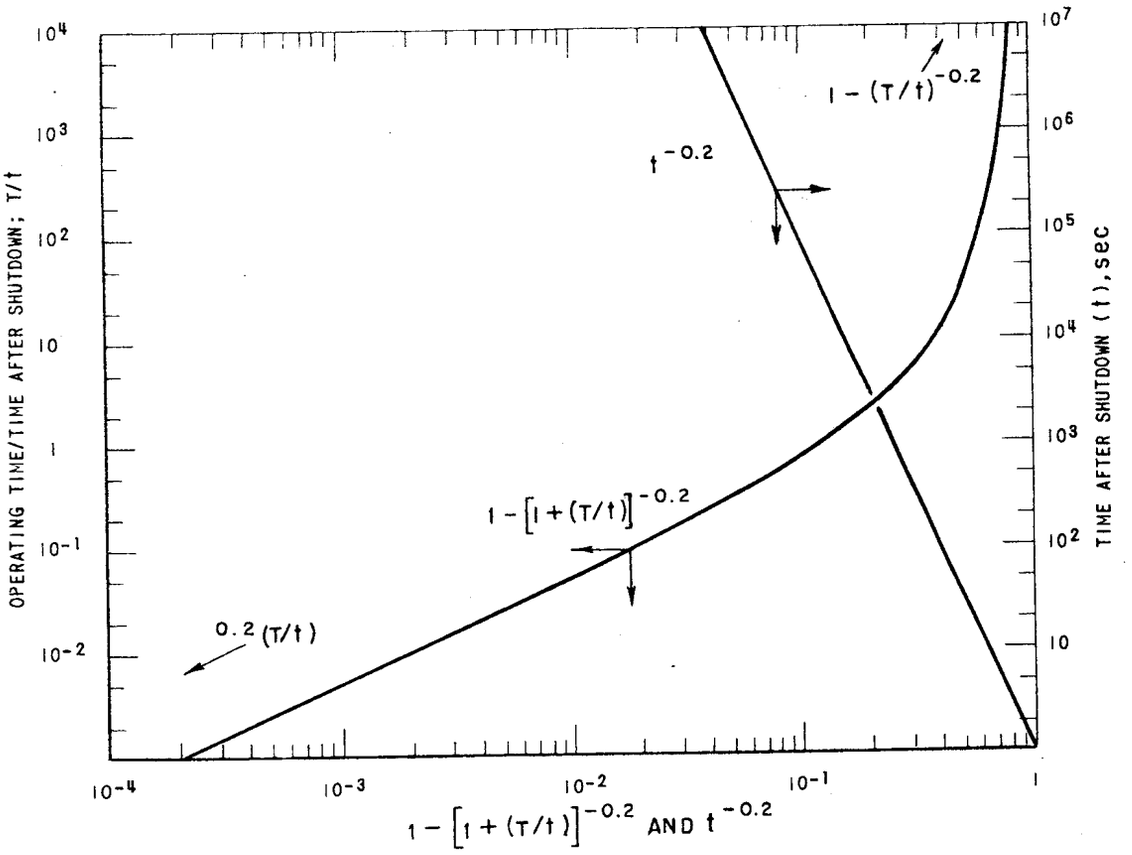

Fig. 8-5 — Factors for calculating power from fission products after shutdown. *Reproduced from Ref. 5.*

8.1.7 ACTIVATION GAMMA-RAY DATA

Table 8-5 lists activation data for some reactor coolant materials. Pure beta emitters are neglected. The activation cross sections for O^{16} and O^{17} are averaged over the fission neutron spectrum since the (n,p) reactions involved have threshold energies in the Mev range.[4]

Table 8-6 is an extensive compilation of activation data for many isotopes produced by capture of thermal neutrons. Gamma-ray activity data are given for both primary and possible secondary products of neutron capture. For shielding applications, pure beta emitters are not important, hence they

Table 8-5 — ACTIVATION DATA FOR SOME REACTOR COOLANTS

Data from Ref. 4, Table 4.1.

Target Isotope	Isotopic Abundance, %	Activation Cross Section, barn	Radioactive Product of Reaction	Half-Life	Energy of Radiation, Mev(γ)	Gammas per Disintegration of Active Atom
Na^{23}	100	0.53[a]	Na^{24}	14.9 hr	2.76; 1.38	1; 1
K^{41}	6.8	1.15[a]	K^{42}	12.4 hr	1.51	0.25
O^{18}	0.204	0.00021[a]	O^{19}	29.4 sec	1.6	0.7
O^{16}	99.8	$\sim 0.019 \times 10^{-3}$[b]	N^{16}	7.4 sec	6.13; 7.10	0.76; 0.06
O^{17}	0.039	$\sim 0.0052 \times 10^{-3}$[b]	N^{17}	4.1 sec	1 (neutron)	1 (neutron)

[a] Neutron activation cross section at 2200 meter/sec.

[b] Fast (n,p) reactions; cross sections averaged over fission spectrum. Data are from Roys and Shure.[37] A previous determination by Henderson and Tunnicliffe[38] gives cross sections of 0.0185×10^{-3} barns for N^{16}, and 0.0093×10^{-3} barns for N^{17}.

Table 8-6—GAMMA-RAY ACTIVITY DUE TO THERMAL NEUTRON CAPTURE

s = second m = minute h = hour d = day y = year * = metastable

Radioactive Isotope	Half-Life	E_γ, Mev	Yield-% per Disinte-gration	Parent Isotope	Isotopic-% or Half-Life	Activation Cross Section, barn
B^{12}	0.027 s	~4.5	~4	B^{11}	81.2	<50 mb
N^{16}	7.4 s	6.1 7.1	55 20	N^{15}	0.37	24 ± 8 μb
O^{19}	29.4 s	1.4	70	O^{18}	0.20	0.21 ± 0.04 mb
F^{20}	10.7 s	1.63	100	F^{19}	100	9 ± 2 mb
Ne^{23}	40.2 s	0.44 1.65	29 1	Ne^{22}	8.8	36 ± 15 mb
Na^{24}	15.1 h	2.76 1.38 4.14	99.96 99.96 0.04	Na^{23}	100	0.53 ± 0.02
Mg^{27}	9.45 m	1.015 0.181 0.834	29 1 70	Mg^{26}	11.3	26 ± 2 mb
Al^{28}	2.3 m	1.78	100	Al^{27}	100	0.21 ± 0.02
Si^{31}	2.65 h	1.26	0.07	Si^{30}	3.12	0.11 ± 0.01
S^{37}	5.04 m	3.12	90	S^{36}	0.016	0.14 ± 0.04
Cl^{38*}	1.0 s	0.66	100	Cl^{37}	24.5	~5 mb
Cl^{38}	37.5 m	2.15 1.65	47 31	Cl^{37} Cl^{38*}	24.5 1 s	0.56 ± 0.12
A^{41}	1.83 h	1.37	99.3	A^{40}	99.6	0.53 ± 0.02
K^{42}	12.46 h	1.53	18	K^{41}	6.91	1.15 ± 0.11
Ca^{47}	4.9 d	1.31 0.82 0.49	71 5 5	Ca^{46}	0.0033	0.25 ± 0.10
Ca^{49}	8.8 m	3.10 4.05	89.78 9.88	Ca^{48}	0.185	1.1 ± 0.1
Sc^{46*}	19.5 s	0.14	100	Sc^{45}	100	10 ± 4
Sc^{46}	85 d	1.12 0.89	99.9 100	Sc^{45} Sc^{46*}	100 19.5 s	12 ± 4
Se^{77*}	17.5 s	0.162	100	Se^{76}	9	7 ± 3
Se^{79*}	3.9 m	0.096	100	Se^{78}	23.5	0.4
Zn^{71*}	3 h	0.38 0.49 0.61	100 100 100	Zn^{70}	0.62	?
Zn^{71}	2.2 m	0.51	100	Zn^{70}	0.62	85 ± 20 mb
Ga^{70}	21 m	1.04	0.8	Ga^{69}	60.2	1.4 ± 0.3
Ga^{72}	14.2 h	0.69[a] 0.89 1.86 2.51	28.2 105 30.3 53.1	Ga^{71}	39.8	5.0 ± 1.0
Ge^{75*}	48 s	0.139	100	Ge^{74}	36.7	?
Ge^{75}	82 m	0.63[a] 0.264	0.80 11.15	Ge^{74} Ge^{75*}	36.7 48 s	0.45 ± 0.08
Ge^{77*}	52 s	0.159	14.2	Ge^{76}	7.7	30 ± 20 mb
Ge^{77}	12 h	0.56[a] 0.79 1.36 2.0	21.6 4.3 4 1	Ge^{76} Ge^{77*}	7.7 52 s (14.2%)	0.2 ± 0.1
As^{76}	26.8 h	2.05 1.40 1.20 0.64 0.55	1 2 9.22 8.78 39.78	As^{75}	100	4.2 ± 0.8
Se^{81*}	56.8 m	0.103	100	Se^{80}	49.8	30 ± 10 mb
Se^{83}	25 m	0.176 0.950	100 100	Se^{82}	9.2	4 ± 2 mb
Br^{83}	2.33 h	0.046	20	Se^{83*} Se^{83}	67 s 25 m	
Kr^{83*}	1.88 h	0.032 0.009	100 100	Br^{83}	2.33 h	

Sc^{47}	3.43	d	0.16	74	Ca^{47}	4.9	d			Br^{80*}	4.5	h	0.048	100	Br^{79}	50.54		2.9 ± 0.5	
Ti^{51}	5.79	m	0.605	1.4	Ti^{50}	5.25		0.14 ± 0.03					0.036	100					
			0.928	4.2						Br^{80}	18.5	m	0.62	14	Br^{79}	50.54		8.5 ± 1.4	
			0.323	95.8											Br^{80*}	4.5	h		
V^{52}	3.76	m	1.44	100	V^{51}	99.8		4.5 ± 0.9		Br^{82}	35.9	h	0.688[a]	152.4	Br^{81}	49.5		3.5 ± 0.5	
Cr^{51}	27.8	d	0.32	10	Cr^{50}	4.31		13.5 ± 1.4					0.817	108					
													1.469	69.8					
Mn^{56}	2.58	h	2.98	0.4	Mn^{55}	100		13.4 ± 0.3		Kr^{79}	34.5	h	0.217[a]	34.4	Kr^{78}	0.35		2.0 ± 0.5	
			2.13	15									0.398	12.7					
			2.65	1.8									0.833	5.84					
			1.81	24															
			0.845	99						Kr^{85*}	4.4	h	0.305	22	Kr^{84}	57		0.10 ± 0.03	
Fe^{59}	45.1	d	0.191	3	Fe^{58}	0.31		0.9 ± 0.2					0.150	78					
			1.29	43						Kr^{87}	78	m	2.57	21.9	Kr^{86}	17.4		60 ± 20	mb
			1.10	57									2.05	3.57					
Co^{60*}	10.5	m	0.058	99.7	Co^{59}	100		16 ± 3					0.85	13.57					
													0.403	86.9					
Co^{60}	5.3	y	1.17	99.9	Co^{59}	100		20 ± 3		Rb^{86*}	1.02	m	0.56	100	Rb^{85}	72.15		?	
			1.33	100	Co^{60*}	10.5	m												
						(99.7%)				Rb^{86}	18.6	d	1.08	10	Rb^{85}	72.15		0.72 ± 0.15	
Co^{61}	1.65	h	0.07	100	Co^{60}	5.28	y	6 ± 2							Rb^{86*}	1.02	m		
Ni^{65}	2.56	h	0.37	4.1	Ni^{64}	1.16		1.6 ± 0.2		Rb^{88}	17.8	m	2.68	6.1	Rb^{87}	27.85		0.12 ± 0.03	
			1.49	24.9									0.91	13.6					
			1.12	18.1									1.85	24					
													4.89	Small					
Cu^{64}	12.87	h	1.34	0.4	Cu^{63}	69		3.9 ± 0.8		Sr^{85*}	70	m	0.233	1.3	Sr^{84}	0.55		?	
Cu^{66}	5.15	m	1.05	9	Cu^{65}	31		1.8 ± 0.4					0.007	84.7					
													0.225	84.7					
Zn^{65}	245	d	1.11	45.5	Zn^{64}	48.9		0.5 ± 0.1					0.150	14					
Zn^{69*}	13.8	h	0.439	100	Zn^{68}	18.6		97 ± 10	mb	Sr^{85}	64	d	0.513	100	Sr^{84}	0.55		1.0 ± 0.3	
As^{77}	38.8	h	0.524	0.52	Ge^{77*}	52	s								Sr^{85*}	70	m		
						(85.8%)										(86%)			
			0.246	1.51	Ge^{77}	12	h			Sr^{87*}	2.8	h	0.388	100	Sr^{86}	9.87		1.3 ± 0.4	
Se^{75}	119.9	d	0.121[a]	24.7	Se^{74}	0.87		26 ± 6		Zr^{95}	63.3	d	0.754	54	Zr^{94}	17.4		0.09 ± 0.03	
			0.265	58.7									0.722	43					
			0.280	17.8															
			0.136	59.9						Zr^{97}	17	h	1.15	80	Zr^{96}	2.8		0.10 ± 0.05	
			0.402	17.8									1.72	20					
													0.58	80					

687863 O - 63 - 42

Table 8-6 — GAMMA-RAY ACTIVITY DUE TO THERMAL NEUTRON CAPTURE (Continued)

s = second m = minute h = hour d = day y = year * = metastable

Radioactive Isotope	Half-Life	E_γ, Mev	Yield-% per Disintegration	Parent Isotope	Isotopic-% or Half-Life	Activation Cross Section, barn
Nb^{94*}	6.6 m	0.0414	99.9	Nb^{93}	100	1.0 ± 0.5
		0.90	~0.1			
Nb^{95*}	84 h	0.235	100	Zr^{95}	63.3 d (3%)	
Nb^{95}	35 d	0.770	99	Nb^{95*}	84 h	
				Zr^{95}	63.3 d (97%)	
Nb^{97*}	60 s	0.747	100	Zr^{97}	17 h	
Nb^{97}	74 m	0.665	100	Nb^{97*}	60 s	
Mo^{93*}	6.8 h	0.26	100	Mo^{92}	15.86	< 6 mb
		0.68	100			
		1.48	100			
Mo^{99}	67 h	0.780[a]	8	Mo^{98}	23.75	0.45 ± 0.10
		0.740	6			
		0.377	1			
		0.041	5			
		0.181	6			
Mo^{101}	14.6 m	0.515[a]	96	Mo^{100}	9.62	0.20 ± 0.05
		0.083	93.5			
		0.896	3.5			
		2.08	8.5			
Tc^{99*}	6.04 h	0.142	1	Mo^{99}	67 h (94%)	
		0.002	99			
		0.140	99			
Tc^{101}	14 m	0.307[a]	87	Mo^{101}	14.6 m	
		0.939	3			
		0.545	10.4			
		0.130	3.5			
Ru^{97}	2.8 d	0.57	1	Ru^{96}	5.5	10 ± 4 mb
		0.325	3.5			
		0.216	95.5			
Tc^{97*}	92 d	0.099	100	Ru^{97}	2.8 d	
		0.090	100			
Cd^{113*}	5.1 y	0.265	0.1	Cd^{112}	24.1	30 ± 15 mb
Cd^{115*}	43 d	1.30	1	Cd^{114}	28.86	0.14 ± 0.03
		0.935	2			
Cd^{115}	53 h	0.033	1	Cd^{114}	28.86	1.1 ± 0.3
		0.523	23.8			
		0.49	12.4			
		0.26	2.32			
In^{115*}	4.5 h	0.335	95	Cd^{115}	53.0 h	
Cd^{117*}	2.9 h	0.84	61	Cd^{116}	7.58	1.5 ± 0.3
		1.27	30			
		1.55	9			
		0.425	61			
		0.281	91			
In^{117*}	1.9 h	0.312	22	Cd^{117*}	2.9 h	
		0.160	23	Cd^{117}	50 m	
In^{117}	66 m	0.562	91	In^{117*}	1.9 h (22%)	
		0.712	9			
		0.160	91			
Cd^{117}	50 m	0.425	100	Cd^{116}	7.58	?
		0.281	100			
Sn^{117*}	14 d	0.562	100	In^{117}	66 m	
		0.160	100			
In^{114*}	50 d	0.192	96.5	In^{113}	4.2	56 ± 12
		0.722	3.5			
		0.556	3.5			
In^{114}	72 s	1.300	0.09	In^{113}	4.2	2 ± 0.6
In^{116*}	54.2 m	0.137[a]	3	In^{115}	95.8	145 ± 15
		1.49	21			
		0.40	25			
		1.27	129			
		2.09	25			
Sn^{113}	112 d	0.400	100	Sn^{112}	0.95	1.3 ± 0.3

Ru^{103}	39.7	d	0.610 0.495 0.055	6.45 90.5 1.09	Ru^{102}	31.5		1.2 ± 0.3		In^{113*}	1.75	h	0.258 0.393 0.135	11 89 11	Sn^{113}	112	d							
Ru^{105}	4.5	h	0.730	100	Ru^{104}	18.7		0.7 ± 0.2		Sn^{117*}	14	d	0.162 0.320 0.159	99 1 99	Sn^{116}	14.24		6 ± 2	mb					
Rh^{103*}	54	m	0.040	100	Ru^{103} Pd^{103}	41 d 17 d (94%)				Sn^{119*}	275	d	0.065 0.024	100 100	Sn^{118}	24.01		10 ± 6	mb					
Rh^{105*}	40	s	0.130	100	Ru^{105}	4.5	h			Sn^{123}	40	m	0.153	100	Sn^{122}	4.71		0.16 ± 0.04						
Rh^{105}	36.5	h	0.310	30	Rh^{105*}	40	s			Sn^{125}	9.5	m	1.39 0.326	1.9 99.7	Sn^{124}	5.98		0.2 ± 0.1						
Rh^{104*}	4.4	m	0.051 1.53	100 0.0065	Rh^{103}	100		12 ± 2		Sb^{125}	2.4	y	0.637[a] 0.175 0.465 0.0354	22 11 60 11	Sn^{125} Sn^{125}	9.5 m 9.5 d								
Rh^{104}	42	s	1.24 0.556	0.11 1.98	Rh^{104*} Rh^{103}	4.4 m 100		140 ± 30		Te^{125}	58	d	0.110 0.0354	100 100	Sb^{125}	2.4	y							
Pd^{103}	17	d	0.498 0.362 0.298	4 2.84 2.05	Pd^{102}	0.96		4.8 ± 1.5		Sn^{125}	9.5	d	1.97 0.81 1.07	1.2 1 3.75	Sn^{124}	5.98		4 ± 2	mb					
Pd^{109*}	4.8	m	0.17	100	Pd^{108}	26.71		?		Sb^{122*}	3.5	m	0.0753 0.0607	100 100	Sb^{121}	57.25		?						
Ag^{109*}	39.2	s	0.0875	100	Pd^{109} Cd^{109}	13.6 h 1.30 y				Sb^{122}	2.8	d	1.137 0.686 1.258 0.566	0.73 3.4 0.66 66.3	Sb^{121} Sb^{122*}	57.25 3.5 m		6.8 ± 1.5						
Pd^{111}	22	m	0.73 0.65 0.56	< 1 < 1 < 1	Pd^{110}	11.81		0.3 ± 0.1		Sb^{124*}	21	m	0.0185	100	Sb^{123}	42.75		30 ± 15	mb					
Ag^{108}	2.3	m	0.60 0.62 0.43	0.22 0.8 0.28	Ag^{107}	51.35		44 ± 9		Sb^{124*}	1.3	m	0.012	100	Sb^{123}	42.75		30 ± 15	mb					
Ag^{110*}	270	d	0.883[a] 0.945 1.382 1.519	203 48 40 8	Ag^{109}	48.65		2.8 ± 0.5		Sb^{124}	60.9	d	1.37[a] 2.09 0.967 0.644 0.725	3.75 49.2 2.16 108.6 16	Sb^{123} Sb^{124*} Sb^{124*}	42.75 21 m 1.3 m		2.5 ± 0.5						
Ag^{111}	7.5	d	0.340 0.243	8 1	Pd^{111}	22	m			Te^{121*}	154	d	0.0818 0.214	100 100	Te^{120}	0.089		?						
Cd^{107}	6.7	h	0.846	< 1	Cd^{106}	1.21		1 ± 0.5		Te^{121}	17	d	0.575 0.506	87 13	Te^{121*}	154	d							
Ag^{107*}	44.3	s	0.094	100	Cd^{107}	6.7	h																	
Cd^{111*}	48.6	m	0.148 0.247	100 100	Cd^{110}	12.4		0.2 ± 0.1																

Table 8-6—GAMMA-RAY ACTIVITY DUE TO THERMAL NEUTRON CAPTURE (Continued)

s = second m = minute h = hour d = day y = year * = metastable

Radioactive Isotope	Half-Life	E_γ, Mev	Yield-% per Disintegration	Parent Isotope	Isotopic-% or Half-Life	Activation Cross Section, barn
Te^{123*}	104 d	0.0887	100	Te^{122}	2.46	1.1 ± 0.5
		0.159	100			
Te^{125*}	58 d	0.110	100	Te^{124}	4.61	5 ± 3
		0.0354	100			
Te^{127*}	105 d	0.089	98	Te^{126}	18.71	90 ± 20 mb
		0.0585	1.5			
Te^{127}	9.35 h	0.418	Small	Te^{126}	18.71	0.8 ± 0.2
		0.370	Small	Te^{127*}	105 d	
		0.170	Small		(98%)	
Te^{129*}	33 d	0.106	100	Te^{128}	31.8	15 ± 5
Te^{129}	74 m	1.12	10.4	Te^{128}	31.8	0.13 ± 0.03
		0.21	1.7	Te^{129*}	33 d	
		0.72	2			
		0.475	17.1			
		0.027	98			
Te^{131*}	30 h	0.180[a]	21.7	Te^{130}	34.5	< 8 mb
		0.239	70			
		1.12	90			
		0.099	84			
		0.446	50			
Te^{131}	24.8 m	0.773	5	Te^{130}	34.5	0.22 ± 0.05
		0.446	45	Te^{131*}	30 h	
		0.147	60		(21.7%)	
		0.099	40			
		0.051	40			
I^{128}	24.98 m	0.540	1.8	I^{127}	100	5.5 ± 0.5
		0.455	17.3			
		0.990	0.2			
Xe^{125}	18 h	0.243	95	Xe^{124}	0.096	?
		0.056	5			
		0.187	5			
I^{125}	60 d	0.035	100	Xe^{125}	18 h	
Xe^{127}	36.4 d	0.368	10	Xe^{126}	0.09	?
		0.170	85			
		0.486	73			
		1.60	76			
		0.130	26			
Ce^{137*}	35 h	0.255	100	Ce^{136}	0.193	0.6 ± 0.2
Ce^{137}	8.7 h	0.445	3	Ce^{136}	0.193	6.3 ± 1.5
				Ce^{137*}	35 h	
Ce^{139*}	55 s	0.740	100	Ce^{138}	0.250	7 ± 5 mb[b]
Ce^{139}	140 d	0.1665	100	Ce^{138}	0.25	0.6 ± 0.3
				Ce^{139*}	55 s	
Ce^{141}	32 d	0.1449	75	Ce^{140}	88.48	0.31 ± 0.10
Ce^{143}	32 h	1.10[a]	6	Ce^{142}	11.07	0.95 ± 0.05
		0.861	17			
		0.351	24			
		0.294	21			
		0.057	36			
Pr^{142}	19.3 h	1.61	2.8	Pr^{141}	100	10 ± 3
Nd^{147}	11.06 d	0.69	3	Nd^{146}	17.26	1.8 ± 0.6
		0.318	20			
		0.165	3			
		0.532	25			
		0.092	60			
Nd^{149}	2.0 h	0.65[a]	15	Nd^{148}	5.74	3.7 ± 1.2
		0.124	81			
		0.285	68			
Pm^{149}	52 h	0.285	100	Nd^{149}	2 h	
		1	100			
Nd^{151}	12 m	0.73[a]	40	Nd^{150}	5.63	?
		0.085	60			
		0.117	120			
		0.421	60			
		1.14	100			
Pm^{151}	27.5 h	0.715[a]	10	Nd^{151}	12 m	
		0.340	42			

			0.200	85					
			0.145	2					
			0.056	4					
Xe^{129*}	8	d	0.0400	100	Xe^{128}	1.919	?		
			0.196	100					
Xe^{133*}	2.3	d	0.232	100	Xe^{132}	26.89	?		
Xe^{133}	5.27	d	0.081	100	Xe^{132}	26.89	0.2 ± 0.1		
					Xe^{133*}	2.3 d			
Xe^{135*}	15.6	m	0.52	100	Xe^{134}	10.44	?		
Xe^{135}	9.2	h	0.370	2	Xe^{134}	10.44	0.2 ± 0.1		
			0.620	3	Xe^{135*}	15.6 m			
			0.250	97					
Cs^{134*}	3.2	h	0.137	0.8	Cs^{133}	100	17 ± 4	mb	
			0.0105	98.2					
			0.127	98.2					
Cs^{134}	2.3	y	0.200[a]	13	Cs^{133}	100	26 ± 5		
			0.801	210	Cs^{134*}	3.2 h			
			1.17	4.02					
			1.37	6.70					
Ba^{131}	11.6	d	1.03[a]	2.9	Ba^{130}	0.101	10.1 ± 1.0		
			0.82	5.6					
			0.495	79.7					
			0.245	17.2					
			0.122	61					
Ba^{133*}	38.8	h	0.276	100	Ba^{132}	0.097	?		
			0.012	100					
Ba^{133}	7.2	y	0.360	96.5	Ba^{132}	0.097	7 ± 2		
			0.070	3.5	Ba^{133*}	38.8 h			
			0.292	3.5					
			0.081	100					
Ba^{135*}	28.7	h	0.268	100	Ba^{134}	2.42	?		
Ba^{137*}	2.60	m	0.661	100	Ba^{136}	7.81	?		
Ba^{139}	85	m	1.43	19	Ba^{138}	71.66	0.5 ± 0.1		
			0.163	85					
La^{140}	40.2	h	2.57[a]	20	La^{139}	99.9	8.4 ± 1.7		
			0.920	40					

			0.177	115					
			0.275	70					
			0.069	105					
Sm^{145}	400	d	0.0613	100	Sm^{144}	3.16	< 2		
Sm^{153}	47	h	0.17	25	Sm^{152}	26.63	140 ± 40		
			0.07	15					
			0.1	53					
Sm^{155}	24	m	1.05	100	Sm^{154}	22.53	5.5 ± 1.1		
			0.246	100					
Eu^{155}	1.7	y	0.102	50	Sm^{155}	24 m			
			0.084	27					
			0.018	27					
Eu^{152}	9.2	h	1.39[a]	1.54	Eu^{151}	47.8	1400 ± 300[b]		
			0.983	21.4					
			0.344	2.8					
			0.122	15.2					
Gd^{153}	236	d	0.1	100	Gd^{152}	0.2	< 125		
Gd^{159}	18	h	0.364	10	Gd^{158}	24.87	4 ± 2		
			0.23	6					
			0.136	4					
			0.079	2					
			0.056	12					
Gd^{161}	3.63	m	0.360	10	Gd^{160}	21.90	0.8 ± 0.3		
			0.102	90					
			0.316	90					
			0.060	10					
Tb^{161}	7	d	0.106[a]	2	Gd^{161}	3.63 m			
			0.0573	18					
			0.0277	27					
			0.0783	5					
Tb^{160}	73	d	0.093[a]	80	Tb^{159}	100	> 22		
			0.976	63					
			1.45	26					
			0.466	39					
			0.297	63					
Dy^{165*}	1.25	m	0.108	90	Dy^{164}	28.18	510 ± 20		
			0.515	6					
			0.361	4					

Table 8-6 — GAMMA-RAY ACTIVITY DUE TO THERMAL NEUTRON CAPTURE (Continued)

s = second m = minute h = hour d = day y = year * = metastable

Radioactive Isotope	Half-Life	E_γ, Mev	Yield-% per Disinte-gration	Parent Isotope	Isotopic-% or Half-Life	Activation Cross Section, barn
Dy^{165}	139 m	0.279[a]	1	Dy^{164}	28.18	2100 ± 300[b]
		0.361	40	Dy^{165*}	1.25 m (90%)	
		1.02	8			
		0.71	2			
		0.094	10			
Ho^{166}	27.2 h	1.378	1	Ho^{165}	100	60 ± 12
		0.080	48			
Er^{169}	9.4 d	0.0084	15	Er^{168}	27.1	2 ± 0.4
Er^{171}	7.5 h	0.308[a]	95	Er^{170}	14.9	9 ± 2
		0.013	3			
		0.126	40			
		0.118	55			
		0.005	65			
Tm^{170}	127 d	0.084	24	Tm^{169}	100	118 ± 30
Yb^{169}	32 d	0.0084[a]	60	Yb^{168}	0.14	11000 ± 3000[b]
		0.094	60			
		0.118	60			
		0.20	50			
		0.31	40			
Yb^{175}	4.1 d	0.396[a]	10	Yb^{174}	31.84	60 ± 40
		0.144	5			
		0.251	2			
		0.138	3			
		0.114	13			
Yb^{177}	1.8 h	1.24[a]	4	Yb^{176}	12.73	5.5 ± 1
		0.140	1			
		0.147	9			
		0.118	3			
Lu^{176*}	3.7 h	0.089	90	Lu^{175}	97.4	35 ± 15
Lu^{177}	6.7 d	0.321	2	Lu^{176}	2.6	4000 ± 800
		0.208	2	Yb^{177}	1.8 h	
		0.072	3			
		0.250	3			
		0.113	5			
Os^{185}	95 d	0.879[a]	15	Os^{184}	0.018	<200
		0.233	2			
		0.160	2			
		0.646	85			
Os^{191*}	14 h	0.074	100	Os^{190}	26.4	?
Ir^{191*}	4.9 s	0.042	100	Os^{191}	16 d	
		0.129	100			
Os^{193}	31.5 h	0.387[a]	5	Os^{192}	41	1.6 ± 0.4
		0.460	5			
		0.281	12			
		0.139	7			
		0.073	36			
Ir^{192*}	1.45 m	0.056	100	Ir^{191}	38.5	260 ± 100
Ir^{192}	74.5 d	0.485[a]	208	Ir^{191}	38.5	700 ± 200
		0.613	23	Ir^{192*}	1.45 m	
		1.06	0.04			
Ir^{194}	19 h	2.05[a]	0.14	Ir^{193}	61.5	130 ± 30
		1.66	8.9			
		1.18	9.4			
		0.643	18.5			
		0.328	19.3			
Pt^{193*}	3.5 d	0.130	100	Pt^{192}	0.78	90 ± 40
Pt^{195*}	~6 d	0.130	60	Pt^{194}	32.8	?
		0.031	40			
		0.099	40			
Pt^{197}	18 h	0.279	0.9	Pt^{196}	25.4	0.80 ± 0.10
		0.191	10.6			
		0.077	99.1			
Pt^{199}	31 m	0.96[a]	3	Pt^{198}	7.2	3.9 ± 0.8
		0.54	41			
		0.197	81			
		0.246	42			
		0.316	41			

Hf^{175}	70	d	0.430 0.089 0.342	1.5 13.7 97.5	Hf^{174}	0.19		?		Au^{199}	3.15	d	0.209 0.050 0.159	3.7 20.6 89.9	Pt^{199}	31	m			
Hf^{180*}	5.5	h	0.444 0.333 0.216 0.093 0.0576	80 20 20 80 100	Hf^{179}	13.75		?		Au^{198}	2.7	d	1.089 0.4118	0.16 99.018	Au^{197}	100		96	±	10
Hf^{181}	44.6	d	0.482[a] 0.137 0.0039 0.346	89.3 110 1 13.2	Hf^{180}	35.25		10	± 3	Hg^{197*}	24	h	0.164 0.133	96.6 96.6	Hg^{196}	0.146		?		
Ta^{182*}	16.5	m	0.180	100	Ta^{181}	100		30	± 10	mb	Hg^{197}	65	h	0.191 0.077	1.2 100	Hg^{197*}	24 h (96.6%)			
Ta^{182}	115	d	0.229[a] 0.100 0.084 1.289	45 65 55 94	Ta^{181} Ta^{182*}	100 16.5 m		19	± 7		Au^{197*}	7.4	s	0.407 0.130 0.277	2 1.4 1.4	Hg^{197*}	24 h (3.4%)			
W^{181}	140	d	0.152 0.136	0.176 0.114	W^{180}	0.135		10	± 10		Hg^{203}	45.4	d	0.279	100	Hg^{202}	29.8		3.8	± 0.8
W^{185*}	1.7	m	1.30 1.65	100 100	W^{184}	30.6		2.1	± 0.6		Hg^{205}	5.5	m	0.203	Small	Hg^{204}	6.85		0.43	± 0.10
W^{187}	24	h	0.686 0.480 0.206 0.072 0.132	12 8 5 3 3	W^{186}	28.4		34	± 7		Tl^{204}	3	y	0.38	0.008	Tl^{203}	29.5		8	± 3
Re^{186}	91	h	0.768 0.123 0.137	0.05 2 22	Re^{185}	37.07		100	± 20		Th^{233}	23.5	m	0.662 0.448 0.350 0.172 0.098	0.05 0.10 0.004 0.03 0.25	Th^{232}	100		7.34	± 0.15
Re^{188*}	18.7	m	0.060 0.105	100 100	Re^{187}	62.93		?			Pa^{233}	26.95	d	0.417[a] 0.104 0.313 0.058 0.028	20 35 80 111 39	Th^{233}	23.5	m		
Re^{188}	17	h	1.96[a] 0.633 0.155	0.20 1 9	Re^{187} Re^{188*}	62.93 18.17 m		75	± 15		U^{239}	23.5	m	0.075	100	U^{238}	99.274		2.76	± 0.09
											Np^{239}	2.33	d	0.067[a] 0.285 0.105 0.228	62 87 30 4	U^{239}	23.5	m		

[a]Effective value.
[b]Reactor neutrons.

are not included. Activation cross sections are compiled from BNL-325.[34] The comments given in the introduction to the section "Thermal Cross Sections" in BNL-325 apply.

Most of the radioactive isotopes listed in Table 8-6 are formed directly as a result of thermal neutron capture by the parent isotope. The activation cross sections listed refer to such direct formation. If the radioactive isotope is formed by the decay of a previously produced radioactive isotope, the half-life of the immediate parent is listed rather than an isotopic abundance.

The half-life values are taken from the Trilinear Chart of Nuclides.[35] Energies of the photons emitted, and their respective percentage yields per disintegration, are taken from Refs. 35 and 36. The superscript "a" indicates that gamma-ray energies and yields are effective values obtained by summing yields of individual gammas and assigning to them the highest energy represented within the group. If the yield of a gamma ray is less than 1% per disintegration and it is not the highest energy gamma ray given off, it is omitted. If a gamma ray is the highest energy photon given off and it has appreciably higher energy than the next lower one, it is included even if its yield is less than 1%.

8.1.8 CROSS SECTIONS FOR PHOTONEUTRON PRODUCTION

The cross sections for photoneutron production for deuterium and beryllium are plotted in Figs. 8-6 and 8-7, respectively.*

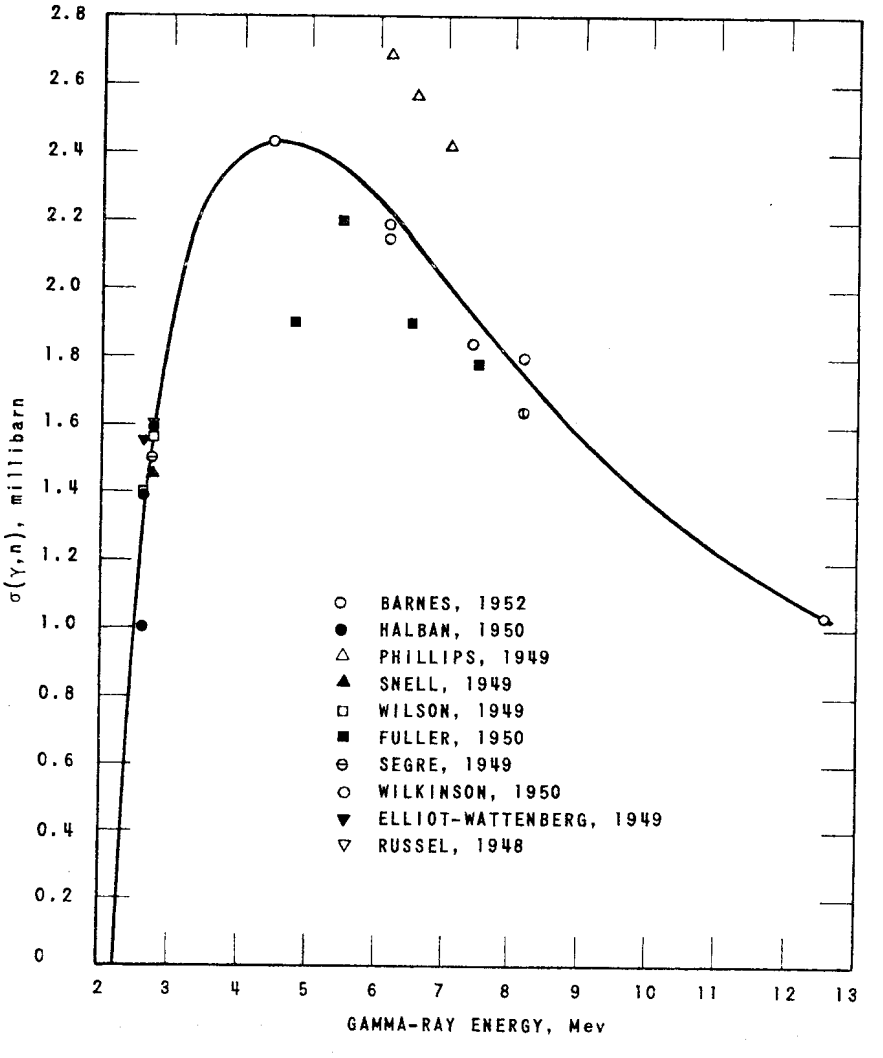

Fig. 8-6 — Photoneutron production cross section for deuterium.

*Private communication, R. M. Freestone, ORNL, April, 1961.

Source of Data for Fig. 8-6

C. A. Barnes, et al., *Phys. Rev.*, 86: 359, (1952).
H. Halban, 1950; cited by W. F. Hornyak, et al., *Rev. Modern Phys.*, 22: 296, (1950).
J. A. Phillips, et al., *Phys. Rev.*, 80: 326, (1950).
A. H. Snell, et al., *Phys. Rev.*, 80: 637, (1950).
R. Wilson, et al., *Nature*, 163: 245, (1949).
E. G. Fuller, *Phys. Rev.*, 79: 303, (1950).
E. Segre; cited by E. Guth and C. Mullin, *Phys. Rev.*, 76: 234, (1949).
D. H. Wilkinson; cited by Hornyak, et al., *Rev. Mod. Phys.*, 22: 296, (1950).
L. G. Elliott and A. Wattenberg, cited by Hornyak, et al., *Rev. Modern Phys.*, 22: 296, (1950).
B. Russel, et al., *Phys. Rev.*, 73: 545, (1948).

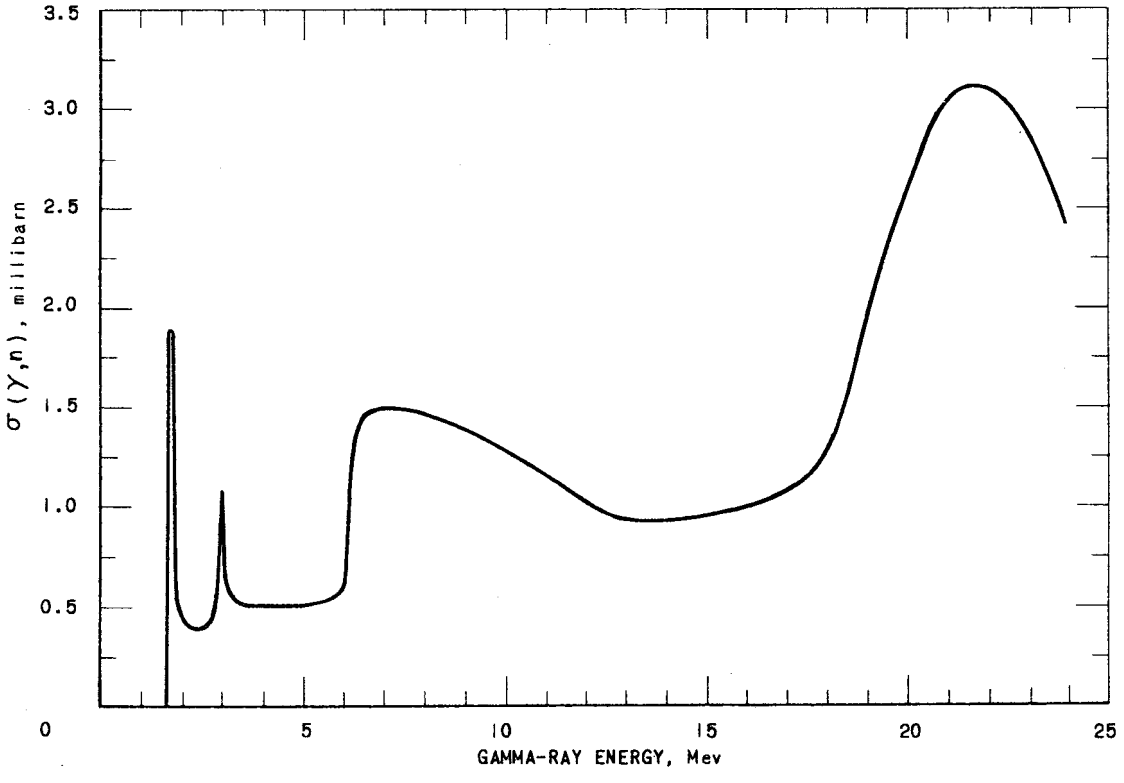

Fig. 8-7 — Photoneutron production cross section for beryllium.

8.2 NEUTRON CONSTANTS

This section is limited to effective constants useful for hand calculations in shield design. Appropriate techniques are presented by Avery, et al.,[3] Duncan and Whittum,[39] and Grotenhuis.[5]

8.2.1 ATTENUATION OF FISSION NEUTRONS IN WATER

Figure 8-8 shows plots of centerline attenuation data for water measured in the Bulk Shielding Facility at ORNL.[40] The change in slope of the thermal neutron flux at about two meters from the reactor indicates that beyond this point more of the thermal neutrons are due to photoneutrons than to the slowing-down of fission neutrons from the reactor.

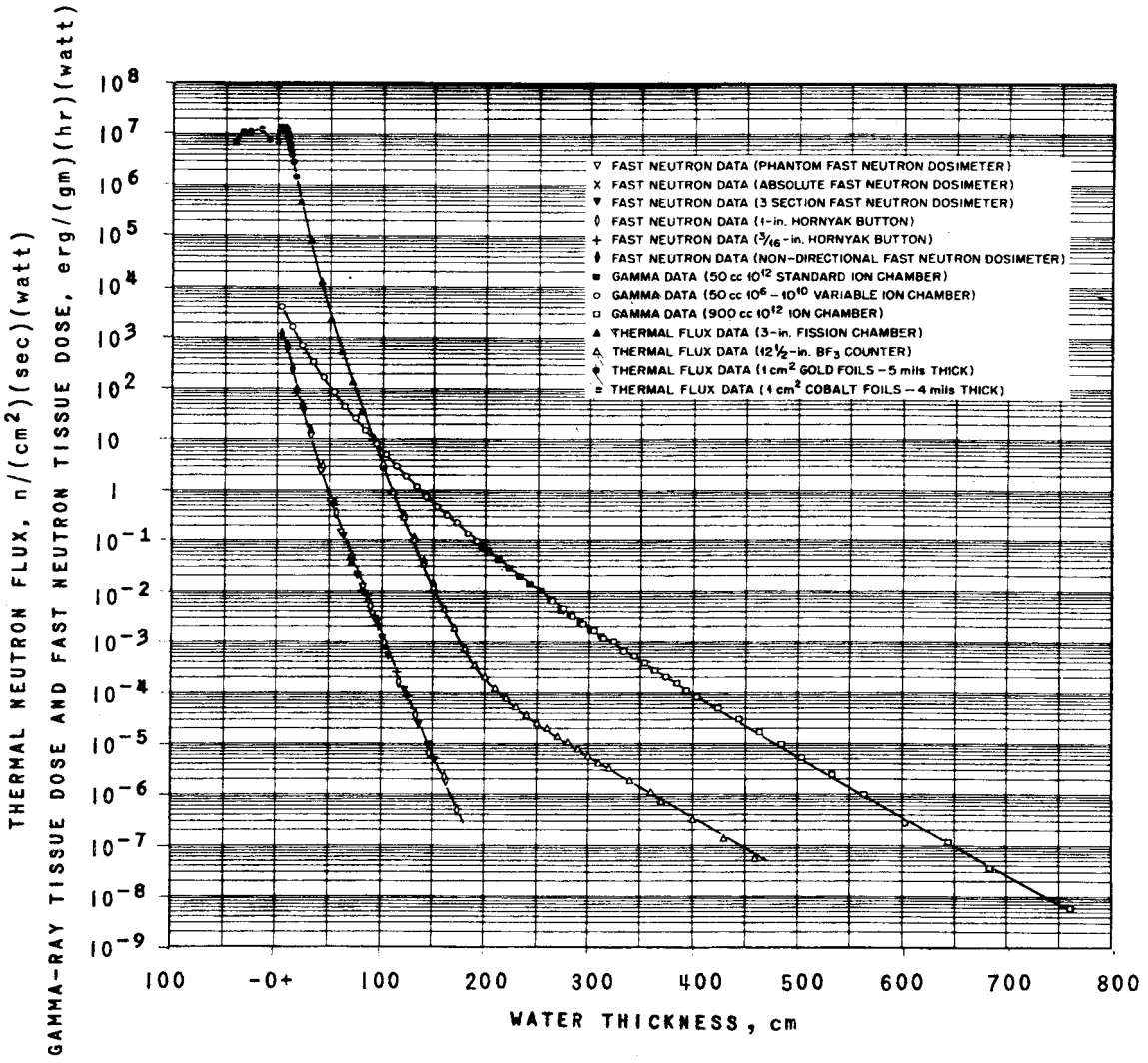

Fig. 8-8 — Neutron and gamma-ray attenuation in water at centerline of Bulk Shielding Facility at ORNL. *Reproduced from Ref. 40.*

A multigroup analysis of attenuation of fission neutrons in water using the P1MG Code is reported by Anderson and Shure[41] and compared with experiments and calculations using the "moments" method. Duncan and Whittum[39] fit an attenuation kernel calculated by the moments method with the sum of two exponentials:

$$4\pi x^2 \text{ (Dose Rate, mrep/hr)} = 0.0102 \left(e^{-0.129x} + e^{-0.1091x}\right)$$

and compare it with the BSF curve (Fig. 8-8).

8.2.2 REMOVAL CROSS SECTION

The removal cross section, originally defined by Albert and Welton,[42] is a parameter used widely in fast neutron attenuation calculations. It is a measure of the ability of a material to remove a fast neutron from further consideration as a fast neutron for shielding attenuation purposes. This involves not only the interaction of the neutron with an atom of the material, but also its subsequent interaction with the atoms of a hydrogenous material. Neutrons which are either degraded in energy by inelastic scatterings, or deflected by wide angle elastic scatterings in the material, are unlikely to penetrate large distances into a medium such as water, or a concrete which contains several atom-per cent of hydrogen.

Table 8-7 lists the removal cross sections determined in the Lid Tank Facility at ORNL by analysis of neutron attenuation measurements in water beyond slabs of various materials.[43] Figure 8-9 is a plot of the removal cross section of various elements as a function of atomic weight. The smooth variation with atomic weight indicates that removal cross sections may be estimated with reasonable accuracy.

Table 8-7—REMOVAL CROSS SECTIONS FOR VARIOUS MATERIALS

Data from Ref. 43.

Material	σ_R, barn	N_0 at 20°C, atom/cm^3	Σ_R, cm^{-1}
Hydrogen	1.00 ± 0.05	—	—
Deuterium	0.92 ± 0.10[a]	—	—
Lithium	1.01 ± 0.04	0.0460×10^{24}	0.046
Beryllium	1.07 ± 0.06	0.120	0.128
Boron	0.97 ± 0.10	0.139	0.135
Carbon (Graphite)	0.72 ± 0.05	0.113	0.081
Oxygen	0.92 ± 0.05	—	—
Fluorine	1.29 ± 0.06	—	—
Aluminum	1.31 ± 0.05	0.0603	0.079
Chlorine	1.2 ± 0.8	—	—
Iron	1.98 ± 0.08	0.0848	0.168
Nickel	1.89 ± 0.10	0.0913	0.173
Copper	2.04 ± 0.11	0.0846	0.173
Zirconium	2.36 ± 0.12	0.0423	0.10[b]
Tungsten	3.13 ± 0.25	0.0631	0.198[c]
Lead	3.53 ± 0.30	0.0330	0.116
Bismuth	3.49 ± 0.35	0.0282	0.098
Uranium	3.6 ± 0.4	0.0473	0.17
Boric Oxide (B_2O_3)	4.30 ± 0.41	—	—
Boron Carbide (B_4C)	5.1 ± 0.4	—	—
Fluorothene (C_2F_3Cl)	6.66 ± 0.8	—	—
Heavy Water (D_2O)	2.76 ± 0.11	—	—
Lithium Fluoride (LiF)	2.43 ± 0.34	—	—
Oil (CH_2)	2.84 ± 0.11	—	—
Paraffin ($C_{30}H_{62}$)	80.5 ± 5.2	—	—
Perfluoroheptane (C_7F_{16})	26.3 ± 0.8		

[a]Calculated; $\sigma_R(D_2O) = 2.76$ b.
[b]Value given by Miller.[44]
[c]Value given by Miller.[45]

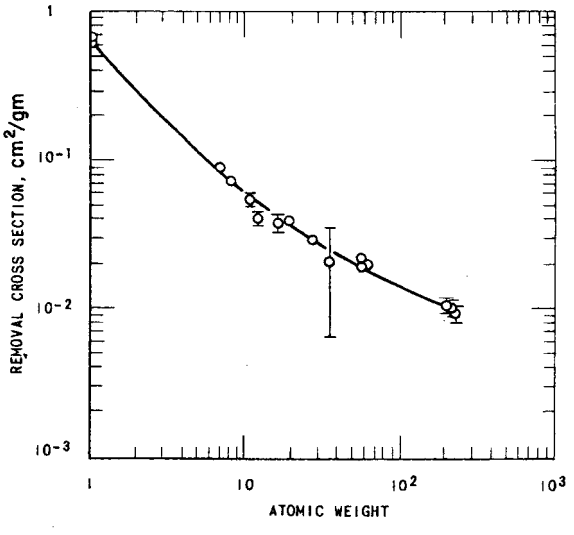

Fig. 8-9—Experimental removal cross section as a function of atomic weight for various elements. *Data from Ref. 43.*

8.2.3 CONVERSION FACTORS: NEUTRON FLUX-TO-DOSE

Absorbed dose of any ionizing radiation is the energy imparted to matter by ionizing particles per unit mass of irradiated material at the place of interest. The accepted unit of absorbed dose is the rad. One rad equals 100 ergs/gm.

The definition of the rad does not specify the target medium nor the type of ionizing radiation; therefore, a quantity known as the Relative Biological Effectiveness (RBE) is used to indicate the effectiveness of absorbed dose in tissue, depending upon the type of radiation. Biological dose is expressed in rems, and is equal, numerically, to the product of the dose in rads and the value of the RBE for the particular type and energy of radiation.

The RBE for hard gamma rays is unity; for neutrons, it is a function of neutron energy, as shown in Table 8-8.

Table 8-8—RELATIVE BIOLOGICAL EFFECTIVENESS (RBE) FOR NEUTRONS AS A FUNCTION OF ENERGY

Reproduced from Ref. 47.

Neutron Energy, Mev	RBE
Thermal	3
0.0001	2
0.005	2.5
0.02	5
0.1	8
0.5	10
1.0	10.5
2.5	8
5.0	7
7.5	7
10	6.5

In Fig. 8-10, the first collision dose rate for neutrons (dose imparted to a small volume of tissue) is given in millirems/hr as a function of neutron energy. It is obtained by multiplying the first collision dose, which includes all of the energy imparted by the neutron to heavy ionizing particles, by the appropriate RBE.

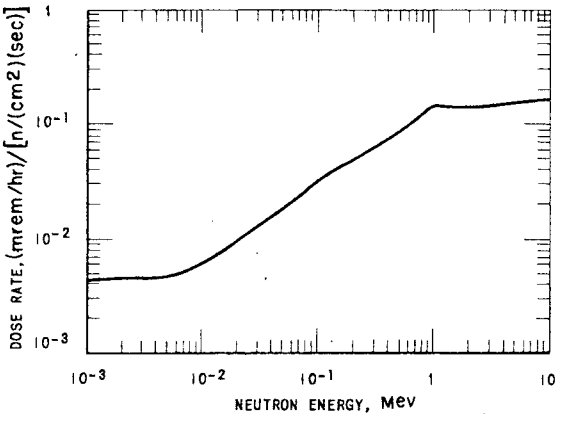

Fig. 8-10—Conversion between neutron flux and biological dose. *After Snyder and Neufeld; reproduced from Ref. 3.*

Depth dose curves have been computed by Snyder[46] using a Monte Carlo method and are reported in the NBS Handbook 63.[47] The depth dose refers to the energy imparted to tissue as a function of depth beneath the surface, due to all primary and secondary ionizing events throughout the tissue body.

The historical unit of dose, the roentgen, is defined as the amount of X-ray or gamma radiation which will produce ions carrying one electrostatic unit of charge in 0.001293 gm of dry air.[48] The dose delivered by one roentgen of such radiation to tissue is equal to 0.93 rad.

8.3 GAMMA-RAY CONSTANTS

The theory of gamma-ray attenuation has been treated extensively in the literature (see Refs. 1, 49, 50, 51, and 52). The data presented in this section are tabulated for discrete gamma-ray energies so that they may be applied in calculations using line spectra.

8.3.1 TOTAL GAMMA-RAY ATTENUATION COEFFICIENT

Table 8-9 gives total gamma-ray attenuation coefficient, μ/ρ, for some common materials.[53] The product of these numbers and the density of the material gives the familiar total cross section, μ_t, (Table 8-10).

8.3.2 ENERGY ABSORPTION COEFFICIENT

Only a fraction of the events represented by the total attenuation cross section actually removes the gamma-ray. In particular, Compton scattering can cause a change in the direction and the energy of a photon without absorbing it. The energy absorption coefficient is a measure of the fraction of the gamma-ray energy which is converted from radiant energy into heat:

$$\phi(E)\ [\text{Mev}/(\text{cm}^2)(\text{sec})]\ \mu_e(E)[\text{cm}^{-1}] = \text{Heat Generation Rate}\ [\text{Mev}/(\text{cm}^3)(\text{sec})]$$

Table 8-11 lists energy absorption mass attenuation coefficients (μ_e/ρ). The product of these coefficients and the density of the material gives the energy absorption cross section, μ_e, (Table 8-12).

8.3.3 BUILDUP FACTORS

Since not all gamma interactions are absorptive, and some scattered radiation may ultimately penetrate a shield, a numerical correction is commonly used in attenuation calculations. The uncollided flux is calculated using total cross sections, and then multiplied by the appropriate buildup factor to give a more realistic value of the transmitted flux. Buildup factors have been determined theoretically[54] by Monte Carlo calculations and by the method of moments. The buildup factor (B) is a function of the distance (x) into the shield, measured in mean free paths, ($\mu_t x$), as well as of the particular material and gamma-ray energy.

Table 8-13 gives a set of dose buildup factors for a point isotropic source, applicable for shields at least one mean free path in thickness.[55] Table 8-14 gives coefficients A_1, $-a_1$, and a_2, for an analytical fit to the buildup factor:[50]

$$B(\mu_t x) = A_1 \exp(-a_1\mu_t x) + A_2 \exp(-a_2\mu_t x)$$

where

$$A_2 = 1 - A_1$$

Values have been calculated[54] for energy and energy absorption buildup factors, and for plane monodirectional sources.

8.3.4 CONVERSION OF GAMMA-RAY FLUX TO DOSE RATE

The curves in Fig. 8-11 can be used to obtain gamma-ray dose rate as a function of gamma-ray flux of a particular energy expressed either in terms of photons/(cm^2)(sec) or Mev/(cm^2)(sec).

Table 8-9—TOTAL MASS ATTENUATION COEFFICIENTS (μ/ρ)

(in cm^2/gm)

Data from Ref. 53.

Material	Gamma-Ray Energy, Mev																	
	0.1	0.15	0.2	0.3	0.4	0.5	0.6	0.8	1.0	1.25	1.5	2	3	4	5	6	8	10.0
H	.295	.265	.243	.212	.189	.173	.160	.140	.126	.113	.103	.0876	.0691	.0579	.0502	.0446	.0371	.0321
Be	.132	.119	.109	.0945	.0847	.0773	.0715	.0628	.0565	.0504	.0459	.0394	.0313	.0266	.0234	.0211	.0180	.0161
C	.149	.134	.122	.106	.0953	.0870	.0805	.0707	.0636	.0568	.0518	.0444	.0356	.0304	.0270	.0245	.0213	.0194
N	.150	.134	.123	.106	.0955	.0869	.0805	.0707	.0636	.0568	.0517	.0445	.0357	.0306	.0273	.0249	.0218	.0200
O	.151	.134	.123	.107	.0953	.0870	.0806	.0708	.0636	.0568	.0518	.0445	.0359	.0309	.0276	.0254	.0224	.0206
Na	.151	.130	.118	.102	.0912	.0833	.0770	.0676	.0608	.0546	.0496	.0427	.0348	.0303	.0274	.0254	.0229	.0215
Mg	.160	.135	.122	.106	.0944	.0860	.0795	.0699	.0627	.0560	.0512	.0442	.0360	.0315	.0286	.0266	.0242	.0228
Al	.161	.134	.120	.103	.0922	.0840	.0777	.0683	.0614	.0548	.0500	.0432	.0353	.0310	.0282	.0264	.0241	.0229
Si	.172	.139	.125	.107	.0954	.0869	.0802	.0706	.0635	.0567	.0517	.0447	.0367	.0323	.0296	.0277	.0254	.0243
P	.174	.137	.122	.104	.0928	.0846	.0780	.0685	.0617	.0551	.0502	.0436	.0358	.0316	.0290	.0273	.0252	.0242
S	.188	.144	.127	.108	.0958	.0874	.0806	.0707	.0635	.0568	.0519	.0448	.0371	.0328	.0302	.0284	.0266	.0255
A	.188	.135	.117	.0977	.0867	.0790	.0730	.0638	.0573	.0512	.0468	.0407	.0338	.0301	.0279	.0266	.0248	.0241
K	.215	.149	.127	.106	.0938	.0852	.0786	.0689	.0618	.0552	.0505	.0438	.0365	.0327	.0305	.0289	.0274	.0267
Ca	.238	.158	.132	.109	.0965	.0876	.0809	.0708	.0634	.0566	.0518	.0451	.0376	.0338	.0316	.0302	.0285	.0280
Fe	.344	.183	.138	.106	.0919	.0828	.0762	.0664	.0595	.0531	.0485	.0424	.0361	.0330	.0313	.0304	.0295	.0294
Cu	.427	.206	.147	.108	.0916	.0820	.0751	.0654	.0585	.0521	.0476	.0418	.0357	.0330	.0316	.0309	.0303	.0305
Mo	1.03	.389	.225	.130	.0998	.0851	.0761	.0648	.0575	.0510	.0467	.0414	.0365	.0349	.0344	.0344	.0349	.0359
Sn	1.58	.563	.303	.153	.109	.0886	.0776	.0647	.0568	.0501	.0459	.0408	.0367	.0355	.0355	.0358	.0368	.0383
I	1.83	.648	.339	.165	.114	.0913	.0792	.0653	.0571	.0502	.0460	.0409	.0370	.0360	.0361	.0365	.0377	.0394
W	4.21	1.44	.708	.293	.174	.125	.101	.0763	.0640	.0544	.0492	.0437	.0405	.0402	.0409	.0418	.0438	.0465
Pt	4.75	1.64	.795	.324	.191	.135	.107	.0800	.0659	.0554	.0501	.0445	.0414	.0411	.0418	.0427	.0448	.0477
Tl	5.16	1.80	.866	.346	.204	.143	.112	.0824	.0675	.0563	.0508	.0452	.0420	.0416	.0423	.0433	.0454	.0484
Pb	5.29	1.84	.896	.356	.208	.145	.114	.0836	.0684	.0569	.0512	.0457	.0421	.0420	.0426	.0436	.0459	.0489
U	1.06	2.42	1.17	.452	.259	.176	.136	.0952	.0757	.0615	.0548	.0484	.0445	.0440	.0446	.0455	.0479	.0511
Air	.151	.134	.123	.106	.0953	.0868	.0804	.0706	.0655	.0567	.0517	.0445	.0357	.0307	.0274	.0250	.0220	.0202
NaI	1.57	.568	.305	.155	.111	.0901	.0789	.0657	.0577	.0508	.0465	.0412	.0367	.0351	.0347	.0347	.0354	.0366
H_2O	.167	.149	.136	.118	.106	.0966	.0896	.0786	.0706	.0630	.0575	.0493	.0396	.0339	.0301	.0275	.0240	.0219
Concrete[a]	.169	.139	.124	.107	.0954	.0870	.0804	.0706	.0635	.0567	.0517	.0445	.0363	.0317	.0287	.0268	.0243	.0229
Tissue	.163	.144	.132	.115	.100	.0936	.0867	.0761	.1683	.0600	.0556	.0478	.0384	.0329	.0292	.0267	.0233	.0212

[a]Type 04.

Table 8-10 — TOTAL GAMMA-RAY ATTENUATION CROSS SECTIONS (μ_t)

(in cm^{-1})

Material	Density, gm/cm^3	Gamma-Ray Energy, Mev																	
		0.1	0.15	0.2	0.3	0.4	0.5	0.6	0.8	1.0	1.25	1.5	2	3	4	5	6	8	10.0
Be	1.85	.244	.220	.202	.1748	.1567	.1430	.1323	.1162	.1045	.0932	.0849	.0729	.0579	.0492	.0433	.0390	.0333	.0298
C	2.25	.335	.302	.275	.239	.2144	.1958	.1811	.1591	.1431	.1278	.1166	.0999	.0801	.0684	.0608	.0551	.0479	.0437
Na	.9712	.147	.126	.115	.099	.0886	.0809	.0748	.0657	.0590	.0530	.0482	.0415	.0338	.0294	.0266	.0247	.0222	.0209
Mg	1.741	.279	.235	.212	.185	.1643	.1497	.1384	.1217	.1092	.1975	.0891	.0770	.0627	.0548	.0498	.0463	.0421	.0397
Al	2.70	.435	.362	.324	.278	.2489	.2268	.2098	.1844	.1658	.1480	.1350	.1166	.0953	.0837	.0761	.0713	.0651	.0618
Si	2.42	.416	.336	.303	.259	.2309	.2103	.1941	.1709	.1537	.1372	.1251	.1082	.0888	.0782	.0716	.0670	.0615	.0588
P	1.83	.318	.251	.223	.190	.1698	.1548	.1427	.1254	.1129	.1008	.0919	.0798	.0655	.0578	.0531	.0500	.0461	.0443
S	2.07	.389	.298	.263	.224	.1983	.1809	.1668	.1463	.1314	.1176	.1074	.0927	.0768	.0679	.0625	.0588	.0551	.0328
K	0.87	.187	.130	.110	.092	.0816	.0741	.0684	.0599	.0538	.0480	.0439	.0381	.0318	.0284	.0265	.0251	.0238	.0232
Ca	1.55	.369	.245	.205	.169	.1496	.1358	.1254	.1097	.0983	.0877	.0803	.0699	.0583	.0524	.0490	.0468	.0442	.0434
Fe	7.86	2.704	1.438	1.085	.833	.7223	.6508	.5989	.5219	.4677	.4174	.3812	.3333	.2837	.2594	.2460	.2389	.2319	.2311
Cu	8.933	3.814	1.840	1.313	.965	.8183	.7325	.6709	.5842	.5226	.4654	.4252	.3734	.3189	.2948	.2823	.2760	.2707	.2725
Mo	9.01	9.280	3.505	2.027	1.171	.8991	.7668	.6857	.5838	.5181	.4595	.4208	.3730	.3289	.3144	.3099	.3099	.3144	.3190
Sn	7.298	11.53	4.109	2.211	1.117	.795	.6466	.5663	.4722	.4145	.3656	.3350	.2978	.2678	.2591	.2591	.2613	.2686	.2795
I	4.94	9.040	3.201	1.675	.815	.563	.4510	.3912	.3226	.2821	.2480	.2272	.2020	.1828	.1778	.1783	.1803	.1862	.1946
W	19.3	81.25	27.79	13.66	5.655	3.358	2.413	1.949	1.473	1.235	1.050	.9496	.8434	.7817	.7759	.7894	.8067	.8453	.8975
Pt	21.37	101.51	35.05	16.99	6.924	4.082	2.885	2.287	1.710	1.408	1.184	1.071	.9510	.8847	.8783	.8933	.9125	.9574	1.019
Tl	11.86	61.20	21.35	10.27	4.104	2.419	1.696	1.328	.9773	.8005	.6677	.6025	.5361	.4981	.4934	.5017	.5135	.5384	.5740
Pb	11.34	59.99	20.87	10.16	4.037	2.359	1.644	1.293	.9480	.7757	.6452	.5806	.5182	.4774	.4763	.4831	.4944	.5205	.5545
U	18.7	19.82	45.25	21.88	8.452	4.843	3.291	2.543	1.780	1.416	1.150	1.025	.9051	.8322	.8228	.8340	.8509	.8957	.9556
NaI	3.667	5.757	2.083	1.118	.568	.407	.3304	.2893	.2409	.2116	.1863	.1705	.1511	.1346	.1287	.1272	.1272	.1298	.1342
H_2O	1.00	.167	.149	.136	.118	.106	.0966	.0896	.0786	.0706	.0630	.0575	.0493	.0396	.0339	.0301	.0275	.0240	.0219
Concrete[a]	2.35	.397	.327	.291	.251	.2242	.2045	.1889	.1659	.1492	.1332	.1215	.1046	.0853	.0745	.0674	.0630	.0571	.0538

[a]Type 04.

Table 8-11—ENERGY ABSORPTION MASS ATTENUATION COEFFICIENT $(\mu_e/\rho)^a$

(in cm^2/gm)

Material	Gamma-Ray Energy, Mev																	
	0.1	0.15	0.2	0.3	0.4	0.5	0.6	0.8	1.0	1.25	1.50	2	3	4	5	6	8	10.0
H	.0411	.0487	.0531	.0575	.0589	.0591	.0590	.0575	.0557	.0533	.0509	.0467	.0401	.0354	.0318	.0291	.0252	.0255
Be	.0183	.0217	.0237	.0256	.0263	.0264	.0263	.0256	.0248	.0237	.0227	.0210	.0183	.0164	.0151	.0141	.0127	.0118
C	.0215	.0246	.0267	.0288	.0296	.0297	.0296	.0289	.0280	.0268	.0256	.0237	.0209	.0190	.0177	.0166	.0153	.0145
N	.0224	.0249	.0267	.0288	.0296	.0297	.0296	.0289	.0280	.0268	.0256	.0236	.0211	.0193	.0180	.0171	.0158	.0151
O	.0233	.0252	.0271	.0289	.0296	.0297	.0296	.0289	.0280	.0268	.0257	.0238	.0212	.0195	.0183	.0175	.0163	.0157
Na	.0289	.0258	.0266	.0279	.0283	.0284	.0284	.0276	.0268	.0257	.0246	.0229	.0207	.0194	.0185	.0179	.0171	.0168
Mg	.0335	.0276	.0278	.0290	.0294	.0293	.0292	.0285	.0276	.0265	.0254	.0237	.0215	.0203	.0194	.0188	.0182	.0180
Al	.0373	.0283	.0275	.0283	.0287	.0286	.0286	.0278	.0270	.0259	.0248	.0232	.0212	.0200	.0192	.0188	.0183	.0182
Si	.0435	.0300	.0286	.0291	.0293	.0290	.0290	.0282	.0274	.0263	.0252	.0236	.0217	.0206	.0198	.0194	.0190	.0189
P	.0501	.0315	.0292	.0289	.0290	.0290	.0287	.0280	.0271	.0260	.0250	.0234	.0216	.0206	.0200	.0197	.0194	.0195
S	.0601	.0351	.0310	.0301	.0301	.0300	.0298	.0288	.0279	.0268	.0258	.0242	.0224	.0215	.0209	.0206	.0206	.0206
A	.0729	.0368	.0302	.0278	.0274	.0272	.0270	.0260	.0252	.0242	.0233	.0220	.0206	.0199	.0195	.0195	.0194	.0197
K	.0909	.0433	.0340	.0304	.0298	.0295	.0291	.0282	.0272	.0261	.0251	.0237	.0222	.0217	.0214	.0212	.0215	.0219
Ca	.111	.0489	.0367	.0318	.0309	.0304	.0300	.0290	.0279	.0268	.0258	.0244	.0230	.0225	.0222	.0223	.0225	.0231
Fe	.225	.0810	.0489	.0340	.0307	.0294	.0287	.0274	.0261	.0250	.0242	.0231	.0224	.0224	.0227	.0231	.0239	.0250
Cu	.310	.107	.0594	.0368	.0316	.0296	.0286	.0271	.0260	.0247	.0237	.0229	.0223	.0227	.0231	.0237	.0248	.0261
Mo	.922	.294	.141	.0617	.0422	.0348	.0315	.0281	.0263	.0248	.0239	.0233	.0237	.0250	.0262	.0274	.0296	.0316
Sn	1.469	.471	.222	.0873	.0534	.0403	.0346	.0294	.0268	.0248	.0239	.0233	.0243	.0259	.0276	.0291	.0316	.0339
I	1.726	.557	.260	.100	.0589	.0433	.0366	.0303	.0274	.0252	.0241	.0236	.0247	.0265	.0283	.0299	.0327	.0353
W	4.112	1.356	.631	.230	.121	.0786	.0599	.0426	.0353	.0302	.0281	.0271	.0287	.0311	.0335	.0355	.0390	.0426
Pt	4.645	1.556	.719	.262	.138	.0892	.0666	.0465	.0375	.0315	.0293	.0280	.0296	.0320	.0343	.0365	.0400	.0438
Tl	5.057	1.717	.791	.285	.152	.0972	.0718	.0491	.0393	.0326	.0301	.0288	.0304	.0326	.0349	.0354	.0406	.0446
Pb	5.193	1.753	.821	.294	.156	.0994	.0738	.0505	.0402	.0332	.0306	.0293	.0305	.0330	.0352	.0373	.0412	.0450
U	9.63	2.337	1.096	.392	.208	.132	.0968	.0628	.0482	.0383	.0346	.0324	.0332	.0352	.0374	.0394	.0443	.0474
Air	.0233	.0251	.0268	.0288	.0296	.0297	.0296	.0289	.0280	.0268	.0256	.0238	.0211	.0194	.0181	.0172	.0160	.0153
NaI	1.466	.476	.224	.0889	.0542	.0410	.0354	.0299	.0273	.0253	.0242	.0235	.0241	.0254	.0268	.0281	.0303	.0325
H_2O	.0253	.0278	.0300	.0321	.0328	.0330	.0329	.0321	.0311	.0298	.0285	.0264	.0233	.0213	.0198	.0188	.0173	.0165
Concrete	.0416	.0300	.0289	.0294	.0297	.0296	.0295	.0287	.0278	.0272	.0256	.0239	.0216	.0203	.0194	.0188	.0180	.0177
Tissue	.0271	.0282	.0293	.0312	.0317	.0320	.0319	.0311	.0300	.0288	.0276	.0256	.0220	.0206	.0192	.0182	.0168	.0160

[a]Calculated from data of Grodstein[53] by Blizard, et al., ORNL.

Table 8-12—GAMMA-RAY ENERGY ABSORPTION CROSS SECTION (μ_e)

(in cm^{-1})

Material	Density, gm/cm^3	Gamma-Ray Energy, Mev																	
		0.1	0.15	0.2	0.3	0.4	0.5	0.6	0.8	1.0	1.25	1.50	2	3	4	5	6	8	10.0
Be	1.85	.0339	.0401	.0438	.0474	.0487	.0488	.0487	.0474	.0459	.0438	.0420	.0389	.0339	.0303	.0279	.0261	.0235	.0218
C	2.25	.0484	.0554	.0601	.0648	.0666	.0668	.0666	.0650	.0630	.0603	.0576	.0533	.0470	.0427	.0398	.0374	.0344	.0326
Na	.9712	.0281	.0251	.0258	.0271	.0275	.0276	.0276	.0268	.0260	.0250	.0239	.0222	.0201	.0188	.0180	.0174	.0166	.0163
Mg	1.741	.0583	.0481	.0484	.0505	.0512	.0510	.0508	.0496	.0481	.0461	.0442	.0413	.0374	.0353	.0338	.0327	.0317	.0313
Al	2.70	.1007	.0764	.0743	.0764	.0775	.0772	.0772	.0751	.0729	.0699	.0670	.0626	.0572	.0540	.0518	.0508	.0494	.0491
Si	2.42	.1053	.0726	.0692	.0704	.0709	.0702	.0702	.0682	.0663	.0636	.0610	.0571	.0525	.0499	.0479	.0469	.0460	.0457
P	1.83	.0917	.0576	.0534	.0529	.0531	.0531	.0525	.0512	.0496	.0476	.0458	.0428	.0395	.0377	.0366	.0361	.0355	.0357
S	2.07	.1244	.0727	.0642	.0623	.0623	.0621	.0617	.0596	.0578	.0555	.0534	.0501	.0464	.0445	.0433	.0426	.0426	.0426
K	0.87	.0791	.0377	.0296	.0264	.0259	.0257	.0253	.0245	.0237	.0227	.0218	.0206	.0193	.0189	.0186	.0184	.0187	.0191
Ca	1.55	.172	.0758	.0569	.0493	.0479	.0471	.0465	.0450	.0432	.0415	.0400	.0378	.0357	.0349	.0344	.0346	.0349	.0358
Fe	7.86	1.769	.6367	.3844	.2672	.2413	.2311	.2256	.2154	.2051	.1965	.1902	.1816	.1761	.1761	.1784	.1816	.1879	.1965
Cu	8.933	2.769	.956	.5306	.3287	.2823	.2644	.2555	.2421	.2323	.2206	.2117	.2046	.1992	.2028	.2064	.2117	.2215	.2332
Mo	9.01	8.307	2.649	1.270	.5559	.3802	.3135	.2831	.2532	.2370	.2234	.2153	.2099	.2135	.2253	.2361	.2469	.2667	.2847
Sn	7.298	10.721	3.437	1.620	.6371	.3897	.2941	.2525	.2146	.1956	.1810	.1744	.1700	.1773	.1890	.2014	.2124	.2306	.2474
I	4.94	8.704	2.752	1.284	.494	.2910	.2139	.1808	.1497	.1354	.1245	.1191	.1166	.1220	.1309	.1398	.1477	.1615	.1744
W	19.3	79.362	26.171	12.178	4.439	2.335	1.517	1.156	.8222	.6813	.5829	.5423	.5320	.5539	.6002	.6466	.6852	.7527	.8222
Pt	21.37	99.264	33.252	15.365	5.599	2.949	1.906	1.423	.9937	.8014	.6732	.6261	.5984	.6326	.6838	.7330	.7800	.8548	.9360
Tl	11.86	59.976	20.364	9.381	3.380	1.803	1.153	.8515	.5823	.4661	.3866	.3570	.3416	.3605	.3866	.4139	.4198	.4815	.5290
Pb	11.34	58.889	19.879	9.310	3.334	1.769	1.127	.8369	.5727	.4559	.3765	.3470	.3323	.3459	.3742	.3992	.4230	.4672	.5103
U	18.7	180.08	43.702	20.495	7.330	3.890	2.468	1.810	1.174	.9013	.7162	.6470	.6059	.6208	.6582	.6994	.7368	.8284	.8864
NaI	3.667	5.376	1.745	.8214	.3260	.1988	.1503	.1298	.1096	.1001	.0928	.0887	.0862	.0884	.0931	.0983	.1030	.1111	.1192
H_2O	1.00	.0253	.0278	.0300	.0321	.0328	.0330	.0329	.0321	.0311	.0298	.0285	.0264	.0233	.0213	.0198	.0188	.0173	.0165
Concrete	2.35	.0978	.0705	.0679	.0691	.0698	.0697	.0693	.0674	.0653	.0639	.0602	.0562	.0508	.0477	.0456	.0442	.0423	.0416

687063 O - 63 - 43

Table 8-13—DOSE BUILDUP FACTOR B(μ_tx) FOR A POINT ISOTROPIC SOURCE

Data from Ref. 55.

Material	μ_tx	Gamma-Ray Energy, Mev							
		0.5	1.0	2.0	3.0	4.0	6.0	8.0	10.0
Water	1	2.52	2.13	1.83	1.69	1.58	1.46	1.38	1.33
	2	5.14	3.71	2.77	2.42	2.17	1.91	1.74	1.63
	4	14.3	7.68	4.88	3.91	3.34	2.76	2.40	2.19
	7	38.8	16.2	8.46	6.23	5.13	3.99	3.34	2.97
	10	77.6	27.1	12.4	8.63	6.94	5.18	4.25	3.72
	15	178	50.4	19.5	12.8	9.97	7.09	5.66	4.90
	20	334	82.2	27.7	17.0	12.9	8.85	6.95	5.98
Aluminum	1	2.37	2.02	1.75	1.64	1.53	1.42	1.34	1.28
	2	4.24	3.31	2.61	2.32	2.08	1.85	1.68	1.55
	4	9.47	6.57	4.62	3.78	3.22	2.70	2.37	2.12
	7	21.5	13.1	8.05	6.14	5.01	4.06	3.45	3.01
	10	38.9	21.2	11.9	8.65	6.88	5.49	4.58	3.96
	15	80.8	37.9	18.7	13.0	10.1	7.97	6.56	5.63
	20	141	58.5	26.3	17.7	13.4	10.4	8.52	7.32
Iron	1	1.98	1.87	1.76	1.55	1.45	1.34	1.27	1.20
	2	3.09	2.89	2.43	2.15	1.94	1.72	1.56	1.42
	4	5.98	5.39	4.13	3.51	3.03	2.58	2.23	1.95
	7	11.7	10.2	7.25	5.85	4.91	4.14	3.49	2.99
	10	19.2	16.2	10.9	8.51	7.11	6.02	5.07	4.35
	15	35.4	28.3	17.6	13.5	11.2	9.89	8.50	7.54
	20	55.6	42.7	25.1	19.1	16.0	14.7	13.0	12.4
Tungsten	1	1.28	1.44	1.42	1.36	1.29	1.20	1.14	1.11
	2	1.50	1.83	1.85	1.74	1.62	1.43	1.32	1.25
	4	1.84	2.57	2.72	2.59	2.41	2.07	1.81	1.64
	7	2.24	3.62	4.09	4.00	4.03	3.60	3.05	2.62
	10	2.61	4.64	5.27	5.92	6.27	6.29	5.40	4.65
	15	3.12	6.25	8.07	9.66	12.0	15.7	15.2	14.0
	20	—	7.35	10.6	14.1	20.9	36.3	41.9	39.3
Lead	1	1.24	1.37	1.39	1.34	1.27	1.18	1.14	1.11
	2	1.42	1.69	1.76	1.68	1.56	1.40	1.30	1.23
	4	1.69	2.26	2.51	2.43	2.25	1.97	1.74	1.58
	7	2.00	3.02	3.66	3.75	3.61	3.34	2.89	2.52
	10	2.27	3.74	4.84	5.30	5.44	5.69	5.07	4.34
	15	2.65	4.81	6.87	8.44	9.80	13.8	14.1	12.5
	20	2.73	5.86	9.00	12.3	16.3	32.7	44.6	39.2
Uranium	1	1.17	1.31	1.33	1.29	1.24	1.16	1.12	1.09
	2	1.30	1.56	1.64	1.58	1.50	1.36	1.27	1.20
	4	1.48	1.98	2.23	2.21	2.09	1.85	1.66	1.51
	7	1.67	2.50	3.09	3.27	3.21	2.96	2.61	2.26
	10	1.85	2.97	3.95	4.51	4.66	4.80	4.36	3.78
	15	2.08	3.67	5.36	6.97	8.01	10.8	11.2	10.5
	20	—	—	6.48	9.88	12.7	23.0	28.0	28.5

Table 8-14—COEFFICIENTS FOR AN ANALYTIC FIT TO BUILDUP FACTOR EQUATION

Reproduced, in part, from data of Ref. 51.

Material		Gamma-Ray Energy, Mev							
		0.5	1	2	3	4	6	8	10
Water	A_1	—	13.5	8.1	5.6	4.5	3.4	2.8	2.5
	$-a_1$	—	0.100	0.068	0.059	0.0555	0.0525	0.05	0.0473
	$+a_2$	—	0.010	0.0405	0.073	0.11	0.156	0.17	0.1719
Aluminum	A_1	—	8.0	5.5	4.5	3.8	3.1	2.3	2.25
	$-a_1$	—	0.11	0.082	0.074	0.066	0.064	0.062	0.060
	$+a_2$	—	0.044	0.093	0.116	0.130	0.152	0.150	0.128
Iron	A_1	10.0	8.0	5.5	—	3.75	2.9	2.35	2.0
	$-a_1$	0.0948	0.0895	0.0788	—	0.075	0.0825	0.0833	0.095
	$+a_2$	0.012	0.04	0.07	—	0.082	0.075	0.0546	0.0116
Tungsten	A_1	—	3.3	2.9	2.7	2.05	1.2	0.7	0.6
	$-a_1$	—	0.043	0.069	0.086	0.118	0.171	0.205	0.212
	$+a_1$	—	0.148	0.188	0.134	0.070	0.00	0.052	0.144
Lead	A_1	1.65	2.45	2.60	2.15	1.65	0.96	0.67	0.50
	$-a_1$	0.032	0.045	0.071	0.097	0.123	0.175	0.204	0.214
	$+a_2$	0.296	0.178	0.103	0.077	0.064	0.059	0.067	0.08
Concrete	A_1	12.5	10.0	6.3	4.7	3.9	3.1	2.7	2.6
	$-a_1$	0.11	0.088	0.069	0.062	0.059	0.059	0.056	0.050
	$+a_2$	0.01	0.029	0.058	0.073	0.079	0.083	0.086	0.084

Note: Reference 51 includes a discussion of the errors involved in these analytical fits. In general, the errors are less than a few per cent and, in no case, greater than 8%.

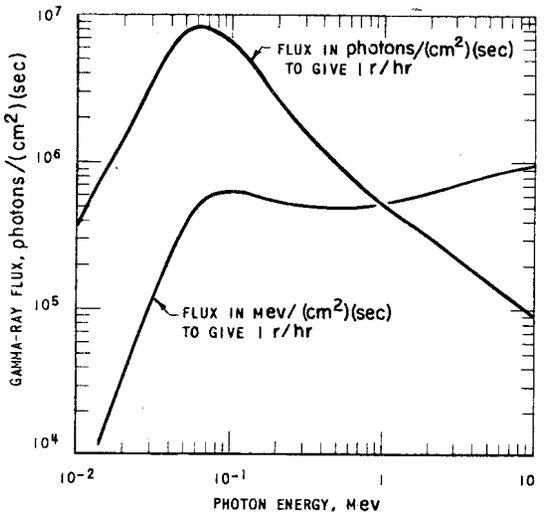

Fig. 8-11—Gamma flux to give 1 roentgen/hr.

8.4 SHIELDING PROPERTIES OF CONCRETES

One of the uncertainties in shield design work has been the variation in content of the various concretes. This is particularly true of the water content, which has the vital role of a moderator in the concrete. In cases where water retention is not known, two or three values are assumed. The resulting constants indicate a range of numbers with the parameter being water content.

8.4.1 PHYSICAL COMPOSITIONS

The various concretes considered, their densities and mix proportions are listed in Table 8-15. Table 8-16 gives a detailed breakdown of the elemental compositions of the concretes upon which the calculations of the cross sections are based.

8.4.2 NUCLEAR CONSTANTS

Neutron constants for the concretes are presented in Table 8-17. The values for the age to thermal energy (τ), and the two-group fast neutron diffusion coefficient (D_f) are approximate, but form a consistent set for purposes of comparison. Measured removal cross sections, Σ_R, and fast neutron relaxation lengths, λ, are included.

Table 8-18 gives the effective thermal neutron absorption cross section, Σ_a, and the effective number of gamma-ray photons emitted per neutron capture, N(E), for a four-line gamma energy spectrum.

Gamma-ray attenuation coefficients for ordinary concrete (Type 04) are included in Tables 8-9 and 8-10.

8.4.3 TEMPERATURE DEPENDENCE OF REMOVAL CROSS SECTION

The shielding effectiveness of a concrete depends heavily on the water content. The quantity of contained water decreases as the concrete is heated, changing the value of the removal cross section. Table 8-19 lists measured fast neutron relaxation lengths for four types of concrete as a function of temperature.

8.5 CONVERSION FACTORS USEFUL IN SHIELDING CALCULATIONS

Table 8-20 lists energy and power conversion factors which are occasionally of use in shielding calculations.

Table 8-15—COMPOSITION AND DENSITY OF VARIOUS CONCRETES

Concrete	*Symbol	Density		Composition, lb/yd³					Ref.
		gm/cm³	lb/ft³	Water	Cement	Aggregate	Steel Punchings	Total	
Ordinary									
1	01	2.33	145	—	—	—	—	—	56
2a	02-a	2.3	144	260	318	3300 (Sand and Gravel)	—	3878	56
2b	02-b	2.22	139	—	—	—			
3	03	2.39	149	—	—	—	—	—	57
4	04	2.35	147	—	—	—	—	—	58
5 (Harwell)	05	2.5	156	—	—	—	—	—	3
6 (APDA)	06	1.25-1.4	78-88	0.231 vf	0.256 vf	0.513 vf (Diatomaceous Earth)	—	—	59
7(APDA)	07	2.1-2.24	130-140	373	525	1.39 (Plastiment) 2032 (Serpentine) 956 (Sand)	—	3887	59
Ferrophosphorus									
1a	FP-a	4.68	292	384	730	6870 (Ferrophosphorus Slag)	—	7894	‡
1b	FP-b	4.57	285	—	—	—	—	—	—
2 (Hanford Shield Test)	FP-HW	4.84	302	396	752	7000	—	8148	60
Barytes									
1a	BA-a	3.46	216	370	550	4980 ($BaSO_4$ Ore)	—	5900	56,61
1b	BA-b	3.35	212	—	—	—	—	—	—
2	BA-H	3.757	223	—	—	—	—	—	3
Magnetite									
1a (EBWR Shield)	M-a	3.62	226	330	875	4900 (Magnetite Ore)	—	6105	62,63
1b	M-b	3.52	220	—	—	—	—	—	—
2 (Hanford Shield Test)	M-HW	3.29	205	—	—	—	—	—	64
Ilmenite									
1 (New York State)	I-1	3.68	230	—	—	—	—	—	65†
2 (Swedish)	I-2	3.62	226	—	—	—	—	—	66†
3 (NRU Shield)	I-NRU	3.52	220	170	564 + 2 bags Intrusion Aid	3182 (Ilmenite) 780 (Magnetite Sand)	—	—	67
Magnetite and Steel Punchings									
1a (MIT Reactor Shield)	MS1-a	4.5	280	333	550	3310 (Magnetite Ore)	3360	7553	62
1b	MS1-b	4.4	274	—	—	—	—	—	—
2a (EBWR Shield)	MS2-a	4.74	295	340	940	1900 (Magnetite Ore)	4800	7980	62,63
2b	MS2-b	4.64	290	—	—	—	—	—	—
Limonite and Steel Punchings									
1a (CP-5 Shield)	LS-a	4.64	289	347	980	1825 (Limonite Ore)	4680	7832	††
1b	LS-b	4.54	283	—	—	—	—	—	—
2 (Brookhaven)	LS-BR	4.33-4.49	270-280	330	750	2200 (Limonite) 10 (Plastiment Liquid)	4300	—	68

* Where appearing, "a" and "b" indicate 100% and 50% water retention, respectively.
† Ilmenite Ore substituted for Magnetite in M-a.
‡ Victor Chemical Works, Chicago, Illinois.
†† Spectrochemical Analysis by Hanford, unpublished.

Note: vf = Volume fraction in mix.

Table 8-16—ELEMENTAL COMPOSITION OF ORDINARY CONCRETES AND HEAVY CONCRETES WITH AND WITHOUT STEEL PUNCHINGS

(in gm element/cm^3 concrete)

Heavy Concretes with Steel Punchings						
Element	MS1-a	MS1-b	MS2-a	MS2-b	LS-a	LS-b
H in water	0.0221	0.0110	0.0224	0.0112	0.0228	0.0114
in ore	—	—	—	—	0.172	
O in water	0.176	0.0882	0.0180	0.0898	0.182	0.0911
in ore	0.725		0.347		0.408	
in cement	—	—	0.201		0.209	
Mg in ore	0.0179		0.0102		—	—
in cement	0.0040		0.0067		0.007	
Al in ore	0.0417		0.0239		0.0043	
in cement	0.0139		0.0236		0.0245	
Si in ore	0.0230		0.0132		0.0043	
in cement	0.0350		0.0599		0.0623	
S	—	—	—	—	—	—
K	—	—	—	—	0.0043	
Ca in ore	0.0113		0.00646		—	—
in cement	0.1480		0.251		0.261	
Ti	0.130		0.074		—	—
P	0.0003		0.00017		—	—
V	0.0046		0.0026		0.0043	
Fe in ore	1.127		0.645		0.633	
in cement	0.009		0.0156		0.0162	
in punchings	2.002		2.851		2.772	
Zn					0.0043	
p, gm/cm^3	4.5	4.4	4.74	4.64	4.64	4.54

Ordinary Concretes								
Element	01	02-a	02-b	03	04	05	06	07
H	0.00484	0.023	0.0144	0.020	0.013	0.022	0.034	0.033
O in water	0.0384	0.183	0.114	0.159	0.103	1.231	0.793	1.07
in dry mix	1.1106	1.037	1.036	0.957	1.062			
C	0.130	0.0023		0.118	—	0.008	—	0.002
Mg	0.00486	0.005		0.057	0.006	0.002	0.003	0.281
Al	0.0119	0.078		0.085	0.107	0.131	0.025	0.040
Si	0.438	0.775		0.342	0.737	0.63	0.417	0.435
S	0.00192	—	—	0.007	0.003	0.0037	—	—
K	—	0.0299		0.004	0.045	0.025	—	0.008
Ca	0.581	0.100		0.582	0.194	0.242	0.001	0.141
Fe	0.00726	0.032		0.026	0.029	0.122	0.013	0.064
Na	—	0.0368		—	0.400	0.029	—	0.008
Ti	—	—	—	—	—	0.017	—	trace
Mn	—	—	—	—	—	0.045	—	trace
Ni	—	—	—	—	—	—	—	0.002
P	—	—	—	—	—	—	—	trace
Cl	—	—	—	—	—	—	—	trace
Zr	—	—	—	—	—	—	—	trace
Cr	—	—	—	—	—	—	—	trace
B	—	—	—	—	—	—	0.010	0.002
ρ, gm/cm^3	2.33	2.30	2.22	2.39	2.35	2.5	1.3	2.1

Heavy Concretes												
Element	FP-a	FP-b	FP-HW	BA-a	BA-b	BA-H	M-a	M-b	M-HW	I-1	I-2	I-NRU
H in water	0.0253	0.0127	0.021	0.0243	0.0122	0.0097	0.0217	0.0109	0.015	0.0217	0.0217	0.008
O in water	0.202	0.101	—	0.194	0.0972	—	0.174	0.087	—	0.174	0.174	—
in ore	—	—	0.322	0.828		0.987	0.894		1.279	1.037	0.916	1.191
in cement	0.156		—	0.118		—	0.187		—	0.187	0.187	—

Mg in ore	—	—	—	—	—	—	0.0263	—	0.280	0.0139	—
			0.006								0.053
in cement	0.00522		—	0.00396		—	0.0063	—	0.0063	0.0063	—
								0.184			
Al in ore	—	—	—	—	—	—	0.0614	—	—	—	—
			0.009			0.017					0.075
in cement	0.0183		—	0.0139		—	0.0220	—	0.022	0.022	—
Si in ore	—	—	—	—	—	—	0.0339	—	0.047	—	—
			0.090			0.250		0.129			0.122
in cement	0.0465		—	0.0352		—	0.0567	—	0.0557	0.0557	—
P	1.206		1.049	—	—	—	0.0004	—	—	—	—
S	—	—	0.004	0.361		0.250	0.0052	—	—	—	—
Ca in ore	—	—	—	0.0203		—	0.0166	—	—	0.0012	—
			0.203			0.205		0.220	—	—	0.113
in cement	0.195		—	0.148		—	0.234	—	0.234	0.234	—
Ti	—	—	0.042	—	—	—	0.192	—	0.998	0.914	0.513
V	—	—	0.084	—	—	—	0.0113	—	—	—	—
Cr	—	—	0.084	—	—	—	0.00575	—	—	—	—
Mn	—	—	0.013	—	—	—	0.0067	—	0.0247	0.0305	—
Fe in ore	2.814		—	0.150		—	1.661	—	0.583	1.001	—
			2.823			0.825		1.46			1.39
in cement	0.0121		—	0.00917		—	0.0145	—	0.0145	0.0145	—
Ba	—	—	—	1.551		0.997	—	—	—	—	—
Ni	—	—	0.017	—	—	—	—	—	—	—	—
Cu	—	—	0.008	—	—	—	—	—	—	—	—
Mo	—	—	0.042	—	—	—	—	—	—	—	—
C	—	—	0.004	—	—	0.0323	—	—	—	—	0.019
ρ, gm/cm^3:	4.68	4.57	4.84	3.46	3.35	3.57	3.62	3.52	3.29	3.62	3.62	3.5

Table 8-17—NEUTRON CONSTANTS FOR CONCRETE

Concrete[a]	Density, gm/cm^3	κ_{th}, cm^{-1}	D_{th}, cm	Σ_R, cm^{-1}		λ, cm (Exptl.)	$1/\lambda$	τ, cm^2	D_f, cm
				Calc.	Exptl.				
01-a	2.33	0.0778	0.968	0.074	0.083[b]	11.1	0.090	349	1.40
b	—	—	—	0.072	—	—	—	581	—
c	—	—	—	—	—	—	—	1370	—
02-a	2.30	0.139	0.484	0.085	—	—	—	101	1.14
b	2.20	0.0993	0.749	0.075	—	—	—	205	1.51
c	—	—	—	—	—	—	—	1530	2.04
03-a	2.39	0.137	0.512	0.084	0.086	—	—	119	1.23
b	—	—	—	—	—	—	—	222	1.39
c	—	—	—	—	—	—	—	1250	1.65
04-a	2.35	0.112	0.688	0.079	—	—	—	179	1.31
b	—	—	—	—	—	—	—	316	1.57
c	—	—	—	—	—	—	—	1450	1.73
06	1.30	0.968	0.406	0.061	—	—	—	—	—
07	2.09	0.474	0.378	0.084	—	—	—	—	—
FP-a	4.68	0.518	0.344	0.13	0.15[b]	—	—	51.6	—
b	4.57	0.442	0.463	0.12	—	—	—	92.4	—
c	—	—	—	—	—	—	—	275	—
FP-HW	4.82	0.502	0.358	0.125	0.131	7.19	0.139	86.9	1.10
BA-a	3.50	0.212	0.440	0.093	—	8	0.125	179	1.29
b	3.39	0.162	0.667	0.082	—	—	—	1650	1.62
BA-H	3.575	0.155	0.912	0.064	—	—	—	75.4	—
M-a	3.55	0.375	0.393	0.11	—	—	—	141	—
b	3.45	0.314	0.540	0.10	—	—	—	708	—
M-HW	3.29	0.289	0.482	0.098	—	8.75	0.114	—	—
I-1	3.50	0.450	0.419	0.11	—	—	—	—	—
2	3.76	0.493	0.401	0.11	—	—	—	—	—
I-NRU	3.44	—	—	0.098	—	13.4	0.075	—	—
MS1-a	4.5	0.504	0.365	0.13	—	—	—	69	—
b	4.4	0.436	0.472	0.12	—	—	—	131	—
c	—	—	—	—	—	—	—	713	—
MS2-a	4.70	0.532	0.337	0.12	—	—	—	56	0.814
b	4.60	0.458	0.445	0.11	—	—	—	113	0.932
c	—	—	—	—	—	—	—	958	1.00
LS-a	4.54	0.511	0.340	0.12	0.114[b]	—	—	—	—
b	4.44	0.437	0.455	0.11	—	—	—	—	—
LS	4.24	—	—	—	—	7.7	0.130	—	—
LS	4.15	—	—	—	—	7.9	0.126	—	—

[a]Assumed Water Retention: a = 100%; b = 50%; c = 0%.
[b]ANL Shield Facility.[69]

Note: κ_{th} = Reciprocal diffusion length for thermal neutrons. D_{th} = Diffusion coefficient for thermal neutrons.

Table 8-18—CAPTURE GAMMA-RAY SPECTRA OF CONCRETES

Concrete[a]	Σ_a^b, cm^{-1}	N(E)						
		1 Mev	2 Mev	3 Mev	4 Mev	6 Mev	8 Mev	10 Mev
01	0.0059	0.355	1.29	0.676	0.715	0.408	0.0332	0.0003
02-a	0.0094	0.546	0.533	0.739	0.447	0.143	0.0542	0.0004
02-b	0.0074	0.694	0.678	0.668	0.569	0.182	0.0689	0.0005
03	0.0097	0.374	0.911	0.751	0.483	0.284	0.0514	0.0003
04	0.0086	0.675	0.765	0.694	0.595	0.217	0.0618	0.0004
FP-a	0.0924	0.871	0.655	0.373	0.302	0.258	0.312	0.0016
b	0.0903	0.890	0.670	0.359	0.308	0.264	0.319	0.0016
BA-a	0.0197	0.279	0.274	0.426	0.483	0.204	0.092	0.0008
b	0.0176	0.313	0.307	0.357	0.541	0.229	0.103	0.0009
M-a	0.0553	0.676	0.721	0.325	0.240	0.304	0.296	0.0020
b	0.0534	0.700	0.747	0.301	0.249	0.315	0.307	0.0020
I-1a	0.0848	0.568	1.34	0.242	0.250	0.636	0.0783	0.0018
2a	0.0975	0.599	1.25	0.248	0.248	0.588	0.116	0.0018
MS1-a	0.0939	—	0.225	—	0.247	0.289	0.435	—
b	0.0897	—	0.208	—	0.251	0.295	0.445	—
MS2-a	0.0953	0.705	0.647	0.304	0.234	0.271	0.339	0.0020
b	0.0933	0.720	0.661	0.290	0.239	0.277	0.346	0.0020
LS-a	0.0888	0.713	0.600	0.315	0.237	0.245	0.352	0.0019
b	0.0868	0.729	0.614	0.299	0.243	0.251	0.360	0.0020

[a]Assumed water retention: a = 100%; b = 50%.

[b]Σ_a = Thermal neutron absorption cross section at 20°C corrected (0.8862) for 1/v absorption in a Maxwell distribution.

Table 8-19—MEASURED RELAXATION LENGTHS FOR SEVERAL CONCRETES AS A FUNCTION OF CONCRETE TEMPERATURE

Concrete Type	Density, gm/cm^3	Temperature						Ref.
		Unheated	100°C	175°C	200°C	300°C	320°C	
Iron-Limonite	4.23	7.8	8.4	9.7	—	—	10.1	70
Magnetite-Limonite	3.39	9.0	10.2	11.5	—	—	11.1	70
Magnetite	3.29	8.75	9.52	—	9.75	10.1	—	71
Ferrophosphorus	4.83	7.19	7.75	—	8.06	—	8.26	72
Ordinary	2.34	12.1	12.8	—	13.0	13.4	—	73

Table 8-20—CONVERSION FACTORS

Multiply	By	To Obtain
Mev	1.517×10^{-16}	Btu
Mev	4.44×10^{-20}	kw-hr
Mev	3.83×10^{-14}	gm-cal
Mev	1.602×10^{-6}	ergs
ergs	6.24×10^{5}	Mev
ergs	9.49×10^{-11}	Btu
ergs	2.78×10^{-14}	kw-hr
ergs	2.39×10^{-8}	gm-cal
gm-cal	2.61×10^{13}	Mev
gm-cal	3.97×10^{-3}	Btu
gm-cal	1.163×10^{-6}	kw-hr
gm-cal	4.18×10^{7}	ergs
kw-hr	2.25×10^{19}	Mev
kw-hr	3.41×10^{3}	Btu
kw-hr	8.60×10^{5}	gm-cal
kw-hr	3.60×10^{13}	ergs
Btu	6.59×10^{15}	Mev
Btu	2.93×10^{-4}	kw-hr
Btu	252	gm-cal
Btu	1.055×10^{10}	ergs
watts	6.24×10^{12}	Mev/sec
Mev/sec	1.602×10^{-13}	watts
Btu/sec	1.055×10^{3}	watts
Mev/(cm^2)(sec)	1.485×10^{-10}	watts/ft^2
Mev/(cm^2)(sec)	1.409×10^{-13}	Btu/(ft^2)(sec)
kw/ft^2	3.42×10^{3}	Btu/(ft^2)(hr)
watts/cm^2	3.18×10^{3}	Btu/(ft^2)(hr)
Mev/(cm^3)(sec)	4.54×10^{-9}	watts/ft^3
Mev/(cm^3)(sec)	4.30×10^{-12}	Btu/(ft^3)(hr)
kw/liter	9.7×10^{-4}	Btu/(ft^3)(hr)

REFERENCES

1. H. Goldstein, *The Fundamental Aspects of Reactor Shielding*, (Reading, Mass.: Addison Wesley Publishing Company, Inc., 1959).
2. B. T. Price, C. C. Horton and K. T. Spinney, *Radiation Shielding*, (New York: Pergamon Press, 1957).
3. A. F. Avery, et al., *Methods of Calculation for Use in the Design of Shields for Power Reactors*, AERE-R-3216, (February, 1960).
4. T. Rockwell, III (ed.), *Reactor Shielding Design Manual*, TID-7004, (March, 1956).
5. M. Grotenhuis, *Lecture Notes on Reactor Shielding*, ANL-6000, (March, 1959).
6. H. Goldstein, *The Attenuation of Gamma Rays and Neutrons in Reactor Shields*, Chap. 3: *Sources of Neutrons and Gamma Rays*, p. 33, (1957).
7. R. L. Gamble, *Prompt Fission Product Gamma Rays from Uranium-235*, Reactor Shielding Information Meeting, May 12-13, 1955, Fort Belvoir, Virginia, WASH-292, Pt. 3, 28, (September, 1955).
8. H. W. Bertini, et al., *Basic Gamma-Ray Data for ART Heat Deposition Calculations*, ORNL-2113, (October 3, 1956).
9. Matts Roos, *Sources of Gamma Radiation in a Reactor Core*, J. Nuclear Energy, Part B: Reactor Technology, 1: 98-104, (1959).
10. F. C. Maienschein, et al., *Energy Spectra of Fission-Associated Gamma Radiation*, Proc., 1958 Geneva Conference, 15: Paper No. 670, p. 368.
11. V. V. Sklyarevskii, D. E. Fomenko and E. P. Stepanov, *Investigation of U^{235} Fission γ-Rays in the Energy Region up to 250 kev*, Soviet Physics-JETP, 5: No. 2, 220-225, (1957). Russian Ref. JETP, 32: 256-262.
12. J. G. Carver, *U^{235} Fission Gamma Ray Source Data*, XDC-60-11-63, (October, 1960).
13. F. C. Maienschein, et al., *Gamma Rays Associated with Fission*, Proc., 1958 Geneva Conference, 15: Paper No. 670, p. 366.
14. M. R. Smith, *Distribution of the Energy per Fission for U^{235}*, GEANP (to be published).
15. F. C. Maienschein, R. W. Peele and T. A. Love, *Recent Fission Gamma Ray Spectral Measurements*, Papers from Seventh Semiannual Shielding Information Meeting, XDC-60-6-70, Paper No. 3, (October 1959).
16. I. J. MacBean, *Energy Release from Fission Product Decay*, AERE-R-3033, (September, 1959).
17. J. Howlett, et al., *Tables of Fission Product Activities After Irradiation and Decay*, AERE-T/R 589, (October, 1950).
18. J. O. Blomeke and M. F. Todd, *U^{235} Fission Product Production as a Function of Thermal Neutron Flux, Irradiation Time and Decay Time*, ORNL-2127, Pt. 1, 1-2: (August 19, 1957).
19. L. Burris, Jr. and I. G. Dillon, *Estimation of Fission Product Spectra in Discharged Fuel from Fast Reactors*, ANL-5742, (July, 1957).
20. J. F. Perkins and R. W. King, *Energy Release from the Decay of Fission Products*, Nuclear Sci. and Eng., 3: No. 6, 726-46, (June, 1958).
21. W. Zobel, et al., *Characteristics of Fission Product Gamma Rays Emitted from 1 to 1800 Sec After Thermal Fission of U^{235}*, ORNL-2609, (October 28, 1958), pp. 50-51.
22. M. R. Smith, *The Activity of the Fission Products of U^{235} (Program 408)*, XDC-60-1-157, (December, 1959).
23. W. E. Knabe and G. E. Putnam, *The Activity of the Fission Products of U^{235}*, APEX-448, (October, 1958).
24. E. Troubetzkoy and H. Goldstein, *A Compilation of Information on Gamma-Ray Spectra Resulting from Thermal-Neutron Capture*, ORNL-2904, (January 18, 1961).
25. J. D. Anderson, et al., *Inelastic Scattering of 14-Mev Neutrons from Carbon and Beryllium*, Phys. Rev., 111: No. 2, 572-574, (1958).
26. E. S. Troubetzkoy, *Fast Neutron Cross Sections of Iron, Silicon, Aluminum, and Oxygen*, NDA-2111-3, C: (November 1, 1959).
27. J. F. Scoles, *Calculated Gamma Ray Spectra from U^{235} Fission Products*, NARF-58-37-T, (August 29, 1958).
28. J. R. Stehn and E. F. Clancy, *Fission Product Radioactivity and Heat Generation*, Proc., 1958 Geneva Conference, 13: Paper No. 1071, p. 49.
29. F. H. Clark, *Decay of Fission Product Gammas*, NDA-27-39, (1954).
30. R. L. Caldwell, W. R. Mills, Jr. and J. B. Hickman, Jr., *Gamma Radiation from Inelastic Scattering of 14-Mev Neutrons by the Common Earth Elements*, Nuclear Sci. and Eng., 8: No. 3, 173-182, (September, 1960).
31. W. Zobel and T. A. Love, *Time and Energy Spectra of Fission-Product Gamma Rays Measured at Short Times After Uranium Sample Irradiations*, Applied Nuclear Physics Division Annual Report for the Period Ending September 10, 1956, ORNL-2081, p. 95.
32. K. Way and E. P. Wigner, *Radiation from Fission Products*, Phys. Rev., 70: 115, (1946).
33. J. W. Butler and M. Grotenhuis, *The Decay of Fission Product Activity for Cyclic Operation of a Reactor*, Nuclear Sci. and Eng., 3: No. 1, 47, (January, 1958).
34. D. J. Hughes and R. B. Schwartz, *Neutron Cross Sections*, BNL-325, (July, 1958).
35. W. H. Sullivan, *Trilinear Chart of Nuclides*, (2nd Rev.), USAEC, (January, 1957).
36. *The Reactor Handbook*, Vol. 1: Physics, AECD-3645, (1955), pp. 158ff.
37. P. A. Roys and K. Shure, *Production Cross Section of N^{16} and N^{17}*, Abstracts, 1958 Annual Meeting of the American Nuclear Society, Los Angeles, Paper No. 3-8, (June, 1958).
38. W. J. Henderson and P. R. Tunnicliffe, *The Production of N^{16} and N^{17} in the Cooling Water of the NRX Reactor*, Nuclear Sci. and Eng., 3: No. 2, 145, (February, 1958).
39. D. S. Duncan and H. O. Whittum, Jr., *Application of Fast Neutron Removal Theory to the Calculation of Thermal Neutron Flux Distributions in Reactor Shields*, NAA-SR-2380, (July 1, 1958).
40. *Attenuation in Water of Radiation from the Bulk Shielding Reactor: Measurements of the Gamma-Ray Dose Rate, Fast-Neutron Dose Rate and Thermal Neutron Flux*, ORNL-2518, (July 8, 1958).
41. D. C. Anderson and K. Shure, *Calculation of Thermal Neutron Fluxes in Primary Shields*, WAPD-TM-193, (November, 1959).
42. R. D. Albert and T. A. Welton, *A Simplified Theory of Neutron Attenuation and Its Application to Reactor Shield Design*, WAPD-15, (November 30, 1950).
43. G. T. Chapman and C. L. Storrs, *Effective Neutron Removal Cross Sections for Shielding*, AECD-3978, (ORNL-1843), (September 19, 1955).
44. J. M. Miller, *Neutron Physics Division Annual Progress Report for Period Ending September 1, 1959*, ORNL-2842, (November 16, 1959), p. 168.
45. J. M. Miller, *Effective Removal Cross Section of Tungsten*, Applied Nuclear Physics Division Annual Report for the Period Ending September 1, 1957, ORNL-2389, (September 1, 1957), p. 187.
46. W. S. Snyder and J. Neufeld, *On the Passage of Heavy Particles Through Tissue*, Radiation Research, 6: 67-78, (1957).
47. *Protection Against Neutron Radiation Up to 30 Million Electron Volts*, U. S. Department of Commerce, NBS Handbook No. 63, (November 22, 1957), p. 39.
48. *Report of the International Commission on Radiological Units and Measurements (ICRU)*, U. S. Department of Commerce, NBS Handbook 62, (1956).
49. H. Goldstein and J. E. Wilkins, Jr., *Calculations of the Penetrations of Gamma Rays – Final Report*, NYO-3075, (June 30, 1954).
50. U. Fano, *Gamma-Ray Attenuation*, The Reactor Handbook, Vol. 1: Physics, AECD-3645, (1955), Chap. 2.3, p. 637.
51. J. J. Taylor, *Application of Gamma-Ray Build-up Data to Shield Design*, WAPD-RM-217, (January 28, 1954).
52. G. W. Grodstein, *X-Ray Attenuation Coefficients from 10 kev to 100 Mev*, NBS Circular 583, (April 30, 1957), Chaps. 1-3.
53. Ibid., Table 8-40.

54. Rockwell, op. cit., Ref. 4, pp. 113ff.
55. Goldstein and Wilkins, op. cit. Ref. 49, Chaps. 7-8.
56. Reactor Handbook, op. cit., Ref. 36, p. 674.
57. Zobel and Love, op. cit. Ref. 31, p. 161.
58. Grodstein, op. cit. Ref. 52, p. 50.
59. H. E. Hungerford, R. F. Mantey and L. P. Van Maele, *New Shielding Materials for High Temperature Application*, Nuclear Sci. and Eng., 6: No. 5, 396-408, (November, 1959).
60. D. E. Wood and E. D. Peterson, *Neutron Attenuation in Magnetite Concrete Heated to 200°C*, HW-55372, (March 25, 1958).
61. Reactor Handbook, op. cit., Ref. 6, pp. 726-727.
62. E. Creutz and K. Downes, *Magnetite Concrete for Radiation Shielding*, J. Appl. Phys., 20: 1236, (1949).
63. M. Grotenhuis and J. W. Butler, *Experimental Boiling Water Reactor (EBWR) Shield Design*, ANL-5544, (August, 1956).
64. D. E. Wood, *Neutron Attenuation of Magnetite Concrete Heated to 100°C*, HW-53395, (October, 1957).
65. Dana's System of Mineralogy, (New York: John Wiley and Sons; 7th edition), Vol. 1, Section 4415, New York State Ore, Analysis No. 11, p. 537.
66. Ibid., Sundsvale (Sweden) Ore, Analysis No. 3, p. 537.
67. J. M. Robson, *The Attenuation of Neutrons by the Side Shield of the NRU Reactor*, CRP-860b, (October, 1959).
68. John Ruddy, BNL, unpublished data.
69. M. Grotenhuis, *Shielding Experiments*, Nuclear Reactor Experiments (Princeton, New Jersey: D. Van Nostrand Co., 1958), Chap. 6.2, p. 172.
70. W. L. Bunch, *Attenuation Properties of High Density Portland Cement Concretes as a Function of Temperature*, HW-54656, (January 22, 1958), p. 41.
71. D. E. Wood, *The Effect of Temperature on the Neutron Attenuation of Magnetite Concrete*, HW-58497, (December, 1958).
72. E. G. Peterson, *Shielding Properties of Ferrophosphorus Concrete as a Function of Temperature*, HW-64774, (July 15, 1960).
73. E. G. Peterson, *Shielding Properties of Ordinary Concrete as a Function of Temperature*, HW-65572, (August 2, 1960).

Section 9

CONSTANTS RELATED TO INTERPRETATION OF EXPERIMENTAL DATA

This section summarizes those constants necessary to the interpretation of counting data, and the properties of neutron sources. Included is a review of the flux perturbations caused by detecting foils, the interpretation of cadmium-covered counting data, scintillator constants and gas constants appropriate to counting chambers, range-energy relationships, and atomic and molecular stopping cross sections. Constants related to the absorption and scattering of alpha and beta radiation in foil counting, and of the charged recoil or reaction particles in neutron counting, are outlined in Sections 9.5 and 9.6. Spectra and/or yields of both artificial and spontaneous fission neutron sources are tabulated.

9.1 FOIL ACTIVATION DATA

Measurements of absolute flux or neutron density generally perturb the measuring medium enough to require extrapolation of the data to an essentially unperturbed condition. When such measurements are made by foil irradiations, extrapolation to zero foil mass (the unperturbed condition) all too often becomes self-defeating because the measured quantity (foil activation) is directly proportional to the foil mass, while statistical errors are inversely proportional to the square root of the activation. An alternate to the experimental approach is the theoretical prediction of the unperturbed flux in terms of the foil constants and the properties of the measuring medium.

Usually, the perturbing effects are divided into two terms: (1) self-shielding, which describes the shielding of the inner layers by the outer layers of the foil; and (2) outer flux perturbation, which describes the depletion of the neutron density in the medium surrounding the foil due to absorption by the foil. Much of the work presented here on self-shielding and outer flux perturbations is based on papers by Vigon and Wirtz,[1] Meister,[2–5] and a selected review of these papers by Wirtz and Beckurts.[6]

9.1.1 CROSS SECTIONS AND NEUTRON SPECTRA

Expressions for the self-shielding and the outer flux perturbation are given in terms of the variable, $\tau = t\Sigma_a$. The value of Σ_a for any given foil depends on the neutron spectrum in which the foil is irradiated, and on the microscopic reaction cross section, $\sigma(E)$.

Reaction rates, R, in infinitely dilute absorbing samples are defined in terms of the reaction cross section, and the "true" flux:*

$$R = \int_0^\infty \sigma(E)\ \phi(E)\ dE = \int_0^\infty \sigma(E)\ \frac{dn}{dE}\ \sqrt{\frac{2E}{m}}\ dE$$

*"True" flux = (neutron density/cm^3)(mean value of neutron velocity). "Conventional" of "2200 meter/sec" flux = (neutron density/cm^3) ($v_0 = 2.2 \times 10^5$ cm/sec). It is related to the "true" flux by the ratio: $\phi_{true}/\phi_{conven.} = \sqrt{4T/\pi T_0}$ which, for a room-temperature Maxwellian distribution ($T = T_0 = 273.6°K$), reduces to 1.128.

It is often convenient to divide the flux into two parts: a Maxwellian of temperature T ("thermal flux") in which

$$\frac{dn}{dE} = \frac{2N}{\sqrt{\pi}} E_0^{-3/2} \sqrt{E}\, e^{-E/E_0} \qquad \text{for the range } 0 \leq E \leq 5kT,$$

and a 1/E slowing-down tail ("epithermal flux") with

$$\frac{dn}{dE} = \beta \frac{1}{E} \qquad \text{for the range } 5\ kT \leq E,$$

where $E_0 = kT$; β is a measure of the relative value of the epithermal flux;[7,8] and

$$N = \int_0^\infty \frac{dn}{dE}\, dE$$

is the total neutron density per cubic centimeter. The normalization, β, is often given in terms of the fractional neutron density in the epithermal region, relative to the total neutron density by Westcott's "r" function. The latter can be determined from measured cadmium ratios. The relations between "r" and the measured subcadmium ratio are given in Section 3.2.2.

Most detecting foils have resonances at energies much higher than the 5 kT value used to define thermal and epithermal flux. Narrow, well-spaced, single-level, Breit-Wigner-type resonances exhibit a $1/\sqrt{E}$ behavior at energies well below the resonance energy, and an $E^{-3/2}$ behavior at energies much higher than the resonance energy.[8] Any departure from the $1/\sqrt{E}$ law in the thermal region is expressed by Westcott's "g(T)" function and in the epithermal region by his "s" function (see Section 3.2.2). The total cross section used in computing reaction rates is the sum of all the resonance contributions (resonance integral), and the $1/\sqrt{E}$ contribution in the thermal and the epithermal regions. Some tabulations of resonance integrals include the $1/\sqrt{E}$ contribution in the epithermal region; others may include this contribution but only from the effective cadmium cutoff energy (rather than 5 kT).

9.1.2 SELF-SHIELDING FUNCTION

The self-shielding function, $G(\tau)$, is defined as the ratio of the average flux through the volume, to the average flux over the surface of the foil:

$$G(\tau) = \bar{\phi}_V / \bar{\phi}_S \tag{9-1}$$

The average flux through the volume, in turn, is related to the activation, C, by:

$$C = \tau \bar{\phi}_V \tag{9-2}$$

where τ is the foil thickness in absorption lengths (the product of the foil thickness, t, and the macroscopic activation cross section, Σ_a). The activation of successive foil layers can be computed by expanding the average surface flux in terms of its angular components, $P_\ell(\cos\theta)$ with coefficients K_ℓ. The total activation is then the integral over the differential activation of the various layers and summed over all the angular components:[1]

$$C = \sum_\ell (2\ell + 1)\, K_\ell \int_0^t \int_0^{\pi/2} [\exp(-x\, \Sigma_a'/\cos\theta)]\, P_\ell(\cos\theta) \sin\theta\, \Sigma_a\, d\theta\, dx$$

where Σ_a' is the total absorption cross section, including (n,p), (n,2n), etc., processes. For the general case, $\Sigma_a \simeq \Sigma_a'$, integration gives the self-shielding as:

$$G(\tau) = \frac{1}{\tau} \frac{\left\{\left[\frac{1}{2} - E_3(\tau)\right] K_0 + 3\left[\frac{1}{3} - E_4(\tau)\right] K_1 + \ldots\right\}}{\int_0^{4\pi} \phi_S(\cos\theta)\, d\Omega}$$

where

$$E_n(\tau) = \int_1^\infty \frac{e^{-\tau x}}{x^n}\, dx$$

is the exponential integral of order n. For convenience, the first four orders of this function are tabulated in Section 9.1.8. In an isotropic flux the higher terms are small, and to a good approximation, only the K_0 term need be considered:

$$G(\tau) = \frac{1}{\tau}\left[\frac{1}{2} - E_3(\tau)\right] \tag{9-3}$$

Equation (9-3) was first derived by Bothe[9] in terms of $E_1(\tau)$.

In moderately thin foils ($\tau < 0.05$), the self-shielding can be very closely approximated by:

$$G(\tau) = 1 - \tau(1 - \log \tau)$$

It should be pointed out that the often-used phrase: "the activation of a 1/v absorber is proportional to the neutron density" is true only in the limiting case of $\tau \to 0$ and $G(\tau) \to 1$.

9.1.3 SELF-SHIELDING IN RESONANCE ACTIVATION

Most resonances are so narrow that an individual foil is not greatly affected by its own outer flux perturbation at the resonance energy since neutrons at this energy have only one mean free path before being removed either by slowing down or by capture. As a first approximation, the value of Σ_a and hence, the value of τ, might be averaged over the resonance, and the self-shielding computed according to Eq. (9-3).

A better approximation is given by Trubey, Blosser, and Estabrook.[10] Assuming a narrow, single-level, Breit-Wigner-type resonance, their results give the self-shielding as:

$$G_r(\tau) = \frac{\tau_r}{2}\int_{\frac{1}{2}\tau_r}^{\infty} y^{-2}\, e^{-y}\, [I_0(y) + I_1(y)]\, dy \tag{9-4}$$

where τ_r is the foil thickness at the peak of the resonance, and $I_0(y)$ and $I_1(y)$ are modified Bessel functions of the first kind and of the zeroth and first orders, respectively.[11] In the limiting cases of very thick or very thin foils, they give

$$G_r(\tau) = \frac{4}{3\sqrt{\pi}}\frac{1}{\sqrt{\tau_r}} \qquad \text{for thick foils}$$

$$G_r(\tau) = 1 + \frac{\tau_r \ln \tau_r}{4} - 0.3274\, \tau_r \qquad \text{for thin foils}$$

For foils of intermediate thickness, they did a numerical integration of Eq. (9-4). Their results, along with some of their measurements, are shown in Fig. 9-1.

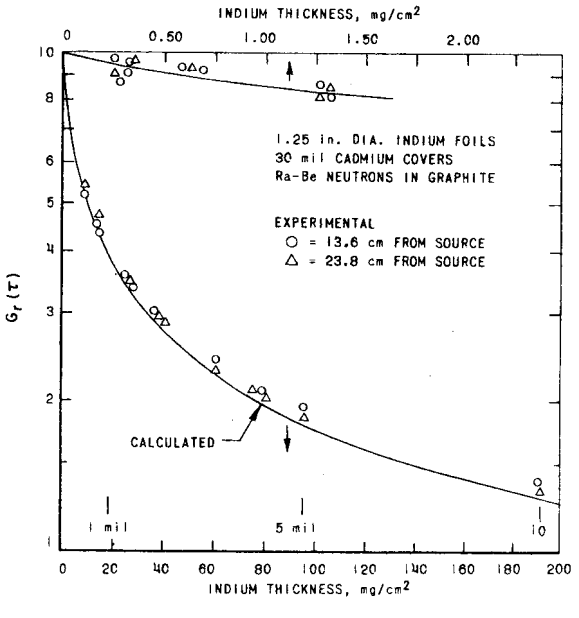

Fig. 9-1—Resonance self-shielding function, $G_r(\tau)$, vs. indium thickness in an isotropic flux. *Reproduced, in part, from Ref. 10.*

9.1.4 OUTER FLUX PERTURBATIONS

In the medium surrounding an absorbing foil, there is a net neutron current toward the foil as well as a depletion of the neutron density. It is customary to consider the foil as a negative source of neutrons whose strength is determined by the total number of neutrons absorbed per unit foil surface area per second. As a first approximation, diffusion theory can be used to predict the flux distribution from such a negative source. For those cases where the dimensions of the foil are comparable to the transport or diffusion lengths of the scattering medium: (1) the theory must either be modified, or (2) the more sophisticated techniques of transport or Monte Carlo theory are better used.

The outer flux perturbation, $F(\gamma,\tau)$, is defined as the ratio of the activation of a foil in the perturbed flux, to that which would result in an unperturbed flux. Neglecting the introduction of angular components in the flux, due to absorption by the foil, the outer flux perturbation can be expressed as the ratio of the average surface flux, to the originally unperturbed flux, ϕ_0:

$$F(\gamma,\tau) = \bar{\phi}_S/\phi_0 \tag{9-5}$$

where the properties of the medium are contained in the argument: $\gamma = \Sigma_{scat}/\Sigma_{tot}$. Ritchie and Eldridge[12] have reviewed a number of calculations for $F(\gamma,\tau)$ and note that they can be written in the common form:

$$F(\gamma,\tau) = \left\{1 + \left[\frac{1}{2} - E_3(\tau)\right] g(\gamma,\tau)\right\}^{-1} \tag{9-6}$$

where the functional form of $g(\gamma,\tau)$ depends on the method of calculation. Table 9-1 lists the theoretical expressions for the g-function employed by various investigators.

Table 9-1—EXPRESSIONS FOR THE g-FUNCTION

Author	Expression[a]	Range	Remarks
Bothe,[9] modified by Tittle[13]	$(3/2)\ (L/\lambda_{tr})\ [R/(R+L)] - 1$	$R \gg \lambda_s$	—
Vigon-Wirtz[1]	$(3/2)\ (L/\lambda_{tr})\ [1 - \exp(-0.85R/L)] - 1$	$R \gg \lambda_s$	—
Wirtz-Beckurts[6]	$(3/2)\ (L/\lambda_{tr})\ [1 - \exp(-0.85R/L)] - \{[1 - 3E_4(\tau)]/[1 - 2E_3(\tau)]\}$	$R \gg \lambda_s$	The term enclosed in braces = 0.77 ± 0.03 for $\tau \leq 0.05$; = 1.00 for $\tau \geq 5$
Wirtz-Beckurts[6]	$(3/2)\ (L/\lambda_{tr})\ [1 - \exp(-R/L)] - 0.12$	$R \gg \lambda_s$	Empirical formula based on measurements by Meister[2]
Bothe[9]	$0.68\ (R/\lambda_s)$	$R \ll \lambda_s$	—
Tittle[13]	$0.68\ (R/\lambda_{tr})$	$R \ll \lambda_s$	—
Meister[3b]	$(4/3\pi)\ (R/\lambda_s)\ \zeta_0(\tau)\ [1/2 - E_3(\tau)]^{-1}$	$R \ll \lambda_s$	—
Skyrme,[14] modified by Ritchie-Eldridge[12]	$(3/2)\ (L/\lambda_{tot})\ S(2R/L) - K\ [(2R/\lambda_s), \gamma]$	All R's	$S(x) = 1 - (4/\pi) \int_0^1 (1-t^2)^{1/2}\ e^{-xt}\ dt$ $K \approx (1/15)\ (2R/\lambda_s)$ for $2R \leq \lambda_s$ $K \approx 0.15$ for $2R \gg \lambda_s$

[a]The terms λ_{tr}, λ_s, and L, are the transport, scattering, and diffusion lengths in the medium; R and τ are the foil radius and thickness (in absorption lengths).

[b]Values of Meister's $\zeta_0(\tau)$ function are given in Table 9-5. As used by Wirtz-Beckurts, this function has the value: $2[1/2 - E_3(\tau)]$.

In addition to the results quoted in Table 9-1, Ritchie and Eldridge[12] have made a transport theory calculation of this function for discs of infinite radii. To adapt their results to finite discs, they suggest multiplying by a fraction determined from Skyrme's work:[14]

$$g = g^{\infty}_{R\text{-}E}\ (g^{R}_{S}/g^{\infty}_{S})$$

where the superscripts R and ∞ indicate the foil radius, and the subscripts R-E and S refer to the results of Ritchie-Eldridge, and Skyrme, respectively. Selected values are listed in Table 9-2. It will be noted from the numerical values in this table that to a good approximation:

$$g^{\infty}_{R\text{-}E} \simeq (3/2)\ (L/\lambda_{total})$$

Table 9-2—VALUES OF $g^{\infty}_{R\text{-}E}$ AND THE RATIO $(g^{R}_{S}/g^{\infty}_{S})$

$g^{\infty}_{R\text{-}E}$						$(g^{R}_{S}/g^{\infty}_{S})$[a]		
(L/λ_{tot}) =	16	12	8	6	4	(L/λ_{tot}) =	16	4
τ = 0.001	23.78	17.76	11.75	8.727	5.687	(2R/L) = 0.01	0.0038	0.0034
0.01	23.73	17.73	11.70	8.683	5.642	0.02	0.0073	0.0068
0.10	23.54	17.53	11.52	8.501	5.470	0.05	0.0190	0.0171
0.20	23.44	17.43	11.42	8.408	5.383	0.10	0.0381	0.0376
0.50	23.29	17.28	11.28	8.269	5.255	0.20	0.0760	0.0735
1.00	23.18	17.18	11.17	8.172	5.168	0.50	0.184	0.173
2.00	23.10	17.10	11.10	8.104	5.106	1.00	0.318	0.311
5.00	23.07	10.07	11.07	8.076	5.080	—	—	—

[a]Computed from Table 9-1.

and

$$(g^{R}_{S}/g^{\infty}_{S}) \simeq 0.35\ (2R/L)$$

or combined

$$g \simeq 1.05\ (R/\lambda_{total})$$

The results of Meister's measurements are compared with the various calculations in Fig. 9-2.

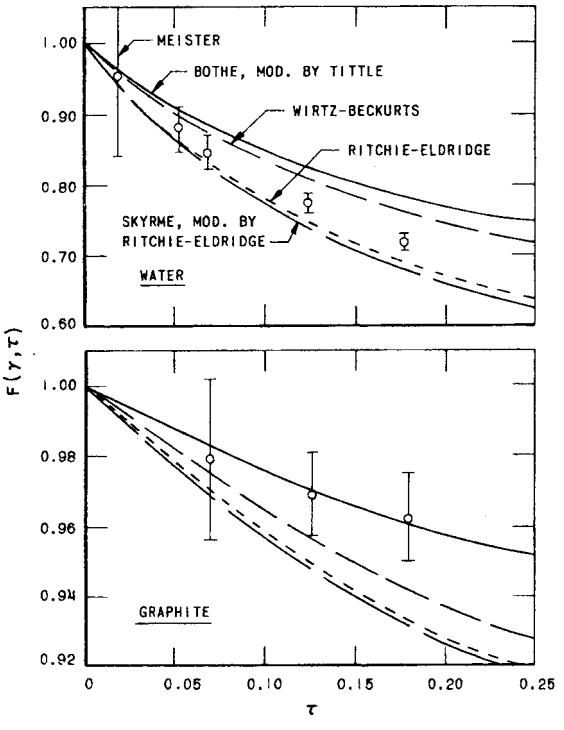

Fig. 9-2—Calculated vs. measured outer flux perturbations in water and in graphite for 1.2 cm radius indium foils.

9.1.5 INTEGRAL FLUX PERTURBATIONS

The relation between experimentally measurable activation and the initially unperturbed flux is obtained by combining Eqs. (9-1), (9-2), (9-3), and (9-6):

$$C = \tau\, G(\tau)\, F(\gamma,\tau)\, \phi_0$$

$$= \frac{(1/\tau)\,[(1/2) - E_3(\tau)]}{1 + [(1/2) - E_3(\tau)]\, g(\gamma,\tau)}\, \phi_0 \qquad (9\text{-}7)$$

687863 O - 63 - 44

Dalton and Osborn[15] performed a very general transport theory calculation of the "flux" ratio, $\bar{\phi}_v/\phi_0$, for the case of a cylindrical detector. As used here, the average volume flux is proportional to the activation. The calculation allowed for isotropic scattering in the foil, and anisotropic scattering in the surrounding medium. Unlike previous work in this field, their expression was not separated into a self-shielding factor and an outer flux perturbation. Figure 9-3 shows the flux ratios obtained with coin- and with wire-shaped detectors in graphite and in water.

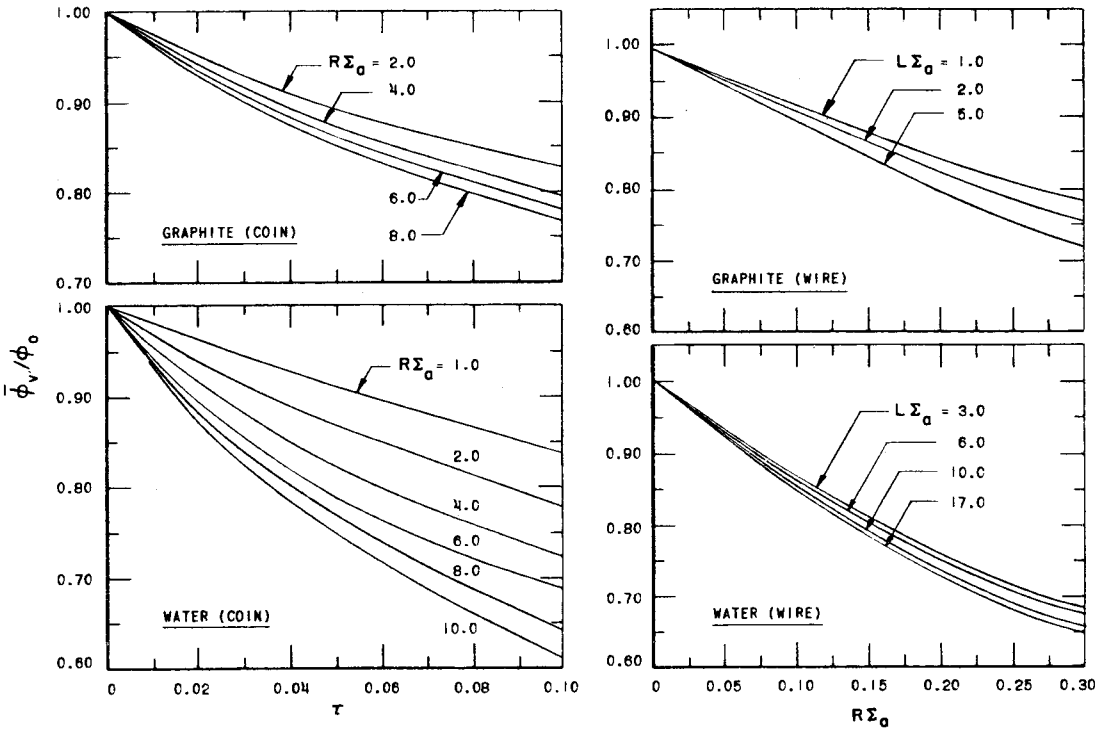

Fig. 9-3 — Flux ratios for coin- and wire-shaped foils in water and in graphite. *Reproduced from Ref. 15.*

Sola,[16] Thompson,[17] Meister,[2] and Zobel,[18] have measured integral flux perturbations in water (or paraffin) and in graphite. Their results are plotted in Fig. 9-4; included for comparison are calculations by Ritchie and Eldridge,[12] and Dalton and Osborn.[15] The measurements in water by Meister were made first in a void in the medium where no outer flux perturbation existed (only self-shielding), and then in the medium where both effects were present. Other experimental results[19] approximate the theoretical values of Ritchie, and the measured values of Sola and Meister, to the extent that these numbers can be assumed correct to within 3%.

There is one significant difference between theories. For a given τ, the Dalton-Osborn calculation gives equal integral flux perturbations for any combination of R and Σ_a, provided the product remains constant; other theories require R invariant.

9.1.6 FLUX DISTRIBUTION SURROUNDING A FOIL

Several theoretical expressions have been derived to calculate the flux perturbation caused by a foil at a specific point in the surrounding medium. This information is required to establish the minimum spacing between foils consistent with a given error in the measurements of the unperturbed flux.

For distances, z, greater than a scattering length, λ_s, from the foil surface, diffusion theory calculations by Vigon and Wirtz[1] give:

$$\phi(z) = \left\{1 - \frac{(L/\lambda_{tr})\, f(\tau)\, [\exp(-z/L) - \exp(-\sqrt{R^2 + z^2}/L)]}{1 + (L/\lambda_{tr})\, f(\tau)\, [1 - \exp(-R/L)]}\right\} \phi_0$$

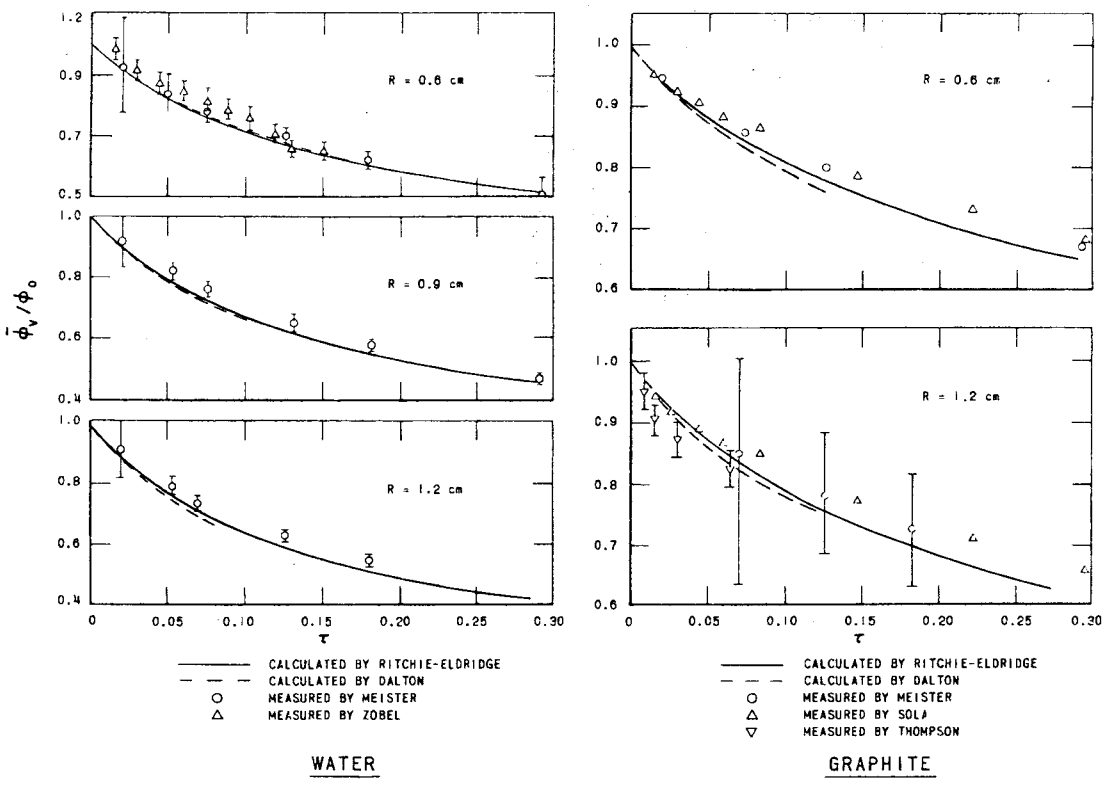

Fig. 9-4—Measured and calculated integral flux perturbations in water and in graphite for various foil radii.

For $z < \lambda_s$, the modified diffusion theory of Meister[4] gives:

$$\phi(z) = \frac{1 + E_2(\tau) + \beta[1 - E_2(\tau/\beta)]}{2 + (R/\lambda_{tr})\,\zeta_0(\tau)}\,\phi_0$$

In these expressions, ϕ_0 is the value of the unperturbed uniform (but not necessarily isotropic) flux prior to foil insertion; L and λ_{tr} are the diffusion and the transport lengths in the medium; R is the foil radius; Meister's $\zeta_0(\tau)$ function is given in Table 9-5;

$$\beta^2 = \frac{z^2}{R^2 + z^2}$$

and the relation for $f(\tau)$, originally given by Vigon and Wirtz, but later modified by Wirtz and Beckurts[6] is:

$$f(\tau) = \frac{(1/2) - E_3(\tau)}{(1/3) + E_4(\tau)}$$

In Fig. 9-5, the results of both theories are compared with the transport calculations of Dalton and Osborn,[15] and the measurements of Meister,[4] for the cases of water and graphite. The measurements in graphite are exceptionally well fitted to a curve (dashed line) which joins diffusion theory at large distances (Curve A), with the Meister theory (Curve C) close to the foil. The corresponding results for water are shown as Curve D (diffusion theory), and Curve E (Dalton and Osborn theory).

9.1.7 FOIL COVERS

Foil covers are used to shield a detecting foil from neutrons within particular energy regions. Very thin covers absorb neutrons in direct proportion to their thickness. Thicker covers, more typical

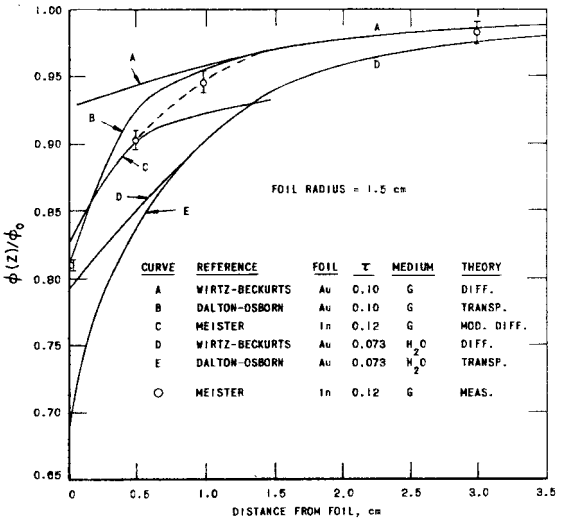

Fig. 9-5—Calculated vs. measured flux surrounding a foil.

for practical cases, absorb neutrons according to $[(1/2) - E_3(\tau)]$, thereby attenuating the neutron flux incident on the detecting foil by the factor:

$$1 - \alpha = 2\ E_3(\tau_c)$$

where τ_c is the cover thickness, in absorption lengths, for the neutron energy under consideration. Within this energy region, the activation of the inner foil is given by:

$$C_{covered} = \tau G(\tau)\ F(g, \tau + 2\tau_c)\ 2\ E_3(\tau_c)\ \phi_0 \qquad (9\text{-}8)$$

where τ is the thickness, in absorption lengths, of the detecting foil.

Resonance Covers. Resonance absorption by covers having large resonances, i.e., gold or indium, is primarily a surface effect. Such covers will effectively remove all resonance energy neutrons from the detecting foil. The consequent reduction in activation between the covered foil and a bare foil is used as a measure of the resonance flux. The predicted activation is given by the combination of Eqs. (9-4) and (9-8).

Cadmium Covers. Cadmium covers shield the foil from flux at energies less than 0.4 ev. They are used to determine the thermal and the epithermal flux components. "Thermal" and "epithermal" flux, as used here refer, respectively, to the flux below and above the effective cadmium cutoff energy. Two quantities are usually defined:

The cadmium ratio:

$$C.R. = \frac{\text{uncovered activity}}{\text{covered activity}} = \frac{\text{(thermal + epithermal) activity}}{\text{epithermal activity}}$$

and the subcadmium fraction:

$$C.F. = \frac{\text{(uncovered − covered) activity}}{\text{uncovered activity}} = \frac{\text{thermal activity}}{\text{(thermal + epithermal) activity}}$$

Difference measurements with and without cadmium covers are made to establish the thermal activity in the presence of appreciable epithermal flux, or vice versa. Martin[20] has measured the contribution to the total activation by thermal neutrons transmitted through various thicknesses of cadmium onto an indium foil. His results are reproduced in Fig. 9-6. The corresponding contribution to the total activation by epithermal neutrons was measured in graphite by Martin, and in water by Blosser and Trubey.[21] The data are plotted in Figs. 9-7 and 9-8, respectively.

The ratio of the epithermal component of the total activation of an uncovered foil, to the epithermal activation of the covered foil is referred to as the cadmium correction factor, $F_{Cd}(t)$. This factor is a function of the cadmium thickness t, the neutron flux spectrum and its angular distribution, and the foil material, size, and shape.

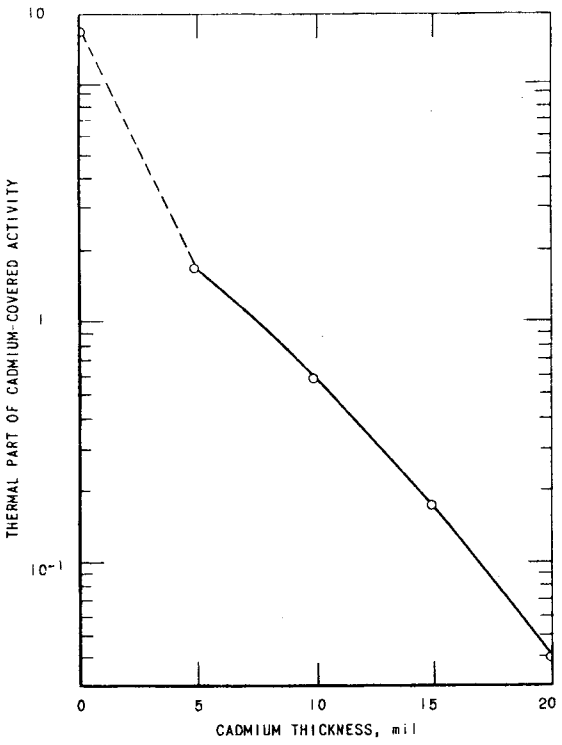

Fig. 9-6 — Thermal neutron activation of cadmium-covered indium foils. *Reproduced from Ref. 20.*

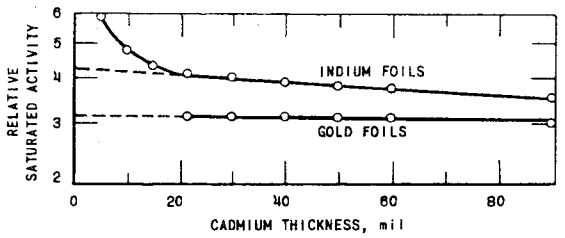

Fig. 9-7 — Epithermal neutron activation of cadmium-covered indium and gold foils in graphite. *Reproduced from Ref. 20.*

Fig. 9-8 — Epithermal neutron activation of cadmium-covered indium foils in water. *Reproduced from Ref. 21.*

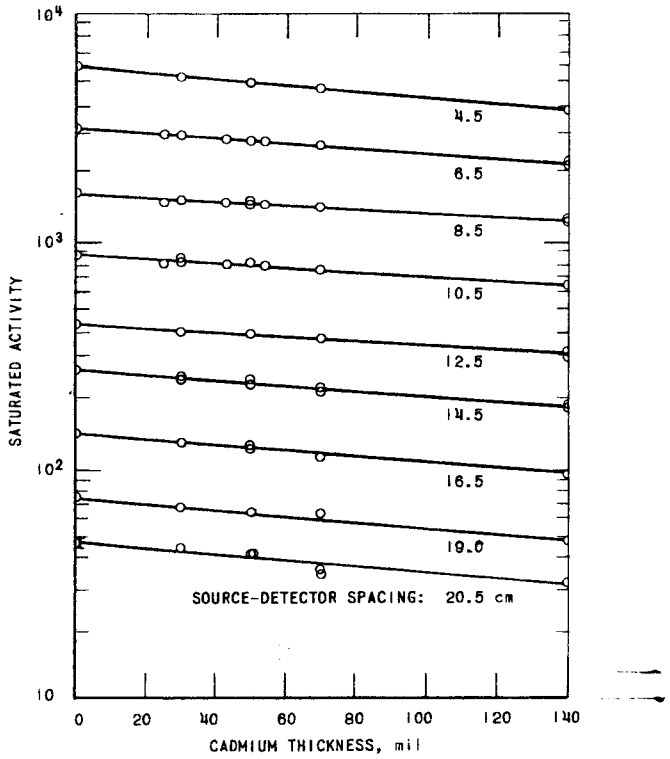

For isotropic fluxes, Branch[22] gives the expression:

$$F_{Cd}(t) = 1/E_2(\tau_{Cd})$$

where τ_{Cd} is the effective cadmium thickness for the epithermal neutrons in the cadmium cover. This expression does not account for scattering in the cadmium. The epithermal activation of an uncovered foil is obtained by linear extrapolation of the measured total activation of a covered foil to zero cadmium thickness, as indicated by the dashed line in Fig. 9-7. Table 9-3 lists the experimentally determined cadmium correction factors for indium foils with cadmium covers 40 mil thick.

Table 9-3—CADMIUM CORRECTION FACTORS (F_{Cd}) FOR 40 MIL THICK CADMIUM COVERS ON INDIUM FOILS

Indium Foil		Medium	Approx. C.R.	Source-Detector Separation,[a] cm	F_{Cd}	Ref.
Thickness, mg/cm^2	Size, cm					
96.1	3.2 (dia.)	Graphite	—	13.6	1.128[b]	10
96.1	3.2 (dia.)	Graphite	—	23.8	1.131[b]	10
96.1	3.2 (dia.)	Graphite	—	34.0	1.129[b]	10
96.1	3.2 (dia.)	Graphite	—	44.1	1.137[b]	10
96.1	3.2 (dia.)	Graphite	—	64.4	1.141[b]	10
1.28	3.2 (dia.)	Graphite	—	13.6	1.109[b]	10
0.59	3.2 (dia.)	Graphite	—	13.6	1.123[b]	10
3.59	2 × 3.1	Water	10	—	1.077	20,23
58.8	3.02 (dia.)	Water and Solutions	10	—	1.120	20,24
93.5	4 × 6.35	Water	10	—	1.20	20,25
94.5	4 × 6.35	Graphite	50	—	1.150	20,26
94	1.00 × 1.00	Graphite	6	—	1.098	20
88	1.00 × 1.00	Graphite	6	—	1.094	20
69	1.00 × 1.00	Graphite	6	—	1.09	20
29	1.00 × 1.00	Graphite	6	—	1.09	20
88	1.00 × 1.00	Graphite	16	—	1.095	20
88	0.20 × 1.00	Graphite	6	—	1.10	20
20	1.8 (dia.)	Hole in Graphite[c]	48	—	1.065	2
300	1.8 (dia.)	Hole in Graphite	48	—	1.088	2
20–300	1.8 (dia.)	Paraffin	28[d]	—	1.05	2

[a]ORNL data uses the distance from the radium-beryllium source in the Standard Pile to the detector.
[b]Average value of the ORNL data least-squares-fit to a third-order exponential integral and to a simple exponential.
[c]Foils exposed in a void space in a graphite block to eliminate outer flux perturbation.
[d]Foil in center of paraffin cube, 17 cm on a side with two sources, 20 cm beyond opposite faces of the cube.

A comprehensive study of the effect of cadmium covers in water has been made by Blosser, Trubey, and Estabrook at ORNL.[10,21] Their results, as evaluated from the data in Fig. 9-8, are shown in Fig. 9-9 for indium foils (5 mil thick; 96.1 mg/cm^2) with cadmium covers (40 mil and 140 mil thick).

The correction factor as a function of detecting foil thickness for three different thicknesses of cadmium covers has been determined by Tittle.[13,27] His results are reproduced as Fig. 9-10.

Effective Culoff Energy. The effective cutoff energy, E_{CO}, is defined as the energy of the step in an idealized step function-type filter with $\Sigma_a = 0$ for $E < E_{CO}$, and $\Sigma_a = \infty$ for $E > E_{CO}$. The activation of a foil covered with such a filter is identical to that of a cadmium-covered foil.

Stoughton, Halperin, and Lietzke[28] have published extensive tables of the effective cutoff energy calculated for point 1/v absorbers inside spherical and cylindrical cadmium covers. They assumed that the neutron spectrum was a Maxwellian plus a 1/E component whose flux ratio, r, could be varied. A selection of their results for different Maxwellian temperatures, using both boron and cadmium covers, is given in Table 9-4. Dayton and Pettus[29] have calculated effective cutoff energies in slab geometry. Their results are shown in Fig. 9-11.

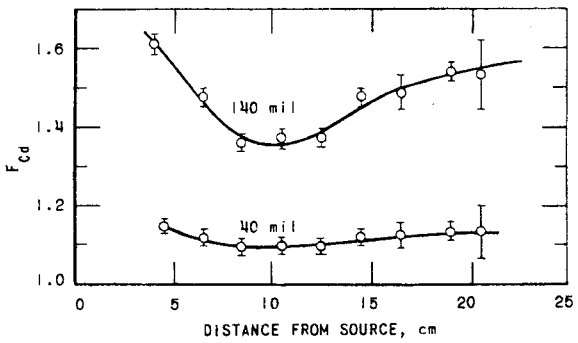

Fig. 9-9 — Cadmium correction factor, F_{Cd}, as a function of distance from source in water for indium foils (5 mil thick) with cadmium covers (40 mil and 140 mil thick). *Reproduced from Ref. 21.*

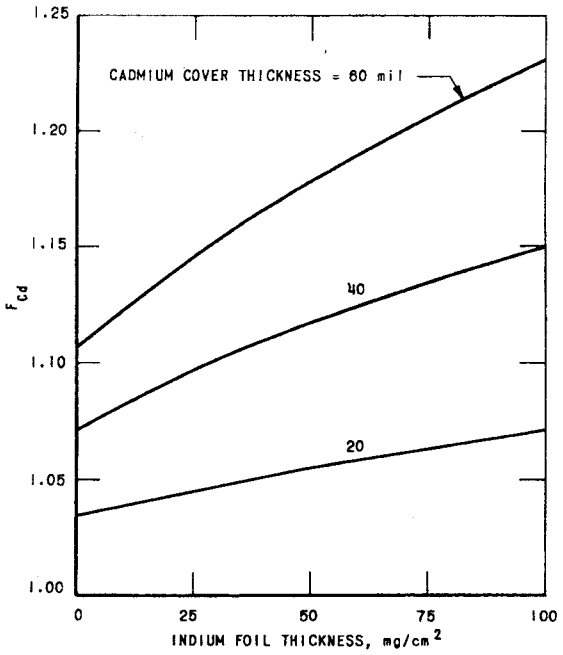

Fig. 9-10 — Cadmium correction factor for indium foils as a function of detecting foil thickness. *Reproduced from Ref. 27.* ⟶

Table 9-4 — EFFECTIVE CUTOFF ENERGY FOR CYLINDRICAL CADMIUM AND BORON COVERS

(Cylinder Height = 2 × Diameter)

Cadmium Thickness, mil	r = 0		r = 12		r = 20	
	E_{CO}	Frac.	E_{CO}	Frac.	E_{CO}	Frac.
Cadmium; E_m = 0.0253 ev						
10	0.387	0.061	0.173	0.358	0.148	0.482
20	0.452	0.066	0.431	0.075	0.419	0.082
40	0.547	0.071	0.547	0.071	0.547	0.071
100	0.718	0.076	0.718	0.076	0.718	0.076
Cadmium; E_m = 0.05 ev						
10	—	—	0.206	0.347	0.189	0.466
20	—	—	0.429	0.079	0.416	0.088
40	—	—	0.545	0.072	0.545	0.072
100	—	—	0.719	0.076	0.718	0.076
Boron; E_m = 0.0253 ev						
Boron Thickness, mg/cm^2						
20	0.20	0.16	0.040	0.42	0.040	0.44
40	0.29	0.25	0.073	0.57	0.68	0.60
100	0.79	0.34	0.25	0.55	0.173	0.62
1000	61.4	0.37	61.2	0.37	61.2	0.37
Boron; E_m = 0.35 ev						
20	—	—	0.041	—	—	—
40	—	—	0.086	—	0.082	—
100	—	—	0.206	—	0.165	—
1000	—	—	63.7	—	63.7	—

Note: E_m is the Maxwellian characteristic energy, kT, or the energy corresponding to the most probable velocity; r is the ratio of the Maxwellian flux to the 1/E flux; and Frac. is the fraction of reactions that occur below the cutoff energy.

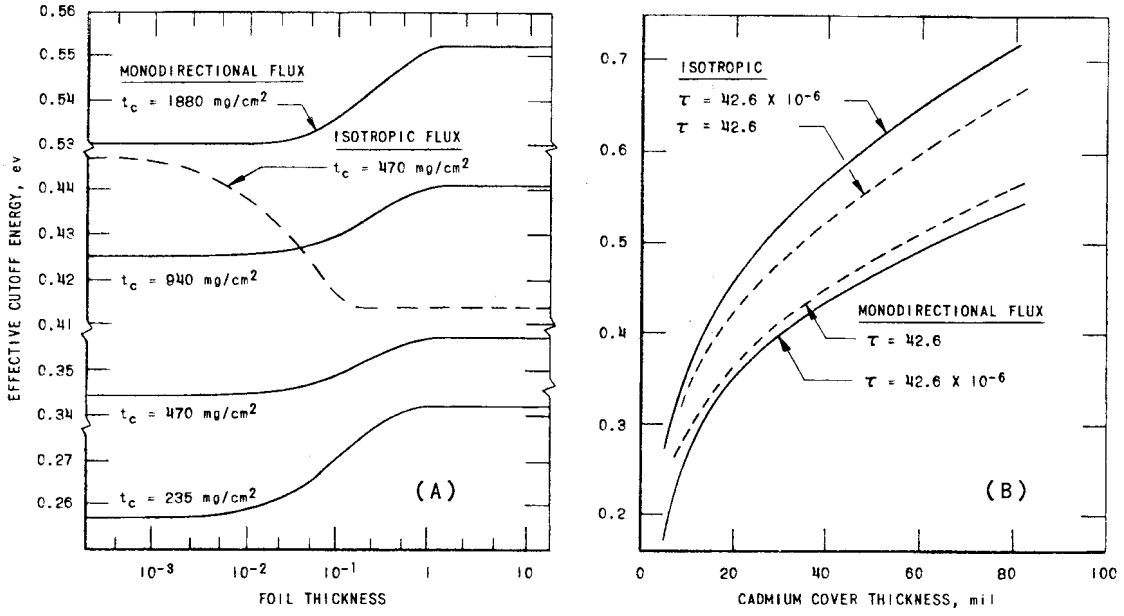

Fig. 9-11 —Effective cutoff energy as a function of (A) foil thickness, τ, and (B) cadmium cover thickness, t_c, for 1/v absorbers. *Data from Ref. 29.*

9.1.8 EXPONENTIAL INTEGRALS AND ASSOCIATED FUNCTIONS

The values of the first four orders of the exponential integral as computed by Schlosser[30] and by Trubey[30] and defined in Section 9.1.2 are listed in Table 9-5 for a variety of arguments. Also included is the first-order absorption term, $(1/2) - E_3(\tau)$; the self-shielding function, $G(\tau) = [(1/2) - E_3(\tau)]/\tau$; the second-order correction term, $[(1/3) - E_4(\tau)]$; and Meister's $\zeta_0(\tau)$ function.

9.1.9 FOIL MATERIALS AND PROPERTIES

Table 9-6 lists the properties of certain materials commonly used as thermal- and resonance-energy neutron-detecting foils. Although more extensive lists exist,[31–33] this selection is based primarily on availability, feasibility of measuring the indicated radioactivity in the presence of certain natural contaminants, reasonable half-lives and cross sections, and, to a lesser extent, on experience. Columns (4) through (7) list the most intense decay components and the frequency of their occurrence per unit parent atom decay. Cross sections listed in columns (8) and (9) are measures of the usefulness of a given isotope in any particular application. Energies of the three largest resonances for each isotope are listed in column (10), and the area under each single resonance in column (11). This area, proportional to the activation probability within a single resonance, was computed assuming a narrow, Breit-Wigner type resonance. Column (12) is the measured area under all resonances in the particular isotope. All resonance parameters and cross sections are taken from Ref. 34.

Properties of certain useful threshold-detecting foils are listed in Table 9-7. Near threshold, most of the (n,p) and (n,2n) cross sections increase almost linearly with energy. The threshold energies were determined by linear extrapolation of the measured cross sections. The cross sections at three times the threshold (a convenient, though arbitrary energy) are listed in column (9) to facilitate a relative comparison among foils.

Table 9-5—EXPONENTIAL INTEGRALS AND ASSOCIATED FUNCTIONS

τ	$E_1(\tau)$	$E_2(\tau)$	$E_3(\tau)$	$E_4(\tau)$	$(1/2) - E_3(\tau)$	$G(\tau)$	$(1/3) - E_4(\tau)$	$\xi_0(\tau)$
0.001	6.332	0.9927	0.4990	0.3328	0.0009960	0.9960	0.0004995	—
0.002	5.639	0.9867	0.4980	0.3323	0.001986	0.9930	0.0009980	—
0.005	4.726	0.9714	0.4951	0.3308	0.004922	0.9844	0.002488	—
0.010	4.038	0.9497	0.4903	0.3284	0.009723	0.9723	0.004951	—
0.020	3.355	0.9131	0.4810	0.3235	0.019032	0.9516	0.009807	0.0453
0.030	2.959	0.8817	0.4720	0.3188	0.02800	0.9333	0.014571	—
0.050	2.468	0.8278	0.4549	0.3095	0.04508	0.9016	0.02384	0.1054
0.075	2.087	0.7712	0.4350	0.2984	0.06505	0.8673	0.03496	—
0.10	1.8229	0.7225	0.4163	0.2877	0.08371	0.8371	0.04560	0.1908
0.20	1.2227	0.5742	0.3519	0.2494	0.14805	0.7403	0.08389	0.3276
0.30	0.9057	0.4691	0.3000	0.2169	0.2000	0.6667	0.11640	0.435
0.50	0.5598	0.3266	0.2216	0.16524	0.2784	0.5568	0.16809	0.590
0.75	0.3403	0.2171	0.15477	0.11876	0.3452	0.4603	0.2146	—
1.00	0.2194	0.14850	0.10969	0.08606	0.3903	0.3903	0.2473	0.804
1.20	0.15841	0.11110	0.08393	0.06682	0.4161	0.3468	0.2665	—
1.30	0.13545	0.09644	0.07358	0.05896	0.4264	0.3280	0.2744	—
1.40	0.11622	0.08389	0.06458	0.05206	0.4354	0.3110	0.2813	—
1.50	0.10002	0.07310	0.05674	0.04601	0.4433	0.2955	0.2873	—
2.0	0.04890	0.03753	0.03013	0.02502	0.4699	0.2349	0.3083	—
2.5	0.02491	0.019798	0.016295	0.013782	0.4837	0.19348	0.3196	—
3.0	0.013048	0.010642	0.008931	0.007665	0.4911	0.16359	0.3257	—
3.5	0.006970	0.005802	0.004945	0.004296	0.4951	0.14144	0.3290	—
4.0	0.003779	0.003198	0.002761	0.002423	0.4972	0.12431	0.3325	—
5.0	0.0011483	9.965×10^{-4}	9.965×10^{-4}	7.830×10^{-4}	0.4991	0.09982	0.3325	—
6.0	3.601×10^{-4}	3.183×10^{-4}	2.846×10^{-4}	2.570×10^{-4}	0.4997	0.08329	0.3331	—
7.0	1.1548×10^{-4}	1.0351×10^{-4}	9.366×10^{-5}	8.543×10^{-5}	0.4999	0.07142	0.3332	—
8.0	3.767×10^{-5}	3.414×10^{-5}	3.1180×10^{-5}	2.867×10^{-5}	0.5000	0.06250	0.3333	—
9.0	1.2447×10^{-5}	1.138×10^{-5}	1.0479×10^{-5}	9.701×10^{-6}	0.5000	0.05556	0.3333	—
10.0	4.157×10^{-6}	3.830×10^{-6}	3.549×10^{-6}	3.304×10^{-6}	0.5000	0.05000	0.3333	—
12.5	2.774×10^{-7}	2.592×10^{-7}	2.432×10^{-7}	2.289×10^{-7}	0.5000	0.44000	0.3333	—
15.0	1.918×10^{-8}	1.8108×10^{-8}	1.7140×10^{-8}	1.6267×10^{-8}	0.5000	0.03333	0.3333	—
17.5	1.3609×10^{-9}	1.2939×10^{-9}	1.2330×10^{-9}	1.1774×10^{-9}	0.5000	0.02857	0.3333	—
20.0	9.835×10^{-11}	9.405×10^{-11}	9.009×10^{-11}	8.644×10^{-11}	0.5000	0.02500	0.3333	—
25.0	5.349×10^{-13}	5.157×10^{-13}	4.978×10^{-13}	4.811×10^{-13}	0.5000	0.02000	0.3333	—

Table 9-6—SOME USEFUL THERMAL- AND RESONANCE-DETECTING FOILS AND THEIR PROPERTIES

(1)	(2)	(3)	(4)	(5)	(6)	(7)	(8)	(9)	(10)	(11)	(12)
Isotope and Reaction	Natural Abundance, %	Beta Radiation[a]			Gamma Radiation[a]		Cross Section, barn		Resonance Properties		
		Half-Life	Max. Energy, Mev	Intensity,[b] %	Energy, Mev	Intensity,[b] %	Isotope[c]	Element[c]	Resonance Energy, ev	Single[d] Resonance, b	Meas. Total Resonance Integral, b
$Mn^{55}(n,\gamma)Mn^{56}$	100	2.58 hr	2.85	60	0.85	70	13.3 ± 0.2	13.2 ± 0.2	337	—	7.7 ± 0.5
	—	—	1.05	25	—	—	—	—	—	—	—
$Rh^{103}(n,\gamma)Rh^{104}$	100	4.4 min[e]	none	—	0.077 & 0.051[f]	99	12 ± 2	194 ± 4	1.257	1005	656
	—	44 sec	2.5	98.5	0.556	1.4	—	—	—	—	—
$Ag^{107}(n,\gamma)Ag^{108}$	51.35	2.3 min	1.77	98	0.63	1.0	45 ± 4	64.8 ± 0.4	16.5	76.6	75
	—	—	—	—	—	—	—	—	41.5	5.95	—
	—	—	—	—	—	—	—	—	51.4	15	—
$Ag^{109}(n,\gamma)Ag^{110}$	48.65	253 day	0.087	58	0.61	1	3.2 ± 0.4	—	5.20	870	1160
	—	—	—	—	—	—	—	—	30.5	14.2	—
	—	—	—	—	—	—	—	—	40.2	6.1	—
$In^{115}(n,\gamma)In^{116m}$	95.77	54.05 min	1.0	51	1.27	75	155 ± 10	191 ± 3	1.457	2810	3500
	—	—	0.87	28	2.09	25	—	—	3.86	43.5	—
	—	—	0.6	21	—	—	—	—	9.12	41.5	—
$Dy^{164}(n,\gamma)Dy^{165}$	28.18	139.2 min	1.25	—	0.095	—	2000 ± 200	936 ± 20	none	—	—
	—	—	0.88	—	0.361	—	—	—	—	—	—
$Ir^{191}(n,\gamma)Ir^{192}$	38.5	74.3 day	0.67	48	0.47 & 0.32[f]	48	700 ± 200	440 ± 20	0.654	2380	3500
	—	—	0.53	41	0.32 & 0.60[f]	41	—	—	5.36	438	—
$Ir^{193}(n,\gamma)Ir^{194}$	61.5	19 hr	2.24	66	—	—	130 ± 30	—	1.303	1080	1370
	—	—	1.91	15	0.33	20	—	—	40.4	36.5	—
	—	—	0.98	10	2.05	9	—	—	—	—	—
$Au^{197}(n,\gamma)Au^{198}$	100	2.7 day	0.96	98.6	0.412	99	96 ± 10	98.2 ± 0.5	4.906	1180	1558
	—	—	—	—	—	—	—	—	61.2	36.2	—

[a]Only the most intense radiation is listed.
[b]Intensities are given per unit parent atom decay.
[c]2200 meter/second neutrons.
[d]Calculated from single-level resonance parameters given in Ref. 34.
[e]99+% of the 4.4-minute activity decays to the 44-second activity.
[f]Cascade transition.

Table 9-7—SOME USEFUL RESONANCE-DETECTING FOILS AND THEIR PROPERTIES

(1)	(2)	(3)	(4)	(5)	(6)	(7)	(8)	(9)	(10)
Isotope and Reaction	Natural Abundance, %	Beta Radiation[a]			Gamma Radiation[a]		Threshold Properties		
		Half-Life	Max. Energy, Mev	Intensity, %	Energy, Mev	Intensity,[a] %	Energy, Mev	Cross Section,[b] mb	Average,[c] mb
$S^{32}(n,p)P^{32}$	95.02	14.2 day	1.71	100	None	—	1.0	120	62 ± 2
$Fe^{56}(n,p)Mn^{55}$	91.68	2.58 hr	2.85	60	0.85	70	2.1	15	0.87 ± 0.4
	—	—	1.05	25	—	—	—	—	—
$F^{19}(n,2n)F^{18}$[d]	100	112 min	0.65[e]	97	None	—	10.4	—	—
$O^{16}(n,2n)O^{15}$[f]	99.96	2 min	1.72[e]	100	None	—	16.5	—	—
$Si^{28}(n,p)Al^{28}$	92.18	2.27 min	2.88	100	1.78	100	4	600	—
$C^{12}(n,2n)C^{11}$	98.89	20.4 min	0.98[e]	99	None	—	20.2	—	—
$Al^{27}(n,p)Mg^{27}$	100	9.45 min	1.75	58	0.84	70	1.8	32	3.43
	—	—	1.59	42	1.01	30	—	—	—
$P^{31}(n,p)S^{31}$	100	2.62 sec	1.49	99.9	None	—	1.0	65	30 ± 3

[a]Only the most intense radiation is listed. Intensities are given per unit parent atom decay.
[b]Cross section determined at three times the threshold energy by linear extrapolation of measured cross section.
[c]Average is taken over a fission spectrum.
[d]Used as CaF.
[e]Positron decay.
[f]If used in the form of cellophane, there is a 20.4-min positron decay due to $C^{12}(n,2n)C^{11}$ reaction.

9.2 CHARACTERISTICS OF PHOTOMULTIPLIER TUBES AND SCINTILLATORS

Scintillation detectors have become one of the standard tools for obtaining experimental data. Characteristics of some common photomultiplier tubes and scintillators are presented here. Detailed studies of the physics and performance characteristics of the various types of phototubes and phosphors are reported in Refs. 35, 37, and 38, inclusively.

9.2.1 PHOTOMULTIPLIER TUBES

Table 9-8 lists the characteristics of representative photomultiplier tubes. Except where noted, all tubes are 2 in. nominal diameter, head-on, semi-transparent photocathode devices having an S11 response[39] which peaks between 3900 Å and 4900 Å, with a full-width half-maximum of about 100 Å. The data are reproduced from Refs. 40 and 41, and from manufacturers' literature. Additional data on these and other tubes are reported in Refs. 37, 38, and 42.

The following brief comments are made with reference to Table 9-8. Up to a certain maximum current which is given in column (3), the current rises linearly with the light incident on the photocathode. At higher light intensities, the current approaches a saturation value, given in column (4). Columns (6) and (5) give, respectively, values of the r.m.s. variation of the electron transit time through the tube, for illumination of a fraction, or of the whole photocathode. The listed values are accurate to about 50%, but do give the approximate magnitude of the pulse rise time of the tube. Two components contribute to this variation in the transit time: the pulse width for a single initial electron leaving the photocathode as shown in column (7), and the velocity spread of all the electrons contributing to the output pulse.

Table 9-8—CHARACTERISTICS OF SOME REPRESENTATIVE PHOTOMULTIPLIER TUBES

Data from Refs. 40 and 41.

(1)	(2)	(3)	(4)	(5)	(6)	(7)	(8)	(9)	(10)	
Mfr. & Serial No.	Current Gain	MLPC,[a] ma	SPC,[b] ma	(ϵ_{tot}),[c] mμs	(ϵ_{part}),[d] mμs	(λ_{out}),[e] mμs	Cathode Material	Dark Current,[f] lumen	Limiting Sensitivity, amp/lumen	Remarks
RCA 6810A	10^8	500	1200 (3800 v)	1.2	0.6(1/4)	0.7	Sb-Cs-O	1.1×10^{-9}	2×10^4	Sensitivity at 2000 v is 1800 amp/lumen with 14 dynodes, and 50 amp/lumen with 10 dynodes.
(C 7187)	—	—	—	—	0.4(3/4)	—	—	—	—	
RCA 7265 (C 7237)	10^8	500	1200 (3800 v)	1.2	—	0.7	Multi-alkali	2×10^{-10}	—	—
Dumont K1549	6×10^6	300 (1890 v)	500 (1890 v)	1.7	—	—	—	—	—	—
EMI 9534	2×10^7	50 (2500 v)	150	2.0	—	2.5	Sb-Cs-O	10^{-9}	2×10^3	—
RCA 7264 (C 7251)	10^8	500	1200 (3800 v)	1.2	0.25(3/4)	0.7	—	1.1×10^{-9}	—	Spherical end window.
Amperex 56AVP	2×10^8	250	1000	0.9	—	—	—	—	—	—
RCA 931A	3.8×10^6	10	100	0.5 (150 v/ stage)	—	3.0 (150 v/ stage)	—	2.5×10^{-9}	—	Internal photocathode.
RCA 5819	2.3×10^6	10	100	1.6	0.5(1/2)	3.0	—	8.5×10^{-10}	—	Curved photocathode.
RCA 6655A	4.4×10^6	10	100	1.2	—	3.0	—	8.5×10^{-10}	—	Curved photocathode.
RCA 6342A	7.3×10^5	10	100	1.2	—	3.0	—	2×10^{-9}	—	Curved photocathode.
RCA 6903	4×10^5	10	100	12	0.6(1/2)	3.0	—	10^{-9}	—	Similar to 6655 with S-13 response.
Dumont 6292	2.8×10^6	6	20	3.7	1.6(1/2)	10	Sb-Cs-O	2×10^{-10}	2×10^3	—
EMI 6097	10^8 (2900 v)	100	500	2.7	—	5.5	Sb-Cs-O	2×10^{-10}	8×10^3	—

[a] Maximum linear pulse current.
[b] Saturation pulse current.
[c] r.m.s. transit time dispersion, full cathode.
[d] r.m.s. transit time dispersion for indicated fraction of photocathode radius.
[e] r.m.s. width of single electron pulse at output.
[f] Minimum typical dark current input.

9.2.2 NEUTRON-DETECTING SCINTILLATORS

Absolute measurements of neutron intensity and energy with proton recoil scintillators are generally difficult because of the uncertainties in crystal response, and in crystal and photocathode nonuniformities. Calculations[43] and measurements[44] for anthracene indicate that about 55 ev of energy is absorbed by the phosphor for each photon produced. When coupled to the photocathode with about a 50% light collection efficiency and an 11% photocathode quantum efficiency (corresponding to a 50 μa/lumen photocathode sensitivity), the total absorption of 1 Mev produces about 10^3 photoelectrons.

Solid, liquid, and gas scintillators have been used as proton recoil devices for determining the energy and the intensity of neutrons. Performance characteristics of selected phosphors are listed in Table 9-9.

Table 9-9—CHARACTERISTICS OF SOME REPRESENTATIVE ORGANIC SCINTILLATORS

Data from Ref. 40.

Phosphor[a]	Electrons/cm^3 ($\times 10^{23}$)	Hydrogen atoms/cm^3 ($\times 10^{22}$)	RPAR[b]	S.D.T.,[c] mμs	τ/R'(E),[d] mμs-Mev per photoelectron
Anthracene	4.0	4.2	1.00	35	0.035
Stilbene	4.0	4.7	0.40	6	0.015
Quaterphenyl	~3.5	~3.9	0.85	4.2	0.005
Xylene + p-terphenyl(5) + dibiphenyloxazole(BBO) (0.015)	2.8	4.9	0.5	4.2	0.008
Toluene + p-terphenyl(9)	2.8	4.5	0.5	4.2	0.004
Phenylcyclohexane + p-terphenyl(5) + diphenyloxazole benzene (POPOP)	3.0	5.5	0.54	~3	0.006
Triethylbenzene + p-terphenyl(5)	2.9	5.7	0.5	~3	0.006
Isopropylbiphenyl + p-terphenyl(5)	3.2	4.7	0.5	—	—
Polystyrene + p-terphenyl (2.5)	3.2	4.7	0.3	~3	0.01
Polyvinyltoluene + p-terphenyl	2.8	4.8	0.3	~3	0.01

[a]Solute contents given in grams per liter, where designated.

[b]Relative pulse amplitude response to electrons in small scintillators, compared to anthracene.

[c]Scintillation decay time.

[d]Ratio between scintillation decay time and the number R'(E) of photoelectrons released per Mev of electron energy absorbed in the phosphor.

For recoil protons or other heavy-charged particles, the photoelectron production per Mev of energy absorbed, R'(E), must be corrected for the nonlinear response of the phosphor. There is also a variation of R'(E) of as much as 25% among combinations of the same type of crystal and phototube. This is due to differences in spectral response and sensitivity of phototubes, and the size, purity, and optical efficiency of the phosphors. At lower neutron energies (<~200 kev), the recoil proton does not have sufficient energy to produce a statistically significant number of photoelectrons at the photocathode. At thermal energies, the charged particle reactions are generally used to produce either protons or alpha particles which can be detected. Table 9-10 lists some properties of certain heavy-charged particle scintillation detectors.

Table 9-10—CHARACTERISTICS OF SOME LOW-ENERGY NEUTRON DETECTORS

Data from Ref. 40.

Reaction	Detected Particle	Detected[a] Particle Energy, Mev	Scintillator	S.D.T.,[b] mμs	$(\tau/R)^c$
$B^{10}(n,\alpha\gamma)Li^7$	γ	0.48	NaI(Tl)	250	0.25
$Li^6(n,\alpha)H^3$	α, H^3	4.85	LiI(Eu)	2000	0.5
$K^{39}(n,p)A^{39}$	p	0.20	KI(Tl)	1000	10
$B^{10}(n,\alpha\gamma)Li^7$	α	2.3	He + Xe (>10%) (Quaterphenyl wave length shifter)	<15	<0.007
$He^3(n,p)H^3$	p	0.77	He + Xe (>10%) (Quaterphenyl)	<15	<0.02

[a]For incident thermal neutrons.
[b]Scintillation decay time.
[c]Scintillator decay time, τ, per photoelectron produced, R, in mμs/photoelectron.

9.2.3 GAMMA-DETECTING SCINTILLATORS

Three factors must be considered when making gamma-ray intensity and energy measurements with scintillation spectrometers:

(1) Energy-dependent efficiency of the detector
(2) Compton scattering and photofraction
(3) X-ray escape

A most convenient and sensitive gamma detector is the thallium-activated NaI crystal, optically coupled to a photomultiplier tube. Data given here on efficiencies, Compton scattering, and X-ray escape, are therefore primarily limited to this type of crystal.

Detecting Efficiency. Three processes compete in absorbing the gamma-ray energy: photoelectric absorption, Compton scattering, and pair production. The energy dependence of the various cross sections, and the physical dimensions of the crystal (in absorption mean free paths), determine the intrinsic efficiency of the scintillator. The "intrinsic efficiency" is defined as the ratio of the number of photons which produce detectable output pulses, to the total number incident on the crystal surfaces. The individual and the total cross sections for gamma-ray absorption in NaI(Tl) are listed in Table 9-11.

Extensive tables and graphs of efficiencies for various crystal sizes and detecting geometries can be found in Refs. 35, 37, and 45. Representative data are reproduced in Fig. 9-12, which shows the energy dependence of the "Source Intrinsic Efficiency at Zero Distance." This is the ratio between the number of detected gamma-rays, and the total emission rate of a monochromatic isotropic source immediately at the surface of the crystal. These data represent the results of approximately 10,000 Monte Carlo case histories.

Photofraction and Photo Peak Efficiency. Except for very low (< 20 kev) and very high (> 10 Mev) gamma-ray energies, where the mechanics of energy loss and subsequent light production are not clearly understood, the amount of light produced by the crystal, and hence, the amplitude of the output

Table 9-11 — GAMMA-RAY ATTENUATION COEFFICIENTS FOR SODIUM IODIDE–0.1% THALLIUM-ACTIVATED CRYSTALS

Data from Ref. 35.

Photon Energy, Mev	Scattering, cm^{-1}		Photoelectric K, L, and M Shells, cm^{-1}	Pair Production, cm^{-1}		Total Inelastic Cross Section, cm^{-1}	
	Coherent	Incoherent		Nucleus	Electron	0.1% Tl Correction	NaI – 0.1 Tl
0.01	8.3858	0.6048	448.3	—	—	0.28150	448.90
0.01268	—	0.5990	200.1	—	—	0.14535	200.70
0.015	5.1538	0.5945	140.7	—	—	—	141.29
0.01537	—	0.5912	125.5	—	—	0.51057	126.09
0.020	3.5429	0.5841	62.14	—	—	0.24583	62.72
0.030	1.9424	0.5635	18.94	—	—	0.078539	19.50
0.03323	1.80095	0.5576	13.99	—	—	—	14.55
0.03323	1.80095	0.5576	110.88	—	—	—	111.44
0.040	1.37061	0.5458	66.36	—	—	0.035084	66.91
0.050	0.88574	0.5296	36.42	—	—	0.018428	36.95
0.060	0.64993	0.5148	22.12	—	—	0.011024	22.635
0.080	0.39644	0.4883	9.997	—	—	0.004991	10.485
0.08584	—	0.4820	5.774	—	—	0.004131	6.256
0.08584	—	0.4820	5.798	—	—	0.028292	6.280
0.10	0.27265	0.4646	5.325	—	—	0.018908	5.790
0.15	0.125744	0.4190	1.6716	—	—	0.006612	2.0906
0.20	0.736885	0.3836	0.7397	—	—	0.003176	1.1233
0.30	0.338967	0.3334	0.2386	—	—	0.0012696	0.5720
0.40	0.019159	0.2995	0.10658	—	—	0.0007541	0.4061
0.50	0.0131166	0.2731	0.05775	—	—	0.0005231	0.33085
0.60	0.0085479	0.2525	0.03702	—	—	0.0004112	0.28952
0.80	0.0053056	0.2219	0.019255	—	—	0.0003019	0.24116
1.0	0.0026528	0.1995	0.01244	—	—	0.0002476	0.21194
1.5	0.00176852	0.16197	0.006072	0.002659	—	0.0001862	0.17070
2.0	0.00073688	0.13822	0.003851	0.009008	—	0.0001657	0.15108
3.0	—	0.10872	0.00237	0.02347	0.0000103	0.000154	0.13457
4.0	—	0.09057	0.001629	0.03676	0.0000590	0.000153	0.12902
5.0	—	0.07818	0.001185	0.04798	0.0000103	0.000155	0.12745
6.0	—	0.06903	0.001037	0.05727	0.000148	0.000159	0.12748
8.0	—	0.05650	0.000740	0.07247	0.000295	0.000166	0.13001
10.0	—	0.04809	0.000593	0.08517	0.000590	0.000178	0.13444
15.0	—	0.03555	0.000444	0.10997	0.001033	0.000202	0.14700
20.0	—	0.028543	0.000296	0.12767	0.001475	0.000223	0.15798
30.0	—	0.020755	—	0.15350	0.001918	0.000254	0.17617
40.0	—	0.016477	—	0.16974	0.002507	0.000277	0.18872
50.0	—	0.013749	—	0.18450	0.002803	0.000294	0.20105
60.0	—	0.011845	—	0.19335	0.003098	0.000307	0.20829
80.0	—	0.009323	—	0.20811	0.003540	0.000328	0.22097
100.0	—	0.007744	—	0.21845	0.003983	0.000342	0.23018

pulse, is approximately proportional to the energy lost by the gamma-ray within the crystal. Nonlinearities are small and only recently have they been studied in any detail.[35]

Of all gamma-rays detected by the crystal, only a fraction, known as the "photo-fraction," lose all their energy in the crystal. Total energy loss results in the "full energy peak," a Gaussian distribution of light outputs and consequent pulse heights whose mean amplitude is proportional to the incident gamma energy. Partial energy loss within the crystal contributes to the "Compton distribution." The photofraction is defined as the fraction of the total observed counts which contribute to the full energy peak. Figure 9-13 shows the calculated and measured photofractions for right cylindrical NaI(Tl) scintillators.

The photopeak efficiency is the ratio between the gamma-rays which lose all their energy in the crystal, and the total number of incident gamma-rays. Figure 9-14 shows the dependence of this quantity on the gamma-energy and counting geometry for a right cylindrical NaI(Tl) crystal (1.50 in. dia. × 1 in. long). Similar data for crystals of various sizes are published in Ref. 37.

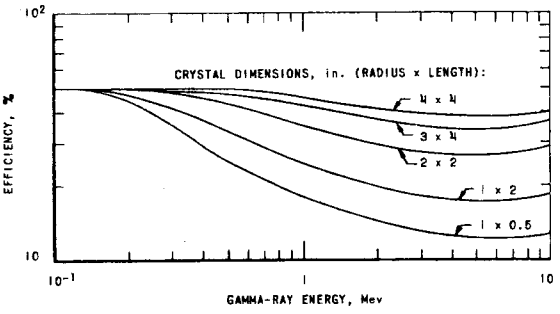

Fig. 9-12—Intrinsic efficiencies of NaI(Tl) gamma scintillators. *Data from Refs. 35, 37, and 45.*

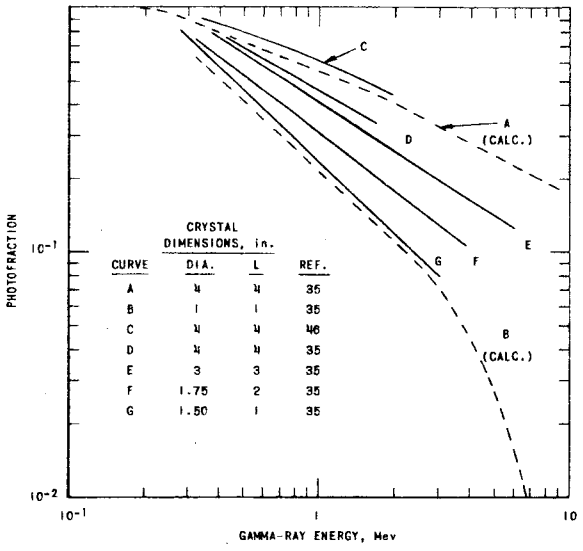

Fig. 9-13—Calculated and measured photofractions for cylindrical NaI(Tl) scintillators.

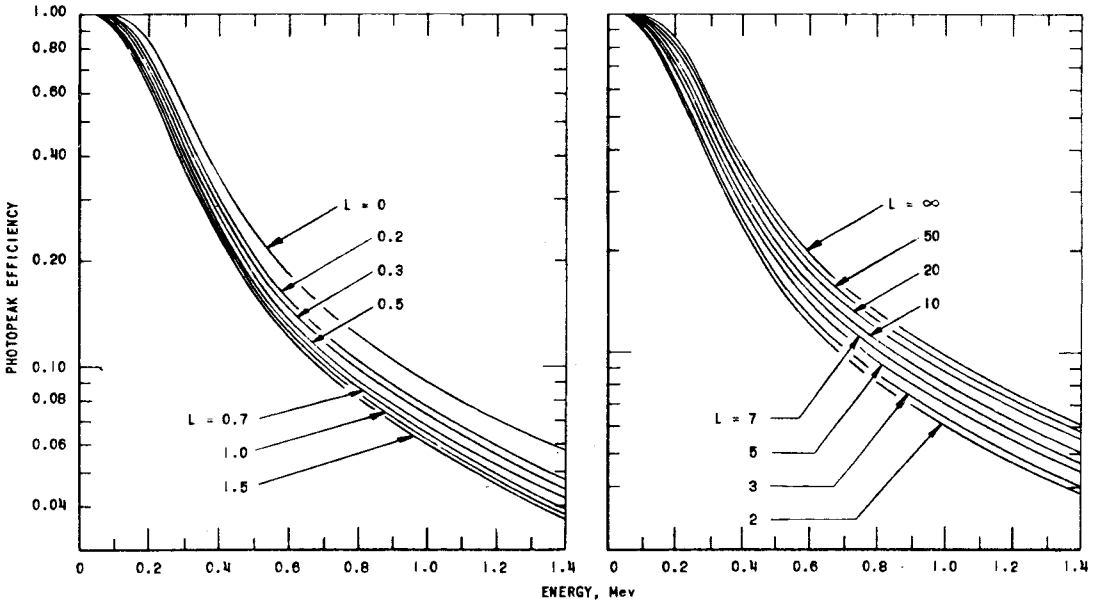

Fig. 9-14—Calculated photopeak efficiency as a function of energy and distance, L, from source to NaI(Tl) crystal (1.50 in. dia. × 0.50 in. long). *Reproduced from Ref. 47.*

X-Ray Escape Peak. In the measurement of low-energy ($E \lesssim 150$ kev) gamma-ray intensities with NaI(Tl) crystals, the area under the photopeak does not represent all of the absorbed gamma-ray energy, despite the absence of Compton scattering. This is due to the re-emission of an iodine K-shell X-ray which frequently occurs after the absorption of a gamma-quantum on the crystal surface. Two peaks are observed in the resulting pulse height distribution: one corresponding to the photopeak of the incident gamma-ray and the other at an energy 33.2 kev less than the photopeak. The difference in energy is accounted for by the iodine K-shell X-ray which escapes from the crystal. Intensity determinations from measurements of the area under the true photopeak must be corrected for the escape peak; under certain conditions the correction may be as much as 40%.

Figure 9-15 shows this correction, in terms of the photopeak area, for an infinitely thick crystal and three different source-detector geometries. "Escape peak" and "full energy peak" refer to the area under the two peaks in the pulse height distribution.

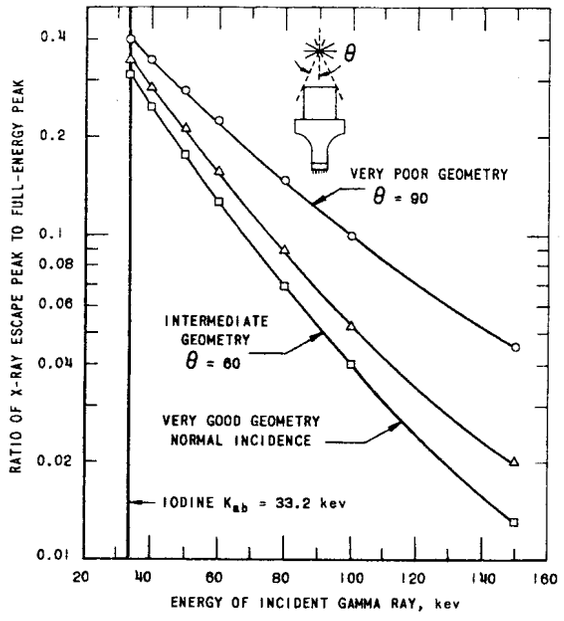

Fig. 9-15—Ratio of escape peak to photopeak in an "infinitely thick" NaI(Tl) scintillator. *Reproduced from Ref. 35.*

9.2.4 CHARGED-PARTICLE DETECTING SCINTILLATORS

Both organic and inorganic phosphors are in common use as beta- and alpha-particle scintillators. As a beta detector, anthracene has been the most extensively studied; it is used as a standard for evaluation of the other types of scintillators. Such comparisons are necessarily limited to energies greater than about 100 kev, the minimum energy required to produce a statistically significant number of photoelectrons at the photocathode. The absolute efficiency of anthracene has been measured as being anywhere from 1 to 10%, depending on the perfection and size of the crystal, and on the uniformity and type of the photocathode. Table 9-12 lists selected characteristics of certain phosphors.

At very low electron energies, the pulse height output is a nonlinear function of electron energy. Apparently there are surface effects such as loss by radiation from the bombarded face, and quenching due to surface impurities or dislocations. Linear extrapolation of the high-energy response gives a 24-kev intercept in anthracene. The same type of nonlinearity has been observed for heavier-charged particles at all energies in most of the organic phosphors. The response of anthracene as a function of energy for different charged particles is shown in Fig. 9-16.

Much recent work has been reported for CsI(Tl). Calculated and measured response of this phosphor to charged particles is shown in Fig. 9-17.

9.3 GAS CONSTANTS FOR NEUTRON DETECTORS

Direct neutron detection is usually based on a measurement of the ionization caused by a charged particle resulting from a scattering or capture event. The mechanics of pulse formation by the ions in a chamber depend on (1) the properties of the radiator or target used to produce the charged particles; (2) the chamber geometry; (3) the mode of operation (ion, proportional or saturation) of the chamber; and (4) the physical constants of the chamber gas.

The influence of the radiator properties on the energy and angular distribution of charged particles can be determined from the range-energy relationships, or from the atomic or molecular stopping power of the radiator material. Loss of energy by the charged particle, both outside of the sensitive volume and in the chamber walls, has been treated by Rossi and Staub,[49] Skyrme, Tunnicliffe and Ward,[50] and by Rembser.[51] Excellent discussions of the dependence of pulse shapes and collection

687863 O - 63 - 45

Table 9-12—SOME USEFUL CHARGED PARTICLE-DETECTING PHOSPHORS

Data from Ref. 37 except as noted.

Type	Phosphor or Solvent	Density, gm/cm^3	Relative Pulse Height[a]	Decay Time, mμs	Wave Lengths of Maximum Emission, Å	Remarks
Inorganic Crystal	NaI(Tl)	3.67	800	250	4100	Hygroscopic
	ZnS(Ag)	4.10	800 (β), 1400 (α)	70, 900[b]	4500	Multi-crystalline powder
	ZnS(Cu)	4.10	800 (β), 1200 (α)	~1000	5200	Multi-crystalline powder
	KI(Tl)	3.13	200	<1000	4100	Phosphorescent
	$CaWO_4$	6.03	400	~4,000	4300	Small crystals
	$CaWO_4$	7.90	500	~6,000	5200	Small crystals
	CsI(Tl)[c]	4.51	350	1200	4100–5700	—
Organic Solids	Anthracene ($C_{14}H_{10}$)	1.25	100	23–38	4450	—
	p-terphenyl	1.23	40	4.5	3900; 4100	—
	trans-Stilbene	1.16	60	3–8.2	3850	—
Organic Liquids	Xylene[d,e]	0.86	40	—	3250–4000[f]	—
	Xylene[d,g]	—	44	—	—	—
	Toluene[d,g]	0.87	61	<2.9	4320	—
	Toluene[h]	—	54	3.0	3820	—
Organic Plastics	Polystyrene[d,i]	1.06	36	2.2	4150	—
	Polystyrene[d,j]	—	39	4.0	4450	—
	Polyvinyltoluene[d]	—	51	—	4300	—
	p-xylene[i]	—	70	—	—	—

[a] Anthracene taken as 100 for well-collimated monoenergetic high energy electron beam. Statistical spreads in the relative pulse height may be as large as 25% because of the intrinsic resolution of the phosphor, variations in photocathode quantum efficiencies, and variations in the optical coupling coefficient.

[b] Y. Koechlin, L. Koch, and A. Lansiart, "Etat Actual du Developpement des Compteurs a Scintillation en France," CEA-980 (1958) Centre D'Etudes, (Saclay) Report.

[c] C. T. Schmidt, IRE Trans. on Nuclear Sci., NS-7, 25, (1960).

[d] Primary solute is p-terphenyl.

[e] Secondary solute is α NPO = 2-(1-naphthyl)-5-phenyloxazole.

[f] Spectral range.

[g] Secondary solute is POPOP = 1,4-di-2-(5-phenyloxazole)-benzene.

[h] Primary solute is PBD = 2-phenyl-5-(4-biphenyl)-1,3,4-oxadiazole.

[i] Primary solute is PPO = 2,5-diphenyloxazole (most soluble of primary solutes).

[j] Secondary solute is TPB = 1,1,4,4, tetraphenyl-1,3-butadiene.

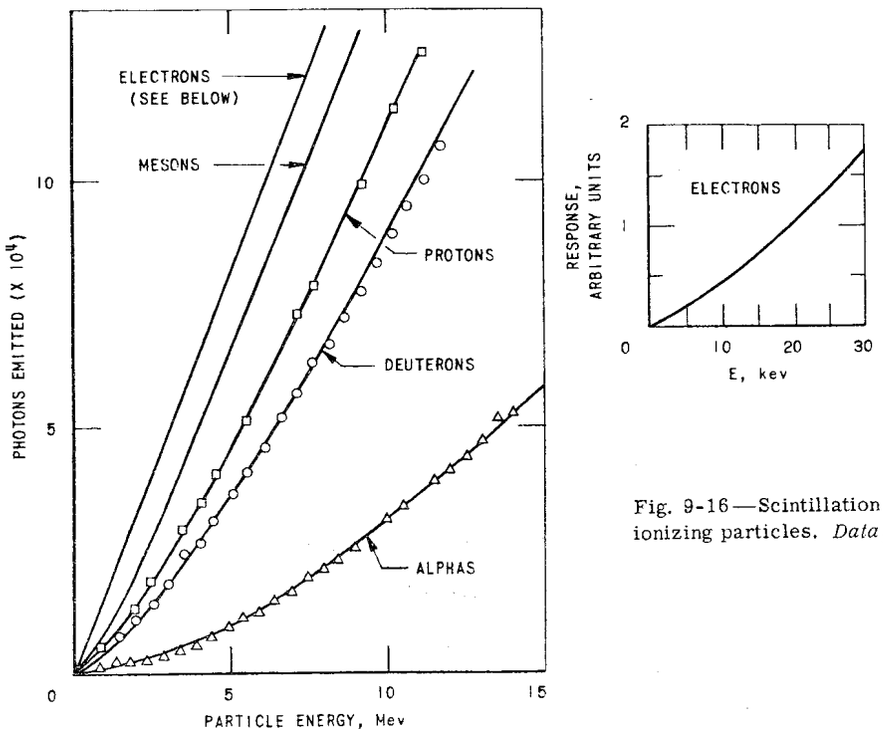

Fig. 9-16—Scintillation response of anthracene to ionizing particles. *Data from Ref. 37.*

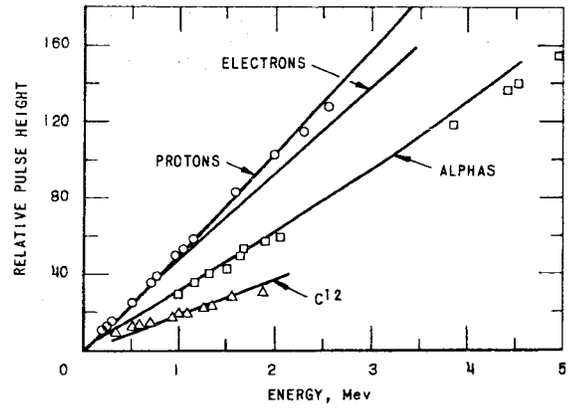

Fig. 9-17—Scintillation response of CsI(Tl) (normalized to proton data). *Reproduced from Ref. 48.*

times on chamber geometry and mode of operation are given in various books and review articles on the subject.[49,52–59] Gas constants associated either directly or indirectly with the pulse formation and collection are discussed in this section. The range and energy losses by charged particles in these gases are discussed in Section 9-4.

9.3.1 DIFFUSION COEFFICIENTS, MOBILITIES, AND DRIFT VELOCITY OF HEAVY IONS

The motion of electrons or ions in the chamber gas is described by the equation:[49,56]

$$\frac{dn}{dt} = D\nabla^2 n - \nabla (n \vec{w})$$

where D = diffusion coefficient of particle in the gas, cm^2/sec
n = density of gas particles
$\vec{w}$ = drift velocity of particle, cm/sec

The drift velocity depends on the ion mobility, μ [cm^2/(volt)(sec)(mmHg)], and the strength of the electric field, X (volts/cm). For heavy positive or negative ions, the drift velocity in the direction of the electric field of strength X is given by

$$w_{\pm} = \mu_{\pm} \frac{X}{p}$$

where $\mu_{\pm}$ is the mobility for positive or negative ions, and p is the gas pressure in atmospheres.

Diffusion coefficients and mobilities for heavy ions are listed in Table 9-13. The change of ion mobility with mass for several gases is shown in Fig. 9-18. Due to the strong interaction between the

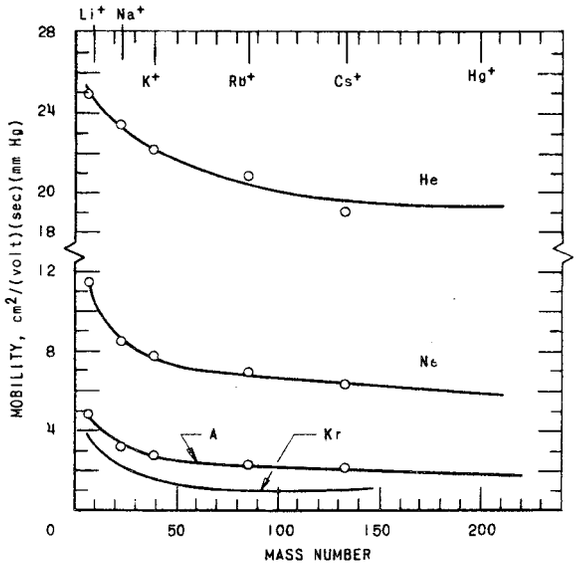

Fig. 9-18—Mobility of ions with mass M in various gases at NTP. *Data from Refs. 56 and 61.*

Table 9-13—DIFFUSION COEFFICIENTS (D) AND MOBILITIES (μ) OF HEAVY IONS AT NTP[a]

Gas	Ion	cm^2/sec		$cm^2/(volt)(sec)(mm\ Hg)$	
		D_+	D_-	μ_+	μ_-
H_2	H_1	0.129 (0.123)[b]	0.145 (0.19)[b]	18.3[c]	—
	H_2	—	—	13.9[c]	—
	H_3	—	—	22.0[c]	—
He	He_1	0.421	—	10.8[d]	—
	He_2	—	—	20.3[d]	—
	Li	—	—	26.0[e]	—
	Hg	—	0.039[a,b]	19.6[f]	—
O	O_2	0.027[a,b]	0.042[a,b]	1.90[g]	1.84
N	N_2 or N_4	0.030[a,b]	0.041[a,b]	2.6	—
Ne	Ne_1	0.016	—	4.3[d]	—
	Ne_2	—	—	6.5[d]	—
	Hg	—	—	5.95[f]	—
	Na	—	—	11.7	—
A	A_1	0.062	—	1.64[d,g]	—
	A_2	—	—	2.7[d]	—
	Hg	—	—	1.84[f]	—
	K	—	—	3.7	—
K	K	—	—	0.90[g]	—
Xe	Xe_1	0.016	—	0.58[g,h]	—
	Xe_2	—	—	0.79[h]	—
	Cs	—	—	1.31	—
Hg	Hg	~0.016	—	0.29[g]	—
Kr	Kr	0.022	—	0.90[h]	—
	Kr_2	—	—	1.21[h]	—
	Rb	—	—	0.21	—
CO	CO	—	—	1.6[g]	—
CO_2	CO	0.024[a,b]	0.026[a,b]	1.1	1.15
	CO_2	—	—	0.96	0.96
Air	N_2 or O_2	0.029[a,b]	0.043[a,b]	0.18	2.5
SF_6	SF_6	—	—	0.45[g]	—
H_2O	—	—	—	0.47	0.58
Cl	Cl_2	—	—	0.74	0.74
C_2H_5	OH	0.105	—	0.35	0.35

[a]Data from A. von Engel, Ionized Gases, (Oxford: Clarendon Press, 1955), except as noted.

[b]N. A. Kapzow, Elektrische Vorgange in Gasen und Vakuum, Hochschulbucher fur Physik, Vol. 15, (Berlin: Deutscher Verlag der Wissenschaften, 1955).

[c]E. A. Mason and J. T. Vanderslice, Phys. Rev. 114, 497, (1959).

[d]L. M. Chanin and M. Biondi, Phys. Rev., 94, 910, (1954).

[e]K. Hoselitz, Proc. Roy. Soc. (London), A177, 200, (1941).

[f]L. M. Chanin and M. A. Biondi, Phys. Rev., 106, 473, (1957).

[g]E. W. McDaniel and M. C. R. McDowell, Phys. Rev. 114, 1028, (1959).

[h]Ref. 61.

ions and the surrounding gas atoms or molecules, the mobility of ions in their parent gas is generally somewhat less than in a foreign gas. In extremely pure gases, the negative ions have about the same mobility as the positive ions. The values listed in Table 9-13 are generally valid for both cases. For further discussion see Ref. 60.

Polar impurities in the gas tend to make the mobilities of the negative and positive ions unequal. In air and other gases, where oxygen and water vapor are the chief impurities the positive ions are slower, while in the presence of alcohol, for example, they may have higher mobilities than the negative ions. The values in Table 9-13 do not apply at very high X/p, when the drift velocity of the ions is not proportional to X/p, but tends to fit a law of the form $v \sim (X/p)^{1/2}$.

In mixtures of two gases, A and B, the positive ion mobility obeys Blanc's Law:[62]

$$\frac{1}{\mu} = \frac{f_A}{\mu_A} + \frac{1 - f_A}{\mu_B}$$

where f_A is the fractional concentration of gas A. Experimental verification of Blanc's Law has been limited to very large and very small fractional concentrations. At intermediate concentrations, deviations as large as 6% have been observed.[63,64]

9.3.2 DRIFT VELOCITY OF ELECTRONS

There is no precise expression for the drift velocity of electrons in various gases. One simplification often used assumes that the elastic scattering length, λ, is independent of the electron velocity, and that it is possible to ascribe a mean absolute velocity, u, to all the electrons. To a good approximation, the electron drift velocity is given by:

$$w_e = \frac{2e}{3m} \frac{X}{p} \frac{\lambda}{u}$$

where X/p is the electric field strength per unit gas pressure; and e and m are the electron charge and mass, respectively.

The drift velocity is shown to increase with field strength and with scattering mean free path, and to decrease as the mean value of its absolute velocity, u, increases. This can be explained, qualitatively, by the fact that the velocity and direction of slow-moving electrons are more effectively influenced by an external field while traveling through a mean free path than are those of fast-moving particles.

Figure 9-19 shows, for example, that in pure inert argon gas, the drift velocity of electrons is relatively low, due, probably, to the lack of inelastic scattering. Mean electron velocities, u, are therefore very high, and w_e is correspondingly low.

With the addition of air or N_2 impurities into argon, inelastic scattering at low electron energy is introduced by the rotational and vibrational levels of the molecules. The consequent higher scattering length and lower mean velocity of the electrons both result in an increase of the drift velocity. Considerable advantage can be taken of this fact in the construction of fast chambers.

As evidenced by Figs. 9-19 and 9-20, increasing mean velocity and decreasing scattering mean free path cause the characteristic bending over of the drift velocity curve at high field strength.

9.3.3 IONIZATION POTENTIALS

Reynolds, et al.,[66] used the experimental data of Walske[67] to evaluate the average ionization potential, I, for gaseous elements (of charge Ze) as a function of incident proton energy. Their results are shown in Fig. 9-21.

Direct measurements have been made of the energy of electrons and of alpha particles required to produce one ion pair in various gases. The data listed in Table 9-14 have been selected from a compilation of these measurements made by Jesse and Sadauskis[68] and reviewed by Fulbright.[52]

Hurst and Strikler[69] have reported a number of values of the average energy, W_{ij}, required for alpha particles to produce an ion pair in various mixtures of two gases. Their results are shown in Fig. 9-22. In the figure:

$$Z''_{ij} = \frac{P_i}{P_i + (f_j/f_i)P_j}$$

where P is the partial pressure; f is the empirical weighting constant; and the subscripts i and j denote the types of gases being mixed. The measured ratio, f_j/f_i, for different gases is listed in Table 9-15.

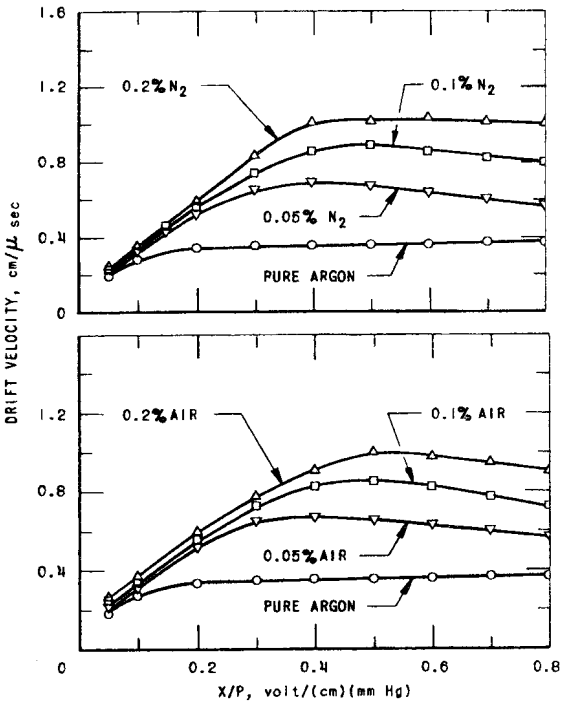

Fig. 9-19—Measured electron drift velocity in argon-nitrogen, and in argon-air mixtures. *Reproduced from Ref. 65.*

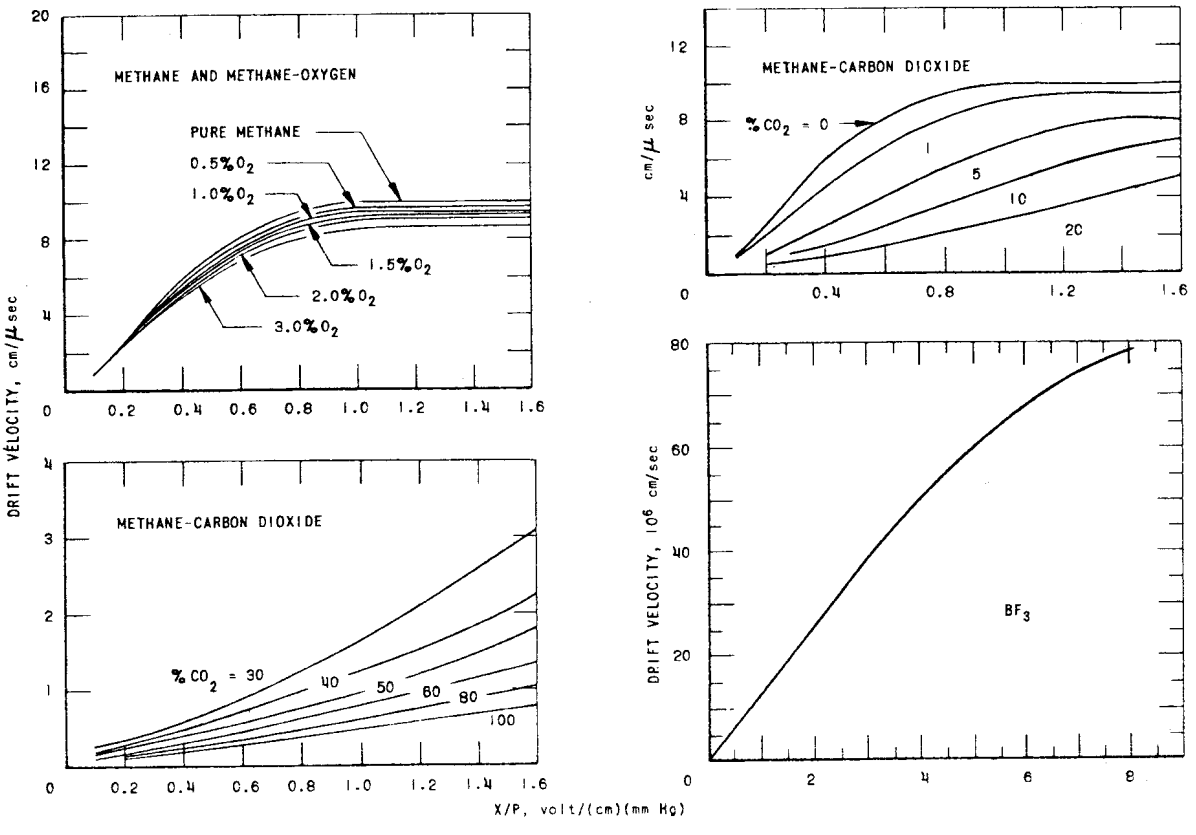

Fig. 9-20—Measured electron drift velocity in pure gases and gas mixtures. *Reproduced from Refs. 49 and 65.*

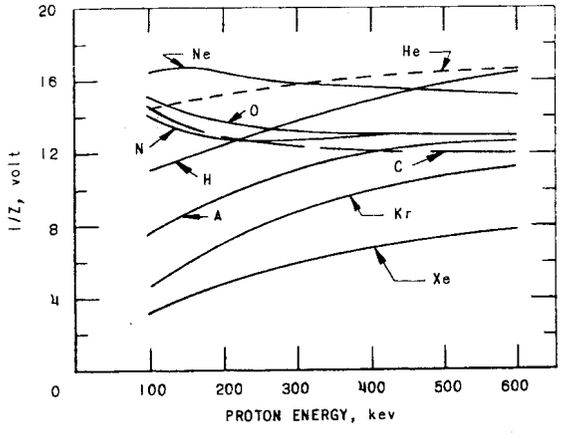

Fig. 9-21—Average ionization potential of gaseous elements as a function of proton energy. *Reproduced from Ref. 66.*

Table 9-14—ABSOLUTE VALUES OF THE ENERGY REQUIRED TO PRODUCE ONE ION PAIR IN DIFFERENT GASES

Data from Refs. 52 and 68.

Gas	w_e, ev	w_α, ev
Hydrogen	36.9	36.6
Helium	41.3	44.4
Nitrogen	34.9	36.3
Oxygen	31.3	32.1
Neon	35.9	36.8
Argon	26.3	26.25
Krypton	24.4	24.1
Xenon	22.1	21.9
Air	34.2	35.2
CO_2	32.7	34.15
Methane (CH_4)	28.1	29.1
Ethylene (C_2H_4)	26.4	28.0[a]
Acetylene (C_2H_2)	26.1	27.5[a]
Ethane (C_2H_6)	24.6	26.6[a]

[a]Average values for polonium alphas.

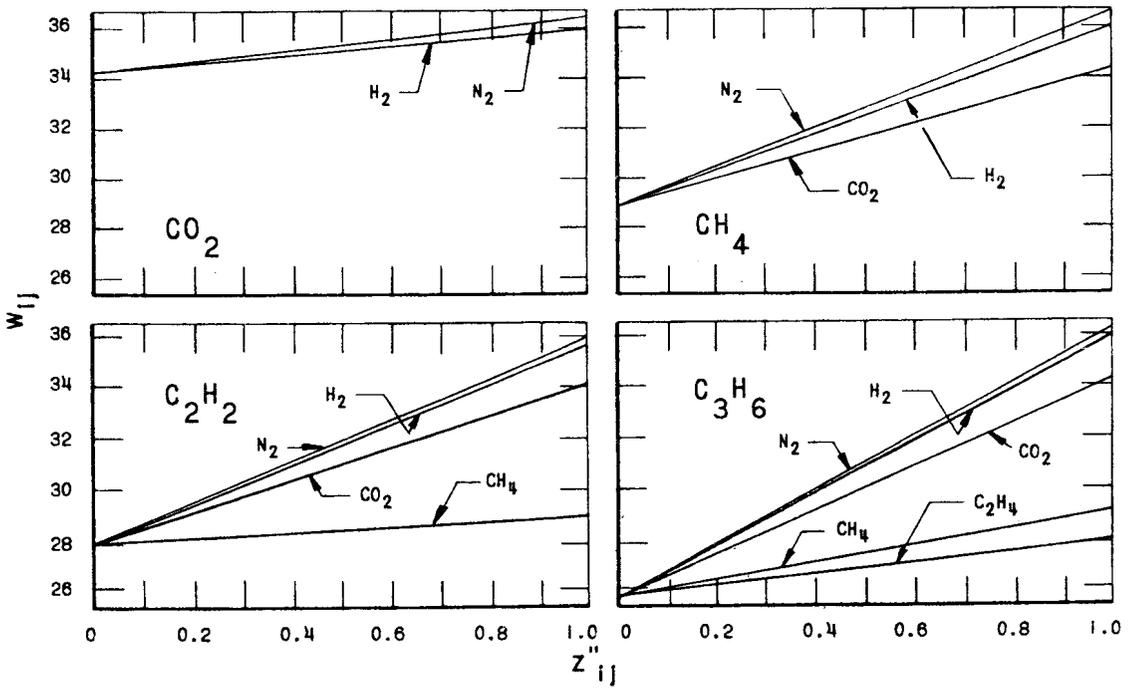

Fig. 9-22—Average energy, W_{ij}, required to produce one ion pair in a mixture of two gases. *Reproduced from Ref. 69.*

Table 9-15—MEASURED VALUES OF THE RATIO f_j/j_i

Data from Ref. 69.

Mixture		f_j/f_i
Gas i	Gas j	
N_2	CH_4	1.65 ± 0.06
N_2	CO_2	1.6 ± 0.2
N_2	C_2H_4	3.2 ± 0.1
N_2	C_3H_6	4.50 ± 0.14
CO_2	CH_4	1.50 ± 0.06
CO_2	C_2H_4	1.67 ± 0.05
CO_2	C_3H_6	2.5 ± 0.1
CH_4	C_2H_4	2.0 ± 0.5
CH_4	C_3H_6	2.3 ± 0.2
C_2H_4	C_3H_6	1.3 ± 0.15
H_2	CO_2	3.5 ± 0.9
H_2	CH_4	3.8 ± 0.15
H_2	C_2H_4	7.2 ± 0.2
H_2	C_3H_6	9.0 ± 0.25

9.4 RANGE-ENERGY RELATIONS AND ATOMIC STOPPING CROSS SECTIONS

Several comprehensive and authoritative reviews of range-energy relations have been published in the open literature.[70–74] Selected data on stopping powers and ranges used in neutron detection and spectroscopy are discussed in this section.

9.4.1 ENERGY LOSS BY HEAVY IONS

Excluding fission fragments, the average energy lost per centimeter of path length of an ion of mass M, velocity v, and charge ze, in a stopping material having NZ electrons/cm^3, is given by the well-known Bethe formula:[72]

$$-\frac{dE}{dx} = \frac{4\pi^2 z^2 e^4}{mv^2} NZ \left[\log\left(\frac{2mv^2}{I}\right) - \log(1-\beta^2) - \beta^2\right]$$

where N = number of target atoms per cm^3
m = electron mass
I = mean excitation potential
β = v/c, the particle velocity divided by that of light

The value of (1/N)(dE/dx), i.e., the energy loss per centimeter path length per unit atom density, is known as the atomic stopping power. Tables 9-16, 9-17, and 9-18 list the values of the stopping power as a function of energy for different ions in different gases, and the range determined from the integral over the energy.

9.4.2 ENERGY LOSS BY ELECTRONS

Energy losses by electrons and by fission fragments are cases of extremely light and heavy particles. Electron losses at energies less than about 1 Mev are due primarily to ionization so that $(-dE/dx) \sim (NZ/E)$, while at higher energies losses by Bremsstrahlung become large and $(-dE/dx) \sim (NZ^2E)$.[77] In addition, electrons may lose sizable fractions of their energy in a single collision which results in large straggling of energy loss. Bohr points out that the average energy loss is consider-

Table 9-16 — ATOMIC STOPPING POWERS FOR LOW-ENERGY PROTONS [10^{-15}(ev)(cm^2)/atom]

Data from Refs. 66 and 72.

Energy, kev	H_2	He	N_2	O_2	Air_2	C	A	Ne	Kr	Xe
30	5.84 ± 3.4	—	16.1 ± 2.6	—	15.5 ± 2.6	—	—	—	—	—
40	6.25 ± 3.4	6.67 ± 3.4	17.1 ± 2.6	15.2 ± 2.6	16.48 ± 2.6	—	31.4 ± 2.6	10.6 ± 2.6	35.6 ± 2.7	50.0 ± 2.7
50	6.43 ± 3.4	6.97 ± 3.4	17.8 ± 2.6	16.4 ± 2.6	17.16 ± 2.6	—	33.4 ± 2.6	11.9 ± 2.6	38.3 ± 2.7	52.6 ± 2.7
60	6.45 ± 3.4	7.22 ± 3.4	18.2 ± 2.6	16.9 ± 2.6	17.7 ± 2.6	—	34.3 ± 2.6	12.8 ± 2.6	39.8 ± 2.7	53.5 ± 2.7
70	6.36 ± 3.4	7.33 ± 3.4	18.5 ± 2.6	17.15 ± 2.6	17.9 ± 2.6	—	34.4 ± 2.6	13.45 ± 2.6	40.5 ± 2.7	53.5 ± 2.7
80	6.23 ± 3.4	7.37 ± 3.4	18.5 ± 2.6	17.25 ± 2.6	17.87 ± 2.6	—	34.1 ± 2.6	13.95 ± 2.6	40.5 ± 2.7	53.2 ± 2.7
90	6.04 ± 3.4	7.37 ± 3.4	18.25 ± 2.6	17.25 ± 2.6	17.72 ± 2.6	—	33.5 ± 2.6	14.3 ± 2.6	40.3 ± 2.7	52.0 ± 2.7
100	5.83 ± 3.4	7.30 ± 3.4	17.9 ± 2.6	17.17 ± 2.6	17.5 ± 2.6	16.25 ± 2.1	32.6 ± 2.6	14.6 ± 2.6	39.8 ± 2.7	50.6 ± 2.7
150	4.70 ± 2.7	6.37 ± 2.7	16.1 ± 1.7	16.13 ± 1.7	15.98 ± 1.7	14.6 ± 2.1	28.2 ± 1.7	14.6 ± 1.7	35.0 ± 1.8	45.2 ± 1.8
200	3.90 ± 2.7	5.55 ± 2.7	14.2 ± 1.7	14.70 ± 1.7	14.21 ± 1.7	12.70 ± 2.1	24.5 ± 1.7	14.10 ± 1.7	30.7 ± 1.8	41.8 ± 1.8
250	3.33 ± 2.7	4.91 ± 2.7	12.5 ± 1.7	13.26 ± 1.7	12.74 ± 1.7	11.28 ± 2.1	21.6 ± 1.7	13.20 ± 1.7	27.4 ± 1.8	38.6 ± 1.8
300	2.91 ± 2.7	4.41 ± 2.7	11.2 ± 1.7	11.99 ± 1.7	11.56 ± 1.7	10.20 ± 2.1	19.5 ± 1.7	12.34 ± 1.7	25.1 ± 1.8	35.8 ± 1.8
350	2.60 ± 2.7	4.01 ± 2.7	10.13 ± 1.7	11.01 ± 1.7	10.60 ± 1.7	9.30 ± 2.1	17.9 ± 1.7	11.50 ± 1.7	23.3 ± 1.8	33.4 ± 1.8
400	2.35 ± 2.7	3.69 ± 2.7	9.34 ± 1.7	10.23 ± 1.7	9.79 ± 1.7	8.54 ± 2.1	16.6 ± 1.7	10.75 ± 1.7	22.0 ± 1.8	31.4 ± 1.8
450	2.14 ± 2.7	3.42 ± 2.7	8.62 ± 1.7	9.45 ± 1.7	9.05 ± 1.7	7.94 ± 2.1	15.55 ± 1.7	10.15 ± 1.7	20.9 ± 1.8	29.8 ± 1.8
500	1.97 ± 2.7	3.18 ± 2.7	8.08 ± 1.7	8.84 ± 1.7	8.39 ± 1.7	7.38 ± 2.1	14.7 ± 1.7	9.58 ± 1.7	19.9 ± 1.8	28.6 ± 1.8
550	1.82 ± 2.7	2.99 ± 2.7	7.61 ± 1.7	8.38 ± 1.7	7.9 ± 1.7	6.95 ± 2.1	13.9 ± 1.7	9.09 ± 1.7	19.1 ± 1.8	27.4 ± 1.8
600	1.70 ± 2.7	2.81 ± 2.7	7.21 ± 1.7	7.91 ± 1.7	7.51 ± 1.7	6.55 ± 2.1	13.3 ± 1.7	8.65 ± 1.7	18.4 ± 1.8	26.4 ± 1.8

Molecular Stopping Powers for Low-Energy Protons [10^{-15}(ev)(cm^2)/atom]

Energy, kev	CH_4	C_2H_2	C_2H_4	C_6H_6	H_2O	NH_2	NO	CO_2	N_2O
30	37.4 ± 2.6	43.4 ± 2.6	—	116.0 ± 2.6	—	29.7 ± 2.6	—	—	—
40	39.7 ± 2.6	47.4 ± 2.6	54.4 ± 2.6	126.0 ± 2.6	25.0 ± 2.6	32.0 ± 2.6	32.6 ± 2.8	44.2 ± 2.6	47.0 ± 2.8
50	40.9 ± 2.6	49.5 ± 2.6	57.4 ± 2.6	133.0 ± 2.6	26.1 ± 2.6	33.6 ± 2.6	34.5 ± 2.8	46.8 ± 2.6	48.6 ± 2.8
60	41.3 ± 2.6	49.8 ± 2.6	58.7 ± 2.6	135.7 ± 2.6	26.9 ± 2.6	34.6 ± 2.6	35.7 ± 2.8	48.4 ± 2.6	49.9 ± 2.8
70	41.2 ± 2.6	49.2 ± 2.6	58.8 ± 2.6	135.5 ± 2.6	27.5 ± 2.6	34.7 ± 2.6	36.4 ± 2.8	49.6 ± 2.6	50.5 ± 2.8
80	40.8 ± 2.6	48.0 ± 2.6	58.0 ± 2.6	134.4 ± 2.6	27.6 ± 2.6	34.4 ± 2.6	36.6 ± 2.8	50.2 ± 2.6	50.9 ± 2.8
90	40.0 ± 2.6	46.7 ± 2.6	56.7 ± 2.6	133.5 ± 2.6	27.5 ± 2.6	33.9 ± 2.6	36.6 ± 2.8	50.5 ± 2.6	51.0 ± 2.8
100	38.9 ± 2.6	45.0 ± 2.6	55.5 ± 2.6	131.7 ± 2.6	27.3 ± 2.6	33.5 ± 2.6	36.4 ± 2.8	50.5 ± 2.6	50.7 ± 2.8
150	33.6 ± 1.7	38.5 ± 1.7	48.8 ± 1.7	116.5 ± 1.5	24.7 ± 1.7	30.1 ± 1.7	33.2 ± 1.9	47.1 ± 1.7	47.0 ± 1.9
200	28.6 ± 1.7	32.9 ± 1.7	41.4 ± 1.7	102.0 ± 1.5	22.0 ± 1.7	25.6 ± 1.7	29.7 ± 1.9	42.5 ± 1.7	42.0 ± 1.9
250	24.8 ± 1.7	29.0 ± 1.7	36.1 ± 1.7	89.2 ± 1.5	19.7 ± 1.7	22.3 ± 1.7	26.7 ± 1.9	38.1 ± 1.7	37.6 ± 1.9
300	22.0 ± 1.7	25.9 ± 1.7	32.0 ± 1.7	79.8 ± 1.5	17.9 ± 1.7	19.9 ± 1.7	24.1 ± 1.9	34.6 ± 1.7	34.0 ± 1.9
350	19.8 ± 1.7	23.5 ± 1.7	28.8 ± 1.7	72.2 ± 1.5	16.2 ± 1.7	17.9 ± 1.7	22.0 ± 1.9	31.6 ± 1.7	31.0 ± 1.9
400	18.1 ± 1.7	21.4 ± 1.7	26.2 ± 1.7	66.3 ± 1.5	15.0 ± 1.7	16.4 ± 1.7	20.3 ± 1.9	29.2 ± 1.7	28.6 ± 1.9
450	16.65 ± 1.7	19.7 ± 1.7	24.1 ± 1.7	61.4 ± 1.5	13.9 ± 1.7	15.1 ± 1.7	18.9 ± 1.9	27.0 ± 1.7	26.6 ± 1.9
500	15.5 ± 1.7	18.4 ± 1.7	22.4 ± 1.7	57.3 ± 1.5	13.0 ± 1.7	14.0 ± 1.7	17.6 ± 1.9	25.2 ± 1.7	25.0 ± 1.9
550	14.5 ± 1.7	17.2 ± 1.7	20.9 ± 1.7	53.9 ± 1.5	12.2 ± 1.7	13.1 ± 1.7	16.6 ± 1.9	23.7 ± 1.7	23.5 ± 1.9
600	13.6 ± 1.7	16.2 ± 1.7	19.6 ± 1.7	51.0 ± 1.5	—	12.3 ± 1.7	15.7 ± 1.9	22.4 ± 1.7	22.2 ± 1.9

Note: Errors are relative to the stopping powers, in per cent.

ably larger than the most probable energy loss, the latter being more nearly the experimentally measured quantity and given by:[70,78]

$$-\frac{dE}{dx} = \frac{2\pi e^4}{mv^2} NZ \left[\log \frac{mv^2 W}{I^2 (1-\beta^2)} + (1-\beta^2) - \delta \right]$$

where $W = \frac{1}{2}(E - mc^2)$ = maximum energy transfer in a single electron scattering event

δ = a density effect that depends on the stopping material. Extensive density data are given in Ref. 78.

I = the ionization energy

Stopping powers for electrons in several solids and gases are given by Marinelli[79] and Sternheimer.[78] Their data are reproduced in Figs. 9-23 and 9-24.

9.4.3 ENERGY LOSS BY FISSION FRAGMENTS

Unlike electrons and heavier ions for which most of the ionization occurs near the end of their ranges, fission fragments start with a charge of ~20 and produce most of the ionization at the begin-

ning of their range. As the fragment loses energy, it also loses part of its charge through recombination with electrons.

The energy lost per centimeter of range is determined by two factors: (1) ionization predominates for high velocities and high charge; and (2) nuclear collisions become significant in terms of energy loss (1 to 7 Mev/collision) at lower energies. Bethe and Ashkin[70] give the energy loss as:

$$-\frac{dE}{dx} = \frac{4\pi z^2 e^4}{mv^2} NZ \left\{ \left(\frac{\bar{z}}{z}\right)^2 \log \frac{1.123\ mv^3}{I\ e^2\ \bar{z}} + \left(\frac{m}{M^2}\right) Z \log \left[\frac{M\ M_2\ v^2\ \alpha}{z\ Z\ e^2\ (M + M_2)} \right] \right\}$$

Table 9-17—STOPPING POWERS OF HIGH-ENERGY PROTONS AND ALPHA PARTICLES IN CERTAIN GASES AND VAPORS RELATIVE TO AIR

Data from Ref. 75.

Range, cm:	1	2	4	10	20	40	100	200
Energy:								
proton, Mev:	0.55	0.9	1.4	2.45	3.7	5.5	9.25	13.65
alpha, Mev:	1.9	3.4	5.5	9.7	14.5	—	—	—
Gas								
H_2	0.25	0.23	0.218	0.205	0.198	0.191	0.195	0.18
He	—	—	0.18	—	—	—	—	—
(C)	0.47	0.467	0.464	0.459	0.456	0.453	0.448	0.445
CH_4	0.97	0.927	0.90	0.87	0.852	0.835	0.818	0.805
Air (O_2, N_2)	1	1	1	1	1	1	1	1
Ne	—	—	0.62	—	—	—	—	—
A	—	—	0.87	—	—	—	—	—
Kr	—	—	1.46	—	—	—	—	—
Xe	—	—	1.88	—	—	—	—	—
Vapor								
H_2O	0.757	0.737	0.725	0.712	0.705	0.698	0.692	0.687
C_2H_6O	2.22	2.16	2.12	2.07	2.04	2.01	1.99	1.97

Table 9-18—STOPPING POWERS FOR He, N, AND Ne IONS IN VARIOUS GASES [10^{-15}(ev)(cm^2)/atom]

Data from Ref. 76.

Ion	E, kev	Gas			
		Hydrogen	Helium	Air	Argon
Helium	150	8.6	10.2	30.6	53.3
	175	9.4	11.0	43.3	57.0
	200	10.2	11.7	33.7	60.0
	250	11.0	13.2	36.3	66.0
	300	11.4	14.4	38.5	71.0
	350	11.9	15.5	40.5	75.0
	400	12.3	16.7	42.3	79.0
Nitrogen	150	12.7	16.7	—	—
	175	13.3	17.7	—	—
	200	13.8	18.7	52.6	90
	250	15.2	20.5	59.0	102
	300	17.0	22.2	64.5	114
	350	17.7	23.7	70.0	125
	400	18.5	25.0	74.5	135
Neon-20	150	—	10.5	—	—
	175	6.9	11.8	—	—
	200	7.3	12.8	41	63
	250	7.9	14.3	46	70
	300	8.8	16.0	50.5	77
	350	9.6	17.5	54.5	83
	400	10.3	18.0	58	86

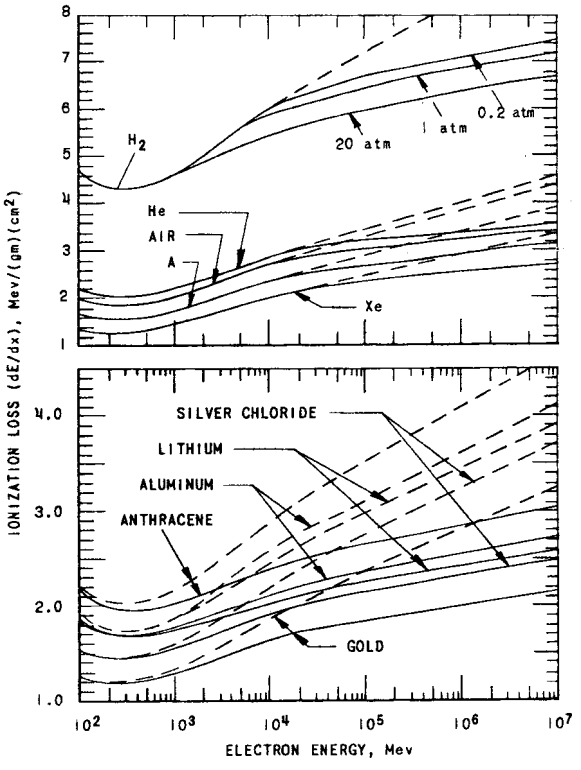

Fig. 9-23—Ionization loss of electrons in various gases and solids. Dashed curves give the values of (1/N)(dE/dx) which would be obtained without the density effect. *Data from Ref. 78.*

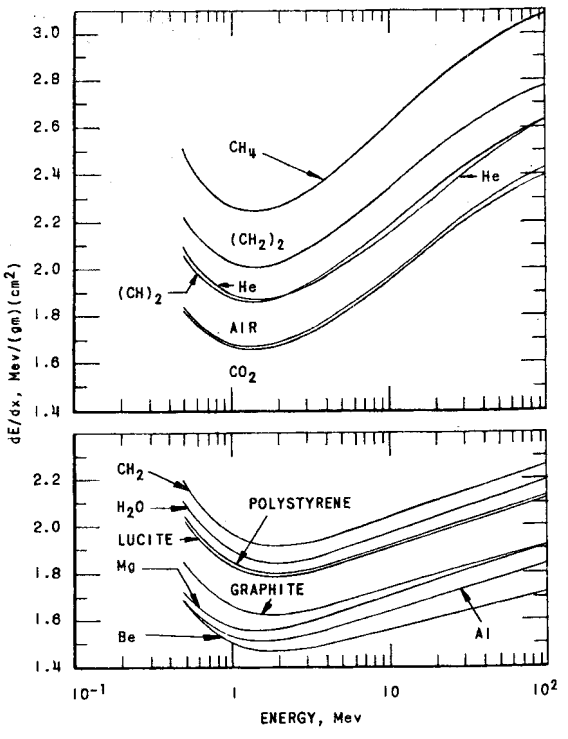

Fig. 9-24—Stopping powers for electrons in various gases, liquids, and solids. *Data from Ref. 79.*

where M = mass of the fragment
v = velocity of the fragment
ze = total charge of the fragment
M_2 = mass of the stopping material
Ze = total charge of the stopping material
I = excitation potential of the stopping material
m = electron mass
α = an impact parameter
$\bar{z}$ = average fragment charge given approximately by: $\bar{z} = (z)^{1/3}\ \hbar v/e^2$

Energy lost by ionization (the first term), is the same as that for protons and alpha particles, and the energy lost by nuclear collisions (the second term) depends on how strongly nuclear scattering is screened by the atomic electrons.

Assuming $\bar{z} \sim v$ and the range is proportional to v^3 (Geiger relation), the ratio of the ranges of a fragment and an alpha particle of the same velocity is:

$$\frac{R_F}{R_\alpha} = \frac{7A}{z^{2/3}}\left(\frac{e^2}{\hbar v}\right)^2$$

where A is the mass number of the fragment.

Energy losses by fission fragments have been determined by Lassen[80] and are shown in Fig. 9-25. The conversion from range to energy (or velocity) for argon is shown in Fig. 9-26.

9.4.4 STOPPING POWER CONVERSION FACTORS

Atomic and molecular stopping powers are usually expressed in units of 10^{-15}(ev)(cm^2)/atom, or (kev)(cm^2)/mg. Table 9-19 lists conversion constants for several materials. Conversion factors for gases at NTP into units of ergs/cm or kev/cm are listed in Table 9-20.

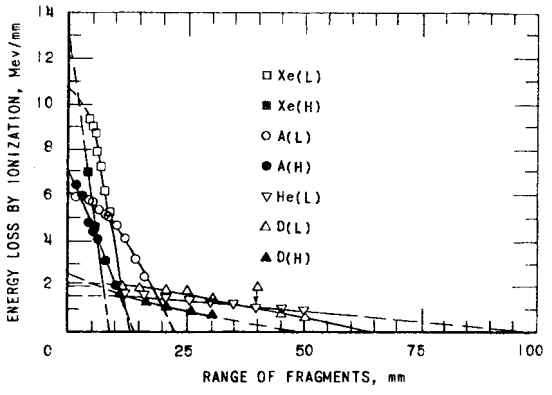

Fig. 9-25—Ionization density vs. range for median-light and median-heavy fission fragments in deuterium, helium, argon, and xenon at NTP. *Reproduced from Ref. 80.*

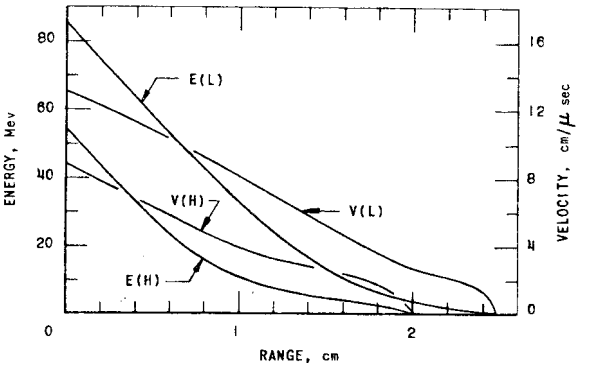

Fig. 9-26—Range of median-light (L) and median-heavy (H) fission fragments in argon at NTP. *Reproduced from Ref. 80.*

Table 9-19—CONSTANTS FOR CONVERSION OF STOPPING CROSS SECTION TO RATE OF ENERGY LOSS[a]

Data from Ref. 81.

Stopping Material	A	Stopping Material	A
H	598	Ti	12.57
Li	86.8	V	11.82
Be	66.8	Ni	10.26
C	50.1	Cu	9.48
N	43.0	Zr	6.60
O	37.6	Mo	6.28
Al	22.3	Ta	3.33
Sc	13.40	Au	3.05

[a]To obtain dE/dx in units of (kev)(mg)/cm^2, multiply the stopping cross section, in units of 10^{-15}(ev)(cm^2)/atom, by A.

Table 9-20—CONVERSION FACTORS FOR EXPRESSING STOPPING POWER IN VARIOUS UNITS

Data from Ref. 76.

Given units	Units desired			
	$\frac{(kev)(cm^2)}{mg}$	$\frac{(ev)(cm^2)}{atom}$	ergs/cm at NTP[a]	kev/cm at NTP
$\frac{(kev)(cm^2)}{mg}$	H_2 1	1.673×10^{-18}	1.440×10^{-10}	0.0899
	He 1	6.645×10^{-18}	2.881×10^{-10}	0.1786
	Air 1	24.05×10^{-18}	2.070×10^{-9}	1.293
	Argon 1	66.29×10^{-18}	2.855×10^{-9}	1.782
$\frac{(ev)(cm^2)}{atom}$	5.977×10^{17}	H_2 1	8.610×10^{7}	5.375×10^{16}
	1.505×10^{17}	He 1	4.305×10^{7}	2.688×10^{16}
	0.4158×10^{17}	Air 1	8.610×10^{7}	5.375×10^{16}
	0.1508×10^{17}	Argon 1	4.305×10^{7}	2.688×10^{16}
erg/cm at NTP	69.42×10^{5}	1.162×10^{-8}	H_2 1	6.243×10^{8}
	34.95×10^{5}	2.323×10^{-8}	He 1	6.243×10^{8}
	4.828×10^{5}	1.162×10^{-8}	Air 1	6.243×10^{8}
	3.498×10^{5}	2.323×10^{-8}	Argon 1	6.243×10^{8}
kev/cm at NTP	11.12	1.861×10^{-17}	1.602×10^{-9}	H_2 1
	5.599	3.722×10^{-17}	1.602×10^{-9}	He 1
	0.7734	1.861×10^{-17}	1.602×10^{-9}	Air 1
	0.5612	3.722×10^{-17}	1.602×10^{-9}	Argon 1

[a]NTP = 0°C, 760 mm Hg.

9.4.5 RANGE-ENERGY RELATIONS

The range of a charged particle in matter is defined as the integral (usually numerical) of the reciprocal stopping power over the energy from zero to the incident particle energy. A useful nomograph (Fig. 9-27) for determining the ranges of the various types of particles (exclusive of electrons and fission fragments) is given by Bethe and Ashkin.[70] More detailed proton range data, particularly at the lower energies, are given by Whaling,[72] and are reproduced in Table 9-21.

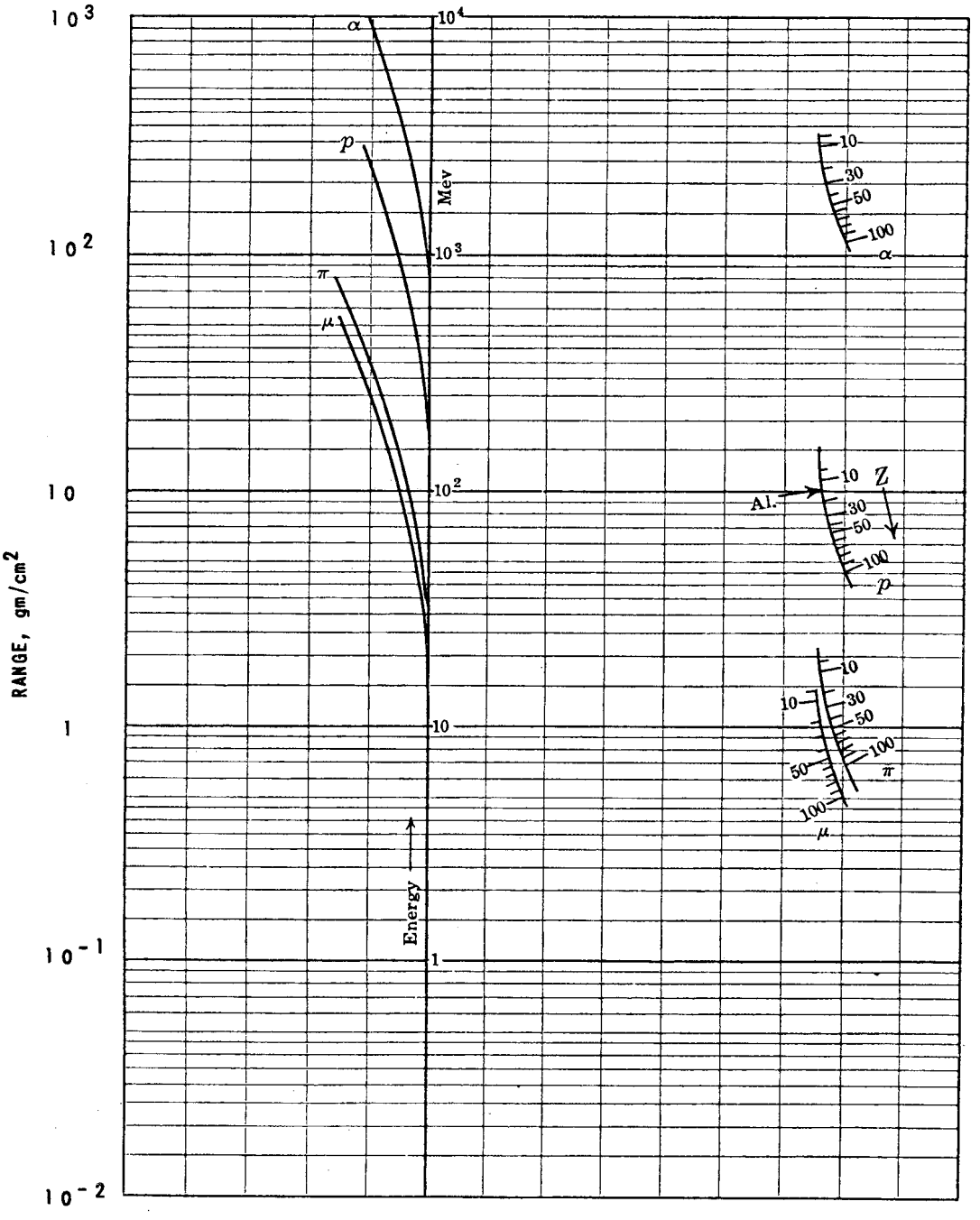

Fig. 9-27—Nomograph for approximate determination of range-energy relationships according to R. R. Wilson. (To use, connect range, energy, and Z by a straight line.) *Reproduced from Ref. 70.*

Table 9-21—MEAN PROTON RANGES FOR VARIOUS GASES AT NTP

Data from Ref. 72.

E_p, Mev	H_2, cm	He, cm	Be, mg/cm^2	N_2, cm	O_2, cm	Ne, cm	Al, mg/cm^2	A, cm	Cu, mg/cm^2	Kr, cm	Xe, cm	Au, mg/cm^2	H_2O vapor, cm	CH_4, cm	CO_2, cm	Air, cm
0.040	0.174	0.346	—	0.0459	0.0561	—	—	0.0535	—	—	—	—	—	0.0424	0.0361	0.0600
0.045	0.190	0.375	—	0.0575	0.0623	—	—	0.0597	—	—	—	—	—	0.0474	0.0406	0.0658
0.050	0.205	0.404	—	0.0632	0.0684	—	—	0.0656	—	—	—	—	—	0.0523	0.0449	0.0715
0.055	0.220	0.433	—	0.0687	0.0744	—	—	0.0715	—	—	—	—	—	0.0571	0.0491	0.0772
0.060	0.236	0.461	—	0.0742	0.0802	—	—	0.0772	—	—	—	—	—	0.0619	0.0532	0.0828
0.065	0.251	0.488	—	0.0796	0.0861	—	—	0.0830	—	—	—	—	—	0.0667	0.0572	0.0883
0.070	0.266	0.515	—	0.0849	0.0918	—	—	0.0888	—	—	—	—	—	0.0715	0.0612	0.0938
0.075	0.282	0.541	—	0.0902	0.0976	—	—	0.0946	—	—	—	—	—	0.0763	0.0651	0.0994
0.080	0.297	0.568	—	0.0955	0.103	—	—	0.100	—	—	—	—	—	0.0811	0.0691	0.105
0.085	0.313	0.594	—	0.101	0.109	—	—	0.106	—	—	—	—	—	0.0859	0.0730	0.110
0.090	0.329	0.621	—	0.106	0.115	—	—	0.112	—	—	—	—	—	0.0908	0.0769	0.116
0.095	0.346	0.648	—	0.112	0.120	—	—	0.118	—	—	—	—	—	0.0957	0.0808	0.121
0.100	0.362	0.674	0.16	0.117	0.126	0.372	0.26	0.124	0.552	0.119	0.087	1.32	0.165	0.101	0.0847	0.127
0.15	0.551	0.963	0.24	0.175	0.185	0.504	0.38	0.188	0.770	0.172	0.128	1.76	0.239	0.154	0.125	0.186
0.20	0.780	1.29	0.32	0.240	0.249	0.639	0.51	0.263	0.992	0.233	0.173	2.19	0.323	0.218	0.169	0.253
0.25	1.05	1.67	0.42	0.314	0.320	0.784	0.65	0.348	1.22	0.300	0.242	2.61	0.417	0.292	0.218	0.328
0.30	1.37	2.09	0.52	0.398	0.398	0.939	0.80	0.444	1.46	0.374	0.275	3.05	0.521	0.376	0.272	0.410
0.35	1.73	2.56	0.63	0.491	0.484	1.10	0.96	0.549	1.72	0.454	0.332	3.52	0.637	0.470	0.332	0.500
0.40	2.13	3.07	0.76	0.593	0.576	1.28	1.13	0.663	1.99	0.540	0.393	4.02	0.764	0.574	0.398	0.598
0.45	2.57	3.62	0.89	0.703	0.676	1.47	1.31	0.786	2.26	0.632	0.458	4.55	0.902	0.687	0.468	0.702
0.50	3.05	4.21	1.03	0.821	0.783	1.67	1.50	0.916	2.55	0.727	0.527	5.10	1.05	0.809	0.544	0.814
0.55	3.57	4.85	1.19	0.947	0.897	1.88	1.70	1.05	2.86	0.828	0.600	5.68	1.21	0.940	0.624	0.923
0.60	4.12	5.53	1.35	1.08	1.02	2.10	1.91	1.20	3.17	0.933	0.676	6.29	1.38	1.08	0.709	1.06
0.65	4.72	6.25	1.52	1.22	1.14	2.34	2.13	1.35	3.50	1.04	0.756	6.92	1.56	1.23	0.799	1.19
0.70	5.35	7.01	1.69	1.37	1.27	2.58	2.35	1.51	3.84	1.15	0.840	7.57	1.75	1.38	0.893	1.33
0.75	6.02	7.81	1.88	1.52	1.41	2.84	2.58	1.67	4.20	1.27	0.927	8.24	1.95	1.55	0.992	1.48
0.80	6.72	8.65	2.07	1.69	1.56	3.11	2.83	1.84	4.56	1.39	1.02	8.94	2.15	1.73	1.09	1.63
0.85	7.46	9.54	2.28	1.86	1.71	3.39	3.08	2.02	4.93	1.51	1.11	9.65	2.37	1.91	1.20	1.79
0.90	8.24	10.5	2.58	2.03	1.86	3.68	3.34	2.20	5.32	1.64	1.20	10.4	2.60	2.10	1.31	1.96
0.95	9.06	11.5	2.70	2.22	2.02	3.98	3.61	2.39	5.71	1.77	1.30	11.1	2.83	2.30	1.43	2.13
1.00	9.91	12.5	2.92	2.41	2.18	4.29	3.89	2.58	6.12	1.91	1.41	11.9	3.08	2.51	1.55	2.31
1.5	20.2	24.6	5.56	4.63	4.07	7.93	7.14	4.86	10.7	3.44	2.57	20.4	5.95	5.02	2.97	4.43
2.0	33.8	40.4	8.91	7.42	6.55	12.5	11.2	7.66	16.3	5.27	3.99	30.3	9.60	8.24	4.76	7.13
2.5	50.6	60.0	13.0	10.7	9.52	17.9	16.1	10.9	22.7	7.40	5.64	41.9	14.0	12.2	6.83	10.4
3.0	70.3	82.8	17.7	14.6	13.0	24.0	21.7	14.7	30.0	9.79	7.47	54.7	19.2	16.7	9.31	14.2
3.5	92.8	109	23.0	19.0	16.9	30.9	27.9	18.9	38.2	12.4	9.51	68.9	25.0	22.0	12.1	18.5
4.0	118	138	29.0	23.9	21.3	38.5	34.9	23.6	47.2	15.3	11.7	84.1	31.5	27.9	15.3	23.3
4.5	146	171	35.4	29.3	26.1	47.0	42.7	28.8	57.0	18.5	14.1	100	38.8	34.5	18.7	28.5
5.0	177	206	42.9	35.2	31.4	56.0	51.1	34.3	67.6	21.9	16.6	118	46.7	41.6	22.5	34.3
5.5	210	245	50.8	41.6	37.1	65.9	60.2	40.2	78.9	25.5	19.3	136	55.3	49.4	26.6	40.5
6.0	246	287	59.1	48.5	43.2	76.4	70.0	46.7	91.0	29.3	22.2	156	64.5	57.8	31.0	47.2
6.5	285	331	67.8	55.8	49.7	87.7	80.4	53.5	104	33.4	25.3	176	74.4	66.7	35.7	54.3
7.0	326	379	76.9	63.6	56.7	99.6	91.5	60.7	118	37.8	28.5	198	85.0	76.3	40.8	61.9
7.5	370	430	68.5	71.9	64.0	112	103	68.3	132	42.3	31.8	220	96.2	86.5	46.1	70.0
8.0	417	483	96.5	80.7	72.0	125	115	76.4	147	47.1	35.4	243	108	97.2	51.7	78.5
8.5	466	539	107	89.9	80.2	139	128	84.8	163	52.2	39.1	267	120	108	57.6	87.4
9.0	518	598	118	99.6	88.8	154	142	93.7	180	57.4	42.9	292	133	120	63.9	96.7
9.5	572	660	129	110	97.8	169	156	103	197	62.9	46.9	319	147	133	70.4	106
10.0	628	724	140	120	107	185	171	113	215	68.7	51.1	345	161	146	77.2	117

Extensive tables of electron ranges in various materials have been compiled by Nelms;[82] selected data are plotted in Fig. 9-28. Electron ranges in aluminum vs. electron momentum are given by Ward and Marshall,[83] and are reproduced in Fig. 9-29.

Ranges of the median-light and the median-heavy fission fragments, as measured by Fulmer,[84] are shown in Figs. 1-3 and 1-4 of Section 1.

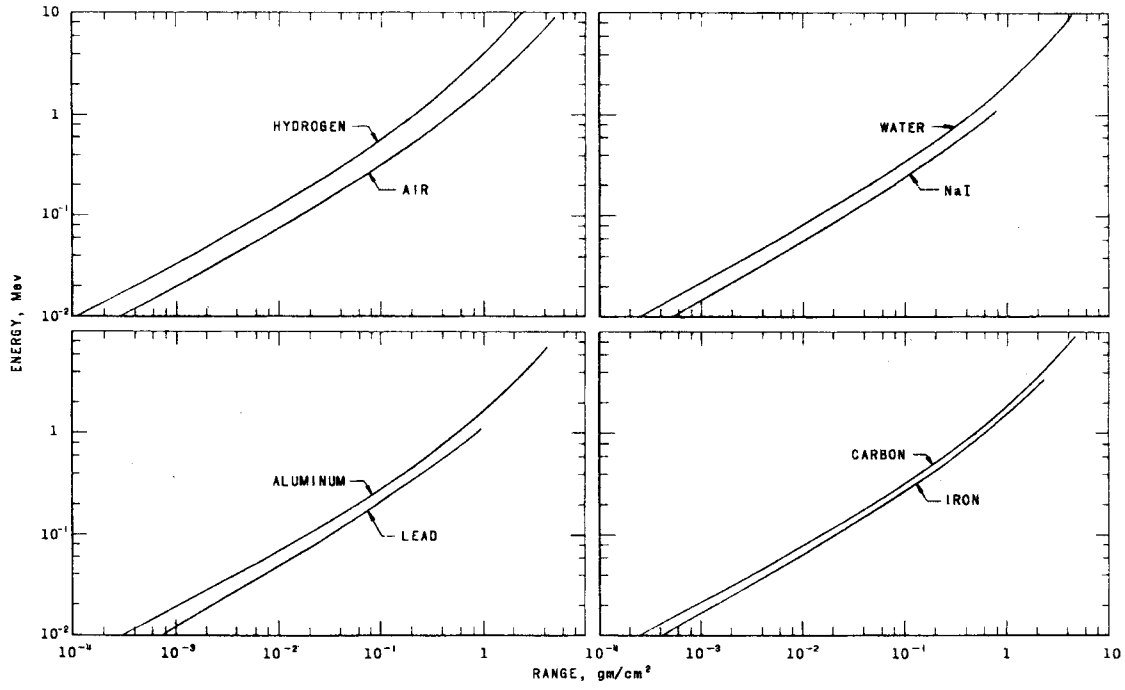

Fig. 9-28—Range of electrons in various materials. *Data from Ref. 82.*

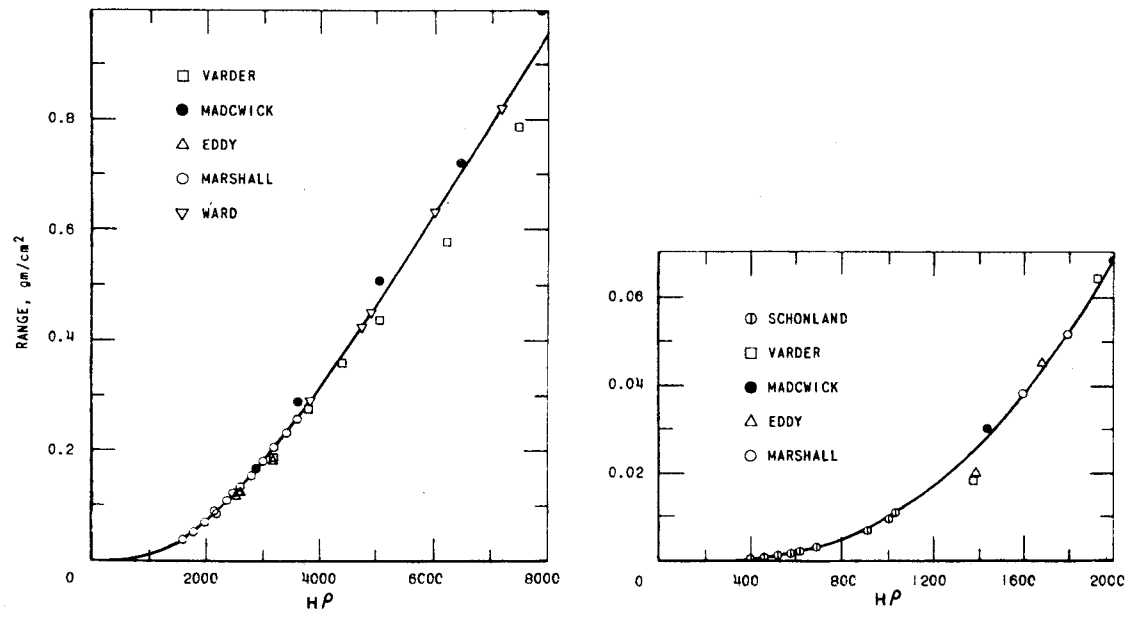

Fig. 9-29—Extrapolated range of electrons in aluminum. Hρ is the product of the radius of electron path and the magnetic field strength. *Reproduced from Ref. 83.*

9.5 RADIATOR AND COUNTER PROPERTIES FOR NEUTRON DETECTION

Proton-recoil techniques are used extensively in detection of high-energy (E > ~100 kev) neutrons. At lower energies, use of the exothermic charged particle reactions are often more practical, particularly the B^{10} (n,α) Li^7 reaction.

Some of the properties of these radiators are outlined in Sections 9.5.1 and 9.5.2. Corrections for thick and thin radiators are given in Sections 9.5.3 and 9.5.4. Radiators containing carbon may require a further correction to the count rate to account for the recoil carbon nuclei.

9.5.1 PROPERTIES OF NON-FISSION RADIATORS

The extensive energy interval through which the B^{10} cross section exhibits a 1/v dependence, and the absence of any strong resonances, make it one of the most widely used and exhaustively studied neutron detectors. Lithium-6 also has a favorable thermal capture cross section but has been used principally in scintillators, largely due to the fact that no suitable gaseous forms of Li exist. Properties of several materials suitable as charged particle sources are listed in Table 9-22.

Table 9-22—PROPERTIES OF NON-FISSION RADIATORS

Data from Refs. 34, 55, 85, and 86.

Material	Reaction	Q Value,[a] Mev	Resonance,[a,b] Energy Mev	Cross Section[a]		Most[c] Useful Energy Range
				At 3 Mev, mb	At 2200 m/s, b	
He^3	(n,p)	0.764	~1.6	550	5400	0.1–1 Mev
Li^6	(n,α)	4.78	0.27	150	945	0.4 ev–2 Mev
B^{10}	(n,α)	2.79	1.85	150	4010	0–5 Mev
N^{14}	(n,p)	0.627	0.49, 0.64	20	1.75	0.1–5 Mev
Cl^{35}	(n,p)	0.62	—	—	0.3	—

[a]Ref. 34.
[b]Ref. 55.
[c]Refs. 85 and 86.

In 93.5% of the B^{10} (thermal n,α) reactions, the resultant excited state of Li^7 decays to the ground state by the emission of a 0.48-Mev gamma ray. The excited state yield varies with energy and drops to 35% at 2 Mev.[86] The He^3 reaction has been reviewed by Bromley and Almquist.[87]

9.5.2 PROPERTIES OF FISSIONABLE LININGS

Materials suitable for fission counters are listed in Table 9-23. Threshold energies are estimated from linear extrapolation of data given in ENL-325.[34] Photofissions are not included owing to their generally high (>5 Mev) threshold energies. Alpha emission half-lives are included to facilitate assessment of the alpha pile-up problem. Cross sections for most threshold detectors increase approximately linearly with energy up to about 3 Mev where they level off. This makes the cross section at twice the threshold energy a convenient, though arbitrary, reference for purposes of comparison.

9.5.3 CORRECTIONS FOR THICK PROTON RECOIL RADIATORS

Proton recoils from solid or liquid radiators must be corrected for the absorption of the proton as it traverses the target material. A thick target is defined as one that is thicker than the maximum proton range, but not so thick that the neutron energy distribution is changed. Under these conditions, the recoil proton spectrum into the chamber will be independent of radiator thickness. For a collimated incident neutron beam having neutron energy E_0, Feather[88] has shown that the number of pro-

tons leaving the target per second which have lost less than some fraction ($f = E_B/E_0$) of their energy is:

$$C(E_B) = \frac{\phi}{3} A \Sigma_H R(E_0) (1 - f^{3/2})^2$$

where $C(E_B)$ is proportional to the observed count rate above a bias point corresponding to E_B; ϕ is the incident neutron flux; A and Σ_H are the area and macroscopic cross section for n-p scattering of the radiator; and $R(E_0)$ is the range of the most energetic proton. The Geiger range-energy relation: $[R(E_i) = KE_i^{3/2}]$, was assumed to hold. Figure 9-30 shows the calculated counter efficiency, $C(E_B)/\phi$, for different fractional energy losses, f, in a polyethylene radiator.

Table 9-23 — FISSION THRESHOLD ENERGIES AND CROSS SECTIONS OF MATERIALS FOR FISSION COUNTERS

Data from Refs. 34, 86, and 89.

Isotope	Threshold Energy (E_0), Mev	Cross Sections			Half-Life, yr
		At $2E_0$, mb	At 3 Mev, mb	At Thermal Energy, b	
Th^{232}	1.25	120	140	—	1.4×10^{10}
Pa^{231}	0.42	550	1100	—	3.4×10^{4}
U^{233}	Thermal	—	1900	530	1.6×10^{5}
U^{234}	0.26	400	1500	—	2.5×10^{5}
U^{235}	Thermal	—	1300	580	7.1×10^{8}
U^{236}	0.70	600	850	—	2.4×10^{7}
U^{238}	1.25	550	550	—	4.5×10^{9}
Np^{237}	0.32	850	1500	—	2.2×10^{6}
Pu^{239}	Thermal	—	2000	750	2.4×10^{4}

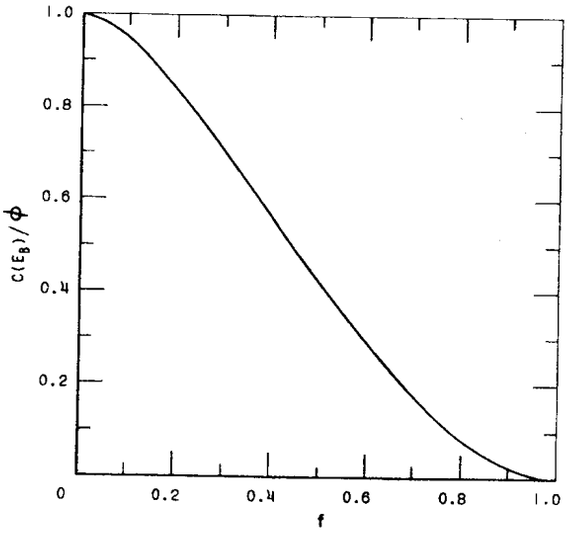

Fig. 9-30 — Calculated counter efficiency, $C(E_B)/\phi$, for different fractional energy losses, f, in a polyethylene radiator. *Reproduced from Ref. 56.*

9.5.4 CORRECTIONS FOR THIN RADIATORS

Formulae for correcting the energy distribution of emerging protons from thin radiators (thickness < max. proton range) have been developed by Moyer, and by Kronenberg and Murphy. The formula of Moyer[90] for thin targets relates the observed count rate to the collimated incident neutron flux. He finds the counting efficiency [the ratio of observed count rate, $C(E_B,S)$, to true flux, $\phi(E_B)$] above a bias point corresponding to E_B for a radiator of thickness S, is given by:

$$\frac{C(E_B,S)}{\phi(E_B)} = \frac{1}{2} \Sigma_H A R(E_B) \frac{S}{R(E_n)} \left\{1 + \frac{S}{R(E_n)} - \frac{9}{5}\left[\frac{S}{R(E_n)}\right]^{3/2}\right\}$$

687863 O - 63 - 46

where Σ_H is the macroscopic n-p scattering cross section of the target; E_B and E_n are the bias and incident neutron energies, respectively (E_n is also the maximum recoil proton energy); A is the area of the radiator; and R is the proton range in the radiator. This ratio is plotted in Fig. 9-31 as a function of neutron energy for various polyethylene radiator thicknesses.

In the limit of thick targets, $S > R(E_n)$, the equation reduces to:

$$\frac{C(E_B)}{\phi(E_n)} = \frac{1}{10} \Sigma_H A R(E_B)$$

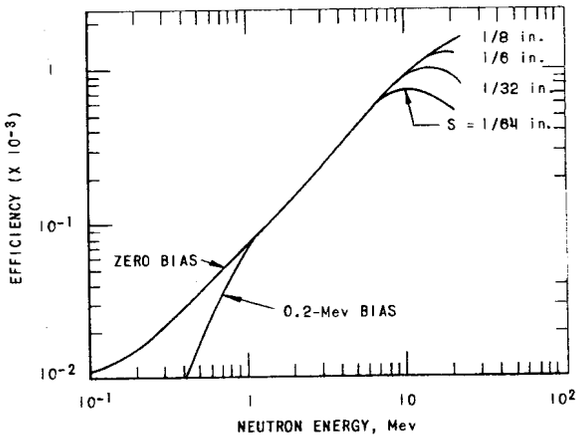

Fig. 9-31—Calculated efficiency, $C(E_B)/\phi$, for different thicknesses of polyethylene radiator. *Reproduced from Ref. 90.*

Kronenberg and Murphy[91] have treated the general case of proton recoils resulting from a continuous neutron spectrum. The limiting case for monoenergetic neutron irradiation (corresponding to Moyer's work) gives the number of protons with energy between E and E + dE leaving the surface of the radiator as

$$\frac{dN}{dE} = \frac{\Sigma_H A F(E) E^{-\nu}}{4K} \left(\frac{E_n - E}{E_n}\right)$$

where F(E) is the fraction of incident neutrons with energy greater than E and represents the total number of parents for the protons which ultimately leave the radiator, and K and ν are the constants that best describe the proton energy loss as a function of energy:

$$\frac{dE}{dx} = KE^{-\nu}$$

The differential distribution in terms of the bias energy, E_B, for different energy incident neutrons is shown in Fig. 9-32.

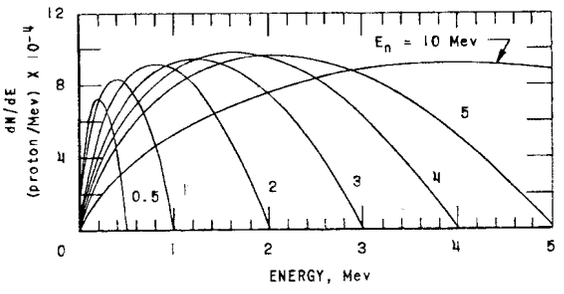

Fig. 9-32—Differential recoil proton pulse height distribution leaving the surface of a Plexiglas slab for various incident neutron energies. Normalized to 1 n/(cm^2)(sec). *Reproduced from Ref. 91.*

The total number of protons leaving the target is obtained by integration over all proton energies. By choosing the range such that $\nu = 0.7$, the resulting integral is identical to Moyer's expression. The Geiger relation for the range ($R \sim E^{3/2}$) gives $\nu = 0.5$.

The more general case treated by Kronenberg and Murphy is for a fission spectrum of collimated incident neutrons. Figure 9-33 shows the differential pulse height distribution of recoil protons leaving the surface of a Plexiglas slab for a fission spectrum of incident neutrons.

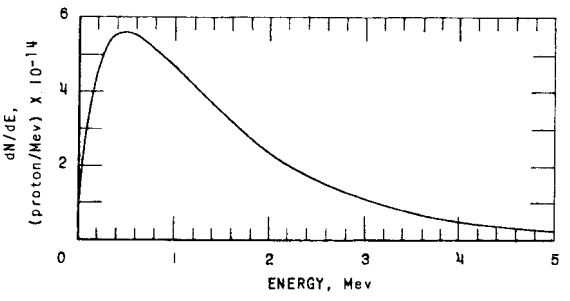

Fig. 9-33 — Differential recoil proton pulse height distribution leaving the surface of a Plexiglas slab for a fission spectrum of incident neutrons. Normalized to 1 n/(cm^2)(sec). *Reproduced from Ref. 91.*

9.6 ABSOLUTE FOIL COUNTING

One method employed to determine absolute neutron fluxes is to measure the absolute activity of a foil irradiated in the flux for a known time. The measured count is corrected for irradiation time, decay after irradiation, decay during counting, dead time losses in the counter, foil self-shielding and outer flux perturbations. Other corrections include the absorption and scattering of the measured radiation by the foil, the air and the counter window, the geometry and efficiency of the detector, back-scattering of the sample support, and additional radiations resulting from impurities in the foil. These effects are discussed at length in Refs. 92 through 96. This section is limited to factors dependent upon the properties of the foil and its support: self-absorption, self-scattering, and back-scattering.

9.6.1 ABSOLUTE BETA COUNTING

An expression giving the total count rate, with back-scattering from the sample and its support, and absorption in the sample, the air, and the counter window included, has been given by Libby.[95] A sample of area A(cm^2), undergoing σ disintegrations per minute per milligram will produce:

$$R = \frac{A\sigma}{G}\left[1 + \frac{\eta}{2}\exp\left(-\ell/\lambda_w\right)\right]\exp\left(-\ell/\lambda\right)\left[1 - \exp\left(-x/\lambda_s\right)\right]$$

counts per minute in a 100% efficient cylindrical counter with an air path plus window thickness of ℓ mg/cm^2. $G = 4\pi/\Omega$ is the geometry factor, where Ω is the solid angle subtended by the sensitive volume of the counter. λ is the mean free absorption length for the radiation being counted, with the subscripts s and w denoting the sample and the window, respectively. η is the (dimensionless) back-scattering coefficient indicating the relative intensity of the back-scattered radiation compared to the intensity of the direct radiation. x is the sample thickness in mg/cm^2.

The equation was derived by assuming that the absorption length for the back-scattered betas is one-half as long as before the scattering process. Such an assumption generally applies for absorbing materials with $Z > 15$.

For close geometry (solid angle subtended by the counter approaches 2π), an empirical relation for the back-scattering coefficient is given by Libby:

$$\eta = 0.65\left[1 - \exp\left(-\bar{Z}/35\right)\right]$$

where $\bar{Z}$ is the average atomic number of the sample on a weight average basis. In most practical decay schemes with maximum beta energy E_0 (in Mev), electron ranges obey the Geiger relation so that λ may be approximated by:

$$\lambda = 55\ E_0^{3/2}\ \text{mg/cm}^2$$

In general, the absorption length depends on the shape of the distribution and the maximum beta energy. The above expressions are valid only for a single beta group having an "allowed" shape. It is

also inferred that the detector response to gamma radiation has been accounted for. Correction factors necessary to account for complex decay schemes (such as indium) usually have to be established experimentally.

Koontz, et al.,[96] have defined separate correction factors, f_s, f_b, and f_γ, and their product as:

$$f_s = \frac{\text{counting rate with self-absorption and self-scattering}}{\text{counting rate without self-absorption and self-scattering}}$$

with f_b and f_γ analogously defined to describe the effect on the observed count caused by back-scattering and by an additional gamma count rate, respectively.

Measurements of these correction factors were made with a 2π windowless counter ("good geometry"), and with small foils placed 2.2 cm from the end of a G-M counter ("bad geometry"). The fractional change in count rate is shown in Fig. 9-34. "Good geometry" shows only the scattering and absorption of the emitted betas within the foil. Under the "bad geometry" conditions, the scattering and absorption of the air and tube window are also included. The total correction factor, including gammas and the back-scattered betas from a thick silver backing, is shown in Fig. 9-35. In this case, the difference between the two geometries is a measure of the scattering and absorption of the air and the counter window.

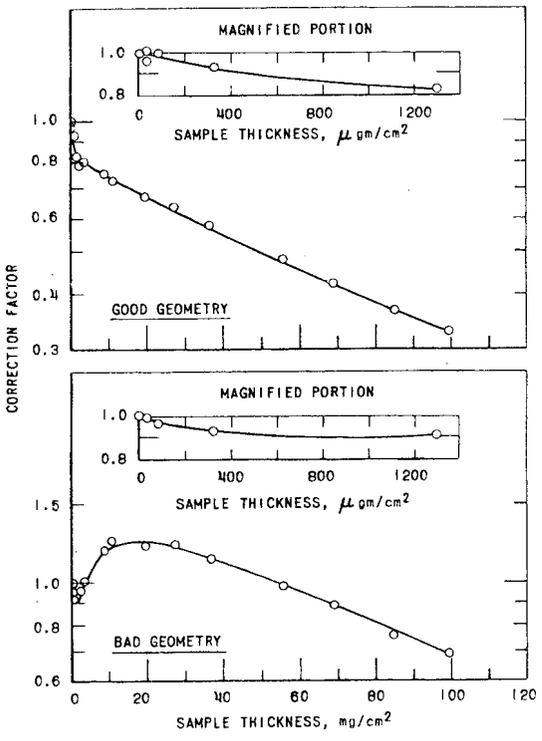

Fig. 9-34—Correction factor, f_s, for absorption and scattering of indium beta radiation. *Reproduced from Ref. 96.*

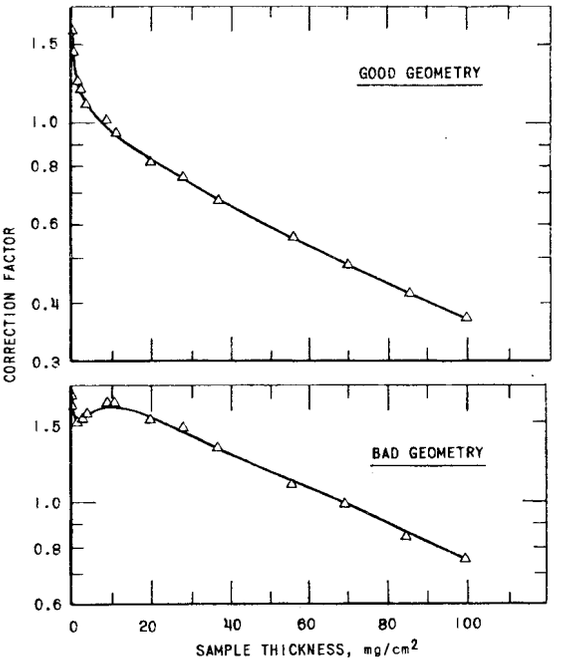

Fig. 9-35—Total correction = $f_s f_b f_\gamma$ for self-absorption and self-scattering from an indium foil; for backscattering of a thick silver foil backing; and for additional counts due to gamma radiation. *Reproduced from Ref. 96.*

For general counting geometries other than used by Koontz, et al., Tsvetaeva and Brusentsya[97] give an approximate correction to the counting rate due to the absorption of the air and the counter tube window (again a G-M tube):

$$\frac{1}{f_a f_w} = 2^{(t_w + t_a)/d_{1/2}(E_0)}$$

where t_w and t_a are the thicknesses of the detector window and the air gap between sample and detector in mg/cm^2; and $d_{1/2}(E_0)$ is the thickness of a layer of material (air plus window) in which one-half

of the detected radiation with maximum beta energy E_0 is absorbed. The values of $d_{1/2}(E_0)$ for various end point beta energies have been determined by a number of authors;[97-99] typical results are shown in Fig. 9-36. In the most recent work (Ref. 97), the correction for air absorption and scattering was determined by measurements first in a vacuum, then in air at atmospheric pressure. These results are shown in Fig. 9-37.

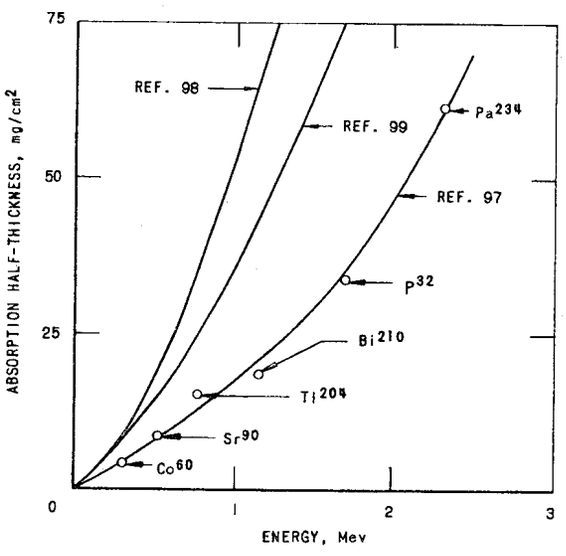

Fig. 9-36—Absorption half-thickness, $d_{1/2}(E_0)$, for various end point beta energies. *Reproduced from Ref. 97.*

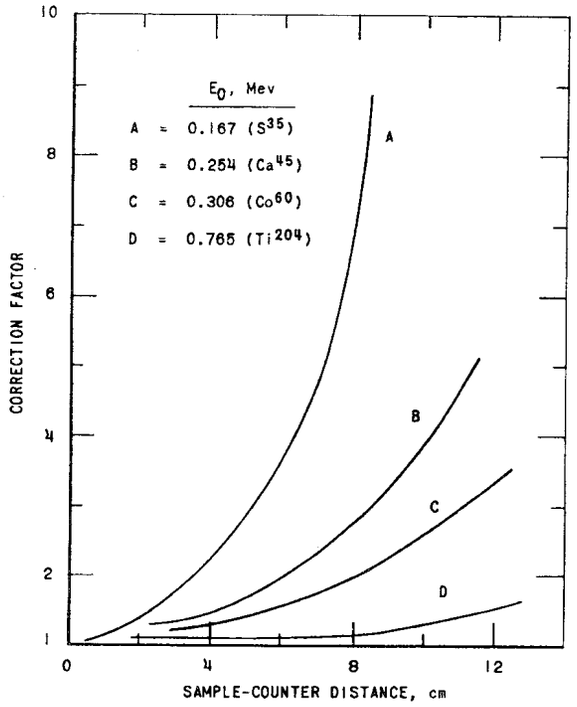

Fig. 9-37—Correction factor for air scattering and absorption for various end point energies. *Reproduced from Ref. 97.*

Bayhurst and Prestwood[100] point out that in determining the counting efficiencies, the average energy of the electrons is more important than the maximum energy. They give graphs for converting the maximum energies into average energies for various values of the atomic number. In addition, they give a diagram relating the maximum beta energy of forbidden transitions to that of allowed transitions, for the same counting efficiency. In the case of complex beta spectra, the average energy is obtained from an intensity weighting of each beta group.

Figures 9-38 and 9-39 show the counting efficiency as a function of average energy and of sample thickness, as given by Bayhurst and Prestwood. These curves are valid only for the equipment and geometry used by the authors, but they have general significance for evaluating the relative efficiencies for the various beta emitters. Nuclides with more than one beta group have only the value for the most abundant group plotted in Fig. 9-38. The contributions of the less-abundant groups have been subtracted from the experimentally determined total.

9.6.2 ABSOLUTE ALPHA COUNTING

Corrections appropriate to alpha counting are very similar to those applied to beta counting. Because the range of the alpha particle is much shorter than that of beta particles, more care must be taken to achieve the same degree of accuracy. The nature of alpha particle scattering is such that these losses will be negligible in "low geometry" counters, i.e., counters whose apertures are approximately 1% of the total solid angle.

Back-scattering. The back-scattering of alpha particles from various mounting materials was investigated by Crawford.[101] The sample was considered to be spread evenly in a thin layer on a backing material. Table 9-24 lists the results in terms of the ratio of the back-scattering in selected materials, to that of gold taken as a standard.

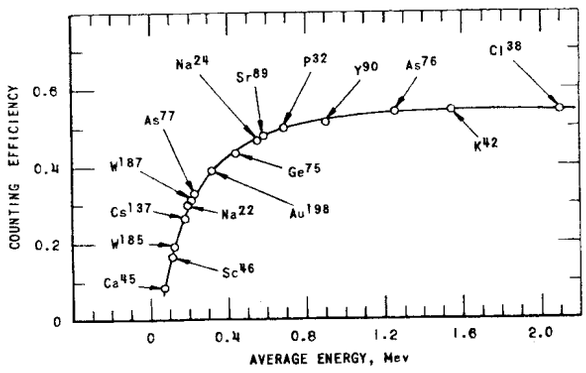

Fig. 9-38—Counting efficiency in 4π geometry for a standard sample (8.3 mg/cm^3). *Reproduced from Ref. 100.*

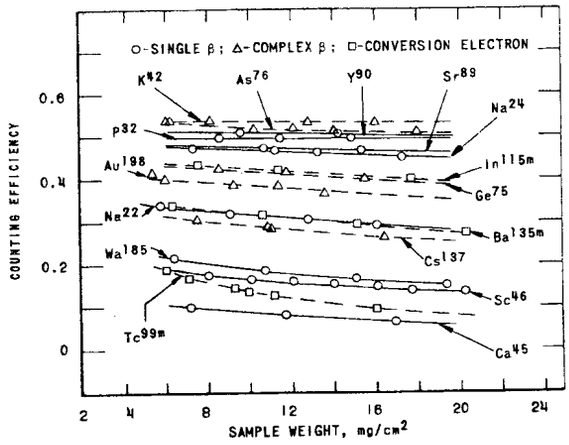

Fig. 9-39—Counting efficiency in 4π geometry for different sample thicknesses. *Reproduced from Ref. 100.*

Table 9-24—BACK-SCATTERING OF ALPHA PARTICLES (Pu^{239}) FROM VARIOUS BACKING MATERIALS

Data from Ref. 101.

Sample Mount Material	Back-scattering
Au[a]	1.00
Pt	0.99
U_3O_8	0.894
SiO_2 quartz	0.19
Al	0.23
Be	0.10

[a]Au taken as a standard.

The absolute value of the ratio of the back-scattering in gold (ratio of counts observed to true counts without back-scattering) was found to be 1.032. This value is in close agreement with the value of approximately 1.04 for Pt obtained by Cunningham, et al.[102] The relative values for alpha particle back-scattering in platinum and quartz (Table 9-24) are also in agreement with his experimental values.

The back-scattering coefficients listed in the table were determined with Pu^{239} alpha particles (range in air = 3.68 cm). Corrections for different energy alpha particles may be accomplished by the quantity:

$$\frac{f}{f_0} = \frac{R_0/\rho_0}{R/\rho}$$

where R and R_0 are the ranges in air of the sample and the standard, respectively, and:

$$\rho = \frac{2\,(1-k)}{k^2}\ln(1-k) + \frac{2-k}{k}$$

where k is the ratio between the maximum distance that the alpha particle can travel and still produce a detectable count in the backing material, and the corresponding distance in air. ρ_0 has an analogous definition but applies to the standard.

Self-Absorption. Steinberg[47] has calculated the fraction of alpha counts lost in a 2π counter due to absorption within the alpha-emitting sample:

$$\text{Fraction lost} = \frac{1}{2}\frac{t}{R}$$

where t is the sample thickness; and R is the effective range of the alpha particle in the source material, i.e., the maximum distance the particle can travel and still produce a detectable event.

9.7 NEUTRON SOURCES

A number of comprehensive reviews of measurements of the spectra and yields of available neutron sources have been published.[103–107] The periodic performance of these surveys, particularly of the (α,n) and the (γ,n) sources, is evidence of the difficulties associated with these measurements. Detailed reviews of the physics of the (p,n) and (d,n) reactions are the subject of a series of papers in the Handbuch der Physik,[107–109] and elsewhere.[110–113] Extensive tables giving the relation between the incident charged particle energy, the energy of the emitted neutron, and the angle between the two, have been published in Refs. 114 through 120.

9.7.1 SPECTRA OF (α,n) SOURCES

Only recently has there been any reasonable agreement between measurements of the spectrum for a given type of natural α,n reaction. In part, the difficulty has been in obtaining homogeneous mixing of a uniformly fine radioactive salt with the powdered target material. Except for a Po^{210} source, the daughter activities in the source build up with time. Generally, the alphas in the daughter activity have different energies than the parent so that the resulting neutron spectrum changes accordingly. Po^{210} decays directly to the ground state of stable Pb^{206}, and so the alpha particle can be used as a standard (E_α = 5.3056 ± 0.0006 Mev).[121] The short half-life (138 days) precludes the use of Po^{210} in certain applications. Calculated and measured spectra for the various Po^{210} sources are shown in Figs. 9-40 through 9-43.

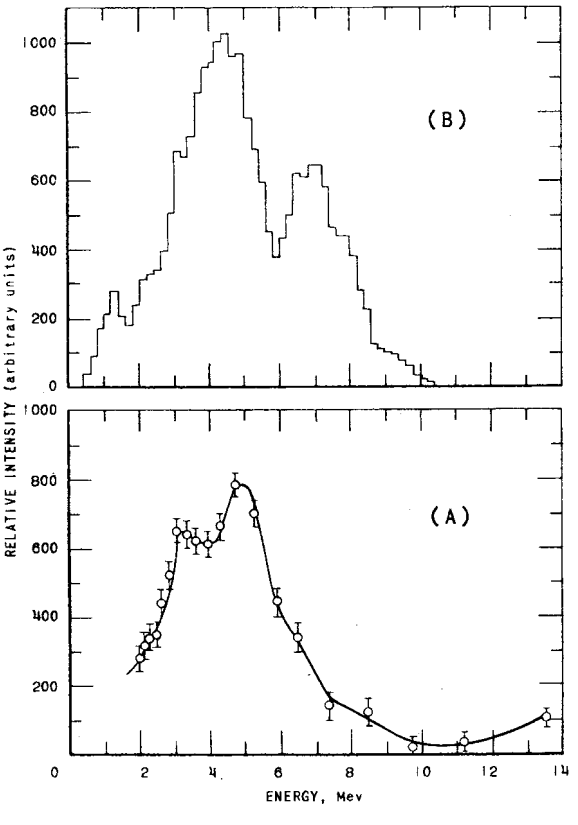

Fig. 9-40—Neutron spectrum from a Po-α-Be source measured by (A) time-of-flight and (B) photographic emulsion methods. *Reproduced from Refs. 122 and 123.*

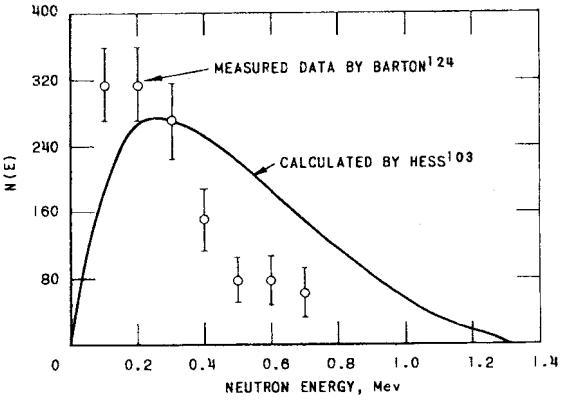

Fig. 9-41—Neutron spectrum from a Po-α-Li^7 source. *Reproduced from Ref. 103.*

The long half-life of Ra^{226} (1,622 years) makes it very desirable as an alpha emitter for neutron sources, but the changing composition of alpha-active daughters in the Ra source material results in a corresponding change of spectrum. Equilibrium is established between Ra^{226} and all its daughter substances after about one month, but 100 years are required before equilibrium is achieved with the 138-day Po^{210} (through the 19.4-year Pb^{210}). The calculated spectrum for a young (1 month old) source is compared to a measured value in Fig. 9-44.

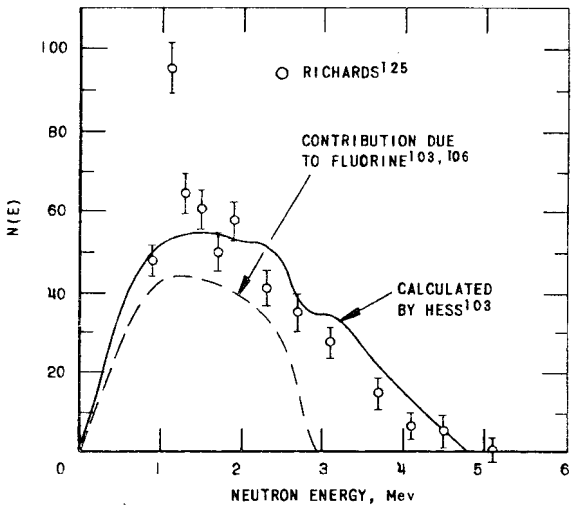

Fig. 9-42—Neutron spectrum from a Po-α-BF_3 source. *Reproduced from Ref. 106.*

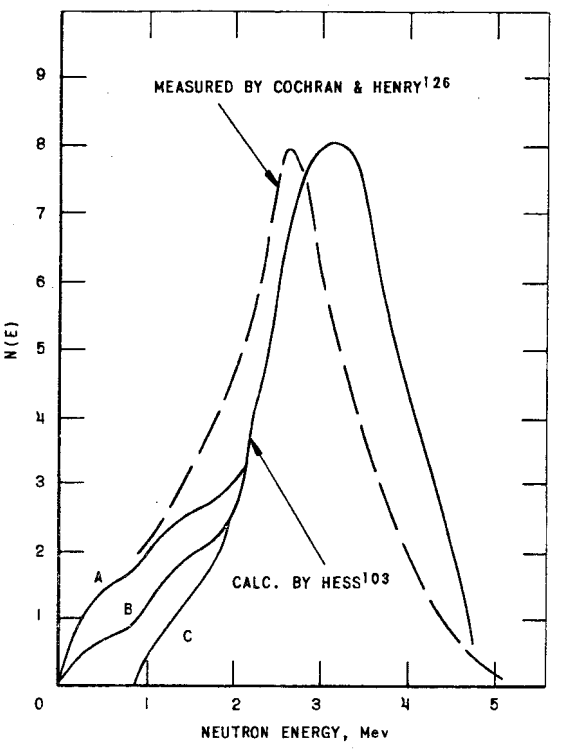

Fig. 9-43—Neutron spectrum from a Po-α-B source. Curves A, B, and D, calculated for 20%, 10%, and 0% of reactions proceeding to the 2.31-Mev state of the daughter nucleus, N^{14}. *Reproduced from Ref. 103.*

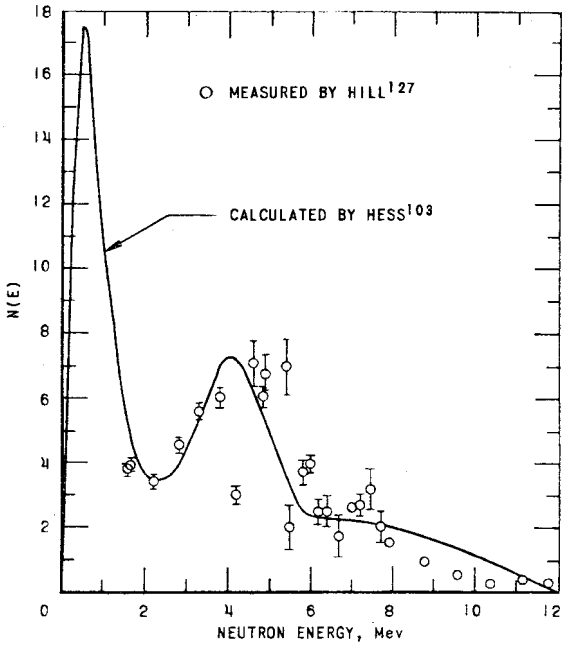

Fig. 9-44—Neutron spectrum from a Ra-α-Be source. *Reproduced from Ref. 103.*

With the increased availability of the transuranium elements in large quantities, Pu^{239} (24,300-year half-life) alloyed with Be as $PuBe_{13}$ offers relatively moderate yields with small gamma backgrounds. The calculated and measured spectrum from such a source is shown in Fig. 9-45.

All but two of the daughter activities in the 22-year Ac^{227} decay chain are alpha active. However, unlike Ra^{226} where the buildup of Po^{210} is determined by the long-lived Pb^{210} (19.4 years) decay in the chain, these activities are relatively short-lived and equilibrium is attained in a relatively short time. The measured spectrum of an equilibrium Ac^{227}-α-Be source is shown in Fig. 9-46.

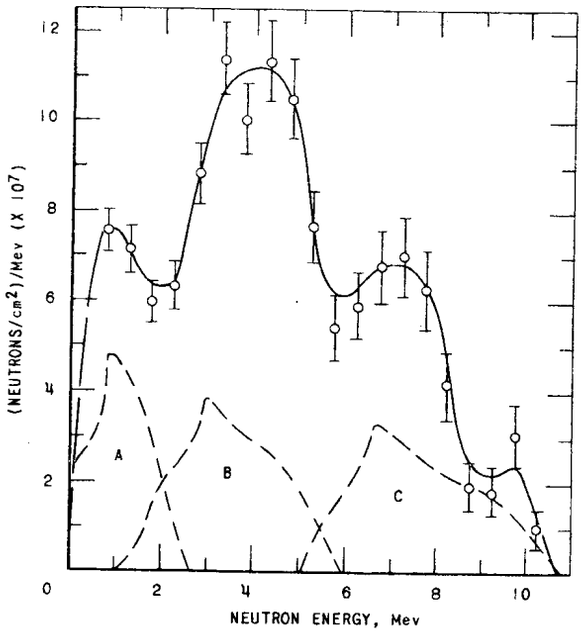

Fig. 9-45—Neutron spectrum from a Pu-α-Be source. Curves A, B, and C are the calculated neutron distributions associated with the 7.5-Mev, 4.5-Mev, and the ground state, respectively, of the daughter nucleus, C^{12}. *Reproduced from Ref. 128.*

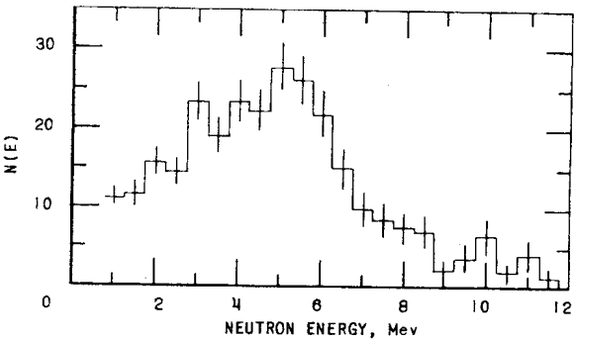

Fig. 9-46—Neutron spectrum from an equilibrium Ac-α-Be source. *Reproduced from Ref. 129.*

9.7.2 YIELDS OF (α,n) SOURCES

Absolute yield measurements of the natural alpha emitting neutron sources are not only difficult to measure accurately, but often change with time, as does their neutron spectrum. Many standard sources are made of an alloy of $RaBe_2$ mixed with Be powder, and their yields vary from 485 to 552 neutrons/10^6 alphas, depending on the Po^{210} content. Runnalls and Boucher[130] have derived an empirical relation between the maximum yield from a thick target, n_{max}, and the alpha particle energy, E, for Be:

$$n_{max} = 0.152\ E^{3.65} \text{ neutrons}/10^6 \text{ alpha particles}$$

Calculated and measured yields of the Ra^{226}-α-Be chain are given in Table 9-25. Calculated yields were obtained using the relation of Runnalls and Boucher. Decay properties are from Strominger, Hollander and Seaborg.[131]

Details of the Ac^{227}-α-Be chain are given in Table 9-26.

Runnalls and Boucher have also published measured and calculated yields for Pu-α-Be, Am-α-Be, and Cm-α-Be sources. The data are listed in Table 9-27; decay properties are from Ref. 131.

The relative yields of mixtures of Pu and Be are given by the relation;

$$\frac{n}{n_{max}} = \frac{N\,S_{Be}}{N\,S_{Be} + S_{Pu}}$$

Table 9-25—DECAY CHAIN OF Ra^{226}-α-Be NEUTRON SOURCE

Data from Ref. 106, except as noted.

Source	Half-life	Emitted Particle		Yield, neutrons/10^6 alphas	
		Type	Energy, Mev	Calc.	Meas.
Ra^{226}-Be	1622 yr	α	4.777	46	—
Em^{222}-Be	3.82 day	α	5.486	76	—
Po^{218}-Be	3.05 min	α	5.998	105	—
Pb^{214}	26.8 min	β^-	1.03	—	—
Bi^{214}	19.7 min	β^-	3.18	—	—
Po^{214}-Be	164 μsec	α	7.680	258	—
Pb^{210}	19.4 yr	β^-	0.017	—	—
Bi^{210}	5.0 day	β^-	1.17	—	—
Po^{210}-Be	138.4 day	α	5.3056[a]	67	72[b]
Pb^{206}	Stable	—	—	—	—
Equilibrium Neutron Yield				522	485 to 552

[a]Recommended international standard, Ref. 121.
[b]Ref. 138.

Table 9-26—DECAY CHAIN OF Ac^{227}-α-Be NEUTRON SOURCE

Data from Ref. 106.

Source	Half-life	Emitted Particle		Yield, neutrons/10^6 alphas
		Type	Energy, Mev	
Ac^{227}	22 yr	β^-	0.045	—
Th^{227}-Be	18.6 day	α	5.90	99
Pa^{223}-Be	11.2 day	α	5.65	84
Em^{219}-Be	3.92 sec	α	6.71	158
Po^{215}-Be	1830 μsec	α	7.365	222
Pb^{211}	36.1 min	β^-	1.4	—
Bi^{211}-Be	2.16 min	α	6.56	146
Tl^{207}	4.76 min	β^-	1.44	—
Pb^{207}	Stable	—	—	—
Equilibrium Neutron Yield				709

Table 9-27—MISCELLANEOUS α-Be NEUTRON SOURCE YIELDS

Data from Refs. 130 and 131.

Source	Half-life	Energy Intensity		Yield, neutrons/10^6 alphas	
		Mev	%	Calc.	Meas.
Pu^{239}-α-Be	24,400 yr	5.147	72.5	60	60 ± 2
Am^{241}-α-Be	458 yr	5.477	85	35	74 ± 2
Cm^{242}-α-Be	162.5 day	6.110	73.7	—	112 ± 3

where N is the ratio of Be atoms to total source atoms, and S_{Be} and S_{Pu} are the atomic stopping powers of Be and Pu (0.60 and 4.6), respectively. The most intense Pu alpha particle has an energy of 5.147 Mev (the average intensity of all alpha groups is 5.139 Mev), so that n_{max} is computed as 60 neutrons/10^6 alphas. Calculated neutron yields for different Pu-α-Be atom fractions are given in Table 9-28.

A number of miscellaneous neutron sources of practical interest are listed in Table 9-29.

Table 9-28—CALCULATED NEUTRON YIELDS FROM MIXTURES OF Be AND Pu

Data from Ref. 132.

Be Atom Fraction	Neutrons/ 10^6 alphas	Neutrons/sec/ 6.02×10^{23} atoms
0.10	1.26	6.2×10^5
0.20	2.77	12.0
0.30	4.60	17.4
0.40	6.92	22.5
0.50	9.88	26.8
0.60	14.0	30.4
0.70	19.3	31.5
0.80	27.5	29.3
0.90	41.1	22.3
1.00 (pure Be)	68.0	—

Table 9-29—MISCELLANEOUS (α,n) NEUTRON SOURCE YIELDS

Source	Yield, Neutrons/10^6 alphas	Neutrons/μc/sec	Ref.
Po^{210}-α-Li	4.7	—	133
Po^{210}-α-B	19	—	106, 133, 134
Po^{210}-α-F	10.4	—	103, 133
Po^{210}-α-BF_3	13.5	—	103
Po^{218}-α-B	40	—	107
Ra^{226}-α-B	—	6.8	105
Ra^{226}-α-BeF_4	100	2.53	105
Bi^{214}-α-B	100	—	107
Em^{222}-α-B	30	—	107

9.7.3 PHOTONEUTRON SOURCES

The threshold energy for the (γ,n) reactions of all nuclei available in sufficient amounts to make them practical as photoneutron sources is well above 5 Mev, except for Be^9 and H^2. This is far beyond the energy region of γ-rays from most of the radioactive isotopes. Thus H^2 (threshold energy = 2.226 Mev) and Be^9 (threshold energy = 1.666 Mev) are used in practical designs for radioactive photoneutron sources. The energy of a neutron produced in a (γ,n) reaction is approximately given by an expression of the form (see, for example, Ref. 106):

$$E_n = a + b \cos \psi$$

where $$a = \frac{A-1}{A}\left[E_\gamma - Q - \frac{E_\gamma^2}{1862\,(A-1)}\right]$$

$$b = \frac{E_\gamma}{A}\left[\frac{2(A-1)\,(E_\gamma - Q)}{931\,A}\right]^{1/2}$$

and A = mass of the target nucleus
E_γ = energy of the γ-ray, in Mev
Q = threshold energy, in Mev
ψ = angle between the flight paths of the γ-ray and the emitted neutron

For monochromatic incident γ-rays, the energy spread of the neutron distribution is 2b. In most practical cases, the energy spread is much greater due primarily to the energy loss of neutrons and γ-rays in scattering processes in the source. A survey of the characteristics of photoneutron sources, including an extensive bibliography, is given in Ref. 106. Some of these data are reproduced in Table 9-30.

Table 9-30—CHARACTERISTICS OF PHOTONEUTRON SOURCES

Data from Refs. 106 and 135.

γ-Emitter	Half-life	γ-Ray Energies above (γ,n) threshold, Mev	Percent of Total γ-Ray Yield	Neutron Energy, Mev				Yield/gram at 1 cm for a 1-curie source, $\times 10^{-4}$	
				H^2 Target		Be^9 Target			
				Calc.	Obs.	Calc.	Obs.	H^2 Target	Be^9 Target
Na^{24}	15.05 hr	2.757	100	0.29	0.22	0.966	0.83	27	13
Al^{28}	2.27 min	1.782	100	—	—	0.1	—	—	—
Cl^{38}	37.29 min	2.15	60	—	—	0.43	—	—	—
Mn^{56}	2.58 hr	1.77	20	—	—	0.93	0.15	—	—
		2.06	13	—	—	0.35	0.3	—	2.9
		2.88	1	0.35	0.22	1.08	—	0.31	—
Ga^{72}	14.3 hr	1.87	4	—	—	0.18	—	—	5.9
		2.21	16	—	—	0.48	—	—	3.7
		2.51	13	0.14	0.13	0.75	—	6.0	—
As^{76}	26.8 hr	1.77	—	—	—	0.093	—	—	—
		2.06	4	0.5	—	0.35	—	—	—
Y^{88}	104 day	1.85	99	—	—	0.17	0.16	—	10
		2.76	1	0.26	—	0.97	0.22	0.3	13
In^{116m}	54 min	2.09	12	—	—	0.38	0.30	—	0.82
Sb^{124}	60 day	1.69	—	—	—	0.030	0.029	—	15
		2.09	—	—	—	0.38	—	—	—
La^{140}	40 hr	2.55	3	—	—	0.75	0.62	—	0.28
Pr^{144}	17.5 min	2.18	44	—	—	0.46	—	—	0.08
Ra^{226}	1622 yr	1.69	—	—	—	0.021	—	—	—
(and daughters)		1.76	—	—	—	0.084	—	—	—
		1.82	—	—	—	0.14	—	—	3
		2.09	—	—	—	0.38	—	—	3.5
		2.2	—	—	—	0.48	—	—	—
		2.42	—	0.096	0.12	0.67	—	0.1	—
Ra^{228}	6.7 yr	1.8	—	—	—	0.12	—	—	—
(and daughters)		2.2	—	—	—	0.48	—	—	—
		2.6	—	0.2	0.2	0.85	0.83	9.5	3.5

Corrections to the thick target yields listed in Table 9-30 may be computed from γ-ray attenuation data given in this book, or from such linear attenuation coefficients given by Davison and Evans.[136] For non-slab geometries, corrections may be computed from tables by Case, et al.[137] Application of any given type of photoneutron source may be considerably limited because of the small (γ,n) cross section (usually on the order of millibarns), and the high γ-background peculiar to these types of sources.

9.7.4 SPONTANEOUS FISSION SOURCES

Properties of spontaneous fission neutron sources are given in Table 9-31. Yields per gram per second of source material were computed from the listed half-lives and neutrons/fission.

Table 9-31—PROPERTIES OF SPONTANEOUS FISSION NEUTRON SOURCES

Nuclide	Spontaneous Fission Half-life[a]	Decay Properties[b]		Neutrons per fission[c]	Neutrons per gram of source per second
		Particle	Half-life		
Md^{256}	3.5 hr	E.C.	~30 min	—	—
Fm^{256}	3 hr	—	—	—	—
Fm^{255}	>60 yr	α	21.5 hr	—	—
Fm^{254}	246 day	α	3.24 hr	4.05 ± 0.19	3.16×10^{14}
Fm^{252}	>8 yr	α	30 hr	—	—
E^{254}	1.5×10^5 yr	β^-	39 hr	—	—
		α	480 day	—	—
E^{253}	3×10^5 yr	α	20.03 day	—	—
Cf^{254}	85 × 15 day	—	—	3.90 ± 0.14	8.78×10^{14}
Cf^{252}	66 × 10 yr	α	2.6 yr	3.84 ± 0.12	3.07×10^{12}
Cf^{250}	$(1.5 \pm 0.5) \times 10^{14}$ yr	α	10.9 yr	—	—
Cf^{249}	1.5×10^9 yr	α	360 day	—	—
Cf^{248}	7×10^3 yr	α	350 day	—	—
Cf^{246}	2100 ± 300 yr	α	35.7 hr	2.92 ± 0.19	7.5×10^{10}
Bk^{249}	6×10^8 yr[d]	α,β^-	314 day	3.72 ± 0.16	3.32×10^5
Cm^{250}	2.3×10^4 yr[b]	—	—	—	—
Cm^{248}	4.6×10^6 yr[b]	α	4.7×10^5 yr	—	—
Cm^{246}	3×10^7 yr	α	6600 yr	—	—
Cm^{244}	1.4×10^7 yr	α	17.9 yr	2.82 ± 0.09	1.09×10^7
Cm^{242}	7.2×10^6 yr	α	162.5 day	2.59 ± 0.11	2×10^7
Cm^{240}	1.9×10^6 yr	α	26.8 day	—	—
Am^{241}	$\geq 1.4 \times 10^{13}$ yr[d]	α	458 yr	3.14 ± 0.05	—
Pu^{244}	$(2.5 \pm 0.8) \times 10^{10}$ yr	α	~7.6×10^7 yr	—	—
Pu^{242}	$(7.25 \pm 0.3) \times 10^{10}$ yr	α	3.79×10^5 yr	2.28 ± 0.13	1.7×10^3
Pu^{240}	1.2×10^{11} yr	α	6600 yr	2.23 ± 0.05	1.02×10^3
Pu^{239}	5.5×10^{15} yr	α	24400 yr	2.90 ± 0.04[e]	3.0×10^{-2}
Pu^{238}	4.9×10^{10} yr	α	86.4 yr	2.28 ± 0.10	2.5×10^3
Pu^{236}	3.5×10^9 yr	α	2.85 yr	2.17 ± 0.20	3.5×10^4
Np^{239}	$>5 \times 10^{12}$ yr	β^-	2.3 day	—	—
Np^{237}	$>4 \times 10^{15}$ yr	α	2.2×10^6 yr	—	—
U^{238}	8×10^5 yr	α	4.51×10^9 yr	2.30 ± 0.20	1.6×10^{-2}
U^{236}	2×10^{16} yr	α	2.39×10^7 yr	1.58 ± 0.15[d]	4.4×10^{-3}
U^{235}	1.8×10^{17} yr	α	6.8×10^8 yr	2.47 ± 0.03[e]	8×10^{-4}
U^{234}	1.6×10^{16} yr	α	2.5×10^5 yr	1.63 ± 0.15	5.8×10^{-3}
U^{233}	$\geq 3 \times 10^{17}$ yr[d]	α	1.6×10^5 yr	2.51 ± 0.03[e]	—
U^{232}	$(8 \pm 5.5) \times 10^{13}$ yr	α	74 yr	—	—
Pa^{231}	$\geq 10^{16}$ yr[d]	α	3.43×10^4 yr	—	—
Th^{232}	$<10^{21}$ yr	α	1.4×10^{10} yr	—	—
Th^{230}	$\geq 1.5 \times 10^{17}$ yr	α	8.0×10^4 yr	1.24 ± 0.15[d]	—

[a]From E. K. Hyde and G. T. Seaborg, "The Transuranium Elements," Handbuch der Physik, S. Flugge (ed.), 42, 205, (1957); also from M. H. Studier and J. R. Huzenga, Phys. Rev., 95, 545, (1945), except as noted.

[b]Ref. 131.

[c]For spontaneous fission, except as noted; from A. Kraut, Nukleonik, 2, 105, (1960).

[d]For neutron induced fission; from A. Kraut, ibid.

[e]For spontaneous fission; from I. Halpern, Ann. Rev. Nuclear Sci., 9, 245, (1959).

REFERENCES

1. M. A. Vigon and K. Wirtz, *Zur Theorie der Sondenstörungen im Neutronenfeld*, Z. Naturforsh, 9a: 286, (1954).
2. H. Meister, *Aktivierungsstorung von Indiumfolien im Neutronenfeld*, Z. Naturforsh, 10a: 669, (1955).
3. H. Meister, *Zur Theorie der Storung kreisscheibenformiger Neutronensonden, deren Radius klein gegen die Streuweglange der Umgebung ist*, Z. Naturforsh, 11a: 347, (1956).
4. H. Meister, *Storung der Neutronendichte im der Umgebung einer absorbierenden Sonde*, Z. Naturforsh, 11a: 356, (1956).
5. H. Meister, *Numerische Berechnung der Storung einer unendlich ausgedehnten scheibenformigen Neutronensonde nach der Transport Theorie*, Z. Naturforsh, 11a: 579, (1956).
6. K. Wirtz and K. H. Beckurts, *Elementare Neutronenphysik*, (Berlin: Springer, 1958).
7. C. H. Westcott, *Specification of Neutron Flux and Nuclear Cross Sections in Reactor Calculations*, J. Nuclear Energy, 2: 59, (1955); C. H. Westcott, *Effective Cross Section Values for Well-Moderated Thermal Reactor Spectra*, CRRP-787, (1958); C. G. Campbell and R. G. Freemantle, *Effective Cross Section Data for Thermal Reactor Calculations*, AERE RP/R 2031, (1957).
8. R. W. Stoughton and J. Halperin, *Heavy Nuclide Cross Sections of Particular Interest to Thermal Reactor Operation: Conventions, Measurements and Preferred Values*, Nuclear Sci. and Eng., 6: 100, (1959).
9. W. Bothe, *Zur Methodik der Neutronensonde*, Z. Physik, 120: 437, (1943); English translation in CP-2964, (1945).
10. D. K. Trubey, T. V. Blosser, and G. M. Estabrook, *Correction Factors for Foil-Activation Measurements of Neutron Fluxes in Water and Graphite*, ORNL-2842, (1959), p. 204.
11. See for example: H. B. Dwight, *Mathematical Tables of Elementary and Some Higher Mathematical Functions*, (2nd ed.; New York: Dover Publications, 1958), p. 183.
12. R. H. Ritchie and H. B. Eldridge, *Thermal Neutron Flux Depression by Absorbing Foils*, Nuclear Sci. and Eng., 8: 300, (1960).
13. C. W. Tittle, *Slow-Neutron Detection by Foils–II*, Nucleonics, 9: No. 1, 60, (July, 1951).
14. T. H. R. Skyrme, *Reduction in Neutron Density Caused by an Absorbing Disk*, MS-91 (Canada), undated.
15. G. R. Dalton and R. K. Osborn, *Flux Perturbations by Thermal Neutron Detectors*, Nuclear Sci. and Eng., 9: 198, (1961).
16. A. Sola, *Flux Perturbation by Detector Foils*, Nucleonics, 18: No. 3, 78, (1960).
17. M. W. Thompson, *Some Effects of the Self-Absorption of β-Rays and Neutrons in Neutron-Detecting Foils*, AERE RE/R 1549; also, J. Nuclear Energy, 2: 286, (1956).
18. W. Zobel, *Determination of Experimental Flux Depression and Other Corrections for Gold Foils Exposed in Water*, ORNL-2842, (September, 1959), p. 202; Trans. Am. Nuclear Society, 3: 168, (1960).
19. T. L. Gallagher, *Foil Depression Factors for Indium Disk Detectors*, Nuclear Sci. and Eng., 3: 110, (1958); E. D. Klema and R. H. Ritchie, *Thermal Neutron Flux Measurements in Graphite Using Gold and Indium Foils*, Phys. Rev., 87: 167, (1952).
20. D. H. Martin, *Correction Factors for Cd-Covered-Foil Measurements*, Nucleonics, 13: No. 3, 52, (March, 1955).
21. T. V. Blosser and D. K. Trubey, *An Investigation of the Slowing Down of Fission Neutrons in Water*, ORNL-2842, (November, 1959), p. 109.
22. G. M. Branch, *Neutron Temperature Measurements in Graphite and in a Uranium-Graphite Reactor*, MDDC-747, (October, 1946).
23. R. L. Walker, *Absolute Calibration of a Ra-Be Neutron Source*, MDDC-414, (September, 1945).
24. J. E. Dacey, R. W. Paine, Jr., and C. Goodman, *Shielding Properties of Various Materials Against Neutrons and Gamma Rays; Neutron Shielding Studies*, MIT Technical Report No. 23, NP-1243, (October, 1949).
25. J. H. Rush, *Range of a Ra-α-Be Neutrons in Water*, Phys. Rev., 73: 271, (1948).
26. J. W. Kunstadter, *A Correction to be Applied to the Activity of Neutron-Activated Cadmium-Covered Indium Foils*, Phys. Rev., 78: 484, (1950).
27. C. W. Tittle, *Slow-Neutron Detection by Foils-I*, Nucleonics, 8: No. 6, 5, (June, 1951).
28. R. W. Stoughton, J. Halperin, and M. P. Lietzke, *Effective Cadmium Cutoff Energies*, ORNL-2823 and Supplement, (March, 1960).
29. I. E. Dayton and W. G. Pettus, *Effective Cadmium Cutoff Energy*, Nucleonics, 15: No. 12, 86, (December, 1957).
30. D. K. Trubey, *Table of Three Exponential Integrals*, ORNL-2750, (July, 1959); also private communication from J. E. Schlosser, Hanford, (December, 1960).
31. J. B. Marion and J. M. Fowler (eds.), *Fast Neutron Physics–Part I*, (New York: Interscience Publishers, Inc., Copyright 1960).
32. P. R. Byerly, Jr., *Radioactivation Methods of Determining Neutron Flux*, ibid., Ref. 31, p. 657.
33. O. U. Anders, *Neutron-Activation Sensitivities*, Nucleonics, 18: No. 11, 178, (November, 1960).
34. D. J. Hughes and R. B. Schwartz, *Neutron Cross Sections*, BNL-325 (2nd ed., 1958), and Supplement No. 1, (1960).
35. C. Crouthamel, *Applied Gamma-Ray Spectrometry*, (New York: Pergamon Press, 1960).
36. S. Flugge (ed.), *Handbuch der Physik*, (Berlin: Springer, 1958).
37. W. E. Mott and R. B. Sutton, *Scintillation and Cerenkov Counters*, ibid., Ref. 36, 45: p. 86.
38. Proceedings of Scintillation Counter Symposia: Second Symposium: W. H. Jordon, AECU-583, (October, 1949); Third: Nucleonics, 10: No. 3, 32-41, (March, 1952); Fourth: Nucleonics, 12: No. 3, 13-56, (March, 1954); Fifth: IRE Trans. on Nuclear Sci., NS-3, (1956); Sixth: IRE Trans. on Nuclear Sci., NS-5, (1958); Seventh: IRE Trans. on Nuclear Sci., NS-7, No. 2-3, (1960).
39. *Technical Data Electron Tubes*, Tung-Sol Electric, Inc., Newark, N. J. (1951), Plate No. 3487.
40. J. H. Neiler and W. M. Good, *Time of Flight Techniques*, ibid., Ref. 31, p. 509.
41. J. Sharpe and E. E. Thomson, *Photomultiplier Tubes and Scintillation Counters*, Proc., 1958 Geneva Conference, 14: Paper No. 1465, p. 311.
42. G. A. Morton, *Recent Developments in the Scintillation Counter Field*, Proc., 1955 Geneva Conference, 14: Paper No. 61, p. 246.
43. F. D. Brooks, *Organic Scintillators*, Progress in Nuclear Physics, 5: (London: Pergamon Press, 1956).
44. G. T. Wright, *Absolute Quantum Efficiency of Photofluorescence of Anthracene Crystals*, Proc., Phys. Soc. (London), 68B: 241, (1955).
45. W. F. Miller and W. J. Snow, *Energy Loss Spectra for Gamma Rays in NaI*, Rev. Sci. Inst., 31: No. 1, 39, (January, 1960).
46. N. E. Scofield, *A Technique for Unfolding Gamma-Ray Scintillation Spectrometer Pulse-Height Distributions*, USNRDL-TR-447, (June, 1960).
47. E. P. Steinberg, *Interpretation of Counting Data*, ANL-5622, (September, 1956).
48. A. Meyer and R. B. Murray, *Scintillation Response of Activated Conic Crystals to Charged Particles*, Proc., Seventh Scintillation Counter Symposium, IRE Trans. on Nuclear Science, NS-7, No. 2-3, 22, (1960).
49. B. B. Rossi and H. H. Staub, *Ionization Chambers and Counters*, National Nuclear Energy Series, (New York: McGraw-Hill Book Co., Inc., 1949), Div. V, 2.
50. T. H. R. Skyrme, P. R. Tunnicliffe, and A. G. Ward, *A Proportional Counter for Neutron Flux Measurements in the Energy Range 0.1 to 1 Mev*, Rev. Sci. Inst., 23: 204, (May, 1952).
51. J. Rembser, *Wand-und Endeffekte in zylindrischen NeutronenstoBzahlem*, Nukleonik, 1: 167, (1959).
52. H. W. Fulbright, *Ionization Chambers in Nuclear Physics*, ibid., Ref. 36, 45: p. 1.
53. S. A. Korff, *Geiger Counters*, ibid., Ref. 36, 45: p. 52.

54. S. C. Curran, *The Proportional Counter as Detector and Spectrometer*, ibid., Ref. 36, 45: p. 174.
55. H. H. Staub, *Detection Methods*, Experimental Nuclear Physics, E. Segre (ed.), (New York: John Wiley and Sons, Inc., 1953), 1: Part I, p. 1.
56. D. H. Wilkinson, *Ionization Chambers and Counters*, (Cambridge: University Press, 1950). See also A. M. Tyndall, *The Mobility of Positive Ions in Gases*, (Cambridge: University Press, 1938).
57. References listed on pp. 232 to 235 in W. D. Allen, *Neutron Detection*, (New York: Philosophical Library, 1960).
58. A. T. G. Ferguson, *Gas Recoil Counters*, ibid., Ref. 31, p. 179.
59. R. W. Lamphere, *Fission Detectors*, ibid., Ref. 31, p. 449.
60. E. U. Condon and H. Odishaw, *Handbook of Physics*, (New York: McGraw-Hill Book Co., 1958), Chap. 10, pp. 4-159.
61. L. N. Chanin and M. A. Biondi, *Mobilities of Mercury Ions in Helium, Neon and Argon*, Phys. Rev., 107: 1219, (1957).
62. M. Lax, *Generalized Mobility Theory*, Phys. Rev., 109: 1921, (1958).
63. M. A. Biondi and L. N. Chanin, *Deviations from Blanc's Law of Ionic Mobilities: Ne^+ in Neon-Helium Mixtures*, Phys. Rev., 100: 1230, (1955).
64. T. Holstein, *Mobility of Positive Ions in Gas Mixtures*, Phys. Rev., 100: 1230, (1955).
65. T. E. Bortner, G. S. Hurst, and W. G. Stone, *Drift Velocities of Electrons in Some Commonly Used Counting Gases*, Rev. Sci. Inst., 28: No. 2, 103, (February, 1957).
66. H. K. Reynolds, et al., *The Stopping Cross Section of Gases for Protons*, 30-600 kev, Phys. Rev., 92: 742, (1953).
67. M. C. Walske, *The Stopping Power of k-Electrons*, Phys. Rev., 88: 1283, (1952).
68. W. P. Jesse and J. Sadauskis, *Ionization in Pure Gases and the Average Energy to Make an Ion Pair for Alpha and Beta Particles*, Phys. Rev., 97: 1668, (1955).
69. G. S. Hurst and T. D. Strikler, *Penetration of Charged Particles in Matter*, Nuclear Science Series Report No. 29, National Academy of Sciences, National Research Council Publications No. 752, (1960), p. 134.
70. H. A. Bethe and J. Ashkin, *Passage of Radiation Through Matter*, Experimental Nuclear Physics, E. Segre (ed.), (New York: John Wiley and Sons, Inc., 1953), 1: Part II, p. 166.
71. S. K. Allison and S. D. Warshaw, *Passage of Heavy Particles Through Matter*, Rev. Mod. Phys., 25: No. 4, 779, (1953).
72. W. Whaling, *The Energy Loss of Charged Particles in Matter*, ibid., Ref. 36, 34: p. 193.
73. H. A. Bethe, *The Range-Energy Relation for Slow Alpha-Particles and Protons in Air*, Rev. Mod. Phys., 22: No. 2, 213, (1950).
74. M. S. Livingstone and H. A. Bethe, *Nuclear Physics*, Rev. Mod. Phys., 9: No. 3, 245, (1937).
75. W. E. Stephens and H. Staub, *Cloud Chamber Detection*, ibid., Ref. 31, p. 335.
76. P. K. Weyl, *The Energy Loss of Hydrogen, Helium, Nitrogen and Neon Ions in Gases*, Phys. Rev., 91: 289, (1953).
77. S. E. Liverhant, *Elementary Introduction to Nuclear Reactor Physics*, (New York: J. Wiley and Sons, 1960).
78. R. M. Sternheimer, *The Density Effect for the Ionization Loss in Various Materials*, Phys. Rev., 88: 851 (1952).
79. L. D. Marinelli, *Radiation Dosimetry and Protection*, Annual Reviews of Nuclear Science, (Stanford, California: Annual Reviews, Inc., 1953), 3.
80. N. O. Lassen, *On the Energy Loss by Fission Fragments Along Their Range*, Kgl. Danske Videnskab. Selskab, Mat.-Fys. Medd., 25: No. 11, (1950).
81. J. H. Coon, *Targets for the Production of Neutrons*, ibid., Ref. 31, p. 677.
82. A. T. Nelms, *Energy Loss and Range of Electrons and Positrons*, National Bureau of Standards Circular 577, (1956).
83. A. G. Ward and J. S. Marshall, *Absorption Curves and Ranges for Homogeneous Beta-Rays*, Can. J. Res., 15: Sec. A, 39, (March, 1937).
84. C. B. Fulmer, *Scintillation Response of CsI (Tl) Crystals to Fission Fragments and Energy vs Range in Various Materials for Light and Heavy Fission Fragments*, Phys. Rev., 108: 1113, (1957).
85. J. E. Perry, Jr., *Neutron Flux Measurements*, ibid., Ref. 31, p. 623.
86. H. H. Barschall, *Detection of Neutrons*, ibid., Ref. 36, 45: p. 437.
87. D. A. Bromley and E. Almquist, *He^3 Induced Reactions*, Reports on Progress in Physics, 23: 544-629, (1960).
88. N. Feather, British Atomic Energy Project Report, Br. 512, (September, 1944), as reported by Wilkinson, Ref. 56.
89. R. T. Siegel, *High-Energy Neutron Detectors*, ibid., Ref. 36, 45: p. 487.
90. B. J. Moyer, *Survey Methods for Fast and High-Energy Neutrons*, Nucleonics, 10: No. 5, 14, (May, 1952).
91. S. Kronenberg and H. M. Murphy, Jr., *Energy Spectrum of Protons Emitted from a Fast-Neutron-Irradiated Hydrogenous Material*, Radiation Research, 12: 728, (1960).
92. D. W. Engelkemeir, et al., *Investigation of the Effects on β Counting of Self-Scattering due to Source Weight*, National Nuclear Energy Series, (New York: McGraw-Hill Book Co., 1951), Div. IV, 9: Book I, p. 56.
93. L. R. Zumwalt, *Absolute Beta Counting Using End-Window Geiger-Mueller Counters and Experimental Data on Beta-Particle Scattering Effects*, AECU-567, (September, 1949).
94. H. O. Anger, et al., *Conference on the Absolute Beta Counting*, Preliminary Report No. 8, National Research Council, Committee on Nuclear Science, (1950).
95. W. F. Libby, *Simple Absolute Measurement Technique for Beta Radioactivity*, Anal. Chem., 29: 1566, (1957).
96. R. L. Koontz, M. A. Greenfield, and A. A. Jarrett, *Absolute Thermal Neutron Determination, Part II: Absolute Beta Counting of Indium Foils*, NAA-SR-1137, (October, 1955).
97. N. E. Tsvetaeva and M. N. Brusentsya, *Measurement of Beta Activity in a Counter*, Atomnaiia Energiia, 4: 583, (1958); English Translation in Soviet J. of Atomic Energy, 4: No. 6, 767, (June, 1958).
98. N. G. Gusev, *Handbook on Radiation and Protection*, (Moscow, USSR: Medgiz, State Publishers of Medical Literature, 1956).
99. V. Bochkarev, et al., *Measurement of the Activity of Data on Beta and Gamma Sources*, (USSR: Academy of Science Press, 1953).
100. B. P. Bayhurst and R. J. Prestwood, *A Method for Estimating Beta-Counting Efficiencies*, Nucleonics, 17: No. 3, 82, (March, 1959).
101. J. A. Crawford, *Theoretical Calculations Concerning Back-Scattering of Alpha Particles*, The Transuranium Elements, G. T. Seaborg, J. J. Katz, W. M. Manning (eds.), (New York: McGraw-Hill Book Co., 1949), Div. IV, 14-B, Part II, pp. 1307-1326.
102. B. B. Cunningham, A. Ghiorso and J. C. Hindman, *Back-Scattering of Pu^{239} Alpha Particles from Platinum*, The Transuranium Elements, G. T. Seaborg, J. J. Katz, W. M. Manning (eds.), (New York: McGraw-Hill Book Co., 1949), Div. IV, 14-B: Part II, pp. 1192-1196.
103. W. N. Hess, *Neutrons from (α,n) Sources*, Ann. Phys., 6: 115, (1959).
104. U. S. National Committee on Radiation Protection and Measurements, National Bureau of Standards Handbook, No. 72, (1960).
105. B. T. Feld, *The Neutron*, Experimental Nuclear Physics, E. Segre (ed.), (New York: John Wiley and Sons, Inc., 1953), II, p. 357.
106. A. O. Hanson, *Radioactive Neutron Sources*, ibid., Ref. 31, p. 3.
107. E. Amaldi, *The Production and Slowing Down of Neutrons*, ibid., Ref. 36, 38: Part II, 1, (1959).
108. W. E. Burcham, *Nuclear Reactions, Levels, and Spectra of Light Nuclei*, ibid., Ref. 36, 40: 1, (1957).
109. B. B. Kinsey, *Nuclear Reactions, Levels, and Spectra of Heavy Nuclei*, ibid., Ref. 36, 40: 202, (1957).
110. R. M. Frank and J. L. Gammel, *Inelastic Scattering of Protons and Neutrons by Deuterons*, Phys. Rev., 93: 463, (1954).
111. B. H. Bransden and E. H. S. Burhop, *The Disintegration of the Deuteron by Neutron Impact*, Proc., Phys. Soc. (London), A63: 1337, (1950).

112. A. O. Hanson, R. F. Taschek, and J. H. Williams, *Monoergic Neutrons from Charged Particle Reactions*, Rev. Modern Phys., 21: 635, (1949).
113. J. Monahan, *Kinematics of Neutron-Producing Reactions*, ibid., Ref. 31, p. 49.
114. J. E. Brolley, Jr. and J. L. Fowler, *Monoenergetic Neutron Sources: Reactions with Light Nuclei*, ibid., Ref. 31, p. 73.
115. J. B. Marion, *Monoenergetic Neutron Sources: Reactions with Medium-Weight Nuclei*, ibid., Ref. 31, p. 113.
116. J. H. Gibbons and H. W. Newson, *The Li^7 (p,n) Be^7 Reaction*, ibid., Ref. 31, p. 133.
117. A. S. Langsdorf, Jr., J. E. Monahan, and W. A. Reardon, *A Tabulation of Neutron Energies from Monoergic Protons on Lithium*, ANL-5219, (January, 1954).
118. J. B. Marion and B. Allen, *A Tabulation of Neutron Energies from Various Charged Particle Reactions*, NP-6710, (August, 1955).
119. C. Wong, et al., *Neutron Spectra from the p + d Reaction*, Phys. Rev., 116: 164, (1959).
120. L. Cranberg and R. K. Smith, *Breakup of Deuterons by Protons*, Phys. Rev., 113: 587, (1959).
121. C. P. Browne, et al., *Comparison of Po^{210} Alpha-Particle Energy with the Li^7 (p,n) Be^7 Reaction Threshold Energy*, Phys. Rev., 120: 905, (1960).
122. A. I. Vretennikov and V. Ia. Averchenkov, *20-Channel Time Analyzer for Selecting Fast Neutrons by Their Time of Flight*, Priobary I Tekhnika Eksperimenta, 3: 48, (1958); also, Inst. and Exp. Techniques, 3: 371, (1958).
123. I. Medveczky, *Investigation of the Energy Spectrum of Neutrons from a Po-Be Source with the Photographic Emulsion Method*, Acta Physica, Acad. Sci. Hung., 6: 61, (1957).
124. D. M. Barton, *Measurement of the Neutron Spectrum from a Po-Li^7 Neutron Source*, LA-1609, (July, 1953).
125. H. T. Richards, *Po Alphas on BF_3 as a Neutron Source*, MDDC-472, (May, 1944).
126. R. G. Cochran and K. M. Henry, *Proton Recoil Fast-Neutron Spectrometer, Part II: Experimental*, Rev. Sci. Inst., 26: No. 8, 757, (August, 1955).
127. D. L. Hill, *Studies with the Ranger*, AECD-1945(Rev.), (April, 1947).
128. L. Stewart, *Neutron Spectrum and Absolute Yield of a Plutonium-Beryllium Source*, Phys. Rev., 98: 740, (1955).
129. W. R. Dixon, A. Bielesch, and K. W. Geiger, *Neutron Spectrum of an Actinium-Beryllium Source*, Can. J. Phys., 35: No. 6, 699, (1957).
130. O. J. C. Runnalls and R. R. Boucher, *Neutron Yields from Actinide-Beryllium Alloys*, Can. J. Phys., 34: No. 9, 949, (1956).
131. D. Strominger, J. M. Hollander, and G. T. Seaborg, *Table of Isotopes*, Rev. Modern Phys., 30: No. 2, Part 2, 585, (1958).
132. R. E. Tate and A. S. Coffinberry, *Plutonium-Beryllium Neutron Sources, Their Fabrication and Neutron Yield*, Proc., 1958 Geneva Conference, 14: Paper No. 700, p. 427.
133. E. Segre and C. Wiegand, *Thick-Target Excitation Functions for Alpha Particles*, MDDC/185, (September, 1944).
134. R. L. Walker, *The (α,n) Cross Section of Boron*, Phys. Rev., 76: 244, (1949).
135. A. Wattenberg, *Photo-Neutron Sources*, Preliminary Report No. 6, NP-1100, (July, 1949).
136. C. M. Davison and R. D. Evans, *Gamma-Ray Absorption Coefficients*, Rev. Modern Phys., 24: 79, (1952).
137. K. M. Case, F. deHoffmann, and G. Placzek, *Introduction to the Theory of Neutron Diffusion*, (Washington: U. S. Government Printing Office, 1953).
138. J. H. Roberts, *Neutron Yields of Several Light Elements Bombarded with Polonium Alpha Particles*, MDDC-731, (Declassified: January, 1947).

Section 10

DIGITAL COMPUTER CODES

The digital computer codes summarized in this section have been selected on the basis of general utility and availability. Consistent with the nature of this edition, the scope of the compilation is limited to reactor physics programs in production and described in the open literature.* No attempt was made to include engineering codes or general mathematical routines often used in reactor design calculations.

Some highly useful codes no doubt have been overlooked. It is expected that these oversights can be included in subsequent editions.

The format employed throughout this section is as follows. Codes are grouped and listed in alphabetical order under headings which identify the subject matter treated, rather than the computer or mathematical theory used. These groupings are necessarily arbitrary and are not meant to be restrictive, since many codes might well be included under several headings.

Each code summary includes: code designation; description of code; input information required; output available; and related codes. Superscript numerals appearing in the text correspond to references cited in the tabulation of supplementary information at the end of each code grouping. Also included in these supplementary tables are: the name of the originating installation, a description of the machine configuration required, and an estimated problem running time or the time used for a "typical problem."

10.1 PARAMETER EVALUATION AND WEIGHTING PROCEDURES

This section is comprised of codes developed for the treatment of the slowing-down of neutrons; the calculation of parameters used in the determination of the infinite multiplication factor, k_∞; and the computation of weighting functions for averaging cross sections and related quantities.

10.1.1 RESONANCE ESCAPE AND RESONANCE REGION AVERAGES

Codes described in this category are concerned with the problem of estimating, for a given configuration of resonant absorbers in a scattering medium, the probability of a neutron escaping capture in passing through the resonance region. Computation of the effective resonance integral associated with a given configuration is also included.

*Previously published compilations of nuclear code abstracts are: A. Radkowsky and R. Brodsky, "A Bibliography of Available Digital Computer Codes for Nuclear Reactor Problems," AECU-3078, (October, 1955); and V. Nather and W. Sangren, "Abstracts—Nuclear Reactor Codes," Comm. Assoc. for Comp. Mach., Vol. 2, No. 1, (January, 1959), with updated index, Vol. 3, No. 1, (January, 1960).

687863 O - 63 - 47

NUREP

Description

NUREP[1,2,3] is the NYU Monte Carlo Program, REP, that estimates the resonance escape probability in a two-dimensional, periodic reactor lattice. Two code versions are available: (1) NREP1 for a rectangular array of concentric, circular annuli, or a set of infinite slabs; and (2) NREP2 for a rectangular lattice composed of subrectangles. Each geometric region is a homogeneous mixture of nuclides. Restrictions permit no more than five nuclides per mixture, nor more than ten different mixtures.

The calculation follows the life of a neutron in an energy range (E_{max},E_{min}) containing resonances of U^{238}. Initial position and direction of the neutron (or history) are chosen at random. The initial energy of the neutron is chosen in the interval $(0,E_{max})$ on the assumption that it has been slowed down from higher energy with no appreciable absorption. The motion of this neutron through the infinite array of cells in the lattice is simulated by translating it, without change in direction, to the opposite boundary of the basic working cell upon attempt to escape. In the event of collision with a nuclide, a particular isotope is chosen for the event; the emergent parameters and appropriate energy loss of the neutron are then determined. The code abandons a history when the neutron energy falls below E_{min}.

Each history has a weight, initially one, associated with it. Upon collision of the neutron, this weight is multiplied by the probability of survival, σ_s/σ_t, at that event; σ_s and σ_t are the microscopic scattering and total cross sections, respectively. The average of all final weights is the estimate of the resonance escape probability, i.e., the fraction of neutrons surviving slowing down into the interval $(0,E_{min})$. Pertinent data for the absorption distributions are collected at each event in each history, and are printed at the end of the problem.

Only elastic scatterings, isotropic in the center-of-mass system, are considered. The target nuclide of each collision is assumed to be at rest; however, Breit-Wigner resonance scattering and absorption cross sections are Doppler-broadened to account for the motion of the resonance nuclide.

The code will treat up to 60 known resonances; higher resonances, if desired, are treated statistically. Upon collision with the resonance nuclide at an energy between two adjacent resonances, the cross section taken is the sum of the background and contributions from these two resonances. The scattering cross section for the resonance nuclide includes interference between resonance and potential scattering; interference between resonances is neglected.

The parameters for the high-energy U^{238} resonance structure are given statistically in NUREP. For convenience, these resonances are uniformly spaced and have a constant gamma width. The neutron width is determined from the Porter-Thomas distribution.

Input Information Required

1. Problem identification and code option (NREP1 or NREP2).
2. Temperature (°K).
3. Energy range (E_{max}, E_{min}).
4. Number of histories to run.
5. Description of nuclide mixtures (≤ 10); number of nuclides in mixture (≤ 5); and concentration of each.
6. Material description of regions (≤ 15).
7. Potential scattering cross section, σ_s; absorption cross section, σ_a, at 1 ev; $\xi\sigma_s$; and mass M for every nuclide present.
8. Parameters associated with resonances ($\leq$ 60 resonances).
9. Specification of geometry (3 options: slab, staggered or unstaggered rods, for NREP1; 1 option: rectangles, for NREP2).
10. Restart option.

Output Available

Output is on-line.

1. Resonance escape probability, and probable error after every 1,024 histories.
2. The final resonance escape probability and probable error.

3. Absorption distribution over 16 energy intervals within each region.
4. Absorption distribution for each region.
5. Spatial distribution of absorptions for each of 10 equal volume elements in each absorbing region.

Rerun cards are punched at intervals of 1,024 histories and at the end of each problem.

Related Codes

Modifications of NREP1 and NREP2 to allow more than one isotope of the resonance absorber have been made by Berwind.[4] The modified versions are NREP3 and NREP4, respectively.

QUERY

Description

QUERY[5] calculates the resonance escape probability for a lattice using the tables of Adler, Hinman, and Nordheim.[6] Three reactor compositions are allowed: homogeneous, heterogeneous metal fuel, and heterogeneous oxide fuel.

It has been shown[7] that the resonance integral for fuel lumps in a lattice can be calculated in the same manner as the resonance integral for a single isolated lump by use of the concept of an effective average chord length, thus reducing a lattice calculation to an equivalent isolated lump calculation.

The resonance integral for each resolved resonance may be calculated by the NR (narrow resonance) or NRIA (narrow resonance infinite mass) approximation.

In the unresolved resonance range, the Porter-Thomas distribution is used to determine the neutron widths and subsequent integrations are performed using the referenced tables.[6]

Input Information Required

Problem parameters to be specified are:

1. Number of resonances, (≤ 99).
2. Reactor composition (3 options).
3. Effective average chord length, $\bar{r}$.
4. Geometry (cylindrical, slab, spherical).
5. Temperature.
6. Potential scattering cross section.
7. Moderator total cross section.
8. $\xi\sigma_s$.
9. Approximation type (NR or NRIA).
10. Number density, and atomic weight of absorbers.
11. Volume absorption term, A_3, in a metal fuel NRIA calculation.
12. Resonance parameters for each resolved resonance.
13. Data for unresolved resonances.

Output Available

1. Input data are printed.
2. The following are printed for each resolved resonance:

Γ = total width.

$$\sigma_0 = \frac{2.6 \times 10^6}{\text{E (of resonance)}} \frac{\Gamma_{\text{neutron}}}{\Gamma}.$$

A_V = volume contribution term.

A_S = surface contribution term.

$A = A_V + A_S$.

p = resonance escape probability.

3. The sum of the A values and the resonance escape probability for the set of resolved resonances.
4. The energies at which the integrands were evaluated are tabulated for each unresolved resonance calculation.
5. Values of A_v and A_s corresponding to the energies in (4), together with approximate values obtained by omitting both the integration over the Porter-Thomas distribution and Doppler broadening.
6. Results of the integrations, together with the unresolved resonance escape probability.

Related Codes

Similar programs have been reported for the Mercury computer at Harwell.[8] These programs evaluate the resonance escape probability and self-shielding factors for two lattice configurations: alternating parallel slabs of fuel and moderator, and parallel cylindrical fuel rods regularly spaced in the moderator.

The EXSLOWEQ code[9] includes a general treatment of the problem of slowing down through the resonance region. This FORTRAN program computes the neutron flux and slowing-down density for an infinite, homogeneous medium consisting of a single moderator and a resonance absorber. The code can be used to calculate appropriate temperature-dependent, multigroup cross sections.

SUPPLEMENTARY INFORMATION

Code Name	Related Codes	Originating Installation	Machine Configuration	Running Time	References
NUREP		New York University	IBM-704 with 32K core memory, 2 tape units.		1. R. D. Richtmyer, R. Van Norton and A. Wolfe, "The Monte Carlo Calculation of Resonance Capture in Reactor Lattices," Proc., 1958 Geneva Conference, 16, Paper No. 2489, p.180. 2. R. Van Norton, "A Preliminary Description of an NYU Resonance Escape Probability Monte Carlo Program (704)," NYU S-570905.
	NREP1	Westinghouse Electric Corp., Bettis Atomic Power Laboratory		90 min for 10,000 histories.	3. H. J. Berwind, "NUREP–The NYU Resonance Escape Probability Program for the IBM-704," WAPD-R(B)-93, (May, 1960).
	NREP2			150 min for 10,000 histories.	
	NREP3				4. H. J. Berwind, "NUREP Modification," WAPD-R(B)-150, (October, 1960).
	NREP4				
QUERY		Combustion Engineering, Inc., Nuclear Division	IBM-704 with 32K core memory, 2 tape units.	1-2 min for homogeneous reactor; 5-6 min for heterogeneous reactors.	5. "An IBM-704 Program for Calculating Effective Resonance Absorption Cross-Sections by the Narrow Resonance or Narrow Resonance Infinite Mass Approximation," CEND-94, Quarterly Progress Report, (Nov. 1, 1959 to Jan. 31, 1960). 6. F. T. Adler, G. W. Hinman and L. W. Nordheim, "The Quantitative Evaluation of Resonance Integrals," Proc., 1958 Geneva Conference, 16, Paper No. 1988, p.155. 7. "Study of Slightly-Enriched Uranium-Water Lattices with High Conversion Ratio," Quarterly Progress Reports, NYO-2701 (May 1 to July 31, 1959); NYO-2702 (August 1 to October 31, 1959).
	Harwell Programs	Atomic Energy Research Establishment, Harwell, England	Ferranti-Mercury.	35 min with Doppler-broadening; 3 min without.	8. A. J. Taylor, "A Programme for the Evaluation of Resonance Escape Probabilities and Self-Shielding Factors in Hydrogen Moderated Lattices," AERE-R3364, (June, 1960).
	EXSLOWEQ	University of Illinois	IBM-704 (FORTRAN).	15 min.	9. F. T. Adler, "Exact Solution of the Slowing Down Problem," (In Press.).

10.1.2 SLOWING-DOWN TREATMENTS

The following codes may be used to compute the slowing-down distribution of neutrons in a moderating medium. A variety of geometric configurations and approximation methods are considered.

CASINO 13

Description

CASINO 13[10] is a Monte Carlo code that computes the slowing down of neutrons in an infinite, heterogeneous lattice of concentric, cylindrical fuel assemblies.

Neutrons are started at fission energies, and their histories are computed as they undergo elastic collisions until thermalization and eventual termination occur. At each collision, a scattering mass is determined for the targets present as a function of the neutron energy. Scattering is assumed to be isotropic in the center-of-mass system at all energies, and isotropic in the laboratory system for energies above 1 ev. In the thermal energy range, the moderator atoms are assumed to have a Maxwellian velocity distribution. At higher energies, the moderator atoms are assumed to be stationary. Absorptions are accounted for by a weighting procedure.

The fundamental geometry in the calculation for the determination of the positions of neutrons is that of a cylindrical assembly in the center of a rectangular cell. In the final results, this geometry is transformed into a hexagonal lattice configuration and fluxes are given as functions of energy, position, and angle for a sector of this lattice.

Input Information Required

1. Description of isotopic mixtures (≤ 5): energy-dependent cross sections, and isotopic concentrations.
2. Description of regions (≤ 12): dimensions, mixture identification, and source location.
3. Energy levels: below which target motion occurs, and below which target mass is to be adjusted.
4. Output edit options: regions and energy groups for which the flux is to be tabulated.

Output Available

1. Three orthogonal components of neutron age for four values of energy (i.e., x,y,z components).
2. Three orthogonal components of migration area, M^2.
3. The flux is tabulated for 18 energy groups and for a maximum of 32 spatial regions, including a maximum of 12 regions within the fuel assembly, for fixed directions.
4. The number of fissions and absorptions in each of the components of the fuel assembly and in the surrounding moderator are tabulated according to energy into thermal absorptions (below 0.56 ev) and fast absorptions (above 0.56 ev). These quantities permit the determination of the thermal utilization and k_∞.

MUFT-4

Description

The MUFT-4[11] code computes for a given Fourier mode, the P_0 and P_1 components as functions of energy for neutrons slowing down from a plane source in an infinite, homogeneous medium. The solution may also be regarded as giving the P_0 and P_1 components of a multigroup flux in an infinite slab having a cosine source shape, provided the source and the fluxes vanish at the same extrapolated distance independent of energy. Few-group constants are obtained by averaging over the calculated neutron spectrum.

The basis of the calculation procedure is the P_1 or B_1 approximation[12] to the Fourier transform with respect to space of the one-dimensional Boltzmann equation. The moderation is accounted for by

hydrogen and non-hydrogenous components. Within the given approximation (P_1 or B_1), hydrogen moderation may be treated either exactly or according to the Selengut-Goertzel approximation. Non-hydrogenous or heavy element slowing down may be computed by either the age or Greuling-Goertzel approximations. Leakage and inelastic scattering contributions are included.

Resulting from the above considerations are five equations[13] for the following quantities:

$F = F_0(u)$
$J = -iF_1(u)$
$\eta = \int_0^u du' \, \Sigma_H(u') \exp[-(u-u')] \, F_0(u')$
$\rho = -i\int_0^u du' \, \Sigma_H(u') \exp[-\frac{3}{2}(u-u')] \, F_1(u')$
q = slowing down due to non-hydrogenous elements

where $F_0(u) = P_0$ component or flux at lethargy u
$F_1(u) = P_1$ component or current at lethargy u
i = imaginary unit
Σ_H = hydrogen macroscopic scattering cross section

The group equations are formed by averaging the five equations over lethargy intervals. In the averaging procedure, provisions are made for the treatment of resonance effects. The NRIA approximation is used (see Section 3.6.3).

The group equations are solved for each of the J groups ($J \leq 100$). Few-group data are then computed.

Input Information Required

In most cases, the user will have a library tape, LTP1,[14] containing the following data: MUFT-4 program; lethargy increments; microscopic cross sections; resonance parameters, including absorption parameters and fission-to-absorption ratios; inelastic scattering matrix; and source spectra for 54 groups.

The following additional input information is required:

1. Approximation options: P_1 or B_1, Selengut-Goertzel or exact; age or Greuling-Goertzel. Constants are not available on the currently distributed tape for the Greuling-Goertzel option.
2. Buckling (B^2). B^2 cannot equal zero if the B_1 option is used.
3. Total number of elements (≤ 15), and the densities for each.
4. Break points or group numbers to determine few-group structure.
5. L-factors (i.e., the self-shielding numbers) – at least one for each element which has resonance data in the library, but not more than eight per group.

Output Available

Three types of edit are available for output printing:

Edit 1 prints three sets of few-group parameters representing three, two, and one fast group sets. The few-group parameters are:

D = diffusion constant
Σ_a = absorption cross section
Σ_r = removal cross section to group immediately below
$\nu\Sigma_f$ = ν times the fission cross section

Edit 2 prints the information in Edit 1, and for the three sets of few-group data:

Σ_f = fission cross section
$T = D/(\Sigma_a + \Sigma_r)$
$P = \Sigma_r/(\Sigma_a + \Sigma_r)$
τ = age
Γ = total average flux for a group
$\alpha = \nu\Sigma_f\Gamma$
$\beta = \Sigma_f\Gamma$
Λ = total average current for a group
$\Xi = \Sigma_a\Gamma$
γ = total average source for a group
F, J, η, ρ, and q for each of the 54 groups

Edit 3 prints the information in Edits 1 and 2, and, for each group and selected element i:

Σ_f^i and $\nu\Sigma_f^i$
Σ_a^{ri} = resonance absorption cross section
Σ_a^{si} = non-resonance absorption cross section
$\alpha^i = \nu\Sigma_f^i\Gamma$
$\beta^i = \Sigma_f^i\Gamma$
$\Xi^i = \Sigma_a^i\Gamma$
$(\eta + q)^i$ = resonance absorption spectrum

Related Codes

Versions of the MUFT code are also available for the IBM-650 and Philco-2000 machines. These are MUFT-III and MUFT-5, respectively.

FORM,[15] is a FORTRAN version of MUFT written for the IBM-709. It includes options that permit up to 24 few-group schemes, and changing of cross sections at "execute" time.

P1MG

Description

P1MG[16] is a one-dimensional, multigroup code based on the P_1 equations in a Greuling-Goertzel approximation.[17] These equations are integrated over each non-thermal group for a given energy group structure. The absorption terms are split into smooth and resonance components and are treated in the MUFT-4 manner.[11] Average thermal parameters are not computed and are assumed to be given. Assuming spatial separability, bucklings for the transverse directions are used to reduce the spatial variation to a one-dimensional variation.

A three-point equation relating the flux at adjacent points within a homogeneous medium, for each group, is obtained by replacing the derivatives in the P_1 equations by central difference approximations. With appropriate group-dependent boundary conditions, and consistent interface conditions, this equation is solved by an iterative process.

The iterative process starts with a guess for the source in the first group and the difference equation for the first group is solved. This, in turn, permits the determination of the source for the second group and the second group equation is solved. This is continued until all the groups have been computed; then the improved source and a parameter, λ, which is the total fission source in the assembly, are determined. The process is repeated until set criteria on λ are met. Extrapolation for the source determination is available, and in general, the convergence and extrapolation procedures are like the WANDA code (Section 10.2).

Boundary conditions available are in the form:

$$\frac{d\phi^j}{dx} + C_{L,R}\,\phi^j = 0$$

where j refers to the group number; ϕ is the neutron flux, and the subscripts (L,R) refer to left-hand or right-hand boundaries. C_L must be zero for a cylinder or sphere (i.e., flux derivative is zero at the origin), but it can have any value for a slab. C_R can be any value independent of C_L.

Input Information Required

1. Total number of groups (≤ 80), points (≤ 200), regions (≤ 15).
2. Geometry (slab, cylinder, or sphere), corresponding transverse and resonance bucklings, mesh sizes, and boundary conditions.
3. Thermal cross sections, isotopic densities, source distribution guess, eigenvalue guess, few-group structure.
4. Convergence option (eigenvalue or pointwise).

Output Available

On-line edits are:

1. Input data.
2. Sequence of eigenvalues leading to a converged value.

Six types of edits are available for off-line printing:

Edit 1: Converged eigenvalue, normalized source, region source averages, and flux for groups specified at each point.

Edit 2: Slowing-down densities for each isotope, at each point, and currents for all the midpoints for each group specified.

Edits 3,4,5,6: Diffusion coefficients; removal, absorption, and ν times fission cross sections; flux for each point for the three varieties of few-group structure; and regionwise fast and thermal absorption totals.

Related Codes:

The P1MG1 version requires that the microscopic data for the thermal group be contained in the library. P1MG2 requires that thermal macroscopic cross sections be supplied as problem input. A version called P1MG3 is available for the Philco-2000 computer.

PROGRAM 0159

Description

PROGRAM 0159[18] is a Monte Carlo code for the study of the behavior of fast neutrons in a finite cylinder in which tubular regions are embedded. (The tubular regions with axes parallel to the axis of the containing cylinder, may be filled with any material.)

The program computes the escape spectrum, the absorption spectrum, and slowing-down probability. Spatial distribution of absorption, slowing-down events, and the fast neutron escape fractions for each tube, are also determined.

The above data are generated by following the histories of neutrons, emitted from a monoenergetic point source located in a specified tube, throughout their slowing down to a specified cutoff energy, escape, or absorption. Neutron slowing down is assumed to result from elastic collisions isotropic in the center-of-mass system. A weight, W, is assigned to each collision. An escape event after the n*th* collision is tallied with the weight:

$$W_E = \prod_{\ell=1}^{n} \left(\frac{\Sigma_s}{\Sigma_t}\right)_\ell$$

where Σ_s and Σ_t are the scattering and total cross sections for the region in which the ℓ*th* collision occurred. Similarly, non-fission and fission absorption weights W_{NF} and W_F, respectively, are:

$$W_{NF} = \left(\frac{\Sigma_a - \Sigma_f}{\Sigma_t}\right)_n \prod_{\ell=1}^{n-1} \left(\frac{\Sigma_s}{\Sigma_t}\right)_\ell$$

$$W_F = \left(\frac{\Sigma_f}{\Sigma_t}\right)_n \prod_{\ell=1}^{n-1} \left(\frac{\Sigma_s}{\Sigma_t}\right)_\ell$$

where Σ_a and Σ_f are the absorption and fission cross sections, respectively, in the region at the n*th* collision.

Input Information Required

1. Number of neutron histories.
2. Source locations and energy.
3. Energy cutoff.

4. Composition of material in the various regions (< 40 elements).
5. Microscopic cross sections.
6. Geometrical data, including specifications for the spatial output.

Output Available

For each of the 20 lethargy groups:

1. Non-fission absorptions.
2. Fission absorptions.
3. Escape fractions.
4. Slowing-down probabilities.

The assembly is divided into a maximum of 100 (10 axial and 10 radial) subregions. Spatial averages are computed for each subregion, and these averages are used to construct a histogram for the spatial distributions of each of the 20 groups.

PROGRAM 0329, 0366

Description

PROGRAM 0329, 0366[19] is a Monte Carlo code that computes the neutron slowing-down probability, cumulative absorption fraction, and end-leakage spectrum in any lattice of finite length which may be generated by a three-region, hexagonal translation cell of the same finite length.

Neutrons with a given energy are started from a given point source position. In PROGRAM 0329, the slowing-down history of a neutron is stopped when the lethargy exceeds a given cutoff value or the neutron escapes from the lattice. In PROGRAM 0366, the neutron history is stopped when the number of collisions equals a preset collision cutoff number, or the neutron escapes from the lattice. Thus PROGRAM 0366 permits study of lethargy-increase distribution at scattering for a given incident lethargy, and also gives the contribution to end-escape from a given order of scattering. Only elastic collisions isotropic in the center-of-mass system are considered in the slowing-down model.

Input Information Required

1. Number of neutron histories.
2. Lethargy points (≤ 201) at which cross sections are given and the slowing-down count is made.
3. Lethargy levels (≤ 21) between which escape counting is performed.
4. Materials used (≤ 30).
5. Source lethargy and position; cutoff lethargy.
6. Cell dimensions.
7. PROGRAM 0366 requires the designation of a collision cutoff number.

Output Available

1. Slowing-down probability for a maximum of 200 lethargy intervals.
2. Capture spectrum and fission absorption spectrum histograms for a maximum of 200 lethargy intervals; also the cumulative, and density distributions for each.
3. End-escape spectrum for a maximum of 20 lethargy intervals.
4. Distribution of the lethargy change in scattering at a given lethargy.

RDR 5

Description

The RDR 5[20] code obtains accurate numerical solutions to neutron transport problems involving slowing down of neutrons in multiregion slab geometry. At each lethargy u, it obtains the spatial dependence for a ten-discrete-direction approximation to the vector flux.

To obtain the difference equations solved by the code from the Boltzmann equation for slab geometry, it is necessary to approximate a double integral over lethargy and direction, this integral representing the scattered-in neutrons. The integration over direction is replaced by a 10-point double Gauss or single Gauss quadrature approximation. The integral over lethargy is approximated by a sum over discrete values of lethargy, and involves a specified set of transfer coefficients. These coefficients define the transfer of neutrons from all lower lethargy groups to the particular group under consideration.

Two types of spatial approximation are available with respect to the behavior of the flux between two adjoining space mesh points: (A) linear, or (B) exponential.

For a given lethargy, the difference equations and boundary conditions are used to compute the flux at each point in the space mesh for each of the relevant directions. Convergence is achieved in a group (3 to 8 iterations required) when

$$\frac{\text{Flux (new)} - \text{Flux (old)}}{\text{Flux (new)}} < \epsilon$$

for every space point and direction.

The boundary conditions are represented by a set of parameters which allow reflecting boundaries, free boundaries, a specified incoming flux, or a combined reflecting boundary condition with a plane source.

At present, there are three versions of RDR 5: A, B, and C. Version A uses spatial approximation (A) and double Gauss quadrature; Version B uses spatial approximation (B) and double Gauss quadrature; and Version C uses spatial approximation (B) and single Gauss quadrature.

Input Information Required

The input for RDR 5 is divided into three parts:

Part I specifies the number densities of the isotopes (≤ 8) in the various compositions (≤ 6), and the number of groups (≤ 99).

Part II is divided into four sections for the specification of:

1. Mesh size, arrangement of compositions, and spatial dependence of the fission source. The number of regions may be ≤ 99, but the number of points used is related to the number of regions by: (number of points) + 0.4 (number of regions) ≤ 299.
2. Angular and lethargy variation of fission source.
3. Boundary conditions, and convergence parameter, ϵ.
4. Output edit options.

Part III lists the isotopic cross sections, and transfer numbers that represent the differential scattering cross section.

Output Available

There are three options for editing the output:

Option 1 provides a list of values of the scalar flux and current for each space coordinate, and the average flux in each region.

Option 2 edits the total source in a group.

Option 3 gives a list of values of the vector flux at each of the ten angles for each space coordinate.

Any one of these three options may be selected for specified groups, or all of the groups.

Related Codes

RDR 5 can be made equivalent to a P_9, or a double-P_4 code by reinterpreting the weights used in the quadrature formula for angular integration.[21] The reinterpretation also involves the termination of the series expansion of the scattering kernel at the proper term.

To determine the group transfer coefficients used as input in RDR 5, assumptions have to be made regarding the lethargy dependence of the cross sections and flux in a lethargy interval. These assumptions are discussed in general terms, in Ref. 21, and, in particular, as they apply to the PREP code[22] which is used to produce transfer coefficients for input to RDR 5.

SUPPLEMENTARY INFORMATION

Code Name	Related Codes	Originating Installation	Machine Configuration	Running Time	Reference
CASINO 13		E. I. duPont de Nemours & Co., Savannah River Laboratory	IBM-704 with 16K core memory, 2 tape units.	35 min for 600 neutrons with 50 energy groups, 12 directions, 9 regions.	10. W. V. Baxter, "A Monte Carlo Code for Transport of Neutrons," DP-446, (December, 1959).
MUFT-4		Westinghouse Electric Corp., Bettis Atomic Power Laboratory	IBM-704 with 8K core memory, 2 tape units.	1 min.	11. H. Bohl, Jr., E. N. Gelbard and G. H. Ryan, "Muft-4 Fast Neutron Spectrum Code for IBM-704," WAPD-TM-72, (July, 1957). 12. "Reactor Physics Constants," ANL-5800 (1st ed.), p.150.
	MUFT-III MUFT-5		IBM-650. Philco-2000.	5 min.	13. R. L. Hellens, R. W. Long and B. H. Mount, "Multigroup Fourier Transform Calculation Description of Muft III Code," WAPD-TM-4, (July, 1956). 14. A. F. Henry, "54-Group Library for P-1 Programs," WAPD-TM-224, (April, 1960).
	FORM	North American Aviation Inc., Atomics International Division	IBM-709 with 32K core memory, 4 tape units (FORTRAN).	<1 min.	15. D. J. McGoff, "FORM-A Fourier Transform Fast Spectrum Code for the IBM-709," NAA-SR-Memo-5766, (September, 1960).
P1MG		Westinghouse Electric Corp., Bettis Atomic Power Laboratory	IBM-704 with 16K core memory, 1 drum unit, 10 tape units.	45 min for 54 groups 15 regions, 200 points.	16. H. Bohl, Jr., et al., "P1MG-A One-Dimensional Multigroup P_1 Code for the IBM-704," WAPD-TM-135, (July, 1959). 17. E. Greuling, F. Clark and G. Goertzel, "A Multigroup Approximation to the Boltzmann Equation for Critical Reactors," NDA 10-96, (1953).
	P1MG 1 P1MG 2 P1MG 3		Philco-2000.		
PROGRAM 0159		General Electric Co., Aircraft Nuclear Propulsion Dept.	IBM-704.	20 min for 1000 histories.	18. J. R. Beeler and D. R. Martin, "Interim Report on the Heterogeneous Slowing Down Program 0159," XDC-60-5-52, (March, 1960).
PROGRAM 0329, 0366		General Electric Co., Aircraft Nuclear Propulsion Dept.	IBM-704, 3 tape units.	20 min for 1000 histories.	19. J. R. Beeler and J. M. Lutz, "Slowing Down Probability in a Lattice Generated by a Three-Region Cell of Finite Length," XDC-59-7-57, (January, 1959).
RDR 5		U. S. Navy Department, David W. Taylor Model Basin	NORC.		20. C. W. Dawson, "Multigroup Transport Code RDR 5," David W. Taylor Model Basin, AML Report 103, (May, 1960). 21. R. C. Gast, "A P-9 Multigroup Method for Solution of the Transport Equation in Slab Geometry," WAPD-232, (May, 1960).
	PREP				22. H. J. Amster and L. M. Culpepper, "The PREP Code for Calculating Group and Angle Transfer Cross Sections of Elastic Scattering for the RDR 5 Transport Code on the NORC Computer," WAPD-TM-117, (February, 1958).

10.1.3 THERMAL PARAMETERS AND SPECTRUM CALCULATIONS

The codes in this section may be employed to determine for moderating materials the neutron energy distribution over which cross sections may be averaged to obtain parameters in the thermal energy range.

COGENT

Description

The COGENT[23] code is primarily intended to solve the problem of neutron space-energy distribution with hydrogen moderation. The code solves the one-dimensional neutron diffusion equation for 30 coupled energy groups with specified external neutron sources. The sources may vary in energy and space.

The boundary conditions may be: flux equal zero, current equal zero, or the logarithmic condition, at the exterior or right-hand boundary for all geometries. The same conditions are available for the left-hand boundary in the slab case, but in spherical or cylindrical geometry the current equal zero condition is required.

The macroscopic constants for each region are determined from the microscopic cross section library. The input moderator temperature is used as an index to select the 30×30 scattering matrix from the COGENT library. The scattering matrix entries are normalized to the hydrogen content in the region. A hydrogen gas model was used to construct the scattering matrices.

With all constants and sources determined for a specified set of mesh points and boundary conditions, the code solves for the multigroup flux in an iterative manner. Iterations are continued until the convergence criterion on the ratio of ϕ_{new}/ϕ_{old} is satisfied for all groups and all points. If convergence is not achieved after 200 iterations through the groups, the calculation is stopped and the results are printed. An extrapolation procedure is incorporated in the code to speed convergence.

There are provisions for stopping and restarting a given problem at approximately the same stage of computation.

Input Information Required

1. Geometry (slab, cylinder, sphere.)
2. Number of regions (≤ 4).
3. Number of points (≤ 101).
4. Number of isotopes (≤ 10).
5. Lateral buckling, B^2.
6. Hydrogen moderator temperature.
7. Convergence criterion.
8. Extrapolation factor.
9. Initial flux guess (3 options).
10. Source specification (4 options).
11. Output edit options.
12. Regional parameters: mesh width, and isotope concentrations.

Output Available

1. All input data are printed.
2. If the problem has converged:
   a. Fluxes at each point for each group.
   b. One-group fluxes at each point.
   c. Average diffusion coefficient at each point.
   d. Average cross sections per point per isotope, if requested.
   e. Flux plot per group, if requested.
3. If the problem has not converged after 200 iterations:
   a. Flux edit for the 199*th* iteration.
   b. Flux edit for the 200*th* iteration.
   c. Convergence of the 199*th* and 200*th* iterates.

ROUTINE II

Description

The ROUTINE II[24] code computes the infinite, homogeneous medium neutron energy distribution in equilibrium with light- or heavy-water moderators. The effects of chemical binding, moderator temperature, and absorptions are included.

The code is based on the methods developed by Brown and St. John,[25] and Brown,[26] for calculation of neutron energy spectra in D_2O and H_2O. The results of these calculations indicate a neutron spectrum composed of a Maxwellian-like distribution at low energy, and 1/E tail at high energy.

The code computes the energy distribution in the "Maxwellian-like" region by considering the distribution as a 28-component vector (28 energy groups are used). A source term is provided by treating neutrons scattered down from the 1/E tail as source neutrons. The resulting matrix equation is solved iteratively.

Provisions are made for variations of effective absorption cross sections in the assembly, moderator temperature, effective mass of the deuteron, and specification of parameters in the functional form of the scattering cross section.

Input Information Required

1. Mass of target.
2. Effective mass of target.
3. Velocity intervals.
4. kT(ev).
5. Three parameters which specify the best fit to the scattering cross section formula.
6. Source, and absorption cross section for each velocity interval.
7. Energy limits on the Maxwellian range to be considered.

Output Available

The neutron distribution for the 28 groups is punched on a set of cards. These cards may be listed on an IBM-407 printer.

SOFOCATE

Description

The SOFOCATE[27] code solves a revised Wigner-Wilkins differential equation, and thermal constants are averaged over the flux spectrum given by the solution.

Wigner and Wilkins[28] derived a differential equation which determines the energy spectrum of neutrons in equilibrium with a hydrogen-moderated, homogeneous medium. The derivation is based on the medium being infinite, the moderator having a constant scattering cross section, and an absorption cross section obeying the 1/v law. Chemical binding effects are not included.

The same form of differential equation is obtained in SOFOCATE by redefining the ratio of absorption to scattering (γ in Ref. 28), as an "arbitrary" function, C(E), of energy E. This function may include leakage effects.

The function C(E) and an energy-dependent diffusion coefficient D(E) are computed from input data. The coefficient D(E) is computed from the Selengut-Goertzel approximation. After C(E), D(E), and related coefficients are computed, the differential equation is solved numerically by the Milne method.

The solution to the Wigner-Wilkins equation approaches a Maxwellian as the absorption and leakage approach zero. The code does not solve this particular case numerically, but averages over Maxwellians may be obtained since provisions are made to generate a Maxwellian flux from a formula.

Averages of cross sections, diffusion coefficients, and related quantities, are then computed over the determined flux spectrum. A five-point quadrature formula is used.

Input Information Required

1. Maximum energy (≤ 2 ev).
2. Temperature, °K.
3. Microscopic cross sections for material i (i = 0,1... 99).
4. Atomic density, N_i, for each material.
5. Buckling, B^2.
6. Value of ν_i for fissionable materials.
7. Average cosine, $\bar{\mu}$.
8. Choice of mesh spacing in energy (fine or coarse).
9. Materials for which averages, over the solution or a Maxwellian, of the cross sections are desired.
10. Material coefficients and constants to compute $C_i(E)$.

Output Available

1. Number density, N(E).
2. Flux, $E^{1/2}$ N(E).
3. The product of energy and flux, $E^{3/2}$ N(E).
4. Absorption and fission cross sections,

$$\bar{\sigma}^{\,i}_{a,f} = \frac{\int_0^{E_{max}} C_i(E)\, N(E)\, dE}{\int_0^{E_{max}} E^{1/2}\, N(E)\, dE},$$

for the materials (i.e., i values) requested.

5. Average diffusion coefficient,

$$\bar{D} = \frac{\int_0^{E_{max}} E^{1/2}\, D(E)\, N(E)\, dE}{\int_0^{E_{max}} E^{1/2}\, N(E)\, dE}$$

6. Macroscopic values $\bar{\Sigma}_a$ and $\nu\bar{\Sigma}_f$.

Related Codes

The DONATE[29] and the KATE 1[30] codes perform similar computations on the IBM-650, and the Philco-2000 machines, respectively.

SPECTRUM

Description

The SPECTRUM[31] code computes the infinite-homogeneous-medium thermal neutron spectrum (flux per unit energy versus energy), for a medium consisting of a single moderator and up to twenty absorbers. The code solves the equation:[32,33]

$$\left[\sum_\alpha N_\alpha \sigma_\alpha(E) + N_H \int_0^{E_{max}} \sigma(E \rightarrow E^1)\, dE^1\right] \phi(E) = N_H \int_0^{E_{max}} \sigma(E^1 \rightarrow E)\, \phi(E^1)\, dE^1 + N_H \sigma_S\, S(E)$$

where: N_α = atom density of αth absorber
N_H = moderator atom density
$\sigma_\alpha(E)$ = microscopic absorption cross section for αth absorber
$\sigma(E \rightarrow E^1)$ = microscopic energy transfer cross section for moderator
σ_S = free atom microscopic scattering cross section for moderator
E_{max} = cutoff energy
$S(E)$ = energy distribution of neutrons scattered into the interval $0 < E < E_{max}$ from energies above E_{max}

The integrals in the equation are replaced by sums, and the resulting system of equations is solved by an iterative procedure. The constraining conditions of neutron conservation and detailed

balance are satisfied at each iteration. Iterations continue until either the convergence criterion on the ratio of two successive iterates is met, or 100 iterations are performed.

Input Information Required

1. A set (≤ 75) of energies, E_i, and associated values of $S(E_i)$, $\sigma_\alpha(E_i)$, and $\sigma(E_i \rightarrow E_j)$.
2. Temperature, kT(ev).
3. Values of N_α, N_H, and σ_s.
4. Convergence criterion.
5. Initial guess for the flux spectrum, if not to be computed from Maxwellian.

Output Available

1. All input information is printed.
2. Convergence tests.
3. Flux per unit energy.
4. Flux times energy.

Related Codes

A number of codes useful in preparing the input cross sections, $\sigma(E_i \rightarrow E_j)$, are described in Ref. 31.

SYZYGY

Description

SYZYGY[34] computes the energy and spatial distribution of the neutron flux in the vicinity of the juncture of two media of different temperatures. Three system geometries are treated:

1. An infinite plane separating media at temperatures T_1 and T_2.
2. An infinite slab at temperature T_1, embedded in an infinite medium at temperature T_2.
3. An infinite circular cylinder at temperature T_1, surrounded by an infinite medium at temperature T_2.

Using the non-absorbing heavy gas approximation with the P_1 approximation, a differential equation[35] is obtained for the flux as a function of energy and position which involves the characteristics of the media as parameters. The solution to this equation, or the flux, is represented by an infinite series. The SYZYGY code calculates the various terms in the given series and approximates the sum of the series.

Input Information Required

1. Energy structure (≤ 275 points).
2. System geometry.
3. Number of terms of the series to be included.
4. Normalization constant and initial values for the flux.
5. Option to provide output information on punched cards.
6. Option to print flux at selected intervals.
7. Mesh spacing within each region (≤ 25 points/region).
8. Temperature, diffusion coefficient, and $\xi\sigma_s$ for each region.

Output Available

The output is on two tapes and the on-line printer. One tape contains the flux spectra and 1/v detector reaction rates. The other tape contains intermediate quantities which make up the flux values. All input data are printed on-line.

TEMPEST

Description

The TEMPEST[36] code computes the neutron energy spectrum based upon the Wigner-Wilkins[28] light-moderator equation, the Wilkins[37] heavy-moderator equation, or the formula for the Maxwellian distribution.

In both Wigner-Wilkins and Wilkins approximations, the code solves a Riccati-type differential equation. The solution is then used to construct the neutron energy spectrum and neutron flux energy spectrum.

Macroscopic and microscopic cross section averages over the computed neutron flux spectra are also obtained.

Input Information Required

The energy-dependent data for various elements are available in a prepared library. This library is in both decimal and binary form. The total number of cross sections tabulated in the library must not exceed 5000. The number of elements must not exceed 300. There is a routine available which produces a TEMPEST library from a set of energy-dependent cross sections. With the use of the library, the input information is limited to:

1. List of elements to be used.
2. Type of calculation (3 options).
3. Cross sections to be spectrum averaged.
4. Energy interval, ($E_{max} \leq 2$ ev).
5. Buckling.
6. Temperature, °K.

Output Available

1. The library is printed, if desired.
2. All input is printed.
3. Table of E(ev); N(E) = neutron energy spectrum; ϕ(E), the neutron flux energy spectrum = $\sqrt{E}$ N(E); and Eϕ(E).
4. Total flux, average diffusion coefficient, average transport cross section, average macroscopic absorption and average ν times fission cross sections, the averages being with respect to ϕ(E).

TRAM

Description

TRAM[38] is a three-dimensional code for the determination of spatial and spectral variations in neutron populations below 100 ev in hydrogen-moderated assemblies.

The computations are carried out by a non-branching Monte Carlo method in which the principal random variables are realized by a random address technique.

The geometry considered consists of zones bounded by planes and/or elliptical (circular) cylinders (axis of cylinder parallel to z-axis). A material region comprises one or more zones. The bounding surface of a zone may be denoted as trapping, reflecting, or transmitting. The trapping of a particle at a surface is recorded in one of two registers which may represent absorptions and leakage, respectively.

Source neutrons are generated with a uniform distribution inside each material region, with region-dependent source rate. The source energy is stochastically determined by assuming that a particle of 100-ev incident energy has just been scattered by hydrogen. Five types of hydrogen scattering are used in various proportions in the 32 energy groups considered to provide a model for proton thermal motions and chemical binding. The 32-group structure of the code is fixed. This model

687863 O - 63 - 48

(it is reported) gives infinite medium spectra and diffusion lengths in agreement with experimental values.

All other elements are assumed to scatter isotropically in the laboratory system without energy change.

The program permits operation in a two-dimensional mode (i.e., all particles are generated with $z = 0$), a one-group mode, and choice of temperature for the Maxwellian distribution (68°F or 520°F).

Input Information Required

1. Microscopic scattering and absorption cross sections for the elements (≤ 12) used, and the composition of the materials (≤ 20) which are made up from these elements.
2. Definition of the bounding surfaces (≤ 50) for the zones, and specification of the type of boundary activity (the reflecting type of boundary activity applies to a circular cylinder only).
3. Source assignments for various regions.
4. Number of runs, output and operating options to be used, and necessary restart information.

Output Available

Except in the tracing mode when each complete particle history is obtained, the following information is printed after each run:

1. Problem and run identification.
2. Number of histories generated.
3. Number of particles annihilated.
4. Number of particles in trap registers 1 and 2.
5. Number of random variables used.
6. Number of captures in each material.
7. Normalized total path lengths traversed.
8. Averages of accumulated path lengths, and capture rates.

The input is printed on the initial run of a problem. If specified, a statistical edit is printed after each 25 runs.

SUPPLEMENTARY INFORMATION

Code Name	Related Codes	Originating Installation	Machine Configuration	Running Time	References
COGENT		Combustion Engineering, Inc., Nuclear Division	IBM-704 with 16K core memory, 5 tape units, 1 drum unit.	40 min.	23. R. L. Ellis, R. B. Kellogg and B. J. McGovern, "COGENT-A One-Dimensional Multigroup Code for the Calculation of Neutron Space-Energy Distributions," TID-11026 (MPC-18), (July, 1960).
ROUTINE II		E. I. duPont de Nemours & Co., Savannah River Laboratory	IBM-650.	30 min.	24. J. C. English, "IBM-650 Routine II Neutron Energy Spectra in Water," DP-222, (July, 1957). 25. H. D. Brown and D. S. St. John, "Neutron Energy Spectrum in D_2O," DP-33, (February, 1954). 26. H. D. Brown, "Neutron Energy Spectra in Water," DP-64, (February, 1956).
SOFOCATE	 DONATE KATE-1	Westinghouse Electric Corp., Bettis Atomic Power Laboratory	IBM-704 with 8K core memory, 5 tape units IBM-650. Philco-2000.	0.5 min.	27. H. Amster and R. Suarez, "The Calculation of Thermal Constants Averaged over a Wigner-Wilkins Flux Spectrum: Description of the SOFOCATE Code," WAPD-TM-39, (January, 1957). 28. E. P. Wigner and J. E. Wilkins, Jr., "Effect of the Temperature of the Moderator on the Velocity Distribution of Neutrons with Numerical Calculations for H as Moderator," AECD-2275, (September, 1944). 29. H. Amster and R. Suarez, "Distribution of Neutrons at Thermal Energies: Description of DONATE Code," WAPD-PM-45, (May, 1956). 30. H. Amster and J. Callaghan, "KATE-1, A Program for Calculating Wigner-Wilkins and Maxwellian-Averaged Thermal Constants on the Philco-2000," WAPD-TM-232, (October, 1960).
SPECTRUM		General Dynamics Corp., General Atomics Division	IBM-704 with 32K core memory, 2 tape units (FORTRAN).	1–2 min.	31. D. H. Perkel, "A Family of Thermalization Codes," GAMD-754 (Rev.), AECD-4296, (July, 1959). 32. M. S. Nelkin, "A 704 Program for Computing Thermal Neutron Spectra in Infinite Homogeneous Media," AECU-4155, (November, 1958). 33. M. J. Poole, M. S. Nelkin and R. S. Stone, "The Measurement and Theory of Reactor Spectra," Progress in Nuclear Energy (New York: Pergamon Press, 1958), Series I: Physics and Mathematics, Vol. 2, p.96.

SUPPLEMENTARY INFORMATION (Continued)

Code Name	Related Codes	Originating Installation	Machine Configuration	Running Time	References
SYZYGY		General Electric Co., Hanford Atomic Products Operation	IBM-709 with 32K core memory, 2 tape units (FORTRAN).	3 min.	34. J. E. Schlosser, "SYZYGY, A Code for Calculating the Thermal Neutron Flux Spectrum Near a Temperature Discontinuity," HW-61042, (August, 1959). 35. Nuclear Physics Research Quarterly Report, HW-51983, (August, 1959), pp. 9-10.
TEMPEST		North American Aviation, Inc., Atomics International Division	IBM-709, 7090 (FORTRAN).		36. R. H. Shudde and J. Dyer, "TEMPEST, A Neutron Thermalization Code," NAA Program Description, Decks No. 3W-354, (September, 1960). 37. J. E. Wilkins, Jr., "Effect of the Temperature of the Moderator on the Velocity Distribution of Neutrons for a Heavy Moderator," CP-2481, (November, 1944).
TRAM		General Electric Co., Knolls Atomic Power Laboratory	IBM-704 with 32K core memory, 3 tape units. Philco-2000.	2 hr.	38. M. A. Martino and W. W. Stone, "TRAM, A Monte Carlo Thermal Neutron Code for the IBM-704," KAPL-2039, (June, 1959).

10.1.4 FLUX COMPUTATIONS, WEIGHTING, AND DISADVANTAGE FACTORS

Codes for the solution of the P_n approximation to the Boltzmann equation for various material configurations are described. These, and the other codes listed, obtain flux distributions which may be used to define "average" or "homogeneous" properties for complex configurations and/or to compute heavy absorber effects near or at the surface of a material discontinuity. Codes for the calculation of lattice parameters are included here also.

CEPTR

Description

The CEPTR[39] code solves numerically the equations for the P_3 approximation to the monoenergetic transport equation in cylindrical geometry.

Difference equations relating neighboring points are obtained from the P_3 differential equations by means of a truncated Taylor series at each point in a mesh.

The difference equations are solved by using starting values consistent with the boundary conditions at the outer boundary and working toward the origin. One particular solution and three homogeneous solutions are constructed. A linear combination of homogeneous solutions and the particular solution is made to satisfy the flux condition at the origin to a high degree of precision. The boundary condition at the origin is the zero gradient of the scalar flux. At the outer edge, one of three conditions may be specified: reflecting, vacuum, or zero gradient.

The external source is assumed to be isotropic; any region may be a void having zero cross sections.

Input Information Required

1. Total number of regions (≤ 10) of homogeneous material.
2. Total number of mesh intervals M, ($2 \leq M \leq 150$).
3. Designation of outer boundary condition (reflecting, vacuum, or zero gradient at edge of cell).
4. Source specification (pointwise or regionwise).
5. Mesh intervals and spacing in each region.
6. Total cross section for each region.
7. Scattering cross section angular components (4) for each region.

Output Available

1. Restatement of all input information.
2. Six directional flux components at every point, together with the radius, region number, and point number associated with the given point.
3. Average scalar flux for each region.
4. Sum of absorptions and leakage in each region.
5. Integrated sources for the individual regions.
6. Total integrated source, and absorptions plus leakage for all regions.
7. Error estimate checks.

FLIP

Description

The FLIP[40] code solves the one-velocity, one-dimensional transport equation with isotropic source for slab geometry in the P_L^{41} and double-P_L^{42} approximations. The results of the computation permit the determination of average parameters and replacement of multiregion systems by "equivalent" simpler systems.

Coupled systems of differential equations are obtained from expansions of the flux and scattering cross section in Legendre polynomials. These differential equations are solved by an iterative procedure. Convergence is achieved when, for all mesh points:

$$|\lambda_n^k - 1| < \epsilon$$

where $\lambda_n^k = \dfrac{k\textit{th} \text{ iterate of the scalar flux at the } n\textit{th} \text{ mesh point}}{(k-1)\textit{th} \text{ iterate of the scalar flux at } n\textit{th} \text{ mesh point}}$, ϵ being preassigned.

FLIP does P_3, P_5, P_7, double-P_1, double-P_2, and double-P_3 calculations. The two versions of the code, FLIP 1 and FLIP 2, differ in the options available for boundary conditions. In FLIP 1, either the directional flux or the current must vanish at each boundary. In FLIP 2, "gray" boundary conditions may be used, but only the double-P_1 approximation is available.

Input Information Required

FLIP 1:

1. Approximation type.
2. Number of regions (≤ 50).
3. Number of points (≤ 50).
4. Mesh spacing.
5. Fuel region designations.
6. Interface coordinates.
7. Boundary conditions (left, right, symmetric, non-symmetric).
8. Input type (regular or direct).
9. Output type (4 types).
10. Source type (regionwise or pointwise).
11. Convergence criterion.

Depending on the input type, cross sections or quantities derived from cross sections must be supplied. The regular input requires Σ_a and components of Σ_s consistent with the approximation selected; the code then computes the coefficients used in the differential equation. In the direct input, these coefficients are supplied by the user.

FLIP 2:

As in FLIP 1, except that the maximum number of regions is 25; the maximum number of points is 251; and the "gray" boundary condition coefficients must be specified.

Output Available

1. Restatement of input information.
2. Coefficients in the equations computed from the cross sections for each region and for each expansion index used in the approximation.
3. Converged fluxes for each point.
4. For each region, the integral of the scalar flux, and the integral of Σ_a weighted by the scalar flux.
5. Sums of the integrals in (4) over various regions.
6. Balance checks.

Related Codes

The SIMPL-1 and SIMPL-2 codes[43] solve the P_3 and double-P_1 equations in a similar fashion.

HOBO (RE 184)

Description

The HOBO[44] code does a fundamental mode calculation using either the asymptotic transport theory approximation, or the diffusion theory approximation for the buckling. In these calculations, Selengut-Goertzel slowing down may be included and adjoint fluxes may be calculated.

The necessary averaging of cross sections over the composition is also performed by the code and this portion of the code may be used independently of the succeeding calculations.

An iterative procedure is used. From an initial guessed value of the buckling, κ^2, multigroup fluxes are computed. Using these fluxes, the total source is computed and from this source a new value of κ^2 is determined. This process continues until the source equals unity within a prescribed convergence criterion.

Input Information Required

1. Volume fraction for each material z ($1 \leq z \leq 20$).
2. For each energy group j ($1 \leq j \leq 20$): the absorption cross section, transport cross section, ν times the fission cross section, elastic scattering cross section, and inelastic scattering cross sections from group k to group j ($k < j$), for each material.
3. Energy intervals defining the group structure.
4. Fraction of fission spectrum in each group.
5. Convergence criterion.
6. Buckling approximation form, and an initial guess of the buckling value.

Output Available

The converged values of κ or κ^2, scaled total source, and scaled flux for each group are punched. When adjoint fluxes are computed, they are punched in order of increasing energy, and the total source is replaced by a sum over the groups of the group adjoint flux times the group fission fraction.

I_2

Description

The I_2 program[45] treats the analytic solution of the P_3 approximation to the Boltzmann equation in cylindrical geometry.

Using the P_3 approximation and infinite cylindrical geometry, the transport equation is reduced to a set of coupled, second-order differential equations for the flux moments. The solutions to this set are linear combinations of Bessel functions. The conditions of continuity of all flux components at interfaces between regions, and the boundary condition of zero current at the outer edge, permit the determination of the coefficients in the solutions. For a sizable system of concentric annuli, a large system of simultaneous equations would have to be solved. (To avoid this large system of equations, a method due to Weil[46] is used. This method allows the reduction in the equation system size, and improves the accuracy.) Uniform isotropic sources are assumed, and at least one region must have a non-zero source. Zero absorption regions are not permitted.

Input Information Required

1. Problem parameters: identification, input and output options, number of regions N($3 \leq N \leq 50$), number of materials (≤ 10), and number of points at which flux and current are to be computed.

2. Material data: absorption cross section, scattering cross section, and diffusion coefficient, if scattering is isotropic; if scattering is anisotropic, the first three Legendre components of the scattering cross section.
3. Specification of the regional dimensions, material composition, and source.

Output Available

The three output options available are called short, intermediate, and long programs. The short program computes the average flux within a region, average non-moderator and moderator fluxes, a cell correction, and an absorption check. The intermediate program gives the short program information plus the total flux and radial current. The long program includes the intermediate program and produces higher flux moments and the total angular flux.

Related Codes

An IBM-650 version of this code is entitled P_3.[47]

IDIOT

Description

The IDIOT[48] code computes lattice parameters for a unit lattice cell. The fuel assemblies in the cell can be either a cluster of rods or a series of concentric cylinders.

A P_3 code[49] is used to compute the average thermal flux in a region. This flux is used in the subsequent calculations for the thermal utilization, f, and the lattice diffusion length, L_T^2. The P_3 part of the code may be used independently.

A combination of theoretical, semi-empirical, and empirical formulae is used to calculate: the Fermi age, τ; streaming correction to the diffusion length and age; first flight collision probabilities; fast effect, ϵ; η; effective resonance integrals, RI; resonance escape probability, p; Doppler coefficients for U^{238}; and age of resonance neutrons. These parameters are then used to calculate:

$$k_\infty = \eta f p \epsilon$$

for the lattice;

$$k_{eff} = k_\infty \exp(-\tau B^2)/(1 + B^2 L_T^2)$$

for a reactor of geometrical buckling, B^2; and the conversion ratio, C_0, for the reactor.

The IDIOT code also produces a set of average cross sections that have been flux- and volume-weighted over the unit lattice cell.

The limitations of the code are: a maximum of four uranium regions for concentric cylinder geometry; two rings of fuel rods in the case of cluster geometry; a neutron temperature of $\leq$1280°C in any fuel region; and a maximum of sixteen regions in the unit cell.

Input Information Required

The code contains a library of two-group data for a given set of fifteen materials. The nuclear data may be changed at the will of the user, but the atomic mass numbers assigned to the various materials must be kept the same. (Note: It is possible to use a heavy material with an atomic mass different from the specified value by adjusting the density of the material such that the "atoms/cc" will be computed correctly by the code.)

Other input information relates to the geometric description of the problem to be solved.

There are options whereby certain parts of the calculations may be omitted; for example, ϵ and p may be set equal to unity.

Output Available

Normal output consists of the following listings:

1. Input quantities.
2. Radius, average flux, thermal utilization, neutron temperature, volume fractions, atomic mass numbers, and cross sections for each region used in the P_3 subroutine, and a flux traverse.
3. Maxwellian-averaged cross sections, epithermal ratio, Westcott cross sections for each region; and the collision probability, inelastic collision probability, ratio of fast-to-thermal fissions, effective surface of fuel, mass of uranium, effective resonance integral, cell-averaged cross sections and diffusion coefficient, η, ϵ, f, p, L^2, τ, k_∞, k_{eff}, B^2, streaming corrections, migration area, and conversion ratio.

Additional information may be obtained which consists of volume and surface parts of the resonance integral, effective resonance integral, and special functions necessary to calculate the resonance escape probability.

RANCH

Description

The RANCH[50] program provides a numerical solution to the one-dimensional, one-velocity, neutron transport equation for slab geometry with anisotropic scattering. The source is assumed to be isotropic, but may vary with position.

The boundary conditions permitted are: two reflecting boundaries; one reflecting boundary and a specified incident vector flux at the other boundary; and incident vector flux specified at both boundaries.

Having assumed a form for the scattering kernel, $P(x,\mu,\mu')$, for scattering from direction $\cos^{-1}\mu'$ into direction $\cos^{-1}\mu$, the scattering integral is replaced by a double Gauss quadrature formula involving the vector flux, $F(x,\mu)$, at 2L angular directions in the range $-1 \leq \mu \leq 1$. Using the trapezoidal rule to integrate the resulting first-order differential equations in the space variable x, a set of difference equations is obtained for the vector flux, $F_{j,\lambda}$ at the points $x = x_j$, $\mu = \mu_\lambda$, where $j = 1,2,3,\ldots N$, and $\lambda = 1,2\ldots,2L$.

The set of difference equations is solved by an iterative process accelerated by an over-relaxation scheme.

Input Information Required

For each region (≤ 50):

1. Total and scattering cross sections.
2. Parameters to specify the scattering kernel.
3. Mesh size (constant within each region).
4. Source density (regionwise or pointwise).

Problem parameters:

1. Number of angles (2L) at which vector flux is to be calculated (2L = 4,6,8,10,12).
2. Over-relaxation parameter.
3. Convergence parameter.
4. Flux print option.
5. Option to change from Gaussian quadrature to formula supplied by problem requestor.
6. Boundary conditions.

Output Available

1. Edit of input information.
2. Scalar fluxes, vector fluxes, and integral of source over each region.
3. Integral of scalar flux times the absorption over each region.
4. Angular moments of the vector flux.

Related Codes

The HERD[51] programs use the same methods to solve the one-dimensional, one-velocity, neutron transport equation with isotropic scattering.

RDR 4

Description

The RDR 4[52,53] code solves the monoenergetic, one-dimensional, slab geometry, transport equation with anisotropic scattering and isotropic regional sources. Three choices of boundary conditions are available: two reflecting boundaries; two free boundaries; or one reflecting and one free boundary. The angular integration is carried out using one of the L = 8, 10, or 12 angular point, double Gauss quadrature formulas, corresponding to a P_7, P_9, or P_{11} computation, respectively.

Input Information Required

For each region (≤ 90):

1. Number of lattice points, including both endpoints, m.
2. Distance between lattice points, Δx.
3. Total macroscopic cross section in the region times lattice spacing, $\Delta x \Sigma_t$.
4. Ratio of macroscopic scattering (non-removal) cross section, to total cross section, Σ_s/Σ_t.
5. Ratio of total source in region, to total cross section, S/Σ_t.
6. Coefficients of P_1 and P_2 terms in the expansion of Σ_s in terms of Legendre polynomials P_n, a_1, and a_2.
7. Guess for average vector flux at left and right boundaries of region, F_L and F_R.

Output Available

1. Values of Σ_s/Σ_t, S/Σ_t, a_1, and a_2, from input.
2. Scalar flux, average scalar flux for each region and transformed space coordinates:

$$\bar{x} = \int_0^x \Sigma_t(y)dy$$

3. Angular flux.

ROUTINE V

Description

ROUTINE V[54] computes an analytic multigroup approximation to the Boltzmann equation for reactor cells with cylindrical symmetry.

Five energy groups are treated. The P_3 approximation is used in the lowest energy group, and the P_1 approximation is used in the four higher energy groups. Up-scattering is permitted only from the lowest energy group to the group immediately above it; down-scattering is allowed from every one of the higher energy groups to the group immediately below it.

The group structure is not fixed. Isotropic sources are assumed.

The five-group approximation and the method used to approximate the angular distribution in the various groups leads to a system of 14 differential equations. To facilitate the solution of these equations, the cross sections and sources are assumed constant in a given space interval (r_i, r_{i+1}). Using the usual continuity interface and cell boundary conditions, the solution of the system of equations is obtained as a sum of Bessel functions, and this form is used to calculate the fluxes.

Input Information Required

1. Region specification (2 regions).
2. Group structure (5 groups).
3. Macroscopic reaction cross sections for each group and region.
4. Sources.
5. Number of points per region.
6. Points at which total flux in a group is to be printed.

Output Available

1. Total flux for the group at every point specified in a region.
2. Integral of the flux over the region.
3. Average value of total flux in the region.
4. Total absorption (capture plus fission) for each group in the region.
5. Flux integrals over the cell for each group.
6. Cell absorptions per group.
7. Thermal utilization.
8. Total neutron production.

SLOP-1

Description

SLOP-1[55] is a one-dimensional, thermal, multigroup program for the computation of the thermal flux level and energy spectrum as a function of position in a heterogeneous array of diffusing media.

The particular version of the program discussed here contains: (1) a P_1 and double-P_1 treatment of slab problems; and (2) a P_1 approximation for cylinders and spheres.

The major limitations of SLOP-1 are: (1) isotropic slowing down into the thermal group; (2) regionwise constant slowing down; (3) no transverse buckling; and (4) one moderating material in any problem. All regions must be at the same temperature.

The transfer matrices in all SLOP-1 libraries are limited to hydrogen moderation. However, with transfer matrices properly chosen, the program could be used to treat any mixture of which one moderating component is much lighter than all others.

A set of difference equations representing the double-P_1 approximation is obtained by integrating over a given energy structure, and using a three-point, central difference formula to account for spatial variations. The P_1 approximation is represented by a special case of these equations.

Three modes of operation (Gears) are available, and are controlled through input specification. Gear One is used for P_1 calculations. For a given set of starting values and boundary conditions, the flux, F_{0n}^m, and the current, F_{in}^m, are computed for all spatial mesh points, n, at each energy mesh point, m. Convergence is achieved when, for all spatial mesh points:

$$|1 - \epsilon_1| < (I_n^t / I_n^{t-1}) < |1 + \epsilon_1|$$

where I_n^t = absorption rate after t sweeps of the energy mesh points; and
ϵ_1 = specified convergence parameter.

Gear Two computes F_{0n}^m, F_{1n}^m, and the higher moments of the flux: F_{2n}^m, F_{3n}^m. An additional iteration occurs at each energy mesh point m before proceeding to the next energy, m + 1, with the same procedure as in Gear One. Convergence criterion is the same as in Gear One except that the parameter ϵ_2 is used.

Gear Three is used for double-P_1 calculations and solves for the same quantities as Gear Two. Iterations are performed for each energy until

$$\left|1 - \max_n, \min_n (F_{0n}^{\ell} / F_{0n}^{\ell-1})\right| < \delta$$

where ℓ is the energy iteration index, and δ is the specified convergence parameter. Finally, Gear One-type convergence, with a convergence parameter ϵ_3 must be satisfied.

Extrapolation procedures are available in all Gears. With proper specification, computation may be started in any Gear, and any Gear may be skipped.

The P_1 calculations employ boundary conditions of the type:

$$F_1^m = C_0^m \; F_0^m$$

where C_0^m is an input number.

Blackness theory boundary conditions may be used in the double-P_1 calculations. In this event, eight constants are specified for each energy m.

Various average quantities and few-group constants may be obtained from the computed distributions.

Input Information Required

Problem parameters and controls:

1. Total number of energy points (≤ 50).
2. Number of space points, N, excluding the origin ($2 \leq N \leq 250$ for P_1; $2 \leq N \leq 150$ for double-P_1).
3. Number of regions (≤ 25), and geometry (slab, cylinder, sphere).
4. Temperature of all regions.
5. Parameters for Gear control and convergence.
6. Parameter specifying data library to be used.
7. Boundary condition constants. A provision in the code allows one set of eight constants to serve for all the M energies.
8. Parameter designating output edit.
9. Breakpoints to specify few-group or multigroup structure.

Region Parameters:

1. Definition of regions in terms of spatial mesh point numbers.
2. Mesh size.
3. Total number of isotopes (≤ 15).
4. Source distribution.
5. Region composition.
6. Flux guess (may be specified pointwise, or taken from previous problem).

Output Available

On-line output consists of an edit of the input data and an indication of convergence after each energy mesh traverse.

Three general classes of final information edit are available for off-line printing: (1) one-group edits; (2) few-group edits; and (3) multigroup edits. The information to be printed by each class is optional and may include any or all of the following: the flux, the second moment of the angular flux, the current, the third moment of the angular flux, cross section averages, average diffusion coefficients, and few-group scattering matrices.

Related Codes

The ECESS[56] program is used to compute the hydrogen scattering matrices used as input data for SLOP-1. ECESS calculates from the transport equation P_0 through P_3 transfer matrices, using the thermal energy monatomic gas model, with parameters of temperature, t, and the ratio of atomic mass to neutron mass, M/m.

TUT-T5

Description

TUT-T5[57,58] is a Monte Carlo code that calculates, for a one-energy model, a regionwise distribution of neutron capture probabilities in a two-dimensional, rectangular cell. The results of the calculation may be used to determine capture ratios for materials (thermal utilization), in a lattice where diffusion theory approximations may not be sufficiently accurate.

The mathematical model is the monokinetic Boltzmann equation with a region-dependent source; hydrogen scattering is assumed linear in the cosine of the scattering angle; and scattering of other elements is assumed isotropic.

The solution, or the code, is based on a Monte Carlo method in which random particle life histories are simulated using pseudo-random numbers, and the integrals defining the capture probabilities are estimated by averages of weighting functions (random variables) associated with the histories.

The random variable used in TUT-T5, sums the distance traveled by the neutrons in the various regions. These sums are used to estimate the integral of the flux over the given region. Multiplication by appropriate capture cross sections gives the capture probabilities.

The geometric configuration considered consists of an infinite lattice of rectangular cells in the x-y plane. Each of these cells is divided into four quarter-cells. Calculations are then done on each quarter-cell which may contain as many as 32 subrectangles considered as a separate region. Material compositions may be defined over any collection of these subregions.

Input Information Required

1. Coordinates of the quarter-cells.
2. For each region (≤32): dimensions, boundary conditions at each edge, source, and composition identification.
3. Cross sections for each composition (number of compositions ≤ number of regions).

Output Available

1. For each experiment consisting of ≤1000 histories, estimates of capture probabilities for each composition.
2. The mean capture probability for all experiments and associated statistical data and deviations.

Related Codes

NYU TUT-704[59] is a related Monte Carlo code.

TRAC-1,[60] programmed for the Philco-2000 machine, computes for each composition: (1) the epithermal capture probabilities integrated over the entire epithermal energy spectrum; and (2) thermal capture probabilities, if desired. In addition, improvements have been incorporated such that when the equivalent TUT-T5 problem is run with the TRAC-1 code, the running time is reduced.

SUPPLEMENTARY INFORMATION

Code Name	Related Codes	Originating Installation	Machine Configuration	Running Time	References
CEPTR		Combustion Engineering, Inc., Nuclear Division	IBM-704 with 32K core memory, 2 tape units.	1–2 min.	39. P. B. Daitch, B. J. McGovern and M. Schilder, "CEPTR–An IBM-704 Code to Solve the P_3 Approximation to the One-Velocity Transport Equation in Cylindrical Geometry," MPC-20, (September, 1959).
FLIP	FLIP 1 FLIP 2 SIMPL-1 SIMPL-2	Westinghouse Electric Corp., Bettis Atomic Power Laboratory	IBM-704 with 32K core memory, 1 tape unit. IBM-704.	10 min.	40. B. L. Anderson, et al., "FLIP–An IBM-704 Code to Solve the P_2 and Double-P_2 Equations in Slab Geometry," WAPD-TM-134, (March, 1959). 41. "Reactor Physics Constants," ANL-5800, (1st ed.), p. 150. 42. Ibid, p. 324. 43. L. M. Culpepper, et al., "The IBM-704 SIMPL Codes," WAPD-TM-107, (January, 1958).
HOBO (RE 184)		Argonne National Laboratory	IBM-650; IBM-704	3–5 min; 3–5 sec.	44. AMD Program Library File RE 184; RE 247.
I_2	 P_3	General Electric Co., Aircraft Nuclear Propulsion Department General Electric Co., Vallecitos Atomic Power Laboratory	IBM-704 with 8K core memory, 1 tape unit. IBM-650.	20 sec. 10 min.	45. R. R. McCready and D. B. Vollenweider, "An IBM-704 Program for the Solution of the Neutron Transport Equation in Fifty Concentric Cylindrical Annuli by the Weil Method, Program I_2," APEX-468, (September, 1959). 46. J. W. Weil, "Neutron Flux Distribution Calculations Using the P_3 Spherical Harmonics Method," KAPL-1173, (July, 1954). 47. IBM-650 Library Program 8.2.014.
IDIOT		General Electric Co., Hanford Atomic Power Laboratory	IBM-709 (FORTRAN).	1–2 min.	48. C. R. Richey, "IDIOT–A Lattice Parameter Code for the IBM-709," HW-63411, (January, 1960). 49. D. D. Matsumoto and C. R. Richey, "Program on the 709 Digital Computer of the P_3 Approximation to the Boltzmann Equation in Cylindrical Geometry," HW-60781, (June, 1959).
RANCH		Westinghouse Electric Corp., Bettis Atomic Power Laboratory	IBM-704 with 32K core memory, 1 tape unit.	3 min.	50. L. A. Hageman and J. T. Mandel, "RANCH, An IBM-704 Program Used to Solve the One-Dimensional, Single Energy Neutron

	HERD		IBM-704 with 16K core memory.	0.5–5 min.	Transport Equation with Anisotropic Scattering," WAPD-TM-268, (February, 1961). 51. L. A. Hageman, "HERD-1,2 and 3–IBM-704 Codes Used to Solve the One-Dimensional, One-Velocity Transport Equation with Isotropic Scattering," WAPD-TM-162, (January, 1959).
RDR 4		U. S. Navy Department, David W. Taylor Model Basin	NORC.		52. C. W. Dawson and E. H. Bareiss, "RDR 4 Instruction Manual, David W. Taylor Model Basis One-Dimensional, One-Group Transport Theory Routine No. 4 for Nuclear Reactor Design," David W. Taylor Model Basin Report 1100, (December, 1956). 53. E. H. Bareiss, "Flexible Transport Theory Routines for Nuclear Reactor Design," David W. Taylor Model Basin Report 1030, (December, 1956).
ROUTINE V		E. I. duPont deNemours & Co., Savannah River Laboratory	IBM-650 with floating point hardware.	20 min.	54. R. R. Haefner, "IBM-650 Routine V, A Multigroup P_3 Program for the Neutron Transport Equation," DP-427, (October, 1959).
SLOP-1	ECESS	Westinghouse Electric Corp., Bettis Atomic Power Laboratory	IBM-704 with 16K core memory, 9 tape units. IBM-704 with 8K core memory, 3 tape units.		55. H. Bohl, et al., "SLOP-1 A Thermal Multigroup Program for the IBM-704," WAPD-TM-188, (October, 1960). 56. W. W. Clendenin and G. R. Culpepper, "ECESS An IBM-704 Program Computing Transport Equation Coefficients for Monatomic Gas Moderator in the Thermal Energy Region," WAPD-TM-200, (April, 1960).
TUT-T5		Westinghouse Electric Corp., Bettis Atomic Power Laboratory	IBM-704 with 32K core memory, 2 tape units.	1–2 hr.	57. J. Spanier, H. Kuehn and W. Guilinger, "TUT-T5, A Two-Dimensional Monte Carlo Calculation of Capture Probabilities for the IBM-704," WAPD-TM-125, (November, 1959). 58. J. Spanier, "The Physics and Mathematical Analysis for the TUT-T5 Monte Carlo Code," WAPD-TM-186, (January, 1960).
	NYU TUT-704	New York University.	IBM-704, UNIVAC 1.		59. A Rotenberg, A. Lapidus and R. Richtmyer, "A Monte Carlo Calculation of Thermal Utilization," NYO-7976, (January, 1958).
	TRAC-1	Westinghouse Electric Corp., Bettis Atomic Power Laboratory	Philco-2000 with 4 tape units.	20–40 min.	60. H. J. Berwind and J. Spanier, "TRAC-1, A Monte Carlo Philco-2000 Program for the Calculation of Neutron Capture Probabilities," WAPD-TM-229, (March, 1961).

10.2 CRITICALITY SEARCH AND REACTIVITY CALCULATIONS

The majority of the codes in this section solve the multigroup set of diffusion equations:

$$D^j \nabla^2 \phi^j - \Sigma^j \phi^j + S^j = 0$$

where j represents the energy group, (j = 1,2 ... J, with J the thermal group)

D^j = diffusion coefficient
ϕ^j = neutron flux
Σ^j = cross section representing total removal
S^j = total source

The codes differ primarily in their definition of Σ and S, the methods of solution, boundary conditions available, the scope of problem parameters allowed, and the parameters that are varied to achieve criticality.

Other definitions which can be more appropriately included here are:

B_j^2 = transverse buckling
Σ_a^j = absorption cross section = $\Sigma_c^j + \Sigma_f^j$
Σ_t = total cross section
$\Sigma_s^{j\to k}$ = cross section for scattering from group j into group k
χ^j = fraction of fission neutrons born in group j
Σ_f^j = fission cross section
ν = average number of neutrons emitted per fission
ξ = lethargy gain per collision

10.2.1 ONE-DIMENSIONAL GEOMETRIES

AIM-5

Description

In this diffusion theory code:[61]

$$\Sigma^j \equiv D^j B_j^2 + \Sigma_a^j + t_j \Sigma_p + \sum_{k=j+1}^{\underline{M}} \Sigma_s^{j\to k}$$

where $t_j\Sigma_p$ = distributed poison cross section in group j
$\underline{M}$ = minimum (J, j plus the number of groups into which down-scattering is allowed)

$$S^j \equiv \chi^j \sum_{k=1}^{J} \frac{(\nu\Sigma_f)^k \phi^k}{\lambda} + \sum_{k=\overline{M}}^{j-1} \Sigma_s^{k\to j} \phi^k$$

where $\overline{M}$ = maximum (1, j minus the number of groups into which down-scattering is allowed)
λ = the eigenvalue.

The finite difference equations and the method of solution are the same as those in the WANDA[91] programs.

At the external boundaries, the conditions available are:

(1) $\phi^j = 0$;

(2) $\frac{d\phi^j}{dr} = 0$;

(3) $\phi^j + \frac{\omega^j d\phi^j}{dr} = 0$; and

(4) $\phi^j = \omega_3^j$.

If condition (4) is used and unless all ω_3^j are zero, a "one iteration" problem is indicated.

The two convergence criteria defined in the WANDA description are applicable here also, as is the linear extrapolation of the source term. In AIM-5 however, it is assumed that the extrapolation factor $\theta_i = 0$ for the first two iterations, (i = 1,2), and it is possible to specify one value of θ that is used for $i \geq 3$, or to specify a sequence of 20 values to be used. The code value of $\theta = 0.8$ may be used, if desired.

Five different types of criticality search may be made:

(1) Buckling (in particular regions or over the entire reactor).
(2) Homogeneous poison (in particular regions or over the entire reactor).
(3) Dimension (in particular regions or over the entire reactor, Δr constant).
(4) Position of a poison boundary.
(5) Position of a fuel boundary.

Types (4) and (5) are searches for the position of an interface between two regions, both having the same value for Δr. In all cases, the search is made for an eigenvalue of unity. If another value is desired, it must be indicated in the input. A maximum number of iterations or fulfillment of the convergence requirement, $|1 - \lambda| \leq \epsilon_2$, will terminate the criticality search.

Input Information Required

Problem parameters:

1. Geometry (slab, cylinder, or sphere).
2. Boundary conditions.
3. Convergence criteria, ϵ_1 and ϵ_2.
4. Source extrapolation factor or factors.
5. Output print options (eigenvalue only, or fluxes and eigenvalue; every point or every other point, specified groups only, normalized or not).
6. Source guess option (by region, by point, or from previous problem).
7. Buckling (by region or over entire reactor, group dependent or not).
8. Input print option.
9. Checks desired (yes, no, or compute peak-to-average ratios).
10. Number of regions (≤20).
11. Number of points (≤239).
12. Number of lethargy groups (≤12).
13. Number of groups into which down-scattering is allowed (≤11).
14. Flux normalization options (specified point, maximum flux, or no normalization).
15. Adjoint flux options (real and adjoint, adjoint only, adjoint not required, punch cards or not).
16. Criticality search options (type of search, control regions, maximum number of iterations in a search, eigenvalue desired if other than unity).
17. Maximum number of iterations in the flux calculations.
18. S_n restart dump option and associated S_n parameters.
19. Value of radius at the origin, region identification, and the mesh size, Δr, for each region.

Material properties:

1. Values of D, Σ_a, $\nu\Sigma_f$, $\Sigma_s^{k\to j}$ for each material or each region and each energy group.
2. Poison cross section, Σ_p, for each region.
3. Fission spectrum χ^j, j = 1,2 ... J.
4. Poison fractions t_j, j = 1,2 ... J.

A library of cross section data for up to 20 materials may be loaded initially, and materials selected as needed for subsequent problems. A material number must be specified for each region.

If a given case is specified and the following problem has input data in common, this common information need not be specified. In addition, the source computed for one problem may be used as a source guess for the next problem.

Output Available

In all cases, the input options chosen are printed. Optionally, a complete listing of the input data is provided.

In all cases, the eigenvalue is printed and a listing of the normalized sources and fluxes may be obtained if requested; the fluxes obtained are either for all groups or for specified groups, and either for all points or at every other point.

687863 O - 63 - 49

An additional option provides average regional source values, regional volumes, flux integrals, and leakage and removal for each region and each group. The peak-to-average flux ratio for each fuel region, or over the entire reactor in the thermal group, may be requested also.

Related Codes

If an adjoint flux is requested, cards may be punched for later use as input data for the perturbation code PERT.[62] Cards are punched also as input data for the SNG code if a later S_n program run is requested.

DMM

Description

In the DMM[63,64] diffusion theory code, Σ^j is an input quantity, and

$$S^j \equiv \chi^j \frac{P}{K} + \sum_{k=1}^{j-1} T^{k\to j}\,\phi^k$$

where

$$P = \sum_{j=1}^{J} F^j\,\phi^j$$

$T^{k\to j}$ and F^j are input quantities representing the general $\Sigma_s^{k\to j}$ and $\nu\Sigma_f^j$, respectively; and K is the normalization factor defined to satisfy the condition:

$$\int_0^R P(r)dv = \text{volume of reactor}$$

The boundary conditions available are of the form:

$$(1 - B^j)\, D_b^j\, (\phi')^j = [(1 - B^j)\, D_b^j + B^j\, (|r_b - r'|)]\, \phi_b$$

where the primed quantities refer to values at the first interior point, and the subscript b refers to the boundary point values; B^j are input quantities.

Given a preliminary set of point values for either P_n or ϕ_n^j, the group equations are solved in turn for j = 1,2 ... J, and a value of K and a new set of P_n values are obtained. To accelerate convergence, $\tilde{P}_n$ values are used in place of P_n where

$$\tilde{P}_n^i = P_n^i + \omega(P_n^i - P_n^{i-1})$$

with ω specified as input data; i is the iteration index.

The convergence criterion employed is:

$$|K_i - K_{i-1}| \le \epsilon$$

where ϵ is an input parameter.

Input Information Required

Problem parameters:

1. Problem identification number.
2. Number of energy groups J, regions L, and mesh points N, to be used, $\{3N + 2L + J\,[4 + N + (L/2)\,(J + 5)] \le 1601\}$.
3. Geometry (slab, cylinder, or sphere).
4. Acceleration variable, ω.
5. Convergence criterion, ϵ.
6. Region definitions (i.e., number of points and interface designation). The mesh spacing is constant within a region.

7. Boundary condition parameters, B^j, for each boundary, for each group.
8. Initial guess for the flux, ϕ_n^j, if desired.

Material properties for each region:
1. Values of $\nu\Sigma_f$, D, Σ, and $\Sigma_s^{k\to j}$ (k = 1,2, ... j – 1), for each group.
2. Fission spectrum χ^j, j = 1,2, ... J.

Output Available

A card is punched after the second and each succeeding iteration, giving the problem number and values of K^i, K^{i-1}, and $(K^i - K^{i-1})$. After convergence is achieved, the fluxes, ϕ_n^j, may be punched with proper identification. The console setting may be used at any time to initiate a stop at the end of the current iteration, with the option of punching the flux values of that iteration.

Related Codes

MCC[65,66] is an amended version of the DMM program, with an improved treatment of regional boundaries.

DSN

Description

The DSN[67–69] code solves the neutron transport equation, using an angular segmentation method.

This code will solve the stationary (time-independent) problems restricted to the one-dimensional geometries and the special time-dependent case to be described later. It limits itself to the use of discrete neutron energy groups and isotropic emission. A form of linear anisotropic neutron scattering is available.

The neutron flux, $\phi^j(r)$, and the current, $J^j(r)$, are defined in terms of the angular neutron flux,

$$\phi^j(r,\mu),\ (-1 \le \mu \le 1)$$

as

$$\phi^j(r) = \frac{1}{2}\int \phi^j(r,\mu)\, d\mu$$

and

$$J^j(r) = \frac{1}{2}\int \mu\, \phi^j(r,\mu)\, d\mu$$

where μ is the direction cosine with respect to the positive r direction. The flux and current are then functions of position and energy group alone.

If the time-dependent case $\phi^j(r,\mu,t)$ can be approximated by $\phi^j(r,\mu)\exp(\alpha t)$, the time-dependent equations may be reduced to the time-independent equations with Σ_{tr}^j replaced by $\Sigma_{tr}^j + (\alpha/v^j)$, where α now is the eigenvalue, and v^j the energy group velocity.

In the DSN equations, the source S^j may be written:

$$S^j \equiv Q^j + \chi^j \sum_{k=1}^{J} \nu\Sigma_f^k\, \phi^k + \sum_{k=1}^{J} \Sigma_s^{k\to j}\, \phi^k$$

where Q^j is a specified independent source and may or may not be present denoting the inhomogeneous or homogeneous problem.

Typical homogeneous problems that can be solved are:
(1) Critical dimension problems in which some dimension is varied until a stationary solution is found.
(2) Critical concentration problems in which the proportion of a particular material is varied.
(3) Reactivity problems in which ν is divided by k, and k is varied.

The boundary condition at r = 0 is assumed always perfectly reflective for the cylindrical and spherical problems. For the plane cases, there are two other options: $\phi^j(0,\mu^{in}) = 0$, the free boundary condition; and $\phi^j(0,\mu^{in}) = \phi^j(R,\mu^{out})$, the periodic boundary condition. The outer boundary condition may be zero inward flow, perfect reflection, or slab periodicity.

In the DSN code, the μ-interval (−1,1) is divided into n segments (n even) of equal length 2/n. An average value of the angular flux, $\phi^j(r,\bar{\mu})$ is defined for each μ-interval. The $\bar{\mu}$, and the weight associated with each $\bar{\mu}$, have been determined to satisfy neutron conservation and the diffusion theory condition for the second angular moment of the flux.

The DSN equations are solved by an iterative procedure on the source term. The iteration starts with an initial trial source function, and a guess for the eigenvalue, if any. Starting with a selected energy group, each group flux in turn is computed. The number of iterations required per group is determined by the accuracy achieved. An input parameter, ϵ, specifies the accuracy desired in each group for a fixed eigenvalue. Before the procedure is repeated for all groups, an improved estimate for the eigenvalue, if any, is obtained usually by an empirical formula based on the neutron balance in the system. The iterative procedure is terminated when the specified accuracy, ϵ, is achieved in fewer than three runs through the groups with a new eigenvalue.

The code is written in the FLOCO-II language developed at Los Alamos for use on the IBM-704. It is a symbolic "load and go" system, including specialized program and data input-output facilities.

Input Information Required

Problem parameters:

1. Problem identification.
2. Problem type (real or adjoint, reactivity, time dependent, concentration, or dimension).
3. Geometry (slab, cylinder, or sphere).
4. Boundary conditions.
5. Initial source guess.
6. Order of the S_n approximation.
7. Number of regions.
8. Number of mesh intervals.
9. First and second guess for the eigenvalue.
10. Convergence criterion, ϵ.
11. Number of energy groups, and specification of a base group.
12. Indices to specify the cross section matrix.
13. Material composition throughout the reactor.
14. Options and specifications for Q.
15. Specification of a fixed k or α, if desired.

Material properties:

1. Values of $\nu\Sigma_f$, Σ_{tr}, and $\Sigma_s^{k\to j}$ for each material and each energy group.
2. Fission spectrum χ^j, j = 1,2 ... J.
3. Velocities v^j, j = 1,2 ... J, if an α calculation is desired.
4. Concentration or dimension modifiers if a concentration or dimension problem is desired.
5. Second transfer matrix, $\Sigma_{sst}^{k\to j}$, if linear anisotropic scattering is to be included.

Output Available

After each iteration, an on-line monitor prints:

1. Outer iteration count.
2. Inner iteration count.
3. ϵ^i.
4. Eigenvalue.
5. Derivative of eigenvalue with respect to λ (λ is defined as the total neutron population decay factor).
6. Neutron balance.
7. λ^i.

Similar group monitor lines may be printed on-line, if desired.

The final print lists:
1. Input information.
2. Storage map.
3. All iteration monitor lines.
4. Source at r = 0, and r = R.
5. Effective cross sections.
6. At each mesh point: the mid-point of the mesh interval, fission density, volume element, and neutron flux associated with that interval.
7. A reaction summary print.

Related Codes

The SNG and SNK codes are predecessors of the DSN code at Los Alamos. A version of the SNG code has been written for the Mercury machine at Harwell.[70]

PROGRAM S-VII[71] is similar to DSN. It uses a variational formulation, and includes simultaneous calculation of real and adjoint flux, both isotropic and anisotropic transfer, and first-order perturbation computations.

The CELCOR[72] program uses the S_n method for S_2 through S_{16} cell correction calculations in any of the three standard geometries. It also provides a restricted form for cell correction calculations in two-dimensional, slab geometry.

F2

Description

The F2 code is a two-group, neutron diffusion program,[73] with alternatives including the solution of the adjoint equations or the one-group equation.

For group 1:

$$\Sigma^1 \equiv D^1 B_1^2 + \Sigma_a^1 + \Sigma_s^{1\to 2};\ S^1 \equiv \frac{\chi^1}{k} \sum_{j=1}^{2} \nu \Sigma_f^j \phi^j + \bar{S}^1$$

For group 2:

$$\Sigma^2 \equiv D^2 B_2^2 + \Sigma_a^2;\ S^2 \equiv \frac{\chi^2}{k} \sum_{j=1}^{2} \nu \Sigma_f^j \phi^j + \Sigma_s^{1\to 2} + \bar{S}^2$$

where $\bar{S}^1$ and $\bar{S}^2$ are the external source terms for the groups, and k is the eigenvalue.

At the inner and outer boundaries, an albedo boundary relating the current-in to the current-out is imposed:

$$A_{\substack{\text{in}\\\text{out}}}^j = [\phi^j \mp 2D^j(d\phi^j/dr)]/[\phi^j \pm 2D^j(d\phi^j/dr)]$$

Continuity of flux and current is assumed at internal interfaces.

Four convergence tests are incorporated in the code:

(1) Mean square:

$$\sum_n \{r_n^\mu [(F_n^+)^i - (F_n^+)^{i-1}]^2 + r_{n+1}^\mu [(F_{n+1}^-)^i - (F_{n+1}^-)^{i-1}]^2\} \frac{\Delta r}{2} < \epsilon$$

(2) Maximum difference:

$$|(F_n^\pm)^i - (F_n^\pm)^{i-1}| < \epsilon \text{ for all n}$$

(3) Reactivity:

$$\left|1 - \frac{k^i}{k^{i-1}}\right| < \epsilon$$

(4) Maximum number of iterations: i = I

where F represents the fission density (the + and – superscripts indicate right and left, respectively); i is the iteration number; n, the point index; μ, an integer designating geometry; and ϵ, an input parameter.

Any one of tests (1), (2), and (3) must be satisfied or the maximum number of iterations, test (4), will terminate the problem.

Input Information Required

The F2 code was designed for parameter studies. Accordingly, the input for each problem need only include changes in data from those used in the preceding problem.

Problem parameters:

1. Problem identification.
2. Number of regions ($\leq$50).
3. Type of problem (two-group real, two-group adjoint, one-group).
4. Geometry μ (slab, cylinder, sphere).
5. Buckling options (calculate B_j^2 with or without extrapolation distance, B_j^2 an input parameter for problem or for each region).
6. Boundary condition options [$(d\phi/dr)|_{r=0} = 0$ for cylinder and sphere; $\phi(0) = 0$ for slab, and $\phi(R) = 0$ for all cases; specified albedos; specified flux ratios].
7. Boundary crossing options (extra mesh points at each interface, extra mesh points at outer boundaries, no extra points).
8. External source option (no external source, external source specified for each region or each point).
9. Convergence tests to be exercised.
10. Normalization factor for fluxes (average over core of fast flux, fast flux at specified point, average over specified material of slow flux).
11. Output option to include flux photograph.
12. Perpendicular dimensions and reflector savings.
13. Properties of regions: interfaces, number of intervals (sum $\leq$ 100), material designation ($\leq$50), and group buckling factors.

Material properties:

1. Material identification and its two-group constants: D^1, D^2, Σ_a^1, Σ_a^2, $\nu\Sigma_f^1$, $\nu\Sigma_f^2$, $\Sigma_s^{1\to2}$.
2. The source spectrum for each material and each group: $\bar{S}^1$, $\bar{S}^2$. If both $\bar{S}^1$ and $\bar{S}^2$ are zero for all regions, $\bar{S}^1$ is replaced by 1.

Output Available

For each problem, a print-out of:

1. Input data.
2. Eigenvalue for each iteration.
3. Radius, converged fluxes, and fission density at each point.
4. Material or region volumes, and average fluxes for each region and each energy.

In addition, if a group of problems is done consecutively, a group summary print-out is made listing the problem identification, eigenvalue, fission density, and perpendicular dimensions of each.

Related Codes

The F2, C_2,[74] and I_2 (Section 10.1.4) programs, have been incorporated into a general reactor analysis code, GEORGE,[75] for processing reactor design problems.

The C_2 code computes the reactivity of a bare, homogeneous, cylindrical reactor, assuming energy loss by isotropic elastic scattering. Slowing-down densities are computed using either modified age theory or Coveyou-Macauley theory, and Maxwell-averaged cross sections in the thermal group are obtained from a tape library[76] as a function of temperature. The flux at the nineteen levels plus the thermal group is used to compute two-group constants for the F2 code. The I_2 program may be used to calculate thermal disadvantage factors for C_2.

The GEORGE program uses an iterative loop between the C_2 composition calculation, and F2 radial and longitudinal calculations, to find consistent reflector savings.

FIRE

Description

FIRE is a one-dimensional, diffusion theory program[77,78] that provides for inelastic scattering and for hydrogen and continuous slowing down. In this program:

$$\Sigma^j \equiv \Sigma_a^j + \sum_{\substack{k=1 \\ k\neq j}}^{j} b^{j\to k}\,\Sigma_s^j$$

where

$b^{j\to k}$ = transfer coefficient

and

$$S^j \equiv q_1^j - q_2^j + H_1^j - H_2^j + I^j + \nu\chi^j S$$

where q represents the continuous slowing-down source

$q_2^j = \xi\Sigma_{t2}^j\ \phi_2^j$ at the upper end, u_2, of each lethargy group

H = hydrogen source

$H_2^j = e^{-u_2}\sum_{k=j}^{J} m^k\ \Sigma_{SH}^k\ \overline{\phi}^k$

$H_1^j = e^{-u_1}\sum_{k=j+1}^{J} m^k\ \Sigma_{SH}^k\ \overline{\phi}^k$

with

$$m^j = \int_{u_1}^{u_2} e^u\,du$$

and I = source due to inelastic scattering

$$I^j = \sum_{\substack{k=1 \\ k\neq j}}^{J} a^{k\to j}\,\Sigma_s^k\ \overline{\phi}^k$$

where $a^{k\to j}$ = transfer coefficient from k to j

$S = \int_u \Sigma_f\,\phi(u)\,du$

ν = the eigenvalue

Continuity of flux and current is assumed at all interfaces. The boundary conditions for cylinder and sphere are zero current at r = 0, and zero flux at the extrapolated outer boundary (energy-dependent). For the slab, two options are available for the flux at the inner boundary: the flux is zero, or the current is zero; the zero flux (energy-dependent) condition is used at the extrapolated outer boundary.

The program tests for convergence as follows:

$$|S_n^i - S_n^{i-1}| < \epsilon, \text{ for all n}$$

and

$$|\nu^i - \nu^{i-1}| < \epsilon$$

where ϵ is specified as input; n is the point; and i is the iteration index.

A variable geometric buckling approximation procedure for bare reactors has been added to the original FIRE code.

Input Information Required

Problem parameters:

1. Number of space points (≤180).
2. Number of regions (≤12 for ≤40 groups; ≤24 for ≤20 groups).

3. Number of elements (≤200).
4. Number of lethargy groups (≤40).
5. Geometry (slab, cylinder, sphere).
6. Hydrogen identification and indicator (if non-standard).
7. Punch option (if cards are to be punched for subsequent use).
8. Regional properties (boundaries, point spacing, elements and concentrations of each present). A variable mesh size may be used.

Material properties specified on the microscopic library tape:

1. Tape identification.
2. Lethargy widths u^j; hydrogen scattering probabilities, σ_{SH}^j; and the neutron fission spectrum fractions, χ^j; for each group.
3. Identification of the elements, and microscopic cross sections: $\xi\sigma_t$, σ_a, σ_{tr}, σ_f, $\sigma_s^{j\to k}$, for each group, and for each element. The cross section input is in the same form as that required by the DSN code (Section 10.2.1).

Output Available

1. Final fluxes.
2. Power distribution.

GNU II

Description

This program[79,80] is incorporated into the MAGNUM[81] reactor survey system to solve the one-dimensional, age-diffusion equation for a slab, cylinder, or sphere. Here

$$\Sigma^j \equiv D^j B_j^2 + \Sigma_a^j + \sum_{k=4}^{9} \Sigma_s^{j\to k}$$

where the source groups for inelastic scattering are limited to groups 1-6; consequently, the last term equals zero for $j > 6$.

$$S^j \equiv -\frac{\partial q}{\partial u_j} - \frac{\partial \eta}{\partial u_j} + \frac{\chi^j}{k_{eff}} \sum_{k=1}^{J} (\nu \Sigma_f)^k \phi^k + \sum_{k=1}^{6} \Sigma_s^{k\to j}$$

for nonthermal groups; and

$$S^J \equiv q + \eta$$

for thermal groups; where q represents the slowing-down density due to elastic scattering by materials other than hydrogen, and η represents the same scattering by hydrogen. In the expression for S^j, the last term equals zero for $4 < j < 9$.

The solution of the difference equations follows an iterative procedure. An initial fission source distribution is assumed. The equations are solved for each group, in turn, using neutrons slowed down from the previous group and inelastically scattered into the group as additional contributions to the source. The new source distribution is computed and compared to the old distribution at each point. The problem is solved when the absolute value of the difference at each point is less than δ, an input parameter. Options permit stopping after a fixed number of iterations, or after the change in k_{eff} over an iteration is less than δ.

Continuity of flux and current is required at each interface. The boundary conditions at the edges may be either zero flux or zero current.

The criticality search subprogram can be used to obtain a specified k_{eff}. This is accomplished by adjusting any one of the parameters: atomic densities of as many as ten isotopes in selected regions, the dimensions of one or more regions, or the position of a control rod represented by a single isotope.

With the buckling iteration subprogram,[82] GNU is used to estimate from the solution of one geometry, the proper values of the transverse buckling constants, by groups, for the complimentary geometry.

This is an iterative procedure and is carried out until the buckling and k_{eff} values converge within the specified convergence criterion.

The burnout program available with GNU is described in Section 10.3.2.

Input Information Required

Problem parameters:

1. Problem identification.
2. Number of regions (≤ 20).
3. Geometry (slab, cylinder, or sphere).
4. Inelastic scattering option.
5. Buckling options (by groups, regions, or combination), and values.
6. Initial source options (flat, input, output from previous problem, input to be reduced by r factor), and source guess if it is to be input data.
7. Cross section print option.
8. Output options.
9. Convergence test option (on k_{eff}, or on k_{eff} and point sources), and criterion.
10. Boundary conditions.
11. Exit option (to another GNU problem, to criticality search,[80] to burnout calculation, to buckling calculation[82]).
12. Groups for which fluxes are to be printed, or over which sums are to be computed.
13. Mesh point value at interfaces (a total of 250 mesh points is allowed).
14. Group structure.
15. Materials used and the atomic densities of each for each region.

A library of microscopic cross sections,[79] defined at 269 points of the lethargy interval corresponding to 10 Mev-0.025 ev, is maintained for generating the multigroup cross sections for GNU. Four microscopic cross sections: $\xi\sigma_t$, σ_a, $\nu\sigma_f$, and $3\sigma_{tr}$, are listed in each interval.

Output Available

The basic output lists the input, the fissionable volume, k_{eff}, and the neutron balance check value for each iteration. Other output, optionally available includes:

1. Power density distribution.
2. Neutron flux space-lethargy distribution.
3. Flux integrated over selected lethargy intervals.
4. Neutron absorptions, escapes, degradations, fissions by region for each group, over all groups.
5. Neutron balance by group.
6. Total absorptions in each region for each of up to 20 selected isotopes.
7. The conversion ratio.
8. Macroscopic few-group cross sections computed from flux-weighted average values of the cross sections used.

Related Codes

A modified version of the MAGNUM code has been prepared to utilize an IBM-704 with a 32K core memory.

PROD II

Description

This code[83,84] is an age-diffusion program providing for both inelastic scattering and the Selengut-Goertzel approximation to account for slowing down by hydrogen.

$$\Sigma^j \equiv D^j B^2 + \Sigma_a^j + \sum_{k=j+1}^{\min(J,8)} \Sigma_s^{j\to k} + \Sigma_{sl}^j$$

$$S^j \equiv -\frac{\partial q}{\partial u_j} - \frac{\partial \eta}{\partial u_j} + \Sigma_{sl}^{j-1}\,\phi^{j-1} + \nu\chi^j \sum_{k=1}^{J} \Sigma_f^k\,\phi^k + \sum_{k=1}^{\min(j-1,7)} \Sigma_s^{k\to j}\,\phi^k$$

for nonthermal groups; and

$$S^J \equiv q + \eta + \Sigma_{sl}^{J-1}\ \phi^{J-1} + \nu\chi^J \sum_{k=1}^{J} \Sigma_f^k\ \phi^k + \sum_{k=1}^{\min(j-1,7)} \Sigma_s^{k\to j}\ \phi^k$$

for the thermal group, $j = J$,

where $\frac{\partial \eta}{\partial u_j} = \Sigma_{sH}^j\ \phi^j - \eta^{j-1}$, $\eta^0 = 0$, and Σ_{sH}^j is the macroscopic hydrogen scattering cross section

η represents the slowing-down density due to hydrogen
q represents the slowing-down density due to elastic scattering by other materials
Σ_{sl} = slowing-down cross section
u_j = lethargy for group j

Boundary conditions require continuity of current and flux at interfaces. For the cylindrical and spherical problems, $r = 0$ is always assumed to be the center of the reactor, and $\phi'(0) = 0$. For the slab, a choice of the two conditions: $\phi(0) = 0$, or $\phi'(0) = 0$, is available. At the outer edge, $r = R$, $\phi(R) = 0$, or

$$D^j \frac{d\phi^j}{dr}\bigg|_R = -\Gamma^j\ \phi^j$$

in which case the cross sections used in the calculation of Γ^j are those of the material outside the last region:

$$\Gamma^j = (D^j\Sigma^j)^{1/2}$$

Owing to limitation of storage space in the IBM-650, the code is divided into two parts. The first part solves for the flux, using an approximation to the fission source, S_n^i. The second part computes the power for each mesh point and from this, the values of ν_c and S_n^{i+1}.

The Multigroup Calculation and the Power Calculation may be used in succession to iterate on the source guess until the power output is as close to the source input as desired.

Input Information Required

Problem parameters:

1. Problem identification.
2. Number of regions ($\leq$50).
3. Number of groups ($\leq$50).
4. Number of mesh points (points + regions $\leq$ 98; or if inelastic scattering is included, points <50).
5. Mesh point spacing and number of points for each region.
6. Geometry (sphere, cylinder, slab).
7. Boundary condition options.
8. Selengut-Goertzel and inelastic scattering options.
9. Initial source guess.
10. Volume of reactor.
11. Specification of core regions.
12. Lateral buckling.
13. Power factor for scaling purposes.

Material properties:

1. Lethargy widths, Δu_j, and exp $(-\Delta u_j)$ for each group, and the fission spectrum fractions, χ^j.
2. Values of D, Σ_a, Σ_f, Σ_{sH}, $\Sigma_{sl}^{j\to j+1}$, $\Sigma_s^{j\to k}$ for each material and each group, if required by options.

Output Available

1. Fluxes at each point for each group.
2. Fission sources at each point normalized such that the integral over the core volume is equal to unity.
3. Average number of neutrons, ν_c, emitted per fission required to maintain criticality.
4. $k = 2.5/\nu_c$.

Related Codes

VALPROD[85] is a revision of the PROD II code. It is designed to solve problems consecutively by permitting the use of the power distribution from one problem as source guess for the next problem. Automatic convergence criteria are included.

Descendants of VALPROD include VALPROD IB and IIB. Both versions allow up to 99 groups. VALPROD IIB provides for semi-automatic Chebyshev acceleration in the source iteration.

VAPOR is designed to reduce running time by restricting the number of groups and points.

FAF[86] provides for a gradient boundary condition at region interfaces and a continuous variation of composition within a region (IBM-650 Model A4).

The PERCOLATOR and the BD-1 codes are used alternately with VALPROD to compute void distributions for a boiling reactor model.

REX

Description

The REX[87] series of one-dimensional, diffusion theory codes provide the real or adjoint solution for a slab, cylinder, or sphere. In these codes:

$$\Sigma^j \equiv D^j B^2 + \Sigma_a^j + \sum_{k=j+1}^{\min(j+G,J)} \Sigma_s^{j\to k}$$

where G is the number of groups into which downscattering is considered ($G \leq 6$), and

$$S^j \equiv \chi^j \sum_{k=1}^{J} \nu\Sigma_f^k \phi^k + \sum_{k=\max(1,j-G)}^{j-1} \Sigma_s^{k\to j} \phi^k$$

In the numerical solution, the set of J-coupled, difference equations is solved by iteration. With the initial composition and fission source approximation given, the difference equations are used to calculate the fluxes and their related fission source terms. These, in turn, are used to compute new fluxes and thence new source terms. This iteration is termed a minor cycle and is repeated until

$$|IS_f^i(\ell) - IS_f^{i-1}(\ell)| < \delta$$

where $IS_f(\ell)$ represents the integral of the fission source in region ℓ; i is the iteration or minor cycle index; and δ is an input parameter. This criterion must be met for each region, after which a criticality test is made which requires

$$|1.0 - \sum_{\substack{\text{core}\\\text{regions}}} IS_f^m(\ell)| < \epsilon$$

where m represents the major cycle index, and ϵ is an input parameter. If the reactor is not critical, the composition of the core regions is varied and a new minor cycle initiated. This iterative change in composition is called a major cycle.

Boundary conditions for interfaces are the standard continuity of flux and current conditions. For the cylinder and sphere, the boundary conditions are fixed with the current zero at r = 0, and the flux zero at the outer edge.

For the slab, either the flux or current may be zero at both boundaries. In the slab programs provision has been made to allow iteration on buckling rather than on composition, if desired.

Inpul Information Required

Problem parameters:

1. Code desired.
2. Problem and cross section set identification.
3. Number of energy groups (≤20), and down-scattering recipients (≤6).
4. Number of core regions.
5. Total number of regions (≤10).

6. Number of subintervals in each region (total <99).
7. Number of materials to be used (≤ 10).
8. Radii of region interfaces.
9. Volume fractions for each material included in each region.
10. Standard configuration for core regions, s_ℓ. The volume fraction of a material in a core region is computed as $VF(z) = c^m s_\ell [VF(z)]_{fuel} + (1 - c^m s_\ell) [VF(z)]_{diluent}$, where c is a concentration factor which may be varied to achieve criticality in a composition.
11. Initial composition.
12. Convergence criterion, δ.
13. Criticality criterion, ϵ.
14. Initial step function fission source for each region.
15. If a cylinder, the height to be used over the reactor is to be specified; if a slab, B^2 over the reactor and boundary conditions are required.

Material properties:

1. Values of $\Sigma_a + \sum_{k=j+1}^{\min(j+G,J)}$, $\Sigma_s^{j\to k}$, $3\Sigma_{tr}$, $\nu\Sigma_f$, $\Sigma_s^{j\to k}$, and Σ^{total}, for each material and each group. The quantity, Σ^{total} = sum of all cross sections, is used as a check on the cross section input.
2. Fission spectrum fractions χ^j, j = 1,2, ... J.

Problems, and cross section sets, may be merged on their respective tapes since the program searches for both the problem and cross section input after trying to do the problems consecutively.

Output Available

1. k_{eff} for each minor cycle.
2. Composition value for each major cycle.
3. Critical fission sources for each point.
4. Fission source integrals for each region.
5. Flux values for each point and each energy group.
6. Flux integrals and leakage terms for each region and group.

Related Codes

RE 122 is an IBM-704 version with a larger variety of boundary conditions and other minor modifications.

UNCLE III, IV

Description

UNCLE III[88] solves the one-group, one-dimensional, diffusion equation:

$$\frac{d^2\phi(x)}{dx^2} + [B^2(x) - B_0^2]\,\phi(x) = 0,$$

where B_0^2 is a poison parameter calculated by the routine to produce criticality.

The extrapolated Liebmann method is used with the boundary condition $\phi = 0$ at both end points. The number of grid intervals must be less than or equal to 36.

The UNCLE IV[89] program obtains the solution of the diffusion equation:

$$\nabla^2\phi(r) + B^2\phi(r) = 0$$

for cylindrical geometry. The solution is obtained by integration of a difference equation with radial symmetry assumed:

$$\phi(0) = 1$$

$$\lim_{r \to 0} \frac{1}{r} \frac{\partial \phi}{\partial r} = \frac{\partial^2 \phi}{\partial r^2}$$

and

$$\phi(R) < 10^4$$

The difference equation is solved at each of 64 uniformly-spaced grid points. Any of three parameters may be varied to achieve criticality: a uniform poison in all regions, the buckling in specified regions, or the interfaces between regions.

Input Information Required

Problem parameters:

For UNCLE III: reactor height and buckling terms at each grid point.

For UNCLE IV: interface coordinates, parameters to be varied, and the buckling terms for each region (<6).

Output Available

For UNCLE III, the punched output consists of the buckling and flux terms for each point, the reactor height, poison value, number of points, and iteration number, at each iteration.

For UNCLE IV, the problem identification, buckling, and outer boundary values of each region, and every fourth value of the flux, are punched for each iteration.

These cards can then be listed on an IBM-407 printer.

VARI-1

Description

This program[90] for the one-dimensional, age-diffusion theory solution, is similar to the GNU II code. It provides for slab, cylinder, or sphere problems with

$$\Sigma^j \equiv D^j B_j^2 + \Sigma_a^j$$

$$S^j \equiv -\frac{\partial q}{\partial u_j} - \frac{\partial \eta}{\partial u_j} + \frac{\chi^j}{k_{eff}} \sum_{k=1}^{J-1} \nu \Sigma_f^k \phi^k + \Sigma_f^J \phi^J$$

for non-thermal groups; and

$$S^J \equiv q + \eta$$

for thermal groups; where q represents the slowing-down density due to elastic scattering by materials other than hydrogen, and η represents the same scattering by hydrogen.

At both edges of the reactor, any of the boundary conditions: zero flux, zero current, or zero flux at an extrapolated boundary, may be employed. At an interface, both flux and current are required to be continuous.

The difference equations are solved by an iterative procedure as follows. An initial source distribution is specified. The fluxes are computed through each energy group using neutrons slowed down from the previous group as additional contributions to the source. After the fluxes have been obtained for the highest thermal group, a new source distribution is completed and the number of fissions produced can be calculated. This quantity divided by the fissionable volume is the value of k_{eff} for this iteration. The new source distribution is compared to the source distribution computed after the pre-

vious iteration. The problem is solved when the absolute value of the difference at each point is less than δ, an input parameter. Options permit stopping after a fixed number of iterations, or after the change in k_{eff} over an iteration is less than δ. At this point, the value of k_{eff} may not be sufficiently near the desired value and the program proceeds to vary the specified parameters — regional dimensions or material concentrations — to achieve the specified value of k_{eff}.

Input Information Required

Problem parameters:

1. Problem identification.
2. Number of regions ($\leq$20).
3. Geometry (slab, cylinder, sphere).
4. Buckling options (by groups, by regions).
5. Initial source options (flat, input, output from previous problem).
6. Print options.
7. Convergence test option (on k_{eff}, on k_{eff} and point source), and convergence criterion.
8. Boundary conditions.
9. Number of fissionable materials ($\leq$4).
10. Number of thermal groups ($\leq$12).
11. Self-shielding option.
12. Regional descriptions including region boundaries, mesh increments, buckling, materials used, and the atomic densities of each.
13. Parameters to be varied, and k_{eff} desired if convergence to a particular k_{eff} is required.

Output Available

1. Input data.
2. Optional printing of microscopic and macroscopic cross sections.
3. k_{eff}.
4. Flux distributions.
5. Balance integrals.
6. Power densities for the thermal groups.

Related Codes

Codes from which VARI-1 evolved include PROBE I and PROBE II, both originally coded for the IBM-701.

WANDA

Description

WANDA-4[91,92,93] is the few-group, diffusion theory code described here as representative of the WANDA family of codes. In this code, applicable to slab, cylinder, and sphere problems:

$$\Sigma^j \equiv D^j B^2 + \Sigma_a^j + \Sigma_s^{j \to j+1} + t_j \Sigma_p$$

where Σ_p = a smeared poison cross section representing control rods
t_j = fraction of the poison appearing in group j

and

$$S^j \equiv \frac{\chi^j G}{\lambda} + \Sigma_s^{j-1 \to j} \phi^{j-1}$$

where

$$G = \sum_{j=1}^{J} \nu \Sigma_f^j \phi^j$$

and λ is the eigenvalue.

The diffusion equations are replaced by a set of coupled difference equations. The operator in the diffusion equations is replaced by a central difference formula; at interior interfaces it is required that flux and current be continuous; and at exterior boundaries, the flux or its derivative is set equal to zero. The resulting matrix equation is inverted by sweeping the mesh out and back, and the group equations are solved in order. The eigenvalue is computed as

$$\lambda = \int_{vol} G(r)\, dV$$

Two criteria may be used to determine convergence. The first, "eigenvalue convergence," requires that

$$\left|\frac{\lambda_i - \lambda_{i-1}}{\lambda_i}\right| \leq \epsilon_1$$

for two successive iterations. The second, "pointwise convergence," requires that

$$\frac{(\bar{\lambda}_i - \underline{\lambda}_i)}{\bar{\lambda}_i} \leq \epsilon_2$$

for two successive iterations, where

$$\bar{\lambda}_i = \max_r [G_i(r)/G_{i-1}(r)]$$

and

$$\underline{\lambda}_i = \min_r [G_i(r)/G_{i-1}(r)]$$

The convergence criteria, ϵ_1 and ϵ_2, are specified as problem input, and i is the iteration index. An extrapolation process has been incorporated to accelerate convergence whereby

$$\frac{G_i(r)}{\lambda_i} + \theta_i \left[\frac{G_i(r)}{\lambda_i} - \frac{G_{i-1}(r)}{\lambda_{i-1}}\right]$$

is used in iteration (i + 1), rather than $G_i(r)/\lambda_i$. Either a fixed value of $\theta_i (i \geq 2)$, may be supplied as input, or the code will compute a sequence of values based on Chebyshev polynomials.

This code will vary the buckling or poison cross section in all regions, or any subset of regions chosen, or the boundary separating two regions, to search for a specified critical eigenvalue $\pm \epsilon_1$. Values of buckling or poison which cause Σ^j to become negative are not allowed. The control boundary may not cross an interface or delete a region.

Input for one problem may be saved and used for the succeeding problem with changes in input data only specified. The converged source of one problem may be used as the input source guess for a succeeding problem.

Input Information Required

Problem parameters:

1. Number of material compositions (≤35).
2. Number of regions (≤35).
3. Number of groups (≤4).
4. Geometry (slab, cylinder, sphere).
5. Boundary conditions.
6. Convergence criteria (ϵ_1 is also used to terminate a criticality search problem).
7. Region descriptions (material composition identification, interface designation, and mesh size).
8. Source extrapolation factor, θ.

Material properties:

1. Values of D, Σ_a, $\nu\Sigma_f$, $\Sigma_s^{j\to j+1}$ for each composition* and each group, with the exception of the thermal group where a composition source guess may be supplied in place of $\Sigma_s^{j\to j+1}$. If desired, the source guess may be specified pointwise.

*The WANDA-3 code can be used if pointwise specification is desired.

2. Buckling input. This may be specified as one-value, regionwise, or pointwise, and may be given individually for each group, if desired.
3. Fission spectrum fractions χ^j, j = 1,2, ... J.
4. Poison fractions t_j, j = 1,2, ... J.

If an eigenvalue search is to be undertaken, additional input is required that specifies the parameter to be varied, the regions concerned, a second guess or guesses for that parameter, and the critical eigenvalue desired.

Output Available

1. Input edit.
2. Sequence of eigenvalues leading to the converged eigenvalue, along with the control parameter values for each sequence in a search.
3. Region integrals of the source and fluxes.
4. Regional checks.

Optionally, the pointwise source and flux values can be printed, and/or plotted, and/or punched on binary cards in a form suitable for the P_1 code, P1MG (Section 10.1.2).

Related Codes

An IBM 704 adjoint code equivalent of WANDA has been prepared under the name EDNA.

Two similar few-group, one-dimensional codes have been prepared for the IBM-650: (1) ENSIGN, a fixed point, 4-group version for rectangular and cylindrical geometries only; and (2) LIL ABNER,[94,95] which uses the IBM Interpretive Floating Point System.

The LIL ABNER code provides for 1 to 8 energy groups, three geometries, and a maximum of 10 regions and 100 mesh points. As in WANDA, neutrons are allowed to scatter only into the next lower energy group. A source extrapolation procedure is included. Boundary conditions are: zero flux or zero flux derivative, and any of the three geometries: slab, cylinder, or sphere, may be considered.

The Philco-2000 version of WANDA, known as WANDA 5,[96] allows as many as 500 mesh points and 100 regions.

ZOOM

Description

The ZOOM code is available for three machines: IBM-704,[97] IBM-709[98,99] and IBM-7090. The IBM-709 version is described here. In this code:

$$\Sigma^j \equiv \Sigma_a^j + \Sigma_f^j + \sum_{\substack{k=1 \\ k\neq j}}^{J} \Sigma_s^{j\to k} + \left\{(1+2a)\left(\frac{\pi}{L_Z + 2\ell_R D^j}\right)^2 + (1-2a)\left(\frac{\pi}{L_Y + 2\ell_R D^j}\right)^2\right\}(1-a)D^j$$

where a = geometry indicator (a = 0 for slab; a = ½ for cylinder; a = 1 for sphere)

L_Z, L_Y = problem dimension in the Z and Y directions, respectively

ℓ_R = boundary condition constant at the exterior boundary (i.e., $\ell_R D^j(R)$ is the energy-dependent extrapolation length)

and

$$S^j \equiv \sum_{\substack{k=1 \\ k\neq j}}^{J} \Sigma_s^{k\to j}\,\phi^k + \frac{\chi^j}{\lambda}\sum_{k=1}^{J}(C + DE^k)\,\Sigma_f^k\,\phi^k$$

where $C + DE^j$ = the mean value of C + DE in group j. (C, D are constants. E is the energy value; this factor is a correction to account for the variation of neutrons per fission, with the energy of the neutron causing the fission.)

λ = the eigenvalue.

The boundary conditions applied require a zero derivative of the flux at r = 0 for cylindrical and spherical geometry; for the slab, this condition or an energy-dependent extrapolation length is allowed. At the r = R boundary for all geometries, the energy-dependent extrapolation length condition is applied. Continuity of flux and current at interfaces is required.

A procedure has been incorporated to perform inner iterations on flux values within energy groups, for all groups below a specified group, until one of two convergence criteria is met.

$$\left(\sum_n \left|\phi_n^i - \phi_n^{i-1}\right| \Big/ \sum_n \left|\phi_n^i\right|\right) < \epsilon_1$$

where ϵ_1 is an input parameter; or i, the iteration index $\geq$ a maximum I, also specified as an input parameter. Here, n is the point index.

A linear combination of the source values from previous iterations is used to calculate the source value for the succeeding iteration. These outer iterations use the following test for convergence:

$$\left(\sum_n \left|\phi_n^{i,m} - \phi_n^{i,m-1}\right| \Big/ \sum_n \left|\phi_n^{i,m}\right|\right) < \epsilon_2$$

where ϵ_2 is an input parameter, and m is the outer iteration index.

Input Information Required

Problem parameters:

1. Problem identification.
2. Number of materials ($\leq$15).
3. Number of intervals ($2 \leq k \leq 40$).
4. Number of energy groups ($\leq$18).
5. Number of energy groups over which inner iterations are desired.
6. Number of the maximum energy group over which power is to be summed.
7. Geometry (slab, cylinder, sphere).
8. Boundary condition constants.
9. Problem dimensions.
10. C, D = the constants used in $C + DE^j$.
11. Convergence criteria.
12. Initial value of eigenvalue.
13. Power normalization factor.
14. Radius associated with each point.
15. Maximum degree of the Chebyshev polynomial for use in the source extrapolation procedure.

Material properties:

1. The material density, N, and the microscopic cross sections σ_a, σ_f, σ_{tr}, σ_s, for each material and energy group.
2. Transfer functions, μ, and cell factors, X, for each material and group.
3. Volume fractions, V, of each material, z, associated with each point, such that:

$$\Sigma_{tr} = \sum_z V_z N_z \sigma_{tr}^z$$

$$\Sigma_a,\ \Sigma_f = \sum_z V_z N_z X_z (\sigma_a^z,\ \sigma_f^z)$$

$$\Sigma_s^{j\to k} = \sum_z V_z N_z \mu_z^{j\to k} X_z \sigma_s^z$$

4. Fission spectrum fractions χ^j, j = 1,2 ... J.
5. Energy E_j, j = 1,2 ... J, as used in the quantity $C + DE^j$.

Energy groups in this code are numbered in order of increasing energy. Use of a library tape of material cross sections is optional.

687863 O - 63 - 50

Output Available

1. Input data.
2. Value of k_{eff} and number of inner iterations for each power cycle.
3. Converged flux values for each point and each group.
4. Radii and power associated with each interval and over the entire reactor.
5. For each point:

$$\sum_j \Sigma_f^j(n)\phi^j(n-1);$$

$$\sum_j \Sigma_f^j(n)\phi^j(n); \text{ and}$$

$$\sum_j [(C + DE^j)\ \Sigma_f^j(n)\phi^j(n)]$$

Sense switch options permit termination and edit at the next outer iteration, flux edit for every outer iteration, a monitor print of the eigenvalue, and suppression of inner iterations.

SUPPLEMENTARY INFORMATION

Code Name	Related Codes	Originating Installation	Machine Configuration	Running Time	References
AIM-5		North American Aviation, Inc., Atomics International	IBM-704 or 709 with 32K core memory, 2 tape units, 1 additional tape unit for adjoint or "RESTART DUMP" option (FORTRAN).		61. H. P. Flatt and D. C. Baller, "AIM-5, A Multigroup One-Dimensional Diffusion Equation Code," NAA-SR-4694, (March, 1960).
	PERT		IBM-7090 with 32K core memory, 2 tape units (FORTRAN).		62. H. P. Flatt, "PERT, A Perturbation Theory Code." NAA Program Description (February, 1961).
DMM		American Standard Corp., Burroughs Corp. IBM Corp.	IBM-650 with floating point arithmetic and index registers.	30–130 sec/iteration.	63. IBM-650 Library File 8.2.015. 64. J. Franklin and E. J. Leshan, "A Multigroup, Multiregion, One-Space Dimensional Program Using Neutron Diffusion Theory," ASAE-4, (April, 1957).
	MCC	Burroughs Corp., Professional Services Department	B-205 with 1 tape unit.		65. D. Burns, J. N. Franklin and W. Taylor, "Multigroup Criticality Computations on the Burroughs 205 System for Heterogeneous Reactors Using the Diffusion Approximation," No. 44, NES-001, (June, 1959).
			B-220 with 5K core memory.		66. D. Burns and J. Allen, "Multigroup Criticality Computations on the Burroughs 220 System for Heterogeneous Reactors Using the Diffusion Approximation," No. 76, NES-002. (September, 1960).
DSN		Los Alamos Scientific Laboratory	IBM-704.	≈30 min; 0.02 sec/point/group/iteration, with ≈70 iterations for fast systems and ≈200 for slow neutron systems.	67. B. Carlson, C. Lee and J. Worlton, "The DSN and TDC Neutron Transport Codes," LAMS-2346, (February, 1960). 68. B. Carlson, C. Kazek and C. Lee, "Numerical Solution of Transient and Steady-State Neutron Transport Problems," LA-2260, (May, 1959).
	SNG SNK				69. B. Carlson and G. Bell, "Solution of the Transport Equation by the S_n Method," Proc. 1958 Geneva Conference, 16, Paper No. 2386, p. 535.
	Mercury S_n	Atomic Energy Research Establishment, Harwell, England	Ferranti-Mercury.	2 sec/point/group/iteration.	70. H. E. Wrigley, "A Program for Solving the Neutron Transport Equation by Carlson's S_n Method on the Ferranti-Mercury Computer, AERE T/R 2789, (December, 1958).

SUPPLEMENTARY INFORMATION (Continued)

Code Name	Related Codes	Originating Installation	Machine Configuration	Running Time	References
DSN (Contd.)	PROGRAM S-VII	General Electric Co., Aircraft Nuclear Propulsion Department	IBM-704.		71. B. H. Duane, "Neutron and Photon Transport Plane-Cylinder-Sphere GE-ANPD Program S Variational Optimum Formulation," XDC 59-9-118, (January, 1959).
	CELCOR	The Martin Co., Nuclear Division	IBM-709 with 32K core memory, 7 tape units (FORTRAN).	10 min/cell.	72. G. A. Cannon, "APWRC-CELCOR, A FORTRAN II Program for Multiple Lethargy Lead P1 or S2 to S16 DSN Cell Corrections in Cylindrical, Spherical and One or Two Dimensional Slab Geometry," MND-C-2459, (December, 1960).
F2		General Electric Co., Aircraft Nuclear Propulsion Department	IBM-704 with 8K core memory, 6 tape units, and optional use of CRT.	30 sec.	73. F. B. Smith, "F2 Two-Group Neutron Diffusion Program," APEX-539, (August, 1958).
	C_2				74. D. B. Vollenweider, "Bare Reactor Program (IBM-704 Program C2)," APEX-418, (July, 1957).
	GEORGE			10 to 20 min.	75. T. A. Hoffman and W. B. Henderson, "General Reactor Analysis Computer Program for the IBM-704, Program GEORGE," APEX-543, (October, 1959).
					76. K. A. Paine, "Nuclear Data Tape Program (IBM-704 Program NDTP)," APEX-574, (October, 1960).
FIRE		Los Alamos Scientific Laboratory	IBM-704 with 8K core memory, 2 tape units, and 1 drum unit.	1–2 min.	77. C. B. Mills and F. Brinkley, "A One-Dimensional Intermediate Reactor Computing Program," LA-2161, (March, 1959).
			IBM-704 with 32K core memory, 3 tape units.	May run one hour or more with up-scattering.	78. Ibid, Supplement, LA-2161, (March, 1960).
GNU II (MAGNUM)		General Motors Corp., Research Laboratories	IBM-704 with 8K core memory, 7 tape units, and 1 drum unit.	GNU II 3 min. Criticality search 12 min. Buckling iteration 40 min.	79. C. L. Davis, J. M. Bookston and B. E. Smith, "GNU II, A Multigroup One-Dimensional Diffusion Program for the IBM-704," GMR-101, (November, 1957).
					80. J. M. Bookston and C. L. Davis, "An IBM-704 Program for Criticality Search on Reactor Parameters," GMR-102, (November, 1957).
					81. C. B. Leffert, "Instruction Manual for the GM Nuclear Reactor Code System MAGNUM," GMR-100, (1958).
					82. B. E. Smith, "Buckling Iteration Program," GMR-104, (November, 1957).
	MAGNUM 32K	Internuclear Co.	IBM-704 with 32K core memory.		

PROD II		General Electric Co., Knolls Atomic Power Laboratory	IBM-650.	1 min/iteration, 1 group.	83. C. J. Habetler, "One-Space-Dimensional Multigroup for the IBM-650 Part I Equations," KAPL-1415, (December, 1955). 84. V. A. Walbran, "One-Space-Dimensional Multigroup for the IBM-650 Part II Machine Program," KAPL-1531, (April, 1956).
	VALPROD	General Electric Co., Vallecitos Atomic Laboratory			85. C. M. White, "VALPROD, A Revision of the PROD II 650 Multigroup Program," GEAP-0952, (January, 1957).
	VALPROD IB, IIB			2 min/iteration, 3 groups.	
	VAPOR			0.5 min/iteration, 3 groups.	
	FAF		IBM-650, Model A4.	0.5 min iteration, 3 groups; ~4 min.	86. R. H. Stark and C. M. White, "FAF, A Multigroup Program for the IBM-650 Model A4," GEAP-3048.
	PERCOLATOR BD-1	American Standard Corp., Atomic Energy Division		1.5 min/iteration.	
REX		Argonne National Laboratory	UNIVAC with 7 tape units.	20 min/problem.	87. M. K. Butler and J. M. Cook, "UNIVAC Programs for the Solution of One-Dimensional Multigroup Reactor Equations," ANL-5437, (October, 1956).
	RE 122		IBM-704 with 8K core memory, 4 tape units.		
UNCLE III		E. I. duPont de Nemours & Co., Savannah River Laboratory	IBM-650.	5 sec/iteration.	88. IBM-650 Program Library 8.2.012.
UNCLE IV				2.5 min/problem.	89. IBM-650 Program Library 8.2.018.
VARI-1		Curtiss Wright Corp., Research Division	IBM-704 with 8K core memory, 1 drum unit, 7 tape units.		90. J. M. Fontana, F. J. Casagrande and W. J. Roberts, "VARI-1, A One-Dimensional Variable Geometry Multigroup Nuclear Diffusion Code," CWR 900-12, (June, 1959).
	PROBE I; PROBE II		IBM-701.		

SUPPLEMENTARY INFORMATION (Continued)

Code Name	Related Codes	Originating Installation	Machine Configuration	Running Time	References
WANDA		Westinghouse Electric Corp., Bettis Atomic Power Laboratory	IBM-704 with 8K, 16K, or 32K core memory, 1 tape unit.	Varies from a few seconds to 1 hr or more. Problems with 150 mesh points and no criticality search usually require 2 min.	91. O. J. Marlowe, et al., "WANDA–A One-Dimensional Few-Group Diffusion Equation Code for the IBM-704," WAPD-TM-28, (November, 1956). 92. O. J. Marlowe and E. M. Gelbard, "WANDA–A One-Dimensional Few-Group Diffusion Equation Code for the IBM-704," WAPD-TM-28 Addendum, (September, 1957). 93. O. J. Marlowe, "WANDA–A One-Dimensional Few-Group Diffusion Equation Code for the IBM-704," WAPD-TM-28 Addendum 2, (July, 1959).
	EDNA		IBM-704.		
	ENSIGN		IBM-650.		
	LIL ABNER		IBM-650.	1 hr for 2 groups 100 points, 7 iterations.	94. H. Bohl, E. Gelbard and R. Suarez, "A Few-Group One-Dimensional Code for IBM-650," WAPD-TM-3, (July, 1956). 95. IBM-650 Program Library 8.2.007.
	WANDA-5		Philco-2000.		96. O. J. Marlowe and M. C. Suggs, "WANDA 5, A One-Dimensional Neutron Diffusion Equation Program for the Philco-2000 Computer," WAPD-TM-241, (November, 1960).
ZOOM		Lawrence Radiation Laboratory	IBM-704 with 8K core memory, 6 tape units.	10 min.	97. R. N. Stuart, et al., "ZOOM–A One-Dimensional Multigroup Neutron Diffusion Theory Reactor Code for the IBM-704," UCRL-5293, (November, 1958).
			IBM-709, 7090, with 2 tape units.	IBM-709 code runs 5–10 times as fast as 704 version.	98. S. P. Stone, E. T. Collins and S. R. Lenehan, "9-ZOOM–A One-Dimensional, Multigroup, Neutron Diffusion Theory Reactor Code for the IBM-709," UCRL-5682, (August, 1959). 99. S. P. Stone, "9-ZOOM–A One-Dimensional, Multigroup Neutron Diffusion Theory Reactor Code for the IBM-709," UCRL-5682 Supplement 1, (July, 1960).

10.2.2 TWO-DIMENSIONAL GEOMETRIES

ANGIE

Description

ANGIE[100,101] is the two-dimensional counterpart of the ZOOM code for a rectangular network of x-y or r-z coordinates. The IBM-709 version, 9 ANGIE,[102] is described here.

A second-order difference approximation is used, and the scattering of neutrons is restricted to occur between a group and the one immediately above it in energy, or the two immediately below it.

The solution of the difference equations is obtained by a modified Peaceman-Rachford iteration procedure.* This program does not use the ZOOM "inner iteration" technique in each energy group, but does include the power extrapolation procedures of the ZOOM program.

Energy-dependent extrapolation boundary conditions are applied at all outer boundaries except at the r = 0 symmetry boundary in r-z coordinates; in addition, the energy-dependent extrapolation boundary condition may be applied to selected interior "rod" regions.

Input Information Required

Problem parameters:

1. Problem identification.
2. Number of materials, L_{max}, and regions, R_{max}, ($L_{max}\ R_{max} \leq 6000$).
3. Specification of mesh points (≤ 2000, ≤ 100 in any one direction).
4. Coordinate system (r-z or x-y).
5. Number of energy groups (≤ 18). Energy groups are numbered in order of increasing energy.
6. Exterior boundary condition constants for each energy.
7. Interior rod region boundary condition constants for energy groups and mesh points concerned.
8. Convergence criterion, ϵ.
9. Initial value for the eigenvalue.
10. Power normalization factor.
11. Maximum degree of Chebyshev polynomial for use in the source extrapolation procedure.

Material properties:

1. Atomic density, N, and the microscopic cross sections σ_a, σ_f, σ_s, σ_{tr}, for each material and each energy group.
2. Transfer fractions, μ, for each material.
3. Volume fraction, V, of each material associated with each region such that volume-averaged regional cross sections may be computed.
4. Fission spectrum fractions χ^j.
5. Energy E_j, as used in the $C + DE^j$ function correlating the total neutrons per fission with the energy of the neutron causing the fission.

Provisions are included for obtaining starting fluxes from a suitable, previous problem.

Output Available

Tape output includes a preliminary listing of the input, and a "picture" of the two-dimensional region layout. Upon convergence, there is available for off-line printing a tape listing of the effective multiplication constant, all fluxes, and several forms of spatial power and absorption distributions. This final edit may be forced for any iteration cycle.

On-line monitoring of the problem is provided.

*D. W. Peaceman, H. H. Rachford, Jr., "The Numerical Solution of Parabolic and Elliptic Differential Equations," J. Soc. Ind. Appl. Math., 3: (March, 1955).

Related Codes

Two codes, SOPHIST I and II, compute the multigroup input data required for ZOOM and ANGIE.

A program for solving the multigroup diffusion problem over either the x-y or r-z networks has also been prepared for the Mercury computer.[103]

CURE

Description

CURE[104] is the two-dimensional, multigroup program coded for KAPL by the Computer Usage Company and the National Bureau of Standards. Three coordinate systems are included: x-y, r-z, and r-θ. Irregular outer boundaries, variable mesh spacing, and point deletions are permitted.

In the CURE code:

$$\Sigma^j \equiv \Sigma_a^j + \Sigma_s^{j\to j+1} + D^j B^2$$

and

$$S^j \equiv \chi^j P + \Sigma_s^{j-1\to j}\,\phi^{j-1} + [1 - \exp(-\Delta u^j)]\,\eta^{j-1} + \sum_{k=1}^{j-1} \Sigma_s^{k\to j}\,\phi^k$$

where

$$P = \nu \sum_{j=1}^{J} \Sigma_f^j\,\phi^j$$

"Few-group" calculations are distinguished from "multigroup" calculations by the manner in which the source term is calculated. In "few-group" calculations, the last two terms of the source equation, representing the sources due to hydrogen slowing down and inelastic scattering, do not appear.

To solve the group diffusion equation, a grid is superimposed on the reactor plane. Material boundaries, and outer boundaries where boundary conditions are specified, must lie on grid lines. At each node of the grid, the equation is reduced to a difference equation involving the node and its nearest neighbors. If there are N points in the mesh, N simultaneous equations are solved. A generalized Peaceman-Rachford iteration scheme is used on the fluxes,* while the fission source extrapolation routine employs the "best strategy" technique of Stiefel.

For the first double sweep of the first Peaceman-Rachford cycle, an error E^1 is determined as:

$$E^1 = \sum_n (|\phi_n^{1/2} - \phi_n^0| + |\phi_n^1 - \phi_n^{1/2}|)$$

and after each cycle m, E^m is calculated:

$$E^m = \sum_n (|\phi_n^m - \phi_n^{m-1/2}| + |\phi_n^{m-1/2} - \phi_n^{m-1}|)$$

The flux is considered adequately converged when $E^m < \xi E^1$; ξ is an input parameter.

The fission source extrapolation routine employs three successive fission distributions and these outer iterations are terminated when either the iteration index i = p, or

$$\sum_n (\mathscr{S}_n^i - \mathscr{S}_n^{i-1})^2 < \epsilon$$

where p and ϵ are input parameters, and $\mathscr{S}$ is the volume-weighted fission source at node n.

Boundary conditions that may be applied at irregular outer boundaries are: flux zero, flux given, current zero, ratio of current to flux = a constant Z^j ($Z^j = \sqrt{\Sigma^j D^j}$ is based on an infinite blanket with exponential flux decay), and, in r-θ problems on lines of constant θ, a periodic flux and current condition.

*A code was also prepared using the extrapolated Liebmann flux iteration technique.

In a 3-group problem, macroscopic cross sections may be either given directly as input, or calculated from basic composition input data based on the prescription by Deutsch.*

For multigroup problems, the macroscopic cross sections are computed from a specification of the materials and library of microscopic cross sections.

Input Information Required

Problem parameters:

1. Problem number.
2. Maximum number of points in any row and in any column.
3. Geometry specification (x-y, r-z, r-θ).
4. Number of energy groups skipped before $\Sigma_f^j \neq 0$, and total number of groups.
5. Periodic option (yes or no).
6. Inelastic scattering option (yes or no). Inelastic scattering may be considered from the first six groups only.
7. Source-flux guess option (available or not).
8. Perpendicular buckling.
9. Upper bound on number of flux iterations for any group per outer iterations.
10. Peaceman-Rachford iteration parameters.
11. Peaceman-Rachford convergence factor.
12. Source extrapolation parameter.
13. Power convergence factor.
14. Cross section option (0 = calculated, 1 = input).
15. Maximum fuel region index.
16. Water density factor.

Configuration data:

1. Boundary point specifications and associated boundary conditions.
2. Mesh point and material designations.
3. Special, superimposed, thin region definitions and identification.

Cross section specifications required for "few-group" problems, with cross section option = 0:

1. Problem number.
2. General temperature.
3. For each material: the material index, the volume associated with the material, a special temperature if desired, age option, xenon option, thin region index, epithermal unshielding factors, element identifications, and volume of each element included in this material.

Cross section specifications required for "few-group" problems, with cross section option = 1:

For each material: D^j, Σ^j, $\Sigma_s^{j-1\to j}$, Σ_f^j, and Z^j for each group.

For multigroup problems that compute macroscopic cross sections from problem input data and a microscopic cross section library:

1. Problem number.
2. General temperature.
3. For each material: the material index, slowing-down parameters (may be group dependent), self-shielding factors, element identification, volume fraction, and self-shielding factors associated with each element included in this material.
4. Fission spectrum fractions χ^j, j = 1, 2 ... J.

A maximum of 40 different materials is allowed.

Output Available

Edited output includes:

1. Reactivity index.
2. Flux and power map for final outer iteration.
3. Average flux per unit core volume for each material.
4. Macroscopic cross sections.

*R. W. Deutsch, "Computing 3-Group Constants for Neutron Diffusion," *Nucleonics, 15:* No. 1,(January, 1957).

5. Power and flux convergence data, including for each energy group: the number of double mesh sweeps for each outer iteration, last E^i value, and a neutron balance; also a measure of the convergence of the outer iteration and the coordinate indices of the point at which the most change in $\mathscr{S}$ occurred over the past iteration.

Optional output includes all input data and collapsed meshes of coordinates, indices, control words, difference equation coefficients, volume weights, material indices, and boundary conditions.

Related Codes

The original CURE code made available was for an 8K, 6-tape, IBM-704 and handled "few-group" problems only. Later, two versions[105] were introduced specifically for the 32K machine. The first version quintupled the number of mesh points allowed and handles 1 to 50 groups. The second version doubled the mesh points allowed, halved the number of tape units required, and approximately halved the running time per outer iteration; it handles 1 to 3 groups. In addition, both versions incorporate a number of refinements, including the Shinn version of the flux iteration reported to run 16% faster.

The multigroup version of the CURE code, CUREM, solves for 3 to 50 groups in the real case, or for 10 to 50 groups in the adjoint case. A different program tape must be used for each case, and seven tapes are required for the adjoint program.

A 3-group perturbation code utilizes CURE real and adjoint binary output tapes as input. This program, PSP,[106,107] computes the reactivity increments over regions specified. The code permits 40 different sets of cross section changes and 199 regions for summation.

KAPL-originated versions of CURE are described under CUREBO (Section 10.3.3).

EQUIPOISE

Description

EQUIPOISE[108] is a two-group, two-dimensional, diffusion theory code for cylindrical geometry.

Five-point difference equations are used to solve the 2-group neutron diffusion equations. Either of two procedures may be employed. In the usual case, the eigenvalue, λ (= ratio of neutron absorption plus leakage to neutron production), is computed by substituting an initial flux guess into the equations, applying the boundary conditions, and then adding all of the equations for the mesh points. This value of λ is then inserted into all of the equations and the fast and thermal fluxes at all points in the mesh are computed. Having a complete new set of fluxes allows the calculation of a new eigenvalue and repetition of the process, until convergence is obtained.

An alternative procedure is to fix the eigenvalue and compute the fluxes until the ratio of successive flux values is everywhere the same. The fluxes are normalized to a value of 100 for the thermal flux at an arbitrary interior point.

If a problem is being solved with a fixed eigenvalue, the calculation stops when:

$$\frac{\rho_{max} - \rho_{min}}{0.5\,(\rho_{max} + \rho_{min})} < \epsilon$$

where

$$\rho = \frac{\phi^{i}_{unnormalized}}{\phi^{i-1}_{normalized}}$$

is calculated for each point.

Three types of boundary conditions are possible: zero flux, zero current, and constant flux, along the entire edge of the mesh. If a constant flux condition is selected, the fixed eigenvalue iteration procedure must be used and no interior normalization point should be specified.

The calculation procedure is accelerated by use of the extrapolated Liebmann process, designated by EL; here

$$\phi^{i}_{EL} = (1-\beta)\,\phi^{i-1}_{EL} + \beta\phi^{i}$$

where ϕ^i are the flux values as calculated in the *ith* iteration, and β is a number between 1 and 2. In the code, β is determined as

$$\beta = 2 - \sqrt{2}\left[\left(\frac{\pi}{M}\right)^2 + \left(\frac{2.405}{N}\right)^2\right]^{1/2}$$

where M and N are the number of intervals in the axial and radial directions, respectively. The number of axial intervals is doubled if either the top or bottom boundary is a symmetry boundary. Negative fluxes are not permitted. If a negative flux is calculated, a β halfway between the present β and 1 is used, and this reduction is continued as required to produce all $\Phi \geq 0$. Provision is made to attempt restoration of the original β value every tenth iteration.

Two convergence criteria are included. The first requires

$$\left|\frac{\lambda_{max} - \lambda_{min}}{\lambda}\right| < \epsilon$$

The second requires

$$\left|1 - \frac{\phi^i_{unnormalized}}{\phi^{i-1}_{normalized}}\right|_{max} < \epsilon$$

where ϵ is an input quantity. If the first convergence criterion is met, five sweeps through a group are made before moving to the other group. Only after a total of 30 sweeps, 15 through each group, is the eigenvalue recalculated.

Oscillations in λ and the fluxes have been observed and appear to be due to the loss of significant figures.

Input Information Required

Problem parameters:

1. Problem identification.
2. Number of rows and columns to be included in the mesh (each ≤ 25).
3. Coordinates of the normalization point.
4. Flux guess option (result of previous case; specified as input).
5. Source print option (value of source printed for each mesh point; source calculation omitted).
6. Convergence option (λ convergence only required; both λ and ϕ convergence required).
7. Criticality option ($\lambda = 1.0$ and problem is solved for flux only; λ not held constant).
8. Boundary condition indicators for top, right, and bottom boundaries.
9. Convergence criterion, ϵ.
10. Extrapolated Liebmann coefficient, if an input parameter.

Mesh specifications:

1. Increments in the axial and radial directions.
2. Region specifications (i.e., coordinates) and associated cross sections, including D_F, D_S, Σ_F, Σ_S, $\nu\Sigma_{fF}$, and $\nu\Sigma_{fS}$; the resonance escape probability p; and the initial flux guesses ϕ_F and ϕ_S.

Output Available

The code prints on-line the problem input data with the exception of the options requested; and the convergence levels and eigenvalue estimate for every tenth iteration and final iteration. After the last iteration, the ratio of absorptions calculated on the basis of unnormalized fluxes for this iteration, to absorptions calculated on the basis of the normalized fluxes for the previous iteration, is also printed as "flux ratio."

Other output available for off-line printing includes the normalized fast and slow flux values at each point; the total production, absorption, and the leakage at each boundary in each group; the fast and slow absorption by region; and the source density at each quadrant of each mesh point.

Related Codes

EQUIPOISE-2^{109} is an IBM-7090 version of EQUIPOISE.

FLEER

Description

FLEER[110] is a three-group, two-dimensional, diffusion theory program. The equations solved are:

$$-D^1 \nabla^2 \phi^1 + \Sigma^1 \phi^1 = \nu (F^2 \phi^2 + F^3 \phi^3)$$

$$-D^2 \nabla^2 \phi^2 + \Sigma^2 \phi^2 = \Sigma_s^{1\to 2} \phi^1$$

$$-D^3 \nabla^2 \phi^3 + \Sigma^3 \phi^3 = \Sigma_s^{2\to 3} \phi^2$$

where ϕ^j is the flux in the j*th* group; D^j, Σ^j, and F^j, are the diffusion, total removal, and fission cross sections; $\Sigma_s^{j-1\to j}$ is the slowing-down cross section from group j − 1 to group j; and ν is the eigenvalue.

These equations are approximated by finite difference equations at each point of a triangular mesh with uniform spacing. The outer boundary of the mesh must be a parallelogram. A 120° periodic boundary condition may be applied on the left and bottom sides to simulate a hexagonal reactor configuration, if desired. The finite difference equations at a point in the interior of the mesh involve the six neighboring points and the coefficients used are related to the material properties of the surrounding six sextants.

Other boundary conditions available include: zero flux, zero current, and

$$-D^j \frac{\nabla \phi^j}{\phi^j} = \sqrt{\Sigma^j D^j}\, \phi^j$$

as used in most KAPL codes.

A special version of the WOX6 cross section routine is used to calculate the cross sections for the thermal, epithermal, and fast groups. The WOX6 routine is based upon the prescription of Deutsch, and versions of the routine have been used in the CURE (Section 10.2.2) and CUREBO (Section 10.3.2) programs.

A line relaxation is used for the flux iterations in each group which are terminated at "i" sweeps when any of the following is satisfied:

(1) i = i max, where i max is supplied as input for each group.
(2) $R^i \le s$, where $R^i = \sum_{\text{all points}} |\phi^i - \phi^{i-1}|$, and s is an input parameter.
(3) $R^i/R^1 \le \epsilon(m)$, where m is the power iteration index, and $\epsilon(m)$ is supplied as input.

When the flux iteration criteria have been satisfied in all three groups, a new source is calculated for group one, and ν is calculated. The new source is then extrapolated by use of Chebyshev polynomials. After each power iteration, the latest flux and source values are written on tape and the program may either edit these values or continue until $|\nu^m - \nu^{m-1}| < q$ for two consecutive iterations; q is an input number.

Input Information Required

For WOX6:

The input consists of two parts. Part one is the material-independent input and includes:

1. Problem identification.
2. Buckling.
3. General temperature.
4. Options for cross section calculation.
5. Fraction of steady-state reactor power reduction used in peak xenon calculation.

Part two consists of a material-dependent input table. The table includes:

1. For each material: material index, volume, temperature, age option, F or control rod equivalence factors, xenon option, operating power or xenon concentration, specific moderator density, and thin region theory options.

2. Effective mass of fuel and burnable poison, for each core material. It is assumed that the fuel is U^{235}, and the burnable poison is B^{10}.
3. Volume fractions of water, zirconium, aluminum, iron, Zircaloy, Inconel, polyethylene, and stainless steel in each material.

For FLEER:
1. Specification of the flux guess, if used.
2. Mesh spacing. Point mesh may contain up to 14,000 points.
3. Boundary conditions.
4. Relaxation factors for the groups.
5. Acceleration parameters (if desired).
6. Convergence criteria.
7. Detailed description of material composition and geometric configuration of the mesh.

Output Available

The on-line output consists of convergence summaries that include:
1. Problem identification.
2. Number of outer iterations.
3. Value of the eigenvalue, ν.
4. $k_{eff} = 2.46/\nu$.
5. $\sum_{\text{all points}} |S^{i*} - S^{i-1}|^2$, where S* represents the unextrapolated source value for group one, and S the extrapolated value.
6. ν_{max} and ν_{min}, where $\nu_{max,\,min} = \nu^i \, (S^{i-1}/S^{i*})_{max,\,min}$ for all points.
7. $(1/2\nu)\,(\nu_{max} - \nu_{min})$.
8. Source extrapolation parameters.
9. Number of inner iteration mesh sweeps.
10. Residual values.
11. Calculated acceleration parameters.

The off-line output includes, in addition:
1. WOX6 output.
2. Topological material mesh.
3. Relative power at each point.
4. Group fluxes at each point.
5. Volume of each material present.
6. Total volume of fuel material.
7. Group-dependent flux integrals.
8. Material power fractions.
9. Power densities.

MUG II

Description

MUG II is a two-dimensional, multigroup program[111,112] designed for the three coordinate systems (x-y, r-z, r-θ), and is the basis of the later TOSPY, CURE, and PDQ programs, which are also described in this section. In the MUG II program

$$\Sigma^j \equiv [w_2^j(\Delta u/\xi\Sigma_s)^j]^{-1} + \Sigma_a^j + D^j B^2$$

and

$$S^j \equiv \left(\frac{1 + (w_1/w_2)}{\Delta u}\right)^j q_{j-1} + \frac{\chi^j \mathscr{S}}{\Delta u^j}$$

when ϕ is defined as flux per unit lethargy; or

$$\Sigma^j \equiv \left(\frac{\xi \Sigma_s}{\Delta u}\right)^j + \Sigma_a^j + D^j B^2$$

and

$$S^j \equiv \left(\frac{\xi \Sigma_s}{\Delta u}\right)^{j-1} \phi^{j-1} + \chi^j \mathcal{S}$$

when ϕ represents the flux in the group. $\mathcal{S}$ represents the fission distribution. An input parameter determines the numerical approximation used.

At any boundary of the $x_1 - x_2$ geometry, the boundary condition: zero flux, or constant current-to-flux ratio, may be employed. A third possibility for boundaries of constant x_2 is, for any given x_1 and energy, the flux and the normal derivative at both boundaries of x_2 are equal. This is the periodic condition.

The neutron flux for a particular group is determined by iteration on a guess. The error criterion $\mathcal{A}$, an input quantity, is used as a convergence test for group flux iterations as follows:

$$E^i = \sum_n |\phi_n^i - \phi_n^{i-1}| < \mathcal{A}$$

A second condition included to terminate these iterations is:

$$E^i < E^1/20$$

When a power iteration is done, the fluxes and powers are available for editing or use as input to a succeeding run.

A version of the MUG II code provides for the Selengut-Goertzel treatment of hydrogen scattering for the case of hydrogen-moderated reactors.

Convergence in r-θ geometry is extremely slow near the origin. A procedure is available which permits one-dimensional calculations for the closely-packed origin over a period determined by the operator. This procedure effects a reduction in running time and does not affect the accuracy in the final runs.

Input Information Required

1. Specification of geometry.
2. Location of interfaces and mesh points. Mesh size must be constant along each axis, and, at most, seven regions are permitted along each axis.
3. Material composition of each region.
4. Boundary conditions.
5. Convergence criterion.

Output Available

The following are available for editing after each power iteration:

1. Problem parameters.
2. Group fluxes for each mesh point.
3. Group flux integrals for each iteration.
4. Value of power at each point.

Related Codes

The UNIVAC two-dimensional code TOSPY is an extension of MUG II to include thin regions, such as H_2O gaps and control rods, and variable mesh spacing.

PDQ 2

Description

This two-dimensional code[113,114] solves the one- to four-group neutron diffusion equations over a rectangular region of the x-y or r-z plane. The equations solved use:

$$\Sigma^j \equiv D^j B^2 + \Sigma_a^j + \Sigma_s^{j \to j+1}$$

$$S^j \equiv \frac{\chi^j \psi^j}{\lambda} + \Sigma_s^{j-1 \to j} \phi^{j-1}$$

$$\psi^j \equiv \sum_{k=1}^{j} \nu \Sigma_f^k \phi^k$$

where λ is the eigenvalue.

The two-dimensional rectangular region, R, is composed of diffusion regions and rod regions. The flux and current are continuous across any interface between two diffusion regions. The flux for one or more groups is not defined interior to rod regions, but is set to satisfy the boundary condition: ratio of current-to-flux is an input constant along these boundaries. For all other groups, the region is treated as a diffusion region. The only restriction on the placement of rod regions is that no two rod regions intersect or have a common boundary.

The external boundary conditions which may be used are the zero flux condition, or the symmetry condition, $d\phi/dr = 0$. The symmetry condition is applied one-half an interval inward from the external boundary so that the flux values at the boundary point and at the first interior point are equal.

A mesh of vertical and horizontal lines is imposed on the rectangular region, R, so that all internal and external boundaries lie exactly on mesh lines. The differential equations are then approximated by difference equations using five-point formulae. Using the Young-Frankel successive over-relaxation method with approximate values of λ, the flux, and source at each mesh point, the mesh is swept and solved for improved values of the group j flux. Each sweep constitutes an inner iteration, and inner iterations are continued in each group until the flux at each point is non-negative and the residual

$$R^i = \sum_n |\phi_n^{i+1} - \phi_n^i| < \epsilon' R^0$$

where ϵ' is the larger of 0.05 and the input parameter ϵ.

At this point, calculation in group j + 1 is begun with the latest values of ϕ^j and approximate values of ϕ^{j+1}. After a set of inner iterations has been performed in each group, a new source approximation, and a new λ are calculated. Use of a source extrapolation technique based on Chebyshev polynomials is included to accelerate convergence.

The criterion for stopping the outer iterations is:

$$[(\bar{\lambda})^m - (\underline{\lambda})^m]/\lambda^m \leq 2\,\epsilon^2$$

where m is the outer iteration index, and

$$(\bar{\lambda})^m = (\lambda)^{m-1} \max_n [(\psi)_n^m/(\psi^*)_n^{m-1}]$$

$$(\underline{\lambda})^m = (\lambda)^{m-1} \min_n [(\psi)_n^m/(\psi^*)_n^{m-1}]$$

with $(\psi^*)_n^{m-1}$ being the extrapolated source approximation.

The code will perform a special type of mesh sweep in square x-y problems which are symmetric with respect to the diagonal. This results in a considerable reduction in running time.

In the case of one-group, homogeneous source problems, the source approximation used at each point is the numerical average of the input flux approximations for the compositions in the four quad-

rants about the point, multiplied by the weighted average of the four values of $\nu\Sigma_f$. The code finds the flux corresponding to this source which meets the condition:

$$R^i = \sum_n |\phi_n^{i+1} - \phi_n^i| \leq \epsilon$$

and then averages and edits this flux.

Input Information Required

Problem parameters:

1. Problem identification.
2. Geometry option (x-y or r-z).
3. Special source calculation option (source values for each mesh quadrant may be computed for off-line punching or printing, if desired).
4. Edit options (flux edits for any group or the standard source edit may be bypassed).
5. Symmetry option.
6. Number of groups (≤ 4).
7. Number of compositions (≤ 35), and the definitions of the compositions, i.e., composition number and indices of columns and rows forming its boundaries.
8. Definitions of the mesh, i.e., mesh interval and column index at which interval changes. The total number of interior mesh points allowed by the code depends upon the core storage of the IBM-704 being used. The maximum number is 1,250 for a 4K core; 2,500 for an 8K core; 3,750 for a 16K core; and 6,500 for a 32K core.
9. Boundary condition parameters.
10. Buckling.
11. Initial approximation to the eigenvalue.
12. Convergence criterion, ϵ.

Material properties for each composition:

1. Values of D, Σ_a, $\Sigma_s^{j\to j+1}$, and $\nu\Sigma_f$, for each energy group except $j = J$; D^J, Σ_a^J, and $\nu\Sigma_f^J$, for the thermal group.
2. Input flux approximation for each group. If $D^j = 0$, ϕ^j must equal zero, and Σ^j is replaced by C^j, the constant for the logarithmic derivative condition to be applied at the boundaries of this composition.
3. Fission spectrum fractions: χ^1, χ^2, χ^3. The requirements imposed on the fission spectrum are $\chi^1 = 1$ for $J = 1$; and

$$0.95 < \sum_{k=1}^{J-1} \chi^k < 1.05, \text{ and } \chi^J = 0 \text{ for } J > 1$$

There is a limitation on the total amount of input which may be used. The total of all quantities in the input, including card numbers, must not exceed 2,400.

Output Available

1. All input data are edited on-line, including a printed "picture" of the composition layout. This is limited by the width of the paper to the first 58 columns.
2. Results of the omega routine which estimates the optimum values of ω for use as overrelaxation factors.
3. Condensed results of each outer iteration, including initial and final residuals, number of inner iterations computed in each group, $\bar{\lambda}$, λ, $\underline{\lambda}$, and source extrapolation values.
4. Integrated areas, integrated and averaged final flux and source values.

The edit of the final flux and source is written on tape for off-line printing.

A binary tape of final fluxes may be written and used as the input flux approximation for another problem provided the problems contain the same number of groups, the same number of points in each coordinate direction, and the same external boundary conditions.

Related Codes

The PDQ-3 code[115] reduces the machine running time primarily through use of a line-relaxation rather than a point-relaxation iteration scheme. It treats x-y geometry only, and permits non-zero values of the fission spectrum in the thermal group. χ^j may be specified by composition, if desired, as required for adjoint calculations.

PDQ-3 integrates and averages over particular regions specified in the input data, and pointwise editing is done only in those groups and regions specified. In addition, flux-weighted values of the composition-dependent parameters are edited at the end of each problem.

PDQ-4 is a modified version of PDQ prepared for the Philco-2000 machine.

TDC

Description

TDC[67–69] is the two-dimensional, cylindrical geometry counterpart of DSN (Section 10.2.1).

The integrations are performed starting with the top slice of the cylinder. Each slice is treated as in the DSN cylindrical case, except that there is neutron flow in at the top surface and out at the bottom of each slice. When the integrations for the bottom slice have been performed, the bottom boundary conditions are applied and the whole process repeated, now going from bottom to top with neutron flow in at the bottom and out at the top of each slice. In total, therefore, there are twice as many integration directions in TDC as in the DSN cylindrical case.

The following problems may be solved:

(1) Critical dimension problems in which thicknesses of zones (either cylindrical shells, slices, or both) may be varied until criticality is achieved.
(2) Critical concentration problems in which the proportions of specified materials are varied.
(3) Reactivity problems in which ν is divided by k, and k is varied.
(4) Exponential rate problems in which α is the eigenvalue [the time variation given by exp (αt)].

The boundary condition at r = 0 is assumed reflective; the boundary condition at the bottom surface may be specified as zero flux, or perfect reflection. If the cylinder is symmetric about a central plane perpendicular to the axis, that plane is at the bottom. The top and free surface boundary conditions may specify zero flow or reflection; this is not perfect reflection but correct as far as the current is concerned.

The code is written in the FLOCO II language developed at Los Alamos for use on the IBM-704. It is a symbolic "load and go" system, and includes specialized program and input-output facilities.

Input Information Required

Problem parameters:

1. Problem identification.
2. Problem type (real or adjoint, reactivity, time-dependent, concentration, or dimension).
3. Boundary conditions.
4. Initial source guess.
5. Order of the S_n approximation.
6. Number of regions (radial and axial).
7. Number of mesh intervals (radial and axial).
8. First and second guess for the eigenvalue.
9. Convergence criterion, ϵ.
10. Number of energy groups and specification of a base group.
11. Indices to specify the cross section matrix.
12. Material composition throughout the reactor.
13. Q options and specifications for a distributed source or an isotropic boundary source at top and/or free boundary.
14. Specification of a fixed k or α, if desired, for calculation of a different eigenvalue.

687863 O - 63 - 51

Material properties:
1. Values of $\nu\Sigma_f$, Σ_{tr}, $\Sigma_s^{k\to j}$, k = 1,2, ... J, for each material and each energy group.
2. Fission spectrum fractions χ^j.
3. Velocities, v^j, if an α calculation is specified.
4. Concentration or dimension modifiers, if a concentration or dimension problem is requested.

Output Available

After each iteration, an on-line monitor print consists of:
1. Number of outer iterations.
2. Number of inner iterations.
3. Indication of convergence.
4. Value of the eigenvalue.
5. Derivative of the eigenvalue with respect to λ. (λ is defined as the total neutron population decay factor.)
6. Neutron balance.
7. Value of λ.

The tape edit for off-line printing contains:
1. Input data.
2. Storage map.
3. All iteration monitor lines.
4. Source at r = 0 and r = R.
5. Effective cross sections.
6. For each mesh point: the mid-point of the interval, fission density, volume element, and neutron flux associated with that interval.
7. Reaction summary table.

An on-line group monitor print may be obtained after each group iteration, if desired. This monitor line lists the group number, the group scale factor, neutron balance, leakage, collisions, sources, and error indicators.

Related Codes

The SYNFAR[116] program uses the one-dimensional, S_n or P_1 method to synthesize two-dimensional flux and reactivity. It solves either the static or dynamic equations.

UNCLE I, II

Description

UNCLE I and II[117,118] codes solve the one-group, two-dimensional, diffusion equation in cylindrical (r-z) and planar (x-y) geometry, respectively.

The equation solved is:

$$\nabla^2 \phi(x_1, x_2) + [B^2 (x_1, x_2) - B_0^2] \phi(x_1, x_2) = 0$$

where B_0^2 is a poison added uniformly in the space to produce criticality.

The extrapolated Liebmann method is used with the boundary conditions of zero flux at both x_2 boundaries and at the outer boundary in the x_1 direction, and zero current at the $x_1 = 0$ boundary.

The solution is obtained over a network of nine points in the x_1 direction, and sixteen points in the x_2 direction.

Input Information Required

1. Problem number.
2. Grid spacing in each direction.
3. Buckling terms.

Output Available

The problem identification, buckling terms, and flux terms at each iteration are punched for listing on an IBM-407 printer.

687863 O - 63 - 52

SUPPLEMENTARY INFORMATION

Code Name	Related Codes	Originating Installation	Machine Configuration	Running Time	References
ANGIE		Lawrence Radiation Laboratory	IBM-704 with 8K core memory, 1 drum unit, 6 tapes.	About 1 hr for 2-group problems/ 2000 mesh points.	100. R. Stuart and S. Stone, "ANGIE, A Two-Dimensional, Multigroup, Neutron Diffusion Code for the IBM-704," UCRL-5019, (1957).
			IBM-709 with 32K core, memory, 6 tapes, 2 channels.	About twice as fast as 704 version.	101. UCRL-5019 Supplement. 102. S. Stone and R. Lingenfelter, "Neutron Diffusion Theory Programs and Their Application to Simple Critical Systems," UCRL-5913, (March, 1960).
	SOPHIST I, II 2-D Multigroup Diffusion	Atomic Energy Research Establishment, Harwell, England	Ferranti-Mercury.		103. A. Hassitt, "A Programme for Solving the Multigroup Neutron Diffusion Equations in Two Space Dimensions on the Ferranti-Mercury Computer," AERE T/R 2487, (February, 1958).
CURE		General Electric Co., Knolls Atomic Power Laboratory	IBM-704 with 8K core memory, 6 tape units.		104. E. Wachspress, "CURE, A Generalized Two-Space Dimension Multigroup Coding for the IBM-704," KAPL-1724, (April 1, 1957).
			IBM-704 with 32K core memory, 3 tape units.	5 min, plus 1 min/ outer iteration.	105. F. Trantham, "CURE, A Two-Space Dimension, Multigroup Code for the IBM-704," APEX 452, (August, 1958).
	CUREM		IBM-704 with 32K core memory, 6 tape units.	8 min, plus 2 min/ outer iteration.	Ibid, Ref. 104, Modification No. 2, (September, 1958).
	PSP	U. S. Navy Department, David Taylor Model Basin	IBM-704 with 8K core memory, 5 tape units.	5 min.	106. "704 Perturbation Calculation (PSP)," AECU-4321, (1959). 107. M. Jackson, "704 Perturbation, AML Problem 840-121," AML Report 60, (October, 1957).

EQUIPOISE		Oak Ridge National Laboratory	IBM-704 with 8K core memory, 1 drum unit, 7 tape units (FORTRAN).	10–15 min for a full mesh (25 × 25) or about 100–150 iterations.	108. M. L. Tobias and T. B. Fowler, "EQUIPOISE, An IBM-704 Code for the Solution of Two-Group Two-Dimensional, Neutron Diffusion Equations in Cylindrical Geometry," ORNL-2967, (November, 1960).
	EQUIPOISE 2	Oak Ridge National Laboratory	IBM-7090 with 7 tape units (FORTRAN).	1–3 min for a 1000-point problem.	109. T. B. Fowler and M. Tobias, "EQUIPOISE-2; A Two-Dimensional, Two-Group, Neutron-Diffusion Code for the IBM-7090 Computer," CF 60-11-67, (November, 1960).
FLEER		General Electric Co., Knolls Atomic Power Laboratory	IBM-704 with 32K core memory, 7 tape units, 1 drum unit. Philco-2000.	40 min for a 1000-point problem.	110. J. L. Fletcher, et al., "FLEER: A Two-Dimensional Triangular Mesh Diffusion Program for the IBM-704," KAPL-2086, (May, 1960).
MUG II		General Electric Co., Knolls Atomic Power Laboratory	UNIVAC I with 7 tape units.	5 hr for 15-group problem on 30 × 30 mesh.	111. R. H. Stark, "Preparation of Input Data for Two-Space-Dimension Multigroup," KAPL-1068, (October, 1954).
	TOSPY				112. G. M. Roe, "Adaptation of Multigroup Methods to Cylindrical Geometries," KAPL-950, (September, 1954).
PDQ 2		Westinghouse Electric Corp., Bettis Atomic Power Division	IBM-704 with 4K, 8K, 16K, or 32K core memory, 6 tape units, 1 drum unit.	1 hr.	113. G. Bilodeau, et al., "PDQ, An IBM-704 Code to Solve the Two-Dimensional Few Group Neutron Diffusion Equations," WAPD-TM-70, (August, 1957).
					114. R. Varga, "Numerical Solution of the Two Group Diffusion Equations in x-y Geometry," WAPD-159, (August, 1956).
	PDQ-3		IBM-704 with 32K core memory, 8 tape units.	40 min.	115. W. Cadwell, "PDQ-3, A Program for the Solution of the Neutron Diffusion Equations in Two Dimensions on the IBM-704," WAPD-TM-179, (March, 1960).
	PDQ-4		Philco-2000.		

SUPPLEMENTARY INFORMATION (Continued)

Code Name	Related Codes	Originating Installation	Machine Configuration	Running Time	References
TDC		Los Alamos Scientific Laboratory	IBM-704.	0.02 sec/point group/iteration with ~70 iterations for fast systems, and ~200 iterations for slow neutron systems.	67. B. Carlson, C. Lee and J. Worlton, "The DSN and TDC Neutron Transport Codes," LAMS-2346, (February, 1960). 68. B. Carlson, C. Kazek and C. Lee, "Numerical Solution of Transient and Steady-State Neutron Transport Problems," LA-2260, (May, 1959). 69. B. Carlson and G. Bell, "Solution of the Transport Equation by The S_n Method," Proc. 1958 Geneva Conference, 16: Paper No. 2386, p. 535.
	SYNFAR	The Martin Company, Nuclear Division	IBM-7090 with 32K core memory, 7 tape units (FORTRAN).	5 min.	116. D. H. Frederich, "APWRC-SYNFAR, A Fortran II Program for Two Dimensional Static or Dynamic Synthesis Using P1 or S2-S16 DSN Flux or Adjoint in Slab, Cylindrical, or Spherical Geometry," MND-C-2460, (January, 1961).
UNCLE I UNCLE II		E. I. DuPont de Nemours & Co., Savannah River Laboratory	IBM-650.	20 sec/iteration; ≈ 30 iterations/problem.	117. IBM-650 Program Library, 8.2.010. 118. IBM-650 Program Library, 8.2.011.

10.2.3 THREE-DIMENSIONAL GEOMETRIES

TKO

Description

The TKO code[119,120] solves the few-group, time-independent, diffusion equations in x, y, z geometry. The solution is obtained over a rectangular parallelepiped which is symmetric with respect to the plane x = y. The region of solution is thus an isosceles-right-triangular prism with a symmetry condition applied across the diagonal surface of the prism.

The equations use

$$\Sigma^j \equiv \Sigma_a^j + \Sigma_s^{j\to j+1}$$

and

$$S^j \equiv \frac{\chi^j \psi}{\lambda} + \Sigma_s^{j-1\to j}\,\phi^{j-1}$$

where

λ = the eigenvalue

$$\psi = \sum_{j=1}^{J} \nu\Sigma_f^j\,\phi^j$$

with the following restrictions:

(1) $1 \le J \le 4$.

(2) $\chi^J = 1$ for $J = 1$.

(3) $\sum_{j=1}^{J-1} \chi^j = 1$ and $\chi^J = 0$ for $J > 1$.

The parallelepiped is divided into a number of diffusion regions and rod regions. The current and flux are continuous across any interface between two diffusion regions. For one or more groups, the flux at the boundary of a rod region satisfies the condition: ratio of current-to-flux is a constant. For all other groups, the rod region is treated as a diffusion region. Either a zero flux or a zero current condition may be applied at each external boundary.

The differential equations are solved numerically by imposing a mesh of horizontal and vertical planes on the parallelepiped, and replacing the differential equations with seven-point difference equations at the points of intersection of the mesh planes.

The subsequent inner and outer iterations are analogous to the iterative procedures used in the PDQ code (see Section 10.2.2). The mesh is swept, computing the fluxes for j = 1. During each sweep, the residual

$$R^i = \sum_n |\phi_n^i - \phi_n^{i-1}|$$

is calculated; n is the point, and i is the inner iteration index. The Young-Frankel successive overrelaxation method is employed for these inner iterations which are continued until

$$R^i \le 0.05R^1 \qquad \text{for } J > 1$$

or

$$R^i \le (2 - \omega^i)\,\epsilon \qquad \text{for } J = 1$$

where ω is the overrelaxation factor, and ϵ is an input parameter. The requirement of non-negative flux values may necessitate additional iterations.

The inner iterations are completed on succeeding groups until all groups have been processed. The resulting fluxes are then used to compute an improved source approximation, ψ^m, where m is the outer iteration index. A new eigenvalue and corresponding bounds are calculated from the formulae:

$$\left(\lambda\right)^m = \left(\lambda\right)^{m-1}\left[\sum_n \left(\psi_n^m\right)^2 \Big/ \left(\sum_n \psi_n^{m-1}\,\psi_n^m\right)\right]$$

$$(\bar{\lambda})^m = (\lambda)^{m-1}\ \max_n\ (\psi_n^m/\psi_n^{m-1})$$

$$(\underline{\lambda})^m = (\lambda)^{m-1}\ \min_n\ (\psi_n^m/\psi_n^{m-1})$$

If the inequality

$$\epsilon^m = \frac{(\bar{\lambda})^m - (\lambda)^m}{(\lambda)^m} \leq 2\ \epsilon^2$$

is satisfied, the problem is considered converged. If not, the source is extrapolated, using an acceleration technique based on Chebyshev polynomials, and an approximation to the homogeneous spectral norm of the outer iteration matrix. The approximation, $\bar{\sigma}$, may be given as input information, or calculated by the program.

Input Information Required

Problem parameters are:

1. Problem identification.
2. Edit options (flux edits for any group or the source edit may be bypassed).
3. Number of groups (≤ 4).
4. Definitions of the mesh, i.e., the sequence of mesh intervals in both the x and y directions, and the z direction. The number of points is limited to 2,675 and 4,725 on 16K and 32K computers, respectively.
5. Number of compositions (≤ 511), and the definition of each material composition over the mesh.
6. Boundary condition parameters.
7. Initial approximation to the eigenvalue.
8. Convergence criterion, ϵ.

Material properties for each composition:

1. Values of D, Σ_a, $\Sigma_s^{j\to j+1}$, and $\nu\Sigma_f$, for each energy group except j = J; D^J, Σ_a^J, and $\nu\Sigma_f^J$, for the thermal group.
2. Input flux approximation for each group. If $D^j = 0$, ϕ^j must equal zero and Σ_a^j is replaced by C^j, the constant for the logarithmic derivative condition to be applied at the boundaries of this region for this group.
3. Fission spectrum fractions: χ^1, χ^2, χ^3; $\chi^J = 0$ is a restriction of the code.

Output Available

The on-line output includes:

1. Problem identification.
2. Results of omega routine.
3. Condensed results of each outer iteration, including initial and final residuals, number of inner iterations performed in each group, indication of the occurrence of negative flux values, values of m, $(\bar{\lambda})^m$, $(\underline{\lambda})^m$, λ, and ϵ^m, source extrapolation coefficients α^m and β^m, renormalization factor, and value of $\bar{\sigma}$ used.
4. Indication of restarts initiated or forced edits.

All of the input data are edited off-line, including a printed "picture" of the composition layout. The off-line edit, in addition, provides the composition-integrated volumes, composition-integrated and averaged flux and source values, and the flux and source vectors called for by the input edit option parameters. The pointwise values are edited to form a "picture" of each x-y plane. Each page is labeled with the problem identification, group number, plane number, final eigenvalue, row and column identification, and the page number.

For 2-, 3-, and 4-group problems, the flux values may be saved and used to provide a pointwise input flux guess for a subsequent problem, provided the problems have the same number of groups, mesh planes in each coordinate direction, and rod regions with interior points are similarly placed in the mesh.

A preliminary input edit may be written immediately after the input is read. This allows the problem originator to examine these edits before proceeding.

TRIXY

Description

TRIXY is a three-dimensional, diffusion theory, Cartesian coordinate system code[121,122] with:

$$\Sigma^j \equiv \Sigma_a^j + \Sigma_s^{j\to j+1}$$

and

$$S^j \equiv \chi^j \mathscr{S} + \Sigma_s^{j-1\to j}\,\phi^{j-1}$$

where $\mathscr{S}$ represents the accelerated normalized power distribution.

The difference equations are obtained by integrating the group diffusion equation over the volume associated with each point. Assuming S^j is known, this system of linear algebraic equations with $x_1 \cdot x_2 \cdot x_3$ unknowns is solved by the accelerated Liebmann technique, with a renormalization factor applied to ensure neutron balance.

Group iterations are carried out in order of increasing j. A group iteration consists of as many mesh sweeps as are required to satisfy any of the convergence criteria:

$$\epsilon_1^i = \sum_n \left(\phi_n^{j,i} - \phi_n^{j,i-1}\right)^2 \le \delta_1^j$$

where δ_1^j for each group is specified as input data, or

$$\epsilon_1^i \le \epsilon_1^1/C$$

or

$$i = I_{max}$$

where C is a predetermined parameter and I_{max} is the number of sweeps allowed.

A run m consists of flux iterations over all groups followed by a calculation of the power distribution normalized to 1 neutron/(sec)(cm^3 of core). Iteration on power is terminated after run m provided

$$\epsilon_2^m = \sum_n |\bar{\mathscr{S}}_n^m - \mathscr{S}_n^{m-1}| \le \delta_2$$

where the bar indicates no acceleration factor has been applied, and δ_2 is specified as an input parameter.

An acceleration factor, ω, is used for the power iteration as follows:

$$\mathscr{S}_n^m = \mathscr{S}_n^{m-1} + \omega\,(\bar{\mathscr{S}}_n^m - \mathscr{S}_n^{m-1})$$

Boundary conditions are specified independently for each face of the rectangular parallelepiped. The conditions may be: zero flux or constant outward current-to-flux ratio.

Scattering is restricted to degradation from the next higher energy group.

Adjoint fluxes may be computed, provided Σ_t^j/Σ_t^j is independent of position throughout the core portion of the mesh.

The program can be run on an 8K, 16K, or 32K IBM-704 computer with appropriate mesh limitations; for a 32K machine, the product of the number of mesh points perpendicular to the x_2 and x_3 axes must be < 4,000. Up to 975 material compositions are permitted within the mesh, and 3,000 within the

file of cross section records. Up to six energy groups may be used and the product of the number of mesh points and energy groups is limited to 150,000. There may be up to 72 mesh planes perpendicular to any of the three axes.

Input Information Required

Problem parameters:

1. Indices for each of the three dimensions (x_1, x_2, x_3).
2. Flux convergence criteria, δ_1^j, for each group.
3. Power convergence criterion, δ_2.
4. Description of the core, including volume, group number of highest energy group where fissions may occur, and the six mesh planes bounding all fissionable material.
5. Composition identification of reflector current-to-flux ratio boundary conditions.
6. Specification of configurations of materials (lists A and B).
7. Mesh point spacings.
8. Input control data for the edit routine, including selected columns, regions, and groups for flux, flux integral, and power density and power integral printouts.
9. Power guess, either available from a previous problem, or a rough power guess supplied for a coarse mesh.

The library tape contains a file of configurations and files of cross section data.

A configuration is an area of uniform material composition in a plane normal to the x_3 axis. Each configuration is a record in the configuration file. Lists A and B of input information are used to project these plane figures into three-dimensional volumes. List B is the control rod list and the control rod configurations are superimposed upon the list A configurations.

Each cross section file contains four records:

1. Identification number, number of energy groups (≤ 6), fission spectrum fractions χ^j, and number of words in each record in the file.
2. Values of D^j, Σ^j, $\Sigma_s^{j-1\to j}$, Σ_f^j for all compositions containing fuel, in order of increasing composition index.
3. Values of D^j, Σ^j, $\Sigma_s^{j-1\to j}$, for all non-fissionable compositions, in order of increasing composition index.
4. Outgoing current-to-flux ratios for various reflector compositions; J values are listed for each composition, in order of increasing composition index.

The composition index is specified in lists A and B for proper assignment of material cross sections.

Output Available

Seven different items of output may be requested. These are combinations of the following data:

1. Power densities for each point, followed by the power integral and the power density of the column either for all planes perpendicular to x_1 or selected columns.
2. Power integral for every column for all planes perpendicular to x_1.
3. Power density for every column for all planes perpendicular to x_1.
4. Number of fissions per source neutron for each group followed by the total.
5. Flux integral for each composition for each group.
6. Average flux for each composition for each group.
7. Flux for each point for specified groups for all planes perpendicular to x_1 or selected columns.

The criticality and source error are printed for each source iteration.

UFO

Description

UFO is a few-group program[123] with

$$\Sigma^j \equiv \Sigma_a^j + \Sigma_s^{j\to j+1}$$

and

$$S^j \equiv \chi^j \mathscr{F} + \Sigma_s^{j-1 \to j} \phi^{j-1}$$

where

$$\mathscr{F} = \nu_c \sum_{k=1}^{J} \Sigma_f^k \phi^k$$

Boundary conditions at each face of the parallelepiped may be given as zero flux, zero current, or a specified ratio of outward current-to-flux.

The differential equation for each group is represented by a set of seven-point difference equations relating the fluxes at the mesh points of the rectangular mesh (x_1, x_2, x_3). The coefficients are determined by integrating the diffusion equation over the eight octants at the mesh point.

The multigroup difference equations are solved by using an accelerated Liebmann flux iteration procedure. Inner (flux) iterations for each group are terminated when

$$\epsilon^i = \sum_n |\phi_n^i - \phi_n^{i-1}| \leq \epsilon$$

$$\epsilon^i \leq \xi \epsilon^1$$

or

$$i = I$$

Values of ϵ and I are group-dependent and may be specified as input parameters, or supplied by the program. ξ may be given as a constant c; as a step function with one value, a, for the first two outer iterations and a second value, c, for later iterations; or as a linear function of outer iterations, m, subject to a constant cutoff value:

$$\xi = \max [a - b\,(m-1),\ c] \qquad \text{for } b > 0$$

$$\xi = \min [a - b\,(m-1),\ c] \qquad \text{for } b < 0$$

Values of a, b, and c may be specified as input parameters, or provided by the program.

The Liebmann acceleration factors, ω^j, may be specified as input or calculated by the code from estimates of the spectral norm of the matrix corresponding to these difference equations.

When all groups have successively met the convergence criteria, a new source is calculated. In the source recalculations or outer iterations, a three-term extrapolation formula is used. The formula is applied at the second or third source iteration, depending on whether or not an estimate of the "dominance ratio," λ^1/λ^0, is supplied. The accelerated source iterations generate Chebyshev polynomials of increasingly higher order. The newly calculated sources are then used as source guesses for the next outer iteration and the program proceeds through outer and inner iterations until the termination criteria are met.

The outer iterations are terminated when

$$\frac{\nu_{max} - \nu_{min}}{\nu_c} \leq E_R$$

or

$$\sum_n (\bar{\mathscr{F}}_n - \mathscr{F}_n)^2 \leq E_S$$

If neither E_R nor E_S is specified as an input parameter, manual termination is necessary.

Input Information Required

Problem parameters:

1. Problem identification.
2. Number of groups (≤ 5).
3. Group number below which no fissions occur.

4. Number of compositions (≤ 512).
5. Index of last mesh plane in each coordinate direction.
6. Boundary condition parameters.
7. Convergence criterion for the error ratio, E_R.
8. Optional input parameters (assumed values given in parentheses):

χ^j = fission spectrum fractions ($\chi^1 = 1$; $\chi^{j\neq 1} = 0$).
ϵ^j = flux convergence criterion (0).
I = maximum number of flux sweeps (0).
a_S = 2/"dominance ratio" (computed).
E_S = source convergence criterion (0).
c,a,b = flux convergence parameters (0.05;0;0; if a_S specified; 0.05;0.005;0; otherwise).
Z = value of flux residual below which residual calculation will be computed for every sweep, rather than every fifth sweep (100).
ω^j = accelerated Liebmann factors (computed).

9. Definitions of the mesh, i.e., mesh intervals in each of the three coordinate directions.
10. Description of the composition planes.

Material properties for each composition:
1. Values of D, Σ_a, $\Sigma_s^{j\rightarrow j+1}$, and $\nu\Sigma_f$, for each energy group except j = J; D^J, Σ_a^J, and $\nu\Sigma_f^J$, for the thermal group.
2. Input flux approximation for each group for the initial iteration.

Certain parameters may be changed during the running of the problem. This is especially useful where the choice of parameters may be determined on the basis of early output, and affords the opportunity for correction of poor estimates.

The number of mesh planes is limited by: $(I)(J) \leq 4{,}000$; $(J)(K) \leq 4{,}000$; where I-1, J-1, and K-1, are the number of mesh planes interior to the reactor region for the x_1, x_2, and x_3 directions, respectively.

The number of mesh points and point types, Q, is limited by: $(I)(J)(K) + Q \leq 17{,}000$; $2(I-1)(J-1)(K-1) + 7Q \leq 30{,}200$.

Additional memory space is achieved by keeping tables of coefficients with separate entries only for distinct point types. The point-type index is coded into the flux value of the point. The total number of point types must not exceed 1,900.

If there is insufficient storage, this fact will be printed and the calculation stopped.

Output Available

The on-line output lists:
1. Problem identification.
2. Overrelaxation factors (if supplied).
3. Spectral norm and overrelaxation factor (if calculated).
4. Source calculation results including the outer iteration number; error ratio, E_R; sum of residuals squared; and values of ν_c, ν_{max}, ν_{min}, and $1/\nu_c$.
5. Summary of flux iterations, including for each group: final flux residual E^I, E^I/E^1; number of inner iterations; exit criterion; and value of I.
6. Value of a_S (if calculated).
7. Numbers of tape units containing the most recent source/flux values.

The off-line edit lists:
1. Input data, including topological material edit, macroscopic cross sections, and flux guesses.
2. On-line output described above.
3. Total fissionable volume.
4. Total number of points of different types.
5. Final source and group fluxes (pointwise for each plane).
6. Source integrals.

SUPPLEMENTARY INFORMATION

Code Name	Related Codes	Originating Installation	Machine Configuration	Running Time	References
TKO		Westinghouse Electric Corp., Bettis Atomic Power Division	IBM-704 with 16K or 32K core memory, 7 tape units.	1.5 hr.	119. W. R. Cadwell, "TKO, A Three-Dimensional Neutron-Diffusion Code for the IBM-704," WAPD-TM-143, (October, 1959). 120. W. R. Cadwell, "The TKO-1 Code," WAPD-T-926, (December, 1958).
TRIXY		General Electric Co., Knolls Atomic Power Laboratory General Electric Co., Flight Propulsion Laboratory Department	IBM-704 with 8K, 16K, or 32K core memory, 6 tape units.	2-3 hr.	121. P. Greebler, "TRIXY, A Computer Program for Multigroup Nuclear Reactor Calculations in Three Space Dimensions," KAPL-1549, (August, 1956). 122. F. Banan, et al., "TRIXY Multigroup Analysis of Nuclear Reactors in Three Space Dimensions," R59FPD936, (April, 1960).
UFO		General Electric Co., Knolls Atomic Power Laboratory	IBM-704 with 32K core memory, 1 drum unit, 8 tape units.	2 hr.	123. E. Auerbach, J. Jewett and M. Ketchum, "UFO, A Three-Dimensional Neutron Diffusion Code for the IBM-704," KAPL-1999, (March, 1959).

10.3 REACTOR DYNAMICS AND CONTROL

The codes described in this section treat the short- and the long-term behavior of reactors. Material inventories over the reactor lifetime are computed by the depletion codes. The kinetics programs facilitate studies of reactor stability and control, and other programs evaluate control rod systems or cells.

10.3.1 CONTROL CELLS AND WORTH EVALUATION

Only those codes specifically designed to determine the worth of control assemblies are included in this section. Many codes developed primarily for other uses can be applied to this problem as well. Some of these may be found in Sections 10.1.3, 10.1.4, and 10.2.

SCRAM I

Description

The SCRAM I code[124] employs a modified two-group theory[125] to compute the gross rod worth of a central, cylindrical control rod plus M identical rods in a ring concentric to the central rod. The code is applicable only to a bare, cylindrical reactor with cylindrical rod configuration; non-circular rods must be approximated by equivalent cylinders. Control rods may be solid or cylindrical shells filled with moderating material. The absorbing material is considered black to thermal neutrons, and to have no effect on fast neutrons.

The reactivity worth of the rod(s) is defined by:

$$\rho = \frac{(\nu_c^f/\nu) - (\nu_c^0/\nu)}{(\nu_c^0/\nu)}$$

The code computes values of

$$\frac{\nu_c}{\nu} = \frac{1}{k_{eff}}$$

The first value computed (ν_c^0/ν), corresponds to no rods in the reactor. It is obtained from a modified two-group formula for k_{eff} which includes contributions from fast (k_f), and thermal (k_{th}) multiplication factors. Other values of (ν_c/ν) are tried, and k_f and k_{th} modified accordingly, until a value of (ν_c^f/ν) is obtained which satisfies the criticality determinant for the reactor with the rods inserted.

Input Information Required

1. Number of rods in the ring, ring radius, and rod radius.
2. Reactor radius, reflector savings, and axial buckling.
3. For the reactor core: resonance escape probability; fast fission factor; Fermi age = τ; diffusion length; fast (D_f) and thermal (D_{th}) diffusion coefficients; k_f; and k_{th}.
4. For the rods: Fermi age, and fast diffusion coefficient.

Output Available

The output is on punched cards which contain:

1. Input data.
2. Sequence of values of $(\nu_c^0/\nu) \ldots (\nu_c^f/\nu)$, and critical determinant values for all iterations.
3. Final values of the material buckling; ρ; and k_{eff}.

Related Codes

Similar calculations are performed by the following codes: PPCo 10-006, PPCo 10-009, and PPCo 10-010.

SUPPLEMENTARY INFORMATION

Code Name	Related Codes	Originating Installation	Machine Configuration	Running Time	References
SCRAM I		Alco Products, Inc.	IBM-650.	5 min.	124. P. V. Oby, "SCRAM I: Control Rod Worth Calculation on the IBM-650," APAE Memo 89, (April, 1957). 125. R. L. Murray and J. W. Niestle, "Reactor Control Rod Theories," Nucleonics, 13: No. 2, 18, (February, 1955).
	PPCo 10-006 10-009 10-010	Phillips Petroleum Co., (NRTS)	IBM-650.	2 min/ν value. 1 min/ν value. 2 min/ν value.	

10.3.2 BURNUP

The following codes compute changes in reactivity and material concentrations due to fuel depletion, poison buildup, breeding, and conversion over the operating lifetime of a reactor. The criticality programs in Section 10.2 are often used as subprograms.

BOUT AND BOUT II

Description

The application of the BOUT and BOUT II codes[126] is limited to reactor models containing a single fuel, or a single fuel and a single burnable poison.

Given fuel, burnable poison, and fission product concentrations over the reactor, the routines, NEXT and HUF, calculate the cross-section input to the PROD II diffusion code (Section 10.2.1). PROD II computes the critical position of the control regions. These results are used by the BOUT program to calculate values of fuel, burnable poison, and fission product concentrations, remaining in the reactor. This procedure is repeated for each successive time step until the excess reactivity in the reactor is depleted.

There is provision for either steady-state or a peak-xenon specification.

The BOUT II code incorporates fuel self-shielding.

Input Information Required

Problem parameters to be specified at each time step:

1. Total fuel burned out.
2. Fission products (equivalent B^{10}) formed.
3. Total power.
4. Ratio of poison-to-fuel absorption cross sections.
5. Self-shielding factor for poison under full power.
6. Factor to give equivalent poison self-shielding under shutdown.

Parameters required at each time step for each region of the reactor model:

1. Burnable poison self-shielded for the "hot" condition.
2. Burnable poison self-shielded for the "cold" condition.
3. Fraction of original burnable poison remaining.
4. Fraction of original fuel loading remaining.
5. Fuel and burnable poison originally present.
6. Volume of the region.
7. Ratio of 2nd group flux to 3rd group flux, neglecting leakage in group 3.

Output Available

The following data are punched for each time step:

1. Fraction of power in each region.
2. Sum of power fractions over successive regions from center of reactor through each region.
3. Average power density in each region.
4. Fuel in each region.
5. Fractions of original fuel, fission products, and burnable poison remaining.
6. "Hot" and "cold" burnable poison in each region.

BOX

Description

BOX is a one-dimensional, three-energy-group code[127] that computes flux distributions throughout the life of highly enriched, water-cooled, water-moderated reactors.

The cross sections and related group constants are obtained by averaging nuclear cross section data over the appropriate energy group as in the CURE program (Section 10.2.2). The neutron fluxes and the eigenvalue are then obtained by numerical approximations to the solution of the three-group diffusion theory equations. The code for this section is a modification of the WANDA program (Section 10.2.1). The code allows for slab, cylindrical, or spherical geometry, and for the flux or the derivative of the flux to vanish at the boundaries as boundary conditions.

Reactor control rods are represented by the "window shade" technique, an area absorption method. Instead of considering the actual rod geometry, the source neutrons are reduced by a rod-absorption factor dependent on the core and rod composition, rod geometry, and rod interaction effects. A depletion calculation is performed when a rod position yields minimum departure from criticality. This depletion calculation permits separate fuel and poison self-shielding but assumes the same ratio of epithermal-to-thermal absorption for fuel and poison.

Fission product buildup is calculated on the assumption of a constant fuel volume determined by the initial loading, and is a function of the fuel depletion factor in a region. Effects of epithermal fission and capture are ignored. The depleted fuel and poison masses are then used to compute a new set of cross sections and group constants for the next time step.

At each time step, the flux distribution and eigenvalue are determined for steady-state xenon depletion, for peak xenon override with control rods entirely withdrawn, and for cold shutdown conditions. This is repeated for as many depletion steps as desired.

A general temperature may be specified for all regions, or a specific temperature for any one or all regions. Age factors may be supplied as input data, or the code will calculate them as a function of the fraction of water specified. All materials must include either some fraction of water or values for the ages for groups 1 and 2.

Input Information Required

Problem parameters:

1. Initial fuel and poison masses.
2. Initial fractional power distribution.
3. Initial fuel and poison concentration factors.
4. Amount of fuel depleted in each time step.
5. Geometry (slab, cylinder, sphere).
6. Number of regions ($\leq$250).
7. Number of mesh points ($\leq$250).
8. Boundary conditions to be applied.
9. Convergence criteria.
10. Extrapolation factors for the source iteration procedure.

Output Available

1. Cross section and related group constants for each region.
2. Converged eigenvalue, flux and source distributions, region flux and source integrals and volumes, for each 3-group calculation.
3. Depleted fuel and poison masses, and depletion factors for each time step.

Provision is included for punching of restart data before each depletion calculation.

BURNOUT

Description

The BURNOUT code[128] was prepared for use in conjunction with the one-dimensional, multigroup diffusion code GNU (Section 10.2.1).

A GNU calculation provides the flux distribution throughout the reactor. The results are used by BURNOUT to solve the series of 15 simultaneous differential equations describing the production, absorption, and beta decay, thereby furnishing new values of nuclide concentrations in the various reac-

tor regions. This information is used in a second GNU calculation to determine the flux distribution to be used for the next time step, and so on. The assumption is made that the flux distribution is constant throughout a time step.

Elements that may be included are Th^{232}, Pa^{233}, U^{233}, U^{234}, U^{235}, U^{238}, Np^{239}, Pu^{240}, Pu^{241}, I^{135}, Xe^{135}, Pm^{149}, Sm^{149}, and a fictitious element to account for fission products.

A xenon override test may be applied at specified time steps. In this case, the burnout equations are solved with a zero flux level for a specified number of hours and the densities are modified appropriately. A GNU calculation then determines whether the reactor would be supercritical. If not, the computation may either stop or return to assume the densities used previous to the test and continue.

Input Information Required

1. Time (in days) for which the time steps are to be calculated (≤10 values).
2. Cross section print-out option (macroscopic cross sections may be printed, if desired).
3. Flux print option (a GNU print option).
4. Power levels for each time step.
5. Chains to be considered (≤6), i.e., Th^{232}, U^{235}, etc.
6. Gas diffusion constants (≤3), (these are used to modify the decay constants).
7. Atomic weights for mass print-outs.
8. Stop options.
9. Criticality options.
10. Lateral dimension of reactor.
11. Xenon test options.
12. GNU input specifications.

Output Available

1. Input information.
2. Value of k_{eff} for each GNU iteration.
3. For each completed GNU calculation: power density distribution; absorptions and fissions by regions and by elements; and table of masses by element and region.
4. For each time step, a table of atomic densities constructed from the solution of the burnout equations.

CANDLE 1

Description

CANDLE[129–131] designates a series of one-dimensional, depletion programs. This description will pertain to CANDLE 1 except as the CANDLE 2 and CANDLE 3 modifications are noted.

CANDLE 1 assumes, initially, that the elements comprising a region are uniformly distributed. The 4-group diffusion equations of WANDA[91] are used.

When criticality is attained, the fluxes in each group are normalized to a specified total power output and used in the isotopic-density equations to compute new isotopic number densities at each mesh point. These equations have the general form:

$$\frac{dN_n^M}{dt} = -\lambda^M N_n^M(t) - N_n^M(t)\left(\sum_{j=1,2,3} \sigma_a^{M,j}\,\phi_n^j + g^{M,4}\,\sigma_a^{M,4}\,\phi_n^4\right) + \lambda^{M-1}\,N_n^{M-1}(t) + N_n^{\overline{M}}(t)\left(\sum_{j=1,2,3} \sigma_a^{\overline{M},j}\,\phi_n^j + g^{\overline{M},4}\,\sigma_a^{M,4}\,\phi_n^4\right)$$

where N_n^M, N_n^{M-1}, and $N_n^{\overline{M}}$ are the isotopic densities of different isotopes M at mesh point n; λ is the decay constant; and $\sigma_a (= \sigma_c + \sigma_f)$, the microscopic absorption cross section. The constant, g^4, is the thermal self-shielding factor.

In solving the isotopic density equations, it is assumed that the flux is constant over a time interval. These isotopic densities and the microscopic cross sections are used to calculate new group constants for each mesh point. Special formulas are used for $\Sigma_s^{3\to4}$ and Σ_a^3 to account for the variable self-

shielding of the resonance absorption when U^{238} is present. The criticality search can then be carried out for the next lifetime stage.

A maximum xenon override test can be performed at the end of any burnout stage. An eigenvalue is computed under the condition of no external control (i.e., with all control poison removed, or with the control buckling equal to the specified "end of life" buckling). If this eigenvalue is ≤ 1, it is not possible to override peak xenon and the computation may terminate at this point; if >1, a criticality search can be done.

"End of life" options included are:

(1) When it is no longer possible to override peak xenon.
(2) When it is no longer possible to override equilibrium xenon.
(3) When a specified number of time steps have been completed.
(4) When any one of the number densities of the burnable elements becomes negative.
(5) When any of the group cross sections becomes negative.

Input Information Required

Problem parameters:

1. Problem identification.
2. Number of mesh points (≤ 251; must be odd).
3. Number of regions (≤ 25).
4. Geometry (slab, cylinder, sphere).
5. Boundary conditions.
6. Convergence test to be employed and criteria ϵ_1, ϵ_2.
7. Number of energy groups (4 for CANDLE 1).
8. Extrapolation factors.
9. Buckling options (group or region variable).
10. Criticality search parameter (buckling, poison, boundary), and initial guess.
11. Height (if not to be calculated).
12. Number of elements.
13. Number of self-shielding factors ($\neq 1$).
14. Number of time steps (≤ 25).
15. Δt (sec), and power (watts), for each time step.
16. Region definitions (interface point numbers, mesh widths and control region identifiers).
17. Xenon option (% by which flux is to be reduced, Δt for xenon buildup, and time steps for use).
18. Source guess.
19. Edit options.

Material properties:

1. Isotopic densities, self-shielding factor ($\neq 1$) and thermal cross sections (σ_{tr}, σ_a, $\nu\sigma_f$, σ_f) for the elements specified. Fast cross sections are available in the CANDLE library.
2. Fission spectrum fractions (χ^1, χ^2, χ^3).
3. Values of the fractions of Σ_p (t^1, t^2, t^3).
4. Value of Σ_p for each region.
5. Values for resonance escape for U^{238} for each region (= 1 if region does not contain U^{238}).

If desired, a completed problem may be modified and the problem continued.

Output Available

The supervisory output is printed on-line and includes:

1. Region-group data for time zero.
2. Values of control parameters and associated eigenvalues.
3. Region and total integrals of source-normalized power.
4. Isotopic densities of fissionable elements.
5. When the maximum xenon override test is used, control parameters, eigenvalues, pointwise and integrated power values are available.

In addition, any or all of the following may be selected for any or all time steps:

1. Control parameters and eigenvalues.
2. Values of $\Sigma_s^{j\rightarrow j+1}$, Σ_a, $\nu\Sigma_f$, and D, for each point and each group.
3. Values of the source and flux for each point and each group.

687863 O - 63 - 53

4. Values of the power for each fissionable element, total power for each point, and region and total integrals.
5. Values of region and total integrals of isotopic densities of the fissionable elements.
6. Values of isotopic densities of the time-dependent elements for each point (U^{235}, U^{236}, U^{238}, Pu^{239}, Pu^{240}, Pu^{241}, Pm^{149}, I^{135}, Sm^{149}, Xe^{135}, fission products, B^{10}, and a second burnable poison).

Related Codes

CANDLE 2 differs from CANDLE 1 as follows:
1. Provision has been made for a 2-group option.
2. The fast cross section library has been improved.
3. The input has been modified (iodine yield is supplied as problem input, and two self-shielding factors must be specified for certain elements).
4. An average power is included as output.
5. Operating instructions have been revised.

CANDLE 3 differs from CANDLE 2 as follows:
1. Provision has been made to calculate a pointwise varying, group-dependent buckling for the diffusion equations as a function of the fuel fraction.
2. A change allowing more flexibility in the boundary-search option has been included.
3. The buckling and poison criticality search options are not included.
4. Input and output modifications are included to permit input of coefficients for a "polynomial buckling" option, and output of the buckling values.

A version of CANDLE is also available for the Philco-2000 computer.[132]

CUREBO

Description

The CUREBO[133] code consists of three major parts:
(1) Calculation of the cross sections for the reactor regions (WOX7).
(2) Solution of the multigroup diffusion equations in two-space dimensions for the reactor (CURE, Section 10.2.2).
(3) Calculation of fuel and poison depletion as a result of steady-state operation of the reactor (BO 2).

The depletion calculations (BO 2) may be one of three types, depending upon the location of the burnable poison in the region: (1) discrete poison, where all the burnable poison is subject to a self-shielding factor different from the fuel self-shielding factor; (2) homogeneous poison, where all of the burnable poison is subject to the same self-shielding factor as the fuel; or (3) combination poison, where some of the burnable poison is subject to the fuel self-shielding factor, and the remainder to a different self-shielding factor.

WOX7 calculates neutron cross sections based upon the Deutsch prescription. It is assumed that the fuel is U^{235} and the burnable poison is B^{10}. Effective masses of fuel and poison in core materials are calculated from actual masses. The effective neutron temperature, thermal cutoff, and age factors are determined before the 3-group cross section calculations are performed. Optional calculations permit rod representation by the "cylindrical shell" or "window shade" model, and any of four xenon representations for each core region: no xenon, steady-state xenon, peak xenon, or transient xenon.

The CURE codes included in CUREBO are modifications of the CURE few-group code as originally developed by Computer Usage for KAPL (Section 10.2.2). The five current versions of KAPL CURE, as used in CUREBO, are:

CURE 1CT – does not use drums; uses 6 tape units; number of points $\leq$3,294; slow Peaceman-Rachford flux calculation.

CURE 1C – uses drums; 6 tape units; number of points $\leq$2,046; slow Peaceman-Rachford flux calculation.

CURE 2CT – does not use drums; uses 7 tape units; number of points $\leq$3,236; limited to full rectangular meshes in x-y or r-z geometry; fast Peaceman-Rachford flux calculation.

CURE 2C – uses drums; 7 tape units; number of points ≤2,046; limited to full rectangular meshes in x-y or r-z geometry; fast Peachman-Rachford flux calculation.

CURE 3CT – modified line inversion technique used for flux calculation; limited to periodic x-y geometry; number of points ≤3,249; uses 6 tape units.

When any of several CURE tapes is usable, the most restrictive code tape is the fastest.

Input Information Required

Problem parameters to be specified for WOX7 and BO 2 are:

1. General temperature.
2. Regional properties including region index, region volume, initial discrete poison ratio, temperature, age, self-shielding, and xenon options; actual mass of U^{235} or B^{10} in region; volume fractions of water, zirconium, aluminum, iron, stainless steel, Zircaloy, ethylene, Inconel, and void, for the region; and specific moderator density.
3. Values of ν(critical) calculated by CURE which will initiate the depletion calculation, and the fuel depletion factor to be used to calculate the new fuel and poison concentrations in the depletion code.
4. CURE general mesh description, boundary condition specifications, point and material specification, and special configuration descriptions.

Output Available

On-line output consists of iteration summaries of each CURE iteration. Each summary includes:

1. Value of k_{eff}.
2. Flux convergence summaries by groups.
3. Estimate of flux error and related iteration parameters.
4. Machine error indicators.

Off-line printing consists of:

1. The WOX7 output, including the macroscopic uranium cross section, average absorption cross section, and xenon cross section, for each region; temperatures; all cross sections as they are prepared for the CURE code; thickness of all designated "thin regions"; control rod equivalence factors; and the CURE input edit.
2. The CURE output, including the iteration summaries as printed on-line; material, power, and flux maps; integrated region volumes; fluxes for each of the first three energy groups; power fractions; and power density.
3. The BO 2 input edit and output, including concentration of fuel and of poison, and depleted mass of fuel and of poison, in each region.

Optional output that may be printed consists of:

1. CURE coefficient edit.
2. Topological point and point-type edits.
3. Plain source, plain flux, and plain power edits.
4. WOX7 input edit (if decimal input is used).

Punched card output, supplied by BO 2, is used as the binary input for WOX7 to continue the calculation for the next time step.

DRACO

Description

DRACO[134] is a three-dimensional, few-group depletion code. Group cross sections and related constants are calculated and used in solving the modified neutron diffusion equations of TKO (Section 10.2.3). The resulting fluxes are normalized to a specified output power. Assuming these fluxes are constant over the specified "time step," new isotopic densities are computed for the time-dependent elements. The isotopic densities of time-independent elements are specified for each time step and are assumed constant within a composition. The code handles either two- or four-energy-group calcula-

tions. Microscopic cross sections for the three fast neutron energy groups are included in the program. The thermal cross sections and the resonance escape probability of U^{238} and thermal self-shielding factor (where applicable), are specified as input for each time step.

Zero flux or zero current boundary conditions may be imposed at any outer boundary. The logarithmic derivative condition may be applied at the boundaries of a "rod" region.

A mesh is imposed by defining a set of x, y, and z coordinate axes, and spacing horizontal and vertical planes along these axes. With ss, tt, and uu referring to the index of the last plane in the x, y, and z coordinate directions, respectively, the following conditions must be met:

(1) ss = tt.
(2) $3 \leq$ ss, uu ≤ 28.
(3) $\frac{1}{2}$ (ss) (ss-1) (uu-1) $\leq$2,685 (16K machine); 4,750 (32K machine).
(4) the plane x = y is a plane of symmetry.

A mesh rectangular parallelepiped is defined by its eight vertices. A composition made up of one or more mesh rectangular parallelepipeds, is identified by the material contained in that region. A maximum of fifty compositions may be handled; any of thirty elements may be included.

A maximum xenon calculation, DRACO 2, may be performed at any time step except zero. The power-normalized fluxes of the requested time step are reduced by a specified percent and are used to calculate new isotopic densities for a specified interval of time. The neutron diffusion equations are solved with the cross sections and related group constants corresponding to these new densities. The resulting source-normalized fluxes are averaged for each mesh rectangular parallelepiped and normalized.

Input Information Required

Problem parameters:

1. Problem identification.
2. Code identification.
3. Number of groups (2 or 4).
4. Number of compositions ($\leq$50).
5. Number of planes in x and y, and z coordinate directions.
6. Boundary conditions.
7. Initial flux picture, sigma, and omega print options.
8. Number and size of time step.
9. Power in watts.
10. Initial eigenvalue guess.
11. Convergence criterion.
12. Mesh description.
13. Composition description.
14. Initial flux guess.

Material properties:

1. Thermal microscopic cross sections (σ_{tr}, σ_a, σ_f, and $\nu\sigma_f$), isotopic densities, and thermal self-shielding factors, for each element.
2. Fission spectrum fractions (χ_1, χ_2, χ_3) for 4-group problems, or (χ_1) for 2-group problems.
3. Poison fractions (t_1, t_2, t_3, t_4) for 4-group problems, or (t_1, t_2) for 2-group problems.
4. Iodine yield for elements U^{235}, U^{238}, Pu^{239}, and Pu^{241}.
5. Resonance escape probability of U^{238}, and homogeneous poison for each composition.
6. Constants to be applied at logarithmic derivative or "rod" region boundaries.

Output Available

When requested, a "picture" representation of the composition numbering for the entire region under consideration may be obtained immediately after the input has been processed (for checking purposes), or at the end of a time step calculation.

During a time step calculation, the following information is printed on the on-line printer:

1. Composition values of D, Σ_a, $\nu\Sigma_f$, and $\Sigma_s^{j\rightarrow j+1}$ at time step zero.
2. Omegas, eigenvalues, and associated information, from each iteration.
3. Composition-integrated volume, and composition-integrated and averaged fluxes, for each group.

4. Percentage of power for each fissionable element in each composition, and the percentage of power contributed by each composition.
5. Normalization factor used to obtain the power-normalized fluxes.

The edits available from the binary tape with DRACO 3 allow printing of data from selected rectangular parallelepipeds, including:

1. Point fluxes for specified groups.
2. Point power values.
3. Power produced by a specified element, or total power.
4. Initial isotopic densities of any selected time-dependent element.
5. Macroscopic data for any group.

Also available are edits of:

1. Composition-averaged initial isotopic densities of the time-dependent elements for each composition, or over the entire region.
2. Final integrated isotopic densities.
3. Integrated power for each fissionable element for each composition, and over the entire region; the total integrated power for each composition, the composition volumes, and the total volume.
4. Average block "stick" power.
5. Average point "stick" power, or for any specified "sticks" the point power for each point of the "stick."

GPR

Description

The GPR code[135] computes the material and reactivity balance in a plutonium recycle system under conditions of steady-state operation and linearly-graded irradiation.

Recycle process losses may be computed on the basis of either uniform or two-region spike enrichment. The two regions – feed and recycle – may have different flux levels, neutron spectra, heat generation, and exposures.

The effective cross sections used are those due to Westcott (Section 3.2.2), and are defined by specification of temperature and the proportion of epithermal neutrons in the spectrum.

For the case of a uniformly enriched reactor, the exposure, T, is calculated by a Newton-Raphson iteration scheme, using input parameters and calculated cross sections. The results are used to compute the steady-state and discharge concentrations of fuel isotopes and process losses. A set of thermal cross sections is generated and inserted in the calculation to yield η, f, and p.

If spike analysis is desired, a new spectral index is calculated based on the amount of feed displaced by the spike material. This value is used to calculate a new set of cross sections and new exposure, and the entire process is repeated until convergence is obtained.

Input Information Required

The significant input parameters are:

1. Reactivity.
2. Fast effect.
3. Proportion of epithermal neutrons in the spectrum.
4. Westcott parameters g and s, both functions of the neutron temperature.
5. Absorptions in non-fuel materials.
6. Loss rates.
7. Initial U^{235} enrichment in the feed.

Output Available

1. Values of η, f, p.
2. Regional and reactor-averaged isotopic concentrations.

TURBO

Description

TURBO[136] is the two-dimensional counterpart of the one-dimensional, depletion code, CANDLE. Two or four groups may be used. The neutron flux values are computed in either x-y or r-z geometry by using a modification of PDQ (Section 10.2.2).

The flux values obtained from the spatial calculation are normalized to a specified power output. Assuming flux and power to be constant for a specified time step, the isotopic densities are recomputed for certain fuel and fission elements. The time-dependent elements considered are U^{235}, U^{236}, Pu^{239}, Pu^{240}, Pu^{241}, Pr^{149}, Sm^{149}, I^{135}, Xe^{135}, fission products, B^{10}, and a second burnable poison. The depletion equations used in calculating the densities have the general form:

$$\frac{dN_n^M}{dt} = -\lambda^M N_n^M(t) - N_n^M(t)\left(\sum_{j=1}^{J-1} \sigma_a^{M,j}\phi_n^j + g^M\sigma_a^{M,J}\phi_n^J\right) + \lambda^{M-1} N_n^{M-1}(t) + N_n^{\overline{M}}(t)\left(\sum_{j=1}^{J-1} \sigma_a^{\overline{M},j}\phi_n^j + g^{\overline{M}}\sigma_a^{\overline{M},J}\phi_n^J\right)$$

where N_n^M, N_n^{M-1}, and $N_n^{\overline{M}}$ are the isotopic densities of different isotopes at mesh point n; λ is a decay constant; σ_a is the microscopic absorption cross section; and g is the thermal self-shielding factor.

At this point, the calculation for this time step is complete. These results must be reviewed to determine the course of action for the next time step. Input adjustments allowed between time steps include changes in the length of the time step, the specified power, thermal microscopic cross sections, and self-shielding factors, transverse buckling, homogeneous poison, logarithmic derivative conditions, and isotopic densities of those elements whose concentrations are not time-dependent. At the end of each time step, a history tape contains all the information needed to continue to the next time step; a second tape contains information already calculated which may be edited selectively.

The cross section and other material-group-dependent parameters required for the spatial calculation are computed at each succeeding time step. In calculating these four-group quantities, the resonance escape of U^{238} and thermal self-shielding are taken into account. The two-group constants are obtained by collapsing the three fast groups into one fast group, the thermal group constants remaining unchanged.

Self-shielding for U^{235}, B^{10}, and the second burnable poison are given as a function of their depletion:

$$N^M(t)\, g^M(t) = N^{Ma} g^{Ma} + N^{Mb}(t)\, g^{Mb}$$

where N^{Ma} is the initial density of isotope M; and $N^{Mb} = N^M(t) - N^{Ma}$; g^{Ma} and g^{Mb} are specified in the input.

A maximum xenon calculation is available in which the flux or power level at a given time step is reduced by a specified fraction and used to deplete the isotopic densities over a specified time interval.

Input Information Required

Problem parameters:

1. Problem identification.
2. Geometry option (x-y or r-z).
3. Symmetry option (for 45° symmetry).
4. Maximum xenon option.
5. Number of groups (2 or 4).
6. Number of compositions ($\leq$35).
7. Boundary conditions.
8. Buckling parameters.
9. Initial eigenvalue.
10. Convergence criterion.
11. Time step number, size of step, power in watts, power fraction for use in calculating maximum xenon.

12. Mesh description. The number of mesh points is limited by the size of the core memory: 8K ≤ 2,500; 16K ≤ 3,750; and 32K ≤ 6,500.
13. Composition description.
14. Flux guess.

Material properties:
1. Fission spectrum fractions (χ^1, χ^2, χ^3).
2. Poison fractions (t^1, t^2, t^3).
3. Thermal cross sections (σ_{tr}, σ_a, σ_f, $\nu\sigma_f$).
4. Iodine yield.
5. Resonance escape probability for U^{238}, and the homogeneous poison Σ_p for each composition.
6. Number densities, self-shielding factors, and the constants for the logarithmic derivative condition of the "rod" regions.

Output Available

For each calculation, a supervisory on-line print lists:
1. Composition cross sections, and "picture" (initial time step only).
2. Eigenvalues of the iterations.
3. Composition flux averages from PDQ computation.
4. Fraction of power generated by each fissionable element for each composition.
5. Fraction of total power generated in each composition.

The requestor may select for printing or for punching:
1. Power in each of the four quadrants about a point.
2. Normalized power at each point.
3. For each rectangle: isotopic densities, fission energy produced, normalized or unnormalized power, or the fast macroscopic cross sections.
4. Pointwise flux for any specified group, and pointwise sources.
5. Values of isotopic number densities of a specified element, and integrated isotopic number densities, at the beginning of a time step.
6. Flux-weighted average cross sections.
7. Final isotopic number densities, or integrated number densities.

Related Codes

PROP will read the power data output from TURBO, and compute the normalized power at each fuel point in each plane selected as input to the JET thermal survey code.

A version of TURBO is also available for the Philco-2000 computer.[132]

SUPPLEMENTARY INFORMATION

Code Name	Related Codes	Originating Installation	Machine Configuration	Running Time	References
BOUT BOUT II NEXT HUF		General Electric Co., Knolls Atomic Power Laboratory	IBM-650.		126. O. A. Sappington, et al., "Three-Group Burnout Codes for use with PROD II," KAPL-M-MAA-1, (May, 1957).
BOX		General Electric Co., Knolls Atomic Power Laboratory	IBM-704 with 16K core memory, 1 drum unit, 3 tape units.	10 min/depletion step for 34 regions, 100 mesh points.	127. "Reactor Technology Quarterly Report No. 7 Physics," KAPL-2000-4, (December, 1958).
BURNOUT		General Motors Corp., Research Laboratories	IBM-704 with 8K core memory, 6 tape units, 1 drum unit.	50 min.	128. J. M. Bookston, "Reactor Material Burnout Program," GMR 103, (November, 1957).
CANDLE 1 CANDLE 2 CANDLE 3 CANDLE		Westinghouse Electric Corp., Bettis Atomic Power Laboratory	IBM-704 with 8K core memory, 4 tape units, 1 drum unit. Philco-2000 with 32K core memory, 16 tape units, 8 index registers.	15 min to 4 hr; average: 30 min. 2 to 10 min.	129. O. J. Marlowe and P. A. Ombrellaro, "CANDLE–A One-Dimensional Few-Group Depletion Code for the IBM-704," WAPD-TM-53, (May, 1957). 130. O. J. Marlowe and P. A. Ombrellaro, "CANDLE 2," WAPD-TM-53, Addendum 1, (October, 1957). 131. L. M. Culpepper, "CANDLE 3," WAPD-TM-53, Addendum 2, (October, 1957). 132. O. J. Marlowe, "Nuclear Reactor Depletion Programs for the Philco-2000 Computer," WAPD-TM-221, (January, 1961).
CUREBO	CURE 1CT 1C 2CT 2C 3CT	General Electric Co., Knolls Atomic Power Laboratory	IBM-704 with 32K core memory plus 6 tape units; 1 drum unit, 6 tape units; 7 tape units; 1 drum unit, 7 tape units; 6 tape units.		133. J. A. Archibald, Jr., "CUREBO: A Generalized Two-Space-Dimensional Coding with Cross Section and Depletion Calculations for the IBM-704," KAPL-1885, (April, 1959).
DRACO	DRACO 1 DRACO 2 DRACO 3	Westinghouse Electric Corp., Bettis Atomic Power Laboratory	IBM-704 with 16K or 32K core memory, 1 drum unit plus 9 tape units; 10 tape units; 9 tape units.	2 hr/time step for 2 groups, 3000 points.	134. D. S. McCarty and C. M. King, "DRACO–A Three-Dimensional Few-Group Depletion Code for the IBM-704," WAPD-TM-137, (December, 1958).

GPR		General Electric Co., Hanford Atomic Products Operation	IBM-650. IBM-709 (FORTRAN).	1.5 to 3 min for uniform enrichment; 3 to 6 min for spike case. 2 sec/case.	135. R. E. Peterson and G. S. Busselman, "A Generalized Calculation of Material and Reactivity Balance in Recycled Plutonium Reactors," HW-54074, (January, 1958).
TURBO	TURBO 1 TURBO 2 TURBO 3 TURBO 4 TURBO 5 PROP JET	Westinghouse Electric Corp., Bettis Atomic Power Laboratory	IBM-704 with 8K core memory plus 9 tape units; 10 tape units; 9 tape units.	1.5 hr/time step.	136. J. B. Callaghan, et al., "TURBO–A Two-Dimensional Few-Group Depletion Code for the IBM-704," WAPD-TM-95, (November, 1957).
	TURBO		Philco-2000 with 32 core memory, 16 tape units, 8 index registers.	10 to 30 min.	132. O. J. Marlowe, "Nuclear Reactor Depletion Programs for the Philco-2000 Computer," WAPD-TM-221, (January, 1961).

10.3.3 ISOTOPE PRODUCTION

Isotope production is generally computed from sets of coupled first-order differential equations; consequently, any of the available mathematical subroutines for this purpose could be adapted to this problem. Some of the codes in Section 10.3.2 also include a treatment of this subject. The following codes were developed specifically for studies of isotope production.

CRUNCH

Description

The CRUNCH code[137,138] was developed for parameter studies of the production of transplutonic elements; in particular, Cf^{252} production from successive neutron capture in Pu^{242} and its reaction products. The method employed is general and can be applied to other physical and chemical first-order reactions.

The general equation for representing the amount of any isotope of the chain as a function of time for constant flux is:

$$\frac{dN_i}{dt} = P_i N_{i-1} - r_i N_i$$

where P_i represents the production cross section, and may be either λ_{i-1} for beta decay, or $\sigma_{c,i-1}\Phi$ for neutron capture, but not both simultaneously; and r_i represents a removal cross section that can be any part, or all of

$$\lambda_i + \sigma_{c,i}\Phi + \sigma_{f,i}\Phi$$

depending on the particular isotope, i. The values λ, σ_c, and σ_f, are the decay constant, radiative capture cross section, and fission cross section, respectively. Only unbranched chains are considered. It is possible to include alpha decay by treating it as a fictitious, self-repeating, beta decay chain.

The average cross section of the material present, and the heat generation rate in kilowatts, are calculated for use in nuclear calculations.

To avoid repeated roots, such as occur when alpha decay is considered, it is necessary to alter by a small amount the removal cross sections in each cycle. In order that these alterations have negligible effect, and that cases of very short neutron exposure times and very long chains can be calculated without loss of significance, the code has been written in double precision arithmetic.

The calculation part of the code has been written as a FORTRAN II subroutine for use in more complex calculations.

Input Information Required

1. Title, time, flux, and number of reactions to be considered (≤ 50).
2. For each reaction in the order of occurrence: initial concentration (N_i); radiative capture cross section ($\sigma_{c,i}$); fission cross section ($\sigma_{f,i}$); decay time (λ_i); and designation of propagation form (beta decay or neutron capture).
3. Option to vary time and/or flux on a given chain of reactions; if used, necessary input data must be prescribed.

Output Available

The output information lists the input data, neutron flux, time, average cross section, power, and the amount of each element at the end of the specified time.

Related Codes

Similar codes are available for the Ferranti-Mark I and Ferranti-Mercury computers. These have been designated OTHER POISONS[139] and POISON'S CALCULATION, MARK 2.[140]

SUPPLEMENTARY INFORMATION

Code Name	Related Codes	Originating Installation	Machine Configuration	Running Time	References
CRUNCH		Oak Ridge National Laboratory	IBM-704 with 8K core memory, 1 tape unit (FORTRAN).	3 sec/reaction.	137. M. P. Lietzke and H. C. Claiborne, "CRUNCH: An IBM-704 Code for the Calculation of N Successive First Order Reactions," ORNL-2958, (November, 1960). 138. H. C. Claiborne and M. P. Lietzke, "Californium Production in the High Flux Isotope Reactor," CF-59-8-125, (August, 1959). 139. E. G. H. Crouch, "Calculation of Fission Product Accumulation," AERE T/M 159, (March, 1958). 140. E. G. H. Crouch, "A Program for the Calculation of Fission Product Accumulation," AERE T/M 174, (February, 1959).
	OTHER POISONS	Atomic Energy Research Establishment, Harwell, England	Ferranti-Mark I.	1 to 1.5 hr.	
	POISON'S CALCULATION, MARK 2		Ferranti-Mercury.		

10.3.4 REACTOR KINETICS AND TRANSFER FUNCTIONS

This section contains codes that solve the space-independent, one-energy group, reactor kinetics equation systems. These systems, given as Eqs. (5-50) and (5-51) of Section 5.3.2, are repeated here for convenience:

$$\frac{dn}{dt} = [k_{eff}(1-\beta) - 1]\frac{n}{\ell} + \sum_{i=1}^{I} \lambda_i C_i$$

$$\frac{dC_i}{dt} = \frac{k_{eff}\beta_i n}{\ell} - \lambda_i C_i \qquad (10\text{-}1)$$

and

$$\frac{dn}{dt} = (\rho - 1)\frac{\beta n}{\ell} + \sum_{i=1}^{I} \lambda_i C_i$$

$$\frac{dC_i}{dt} = \beta_i \frac{n}{\ell} - \lambda_i C_i \qquad (10\text{-}2)$$

A frequently used modification of the first system is

$$\frac{dn}{dt} = \frac{k_{ex} n}{\ell} - \sum_{i=1}^{I} \frac{dC_i}{dt}$$

$$\frac{dC_i}{dt} = (1 + k_{ex})\beta_i \frac{n}{\ell} - \lambda_i C_i \qquad (10\text{-}3)$$

where the nomenclature applicable to this section are defined:

n = neutron density.
Δn = variation in the neutron density over a time interval.
k_{eff} = effective multiplication constant.
$k_{ex} = k_{eff} - 1$.
β = delayed neutron fraction.
a_i = relative yield of the *ith* delayed neutron group.
$\beta_i = \beta a_i$, delayed neutron fraction for *ith* delayed neutron group.
λ_i = decay constant of the *ith* delayed neutron group.
C_i = density of precursors for the *ith* delayed neutron group.
I = total number of delayed neutron groups.
ℓ = prompt neutron lifetime.
$\rho = k_{ex}/k_{eff}$ = reactivity; [$\rho = k_{ex}/(k_{eff}\beta)$, reactivity in dollars].
t = time.
Δt = time interval.
S = external source term.

A zero subscript to any of the above quantities indicates an initial value. External source terms are often included in the neutron density equation.

Additional codes included pertain to the computation of the reactor transfer function on the basis of the above equations and a feedback function.

AIREK II, AIREK III

Description

The AIREK[141,142] codes solve the kinetic system, Eq. (10-2), coupled with differential equations that describe the feedback as a function of the neutron density. If F represents the feedback quantity, the following relation is assumed:

$$\frac{dF}{dt} = c_1 F + c_2 n(t) + c_3 n(0)$$

where c_1, c_2, c_3 are input parameters. The feedback equation with $c_3 = 0$ has the same form as the delayed precursor equation; this fact is utilized in the subsequent solution.

AIREK II solves the coupled system using a fourth-order Runge-Kutta method. AIREK III obtains a substantially improved numerical solution by using a modified system and a fifth-order Runge-Kutta procedure. The modified system is derived by assuming $n(t) = \exp[J(t)]$, and dividing Eq. (10-2) by $n(t)$.

Several subroutines are available to handle various forms of ρ for both programs:

$\rho = \rho_0$, where ρ_0 = a fixed step input reactivity.
$\rho = \rho_0 + \sum_m D_m F_m$, with D_m given as an input constant.
$\rho = \rho_0 + f(t)$, with $f(t)$ defined as straight-line segments or a trigonometric function.
$\rho = \rho(t)$; values of $\rho(t)$ are listed in tabular form.

Input Information Required

1. Total number of delayed neutron groups ($0 < I \leq 25$).
2. Number of feedback equations ($0 \leq m \leq 49 - I$).
3. Values of Δt, Δt_{max}, Δt_{min}, β, ℓ, S, n_0, a_i.
4. Reactivity parameters.
5. Coefficients for feedback equations.
6. Parameters that permit adjustment of interval size.

Output Available

Values of n; inverse period; C_i; and feedback variables (F_m); as functions of time.

BUM, RE 132

Description

The BUM[143,144] program computes the vector transfer function, LP(s), where

$$\frac{1}{LP(s)} = \frac{1}{ZP(s)} - TF(s)$$

and

ZP(s) = zero power transfer function
F(s) = transfer function of the feedback loop
T = constant

By the use of Laplace transforms on the kinetic system Eq. (10-1)

$$\frac{1}{ZP(s)} = \frac{s\left[\ell + k_{eff} \sum_{i=1}^{6} \frac{\beta_i}{s + \lambda_i}\right] - (k_{eff} - 1)}{1 - s \sum_{i=1}^{6} \frac{\beta_i}{s + \lambda_i}}$$

with s being the transform variable; $s = i\omega$, for sinusoidal reactivity input of frequency ω.

The code combines the above expression for 1/ZP(s) with the following expressions for F(s):

$$F(s) = \frac{\sum_{j=0}^{J} a_j s^j}{\sum_{j=0}^{J} b_j s^j} \tag{A}$$

$$F(s) = \sum_{m=1}^{3} A_m \frac{\prod_{L=1}^{3} (1 + T_{m,L}\, s)}{\prod_{L=1}^{3} (1 + T_{m+3,L}\, s)} \tag{B}$$

where a_j, b_j, A_m, $T_{m,L}$, and $T_{m+3,L}$, are coefficients related to material properties.

Input Information Required

For the IBM-650, where form (A) of F(s) is always used:
1. Prompt neutron lifetime.
2. Number of energy groups ($J \leq 10$).
3. Values of $\omega(\leq 10^8)$; k_{ex}; λ_i ($i \leq 6$); β_i; a_j; b_j; and $T(\leq 10^5)$.

For the IBM-704:
1. Prompt neutron lifetime.
2. Number of energy groups ($J \leq 30$).
3. Number of (≤ 500) and values of ω.
4. Values of k_{ex}; T; λ_i; and β_i.
5. Total number of delayed neutron groups ($I \leq 30$).
6. Depending on the form of F(s) used: a set of values a_j, b_j, for form (A); or a set of values $A_m (m \leq 3)$, $T_{m,L}$, $T_{m+3,L}$ for form (B).

Output Available

The modulus, amplitude, and decibel value of 1/ZP(s), LP(s), and TF(s), are computed for each value of ω. The IBM-704 prints phase angles of the three quantities in radians and in degrees. The IBM-650 punches angles in either degrees or radians.

K-CODE, ARK-1

Description

The K-CODE[145,146] determines for an element of reactor volume the neutron flux from the simultaneous solution of the diffusion equation, delayed neutron equations, and temperature feedback equations. These equations are solved in the dimensionless forms:

$$\frac{d\psi_1}{dt} = A\psi_1 + B \sum_\mu f_\mu \psi_\mu$$

$$\frac{d\psi_\mu}{dt} = \lambda_\mu (a\psi_1 - \psi_\mu)$$

$$\frac{d\psi_\nu}{dt} = \lambda_\nu (\psi_1 - \psi_\nu) - d_\nu D(t)$$

where ψ_1 = relative neutron flux, ϕ/ϕ_0
ψ_μ = relative precursor concentration, $C_\mu/C_{\mu 0}$
ψ_ν = relative temperature, $T_\nu/T_{\nu 0}$

$$A = \frac{1-\beta}{\beta} a\, B - \frac{1}{\ell} (1 + b\, L_0^2 B_g^2)$$

$$B = \frac{\beta b}{\ell} (1 + L_0^2 B_{g0}^2) \exp [-\tau (B_g^2 - B_{g0}^2)]$$

λ_ν = thermal relaxation constant of the *vth* material
d_ν = weighting factor for the temperature increment of the *vth* material
D(t) = increment of temperature for an external source
ℓ = neutron lifetime
C_μ = concentration of the precursors of the μth group of delayed neutrons
$= C_i/[\rho \exp(-\tau B_g^2)]$
$f_\mu = a_i$
$\lambda_\mu = \lambda_i$
L = diffusion length
B_g^2 = effective leakage buckling
τ = Fermi age

and a and b are factors used to express the temperature dependence of the absorption rate and core parameters. Steady-state quantities are designated by a zero subscript.

The equations are solved by iteration of a difference formula. Three iterations are completed for each time step. An alternate form of the neutron equation:

$$\psi_1 = \frac{B}{A} \sum_{\mu} f_\mu \psi_\mu$$

may be used for flux transients of long duration.

If the buckling and diffusion length remain constant during the time increment, the equations reduce to those used in the ARK-1 code.[147] This code uses a fourth-order Runge-Kutta integration method.

Input Information Required

1. Problem parameters: τ, ℓ, f_μ, λ_μ, β.
2. Material properties: λ_ν, d_ν, a, b.
3. Initial values of diffusion length, relative flux and its time derivative, and time-dependent values of B_g^2 and D.

The values of $B_g^2(t)$ and D(t) are listed in tabular form and a linear interpolation formula is used within the program.

The ARK-1 version requires a slightly modified input.

Output Available

Values of ψ_i, T_ν, and C_μ, are given as functions of time.

RE 29, RE 129

Description

Both of these codes[148,149] solve the kinetics system Eq. (10-3) for n(t), given k_{ex}.

Both sides of Eq. (10-3) are integrated with respect to t, and the quantities under the integral signs are replaced by linear approximations valid in the interval Δt under consideration. From the resulting expressions, $n(t_j)$ is determined successively for a set of time values, t_j.

There are many versions available for the form of k_{ex} to be used; some are:

(1) $k_{ex} = At + B \int_0^t n\,dt$.

(2) $k_{ex} = At + B(n-1)$ for $t < t_0$.

$= B(n-1)$ for $t \geq t_0$.

(3) k_{ex} specified at discrete time points.

(4) $k_{ex} = \sum_m A_m (t - t_0)^m + \sum_m B_m \left(\int_0^t n\,dt\right)^m$, and

$\ell = \sum_m L_m \left(\int_0^t n\,dt\right)^m$ for $m = 0,1, \ldots 4$

Options (1), (2), and (3) are coded for the IBM-650; options (1), (3), and (4) are available for the IBM-704.

For problems involving an initial step or ramp change in k_{ex}, an optional, artificial start routine is provided to compute the initial values of (dC_i/dt) and Δn.

Input Information Required

1. Number of delayed neutron groups ($\leq$18 for RE 29; $\leq$100 for RE 129).
2. Values of β_i, λ_i, S, Δt; artificial start and print options.
3. Initial values for n, Δn, k_{ex}, (dC_i/dt).
4. Form of k_{ex} to be used and related coefficients, tables, convergence and termination criteria.

The code permits change of coefficient values in the form of k_{ex} at selected time values during the running of a problem.

Output Available

1. Edit of input data.
2. Values of t, an edit of n, $[n/(dn/dt)]$, k_{ex}, and $\int_0^t ndt$, for each time specified by the print option.

In addition, version (4) prints the computed neutron lifetime.

RE 126, RE 135

Description

These codes[150] solve the kinetics system Eq. (10-1), with a source term for a specified reactivity step. The solution is accomplished by obtaining the roots, s_j, of the inhour equation and inserting these in an equation of the following form to determine the neutron density:

$$\frac{n(t)}{n_0} = \sum_{j=1}^{I+1} A_j + B_j) \exp (s_j t) + C$$

A_j, B_j, and C are determined from λ_i, β_i, ℓ, s_j, and $k_{ex,0}$, the form depending on whether the equilibrium or non-equilibrium precursor problem is treated.

RE 126 performs this calculation for the case of a reactivity step with equilibrium precursors; both non-zero and zero final reactivity are treated.

RE 135 computes the reactivity step case with non-equilibrium precursors. It is assumed that the reactor has been operating at steady power, n_0, for a buildup time of T_B seconds. The precursor concentrations are given by:

$$C_{i0} = \frac{k_{eff,0}\beta_i n_0}{\ell\lambda_i} [1 - \exp (-\lambda_i T_B)]$$

Both codes use an iterative procedure to determine the roots of the inhour equation. The problem is terminated when the difference between the reactivity determined by the roots and the specified final reactivity value, ρ_f, is a minimum.

Input Information Required

1. Number of delayed neutron groups ($I \leq 30$).
2. Values of λ_i, β_i, ℓ, $k_{ex,0}$, ρ_f.
3. Number of time steps (≤ 500).
4. Time values (t).

RE 135 requires, in addition, the buildup time values (T_B).

Output Available

1. Input information.
2. Roots s_j.
3. Coefficients A_j and B_j.
4. Number of iterations and indication of convergence achieved.
5. For each time value: $(1/n_0)(dn/dt)$, (n/n_0), $[n/(dn/dt)]$, and deviation from the asymptotic period.

RE 135 prints the output information for the equilibrium case as well as the non-equilibrium or precursor buildup case.

RE 138

Description

RE 138[151] calculates the excess reactivity using Eq. (10-1) with I delayed neutron groups, given the neutron density as a function of time. Defining

$$\alpha(t) = \frac{dn}{dt}\frac{1}{n}$$

$$d_i(t) = \frac{\ell\lambda_i}{\beta_i}\frac{C_i}{n}$$

evaluating the neutron density equation at t_j and t_{j+1}, and subtracting the result yields:

$$\ell\Delta\alpha_j = (1-\beta)\,\Delta k_j + \sum_{i=1}^{I}\beta_i\,\Delta d_{ij}$$

Assuming that the neutron density can be represented by

$$n = n_j \exp\left[\bar{\alpha}_j(t-t_j)\right]$$

in the interval,

$$t_j \le t \le t_{j+1}$$

where

$$\bar{\alpha}_j = \frac{1}{\Delta t_j}\ln\left(\frac{n_{j+1}}{n_j}\right)$$

and

$$\alpha_j = \frac{\bar{\alpha}_{j-1} + \bar{\alpha}_j}{2}$$

the precursor equations can be integrated for Δd_{ij}. This value is substituted in the neutron formula to obtain Δk_j.

Input Information Required

1. Problem identification.
2. Number of delayed neutron groups ($I \le 25$).
3. Values of λ_i and β_i.
4. Prompt neutron lifetime.
5. Initial reactor period ($1/\tau$).
6. Form assumed for density of neutron precursors (steady-state or asymptotic).
7. Number of regularly-spaced points, and neutron density for each point (n_j).
8. Time step (Δt).

Output Available

Values of k_{ex}, (dk_{ex}/dt), (d^2k_{ex}/dt^2), reactor period, and $\int_0^t n\,dt$, are listed for each time value.

RE 171

Description

This program[152] calculates the excess reactivity, using the kinetics system Eq. (10-3) with I delay groups, given the neutron density as a function of time.

The method of solution depends on the integration of the precursor equations over the time interval, Δt. In performing this integration, the variation of k_{ex} and n is assumed linear.

The solution is advanced by alternately calculating the quantities k_{ex} and $[\ell(dC_i/dt)]$ at each time step, based upon values from the previously calculated time step.

The derivatives of k_{ex} are formed using a three-point difference formula. The integral is computed by trapezoidal integration.

Input Information Required

1. Initial value of k_{ex}.
2. Prompt neutron lifetime.
3. Asymptotic period.
4. Number of delay groups ($I \leq 30$).
5. Values of λ_i and β_i.
6. Number of points, and the neutron density (n_j) for each point.
7. Time steps. A series of different values of Δt may be used throughout a problem.

Output Available

Values of k_{ex}, (dk_{ex}/dt), (d^2k_{ex}/dt^2), and $\int_0^t n dt$, are listed for each time value.

Related Codes

RE 171 is an IBM-704 version of an earlier AVIDAC program, RE 31.

687863 O - 63 - 54

Code Name	Related Codes	Originating Installation	Machine Configuration	Running Time	References
AIREK II AIREK III		North American Aviation, Inc., Atomics International Division	IBM-704, 709 with 8K core memory (FORTRAN).	10 time increments/sec for six delayed neutron groups and two feedback equations.	141. A. Schwartz, "Generalized Reactor Kinetics Code AIREK II," NAA-SR-Memo-4980, (February, 1960). 142. A. Schwartz, "Fifth-order Runge-Kutta Numerical Integration Formulas," Subtitle: "Generalized Reactor Kinetics Code, AIREK III," Atomics International Memorandum.
BUM RE 132		Argonne National Laboratory	IBM-650. IBM-704 with 8K core memory, 1 tape unit.	15 sec/frequency. 1 sec/frequency.	143. J. Koerner, "The Transfer Function Problem Programmed for the 650," Reactor Engineering Division Memorandum, (August 19, 1958). 144. C. E. Cohn and J. A. Thie, "A Transfer Function Code (RE 132) for the IBM-704," Reactor Engineering Division Memorandum, (August 19, 1958).
K-CODE ARK-1		E. I. DuPont de Nemours & Co., Savannah River Laboratory Armour Research Foundation	IBM-650.	32 sec/time increment.	145. H. D. Brown, "A General Treatment of Flux Transients," Nuclear Sci. and Eng., 2, No. 5, 687, (September, 1957). 146. IBM-650 Program Library 8.2.008. 147. T. Englehart and W. E. Loewe, "The ARK-1 Code," Appendix of AECU-3659, (February, 1958).
RE 29 RE 129		Argonne National Laboratory	IBM-650. IBM-704 with 8K core memory, 1 tape unit.	10 min for 250 time intervals. 1 min/1000 time intervals.	148. R. O. Brittan, "Some Problems in the Safety of Fast Reactors," ANL-5577, (May, 1956). 149. AMD Program Library RE 129.
RE 126 RE 135		Argonne National Laboratory	IBM-704 with 8K core memory, 1 tape unit (FORTRAN).	3 sec/15 delay groups, 20 time values. 1 min/15 delay groups, 20 time values.	150. C. E. Cohn and B. J. Toppel, "IBM-704 Codes for Reactivity Step Calculations (RE 126 and RE 135)," ANL-6134, (March, 1960).
RE 138		Argonne National Laboratory	IBM-704 with 8K core memory, 1 tape unit (FORTRAN).	1 sec/time interval.	151. AMD Program Library RE 138.
RE 171	RE 31	Argonne National Laboratory	IBM-704 with 8K core memory, 1 tape unit. AVIDAC (GEORGE)	3 min/40 values of k_{ex}.	152. AMD Program Library RE 171.

10.4 REACTOR HAZARDS AND SAFETY

The codes in this section are used to evaluate potential reactor hazards by taking into account the interrelationship of thermodynamic, hydrodynamic, and nuclear characteristics of a reactor system.

AX-1

Description

AX-1[153] computes the variation in time and space of the specific energy, temperature, pressure, density, and velocity of a spherically-symmetric, super-prompt critical system. As a function of time, it computes the inverse period (α), the power, the total energy, and the position of the boundaries of the various shells into which the system has been subdivided. All delayed neutron effects are ignored, and no allowance is made for transfer of heat by conduction or radiation.

The neutronics portion of the program is always done using the S_4 approximation. It supplies to the succeeding portions of the program the $\alpha(= k_{ex}/\ell)$ corresponding to that specific configuration. It also supplies a relative power distribution to be used in assigning the increase in energy within each spherical shell or mass point.

The program proceeds into the hydrodynamic and thermodynamic portions. For short time intervals (Δt), the inverse period (α) is considered to remain constant while the power varies as exp ($\alpha \Delta t$). From the pressure gradients in the system, the average accelerations of the mass points are computed and, hence, the new velocities at the end of a time interval. These, in turn, lead to the new radial positions of each shell boundary at the end of a time interval.

The energy added during the time interval is distributed among the shells in accord with the previously calculated fission distribution. By allowing for the work done by or on a shell in expansion or compression, the net change in internal energy is computed, and from the internal energy, a new pressure and temperature. In the AX-1 program, hydrodynamic pressure is a linear function of density and temperature, while the specific heat at constant volume is assumed a linear function of temperature. The coefficients in these assumed linear forms are allowed to vary from shell to shell, but no provision is made for mixing several substances within a shell to generate average values.

The thermodynamic equations are solved by an iterative procedure. The so-called viscous pressure, devised by von Neumann and Richtmyer, is included to permit thermodynamic and hydrodynamic calculations in the presence of a steep shock front. The total pressure is the sum of the hydrodynamic pressure, P_H, and the synthetic viscous pressure, P_V.

When calculation of the thermodynamic and hydrodynamic changes over the time interval is complete (a hydrocycle), a series of tests are run and the program either proceeds with another hydrocycle, or goes back to the S_4 neutronics calculation. The code examines the rate of change of certain parameters and varies the Δt of a hydrocycle, or the number of hydrocycles per neutron cycle accordingly.

Input Information Required

1. Description of regions ($\leq$39): dimensions, composition identification ($\leq$8), number of mass points, and associated temperature, density, velocity, and fission source.
2. Initial reactivity, if desired (code will then adjust dimensions to give this value).
3. Initial reactor power level.
4. Material parameters for the S_n calculation, including cross section values and velocity associated with each energy group ($\leq$7).
5. Values of the coefficients and constants required for the pressure, temperature, density, specific heat, and other relationships incorporated.
6. Convergence and test criteria.

Output Available

1. Input data.
2. Initial k_{eff}.
3. For each S_n calculation: a short print-out listing the time, total energy, power, inverse period, and time interval and criterion for stability of the hydrodynamic calculation.
4. Optional: a long print-out listing total energy, kinetic energy, and checks on the energy computation; and density, radius, velocity, pressure, internal energy, and temperature, of each mass point.

Related Codes

The HATCHET code[154] is derived from AX-1 and was designed to calculate the burst characteristics of a particular pulsed reactor. This reactor model consists of a series of spherical shells which are not in physical contact. The code allows three energy groups and six materials in the reactor. The iterative procedure is based on convergence to a new temperature, rather than to a new pressure as in AX-1. Thin shell theory is introduced to describe the movement and state of the concentric shells comprising the reactor. The input and output are similar to AX-1.

SUPPLEMENTARY INFORMATION

Code Name	Related Codes	Originating Installation	Machine Configuration	Running Time	References
AX-1		Argonne National Laboratory	IBM-704 with 8K core memory, 2 tape units (FORTRAN).	1 hr.	153. D. Okrent, et al., "AX-1, A Computing Program for Coupled Neutronics-Hydrodynamics Calculations on the IBM-704," ANL-5977, (May, 1959).
	HATCHET	Aerojet-General Corp., Aerojet-General Nucleonics	IBM-704 with 8K core memory, 2 tape units (FORTRAN).	40 min/energy group.	154. J. P. Lehman, "HATCHET, A Coupled Neutronics-Hydrodynamics Code to Calculate Burst Characteristics for a Pulsed Reactor for IBM-704," AN-237, (September, 1960).

10.5 SHIELDING

The codes in this section are used to estimate the heat generation rates and/or radiation levels for either neutrons or gamma rays at specified distances from sources. These sources are often derived from the results of criticality computations.

GRACE I

Description

The GRACE I code[155] computes the gamma-ray flux distribution in a multiregion, finite or semi-infinite, slab shield. The results are converted to either dose rates or heat generation rates, as desired. In each region, a uniform or an exponential source distribution may or may not be specified. Furthermore, if a source region radius is specified, the program will assume a truncated-cone geometry for that source, with the detector located at the apex of the cone. The cone angle is defined in terms of the source radius and the distance from the detector to the closest surface of the source.

A single material buildup factor is used to compute the flux distribution at a particular location in the shield from a given source region. This buildup factor may be specified as: (1) a single buildup factor for each region, or (2) a set of buildup factors, each corresponding to a source region.

Input Information Required

The input consists of library data and problem data. The library data include energy- and material-dependent constants.

1. Number of energy groups (≤20).
2. Number of materials (≤10).
3. Buildup factors (≤5).
4. Mass absorption coefficients.
5. Energy produced per neutron capture.

The problem data include:

1. Number of regions (≤30).
2. Thermal neutron flux at the inner and outer boundary of the source regions.
3. Radius of source regions for use in the truncated cone calculation.
4. For each material region: thickness, material type, number of mesh points (≤10), buildup factor-type, type of source, macroscopic absorption cross section, and density.

Output Available

Upon completion of the calculations for the total heat generation rates or dose rates in a given material region, either an energy or region print, or both, may be obtained. The energy print gives, at each mesh point, the total heat generation or dose rate distributed among the various energy groups. The region print gives, at each mesh point, the total heat generation rate or dose rate distributed among the various source regions.

A final print gives the total heat generation rate or dose rate at each point.

Related Codes

The GRACE II[156] code is a similar program written for spherical and cylindrical geometries.

HIGH ENERGY SPECTRA MONTE CARLO PROGRAM

Description

This Monte Carlo program[157] computes high-energy spectra in a system composed of concentric, infinite cylinders surrounded by an outer material with square or rectangular boundaries.

A specified number of fission neutrons born in the fissile materials, together with descendants, are tracked, one-by-one, through the system until they are absorbed, lost by leakage through the lattice boundary, or their energies fall below a specified cutoff energy. The neutrons may be started from any region within the cell. In the range 0-4 Mev, they are chosen from a cumulative probability distribution function of the Cranberg fission spectrum. Above 4 Mev, a negative exponential distribution is used to represent the fission spectrum.

The techniques of Russian roulette and neutron splitting are incorporated in the tracking routine to force neutrons to migrate toward regions of interest, and to reduce the number tracked in less important regions.

The nuclides available with the program: nickel, chromium, iron, hydrogen, aluminum, oxygen, deuterium, carbon, U^{235} and U^{238}, cover the range 0.01 to 14.0 Mev. Thirty-two equiprobable values of the scatter angle and corresponding energy reduction factor are used for the angular distribution of elastically scattered neutrons. Inverse mean free paths for the material regions used are calculated for each energy level. The nuclear reaction that occurs at each collision is determined by using a random number together with the cross section at the neutron's energy band in the material. The cross sections are obtained from the calculated inverse mean free paths.

The total neutron flux is automatically tabulated over every material. An entirely independent set of concentric annular regions may be used to score the average collision density. The neutron collision densities for the cutoff neutrons, and their positions and directions, are also tabulated for specified energy bands below cutoff energy.

Input Information Required

1. Problem identification.
2. Number of fission neutrons to be started.
3. Cutoff energy to be used.
4. Description of fission strength over the regions; each problem must have at least two fission strength regions which must cover the complete area inside the cell boundary.
5. Cross section energy band table, if different from that included on program tape.
6. Energy band table to be used for tabulating or scoring.
7. Table of weights and radii dividing the system into regions for neutron splitting and Russian roulette.
8. Description of material regions.
9. Regions to be used in tabulating collision results.
10. Table of track lengths used to limit the track length in a material region.
11. Definition of the materials: nuclide constituents.

Output Available

1. For each region specified and each energy level: tables of total neutron flux, inverse mean free paths, and collision densities.
2. Optional: tabulations of neutron collision densities below cutoff energy, and distribution of track lengths over the maximum prescribed for inclusion in neutron flux scoring.

Related Codes

Basic data for the nuclides included are processed by other AWRE programs[158] into suitable form for Monte Carlo calculations.

MIS

Description

The MIS code[159] is used for neutron shielding calculations in multiple-layer, spherical geometry. The code uses Monte Carlo methods, and includes provisions for inelastic and anisotropic scattering.

The code calculates average track length per neutron per energy group in each region. This is converted to flux by dividing the track length by the volume of the region and the region weighting factor. MIS I is used for equally-spaced energy groups, and MIS II for equally-spaced lethargy groups.

The reactor shielding configuration consists of a source distributed uniformly per unit volume in a spherical core. The core is surrounded by concentric, spherical shells of different shielding materials. The core and the shielding shells may consist of single materials or mixtures of materials.

The code recognizes three types of boundaries: physical boundaries, flux boundaries, and doubling boundaries. Flux and doubling boundaries may be placed at arbitrary distances from the center of the configuration. Every physical and every doubling boundary is automatically assumed to be a flux boundary as well.

Particles are born with uniform probability per unit volume in the source region. The direction of motion and the energy of the particle are calculated for a given random number ξ. The distance the neutron will travel to the next event is distributed according to

$$P(x)\,dx = e^{-x}\,dx$$

where x = mean free path of the neutron.

The type of event is decided after the position of the next event is determined: inelastic, isotropic elastic, or anisotropic elastic scattering; or absorption of the particle. Leakage is determined by the position of the particle. A new energy and direction of the particle are then chosen for the scattering processes.

Source particles may be introduced at arbitrarily located surfaces if the "doubling" scheme is sacrificed.

Input Information Required

1. Number of flux regions.
2. Energy limits and group structure.
3. Fission spectrum and inelastic spectrum definitions.
4. "Doubling" parameters.
5. Total number of particles to be considered.
6. For each physical region: number of inelastic scatterers, isotropic and anisotropic scatterers, total and scattering cross sections for the composition.
7. For each element and energy group: tables of inelastic, isotropic and anisotropic cross sections.
8. For each boundary: the boundary type and the radius squared.

Output Available

1. Current in both directions across each flux boundary.
2. Number of neutrons absorbed and degraded in each region.
3. Number of neutrons at the outer boundary.
4. If "doubling" boundaries are used: the number of neutrons that died and the number that "doubled" at each "doubling" boundary.
5. For each energy group: current at the outer boundary, average track length per neutron for each region, neutron flux for each region, and standard deviation of the track length and the flux.

NIOBE

Description

The NIOBE code[160] performs numerical integration of the Boltzmann equation in a finite, multilayered, spherically symmetric configuration.

The code will calculate at all interior and surface points the angular distributions, total fluxes and currents for neutrons (or photons), as a function of energy (or wave length).

The code consists of two parts: the slowing-down treatment, and the "one-velocity" problem. In the slowing-down treatment, both elastic and inelastic scattering are considered. Special methods are included for Li and Be inelastic scattering as well as a statistical model for heavier materials.

The treatment of the "one-velocity" equation is as follows: assuming a value for the angular flux, the equation is solved by integrating along the characteristics; this process is continued until a specified convergence is achieved. In the "one-velocity" solution, Lagrange interpolation up to order fifteen is used on the angular variable and Gaussian quadrature formulae are used for the integrations.

Input Information Required

1. Total and scattering cross sections. (A maximum of five materials is permitted in each region. Up to fifty regions may be handled).
2. Legendre coefficients of the differential scattering cross section (up to order 19).
3. Appropriate data for inelastic scattering. Data are tabulated as functions of energy. The required set of values is computed from this tabulation.
4. Radiation source may be specified either as incident on the configuration, or internally distributed.

Output Available

1. At each radial point ($\leq$200), the angular neutron (or gamma) flux in a maximum of 16 directions and at a maximum of 200 energy values. The energy values may be spaced equally in increments of ln(E) for neutrons, or spaced equally in wave lengths for photons.
2. At every point: an integral over energy of the total flux times an arbitrary response function, i.e., dose activation.

RE 34

Description

The RE 34 code[161] solves the one-dimensional, multigroup, diffusion equation system:

$$\nabla(D^j \nabla \phi^j) - \sigma^j \phi^j + S^j = 0$$

in slab, cylindrical, or spherical geometry. In the equation system, j represents the energy group, and

$$S^j = s^{j-1} \sigma^{j-1} \phi^{j-1} \text{ for } j = 2,3 \ldots J$$

where σ^j is the group removal cross section, s^j the transfer fraction, and D^j the diffusion coefficient. S^1 is prescribed as input.

In the numerical solution of the problem, the diffusion equation system is replaced by a set of J-coupled, difference equations.

Any one of three boundary conditions may be used at the inner boundary. The derivative of the flux may be set to zero, the flux value may be specified, or for $r \neq 0$ the "black boundary" condition may be imposed. At interfaces, continuity of flux and current, or a "black boundary" condition may be chosen.

At the outer boundary, the flux or derivative of the flux may be equal to zero, or the "black boundary" condition may be applied.

Input Information Required

Problem parameters:
1. Problem identification.
2. Geometry (slab, cylinder, sphere).
3. Number of energy groups.
4. Number of material regions.
5. Outer radius.
6. Interval size and number of intervals in each region.
7. Point-by-point source distribution for the highest energy group.

Group-region parameters:
1. Boundary condition indicators.
2. For each group and region: cross sections and related quantities, D, σ, and s.

Output Available

1. Input data.
2. Group flux distributions.
3. For each region and each group: flux integrals, neutron leakages, and balance checks.
4. Values of current at "black boundaries," and at the outermost boundary.

RE 157

Description

The RE 157 program[162] is designed to calculate $\phi_\gamma(a)$, the capture gamma-ray flux at the outer surface, a, of a shield, resulting from an exponentially varying thermal neutron flux, $\phi(x)$, in the adjoining slab.

If $\phi(0)$ is the thermal neutron flux at the interface, then

$$\phi(x) = \phi(0) \exp(\kappa x), \quad 0 \leq x \leq t$$

where κ is the exponential slope of the thermal flux. A linear buildup factor $(1 + \mu x)$ is used for gamma radiation in the slab and shield, where $\mu(E)$ is the gamma-ray total cross section for a given energy E in the material.

Using these assumptions, analytic expressions are obtained for $\phi_\gamma(a)$ which are evaluated by the machine.

Input Information Required

1. Volume source.
2. Value of κ.
3. Thickness of the slab and shield.
4. Value of $\mu(E)$ for the slab and shield.

Output Available

The input information and values of $\phi_\gamma(a)$.

SHIELDING 09-0

Description

SHIELDING 09-0[163] computes the contribution of the once-scattered radiation to the total dose rate, for an anisotropic point source of fast neutrons recorded by an unshielded isotropic detector, when both source and detector are immersed in a homogeneous, infinite medium.

If the source energy spectrum is discrete, the dose rate associated with the total, once-scattered particle flux arriving at the detector is given by:

$$D = \frac{nR^2}{\rho} \sum_{j=1}^{J} K(E_j) \int_{\gamma_0}^{\pi} \int_{\beta_0}^{\pi-\gamma} \int_{0}^{2\pi} \frac{D_R(E_j,\gamma,\psi)}{K(E_j^s)} \exp\left\{\frac{-\rho}{\sin(\gamma+\beta)}\left[k_1\,\Sigma(E_j)\sin\beta + k_2\,\Sigma(E_j^s)\sin\gamma\right]\right\} \frac{d\sigma(E_j,\theta)}{d\Omega}\, d\gamma\, d\beta\, d\psi$$

where
- n = scatterer density of the medium.
- R = radius of sphere. The direct beam dose rate at the surface of this sphere defines the source.
- ρ = distance between point source and point detector.
- $D_R(E_j,\gamma,\psi)$ = direct-beam dose rate due to neutrons of energy E_j.
- $K(E_j)$ = conversion factor: dose rate to particle flux.
- $K(E_j^s)$ = conversion factor: scattered particle flux of energy E_j^s to dose rate.
- γ = angle between direction of unscattered radiation leaving the source, and source-detector axis.
- β = angle between direction of radiation scattered to detector, and source-detector axis.
- ψ = angle between x axis and projection of r_1 on x-y plane, where r_1 is the distance between the point source and the scattering point.
- k_1, k_2 = screening constants, allowing for the inclusion or exclusion of the attenuation due to the medium.
- $\Sigma(E_j), \Sigma(E_j^s)$ = total macroscopic cross section of the medium for the unscattered and once-scattered energy intervals, respectively. These are total absorption coefficients when applied to gamma shielding.
- $\frac{d\sigma(E_j,\theta)}{d\Omega}$ = probability that a neutron with energy E_j will scatter into a unit solid angle about θ, given as a third-degree polynomial in cos θ with the coefficients functions of E_j.

Trapezoidal quadrature is used to evaluate the integrals.

Input Information Required

1. Values of n and R.
2. Detector point coordinates.
3. Number of initial energy levels (≤10).
4. Values of E_j, $\Sigma(E_j)$, k_1, and k_2.
5. Tables of angular intervals and dose rate fractions.
6. Coefficients for determining values of $(d\sigma/d\Omega)$, E_j^s, $\Sigma(E_j^s)$, and $K(E_j)$.
7. Parameters for application of quadrature formula.

Output Available

1. Once-scattered dose rate for each source energy.
2. Total dose rate for all source energies at the detector point.

Related Codes

SHIELDING 05-0[164] is a similar program for calculating gamma-ray dosage. Modifications have been made in the computation of the E_j^S and $K(E_j)$ values, and the Klein-Nishina formula is used for $(d\sigma/d\Omega)$.

Two other programs, SHIELDING 07-1[165] and 10-0[166], are used for the shielded point detector case to calculate gamma-ray and fast neutron dosage due to both direct beam and once-scattered radiation.

SHIELDING 12-0

Description

The SHIELDING 12-0 program[167] computes the gamma-ray flux, energy absorption rate, or dose rate from an isotropic point source of photons having J initial energy levels.

The total dose rate from an isotropic point source in an infinite, attenuating, homogeneous medium is given by the sum over the energy levels of

$$D_\gamma(E_j) = \frac{B[\rho\Sigma(E_j)]\, K(E_j)\, S(E_j) \exp\,[-\rho\Sigma(E_j)]}{4\pi\rho^2}$$

where $B[\rho\Sigma(E_j)]$ = buildup factor. Empirical expressions for computing buildup factors are taken from Goldstein and Wilkins.[168]

$K(E_j)$ = conversion factor: photon flux to energy absorption rate or dose rate.

$S(E_j)/4\pi\rho^2$ = photon flux at the surface of a sphere of radius ρ about an isotropic point source in a non-attenuating medium.

$\Sigma(E_j)$ = linear total absorption coefficient.

Dose rate calculations for multiple-layer shields require specification of the thickness of each material. This is accomplished by use of material path fractions, θ_m. The source-receiver distance, ρ, multiplied by the material path fraction, θ_m, equals the thickness of material m, and $\Sigma(E_j)$ is replaced by the sum over m of $\theta_m[\Sigma(E_j)]_m$. Buildup factors are appropriately modified. The code considers also the case of material combinations, and the buildup factors are computed taking this into account.

Input Information Required

1. Number of initial energy levels ($J \leq 20$).
2. Number of materials (≤ 20).
3. Distance between point source and receiver.
4. For each energy level: source intensity, conversion factor, ratio of Compton scattering to total attenuation coefficient, path fraction, screening constants, buildup factor coefficients, and gamma-ray linear absorption coefficients for the materials, or material combinations encountered.

Output Available

Values of $D_\gamma(E_j)$, and the sum of the $D_\gamma(E_j)$.

SPAN-2

Description

The SPAN-2 code[169] calculates the uncollided gamma flux at a point outside a right circular cylinder. The cylinder is surrounded radially by cylindrical shell shields, and axially (above) by plane slab shields. The source contained in the cylinder is assumed to vary in the radial and axial directions only.

The uncollided flux is given by:

$$\phi = \frac{1}{4\pi}\int_0^{2\pi} d\theta \int_0^{R_c} r\, dr \int_{-H/2}^{H/2} dz\, \frac{S(r,z)}{D^2} \exp\left[-\left(\sum_{n=1}^{N_s} \mu_n^s D_n^s + \sum_{m=1}^{N_t} \mu_m^t D_m^t\right)\right]$$

where S(r,z) = source.
D = distance from point P in the core, to the field point P_f.
D_n^s = distance traveled through the *nth* cylindrical shield in moving from P to P_f.
D_m^t = distance traveled through the *mth* slab shield in moving from P to P_f.
μ_n^s = attenuation coefficient for *nth* cylindrical shield region.
μ_m^t = attenuation coefficient for *mth* slab shield.
R_c = radius of the core.
H = height of the core.

Three cases are considered:
(1) The ray from P to P_f does not pass through any top shields. In this event:

$$\sum_{m=1}^{N_t} \mu_m^t D_m^t = 0$$

(2) The ray from P to P_f does not pass through any side shields. In this event:

$$\sum_{n=4}^{N_s} \mu_n^s D_n^s = 0$$

(3) The ray from P to P_f passes through both top and side shields.

SPAN 2 performs the integrations numerically by use of Gauss quadrature of orders 9, 12, 9, in the r, z, and θ directions, respectively.

The library contains the microscopic cross sections of ten materials: H, O, Zr, C, Fe, Al, U, Pb, concrete, and H_2O. The code uses the library to compute the energy level attenuation factors for each region.

Input Information Required

1. Problem identification.
2. Source identification.
3. Number of energy levels (≤30).
4. Number of side and top shields (≤28).
5. Thickness of top, side, and bottom reflectors.
6. Integration limits for the r, z, and θ integrations.
7. Description of core, including number of regions, number and identification of materials contained in each region.
8. Description of shields, including number and the number and identification of materials (≤9) contained in each shield.
9. Number densities of the materials in the shield regions.
10. Coordinates of the field points (≤100) at which the uncollided flux is to be calculated.

The code is designed to obtain the source distribution from either a TURBO tape 7 (Section 10.3.2), or punched cards. Restart procedures are also incorporated.

Output Available

1. Core height and radius.
2. Table of source strengths in r and z directions at point of integration within the core.
3. Material compositions of the core, reflector, top and side shields.
4. Value of flux at each field point specified.

Related Codes

SPIC-1[170] calculates the fast neutron dose rate or the thermal neutron flux in water outside a right circular cylinder. It is essentially a modification of SPAN 2.

The fast neutron dose rate, or thermal neutron flux in water is approximated by a fit of the form

$$a_1\phi_1 + a_2\phi_2 + a_3\phi_3$$

where ϕ_1, ϕ_2, and ϕ_3 have the same form as the ϕ of SPAN 2, and a_1, a_2, and a_3, are empirically-determined constants.

Any one of three libraries may be used to calculate the attenuation factor. The first is for the fast neutron dose rate in water; the second is for the thermal neutron flux in low-temperature water (20°C); and the third is for the thermal neutron flux in high-temperature water (230°C – 290°C).

Effective removal cross sections are used for all elements except water and hydrogen. The values for water and hydrogen are determined empirically.

SUPPLEMENTARY INFORMATION

Code Name	Related Codes	Originating Installation	Machine Configuration	Running Time	References
GRACE I GRACE II		North American Aviation, Inc., Atomics International Div.	IBM-704, 709, with 8K core memory (FORTRAN). IBM-709 with 16K core memory (FORTRAN).	1 min.	155. D. S. Duncan and A. B. Speir, "GRACE I An IBM-704-709 Program Designed for Computing Gamma-Ray Attenuation and Heating in Reactor Shields," NAA-SR-3719, (January, 1959). 156. D. S. Duncan and A. B. Speir, "GRACE II An IBM-709 Program for Computing Gamma-Ray Attenuation and Heating in Cylindrical and Spherical Geometries," NAA-SR-Memo-4649, (November, 1959).
HIGH ENERGY SPECTRA MONTE CARLO PROGRAM		Atomic Energy Establishment, Winfrith, England.	IBM-709 with 4 tape units.	~100,000 collisions/hr.	157. S. Francescon, "A Monte Carlo Program for Calculating High Energy Spectra in Cylindrical Geometry on the IBM-709 Computer," AEEW-R 45, (October, 1960). 158. J. B. Parker and K. Parker, "The Preparation of Nuclear Data for Use in Neutronic Calculations on High Speed Computers," AWRE 0-20/60, (June, 1960).
MIS		Nuclear Development Corp. of America.	DATATRON.		159. F. J. Oswald and R. Schaffer, "Description of MIS, A Monte Carlo Inelastic Scattering Code for the DATATRON Computer," NDA 2-66, (June, 1957).
NIOBE		Nuclear Development Corp. of America.	IBM-704 with 32K core memory, 10 tape units. IBM-7090 with 10 tape units.	15 hr for an 85-point, 81-energy value, 8-angular ray problem. 2.5 hr for same type problem.	160. S. Preiser, et al., "A Program for the Numerical Integration of the Boltzmann Transport Equation–Niobe," ARL 60-314, (December, 1960).
RE 34		Argonne National Laboratory	IBM-704 with 8K core memory.	1-2 min.	161. M. K. Butler and J. M. Cook, "RE 34, An IBM-704 Reactor Shielding Program," ANL-5859, (June, 1959).
RE 157		Argonne National Laboratory	IBM-704 with 8K core memory.	0.5 sec.	162. AMD Program Library RE 157.

SHIELDING 09-0 05-0 07-1 10-0		General Electric Co., Aircraft Nuclear Propulsion Department	IBM-704 with 8K core memory.		163. J. W. Haffner, J. J. Loechler and J. E. MacDonald, "IBM-704 Program Report, Aircraft Nuclear Propulsion Shielding Program 09-0," APEX-533, (December, 1958). 164. J. J. Loechler, J. E. MacDonald and H. M. VanValdenberg, "704 Program Report, Aircraft Nuclear Propulsion Shielding Program 05-0," XDC-59-8-218, (July, 1959). 165. J. J. Loechler and J. E. MacDonald, "IBM-704 Program Report, Aircraft Nuclear Propulsion Shielding Program 07-1," XDC-60-3-103, (February, 1960). 166. J. W. Haffner, J. J. Loechler and J. E. MacDonald, "IBM-704 Program Report, Aircraft Nuclear Propulsion Shielding Program 10-0," APEX-503, (March, 1958).
SHIELDING 12-0		General Electric Co., Aircraft Nuclear Propulsion Department	IBM-704 with 8K core memory, 2 tape units.		167. W. E. Edwards and J. J. Loechler, "Shielding Computer Program 12-0 Gamma Ray Penetration Point Source," APEX 404, (August, 1958). 168. H. Goldstein and J. E. Wilkins, Jr., "Calculations of the Penetrations of Gamma Rays," NYO-3075, (June, 1954).
SPAN-2 SPIC-1		Westinghouse Electric Corp., Bettis Atomic Power Div.	IBM-704 with 32K core memory, 2 tape units. IBM-704 with 32K core memory, 2 tape units.	4 min/energy level for a 20-field-point problem with 10 side and 10 top shields. 6.5 min.	169. P. A. Gillis, T. J. Lawton and K. W. Brand, "SPAN-2 An IBM-704 Code to Calculate Uncollided Flux Outside a Circular Cylinder," WAPD-TM-176, (August, 1959). 170. P. Gillis, "SPIC-1 An IBM-704 Code to Calculate the Neutron Distribution Outside a Right Circular Cylindrical Source," WAPD-TM-196, (November, 1959).

SUBJECT INDEX

A

Absorption escape probability
  definition, 3.6.3.2
Activation
  See Foil activation
Age
  beryllium, 3.4.2
  calculation methods, 3.4.2, 3.5.3
  carbon-hydrogen mixtures, 3.4.2
  computer program for Fourier transform of slowing down distribution, 3.5.1
  concrete, 8.4.2
  definition, 3.4.2
  diphenyl, 3.4.2
  equation for mixtures, 3.5.3
  equivalence method, 3.5.3
  graphite and graphite-bismuth mixtures, 3.4.2
  graphite-uranium lattices, 4.5.3.3
  heavy water-uranium lattices, 4.5.4.2
  heavy water-UO_2 lattices, 4.5.4.2
  measurement by pulsed neutron method, 5.3.8
  moments and age in graphite and graphite-bismuth mixtures, 3.4.2
  moments for slowing-down distributions from fission sources, 3.4.4
  moments from fission sources, 3.4.2
  non-fission neutrons in various media, 3.4.3
  P_1 approximation, 3.5.3
  sensitivity to variations of cross sections in water, 3.4.3
  two-group as function of buckling, 3.5.3
  two-group Fermi age relationship for heavy water system, 3.5.3
  U^{233} fission neutrons in water, 3.4.4
  U^{235} fission neutrons in water, 3.4.4
  water-heavy water mixtures, 3.4.2
  water-metal mixtures and lattices, 3.4.2, 3.5.3
Age-diffusion equation
  multigroup calculations, 6.1.1
Alpha particles
  absolute foil counting, 9.6.2
  back-scattering, 9.6.2
  ion pair production energy requirements in gases, 9.3.3
  range, 9.4.1
  self-absorption, 9.6.2
  stopping powers, 9.4.1
Asymptotic period
  deviation from observed period, 5.3.4, 5.3.5
  inhours per percent of reactivity for various fast assemblies, 7.3.2
  reactivity as function of asymptotic period and effective delayed neutron fraction for fast systems, 7.3.2
  reactivity as function of asymptotic period and neutron lifetimes for Pu^{239}, U^{233}, and U^{235}, 5.3.2
  reactivity as function of asymptotic period for various ZPR-III assemblies, 7.3.2
  reactivity error as function of asymptotic period error, 5.3.4
  source effects, 5.3.5
Autocorrelation function
  See Noise

B

Beta particles
  absolute foil counting, 9.6.1
  absorption half-thickness for endpoint energies, 9.6.1
  counting correction factors, 9.6.1
  counting efficiency, 9.6.1
  decay half-lives for isotopes used in detecting foils, 9.1.9
  maximum energy for isotopes used in detecting foils, 9.1.9
  prompt fission emission, 1.2.2

687863 O - 63 - 55

Blanc's law
statement of law, 9.3.1
Boltzmann equation approximation comparisons for fast systems
comparison of diffusion theory, S_4, and Serber-Wilson methods, 7.4.1
fundamental mode analysis, 7.4.1
relative error in criticality calculation as function of SNG order, 7.4.1
Buckling
beryllium-uranium homogeneous cores, 3.7.11
beryllium-uranium lattices, 4.5.7
effect on D_F in uranium-water mixtures, 3.5.3
effect on fast removal cross section in water, 3.5.3
effect on two-group age in water, 3.5.3
equivalence of radial buckling for octagon and circle, 6.3.3
fast systems of mixtures of fissionable and fertile materials, 7.2.6
function of core and central control rod radii, 5.1.4
graphite-uranium lattices, 4.5.3.1, 4.5.3.2, 4.5.3.3
heavy water-uranium lattices, 4.5.4.1, 4.5.4.2
heavy water-UO_2 lattices, 4.5.4.2
intermediate graphite reactors, 6.3.3
measurement by pulsed neutron method, 5.3.8
various intermediate reactor systems, 6.1.3
water-ThO_2-UO_2 lattices, 4.5.5
water-uranium lattices, 4.5.1.1, 4.5.1.2, 4.5.2
Buildup factors
coefficients for analytic fit to buildup factor equation, 8.3.3
dose buildup factor for point isotropic source, 8.3.3
gamma rays, 8.3.3
Burnable poisons
combinations with two different self-shielding factors, 5.2.8
epithermal absorption, 5.2.8
materials, 5.2.8
non-uniform burnup, 5.2.8
power distribution as function of time, 5.2.8
power flattening, 5.2.8
self-shielded poisons, 5.2.8
self-shielding factor, 5.2.8
space- and time-dependent problems, 5.2.8

C

Cadmium correction factor
as function of indium foil distance from source, in water, 9.1.7
as function of indium foil thickness, 9.1.7
cadmium covers on indium foils, 9.1.7
definition, 9.1.7
Cadmium effective cutoff energy
definition, 9.1.7
for cadmium and boron covers as function of cover thickness and Maxwellian temperature, 9.1.7
Cadmium ratio
boron-poisoned solutions of $UO_2(NO_3)_2$, 3.7.1.6
definition, 9.1.7
intermediate graphite-moderated, beryllium-reflected reactors, 6.3.3
TREAT core, 3.7.12
water-ThO_2-UO_2 lattices, 4.5.5
water-uranium lattices, 4.5.1.1, 4.5.1.2, 4.5.1.3
Capture-to-fission ratio (α)
Pu^{239} and U^{235}, as function of position in EBR-I, 7.2.10
values for various materials as function of energy, 2.2.1
Chemical binding
See also Kernels (thermal scattering) and Thermalization
calculations for water, 3.1.3.5
energy transfer and angular distribution for crystals, gases, and liquids, 2.4.1, 2.4.2
Collision density
integral equation, 3.6.3.1
solutions for special cases, 3.6.3.2
Computer codes (described)
AIM-5, 10.2.1
AIREK II, 10.3.4
AIREK III, 10.3.4
ANGIE, 10.2.2
ARK-1, 10.3.4
AX-1, 10.4
BOUT, 10.3.2
BOUT II, 10.3.2
BOX, 10.3.2
BUM, 10.3.4
BURNOUT, 10.3.2
CANDLE 1, 10.3.2
CASINO 13, 10.1.2
CEPTR, 10.1.4
COGENT, 10.1.3
CRUNCH, 10.3.3
CURE, 10.2.2
CUREBO, 10.3.2
DMM, 10.2.1
DRACO, 10.3.2
DSN, 10.2.1
EQUIPOISE, 10.2.2
F 2, 10.2.1
FIRE, 10.2.1
FLEER, 10.2.2
FLIP, 10.1.4
GNU II (MAGNUM), 10.2.1
GPR, 10.3.2

Computer codes (described) (Continued)
GRACE I, 10.5
HIGH ENERGY SPECTRA MONTE CARLO PROGRAM, 10.5
HOBO (RE 184), 10.1.4
I_2, 10.1.4
IDIOT, 10.1.4
K-CODE, 10.3.4
MAGNUM (GNU II), 10.2.1
MIS, 10.5
MUFT-4, 3.5.1, 10.1.2
MUG II, 10.2.2
NIOBE, 10.5
NUREP, 10.1.1
PDQ 2, 10.2.2
P1MG, 10.1.2
PROD II, 10.2.1
PROGRAM 0159, 10.1.2
PROGRAM 0329, 10.1.2
PROGRAM 0366, 10.1.2
QUERY, 10.1.1
RANCH, 10.1.4
RDR 4, 10.1.4
RDR 5, versions A, B, and C, 10.1.2
RE 29, 10.3.4
RE 34, 10.5
RE 126, 10.3.4
RE 129, 10.3.4
RE 132, 10.3.4
RE 135, 10.3.4
RE 138, 10.3.4
RE 157, 10.5
RE 171, 10.3.4
RE 184 (HOBO), 10.1.4
REX, 10.2.1
ROUTINE II, 10.1.3
ROUTINE V, 10.1.4
SCRAM I, 10.3.1
SHIELDING 09-0, 10.5
SHIELDING 12-0, 10.5
SLOP-1, 10.1.4
SOFOCATE, 10.1.3
SPAN-2, 10.5
SPECTRUM, 10.1.3
SYZYGY, 10.1.3
TDC, 10.2.2
TEMPEST, 10.1.3
TKO, 10.2.3
TRAM, 10.1.3
TRIXY, 10.2.3
TURBO, 10.3.2
TUT-T5, 10.1.4
UFO, 10.2.3
UNCLE I, 10.2.2
UNCLE II, 10.2.2
UNCLE III, 10.2.1
UNCLE IV, 10.2.1
VARI-1, 10.2.1
WANDA, 10.2.1
ZOOM, 10.2.1

Computer codes (related)
(Code to which related appears in parentheses)
2-D MULTIGROUP DIFFUSION (ANGIE), 10.2.2
BD-1 (PROD II), 10.2.1
C_2(F2), 10.2.1
CANDLE (CANDLE 1), 10.3.2
CANDLE 2 (CANDLE 1), 10.3.2
CANDLE 3 (CANDLE 1), 10.3.2
CELCOR (DSN), 10.2.1
CURE 1C (CUREBO), 10.3.2
CURE 1CT (CUREBO), 10.3.2
CURE 2C (CUREBO), 10.3.2
CURE 2CT (CUREBO), 10.3.2
CURE 3CT (CUREBO), 10.3.2
CUREM (CURE), 10.2.2
DONATE (SOFOCATE), 10.1.3
DRACO 1 (DRACO), 10.3.2
DRACO 2 (DRACO), 10.3.2
DRACO 3 (DRACO), 10.3.2
ECESS (SLOP-1), 10.1.4
EDNA (WANDA), 10.2.1
ENSIGN (WANDA), 10.2.1
EQUIPOISE-2 (EQUIPOISE), 10.2.2
EXSLOWEQ (QUERY), 10.1.1
FAF (PROD II), 10.2.1
FLIP 1 (FLIP), 10.1.4
FLIP 2 (FLIP), 10.1.4
FORM (MUFT-4), 10.1.2
GEORGE (F2), 10.2.1
GRACE II (GRACE I), 10.5
HARWELL PROGRAMS (QUERY), 10.1.1
HATCHET (AX-1), 10.4
HERD (RANCH) 10.1.4
HUF (BOUT), 10.3.2
JET (TURBO), 10.3.2
KATE-1 (SOFOCATE), 10.1.3
LIL ABNER (WANDA), 10.2.1
MAGNUM 32K (GNU II), 10.2.1
MCC (DMM), 10.2.1
MERCURY S_n (DSN), 10.2.1
MUFT-III, (MUFT-4), 10.1.2
MUFT-5 (MUFT-4), 10.1.2
NEXT (BOUT), 10.3.2
NREP 1 (NUREP), 10.1.1
NREP 2 (NUREP), 10.1.1
NREP 3 (NUREP), 10.1.1
NREP 4 (NUREP), 10.1.1
NYU-TUT-704 (TUT-T5), 10.1.4
OTHER POISONS (CRUNCH), 10.3.3
P_3 (I_2), 10.1.4
P1MG1 (P1MG), 10.1.2
P1MG2 (P1MG), 10.1.2
P1MG3 (P1MG), 10.1.2
PDQ 3 (PDQ 2), 10.2.2
PDQ 4 (PDQ 2), 10.2.2
PERCOLATOR (PROD II), 10.2.1
PERT (AIM-5), 10.2.1

Computer codes (related) (Continued)
POISON'S CALCULATION, MARK 2 (CRUNCH), 10.3.3
PPCo 10-006 (SCRAM I), 10.3.1
PPCo 10-009 (SCRAM I), 10.3.1
PPCo 10-010 (SCRAM I), 10.3.1
PREP (RDR 5), 10.1.2
PROBE I (VARI-1), 10.2.1
PROBE II (VARI-1), 10.2.1
PROGRAM S-VII (DSN), 10.2.1
PROP (TURBO), 10.3.2
PSP (CURE), 10.2.2
RE-31 (RE 171), 10.3.4
RE 122 (REX), 10.2.1
SHIELDING 05-0 (SHIELDING 09-0), 10.5
SHIELDING 07-0 (SHIELDING 09-0), 10.5
SHIELDING 10-0 (SHIELDING 09-0), 10.5
SIMPL-1 (FLIP), 10.1.4
SIMPL-2 (FLIP), 10.1.4
SNG (DSN), 10.2.1
SNK (DSN), 10.2.1
SOPHIST I (ANGIE), 10.2.2
SOPHIST II (ANGIE), 10.2.2
SPIC 1 (SPAN 2), 10.5
SYNFAR (TDC), 10.2.2
TOPSY (MUG II), 10.2.2
TRAC-1 (TUT-T5), 10.1.4
TURBO (TURBO), 10.3.2
TURBO 1 (TURBO), 10.3.2
TURBO 2 (TURBO), 10.3.2
TURBO 3 (TURBO), 10.3.2
TURBO 4 (TURBO), 10.3.2
TURBO 5 (TURBO), 10.3.2
VALPROD (PROD II), 10.2.1
VALPROD IB (PROD II), 10.2.1
VALPROD IIB (PROD II), 10.2.1
VAPOR (PROD II), 10.2.1
WANDA-5 (WANDA), 10.2.1
Computing codes (by subject)
burnup, 10.3.2
control cells and worth evaluation, 10.3.1
disadvantage factors, 10.1.4
flux, 10.1.4
hazards and safety, 10.4
isotope production, 10.3.3
kinetics, 10.3.4
reactivity and criticality search, one dimensional geometry, 10.2.1
reactivity and criticality search, two dimensional geometry, 10.2.2
reactivity and criticality search, three dimensional geometry, 10.2.3
resonance escape and resonance region averages, 10.1.1
shielding, 10.5
slowing down, 10.1.2
spectrum, 10.1.3
thermal parameters, 10.1.3
transfer functions, 10.3.4
Concretes
densities, 8.4.1, 8.4.2
elemental compositions, 8.4.1
gamma-ray attenuation coefficients, 8.3.1
mix proportions, 8.4.1
nuclear constants, 8.4.2
relaxation lengths of fast neutrons, 8.4.2, 8.4.3
shielding properties, 8.4
Control
absorption area for black bar, 5.1.3
absorption area for black cross, 5.1.3
absorption area method, 5.1.3
age-diffusion theory for slab control, 5.1.6
buckling as function of core and central rod radii, 5.1.4
calculated and experimental rod worths, 5.1.5
control cell method including epithermal absorption, 5.1.6
control cells, 5.1.5
control sheets in slab reactor, 5.1.5
edge correction for hafnium slab, 5.1.3
effective radii, 5.1.2, 5.1.3
effective radii nomogram for black rectangular bars, 5.1.2
effectiveness of eccentric rod, 5.1.4
effectiveness of partially withdrawn rods, 5.1.4
effectiveness of rods in bare versus reflected reactors, 5.1.4, 5.1.5
flux peaking in water channels, 5.1.6
interaction effects of control rods, 5.1.5
interaction of two cylindrical control rods, 5.1.5
linear extrapolation distance for Milne's problem, 5.1.1
linear extrapolation distances for various configurations, 5.1.1
multigroup calculations, 5.1.6
neutron collision probabilities in infinite cylinders, 5.1.1
Nordheim-Scalletar method, 5.1.5
one-group diffusion calculations, 5.1.5
poison cross section for cross rods, 5.1.5
reactivity effects of cylindrical rods, 5.1.4
reactivity versus number of rods, 5.1.5
relative effectiveness for various shapes of black bodies, 5.1.2, 5.1.3
small-source theory for heterogeneous reactors, 5.1.7
thin absorbers, 5.1.6
two-group diffusion theory, 5.1.5, 5.1.6
two-group perturbation theory, 5.1.6
Conversion factors
energy and power conversion factors, 8.5
energy-lethargy conversion tables, 1.3.2
gamma flux-to-dose, 8.3.4
neutron flux-to-dose, 8.2.3
stopping power to energy loss, 9.4.4

Counters
See Radiators and Scintillators
Coupled fast-thermal systems
ZPR-III critical experiment, 7.2.11
ZPR-V critical experiment, 7.2.11
Critical dimensions
See Critical parameters and Integral data ...
Critical masses
See Integral data ...
Critical parameters
air gap effects on uranium-beryllium oxide reactors, 3.7.11
annular cores, aqueous solutions of UO_2F_2 and U_3O_8, 3.7.6
aqueous solutions enriched in U^{233}, 3.7.13
aqueous solutions enriched in U^{235}, 3.7.1
aqueous solutions of plutonium nitrate, 3.7.14
aqueous solutions of UO_2F_2, 3.7.1.1, 3.7.1.4, 3.7.1.5
aqueous solutions of $UO_2(NO_3)_2$, 3.7.1.4, 3.7.1.6
beryllium oxide-uranium reactors, 3.7.11
circulating and non-circulating aqueous solutions of UO_2SO_4; heavy water reflected, 3.7.4
critical mass as function of H/U^{235}, 3.7.9
fitting formula for cylinders, aqueous solutions of UO_2F_2, 3.7.1.2
graphite-moderated, foil-fueled reactors, 3.7.12
graphite-reflected, heavy water solutions of UO_2F_2, 3.7.10.2
heavy water solutions of UO_2F_2, 3.7.10.1
interacting arrays of vessels, aqueous solutions of UO_2F_2, 3.7.5
Los Alamos water boiler experiments, 3.7.1.7
paraffin and UF_4 mixtures, 3.7.9
plastic-water reflected, aqueous solution of UO_2F_2, 3.7.1.3
reflector composition and dimension effects on aqueous solutions of uranium salts, 3.7.2, 3.7.2.1, 3.7.2.2, 3.7.2.3, 3.7.4
reflector void effects on aqueous solutions of $UO_2(NO_3)_2$, 3.7.2.1
slurries of water-UO_3, 3.7.8
temperature effects, 3.7.1.1, 3.7.4, 3.7.12, 3.7.13
Cross sections
Amster's compilation of average thermal values, 3.2.3
aqueous moderator values for spectrum calculations, 3.1.3.5
calculation of effective thermal, using heavy monatomic gas model, 3.2.1
coefficients for determination of effective thermal, 3.2.1, 3.2.2
comparison in hydrogenous media, 3.3.3
determination by computer codes, 3.2.4
fast effect values, 4.3.1
gamma-ray absorption in NaI(Tl), 9.2.3
isotopes used in detecting foils, 9.1.9
materials for fission counters, 9.5.2
one-group for ϵ computations, 3.6.2
2200 m/s values, 2.1
Westcott's convention for effective thermal, 3.2.2
Cross sections (absorption)
average macroscopic times average neutron velocity for beryllium, 3.3.1.2
fission products, 5.2.2
Pa^{233}, 5.2.3, 5.2.5
plutonium isotopes, effective, 5.2.5
Sm^{149}, 5.2.1
thermal neutrons in concrete, 8.4.2
uranium isotopes, effective, 5.2.4, 5.2.5
water, 3.1.7.2
Xe^{135}, 5.2.1
Cross sections (activation)
fast reactor spectra, 7.2.9
fission spectrum, 7.2.9
isotopes produced by thermal neutron capture, 8.1.7
reactor coolant materials, 8.1.7
Cross sections (capture)
as function of energy, 2.3
effect on flux age, 3.4.3
effective group, 6.2.1
fission product, intermediate to fast energy range, 6.2.2
moderators, measurement of effective, pulsed neutron method, 5.3.8
Np^{239}, effective, 5.2.5
one-group values for fast fission factor computation, 3.6.2
plutonium isotopes, effective, 5.2.5
Pu^{240}, effective, 5.2.6
Pa^{233}, effective, 5.2.5
thorium isotopes, effective, 5.2.5
uranium isotopes, effective, 5.2.4, 5.2.5
Cross sections (fission)
as function of energy, 2.2.2
average, fission spectrum neutrons above U^{238} fission threshold, 7.2.9
effective group, 6.2.1
fission detector ratios as function of composition of fissionable and fertile materials, 7.2.4, 7.2.6
fission detector ratios in uranium equilibrium spectrum flux, 7.2.6
one-group values for fast fission factor computations, 3.6.2
plutonium isotopes, effective, 5.2.5
uranium isotopes, effective, 5.2.4, 5.2.5
Cross sections (multigroup)
ANL 4-, 10-, 11-, 13-, and 16-group sets, 7.1.2

Cross sections (multigroup) (Continued)
fast and epithermal for equivalence factor computations, 3.5.3
fast group for water and water-uranium mixtures, 3.5.3
few-group, 3.5.2, 3.5.3, 7.1.3
four-group for fast-thermal coupled system calculation, 7.2.11
LASL 6-, 10-, and 16-group sets, 6.1.3, 7.1.2
MUFT 54-group library, 3.5.1
multigroup calculations in finite media, 3.6.4.7
multigroup equations, 7.1.1
USSR 9-group set, 7.1.2
Cross sections (photoneutron production)
beryllium, 8.1.8
deuterium, 8.1.8
Cross sections (removal)
as function of atomic weight, for shielding attenuation calculations, 8.2.2
average, for fission spectrum neutrons above U^{238} and Np^{237} fission thresholds, 7.2.9
concretes, 8.4.2
fast neutrons in water as function of buckling, 3.5.3
fast neutrons in water-uranium and water-UO_2 mixtures, 3.5.3
temperature dependence in concrete, 8.4.3
various isotopes, for shielding attenuation calculations, 8.2.2
Cross sections (scattering)
angular distribution as a function of energy, 2.4.3
as function of energy and angle, 2.4
effect on flux age, 3.4.3
effective group, 6.2.1
inelastic (n,γ) for 14-Mev neutrons, 8.1.4
non-elastic for uranium, 3.6.2
one-group values for fast fission factor computation, 3.6.2
partial inelastic for fissionable isotopes as function of incident energy, 2.4.2
total inelastic for fissionable isotopes as function of incident energy, 2.4.2
U^{238} inelastic in uranium equilibrium spectrum flux, 7.2.6
Cross sections (total)
stainless steel, 2.4.3
water, 2.4.1
Cross sections (transport)
average, for fission spectrum neutrons above U^{238} and Np^{237} fission thresholds, 7.2.9
average microscopic for various materials in fast and epithermal groups, 3.5.3
average values for hydrogen in water as function of $\beta\gamma$ and kT, 3.3.4
comparison in hydrogenous media, 3.3.3
thermal values for hydrogen, 3.3.3

D

Detector ratios
fast reactor systems, 7.2.4
Diffusion coefficient
discussion, 3.3.2.2
fast coefficient for concrete, 8.4.2
measurement by pulsed neutron method, 5.3.8
method of equivalence factors, 3.5.3
thermal coefficient for beryllium, 3.3.1.2
thermal coefficient for concrete, 8.4.2
Diffusion constants
See also Diffusion coefficient, Diffusion cooling, Diffusion length, and Transport mean free path
anisotropy effect on slowing-down area in lattices, 4.4.2
average values of $E^{-1/2}$ as function of $\beta\gamma$ and kT, 3.3.4
diffusion theory analysis, 4.4.2
discussion, 3.3, 3.3.2.2, 4.4
in hydrogenous moderators as function of $\beta\gamma$ and kT, 3.3.4
measurement by pulsed neutron method, 5.3.8
non-thermal for multigroup theory, 3.5
one- and two-group representations, 3.5.3
reactor hole effects, 4.4.3
temperature coefficients for diffusion length in water, 3.3.2.1, 3.3.2.2
thermal-group diffusion parameters, 3.3
thermal neutrons in beryllium, 3.3.1.2
thermal neutrons in beryllium oxide, 3.3.1.3
thermal neutrons in graphite, 3.3.1.1
thermal neutrons in moderators containing absorbers, 3.3.4
thermal neutrons in non-equilibrium environments, 3.3.5
thermal neutrons in water and other hydrogenous moderators, 3.3.2.2, 3.3.3
transport theory analysis, 4.4.2
variation with buckling in water-uranium mixtures, 3.5.3
Diffusion cooling
coefficient measurement by pulsed neutron method, 5.3.8
discussion, 3.3.1.2
Diffusion length
discussion, homogeneous systems, 3.3, 3.3.4
empirical formulas for thermal neutrons in water, 3.3.2.1
graphite-uranium lattices, 4.5.3.3
Hanford reactors, 3.3.1.1
heavy water-uranium lattices, 4.5.4.2
heavy water-UO_2 lattices, 4.5.4.2
measurement by pulsed neutron method, 5.3.8
natural uranium in equilibrium spectrum flux, 7.2.6

Diffusion length (Continued)
streaming correction factors for diffusion in graphite, 3.3.1.1
temperature coefficients for thermal neutrons in water, 3.3.2.1
thermal neutrons in beryllium, 3.3.1.2
thermal neutrons in beryllium oxide, 3.3.1.2
thermal neutrons in concrete (k), 8.4.2
thermal neutrons in graphite, 3.3.1.1
thermal neutrons in hydrogenous moderators, 3.3.3
thermal neutrons in water, 3.3.2.1, 3.3.4
with anisotropy, 4.4.2
with no anisotropy, 4.4.1
Disadvantage factor
diffusion theory, 4.1.1
double-P_n method, 4.1.2
effects of spectral hardening, 4.1.6
formulas for thermal utilization, 4.1.1.1
from considerations of rod blackness and extrapolation length, 4.1.5
graphite-uranium lattices, 4.5.3.3
heavy water-uranium lattices, 4.5.4.1, 4.5.4.2
integral transport theory, 4.1.4, 4.1.4.1, 4.1.4.2
intermediate graphite-U^{235} foil reactors, 6.3.3
phenomenological and approximate formulae, 4.1.7
radial flux distribution in rods, 4.1.7.1
resonance, 4.2.6
Serber-Wilson method in slab geometry, 4.1.4.3
spherical harmonic method, 4.1.2, 4.1.3, 4.1.7.2
thermal self-shielding factor for lumps, 4.1.7.3
water-ThO_2-UO_2 lattices, 4.5.5
water-uranium lattices, 4.5.1.1
water-UO_2 lattices, 4.5.2
Doppler effect
broadening and scattering interference effects, 3.6.4.3
coefficients of UO_2 and hafnium in intermediate reactors, 6.2.1
fast reactors, 7.3.3
intermediate reactors, 6.2.1
ZEUS-3B experiment, 7.3.3
ZPR-III experiment, 7.3.3

E

Effective mass
calculations for water and heavy water, 3.1.3.5
Electrons
drift velocity, 9.3.2
energy losses, 9.4.2
ion pair production energy requirements in gases, 9.3.3
ionization losses, 9.4.2
range, 9.4.5
stopping power, 9.4.2
Equivalence factors
heavy water mixtures, 3.5.3
water mixtures, 3.5.3
Eta (neutrons emitted per absorption), 2.2.1, 3.6.5, 5.2.4
Excursions (reactor)
above prompt critical, 5.5.1
burst width as function of period, 5.5.1
conduction boiling model, 5.5.2
Corben model, 5.5.2
EBR-I experiments, 7.3.4
general considerations, 5.5.1
Godiva burst experiments, 7.3.4
homogeneous reactors, 5.5.2
kinetic equations, simplified, 5.5.1
non-empirical methods for analysis, 5.5.2
prompt negative temperature coefficients of reactivity, 5.5.3
reactivity insertion at constant rate, 5.5.1
reactivity insertion by ramp rate, 5.5.2
reactivity insertion by step rate, 5.5.1
reactivity reduction mechanism, 5.5.1
reflector delayed neutrons, 5.5.2
relationships among compensated reactivity, energy, fuel surface temperature, period, power, and pressure, 5.5.2, 5.5.3
SPERT-I core characteristics, 5.5.2
TREAT core characteristics, 5.5.3
TREAT transient experiments summary, 5.5.3
TRIGA core characteristics, 5.5.3
TRIGA transient experiments summary, 5.5.3
water reactors, 5.5.2
Exponential integral
definition, 9.1.2
table, 9.1.8
Extrapolation length
as function of H/U ratios, 3.7.1.4
fast dilute systems, 7.2.8
fast high-density systems, 7.2.7
linear, for control elements, 5.1.1

F

Fast effect
calculations for infinite homogeneous systems, 3.6.2
collision probabilities, 4.3.1, 4.3.4
cross sections, 4.3.1
fast conversion ratio, 4.3.1, 4.3.2
fast effect factor, 3.6.1
fast effect factor in beryllium and beryllium oxide, 3.6.2

Fast effect (Continued)
fast fission factor, 3.6.1, 3.6.2, 4.3, 4.3.1
fast fission factor as function of fast fission ratio, 4.3.2
fast fission factor for graphite-uranium lattices, 4.5.3.3
fast fission factor for heavy water-uranium lattices, 4.5.4.2
fast fission factor for heavy water-UO_2 lattices, 4.5.4.2
fast fission factor for water-uranium lattices, 4.5.1.1
fast fission ratio, 4.3.1, 4.5.1.2, 4.5.2
fast leakage effect, 4.3.3
formulas, 4.3.1, 4.3.2
heterogeneity effects, 4.3.4
interaction, 4.3.4
one-group formulation, 3.6.2
water mixtures of uranium metal and uranium oxide, 3.5.3
Fission
average energy of neutrons, 1.3.1
average neutron yield per neutron absorbed (η), 2.2.1
delayed neutrons, 1.4
energetics, 1.2.1
prompt beta emission, 1.2.2
prompt gamma emission, 1.2.2
prompt neutron spectrum, 1.3.1, 1.3.2
Fission products
buildup of total fission product poisoning, 5.2.2
chains, 1.2.3
cross sections, 5.2.2
cross sections as function of burnup, 5.2.2
decay of gamma rays, 8.1.5
decay of gross ($\gamma + \beta$) fission product energy release, 8.1.6
delayed gamma ray energy per fission, 8.1.2
empirical formula for decay of gross ($\gamma + \beta$) fission product energy release, 8.1.6
energy, 1.2.1
energy loss as function of range, 9.4.3
energy loss by ionization, 9.4.3
equilibrium concentrations, 5.2.2
equilibrium gamma ray energy per fission, 8.1.2
integrated energy generation after reactor shutdown, 8.1.6
ionization density as function of range, 9.4.3
mass, 1.2.1
mass ratio, 1.2.1
non-saturating poisons, 5.2.2
poisoning effect on η in $Th^{232}-U^{235}$ systems, 5.2.4
poisoning in Pu^{239}, U^{233}, and U^{235}, 5.2.2
power generation after reactor shutdown, 8.1.6
pseudo-element calculations, 5.2.2
pseudo-fission products, 5.2.2
range, 1.2.4
resonance absorption, 5.2.2
resonance integral, 5.2.2
yields: cumulative, direct, and total chain, 1.2.3, 5.2.2
Flux distribution
aqueous moderators, 3.1.7.1
fission-to-equilibrium spectra comparison for beryllium, 3.6.2
Fourier transforms of infinite medium point source kernel, 3.4.1.1
minimum-critical-mass experiment, 3.7.7
radial flattening in water-uranium solution in cylindrical core, 3.7.7
spatial distribution of sources in absorbing medium, 3.1.5.2
temperature discontinuity between media, 3.1.5.1
Foil activation
activation of cadmium-covered indium and gold foils by epithermal neutrons, 9.1.7
activation of cadmium-covered indium foils by thermal neutrons, 9.1.7
activation and initially unperturbed flux relation, 9.1.5
cadmium correction factor as function of indium foil distance from source, in water, 9.1.7
cadmium correction factor for cadmium-covered indium foils, 9.1.7
cadmium correction factor for indium foils as function of foil thickness, 9.1.7
"conventional" flux, 9.1.1
effective cutoff energy definition, 9.1.7
effective cutoff energy for cadmium and boron covers as function of cover-thickness and Maxwellian temperature, 9.1.7
flux distribution surrounding a foil, 9.1.6
flux ratios for foils in water and in graphite, 9.1.5
foil covers discussion, 9.1.7
g-functions for outer flux perturbations, 9.1.4
integral flux perturbations, 9.1.5
integral flux perturbations as function of foil radii, 9.1.5
Meister's ξ_0 (τ) function for flux distribution surrounding a foil, 9.1.8
nuclear properties of selected detecting foil materials, 9.1.9
outer flux perturbations, 9.1, 9.1.1, 9.1.4
resonance energy of isotopes used in detecting foils, 9.1.9
resonance self-shielding function as function of indium thickness, 9.1.3
self-shielding approximation for thin foils, 9.1.2
self-shielding function, 9.1.2

Foil activation (Continued)
self-shielding function approximation, 9.1.8
self-shielding in resonance activation, 9.1.3
self-shielding second-order correction term, 9.1.8
threshold energy and cross sections for isotopes used in detecting foils, 9.1.9
"true" flux, 9.1.1
Foil counting
absolute alpha counting, 9.6.2
absolute beta counting, 9.6.1
absolute beta counting corrections, 9.6.1
absolute neutron flux counting, 9.6
absorption half-thickness for endpoint beta energies, 9.6.1
alpha back-scattering from various backing materials, 9.6.2
alpha self-absorption, 9.6.2
beta counting efficiency as function of energy, 9.6.1
beta counting efficiency as function of sample thickness, 9.6.1
Four-factor formula
neutron chain process description, 3.6.1
Fourier transforms
diffusion (Yukawa) kernel, 3.4.1
Gaussian (Fermi) kernel, 3.4.1
neutron slowing-down distribution computer program, 3.5.1
slowing-down kernels, 3.4.1, 3.4.1.1, 3.4.4
transport kernel, 3.4.1
Fuel solutions
critical parameters, 3.7

G

Gamma detection
See Radiators and Scintillators
Gamma rays
buildup factors, 8.3.3
capture spectra for concretes, 8.4.2
coefficients for analytic fit to buildup factor equation, 8.3.3
dose buildup factor for point isotropic source, 8.3.3
energy absorption cross sections, 8.3.2
energy absorption mass attenuation coefficient, 8.3.2
energy and intensity for isotopes used in detecting foils, 9.1.9
photon energy yield in percent per disintegration, from thermal neutron capture, 8.1.7
total attenuation cross sections, 8.3.1
total mass attenuation coefficient, 8.3.1
Gamma rays (fission products)
delayed energy per fission, 8.1.2
energy decay rate as function of reactor shutdown time, 8.1.5
equilibrium energy per fission, 8.1.2
Gamma rays (prompt)
average number of photons per neutron capture, 8.1.3
energy of photons per fission, 1.2.2
fission spectrum of photons, 1.2.2, 8.1.1
inelastic scattering cross sections for 14-Mev neutrons, 8.1.4
maximum energy from neutron capture by various nuclei, 8.1.3
number of photons per fission, 1.2.2
photon spectrum from neutron capture, 8.1.3
total prompt energy per fission, 8.1.1
Gas constants
average energy to produce one ion pair in gases, 9.3.3
average ionization potential of gaseous elements as function of proton energy, 9.3.3
Blanc's law, 9.3.1
characteristics of charged-particle detecting phosphors, 9.3.1
diffusion coefficients for heavy ions, 9.3.1
drift velocity of electrons in gases, 9.3.2
drift velocity of heavy ions, 9.3.1
mobility of heavy ions, 9.3.1
mobility of ions in gases as function of ion mass, 9.3.1

H

Half-lives
beta-emitting isotopes used in detecting foils, 9.1.9
decay chain of Ra^{226}-α-Be neutron source, 9.7.1
delayed neutron, 1.4.1
delayed photoneutrons in beryllium from U^{235} fission products, 1.4.3, 5.3.9
delayed photoneutrons in heavy water from U^{235} fission products, 1.4.3, 5.3.9
gamma-emitting isotopes used as photoneutron sources, 9.7.3
isotopes produced by thermal neutron capture, 8.1.7
spontaneous fission for various isotopes, 1.6, 9.7.4
Holes in reactor
See Diffusion constants, Reactivity effects, and Reflectors

I

Inelastic scattering
See also Cross sections (scattering)
energy transfer for fissionable isotopes, 2.4.2

Infinite multiplication factor
four-factor formula $k_\infty = \epsilon\ p\ \eta\ f$, 3.6
heavy water-uranium lattices, 4.5.4.2
heavy water-UO_2 lattices, 4.5.4.2
water-ThO_2-UO_2 lattices, 4.5.5
water-uranium lattices, 4.5.1.1
Inhomogeneity effect in fast reactors
large fast assembly, 7.2.3
ZPR-III systems, 7.2.3
Integral data (fast systems)
EBR-II, 7.2.1
empirical correlations for predicting criticality, 7.2.1
Enrico Fermi Reactor mock-up, 7.2.1
Godiva, 7.2.1
Jemima, 7.2.1
Jezebel, 7.2.1
plutonium cores, as function of diluent material, 7.2.1
plutonium high-density cores, 7.2.1
plutonium high-density cores in extreme geometry, 7.2.1
Pu^{239} core, as function of reflector material, 7.2.1
Popsy, 7.2.1
Topsy, 7.2.1
uranium cores, as function of various enrichments and diluents, 7.2.1
uranium cores, for various core and blanket material compositions; ZEUS experiments, 7.2.1
U^{233} cores, as function of reflector material, 7.2.1
U^{235} cores, as function of core dimensions, 7.2.1
U^{235} cores, as function of natural uranium reflector thickness, 7.2.1
U^{235} cores, as function of reflector material and thickness, 7.2.1
U^{235} cores in extreme geometry, 7.2.1
U^{235} cores with water and graphite reflectors, 7.2.1
U^{235} high-density annular cores, as function of reflector materials, 7.2.1
U^{235}-plutonium cores containing Pu^{240}, 7.2.1
ZPR-III, 7.2.1
ZPR-III fast-thermal coupled critical experiment, 7.2.11
Integral data (intermediate systems)
beryllium-plutonium homogeneous reactors, 6.4
beryllium-uranium heterogeneous reactors, 6.3.1
beryllium-uranium homogeneous reactors, 6.4
beryllium oxide-uranium heterogeneous reactors, 6.3.2
beryllium oxide-uranium homogeneous reactors, 6.4
graphite-uranium heterogeneous reactors, 6.3.3
graphite-uranium heterogeneous reactors with gaps between core and reflector, 6.3.3
graphite-uranium homogeneous reactors, 6.4
heavy water-UO_2F_2 reactors, 6.3.5, 6.4
hydrogen-plutonium heterogeneous reactors, 6.3.4
hydrogen-UO_2F_2 reactors, 6.3.4, 6.4
Integral data (thermal systems)
aqueous slurries of UO_3, 3.7.8
aqueous solutions of plutonium nitrate, 3.7.14
aqueous solutions of UO_2F_2, 3.7.1.1, 3.7.1.2, 3.7.1.3, 3.7.1.4, 3.7.1.5, 3.7.2.1, 3.7.2.2, 3.7.2.3, 3.7.3, 3.7.5, 3.7.6, 3.7.7, 3.7.13
aqueous solutions of $UO_2(NO_3)_2$, 3.7.1.6, 3.7.2.1, 3.7.13
aqueous solutions of UO_2SO_4, 3.7.4
aqueous solutions of U_3O_8, 3.7.6
beryllium oxide fueled with foils of uranium, 3.7.11
beryllium-uranium lattices, 4.5.7
discussion, heterogeneous systems, 4.5
discussion, homogeneous systems, 3.7
graphite fueled with foils of uranium, 3.7.12
graphite-uranium lattices, 4.5.3
heavy water-ThO_2-UO_2 lattices, 4.5.6
heavy water-uranium lattices, 4.5.4
Los Alamos Water Boiler, 3.7.1.7
paraffin-UF_4 mixtures, 3.7.9
water-ThO_2-UO_2 lattices, 4.5.5
water-uranium lattices, 4.5.1
water-UO_2 lattices, 4.5.2
Intermediate reactors
definition, 6
Isotope buildup (thorium-uranium chain)
batch irradiation of Th^{232}, 5.2.3
buildup from Th^{232} enriched in U^{235}, 5.2.4
concentration of heavy isotopes produced in thorium reactors, 5.2.3
concentration of heavy isotopes produced in thorium-uranium reactors, 5.2.4
constant power operation, 5.2.4
continuous irradiation, 5.2.3
cross sections for Pa^{233}, 5.2.3
cycled irradiation of Th^{232}, 5.2.3
cycled versus uninterrupted isotope production, 5.2.3
distribution of uranium isotopes in thorium slug, 5.2.3
effect of fission product poisoning, 5.2.4
effective cross sections of uranium isotopes, 5.2.4, 5.2.5
equilibrium concentrations, 5.2.4
isotope concentration as function of flux and processing time, 5.2.3
Pa^{233}-U^{233} ratio as function of flux and time, 5.2.3

Isotope buildup (thorium-uranium chain) (Continued)
reactivity as function of buildup of uranium isotopes, 5.2.4
resonance integral values for Pa^{233}, 5.2.3
schematic of chain, 5.2.3
summary of Th^{232} irradiation data, 5.2.3
variation of η in Th^{232}-U^{235} system, 5.2.4
variation of fuel composition in uranium recycle operation for thorium-heavy water reactor, 5.2.4
variation of fuel composition in uranium recycle operation for thorium oxide-water reactor, 5.2.4
Isotope buildup (uranium-plutonium chain)
See also Plutonium recycle
Am^{243} production as function of Pu^{239} irradiation time at fixed flux, 5.2.5
basic constants for calculation, 5.2.5
Cm^{244} production as function of Pu^{239} irradiation time at fixed flux, 5.2.5
distribution of plutonium isotopes in NRX rod, 5.2.5
effective cross sections, 5.2.5
effective Pu^{240}, irradiation dependence, 5.2.6
effective time-average cross sections for Pu^{239} and Pu^{240}, 5.2.5
isotope analysis of irradiated plutonium samples, 5.2.5
nuclear reactions in U^{238}, 5.2.5
reactivity as function of cooling time, 5.2.5
reactivity as function of plutonium isotope buildup, 5.2.5
reactivity effect of Np^{239}, 5.2.5
schematic of chain, 5.2.5
U^{235} burnup as function of nvt for natural uranium irradiation, 5.2.5

K

Kernels
diffusion (Yukawa), 3.4.1
Fourier transform for fission neutrons slowing down in water, 3.4.4
Fourier transform of the infinite medium, point source, 3.4.1.1
Gaussian (Fermi), 3.4.1
moments for slowing down in various media from fission sources, 3.4.2
neutron collision density, 3.6.3.1
non-leakage probability for a 2-Mev source in heavy water, 3.4.1.1
transport, 3.4.1
Kernels (thermal scattering)
See also Chemical binding and Thermalization
effective mass approximations to chemical binding in water, 3.1.3.5
hard spheres of heavy mass, 3.1.3.2
hard spheres of unit neutron mass, 3.1.3.1
heavy crystalline moderator, 3.1.3.3
scattering in water, 3.1.3.4
Ki_3 functions
table, 4.2.3
Kinetics
See also Asymptotic period, Excursions (reactor), and Stability (reactor)
discussion, 5.3
equations, 5.3.2, 5.5.1
fast reactor kinetics, 7.3.4

L

Lethargy
energy-lethargy conversion tables, 1.3.2
Logarithmic energy loss
average loss per collision (ξ), 2.1

M

Mass
See Effective mass
Material replacement
reactivity effects on various fast assemblies, 7.2.5
Median-energy-of-fission
as function of BeO/U^{235} ratios in intermediate reactors, 6.4
intermediate reactors, 6.3.1
Migration area
water-ThO_2-UO_2 lattices, 4.5.5
water-uranium lattices, 4.5.1.1
Moments
slowing-down, distribution from fission sources, 3.4.4
slowing-down, for graphite and graphite mixtures, 3.4.2
slowing-down, for various C/H ratios of unit mass density, 3.4.2
Multigroup constants for fast reactors
discussion, 7.1
Multigroup diffusion theory
See also Cross sections (multigroup)
capture effects on cross section calculations, 3.5.3
definition of group cross sections, 7.1.1
equations, 7.1.1
fast group constants by method of equivalence factors, 3.5.3
modification for finite media neutron resonance, 3.6.4.7
MUFT 54-group library, 3.5.1
non-thermal parameters, 3.5
Multigroup notation
cross section equations, 7.1.1
diffusion equations, 7.1.1
transport equations, 7.1.1

Multigroup transport theory
DSN method, 7.1.1
S_n method, 7.1.1
transport equations, 7.1.1

N

Narrow resonance approximations
See Resonance absorption
Neutron attenuation
fission, in water, 8.2.1
kernel, 8.2.1
moments calculation for fission, in water, 8.2.1
multigroup analysis for fission, in water, 8.2.1
Neutron detection
See Radiators and Scintillators
Neutron lifetime
effect on period, 5.3.5
measured values, 5.3.1
measurement by pulsed neutron method, 5.3.8
one-group theory, 5.3.1
perturbation theory, 5.3.1
prompt, measurements for fast systems, 7.3.1
prompt, ZPR-III fast-thermal coupled critical experiment, 7.2.11
SPERT-I Reactor, 5.5.2
TREAT Reactor, 5.5.3
two-group theory, 5.3.1
Neutron temperature
effect on flux distribution, 3.1.7.1
effect on integral data of beryllium oxide intermediate reactors, 6.3.2
effect on integral data of graphite intermediate reactors, 6.2.3
measured and calculated values comparison in aqueous moderators, 3.1.7.1
Neutrons (delayed)
absolute fission yield, 1.4.1
decay constant, 1.4.1
effective fraction, age theory equations, 5.3.1
effective fraction, diffusion theory equations, 5.3.1
effective fraction, fast reactors, 7.3.2
emission, 1.4
formula for effective fraction, 7.3.2
Fourier transforms of slowing-down kernels, 3.4.4
fraction, 1.4.1
fraction, aqueous solution of UO_2F_2, 5.3.1
fraction, Los Alamos Water Boiler, 5.3.1
fraction, TREAT and TRIGA Reactors, 5.5.3
half-life of parent, 1.4.1
mean energy, 1.4.2
multigroup distribution, 7.3.2
reactivity as function of asymptotic period and effective fraction for fast systems, 7.3.2
relative abundance, 1.4.1
Neutrons (fission)
average energy, 1.3.1
emission, 1.5
number per fission as function of incident neutron energy, 1.5.1, 1.5.2
probability function, P_ν, for emitting ν neutrons per fission, 1.5.3
Neutrons (prompt)
emission, 1.5
fission spectrum, 1.3, 1.3.1, 1.3.2
Neutrons (pulsed)
age equation, 5.3.8
diffusion cooling, 5.3.8
diffusion equation, 5.3.8
diffusion parameter measurements, 5.3.8
effective cross section measurement for moderators, 5.3.8
slowing-down time spectrometer, 5.3.8
thermalization time constants, 5.3.8
time to establish fundamental mode as function of buckling for beryllium, 5.3.8
Noise
See also Rossi alpha
autocorrelation function, 5.3.7
fluctuation experiments, 5.3.7
power spectrum, 5.3.7
signal-to-noise ratio by means of oscillator, 5.3.7
variance-to-mean experiment, 5.3.7
Nuclear temperatures, 2.4.2

P

Period
See Asymptotic period
Perturbation
g-functions for outer flux perturbations caused by absorbing foils, 9.1.4
outer flux perturbation caused by absorbing foils, 9.1.4
Photomultiplier tubes
characteristics, 9.2.1
Photoneutrons
effectiveness factor, 5.3.9
half-lives in beryllium from U^{235} fission products, 5.3.9
half-lives in heavy water, 1.4.3
half-lives in heavy water from U^{235} fission products, 5.3.9
mean lives in beryllium, 1.4.3
yields in beryllium and heavy water, 1.4.3
Photons
See Gamma rays, Gamma rays (fission products), and Gamma rays (prompt)

Placzek function
definition, 3.6.3.2
variation with the mass number, 3.6.3.2
Plutonium recycle
fuel cycle management examples, 5.2.7
graphite reactors, 5.2.7
heavy water reactors, 5.2.7
water reactors, 5.2.7
Power flattening
See Burnable poisons
Protons
range in various gases, 9.4.1, 9.4.5
stopping power, 9.4.1

R

Radiation dose
conversion of gamma flux to dose rate, 8.3.4
conversion of neutron flux to dose rate, 8.2.3
depth dose, 8.2.3
first collision dose rate for neutrons as function of energy, 8.2.3
rad, 8.2.3
relative biological effectiveness for neutrons as function of energy, 8.2.3
rem, 8.2.3
roentgen, 8.2.3
Radiators
corrections for thick proton recoil, 9.5.3
corrections for thin, 9.5.4
differential recoil proton pulse height distribution, 9.5.4
efficiency in polyethylene, 9.5.4
fission threshold energies and cross sections for fission counter materials, 9.5.2
properties of fissionable linings, 9.5.2
properties of non-fission, 9.5.1
Range-energy relations for charged particles
electrons, 9.4.2, 9.4.5
factors for converting stopping power to energy loss, 9.4.4
factors for converting stopping power units, 9.4.4
fission fragments, 1.2.4, 9.4.3
heavy ions, 9.4.1
nomograph, 9.4.5
protons, 9.4.5
Reactivity effects
See also Burnable poisons, Control, Isotope buildup . . . , and Temperature effects
as function of buildup of plutonium isotopes, 5.2.5
as function of buildup of uranium isotopes, 5.2.4
as function of control rod separation, 5.1.5
as function of material composition in intermediate reactors, 6.3.1
as function of number of control rods, 5.1.5
burnable poisons, 5.2.8
change as function of control rod radius and depth of penetration, 5.1.4
holes in reflector, 3.7.3
inhomogeneity effect in fast systems, 7.2.3
material replacement effects on various fast assemblies, 7.2.5
measurements by pile oscillator, 5.3.7
radial water reflector, 3.7.1.6
reflector level in HRE-1, 3.7.4
relative effects of slab and cross control rods, 5.1.3
SPERT-I Reactor, 5.5.2
Reflector savings
beryllium-uranium lattices, 4.5.7
fast high-density systems, 7.2.7
fast dilute systems, 7.2.8
intermediate beryllium-plutonium reactors, 6.4
water-ThO_2-UO_2 lattices, 4.5.5
water-uranium lattices, 4.5.1.1, 4.5.1.2, 4.5.2
Reflectors
composition and thickness effects on critical parameters of water solutions of uranium salts, 3.7.2, 3.7.2.1, 3.7.2.2, 3.7.2.3
core critical height variation with graphite thickness, 3.7.11
critical parameters of water-metal solutions versus bottom reflector structure, 3.7.2, 3.7.2.2, 3.7.2.3
level effects in HRE-1, 3.7.4
properties of radial, 3.7.2.1
reactivity effects of holes, 3.7.3
reactivity worth of radial water, 3.7.1.6
void effects, 3.7.2.1
Resonance absorption
correction factor for fluctuations in neutron width, 3.6.4.1
Doppler broadening, 3.6.4.3, 4.2.5
effective group resonance integrals, 6.2.1
energy self-shielding, 6.1.2
escape probabilities in fuel mixtures, 3.6.4.8
escape probabilities in water mixtures of uranium and uranium oxide, 3.5.3
escape probability calculation, 3.6.4.8
escape probability computed by synthetic-kernel methods, 3.6.3.2
fission products, 5.2.2
in homogeneous mixtures of hydrogen and U^{238}, 3.6.4.5
in infinite homogeneous medium, 3.6.3, 3.6.4
integral computations over isolated resonances, 3.6.4.6
integral values for Pa^{233}, 5.2.3
integrals in homogeneous mixtures, 3.6.4.4
integrals for infinite dilution, 3.6.4.1
modifications for finite media, 3.6.4.7

Resonance absorption (Continued)
narrow resonance approximations to the resonance integral, 3.6.4.2, 3.6.4.3, 3.6.4.5, 4.2, 4.2.2.1, 4.2.2.3
resonance properties for isotopes used in detecting foils, 9.1.9
Resonance absorption (heterogeneous systems)
Dancoff-Ginsburg correction for shadowing, 4.2.3
disadvantage factors, 4.2.6
equivalence principles for heterogeneous and homogeneous systems, 4.2.2, 4.2.2.1, 4.2.2.3
escape probability, 4.2
escape probability in graphite-uranium lattices, 4.5.3.3
escape probability in heavy water-uranium lattices, 4.5.4.2
escape probability in heavy water-UO_2 lattices, 4.5.4.2
escape probability methods in isolated lumps and lattices, 4.2.2.3
escape probability by Monte Carlo calculation, 4.2.4
escape probability by variational method, 4.2.2.3
escape probability in water-ThO_2-UO_2 lattices, 4.5.5
escape probability in water-uranium lattices, 4.5.1.1
geometrical corrections, 4.2.2.3
integral empirical formulas, 4.2.7
integrals as function of lower energy limit, 4.2.1
integrals for graphite-uranium lattices, 4.5.3.3
integrals for heavy water-uranium lattices, 4.5.4.2
integrals for heavy water-UO_2 lattices, 4.5.4.2
integrals for isolated lumps, 4.2.1
integrals for U and UO_2 as functions of temperature, 4.2.1
integrals for U^{238}, 4.2.1
penetrability factors, 4.2.2.3
Resonance escape probability
See Resonance absorption
Resonance integrals
See Resonance absorption
Rossi alpha
noise experiment, 5.3.7
values for various fast systems, 7.3.1
ZPR-III fast-thermal coupled critical experiment, 7.2.11

S

Samarium fission product effect
concentration as function of flux and time, 5.2.1
cross sections, 5.2.1
equations, 5.2.1
yield, 5.2.1
Scintillators
characteristics of low-energy neutron detectors, 9.2.2
characteristics of organic, 9.2.2
charged-particle detectors, 9.2.4
Compton scattering, 9.2.3
efficiency, detecting, 9.2.3
efficiency, gamma-detecting, 9.2.3
efficiency, "intrinsic," 9.2.3
efficiency, photopeak, 9.2.3
gamma attenuation coefficients for NaI(Tl) crystals, 9.2.3
gamma-detecting, 9.2.3
pair production, 9.2.3
phosphor characteristics, 9.2.4
photoelectric absorption, 9.2.3
photofraction, 9.2.3
response of anthracene and CsI(Tl) to ionizing particles, 9.2.4
X-ray escape peak, 9.2.3
Shape factor
definition, 7.2.2
fast cylindrical assemblies, as function of L/D, 7.2.2
power distribution, 7.2.2
Slowing-down parameters
macroscopic per fissile atom, partition ratio, 3.7
in well-moderated media, 3.4
Slurries (aqueous)
critical parameters of UO_3, 3.7.8
Small-source theory
See Control
Snell experiment, 7.2.6
Sources (α,n)
neutron spectra, 9.7.1
neutron yield from decay chain of Ra^{226}-α-Be and Ac^{227}-α-Be, 9.7.2
neutron yields, 9.7.2
Sources (d,n), 9.7
Sources (γ,n)
gamma energies and yields above (γ,n) threshold for H^2 and Be^9 targets, 9.7.3
half-lives of isotopes used as photoneutron sources, 9.7.3
neutron energy as function of gamma energy for H^2 and Be^9 targets, 9.7.3
neutron yield for various gamma-emitters and H^2 and Be^9 targets, 9.7.3
threshold energies for (γ,n) reactions, 9.7.3
Sources (n,2n)
ratio of secondary to primary in beryllium-uranium mixtures, 3.6.2
Sources (p,n), 9.7
Sources (spontaneous fission)
decay properties for spontaneous fission of various isotopes, 9.7.4

Sources (spontaneous fission) (Continued)
neutrons per fission, 9.7.4
neutrons per gram of source per second, 9.7.4
Spectra (thermal neutron)
angle-independent Boltzmann equation, 3.1.1
comparison in a crystalline and gaseous moderator, 3.1.4.6
comparison of normalized fission to equilibrium in beryllium, 3.6.2
effective mass approximations to chemical binding in water, 3.1.3.5
empirical description, 3.1.6
experiments, 3.1.7
fitting to Monte Carlo results, 3.1.6.1
general methods of solution of angle-independent Boltzmann equation, 3.1.2
in medium with temperature discontinuity, 3.1.5.1
in polyethylene, 3.1.7.3
in water, 3.1.7.1, 3.1.7.2, 3.1.7.3
in water-moderated multiplying media, 3.1.7.2
in water-natural uranium lattices, 3.1.7.4
in water poisoned with boric acid, 3.1.7.1
in zirconium hydride, 3.1.7.3
infinite homogeneous medium, 3.1.1
moderation by hydrogen bound in an oscillator potential well, 3.1.4.5
moderation by a monatomic heavy gas, 3.1.4.2, 3.1.4.3
moderation by monatomic hydrogen gas, 3.1.4.1
Monte Carlo calculations, 3.1.6.1
neutron thermalization equations, solutions in special cases, 3.1.4
scattering in water, 3.1.3.4
scattering kernels, 3.1.3
spatial distribution of sources, effect of, 3.1.5.2
Wilkins equation, variational solution, 3.1.4.4
Spectra-related constants (fast neutrons)
cross section ratios for fast systems, 7.2.4
fast fission cross section ratios as function of composition of fissionable and fertile materials, 7.2.6
fast fission cross section ratios in uranium equilibrium spectrum flux, 7.2.6
Spectrometers
slowing-down time, 5.3.8
Spontaneous fission
delayed neutron yield, 1.4.1
half-lives, 1.6
number of neutrons per fission (ν), 1.5.1, 1.5.2
spectrum, 1.3.1
Stability (reactor)
asymptotic, 5.4.1
autonomous system, 5.4.1
boiling water, feedback model, 5.4.2
boiling water, hydraulic instabilities, 5.4.2
boiling water, natural and forced circulation, 5.4.2
boiling water, transfer function for EBWR, 5.4.2
circulating fuel, 5.4.4
discussion, 5.4.1
EBR-I experiments, 7.3.4
flux-tilt instability, 5.4.2
instability threshold, 5.4.2
linear, 5.4.1
linear feedback, 5.4.1
noise effect, 5.4.2
non-linear, 5.4.1
non-linear feedback, 5.4.1
orbital, 5.4.1
prediction of performance at higher powers, 5.4.2
stochastic instability, 5.4.2
xenon instability, 5.4.3
Stopping cross section
See Range-energy relations for charged particles
Stopping power
See Range-energy relations for charged particles

T

Temperature effects
beryllium oxide experiment on Hot Box, 6.2.3
critical fuel concentration in HRE-1, 3.7.4
critical mass of graphite-U^{235} reactor, 3.7.12
critical parameters in aqueous solutions of UO_2F_2, 3.7.1.1, 3.7.13
diffusion length in hydrogenous mixtures, 3.3.3
diffusion length in water, 3.3.2.1
SPERT-I Reactor, 5.5.2
thermal diffusion constants in beryllium, 3.3.1.2
TREAT Reactor, 3.7.12, 5.5.3
TRIGA Reactor, 5.5.3
water-UO_2 lattices, 4.5.2
Thermal utilization
See also Disadvantage factor
effective value of ηf, 3.6.5
Thermalization
See also Chemical binding and Kernels (thermal scattering)
coefficients for gas model, 3.1.4.2
homogeneous media calculations, 3.1
parameters for aqueous moderators, 3.1.6.1, 3.1.7.1
Thermalization time constants
See Neutrons (pulsed)

Thorium conversion
See Isotope buildup (thorium-uranium chain)
Transfer function
boiling water reactor, 5.4.2
definition, 5.3.3
effect of source, 5.3.6
equations, 5.3.3
magnitude and phase angle without feedback for Pu^{239}, U^{233}, and U^{235}, 5.3.3
Transport mean free path
discussion, 3.3, 3.3.2.2
fission neutrons in heavy water-water mixtures, 3.4.2
thermal neutrons in beryllium, 3.3.1.2
thermal neutrons in diphenyl, 3.3.4
thermal neutrons in Dowtherm A, 3.3.3
thermal neutrons in graphite, 3.3.1.1
thermal neutrons in heavy water, 3.3.1.4
thermal neutrons in hydrogenous moderators, 3.3.3, 3.3.4
thermal neutrons in mixtures of moderators containing absorbers, 3.3.4
thermal neutrons in water, 3.3.2.2
Transport scattering factor $(1-\bar{\mu}_0)$ table, 2.1

W

Westcott's formulation
table of g and s coefficient values, 3.2.2
Wilkin's equation
variational solutions, 3.1.4.4

X

Xenon fission product effect
cross sections, 5.2.1
equations, 5.2.1
instability, 5.4.3
saturation, 5.2.1
shutdown, 5.2.1
step function change in flux, 5.2.1
translation time, 5.2.1
universal xenon curve, 5.2.1
yield, 5.2.1

U.S. GOVERNMENT PRINTING OFFICE : 1963 O—687863